Proceedings of the 37th International Symposium on Automation and Robotics in Construction (ISARC 2020)

From Demonstration to Practical Use
- To New Stage of Construction Robot -

Kitakyushu, Japan, October 27-28, 2020

37th ISARC 2020 Online

International Association for Automation and Robotics in Construction

I.A.A.R.C.

Knowledge and Competence

Kazuyoshi Tateyama
Ritsumeikan University
Japan

Kazuo Ishii
Kyushu Institute of Technology
Japan

Fumihiro Inoue
Shonan Institute of Technology
Japan

ISBN 978-952-94-3634-7

1. Edition 2020

Cover design: Masaharu Moteki

Preface

The 1st International Symposium on Automation and Construction (ISARC) was held at Carnegie Mellon University in Pittsburgh, Pennsylvania, USA in 1984. Since then, ISARC has been held all over the world every year to exchange information about the development and practical use of construction robot technology among industry experts, academic researchers and individuals with novel ideas for all fields of construction, civil and building engineering, machine automation, robotics applications to construction, information technologies, planning, logistics, etc.

ISARC has been held in Japan four times so far, but it has not been held here since 2006, because the momentum for the development of construction robots declined rapidly with the economic downturn around 2000. We were very pleased to learn that we would be able to hold the 37th ISARC in Japan in 2020 after 14 years thanks to the recent increase of momentum in the development of construction robots.

For the symposium, we had planned and prepared to organize not only research presentations, but also key note lectures, technical exhibitions and technical visits related to construction robots in use on the island of Kyushu, in the western part of Japan. Last December, we started a call for papers, and more than 390 abstracts were received from 33 countries.

Unfortunately, the infectious disease caused by COVID-19, which started at the end of last year, quickly spread throughout the world, and many people are still suffering from its effects. We would like to express our heartfelt sympathy to all the people who are in a severe situation, including those who have lost loved ones and/or have been infected by the disease.

There is still no clear end in sight to COVID-19. For this reason, in May of this year, we decided to hold the symposium online and immediately started the preparations for an online symposium. However, we had neither the experience nor the know-how to organize an online international symposium. Therefore, our original plan was not necessarily a very productive one. Under these circumstances, we received tremendous support from the IAARC Board members and were able to hold the online symposium successfully. We would like to extend our sincere gratitude to them for their kindness and great cooperation.

Although the number of submitted papers decreased, due to changes related to an online symposium, we still received 221 full papers from 23 countries. We believe that this symposium was very fruitful in terms of cross-national technical exchange among all the participants.

Finally, I would like to express our deepest gratitude to the members of the Japanese local committee for all the work they did with us in planning and preparing for this symposium. I believe that the efforts of all the people involved in this symposium will greatly contribute to the further evolution of construction robots.

Kazuyoshi Tateyama
Chair, 37th ISARC
Professor, Ritsumeikan University, Japan

Introduction

This publication is the Proceedings of the 37th International Symposium on Automation and Robotics in Construction (ISARC). The symposium was held online during 27-28 October 2020. The Proceedings include an illustrated review of the program, the names of organizations and persons who contributed to the technical program, and the 221 technical papers from 23 countries authored for this international meeting.

The manuscripts were presented during 57 sessions on 3 tracks, among them: automation and robotics, building information modeling (BIM), inspection and monitoring, artificial intelligence and machine learning, construction management, safety and health, data sensing and analysis, mixed Realities (AR/VR), control technology, education, environmental sensing and modeling, human sensing and monitoring, IT supported system, database, big data, lean, logistics, prefabrication, modularization, leaning/AI/recognition, human-computer interaction, measurement, modeling and management, new application field of construction robots and machines, risk management, robot and interface design, and robot construction.

Please note: All ISARC proceedings since 1984 are available at no cost at http://www.iaarc.org.

We are very grateful for the support of so many. Thank you!

Prof. Kazuyoshi Tateyama, Ritsumeikan University, Japan (Chair)
Prof. Kazuo Ishii, Kyushu Institute of Technology, Japan (Co-Chair)
Prof. Fumihiro Inoue, Shonan Institute of Technology, Japan (Co-Chair)

Acknowledgements

Symposium host:	The International Association for Automation and Robotics in Construction
	Japanese Council for Construction Robot Research
Symposium sponsors:	Council for Construction Robot Research
	The International Association for Automation and Robotics in Construction
Symposium co-sponsors:	Advanced Construction Technology Center
	Architectural Institute of Japan
	Japan Robot Association
	Japan Construction Machinery and Construction Association
	Japan Society of Civil Engineers
	City of Kitakyushu
	The Robotics Society of Japan
Symposium cooperation:	The Institute of Electrical Engineers of Japan
	Japan Association of Surveyors
	Japan Association for the Unmanned Construction
	Japan Federation of Construction Contractors
	The Japanese Geotechnical Society
	The Japan Society of Mechanical Engineers
	The Japan Society for Precision Engineering
	Kitakyushu Convention & Visitors Association
	The Society of Instrument and Control Engineers
	Sabo & Landslide Technical Center
	New Unmanned Construction Technology Research Association
	Ritsumeikan University
	The Kajima Foundation
	Rent All Scholarship Foundation
Symposium support:	Ministry of Land, Infrastructure, Transport and Tourism

Local Organizing Committee

Chair	Kazuyoshi Tateyama, Ritsumeikan University, Japan
Co-Chair	Fumihiro Inoue, Shonan Institute of Technology, Japan
Co-Chair	Kazuo Ishii, Kyushu Institute of Technology, Japan

Program committee

Chair	Hisashi Osumi, Chuo University, Japan
Co-Chair	Kazuo Kikawada, Hazama Ando Corporation, Japan
Co-Chair	Fumihiro Inoue, Shonan Institute of Technology, Japan
Co-Chair	Mitsuo Kamesaki, Waseda University, Japan

Award committee

Chair	Miho Makatayama, Building Research Institute, Japan

Publication committee

Chair	Masamitsu Kurisu, Osaka University, Japan

Web-management

Chair	Takaaki Yokoyama, Ritsumeikan University, Japan

International relations

Chair	Hiroshi Furuya, Obayashi Corporation, Japan

Finance

Chair	Hiroki Murakami, IHI Corporation, Japan

Secretary-general

Masaharu Moteki, Advanced Construction Technology Center, Japan

Technical Committee

Tatsuo Arai	The Univ. of Electro-Communications
Mantha Bharadwaj	New York Univ. - Abu Dhabi
Thomas Bock	Technical University Munich
Frederic Bosche	University of Edinburgh
Ioannis Brilakis	University of Cambridge
Alessandro Carbonari	Polytechnic University of Marche
Daniel Castro	Georgia Institute of Technology
Soungho Chae	Kajima Corporation
Hung-Ming Chen	Ntl Taiwan Univ. Science & Tech.
Po-Han Chen	Ntl Taiwan University
Yong Cho	Georgia Institute of Technology
Satoru Doi	Obayashi Corporation
Chen Feng	New York University
Yutaro Fukase	Shimizu Corporation
Hiromitsu Fujii	Chiba Institute of Technology
Hiroshi Furuya	Obayashi Corporation
Borja Garcia de Soto	New York University - Abu Dhabi
Jozef Gasparik	Slovak University of Technology
Quang Ha	University of Technology, Sydney
Daniel Hall	ETH Zurich
Kouji Hamada	Obayashi Corporation
Amin Hammad	Concordia University
Takeshi Hashimoto	Public Works Research Institute
Shigeki Hiraoka	Topcon Corporation
Daehie Hong	Korea University Seoul
Koji Ihara	Asunaro Aoki Construction Co., Ltd.
Ryusei Ikeda	East Nippon Expressway Co., Ltd.
Fumihiro Inoue	Shonan Institute of Technology
Genya Ishigami	Keio University
Kazuo Ishii	Kyushu Institute of Technology
Fumio Itoh	Japan Construction Machinery and Construction Association
Yonghoon Ji	Japan Advanced Inst. Science & Tech.
Vineet Kamat	The University of Michigan
Mitsuhiro Kamezaki	Waseda University
Kazuito Kamiyama	Takenaka Corporation
Kazuya Kikawada	Hazama Ando Corporation
Huoungkwan Kim	Yonsei University
Shigeo Kitahara	Kumagai Gumi Co., Ltd.
Taizo Kobayashi	Ritsumeikan University
Markus König	University of Bochum
Masamitsu Kurisu	Osaka University
Soonwook Kwon	Sungkyunkwan University
Junbok Lee	Kyung Hee University
Nan Li	Tsinghua University
Miho Makatayama	Building Research Institute
Leonardo Messi	Polytechnic Univ. of Marche
Naoki Mori	Taisei Corporation
Masaharu Moteki	Advanced Construction Technology Center
Hiroki Murakami	IHI Corporation
Keiji Nagatani	The University of Tokyo
Satoshi Nakamura	Tokyu Construction
Takahiro Nakamura	Kajima Corporation
Tadashi Narise	Maeda Corporation
Yasutoshi Nomura	Ritsumeikan University
Ken Ooi	Komatsu Ltd.
Makoto Oshio	Kajima Corporation
Hisashi Osumi	Chuo University
Benny Raphael	I.I.T. Madras
Saiedeh Razavi	McMaster University
Kazuyuki Sano	Taisei Corporation
Anoop Sattineni	Auburn University
Isaac Shabtai	Israel Institute of Technology
Yasuyuki Shingu	Shimizu Corporation
Shinya Suzuki	Toda Corporation
Piotr Szynkarczyk	Industrial Research Institute for Autom. & Measurement
Hiroki Takabayashi	aT ROBOTICS Inc.
Manabu Takeishi	Hazama Ando Corporation
Toshinari Tanaka	Port & Airport Research Inst.
Jochen Teizer	University of Bochum
Yelda Turkan	Oregon State University
Takao Ueno	Tokyu Construction
Kazunori Umeda	Chuo University
Tomohiro Umetani	Konan University
Enrique Valero	University of Edinburgh
Frans van Gassel	Eindhoven Univ. of Technology
Koshy Varghese	I.I.T. Madras
Józef Wrona	Wajskova Technical Academia
Hiroshi Yamamoto	Komatsu Ltd.
Shinya Yamamoto	Shimizu Corporation
Takaaki Yokoyama	Ritsumeikan University
Zhenhua Zhu	Wisconsin University

Program Schedule

JST*	Tuesday October 27	Wednesday October 28
08:00 – 13:00	Opening Ceremony *Tucker-Hasegawa 2020 Award Keynote Lecture* Academic Presentations	Academic Presentations
14:00 – 15:00	Keynote2	Keynote3
15:00 – 19:00	Academic Presentations	Academic Presentations Award and Closing Ceremony
20:00 – 23:00	Academic Presentations	

*Japan Standard Time

Keynote

Tucker-Hasegawa 2020 Award Keynote Lecture

Hyoungkwan KIM

Professor at Yonsei University, Korea

Smart Safety Assurance for Temporary Structures

Temporary structures on construction sites has been the major cause of worker fatalities. According to a Korean statistics report, about 300 people are losing precious lives each year due to accidents involving temporary structures. A new research program was launched this year to develop a smart safety assurance system that recognizes, evaluates, and predicts accident risks that may occur during the installation, dismantling, and operation of temporary structures. It is a part of the smart construction initiative sponsored by the Korean Ministry of Land, Infrastructure, and Transport, and the Korea Agency for Infrastructure Technology Advancement. The program was designed for developing technologies such as deep learning-based hazard identification, augmented reality-based risk warning, and smart mobility for intelligent sensing of construction sites, with a total budget of ₩12.5 billion ($10.5 million) over six years. The program has a clear goal of reducing the number of accidents related to temporary structures by more than 25% through the creation of a new construction culture, safety-related policies, and safety-related industries.

Speaker profile:

Hyoungkwan KIM, Ph.D. is a Professor of the School of Civil and Environmental Engineering at Yonsei University, Korea. His areas of research include construction automation, infrastructure adaptation to climate change, and project finance. He is the principal investigator of a $10.5 million research program titled “Smart Safety Assurance for Temporary Structures,” which is a part of smart construction initiative sponsored by the Korean Ministry of Land, Infrastructure, and Transport, and the Korea Agency for Infrastructure Technology and Advancement. He serves as Vice- President for the International Association for Automation and Robotics in Construction (IAARC), and Associate Editor for Journal of Computing in Civil Engineering, American Society of Civil Engineers (ASCE). He also served as Secretary General for Association for Engineering Education in Southeast Asia and the Pacific (AEESEAP). He has received six excellent teaching awards and an excellent research award from Yonsei University. More information on Prof. Kim can be found at: http://aim.yonsei.ac.kr.

Keynote 2

Naoki SATO

Director of the Space Exploration System Technology Unit, The Japan Aerospace Exploration Agency (JAXA), JAXA Space Exploration Center (JSEC), Japan

International Space Exploration and Japanese Lunar Activities

JAXA is engaged in international collaborations to tackle the challenge of human and robotic exploration missions in and beyond low-Earth orbit (LEO). The current focus is exploration missions to the Moon and Mars, targeting future human activities. His presentation introduced Japan's current exploration activities and JAXA's future plans and studies beyond the Earth orbit with the context of international coordination. Especially for the lunar surface activities, the concept study of the lunar base construction, which JAXA had conducted with a group of construction-related companies across Japan, was introduced along with the technological development.

Speaker profile:

Naoki SATO graduated from the Aeronautics Engineering Department, Kyusyu University in 1986, and gained a master degree of applied engineering of Kyusyu University in 1988. In the same year, he entered the National Space Development Agency of Japan (predecessor of JAXA). From 1990 he had been involved in the International Space Station program for about 16 years. Afterwards, he has been working for the international space exploration program formulation. Since April 2018 he is the current ISECG chair and since July 2018 he was assigned as the Director of the Space Exploration System Technology Unit of JAXA Space Exploration Center (JSEC).

Keynote 3

Yasushi NITTA

Director for Construction Equipment and Safety Planning Office, Policy Bureau, Ministry of Land, Infrastructure, Transport and Tourism, Japan

Initiatives for Robot Introduction in Japanese Public Works

The Japanese society faces various social issues such as frequent occurrences of earthquakes, eruption of volcanoes, floods, landslides, etc., resulting in the deterioration of the infrastructure. Japan also sees a reduction of the working population in the construction industry. In his speech, he introduced initiatives for the social implementation of robots and information and communication technologies in the Japanese construction industry, including the Ministry of Land, Infrastructure, Transport and Tourism (MLIT).

Speaker profile:

After graduating from University of Tsukuba in 1994, Dr. Yasushi NITTA joined the Ministry of Land, Infrastructure, Transport and Tourism (MLIT). There he is widely engaged in policy planning, public works and R&D in the various departments, such as MLIT Headquarters, Regional Development Bureau, National Road Office, National Research Institutes (PWRI, NILIM), Advanced Construction Technology Center (ACTEC). He is especially responsible for the planning and operation of on-site verification projects to promote the introduction of robots to the infrastructure department, development/deployment/budgeting/operation of disaster

countermeasure machines, and nationwide deployment of machine construction (i-Construction) using 3D data. Dr. NITTA is also engaged in establishing technical standards for the purpose, demonstrating ultra-long-distance unmanned construction technology, and flood control as an international emergency relief team.

Video list

Construction robots in Japan

1. **Sea Experiment on Tele-operation System of Underwater Excavator**
   National Institute of Maritime, Port and Aviation Technology,
   Port and Airport Research Institute,
   Infrastructure Digital Transformation Engineering Department
2. **Development of Heavy Carrier Robot for Shallow Water Area**
   New Unmanned Construction Technology Research Association
3. **Tunnel RemOS-WL**
   Kanamoto Co., Ltd.
4. **kana Robo – Robo-Construction System –**
   Kanamoto Co., Ltd.
5. **kana Robo – Robo-Construction System 2 –**
   Kanamoto Co., Ltd.
6. **ROBO CONSTRUCTION – DokaBOri Training –**
   Fujiken Co,Ltd.
7. **"A4CSEL" at the Seisho Test and Practice Field**
   KAJIMA CORPORATION
8. **Pursuing "Zero Ground Subsidence" in Shield Tunneling**
   TAC Corporation
9. **Automatic Dam Concrete Placing System**
   SHIMIZU CORPORATION
10. **Automatic Tunnel Lining Concrete Placing System**
    SHIMIZU CORPORATION
11. **A robot that assists in plotting**
    SHIMIZU CORPORATION
12. **Development of IT construction system by Robot**
    Public Works Research Institute
13. **Demonstration of autonomous excavation, loading and unmanned bulldozer. (CEATEC2018)**
    Komatsu Ltd., Office of CTO
14. **Smart Construction Concept, Future image. (CEATEC2018)**
    Komatsu Ltd., Office of CTO
15. **BE A HERO, Future image**
    Komatsu Ltd., Office of CTO
16. **DEEP CRAWLER - Crawler type ROV**
    WAKACHIKU CONSTRUCTION Co., Ltd.
17. **What is dredging? - A job that protects the safety of the sea**
    WAKACHIKU CONSTRUCTION Co., Ltd.
18. **Robotic rubble-mound mechanized construction system**
    PENTA-OCEAN CONSTRUCTION CO., LTD.
19. **Rotation Control Device for Lifting Cargo**
    WAKACHIKU CONSTRUCTION Co., Ltd.
20. **Automatic operation system of the construction machine (Vibrating roller・Bulldozer)**
    HAZAMA ANDO CORPORATION

Table of Contents

Improving Construction Demonstrations by Integrating BIM, UAV, and VR

K. C. Wang[a], R. J. Gao[a], S. H. Tung[a] and Y. H. Chou[a]

[a]Department of Construction Engineering, Chaoyang University of Technology, Taiwan
E-mail: wkc@cyut.edu.tw, a0988554148@gmail.com, s10811614@gm.cyut.edu.tw, a36153615@gmail.com

Abstract –

In recent years, building information modeling (BIM) has been widely used to create animated simulations for engineering demonstrations. On-site engineers often employ animations generated using a BIM system to explain the current project status to their managers, so that the managers can grasp the actual project status. However, the fidelity of the terrain models built using BIM is relatively low, and the modeling process is labor-intensive. These factors negate the advantages of BIM. To overcome these problems, in this study, images of an engineering site are captured using Unmanned Aerial Vehicle and are subsequently used to generate a landscape terrain model of the area surrounding the engineering site by means of image comparison and GPS positioning techniques. The terrain model and the BIM main simulation model are integrated to present the actual site condition. In addition, to further enhance the realism of the integrated model, this study introduces the integrated model into the virtual reality (VR) environment to present the construction site. The manager can check the construction progress of the project easily without having to visit the project site.

To test the feasibility of the proposed method, it is applied to a bridge construction project. The results indicate that the aerial photos captured using Unmanned Aerial Vehicle can be converted into point cloud models and mesh segmentation models. Both types of models can be imported and integrated into BIM software. However, if other renderings (such as Lumion) or VR software (such as Fuzor) are to be used for further animation production, the photos captured using Unmanned Aerial Vehicle can only be converted into mesh segmentation models before importing them for use in subsequent applications.

Keywords –

Building Information Modeling; Unmanned Aerial Vehicle; Virtual Reality, Construction Demonstrations

1 Introduction

Building information models (BIM) have been increasingly adopted to enable construction project presentations through animated simulations. On-site construction projects are usually modeled using BIM with animations to intuitively display the expected final product of a project to managers, allowing managers to understand and manage project progress.

The applications of BIM has also been extended in addition to its common use in animation and four-dimensional simulations[1,2,3]. To achieve satisfactory BIM presentations, using BIM, engineers build a model of the construction site in question and combine it with another model that simulates the surrounding area. However, BIM-simulated terrain models are usually inaccurate, and their construction incurs considerable financial and labor costs, consequently reducing the benefits of BIM displays.

Recently, the rapid advancement of unmanned aerial vehicles (UAV) has enabled the industry and academia in Taiwan to integrate aerial photography with aerial photogrammetry software to create three-dimensional (3D) models[4,5,6]. Numerous studies have proposed route planning suggestions for UAV used in modeling and aerial photography[6]. However, several questions remain unanswered regarding integration between UAV imagery and BIM, including differences between various aerial photogrammetry software programs, UAV 3D modeling procedures, and approaches to integrating UAV 3D models with BIM.

Instead of selecting commercially available UAV photogrammetry software (e.g., Altizure and Contextcapture), this study built models of the project site and its surrounding area simply by using Pix4D and Recap. Subsequently, the constructed terrain model was incorporated into BIM software. The resultant model accurately displayed the actual on-site conditions; different software programs were imported into the model to verify its rendering feasibility.

2 Literature Review

2.1 Display of BIM animation and virtual reality environments

Conventional two dimensional and 3D modeling methods fail to comprehensively display a building. No existing BIM software program can accurately reflect the actual materials or establish a complete 3D scene. Generally, a 3D scene comprises streets, surrounding buildings, cars, pedestrians, trees, and animations. The use of rendering on a virtual scene, which can be realized through a combination of walkthroughs and virtual reality (VR) technologies, creates a realistic scene that offers immersive user experiences [7].

Scholars have incorporated BIM animation into VR in practice; for example, Hu and Wang [8] integrated a tunnel BIM, collision parameters, and remote-control car models with VR to create a third-person VR walkthrough.

2.2 UAV image-based 3D models

UAV photogrammetry 3D models have often been combined with BIM models.Wen et al [4] adopted UAV and augmented reality technologies to construct BIM models. They used a UAV to obtain images of surroundings and established real-time augmented reality markers in a positioning system, after which a BIM model was imported to allow the UAV to instantly combine the BIM with its surrounding area as it flew.

Karachaliou et al [5] preserved cultural heritage buildings by integrating UAV technologies with BIM. Specifically, they obtained indoor data of the target building by integrating a UAV-generated external model with laser scanning and photogrammetry. Next, a BIM was constructed using Autodesk Revit. Through this approach, Karachaliou et al. [5] effectively recorded cultural heritage buildings with complex scales or forms in a museum.

Comparing a conventional model with a UAV imagery-constructed model, Liu [6] discovered that the construction of a conventional environment model involved complex measurement procedures; by contrast, measurements and geographic data can be simultaneously obtained, with the flight route determined, as UAV images were captured. Additionally, UAV can capture images of hazardous regions where human cannot approach and accurately reveal the surrounding terrain.

Researchers of most UAV studies have recognized that UAV-constructed 3D models more accurately present an environment than conventional models do. However, researchers have rarely discussed the overall process of combining UAV imagery with BIM and the subsequent application of rendering software for animation production.

3 Method of integrating BIM, UAV, and VR

This study integrated BIM with UAV and VR technologies to facilitate the presentation and simulation of construction projects; the procedures are presented in Figure 1. UAV images were used to construct 3D models through the separate application of two UAV photogrammetry software programs (i.e., Recap and Pix4D). Subsequently, CloudCompare was used to crop and export a point cloud model with triangle meshes. The exported model was merged with a BIM model, after which Lumion and VR software were run to perform rendering and make animations.

This process is detailed in six subsections, namely “BIM model,” “Aerial 3D model construction using Pix4D,” “Aerial 3D model construction using Recap,” “Point cloud models cropping,” “Integration of aerial 3D models with the BIM,” and “Rendering and animation production.”

3.1 BIM construction

The BIM of a bridge was constructed before being combined with UAV images. This bridge model encompasses basic components including piers, roads, pylons, and steel cables. However, numerous parts of the bridge cannot be established using basic components separately such as pillars, beams, boards, or walls. Therefore, these parts were constructed using grouped components and later integrated into the project.

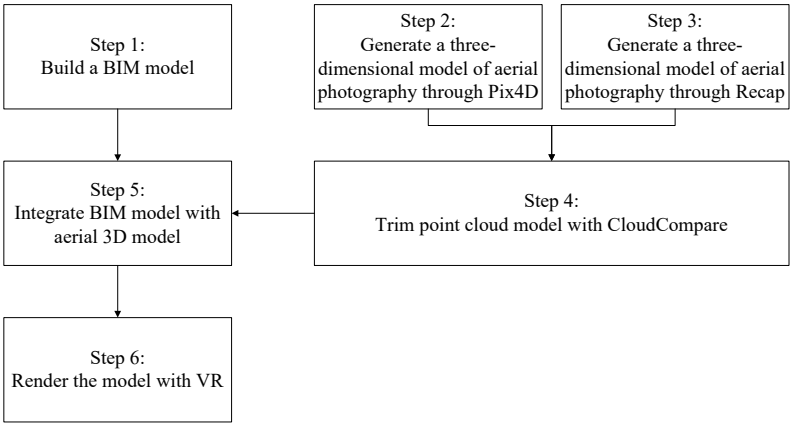

Figure 1. Architecture of integrating of BIM and 3D model

3.2 Aerial 3D model construction using Pix4D

As an aerial photogrammetry software suite, Pix4D can locate UAV-captured images on a coordinate system. After images were imported, this study set the imaging parameters to produce a point cloud model and 3D model.

3.3 Aerial 3D model construction using Recap

Recap is another point cloud processing software program. UAV-captured images were first imported into the software program before a point cloud model was generated using the built-in global positioning system. Furthermore, because Recap is developed by Autodesk, it is more compatible with BIM software than Pix4D is.

3.4 Point cloud model cropping

This study used CloudCompare to crop the 3D models established using Pix4D and Recap. When empty areas are present in the background, CloudCompare allows users to select a few point clouds of the surrounding terrain and fill in these areas through stitching. The software program also hides the area that requires no cropping, making the cropping process easier.

3.5 Integration of aerial 3D models with the BIM

Aerial 3D models must be accurately merged with the BIM model, during which time a point cloud model should be imported into Revit. Currently, only Recap-produced point clouds are compatible with Revit. Because manually aligning the point clouds with the host model does not provide sufficient accuracy, this study redefined the host model position in the Revit project by setting the project base points. This study also relocated the Recap origin to the target position where the point cloud was to be combined the BIM.

The integrated model can be exported to various formats according to different needs. An advantage of combining point cloud data with a host BIM on Revit is that existing BIM software programs can directly import the integrated model into rendering software by using Revit plug-ins. Moreover, these software programs enable simultaneous model revision and rendering as well as the production of animation or a VR display.

3.6 Rendering and animation production

If the integrated model is displayed in a walkthrough on Revit, the fidelity to the terrains and on-site conditions may is inadequate. To improve the fidelity of the terrain model and host BIM, this study displayed the models using Fuzor.

4 Case study

This case study was of a bridge construction project in central Taiwan. In the following subsections, this study describe the construction of a terrain model based on UAV images and its integration with a host model. This study discuss the process by which the fidelity of the integrated model was improved by using rendering software.

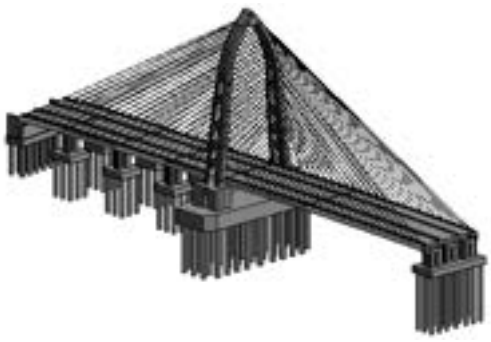

Figure 2. BIM model of case study

4.1 BIM of the bridge

The BIM of a cable-stayed bridge was established. As mentioned, bridges cannot be drawn with basic components used in drawing housing structures, which are composed of pillars, beams, boards, and walls. Therefore, this study divided the bridge into piers, roads, pylons, and cables and built each family components respectively.

4.2 Aerial 3D modeling on Pix4D

On-site images taken by the UAV were imported into Pix4D for 3D modeling in the following four steps:

1. Image importing: The UAV captured on-site orthophotos, oblique photos, and panoramic photos. These photos were then imported into a Pix4D project.
2. Image parameter settings: Image parameters were set after importing was conducted. Because the UAV simultaneously took pictures and recorded their coordinates, the coordinates were already stored in Pix4D in the image importing process. Accordingly, the World Geodetic System 84 (WGS84) was selected in the coordinate system; the coordinate unit was set to m, and the edited coordinate data were directly exported (Figure 3).

Figure 3. Image parameter settings

3. Point cloud modeling: After 3D modeling was completed, the photography methods were set to orthophotography and oblique photography. A point cloud model was then generated, after which two options were available, namely “export the point cloud” and “export the triangle mesh” (Figure 4).

Figure 4. Modeling method settings

4. Exporting the point cloud to CloudCompare: When the terrain in question is vast, the resulted point cloud can be susceptible to the Earth’s curvature and becomes imprecise. To avoid such a problem, repeat Step 3 several times to generate a point cloud and cropped and stitched it using CloudCompare to better reflect the actual terrain.

4.3 Aerial 3D modeling on Recap

On-site images taken by the UAV were imported into Recap for 3D modeling in the following four steps:

1. Photography mode setting: When creating a new project, the user must choose either the “Object” (for general objects) or “Aerial” (for terrains) photography mode for 3D modeling. Because terrain photos were taken by a UAV, “create 3D aerial” was selected to construct a 3D terrain model (Figure 5).

Figure 5. Selecting the Aerial mode

2. Image importing and coordinate settings: To create a 3D terrain model, images were imported (Figure 6);

subsequently, coordinates can be set for the imported images. Notably, our UAV already attached coordinates to images it captured. Consequently, this study only had to choose the coordinate system of the target location (WGS84) when setting coordinates for the project.

3. Point clouds generation: In this step, a point cloud model was constructed. When the model is being exported, .rcp or .rcs formats can be selected to facilitate the subsequent combination with the Revit host model.
4. Point cloud exporting to CloudCompare: Although point cloud clipping and deleting is allowed on Recap, this software focuses on point cloud creation. To obtain an accurate point cloud, this study used CloudCompare to clean up the point cloud, whereby the point cloud model was cropped and modified.

4.4 Point cloud cropping

This study cropped and modified point clouds using CloudCompare to facilitate the subsequent display of an integrated host model. Because the point cloud failed to present vegetation realistically, such parts in the point cloud was cropped out. However, such practice resulted in empty areas in the model (Figure 7); therefore, nearby point clouds were used to perform stitching and fill in these empty areas. When each area is being filled in, at least three base points must be selected, after which the software automatically aligned the clouds with corresponding areas to complete the stitching (Figure 8). The stitching area between the point cloud model and host model was also modified so that other software programs could be used subsequently to more realistically present vegetation.

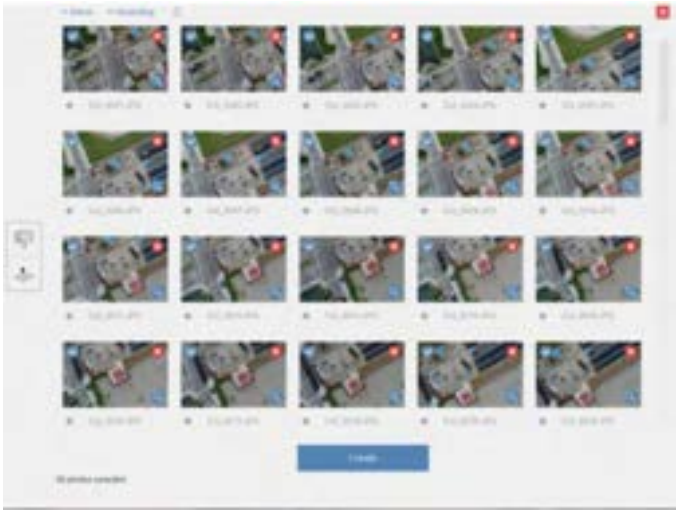

Figure 6. Terrain image importing

Figure 7. Comparison between uncropped and cropped terrain point clouds

Figure 8. Filling up the empty areas

4.5 Integration of the aerial 3D models with the BIM

In this study, the host model of the bridge was built using Autodesk Revit. The aforementioned point cloud 3D model was imported into Revit to merge it with the host model. However, the point cloud exported using Pix4D was incompatible with Revit. Therefore, this study used the origin-updating command in Recap to relocate the origin in the stitching area (Figure 9). By updating the project base points, this study moved the bridge model origin in the stitching area to align the point cloud model origin with the host model origin. When the cloud point was being imported, the option "Origin to Origin" was selected to facilitate the precise combination of the two models, as illustrated in Figure 10.

Figure 9. Updating the origin of the point cloud model

Figure 10. Integration of the point cloud model with the host model

4.6 Rendering and animation production

To further enhance the fidelity of the terrain model and BIM, this study displayed the model using a VR software program termed Fuzor. After the terrain model was merged with the BIM, a plug-in was employed to convert the integrated model for use on Fuzor, whereby the model can be instantly modified and synchronized with Fuzor models. Fuzor were then used to add elements such as trees, cars, and pedestrians in the model. Finally, rendering was implemented and landscape elements were added to create a complete and realistic scene. Subsequently, walkthrough animations or VR environments, which provides immersive experiences,

may be created using Fuzor, allowing users to better understand the project status.

5 Conclusion

This study was of a bridge construction project in central Taiwan. In the following subsections, this study describe the construction of a terrain model based on UAV images and its integration with a host model. This study discuss the process by which the fidelity of the integrated model was improved by using rendering software.

5.1 Comparison of terrain modeling procedures

According to the comparison between terrain modeling procedures in Pix4D and those in Recap, the following advantages and drawbacks were determined.

1. Pix4D terrain modeling
   (1) The triangle mesh is delicate: After generating the point cloud on Pix4D, the user can reduce the size of each triangle by adjusting related parameters. Therefore, the exported triangle mesh is more delicate, contributing to a better visual effect during animation display.
   (2) The point cloud is complete: After the UAV-captured terrain images are imported, the point cloud generated by Pix4D is not affected by overlap rate, allowing researchers to create a point cloud model. By contrast, in Recap, a point cloud model cannot be generated if the overlap rate is low.
2. Recap terrain modeling
   (1) Higher compatibility with BIM software programs: Because Recap was developed by Autodesk, the Recap-derived point cloud is compatible with other Autodesk-developed BIM software programs. By contrast, the Pix4D-constructed point cloud must be converted into a compatible format using Recap before being integrated with a Revit model.
   (2) Ability to redefinition the origin: After creating a point cloud model, Recap can update its origin, allowing the model to be accurately merged with a host BIM. By contrast, Pix4D does not have this origin-updating feature.

5.2 Rendering and animation production

After the terrain model and host BIM are integrated, Lumion and Fuzor may be more suitable options for model rendering and animation display compared with Enscape, which fails to display a terrain model when the model is imported. To use the coordinate alignment function on Lumion, the host BIM and point cloud must be exported to the .fbx format and a triangle mesh, respectively. By contrast, Fuzor can simultaneously display terrain models without changing the file format.

After the fidelity of the terrain and host BIM is improved, the models are ready for animation production and VR environment import. The use of VR technology to present the construction site can provide an immersive experience, enabling users to clearly preview the expected final product and monitor construction progress. The strengths of Fuzor are further demonstrated through its functions of five-dimensional display of construction simulation, conflict detection, and animation production.

References

[1] Li K.F, Analyzing scheduling activities based on BIM models,National Central University Graduate Institute of Construction Engineering and Management Thesis,2014.

[2] Lin Z.H, Using Ontology and BIM to Coordinate Trades of the Interior Renovation Project,National Cheng Kung University Department of Civil Engineering Thesis,2016.

[3] Hsu C.W, 4D Automatic Scheduling in High-Tech Facility Construction,National Taiwan University Department of Civil Engineering Thesis,2016.

[4] Wen M.Z, Lai J.S, Han J.Y, Chang W.Y, Liu Y.C, Kang S.C, Hsieh C.T, Tan Y.C, Huang C.C, Lee F.Z, Lin Y.T Lin Franco, Chang R.T, Application Of UAV Imaging Technology To River Flood Simulation, Journal of the Chinese Institute of Civil & Hydraulic Engineering,Volume27,Issue3,Page 231-240,2015.

[5] Karachaliou E, Georgiou E, Psaltis D, Stylianidis E, UAV FOR MAPPING HISTORIC BUILDINGS: FROM 3D MODELLING TO BIM, 8th Intl. Workshop 3D-ARCH "3D Virtual Reconstruction and Visualization of Complex Architectures",2019.

[6] Liu T.Y, Application of Unmanned Aerial Vehicle on Image Analysis of Landscape Survey,National Chung Hsing University Program of Landscape & Recreation Thesis,2018.

[7] Li S and Wang J, Research on integrated application of virtual reality technology based on BIM, 2016 Chinese Control and Decision Conference (CCDC),2016

[8] Hu M and Wang Y, Research on Urban Tunnel Lifecycle Management Based on BIM, 2SHU-UTS SILC Business School, Shanghai University, Shanghai, China, 2016 3rd International Conference on Economics and Management,2016.

Using Virtual Reality and Augmented Reality for Presale House Customer Change

Ouedraogo Ben Amed[a], Li-Chuan Lien[a], Unurjargal Dolgorsuren[a], Yan-Ni Liu[b]

[a]Department of Civil Engineering, Chung Yuan Christian University, Taoyuan, Taiwan.
[b]Create Your Worth Technology, Ltd
E-mail: lclien@cycu.edu.tw, cywtcgs@gmail.com

Abstract –

Using Building Information Modeling (BIM) technology, a unique virtual model of a project can be created, which will allow all parties involved in the design process of project members (owners, architects, engineers, contractors, sub-contractors and suppliers) to collaborate more precisely and more effectively than using traditional processes. The collaboration of the different parties must be linked by a functional system with the presence of software, the team members constantly refine and adjust their portions according to the project specifications and design modifications to guarantee that the model is as precise. Augmented Reality (AR) in turn can bridge the cognitive gap between pre-sale products and real products. Although the presence of Augmented Reality (AR) and Virtual Reality (VR) is necessary, it is necessary to establish a system that directly connects AR, VR, the company, clients, investors and various construction documents. This VR system will be used in the functions of the pre-sale houses between companies, owners and investors. The project that will be used for this study is a building of five floors and two basement located in the District of Zhonghe in Taiwan. As the result showed, for the presentation of the presale house, the technique of the Event-Driven Process Chain (EPC) diagram is used including the import and export of several files. In addition the diagram system gives customers the opportunity to make changes regarding materials, design and time liner in future construction. These different changes made by the customers and approved by the company will generate consequences for the initial contract drawn up by the company. The software Fuzor to ensure the realization of the VR and AR while maintaining a concordance of the different stages of the diagram. To satisfy the requests of the ownership of, the project price and timing, Navisworks and Revit have also allowed the good management of the project. The EPC diagram will have two alternatives, the first alternative will be proposed by the company according to the demand on the market. Then follow the second alternative, this will be the new proposals suggested by the customers after consulting the proposals of the company using VR and AR. At the end of these various changes by the EPC system the prices of materials, other design, the implication of equipment, labor, materials and subcontractors will be updated according to the proposal of the owner.

Keywords –

Augmented Reality (AR); Virtual Reality (VR); Presale House; Building Information Modeling (BIM); Event-driven Process Chain (EPC) concept.

1. Introduction

In the 1960s, rapid economic development in several Asian countries, including Taiwan, Hong Kong, China, Singapore, South Korea, Indonesia and Malaysia, led to an explosion in demand for housing in several major cities. This growth in housing demand also reflected the economic status of these countries [1]. The solution to this growing demand, a unique and innovative presale housing system was developed, and has been adopted and developed since then. These house pre-sales refer to the contractual sales of housing before the construction of the construction project, i.e. the management companies design a building and start to build or before construction try to make offers to customers for the purchase of their houses. With this system, companies can receive pre-contracts which will allow them to finance future construction. Some customers in order to guarantee a good future for their families will be interested, the pre-sale accommodation can be purchased at a reduced price and they acquire property rights in advance. In addition, home buyers can participate in and oversee the advancement through the VR and AR of the housing project to secure their property rights at the end of the project, and even make proposals during construction [1]. Use to gain customer trust. This requires creating beautiful reception centers and hiring professional real estate sales agents. This

strategy requires a lot of expense, which is a major drawback for companies. Through architectural models, a plan for implementing 3D product perspectives and models coupled with examples of housing, the companies are trying to improve the understanding of investors and customers to stimulate purchase intention. Many customers are dissatisfied after the construction of their infrastructure works, most of these problems are due to the fact that the owner does not really know what his project will look like after construction and the delay in construction. To solve this problem new technique have been developed in this study [2].

2. Presale house presentation

2.1 Research content

The concept of the Event-driven Process Chain (EPC) diagram will be used for the presentation of the presale house.

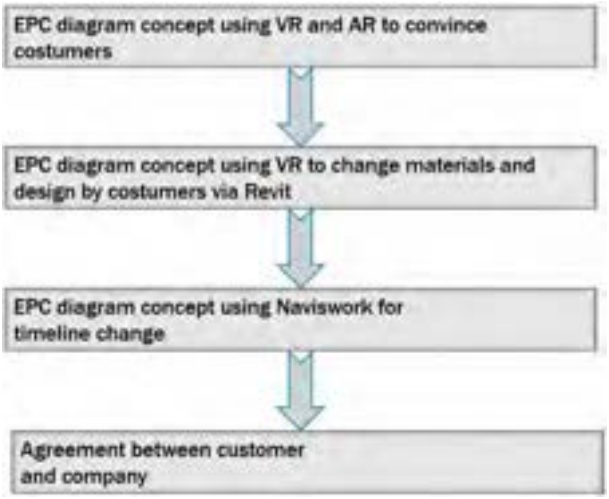

Figure 2.1. Work process

This diagram highlights an intersecting connection between the different parts of the construction. The objective is to convince the owner or investors to buy or place an order before finalizing the construction.

2.2 Diagram of the presale house presentation

In this study for a good presentation and convincing of the presale house, the concept EPC was used. The EPC is a flowchart for business process modeling for product management through multiple partners. EPC can be used to configure company resource planning execution with the aim of structuring all the details in time and in their place, and for business process improvement. Used to control an autonomous workflow instance in work sharing represent in Figure 2.2.

In this study Events are passive elements in event-driven process chains. That event describes under what circumstances a function or a process works or which state a function (Navisworks, Revit, Fuzor) or a process results in. Then the function described below.

Figure 2.2. Event-driven Process Chain

The function of the figures used:

- Event and result event
- Information: output and input documents
- Function
- Supporting system
- Organizational unit type

Figure 2.3 explains the strategies implemented to present the 3D model by the company to the owners. This strategy involves the creation of a 3D animation of the project from the Revit file.

The experimentation is based on a construction project in the district of zhonghe. The project comprises a building of five (5) floors and two bases for habitation. The building will be built in a residential area. The two bases will be used for parking. This experiment will focus on the project information.

In this study the responsibility is to convince the customers or investors to buy or rent the room (building) during or before the construction phase. To convince customers or investors several ideas has been established in which softwires and new technologies will be use.

Owner of the entire building: The whole building belongs to a single structure and all decisions will be specific to these people.

Inspection by Virtual Reality: Step1 owners order to company using Fuzor

In this first step the company uses Fuzor software for a complete presentation of the building to the owners. This presentation concerns the exterior and interior designs. This function will obviously need supporting systems and information (input documents function). This is how the second and the third step, which are respectively construction type to the company, Step2 and Virtual view to the company Step3, will take

place.

In Step 3 the first presentation will be done by VR BOX headset. This involves the use of the Fuzor application on smart phone. First use the Fuzor software to output the construction file in FZM format, then transfer it to the smart phone, then open the file using the Fuzor application. The owner can start to see the virtual view of his future home. The Fuzor 3D view, the company will use the synchronization system from the Revit software to open the project.

This synchronization system is very important because it will facilitate the work when the owner will make a decision regarding a change. After the synchronization the file of the project will be opened on Fuzor.

For the good vision of the project, the environment in which the project will be implemented will be presented to the owner with the presence of his future building. This presentation will be done by Mixed Reality (MR) [4]. The 3D photo model (presented in Figure 2.4 and 2.5) of the construction environment produced by the Bentley contextcapture software which was the subject of the first part of this study.

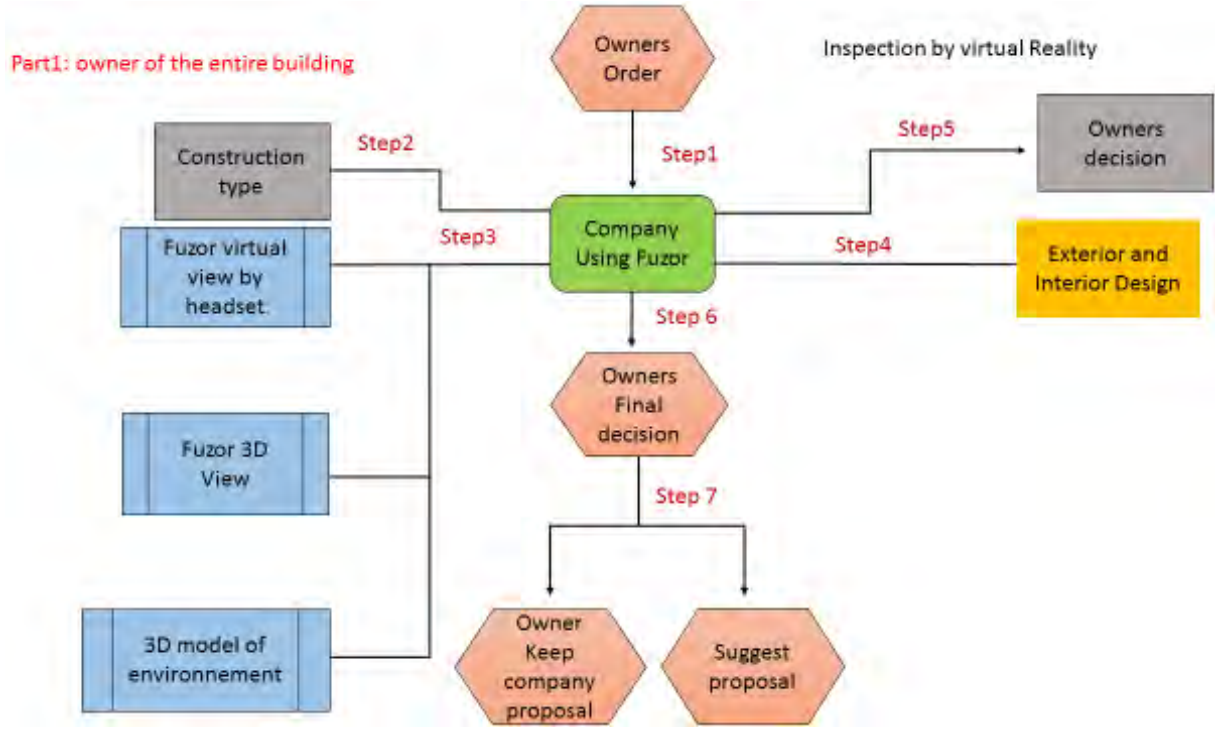

Figure 2.3. Inspection by Virtual Reality

Figure 2.4.3D photo model Augmented Reality1

Figure 2.5.3D photo model Augmented Reality2

For this fact the 3Dmax software will be used, initially the two files will be input in the software 3Dmax namely the format FBX coming from Bentley context capture and the format FBX of the construction coming from Fuzor. In the 3DMax software the 3D model of the construction will be positioned exactly in the space dedicated to the implementation of the project, this is illustrated in Figure 2.6 [5].

MR shows in Figure 2.6 technology allow real and virtual elements to interact with one another and the user to interact with virtual elements like owners viewing their construction in real world. How does MR work? There must be an MR device, either a headset or translucent glasses, in this VR BOX study was used to create the experience [6].

Figure 2.6. Mixed Reality

Using much more processing power than VR, Augmented Reality (AR) and AR technology connects the virtual and real worlds in a single connected experience like combining two visions into one using visual / gesture recognition technology / voice via headset or a pair of motion controllers. In this project, the mixed product was used to introduce the owner to the environment of his new construction. To allow him to understand the situation in which his future building will be presented. Since AR maintains a connection with the real world, it is not considered as a completely immersive experience [7]. In a MR environment, wherever user go and watch when he wear MR technology, the 3D content allow him to meet in space will react in the same way as in the real world under these conditions the owners are assured of see their construction in a real and precise event. In this example study, an object will approach the owner when it changes movement, the object will approach and interact with it [8].

Step 4 will be the subject of the design, i.e. the exterior and interior design. This will be about what types of materials to use.

Step 5 represents an output of the files used in the different software from the information received beforehand for the development of the project.

After submitting the details of the project to the owners, Step 6 will be the owner's decision. The decision of the owner will either keep the proposal of the company or give his own suggestions to change the design, Step 7 shows. If the owner decides to make changes this leads to called Change in Materials and Prices.

3. Change in materials and prices

3.1 The cost of the materials of the structure:

Construction materials are priced by weight or number that of structural steel is normally priced by weight, so it is important to have a clear idea of the structural sections that will be used and the meaning of the lettering of each section to establish an accurate estimate [9].

These structural sections are already chosen according to the construction model established beforehand by the company as shown in Figure 3.1.

Type	Diameter / mm	Pipe cost / $/m	Installation cost / $/m	Total cost / $/m
PVC-1075	75	6,47	12,53	19
PVC-10110	110	11,91	13,5	25,41
PVC-10140	140	18,32	14,34	32,66
PVC-10200	200	30,66	16,11	46,77
PVC-10315	315	60,2	19,74	79,94
PVC-10400	400	95,3	22,64	117,94
HDPE-1075	75	8,85	12,53	21,38
HDPE-10110	110	15,1	13,5	28,6
HDPE-10140	140	20,9	14,34	35,24
HDPE-10200	200	36,69	16,11	52,8
HDPE-10315	315	75,52	19,74	95,26
HDPE-10400	400	119,4	22,64	142,04
HDPE-101000	1000	771,13	57,73	828,86
STEEL75	76	46,74	12,56	59,3
STEEL110	110	53,11	13,27	66,38
STEEL160	160	77,12	14,69	91,81
STEEL200	200	96,51	16,2	112,71
STEEL315	315	139,36	19,84	159,2
STEEL400	400	177,18	23,37	200,55
STEEL1000	1000	405,47	58,71	464,18

Figure 3.1.MEP materials cost

3.2 The cost of the materials of the mechanical, electrical, and plumbing (MEP):

The construction obviously needs a mechanical part in its structuring, the mechanical parts are generally subcontracted to mechanical specialties, which prepare detailed quotes for the plumbing and heating, ventilation and air conditioning (HVAC) systems, this part plumbing promotes comfort in the management of the structure. To accurately estimate plumbing costs, construction contributor must therefore have field experience and a good knowledge of various plumbing systems, materials, labor and equipment, as well as " an understanding of the design and internal and external specifications of the structure. This simply transfers the

preparation of the detailed estimate to another party, but this does not eliminate the need to estimate and analyze the prices indicated by the engineers [11].

Figure 3.2, relates the finalization of the owner decision regarding the change of materials.

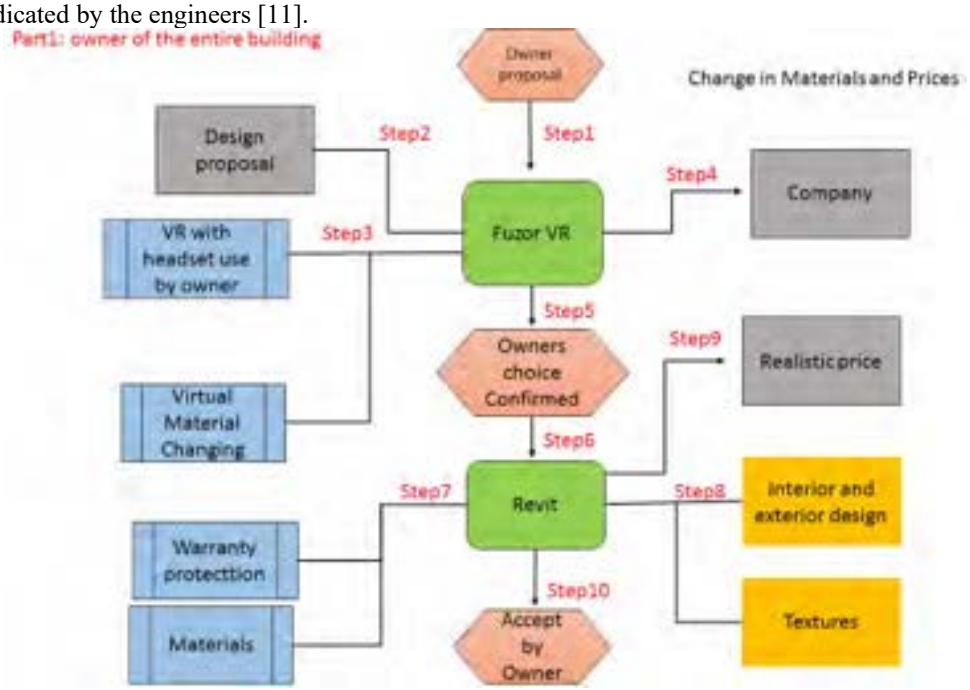

Figure 3.2. Change in Materials and prices

Step 1 explains the changes proposed by the owner. These different changes suggested by the owner will be recorded in project document at Step 2. Fuzor software by VR function will help the owner to make these changes while taking into account the material already submitted by the company.

Step 3 demonstrates the change in the model by the owner. This is done from the VR Box headset or directly on the Fuzor software, and from the already done synchronization above the materials that are changed or created directly translates to the main model of Revit, Figure 3.3 shows a synchronization view between Fuzor and Revit.

Figure 3.3. Synchronization between Fuzor and Revit

In this project the owner has had to change the design exterior first by modifying by itself the shape of the wall. For the modification, the owner prefers to insert a balcony at each floor, illustrate in Figure 3.4.

Figure 3.4. Design change

3.3 Interactive clash management:

The functioning of the interactive clash defines interference and proximity tolerances. To start it, it is necessary to select sections of the building, systems or types of objects to compare, then define the tolerance and execute the conflict check [13]. This procedure will allow Fuzor to list all the conflicts according to defined criteria and lists them in the conflict interface. By clicking on any conflict in the list, accessing this conflict results in highlighting the objects in conflict. After the different changes the clash management system (tolerances 0.83) of Fuzor was used to detect the

presence of indifference in the design. Figure 4.16. Shows that there is no clash problem after changing the facade of the wall by including several balconies, the same result is observed at the change of the exterior texture from yellow to blue. But after changing the size of the wall inside the level 2 chamber, a clash was detected. This was the subject of a bug fix on the Revit software. This error is mentioned in Figure 3.6 in red object [13].

Step 4 will contain data collection after the various modifications. This document contains the price, the size, and the colors of the different materials. This document will be used by the company later to fix the prices and the timeline of execution of the works.

At Step 5, the different changes are finished, and the owner is satisfied with the design of its construction. The company has confirmation from the owner about the texture, the choice of materials and the modeling of the construction.

In Step 6 the changes will be transferred to the Revit software for price validation, material verification and their warranty. This transfer between the two programs is already established by the plugin system in the previous steps.

Step 7 All materials used in the project are chosen according to their quality. These qualities are closely linked to their guarantee, the objective is to present an excellent project in the choice of materials and economically favorable.

In step 8 usually the owners are more focused on the appearance of their home, regarding the exterior and interior design, the texture. These different elements are crucial in the context to convince them. It is to this extent that very special importance was devoted to this part. The interior design can easily be modified if the need arises. The size of furniture, doors, windows etc.… can be altered. Partitions can be moved and rearranged. Making these changes in Revit is very simple and does not require much time either. It is possible to replicate and resize furniture without much effort.

For the realistic price in Step 9, the construction cost estimate is the process of forecasting the cost of construction of a physical structure that is established according to needs and modalities.

4. TimeLine management for presale house presentation

4.1 The setting of the timeline by the company

This diagram (Figure 4.1) presents a flexibility of work between the owner, the company and the different working associates. This is a method which gives the choice to all the participants of the project to freely express for a more balanced management of working time. This diagram is presented in several steps that will often require the desires of the owner.

Step 1: In the first step the company will be the source of manipulation of documents, software and agreements collected at stakeholder level for an adequate balance of the progress of the project.

Step 2, in this part the NWD format to collect at Revit level will import into Navisworks as the diagram specifies.

Step 3, the 3D model of the building space already produced will be used to show the evolution and timing of the building to the owner. This part is a mix of the model produced by Revit and the 3D model produced by Bentley contextcapture. This technique aims to present the owner in what environment will present his new construction. This will also prove the credibility of the planning that will be made later and show the conditions of the realization of the project. Then in the setting of the timeliner organization unit of Step 4 will be a major factor, which are the structure of the building and the MEP. In Step 5, project planning is a crucial element in the relationship between the owner and the company. In Step 6 it will be necessary to transfer to the owner online each step of execution of the project. This will enable him to follow in progress the different phases of the workings. This also aims at pushing the company to respect the deadlines.

In Step 7 after having shown the owner the time of execution of the work he can accept or propose another schedule that suits him. If the owner accepts the schedule of the company the work will take place as such. If the owner suggests another period for the planning this leads to the Timeline B Figure 4.1, which is timelines B.

Timeline B, explains in detail if the owner decides to give a new schedule of the final delivery of the project.

Step1, in this part the owner has decided to change the time of the construction for personal reasons. Consequently, the owner must provide its period of the end of the works. This calendar will be first examined by the company for its feasibility.

In the second Step, the company received the owner's claims, this information was input into the Navisworks software and later produced data.

In order to carry out Step 3 which changes the planning, Step 4 concerning the organization unit (labor, material, equipment, and subcontractor) will be crucial elements. First of all, the different elements that must be influenced by the change of the schedule must be defined.

4.2 A specific part of the building belonging to the owner

Alternative 2: A room or floor level owned by the owner

The inspection of the reality virtual is the same thing as that of the owner for all the building. The parameterize and the use of the files remains the same, in Figure 4.2.

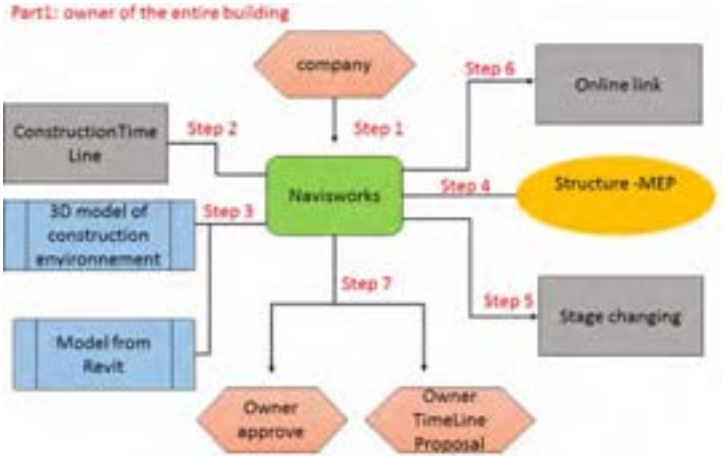

Figure 4.1. Timeline B

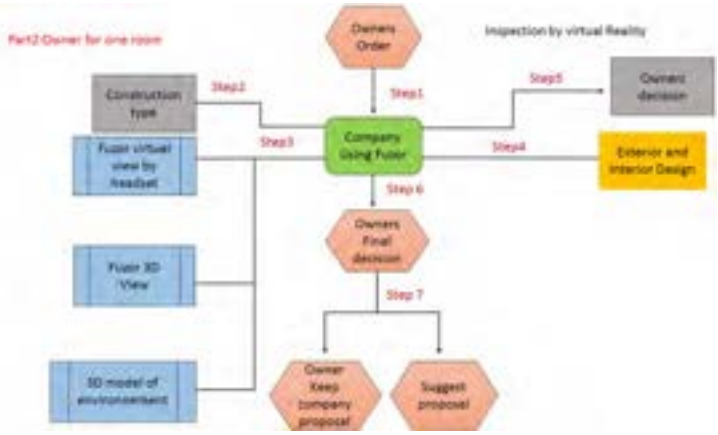

Figure 4.2. Inspection by Virtual Reality

The price and setting of the materials remains the same, except that the setting will not take into account the exterior design, in Figure 4.3. The timeliner of Navisworks will be the same, except that the owner will have no suggestion to make compared to the time of execution.

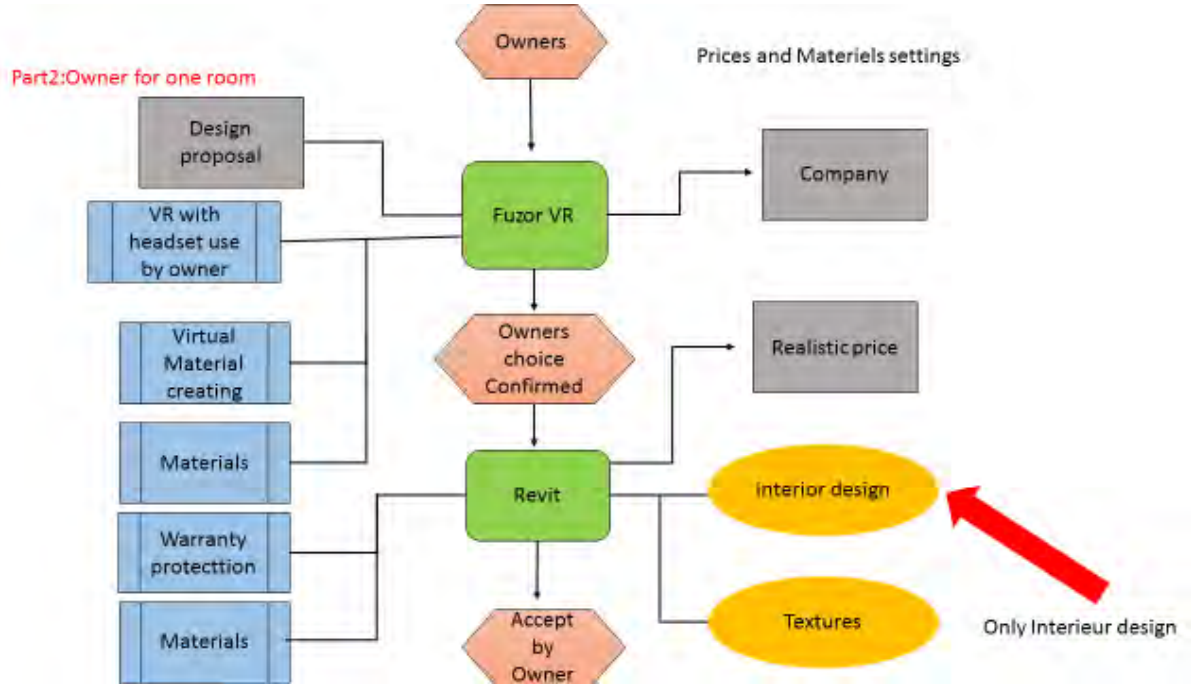

Figure 4.3. Prices and Materials settings

5. Discussion

After having given the owners of the project the choice of design, time and materials, the observation was made in relation to the price because the customer will always want what is comfortable and durable but do not want to invest the necessary money. So to facilitate partnership it was necessary to try to involve the catalogs of the materials. This catalog will be considered as a trust course between the different partners. It should also be emphasized that the use of VR for the presentation of the presale house is a very positive idea for future of owners. They note the perception of their future home and suggestions if possible. Regardless of budget, just about every

developer, realtor, architect, or interior designer can take advantage of VR and AR to showcase a project inside.

VR can show off a project at any stage, from pre-construction to proposed renovations and upgrades. VR with the synchronization system can be customized and quickly updated, complete with interactive components that allow prospective homeowners or builders to change finishes, fabrics, layout ideas, and more. Whether it is the structural part or the MEP, everything is detailed in the report to submit to the owner.

In the analysis of this study of EPC diagram, the observation is that whenever the time of construction has been changed by the owner the load of labor has increased considerably. This means that the company needs to be more lenient in partnering with the subcontractors for efficient execution and on time.

5.1 Conclusion

Traditional way presents many disagreements between costumers and company Owners can make change at the project to solve disagree and delay problems. This study has also allowed to identify some concerns of the owners in the future, about comfort and safety.

In this study the contribution was considerable compared to the previous researches on which the study is focused. The advantage is the technique and the software used allowed efficiency in the study, less time was used compared to the other researches. The major advantage is gaining trust among owners and investors.

5.2 Future work

Future research will be based on the difficulties encountered in the execution of these projects. In addition the new ideas will come from the suggestions given by the different partners for the good execution.

Create a function that allows the owner of a single room or a single level of construction to suggest the construction time.

Using the system of a mobile phone application, project participants can easily view, add a profile to the system and set permissions for what new employees are allowed to do, while following the roadmap of the project. Additionally, tools can be labeled with QR codes to ensure they are easy to find.

Developing a function to adjust parameters such as the number of workers, available equipment and construction materials can be done to show how these changes would affect the cost of the project with a connection of Navisworks and Revit to control the data and the time required for completion.

References

[1] Kalloc Studios Asia Limited Unit 321, 3/F, Building 16W, Phase 3 Hong Kong Science Park, Shatin N.T. Hong Kong. www.kalloctech.com

[2] Niu, S; Pan, W; Zhao, Y. A virtual reality integrated design approach to improving occupancy information integrity for closing the building energy performance gap. Sust. Cities Soc. 2016, 27, 275–286.

[3] Vergara, D; Rubio, M.P; Lorenzo, M. On the design of virtual reality learning environments in engineering. Multimodal Technol. Interact. 2017, 1, 11.

[4] https://www.autodesk.com/solutions/bim/hub/the-future-of-construction-manufacturing-vs-building

[5] http://www.create-architecture.com/services/virtual-reality-bim/

[6] https://www.3deling.com/registered-point-cloud/?gclid=Cj0KCQiA2o_fBRC8ARIsAIOyQ-nA4YUk4nxtGqLV6_Q5gz8oFoKPX7N2zZMArxJBi1j1_dr5FPXFtukaAp5OEALw_wcB

[7] https://www.spar3d.com/news/software/atom-view-quantum-leap-point-cloud-visualization/

[8] https://knowledge.autodesk.com/support/revit-products/learn-explore/caas/CloudHelp/cloudhelp/2018/ENU/Revit-Model/files/GUID-B89AD692-C705-458F-A638-EE7DD83D694C-htm.html

[9] https://knowledge.autodesk.com/support/revit-products/learn-explore/caas/CloudHelp/cloudhelp/2018/ENU/Revit-Model/files/GUID-B89AD692-C705-458F-A638-EE7DD83D694C-htm.html

[10] https://knowledge.autodesk.com/support/revit-products/learn-explore/caas/CloudHelp/cloudhelp/2018/ENU/Revit-Model/files/GUID-D179BB6C-5528-498F-9413-00237092C2FA-htm.html

[11] https://www.mgfx.co.za/blog/building-architectural-design/use-revit-live-set-virtual-reality-vr-experience-using-htc-vive/

[12] https://rennie.com/nataliegenest/posts/the-pros-and-cons-of-buying-pre-sale-homes

[13] https://en.wikipedia.org/wiki/Event-driven_process_chain

Virtual Prototyping-Based Path Planning of Unmanned Aerial Vehicles for Building Exterior Inspection

Z.J. Zheng[a], M. Pan[a] and W. Pan[a]

[a] Department of Civil Engineering, The University of Hong Kong, Hong Kong SAR, China
E-mail: zhengzj@connect.hku.hk, panmi@connect.hku.hk, wpan@hku.hk

Abstract –

Proper building maintenance is critical to ensuring the well-being of citizens and sustainable development of the urban environment. For high-rise high-density cities, one challenge to building maintenance concerns the inspection of building exteriors, which has been mostly done manually but is of highly risky, labor-intensive, and error-prone. Unmanned aerial vehicles (UAVs) have the potential to support building exterior inspection in a safe and efficient way. However, the effective application of UAVs for exterior inspection is hindered by path planning problems in high-rise high-density urban areas. Previously developed path planning algorithms are constrained by algorithmic complexity and cannot be implemented in a large three-dimensional space. Besides, path planning assisting tools available in the market that supported by Google Earth Pro can hardly assure high accurate results. In this paper, a new virtual prototyping-based path planning system is developed for UAVs for building exterior inspection in high-rise high-density urban areas. Unreal Engine as a widely-used game engine was applied. The system provides a realistic game world to simulate real-world activities, which enables operators to design UAV paths like playing games. The flight paths and viewpoints can be repeatedly tested in a gaming context until requirements are satisfied. The system integrates expert knowledge through "human in the loop" and realistic information on the virtual environment featured with repeatability. The system thereby greatly alleviates the risks that are induced by physical constraints in the real world when adopting UAV, and thus should significantly improve the effectiveness and efficiency of building exterior inspection.

Keywords –

Unmanned aerial vehicles (UAVs); Path planning; Building exterior inspection; Virtual prototyping; Human in the loop

1 Introduction

The importance of proper maintenance of buildings has been widely recognized to ensure that buildings are function effectively and efficiently for well-being of citizens and sustainable development of the urban environment [1]. For high-rise high-density cities like Hong Kong, one of the most challenging issues with maintenance is the inspection of building exteriors. Visual inspection by professionals is the most common method, but is highly risky, labor-intensive, and error-prone. Tools, such as telescopes and cameras, are applied to help inspectors. Still, they are limited in the distance and inefficiency until the commercialization of Unmanned Aerial Vehicles (UAVs).

UAVs refer to an aircraft that is operated with no pilot on board, also termed as drones or Unmanned Aerial Systems (UASs) [2]. UAVs have great potentials in the construction industry [3]. When paired with video recording and digital cameras, UAVs could provide professionals with an aerial perspective to overcome the inaccessible areas without compromising their safety. UAVs enable various types of surveying services for professionals [2]. Despite the well-demonstrated benefits in reduced labor, cost and risk, there are issues hindering the effective application of UAVs. A critical one is path planning, which is closely related to UAV performance and usually done by drone operators. Due to the flight time limitation, operators could make limited adjustments during operation. It is a sophisticated task to plan paths and viewpoints in a highly accurate manner to avoid collision and invalid data collection, which is even more difficult in high-rise high-density urban contexts like Hong Kong. Especially for tasks such as building exterior inspection (e.g. crack and loose object detection). Moreover, poor path planning could result in distorted images captured from inappropriate viewpoints that further induce false positives [7].

Previously developed path planning methods, such as Dijkstra algorithm [8], A* [9], and D* [10], focus on the optimization of path distance by considering physical constraints in mathematics. These methods well tackle

the distance and obstacle problems, but seldomly address the data effectiveness with the environment in high abstraction. In addition, path planning for UAVs requires the exploration of three-dimensional (3D) space. Many existing algorithms are constrained with its space complexity such as A*, since desktops cannot offer enough memory to store all generated nodes if it needs to explore a large space. Simulation-based methods are preferable to investigate the mechanisms behand path planning for UAVs cost-effectively. Particularly, virtual prototyping offers a favorable platform to animate the real world by using advanced game engines for optimization and visualization. By integrating expert knowledge and experience through "human in the loop" [11], virtual prototyping can be used to handle complex tasks in uncontrollable environments. Nevertheless, there is still lack of knowledge of how to effectively use virtual prototyping for UAV path planning.

Therefore, this paper aims to develop a new virtual prototyping-based path planning system for UAVs, within the context of building exterior inspection in high-rise high-density urban areas. Unreal Engine as a widely-used game engine was applied. Drone operators can simulate flight tasks such as playing games in the simulation system, e.g. controlling the virtual drone to fly in the game environment with virtual cameras providing real-time images and videos. The flight paths and viewpoints can, therefore, be repeatedly tested in a gaming context until requirements are satisfied.

2 Literature Review

2.1 UAV for Exterior Inspection

UAVs originated from the military in 1916 [12], which has not been popularized until UAVs commercialization companies grow up in recent years. Later on, commercial companies, like DJI, made the UAVs commercialized and accessible to the public by providing low-price UAVs that are easy to operate. Owing to the aerial perspective that enables a broad variety of surveying services, UAV has gained considerable interest in the construction industry. One of the important applications is the exterior inspection of buildings. Caballero et al [3] developed a vision-based method to estimate the real motion of an UAV and applied it to the external building inspection. Emelianov [4] inspected the building facades by aerial laser using an UAV for difficult site conditions. Ellenberg [5] detected masonry cracks with visual images captured by an UAV. These applications promote the productivity of building inspection works and greatly reduce the risk of relevant workers. However, there are still some issues that need to be tackled, such as path planning and data effectiveness. Most commercial UAVs have a minimal capacity on flight time, which is usually less than 30 minutes. Path planning is, therefore, critical to not only avoid obstacles but also reduce unnecessary adjustments when operating UAVs [2]. Otherwise, the UAV operator has to abort the task frequently to change batteries, which no doubly decreases the productivity of inspection works.

2.2 Path Planning Methods for UAV

Considerable research has been conducted on the topic of path planning. Many reported methods for path planning are based on mathematics like Dijkstra's algorithm [8], A* [9], D* [10], rapidly-exploring random tree (RRT) [14], bath informed trees (BIT*) [15]. These algorithms can be used to address obstacles and distance problems, which have been successfully applied in game development and robotics for path planning. However, for tasks in building exterior inspection, an essential consideration is imaging effects that are greatly influenced by viewpoints, view angles, and light [2]. Previous path planning algorithms cannot take such constraints into account.

Therefore, in UAV applications in the construction industry for surveying and inspection, path planning tasks are usually conducted manually, which is highly related to operators' experiences. In addition, some operators use the waypoint method assisted by Google Earth Pro, which however has the accuracy issues [16]. The reported root mean square error (RMSE) of its control point is around 24.1m in developed countries and 44.4m in developing countries [16]. Other path planning tools on the market that are developed based on Google Earth Pro service have similar accuracy limitations. For high-rise high-density cities like Hong Kong, accuracy is a critical aspect when adopting UAVs to avoid accidents and improve data effectiveness. There is an urgent need for a user-friendly and accurate path planning tool that can help operators to effectively and efficiently design UAV paths for missions.

2.3 Virtual Prototyping in the Construction Industry

Virtual prototyping refers to the process of constructing and testing a digital mock-up to present, analyze, and test life-cycle aspects [17]. The development of building information modeling (BIM) promotes the application of virtual prototyping in the construction industry, which has been widely reported to increase productivity in design [18], manufacturing [19], construction [20] and maintenance stages [21]. Recently, virtual reality (VR) and augmented reality (AR) supported by powerful game engines are gaining increasing interest in both practice and research in the construction industry. For example, Du et al. [22] developed a real-time synchronization method between

BIM data and VR environment for collaborative decision. Cao et al. [23] adopted VR to study indoor fire evacuation and found out that people under the file emergency condition spent more time in finding their way to exit the building that those under control condition. Shi et al. [24] applied VR for impact assessment of construction workers' fall risk behavior, which demonstrates the effectiveness of using VR in safety studies. Webster et al. [25] developed an AR system for the construction, inspection, and renovation of architectural structures, which improved the construction of performances. Wang et al. [26] integrated AR with BIM to control the onsite construction progress, which demonstrated how AR and BIM can improve the way the information is accessed. With the development of game engines, virtual prototyping has demonstrated its greater potentials for the construction industry.

3 System Architecture

The overall system architecture by using a game engine for UAV path planning for building exterior inspection is proposed in Figure 1, including building environment model structure, game engine structure, device structure and professional structure. In building environment model structure, professional software provides 3D building and environment models, such as 3ds Max, Revit, Rhino 3D, etc. Game engine is the core of the system architecture that consists of a game world and three plugins: a UAV simulator, a model converter, and a path generator. Device structure consists of a remote controller and an UAV. In the human structure, relevant professionals (operators) could assess paths and viewpoints according to their expert knowledge.

The proposed system functions with three stages. Firstly, building environment models will be imported to the game engine by the model converter plugin, which provide the main contents of the game world. Secondly, remote controller will be linked to the game engine by the UAV simulator plugin. The remote controller enables professionals to control a virtual UAV in the game world to simulate the inspection task. The flight paths and viewpoints are repeatedly tested until all requirements are satisfied. Finally, the path generator plugin will generate a path planning file that can be directly used in a real UAV for automated operation.

4 System Development

To develop the system based on the proposed architecture shown in Figure 1, this research is based on the Unreal Engine as it is open source and one of the most popular game engines. The following sub-sections describe the design and development of three major components in the game engine, namely a UAV simulator, a model converter, and a path generator.

4.1 UAV Simulator

UAV simulators are usually designed for testing, operational training and research because of its cost-effectiveness and safety assurance. There are more than 20 types of UAV simulators reported in history [27]. By considering its openness, functions and stability, this research adopted the Microsoft AirSim UAV simulator built on Unreal Engine, shown in Figure 2 [28]. AirSim provides a broad variety of sensor simulations including camera, infrared camera, distance sensor, barometer and so on, which together with Unreal Engine could develop a realistic game world as shown in Figure 3. These sensors can greatly help the operators to make sophisticated mission planning tasks e.g. UAV path planning for building inspection in a cost-effective, safe and robust manner.

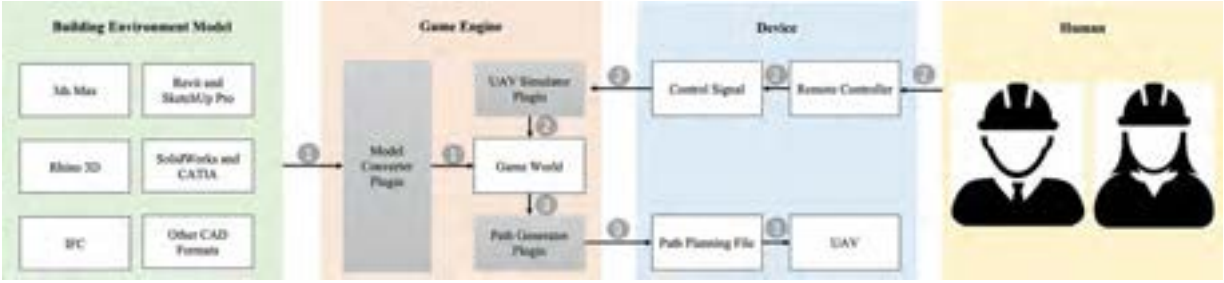

Figure 1. System architecture of the Virtual Prototyping-Based Path Planning for UAV

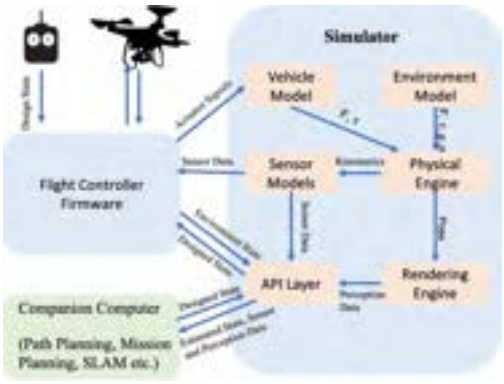

Figure 2. AirSim simulator architecture (reproduced from [28])

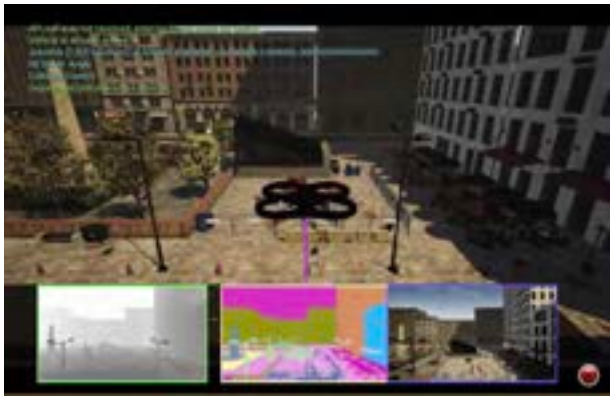

Figure 3. Game world in Unreal Engine

4.2 Model Converter

The model converter enables users to import building and environment models from other professional software. The model converter in the developed system is based on the DataSmith module in Unreal Engine, which supports model importation from a broad variety of professional software (e.g. 3ds Max, Revit and Rhino 3D) [29]. The model converter makes it convenient to build a game world in Unreal Engine based on building and environment models that are commonly available from the design stage of a construction project.

4.3 Path Generator

The path generator plugin records the UAV waypoints, view angles, actions (e.g. take an image or video) and speeds in the game world when professionals are testing paths and viewpoints. After the playing process, the path generator will output a path planning file that can be used in a real UAV, shown in Figure 4. In this research, DJI Matrice 210 V2 RTK (Figure 5) was used, and the path file is generated according to the requirements of DJI products. For example, the North East Down (NED) Coordinate System is applied in the developed path planning system, while geodetic datum is required as input coordinates by DJI products. Thus, the axes conversion [30] is needed during the path file generation, as shown in Figure 4. When the developed system is used for other types of UAVs, the path generator can be easily extended to generate a new path file according to specific requirements by other types of UAVs.

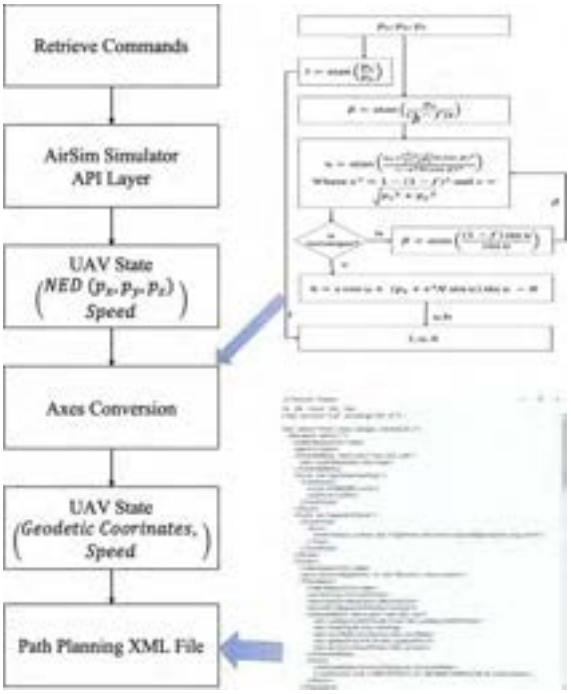

Figure 4. Procedure of path recording and file generation

Figure 5. DJI Matrice 210 V2 RTK used for the study

5 System Demonstration

In this section, demonstration of the developed virtual prototyping-based UAV path planning system was conducted for building exterior inspection, including viewpoint selection and path generation. To illustrate the effectiveness of the developed system, results from virtual prototyping-based method are analyzed and compared with results from using A* method [31] that is the most widely used algorithm for path planning [32].

5.1 Viewpoint Selection

To ensure a virtual camera in the game world can function like a physical camera in the real world, specifications of the virtual camera should be set up like the physical ones, e.g. field of view (FOV), aspect ratio, lens, etc. After that, the virtual camera can be used to test the locations and view angles of viewpoints (Figure 6). When the inspection area is larger than the FOV, more than one viewpoint should be used to cover the whole area, and overlaps could be tested at the same time.

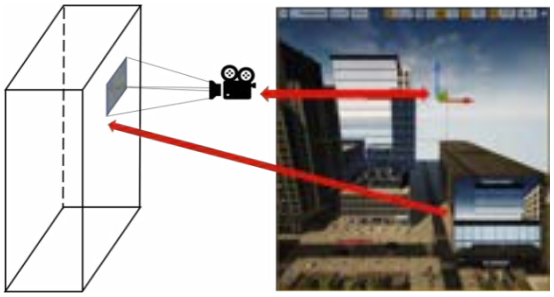

Figure 6. Viewpoint selection

5.2 Path Generation

As the space and the number of viewpoints increases, the challenge of adopting A* method will dramatically increase due to the algorithm complexity [31]. On the contrary, the virtual prototyping-based method is nearly not constrained in such cases. To avoid the problem of out of memory when adopting A* method, the comparative analysis is conducted with a single-viewpoint case. Results are shown in Figure 7, Figure 8 and Table 1.

Figure 7. Path generated by the developed system (shown by green line)

Figure 8. Path generated by A* (shown by red line)

Table 1. Geometry Comparison

Method	A*	Proposed Method
Start Point	(0, 0, 0)	(0, 0, 0)
Middle Points	(-0.9, 0.1, -5.0)	(0, 0, -48.8)
	(1.6, 2.6, -12.5)	(39.6, 0, -48.8)
	(6.6, -2.4, -27.5)	-
	(26.6, -2.4, -27.5)	-
	(41.6, -7.4, 32.5)	-
Viewpoint	(39.6, -22.3, -48.8)	(39.6, -22.3, -48.8)
Distance	88.7	110.7

Notes: local north, east, down (NED) coordinates and international system of units (IS)

In general, the path generated by the proposed visual prototyping-based method (Figure 7) has less twists and turns compared with the path generated by A* method (Figure 8). When implementing A*, the exploration space is discretized into 3D grids. By searching the whole 3D grids, A* method can usually find a shorter path (shown in Table 1) with more twists and turns by linking nodes in the 3D grids, compared with the proposed visual prototyping-based method. If the twists and turns are extremely irregular, UAVs cannot flight as the designed path due to motion constraints [33]. Besides, the path generated by the proposed method (Figure 8) crossed less dangerous areas (e.g. roads) compared with A* method

(Figure 7). The developed system provides a realistic game world for relevant professionals to design a path for UAVs in building exterior inspection like playing games. By implementing "human in the loop", the developed system can easily take more constraints into consideration by integrating expert knowledge and experience.

6 Discussion

Manual visual-based building exterior inspection is usually labor-intensive, time-consuming, error-prone and highly risky. As the low-price commercial UAVs are popularized, professionals start to use UAVs for building exterior inspection works, which brings in benefits including enhanced safety and efficiency. However, in high-rise high-density cities like Hong Kong, the complex flight environments require a more accurate path planning method that can help professionals to design path for their inspection task to avoid accidents (e.g. collision). Previously developed path planning methods like A* [9] well tackle the distance problem but cause too many twists and turns on a path. In addition, these mathematically based path planning methods like A* have a bottleneck on algorithmic complexity when they need to be applied in a large 3D space. The required computing time is too long, or the required memory space is too large [31]. Also, these algorithms seldomly considered the data effectiveness (e.g. image distortion and light effect). Therefore, these path planning algorithms are seldom adopted for inspection tasks in the construction industry.

Virtual prototyping enabled by game engines offers a realistic game word to simulate detailed activities in the real world. The virtual prototyping-based path planning method developed in this paper enables professionals to design UAV paths for their inspection tasks like playing games. The new method not only overcomes the bottleneck of algorithmic complexity of previous algorithms [31], but also takes into consideration more constraints (e.g. dangerous area, images distortion and light effect) by taking the advantage of expert knowledge through "human in the loop". Compared with path planning tools that are supported by Google Earth Pro, the developed system has a higher level of accuracy because the game world is constructed using accurate BIM models.

The developed path planning system involves game engine, UAV and professionals, which can be extended for more general applications in the construction industry. First, game engine can be used for mission planning for robotics. As the development of automation and control technology, adopting robotics has great potentials to improve the productivity in the construction industry [34][35] Robots can be trained, tested and assigned tasks by a game engine. Second, a cyber-physical system for construction management or even smart city management can be built by synchronization between the real and game worlds. Third, human can also be linked to the game world to maximize the power of human/hardware-in-the-loop (HHITL) [36]. For example, a professional can use remote controller to control a robot to conduct a task in a game environment for once, then the robot can learn how to conduct the task in the real world by itself through imitation learning [37].

7 Conclusions

Building exterior inspection using UAVs is widely recognized around the world in recent years, because of a broad variety of benefits including low cost, high safety and efficiency. However, there has been no user-friendly tool that can help professionals with path planning in an accurate and efficient manner. In this paper, a new virtual prototyping-based path planning system is developed for UAVs. It helps professionals to design an accurate path for inspection tasks efficiently. The new method will not only overcome the algorithm complexity problem that exists in many previously developed path planning algorithms, but also provide a higher level of accuracy than the path planning assisting tools available in the market do.

The developed path planning system can be easily extended for other mission planning tasks for robotics in the construction industry. Furthermore, it can also be developed into a cyber-physical system for construction management or even smart city management. These extensions will be explored in future research.

Acknowledgements

The work presented in this paper was supported by a grant from the Research Impact Fund of the Hong Kong Research Grants Council (Project No.: HKU R7027-18).

References

[1] Yiu, C. Y. Building depreciation and sustainable development. *Journal of Building Appraisal,* 3(2): 97-103, 2017.

[2] Rakha, T. and Gorodetsky, A. Review of Unmanned Aerial System (UAS) applications in the built environment: Towards automated building inspection procedures using drones. *Automation in Construction*, 93: 252-264, 2018.

[3] Caballero, F., Merino, L., Ferruz, J. and Ollero, A. April. A visual odometer without 3D reconstruction for aerial vehicles. Applications to building inspection. In *Proceedings of the 2005 IEEE International Conference on Robotics and*

Automation, pages: 4673-4678, IEEE, 2005.

[4] Emelianov, S., Bulgakow, A. and Sayfeddine, D. Aerial laser inspection of buildings facades using quadrotor. *Procedia Engineering*, 85:140-146, 2014.

[5] Ellenberg, A., Kontsos, A., Bartoli, I. and Pradhan, A. Masonry crack detection application of an unmanned aerial vehicle. In *Computing in Civil and Building Engineering,* pages: 1788-1795, 2014.

[6] Pan, M. and Pan, W. Stakeholder perspectives on the future application of construction robots for building in a dialectical system framework, *Journal of Management in Engineering*, 36(6): 04020080, 2020.

[7] Martinez-De Dios, J.R. and Ollero, A. Automatic detection of windows thermal heat losses in buildings using UAVs. In *2006 world automation congress,* pages: 1-6, IEEE, 2006.

[8] Dijkstra, E.W. A note on two problems in connexion with graphs. *Numerische mathematik*, 1(1):269-271, 1959.

[9] Hart, P.E., Nilsson, N.J. and Raphael, B. A formal basis for the heuristic determination of minimum cost paths. *IEEE transactions on Systems Science and Cybernetics*, 4(2): 100-107, 1968.

[10] Stentz, A. Optimal and efficient path planning for partially known environments. In *Intelligent Unmanned Ground Vehicles,* pages: 203-220, Springer, Boston, MA, 1997.

[11] Fales, R., Spencer, E., Chipperfield, K., Wagner, F. and Kelkar, A. Modelling and control of a wheel loader with a human-in-the-loop assessment using virtual reality. *Journal of Dynamics Systems, Measurement, and control*, 127(3): 415-423, 2005.

[12] ICAO. *Unmanned Aircraft Systems (UAS)*. International Civil Aviation Organization, 2011.

[13] Abd Algfoor, Z., Sunar, M.S. and Kolivand, H., 2015. A comprehensive study on pathfinding techniques for robotics and video games. *International Journal of Computer Games Technology*, 2015.

[14] LaValle, S.M. Rapidly-exploring random trees: A new tool for path planning, *Research Report 9811*, 1998.

[15] Likhachev, M., Gordon, G.J. and Thrun, S. ARA*: Anytime A* with provable bounds on sub-optimality. *In Advances in neural information processing systems*, pages: 767-774, 2004.

[16] Potere, D. Horizontal positional accuracy of Google Earth's high-resolution imagery archive. *Sensors,* 8(12): 7973-7981, 2008.

[17] G.G. Wang. Definition and review of virtual prototyping, J. *Computing and Information Science in Engineering,* 2(3): 232–236, 2002.

[18] M. Nasereddin, M.A. Mullens, D. Cope. Automated simulator development: a strategy for modeling modular housing production. *Automation in Construction*, 16(2): 212–223,2007.

[19] S.H. Han, M. Al-Hussein, S. Al-Jibouri, H. Yu. Automated post-simulation visualization of modular building production assembly line, *Automation in Construction,* 21:229–236, 2012.

[20] X. Li, S.H. Han, M. Gül, M. Al-Hussein. Automated post-3D visualization on ergonomic analysis system for rapid workplace design in modular construction. *Automation in Construction*, 98: 160–174, 2019.

[21] De Sa, A.G. and Zachmann, G. Virtual reality as a tool for verification of assembly and maintenance processes. *Computers & Graphics,* 23(3):389-403, 1999.

[22] Du, J., Zou, Z., Shi, Y. and Zhao, D. Zero latency: Real-time synchronization of BIM data in virtual reality for collaborative decision-making. *Automation in Construction,* 85: 51-64, 2018.

[23] Cao, L., Lin, J. and Li, N. A virtual reality based study of indoor fire evacuation after active or passive spatial exploration. *Computers in Human Behavior,* 90: 37-45, 2019.

[24] Shi, Y., Du, J., Ahn, C.R. and Ragan, E. Impact assessment of reinforced learning methods on construction workers' fall risk behavior using virtual reality. *Automation in Construction,* 104: 197-214, 2019.

[25] Webster, A., Feiner, S., MacIntyre, B., Massie, W. and Krueger, T. Augmented reality in architectural construction, inspection and renovation. *In Proc. ASCE Third Congress on Computing in Civil Engineering,* pages: 996, 1996.

[26] Wang, X., Truijens, M., Hou, L., Wang, Y. and Zhou, Y. Integrating Augmented Reality with Building Information Modeling: Onsite construction process controlling for liquefied natural gas industry. *Automation in Construction,* 40: 96-105, 2014.

[27] Mairaj, A., Baba, A.I. and Javaid, A.Y. Application specific drone simulators: Recent advances and challenges. *Simulation Modelling Practice and Theory*, 2019.

[28] Shah, S., Dey, D., Lovett, C. and Kapoor, A. Airsim: High-fidelity visual and physical simulation for autonomous vehicles. *In Field and service robotics,* pages: 621-635, Springer, Cham, 2018.

[29] Engine, U., 4. Document, "DataSmith".

[30] Wikipedia, Geographic coordinate conversion. Accessed date August 26, 2020. https://en.wikipedia.org/wiki/Geographic_coordinate_conversion

[31] Brewer, D. 3d flight navigation using sparse voxel octrees. *Game AI Pro 3: Collected Wisdom of Game*

AI Professionals, 2017.
[32] Russell, S. and Norvig, P. Artificial intelligence: a modern approach, 2002. Online: https://storage.googleapis.com/pub-tools-public-publication-data/pdf/27702.pdf
[33] Laumond, J.P. ed. *Robot motion planning and control,* Volume 229, Berlin: Springer, 1998.
[34] Yang, Y., Pan, M. and Pan, W. 'Co-evolution through interaction of innovative building technologies: The case of modular integrated construction and robotics. *Automation in Construction,* 107: 102932, 2019.
[35] Pan, M., Linner, T., Pan, W., Cheng, H. and Bock, T. Structuring the context for construction robot development through integrated scenario approach. Automation in Construction, 114: 103174, 2020.
[36] Masone, C., Franchi, A., Bülthoff, H.H. and Giordano, P.R. October. Interactive planning of persistent trajectories for human-assisted navigation of mobile robots. *In 2012 IEEE/RSJ international conference on intelligent robots and systems,* pages: 2641-2648, IEEE, 2012.
[37] Schaal, S. Is imitation learning the route to humanoid robots?. *Trends in cognitive sciences,* 3(6): 233-242, 1999.

Near Real-Time Monitoring of Construction Progress: Integration of Extended Reality and Kinect V2

Ahmed Khairadeen Ali[a], One Jae Lee[b] and Chansik Park[a]

[a]School of Architecture and Building Sciences, Chung-Ang University, Seoul 06974, Republic of Korea
[b]Haenglim Architecture and Engineering Company, 201, Songpa-daero, Songpa-gu, Seoul, 05854, South Korea
E-mail: ahmedshingaly@gmail.com, o.lee@haenglim.com, cpark@cau.ac.kr

Abstract –

Construction progress monitoring and visualization have recently undergone advanced development. However, the data exchange process between construction offices and jobsites still lacks automation and real-time data records. Furthermore, an information gap between construction offices and jobsite activity persists, and progress inspectors still need to visit jobsites to check progress and assign quality ratings. Therefore, this research proposes a near real-time construction progress monitoring system called (iVR), which integrates 3D scanning, extended reality, and visual programming to visualize interactive onsite inspection and provide numeric data. The iVR system contains four modules: 1) recording jobsite activity through 3D scan (iVR-scan); 2) processing and converting 3D scan data into a 3D model (iVR-preparation); 3) immersive virtual reality inspection in the construction office (iVR-inspect); and 4) visualizing inspection feedback on the construction jobsite using augmented reality (iVR-feedback). In other words, 3D laser scanners first capture an activity point cloud and the iVR-preparation algorithm processes and converts the point cloud into a 3D model that is sent to the construction office's BIM cloud. Then, the proposed VR mode in iVR-inspect enables a quality assurance inspector to trace workflow, compare current project progress with blueprints, measure objects, and add text or design notes to 3D models to improve the site management and decision-making quality. Finally, iVR-feedback sends inspection reports to jobsite workers, who can visualize them in an augmented reality mode integrated with graphical algorithms. An experimental laboratory trial is presented in this paper to validate the concept; the iVR system for progress monitoring successfully generated the required results. The proposed system has the potential to help progress inspectors and workers complete quality and progress assessments and decision making through the development of a productive and practical communication platform. It compares favourably to conventional manual monitoring or data capturing, processing, and storing methods, which have storage, compatibility, and time-efficiency issues. Moreover, iVR minimizes physical interactions between workers and QA inspectors, thus creating healthier construction jobsites that are characterized by minimal human interaction. Finally, the same approach can be applied to more complex construction activities with movable natures.

Keywords –

Kinect Camera; Augmented Reality; Virtual Reality; Building Information Modeling; Progress Monitoring

1 Introduction

Building Information Modelling (BIM) technology, a recent trend in the construction industry, is an exciting solution for achieving automation in construction project progress monitoring. BIM is a rich source of 3D geometry-related information, such as architecture, structure, and MEP; furthermore, it enables knowledge sharing and interoperability over a building's lifecycle [1–3].

Engineers at a construction site find it challenging to manage a complicated BIM model and recognize the necessary attributes in the model [4,5]. Since BIM models are stored on servers or separate computers, they are often not updated synchronously on the jobsite. In other words, the transfer of knowledge from the design office to the engineering office on the construction site is significantly delayed [6]. This delay is crucial in certain projects, such as rapidly tracked projects, where planning and construction occur simultaneously. Slower data exchange results in project slowdown or rework [7]. This implies a need for real-time data exchange between building and planning offices [8]. Therefore, designing a near real-time system for tracking construction projects and closing the distance between jobsite operation and construction offices is necessary.

The aim of this study is to evaluate the degree to

which virtual reality systems can be integrated into and affect state-of-the-art construction progress monitoring workflows. This research demonstrates the degree to which mixed reality equipment and 3D laser scanning embedded in visual programming can solve these problems; furthermore, it assesses the effectiveness of the proposed device and framework. We aim to reduce the distance between the jobsite and the construction office, and establish a framework that can provide near real-time progress tracking and data quality control between the construction office and jobsite activities. Therefore, we developed a near real-time progress monitoring system called iVR that consists of four modules: 1) the iVR-scan module monitors jobsite activity using a Kinect scanner, 2) the iVR-prepare module converts captured point cloud data into a 3D model and sends it to the construction office, 3) the iVR-inspect module utilizes virtual reality to help inspectors check activity quality and write review comments, and 4) the iVR-feedback module utilizes augmented reality to visualize inspectors' review reports on jobsites. The iVR system underwent laboratory testing and produced successful results. This system can aid quality inspectors monitor jobsites from construction offices in near real-time, eliminating the need to visit jobsites. Thus, inspectors can monitor multiple activities over a shorter period compared to conventional quality inspection methods. Furthermore, iVR can contribute to a healthier construction environment by reducing human interaction between construction jobsite workers and quality inspectors in the office.

2 Literature Review

Point cloud has been used in different phases of the construction industry for planning and design; production and development; operation and maintenance; etc. [2]. During the planning and design process, point cloud helps in the reconstruction of 3D site models and existing buildings [2,4]. Suitable data acquisition process and devices for construction work include 3D laser scanning, photogrammetry, videogrammetry, and RGB-D and stereo cameras [3].

The Kinect 3D scanner uses the same technology that a mid-range 3D scanner, projector, or infrared camera might use to measure the depth of, and around, an object [9]. The two cameras of the Kinect enable it to scan almost every item in 3D with good precision. The Kinect cameras have been used in the detection and evaluation of construction sites, product identification, materials and labor [2,10], safety monitoring [11] and reconstruction [8]. Many simultaneous localization and mapping (SLAM) programs have used sparse maps to identify and concentrate on real-time monitoring [7]. Other approaches have been used for point-based reconstruction [5]. Kinect cameras reconstruct surfaces more reliably, based on real-world geometry; thus, they exceed point-based representations [7,8].

Immersive modeling increases the understanding of complex construction processes and facilitates the assessment of project situations at reduced costs and interference levels [12,13]. Furthermore, it enables synchronous cooperation between different stakeholders in planning and design [14,15]. The use of virtual reality during the design process has yielded significant improvements in design, which increase workers' safety during construction [16,17].

Laser scanning data are commonly used for dimensional and surface quality assurance in several civil applications and project quality management [18–20]. We propose a precise and effective laser scanning-based technique to reduce the distance between office and construction worksites by combining Kinect 3D scanning and extended reality for a near real-time dimensional and surface quality control approach.

3 Methodology

The research methodology's design and selection were divided into three steps. First, we analysed the current best practice in construction jobsite progress monitoring and selected the best technologies to achieve its objectives. Second, we developed a progress monitoring system called iVR. Finally, we validated the system with a laboratory test and analysed the results for development (Figure 1).

This research proposes a progress monitoring system, iVR, using extended reality and laser scanning. The proposed system consists of four modules: site model capture using 3D laser scanners (iVR-scan); conversion of point cloud into 3D mesh (iVR-preparation); Quality Assurance (QA) inspection and feedback report generation using VR (iVR-inspection); and visualizing inspection feedback on the jobsite using AR (iVR-feedback) (Figure 2).

Figure 1. Research methodology design and selection

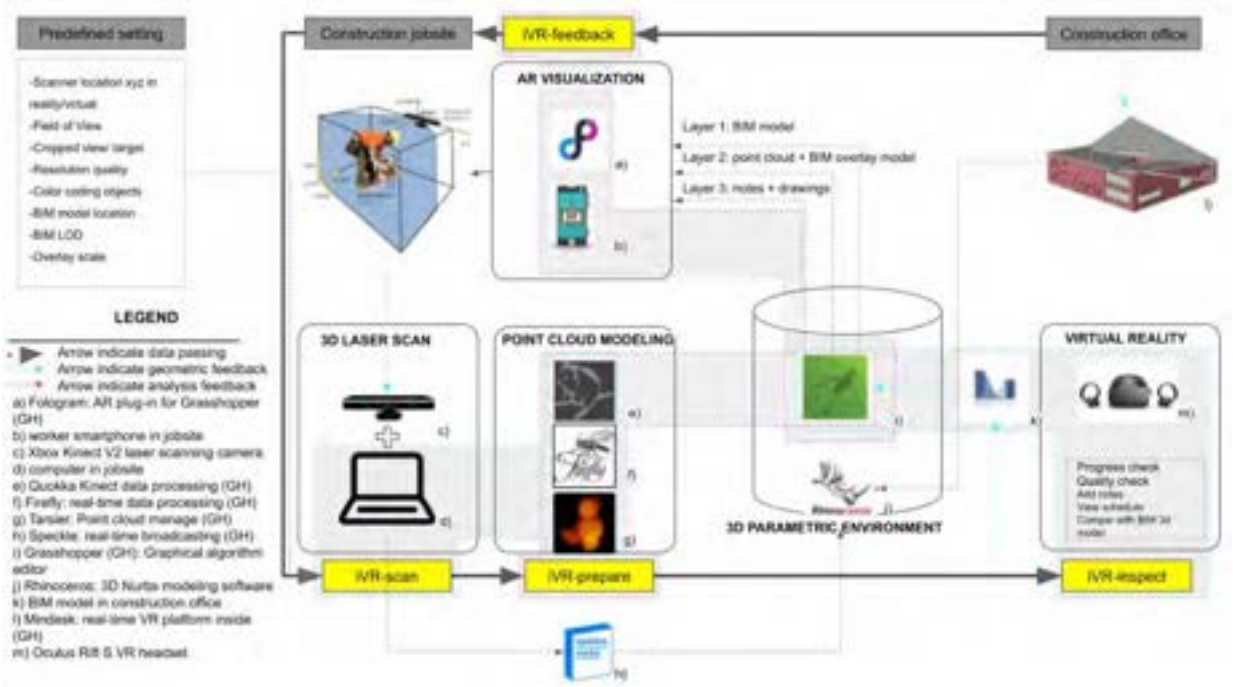

Figure 2. iVR system architecture connection loop between construction jobsite and construction office

3.1 iVR-scan

In this module, a laser scanner installed on the jobsite tracks an operation and sends live scanning data to the building office. This module focuses on the location, path, type of laser scanner, software, and hardware needed to complete this process.

This research used the Kinect V2 [21] [21], offering live scanning, as a 3D laser scanner. (Lidar + photogrammetry = Kinect 3D scan) represents the combination of cameras and sensors for target observation and distance recognition, thus building this research's concept.

The Kinect 3D scanner uses the same technology that is used by a mid-range 3D scanner, camera, or infrared camera to calculate the depth field of, and around, an object. The two "cameras" of the Kinect enable accurate 3D scanning of almost all items.

The scanning process for the target item is as follows: 1) Assign a position for the laser scanner in the BIM area, using the everyday operation optimizer iVR-scan position tool; 2) Set up the laser scanner and direct it toward target objects on the construction site; 3) Connect Kinect V2 to the Grasshopper PC Graphical Algorithm Editor [22,23] in the commercially developed software Rhinoceros [24]. Three point cloud libraries (Quokka [25], Tarsier [26], and Firefly [27]) in Grasshopper manage point cloud data and convert them into point, color, and GPS coordination in order to process the model in real time. Then, the Speckle cloud [28] sends cloud point data from the jobsite to the Grasshopper Rhinoceros in the development office, which gets synchronized and updated per time cycle.

3.2 iVR-preparation

The built algorithm in iVR-preparation processes these data in the construction office as follows, before the inspector gets access to the point cloud data collected from the jobsite: Step 1) Using the Speckle data receiver to receive point cloud data from job PC; Step 2) Building a visual algorithm that coordinates and compares point cloud colours, points, and GPS with the BIM model; Step 3) iVR-crop the selected item from the scanned scene, utilizing colour coding to minimize computational data and the time spent on further measures; Step 4) iVR-preparation uses Alpha shape matching cube mathematical logic [29] and a ball pivoting algorithm [30,31] to convert the point cloud into a 3D mesh object; Step 5) To reduce computational data and time spent, iVR-preparation uses a bounding box to include the produced 3D mesh; Step 6) iVR-preparation contrasts the cloud bounding point box with the BIM model and analyzes the operation's progress.

3.3 iVR-inspect

In this module, 3D mesh is aligned with the BIM model that was developed in iVR-preparation. A progress tracking investigator attaches the virtual reality (VR)

headset to the Rhinoceros area and starts reviewing progress details obtained from the jobsite in VR technology. In general, the iVR-inspection module process is as follows: 1) Aligning the 3D mesh with the BIM model that was developed in iVR-preparation; 2) Linking the VR headset to the virtual reality and set layout design, size, and colors; 3) The controller monitors progress checks, building accuracy, and quality checks; 4) The progress monitoring inspector composes notes, highlights items, and draws illustration types as input; 5) Sending a fresh dataset kit back to the jobsite.

The reason we chose the VR inspection method rather than conventional site visits or BIM versus point cloud screen checking is to give the progress monitoring inspector the capability and power of immersive reality, thereby increasing inspection rate, speed, and accuracy.

Finally, after the progress monitoring inspector completes the progress and quality checks, draws illustrations, and writes comments, iVR-inspection sends multilayer data, including the BIM model, overlay model, comments, drawings, and an accomplishment report to iVR-feedback.

3.4 iVR-inspect

In this module, iVR-feedback uses the Fologram library [32] in Grasshopper Rhinoceros to simulate the inspector's files on the jobsite by utilizing extended reality. The iVR-feedback workflow consists of: 1) A worker's phone is registered with the Fologram tool in the construction office to receive live data; 2) The progress monitoring inspector sends BIM models, comments and sketches, output reviews, and overlay models to a mobile phone on the jobsite via Fologram; 3) A jobsite worker visualizes all the data received via mobile phone in extended reality. Using the parametric models representing the architecture, an immersive holographic instruction set is generated. Fologram synchronizes the geometry created on virtual reality devices through a local Wi-Fi network in a Rhinoceros or Grasshopper file. If a consumer makes improvements to a pattern in Rhinoceros or Grasshopper, those changes will be observed and forwarded to all related extended reality apps, thus allowing users to display digital models in a physical environment and on-scale, while making changes to these models using common, powerful CAD software devices. This tool inspector can also monitor whether a worker uses Fologram to correctly view comments using data from a jobsite; this is a very important benefit of iVR-feedback.

4 Case Study

A laboratory test was designed to simulate a specific activity's quality inspection between the jobsite and the construction office in order to validate the proposed iVR system. All four phases of iVR were introduced in this case study, and the time spent on each phase as well as their accuracy and practicality were reported to facilitate further device growth. The target activity in this research comprised six boxes (20 x 30 x 20 cm) laid in two columns with three boxes on each side of the construction. The target activity was designed in a BIM environment; Styrofoam boxes were used to represent the jobsite (Figure 3) in the laboratory.

The construction site working environment is constantly changing and therefore it is challenging to maintain a constant network between different devices. In the case study one operator runs the iVR-scan that consists of a Kinect V2 camera connected to iVR platform on a portable computer. The computer specifications used in the case study are: (processor: intel core i7 cpu, installed ram 32 gb, graphic card: nvidia GeForce gtx 1060 3gb) which registered 3d point cloud data from target activity in the jobsite. Next, the iVR-prepare cropped the point cloud scene and converted the targeted object into 3D mesh and sent it to the Construction office using Speckle doc cloud synchronizer between two iVR platforms using Wi-Fi internet. After that, the iVR-inspect used VR technology to check quality, insert notes, check progress rate and draw comments and send it to iVR-feedback. In the case study, a smart phone with 4G Wi-Fi was used in iVR-feedback to receive data from the construction office and visualize them in the jobsite. It is essential that both construction offices and iVR-scan are connected to the same wifi host. Finally the worker successfully visualized the inspector report in using AR technology as illustrated in Figure 3.

It takes about 17 minutes to finish one loop of iVR data exchange. It took 23 minutes for the inspector to comment using VR in iVR-inspect and for the worker to provide feedback visualization in iVR-feedback. In total, the laboratory test took about 40 minutes.

First, the laboratory research for the case study began by targeting one pile of boxes for 3D laser scanning, collecting 3D geometry vertices, and documenting the point cloud using Kinect V2 (seconds time). The Qualla library was used to control point cloud resolution to manage the processing and time required for computational data. Next, a cropping box was created containing only selected items (in our case, concrete columns) for the next stage in order to minimize processing time and remove the unwanted items that were scanned from the point cloud, as seen in the iVR-scan module section of Figure 3.

Next, iVR-preparedness monitors point clouds at any interval and updates current point clouds as a loop. In this case study, the interval for updating was set at 17 minutes. As described in the methodology, iVR-preparation used ball pivot algorithms to convert concrete column point

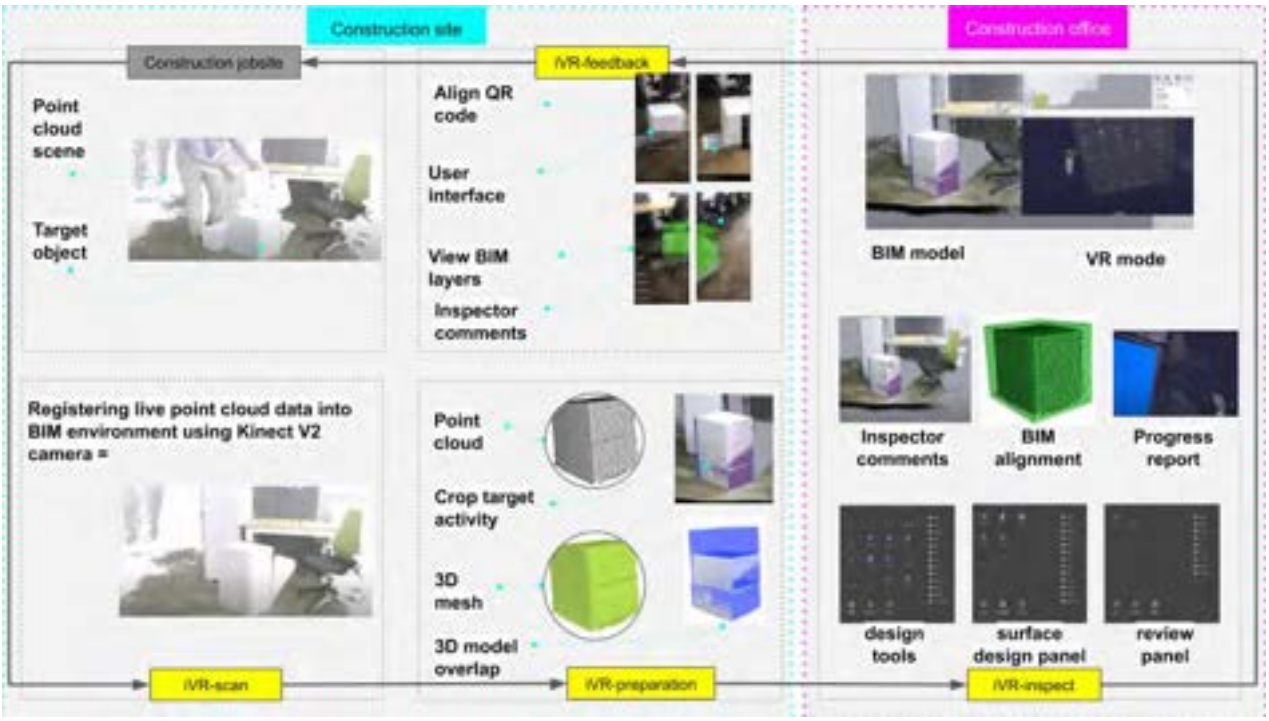

Figure 3. Case study lad test of column monitoring and quality check in near real-time using iVR system

clouds into 3D mesh. Using the Speckle cloud 3D model synchronizing device and overlaying it with the BIM model in the Grasshopper Rhinoceros program as seen in Figure 3, the iVR-preparation module was sent to the development office after the 3D mesh and the point cloud.

After that, progress monitoring inspectors receive point cloud and 3D mesh data in the building office using Grasshopper Rhinoceros and the Speckle data receiver tool. This research used Oculus Rift S [33] [32] to test iVR-inspection. The progress monitoring inspector simulated the 3D model in virtual reality, taking measurements, writing notes, checking development and consistency, taking snapshots of the required information, and producing development reports, as shown in the iVR-inspection module section of Figure 3.

Finally, the iVR-feedback algorithm sends inspectors' progress reports back to the worksite using Fologram's augmented reality platform in Grasshopper Rhinoceros. Workers on the site get progress sheet reports that include

BIM models, feedback, sketches, and accomplishment pace, and overlay models. Notice that external details can often be added to progress reports, including job venue, mission independency, timetable, and building methods. In construction offices, workers' phones and receiver Fologram devices should be connected to the same Wi-Fi network for AR operation. In this case study, iVR-feedback effectively visualized input details on the construction site, allowing workers to check observations from the progress inspector in the overlay model and follow up on the relevant revised information requested by the progress inspector, as seen in the iVR-feedback section of Figure 3.

Figure 3. Case study lab test of iVR progress monitoring using extended reality and data exchange between construction jobsite and office.

5 Discussion

The adopted case study to track the concrete columns' progress showed that the new program can accommodate more complex and robust worksite construction. The iVR program successfully captured tracking data, analysed it, produced a progress inspector's report, and returned it to the construction worksite for input. Through iVR-inspect, auditors can harness the power of augmented reality to observe concrete columns from different angles and take samples that are out of the scope of conventional methods. This research argues that using iVR at the progress monitoring stage could improve decision making and result in a better product in a shorter time span and with the lesser human resources. The study also argues that this approach reduces humans' physical contact, which helps maintain social distancing measures to reduce the spread of infectious diseases, such as the COVID-19 pandemic [95]. The innovative methods, algorithms, and technologies developed in this research distinguish it from past research. Hence, this study makes several significant contributions.

First, the 3D laser scanner is directly connected to the

BIM environment in this research. A medium platform is not required, whereas other frameworks developed by researchers need a medium platform to convert scanned data into point cloud or massing geometry.

Second, the iVR system eliminates file format compatibility issues as every hardware and software is connected directly to the Grasshopper Rhinoceros' visual program. Many progress tracking models, on the other hand, involve various scanning tools in a range of formats (xyz, ply, pts, e57, las, and laz) and BIM-type formats (3dm, dwg, obj, ifc, rvt, and nwd); these variations in file format pose consistency concerns and can also trigger data fragmentation or failure due to the need for specific versions or data processing.

Third, data storage in the BIM environment is managed and controlled in iVR. To import or export information, Kinect apps, the VR headset, and Fologram are connected to the BIM environment, which make them extremely light and easy to work with. However, other state-of-the-art data management tracking exists in the scanning business' cloud or on handheld devices, which is inefficient because the customer has to link the processed point cloud data with another data cloud or other BIM applications to track the operation's progress.

In the case study, the accuracy of registered data in the iVR-scan was +- 3 mm compared to the actual measurements. The laser scanned data accuracy depends on various factors including: distance between target object and laser scanner, colour, scale, rotation of the target object, and the lamination of the room. The backside of the target object is not registered by the laser scanner therefore the 3d model of target object misses the backside which is one of the limitations of fixed laser scanners in the jobsite. The point cloud registered in the iVR-scan can is colour coded also which can help iVR-inspect differentiate different objects using associated colour code. The scale factor remained fixed to 1 to 1 throughout the iVR loop to maintain accuracy and data management. There was no data loose during the iVR loop except when iVR-prepare crop the scene point cloud and detach target object from the rest of the point cloud to reduce computation time. The system needs to be tested on a variety of construction activities with different object scales and colour to compare accuracy and efficiency of iVR.

6 Conclusion

Despite critical advancements in 3D scanning and photogrammetry techniques for tracking building progress, traditional quality control and progress testing often entail manual inspection or data analysis, which takes a long time to track and relies on conventional methods. A near real-time project monitoring tool (iVR) has been developed and tested to address this issue. The vital benefits of iVR are summarized, based on the findings, as follows:

(A) The study indicates that the device significantly reduces the information gap between the development office and jobsite; the collection, sharing, and computation of data requires fewer resources and time.

(B) Immersive, interactive, and augmented technologies allow investigators and workers to visualize tasks from perspectives that are unfeasible with traditional approaches; they enable effective interaction and an almost tangible approach to the data by providing investigators and workers with the appropriate means to sketch, report, and add data.

(C) Using iVR, inspectors can monitor several activities in a short period while remaining in the construction office. Furthermore, it can reduce human resources and improve quality and production.

(D) The system can ensure social distancing and minimize human activity among staff and construction officers, which might further mitigate the spread of infectious diseases on building sites during the ongoing COVID-19 pandemic.

To conclude, iVR's potential for progress tracking at the construction level was identified and validated with a laboratory-tested case study. This method will be presented in the future as a tab plug-in to commercial software applications; it will improve the progress tracking inspection process. The methodology's scope in the architectural field is limited to activity geometry, such as construction progress monitoring; however, in the future, it could be expanded to also include progress tracking (photogrammetry + Real 3D scanner), material tracking (GPS, RFID), worker tracking (RFID), and equipment tracking (GPS and distributed sensors). The iVR-scan is currently only applicable to jobsite target activity; however, it can be extended to not only focus on object quality checks, but can also consider human activity, such as human recognition and skeletonizing, to identify human figures and track skeleton images of people moving within the Kinect field of view. In iVR-preparation, generated reports could be integrated with BIM schedule targeted activity reports to give feedback to 4D BIM, facilitating automatic updates and increasing automation in QA inspection.

Data Resources

All of the iVR project's visual program algorithms and datasets are stored in the Mendeley Data repository https://data.mendeley.com/datasets/g2xh9k5yzy/1, and

the results that are presented in this paper can be reproduced by following the readme file instructions or the methodology that this paper explained. Case study video footage can be found using these links: https://www.youtube.com/watch?v=jjT40j6UATw; https://www.linkedin.com/posts/ahmed-khairadeen-ali-09631791_cad-digitalconstruction-openbim-activity-6668921608612253696-RBeS; and https://www.linkedin.com/posts/ahmed-khairadeen-ali-09631791_openbim-dynamo-digitalconstruction-activity6674930637192998912-ASWP.

Acknowledgement

This study was financially supported by the National Research Foundation of Korea (NRF) grant funded by the Korea government Ministry of Science and ICT (MSIP) [No. NRF-2020R1A4A4078916]. This research was also supported by Haenglim Architecture and Engineering Company. The first author would like to thank Chung Ang University and the Korean Government Scholarship program.

References

[1] R. Volk, J. Stengel, F. Schultmann, Building Information Modeling (BIM) for existing buildings — Literature review and future needs, Autom. Constr. 38 (2014) 109–127.

[1] R. Volk, J. Stengel, F. Schultmann, Building Information Modeling (BIM) for existing buildings — Literature review and future needs, Autom. Constr. 38 (2014) 109–127. https://doi.org/10.1016/j.autcon.2013.10.023.

[2] D. Rebolj, Z. Pučko, N.Č. Babič, M. Bizjak, D. Mongus, Point cloud quality requirements for Scan-vs-BIM based automated construction progress monitoring, Autom. Constr. 84 (2017) 323–334. https://doi.org/10.1016/j.autcon.2017.09.021.

[3] M.-K. Kim, J.C. Cheng, H. Sohn, C.-C. Chang, A framework for dimensional and surface quality assessment of precast concrete elements using BIM and 3D laser scanning, Autom. Constr. 49 (2015) 225–238.

[4] A. Braun, S. Tuttas, A. Borrmann, U. Stilla, Improving progress monitoring by fusing point clouds, semantic data and computer vision, Autom. Constr. 116 (2020) 103210. https://doi.org/10.1016/j.autcon.2020.103210.

[5] C. Zhang, D. Arditi, Automated progress control using laser scanning technology, Autom. Constr. 36 (2013) 108–116.

[6] I. Brilakis, H. Fathi, A. Rashidi, Progressive 3D reconstruction of infrastructure with videogrammetry, Autom. Constr. 20 (2011) 884–895. https://doi.org/10.1016/j.autcon.2011.03.005.

[7] D. Chekhlov, M. Pupilli, W. Mayol-Cuevas, A. Calway, Real-Time and Robust Monocular SLAM Using Predictive Multi-resolution Descriptors, in: G. Bebis, R. Boyle, B. Parvin, D. Koracin, P. Remagnino, A. Nefian, G. Meenakshisundaram, V. Pascucci, J. Zara, J. Molineros, H. Theisel, T. Malzbender (Eds.), Adv. Vis. Comput., Springer, Berlin, Heidelberg, 2006: pp. 276–285. https://doi.org/10.1007/11919629_29.

[8] H.P.H. Shum, E.S.L. Ho, Y. Jiang, S. Takagi, Real-Time Posture Reconstruction for Microsoft Kinect, IEEE Trans. Cybern. 43 (2013) 1357–1369. https://doi.org/10.1109/TCYB.2013.2275945.

[9] P. Henry, M. Krainin, E. Herbst, X. Ren, D. Fox, RGB-D mapping: Using Kinect-style depth cameras for dense 3D modeling of indoor environments, Int. J. Robot. Res. 31 (2012) 647–663. https://doi.org/10.1177/0278364911434148.

[10] Sacks R., Navon R., Brodetskaia I., Shapira A., Feasibility of Automated Monitoring of Lifting Equipment in Support of Project Control, J. Constr. Eng. Manag. 131 (2005) 604–614. https://doi.org/10.1061/(ASCE)0733-9364(2005)131:5(604).

[11] N. Khan, A.K. Ali, M.J. Skibniewski, D.Y. Lee, C. Park, Excavation Safety Modeling Approach Using BIM and VPL, Adv. Civ. Eng. 2019 (2019) e1515808. https://doi.org/10.1155/2019/1515808.

[12] J.M. Davila Delgado, L. Oyedele, T. Beach, P. Demian, Augmented and virtual reality in construction: Drivers and limitations for industry adoption, J. Constr. Eng. Manag. 146 (2020) 04020079.

[13] S.A. Miller, R. Abovitz, System and method for augmented and virtual reality, 2020.

[14] M. Noghabaei, A. Heydarian, V. Balali, K. Han, A Survey Study to Understand Industry Vision for Virtual and Augmented Reality Applications in Design and Construction, ArXiv Prepr. ArXiv200502795. (2020).

[15] M. Noghabaei, A. Heydarian, V. Balali, K. Han, Trend Analysis on Adoption of Virtual and Augmented Reality in the Architecture, Engineering, and Construction Industry, Data. 5 (2020) 26.

[16] J. Labovitz, C. Hubbard, The Use of Virtual Reality in Podiatric Medical Education, Clin. Podiatr. Med. Surg. 37 (2020) 409–420.

[17] M.M.A. da Cruz, A.L. Ricci-Vitor, G.L.B. Borges, P.F. da Silva, F. Ribeiro, L.C.M. Vanderlei, Acute hemodynamic effects of virtual reality based-therapy in patients of cardiovascular rehabilitation: cluster randomized crossover trial, Arch. Phys. Med. Rehabil. (2020).

[18] S.K. Vasudevan, K. Venkatalachalam, S.A. Preethi, G. Mithula, G. Navethra, K. Nagarajan, An interactive and innovative application for hand rehabilitation through virtual reality, Int. J. Adv. Intell. Paradig. 15 (2020) 252–272.
[19] R. Tilhou, V. Taylor, H. Crompton, 3D Virtual Reality in K-12 Education: A Thematic Systematic Review, in: Emerg. Technol. Pedagog. Curric., Springer, 2020: pp. 169–184.
[20] E. Rho, K. Chan, E. Varoy, N. Giacaman, An Experiential Learning Approach to Learning Manual Communication through a Virtual Reality Environment, IEEE Trans. Learn. Technol. (2020).
[21] Amazon.com: Kinect for Windows: Computers & Accessories, (n.d.). https://www.amazon.com/Microsoft-L6M-00001-Kinect-for-Windows/dp/B006UIS53K (accessed May 19, 2020).
[22] Grasshopper - algorithmic modeling for Rhino, (n.d.). https://www.grasshopper3d.com/ (accessed May 22, 2020).
[23] A.K. Ali, H. Song, O.J. Lee, E.S. Kim, H.H. Mohammed Ali, Multi-Agent-Based Urban Vegetation Design, Int. J. Environ. Res. Public. Health. 17 (2020) 3075. https://doi.org/10.3390/ijerph17093075.
[24] Rhino 6 for Windows and Mac, (n.d.). https://www.rhino3d.com/ (accessed May 22, 2020).
[25] alhadidi, QUOKKA PLUGIN (REAL-TIME 3D SCANNING), Suleiman Alhadidi. (2017). http://alhadidi.com/quokka-plugin-real-time-3d-scanning/ (accessed May 22, 2020).
[26] camnewnham / tarsier — Bitbucket, (n.d.). https://bitbucket.org/camnewnham/tarsier/src/master/ (accessed May 22, 2020).
[27] Firefly Experiments, Firefly Exp. (n.d.). http://www.fireflyexperiments.com (accessed May 22, 2020). [28] Speckle Docs / Grasshopper Basics, (n.d.). https://speckle.systems/docs/clients/grasshopper/basics/ (accessed May 22, 2020).
[29] CGAL 5.0.2 - 3D Alpha Shapes: User Manual, (n.d.). https://doc.cgal.org/latest/Alpha_shapes_3/index.html (accessed May 22, 2020).
[30] W. Lu, L. Liu, Surface reconstruction via cooperative evolutions, Comput. Aided Geom. Des. (2020) 101831.
[31] M. Zhang, Y. Rao, J. Pu, X. Luo, Q. Wang, Multi-data UAV Images for Large Scale Reconstruction of Buildings, in: Int. Conf. Multimed. Model., Springer, 2020: pp. 254–266.
[32] Fologram | Food4Rhino, (n.d.). https://www.food4rhino.com/app/fologram (accessed June 11, 2020).
[33] Oculus Rift S: VR Headset for VR Ready PCs | Oculus, (n.d.). https://www.oculus.com/rift-s/?locale=en_US (accessed June 6, 2020).

VRGlare: A Virtual Reality Lighting Performance Simulator for real-time Three-Dimensional Glare Simulation and Analysis

Kieran W. May[a], James Walsh[a], Ross T. Smith[a], Ning Gu[a], Bruce H. Thomas[a]

[a] Australian Research Centre for Interactive and Virtual Environments,
University of South Australia, Mawson Lakes, Australia
E-mail: kieran.may@mymail.unisa.edu.au, {james.walsh, ross.smith, ning.gu, bruce.thomas}@unisa.edu.au

Abstract -

Lighting performance simulators play an important role in the architectural design process, as it provides the means to address lighting design issues early within the design stage of a construction project life-cycle. Currently, several lighting performance simulators provide support for glare simulation and analysis; however, they are primarily limited to two-dimensional desktop displays and not capable of simulating glare in real-time. Furthermore, the quantitative data produced from these simulators consist of reports, complex numerical data-sets, two-dimensional graphs, and charts, which creates a divergence between the data produced and the three-dimensional context of the building. As a result, analysis of glare data generally requires specialists such as experienced architects who have an extensive background in interpreting these two-dimensional data-sets. In order to overcome the aforementioned issues, we present VRGlare: an immersive Virtual Reality lighting performance simulator capable of real-time glare simulation and analysis. In addition to semi-realistic lighting renderings, this research proposes four visualisation techniques to represent glare within an immersive three-dimensional context. We also present two multi-sensory approaches designed to re-create the physical discomfort that occurs when experiencing glare. This paper provides an overview of the developed simulator which includes the hardware, software, algorithms, visualisations, and multi-sensory representation of glare discomfort.

Keywords -

Virtual Reality; Lighting Performance Simulation; Immersive Glare Visualisation; Glare Analysis; Building Information Modelling

1 Introduction

Sufficient work-place lighting is an essential requirement for workers who spend multiple hours on a computer per day. Previous studies have demonstrated visual discomfort in the workplace has a negative impact on a worker's overall level of productivity, performance, and overall job satisfaction [1, 2]. The physical symptoms associated with visual discomfort include eye-strain, headaches, fatigue, red, sore, itchy, watering eyes, and lighting sensitivity. Visual discomfort can occur in workplaces due to various factors associated with lighting including uniformity, glare, veiling reflections, shadows, and flicker [3]. As a result, providing architects with the necessary tools to mitigate visual discomfort during their design process is required. With the continuous advancements of Lighting Performance Simulators (LPS) in recent years, LPS has become an increasingly used tool for architects to plan and design their ideal lighting layout. A LPS can be defined as a software system that provides the ability to simulate, analyze, and assess the performance of lighting through realistic simulations, algorithms, and large subsets of data. Currently, several LPS systems provide support for glare simulation and analysis, however, they are primarily limited to two-dimensional desktop displays and not capable of simulating glare in real-time. Furthermore, the quantitative data produced from these simulators consist of reports, complex numerical data-sets, two dimensional graphs, and charts, which creates a divergence between the data produced and the three-dimensional context of the building. These traditional methods of representing glare data were based on the limitation that computers lacked the hardware capability to simulate lighting data in real-time. However, as processing speed and power of computers rapidly advances [4], glare simulators will transition from requiring lengthy calculation processes to real-time simulation of data. As a result, new and improved methods for representing glare will be introduced over-time rendering previous methods obsolete. In order to overcome the aforementioned issues, we present VRGlare: an immersive LPS capable of real-time simulation and visualisation of Glare for lighting design and analysis. The proposed system utilizes Virtual Reality (VR) to improve the spatial awareness, and presence [5] lacking in modern PC-based LPS. A set of five immersive visualisations were developed and presented in this paper to demonstrate the potential of using VR for real-time glare simulation and analysis. Due to the dynamic range of current head-mounted displays (HMDs), it is not possible to experience glare discomfort in VR. Therefore, we present two multi-sensory approaches to achieve recreation of glare discomfort in VR using haptic and audio interfaces.

The specific contributions of this paper are:

- A **real-time Virtual Reality Glare simulator** for immersive glare analysis and design.
- A set of **five visualisation techniques** to represent glare within a real-time immersive environment.
- Two methods for **representing glare discomfort through multi-sensory** approaches.

2 Related Work

Despite the rapid hardware advancements of computers in the last decade, limited investigations have been conducted on real-time simulation of glare data for lighting analysis and design. Moreover, no prior research exists on exploring the use of immersive three-dimensional visualisation techniques to create a direct link between glare data produced and the three-dimensional context of the building. As a result, the related works discussed in this section consists mostly on previous research exploring the integration of immersive displays for lighting performance simulation and analysis. The specific research addressed includes the following areas associated with immersive lighting performance: artificial and natural lighting design, day-lighting analysis, and energy cost and consumption. We also provide a brief overview of the historical research developments for LPS, and describe a modern commercial LPS which supports glare simulation and analysis: DIALux.

2.1 Immersive Lighting Performance tools for Simulation and Analysis

In recent years, researchers have begun exploring the integration of Virtual and Augmented reality (AR) with Building Information Modelling (BIM) for lighting design and analysis. BIM is described as a process where building information related to a project's activities is directly linked with a corresponding three-dimensional virtual CAD model. BIM has the potential to be a valuable tool for improving the accuracy of future lighting simulations as non-geometrical factors such as material can have a considerable impact on lighting performance. One of the earliest works using immersive displays for lighting analysis was achieved by Sheng et al. [6] who built a multi-projector AR table-top visualisation system capable of simulating artificial and natural lighting of buildings. The developed prototype was capable of simulating the effects of day-lighting over a 24 hour day-time cycle. Similarly, Natephra et al. [7] developed a BIM-based lighting design feedback (BLDF) prototype targeted towards immersive visualisation using VR. The motivation for developing BLDF was to address flaws associated with previous LPS tools. The authors noted one of the key improvements of their prototype was the implementation of a built-in system to calculate and provide information relating to lighting energy cost and consumption. The results from a case-study conducted demonstrated BLDF was capable of providing stakeholders with an increased level of satisfaction and understanding for perceiving and optimizing lighting conditions to improve lighting design, and mitigate energy costs for future occupants. The authors discussed one of the future directions of their work is to incorporate support for glare simulation and analysis. More recently, Wong et al. [8] developed an immersive lighting visualisation tool incorporating VR and aspects of BIM. This was achieved by linking lighting simulation data obtained from DIALux with the Unity 3D Game Engine to handle VR visualisation and interaction. The results of this research concluded that the system was capable of producing realistic lighting rendering effects and provided the appropriate feedback for users to make informed lighting decisions. Immersive VR daylighting analysis and simulation tools such as RadVR [9] have also demonstrated VR as an effective medium to improve spatial understanding of tasks, improve navigation, and sun position analysis in comparison to PC oriented LPS tools. Representation of daylighting data using RadVR was achieved through two-dimensional heatmaps which incorporated a three colour gradient palette consisting of blue as the minimum value, yellow as the median, and red as the maximum. Birt et al. [10] performed a comparability study aimed at assessing the advantages and disadvantages of using VR for lighting simulation and analysis compared to AR. The results of this research showed VR was most efficient for lighting visualisation and provided a more realistic reconstruction of the real world, whereas AR improved the manipulability of the system, enhanced creativity, and improved participants confidence of the design.

2.2 Commercial Glare Simulation and Analysis applications

The history of lighting performance simulators dates back as early as 1970s when researchers begun developing algorithms to predict luminance and illuminance levels of natural, and artificial light sources [11]. Due to the limited computational power at this time, data was primarily represented numerically. By the 1990s, computer hardware became advanced enough to allow lighting simulators to produce semi-realistic rendered images of lighting. However, these simulators still primarily relied on representing data through numerical datasets, and two-dimensional images and drawings such as isolines. The 1990s also saw the introduction of Radiance: a LPS capable of simulating glare [12], luminance, and illuminance levels [13]. The lighting engine utilized a backwards ray-tracing approach to produce semi-realistic lighting simulations of CAD models. Among numerical datasets, Radiance also utilized semi-realistic static images to visualise lighting data. These images could be overlayed with different visualisations such as false-colour images or contour lines. Radiance was later open-sourced and is still widely utilized as both a lighting analysis tool and backend lighting engine to several LPS systems. Modern commercial LPS applications such as DIALux[1] provides support for calculation, and analysis of glare, daylighting, and artificial

[1]https://www.dialux.com/en-GB/

lighting analysis, energy consumption, among a variety of other features. The software integrates CAD support allowing users to design buildings directly through their software, or import CAD models and BIMs using the Industry Foundation Class. DIALux utilizes LUMSearch: a catalogue search engine to support the integration of a comprehensive range of lighting fixtures. However, despite the significant computational hardware advancements over-time, lighting visualisations in DIALux still primarily consist of traditional approaches for representing glare. These approaches include isolines, numerical data-sets, two-dimensional graphs and charts, static three-dimensional false-colour images and lighting renderings, and auto-generated reports. Although these traditional methods of representing glare data are still effective, users lack the in-situ awareness of the building which we believe can potentially lead to misinterpretation of data. Furthermore, calculation of glare data requires a lengthy calculation process and isn't capable of real-time. We believe real-time simulation of glare data is necessary to provide a more precise representation of glare data resulting in users making more informed lighting decisions.

3 System Overview

3.1 Hardware

The VR technology used to run VRGlare consisted of a standard HTC Vive[2] setup. We also experimented with the Pimax 5K Plus[3] HMD capable of producing a 170 degree field of view (FOV), and 2560x1440 resolution on each lens. However, due to the significantly higher performance demands of the Pimax we primarily used the Vive. A powerful PC was used to handle the high processing and memory demands of VRGlare. The specifications of the PC consisted of an Nvidia GeForce RTX 2080 Graphics Card with an Intel(R) Core(TM) i7-9700 CPU @ 3.00GHz processor and 16GB RAM. Two standard HTC Vive controllers with 6DOF tracking were used as the input devices.

3.2 Lighting Performance Simulator: VRGlare

In order to develop our own glare visualisation techniques, we designed and built our own custom LPS which we called VRGlare. VRGlare was developed using the Unity 3D game engine, and the software was programmed entirely in C#. The lighting rendering system was based off Unity's High Definition Rendering Pipeline described in Section 3.5.1, and initial lumen calculations were based off Unity 3D's built-in lighting integration. The SteamVR library was incorporated to provide VR support, and the 3D User Interaction Toolkit [14] to provide basic VR interaction. The specific motivation for building our own custom LPS was due to other open-source solutions not providing real-time simulation capability, lacked VR support, or did not provide access to their rendering system to build custom visualisation techniques.

[2]https://www.vive.com/
[3]https://www.pimax.com/pages/5k-plus-bundle

3.3 Glare Calculations

3.3.1 Real-time calculation Algorithm

The following four-step algorithmic approach is utilized in VRGlare to achieve a real-time simulation of glare data.

1. At run-time, all objects within the Virtual Environment (VE) are broken down into smaller submeshes. **(Re-calculated once every 500ms)**
2. Lux is calculated for each submesh by casting a ray from each light source to all submeshes within the light sources range.
3. Retrieve all active submeshes within the user's view frustum.
4. Re-calculate glare for each sub-mesh using the UGR equations shown below.

3.3.2 Unified Glare Rating

The Unified Glare Rating (UGR) [15] illustrated in equation 1 is utilized in our LPS to calculate glare discomfort. The UGR equation is used to determine the likelihood of a luminaire causing glare discomfort to surrounding objects. UGR outputs values generally range from < 10 being imperceptible, to > 28 being uncomfortable (see Table 1).

$$UGR = 8log[0.25/Lb \sum(L^2\omega/p^2)] \quad (1)$$

Where Lb is the background luminance, L is the luminance of the luminous parts of each luminaire in the direction of the observer's eye, ω is the solid angle of the luminous parts of each luminaire at the observer's eye, and p is the Guth position index for each luminaire.

Table 1. This table demonstrates the range of values outputted by the UGR equation and its associated description. The corresponding RGB values used in the heat-map visualisation described in Section 3.5.2 are shown on the right-most column (The RGB colours in the table may differ from the generated colours in the system).

UGR Rating	UGR Description	Heat Map RGB
<10	Imperceptible	0, 34, 255
>10 <15	Just perceptible	0, 255, 255
>15 <18	Perceptible	0, 255, 125
>18 <21	Just acceptable	0, 255, 0
>21 <24	Unacceptable	0.35, 0.72, 0.188
>24 <28	Just uncomfortable	0.7, 0.72, 0.188
>28	Uncomfortable	1, 0, 0.188

3.4 Bench-markings: Performance Analysis

The capability and performance of VRGlare was measured through a series of stress-tests designed to determine how many glare calculations points the system was capable of handling in real-time. The structure of these tests consisted of spawning an increasing amount of light sources, and virtual objects within the users FOV. To maintain a consistent amount of submeshes, we re-used the same object for each trial. The heatmap visualisation later described in Section 3.5.2 was used as the primary glare visualisation technique throughout the tests. The hardware specifications used in these tests are described in Section 3.1, with the exception of the Pimax 5K which was substituted with a standard HTC Vive HMD. The overall results demonstrated VRGlare performed reasonably well (45 FPS) with 5 light sources, and 50 objects (1300 submeshes) within the user's FOV. A full breakdown of the bench-marking results are described in Table 2.

Table 2. Benchmarking results for heatmap visualisation

Objects In FOV	Light Source	Sub-Meshes	Rays Casted	Frames per second
1	1	26	27	90
10	2	260	552	85
10	5	260	1305	50
20	5	520	2605	48
20	10	520	5210	46
50	5	1300	6505	45
50	10	1300	13010	27
75	10	1950	19510	15
100	10	2600	26010	10
100	20	2600	52020	<5

3.5 Glare Visualisation Techniques

In this section we provide an overview of the visualisations and multi-sensory approaches used in VRGlare to represent glare within an immersive three-dimensional environment. The visualisations described consist of a standard semi-realistic lighting rendering, real-time heatmaps, three new visualisations, and two multi-sensory glare discomfort techniques. Each section provides an overview of each technique which includes the design motivations, partial implementation details, advantages, disadvantages, and potential uses.

3.5.1 Semi-realistic Lighting Visualisation

The semi-realistic lighting visualisation is designed to present a standard semi-realistic rendering of the generated lighting, and glare present within the VE. This is achieved through Unity's built-in High Definition Rendering Pipeline (HDRP) which handles the backend rendering calculations. A number of variables such as the intensity, position, and orientation of natural, and artificial light sources within the VE are used to calculate lighting. Additional object parameters such as materials are also considered to generate semi-realistic glare rendering. Furthermore, the HDRP combines semi-realistic shaders, and global illumination algorithms to simulate direct and indirect lighting phenomenons such as glare, shadows, reflectiveness, and light ray bouncing.

Figure 1. This image presents the standard HDRP Lighting Visualisation: which is a realistic representation of Glare within the scene. Lights are set to 800 lumens and a 3 meter range.

The motivation for utilizing the HDRP as our default visualisation is to present a semi-realistic recreation of the expected lighting produced based on a given lighting design. Additional four-dimensional support has been integrated into the system allowing users to simulate the lighting at specific times throughout the day. The combined use of Unity's HDRP with VR also allows users to experience the interior lighting of a building from a first-person perspective. VR locomotion techniques such as teleportation has also been implemented in VRGlare to provide a non-disorienting approach to navigate throughout the building. We believe this visualisation could be particularly useful for architects to gather lighting feedback from client(s) and other stakeholders associated with the development of the building. The disadvantages of using a default lighting visualisation mainly stems from the user's inability to accurately determine whether the intensity of glare present inside the VE is acceptable or not. As a result, we present our implementation of four visualisations, and two multi-sensory approaches to overcome this specific problem. Furthermore, the HDRP utilizes separate algorithms for glare calculation as opposed to the UGR standards described in section 3.3. This results in less-accurate representation of glare depicted in the rendering as opposed to our other propose visualisations which utilize the standardized UGR equations to calculate glare.

Figure 2. This image presents the heatmap Lighting Visualisation: which generates a three-dimensional heatmap to represent the amount of Glare within the scene. Lights are set to 800 lumens and a 4 meter range.

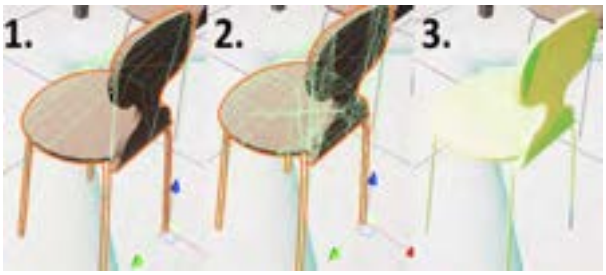

Figure 3. This diagram shows the process of superimposing heatmaps onto virtual objects. *1)* A standard object with a mesh collider is placed into the VE, *2)* The object is sliced into twenty-three submeshes, *3)* Calculations are performed and the generated heatmap is superimposed over the object.

3.5.2 Realtime Heatmap Visualisation

The real-time heatmap visualisation utilizes false-colour images to represent the intensity of glare within the user's FOV. The corresponding RGB colours used in the heatmaps to represent glare intensity follow a four colour gradient palette illustrated in Table 1. At run-time, all objects within the VE are broken down into sub-meshes, these sub-meshes are then used to calculate glare for multiple surface points of an objects. Once these calculations have taken place, the generated heatmaps are superimposed over objects within the VE providing glare feedback to the user (See Figure 3). Unlike previous LPS which require lengthy re-calculation processes whenever a change occurs to the building design, VRGlare is capable of producing calculations in real-time. This means when an object or light source properties are manipulated within the VE, the heatmaps will automatically and simultaneously update in real-time. Prior use of heat-map or false-colour visualisations to represent data on surfaces has been demonstrated as an effective approach to convey feedback due to its high-level of detail, and simplistic readability [16]. Heatmap visualisations provide a simple yet in-depth representation of glare data by revealing the glare intensities for all possible surfaces within the user's FOV using a colour-coded visualisation. The simplistic nature of heatmaps allows interpretation of glare data to be achieved without necessarily requiring an architect or interior designer to analyze data. The trade-off associated with using real-time heatmap visualisations results in users losing the semi-realistic aspects for both the lighting rendering and graphics within the scene. This is due to the visualisation technique superimposing RGB colour-coded heatmaps over the virtual objects thus obstructing the natural material of the objects, and as a result creating an inaccurate representation of how the expected lighting would appear within the building.

Heatmap Visualisation Extension: MirrorViz

MirrorViz is a tool developed as an extension to the real-time heatmap visualisations. The motivation for MirrorViz is that it allows users to overcome the trade-off limitation associated with being unable to experience the realistic-lighting rendering effects when using heatmaps. MirrorViz overcomes this limitation by attaching a 'mirror' to the user's hand which acts as a gateway between the heatmap and semi-realistic lighting rendering effects of the VE.

Figure 4. This image presents MirrorViz: an extension to the heatmap visualisation technique

3.5.3 Bendrays Visualisation

The Bendrays visualisation technique is loosely based off the previously developed interaction technique Bendcast[17]. Bendrays represents glare by casting multiple rays from the user's hand to objects within the user's FOV. The rays bend towards object surfaces that produce a UGR value greater than the glare discomfort threshold set by the user. The casted rays are represented as red bezier curves which bends towards objects based on the angle between the user's hand and the given object. This process provides a natural way of casting multiple rays from the user's hand without obstructing the user's perspective.

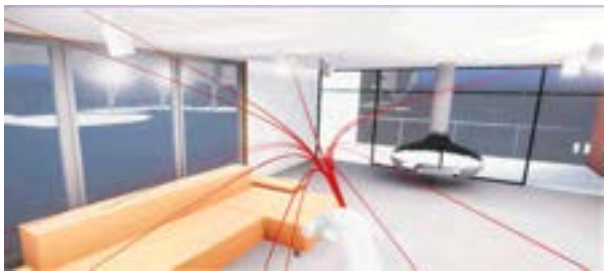

Figure 5. This image presents the Bendrays Lighting Visualisation: (Settings Lights 800 Lumens, 3 meter range in the scene. Rays bend to spots with > 30 UGR

Figure 6. Animated Arrows visualisation. Top image shows the visualisation with a UGR > 24 whereas the bottom image contains a UGR threshold of > 0

The design motivations which led to the development of the Bendrays visualisation stems from addressing the fundamental limitation of heatmaps which results in users being unable to experience the semi-realistic lighting rendering and graphics provided by Unity's HDRP. Due to the high memory usage of the Bendrays algorithm, Bendrays can negatively impact the performance of the real-time simulator when a large number of objects exceeding the glare threshold are present within the user's FOV. Additionally, in this scenario, the large number of rays produced can potentially obstruct the user's perspective and reduce the readability levels of the visualisation. Lastly, based on our informal observations we believe Bendrays is unable to provide the level of detail compared to the heatmap visualisation and as a result interpretation of data is not as intuitive.

3.5.4 Animated Arrows Visualisation

Animated arrows is a volumetric glare visualisation designed to represent glare discomfort through virtual arrow cues. The generated arrows are omitted from a given light source to any light ray hit surfaces within the user's FOV that exceeds the glare threshold set by the user. The trajectory for the animated arrows is achieved by casting rays from the light source to all submeshes within the users FOV. Using this trajectory, the arrow follows the path of the casted ray until it hits the surface of the mesh. Once the animated arrow collides with the mesh, the object's material is momentarily replaced with a generated heatmap. Finally, the animation will reset after a specified amount of time set by the user and repeat the animation cycle over. Additional parameters can be modified by the user such as the speed of the animation, or the amount of arrows produced by modifying the glare threshold. Animated Arrows provides a unique approach to represent glare data as it allows the user to visualise the entire process of a light-ray being cast from the origin light source to the surface it hits. Due to the additional background information provided, we believe this visualisation not only allows users to visualise glare data, but also provides an approach for users to gain a more detailed understanding of the entire process that's causing the glare to occur. As a result, we believe animated arrows can be a particularly useful tool for re-designing artificial light sources to mitigate glare, especially for users who may not have an extensive background in lighting design. Our current implementation of animated arrows utilizes a performance heavy-algorithmic approach. This can specifically becomes an issue if a large amount of objects exceeding the glare threshold are present in the users FOV. The outcome in this scenario would result in the visualisation producing potentially hundreds of animated arrows causing the applications frame rate to drop. Similarly to the Bendrays visualisation, the large amount of arrows produced may result in the visualisation becoming distracting to the users, and partially obstruct the user's FOV resulting in decreased readability levels as depicted by Figure 6. Lastly, based on our informal observations we believe representation of glare data is not as intuitive as the heatmap visualisation. This is primarily due to the user being required to wait for the animation to complete its cycle in order to interpret the glare data from the generated heatmap.

3.6 Multi-sensory Glare Discomfort Representations

Currently, LCD and other related displays do not provide the required dynamic range for reproducing the vi-

sual discomfort phenomena that occurs when a user experiences glare in VR. Therefore, in order to recreate the physical discomfort associated with experiencing glare we propose two multi-sensory approach of representing glare discomfort.

Table 3. Audio and Haptic feedback table

UGR Rating	UGR Description	Mean Pitch Frequency (Sine)	Mean Pitch Frequency (Triangle)	Vibration Freq
<10	Imperceptible	97.8 Hz	151.8 Hz	20 Hz
>10 <15	Just perceptible	127 Hz	224.8 Hz	30 Hz
>15 <18	Perceptible	154.2 Hz	270 Hz	50 Hz
>18 <21	Just acceptable	191.2 Hz	502 Hz	70 Hz
>21 <24	Unacceptable	313.4 Hz	899.2 Hz	100 Hz
>24 <28	Just uncomfortable	494.2 Hz	1152.2 Hz	150 Hz
>28	Uncomfortable	1057 Hz	1794.4 Hz	255 Hz

3.6.1 Audio-based Discomfort Representation

Our first approach utilizes an audio-based interface designed to re-create glare discomfort by stressing the user through audio cues. This is achieved by producing varying pitches of three-dimensional frequencies based on the amount of glare visible within the user's FOV. The algorithm is described as followed: firstly, the UGR calculation is performed to determine the amount of glare associated with each object present in the user's FOV. Next, a three-dimensional audio source is placed at the position of the produced glare sources. Finally, the audio source outputs a three-dimensional sound at a specific frequency based on the amount of glare produced by a given object. The frequencies obtained as illustrated in Table 3 were collected by running a pilot study where participants (n=5) were instructed to change the Hertz frequency to match the description described in the UGR discomfort-scale. The mean pitch was then calculated from the data-set and used to determine the frequencies of the sounds produced by the simulator. Another design motivation for developing this technique was to provide users with an approach to represent discomfort levels of glare in the VE without having to visually the experience the glare. One particular scenario where this technique could be used is to provide 360 degree glare feedback, this would allow a user to gain an understanding of objects producing glare behind or outside the users FOV. The disadvantages with using an audio-based interface to represent glare is primarily associated with the difficulty required to accurately interpret data and locate the origin of a glare source. To resolve this issue, we propose using the audio interface concurrently with a visualisation technique.

3.6.2 Haptic-based Discomfort Representation

In addition to an audio-based glare discomfort technique, we also experimented with an alternative multi-sensory approach which utilizes haptic feedback to convey glare discomfort through vibrations. This is achieved by outputting vibrations ranging in intensity values based on the amount of glare present within the user's FOV. The hardware to achieve this consisted of two HTC Vive Controllers, each capable of producing vibrations ranging between 0-255 Hertz. The motivation for developing this technique was strictly to experiment with alternative multi-sensory approaches to represent glare. Based on our initial informal observations we believe vibrations are not as an effective sensory modality for reproducing the physical discomfort of glare in comparison to an audio-based interface. However, we believe this proof of concept could be potentially used to capture glare discomfort feedback in a less physically distressing manner. The hardware used to output haptic-feedback also plays a key role in how effective the technique will perform. In our case, we used the HTC Vive Controllers which was limited to producing a maximum of 255 Hertz on each hand.

4 Future Directions

The immersive glare-based simulation and visualisations presented in this paper is one aspect of a more compact immersive LPS prototype we built. The future directions of this work aims to conduct a formal user study to evaluate all aspects of our immersive lighting simulator which includes interior/exterior lighting design and simulation, daylight analysis, energy consumption, and cost analysis. We also aim to explore the advantages and disadvantages of using immersive displays and six degrees of freedom input devices compared to a standard PC-mouse desktop setup for lighting analysis, and design. Current implementations of our system is limited to a uni-directional exchange of data between Revit and Unity using the Industry Foundation Class. A future direction could be to develop a workflow that creates a real-time bi-directional exchange of BIM data between Revit and Unity. Finally, using the ZED Mini depth-sensor we aim to incorporate Mixed Reality support into our system. This will allow users to navigate between AR and VR perspectives which has previously been identified as a potentially valuable tool for lighting analysis, and design[10].

5 Conclusion

This paper presented VRGlare: An immersive Lighting Performance Simulator supporting real-time glare simulation and analysis through the integration of Virtual Reality. In summary, we discussed the hardware, algorithms, equations, visualisations, and multi-sensory representations of

glare in respect to the simulator. Five visualisation techniques were presented capable of representing glare and providing feedback to the user in a simplified, and effective manner. We also presented two multi-sensory glare discomfort techniques using an audio and haptic-based interfaces designed to simulate the physical discomfort caused when experiencing glare. Lastly, we discussed the limitations associated with our simulator, future directions, and goals. Our hope is that this work will act as a stepping stone towards the future research and development of using three-dimensional visualisation techniques for real-time lighting performance simulation.

6 Acknowledgement

This work was supported by the Innovative Manufacturing Cooperative Research Centre whose activities are funded by the Australian Commonwealth Government's Cooperative Research Centres Programme, the Australian Research Council. The IVE: Australian Research Centre for Interactive and Virtual Environments at the University of South Australia has been working with CADwalk Global[4] as part of this project.

References

[1] GV Hultgren and B Knave. Discomfort glare and disturbances from light reflections in an office landscape with crt display terminals. Applied Ergonomics, 5 (1):2–8, 1974.

[2] Jeffrey Anshel. Visual ergonomics in the workplace: How to use a computer and save your eyesight. Performance+ Instruction, 33(5):20–22, 1994.

[3] Peter Robert Boyce. Human factors in lighting. Crc Press, 2014.

[4] Charles E Leiserson, Neil C Thompson, Joel S Emer, Bradley C Kuszmaul, Butler W Lampson, Daniel Sanchez, and Tao B Schardl. There's plenty of room at the top: What will drive computer performance after moore's law? Science, 368(6495), 2020.

[5] Yu Shu, Yen-Zhang Huang, Shu-Hsuan Chang, and Mu-Yen Chen. Do virtual reality head-mounted displays make a difference? a comparison of presence and self-efficacy between head-mounted displays and desktop computer-facilitated virtual environments. Virtual Reality, 23(4):437–446, 2019.

[6] Y. Sheng, T. C. Yapo, C. Young, and B. Cutler. A spatially augmented reality sketching interface for architectural daylighting design. IEEE Transactions on Visualization and Computer Graphics, 17(1):38–50, 2011.

[7] Worawan Natephra, Ali Motamedi, Tomohiro Fukuda, and Nobuyoshi Yabuki. Integrating building information modeling and virtual reality development engines for building indoor lighting design. Visualization in Engineering, 5(1):1–21, 2017.

[8] MO Wong, J Du, ZQ Zhang, YQ Liu, SM Chen, and SH Lee. An experience-based interactive lighting design approach using bim and vr: a case study. In IOP Conference Series: Earth and Environmental Science, volume 238, page 012006. IOP Publishing, 2019.

[9] Mohammad Keshavarzi, Luisa Caldas, and Luis Santos. Radvr: A 6dof virtual reality daylighting analysis tool. arXiv preprint arXiv:1907.01652, 2019.

[10] James Birt, Patricia Manyuru, and Jonathan Nelson. Using virtual and augmented reality to study architectural lighting. In International Conference on Innovation, Practice and Research in the Use of Educational Technologies in Tertiary Education, pages 17–21, 2017.

[11] CGH Plant and DW Archer. A computer model for lighting prediction. Building Science, 8(4):351–361, 1973.

[12] Gregory Ward. Radiance visual comfort calculation. volume 6, 1992.

[13] Gregory J Ward. The radiance lighting simulation and rendering system. In Proceedings of the 21st annual conference on Computer graphics and interactive techniques, pages 459–472, 1994.

[14] Kieran May, Ian Hanan, Andrew Cunningham, and Bruce Thomas. 3duitk: An opensource toolkit for thirty years of three-dimensional interaction research. In 2019 IEEE International Symposium on Mixed and Augmented Reality Adjunct (ISMAR-Adjunct), pages 175–180. IEEE, 2019.

[15] Commission Internationale de L'Eclairage. Cie 117-1995 discomfort glare in interior lighting, 1995.

[16] Leland Wilkinson and Michael Friendly. The history of the cluster heat map. The American Statistician, 63(2):179–184, 2009.

[17] Kai Riege, Thorsten Holtkamper, Gerold Wesche, and Bernd Frohlich. The bent pick ray: An extended pointing technique for multi-user interaction. In 3D User Interfaces (3DUI'06), pages 62–65. IEEE, 2006.

[4]Gerhard Kimenkowski and Stephen Walton, Project Managers for CADwalk Global - https://www.cadwalk.global/

Development of an Augmented Reality Fitness Index for Contractors

Hala Nassereddine[a], Wafik Lotfallah[b], Awad Hanna[c], and Dharmaraj Veeramani[d]

[a]Department of Civil Engineering, University of Kentucky, USA
[b]Department of Mathematics, American University in Cairo, Egypt
[c]Department of Civil and Environmental Engineering, University of Wisconsin–Madison, USA
[d]Department of Industrial and Systems Engineering, University of Wisconsin–Madison, USA
E-mail: hala.nassereddine@uky.edu, lotfallah@aucegypt.edu, ashanna@wisc.edu, raj.veeramani@wisc.edu

Abstract –

Construction, one of the most information-intensive industries, plays a vital role in the prosperity of nations and is expected to grow to new heights. This significant expansion, along with the increased complexity and sophistication of construction projects and rapid advances in emerging technologies, has fueled construction companies' interest in innovation as a source of competitive advantage. Augmented Reality (AR), a pillar of Industry 4.0, is an emerging technology that is gaining traction in construction. AR can be described as both an information aggregator and a data publishing platform that allows the user to (1) passively view displayed information, (2) actively engage and interact with published content, and (3) collaborate with others in real-time from remote locations. The objective of this paper is to develop an Augmented Reality Fitness Index (ARFI) to assess the suitability and applicability of AR for contractors in the construction industry. The rationale behind the proposed index is to understand the perception of stakeholders regarding the eligibility of AR in the construction industry and to investigate the potential degree of usage of AR throughout the seven phases of the lifecycle of a construction project: conceptual planning, design, pre-construction planning, construction, commissioning, operation and maintenance, and decommissioning. From the literature review, 43 AR use-cases were identified and grouped into the seven phases of a construction project. A survey was then developed to capture contractors' level of familiarity with AR in construction, level of usage of AR in construction, and perceived possible use of each AR use-cases. Next, contractors' perceived relevance of each of the 43 AR use-cases was obtained by surveying a group of subject matter experts. Using the collected data, a mathematical model was developed to compute an ARFI for each phase. The computed ARFI is used as an indication to guide the implementation of AR in construction.

Keywords –

Augmented Reality; Fitness Index; Contractors; Mathematical Model

1 Introduction

Construction, one of the most information-intensive industries, is a major contributor to the prosperity of nations and a sector that is expected to continue to grow [1]. This growth, along with the increased complexity of construction projects and rapid advances in digital technologies, heralds an increased interest by construction companies to innovate and transform their business-as-usual to remain competitive [2]–[5]. One emerging technology that is gaining interest in construction is Augmented Reality (AR). AR, a pillar of the fourth industrial revolution (Industry 4.0), both an information aggregator and a data publishing platform that allows the user to (1) passively view displayed information, (2) actively engage and interact with published content, and (3) collaborate with others in real-time from remote locations [1].

Various research efforts have investigated the potential use and impact of AR on construction projects. Some studies explored AR use-cases in specific phases of the construction project lifecycle, and others developed prototypes to investigate the impact AR on construction projects. While these efforts are critical to understanding the potential of the technology, they don't measure the degree of fitness of AR in construction. Therefore, the objective of this paper is to develop an Augmented Reality Fitness Index (ARFI) to assess the suitability and applicability of AR throughout the construction project lifecycle, using data collected from contractors.

2 Research Methodology

The methodology employed to fulfill the main goal of the research encompasses the following sub-goals. First,

a comprehensive and thorough review of the existing literature is conducted to extract AR use-cases. These AR use-cases are then mapped across the project lifecycle. The lifecycle of a construction project consists of a series of phases, and the literature review showed that there is no single definition for what the phases are. The project phases adopted in this research are those introduced by [6] and are as follows: 1) Conceptual Planning, 2) Design, 3) Pre-Construction Planning, 4) Construction, 5) Commissioning, 6) Operation and Maintenance, and 7) Decommissioning. Once the AR use-cases were identified, a survey was developed and distributed to contractors to collect their perception of AR in construction. The data collected from the survey was then analyzed, and a mathematical model was developed to compute an Augmented Reality Fitness Index for each phase of the construction project lifecycle.

3 Augmented Reality Use-Cases

Research studies by [7]–[35] were reviewed, and 43 AR use-cases were identified and grouped into the seven AR phases, as shown below. *P1* is Conceptual Planning, *P2* is Design, *P3* is Pre-Construction Planning, *P4* is Construction, *P5* is Commissioning, *P6* is Operation and Maintenance, and *P7* is Decommissioning:

P1 Real-time visualization of conceptual projects
P1 Overlaying 4D content into real-world (or physical objects) such as traffic flow, wind flow, etc.
P1 An understanding of how the desired project connects with its surroundings
P2 Overlay of 3D models over 2D plans (i.e. Design [or project] visualization in the office over 2D plans)
P2 Design (Project) visualization at full scale on-site
P2 Virtual tours for clients while on-site or in the office (AR walk-through)
P2 Real-time design change (material selection, design functionalities)
P3 Clash detection
P3 Early identification of design errors
P3 Constructability Reviews during design
P3 Full-scale site logistics (virtually locate equipment, trailers, laydown areas, storage, etc.)
P3 Space Validation and Engineering Constraints Checks (collaboratively locate and operate virtual construction equipment, such as cranes)
P3 Virtual planning and sequencing
P3 Safety orientation (do safety orientation in an augmented virtual environment)
P3 AR-simulation based safety training programs for workers
P4 Visualizing layout and integration of prefab components in the shop
P4 Site layout without physical drawings
P4 4D Simulations on-site (augmented simulated construction operations)
P4 Monitoring the progression of workflow and sequence
P4 Visualization of augmented drawings in the field
P4 On-site inspections
P4 Remote site inspection
P4 Visualization of underground utilities
P4 Visualization of the proposed excavation area
P4 Visualization of the construction systems/work (i.e. MEP, structural, etc.)
P4 Planning the positioning and movement of heavy/irregular objects/equipment
P4 Real-time support of field personnel
P4 On-site safety precautions (site navigation and in-situ safety warning)
P4 Augmented Mock-ups
P4 Construction progress visualization and monitoring
P4 On-site material tracking
P4 Create design alternatives on-site
P4 Visualization of augmented work instructions/manuals/procedures in the field
P4 Real-time visualization, review, and analysis of data associated with a particular worker, equipment, construction system, etc.
P5 On-site inspection/Punchlists
P5 Remote site inspection
P6 Availability of Maintenance information
P6 Locate building systems that need maintenance without destructive demolition or further survey work
P6 Refurbishment visualization
P6 Real-time support of engineers and technicians
P6 Training for maintenance and repair
P7 Remodeling visualization
P7 Evaluation of the new facility/installations over the existing one

4 Data Collection

4.1 Survey

Once the 43 AR use-cases were identified, a survey was developed, tested, and distributed to contractors. The survey was designed to capture the following data:

1. Respondent's level of familiarity of AR in the context of the construction industry measured on the following scale: (0) never heard of it; (1) vaguely heard of the term before; (2) basic understanding; (3) good understanding; and (4) very good understanding.
2. Respondent's level of usage of AR in the context of the construction industry measured on the following scale: (0) have not experienced AR before and not interested in the technology; (1) have not

experienced AR before but interested in the technology; (2) explored/ exploring AR applications; (3) tested/ testing AR applications; and (4) have used AR on at least one construction project.

3. Contractor's approximate average annual revenue in the last three years (measure in U.S. dollars).
4. Respondent's perceived level of usage of each of the 43 AR use cases measured on a five-point Likert scale of (1) very low; (2) low; (3) moderate; (4) high; and (5) very high. Respondents could also select "N/A" (coded as 0) if they don't think an AR use-case will be used.

4.2 Data Characteristics

A total of 46 responses were collected. Survey results showed that 13% of respondents had vaguely heard of AR, 2% had a basic understanding, 14% had a good understanding, and the remaining 17% had a very good understanding of the technology. When asked about their usage of AR in construction, 13% indicated that they had not experienced AR before but are interested, 8% stated that they had explored/are exploring AR applications, 11% mentioned that they had tested/are testing AR application, and the remaining 14% reported that they had used AR on at least one construction project. It should be noted that none of the respondents indicated that they had not heard of AR before or are not interested in the technology, proving that AR is a promising technology in construction.

4.3 Data Analysis

Researchers indicated that the perception of users of a technology is influenced by the users' familiarity and degree of usage of the technology [36], [37]. Therefore, before developing the mathematical model, the relationship between:

1. The respondent's perception of an AR use-case and the respondent's familiarity with AR
2. The respondent's perception of an AR use-case and the respondent's usage of AR

were evaluated using the Kruskal-Wallis H test and Kendall's tau-b. Additionally, the impact of the economic volume of the respondents (i.e. average annual revenue) on the respondent's perception of an AR use-case was also investigated using Kruskal-Wallis H test.

The analysis of these three relationships resulted in significant p-values, providing statistical evidence at the 95% confidence level that the respondent's perceived level of usage of each AR use-case differs across the different levels of familiarity and usage of AR and the economic volume of the company.

5 Augmented Reality Fitness Index (ARFI)

The objective is to develop an Augmented Reality Fitness Index (ARFI) to assess the suitability and applicability of AR in the construction industry using contractors' data. Using the data collected for the survey and the statistical relationships that were identified in the previous sections, this section outlines the steps undertaken to develop the mathematical model.

5.1 Motivation

ARFI is a proposed measure on a normalized scale from 0 to 1 of the usage potential of AR in a particular construction phase and throughout the lifecycle of a construction project. The rationale behind the proposed index is to understand the perception of contractors regarding the eligibility of AR in the construction industry and to investigate the potential degree of usage of AR throughout the seven phases of the lifecycle of a construction project. ARFI in each phase is computed as a weighted average of the usage potential of the technology's identified use-cases in that phase and based the perceived relevance of each use-case.

The usage potential (UP_j) of an AR use-case j is calculated as a weighted average of the perceived possible use of this use-case in its corresponding phase obtained from the survey. However, this variable is subjective by nature and differs among respondents. To reduce the influence of this subjectivity, the perceived possible use of an AR use-case j is, therefore, subsequently weighted based on three variables: familiarity with AR, current usage of AR, and economic volume of the respondent. These three variables are combined into one variable, namely the response weight (w_i), which is used to weigh the perceived possible use of an AR use-case corresponding to respondent i.

Contractors' perceived relevance of an AR use-case j was obtained by surveying a group of subject matter experts on each of the 43 identified use-cases.

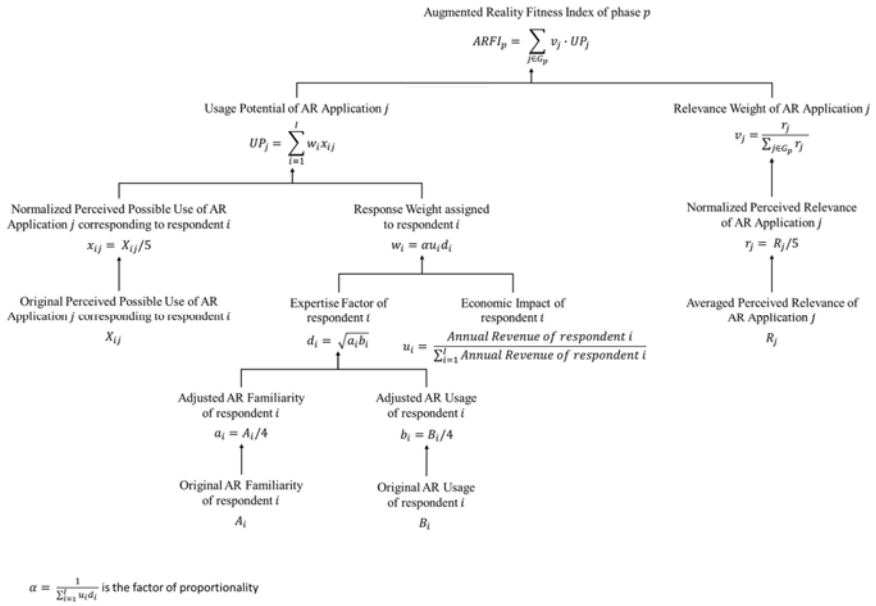

Figure 1. Breakdown of the Augmented Reality Fitness Index Mathematical Model

5.2 Mathematical Formulation

The model computes for each phase p of the lifecycle of a construction project a corresponding Augmented Reality Fitness Index, $ARFI_p$.

$ARFI_p$ is based on the evaluation of the weighted usage potential of a set of AR use-cases in phase p. In the following, J denotes the total number of AR use-cases ($J = 43$), and G_p (with $1 \leq p \leq 7$) denotes the disjoint sets of AR use-cases within a phase p, with:
$G_1 \cup G_2 \cup G_3 \cup G_4 \cup G_5 \cup G_6 \cup G_7 = \{1, 2, 3, \dots, 43\}$,
where:
$G_1 = \{1, 2, 3\}$, $G_2 = \{4, 5, 6, 7\}$, $G_3 = \{8, 9, \dots, 15\}$, $G_4 = \{16, 17, \dots, 33\}$, $G_5 = \{34, 35\}$, $G_6 = \{36, 37, \dots, 41\}$, and $G_7 = \{41, 42\}$ represent the sets of AR use-cases in the Planning Phase, Design Phase, Pre-Construction Phase, Construction Phase, Commissioning Phase, Operation and Maintenance Phase, and Decommissioning Phase, respectively.

The model used to calculate $ARFI_p$ is defined as:

$$ARFI_p = \sum_{j \in G_p} v_j \cdot UP_j \quad (1)$$

where:

- p denotes the number of phases of the lifecycle of a construction project ($1 \leq p \leq 7$),
- UP_j denotes the usage potential of AR use-case j, and
- v_j denotes the relevance weight of AR use-case j, with $v_j \geq 0$ and $\sum_{j \in G_p} v_j = 1$.

The underlying assumption here is that the index $ARFI_p$ solely depends on the AR use-cases in phase p. To compute this index, we need to determine the values of UP_j and v_j.

5.2.1 Usage Potential of AR Use-case *j*

The Usage Potential of AR of use-case j is defined as:

$$UP_j = \sum_{i=1}^{I} w_i x_{ij} \quad (2)$$

where:

- I denotes the number of respondents,
- x_{ij} denotes the normalized perceived possible use of an AR Use-case j corresponding to respondent i. These normalized values are calculated using $x_{ij} = X_{ij}/5$, with X_{ij} being the original perceived impact of a barrier k corresponding to respondent i, where $X_{ij} \in \{0, 1, 2, 3, 4, 5\}$. And,
- w_i is a response weight assigned to respondent i, with $\sum_{i=1}^{I} w_i = 1$.
- w_i is computed based on the following four variables, A_i, B_i, and u_i, where:
- A_i is the AR familiarity of respondent i, with $A_i = \{0, 1, 2, 3, 4\}$,
- B_i is the AR Usage of respondent i, with $B_i = \{0, 1, 2, 3, 4\}$, and
- u_i is the economic impact of respondent i, with

$$u_i = \frac{Annual\ Revenue\ of\ respondent\ i}{\sum_{i=1}^{I} Annual\ Revenue\ of\ respondent\ i}$$

It should be noted that none of the respondents selected 0, and therefore, original values did not need to be adjusted to account for zeroes. Original values were normalized, and as a result, the following variables are defined:

- a_i is the adjusted AR familiarity of respondent i, where $a_i = A_i/4$, so $a_i \in \{0.25, 0.5, 0.75, 1\}$, and
- b_i is the adjusted AR Usage of respondent i, where $b_i = B_i/4$, so $b_i \in \{0.25, 0.5, 0.75, 1\}$.

The variables a_i, and b_i are then combined into a new variable, d_i, which represents the "expertise factor" of respondent i. d_i is calculated as the geometric mean of a_i and b_i, i.e.

$$d_i = \sqrt{a_i b_i}.$$

As shown in Figure 2 the geometric mean (right) gives smaller weights to respondents with lower expertise in comparison to the arithmetic mean (left).

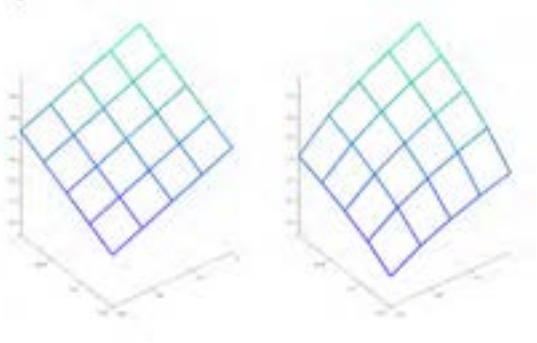

Figure 2. Effect of Using geometric mean on the expertise factor, d_i, for $a_i = 1$

For each respondent i, w_i is then assumed to be proportional to u_i (their economic impact) and d_i (their expertise factor). Therefore:

$$w_i = \alpha u_i\ d_i$$

α is then calculated by:

$$1 = \sum_{i=1}^{I} w_i = \alpha \sum_{i=1}^{I} u_i d_i.$$

Thus,

$$\alpha = \frac{1}{\sum_{i=1}^{I} u_i d_i}$$

and,

$$w_i = \frac{u_i d_i}{\sum_{i=1}^{I} u_i d_i} = \frac{u_i \sqrt{a_i b_i}.}{\sum_{i=1}^{I} u_i \sqrt{a_i b_i}.} \quad (3)$$

5.2.2 Perceived Relevance of AR Use-case *j*

The Usage Potential of an AR use-case j, UP_j, obtained from equation (2) is then weighted using the perceived relevance of that AR use-case j. R_j denotes the perceived relevance of each AR Use-case j obtained by averaging the responses of a group of 10 subject matter experts, where $0 \le R_j \le 5$. These rates were then normalized to r_j, with $0 \le r_j \le 1$. Therefore, for each AR use-case j, $r_j = R_j/5$.

For each AR use-case j, the relevance weight v_j is assumed to be proportional to r_j. Therefore, $v_j = \beta r_j$, and similar to α, β is calculated by:

$$\beta = \frac{1}{\sum_{j \in G_p} r_j}$$

thus,

$$v_J = \frac{r_j}{\sum_{j \in G_p} r_j} \quad (4)$$

Consequently,

$$ARFI_p = \sum_{j \in G_p} \frac{r_j}{\sum_{j \in G_p} r_j} \sum_{i=1}^{I} \frac{u_i \sqrt{a_i b_i}.}{\sum_{i=1}^{I} u_i \sqrt{a_i b_i}.} x_{ij} \quad (5)$$

5.3 Model Validation

The objective of the mathematical model is to reduce the subjectivity of the data by adjusting the answers of the respondents based on their level of familiarity and usage of AR in construction. An important question arises as to how to prove that the methodology employed to develop the model is effective. [38] noted that simulations provide a powerful technique for answering this question. Therefore, a simulation study was designed to evaluate the mathematical model developed and to compare it to competing approaches, i.e. using the arithmetic mean instead of geometric. The objective of the simulation is to prove that the values computed from the model are more representative than the observed raw data collected from the survey.

The Latin-Hypercube Sampling (LHS) experimental design technique in Python was used to run the simulation 1,000 times in a Monte Carlo Fashion.

Four datasets are generated in this simulation: the assumed *true* dataset, the *observed* dataset, the *arithmetic-based modeled* dataset, and the *geometric-based modeled* dataset. The *observed* dataset was generated by adding noise to the *true* dataset, and it represents the data collected from the survey. The *arithmetic-based modeled* dataset was generated by

adjusting the *observed* dataset using the arithmetic mean (i.e. $d_i = \frac{a_i+b_i}{2}$). The *geometric-based modeled* dataset was generated by adjusting the *observed* dataset using the geometric mean (i.e. $d_i = \sqrt{a_i b_i}$).

In order to evaluate the effectiveness of each model, the squared deviations between 1) *observed* and *true* values, 2) *arithmetic-based modeled* and *true* values, and 3) *geometric-based modeled* and *true* values were calculated. Results showed that the deviation between the *geometric-based modeled* and *true* values is statistically significantly less than the other two deviations, justifying the use of the geometric mean.

6 Discussions

ARFI in each phase is computed using equation (5), and the values are displayed in Table 1 and illustrated in Figure 3.

Table 1. $ARFI$ values for each phase

Phase	ARFI
Conceptual Planning	0.743
Design	0.768
Pre-Construction Planning	0.719
Construction	0.709
Commissioning	0.589
Operation and Maintenance	0.701
Decommissioning	0.646

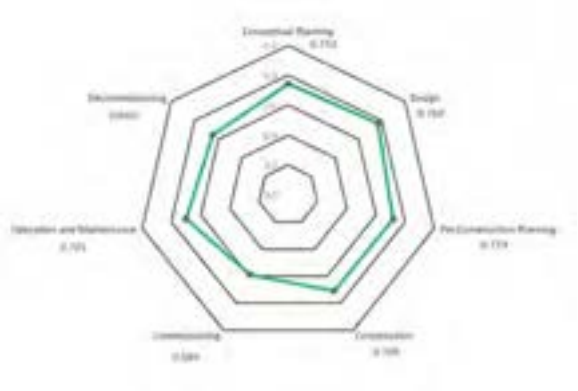

Figure 3. A radar chart of $ARFI$ values throughout the construction project lifecycle

It can be shown from Table 1 and Figure 3 that all ARFI values are greater than 0.5 indicating the potential of AR in construction. According to contractors, AR is perceived as the highest fitness index in Design (0.743), followed by Conceptual Planning (0.743), Pre-Construction Planning (0.719), Construction (0.709), Operation and Maintenance (0.701), Decommissioning (0.646), and finally commissioning (0.589).

These results highlight the importance of integrating AR throughout the entire lifecycle, placing a greater emphasis on early phases. Although the ARFI values were computed from the perspective of contractors, the construction phases – which traditionally is the most relevant phase for contractors – did not have the highest ARFI value. This shows that contractors are aware of the need to integrate AR early in the project for the later project phases to reap the benefits. The results also suggest that the construction industry is shifting the traditional delivery systems as contractors' involvement and engagement in the early phases of the project is increasing.

7 Conclusions

AR is a promising technology in the construction industry. While previous research efforts have investigated specific AR use-cases, this paper investigated the fitness and applicability of AR throughout the seven phases of the construction project lifecycle. Forty-three AR applications were identified from the extant literature and were grouped into the seven phases. Next, a survey was developed to collect contractors' perceptions of the potential of AR in construction, and 46 responses were collected. Data summary showed that all respondents had some level of familiarity with AR in the context of the construction industry, and the majority had previously used the technology to some extent. Statistical analyses showed that the respondent's perception of the potential use of an AR use-cases depends on three variables: 1) the respondent's familiarity with AR, 2) the respondent's usage of AR, and 3) the company's economic volume. A mathematical model, ARFI, was then developed to compute an AR fitness score between 0 and 1 for each phase of the project lifecycle. The calculated ARFI values were all greater than 0.5, indicating that AR can be well integrated into all phases. Additionally, while ARFI was developed using contractors' data, construction did not have the highest ARFI value. Early project phases, namely design, conceptual planning, and pre-construction planning, had an ARFI score slightly higher than construction, indicating contractors' awareness of the potential of AR and increased involvement in early phases. Future work can survey other stakeholders, including Architect/Engineers, subcontractors, facility managers, and owners, and investigate variations of stakeholders' perceptions of the fitness of AR.

References

[1] Nassereddine H. Veeramani D. and Hanna A. Augmented Reality-Enabled Production Strategy

Process. *In Proceedings of the International Symposium on Automation and Robotics in Construction*, 36:297–305, 2019.

[2] El Jazzar, M., Piskernik, M. and Nassereddine, H. Digital twin in construction: an empirical analysis. In *EG-ICE 2020 Proceedings: Workshop on Intelligent Computing in Engineering*, pages 501–510, Berlin, Germany, 2020.

[3] Bou Hatoum, M. and Nassereddine, H. Developing a framework for the implementation of robotics in construction enterprises. In *EG-ICE 2020 Proceedings: Workshop on Intelligent Computing in Engineering*, pages 453–462, Berlin, Germany, 2020.

[4] Nassereddine, H., Schranz, C., Bou Hatoum, M., & Urban, H. A comprehensive map for integrating augmented reality during the construction phase. In *Creative Construction e-Conference 2020*, pages 56–64, Budapest, 2020.

[5] Nassereddine H., El Jazzar M. and Piskernik M. Transforming the AEC industry: a model-centric approach. In *Creative Construction e-Conference 2020*, pages 13–18, Budapest, 2020.

[6] Nassereddine H. M. Design, Development and Validation of an Augmented Reality-Enabled Production Strategy Process for the Construction Industry. *The University of Wisconsin-Madison*, Dissertation, 2019.

[7] Webster A. Feiner S. MacIntyre B. Massie W. and Krueger T. Augmented reality in architectural construction, inspection and renovation, in *Proceedings of ASCE Third Congress on Computing in Civil Engineering*, 1:996, 1996.

[8] Thomas B. Demczuk V. Piekarski W. Hepworth D. and Gunther B. A wearable computer system with augmented reality to support terrestrial navigation. *In Digest of Papers. Second International Symposium on Wearable,* pp. 168–171. IEEE, 1998.

[9] Thomas B. Piekarski W. and Gunther B. Using augmented reality to visualise architecture designs in an outdoor environment. *International Journal of Design Computing Special Issue on Design Computing on the Net (DCNet)*, (1)4, 1999.

[10] Dunston P. S. Billinghurst M. Luo Y. and Hampson B. Virtual visualization for the mechanical trade. *In Proceedings of International Symposium on Automation and Robotics in Construction (ISARC),* pp. 1131–1136, 2000.

[11] Kensek K. Noble D. Schiler M. and Tripathi A. Augmented Reality: An application for architecture. *Computing in Civil and Building Engineering (2000)*, pp. 294–301, 2000.

[12] Hammad A. Garrett J. H. and Karimi H. A. Potential of mobile augmented reality for infrastructure field tasks. *In Proceedings of the 7th International Conference on 3D Web Technology,* 2002.

[13] Roberts G. Evans A. and Dodson A. The Use of Augmented Reality, GPS and INS for Subsurface Data Visualisation, *In FIG XXII International Congress*, pp. 12, 2002.

[14] Dias J. M. S. Capo A. Carreras J. Galli R. and Gamito M. A4D: augmented reality 4D system for architecture and building construction. *In Conferencia Virginia tech*, 2003.

[15] Wang X. and Dunston P. S. Design, strategies, and issues towards an augmented reality-based construction training platform. *Journal of information technology in construction (ITcon),* 12(25):363–380, 2007.

[16] Shin D. H. and Dunston P. S. Identification of application areas for Augmented Reality in industrial construction based on technology suitability. *Automation in Construction,* (17)7:882–894, 2008.

[17] Behzadan A. H. and Kamat V. R. Interactive augmented reality visualization for improved damage prevention and maintenance of underground infrastructure. *In Construction Research Congress 2009: Building a Sustainable Future*, pp. 1214–1222, 2009.

[18] Golparvar-Fard M. Peña-Mora F. and Savarese S. D4AR–a 4-dimensional augmented reality model for automating construction progress monitoring data collection, processing and communication. *Journal of information technology in construction*, 14(13):129–153, 2009.

[19] Helmholt K. A. Hoekstra W. and van Berlo L. C2B: Augmented reality on the construction site. *In Proceedings of the 9th International Conference on Construction Applications of Virtual Reality. Sydney, Australia*, pp. 5–6, 2009.

[20] Akyeampong J. Udoka S. and Park E. A Hydraulic Excavator Augmented Reality Simulator for Operator Training. *In Proceedings of the 2012 International Conference on Industrial Engineering and Operations Management*, 2012.

[21] Yeh K. C. Tsai M. H. and Kang S. C. On-site building information retrieval by using projection-based augmented reality. *Journal of Computing in Civil Engineering,* 26(3):342–355, 2012.

[22] Park C. S. and Kim H. J. A framework for construction safety management and visualization system. *Automation in Construction*, 33:95–103, 2013.

[23] Park C. S. Lee D. Y. Kwon O. S. and Wang X. A framework for proactive construction defect management using BIM, augmented reality and ontology-based data collection template. *Automation in Construction*, 33:61–71, 2013.

[24] Rankohi S. and Waugh L. Review and analysis of augmented reality literature for construction industry. *Visualization in Engineering*, 1(1):9, 2013.

[25] Wang X. Love P. E. D. Kim M. J. Park C. S. Sing C. P. and Hou L. A conceptual framework for integrating building information modeling with augmented reality. *Automation in Construction*, 34:37–44, 2013.

[26] Danker F. and Jones O. Combining Augmented Reality and Building Information Modelling-An industry perspective on applications and future directions, 2014.

[27] Zollmann S. Hoppe C. Kluckner S. Poglitsch C. Bischof H. and Reitmayr G. Augmented reality for construction site monitoring and documentation. *In Proceedings of the IEEE*, (102)2:137–154, 2014.

[28] Meža S. Turk Ž. and Dolenc M. Measuring the potential of augmented reality in civil engineering. *Advances in Engineering Software*, 90:1–10, 2015.

[29] Bluebeam, Inc. No Plans, No Problem: Building With AR, 2016. On-line: https://www.youtube.com/watch?v=X_XSUcq3YDE, Accessed: 09/06/2020.

[30] Ghaffarianhoseini A. *et al.* Integrating Augmented Reality and Building Information Modelling to Facilitate Construction Site Coordination. *In Proceedings of the 16th International Conference on Construction Applications of Virtual Reality*, 2016.

[31] Woyke E. Augmented reality could help construction projects finish on time and within budget, *MIT Technology Review*, 2016. On-line: https://www.technologyreview.com/s/602124/augmented-reality-could-speed-up-construction-projects/. Accessed: 09/06/2020.

[32] Chalhoub J. and Ayer S. K. Mixed Reality for Electrical Prefabrication Tasks, *Computing in Civil Engineering 2017*, pp. 76–83, 2017.

[33] Heinzel A. Azhar S. and Nadeem A. Uses of Augmented Reality Technology during Construction Phase, *In Revolutionizing the Architecture, Engineering and Construction Industry through Leadership, Collaboration and Technology*, 2017.

[34] Kivrak S. and Arslan G. Using Augmented Reality to Facilitate Construction Site Activities. *Advances in Informatics and Computing in Civil and Construction Engineering*, pp. 215–221, 2019.

[35] Chandarana S. Shirke O. and Desai T. Review of Augmented Reality Applications: Opportunity Areas & Obstacles in Construction Industry, n.d.

[36] Madadi Y. Iravani H. and Nooghabi S. N. Factors effective on familiarity and usage of information and communication technology (ICT) University College of Agriculture and Natural Resources, University of Tehran, Iran. *In Procedia-Social and Behavioral Sciences*, 15:3625–3632, 2011.

[37] BrckaLorenz A. Haeger H. Nailos J. and Rabourn K. Student perspectives on the importance and use of technology in learning. *In Annual Forum of the Association for Institutional Research*, 31, 2013.

[38] Hallgren K. A. Conducting simulation studies in the R programming environment. *Tutorials in quantitative methods for psychology*. 9(2): 43, 2013.

A Method to Produce & Visualize Interactive Work Instructions for Modular Products within Onsite Construction

Raafat Hussamadin[a], Jani Mukkavaara[a], Gustav Jansson, Ph.D.[a]

[a] Department of Civil, Environmental and Natural Resources Engineering, Luleå University of Technology, Sweden
E-mail: Raafat.Hussamadin@ltu.se, Jani.Mukkavaara@ltu.se, Gustav.Jansson@ltu.se

Abstract –

Well detailed, informative and accurate work instructions are a necessity to mitigate delays in construction. Today, this is done through a combination of shop drawings, documents, sheets, work pre-planning meetings and onsite verbal work instructions to transfer knowledge and information between all actors. Due to the subjectivity of these methods, many incorrect assumptions and man-made errors originated from miscommunication and misinterpretation can occur. Such issues are tough to identify prior to their occurrence on construction sites, leading to construction delays. Virtual Reality (VR) technology can simulate and visualize assembly processes using Standard Operating Procedure (SOP). The visualization aims to ensure a quality communication with skilled workers and to aid their interpretation of SOPs by reducing assumptions. As a result of a more effective education, it can support the collaboration between actors. Utilization of SOPs for visualization of Work Instructions (WI) and assembly processes are important, because many process WIs on construction sites are repetitive. Modularity can increase the efficiency by supporting instancing and variation creation of construction tasks and products. Interactivity can support the continuously changing status and demands of construction sites.

A method has been iteratively developed to support visualization of modular and interactive SOPs within the context of industrialized house-building (IHB), to increase the quality and consistency of communication at construction sites. Concurrently to development of the method, a prototype using VR technology was developed. Interactive functionalities along with VR technology make it possible to adjust SOP and WI modules to suit the demands and conditions of the construction site, including real-time. As a result, the developed method is responsive and adjustable to conditions such as weather, man-made errors, assembly re-sequencing and re-scheduling. Combining product design, SOPs, WIs and assembly process in early stages of construction has shown to help identify potential issues and aid in planning for cautious measurements. Results show that by using the developed method, skilled workers were able to identify occurring miscommunications, and misinterpretations between them, site managers and foremen as well as ensuring their understanding.

Keywords –

Virtual Reality; Standard Operation Procedure; Work Instruction; Process Visualization; Interactive; Modular

1 Introduction

Usage and distribution of information within offsite manufacturing by having Standard Operating Procedures (SOP) and Work Instructions (WI) have improved the manufacturing workflow in industrialized house-building (IHB). This has however not been well translated to onsite construction, which has been lacking in development efficiency and has become a bottleneck. A well detailed SOP and WI, that are thoroughly and correctly communicated is a necessity to mitigate onsite construction delays.

The difference between the usage of SOP and WI in offsite manufacturing compared to onsite construction has been significant. Standardization reduces the complexity of information flows and its coordination [1]. With adoption of assembly line manufacturing and increased standardization, IHB has optimized offsite manufacturing tasks, resource flow, and repetitive assembly processes for the skilled workers. IHB has invested time and resources to create high quality SOPs and WIs that are thoroughly communicated to the associated skilled workers. This has however not been translated to a construction site in which the flow-oriented workflow meets the project-oriented workflow. Skilled workers on construction sites perform a variety of tasks and often have a limited holistic view of the project. This is due to only performing their allocated tasks and becoming indifferent to assembly sequence, schedule, construction quality and other tasks, leading to the hampering of progress and an increase in waste [2]. Current document-based WIs are time consuming, error

prone, and inconsistent, leading to miscommunications and misinterpretations, which causes delays [3]. With one of the reasons being that many of the skilled workers are contractors, requiring reintroduction to SOPs and WIs of the said project and company, reducing the long-term sustainability benefits that can be acquired from a SOP and WI.

WIs are communicated through a combination of shop drawings, text documents, sheets, and meetings. This means that the recipient of the information, engineers and skilled workers, must interpret the information and create a visual image of the construction, its assembly sequence and its tasks. Due to the risk of misinterpretation, and in turn assembly errors, WIs are communicated to skilled workers mainly through verbal communication [3], resulting in the verbal communication often being a time-consuming and inefficient communication method [4]. Verbal communication of WIs leads to skilled workers having many uncertainties and misinterpretations, including assembly sequence, task instructions, and resource usage [5]. Uncertainty prevents them from recognizing potential problems, communicating potential improvements and simultaneously reduces their motivation [2,5].

The purpose of this study is to iteratively develop a method for the creation of modular interactive visualization of SOPs and WIs within the context of IHB. With the aim of increasing the quality of communication at construction sites, a prototype based on game engine technology was developed and evaluated to reduce man-made errors in construction sites.

2 Research Approach

The study has been conducted with a design science (DS) approach by Hevner [6], to develop the knowledge and understanding of the problems within the field by iteratively building a prototype. Data collection methods were semi-structured interviews, observations, meetings and supplemented by a literature review. The primary activities in DS research are the designing, building and evaluation of prototypes [7]. Prototypes can comprise processes, models, methods, and software. This paper uses DS to describe the development of a software prototype for modular and interactive visualization SOP and WI, and to propose a method based on this process.

To support the development of the method and its evaluation, a study was conducted in multiple IHB construction projects. These projects were selected for the study due to them having new assembly processes for onsite construction, meaning that SOPs and WIs for said assemblies were under development. In an iterative process, the method was designed and built for evaluation of construction sites works in collaboration with site managers and foremen. Using results from the evaluation of the prototype, the method was further developed for upcoming projects. Skilled workers were collaborated with within the later stages of the development, only when a certain maturity had been achieved.

Semi-structured interviews with process development engineers, site managers, foremen and skilled workers were used to identify the information flow within the company, the perception of the prototype, and for comparison of the prototype with text based WIs as well as mapping and development of assembly sequence, SOPs and WIs.

3 Theory

3.1 Standard Operating Procedure & Work Instruction

Standard Operating Procedure (SOP) is a means of documentation that describes the best-known practices within a specific company, often in the form of text-based documents. A company can use SOPs to achieve a reduction in scheduling waste, quality issues and environmental impacts, while simultaneously increasing the safety and consistency of assembly processes [2,8]. SOPs also benefits the company by encouraging the documentation of information resulting in knowledge staying within the company [2,8].

A SOP can include working methods, precautions, task durations, preparatory tasks, step-by-step instructions, resources, etc. [9]. The step-by-step instructions contain a specific start point and a description of each sequenced instruction, where a group of instructions is a WI. A SOP must be user-friendly, easy to understand and must be easily revisable [2].

Work instruction (WI) is an approach to manage the dissemination of information and knowledge within companies [10] and the best practices of work [11]. During its life-cycle, a WI goes through three phases, creation, use and maintenance phase [12]. The creation phase consists of product information, such as 3D models and shop drawings, and resource information such as tools, machinery, skilled workers, and process information that contain step-by-step instruction of the assembly process and construction rulesets [11,12]. Under the use phase, a WI is performed by skilled workers to support the sequenced assembly tasks with guided step-by-step instruction [12].

Process modularity improves the adaptability of a product, its requirements and standardization by simplifying the re-sequencing and addition of new modules to the assembly sequence [13]. It further improves the possibility of parallel assembly, hence reducing lead times [14]. Modular processes are built on

three principles [15]:

- Standardization: Breakdown of a standard process into main sub-processes and instance sub-processes that can be derived and customized from the main sub-processes.
- Re-sequencing: Reordering of sub-processes.
- Postponement: Postponing instance sub-processes to increase flexibility.

3.2 Visualization & Interactivity of Modular SOP

Visualization is an effective method for introducing SOP to construction sites, where it can improve the understanding of construction aims, standards, quality, safety instructions, assembly sequence, schedule, and potentially give an improved holistic view of the construction project [2,16]. With the aim to reduce man-made errors, due to miscommunication and misinterpretation and prior expertize [2], an animated SOP and WI can enhance the holistic view of a project. In comparison to documents and static-pictures, animations are more effective, particularly when combined with realistic graphics and task instructions [17,18]. The improved holistic view and better understanding of construction tasks conducted by other skilled workers can encourage communication, and improve motivation, which can lead to further development of SOP and WI [2,5]. Text based SOP documents are more cognitively demanding, followed by pictures [10], whilst animation could reduce cognitive demand [17]. Visualization might also reduce language gaps, as they simplify communication of important information [8].

WIs require a combination of paper documentations, such as shop drawings and text-based instructions, risking misinterpretations due to subjectivity. Therefore, WIs are instead often delivered via verbal communication to skilled workers by foremen [11]. In a study comparing instructional texts, diagrams and animations for assembly tasks, visualization of WI through animations showed an increase of step-by-step instructions understanding, leading to less man-made errors, increases in efficiency and accuracy of process assembly for the novice users [17].

Best practice changes, design changes and personal changes require revisions and re-education of WI documentations to reflect the changes. These modifications to WI are performed in the maintenance phase [12]. Therefore, effective communication, where information is filtered according to the need of every actor, can improve lead times [17].

4 Development of the method

Real-time visualization of assembly processes with game engine technology can visualize SOPs and WIs. Game engine technology, through Unity, see Figure 1, was used due to its possibility for real-time rendering of realistic environments and models in combination with scripting to create interactivity and modularity as well as for its capability of developing and distributing the prototype to a variety of IT-platforms.

4.1 Development of SOP & WI

Due to the assembly process being a new roof solution within the studied company, no registered SOPs or WIs existed beforehand. Their development started with usage of a detailed 3D-model (with 6565 components) and shop drawings of the roof. In collaboration with process development engineers, site managers and foremen, the assembly process was iteratively mapped, modified and optimized. The mapping led to the possibility of identifying main and repetitive SOPs, WIs, instructions and some foreseeable issues that could occur, mainly due to their limited tolerance values, weather or logistics.

A total of 8 pre-defined main SOP modules were mapped and developed for the roof assembly sequence. These SOPs clarify the WIs required to be performed together with the information needed for a successful onsite construction. Therefore, emphasis on their development, content of information and visualization has been a major focal point. This was conducted through quality control procedures, where the prototype was evaluated by professionals with several roles using different IT-platforms. Every main SOP contains information about its title, a description and a list of sequenced WIs. The main SOPs were utilized to create a total of 25 SOP instances for the roof sequence assembly.

Similar to the described SOP above, a total of 26 pre-defined main WI modules, with 237 instances, were developed for the roof assembly sequence. Every main WI contains information about its title, a description and a sequenced list of step-by-step instructions.

A total of 6102 components have received instructions and animation information. A component (e.g. a single roof truss) contains a 3D model representing its geometrical, positional and rotational data as well as an instruction template. For reusability of information, component information is modularized using instructional templates, with a total of 18 main templates developed for the roof assembly sequence. A template consists of data about instruction, including descriptions, materials, tools, machinery and precautional notes. Each listed instruction has its template parameters gathered, sequenced and sorted in lists available to associated WI. Additionally, the instruction template describes how and

when an animation should occur. This is described using four parameters: task duration, sequence type, adaptive position and adaptive rotation.

Adaptive position and rotation are three-dimensional vector values that indicate how far from the original position and rotation the animation should start.

Sequence type parameter modifies the relation of an instruction with other instructions under the same WI, as in, it makes it possible for the developer to decide when the sequences are animated, from sequence to sequence. The developer can give the user the choice to decide when to start a specific animation by setting its sequence type value in instruction to wait for user input, OnClick, (indicated by a mouse icon, Figure 2). In some cases, it might be preferable to start the next sequenced animation immediately when the previous animation is done instead of requiring user input. The developer can for such cases set the sequence type value in an instruction to wait and be played when the previous animation is done, AfterPrevious, (indicated by a clock icon, Figure 2). For cases where multiple animations should be played simultaneously, such as repetitive screwing of multiple screws, the developer can set the sequence type value in instruction to play the animation when the previous sequence animation starts playing, WithPrevious, (indicated by an arrow icon, Figure 2).

Alternative Sequences (AS) are pre-prepared solutions or modifications to foreseeable changes or issues that can be required to conduct a SOP correctly. From meetings and observations, AS has been identified as a possible interactive functionality where it opens the possibility to develop SOPs and visualize alternative construction solutions that existed but were not included.

AS is integrated with the modularity and interactivity of the method to allow the selection between multiple assembly sequence alternatives. AS modifies the WI sequence within a specific SOP, indicated by the circle icon as seen in Figure 2. Due to AS modifying data within SOPs in real-time, having and caching lists of precaution notices, task durations and resources, which according to theories mentioned before exist in SOP is no longer possible. The information has instead been moved to the individual instructions. With that, SOP now has access to this data through its list of WI, meaning that it dynamically collects data from instructions in accordance with the animation. These dynamically generated lists can later be presented to the user. As it is built on using modular WIs, it is possible for the user to swap modules of WI with other modules.

Sequence details are parameters available within SOPs. The parameter can modify the sequence type and task duration values for all instructions of the SOP. Sequence details were developed to utilize the instances and modularization of SOP by making it possible to use a single SOP in multiple different levels of detail, instead of being required to recreate the SOP or a variety that needs to be modified manually. As an example, in Figure 2, the SOP “Roof Cassette Montage” is using a sequence detail value of Low Detail, while “Roof Cassette & Gable Montage” is using Normal Detail. Both of the SOPs contain instances of the same main WI “Roof Cassette Assembly”, we can however see that their instructions have different sequence types due to their sequence detail.

Sequence details follow rulesets defined by the developer to determine how the sequence type and task duration modifications occur. A ruleset can be based on fixed values but also instructions sequence order, such as first or last sequence. By default, a higher sequence detail value results in fewer simultaneous but more total animations. This corresponds to a more detailed instruction with more steps. Example of a sequence detail ruleset:

- Very High Detail: All Sequence Types to OnClick
- High Detail: WithPrevious to AfterPrevious
- Normal Detail: Preassigned values
- Low Detail: OnClick to AfterPrevious & AfterPrevious to WithPrevious
- Very Low Detail: All Sequence Types to WithPrevious

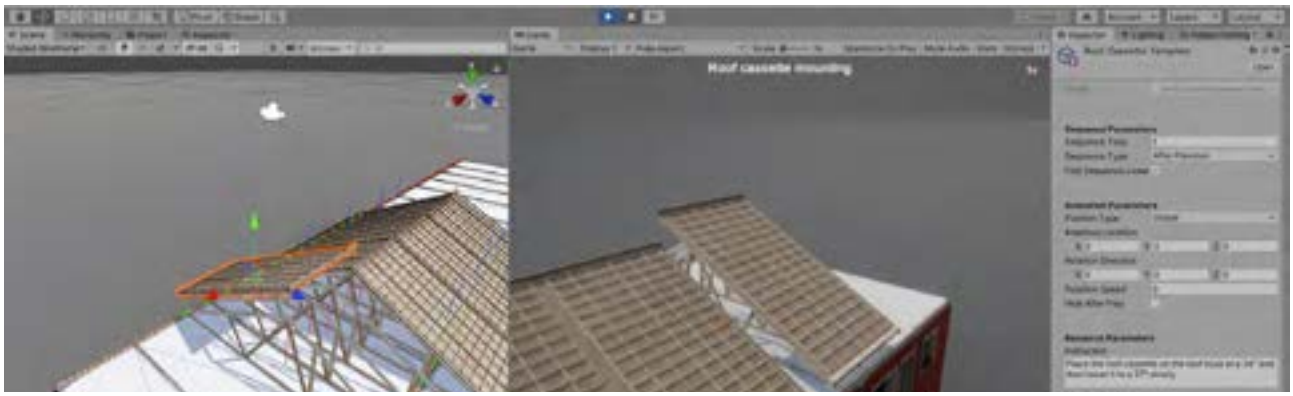

Figure 1. Prototype in Unity. Selected roof cassette (left, Scene tab) is using a Roof Cassette template (right, Inspector tab). Template information is utilized to visualize it (middle, Game tab).

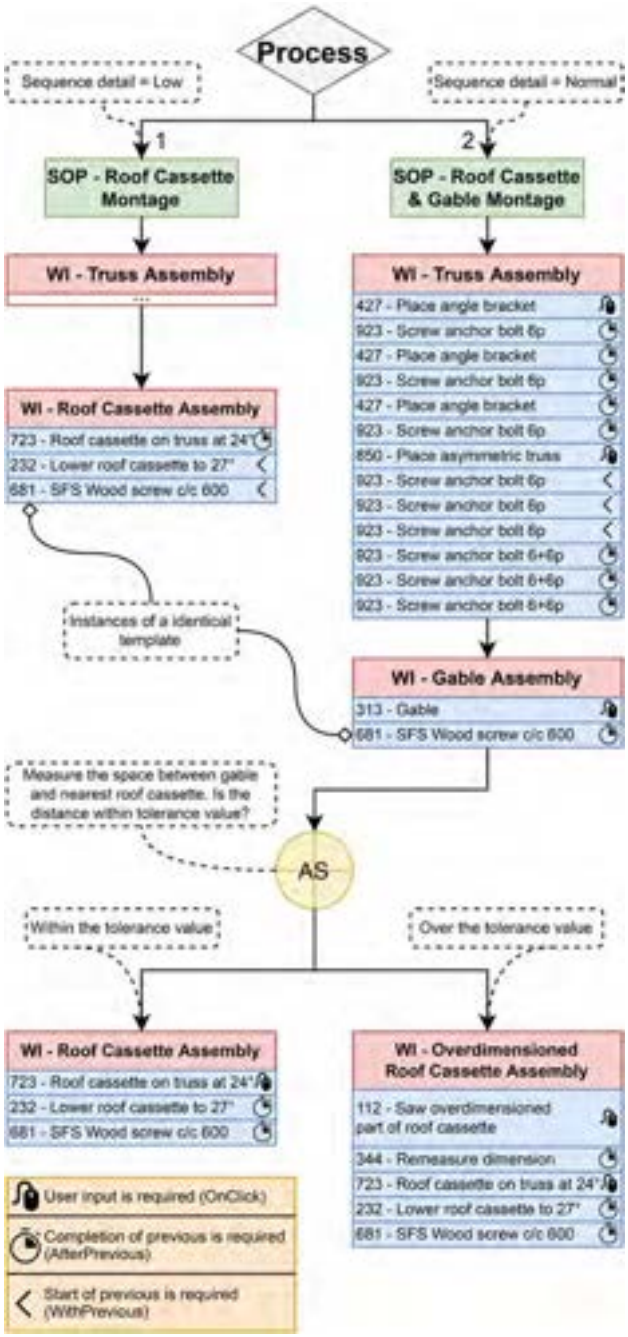

Figure 2. Data model for the developed conceptual model, identifying relations for SOP instances, WI instances, AS and instructional templates. Sequence type and sequence detail effect on instruction templates is also visualized in the diagram.

The use of modularity has been an essential factor for the development of SOPs, WIs and instruction templates. It has aided in the reduction of data redundancy by supporting reuse, updating and maintenance with the prototype. The main SOPs, WIs and instructional templates are developed from scratch. Variants and copies of SOPs as well as WIs are instanced, giving the potential to modify and update the main SOPs and WIs to automatically push the changes to all instances. Examples of main and instanced SOPs include the SOP "Roof Cassette Montage", which is a main SOP, and the SOP "Roof Cassette & Gable Montage", which is a variant from it (where a WI and an AS module are added to it), see Figure 2.

As for instructional templates, the components are using templates to pull data. The SOPs, WIs and template-based instructions are interchangeable, organizable and are decoupled from other SOPs, WIs and templates respectively. Modularization of instruction templates is developed to avoid the need of component instancing and data pushing. For example, 3 components in 2 main WIs are using an identical template "681 – SFS Wood screw c/c 600", as seen in Figure 2. This is desirable because components, in addition to containing identical data, also contain multiple unique data, such as geometrical, positional and rotational data.

4.2 Interactive prototype development

The developed method workflow is divided into 5 phases. First, the initiation phase, see green in Figure 4, where additional data is generated and cached for core functionalities of the prototype. It starts with initializing all components, SOPs, WIs, and instructions. Each SOP that has its sequence detail value changed from normal, gets its instruction sequence type values modified (OnClick, AfterPrevious, WithPrevious). That occurs according to the sequence detail as well as pre-defined rulesets by the developer. To identify animation paths for each component, their original position and rotation data (originalPosition & originalRotation) are cached. Afterwards, through addition with the adaptive values (adaptivePosition & adaptiveRotation), the start position and rotation (startPosition & startRotation) are calculated. Direction of the local axis is considered into the calculation, when the local option is selected. For each instruction not played simultaneously (Sequence Type != WithPrevious), it has its next sequence instruction checked, if any exist, to find out if that instruction needs to be simultaneously played (Sequence Type = WithPrevious). The instruction is added to a list of instructions planned to be animated simultaneously with the original instruction (simultaneousInstructions list), the method loops continuously until either finding no more sequenced instruction or finding a non-simultaneous instruction. The method, lastly in the first phase, disables and hides all component instructions for them to be later enabled and displayed when animated.

The second phase, see orange in Figure 4, focuses on searching for the next sequenced instruction within SOP-WI. A procedure to search for the next sequence starts.

This procedure can be called for multiple reasons, including when the user tries to view the next sequenced instruction. The SOPs, WIs and instructions are sequentially organized. Therefore, using current instructions sequence index + 1 in comparison with the total number of instructions within the WI, it is identified if there are more instructions available to be selected. However, if there are no more instructions available, using current WI sequence index + 1 in comparison with the total number of WI within the SOP identifies if there are more WIs available to be selected. The method selects found WI and selects the first available instruction. Otherwise, if none is found, using the current SOP sequence index + 1 in comparison with the total number of SOPs within the Process identifies if there are more SOPs available to be selected. If the method finds a new SOP, it gets selected together with the first sequenced WI/AS, with also a selection of the first instruction in case of it being a WI. The user is prompted to select one of the available AS options, if the first sequence was instead an AS, Figure 3. When none of the above processes can find a new instruction, the method identifies that no more instructions are available.

For the third phase, see blue in Figure 4, to start, the second phase must find a new instruction. The method utilizes the components' instruction data to animate them accordingly. The method ensures to loop through and animate all components if the instruction has simultaneously planned instructions to be animated (simultaneousInstructions list), else it only animates the selected instructions. The selected instruction is moved to its start position and rotation (startPosition & startRotation) and is made visible to the user. Through linear interpolation, it is possible (with a timer counting the duration of instruction animation as an interpolant) to calculate and animate a moving and rotation pattern for the component. This is a continuous process, until the component reaches its original position and rotation (originalPosition & originalRotation). Using the method in the second phase, the next sequenced instruction is searched. If found, and found instruction is planned to be animated immediately afterwards (Sequence Type = AfterPrevious), the next sequenced instructions animation is started.

Figure 4. AS, user selects a WI from list to modify current SOP. Including step-by-step instructions.

The fourth phase, see yellow in Figure 4, is simultaneously run with the third phase. This phase moves the camera to target the animated components. Using an orbit camera, it is possible, by moving the camera target, to rotate around and view the current instruction. An orbit camera also opens the possibility to zoom in/out (distance parameter). To customize and pre-define the camera viewpoint, two new parameters were added in the prototype to each component of all instructions, rotation (x & y) and distance. Through linear

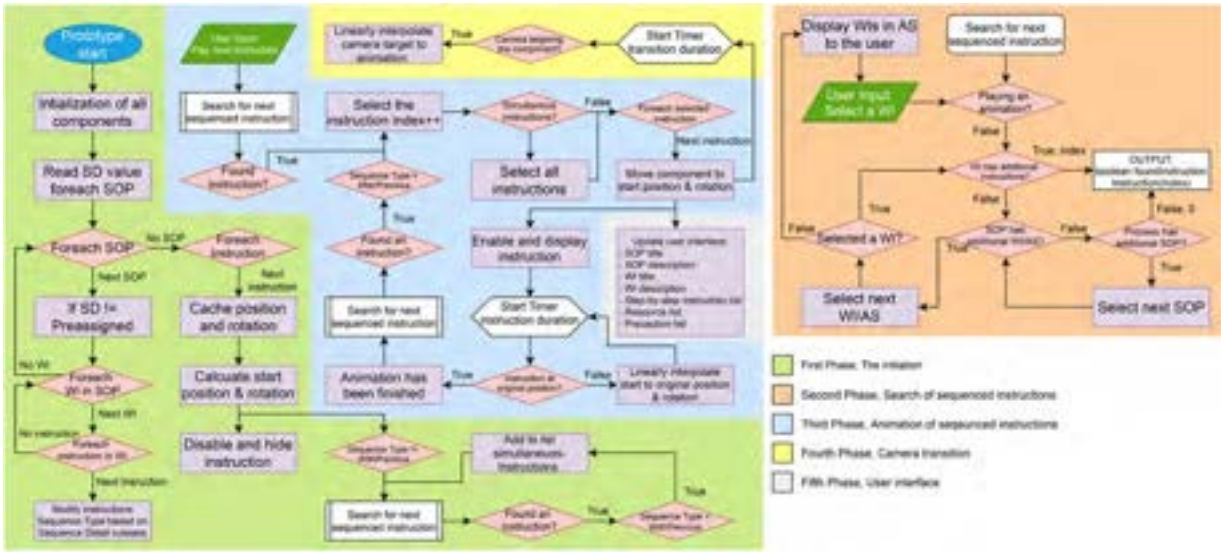

Figure 3. Flowchart of the prototype using the iteratively developed method.

interpolation, in combination with a transition duration timer as the interpolant, the camera glides to its target from its current position to its target position. In addition, linear interpolation occurs even for rotation and distance, ensuring a smooth rotation and modification of the camera's distance to the component's values.

The fifth phase, see gray in Figure 4, runs simultaneously with the second phase. This phase ensures that the user interface is functioning and displaying updated information. The user interface, Figure 5, to not overload the user, only presents the basic information. With additional information being only available when requested by the user. With each newly started animation of a component, its instruction data with description, resources and precautions are added to a list and presented to the user when requested. When a new SOP or WI is selected, the SOP and WI titles as well as descriptions are updated and can be presented to the user. The list is cleared when the selected SOP changes. Combining it all together results in a prototype that can be exported and utilized by a variety of devices for usage in construction sites, see Figure 5.

Figure 5. Prototype running on Android smartphone.

5 Discussion & Conclusion

According to the study, onsite construction at an IHB company has shown to utilize many repetitive processes as well as variants of these processes. Development of a method for the conception and usage of modular SOPs (main & instances), WIs (main & instances) and instructional templates has opened the possibility for reuse of information and experience within multiple construction projects, reducing data redundancy and in turn even decreasing lead times. Reusability of modular AS has encouraged the IHB company to increase their SOP quality by putting more resources into their development and identifying foreseeable issues.

Interactively defining modular SOPs, WIs and instructions has shown the potential to simplify and streamline the assembly sequence process with data within SOPs, etc. The structure of main and instances as well as templates ensured that modifications to mains and templates updated all instances accordingly, aside from unique values within said instances. The interactive modularity has aided the creation of unique variants for mains and templates that later can be utilized in the creation of instances and their connection to components, respectively.

Interactive visualization of modular SOPs, WIs and instructions with user inputs, accurate information and animations have been described by interviewees using the prototype as a usable and useful tool. This, combined with 3D models, potentially gives an improved holistic view of the construction project, assembly process sequence as well as step-by-step instructions that otherwise with many shop drawings and information sources was difficult to obtain. It has assisted the communication between site managers, foremen and skilled workers, resulting in earlier identification of misinterpretations and misassumptions that traditionally instead were identified during the assembly process by foremen. For inexperienced skilled workers and new processes, visualization of the assembly sequence is seen as a massive help in describing and educating how an assembly is correctly performed. Also, ensuring that site managers, foremen and skilled workers have a similar understanding of the construction's assembly processes. Reducing communication deficiencies that can occur due to actors having different backgrounds, experiences or standards is a key to reducing man-made errors. This is supported by theory, as 3D models and good quality instructions could be used for training of new assembly processes as well as for new skilled workers [3]. According to interviewees, inclusion of the developed prototype as a complimentary data source in construction site has shown to bring the typically occurring misinterpretations and misassumptions into the open. With many of them being due to usage of outdated and incorrect versions of the text-based instructions. Prior to usage of the prototype, interviewed skilled workers were certain that their processes were up to the standard set by the company. However, after inclusion of the prototype, they were able to identify multiple processes that are being conducted differently, noting that this is how they used to do it before.

Development of SOPs, WIs and instructions combined with detailed 3D models has been shown in the study to aid project engineers in the identification and mapping process of assembly sequences, their optimization possibilities, sequence errors as well as possible misinterpretations in early stages of the development. Leading to an improved holistic view for process sequence of the construction when the

information is joined together and in turn minimizing possible process errors by improving planning for parameters such as object collisions, zones (reachable & unreachable), avoidance of uncomfortable and risky working conditions. Many of these optimizations and sequence errors are traditionally identified at later stages by foremen and skilled workers, which are often communicated to project engineers. The prototype is expected to increase the construction efficiency by:

- Reducing the required education time of inexperienced skilled workers.
- Reducing misunderstandings and misinterpretations of the standardized processes.
- Visualization of critical sequences, safety instructions, tools and materials.
- Simplifying the conduction of self-control.
- Assisting the daily follow-up of construction job planning.

As a complementary result of the study, improved feedback loops between skilled workers and engineers was observed at early stages using the developed prototype, for assisting in assembly sequence and construction processes.

Acknowledgements

This research study was made in the research project Connected Building Site funded by the Swedish Governmental Agency for Innovation (VINNOVA). Connected Building site is a testbed on digitization of construction with a focus on site planning, production and supply. We thank interviewees as well as construction companies for their incentive and effort.

References

[1] Slack N, Chambers S, Johnston R. Operations management / Nigel Slack, Stuart Chambers, Robert Johnston. 2004.

[2] Nakagawa Y. Importance of standard operating procedure documents and visualization to implement lean construction. In: 13th International Group for Lean Construction Conference: Proceedings. 2005. p. 207–15.

[3] Mourgues C, Fischer M. A product / process model-based system to produce work instructions. Manag IT Constr Constr Tomorrow. 2010;

[4] Davenport TH, Prusak L. Working knowledge: how organizations manage what they know. Choice Rev Online. 1998;35(09):35-5167-35–5167.

[5] Mourgues C, Fischer M, Hudgens D. USING 3D AND 4D MODELS TO IMPROVE JOBSITE COMMUNICATION – VIRTUAL HUDDLES CASE STUDY. In: CIB 24th W78 Conference & 14th EG-ICE Workshop & 5th ITC@ EDU Workshop,. 2007. p. 91–7.

[6] Hevner AR. A Three Cycle View of Design Science Research. Vol. 19, Scandinavian Journal of Information Systems. 2007.

[7] Hevner AR, March ST, Park J, Ram S, Ram S. Research Essay Design Science in Information. MIS Q. 2004;28(1):75–105.

[8] Bergerova K. Standard Operating Procedures at Skanska Standardization and continuous improvement in the construction industry. 2010.

[9] Nakagawa Y, Shimizu Y. Toyota Production System Adopted by Building Construction in Japan 817 TOYOTA PRODUCTION SYSTEM ADOPTED BY BUILDING CONSTRUCTION IN JAPAN. Vol. 12, Proceedings IGLC. 2004.

[10] Li D, Mattsson S, Salunkhe O, Fast-Berglund A, Skoogh A, Broberg J. Effects of Information Content in Work Instructions for Operator Performance. Procedia Manuf. 2018;25:628–35.

[11] Mourgues C, Fischer M, Kunz J. Method to produce field instructions from product and process models for cast-in-place concrete operations. Autom Constr. 2012;22:233–46.

[12] Serván J, Mas F, Menéndez JL, Ríos J. Using augmented reality in AIRBUS A400M shop floor assembly work instructions. AIP Conf Proc. 2012;1431(April):633–40.

[13] Tu Q, Vonderembse MA, Ragu-Nathan TS, Ragu-Nathan B. Measuring modularity-based manufacturing practices and their impact on mass customization capability: A customer-driven perspective. Decis Sci. 2004;35(2):147–68.

[14] Lennartsson M, Björnfot A. Step-by-Step Modularity-a Roadmap for Building Service Development. Development Lean Construction Journal. 2010.

[15] Feitzinger E, Lee HL. Mass Customization at Hewlett-Packard: The Power of Postponement Harvard Business Review. 1996.

[16] Moser L, Santos A. Exploring the role of visual controls on mobile cell manufacturing: A case study on drywall technology. Int Gr Lean Constr. 2003.

[17] Watson G, Butterfield J, Curran R, Craig C. Do dynamic work instructions provide an advantage over static instructions in a small scale assembly task? Learn Instr. 2010;20(1):84–93.

[18] Höffler TN, Leutner D. Instructional animation versus static pictures: A meta-analysis. Learn Instr. 2007;17(6):722–38.

A Framework for Augmented Reality Assisted Structural Embedment Inspection

Jeffrey Kim[a] and Darren Olsen[a]

[a]McWhorter School of Building Science, Auburn University, United States
E-mail: jeff.kim@auburn.edu, dao0002@auburn.edu

Abstract –

Embedments (embeds) placed in concrete or masonry structures are used extensively in construction to connect the final product of one trade-contractor's work to another and are therefore, a critical coordination facet for most construction projects. A failure in this coordination usually leads to lost productivity. Therefore, the need to productively improve the installation quality is paramount. A between-groups experimental study was designed to measure embed placement accuracy within an experimental space. One group inspected the work with a 2-dimensional set of construction plans while another group carried out the work with the assistance of an augmented reality (AR) inspection tool. An AR headset was used that presented a parametric model as a visual overlay on the walls of the experimental space. In this way, the embed placement accuracy could be inspected. The results indicated that accuracy was weakly significant between the two methods of embed inspection. However, a shortcoming discovered during the research required the precision of the AR tool to be tuned because of an image drift within the AR visualization. This paper analyzes the AR shortcoming, differences in accuracy, proposes reasons for the differences, and addresses the accuracy trade-off in a broader context of the framework.

Keywords –

Augmented Reality; Productivity; Construction Inspections; Embeds

1 Introduction

Construction coordination is a risk that is customarily assigned to the construction manager of a project. While the construction manager is often rewarded commensurate with accepting this risk, there is often a desire for them to develop better ways to manage this risk. Pre and post construction inspections are one way that construction managers have mitigated their risk, but sometimes this process fails. Sometimes, a lack of time becomes the root cause [1] and defects end up costing the project time and money.

In this research, we explore a framework that addresses inspection defects with the understanding of the pivotal role that this process plays in a project's productivity and for its success.

2 Background and Rationale

Concrete and masonry anchors are commonly used for the attachment of other structural members to concrete and masonry. In construction and civil engineering disciplines they are commonly called embedments (embeds). It is best if they can be installed prior to the completion of the concrete or masonry structure [2]. Failure to place embeds prior to the concrete or masonry construction can be problematic for several reasons [3], [4], some of which include:

1. Drilling holes for a post-installation anchor will often hit or compromise the internal steel reinforcing
2. Lost time to re-design and retrofit the structure for a post-installation anchor
3. Added cost of re-design and specialized post-installation anchors

Augmented reality (AR) is a technology that is used to add supplemental information to a real-world view [5]. By adding this meta-information to a person's perception of the real-world view, more insight may be gained by the viewer of what is being observed [6]. AR is quickly finding practicality in the construction industry and some researchers are beginning to refine the ways by which AR can be used for inspection of defects [4]. When inspectors can gain additional insights about what they are observing, they can enhance their work and help to resolve issues prior to construction, when cost and time are less vulnerable to inflationary change [7].

The process of embed placement prior to the construction of concrete and masonry structures is one such situation on a construction project that is

vulnerable to cost and time inflation if they are missed or improperly installed. Therefore, the need for this research was determined based on this observed dilemma and the aim for this research is to use AR technology to assist an inspector in the process of defect detection of embed placement.

3 Methodology

This study was conducted using a between-groups design. One group of randomly selected students were chosen to perform an inspection of installed embeds using 2-dimensional (2D) embed placement drawings. The other group was randomly selected to conduct the same inspection using an AR inspection tool. The following section describes the setting, tools, and procedures that each group was to follow.

3.1 Demographics

A convenience sample was used consisting of postsecondary students in a construction management program in the Southeastern United States. These students were requested to participate in this study at a normally scheduled class time. Students in this CM program, at this point and time in their academic career, have taken plan reading courses, understand building information modeling practices, and several of the students have had some construction-related internships.

3.2 Setting

The study was conducted in a vacant space within the academic building where the students take their classes. This indoor space is approximately 54'-0" long (16.5 m) and 12'-6" wide (3.8 m). The height of the room is 17'-0" (5.2 m) with no finished ceiling – all MEP equipment, conduit, and piping are exposed. On the long side of the room is a 30'-8" x 12'-6" (9.4 m x 3.8 M) window wall, which does not have any window treatments and allows an abundance of outdoor natural light within the space. Refer to Figure 1 for a composite layout of the experiment room.

Figure 1. Rendering of the experiment room

The room in Figure 1 has exposed masonry walls and provided a setting to place mockup embeds on the walls of the space. A parametric model of the room was created in *Autodesk's Revit* and embeds were positioned throughout the room as shown in the closeup rendering of one side of the room (see Figure 2).

Figure 2. Closeup within the parametric model of experiment room showing embed placement

Some embeds were designed to simulate steel angles (colored yellow) and others were designed to simulate flat plates (colored green). Upon completing the parametric model, the embed coordinates were loaded into a total station and the researchers positioned the mockup embeds within the room to match their locations in the parametric model.

3.3 The Embeds

The mockup embeds were fabricated from colored cardboard and matched the color of the embeds in the rendering shown in Figure 2. A *Microsoft* first generation *HoloLens* was used for the AR inspection. The researchers used *HoloLive* and *Visual Live* to upload the model into the HoloLens and for the inspection of the mockup embeds. Figure 3 illustrates the workflow involved in transitioning the parametric model coordinates to the total station that was used to layout the mockup embeds in the experiment room.

Figure 3. Workflow for migrating parametric model information to a total station for embed layout

The researchers preselected that some of the embeds would be placed with identifiable issues. The student-inspectors would have to identify these preselected issues. These issues are summarized below along with the frequency of their use identified in Table 1. The embed issues (listed below) were categorized into three *Issue Categories*.

1. Embed was installed with no issues
2. Embed was installed but has a placement issue
3. Embed was NOT installed

Table 1. Embed configuration

Embed ID	Status	Color	Issue Category
10	Installed	Yellow	1
12 Left	Missing	Yellow	3
12 Right	Installed	Yellow	1
14	Installed	Yellow	1
15	Missing	Yellow	3
16	Missing	Yellow	3
21	Installed	Yellow	1
23	Installed	Yellow	1
A	Installed	Green	1
B	Installed	Green	1
D	Installed	Greed	1
G	Installed	Green	1
P	Missing	Green	3
Q	Installed	Green	1
S	Installed	Green	1
TOTAL 15 Embeds			

Lastly, once the coordinates for each embed was determined, the researchers affixed the mockup embeds to the wall as shown in Figure 4.

Figure 4. Mockup embeds placed in the experiment room (descriptions are shown for clarity but were not included in the experiment room)

3.4 2D Embed Placement Drawings

The parametric model was used to create 2D embed placement drawings. These drawings were printed on 8 ½" x 11" paper without color. The 2D drawings used interior elevations and annotated dimensions to locate the embed within the experiment room. An example of the 2D embed placement drawing is shown in Figure 5.

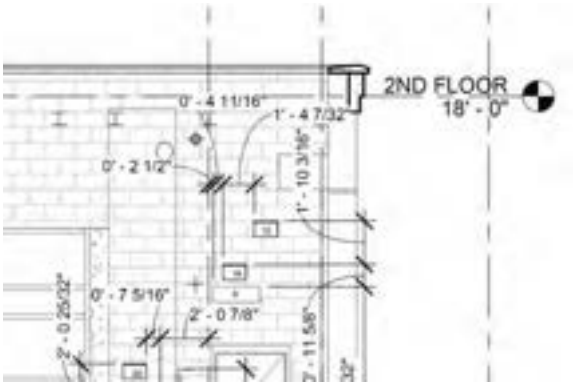

Figure 5. Partial image of 2D embed placement drawings

Students using the 2D placement drawings were to visually compare what they observed on the 2D drawings, matching to what was installed within the experiment room.

3.5 AR Inspection

Students using the HoloLens were to visually observe where they perceived a difference between the image rendered in the HoloLens' overlay of the room to the installed condition within the experiment room. Figure 6 shows what an inspector using the HoloLens would see when inspecting embeds in the experiment room.

Figure 6. Framework of inspecting embeds using AR

The use of the HoloLens in this way allowed for the student inspector to view the correct placement through a model of the room that was superimposed on the visual of the *real-world* experiment room.

3.6 Experiment Procedures

As mentioned, this experiment was designed as a between-groups procedure. The students were randomly selected to conduct an inspection of the experiment room's embed layout using either 2D embed placement drawings or using the HoloLens for inspection.

All students were asked to record their findings on a paper inspection sheet. Because AR does not completely replace the view of the user, the student inspectors were able to report their findings on the paper inspection sheet. Both groups of students used the same type of inspection sheet to record their findings. The inspection sheet contained numbers ranging from 1 to 31 and letters A through Z. With both methods, if the student identified an error, they were asked to record the problem on the inspection sheet with the associated embed identification (number or letter). There were more numbers and letters on the inspection sheet than were embeds placed within the experiment room. This open-endedness was purposefully designed to control for a situation where students may assume that all embeds on the inspection sheet needed to be identified to properly complete the inspection. All inspection sheets were collected and tabulated at the end of the experiment.

4 Data and Results

A total of 46 students participated in the experiment. 25 students used the 2D embed placement drawings to conduct the inspection while 21 students used the AR inspection method.

Table 2 tabulates the error frequency for each of the 15 embeds used in this experiment grouped by inspection method. An error was determined if the student inspector did not accurately identify the installation state of the mockup embeds. While conducting the experiment, some students using the AR inspection reported seeing illusions that obscured the reality of what was installed within the experiment room. The researchers identified these visual anomalies as *mirages* in Table 2. The frequencies identified for the *AR Inspection Errors* is independent of the *AR Mirage Errors*.

Table 2. Embed error frequency for each inspection method

Embed ID	2D Embed Placement Drawings Errors (n=25)	AR Inspection Errors (n=21)	AR Mirage Errors
10	1	1	-
12 Left	-	-	-
12 Right	-	-	-
14	3	4	1
15	24	11	1
16	-	4	1
21	22	1	-
23	-	1	-
26	-	-	1†
A	-	-	-
B	-	-	-
D	-	-	-
G	-	1	1
P	1	5	1
Q	-	1	-
S	-	2	2

† denotes an embed that was identified as a mirage and not a part of the experiment.

The researchers tabulated the errors per embed ID and calculated an accuracy score for each inspection method. The average accuracy for the 2D embed placement drawings was 86.4 out of a possible perfect score of 100. The average accuracy for the AR inspection method (not including the observed mirages) was 90.2 out of a possible perfect score of 100. A Two-Sample T-Test was calculated for the difference between the two averages. Eight outlier results were

excluded to correct for skewness of the data. Assuming a Confidence Interval percentage of 95% (*CI*=95%) then $t_{(38)}$=-2.281802, p=0.0342029 ($p \leq 0.05$), resulting in a weak significance in the difference between the two averages.

5 Discussion

The weak significance resulting from the difference between the average accuracy scores for both methods leads to a conclusion that is somewhat indeterminant. In this section, the impact of the results are discussed along with suggestions for the outcome.

5.1 Visibility

The experiments were conducted during day-light hours. With the room lighting and the allowable natural light in the room, there were no significant shadows or dark areas of the room that could notably affect either method of visual inspection. Despite this fact, the data indicate that identification of embeds "15" and "21" were more successful when the AR method of inspection was used. Embed "15" was accurately reported 4% of the time using the 2D placement drawings and 48% using the AR inspection. Embed "21" was accurately reported 12% of the time using the 2D placement drawings and 95% using the AR inspection. Both embeds were simulated steel angles (yellow) and place in a *side* view when observed from the elevation view of the wall (example embed "15" shown in Figure 7). One embed was missing (embed "15") and the other was installed (embed "21" see Figure 8).

Figure 7. Placement of embed "15" (side view)

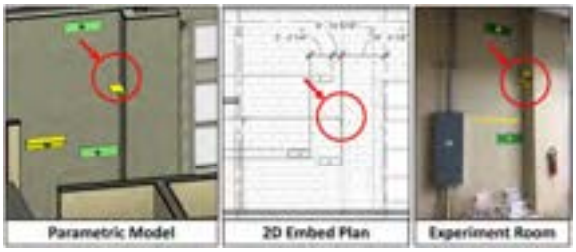

Figure 8. Placement of embed "21" (side view)

The low profile of these embeds on the 2D placement plans made it difficult to verify, especially when the embed was missing, as is the case for embed "15". This condition is a reality for most construction projects. If an inspector takes 2D plans to the field for inspection and only observes what is available to them in an *elevation* view without querying for alternate *detail* views – omissions can occur. With the AR inspection, the original model is available, and an infinite amount of *views* are available to them by simply adjusting their physical position on the construction site – much like an inspector naturally does to inspect installed work at a construction project. Lastly, although the condition was not tested in this study, the embeds tend to be distinguished during the inspection process because a *colored* view was available during the inspection process using the HoloLens. Conversely, the monochromatic view when looking at 2D construction plans does not have this advantage which is why most inspectors tend to highlight their inspection drawings with colored annotations.

5.2 Accuracy

The findings are not strongly significant for the AR inspection method and the data indicate that the 2D embed placement plans were in most cases equally accurate. Aside from the visibility issue discussed for embeds "15" and "21" in the previous subsection, most of the time, the 2D plan inspection method had slightly fewer errors. For instance, embed "16" was a missing embed and was erroneously reported five times with the AR method. It was not erroneously reported using the 2D plan method. Additionally, embed "P" was also a missing embed and erroneously reported once with the 2D plan method and five times with the AR method. Nothing was controlled in the experiment to gather data for these occurrences; however, it is speculated that something within the AR inspection distracts the viewer while performing their inspection. As will be discussed in the next subsection, illusions were noted that caused some misreporting during the inspection process for the AR inspectors.

5.3 Mirages

During the AR inspection, it was anecdotally noted to the researchers that in some cases, the student inspectors could not see the embed or that there appeared to be an embed present, when in fact it was not. The researchers allowed for this condition by having the student inspectors note the aberrations in their inspection reports. As seen in Table 2, this occurred eight times. In two cases, a missing embed was not accurately identified as missing and in the remaining six cases, the embed was present but was missed in the inspection report.

During the experiment, the researcher needed to continually adjust the HoloLens for a condition called "drift" [8]. Drift was identified by the student inspectors as they conducted their inspection and would notice that the image of the model in the HoloLens was not superimposed accurately within the experiment room. In some cases, the difference was slight – enough so that the inspection could continue without stopping the experiment. At other times, the drift was noticeably distracting to the point that a satisfactory reporting could not be made. It is surmised that this condition was responsible for the mirages present during the inspection. This condition is not localized to the HoloLens, it is in fact a common issue within the AR discipline [9].

5.4 Limitations

While the researchers sought to minimize the conditions of the study that could adversely affect the results, upon completion of the experiment some elements became known that should be considered if the study were to be repeated.

5.4.1 Color and Shape

The researchers did not collect data explicitly regarding the shape and color of the embeds used in this experiment. In fact, the color of the embed was not typical to the actual color of an embed installed on a construction project (see Figure 9).

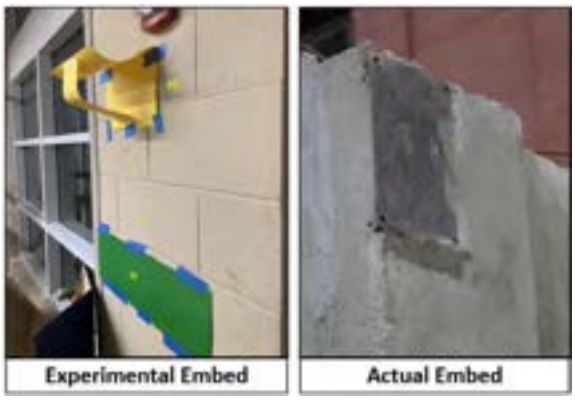

Figure 9. Visual comparison of experimental embed and an actual embed.

The difference between the two images in Figure 9 is obvious. Because this study was designed to establish a framework for future experimentation, it was not necessary to obtain data from actual conditions just yet. In future studies, the color of the surrounding material (concrete, stone, masonry, etc.) may not have enough contrast to make a successful inspection. Therefore, a consideration of the color of the embed and the color of the surrounding materials would be prudent.

5.4.2 Student Work Experience

This study was conducted with a convenience sampling that is not representative of practitioners in the construction industry. While the students that volunteered for this study do have some construction knowledge and skills, they lack experience and advanced visualization skills that more seasoned practitioners may have [6]. Consequently, the results when practitioners are involved in the study may yield different results. Again, future iterations of this study should be conducted with practitioners to obtain more practical results in the accuracy of inspection using the two methods.

5.4.3 Image Drift

Image drift is an issue when working with AR [8], [9]. This study did not collect data for this condition, including its effect on accuracy. However, a more detailed study should be attempted that ascertains the accuracy of the HoloLens when used for inspection, controlling for variables such as lighting (natural and artificial), temperature, reflectivity, and other items that may affect the visual acuity of the inspector.

6 Conclusions and Future Work

This experiment yielded a significance that was weak in terms of accuracy when student inspectors were

trying to identify errors in embed placement. The data however, eluded to some interesting points about using AR as an inspection tool for embed inspections, and quite possibly for other types of inspections as well. In this study, the researchers aimed to create a framework that could be used in ongoing and future studies where AR is used to assist a construction inspector. One key finding that was advantageous when inspectors used the AR method was the visibility of certain elements that were difficult to find on a 2D plan. The drawback with using plans has always been the experience of the person reading and interpreting them [10]. In a time within the construction industry when many seasoned professionals are departing from the workforce [11], either through retirement or disability, their replacements (recent academic graduates) lack the experience to accurately perform these inspections at the same level as their predecessors. This experience gap creates a challenge and an opportunity that the construction industry has always seemed to face. When compared to other non-farming industries, the construction industry's productivity has not made significant improvements [12]. Similarly, the industry's focus on research and development has been paltry – yet may be improving slowly [13]. Therefore, the overarching goal for this research study was to set forth a framework that can improve accuracy, productivity, and fill the ever-widening skills gap in a small part of the construction process.

The researchers acknowledge that the practicality of this tool is *experimental* at the moment, however, through continued field experimentation and with the continual improvement in the hardware and software, there is promise for more advantageous results for the AR method.

Lastly, the researchers would like to express that future developments in this research will include an approach toward having the AR make use of artificial intelligence (AI) for the automatic recognition of embed placement errors. The inspector's attention could be drawn to errors that the AI finds, allowing the inspector to focus more on the serious problems and waste less time on the embeds that meet a certain threshold for accuracy. This process, if perfected, could save a tremendous amount of time for inspectors to perform more worthwhile tasks.

References

[1] D. D. de Saram and S. M. Ahmed, "Construction Coordiantion Activities: What is Important and What Consumes Time," *J. Manag. Eng.*, vol. 17, no. October, pp. 202–213, 2001.

[2] M. Saleem, W. A. Al-Kutti, N. M. Al-Akhras, and H. Haider, "Nondestructive Testing Procedure to Evaluate the Load-Carrying Capacity of Concrete Anchors," *J. Constr. Eng. Manag.*, vol. 142, no. 5, pp. 1–8, 2016.

[3] B. A. Mohr and S. K. Harris, "Marrying Steel to Concrete: A Case Study in Detailing," *Struct. Mag.*, no. November, pp. 34–36, 2011.

[4] O. S. Kwon, C. S. Park, and C. R. Lim, "A defect management system for reinforced concrete work utilizing BIM, image-matching and augmented reality," *Autom. Constr.*, vol. 46, pp. 74–81, 2014.

[5] R. Azuma, "A survey of augmented reality," *Presence Teleoperators Virtual Environ.*, vol. 6, no. 4, pp. 355–385, Aug. 1997.

[6] J. Kim and J. Irizarry, "Evaluating the Use of Augmented Reality Technology to Improve Construction Management Student's Spatial Skills," *Int. J. Constr. Educ. Res.*, 2020.

[7] C. Thomsen and S. Sanders, *Program Management 2.0: Concepts and strategies for managing building programs (revised)*. The Construction Management Association of America Foundation, 2011.

[8] Y. Liu, H. Dong, L. Zhang, and A. El Saddik, "Technical evaluation of HoloLens for multimedia: A first look," *IEEE Multimed.*, vol. 25, no. 4, pp. 8–18, 2018.

[9] R. Azuma, Y. Baillot, R. Behringer, S. Feiner, S. Julier, and B. MacIntyre, "Recent Advances in Augmented Reality.," *IEEE Comput. Graph. Appl.*, vol. 21, no. 6, p. 34, Nov. 2001.

[10] M. Alias, T. R. Black, and D. E. Gray, "Effect of instruction on spatial visualization ability in civil engineering students," *Int. Educ. J.*, vol. 3, no. 1, p. 12, 2002.

[11] McGraw Hill Construction, *Construction Industry Workforce Shortages: Role of Certification, Training and Green Jobs in Filling the Gap*. 2012.

[12] L. Sveikauskas, S. Rowe, J. Mildenberger, J. Price, and A. Young, "Productivity Growth in Construction," *J. Constr. Eng. Manag.*, vol. 142, no. 10, p. 04016045, Oct. 2016.

[13] JBKnowledge, "The 6th Annual Construction Technology Report," 2017.

Towards Circular Economy in Architecture by Means of Data-driven Design-to- Robotic-Production

G. Nazzarri [a] and H. Bier [a]

[a] Robotic Building, Faculty of Architecture, University of TU Delft, Netherlands

E-mail: H.H.Bier@tudelft.nl

Abstract –

While the global impact of plastic waste is increasingly concerning, the application of reused materials in the built environment remains little explored. This paper presents research into the reuse of plastic in architecture by means of computational design and robotic fabrication. Design possibilities using reclaimed plastic artefacts were explored by testing their structural stability and robotically modifying them in order to create a pavilion. While the design conceptualization started with the reclaimed material and the analysis of its potential, the digital workflow involved generative and performance- driven design, structural optimization and geometry generation for robotic fabrication.

Keywords –

Robotic fabrication; Circular economy; Reuse; Plastic; Pavilion; Computational design; Waste control; Human-Robot Collaboration

1 Introduction

Applications of Industry 4.0 technologies, such as automation, Internet of Things (IoT), and cyber-physical systems [3] are relatively new in architecture but they have already proven to revolutionize the way architects think and practice.

For instance, Design-to- Robotic-Production (D2RP) approaches developed at TU Delft since 2014 establish a feedback loop between the design and the production of the 1:1 scale building components [1].

This implies that the initial generative design is optimized in order to address functional, structural, environmental, material, etc. requirements and then converted into robotic tool paths to add, remove or transform materials according to requirements.

The challenge is to identify tasks that can be robotized and develop future interaction scenarios between humans and robots. In this paper, work is presented that explores both while taking the challenges of circular economy into account.

2 Circular Economy

Plastics production has increased twentyfold since 1964, reaching 311 million tons in 2014 [4].

Despite the economic crisis, the world plastics request is continuously increasing and it is expected to almost quadruple by 2050. With the increase of the plastic production, the plastic waste increases as well, so much that the ocean is expected to contain by 2050, more plastic waste (by weight) than fish.

Figure 1. The plastic container is tested for structural strength

Currently, this problem is addressed on two levels, firstly the manufacturing of plastic materials from oil is gradually replaced with renewable bio-sourced materials; secondly the recycling or reusing products is considered. When recycling is not the best option because soiled plastics and multi-layered plastic products may not be suitable or difficult i.e. expensive to be recycled, reuse is considered (Fig. 1).

The research presented in this paper explores how by employing D2RP methods and by applying circular economy principles [5], thus reusing objects otherwise designated for the landfill, an approach that can be

applied to various geometries is developed and tested.

The reused objects were searched for in a traditional manner, by going to stores and selecting potentially usable components.

Figure 2. Development of the node from the unrecyclable plastic container using a combination of D2RP and traditional methods

Considering the potential of IoT to connect the D2RP system with materials that are provided with unique identifiers (UIDs) and filter databases for specific plastic materials and products catalogued with respect to their physical and chemical characteristics, it is conceivable that a variety of designs for diverse functions could be easily generated.

2.1 Architectural Structure

From an array of available components, several have been structurally tested and the unrecyclable drill container, which has been chosen to be used in the design, showed a peak close to 80 kg (Figure 1). The test highlighted that the base is the weaker part of the element.

By developing joints (Figure 2) from the drill container that could connect linear frame elements (of Polyvinylchloride or PVC pipes for water supply) with a membrane (of semi-open water repellent fabric) a pavilion has been created (Figure 3).

The vaulted structure has a double-curvature that increases the structural performances. Once inflated, the designed mesh is improved using the Mesh Machine component after which it is tessellated with the Dual Graph component. Joints, PVC pipes, and membrane are then placed resulting in a pavilion that serves as event space.

In order to test structural stability, the mechanical properties of the materials were retrieved from CES Edupack 2018 and used as input for the structural analysis. Furthermore, the structure was analyzed in the Grasshopper plugin Karamba 3D. The latter, being embedded in the parametric design environment of Grasshopper, gives the possibility to combine parametric 3D models with finite element calculations.

Following up the structural analysis, joints, PVC pipes and membrane were further developed and tested. The node was developed by removing and folding parts, so that the folded part of one component fits perfectly into the cut part of another component. The connection is then secured by rivets (Figure 2).

With the robot, the component can be cut at a specific optimum angle in a precise and accurate way. Because of the complexity of the geometry, all the components that form the connections need to be custom cut at a specific angle, thus the use of robotic fabrication will make the process more accurate and faster compared to traditional methods.

The workflow involved several steps such as robotic cutting (drilling holes and material removal), manual folding (with a heat gun), manual gluing of the washers and connecting parts with rivets using pop rivet gun.

While the robotic tool path was integrated into only one path for drilling holes and milling i.e. cutting, which made the process faster and more efficient, the folding of the material of the component itself, the gluing and connecting with rivets remained manual.

Figure 3. Generative design optimized in order to address functional, structural, environmental, material, etc. requirements

The robotization of the folding, gluing, and connecting with rivets would have required additional investigation, which due to time constraints has only been simulated as robot-robot cooperation and envisioned as Human-Robot Collaboration (HRC).

2.2 Human-Robot Collaboration

In order to semi-automate the fabrication of the node, a multi-robot setup has been proposed in combination with an HRC approach. In this context, HRC is defined as work performed simultaneously and co-located by a robot and an operator during production [2].

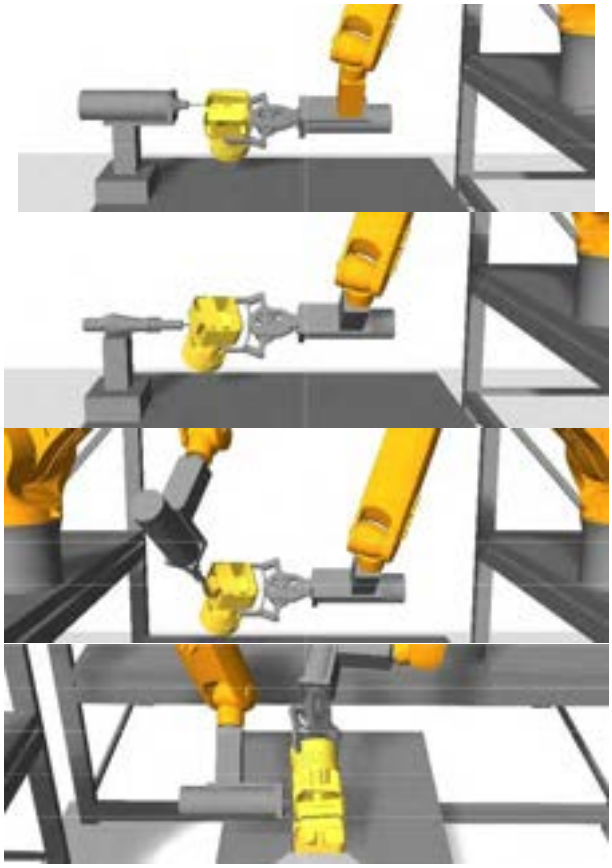

Figure 4. Picking of the first component using the master robot, which is equipped with a gripper, moving then the object around the milling tool and performing the necessary material removal (first image), heating (second image), folding (third image) and placing the rivets (fourth image).

The fabrication sequence of the joints includes two fixed tools, a milling tool and a heat gun, and two moving tools, a gripper and a bolting tool. Hence the component will not be fixed in front of the robot as in the first scenario but it will be moving with it.

The first step of the fabrication sequence will consist in picking up the first component using the master robot, which is equipped with a gripper, moving then the object around the milling tool and performing the necessary material removal (Figure 5).

After that, the object is positioned in front of the heat gun, in order to heat the folding line of the component for one or two minutes, time enough for the plastic to become malleable and for the second robot to come in and easily fold the material using a gripper. The above-mentioned sequence between the two robots is repeated for all the other components.

The last step of the fabrication sequence regards the connection of the objects to each other. The connection will be performed by the second robot, which is equipped with a bolting tool, in collaboration with the master robot, which will hold the component in place.

This proposed HRC approach relies on practical methods facilitating collaborative sawing [7], collaborative polishing [8], etc. It involves limited Artificial Intelligence (AI) that enables the physical collaboration between two robots [7].

This approach is transforming the D2RP process of the joints into a choreography of two cooperating robotic arms alternating their roles along the fabrication process.

In this context, the human may not only orchestrate the sequence of actions implemented by the robots but may help with tasks that could be easier implemented by humans as for instance, inserting the rivets in the holes.

3 Future Steps: Cyber-physical Systems

While the presented research has taken advantage of D2RP and explored the potential of human-robot cooperation, it has not exploited the potential of IoT, which allows selection of materials form a vast variety of materials appropriate for circular economy approaches.

It furthermore, speculated but did not develop and test HRC approaches, which have the potential to make the sequence and safety of human-robot interaction possible.

Figure 5. Simulated and prototyped subtractive D2RP link the virtual and the physical worlds

Both involve tagging and tracing, machine and deep learning in order to establish a cyber-physical system that in time could become an automation ecosystem, wherein architects and constructors collaborate with robots and

customers can purchase online customizable designs using an automated marketing platform that puts the manufacturing plant in action.

The virtual and the physical D2RP&O processes are linked (Fig. 5) and need to take into account the inherent multifaceted nature of building from the early design to the latest building operation phase. Challenges in terms of scale, multi-tool and multi-robot production and operation need to be examined in order to achieve chained processes by linking virtual models (such as Rhino 3D model with Grasshopper plug-ins such as Millipede, Ladybug, etc. for simulating structural and environmental performance) with robotic devices. The aim is to develop/implement chained D2RP&O processes in which robots take specific roles while all (human and non-human) members of the setup including respective (virtual and physical) systems receive feedback at all times.

4 Acknowledgements

This paper builds up on knowledge developed in the Robotic Building group at TU Delft since 2014. It has profited from the input of tutors Sina Mostafavi and Fred Veere and the use of the Robotic Building lab managed by Vera Laszlo.

References

[1] Bier. *Robotic Building*, Springer International Publishing, 2018.

[2] Kolbeinsson, Lagerstedt and Lindblom. Foundation for a classification of collabora-tion levels for human-robot cooperation in manufacturing. *Production & Manufacturing Re-search*, 7:1, 448-471, 2019.

[3] Hermann, Pentek and Otto. Design Principles for Industrie 4.0 Scenarios. In *49th Hawaii International Conference on System Sciences (HICSS),* pages 3928-3937, Koloa, Hawaii, 2016.

[4] Ellen MacArthur Foundation. The new plastics economy: Rethinking the future of plastics & Catalysing action. Online: http://www.ellenmacarthurfoundation.org/publications, , Accessed: 10/05/2019

[5] Geissdoerfern, Savaget, Bocken and Hultink. The Circular Economy – A new sustainability paradigm?. *Journal of Cleaner Production*, 143:757–768, 2017.

[6] CES Edupack 2018. Granta Design Limited, 2018.

[7] Peternel, Tsagarakis and Ajoudani. A Human-Robot Co-Manipulation Approach Based on Human Sensorimotor Information. In *IEEE Transactions on Neural Systems and Rehabilitation Engineering,* vol. 25, no. 7, pages 811-822, 2017.

[8] Peternel, Tsagarakis, Caldwell and Ajoudani. Robot adaptation to human physical fatigue in human–robot co-manipulation. In *Autonomous Robots 42,* pages 1011–1021, 2018.

Automated Pavement Marking Defects Detection

Andrea Leal Ruiz[a] and Hani Alzraiee[b]

[a]Department of Civil and Environmental Engineering, California Polytechnic State University, USA
[b]Department of Civil and Environmental Engineering, California Polytechnic State University, USA
E-mail: alealrui@calpoly.edu, halzraie@calpoly.edu

Abstract –

In 2018, the United States Department of Transportation Federal Highway Administration reported that Americans traverse over 1,000 miles a month on average. Maintenance of pavement marking conditions is crucial to creating a safe driving environment. Traditionally, pavement markings are assessed periodically through manual road inspectors. This method is time consuming and ineffective in capturing the deterioration of the pavement markings throughout their service life. The incorporation of Unmanned Aerial Vehicles (UAVs) and machine learning techniques provide promising ground to detect pavement marking defects. The study proposes a system based on Deep Convolutional Neural Network (DCNN) that can collect, store, and process data to predict pavement marking conditions throughout their service life. The developed pavement marking detection tool has four stages. The Data Collection stage consists of obtaining images using different methods. In the Classification stage, a method for assessing the defects from images is created based on current methods by Departments of Transportation (DOTs) and the Manual on Uniform Traffic Control Devices (MUTCD). The third phase— the Model Development and Data Processing— and the Model Testing phase are to train and test the model using a multi-level classification program and complex algorithms to process the data collected and output a result. The system was implemented, and the preliminary results show that the model can identify and classify the pavement marking defects. The developed system will help transportation authorities identify and forecast future deteriorating rates and intervention timing.

Keywords –

Automation; Construction; Data Acquisition; Transportation

1 Introduction

Road pavement markings are a characteristic of road design that influence drivers' perception of roadway alignment and the ability to maintain safe vehicle positioning [8, 17]. Features such as edge lines, centerline, lane lines, and other pavement markings guide users and provide physical and intuitive barriers that ensure road safety and reduction in traffic congestion [17]. When strategically placed, pavement markings ensure adherence to speed limits [3, 21]. Environmental factors and wear from vehicle contact, as well as misplaced markings, call for the inspection and maintenance of these road markings [21].

The current practices of pavement marking inspection are mainly done manually. Manual inspection techniques such as Visual Nighttime Inspection, Measured Retroreflectivity, Expected Service Life, and Blank Replacement methods are a few of the vision-based techniques employed by DOTs to assess and evaluate pavement marking conditions [9]. Handheld devices, measurements, and Senior Citizen vision characterize these methods. These manual methods allow for high subjectivity and rely on trained inspectors that must go through training to follow the appropriate protocols. These visual assessment techniques require investing time, money, and resources. These processes often require workers to drive in nighttime conditions, evaluate, and record pavement conditions that pose public and individual safety risks.

Experimental studies have found short-term and long-term reductions in speed along hazardous curves by installing and maintaining pavement markings [21, 3]. Drops in speed from 41.3 to 33.9 miles per hour were attributed to pavement markings "designed to make the roadways appear narrower at the beginning of the curves." Other sites saw up to a 50% increase in adherence to advisory speed after the pavement marking installations [3]. Additional pavement markings in 42 sites in advance of roundabouts and termination of high-speed roads saw a 52% reduction in crashes after 2 years. Verbal and symbolic pavement markings consisting of the word "SLOW" and a left curve arrow installed before entering sharp horizontal curves also saw significant reductions in average vehicle speeds [3]. Earlier studies showed crash reductions after the installation of edge lines ranging from 19% to 46% [7, 19]. Despite differences in modern days traffic, vehicle design, and design speeds, more studies continue to report crash reductions as a result of

pavement markings. Particularly, a study across 10 states found crash reductions of 36% after installing edge lines and an average of 21% attributed to pavement markings overall [4, 22].

There are two ways of assigning pavement marking defects: manual and automated. A manual evaluation of pavement markings from photogrammetry data would be highly subjective and time-consuming, thus an automated identification method presents an efficient and reliable alternate [2, 13]. This paper aims to propose an innovative UAV-based Pavement Marking Identifier Tool using a deep learning technique that automatically identifies the pavement marking defects. The tool uses data collected from Google Maps to train and test the model. This stage of the research looks at the applicability and efficiency of the technique.

2 Literature Review

2.1 Overview

An assessment of the effects of pavement markings on road safety reveals the importance of identifying and addressing current defects and missing pavement markings. Efforts are underway to mitigate the risks of missing important pavement markings and those in poor condition. For example, the Michigan Department of Transportation (MDOT) plans to require wrong-way arrows at all target exit ramps [18]. At paired exit/entrance ramps, the left turn into the exit has resulted in several fatal crashes. By installing pavement marking extension lines, vehicles could be guided into the correct ramp. They are considered a low-cost treatment with a benefit-cost ratio of 45.9 and the potential to reduce traffic-related deaths and increase road safety [3, 18]. A study was also conducted to assess whether pavement markings before wrong way entries in two sites were in good condition, or at all present [14]. The study found that both sites lacked pavement markings, such as Wrong-Way Arrows and stopping lines, which are linked to a reduction in fatal crashes. Also, in 2004, the Missouri Department of Transportation began implementing lane departure countermeasures consisting of pavement markings such as edge lines, centerlines, and skip lines, as well as other road features focused on lane departure countermeasures [8]. As a result, from 2005 to 2007, there was a 25 percent reduction in lane departure fatalities. Pavement markings wear out due to constant vehicle contact and weathering and therefore require inspection and maintenance. Given the role they play in road safety and the limited resources some cities struggle to keep pavement markings up to the standards due to limited resources. In addition, prioritizing pavement repair and maintenance in a very efficient way is critical for decision-makers to plan future budget allocation and prioritizing road maintenance.

2.2 Data Acquisition

New technologies of real-time data collection such as drones are an increasingly popular technology in construction and transportation [5, 19]. A recent study developed a framework for using UAVs in transportation, which defined the drone block as (1) flight planning, (2) flight implementation, and (3) data acquisition [15]. This framework was implemented by a later study to capture images of pavement defects [14]. This study outlined the importance of taking weather conditions and flight restrictions into account in the flight planning process. This ensured optimized visuals and adherence to regulations. For flight implementation, flights can be conducted manually or autonomously. For automated surveys, an advanced image processing algorithm is required such as Support Vector Machines (SVM) or Structure from Motion (SfM) [12, 13, 2]. These machine learning algorithms allow UAVs to quickly identify the presence of defects and cracks on the road, although they have yet to be implemented to detect defects in pavement markings. The SfM is an innovative photogrammetry method used to transform photo data sets into 3D models; however, research on its applications for road pavement is limited [13]. The data acquisition consists of captured images by the drones. These images are deemed adequate for analyzing and monitoring the condition of unpaved roads [23] and road pavement distresses [13], but there is very limited research in its applications to pavement markings. Data collection via UAVs also mitigates the risks associated with workers in high traffic zones [14].

2.3 Data Processing and Inferencing

Data processing and analysis is critical in developing an automated defects detection system. Efficient data extraction, noise removal, and storage are necessary components to have a functioning system [15]. Manual evaluations of the drone-captured images based on visual observations are associated with high levels of subjectivity, and low production rates [13]. For example, in a study analyzing the condition of road pavement, different crack types were assigned different ratings to assess and prioritize remedial actions according to the severity and average traffic volume [2]. Due to limited resources and a large area to cover, metric accuracy must be consistent [13]. Therefore, automated identification methods and severity numerical index assignments are considered a fundamental goal in transportation efforts to maintain the assets. Autonomous surveys incorporating machine learning algorithms can process the images automatically to identify the distress type [13]. A study that incorporated a UAV-based system with a machine learning algorithm observed an accuracy in pavement

crack identification of 90.16 [12].

Other studies incorporating the use of multi-level classification and deep machine learning to develop predictive models for addressing pavement defect repairs and maintenance continue to advance [25]. These improvements in machine learning models are pivotal to the development of smart cities and autonomous vehicles. Furthermore, deep convolution neural networks (DCNNs) have been implemented to detect pavement cracks and reduce noise [24]. Using datasets for training and testing models set the basis for a system that can characterize road conditions [25].

Multiple studies have also incorporated a Geographic Information System (GIS) to enable automatic visualization of road conditions and automated pavement management [2, 12, 16, 6, and 20]. This system can be used to position classified images into Google Maps [12] and can cover thousands of miles of roadways as well as smaller volume roads [14]. GIS has spatial analysis capabilities that can integrate the graphical display of pavement condition and the assigned prioritization based on classification to facilitate pavement management operations [6, 20]. Currently, the system cannot predict the rate of deterioration of pavement marking based on its current condition but using a Matlab-GIS-based application, it can rate the condition of road segments [2]. Studies integrating this system for the inspection of pavement markings are very limited.

3 Methodology

The proposed framework for the pavement marking identifier tool is outlined in Fig.1. The framework encompasses four stages: (1) data collection using UAV, (2) data classification, (3) model development and training, and (4) model testing.

3.1 Data Collection

In the proposed framework, the data concerning pavement marking condition is collected using either a UAV or a Light Detection and Ranging (LIDAR) device. In this paper, the authors are using the UAV method given the high number of images that can be collected in a short time. For training and testing the model, two sets of data are required. The authors used Google maps and the Google search engine to collect images that show the defects as highlighted in Table 1.

3.2 Data Classification

The data classification phase consists of developing terminology that informs developed framework users of the pavement marking defects present in a surveying site. These terms, as specified in Table 1, are designed to provide a visual evaluation based on criteria outlined in the MUTCD. Per the standards, all lines must be continuous, and uniform in shape. Class 3, 7, and 8 defects address this standard. Lines must also have clear and sharp square edges, as well as be parallel to each other with discernible space. Class 1, 2, 4, 5 address this. Marking visibility and obstruction are addressed in defect classes 6 and 9.

Based on these standards, the set of defects was developed to inform the user when a pavement marking did not fall within these guidelines, as seen in Table 1. This study categorizes the images by lane feature and the associated defect type. These terms can be modified or expanded to suit the needs of any given road segment or the regulations of a company or department of transportation. The output is the class type.

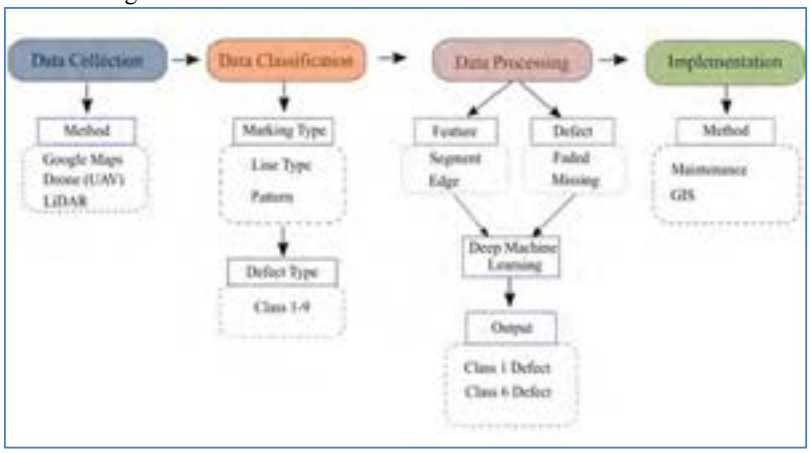

Figure 1. Automated System for Identifying Pavement Marking Defects

Table 1. Classes of Defects

Class Type	Feature
Class 1	Edge Missing
Class 2	Corner Missing
Class 3	Segment Missing
Class 4	Edge Faded
Class 5	Corner Faded
Class 6	Segment Faded
Class 7	Misalignment
Class 8	Cracking
Class 9	Ghost Marking

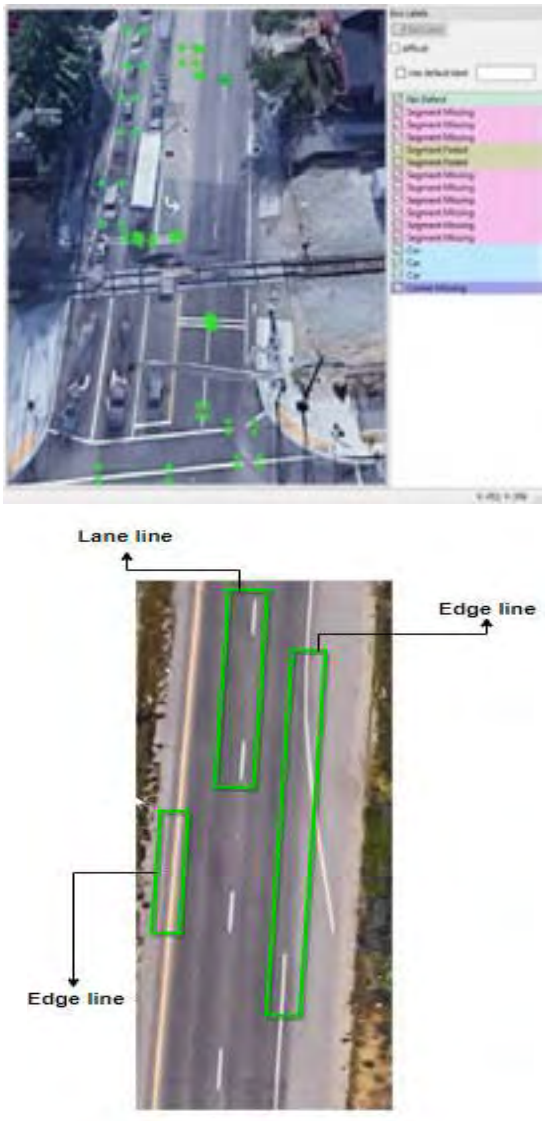

Figure 2. Pavement Marking Annotation and Data Preparation for Model Training

For purposes of this study, lane type identification was added to ensure that the labeling algorithms can differentiate between spacing between dashed center lines and faded sections along a continuous edge line. As seen in Fig. 2 a multilevel classification software was employed in this study in order to annotate the features of the road segment onto the image. This step is essential in developing a reliable and consistent algorithm-based system for future automated classification of roads. The annotations made must be precise and consistent to increase confidence levels. The second round of annotations classifies the markings based on defect types from Table 1. The pavement markings from the training and testing data must be fully categorized to be processed correctly according to MUTCD standards.

3.3 Model Development and Data Processing

3.3.1 Model Development

The model used to detect the objects in the test images was based on a region proposing convolutional neural network (RCNN) written in python. This model initially had the original settings of a pre-trained model called the "faster_rcnn_inception_v2" model from tensor flow's library of packaged models open to anyone for usage and particular implementation. The layers of the neural network were pre-defined for optimal speed and result, and required weights adjusted and optimized for the pavement images.

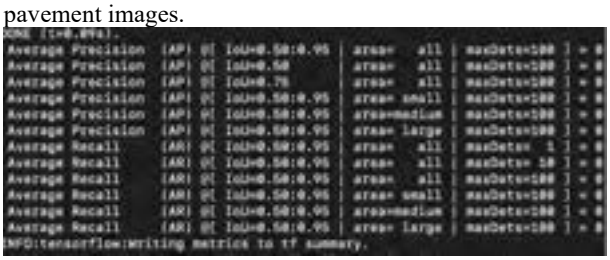

Figure 3. Deep Learning Model Precession Data

3.3.2 Model Training

For this study, this model was trained to identify the specific features of the pavement images. The model was trained using a dataset named pavement marking images (PMI). The model was fed aerial images from Google Maps, which are accessible to all and contain data from roads all over the world. These are updated about every 1-3 years, which renders the satellite-images mostly accurate. Images were captured along the highways of San Luis Obispo County, CA, which were manually inspected and annotated according to the lane type, as seen in Fig. 1, and the defects identified. A multi-level classification program was used in this process.

To train this model, each image's data is passed through the network. Once all the images go through the network, this is considered an epoch. After each epoch,

the weights of the network are changed slightly to yield better predictions on all of the data. 100 training images were collected and annotated and 50 images more were selected for testing.

3.4 Model Testing

The model was only given 80 training images and 20 test images. A snapshot of the model results is shown in Fig. 3. The results of the Validation Data are outlined in the Preliminary Results and Analysis section of this report.

Once all the training and testing images have been processed, the images captured by a UAV, or similar technology, can be automatically processed using complex computer vision algorithms to extract multiple features from the images captured. If these images are annotated consistently and with reduced background noise, the output should be accurate and reliable. The coded data from the collection and classification stage is processed, and its output informs what type of defect, if any, is found along a given road segment.

4 Preliminary Results and Analysis

This study presented preliminary results of the proposed system that automatically predict the pavement marking condition. The proposed deep learning model was trained with a sample of annotated images, and another sample was used for testing purpose. The model was able to predicate road segments with and without pavement marking defects. A group of the defects classified as corner faded and missing were identified with an accuracy of 50% to 80% as shown in Figure 4. Although the model was intended to generate preliminary results using machine learning technique, the results still showed promising trends and levels of confidence for expansion and fine-tuning. The model projected higher accuracy in detecting larger features than small and medium ones. This was expected because larger objects in the image contain more pixels which inform the object detector of what defect it might be, than small and medium-sized features. These results will guide the manual annotation of additional sets of data to enhance the model prediction algorithm. Annotating defects in images, and ensuring less noise within the boundary circling the defects was found to be critical for the model accuracy.

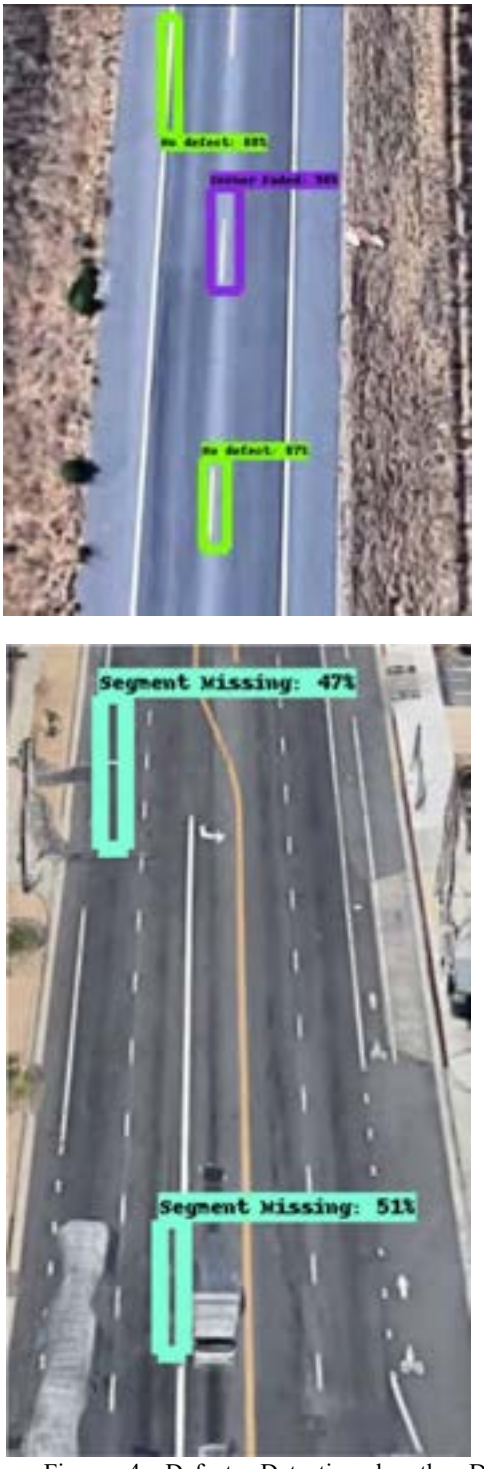

Figure 4. Defects Detection by the Deep Learning Model

Despite the small number of data sets used to train and test the model, the deep learning model was able to

predict road pavement defects with over 50% confidence. In some instances, it predicted the defects with 80% confidence, as shown in Fig. 4. These results also yield increased confidence in identifying pavement markings without defects. This was expected since faded segments vary in levels of marking deterioration and visibility, while pavement markings in good condition are similar in contrast to the pavement in their clean-cut edges. The results of the model were validated manually by comparing the model outcomes with the manually annotated images.

These results inform us of the current condition of pavement markings in the area, as well as which road segments require immediate attention, and which should be monitored. The preliminary state of these results cannot replace traditional methods for pavement marking inspection, but it can still inform road agencies of which road segments output the most defects in an initial site survey using a drone. By expanding the training and testing data, these results could be used to predict the remaining service life of each road segment captured.

Lastly, the results of this pavement marking identifier tool are expected to show an increase in safety, a reduction of labor and equipment-associated costs, a fast identification of defects, and expedited repairs.

5 Conclusion

In this paper, a method for assessing and predicting pavement marking defects using machine learning was presented. Images extracted from a satellite imagery web-mapping service were processed to create a dataset of over 100 annotated images. For image optimization, images compiled were carefully annotated to ensure noise reduction, consistency, and proper labeling. The method employed in this paper used images in PASCAL VOC in a multi-level classification program. For image annotations, tighter rectangles enclosing road features were found to produce results that are more accurate. The preliminary results show higher accuracy and detection for larger segments and most common features. These show potential in an integrated manual identification of pavement marking defects and a python-based image extractor software. Future research will be focused on integrating retroreflectivity analysis and reading into the model to better resemble the standard maintenance protocols used by departments of transportation. This will result in a comprehensive system for assessing, monitoring, and maintaining roads. By implementing this model, drones can automatically detect and classify the pavement marking defect classes. The machine-learning-based methods employed in this research are accessible, cost-effective, and relatively safe to conduct pavement marking assessments and evaluations. With enough data and proper annotation, the model developed can detect marking defects from an aerial view using different camera views. This reduces labor and equipment costs otherwise incurred from manual inspection and reduces the risk of construction-related accidents from placing workers in high-speed roads. The improvement of machine learning models for maintaining pavement markings up to standard is essential for the digital maps integrated into the programming of AV's to detect road surface markers (RSMs). By maintaining roads up to MUTCD standards, AV machine learning can detect the necessary road features to allow for the integration of autonomous vehicles on our roads. Improved roads pave the way for improved cars, transportation systems, and societies.

In the future, this study will be extended to address the relationship between road defects and road pavement marking defects. Many studies suggest that the causes that contribute to pavement defects also contribute to pavement marking defects.

Acknowledgment

This research is supported by Research, Scholarly, and Creative Activities grant program from California Polytechnic State Univeristy.

References

[1] Abkowitz, M., Walsh, S., Hauser, E., and Minor, L. (1990). "Adaptation of Geographic Information Systems to Highway Management." *Journal of Transportation Engineering*, 116(3), 310–327..

[2] Adu-Gyamfi, Y. O., Tienaah, T. O., Attoh-Okine, N. undefined, and Kambhamettu, C. undefined. (2014). "Functional Evaluation of Pavement Condition Using a Complete Vision System." *Journal of Transportation Engineering*, 140(9), 04014040–1-04014040–10.

[3] Agent K. Transverse Pavement Markings for Speed Control and Accident Reduction. Transportation Research Record, Issue 773, 1980, pp 11-14.

[4] Bali, S., R. Potts, A. Fee, I. Taylor, and J. Glennon. Cost-Effectiveness and Safety of Alternative Roadway Delineation Treatments for Rural Two-Lane Highways. Publication FHWA-RD-78-50. Federal Highway Administration, U.S. Department of Transportation, Washington, D.C., 1978

[5] Ball, M. (2016). "State DOTs Using Drones to Improve Safety, Collect Data and Cut Costs." *The magazine for civil & structural engineers*.

[6] Bandara, N. "Pavement Maintenance Decision Making Using Geographic Information Systems."2000 Annual Conference Abstracts - Canadian Society for Civil Engineering, 324-324.

[7] Basile, A.J. Effect of Pavement Edge Markings on

Traffic Accidents in Kansas. In Highway Research Board Bulletin 308, Highway Research Board, National Research Council, Washington, D.C., 1962, pp. 80-86.

[8] Carlson, P. J., Park, E. S., and Andersen, C. K. (2009). "Benefits of Pavement Markings." *Transportation Research Record: Journal of the Transportation Research Board*, 2107(1), 59–68.

[9] Carlson, P. J., Schertz, G., et al. (2014). "Methods for Maintaining Pavement Marking Retroreflectivity." *Texas A&M Transportation Institute.*

[10] Congress, S. S. C., and Puppala, A. J. (2019). "Novel Methodology of Using Aerial Close Range Photogrammetry Technology for Monitoring the Pavement Construction Projects." *Airfield and Highway Pavements 2019*.

[11] Cuelho, E., Stephens, J., and McDonald, C. (2003). "A Review of the Performance and Costs of Contemporary Pavement Marking Systems." Montana. Dept. of Transportation. Research Section.

[12] Ersoz A. and Pekcan O. "Unmanned Aerial Vehicle Based Pavement Crack Identification Method Integrated with Geographic Information Systems." Transportation Research Board 96th Annual Meeting, Transportation Research Board, 2017, 2p

[13] Inzerillo L. and Di Mino G. Image-based 3D reconstruction using traditional and UAV datasets for analysis of road pavement distress. *Automation in Construction*, *96*, 457-469.

[14] Jalayer M. and O'Connell M. et al. "Application of Unmanned Aerial Vehicles to Inspect and Inventory Interchange Assets to Mitigate Wrong-Way Entries." Transportation Research Board 98th Annual Meeting, Transportation Research Board, 2019, 16p.

[15] Khan, M. A., W. Ectors, T. Bellemans, D. Janssens, and G. Wets. UAV-Based Traffic Analysis: A Universal Guiding Framework Based on Literature Survey. Transportation Research Procedia, Vol. 22, 2017, pp. 541–550

[16] Kmetz, Robert J., "GIS Based Pavement Maintenance: A Systematic Approach". *College of Technology Directed Projects*. Paper 36.

[17] Montebello D. and Schroeder J. (2012). "Cost of Pavement Marking Materials." Minnesota Department of Transportation.

[18] Morena, D., and Leix, T. (2012). "Where These Drivers Went Wrong." *U.S. Department of Transportation/Federal Highway Administration*

[19] Musick, J. V. Effect of Pavement Edge Marking on Two-Lane Rural State Highways in Ohio. Highway Research Board Bulletin 266, 1962, pp. 1-7.

[20] Parida, M. (2005). Enhancing Pavement Management Systems Using GIS. Proceedings of the Institution of Civil Engineers, Vol. 158(2),107-113.

[21] Retting R. and Farmer C. "Use of Pavement Markings to Reduce Excessive Traffic Speeds on Hazardous Curves." ITE Journal, Institute of Transportation Engineers (ITE), Volume 68, Issue 9, 1998, 6 p.

[22] T. Miller. "Benefit-Cost Analysis of Lane Marking." In Transportation Research Record 1334, Transportation Research Board, National Research Council, Washington, D.C., 1991, pp. 38-45

[23] Zhang, C. (2008) "A UAV-based photogrammetric mapping system for road condition assessment" *Proceedings of International Archives of Photogrammetry and Remote Sensing*, Beijing, China, 3-11 July 2008, pp. 627-632.

[24] Zhang, L., Yang, F., Zhang, Y. D., and Zhu, Y. J. (2016). "Road crack detection using deep convolutional neural network." *IEEE International Conference on Image Processing (ICIP)*.

[25] Zhang, A., K. C. P. Wang, Y. Fei, Y. Liu, C. Chen, G. Yang, J. Q. Li, E. Yang, and S. Qiu. Automated Pixel-Level Pavement Crack Detection on 3D Asphalt Surfaces with a Recurrent Neural Network. Computer-Aided Civil and Infrastructure Engineering, Vol. 34, No. 3, 2019, pp. 213–229.

An Assistive Interface of a Teleoperation System of an Excavator by Overlapping the Predicted Position of the Arm

Y. Okawa[a], M. Ito[a], R. Sekizuka[b], S. Saiki[c], Y. Yamazaki[c] and Y. Kurita[a]

[a]Graduate School of Advanced Science and Engineering, Hiroshima University, Japan
[b]Graduate School of Engineering, Hiroshima University, Japan
[c]Kobelco Construction Machinery Co., Ltd., Japan
E-mail: yuzukiokawa@hiroshima-u.ac.jp, itoma@hiroshima-u.ac.jp,
ryotasekizuka@hiroshima-u.ac.jp, ykurita@hiroshima-u.ac.jp

Abstract -

A teleoperated hydraulic excavator is introduced to perform safe and quick restoration work in sites affected by disasters. However, the current efficiency of this system is approximately 40–60%, compared to boarding an actual hydraulic excavator, because of the communication delay. To reduce this delay, we developed a system that can display the predicted position of the excavator attachment to the operator. For predicting the movement of the hydraulic excavator relative to the lever input, it is necessary to consider the dynamic characteristics of the hydraulic excavator. In this study, the dynamic characteristics of the turning motion of the hydraulic excavator were assumed to be the first-order delay with a dead time system, followed by the construction of the turning motion simulator of the hydraulic excavator. Through an experiment in which the bucket tip was stopped toward the target position, the operational time was confirmed to be significantly shortened by displaying the predicted position.

Keywords -

Teleoperated hydraulic excavator; Swinging motion; Interface; Communication delay

1 Introduction

Hydraulic excavators often operate in dangerous locations, such as disaster sites. Recently, teleoperated hydraulic excavators have been introduced and have gradually become mainstream, through which several unmanned construction works have been carried out [1, 2, 3]. However, it is believed to have approximately 40–60% work efficiency compared to an actual machine boarding. Thus, the performance improvement of the teleoperated hydraulic excavator is necessary. Communication delays are one of the factors that reduce work efficiency. Michael et al. [4] investigated the effect of time delay on the surgical performance of teleoperated surgery and confirmed that the accuracy of moving the remote surgery robot decreased as the time delay increased. In the teleoperated system of a hydraulic excavator, Sugawara et al. [5] achieved high picture quality with low image delay and confirmed the operational efficiency improvement through simulation. However, for a teleoperated hydraulic excavator, which is supposed to be utilized in various work sites, secure and stable communication cannot always be guaranteed. Consequently, eliminating communication delay is challenging. Therefore, a technique that can improve work efficiency, even when communication delay exists, is necessary. Richter et al. [6] developed a system to predict a position without time delay to an operator in a teleoperated manipulation robot. When positioning was difficult, the ring was picked up by one arm and placed back after passing it to another arm. By evaluating the operating hours, with and without the proposed system, a significant difference was confirmed. Walker et al. [7] showed that the operation could be facilitated using a virtual aerial robot, which can provide information regarding where and how the robot finally reaches a position. However, to the best of our knowledge, the prediction superposition technique has not been applied to the teleoperated hydraulic excavators yet.

In this study, we propose a teleoperated system for hydraulic excavators that can overlap the predicted position of the arm with the operation input. We focus on the turning motion of the hydraulic excavator and verify the effectiveness of our proposed method through simulation. First, a simulator of a teleoperated hydraulic excavator was generated; then, the overlapping system for the arm predicted position was mounted for the turning operation. Finally, the difference in the work efficiency with and without the existence of the proposed system was experimentally verified.

2 Simlation of overlapping the predicted position of the arm

A simulator was developed to confirm the effectiveness by the overlapping predicted position and by displaying it in the turning operation of a teleoperated hydraulic excavator. A hydraulic excavator was installed in a three-dimensional virtual space using the Unity game engine. A joystick (Logitech Extreme 3D Pro) was used as an operator interface. It was possible to turn the simulated hydraulic excavator by tilting the joystick to the right and left like the operation lever of an actual machine. The transfer function G(s) of the teleoperated system was approximated by the first-order delay with the dead time

system, as shown in Equation 1. Here, the input was the operation quantity, and the output was the turning angular velocity of the hydraulic excavator, where K, T, and L represent the system gain, time constant, and dead time, respectively.

$$G(s) = \frac{K}{1+Ts}e^{-Ls} \quad (1)$$

The communication delay caused by the teleoperated system of the hydraulic excavator is demonstrated in Figure 1. If the communication delay, L_1, is known, the relationship between the operation input and predicted position can be expressed by the following transfer function, $G_{pre}(s)$.

$$G_{pre}(s) = \frac{K}{1+Ts}e^{-(L-L_1)s} \quad (2)$$

Using the transfer function of Equation 2, the predicted angular velocity was derived from the master input, as shown in Figure 2, and displayed as translucent in Figure 3.

Figure 1. Delay occurred in teleoperated excavators

Figure 2. Derivation method of predicted turning speed

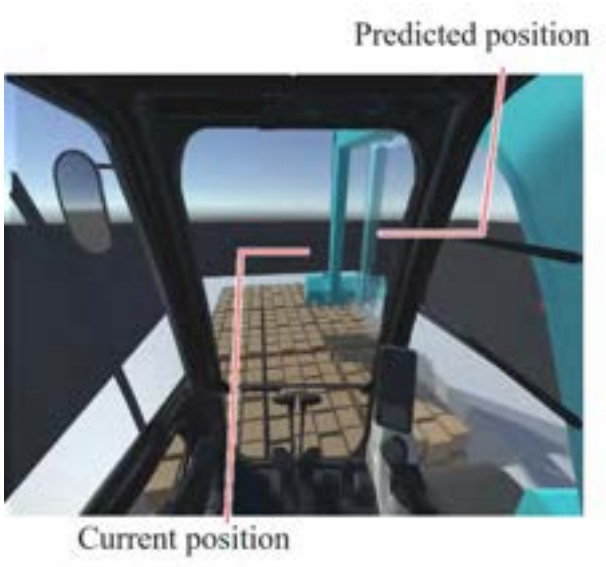

Figure 3. Presentation of predicted position of the attachment in the simulator

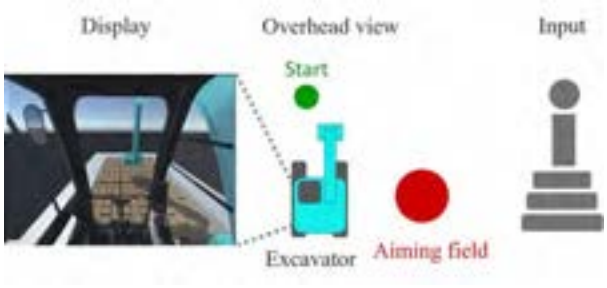

Figure 4. Initial state of the pointing task

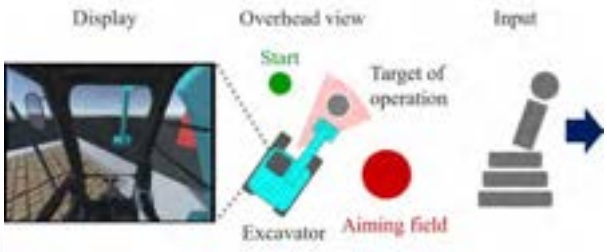

Figure 5. Turning operation state of the pointing task

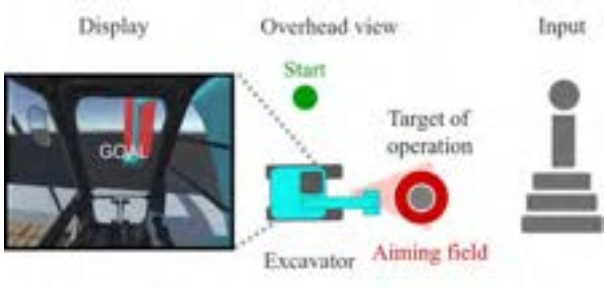

Figure 6. End state of the pointing task

3 Experiment

3.1 Procedure

Using the simulator, a pointing experiment was conducted, in which the bucket tip was turned to the red pole (target position) and stopped. The task started with the state shown in Figure 4 and the subject operated the joystick to turn the hydraulic excavator as shown in Figure 5. Once the target position was reached, the word "GOAL" was displayed on the screen as shown in Figure 6, indicating the completion of a task. The target positions were 30°, 60°, and 90° angles. These were used ten times each for thirty trials forming a task set, and the trial order was randomized. The measured items were the operation time of each task. The subjects performed the above set under the following three conditions.

1. Without dead time and without predicted position display (WOd+WOp)
2. With dead time and without predicted position display (Wd+WOp)
3. With dead time and with predicted position display (Wd+Wp)

Condition 1 assumes the case of operating an actual hydraulic excavator; condition 2 assumes the case of operating a teleoperated hydraulic excavator; condition 3 assumes the case of operating a teleoperated hydraulic excavator by overlapping the predicted position of the arm.

By comparing these three conditions, it was verified how close the working time approaches were in the boarding operation by overlapping the predicted position of the arm in the teleoperated system. Regarding L and T, we set them based on the assumption of an actual machine with a 13-ton excavator, as shown in Table 1, which presents all the relevant parameter values. The communication delay, L_1, was set to 0.26 (s). The subjects were ten healthy persons (Average age 22.7 ± 1.50 years). Before initiating the experiment, the subjects were instructed to finish the task as soon as possible and informed that the target position was on the right side. To eliminate the order effect, the execution order of the above three conditions were randomly made for each subject. Moreover, all subjects performed the test after sufficient practice and agreed to informed consent beforehand based on the Helsinki Declaration.

Table 1. Experiment parameters

	L(s)	T(s)
Acceleration	0.576	1.207
Deceleration	0.422	0.685

3.2 Result

The results of the simulation experiment were shown in Table 2 and Figure 7. For each condition and target position, the average operation time of each subject, as well as that of all subjects, were obtained. Applying the Fisher's LSD test ($\alpha = 0.05$ significant level) revealed that there existed significant differences between Wd + WOp and Wd + Wp at 30° and 90°. Furthermore, a significant difference between the conditions of WOd + WOp and Wd + WOp was confirmed at 30° and 90°. No significant difference was found between the WOd + WOp and Wd + Wp conditions. Detailed statistical results are given in Tables 3, 4, and 5.

Table 2. Result of the experiment

	WOd+WOp	Wd+WOp	Wd+Wp
30°	2.89 ± 0.51	3.93 ± 0.67	3.27 ± 0.67
60°	3.73 ± 0.41	4.17 ± 0.77	3.75 ± 0.59
90°	4.42 ± 0.49	5.69 ± 0.98	4.93 ± 0.63

Table 3. Result of the t-test (WOd+WOp, Wd+WOp)

	degree of freedom	p-value
30°	18	1.00×10^{-3}
60°	18	0.14
90°	18	1.00×10^{-3}

Table 4. Result of the t-test (Wd+WOp, Wd+Wp)

	degree of freedom	p-value
30°	18	3.0×10^{-2}
60°	18	0.15
90°	18	4.00×10^{-2}

Table 5. Result of the t-test WOd+WOp, Wd+Wp)

	degree of freedom	p-value
30°	18	0.20
60°	18	0.96
90°	18	0.16

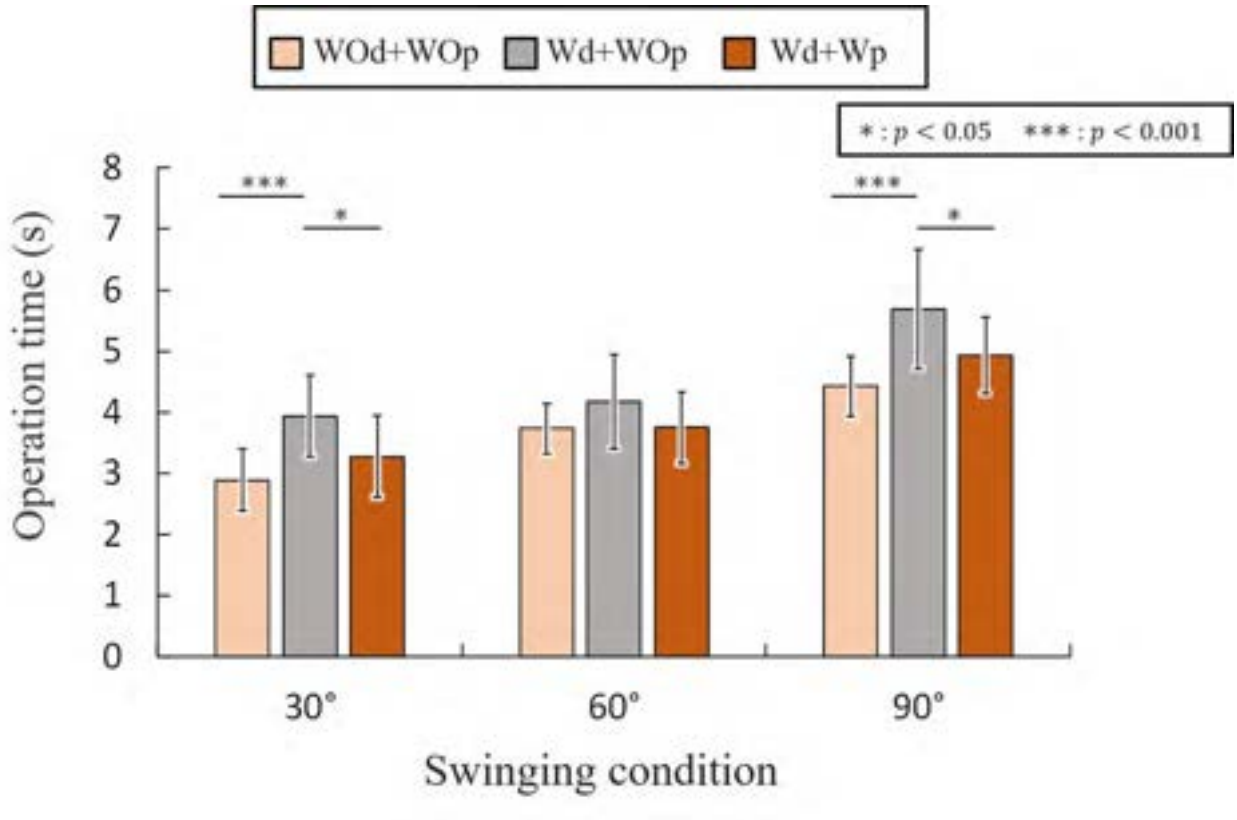

Figure 7. Result of the experiment

3.3 Discussion

This study verified the effectiveness of overlapping the predicted position of the arm in the turning operation using a simulator. The experimental results confirmed that the turning operation time was decreased at 30° and 90° by overlapping the predicted position on Wd + WOp. Moreover, the decreasing tendency of the operation time can be observed even at 60°, although the significance of this tendency could not be confirmed. As seen from Figure 7, it is confirmed that the operation time of Wd + Wp approached that of WOd + WOp. However, some subject commented after the trial that, "The predicted position was always overlapped, and I thought it was in the way.". We think that determining which position should be viewed and which should be operated was challenging when the predicted position overlapped with the current position. Therefore, the work efficiency is thought to be further improved by investigating the display technique of the prediction position, and that it may approach the turning work efficiency of WOd + WOp. Concretely, when the distance between the predicted position and the present position approaches, the predicted position will not be displayed.

4 Conclusion

In this study, the overlapping effects of the predicted position of the arm of the teleoperated hydraulic excavator was verified, during the turning operation, through simulation. The experimental results confirmed that the turning work efficiency, decreased by becoming tele-operational, approached the efficiency of the boarding operation by overlapping the predicted position of the arm. There is the problem of the predicted position on the screen blocking the current arm position. In the future, work efficiency could be further improved by examining the display technique. Furthermore, installing on the actual teleoperated system of the hydraulic excavator is a future investigation topic. With the moment of inertia changes caused by the inclination of the machine body and the weight of the loaded soil, it is necessary to improve the accuracy of the predicted arm position in the actual teleoperated system of the hydraulic excavator.

References

[1] Kazuhiro Chayama, Akira Fujioka, Kenji Kawashima, Hiroshi Yamamoto, Yasushi Nitta, Chikao Ueki, Atsushi Yamashita, and Hajime Asama. Technology of

unmanned construction system in japan. *Journal of Robotics and Mechatronics*, 26(4):403–417, 2014.

[2] Eiji Egawa, Kensuke Kawamura, Masaharu Ikuta, and Takayuki Eguchi. Use of construction machinery in earthquake recovery work. *Hitachi Review*, 62(2): 136–141, 2013.

[3] Yuji Hiramatsu, Takashi Aono, and Masami Nishio. Disaster restoration work for the eruption of mt usuzan using an unmanned construction system. *Advanced Robotics*, 16(6):505–508, 2002.

[4] Michael D Fabrlzio, Benjamin R Lee, David Y Chan, Daniel Stoianovici, Thomas W Jarrett, Calvin Yang, and Louis R Kavoussi. Effect of time delay on surgical performance during telesurgical manipulation. *Journal of endourology*, 14(2):133–138, 2000.

[5] Kazuhiro Sugawara, Kazunori Hoshino, Hiroshi Ogura, Keisuke Inata, and Takashi Takeuchi. Long-distance remote control system of hydraulic excavator. *Journal of the Society of Instrument and Control Engineers*, 55(6):519–522, 2016 (in Japanese).

[6] Florian Richter, Yifei Zhang, Yuheng Zhi, Ryan K Orosco, and Michael C Yip. Augmented reality predictive displays to help mitigate the effects of delayed telesurgery. In *International Conference on Robotics and Automation*, pages 444–450. IEEE, 2019.

[7] Michael E Walker, Hooman Hedayati, and Daniel Szafir. Robot teleoperation with augmented reality virtual surrogates. In *14th ACM/IEEE International Conference on Human-Robot Interaction*, pages 202–210. IEEE, 2019.

Development of Rotary Snow Blower Vehicle Driving Support System using Quasi-Zenith Satellite on the Expressway in Japan

Katsuyoshi Abe [a*], Atsushi Ichikawa [b], Toshiaki Itou[c] and Keigo Kurihara[d]

[a※]Hokkaido Regional Head Office, East Nippon Expressway Company Limited, Japan
k.abe.ag@e-nexco.co.jp
[b] Hokkaido Regional Head Office, East Nippon Expressway Company Limited, Japan
[c] Nexco-Engineering Hokkaido Co., Ltd
[d] Nexco-Engineering Hokkaido Co., Ltd.

Abstract

The rotary snow blower vehicle operated for removing accumulated snow on road shoulders must be performed even in the conditions of a poor visibility due to a snowstorm or road markings completely covered by snow. The operators of the vehicle have to pay full attention to avoid contacting road structures and ordinary cars passing just beside the snow removal vehicle. Therefore, we have developed a high-precision snow removal vehicle positioning device using a quasi-zenith satellite and a high-precision expressway map for the first time in Japan. The device can indicate precisely the exact position of the snow blower vehicle on expressways in real time and the operator can drive the vehicle by watching a monitor showing the assistant information provided by the device. The error of the indicated location would be relatively small such as less than a few ten centimeters and several tests have been carried out in a special test field and on the expressway in Hokkaido

Keywords –

Quasi-zenith satellite based driving support system; Snow and ice countermeasure

1. Introduction and background

Since most of the expressways operated by East Nippon Expressway Company (NEXCO East) pass through snowy areas, one of the biggest challenging operational tasks is to ensure smooth and safe traffic even in cold winter.

However, as Japanese future population is in decline, it is anticipated that skilled workers will be aging and it will be difficult to secure the required workers. Since it is expected that snow and ice countermeasures will need to be performed by workers with lesser skills in the future, it is necessary to create an environment that enables such work to be performed more safely and reliably than at present.

In addition, snow and ice countermeasures on expressways involves various types of work and requires skilled operators. The visibility in the environment is particularly bad during snowfall and in snowstorms, and it is difficult for snow and ice work vehicle operators to determine the position of their vehicles on the road at such times, and this labor-intensive work requires the operators to pay close attention to avoid colliding with general vehicles and road structures.

The scarcity of skilled workers in the future is expected to inevitably require this work to be performed by unskilled workers. As such, it is necessary to create an environment where even unskilled operators can perform the work safely and reliably, and this required aiming to provide support for operators by means of driving support technology.

Therefore, we have developed a high-precision snow removal vehicle positioning device using a quasi-zenith satellite and a high-precision expressway map for the first time in Japan. As Wang & Noguchi (2019) reported, the satellite is going to be used in the Japanese agriculture. The device can indicate precisely the exact position of the rotary snow removal vehicle on expressways in real time and the operator can drive the vehicle by watching a monitor showing the assistant information provided by the device. The error of the indicated location would be relatively small such as less than a few ten centimeters and several tests have been carried out in a special test field. In addition one of the tests was conducted on the

expressway in Hokkaido.

In this report, we would like to outline this novel approach to provide a real time exact location on the expressway by comparing a quasi-zenith satellite information with a high-precision map data and some representative test results are going to be explained.

Figure-1. Snow and ice countermeasure work on the expressway (snow blowing work)

Figure-2. Expressway during snowstorm

2. Outline of the developed system

Snow blowing work is performed while running at low speed between the white line of the shoulder and the curb of the shoulder, and the operator of the rotary snow blower vehicle must take care that the vehicle does not run outside the white line on the shoulder into the vehicle lane or collide with guardrails on the shoulder of the road. Using a quasi-zenith satellite positioning device and a high-precision map of the curb, it is possible to continually identify the positional relationship between the rotary snow blower vehicle and the shoulder white line and curb when the vehicle is running out of bounds into the lane or colliding with the guardrails. In this study, we developed a system to warn the operator of a rotary snow blower vehicle when the vehicle was running out of the shoulder area. (Figure-3)

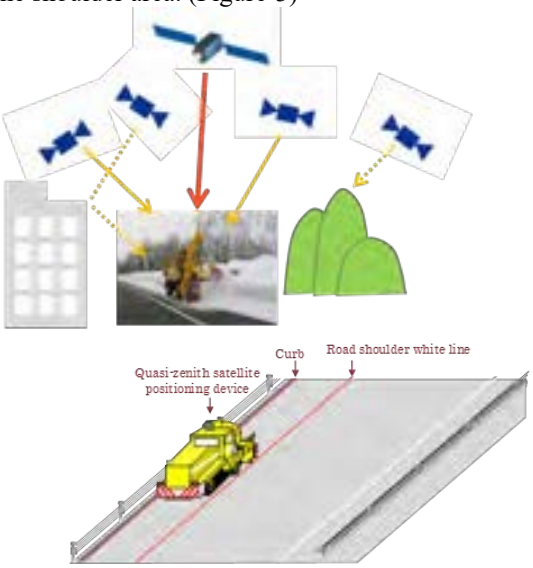

Figure-3. Narrow working range of rotary snow blower vehicle

3. Creation of high-precision maps

3.1 Map creation range

The road features required for snow blower work were created as map information from high-precision three-dimensional point group data by a mobile mapping system (MMS) to create the three-dimensional maps. The target section is 3.0 km (32.4 KP to 35.4 KP) of the outbound lane between the Iwamizawa Interchange and Iwamizawa Service Area on the Hokkaido Expressway. (Figure-4)

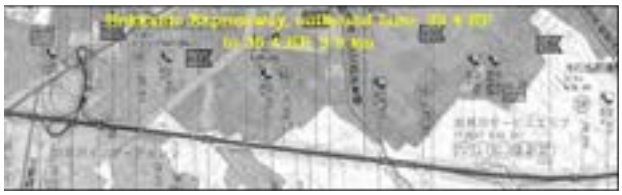

Figure-4. High-precision map creation range

3.2 Mapped road features

The features required for monitoring when the rotary snowblower vehicle runs out of bounds into the vehicle lane and the road features required to avoid colliding with vehicles and blown snow when removing snow are mapped from the high-precision three-dimensional point

group data.(Figure-5)

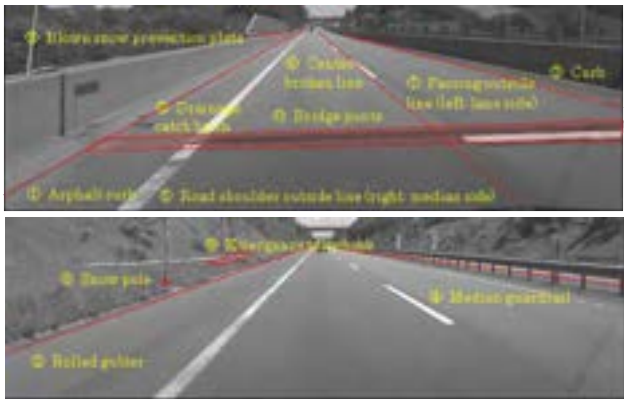

Figure-5 Mapped features

4. Guidance system

4.1 System screen

The system recognizes the running position of the rotary snow blower vehicle from the satellite information and uses the result of collation with the map data to provide guidance for the snow removal work by judging when the vehicle is running out of bounds. The system screen is composed of two screens, a 2D display and a 3D display, and the 3D display screen also displays various types of information about objects requiring caution to make it easier to understand the vehicle's current position and the situation ahead of the vehicle. (Figure-6)

Display description

① 3D display area	Displays an image of the vehicle viewed from behind. Displays the curb ahead and objects requiring caution, and the white lines turn red when the vehicle runs outside the lines on the left or right. The blue line indicates the front position of the vehicle.
② 2D display area	Displays an image of the vehicle looking down on it from directly above. The white lines turn red when the vehicle runs outside the lines on the left or right. There is no display of objects requiring caution.
③ Outside the road shoulder warning information	A warning is displayed when there is an object requiring caution outside the road shoulder 30 m ahead of the vehicle.
④ Road warning information	A warning is displayed when there is an object requiring caution in the road 30 m ahead of the vehicle.
⑤ Running status	When the vehicle is running in the shoulder lane (within the white lines), "OK" is displayed, and when the vehicle runs outside the lane, "OUT" is displayed in red letters. An arrow is displayed indicating the side on which the vehicle ran outside the lane.
⑥ Left clearance (out-of-bounds width)	Displays the clearance to where the left side of the vehicle runs outside its lane. When vehicle is outside its lane, the background turns red and the distance outside the lane is displayed.
⑦ Right clearance (out-of-bounds width)	Displays the clearance to where the right side of the vehicle runs outside its lane. When vehicle is outside its lane, the background turns red and the distance outside the lane is displayed.
⑧ Skew running angle	Displays the skew running angle of the vehicle.
⑨ Road shoulder width	Displays the width of the road shoulder at the point where the running vehicle is located.
⑩ Current time	Displays the current time received from the satellite.
⑪ Reception status display	Displays the reception status and type of position information output from the receiver.
⑫ Sound switching	Switches the warning sound ON and OFF.
⑬ Settings	Switches to the setting screen for vehicle information.

Figure-6. System screen

4.2 System operation when a warning is issued

As shown in Figure-7, in both the 2D and 3D screens, when the vehicle goes out of bounds, the white line on the side the vehicle went out on changes to a red line, “OUT” is displayed in the “Running status” display field, an arrow (⇒) is displayed indicating the side the vehicle went out on, and the amount the vehicle went out of bounds is displayed in meters in red in the "Clearance width (out-of-bounds width)" display field.

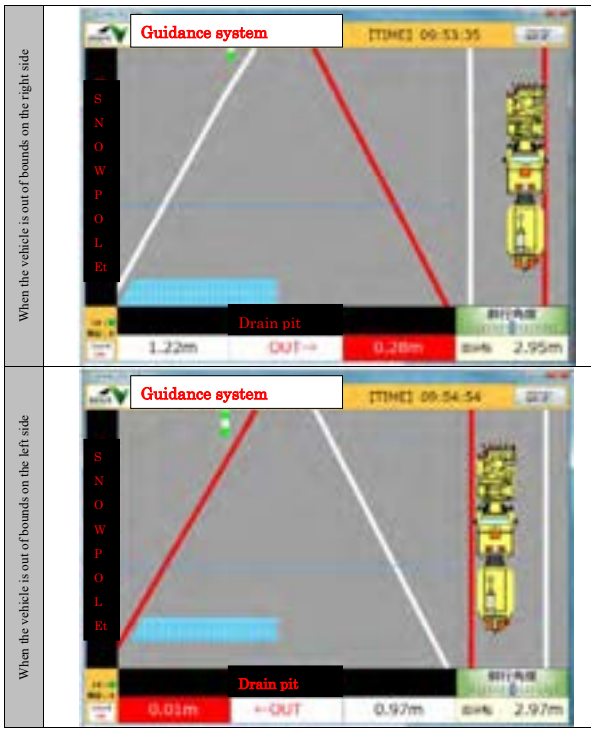

Figure-7. System operation when a warning is issued

5. Trial test results

A trial test of the system was performed by running the rotary snow blower vehicle equipped with high-precision positioning equipment and a work guidance system on the shoulder of a road. The test was performed on the shoulder of the outbound lane on a section of the Hokkaido Expressway from the Iwamizawa Interchange to the Iwamizawa Service Area. The trial method involved installing the system equipment and video cameras on a rotary snow blower vehicle in the maintenance yard at the Iwamizawa Interchange, then after moving to the shoulder of the main lane (Iwamizawa Interchange to Iwamizawa Service Area), the rotary snow blower vehicle was run at actual working speed, and system log data and video camera images were recorded.

The method used to verify the trial results was to calculate the error between the system and the actual measurement values from the recorded system log data and each video camera image, and extract and verify the evaluation target section as representative points.

The trial test resulted in an average error value of approx. 0.2 m. By road structure, the error for embankments section was 0.19 m, the error for cuttings section was 0.22 m, and the accuracy of embankments was higher due to the better satellite reception environment. (Figure-8)

The target error of this system is set at 0.2 m, and the above results were almost satisfactory. Therfore, operator would trust the system and could keep the vehicle in an expressway shoulder based on the guidance imformation.

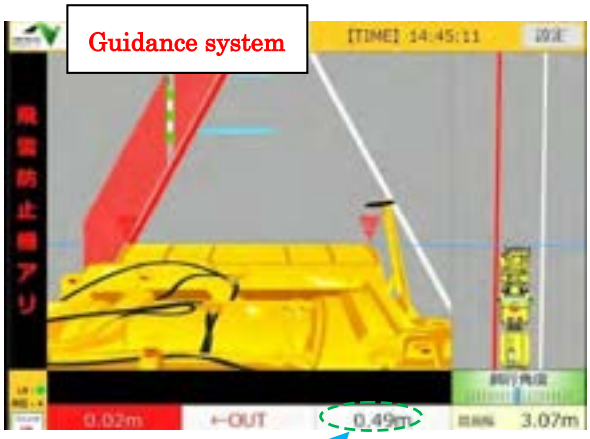

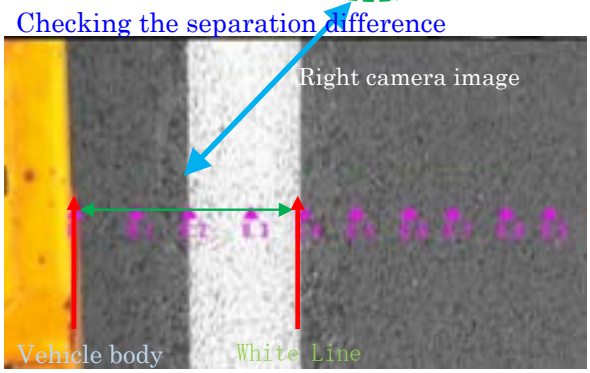

Road structure	System error (m)	
	Average value	Sample
Overall	0.22	171
Embankment	0.19	27
Cutting	0.22	144

Figure-8. Trial test verification method and system errors

6. Conclusion

The developed guidance system could provide resonable results to assit snow blowing operation. We are now under additional testing for improving its further accuracy and plan to use the system practically at the end of 2020.

The system can achieve both providing safer winter expressway for drivers and reducing the burden of the snow blower operatiors, so we are making best effort to complete this project. In additon, we are going to challenge to develop an automonous snow blower based on the quasi-zenith satelite system as the second stage of the project.

Acknowledgement

The authors wish to acknowledge Dr Noboru Noguchi, Professor of Hokkaido University -, for his advice on the quasi-zenith satellite based precise position system in this study

References

[1] WANG, H. & NOGUCHI, N. (2019). Navigation of a robot tractor using the Japanese quasi-zenith satellite system (part1), Journal of the Japanese society of agricultural machinery and food engineers, 81(4) 250-255.

A Systematic Review of the Geographic and Chronological Distributions of 3D Concrete Printers from 1997 to 2020

Jihoon Chung[a], Ghang Lee[a], and Jung-Hoon Kim[b]

[a]Architecture and Architectural Engineering, Yonsei University, South Korea
[b]Civil and Environmental Engineering, Yonsei University, South Korea
E-mail: j_chung@yonsei.ac.kr, glee@yonsei.ac.kr, junghoon@yonsei.ac.kr

Abstract –
Although several previous studies have reviewed 3DCPs, they have been based on few cases and do not include the latest 3DCPs. This study analyzed 139 academic papers and 98 types of three-dimensional concrete printers (3DCPs) developed from 1997 to 2020 through a systematic literature review. A chronological distribution analysis showed that the number of papers and printers suddenly increased after 2012. Most papers (89%) and 3DCPs (86%) were produced from 2012 to 2020. A geographic distribution analysis showed that while Switzerland published more papers than the US, the latter developed more than twice as many 3DCPs than Switzerland. The difference is attributed to who led the development: the industry (US) or academia (Switzerland). Among nozzle-traveling 3DCPs, gantry and cable-suspended platforms were the most common types for some time, but the robotic arm type has spread considerably in the last five years. Since 2013, mobile and collaborative 3DCPs have also increased.

Keywords –
Concrete; 3D Printing; Additive Manufacturing; Technical Specification

1 Introduction

Over the last 30 years, additive manufacturing has been explored to improve construction safety, reduce construction time and production costs, and produce geometrically challenging building elements [1]. In 2012, the number of 3D concrete printers (3DCPs) suddenly increased [2, 3]. Early 3DCPs included contour crafting [4] and D-Shape [5].

Recently, 3DCPs have evolved to support large-scale 3D printing [2, 6]. For example, the Institute for Advanced Architecture of Catalonia [7] developed a family of small-scale mobile robots, each of which can perform a specific task during construction. Keating et al. [8] employed a robotic arm system with a long reach and a terrestrial mobile system as a platform to maximize the building size. Zhang et al. [9] utilized multiple mobile robot printers to collaboratively print a large structure. DediBot [10, 11] adopted an aerial drone-based system to overcome the limitations of conventional 3D printing devices.

Although several studies have comparatively reviewed 3DCPs, none have analyzed their geographic or chronological distributions. This study examined the geographic and chronological distributions of studies and 3DCPs through a systematic literature review of 139 academic papers and 98 types of 3DCPs published from 1997 to 2020. The year 1997 was selected as the starting point because the earliest paper found was published in that year.

The rest of this paper is divided into five sections. Section 2 presents a review of previous studies related to the field and identifies their limitations. Section 3 describes the overall design of the literature search. Section 4 reports the results of the analysis. Section 5 discusses the current status and future directions of the technology. Section 6 summarizes the results and concludes the paper.

2 Previous Studies

Previous studies comparatively reviewing 3DCPs are characterized by two main limitations. First, they have been based on only a few cases. Lim et al. [1] comparatively analyzed only four types of 3DCPs: Pegna [12], contour crafting [13], concrete printing [14], and D-Shape [15]. Ma et al. [16] and Zhang et al. [17] analyzed three types: contour crafting, D-Shape, and concrete printing. Bhardwaj et al. [18] reviewed six 3DCPs, and Paul et al. [19] reviewed 10. Second, diverse 3DCPs have recently been developed, such as multiple mobile printers, aerial drone-based systems, and entrained reinforcement cable systems. These new 3DCPs have not been included in previous analyses, although some studies were published in the past couple of years. Moreover, Chung et al. [20] recognized that new 3DCPs could not be properly categorized using the existing classification system for 3D printers and proposed a new classification

system; however, the classification was based on only 12 relevant papers.

3 Literature Search Method

A systematic literature review (SLR) is a widely used review method in the medical and management fields [21, 22], as well as in the construction field [23, 24]. SLRs aim to minimize bias through exhaustive literature searches related to a specific research question [22, 25, 26].

This study followed the SLR method proposed by Saade et al. [24], Tranfield et al. [22], and Wohlin [26] and used two methods: a keyword-based search and snowballing—a method for finding additional references through the reference lists of identified papers. Figure 1 describes the flowchart of the keyword-based search and snowballing.

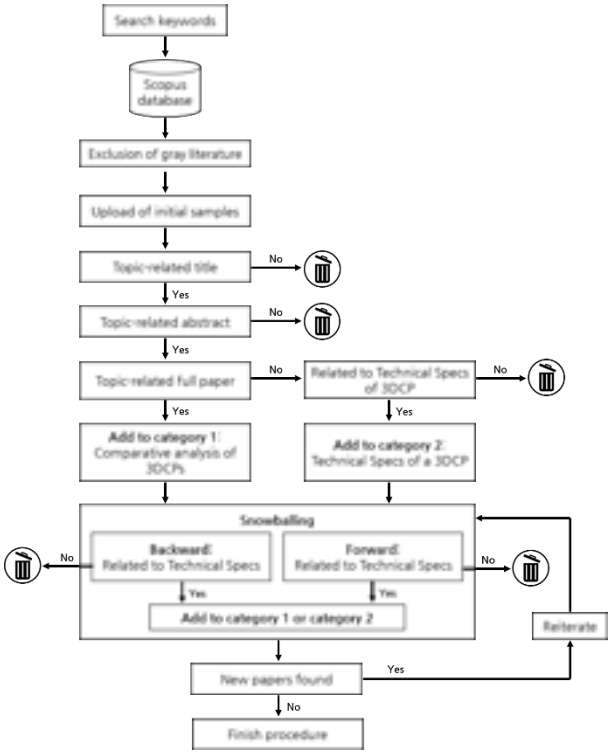

Figure 1. Flowchart of the literature search

The literature search was performed in two steps. The research question on which the search was based was, "What are the geographic and chronological distributions of 3DCPs from their early days to date?" The keyword string [("concrete" AND "3D printing") OR ("additive" AND "manufacturing")] was used to search relevant papers in the Scopus database [27]. To collect as many papers as possible, we intentionally left out specific keywords, such as "classification" or "property," and used generic terms, such as "concrete," "3D printing," "additive," and "manufacturing." Only peer-reviewed journal papers in English were included in the review.

Initially, 433 papers were collected through the keyword search. Irrelevant papers were excluded by reviewing the titles (247 papers), the abstracts (75 papers), and the contents of the full papers (47 papers). The exclusion was performed conservatively. The remaining 64 papers were divided into two categories: a comparative analysis of 3DCPs (29 papers) and a group of studies focusing only on the technical specifications of a 3DCP (35 papers).

Snowballing was then applied. This method is divided into forward and backward snowballing. Forward snowballing identifies studies citing a paper under examination. Backward snowballing identifies studies cited in a paper under examination. Both methods were iterated until no more papers were found. In the first iteration, six papers were added to the first category (comparative analysis), and 51 were added to the second category (technical specifications). A second iteration was then conducted based on these 57 papers, identifying 18 papers, all belonging in the second category. A third iteration returned only one paper, also of the second category. No new papers were found in the fourth iteration, and the process was terminated. In total, the snowballing method identified six papers for the first and 69 papers for the second category. Overall, 139 papers were identified by the two search methods.

4 Results

4.1 Chronological Distribution of Publications

The chronological distribution of the collected papers shown in Figure 2 indicates a growing interest in 3D concrete printing technology. As previously stated, the earliest paper found was published in 1997. Only five papers were published from 1997 to 2004, and 10 papers were published between 2005 and 2012. After 2012, the number of papers suddenly increased, with 89% (124) of the collected papers published from 2013 to 2020. There has been an upsurge in the number of published papers per year (an average of 15.5 papers per year) during the last eight years. This reflects the increasing interest in 3DCPs and 3D printers in general since 2012. One directly related event is U.S. President Barack Obama's speech about 3D printing as the future in February 2013 [28].

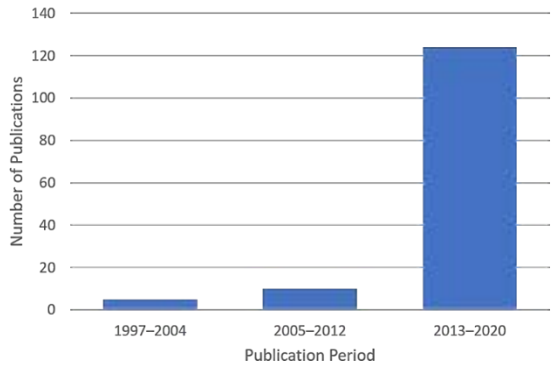

Figure 2. Chronological distribution of publications

4.2 Geographic Distribution of Publications

Figure 3 shows the number of publications per country. The assignment of publications to countries is based on the affiliation of the first author only. As shown in the figure, Switzerland and the US contributed the most publications related to 3DCPs, followed by Germany, France, and the UK.

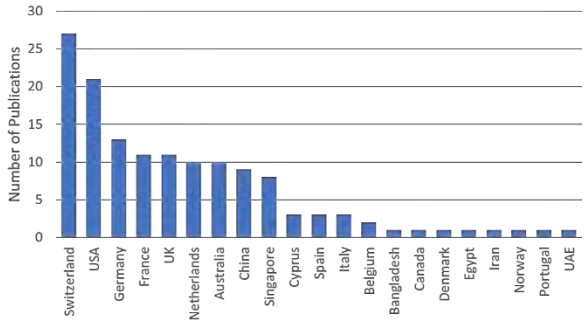

Figure 3. Geographic distribution of publications

4.3 Chronological Distribution of 3DCPs

An analysis of the selected papers identified 98 types of 3DCPs. Figure 4 shows their chronological distribution. Only two were developed from 1997 to 2004, and 12 were proposed between 2005 and 2012. Most (84) 3DCPs were proposed from 2013 to 2020, accounting for 86% of the identified cases. This shows that the number of proposed 3DCPs per year (12.25 per year on average) has substantially increased during the last eight years. This trend is in line with the number of relevant publications and conforms the findings of previous studies [2, 3].

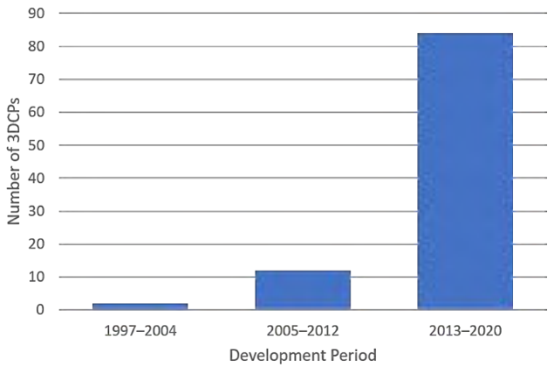

Figure 4. Chronological distribution of 3DCPs

4.4 Geographic Distribution of 3DCPs

Figure 5 shows the number of 3DCPs per country. Many 3DCPs were developed in the US, China, and Germany. An interesting discrepancy can be observed between the number of papers and the number of 3DPCs per country. Although more papers were published in Switzerland than in the US, the number of printers developed in the US was more than double that in Switzerland. This is because many 3DCPs in the US were developed by companies, which tend not to publish their outcomes. In contrast, 3DCPs in Switzerland were developed by research institutions, which are encouraged to publish their work.

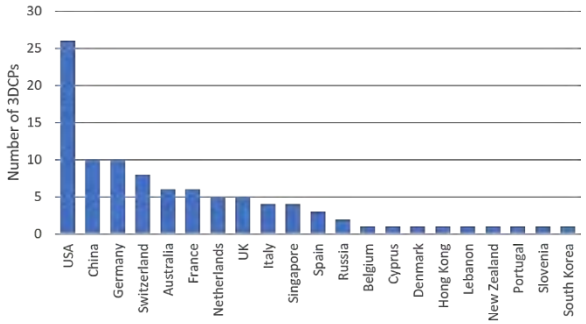

Figure 5. Geographic distribution of 3DCPs

4.5 Distribution of Nozzle-Traveling 3DCPs

To identify chronological trends, 3DCPs were classified based on the classification system proposed by Chung et al. [20]. One of the classification criteria in this system is a type of nozzle-traveling system. Figure 6 shows that the most widely used system has employed a gantry method to move a nozzle since 1997 with some intervals. A cable-suspended platform was the most common system between 2004 and 2010; however, since 2012, the gantry type has become the most

common, and several new types of nozzle-traveling systems, such as the scara, delta, crane, and robotic arm types, have emerged. Especially the number of robotic arm type systems has substantially increased during the last five years. This is because this type can extend the printing range without requiring a massive external framework to support the print nozzle [9]. Considering this tendency, it is possible that the number of robotic arm systems will exceed gantry-based systems in the future.

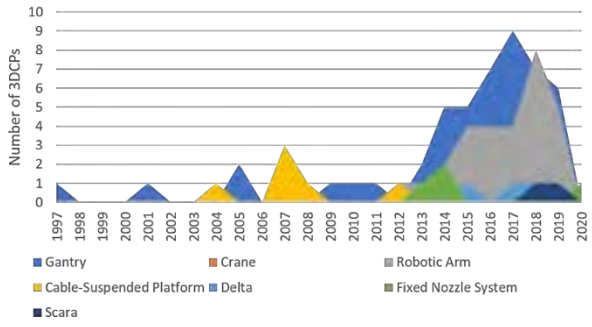

Figure 6. Chronological distribution of nozzle-traveling 3DCPs

4.6 Distribution of Mobile 3DCPs

Another classification criterion is the mobility of the building platform, which means a movable platform equipped with a terrestrial mobile system or an aerial drone-based system. Figure 7 shows that although the fixed system remains the most common system, terrestrial mobile and aerial drone-based systems have printed larger building volumes since 2013. These systems do not require planning or specific infrastructure on the construction site, such as cranes [29, 8]. Given that it enables fully autonomous on-site fabrication, the mobile system can become central to developing 3D concrete printing systems in the future instead of the fixed system. Our analysis also revealed combinations of the nozzle-traveling and mobile platforms: 75% of the terrestrial mobile systems employ robotic arms, and all aerial drones employ fixed nozzles.

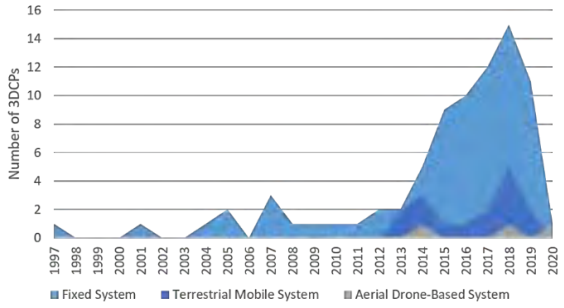

Figure 7. Chronological distribution of mobile 3DCPs

4.7 Distribution of Collaborative 3DCPs

Figure 8 shows the chronological distribution of collaborative robots identified in the 3DCP collection. Eight collaborative 3DCPs have been developed in the last eight years. Although single 3DCPs still represent the most common system, some systems have adopted multiple robots to collaboratively print large-scale structures without increasing the size of the robots. Several researchers have predicted that the collaboration capability of 3DPCs will be a key feature of the technology in the future [2, 8, 9]. Collaborative 3DCPs can be grouped into two types. The first is a collection of different robots designed to perform each task of a series of printing processes. An example is minibuilders composed of three robots [7]. The second type comprises identical robotic 3DCPs simultaneously crowd-printing different parts of a large-scale structure.

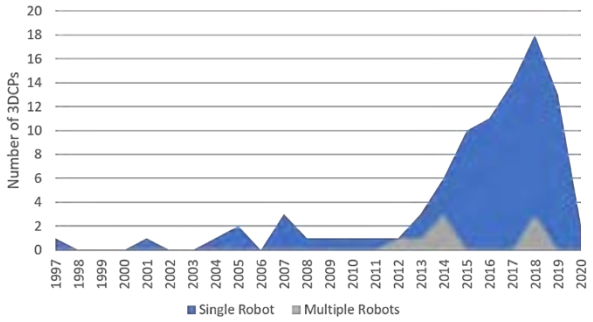

Figure 8. Chronological distribution of collaborative 3DCPs

5 Current Status and Future Directions

This section discusses the current status and future directions of 3DCP technology with regard to nozzle-traveling systems, building platform mobility, and collaborative printing.

Regarding the nozzle-traveling system, the gantry and robotic arm types are currently the most popular. However, most nozzle-traveling systems are designed to print small- or medium-sized structures off site or at fixed locations. To enable 3D-printing of large-scale structures on site in the near future, the development of nozzle-traveling systems on mobile platforms with collaborative printing functionality will be inevitable.

Regarding the mobile platform, although terrestrial mobile and aerial drone-based systems have been developed since 2013, they are still in an early stage. Even if several terrestrial mobile systems were employed on a construction site, they would only be operated on flat concrete slabs. Aerial drone-based systems, on the other hand, are characterized by limited payloads and

unstable printing. If they are to be used in real construction projects, these issues must be addressed.

Regarding collaborative printing, although the number of studies on crowd-printing robots has increased, Nanyang Technological University is the only institution that has implemented the collaborative system—and only in a laboratory environment. To raise collaborative printing to a practical level, more studies on robot localization and nozzle trajectory planning are required.

6 Conclusion

This systematic literature review was conducted to address the limitations of previous studies: few reviewed cases and no reviews of new 3DCPs. The collected 139 papers and 98 types of 3DCPs and the analysis results can be used as a basis for developing a technical specification framework of 3DCPs.

The results show a dramatic increase in the numbers of papers and printers developed after 2012, accounting for an average of 15.5 papers and 12.25 3DCPs per year. Although Switzerland boasts the most publications, the US is home to more printers developed. This is because many manufacturers in Switzerland have been research institutions, which tend to publish their outcomes, whereas many manufacturers in the US have been companies, which do not. The robotic arm type of 3DCP has gained considerable popularity in the last five years, in contrast to the cable-suspended platform. Some types of mobile and collaborative 3DCPs have been adopted since 2013. Given that these types offer greater printing efficiency as relatively new technologies, they can become central to the future development of 3DCP systems.

In the future, we plan to identify the properties of 3DCPs based on a comparative analysis of 35 review papers and 98 types of 3DCPs. We also plan to develop and validate a technical specification framework by conducting surveys or focused group interviews. A technical specification framework can be used as a reference for 3DCP developers and users.

Acknowledgment

This research was supported by a grant (20AUDP-B121595-05) from the Urban Architecture Research Program funded by the Ministry of Land, Infrastructure and Transport of the Government of the Republic of Korea.

References

[1] Lim S., Buswell R. A., Le T. T., Austin S. A., Gibb A. G. F., and Thorpe T. Developments in construction-scale additive manufacturing processes. *Automation in Construction*, 21(1):262–268, 2012. doi: 10.1016/j.autcon.2011.06.010.

[2] Labonnote N., Rønnquist A., Manum B., and Rüther P. Additive construction: State-of-the-art, challenges and opportunities. *Automation in Construction*, 72:347–366, 2016. doi: 10.1016/j.autcon.2016.08.026.

[3] Tay Y. W. D., Panda B., Paul S. C., Noor Mohamed, N. A., Tan, M. J., and Leong, K. F. 3D printing trends in building and construction industry: a review. *Virtual and Physical Prototyping,* 12(3):261-276, 2017. doi: 10.1080/17452759.2017.1326724

[4] Khoshnevis B. Automated construction by Contour crafting—related robotics and information technologies. *Automation in Construction*, 13(1):5–19, 2004. doi: 10.1016/j.autcon.2003.08.012.

[5] Dini E., Chiarugi M., and Nannini R. *Method and Device for Building Automatically Conglomerate Structures*, volume US20080148683A1. US Patent, United States, 2006.

[6] Paolini A., Kollmannsberger S., and Rank E. Additive manufacturing in construction: A review on processes, applications, and digital planning methods. *Additive Manufacturing*, 30, 2019. doi: 10.1016/j.addma.2019.100894.

[7] IAAC. Small robots printing large-scale structures. On-line: https://iaac.net/project/minibuilders/, Accessed: 15/06/2020.

[8] Keating S. J., Leland J. C., Cai L., and Oxman N. Toward site-specific and self-sufficient robotic fabrication on architectural scales. *Science Robotics*, 2(5), 2017. doi: 10.1126/scirobotics.aam8986.

[9] Zhang X., Li M., Lim J. H., Weng Y., Tay Y. W. D., Pham H., and Pham Q. C. Largescale 3d printing by a team of mobile robots. *Automation in Construction*, 95:98–106, 2018. doi: 10.1016/j.autcon.2018.08.004.

[10] DediBot. Open-ended additive manufacturing (OAM). On-line: http://www.dedibot.com/en/product/detail/19, Accessed: 15/06/2020.

[11] TCTMagazine. Dedibot showcase flying 3d printer at tct asia 2018. On-line: https://www.tctmagazine.com/tct-events/tct-asia/dedibot-showcase-flying-3d-printer-at-tct-asia-2018/, Accessed: 15/06/2020.

[12] Pegna J. Exploratory investigation of solid freeform construction. *Automation in Construction*, 5(5):427–437, 1997. doi:10.1016/S0926-5805(96)00166-5.

[13] Khoshnevis B., Hwang D., Yao K., and Yeh Z. Megascale fabrication by contour crafting. *International Journal of Industrial and Systems Engineering*, 1(3): 301–320, 2006.

[14] Lim S., Le T., Webster J., Buswell R., Austin A., Gibb A., and Thorpe T. Fabricating construction components using layered manufacturing technology. In *Global Innovation in Construction Conference*, pages 512–520, 2009.

[15] Dini E. D-shape. On-line: https://d-shape.com/, Accessed: 15/06/2020.

[16] Ma G., Wang L., and Ju Y. State-of-the-art of 3d printing technology of cementitious material—an emerging technique for construction. *Science China Technological Sciences*, 61(4):475–495, 2018. doi: 10.1007/s11431-016-9077-7.

[17] Zhang J., Wang J., Dong S., Yu X., and Han B. A review of the current progress and application of 3d printed concrete. *Composites Part A: Applied Science and Manufacturing*, 125, 2019. doi: 10.1016/j.compositesa.2019.105533.

[18] Bhardwaj A., Jones S. Z., Kalantar N., Pei Z., Vickers J.,Wangler T., Zavattieri P., and Zou N. Additive manufacturing processes for infrastructure construction: A review. *Journal of Manufacturing Science and Engineering*, 141(9), 2019.

[19] Paul S. C., van Zijl G. P. A. G., Tan M. J., and Gibson I. A review of 3d concrete printing systems and materials properties: Current status and future research prospects. *Rapid Prototyping Journal*, 24(4):784–798, 2018. doi: 10.1108/RPJ-09-2016-0154.

[20] Chung J., Lee G., Kim J., and Choi J. A comparative analysis of the classification system for three-dimensional concrete printers. *Korean Journal of Construction Engineering and Management*, 21(2):3–14, 2020.

[21] Delbufalo E. Outcomes of inter-organizational trust in supply chain relationships: a systematic literature reviewand a meta-analysis of the empirical evidence. *Supply Chain Management: An International Journal*, 17(4):377–402, 2012.

[22] Tranfield D., Denyer D., and Smart P. Towards a methodology for developing evidence-informed management knowledge by means of systematic review. *British Journal of Management*, 14(3):207–222, 2003. doi:10.1111/1467-8551.00375.

[23] Pomponi F. and Moncaster A. Embodied carbon mitigation and reduction in the built environment – what does the evidence say? *Journal of Environmental Management*, 181:687–700, 2016. doi: 10.1016/j.jenvman.2016.08.036.

[24] Saade M. R. M., Yahia A., and Amor B. How has LCA been applied to 3d printing? a systematic literature review and recommendations for future studies. *Journal of Cleaner Production*, 244:118803, 2020. doi: 10.1016/j.jclepro.2019.118803.

[25] Cook D. J., Mulrow C. D., and Haynes R. B. Systematic reviews: synthesis of best evidence for clinical decisions. *Annals of internal medicine*, 126(5):376–380, 1997.

[26] Wohlin C. Guidelines for snowballing in systematic literature studies and a replication in software engineering. In *Proceedings of the 18th International Conference on Evaluation and Assessment in Software Engineering*, pages 1–10, London, England, United Kingdom, 2014.

[27] Scopus. Document search. On-line: https://www.scopus.com/, Accessed: 15/06/2020.

[28] Gross D. Obama's speech highlights rise of 3-d printing. On-line: https://edition.cnn.com/2013/02/13/tech/innovation/obama-3d-printing/index.html, Accessed: 15/06/2020.

[29] Furet B., Poullain P., and Garnier S. 3d printing for construction based on a complex wall of polymerfoam and concrete. *Additive Manufacturing*, 28:58–64, 2019. doi: 10.1016/j.addma.2019.04.002.

Towards High-Quality Road Construction: Using Autonomous Tandem Rollers for Asphalt Compaction Optimization

J. Husemann[a], P. Wolf[a], A. Vierling[a], K. Berns[a], and P. Decker[b]

[a]Robotics Research Lab, TU Kaiserslautern, Germany
[b]BOMAG GmbH, Germany
E-mail: {husemann, patrick.wolf, vierling, berns}@cs.uni-kl.de, peter.decker@bomag.com

Abstract -

Autonomous road construction offers the possibility to improve the demanding and error-prone process of road compaction. Compaction results and surface coverage are optimized through the coordination of automated tandem rollers. This paper evaluates the impact of different road compaction strategies, ambient influences, and coordination errors on the resulting road. Thereby, suitable compaction parameters for track length, or number of rollers are determined. The concept has been validated in a simulated road construction environment. Additionally, real compaction tests have been performed using autonomous tandem rollers.

Keywords -

Off-road robotics; Behavior-based control; Automated road construction
Topics: (B-1), (B-2)

1 Introduction

Recent construction robotics proceeds towards the complete automation of demanding tasks as high-quality road construction [1, 2, 3, 4]. Thereby, the efficiency, safety, and quality of processes are increased while errors can be reduced. The area of road construction can profit from automation in particular because a fleet of machines has to be coordinated according to time restrictions, and spatial coverage to fulfill clearly defined tasks.

The automation of road work depends on the local construction and communication infrastructure and AI skills of construction robots. The project *Autonomous Mobile Machine Communication for Off-Road Applications* (5G-AMMCOA) funded by the German Federal Ministry of Education and Research (BMBF) targets key topics. The project demonstrators are two pivot-steered BOMAG tandem rollers BW 154 and BW 174 which have been equipped for autonomous operation.

This paper presents a set of improvements to increase the quality and efficiency of a road construction scenario. Furthermore, tests using different roller and road setups are done to conclude a setup for efficient road construction. Sect. 2 presents the state of the art of autonomous street construction. Sect. 3 gives an insight into the road model used for task distribution. Details on the road construction approach are provided in Sect. 4. Details on the robot control approach are stated in Sect. 5 including pivot point selection and multi-field compaction. In Sect. 6 handling of communication errors and task abortion criteria are presented. Finally, simulation and real-world experiments are shown (Sect. 7) followed by a summary and conclusion (Sect. 8).

2 Related Work

Current research aims to improve the quality of road construction processes. Cutting edge technologies as Blockchain and Machine Learning are deployed to improve road construction documentation and monitoring and prevent documentation frauds [5]. Also, road construction efficiency can be improved using the Internet of Things and Industry 4.0 techniques [6]. Additionally, the context-realistic training of construction site personnel as tandem roller operators using Virtual Reality and simulation is of importance to improve the quality [7].

Besides this, research targets the automation of the overall road construction process including the construction machinery as compactors. The automation of tandem rollers and the coordination with a paver was investigated by [3, 8]. Real-time path-planning and data exchange of compactors were investigated in the *SmartSite* project [2]. The follow-up project *Road Construction 4.0* aims to further improve the intelligent control of construction processes [9]. A behavior-based multi-robot coordination approach exploiting 5G-communication was presented in [4]. Additionally, assistance functionality for road construction tooling as automated edge cutting or autonomous collision prevention aid during reverse drive operations has been published in [10].

3 Road Model

The autonomous road construction approach involves a fleet of machines, as tandem rollers, feeders, pavers, and trucks. In the following, the tandem roller automation is targeted. Thereby, the tandem rollers share data with the paver to update a road model and coordinate themselves

accordingly. The road model utilized by the robot control approach is described by [4]. The model considers a spatial description of the individual road segments as lanes, fields, tracks, seams, and edges.

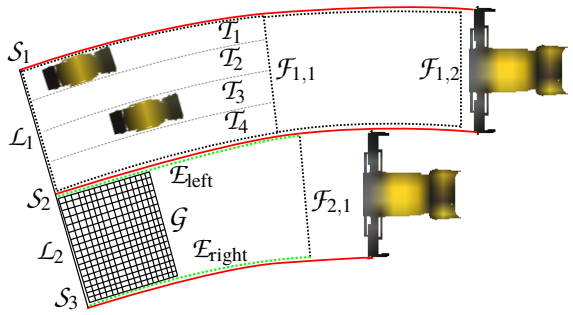

Figure 1. Road model for compaction planning. The road $\mathcal{R}$ has lanes $\mathcal{L}$, seams $\mathcal{S}$, fields $\mathcal{F}$, edges $\mathcal{E}$, grids $\mathcal{G}$, and tracks $\mathcal{T}$ [4, p. 955].

Further, the temperature of the road is considered since sufficient compaction is only possible within a given temperature span and therefore time duration.

The temperature visualization scheme is depicted in Fig. 2a. The road's amount of compaction is estimated through the number of transitions as shown in Fig. 2b. Resulting from current compaction status and temperature, the criticality for ongoing compaction can be determined. The compaction priority visualization can be seen in Fig. 2c. Areas with a low temperature and low compaction amount are visualized orange (high criticality) while hot areas or compacted areas are green (low criticality).

(a) Road temperature model (blue: cold asphalt $\leq$80 °C, pink: hot asphalt $\geq$160 °C).

(b) Compaction transition count (red: 0 transitions, green: $\geq$ 5 transistions)

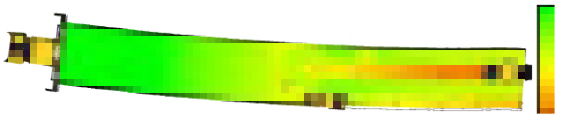

(c) Compaction priority visualization (green: low priority 0, orange: high priority 1).

Figure 2. Road visualization.

4 Road Construction Approach

The tandem rollers use a distributed, behavior-based control approach [4]. Thereby, several extensions help to improve the compaction result as a more dedicated pivot point selection, multi-field compaction, and the consideration of overtaking maneuvers for a larger group of robots located within the same area.

4.1 Pivot point selection

During road construction, rollers move back and forth between two reversing points: one close to the paver, one further away. The reversing points in a track move forward, as the paver moves forward. The close reversing point will have approximately the same distance to the paver every time, assuming a constant temperature of the delivered material and a continuous material stream. Since the close reversing point is in very hot material, drivers usually make a small curve towards the end of the track. This leaves the wave of material in front of the drum in an angle to the next pass on this position, resulting in a better distribution of the material wave. Otherwise, the next pass could not distribute the material and a permanent wave in the road would be the result. The further reversing points can be chosen on the base of the track length.

Figure 3. Visualization of the reversing points close to the paver from a real world example.

Fig. 3 visualizes the close reversing points in a real world scenario. The building direction is from left to right. One can see how the close reversing points move from right to the left side as the roller changes the track to keep up with the paver. In the middle, there was a temporary paver stillstand due to a lack of material and the roller had

Figure 4. Spatial road visualization with pivot point (blue diamond), support points (track 1), and turn-in point (end point, track 2).

to pass some time resulting in an accumulation of close reversing points. After the stillstand the order in which the roller compacts the tracks change from right to left, to left to right. This is because the curvature of the road has changed and so did the cross slope. The roller always wants to start on the lower side of the road, building a foundation to compact against when moving up.

A lane, a set of support points, is generated to control the autonomous tandem roller. Since abrupt steering maneuvers damage the asphalt surface, sudden steerings have to be avoided. A smooth roller trajectory can be achieved on a track as depicted in Fig. 4. Therefore, a pivot point P_t as a turning point for moving to the next track has to be determined with a minimum distance of d_{min} to the end of the track. The value of d_{min} depends on the track width w_{track} and maximum allowed steering value $c_{\text{track, max}}$. The BW 154 has a drum width of $w_{\text{drum}} = 1.5\,\text{m}$ and a maximum curvature of

$$c_{BW154,\,max} = \frac{\tan\left(22°\right)}{1.35\,\text{m}} = 0.299\frac{1}{\text{m}} \tag{1}$$

In the particular case follows $w_{\text{track}} = 1.3\,\text{m}$ (resulting from the track overlap), and $c_{max} = 0.1\,\frac{1}{\text{m}}$ to prevent sudden steering movements. In contrast to track switching, a turn in maneuver is executed at the front of each track.

4.2 Multi-field optimization

A suggested extension to the compaction process is multi-field optimization. The paver continuously lays out asphalt which can be structured into fields $\mathcal{F}$. For a slower compaction process resulting from a small number of rollers, it may also occur that the tracks $\mathcal{T}_{i+1,j}$ of the field $\mathcal{F}_{i+1}$ already cool down without being compacted accordingly. This results from rollers that are still occupied with the tracks $\mathcal{T}_{i,j}$ of the previous field $\mathcal{F}_i$ (Fig. 5a). Due to the low compaction amount of the field $\mathcal{F}_{i+1}$, a track of $\mathcal{F}_{i+1}$ may have a higher priority as the tracks of $\mathcal{F}_i$.

(a) No multi-field optimization: the front field cools down since the current field is finished first.

(b) Multi-field o ptimization, t he f ront fi eld is in cluded in to the compaction task.

Figure 5. Priority map visualization.

Multi-field o ptimization i s u sed t o a void insufficient compaction. Therefore, previous tracks $\mathcal{T}_{i,j}$ of the field $\mathcal{F}_i$ are included into the current compaction task (Fig. 5b). The compaction of track $\mathcal{T}_{i+1,j}$ also blocks $\mathcal{T}_{i,j}$ since the vehicle needs the track to adjust to the task. Accordingly, track $\mathcal{F}_{i,j}$ is only added to the task if its compaction is not finished yet. Furthermore, it is checked if the task is currently blocked by another roller. By that, it is avoided that the temperature of the unfinished field $\mathcal{F}_i$ drops below the minimum compaction temperature threshold while the rollers are compacting field $\mathcal{F}_{i+1}$. Further, the optimization prevents the adjustment of a task on any unfinished fields. Besides, it is more time-efficient since two tracks are compacted while only adjusting to the task once.

5 Robot Control

The following section proposes further navigation-based robot control add-ons. Such are overtaking maneuvers of other machines in blocked sections and an improved path planning for refueling of water and diesel.

5.1 Overtaking and local trajectory adaptation

An alternative pathway for traveling can be computed as follows (Alg. 1). Considering the field the roller is positioned on it is calculating a path to field $\mathcal{F}_{i-1}$ in front of the targeted field of the next task $\mathcal{F}_i$. Using the information saved in the road model a working begin $\mathcal{F}_w$ is defined. This is the first field of the road which is not finished due to its temperature and compaction value. A field is considered as finished if the temperature is too low or the compaction amount is sufficient. If a roller's position $\mathcal{F}_i$ is behind the working begin ($i < w$) it approaches $\mathcal{F}_w$ by following the points saved in the tracks $\mathcal{T}_{i+1,t-1}$ to $\mathcal{F}_{w-2,t-1}$ where t is the number of tracks.

Algorithm 1: Pseudo code for calculation of avoidance points.

```
if current field id < working begin then
    drive to working begin;
end
if task's field id - current field id > 2 then
    for i = task's field id; i < current field id; i++ do
        add avoidance points of field i to target points;
    end
end
add task points to target points;
```

It is ensured that the rollers are always taking a path in driving direction right on the road by taking the points of the track with the highest ID. The tracks are numbered from left to right and split a field into longitudinal overlapping paths, which are driven by the rollers. This ensures that the driven path is never blocked by a roller driving in the opposite direction.

Next, a path to the task's field has to be determined while not interfering with other rollers currently performing tasks. Usually, the number of rollers compacting a

field at the same time is limited by the number of tracks. Additional rollers can be exploited by compacting fields further ahead. Since rollers are occupying the access route it is not necessarily possible to approach the task directly. Based on the number of fields between the current vehicle position and the target field of the task it can be determined if it is necessary to task evasive actions. If the number of fields between the current vehicle field $\mathcal{F}_i$ and the targeted field of the task $\mathcal{F}_k$ is smaller than two, the task can be approached directly. This is the case since task $\mathcal{T}_{k,j}$ is blocking all neighboring tracks, including the tracks on $\mathcal{F}_{i+1}$ which could be needed to approach the task. If the number of tracks between $\mathcal{F}_i$ and $\mathcal{F}_k$ is larger, other rollers may be occupying the tracks needed to approach the task directly. In this case, an avoidance lane is used which is located on the side of the road. In the case that a roller is required to take the avoidance lane, a request is sent to the paver. The paver is handling the assignment of this avoidance lane in the same way as the handling of the tracks. When performing an evasion maneuver a roller on-field $\mathcal{F}_i$ is aiming for the avoidance points of $\mathcal{F}_{i+1}$ and re-enters the road at $\mathcal{F}_{k-1}$. Afterward, the task can be directly approached.

5.2 Refueling

It is necessary to ensure the water and fuel supply of the rollers to achieve a successful compaction process. For this purpose, it is necessary to periodically send rollers to a refill station. Since the limiting factor of the compaction process is the slow speed of the paver, the refill process should not interrupt the compaction of the road. Typically at most one roller should perform a refill task at a time to secure ongoing compaction.

The refill task is assigned similarly to the standard compaction task. The fill levels of fuel and water of all rollers are monitored at the paver. The paver is creating and assigning the refill tasks based on the fill levels and two thresholds t_{refill} and t_{critical}. A roller is ready to be assigned a refill task in case the fill level is below t_{refill}. The t_{critical} threshold defines the fill level when the roller cannot perform any compaction tasks anymore before refueling. Therefore, each fill level is checked before assigning a new compaction task and refueling is started if at least one roller is fallen short of t_{refill}. Below a specific roller count, only one refill task can be performed at the same time. Accordingly, it is checked if a refill task is currently running. If this is the case, a second refuel task is not assigned and the assignment of the compaction tasks continues. In contrast, if no refill task is running, the roller with the lowest fill level starts refueling. The only case where more than one refill task can be performed similarly is the situation where multiple rollers fall below $t_{critical}$. In this case, the task is assigned independently of the currently running tasks, since the roller is incapable to perform other tasks anymore.

A roller with an assigned refill task follows the previously compacted road up to the road's begin using the points of $\mathcal{T}_{i-1,0}$ to $\mathcal{T}_{0,0}$. $\mathcal{T}_i$ denotes the field where the roller is currently placed on. The overtaking mechanism is used to avoid mutual interference at other field locations that have to be passed. A predefined path is driven which leads to the corresponding refill station after reaching the road's begin. Similarly, after refueling is finished, the roller navigates back to the entry point of the road $\mathcal{F}_w$.

6 Error Handling

A major issue in the communication between rollers and pavers is the handling of message loss and robot control failures. Those problems occur unintended and can consequently not be avoided. Typical situations are a data loss in the communication interface or safety-critical events as construction workers on the road which cause a safety stop of a roller. Therefore such events need to be explicitly regarded by the robot control to prevent a standstill of construction. This includes dynamically adding and removing rollers from the road works.

6.1 Communication failures

Rollers are continuously communicating with the paver and other rollers during the compaction process. Rollers are periodically sending the status of their currently assigned tasks. This is used for calculating new compaction tasks and monitor the state and finished tasks. Additionally, these updates are used as an acknowledgment mechanism to register whether an assignment message is received successfully. Besides, the messages are used to monitor if a roller is still active. If the paver's remote interface does not receive a status update of a roller for a set period t_{active} the roller is set to inactivity. Consequently, it is no longer part of the task assignment process. As soon as the roller is resuming the data transmission, it is reintroduced into the compaction process and can again receive tasks. Thus, t_{active} has to be chosen in a way that rollers can complete their current task before the threshold time is exceeded. A larger threshold is used for refill tasks (around 30 min) since they require a larger time duration due to the potentially large travel distance and the refilling time.

6.2 Task abortion criteria

Task abortion criteria are defined in addition to the communication failures. These should guarantee the revival of the process if an unforeseen event occurs as a roller does a safety stop. Even though the collision of the rollers is prevented by safety systems [11, 12], this does not resolve the problem that a path is not traversable. It is possible to

define upper bounds which should not be exceeded since the time needed to perform a compaction task does not vary considerably. It can be estimated based on the track length and roller's velocity. Therefore, the task is aborted and the roller moves back to the starting point of the task if the execution of a compaction task exceeds this time. Consequently, a new task can be assigned.

7 Experiments

A series of simulated and real-world compaction tests have been performed to evaluate the road construction result. The robot control was implemented using Finroc, a C++/ Java-based framework for intelligent robot control [13]. For simulation, Unreal Engine 4 was used which interacts with the control framework using an interface plugin [14].

Simulated compactions trials were performed on a static test road and the virtual B10 highway, Germany. In a long-term test, a road segment of 800 m with a field width of 7.5 m was compacted. Thereby, the number of rollers and the general road layout data structure were adapted to evaluate the impact on the compaction result (Fig. 6). In a second series, both tandem rollers BW 154 and BW 174 of the 5G-AMMCOA project compacted a road on the ZAK test environment, Germany (Fig. 7). Approximately, 300 m road with a width of 6.5 m have been processed.

Figure 6. Simulated autonomous road compaction tests on the B10 highway using a varying number of rollers and field length.

Figure 7. Autonomous compaction trial on ZAK road using the tandem rollers BW 154 and BW 174.

7.1 Single field compaction

In the first series of experiments, the influence of different numbers of tracks and rollers on the compaction time of a single field is shown. For this, a set of rollers is compacting a static street segment with a length of 25 m. The tests aim to show the advantages of additional rollers on the compaction time of single fields (Table 1). The tests were performed simulating an ambient temperature of 20 °C, and a wind velocity of 5 m/s. To reach the targeted compaction value each track had to be driven two times. Driving a single track on this street approximately takes one minute plus some additional time for the task approach.

Using just one roller, it was not possible to completely compact fields with more than four tracks before the asphalt is cooled down below the stop temperature of 80 °C. Also, it can be seen that a third roller has no impact on the compaction of a field with four tracks since the field overlap limits the space to two rollers at the same time. On larger track numbers, the advantage of additional rollers can be seen on the compaction duration of the field.

Table 1. Compaction duration for different track parametrization and varing roller counts.

# rollers	# tracks	duration [s]
1	4	630
2	4	360
3	4	360
1	5	–
2	5	540
3	5	350
1	6	–
2	6	600
3	6	420

7.2 Simulated B10 compaction

In the simulation, a paver laid out asphalt on the virtual B10 highway. Hereby, each test run was repeated with different test parameters as the number of rollers, compaction field length, and ambient conditions. Each test was running for approximately 30 min creating a road segment of 250 m length. A base course was paved which had a width of 7.5 m resulting in four tracks. The ambient conditions are an initial temperature of 20°C and wind velocity 5 m/s.

Number of Rollers In the first tests a fixed field length of 25 m is used and the number of rollers is varied. Thereby, it was not possible to sufficiently compact the road using a single roller only since the maximum area the roller can compact in a given time is lower than the area created by the paver. Therefore, after successfully compacting the first fields, the single roller is not able to finish the later fields before cooling off. Using two or three rollers, it

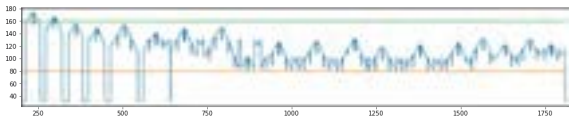

(a) Temperature measurements single roller trajectory over time.

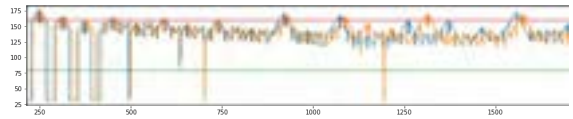

(b) Temperature measurements dual roller compaction over time.

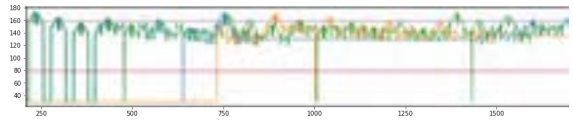

(c) Temperature measurements three roller compaction over time.

Figure 8. Compaction temperature for the tests with one (a), two (b), and three (c) rollers. The top straight line represents the start temperature (160 °C) the bottom line the stop temperature (80 °C).

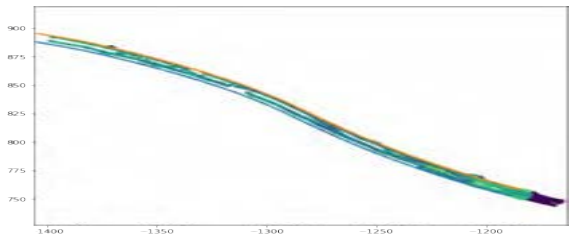

(a) Temperature-trajectory plot single roller test.

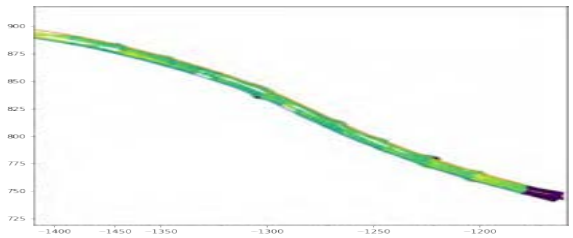

(b) Temperature-trajectory plot dual roller test.

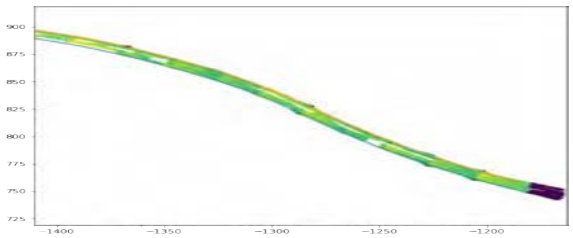

(c) Temperature-trajectory plot three roller test.

Figure 9. Temperature plot according to the roller trajectories. Light green depicts a high temperature (160 °C), purple is below the stop temperature (80 °C).

was possible to compact the road within the temperature windows. However, it should be mentioned, that due to the short test duration, no refills had to be performed. Upcoming refill tasks might negatively affect dual roller performance because the scenario changes to a single roller case in-between. Due to this, the deployment of a third roller is recommended in this scenario.

Fig. 8 depicts the surface temperatures measured by the rollers. It can be seen, that in the single roller case, the roller operates most of the time close to the lower compaction threshold temperature of 80 °C. After a while, the roller always compacts tracks which are close to the stop temperature, since they are the most urgent ones. Fig. 9 plots the temperature data against the spatial position of each roller. It can be seen that the overall track temperature is colder (in the visualization more bluish) than in the multi-roller tests. Also, at a later position on the road, only two of four tracks are compacted. In the temperature visualization of multiple roller tests (Fig. 8b-c), it can be seen that the track's temperature is usually close to the start temperature (160 °C). This provides some buffer time for unforeseen delays. Additionally, it can be observed, that in the three roller tests idle times appear in the temperature plot since no task is valid at the moment. In such a situation, the roller has the default behavior to iron a part of the road until a new task becomes available. Temperature data is measured at the kinematic center of the roller. Therefore, some gaps appear in the multi roller spatial plot. This results from the length and width of the roller.

Field length In another trial, the impact of the field length is considered. In addition to the standard field length of 25 m, two additional runs are performed using field lengths of 12.5 m, and 50 m. In general, the desired compaction was achieved in all three road setups.

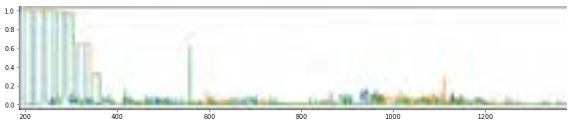

(a) Compaction criticality for a field length of 12.5 m

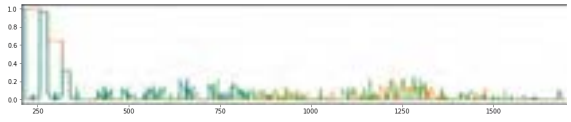

(b) Compaction criticality for a field length of 25.0 m

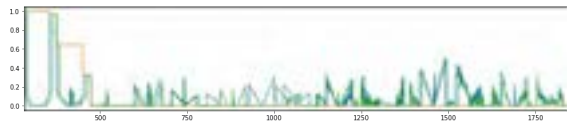

(c) Compaction criticality for a field length of 50.0 m

Figure 10. Critically of the for a field length of 12.5 m (a), 25 m (b) and 50 m (c)

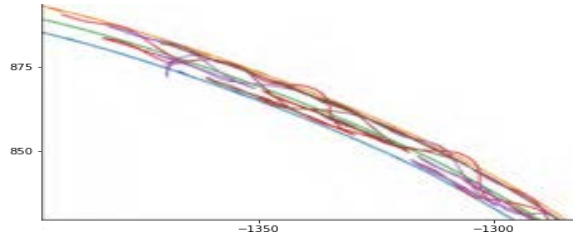

(a) Trajectories for a field length 12.5 m

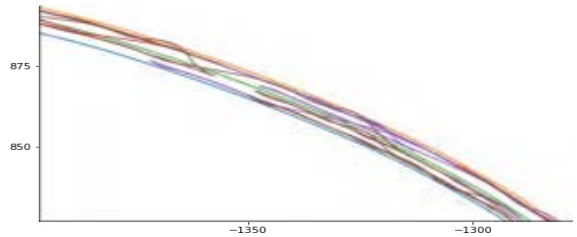

(b) Trajectories for a field length 25.0 m

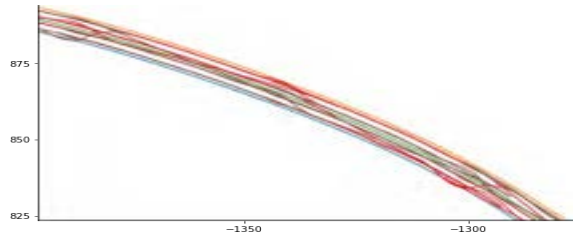

(c) Trajectories for a field length 50.0 m

Figure 11. Driven trajectories for different field length.

Anyways, the different layouts had various advantages and disadvantages.

In the tests with a short field length, the approach seemed to be much more reactive. The tracks are finished faster and are mostly compacted at high temperatures. This can be seen in the plots of the track criticality value of the road. The critical value is a combination of the temperature and the current compaction, indicating how critical the compaction of a track is at the moment (see Fig. 10). A roller has to wait shorter for a smaller field length to start the compaction than for a larger field length. A major issue is the approach of a task start destination. On one side, the number of task approaches is doubled, since the number of tracks is double. However, the main issue with the task approach is, that the maneuvering needs space in front of the track which should be compacted Fig. 11. The needed space behind the field is larger than the field length of 12.5 m. By that, when approaching a task at field $\mathcal{F}_i$, both the corresponding tracks of $\mathcal{F}_{i-1}$ and $\mathcal{F}_{i-2}$ have to be blocked, while the tests with higher field length only require to block the tracks of $\mathcal{F}_{i-1}$. Driven trajectories are easier to perform using the 50 m fields because less steering are needed Fig. 11. In contrast, the critically of the compacted asphalt is higher in these tests (Fig. 10c) due to the increased time to travel to a track. This is the case due to the larger temperature differences between the start and the end of the field. It also leads to a later beginning of the compaction, since the compaction is started after the average temperature of the track is below the start temperature of 160°C. Finally, another disadvantage is that the number of tracks available for compaction is low and that additional rollers are not exploited. In long term tests a field length of 25 m has achieved the best results.

7.3 Ambient Influences

The time available to compact a field is strongly dependent on the ambient temperature and wind velocity. For simulation, an estimation of the temperature is done. In the real scenario, the temperature is updated using the measurements of the rollers in addition to the model. To show the importance of ambient influences, the available simulated compaction time is shown for different conditions (Table 2).

Table 2. Compaction time based on ambient influences.

temperature [°C]	wind velocity [m/s]	duration [s]
10	5	580
20	5	630
30	5	690
20	10	400
20	20	240

7.4 Real-world ZAK compaction

Finally, tests on the real machine were performed. A single roller was compacting a road consisting of one field (Fig. 12) using the best performing setup from the simulation tests. In general, the roller was able to compact the field as expected and all timing and temperature constrains were fulfilled. However, the accuracy of the trajectories is lower than in simulation and has to be regarded more careful in future. Also, the steering actions are often too large which is not desired when driving on hot asphalt.

Figure 12. Track compaction trajectory of the ZAK test using BW 174 on a single track.

8 Conclusion

This paper presented different extensions to improve the results of autonomous road compaction, regarding the road mode, robot control optimization, and error handling. The impact of different parameters as number of rollers,

field length, and ambient conditions was evaluated within a series of autonomous compaction trials in simulation and real world. The number of required number of rollers and the impact of different field length have been discussed.

Future work aims to consider trucks properties into the compaction planning. So, varying asphalt installation temperatures resulting from transport are included into planning. Also, real-world autonomous compaction tests on hot asphalt are targeted and the impact on sensor quality and the control behavior further examined.

References

[1] S. Deb. Automation and robotics based technologies for road construction, maintenance and operations. The Masterbuilder, pages 44–50, April 2013.

[2] R. Kuenzel, J. Teizer, M. Mueller, and A. Blickle. SmartSite: Intelligent and autonomous environments, machinery, and processes to realize smart road construction projects. Automation in Construction, 71(Part 1):21 – 33, 2016. The Special Issue of 32nd International Symposium on Automation and Robotics in Construction.

[3] C. Halbrügge and B. Johanning. Automatisierte Asphaltverdichtung mit schemelgelenkten Tandemwalzen. ATZoffhighway, 8(2):56–67, Jul 2015.

[4] P. Wolf, T. Ropertz, A. Matheis, K. Berns, and P. Decker. Distributed coordination and task assignment of autonomous tandem rollers in road construction scenarios. In 36th International Symposium on Automation and Robotics in Construction (ISARC 2019), pages 953–960, Fairmont Banff Springs Hotel, Banff, AB, Canada, May 21–24 2019.

[5] R. Shinde, O. Nilakhe, P. Pondkule, D. Karche, and P. Shendage. Enhanced road construction process with machine learning and blockchain technology. In 2020 International Conference on Industry 4.0 Technology (I4Tech), pages 207–210, 2020.

[6] J. Axelsson, J. Fröberg, and P. Eriksson. Towards a system-of-systems for improved road construction efficiency using lean and industry 4.0. In 2018 13th Annual Conference on System of Systems Engineering (SoSE), pages 576–582, 2018.

[7] V. Faridaddin, A. K. Langroodi, D. Makarov, and S. Miller. Context-realistic virtual reality-based training simulators for asphalt operations. In Mohamed Al-Hussein, editor, Proceedings of the 36th International Symposium on Automation and Robotics in Construction (ISARC), pages 218–225, Banff, AB, Canada, May 2019.

[8] C. Halbrügge, B. Johanning, and A. Römer. Automatisierte Maschinenführung von Straßenwalzen. BauPortal, 4:35–37, June 2015.

[9] A. Ulrich, M. N. Tamo, V. Farbischewski, and M. Watermann. Autonom arbeitende Maschinen im Straßenbau. Forschungsprojekt schafft Voraussetzungen für erfolgreichen Einsatz. VDBUM Info, pages 30–33, September / Oktober 2018.

[10] P. Wolf, A. Vierling, J. Husemann, K. Berns, and Peter Decker. Extending skills of autonomous off-road robots on the example of behavior-based edge compaction in a road construction scenario. In K. Berns at. al., editor, Commercial Vehicle Technology 2020. Proceedings of the 6th Commercial Vehicle Technology Symposium – CVT 2020, Kaiserslautern, Germany, March 10–12 2020. Commercial Vehicle Alliance Kaiserslautern (CVA), Springer Vieweg.

[11] P. Wolf, T. Ropertz, K. Berns, M. Thul, P. Wetzel, and A. Vogt. Behavior-based control for safe and robust navigation of an unimog in off-road environments. In K. Berns at. al., editor, Commercial Vehicle Technology 2018. Proceedings of the 5th Commercial Vehicle Technology Symposium – CVT 2018, pages 63–76, Kaiserslautern, Germany, March 13–15 2018. Commercial Vehicle Alliance Kaiserslautern (CVA), Springer Vieweg.

[12] T. Ropertz, P. Wolf, and K. Berns. Behavior-based low-level control for (semi-) autonomous vehicles in rough terrain. In Proceedings of ISR 2018: 50th International Symposium on Robotics, pages 386–393, Munich, Germany, June 20–21 2018. VDE VERLAG GMBH.

[13] M. Reichardt, T. Föhst, and K. Berns. Introducing FINROC: A Convenient Real-time Framework for Robotics based on a Systematic Design Approach. Technical report, Robotics Research Lab, Department of Computer Science, University of Kaiserslautern, Kaiserslautern, Germany, 2012.

[14] P. Wolf, T. Groll, S. Hemer, and K. Berns. Evolution of robotic simulators: Using ue 4 to enable real-world quality testing of complex autonomous robots in unstructured environments. In F. De Rango, T. Ören, and M. Obaidat, editors, Proceedings of the 10th International Conference on Simulation and Modeling Methodologies, Technologies and Applications (SIMULTECH 2020), pages 271–278. INSTICC, SCITEPRESS – Science and Technology Publications, Lda, July 8–10 2020.

Ontology-Based Decoding of Risks Encoded in the Prescriptive Requirements in Bridge Design Codes

F. Hassan[a] and T. Le[b]

[a]Ph.D. Student, Glenn Department of Civil Engineering, Clemson University, Clemson, SC, USA
[b]Assistant Professor, Glenn Department of Civil Engineering, Clemson University, Clemson, SC, USA
E-mail: fhassan@g.clemson.edu, tuyenl@clemson.edu

Abstract –

Bridge designs are typically governed by a voluminous set of requirements in various design standards and codes. The requirements are aimed at ensuring the structural safety against different environmental risks experienced by a bridge facility during its service life. The requirements provided in the bridge design standards are generally prescriptive in nature that do not explicitly specify the types of risks addressed in them. As a result, the understanding of the risks hidden in the requirement text is solely associated with the individual designer who often lacks adequate training in interpreting the risks addressed in prescriptive requirements. The conventional practice of manual identification of risks encoded in the prescriptive provisions requires much effort, domain knowledge and may include human errors as well. Little attention has been paid towards automated identification of risks encoded in the prescriptive requirements. The paper presents an ontology-based risk decoding model to decode the risks implied in the prescriptive requirements. The risks included the earthquake, flood, wind, fire, vessel collision, blast loading, temperature and overloading. An ontology for conceptualizing the domain knowledge of the eight risks was first developed. The ontology-based decoding model ranks the risks for a prescriptive requirement by measuring the semantic similarity between the requirement and the risk ontology. The model was tested on the AASTO bridge design specifications and evaluated in terms of Spearman, Kendall tau and Pearson rank correlation test. This study is expected to assist the designers in the improved understanding of risks encoded in prescriptive design standards.

Keywords –

Bridge design;Prescriptive requirements; Design standards; Environmental risks; Natural language processing; Deep learning

1 Introduction

Bridge designs are generally carried out in accordance with a set of requirements specified in the design codes and standards [1]. The primary goal behind these requirements is to ensure the structural stability and durability of the bridge against several environmental risks [2]. The major risks experienced by the bridges are flood, earthquake, wind, fire, etc. In order to execute a safe and reliable design, the precise understanding of the requirements is very crucial [1]. The requirements currently available in the bridges design codes are mostly described in a prescriptive manner where the main intention or the objective behind the requirement is not clearly stated [3]. Accordingly, there is a need for an automated framework which can decode the risks hidden in the text of prescriptive requirements.

The accurate decoding of the risks in the prescriptive requirements is very important to produce a design that can enable the safety of the bridge against all hazards or risks [4]. The prescriptive requirements are typically produced by the code writers with years of experience in the industry and research. In addition, a detailed study of the past failures along with the full-scale testing of the proposed models are also performed while designing the prescriptive requirements [5]. The code writers only present the final criteria for the safest designs without providing any information regarding the types of risks considered while developing that criteria. For instance, the prescriptive requirement *"The maximum girder spacing shall not exceed 10½ ft."* may fulfill the design requirements against overloading, earthquake, and flood but may not fulfil the performance required against the fire risk. Another requirement *"The spacing of intermediate bracing shall not exceed 20 ft."* may achieve the goals of flood, wind, and earthquake risks while the fire, temperature and overloading risks may not be mitigated by implementing this requirement. However, such information of the risks is not provided in the

requirement text. Since many prescriptive requirements have certain limitations in terms of risks, the implementation of the prescriptive requirements without understanding the risks addressed in them may result in the scenarios where a few risks may be go unchecked in the bridge design [6]. Young engineers in the industry mostly lack the experience and knowledge required for understanding the risks encoded in the prescriptive requirements. The blind implementation of the prescriptive requirements by young engineers without understanding the objectives and performance level implied in the requirement may result in an unsafe design. In addition, since the objectives covered in the prescriptive require are not known, it is difficult in international construction industry to establish an equivalence between two different criteria stated in codes of two different countries [7]. Therefore, a risk decoding model is required that can precisely decode the risks encoded in the prescriptive requirements.

The current body of knowledge lacks methods to address the issue of risks hidden in the prescriptive requirements. To fill the gap, this study has attempted to develop an automated ontology-based risk decoding model using the linguistic methods such as vector space models and ontologies. A detailed ontology covering the domain knowledge of the eight risk categories was first developed. The risk categories included earthquake, flood, wind, fire, vessel collision, blast loading, temperature and overloading. Following this, the trained vector space model and ontology were employed to decode and rank the risks encoded in the prescriptive requirements according to the semantic similarity of the requirement text and the risk ontology.

2 Background

2.1 Risks in bridge design codes

The risks involved in the bridge design are controlled and mitigated by the implementation of requirements available in the design codes [1]. The bridge design codes generally include two types of requirements; (1) prescriptive requirements, and (2) performance-based requirements [8]. The prescriptive requirement only states the acceptable solution without indicating the performance level while the performance-based requirements specifies the performance level required without providing any prescription or solution. The prescriptive requirements can further be classified into two categories. The first category is when the quantitative prescription is explicitly stated, for example, *"The maximum girder spacing shall not exceed 10½ ft."*. The second type is when the relevant code or method is specified to be followed in design, for example, *"The deck overhang shall be designed in accordance with Section 13 of the LRFD Specifications."* Since the goals or intention behind the recommendations in prescriptive requirements are not specified, the young designers often assume that the requirements cover all the risks. However, this is not the case for the prescriptive requirement since prescriptive requirements always have certain limitations as well [4]. The implementation of the requirement for a scenario for which is not designed often results in the failure in achieving the required performance. Therefore, the decoding of the risks is very important to ensure that the requirements are applied to the scenarios for which they are actually designed.

2.2 Text processing using ontologies

Ontologies are the knowledge representation methods widely used to present the domain knowledge shared among different systems [9]. Ontologies are employed to provide the background knowledge in a machine-readable format for the development of several automated systems for text classification, word sense disambiguation, etc. [10]. The representation of knowledge in the form of concepts in ontologies enables the reuse of the ontologies for other systems [11]. Concepts are the domain entities which are represented in a hierarchical form in ontologies. The relationships are used to define the type of connections between the different concepts and sub-concepts. Ontologies can also play a key role in text processing. For instance, the ontologies can be used to represent the features of a text document. The extracted features can then be used to classify or rank the labels using a machine learning algorithm [12]. In addition, ontologies can also be used to represent the domain knowledge of class labels. The developed ontologies of the labels can then be used to analyze the documents followed by the assigning of labels or ranks [13].

2.3 Related studies

Several researchers have studied the limitations pf the prescriptive requirements, however, most studies have been focused on the addressing a few specific limitations such as design hinderance while many other limitations such as absence of risk information in prescriptive requirement have not received the equal attention. For instance, [14] studied the limitation of the prescriptive codes in addressing the fire risk. As a solution, the authors stressed upon the improvement of current prescriptive codes, ensuring their proper implementation along with the promoting the fire education. Another study by [15] highlights the limitations of the prescriptive codes in introducing innovative solutions to mitigate problems associated with the climate change. A five-step solution was

provided by the author to control the degradation of environment due to the use of specific materials prescribed in the prescriptive requirements. [16] also addressed the same limitation of hinderance in using alternative methods to improve the project performance in design-bid-build and design-build projects. The study carried out the textual analysis of the performance-based requirements provided in the Swedish design-build contracts.

Prescriptive requirements in the transportation domain also presents the same limitation of disallowing the innovative solutions. Since manufacturers have to follow the prescriptive dimension and weight requirements, they cannot practice new solutions to reduce the road accidents. [17] suggested a performance-based system to address this limitation. The developed regulatory system requires the certification of vehicles as well as operators to meet the approval requirements. [18] highlighted the increase in accidents in Malaysia due to not allowing the new alternative methods in design to prevent the accidents. The author studied the limitations in the prescriptive codes of Malaysia and explored the potential opportunities of improvement by comparing it with the well-established performance-based specifications implemented in Australia. [19] also highlights the limitations of prescriptive requirements in dealing with the complex risks such as blast loading and fire.

Many studies have investigated the limitation of prescriptive requirements in hindering the innovation. However, despite the significant importance, the limitation of prescriptive requirement in specifying the performance level or risk information have not been studied yet. The current study is aimed at developing an automated framework to decode the goals implied in the prescriptive requirements.

3 Methodology

The methodology adopted in this study comprised four major steps illustrated in Figure 1. Firstly, an ontology reflecting the essential semantic knowledge associated with the eight environmental risks was produced. Following this, a vector space model was trained using a domain specific corpus. The third step includes the computation of the semantic similarity scores between the requirement text and the risk categories. After ranking of risks according to the similarity scores, the model was evaluated using different rank correlation coefficients.

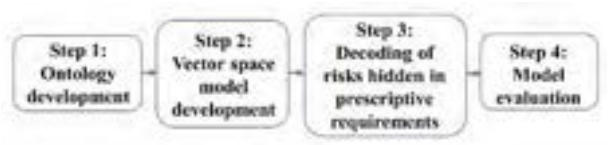

Figure 1. Methodology of the ontology-based risk decoding model

3.1 Step 1: Ontology development

Before development of ontology, the major risks involved in the bridge designs were identified. Upon reading of the relevant published articles, following eight (08) major risks were identified: flood, wind, earthquake, fire, temperature, vessel collision, overloading, and blast loading. A detailed ontology to model all the domain specific knowledge of each of the eight risk categories was developed. The four steps involved in the ontology development are explained below.

1. ***Identification of purpose:*** In the first step, the reason behind the development of ontology was explicitly defined. The ontology developed in this study was aimed to decode the environmental risks hidden in the prescriptive requirements.
2. ***Identification of concepts and sub-concepts:*** The second step involved the identification of all concepts and sub-concepts related to each of the eight risk categories covered in this study. The bridges design codes and published articles were used to identify the concepts and sub-concepts. For instance, 'liquefaction" and 'cyclic loading" is related to earthquake, so these concepts were present under the earthquake category in the risk ontology.
3. ***Identification of relations:*** The third step is aimed at defining the relationships between the concepts and sub-concepts in the ontology.
4. ***Ontology modeling:*** Finally, the concepts and sub-concepts were modeled in the protégé tool to produce the final ontology.

Figure 2 illustrates a partial ontology of a risk category "flood'. The ontology of a risk category mainly shows the essential semantic knowledge associated with the risk category in a hierarchical form. As shown, all the sub-concepts below a particular sub-concept provides additional information regarding the upper concept. The higher concepts are the abstract ones while the lower concepts in the ontology provides detailed knowledge of the upper concepts. Each of the eight risk categories has a different number of sub-concepts below it in the ontology depending on the semantic knowledge required to present the risk category.

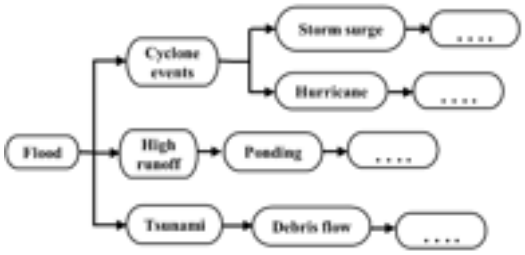

Figure 2. Partial ontology of risk category 'flood'

3.2 Step 2: Vector space model development

Several bridge design codes, standards and the published articles were collected to build a vector space model to learn the semantic meanings of the technical terms used in the design codes. The design codes of ten different state department of transportation (DOT) as well the U.S. DOT was employed to develop the corpus for the training of vector space model. The tables and equations were excluded from the corpus since they are not supported by the natural language processing (NLP) methods. The final corpus used in the training process comprised a total of approximately 1 million words. The domain-specific corpus was pre-processed by implementing the following NLP methods; (1) Lowercasing: The complete corpus was converted into a lowercase format to consider similar meaning words such as "Cracking" and "cracking" as one word. (2) Tokenization: The whole corpus was transformed into a sequence of tokens where a token could be a word, a number or a punctuation. (3) Lemmatization: Lemmatization was performed to convert different grammatical forms of a single word into the root form, for instance, "cracks", "cracked", and "cracking" was converted to the root word "crack".

After pre-processing of the corpus, the wor2vec algorithm was applied to build a vector space model. Both architectures of the word2vec including continuous bag-of-words (CBOW) and hierarchical skip-gram algorithm were applied [20]. Both algorithms have reported comparable performance in the literature [20]. The whole vocabulary in the corpus was presented on a high-dimensional vector space where each unique word holds a unique vector. The distance between the vectors on vector space indicates the semantic similarity between the corresponding words. The training of the vector space model includes the tuning of several parameters such as window size (number of co-occurring words examined in analysing the semantic meaning of a word), vector dimensionality (dimensions of each word vector), frequency threshold (minimum frequency of a word required to include the word in the training process). Different values of the vector dimensionality ranging from 300 to 1200 were tested in this study to determine the optimal value. The window size and frequency threshold considered in all the experiments were 10 and 1 respectively.

3.3 Step 3: Decoding of the risks hidden in prescriptive requirements

The risk decoding approach adopted in this study is the similarity-based. The similarity scores indicating the semantic similarity between the requirement text and the risk ontology were first determined. Based on the similarity scores, the risks encoded in the requirement were ranked in the descending order of relevance. The details of the two steps are provided as follows.

3.3.1 Measurement of the similarity scores

The trained vector space model was employed to compute the similarity score of each term in the requirement and each concept in the ontology. Cosine similarity function was applied for the computation of similarity scores. Cosine similarity computes the angle between the two vectors where a smaller angle shows higher similarity between the corresponding words. The detailed risk ontology and the prescriptive requirement were provided as input to the risk decoding model where the semantic similarity between each word of the requirement and each concept of the ontology were computed using the trained vector space model. After similarities calculation, the similarity values of all terms in a requirement with a specific concept were then summed up to get the total similarity value for the requirement with that specific ontology concept. Since the current study is focused on the decoding of risks which are present at the level 1 of ontology, the similarity scores at the level 1 of ontology are determined by adding the similarity scores of all the concepts below that level 1 concept. Each level 1 concept includes a different number of concepts below it in ontology, therefore, the total similarity values are normalized by the frequency or number of nodes below each level 1 node of ontology. The mean normalized method was applied to compute the total similarity score at the level 1 of ontology. Eq. 1 was used for the computation of mean normalized scores. A total of eight mean normalized scores were obtained where each value corresponds to the total semantic similarity score of the requirement with a specific level 1 concept.

$$mean\ normalized\ score\ = \frac{\sum_{n=1}^{N}(\sum_{t=1}^{T} s_{tc})_k}{N} \quad (1)$$

Where s_{tc} indicates the semantic similarity score of the term *'t'* in the requirement and concept *'c'* in the ontology, *'T'* indicates the total number of terms in a specific requirement, *'N'* indicates the total number of concepts below a level 1 concepts in ontology.

3.3.2 Ranking of the risks

Once the total similarity scores of a requirement with the eight risk factors at level 1 of ontology are calculated, the risk factors are ranked in descending order of relevance. The risk category revealing the highest total mean normalized score was assigned the rank 1 while the remaining categories are ranked from 2 to 8 according to the total similarity scores.

3.4 Step 4: Model evaluation

The risk decoding model was evaluated on a test dataset of 151 prescriptive requirements. The test dataset was manually labeled with the ranks of risks according to the content of the requirement. The performance of the model was evaluated using different rank correlation tests including Spearman, Kendall tau and Pearson rank correlation tests (as shown in Eq. 2-4). The rank correlation value shows the level of agreement between the actual ranks and the predicted ranks. A value of 1 indicates a complete agreement while a value of -1 indicates a complete disagreement between the two sets of ranks.

$$Spearman = r_s = 1 - \frac{6\sum_{i=1}^{n}(x_i - y_i)^2}{n^3 - n} \quad (2)$$

$$Kendall\ tau = r_k = \frac{2}{n(n-1)}(|C| - |D|) \quad (3)$$

$$Pearson = r_p = \frac{n\sum x_i y_i - \sum x_i y_i}{\sqrt{n\sum x_i^2 - (\sum x_i)^2}\ \sqrt{n\sum y_i^2 - (\sum y_i)^2}} \quad (4)$$

where *'x_i'* and *'yi'* are the ranks of a risk category *'i'* in group 1 and 2, 'n' indicates the number of predefined risk categories, *'C'* is set of concordant pairs, and *'D'* is set of discordant pairs.

4 Results and Discussion

This section presents the results of the experiments carried out to evaluate the performance of the risk decoding model. Two different architectures of the word2vec such as CBOW and skip gram algorithm were used to compute the semantic similarities of the requirement terms and the ontology concepts. For each algorithm, four vector space models were developed using a different value for vector dimensionality ranging from 300 to 1200. The window size and minimum threshold value of 15 and 1 respectively were same in all the experiments.

Table 1 presents the results of the risk decoding model using the CBOW algorithm for the similarity computation. The results show that performance of the model was increased with the increment of vector dimensionality until 900. The performance was decreased as the value of vector dimensionality was further increased from 900 to 1200. The highest spearman, Kendall tau and Pearson correlation coefficient of 0.30, 0.23, and 0.29 was achieved with the vector dimensionality of 900 whereas the lowest spearman, Kendall tau and Pearson correlation coefficient of 0.24, 0.19, and 0.23 was achieved with the vector dimensionality of 300.

Table 1. Performance of the ontology-based risk decoding model using CBOW algorithm for similarity computation

Vector dimensionality	Spearman	Kendall tau	Pearson
300	0.24	0.19	0.23
600	0.29	0.22	0.28
900	030	0.23	0.29
1200	0.26	0.20	0.25

Table 2 presents the results of the risk decoding model using the skip gram algorithm for the similarity computation. The same trend as previously seen with the CBOW was observed with the skip gram as well. However, unlike CBOW, the performance of the skip gram model did not change significantly while varying the value of vector dimensionality. A minor increment has been observed till vector dimensionality of 900, however, a decrease in performance was observed for higher values. The skip gram also revealed the highest Spearman, Kendall tau, and Pearson correlation coefficient of 0.64, 0.51, and 0.63 respectively at the vector dimensionality of 900. Among the two word2vec algorithms, the performance exhibited by the skip gram was almost twice better than that achieved by the CBOW algorithm.

Table 2. Performance of the ontology-based risk decoding model using skip gram algorithm for similarity computation

Vector dimensionality	Spearman	Kendall tau	Pearson
300	0.63	0.51	0.62
600	0.62	0.50	0.61
900	0.64	0.51	0.63
1200	0.63	0.51	0.62

4.1 Model performance for different risk categories

The performance of the model in terms of each risk category was further investigated using the best model of skip gram for similarity computation. Figure 3 shows the mean deviation of the predicted ranks from the actual ranks. As shown, the risk categories such as 'temperature' and 'fire' performed the best among the eight categories. For temperature, the mean deviation of 0.23 shows that the model predicts the correct rank for

temperature category most of the times. No risk category exhibited a mean rank deviation of above 2 which proves the adequacy of the model.

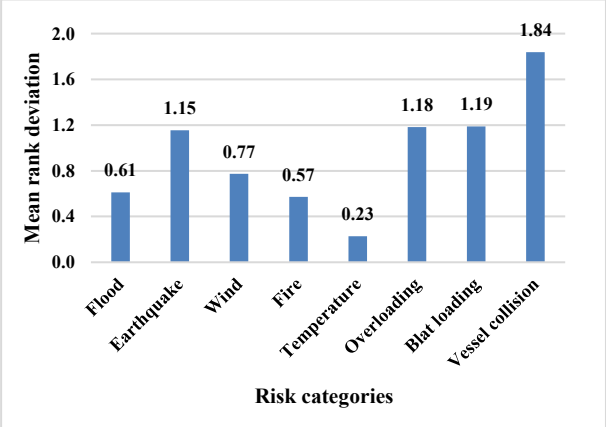

Figure 3. mean deviation of the predicted ranks from actual ranks

5 Conclusion

Bridge design are performed according to the requirements presented in the design codes and standards. However, the requirements are mostly prescriptive in nature where the main objectives or risks addressed in the requirements are not clearly specified. As a result, the designers often face challenges in estimating the limitations and performance level implied in the prescriptive requirements. The study has produced an automated framework using the vector space models and ontologies which can decode the risks encoded in the prescriptive requirements.

An ontology covering the domain specific knowledge associated with the eight risk categories was first developed. In addition, a vector space model was trained on a corpus of approximately 1 million words using the CBOW as well as skip gram algorithm. The model was validated on the unseen prescriptive requirements extracted from the AASHTO bridge design specifications. The experiments revealed that the skip gram algorithm performed better than the CBOW algorithm. The performance exhibited by the skip gram algorithm was double than the performance achieved by the CBOW algorithm. Moreover, the performance was found to be increasing with the increment in the size of word vector dimensions till 900, however, the performance was decreased for higher vector dimensionality values. The overall highest Spearman, Kendall tau, and Pearson correlation coefficient of 0.64, 0.51, and 0.63 respectively was reached by the skip gram model for the similarity computation at the vector dimensionality of 900. Comparing the risk categories, the 'temperature' category performed the best where the model predicted the correct rank in most cases. The model showed the mean rank deviation of 0.23 for the temperature category while the highest mean rank deviation of 1.84 was exhibited by the 'vessel collision' category.

The study has certain limitations in terms of performance. The current model uses the simple mean method to compute the total semantic similarity. In future, the authors will investigate different averaging methods such as weighted average and Bayesian average for the computation of the total similarity scores to examine the improvement in performance. A threshold analysis by setting of a threshold value to exclude the similarity scores of the irrelevant concepts may also improve the performance of the model. In addition, the authors will develop a larger dataset for the training of vector space model to examine if the performance can be improved by using a large dataset.

References

[1] Pritchard, R. W. 2011 to 2012 Queensland floods and cyclone events: Lessons learnt for bridge transport infrastructure. *Australian Journal of Structural Engineering*, *14*(2), 167–176, 2013.

[2] Björnsson, I. Holistic approach for treatment of accidental hazards during conceptual design of bridges – A case study in Sweden. *Safety Science*, *91*, 168–180, 2017.

[3] Patil, S. S., & Molenaar, K. R. Risks associated with performance specifications in highway infrastructure procurement. *Journal of Public Procurement*, *11*(4), 482–508, 2011.

[4] Björnsson, I. From Code Compliance to Holistic Approaches in Structural Design of Bridges. *Journal of Professional Issues in Engineering Education and Practice*, *142*(1), 1–6, 2016.

[5] Bulleit, W. M. Structural building codes and communication systems. *Practice Periodical on Structural Design and Construction*, *17*(4), 147–151, 2012.

[6] Kobyliński, L. New Generation Stability Norms-How to Approach the Task. *Polish Maritime Research*, *25*(s1), 56–62, 2018.

[7] Foliente, G. C. Developments in performance-based building codes and standards. *Forest Products Journal*, *50*(7–8), 2–11, 2000.

[8] Hurd, M. E. Quantitative Design Decision Method : Performance-Based Design Utilizing A Risk Analysis Framework, 2012.

[9] Qin, C., Zhao, P., Mou, J., & Zhang, J. Construction of personal knowledge maps for a peer-to-peer information-sharing environment. *Electronic Library*, *36*(3), 394–413, 2018.

[10] Allahyari, M., Pouriyeh, S., Kochut, K., & Reza, H. A Knowledge-based Topic Modeling Approach for Automatic Topic Labeling. *International Journal of Advanced Computer Science and Applications*, *8*(9), 335–349, 2017.

[11] Chang, Y. H., & Huang, H. Y. An automatic document classifier system based on Naïve Bayes classifier and ontology. *Proceedings of the 7th International Conference on Machine Learning and Cybernetics, ICMLC*, *6*(July), 3144–3149, 2008.

[12] Lee, Y. H., Tsao, W. J., & Chu, T. H. Use of ontology to support concept-based text categorization. *Lecture Notes in Business Information Processing*, *22 LNBIP*, 201–213, 2009.

[13] Yu, F., Zheng, D. Q., Zhao, T. J., Li, S., & Yu, H. Text classification based on a combination of ontology with statistical method. *Proceedings of the 2006 International Conference on Machine Learning and Cybernetics*, *2006*(August), 1042–1047, 2006.

[14] Tavares, R. M. An analysis of the fire safety codes in Brazil: Is the performance-based approach the best practice? *Fire Safety Journal*, *44*(5), 749–755, 2009.

[15] Francart, N., Larsson, M., Malmqvist, T., Erlandsson, M., & Florell, J. Requirements set by Swedish municipalities to promote construction with low climate change impact. *Journal of Cleaner Production*, *208*, 117–131, 2019.

[16] Bröchner, J., & Silfwerbrand, J. Performance of performance specifications in design-build highway projects. *Construction Economics and Building*, *19*(2), 111–125, 2019.

[17] Calvert, F. Improving Regulation of Heavy Vehicles: Performance-Based Standards. *8th International Symposium on Heavy Vehicle Weights and Dimensions*, *61*(0), 2004.

[18] Osmin, M. S. The Opportunities and Challenges Overview: Implementing Performance Based Standards Regulation for High Capacity Passenger Vehicle in Malaysia, (82005), 2017.

[19] Thompson, B. P., & Bank, L. C. Risk perception in performance-based building design and applications to terrorism-resistant design. *Journal of Performance of Constructed Facilities*, *21*(1), 61–69, 2007.

[20] Mikolov, T., Chen, K., Corrado, G., & Dean, J. Efficient estimation of word representations in vector space. *1st International Conference on Learning Representations, ICLR 2013 - Workshop Track Proceedings*, 1–12, 2013.

Current Status of Unmanned Construction Technology Developed using a Test Field System

Koji.Ihara[a] and Takeshi.Tamura[b]

[a] ASUNARO AOKI CONSTRUCTION CO.,LTD.Japan
[b] UNZEN RESTORATION WORK OFFICE All Rights Reserved.Japan

koji.ihara@aaconst.co.jp, tamura-t8915@mlit.go.jp

Abstract –

Unmanned construction work is civil engineering work carried out by remotely operating construction machinery located in a caution zone (a zone whose entry is prohibited or restricted), thus enabling the operator to perform remote work from inside the safe area without any need to enter the caution zone.

This technology came into being as a result of a proposed public offering of technology from each civilian company, which utilized the test field* of January 1994, and also technology verification at the site. From then onward to the present time, new technology was acquired continuously, then it evolved, and spread throughout Japan.

This paper describes the birth of unmanned construction, the development of related technology, and the trend of current technology.

***A system for constructing a life-size building intended for increasing the degree of completeness through technology verification in the field.**

Keywords –

Unmannde Contruction; Remote control; Operation guidance; Wireless communication; Safety monitoring

1 Description of unmanned construction

This unmanned construction technology consists of construction machinery that is operated remotely, and supporting equipment for operating remote operation of this machinery (Figure 1).

Also, it is necessary to arrange the shape of the the civil engineering structure and equipment constructed in the caution zone, and also the quality confirmation method.

A description of each item is set out below.

1.1 History of unmanned construction

Work using remote-operated construction machinery commenced in 1969. In this case, land reclamation was carried out on the Joganji-gawa River in Toyama Prefecture using an amphibious bulldozer (Figure 2). Subsequently, the use of remote operation was extended to land type back hoes, bulldozers and dump trucks.

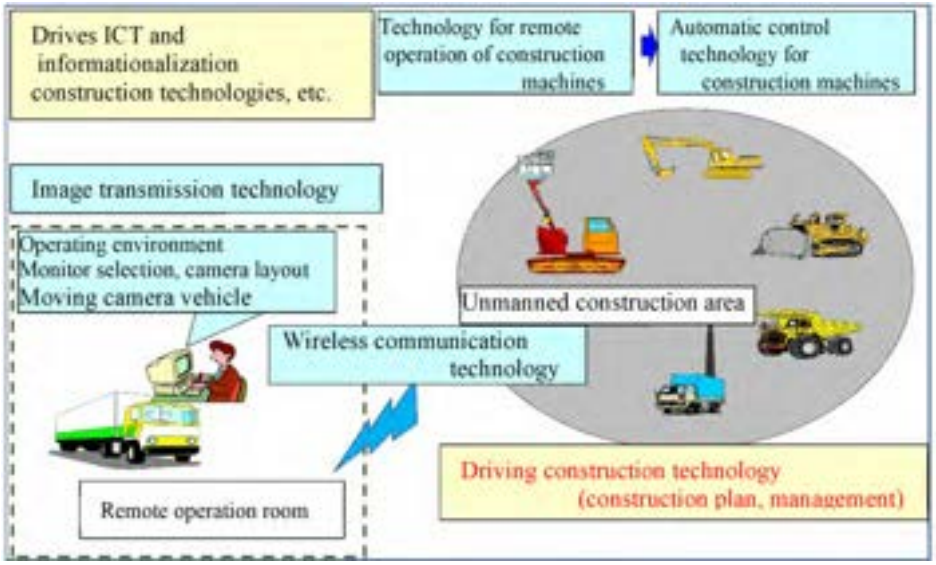

Figure 1. Unmanned Construction Technology

Figure 2. AMPHIBIOUS BULLDOZER

1.2 The birth of unmanned construction

A test field system tests new technology at the jobsite, in order to confirm its integrity.

In the case of the test field at Mt. Unzen-Fugendake, because mudslides occurred due to the increase in volcanic activity, and sand and soil accumulated in sand ponds, it is necessary to urgently remove boulders and also sand and soil. Because it is difficult to carry out construction using manned machinery, topics are assigned such as the acquisition of technology for continuous excavation and removal of soil by unmanned construction (Table1).

Table 1. Technical subject of a test field ［1］

	Contents of a technology	Technological standard
①	Excavatingand carriage accompanied by the smash at the condition and moreover, of a rock that isn't uniform	A pellet smash as much as 2 in diameter - 3 m is possible
②	A temperature in a spot is prepared to the humidity conditions.	It has been possible to operate even the condition as much as 100 ℃ of a temperature, 100 % of the humidity temporarily as a peripheral condition
③	The remote control can do a building machine.	Equal to or more than 100 m of remote control is possible.

In response to this emergency technology, public offering of technology that could be used together with procurable technology were selected, and then grouped together. The base machines consisted of large, remote operation type construction machines (bulldozers, backhoes, dump trucks) grouped together. As the operation support equipment, an ITV camera was used for securing adequate visibility over an operation distance of 100 m. Also, because the operation signals transmitted to and from the construction machines, and the image information obtained from the camera is transmitted wirelessly, wireless relay facilities for preventing instantaneous shutdown of wireless transmission, mobile camera vehicles which compensate for the dead angle of the camera image, remote operation rooms, and other ancillary facilities that are peculiar to unmanned construction were installed (Figure 3).

Figure 3. Relay vehicle＆camera car

At the commencement of construction, work is extremely difficult to carry out, even in the case of excavation work which is considered to be easy work.

Examples include radio interference, power source problems, a breakdown due to impact during construction, and problems concerning contact between construction machines at the in the dead angle of the camera. Upon completion of the test construction it was determined that excavation work could be carried out.

2 Improved technology used at Mt. Unzen-Fugendake

At Mt.Unzen-Fugendake, there is a danger of the lava dome collapsing, even at present. For this reason, a sand arrestation facility was fabricated using unmanned operation, from August 1994 corresponding to the completion of a test construction under the field system, to the present day. Concerning unmanned construction which has been employed in the Unzen region over the past 50 years, it was considered necessary to make technology improvements in communication by using a variety of sand arrestation structures and also the positional relationship between the safety zone and the work location. Also, on the other hand, equipment and other items for performing quality control was installed on trial. These items basically consist of existing useful technology that has been converted into remote technology.

For this reason, “unmanned construction” has been used from August 1994, corresponding to the completion of test construction, to the present day. This technology has been improved according to changes in the situation of the work, such as the object of construction or the operation position. Also, whenever new technology was employed, it was corrected and verified at the jobsite and its effectiveness confirmed.

2.1 Application to a variety of sand arrestation structures

Excavation technology that was confirmed by test construction was developed to the final structure.

2.1.1 Construction of a weir using the RCC method

The RCC (Roller Compacted Concrete) method which enables construction work to be performed by improving earthmoving machines was adopted. To enable this method to be used, vibration rollers, water spraying vehicles, cleaning cars, and sand and soil formwork shaping machines were developed. (Figure 4)

Figure 4. Building of RCC

2.1.2 Building of a steel slit dam

In the construction of a steel open type dam, transportation and installation were carried out, taking into consideration the shape of the steel slit. The dam was fixed by using high-fluidity concrete. Also, conveying of the concrete, conveying of the concrete to be laid, laying of the concrete, and surface-finishing were carried out. (Figure 5).

Figure 5. Building of a steel slit dam

2.2 Operating method

The operating methods are classified as shown in Table 2.

Table 2. operating method

	Watching operation	Monitor operation		
Form of construction work	It operates directly.	Monitor operation	Utilization of a becoming ICT	Utilization of TCP/IP
Overview	Watching operation	It operates while seeing the monitor of a camera.		
		-		Utilization of TCP/IP
Overview of the construction system of becoming of the unmannedness	Independent work of a remote type operation machine	Direct method A remote type construction machinery communicates with an operation place directly. Relay method An operation place and remote type operation machine are done through a relay-aircraft.	Utilization of a becoming ICT GNSS measure uses a technology and guidance equipment.	Utilization of TCP/IP It adopts a wireless LAN to the operation and transmission of the picture information.

2.3 Quality control

In Japan, the control outline was formulated in 2012. Presently, “Compaction control using TS-GNSS” has come into general use. When compaction was carried out in the Unzen zone using unmanned operation, it was used from 1995 as RCC method concrete laying control and also compaction control using a GPS in 1999 (Figure 6, Figure 7).

When an unmanned operation was performed at Mt. Unzen-Fugendake, concrete laying control using a GPS occurred in 1995. In 1999 compaction control took place using an GPS.

In this way, when unmanned operation was performed at Mt. Unzen-Fugendake,new technology was introduced proactively, enabling the performance to be confirmed. As a result, the spread of new technology advanced (Figure 8, Figure 9).

Subsequently as well, efforts were made to promote remote operation of surveying equipment, flat plate loading tests, and core boring machines.

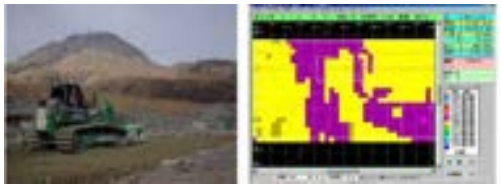

Figure 6. Management of an leveiing

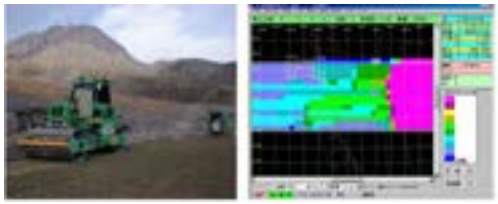

Figure 7. Management of an compaction

Figure 8. Remote control type measure equipment

Figure 9. Measuring machine of a remote control type bearing power of groun

3 Information transmission base of a new technology

Building of becoming of the unmannedness was established by a thing such as it develops Unzen Fugendake as a base in various parts of Japan and that technology feeds back into Unzen Fugendake again with a technology.

Also, we used it at an early stage such as compaction control using GPS to verify its performance.

3.1 Whole country spread of building of becoming of the Unmanned Construction Technology

Building of becoming of the unmannedness of an Unzen area makes it the causing place of a nucleus technology, and that technology is developed in the volcanic disaster / landslide disaster of various parts of Japan (figure 10).Also, also, that disaster occurrence form is done to the improvement adjusted to the characteristic of each place to be different respectively.

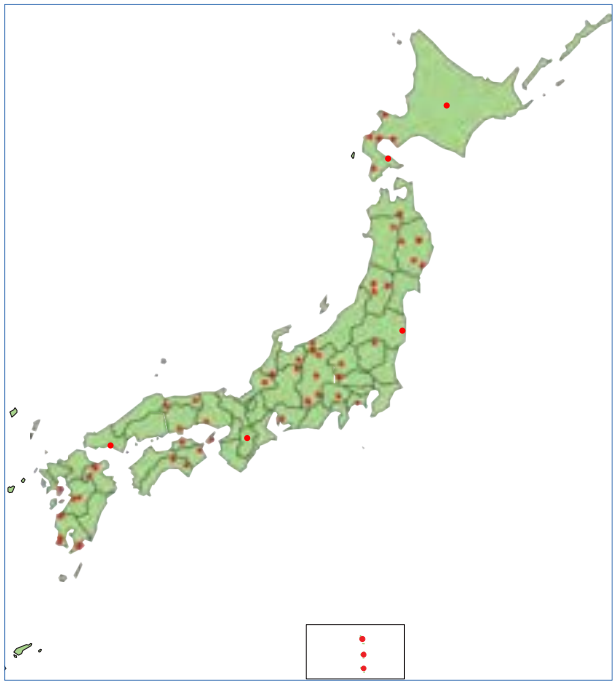

Figure 10. Building of becoming of the unmannedness implemented in Japan

4 Recent situation concerning unmanned operation at Mt. Unzen-Fugendake

Preparation of a sand arrestation on a dry river bed at Mt. Unzen-Fugendake is advancing, and the object of unmanned construction also changes. Very recently, this work consists of reinforcement work for existing sand arrestation facilities. Compared with the previous operations, it can be seen that this work is carried out on a narrow working area. When carrying out unmanned construction in the applicable zone, technology will be updated.

A description of the latest technology is set out below.

4.1 Construction technology

The most up-to-date technology is used. at Mt. Unzen-Fugendake.

4.1.1 Machine control bulldozer

An operation guidance system is provided as standard. Regarding control of the blade of the bulldozer that determines the quality of the concrete compaction, a automatic control system is used.

4.1.2 Compaction using a Excavator

When performing compaction work in confined spaces, a excavator bucket with compaction equipment was used in order to regulate the compaction time (Figure 11) .

Figure 11. Bucket total firming equipment

4.1.3 Surveying by using TS tracking and electronic reference points

In order to increase the accuracy of UAV surveying, it is necessary to use the altitude points (verification points and evaluation points) inside the measurement points. In order to reduce the number of measurement points inside the prohibited zones, the number of elevation points was reduced by measuring the position of the camera mounting on the UAV, by means of an automatic tracking total station. Regarding the evaluation points, a device that measures the self-coordinates by static conveying, of a remotely operated type construction machine was installed on a remote-operated construction machine. (Figure 12).

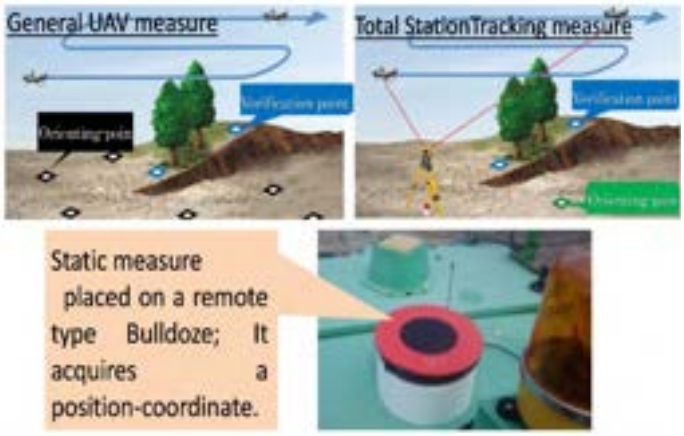

Figure 12. Electronic tacheometer tracking and UAV measure by an electronic reference mark

4.2 Safe watch

When carrying out unmanned construction at Mt. Unzen-Fugendake, it is important to carry out safety monitoring as well. The greatest danger is that of the lava dome collapsing. Consequently, visual monitoring and image monitoring were carried out.

4.2.1 Securing visibility by image clarification processing

Much fog and mist envelope the Mt. Unzen-Fugendake zone, posing an impediment to monitoring. For this reason, image processing was performed to determine whether foggy or misty areas are thin or dense, and also whether the distance is near or far, in order to improve the visibility of misty areas (Figure 13).

Figure 13. Securance of the visibility by processing of becoming of the image clearness

4.2.2 Obtaining an early grasp of an earthquake

There is a danger of the lava dome collapsing due to an earthquake. For this reason, an integrated type quake detection system has been installed in the operation room to permit earthquake monitoring (Figure 14).

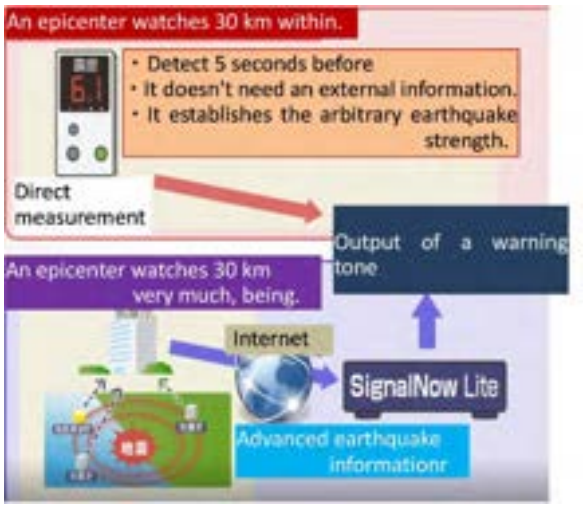

Figure 14. Earthquake watch

5 Conclusion

Even after the eruption of Mt. Unzen-Fugendake, Japan has been fraught with many disasters such as the eruption of Mt. Usu, the Mid-Niigata Prefecture Earthquake, the Iwate-Miyagi Inland Earthquake, and the Great East Japan Earthquake. As a result of the adoption of unmanned constructions, the regions concerned quickly recovered from the disasters.

In this way, unmanned construction enabled quick action to be taken for all disaster regions in Japan. This is because even after the end of the test field system, unmanned operation was performed continuously at Mt. Unzen-Fugendake, and also because efforts were made to realize performance improvement. Also, in recent years, informationalization construction as well is used in advance at Mt. Unzen-Fugendake enabling the performance to be confirmed. It also performs an important role with respect to new technology in the construction zone at Mt. Unzen-Fugendake.

However, at Mt. Unzen-Fugendake, there still exists the danger of an avalanche due to the collapse of the lava dome, and also apprehension concerning the possibility of the disappearance of the unmanned construction jobsite when the scheduled sand arrestation facility is completed.

Japan, from its national land consisting of location, terrain, geology, and also its natural conditions, is considered to be a fragile land from the viewpoint of natural disasters including earthquakes, typhoons, and localized torrential rain. It is also considered that the securing of a providing ground for unmanned construction, which is effective technology for recovery from a disaster, is important for to the future development of civil engineering.

References

[1]UnzenRestoration Project Office. *Proiect Outline Striving Toward a Disaster-Resistant Country*:3-4, 2011

[2] Takashi Yamaguti. It takes for a countermeasure for the Tarumaezan volcanic explosion urgency decrease disaster. In *Erosion control and riparian work Vo.47*;Pages 47-50,2014.4

Remote Control Demonstration of the Construction Machine Using 5G Mobile Communication System at Tunnel Construction Site

Ken Takai [a], Hiroaki Aoki [a], Yusuke Tajima [b] and Michinobu Yoshida[c]

[a]Technology Center, Taisei Corporation

[b]Advanced Technology Department Division, SoftBank Corp.

[c]Kanamoto Co., Ltd

E-mail: takai@bcd.taisei.co.jp, aoki-h@ce.taisei.co.jp, yusuke.tajima@g.softbank.co.jp, yoshida@kanamoto.co.jp

Abstract –

Since March 2020, 5G has been commercialized mainly in urban areas in Japan, and 5G communication infrastructure demonstration tests are actively conducted among various industries such as telecommunications carriers and construction industries.

The authors installed a portable 5G base station close to tunnel portal in "Subcontracting for research and study of technical conditions, etc. for a fifth-generation mobile communication system (Hereafter, 5G). This can handle simultaneous connection requests from various terminals" (Hereafter, 5G demonstration experiment) of the Ministry of Public Management, Home Affairs, Posts and Telecommunications in fiscal 2019, and constructed a high-quality radio wave environment in the tunnel pit, and carried out various experiments to improve working environment such as safety.

This paper describes an experiment in which a long-distance running and lifting work of a construction machine succeeded by remote control, while a high quality radio wave environment was constructed in a tunnel construction site by 5G, and clear multiple images which can surely carry out remote control, and other support information were acquired.

Keywords –

fifth-generation mobile communication system(5G); construction machinery; remote control

1 Summary

Standardization of the next generation mobile communication standard (Hereinafter abbreviated as "5G") is advanced in 3GPP (3rd Generation Partnership Project) which decides the world standard of the mobile communication.

5G can realize high speed and large capacity (eMBB: enhanced Mobile Broadband: up to 10 Gbps or higher), ultra-low delay (URLLC: Ultra-Reliable and Low Latency Communications: One-way transmission delay of 1 ms or less), and multiple simultaneous connections (mMTC: massive machine type communication: 1 million devices/km^2), and is expected to be used not only in conventional communications not only for smartphones but also in various industrial fields [1].

In recent years, there has been a strong movement to improve productivity at construction sites through ICT (information and communication technology) based on the "i-Construction (i-Con)" advocated by the Ministry of Land, Infrastructure, Transport and Tourism. Many IoT and ICT equipment easily used on site, have been introduced and put into operation.

However, even before i-Con was proposed, there was a method using IoT and ICT, which is the focus of this paper, unmanned construction by remote control of construction machinery (Figure 1).

Figure 1. Status of unmanned construction

This method is used at the restoration of natural disasters and in severe places such as radioactive environment, etc., where safety is concerned when person enters and work, and using radio-controlled construction machines communicating by radio and camera images for confirming the construction situation. Therefore, the construction of wireless infrastructure is a very large technical element for this method.

If radio-controlled construction equipment cannot be operated smoothly due to the quality of the wireless infrastructure, or if the quality of camera images for acquisition of construction information is deteriorated, the construction efficiency is affected and construction becomes difficult. Therefore, the present unmanned construction is often carried out in the range of about 150 m in which radio wave surely reaches by utilizing Wi-Fi, etc.

Unauthorized and inexpensive Wi-Fi is said to have a considerable merit, but in reality, there are not many works that can be done within the range of one Wi-Fi communication device.

Even if authorization is necessary, infrastructure which can stably communicate in a wide range will be required in future. Therefore, the experiment was also carried out from the viewpoint of whether the new communication means of 5G can become the communication infrastructure for the remote control of the construction machinery.

Figure 2. Image of remote control

2 Outline of experiment and demonstration site

The Japan islands are divided into the Pacific Ocean side and the Sea of Japan side by chain of mountains. Population tends to be concentrated in lowlands on the sea side and basins in mountains.

Because 70% of the land is mountain and hilly land occupy geomorphologically, the transportation infrastructure between cities in the lowland and basin passes through the mountain.

Since old times, the transportation network has been constructed by cutting down the mountain. In recent years, transportation networks in mountainous areas have been disrupted by disasters caused by abnormal weather.

Losses due to these disasters have social and economic impacts not only on damaged transportation infrastructure facilities but also on the isolation of regions. Therefore, it is highly necessary that the tunnel is newly constructed or improved as a review of the transportation network

The reason we selected "tunnel" is because 1) we thought that tunnels are indispensable infrastructure for modern society as railway transportation infrastructure such as subway and life infrastructure such as water supply and sewerage; and 2) important as social capital in urban areas.

Since the radio wave has the property of reflection and transmission, we thought that it was interesting in the aspect of how much radio wave reaches by repeating reflection and transmission in the tunnel environment.

From such background, this experiment was carried out on a subject of "tunnel", assuming actual possible phenomena, and considering to propose a solution. As shown in Figure 3, it is assumed that a site survey and response are carried out when an inaccessible place occurs in a tunnel. A 5G base station is installed near the entrance (Hereinafter, the pit mouth) of the tunnel, and radio waves are outputted toward the tunnel pit. We decided to carry out remote control of the construction equipment within the range of radio waves.

At present, when such a situation occurs, preliminary investigation and consultation with experts are carried out as much as possible, but there are cases in which eventually carried out by human power. In the future, these cases should be avoided from the viewpoint of worker safety, and they should be dealt with by IoT/ICT or 5G communication technology. This experiment is considered to be a practical use case.

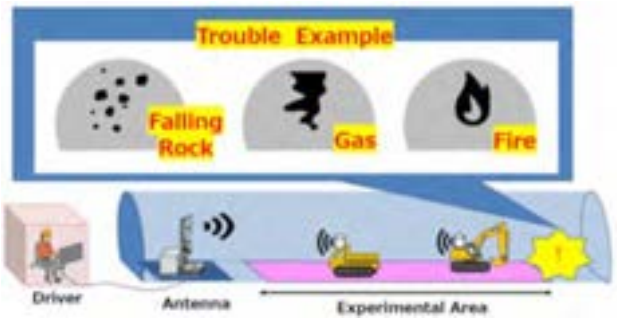

Figure 3. Outline of this experiment

In the experiment, we mainly carried out the following two points.

1. 5G radio wave propagation characteristics (reach distance)
   A 5G radio base station was installed near the tunnel portal to the face, and determined the experimental area by measuring where it reaches in the tunnel.

2. Remote operation of construction machinery The remote control of the construction machine was carried out in the experimental area. (4-ton class crawler carrier and 12ton class hydraulic excavator

2.1 Experimental Location

Project names: Hokkaido Shinkansen Line, Shiribeshi Tunnel (Ochiai)
Owner: Japan Railway Construction, Transport and Technology Agency (JRTT)
Contractor: Taisei, Sato, Tanaka, Horimatsu JV
Construction period: March 26, 2015 - June 24, 2022
Main construction: Tunnel excavation 4,865 m (Standard cross section: 65 m2)

2.2 Use of portable base stations

In conventional mobile communications, in order to deal with data communication traffic of mobile phones such as smart phones, base stations are often installed mainly from urban areas where the number of users is large. On the other hand, in 5G, by utilizing the features of eMBB, URLLC, and mMTC, it is considered that IoT (Internet of Things) will become the mainstream along with smartphone.

However, when it is applied to IoT, not only in urban areas but also in suburban areas where the number of users is relatively small, a large amount of traffic processing will be periodically required. Construction sites are one of such IoT use cases, but constructing new base stations in suburban areas requires more time and cost than constructing in urban areas.

In this experiment, we used a portable 5G base station developed by Softbank Corporation, which can construct a local 5G communication infrastructure (Figure 4). In this base station, not only antennas and radios but also core equipment in the data center can be arranged in the field. Therefore, in the field, the collected data can be processed at high speed and in a complicated manner.

And, if prior adjustment such as license application is completed, 5G communication area can be rapidly developed in a few days, and will be suitable network solution for the development of IoT to the suburb.

Figure 4. Portable 5G facility installed in the tunnel (4.85 Ghz, 120 W).

2.3 Use of on-board remote-controlled robots

For the remote control, we used the construction machine mounted remote control robot (hereinafter referred to as Robot) developed by Kanamoto Co., Ltd. The experiment was carried out by mounting this robot on each of the two construction machines mentioned above.

The robot is a humanoid twin-arm bipedal robot (Figure 5) with the total length of about 1.5 m and the weight of about 20 kg, which can be installed in the operator's seat of a construction machine. (conversion to radio-controlled equipment). By transmitting the image mounted on the construction machine in real time from the driver's viewpoint and transmitting the state of inclination and vibration of the vehicle to the driver's seat bilaterally, the system is capable reproducing the driving remotely feeling close to the real machine.

In addition to such reproducibility, it is highly possible to respond more quickly than the method of procuring radio-controlled construction machinery with limited number of units. For the construction site, there is an economical merit that the construction machinery in the site can be utilized. In this experiment, it was also the first execution to control the Robot by 5G communication in the environment in which the visual observation was not effective at all.

Figure 5. Robot

2.4 Use of Human Body Detection Cameras

There is a report from advanced driver-assistance systems (ADAS) to support the driving operation of the driver of the car that the number of "Rate of contact accidents with people" is decreasing in the cars equipped with "Human body detection system". ADAS is a function to automatically stop a vehicle when a person is detected in a traveling direction by a camera mounted on an automobile, and is an epoch-making technology to improve safety of a driver and a pedestrian.

One of the three major industrial accidents in the construction industry is "construction machinery", and there are many reports of cases in which people and machines come into contact. Taisei Corporation is developing technology to eradicate this disaster.

In this experiment, we plan long distance running by remote control by crawler dump with high rough terrain running performance as an initial action. We also assumed that it was necessary to explore whether there were people left in the tunnel in an emergency. In this experiment, we used a technology that automatically stops construction machinery by sending a stop signal to the construction machinery side when a person enters the movable range of the construction machinery during remote control.

Figure 6. Human body detection camera
(Above: Detected human body)

3 Experiments and Results

Troubles such as “fire”, “toxic gas”, and “rockfall” shown in Figure 3 are supposed in a tunnel pit, which is difficult for a human to approach. For such trouble, the experiment was carried out by the following procedure. (This is an assumption and is not related to the experimental site.)

3.1 Experimental Scenarios

1. Portable 5G base station installed near the tunnel portal

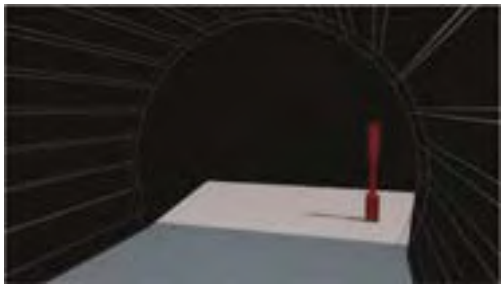

2. Investigation by crawler carrier. In addition to cameras, gas detectors and scanners are installed on vehicles.

3. Since the vehicle has high traveling performance, it is possible to search for long distance while avoiding obstacles

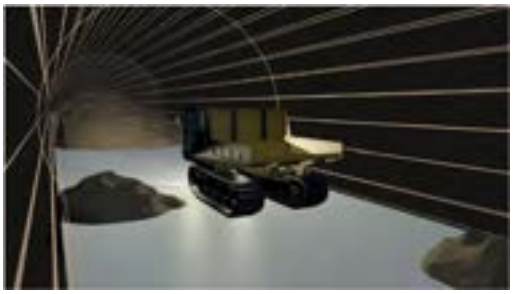

4. A loading machine is installed to remove the obstacle

5. Image of Obstacle Removal

6. Removal completed. go further into

3.2 5G Radio Wave Propagation Characteristics (reach distance)

A radio wave measuring vehicle was used to measure the processing speed (UL side throughput) of the 5G radio wave in the tunnel pit for each distance. The results are shown in Figure 7.

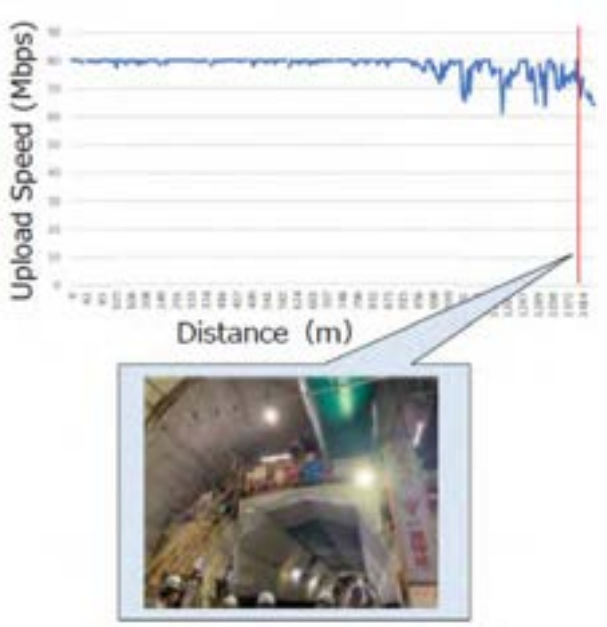

Figure 7. Measured results of the distance reached.

The site had a section including a curve (R = 6,500 m), and it was an environment in which the back side could not be viewed directly, and in addition, it was an environment in which materials and equipment for construction were placed. Therefore, in the preliminary examination, the reach distance of several hundred meters was estimated. However, actually, the radio wave reached far exceeding it. At the 1,400 m point, the "tunnel lining form" which covers most of the tunnel section is located (Therefore, the radio measurement vehicle was

not measured on the face side.), and the processing speed is expected to drop rapidly beyond this point.

3.3 Remote Control of Construction Machinery

Two models shown in Figure 8 and 9 were remotely operated

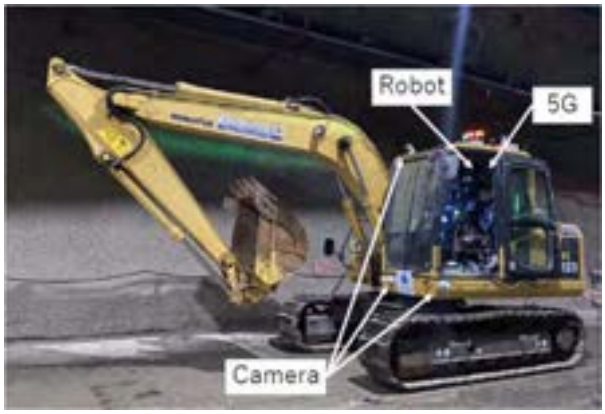

Figure 8. 12ton class hydraulic excavator

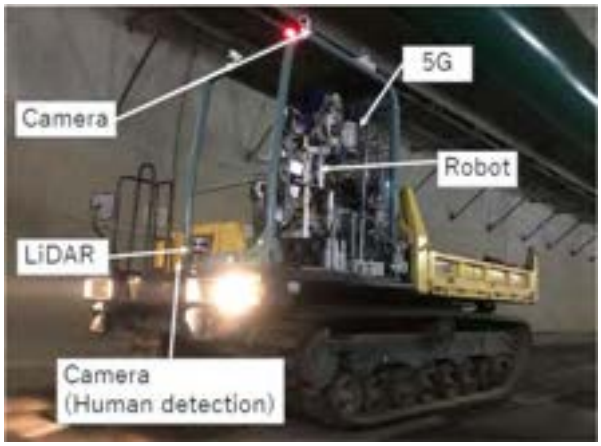

Figure 9. 4ton class crawler career

The remote control which steers while watching the video information is usually carried out by in-vehicle video and bird's-eye view video. However, it is difficult to make a large numbers of birds-eye image acquisition facilities for remote control, because of technical and economic difficulties.

Therefore, in this experiment, by taking advantage of the feature of large-capacity 5G communication, by adding a large amount of sensor information in addition to in-vehicle video as in the past, all remote operation support information was installed in the vehicle, and no birds-eye view video was used (Figure 10).

Figure 10. Remote operation support information

Table 1 lists the remote operation support information for this experiment. Here are two sensors to be noted.

One is the detection of obstacles on the tunnel wall and ahead from the large-capacity point cloud information obtained by sensing with Lidar (Generic 16 Line). The other is the adoption of the human body detection system by AI developed by Taisei Corp.

In both systems, smooth transmission and reception are difficult using conventional Wi-Fi and low-power communication, but 5G communication is possible.

Table 1. List of Remote Operation Support Information.

type	Direction	Units	Capacity (bps)
Vehicle Camera	Up	4	60M
Robot Control	Down	1	40K
Vehicle Vibration	Up	1	40K
Lidar	Up	1	70M
Human detection	Up	1	15M

Each construction machine was able to carry out the following by remote control. Both were successful without birds-eye view (Figure 11).

1. A crawler carrier ran 1,400 m by remote control.

2. 2) Hydraulic shovel: lifted and moved 1ton sandbag by remote control.

Figure 11. experiments

4 Conclusion

The verification of the portable 5G facility was carried out in the tunnel environment this time, following the external environment in fiscal 2018 [2]. From the result, it is considered a communication infrastructure which can be adapted to many construction sites.

In the construction site, the construction is started by improving temporary facilities in accordance with the construction contents. In order to advance the ICT in the construction field, "temporary communication" will be necessary in future, and the possibility that 5G will become highly influential in the selection of the communication radio wave.

The case verified this time is the technology which can be utilized for investigation of tunnel disaster and emergency work even in the present stage, and it is considered to be one of the effective utilization of 5G. We would like to continue our research on the improvement of construction productivity using 5G.

I would like to take this opportunity to thank all of you who are participating in and cooperating with this experiment.

References

[1] ITU-R M. 2083 – 0: "IMT Vision – Framework and overall objectives of the future of development of IMT for 2020 and beyond", Sep. 2015.

[2] Aoki et al., Construction of Construction Production System using (5G) (CHAPTER 1), JSCE Annual Lecture, Sep. 2019

Sea Experiment on Tele-operation System of Underwater Excavator

Tsukasa Kita[a], Taketsugu Hirabayashi[a], Atsushi Ueyama[b], Hiroshi Kinjo[c], Naoki Oshiro[c], and Nobuyuki Kinjo[d]

[a]Frontier technology and engineering Department, Port and Airport Research Institute, Japan
[b]Kyokuto Co., Ltd, Japan
[c] Faculty of Engineering, University of the Ryukyus, Japan
[d]Okinawa General Bureau, Japan
E-mail: mailto:kita-t@p.mpat.go.jp,

Abstract –

We have developed a remote operation support system for underwater excavators and conducted Sea experiments. Underwater excavators have been operated by divers boarding on them. Their main task is levelling rubble mounds of port structures in Okinawa, Japan. However, in recent years, remote control is required due to the decrease in the number of the divers. Therefore, we have been developing tele-operation support system for underwater excavators. This system integrates three elemental technologies such as "Underwater Information Presentation" that serves as a display interface, "Measurement Method of Mound Shape" and "Attachment for levelling works operated with simple input". So far, we conducted elemental tests of each technology underwater and on land to confirm their usefulness.

In this report, we performed experiments using this system in the sea. First, the elemental test of the attachment was performed by boarding operation of divers. The purpose of the attachment is to perform levelling works without difficult input for position adjustments in order to improve the work efficiency of remote operations. The purpose of the tests is to evaluate the performance of the attachment alone. The measurement items are the varies of mound height and the working time. As the results, the attachment was confirmed to be able to submerge the mound and the operability in the sea is the same as that on land. Next, a remote operation test simulating levelling works was conducted to measure the work accuracy and the work efficiency. As the results, by adding a mechanism to move stones to depressions, this system is demonstrated to level the mound from unevenness of ±30 cm to that of ±10 cm. In addition, it is confirmed that the working times with the system depends on the operators' experiences of tele-operations more than that of boarding operations.

From the above, the proposed system is demonstrated to be useful for levelling works of mounds by tele-operated underwater excavators.

Keywords –

Tele-Operation; Underwater Construction; Port Construction;

1 Introduction

Underwater excavators have been adopting for a long time in port constructions in Okinawa, Japan. They are similar in shapes and mechanisms to those on land. However, their hydraulic systems are powered by electric motors. Therefore, they have cables to supply the electric power for the motors from ships. They have been controlled by divers on their cockpits in the sea.

Their main task is levelling works of rubble mounds underlying port structures. They perform the works by pressing the backs of buckets against the mounds or moving stones to depressions (shown in Figure 1).

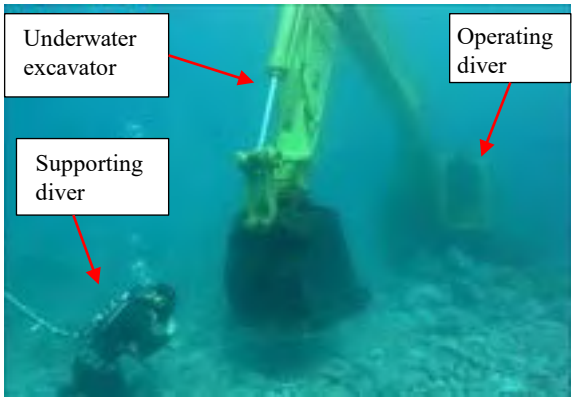

Figure 1. Conventional Levelling work of mound by divers using underwater Excavator

At present, there are two problems. One is that these operations require huge efforts for the safety management. Muddy sea water in construction sites prevents operators from grasping conditions of mounds. Thus, they have to be supported by other divers. The supporting divers change positions of stakes and check unevenness of the mounds. Therefore, they have to stay nearby the vehicles. For this reason, safety checks must be conducted Strictly. Secondary, the work productively is not high due to work suspensions caused by restrictions on dive times or sea conditions. Due to these backgrounds, in order to improve the safety and the efficiently, remote-controlled constructions are required.

Therefore, we have been developing a tele-operating support system for underwater excavators.

2 Tele-operation Support System

An outline of our system is shown in Figure 2.

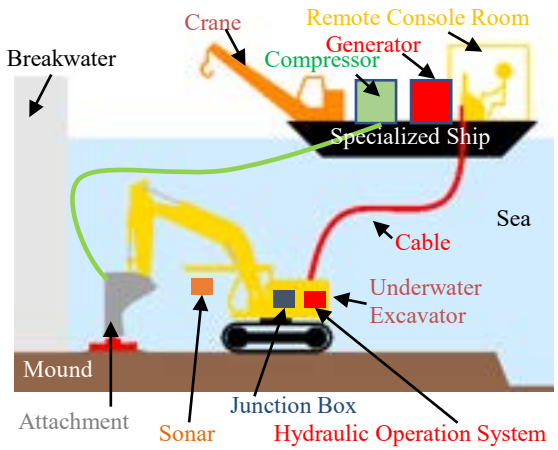

Figure 2. Image of Tele-operation system of underwater excavator

Tele-Operation of underwater excavators is implemented by installing proportional solenoid valves in the pilot hydraulic circuits. Operators use remote consoles on ships, and control the valves by electric signal. Then, the flow rates of the pilot circuits vary and drive the main spool valves. In this way, the flow rates of hydraulic oil are controlled, and operate the hydraulic cylinders.

In addition, we proposed Tele-operation Support System composed of three elemental technologies which are "Underwater information presentation", "Measurement Method of Mound Shape", and "Attachment for levelling works operated with simple input" (shown in Figure 3).

2.1 Underwater Information Presentation

This is an interface that shows work information to remote operators on a ship. It is difficult to visually recognize the position and the orientation of a underwater construction equipment from the ship due to turbidity.

Therefore, the posture of the excavator is calculated with data measured by sensors installed on the vehicle. stroke sensors for cylinders, a gyro sensor, an inclinometer, a geomagnetic compass, a depth gauge, an underwater acoustic positioning device, an encoder etc. are installed (shown in Figure 4).

On the ship, there are a remote console and 3 monitors showing cross-sectional views, bird's-eye views and top views (shown in Figure 5). In addition to them, design information input in advance are also displayed (shown in Figure 6). This allows the operators to work without directly watching the work area in the sea.

So far, an installation test has been performed in actual construction site to verify the robustness of the underwater information presentation alone [1]. In the test, an operating diver ridded on an underwater excavator and performed the conventional levelling work of a mound. The information presentation monitor was installed in the

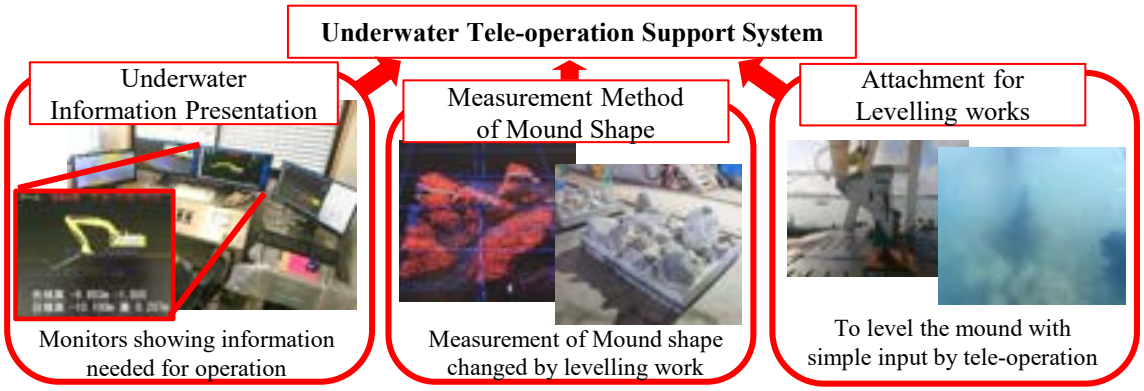

Figure 3. Three elemental technologies for Underwater Tele-operation Support system

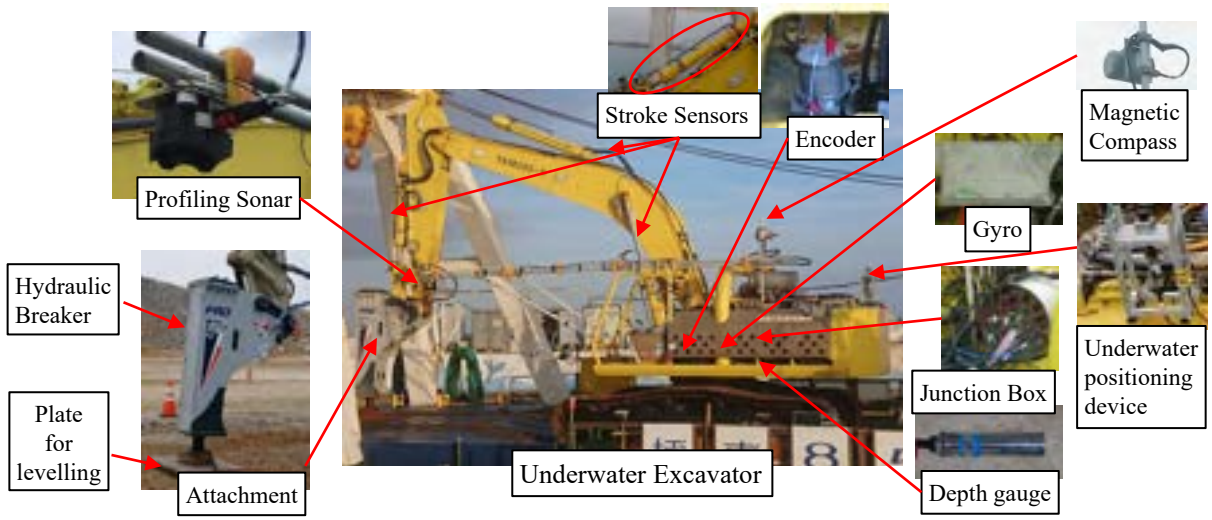

Figure 4. Sensors installed on excavator for underwater information presentation system

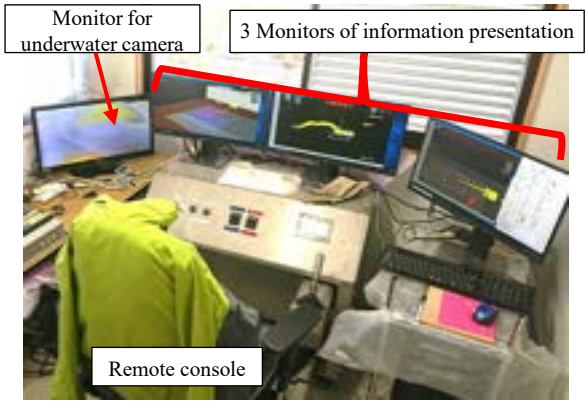

Figure 5. Monitors for underwater information presentation system on remote console room

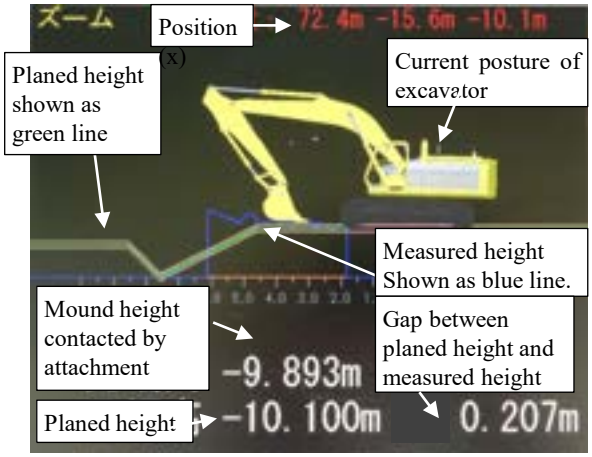

Figure 6. Cross section view of underwater information presentation system in remote console room

cockpit and was used by the diver as a reference for operation. As a result, there was no failure of equipment such as sensors. However, the position measured by the sensor was not correct. The horizontal distance between the ship and the equipment was several meters, but the measured results were often over a hundred meter. This is due to the characteristics of the underwater acoustic positioning system. This system installs a reference station on the ship and a target station on the vehicle. The position is detected by performing triangulation with sound waves between the stations. In this experiment, the sound waves may be blocked by the bubbles from the diver's breathing. Thus, the sound waves may not reach the reference station directly from the target station. At that time, the wave reflected on existing caissons or the seabed may be measured and mistakenly recognized as the direct sound wave. For the reasons, it is considered that the measured values differ from the actual positions. In the experiments conducted in this study, in order to mitigate the effect of bubbles, the installation position of the underwater acoustic positioning system was moved to the rear end of the body.

2.2 Measurement Method of Mound Shape

The height of mounds changes from moment to moment due to the works. Therefore, it is necessary to measure the mound height during the levelling works. We implemented two methods in the system. One is the way using a profiling sonar. Profiling sonars are time-of-flight distance meter using sound waves. Acoustic sensors are less susceptible to turbidity than optical devices such as laser scanners. Therefore, sonars are often used for underwater measurements.

From this measurement, the difference between the mound surface and the target height can be calculated.

The calculation result is shown on the monitors of underwater information presentation and serves as a substitute for the stake. This eliminates the need for the supporting divers to stay in the sea for the staking. This is essential for remote control constructions. In this study, M3 sonar (from Kongsberg Maritime Ltd.) was adopted in consideration of the time required for measurement. The sonar measures the coordinates of 128 points on one cross section up to 40 Hz.

The profiling sonar was installed as shown in Figure 7. The measurements are performed at each time when a certain range end. The sensor was moved with the rotations of the upper part of the excavator to measure the height of the mound surfaces.

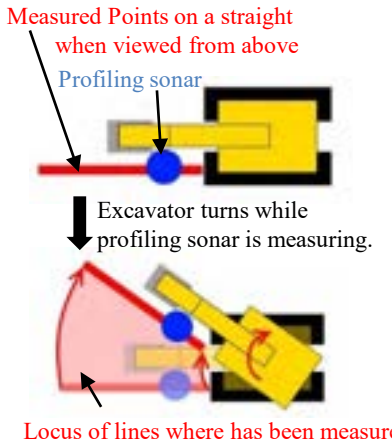

Figure 7. Top view image of position where Profiling sonar installed and the method to measure the height of mound surface

In order to confirm the measurement accuracy, an elemental test was conducted in a water tank [2]. The profiling sonar measured the flat bottom surface of a water tank and mound model in the tank. The mound model was made of rubble stones which are same size as stones of actual rubble mounds in Okinawa, Japan.

As the result, it was apparent that it is possible to recognize the shape of the bottom surface. However, we cannot grasp the contour shape of each stone. This is because the gap between stones could not be measured accurately. In addition, it cannot measure the height under the tip of the arm. Therefore, we cannot judge the completion whether the pressed points get within the acceptable hight. Hence, we examined another way to measure the mound height.

Another method for measuring the height of mounds is to measure by contacting the tip of arms of excavators against mounds. When the attachment is pressed against mounds, the height of the tip calculated by the information presentation system is same as the mound height. It has been shown from the results of previous experiments that this method can measure the mound height with an average error of 31 mm. However, this method can measure only one point in one measurement. Hence, it is not suitable for surface measurement. Therefore, we use the two measurement methods properly depends on the purpose.

2.3 Attachment for levelling work operated with simple input

For the purpose of improving the work efficiency, we examined an attachment that can level mounds without delicate input based on detailed topographic information.

So far, a remote operation test was conducted with a combination of elemental technologies which are "Underwater Information Presentation" and "Measurement Method of Mound Shape". In the test, a stone placed on a flat floor was grasped with a fork grab and moved to a predetermined place. we evaluated the working time depends on the observation method. As a result, it takes 1.8 times longer to perform the work with the profiling sonar, compared with the case of directly visual observation on land. It is considered because the contour of the stone is unclear, and it takes time to perform the operation of positioning for gripping. Therefore, we developed "attachment operated with simple input" for the purpose of improving the work efficiency.

In this system, we proposed a mechanism to attach a plate to the tip of a hydraulic breaker (shown in Figure 4). Not only the static load of the machine, but also the dynamic load of a breaker pushes down protuberances of mounds to perform levelling works. On the other hand, this attachment does not have the ability to raise the lower part than the plan.

An element test was conducted on this device to perform levelling works on a rubble mound installed in the air, to confirm its performance [3]. As a result, it was revealed that the attachment has an ability to level to bring down to the target height from +30cm height.

In addition, we conducted element tests of the proposed attachment in the sea. The purpose of the experiments was to confirm whether the attachment has the ability to level the mound in the sea and the time required for the work. The experiments were carried out at a rubble mound in Hirara Port in Okinawa, Japan. The top surface had a water depth of about 5 m, and unevenness of ±30 cm.

In the experiment, the attachment was equipped on an underwater excavator TKM200-9 (owned by Kyokuto Co., Ltd) whose operating mass is about 20 tons. A diver boarded on and operated it. The diver had experience of controlling underwater excavators in normal tasks. The work was done according to the instructions of an

assistant diver.

The attachment banged the mound for 5 seconds and paused. Then, we measured the mound height. We alternated 5 seconds of beating and measuring for 6 times at the same point. As a result, it was shown that the mound surface could sink 11 cm in 5 seconds and 25 cm in 30 seconds.

In addition, an experiment simulating a continuously work in a range of 2m x 5m was also conducted. In this experiment, we could not recognize the height because we did not stake. Hence, the time for each impact was fixed at 5 seconds. The assisting diver instructed the banging position and the posture of the front part (arm, boom and bucket cylinder). As the result, the working time was the same as the land test if supporting divers guided them. It was confirmed that no deterioration in operability in the sea due to the attachment was observed.

3 Performance test of the remote-control support system in the sea

In order to examine the performance of the remote-control support system, performance tests were conducted in the sea (shown in Figure 8). The experiment was carried out at a caisson mound at Hirara Port. The top is about 8.7m deep. The working areas were 5m x 7m areas on the top of the mound. In the initial state, the top of the mound had unevenness of about ±30cm from the target height. The target of the works is to level unevenness within ±10 cm in the working area.

In the levelling works, the attachment banged a point of the mound until the height gets within the acceptable height. The operator confirmed the completion by watching the cross-sectional view showing the hight of the tip of the attachment contacting with the mound. After that, the attachment was moved to another unlevelled point. The layout is shown in Figure 9. The work procedure is shown in Figure 10.

Figure 8. Captures of sea experiments (left figure; Excavator craned into the sea, right figure; Excavator working without divers on cockpit)

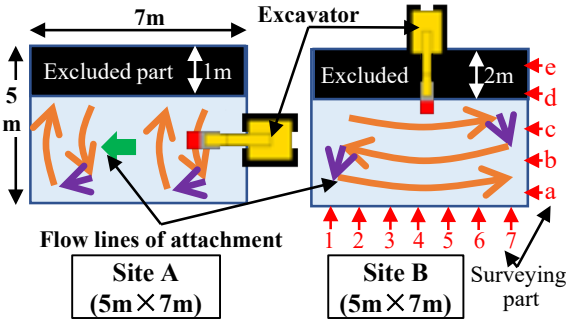

Figure 9. Layout of levelling tests of Site A (left figure) and Site B (right figure)

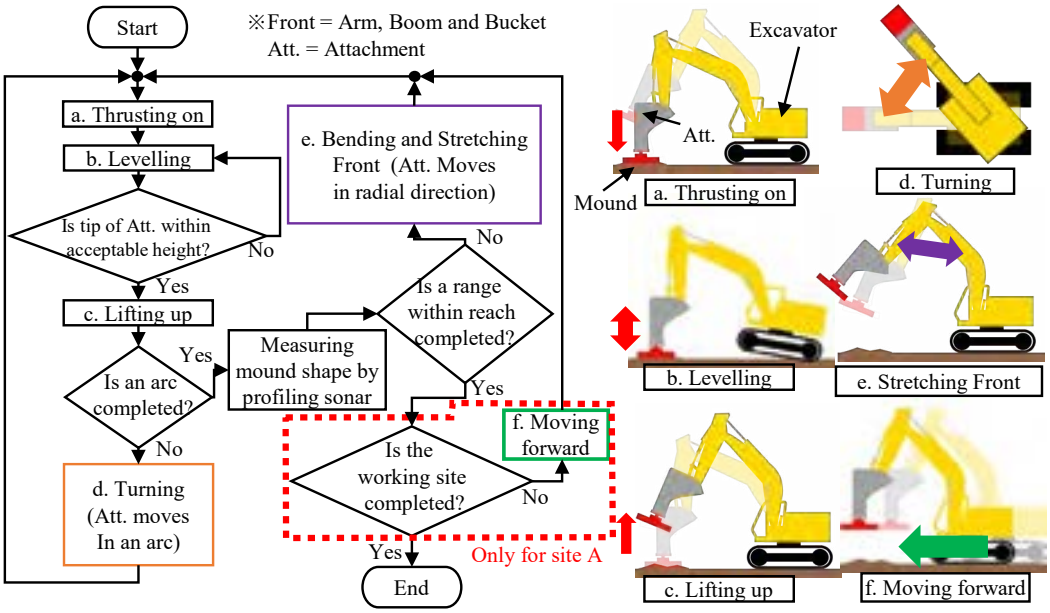

Figure 10. Procedure of levelling tests of mound using tele-operated underwater excavator

The right part of Site A was over 30cm higher than the target height in the initial state. Therefore, it was not possible to make it sink to the target height with the attachment. Therefore, the range was excluded from the evaluation of the work efficiency. On site B, a range in front of the vehicle was excluded from the evaluation. This is because it was out of the working range of the arm.

In Site A, the test is performed by an operator who is an underwater excavator operator and has no remote-control experience. On the other hand, an operator on Site B is not an operator boarding on underwater excavators, but has experiences of remote operations.

3.1 Accuracy of Mound Height

From the results, we assessed the accuracy of the mound height after the works. Before and after the experiment, the mound height was measured by divers using an underwater levelling instrument (shown in Figure 11). Figure 12 and Table 1 show the hight of the Site A after the test. The grey cells in the table are the excluded part. As the results, some points that were higher than the acceptable range remained. The point in yellow circle in Figure 12 is because the initial height was +40 cm from the target. Thus, the attachment could not enough subduct. The part shown in the red circle is because the operator did not bang there due to misunderstanding that it was out of the working range.

Figure 11. Captures of measurements before (left figure) and after (right figure) experiments

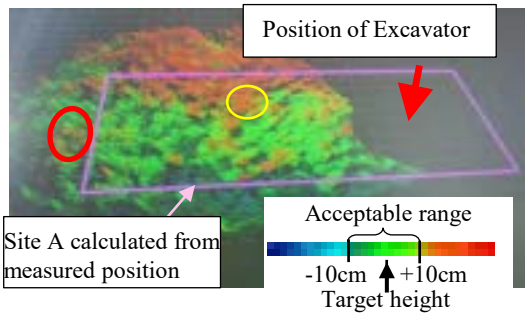

Figure 12. Bird-view of the Site A after experiment shown on monitor of "Underwater Information Presentation"

Table 1. Unevenness from target height surveyed after experiment on Site A

Height [cm]	7	6	5	4	3	2	1
e	23	12	22	21	8	20	25
d	19	10	6	20	5	-2	7
c	14	7	2	-5	-5	6	7
b	2	10	2	4	-3	5	10
a	1	-2	6	-9	9	0	5

The misunderstanding was caused by the measurement error of the horizontal position of the vehicle. That can be dealt with by setting a larger construction range.

In addition, the average height is 0.03m higher than the planed height and the deviation σ was calculated to 0.05m excluding the points in the red and yellow circles. If the mound shape after the work has a normal distribution, 68 % of the mound is within 1σ (-0.02m to +0.08m) in height and 95% of that is within 2σ (-0.07m to +0.13m).

On Site B, 3 survey points were measured -10cm or lower than the planed height. Table 2,3 show the measured height by divers before and after the experiments. Figure 13 shows that measured by the profiling sonar.

The points in black circle in Figure 13 are a missing measurement. The initial height is so low that the sonar cannot measure it hiding behind the rock in front. The points in yellow circles are considered to be the result of striking too much.

Table 2. Unevenness from target height surveyed before experiment on Site B

Height [cm]	7	6	5	4	3	2	1
e	17	30	5	13	28	18	42
d	-6	62	52	32	18	24	22
c	32	31	38	13	38	6	-18
b	-6	35	36	-1	13	33	27
a	-4	24	11	38	21	29	42

Table 3. Unevenness from target height surveyed after experiment on Site B

Height [cm]	7	6	5	4	3	2	1
e	17	34	21	11	30	16	27
d	-11	38	42	29	18	22	5
c	-12	1	-3	6	-1	-10	-17
b	-18	0	0	-2	-15	-5	-1
a	-9	-6	-2	0	-8	2	-2

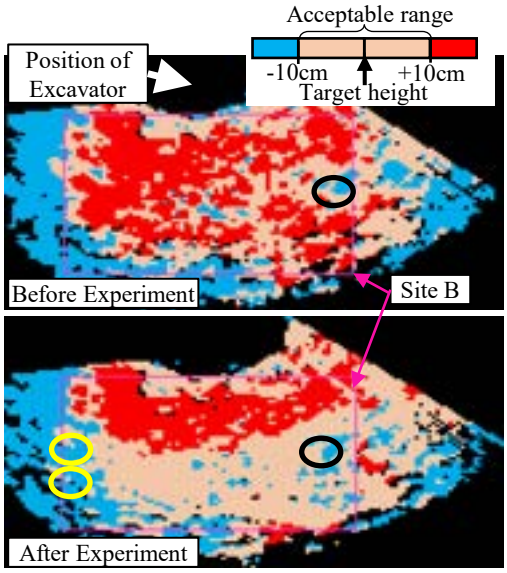

Figure 13. Top view of mound height on Site B measured by profiling sonar before (the upper) and after (the lower) experiment

Since the attachment has only a mechanism that depresses mounds by vibrations, it is necessary to install another function that raises depressions. If the out-of-range points are excluded, the average height is 0.02 m lower than the planed height and the deviation σ is 0.04 m. It means that 95% of the mound is within the range of -0.09 m to +0.05 m in height.

From the results, by taking above measures, underwater excavators with the tele-operation support system seems to have enough performance to level the unevenness of the mounds within ±10 cm from that within ±30 cm.

3.2 Working time

We investigated the work efficiency of the remote operation. The working times in the tests were decomposed into that of each input action. The working time was analysed from the video movie which recorded in the remote-control room on the ship. Figure 14 shows the working times of each items to level one point off.

In the experiment on Site A, the working time was 44 minutes 33 seconds for the work area of about 28 square meters. There are 34 points banged by the attachment, and 0.82 square meters are levelled once.

Site B had the work range of about 21 square meters and had a work time of 20 minutes 39 seconds. The number of banged points is 29, which averages 0.72 square meters.

As the results, the working times of A were longer than that of B in all items. It is considered that the effect of "training for tele-operation" is larger than that of "training of operation of underwater excavators itself". This difference is considered to be due to the fact that the operator engaged in remote operations had empirically predicted and recognized the movement of the equipment with respect to the lever input amount.

In addition, we compared the working time of the boarding-operating work with the supporting diver written in Section2.3. The working times to level depend more strongly on the conditions of the mounds than on the operation method. Therefore, the times of levelling were not taken into account to compare them. Tele-operation support system with highly trained operators was demonstrated to be able to increase the efficiency of the levelling works.

The tele-operating works by operators with great experience of tele-operation is faster than the boarding-operating works in the tests.

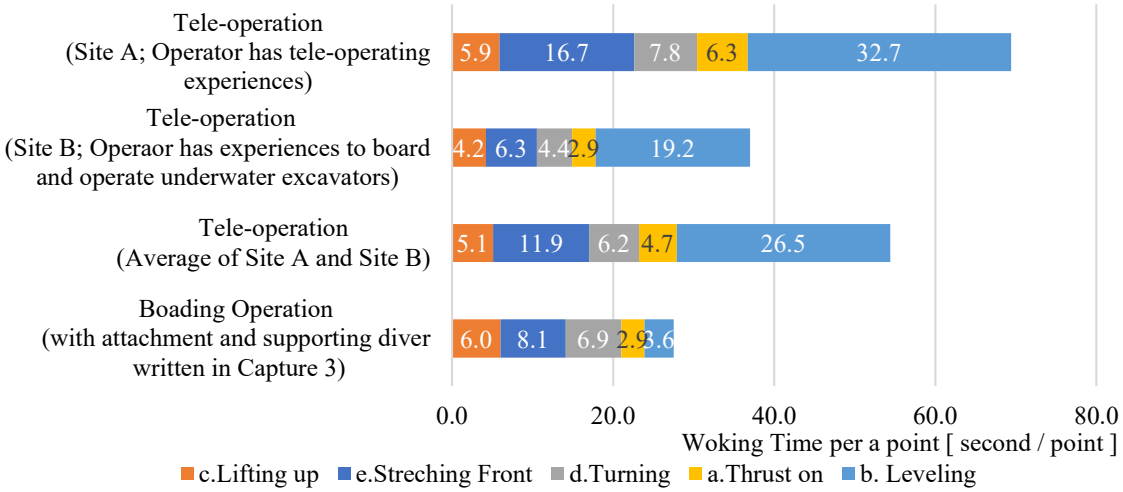

Figure .14 Working times of levelling works using underwater excavator

4 Conclusion

In order to improve the safety and the productivity of underwater constructions, we conducted the study and the sea experiments on remote operation of the underwater excavators.

We proposed a remote operation support system made up of the three elemental technologies. The elemental technologies are ”Underwater Information Presentation,” "Measurement Method of Mound Shape" and "Attachment for levelling works operated with simple input".

In order to assess the performance of the remote-control support system, we conducted the sea experiments simulating the levelling works on the mounds in the sea. The results are shown below.

- The proposed attachment has the ability to level the unevenness of rubble mounds in the sea. The performance to depress mound height was 11 cm in 5 seconds, and 25 cm in 30 seconds.
- Turbidity caused by the attachment is not more terrible than that of conventional works.
- For 28 survey points on Site A, there were 3 points of +10cm or higher than the planed height. Taking measures that set larger work ranges than the target may get rid of the remaining caused by the error of measured position of the vehicle.
- On Site A, the average height was 0.03m higher than the planed height and the deviation σ was calculated to 0.05m without exceptional points.
- For 21 survey points on Site B, there were 3 points of -10 cm or lower than the planed height. It is necessary to add another mechanism to move stones to places whose height are low.
- Excluding exceptional points, the average height after the tests on Site B was 0.02 m lower than the planed height and the deviation σ was 0.04 m.
- Working time was 65 minutes 12 seconds for the total work area of about 49 square meters, which was 45.1 square meters per unit time.
- When the operator with remote-operating experiences performed the simulating task with remote-operating system, the working time is shorter than that performed by the operator with the conventional boarding work. The work efficiency by remote-control is considered to depend on the skill level of the operator.
- By improving the attachment, remote-operated excavators are demonstrated to be able to level unevenness of the top surface of mounds within ±10 cm in the sea.

As the next step, we plan to study and sea experiments on an attachment to move stones into lower place than planed mound.

References

[1] Hirabayashi T., Kita T., Yoshie M., Ueyama A., Suzuki M., Kinjo H., Oshiro N. and Kinjo N. Examination of Adaptation of Information Presentation System for Underwater Excavator. The 18th Symposium on Construction Robotics in Japan, O3-3, 2018.

[2] Hirabayashi T., Kita T., Yoshie M., Ueyama A., Suzuki M., Kinjo H., Oshiro N. and Kinjo N. Development of Tele-operation System for Underwater Excavator～Addition of profile sonar for mound measurement～. The 19th Symposium on Construction Robotics in Japan, O3-2, 2019.

[3] Kita T., Hirabayashi T., Yoshie M., Ueyama A., Suzuki M., Kinjo H., Oshiro N. and Kinjo N. Development of Tele-operation System for Underwater Excavator ～ Support Device using Hydraulic Breaker～. The 19th Symposium on Construction Robotics in Japan, O3-3, 2019.

Automation and Operation Record of Large Overhead Crane for Segment Transportation

Yasushi Nishizaki [a], Koki Takahashi [a] and Takashi Fukui [a]

[a]Tokyo Outer Ring Road Main Tunnel, South Route, Tomei North Project, Kajima Corporation, Japan
E-mail: nishizay@kajima.com, koki@kajima.com, fukuita@kajima.com

Abstract –

The wall of the shield tunnel body is made by assembling panels called segments into a ring shape. For the segment transportation in this site, quick, accurate and safe operation is required in each device mainly using a crane. However, in recent years, it is difficult to secure human resources due to the aging of skilled workers, and automation of segment transport equipment has become an urgent issue.

In this paper, we decided to work on automation of a 40t large overhead crane. The focus of this effort was to investigate an automatic gripping device that can handle various types of segments with different shapes, to study the selection and arrangement of sensors that achieve both high-precision positioning and fail-safe functions, and to efficiently use segments in narrow spaces. This is the construction of a management system using a color code for transporting to a computer.

As a result, the number of workers was reduced by automatic operation, and rework due to human error in selecting the carry-in / carry-out segment was eliminated, and productivity was improved through labor savings. In addition, it eliminates damage to the segments due to erroneous operations and contributes to ensuring quality.

Keywords –

large overhead crane (load limit:40t);
Autonomous conveying technology;
underground expressway construction site

1 Introduction

In this work, the main line tunnel is being constructed from the intersection of the Tomei Expressway and the Nogawa River in Okura, Setagaya-ku to Inokashira-dori, Kichijoji, Musashino-shi, as part of the Tokyo Outer Ring Road extending from the Kan-Etsu Expressway to the Tomei Expressway, by the EPB shield tunneling method (Figure 1). This work is characterized by a large section (outer diameter: 16.1 m), long distance (9 km), and high-speed excavation.

The walls of the shield tunnel body are made by assembling panels called segments in a ring shape. At the construction site, segments are carried mainly by using cranes, which requires quick and accurate operation. In recent years, however, the aging of skilled workers has made it difficult to secure human resources, so there is an urgent need to automate the cranes. Therefore, this project worked on the automation of 40t large overhead cranes to be used for carry-in, storage, and carry-out of segments in the segment stockyard. This paper reports on how this project was planned and the actual operation results.

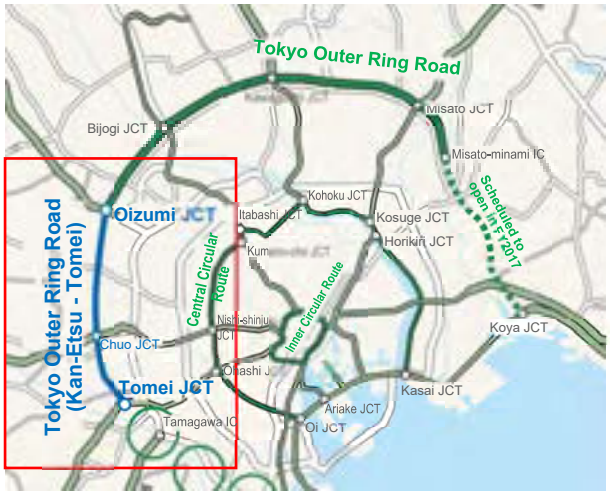

Figure 1. Map of construction location

2 Construction Overview

2.1 Overall Construction Overview

Construction name: Construction Work of the Tokyo Outer Ring Road Main Line Tunnel (Southbound) Tomei Expressway North Route
Orderer: Tokyo Outer Ring Road Construction Office, Kanto Branch, East Nippon Expressway Company Limited

Contractor: Specific Construction Work Joint Venture of Kajima, Maeda, Sumitomo Mitsui, Tekken, and Seibu
Construction area: from Okura, Setagaya-ku, Tokyo to Kichijoji Minami-cho, Musashino-shi, Tokyo
Construction outline

- Section size
  Outer diameter of tunnel: φ15.8 m
  Inner diameter of tunnel: φ14.5 m
  Outer diameter of shield machine: φ16.1 m (largest in Japan)
- Excavation length: 9,155 m
- Construction method: EPB shield tunneling method
- Horizontal alignment: R = 643 m (minimum)
- Earth covering: 38.3 (at the riverbed of Nogawa River) to 55.7 m
- Longitudinal slope: 0.3 to 1.5%
- Cross Passage: 5 locations
- Underground junction: 1 location

2.2 History of Introduction of Automated Overhead Cranes

A multi-shelf automated warehouse is an example of equipment that automatically carries segments in and out. Such warehouses are well-proven and technically established, but if used in construction work that handles large segments such as this project, the following problems arise:

1. The multi-shelf warehouse for large segments requires a large frame structure and consequently large support piles, which increases the construction period and cost.
2. The large frame structure also reduces the advantage of a small footprint of the multi-shelf warehouse.
3. The equipment (a stacker crane) cost is also high (about 2.5 times that of an overhead crane) because it handles heavy loads.

An overhead crane can move freely in three dimensions and function equivalently to a multi-shelf warehouse. Since the overhead crane does not require any special structure, it can shorten the construction period and reduce the cost, and is highly applicable to other similar construction works. Therefore, although it was an unprecedented attempt, this project worked on the automation of overhead cranes as equipment that can automatically carry in and out even large segments instead of a multi-shelf automatic warehouse.

2.3 Segment Overview

In this project the tunnel is constructed by using segments of different materials and widths depending on the purpose and conditions at each location. Over 70,000 segments must be brought in to construct a total of 5,676 rings over the total tunnel length of 9,155 m (Table 1)

Table 1. Segment overview

RC segment		◆ Reinforced concrete structure ◆ Has high rigidity and excellent compression resistance and durability; Used for standard sections across the entire tunnel Number of rings: 4,247 Number of divisions: 13 pcs/ring Weight: Approx. 10 ton/pc
Composite segment		◆ Hybrid structure of steel and concrete ◆ Used in areas where high-rise buildings causing high loads may be constructed Number of rings: 628 Number of divisions: 13 pcs/ring Weight: Approx. 11 ton/pc
Steel segment		◆ Box structure made of steel plates ◆ Used for lateral connecting galleries requiring openings and underground widened sections that need to be cut to be removed Number of rings: 801 Number of divisions: 13 or 14 pcs/ring Weight: Approx. 5 ton/pc

2.4 Overview of Segment Stockyard

Figure 2 and 3 show the workflow from carry-in to carry-out in the segment stockyard.

Segments are transported by trailer, and then picked up, carried in, and stored in the segment stockyard by the overhead cranes. In order to prevent the load from collapsing during transportation, the segments are stacked in only two tiers. In the stockyard, however, segments are stacked in four tiers in principle, and so three rows are used for one ring. In the tunnel, since a precast RC invert is to be installed when assembling segments, it is efficient to also carry in and store RC inverts in the segment stockyard and carry one out together with segments. Therefore, a RC invert storage area is also provided in the segment stockyard. The stockyard as a whole can store segments for 10 rings and RC inverts for eight rings (Figure 4).

Segments stored in the segment stockyard are picked up by the overhead cranes and placed on a temporary receiving pedestal (hereafter, “temporary receiving setter”) to be carried out. The segments placed on the temporary receiving setter are transferred to a transport carriage to be carried into the tunnel. Once the segments are carried out of the segment stockyard, their order cannot be changed in the tunnel. Therefore the segments must be carried out in the order of assembly.

Table 2 shows the mechanical specifications for the overhead crane body. Two overhead cranes are installed in order to shorten the cycle time by alternately carrying in and out segments, eventually enabling high-speed excavation (Figure 5).

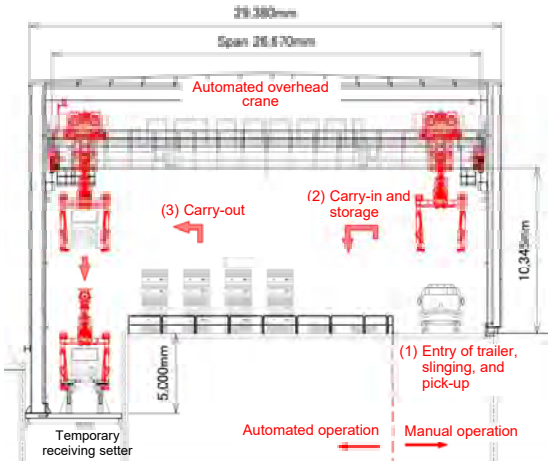

Figure 2. Carry-in/out of segments using overhead cranes

Table 2. Mechanical specifications for overhead crane

Item		Specifications
Rated values	Load	40 t
	Hoisting speed	0.172 m/s
	Traverse speed	0.417 m/s
	Travel speed	0.417 m/s
Wire rope		Type B: IWRC 6 × Fi (29) 8 hooks × 20 mm
Construction	Span	26.67 m
	Crane girder length	27.17 m
	Lifting height	14.25 m
	Crane girder height	10.345 m
Motor	For hoisting	2 × 45 kW
	For traverse motion	2 × 2.2 kW
	For traveling	2 × 5.5 kW
Drum	Hoisting drum	PCD φ540 mm
Sheave	Hoisting sheave	PCD φ558, 400 mm
	Equalizer sheave	PCD φ400 mm

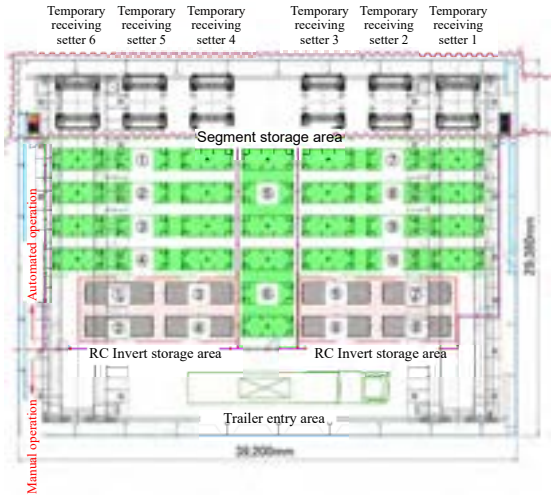

Figure 4. Plan view of segment stockyard

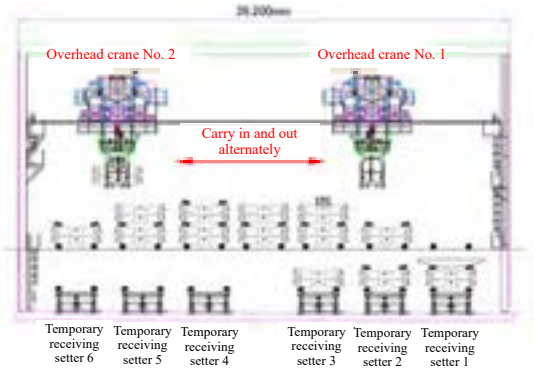

Figure 5. Vertical section of segment stockyard

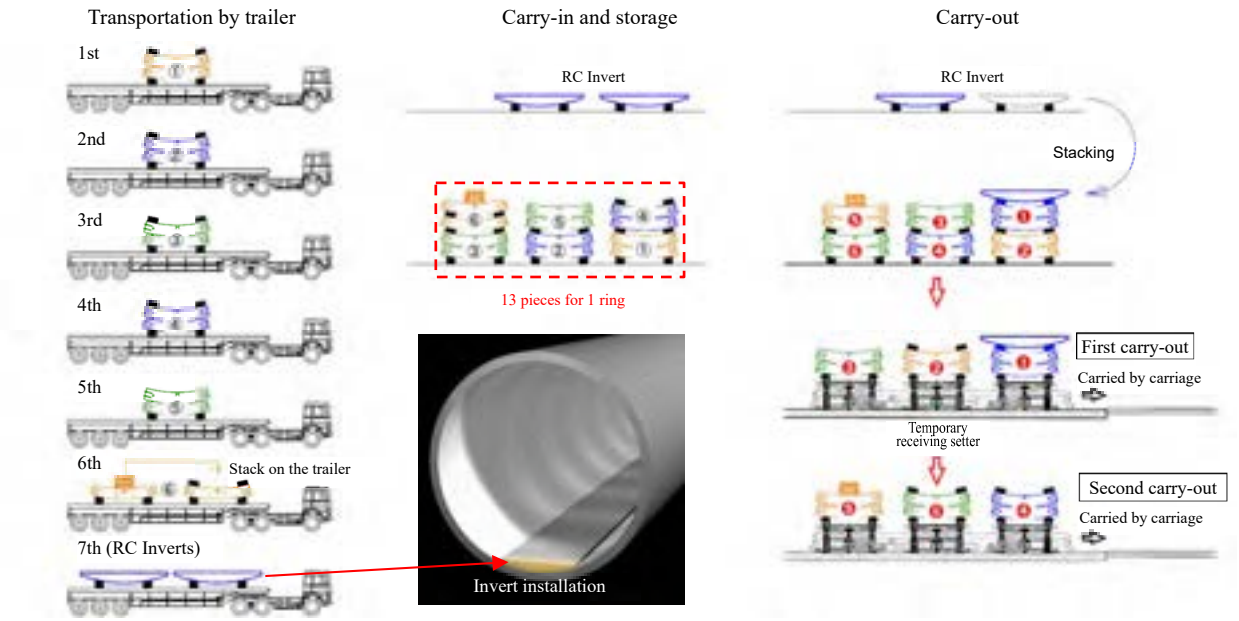

Figure 3. Workflow from carry-in to carry-out in segment stockyard (for one ring)

3 Automated Equipment

3.1 Overview of Automated Cranes

3.1.1 Scope of automation

This time, segments are picked up manually from trailers. This is because there are various shapes of trailers and segments and therefore positioning is difficult, and also the segments brought in by trailers must be checked for damage, requiring human intervention.

After segments are picked up and moved to the storage area, carry-in, inventory management, and carry-out are performed automatically.

3.1.2 System Configuration

Figure 6 shows the system configuration of the automated overhead cranes. The system consists of overhead crane and segment grabs equipped with various sensors and control devices necessary for automation, a management system that issues transport instructions, and a ground control panel that exchanges signals with each piece of equipment.

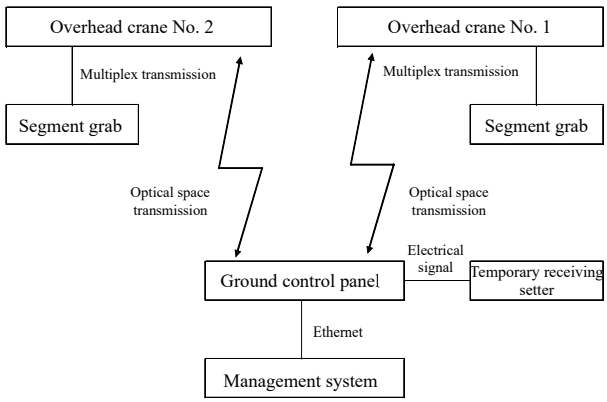

Figure 6. Configuration of automated crane system

3.2 Overhead Crane

3.2.1 Basic Configuration

Table 3 lists the sensors mounted on the overhead crane body for the purpose of automation, and Figure 7 shows the layout.

The position coordinates of the overhead crane were measured by using a laser rangefinder for the travel and traverse directions, and by using an encoder for the hoisting and lowering directions.

Table 3. List of overhead crane sensors

Intended use	Qty.	Model	Intended use of signals	Mounting position and specifications
Hoisting sensor				
Encoder for hoisting position detection	2	MRE-G160SP061FKB (NSD)	For hoisting position detection	Mounted on hoisting drum
Normal upper limit (for origin correction)	2	PSKU-110CO (YE CONTROL)	For correction of hoisting position detection encoder For automated operation control	Weight type
Upper and lower hoisting cam limit switch	2	Supplied with hoist		
Emergency upper limit	2	Supplied with hoist	For master interlock	
Load detector	2	DLS-5033A-1		
Traverse motion sensor				
Laser rangefinder for traverse position detection	1	DL100 (SICK)	For traverse position detection	Mounted on girder With reflector mounted on traverse grab Reflector: 0.5 × 0.5 m
Traverse limit	2	PIKU-110 (YE CONTROL)	Triggers emergency stop when open	
Magnetic proximity switch for traverse position detection	5 (3)	PSMM-R3E1H (YE CONTROL)	For speed monitoring before traverse limit and trailer area detection Triggers emergency stop upon detecting abnormal speed while open	Sensor: Mounted on girder (3 sensors for overhead crane No. 2)
Magnet for magnetic proximity switch for traverse position detection	1	PSMM-M450T (YE CONTROL)	For speed monitoring before traverse limit and trailer area detection Triggers emergency stop upon detecting abnormal speed while open	Magnet: Mounted on traverse grab
Travel sensor				
Laser rangefinder for travel position detection	2	DL100 (SICK)	For travel position detection	Mounted on girder With reflector mounted on soundproof house wall Reflector: 1 × 1 m
Travel limit	1	PIKU-110 (YE CONTROL)	Triggers emergency stop when open	
Magnetic proximity switch for travel position detection	9 (7)	PSMM-R3E1H (YE CONTROL)	For speed monitoring before travel limit Triggers emergency stop upon detecting abnormal speed while open	Sensor: Mounted on travel girder (7 sensors for overhead crane No. 2)
Magnet for magnetic proximity switch for travel position detection	9 (7)	PSMM-M450T (YE CONTROL)	For speed monitoring before travel limit Triggers emergency stop upon detecting abnormal speed while open	Magnet: Mounted on soundproof house wall (7 magnets for overhead crane No. 2)
Others				
Optical space transmission device	1 pair (2 units)	BWF-3EA/B (Hokuyo)	For overhead–ground transmission: 1 pair	Crane-ground transmission
Anti-collision detector	1	TCR-30L3 (Toyo Electric)	For collision prevention between cranes	Mounted on girder With reflector mounted on counterpart crane

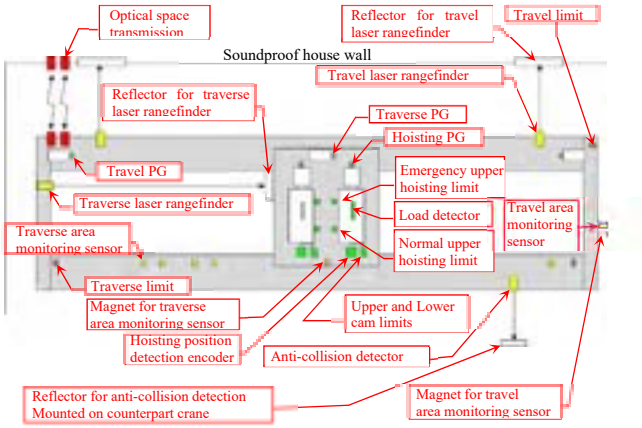

Figure 7. Layout of overhead crane sensors

3.2.2 Positioning Accuracy

The stopping accuracy of the overhead crane must be set to the target value ±50 mm, considering the possibility of interference between the segment to be carried into the tunnel and other equipment. Since high-precision positioning control is required, vector control with PG (pulse generator), which can output stable torque even at low speeds, is used to control the electric motor (Table 4).

Table 4. Specifications for overhead crane motor

Intended use	Qty.	Model	Output (kW)	Control method
Electric hoisting motor	2	For hoist 180Fr	45	Yaskawa Matrix Converter U1000 80 kVA Vector control with PG PG: MSK-510-1024 (1024 pulse/rev)
Electric traverse motor	2	CNVM3-6120-AP-B-21	2.2	Yaskawa Matrix Converter U1000 8 kVA Vector control with PG PG: ERN1330 (1024 pulse/rev)
Electric travel motor	2	CNVM8-6165-AP-B-25	5.5	Yaskawa Matrix Converter U1000 12 kVA Vector control with PG PG: ERN1330 (1024 pulse/rev)

3.2.3 Safety Functions

The following safety functions are provided so that the automated operation of the overhead cranes is stopped if the positions of the cranes cannot be measured accurately due to failure in the laser rangefinder or encoder measuring the positional coordinates of the cranes.

1. Positioning monitoring
   If the deviation between the integrated value of the vector control PG and the value measured by the laser rangefinder, for the travel and traverse directions, or the deviation between the command value from the management system and the value measured by the encoder, for the hoisting and lowering directions, exceeds a certain value during positioning, it is regarded as a position detection error and the overhead crane is stopped.
2. Area monitoring
   The area is monitored by magnetic detection sensors to prevent the overhead cranes from continuing automated operation after deviating from the predetermined area. These sensors are installed near the boundary between the manual and automated operation areas and that between the working areas of the two overhead cranes.Figure 8 shows the area monitoring plan diagram.
   A magnetic detection switch for monitoring deceleration is installed in front of the segment storage area at the end of each area. If the overhead crane is traveling or traversing faster than the rated speed when detected by the sensor, it is judged to be abnormal and the crane is stopped. This ensures that overhead cranes approaching an area boundary are decelerated without fail.
   If the overhead crane continues traveling or traversing even after reaching the segment storage area at the end of each area, the limit magnetic detection switch (or the limit switch for the travel and traverse ends) judges it as an overrun and stops the crane. The limit magnetic detection switch acts as an electric stopper and is set to the position such that the overhead crane stops before hitting against the mechanical stopper.

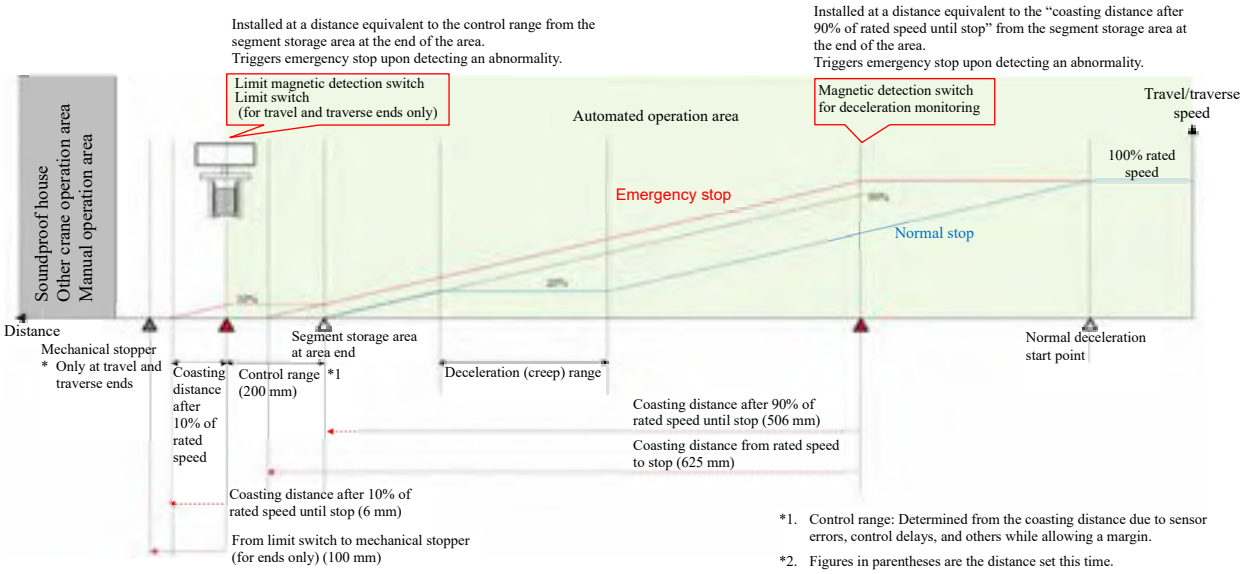

Figure 8. Area monitoring plan diagram

3.3 Segment Grab

Transportation of segments using a crane used to be performed by manually slinging the segments on a sling or the like. This time, a segment grab was newly developed as an automated segment slinging device.

Figure 9 shows the mechanical drawing and Table 5 lists the mechanical specifications for the segment grab. The segment grab is used as a slinging tool by hanging it on the hook of the automated overhead crane. However, the hook would rotate freely if left as it is, so it is pinched with plates to prevent rotation.

In order to align the center of gravity between the segment grab and the segments even for those with different widths, the segments are sandwiched by two arms in the lateral direction and then placed on the grabbing jaws. The grabbing jaws that support segments are fitted with rubber plates, and the arms and the grabbing detection bar that come into contact with the segments are fitted with MC nylon plates (friction reducing plates), in order not to damage the segments during lifting. Photo 1 shows the segment grab grabbing segments.

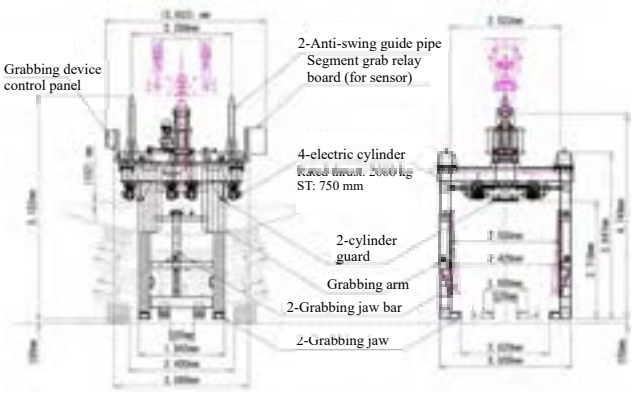

Figure 9. Segment grab drawing

Table 5. Mechanical specifications for segment grab

Item		Specifications
Rated load		33 t
Opening/closing speed		75 mm/sec × 2 (9.0 m/min)
Arm opening		520 to 2,020 mm
Arm length		3,547 mm
Arm width		1,950 mm
Jaw length		240 mm
Own weight		6,800 kg
Electric cylinder	Power supply	3-phase, 400 V, 50 Hz
	Stroke	750 mm
	Motor capacity	2.2 kW × 2 units × 2 arms
	Rated thrust (per piece)	2,000 kgf
	Accessories	Thrust detector Rotary encoder Stroke adjustment LS

In addition, anti-swing guide pipes are installed on the segment grab, which fit into the sheath pipes on the overhead crane when the grab is hoisted to the upper limit, preventing the load from swinging during traverse motion. Although it is necessary to hoist up the grab to the upper limit each time before making traverse motion, this enables high-speed traverse motion and highly accurate positioning.

Table 6 lists the sensors mounted on the segment grab, and Figure 10 shows the layout.

The grabbing sensors detect that the segments are sandwiched by the arms, and the loading sensors detect that the segments are engaged with the jaws. Both types of sensors work together to detect that the segments are securely grabbed.

The pocket collision and bottom collision detection sensors are provided to prevent contact between the segment grab and the segment, RC invert or any obstacle in the event of an abnormality in positioning or an unexpected incident.

The grab opening detectors are provided to detect the cylinder strokes of the left and right arms and are used for positioning correction in the traverse direction (Figure 11). In particular, when picking up segments from a trailer by manual operation, the center cannot be aligned precisely between the segment grab and segments, causing a difference in the strokes of the left and right arms. If the segments are carried in such a state, the center of the segments will deviate from the target position because the positioning is performed using the center of the segment grab as the reference. In order to prevent this, the strokes of the left and right arms are detected when grabbing the segments, and the traverse distance is corrected during positioning by the difference between the strokes.

Photo 1. Segment grab grabbing segments

Table 6. List of segment grab sensors

Name	Qty.	Model	Intended use of signals	Notes
Electric cylinder	4	LPTC2000H7.5V LRIJF-TK (Tsubaki E&M)	For opening/ closing the grab	With thrust detector, rotary encoder, and stroke adjustment LS
Hole detection photoelectric switch	6	PEY-155C (Hokuyo)	For detecting obstacles when opening/closing the grab	Light projector/receiver
Loading detection proximity switch	2	E2E-X3D1 (Omron)	Loading detection	
Grabbing detection proximity switch	2	E2E-X10D1 (Omron)	For grabbing detection	
Bottom collision detection photoelectric switch	16	PZ-G41N (Keyence)	For detecting obstacles under the grab	
Pocket collision detection photoelectric switch	16	PD5-1MC (Hokuyo)	For detecting obstacles when lowering the grab	

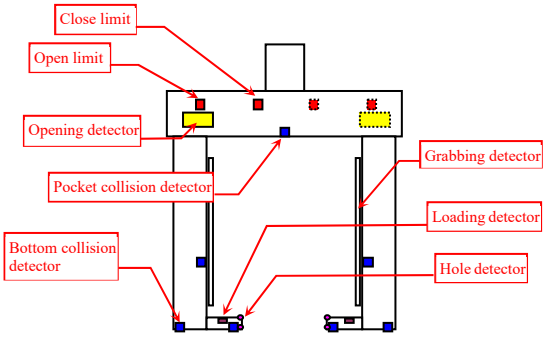

Figure 10. Layout of segment grab sensors

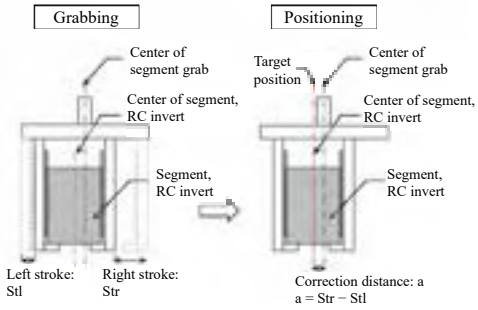

Figure 11. Positioning correction in traverse direction

3.4 Picking Up and Attitude Detection of Segments

It is impossible to position the trailer strictly at right angles to the overhead crane or load segments exactly parallel to the trailer, and consequently, segments are angularly misaligned with the segment grab. As the segment grab is suspended by wires, it rotates to align with the segments upon grabbing the segments, but when the grab is hoisted up to the upper limit, the guide pipes on the grab fit into the anti-swing sheath pipes, so that the angular deviation is corrected (Figure 12).

3.5 Management System

The management system consists of a survey system and an ordering system. The configuration of the management system is shown in Figure 13.

The survey system plans the allocation of future segments based on the survey results of the tunnel alignment and the design alignment plan.

The ordering system orders the factory to ship the segments planned to be allocated by the survey system, and at the same time, specifies the loading order of the segments onto the trailer according to the types of segments, and is also able to check whether the segments are loaded onto the trailer in the specified order at the time of shipment from the factory.

The automated overhead crane automatically determines where to store the segments in the stockyard from the information on the segments brought in by trailers and that on the inventory in the stockyard. In addition, it automatically selects the segments to be carried out according to the allocation plan and transports them from the stockyard to the temporary receiving setter.

The color code shown in Figure 14 was adopted as a marker to identify each segment and RC invert. A color code sticker which identifies the segment type is attached to the side of each segment at the factory, and the color code is read by the camera on a tablet terminal at the site so that the automated overhead crane recognizes the type of the segment brought into the stockyard. Unlike barcodes and QR codes, multiple color codes can be read from a distance at a time, which is ideal for identifying stacked large segments such as those in this case.

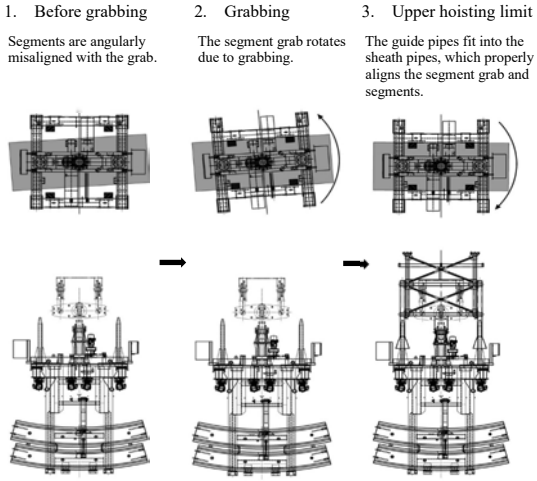

Figure 12. Angular misalignment correction flow for segments

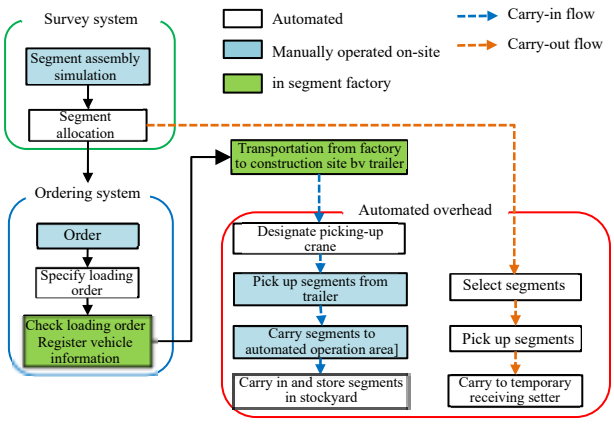

Figure 13. Configuration of management system

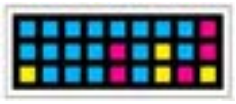

Figure 14. Color code

3.6 Safety Measures

In order to prevent accidents such as people getting caught in the overhead crane during automated operation, fences are installed at the boundary between the automated and manual operation areas. However, to allow people to enter the automated operation area for maintenance, open/close doors are provided at some points of the fences. A lockable open/close detection sensor is also mounted on each door in order to prevent people from accidentally entering the area during automated operation (Figure 15). If any door opens during automated operation, the overhead cranes are stopped. Furthermore, to ensure safety, people entering the automated operation area are obliged to carry the key of the open/close detection sensor with them so that the automated operation of the cranes cannot be restarted until they leave the area.

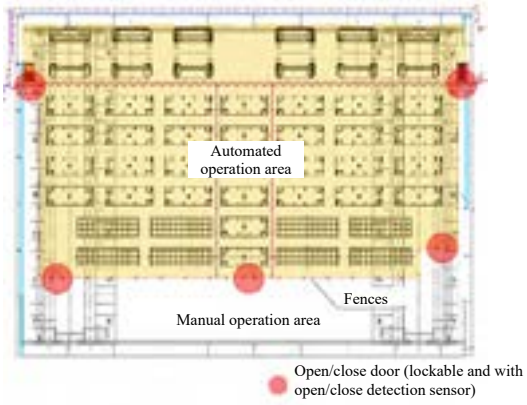

Figure 15. Layout of fences and doors with open/close sensors

4 Actual Operation Results

4.1 Productivity Improvement

4.1.1 Labor saving and reduced dependency on personnel

As a result of the introduction of automated overhead cranes, all the segment stockyard operations were automated except unloading of segments from the trailer, which required only two operators. Before these cranes were introduced, it had been assumed that a total of six operators would be required, two for each of the two overhead cranes and two for the temporary receiving setter. Thus, the use of automated overhead cranes improved productivity by saving labor.

This project significantly improved productivity also by reducing labor hours due to the reduced thinking time required for determining where to store segments and identifying the segments to be carried out, and by reducing the dependency on personnel so that even operators without specialized knowledge or advanced skills can perform the operations.

4.1.2 Reduction of losses due to rework

If a wrong segment is carried into the tunnel, the segment must be replaced, requiring shield excavation to be stopped. This would cause various losses, such as the stand-by hours of excavation operators and cancellation of materials and vehicles. In the case of a large-scale construction work like this, the cost incurred would be enormous.

The segment selection function of the automated overhead crane has been working without requiring any rework until now.

4.2 Quality Assurance

While ensuring a positioning accuracy of ±50 mm, this project achieved automated transportation, and prevented malfunctions by means of various sensors and prevented erroneous operation by humans. The system has not caused any damage, such as cracking and chipping, to segments until now. The project has successfully built equipment that can make a significant contribution to quality assurance.

4.3 Improved Safety

In automated operation, the overhead cranes (machine) and segments and RC inverts (load) are completely separated from humans, eliminating the risk of man-made disasters and contributing to improved safety.

5 Conclusion

This project introduced automated transportation using overhead cranes, which was unprecedented in the carry-in/out of segments for shield construction work. The system improved the on-site productivity and safety, and also contributed to quality assurance. The automated overhead crane we developed can handle segments of different widths and shapes, and is highly applicable to other similar construction works.

We will continue to work on improving the efficiency of construction work on-site in order to address the shortage of human resources due to the declining birthrate and aging population.

Development of an Automated Angle Control System to Improve Safety and Productivity

Tsuyoshi Fukuda[a], Takumi Arai [a], Kousuke Kakimi [a], and Keishi Matsumoto [b]

[a]Shimizu Corporation, Japan
[b]SANDVIK Corporation SMRT Company, Japan
E-mail: tys.fukuda@shimz.co.jp, t_arai@shimz.co.jp, kakimi_kousuke@shimz.co.jp, keishi.matsumoto@sandvik.com

Abstract –

Currently, the high demands and needs to improve productivity and labor-saving in construction industries leads to many automation and mechanization. This report aims to address the shortage of skilled worker in the future as well as improvement of safety, productivity and quality. Comprehensive collection and utilization of information were carried out and with target to eliminate the over reliance of experience worker in mountain tunneling, "Automated Angle Control System" technology was developed to reduce the overbreak of tunnel during excavation. The concept of this method is to ensure that the productivity of drilling for blasting operation will not be influenced by the worker skills. This system was tested in Shin-Tomei Expressway Takatoriyama west tunnel construction project and results confirmed that the system successfully minimized the overbreak of tunnel during excavation. The authors hope that this report will contribute to the improvement of safety and productivity.

Keywords –

automated angle control system; overbreak; drilling energy; safety; productivity

1 Introduction

Over 40 years have elapsed since the introduction of the New Austrian Tunneling Method in Japan; notable advancements have been achieved with respect to the construction methods. However, reliance of experience and instinct of skilled workers still remain because of the heterogeneity and uncertainty of the ground conditions (bedrock) which is the primary material of the tunnel, whereas bridges and framework structures use concrete and other materials of consistent quality and standards.

The recent use of machines and automation to boost productivity, including reduced labor and improved construction methods, is a demand of the times and merits active involvement. In addition, the nature of public construction projects dictates that projects be implemented with greater transparency and objectivity.

Against this background, this paper strives to collect and utilize as much objective information as possible with the aim of achieving construction that does not rely on experience or instinct, resolving the future shortage of skilled laborers, and improving safety, productivity, and quality. To meet these objectives, the authors developed the automated angle control system as a technology for reducing overbreak in mountain tunnels.

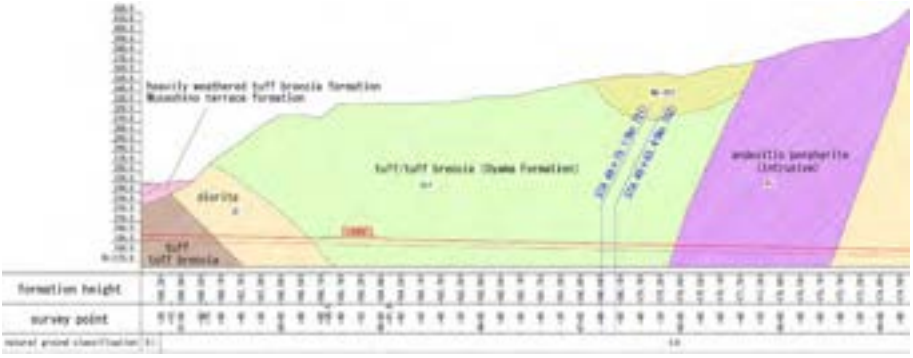

Figure 1. The geological profile and demonstration test area (outbound lane).

The concept of this overbreak reduction technology aims at improved productivity unaffected by skilled labor in explosive drilling and achieves the designed cross-section while allowing accurate formation with minimal overbreak. This reduces the occurrence of mucks as well as shortens time required for mucking and shotcrete. Moreover, it also has the benefit of preventing ground from loosening by smoothing the excavation surface. Additionally, this technology can be used effectively to serve as a safety indicator for preventing accidental flaking of the face as it is possible to understand its ground morphology by using the drilling energy obtained as a byproduct of the drilling work required for explosive drilling.

This paper will report on the results of the demonstration tests conducted in the Mt. Takatoriyama west tunnel construction project.

2 Construction Site Details and Geology of the Demonstration Test Area

Takatoriyama Tunnel is a twin-bore tunnel comprising two highway lanes, which connect the cities of Hadano and Isehara, and has a total length of 3.9 km. Its internal cross-sectional area is 80 m2, and the tunnel extensions on the western side measure 1,573 and 1,609 m for the inbound and outbound lanes, respectively, with downslopes of 2% being observed in both the lanes. The geological profile and demonstration test area are presented in Figure 1. The system trials were initiated in tuff and tuff breccia (Oyama Formation) that are suitable for blasting and proceeded while trying to adjust the system functions. Further, 14-m zones of STA.46+79.1–STA.46+65.4 is designated as demonstration test areas and validated the effectiveness of the system. The demonstration test area is primarily characterized by distributed weathered tuff, with a tunnel face evaluation grade point of 41–44 belonging to CII of the ground classification.

3 Automated Angle Control System

This system is characterized by its ability to reduce overbreak without skilled labor and to prevent face accidents by utilizing drilling energy. Figure 2 gives an overview of the entire automated angle control system.

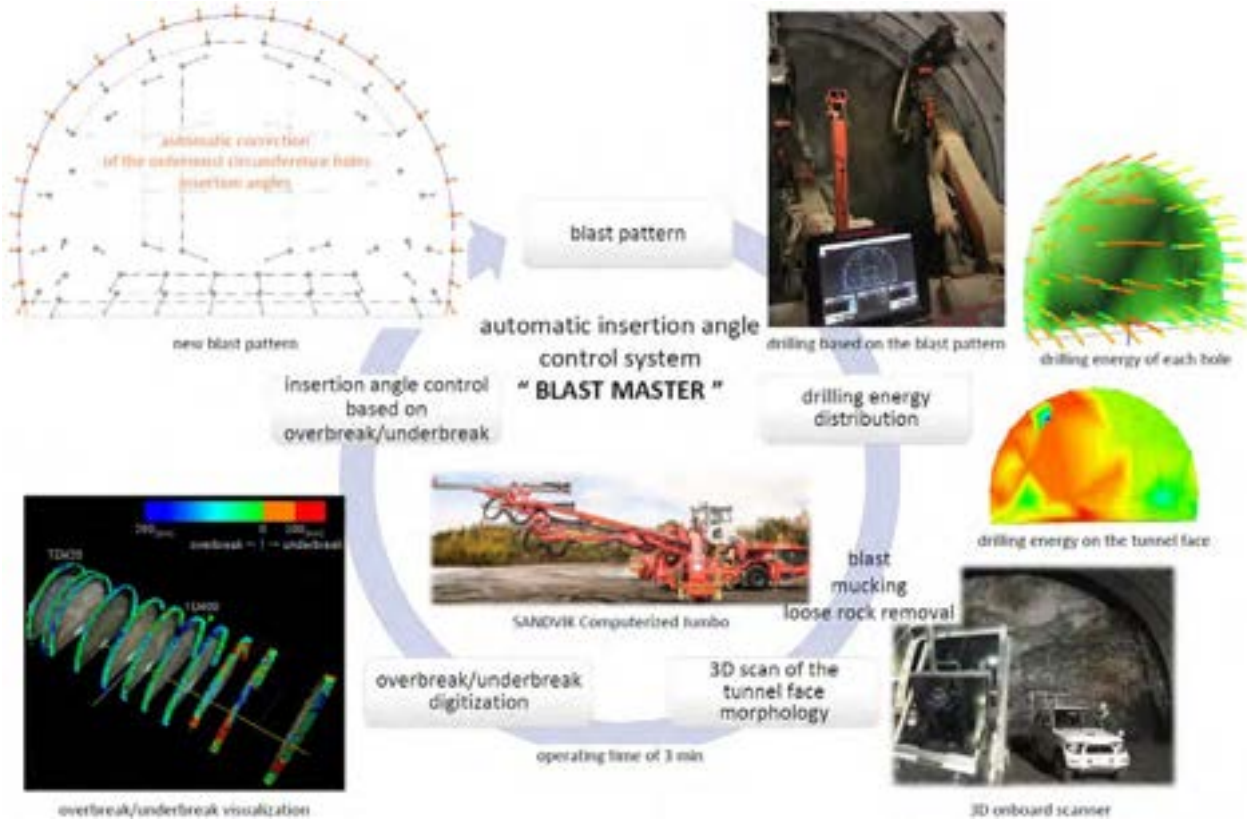

Figure 2. Overview of the automated angle control system.

3.1 Overbreak reduction technology without the need for skilled labor

The authors believe that there are limits for the reduction of overbreak even if a computerized drill jumbo is used to improve the drilling accuracy based on the predefined blast patterns because of the influence of the ground heterogeneity and bedrock fissures. The results supporting this assumption have been obtained from a previous report (1) (2).

Conventionally, the skills of experienced workers are relied on to reduce the overbreak in heterogeneous ground. Our system (Figure 2) solves this issue. The overbreak reduction mechanisms (steps) can be given as follows:

Step I: A blast pattern is created and displayed it on the computerized drill jumbo operating screen (the initial blast pattern is set based on the prior experience and ground strength).

Step II: The jumbo operator accurately performs face drilling based on the generated blast patterns (at this time, the drilling energy is automatically calculated and recorded).

Step III: After charging, blasting, and mucking, scaling will be carried out to ensure the safety of the tunnel face area is confirmed. Subsequently, a three-dimensional (3D) onboard scanner is set in front of the tunnel face, and the face morphology is scanned immediately after the excavation (with a duration of approximately 3 min).

Step IV: The scan result is digitized and examined on the spot to confirm the overbreak/underbreak amounts (underbreaks are eliminated on the spot).

Step V: The corrected drilling angle value is automatically calculated from the predefined correction value derived from the relationship between overbreak amount and drilling angle (the corrected value does not rely on the ground morphology).

Step VI: The corrected value is utilized in the blast patterns of the next cycle, automatically generating the subsequent blast pattern (go to Step II).

3.2 Technology for preventing face accidents by utilizing drilling energy

As indicated in Step II above, face drilling based on the blast patterns also records the drilling energy distribution in the depth direction of the drilling positions as shown in Figure 3. Figure 4 shows the face as seen from the ground.

The drilling energy distribution map shown in Figure 4 is generated by calculating the mean of the drilling energy data obtained 0.5m below the face surface or deeper and projecting the result of each drilled hole onto the face surface. The parts that are relatively shallow from the face surface (less than 0.5 m

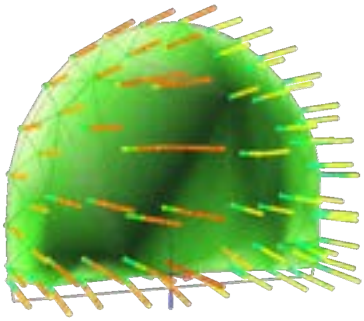

Figure 3. Face drilling in action

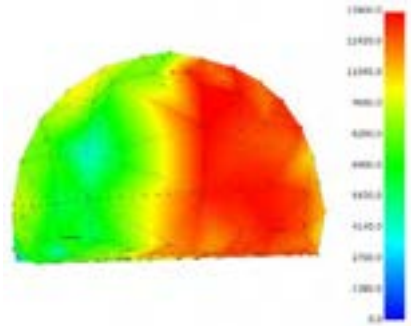

Figure 4. Distribution of drilling energy at completion of drilling

Figure 5. Map streamed to computer jumbo screen

Figure 6. Face monitoring personnel monitors the face

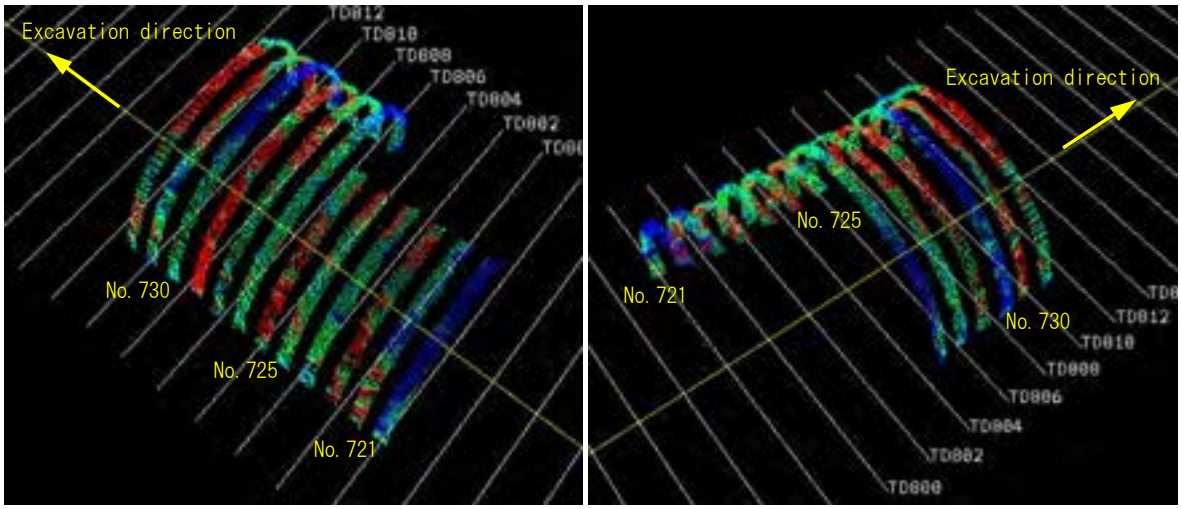

[Left wall] [Right wall]

Figure 7. Measurement results of the 3D scanner used in the demonstration test area

from the surface) are excluded from the evaluation data set because previous blasts and face sprayed concrete can obscure the true ground morphology. Figure 4 is automatically generated at the completion of face drilling.

A face drilling energy distribution map generated such as the one shown in Figure 5 gives an objective indication of the ground morphology distributed along the face, which is referred to as a face safety index in this system, and is used to prevent face accidents.

When the drilling work has been completed, a drilling energy distribution map is generated, after which the face safety index is immediately and automatically streamed to mobile devices such as smartphones and tablets of all tunnel construction personnel, including face monitoring personnel, jumbo operators, and JV personnel. This allows all personnel to continue working with the latest face information. Figure 6 shows the face monitoring personnel observing the face while checking the face safety index.

4 Automatic Drilling Angle Control System Demonstration Test Results

The results from the 3D scanning employed in the demonstration test area are presented in Figure 7. The red and blue colors represent the underbreaks and overbreak, respectively, enabling us to understand the overbreak and underbreak locations. The maximum and mean overbreak based on the obtained scanned data organized in a time series are presented in Figure 8. The following can be stated based on the results obtained from Figures 7 and 8.

No. 721 can be attributed to explosive drilling from the initial blast pattern (set by considering the past experience and ground strength), with all the drilling angles in the outermost circumference drilled at the same angle. The maximum and mean overbreaks were 67.0 and 30.2 cm, respectively, with an increase in the crown area.

Subsequently, the drilling angle of the outermost circumference was individually corrected using the results obtained from the overbreak/underbreaks in No. 721–724. Thus, it can be confirmed that No. 725 showed the lowest number of underbreaks and the overbreak considerably decreased. The maximum and mean overbreaks were 21.0 and 6.6 cm, respectively, with decreases of approximately 69% and 78%, respectively, when compared with the results obtained from the initial blast pattern.

Based on the drilling performance of the entire demonstration test section, it can be assumed that by operating the system several times, it is possible to reduce the effect of excessive overbreak and smooth the excavation surface.

Figure 9 shows the statistical treatment of the relation between the corrected drilling angle of the outermost circumference among all the drilling results in the demonstration test area and the overbreak volume generated from that drilling angle. Despite the lack of sufficient drilling results for obtaining a definitive evaluation, an overbreak value of zero is predicted at a drilling angle of 2°–4°. Therefore, planning with a blast pattern involving drilling angles of 2°–4° is a logical choice for future drilling in a geological terrain similar to that of the Takatoriyama Tunnel (i.e., tuff breccia).

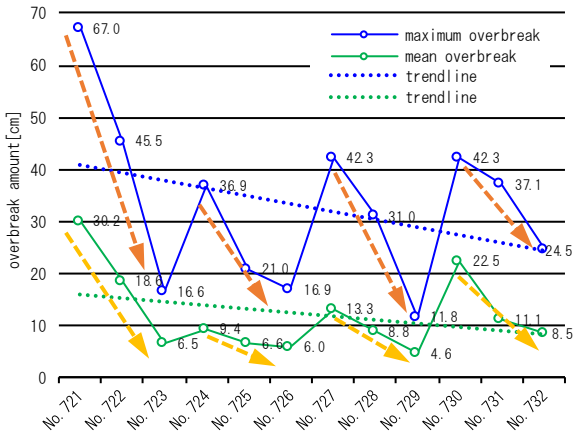

Figure 8. Overbreak reduction effects (tuff/tuff breccia)

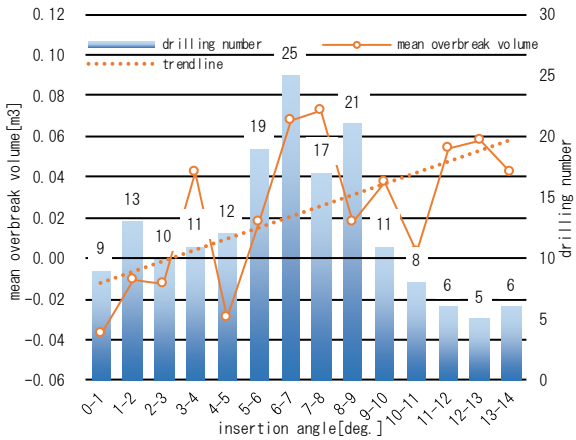

Figure 9. Relation between the drilling angle and overbreak amount (tuff/tuff breccia)

5 Summary

The implementation of the automated drilling angle control system in multiple drilling cycles confirmed a reduction in the maximum and mean overbreak by approximately 69% and 78%, respectively. These values are observed to vary based on the ground conditions (e.g., ground heterogeneity and influence of rock fractures).

Although the effectiveness of overbreak reduction differ based on the ground conditions, this test demonstrate that the system can effectively decrease the overbreak amount without relying on skilled labor forces.

Based on these results, the authors expect to find the most suitable drilling angle and angle correction logic by applying this system to the various ground conditions.

Face drilling energy is used to objectively show the ground conditions distribution in the face, which is regarded as a “Face Safety Index” in this system and used to prevent tunnel face accidents.

While the authors do not consider this index to be an absolute assurance of safety, it has been recognized as a means for offering peace of mind by providing tunnel work personnel, such as face monitoring personnel and workers at the tunnel face, with the most recent ground conditions information that cannot be obtained by visual observation alone, as soon as the drilling work is completed.

References

[1] Okawa, R., Yamabe, K., Arai, T., Otsubo, H., Kakimi, K., Fukuda, T. Overbreak reduction during explosive drilling based on an Automated Insertion Angle Control System, VI-459, 2019.9.

[2] Okawa, R., Yamabe, K., Otsubo, H., Arai, T., Kakimi, K., Fukuda, T. Proposal of a Novel Evaluation Method for using Drill Jumbo Machine Data, VI-460, 2019.9.

Automated Detection for Road Marking Quality, using Visual Based Machine Learning

Firas.Habbal [a], Fawaz.Habbal [a], Abdulla.Alnuaimi [b], Shafya.Alkheyaili [b], Ammar.Safi [b]

[a]Department of Management College of Business,
International learning institute, United Arab of Emirates
[b]Ministry of Infrastructure Development, United Arab of Emirates
E-mail: firas.habbal@iqli.net, fawaz.habbal@iqli.net, Abdulla.alnuaimi@moid.gov.ae,
Shafia.Alkheyaili@moid.gov.ae, ammar.safi@moid.gov.ae

Abstract –

Most of the cities road marking inspection is performed manually and considered an ideal candidate for automation because it is a labour-intensive process. We propose a solution based on automated quality assessment tool for road marking to detect and qualify road marking characteristics. Our data inventory and data collection approach work on images collected from a camera mounted on vehicle or drone. We use an automated procedure to choose images suitable for inspection based on road marks conditions. From the selected data we segment the ground and detect three different parameters; road markings conflicts, missing road markings, and road marking reflectivity.

We describe convolutional neural network and image classification algorithms that identifies road marks conflicts, visibility, missing road markings. We also discuss the problem of evaluate the quality of the existing road markings, conserve human and financial resources that is caused by on-site inspections, reduce improper manipulation of road marking (human errors), and prompt jobsite management to focus on promoting fine workmanship of road marking during the execution and train the classifier. We present results from the prototype that shows the detection of the three trained parameters mentioned above. Finally, we show results computed using our method over a subset of a citywide urban and non-urban road network.

Keywords –

Road Marking; Road Detection; Automated Roads Evaluator; Focal Point Detection

1 Introduction

For at least two decades, the development of transportation systems has led to the development of embedded applications allowing to improve the driving comfort and to minimize the risk level of hazardous areas. More specifically, the researches in intelligent and Advance Driving Assistance Systems have provided a great number of devices on many types of automatic vehicle guidance and security systems such as obstacle detection and tracking [1], road visibility measurement [2], pedestrian detection, road departure warn- ing systems. However, one of the first embedded system that was studied is probably the lane detection system. This application is usually based on road marking detection algorithms. [3]. This system is also one of the most important sources of information in order to build a local perception map of an environment surrounding an ego-vehicle. Indeed, this information provides relative vehicle location information to all other perception systems (obstacles, road signs, ...) that need to know the road and lanes attributes. For this reason, the system must be as robust as possible. Moreover, for several year, it appears evident the automation of the driving task is probably a solution in the reduction of the road injuries. But for automated or partially automated driving task, the road marking and lane localization are very important and provide a critical information. This information needs to be really accurate, certain, reliable in order to achieve some manoeuvers like lane changes or generate safe path planing (co-pilot) [4].

The research and the study proposed in this paper are directly dedicated to this important topic of road markings detection and tracking, and lanes estimation for automated and/or partially automated driving applications. Our objective is to provide an assessment of the road surface attributes (road markings attributes, type of road marking, number of lane and characteristic of lanes). This method is based on use of one or several embedded cameras.

Most of the algorithms are basically based on a three-step scheme summarized as follows. First, images are processed in order to extract road marking features. Second, extracted primitives are analyzed in order to extract point distributions corresponding to a road

marking. And finally, in a third step, extracted and validated points are used to extract lane shape. In some previous work [5], the first extraction part has been studied, tested, and evaluated in order to determine the best way to extract road marking primitives. In this paper, a double extraction strategy is proposed to achieve the discrimination of the points for marking points and non-marking points. To guaranty the robustness of our approach, we proposed in addition a performance evaluation protocol for the first road primitive's extraction stage based on the use of the SiVIC platform, which is presented in [6]. This protocol provides an accuracy measurement of the clustering and robustness relatively to a clustering threshold.

In this paper, we present several significant improvements of the original method proposed by S. S. Ieng and D. Gruyer in [7]. The global scheme is the same one, but some enhancements have been done in each part. For instance, the combination strategy of several extractors, the management of the primitives in the detection stage, and the lane and markings estimation in the lane estimation part has been modified. In addition, instead of imposing a very discriminative threshold into the extraction part, we propose the use of the intensity of the extracted point into both the detection and the estimation parts. Lane marking detection, originally based on the study of a histogram containing projected points, is now made by using the same type of histogram but where the projected point is weighted in function of their uncertainty. Moreover, the poly-fitting mechanism has been replaced by a weighted poly-fitting, for the same reason. Higher is the extracted intensity points, more strongly weighted are these points in the estimation process. To robust our approach and avoid false alarms, distribution points which are not satisfying very discriminative criteria for peak clustering are submitted to a robust weighted poly- fitting.

2 Literature Review

2.1 Image Amendment

Because of the point of view impact, it is troublesome and dreary to discover the path of the street just from the first front view. To relieve this issue, we utilize differentiate viewpoint imaging strategies to make an all-encompassing perspective in the city. To do this, we have to figure the homograph network that maps the picture in the essential plane (essential camera pivot) to the vertical virtual camera. This transformation to IPM depends on the alignment boundaries of the network camera, the tallness of the camera over the ground, and the perspective of the camera comparative with ground. This implies the IPM is good with all camera designs in light of the fact that the homograph lattice is evaluated. Take these boundaries as indicated by [19] and change them separately for each shading channel of the picture. On the off chance that the skyline is known, the piece of the picture that contains the sky territory doesn't contain any valuable data identified with the street sign and is evacuated for additional thought.

2.2 Image Improvement

We improve feathered creatures eye picture differentiate by changing over shading esteems utilizing versatile limited complexity histogram evening out (CLAHE). This progression is important to evacuate the difference in the picture brought about by over the top sunlight-based light or. Nonetheless, the improved street picture may in any case experience the ill effects of extreme plan data, which might be unseemly for identifying street signs and may prompt mistaken street mark region proposition. To mitigate this issue, we utilize a snappy two-dimensional channel with portrayed advancements to expel structure data from perception while safeguarding edge data. From that point forward, we propose to use on-board data to improve street marker limits. Such an improvement would improve street marker recuperation results for various lighting conditions and assurance settled street mark zone recommendations at the territory identification stage. Along these lines, a top-notch edge map is separated utilizing the quickest edge locator proposed by Dollar et al. This edge discoverer depends on organized backwoods; it works at 60 fps and is impervious to different light conditions. In spite of the fact that this presents a method of producing material suggestions from edges, this calculation doesn't exhibit the precision of item recommendations good for our specific reason. Therefore, we propose an elective way to deal with recommendations of adjoining territories for recognizing street markings.

2.3 Recognizing Regions

Before we proceed onward to the subtleties of the last period of the field recommendation calculation [10], first depict a portion of the highlights that are helpful for expelling guide zones from the street surface.

1. Street signs are normally light and, in this manner, have a higher incentive than their sides. This expands their permeability and the probability that the driver will really feel them. Likewise, traffic signs are typically geometric and here and there painted in various hues.
2. Traffic signals are typically neighbourhood inside the road with long numbers (which are bigger than the width) to make it obvious to the driver in spite of the fast.
3. Some traffic signs have a lot of signs or text.

For this situation, all their contacts are near one another to guarantee that their mediator will be

equivalent to the street checking. Keeping these properties in mind helps us to develop a robust road marking detection algorithm.

Our zone helps cut the picture of ROI discovery in zones that are acceptable possibility for street signs. Traffic scene symbolism, particularly in urban zones, includes a ton of things, for example, vehicles, individuals, trees, which are not important to us, wiping out most zones where street signs are not noticeable. Improves framework execution. We depend on the distinguishing proof of fascinating territories; street signs are in every case splendid around them since they are intended to look simple. For this reason, we utilize Fixed Additional Areas (MSER) to distinguish territories of intrigue that are street markers for our situation. The MSER is an associated locale, and the pixels in the districts are consistently more splendid or darker than the pixels inside the range. There are compelling calculations for processing MSER. We identify MSER in precise road see pictures. Alongside certain regions of different pieces of the scene, practically all zones with street signs were found. Be that as it may, these phony disclosures don't cause any issues in our calculation as they are detached at a later stage. MSER is steady in splendid and recognizable changes. In the writing, variable similitude of direction is acquired by adding circles to MSER areas, changing over curved districts into roundabout districts, and finding nearby element vectors. For our situation, in any case, rotational shakiness is unfortunate since it causes discovery. Street signs on the contrary roadside.

2.4 Focal Point Detection

We separate a lot of highlight focuses from the districts of intrigue registered as clarified previously. To empower constant calculation without the utilization of GPUs, we utilize the FAST corner locator proposed by Rosten et al [18]. Quick has been accounted for to be around multiple times quicker than the Harris corner locator, and multiple times quicker than SIFT. Repeatability of highlight discovery is accounted for better than, and even under the least favourable conditions practically identical to, the SIFT key focuses indicator. We apply the FAST corner finder on the locales of intrigue recognized on the redressed pictures.

2.5 Highlight Extraction

Every POI is gravitated toward an illustrative descriptor. We figure the histogram of the objective expressive (HOG) for every POI. The descriptor of the HOG comprises of a quality vector with 128 measurements, determined utilizing the "best" approach at picture scales around explicit scales and POIs. Deciding these best scales and bearings is a long count. Given the necessary speed, we draw the HOG work vector with 3 fixed scales and 1 fixed bearing. For each scale, a 128-dimensional trademark is determined for every POI. By taking a gander at the included highlights at various scales, we get the last 384-dimensional element vector for every POI. For every single model picture, the arrival on speculation with traffic signals is gotten from reality on troublesome ground. Following the upgrades, POIs in the ROI named the pictures all things considered. From that point onward, the component vector is utilized for all POIs. All highlights are put away as vector reconciliation model pools and related POIs [20].

2.6 Solid twofold picture

The significant data of primary property on how we can expel street signs [11]. Since the street signs are more brilliant than the territory around them, the top channel utilized in it tends to be utilized to feature territories of intrigue. The top warmth channel has the state of a rectangular progression capacity and channels the closest neighbour. Practically speaking, nonetheless, the top warmth channel produces inadmissible outcomes when seen to some degree because of obscure or outrageous light conditions. Furthermore, the channel is delicate to reaction boundary settings.

2.7 Merging of Regions

The third property gives us bits of knowledge into the reconciliation of recommendations in the region. We can see that some sign-based street markers have numerous associations. While some examination sums up territory recommendations by depicting bunch requirements and others treat every area exclusively, we propose a superior answer for this test. Specifically, we use commotion (DBSCAN) with nearby thickness-based bunching of uses created by Torr et al. Basically, DBSCN is a grouping calculation that makes bunches from high-thickness models dependent on the local range, where searches are performed and the base number of explicit focuses in the group less TS. This calculation accomplishes the base number of focuses by choosing any point in the informational collection and imitating the current group from the current bunch point with the minP ts limitation. At the point when the calculation leaves the focuses to be added to the group, any new point is at long last chosen and the procedure is rehashed. Be that as it may, the calculation becomes flimsy when the limit purposes of neighbouring groups are recognized. The depicted places of business this issue and shows the exhibition of visual execution contentions for information with neighbouring bunches. This makes thickness based grouping a powerful acclimation to accomplish a lot of locales that have a place together and have a place with a similar class. The grouping

calculation is applied to the inside directions of the considerable number of proposals of the street checking zones in the wake of separating the wrong regions. The utilization of thickness-based grouping disposes of the need to consider every locale separately and combine districts utilizing experimentally decided imperatives.

While path identification has been seriously read for a considerable length of time, the recognition of other street signs, (for example, representative and finished) has pulled in little consideration. To tackle the issue of finding street signs, numerous strategies depend on starter data about the area of paths. In any case, path exactness may antagonistically influence the acknowledgment of other street signs. Tao et al. He noticed the requirement for autonomous distinguishing proof of street signs and proposed an elective calculation to recognize and distinguish street signs. This methodology influences the recently applied IPM procedure to manage point of view impacts. From that point forward, numerous ROIs are recovered as MSER.

In this way, the FAST component identifier is utilized to remove the objects of intrigue, and the arranged inclination histogram (HOG) is utilized as a handle to make an example for each class. The layout picture is then contrasted with each picture in the format, and the class mark is doled out by looking at the vectors of the test highlights and each picture in the layout. Despite the fact that the creators report victory, this strategy depends on the precision of an exceptionally quick FAST finder and extricating substantial HOG capacities is computationally costly. On the other hand, [15], Perform low-level preparing to remove ROI from IPM pictures to distinguish target street signs. Recuperated ROIs are breaking down and distinguished dependent on rakish direction and bead size. In spite of the fact that this work has yielded good subjective outcomes, no quantitative appraisal is justified. Moreover, another calculation ought to be liable for recognizing a specific sort of street marker, which brings about lower adaptability. Correspondingly, it tries to expand the unwavering quality of the calculation by separating street markers into text and representative street markers. Text-markers are recognized utilizing the optical character acknowledgment calculation, while character-based markers are distinguished by extricating the HOG highlights ordered utilizing the support vector machine (SVM). In any case, a slight improvement in the proposed calculation doesn't legitimize the need to process street markers independently, prompting computational repetition.

In contrast to physically made assignments, whose exhibition relies upon their planned reason, classifiers have demonstrated their dependability for some PC vision applications dependent on fake neural system extraction (ANN) devices and AI. Various works have endeavoured to utilize neural systems to improve the discovery and recognizable proof of street markers. For instance, [17] the creators propose to utilize the coordinating edge in the IPM picture to discover likely contender to submit to a prepared neural grouping.

This strategy shows great quality against various states of light, climate and street surface. This is the primary method to utilize completely associated neural systems to perceive street signs. Rather than completely associated neural systems, virtual neural systems (CNN) have performed better in characterization results because of their capacity to remove increasingly powerful portrayal highlights. Be that as it may, with current ExxonMobil or VGGNET models, such a profound CNN as a rule requires a great deal of preparing information and is regularly executed on costly GPUs, permitting the vehicle circuit but there is more weight. Following this rationale, Chen and so on. Proposed a calculation that utilizes the Being Object Detector to give proposals to various potential areas with similitudes to the district's images. These up-and-comer territories are additionally grouped by the PCA Network (PCENT). PCN8 is a sort of profound learning system that utilizes PCA channel bank as opposed to confounding layers like CNN. As a rule, PCANet is a lightweight rendition of CNN that is basically basic and has demonstrated to be a compelling technique for picture arrangement. The impediment of the proposed approach is that a fixed number of BNB lines (30 offensive up-and-comers) are drawn per outline, which frequently prompts computational repetition, as the quantity of street signs from the survey perspective never increments. Doesn't reach such huge numbers of locales.

Another disadvantage is that the street markings are not set accurately and regularly the determined bouncing box contains other disconnected articles. Simultaneously as our work, Hyeon et al. We have built up an elective framework for perceiving and perceiving street markings. This technique varies from multiple points of view. Extraction of associated sets is finished utilizing Gaussian diff rather than MSER. Locale put together gathering is accomplished based with respect to curved conditions while depending on thickness-based gathering. Arbitrary woodland is utilized for characterization errands. Rather, utilize further developed AI strategies. Likewise, this paper groups perceived regions into image based or text-based street markings, however the client needs to accomplish more acknowledgment. This technique, then again, treats all street markings similarly and perceives an unmistakable class of all street markings presented. Intrigued per users are urged to think about this synchronous work too. To beat the previously mentioned downsides of the current techniques, we propose a calculation that gives superior on complex datasets. Our commitment comprises of three sections.

We give a framework that dependably recognizes street markings in pictures. Wireframes process a few pictures in equal without expanding the calculation time. This commitment guarantees that street markings are distinguished under various lighting conditions and uses thickness-based bunching to amass street markings. These disposes of the need to process character and text territories independently and utilizes AI procedures to perceive street markings. Notwithstanding PCANet, it proposes a little CNN and gives an iterative answer for improve and keep up the steadiest districts.

2.8 Runtime Template Corresponding

We presently go to the execution coordinating calculation that improves the score. The means recorded in the past areas. Amendment, MSER check, sharp edge location and HOG-explicit computations are performed on each test symbol. The test pictures are uncovered based on POI after indication discovery. In the road see picture, there might be a wide range of traffic signs. What's more, one sort of image can show up in numerous spots in a picture. In this way, each example may have more than one comparing patch in the test picture. Moreover, P.O.I. The identifier doesn't have a redundancy of 100 reiterations, subsequently, a portion of the POI tests found in the test picture don't show up in the example, etc. Accordingly, the test picture for the most part has a similar POI substrate as the POI substrate in the example. There are two stages in our calculation to ascertain this comparability. In the first place, we acquire a positive POI coordinate dependent on their component vector, and second, we improve the outcome utilizing an auxiliary coordinating calculation that coordinates the 2D geometry of the POI in the street sign [3].

3 Research Methodology

Our aim of this research is to develop an automated road marking detector based on multi-deep learning algorithms to detect and qualify the road marking conditions in which is evaluated the best selected road marking that fulfil the future autonomous vehicles needs and requirements, by utilizing deep learning algorithms. Using convolutional neural network and image classification technologies, the proposed prototype system first receives digital images of finished road marking surface and do the images processing and analysing to capture the road marking characteristics.

Those characteristics are then evaluated to determine the quality level of road marking conditions. System will be trained by multi-real cases as well as demonstrated through three real cases to show how it works. In the end, a test comparing the assessment results between the proposed system and expert inspection will be conducted to enhance the accountability and accuracy of the proposed mechanism.

Our system consists of training and testing phases. The input to the training phase is a set of images with ground truth masks and labels of the road markings as shown in Figure 1.

Figure 1. Template Images

We will call these training images as template images henceforth since these are used as templates for the road marking detection.

For each template image, we first perform rectification to compensate the lens and perspective

distortions. Within the regions of interest containing the road markings, a set of points of interest (POI) are detected, for which we use FAST corner detectors [15]. A Histogram of Oriented Gradients (HOG) [16] feature vector is extracted for each POI and the template set is built using the locations and the feature vectors of the POIs extracted from all template images for the particular type of road marking.

During runtime, the same steps are repeated for each frame of the testing video, captured pictures and a set of POIs and their feature vectors are extracted, except that the regions of interest are detected automatically. Subsequently, we find multiple matching candidates for each POI in each template image. Lastly, a convolutional neural network and image classification algorithms are employed to test if a subset of the matched POI pairs forms a road marking the same as the ones in the template images.

3.1 Image Rectifications

The camera we use is mounted on a rooftop rack and focuses to the front of the vehicle. Because of this low perspective, there is a huge point of view contortion with separation. We correct the picture utilizing a reverse point of view change that altogether diminishes this mutilation. Converse viewpoint changes have likewise been utilized widely in past work on street stamping identification [16], [4]. The reverse point of view change is a lattice which just relies upon the camera adjustment, the tallness of the camera over the ground, and the review edge of the camera θ regarding the ground Figure 2. Applying the lattice changes an information picture to a feathered creatures eye see. A case of such a fowl's eye see is appeared in Figure 3. Note that the change boundaries are adjusted beforehand accepting the ground is level, as opposed to aligned in real-time. Subsequently

the paths might be not ideal equal in the winged animals eye see when the vehicle is on slopes or has pitch and move developments. Acquiring the flying creatures eye see permits us to legitimately figure the slope on this picture to get the HOG descriptors. Without the winged creatures eye see, we would have been compelled to utilize an anisotropic angle administrator to represent the point of view twisting.

Figure 2. The setting of Cameras

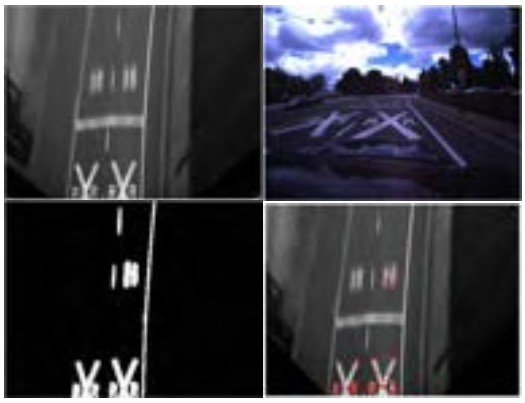

Figure 3. Image Detection multi views

3.2 Region of Interest Detection

Our region of interest (ROI) detector helps prune the image to portions which are good candidates for being road markings. Since a traffic scene image, especially in urban areas, will contain many objects such as vehicles, people, trees etc., which are not of interest to us, removing most of these areas where road signs are not likely to occur improves the efficiency of our system considerably.

We base our recognition of interesting regions on the perception that street signs are consistently more brilliant than their prompt environmental factors since they are intended to be seen without any problem. To this end, we utilize Maximally Stable Extremal Regions (MSERs) [17] to identify locales of intrigue, which are putative street markings for our situation. A MSER is associated district that is extremal as in the pixels inside the locales are consistently more splendid or darker than the pixels on the limit. Proficient calculations for processing MSERs exist. We recognize MSERs on the redressed street scene pictures.

MSERs are steady across brightening and perspective changes. In the writing, perspective invariant coordinating is accomplished by fitting circles to the MSER areas, changing the oval districts to roundabout locales, and extricating nearby component vectors [15]. Be that as it may, for our situation, the subsequent revolution invariance is bothersome as it would prompt discovery of street markings in the contrary roadside too. A model is appeared in Figure 4, where there is a left go sign in the contrary path. Subsequently, we don't change the MSERs into circular districts.

3.3 Runtime template matching

We currently continue to the runtime coordinating calculations that perceive the street markings. The means referenced in the past areas viz. correction, MSER identification, Quick corner discovery, and Hoard descriptor calculation are performed on each test picture. The signs in the testing pictures are then recognized and distinguished dependent on the POIs.

In a street scene picture, there might be numerous diverse street signs. Additionally, a solitary sort of street stamping may show up at different areas in a picture. In this way, every layout may have numerous coordinated fixes in a test picture. Furthermore, since the POI identifier doesn't have 100% repeatability, a portion of the POIs distinguished in the test picture may not be recognized in the layout picture and the other way around. Subsequently, there is generally a subset of POIs in the test picture that coordinate a subset of the POIs in the layout. Our calculation to process this coordinating comprises of two stages. Initially, we find putative coordinating sets of POIs dependent on their element vectors, and second, we refine the outcome through an auxiliary coordinating calculation that coordinates the 2D geometry of the POIs inside the street checking.

4 Dataset

To the best of our knowledge, currently there is no dataset that is designed for evaluating the performance of road marking detection and recognition. Hence, we collected our data using a mounted camera on a rack of a vehicle or drone and facing forwards. The vehicle was driven on urban and non-urban roads in Dubai and Sharjah Emirates, UAE under various road conditions. We manually annotated a subset of the road markings appearing in the captured images. We hope that this extensive dataset will provide a fruitful benchmark for other researchers working on this problem. An example of an annotated template image is shown in Figure 4.

Figure 4. Annotated template

5 Experiments & Findings

We tested our algorithm on the dataset described above. Our algorithm uses OpenMP for parallelization in the feature extraction stage. A value of 1.3 was used for the α threshold from (1), while the value for the β parameter from Section IV-B was set to 0.01.

Figure 5. Detection Segments

Fig. 5 Unqualified Detected Segments left side the wrong road marking and right side the template images

Our system currently depends on two manually selected threshold values, the α parameter of (1) and the β parameter of section IV-B. It is future work to automatically select these parameter values and adapt them online for different test conditions. We currently observe that the values used in our experiments presented above are applicable in a wide range of scenarios including large variations in road marking conditions.

Our system works robustly for complex road markings, but the false positive rate is higher for simpler markings such as forward arrows. Finding a tighter cost function that alleviates this problem is part of future work.

In our experiment, we select several images as the templates, which contain different types of road markings including pedestrians' crosswalks, intersections, and roundabouts. Our algorithm achieves a true positive rate of 90.1% and a false positive rate of 0.9%, indicating that false positive detections occur only very rarely. We found that our algorithm could also detect and recognize road markings clarity in case of sand dunes / snow accumulation.

In our system, we trace and obtain several segments that contains unqualified road markings as shown in figure 5.

Acknowledgment

This research is financially supported by Ministry of Infrastructure Development in United Arab of Emirates and International Group of Innovative Solutions. LLC.

References

[1] J.-P. Tarel, S.-S. Ieng, and P. Charbonnier, "Using Robust Estimation Algorithms for Tracking Explicit Curves," in *ECCV 2002*, ser. Lecture Notes in Computer Science, A. Heyden, G. Sparr, M. Nielsen, and P. Johansen, Eds. Springer Berlin / Heidelberg, 2002, vol. 2350, pp. 492–507, 10.1007 3-540-47969-4 33. [Online]. Available: http://dx.doi.org/10.1007/3-540-47969-4 33

[2] R. Sittler, "An optimal data association problem in surveillance theory," *IEEE transactions on military electronics*, vol. 8, no. 2, pp. 125–139, 1964.

[3] M. Bertozzi and A. Broggi, "Gold: a parallel real-time stereo vision system for generic obstacle and lane detection," *IEEE Transactions on Image Processing*, vol. 7, no. 1, pp. 62 –81, Jan. 1998.

[4] B. Vanholme, D. Gruyer, S. Glaser, and S. Mammar, "A legal safety concept for highly automated driving on highways," in *Intelligent Vehicles*

Symposium (IV), 2011 IEEE. IEEE, 2011, pp. 563–570.

[5] E. Pollard, D. Gruyer, J. Tarel, S. Ieng, and A. Cord, "Lane marking extraction with combination strategy and comparative evaluation on synthetic and camera images," in *Intelligent Transportation Systems (ITSC), 2011 14th International IEEE Conference on*. IEEE, 2011, pp. 1741–1746.

[6] D. Gruyer, S. Glaser, and B. Monnier, "Sivic, a virtual platform for adas and padas prototyping, test and evaluation," in *FISITA 2010 World Automotive Congress, Budapest, Hungary*, 2010.

[7] S. Ieng, J. Vrignon, D. Gruyer, and D. Aubert, "A new multi-lanes detection using multi-camera for robust vehicle location," in *Proc. on thee IEEE Intelligent Vehicles Symposium*. IEEE, 2005, pp. 700–705.

[8] M. Burrow, H. Evdorides, and M. Snaith. Segmentation algorithms for road marking digital image analysis. In Proceedings of the Institution of Civil Engineers-Transport, volume 156, pages 17–28. Thomas Telford Ltd, 2003.

[9] T.-H. Chan, K. Jia, S. Gao, J. Lu, Z. Zeng, and Y. Ma. Pcanet: A simple deep learning baseline for image classification? In Transactions on Image Processing, 24(12):5017– 5032, 2015.

[10] K. N. Chaudhury, D. Sage, and M. Unser. Fast bilateral filtering using trigonometric range kernels. In Transactions on Image Processing, 20(12):3376–3382, 2011.

[11] T. Chen, Z. Chen, Q. Shi, and X. Huang. Road marking detection and classification using machine learning algorithms. In IV, 2015.

[12] M.-M. Cheng, Z. Zhang, W.-Y. Lin, and P. Torr. Bing: Binarized normed gradients for objectness estimation at 300fps. In CVPR, 2014.

[13] P. Dollar and C. L. Zitnick. Structured forests for fast edge ´ detection. In ICCV, 2013. [7] P. Dollar and C. L. Zitnick. Fast edge detection using struc- ´ tured forests. ArXiv, 2014.

[14] S. Ghosh and K. N. Chaudhury. On fast bilateral filtering using fourier kernels. In Signal Processing Letters, 23(5):570– 573, 2016.

[15] J. Greenhalgh and M. Mirmehdi. Automatic Detection and Recognition of Symbols and Text on the Road Surface, pages 124–140. Springer International Publishing, 2015.

[16] D. Hyeon, S. Lee, S. Jung, S.-W. Kim, and S.-W. Seo. Robust road marking detection using convex grouping method in around-view monitoring system. In IV, 2016.

[17] A. Kheyrollahi and T. P. Breckon. Automatic real-time road marking recognition using a feature driven approach. In Machine Vision and Applications, 23(1):123–133, 2012.

[18] E. Rosten, R. Porter, and T. Drummond. Faster and better: A machine learning approach to corner detection. IEEE Trans. Pattern Analysis and Machine Intelligence, 32:105–119, 2010.

[19] T. Wu and A. Ranganathan. A practical system for road marking detection and recognition. In IV, 2012.

[20] J. Matas, O. Chum, M. Urban, and T. Pajdla. Robust wide baseline stereo from maximally stable extremal regions. In Proceedings of the British Machine Vision Conference, pages 414–431, 2002

[21] M. Bertozzi, A. Broggi, and A. Fascioli. Stereo inverse perspective mapping: theory and applications. Image and Vision Computing, 8(16):585–590, 1998.

[22] N. Dalal and B. Triggs. Histograms of oriented gradients for human detection. In *IEEE Conference on Computer Vision and Pattern Recognition*, pages 886–893, 2005.

[23] E. Rosten, R. Porter, and T. Drummond. Faster and better: A machine learning approach to corner detection. *IEEE Trans. Pattern Analysis and Machine Intelligence*, 32:105–119, 2010.

[24] J. Matas, O. Chum, M. Urban, and T. Pajdla. Robust wide baseline stereo from maximally stable extremal regions. In *Proceedings of the British Machine Vision Conference*, pages 414–431, 2002.

A Construction Progress On-site Monitoring and Presentation System Based on The Integration of Augmented Reality and BIM

Sheng-Kai Wang [a] and Hung-Ming Chen [b]

[a] Graduate Student, Department of Civil and Construction Engineering, National Taiwan University of Science and Technology
[b] Professor, Department of Civil and Construction Engineering, National Taiwan University of Science and Technology
E-mail: M10605510@mail.ntust.edu.tw, hungming@mail.ntust.edu.tw

Abstract –

An on-site construction progress monitoring and presentation system is herein developed that overlays the virtual building information model (BIM) onto the real-time scene of the construction site using augmented reality (AR). The system utilizes the novel AR technology of simultaneous localization and mapping (SLAM), which is a real-time positioning technology based on visual-inertial odometry and point cloud map construction. Based on the scanned 3D environment point cloud and the adopted plane detection method, the indoor positioning is first initialized by attaching a virtual BIM component, which is set up on the centerline for alignment, to the corresponding real component at the actual site environment. Then, according to the completion surface of the actual object, the parameters of the position offset are kept adjusted at different construction stages, so the model can remain in position with the current scene. In this manner, the 3D BIM will be superimposed and displayed on the real-time view of the site based on the device's understanding of the environment through the recorded point cloud map using SLAM. In addition, the system also provides application modules for monitoring the project progress on-site. The on-site engineer can perform data collection through the designed system by interacting with virtual objects, with visual feedback provided for monitoring progress and evaluating project performance. To monitor the progress of a construction project on-site in real time, a method is proposed to quickly update the SLAM-based indoor positioning for adapting to a changeable construction environment. This compensates for the lack of visualization in the current construction management methods.

Keywords –

Augmented reality; Simultaneous localization and mapping; BIM; Construction progress management

1 Introduction

Augmented reality (AR) has many applications in the field of civil engineering, where the aim is to calculate the user's orientation and position to superimpose virtual objects and information onto the real world through a display device, thereby providing the user with the corresponding 3D model information and spatial details of the project site. The augmented reality positioning mode differs according to the location and use, in addition to variations in the resulting usage restrictions.

In the life cycle of construction projects, as building information modeling (BIM) is gradually maturing and being promoted, the combination of AR and BIM can be used to display increasing amounts of building information. Through visualization technology, the use of traditional 2D drawings has been traded for a more intuitive 3D model, and by combining the model with the actual scene to aid in decision-making, the design, materials, and configuration can be checked whether they are congruent with the designer's concept. If there are issues with the construction, immediate modifications can be made, thereby greatly reducing the errors during design, and reducing the cost and time of retrofitting after construction completion. While some previous studies have attempted to apply AR to the field of architectural engineering [1-3], the applications have been mostly limited to outdoor construction sites or existing construction sites.

Furthermore, in the project life cycle, the construction stage is where most changes occur and is the stage most prone to errors, with immediate corrections being challenging. Once the procedures have errors, the domino effect caused by errors will cause significant

delays and cost increases. Therefore, the accuracy of message transmission of relevant construction operations, flow processes, and information between various construction units appears to be particularly important. A closer look at the construction on-site environment can reveal several characteristics such as a "harsh environment", "many on-site stacking objects and construction equipment", "huge and rapid changing construction environment", "difficulty in equipment setup, update, and maintenance" and "uncertainty in environment situation". As a result, the positioning of an AR system on a construction on-site becomes a major challenge. For many of the technologies used in augmented reality such as GPS, marker indoor positioning, Bluetooth, Wi-Fi, and RFID, the use of some external sensor devices to initialize the AR system is required. Additionally, apart from inadequacies in efficiency and accuracy as well as a higher cost, for the rapid vicissitude of the construction environment, there is a need to set up a device such as a Bluetooth device for positioning, along with installation difficulties and the time-consuming and complex maintenance and updating. In traditional construction management, for progress tracking and checking the construction tasks, there is a need to manually collect data, illustrations, and other information from all construction units, which, can be a quite time-consuming and labor-intensive operation. Presentations through text and data do not provide adequate visualization for the on-site personnel. There is not enough specific intuition. It is not easy to immediately present the work tasks in progress within the local space, and for professionals from different backgrounds, further errors may result in message uploading[4]. Even with the assistance of 3D simulation in BIM, the construction personnel still have to rely on their spatial reasoning and map out the illustrations or 3D models to the physical space, and thus, real-time discussions cannot be made timely on-site, thereby further affecting the time and cost. Meža [5] used AR for the visualization of the preliminary design and the monitoring of the construction on-site, and when compared with other applications, AR was found to effectively and drastically improve the intelligibility of information.

This study attempts to apply an existing AR framework and propose a set of construction management systems based on AR and BIM that are suitable for the construction stage. Through the visual tracking of simultaneous localization and mapping (SLAM) and AR system initialization based on dynamic reference benchmarks in response to the rapid changes and uncertainties of the construction environment, when the construction environment changes drastically, the BIM model is quickly fitted and positioned to improve the updating efficiency. In combination with construction management, interaction with the BIM model is conducted through AR for comparing the pre-planned construction progress with the actual progress on-site as reported by on-site personnel, as well as providing assistance in checking construction tasks. As compared with traditional construction management, visualization technology can be used to enable on-site personnel to view progress more intuitively and accurately, and to look for possible problems or risks in advance.

2 Objective

A "construction progress integrated management system based on augmented reality technology" is herein created with the aim to integrate the ARKit augmented reality framework as developed by Apple Inc., BIM, and construction management concepts, and present them on the site at the construction stage. Apart from the electronic construction management data collection and incorporating progress calculation functions into the system framework, this study proposes a model positioning and fitting system framework that is suitable for an indoor construction site through existing AR tools. The target application is under construction project sites.

For the model positioning and fitting operation flow process, first, due to the unpredictable on-site environment and the characteristics of environmental changes at the construction stage, the on-site configuration cannot be accurately predicted and no fixed object can be used as a positioning reference point. Thus, the pre-setting of a reference point is challenging and it is necessary to set a dynamic reference plane when positioning the BIM model, whereby the plane is used as the basis for initializing the model positioning. This reference plane can be dynamically determined according to the instantaneous configuration of the on-site environment and the offset position can be measured using the setting position in the original model. Then, the visual-inertial odometry (VIO) technology in ARKit is used to perform the positioning and feature point mapping of the AR system initialization in an uncertain space environment, and to create fitting-assisted reference components through existing structures or objects on-site during the mapping process. In this process, the reference components are used as fitting corrections for the 3D model when drifting is generated when a device is moved. Finally, the plane detection technology is used to pre-set the corresponding position of the initial dynamic reference plane in the BIM model onto the actual site. By entering the position parameters in advance, the AR system initialization is completed as the 3D model is fitted onto a relative spatial position. The operation preprocessing flow process for the initialization is shown in Figure 1. Through this process, quick dynamic positioning and fitting of the model can

be achieved. Subsequently, the model repositioning and fitting can be carried out according to the recorded feature point maps in response to the changing construction environment, thereby improving the efficiency of system initialization and achieving a marker-less indoor positioning. The actual operating process is shown in Figure 2.

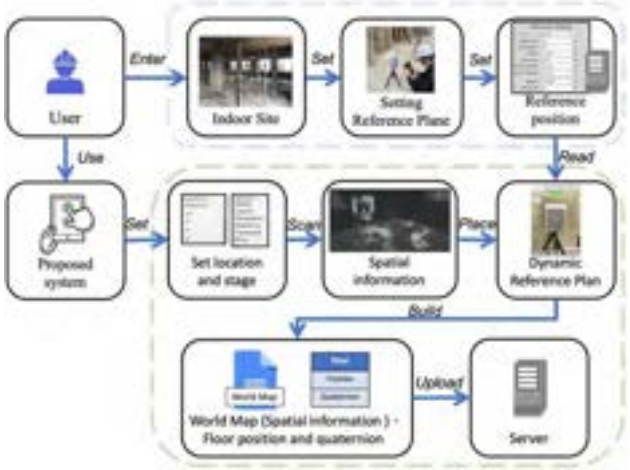

Figure 1. The pre-setting process of the proposed system.

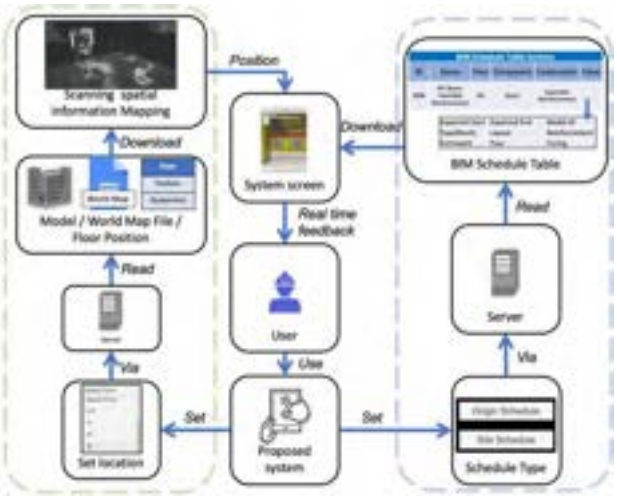

Figure 2. The operating process of the proposed system.

Finally, the BIM model and the construction schedule are integrated to achieve a mechanism for automatic collection of construction task data, daily management operations, information transfer, progress information visualization, and feedback. The mechanism further improves the project AR management framework that is lacking in relevant literature for traditional construction management.

The construction progress integration management system using AR will take the construction of a reinforced concrete (RC) as an example. Main construction operation tasks are divided into lofting, steel bar binding, formwork assembly, grouting, and concrete curing. To verify the proposed system, the positioning is subjected to a verification test on an actual site to monitor whether the BIM models can be efficiently fit to the site and are not affected by the work surface at various construction stages, and whether the system positioning accuracy is sufficient to meet the site requirements. Moreover, through the system display and comparison with the traditional construction management methodology, the proposed system is demonstrated to integrate planning and actual site information, and display this data on an AR device. The progress summary information is displayed using different colors corresponding to construction status, and it is verified that the user can perform queries and comparisons on construction task progress with the use of virtual reality as well as efficiently check construction tasks.

3 System Requirements and Mechanisms

To achieve these objectives, the functional requirements of the system are investigated, with Unity3D and ARKit frameworks used as the system development platforms. These analysis functions include the AR indoor positioning process based on SLAM visual inertia, system pre-position operation test, reference plane design and deployment rules, preprocessing of the BIM model, and the BIM model component information and progress information storage framework. The following subsections focus on introducing the functional analysis and proposed system methodology.

3.1 BIM model preprocessing

To achieve the “construction progress integration management system based on augmented reality technology” as mentioned in the aim of this study, the proposed system needs to establish a BIM model using 2D illustrations. Analyzing the project scale, characteristics, management organization, management method, and work breakdown structure diagram of the RC structure, the scope when operating the system will provide visual feedback to users based on the floor level. To reduce the burdens on the display and storage space of the device, the pre-position processing of the BIM model segments the 3D model into floors, and stores them on the server for users to download. The primary pre-setting process is shown in Figure 3.

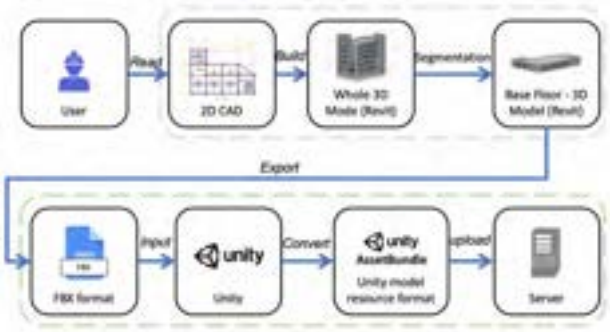

Figure 3. Pre-setting process of the BIM model.

3.2 Augmented reality indoor positioning

The ARKit framework is used as a development tool in iOS. ARKit is a framework based on SLAM combined with an inertial measurement unit (IMU). SLAM refers to a camera device equipped with a lens determining its own position and stance (sensors) by repeatedly observing environmental feature points (e.g., ground surface, walls, columns, etc.) during a movement process, starting from an unknown location in an unknown environment, and then calculating the feature point coordinate data intercepted from the image by its own position and stance to construct the feature point map, thereby achieving the self-positioning and mapping.

3.2.1 ARKit framework

SLAM has mostly resolved the two problems of positioning and mapping. “Positioning” refers to the device location as self-estimated in its environment at that moment, while “mapping” (a.k.a. feature points or a point cloud map) refers to the model of the identified local environment, i.e. the environmental map with incremental feature points as found through continuous movement and repeated observation of environmental features using positioning. The visual SLAM processing procedure is divided into five steps: (1) camera information image sequence acquisition and access, (2) visual-inertial odometry (VIO), (3) calculation optimization of device position and stance, (4) closed-loop detection of repeated observations, and (5) feature point mapping. In the ARKit, stance estimation of the IMU has been added into the second step of SLAM to measure the acceleration and angular velocity of the device, and through Kalman filtering the most accurate position of the device is obtained. Through a combination of the camera and inertial sensor, the estimation errors are lowered to increase the positioning accuracy. In the framework of ARKit, feature points captured by each image will be stored as anchors attributes, indicating that there is an anchor list for tracked positions or objects as detected on the map., If images that are being taken are repeatedly identified, the device location can be repositioned.

3.2.2 Plane detection

As mentioned above, many feature points can be extracted from the camera images to develop a tracking and positioning feature point map. Under this framework, these feature points not only can be used for estimating the device position, any three extracted points can form a plane, and then these triangular planes is subjected to processing through an algorithm and several plane optimizations. Finally, a sufficient number of planes can be used to estimate the real physical plane. Through the estimated plane, model components can be placed at the captured anchor position through interaction with the AR system.

3.2.3 Analysis of feature point mapping

Based on the abovementioned positioning theory of SLAM under the ARKit framework, an analysis is conducted on the construction and operation behavior of the feature point mapping, and the results of a test of using the device movement rate for positioning and mapping, as well as using the measurement mode on the construction site, are presented as shown in Figure 4 and Figure 5.

Figure 4. Actual environment.

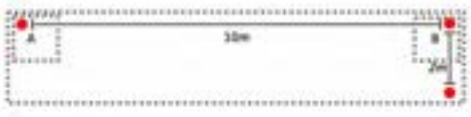

Figure 5. Schematic top-view.

From multiple test results, the movement rate and 3D error with a varying number of intercepted feature points was obtained (Figure 6). Under the same movement range, it can be found that there are more feature points

intercepted at a slower movement rate, and the accuracy in positioning and mapping is also relatively higher. For the variance in errors with the number of feature points found via interception corresponding to the fitted model, it can be found that the errors generated at movement rates less than 0.5 m/s gradually converge to approximately 1% of the overall movement distance. Therefore, when the camera intercepts the feature points, blurring will increase in the camera due to the high-speed movement, which will cause errors in positioning and mapping. At slow movement speeds (approximately 0.5 m/s), the generated errors begin to converge, and the resulting error falls to around 1% of the movement distance. Errors in a very harsh environment can almost be on the order of inches [6].

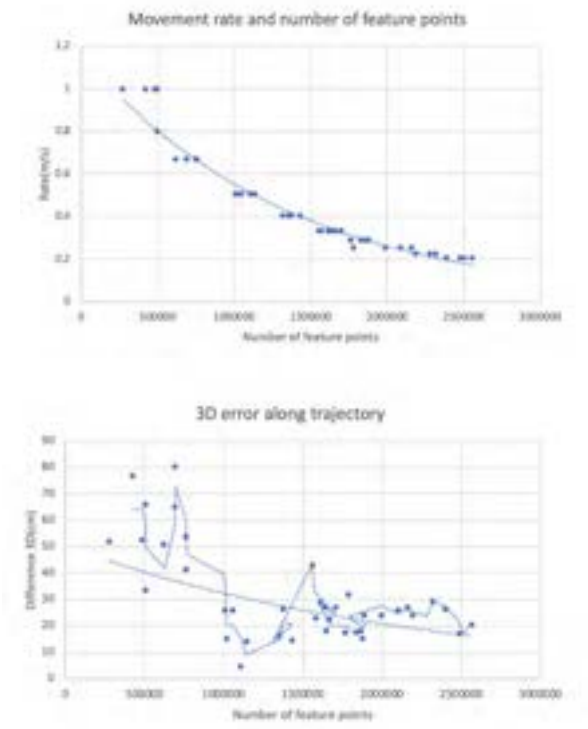

Figure 6. Movement (top) and 3D error (bottom) with number of feature points.

3.3 BIM model fitting mechanism

The model fitting mechanism is mainly to align one of the BIM model components with the corresponding real object for placement, and then to use the relative relationship between a single component of the BIM model and the entire model to fit the entire model on the map of feature points, thereby superimposing the model on the site. However, due to the unpredictable construction environment and characteristics such as environmental changes at the construction stage, the on-site configuration cannot be predicted and no fixed objects on the site can be used as positioning reference points for the feature point map. Therefore, a dynamic reference plane is required as a reference point for position initialization. This reference plane can be dynamically configured according to the configuration of the site environment at the time of initialization. When configuring the reference plane, the positional distance difference $\Delta \boldsymbol{R}$ from the reference plane in the BIM model is measured via centering and leveling operations, as shown in Figure 7. Finally, the offset data is recorded in the database. When fitting the model, the model file is first downloaded from the server according to the selected plane position and stage. Then, the system will first read the coordinate $\boldsymbol{P}$ and angle $\boldsymbol{Q}$ of the previously loaded model. Next, the selected virtual reference plane is aligned and placed on the actual reference plane; during the placement, angles $\boldsymbol{P}'$ and $\boldsymbol{Q}'$ (see Equation (1)) are obtained. Finally, the angle rotations of $\Delta \boldsymbol{Q}$ (see Equation (2)) and the model position movement distance of ΔP for the reference plane offset of $\Delta \boldsymbol{R}$ will be first calculated and then uploaded together to the server as the basis for the model fitting (see Equation (3)).

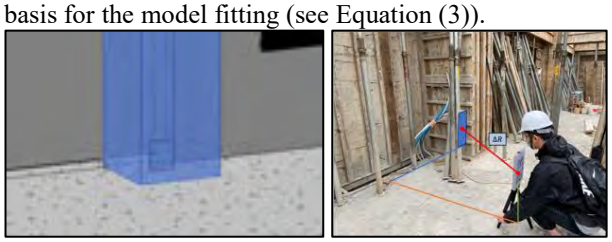

Figure 7. BIM model reference (left) and actual environment (right).

$$Q'\,[x' \quad y' \quad z' \quad w'] = \Delta Q \times Q[x \quad y \quad z \quad w] \tag{1}$$

$$\Delta Q = Q \times Q'^{-1} \tag{2}$$

$$\Delta P = |P - P'| + \Delta R \tag{3}$$

3.4 Integrating BIM model data and progress schedule data

During the construction project, due to the influence of different factors, each in progress construction task can either be ahead of schedule, behind schedule, or on schedule, further affecting the start of relevant subsequent tasks. As a result, the actual construction operations will change from the initial construction plan. Essentially, construction management and control are based on contracts that use the project schedule as a foundation, while for the proposed system, the user continuously updates the actual progress of work tasks on the BIM model via the AR system, as the BIM model components in the system framework are associated with their corresponding work tasks. Given that a user continuously interacts with the model to enter the actual construction progress to dynamically update the schedule,

this dynamic update is based on the successive relationship of construction operation tasks. The overall schedule obtained is thus a real-time prediction of the overall construction length based on actual project progress. Estimations for subsequent tasks can be based on this dynamic scheduling and in the same manner, engineering performance evaluations can be implemented based on planning and actual on-site scheduling; early deployment and improvement can be made on subsequent implementation of the same standard layer using AR feedback for the actual situations that have happened on the site. The operating mechanism of the real-time dynamic update for the construction schedule is shown in Figure 8.

Figure 8. Operating mechanism of the real-time dynamic update for the construction schedule.

4 Application Scenarios

Based on the prototype system developed, four types of application modes that meet the practical requirements are proposed for integrating the virtual and real environments: (1) interface conflict and positional views, (2) component data presentation and task checklist, (3) construction progress presentation and progress comparison, and (4) presentation of affected construction tasks and construction simulation. These modes are applicable for the construction life cycle and acceptance and review stages, with the mode adjustable depending on the degree of detail in the BIM model and operation requirements. It is not necessary that one type of mode can only support operation in one stage. Below is a detailed display and description of these four modes following the characteristic classification of system operations.

4.1 Interface conflict and positional views

The first application mode is used for presentation before the construction of the structure begins. Surrounding a construction site, there are mostly existing buildings or structures such as adjacent houses, slopes, roads, and other structures. The aim of this application mode is to alleviate the ecological impact from the project site and to investigate countermeasures by viewing possible affected location (e.g. surrounding adjacent houses, slopes, channels, and other existing structures) before the construction starts, as well as confirming the construction disturbance range (e.g. construction access roads, earthwork, and material stacking areas, etc.) to determine the project configuration and for moving line planning. For the case study introduced in the present study, it can be clearly seen that there are slopes and existing channels surrounding the future water collecting well, as shown in Figure 9. Through the repetitive detection of the AR, the relative height of the water collecting well with actual possible affected location can be more clearly seen to discover problems in advance. The evaluation via repetitive detections determines whether the original design or construction plan needs to be further adjusted. During construction, this application mode can assist in confirming whether the depth after excavation is sufficient, as shown in Figure 10, and at the construction stage for the structure, this application can also assist in confirming the location of completed components on the site, as shown in Figure 11 for reference.

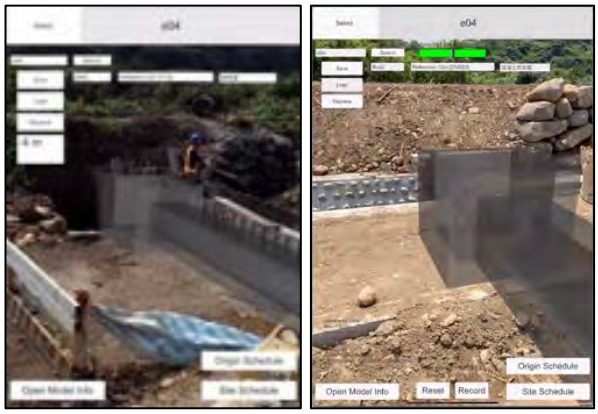

Figure 9. The elevation of the water collecting well and possible a location.

Figure 10. Excavation depth confirmation on the construction site.

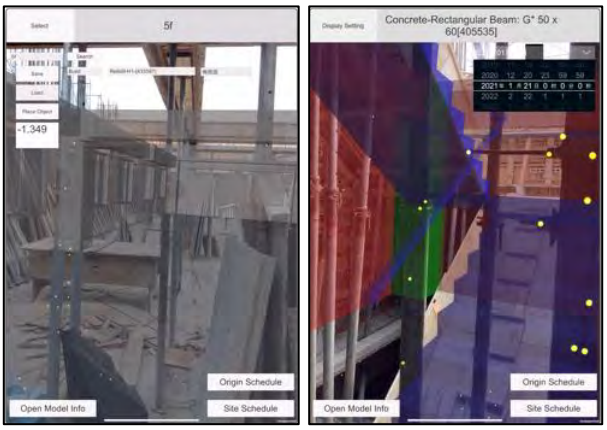

Figure 11. Indoor location assistance for the RC structure construction.

4.2 Component data presentation and checking form

The second mode is to tap and interact with the model after it is superimposed to present relevant information for the selected component. Apart from the attribute parameters and associated construction progress item information, the main presentation content also can have various attached documents according to the component type or usage requirements. Due to the association between components and progress, a user can therefore mark the completion of a system component directly as a unit for a construction task and be provided the construction progress. The information on the progress of components that can be provided to the user based on the ARKit real-time positioning when the system is operating at the construction stage is given below. The application procedure as follows:

1. When a project enters the construction stage, the user enters the location where a task is to be completed and then checks the task when completed to ensure the quality of project work.
2. The user moves toward the component to be checked after the completion of system positioning.
3. Attributes and progress information for the component can be obtained by tapping the component on the device screen.
4. When the quality audit confirms that there are no errors, the task for that component will be marked as complete and updated. At this point of time, following the date of checking, the progress for that will be determined as either ahead, on , or behind schedule. The system will update the dynamic progress schedule for subsequent associated work tasks according to the date of checking, so that the user can estimate future progress, as shown in Figure 12.

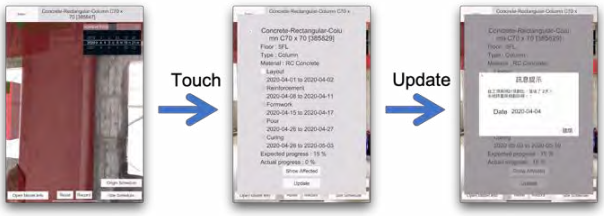

Figure 12. Component information query and task checklist.

4.3 Construction progress presentation and progress comparison

The third mode is to superimpose the actual objects with the virtual objects and view the current construction progress overview based on the schedule, where yellow, green, and red indicate in progress, complete, and delayed, respectively, as shown in Figure 13 (left). Moreover, this mode compares progress with the planning schedule and the actual checking date. It presents whether each work task in the past is ahead of schedule (green), on (yellow), or behind schedule (red), as shown in Figure 13 (right). On site, a user can carry out the presentation and review whether there are conflicts on the moving lines and configurations to adjust the schedule and for early deployment of subsequent work tasks.

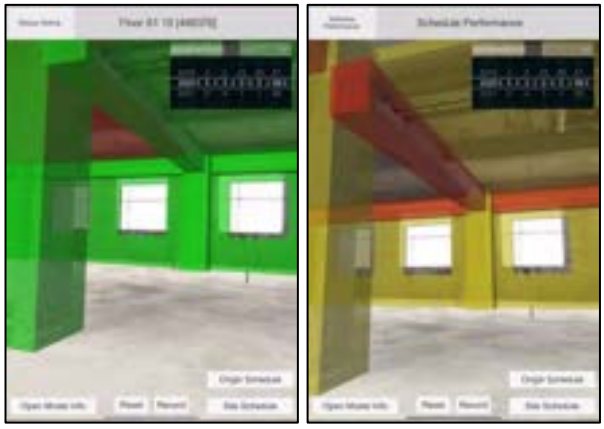

Figure 13. On-site progress presentation (left) and comparison of progress (right).

4.4 Presentation of affected construction tasks and construction simulation

The fourth mode considers the sequence of planned work processes and uses blue as the color for the work task component to be implemented in the future, so that the user can perform construction simulations on site, as shown in Figure 14 (left). Furthermore, following the results of using the previous several modes in sequence,

for the components that are likely to be subsequently affected due to delays in the work process, the components are presented in orange, as shown in Figure 14 (right), giving the user a visual reference beyond than numerical data and text.

Figure 14. A construction simulation (left) and an affected work task (right).

5 Conclusions

This study proposed the "A Construction Progress On-site Monitoring and Presentation System Based on the Integration of Augmented Reality and BIM". The aim was to carry out the positioning of an AR system at a construction site through the ARKit framework based on SLAM for an indoor site at the construction stage, and be able to respond to unknown and rapid changes in the harsh site environment. Under different construction stages, the dynamic reference plane without pre-setting additional sensor devices conducts rapid system positioning initialization. The indoor position is located by visually scanning the site environment characteristics, and then, by downloading the BIM-related information and progress information from the database, a virtual and real integration mode on site allows for viewing the elevation, position, and progress of components. Furthermore, data collection is conducted through user interaction with the AR system, and the collected data is integrated to provide visualized feedback functions, such as a comparison on the difference between planning and on-site actual progress and construction simulations. Adaptability, immediacy, synchronization, and convenience as provided by the proposed system can improve the efficiency of on-site construction personnel in understanding the progress, in planning, and in decision-making. Through the combination of AR and indoor positioning, the proposed BIM information on-site visualization can improve the existing BIM visual model, and can effectively and quickly collect and acquire information, thereby reducing complicated operations and the required time. Through the real-time visual feedback on site, the virtual and actual scenes can be superimposed on a single screen simultaneously, therefore supporting on-site construction monitoring and discussion. The future development of the system will be further integrated with computer vision for automatically identifying the completion rates of all BIM overlaid components in a scene through deep learning based AI.

6 References

[1] Golparvar-Fard, M., F. Pena-Mora, and S. Savarese, D4AR–a 4-dimensional augmented reality model for automating construction progress monitoring data collection, processing and communication. Journal of information technology in construction, 2009. 14(13): p. 129-153.

[2] Feng, C. and V.R. Kamat. Augmented reality markers as spatial indices for indoor mobile AECFM applications. in Proceedings of 12th international conference on construction applications of virtual reality (CONVR 2012). 2012.

[3] Bae, H., M. Golparvar-Fard, and J. White, High-precision vision-based mobile augmented reality system for context-aware architectural, engineering, construction and facility management (AEC/FM) applications. Visualization in Engineering, 2013. 1(1): p. 3.

[4] Kang, J.H., S.D. Anderson, and M.J. Clayton, Empirical study on the merit of web-based 4D visualization in collaborative construction planning and scheduling. Journal of Construction Engineering and Management, 2007. 133(6): p. 447-461.

[5] Meža, S., Ž. Turk, and M. Dolenc, Measuring the potential of augmented reality in civil engineering. Advances in Engineering Software, 2015. 90: p. 1-10.

[6] Hasler, O., S. Blaser, and S. Nebiker, IMPLEMENTATION AND FIRST EVALUATION OF AN INDOOR MAPPING APPLICATION USING SMARTPHONES AND AR FRAMEWORKS. International Archives of the Photogrammetry, Remote Sensing & Spatial Information Sciences, 2019.

Rule-Based Generation of Assembly Sequences for Simulation in Large-Scale Plant Construction

J. Weber[a], J. Stolipin[b], U. Jessen[b], M. König[a] and S. Wenzel[b]

[a]Chair of Computing in Engineering, Ruhr-University Bochum, Germany
[b]Department of Organization of Production and Factory Planning, University of Kassel, Germany
E-mail: jan.m.weber@rub.de, jana.stolipin@uni-kassel.de, jessen@uni-kassel.de, koenig@inf.bi.rub.de, s.wenzel@uni-kassel.de

Abstract –
The efficient construction of large industrial plants (e.g. concrete plants, chemical plants) in high quality requires precise planning and execution of the individual logistics and assembly steps. For this purpose, detailed step-by-step instructions should be prepared that can be clearly interpreted and thus implemented by the staff on site carrying out the work. Especially meaningful and project-specific assembly instructions are very important. In some cases, digital plant models are already being used to visualize the assembly sequences. The individual steps of assembly are animated together with the associated plant elements, staff and other resources. However, the exact assembly sequence has to be specified by a production engineer. This paper presents an approach for semi-automatic generation of step-by-step instructions for assembly in large-scale plant construction. Basic information for the assembly of a plant can already be taken from digital (BIM) models (BIM: Building Information Modeling). They include, e.g., information on components, construction details and connections. Based on this information, specific assembly sequences can be defined as rules for various plant groups. These rules are collected in a central database and provided for further use. An example shows how individual assembly sequences can be generated based on a digital plant model using the rule set. The results can be made available as 4D animations to the involved employees on the construction site. The assembly sequences defined for a project can provide useful support for planning the processes on the construction site (assembly, transport and storage of building elements). A simulation provides the validation of the planning created for this project and therefore also the validation of the defined assembly processes.

Keywords –
Logistics Scheduling; 4D BIM; Plant Construction; Assembly Sequencing; Simulation

1 Introduction

Precisely coordinated individual construction site logistics are of great importance for the efficient and cost-effective handling of large-scale plant construction projects, especially when the transport and storage of very sensitive and large components are involved. Planning includes the selection, design, dimensioning and optimization of processes, material flows and resources. Depending on the complexity of the large plant, many different boundary conditions must be considered in the project-specific planning of site logistics. Therefore, planning is a very error prone and time-consuming process, exacerbated by the fact that it is usually performed manually. Even for the most motivated companies, the effort required for the first draft of a schedule can be so taxing that resources for an improved schedule are not available [1]. The automated planning and control of construction site logistics for such large-scale projects have not been sufficiently supported by digital planning tools so far. Today, planning and control of construction site logistics require extensive project experience. If transport and storage conditions are not properly analyzed and adhered to, not only can installation delays occur, but also damage to sensitive system components. In the worst case, reworking or complete disassembly may be necessary. In order to ensure that components are only delivered when they can be stored as required or directly installed, it is necessary to know the exact sequence of construction in advance.

Digital models have also been used for several years in large-scale plant construction for the planning and prefabrication of plant components. However, the digital models are hardly used on site, e.g. for controlling processes on the construction site. Even though digital building models do exist, only low-detailed assembly sequences, if any, are currently created by hand and given to the workers carrying out the work in the form of a manual, but the sequences are usually only determined

on site. Even if plant components can be visualized on the construction site with the aid of mobile devices, there is currently no IT-supported assistance for compliance with a previously created assembly sequence. Certain information for the exact planning of the construction sequence is already available on the basis of the digital model or can be supplemented by categorizations based on our previous work [2]. However, the existing information is not sufficient for an assembly sequence and has to be systematically supplemented and properly linked.

In our approach, we use geometric attributes and other IFC (Industry Foundation Class) model information in conjunction with a model-specific set of rules to create an assembly sequence that can be transferred into a 4D model by adding the respective performance factor. On this basis, the warehouse logistics, means of transport and shift schedules of the construction workers required for the respective component and assembly tasks can be planned.

2 Related Work

In contrast to industrial production, there are significantly more uncertain factors in construction projects that need to be taken into account during the planning stage and to which a quick and efficient response is required. The basis for the execution of a construction project is the schedule, which is nowadays manually defined by project managers based on their experience and linked to the construction elements. Even the linking of costs and schedules is still done manually today [3]. This is a time-consuming planning process. The project plan is only adjusted in case of interruptions due to due to material shortages caused by delivery delays, lack of storage space or weather conditions [4]. In a global view of construction projects, little attention is given to the logistics on the construction site. Thus, unforeseen events cause delays to the entire project schedule. These delays could be minimized by an iterative re-planning of the project plan based on the current construction status.

In the construction industry, the transition to digital construction planning is mainly taking place with the help of BIM. The BIM methodology allows a seamless transfer of construction project information throughout the entire product life cycle. This is achieved by linking geometry information with other relevant information. With the right BIM management software, this linked data can be used for visualization, checking for compliance with rules, collision detection, assignment of schedules to components (4D), cost estimation (5D) and the generation of construction plans.

As part of our research, we have already developed an approach for linking BIM with logistics information, especially for large-scale plant construction. We created the method of classifying required logistics information for each element and storing it in form of an OWL-formatted ontology (OWL: Web Ontology Language) [2]. A created ontology represents a knowledge model with information for planning and controlling logistical processes on the construction site. The information in this ontology forms the foundation for the generation of assembly sequences in a construction project as used in the methodology presented in this paper. With the help of BIM management software and the extension developed, it is possible to assign any elements to these categories, thus enabling identification for our methodology presented in this work.

In contrast to the collision database shown in this paper, Borrmann and Schraufstetter implemented in their research metric operators of an SQL (Spatial Query Language) with octree and B-Rep approaches to reflect distance relationships between spatial objects [5]. Daum and Borrmann extended this SQL-based approach by a method for its topological and directional predicates which operates directly on the boundary representation [6]. Liu, Lei et al. developed an automatic scheduling approach exclusively for panelized construction in residential buildings [7].

3 Methodology

We developed an approach consisting of two steps to determine an automatic assembly sequence. In a first step, a sequencing of element by element according to the ascending Z-axis is generated. Basically, this procedure is logical for most elements, as the lower edge of an element usually rests on the upper edge of the element below. However, when generating assembly sequences based exclusively on the Z-coordinate of elements, it becomes apparent that logical errors can occur, for example when elements are levitating without being connected to a support structure.

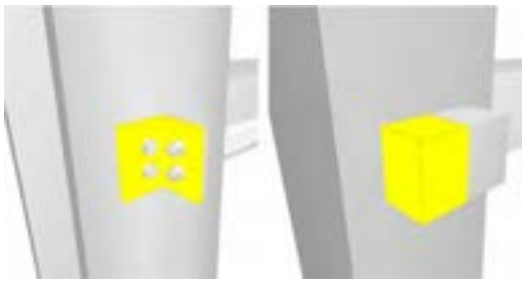

Figure 1. Model elements and corresponding bounding boxes

Therefore, in a second step it is necessary to determine whether all elements located under or next to an element and touching the element in question have already been

built. Although there is the possibility to link elements in construction software, these links are not necessarily created for each element. Thus, we determine such links for any IFC model ourselves. To determine these links between elements, we use the bounding boxes of the elements and define an offset within other elements as shown in Figure 1. We then compare the bounding boxes of each element with those of all other elements and check for overlaps. In the example above (Figure 1), a collision is found between the angle cleats and the database. This is to achieve that in the best case all elements can be automatically assigned to a category with the help of regular expressions. Once this step is completed, the user can display all elements that could not be automatically assigned and thus the user can assign them manually to the categories of ontology. If desired, the manual assignment can be performed globally for the entire model, if elements with similar names are present. The available categories are taken from a direct connection to an *Apache Jena FUSEKI*

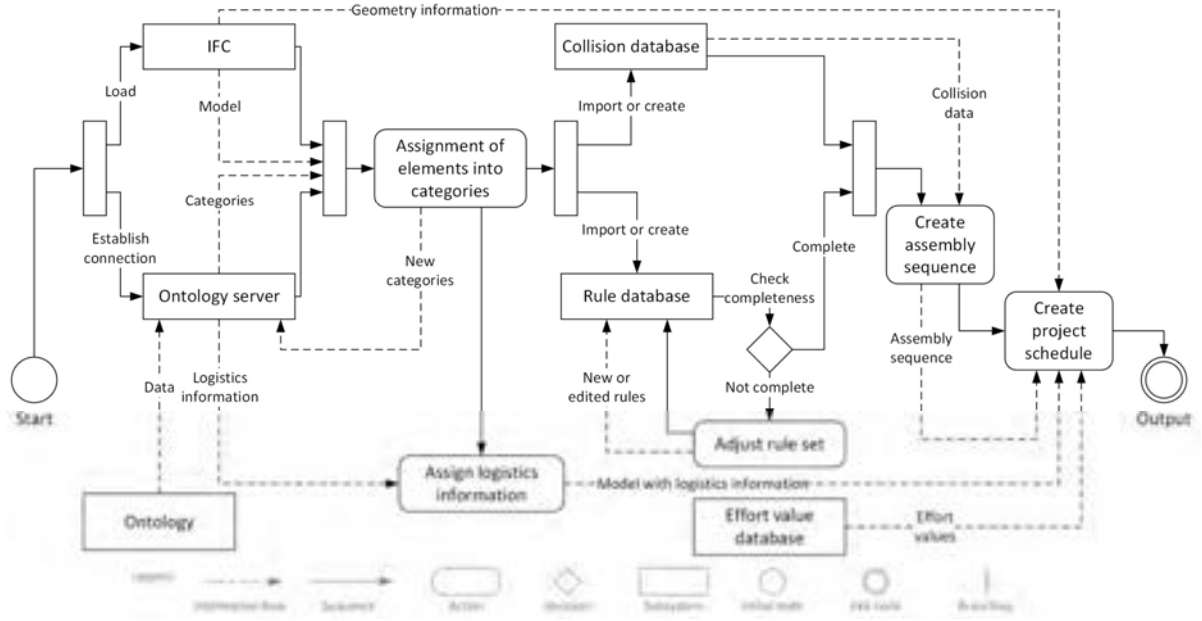

Figure 2. General methodology

column, due to a defined offset which slightly enlarges the bounding boxes, but not between both angle cleats. Using these overlaps, a collision database is created in which all collisions per building element are recorded. This procedure offers a great performance advantage for the actual creation of the construction manual, as the database only needs to be created once for each model and thus in the following steps different rule sets can be applied and tested with little time expenditure. As soon as the rule sets have been defined correctly, i.e. completely, the construction sequence for each element can be determined. In doing so, each foundation is considered separately so that processes can easily be parallelized if necessary.

To be able to assign the construction rules to the individual building elements, these building elements must first be assigned to the ontology categories. We have provided two different methods for this: On the one hand, an automatic assignment can be carried out using regular expressions. These regular expressions must either be stored in the ontology for each category or can be defined in a *JSON* (JavaScript Object Notation) ontology server, where a created ontology is uploaded (see Figure 2). If a required category is not available in the ontology, it can be created directly via the software extension developed by us and transferred to the ontology. After all elements have been assigned to a category, an assembly sequence can be defined using the rule database and collision database. The creation of the rule database and the creation of the assembly sequence is explained in the next chapter. The assembly sequence as well as the logistics information per element can be provided at the output. With the help of a provided effort value database it is also possible to create a schedule for the construction process from the assembly sequence and to validate it together with the geometric information from the 3D model in a simulation study, see chapter 5.

4 Automatically Generated Assembly Sequencing

To specify a construction sequence, a rule database is required in addition to a collision database and components classified in categories of the created

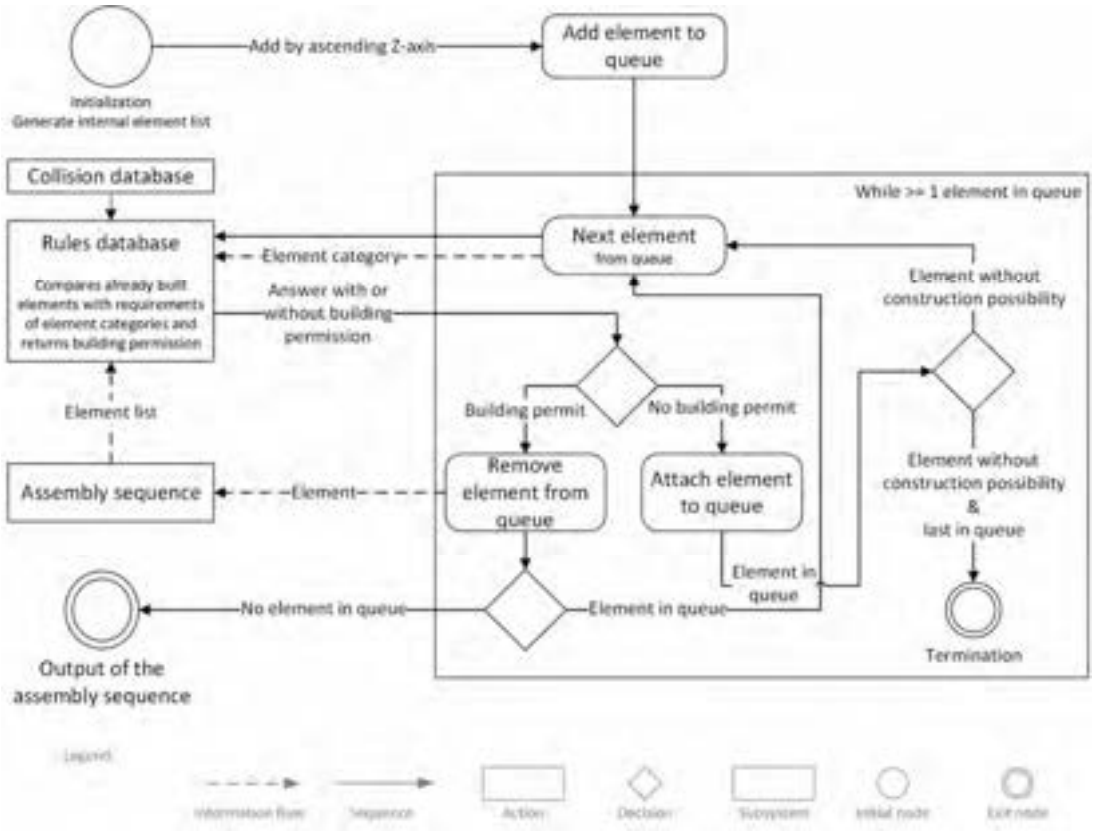

Figure 3. Rule-based assembly sequencing methodology flowchart

ontology. The rule database contains rules for assigning certain numbers of components to other components with AND connections. For each component, different rules can be linked together in the form of OR links. Since this is not a physics simulation, any torques occurring on components are not tolerable and must therefore be prevented by the rule set.

As an example, the rule set for the construction of a beam disregarding joining elements is shown below. The following rules apply to the construction of a beam:

Column(2)
∨
Column(1) ∧ Beam(1)
∨
Beam(2)

Figure 4. Example rules

The beam can therefore be attached either to two columns, one column and one beam, or to two beams as shown in Figure 4. This ensures that there are always two supports for the beam, so that no moments can occur at the supporting structure or the beams themselves and allowable moments in beams [8] and other parts can be neglected. When the rule set is defined, the construction manual can be generated. As shown in Figure 3, we start our rule-based assembly sequencing with the generation of an internal object list. This list contains all building elements which are then added to a queue by their ascending Z-axis. This ensures that the order of the objects is as close as possible to the actual order because we focus on buildings that are generally built from the bottom to the top. For a bridge construction, for example, two-way sorting would be necessary. Now the next element is taken from the queue in a loop and its category is passed to the rule database. The rules database compares already built elements with the requirements of the category of this element and returns a building permission or not. If the element receives a building permission, it will be appended to the building order. In the next step (not shown in the figure), the system always checks directly, independently of the queue, whether neighboring fastening elements (bolts, angle cleats and welds) can be built according to the rule set. If so, all required fastening elements will be immediately attached to the element to be fastened in the construction sequence, followed by the element to be attached. If the element has not received a building permission, it will be reattached to the queue. If there are no further building permissions and it is the last element in the queue, the rule set used will not be sufficient and the generation of the assembly sequence will be aborted. Otherwise, the element is

reattached to the queue so that it can be built later. If the element has received the building permission, it will be added to the building order. The construction sequence also serves the rule database as a basis for the decision. If there are no more objects in the queue, the assembly sequence can be output.

4.1 Case Study 1 – Simple Steel Construction Model

For the validation of our methodology, a simple steel construction model containing 78 elements is used as shown in Figure 5. Despite its low complexity, the design features correspond to an actual steel construction model. The model has two storage areas and simple steel structure on top of a concrete foundation. The steel construction consists of four columns and five beams with two concrete slabs on top, 60 bolt connections (in 30 groups), 16 angle cleats, 16 anchor rods and six steel plates (two of which are already welded to a beam before installation (pre-assembled)).

Figure 5. Overview of the simple model

After completion, this model is exported in IFC format and finally imported into *DESITE MD*. Using the software we developed, the elements of the model are then divided into categories of the ontology according to the methodology [2]. This is achieved using the implemented procedure, which matches elements by their names using regular expressions and automatically categorizes them. The collision database is created with an offset between elements of −0.02 m for the bolts and 0.03 m for all other elements. The collision database is checked against the model to ensure that all elements have collisions and that all elements of the model are considered in the later generated assembly sequence. Afterwards the rules for the assembly manual are defined. These can be quickly and easily adapted by using our rule editor. Once the rule set is defined, it is tested by creating an assembly based on it. To check the correctness of the rules, it has to be possible to create an assembly instruction in the first instance without causing any errors.

In the second step, the correctness of the building sequence is checked by an expert. Special attention is paid to whether the sequence is logical and consistent, for example, that no elements are built until elements that were not previously required have been built and thus no elements are levitating. If problems are found during the check, the rule set will be adjusted and then re-tested. Here, both the linking rules and the prioritization can be modified. To clarify the dependencies between the elements and to identify possible sources of error, the construction plan can be visualized as a Work Breakdown Structure (WBS). Figure 6 shows an example of the construction plan for a beam:

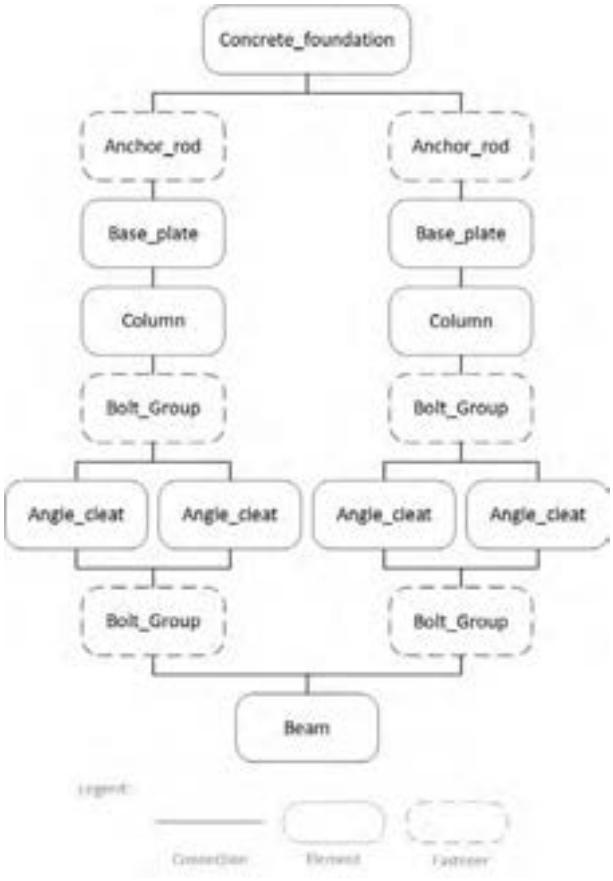

Figure 6. WBS graph of a beam

To build the beam, 15 additional elements are required, with the dashed elements representing connecting elements. Thus, the WBS shows the connection concept and not the construction sequence, since, for example, the final beam is first inserted and then directly bolted to the bolts. The advantage of the WBS illustration is that parallel processes can be identified. In addition, it offers the possibility to develop strategies to compensate for bottlenecks in a WBS branch by first building other branches for which all materials are available.

4.2 Case Study 2 – Complex Model

Once the assembly schedule for *Case Study 1* has been successfully created, we test the developed rule set on a more complex real model. The complex model is a section of a plant construction project of *thyssenkrupp Industrial Solutions* and contains 780 elements. To ensure general compatibility, the model is reduced to a steel construction tower as shown in Figure 7. The model consists of 16 concrete elements, 16 anchor rods, 4 base plates, 4 columns, 8 beams, 14 vertical bracings, 114 plates and 221 miscellaneous elements, connected with 94 bolt assemblies and 216 weld connections. Since the model was engineered in *Trimble Tekla Structures*, it has a completely different terminology. Therefore, the first step is to adjust the regular expressions to assign the categories of the created ontology. The first attempt to create an assembly sequence shows that the previously developed set of rules is not sufficient. A closer examination of the issue reveals that the existing categories of the ontology are also not sufficient.

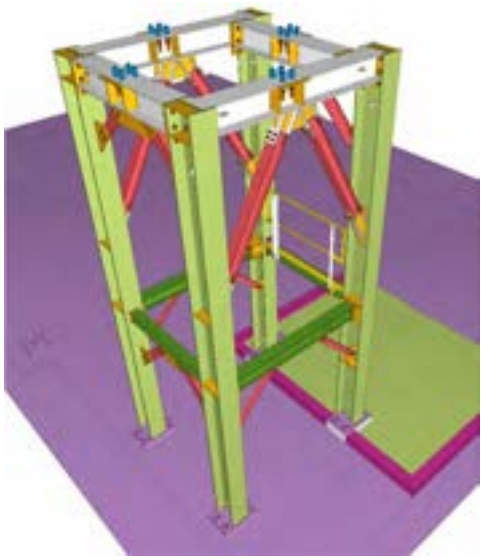

Figure 7. thyssenkrupp steel construction tower

Therefore, different categories are created via the communication link to the ontology server (as shown in Figure 2), especially for the fasteners that were previously assigned to only one category.

Based on this, the rule set is extended and tested using the collision database. After a few iterations the assembly sequence can be correctly created. This comprises 713 individual steps. However, a detailed step-by-step analysis shows that the assembly sequence for the diagonal beams is not logical, because one end of each beam has no direct connection. This problem is solved by recreating the collision database with a lower offset of 0.015 m to prevent the detection of a false number of required building elements in the surrounds.

5 Detailed Validation using Simulation

The detailed validation of the method for creating the assembly sequence is carried out with the help of discrete event simulation. For this purpose, the processes on the construction site are first planned. The generated assembly sequence is an essential prerequisite for a detailed analysis of the construction site assembly and the logistics processes. Using a generated assembly sequence (e.g. the simple model of Case Study 1 with 78 elements), a detailed BIM-based model and related information from the developed ontology, planning of processes on the construction site is carried out. For this purpose, different planning scenarios are defined for the processes on the construction site. In the planning scenarios the construction and logistics activities as well as the planning-relevant properties of the construction elements and materials of the building project are considered. For the creation of the scenarios, the assembly sequences specified by the construction plan and the dates of delivery of building materials are considered in detail. For the representation of scenarios, *Gantt* charts are used in planning. In the *Gantt* diagram, the individual deadlines of the planned processes on the construction site (such as transport, storage, and assembly) and the delivery schedules are coordinated. In addition, information from the ontology (e.g. requirements of building materials for storage and transport on the construction site) and formal descriptions of the processes are used to design the processes.

To enable simulation to validate the automatically generated assembly sequences, the defined processes on the construction site (such as the sequence of assembly, transport and storage) as well as the use of available resources (such as storage areas or transport equipment) need to be modeled. The planned processes, restrictions and resources can then be validated by simulation. For this purpose, material flow simulation models are built in *AnyLogic* based on the supplemented BIM model. Validation scenarios are experimentally examined using the simulation model. The simulation model provides valuable performance data in advance of construction activities and checks the planned equipment of the construction site (material flow and storage technology) and the planned deadlines.

In the following, this simulation-supported procedure is discussed for Case Study 1 – Simple Steel Construction Model (see Figure 8). For the execution of the simulation-supported validation of the construction manual, in addition to the data from the BIM model, the layout and the prepared construction plan (see section 4.1), assumptions are made regarding the dates of delivery of the components, personnel deployment and resources on the construction site. When designing the planning scenarios, it is necessary to know the exact construction sequence and deliveries in advance, because

they are coordinated with each other and thus transports and storage on the construction site need to be planned.

Information on material and resource requirements for each process (e.g. storage conditions for steel beams) from the ontology (see [2]) is used to design transport and storage.

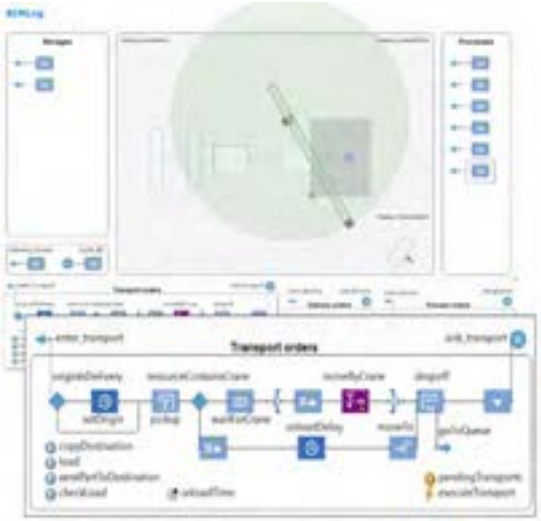

Figure 8. Example simulation model for Case Study 1 – Simple Steel Construction Model

In the simulation model (Figure 8) the layout, the positions of the six assembly locations of the elements, and the project-relevant processes (such as the assembly queues in the *Processes* area and the storages in the *Storages* area) are formalized. The processes sequences (transport by crane, deliveries to the construction site, as well as assembly and pre-assembly) are built in the simulation model (see Figure 8). The modeled processes conform to the generally valid process description at the construction site. They can therefore be extended, adapted and reused for new construction projects or planning scenarios. The relevant process sequences are used in the simulation according to the planning scenario.

The resources planned for the project are one crane, one crane operator, and one worker. The planning data from a defined scenario is implemented in the simulation model as tables, e.g. bill of materials for each construction process, scheduled deliveries to the construction site, scheduled start times of construction processes, transport processes and warehouse processes as well as resources scheduled for the processes. The simulation ensures that the components will only be delivered if they can be stored or installed directly. The simulated process times of the assembly processes are entered into a table during the simulation run, so that the duration of the individual construction processes and the total duration of the project can be estimated. An animation of the processes illustrates the approximate sequence of logistics processes on the construction site.

To evaluate the planning scenario, in addition to the simulated process times, key performance indicators, such as the utilization of resources (in percent) or the utilization of storage areas (in storage units) are calculated over the entire duration of the simulated project. The simulation-based validation provides a consistent and valid logistics model that can also be used to control logistics on the construction site. In case 1, the simulation points out that the crane, the crane operator, and the employee are almost always working at 100% capacity at the beginning of the simulated time (see Figure 9). This indicates that a new scenario with a second crane could lead to a better utilization of resources and personnel. Therefore, this scenario with two cranes is also being tested in a simulation study. The use of two cranes for Case 1 leads to a reduction of the simulated project time. However, this scenario is not regarded to be economical.

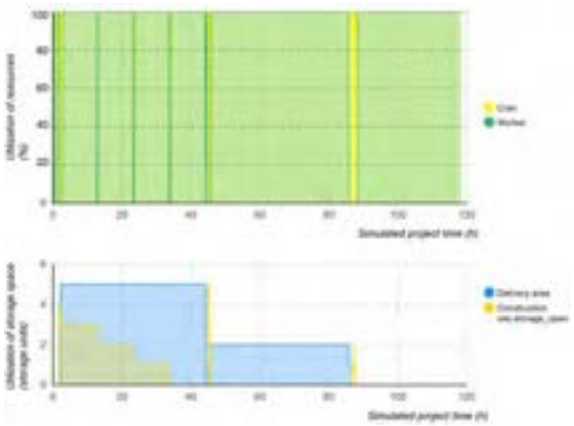

Figure 9. Utilization of resources (%) and utilization of storage space (storage units)

In the first scenario with one crane, the simulation carried out shows the utilization of the storage areas as an example. At the beginning of the construction processes the delivery area is highly utilized and the construction site storage (open storage) only stores a few parts over simulated project time (max. five storage units). Thus, the simulation provides the requirements for dimensioning of storage areas on the construction site (see Figure 9).

6 Conclusion & Outlook

Our approach demonstrates that creating step-by-step instructions for IFC files from any source works very well even at this early stage. The main effort lies in the categorization of the elements. Depending on the source of the IFC file, this can be greatly simplified and thus accelerated by using regular expressions. However, regular expressions can only be used across projects for models in which elements of the same type also have a

similar name. Therefore, it is very important that the models or their elements are always classified in the same way. If a uniform classification is not available, a manual revision based on given guidelines must be carried out. To avoid this problem, interfaces to different modeling tools must be developed. These interfaces could be designed in such a way that they provide more information than the respective IFC export function provides. In addition, this also eliminates the need to create a collision database, since the links between components can usually be determined directly by the design software. This is particularly advantageous for components with a more complex geometry, such as angled pipe connections or reinforcement meshes. Bidirectional communication is also conceivable. With a sufficient number of previous design projects and thus maintenance of the ontology as well as regular expressions it will be possible to generate the design instruction with a single click. In addition to the application for simulation, cost estimation [3] is also possible.

To evaluate our methodology in terms of its practical applicability, we have presented it to seven experts from the industry. The experts are representatives of companies from the fields of plant construction and logistics. They agree that detailed digital construction site logistics planning is of high importance or is becoming increasingly important. The participants in the evaluation survey are convinced that enriching the BIM model with information on construction site logistics will offer their companies advantages in future in the exchange between company departments and project partners. In their opinion, this information should also be available in digital form directly on the construction site. The semi-automatic generation of step-by-step construction instructions is less or not important for two in seven participants in the evaluation survey, while five in seven rate it as important or very important. However, all respondents agree that semi-automatic generation of schedules is very helpful for their companies.

The high potential lies in the iterative construction process and construction logistics planning which is made possible by our methodology. This iterative planning requires that the current state of construction is known accurately at all times. There are already many established possibilities for this today, by means of automated continuous construction progress monitoring [9]. As soon as an interface for communication with the simulation tool has been developed, it is possible to generate the simulation model semi-automatically. In the end, a decision maker will still make the final choice for the preferred scenario. In this way, in case of delays due to bad weather or delayed deliveries, damaged material etc., alternative strategies can be developed in a short time and with little manpower, which ensures an efficient construction process despite the disruption and also minimizes otherwise occurring delays in the best possible way.

7 Acknowledgements

The results presented in this paper originated in the joint research project "*BIMLog* - BIM-Based Logistics Planning and Control in Large-Scale Plant Construction" at the *University of Kassel* and the *Ruhr-Universität Bochum*.

This research project (19720 N) has been carried out within the *Industrial Collective Research* (IGF) and has been funded via the *German Federation of Industrial Research Associations* (AiF) by the *Federal Ministry for Economic Affairs and Energy* (BMWi) on the basis of a decision of the *German Bundestag* and on behalf of *Bundesvereinigung Logistik* (BVL) *e.V.* (German Logistics Association). We would also like to thank *thyssenkrupp Industrial Solutions*, who kindly provided the model for Case 2, and *Doosan Lentjes* for supporting our research activities with data and expert knowledge of large-scale plant construction projects.

References

[1] Chevallier N. and Russell A. *Canadian journal of civil engineering*, 6:1059–1077, 1998.

[2] Weber J., Stolipin J., König M. and Wenzel S. Ontology for Logistics Requirements on a 4D BIM for Semi-Automatic Storage Space Planning. In *Proceedings of the International Symposium on Automation and Robotics in Construction (IAARC)*. Banff, AB, Canada, 2019.

[3] Fan S.-L., Wu C.-H. and Hun C.-C. *淡江理工學刊*, 3:223–232, 2015.

[4] Castro-Lacouture D., Süer G., Gonzalez-Joaqui J. and Yates J. *Journal of Construction Engineering and Management*, 10:1096–1104, 2009.

[5] Borrmann A., Schraufstetter S. and Rank E. *Journal of Computing in Civil Engineering*, 1:34–46, 2009.

[6] Daum S. and Borrmann A. *Advanced Engineering Informatics*, 4:272–286, 2014.

[7] Liu H., Lei Z., Li H. and Al-Hussein M. An automatic scheduling approach: building information modeling-based onsite scheduling for panelized construction. In *Proceedings of the Construction Research Congress: Construction in a Global Network*. Atlanta, Georgia, USA, 2014.

[8] American Institute of Steel Construction, Inc. Manual of Steel Construction, 6th Edition, New York, USA, 1966.

[9] Pučko Z., Šuman N. and Rebolj D. *Advanced Engineering Informatics*, 27–40, 2018.

An Analysis of 4D-BIM Construction Planning: Advantages, Risks and Challenges

P. Farnood Ahmadi[a] and M. Arashpour[b]

[a] Department of Construction Management, Planning Engineer, Hickory Group, Melbourne, Australia
[b] Department of Civil Engineering, Monash University, Melbourne, Australia
E-mail: p.farnood@hickory.com.au, Mehrdad.Arashpour@monash.edu

Abstract –

The rapid growth on the field of project management and building information modelling (BIM) has led not only to the enhancement of architectural/structural design, construction methodology and operation of facilities but also to the generating of the new and exciting applications such as 4D simulations, project scheduling and controlling. 4D planning and scheduling is one of the BIM uses based on the BIM guidelines. Poor quality of construction works, and ineffective scheduling and planning can be significantly mitigated by adopting BIM in early design processes. In this paper, the advantages, possible risks of 4D-BIM construction scheduling, existing and future challenges of 4D planning in the construction industry are discussed. First presented is the primary concept of 4D-BIM simulation with its possible applications and capabilities in construction planning. After that, weaknesses and strengths of generation of 4D simulation/animation of the conventional and prefabricated construction building projects according to the construction schedule are analyzed. The results show that the integration of BIM model in the construction program is essential and ensures greater control over the construction projects. Also, it can be concluded that the automation in 4D-planning needs to be more considered and optimized by programing and formulating of construction planning and geometric model creation. Finally, this study contributes to the construction/project managers to improve their management performance and efficiency of works, also this investigation contributes to identify research gaps and opportunities for future study.

Keywords –

Building information modelling (BIM); 4D simulation; Project scheduling; Construction projects

1 Introduction

Nowadays, construction building projects are becoming much more difficult and complex. Prevalent problems regarding construction building projects arising from weak and insufficient connection between design and construction phases due to inefficient transferring of information and data have been reported. Building Information Modelling (BIM) is a digital presentation of functional and physical characteristics of a project which is regarded as a potential solution to challenges within the design and construction stages. Therefore, BIM is a good technology not only in the design stage, but also in the construction stage, provided it ensures time saving and working effectiveness throughout the project life cycle. To create a 4D model, BIM as a powerful planning and 3D modelling tool need to be complemented with a specific planning software package. The 4D model of a project can be developed to simulate a graphical sequence of execution tasks and construction operations, therewith providing the stockholder with a visual and virtual understanding of the construction process [1-3]. 4D-BIM has been used by designers, engineers and planners to optimize design, and to analyze the buildability of a project plan and manage resource requirements [3]. 4D planning and scheduling are some of the BIM use based on the BIM guidelines. Poor quality of construction works, and ineffectual construction planning can be significantly diminished by adopting BIM in the early design process [1, 4]. It should be noted that the virtual project planning and progress reporting are the scheduling-related themes of the construction stage and some of the intent of these themes are safety planning, cost reporting, and equipment machine control. The utilization of 4D-BIM modelling in line with analyzing the effectiveness of delays on the project schedule and tracking the actual progress of the project schedule improved the construction performance. The onsite construction performance can be enhanced by linking building information models with schedules so as describe the: 1) material handling and site logistics 2)

virtual building model 3) site production structures 4) environmental management controls and related equipment [5]. A study presented a BIM-based integrated scheduling approach for detailed scheduling under resource constraint to simplify the automatic generation of the optimum construction schedule for building projects by performing in-depth integration of BIM/project models with process simulation and work break down (WBS) information. The proposed scheduling system can produce schedules for panelized construction. This system facilitates on-site assembly work by lessening human error [2]. The contractors' tender team can use 4D-BIM scheduling in developing executable risk mitigation strategies. In addition to that the advancement of efficient risk mitigation strategies are supported by 4D-BIM tool during the procurement phase of an actual construction project. Using the 4D-BIM tool has some challenges due to the dynamic nature of the procurement phase resulting the 4D model was not an invaluable tool for contractors [6]. A study reported the development of a control method and logistics scheduling for site assembly of Engineer-to-Order (ETO) prefabrication building system using 4D BIM as a mechanism for dealing with the uncertainties in the construction project [7]. 4D-BIM contributes to improve the work-space scheduling and the associated frameworks enable the detection of possible site congestions by utilizing workspace specifications, construction schedule and activities. 4D-BIM tool improves safety planning process by analyzing site-specific temporal and spatial information [8]. Another investigation introduced a framework for automatic scheduling of construction project through automatic data extraction by using BIM. The proposed framework creates a schedule which contains construction tasks, duration and the activity's sequences. The model has some limitations which is related to the scalability and complexity. The model is a simple BIMs with limited details so by increasing its complexity the model requires more time to generate the construction schedule, and finally some practical methods need to be applied to determine the interdependency between activities and associated elements to minimize the use of use input and default settings [9]. An innovative BIM-based management workflow has been suggested which integrates digital programing with BIM to implement cost planning and efficient schedule of building fabric maintenance. In this research Weibull Distribution is utilized to specify the main information about the corrective and preventive maintenance for building fabric components. A case study was conducted for checking the validation of the model and the practicability of the proposed workflow. This study not only reduced the knowledge gap between practical maintenance applications and maintenance theory but also linked the maintenance phase with design and construction phases. The investigation asserted that a lot of manual works related to information flow need to be done such as data gathering, entering details and creation of functions and tables [10].

By considering the development of the abovementioned applications and technologies, this study accomplishes a review of the relevant literature with the following objectives: 1) summarizing the capabilities and applications of integrating BIM/4D-BIM in construction projects; and 2) identifying advantages of integrating BIM/4D-BIM in construction projects; and 3) summarizing the potential risks and challenges in integrating BIM/4D-BIM in construction projects 4) analyzing of previous investigations 5) conducting a case study for validation of results. This paper aims to identify research gaps and opportunities for future study by considering the advantages, risks and challenges of using BIM and 4D-BIM planning in construction projects.

2 The Implication of 4D-BIM in the Construction Projects: Capabilities and Applications

2.1 4D-BIM Capabilities

The increasing utilization of 4D modelling in construction projects emphasizes on chances for using these capabilities in recent digital management system incorporating with role reorganization, workflows and practices providing a tool for onsite monitoring and constructability analysis of construction progress. The 4D-BIM can only be developed by the accretion of three main capabilities as follow, 1) capability is the visualization of space and time relationships of construction project activities, 2) analysis of the construction program to evaluate implementations, and 3) reduction of errors via construction schedule validation to improve the integrity of communications and collaborations between the project team. 4D-BIM capabilities can be dived into two categories: 1) construction scheduling, and 2) site scheduling. Some of the prevalent end points in leveraging 4D-BIM capabilities are exemplified to improve scheduling, monitoring and waste management. Rule-checking method is a 4D-BIM platform with a rule engine which provides a capability to determine effective environmental rules to support a rule-checking method. In this method, a time-space detection would automatically recognise environmental hot-spots and enhance monitoring performance [5]. 4D simulation allows for the investigation of different scenarios to optimize the construction process. The arrival of BIM as a first commercial tool has made this discipline noticeably easier, specifically with the capability to use

BIM to streamline the creation of links between activities and the 3D models. 4D modelling provides some planning capabilities and incorporates the CPM logic into the software [11].

2.2 4D-BIM Applications

4D-BIM is used to identify project clashes by applying the outcomes to the case study in order to assess feasibility of the system and practical applications. The application of BIM technology to task scheduling is an appropriate choice for clarification and organization of the execution scheduling [12]. A communication strategy has been proposed between 4D-BIM and Chronographical scheduling application developed on VBA Excel. The use Chronographical 4D planning and its compatible approaches, not only consider the linearity of team's production and the workspaces, but also make the study of links between activities easier. This modelling simplifies the automation of the 4D-BIM and change management process [11]. 4D-BIM is used to investigate and validate necessary details to incorporate a special type of sensor (ultrawide band localization system) and try to diagnose the right amount of details to capture the movement of equipment, work force and material. In this application, semantic data modelling and data mining have been used. This integration provides a flexible and high-performing pattern recognition methods [13]. A BIM base decision-making framework is proposed to minimise construction waste in design phase and to automate waste analysis by planning the process of work to reduce the material wastes for roof sheathing installation for prefabricated buildings. A hybrid algorithm integrating greedy algorithm and particle swarm is used to optimize material cutting plans for minimising sheathing material waste [14].

Integration of 4D-BIM with as-built photographs using time-laps photos was presented for monitoring of construction progress. Visualization is needed to create an automatic monitoring system, and this could be achievable via creating a 4D-BIM modelling from point cloud images and implementing an image classification for detection of progress and as-scheduled model from BIM. Regarding to this matter a framework is proposed to develop a concept archetype of a hybrid system to demonstrate the capability of processing images of construction site and integration of them with the nD-BIM within a game like VR environment. This framework enables stockholders and construction managers to use an advanced decision-making tool while detecting the inconsistencies in and efficient manner [15]. 4D-BIM is used to illustrate the planning phase to communicate, interact and get the final design approval and construction sequence. For improving the communication of construction planning and sequencing, 4D-BIM is developed to link BIM to the project schedule. in addition to that for generating a cash flow 4D-BIM is linked to the costing data [16]. 4D-BIM is presented as a practical tool for determining construction risks in early stages of construction building projects to take proactive measures in the design and scheduling phase to mitigate site hazards and to plan for safety resource allocations [17, 18].

3 Advantages of Integrating BIM/4D-BIM in Construction Projects

Four case studies demonstrate the time and cost savings realized in using and developing a BIM model for the design, preconstruction, project scheduling and construction phases. As mentioned, some noticeable benefits are realized through the applying of BIM technology in construction projects. The time and cost benefits to the owner were important and the unknown costs that were reduced via visualization, coordination, realisation and detection of clashes and conflicts. Some effective negative issues or risks related to the project planning phase can be controlled or mitigated via using BIM technology such as 1) incomplete documents and design 2) numerous uncoordinated consultants 3) field construction ahead of design 4) owner's frequent design/scop changes and constant design development [19]. One of the most crucial benefits regarding to the integration of BIM within prefabrication is the reduction of disagreement in a final model between manufacturers and designers. Second vital advantage is the simplifying the procurement plan as a united BIM system can facilitate design coordination from the beginning of the project. Early detection of long completion time, exploring design limitations for prefabrications, reducing the fabrication cycle time and coordination errors are also listed as the benefits of integrating BIM in prefabrication industry. The reduction in project duration and the increment in mass customisation are the other advantages of integrating BIM into the design and construction stages of a prefabrication building projects [20]. BIM gives unique opportunities to further harness the performance of prefabricated construction. BIM mitigates the risks of programing in prefabricated construction industry [21].

An study showed that only 7 advantages out of 18 advantages are identified and ranked as important with high value as follow: increase efficiency and productivity in pre-construction and main construction process, determine cost and time related to design changes, rectify clashes in design, enhance and maintain synchronized communication, develop integrated construction planning and scheduling, recognise time-based clashes, track and monitor the progress of project during construction. It should be noted that the benefits are significantly depends on BIM implementation which is

driven by some factors the such as personal commitments, mutual trust/respect, early involvement of project team, capability to use BIM technology [22]. 4D environment planning contributes to plan and manage the construction phases including logistics and operations. Also, the 4D-BIM development allows to status, monitor and update the construction progress. 4D-BIM is a practical tool and technology for development of economic and technical documentation such project schedule to be submitted for a construction project bidding. Visualization of work schedule performs a better control and construction management over the different stages of project. Correct distribution of workers, minimising interferences among different construction tasks and preventing unnecessary overlaps into the various construction sectors are the other benefits of using 4D-BIM. 4D modelling increases and modifies the logical-temporal connections between the various tasks which brings a high level of off-site prefabrication and continues improvement of works [23]. Table 1 illustrates a synopsis of 4D-BIM benefits.

Table 1. A summarised list of 4D-BIM advantages

No.	Advantages of 4D-BIM	Sources in Literature
1	Enhancing the project performance	[24, 25]
2	Efficient planning and scheduling	[25, 26]
3	Detailing the project stages	[25, 26]
4	Generating multiple planned scenarios	[25, 27]
5	Being used for project bidding purposes	[25]
6	Enhancing the ability to adapt future plans and network changes	[25, 28]
7	Utilising 4D-BIM in line with VR and mixed reality technologies	[24, 25]
8	Using 4D-BIM in line with 3D point cloud scanning technology	[25, 29]
9	Being a proactive platform for risk detection	[26, 25]
10	Being proactive in directly advising and addressing on solutions for projects issues	[27, 25]

4 Potential Risks of Integrating BIM/4D-BIM in Construction Projects

BIM risks are defined in two categories: contractual and technical. Lack of designation of possession of the BIM data and protection regarding to the copyright laws and other legal issues are known as the first risk. Determining a person to be responsible to enter the BIM data into the model and ensuring its accuracy and consistency is another contractual risk. Cost and schedule are the other dimensions of BIM and the associated contractual and technological responsibilities are becoming an issue. Many contract administrators require subcontractors to present detailed critical path method plans and related work costs prior to start of the construction project. Having an efficient collaboration to share the risks of using BIM between the project participants is one of the most effective way to coupe with these risks [19]. Misunderstanding of BIM as the potential management barrier leads to serious risks such as hindering the remarkable achievement and benefits of BIM in construction industry. Having no mature dispute resolution mechanism increases the risks of BIM implementation. There are some risks related to the costs and training time due to learning curve which justifies the noticeable decrease in staff member's productivity and performance. Some employers are worry about squandering money and time on labor training. In comparison with conventional methodologies and techniques, the use of BIM increases the costs during the design phase which might increase the risk of BIM implementation. BIM impeding profitability in construction building industry is known as a significant risk. Insufficient standard practices and insurance applicable to BIM implementation brings new risks to all project's participants. Lack of a standard form of contract brings uncertainty regarding to the BIM implementation and to dealing with this uncertainty more money and time is needed to be spent [21].

5 Challenges in Integrating BIM/4D-BIM in Construction Projects

The main Adoption and acceptance of the BIM has been much lower than expected due to the main two reasons, managerial and technical. As the technical sake: a well-organized transactional construction process model is needed to omit data interoperability necessities, the requirement need to be identified that the digital design data is computable, and Practical strategies for deliberate exchanges and integration of meaningful information need to be developed between the BIM components. The managerial reason cluster around use and implementation of BIM. Now, there is no an explicit consensus on how to use or implement BIM. As mentioned, a standardise BIM process need to be

established to define guidelines for its implementation. On the other hand, finding an appropriate time to include and engage project's participants into BIM process will be a serious challenge for owners [19]. The changes in business practices to support BIM process is the most significant challenge in the prefabrication. Changing CAD technology to BIM needs more investment in BIM software, also hardware and training are other two challenges in prefabrication. BIM requires comprehensive knowledge of construction processes, methods and extensive resources. As mentioned, legal and collaborative issues are known as barrier of using BIM in construction projects since using BIM contrasts to assign the responsibility to each party and to define liability issues between the parties. In addition, applying BIM in prefabrication building projects increases the complexity of the model of intellectual property rights [20]. Difficulty in reengineering the current existing process and adaptation to the BIM process is a challenge. Lack of adaption of BIM tools to the building codes to meet the requirements is another barrier for BIM implementation. Increase workload for modelling, resistance to alterations, negative orientation towards data sharing and collaborative working, lack of a well-stablished workflow, lack of an efficient interactivity, lack of sufficient external stimulus, lack of doing research on BIM implementation, costs of tools and hiring BIM specialists, vague economic benefits, lack of protective legislation for protecting the IP rights and lack of BIM standards are listed as BIM challenges in construction building projects [21].

Some stakeholders believe that 4D-BIM is used as a business tool for marketing purposes and that most are not interested to develop a 4D-BIM model as opposed to a 2D program during construction projects which are frequently changing. Previous studies emphasised that some 4D-BIM approaches are constrained due to lack of a cooperative environment. The behaviour and culture of those who involved in BIM processes need to be changed to accept this technology. Modifying of culture can be difficult for those who have accomplished their works in the same method may find it challenging to adapt and accept. Project team and client experiences to implement 4D-BIM are further barriers to the associated technology and process. The size of the organization or company, resources availability and risks of each projects might be effective to the adaption of 4D-BIM technology. Insufficient knowledge and technical matters are two barriers for adoption of 4D-BIM in safety management [30].

6 Analysis of previous investigations

All The database of the selected papers includes 100 articles (including the above cited studies) published from 2010-2020. 4D-BIM Construction Planning, BIM scheduling, 4D planning, 4D scheduling, 4D Construction Planning, 4D-BIM Construction and BIM are used as the search criteria and key words for the advanced search through ScienceDirect website. According to the database of selected papers, as analysis has been done to find the most occurring keywords. VOSviewer, a source graph and network analysis software has been used for this analysis [31].

The outcome is shown in Figure. 1, showing the high occurrence of some words such as building information modelling, BIM implementation, 4D model, construction process, visualization, schedule and etc in 2 various clusters. The size of each circle represents its weight. The higher weight of an item resulted in the larger circle and label of the item. It is quite obvious that the red cluster is the representative of the fourth dimension of 4D-BIM and the most related keywords to this study. 4D model which is grouped by schedule related cluster has the strong direct and indirect connection with building information modelling, collaboration, BIM implementation, adoption, productivity, analysis, cost and time from the green cluster.

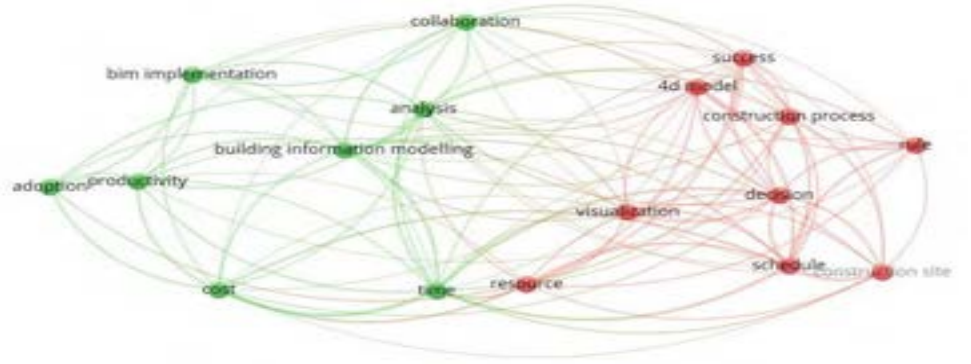

Figure 1. Network representation of keywords re-occurrence in literature

From the above figure, this can be comprehended that 4D modelling as a demanding visualization methodology

is the best solution to visualize the construction process and 2D construction schedule. This would be a practical approach to the successful completion of a construction project, saving time/cost and improving performance of the work, resource management and decision-making process. Automation of construction scheduling as a new approach need more collaboration between different parties to be implemented in construction industry. The adoption of this approach has some benefits like improving the performance of site manufacturing and on-site works, increasing the productivity of works and site safety, and challenges such as BIM implementation and rules as these have been mentioned in literature review.

7 Case Study

The Ovolo Hotel is a 6-storey building including 123-guest room, basement and a ground floor common area. This project is also featured SYNC bathroom pods and prefabricated modules which helped to reduce the construction timeline and fast track the project. Program reduced by up to 30% using fast-track prefabricated system in structure. It should be noted that the prefabricated system design, fabrication and on-site installation always come with BIM modelling. Some advantages, risk and challenges of using prefabricated system integrated BIM are mentioned as follow:

7.1 Advantages of prefabricated system and BIM/4D-BIM in Prefabrication

Time saving is an important advantage of the prefabricated system, for instance, once level 4 is installed and bolted, level 1 can be completely stripped out and the level is ready for fitting out. But in the conventional system fitting out is going to be started about 8 levels below the wet deck. As it is illustrated in Figure 2, you can see that façade is already erected and the fitting out period is reduced by 5 working days in average for each level. The financial advantages of the prefabricated system far outweigh than its drawbacks. It should be noted that the cost of pre-construction works in early stages including design and prefabrication cost is a prefabricated project is significantly higher than pre-works cost in a conventional project, but these costs can be offset in construction stages by proper sequencing and coordinating of off-site and on-site works. Prefabricated system eliminates costs of few trades on site such as façade installation costs which is 60% cheaper than façade installation in a conventional system. Prefabricated system requires less labor on site which means less labor cost in construction period. In terms of safety, the prefabricated system does have some risks both horizontal and vertical. Proper sequencing of loading elements and prefabricated modules on to the job reduces safety-related risks on site. Façade is already installed, and this feature creates full protection. In the prefabricated system there is no form work and back propping, so site is always clean which this increases site safety. As it is mentioned, using the prefabricated modules have noticeable advantages by itself, but by providing an effective sequence of construction/loading and visualizing them construction works can be optimized, and site safety and more time/cost saving can be guaranteed. As the prefabricated system is totally a crane-based system, optimization and visualization of construction sequence and loading plan is highly recommended.

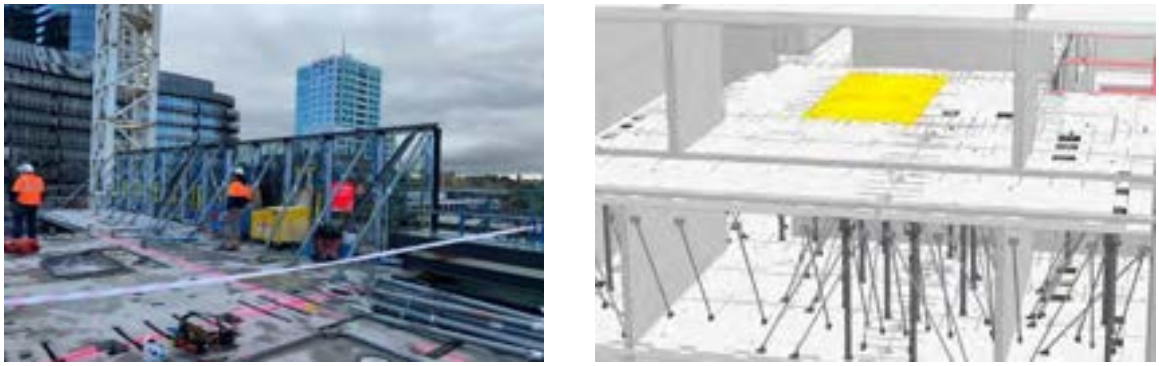

Figure 2. 3D Geometric model of the structure and prefabricated modules

7.2 Challenges/risks of prefabricated system and BIM/4D-BIM in Prefabrication

The main issue in BIM/4D implementation is related to services. Everything related to design such as shop drawings and coordination of shop drawings need to be locked-in early. If all the design related to services is not locked-in on time and early, then technically all penetrations would be wrong due to this fact that all penetrations are casted already in the prefabricated modules. So, any changes need to be captured or any rectifications need to be done early and before pouring

concrete off site. If all related design things are not locked-in enough, all hard works such as over layering, penetrations/service coordination go down to drawings which is required to be checked and reviewed by different groups engaged in a project and this is a very time-consuming process. In a conventional system because everything is in-situ, manipulations and making some changes is possible even in last minutes. But as it mentioned above in the prefabricated system pre-works should be well organized because making changes on site is quite impossible after fabrication of modules. In general, design works in a prefabricated project is more complicated than those in conventional project. To make a prefabricated system perfect, effective and to make key decisions early, less duration should be allocated to the design and material procurement in construction program. For this purpose, in addition to the practical experience, high level of technical knowledge is required in different areas such as creating an effective design (3D model), coordinating of trades off site and planning the construction sequence well enough. Because the prefabricated system method is almost new, labors need to be trained and engineers should teach them the new critical path and sequence of work to change their mind set from conventional to the prefabricated system. In summary, from the above-mentioned challenges and risks in both literature and the case study, it can be concluded that using BIM-4D or in another word visualizing the 3D model contributes a lot in clash detection for early rectifications, optimizes the program of the project from design to construction stages and clarifies construction sequence for engineers, coordinators, managers and labors to streamline the construction process and reduce the associated risks and challenges.

8 Conclusion

The study identified some noticeable advantages, risks and challenges of using BIM/4D-BIM in Construction Projects. The research concludes that the adoption of 4D-BIM in construction industry is highly recommended to improve and facilitate off-site and on-site construction works. Shortening and streamlining the procurement, design, prefabrication and construction duration and process in the project schedule are the significant advantages of 4D-BIM integration in the construction industry. Using BIM/4D-BIM can reduce coordination risks, the fabrication cycle time and risks of programing in construction industry. 4D-BIM enables different project teams to be involved early in design and prefabrication/construction process to detect the existing clashes and design errors. For setting a more realistic target, 4D-BIM contributes to visualize the construction and logistic plan. Some serious risks and barriers are acknowledged such as contractual and technical limitations which lead to legal risks and misunderstanding of BIM/4D-BIM. Implementing BIM/4D-BIM requires enough national and international standard practices, comprehensive practical and technical knowledge in the construction industry. Regarding to technical limitations and practical experiences, the automation of the 4D-BIM is required to optimize and simplify the process for better understanding of clients and subcontractors who are not advanced enough to understand the 4D-BIM concept. By automating the process less time and cost are needed to develop the 4D model and less technical knowledge is needed for model implementation which could lead to more future development and adoption of 4D-BIM.

9 Acknowledgments

The Authors gratefully acknowledge the contribution provided by Hickory Group and Monash University with coordination of the department of civil engineering. Special appreciation goes to Ayman Tawil and Alex Stavrou for their technical assistance.

References

[1] Ganbat T. Chong H. Liao P. Lee C. A Cross-Systematic Review of Addressing Risks in Building Information Modelling-Enabled International Construction Projects. *Archives of Computational Methods in Engineering,* 26:899–931, 2019.

[2] Liu H. Al-Hussein M. Lu M. BIM-based integrated approach for detailed construction scheduling under resource constraints. *Automation in Construction*, 53:29–43, 2015.

[3] Mahalingam A. Kashyap R. Mahajan C. An evaluation of the applicability of 4D CAD on construction projects. *Automation in Construction*, 19:148–159, 2010.

[4] Pezeshki Z. Soleimani Ivari. S.A. Applications of BIM: A Brief Review and Future Outline. *Arch Computat Methods Eng,* 25:273–312, 2018.

[5] Jupp, J. 4D BIM for Environmental Planning and Management. *International High- Performance Built Environment Conference – A Sustainable Built Environment Conference,* Sydney, Australia, Pages 180: 190 – 201, 2017.

[6] Sloot R.N.F. Heutink A. Voordijk J.T. Assessing usefulness of 4D BIM tools in risk mitigation strategies. *Automation in Construction,* 106:102881, 2019.

[7] Bortolini R. Torres Formosoa C. Viana D.D. Site logistics planning and control for engineer-to-order prefabricated building systems using BIM 4D modelling. *Automation in Construction,* 98:248–

264, 2019.

[8] Asadzadeh A. Arashpour M. Li H. Ngo T. Bab-Hadiashar A. Sensor-based safety management. *Automation in Construction,* 113:103128, 2020.

[9] Kim H. Anderson K. Lee S. Hildreth J. Generating construction schedules through automatic data extraction using open BIM (building information modelling) technology. *Automation in Construction,* 35:285-295, 2013.

[10] Chen C. Tang L. BIM-based integrated management workflow design for schedule and cost planning of building fabric maintenance. *Automation in Construction,* 107:102944, 2019.

[11] Mazars T. Francis A. Chronographical spatiotemporal dynamic 4D planning. *Automation in Construction,* 112:103076, 2020.

[12] Candelario-Garrido A. García-Sanz-Calcedo J. Manuel Reyes Rodríguez A. A quantitative analysis on the feasibility of 4D Planning Graphic Systems versus Conventional Systems in building projects. Sustainable Cities and Society,35:378–384, 2017.

[13] Oliveira E. Ferreira Júnior C. Correa F. Simulation of Construction Processes as a Link Between BIM Models and Construction Progression On-site. *Proceedings of the 35th CIB W78 2018 Conference: IT in Design, Construction, and Management.* Pages 11-18, USA, Chicago, 2018.

[14] Liu H. Sydora C. Sadiq Altaf M. Han S. Al-Hussein M. Towards sustainable construction: BIM-enabled design and planning of roof sheathing installation for prefabricated buildings. *Journal of Cleaner Production*, 235:1189-1201, 2019.

[15] Pour Rahimian F. Seyedzadeh S. Oliver S. Rodriguez S. Dawood N. On-demand monitoring of construction projects through a game-like hybrid application of BIM and machine learning. *Automation in Construction*, 110:103012, 2020.

[16] Shou W. Wang J. Wang X. Yih Chong H. A Comparative Review of Building Information Modelling Implementation in Building and Infrastructure Industries. *Archives of Computational Methods in Engineering*, 22:291–308, 2015.

[17] Jin Z. Gambatese J. Liu D. Using 4D BIM to assess construction risks during the design phase. *Engineering, Construction and Architectural Management*, 26 (11): 2637-2654, 2019.

[18] Jin Z. Gambatese J. Liu D. Dharmapalan V. Risk Assessment in 4D Building Information Modelling for Multistorey Buildings. *Proceedings of the Joint CIB W099 and TG59 Conference Coping with the Complexity of Safety, Health, and Wellbeing in Construction.* Pages 84-92, Brazil, Salvador, 2018.

[19] Azhar S. PH.D. A.M.ASCE. Building Information Modeling (BIM): Trends, Benefits, Risks, and Challenges for the AEC Industry. *Leadership and Management in Engineering,* 11:241-252, 2011.

[20] Mostafa S. Pyung Kim k. Tam V. Rahnamayiezekavat P. Exploring the status, benefits, barriers and opportunities of using BIM for advancing prefabrication practice. *International Journal of Construction Management*, 20 (2): 146-156, 2020.

[21] Tan T. Chen K. Xue F. Lu W. Barriers to Building Information Modeling (BIM) implementation in China's prefabricated construction: An interpretive structural modeling (ISM) approach. *Journal of Cleaner Production,* 219:949-959, 2019.

[22] Al-Ashmori Y.Y. Othman I. Rahmawati Y. Mugahed Amran Y.H. Abo Sabah S.H. Darda'u Rafindadi A. Mikic´ M. BIM benefits and its influence on the BIM implementation in Malaysia. *Ain Shams Engineering Journal, 2020.*

[23] Viscuso S. Talamo C. Zanelli A. Arlati E. BIM Management Guidelines of the Construction Process for General Contractors. *Digital Transformation of the Design, Construction and Management Processes of the Built Environment*. Springer, Gewerbestrasse 11, 6330 Cham, Switzerland, 2019.

[24] Higgins P, Cousins PT. Using the CIC PROTOCOL, 1st ed, Westminster: NEC, 2013.

[25] Crowther J. O. Ajayi S. Impacts of 4D BIM on construction project performance. *International Journal of Construction Management, 2019.*

[26] Hardin B. McCool D. BIM and construction management: proven tools, methods, and workflows. 2nd ed. Indiana: Wiley, 2015.

[27] Mordue S. Finch R. *BIM for construction health and safety*, 1st ed. Newcastle upon Tyne: RIBA Publishing, 2015.

[28] Eastman C. Teicholz P. Sacks R. Liston K. *BIM handbook: a guide to building information modelling for owners, managers, designers, engineers, and contractors*. 2nd ed. New Jersey: John Wiley & Sons, 2011.

[29] Han KK, Golparvar-Fard M. Appearance-basedmaterial classification for monitoring of operation-level construction progress using 4D BIM and site photologs. *Automat Constr*, 53:44–57, 2015.

[30] Swallow M. Zulu S. Benefits and Barriers to the Adoption of 4D Modeling for Site Health and Safety Management. Front. Built Environ, 4:86 1-12. 2019.

[31] Oraee M. Hosseini M.R. Papadonikolaki E. Palliyaguru R. Arashpour M. Collaboration in BIM-based construction networks: A bibliometric-qualitative literature review. *International Journal of Project Management*, 35:1288–1301, 2017.

Ontology-based Product Configuration for Modular Buildings

Jianpeng Cao[a] and Daniel Hall[a]

[a]Department of Civil, Environmental and Geomatic Engineering, ETH Zurich, Switzerland
E-mail: cao@ibi.baug.ethz.ch, hall@ibi.baug.ethz.ch

Abstract –

To support mass customization for industrialized construction, researchers and industry have adopted product configuration strategies. Based on the theory of modularization, pre-defined module libraries can be configured into feasible construction projects. However, the digital representation of configuration knowledge is understudied. Current Building Information Modeling (BIM) product modeling does not enable automatic generation and reasoning of configuration solutions for new products. This study proposes an ontology-based strategy to configure modular buildings. The proposed BIM-to-ontology workflow collects and formalizes configuration constraints. In particular, we elaborate on how those constraints can be modeled within the ontology in a modular building case. The ontology maintains the product hierarchy needed for product assembly. Such ontology development can support the rapid development of new products with customized variations. The paper identifies the limitations of the current product modeling approach. The proposed ontology can act as a foundation for BIM-based product platform development and increase the use of mass customization for industrialized construction.

Keywords –

Product configuration; ontology; BIM; Modular buildings

1 Introduction

Although mass production increases production efficiency and product quality, it lacks design flexibility and customization [1]. Increased design flexibility can be achieved through the configuration of standard components and variant components (i.e. modules) via a platform-based strategy [2]. To support the product configuration, a flexible product model is required [3,4]. It should not only describe the product composition in terms of the assemblies, sub-assemblies and parts, but also satisfy configuration reasoning and inference. However, few scholars uncover how product modeling could support the configuration of industrialized construction, especially modular buildings. For example, software vendors often embed a product structure in configuration applications, i.e. component trees and feature models. The structure has no functionalities to specify how a correct product could be configured from the available parts and assemblies. In many industrialized construction settings, the configuration is done manually based on document-based design handbook. The project practitioners need to familiar with the rules and abide by them. Considering the nature of low digitalization and fragmentation of construction information management, the procedure is difficult to implement. There is significant potential risk of rework and changes during the project.

To fix this problem, the authors propose an ontology-based structure to represent the configuration knowledge for modular buildings. The results facilitate the reuse of the configuration knowledge and lay a foundation for technical platform development. The paper is organized as follows. In the next section, strategies for product modeling in the manufacturing industry and the construction industry are first reviewed. Then, the ontology modeling approach is explained. Built upon that, an ontology-based product modeling is adapted to the modular building settings. In the end, a modular building case is used to illustrate how the configuration semantics could be modeled via ontology.

2 Literature Review

2.1 Product Modeling Strategies

Due to trends of product complexity and global manufacturing, the unified product model is becoming increasingly important throughout the product lifecycle. A unified model that supports the integration and transformation of different model views can improve industrial competitive advantage [5].

In the manufacturing industry, bill-of-material (BOM) is the most widely used approach in modelling a product structure. It uses a tree structure to represent the product hierarchy. However, it is not efficient to enable derivative product modelling with an increasing number of variants

[6]. An alternative approach is the Generic bill-of-material (GBOM). GBOM attempts to fix the variants of the product configuration by inheritance. The parameters of primary generic products are passed through the levels of GBOM and inherited by lower level of generic subassembly products [7]. However, GBOM is only able to model a product with a predefined set of components. It cannot support engineer-to-order variants, which are designed according to special customer requirements.

Two approaches – Adaptive generic product structure (AGPS) and product variant master (PVM) –have been developed to solve limitations of engineered-to-order products by categorizing the base models, reused variants and new components [8] [9]. Two types of syntaxes, including "part-of" and "kind-of" are used to model the structures of aggregation and specialization respectively. Rules are set to restrict the variant selection and property determination. The PVM depicts properties, functions and structure of a product at the engineering view and production view, similar to the engineering bill of material (E-BOM) and manufacturing bill of material (M-BOM).

2.2 Product Modeling for Modular Buildings

Unlike products in the manufacturing industry and projects in traditional site-built construction projects, industrialized construction product platforms combine both product-level information and project-level information [10,11]. The hierarchy between components is more important in industrialized construction systems[10,12], compared with site-built construction.

Several researchers have adapted or proposed product modeling structures for use in industrialized construction. Hvam and Thuesen used Product Variant Master (PVM) to represent a product part view [13]. Ramaji et al proposed a Product Architecture Model (PAM) to capture the product information of modular buildings [14]. Both strategies build upon a hierarchical structure [15,16], where modules are defined at different levels of complexity. First, the overall product architecture uses a hierarchical determination for sub-assemblies and parts. Then, the variations of each assembly and part are decided as a set of interchangeable components, which share similar features and functionalities. Finally, the components and related attributes are categorized based on the level of details. The benefits of the hierarchical structure include ensuring easy connection to the information management systems (e.g. ERP and PLM) [17,18], maintaining consistency with the construction classification system (e.g. Uniclass and Omniclass) [19], and providing customization at different hierarchical levels of products [20].

2.3 Current Product Modeling using BIM

Product modeling in the construction industry is implemented in existing BIM applications. Firstly, the architects have a rough design concept of a certain type of modular construction, such as volumetric modular structures. A general building outline can be created as mass models, including facility layout, building shape and direction, floor plan, etc. Secondly, the conceptual design is developed with architectural modules. The modules are categorized by product hierarchy [21]. For example, these modules can contain standalone units (e.g. smaller room pods), components (e.g. level, floor, wall, ceiling components), and/or subcomponents (e.g. pillars, beams, framing studs). Thirdly, the engineering team receives analytical models to conduct structural and mechanical analysis. The generated component-level BIM is validated and optimized in terms of material use and geometric dimensions. This feedback information is incorporated into the BIM with updated parameters. Finally, a detailed design is conducted by production teams to split the components into subcomponents [22].

Due to BIM's low compatibility with the production systems, the subcomponents are usually modeled within the third-party application, such as HSBCAD. The industry foundation classes (IFC) and a documented information exchange manual (IFD) are used to support the information exchange between model views. Beetz et al. developed ifcOWL and a mechanism to transform IFC specification from EXPRESS to OWL [23], which improves knowledge extraction [24], integration [25] and reasoning [26] from BIM. However, a product hierarchy which reflects the product composition is usually not represented in the exported IFC file.

3 Research Approach

3.1 Ontology Modeling

Ontology is widely applied in many industries for domain knowledge management. Due to its formal representation, ontology facilitates the knowledge capture, reuse and integration [27]. The construction of ontology for product configuration has been studied as early as the 1990s [4]. It is applied to manufacturing products, such as Personal Computers (PC) [28], manufacturing machines [29], and automotive [30]. The formal procedures to build an ontology follow five steps [31]: 1. identifying the purpose and scope of ontology; 2. reviewing existing ontologies, taxonomies, or other sources; 3. Enumerating main classes and build corresponding class hierarchy; 4. constructing an ontology in an ontology editor tool (e.g. Protégé); 5. ontology validation. The construction and validation steps are illustrated via an illustrative example in Section

3.1.1 Define Scope and Purpose

This research looks specifically at floor plan configuration. The proposed ontology is built to represent both the building structure / composition and constraints in a well-defined formal semantics to validate a customized configuration. The information involved in the configuration process includes customer requirements and design regulations. Customer requirements specify the acceptable combinations of spatial modules or variations of compositional building elements in the final floorplan design [15]. The design regulations, such as the horizontal stability, can be encoded to validate the customized floorplans.

The intended users of the ontology are customers without sufficient design knowledge. The ontology is maintained by professionals with the means to develop new spatial modules and building elements for their product platforms.

3.1.2 Reuse Existing Ontologies

Building Information Modeling (BIM) applications contain taxonomies and content libraries, which can be extracted to enable ontology construction. Generally, a BIM project contains system families and loadable families. The former one is embedded in the project template with default structures, while the latter is created independently and loaded into projects. Because most BIM libraries do not contain well-defined components for industrialized construction, design teams for modular construction usually need to create customized ones. The customized BIM modules can be reused in different project settings. In this study, a MEP-integrated volumetric unit is defined as the first level hierarchy under the project. Each unit is modeled as sub-project, which can be further linked to the main project. The main project and linked models are stored separately to facilitate the reuse of linked models. The components of volumetric units, such as walls, floors and ceilings are the second level of product hierarchy, which is modeled in the linked project.

To extract the BIM data of the module as well as their components, Revit API is used in this study. First, the volumetric units can be filtered under the category of "RvtLinks". The "RvtLinks" is a built-in category used to represent linked models in the main project file. Then, the linked document is located. The component granularity is extracted from linked document through the "FilteredElementCollector", which provides access to obtain a collection of elements by category.

3.1.3 Build Class Hierarchy

The extracted BIM data, including BIM families, instances and parameters, should be mapped to the ontology structure. The structure of an ontology is constructed as a tree structure of classes, to represent the hierarchy of the modular buildings. The object properties are used to assert relationships between classes. The attributes of each class are modeled as data properties. The mapping relationships are illustrated as BIM family to Ontology class, BIM instance to Ontology individual, BIM parameter to Ontology data property. In addition, some inexplicit relationships in BIM, such as the hosted relationship between opening families (e.g. windows and doors) and wall families, can be mapped to the object properties. The extracted objects are collected as key-value pairs in the C# dictionary, where the keys are unique "ElementId" used to maintain the one-on-one relationship between BIM and ontology, and the values are attributes of elements. The Python module "Owlready" [32] is used to write the BIM data into the ontology.

The above concepts of an ontology contain the basic taxonomy for a configuration problem. However, they are usually not enough to describe complex semantics. These semantics, including the constraints over the product structure, are useful to reason the correctness of a configured solution. The typical constraints for configuration include composition, compatibility, dependency and cardinality [33]. Composition rules define which components are mandatory or optional in the product architecture. The product architecture can be built as a tree structure. A component can be either a root node, an intermediate node or a leaf node. Once a non-leaf component is selected, the direct child component can be automatically added to the product. Compatibility rules define which components cannot exist simultaneously in the product. If a component with a compatibility rule is selected, the system will exclude certain components from the option lists. Dependency rules define which components must belong together in a product. If a component with a dependency rule is selected, the system will add its mated components to the product. Cardinality rules define the required or limited number of components under certain circumstances. The product structure can only represent the existence of a components. A component with a cardinality rule need to be assigned the quantity occurring in the product and checked against its validity.

4 Implementation

To demonstrate the ontology usage, a multi-story modular residential project from a European construction company is used as an illustrative example. The project consists of prefabricated, highly standardized volumetric units that are combined under a set of restrictions to create apartment buildings. Each module is fully designed for certain functionalities. While the product concept is standardized, the individual configuration can vary from the building profile on the selected site, the layout of the apartment on the floor plan, the material

type of façade, the roof types and the balcony types. The project-specific configuration is supported by a library of 3D models in Autodesk Revit that define all relevant design regulations. The BIM content library can be linked to the proposed ontology following the process mentioned above. Then, the project can be configured with the BIM library and reasoned for correctness. Figure 1 shows the classes and object properties in the configuration model.

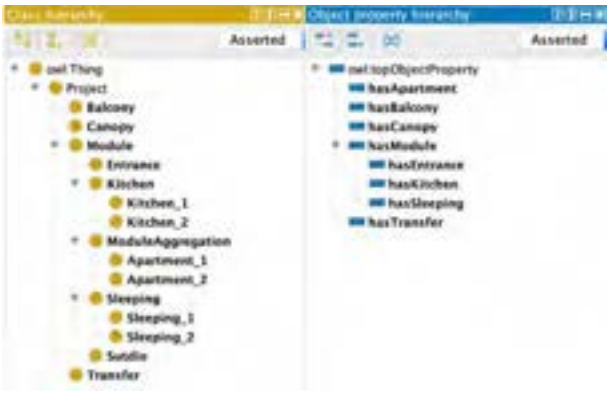

Figure 1. Class hierarchy and object property hierarchy of the modular building

4.1 Composition constraint

"An Apartment_2 is composed of 1) one entrance module; 2) one kitchen module; 3) one sleeping module." The definition of the class "Apartment_2" in Protégé is shown in Figure 2. The "Entrance", "Sleeping", and "Kitchen" are disjointed classes. The "hasEntrance", "hasSleeping" and "hasKitchen" are object properties which map from the apartment class to the corresponding module class. "Exactly" keyword is used to restrict the existence of a certain class.

Figure 2. Composition constraint to define a three-module apartment

4.2 Cardinality constraint

"A two-story modular project is developed for wind loads in terrain type 1, which requires at least five modules in width per floor." The constraint is encoded in SWRL and SQWRL (Semantic Query Enhanced Web Rule Language) as shown in Figure 3. SQWRL support collection operators that provide the grouping and aggregation functionalities. In this scenario, each type of modules, including "Sleeping", "Kitchen" and "Entrance", are grouped and added. Then, the total number of selected modules is compared with the required number of modules based on the design requirements.

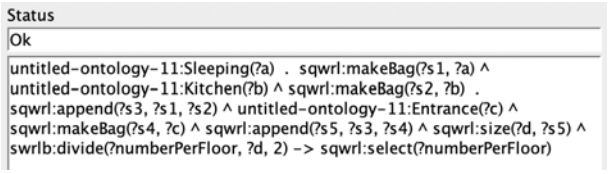

Figure 3. Cardinality constraint to check the required number of spatial modules

4.3 Compatibility constraint

"The Kitchen modules should not be selected to configure a studio apartment". The constraint is defined as a SWRL (Semantic Web Rule Language) as shown in Figure 4 via the SWRLTab of Protégé. The constraint is a conjunction of four positive atoms. The "Project (?x)" and "Kitchen (?m)" represent the instance of project (x) and kitchen (m) respectively, while the "onlyStudio(?x, true)" represents that the project only contains studios. Finally, when the kitchen module (m) is added to the project (x), the "hasModule (?x, ?m)" will be generated automatically. As the consequence of the rule is void, the checker returns an error, representing the event at the left side of arrow cannot occur.

Figure 4. Compatibility constraint to limit the module selection

4.4 Dependency constraint

"If a user specifies an apartment with balcony, the matched canopy will exist in the same configuration." Similar to compatibility constraint, the constraint is defined in the SWRL as shown in Figure 5. For the specified apartment, if a balcony with width equals 1.5 meters is required in the sleeping room. The rule will automatically add the matched canopy and set its width same as the balcony.

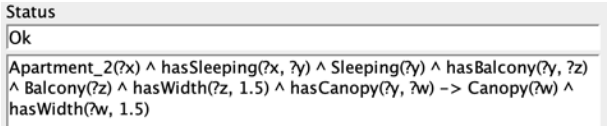

Figure 5. Dependency constraint to select mated

components

5 Discussion

The proposed ontology-based product modeling is a novel approach to represent design information for modular buildings. It is aimed at achieving mass customization by linking customer requirements and design regulations with a predefined module library. The research is built upon the product modularization. With a module library, the various configuration can be achieved. Compared with the PVM and PAM approaches, this ontology-based approach is capable to represent more complex product structures and semantics. Furthermore, the proposed ontology can be well-connected to BIM tools through ifcOWL to avoid reconstruction of taxonomies.

6 Conclusion

Mass customization has been strongly emphasized in the construction industry, especially the industrialized construction. Product configuration is an idea borrowed from the manufacturing industry to achieve mass customization. Similar to the automotive industry, modular buildings can be configured with different categories of modules, such as volumetric units and panels. Compared with the traditional design process, the key benefits of configuration are the fast derivation of product variety to satisfy customer's needs, and the reuse of digital BIM contents to improve design efficiency and product quality. However, the existing product modeling only deals with the categorical classification of product composition, without considering a configurable product structure.

To support the digital representation of configuration knowledge, this research proposes an ontology-based modeling approach. First, it illustrates how configuration tasks can be implemented in a BIM environment via a BIM-to-ontology workflow. Second, the paper focus on how product hierarchical structure and semantical constraints can be modeled in an ontology. A modular building project is used as a case study to explain it in detail. Ultimately, this lays the foundation for the technical configuration platform development.

The research has some limitations. First, the configured product is limited at the floor plan. A wider scope of building products, such as MEP systems, should be included in the configuration process. This might require a better understanding of customer requirements on the building performance. Second, the complex semantics of product configuration has to be manually added into the ontology. Previous scholars have identified that building such large-scale ontology requires domain knowledge, which will take time and considerable resources [34]. Future research direction might be the automatic construction of multi-domain ontology with natural language processing.

References

[1] Barman, S. & Canizares, A. E. A survey of mass customization in practice. *International Journal of Supply Chain Management*, 4:65–72, 2015.

[2] Jensen, P., Olofsson, T., Smiding, E. & Gerth, R. Developing Products in Product Platforms in the AEC Industry. *Computing in Civil and Building Engineering*, 1062–1069, 2014.

[3] Yang, D., Miao, R., Wu, H. & Zhou, Y. Product configuration knowledge modeling using ontology web language. *Expert Systems with Applications*, 36:4399–4411, 2009.

[4] Soininen, T., Tiihonen, J., Männistö, T. & Sulonen, R. Towards a general ontology of configuration. *Artificial Intelligence for Engineering Design, Analysis and Manufacturing*, 12:357–372, 1998.

[5] He, L., Ni, Y., Ming, X., Li, M. & Li, X. Integration of bill of materials with unified bill ofmaterials model for commercial aircraft design to manufacturing. *Concurrent Engineering Research and Applications*, 22:206–217, 2014.

[6] Hegge, H. M. H. & Wortmann, J. C. Generic bill-of-material: a new product model. *International Journal of Production Economics*, 23:117–128, 1991.

[7] Simpson, T. W. Product platform design and customization: Status and promise. *Artificial Intelligence for Engineering Design, Analysis and Manufacturing: AIEDAM*, 18:3–20, 2004.

[8] Brière-Côté, A., Rivest, L. & Desrochers, A. Adaptive generic product structure modelling for design reuse in engineer-to-order products. *Computers in Industry*, 61:53–65, 2010.

[9] Hvam, L., Niels Henrik Mortensen & Riis, J. *Product Customization*, Springer Science & Business Media, Berlin, 2008.

[10] Ramaji, I. J. & Memari, A. M. Product Architecture Model for Multistory Modular Buildings. *Journal of Construction Engineering and Management*, 142:04016047, 2016.

[11] Malmgren, L., Jensen, P. & Olofsson, T. Product modeling of configurable building systems - A case study. *Electronic Journal of Information Technology in Construction*, 16:697–712, 2011.

[12] Giles, H. Prefabricated Construction using Digitally Integrated Industrial Manufacturing. *Enquiry The ARCC Journal for Architectural Research*, 5:226–243, 2008.

[13] Kudsk, A., Grønvold, M. O., Olsen, M. H., Hvam, L. & Thuesen, C. Stepwise Modularization in the

Construction Industry Using a Bottom-Up Approach. *The Open Construction and Building Technology Journal*, 7:99–107, 2013.

[14] Ramaji, I. J., Memari, A. M. & Messner, J. I. Product-Oriented Information Delivery Framework for Multistory Modular Building Projects. *Journal of Computing in Civil Engineering*, 31:04017001, 2017.

[15] Wikberg, F., Olofsson, T. & Ekholm, A. Design configuration with architectural objects: Linking customer requirements with system capabilities in industrialized house-building platforms. *Construction Management and Economics*, 32:196–207, 2014.

[16] Jensen, P., Lidelöw, H. & Olofsson, T. Product configuration in construction. *International Journal of Mass Customisation*, 5:73, 2015.

[17] Mukkavaara, J., Jansson, G., Olofsson, T. & Engineering, N. R. Structuring information from BIM: A glance at bills of materials. in *35th International Symposium on Automation and Robotics in Construction (ISARC 2018)* , 2018.

[18] Boton, C., Rivest, L., Forgues, D. & Jupp, J. Comparing PLM and BIM from the Product Structure Standpoint. *IFIP International Conference on Product Lifecycle Management*, 492:423–432, 2016.

[19] Boton, C., Rivest, L., Forgues, D. & Jupp, J. R. Comparison of shipbuilding and construction industries from the product structure standpoint. *International Journal of Product Lifecycle Management*, 11:191–220, 2018.

[20] Schoenwitz, M., Naim, M. & Potter, A. The nature of choice in mass customized house building. *Construction Management and Economics*, 30:203–219, 2012.

[21] Gosling, J., Pero, M., Schoenwitz, M., Towill, D. & Cigolini, R. Defining and Categorizing Modules in Building Projects: An International Perspective. *Journal of Construction Engineering and Management*, 142:1–11, 2016.

[22] Yuan, Z., Sun, C. & Wang, Y. Design for Manufacture and Assembly-oriented parametric design of prefabricated buildings. *Automation in Construction*, 88:13–22, 2018.

[23] Beetz, J., Van Leeuwen, J. & De Vries, B. IfcOWL: A case of transforming EXPRESS schemas into ontologies. *Artificial Intelligence for Engineering Design, Analysis and Manufacturing: AIEDAM*, 23:89–101, 2009.

[24] Zhang, L. & Issa, R. R. A. Ontology-based partial building information model extraction. *Journal of Computing in Civil Engineering*, 27:576–584, 2013.

[25] Fahad, M. & Bus, N. Integrating BIM and Product Manufacturer Data using the Semantic Web Technologies. *Journal of Information Technology in Construction*, 24:424–439, 2019.

[26] Ma, Z. & Liu, Z. Ontology- and freeware-based platform for rapid development of BIM applications with reasoning support. *Automation in Construction*, 90:1–8, 2018.

[27] Elhakeem, A. & Hegazy, T. Distributed Ontology Architecture for Knowledge Management in Highway Construction. *Journal of Construction Management and Engineering*, 131:168–175, 2005.

[28] Liu, Y., Lim, S. C. J. & Lee, W. B. Product family design through ontology-based faceted component analysis, selection, and optimization. *Journal of Mechanical Design, Transactions of the ASME*, 135:1–17, 2013.

[29] Yang, D., Dong, M. & Miao, R. Development of a product configuration system with an ontology-based approach. *CAD Computer Aided Design*, 40:863–878, 2008.

[30] Liang, J. S. Generation of automotive troubleshooting configuration system using an ontology-based approach. *Computers in Industry*, 63:405–422, 2012.

[31] Zhou, Z., Goh, Y. M. & Shen, L. Overview and Analysis of Ontology Studies Supporting Development of the Construction Industry. *Journal of Computing in Civil Engineering*, 30:1–14, 2016.

[32] Lamy, J. B. Owlready: Ontology-oriented programming in Python with automatic classification and high level constructs for biomedical ontologies. *Artificial Intelligence in Medicine*, 80:11–28, 2017.

[33] Yang, D. & Dong, M. Applying constraint satisfaction approach to solve product configuration problems with cardinality-based configuration rules. *Journal of Intelligent Manufacturing*, 24:99–111, 2013.

[34] Wang, T., Gu, H., Wu, Z. & Gao, J. Multi-source knowledge integration based on machine learning algorithms for domain ontology. *Neural Computing and Applications*, 32:235–245, 2020.

On Construction-specific Product Structure Design and Development: the BIM Enhancement Approach

S.Mansoori, H.Haapasalo and J. Härkönen

Industrial Engineering and Management, University of Oulu, Finland
E-mail: Solmaz.Mansoori@oulu.fi, Harri.Haapasalo@oulu.fi, Janne.Harkonen@oulu.fi

Abstract – The construction industry suffers from low productivity, and the Building Information Modelling (BIM) has not been successful in enhancing the productivity and the flow of information throughout highly fragmented construction projects. Hence, this study aims to facilitate consistency in information and addresses the current gaps in BIM by applying the Productization and Product Structure concept. The study follows conceptual research approach and accordingly, previous studies on productization and product structure are reviewed. The Part-Phase-Elements Matrix is proposed as a construction-specific product structure to facilitate consistency in information and enhance BIM.

Keywords– Productization; Product structure; Information Management; BIM; Construction

1 Introduction

Construction industry is highly fragmented and complex and suffers from low productivity improvement [1]. Building Information Modelling (BIM) has shown some promise to assist in improving productivity [2] but remains essentially ineffective despite the potential of enhancing the collaborative way and providing relevant parties with reliable information [3]. Simultaneously, construction projects suffer from different stakeholders and suppliers using a variety of systems [4] resulting in considerable conflicts when operational integration and automation are needed [5]. Loss of relevant information and data corruption are inevitable in such circumstances. Hence, strong needs exist for a unified concept to organize and manage information, including product and process information to facilitate the integration of construction processes.

With increasing moves toward achieving the concurrent construction goal by advanced BIM [6], the construction industry is getting increasingly similar with manufacturing industry. The current situation in construction is quite alike to the experiences by complex manufacturing companies some decades ago [7]. Considerable interests exist for implementing well-established methods from the manufacturing industries to improve BIM implementation [8]. These have common goals with BIM to ensure process fluency and product data integrity among multiple systems.

Various approaches have been proposed for the purpose of improving BIM. The BIM improvement based on Product Lifecycle Management (PLM) [7], [8], adoption of Industry foundation classes (IFC) as a well-known data model standard to deliver the integrated building information [9], implementing situation based management approaches such as Last Planner [10], proposing a central information repository as a multi-disciplinary collaboration platform [11], and modularization via considering the building as a product [10]. Further, Holzer [12] suggest that BIM should be built so that standardized product data can be derived directly from the model to the existing information systems utilized in the industry, rather than transforming BIM into a construction-dedicated PLM. However, the current research is particularly deficient in construction specific information system considerations.

BIM modelling based on a standardized Product Structure (PS) has been argued to be the missing link between BIM approach and the disconnected construction processes to some extent in the literature [12]–[14]. Product structure is a consistent unit representing a physical or conceptual grouping of product components which can be easily identified and replaced [15]. Product structure is the core entity for the transmission of information across the entire life cycle of a production project system [13] that enables platform-based production, and strengthens stakeholder engagement and cooperation from product development to marketing agents [16]. Indeed, the product structure bridges the development and marketing of new products within the concept of Productization [17].

The productization concept was originally borrowed from managerial texts and mainly used in the service or software industries [18]. The concept has evolved over the years, but at a general level, productization is used in the context of creating products or services and covers all the activities required before a product is ready commercially [19]. Productization also refers to

commercial and technical modelling the offer products according to a consistent product structure [20]. Consequently, product structure plays a key role in the Productization process as a structured product information repository and makes products and related data more systematized and manageable. Despite some researchers having addressed the concept of productization in relation to modelling of products and services and the potential of product structure involving acting as a unified concept to ensure consistency of information, the context of construction industry has only been discussed to a certain extent [21]. Further work is necessary to detail the found links and to establish an equivalent central backbone structure to enhance the implementation of BIM.

This study explores the core of productization concept, and the product structure as an eminent solution to facilitate consistency in information, and hence addresses the current gaps in BIM. This is based on the argument that product structure -focused construction modelling is the missing link of the BIM approach and has potential to improve BIM performance. Addressing the gaps in BIM can support the long-term vision of improving the of product data management in the construction industry. The goal is to create a standardized concept for product information and to provide a mechanism for the effective sharing of product data between different phases of the building lifecycle. The intention is to enable flexibility in how many stakeholders can be involved in a specific project.

The above discussion can be outlined along the following research questions (RQs);

1. How does a conceptual product structure look like in a general level?
2. How can the conceptual product structure support BIM Implementation?
3. How can a specific product structure be formed to enable reliable information exchange between different stakeholders in collaboration?

This study is a conceptual research. The research methodology is presented in section 2. The Literature Review on Productization and Product Structure at the general level forms the basis to answer RQ1. Meanwhile, the literature review on construction project specifications and challenges of BIM implementation in conjunction with the conceptual product structure, offers a response to RQ2 and also supports the creation of a construction-specific product structure that responds to RQ3. Discussion and conclusion are presented in sections 4 & 5 respectively.

2 Methodology

The study follows conceptual research approach. The literature on productization and product structure are reviewed first, while seeking for different approaches to interpret concepts at a general level. A construction specific product structure is designed and developed to support BIM implementation. A three-dimensional matrix to is used to combine product structure, building product library as a structured database, and user specifications layers from various construction project phases.

3 Literature Review

3.1 Productization

The term "productization" has been used interchangeably with standardization, systemization, productivisation, industrialization and commercialization. Productization is seen to mean standardization of the elements in the offering [22] and concern all the activities before the product is ready commercially [19]. Productization is also defined as a transformation process from customer specific (low productized) to standard mass market products (high productized) offering [17], [22], in relation to which rationalization is necessary to produce deliverables from individual level tacit abstract knowledge to organization level easier to communicate knowledge [17], [23]. Productization has been seen as a delivery-oriented concept [24], which enables an optimal balance between customization and standardizationas well as the ability to make and to sell [23].

Productization refers to the conversion of custom or incidental products to standard ones [25]. Considering all the above mentioned, productization id a transformational process in which product information and materials are streamlined, systematized and standardized through replicable methods and transparent format. Productization can be seen as a process that transforms inputs into outputs, which is in line with Transformation-Flow-Value theory proposed [26] in which the production in construction is conceptualized in a way that production is one of the major concepts (transformation from inputs to outputs, as a flow to fulfil customer needs and add value). Figure 1 illustrates productization as portrayed by the literature to provide systematics for the discussion. Indeed, productization contributes through systematization and routines to both efficiency and profitability [27], covers aspects relevant to both new product development and marketing by the product-centric view. Literature on product management [14], [17], [28] further splits productization into technological and commercial perspectives. It is also claimed that productization should be split into Inbound and Outbound activities relating to capacity to produce and sell to build a harmonized development process and

avoid duplicating tasks using existing platforms and modules [18]. The outbound productization aims at improving product value for consumers and providing wider product families to satisfy consumer needs. It is believed that productization should cover both abilities to make and sell by finding a balance between standardization and customization [17] .

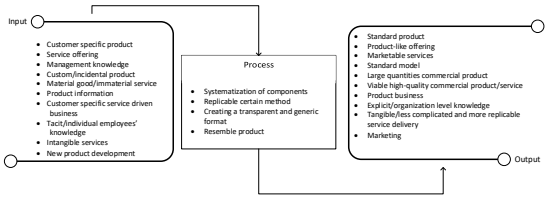

Figure 1. Productization

Evidently, the concept of productization is strongly connected to module-based product development and mass customization (MC). Modularization refers to a product and process structure in which the design elements are divided into modules with well-defined interfaces along a formal architecture [24]. Module based product development is enabler and one of the success factors for MC [29].

MC addresses distinct market requirements and promotes modularization, which can be seen as higher levels of standardization [23]. By increasing the level of productization, the clarity of the offering increases, and becomes more understandable and communicable towards customers [17]. “Successful MC products must be modularized, versatile, and constantly renewed” [29, p. 4]. This is promoted by developing modular product families for the provision of an appropriate variety of products [30] to satisfy customer needs. The concept of productization begins with the core product followed by routines.

3.2 Product Structure

A broad range of definitions for product structure exist in the academic literature [31]. The product structure term is commonly used in various fields under different terms: product architecture [15], configuration model [32], product structure tree [33]and modular product structure [30]. In a general level, product structure is defined as an organized hierarchical classification [34], [35], structural representation [36] and basis for all information of product components (characteristics, technical objects, product functions requirements) [31], [35], [36] and their assembly relationships [15], [31], [37]–[39].

Product structure is a context-dependent explanation of the product’s composition from the elements and the relations between the elements in which all ‘instantiated data’ is managed and stored [40] to realize the product function [41] and form a consistent unit that can be easily identified and replaced [15]. Product structure captures not just the product components’ assembly relationship, but also the data relationship that distinguishes them. “This data materialises as files with revisions and versions" [13, p. 11]. To ensure that product data can be handled well and that the change can be monitored and recorded, the product data should be sorted and managed according to the product structure [39].

Product Data Management (PDM) enriched by unified product structure serves as a central repository of information for process and product history and facilitates integration and data sharing among all business users dealing with products [42]. Several studies have addressed how product structure is the basis for the implementation of product data management (PDM), and fulfils the criteria of generating a manufacturing plan and schedule [39] supports managerial decision-making [39]and collaborative workflow in maintaining all design details up to date [38], so that they are dynamic and reusable.

A generic product structure is a hierarchical structure of either abstract or physical elements [43] which represent the structure of the entire product family and show which modules and part types, or classes are used in the products or a product family [31], [32]. The generic product structure offers information on possible implementations of existing templates in a wide variety of similar products [31]. Opposite of general product structure is a specific or precise product structure in which the information is only limited to a particular product. Specific/precise product structure shows the particular modules and parts, which together form the product [31]. A specific/precise product structure is a set of descriptions of components organized into a part of the hierarchy that is required to create or order the part [44].

Bill of Materials (BOM) is one of the most common product structures which identifies the parent-child relations between product components. BOM is a list of all sub-assemblies, intermediates, parts and materials that form a parent assembly and show the quality of each assembly needed to produce a complete product [45]. The terms product structure and BOM can be used interchangeably in spoken language, however, “The definition of product structure is more comprehensive" [34, p. 54]. At some point during the life of the product development, BOM is regarded as a basic filtered product structure snapshot [35].

BOM itself tends to fall into two main types; Engineering Bill of Material (EBOM) and Manufacturing Bill of Material (MBOM). EBOM is the cornerstone of the “As Designed” Product Structure that describes ‘what’

the product is [46], [47], which is later converted into MBOM. MBOM, refers to 'how' the product is produced and assembled [46] by maintaining manufacturing interactions through the planning of production processes[47]. Also other product structure based BOM categories exist. According to the product structure tree EBOM and MBOM are designed automatically as requested [37]. BOM is the core part of any integration system as a means of communication during product development [48] and it is widely evidenced that the BOM related processes and implementation activities dramatically affect how an organization can run multiple systems like Computer-aided Design (CAD), Product Data Management (PDM), PLM, and (Enterprise Resource Planning) ERP [42].

Product structure can encompass and store various kinds of product information. It is viewed that the product structure description data can be summarized into natural attributes (product and part names, ID, size, material, weight, and origin) and the relevance between the components (father-child relationship between products and parts) [49]. It is also argued that product structure information consisting of product structure decomposition, part ratios and outgoing fractions, help to frame the limits of a system and to model and analyse the subsystems, which can be retrieved from BOM and disassembly BOM [50]. Some academics also suggest an extra node between the product and part nodes and refer to modules [31] or components [37] that can be common or alternative/optional components equipped with configuration rules [43].

3.3 Construction Projects Context

3.3.1 BIM in Construction Project Context

Construction projects have certain properties that complicate their management, to name a few, quite volatile planning environment, evolving production locations, highly fragmented and extremely multidisciplinary non-linear work processes, spatial restrictions, and specific regulations [13]. These properties place difficulties on the construction projects regarding cooperation, accurate exchange of knowledge, and incorporation of various stakeholders.

It is widely acknowledged how the collaboration of numerous multidisciplinary project members through continuous, accurate and real time information sharing, play a vital role in overcoming these difficulties [51]. The ambiguity that surrounds the definition, business value and purpose of BIM impede a common understanding of BIM implementation between stakeholders [52]. Accordingly, the major issue is that "BIM is a powerful but complex technology" [53, p. 321].

The challenges of BIM implementation have been widely discussed in literature. Lack of defined standards and technically integration requirements and management of outcomes as the main barriers to BIM use [2]. BIM implementation faces challenges like the need for a well-design transactional structure and practical strategies for integration and the exchange of information among involved parties, a need for well-developed guidelines, a need for someone to be responsible for the distribution of operational development, cost and to identify a suitable time for the engagement of stakeholders in different segments to exchange the information [3]. Therefore, the challenges to the implementation of BIM with regard to the scope of this study needed to be examined with the capabilities of the construction-specific product structure. In this regard Section 4 presents debate.

3.3.2 Product Structure in Construction Project Context

Product structure concept relating to construction projects follow the general product structure logic in terms of structure and context. A construction project and the related productization mechanism, could be split into capacity to produce (Inbound) and sell (Outbound) activities as proposed by [17]. Harkonen et al. (2018) further modelled the technical product portfolio and commercial product portfolio in the construction project context by simultaneously relating to the development and sales capability activities.

The product structures are generated during the design phase [40], where all necessary stakeholders should be involved to design the product structure according to their requirements [38]. The requirements help to clarify what the product must do, or the qualities of the product. These requirements tend to fall in three categories: functional requirements referring to things the product must do, non-functional requirements referring to qualities the product must have, and constrains referring to context specific limitations that shape the requirements [54]. These requirements must be gathered and categorized according to the customer needs, regional business resources, and context-specific constraints [15]. Nevertheless, product structure might be overloaded with a wide variety of requirements and become difficult to handle should the large number of stakeholders and different domains be considered, meaning all those involved in construction projects. Therefore, also considering the capacity of product structure is vital while attempting to satisfy the various user criteria and the needs of different construction project phases. An unified product structure should be a tradeoff between individual requirements of various stakeholders (differentiation) and keeping standardization and commonality product's components [55].

The next preliminary concept to consider is a

database for potential technical objects that support is among them [2]. General product structure determination proposed by [36] involves arranging functional elements, mapping them to physical components, and defining interface specifications among components, and a technical objects. It is also worth noting that in order to make the database functional, the technical objects library needs to be hierarchically organized in a standard way. Feature templates have been proposed as a database to consist of well-formed, predefined CAD features, attribute aggregations, and constraints enhanced with engineering information and reusable geometric elements [31]. Yet the function models may not have enough structure and integration might be necessary. Accordingly, a construction classification system can be used to provide standardized technical objects, which are coded and organized hierarchically. There are several "construction classification systems" available based on different logics, but the main purpose in all is to classify building artefacts to support reliable information exchange [56]

Comparison between alternative construction classification systems have been investigated, including OmniClass, MasterFormat, UniFormat and Uniclass [57]. The UniFormat classification system is used in this study, as its purpose is to "enhance reporting of design program information, especially for preliminary project descriptions and performance specifications, and provide a basis for systematic filing information for facility management, drawing details, BIM objects, and construction market data" [58, p. 1]. This is in line with objectives of this paper. In this classification system, the building elements are hierarchically grouped into three levels of major group elements, group elements, and individual elements [59]. These three dimensions need to be acknowledged simultaneously to ensure coherent, reliable and structured knowledge to be shared by various stakeholders in the construction project life cycle phases.

A Part Template Matrix has been proposed for a generic product structure, which nicely visualizes dependencies and affiliations between feature templates and product structure [31]. Inspired by that, this study aims to enhance the proposed matrix using standardized and structured database as the source of all applicable individual element level building artefacts.

4 Results and Discussion

4.1 Conceptual Product structure and BIM

The content and structure of the product structure have been discussed in the literature based on hierarchical elements and also on the basis of information within each element. Figure 2 depicts a product structure from the hierarchical elements of the product (Left) and their respective units of information (right). The illustration is inspired by the previous research regrading product structure in general level.

The product part-of hierarchy structure starts with the product family including different products and displays alternate modules and component forms (parts) that could potentially be used in the products, or the product family. Information units correspond to elements of the product structure illustrated in on the right side of figure 2. Information of possible variety of products (Product Data layer) is stored as a generic product structure which includes several different specific products structures (BOM). Next level is the assembly process layer that includes a collection of component descriptions required to build or order a part. In this level, specific EBOM and MBOM describes 'what' the product is and 'how' the product is produced and assembled. Detailed information of the parts is stored within the elements layer to specify the characteristics used for grouping or separating.

The findings indicate that a product structure consist of comprehensive information regarding product and production process with a clear structure of relations between detail information. Meanwhile, information can be tracked and reused from product data, process and elements layer of product structure. The centralized and standardized product structure makes it accessible and easy to follow as a consistent information unit for all the stakeholders involved in the lifecycle of construction projects. In short, a product structure with a well-designed structure can provide a platform for continuous, accurate and real-time information that can be used in collaboration with numerous stakeholders.

Regarding "BIM" implementation, the mentioned gaps in could be well addressed with the potential of the product structure discussed in literature promoting standardization, collaborative exchange of reliable information and integration of multidisciplinary stakeholders. The flow of information about elements and their relationship, production process, specific product and product family will be available via a product structure.

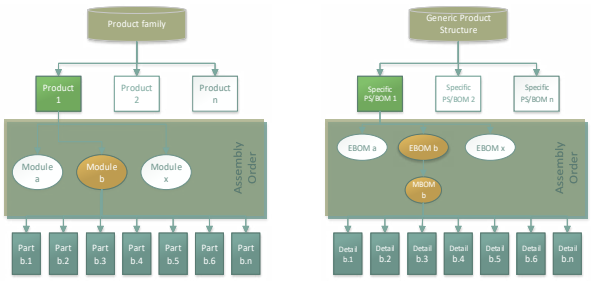

Figure 2. Product Structure from hierarchical elements of the product (Left) and their respective units of information (right).

4.2 Construction Specific Product Structure

The construction projects' specifications are considered to develop a construction specific product structure, since the product structure is a context-specific phenomenon itself that can be interpreted differently through the project life cycle with various disciplines and stakeholders involved in the project.

In this regard, the findings indicate that the product structure could be developed to be used from both technical and commercial standpoints. The conceptually illustrated product structure (Figure 2) was developed to be used for technical and commercial purposes. Involvement of stakeholders and related well-defined requirements within the early stages of construction projects enhance product structure functionality. Hierarchically structured and standard library of building objects further facilitate efficient information exchange among stakeholders.

Accordingly, the product structure is enriched first by the standard construction object library which consist three layer of details including major group elements, group elements, and individual elements. These three levels may well correspond to product structure hierarchy levels of product, modules, and parts. A Matrix based model is used to explain corresponding dimensions and their interactions.

Using a standardized and structured database as the source of all applicable individual element level building artefacts in bottom of product structure will enhance collaborative exchange of reliable information and integration of multidisciplinary stakeholders. This approach provides a basis for systematic flow of information across project and add an appropriate classification of elements.

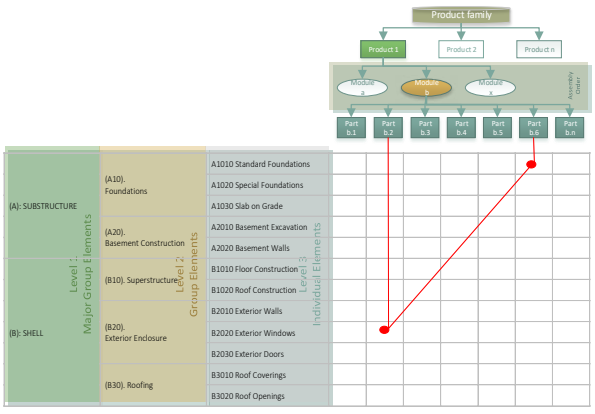

Figure 3. Part-Elements Matrix

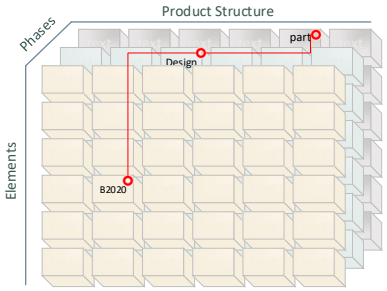

Figure 4. The Part-Phase-Elements Matrix

So far, Part-Elements Matrix is able to integrate PS and library elements. To make the Part-Elements Matrix usable for involved parties acros different stages of the project, third dimension is needed to illustrate the potential inclusion of unlimited users from different disciplines within the construction phases (Figure 4). The addition of user dimension, in other words, allows the collaborative use of the proposed Part-Elements Matrix. The proposed matrix has added new dimensions called Phase Layer. As a result, the 3-dimentional Part-Phase-Elements Matrix has formed demonstrating the relationship between the parts, elements, and users. The Part-Phase-Elements Matrix has Part-Elements Matrix capacities as a basis and allows stakeholder engagement to enhance BIM as well.

The Part-Phase-Elements Matrix shows the relationship between the part and the correlated elements that exist in the object library. In the meantime, the phases layer indicates that the stakeholder involved in the second phase of the project (design) is the corresponding user. In the example given in figure 4, the element no. B2020 related to Part (x) from PS, is used by a user from Design phase. This type of relational information. The proposed Part-Phase-Elements Matrix has the potential to facilitate consistency in information and enhance BIM as a construction-specific product structure.

5 References

[1] C. Boton, L. Rivest, D. Forgues, and J. Jupp, "Comparing PLM and BIM from the Product Structure Standpoint," in *Product Lifecycle Management for Digital Transformation of Industries*, vol. 492, Springer International Publishing, 2016, pp. 443–453.

[2] C. M. Eastman, C. Eastman, P. Teicholz, R. Sacks, and K. Liston, *BIM Handbook: A Guide to Building Information Modeling for Owners, Managers, Designers, Engineers and Contractors*. Wiley, 2008.

[3] S. Azhar, "Building information modeling (BIM): Trends, benefits, risks, and challenges for the AEC industry," *Leadership and management in engineering*, vol. 11, no.

3, pp. 241–252, 2011.
[4] D. Bryde, M. Broquetas, and J. M. Volm, "The project benefits of building information modelling (BIM)," *International journal of project management*, vol. 31, no. 7, pp. 971–980, 2013.
[5] C. Merschbrock and B. E. Munkvold, "A Research Review on Building Information Modeling in Construction-An Area Ripe for IS Research," *Communications of the Association for Information Systems*, vol. 31, 2012
[6] B. Succar, "Building information modelling maturity matrix," in *Handbook of Research on Building Information Modeling and Construction Informatics: Concepts and Technologies*, IGI Global, 2010, pp. 65–103.
[7] J. R. Jupp and M. Nepal, "BIM and PLM: Comparing and Learning from Changes to Professional Practice Across Sectors," in *Product Lifecycle Management for a Global Market*, vol. 442, Springer, 2014, pp. 41–50.
[8] S. Aram and C. Eastman, "Integration of PLM Solutions and BIM Systems for the AEC Industry," presented at the 30th International Symposium on Automation and Robotics in Construction and Mining, Canada, 2013.
[9] C. Fu, G. Aouad, A. Lee, A. Mashall-Ponting, and S. Wu, "IFC model viewer to support nD model application," *Automation in Construction*, vol. 15, no. 2, pp. 178–185, Mar. 2006.
[10] S. Bertelsen, "Modularisation: A Third Approach to Making Construction Lean?," presented at the 13th International Group for Lean Construction Conference, Sydney, 2005, pp. 81–88.
[11] V. Singh, N. Gu, and X. Wang, "A theoretical framework of a BIM-based multi-disciplinary collaboration platform," *Automation in Construction*, vol. 20, no. 2, pp. 134–144, 2011.
[12] D. Holzer, "Fostering the Link from PLM to ERP via BIM: The AEC Industry in Transition," in *Product Lifecycle Management for a Global Market*, vol. 442, Springer, 2014, pp. 75–82.
[13] C. Boton, L. Rivest, D. Forgues, and J. R. Jupp, "Comparison of shipbuilding and construction industries from the product structure standpoint," *IJPLM*, vol. 11, no. 3, p. 191, 2018.
[14] J. Harkonen, A. Tolonen, and H. Haapsalo, "Modelling of Construction Products and Services for Effective Productisation," *MNG*, vol. 13, no. 4, pp. 335–353, Dec. 2018.
[15] F. Belkadi *et al.*, "Co-Definition of Product Structure and Production Network for Frugal Innovation Perspectives: Towards a Modular-based Approach," *Procedia CIRP*, vol. 50, pp. 589–594, 2016.
[16] M. Gunzenhauser and L. Bongulielmi, "Global Product Structure Matrix: An Integrated Component of a Variable Process Model for Global Platforms," presented at ICED' 07, Paris, France, Aug. 2007, pp. 1–12.
[17] H. Simula, T. Lehtimäki, and J. Salo, "Re-thinking the product – from innovative technology to productized offering," in *Proceedings of the 19th International Society for Professional Innovation Management Conference*, Tours, France, 2008.
[18] K. Valminen and M. Toivonen, "Seeking efficiency through productisation: a case study of small KIBS participating in a productisation project," *The Service Industries Journal*, vol. 32, no. 2, pp. 273–289, Feb. 2012.
[19] C. Pyron, J. Prado, and J. Golab, "Test strategy for the PowerPC 750 microprocessor," *IEEE Des. Test. Comput.*, vol. 15, no. 3, pp. 90–97, 1998.
[20] J. Harkonen, A. Tolonen, and H. Haapasalo, "Service productisation: systematising and defining an offering," *Journal of Service Management*, vol. 28, no. 5, pp. 936–971, 2017.
[21] J. Harkonen, E. Mustonen, and H. Haapasalo, "Construction related data management-classification and description of data from different perspectives," presented at the Management, Knowledge and Learning International Conference, Piran, Slovenia, 2019.
[22] K. Guvendiren, S. Brinkkemper, and S. Jansen, "Productization of an IT service firm," presented at the 5th International Conference on Software Business (ICSOB), Paphos; Cyprus, 2014, vol. 182 LNPIB, pp. 115–131.
[23] Ying Zhang, Nan Zhang, and Li-ling Sun, "Research on the method in aerospace computer productization," in *2017 6th International Conference on Industrial Technology and Management (ICITM)*, Cambridge, United Kingdom, Mar. 2017, pp. 114–117.
[24] S. Kuula, H. Haapasalo, and A. Tolonen, "Cost-efficient co-creation of knowledge intensive business services," *Serv Bus*, vol. 12, no. 4, pp. 779–808, Dec. 2018.
[25] W. Leenen, K. Vlaanderen, I. van de Weerd, and S. Brinkkemper, "Transforming to Product Software: The Evolution of Software Product Management Processes during the Stages of Productization," in *Software Business*, vol. 114, Springer, 2012, pp. 40–54.
[26] L. Koskela, "An exploration towards a production theory and its application to construction," Doctoral Dissertation, Technical Research Centre of Finland, Espoo, 2000.
[27] E. Jaakkola, "Unraveling the practices of 'productization' in professional service firms," *Scandinavian Journal of Management*, vol. 27, no. 2, pp. 221–230, Jun. 2011.
[28] A. Tolonen, J. Harkonen, and H. Haapasalo, "Product Portfolio Management-Governance for Commercial and Technical Portfolios over Life Cycle," *Technology and Investment*, vol. 05, no. 04, pp. 173–183, 2014.
[29] G. Da Silveira, D. Borenstein, and F. S. Fogliatto, "Mass customization: Literature review and research directions," *International Journal of Production Economics*, vol. 72, no. 1, pp. 1–13, 2001.
[30] M. Windheim, E. Greve, and D. Krause, "Decisive economies and opportunity cost of modular product structure alternatives: An empirical case study," in *2017 IEEE International Conference on Industrial Engineering and Engineering Management (IEEM)*, Singapore, Dec. 2017, pp. 1636–1640.
[31] A. Christ, V. Wenzel, A. Faath, and R. Anderl, "Integration of Feature Templates in Product Structures Improves Knowledge Reuse," in *Proceedings of the World Congress on Engineering and Computer Science, WCECS*, San Francisco, USA, Oct. 2013, vol. 2, p. 9.
[32] T. Mannisto, H. Peltonen, A. Martio, and R. Sulonen, "Modelling generic product structures in STEP," *Computer-Aided Design*, vol. 30, no. 14, pp. 1111–1118, Dec. 1998.
[33] J. Li, W. Yang, Y. Zhang, Y. Pei, Y. Ren, and W. Wang,

"Aircraft vulnerability modeling and computation methods based on product structure and CATIA," *Chinese Journal of Aeronautics*, vol. 26, no. 2, pp. 334–342, 2013.

[34] A. Brière-Côté, L. Rivest, and A. Desrochers, "Adaptive generic product structure modelling for design reuse in engineer-to-order products," *Computers in Industry*, vol. 61, pp. 53–65, 2010

[35] R. Pinquié, L. Rivest, F. Segonds, and P. Véron, "An illustrated glossary of ambiguous PLM terms used in discrete manufacturing," *IJPLM*, vol. 8, no. 2, p. 142, 2015.

[36] C.-H. Chu, Y.-P. Luh, T.-C. Li, and H. Chen, "Economical green product design based on simplified computer-aided product structure variation," *Computers in Industry*, vol. 60, no. 7, pp. 485–500, 2009

[37] N. Y. Lu, F. Y. Liu, and T. Shay, "A Product Structure Management Method Based on Ajax," *AMR*, vol. 201–203, pp. 744–749, 2011

[38] G. Şenaltun and C. Cangelir, "DMU Management – Product Structure and Master Geometry Correlation," presented at the 20th ISPE, 2013, pp. 353–360

[39] Wu Binbin, Zhao Gang, and Yu Yong, "Research on constructing product structure of large airliners based on configuration item," in *ICSEM*, Guiyang, China, 2011, pp. 364–367.

[40] M. Tichem and T. Storm, "Designer support for product structuring—development of a DFX tool within the design coordination framework," *Computers in Industry*, vol. 33, no. 2–3, pp. 155–163, Sep. 1997

[41] Y. Wu and F. Kimura, "Conceptual Design of Product Structure for Parts Reuse," in *Advances in Life Cycle Engineering for Sustainable Manufacturing Businesses*, S. Takata and Y. Umeda, Eds. London: Springer London, 2007, pp. 35–40.

[42] H. M. Shih, "Migrating product structure bill of materials Excel files to STEP PDM implementation," *International Journal of Information Management*, vol. 34, no. 4, pp. 489–516, Aug. 2014

[43] K. Sarinko, R. Bjorkstrand, and A. Martio, "An Empirical Study of Requirements Related to Generic Product Structures in CAD-PDM Integration," presented at the ICED 05, Melbourne, Australia, Aug. 2005.

[44] T. Mannisto, H. Peltonen, and R. Sulonen, "View to product configuration knowledge modelling and evolution," in *Proceedings of the AAAI 1996 Fall Symposium on Configuration*, Nov. 1996, pp. 111–118

[45] D. Garwood, *Bills of Material: Structured for Excellence*. Dogwood Publishing Company, 1997.

[46] M. T. Elhariri Essamlali, A. Sekhari, and A. Bouras, "PLM System Support for Collaborative Development of Wearable Meta-Products Using SBCE," in *Product Lifecycle Management in the Era of Internet of Things*, vol. 467, Springer, 2016, pp. 33–42.

[47] E. Tekin, "A Method for Traceability and 'As-built Product Structure' in Aerospace Industry," *Procedia CIRP*, vol. 17, pp. 351–355, 2014.

[48] J. H. Lee, S. H. Kim, and K. Lee, "Integration of evolutional BOMs for design of ship outfitting equipment," *Computer-Aided Design*, vol. 44, no. 3, pp. 253–273, Mar. 2012.

[49] P. Jia, Q. Gao, S. H. Zhang, and G. Liu, "The Study of Mapping Mechanism from Product Structure to R&D Project Tasks," *AMM*, vol. 121–126, pp. 2377–2381, Oct. 2011

[50] J. S. C. Low, W. F. Lu, and B. Song, "Product Structure-Based Integrated Life Cycle Analysis (PSILA): a technique for cost modelling and analysis of closed-loop production systems," *Journal of Cleaner Production*, vol. 70, pp. 105–117, May 2014.

[51] B. Becerik-Gerber and S. Rice, "The perceived value of building information modeling in the US building industry," *Journal of Information Technology in Construction (ITcon)*, vol. 15, no. 15, pp. 185–201, 2010.

[52] D. Zuppa, R. R. A. Issa, and P. C. Suermann, "BIM's Impact on the Success Measures of Construction Projects," in *Computing in Civil Engineering (2009)*, Austin, Texas, United States, Jun. 2009, pp. 503–512.

[53] I. Kaner, R. Sacks, W. Kassian, and T. Quitt, "Case studies of BIM adoption for precast concrete design by mid-sized structural engineering firms," *Journal of Information Technology in Construction (ITcon)*, vol. 13, no. 21, pp. 303–323, 2008.

[54] S. Robertson and J. Robertson, *Mastering the Requirements Process*. Addison-Wesley, 2006.

[55] F. Salvador, "Toward a Product System Modularity Construct: Literature Review and Reconceptualization," *IEEE Trans. Eng. Manage.*, vol. 54, no. 2, pp. 219–240, May 2007.

[56] K. A. Jorgensen, "Classification of Building Object Types: Misconceptions, challenges and opportunities," in *Proceedings of the CIB W78-W102*, Sophia Antipolis, France, Oct. 2011.

[57] K. Afsari and C. M. Eastman, "A Comparison of Construction Classification Systems Used for Classifying Building Product Models," in *52nd ASC Annual International Conference Proceeding*, Provo, Utah, 2016.

[58] UniFormat, "UniFormat™: A Uniform Classification of Construction Systems and Assemblies," Constructions Specification Institute (CSI)/Construction Specifications Canada (CSC), Standard, 2010.

[59] R. P. Charette and H. E. Marshall, *UNIFORMAT II Elemental Classification for Building Specifications, Cost Estimating and Cost Analysis*. US Department of Commerce, Technology Administration, National Institute of Standards and Technology, 1999.

Parametric Structural Design for automated Multi-Objective Optimization of Flexible Industrial Buildings

J. Reisinger[a], M. Knoll[a] and I.Kovacic[a]

[a]Department of Integrated Planning and Industrial Building, Vienna University of Technology, Austria
E-mail: julia.reisinger@tuwien.ac.at, maximilian.knoll@tuwien.ac.at, iva.kovacic@tuwien.ac.at

Abstract -

Individual customer needs and accelerating technological advances in Industry 4.0 are leading to rapid manufacturing changes, thus industrial buildings need to accommodate constantly evolving production processes. The load-bearing structure acts as crucial limiting factor regarding the building's flexibility. As structural performance is highly linked to other design-disciplines, there is a need for integrated computational solutions allowing for performance-oriented structural design and optimization in early-design stage.

In order to address these issues, this paper presents the framework development of an early-stage parametric structural optimization and decision support model for integrated industrial building design. The framework combines architectural, structural, building service equipment and production process planning parameters and evaluates the impact of changing manufacturing conditions on the structural performance, automatically evaluating flexibility metrics to guide the decision-making process towards increased sustainable design. In a case study of ten real industrial construction projects, the interdependencies between discipline-specific data in industrial building design are analysed and collected in a graph data model. The proposed parametric framework is tested on a pilot project from the food production sector. Results validate the efficiency of the framework design and indicate that an optimization of the structural axis grid can save up to 25% of the material demand. A discussion on the results and next steps for further model improvement are presented.

Keywords –

Industrial building design; parametric modeling; performance-based structural design; multi-criteria decision analysis; early design stage; decision support

1 Introduction

Flexibility has become an increasingly important topic in industrial building design. Due to product individualizations, accelerating technological advances in manufacturing planning and shorter production lifecycles industrial buildings strive for highly flexible structures. The load-bearing structure, as the most rigid element with the longest service life in a building, is decisive for the adaptability and transformability of manufacturing systems. Flexible load-bearing structures, which can be implemented by means of wide-span girder systems and different load carrying capacities, can prolong the building's service life without expensive rescheduling measures.

The data and software needed by manufacturing planners differ by the ones from building design and are usually based on special discipline-specific knowledge. Multidisciplinary design teams involve conflicting views of different stakeholders and planning parameters and the prevalent uncertainty associated with multiple discipline-specific models. However, the production owner's demand should be satisfied by cooperating and assessing work of all planning disciplines. Compared with manufacturing services, building components have a much longer lifecycle, though buildings need to supply the interaction between production processes and machines, the building structure and service equipment. Effects of changing production processes on the building structure and consequently on the performance along the whole life cycle of the factory should be simulated and visualized in real time, giving reliable feedback on design-decisions already in early design stage. Therefore, a large quantity of data need to be integrated, although data availability in early design-stage is rare and data exchange between different disciplines rarely exist.

Integrated decision-making systems that provide manufacturing and building criteria is relatively complex, since currently production and building design processes run consecutively, lacking in feedback loops. Additionally, structural considerations usually enter the design process too late and are subservient to

architectural and production goals, leading to suboptimal structures and inflexible floorplans. Thus, environmental and economic aspects such as resource consumption and life-cycle costs could be reduced by collaborative performance-based decision-support systems, optimizing the structural system. However, digital industrial building models do not properly address the interaction between production and building design disciplines, which may later lead to inflexible solutions.

In industrial construction projects, stakeholders are faced with numerous complex design decisions, involving the choice of conflicting variables such as different construction types, production processes or building service equipment (BSE). Multi-criteria decision analysis (MCA) taking into account possible scenarios of production layouts can help to improve the structural performance of production systems. Though, require maximum integration of all stakeholders and a vast amount of data in early design stage. To achieve this integration several architectural, structural and manufacturing aspects and their interrelations need to be considered and new computational strategies developed in order to generate applicable design solutions.

This paper presents ongoing research, conducted within the research project BIMFlexi, which aims to increase the flexibility of industrial buildings towards rapidly changing manufacturing systems in a BIM-based digital platform. This paper explores a novel approach integrating production process planning into performance-based structural design in early design stage of industrial buildings. A framework for a parametric structural design and optimization model in order to allow multi-objective optimization (MOO) with immediate decision support increasing the flexibility of industrial buildings is developed. The parametric model framework is designed to be integrated into the BIM-based digital platform of BIMFlexi in a next step of the research.

In this paper, we first review the state of the art for MCA in industrial building design. We then explore collaborative decision-making problems with focus on structural performance integration (chapter 2). In order to identify relationships between building design and production planning the results of a comprehensive case study, analysing ten real industrial facilities, are summarized in a graph data model. We propose a framework for a parametric structural performance-based design and optimization model that can be used by stakeholders involved in industrial construction projects to support in multi-criteria decision-making in early design stage (chapter 3). The framework is tested on a pilot project and results are discussed (chapter 4). The paper completes with a conclusion and outlook of the next steps. (chapter 5).

2 Literature Review

Research and industry community widely acknowledge the need for flexible and adaptable buildings, contributing to sustainable design choices [1]. Maximizing the flexibility of building structures can minimize costs and time required for rescheduling, but identification of interdependencies among discipline-specific systems bears challenges [2]. Cavalliere et al. [3] develop a BIM-based parametric model for automatic flexibility evaluation for sustainable building design.

Regarding MCA and decision-support systems for production plants, numerous research has been conducted in optimization of manufacturing systems [4-7]. A modular process model taking into account databased interdependencies in factory planning respecting the building is developed by Hawer et al. [8]. Yet, industrial buildings are rarely in research focus [9]. Among the conducted research, several authors proposed models concentrating on industrial building level. Kovacic et al. [10] develop a life-cycle analysis tool for facade-systems of industrial buildings, claiming that decision-making processes require long-term horizons, which, however, still need improvement. Authors in [11] develop an approach for factorial design space exploration supporting in multi-criteria decision-making (MCDM) to study energy performance, environmental impact and cost effectiveness along the life cycle. The author in [12] present a sustainability assessment methodology based on MCDM including factors influencing early design stage of industrial buildings. In [13] a study developed a decision-making model to describe relations between factory buildings, manufacturing equipment, sustainability aspects and the planning process. Other researchers focused on the prediction of the energy efficiency in production facilities [14] or used MCA for space heating system selection in industrial buildings [15]. Methods and models developed for MCA of industrial buildings mostly address energy performance improvement. Less attention is on the structural performance. However, to determine the overall efficiency of industrial buildings a concurrent assessment of the synergy effects of production processes, BSE and the building itself is needed [16].

Current available structural analysis tools are not sufficient for early design stage as their focus is rather on precision than flexibility often lacking in interoperability to other design tools [17]. Few structural analysis methods allow analysis and visualization in a single environment, provide feedback only to the structural engineer himself and do not support an integrated performance improvement [18]. Parametric modeling can support in conceptual design, enabling early integration of engineering-specific knowledge [19] allowing fast variant studies and enabling flexible

exploration of design spaces by varying parameters and their dependencies [20]. Using parametric design tools such as Grasshopper for Rhino [21] or Generative Components [22] provide visual programming environments and allow the integration of structural performance simulations such as Karamba3D [23]. In addition, a number of computational tools supporting MOO are already embedded in traditional parametric modeling software [24], including the generative solver Galapagos [25] for Grasshopper.

Several methods have been used to support integrated design exploration for structural performance with MOO in conceptual stage. Authors in [24] present a case study of a cantilevered stadium roof for early-stage integration of architectural and structural performance in a parametric MOO design tool. In [26] a MOO methodology for structural efficiency and operating energy efficiency focusing on long span building typology is presented. [27] develop a design tool, which parametrically generates and semi-automatically analyzes truss designs with real-time visual structural performance feedback. Mueller and Ochsendorf [18] propose a computational approach in evolutionary design space exploration, combining structural performance and designer preferences. Pan et al. [28] propose a design process for long-span structures composed of a parametric model, a framework of interdisciplinary assessment criteria and MOO with post-processing tools.

The above listed research results are remarkable but focus either on production process modeling or building performance, mostly focusing on energy efficiency. Holistic models receive little attention. Indeed, the focus in early industrial building design should be on the optimization of the load-bearing structure in order to maximize the facilities flexibility, thus prolonging the buildings service life and reduce life-cycle costs.

Hence, this paper deals with the framework development of an early-stage parametric structural optimization and decision support model for integrated industrial building design. It integrates architectural, structural, BSE and production process planning and evaluates the impact of changing manufacturing conditions on the structural performance, automatically evaluating flexibility to guide the decision-making process towards increased sustainable design.

3 Research Methodology

As described in the previous chapter, this paper focuses on the investigation of the interdependencies between building (architecture, structure, BSE) and production (manufacturing program, machine layout and space requirements) data in order to develop a parametric multi-criteria model for structural optimization and decision support. Multi-criteria decision-making requires a vast amount of data in order to come to applicable results. The research is based on a case study to construct a network from direct empirical observations, showing graphical data structure, compactly representing dependencies.

3.1 Use-Case Study

The use-cases under investigation are selected acc. to [29] and are representative for the research objective. Due to different types of production examined – Automotive, Food and Hygiene, Logistic, Metal Processing and Special Products - a diversity is created and not exclusively the needs and objectives of a specific manufacturing sector investigated. The recommendations in [29] are followed with a total number of ten examined use-cases. The purpose of the research is to develop theory, not to test it. The use-cases are selected because the highest density of given information and the best accessibility of data and leading stakeholders was available [30]. Table 1 gives an overview of the examined use-cases.

Table 1. Use-Cases examined

Use-Case	Production Type	Floor Area [m²]	Primary Construction
A	Food	5760	Steel Truss
B	Logistic	5040	Steel Truss
C	Logistic	8064	Timber Girder
D	Metal	16200	Timber Truss
E	Automotive	160704	Steel Truss
F	Metal	2800	Steel Girder
G	Metal	28224	Precast RC Girder
H	Special	1296	Precast RC Girder
I	Metal	6750	Underspanned Timber Girder
J	Special	1992	Steel Truss

3.2 Graph Data Model

We have undertaken a process of creating a graph data model for the representation of interactions between production planning and building design to cover the requirements for the developed parametric model. A graph data structure is naturally defined around graphs, nodes and edges. In the conducted research an attributed graph is used for modeling, describing properties for nodes and edges [31]. The approach consists of two tasks: extracting generic hypothesis-evidence relationships from the case study, concentrating on design variables and parameters and organizing such relationships in a data structure to facilitate quick response using a minimal amount of memory and computational time later on.

The proposed Graph Data Model for integrated industrial building design (GIB) is structured as follows:

- *Nodes:* The design parameters in GIB system include geometric entities (i.e. structural elements), constraints (loads, legal restrictions) or other requirements (i.e. space requirements).
- *Labels:* The nodes are assigned in four labels according to the examined disciplines.
- *Edges:* define the relationship between the nodes
- *Properties:* Nodes or edges maintain a set of attributes (property values) thus allowing storing of relevant data and information.

Figure 1 shows the effective graphic representation of dependencies in integrated industrial building design combining the disciplines of production-, architectural-, structural-, and BSE planning based on the results of the case study. The proposed GIB model is grow- and changeable over time and relationships, nodes, properties and labels can be added or removed. The flexibility and simplicity of the graph data model allows reviewing of the data structure and serves as basis and modeling guide for the parametric script.

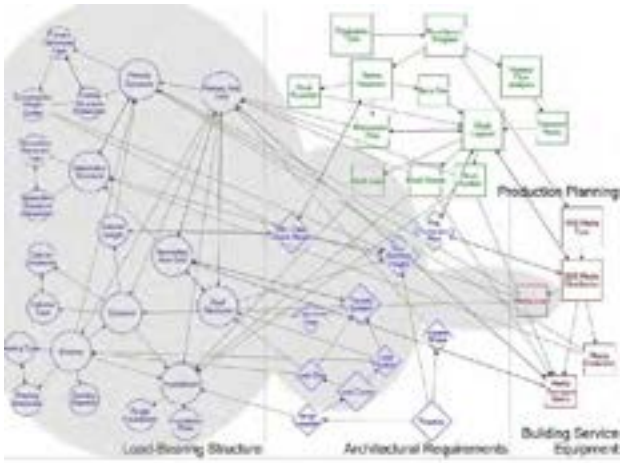

Figure 1. Attributed graph data model for integrated industrial building design (GIB).

Figure 1 additionally highlights the nodes that have already been considered in the status of the parametric framework in grey area. Missing parts, e.g. production- and BSE- entities will be integrated in the next step of the research.

3.3 Model Framework Description

In multi-criteria design analysis, the number of design-options is typically very large and the options not explicitly known. We have developed a framework for a parametric design process in Grasshopper for Rhino [21] in order to find options within the solution space and systemise the appropriate evaluation. Additionally, the Grasshopper components Karamba3D [23] for structural analysis and Galapagos [25] for evolutionary search are used in the parametric design process. Karamba3D allows early-stage structural design, form-finding, and structural optimization. Using a parametric script allows the automatic analysis and optimization of the load-bearing structure in consideration of constraints from other disciplines.

The framework consists of six discrete steps (see Figure 2) that in total comprise the parametric multi-criteria model for structural optimization and decision support:

1. Parameter & Input
2. Geometry & Loads
3. Element Definition
4. Structural Analysis
5. Structural Performance
6. Optimization

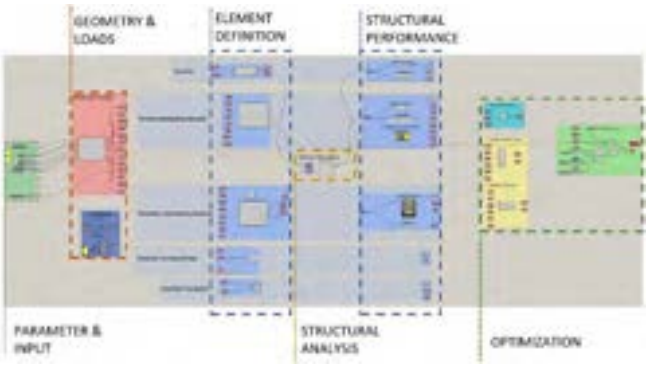

Figure 2. Framework of the parametric grasshopper model containing six steps.

In a first step, the definition of the building's typology takes place by selecting eight design inputs as described in Table 2. The load-bearing element-ranges are defined according to the case-study results.

Table 2. Input variables for the design process

Typology		
	Variable	Range
G1	Prim. Axis Grid (x-axis)	0 – 30m
G2	Prim. Axis Fields	1 – i
G3	Sec. Axis Grid -x	0 – 30m
G4	Sec. Axis Grid -y	1 – j
G5	Hall Headroom	5 - 15m
G6	Max. Building Height	5 - 20m
S1	Primary Structure Type	1-2
S2	Secondary Structure Type	1-2

The design variables for flexible structural industrial building design are defined as the position of the columns representing the axis grid in x- and y- direction, for both the primary and secondary structural system.

Furthermore, an important grid variable represents the z-direction as the free hall headroom inside the building and the outer maximum building height. The primary and secondary structure type can be chosen variable in a range of two pre-defined systems, which are either a truss (Option 1) or girder structure (Option 2).

Following, the base geometry is generated as a wireframe model, according to the definition of the axis grid. Simultaneously, pre-defined loads, obtained from the case study, such as snow load and live loads, dependent from production process and BSE-planning, are applied automatically.

In the third step, the structural elements are generated based on the generated wireframe model. Currently, following structural elements for modeling and calculation are taken in account:

- Primary load-bearing structure
- Secondary load-bearing structure
- Columns
- Bracing system
- Individual foundations
- Concrete foundation plate

After the generation of the structural system with associated elements, the structural analysis is carried out in the fourth step. The pre-dimensioning of the pre-defined elements considering input variables and load-cases takes place. The fitting of the cross-sections is executed with the native cross-section optimizer in Karamba3D.

In the fifth step, the structural performance is carried out. Since as-built structures often differ from idealized finite-element models for structural computation, the elements are re-arranged by considering structural design rules based on gained knowledge during the case study. For further processing, the structural performance is evaluated based on the criteria of utilization and maximum displacement.

The final step contains the calculation of constraints and objectives for design optimization. The optimization step uses Galapagos as an evolutionary algorithm to optimize the design alternative considering the fitness function, as described in the following section.

3.4 Fitness Function and Optimization

In order to allow the optimization of the input variables, the parametric script automatically calculates objectives and constraints of diverse design options. Table 3 shows the set of constraints and objectives considered in the fitness function. The considered constraints are the maximum utilization of the structural elements, the maximum building height and the maximum displacement of the structural system.

The pursued flexibility objectives are the minimization of the structural space requirements in the production hall (F1), the maximization of the free height reserve in the hall (F2), the maximization of the material saving (F3) and the minimization of the structural utilization in order to be able to place additional loads on the system in future without conversion work (F4). The presented objectives are a pre-selection based on a series of interviews with different discipline-specific stakeholders carried out during the case study.

The definition of the flexibility objectives for the fitness-rating is partly based on the method presented in [3], where distance- and percentage-based indicators are presented giving the possibility to determine the flexibility of design alternatives. The distance-based indicator serves for definition of the objective function F2 to maximize the height reserve of the system, whereas the percentage-based indicator is used for the objective functions F1 to minimize the structural space and F4 to minimize the utilization of the structural system. In addition, a reference-value based indicator is defined by putting obtained reference values of the material demand in different production types from the use-case analysis (i.e. average material demand of a structural system) in proportion to the actual material demand of the optimized system. The reference-based indicators serve for the calculation of the objective function F3 to maximize material savings.

Table 3. Constraints and objectives defining the fitness function for flexible industrial building design

Constraints		
	Constraint	Range
C1	Maximum Utilization ≤ 1,0	{0,1}
C2	Building Height ≤ Max. Height	{0,1}
C3	Displacement ≤ Max. Displacement	{0,1}
Objectives		
	Objective	Range
F1	Minimize Structural Space *percentage-based*	{0:1}
F2	Maximize Height Reserve *distance-based*	{0:1}
F3	Maximize Material Saving *reference-value-based*	{0:x}
F4	Minimize Utilization *percentage-based*	{0:1}

During the process, the user is given the possibility to define weighting factors to the different objectives given and these weighting factors are applied to the different objective functions F1 - 4. The weighted objective functions are then gathered in a linear equation describing the function for the fitness rating:

$$Q = \prod Ci * (\sum ajFj) \quad (1)$$

Q *Fitness Rating*
C_i *Constraint [0,1]*

F_j *Fitness indicator*
a_j *Weighting ($\sum a_j=1$)*

4 Results and Discussion

In order to evaluate the accuracy and validity of the proposed framework and the applied fitness function a proof-of concept is performed based on a pilot project. The chosen pilot project is a real production facility from the food and hygiene sector with a total production area of 5.760m² - Use Case A of the Case-Study. The external dimensions of the hall are 48x120m, with a structural axis grid of 12x24m.The building structure was realised as steel truss-system in primary and secondary direction with truss construction heights of 2,4m. The columns consist of pre-cast concrete cross-sections with dimensions of 60x60cm and the bracing system uses end-fixed columns to bear horizontal loads. Figure 3 shows the 3D Visualisation of the Pilot Project and the applied load-areas in Rhino3D, taking into account snow loads and BSE- and production-related loads.

A variant study is carried out in order to obtain and compare analysis and optimization results. The grasshopper script automatically generates and evaluates numerous design options of the pilot project with the goal of optimization of the structural system. After running the analysis and optimization script, the twelve most relevant design options were categorised according to the structural type and examined in detail. Category 1 contains all options with pure truss structures, options of category 2 contain only girder structures and category 3 options represent a set of mixed structures. A balanced objective weighting (each objective 25% importance) has been defined in the proof-of concept.

- PP: Pilot Project – Truss structure
- Cat. 1: Truss structure - primary & secondary
- Cat. 2: Girder structure - primary & secondary
- Cat. 3: Mixed structure

Figure 3. Pilot project model visualisation in Rhino 3D with load distribution.

The optimization results of the best-rated design-option from each category (Cat.1-3) compared to the pilot project (PP) are presented in Table 4.

Table 4. Optimization Results of Proof-of Concept

Options	PP	Cat. 1	Cat. 2	Cat. 3
Variables				
G1 [m]	12	12	12	12
G2 [pc]	4	4	4	4
G3 [m]	24	12	6	12
G4 [pc]	5	10	20	10
G5 [m]	6,35	6,35	6,35	6,35
G6 [m]	9,30	9,30	9,30	9,30
S1 [no.]	1	1	2	1
S2 [no.]	1	1	2	2
Material Demand Results				
steel mass [kg/m²]	45,7	28,7	76,7	89,0
concrete mass [kg/m²]	24,8	25,6	48,9	40,0
Objective Values				
F1	0,94	0,90	0,82	0,90
F2	0,24	0,59	0,59	0,59
F3	1,00	1,27	0,55	0,57
F4	0,91	0,90	0,70	0,76
Fitness Rating				
Q	0,72	0,92	0,67	0,70

Figure 4 presents the best-rated design-option of each category compared to the pilot project in a radar diagram. The objective function of the Material Saving (F3) has a high impact on the performance of the structure.

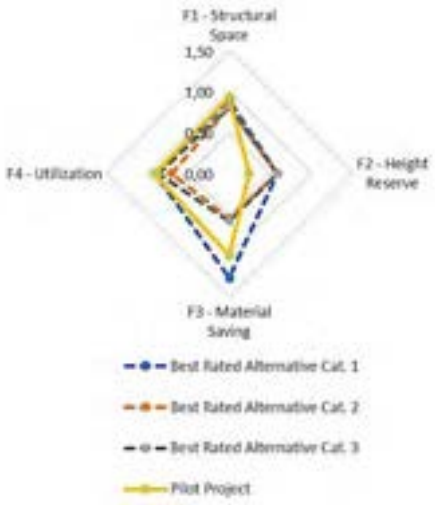

Figure 4. Graphical radar representation of the proof-of concept results.

Table 4 shows that the best rated option with the highest fitness rating is performed by category 1 – the sole truss structure with an axis grid of 12x12m. Highly due to the positive impact of material saving (F3). Results indicate that the Cat. 1 option saves approximately 25% of the structural steel mass compared to the pilot project,

mostly because of the axis grid optimization. Additionally, the structural analysis results in cat.1 increase the utilization of the cross-sections compared to the more conservative cross-section selection in the pilot project. This may also be because during the pilot projects design phase, stakeholders probably may have considered additional design parameters and constraints such as structural reserves, which are not yet represented in the framework of the parametric script.

In category 2, the best-rated option still has a high material demand compared to the pilot project and the positive impact of the Height Reserve (F2), due to girder structures, is not able to compensate this drawback. The bad rating of Material Savings (F3) in category 2 shows that the girder structures are hardly competitive to truss structures due to the high BSE loads.

A mixed structure as analysed in category 3 also has a worse performance compared to the pilot project with a fitness rating of Q=0,70.

In conclusion, results of the variant study show that for the applied load scenario truss structures (Cat.1) are more competitive compared to girder (Cat.2) and mixed (Cat.3) structures. An optimization of the pilot projects performance could be obtained by adjustment of the axis grid in x and y direction.

Regarding the evaluation of the fitness function (Q) and the contained objective functions (F1-4), we observe that the determination of the material saving (F3) has a decisive effect on the performance results (see Figure 4) in comparison to other objectives, considering their narrow value range. Further analysis of the mathematical definition of the objective functions is necessary.

Considering the efficiency of the parametric script, the computational time of approximately 10-15 seconds per option on a standard computational system is improvable but legitimate for a complex structural analysis with parallel optimization.

5 Conclusion

This paper proposed a method to support integrated industrial building design exploration with structural optimization, which is crucial to guarantee the long-term flexibility of factories. In a use-case study, ten real industrial construction projects are analyzed in order to define discipline-specific parameters and their interdependencies in industrial building design. The goal is the development of a computational framework integrating discipline-specific data of production planning, architectural-, structural and BSE design in one holistic model. Parametric modeling combined with structural analysis and optimization algorithms for performance-driven design allows the generation, simulation and optimization of different structural layout options for early decision-making in industrial construction projects.

The developed parametric script considers varying primary and secondary axis grid options with different structural types enabling performance improvement of a building's long-term flexibility. A multi-objective fitness function has been developed rating the flexibility of a building structure and serving as multi-criteria decision support model. A proof of concept on a real pilot project, a food production, was conducted in order to validate the efficiency of the process and show the necessity of extending the parametric framework.

In the next step of the research, the parametric script will be further extended according to the lacking parts of the graph data model, integrating missing production and BSE- data. Furthermore, the mathematical background of the current definition and description of the objectives needs to be further investigated. The mathematical definition of the fitness function and its objectives has to be improved and extended with additional objectives in order to define accurate flexibility statements for all stakeholders. Considering the structural analysis and pre-dimensioning results, an in-depth analysis of the used algorithms in Karamba3D is necessary to cope with utilization fluctuations of the generated structures. The proof of concept will be extended by analysing more case-cases, guaranteeing the robustness of the tool in various production scenarios.

Future work will examine and develop methods to integrate the framework of the parametric model into the BIM-based digital platform by bi-directionally coupling it to BIM, Finite-Element-Method Tools and Virtual Reality software, as aimed in the research project BIMFlexi.

Acknowledgment

The authors would like to acknowledge the support by the Austrian Ministry for Transport, Innovation and Technology through the Austrian Research Promotion Agency FFG for the research project "BIMFlexi" (Grant No. 877159).

6 References

[1] Gosling, J., et al., *Flexible buildings for an adaptable and sustainable future.* Association of Researchers in Construction Management, ARCOM 2008 - Proceedings of the 24th Annual Conference, 2008. **1**: p. 115-124.

[2] Slaughter, E.S., *Design strategies to increase building flexibility.* Building Research & Information, 2001. **29**(3): p. 208-217.

[3] Cavalliere, C., et al., *BIM-based assessment metrics for the functional flexibility of building designs.* Automation in Construction, 2019. **107**: p. 102925.

[4] Francalanza, E., J. Borg, and C. Constantinescu, *Development and evaluation of a knowledge-based decision-making approach for designing changeable manufacturing systems.* CIRP Journal of Manufacturing Science and Technology, 2017. **16**: p. 81-101.

[5] Colledani, M. and T. Tolio, *Integrated process and system modelling for the design of material recycling systems.* CIRP Annals, 2013. **62**(1): p. 447-452.

[6] Kluczek, A., *An Overall Multi-criteria Approach to Sustainability Assessment of Manufacturing Processes.* Procedia Manufacturing, 2017. **8**: p. 136-143.

[7] Deif, A.M., *A system model for green manufacturing.* Journal of Cleaner Production, 2011. **19**(14): p. 1553-1559.

[8] Hawer, S., et al., *An Adaptable Model for the Factory Planning Process: Analyzing Data Based Interdependencies.* Procedia CIRP, 2017. **62**: p. 117-122.

[9] Heravi, G., M. Fathi, and S. Faeghi, *Evaluation of Sustainability Indicators of Industrial Buildings Focused on Petrochemical Projects.* Journal of Cleaner Production, 2015. **109**.

[10] Kovacic, I., L. Waltenbereger, and G. Gourlis, *Tool for life cycle analysis of facade-systems for industrial buildings.* Journal of Cleaner Production, 2016. **130**: p. 260-272.

[11] Lee, B., N. Pourmousavian, and J.L.M. Hensen, *Full-factorial design space exploration approach for multi-criteria decision making of the design of industrial halls.* Energy and Buildings, 2016. **117**: p. 352-361.

[12] Cuadrado, J., et al., *Sustainability-Related Decision Making in Industrial Buildings: An AHP Analysis.* Mathematical Problems in Engineering, 2015. **2015**: p. 1-13.

[13] Chen, D., et al., *Integrating sustainability within the factory planning process.* CIRP Annals - Manufacturing Technology, 2012. **61**.

[14] Bleicher, F., et al., *Co-simulation environment for optimizing energy efficiency in production systems.* CIRP Annals, 2014. **63**(1): p. 441-444.

[15] Chinese, D., G. Nardin, and O. Saro, *Multi-criteria analysis for the selection of space heating systems in an industrial building.* Energy, 2011. **36**(1): p. 556-565.

[16] Gourlis, G. and I. Kovacic, *A study on building performance analysis for energy retrofit of existing industrial facilities.* Applied Energy, 2016. **184**: p. 1389-1399.

[17] Rolvink, A., J. Breider, and J. Coenders, *Structural Components - a parametric associative design toolbox for conceptual structural design*. 2019.

[18] Mueller, C.T. and J.A. Ochsendorf, *Combining structural performance and designer preferences in evolutionary design space exploration.* Automation in Construction, 2015. **52**: p. 70-82.

[19] Sacks, R. and R. Barak, *Impact of three-dimensional parametric modell of buildings on productivity in structural engineering practice.* Automation in Construction, 2008. **17**(4): p. 439-449.

[20] Azhar, S. and J. Brown, *BIM for Sustainability Analyses.* International Journal of Construction Education and Research, 2009. **5**(4): p. 276-292.

[21] Associates;, M. *Grasshopper*. 2020 29.01.2020]; Available from: https://www.rhino3d.com/6/new/grasshopper.

[22] Shea, K., R. Aish, and M. Gourtovaia, *Towards integrated performance-driven generative design tools.* Automation in Construction, 2005. **14**(2): p. 253-264.

[23] Preisinger, C. and M. Heimrath, *Karamba—A Toolkit for Parametric Structural Design.* Structural Engineering International, 2014. **24**(2): p. 217-221.

[24] Brown, N., J. Felipe, and C. Mueller, *Early-stage integration of architectural and structural performance in a parametric multi-objective design tool*. 2016.

[25] Rutten, D., *Galapagos: On the Logic and Limitations of Generic Solvers.* Architectural Design, 2013. **83**.

[26] Brown, N.C. and C.T. Mueller, *Design for structural and energy performance of long span buildings using geometric multi-objective optimization.* Energy and Buildings, 2016. **127**: p. 748-761.

[27] Makris, M., et al., *Informing Design through Parametric Integrated Structural Simulation: Iterative structural feedback for design decision support of complex trusses*. 2013.

[28] Pan, W., et al., *Integrating multi-functional space and long-span structure in the early design stage of indoor sports arenas by using parametric modelling and multi-objective optimization.* Journal of Building Engineering, 2019. **22**: p. 464-485.

[29] Albers, S.K., D; Konradt, U; Walter, A; Wolf, J;, *Methodik der empirischen Forschung*. 2009, Springer Fachmedien Wiesbaden GmbH, Wiesbaden: Gabler Verlag.

[30] Eisenhardt, K.M. and M.E. Graebner, *Theory building from cases: Opportunities and challenges.* Academy of management journal, 2007. **50**(1): p. 25-32.

[31] Angles, R., *A Comparison of Current Graph Database Models*. 2012. 171-177.

Inspection of Discrepancies in Construction Temporary Safety Structures through Augmented Reality

Hashim R. Bokhari[a], Doyeop Lee[a], Numan Khan[a] and Chansik Park[a*]

[a]Department of Architectural Engineering, Chung-Ang University, Seoul, South Korea
E-mail: hashimbokhari@cau.ac.kr, doyeop@cau.ac.kr, numanpe@gmail.com, cpark@cau.ac.kr

Abstract – Construction safety has been a major area for research for an extensive time as the number of accidents, injuries and deaths has not significantly declined, despite strong implementation of safety laws and major efforts of the construction safety professionals. According to the Ministry of Employment and Labor, Korea (MOEL) [1] from 2012 to 2015 the Construction sector occupied the highest percentage of fatalities among all sectors in Korea. Automation of the inspection process of Temporary Safety Structures on Construction sites (TSSC) can reduce fatalities and injuries on work site. This research proposes a unique approach for the safety inspection of TSSC by using an outdoor marker-less AR system along with Structure from Motion (SfM) to reconstruct the 3DCG (3-Dimensional Computer Generated) models by using photographs from different viewpoints. The system(framework) considers area mobility of the inspector and his long relative distance, along with local feature-based image registration technology to target the location for Augmentation of 3DCG models of TSSC. This system would enhance the inspection, verification, and installation of the TSSC and help in ensuring worksite safety of all individuals involved in the construction development process. In future research, a case study would be conducted to confirm the implementation of this framework and integrate other areas for further development.

Keywords –
Instructions; Construction Safety; Inspection; Augmented Reality; Feature-Based Image Matching; Structure from Motion

1 Introduction

Construction worksite safety is a comparatively high researched area, because of the soaring number of fatalities and injuries during development phase of the projects [1] [2]. Construction caused 20.9% of the workplace related fatalities in the United States from 2003 to 2008 (Bureau of Labor Statistics, 2008) (Census of Fatal Occupational Injuries (CFOI) - Current and Revised Data, 2018) and In South Korea it had the highest percentage of fatalities according to the Ministry of Employment and Labor[4]. The processes involved in construction project development should revolve around the central idea of worksite(occupational)safety, as it directly impacts physical human life safety of the workforce and all other humans beings involved in the construction processes, such as management, trades, and logistics teams. Safety can be ensured in certain scenarios by the proper usage of different types of Temporary Safety Structures such as safety fence, struts, guardrails, scaffoldings, handrails, temporary gates, and others. These Temporary Safety Structures on Construction (TSSC) sites require strict monitoring, detailed concentration of the inspector and need to be setup according to the safety design. This makes the safety inspection process a challenge, as construction sites can cover vast areas and site conditions can be unpredictable.

Currently, in most scenarios, the safety inspection is being conducted manually, wherein the safety inspector visits the worksite and enforces legal safety requirements and best practices. The inspector relies on his observation of the entire safety design, installation & verification processes, and his observation of the Temporary Safety Structures on Construction (TSSC), to ensures safety and provides help in avoiding any discrepancies(errors), which can possibly be a major cause for physical bodily harm (injuries) or even deaths on construction worksites. This method typically involves the usage of 2D drawings and requires detailed attention to temporary safety structures on large construction sites. This inspection method requires constant monitoring, strict and lengthier time span, which makes it predisposed to errors, because of the manual nature of the process. The inspector has limitations as a human being, such as concentration span duration and Vision fatigue, such limitations can lead to reduction in the number of discrepancies (errors) detected which in a large scale construction site can be a major cause of safety lapse. Due to these human limitations despite considerable effort from Construction Safety Professionals for worksite safety, the number of fatalities and injuries has not reduced and continues to be

the highest in construction when compared to other industries.

The advancements of technologies for use in construction, such as Augmented Reality, can help improve construction worksite safety. Augmented Reality (AR) is already being actively used in architecture and urban design fields as it can integrate augmentation with the real-world scenes. Through the help of visualization feature of AR[5], construction safety inspection can be improved both at the design stage (3D design visualization) and later at the safety inspection stage for discrepancy monitoring.

Augmented Reality (AR) provides the users (construction professional) with an interactive experience, where the real-world environment and real-world objects are enhanced by computer-generated perceptual information. This proposed framework AR system would integrate real world scenes with 3D (3-Dimensional Computer Graphics) models, to facilitate the possibility of onsite safety inspection. The AR system is to be set for an outdoor environment, specifically for outdoor safety inspection. This is due to the relatively large distance that exists between the user and the 3D model in outdoor AR systems. Such a system would enable the safety inspector to monitor TSSC with the help geometric registration (location-based monitoring). The reference point is the position of the sensor such as GPS or 3D sensor [6], in contrast to when using a marker based method, where the position of the artificial marker servers as the reference point, which is an example of vision-based methods.

Figure 1. Shows a Safety Inspector monitoring Temporary Safety Structures on Construction site

2 Related Work

2.1 Marker-less AR for Inspection

Generally, the proposed system is to be used for outdoor inspection. If a system is sensor based then, one of the key challenges is to get accurate AR. This requires precise tracking of the geometric registration between the live video stream and 3D reconstructed model image. The reference point for geometric registration is proposed to be positioned near (close) to the user (inspector), hence, the sensing errors that can significantly influence the error of the 3D model registration may be reduced. Whereas, in artificial marker-based methods, it is possible to place any large size markers near the target objects. Moreover, the marker needs to be captured properly, with the right angle, by the AR Camera. This imposes limitations on the mobility range of the user and requires placement of a large sized marker. A Marker-Less AR system would enable the Inspector to monitor the construction site from a distance and enhance his mobility. This mobility factor is the primary reason for the advancement of Marker-less AR (which do not require artificial Markers) Technology for example [7], [8] and [9]. The development of a geometric registration method which corresponds point cloud data to natural features of the real world was developed by Yabuki [10]. This method requires natural feature to be continuously captured by the AR Camera, it also requires special equipment to acquire point cloud data, as the system would use to 3D laser scanner to collect the large amount of data for the point cloud.

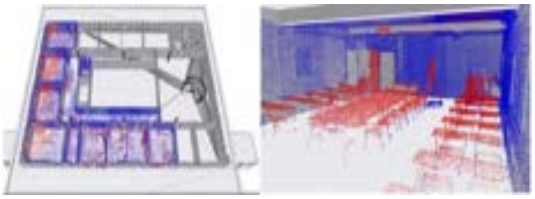

Figure 2. Shows a sample regarding point cloud data & objects segregation for 3D modelling

The 3D Model displayed on the screen uses the equation developed by Zhengyou Zhang [11], where the equation s symbolizes expansion or reduction factor with u and v as the position that draws the object according to the coordinates.

$$s\begin{pmatrix} u \\ v \\ 1 \end{pmatrix} = \begin{pmatrix} f & 0 & c_x \\ 0 & f & c_y \\ 0 & 0 & 1 \end{pmatrix} (R_{3\times3} \quad T_{3\times1}) \begin{pmatrix} X \\ Y \\ Z \\ 1 \end{pmatrix}$$

f denotes the value of the focal length, c_x and c_y determine the coordinates of the center of the image, these values are known as the parameters of the camera where R is rotation matrix and T is the translation matrix of the camera. All these values are known as the external parameters of the camera. The values of X, Y, Z denote the position of the object in the real-world coordinates.

The internal parameter generally remains constant(unchanged), unless camera lens is changed, and can be calculated through camera calibration. Specific to the photograph's viewpoint are the position and posture

data of the camera, for the external parameters. This is the primary reason for the calculation of the external parameters for the AR system. For Marker-based system the calculation takes place via the position of the marker, whereas for marker-less system another calculation method is required. Subsequently, for this study, a novel marker-less based system, along with feature-based image registration technology was used. Additionally, to enhance mobility the system utilizes the sensor-based registration and does not require a marker. The point cloud data used in the system is reconstructed by Structure from Motion (SfM).

2.2 Structure from Motion for 3D modeling

In direct contrast(to Lidar), Structure from Motion(SfM) [12], requires multiple pictures taken from different point of views to create a point cloud data of the TSSC [13]. This a low-cost alternative tool to 3D lasers scanning for creating models [14], it is an emerging method. The system does not utilize any special equipment such as laser scanners.

A major feature of the proposed system is that it does not require any specialized equipment (such as sensors for geomatic-registration between the Augmentations and the real world) as it uses sensor-based registration. Additionally, Artificial Markers are not required (they decrease user mobility and flexibility). Lastly, point cloud data used in this system is reconstructed through SfM and no special equipment such as laser scanners are required. These reconstructed models will be used for 3D model creation.

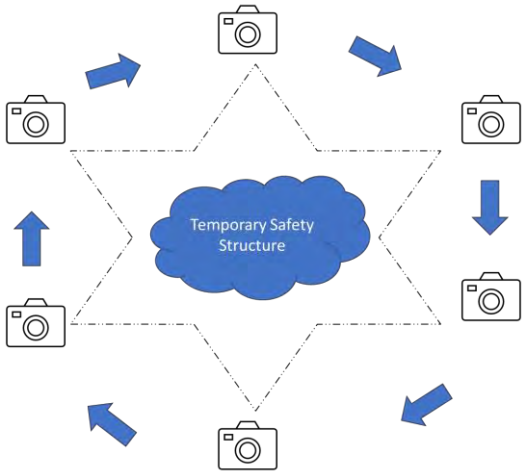

Figure 3. Shows the Image capturing process required for Structure from Motion (SfM)

Figure 4. Shows a sample of different reconstructed models of objects from SfM

This study presents a framework based on a novel marker-less AR system which utilizes local feature-based image registration and Structure from Motion (SfM) technology for discrepancy inspection. The system provides free mobility, reduced limitations, requires less effort and is inexpensive for use in outdoor AR application.

3 Overview of the Proposed System

In this Framework, the proposed system is dived into two sections: Initial-Processing and Core-Processing.

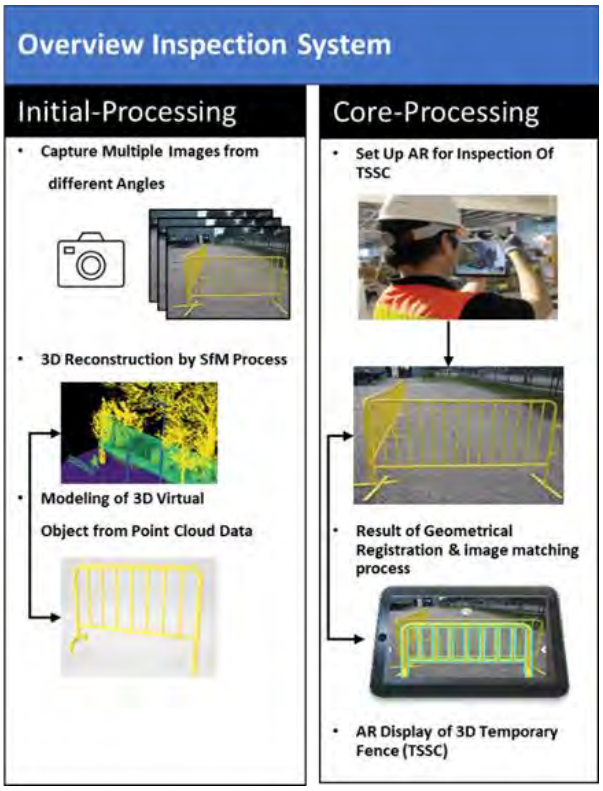

Figure 5. Shows the System Overview

Under the Initial-Process, in the first step, a 3D model of the environment will be reconstructed using the Sfm method, using the pictures taken from multiple viewpoints. The entire data regarding position and orientation of all the viewpoints would be stored in a database. In the second step the coordinates of 3D model generated for augmentation (Safety Fence in this scenario) are to be defined relative to the 3DCG models of the reconstructed environment that was created (reconstructed) using SfM and stored in the database. Finally, the keys point and features from all the pictures used in SfM will be extracted and stored in a separate text file. In addition, the file paths of the all the pictures will be saved in a separate text file.

For the proposed research based framework, the user (inspector) is asked to utilize an advance local feature detector and descriptor known as Speed-Up Robust Features (SURF)[15], as it is based on the improvements from the Scale-Invariant Feature Transform (SIFT) which is used for point detection proposes.

In the Core-Process, Firstly, all the files created in the Initial-Processes step should be imported. Secondly, real time extraction of the features of the live video would be extracted using SURF in real time, the features will then be compared with the features of the stored image in database. Finally, the precise rendering of the 3D virtual objects using position and orientation data of the camera and finding the most similar image in the database will takes place in AR display. For tracking to take place, motion vectors will be calculated by using optical flow. Finally, the calculation of the external parameters would consider internal parameters, Position of points on the screen and the world coordinates of their corresponding points.

To achieve real-time processing, 3 speed enhancement should be applied to processes, firstly, SURF processing, to compare keys features of live video images and all stored images in the database. Secondly, Locality Sensitive Hashing (LSH)[16] algorithm should be applied instead of the full search by linear search algorithms. Finally, a multithreading technique is proposed to be applied for feature extraction during the SURF process. In the Image Registration processing step, the live video images should be trimmed to only process the central area.

3.1 Processes, Software & Libraries

The system design for the proposed project will be implemented using C++ through a combination of multiple open source software applications and libraries. In this context the Initial-Processes will use OpenMVG (Open Multiple View Geometry version 1.6), which is an open source software to conduct Structure from Motion (SfM). Secondly, for 3D modelling Trimble SketchUp (Version 66.1.), which is another opensource software to define the coordinates of the virtual 3D objects.

For Core-Processes OpenCV (Open Source Computer Vision – Version 4.3.0), another opensource library is proposed to be used for live video stream capture and image matching. For Parallel processing

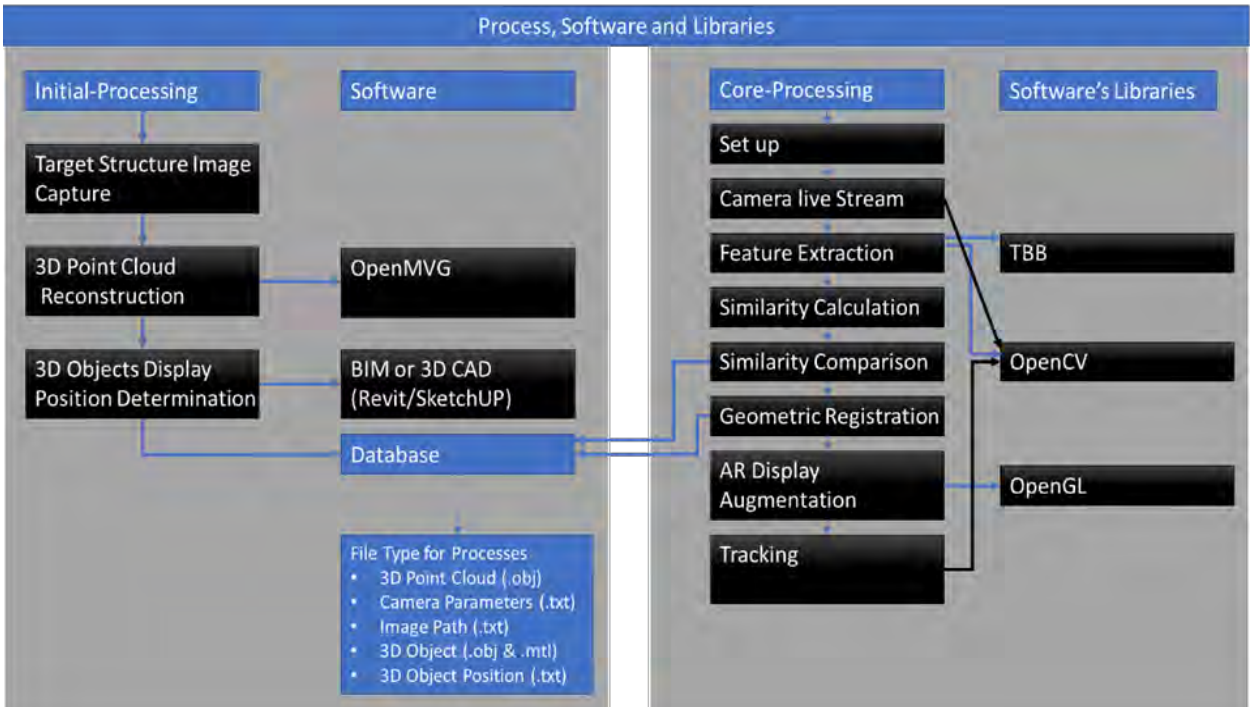

Figure 6. Shows the process, Software and Libraries required for the system

library Threading Building Blocks (2019 Update 8) was used. For Drawing 3D models on the AR display FreeGULT(Version freeglut 3.2.1), it is a toolkit for OpenGL (Open Graphic Library).

4 Designed System Verification Process & Limitations

The 3-step verification process for the proposed system, both the Initial-Processing and Core-Processing need to follow the set 3 steps, for the system to work properly.

Step 1: Location Information and tracking

- Tracking Route of TSSC
- Photography route of SfM
- Registration Position

Step 2: Image Matching

- Live Stream Capture & database Feature Based-Image Matching with SURF

Step 3: Augmented Reality 3D Model Super imposition

- AR Tracking while the User is Walking
- AR Display of Vector Motions
- 3D Model Augmentation

The generated data for each process needs to be saved into the database and will be utilized in the next step until the final step is completed and results are shown.

The proposed system is limited in its geometrical registration to the photography route of the temporary safety facility, this limitation can be overcome by the incorporation of addition photography routes to the TSSC. The 3DCG models face the challenge in tracking due to hand shaking, which can be overcome, by the average of the motion vectors in plural frames can be used when calculating the external parameters, this improvement will require development of new algorithms.

5 Conclusion & Future Research

This research proposes an implementable framework for Inspection of discrepancies in Construction Temporary Safety Structures through Marker-less Augmented Reality, that uses Structure from Motion (SfM) to reconstruct the 3DCG (3-Dimensional Computer Generated) models by using photographs from different viewpoints, along with feature-based image registration technology for construction safety inspection. The system if implemented can enhance the discrepancy monitoring of the Temporary Safety Structures inspection process by providing onsite visual aid of 3DCG models and allow location tracking. The system is limited to photography route and can cover additional routes. In future research, a case study would be conducted to confirm the implementation of the framework, its feasibility as an alternative and further improvements that an enhance the processes, such as blockchain based secure database management system, for the data collection of the system.

Acknowledgement

This work is supported by the Korea Agency for Infrastructure Technology Advancement (KAIA) grant funded by the Ministry of Land, Infrastructure and Transport (Grant 20SMIP-A158708-01).

The researchers would like to thank Mr. Talal Tariq, who is a software developer and Bachelor of Science in Information Technology from the University of Sargodha, Pakistan, for his support during the development of the processes stage for this research project.

References

[1] P. Perttula *et al.*, "Improving the safety and efficiency of materials transfer at a construction site by using an elevator," *J. Constr. Eng. Manag.*, vol. 132, no. 8, pp. 836–843, Aug. 2006, doi: 10.1061/(ASCE)0733-9364(2006)132:8(836).

[2] Z. Zhou, Y. M. Goh, and Q. Li, "Overview and analysis of safety management studies in the construction industry," *Safety Science*, vol. 72. Elsevier, pp. 337–350, Feb. 01, 2015, doi: 10.1016/j.ssci.2014.10.006.

[3] "Census of Fatal Occupational Injuries (CFOI) - Current and Revised Data." https://www.bls.gov/iif/oshcfoi1.htm (accessed Jun. 05, 2020).

[4] B. Jo, Y. Lee, J. Kim, and R. Khan, "Trend Analysis of Construction Industrial Accidents in Korea from 2011 to 2015," *Sustainability*, vol. 9, no. 8, p. 1297, Jul. 2017, doi: 10.3390/su9081297.

[5] A. Fenais, S. M. Asce, S. T. Ariaratnam, F. Asce, and N. Smilovsky, "Assessing the Accuracy of an Outdoor Augmented Reality Solution for Mapping Underground Utilities," 2020, doi: 10.1061/(ASCE)PS.1949-1204.0000474.

[6] V. Bui, N. T. Le, T. L. Vu, V. H. Nguyen, and Y. M. Jang, "GPS-Based Indoor/Outdoor Detection Scheme Using Machine Learning Techniques," *Appl. Sci.*, vol. 10, no. 2, p. 500, Jan. 2020, doi:

10.3390/app10020500.

[7] J. M. Runji and C. Y. Lin, "Markerless cooperative augmented reality-based smart manufacturing double-check system: Case of safe PCBA inspection following automatic optical inspection," *Robot. Comput. Integr. Manuf.*, vol. 64, no. February 2019, p. 101957, 2020, doi: 10.1016/j.rcim.2020.101957.

[8] G. Klein and D. Murray, "Parallel tracking and mapping for small AR workspaces," in *2007 6th IEEE and ACM International Symposium on Mixed and Augmented Reality, ISMAR*, 2007, doi: 10.1109/ISMAR.2007.4538852.

[9] D. Belter and P. Skrzypczynski, "Precise self-localization of a walking robot on rough terrain using parallel tracking and mapping," *Ind. Rob.*, vol. 40, no. 3, pp. 229–237, 2013, doi: 10.1108/01439911311309924.

[10] N. Yabuki, Y. Hamada, T. F.-P. of the 14th I. C. on, and undefined 2012, "Development of an accurate registration technique for outdoor augmented reality using point cloud data."

[11] Z. Zhang, "A flexible new technique for 1. Zhang, Z. A flexible new technique for camera calibration. IEEE Trans. Pattern Anal. Mach. Intell. 22, 1330–1334 (2000).camera calibration," *IEEE Trans. Pattern Anal. Mach. Intell.*, vol. 22, no. 11, pp. 1330–1334, Nov. 2000, doi: 10.1109/34.888718.

[12] M. J. Westoby, J. Brasington, N. F. Glasser, M. J. Hambrey, and J. M. Reynolds, "'Structure-from-Motion' photogrammetry: A low-cost, effective tool for geoscience applications," *Geomorphology*, vol. 179, pp. 300–314, Dec. 2012, doi: 10.1016/j.geomorph.2012.08.021.

[13] "Multiple View Geometry in Computer Vision - Richard Hartley, Andrew Zisserman - Google Books." https://books.google.co.kr/books?hl=en&lr=&id=si3R3Pfa98QC&oi=fnd&pg=PR11&dq=Multiple+View+Geometry,+Cambridge+University+Press&ots=aSxYowadcQ&sig=pIUKR_x3i34dawGqMfA6veSi8Q4&redir_esc=y#v=onepage&q=Multiple View Geometry%2C Cambridge University Press&f=false (accessed Jun. 08, 2020).

[14] T. Nagakura, D. Tsai, and J. Choi, "Capturing History Bit by Bit Architectural Database of Photogrammetric Model and Panoramic Video."

[15] H. Bay, T. Tuytelaars, and L. Van Gool, "SURF: Speeded up robust features," in *Lecture Notes in Computer Science (including subseries Lecture Notes in Artificial Intelligence and Lecture Notes in Bioinformatics)*, 2006, vol. 3951 LNCS, pp. 404–417, doi: 10.1007/11744023_32.

[16] P. Indyk and R. Motwani, "Approximate nearest neighbors," 1998, pp. 604–613, doi: 10.1145/276698.276876.

Status of 4D BIM Implementation in Indian Construction

V.P.C. Charlesraj and T. Dinesh

RICS School of Built Environment, Delhi NCR 201313 India
E-mail: vpcharlesraj@ricssbe.edu.in, dinesh.mc18n@ricssbe.edu.in

Abstract –

Enhanced visualisation is one of the low hanging fruits of BIM implementation. It helps in improving clarity in communications and fosters collaboration & coordination of construction projects for efficient delivery. 4D BIM combines the proposed sequence of work in a project with the 3D parametric digital model of the facility to be built. 4D BIM is highly beneficial both for managing people and materials. It can revolutionise the way facilities are designed, managed and developed. Significant benefits of 4D BIM have been reported in project planning & programming/scheduling, progress monitoring, conflict prevention & resolution, data security and construction safety. 4D BIM also adds value to business by facilitating marketing and sales.

BIM has been primarily used by design & management consultants and some large contractors in India for design optimisation and construction project management. While 4D BIM has the potential to contribute for the efficient project delivery, there is limited literature on the extent of 4D BIM implementation in India. An attempt has been made to investigate the status of 4D BIM implementation in India and study the perceived benefits, barriers and drivers by key stakeholders in the construction sector using a questionnaire survey among clients and contractors.

The results revealed high levels of awareness of 4D BIM, but the usage is low. Plan for usage in the short term is also found to be low. There is no significant difference in perception between the clients and contractors on benefits, barriers & drivers of 4D BIM. *Visualizing the construction flow, Validating the time schedules by simulations* and *Communicating the construction plan* are found to be the most perceived benefits. *Lack of 4D BIM knowledge within internal workforce, Traditional project delivery methods/contract* and *Lack of 4D BIM expertise in the market* have been reported as the critical barriers. The key drivers of 4D BIM are *Government Mandate for 4D BIM* and *Awareness of 4D BIM benefits and ROI*.

Keywords –

4D BIM; Application & benefits; Barriers & challenges; Indian construction

1 Introduction

Construction is the second largest employer next only to agriculture in India and contributes significantly to its GDP. As part of its goal to become a USD 5 trillion economy by 2024, India plans to spend USD 1.4 trillion on its infrastructure in the next five years. The level of complexity of such projects is very high due to international nature in procurement as well as sophisticated client requirements. Efficient project delivery is key in successful completion of these infrastructure projects. Traditional project delivery systems focussed on the iron triangle of project performance, time, cost and scope [1]. Emerging measures such as quality, occupational health & safety and stakeholder satisfaction demand new ways of doing business. Unfortunately, despite the fact that architects, builders and manufacturers fail every day to deliver on schedule, within budget and effectively meet the needs of their customers, not many of them achieve the desired outcomes [2].

Building Information Modelling (BIM) provides a platform for the stakeholders to work collaboratively under a common data environment for better efficiency and results [1]. Global construction projects are evolving day by day, demand for resources is growing, so there is a rising need for a sustainable process for construction scheduling to complete the projects on time within stipulated budget [2]. Design information 3D model can be used for construction planning, where time is added to the model, which is known as 4D BIM. 4D BIM improves the efficiency by reducing wastes and helps in timely completion of projects within budget by controlling the construction schedule and adds value to customers [3]. Despite the potential, it is reported that 4D BIM is not quite widely used by the construction project stakeholders. Hence, it is proposed to assess the extent of usage and understand the perspectives of key stakeholders on benefits, barriers and drivers of 4D BIM [4].

2 Literature Review

Due to increase in the complexity in projects over time, construction planners are being asked to deal with more responsibility and they play a more critical role in built

environment. Gantt chart was developed by Henry Laurence Gantt in 1910 to schedule, coordinate and track the construction sequence over time. It has become the most used scheduling strategy in conjunction with improved techniques [5]. Later, schedulers understood the importance of critical activities and relations among activities, adopted critical path method (CPM), Program Evaluation and Review Technique (PERT) and many more concepts with the help of scheduling software like Microsoft project, Primavera, AstaProject, etc. to create and update schedules by allocating required resources. Traditional methods and today's scheduling software are not directly linked to design or building model [5].

Complex and large projects have different levels of planning like quarterly, monthly and weekly. Effective communication plays a major role in construction planning and guides the projects by facilitating planning & scheduling of the construction works to complete the projects and meet project objectives that include emerging performance measures [1]. Lack of communication will have immediate consequences like rework, non-uniformity, and misapplication of resources which increases the construction time and cost [6].

2.1 4D BIM

4D BIM allows planners to communicate visually and to schedule activities in time and space by linking of construction plan to the 3D model [7]. 4D BIM provides time-related information that is combined with various components of an information model for a specific item or work area that could include specifics of its design and deployment lead time [5]. The information contained in this model also contains the production rate that can be used to help assess the schedule and configure the activities by considering their position and production rate [8].

2.1.1 Project Planning using 4D BIM

Construction planning involves scheduling and sequencing activities in time and space by taking to account available resources, constraints, and other concerns in the process [5]. Traditional methods such as bar charts and the CPM do not consider the spatial configuration associated with these activities. Scheduling is therefore a complex manual job and often does not fully synchronise with the design and makes it difficult for the project stakeholders to easily understand the plan and its impact on the management of site logistics [9]. 4D planning is an extended and deeper version of conventional planning that develops the construction planning to a higher level of detail to provide greater accuracy and less risk. 4D models are also helpful in speeding up the construction process, thereby reducing mistakes and easily eliminating them [7].

To build 4D BIM model, 4D tools requires 3D model from BIM authoring tool and the construction schedule data from scheduling tool. Both the 3D model and construction schedule data are imported into the 4D tool. Then, the scheduler links the “components from the 3D model to the construction activities from the schedule and forms a time-based 4D BIM model [8].

Simulation provides significant guidance and early detection of mistakes in preparation. Instead of making layout mistakes later in the construction phase and trying to fix on-site issues that can be very costly, errors can already be avoided in the design phase [10]. The information that is obtained from the process will be quite large in the early stages by involving all stakeholders and should be collected in depth as the project progresses. It is important to note that 4D BIM refers to a specific way to link data to a knowledge model. The 4D model can be simulated with 'n' sequence number and can make as many changes as possible, and finally created with appropriate 4D sequence simulation [2].

The expertise of contractors is very critical when designing a 4D model for planning processes. If the model is built during the building's design phase, then the contractor can provide valuable feedback on buildability, estimated cost of construction, and sequencing. Also, 4D process planning simulations serve as a communication tool to identify potential bottlenecks and methods to improve coordination between project teams [11].

2.2 Benefits of 4D BIM

4D BIM offers an enhanced vision for planning, constructing and designing, sustaining or developing uniform information model that includes all the relevant information on the life cycle of the project. 4D modelling plays a major role in coordination between planners and customers during the planning phase. This helps project stakeholders spot issues in the construction phase and keep track of progress [5,6]. 4D BIM application helps to build virtual project and stimulate with different scenarios, which give all the stakeholders a better picture to identify the risks in the project at early stage and mitigate those risks by taking corrective measures.

The following key benefits and applicability of 4D BIM have been reported. Visualizing the construction progress at any time with clear look-ahead presentation [6]; Logistics planning (resources flow with in the construction site) [6,14]; Site layout planning (Reduces field interferences which may occur during the execution process, thereby improving the buildability) [6,15]; Location based planning; Clear understanding of the construction process and Construction methodology studies [6]; Validating the time schedules by simulations; Work progress meeting discussions through video for better understanding [16]; Safety planning (Visual representation of the hazards and the safety plan.) [6,18]; Documentation and claim analysis (Pretty easy to prove

who is responsible for the delay and what potential results are anticipated) [19]; Reduction of risk in the project [6]; Enhanced customer satisfaction [6]; Design investigation with schedule simulations which aid to reduce the amount of rework required [6].

2.3 Barriers to 4D BIM Implementation

Despite of benefits that 4D BIM provides to construction industry, still there are few technical and non-technical barriers which are hindering the widespread diffusion of 4D BIM [5]. The extensive adoption of 4D BIM and BIM has more influence on non-technical barriers than on technical barriers. Construction industry realized the value of BIM to an extent and started using it in design phase but BIM usage in production phase for construction planning is growing at slow rate.

Elghaish & Abrishami [20] and Zou et al. [21] reported *challenges related to developing 4D model (model scope, level of detail, temporary components, decomposition and aggregation)* and *lack of proper execution plans, guidelines and standards to follow* as barriers to 4D BIM implementation. Zou et al. [21] also reported *not worth time investment to learn* and *lack of time for employees to learn* as barriers. *Lack of 4D BIM expertise in the market, lack of standards for 4D BIM, difficulty in understanding 4D BIM methods* and *lengthier process of 4D BIM creation* have been reported by Kassem et al. [22]. Kassem et al. [22] and Ahmed et al. [23] identified the following barriers: *lack of demand from the client side to use 4D BIM, high costs to invest in software, high costs for training, lack of 4D BIM knowledge within internal workforce, employee resistance to change from traditional construction planning practices to 4D BIM, traditional project delivery methods/contract,* and *problems with exchanging data between software/Interoperability*.

2.4 Summary

There is a disconnect between the traditional design & planning methods and contemporary planning & scheduling tools. Construction industry realized the value of BIM to an extent and started using it in design phase but BIM usage in planning & production phases is growing at slow rate. Gledson and Greenwood [6] investigated the benefits and applications of 4D BIM in the context of the United Kingdom. Kassem et al. [22] and Ahmed et al. [23] reported the barriers to 4D BIM implementation in the United Kingdom and Qatar respectively. Although 4D BIM has the potential to contribute for the efficient project delivery, it has been observed that country-specific studies have been reported only for UK [6,22] & Qatar [23] and no study has been reported on the extent of 4D BIM implementation in the Indian context. Hence, there is a need to investigate the status of 4D BIM implementation in India and study the perceived benefits & barriers by various stakeholders in the construction sector. An attempt has been made to investigate the extent of 4D BIM usage, perspectives of key stakeholders on 4D BIM in terms of benefits, barriers and drivers in Indian construction.

3 Research Methodology

Identification of various indicators for benefits, barriers and drivers of 4D BIM is done through literature review. BIM functions are used to assess the applicability and benefits. Indicators used in the study are presented in Table 1.

Questionnaire survey-based quantitative approach is used to study the perspectives of the construction professionals on the applicability, benefits, barriers and drivers of 4D BIM.

3.1 Design of Experiment

Target population for this study are clients and contractors in Indian construction industry. Convenient sampling method is used for the selection of respondents.

A questionnaire survey instrument has been developed and deployed online for the survey. This questionnaire is divided into 6 sections, Section 1 contains cover note and a small video on 4D BIM, Section 2 is used to collect the demographic information of the participant and next four sections have questions on applicability of 4D BIM; 4D BIM's perceived benefits over conventional construction planning approaches; Barriers and challenges of 4D BIM adoption; and drivers/solutions for 4D BIM adoption.

Descriptive statistics is used for data analysis. Relative Importance Index (RII) is used to rank the indicators to understand the relative importance as perceived by the respondents [6,23]. *T-test* is used to check the statistical significance of the perceived differences between clients and contractors, if any. Cronbach Alpha is used for internal consistency and data reliability for analysis [6,23].

4 Data Collection and Analysis

The questionnaire instrument is deployed on Google Forms and the enquiries are sent to over 100 prospective respondents (clients & contractors) through Email, LinkedIn, and over phone. There are 38 valid responses received, which includes 17 contractors and 21 clients after continuous follow-up in a span of 4 weeks. Cronbach Alpha is used to evaluate the internal consistency of the instrument and reliability of the data collected for further analysis. The calculated Cronbach Alpha values are presented in Table 2. It is observed that all the values are greater than 0.7, the threshold for social studies, and the data collected is reliable for further analysis [6,23].

Table 1. BIM functions, Barriers and Drivers

BIM Functions	
F01	Logistics planning
F02	Site layout planning
F03	Communicating the construction plan
F04	Planning the construction sequence
F05	Visualizing the construction flow
F06	Location based planning
F07	Validating the time schedules by simulations
F08	Work progress meeting discussions
F09	Safety planning
F10	Documentation and claim analysis
F11	Risk Management
F12	Design investigation with schedule simulations

Barriers to 4D BIM Implementation	
B01	Lack of demand from the client side to use 4D BIM
B02	High costs to invest in software
B03	High costs for training
B04	Lack of 4D BIM knowledge within internal workforce
B05	Lack of 4D BIM expertise in the market
B06	Not worth time investment to learn
B07	Lack of time for employees to learn
B08	Employee resistance to change
B09	Lack of standards for 4D BIM
B10	Challenges related to developing 4D model
B11	Difficulty in understanding 4D BIM methods
B12	Traditional project delivery methods/contract
B13	The lengthier process of 4D BIM creation
B14	Problems with exchanging data between software

Drivers of 4D BIM	
D01	Developing local standards for 4D BIM
D02	Government Mandate for 4D BIM
D03	Improving software functionality
D04	Good support from software vendors
D05	Awareness of 4D BIM benefits and ROI
D06	Availability of 4D BIM expertise in the market

Table 2. Reliability Statistics

Dimensions	Cronbach's Alpha	N of items
Applicability	0.912	12
Relative benefits	0.934	12
Barriers	0.852	14
Drivers	0.856	6
Overall	**0.888**	**44**

5 Results & Discussion

There were 38 valid responses, which include 17 (45%) from contractors and 21 (55%) from clients. Majority of them are from large organisations (76.3%) and others from medium (7.9%) & small (15.8%) organisations. Respondents belong to top management (34.2%), middle management (50%) and operations (15.8%) level in their respective organisations. Construction work experience of the respondents is presented in Figure 1. It can be observed that 40% of the them have more than 10 years and 26% of the respondents have 5-10 years of work experience.

5.1 Awareness & Use of 4D-BIM

It has been observed that majority (68%) of the respondents are aware of 4D BIM and have not used it and 24% are aware and used. Only a little fraction (8%) have responded that they are unaware of 4D BIM (Figure 2). This shows higher level of 4D BIM awareness and lower levels of usage. It has been attempted to understand the plan of the respondents who are aware but have not used 4D BIM. While some of the respondents indicated that they have plans to use 4D BIM in near future (11% within a year & 31% in 1-3 years), a significant 58% of respondents have plans to use 4D BIM after three years only (Figure 3). This implies anticipated lower adoption of 4D BIM in the short run.

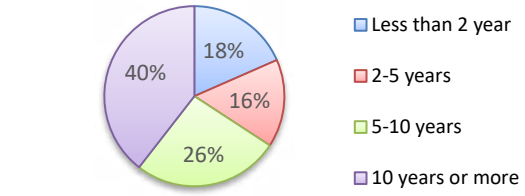

Figure1. Work experience of respondents

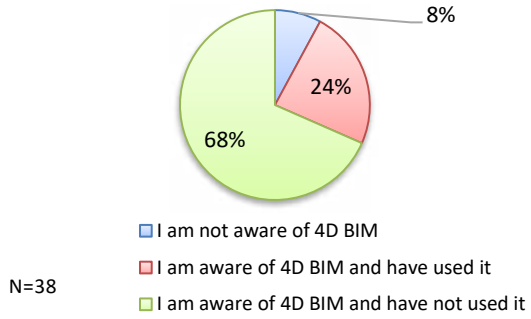

Figure 2. 4D BIM awareness and usage

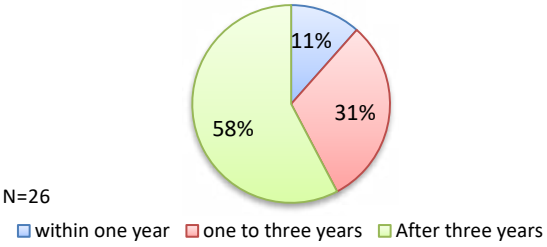

Figure 3. Plan to use 4D BIM

5.2 Applicability of 4D BIM

The participants were asked to provide their opinion on the applicability of 4D BIM by on a five-point Likert scale (Not at all Applicable to Highly Applicable) against various BIM functions as found in Table 1. The frequency distribution of responses as well as RII are presented in Figure 4. It can be noticed from the pattern of responses that the respondents have rated 4D BIM as highly applicable. Among the BIM functions *Visualizing the construction flow (F05), Communicating the construction plan (F03)* and *Validating the time schedules by simulations (F07)* have been found to be the most preferred application of 4D BIM. Even though *Site layout planning (F02)* and *logistic planning (F01)* have been ranked low, they are still very much applicable. In addition, clients have rated *Design investigation with schedule simulations (F12)* very much applicable.

5.3 Relative Benefits of 4D BIM

In response to the question on benefits & usefulness of 4D BIM, the participants rated various BIM functions as found in Table 1 on a five-point Likert scale (Not at all Beneficial to Highly Beneficial). The frequency distribution of responses as well as RII are presented in Figure 5. It can be noticed that the response pattern is similar to the applicability above. *Visualizing the construction flow (F05), Communicating the construction plan (F03)* and *Validating the time schedules by simulations (F07)* have been rated as top benefits of 4D BIM. However, clients perceive that *Design investigation with schedule simulations (F12)* is more beneficial compared to *Communicating the construction plan (F03).* Again, high scores of RII for other indicators reveal the highly beneficial in nature of 4D BIM.

5.4 Barriers to 4D BIM Implementation

The respondents perceive that *Lack of 4D BIM knowledge within internal workforce (B04), Traditional project delivery methods/contract (B12)* and *Lack of 4D BIM expertise in the market (B05)* as the top barriers for the adoption and use of 4D BIM in Indian construction (Figure 6.). This is in response to a question on barriers on a five-point Likert scale of Agreement. *Not worth time investment to learn (B06)* and *Lack of time for employees to learn (B07)* have been rated low as barriers.

5.5 Drivers of 4D BIM

Drivers are key for improved adoption. In response to a question on drivers of 4D BIM on a five-point Likert scale (Very Low to Very High), the respondents rated

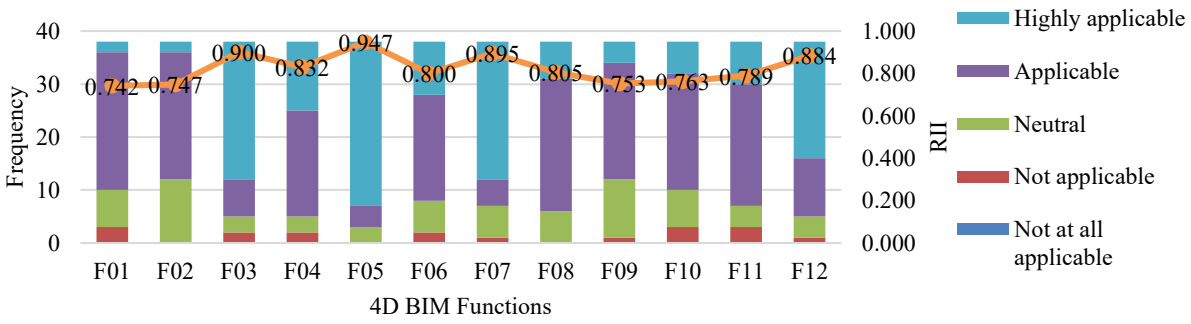

Figure 4. Applicability of 4D BIM

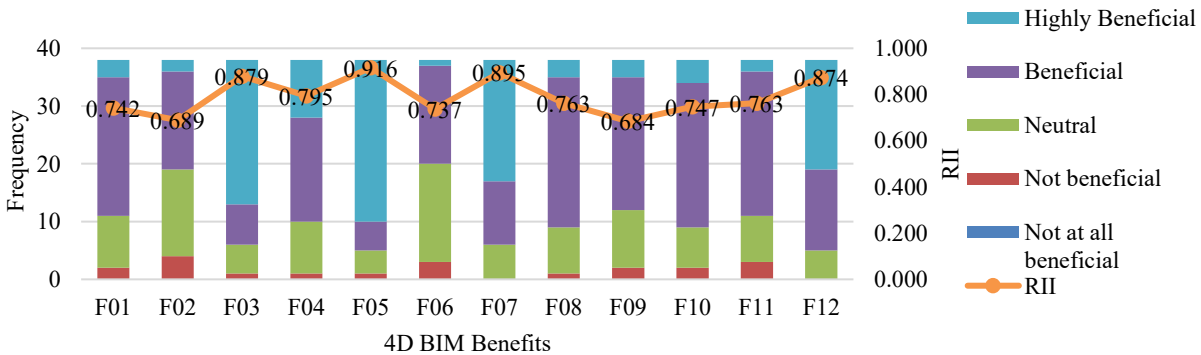

Figure 5. Benefits of 4D BIM

Government Mandate for 4D BIM (D02) as the top driver (Figure 7). Along with D02, *Awareness of 4D BIM benefits and ROI (D05)* and *Availability of 4D BIM expertise in the market* (D06) are also perceived as top drivers for 4D BIM. It can be noticed that *Good support from software vendors (D04)* has been rated lowest.

5.6 Hypothesis Testing

While there has been general agreement among the clients and contractors on their responses with few exceptions, it has been attempted to test this statistically to ensure that this is not by chance. The independent t-test is a statistical test that is used for difference in means [14]. Also, t-test is applicable when there are only two groups to be compared and sample size is very low.

The following hypotheses are tested using t-test for two independent sample assuming equal variance at 5% significance level.

Null hypothesis H0: *There is no significant difference in perceptions of clients and contractors on applicability, benefits, barriers and drivers of 4D BIM in Indian construction.*

Alternate hypothesis H1: *To test the null hypothesis, there is significant difference in the means of Clients and Contractors on applicability, benefits and barriers of 4D BIM functions in construction industry.*

The test results are presented in Table 3. As p-value for all the four variables are greater than 0.05, there is no sufficient evidence to reject H0 and hence H0 is accepted. It implies that the there is no significant difference in perceptions of clients and contractors on applicability, benefits, barriers and drivers of 4D BIM in Indian construction.

Table 3. Results of t-test for null hypothesis

Variables	p-value
Applicability	0.134
Benefits	0.707
Barriers	0.367
Drivers	0.132

However, at indicator level, a statistically significant difference in perception is observed for the barrier, *Lack of time for employees to learn (B07)* between the clients and contractors.

5.7 Discussion

It is indeed an encouraging revelation that there is high level of awareness of 4D BIM in Indian construction. But the challenge is to convert this into adoption and

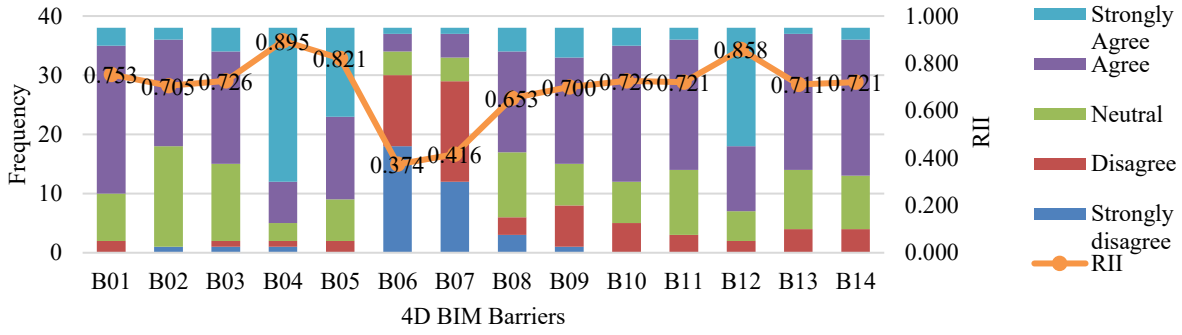

Figure 6. Barriers to 4D BIM implementation

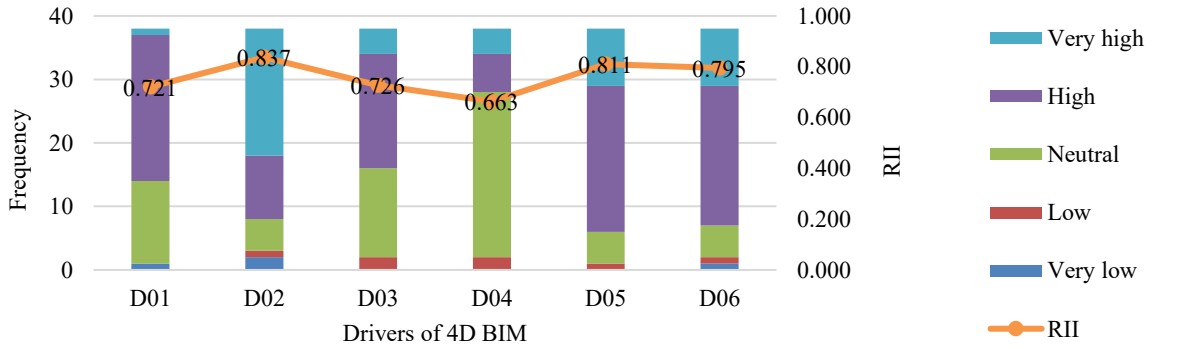

Figure 7. Drivers of 4D BIM

implementation [6]. Despite increased awareness, willingness to use 4D BIM, preferably after three years is not so encouraging. In order to keep up with the global competition as well as to meet the growing demand for infrastructure in India, there is a significant need to embrace 4D BIM sooner than later in Indian construction.

Responses to the application and benefits of 4D BIM *(F05, F03, F07 & F12)* emphasise the need for enhanced visualisation for communication and improved schedule performance. Capacity and capability building through education and training is key to realise these expectations/benefits. This also point towards the digital transformation of construction business in India [2]. Clients focus on *Design investigation with schedule simulations (F12)* over *Communicating the construction plan (F03)* showcases the change in priority of clients to quality designs & timely delivery [24].

It is also important to look at the barriers to 4D BIM adoption. *Lack of 4D BIM knowledge within internal workforce (B04)* calls our attention to training and continuous professional development within the organisations. To overcome the barrier, *Traditional project delivery methods/contract (B12),* innovative procurement methods such as Integrated Project Delivery (IPD) and Smart Contracts with the help of Block Chain can be explored. *Lack of 4D BIM expertise in the market (B05)* demand for educational institutions to relook at the curriculums to ensure that the students graduate with digital skills that are necessary [25]. As *Not worth time investment to learn (B06)* and *Lack of time for employees to learn (B07)* have been rated low as barriers, it seems that the organisations and its employees have mentally prepared to embrace this change.

A closer look at the drivers for the 4D BIM in India reveals that *Government Mandate for 4D BIM (D02)* requires immediate attention. At present, there is no official mandate from the government(s) in India for the use of BIM in construction projects. Other top drivers, *Awareness of 4D BIM benefits and ROI (D05)* demands need for more use cases from India and *Availability of 4D BIM expertise in the market* (D06) points towards education & training for upskilling that shall ensure the supply of talent [24].

It has been observed that the top benefits of 4D BIM identified in India are in line with the UK study [6] except for *logistics planning* (F01) that was rated high in UK. Non-technical barriers such as inefficiency to quantify the tangible benefits and lack of awareness by stakeholders were reported as the critical barriers in UK. In the context of Qatar, in addition to the barriers identified in UK, non-availability of skilled professionals was also found to be critical. In India, use of traditional project delivery methods and lack of demand by clients have been identified as top barriers for 4D BIM adoption in addition to lack of awareness and expertise in 4D BIM.

6 Summary and Conclusions

An attempt has been made to investigate the adoption and implementation of 4D BIM in Indian construction through survey research. The study aimed at assessing the extent of 4D BIM adoption and capture the perceived benefits, barriers and drivers for 4D BIM. The target population for this study was the clients and contractors in Indian construction. One third of the participants responded to the survey and the general pattern in the response revealed that there is high level of awareness on 4D BIM among the clients and contractors in India. Also, most of them plan to use 4D BIM later (after three years) than sooner. It has been found that there is no statistically significant difference between the clients & contractors on their responses.

Visualizing the construction flow (F05), Communicating the construction plan (F03) and *Validating the time schedules by simulations (F07)* have been found to be the top benefits of using 4D BIM. The perceived top barriers for 4D BIM are: *Lack of 4D BIM knowledge within internal workforce (B04), Traditional project delivery methods/contract (B12)* and *Lack of 4D BIM expertise in the market (B05)*. The study also revealed that *Government Mandate for 4D BIM (D02), Awareness of 4D BIM benefits and ROI (D05)* and *Availability of 4D BIM expertise in the market (D06)* are the key drivers for 4D BIM in India. Innovative procurement systems, smart contracts, reinvention of construction education and capacity building & capability development through training can address the changing needs of the clients and contractors for enhanced value creation.

Considering the relatively smaller sample size, the confidence on the conclusions drawn is limited. A wider study among the clients and contractors with increased sample size may reveal greater insight. It is also worth investigating the role of enhanced visualisation for communication in improved schedule performance. Studies on capacity building & capability development would facilitate strategies for supply of necessary talent. Also, the present curriculum in built and natural environment courses may be relooked at to keep up with the demand for digital skills. Policy studies to support government decisions on mandating 4D BIM would be desirable for a roadmap.

7 References

[1] Olanrewaju, A., Tan, S. Y. and Kwan, L. F. Roles of communication on performance of the construction sector. Procedia Engineering, 196: 763–70, 2017.

[2] Dung, D. and Tarar, M. *Impact of 4D Modeling on Construction Planning*. 58, 2012.

[3] Sloot, R. N. F., Heutink, A., and Voordijk, J. T. Assessing usefulness of 4D BIM tools in risk mitigation strategies. *Automation in Construction,* 106:102881, 2019.

[4] Mirzaei, A., Nasirzadeh, F., Parchami Jalal, M., and Zamani, Y. 4D-BIM Dynamic Time-Space Conflict Detection and Quantification System for Building Construction Projects. *Journal of Construction Engineering and Management*, ASCE, 144(7):04018056, 2018.

[5] Hadavi, P., and Tavakolan, M. 4D modeling and BIM-based Project planning using constraint-based simulation for implementation in Iran considering an actual case study. *Construction Research Congress,* CRC 2018, 542–551, 2018.

[6] Gledson, B. J., and Greenwood, D. J. Surveying the extent and use of 4D BIM in the UK. *Journal of Information Technology in Construction*, 21: 57–71, 2016.

[7] Crowther, J., and Ajayi, S. O. Impacts of 4D BIM on construction project performance. *International Journal of Construction Management,* 2019.

[8] Zhang, J., and Li, D. Research on 4D virtual construction and dynamic management system based on BIM. *17th International Workshop on Intelligent Computing in Engineering*, EG-ICE 2010, Nottingham, Tsinghua University, China, 2019.

[9] Álvares, J. S., and Costa, D. B. Construction progress monitoring using unmanned aerial system and 4D BIM. *27th Annual Conference of the International Group for Lean Construction*, IGLC 2019, 1445–1456, 2019.

[10] Boton, C. Supporting constructability analysis meetings with Immersive Virtual Reality-based collaborative BIM 4D simulation. *Automation in Construction*, 96:1–15, 2018.

[11] Wang, Q., Guo, Z., Mintah, K., Li, Q., Mei, T., and Li, P. Cell-Based Transport Path Obstruction Detection Approach for 4D BIM Construction Planning. *Journal of Construction Engineering and Management*, ASCE, 145(3): 04018141, 2019.

[12] Jin, Z., Gambatese, J., Liu, D., and Dharmapalan, V. Using 4D BIM to assess construction risks during the design phase. *Engineering, Construction and Architectural Management,* 26(11), 2637–2654, 2019.

[13] Bortolini, R., Formoso, C. T., and Viana, D. D. Site logistics planning and control for engineer-to-order prefabricated building systems using BIM 4D modeling. *Automation in Construction*, 98: 248–264, 2019.

[14] Deng, Y., Gan, V. J. L., Das, M., Cheng, J. C. P., and Anumba, C. Integrating 4D BIM and GIS for Construction Supply Chain Management. *Journal of Construction Engineering and Management,* ASCE, 145(4): 04019016, 2019.

[15] Getuli, V., and Capone, P. Computational workspaces management: a workflow to integrate workspaces dynamic planning with 4D BIM. *35th International Symposium on Automation and Robotics in Construction,* ISARC 2018, Berlin, Germany, 1117-1124, 2018.

[16] Han, K. K., and Golparvar-Fard, M. Appearance-based material classification for monitoring of operation-level construction progress using 4D BIM and site photologs. *Automation in Construction*, 53, 44–57, 2015.

[17] Kropp, C., Koch, C., and König, M. Interior construction state recognition with 4D BIM registered image sequences. *Automation in Construction*, 86:11–32, 2018.

[18] Park, J., and Cai, H. Framework of dynamic Daily 4D BIM for tracking construction progress through a web environment. *ASCE International Workshop on Computing in Civil Engineering*, IWCCE 2017, Purdue Univ., USA, 193–201, 2017.

[19] Shou, W. C., Wang, J., and Wang, X. Y. 4D BIM for improving plant turnaround maintenance planning and execution: A case study. *35th International Symposium on Automation and Robotics in Construction*, ISARC2018, Berlin, Germany, 1191-1198, 2018.

[20] Elghaish, F., and Abrishami, S. Developing a framework to revolutionise the 4D BIM process: IPD-based solution. *Construction Innovation*, 2020.

[21] Zou, Y., Kiviniemi, A. and Jones, S. W. BIM-based Risk Management: Challenges and Opportunities *Proceedings of 32nd CIB W78 Conf.* 847–55, 2015.

[22] Kassem, M., Brogden, T., and Dawood, N. BIM and 4D planning: a holistic study of the barriers and drivers to widespread adoption. *Journal of Construction Engineering and Project Management*, 2(4):1–10, 2012.

[23] Ahmed, S.M., Emam, H. H., and Farrell, P. Barriers to BIM/4D Implementation in Qatar, *1st Int'l Conference on Smart, Sustainable and Healthy Cities*, (April 2015), 533–547, 2014.

[24] Swallow, M., and Zulu, S. Students' awareness and perception of the value of BIM and 4D for site health and safety management. Journal of Engineering, Design and Technology, 18(2): 414–430, 2019.

[25] Zhang, J. P. and Hu, Z. Z. BIM and 4D-based integrated solution of analysis and management for conflicts and structural safety problems during construction: 1. Principles and methodologies. *Automation in Construction,* 20(2):155–166, 2011.

An Information Quality Assessment Framework for Developing Building Information Models

L.J. Chen[a] and Justin K.W. Yeoh[a]

[a]Department of Civil and Environmental Engineering, National University of Singapore, Singapore
E-mail: ceecl@nus.edu.sg, justinyeoh@nus.edu.sg

Abstract –

Information Quality Assessment (IQA) is an important, but often overlooked aspect, of the Building Information Modeling (BIM) process. Models with information quality issues, such as incomplete and incorrect information, may cause rework during the design process if detected early. Otherwise errors may propagate downstream, leading to significant cost consequences to stakeholders in the Architecture, Engineering and Construction (AEC) industries. Current approaches of IQA show significant efforts on addressing information completeness issues but are limited when addressing information correctness. Greater understanding of the features of these quality issues is necessary to begin to detect these issues. This paper addresses this problem by proposing an IQA framework that incorporates three identified features: IQ Dimensions, Arity and Data Characteristics. From this framework, 3 classes of algorithms are further defined to detect these features. A validation test was conducted against current modeling guidelines used for BIM quality assurance in both architectural and structural disciplines. The results indicated more than 80% of the rules were able to be categorized using the framework. Guidelines that were not categorized included those that were overly ambiguous, or did not directly involve BIM. The outcome of the paper will enable BIM managers to ensure a fit-for-purpose, quality assured model that can reduce rework, and engender greater trust in the model creation process.

Keywords –

Information Quality Assessment; Features of Quality Issues; Building Information Modeling

1 Introduction

Building Information Modeling (BIM) simulates the construction project in a virtual environment. It provides a platform for collecting building-related information and allows information collaboration between different disciplines [1]. Due to its information-centric characteristics, models with poor information quality may cause significant cost consequences and rework [2][7]. Thus, Information Quality Assessment (IQA) for BIM is essential for stakeholders in the Architecture, Engineering and Construction (AEC) industries to realize the full benefits of BIM.

However, quality assessment is still a crucial and challenging task in BIM project delivery processes. Current ways of auditing for model quality control are manual, and usually involves visual checking of the model [8][9] or comparisons using check lists [6][7]. Such auditing processes tend to be time-consuming and difficult to avoid errors. Other than the tedious process of manually checking the models, there is still a lack of a general framework for defining some information quality criteria such as information correctness or accuracy. This consequently causes ambiguity, and difficulties in identifying model quality issues may arise [3]. Hence, implementing a quality assurance process for BIM requires a significant amount of time and effort from qualified personnel, and despite best efforts, may still lead to errors that may propagate to downstream activities, causing unnecessary rework during design. This then may lead to significant cost consequences to stakeholders. The aforementioned challenges may explain why IQA is often overlooked in the BIM process.

The objective of this paper is to propose an information quality assessment (IQA) framework, by identifying three sets of features related to the IQ dimensions of completeness and correctness, arity, as well as data characteristics. Specific algorithmic approaches can then be identified to detect the model quality issues. Section 3 describes the proposed framework, and section 4 describes the algorithm classes in detail. Validation of the proposed IQA framework is then carried out on a set of BIM modeling guidelines/ quality assurance requirements laid out in the Singapore BIM Guide [7].

2 Literature Review

The information contained within BIM should be

complete and correct to support different BIM use cases such as structural analysis, cost estimation and quantity take off [5]. Therefore, the assessment of BIM information quality is essential to evaluate whether the model is fit-for-purpose. In the following section, a review of the literature will be conducted to show current research efforts on BIM quality assessment.

- **IQ frameworks and quality issues in BIM:** Information Quality (IQ) dimensions help to categorize and identify model quality issues. However, the ambiguity in characterizing IQ dimensions exists in current practice of information quality assessment (IQA) [3]. There is a lack of a general consensus regarding the identification of information quality dimensions as well as an agreed-upon taxonomy of information quality issues. Berard [8] evaluated building design information from 8 quality dimensions: relevance, consistency, correctness, precision, availability, distribution, flexibility and amount of information. Zadeh et al. [9] analyzed facility information quality focusing on information incompleteness and well-formedness. Wang et al. [10] developed a model fitness system to evaluate model quality based on information inconsistency. The differences in IQ dimensions between different studies arise due to the different considerations arising from differing BIM uses. For example, the quality issues such as incorrect placement of model elements and inconsistent naming of attributes are more important during the design collaboration process [10]. On the other hand, during construction management, model information such as scheduling and fabrication type are more important to ensure correct quantities are obtained [11].
- **Information completeness:** Although significant ambiguity exists in current IQA practices, information completeness is one of the most consistently mentioned IQ dimension in the literature [9]. There have been a few of research efforts on checking information quality arising from information completeness. Early studies show that manual checking methods such as using checklists [6][7][12], visual checking [5] and photo-analysis [4] were applied to check for missing information in models. BIM applications such as Solibri Model Checker and iTwo are available to detect missing attributes in building elements. However, a review of previous studies shows that a systematic framework for checking information completeness in BIM has not been discussed widely, and constitutes a research gap to be addressed.
- **Information correctness:** Correct information is vital to fulfil the purposes of building information modeling. It plays a critical role as an IQ dimension in the IQA framework. However, information correctness is a concept with widely varying definitions and meanings. Zadeh et al. [9] discussed information correctness issues as inaccuracy of model attributes specifically for facility management. Berard [8] described correctness as "extent of missing, incorrect outdated design information".

  This inconsistent definition of correctness makes detection and validation of incorrect information in models a difficult problem to solve. Kulusjärvi and Heikki [12] described information correctness checking as "to compare and measure information contained in a BIM against reference information". This reference information can be related documentations, or physical reality [3]. In general, this literature review shows that methods to perform correctness checks are limited to visual checking and use semi-automated ways [9][13].
- **Information Delivery Manual (IDM) and Model View Definition (MVD):** In the study of information systems, the quality of information is a characteristic that should be checked against the information consumers' requirements [14]. Analogously, the aforementioned has been adapted for use in BIM: A good quality model is one with useful information specified by BIM users that is fit-for-purpose. During the BIM development process, model information is typically exchanged downstream for different BIM uses. The current best practice is to specify these exchange requirements in the Information Delivery Manual (IDM). This is a standard methodology for BIM users to specify the information required in BIM for different scenarios [15].

  The current implementation of IDM is to represent information exchange requirements in the format of paper-based documents [16]. Based on the exchange requirements, Model View Definitions (MVDs) would be developed to streamline information specific to the BIM use. However, MVD itself does not guarantee whether the data extracted from model is correct or consistent. Validation still needs to be carried out to check if it conforms to the information constraints or rules specified in exchange requirements [17]. Several research efforts have been made on the development of MVDs from IDM specification [16][18], however the validation of the exchanged information is still an open research question.

3 IQA Framework

The components of the proposed framework for information quality assessment (IQA) of building

Table 1. The proposed framework for information quality assessment

IQ Dimensions	Arity	Data Characteristics	An Example of Quality Issue	Algorithm Classes
Completeness	Element level	Geometry Attributes	Missing and incomplete attributes	class 1
		Non-geometry Attributes	Missing and incomplete attributes	class 1
	Model level	Element	Duplicated elements	class 3a
			Missing elements	class 3b
Correctness	Element level	Geometry Attributes	Length of analytical wire is zero	class 1
		Non-geometry Attributes	Physical-analytical model distance exceeds tolerance	class 2
	Model level	Element	Interference clashes	class 3a
		Relations	Elements are not connected	class 3a
			Mismatch between mapping files in different BIM applications	class 3b

information models (BIM) are as shown in Table 1. The objective of this framework is to categorize quality issues from the perspective of the information requirements of the model. Three features of quality issues are identified: IQ dimensions, Arity and Data Characteristics. Subsequently, specific IQA scenarios may be defined using these three features, and consequently classes of algorithms can be identified to address the quality issue raised. Specific examples of such quality issues are provided in Table 1 as well, where these are common issues faced by experienced structural engineers and BIM managers in actual projects.

- **Information Quality Dimensions:** In the proposed framework, information completeness is defined to mean an element must have complete attributes and values, or a model must contain all relevant elements. In other words, incomplete information refers to missing or incomplete attributes or values in the element or missing elements in the model that should exist according to the design scheme.

  For information correctness, this framework considers elements or models that contain incorrect information such that when they are passed downstream, it affects the performance of the model. For example, a model may contain complete information for structural analysis but if the information is incorrect, then during structural analysis, this may result in incorrect analysis.
- **Arity:** The proposed framework recognizes that quality issues on information completeness and correctness can exist on two levels: on single elements (or a single group of multiple elements) and on a model level. This framework refers to this IQ dimension as its arity. To categorize the arity of these issues clearly, this framework refers to these as Element Level issues and Model Level issues, respectively.

  Information quality on element level focus on the data quality in a single element (or a singular group of elements). This means that some values of the attributes or properties in a specific element in BIM will be checked.

  Model level quality issues refer to issues that exist between multiple elements. In this scenario, the quality auditing task here may involve the checking of the relationship between multiple elements or the existence of several elements in a model.

  One difference between element level and model level issues is the source of information to be checked. In the element level, checking can be done by using information from within a single element, such as the attributes or parameters. While in the model level, checking is performed successfully only when the information from multiple elements

are available and, in some cases, data outside BIM maybe required for checking.

From the viewpoint of quality control, dividing IQ issues into element and model level is an important feature to distinguish the specific IQA scenario. These scenarios are important to identify the appropriate algorithm approach to use.

- **Data Characteristics:** Data characteristics refers to the type of data. From the perspective of data characteristics, this framework considers the following:

1. **Geometry attributes:** properties showing geometry information of physical elements;
2. **Non-geometry attributes:** properties showing non- geometry information of physical elements;
3. **Element:** physical elements in the model;
4. **Relations:** relationships between physical elements;

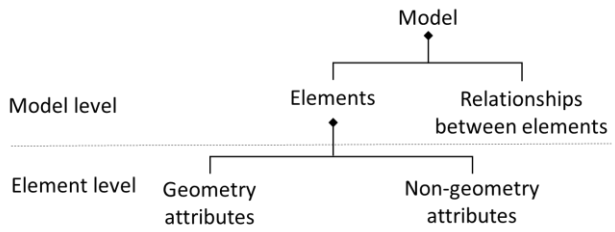

Figure 1. Model Hierarchy

In the model hierarchy shown in Figure 1, "Model" refers to the building information model, and this resides on the highest level. Elements in the model and the relations between these elements are child entities that lie on the second level. Attributes contained within the elements are on the lowest level. Both geometry and non-geometry attributes exist in the element level while existence of the element and the relations between these elements lie on the model level. As IQ issues may arise from different circumstances, issues caused by element attributes can be considered as element level issues and corresponding algorithms can be devised to check this kind of issues.

- **Quality Issues:** In Table 1, examples of common quality issues are listed for different IQA scenarios arising from the structural analysis BIM use. These were identified by experienced engineers and BIM managers in real-world BIM projects. The quality issues mentioned in this framework are categorized according to the features of IQ dimensions, arity and data characteristics. By identifying the features of these quality issues, general approaches for algorithms to detect such quality issues can be developed.

4 Algorithm classification for different IQA scenarios

From the features identified in the framework of Table 1, three classes of algorithms were developed to provide guidance for information quality assessment. Each class of algorithm provides a general approach to detecting the quality issue.

The three classes of algorithms are described in more details below. The description for each algorithm class is also summarized in Table 2, and it is organized by introducing the flowcharts for each algorithm, its features and the IQA scenario it is applied to. Examples are given to illustrate how the assessment can be conducted using the algorithm classes.

- **Class 1 -- Algorithm to check explicit data in a single element:** This class of algorithm can check the explicit data such as values attributes or properties in a single element. Here "explicit data" means the data can be accessed from element directly without any calculations or derivation. It can be applied to check quality issues on information completeness and correctness on element level.

  The procedure of using this algorithm class for checking model information starts from collecting target elements and then examining the specific attributes values for each element. Examples are given here to show how this class of algorithm can be applied to checking model quality issues in two IQA scenarios. When checking information completeness, the algorithm checks whether a specific attribute for an element is missing or the value of the attribute is null. The correctness issues are limit on checking data which are numerical or from string type. When checking correctness issues, it checks whether the value of attributes is within a predefined scope (numerical data) or corresponds with a specific value (string data).
- **Class 2 – Algorithm to check implicit data in a single element:** Checks are based on the implicit data which requires further calculation or derivation from explicit data existing in a single element. This class can be applied to check quality issues on information correctness on the element level.

  The procedure of using class 2 algorithm is very similar to that of algorithm class1, but more complicated with an extra step of calculating the implicit value for the element. Therefore, the function of checking information correctness here is limited to check whether a numerical data is within a predefined scope.

Table 2. Summary of algorithm class

	Algorithm Class 1	Algorithm Class 2	Algorithm Class 3a	Algorithm Class 3b
Description	To check explicit data in a single element	To check implicit data in a single element	To check between multiple elements with native data source within BIM	To check between multiple elements with external data source outside BIM
IQA Scenarios	Information completeness on element level; Information correctness on element level	Information correctness on element level	Information correctness on model level	Information completeness on model level; Information correctness on model level
Flowchart or Conceptual Schema	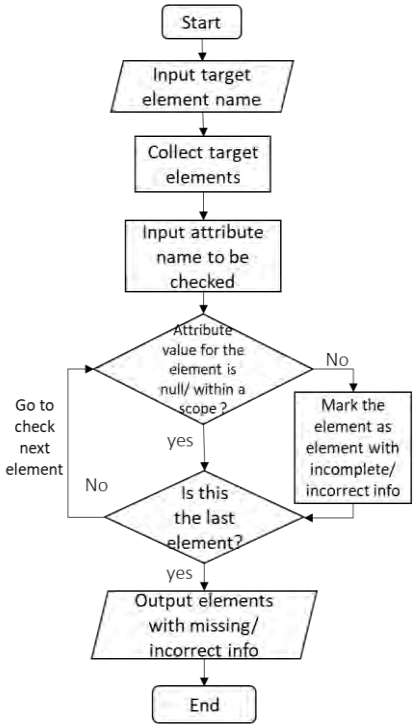	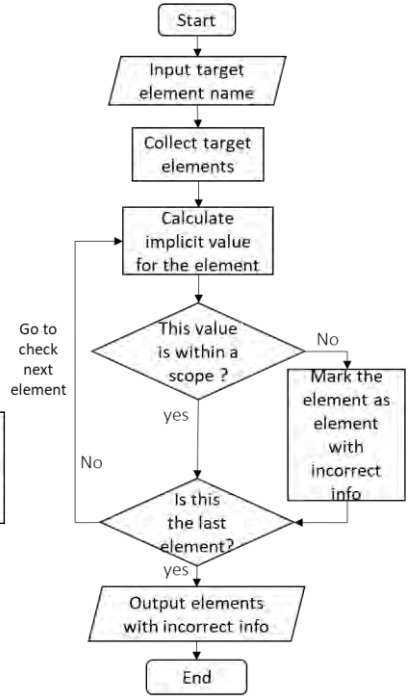	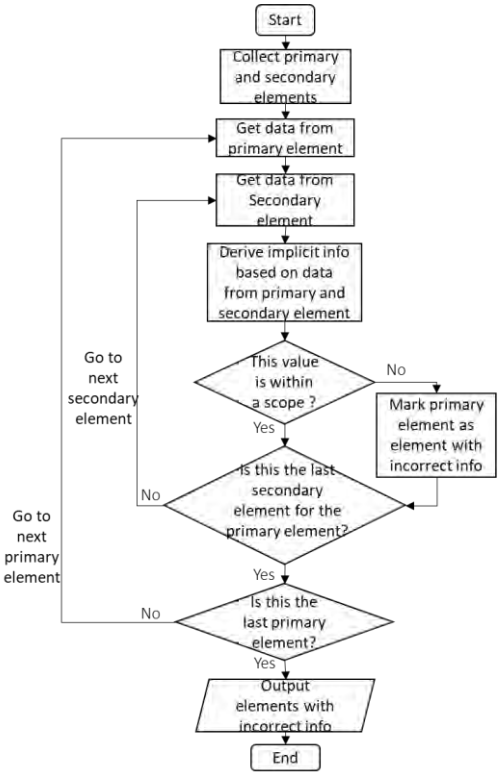	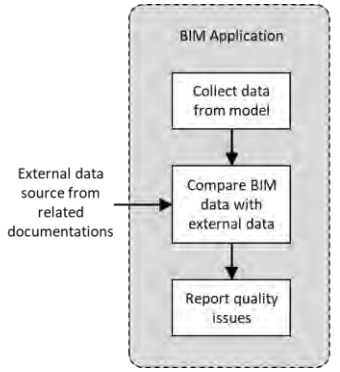

- **Class 3a – Algorithm to check between multiple elements with native data sources within BIM:** This class of algorithm checks information involving multiple elements inside BIM. Checks focus on information correctness issues on model level. Since this class of algorithm checks between multiple elements, it is important to specify the relationship and sequence of elements to be checked. Therefore, a concept shown in Figure 2. specify the "primary and secondary" elements to be checked in this scenario.

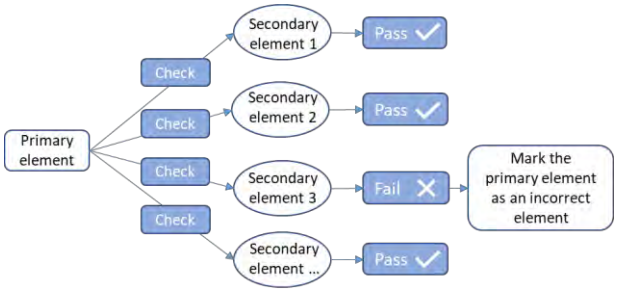

Figure 2. Schematic of checking between primary and secondary elements

The identification of these two element groups depends on what specific quality issues needs to be check. For example, in connection checks, the primary element may be any object which can be connected to other elements. Then the secondary element will be the one close enough to the primary element. During the checking process, primary elements will be collected in the first round. Then in the second round, secondary elements will be collected for each primary element. Checks will be proceeded by obtaining information based on data from the primary element and its secondary elements. Connection checks require the information such as distance between two nodes from different elements. In this case, coordinates of all nodes from both primary and secondary elements will be collected and be used to calculate the distances. The number of checking results depends on the number of secondary elements and if there is at least one result showing two elements did not pass the check. This primary element will be considered as an element with quality issues.

In this algorithm class, checking correctness issues involve the identification of numerical data derived from BIM.

- **Class 3b – Algorithms to check between multiple elements with external data source outside BIM:**
Class 3b requires external data source outside BIM to perform checks. Such algorithms can be applied to check information completeness and correctness on model level. One example can be checking whether there is any missing element in the model. In this case, external data such as 2D CAD drawings may serve as reference information.

Due to the generic nature of procedure, a conceptual schema was given for the instructions of implementation of class 3b algorithms.

5 Validation and discussion

To test the validity of the proposed IQA framework and the algorithm classes derived, the framework was applied to current guidelines for BIM quality assurance. The validation was applied against a set of rules for quality assurance given in Singapore BIM Guide [7]. Both architectural and structural BIM elements were considered in this evaluation. Each rule would be classified according to the specific IQA scenario as well as its corresponding algorithm class. Then the algorithms would be applied to check quality issues against the rules.

A validation set consisting 30 rules from both architectural and structural BIM modeling guidelines was identified and tested on. The applicability rate of the proposed IQA framework to each BIM discipline was calculated (seeing Equation (1)).

$$R_a = \left(1 - \frac{N_u}{N_t}\right) \times 100\% \quad (1)$$

R_a – Applicability rate (%)
N_u – Number of rules categorized to unknown
N_t – Total number of rules tested

The results tabulated in Table 3 indicate more than 80% of rules can be classified through the proposed framework, for both architectural and structural BIM. Results from architectural BIM guidelines show a higher rate of applicability due to greater number of rules on checking spatial information.

Rules categorized as belonging to algorithm class 1 focused on checking existence and correctness of elements attributes such as ID, category, and level information. Compared with the rules in class 1, there were fewer of rules considered to be in class 2 that checks implicit data in elements. The reason can be that quality assurance in this BIM guidelines considers general cases whereas there are no statements on which specific information should be checked. Thus, it would be difficult to decide whether the information to be checked is explicit or implicit. However, in some cases, it was obvious. For example, rules involving checks on distance, areas, and coverage rate etc. were categorized in class 2.

According to the proposed IQA framework, the

Table 3. Validation results

Algorithm Classes	Algorithm Class 1	Algorithm Class 2	Algorithm Class 3a	Algorithm Class3b	Unknown	Applicability Rate, R_a (%)
IQA Scenarios	Information completeness on element level; Information correctness on element level	Information correctness on element level	Information correctness on model level	Information completeness on model level; Information correctness on model level		
Number of architectural BIM rules	6	1	6	2	2	88.2
Number of structural BIM rules	4	0	6	1	2	84.6

quality issues exist not only on element level but also on model level. The validation results demonstrate the current modeling guidelines have many rules for checking information quality on model level. These rules were categorized as class 3a which checks information correctness issues between multiple elements in BIM. Apart from checking data sources within BIM, some rules involving external information source outside BIM were included in class 3b. This indicates checking within single elements on element level is not enough for IQA. Quality issues existing between elements are also important.

Some rules were not able to be classified to any of the IQA scenarios, nor the algorithm classes. One of the reasons is that rule is worded too generally, which may cause ambiguity. For these rules containing general statements, it is not implementable with specific checking methods, nor is it possible to recommend specific instructions. Another reason observed is that some rules have a scope of checking that goes beyond the framework. For example, checking the quality of 2D drawings before exporting to BIM.

6 Conclusion

Good information quality in BIM helps owners in AEC industries realize the full benefits of BIM. Models with poor information quality may cause significant cost consequences. This paper proposed an information quality assessment (IQA) framework to systematically categorize information quality issues existent in BIM. Hence, recommendations for quality control implementation can be formulated. This framework collected quality issues on information completeness and correctness from the perspectives of data arity and data characteristics. Given these features, the quality issues were categorized into IQA scenarios, then corresponding algorithm classes were developed to check said quality issues.

The validation was conducted against current modeling guidelines used for BIM quality assurance in both architectural and structural disciplines. The results indicated more than 80% of rules were able to be categorized using the framework. Further, the rules were shown to fit the IQA scenarios and its corresponding algorithms classes. From the detailed results, it was observed there were fewer rules in class 2 than rules in class 1. This indicated that quality assurance in this set of BIM guidelines consists of general statements on which specific information could not be checked. Thus, it was not possible to determine if the information to be checked was explicit or implicit. It was also observed that there were some rules which were not able to be classified according to any of IQA scenarios. Reasons for this included that rule statement were too general, or

that the content of the rules did not focus on the model or BIM itself, going beyond the scope of this framework.

Thus, the future improvements to the framework should focus on testing more BIM guidelines for quality control to further extend this framework, as well as identifying more classes of algorithms, particularly those identified within class 3b.

In general, the proposed IQA framework is shown to be adequate to guide modeling process, as well as to provide practical guidance for implementation of BIM quality assessment. It enables BIM managers to ensure a fit-for-purpose, quality assured model that can reduce rework, and engender greater trust in the model creation process.

Acknowledgement

The research is supported by the National Research Foundation Singapore, Sembcorp Industries Ltd and National University of Singapore under the Sembcorp-NUS Corporate Laboratory.

References

[1] Zadeh P.A. , Cavka H. B. and Staub-French S. BIM Information Quality Analysis for Space Management. Osaka University, 2016.

[2] Gallaher M. P., O'Connor A. C., Dettbarn J. L., Gilday L.T. *Cost Analysis of Inadequate Interoperability in the us capital facilities industry*. U.S. Department of Commerce, Maryland, U.S., 2004.

[3] Zadeh P.A. , Staub-French S. and Pottinger R. Review of BIM Quality Assessment Approaches for Facility Management. *11th Construction Specialty Conference*, Vancouver, British Columbia, 2015.

[4] Tang P., Anil E. B. Akinci B. and Huber D. Efficient and Effective Quality Assessment of As-Is Building Information Models and 3D Laser-Scanned Data. 2011.

[5] Sacks R., Eastman C., Lee G. and Teicholz P. BIM Handbook – A Guide to Building Information Modeling for Owners, Designers, Engineers, Contractors, and Facility Managers. 2018.

[6] General Services Administration (GSA). GSA Building Information Modeling Guide Series: 08 - GAS BIM Guide for Facility Management. U.S. General Services Administration (GSA), Washington DC, U.S. 2011.

[7] Building and Construction Authority (BCA). *Singapore BIM Guide*, version 2, Building and Construction Authority, Singapore, 2013.

[8] Berard O. BIM for Managing Design and Construction Assessing – Design Information Quality, PhD Thesis, Technical University of Denmark, 2012.

[9] Zadeh P. A., Wang G. Cavka H. B., Staub-French S. and Pottinger R. Information Quality Assessment for Facility Management, *Advanced Engineering Informatics*, 33:181-205, 2017.

[10] Wang J., Wang X., Shou W., Guo J. and Hou L. Development of BIM Model Fitness Review System for Modeling Quality Control, *Computing in Civil and Building Engineering*, 577-584, 2014.

[11] Chen L. and Luo H. A BIM-Based Construction Quality Management Model and Its Applications, *Automation in Construction*, 46:64-73, 2014.

[12] Kulusjärvi H. COBIM: Common BIM Requirements, series 6, 2012.

[13] Becerik-Gerber B., Jazizadeh F., Li N. and Calis G. Application Areas and Data Requirements for BIM-Enabled Facilities Management, *Journal of Construction Engineering and Management*, 138(3):431-442, 2012.

[14] Wang R. Y. and Strong D. M. Beyond accuracy: What Data Quality Means to Data Consumers, *Journal of Management Information Systems*, 12(4): 5-33, 1996.

[15] International Organization for Standardization (ISO), ISO 29481-1:2017 Building information models - Information delivery manual. Part1: Methodology and format, 2017.

[16] Lee Y.C., Eastman C. and Solihin W. An Ontology-Based Approach for Developing Data Exchange Requirements and Model Views of Building Information Modeling, *Advanced Engineering Informatics*, 30(3): 354-367, 2016.

[17] BuildingSmart, Model View Definition (MVD). https://technical.buildingsmart.org/standards/ifc/mvd/, Accessed: 29/05/2020.

[18] Lee G., Park Y. H. and Ham S. Extended Process to Product Modeling (xPPM) for integrated and seamless IDM and MVD development, *Advanced Engineering Informatics*, 27(4): 636-651, 2013.

BIM Based Information Delivery Controlling System

B. Klusmann[a], Z. Meng[a], N. Kremer[b], A. Meins-Becker[a] and M. Helmus[a]

[a]Chair of Construction Management & Economics, University of Wuppertal, Germany
[b] Chair of Design Computation, RWTH Aachen University, Germany
E-mail: klusmann@uni-wuppertal.de, meng@uni-wuppertal.de, kremer@dc.rwth-aachen.de, a.meins-becker@uni-wuppertal.de

Abstract –

The definition of how agreed information deliveries in building projects are achieved and implemented for different objectives and use cases is always a major topic in project management. This procedure is normally specified in accordance with international standards. However, the absence of checklists, guidelines and recommendations for action leads to vaguely defined content and blurred structure of required documents at each building phase. Based on the aspects above, this paper aims to establish standard employer's information requirements (EIR) and BIM execution planning (BEP) during the life cycle of a project and build an online platform for the execution of semi-automatic checking. For this purpose, the existing EIRs and BEPs would be firstly analyzed and compared with each other as well as with other standards. Practical experience is gathered through expert interviews and workshops and complements the comparative analysis. Subsequently, the resulting requirements for EIR and BEP are presented in checklists and guidelines, which form the basis for the development of a controlling instrument. To develop an online tool, the information requirements and test criteria of this instrument are then derived from a database of process modelling from University of Wuppertal (BUW database). Furthermore, a workshop among experts was organized to collect the necessary functions of the software. Eventually, the online platform should consist of two main functions: generation of EIR files in the form of mvd XML according to various BIM objectives and use cases from the client, and the validation of the EIR by comparing IFC files from a contractor with the MVD files. The results of the checking could be BCF files or a final report as possible symbols for a successful information delivery.

Keywords –

Database of Process Modeling; Exchange Requirements; Information Delivery Manual; Model View Definition; Semi-automatic Checking

1 Introduction

In the construction and real estate industry there is an agreement that the highly efficient and accurate exchange of information along the life cycle of a project should be achieved. To carry out a construction project based on building information modeling (BIM), the client should firstly define the employer's information requirements (EIR). The contractors then describe how the BIM objectives and agreed information delivery are achieved and this is implemented in the BIM execution plan (BEP). This procedure is gradually becoming mandatory in different countries depending on their own specifications. For example, in Britain all projects assigned by government should approach the goal of using complete exchangeable BIM models upon common data environment (CDE) for collaboration from April 2016 [1][2]. However, the specific checklists, guidelines and recommendations for action are still missing, so that the content and structure of the necessary documents are currently not clearly defined.

In this research project, detailed information requirements and data delivery processes in BIM-based construction projects will be structured based on use cases from the database of process modelling from University of Wuppertal (BUW database). For each use case, one or more MVD files will be created based on formulated exchange requirement tables. Furthermore, a controlling instrument based on model view definition (MVD) accomplishing the automatic checking will be developed. Finally, an online platform which provides use cases and MVD templates as well as checking functions will be built and published as open resources.

2 State of the Art

To classify the topic, the preliminary work of the University of Wuppertal in the field of process databases and the current standards for information exchange are important. These areas are explained below.

2.1 University of Wuppertal database of Process Modeling

In recent years, the University of Wuppertal has built up a database for processes in the construction and real estate industry. This database is supported by a visualization based on the Business Process Management Notation. Since 2016, this database has been continuously enriched with information on the technical processes through various research projects. The focus was initially on the continuous flow of information in construction projects, answering the following questions: When (time) who (process owner) processes what (information input), after which (other applicable information), why (process goal), to what (information output)? In the course of the Building Information Modeling method, the question of "how" becomes more and more important, since it is an essential aspect of the intended automated information exchange.

The structure of the database and the flow of information with all other linked information currently consists of five levels that represent different levels of detail of the information. The essential levels for the project "BIM based information delivery controlling" are level three, which contains concrete exchange documents or files and the processes for them, and level five, which shows the concrete information requirements (EIR) for the generation of a document or the execution of a process. The structure is shown in a reduced form in Figure 1.

Figure 1. Structure of the University of Wuppertal database

The aim of the process database, which is continuously being developed, is to create the basis for an electronic transmission of information in the construction industry without media format differences. The information the database contains is based on standard processes in the German construction industry and taking into account the various project participants and areas of responsibility, thus serves as a basis for the structured exchange and verification of information.

2.2 Guidelines of BIM use cases

In the course of structuring data for processing within the BIM method, so-called BIM use cases were developed. These use cases always define a certain framework within the existing business process, which is now implemented differently through data exchange within the BIM method. In this way, all relevant exchange processes are to be successively identified, coordinated and adapted. The use cases will be part of the employer's information requirements (EIR) and thus define the contractual relationship between the client and contractor.

Currently, there is no established structure for the implementation of use cases. Within the framework of the project implementation, DIN EN ISO 29481-1 is used as a guideline, which contains information delivery manual (IDM) for building information models [3]. The basic framework for the connection of the data is shown in Figure 2.

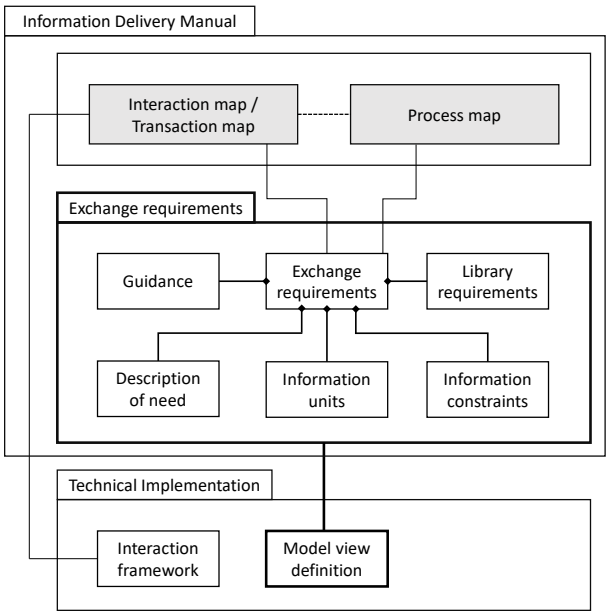

Figure 2. Part of IDM basic framework [3]

This approach is also pursued by the Use Case

Management of Building SMART International [4]. There, building SMART attempts to collect and structure use cases and make them available to the construction and real estate industry. The approach currently differs from that in this research project with the generation of a test file (MVD) being semi-automatic and not having to be carried out manually.

The research team is in close exchange with the use case management of buildingSMART International and the further ISO 29481 development, ensuring that current developments for standardizing the structure of use cases are considered in the project.

2.3 Common Data Environment

The exchange of information within projects is increasingly taking place in common data environments (CDE). CDEs thus serve as a single source of information for the collection, management, exchange and documentation of information, be it graphical information from a model or non-graphical data in various data formats. This shared data environment helps project teams to always have access to all information. To support project workflows, CDE providers offer various modules and functionalities for processing documents and data. In the course of standardization efforts, DIN SPEC 91391 "Common Data Environments (CDE) for BIM projects - Functions and open data exchange between platforms of different vendors" was developed as a first approach. It consists of the two parts "Modules and functions of a common data environment; with digital appendix" [5] and "Open data exchange with common data environments" [6].

The content of DIN SPEC 91391 is the first description of the requirements for manufacturer-independent processing of data within BIM projects. This is important for an implementation of a functioning BIM information delivery controlling in practice, because in this way it can be guaranteed that an open data exchange between different CDE's can be generally valid. A BIM use case is transferred to a CDE use case in a CDE. CDE workflows that support the semi-automatic processing and checking of data are assigned to this CDE use case.

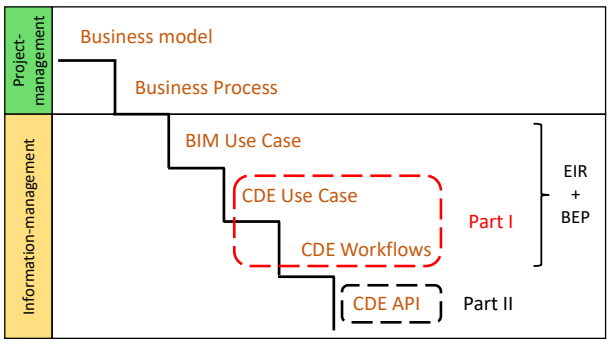

Figure 3. Process detailing from business plan to CDE workflow [5]

According to Figure 3, the areas BIM Use Case, CDE Use Case and CDE Workflow are dealt with in DIN SPEC 91391:1. while the description of the CDE API for the concrete exchange of data is given in DIN SPEC 91391:2. In accordance with DIN SPEC 91391:1, CDE's are divided into three different BIM levels, which represent the different development stages of CDE's. While the common CDE providers currently offer a BIM Level 2 CDE, which in particular provides documents, information containers or nested information containers with metadata, a BIM Level 3 CDE will in future allow direct access to model elements and attributes. The development of a BIM-based information delivery controlling can thus be part of a BIM Level 3 CDE, as it ensures that the information processing requirements of information requests are fulfilled. Accordingly, DIN SPEC 91391 will be considered within the project.

2.4 Information Delivery Manual

In order to describe the concrete information about who delivers what to whom at which point during the life cycle of a project, buildingSMART introduced the information delivery manual (IDM) standard [7]. The IDM plays therefore an important role in specifying the information requirements in tenders, contractors and for guidance in projects [8]. According to ISO 29481-1, the primary IDM components include use case, process map (PM), exchange requirement (ER) and model view definition (MVD). In this case, the user, such as the client, can generate an IDM by defining strategic goals, get machine readable file as MVD, and link IDM to different types of requirements (see Figure 4).

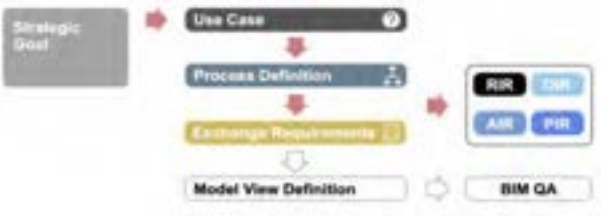

Figure 4. Process of generating IDM and its assignment to various requirements [8]

However, due to the complexity of development process, vague definition for information on exchange as well as lack of physical shared servers and administrator, it is still difficult to implement or share the IDMs under current specifications [1]. To solve these issues, the schema of idmXML is still under development and supposed to be published in ISO 29481-3.

2.5 Model View Definition

When the exchanged information in collaborative work is based on an IFC model, the corresponding partial model in accordance with exchange requirements is able to be expressed as model view definition (MVD) [7]. To allow the quickly mapping of a specific IFC element, the MVD is usually formalized as mvdXML.

The MVD file not only allows the storage of exchange information in a machine-readable format but also enables the checking of IFC files delivered by the contractor. For instance, a MVD checker based on open standard formats for structuring validation rules and BIM collaboration format (BCF) for issue reports was proposed and developed by Zhang, Beetz and Weise [9]. As most of the users are not used to XML format, software suppliers should make more effort in expressing the MVD in a user-friendly way, such as by describing the objective of data exchange [10].

2.6 Linked Data and buildingSMART Data Dictionary

By building a semantic web of data, a machine is able to trace the links between data. Thus, to promote the interoperability of various vocabularies, classification systems, ontologies, etc., the linked data, which origins from semantic web, is introduced in the field of architecture and construction [11].

For international collaboration, the buildingSMART data dictionary (bSDD) was implemented based on the structure from international framework for dictionaries (IFD) and collects tremendous terms and descriptions in multiple languages. It currently contains more than 60,000 concepts and since version 2 X 4 of IFC model serves as a central repository for standard PropertySets (PSet) extensions [12].

The bSDD database is accessable and editable with API. In this project, for example, the GET function by bSDD API is used for extracting all standardized PSets and properties and importing them into University of Wuppertal database, so that the same items would not be created twice. If some attributes or PSets corresponding to specific process in BUW database are created, it is also meaningful to POST the new items into bSDD ensuring that they could be referenced to by other users dealing with similar use case.

3 Concept and methodology

The basic concept of BIM-based information delivery controlling (see Figure 5) consists of three essential steps. Step one consists of a client using an online platform to select BIM use cases to be carried out in the project. The basis for the use cases is the existing BUW database (see section 2.1). The selected BIM Use Cases are provided for the project both as a printed version in the IDM structure and as a digital test file (MVD). In the second step, the contractor will create an IFC model that meets the requirements of the test file. This can be done in any software with IFC export. In the third and last step, the IFC model is checked on the basis of the MVD. During the check, the system checks whether information has been stored within the required fields and whether this information can plausibly describe the required attribute. The check result is returned via a BCF report and a check report.

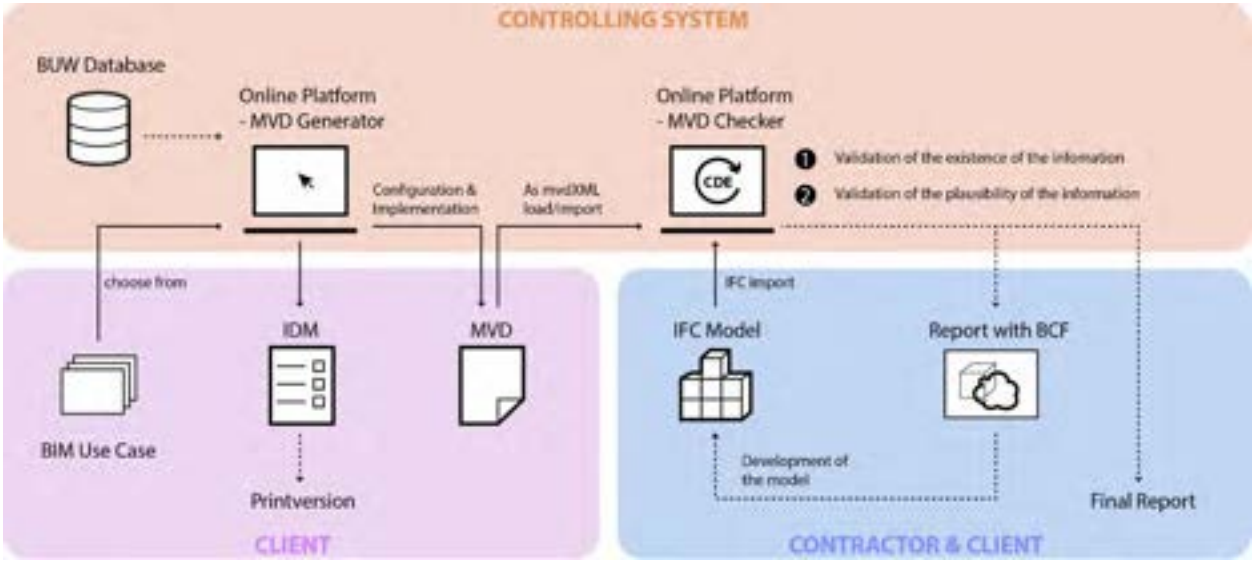

Figure 5. Concept of the BIM Based Information Delivery Controlling System

The Controlling System area is planned as a demonstrator within the project, but will fulfill the requirements for a CDE implementation (see section 2.3).

3.1 Collection of Information

Various methods are used to collect the information required to build BIM use cases. This includes a literature research, a review of existing databases (CAFM Connect, buildingSMART Data Dictionary, Use Case Management bSI) as well as the use cases of clients from BIM pilot projects in practice. In addition, the researched and newly developed use cases were coordinated with partners from industry and local authorities. The development and validation of the information is a continuous process.

3.2 Challenge IFC-connection

Besides the acquisition of information, the biggest challenge is to translate the structured information requirements into the object-based structure according to IFC or to assign the information requirements to the correct objects, generating a functioning inspection file (MVD). This relationship is shown schematically in Figure 6.

The BUW database contains the technical processes that are necessary to fulfill a construction project. The functional processes are mapped to possible objects according to DIN 276 (costs in construction), which in turn are mapped to IFC classes. The complex filtering of possible objects for a process towards a concrete object for a use case is done by building BIM use cases with level 3 processes.

The same structure can be seen in the BIM profiles of CAFM Connect, from which information is taken into account when referencing objects. In addition, the IFC Property Sets (Psets) are imported from the buildingSMART Data Dictionary (bSDD) so that they can also be used when generating the MVD. This ensures that already existing information is processed.

The information requests to be checked are built up by the bSDD both via the processes built up in process levels and via the Psets. The basis for this is a prepared template (see section 4.2). The combination of template and selected processes on process level 3 for the BIM use case leads to the concrete structure of a mvdXML.

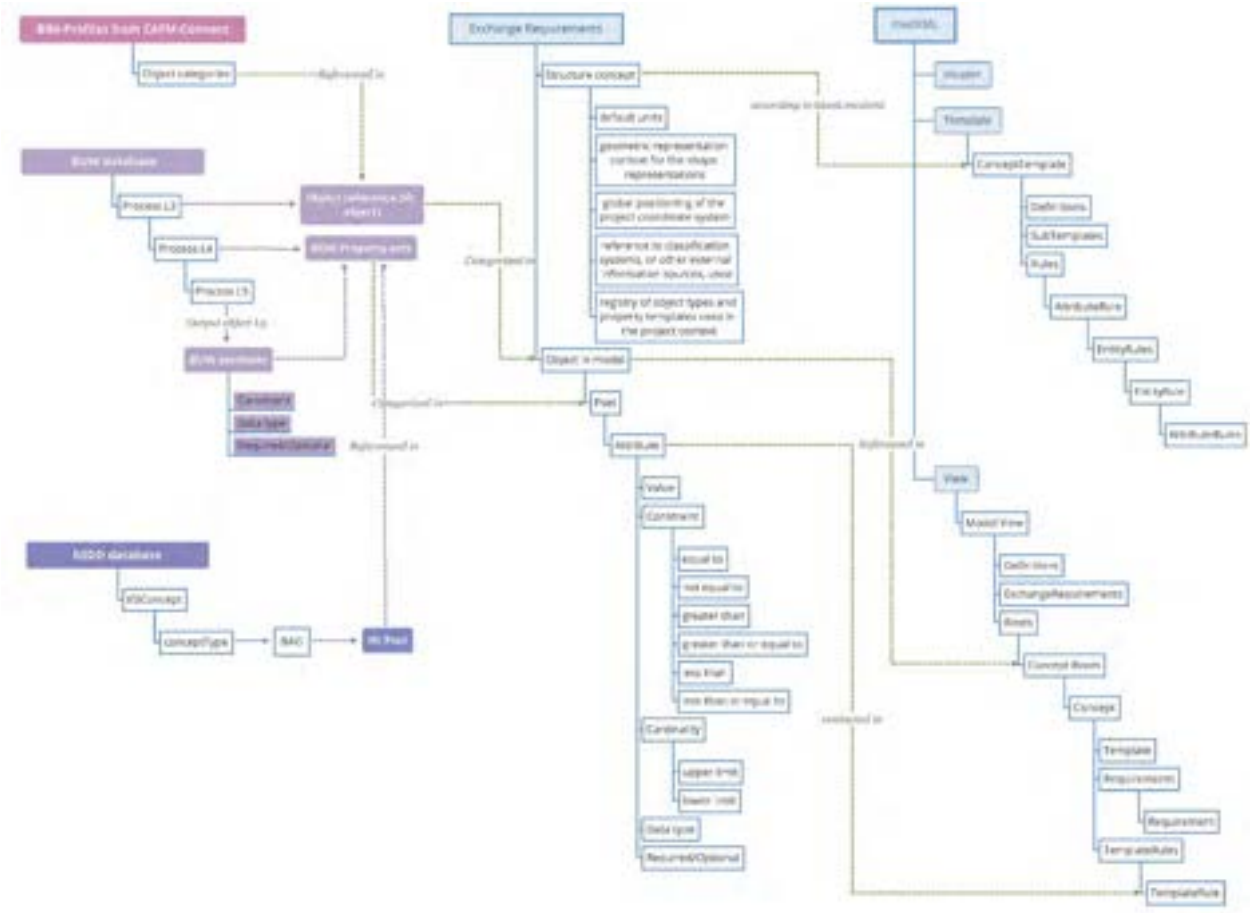

Figure 6. Structure of the data connection for generating mvdXML

4 Implementation

The development of a BIM based information controlling system is carried out in five steps: 1. Establishment of exchange requirements based on specific processes in each use case from BUW database; 2. Generation of MVD files according to exchange requirements; 3. Preparation of IFC model as to be checked file; 4. Examination of IFC file using MVD checker; 5. Building an online platform embedded with all functions. Since the controlling tool is still under test, sample files are taken to explain these implementation procedures in detail.

4.1 Definition and export of exchange requirements

As mentioned in section 2.1, the BUW database contains a tremendous amount of process data, and each use case contains process activity from level 1 to 5, person in charge, relevant object, necessary attributes, etc. Therefore, it is first of all essential to define which items should be contained in exchange requirement table. Because the request of information delivery or file exchange is merely driven by one specific activity at process level 3, only the items at level 3 or its sublevel should be included. To be more specific, process name, person in charge, relevant object, related attributes and property sets are important components in the exchange requirement table. Furthermore, to validate the plausibility of value to the attribute, general conditions should be provided, such as unity, data type, range, cardinality. The exchange requirements are consequently defined by a table or csv file, which forms the basis for generation of MVD (see Figure 6).

4.2 Generation of MVD file

The generation of a computer readable MVDs is based on utilizing predefined mvdXML template files which define the document structure. The template files are filled using exchange requirement information data provided by the BUW database as csv file (Figure 7). This results in standard conformant mvdXML files that can directly be used to validate IFC models.

To be more specific, the process of generating mvdXML itself is carried out in 4 steps: 1. Reading the provided data defined as csv file and extracting all necessary information, such as process name, person in charge, relevant object, IFC object name, property set, attributes and value. 2. Translating the extracted information into structured inputs for the mvdXML template files. 3. Filling the predefined placeholders in the provided template file with translated data. For example, list entries for object references and IFC object names are written into the concept root node. While the entries for property set, property name and all value definition define the constraints in concept nodes. 4. Generating the output files as mvdXML. Multiple mvdXML files are generated for every process name and its associated process owner.

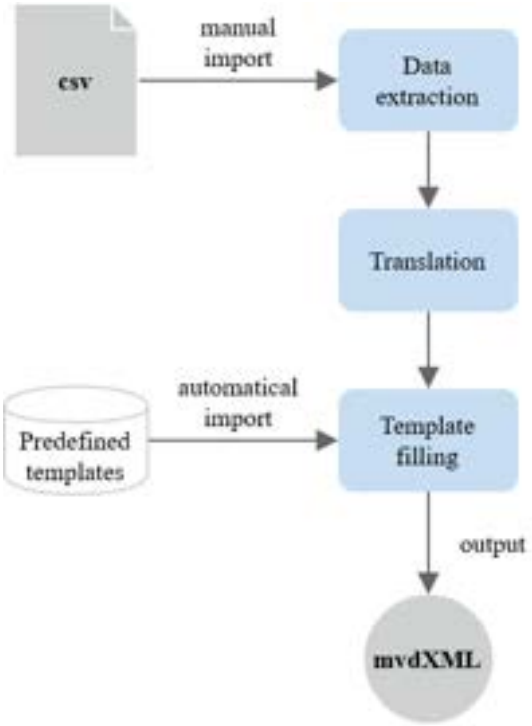

Figure 7. Technical process of generating a mvdXML file

An important aspect of this process is the reduction of effort in generating mvdXML templates by limiting their scope of application on property set definitions. It is possible to get by with a single concept template. However, it is also possible to nest templates in order to allow more complex subdivisions of nodes, as is the case for model view definitions.

Since the generation tool is still in active development, the process has only been applied on the use case ‘facility management’ so far. Further use cases will reveal other possibilities for improvement.

4.3 Preparation of IFC file

The controlling system is developed on the one hand for the client to regulate exchange requirements and to check the IFC file delivered by contractor. On the other hand it also helps the corresponding contractors improve their IFC file before they hand it in to the client. Moreover, to verify the atomization level of this tool, the procedure of importing key attributes in an IFC model should be tested. Hence, it is regarded as an essential part to document the process of preparing the IFC file.

Figure 8. Preview of element "IfcTransportElement-ELEVATOR" with attributes defined by exchange requirements in BIM Vision [13]

Figure 9. Screenshot of result from checking

In this case, the IFC model of a building from the University of Wuppertal is chosen as testing file as a result of its completeness and preciseness. In the very first trial, exclusively one element type (see Figure 8) is used for proof of exchange requirements for facility management. The specific attributes defined in exchange requirements are semi-automatic assigned in Autodesk Revit [14] by importing a shared parameter list.

4.4 Using MVD checker to verify IFC models

The MVD model checker tool is based on the open source software framework bimserver.org [15] . It is a generic tool for verifying IFC model contents for defined exchange requirements using mvdXML [16]. After successful verification, a report is returned as a BCF file, which contains all recognized issues. Consequentially, the MVD model checker has two inputs, the IFC file and mvdXML file and one output, the BCF file.

The controlling tool is still under development, therefore the described validation measures are all based on sample files. These sample files are limited to basic data contents, for example an elevator IFC file and a mvdXML file containing constraints on an IFC transport element. The MVD Model Checker exposes a public REST API which takes the IFC file and mvdXML file as input and returns results as JSON or BCF ZIP formats [17]. After each validation the results are manually examined (see Figure 8). If an unexpected result has been identified, the user can then check the IFC file or mvdXML file and correct errors as appropriate.

To verify the correct behavior of the MVD Model Checker, multiple input files are tested for which the

results can be easily checked manually. That way, for example, a known issue in bimserver.org about IFC inverses has been triggered and was resolved. Boolean string values and complex expressions also have been improved using this method. For the upcoming steps, the difficulty is increased by using more complex IFC and mvdXML files.

4.5 Development of an online platform

Prior to the implementation of this controlling system, a workshop among construction management practitioners was held for coming up necessary functions of the platform and giving those functions priority. Hence, besides the core mechanism of controlling systems which is related to the MVD generator and the MVD model checker, there have been other required functions which were collected in the workshop to be implemented in the platform. The requirements that are rated highest are: automatic choosing of exchange requirement template based on selected use case; test tools are based on open standards and open interface; the application should be possible to reproduce the data records in a way that is understandable to the users, etc.

To realize these functions as well as to combine the MVD generator and checker in one application, a web-based platform is considered to be a suitable tool. The establishment of an online platform will be realized through the following steps: 1. Creating mockups for detailed discussions on user interface design; 2. Using HTML, CSS and JavaScript to build a frontend; 3. Building a backend in Python to drive the MVD model checker and MVD generator. The online platform is still under development and will be published as free resource in the future.

5 Conclusion

The feedback from practice as well as the current topics of the organizations for standardization (ISO, DIN, VDI, buildingSMART) confirm the relevance of the subject in the area of information exchange of the BIM method. In the research project a functioning concept was developed, which is currently in the final phase of implementation, in order to meet the technical and content-related requirements of a semi-automatic BIM-based information supply controlling. The final result of the demonstrator will be provided by the authors via the respective universities and the code will be published.

References

[1] Jeon K. and Lee G. Information Delivery Manual (IDM) Configurator: Previous Efforts and Future Work. In 18th International Conference on Construction Applications of Virtual Reality, Auckland University, New Zealand, 2018.

[2] BSI BIM Level 2 Explained, In EXPLAINED, B. L., British Standards Institution, UK, 2010.

[3] DIN EN ISO. Part 1: Methodology and Format, In ISO 29481-1: Building Information Models-Information Delivery Manual, 2016.

[4] BuildingSMART International: Use Case Management: https://ucm.buildingsmart.org/, Accessed 08/06/2020

[5] DIN Part 1: Components and Function Sets of a CDE with Digital Attachment, In DIN SPEC 91391: Common Data Environments (CDE) for BIM Projects - Function Sets and Open Data Exchange between Platforms of Different Vendors, 2019.

[6] DIN Part 2: Open Data Exchange with Common Data Environments, In DIN SPEC 91391: Common Data Environments (CDE) for BIM Projects - Function Sets and Open Data Exchange between Platforms of Different Vendors, 2019.

[7] Beetz J., Borrmann A. and Weise M. Process-based definition of model content, In Building Information Modeling, Springer, pages 127-138, 2018.

[8] 442 C. T. First WD WI 442023 CEN/TR Guidance for understanding and using EN ISO 29481-1. Working draft, 2019.

[9] Zhang C., Beetz J. and Weise M. Model view checking: automated validation for IFC building models. eWork and eBusiness in Architecture, Engineering and Construction: ECPPM, 14:2014.

[10] Steinmann R. IFC certification of BIM software, In Building Information Modeling, Springer, pages 139-153, 2018.

[11] Pauwels P., Mcglinn K., Törmä S. and Beetz J. Linked data, In Building Information Modeling, Springer, pages 181-197, 2018.

[12] Beetz J. Structured Vocabularies in Construction: Classifications, Taxonomies and Ontologies, In Building Information Modeling, Springer, pages 155-165, 2018.

[13] Bimvision Online: https://bimvision.eu/en/, Accessed: 08/06/2020.

[14] Autodesk Online: https://www.autodesk.com/products/revit/overview, Accessed: 08/06/2020.

[15] Bimserver The open source BIMserver platform. Online: https://github.com/opensourceBIM/BIM-server, Accessed: 20/05/2020.

[16] Oraskari J. OnlineMvdXMLChecker. Online: https://github.com/jyrkioraskari/OnlineMvdXMLChecker, Accessed: 08/06/2020.

[17] mvdXMLChecker OpenAPI Interface. Online: http://lbd.arch.rwth-aachen.de/mvdXML-Checker/apidocs/, Accessed: 08/06/2020.

Development of an Open-source Scan+BIM Platform

Enrique Valero, Dibya D. Mohanty and Frédéric Bosché

School of Engineering, University of Edinburgh, UK

e.valero@ed.ac.uk, d.mohanty@ed.ac.uk, f.bosche@ed.ac.uk

Abstract -

In the last decade, a significant amount of research and development has been conducted at the intersection of Building Information Modelling (BIM) and reality capture data processing, mainly in the two areas often referred to as 'Scan-to-BIM' and 'Scan-vs-BIM'. Interestingly, it appears that all these advances have been made without the availability of any libre, cost-free and ideally open-source software platform that can handle both reality capture data (typically 3D point clouds and images) and Building Information Models. This paper investigates user demands and possible alternative options to develop such a *Scan+BIM* platform to further stimulate research in the field. A set of requirements for such a platform are first identified by means of a questionnaire sent to researchers and industry practitioners. Different software applications, identified from the literature and online, are then assessed against those requirements. A final ranking of these applications is conducted and one suitable solution is identified and suggested for development. The proposed solution combines the OpenInfra Platform, as a BIM and point cloud engine and viewer, and the xBIM Toolkit to provide complementary tools for the BIM engine. This new piece of software is currently under development and the authors intend to make it available to the Construction Informatics community soon.

Keywords -

Reality Capture; Point Clouds; Images; BIM; Engine; Platform; open-source

1 Introduction

The last decade has seen an explosion of research in Construction Informatics. Two fields that have received particular attention are reality capture data processing as well as Building Information Modelling (BIM), the latter being the development of structured data supporting collaborative processes for reliable management of construction projects over their lifecycle [1, 2, 3].

Reality capture technologies have rapidly evolved and are widely used for digital documentation. Digital cameras are now cheap and ubiquitous, and are commonly utilised for the creation of 3D models by means of Structure-from-Motion photogrammetry (PG). Besides, accurate terrestrial laser scanning (TLS) technology is increasingly affordable. Other imaging technologies, such as thermal cameras and ground-penetrating radars, have seen improvements in data quality. And finally, there is an exponential growth in Internet-of-Things (IoT) sensors that can capture various environmental and structural characteristics to be used in the generation of BIM models — and by extension Digital Twins (DTs) — of buildings [4].

These sensors on their own are resulting in a significant increase in data that needs to be curated and processed to extract meaningful information that can support effective design, construction, operation and maintenance of the built environment. The processing of that data along with its structured recording for analysis and efficient retrieval is increasingly considered within a BIM/DT digital framework. While the work conducted here could eventually be extended to a larger set of reality capture data, this paper focuses on 3D (and colour) data acquisition technology, i.e. principally TLS and PG.

Examples of the combined application of TLS/PG and BIM technologies can be found across the lifecycle of built environment assets and can be categorised into three groups [1, 3, 5], discussed in more detail in the following sub-sections: Scan-to-BIM (Section 1.1), Scan-vs-BIM (Section 1.2) and Others (Section 1.3).

1.1 Scan-to-BIM

Scan-to-BIM refers to the process of capturing data of existing built environment assets and producing BIM models representing the *as-is* state of those assets [1, 3, 6, 7, 8]. Although this process has various applications, it is primarily employed for the production of BIM models of existing assets that are then used as a starting point for design of renovation works or for supporting Facilities Management (FM). Scan-to-BIM is an extremely lively field, where academic and private research groups compete in the development of algorithms that automate this process as much as possible (e.g. [9]). While various of the technologies mentioned earlier can be employed in this process, it is notable that the majority of current solutions consider as input laser scanned point clouds [9, 10]. Photogrammetric point clouds and their underlying imagery are also increasingly considered as a valuable input to the scan-to-BIM process [11].

1.2 Scan-vs-BIM

Scan-vs-BIM refers to the process of capturing data of existing built environments and comparing that data against BIM models representing the prior recorded state of those assets [12]. This process has been shown to be of value to progress and quality control during the construction phase of projects, in which case the BIM models are *as-designed* BIM models produced during the design stage [2, 6, 13]. The Scan-vs-BIM process can also be employed to support asset operational monitoring, in which case BIM models are the latest recorded *as-is* BIM models of the assets.

1.3 Others

Other research works also employ reality capture and BIM data, but in different ways. For example, a significant amount of Health & Safety research has been conducted that processes reality capture data (TLS, PG, range cameras, etc.) to detect hazards. In these works, the BIM model of the environment where the sensors are located can be used to provide contextual knowledge to enhance data processing performance [14, 15].

In a different manner, Lovreglio et al. [16] use BIM models and pictures of buildings for the production of Virtual Reality applications to train building occupants in evacuation during earthquakes.

2 Review of Scan Engines, BIM Engines, and Scan+BIM Engines

2.1 Point Cloud Engines

TLS and PG are the two main technologies currently considered in the Architecture, Engineering and Construction (AEC) domain for the acquisition of 3D (i.e. geometric, visual) data of construction assets. For both technologies, the output consists in point clouds containing millions of unconnected 3D points usually enriched with additional data such as: colour, intensity of the received signal, and/or thermal response. Visualisation and navigation of those point clouds are needed for an appropriate understanding and further analysis of the data and processing results.

TLS manufacturers commonly provide users with their own software for data processing and visualisation (e.g. Faro Scene [17], Leica Cyclone [18]). However, these solutions are usually under proprietary (i.e. close-source and non-free) licenses and only allow limited data operations, such as point clouds registration and cleaning. The proliferation of TLS, and therefore the explosion of 3D data processing, have encouraged the development of powerful free and open solutions for 3D data processing and visualisation in the last decade, such as CloudCompare [19] or MeshLab [20].

In the case of photogrammetry, both proprietary software (e.g. RealityCapture [21] and Metashape [22]) and open-source (e.g. Meshroom [23]) are also available for the generation and visualisation of 3D point clouds.

These tools employ well-recognised libraries for handling point clouds, such as PCL [24].

In general, colour information delivered by PG models is more reliable than the colour obtained by TLS devices [25]. However, 3D geometry is less accurate and processes to obtain high resolution point cloud are slower with PG in comparison with TLS.

2.2 BIM Engines

BIM relates to both the creation and the management of structured information on construction projects across the lifecycle of buildings. In BIM processes, visualisation is fundamental for a correct understanding of the asset and its evolution. Therefore, 3D BIM models constitute an ideal visualisation and navigation reference, upon which additional information can be linked, visualise and processed.

A number of BIM engines and viewers have been developed to date, by both academic research teams and leading design software companies, with the purpose of generating, modifying and visualising BIM models. For example, IFC Viewer [26] and the commercialised IFC Engine [27] can load Industry Foundation Classes (IFC) files, visualise the 3D geometry and explore additional non-geometric information through a navigation tree. A more complete solution is delivered by Areddo [28], which is a free but proprietary BIM viewer that can handle IFC files as well as point clouds. Areddo includes additional basic operations like measuring distances and producing cross sections of models. However, this is not an authoring tool, i.e. information cannot be modified. Modification of BIM models, including those stored under the IFC standard, is possible in Autodesk Revit [29], currently the most used tool for the authoring of BIM models. Other related industry proprietary software packages include ArchiCAD [30], and MicroStation [31].

The above solutions, while presenting various levels of capability, are also restrictive because they are proprietary (although some are cost free). Aiming to produce open-source alternatives that could be used, maintained and improved by a community of researchers, alternative solutions for handling and visualising BIM models have been developed in the last decade. This is the case of the xBIM toolkit [32], which includes libraries for the authoring (xBIM Essentials and Geometry) and a Windows Presentation Foundation (xBIM Xplorer) for rendering and visualisation of BIM models based on the IFC open data

schema. Another solution, principally focused on infrastructure, is the OpenInfra Platform [33], which is able to handle BIM models and Geographic Information Systems (GIS) -related data, as well as point clouds (as further discussed below).

A crucial step for the visualisation of the geometry (i.e. 3D models) 'codified' in IFC files is the interpretation of this data and the subsequent generation of renderable models to be shown in a viewer. A variety of libraries have been developed for this purpose in the last decades. Examples of this kind of tools are the open-source ifcOpenShell [34], which is used by the BIM storage and management tool BIMserver [35], or ifcPlusPlus [36] — as well as the xBIM library mentioned above.

2.3 Scan+BIM Engines

Importantly with regard to the focus of this paper, few of the above BIM or point cloud software solutions are able to handle both BIM and point cloud data; and those that do provide various levels of functionalities.

Point clouds can be loaded into Revit, ArchiCAD or Microstation, a feature principally employed to facilitate the production of BIM models of existing structures. In the case of Revit, point clouds need to first be opened with a different piece of software, Autodesk Recap, which exports the data into a unique format readable by Revit. However, the main drawback in all cases is software cost.

As previously mentioned, the cost-free viewer Areddo can be used for visualising both point clouds (in `.pts` format) and BIM models (in `.ifc` format). This tool additionally provides basic functionalities related to visualisation, such as variations in lighting, shadowing effects and navigation; and measuring distances. However, neither point clouds nor 3D models can be modified with Areddo.

Another solution able to deal with point clouds and BIM models is OpenInfra Platform. This modular software, which is still under development, can load BIM models (in `.ifc` format) as well as point clouds (`.e57`).

In summary, it can be observed that, despite the recent explosion in the use of reality capture technologies and BIM methodology for managing buildings over their lifecycle, only a few software packages, mainly proprietary, can handle both reality capture and BIM data, and with limited functionalities in terms of data manipulation (visualisation and authoring for both). Areddo is a visualisation tool that lacks BIM authoring functionalities, and is unable to open standardised formats for point clouds like `.e57`. Besides, like Revit, Areddo is not open-source, which limits the flexibility often required for research.

The research community would be best served by an open-source solution that could handle the two types of data, allowing visualisation and manipulation (i.e. editing/authoring) of both. OpenInfra could be that solution. Although the platform is still under development, it offers great potential since it is both cost-free and open-source and has been conceived as a cluster of interlinked solutions for infrastructure and construction projects, which can be extended with additional tools or features according to the users' needs.

3 User Requirements

The identification of the best way to develop an open-source solution that can effectively handle both types of data first requires that the needs and requirements of its potential final users — i.e. R&D professionals from both academia and construction industry — are brought to light. To this end, an online questionnaire (see Subsection 3.1) has been created and sent to professionals around the world. Results from the questionnaire have then been analysed and the identified requirements are reported in Section 3.2. In Section 4, the existing tools and their functionalities (reviewed earlier) are then juxtaposed to the user requirements to identify the most adequate open-source solution.

3.1 Questionnaire

An online questionnaire was prepared to investigate how R&D professionals, both in industry and academia, work with BIM models and reality capture data. The survey, which can be found in the Annex, enquired about the tools these professionals are currently using, and whether the needs they might have are covered by the software package of their preference.

The questions were divided in three main blocks:

General (Questions 2 - 7): Professional background; experience with reality capture and BIM; their awareness of existing Scan+BIM tools; and their needs and preferences.

BIM functionalities (Questions 8 - 10): Open BIM formats and standards that should be handled by the platform; open mesh geometry formats to be loaded and saved; and the main BIM authoring functionalities (e.g. editing geometric and non-geometric information, changing the topology of the models).

Reality capture functionalities (Questions 11 - 14): 3D and 2D data formats; images and calibration; and functionalities, such as point cloud processing.

A number of questions use a 5-point Likert scale to ask about the criticality of certain functionalities. The scale goes from 1 (not important) to 3 (would be nice) and 5 (critical). For each question the average score is calculated

to help highlight the parameters and requirements which were more relevant to the participants.

The questionnaire was disseminated to academics and construction professionals through specialised mailing lists and social networks (LinkedIn groups and Twitter), reaching more than 35,000 potential users. A total of 31 professionals completed the online questionnaire; 28 of which (90.3%) were academics or researchers and 3 of them (9.7%) worked for construction companies (Question 2). Amongst them, 21 (67.7%) responded to commonly work simultaneously with reality capture data and BIM (Q3).

3.2 Scan+BIM Engine Requirements

3.2.1 General requirements

When asked about their awareness of any 'off-the-shelf' Scan+BIM software platform (Q4), 71% replied negatively. Professionals who gave an affirmative answer to this question (9 out of 31) mentioned Edgewise [37] and Revit [29]. However, only 6 of those 9 people had used those existing solutions.

With respect to their R&D needs (Q5), participants were asked about the size, completeness and format of the datasets handled by such Scan+BIM tool. Table 1 summarises their responses. Note that in this and the following tables, values in bold correspond to those scores higher than the average for the responses to all 7 Likert-type questions, which we refer to as the 'global average'.

As can be seen, participants agreed with the importance of handling open data formats as well as with the development of an open-source tool where other users can contribute. Also, supporting geo-referenced data is appealing to the respondents. However, the score for *handling data from large environments* is below the global average which is $\overline{s} = 3.92$.

Table 1. Question 5: Considering the needs of those responding the questionnaire, "the Scan+BIM software platform should . . . "

Requirement	average	std. dev.
support geo-referenced data	**4.09**	1.14
be able to handle data covering large environments	3.68	1.36
be focused on working with open data formats	**4.55**	0.94
be open-source	**4.14**	1.06

Regarding handling data of different nature (other that point clouds and BIM), 24 participants (>75%) considered that these two sources sufficed (Q6). However, 7 mentioned the advantages of supporting additional data, such as pictures and Geographic Information Systems data.

Finally, from a low level (i.e. software development) perspective, most participants (51%) agreed on the use of the C++ language for the development of the Scan+BIM tool, although some of them (4) mentioned Python as a "versatile and easy to use" alternative (Q7).

3.2.2 BIM functionalities

Regarding the ability of the Scan+BIM platform to handle BIM models, participants were asked about data formats and extra functionalities that they would find of interest for such a tool (Q8). First, when considering the formats and standards proposed in the OpenBIM framework (see Table 2), all respondents essentially agreed about the need to support the `.ifc` format. This is the only standard of the list whose score is higher than the global average $\overline{s} = 3.92$.

Table 2. Question 8: "Regarding the ability of the Scan+BIM platform to handle BIM models, it should support. . . "

Requirement	average	std. dev.
IFC	**4.73**	0.86
IFD	3.45	1.02
MVD	3.35	1.06
BCF	3.38	1.21

In some cases, loading or exporting 3D mesh models could be valuable. Amongst the file formats proposed in Q9, Table 3 shows that `.obj` is the favourite option for those who answered the question.

Table 3. Question 9: "With respect to the ability of handling 3D meshes, the Scan+BIM software platform should support. . . "

Requirement	average	std. dev.
OBJ	**4.24**	1.11
PLY	3.85	1.11
STL	3.75	1.34
VRML	3.5	1.12
COLLADA	3.45	1.36

Finally, the preferred BIM functionalities to be included in the Scan+BIM tool (Q10) are summarised in Table 4. Although most of the proposed features obtained scores above the average, professionals gave priority to the ability of editing the geometry and the topology of BIM objects.

3.2.3 Reality capture functionalities

Following a similar pattern of questions as for the BIM functionalities, the participants were first asked about their

Table 4. Question 10: "Regarding the modification of BIM models, the Scan+BIM software platform should support. . . "

Requirement	average	std. dev.
editing of the geometric information of individual BIM objects (e.g. shape and location)	**4.45**	0.89
editing of the non-geometric information of individual BIM objects	3.77	1.13
editing of the geometric relationships (topology) between BIM objects	**4.23**	1.04
editing of the non-geometric relationships between BIM objects	3.5	1.16
the creation of BIM objects	**3.95**	1.11
the various BIM classifications	**4.23**	1.04

preferred file format for point clouds and pictures (Q11). As illustrated in Table 5, amongst the proposed point cloud file formats, most participants highlighted XYZ, PTS, PTX and E57 as being most important, with values above the global average ($\overline{s}$ = 3.92). Regarding the proposed formats for pictures storage, these obtained lower scores than the alternatives for point clouds, which could reflect the prioritisation of 3D data. Note that pictures can also be stored in `.e57` files.

Table 5. Question 11: "Amongst the following file formats, the Scan+BIM software platform should support. . . "

Requirement	average	std. dev.
E57	**3.95**	0.99
XYZ	**4.38**	0.89
PTS	**4**	1.09
PTX	**4**	1.05
PLY	3.74	0.85
PNG	3.84	0.93
JPEG	3.9	0.89

With respect to point-cloud related functionalities, the participants were asked about the features enumerated in Table 6 (Q12). The preferred option was the ability *to perform some common processing of point clouds*, followed by *adding or editing per point information*.

The last question of those was about the functionalities of the platform for handling pictures and associated features (Q14). Amongst the proposed operations (see Table 7), the most supported functionality was the *support of calibrated images*, the only requirement of this batch with a score above the average.

Table 6. Question 12: "Regarding point-cloud functionalities, the Scan+BIM software platform should support. . . "

Requirement	average	std. dev.
some common processing of point clouds (e.g. cleaning/filtering, segmentation, other)	**4.57**	0.66
adding/editing per-point information (e.g. additional scalar fields)	**4.19**	0.79
the simulation of the acquisition of point clouds (laser scanning)	3.71	0.98

Table 7. Question 14: "With respect to handling pictures and related features, the Scan+BIM software platform should support. . . "

Requirement	average	std. dev.
(externally) calibrated images	**4**	1.04
editing calibration matrices	3.82	0.94
editing images	3.23	1.20
the simulation of the acquisition of images (with or without calibration matrices)	3.45	0.89

4 Comparison of Existing Data Engines and Proposal of a Scan+BIM Solution

After evaluating the results obtained from the proposed questionnaire, the availability of the required functionalities that scored over the global average was assessed amongst current (commercial or free; closed or open-source) software solutions. In the following subsections, the obtained results are discussed for reality capture engines, BIM engines, and Scan+BIM engines. Note that the software packages are compared as 'out-of-the-box' solutions. The use of libraries or application programming interfaces (APIs) to supplement software functionalities is discussed but not considered in the comparison, since those potential solutions have not been implemented yet and, therefore, are not available for the above-mentioned end users.

4.1 Reality Capture Data Engines

A comparison between a number of solutions was performed to analyse how existing reality capture data engines

met the requirements highlighted in the survey result as per questions 11 (Table 5), 12 (Table 6) and 14 (Table 7). As can be seen in Table 8, CloudCompare, MeshLab, Metashape and ReCap meet most of the requirements. In contrast, Reality Capture and Meshroom do not, on their own, fulfil the needs expressed in the questionnaire. All the engines offer *some common point cloud processing* functionalities like cleaning/filtering or segmentation, which is one of the most desirable and basic requirements. However, another highly scored requirement, *adding/editing per-point information*, is only met by CloudCompare and MeshLab. The reality capture engines were also compared based on the general requirements as per question 5 (Table 1). All the engines can work with open data formats and all support geo-referenced data, except Meshroom. However, only CloudCompare, MeshLab and Meshroom are open-source.

In summary, CloudCompare and MeshLab are the solutions which meet most of the desired requirements; and additionally, these are open-source solutions, enabling further development, if needed.

4.2 BIM Engines

Amongst the software solutions presented in Section 2, conventional BIM engines are compared in Table 8, considering the most voted requirements in questions 8 (Table 2), 9 (Table 3) and 10 (Table 4). The evaluated tools handling uniquely BIM objects are the open-source solutions IFC Viewer, xBIM Xplorer and BIMserver. Although the IFC file format is supported by all, the most voted file format for the storage of meshes (i.e `.obj`) is only supported by BIMServer. Additionally, further editing or creation of BIM objects is not in the scope of any of these engines, that basically act as BIM objects viewers only. However, it is worth mentioning that xBIM Xplorer could take advantage of the xBIM toolkit to supplement its functionalities and provide the user with the ability of modifying BIM elements. With respect to the general requirements of question 5 (Table 1), all engines are open-source and allow working with open data format, supporting geo-referenced data.

Commercial solutions such as Revit, Microstation and ArchiCAD, which are provided by renowned international software corporations, all enable, amongst their numerous functionalities, the usage of point clouds. The tree tools are capable of creating and editing BIM object and conduct some basic processing of point clouds. Microstation and Revit can work with most open data formats, whereas ArchiCAD supports limited open data formats. All three solutions are primarily closed, proprietary BIM engines with the capability of loading and visualising point clouds.

Areddo is a freeware and can visualise point clouds and BIM files. However, the range of file formats that can be opened is limited and no operations can be performed on the objects, either point clouds or BIM models.

In contrast, the OpenInfra Platform can manipulate both point clouds and BIM models and is a free open-source solution, which facilitates the addition of new tools and functionalities to the platform. An important advantage of this solution in contrast to all previous ones is its ability to visualise and modify point clouds (as it uses the CloudCompare engine). But, a limitation of OpenInfra is that it offers no native functionality to create and edit BIM objects.

Overall, as shown in Table 8, Revit, Microstation and ArchiCAD meet most of the requirements pointed out in the questionnaire. Although the IFC file format is supported by all engines, the most voted file format for the storage of meshes (i.e. OBJ) is only supported by Microstation. And functionalities related to the creation and editing of BIM objects are only supported by Revit, ArchiCAD and Microstation. Regarding other general requirements, all engines allow working with open data format and support geo-referenced data.

As evident from the comparison above, solutions able to handle BIM models are clearly separable in two different groups: a first group including solutions that cover more requirements, but are closed, proprietary software (ArchiCAD, Microstation, Revit); and a second group with tools that provide comparatively fewer functionalities, but are these are free and open-source which makes them comparatively more flexible to the needs of researchers (IFC Viewer, xBIM Xplorer, BIMserver and OpenInfra). However, in most solutions enumerated in the first group, additional requirements cannot be implemented, since their source code is not available to the general public. In some cases (e.g. Revit), companies provide APIs that can be used for the implementation of supplementary functionalities, but these can be limited and/or complex. On the other hand, amongst the solutions listed in the second group, only OpenInfra can handle both point clouds and BIM objects, but it lacks object editing functionalities.

Therefore, one good solution identified and suggested for development combines OpenInfra, as a BIM and point cloud engine, and the xBIM toolkit that provides supplementary libraries for the BIM engine such as the (semi-)automatic generation of IFC files.

5 Conclusion

This paper presented the first steps on the development of an open-source Scan+BIM platform. First, the authors reviewed a number of existing alternatives that are able to handle point cloud and BIM data, analysing their advantages and disadvantages were highlighted. Considering the main functionalities provided by these solutions, a questionnaire was then sent to potential users of such platform

Table 8. Assessing existing Scan and BIM Engines against the key requirements identified from the questionnaire.

	Reality capture					BIM			Scan+BIM				
Requirement	CloudCompare	MeshLab	RealityCapture	Metashape	Meshroom	IFC Viewer	xBIM Xplorer	BIMServer	ArchiCAD	Microstation	Revit + Recap	Areddo	OpenInfra
IFC	-	-	-	-	-	✓	✓	✓	✓	✓	✓	✓	✓
OBJ	-	-	-	-	-	×	×	✓	×	✓	×	×	×
editing of the geometric information of individual BIM objects (e.g. shape and location)	-	-	-	-	-	×	×	×	✓	✓	✓	×	×
editing of the geometric relationships (topology) between BIM objects	-	-	-	-	-	×	×	×	✓	✓	✓	×	×
creation of BIM objects	-	-	-	-	-	×	×	×	✓	✓	✓	×	×
the various BIM classifications	-	-	-	-	-	×	×	×	✓	×	✓	×	×
e57	✓	×	✓	✓	×	-	-	-	✓	✓	✓	×	✓
XYZ	✓	✓	×	×	×	-	-	-	✓	✓	✓	×	✓
PTS	✓	✓	×	✓	×	-	-	-	×	✓	✓	✓	×
PTX	✓	✓	×	✓	×	-	-	-	×	✓	✓	×	×
some common processing of point clouds (e.g. cleaning/filtering, segmentation, other)	✓	✓	✓	✓	✓	-	-	-	✓	✓	✓	×	✓
adding/editing per-point information (e.g. additional scalar fields)	✓	✓	×	×	×	-	-	-	×	×	×	×	✓
(externally) calibrated images	×	✓	✓	✓	✓	-	-	-	×	×	✓	×	×
support geo-referenced data	✓	✓	✓	✓	×	✓	✓	✓	✓	✓	✓	×	✓
able to working with open data formats	✓	✓	✓	✓	✓	✓	✓	✓	✓	✓	✓	✓	✓
be open-source	✓	✓	×	×	✓	✓	✓	✓	×	×	×	×	✓

(i.e. academics and construction professionals, principally researchers) to collect their needs and requirements for a Scan+BIM software platform. After analysing the data obtained from the questionnaire, the authors concluded that a combination of available open-source solutions, specifically OpenInfra Platform and xBIM toolkit, would be the starting point for the development of the proposed software platform. The authors are in the process of developing that solution and intend to make it available to the Construction Informatics community soon, for the benefit of the research community in particular.

Acknowledgements

This work was conducted as part of the BIMERR project has received funding from the European Commission's Horizon 2020 research and innovation programme under grant agreement No 820621. The views and opinions expressed in this article are those of the authors and do not necessarily reflect any official policy or position of the European Commission.

References

[1] R. Santos, A. A. Costa, and A. Grilo. Bibliometric analysis and review of Building Information Modelling literature published between 2005 and 2015. *Automation in Construction*, 80:118–136, 2017. doi:10.1016/J.AUTCON.2017.03.005.

[2] H. Son, F. Bosché, and C. Kim. As-built data acquisition and its use in production monitoring and

automated layout of civil infrastructure: A survey. *Advanced Engineering Informatics*, 29(2):172–183, 2015. doi:10.1016/J.AEI.2015.01.009.

[3] J. K. W. Wong, J. Ge, and S. X. He. Digitisation in facilities management: A literature review and future research directions. *Automation in Construction*, 92:312–326, 2018. doi:10.1016/J.AUTCON.2018.04.006.

[4] IET and Atkins. Digital twins for the built environment. Technical report, IET and Atkins, 2018.

[5] J. Yang, M.-W. Park, P. A. Vela, and M. Golparvar-Fard. Construction performance monitoring via still images, time-lapse photos, and video streams: Now, tomorrow, and the future. *Advanced Engineering Informatics*, 29(2):211–224, 2015. doi:10.1016/J.AEI.2015.01.011.

[6] P. Tang, D. Huber, B. Akinci, R. Lipman, and A. Lytle. Automatic reconstruction of as-built building information models from laser-scanned point clouds: A review of related techniques. *Automation in Construction*, 19(7):829–843, 2010. doi:10.1016/J.AUTCON.2010.06.007.

[7] V. Pătrăucean, I. Armeni, M. Nahangi, J. Yeung, and C. Haas. State of research in automatic as-built modelling. *Advanced Engineering Informatics*, 29 (2):162–171, 2015. doi:10.1016/J.AEI.2015.01.001.

[8] Y. K. Cho, Y. Ham, and M. Golpavar-Fard. 3D as-is building energy modeling and diagnostics: A review of the state-of-the-art. *Advanced Engineering Informatics*, 29(2):184–195, 2015. doi:10.1016/J.AEI.2015.03.004.

[9] S. Nikoohemat, A. Diakité, S. Zlatanova, and G. Vosselman. Indoor 3D modeling and flexible space subdivision from point clouds. *ISPRS Annals of Photogrammetry, Remote Sensing and Spatial Information Sciences*, IV-2/W5:285–292, 2019. doi:10.5194/isprs-annals-IV-2-W5-285-2019.

[10] C. Mura, O. Mattausch, and R. Pajarola. Piecewise-planar reconstruction of multi-room interiors with arbitrary wall arrangements. *Comput. Graph. Forum*, 35(7):179–188, 2016. URL `http://dl.acm.org/citation.cfm?id=3151666.3151685`.

[11] S. Tuttas, A. Braun, A. Borrmann, and U. Stilla. Acquisition and consecutive registration of photogrammetric point clouds for construction progress monitoring using a 4D-BIM. *PFG – Journal of Photogrammetry, Remote Sensing and Geoinformation Science*, 85(1):3–15, 2017. doi:10.1007/s41064-016-0002-z.

[12] F. Bosché, A. Guillemet, Y. Turkan, C. T. Haas, and R. Haas. Tracking the built status of MEP works: Assessing the value of a Scan-vs-BIM system. *Journal of Computing in Civil Engineering*, 28(4):1–28, 2014. doi:10.1061/(ASCE)CP.1943-5487.0000343.

[13] M.-K. Kim, Q. Wang, and H. Li. Non-contact sensing based geometric quality assessment of buildings and civil structures: A review. *Automation in Construction*, 100:163–179, 2019. doi:10.1016/j.autcon.2019.01.002.

[14] N. Li, B. Becerik-Gerber, B. Krishnamachari, and L. Soibelman. A BIM centered indoor localization algorithm to support building fire emergency response operations. *Automation in Construction*, 42:78–89, 2014. doi:10.1016/j.autcon.2014.02.019.

[15] J. Teizer. Status quo and open challenges in vision-based sensing and tracking of temporary resources on infrastructure construction sites. *Advanced Engineering Informatics*, 29(2):225–238, 2015. doi:10.1016/J.AEI.2015.03.006.

[16] R. Lovreglio, V. Gonzalez, Z. Feng, R. Amor, M. Spearpoint, J. Thomas, M. Trotter, and R. Sacks. Prototyping virtual reality serious games for building earthquake preparedness: The Auckland City Hospital case study. *Advanced Engineering Informatics*, 38:670–682, 2018. doi:10.1016/j.aei.2018.08.018.

[17] Faro. Scene (version 7.0) [computer software]. `https://www.faro.com/en-gb/products/construction-bim-cim/faro-scene/`, 2020.

[18] Leica. Cyclone (version 9.3.2) [computer software]. `https://leica-geosystems.com/en-gb/products/laser-scanners/software/leica-cyclone`, 2020.

[19] D. Girardeau-Montaut. CloudCompare (version 2.10.2) [computer software]. `https://www.danielgm.net/cc/`, 2020.

[20] P. Cignoni and G. Ranzuglia. Meshlab (version 2016) [computer software]. `http://www.meshlab.net/`, 2020.

[21] Capturing Reality s.r.o. RealityCapture [computer software]. `https://www.capturingreality.com`, 2020.

[22] Agisoft LLC. Metashape [computer software]. `https://www.agisoft.com`, 2020.

[23] AliceVision. Meshroom [computer software]. `https://alicevision.org/#meshroom`, 2020.

[24] R. Bogdan Rusu and S. Cousins. 3D is here: Point Cloud Library (PCL). In *IEEE International Conference on Robotics and Automation (ICRA)*, Shanghai, China, May 9-13 2011.

[25] M. Pepe, S. Ackermann, L. Fregonese, and C. Achille. 3D point cloud model color adjustment by combining terrestrial laser scanner and close range photogrammetry datasets. *World Academy of Science, Engineering and Technology International Journal of Computer and Information Engineering*, 10(11), 2016.

[26] RDF Ltd. IFC Viewer [computer software]. http://rdf.bg/product-list/ifc-engine/ifc-viewer/, 2020.

[27] RDF Ltd. IFC Engine [computer software]. http://rdf.bg/product-list/ifc-engine/, 2020.

[28] Arkey Systems. Areddo [computer software]. https://www.areddo.com, 2020.

[29] Autodesk. Autodesk Revit [computer software]. https://www.autodesk.co.uk/products/revit/overview, 2020.

[30] Graphisoft. ArchiCAD [computer software]. https://www.graphisoft.com/archicad/, 2020.

[31] Bentley. Microstation [computer software]. https://www.bentley.com/en/products/brands/microstation, 2020.

[32] S. Lockley, C. Benghi, and M. Černý. Xbim.Essentials: A library for interoperable building information applications. *The Journal of Open Source Software*, 2(20):473, 2017. doi:10.21105/joss.00473.

[33] H. Hetch and S. Jaud. TUM OpenInfraPlatform: The Open-Source BIM Visualisation Software. In *31. Forum Bauinformatik*, Berlin, Germany, 2019.

[34] T. Krijnen. IfcOpenShell [computer software]. http://ifcopenshell.org, 2020.

[35] The Open Source BIM Collective. Bimserver [computer software]. https://github.com/opensourceBIM/BIMserver, 2020.

[36] Bauhaus University Weimar. ifcPlusPlus [computer software]. http://www.ifcquery.com/, 2020.

[37] ClearEdge 3D. EdgeWise Building [computer software]. https://www.clearedge3d.com/products/edgewise-building/, 2020.

Annex: Scan+BIM Questionnaire

Question 1: I have read and agree the above information and its privacy policy and consent to the BIMERR Consortium using this information for research purposes.

Question 2: What is your professional profile?

Question 3: Does your research and development (R&D) activity require you to work simultaneously with reality capture data (point clouds and/or 2D pictures) and Building Information Models (i.e. semantically rich 3D models)?

Question 4: Are you aware of any 'off-the-shelf' (or at least easily accessible/implementable) Scan+BIM software platform?

Question 5: When thinking about your R&D needs, to which extent do you agree with the following statements about such a Scan+BIM software platform? [1 (disagree) to 3 (partially agree) to 5 (fully agree)]

- The Scan+BIM software platform should support geo-referenced data.
- The Scan+BIM software platform should be able to handle data covering large environments (e.g. urban and regional scale).
- The Scan+BIM software platform should be focused on working with open data formats.
- The Scan+BIM software platform should be open-source.

Question 6: Should the Scan+BIM software platform handle data of different nature (other than point clouds and BIM)?

Question 7: In which language should the Scan+BIM software platform be developed?

Question 8: To which level the following BIM open data formats should be supported by such a Scan+BIM software platform? [1 (not important) to 3 (would be nice) to 5 (critical)]

• IFC • IFD • MVD • BCF

Question 9: To which level the following other mesh geometry open data formats should be supported by such a Scan+BIM software platform? [1 (not important) to 3 (would be nice) to 5 (critical)]

• OBJ • PLY • STL • VRML • COLLADA

Question 10: To which extent do you agree with the following statements about BIM-related functionalities of such a Scan+BIM software platform? [1 (not important) to 3 (would be nice) to 5 (critical)]

- The Scan+BIM software platform supports editing of the geometric information of individual BIM objects (e.g. shape and location).
- The Scan+BIM software platform supports editing of the non-geometric information of individual BIM objects.
- The Scan+BIM software platform supports editing of the geometric relationships (topology) between BIM objects.
- The Scan+BIM software platform supports editing of the non-geometric relationships between BIM objects.
- The Scan+BIM software platform supports the creation of BIM objects.
- The Scan+BIM software platform supports the various BIM classifications.

Question 11: To which level the following Reality Capture open data formats should be supported by such a Scan+BIM software platform? [1 (not important) to 3 (would be nice) to 5 (critical)]

• E57 • XYZ • PTS • PTX • PLY • PNG • JPG

Question 12: To which extent do you agree with the following statements about point cloud-related functionalities of such a Scan+BIM software platform? [1 (not important) to 3 (would be nice) to 5 (critical)]

- The Scan+BIM software platform supports some common processing of point clouds (e.g. cleaning/filtering, segmentation, other).
- The Scan+BIM software platform supports adding/editing per-point information (e.g. additional scalar fields).
- The Scan+BIM software platform supports the simulation of the acquisition of point clouds (laser scanning).

Question 13: Are there other important, possibly critical point cloud-related functionalities that should be available in such a Scan+BIM software platform?

Question 14: To which extent do you agree with the following statements about 2D image-related functionalities of such a Scan+BIM software platform? [1 (not important) to 3 (would be nice) to 5 (critical)]

- The Scan+BIM software platform supports (externally) calibrated images.
- The Scan+BIM software platform supports editing calibration matrices.
- The Scan+BIM software platform supports editing images.
- The Scan+BIM software platform supports the simulation of the acquisition of images (with or without calibration matrices).

BuiltView: Integrating LiDAR and BIM for Real-Time Quality Control of Construction Projects

R. Abbas[a], F.A. Westling[a], C. Skinner[a], M. Hanus-Smith[a], A. Harris[a] and N. Kirchner[b]

[a]Engineering Excellence Group, Laing O'Rourke, Australia
[b]Presien, Australia

Email: {rabbas, fwestling, cskinner,mhanussmith,atharris}@laingorourke.com.au, nathan@presien.com

Abstract -

Global spending on rework in the trillion dollar construction industry is estimated at $570bn of direct costs and $440bn of indirect costs. The cost of rework is on the rise, and the main cause is rooted in quality deviations from construction design. Real-time or even near real-time remote progress monitoring and quality control has the potential to prevent a large portion of defects and enables quick detection and handling of errors that often go undetected for too long. Current procedure still relies on human visual inspections that are costly, in terms of time and human resources, and is subject to human error. Moreover, existing tools and services are limited in the size of data they can handle, as LiDAR data can be gigabits in size with hundreds of millions of unstructured points. The technology often fails at being robust to occlusions and other noise elements commonly found on construction sites. More sophisticated algorithms exist to perform different parts of the required analysis; however, they require a high level of expertise to implement and tailor to different use cases. In this paper, we present BuiltView, an automated progressive assurance platform that allows users to validate and document construction activities on a daily basis. BuiltView can significantly r educe r ework b y accurately and efficiently identifying BIM components and detecting discrepancies between the as-designed data and the as-built data, particularly in terms of geometric compliance. BuiltView is a powerful tool that processes billions of LiDAR points in a very efficient manner. Leveraging sophisticated analytical algorithms, BuiltView calculates accurate dimensions and generates comprehensive user-friendly reports to facilitate communication across the business. We show that BuiltView is a valuable tool for automation of quality assurance and quality control, progress tracking and documentation. Using the tool, builders can significantly reduce costly rework, increase productivity and boost transparency between different project stakeholders, thanks to objective, high-accuracy evidence.

Keywords -

LiDAR; BIM; point cloud; progressive assurance; QA/QC; rework; as-built models; project management

1 Introduction

According to McKinsey and Co, most construction projects are expected to run 20% over schedule, and 80% over budget with 25% of profit lost on defects and rework [1]. Moreover, the overall productivity of the construction industry has increased by a mere 1% over the past two decades [2]. The depressed productivity of construction projects is costing the global economy $1.6 trillion each year [3]. For major contractors in the industry, documenting and maintaining a single source of truth is essential for accountability, quality and efficiency of the work. For effective management of construction projects, this data needs to be timely (up to date), detailed and accurate. Autodesk identified frequent information capture of errors, omissions, and defects as the number one key performance indicator (KPI) for construction contractors [4].

Building information modelling (BIM) is widely used in the construction industry to enhance project performance from design to construction and facilities management (FM). Complimenting BIM, point cloud data obtained from LiDAR (Light Detection and Ranging), images, and videos are able to provide accurate and fast records of the 3D geometries of construction-related objects. Point clouds are a set of data points with (X,Y,Z) coordinates along with hardware-dependent additional information, such as reflection intensity, RGB values, and normals. LiDAR, in particular, is able to provide an accurate 3D digital representation of construction site conditions at millimetre level accuracy. The 3D laser scanning market has doubled over the past four years, evaluated now at almost $6bn, and the demand for LiDAR in construction has almost tripled in just four years (approximately 60%) [5]. With recent research showing the efficacy of LiDAR in construction and its capability to reduce rework by 25% [6], there is no doubt that laser scanning is becoming an essential part of the industry.

The value of LiDAR lies in referencing the resultant point clouds to BIM. Despite the fact that there are many existing software and service providers in this space, there is no state-of-the-art framework that can be readily adopted by building design and construction professionals. In this

space, BuiltView presents an innovative and unique solution to the integration of LiDAR with BIM for construction projects. BuiltView is a digital tool that automatically conducts deviation analysis between the as-designed model and point clouds based on as-built conditions.

By automating deviation analysis and progress checking, BuiltView has provided significant value to Laing O'Rourke through reduced rework and improved productivity (as depicted in Figure 2). Laing O'Rourke is an international engineering enterprise, with roots tracing back a century and a half. It excels at delivering large scale projects in building, transport, power, utilities, mining, and infrastructure.

Since inception, Laing O'Rourke has showcased numerous innovative research and development achievements. One recent example is BuiltView, which provides automated reports to improve client and subcontractor relationships. BuiltView is a key enabler of future digital tools such as smart contracts [7] and scan-to-BIM [8]. This paper leverages in-house case studies from past and current projects to assess the value of BuiltView compared with traditional approaches such as survey reports, spot checks, site walks, and eye-balling discrepancies for as-built model creation.

2 BuiltView

In this section, we present the workflow for BuiltView, its key distinguishing features and how it is of value to a multitude of parties of the construction industry, from subcontractors to site engineers to project managers, clients and stakeholders.

2.1 BuiltView: Main Components

BuiltView is a platform that leverages LiDAR and BIM technologies to provide up-to-date information on as-built conditions compared with the as-designed model requirements. BuiltView's value lies in automating quality checking to enable improved productivity and certainty, reduced rework, faster as-built model creation and improved decision making. The main workflow structure is as follows:

1. *Data acquisition*: The data acquisition phase is not limited to any particular hardware and can range from terrestrial laser scanners to drones and handheld mobile devices. The accuracy of the hardware relates directly to the use case it can serve. For instance, photogrammetry cannot yet support millimetre-level floor flatness analysis. Moreover, progress tracking may not require the high accuracy of survey-grade laser scans.

2. *Data Processing*: The data collected is referenced (or geo-referenced) to existing models and analysed in terms of matching objects and geometric compliance.

3. *Quality Assessment*: Quality is assessed through calculated geometric variances between the point clouds and the model, surface deviations and displacement.

4. *Progress Estimation*: Progress is estimated by comparing the amount of work completed with the amount of work planned, while taking into consideration the quality of the work and any rework required on potential defects.

5. *Visualisation*: Customised reports and dashboards are generated to tailor the visualisation of the results to the audience, e.g. project managers will be interested in overall percentages, whereas engineers will be interested in particular activities.

2.2 BuiltView: Key Innovations

There are commercial software packages and algorithms under research and development that aim at detecting and calculating variances between point clouds and models, or between point clouds themselves. With varying features, integrations and pricing models, we have found BuiltView to be the preferred solution in the following areas.

- *Accurate Metrological Algorithms*: BuiltView leverages proprietary deviation analysis algorithms that are capable of detecting objects in point clouds, in the presence of partial occlusions or other noise elements. It is a uniform platform that is independent of the method of capture. The accuracy of the calculated deviations lies solely in the accuracy of the data.

- *Intelligent Referencing and Geo-referencing*: Anyone familiar with point clouds will admit to the difficulties in referencing point clouds to models manually or even using semi-automated tools. The process is theoretically complex and empirically a combination of trial and error. BuiltView leverages intelligent algorithms that can identify different features in point clouds, for example surfaces, corners, beams, and pipes, to better register the point cloud to the model. This is a game changer for use cases where geo-referencing based on survey-grade control points is not possible, for example, in manufacturing facilities (see Section 3).

- *Intelligent Object Categorisation*: The required point cloud quality parameters are highly dependent on the construction-related element classes. For instance, building tolerances of steel beams are not the same as those of pipes or electrical services. BuiltView has built-in intelligence that allows it to produce conformance reports that are specific to every object class.

This saves engineers a tremendous amount of time in translating the results to tangible actions.

- *Robust Data Processing*: While most existing tools and services are limited in the size of data they can handle, BuiltView works with LiDAR data of the order of hundreds of millions of unstructured points with great ease by leveraging proprietary hierarchical data structuring algorithms for efficient processing and storage.

2.3 BuiltView across the Construction Project Life Cycle

Here we present a closer look at the use of BuiltView across a project's life cycle, as illustrated in Figure 1.

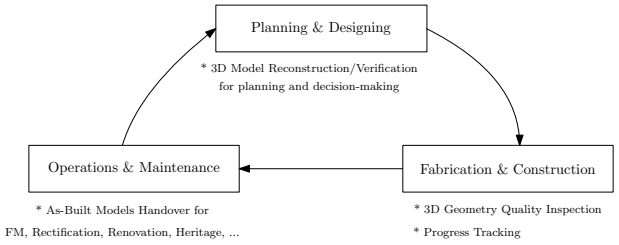

Figure 1. The benefits of BuiltView across the different phases of a construction project

1. *Planning & Design*: This is commonly known in the literature as "Scan-to-BIM", where laser scanning is conducted during the pre-construction phase for site design. This step is crucial for many projects to kick-off the design process with accurate and detailed information. Even when as-built models exist (from previous clients), we find that BuiltView is still invaluable to verify the models quickly, which will serve as a basis for all designs to come. This will be covered in detail in Section 5.
2. *Fabrication & Construction*: BuiltView continues to provide value during the construction phase as a powerful tool to document progress, defects and overall milestones. The nature of the data facilitates communication between different systems (mechanical, electrical, HVAC, etc.) and remote collaboration. The nature of the data, being free of human-error and subjectivity, also facilitates conflict resolution and accountability. This will be covered in Sections 3 and 4.
3. *Operations & Maintenance*: The advantage of laser scanning and the main goal of BuiltView is to close the loop. Laser scanning captures a very high level of detail, and this helps create a permanent as-built record for both owners and facility managers. In the end, this data can help with building operations, renovations, retrofits and future building additions and even demolitions. This will be covered in Section 5.

In the remaining part of this paper, we focus on the three main use cases of BuiltView, namely Quality Assurance and Quality Control (QA/QC), Progress Tracking and Documentation. An overview of the impact BuiltView has had on Laing O'Rourke's projects is depicted in Figure 2.

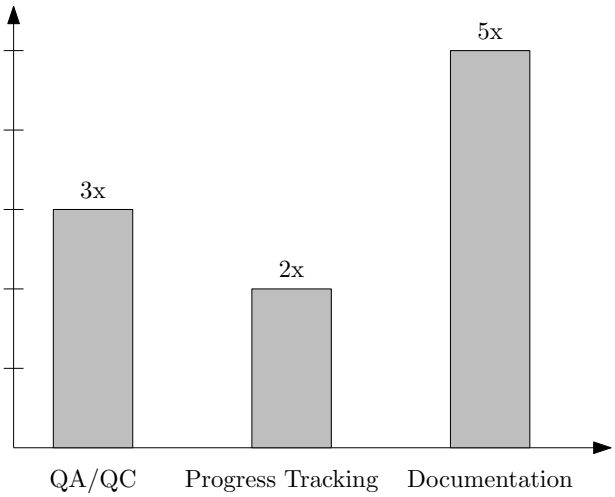

Figure 2. The time savings offered by BuiltView on Laing O'Rourke's past and current projects

3 Quality Assurance and Quality Control

3.1 Traditional QA/QC Workflow

Early identification of defects is critical for quality control because, on average, 6 to 12% of construction cost is wasted due to rework. This is exacerbated when defective components are detected late in the construction process [9]. Traditionally, QA/QC is carried out by periodic site walks and random spot checks that are documented in red-line mark-ups on 2D drawing print-outs. These hard copies are later translated manually in the office into as-built CAD drawings. In other instances, surveyors are sent out to site to check particular areas. The latter is notoriously expensive and is often subject to long turn-around times, leading to delayed detection of defects.

3.2 QA/QC Automation

With BuiltView, LiDAR scans captured with a single site walk can serve a multitude of use cases that can be automatically checked. Laing O'Rourke has successfully

Figure 3. An example of a traditional QA/QC workflow, where deviations are eyeballed in software and measurements are prone to human error.

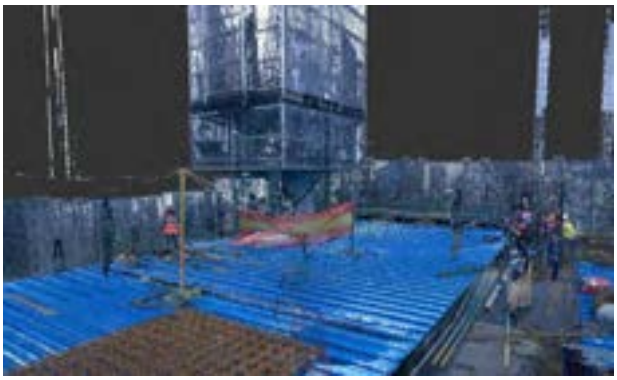

Figure 4. A scan of a 44 level high-rise under construction by Laing O'Rourke.

deployed BuiltView for a number of QA/QC checks listed below.

- *Floor Flatness and Floor Levelness*: BuiltView is capable of replacing manual slab flatness spot checks, based on spirit level and tape measure, with an automated LiDAR-based solution.
- *Reinforcement Steel Bars*: On many projects, BuiltView demonstrated extraordinary capabilities for rebar detection, identification and spacing calculation.
- *Precast Elements*: Precast elements can be checked for quality issues prior to leaving a manufacturing facility - preventing site delays and accelerating rectification.
- *Geometrical Compliance*: Most structural concrete objects - column, beam, wall and slab, and mechanical objects, pipe, duct and cable - can be accurately checked for geometric compliance using BuiltView.

3.3 QA/QC Automation Benefits

- *Floor Flatness and Floor Levelness*: By utilising BuiltView on the 44 level high-rise in North Sydney, Laing O'Rourke mitigated much of the risk associated with the works that followed structural works, for example carpet laying. A scan of the building is shown in Figure 4
- *Reinforcement Steel Bars*: BuiltView demonstrated extraordinary speed and accuracy in counting rebar, computing bar diameter and inter-distances on a large power generation project. The project consisted of 3 million tons of concrete and a total reinforcement weight of 200,000 tons In this environment, assurance checks with minimal labour was highly valued.
- *Precast Elements*: Due to time consuming manual QA processes, it is estimated only 5%-10% of precast units are surveyed in manufacturing facilities prior to delivery. An example of these units is depicted in Figure 6. With BuiltView, this percentage can reach 100% at no additional cost. In practice, BuiltView was used to run automated quality checks on bridge culverts that were scheduled to be installed on a $240 million train bridge project. By detecting defects in a single culvert early in production, BuiltView prevented defects in the remaining 40 precast replicas - preventing rework-related costs and delays.
- *Geometrical Compliance*: By leveraging BuitView as an in-house digital tool for automatically checking geometric compliance (see Figure 5), Laing O'Rourke reduced the turn-around time on as-built validation. Typically, surveyors' reports are based on spot checks of less than 10% of object area. With BuiltView, this percentage can increase to 100% at no additional cost. Moreover, with BuiltView these comprehensive and automated checks allow for a proactive approach to defect identification, allowing for an indirect reduction in total defects and consequent schedule delays.

4 Progress Tracking

4.1 Traditional Progress Tracking Workflow

The process of progress monitoring is traditionally a laborious in construction. Foreman record the work performed on construction sites on a daily and/or weekly basis. Filed reports provide a wide range of data on the available resources, the potential risks, inventories, etc. Nonetheless, these reports cannot capture 3D aspects of the construction work completed and to be completed. They are also prone to human error and aren't frequent

Figure 5. An example of a BuiltView's QA/QC workflow, where deviations are automatically calculated, removing subjectivity in measurements.

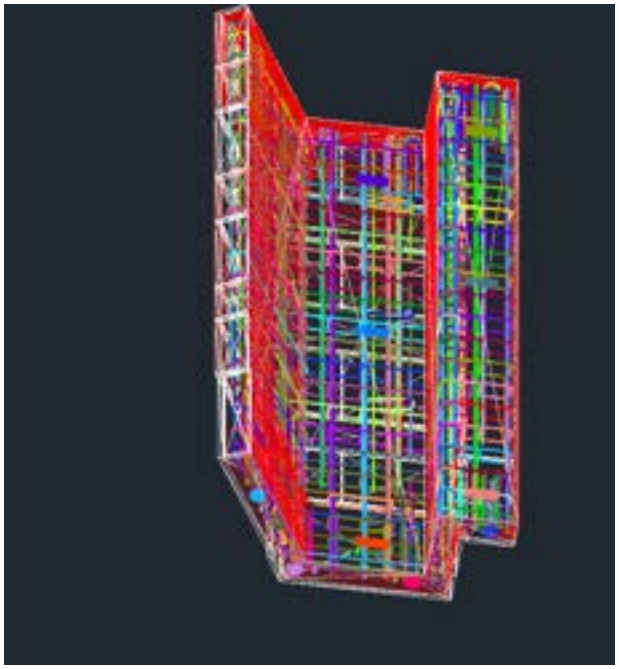

Figure 6. An example of a precast moulds processed by BuiltView for Quality Checks at Laing O'Rourke's manufacturing facility, Explore Industrial Park, UK

enough due to time and cost constraints. This is especially true when multiple site visits are required to collate all data and correct any inaccuracies. Furthermore, significant schedule delays can occur before progress reports can be analyzed and acted upon.

Taking photographs on site is another traditional method of capturing a visual record of on-going progress. Nonetheless, this 2D information is not detailed and comprehensive as 3D geometric data of as-built conditions of construction sites. Consequently, many researcher have directed their work toward generating 3D point clouds from captured photographs, with the aid of photogrammetry and computer vision. The meshes or models generated can be compared with 3D design models and used for automated progress monitoring. However, the capture & analysis process can be laborious.

4.2 Progress Tracking Automation

The traditional process for monitoring progress often prevents corrective actions from taking place in a timely manner, which eventually leads to schedule delays. BuiltView replaces most of these reports (or at least supplements them) with as-built 3D geometric information to minimise delays. By providing reliable progress data of on-site activities, Laing O'Rourke has been able to identify issues that may have caused significant delays. This information is a crucial component of a progress monitoring process as it is timely, detailed, objective, and repeatedly queried at no additional cost. [10].

4.3 Progress Tracking Automation Benefits

BuiltView provides an innovative progress tracking framework that integrates LiDAR and 4D BIM (3D BIM + schedule) [11] as well as 5D BIM (3D BIM + schedule + cost) [12]. Even when BIM is not present in an appropriate format, which is a common aspect of infrastructure and linear projects, BuiltView provides scan to scan comparisons using proprietary point-based algorithm to report temporal changes on projects[13].

Aside from the traditional progress checks of built elements, Laing O'Rourke was successful in tracking earthworks using BuiltView on a 155 km highway upgrade project, one of the largest public infrastructure projects in Australia. By running daily scans and progress checks, the project was capable of accurately detecting schedule delays and make data-based decisions to rectify the issues, boosting overall productivity and mitigating potential budget overruns.

5 BuiltView for Fast, Accurate and Timely Documentation

Data acquisition time for LiDAR in comparison to multiple site walks can be 2-10x faster [14] depending on the hardware used (terrestrial tripods, drones or mobile scanners). As a result, construction professionals are potentially able to document 10x the amount of information [14]. Intuitively, with more high-quality information, data-based decision making becomes easier and more efficient. With BuiltView's high-end processing capabilities, the data size can be reduced by half through de-noising and de-cluttering point clouds and by creating meshes and

Figure 7. An example of point clouds of construction sites, cluttered with equipment and moving personnel.

Figure 8. Multi-Level Buildings can be captured in one day with terrestrial LiDAR scanners, and in under an hour with mobile LiDAR scanners (see Figure 8). Using the correct hardware for the correct use case is a key reason for Laing O'Rourke's success in implementing BuiltView

as-built models. An example of cluttered point clouds is shown in Figure 7.

5.1 As-Built Models for Pre-construction Phase

During the pre-construction phase, the various parties involved in a project collectively define the milestones of the project, based on the expected duration of completion and the available budget. With LiDAR data, heritage buildings were captured with great detail on a number of Australian heritage buildings renewal programs. BuiltView's fast and accurate validation of existing as-built models prior to construction using LiDAR data was invaluable, as it served as the foundation for all works to come. Capturing the intricate architecture of these legacy buildings would have otherwise proven prohibitively slow.

In short, the engineering and risk analysis conducted before starting construction is significantly improved by leveraging accurate as-built data. BuiltView's intelligent system is capable of facilitating the production of as-built models, which clearly improves project performance. In fact, according to recent studies [15], when project definition work is conducted properly, both project schedules and costs are reduced by approximately 20%.

5.2 As-Built Models during Construction Phase

There is a growing requirement for contractors to deliver as-built models during the construction phase or projects, as they progress from one milestone to the next. To streamline this, BuiltView provides a semi-automated workflow for updating the position of BIM components based on point clouds. Compared with manual updates, BuiltView is capable of quickly producing accurate conformance reports that reduce the amount of time designers need to spend eye-balling point clouds to detect variances (see Figure 3. It also reduces the amount of time project engineers have to spend verifying the resulting as-built model from weeks to a few days.

5.3 As-Built Models for Post-construction Phase

It is evident that handover of 3D as-built documentation, whether in the form of a model or a point cloud, is becoming increasingly common in construction contracts. As research and case studies continue to prove the value of objective as-built data, this trend will no doubt continue to grow. As a facilitator of this data, BuiltView is invaluable for closing the loop on learning from one project to the next. We expect opportunities will continue to arise for BuiltView to reduce rework costs, improve productivity and facilitate transparency and accountability within construction. Most recently, following the devastating 2019 Australian Bushfire Season, LiDAR was used to rapidly capture a massive geographic extent for detailed mapping and documentation of the impact of these fires [16]. Laing O'Rourke was appointed by the New South Wales Government of Australia to undertake the first phase of fire recovery clean-up works, and it will leverage BuiltView to rebuild the local community assets with extraordinary performance.

6 Conclusion

In this paper we presented BuiltView, a digital progressive assurance tool that provides construction projects with accurate and timely verification of as-built conditions when compared with design. The tool leverages LiDAR and BIM technologies to provide insights that have been proven useful across multiple project phases and disciplines. Through real-life use cases undertaken at multi-million dollar projects for the international contractor Laing O'Rourke, we showed how BuiltView has been an invaluable asset for reducing rework, boosting productivity, and providing indisputable documentation. By providing an accurate, regular digital representation of

as-built conditions, we believe BuiltView will be a key enabler for digital twins in the near future. Moreover, by providing an accurate, objective measure of construction progress, we forecast that BuiltView will play a key role in enabling the industry-changing efficiencies of smart digital contracts.

References

[1] Rajat Agarwal, Shankar Chandrasekaran, and Mukund Sridhar. Imagining construction's digital future. *McKinsey & Company*, 2016.

[2] Filipe Barbosa, Jonathan Woetzel, Jan Mischke, Maria João Ribeirinho, Mukund Sridhar, Matthew Parsons, Nick Bertram, and Stephanie Brown. Reinventing construction: a route to higher productivity. *McKinsey Global Institute*, 2017.

[3] Lynn Langmade. 7 easy ways to increase construction productivity. *PlanGrid*, 2018.

[4] [report] the kpis of construction. On-line: `http://bim360resources.autodesk.com/optimizing-your-construction-kpi/kpis-of-construction-report`, 04/11/2019.

[5] Industry equipment study. *Survey & Mapping CLEAReport*, 2019.

[6] Qian Wang and Min-Koo Kim. Applications of 3d point cloud data in the construction industry: A fifteen-year review from 2004 to 2018. *Advanced Engineering Informatics*, 39:306–319, 2019.

[7] Jim Mason. Intelligent contracts and the construction industry. *Journal of Legal Affairs and Dispute Resolution in Engineering and Construction*, 9(3): 04517012, 2017.

[8] Richard Laing, Marianthi Leon, John Isaacs, and D Georgiev. Scan to bim: the development of a clear workflow for the incorporation of point clouds within a bim environment. *WIT Transactions on The Built Environment*, 149:279–288, 2015.

[9] Jun Wang, Weizhuo Sun, Wenchi Shou, Xiangyu Wang, Changzhi Wu, Heap-Yih Chong, Yan Liu, and Cenfei Sun. Integrating bim and lidar for real-time construction quality control. *Journal of Intelligent & Robotic Systems*, 79(3-4):417–432, 2015.

[10] Sara Shirowzhan, Samad ME Sepasgozar, Heng Li, John Trinder, and Pingbo Tang. Comparative analysis of machine learning and point-based algorithms for detecting 3d changes in buildings over time using bi-temporal lidar data. *Automation in Construction*, 105:102841, 2019.

[11] Julie Jupp. 4d bim for environmental planning and management. *Procedia engineering*, 180:190–201, 2017.

[12] David Mitchell. 5d bim: Creating cost certainty and better buildings. *RICS COBRA*, pages 1–9, 2012.

[13] Nisha Puri and Yelda Turkan. Bridge construction progress monitoring using lidar and 4d design models. *Automation in Construction*, 109:102961, 2020.

[14] As-builts from point clouds: How maxwell construction is advancing building documentation. On-line:`http://bimlearningcenter.com/`.

[15] James Taylor. *Project scheduling and cost control: Planning, monitoring and controlling the baseline*. J. Ross Publishing, 2008.

[16] Owen F Price and Christopher E Gordon. The potential for lidar technology to map fire fuel hazard over large areas of australian forest. *Journal of environmental management*, 181:663–673, 2016.

Single Shared Model Approach for Building Information Modelling

Simo Ruokamo[a] and Rauno Heikkilä[b]

[a]University of Oulu, Finland & Enterprixe Software Ltd, Finland
[b]University of Oulu, Finland
E-mail: simo.ruokamo@gmail.com, rauno.heikkila@oulu.fi

Abstract –

The current practice for information sharing with building information modelling (BIM) is a distributed data sharing based on conversions. Conversions are problematic due to data loss, redundancy, and conflicting information. A single data schema used by all applications is a requisite for a conversion-free data collaboration. In the study, a software development kit (SDK) was developed, which implements required features and guarantees compatibility between BIM programs. Three independent applications 3DTrussme, Leonardo, and Viewer were developed using SDK. A cloud service for handling the shared model was implemented. In the experiments, Leonardo was used for modelling walls, 3DTrussme for truss design, and Viewer for model viewing. All three applications were using the same shared model on the cloud.

In the experiments, the information exchange occurred without conversions and all data was saved only once on the cloud database. Without conversions and duplicates less conflicts and redundancies occurred, which lead to better data integrity and integration. Using SDK, there was no technical barrier for applications to join the single shared model ecosystem, but a drawback was that existing BIM programs are not compatible without remarkable changes. The performance was acceptable on the test run, but in real use, the size of the model and the number of applications and users, will be much larger. However, a conversion-free single shared model approach can be a possible trend to the development of the next generation BIM as well as a potential alternative for current data sharing methods using distributed files, conversions, and linked data.

Keywords –

Building Information Modelling; Data Conversion; Cloud Services

1 Introduction

The evolution of the building design has developed from handmade paper drawings to a fully digitalized process using computers. In the 1970s, the first 2D CAD (Computer Aided Design) software came to the market and in the 1980s, first pioneers developed 3D design applications for building design. Acronym BIM (Building Information Modelling) is nowadays commonly used for the digitalized information handling and it was probably Jerry Laiserin who first introduced the term BIM [1,2].

A successful collaboration between all stakeholders requires an efficient and functional sharing of the building information [3]. The amount of the BIM data grows significantly during the design and construction stages of the building project. After the construction stage, new information is still created but not at the same rate. Moreover, the flow of the data substantially breaks off when the construction is completed [4]. A continuous information flow is a necessity for improving the data utilizing within facility management [5].

The prevailing practice for data exchange is distributed data management (DDM) approach based on conversions. In general, an exchange format is used for data transfer. Using an exchange format requires two conversions between two applications, but reduces the total amount of import and export formats each application needs to implement [6]. Direct data exchange between native formats requires only one conversion and is less error prone but, on the other hand, each supported format must be programmed.

A conversion-free data exchange requires the use of only one data format. To fully avoid the problem of overlapping and conflicting information, a single data schema is not enough. Separate models, although in the same format, can still include inconsistent data. With the single shared model approach (SSM) no conversions are needed and all information is saved once, which reduces the data complexity and improves the data integrity and integration. The challenge with the single model is

concurrent changes made by different users. Rules must exist for defining which change is valid, when overlapping modifications happen. Figure 1 illustrates the different exchange methods from the perspective of conversions.

Figure 1.The basic differences for the needed conversions with the different data exchange methods. With application to application, the total number of conversions is the largest, whereas with a single shared model no conversions are made.

2 Development of the single shared building information modelling

For a regular user it is common to mix applications, data models, and storages. However, they have their own functions and objectives from a software technology point of view. When application is running, information is available at the main memory of the computer. When application is closed, the data must be stored to permanent storage which can retain its information even when powered off. The interconnection between the permanent storage and application is the data model. A file or database is read into program's run time memory as a data model, then modified during the application run and saved back to the permanent storage.

2.1 Data model and storage

In today's software technology, the common practice for a data model is an object oriented approach [7]. Each different object is encoded as a software class and a requisite set of classes constitutes the whole data model. The class instance is an object that is created from the definition of the class into the data model. Instances get a globally unique identifier when they are created into the data model and one software class can be instantiated as multiple objects, each having a different unique identifier.

The data on the permanent storage is read to object instances and saved back. For instantiating the correct class to the data model the definition of the class must also be saved on the storage. The class instantiating method can be either static or dynamic. With static binding (called also early binding), code of classes must be available when the program is compiled and built. The drawback of the static binding is that every change or addition of a class requires an updated version of the application. Modern programming languages, like Microsoft C# [8], support dynamic binding (called also late binding), which requires the availability of the class not until the application is started. That is a significant difference and makes changes into data model classes much more flexible. A class addition or change does not require a new version of the application.

In a building data model, classes and instances carry the information as a collection of value-name pairs. The IFC (Industry Foundation Classes) is a standardized object-based data format and model maintained by an international non-profit organization called buildingSMART. With IFC, value-name pairs are called property sets [9]. Term attribute is also commonly used with object-based data models. List of classes and properties are not constant which brings up the challenge of the data compatibility. Standards are common languages which realise the universal and admitted understanding for the content of the building information. But standards change slowly and are not adequate for commercial BIM applications since data content advancement is an endless and all the time running process. Therefore the flexibility and extensibility of the information content are key features for the single shared data model. Supporting standardised data is advisable, but by allowing applications to freely specify additional information content, technical barriers are eliminated from the use of a single data model schema. Both the data model and permanent storage must implement freely extendable data content.

The permanent storage can be a database or a file. A database has a more organised data schema and allows partial data access and sharing with several users. The following three alternatives are technically possible as a database schema for storing the data of classes:

1. Separate table for each class with a separate column for each attribute. This schema has traditionally been used.
2. The vertical database schema also called an entity-attribute-value model (EAV) [10].
3. XML schema, where whole data of the class is packed as XML data.

Juola [11] implemented all the three alternatives using a SQL Server database. With separate table for every class it is almost unfeasible to keep tables and columns up-to-date due class changes. Queries are very complicated with the entity-attribute-value schema. The result was, that the XML schema was best suitable for a building data model having always evolving content.

The number of object instances in a data model can grow huge. Some kind of organising and grouping is needed for maintaining the fluent manageability of the model. Objects can be organised based on their material, structural behaviour, type, name, position, feature, or some other data. As a result, the amount of active objects is decreased making the handling of the model more flexible. IFC supports Model View Definition (MVD and Information Delivery Manual (IDM) standards for defining a data subset [12]. Several studies have been made for extracting IFC partial model based on MVD [13].

Hierarchical organisation is a well-known arrangement method, but that method has very rarely been applied among AEC/FM applications. The hierarchical arrangement naturally enables a model division into partial models and hierarchy is simply constructed by defining a parent object for every object. A partial model is then made up of an object and all its descendants at all sub hierarchy levels. The IFC data model has a static and fixed hierarchy of *Project → Site → Building → BuildingStorey → Space* [9]. According to Singh, Gu and Wang [14] a static hierarchy is inadequate and the ordering should be flexible for fulfilling the requirements of users.

2.2 Data sharing

A data concurrency control is essential for the single shared data model. Simultaneous changes to the same data can be handled by an optimistic or pessimistic method [15]. With an optimistic control, it is assumed that conflicting data changes are rare and can be resolved. The pessimistic control is based on data locking, which fully prevents any concurrent data editing. The validity, reliability, and consistency of the information in the building model is best guaranteed by the pessimistic method. Locking the whole model is not realistic, but only a part of the model can be reserved for one user at one time. The hierarchical model arrangement implements partial models that can be reserved and released. The single data model system and hierarchical arrangement with reserving and releasing partial models together make up a pessimistic data concurrency control system for ensuring the validity, reliability, and consistency of the information in the building model.

With the single shared model, all information must be available for all stakeholders without delays and conversions continuously. In the current internet world that is best achieved with a cloud based system. Using the cloud database only is technically possible, but a synchronised local copy gives next advantages:

- Enables incremental updates reducing the amount and size of data transfers [9]. By keeping a change log, only changed data needs to be synchronized between the cloud and local storage.
- The reserved partial model can be first saved to the local storage before publishing it to the cloud. Unfinished work is then not available for other participants.
- Offline working without a connection to the internet is possible with the local synchronized storage.

The cloud storage cannot be accessed like the local storage. User rights on the server cannot be as extensive as they are on the local computer. It would be a clear risk for the security and data integrity to allow public and direct read-write access to the server storage for all. A cloud service implementing only needed functionality ensures that no data corruption occurs due to a false operation. For a safe and secure access to the cloud storage, next functions need to be implemented on the cloud service:

1. Registration of user.
2. Establishing a new model.
3. Getting a list of models available for user
4. Connecting to a model
5. Load for downloading the whole or partial model from the cloud to the local storage.
6. Reservation of the partial model for editing. Reserved part is locked permitting only reading for other users.
7. Releasing and publishing the reserved partial model to the cloud storage.
8. Get changes due to releases made by other users.
9. Adding a new node to the model hierarchy tree.
10. Removing a node form the model hierarchy tree.
11. Disconnect from the shared model and logout from the cloud service.

2.3 Programming principles of the single shared data model system

A derivation programming technique is a common practice with the coding of classes. With derivation, duplicate code for similar classes is avoided, since a derived class inherits everything as default from the parent. Derived classes can develop the inherited content further as much as needed. The amount of software data model classes that are needed during the whole life-cycle of the building is vast. Thus, the development and maintenance of data classes are not tasks for a single software house. However, for ensuring compatibility, base public classes used by all developers are needed. The derivation of new classes must start from public classes, which must implement the required functionality for forcing the compatibility between all developed applications. Especially reading the permanent storage as a data model into runtime memory of the application and saving it back are operations that must only exist on

public classes. Secondly, classes for geometry must be implemented as public classes so that applications can also view non-public class objects that are defined by other applications.

For uniformity, common understanding and ability to co-operate, the amount of public classes should be as large as possible. Many organisations in various countries are developing various BIM standards for diverse purposes [16] and the public classes can be seen as the standardised part. BuildingSMART International has published a few standards for building information content and data exchange [17]. However, also non-standard classes can be made publicly available.

2.4 Arrangement and execution of the experimentation

For a full scale testing of the single shared model system, a cloud service and applications were developed. Cloud service was running on a Windows Server operating system. The web service was implemented using Windows Communication Foundation (WCF) [8]. Storage system used was a relational database Microsoft SQL Server. For the development of applications a public software development kit (SDK) was created including the next four assemblies:

1. Base public classes (BPC) assembly includes base data model classes from which all application specific classes must be derived.
2. A local storage for client (LSC) assembly offers a synchronised local storage for applications.
3. A model toolkit for the client (MTC) implements functionality for synchronising the local and cloud storage.
4. A web service toolkit for the client (WSTC) is a helper assembly simplifying the use of the web service functions.

Three applications were developed using the public SDK. *3DTrussME* is a 3D modelling and structural analysis software for wooden trusses. It has been the first and main testing application for the single shared model system and has a large application specific class library. *3DTrussME* is owned by a Finnish company, Ristek Oy, and the programming is carried out by another Finnish company, Enterprixe Software Ltd [18]. *3DTrussME* is a commercial application currently used in Finland, Norway and Estonia. *Leonardo* is a 3D design application for concrete structures. The development of *Leonardo* is ongoing and it is not yet available for a practical use. The third application used in testing was *Viewer*, which was only used for viewing the model. Figure 2 shows the general arrangement of the testing environment.

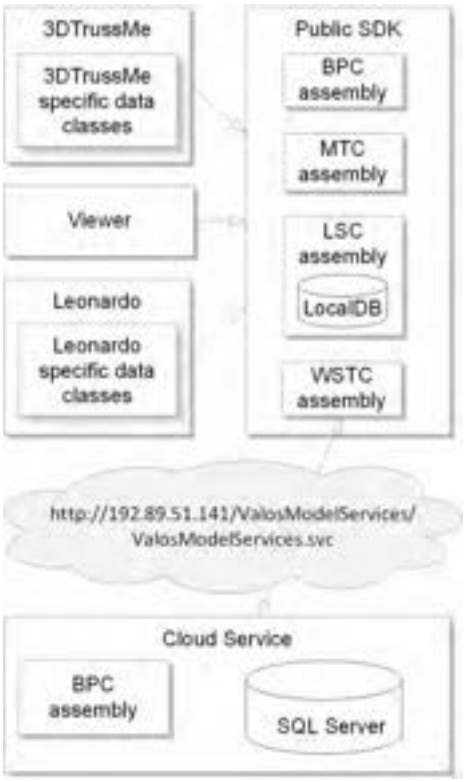

Figure 2. A diagram showing the general arrangement of the testing environment with three applications, public SDK package, and cloud service.

Three users were participating in the test event, one for each application. All three applications were connected to the same shared model on the cloud. *3DTrussME* was used for truss design, *Leonardo* for modelling walls and *Viewer* for viewing the model. The pessimistic concurrency control was in use and partial models were reserved and released. During the test, *Leonardo* data classes were further developed without any compatibility problems for other two applications. The test was executed with steps shown in the next list.

1. Registration of users.
2. A model was established on the cloud database and access to the model for users was granted.
3. User #1 using *3DTrussME* reserved the model, created the base hierarchy and released the model. Fig. 3 shows a screen snapshot after step #3.
4. User #2 using *Leonardo* reserved the *Walls* subtree and started modelling walls. User #1 saw the reservation when getting the latest from the cloud.
5. User #2 finished the modelling of walls, released the node *Walls* and local changes were updated to the cloud model. User #1 updated changes from the cloud and saw the modelled walls. *Leonardo* was using a private wall class, but by using a public wall class instead, walls were available at *3DTrussMe*.

6. User #1 reserved the node *Roof* for truss modelling. User #3 started *Viewer* and saw walls and reservation of the *Roof* node.
7. User #1 noticed that one wall was at wrong position, reserved it, made the correction, and released it.
8. The private data model of Leonardo was further developed by adding new attributes to the wall and by creating a new column class. User #2 started to use the new version of *Leonardo* and updated local model. No compatibility problems or data corruption occurred although *3DTrussMe* used older public wall class and *Leonardo* new changed wall class.
9. User #2 reserved *Walls* and *Columns* node, continued modelling and released nodes.
10. User #1 released Roof node.
11. All users updated their local model and can saw the whole model.
12. All users disconnected from the model and closed applications.

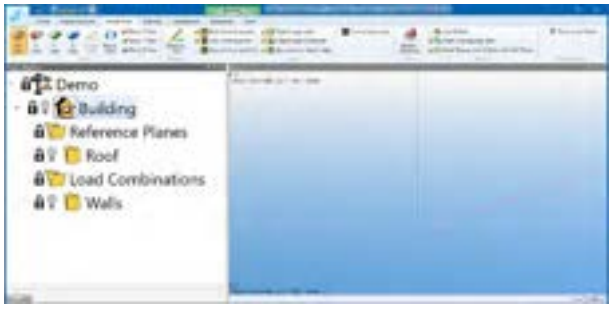

Figure 3. Basic hierarchy after step #3. All nodes are not reserved for changes which is marked as a closed black lock icon in the project explorer tree.

3 Results

As a result of the test execution, a shared model was built up on the cloud. Three applications were using the same shared model on the cloud and all data sharing occurred without conversions and data defects. Figure 4 shows the final model after the execution of the test. The permanent outcome of the executed test was the data stored in the cloud database. Totally five tables were used for data storing:

1. User table for registered users.
2. Model access table for defining the access of users to model.
3. Session table for connected users. With a connection to the model each user gets a session id that identifies the access to one model. Session ids are not permanent and are used instead of credentials after the connection to the model. Session ids are invalidated with disconnect or after defined unused timeout.
4. Event table for the model established, reservation and release events. Events enable the bookkeeping of reserved nodes and incremental updates.
5. Model table for the building model data.

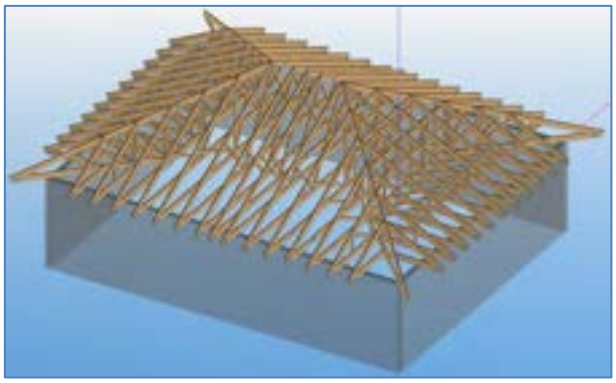

Figure 4. Final model after the execution of the test on *3DTrussME* application.

Just one data format is compulsory for the conversion-free data exchange used. The key points of the specification for a freely expandable data model schema keeping the compatibility backward and forward are as follows:

- The data model schema consists of public part and private application specific portions. All private classes must be derived from public classes.
- Data carriers and all data saving into and reading from the permanent storage are handled by public classes.
- Classes are instantiated using the dynamic binding method.
- Schemas of the data model and permanent storage must enable backward and forward compatibility allowing free changes to the content and number of data classes. This is achieved with a dynamic binding and XML storage format.
- A software development kit (SDK) implements all the key points of this list, and thus, applications developed using SDK automatically realize all key points and are compatible with each other.

Data duplicates are not prevented by using only one data model and storage structure. A single model approach accessed simultaneously by all participants is needed for removing the overlapping information. The following key elements are required for a workable single shared model system:

- The single shared database is placed on the cloud, enabling an equal access for all participants.

- Access control is implemented limiting the entry only for registered and authorized users. Furthermore, access to models per user is controlled.
- All connections to the shared cloud model are performed through a web service that has the required functionality. It is a security risk to allow direct access to the database, which may lead to illegal changes in the database.
- A pessimistic data concurrency control is used.
- An event log keeps track of reservations, releases and data change events enabling the monitoring of the reservation state and incremental updates of the local storage.
- The model arrangement is realized using a hierarchical approach which divides model into numerous and varying size partial models. Those subtrees can be used as units for reservation and for limiting the size of the model that is handled at a time. The hierarchical arrangement is free and the model can be divided as example by design discipline, storey, space or element type using one or combined dimension.
- SDK is used for the development of applications enforcing the compatibility and SDK also eases establishing connections to the single shared model.

4 Conclusions

The presented single data model system is available for all new and old BIM applications. An SDK is free and contains base classes as a start point for the development of application-specific data content. The schema of the data model is version-free allowing changes and additions without breaking the compatibility. In summary, the presented method makes up a conversion-free data exchange solution based on a single extendable data model schema. It is self-explanatory that without conversions all conversion defects will be eliminated. Data duplicates will vanish when a single model schema is extended as a single shared model approach. The data integrity and integration improve when data sharing occurs without conversions and when no overlapping information exists.

To obtain the greatest benefit from the single shared model, software from various disciplines should be available. There is no limit regarding what types of applications can join the ecosystem: the only requirement is to use an SDK. Anyway, many issues can be raised up for the wider industrial use. The incompatibility with the current convention, needed investments and lack of interest hinder the expansion. The reputation and reliability of a new technology is low in the beginning. Rogers [19] divides technology adopters into innovators (2.5%), early adopters (13.5%), early majority (34%), late majority (34%), and laggards (16%). Evidently, the conversion-free single shared model approach needs innovators for the start of the technology expansion.

No commercial single model system for multidisciplinary building information is available. Systems for sharing a model between the same applications have been developed, but none can cross the application boundary. The objective for model sharing with *Tekla*, *Archicad* and *Revit* is to enable multiple people to work simultaneously with the same model. There is no reason to limit the model sharing only between the same applications as long as user and access control prevents conflicting and illegal changes. Indeed, according to Lu, Wu, Chang and Li [21] , there is lack of BIM standards for model integration and management by multidisciplinary teams.

It is a common opinion among the AEC industry and BIM scientists that a single model BIM is an unfeasible solution. According to Day [22], a single building model is only a daydream. On the other hand, Howard and Björk [23] state that a single BIM is the holy grail, but there might not be willingness to achieve it. According to Turk [24], a centralized shared database is impossible but in the future, BIM will approach it. The reasoning for this is mostly not presented by these authors, but model differences between disciplines and the size of model are noted. Because of the rejection of the single BIM model, no research has been conducted of a true single shared model system. Under the umbrella term ‘single BIM’ scientific articles can be found, but they see single BIM as a common repository for distributed data sources. A cloud service or a single address to separate files is only one data delivery tool for distributed information. A true single model system is a shared database that can be accessed simultaneously by several users, and every piece of data is stored only once.

According to Johnson [25], the complexity of design tasks and software evolution raise questions about a single model solution. It is true that tasks performed by engineers and consultants are complex and various. Many kinds of applications are used for design tasks and all software is evolving continuously. However, is that complexity troublesome only for the single shared model approach? The distributed data sharing system uses many data formats and conversions. Is this more complex when compared with the single shared model operating without conversions? Johnson [25] list the next issues for alleviating the skepticism against “One BIM”:

- An open source vendor-neutral elastic data structure.
- Enabling the interoperation of applications from multiple vendors.
- Sharing data in the design ecosystem without explicit import or export.
- Supporting different kind users, tasks, workflows, and stages in the design process.

The presented single shared approach will implement all the above items, but a significant adjustment to current BIM practices and processes must come true.

According to Miettinen and Paavola [2], the benefits of using BIM is often reported by researchers and project participants, but the impact of BIM is difficult to isolate from the success of the entire project. Moreover, increases in the productivity in the construction business have been marginal when compared with other industry sectors [26]. Assuming, that information technology has a notable influence on the improvement of productivity, why has digitalization succeeded in other industry sectors but not in the construction business?

The testing of a software system is not a one-time process. In the test run only three applications and users were involved, but in the reality, many more applications are used with BIM. No technical limit for the number of applications exist, but a growing number of applications and users accessing the same model concurrently can slow down the performance

Microsoft SQL server was used as the cloud storage system and the maximum size of a SQL Server database is 524 272 terabytes [8], which is an incredible amount of information. Before that maximum size limit is reached, other performance issues will probably arise. Client applications do not need to make calls to the cloud service non-stop, but database queries can slow down the cloud service when the database is large. In the test run, there were only three users and one model on the cloud, which naturally cannot show much of the performance for real projects. Microsoft LocalDB was used as a local storage system on the client side. The maximum size of the LocalDB database is 10 GB [8] which is much less than the maximum size of a SQL Server database. Local storage capacity will most obviously be the first bottleneck before any performance problems on the cloud service appear.

An internet service provider (ISP) and independent software vendor (ISV) for web service are needed for offering the cloud service for the single shared model. Figure 5 shows all the major players of the building project. ISVs should not hold a monopoly position in their field of activity. Application development is freely available for all enabling multiple software on the same purpose. Developing the web service can also be done separately by multiple ISVs. There can only exist one public SDK and a private commercial enterprise is not the best ISV for SDK. A public non-profit corporation or alliance would be a better ISV operator for the public SDK.

Allowing all users to change all parts of the model after reservation might not be a desired course of action. As example architects do not usually allow designers from other disciplines to edit architectural plans. By organizing users to groups, more detailed user rights can be implemented. Each group can reserve partial models and control usage rights for other groups. When using both user and group access control the partial model availability can be restricted on many levels.

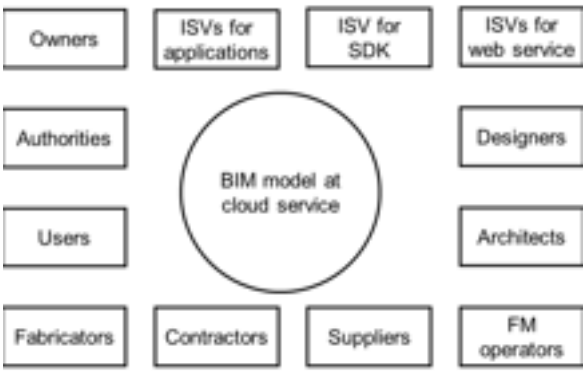

Figure 5. The players around BIM model during the whole life-cycle of the building project.

The main weakness of the single shared model approach is its incompatibility with the currently used data formats. All data classes in current applications must be redone for full compatibility which is likely a threshold for most software houses. Therefore, conversions from existing formats are needed for lowering the obstacle to the presented new single model method; otherwise, it will be isolated without any links to existing systems. Rewriting all IFC classes by starting the derivation from BPC classes could be one solution. After that, importing the IFC files could be done. However, exporting to IFC cannot properly support all the data on a single shared model using a version-free data schema since IFC is not a true open and extendable data format. IFC implements adding new property sets for the objects and the use of IfcProxy for entities that are not defined by IFC [27]. But, this will end up as an outstanding amount of IfcProxies having fully different content if all the native data by all applications is exported. Additionally, updating the schema of the IFC standard will break the compatibility backward and forward, requiring a new version of every application that is using IFC.

References

[1] Laiserin J. LaiserinLetter. 2002; Online: http://www.laiserin.com/features/issue15/feature01.php, Accessed 2013.

[2] Miettinen R, Paavola S. Beyond the BIM utopia: Approaches to the development and implementation of building information modeling. *Automation in Construction*. 2014 7;43:84-91.

[3] Shen W, Hao Q, Mak H, Neelamkavil J, Xie H, Dickinson J, et al. Systems integration and collaboration in architecture, engineering, construction, and facilities management: A review. *Advanced Engineering Informatics* 2010 4; 24(2):196-207.

[4] Xu X, Ma L, Ding L. A framework for BIM-enabled life-cycle information management of construction project. *International Journal of Advanced Robotics Systems* 2014; 11(1).

[5] Nicał AK, Wodyński W. Enhancing Facility Management through BIM 6D. *Procedia Engineering* 2016; 164:299-306.

[6] Isikdag U, Underwood J. Two design patterns for facilitating Building Information Model-based synchronous collaboration. *Automation in Construction* 2010; 19:544-53.

[7] Berdonosov V, Zhivotova A, Sycheva T. TRIZ Evolution of the Object-Oriented Programming Languages. *Procedia Engineering* 2015; 131:333-42.

[8] Microsoft Corporation. Microsoft developer network. 2019; Online: https://msdn.microsoft.com. Accessed 2019.

[9] Eastman C, Teicholz P, Sacks R, Liston K. *BIM Handbook*. Hoboken, New Jersey: John Wiley & Sons, Inc.; 2011.

[10] Nadkarni PM, Marenco L, Chen R, Skoufos E, Shepherd G, Miller P. Organization of heterogeneous scientific data using the EAV/CR representation. *Journal of the American Informatics Association*. 1999; 6(6):478-93.

[11] Rauno Juola. *Rakennuksen tietomallin palvelinpohjaisen tietokannan tallennusratkaisu*. Oulu: University of Oulu, Faculty of Information Technology and Electrical Engineering, Department of Computer Science and Engineering, Computer Science; 2014.

[12] Lee Y, Eastman CM, Solihin W. An ontology-based approach for developing data exchange requirements and model views of building information modeling. *Advanced Engineering Informatics* 2016 8; 30(3):354-67.

[13] Won J, Lee G, Cho C. No-Schema Algorithm for Extracting a Partial Model from an IFC Instance Model. *Journal of Computing in Civil Engineering*. 2013 NOV 1; 27(6):585-92.

[14] Singh V, Gu N, Wang X. A theoretical framework of a BIM-based multi-disciplinary collaboration platform. Automation in Construction 2011 3; 20(2):134-44.

[15] Wette C, Pierre S, Conan J. A comparative study of some concurrency control algorithms for cluster-based communication networks. *Computers & Electrical Engineering* 2004; 30:615-36.

[16] Barbosa MJ, Pauwels P, Ferreira V, Mateus L. Towards increased BIM usage for existing building interventions. *Structural Survey*. 2016;34(2):168-90.

[17] BuildingSMART. buildingSMART International.; Online: http://www.buildingsmart-tech.org/, Accessed 2019.

[18] Jarmo Kajava. *Development of the three-dimensional nail plate structure design software*. Oulu: University of Oulu, Faculty of Technology, Mechanical Engineering; 2017.

[19] Rogers EM. Diffusion of Innovations, 5th edition. New York, USA: Free Press; 2003.

[20] Wong J, Wang X, Li H, Chan G, Li H. A review of cloud-based bim technology in the construction sector. *Journal of Information Technology in Construction*. 2014;19:281-91.

[21] Lu Y, Wu Z, Chang R, Li Y. Building Information Modeling (BIM) for green buildings: A critical review and future directions. *Automation in Construction*. 2017; 83:134-48.

[22] Day M. The trouble with BIM. AECMagazine 2011;.

[23] Howard R, Björk B. Building information modelling – Experts' views on standardisation and industry deployment. *Advanced Engineering Informatics* 2008 4; 22(2):271-80.

[24] Turk Ž. Ten questions concerning building information modelling. *Building and Environment* 2016; 107:274-84.

[25] Johnson BR. One BIM to Rule Them All: Future Reality or Myth? In: Kensek KM, Noble DE, editors. *Building Infromation Modeling: BIM in Current and Future Practice*: John Wiley & Sons; 2014, p. 175-185.

[26] Koskenvesa A. Rakennustyön tuottavuus 1975-2010. *Rakentajan kalenteri* 2011: Rakennustieto Oy; 2011, p. 138-146.

[27] Borrmann A, Beetz J, Koch C, Liebich T, Muhic S. Industry Foundation Classes: A Standardization Data Model for the Vendor-Neutral Exchange of Digital Building Models. In: Borrmann A, König M, Koch C, Beetz J, editors. *Building Information Modeling: Technology Foundations and Industry Practice*: Springer International Publishing AG; 2018, p. 81-126.

Parametric or Non-parametric? Understanding the Inherent Trade-offs between Forms of Object Representation

Chris Rausch[a], Yinghui Zhao[a], Carl Haas[a]
[a]Department of Civil and Environmental Engineering, University of Waterloo
E-mail: chris.rausch@uwaterloo.ca , yinghui.zhao@uwaterloo.ca, chaas@uwaterloo.ca

Abstract –

The need for efficient computing in construction modelling and analysis workflows often requires making tradeoffs between the inherent advantages and disadvantages of different datatypes being generated and managed. This is notably observed in geometry reconstruction (e.g., scan-to-BIM, reverse engineering, etc.), where a tradeoff often occurs between computational efficiency and the choice between increased semantic enrichment or increased representational accuracy (often both cannot be achieved simultaneously). This dichotomy can be generalized as a choice or tradeoff between parametric and non-parametric object representation forms. This paper presents a simple conceptual model for characterizing the datatypes used for representing and defining construction geometry to understand key tradeoffs that exist. First, we survey existing literature across multiple domains to identify and distill key attributes used in characterization according to the terms parametric and non-parametric. Then, we develop and illustrate a conceptual model using an analogy to mathematical expressions vs. discrete digital approximations employed in computer vision (e.g., Gaussian kernel, Hough Transform, and Scale Invariant Feature Transform (SIFT) algorithm). Finally, we outline future research opportunities for improving the state of object representation.

Keywords –

Building Information Modelling; 3D Point Clouds; Data Managements; Geometric Accuracy; Digital Twin; Construction Geometry

1 Introduction

In construction workflows, the virtual representation of physical objects forms the basis for design, communication of product and process requirements, and as-built verification of constructed works. When objects are represented by a set of simple algebraic primitives such as curves, planes, and polysurfaces, an object is said to have a "parametric" form [1]. In contrast, when objects cannot be accurately represented by such primitives, and rely on implicit algebraic forms (e.g., surface normal histograms) or large, non-semantic data structures (e.g., point clouds and meshes), objects are said to be "non-parametric" [2,3]. Computer-aided design (CAD) and building information modelling (BIM) favor parametric representations [2,4], while workflows used for digitization of as-built objects (using tools such as photogrammetry and laser scanning) favor non-parametric representations [3,5]. Practitioners require specific object representations for different purposes across the construction life-cycle. As a result, across the lifecycle of any given project there can exist a wide range of construction elements, components, assemblies, and conditions exhibiting or being represented by parametric and non-parametric forms. This dichotomy exists due to (1) the nuance of methods employed for object representation, (2) inattention or inability to control dimensional variability during construction, and (3) the diversity of geometric forms and conditions that exist across various systems in the AEC industry.

1.1 Geometric Challenges in AEC Related to Parametric and Non-parametric Forms

The premise that geometry can be characterized by a mix of parametric and non-parametric forms has unique implications in Architecture, Engineering, Construction (AEC) that few studies have investigated in detail, but that continues to create challenges for mediation and resolution efforts. Many geometric and topological challenges can be traced to an inability to mediate effectively between parametric and non-parametric domains, as evidenced in the following examples:

- **Existing conditions characterization.** The challenge in these workflows is the process of fusing parametric and non-parametric data stemming from existing conditions and new components or assemblies. This is evidenced particularly in adaptive building reuse where data used to represent existing conditions is most accurately facilitated through non-parametric data. Parameterization of unstructured data can be performed, but often results in a loss of representational accuracy. Examples of as-built conditions which are difficult to parameterize

include large concrete structures, beam camber, rail track levelness, or curvature of free-formed bespoke architectural features.

- **Updating BIM to reflect the as-built status**. The process of updating BIM during construction is complex and subject to varying degrees of accuracy for geometric representation. When objects deviate outside of allowable tolerance thresholds and cannot be accurately or easily represented using parametric primitives, updating the as-designed BIM becomes time-consuming and error-prone.
- **Abstraction of geometric deviations**. While the comparison of 3D sensed data (e.g., point clouds) with BIM has been relied upon in industry for many uses cases, the challenge that still exists is localization, interpretation, and abstraction of discrepancies. While a 3D point cloud can be overlaid on a 3D model to produce a map of geometric deviations, this analysis by itself does not translate into distinct kinematic (i.e., parametric) deviations or non-kinematic (i.e., non-parametric) deviations. The challenge of sensing and interpreting geometric deviations is especially important in repetitive assembly workflows, such as modular construction, where parametric corrections to assembly geometry configuration (i.e., location, orientation, size of objects, etc.) can have a profound impact on manufacturing efficiency and reduction of rework due to dimensional variability.
- **Mixed-form object assembly planning**. Challenges in object assembly planning arise due to varying levels of object regularity, manufacturing processes and dimensional variability. For instance, the assembly of manufactured products into "stick-built" buildings can be particularly challenging since manufactured products are often characterized as being highly parametric with low dimensional variability, while site interfaces are often non-parametric with a high degree of variability [6]. Another example of mixed-form object assembly planning is the optimal packing of irregularly shaped objects into containers, which occurs in nuclear waste disposal. In this case, irregularly shaped objects exhibit non-parametric representations while regularly shaped objects (containers) exhibit parametric representations [7]. These types of packing scenarios are challenging to derive optimized solutions for.

1.2 Problem Statement and Contribution

In light of the challenges with having a mixture of parametric and non-parametric representations in various AEC workflows, this research provides a better understanding into the trade-offs that exist. In some cases, parametric representations might be preferred, while in other cases non-parametric representations might be necessitated. Current classifications and definitions for parametric vs. non-parametric datatypes are verbose, and as a result of the different requirements for datatypes in AEC, navigating this delineation is challenging.

This contribution of this paper is as follows. First, a review of existing classifications for parametric vs. non-parametric entities is explored from a systems-, geometric schema-, semantic information-, and associative modelling-based standpoint. Then, a simple conceptual model is proposed, which captures the intrinsic trade-offs between these representation forms. A demonstration is used to demonstrate how such a model is efficacious for describing these trade-offs. Finally, the implications of this model are discussed, to provide a better understanding into decision making regarding the handling of geometric data in AEC.

2 Delineating between Parametric and Non-Parametric Entities

2.1 Systems Context

The distinction between parametric and non-parametric systems is verbose and multi-variate. In mathematical modelling of systems, the distinction between parametric models and non-parametric models lies with fixity and immutability of system parameters. Parametric models have fixed non-changing parameters for system characterization, while non-parametric models assume that a fixed set of parameters cannot be used for proper system characterization [8]. This notion also appears in robust parameter design [9] where systems are characterized in terms of controllable design aspects, or parameters, and noise variables which are much more challenging and sometimes not feasible to control.

In some cases, non-parametric systems are viewed as having an infinite number of parameters, and since only a finite number of these parameters are used for modelling these systems, the output can change with the same input [10,11]. It should be noted that a clear association of, and connection between the terms *parametric*, *non-parametric*, *stochastic* and *deterministic* for codifying systems cannot be made. For instance, parametric models can be stochastic if the data being observed fits a known distribution with constant variance, and variables are numerical and continuous [12].

Systems can also comprise both parametric and non-parametric attributes, and thus can be considered semi-parametric. The use of *semi-parametric* for domain classification also appears in the context of regression analysis, where a combination of linear and non-linear regression can be useful for statistical inference [13]. The use of localized variables and global parameters define model components that do not change (i.e., global

parameters of an entire population), and model components that do experience variation (i.e., local variable instances of a sample from a population). In addition to describing system certainty, these classes also describe system scale and provide a distinction between design vs. observational attributes.

In summary, the distinction between parametric and non-parametric systems is multi-variate across domains and is based on several factors including modelling approach, system certainty, design vs observational data, and system scale (Figure 1).

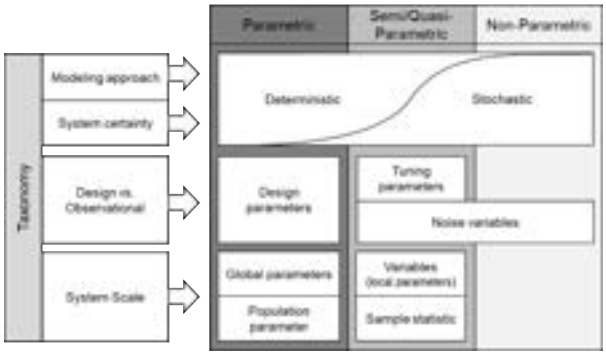

Figure 1. Taxonomy of systems classification in terms of modelling approach, system certainty, design vs. observational data, and system scale.

2.2 Geometric Schema Context

The representation of object geometry using distinct geometric schemas is also verbose and oftentimes unclear. Classification of these schemas are often based on *ambiguity*, *directness*, and *compactness*.

Unambiguous (or complete) representations are used to describe the entirety of a physical object, and underlying primitives or descriptors can be inverted to recreate the exact same object being represented. Unambiguous approaches can be used to provide a one-to-one mapping between objects and their representation [14,15]. Ambiguous representations are often used to distinguish between objects in a very efficient manner [15], even though the descriptors used cannot provide a one-to-one mapping between objects and their representation. Within unambiguous representations, methods can be further classified into implicit and explicit representations. The key difference between these two approaches is the directness for computing objects. Indirect representations use intermediate geometric descriptors such as histograms of normals or curvature to describe objects [1] as compared to explicit methods which directly describe objects using surface (e.g., polysurfaces, meshes), or volumetric (e.g., constructive solid geometry) descriptors [1,5].

A final division between approaches is parametric vs. non-parametric representations. While explicit methods can be either parametric or non-parametric, implicit methods are distinctly not of a parametric form [16]. Parametric representations are more algebraically refined than non-parametric methods, however, they can be more computationally intensive to perform operations on [2]. While this may not be the case for simple primitives such as lines, circles and planes, it is especially true for representing complex geometry, using formats such as polysurfaces, Bezier curves, B-Splines, Non-Uniform Rational Basis Spline (NURBS), and piecewise functions. Non-parametric representations, in contrast, are more computationally efficient, but are more difficult to achieve exact geometric representation. A non-parametric representation can be implicit as in the case of differential properties of a surface of a given location [1], or can also be explicit as in the case of polygonal meshes. The conversion between parametric and non-parametric representations is discussed in [16]. The conversion from parametric to non-parametric is defined as *implicitization* and it is possible to perform for any rational parametric surface of curve. The reverse process, *parameterization*, is not as easy to execute and is not always possible to perform for higher-order descriptors. Parametric representations have become the "quasi-standard" for CAD modelling [2] due to algebraic topology capabilities, while non-parametric representations are preferred in machine vision and as-built modelling systems [5,15] due to computational efficiency.

Despite the existence of classifications for representation schemas such as the one shown in Figure 2, exact definitions and distinctions are at times fuzzy and inconsistent. For instance, some studies state that explicit representations can be either parametric or non-parametric [1,3], while other studies state parametric approaches are always based on implicit methods of describing geometry [17]. This fuzziness stems from the fact that some classifications refer to the datatype itself as the entity being characterized, while other classifications refer to the process taken to derive a datatype as the entity being characterized. In addition, it is difficult to understand clear distinctions between the nature of datatypes with respect to parametric vs. non-parametric attributes. For example, it is well regarded that a representation scheme that allows for modifications of its underlying variables (e.g., control points in NURBS) is parametric. However, the same argument could theoretically be made for meshes (i.e., control vertices can be modified), yet these are clearly defined as being non-parametric schemas. Perhaps there is a theoretical limit to the number of control variables in a representation scheme whereby it starts to become non-parametric. However, no such definitive limit has been (or perhaps can be) defined, which further adds to the existing fuzziness of classification.

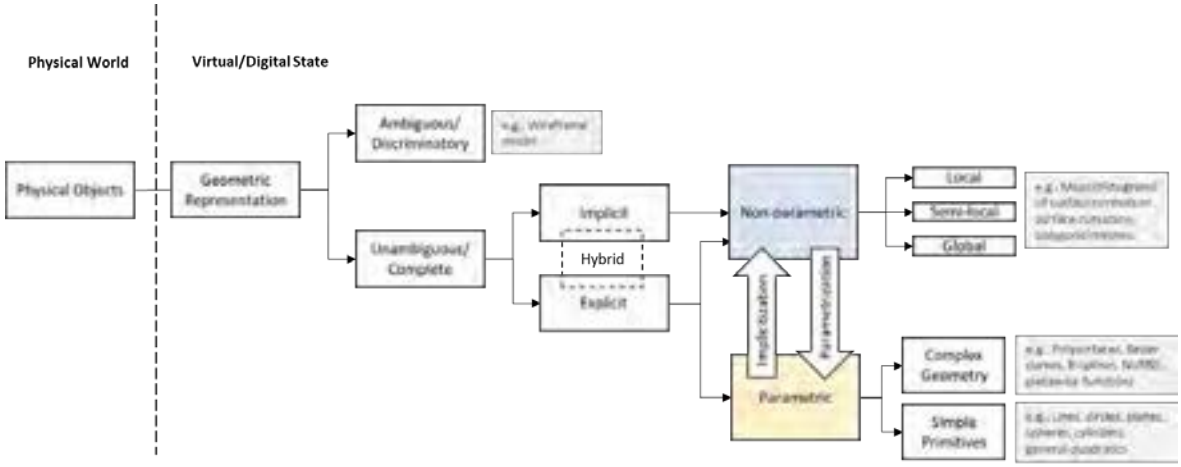

Figure 2. Classification of geometric schemas used to represent physical objects in AEC according to ambiguity, directness, and compactness (adapted from [3] using [1,2,5,14-16]).

2.3 Semantic Information Context

From a building information modelling standpoint, the classification of objects as being parametric extends beyond just representational form and has unique attributes to facilitate use across the entire construction lifecycle. Parametric BIM objects must also include semantic information (parameters) in the form of associated data, rules, topology and material-specific data [4]. Parameters are also used to classify objects into categories, families, types and instances, which is stored as data in the form of text, integers, numbers, area, volume, angles, URLs, or binary data [18]. Across this wide definition of parametric objects in BIM, attributes related specifically to geometry and topology are investigated in this research since they directly affect geometric mediation between objects. Topology describes the spatial relationships between elements that do not change based on changes to geometric parameters of those elements [19]. Topology can relate to the relationship between features of an element (e.g., face to edge), the relationship between elements (e.g., beam to column) or relationship between groups of objects or spaces (e.g., room to room). Topology plays a key role in the way architects and engineers understand the function and expected behavior of building elements. Topology, geometric representation and material properties are distilled into the "semantics" of an object, which can be interpreted as the form, function and behavior of objects and systems of objects [20]. Current modelling practice in construction emphasizes the creation and preservation of semantics by explicitly outlining that building information models must contain parametric intelligence, topological relationships and object attributes [21], otherwise, they are considered no more than 3D geometric models.

2.4 Associative Modelling Context

A fourth context can also be used to describe the delineation of parametric vs. non-parametric entities in AEC. Parametric modelling (or parametric design) involves the use of geometric rules and constraints to embed explicit domain knowledge into BIMs and provides a way for automated design regeneration via an "associative" model [22]. While any CAD modelling system can contain a parametric representation of an object, the following characteristics differentiate parametric modelling systems: users can define custom relationships between features and objects, parameters between objects can be integrated into a system (i.e., a parameter of one object can be used for defining parameters on other objects), parametric definitions are compatible in a system or are otherwise mutually exclusive such that no two parameters create conflicting relationships; geometry should be object or feature-based [22]. This approach to modelling has become very popular in the manufacturing industry and is seen in software such as SolidWorks®. Constraint-based design requires all dimensions of features and parts to be parametrically defined, constrained and related to other features [23], or it is otherwise considered under-constrained, and cannot be realized [24]. While this degree of parametric constraints is not employed in most AEC workflows, the use of associative model does provide a source of additional parametric properties that can be exploited.

2.5 Summary

Exploring a range of contexts reveals a verbose and multi-variate landscape for describing the delineation between parametric and non-parametric entities. Selecting a suitable object representation (whether

parametric or non-parametric) extends beyond just the geometric schema employed, includes semantic information requirements, and might include associative relationships to other objects. In a systems context (2.1), the delineation between parametric and non-parametric is fuzzy (with an intermediate category sometimes being used), and this also translates down to the object level. However, it is clear from the examples of cases where both datatypes exist in AEC, that assessing trade-offs is useful for understanding the inherent benefits and constraints to each datatype. In some cases, parametric object representations are preferred, while in other cases, non-parametric object representations might be required.

3 Proposed Conceptual Model

This research presents a conceptual model to help summarize the key trade-offs between parametric and non-parametric object representations. This model is based on the distinction between analytical expressions and digital approximations that appear in computer vision for pattern and shape recognition processes. As depicted in Figure 3, this model classifies parametric object representations as having many relations between individual datapoints or entities, and are by nature more abstract, while non-parametric object representations have a greater number of unstructured datapoints and are by nature more discrete or approximate.

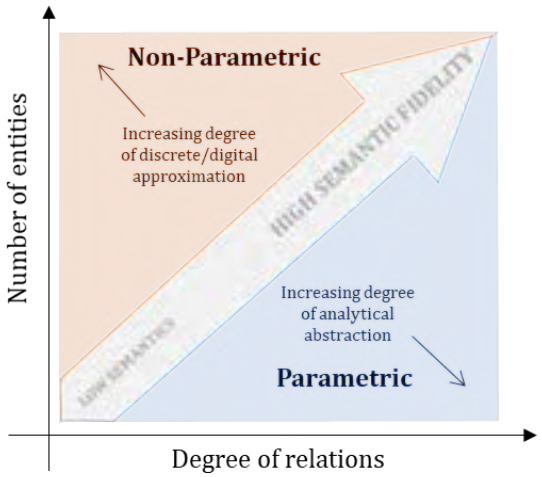

Figure 3. Conceptual model for characterizing the delineation of parametric and non-parametric object representations

3.1 Analogy to Pattern Recognition Techniques

In computer vision, various techniques for pattern recognition can be used to resolutely employ digital approximations of analytical expressions for recognition.

One of the most common methods for shape detection in computer vision is the Hough Transform which detects curves by exploiting the duality between points on a curve and parameters of that curve [25]. It works by first considering the analytical expression of a curve, often in the parametric line form (r, θ), and edge segments of an image given by (x_i, y_i) . The transform is then implemented by discretizing the Hough parameter space over finite intervals of the image, or "accumulator cells". This technique takes an inherently parametric mathematical expression and discretely approximates it in a non-parametric manner to extract and transform information from an image (which itself can also be defined as a non-parametric data source).

Gaussian kernels are another example of discrete approximation used in computer vision to perform an analytical transformation on an image (Figure 4). A more general case of this is convolutional kernels and filters, which transform an expression into a discrete nxn matrix and is convoluted over an image. Discrete approximations such as kernels are efficacious in complex algorithms such as Scale Invariant Feature Transform (SIFT) due to the ability to perform analytical operations in a computationally efficient manner.

In the same way that many pattern recognition techniques transform analytical expressions into discrete approximations, this same analogy can be used to delineate between parametric and non-parametric object representations. On one hand, we can postulate a trend that the more abstract an expression or representation is, the fewer entities are required to relate components together. Conversely however, when these relations are broken and discretized, more discrete values are required to perform a similar level of approximation compared to its analytical counterpart.

Analytical Expression

$$h(u,v) = \frac{1}{2pi\sigma^2} e^{-\frac{u^2+v^2}{\sigma^2}}$$

Discrete Approximation

$$H[u,v] = \frac{1}{273}\begin{bmatrix} 1 & 4 & 7 & 4 & 1 \\ 4 & 16 & 26 & 16 & 4 \\ 7 & 26 & 41 & 26 & 7 \\ 4 & 16 & 26 & 16 & 4 \\ 1 & 4 & 7 & 4 & 1 \end{bmatrix}$$

Figure 4. Analytical Gaussian Expression and its Digital Approximation (i.e., 5x5 Gaussian Kernel)

3.2 Measuring the Degree of Semantic Fidelity

The final component to the proposed model is characterizing the degree of semantic information encapsulated in an object representation. The greater the number of entities and degree of relations between those entities, the greater the semantic fidelity of a representation. In practice, there is a trade-off that occurs between parametric and non-parametric object representations with respect to the degree of semantic encapsulation. This is perhaps most evident when

representing "as-is" objects. While non-parametric object representations are positioned better for obtaining a higher degree of representational accuracy, they cannot be semantically enriched to the same level as parametric object representations. Despite the high level of abstraction in parametric representations and the significant advancements being made to leverage better parametric modelling approaches that maintain representational accuracy of as-is objects, the inability to achieve the same degree of representational accuracy as non-parametric representations restricts its ability to achieve the highest level of semantic fidelity. As such, a notable trade-off occurs between parametric and non-parametric representations with respect to semantics.

4 Demonstrating the Conceptual Model

Previous research has provided information for assessing the trade-offs between geometric schemas (Table 1). Using this breakdown, a simple demonstration can be carried out for the representation of an I-beam element (Figure 5) to show how parametric representations tend to have fewer entities, which are more tightly related. The first digital representation in this figure is a point cloud, which can be obtained by performing sampling reconstruction of existing mathematical descriptions or from reality capture [26]. The other digital representations which are more structured than point clouds are triangular and polygonal (tessellated) meshes. As shown, the point cloud representation has 7296 datapoints (i.e., XYZ points), whereas the triangular mesh contains 1740 datapoints (i.e., triangle vertices), and in the most simplified case, the polygonal mesh structure has 108 datapoints (i.e., polygon vertices). These digital representations are also considered to be non-parametric. As opposed to regular shapes (e.g., rectangular, cylindrical, prismatic, etc.), non-parametric forms cannot be defined parametrically using a shape type and a limited set of parameter values that specifies the object [1]. Figure 5 also depicts two common mathematical representations. Non-Uniform Rational Basis Spline (NURBS) is a common boundary representation, which uses a series of surfaces to completely enclose and represent a given shape. Constructive Solid Geometry (CSG) is a mathematical representation that describes the volume of an object through use of Boolean operations (e.g., addition and subtraction) of simple geometries to create more complex shapes. While CSG has been the preferred method for representing geometry in building information models (BIM) due to its simplistic data structure [1], there are many applications where NURBS are preferred, since it can describe complex geometry more appropriately [21,27]. As shown for the steel beam, the NURBS geometry contains 56 datapoints (i.e., control points), whereas the CSG geometry contains 9 datapoints (3 extrusions built with 3 control points each).

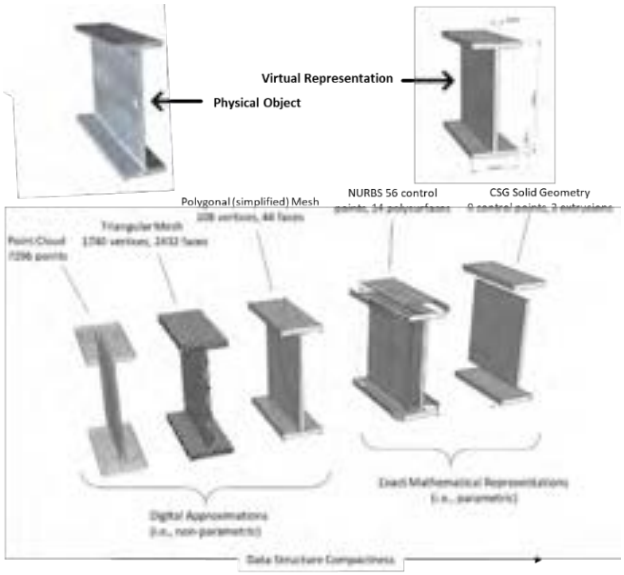

Figure 5. Digital and Mathematical Representations for a Physical Object (Steel Beam Element).

Table 1. Summary of the key trade-offs between geometry representations employed in AEC

Geometry Representation	Geometry Kernel Processing Demand	Continuity	Representational Accuracy (As-is)	Semantic Richness	Exactness for Complex Geometry	Sources
Point clouds	Slow (high computational effort)	Discretized	High	Low	Low	[28]
Mesh	Fast (no interpretation required)	Discretized	Med-High	Low	Med	[28]
BREP	Med (interpretation required)	Exact, continuous	Med	High	High	[17,28]
CSG	Med (interpretation required)	Exact, continuous	Low-Med	High	High	[28]
NURBS	Med (interpretation required)	Exact, continuous	Med-High	High	High	[28]

The general trend for this simple example is that as representation moves from digital to mathematical, it becomes more compact, with fewer entities that are abstractly related. In addition, we can plot each of these geometric descriptors on the conceptual model (Figure 6). One hand the point cloud representation is the most non-parametric with the highest number of entities (which are not related), while the CSG representation is perhaps the most abstract parametric representation. While not directly considered in this example, the Boundary Representation (BRep) geometric schema is another parametric representation which arguably has the highest semantic encapsulation across all geometric schemas. This is because the BRep schema is based on a hierarchical topological structure, with explicit relations between bodies, faces, edges and vertices (refer to [17] for a more detailed breakdown of this schema).

While this example demonstrates how geometric schemas can be characterized using the proposed model, the purpose of the analysis is not to provide a comprehensive (or exhaustive) classification of all possible schemas. However, certain schemas are better suited for more semantic fidelity than others. For instance, given how NURBS and BRep can be discretized by adding additional control points without changing the initial geometry of an object, these representations potentially have the ability to harness the semantic fidelity requirements of a given application as opposed to those of CSG or non-parametric representations.

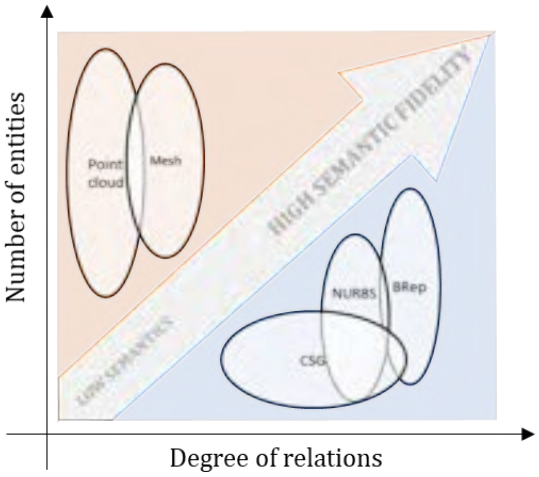

Figure 6. Depicting the Conceptual Model Using Geometric Schemas

5 Conclusions

Within AEC, the choice of object representation form invokes trade-offs with respect to computational efficiency, representational accuracy, and semantic enrichment. Since there remains to be one ubiquitous object representation that can simultaneously meet all of these objectives, the choice of representation will continue to require making trade-offs. Review of existing classifications for object representation reveals that there can be a significant degree of verbosity and ambiguity, further compounding the task of selecting a suitable representation. This paper demonstrates that approaching classification through a parametric vs. non-parametric lens is useful for providing key insight required in selection of a desired object representation. A conceptual model is established by considering two dimensions of an object representation: number of entities used to represent an object and the degree of relations between those entities. These dimensions are fundamental in computer vision for applications such as pattern recognition and shape detection. For instance, the discretization of analytical expressions is a key component to achieving computational efficiency in methods such as the Gaussian kernel, Hough Transform, and Scale Invariant Feature Transform (SIFT) algorithm. In addition to geometric schemas, other attributes can also be described by the proposed model, namely semantic enrichment and associative modelling relationships. These dimensions clearly fit into a parametric vs. non-parametric context within AEC workflows. A functional demonstration using various geometric schemas reveals the trend that parametric representations have a high degree of analytical abstraction, while non-parametric representations have a high degree of digital approximation.

5.1 Future Research Opportunities

In practice, there are numerous workflows which require either parametric or non-parametric representations due to current trade-offs. While this trend is expected to continue, there are opportunities to bridge this gap as evidenced in the following areas of research:

- **'Geometry as a feature'.** Rather than defining objects as an abstraction of geometry, geometry can be viewed as a feature of object. This is already the premise of object-oriented modelling (and is used in IFC, for instance), yet a more concerted focus on this concept can allow for multiple geometric schemas to be used to represent the same object without necessitating the landscape of parametric vs. non-parametric trade-offs.
- **Towards improved geometric schemas.** Current limitations and trade-offs can be addressed by developing new schemas that do not have the limitations of existing schemas. One example is developing a global or 'master' schema that can be modified or updated throughout the lifecycle of AEC projects as required.
- **Developing parametrization methods that preserve fidelity of information.** Rather than converting non-parametric datatypes into a

parametric form at the expense of loss of representational fidelity and semantic information, it is possible to discretize initial parametric forms (e.g., such as NURBS) in such a way that can achieve suitable accuracy while maintaining semantic fidelity.

Acknowledgements

The authors would like to acknowledge the financial support of the Natural Sciences and Engineering Research Council of Canada (NSERC), Mitacs Accelerate and Edge Architects.

References

[1] P. Tang, D. Huber, B. Akinci, R. Lipman, A. Lytle, Automatic reconstruction of as-built building information models from laser-scanned point clouds: A review of related techniques, Autom. Constr. 19 (2010) 829-843.

[2] Y.D. Fougerolle, A. Gribok, S. Foufou, F. Truchetet, M.A. Abidi, Boolean operations with implicit and parametric representation of primitives using R-functions, IEEE Trans. Visual. Comput. Graphics. 11 (2005) 529-539.

[3] V. Pătrăucean, I. Armeni, M. Nahangi, J. Yeung, I. Brilakis, C. Haas, State of research in automatic as-built modelling, Advanced Engineering Informatics. 29 (2015) 162-171.

[4] C. Eastman, C.M. Eastman, P. Teicholz, R. Sacks, BIM Handbook: A Guide to Building Information Modeling for Owners, Managers, Designers, Engineers and Contractors, John Wiley & Sons, 2011.

[5] F. Lafarge, R. Keriven, M. Brédif, Insertion of 3-D-primitives in mesh-based representations: towards compact models preserving the details, IEEE Trans. Image Process. 19 (2010) 1683-1694.

[6] C. Rausch, M. Nahangi, M. Perreault, C.T. Haas, J. West, Optimum Assembly Planning for Modular Construction Components, J. Comput. Civ. Eng. (2016) 04016039.

[7] Y. Zhao, C.T. Haas, A 3D Irregular Packing Algorithm Using Point Cloud Data, ASCE International Conference on Computing in Civil Engineering. (2019).

[8] C.J. Stone, Additive regression and other nonparametric models, The annals of Statistics. 13 (1985) 689-705.

[9] T.J. Robinson, C.M. Borror, R.H. Myers, Robust parameter design: a review, Qual. Reliab. Eng. Int. 20 (2004) 81-101.

[10] J. Kruschke, Doing Bayesian Data Analysis: A Tutorial with R, JAGS, and Stan, Academic Press, 2014.

[11] P.S. Maybeck, Stochastic Models, Estimation, and Control, Academic press, 1982.

[12] R. Nisbet, J. Elder, G. Miner, Handbook of Statistical Analysis and Data Mining Applications, Academic Press, 2009.

[13] D. Ruppert, M.P. Wand, R.J. Carroll, Semiparametric Regression, Cambridge university press, 2003.

[14] C.M. Brown, Some mathematical and representational aspects of solid modeling, IEEE Trans. Pattern Anal. Mach. Intell. (1981) 444-453.

[15] R.J. Campbell, P.J. Flynn, A survey of free-form object representation and recognition techniques, Comput. Vision Image Understanding. 81 (2001) 166-210.

[16] J. Bloomenthal, B. Byvill, Implicit surfaces, Unchained Geometry, Seattle. (2000).

[17] A. Borrmann, V. Berkhahn, Principles of Geometric Modeling, in: Anonymous Building Information Modeling, Springer, 2018, pp. 27-41.

[18] P. Meadati, J. Irizarry, BIM–a knowledge repository, 12 (2010).

[19] W. Jabi, S. Soe, P. Theobald, R. Aish, S. Lannon, Enhancing parametric design through non-manifold topology, Des Stud. 52 (2017) 96-114.

[20] M. Belsky, R. Sacks, I. Brilakis, Semantic enrichment for building information modeling, Computer-Aided Civil and Infrastructure Engineering. 31 (2016) 261-274.

[21] L. Barazzetti, F. Banfi, R. Brumana, M. Previtali, Creation of parametric BIM objects from point clouds using NURBS, The Photogrammetric Record. 30 (2015) 339-362.

[22] G. Lee, R. Sacks, C.M. Eastman, Specifying parametric building object behavior (BOB) for a building information modeling system, Autom. Constr. 15 (2006) 758-776.

[23] K. Chang, C. Chen, 3D shape engineering and design parameterization, Computer-Aided Design and Applications. 8 (2011) 681-692.

[24] J. Monedero, Parametric design: a review and some experiences, Autom. Constr. 9 (2000) 369-377.

[25] D.H. Ballard, Generalizing the Hough transform to detect arbitrary shapes, in: Anonymous Readings in Computer Vision, Elsevier, 1987, pp. 714-725.

[26] L. Linsen, Point Cloud Representation, Univ., Fak. für Informatik, Bibliothek Technical Report, Faculty of Computer …, 2001.

[27] A. Dimitrov, R. Gu, M. Golparvar-Fard, Non-uniform B-spline surface fitting from unordered 3D point clouds for as-built modeling, Computer-Aided Civil and Infrastructure Engineering. 31 (2016) 483-498.

[28] A. Wagner, M. Bonduel, P. Pauwels, U. Rüppel, Representing construction-related geometry in a semantic web context: A review of approaches, Autom. Constr. 115 (2020) 103130.

Development of a Twin Model for Real-time Detection of Fall Hazards

L. Messi[a], A. Corneli[a], M. Vaccarini[a] and A. Carbonari[a]

[a]Polytechnic University of Marche, DICEA Department, Ancona, Italy

l.messi@pm.univpm.it, a.corneli@pm.univpm.it m.vaccarini@univpm.it alessandro.carbonari@univpm.it

Abstract -

The Architecture, Engineering and Construction (AEC) industry is still one of the most hazardous industries in the world. Researchers impute this trend to many factors such as the separation between the phases of safety planning and project execution, implicit safety issues and, most of all, the dynamic and complex nature of construction projects. Several studies show that the AEC industry could greatly benefit of latest advances in Information and Communication Technologies (ICTs) to develop tools contributing to safety management.

A digital twin of the construction site, which is automatically instantiated and updated by real-time collected data, can run fast forward simulations in order to pro-actively support activities and forecast dangerous scenarios. In this paper, the twin model of the Digital Construction Capability Centre (DC3) at the Polytechnic University of Marche (UNIVPM) is developed and run as a mock-up, thanks to the adoption of a serious game engine. This mock-up is able to mirror all the relevant features of a job site during the execution of works from a safety-wide perspective. In such a scenario, virtual avatars randomly explore the construction site in order to detect accessible, unprotected and risky workspaces at height, while warning the safety inspector in case additional safety measures are needed.

Keywords -

Digital Twin; Building Information Modelling; Real-Time Health and Safety Management; Complex Systems

1 Introduction

Nowadays, the AEC industry represents one of the most hazardous productive sectors [1]. In fact, although it employs only about 7% of the world's work force, yet it is responsible for 30–40% of fatalities. Statistics, which are referred to different countries, demonstrate that the construction safety is a perennial global problem.

In the United States, the census data from the U.S. Bureau of Labor Statistics (BLS) showed that as many as 774 workers died from injuries they suffered on construction sites in 2010, accounting for 16.5% of all industries. The fatality rate accounts for 9.8 per 100000 full-time equivalent workers and is ranked the fourth highest among all industries. Within the two decades of 1990 and 2000, more than 26000 U.S. construction workers died at work [2]. That equates to approximately five construction worker deaths every working day. Out of these fatalities, 40% involved incidents were of the type falls from height. Further investigations showed that inadequate, removed, or inappropriate use of fall protection equipment contributed to more than 30% of those falls [2]. Statistics about other countries, such as China [3], United Kingdom [1] and Germany [4], confirm high percentages of fatal accidents in the construction industry and point out falls from height as one of the most frequent causes. As a result, it is evident that the construction industry is far from the vision of "zero accidents/injuries" espoused by many construction-related companies [1].

The high number of fatalities is generally imputed to several causes, such as the separation between the phases of safety planning and project execution [2, 5], implicit safety issues and, most of all, the dynamic and complex nature of construction projects, which require ever-changing safety needs [5]. Construction safety issues can be properly described as complex sociotechnical system [6], which cannot be tackled simply adopting a best-practice approach defined ex ante. Conversely, the answers to such problems can be described as emergent practices [7].

The AEC industry is often regarded as being hesitant in adopting innovative technologies, due to the inherent difficulties of its unstructured and changing environment [1, 8]. Nevertheless, many research studies [9, 10, 11] demonstrate that the application of the latest advances in ICTs in the safety management field can help to proactively respond to hazardous scenarios and enable the shift from reactive to proactive safety management.

1.1 Rule-checking systems

Some research studies [2, 12] apply commercial systems, such as Tekla® [13] and Solibri™ [14], to execute BIM-based rule-checking analysis for the detection of fall hazards. Rules, once they are translated from human language into a computer-readable format, can be executed supporting labor-intensive safety checking tasks in a little time. In this direction, authors in [15] propose an ontology-based approach for construction safety checking, modelling safety constraints with Semantic Web Rule Language (SWRL). The authors, assuming fall from height as a test case, demonstrate the potential of this methodology for the assessment of fall hazard on the base of hole's acceptance criteria defined by safety regulation. In fact in similar circumstances, i.e. when a dimension has to be

compared with a threshold value, a rule-checking system drives to reliable results.

It must be noted that sometimes safety assessment is contextual, that is it depends from complex geometries and spatial dependencies (e.g. non-perpendicular crane cable that lifts up and swings) or ever-changing site conditions (e.g. temporary structures that aid construction processes and are often not modeled). In cases like these, it is hard to define general rules by means of safety checking constraints which cover all possible scenarios; moreover, information provided by a BIM model can result incomplete, inaccurate or not updated. As a consequence, the correctness of the rule-based safety analysis may be largely affected.

1.2 Real-time tracking systems

In some research studies, prototypes of self-updating BIM models based on sensor data for real-time Health and Safety (H&S) management have been developed. The paper [9] proposes an application which aims to improve environmental safety in construction sites; the BIM model displays the latest data from temperature and humidity sensors and the real-time status of various locations, with a focus on the ones affected by atmospheric hazards. Another research work [10] integrates a rule-checking system and a Real-Time Location System (RTLS) to place dynamic virtual fences and to check whether tracked real fences are properly installed. In the system developed in [11], once risks are assigned to building components, a warning can be sent to tracked workers on site in case they come too close to hazards. A requirement for this approach is that hazards are identified and classified in advance.

1.3 Contribution to research

In this work, the development of a digital twin for H&S management in construction sites to prevent falls from height is reported and tested. This approach can be used to complement BIM-based rule-checking systems, which work well when they come to checking compliance with safety codes, regulations and best practices. But, as already stated in Section 1, construction sites represent a type of complex systems and unexpected emerging hazardous scenarios cannot be anticipated unless a digital twin is put in place.

The research study reported in this paper concerns a methodology to develop a digital twin of construction sites, which makes it possible to find out in real-time hazardous scenarios possibly leading to falls from height. A forward-looking simulation approach, run in real-life conditions and implemented in Unity3D^{TM}, and a real-time monitoring sensor network, to update the status of the ever-changing environment and of involved workers, have been integrated and tested in the Digital Construction Capability Centre (DC3) of the Polytechnic University of Marche (UNIVPM at Ancona, Italy).

This paper is organised as follows: Section 2 introduces digital twins as a candidate solution for the management of complexity. Section 3 provides a description of the developed system architecture, whereas in Section 4 simulation and results are reported. Finally, Section 5 is devoted to conclusions.

2 Management of complexity

2.1 Complex systems

2.1.1 Basic of complex systems

A complex system consists of many elements affected by non-linear interactions [16]. As a consequence, small causes may lead to large consequences, and vice versa; this implies no immediate apparent relationship between causes and effects. Interactions, which cause system changes over time, consist of transference of energy or information, usually have a fairly short range and show recurrency, they being affected by loops. Furthermore, the constant flux of energy ensures the survival of a complex system and its history affects the present behaviour. A complex system is usually open or it is hard to define its borders. The scope of such a system is not an intrinsic characteristic, but is usually determined by the purpose of the description and is often influenced by the position of the observer; this process is called framing. Finally, each element ignores the behaviour of the system as a whole and responds only to information that is locally available. The complexity feature emerges as a result of interactions among constituting elements. The most representative examples of complex systems are the human brain, the behaviour of a flock of birds and economic systems of the modern society [16, 17].

The Cynefin framework (Cynefin in Welsh pronounced kunev-in means the multiple factors), introduced in 1999, is a decision-making conceptual structure which proposes strategies to properly tackle each one of the five domains: "simple", "complicated", "complex", "chaotic" and "disordered" [7]. Whereas cause-and-effect relationships can be detected by everyone in the "simple" domain and by experts in the "complicated" one, the same cannot be said in the "complex" one, where the reason why things happen can be understood only in retrospect, causing unpredictability. In the "complex" domain, the Cynefin suggests to probe and sense eventual emergent instructive patterns to be used as responses.

In this research study, the high-level strategy proposed by the Cynefin framework has been assumed. In practice the digital twin, enabling forward-running simulations, makes it possible to "probe and sense" future scenarios;

emergent safety measures can be suggested and applied in real-time.

2.1.2 Complex systems in H&S management

In the AEC industry, safety issues can be regarded as complex sociotechnical systems [6]. Stakeholders include manufacturers, main contractors and subcontractors, design staff, project and site managers. Moreover, construction sites, which are usually interested by crowds of workers, adjacent buildings and facilities, complex weather phenomena, result in a very dynamic operating environment. In other words, the safety status is an emergent property of a system, whose components are subjected to non-linear interactions that cannot be anticipated [18]. In the research study [6], authors have studied a tower crane safety issues as a systemic problem, assuming the safety risk management framework defined by [19] that was specifically developed with complex sociotechnical systems in mind; as a result, a list of factors affecting tower crane safety has been identified.

2.2 Digital twins

2.2.1 Basics of digital twins

The first definition of the concept, nowadays known as the digital twin, was made in 2002 by Michael Grieves, in the context of an industry presentation concerning Product Life cycle Management (PLM) [20]. A digital twin can be defined as a virtual representation of a physical product or process, used to understand and predict the physical counterpart's performance characteristics throughout the product life cycle [21]. To ensure an accurate modeling over the entire lifetime of a product or of its production, digital twins use data from sensors installed on physical objects to determine the objects' real-time performance, operating conditions and changes over time. Using this data, a digital twin evolves and continuously updates to reflect any change to the physical counterpart, creating a closed-loop of feedback in a virtual environment that enables companies to continuously optimize their products, production, and performance at reasonable costs [21].

The statements "digital model", "digital shadow" and "digital twin" are often used as synonyms, although they differ from each other in the level of data integration between the physical and digital counterparts. A "digital model" is a digital representation of an existing or planned physical object that does not use any form of automated data exchange between the physical object and the digital object. If there further exists an automated one-way data flow between the state of an existing physical object and a digital object, one might refer to such a combination as "digital shadow". If further again, the data flows are fully integrated in both directions, one might refer to it as "digital twin" [20].

2.2.2 Digital twins in the AEC industry

In the near future, digital twins are expected to take a center stage in the AEC industry too, advancing rapidly beyond BIM and enabling asset-centric organizations to converge their technologies into a portal or immersive experiences [22]. The result will be better informed decisions to improve network availability, to enhance workers safety, to ensure regulatory compliance and to reduce environmental impacts. Thanks to the application of Artificial Intelligence (AI) and Machine Learning (ML) methodologies, we envisage immersive digital operations, providing analytics visibility and insights to enhance the effectiveness of operations staff and help them anticipate and head off issues before they arise and react more quickly with confidence [22].

A real commitment in this context was demonstrated by the Centre for Digital Built Britain (CDBB) which published, at the end of the year 2018, the Gemini Principles to guide the National Digital Twin and to shape the information management framework that will enable it [23]. The National Digital Twin itself is not intended as a single, monolithic twin of the entire country's infrastructure. Rather, it will be a federation of many twins, representing assets and systems at different levels of granularity, brought together to generate greater value. A first application was developed implementing three interconnected work packages. The first one provides the BIM model of part of the University of Cambridge. The second one regards the integration of data from various sources to enable effective analytics and drive better decisions. Finally, the third one aims to develop novel applications for facility management that exploit the data captured through the digital twin [23].

3 System architecture

3.1 Technology stack

The digital twin model, proposed in this paper, for real-time H&S management is based on the system architecture composed by the following subsystems (see Figure 1):

- a Ultra-wideband (UWB) sensor network for localization;
- Node-RED™ programming tool;
- ArangoDB database;
- Unity3D™ game engine;

The first subsystem consists of a UWB sensor network. This infrastructure is in charge of tracking what workers and equipment are present in the real world's scenario

Figure 1. System Architecture.

and sending data necessary for updating to the main system. An IoT programming tool, namely Node-RED™, wires together the UWB sensor network and the rest of the system's components. ArangoDB, is a database which stores the complete history of coordinates. The hearth of the developed architecture is the serious gaming platform Unity3D™, which hosts the digital twin's simulation environment and enables forward-running simulations to predict hazardous scenarios. In order to enable the safety manager to remotely supervise safety issues, forward simulations' results can be displayed in real-time to an off-site screen (see Figure 1). Furthermore, as soon as any fall hazard is detected, a warning can be immediately sent to the safety manager. This is made possible by sending a message, via SignalR, to Node-RED™, which can trigger an alarm or a smartphone notification (see Figure 1). In this way, the developed system can support real-time H&S management in order to prevent accidents or fatalities.

For the purpose of this paper, the left part of the system architecture (see the continuous-line of the Service box in Figure 1) has been implemented in the Digital Construction Capability Center (DC3).

3.2 Reality mirroring

Real-time sensing is devoted to the continuous mirroring of the digital twin. According to the system architecture depicted in Figure 1, workers involved in on-field activities can be tracked by means of UWB localization systems. This technology leverages the Time of Flight (ToF) technique, which is a method for measuring the distance between two radio transceivers by multiplying the time of flight of the signal by the speed of light. Thus, knowing the position of fixed UWB anchors and operating a trilateration algorithm, the position of any UWB transceivers (tag) can be determined, even if it is moving.

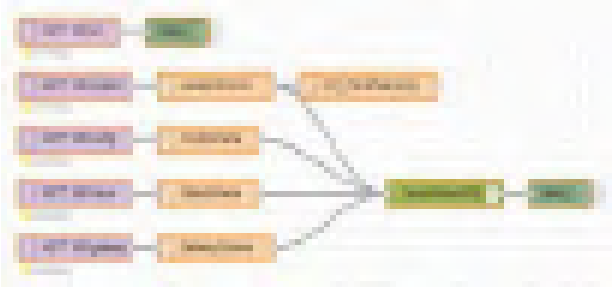

Figure 2. Node-RED flow for storing UWB messages in an ArangoDB collection.

For the purpose of this paper, five anchors were installed in known positions, whereas an UWB tag has been applied to the monitored piece of equipment, that is the ladder, in order to track its position.

In order to wire together hardware devices with the database and again with the Unity3D™ game engine, the flow based graphical programming tool Node-RED™ has been adopted. Node-RED™ is a tool specifically designed for Internet of Things (IoT) applications. In this research, a dedicated Node-RED™ flow wires together the position data coming from the UWB localization system with a database for their storage. The resulting flow built in Node-RED is shown in Figure 2.

During the development of a digital twin, different types of data must be stored and linked together in an emerging way. Therefore, ArangoDB has been selected here, because it is a native multi-model NoSQL open-source database for storing several types of information, including those types typically related to digital twins, such as the complete data history from sensors. Every changes happening in the ArangoDB collection that stores location messages is triggered to the serious gaming engine Unity3D™ by means of the software library SignalR. Hence, sensors data are delivered to the game engine enabling virtual objects' positions to be updated in real-time. As soon as a dangerous scenario is predicted in Unity3D™ by the forward simulations, a real-time notification can be triggered by sending a message to Node-RED™ via SignalR in order to prevent fatal events.

3.3 Implementation of the gaming environment

The use of serious game engines is a promising tool supporting research in real-time control systems, among the others. The first application regarding gaming technology in the area of research was found in the aircraft industry, with the use of Microsoft Flight Simulator for educational purposes [24]. Afterwards, serious game engines had a wide spread for other research purposes such as simulation and analysis, further demonstrating that mere entertainment is not the only feasible, nor the most promising,

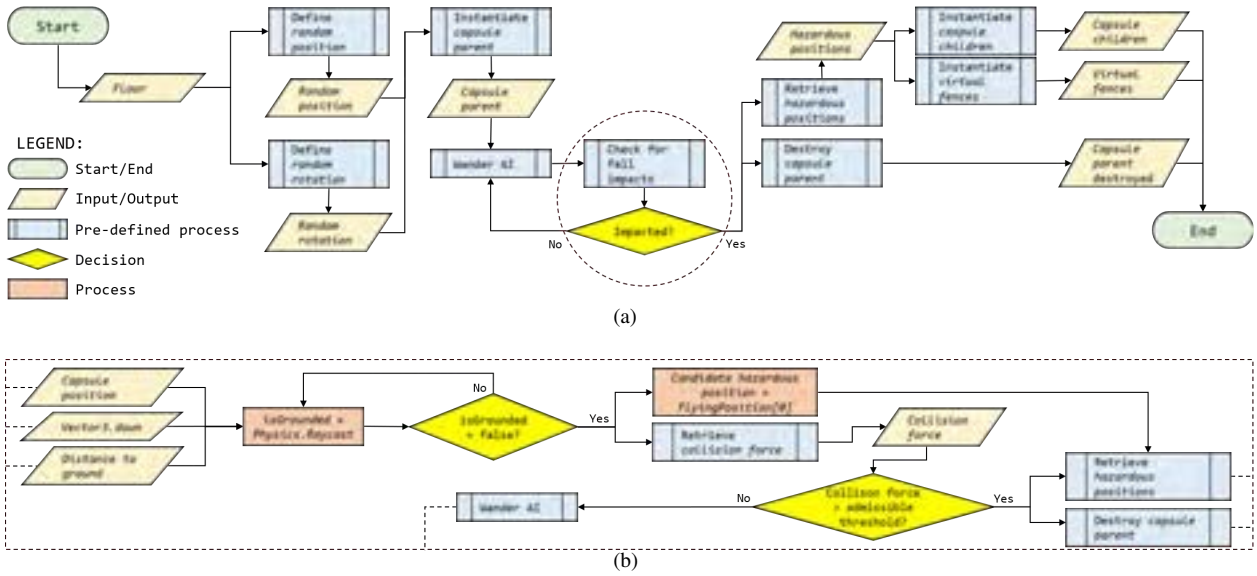

Figure 3. (a) Pseudocode describing the general logic of the digital twin developed in Unity3D^{TM} game engine in order to detect fall hazards; (b) pseudocode describing in details the virtual sensor which checks for fall impacts.

application. The great success of this approach is due to the difficulty of executing real experiments in some fields, especially in H&S management; in fact the need for establishing safe conditions to avoid direct exposure to risks would affect participants behaviour.

In this research study, game technology has been applied to develop the digital twin of a construction site for real-time H&S management. The use of a serious game engine facilitates the modeling of the environment, which includes the physical space, sensors and mechanical physics, and the implementation of simulation. For the purpose of this paper, the gaming platform Unity3D^{TM} has been adopted. The physical space of the digital twin, assumed as case of study, can be directly imported within Unity3D^{TM} as an IFC project with its structure. To this end, an IFC Loader, based on the IFC Engine DLL library [25], has been developed, in order to import topological information, materials properties and all semantic information from the digital model. This tool models the environment using one of the most powerful techniques in solid modelling, that is Boundary Representation (B-Rep). B-Rep represents a solid as a collection of connected surface elements, that is the boundary between solid and non-solid. The digital twin, in order to mimics reality, requires the implementation of human and artificial sensors, known as agents. The sense of sight, for example, must be implemented in digital twins to give humans' avatars the awareness about what is happening around them [26]. In Unity3D^{TM}, this can be done modelling the Field of View (FOV) as a collider by means of a set of quantitative parameters (e.g. FOV angle and elevation angle); a user can see an entity simply if her/his FOV collider intercepts the entity itself. The mechanical physics is a native functionality of game engines; hence, in the game scene every object is affected by gravity and occupies a volume just like in the real world. In details, these properties can be managed by means of the quantitative parameters stored respectively in the rigidbody and collider components of a virtual object. Furthermore, C# advanced programming makes it possible to define, directly in Unity3D^{TM}, a deformation behaviour which acts in response to a rising force applied to an object. To make an example, a ladder could inflect or even break down, if the weight of the overlying avatars is close to or higher than its mechanical strength. To sum up, Unity3D^{TM} hosts the digital twin and can work as a hub that is able to trigger co-simulations related to some specific disciplines and receive back results. In this way, multiple simulators (e.g. fire scenario, plants' functioning, etc.) can be coupled, by means of the models exchange standards (such as Functional Mockup Interface, FMI).

The pseudocode reported in Figure 3(a) describes the general logic at the base of the developed digital twin for real-time identification of fall hazards. At the first instantiation, virtual capsules are generated in a random position and rotation on the surface of a specific floor; instead, at the following instantiations it follows the logic explained below (see the third point in the bullet list). Each of these entities embeds an AI component which allows it to wander and explore the surrounding environment. A virtual sensor, indicated by the red dashed lines in Figure 3(a) and described in details in 3(b), has been implemented in order to evaluate if any possible impact due to a fall can

be harmful and that point must be marked as an hazardous location. To this end, a ray casting algorithm is applied to check if the monitored object is grounded or not; in case of false evidence, which means that the capsule is falling, the first "flying" position is labelled as a candidate hazardous position. The retrieved collision force is then compared with the pain tolerance value of 6 kN, known from literature [27] and regulation [28] about fall-arrest equipment. If the collision force is higher than the admissible threshold, the following events are triggered:

- the point from where the fall has taken place is confirmed as an hazardous position;
- a virtual fence is instantiated in correspondence of the hazardous position as a graphic notification;
- new children capsules are instantiated in the hazardous position with random rotations in order to speed up the exploration of the environment in the nearby;
- the parent capsule is destroyed in order to avoid an overcrowding of capsules.

4 Simulation and results

The system architecture described in Section 3 has been tested in the Digital Construction Capability Centre (DC3), which is a laboratory of the Polytechnic University of Marche in Ancona, Italy. According to the definition of Digital Twin (see Section 2.2.1), the developed digital twin mock-up was meant to replicate the typical environment of the construction site, which continuously changes and evolves. For the purpose of this paper, the works at height scenario has been recreated inside the DC3 laboratory, as well as the evolution of the scene that can be encountered on a construction site.

The top image in Figure 4(a) shows the regular configuration of the DC3 laboratory, in which the floor above the changing room is not accessible since no access path exists; hence, there is no fall hazard affecting that floor area. As shown by the virtual replica of this scenario (see the bottom image in Figure 4(a)), the developed system populates the DC3 digital twin with virtual capsules able to wander on the main floor of the laboratory. It can be noticed that no barrier is suggested by the system and the boundary of the floor on the changing rooms is kept clean.

During the execution of the experiment, a real ladder has been placed connecting the laboratory floor and the floor above the changing room, thus allowing workers to reach that area for any reason, e.g. doing works or temporarily laying materials (see the top image in Figure 4(b)). Any human observer would infer that fall hazards have been generated, because workers reaching the higher level may fall down due to the absence of any barriers. Similarly to reality, wandering virtual capsules may reach the floor above the changing room and fall down (see the bottom image in Figure 4(b)). For each fall event occurring in the digital twin, the virtual sensor (described in Section 3.3 and by Figure 3) compares the collision force generated by each impacted capsule with the pain tolerance value of 6 kN, known from literature [27] and regulation [28] about fall-arrest equipment. As a result, if the collision force exceeds the threshold value, the system notifies that falling capsules have experienced harmful impacts and it infers that fall hazards have been introduced. By picking out the positions from which wandering capsules fall down because no fences are installed (see the top image in 4(b)), the virtual replica suggests that barriers must be placed in these areas (see the bottom image in 4(b)).

As a result, according to the logic described in Section 3.3 falling capsules underpin the real-time detection of fall hazards affecting real workers on site. Virtual fences, highlighted in red in the bottom image in Figure 4(b), have been instantiated in those positions from which harmful impacts have taken place. For the purpose of this paper, 300 virtual capsules, moving with a linear speed of 2 m/s, have been instantiated inside the DC3 twin model. Assuming these conditions and using a laptop equipped by an Intel® Core™ i7-8750H CPU 2.20 GHz processor with 16 GB of RAM memory, the digital twin engine takes on average about 2 minutes, after the ladder positioning, to detect all fall hazards affecting the rooms' top floor and place all the related virtual fences (see the bottom image in Figure 4(b)).

It must be noted that, in case a rule-based safety assessment system was implemented (e.g. labelling any surface above a critical height as an hazardous one) it would always suggest that barriers are needed along the perimeter of the higher floor area. In other words, in the simulated scenario the higher level above the rooms (see Figure 4(a)) would be always labelled as hazardous, even in case it is not accessible because the ladder is not present.

5 Conclusion

This paper proposes a system architecture of a digital twin model for H&S management and implements it for real-time identification of fall hazards. A digital twin mock-up of the DC3 laboratory, developed in Unity3D™, mirrors the construction site by means of a UWB localization system and runs looking-ahead simulation in order to detect fall hazards in near real-time. Especially in large construction sites, notifications of safety needs with a delay of a couple of minutes represent a valuable result if compared to the time usually taken by on-site manager to manually detect all fall hazards. Furthermore, off-site managers can benefit from the opportunity, provided by the developed system, of displaying safety alerts and giving suggestions about mitigation measures. The simulation-

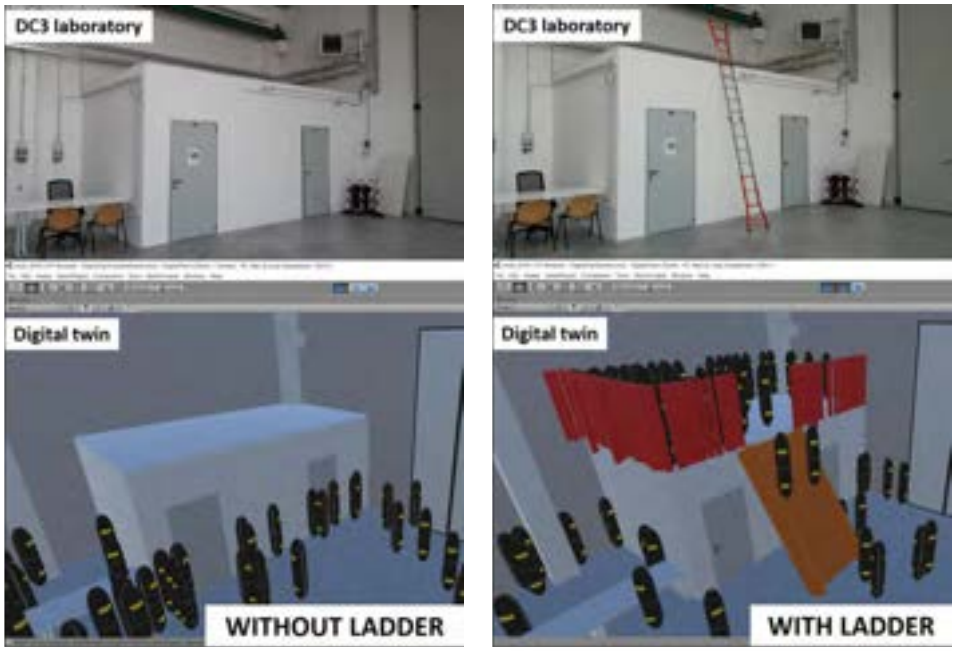

(a) (b)

Figure 4. Construction site for works at height recreated in the DC3 laboratory (top images) compared with its mirroring digital twin (bottom images). The floor above the changing room is not accessible (a) until the ladder has been placed (b).

based approach described in this paper can easily be extended to similar scenarios where the strict application of pre-determined rules cannot work due to the dynamic nature of construction sites. On the overall, simulation results demonstrate that the proposed approach can cover the variety of scenarios in which a rule-based checking systems may fail, since safety assessment is contextual or hard to be modelled by means of pre-determined rules.

References

[1] Zhipeng Zhou, Yang Miang Goh, and Qiming Li. Overview and analysis of safety management studies in the construction industry. *Safety Science*, 72:337–350, 2015. ISSN 18791042. doi:10.1016/j.ssci.2014.10.006. URL `http://dx.doi.org/10.1016/j.ssci.2014.10.006`.

[2] Sijie Zhang, Jochen Teizer, Jin Kook Lee, Charles M. Eastman, and Manu Venugopal. Building Information Modeling (BIM) and Safety: Automatic Safety Checking of Construction Models and Schedules. *Automation in Construction*, 29:183–195, 2013. ISSN 09265805. doi:10.1016/j.autcon.2012.05.006. URL `http://dx.doi.org/10.1016/j.autcon.2012.05.006`.

[3] Hongling Guo, Yantao Yu, and Martin Skitmore. Visualization technology-based construction safety management: A review. *Automation in Construction*, 73:135–144, 2017. ISSN 09265805. doi:10.1016/j.autcon.2016.10.004. URL `http://dx.doi.org/10.1016/j.autcon.2016.10.004`.

[4] Jürgen Melzner, Sijie Zhang, Jochen Teizer, and Hans Joachim Bargstädt. A case study on automated safety compliance checking to assist fall protection design and planning in building information models. *Construction Management and Economics*, 31(6):661–674, 2013. ISSN 01446193. doi:10.1080/01446193.2013.780662.

[5] Sijie Zhang, Kristiina Sulankivi, Markku Kiviniemi, Ilkka Romo, Charles M. Eastman, and Jochen Teizer. BIM-based fall hazard identification and prevention in construction safety planning. *Safety Science*, 72:31–45, 2015. ISSN 18791042. doi:10.1016/j.ssci.2014.08.001. URL `http://dx.doi.org/10.1016/j.ssci.2014.08.001`.

[6] Wei Zhou, Tingsheng Zhao, Wen Liu, and Jingjing Tang. Tower crane safety on construction sites: A complex sociotechnical system perspective. *Safety Science*, 109(June):95–108, 2018. ISSN 18791042. doi:10.1016/j.ssci.2018.05.001.

[7] David J Snowden and M.E. Boone. A Leader's Framework for Decision Making - Harvard Business Review. *Harvard Business Review*, pages 1–8, 2007. ISSN 0017-8012. URL https://hbr.org/2007/11/a-leaders-framework-for-decision-making.

[8] Zhipeng Zhou, Javier Irizarry, and Qiming Li. Applying advanced technology to improve safety management in the construction industry: a literature review. *Construction Management and Economics*, 31(6):606–622, 2013. ISSN 01446193. doi:10.1080/01446193.2013.798423.

[9] Muhammad Arslan, Zainab Riaz, Adnan Khalid Kiani, and Salman Azhar. Real-time environmental monitoring, visualization and notification system for construction H&S management. *Journal of Information Technology in Construction*, 19 (September 2013):72–91, 2014. ISSN 14006529. doi:10.5840/agstm201454111.

[10] Amin Hammad, Shayan Setayeshgar, Cheng Zhang, and Yoosef Asen. Automatic generation of dynamic virtual fences as part of BIM-based prevention program for construction safety. *Proceedings - Winter Simulation Conference*, (December), 2012. ISSN 08917736. doi:10.1109/WSC.2012.6465164.

[11] Chan Sik Park and Hyeon Jin Kim. A framework for construction safety management and visualization system. *Automation in Construction*, 33:95–103, 2013. ISSN 09265805. doi:10.1016/j.autcon.2012.09.012. URL http://dx.doi.org/10.1016/j.autcon.2012.09.012.

[12] Jia Qi, Raja R.A. Issa, Svetlana Olbina, and Jimmie Hinze. Use of building information modeling in design to prevent construction worker falls. *Journal of Computing in Civil Engineering*, 28(5):1–10, 2014. ISSN 08873801. doi:10.1061/(ASCE)CP.1943-5487.0000365.

[13] Trimble Inc. Tekla. URL https://www.tekla.com/.

[14] Nemetschek Inc. Solibri. URL https://www.solibri.com/.

[15] Ying Lu, Qiming Li, Zhipeng Zhou, and Yongliang Deng. Ontology-based knowledge modeling for automated construction safety checking. *Safety Science*, 79:11–18, 2015. ISSN 18791042. doi:10.1016/j.ssci.2015.05.008.

[16] Paul Cilliers. *Complexity & Postmodernism*. 1998. ISBN 0203012259. doi:10.1039/FD9950000C47.

[17] Melanie Mitchell. *Complexity A guided tour*. 2009. ISBN 9789896540821.

[18] Nancy Leveson. A new accident model for engineering safer systems. *Safety Science*, 42(4):237–270, 2004. ISSN 09257535. doi:10.1016/S0925-7535(03)00047-X.

[19] Jens Rasmussen. Risk management in a dynamic society: A modelling problem. *Safety Science*, 27(2-3):183–213, 1997. ISSN 09257535. doi:10.1016/S0925-7535(97)00052-0.

[20] Werner Kritzinger, Matthias Karner, Georg Traar, Jan Henjes, and Wilfried Sihn. Digital Twin in manufacturing: A categorical literature review and classification. *IFAC-PapersOnLine*, 51(11):1016–1022, 2018. ISSN 24058963. doi:10.1016/j.ifacol.2018.08.474.

[21] Siemens Inc. Digital Twin, 2020. URL https://www.plm.automation.siemens.com/global/en/our-story/glossary/digital-twin/24465.

[22] Bentley System Inc. Advancing BIM: Digital Twins. Technical report, Bentley, 2019.

[23] Bentley System Inc. West Cambridge: Developing a digital twin demonstrator The Institute for Manufacturing ' s West Cambridge project is highlighting. pages 92–94, 2017.

[24] William F. Moroney and Brian W. Moroney. Utilizing a microcomputer based flight simulation in teaching human factors in aviation. *Proceedings of the Human Factors Society*, 1:523–527, 1991. ISSN 01635182. doi:10.1518/107118191786754806.

[25] RDF Ltd. IFCEngine DLL Library, 2006. URL http://rdf.bg/product-list/ifc-engine/.

[26] Leonardo Messi, Berardo Naticchia, Alessandro Carbonari, Luigi Ridolfi, and Giuseppe Martino Di Giuda. Development of a Digital Twin Model for Real-Time Assessment of Collision Hazards. pages 14–19, 2020. URL https://doi.org/10.3311/CCC2020-003.

[27] Dave Riches. Analysis and evaluation of different types of test surrogate employed in the dynamic performance testing of fall-arrest equipment CRR 411/2002. 2002.

[28] BS EN 795. BS EN 795:2012, Personal fall protection equipment. Anchor devices. Technical Report 1, 2012.

Automatized Parametric Modeling to Enhance a data-based Maintenance Process for Infrastructure Buildings

Robert Hartung[a], Robin Schönbach[a], Dominic Liepe[a] and Katharina Klemt-Albert[a]

[a]Institute of Construction Management and Digital Engineering, Leibniz Universität Hannover, Germany
E-mail: hartung@icom.uni-hannover.de, info@icom.uni-hannover.de

Abstract –

New innovative and digital approaches, in particular digital methods like Building Information Modeling (BIM), are being used more and more in the Architecture, Engineering and Construction (AEC) Sector. However, most of building operation and maintenance processes still follow conventional processes and are hardly supported by digital databases. Within the widespread field of different infrastructure systems, the railway sector specifically brings a lot of rather old structures and components, which need intense service across their entire lifecycle. Research at Leibniz Universität Hannover explores a fundamental concept for digitally supported maintenance of railway infrastructure to enhance availability, reliability and provide a structured database for the involved stakeholders. Therefore, required methods and processes need to be defined and harmonized for different perspectives like infrastructure operators, monitoring service providers and supervising authorities. Based on digital models, a new approach for a holistic infrastructure management will be introduced and furthermore validated by using a reference project as demonstrator. The paper focuses on the organization, structure and needed level of information within digital models. Further ways of automatization in creation of such models are examined. In conclusion, the risk of damage or breakdown will be reduced and maintenance processes can be initiated on a data-driven basis. By means of this approach, it is possible to change the way from a reactive maintenance processes to efficient repair works in an early stage of damage.

Keywords –

Building Information Modeling; Structural Health Monitoring; shBIM; Digital Maintenance

1 Introduction and Motivation

The German railway and road infrastructure are taking a key role for Germany's economy and public transport, as well as for the European market. Providing a resilient infrastructure is a challenging task with multidimensional complexity [1]. With Germany being in the centre of Europe, six out of nine corridors of the Trans-European Transport Networks (TEN-T) will run across Germany by the estimated completion in 2030. The overall goal is strongly to support the Trans European Internal Market [2]. As shown in Figure 1, Germanys railway network is with more than 33,000 km one of the largest in the European context. This leads on the one hand in high efforts for development and maintenance of the network and its building structures and on the other hand it gives an indication into the complexity of inner-Germanys railway infrastructure.

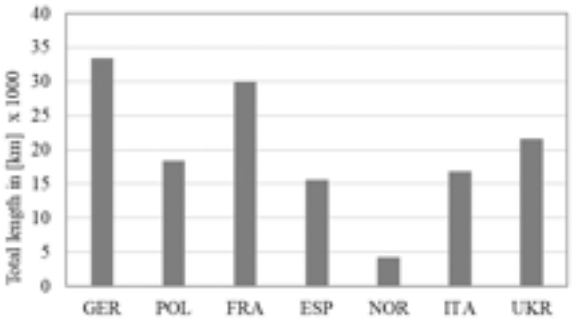

Figure 1. Total length of railway infrastructure in selected European countries, 2016 [3]

With regard to rail, not only the development of new tracks will play an important role in the future. Indeed, retrofitting and especially the maintenance of existing tracks and civil engineering structures like bridges, tunnels or retaining walls will become an enormous challenge for engineering services.

The German railway network operator DB Netz AG is responsible for track maintenance and improvement including civil engineering structures within the infrastructure network in Germany. This covers the responsibilities for the above mentioned 33,000 km tracks, 25,000 bridges and 700 tunnels [4]. The average age of Germany's railway bridges has an age of 73 years with a rising trend.

Bridges are of enormous importance since they are bottlenecks in the infrastructure system. With special regard to railway infrastructure, restrictions or failure in bridge structures have high consequences for the overall track availability and the efficiency of rail-bound traffic. Closed or malfunctioning bridges lead to redirecting trains on non-optimal routes, which leads to a significant loss in the efficiency during operation and high delays.

In order to minimize and prevent the risk of failure, DB Netz carries out a periodic bridge inspection to evaluate the bridge conditions. This binds a high amount of material as well as human resources.

2 Status Quo processes of maintenance

In Germany, the maintenance of civil engineering structures is regulated in a national standard (DIN 1076). Furthermore, there are specific regulations with respect to the infrastructure operator (e. g. Deutsche Bahn, RIL 804 [5]) for Germany's railway network. Due to the later introduced reference project, the aim of the following description of maintenance processes focuses on railway infrastructure in Germany, since the process is highly standardized and regulated by the government.

The established maintenance concepts do not envisage continuous bridge monitoring or condition assessment. The maintenance is usually reactive-oriented and leads to expensive repair works to ensure the system reliability. As can be seen in Figure 2 following the conventional maintenance process results in a periodic assessment of the bridge condition.

The periodic assessment starts with a first obligatory assessment of the bridge structure before start of operation.

The second assessment will be before the end of the warranty period in case of new construction, but in maximum six years after the last assessment. After the end of warranty period the supervision and the assessment will be alternatingly done in a three-year rhythm. The documentation of damages and the information exchange during the process is based on protocols and reports, primarily in paper form or non-object-oriented data bases.

In case of serious damages, solutions for limiting or remedying the damage is approved at a decision conference where all relevant stakeholders are involved. It should be noted, that in all categories the safety of the bridge structure for operation is guaranteed. Otherwise, immediate action would be taken to close the bridge.

Even if small inspections are carried out in the meantime, the periodic condition assessment can lead to a serious lack of information during the inspections. Using Structural Health Monitoring (SHM) in addition to the conventional maintenance process provides a continual assessment in real time (see also Figure 2) [5]. Knowing the real-time-status of the civil engineering structure and evaluating the development in a small-scale, predictive maintenance concepts can be implemented and applied [6]. Appropriate data processing and efficient evaluation mechanisms are required to develop target-orientated treatments.

Data linking between Building Information Modeling (BIM) and Structural Health Monitoring (SHM) to create a holistic data platform with intelligent data organization and data analysis can be a key for a performant status assessment. This new approach is defined as structural health BIM (shBIM) and includes data processing from different sources and different perspectives.

3 Concept shBIM

The key to an innovative digitally supported maintenance approach is a sensor-supported continuous monitoring system, which supports and supplements the traditional manual inspection techniques and leads to a completely new quality of maintenance approaches [7], [8], [9].

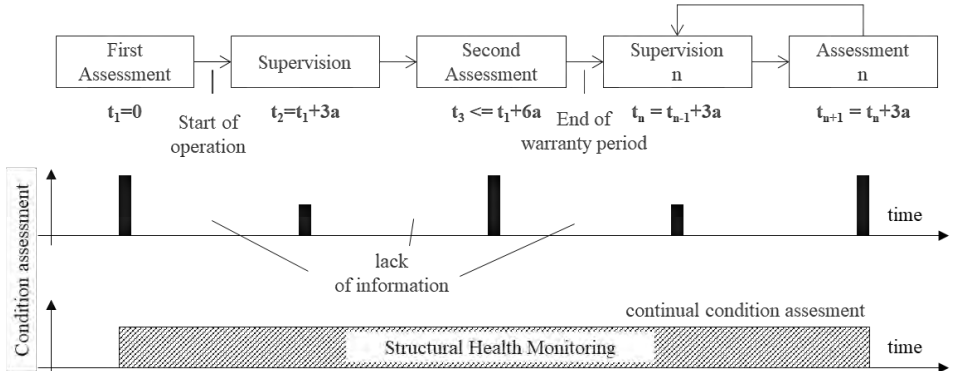

Figure 2. Qualitative degree of condition assessment in the conventional maintenance process (top) compared to a continuous structural health monitoring (bottom)

For this purpose, all information of the inventory, the manual inspection processes as well as from the structure monitoring need to be linked intelligently, edited and provided customized and on demand for the various process stakeholders to enhance the reliability of the rail infrastructure system. The digital method Building Information Modeling provides an ideal conceptual and methodological basis for this collection, linkage and evaluation of multiple data sources and will be extended by the integration of structural health data (monitoring data, inspection data). The overall concept of shBIM is shown in the following Figure 3. The shBIM platform operates as a data hub which is fed by different sources. For generalization, these sources can be defined as three main sources:

First, monitoring data, which includes all data from the SHM systems and dynamic data of the operation phase are linked to an object-oriented building model. The extensive data sets from different monitoring elements like acceleration sensors, strain sensors or temperature sensors will be pre-processed and appropriated for integration in the platform using suitable interfaces (A).

Second, the digital BIM model itself needs to be developed, which includes the information of the infrastructure building and the installed monitoring systems. It contains the object information, geometric information as well as static semantic information and is the central module for the user interface, data visualization and user-oriented data preparation (B).

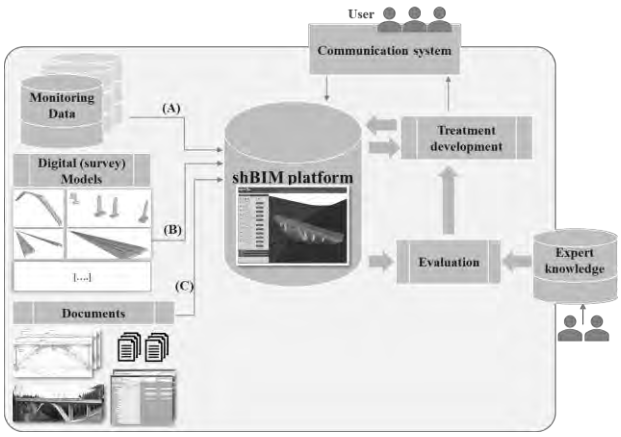

Figure 3. System architecture of the shBIM platform integrating expert knowledge and evaluation processes based on [9]

Third, documents and further data bases, which provide a more detailed description of the construction object, like conventional drawings, photo documentations, reports or maintenance instructions as well as the building documentation of past years, are integrated. They are linked to individual objects or object groups within the shBIM platform (C).

It can be seen that the structuring of the different data sources is strongly dependent on the data sources themselves. Especially for automatization in data analysis and in providing a user-friendly platform, different requirements need to be fulfilled to make evaluations by means of artificial intelligence possible. Merging the information of different sources in an automized way, an evaluation on the health of the examined civil engineering structure can be drawn. The results can be provided for the involved stakeholders to support the maintenance servicing processes. Therefore, also expert know-how can be included in terms of a knowledge-based system. The automated and continuous analysis of the data is used for prediction of probability of occurrence of damage cases as well as for the development of appropriate measures, which are also communicated platform-based. Finally, the information gathered during the service tasks will be recirculated and is used for the assessment of the maintenance measures.

The shBIM approach leads to a comprehensive and user-oriented monitoring data integration. All relevant information is fully integrated into the BIM model and linked to the digital representation objects. To ensure practicability, the question of a convenient level of detail regarding the bridge model needs to be answered. There is a large need for automatization in generating object-oriented models to provide the model as the central data hub to guarantee efficient implementation processes of the existing bridges.

4 Use cases for digital model and needed Information

The use cases for the digital maintenance of bridge structures are diverse. Pursuing different use cases in a digital environment, e.g. manual bridge inspection according to the regulations in RIL 804 [6], supportive monitoring by an SHM system or recalculation to verify the load-bearing capacity of the structure lead to different applications and information densities. However, geometric and semantic requirements of the BIM model need to be formulated for each use case separately.

Important use cases focusing maintenance processes can already be implemented with an abstract information model. An abstract model is defined as a model which consists predominantly of geometric objects without a high demand for geometric detailing, but in accordance to the classification system of Deutsche Bahn. Therefore, the focus is on the semantic description of the objects. It is assumed for use of digital models in maintenance, that the geometry of the components is pushed into the background compared to the specific semantic description [10]. Consequently,

the approach is pursued that abstract geometric objects are sufficient to satisfy the information management in maintenance processes with regard to the introduced structural health monitoring concept. By reducing the geometric detailing, the bridge components can be represented by parameterized objects and thus lead to an enormous time saving in the digital transformation of the documentation of existing bridge buildings. The developed digital models can be integrated as the central data hub for the shBIM platform. Generating the BIM model in an automatized way will reduce errors in manual model creation and enhance efficiency.

- The formulation of the geometric and semantic requirements for each particular use case depends on the internal systems, processes and standardization of the operator. Those are critical input parameters for the automatization process, which will be introduced in the following chapters. The purpose of the abstracted models can be summarized to correspond to the existing standardization of civil engineering structure
- include inventory data for civil engineering structure description
- provide a visual 3D model to improve perception and information management
- allow integration in shBIM-platform for communication and collaboration processes

As already mentioned, this paper focuses on railway infrastructure. However, the developed approach is transferable to any kind of comparable classification system.

5 Concept for parametric modelling

In the following chapter the overall process for an automized abstracted model will be introduced (see Figure 4). In addition, the demonstrated process will be validated on a real reference project within the railway sector in Germany.

5.1 Overall process description

The development of a feasible process for automated model generation is an essential part of the research on digital maintenance of bridge structures. To generate the abstracted models, the approach of parametric modelling with the software Autodesk Revit is used in combination with Dynamo, a visual programming interface. It should be mentioned that the method of visual programming allows an intuitive way of programming, since pre-assembled code blocks are available and can be linked together in a logical way. Instead of having a textual script, the coding follows the logic of the arrangement of the coding blocks (see Figure 5).

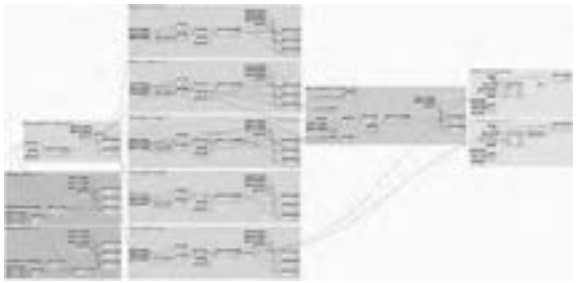

Figure 5. Overview of a part of the script to generate abstracted models using visual programming

This software combination enables the implementation of model generation based on defined geometric and semantic parameters. However, the approach is transferable to alternative software solutions that enable export in open data exchange formats.

At the beginning of the process, the use cases for digital maintenance are defined to obtain the relevant semantic information. In dependence on the semantic description, the possible maximum abstraction level of the building elements is defined, which describe the input parameters for automatization in the modeling process. The abstraction is based on company related specifications, which define structuring and also could include derivations for standard cross sections.

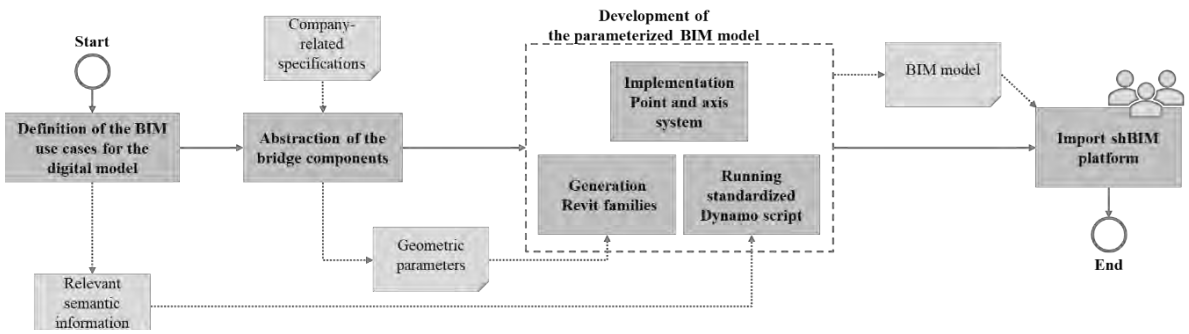

Figure 4. Development process of the abstracted parametrized BIM model

The result of the abstraction is the derivation of geometric input parameters. The development of the parameterized BIM model itself is based on three essential steps. First, the creation of a point-axis-system for the positioning and extrusion of the bridge components need to be set up. The system describes the positioning and the relationships between each abstract component. Components like the abutments can be abstracted as a cube, which follow user-specific input parameters and are placed using a single identification point. Supplementary components like the superstructure, piers and arch are characterized by a start point and an end point, which are represented by the point-axis-system. Between start and end the cross section will be extruded.

The positioning and relationship to other components is realized by the placement of specific points. The arcs are represented in a circle section shaped three-point definition. The extrusion of the rectangle cross section is realized along the curved axis.

Second, the parameterized Revit families based on the identified geometric input parameters from the abstraction process are developed. For cuboid components, the cross section of the element is defined by width and depth. The length of the component is defined due to the length of the corresponding axis.

Third, the creation of a dynamo script that connects the parametric Revit families and the point-axis-system and implements the semantic information from the use cases, has been carried out.

The algorithm goes through the placed families and adds standardized attributes to the components. Then the blank attributes are filled with the values of the specific building. After execution of the script, a geometrically abstracted BIM model is finally generated in an authoring software environment.

An export of the native model to the open standard Industry Foundation Classes (IFC) allows the implementation in the shBIM platform and can be combined with other information such as geodata. This enables the integration of further model data from different disciplines, companies and authoring tools.

In order to be able to practically comprehend the process of geometric abstraction and to demonstrate that a defined information content can be implemented, the development is explained step by step in the following chapter, based on a reference rail infrastructure project.

5.2 Reference project

The *Grubentalbrücke (Railway Bridge Grubental)* is a railway crossing of the "Verkehrsprojekt Deutsche Einheit Nr. 8" (VDE 8), which was completed in 2013. The VDE 8 project is part of an infrastructure program decided by the German government in 1991, to establish the import north-south axis between the cities of Berlin and Munich. The infrastructure is part of the project's subproject 8.1. The Railway Bridge Grubental is one of 24 railway bridges located on the rail route between Nuremberg and Erfurt (see Figure 6), which also interlinks major German cities like Hamburg, Frankfurt and Munich and is of great importance.

The Railway Bridge Grubental is chosen as the reference project since the bridge is characterized by a good data basis and by the existence of an implemented structural health monitoring system. The automated modelling will focus on the geometries of the abutments, piers, superstructure and arch to develop the abstraction process. The implementation of the structural health monitoring components is not part of the automatic process.

Figure 6. Railway Bridge Grubental (left) and the local placement within the high-speed rail network in Germany (right)

5.3 Abstraction of relevant building parts

To start the abstraction process of the Railway Bridge Grubental, two use cases are defined. The exemplary use cases use the semantic information that will be added after the geometric model generation.

Use case A comprises the implementation of a component-specific coding based on the component hierarchy of Deutsche Bahn AG. With the coding it is possible to uniquely identify the individual objects later. This information is model-inherent, directly attached to the component by a corresponding parameter. In addition, almost 450 attributes are taken into account in order to address the maintenance requirements of the existing system with the BIM model. Those parameters can be clustered in different categories. For this use case the cluster results out of the building structure (e.g. abutments, piers, superstructure, etc.), where attributes describe the individual building component in terms of structure, material and environmental conditions. The numerous attributes can be static or be developed dynamically over time. This allows the identification and semantic description of each individual object as

well as the structural health assessment on the level of the component.

Use case B pursues the linking of an as-built drawing in PDF format with the BIM model. Therefore, a unique identification parameter is integrated to the semantic. The linked document can be located on a different location. By mapping the unique object parameter with a document link, a clear allocation is realized.

These use cases have no direct influence on the geometric abstraction, but are intended to show what is possible within linking maintenance information to the model and managing it in the shBIM platform. These use cases present an exemplary method and can be adapted to more detailed considerations.

A geometric abstraction of the Railway Bridge Grubental has been implemented in accordance to the bridge specification regarding the building structure of Deutsche Bahn (see Figure 7). Therefore, it is not important that the exact geometry of the component is created, but their existence is, in order to be identifiable in the classification. The relevant components for the reference project consist of abutments, piers, superstructure and the arch.

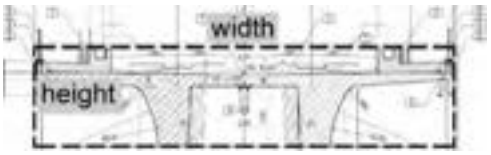

Figure 7. Enveloping rectangle shape to abstract superstructure cross-section

According to the introduced process model, the first step is the description of a point-axis-system for positioning and description of the relationships between the objects (see Figure 8).

A total of 15 points is required to describe the components of the reference railway bridge. For example, the line from point 1 to point 7 is the representation of the superstructure-axis, which is function as extrusion line of the superstructure. The point-axis-system is generated by a standardized dynamo script in accordance to the number and position of the bridge piers. The script acts further as the interface between the developed parameterized Revit families and the point-axis-system. The families are also standardized for cuboid geometries, which have individual compulsion points. The component families are designed in a way that the component is either positioned directly by a pre-defined point in the geometry (abutment) or needs a start and end point to create a corresponding extrusion along the defined axis (piers, superstructure, arch). For the extrusion, an abstracted rectangle cross section as well as the axis itself is parametrized. Focusing on the individual components, they are abstracted in a rectangle shape, so that they take on a simple enveloping shape, here shown using the example of the superstructure.

The superstructure of the reference bridge is a double-webbed slab beam, as continuous beam. The shape is abstracted by stretching a rectangle as a surrounding boundary at the maximum vertical and horizontal shape of the superstructure. The geometric parameters ”height“ and “width“ are created, which define the dimensions of the reduced rectangular cross-section. These parameters are the geometric input for the parameterized Revit families, which can be indicated bridge specific. Using the same method, the other components can also be simplified as cuboid objects, which is the first step to a digital object with a low degree in geometric detailing. The dynamo script has a modular structure and can be supplemented by further components if required or reduced if some components are not needed.

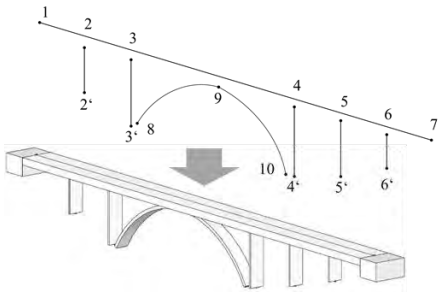

Figure 8. Point and axis system of the abstracted Railway Bridge Grubental and abstract geometric with automated model generation

After the geometry has been created by the script, the semantic information can be added in the next step. For this purpose, an attribute editor forms the end of the algorithm. The attribute editor adds standard attributes from the today’s maintenance system and add the bridge specific values based on a csv-file (use case A). The csv-file is generated as a bridge specific export and is imported as an array to the dynamo procedure afterwards. The last step in accordance to the introduced process is the export of the model for integration to the shBIM platform.

5.4 Evaluation of different Level of Detail

To evaluate the level of detail, a second digital model of the reference railway bridge was modelled in another software tool and has been exported in the open, international standard IFC. This model is characterized by a high level of detail corresponding to the detailed design (see Figure 9). It is used as a reference structure to validate the quality of the abstraction.

Figure 9. Precisely modelled Railway Bridge Grubental on the basis of the detailed design

The validation of the model quality is divided into the criteria of geometric and semantic parameterization and interoperability. During the validation it was checked whether the implemented geometric input parameters like "width_abutment", "height_ superstructure" or "thickness_pier" were generated and transferred correctly.

The model abstraction of the selected bridge components resulted in a reduction of the geometric objects from 4936 of the precise modelling to 9 using the abstract approach. When the two models are overlaid, it becomes clear that the two models differ only in points of geometric detailing of the individual objects and missing equipment components, which are not considered in the abstraction e.g. railings, track, etc. Where in the detailed model the abutments consist out of several components such as swing and chamber walls and the support bench, the abstraction consists of one abutment representation-object. However, bridge specific dimensions such as bridge length, spans, pier heights and the width of the superstructure do not differ from the model based on the detailed design.

The validation of the abstract model with regard to interoperability is of crucial importance. The generated BIM model based on the defined use cases for digital maintenance serves as the data hub in the shBIM platform. Therefore, after integration in the shBIM platform the quality of the abstract BIM model is also validated.

5.5 Integration in shBIM platform

Due to many stakeholders involved in design, construction and operation, this specific platform must guarantee a manufacturer-independent data exchange format, such as the internationally accepted IFC format for open BIM data exchange. The model quality and usability are primarily dependent on the data transfer quality of the interface.

The basis for the development of the shBIM platform is the Common Data Environment (CDE) "Squirrel". To make the abstract model available for maintenance purposes, the last process step is the import of the abstract bridge model into the CDE (see Figure 10) via the open BIM format IFC.

Figure 10. View of the imported BIM model within the CDE-based shBIM platform

On the left side of the user interface, the model structure of the partial model for revisions as well as the partial model management with different functionalities is shown. On the right side, it is possible for each individual user of the CDE to look at the semantics of the bridge elements. Individual elements of the digital bridge model can be selected and therefore their individual properties can be viewed (use case A). Other geometric objects, such as the sensor technology of the SHM system, could also be imported as a separate partial model within the CDE. Specific data, related to the structure or the sensor technology, can be linked to the CDE using a linked data approach (use case B), which means an allocation of each document in the platform to a unique identifier at the building component it belongs to. The overarching objective is to organise and manage all prepared information and processed data within the shBIM concept via the CDE platform. The platform is supposed to support the whole structural health monitoring process of the railway bridge with data and information management throughout the whole life cycle of the railway bridge. Moreover, the shBIM platform will ensure the traceability of edited information and data as well as the documentation of performed maintenance services within the digital BIM model. The access of the shBIM platform is defined via an individual and project-specific authorisation concept.

5.6 Discussion

Deutsche Bahn AG maintains more than 25,000 bridge structures. Detailed 3D modelling for digital maintenance approaches on the basis of the detailed design or even more precisely the actual condition (as built) is economically questionable. The presented approach of abstracted geometric modelling of the bridge using automated generation algorithms shows a method to reduce the effort. It was explained that the semantic information of the digital use cases is in many cases more important for the maintenance processes than the geometric detail depth. In addition, simple

geometric bodies are easier to check during creation and processing. Regarding the interoperability of the models, simple geometry also has advantages. The IFC format has established itself as an international and manufacturer-neutral data exchange format. However, development is ongoing and will continue to be subject to constant changes over the next few years, especially with regard to new infrastructure specifications, which are expected in the next years. Simple geometric shapes guarantee significantly fewer data exchange errors.

Further, the maintenance operator will not be in false expectations due to a reputed exact model. Rather, the stakeholders involved in maintenance are aware that this is an abstraction and that exact geometrical dimensions must be determined, if applicable use cases require a higher level of development. Since bridges along the lifecycle are subjected to modifications, it cannot be assumed, that detailed design from several decades ago and digital models which are based on those, correspond to the status quo. By classifying the bridge types and developing an abstraction standard for each type, an area-wide implementation of automated creation of BIM models for the shBIM platform can be achieved.

Continuous and further detailing of abstract models due to special tasks, such as renewal or repair measures, can be done afterwards.

6 Conclusion and Outlook

In summary the research has shown, that it is possible to highly automate the way of modeling to generate digital models for specific use cases. Abstract models are an adequate option to realize sufficient information management and visualization for various maintenance measures.

However, there is still a lack of description to grasp the manifoldness of bridges and model them in a standardized parametric way. In the next step, the automatization method should be enrolled to a higher number of relevant civil engineering structures from different years of edification and from different structural types to implement specifics in the superstructure and the overall structural system. Open formats can provide a life cycle-oriented, comprehensible and transparent information management in a common data environment, which allows different stakeholders to access. The approach should be exposed for further use cases e.g. the integration of damage assessment and repair measures.

Acknowledgement
This research is supported by the Federal Ministry of Transport and Digital Infrastructure (BMVI) in the funding program mFUND (FKZ: 19F2075A).

References

[1] Klemt-Albert, K., Hartung, R. and Bahlau, S. Enhancing Resilience of Traffic Networks with a Focus on Impacts of Neuralgic Points Like Urban Tunnels. In *Resilience Engineering for Urban Tunnels,* pages 55-70, Reston, USA, 2018.

[2] European Commission. Trans-European transport network (TENtec), https://ec.europa.eu/transport/infrastructure/tentec/tentec-portal/site/index_en.htm, Accessed: 26/05/2020.

[3] Weltbank, World Development Indicators. Länge der Schieneninfrastruktur in ausgewählten Ländern. Online: http://databank.worldbank.org/data/source/world-development-indicators, Accessed: 26/05/2020.

[4] Deutsche Bahn. Infrastrukturzustands- und entwicklungsbericht 2017, *Deutsche Bahn AG*, 2018.

[5] Hartung, R., Senger, L., Klemt-Albert, K. Linking Building Information Modeling and Structural Health Monitoring for reliable railway infrastructure. In *Proceedings of the 29th European Safety and Reliability Conference,* pages 596-603, Hannover, Germany, 2019.

[6] Marx, S., Krontal, L., Tamms, K. Monitoring von Brückenbauwerken als Werkzeug der Bauüberwachung. In *Bautechnik 92 (2),* pages 123-133, Germany, 2015.

[7] Deutsche Bahn Netz AG. Eisenbahnbrücken (und sonstige Ingenieurbauwerke) planen, bauen und instandhalten – Inspektion von Ingenieurbauwerken (8001), *Deutsche Bahn AG,* 2015.

[8] Hartung, R., et. al. Evaluation of Structural Health Monitoring Systems in Bridge Engineering for Increase of Safety in Operations, in *Proceedings of the 30th European Safety and Reliability Conference and the 15th Probabilistic Safety Assessment and Management Conference,* pages 1-8, Venice, Italy, 2020.

[9] Chan, B., Guan, H., et. al. Defining a conceptual framework for the integration of modelling and advanced imaging for improving the reliability and efficiency of bridge assessments. In *Journal of Civil Structural Health Monitoring*, pages 703-714, Berlin/Heidelberg, Germany, 2016.

[10] Isailovic, D., Stojanovic, V., Trapp, M., Richter, R., Hajdin, R., Döllner, J. Bridge damage: Detection, IFC-based semantic enrichment and visualization. In *Automation in Construction*, Vol. 112, Amsterdam, Netherlands, 2020.

Gamification and BIM

Teaching the BIM Method through a Gamified, Collaborative Approach

C. Pütz[a]; C. Heins[b]; M. Helmus[a]; A. Meins-Becker[a]

[a]Chair of Construction Management, University of Wuppertal, Germany
[b] Institute for Database Oriented Design, Jade University of Applied Sciences Oldenburg, Germany
E-mail:puetz@uni-wuppertal.de, Christian.heins@jade-hs.de

Abstract –

Due to the continuous improvement in data acquisition, storage and evaluation, digital technologies are penetrating ever deeper into the operational business of the construction industry. Modern information and communication systems are at the heart of digital working methods. They encompass the factors - People, Processes and Data -, which are all decisive for successful project management. In the context of digitizing a building project, it is necessary to harmonize these factors. When implementing digitization strategies, the focus is often on finding suitable technical solutions and defining processes. However, the human factor continues to play a decisive role in the construction, as a high degree of coordination between the parties involved in the construction process is necessary in order to produce safe and functional unique buildings. In order to establish the methodology of Building Information Modeling successfully in the construction industry in the long term, it is therefore essential to involve the employees in the developments.

The human factor becomes all the more important in large construction projects, which also involve partners across national borders. The approaches to new methods, as is necessary in the case of BIM, sometimes differ greatly due to cultural differences in the international context and cause problems of understanding, even though certain software applications, for example, work perfectly. In addition, employees often experience personal inhibitions that prevent the consistent use of new methods.

The research project "BIM Game", in which partners from several European countries worked together puts the human factor in the forefront of the BIM methodology and develops new ways of communicating the basic ideas of the method already in the education of students. The project focuses on two main points: Firstly, the linking of students via a Learning Management System, which reflects the work in project rooms of a real construction project and thus promotes collaboration. On the other hand, the use of gamification - the application of game elements as known from computer games, for example - to lower inhibition thresholds and increase motivation to deal with the topic. The aim of the project is to teach future project participants how to collaborate in a digital project, rather than merely addressing technical issues. The students slip into different roles and work collaboratively and digitally on a real scenario. They do not receive feedback through classic evaluation systems such as grades, but through badges and the achievement of levels.

Keywords –

collaborative learning platform; learning management system; gamification; BIM Game; game design elements; Building Information Modeling

1 Introduction

The digitization of the construction industry is currently being driven forward primarily by the increasingly widespread use of the methodology Building Information Modeling (BIM). When talking about BIM, the acronym does not mean a software application or the mere work on a 3D model [1]. BIM describes "a collaborative working methodology that uses digital models of a building to consistently capture, manage, and transparently communicate information and data relevant to its lifecycle or to hand it over for further processing." [2] The new working methodology thus requires a holistic approach to planning, construction, operation and dismantling. For the successful implementation of the approach, in addition to suitable software solutions, a cultural change in the construction industry is required. Collaboration on a construction project must be thought of in a team-oriented way in

order to reduce interfaces and enable work in a common data environment (CDE). For this purpose, it is advisable to adapt business processes and familiar forms of cooperation [3].

Working with the BIM methodology therefore requires changes in three areas of current mode of operation. First, processes in the company must be adapted to the new methodology. In many cases, it is first necessary to identify and record the processes currently being carried out. Following this, these processes can be digitized and adapted to work with BIM. In a second step, the implementation of the newly designed processes requires the selection of suitable software offers. The most suitable offer for one's own needs must be selected from the large market for BIM software. For this purpose, prior modelling of the processes is helpful, as these can serve as a kind of demand list for the software selection. The third step that should not be underestimated is the people in the project who have to implement the new processes and use the software. Any well-considered steps in the process and software selection can lose their success if the employees are not appropriately involved in the further development. The discussion about BIM currently focuses mostly on software and processes. Important to remember ist that people traditionally shy away from change [4]. Training in BIM is therefore essential for the successful application of BIM.

There are three ways to prepare personnel for working with the BIM methodology [5]:

1. new employees with appropriate knowledge are hired and implement the specific method in the company
2. BIM skills are purchased through cooperation with external partners
3. Ones own employees are trained in the application of the specific method.

The former variant is often difficult to implement in times of a shortage of junior staff. Employees with BIM skills are in demand on the job market and are difficult to find. Apart from the costs, the purchase of external skills brings with it a certain dependency and is usually associated with trust problems. This strategy can provide an introduction to working with BIM, but it must then be possible to continue the implementation independently. The further training of one's own employees involves a certain amount of effort and requires that acceptance hurdles among employees can be overcome [6].

The BIM Game research project addresses the problem of how to prepare employees in the construction industry for working with the BIM methodology using their own resources and trains students as future employees with BIM competencies. The sluggish implementation of the BIM methodology to date also shows that training courses do not meet the demand [7]. Classical training formats can convey the new form of cooperation in theory, but training based on frontal teaching will not be able to convey practice application in detail.

2 Idea of the BIM Game

The idea of the BIM Game is therefore to rethink training in the field of BIM. Instead of classical lectures, the aim is to teach the method in the cooperative collaboration that the BIM methodology demands. The BIM Game research project, led by gip Besancon, is a cooperation of various universities, colleges, training centers and software companies from five European countries (University of Wuppertal, Jade University of Applied Sciences Oldenburg, Lycee du Bois Mouchart France, Universided de Castilla la Mancha, Université de Liège, datacomp, Pôle énergie Franche Comté). The aim of this inter-European cooperation is to find a common understanding of the BIM methodology and to teach the methodology to students, trainees and experienced professionals in a fun, collaborative way using real-life examples and projects. Regarding the preparation of personnel for working with the BIM methodology it addresses the first and third option. Students should acquire the ability to use BIM in a targeted manner in professional practice in order to establish them as sought-after actors and partners in business and society. Through the involvement of experienced experts, people who are already established on the labour market also learn the superordinate or specific use of BIM.

Playful learning is the most intuitive form of learning that people know. Even at a very young age, new skills are learned through play and adaptation to new challenges is tested [8] [9]. Only with increasing age does learning become less and less playful. The fact that adults still like to play is shown, among other things, by the high user numbers of online games across all ages and genders[10]. The BIM Game makes use of this natural play instinct and thus provides a higher motivation to deal with the topic of BIM and increases the participants knowledge about it. The method behind this is called gamification. Gamification stands for the transfer of typical game design elements into non-game contexts [11]. The goal of gamification is to make everyday training situations, which have nothing to do with games, more interesting by enriching game design elements such as a narrative, avatars, levels, points or badges. The goal is to achieve a change in behaviour and an increase in motivation [12].

Beyond the increase of motivation during the training, the project uses gamification to increase learning effects through the activation of long-term memory. “If you

want to explain something to someone else, you must first understand it yourself, e.g. have read or heard it. Whoever tries out or applies something already links the entire course of events with the actual information, which is why the result is anchored more firmly in the brain as if he had only observed the same result in someone else" [13] This effect is achieved by actively absorbing information through multiple cognitive channels (seeing, applying and experiencing) during the game and by incorporating repetition effects of specific thematic areas throughout the total game. This is to be realized by an active and collaborative processing of application-related building scenarios in an environment embedded by computer game elements. This way of gathering information increases the willingness to learn and lowers the barriers to dealing with the complex topics of the holistic BIM work methodology. The goal is to encourage self-study in a playful way.

2.1 Practical implementation of the project

Between 2016 and 2019, 10 events were organised as part of the BIM Game, which introduced students, trainees and experienced professionals to the BIM methodology in the described collaborative, playful way. Each of these events followed a basically identical structure. To ensure practical relevance, the BIM methodology was taught using scenarios from real professional practice. These scenarios were enriched with game design elements to create a collaborative, playful and motivating learning atmosphere. Figure 1 shows the game design elements integrated in each scenario:

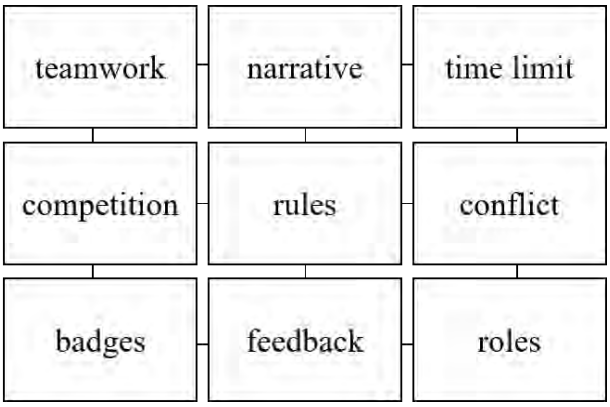

Figure 1. game design elements of scenarios used in the BIM Game

The **narrative** is always based on a scenario of a real construction project. The scenarios correspond to situations from different life cycle phases of a construction project. To classify the scenarios, six life cycle phases from project development to project operation have been defined. This ensures that participants learn that the BIM methodology goes beyond application examples in the planning phase and is relevant for the entire life cycle of a building. The design of the scenarios allowes them to be played through within one day. Depending on the group and event, they can be shortened or extended to half a day or two days by shortening or adding to the task. The content of all scenarios is based on the BIM guidelines ISO 19650. In order to be able to respond individually to the previous knowledge of the different user groups of the BIM Game, each scenario was designed with a unique task and a different focus as well as with different levels of difficulty. All scenarios were developed primarily with the goal of understanding the roles and their tasks in a multinational collaboration in order to strengthen teamwork in an international construction process.

Teamwork is an important part of all scenarios, since BIM projects are never implemented by one person alone, but are always in interdisciplinary teams that have to get along well with each other. Each team member is assigned the **role** of a participant that he or she is not familiar with from the usual project business. An architect, for example, slips into the role of a craftsman, a planning engineer into that of a facility manager. This is intended to create more understanding for the project partners' views of a project. Another aspect of teamwork is **multinational cooperation**. Participants of different nationalities are always mixed so that cooperation with foreign partners, communication in English and the adaptation of different approaches to problems are trained.

Each scenario and each subtask must always be processed within a certain time limit. This simulates the tight schedules of real construction projects and puts the participants under time pressure, which makes cooperation with the project participants indispensable.

For each scenario the participants are given **rules** in the task definition. These can also deliberately contain **conflicts** that need to be resolved within the team and, if necessary, in communication with other participants.

The entire BIM Game and thus also the participation in the individual scenarios is designed as a **competition**. The individual teams compete against each other in the fight for the overall victory. In addition, **badges** are awarded e.g. for the most sustainable project. Winning is always connected with a reward. Extensive **feedback** is given for all teams on the work they have done, which should prepare them for further work with the BIM method.

The central element for the implementation of the scenarios is a digital platform based on common data environments (CDE) from construction projects. The participants process the scenarios completely online

using the platform. They are given the opportunity to communicate via chat functions, files can be stored and exchanged, appointments can be planned and notifications send to others. In order not to prefer a commercial provider of CDE, an open source offer was tailored to the needs of the project. The Learning management system (LMS) nextcloud has been adapted to come close to working in a CDE (see Figure 2).

Figure 2. Extract from the data management area of the platform

The platform serves as a basis and link point for all steps in the scenario processing. The task is provided via nextcloud and all further task parts are organised, processed and completed by the participants via the platform. This set up also made it possible, when organising an event in France, to integrate participants from Spain and Poland who were not on site.

2.2 Example of a scenario

In order to bring closer what exactly a scenario looks like, an example is presented below. In November 2018, 13 students in the field of architecture and civil engineering took part in the described scenario, working in three groups.

In order to bring building product traceability and the application of BIM on the construction site closer, a construction site was simulated in the scenario using Lego bricks. These enabled both a design for a building to be produced and the design to be implemented on the "construction site" within one day. The participants worked through the scenario in the roles of client, BIM manager, architect, engineer, craftsman and supplier. A team of architects and engineers had to develop a design in compliance with budget and sustainability requirements (different stones = different properties). This was implemented "on the construction site". With the help of a BIM viewer, the construction workers could view the design on a tablet and implement it accordingly. Using RFID tags on the individual bricks, the progress of the construction work could be monitored by scanning the tags during installation, then creating an as-built model and tracing the building products in the finished building.

Figure 3. a participant working on the 3D model

The client also acted as a jury in the scenario, evaluating the results and giving feedback to the groups on their solutions (see Figure 4).

Figure 4. client giving feedback to the groups

2.3 Evaluation of events

Selected events were evaluated to continuously improve the scenarios and to check whether the way of teaching the BIM methodology is successful. The evaluation method was based on questionnaires that the participants answered after the scenarios were completed. Over a period of one year and within the framework of four different scenarios, a total of 50 participants were surveyed. The items of the questionnaire were designed as multiple choice questions. Non-symmetrical answer scales were used to avoid an accumulation of neutral answers.

Two aspects were particularly important for the project: Do the participants like the way the method is communicated via collaborative, playful methods and do the participants get a good, lasting impression of the BIM methodology in a short time?

76% of the participants stated that they had gained a good insight into working with the BIM methodology. For the remaining participants, technical problems, e.g.

poor Internet connection, were the main reason why they did not get the desired insight into the methodology. The learning method about collaborative scenarios was positively evaluated by 90% of the participants (see Figure 5).

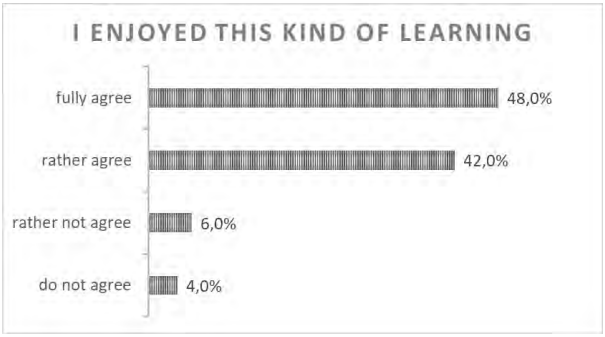

Figure 5. satisfaction of participants with the kind of learning

78% said they had fun and were motivated during the scenario. The idea of competition with other teams motivated 96% of the participants. The gamification method, which has rarely been used in construction training, would be used more frequently by 94% after the BIM game (see Figure 6).

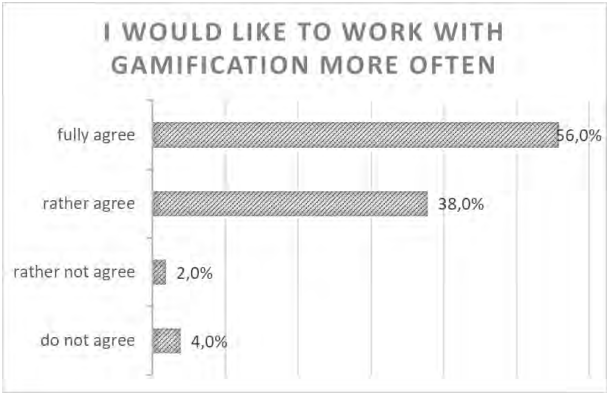

Figure 6. preference of the participants to work with gamification more often

Since it is not only the unique pleasure of teaching that is important for successful application of the BIM methodology, the participants were asked to give their opinion on the durability of what they had learned. More than 70% of the participants stated that they expected the learning content to be more durable than with traditional learning methods. A further 16% rated the durability the same, regardless of the learning methods. The verificaton whether the BIM methodoligy was understood in the context of the scenarios was not done via the questionnaires, but was ensured by presenting the results to the jury.

3 Findings

The study shows that success with the BIM Game has been achieved both in terms of learning the BIM methodoligy and the fun of learning. In comparison to their usual learning settings, the participants were more motivated and felt that they had fun. The playful, collaborative design was also able to help them gain a good insight into working with the BIM methodology and consolidate what they had learned in the long term.

In addition to the positive results of the study, the potential was revealed to make corresponding scenarios more effective in the future. For a digital working method such as BIM, a corresponding equipment of software and hardware is an absolute prerequisite in the learning context. If problems with software or hardware occurred during the events, the positive feedback from the participants decreased. Many training centres and universities have a lot of catching up to do in this area in order to prepare their trainees and students for working life.

Language barriers prevented even more successful results from the participants despite all digitisation. Although collaboration is largely based on technical systems, the simple factor of whether or not participants can talk about complex problems with their counterpart is still an issue that should not be neglected. For a common language on the subject of BIM across national borders, there is also a lack of standardization in the field of BIM. With their understanding of the methodology, each partner works in proprietary systems that inhibit collaborative work. The ISO 19650 standard indeed provides initial guidelines in the direction of standardization, but remains shallow and does not provide enough details to help in the daily work with BIM in the operative business.

4 Conclusion

The study conducted in the context of the BIM Game project shows that alternative learning methods are positively accepted and their application should be further pursued. The implementation of the collaborative working method within the learning phase ensures long-term learning outcomes.

The use of gamification motivates learners to deal with the subject matter more intensely and to get involved with the topic.

5 Suggestions on further research

Within the BIM Game a limited number of game design elements was used. The team was careful in using game design elements to avoid overloading the scenarios.

For future scenarios the use of additional game design elements would be useful, as well as an investigation of how the individual elements work. There has been little research on this so far.

Further information on the project can be found on www.bimgame.eu. The project was co-funded by the Erasmus+ Programme of the European Union.

References

[1] Helmus M. Die Potenziale der Digitalisierung der Wertschöpfungskette Bau entdecken. On-line: http://www.biminstitut.de/start, Accessed: 12/06/2020.
[2] Bundesministerium für Verkehr und digitale Infrastruktur. *Stufenplan Digitales Planen und Bauen*: page 4, Berlin, 2015.
[3] Helmus M. Die Potenziale der Digitalisierung der Wertschöpfungskette Bau entdecken. On-line: http://www.biminstitut.de/start, Accessed: 10/06/2020.
[4] Oakland J. S. and Tanner S. Successful Change Management. *Total Quality Management & Business Excellence*, 18:1-2: 11-12, 2007.
[5] Meins-Becker A. *Die eigenen Digitalisierungsstrategie finden*. Architektenkammer NRW, page 25, Düsseldorf, Germany. 2019.
[6] Hartmann M. *Rekrutierung in einer zukunftsorientierten Arbeitswelt*. Springer Gabler. Hamburg, Germany. 2015.
[7] Helmus M. *BIM-Forschung für kleine und mittlere Unternehmen*. DerBauUnternehmer, 2, 2017.
[8] Oerter R. *Psychologie des Spiels: ein handlungstheoretischer Ansatz*. Quintessenz Verlags-GmbH, München, 1993.
[9] Huizinga J. *Homo Ludens: A Study of the Play-Element in Culture*. Routledge & Kegan Paul Ltd, London, 1949.
[10] Deterding S. Gamification: designing for motivation. *Interactions*, 19(4): 14, 2012.
[11] Deterding S. *From Game Design Elements to Gamefulness: Defining "Gamification"*. In 15th International Academic MindTrek Conference, page 9, Tampere, Finland, 2011.
[12] Sailer M. *Die Wirkung von Gamification auf Motivation und Leistung*. Springer, Wiesbaden, Germany, 2016.
[13] Schroer K. *Die Psychologie des Lernens – Wie funktioniert Lernen?* On-line: https://www.fernstudieren.de/im-studium/effektives-lernen/die-psychologie-des-lernens/, Accessed: 09/06/2020.

Opportunities and Challenges of Digital Twin Applications in Modular Integrated Construction

M.C. Xie[a] and W. Pan[a]

[a]Department of Civil Engineering, The University of Hong Kong, Hong Kong, China
E-mail: mcxie@connect.hku.hk, wpan@hku.hk

Abstract –

Digital twin (DT) is commonly known as a virtual model of a physical object, a process or a system. In order to create DT, the emphasis is on building a Cyber-Physical System (CPS), where information collected from physical processes is used for computation to generate a real-time monitoring cyber model. At the same time, changes of the cyber model will either be used for prediction or reflection in the physical system to achieve the control function. With the development of digital and information communication technologies, DT has been applied in various areas such as manufacturing and aerospace industries. However, studies on the application of DT in the building construction sector were limited. Such studies were particularly rare about volumetric modular building which has attracted a burgeoning interest in both academia and practice globally.

This paper aims to contribute a better understanding of integrating the use of DT for Modular Integrated Construction (MiC) by examining the opportunities and challenges. The paper first reviews the state-of-the-art DT applications across various industries, and then focuses on publications about DT applications in the building construction sector through conducting a systematic search of literature using Scopus. After review and analysis of the identified publications, the paper explores the opportunities and challenges of applying DT in MiC. The review results show that DT is often considered with other digital technologies for integration. A conceptual framework is developed for applying DT in module installation in MiC within the context of Hong Kong as a typical case of high-density cities. Promising opportunities with huge benefits are speculated from the application of DT in MiC, including enhanced coordination of logistics and construction management by using DT to monitor on-site progress during the module installation stage. Nevertheless, challenges are also identified, which exist in not only the sensing technology and cyber system, but also the social-political environment supporting innovation and regulation. The developed framework should provide a useful guide to address the challenges and shape future research on DT in MiC.

Keywords –

Digital Twin (DT); Cyber-Physical System (CPS); Modular Integrated Construction (MiC); Smart Construction

1 Introduction

The construction industry is on a pace from being low-tech towards being innovative, in order to address problems and challenges such as low productivity and profitability and skills shortages facing by the industry [1]. Digital twin (DT) as an emerging digital technology has obtained more and more attention across different industries, particularly in the manufacturing industry over the past few years [2], which can also be a possible solution for the construction industry.

It is acknowledged that the concept of DT was firstly introduced in a presentation by Dr Grieves in 2002, which contains four essential elements of the DT: real space, virtual space and dual links for data transmission between real space and virtual space [3]. After that, the name of DT was raised in a roadmap of National Aeronautics and Space Administration (NASA) to describe a virtual digital product of an aircraft's flight system [4] and has been used ever since. DT is defined as a real-time virtual representation of not only a system, but also a process [5] or a physical object [6].

With the development of digital and information communication technologies, DT has been applied in several industries with wide-ranging demonstrated benefits. For example, the use of DT in the aviation industry helps engineers to quickly find out critical weak spots and to predict the future state of the asset [7]. In the manufacturing industry, DT of a physical product enhances collaboration between customers and designers, where communications are faster and more transparent with the function of automatic real time data acquisition [8]. However, studies on the application of

DT in the building construction sector are limited. Such studies of DT are particularly rare about volumetric modular building construction which has attracted a burgeoning interest in both academia and practice globally. Therefore, this paper aims to achieve the following objectives:

1. Review and elicit the state-of-the-art DT applications particularly in the field of building construction sector;
2. Explore the opportunities and challenges to adopt DT in volumetric modular building construction through the analysis of reviewed publications;
3. Develop a conceptual framework for applying DT in Modular Integrated Construction (MiC) in the context of Hong Kong as a typical case; and
4. Identify current gaps and challenges for future research.

Following this introduction, Section 2 explains the background including the state-of-the-art DT applications across various industries, the context of Hong Kong and delimitation of research scope. Section 3 elaborates the methodological approach for the systematic review. Section 4 presents results of the review on the identified publications, and discusses the results from the perspectives of opportunities, challenges and current research limitations. Section 5 proposes a framework of applying DT in MiC considering the scenario of module installation. Section 6 draws conclusions, as well as recommends prospects for future research.

2 Background

2.1 DT applications across industries

Researchers have contributed to the analysis of publications on DT applications across industries. Tao et al. [9] reviewed fifty papers in the manufacturing industry and found prognostics and health management (PHM) as the most popular application area. Enders and Hossbach [10] provided a cross-industry overview of DT applications, and classified ten industrial sectors where DT is applied, including manufacturing, aerospace, energy, automotive, marine, petroleum, agricultural, healthcare, public sector and mining (see Figure 1), where the manufacturing is the most popular industry applying DT. They also found that the applications of DT can be divided into three purposes including simulation, monitoring and control (see Figure 2).

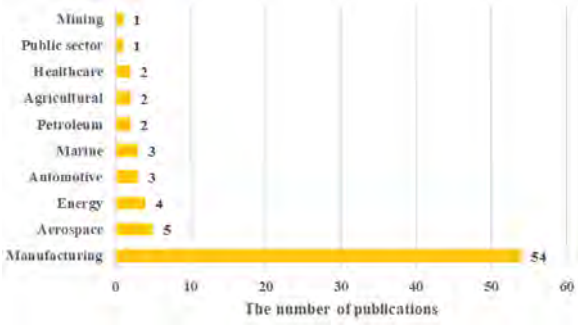

Figure 1. Distribution of relevant publications regarding DT applications across industries identified in the study of Enders and Hossbach [10]

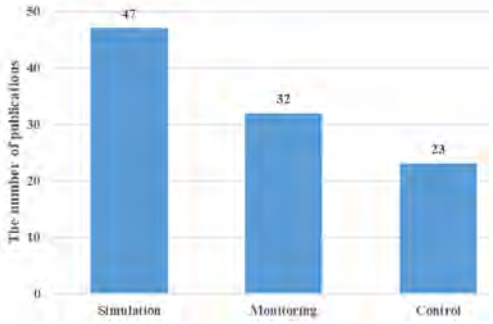

Figure 2. Distribution of relevant publications regarding purposes of DT applications identified in the study of Enders and Hossbach [10]

Even though some studies have been conducted on DT applications in the building sector, most of them focus on post-construction stage so that asset owners can better handle operation and maintenance works. For example, Khajavi et al. [11] established a DT of a building façade in order to collect environmental lighting, ambient temperature and relative humidity, which are used to reduce the overall management and operational cost. Lu et al. [12] developed a DT-enabled anomaly detection system for asset monitoring and validated it in a case study of the heating, ventilation and air-cooling (HVAC) system.

Nevertheless, studies on the application of DT in the building construction sector are limited. The potentials of DT application in MiC are still not clear. Therefore, literature review of relevant publications was carried out in this paper in order to explore opportunities and challenges of DT applications in MiC.

2.2 Hong Kong context

The construction industry in Hong Kong plays an important role in economic growth and social development, which contributed 4.5% of Gross

Domestic Product (GDP) in 2018 [13]. However, the Hong Kong construction industry is facing severe challenges including labour shortage, aging workforce and escalating cost [1]. In order to address these challenges, it was announced in the 2017 and 2018 Policy Address of the Government of the Hong Kong Special Administrative Region (HKSAR) that the Government should lead and promote the adoption of MiC in the construction industry [14, 15].

MiC represents the most advanced level of offsite construction [16], which is first defined by Pan and Hon [17] as "*a game-changing disruptively-innovative approach to transforming fragmented site-based construction of buildings and facilities into integrated value-driven production and assembly of prefinished modules with the opportunity to realise enhanced quality, productivity, safety and sustainability*". MiC is a unique term used in Hong Kong, which belongs to volumetric modular building construction. Compared with conventional construction methods, MiC has distinct characteristics that the majority of on-site works are transferred to a factory for production of modules. In a factory, structural works, architectural works and building service works of modules were completed partially, and then following by transportation of modules to the construction site for installation and assembly. Several MiC pilot projects have been initiated in order to prompt its wide adoption in Hong Kong.

2.3 Delimitation of research scope

In this paper, Hong Kong is selected as a typical case of the high-density city to explore opportunities and develop the conceptual framework for applying DT in MiC. Regarding a building project adopting MiC, the construction lifecycle from offsite production of modules to onsite completion of construction works is the most concerned part, excluding design and operation and maintenance stages. This is because the most significant difference between MiC and conventional construction practices is the change of construction processes. As offsite production of modules in a factory is similar to works in the manufacturing industry, the research scope is limited to onsite works of a MiC project (i.e., module installation and other onsite building works).

3 Methodology

The research approach in this paper for searching and analysing relevant publications and exploring opportunities and challenges of DT applications in MiC, is adopted as proposed by Boje et al. [18]. The overall research methodology process including three steps is provided in Figure 3.

Firstly, publications related to the application of DT in the building construction sector were searched and identified. The search strategy included electronic databases of Scopus. The search terms "digital twin". "building" and "construction" were used to limit the scope. After the initial search, the literatures had to be published in a journal or a conference paper or as a book chapter. Title, keywords, abstract and main contents were then checked to see whether a publication is related to the field of building construction. Secondly, the filtered publications in the first step were reviewed and analysed from the perspectives of time, publication format, topic, consideration of other digital technologies, purpose and potential challenge of DT application in the building construction sector. Thirdly, based on results obtained from the previous two steps, we identified current research gaps, developed a conceptual framework for applying DT in MiC in the context of Hong Kong as a typical case, and explored opportunities and challenges for future research. The original research objectives were considered during each step [19].

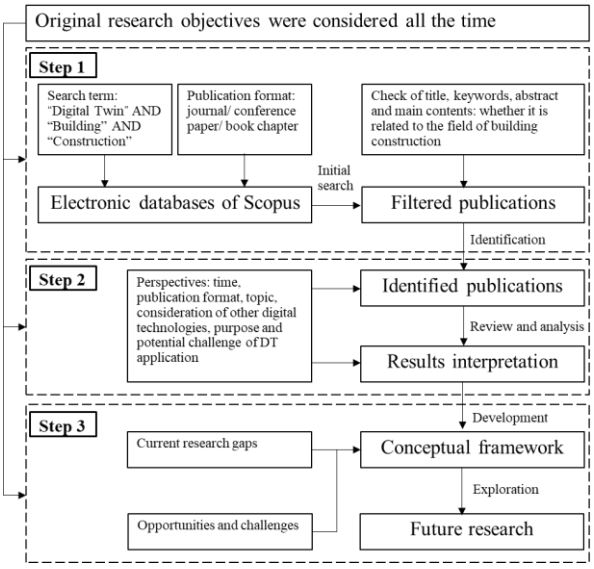

Figure 3. The overall research methodology process in this paper

4 DT applications in the building construction sector

4.1 Review of current practices

The latest search of publications through the electronic databases of Scopus was conducted in June 2020. The selection criteria as elaborated in Section 3 were applied to all papers in the initial search. 46 publications were filtered out for detailed analysis. After title, keywords, abstract and main contents of filtered

publications were checked, there were in total 10 articles identified. All the identified publications are related to the application of DT in the building construction sector. The first related article was published in 2018. The identified publications were evenly split between journal articles and conference papers. Disturbance of publication time and format of the identified publications is provided in Figure 4.

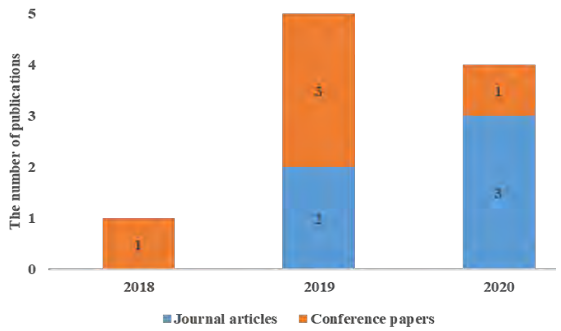

Figure 4. Distribution of publication time and types of the identified publications (as of June 2020)

Three of the identified publications considered the application of DT not only in the construction stage but also in the whole project lifecycle from the planning stage to the operation and maintenance stage [8, 20, 21]. Automated planning and scheduling of works is one of purposes of DT application [18, 22, 23]. Monitoring and assessment of construction performance is achievable with the aid of real-time data capturing from a construction site. One research developed DT of a type of machinery to prevent operation risks [25], while another one developed DT of a type of building material for simulation in order to reduce production time and cost [24]. A summary of different purposes of DT applications in the identified publications is provided in Figure 5.

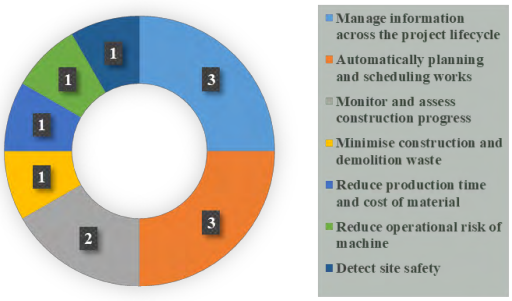

Figure 5. Summary of opportunities of DT applications in the identified publications
Note: numbers in the figure refer to the number of publications

Regarding consideration of other digital technologies, nine publications mentioned about "Building Information Modelling (BIM)", where seven of them considered DT as an evolutional representation of BIM, while the remaining two treated BIM system as a DT [22, 23]. Seven publications [8, 18, 20, 22, 24, 25, 26] included "Internet-of-Things (IoT)" together with sensor in order to collect data from the physical space, but only one of them considered the application of "Wireless Sensor Network (WSN)" for real-time data transmission [25]. Three publications [8, 20, 25] mentioned "cloud platform" when considering storage, analysis, processing and integration of captured data. The concept of "machine learning" was mentioned in three publications [18, 22, 25] so that a self-learning DT can be created. Bevilacqua [20] stated that both Augmented Reality (AR) and Virtual Reality (VR) can benefit from the implementation of DT, as they provide users a more immersed platform to view historical and real-time data. The frequency of other digital technologies, including BIM, IoT/sensor, WSN, cloud platform, machine learning, AR and VR, mentioned in the identified publications is provided in Figure 6.

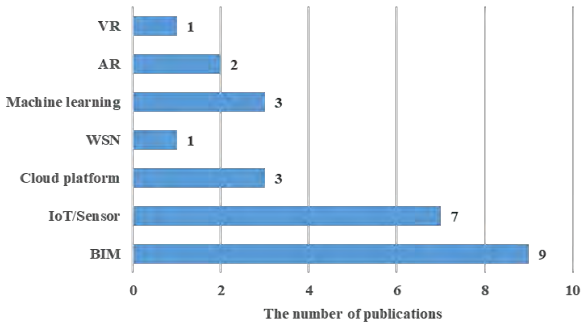

Figure 6. The frequency of other digital technologies mentioned in the identified publications
Notes: VR: Virtual Reality; AR: Augmented Reality; WSN: Wireless Sensor Network; IoT: Internet-of-Things; BIM: Building Information Modelling

Three publications discussed the potential challenges of DT application in the building construction sector [8, 18, 25]. They all mentioned the technology complexity, particularly in the field of sensing technology to gather data on construction site, with the proper consideration of installation and maintenance as well. Development of structuring methods and computing algorithms on the overwhelming amounts of data was also regarded as a common challenge to ensure the high-efficient of data processing. Other potential challenges in terms of the technical level and the social-political level were also

raised as below.

- Lack of sensors with comprehensive capabilities (e.g. integrated measuring distance, temperature, humidity, air quality, etc.) [18];
- Complexity of integration of sensors with different reading frequencies and accuracies (i.e. interoperability) [18];
- Development of reliable and efficient data transmission methods to ensure data connectivity and reduce time delay for further processing [18, 25];
- The existing complex social system [25];
- The dynamic of human interactions with construction activities [25];
- Data privacy (e.g. the sharing of data may need to follow relevant regulations on data privacy) [25]; and
- Data security (e.g. confidential project data needs to be protected during data transmission between real and virtual spaces) [25].

4.2 Opportunities, challenges and limitations

Results of the review on publications related to the application of DT in the building construction sector revealed that relevant researches have been conducted, due to the development of digital and information technologies and demonstration of benefits brought by DT applications across industries. However, only a few researches were conducted in a systematic manner with developed frameworks for DT applications in the building construction sector. Management of information across the whole project lifecycle and automatic planning and scheduling of works are the two most mentioned purposes of applying DT in the building construction sector. The concept of DT was not considered alone, but integrating with at least one existing digital technology. For example, BIM is commonly used as the data model of a building, providing a fundamental basis to develop a DT. Comparatively, DT has extra characteristics of real-time data acquisition through integrating IoT and WSN technologies. Application of DT in the building construction sector has promising benefits such as automated monitoring of site progress and reduced operational risk of machine. However, there are technical and social-political challenges to be addressed including interoperability of various sensors, development of optimised data processing algorithms and data privacy and security issues.

The current research gaps identified from the review are summarised as below for future research.

- The definitions of DT and BIM used in some publications remain identical, which are inaccurate, so a clearer and more uniform definition of DT is needed;
- There is a lack of study on the application of DT in the volumetric modular building construction; and
- There is a lack of empirical evidence to prove benefits of DT application in the building construction sector.

5 A framework of DT application in MiC

In order to apply DT in MiC, the emphasis is on building a Cyber-Physical System (CPS), where information collected from the real space is used for computation to generate a real-time monitoring cyber model. In the meantime, changes of the cyber model will either be used for prediction or reflect in the real space to achieve the control function.

Based on findings in Section 4, a framework of applying DT in MiC is provide in Figure 7. The framework was built in the context of module installation, as it is a unique onsite construction activity compared with conventional construction practices. Interpretation of the framework is provided as below.

1. Firstly, IoT technology is applied on real-time data capturing from labour who is responsible for module installation works, material (i.e. module to be installed) and machinery (i.e. crane) (Sensors supporting wireless transmission of data are required)
2. If BIM containing planning and scheduling of module installation works is available, it will be considered as an input of data source, which is of benefit to enhance logistics coordination
3. WSN or the 5th generation mobile network (5G) is used to ensure transmission and connectivity between the physical space and the cloud platform for storage
4. Computing algorithms are applied for processing data stored in the cloud platform in order to generate real-time DT of module installation process
5. AR, VR and web portal provide construction mangers a user interface to visualize the DT
6. The real-time DT of module installation process has the potentials to provide basic functions including labour safety detection, installation progress monitoring and prediction of required module installation time.
7. The advanced functions may allow construction managers to exert influence on the real space by controlling the DT, through control sensors and a rapid data transmission network. Control sensors include types of buzzing, flashing and vibrating.

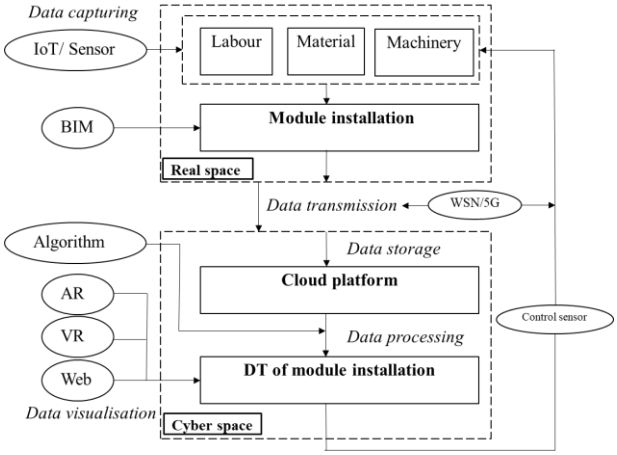

Figure 7. The proposed framework of DT application in module installation of MiC

6 Conclusions

This paper provides an overview of academic publications related to DT applications across industries, particularly in the building industry. The purposes of this paper are to provide a systematic review of application of DT in the building construction sector and to explore opportunities and challenges of applying DT in MiC within the context of Hong Kong as a typical case of high-density cities. Through literature review and analysis of ten publications related to DT applications in the building construction sector, the primary findings are as below.

- Management of information across the whole project lifecycle and automatic planning and scheduling of works are the two most mentioned purposes;
- DT is always integrated with other digital technologies;
- Theoretically, automated monitoring of site progress and reduced operational risk of machine are achievable benefits by adopting of DT; and
- There are technical and social-political challenges to be addressed before adoption of DT.

The framework considering the application of DT in the case of module installation process was proposed based on the findings. Through integrating with other digital technologies in the framework, the DT has potential functions of monitoring, predication and control. In addition to the current generic research gaps for the building construction sector mentioned in Section 5, future research is proposed to explore the following directions about DT applications in MiC:

1. Further literature review and meta-analysis of publications on DT applications in the building construction sector using more electronic databases; and
2. Interviews and focus group discussions with academics and practitioners in the areas of DT and modular building (covering different groups of stakeholders, e.g. client, consultant, contractor) to verify and refine the developed framework.

Acknowledgements

The authors acknowledge support from the Research Grants Council Research Impact Fund of the Hong Kong Special Administrative Region, China (Project Number: HKU R7027-18).

References

[1] Pan W., Yang Y., Zhang Z. and Chan S. *Modularisation for Modernisation: A Strategy Paper Rethinking Hong Kong Construction*, Centre for Innovation in Construction & Infrastructure Development, Hong Kong, 2019.

[2] Salehi M. Bayesian-Based Predictive Analytics for Manufacturing Performance Metrics in the Era of Industry 4.0. Online: https://www.researchgate.net/publication/337167724_Bayesian-Based_Predictive_Analytics_for_Manufacturing_Performance_Metrics_in_the_Era_of_Industry_40, Access: 05/05/2020.

[3] Grieves M. Origins of the Digital Twin Concept. Online: https://www.researchgate.net/ publication/307509727_Origins_of_the_Digital_Twin_Concept, Access 05/05/2020.

[4] National Aeronautics and Space Administration. Draft Materials, Structures, Mechanical Systems, and Manufacturing Roadmap Technical Area 12. Online: https://www.nasa.gov/pdf/501625main_TA 12-MSMSM-DRAFT-Nov2010-A.pdf, Access: 05/05/2020.

[5] Centre for Digital Built Britain. The Gemini Principles. Online: https://www.cdbb.cam.ac.uk/system/files/documents/TheGeminiPrinciples.pdf, Access: 06/05/2020.

[6] Bolton R.N., McColl-Kennedy J.R., Cheung L., Gallen A., Orsingher C., Witell L. and Zaki M. Customer experience challenges: bringing together digital, physical and social realms. *Journal of Service Management*, 29(5): 776-808, 2018.

[7] Arup. Digital twin: towards a meaningful framewok, Online: https://www.arup.com/perspectives/publications/research/section/digital-twin-towards-a-meaningful-framework, Access: 06/05/2020.

[8] Tchana Y., Ducellier G. and Remy S. Designing a unique Digital Twin for linear infrastructures

lifecycle management. *In Proceedings of 29th CIRP Design 2019*, pages 545-549, Portugal, 2019.

[9] Tao F., Zhang H., Liu A. and Nee A.Y.C. Digital Twin in Industry: State-of-the-Art. IEEE Transactions on Industrial Informatics, 15(4): 2405-2415, 2018.

[10] Enders M.R. and Hossbach F. Dimensions of Digital Twin Applications - A Literature Review. *In Proceedings of Twenty-fifth Americas Conference on Information System*, pages 1-10, Cancun, Mexico, 2019.

[11] Khajavi S., Motlagh N.H., Jaribion A. and Werner L. Digital Twin: Vision, Benefits, Boundaries, and Creation for Buildings. *IEEE Access*, 7(-): 147406-147419, 2019.

[12] Lu Q., Xie X., Parlikad A.K. and Schooling J.M. Digital twin-enabled anomaly detection for built asset monitoring in operation and maintenance. *Automation in Construction,* 118(2020): 103277, 2020.

[13] Census and Statistics Department. GDP by major economic activity. Online: https://www.censtatd.gov.hk/hkstat/sub/sp250.jsp?tableID=036&ID=0&productType=8#N3, Access: 06/05/2020.

[14] Chief Executive. The Chief Executive's 2017 Policy Address: Make Best Use of Opportunities Develop the Economy, Improve People Livelihood, Build an Inclusive Society. Online: https://www.policyaddress.gov.hk/jan2017/eng/pdf / PA2017.pdf, Access: 06/05/2020.

[15] Chief Executive. The Chief Executive's 2018 Policy Address: Striving Ahead Rekindling Hope. Online: https://www.policyaddress.gov.hk/2018/eng/pdf/PA2018.pdf, Access: 06/05/2020.

[16] Gibb A.G.F. *Off-Site Fabrication: prefabrication, preassembly, and modularisation*. Whittles Publishing, 1999.

[17] Pan W. and Hon C.K. Modular integrated construction for high-rise buildings. *In Proceedings of the Institution of Civil Engineers-Municipal Engineer*, 171(4): 148-148, 2018.

[18] Boje C., Guerriero A., Kubicki S. and Rezgui Y. Towards a semantic Construction Digital Twin: Directions for future research. *Automation in Construction,* 114(2020): 103179, 2020.

[19] Pan W. A decision support tool for optimising the use of offsite technologies in housebuilding. Online: https://repository.lboro.ac.uk/articles/A_decision_support_tool_for_optimising_the_use_of_offsite_technologies_in_housebuilding/9454214, Access 15/05/2020.

[20] Zhang H., Wei J., Jiao J. and Gao Y. Comprehensive information management analysis of construction project based on BIM. *In Proceedings of International conference on Big Data Analytics for Cyber-Physical-Systems 2019,* pages 1027-1033, Shenyang, China, 2020.

[21] Papadonikolaki E., Leon M., Mahamadu A.M. BIM solutions for construction lifecycle: A myth or a tangible future? *In Proceedings of 11th European Conference on Product and Process Modelling*, pages 321-328, Copenhagen, Denmark, 2018.

[22] Çelik U. 4D and 5D BIM: A System for Automation of Planning and Integrated Cost Management. *In Proceedings of Eurasian BIM Forum,* pages 57-69, Istanbul, Turkey, 2019.

[23] Schimanski C.P. and Monizza G.P. Pushing Digital Automation of Configure-to-Order Services in Small and Medium Enterprises of the Construction Equipment Industry: A Design Science Research Approach. *Applied Sciences*, 9(18): 3780, 2019.

[24] Lydon G.P., Caranovic S., Hischier I. and Schlueter A. Coupled simulation of thermally active building systems to support a digital twin. *Energy and Buildings,* 202(1): 109298, 2019

[25] Bevilacqua M., Bottani E., Ciarapica F.E., Costantino F., Donato L.D., Ferraro A., Mazzuto G., Monteriu A., Nardini G., Ortenzi M., Paroncini M., Pirozzi M., Prist M., Quartrini E., Tronci M. and Vignali G. Digital twin reference model development to prevent operators' risk in process plants. *Sustainability*, 12(3): 1088, 2020.

[26] Akbarieh A., Jayasinghe L.B., Waldmann D. and Teferle F.N. BIM-Based End-of-Lifecycle Decision Making and Digital Deconstruction: Literature Review. *Sustainability*, 12(7): 2670, 2020

Integrating Industry 4.0 Associated Technologies into Automated and Traditional Construction

F.R. Correa[a]

[a]Department of Construction, University of Sao Paulo, Brazil
E-mail: fabiano.correa@usp.br

Abstract –

Nowadays, it is ever more common to find mentions in the scientific literature to a "Construction 4.0". Considering, for instance, Offsite Construction, it is clearer how such concept could be realized. Current widespread adoption of BIM helps but is not enough to realize that end, because it is, in general, limited to information being manually created through authoring software, and consumed for different proposes, such as Clash Detection, or 4D Modeling. Construction 4.0 should transcend the limitations of existing only in cyberspace; it should interact directly with the real environment by means of sensors (gathering data), and remote controlled or autonomous machines, employed as part of the production processes, with Machine Learning algorithms handling the transformation of data into information, and actions. The central element of such approach should be a Digital Twin-driven Cyber-Physical System, which when focused on Construction Phase, would be capable to simulate the dynamics of construction processes. In this position article, an evolution of the concept of Computer-Integrated Construction (CIC) is presented as a possibility in representing and guiding developments associated to the incorporation of different technologies from Industry 4.0 to Construction. A framework where such a system could be applied to Off-site or Automated Construction scenario, and to Traditional Construction scenario as well is proposed. In the latter scenario, common in developing countries, which yet has plenty of (and need for) manual labor in the Construction sector, all those technologies are employed not to reduce jobs, but to augment awareness and eventually to turn the tasks safer for the worker.

Keywords –

Digital Twin; Building Information Modeling; Construction 4.0; Cyber-Physical Systems

1 Introduction

Some years ago, few people thought that the subject of a Fourth Industrial Revolution would be relevant to the Construction sector; one of the first researches to look for signs and directions of it on the industry, didn't found anything that helped towards this end [1]. Nowadays, it is ever more common to find mentions in the scientific literature to a "Construction 4.0", i.e., the application of Industry 4.0 associated technologies to the Construction (Figure 1). Yet, it is still not clear how all those technologies, Cyber-Physical Systems, Digital Twins, Industrial Internet or Internet of Things (IoT), to name just a few, will play a role to transform a sector that has been suffering to find its path towards industrialization.

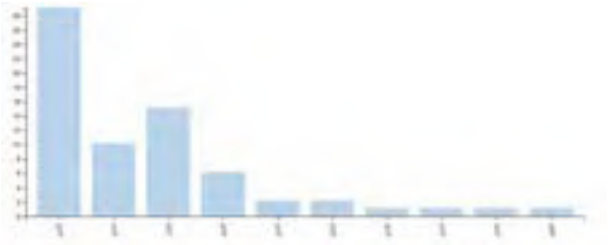

Figure 1. Publications whose subject deals with the concept of Construction 4.0, from Web of Science database.

Both the current importance that Computer-Aided Systems, including PLM (Product Lifecycle Management), has had in Manufacturing Industry [2] and the widespread adoption of its counterpart BIM in the Architecture, Engineering, and Construction (AEC) sector [3], helps but is not enough to realize that end. They are, in general, limited to information being manually created through authoring software, and consumed for different proposes (in case of BIM uses, Clash Detection, or 4D Modeling, for example).

Industry 4.0, as its own name states, is totally focused on manufacturing, i.e., production on a factory,

or more specifically, on a factory with lots of automation that appeared during the Third Industrial Revolution. So, there is this necessity to traverse the cyberspace of digital models of the products towards the control of real machines, or of the entire factory, where happens the production processes.

Such trend aims at reducing time to market, enhance productivity, and achieve mass customization, among other goals. It is the integration of automation in the virtual world, and automation in the real world.

Considering "those aspects of the project that can be designed and managed, i.e., the product (typically a building or plant), the organization that will define, design, construct and operate it, and the process that the organization teams will follow" [4], and the "role of complementarity" that attest to the synergy among Product, Process and Organization [5] ("Manufacturing Technology" being part of the Process), the importance of abstractions or models of those aspects has been increasing. For the goal of a Construction 4.0, it needs a complete virtual or digital representation of the Product, Process and Organization, to be capable to integrate horizontally inside a company, and vertically through the entire supply chain.

Based on a literature review and cross-learning case studies between Manufacturing and Construction Industries [6][7], this position article adopts an evolution of the concept of Computer-Integrated Construction (CIC) as a possibility in representing and guiding developments associated to the incorporation of different technologies from Industry 4.0 to Construction. Industry 4.0, and its inspired Construction 4.0, should be about the integration of virtual and physical, and has in the technology of Digital Twin-driven Cyber-Physical System its most prominent technology.

Although the relevance of such technologies encompasses all the phases in the lifecycle of a building or infrastructure work, due to limited number of pages in that article, the presentation here restricts itself to the Construction Phase. Scenarios where such a framework could be applied to Off-site or Automated Construction in one extreme direction, and on Traditional Construction processes in the other (and the whole spectrum in between), are proposed.

2 Pre-Construction 4.0: Origins of Computer – Integrated Construction (CIC)

Development on Information and Communication Technology (ICT) systems could be traced back to the first hardware that enabled structural calculations, and software that enabled Computer-Aided Drafting systems. It was always done in parallel to innovation in Construction based on new materials, new technology in building systems, and new ways to manage construction processes.

The AEC sector being fragmented as it is, the same happens with its ICT software tools used by different disciplines and professionals. Many researchers were dedicated to the work of integrating the information of those workflows [8]. Construction 4.0 main idea is beyond integration inside virtual world, of the information throughout the lifecycle of the product, the building or infrastructure work: it is the integration of that information with the automation hardware on the shop floor, and the creation of new ways to operate inside an industrialized and automated environment.

There are some similarities between Industry 4.0 paradigm and a popular concept in the 80's, Computer-Integrated Manufacturing (CIM): both incorporate somehow the dynamics of the shop floor computer-based system, towards the goal of automation.

CIM was conceived as an integrated approach to end the 'islands of automation' around Computer-Aided Design (CAD), and Computer-Aided Manufacturing (CAM), and its communication with CNCs machines on the shop floor. The concept took advantage of a digital workflow of information about products and the automated production lines, with machines controlled by computers, and industrial robots: it should integrate and control the machines to produce based on digital information.

The adaptation of that concept to Construction was popular in the 90's, known by the term of Computer Integrated Construction (CIC) [9–11]. It seems that from the researchers inside this theme, there were two approaches:

1. **Focused on the integration between CAD and CAM**: or between design and fabrication – many advanced applications of that era were done without such integration [12]. In the search of that integration in the design phase, it seems also that researchers converged to create object-oriented data schemas and software tools, which in the end became to be known as BIM [13];
2. **Focused on the Digital Fabrication**: whose interest are on Off-site Construction, following assembly on site, and the use of robots and other automated machines – activities of Planning, and Monitoring were done based on digital models.

For the work presented in this article, the latter approach is more relevant. Following that approach leaded to Site Automation [14], Factory Automation System [15], Super Construction Factory [16], or similar approaches, to structure the unstructured onsite environment, so that it would be possible to integrate construction robots without disrupting other workflows around [5].

Such developments by all big Japanese Construction companies, such as Shimizu [17] and Obayashi [18], and replicated by companies of other countries, it should be viewed as a prototype of Construction 4.0, although many of the robots were by then teleoperated. To have a center of operations, and many different digital models, and the assembly of building components itself being done by robots and machines, it had all the elements that comprises the view of the application of Industry 4.0 technologies to Construction.

3 Industry 4.0 Associated Technologies

One way to understand the current drive towards a Construction 4.0 paradigm was presented in the previous section. Today, the maturity of different technologies that could be used in an integrated way allows the development of such future scenario.

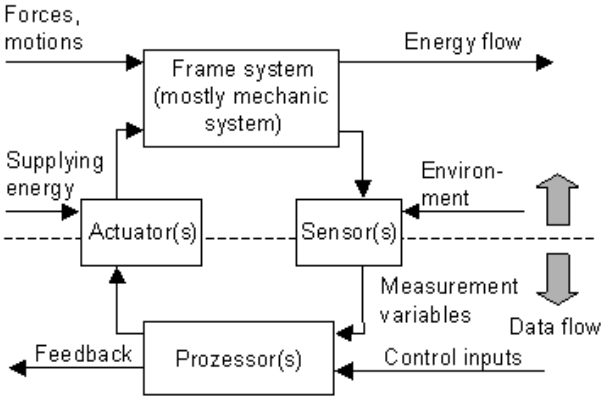

Figure 2. Representation of a mechatronic system [19]

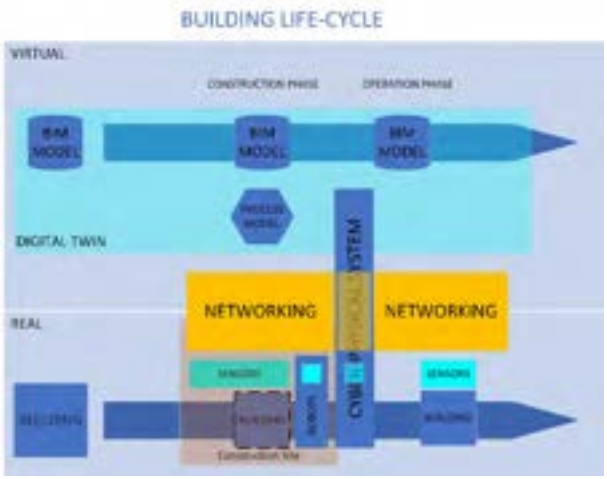

Figure 3. Diagram with the interaction between different Industry 4.0 technologies.

Thinking about construction production as a system, it is interesting to make an analogy with the representation of a mechatronic systems, as shown in Figure 2: 1) Sensor(s); 2) Processor(s); 3) Actuator(s).

Each technology associated to Industry 4.0 paradigm could be viewed as enabling sensing, actuation, and/or processing. The technologies that would be briefly addressed in this section are: Industrial Internet or Internet of Things (IoT), Digital Twins, Machine Learning / Artificial Intelligence Algorithms, and Cyber-Physical System.

Figure 3 illustrate how BIM models changes throughout in the building life cycle in the virtual environment, and its analogous, the physical building is being constructed and operated in the real environment. There is a networking layer that connects both environments, and the sensors that are vital to capture the dynamics of the construction site / shop floor, and the surroundings of robots and of cyber-physical systems, which by its own is driven by digital twins. The hexagon in the figure, bellow the BIM Model in the construction phase, represents the dynamics that are the simulation of the processes, and it enhances the product model, to provide some basis for a digital twin. With it, it is possible to create data and information beyond those produced by the professionals, automatically. In the operation phase, it is only possible to work, if buildings were designed and constructed with embedded sensors, or instrumentalized afterwards, to capture every relevant aspects of its uses.

3.1 Industrial Internet or Internet of Things (IoT)

IoT is about the convergence, where different devices (Things) are capable to communicate one with another over the Internet. They not only communicate; they sense their environment, and they could act over it based on programmed behavior. This “definition” could be stretched to encompass from sensor networks to autonomous systems, and certainly benefit from 5G networks, the existence of Cloud (Edge or Fog) computing nodes, and so on.

It should be the sensing layer, which is essential for whatever scenario of Construction 4.0 that is being proposed. The use of different sensors for tracking people, material, and equipment onsite, and RFID in modular plants could help to leverage the approach to Construction 4.0, producing database for construction processes.

The availability of computational power outside the local where data is collected, and even where it is consumed gives many more possibilities. It is more cost effective.

3.2 Data Analytics: Machine Learning (ML), Artificial Intelligence (AI)

Current successful approach to build complex models is based on data, with Machine Learning (ML) algorithms. It is possible to learn parameters of a parametric model, and to learn the very representation itself.

Machine Learning, or more generally Artificial Intelligence (AI) algorithms could also be used to analyze incoming data, to quantify uncertainty of different scenarios, to propose alternative solutions, and so on.

One necessity with the grow in sensors being used, and data being gathered would be infrastructure to deal with the Big Data Analytics. are analogous to what was presented in the previous sub-section. The differences are the hardware, software and workflow needed to do the same thing in a scalable manner.

3.3 Digital Twins

There is allusions to BIM being the Digital Twin version in the Construction sector, although with different names [20]. Following a PLM approach [2], some works also sees parallel between BIM and PLM. Digital Twins should, in an analogy to object-oriented modeling, provide not only the variables, but also functions pertinent to, and based on those variables. In the case of a building, it should incorporate physics to allow for showing its behavior with software running different simulations [21].

BIM models *per se* should not be considered Digital Twins when the focus of the analysis is the Construction Phase. All uses of BIM models [22] implies taking information from it, quantity takeoff, that generally were inputted by human, and need extra human work to integrate with other databases to achieve the desired result for such utilization – there is no transformation of the data.

So, BIM models, are considered the virtual representation of the Product. In such uses of the model for 4D Planning, 5D cost, it cannot be used *per se* to predict, and it doesn't have dynamic links to account for constant changes in design, planning or construction phases. Those models are created, in general, through human input through authoring software tools, one specific for each discipline, and that need to communicate through interoperable workflows.

Although there isn't general agreement around what BIM is and is not, a process, a 3D digital model of the product with non-geometric and geometric data, or a collection of authoring software tools, here it would follow some VDC practitioners that considers BIM as the digital model, and its uses as part of the VDC practice [4].

Digital Twin should incorporate in its representation functions to transform the initial information and producing result that do not depend only in data, but in inner behavior of the phenomenon modeled.

3.4 Cyber-Physical Systems

The term "Cyber-Physical System" was probably coined by Helen Gill at NSF around 2006 [23]. Figure 4 provides a concept map relating Cyber-Physical Systems to Feedback Systems and Real-Time [24].

Probably an evolution of Distributed Real-Time Embedded Systems (DRE), Cyber-Physical Systems are complex systems, which integrate in its design abstractions of control, system, and software engineering. It is inherently a model-based approach to provide interaction between the physical world and its dynamics, and the cyber or virtual world.

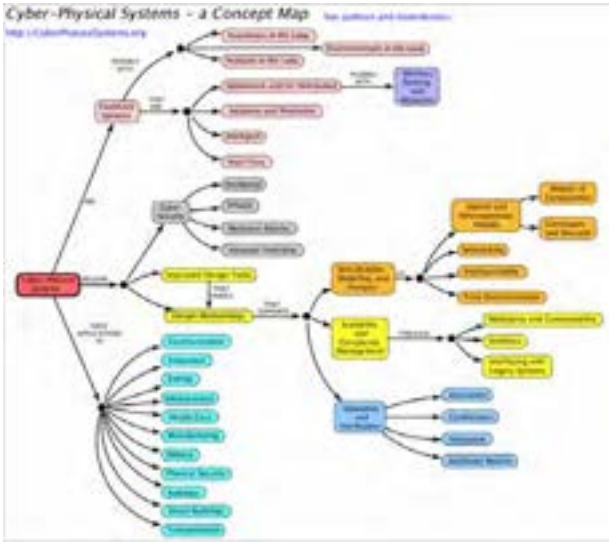

Figure 4. A concept map for Cyber-Physical Systems [24].

It could be driven by Digital Twins or work with other controllers: Additive manufacturing, and construction robots.

4 Construction in the 4.0 era

The challenges in creating a framework, which is valid over the entire spectrum of possibilities of different productions systems in Construction are:

- How to create a Digital Twin of the Manufacturing Technology, or the Virtual Representation of Production Processes;
- How it will behave, its inner dynamics.

It should be a software capable of simulate, at least,

the construction process for each existent building system, allowing predictions in a closed-loop feedback, and possibly in real-time. It will depend on data from sensor networks deployed in production lines for offsite construction (where probably it will be Cyber-Physical System driven by Digital Twins), or on-site, for more traditional production or assembly of modular component.

For the case of the so-called Automated Construction, which we had the Sky-Factories or Site Automation as perfect examples, they already developed such supervisory and control system overseeing the automated processes.

But even for traditional construction in developing countries, that are prone to remain almost that way for the short future, such system could be implemented and used in such a way to give a better understanding to the people making decisions of an uncertainty-bounded possibilities for planning and rescheduling. The technologies adopted should promote the work of people, to make their time more productive, to make their work safer, and make their data-driven decision.

As presented in the previous section, a Digital Twin is the virtual representation of the Production process, when considered only Construction Phase. It represents how raw material and resources such as workers, machines, and so on, are transformed into building components, or the building itself, in such detail that it should be possible to predict the length of time needed to finished each step.

The simulation is the core engine of the proposed framework. Although realistic simulation models of the manufacturing of components in automated lines and considering the human interacting with machines already exist. It could provide scenarios with which to deal during planning, to re-planning during execution.

More challenging is the scenario of simulating traditional construction, in an unstructured environment, with lots of freedom to act. But here it is advocated that with a probabilistic model, constructed over a large collection of data, and individualized to capture each company way of work, could at least provide lower and upper bonds over variables such as cost, amount of human labor needed, alternative plans, risky, and so on.

Example of this approach was set out in [25], and a paper still not published, in which that framework was used over 5-years production data, and results are promising in capturing both the impact of the factory activities, and from panel design in the times in each workstation for wood-framing pre-fabricated homes.

There will be at first, two stages for that approach: 1) gathering data for different construction processes, to build a model or representation based on data [26], instead of expertise from professionals; 2) Application of that model, with real-time data still been gathered, to monitor processes, and to predict future scenarios, and plan in advance for alternative solutions.

Interesting for such approach, is the work that started with Occupancy Grids [27], then evolved to Metric Maps, and algorithms to build such representations at the same time that an autonomous robots navigate knows as SLAM (Simultaneous Localization and Mapping) [28]. Nowadays, SLAM has been used in Construction sector with point-cloud data to produce as-built and as-is BIM models.

It should be possible to decouple complexity on-site by modeling activities individually and allow a simulator for Discrete Event Simulation (DES) like Simphony [29], to add the complexity of interaction, and eventually, movement of resources. In the end, it could constitute a prototype of a library of Construction Processes, based on specific building systems, that could be tailored for each team or construction company, based on historic data of productivity.

5 Scenarios for the Construction 4.0

Two scenarios are being considered, based primarily in the availability of construction work force: 1) Industrialized Scenario, in which there is a lack of construction workers, and the availability of machines and/or construction robots directly responsible to the production process; 2) Traditional Construction Scenario, in which the sector employs a large workforce, but work conditions need to be improved by means of assistive technology.

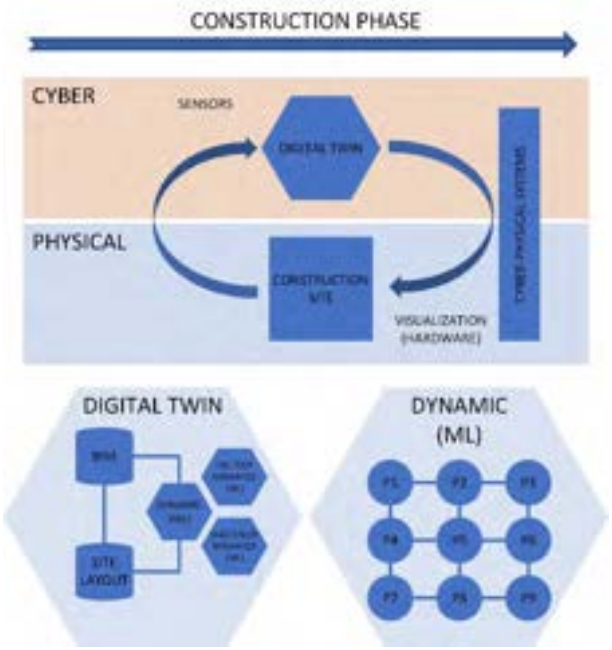

Figure 5. Scenario for Automated Construction.

5.1.1 Industrialized Construction Scenario

Modular, or Off-site Construction in general, could incorporate more straightforwardly Industry 4.0 technologies, although still there is many particularities that should be addressed. There is a large synergy between the different applications, although shop floor in the construction sector, be it for steel-framing, wood-framing, or concrete panels are not very much automated.

Figure 5 represent the industrialized scenario, where there is offsite production, automation in the factory, and eventually construction robots onsite. There are sensors gathering data, monitoring processes, and all data feed in Digital Twin model of the production processes. Those models produce actions to be taken by machines, or equipment which could directly made building components. The bridge between both environments, cyber and physical, is materialized by one or a hierarchical system of Cyber-Physical Systems (CPS), which allows a bidirectional link between BIM model inside the Digital Twin, and the real environment by means of "autonomous" machines.

The more automated the production, the less is the uncertainty, and the final difference between predicted and measured metrics in production. The dynamics would be made of an array, or lattice of production models, with varied dependencies among them, allowing for Machine Learning reasoning.

5.1.2 Traditional Construction Scenario

The main difference between both scenarios is the Cyber-Physical Systems, which are absent in the traditional construction scenario. Moreover, the framework for traditional construction works with human-in-the-loop simulations, as there is not a bidirectional flow of sensor readings and actuation controls between virtual and real environments.

There are countries, mainly developing countries such as Brazil, where there is a real concern regarding substitute Construction workers by robots or machines. Also, workers of the sector receive low wages, and they work in conditions that are potentially dangerous, and hard [30]. For that matter, where there is plenty of (and need for) manual labor in the Construction sector, all those technologies, and the scenario for a Construction 4.0 should be employed to augment and to turn the tasks safer, for the worker.

So, there is an opportunity to change current culture in the sector in those countries, an promote an environment of continuous learning, and to provide better jobs for such individuals by means of using assistive technologies [31][32]. From electric or electronic tools, exoskeletons [33] to facilitate tasks and avoid injuries, tracking systems to manage safety, and so on.

When such approach is deployed integrated with its virtual counterpart to coordinate efforts, to plan and control in a micro-management, it should produce better results.

There are many challenges in this scenario: 1) as it needs more human labor, it increases the number of sensors needed to capture activities on-site – although one could use imaging techniques; 2) the trajectories or the movement of the workforce should allow the identification, at least, of the beginning and the end of each activity in the sequence for the entire production onsite; 3) Those indirect detections could allow the estimation of work complete, and also constitute in historic measurement of productivity; 4) Using Machine Learning algorithms over such databases, it would be possible to incorporate uncertainties in the simulation, and provide worst- and best-scenarios for the planning with human-in-the-loop.

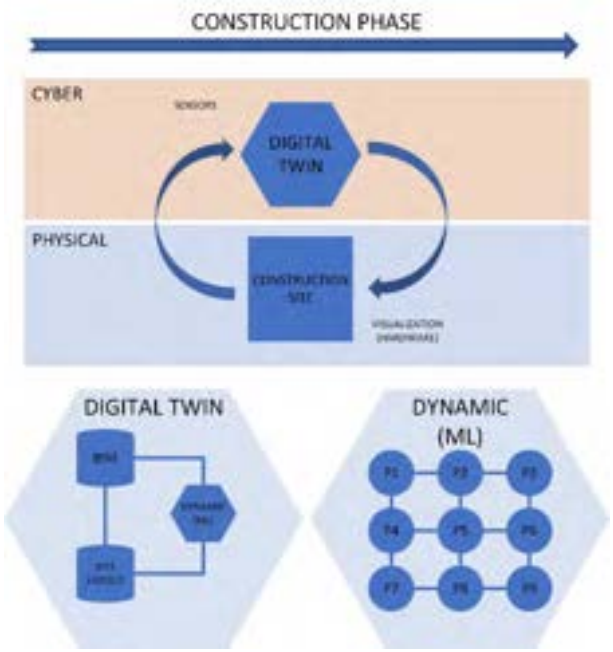

Figure 6. Scenario for Traditional Construction.

It is known that only technology changes would not make a case without addressing how to finance, how to bid public contracts and how to turn it competitive in terms of taxes.

6 Conclusion

In conclusion, a possible Construction 4.0, with two different scenarios that encompasses both Industrialized and Traditional Construction was presented. There should be a large spectrum of applications, in which the assimilation of the different technologies associated to

Industry 4.0 would differ.

As it is based on the digitization process, and its most important piece is the Digital Twin of the Production processes, it is essential that there is a widespread use of sensors to provide real data, and also almost real-time information of the processes, and that planning and control onsite be made in a data-driven approach.

It emphasizes that Construction 4.0 should be a holistic view, to provide a starting point to think about the future of Construction in considering Sustainability, in becoming part of a Circular Economy, and to an approach that considers society and the needs its work force in each different country.

Construction 4.0 won't be relevant without new forms of management and control, that should be proposed to incorporate as a base for a support system a micro-management, with automatic acquisition, and processing of data for the decision-making support system. However, such topic was outside the scope of this article.

References

[1] Oesterreich, T.D., Teuteberg, F.: Understanding the implications of digitisation and automation in the context of Industry 4.0: A triangulation approach and elements of a research agenda for the construction industry. Comput. Ind. 83, 121–139 (2016).

[2] Grieves, D.M.: Virtually Perfect - Driving both lean and innovative products through Product Lifecycle Management. Space Coast Press (2011).

[3] Jung, W., Lee, G.: BIM Adoption Status on SIX Continents. 9, 512–516 (2015).

[4] Kunz, J., Fischer, M.: Virtual Design and Construction: Themes, Case Studies and Implementation Suggestions. (2012).

[5] Bock, T., Linner, T.: Robot-Oriented Design - Design and Management Tools for the Deployment of Automation and Robotics in Construction. Cambridge University Press, New York (2015).

[6] Crowley, A.: Construction as a manufacturing process: Lessons from the automotive industry. Comput. Struct. 67, 389–400 (1998).

[7] Gann, D.M.: Construction as a manufacturing process? Similarities and differences between industrialized housing and car production in Japan. Constr. Manag. Econ. 14, 437–450 (1996).

[8] Aouad, G., Sun, M.: Information modelling and integration in the construction industry: A novel approach. Struct. Surv. 17, 82–88 (1999).

[9] Teicholz, P., Fischer, M.: Strategy for Computer Integrated Construction Technology. J. Constr. Eng. Manag. 120, 117–131 (1994).

[10] Fischer, M., Betts, M., Hannus, M., Yamazaki, Y., Laitinen, J.: Goals, dimensions, and approaches for computer integrated construction. In: Proceedings CIB W 78; Mathur K S, Betts M P, Tham K W (editors); Management of information technology for construction; Singapore, August 1993 (1993).

[11] Wagter, H.: Computer integrated construction. Elsevier (1992).

[12] Yamazaki, Y., Uchiyama, Y., Ito, K., Akimoto, M., Terada, N.: Expert systems and integrated construction planning. Habitat Int. 14, 95–106 (1990).

[13] Yamazaki, Y., Tabuchi, T., Kataoka, M., Shimazaki, D.: 3D/BIM Applications to Large-scale Complex Building Projects in Japan. Int. J. High-Rise Build. 3, 311–323 (2014).

[14] Bock, T., Linner, T.: Site automation - automated/robotic on-site factories. Cambridge University Press (2016).

[15] Yamazaki, Y., Maeda, J.: The SMART system: an integrated application of automation and information technology in production process. Comput. Ind. 35, 87–99 (1998).

[16] Miyakawa, H., Ochiai, J., Oohata, K., Takashi, S.: Application of Automated Building Construction System for High-Rise Office Building. Presented at the (2000).

[17] Tezuka, T., Takada, H.: Robot oriented modular construction system. In: ISARC Proceedings. pp. 123–132. IAARC (1992).

[18] Kudoh, R.: Implementation of an Automated Building Construction System. In: Proceedings 13th International CIB World Building Congress Research and Technology. Development as an investment in the construction industry, 8-9 May 1995, Amsterdam, The Netherlands. pp. 17–28 (1995).

[19] Koriath, H.-J., Neugebauer, R.: Continuing education and training for engineers - mechatronics in a production environment. In: Proceedings CIRP International Manufacturing Education Conference. pp. 337–347 (2002).

[20] Succar, B.: Building information modelling framework: A research and delivery foundation for industry stakeholders. Autom. Constr. 18, 357–375 (2009).

[21] Bernstein, P.G., Jezyk, M.: Models and Measurement: Changing Design Value with Simulation, Analysis, and Outcomes. In: Building Information Modeling - BIM in Current and Future Pratice (2014).

[22] Leicht, R., Niu, M., Messner, J.: Prevalence and value of BIM Uses in Construction. In: International Structural Engineering and

Construction (2017).
[23] Lee, E.A.: The past, present and future of cyber-physical systems: A focus on models, (2015).
[24] Lee, E.: Ptolemy Project - UC Berkely, https://ptolemy.berkeley.edu/projects/cps/.
[25] Correa, F.: Simulating wood-framing wall panel's production with timed coloured petri nets. In: Proceedings of the 36th International Symposium on Automation and Robotics in Construction, ISARC 2019. pp. 1026–1033 (2019).
[26] Abourizk, S.M., Halpin, D.W.: Statistical properties of construction duration data. J. Constr. Eng. Manag. 118, 525–544 (1992).
[27] Elfes, A.: Using Occupancy Grids for Mobile Robot Perception and Navigation. Computer (Long. Beach. Calif). 22, 46–57 (1989).
[28] Thrun, Sebastian; Burgard, Wolfram; Fox, D.: Probabilistic robotics. (2005).
[29] Lee, D.-E., Yi, C.-Y., Lim, T.-K., Arditi, D.: Integrated Simulation System for Construction Operation and Project Scheduling. J. Comput. Civ. Eng. 24, 557–569 (2010).
[30] Manzo, J., Manzo, F.I., Bruno, R.: The potential economic consequences of a highly automated construction industry: What if construction becomes the next manufacturing? (2018).
[31] Rauch, E., Linder, C., Dallasega, P.: Anthropocentric perspective of production before and within Industry 4.0. Comput. Ind. Eng. 139, 105644 (2020).
[32] Longo, F., Nicoletti, L., Padovano, A.: Smart operators in industry 4.0: A human-centered approach to enhance operators' capabilities and competencies within the new smart factory context. Comput. Ind. Eng. 113, 144–159 (2017).
[33] Davila Delgado, J.M., Oyedele, L., Ajayi, A., Akanbi, L., Akinade, O., Bilal, M., Owolabi, H.: Robotics and automated systems in construction: Understanding industry-specific challenges for adoption. J. Build. Eng. 26, 100868 (2019).

System Development of an Augmented Reality On-site BIM Viewer Based on the Integration of SLAM and BLE Indoor Positioning

Yu-Cheng Liu[a], Jhih-Rong Chen[a], and Hung-Ming Chen[b]

[a] Graduate Student, Department of Civil and Construction Engineering, National Taiwan University of Science and Technology
[b] Professor, Department of Civil and Construction Engineering, National Taiwan University of Science and Technology
E-mail: hungming@mail.ntust.edu.tw

Abstract –

Traditionally, when an engineer wants to use Building Information Model (BIM) on-site to support tasks for construction or maintenance, the common approach is to use a tablet or a notebook to run a BIM viewer, thus requiring manual operation for model manipulation. In addition, the BIM presented through the screen and the actual on-site visual are in two separated views, and thus the two are less likely to be synchronized. Augmented Reality (AR) superimposes virtual objects or information that can be interacted with onto real world images or videos. Therefore, this study applied AR to superimpose BIM with an indoor industrial environment for a more immediate and intuitive integration of the physical site and BIM. At present, most applications of combined BIM with AR uses marker or marker-less image recognition to superimpose virtual content using feature points of the marker or object image as an identifier. If the identifier moves outside the device camera view, the virtual content will not appear. With advances in AR, a new AR mode is introduced in this study based on simultaneous localization and mapping (SLAM). Based on this technology, the virtual BIM is placed based on the device's understanding of the environment and then superimposed onto real objects in the scene without any identifiers. A manual method is proposed to align a chosen BIM component to a corresponding real object. Based on the alignment, the system calculates the angle and position to accurately superimpose the BIM on the virtual environment, with these locating characteristics recorded for future use. Since the load and display of an entire BIM model is not necessary and is inefficient in the context of indoor AR applications, the model is divided into room models, and the system only overlays the corresponding room model for a specific room. This is achieved through a combination with the Bluetooth Low Energy (BLE) indoor positioning technology, so that the room in which the user is located can be immediately identified and the corresponding room model can be loaded.

Keywords –

Building Information Model; Augmented Reality; Simultaneous localization and mapping; BLE indoor positioning

1 Introduction

For previous approaches for viewing BIM data, it is generally necessary to use related software, such as Autodesk Revit, Navisworks, Tekla Structures, etc. Moreover, these types of BIM software are traditionally designed for users to operate in an office setting; if it is required to view BIM data during the project maintenance stage, engineering personnel need to configure a lightweight handheld device, such as a tablet or high-end notebook, as a BIM viewing tool. This viewing method results in two problems: (i) BIM software cannot automatically present the model information required by engineering personnel, and (ii) the presented image in the BIM viewing tool and what is visually seen by on-site engineering personnel are two different images, resulting in difficulties in reconciliation.

Recently, Augmented Reality (AR) as a visual technology has risen in prominence. AR can combine the virtual world and the real world on the screen of a specific interactive device. Virtual text, graphics, or 3D models can be superimposed on true images. Based on this technology, the 3D virtual model from BIM can be superimposed onto the image of the project site. There is many applications of Augmented Reality system

development for BIM [1, 2, 3, 4]. For example, during the construction and maintenance stages, an integrated on-site BIM model can be used to present construction progress models at different stages for project management. Additionally, during road maintenance and repair, the state of an underground pipeline can be determined using AR without the need for excavation, thus avoiding losses caused by accidentally excavated pipelines. There also have been broad applications in project operation and maintenance stages, such as in previewing indoor renovations using virtual models or indoor route navigation in large buildings. In essence, AR applications of BIM are typically in indoor environments. Thus, model fitting and accuracy will be a major challenge.

To solve the problem of indoor positioning accuracy, this study uses simultaneous localization and mapping (SLAM) through the combination of visual-inertial SLAM (VI-SLAM) with BIM in AR. SLAM was first proposed in the field of robotics, enabling robots to understand their surroundings during movement, using repeatedly observed feature points to locate their own position (simultaneous localization) and constructing a map based on environmental cognition (mapping). The development process of SLAM also ranges from the earliest sonar and light measurements to the current SLAM based on inertial measurement unit (IMU) and visual measurement technology (VI-SLAM). Recently, an Augmented Reality technology based on VI-SLAM has been developed [5].

This study proposes an overall conceptual framework for a pre-processing system and the user mode. The design of the system concept is conducted according to the abovementioned background and motivation, with the primary application being for the project maintenance stage. To address the effectiveness and localization problems of BIM models for project maintenance when coupled with an on-site inspection, this study introduces AR technology based on SLAM, using its characteristics to optimize the stability and fitness of the AR system as well as for spatial locating via Bluetooth Low Energy (BLE) and acquiring required data through a database. This is so that the cloud data for the room can be loaded immediately to fit the on-site BIM room model.

2 System framework

To effectively meet the abovementioned requirements, a pre-processing (pre-positioning) system is developed before the AR system operation. This pre-processor includes model processing, Internet of Things (IoT) and model data processing, a positioning system, and a model-fitting AR system, with the goal that every building object only needs to be undergo the pre-processing operation once, as well as an AR engineering maintenance system. After completing the pre-processing, the AR system can be used to directly with the model and assist in maintenance operations.

2.1 System pre-positioning operations

This study integrates BLE indoor positioning technology, IoT indoor monitoring technology, and cloud technology as developed previously by our research team, and transplants these technologies to an iOS platform for development. Based on SLAM AR, the Augmented Reality system is redesigned, adding Raspberry Pi into the IoT system for value-added applications to optimize and adjust the BLE positioning mode. The pre-position operation only is required to be performed once, with the expected results obtained without further pre-processing. Before system operation, it is necessary to use Autodesk Revit as a tool to establish the model of a building. This system takes the BIM model of the Second Engineering Building at the National Taiwan University of Science and Technology as an example, with sensors laid out within the required space.

2.2 Model data and sensor data processing

A BIM model has various components such as walls, beams, columns, equipment, etc., and furthermore, every component is configured with numerical data. To import the components contained in a case model into a database, the case statement for itemized components must be exported as a text file. The component data, indoor positioning device and room information, room name, floor number, address, and other related building information are collated into the storage configuration logic of HBase in compliance with the database format used in the laboratory. The component information will be consolidated into an HBase database format through an automated processing program to facilitate future uploading.

For the IoT indoor monitoring data of an on-site room, the perception layer consists of mainly the Arduino microcontroller. Various sensors such as a humidity sensor, water-dripping sensor, and an illuminance sensor are configured with Arduino to collect environmental monitoring data in the space where they are located. The network layer is the XBee communication module, which is connected to the Arduino through the Arduino-XBee Shield to form a ZigBee transmission node with various sensor modules. The Raspberry Pi also needs to be connected to the XBee communication module to form a data-receiving node, transmitting sensor information in the network to the Raspberry Pi through the ZigBee network system. The data is collated and uploaded to HBase via a server-side personal home page (PHP) through a wireless

network, thereby realizing the sensor wireless network transmission framework. The above two data processing flow procedures are shown in Figure 1.

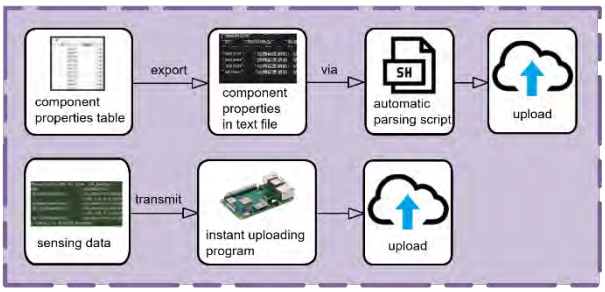

Figure 1. Data processing flow procedures.

2.3 Model processing flow procedure

After a completely established BIM model is exported, problems in material loss are present. If is used directly in the Augmented Reality system, challenges will arise in identifying components. It is necessary to re-render the BIM model material through the 3ds Max material editor and import it into the Unity development platform, so that the identification is correct. An overall BIM model needs to be manually segmented, cutting the model into floor models to be used as floor mini maps of floors. The model is further segmented into room models for the AR system to use for visualization. Finally, the model is converted to a Unity server transfer format through a Unity AssetBundle and uploaded to the server. In future uses, after a user enters the positioned space, the model can be created, deleted, and subjected to other functions during the execution of the AR program through the wireless network, maintaining a stable memory usage in the handheld device. The flow process is shown in Figure 2.

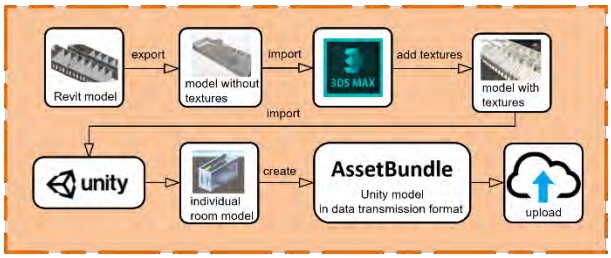

Figure 2. Model segmentation flow process.

2.4 AR pre-processing system

The pre-processing system is used to construct a mapping and record the placement of components. In a fitting operation, when a room to be scanned is entered, the system will first locate the room. After the cloud scanning of spatial points is completed, a selection list of components is produced, and all the components in the room will be listed for the located room. Next, the components to be fit are selected from the list of components. When the model is fit and placed in position visually, the system will calculate the moving distance and rotation angle. When clicking the upload button, the point cloud information file stored in the point cloud map will be uploaded to the server for storage, and the model with the relevant map location information will be stored in the database synchronously. The pre-processing operation procedure is shown in Figure 3.

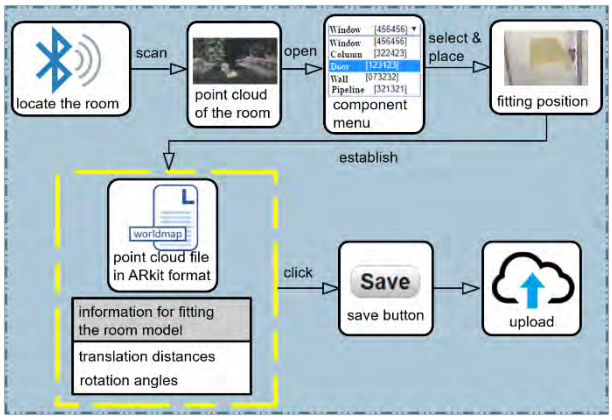

Figure 3. AR pre-processing system operation flowchart.

2.5 AR system operation flow process

The system operation starts mainly after the pre-positioning operations are completed. A user's on-site operation through the proposed system is mainly divided into three parts: indoor positioning, model fitting, and AR presentation. An overall framework of the first two parts is shown in Figure 4.

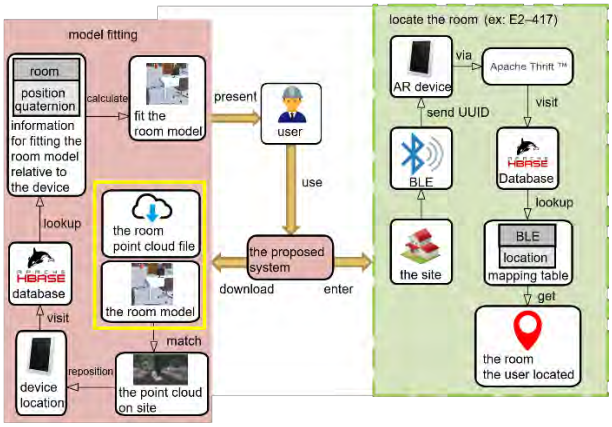

Figure 4. Model fitting flow process (left) and room positioning flow process (right).

In the positioning operation, a user entering the project site can wear a mobile device equipped with the proposed system. The device will receive multiple universally unique identifiers (UUID), with the signal strength transmitted by Beacon devices at each time step. The UUID will be sorted following the received signal strength and ranked from the strongest to the weakest. If the frequency of a Beacon device signal strength per time step is ranked the highest, that UUID will be the UUID of the room. The system will access the Hbase database through functions provided by Apache Thrift, search for the corresponding room position inside the BLE data table, and set it as the system positioning location, as shown in Figure 4 (right).

After a user completes the positioning, the system will download the files corresponding to the room from the server (the point cloud information file that contains the stored point cloud map of the room and the room model file with the pre-position processing). After loading the point cloud information file, the system will compare the feature points in both the point cloud map and the actual environment, and then recalculate the relative position of the device in the point cloud map. Thus, the model will obtain the position and angle of the model relative to the device through the database, and then the room model is fitted to the corresponding position in the point cloud map. The user can see the virtual model overlaid onto the actual environment through the device camera. The flow process is shown in Figure 4 (left).

After the AR model is presented on the system screen interface, users can click on the Revit component model by tapping on the screen. The system will send the Revit ID of the selected components to HBase, search for the corresponding component data parameters, attributes, categories, and other component information via the ID, and transfer the data back to the interface to be viewed by user. From this, if the model is a sensor, the historical data for the sensor can be obtained. Set directly on top of a map, a virtual camera exclusive to the mini map can view the location of the device on the map using an orthographic projection, and thus a mini map navigation mechanism is formed. The complete function flow process is shown in Figure 5.

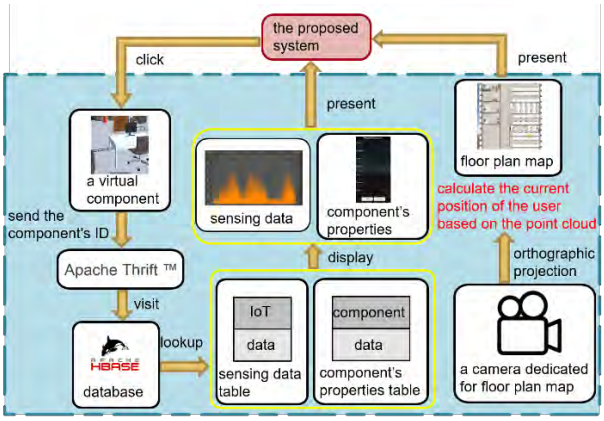

Figure 5. AR presentation flow process.

3 System operation mechanism

The operation mechanism is divided into five sections: BIM model processing method, IoT indoor monitoring sensor group setup, AR preposition processing system mechanism, HBase database configuration, and auxiliary tools.

3.1 BIM model processing method

According to the system requirements, a Revit model of the study site must be first established. Before introducing the BIM model into Unity, the model and component information must first be exported separately. The model must be stored on the HTTP Server in the Unity Asset Bundle format for users to download the model through a wireless network during program execution; component information must be processed before it can be stored in HBase.

Before the Revit model is introduced again into Unity, the model needs to be exported first into a readable format by Unity. The designed system uses the FBX format, while the Revit model is exclusive to the Autodesk software suite. If other software is used for model viewing, the model will not display properly. To resolve this problem, the model must be converted. The designed system uses Autodesk 3D Studio Max (3ds Max) for model conversion.

Considering that the mobile device hardware paired by the user on the project site lacks computational power to process the sizable model and the large-scale rendering of the 3D model, the model is segmented following the room being cut in Revit, as shown in Figure 6.

Figure 6. Schematic diagrams of segmented rooms.

If the attributes of the BIM components are to be imported into the database, processing is necessary. First, the component must have an identifiable code for subsequent component search, and while component itself in Revit is configured with an ID, it is a hidden attribute. At the model establishment stage, the designed system uses the Dynamo extension plug-in to place the attribute members into the ID of each component.

3.2 IoT indoor monitoring sensor group setup

Data transmission of the proposed system uses the Arduino board in combination with sensors, thereby reducing the cost of laying out hardware. The sensor components include an Arduino development board, a number of environmental sensors, the BLE indoor positioning module, and XBee communication module (data transmission). The data processing components include the Raspberry Pi, the XBee communication module (data reception): through the Wi-Fi network module of the Raspberry Pi, the monitoring data received by the XBee module is uploaded to the database storage in the remote server.

3.3 AR pre-processing system mechanism

After entering a room, the positioning of the room can be conducted through this pre-processing system. After confirming the location of the room, the scanning of the point cloud for the 3D space can then be carried out. After the scanning is complete, the point cloud file is uploaded to the server for storage and linked to the database.

Next, it is necessary to record the position of the model in three-dimensional space. First, the user must select the component to be fitted and manually place the component at the true position of the object. Next, the system will calculate the relative position of other remaining components per the position of the manually placed component.

The manual alignment is done through a perpendicular projection from the right center of the screen through a ray. The ray is parallel to the normal vector of the screen plane. If the ray touches the plane of system detection, the right center of the component will be fitted to the position of the system detection ray projection and the model will fit to the parallel plane, as shown in Figure 7.

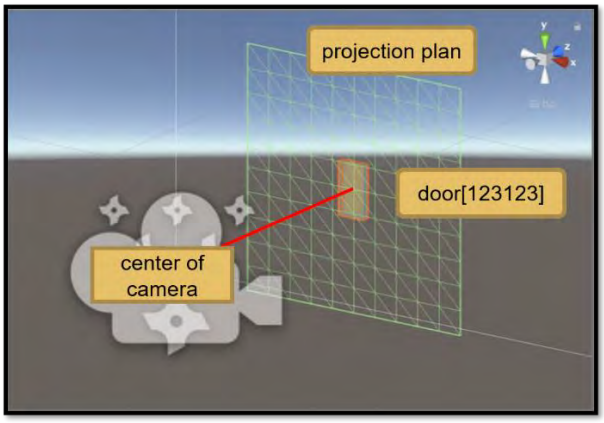

Figure 7. Schematic diagram of the manual model alignment.

After the user performing the pre-positioning enters the room, the system will automatically locate the room where the operator is located, and the room model will be downloaded into the system. After the download is finished, the overall room model will be placed into a point cloud map as a far spot that is invisible to the naked eye. The initial coordinates for this far spot is (10000, 10000, 10000), and for the angle, to avoid the problem of not being able to rotate normally because of gimbal lock, the angle is computed using quaternions with an initial value of (0, 0, 0, 0). When the operator completes the fitting of a single component, the system will calculate record the relative offset of components for the entire room according to the offset of the fitted component. As shown in Figure 8, room model distance before rotating ΔQ is not equivalent to the sub-component distance. After rotating ΔQ, where ΔQ represents relative rotation angle between two components, room model distance is equivalent to the sub-component distance, as shown in Figure 9. The overlaid views in the proposed AR system are shown in Figure 10.

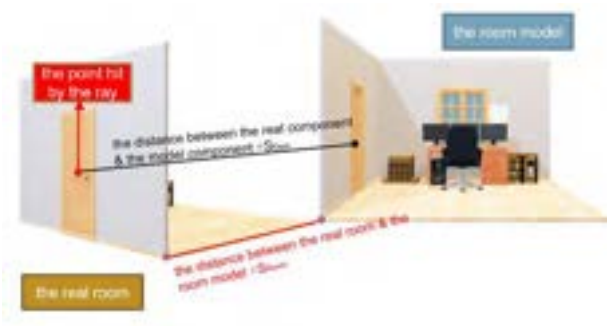

Figure 8. Room model distance before rotating $\Delta \boldsymbol{Q}$ is not equivalent to the sub-component distance.

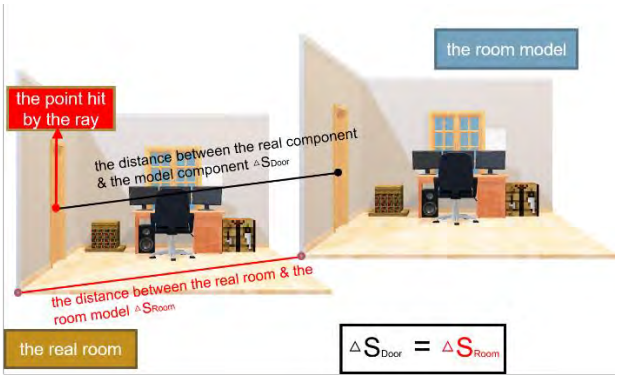

Figure 9. Room model distance after rotating ΔQ is equivalent to the sub-component distance.

Figure 10. The overlaid views in the proposed AR system.

3.4 HBase database configuration

This study assumes that the system application scope is quite large. In practical applications, the dataset may be very large. The designed system adopts Apache HBase, a non-relational database, as a data storage tool, which can allow multiple users to quickly obtain the stored data. The data storage structure is configured according to the system specifications shown in Figure 11.

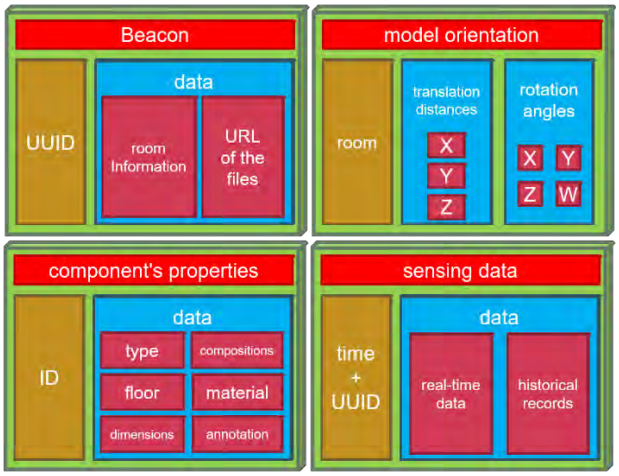

Figure 11. Beacon device data sheet configuration (upper left), model position data sheet configuration (upper right), component information data sheet configuration (lower left), and sensor data sheet configuration (lower right).

3.5 Auxiliary tool mechanism

The AR virtualization for the sensors is similar to presenting the BIM model generally. The sensor models must be first designed and built, as shown in Figure 12. The representative meaning of the models can be intuitively understood by the user.

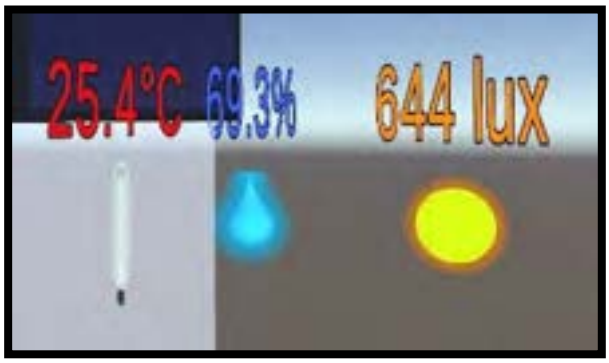

Figure 12. Real-time AR presentation of the sensor measurement data.

When the user taps the model, the system shows the historical data, as shown in Figure 13. To check for abnormal temperatures, the date can be selected. Vertical axis of the chart is the temperature with unit of ℃; horizontal axis is the hours with a range of 0-23.

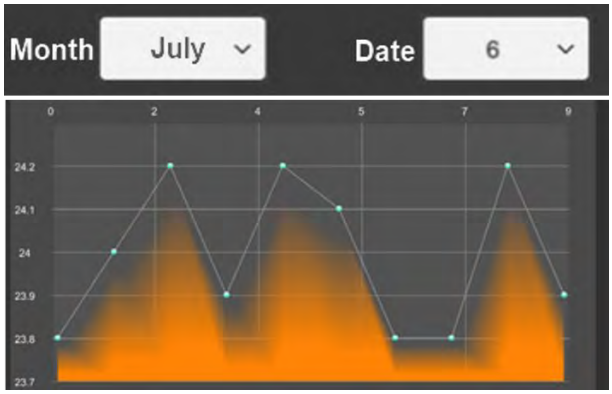

Figure 13. Sensor chart and selection list example.

Users can find a navigation map from the map navigation icon at the lower right of the display. The red sphere is the user's location, which helps the user to understand their current location. After the system locates the room, the system will download the model of the floor from the server and place it on the mini map user interface (UI) layer for viewing. After the room model is completely fitted through the point cloud map, the system will know its relative position between the model and the device. The red sphere is placed on the relative position of the device inside the floor model, and a mini map camera is set directly above the sphere to illuminate the position of the red sphere as an orthographic projection, forming a two-dimensional planar map as shown in Figure 14.

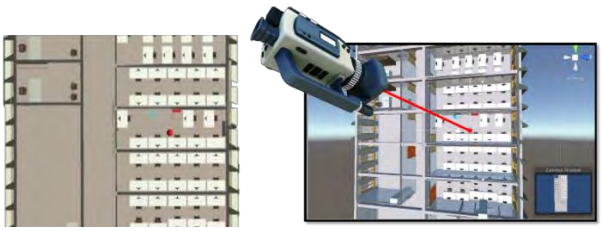

Figure 14. Schematic diagrams of the mini map UI and the orthographic projection mechanism.

4 Verification of system effectiveness

4.1 Effectiveness of program execution

Taking the overall model of the Second Engineering Building as an example, a comparison is conducted on the AR presentations for the unsegmented model and the model placed on the server side after segmentation. The influence of the rendering model on overall system effectiveness is considered, with Xcode Monitor used for monitoring.

iPhone XR is a handheld device with mostly high-end specifications among handheld devices in the current market. The graphics processing has excellent performance in more areas. According to a comparison of the results, the memory usage of the model-processed version is approximately 26.83% of the original model. Using the frame rate to reflect the graphics processing power of the handheld device, the model-processed version reached 205% of the original frame rate, with 60 frames per second (fps) being the current standard of high-resolution TV. Model segmentation is still necessary for the hardware equipment specifications on current handheld devices.

4.2 BLE room positioning verification

For the verifying the indoor positioning of this system, two Beacon devices continuously emitting Bluetooth signals were placed in two adjacent rooms, with the Beacon devices separated by a wooden wall. Enabling the Beacon devices to interact with each other verifies whether the positioned room can be located under the situation where there is mutual interference. Positioning was conducted at the furthest and nearest spots from the Beacon devices in the two rooms and the nearest and furthest positioning results within the same room to calculate the success rate of the positioning. From several tests, an approximate accuracy of 100% accuracy can be obtained.

4.3 Model fitting accuracy

This study conducted a model fitting accuracy test in an office room of the E2 building at Taiwan Tech. The center of a door in the room was taken as the reference point for accuracy measurement. The way to measure fitting accuracy is as follows. Figure 15(a) shows an actual door, with a reference point set at the center of the door. A reference point is also set at the center of the virtual door model. Using the AR pre-processing system for model fitting, shown in Figure 15(b), the reference point has an offset of D1. By comparing the offset of D1 obtained from the observed door at the same actual position, the degree of fitness is calculated in a quantitative approach. The system offsets were measured at two observation points. The first point was at a distance of 109 cm perpendicularly from the reference point of the target component, and the second point was at a distance of 252 cm from the reference point of the target component in the direction of a 60 degrees offset.

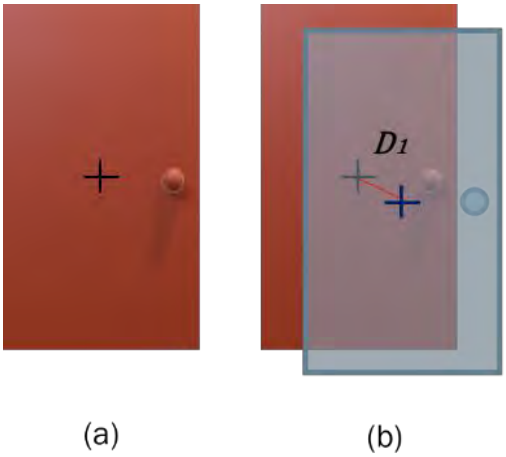

Figure 15. Schematic diagrams of the fitting, with the center of the door taken as the reference points (a) Actual door, (b) fitting of the AR pre-processing system model door.

An average offset can be determined from the statistical results shown in Table 1. The fitting accuracy of the new system can reach errors on the order of millimeters in a single room, with the degree of fitting being more accurate. This degree of errors is acceptable for application at the maintenance stage.

Table 1. Average offset results.

Offset angle	Average offset of x (cm)	Average offset of y (cm)	Normalization of x	Normalization of y
0°	0.0353	0.1623	0.0395%	0.1819%
60°	0.1693	0.2258	0.1898%	0.2531%

5 Conclusions

This study proposes an Augmented Reality system based on SLAM for a marker-less system, and develops a set of AR pre-processing and AR presentation systems to enhance the integration stability of virtual and actual worlds. Moreover, the BIM model and the on-site environment are combined, so that information can be presented to the user on a same interface, information is automatically transmitted to the user, and the complexity of the human-machine interface is reduced, thereby resolving the inconvenience of BIM model on-site operation as mentioned in the study motivation.

Furthermore, in the indoor positioning based on BLE, using a more stable approach than previous research for locating a user's positioned space and loading the room point cloud map and room model based on the positioned room, the subsequent development of AR pre-positioning system and AR presentation system were based on this foundation, thereby reducing system operation complexity. Using rooms to segment the model and point cloud map, pre-storing files in a remote server, and using the database to store the file links and room effectively reduces the system usage space and memory usage during program execution and reduce graphics processing load, thus improving system effectiveness. This framework is taken to propose an augmented reality BIM fitting system that is stable and applicable to a wide range of spaces.

Finally, the designed system uses a Raspberry Pi as the central coordinator. After obtaining all the sensing data, the data is uniformly processed through a regularized program, and then the numerical data is transmitted through the Internet and stored in a database. The integrated application of sensors in augmented reality proactively presents environmental information to the user.

References

[1] C. S. Park, D. Y. Lee, O. S. Kwon, and X. Wang, "A framework for proactive construction defect management using BIM, augmented reality and ontology-based data collection template," Autom. Constr., 2013, doi: 10.1016/j.autcon.2012.09.010.

[2] M. Kopsida and I. Brilakis, "Markerless BIM Registration for Mobile Augmented Reality Based Inspection," in International Conference on Smart Infrastructure and Construction, 2016.

[3] N. Yabuki, A. Motamedi, M. Miyake, and T. Fukuda, "Outdoor Maker-less Augmented Reality System For Visualizing A Building Model And Its Information Using Simultaneous Localization and Mapping," 22nd Int. Conf. Comput. Archit. Des. Res. Asia (CAADRIA 2017), 2017.

[4] P.H. Diao and N.J. Shih, "BIM-based AR maintenance system (BARMS) as an intelligent instruction platform for complex plumbing facilities," Appl. Sci., 2019, doi: 10.3390/app9081592.

[5] J. Polvi, T. Taketomi, G. Yamamoto, A. Dey, C. Sandor, and H. Kato, "SlidAR: A 3D positioning method for SLAM-based handheld augmented reality," Comput. Graph., 2016, doi: 10.1016/j.cag.2015.10.013.

Review of Construction Workspace Definition and Case Studies

K. F. Lai and Y. C. Chan

Department of Civil Engineering, National Taiwan University, Taiwan
E-mail: r08521714@ntu.edu.tw, ychan@ntu.edu.tw

Abstract -

Workspaces in a construction project are considered as critical and limited resources. Since the workspace conflicts cause productivity loss and poor quality, construction researchers have been exploring different workspace definitions and solutions to improve the situations. Construction workspace' function can be classified according to the user's needs and characteristics of activities and can be integrated into 4D BIM simulation. In previous studies, researchers have proposed several different and innovative workspace definition. However, researchers usually only tested their proposed workspace definitions on specific building projects or few particular tasks. It is difficult to tell the effectiveness of the workspace definition when applying to a different construction project or case involving different construction methods. Relevant works of literature regarding construction workspace definitions were collected and discussed in this article to obtain a comprehensive review on this topic. We have applied the proposed definition to the same construction case and also provided an evaluation of their approaches' pros and cons. Then we proposed a criterion of developing proper workspace, so the workspace requirement can be planned based on the project's characteristics and could help the project managers to select the optimum scenario during workspace planning.

Keywords -

Workspace Conflict; Workspace Classification; Conflict Solution; 4D BIM; Conflict Severity

1 Introduction

Various subcontractors have to finish working activities in a space-limited construction site. Each activity requires a certain amount of workspace for workers, equipment areas, etc. Workspace conflicts between activities could result in schedule delays and poor quality. Since there is a rising demand for complicated construction works in the municipal area, the need for a proper construction site layout is crucial to eliminate workspace conflict.

However, it is challenging for the project managers to eliminate the interference caused by workspace conflicts among activities because traditional 2D drawings are not enough to indicate dynamic changes and enough information of equipment's and labors in the construction site.

Therefore, many researchers took efforts to develop techniques such as building information modeling (BIM). The 4D BIM models with schedule management in recent years has been broadly utilized among buildings' life cycle. Researchers also tried to strengthen the techniques of workspace conflict analysis and tried to find better solutions. The studies in the past 20 years covered methods of how to identify the workspace requirement of each activity, how to develop and detect workspace conflict, how to solve the problem before the construction phase starts, and how to simulate dynamic workspace conflict due to dynamic changes.

Since theories of workspace conflict analysis have been evolved for more than 20 years, definitions of workspace has been very different in different studies. While each of these theories of workspace definition can explain some aspects of construction projects, none can successfully be applied to all instances of construction projects. Rather than pursue this further by finding the best definition for all construction projects, we will explore a criterion to select proper definition for workspace conflict analysis by studying and summarizing previous studies from a detailed review covering the different workspace definitions.

2 Literature Review

In this study, we collected previous studies regarding workspace conflict analysis from 2002 to 2018. Table 1 shows a summary of the most important publications in this field and the different factors focusing on by researchers. We will discuss each factor in detail in the following session.

Table 1. Comparison of Previous Workspace Conflict Studies

Reference	Workspace Requirements Definition	Workspace Occupation Representation	Workspace Conflict Detection	Conflict Severity Index	Conflict Severity Quantification	Conflict Solution Strategy
[1]	*	*	*	*		*
[2]	*	*	*	*		
[3]	*	*	*	*		*
[4]	*	*	*			*
[5]		*	*			
[6]	*	*	*	*		*
[7]		*	*	*	*	*

2.1 Workspace Definitions

Workspace definitions are broadly discussed and classified by researchers. Thabet and Beliveau [1] have classified the space into two groups, one is man and equipment, and the other is materials. These two groups are classified according to whether the size of space will be constant or decreased by time. This classification will help to provide the evaluation of the activity's space demand by the sum of quantities from each factors' physical needs and surroundings' needs.

Akinci, Fischer [2] classified construction activities into three categories based on reference object, orientation, and parameters. The categories included macrolevel, microlevel, and paths. Macrolevel spaces referred to huge-scale, such as storage or prefabrication areas. Microlevel spaces were mostly related to building components, and paths were required for transportation. Guo [3] has classified the spaces based on different four users: labor, equipment, materials, temporary facility. Considering whether the space is available for work or not, the space needed for each user could also be defined by space type as the exterior of the job site, the interior of the job site, inside the structure, and space provided by a temporary structure.

Choi, Lee [4] separated the workspace layout by its function or movability. When by function, it includes direct workspace (object space, working space, and storage space); indirect workspace includes set up space, path space, and unavailable space. When workspace defined by movability, it can be separated into fixed workspaces and flexible workspaces**.** The purpose of classification by function is to stand for total workspace definition without missing; moreover, classification by movability is to supply a resolution of workspace conflict after it has been identified.

To deal with dynamic nature in construction sites, Su and Cai [5] proposed two ways of defining workspace: 1) workspace directly created by users, and 2) workspace created based on geometric shapes such as column, sphere, tetrahedron or hexahedron. The latter is based on the simulation of labor workspace or tower crane workspace and provides users to derive workspace with two functions: offset and rotate.

However, the construction layout may be changed by schedule. Dynamic changes based on time flow in a construction site also need to be considered in the use of workspace[2, 6, 7].

Tommelein and Zouein [6] tried to connect the construction layout plan and project schedule plan, which consider the dynamic changes of location and activities in the construction site. Kassem, Dawood [8] suggested providing the definition based on whether the physical change on the construction site was added or not in 4D BIM model. They also defined the object workspace, which represented building elements, and safety workspace that is tolerance between two workspaces, or the distance which objects may fall from height.

Mirzaei, Nasirzadeh [9] defined the varied nature of activities, considering space should be static when the labor crew occupies a place thoroughly during the whole activity duration. Dynamic workspace, on the other hand, represents that the labor crew will move their space during each time interval.

Table 2 shows the collection of workspace definitions from previous studies.

Table 2. Summary of Workspace Definitions

	Definition	Authors
By constant level	Man and Equipment	[1]
By decrease level	Materials	
By users	Labor	[3]
	Equipment	
	Materials	
	Temporary Facility	
By availability	The exterior of Job site	
	Interior of Job site	
	Inside the Structure	
	Space provided by Temporary facility	
By scale	Macrolevel	[2]
	Microlevel	
By function	Direct Workspace	[4]
	Indirect Workspace	

By movability	Fixed Workspace	
	Flexible Workspace	
By geometric shape	Column	[5]
	Sphere	
	Tetrahedron	
By physical change or not	Main Workspace	[8]
	Support Workspace	
By building elements	Object Workspace	
By safety distance	Safety Workspace	
By position changed of labor crew	Dynamic Workspace	[9]
	Static Workspace	

Since there is a variety of workspaces definition, it is crucial to set a flow chart for construction site layout that is useful for specific needs. In the following paragraphs, we will discuss three workspace characteristics proposed by Akinci, Fischer [2], which are generality, reusability, and comprehensiveness.

Generality means we can apply for various workspace requirement, especially for spaces which are related to building components, such as equipment and crews. However, storage areas for materials are also important that should not be ignored. Since some materials are temporary and are waiting to be installed in buildings, but some materials will be left for owners as a backup in the maintenance stage, it is important to set a clear layout easy to separate temporary and permanent materials.

Reusability means construction activity is repeatable or can be done by the same equipment no matter what locations or sizes they have. Usually, Since the construction methods depend on the location and some specific constraints, there will not 100% the same in each location. For example, if there is a window at 20 floors high rise building, but the space beneath the window is not large enough to locate a crane , then the construction method had to changed based on constraints. However, it is too hard to expect what will happen during construction. So, it will be suitable for site managers to follow the most common construction methods for construction.

Comprehensiveness is about the details when it comes to describing the construction methods. The orientation and the volume (length, width, height) of a required workspace should be seen or modified. Each equipment would have its maximum range of workspace. For example, the crane's range can be calculated by the radius chart.

As we've mentioned, these 3 factors are crucial to represent a construction site. In addition, we still notice that it is hard to define the best layout for the construction site, but we can discuss this problem consider the scale.

The case in Guo's research is a 12-story reinforced concrete, and the case in Akinci's research is about the installation of windows in a wall. Since 12-story reinforced concrete is a huge project, so he first classified by major activities survey, reinforced steel, plumb…etc.), then each major activity requires 4 main categories (labor, equipment, materials and set-up space). However, a small construction site is no needed for such a detailed workspace definition. On the other hand, if the layout classification is too simple, some places could be neglected and may become a potential problem. So, it is much proper to define the scope of a construction site in a simpler way first, then give a more detailed classification if necessary.

2.2 Virtual Spatial Collisions

After the workspace definition is decided, workspace for each activity is created for spatial collisions.

According to a 3D bounding volume, three types of space collision detection algorithm can be used in a 3D model, which are bounding spheres (BS), axis-aligned bounding boxes (AABB), and oriented bounding boxes (OBB). The method of bounding spheres is to detect the collision by detecting the sum of two bounding sphere's radius and also the distance between the center of two spheres [10]. Oriented bounding boxes were introduced by Möller and Haines [11], which created minimum bounding boxes around objects without considering the object's axis, and the existence of another axis identified the collision. Axis-aligned bounding boxes need to determine the minimum and maximum coordinate values of the two bounding boxes, which are parallel to their coordinate axes. Figure 1 illustrates three types of collision detection described above.

	Diagram	Collision Condition
Bounding Sphere	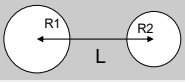	L<R1+R2
Axis-Aligned Bounding Box	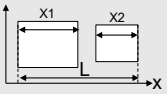	L < X1+X2
Oriented Bounding Box	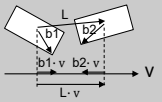	$\|L \cdot v\| < \|b1 \cdot v + b2 \cdot v\|$

Figure 1. Collision conditions

When it comes to the application, axis-aligned bounding boxes (AABB) are used most common on building objects such as beams and columns, most of their shapes are rectangular cuboid. Bounding spheres (BS) methods for workspace conflicts are suitable when there are multiple crane works. But these methods can be combined for specific cases, too. In the installation process of prefabricated steel beams working area, crane work may also affect the installation of the bolt works.

2.3 Moveable Objects

Since the construction site is dynamically changed with schedule, it is critical to detect the resource movement. Previous studies usually assumed that the laborers occupied the whole workspace throughout its duration. However, labors only occupy a part of the needed workspace and change their location all the time. The dynamics of activities should be investigated, and also the patterns of where they start, execute, and end. Few studies have addressed the significance of the activities transition in a required workspace. Mallasi [12] developed 12 execution patterns. Choi, Lee [4] presented the concept of unrealistic workspace problems in Figure 2 which may exist in two activities.

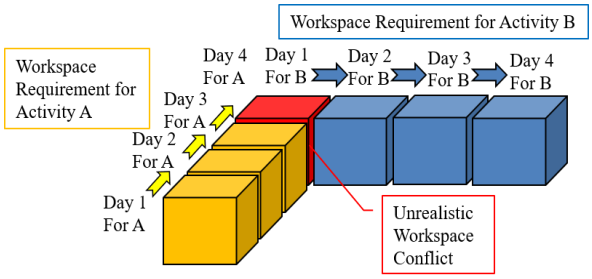

Figure 2. Unrealistic workspace problem modified [4]

The most significant assumption about the construction layout is static. But dynamic changes of the workspace by schedule are also essential when the activities can not be done in a day. If the construction site can be divided into different small spaces, then it will be crucial. This will help when your activity has overlapped other nearby activities' workspace. If both conflict activities can not change each sequence or schedule, then it will be easier to adjust the working sequence and to avoid unrealistic problems.

2.4 Index of Conflict Severity:

The measurements of workspace-conflict need to be qualitative and quantitative.Akinci, Fischen [13] suggested a conflict ratio, which is the ratio between the conflict volume and the required space volume. Guo [3] used the interference space percentage (ISP) and the interference duration percentage (IDP) as two indicators. One is the ratio between the interference space size and the activity's original size, and the other is the ratio between the interference duration and the activity's original duration. Mallasi [12] created a five-criteria quantification index to identify the conflicts. Kassem, Dawood [8] took the congestion severity (CgS %) as the ratio of the sum of the required space and the available space.

The concept of conflict severity can be assessed. However, this indicator cannot quantify the impact of conflicts on project performance. Mirzaei, Nasirzadeh [9] define a new approach to calculate the conflict severity by the labor congestion and conflict space size

Figure 3 shows the different definitions of the conflict severity index.

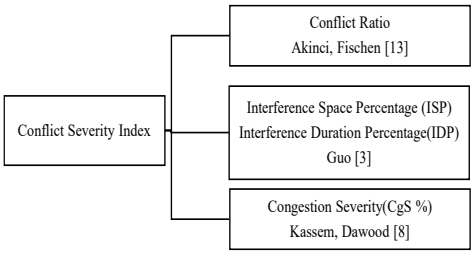

Figure 3. Conflict severity index

In previous studies, several solutions have been derived, but the relationship between the conflict severity and resolution need to be discussed. The goal of conflict severity is to help managers decide the best solution. However, a single number can not reflect the total situation in each study, which may cause the manager hard to decide the best solution. Although in Guo [3] study, ISP and IDP can be calculated and criteria for resolving space conflict are suggested, but there is little discussion on the relationships between these two indicators.

Some studies have suggested congestion as another conflict severity, which is the ratio between the available workspace per person and the minimum workspace required per person.

2.5 Solution For Workspace Conflict

The solution of workspace conflict is crucial since it could help the project managers to raise the working efficiency. Guo [3] not only suggested to change the logical sequence, location, or starting time for conflicting activities to avoid problems but also suggested to recheck the path demand after changing. In a study from Choi, Lee [4], they proposed to change the location of flexible workspace or consider both the schedule plan for critical and non-critical activities. Kassem, Dawood [8]

suggested 2 solutions, first is changing and adjusting the schedule, second is changing and adjusting the physical location and size of workspace.

3 Discussion

The aim of this research was to review previous studies on workspace definitions and conflicts resolutions. Some other factors should be considered and further discussed since there would be some relations between workspace definitions and other factors when conducting conflict analysis.

3.1 4D BIM Applications

Compare to 2D drawing, 4D BIM provides diverse information and visual environment, which can help managers to arrange a proper workspace in the 4D model on a whole scale of the construction site. Most of the previous researches had considered using BIM application programming interface (API) for workspace planning, and this study might help technologists and project managers to follow a criterion for workspace planning by applying BIM API.

3.2 Case studies

Each previous research will choose a case study as their theory's implementation. Now we select the case study in Automated Generation of WorkSpaces Required by Construction Activities by Akinci, Fischer [14], which is about using scissor lift for windows installation.

Figure 4 shows the background of this project. We applied and compared several workspace definitions in the following paragraphs.

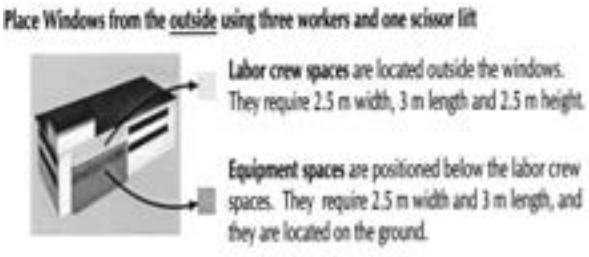

Figure 4. Windows Installation Information [14]

- By scale : This advantage is that we can have a rough range of space sizes for workspace management. Project managers can focus on microlevel spaces, which are the components (windows), equipment(scissor lift), and labors. Its definition seems a little hard and vague to classify whether the items should belong to the macrolevel or microlevel.
- By location: This classification consider whether its the space is exterior or interior of structure/jobsite. However, this does not necessarily needed for a small project since the working and storage area are easy to arrange. It will help if the project's scale is big and the time is long enough so that managers can control all the items in detail.
- By function: The advantage of this definition is that this will help the managers focus more on whether the condition for each workspace is prepared or not to function, rather than to use location or size level as classification.
- By movability: The disadvantage is that this classification may not be so necessary for a small construction project.
- By position changed of labor crew:This can show a dynamic motion for labor workspace by schedule. The feature of this classification is that if the works can not be done in a day, managers can easily understand the work sequence in the schedule. However, if there is no conflict with other activities workspace, then this works sequence seems a little unnecessary.

In this case, we can form up a guideline for planing a proper workspace layout for different kinds of construction sites. Figure 5 shows the workspaces planning into four levels:

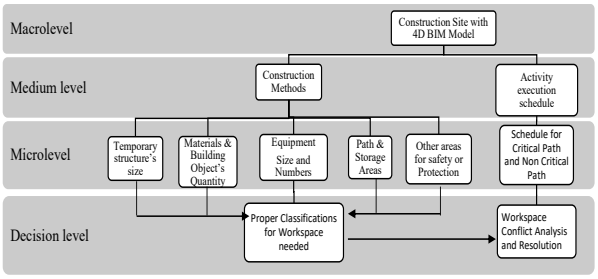

Figure 5. Workspace layout planning flow chart

Macro-level is about choosing types of construction sites, which may be buildings, factories, roads, or other related constructions. The medium level begins to select the construction methods for each activity. Microlevel would let the project manager select necessary and detailed elements to create a proper workspace layout planning in the decision level.

4 Conclusion

This study reviewed the previous research of workspace definitions and conflict resolution. From the literature review, there are different types of workspace

definitions based on several aspects. We also investigate these theories and apply them to a case study. The discussion showed some results that include the pros and cons of whether these factors are necessary for workspace planning. There is no standard answer for classification since each project is unique, a workspace planning flow chart can be helpful to establish a workspace layout with construction methods and quantities of each activities.A proper workspace classification still relies on the degree of understanding among project managers.

However, our study ignores the time-schedule factor, which is a limitation that may somehow affect the result of classification. Future work can focus more on the workspace conflicts of activities in period of time which can discuss a more specific workspace conflict.

Another future research can be further discussed since people can rely more on the development of 4D BIM model. Since BIM model has the function of detecting collision items in design stage, the API developers can improve the function of creating virtual workspace among activities and shows the collisions in the BIM model, and therefore the criterion of workspace layout classification will be more usable for managers to solve the workspace conflict problem.

References

[1] Thabet, W.Y. and Y.J. Beliveau, *Modeling Work Space to Schedule Repetitive Floors in Multistory Buildings.* Journal of Construction Engineering and Management, 1994. **120**(1): p. 96-116.

[2] Akinci, B., et al., *Representing Work Spaces Generically in Construction Method Models.* Journal of Construction Engineering and Management, 2002. **128**(4): p. 296-305.

[3] Guo, S.-J., *Identification and Resolution of Work Space Conflicts in Building Construction.* Journal of Construction Engineering and Management, 2002. **128**(4): p. 287-295.

[4] Choi, B., et al., *Framework for Work-Space Planning Using Four-Dimensional BIM in Construction Projects.* Journal of Construction Engineering and Management, 2014. **140**(9): p. 04014041.

[5] Su, X. and H. Cai, *Life Cycle Approach to Construction Workspace Modeling and Planning.* Journal of Construction Engineering and Management, 2014. **140**(7): p. 04014019.

[6] Tommelein, I.D. and P.P. Zouein, *Interactive Dynamic Layout Planning.* Journal of Construction Engineering and Management, 1993. **119**(2): p. 266-287.

[7] Winch, G.M. and S. North, *Critical Space Analysis.* Journal of Construction Engineering and Management, 2006. **132**(5): p. 473-481.

[8] Kassem, M., N. Dawood, and R. Chavada, *Construction workspace management within an Industry Foundation Class-Compliant 4D tool.* Automation in Construction, 2015. **52**: p. 42-58.

[9] Mirzaei, A., et al., *4D-BIM Dynamic Time–Space Conflict Detection and Quantification System for Building Construction Projects.* Journal of Construction Engineering and Management, 2018. **144**(7): p. 04018056.

[10] Talmaki, S. and V.R. Kamat, *Real-Time Hybrid Virtuality for Prevention of Excavation Related Utility Strikes.* Journal of Computing in Civil Engineering, 2014. **28**(3): p. 04014001.

[11] Möller, T. and E. Haines, *Real-time rendering*. 2002: AK Peters.

[12] Mallasi, Z., *Dynamic quantification and analysis of the construction workspace congestion utilising 4D visualisation.* Automation in Construction, 2006. **15**(5): p. 640-655.

[13] Akinci, B., et al., *Formalization and Automation of Time-Space Conflict Analysis.* Journal of Computing in Civil Engineering, 2002. **16**(2): p. 124-134.

[14] Akinci, B., M. Fischer, and J. Kunz, *Automated Generation of Work Spaces Required by Construction Activities.* Journal of Construction Engineering and Management, 2002. **128**(4): p. 306-315.

A Web-Based Approach to Dynamically Assessing Space Conflicts by Integrating BIM and Graph Database

Wei-Ting Chien[a] and Shang-Hsien Hsieh[a]

[a]Department of Civil Engineering, National Taiwan University, Taipei 10617, Taiwan
E-mail: r06521604@caece.net, shhsieh@ntu.edu.tw

Abstract –

Construction activities require materials or resources to be arranged while planning the route of how these materials or resources can be transported is not a simple process. Traditionally, subcontractors will arrange a daily meeting and negotiate the desired space on site for the next day's resource transporting. However, many of them only use 2D drawings or aerial images while discussing the routes which lack an accurate calculation on space conflicts. In this paper, an approach combining Building Information Modelling (BIM) and Graph Database (GraphDB) is proposed. With the help from 3D BIM models, the coordinates of resource transporting routes can be first extracted and further analysed by the proposed approach. From the result, the collisions along the planning routes can be detected to assist in making a proper transporting plan. In addition, a web-based platform is developed for validation of this approach. Because the platform is a shared one, each user can arbitrarily plot their desired transporting routes in the model at any time. As long as the actual transporting schedule is known for the corresponding route, the platform can dynamically and instantly inspect whether the desired routes will collide with others. In this way, we can eliminate conflicts prior to the start of those activities and potential delay in the construction process can be reduced.

Keywords –

Building Information Modelling; Construction Conflicts; Construction Management; Separating Axis Theorem; Graph Database

1 Introduction

Construction is a complex process which requires a proper plan prior to its commencement. A proper construction plan can assure the owner of the construction's quality and punctuality while a poor plan can not only cause time overrun but also induce a waste of investment. In an attempt to make a decent plan, several issues should be addressed first, including resource shortage, labour shortage, workspace conflicts, and activity sequence conflicts. With the advent of Building Information Modelling (BIM) and other 3D digitalisation technologies, workspace conflicts and other geometric-related issues can be detected and mitigated. For example, Moon et al. [1] demonstrated that using an algorithm along with the model bounding box concept can assist in determining the adjacency distance between two conflict points. With the information as to where the conflict occurs and the percentage of conflict between two workspaces, the conflicts can be handled and reduced in advance. Similarly, Wu et al. [2] used 4D simulations and colour visualisation techniques on the BIM model to detect space conflict while the required workspace for activity was categorised into five types. In addition, some recent research concerned that the movement of workers could potentially raise workspace conflicts. Therefore, Mirzaei et al. [3] defined 16 execution alternatives for workers' movement patterns and developed a quantification system for calculating the workspace conflict impact level on the project through 4D BIM simulations.

As plenty of research is already concentrating on workspace management, another group of research is focusing on construction materials management. For example, Said and El-Rayes [4] presented an optimised model for making critical decisions on construction logistics while considering both material procurement and material storage on construction sites. Golkhoo and Moselhi [5] proposed a multi-layer perceptron approach to create an optimised material delivery schedule. This schedule enabled contractors to not only procure construction materials with minimum expenditure but also avoid shortage or surplus issues. Although the aforementioned research has helped materials be managed properly on site, little research is concentrating on how the materials can be transported safely from the staging area to the activity execution area in a construction site. Unlike the workspace for each activity which can be defined earlier within the construction plan, material transporting routes are normally assigned by the day before the corresponding activity executes. Furthermore, the transporting routes are not determined

by only one person such as the project manager. Instead, the routes are selected by different subcontractors who are in charge of those activities. In this case, a process is required for enabling users to dynamically assign their routes and automatically detect the route collisions. In addition, a shared platform for multiple users to coordinate their route collision detection is desired.

In this paper, an approach integrating BIM, Separating Axis Theorem (SAT) and Graph Database (GraphDB) is proposed for automatic route collision detection. SAT supports the detection as to whether two objects collide. GraphDB offers an efficient way of storing and extracting the assigned route data and the relationships among activities, materials and routes. BIM serves a visualisation platform and provides data related to the facilities under construction. With the development of a web-based BIM model viewer, all subcontractors are allowed to assign their desired transporting routes by drawing them directly in the BIM model. The viewer will automatically calculate and check whether the newly assigned route collides with the existing routes created by the previous users. In this way, the subcontractors will be able to plan their material transporting routes without requiring that all subcontractors be gathered in the same physical space. As long as they have access to the Internet, they can have discussions about route planning on the proposed platform with automatic route collision detection supported.

2 Methods for Route Conflict Detection

To develop an approach for assessing route conflict, the core algorithm for examining the collisions of objects needs to be proposed first. In this research, SAT is selected to achieve this. On the other hand, how to efficiently and accurately store and extract the route and collision data is another crucial part. Therefore, a graph database is adopted to enhance the efficiency of using the collected data.

2.1 Separating Axis Theorem

SAT is aiming at detecting collisions of two objects by examining if any separating line or plane exists between the objects [6]. The theorem can be applied to both 2D and 3D objects. It says if two 2D objects do not collide with each other, there must be at least one line which can separate the two objects without any intersections (Figure 1). That line is called a separating line. Equivalently, 3D objects can be deemed as not colliding by finding at least one separating plane to separate them from overlapping (Figure 1). As implied, there can be more than one separating line or plane for two separate objects. For example, those dashed lines in 2D object illustration shown in Figure 1 are also separating lines. However, finding all of them is not our intention. Efficiently identifying one existing separating line or plane is sufficient to say that two objects are not colliding. Therefore, SAT allows for a rule-based algorithm to significantly narrow down the necessary lines or planes for checking. The algorithm proposes 4 and 15 equations, respectively, for checking whether the 2D and 3D objects are colliding with each other. Each equation represents an examination of one possible separating line or plane. If any of the equations is fulfilled, that means the corresponding line or plane succeeds in separating the two objects and the two objects are proved to be not colliding. In other words, if all of the equations cannot be fulfilled, the objects are proved to be colliding with each other. This strategy saves us a significant amount of time because only 4 lines or 15 planes need to be checked for every collision examination. There exists numerous possible lines or planes to separate two objects whereas this algorithm allows us to inspect just a few lines or planes to guarantee an accurate result as to whether the two objects are colliding or not. For details about the equations, please refer to the tutorial document by Johnny Huynh [6].

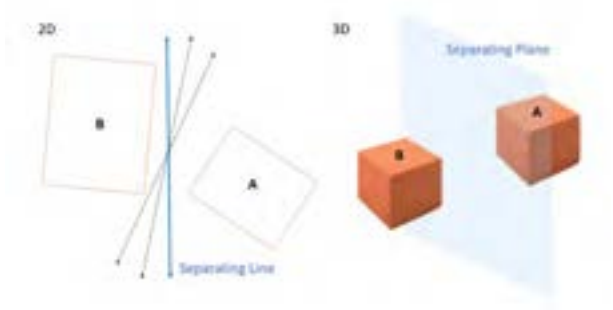

Figure 1. Separating axis theorem illustration

In this research, 3D object collision examination from SAT is applied. A material transporting route is approximately represented by a set of cuboids as shown in Figure 2. In other words, each route can be checked whether they are colliding with other routes simply by examining whether any cuboid in the set of targeting routes is colliding with another route's set of cuboids. For ease of generating a set of cuboids, a central curve of the route should be given first. After that, the curve is further segmented into a list of lines. This is a way of simplifying the curve representation and the point density value can be either specified by the computers automatically or assigned by the users based on their own preference. As the curve is already transformed into a list of segmented lines, determining the width and height of each segment is crucial since the ultimate goal is to transform them into a set of cuboids. Therefore, the width and height of the object using this route can be taken into consideration. For example, assume that the route is assigned for some heavy vehicles to drive through, then the width and

height of the vehicle should be taken into calculation in the collision examination. To achieve this, the segmented lines are horizontally expanded by half of the vehicle width on both sides to represent the total width needed while the vehicle is taking this route. Likewise, the curve is also expanded vertically by the vehicle height to provide the height for the vehicle to pass. In this case, with the segment length already determined in segmenting the curve, a cuboid for every segment can be generated as shown in Figure 2. While each route is transformed into this form of representation, SAT can be applied for checking whether the created routes are colliding with one another.

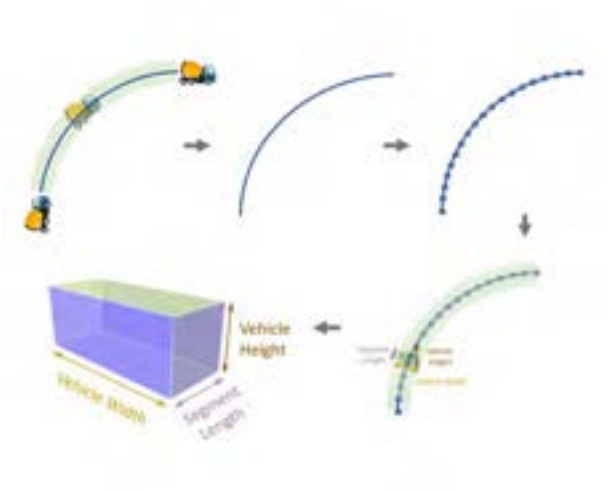

Figure 2. A demonstration of how a route is generated for applying SAT

2.2 Graph Database

Graph database is a database which uses graph as the main structure of storing and querying data [7]. While a graph is generally formed by nodes and edges, it has a greater ability of revealing and explaining complicated relationships among all data. This relatively new concept or technology can be applied to various fields. For example, Sadowski and Rathle [8] proposed using a graph database for finding common patterns from three of the most damaging types of fraud. Cattuto et al. [9] presented a time varying graph database structure for efficiently querying the social network formed with high-resolution records of human activities extracted from mobile devices and sensors. In the field of construction or BIM, Ismail et al. [10] suggested that the 3D IFC models should be automatically transformed into the graph database structure which enables users to manage and analyse the huge amount of building data and complicated relationships. The application of the graph database depends on how to define and manage the nodes and edges.

In this research, three types of nodes are specified, including material, activity and route, which are assigned in green, yellow and blue colour, respectively (Figure 3). Prior to the collision examination, where the route starts and where it ends should be defined first. In this research, it is intended to detect whether a collision may happen while a material is transported from the staging area to the activity area. Therefore, the route's start node is assigned as the staging area and the route's end node is deemed as the activity area likewise. Both nodes encompass the coordinate information of the corresponding area. After the start and end nodes are determined, the route's intermediate nodes are specified by users' drawing of needed transporting routes in the BIM model. As mentioned before, the drawn curve is first interpreted by a list of points and segmented lines. Each point's coordinates are stored in each intermediate node. Furthermore, while the next step is to expand the segmented lines and transform them into a set of segmented cuboids, the information of each cuboid, including width, length, height, can also be stored in the edge (path relationship) between each pair of two adjacent nodes. In this way, each chain in the database can indicate a route for examination and it already contains sufficient information for SAT collision detection including the dimension of each cuboid and its coordinates. Two example chains are illustrated in Figure 3.

After the route data are stored in the database, having them efficiently extracted for SAT examination is another critical part. Taking advantage of the structure of graph database, we can read the cuboid data with just a few lines of code, for example:

```
MATCH (m{name: "<material name>"})-
[rs*]-(a{name: "<activity name>"})
RETURN rs
```

In the above code, m and a are representing the material and activity nodes respectively. Rs* indicates all the relationships along the path from node m to node a. When "return rs" is called at the very end of the code, all the relationships are extracted and returned from the database. In addition, by taking the cuboid coordinates and dimension properties from the relationships (edges), 15 equations can be applied to each pair of cuboids to check whether they are colliding with each other. If any two cuboids are colliding; for example, the two relationships highlighted in pale red in Figure 3 are colliding, then the start nodes of the two relationships will be linked together by an extra relationship called conflict. This relationship is used as an indicator of collision between the two routes to help users identifying all the colliding routes by a few lines of code:

```
MATCH(a1:ACTIVITY)-[:PATH*]-()-
```

```
[rs:CONFLICT]-()-[:PATH*]-
(a2:ACTIVITY) RETURN a1,a2
```

In this graph structure, each pair of colliding routes can be detected. The code mentioned above is basically traversing the graph from one activity node to another and finding paired activities with a conflict relationship as a part of the path. For example in Figure 4, if activity 1 (a1) is able to reach activity 2 (a2) in the graph, the path must contain the conflict relationship because any route chain is independent of others in the very beginning until an extra conflict relationship is established. Therefore, by using this approach, users like subcontractors can make a better material transporting plan by detecting any conflicts in advance.

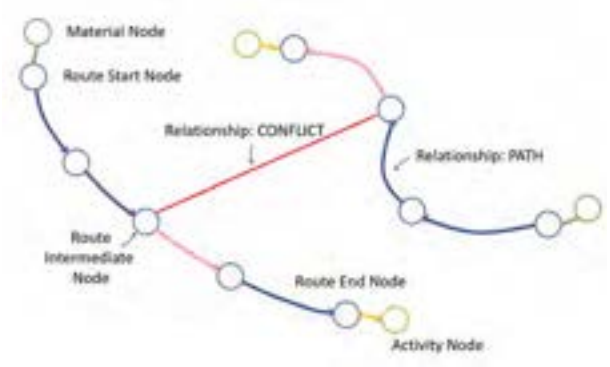

Figure 3. The structure of route data stored in graph database

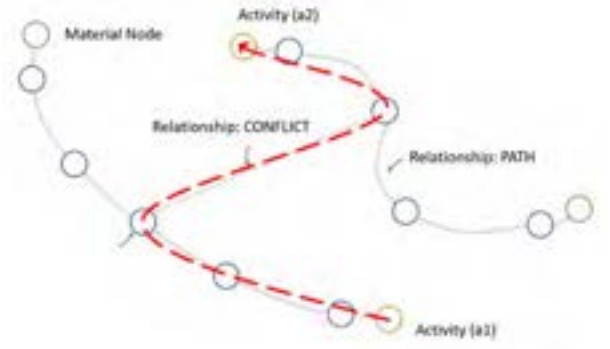

Figure 4. Example for finding colliding routes by traversing the graph

3 Web-based Collaborative Platform

In this research, a web-based collaborative platform is developed for detecting the occurrence of route collisions and making a better material transporting plan. Therefore, a Javascript library called React.js is selected to be the main language for building the whole website. For styling-related works, Bootstrap is adopted by virtue of its convenience. Furthermore, a BIM model viewer should also be provided for reference while users are drawing their material transporting routes. Therefore, a web-based BIM model viewer called Autodesk Forge is employed. The whole viewer is based on another Javascript library called Three.js which is mainly responsible for 3D objects' rendering. For the users' drawn routes, Three.js also helps in displaying them on the 3D models. Regarding backend, Node.js is chosen as the main language handling server-side requests and responses. It is also used for connecting with the graph database management system called Neo4j which assists in creating a database instance and managing the behaviour of the database. The frontend and backend architecture of the platform from the language perspective is shown in Figure 5.

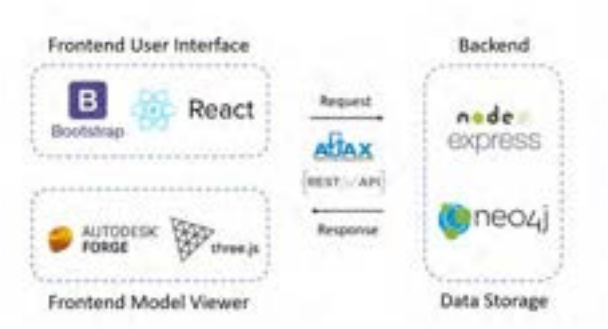

Figure 5. Frontend and backend architecture from the language perspective

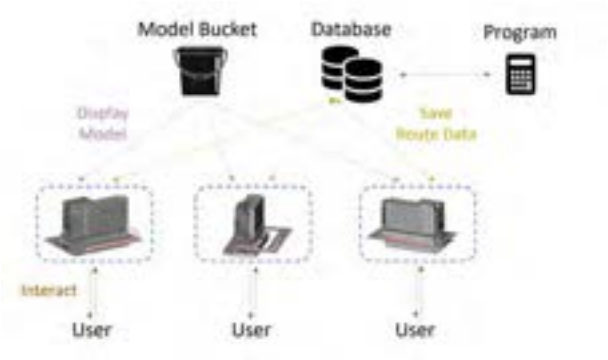

Figure 6. Data flow architecture for the web-based platform

The data flow for the platform (Figure 6) can be split into two parts. The first part concerns 3D BIM models and non-geometric data related to them. For the use of Autodesk Forge, models need to be uploaded to the buckets created in Autodesk server. When models are already in buckets, they can be displayed on any web pages as long as that page contains the configured Forge model viewer. The other part concerns the data related to material, activity and route. As mentioned before, material and activity nodes should be created first with their own coordinates. Those data are stored in the graph database instance as nodes. With that all done, users are

allowed to draw their own material transporting routes and those routes are then transformed into intermediate nodes and links stored in the database. In addition, the moment the route data are stored in the database, the collision examination function written in another javascript program is triggered to check whether there are collisions. If the result is positive, the program automatically creates new conflict relationships between each pair of colliding routes and notifies the frontend Three.js program to display the colliding routes in the 3D model using some conspicuous colours. In this way, users can have clear grasp of which routes are acceptable and which routes need modification.

4 Demonstration

The proposed approach is demonstrated using a prefabricated construction building. In prefabricated construction, most structural components are preliminarily assembled at the manufacturing site. With all processes being completed, the components are further transported to the real construction site for final assembly. Without massive works for on-site grouting, lifting and installing the assembled structures to their designed location can occupy the primary workflow. In this research, the BIM model of the civil engineering research building at National Taiwan University is used. For the purpose of demonstration, the model is filtered and contains only the first floor and the basement. Along the both sides of the building, there are several beams requiring installation for resisting the loading from upper levels. In order to transport the beam from its staging area to the location it was designed, a transporting plan and collision examination should be made first to ensure a smooth process.

The proposed platform is developed to assist in making collision examinations to ensure proper material transporting plans. In the beginning, the platform offers a panel for inputting information including name and execution period of the targeting activity. In addition, the location of the activity should also be assigned by clicking on the 3D model. The program then automatically extracts the coordinates of the clicked point and wraps all the information of the activity into the activity node. Similarly, information such as name and location of a material should be inputted from the platform likewise. Most importantly, relationships between activities and material need to be specified to indicate which material will be used by which activity. With all these prerequisites defined, users can start making the collision examination. By selecting the activity name, the place the activity takes place, the material to be transported and the heavy equipment to use, the system will then be notified about the start point, end point, width and height of the creating route. For easy specification of the equipment, the system has already embedded some crane trucks with its dimension (e.g. HD65 4x2 and HD120 4x2 in Figure 7) for users to select.

From the previous step, the system knows which material and activity the creating route is for. Since the coordinates of the two activities were also defined previously, the start point and destination of the route can be easily displayed in the digital model as the two dark green spheres shown in Figure 8. These actions are for helping users manage the route direction intuitively. After careful consideration, users can draw their own routes as the intermediate points between the start and end green spheres as shown in Figure 8. Once the users finish creating the route and click on the finish button, the data storage process and the collision examination are triggered. If the examination program detects any collision, the colliding routes are displayed with different colours in the BIM model as demonstrated in Figure 9. This collision examination not only detects the geometric overlapping but also takes into account the time period of the routes. Even if the two routes are detected to have geometrical collision, as long as they are not executed at the same time, they would not be considered as having collision by the system. In Figure 9, the system shows that the red and blue routes are colliding on the right side of the building to inform the user to handle the conflict prior to the start of the transporting process.

Figure 7. Selection panel for creating a route

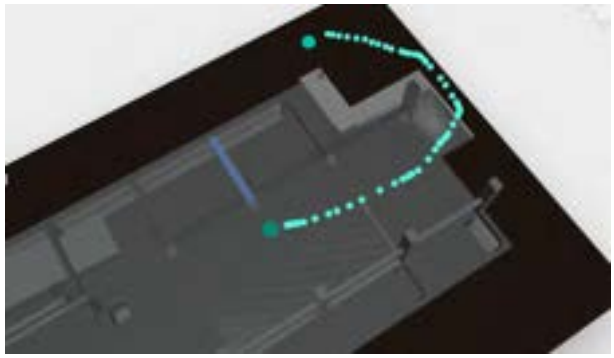

Figure 8. Route drawing demonstration

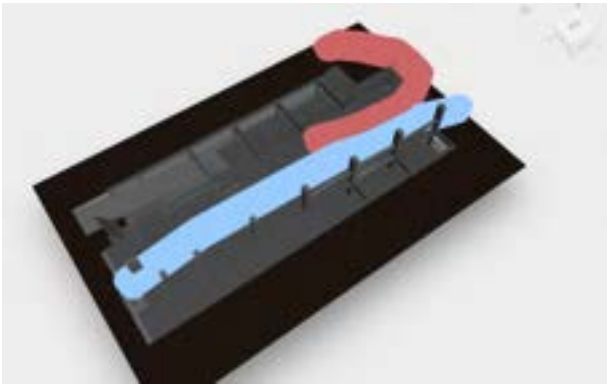

Figure 9. Result for collision examination

5 Conclusion

Construction is a complicated process which often involves different kinds of conflicts. In order to mitigate the negative impact the conflicts can make on a project, a construction plan is required for assuring every activity can be smoothly executed. As space conflict is one of the most common conflicts seen in many construction sites, plenty of research has already addressed it. However, research dealing with material transporting conflict is seldom seen although this kind of conflict is still frequently happening and may cause time overrun of a project. In view of this, this research proposes an approach that integrates BIM, SAT and GraphDB for automatically examining potential colliding routes of transporting construction materials. The result from the conflict examination can further assist the managers in modifying some improper material transporting routes. Furthermore, a web-based coordination platform is developed with the proposed approach to help authorised subcontractors view the BIM model and create their own transporting route plans. As long as they input the necessary information regarding the activity, material and equipment in advance, they are allowed to draw their own routes. The system then automatically checks whether a newly created route is colliding with the existing routes previously created by other users. In this way of coordination, subcontractors can make sure their material transporting routes are exempt from having conflicts with others and do not need to plan a meeting in which everyone is usually asked to use 2D drawings for resolving conflicts. This platform offers an accurate and convenient tool to detect the route conflicts and assist in making a better material transporting plan.

References

[1] Moon, H., Dawood, N., & Kang, L. (2014). Development of workspace conflict visualization system using 4D object of work schedule. *Advanced Engineering Informatics*, *28*(1), 50-65.

[2] Wu, I., & Chiu, Y. (2010). 4D Workspace conflict detection and analysis system. *Proceedings of the 10th International Conference on Construction Applications of Virtual Reality*, November 4-5, 2010, Sendai, Japan.

[3] Mirzaei, A., Nasirzadeh, F., Parchami Jalal, M., & Zamani, Y. (2018). 4D-BIM dynamic time–space conflict detection and quantification system for building construction projects. *Journal of Construction Engineering and Management*, *144*(7), 1-14.

[4] Said, H., & El-Rayes, K. (2011). Optimizing material procurement and storage on construction sites. *Journal of Construction Engineering and Management*, *137*(6), 421-431.

[5] Golkhoo, F., & Moselhi, O. (2019). Optimized material management in construction using multi-layer perceptron. *Canadian Journal of Civil Engineering*, *46*(10), 909-923.

[6] Huynh, J. (2009). Separating axis theorem for oriented bounding boxes. Available from*: jkh.me/files/tutorials/Separating%20Axis%20Theorem%20for%20Oriented%20Bounding%20Boxes.pdf*.

[7] Graph Database. (2020). In Wikipedia. Retrieved on June 10, 2020 from https://en.wikipedia.org/wiki/Graph_database.

[8] Sadowski, G., & Rathle, P. (2015). Fraud detection: Discovering connections with graph databases. *White Paper, Neo Technology*, CA, USA.

[9] Cattuto, C., Quaggiotto, M., Panisson, A., & Averbuch, A. (2013, June). Time-varying social networks in a graph database: a Neo4j use case. *Proceedings of the First International Workshop on Graph Data Management Experiences and Systems,* Jun 22-27, 2013 New York, USA (pp. 1-6).

[10] Ismail, A., Nahar, A., & Scherer, R. (2017). Application of graph databases and graph theory concepts for advanced analysing of BIM models based on IFC standard. *Proceedings of the 24th International Workshop on Intelligent Computing in Engineering (EG-ICE 2017), July 10-12, 2017, Nottingham, UK*.

Deployment of a Standardized BIM Modeling Guideline for the Planning and Construction Industry

G. Hort, D. J. Feller, A. Meins-Becker and M. Helmus

Chair of Construction Management and Economics, University of Wuppertal, Germany
E-mail: Celikdis@uni-wuppertal.de, Feller@uni-wuppertal.de, A.Meins-Becker@uni-wuppertal.de, Helmus@uni-wuppertal.de

Abstract –

The BIM method is perceived as a synonym for the digitalization of the construction industry. The application of this method enables most of all, the consistent and uniform information management and therefore affords a more efficient communication and collaboration environment to all participants in the life cycle of the respective property. Due to the essential role of the building data model within the BIM method, the requirements for modeling at each level must be clarified in detail before modeling. Some companies have internally developed and documented those requirements in their own modeling guidelines. However, small and medium-sized companies often cannot afford the personnel capacity to do likewise.

The development and provision of a standardized guideline for the modeling of building data models by a neutral institution in cooperation with partners from science and economy intends to create a general foundation for the building industry in that manner. The aim of this guideline is to deliver a general framework for the creation of uniform and standardized building models. For this purpose, general regulations, such as the instruction for naming conventions, structure of the project models regarding different planning domains, or more specifically the description of the modeling of individual units, are documented. Within the scope of model elements, the guideline provides the identification in different classification systems as well as the description of the geometric representation along the levels of geometry and a detailed enumeration of the information requirements with the allocation of responsibilities for information delivery and integration for each element. Therefore, the application of this guideline for the modeling of a building data model supplies a clean information management as a basis for a consistent data transfer between different project participants. The application of the BIM Modeling Guideline as part of the exchange information requirements (EIR) is conceivable. Moreover, the provision of this standardized modeling guideline could also serve as a basis for further development within institutions.

Keywords –

Building Information Modeling; Modeling Guideline; Standardization; BIM Model; Level of Geometry; Level of Information

1 State of affairs

A successful and consistent application of the BIM method throughout the entire life cycle of a real estate depends to a large extent on the coordination of the parties involved with regard to the exchange of data and its contents [1]. In addition to the necessary level of detail of the geometric representation and the attributes, this also includes the general organization and structuring of the project as well as the various models to be created. As a result of the prominent role of the building data model when using the BIM method as the lynchpin of information management, it is necessary to create a uniform structure and defined contents for building data models and to set standards for the modeling of building data models in order to create clarity and transparency for all project participants. Such a procedure is usually documented within the framework of a modeling guideline [2].

Research has shown that SMEs in particular do not have the personnel and time capacities to create their own modeling guidelines, whereas many large companies have already started to document their own modeling standards in the form of modeling guidelines, which are continuously updated. The modeling guidelines created in this way are to be regarded as proprietary, as they describe the way of working on the basis of own processes and workflows. Furthermore, the depth of description of modeling guidelines must be considered, since the scope varies in from a pure description of the application of a specific modeling software to a detailed description of the data exchange. The use of external modeling guidelines is therefore not necessarily useful or

feasible. This fact also indicates that there is no company-wide uniform understanding in the German construction industry of the relevant content and the necessary detailing depth of a modeling guideline.

If a company was to develop such a specific modeling guideline, it is still possible that it is not or not sufficiently communicated and coordinated with the project participants. For the successful use of a modeling guideline in a BIM project, it should therefore be agreed upon by all project participants prior to the project start [3].

The development of a standard for the modeling of building data models with the essential specifications and a basis of information requirements on the model element level should serve as a basis for project- and application-specific requirements which should be supplemented if necessary. This basis essentially brings about two changes: On the one hand, not every company would have to think internally about the same or similar BIM goals and the modeling guidelines necessary for implementation. On the other hand, additional work would be reduced by adapting or revising the information structures by project participants when transferring or enriching information. Thus, a standard with regard to the involvement of SMEs and a holistic use of the BIM method over the entire life cycle of a real estate would be advantageous.

2 Development of a standardized BIM Modeling Guideline

Within the scope of the research project "Development of a standardized BIM Modeling Guideline" by the BIM Institute of the University of Wuppertal, the authors, in cooperation with the Technical University of Darmstadt and 17 other partners from the economy, are working on the development of a practical approach to the problems described in Chapter 1. The aim is to create a generally applicable modeling guideline, which defines and describes the basic working methods and specifications as well as the contents and the requirements for the contents of a building information model in a software-neutral way.

The business size of the participating companies in the project vary from large companies to SMEs, which provide planning and construction services at the core of their activities, supplemented by software providers with a focus on BIM content and consulting enterprises. This diversified mix of participating companies allows the identification of a comprehensive cross-section of the current handling of modeling guidelines and modeling in the context of BIM in Germany in general. In addition, the composition of the participating partners enables the consideration of a multitude of perspectives of participants within BIM projects. All companies have already gained experience with the BIM method or are actively implementing it. Figure 1 displays an overview on the respective background of provided modeling guidelines from the project partners.

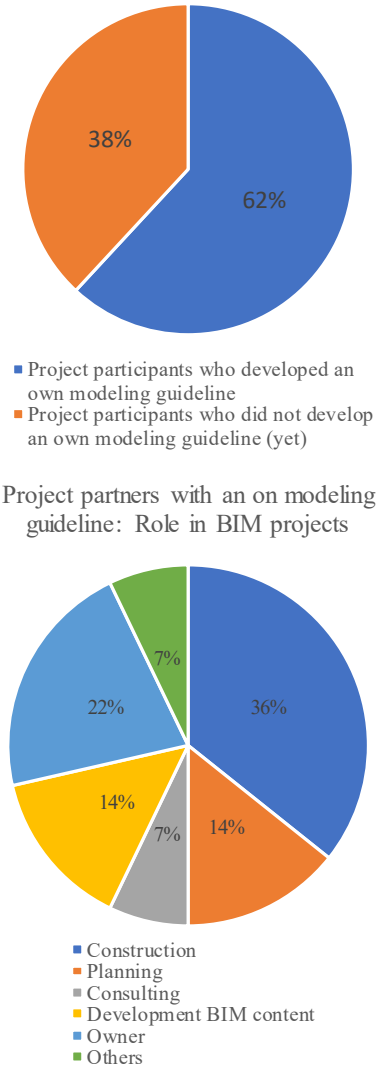

Figure 1. Provided modeling guidelines and their respective background

For the development of the standardized BIM Modeling Guideline, the first step was to analyse the modeling guidelines provided by the project partners, if they have one, and to catalogue content using defined criteria. Some partners, who do not have such a documentation, but implement their own modeling standards, were interviewed for this purpose. The consolidation and analysis of the respective working basis thus provides a view of the best practice currently being lived and implemented within BIM projects and was used as a starting point and working basis for the BIM Modeling Guideline to be created as the project

progressed. The analysis was used to develop an initial definition of the contents and the need for regulation of such a modeling guideline, which was discussed and fixed in an exchange with the project partners: in addition to the description of basic and general principles and specifications for the modeling with the aim of ensuring a clean project and model structure, for example for the coordination of the specialist models of different planning disciplines, content requirements (information requirements) for the building information model to be created are described and additional modeling recommendations are provided. The latter results in a comparison of different working approaches, which can be selected project-specific and according to requirements, for the users, as well as for inexperienced users a simplification of the entry into this complex topic. Considering product neutrality with regard to the use of various modeling applications, the contents are described in such a way that they can always be implemented.

3 Structure of the BIM Modeling Guideline

The BIM Modeling Guideline is divided into a main document and currently into three appendices: the main document of the BIM Modeling Guideline sets a general and descriptive framework around the topic of modeling construction data models using the BIM method. The introductory part of the document describes the motivation and the objectives for the preparation and usage of the document and also clarifies the added value of the application of a (standardized) modeling guideline through cross-institutional standardization of the project and model structure and the model contents. For this purpose, the modeling fundamentals are described with the essential basic principles of model creation, i.e. that the building data model is to be used as the only source for the derivation of plans and documents according to the principle of Single Source of Truth (SSoT), that it is to be modelled according to the actual building process, that the model elements are to be modelled and classified with the appropriate tools and that the data are to be maintained consistently and checked for completeness and correctness before data transfer. In addition to these basic principles, further rules to be considered are listed, such as the handling of model units, schematic representations, labels and regulations, which are particularly necessary for the communication and coordination between non-proprietary authoring systems. These include, naming conventions that must be consistently adhered to for file names, storey definition and the names of model elements and their attributes, or which describe the coordination of the technical implementation of combining different models into one project. Furthermore, the creation of a so-called coordination body is intended to aid bringing together different specialist models to form a central interdisciplinary coordination model, which defines the point of insertion and the reference to the geometric project zero point and serves as the basis for a correct and interdisciplinary quality control. Moreover, modeling specifications on object level for rooms and building elements in general are mentioned, which are especially relevant for a clean geometric mapping and a clean derivation from the geometry, such as that the acidic intersections of the elements or the elements must not be modelled twice. After the description of these modeling definitions follows a list of project-specific aspects to be defined, which have to be agreed upon and documented with all participants before and during the modeling, such as the project structure, the definition of the classification system to be applied or the insertion point.

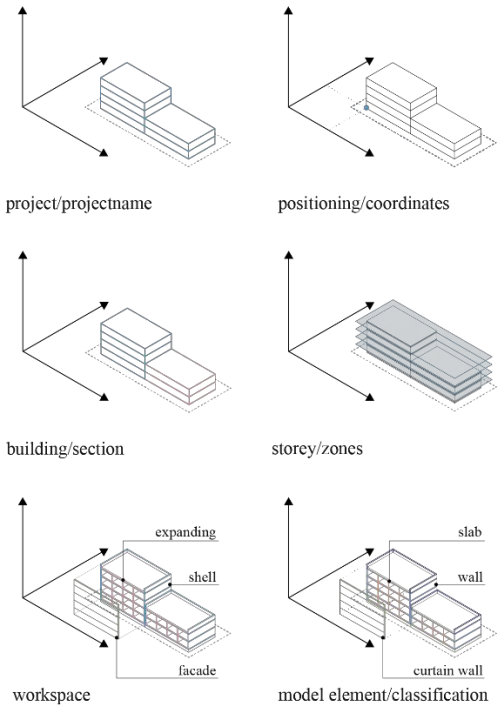

Figure 2. Content of the BIM Modeling Guideline - main document

The main document concludes with some modeling recommendations that have proven themselves in practice, but which are highly dependent on the software and the method (open BIM/closed BIM) and therefore cannot be formulated as a general rule. Topics such as the placement of model elements in the right floors, the extension of vertical and horizontal elements, the handling of multi-layered model elements or baselines are explained and have to be considered.

Appendices 1 and 2 represent user-supporting

documents within the BIM Modeling Guideline: Appendix 1 provides the user with a comprehensive checklist for the definition and documentation of the project organization within a BIM project as an orientation aid. The contents of the main document are divided up and structurally prepared according to the specific topic, so that the project group can implement it quickly and easily.

Appendix 2 takes up the necessary designation system (codification) for models and model elements (beyond the respective classification identifiers) described in the main document and offers detailed suggestions for this. A consistent codification of the model elements as well as of the individual models throughout the entire duration of the project enables, among other things, a simplified and transparent data management [4].

Appendix 3 of the Modeling guideline describes the requirements for the model elements of the architecture, both for the geometric and for the informatic representation. The model elements were catalogued and described in detail depending on the respective workspace: In addition to the respective identifiers of different classification systems (IFC, DIN276, OmniClass, Uniclass) and the graphical representation of the model element, a model element-specific list of the geometric level of detail and the information requirements is provided, depending on the level of detail, Level of Geometry (LoG) or Level of Information (LoI). The geometric level of detail therefore describes the geometric representation of the object to be modelled along the LoG scale from 100 to 500 in keywords, also naming contents that are not to be modelled. The information requirements are described in tabular form along the LoI scale from 100 to 500, considering the designation, the data format and the SI unit. In addition, example values are given for each information requirement. A matrix is used to assign the information requirements to the level of detail. An essential aspect to be considered within the scope of the information requirements is the definition of the information supplying (information generating) and information implementing (information modeling) responsibilities. Considering the project-specific constellations of different participants and different scopes of services, these contents are to be defined in a project-proprietary manner. The modeling guideline and Appendix 3 offer suggestions for the respective spheres of responsibility for each information requirement and model element. The information requirements described in this appendix also represent those information requirements which are to be regarded as fundamental, viz. BIM application-neutral. The consideration of BIM application-specific information requirements is therefore not covered by the current status of the BIM Modeling Guideline.

In the further course of the project, a further document will be prepared which describes the requirements for the model elements of the technical building equipment, whereby the structure and design of this catalogue of requirements will correspond to those of Appendix 3.

4 Benefits

As a result of the development, documentation and provision of the BIM Modeling Guideline, a software-neutral guideline for the modeling of building data models will be made available, which aims to enable and establish transparent information and consistent data management. As a result of the description of project-specific requirements up to the detailed processing of the information requirements for each model element, a working and communication basis is also provided, which can be used or taken as a basis for the tendering and contracting of planning services: both contracting parties start from the same point of understanding and communicate a transparent performance picture along the BIM Modeling Guideline, whereby the understanding of both the expected and the owed performance can be discussed and defined more clearly than ever [5].

Due to its general nature, the BIM Modeling Guideline can also be used for all BIM projects that have chosen object-oriented modeling as the basis for information management, whereby the specification of the authoring software used and the associated processes such as the creation of a model, data transfer or communication may be necessary. The present modeling guideline is therefore particularly suitable as a basis for the development of an institutional modeling guideline for the users or the target groups, which usually use software applications already in use due to their own preferences, existing license agreements or lock-in effects. A one-time adjustment of the BIM Modeling Guideline to the own structures therefore leads to a standardization of all future projects. The shortage of resources of many SMEs for the documentation of their own modeling standards in their own modeling guidelines, as described in Chapter 1, is significantly reduced by the provision of the BIM Modeling Guidelines. This reduced, one-time effort for the adaptation to the own structures is then to be contrasted with the synergy and efficiency effects in future projects.

5 Outlook

In addition to Appendix 4 (Catalogue of Requirements for Model Elements of the Technical Building Equipment) already mentioned in Chapter 2, the BIM Modeling Guideline is to be used and validated in various pilot projects. For this purpose, the authors are in

contact with some of the project participants and other external parties interested in such an implementation. The knowledge und results gained in the course of the practical application enables a determination of the quality, applicability and practicability of the current state of work, which in return allow the derivation of indication and control measures for a revision of the BIM Modeling Guideline. The application in pilot projects promises, beyond the improvement of the quality of the documents, an increased acceptance of these documents, since the BIM Modeling Guideline would thus already be tested in practice in the first stages.

In the further course of the project, the developed modeling guideline is to be transferred to a database in order to make the content more flexibly available. In addition to the provision of the entire modeling guideline (as currently available), the possibility of exporting specific subsets of information requirements via various filters is to be created. By processing the data and integrating these filters, the infrastructure to provide BIM application-specific data packages is created. In this way, it is possible to export exchange requirements per BIM application according to requirements, or conversely, to derive BIM application-specific modeling guidelines. This last step is optional in the context of this project, since the definition of information requirements per BIM application is not part of the project.

Based on the creation of the database and the possibility to output structured data, the aim of the project is to transfer the information into various modeling software. For this purpose, the import requirements for each modeling software are currently being analyzed and the resulting structures are being set up in order to be able to implement such a mapping of the data in the target system. The development of this communication bridge between modeling guidelines (database) and modeling software results in an added value for the user of the BIM Modeling Guideline due to an automated, requirement-oriented mapping of necessary information requirements per model element.

Furthermore, the development of model review rule sets, for example for model checker applications, based on the defined requirements according to the BIM Modeling Guidelines, is to be implemented on the export of the mentioned structured data. The authors are currently analyzing the model import and the systematic structure of the test data and already available model review rules of various applications. As a result of the generation of model review rule sets based on the contents of the BIM Modeling Guideline, the user is enabled to review a model created or received at different points in time of the project (depending on agreed or defined levels of detail) for completeness and/or correctness. The client is thus given the opportunity to track the actual state of work of the planning project participants and to initiate corrective measures if necessary.

6 Notes

As a result of the ongoing project work, updated versions of the modeling guideline including all appendices are developed and made available. When applying the modeling guideline, it is therefore recommended to check that the respective version is up-to-date before using it and to exchange respective documents if necessary. The latest version of the documents can be downloaded free of charge in German language from the authors' homepage.[1]

References

[1] Arbeitsgruppe Hochbau im Arbeitskreis Digitalisiertes Bauen im Hauptverband der Deutschen Bauindustrie e.V. (Hrsg.), BIM im Hochbau. Technisches Positionspapier der Arbeitsgruppe Hochbau im Arbeitskreis Digitalisiertes Bauen im Hauptverband der Deutschen Bauindustrie e.V., S. 4, Berlin, 2018

[2] VDI 2552-2, Building information modeling. Terms and definitions, 2018

[3] Bauen Digital Schweiz (Hrsg.), BIM Vertrag, Rollen, Leistungen. Merkblatt, S. 6, 2018

[4] Bauen Digital Schweiz (Hrsg.), BIM Workbook – Verständigung. Hilfestellung zum Entwerfen und Planen mit der Methode BIM, S. 42, 2018

[5] Baunetz Wissen, Welche Arten von BIM-Daten gibt es?, Online: https://www.baunetzwissen.de/bim/fachwissen/grundlagen/welche-arten-von-bim-daten-gibt-es-5262646, abgerufen am: 14.06.2020

[1] http://www.biminstitut.de/forschung/downloads

Design for Digital Fabrication: an Industry needs Analysis of Collaboration Platforms and Integrated Management Processes

Ming Shan Ng[a], Marcella M. Bonanomi[a b], Daniel M. Hall[a] and Jürgen Hackl[c]

[a]Chair of Innovative and Industrial Construction, ETH Zürich, Switzerland
[b]Polis-Lombardia, Italy
[c]School of Engineering, University of Liverpool, U.K.

ng@ibi.baug.ethz.ch, bonanomi@ibi.baug.ethz.ch, hall@ibi.baug.ethz.ch, hackl@liverpool.ac.uk

Abstract -

Digital Fabrication is an emerging systemic innovation in the architecture, engineering and construction sector. However, the design process for digital fabrication lacks an integrated management process or digital collaboration platform. One reason may be a lack of industry stakeholder needs for such processes and platforms. To explore and facilitate such solution in the current practice, more information about the socio-technical industry requirements on such solution and its implementation to support and manage the BIM-based design process of digital fabrication is needed. To fill this gap, this work conducts an industry-needs analysis through content analysis and an online survey of 144 project stakeholders. Based on the results, this work identifies the most needed fabrication-related information, tools and roles at different design stages and the requirements of platform-based management, which include a common virtual environment for collaboration and a common data environment for data management. Moreover, this work shows that fabrication-related information and new roles are required by project stakeholders since the early design stage. The paper concludes by proposing a conceptual management framework for BIM-platform-based integration for design for digital fabrication in construction projects and identifying potential future research directions on the topic.

Keywords -

BIM, platforms, digital fabrication, design process, project management, survey

1 Introduction

Digital fabrication is an emerging systemic innovation in the architecture, engineering and construction (AEC) sector. In this work, digital fabrication refers to the aspects of industrialised construction, off-site fabrication and /or modular construction that connect design and construction with a digital thread using an integrated process that controls machinery during fabrication tasks [1]. Despite many research and demonstration projects [2], the industry is slow in adopting and implementing digital fabrication due to identified barriers such as skeptical attitude towards DFAB from project stakeholders and complexity in managing process and deliverables [3]. Furthermore, digital fabrication changes the requirements of the design process and requires a new framework in which to guide collaboration between designers and fabricators [4].

To facilitate the design process of digital fabrication, scholarship to date has proposed adoption of new management models such as lean design management and new design approaches such as design for manufacture and assembly (DfMA). These efforts have attempted to bring downstream fabrication information into the upstream design process. The objective of these methods is to facilitate process integration in design and construction [5]. However, an integrated management process specific to digital fabrication does not yet exist.

In addition, there are few digital collaboration platforms available to facilitate an integrated design process for digital fabrication. Digital collaboration platforms are cloud-based platforms for multidisciplinary stakeholders to co-create design deliverables in the design process for tendering and construction. Digital fabrication requires a restructured collaboration process that can support new stakeholders' early involvement and break the wall between design and construction for collective knowledge exchange [2]. Digital fabrication should also connect to ongoing AEC digitalisation approaches such as Building Information Modelling (BIM). Both digital fabrication and BIM aim to help to improve various aspects of integration and foster systemic innovation in the current practice [6]. However, both approaches require a change in management of project life-cycle from planning to construction [2, 7]. Furthermore, the adoption of digitalisation is slow compared to many other industries in the current practice [8, 9]. Nevertheless, a BIM-based collaborative design platform that can support collaborative design for digital fabrication in construction does not yet exist [5]. One potential reason for this is that industry requirements for such platforms are not yet identified.

To fill this gap, this work aims to investigate and analyse the industry requirements for BIM-based collaboration platforms and platform-based integrated management for design for digital fabrication. Based on the industry needs

analysis, this work presents a conceptual framework that manages BIM-based collaborative design process of digital fabrication in projects. To do so, the authors first conduct content analysis of literature review to identify and categorise the requirements of such platforms. The identified requirements are composed in a questionnaire for an online survey of industry experts who have experience in the design and/or construction processes of digital fabrication. Based on the survey results, the authors analyse the industry requirements for such platforms and platform-based management for the design process of digital fabrication. The authors then develop a conceptual management framework for platform-based integration in response to the survey results and the industry needs analysis to address the industry requirements.

This work is organised as follows. Section 2 provides a brief overview of digital fabrication and BIM-based collaboration platforms. Section 3 contains a description of the research design and the survey. Section 4 presents the findings of the conducted survey and the industry needs analysis. Subsequently, Section 5 proposes a conceptual framework for platform-based integration and identifies future research. Section 6 concludes with remarks and suggestions for further work.

2 Background

The architecture, engineering and construction (AEC) sector has been fragmented vertically in processes from design to construction, horizontally among project teams, and longitudinally across projects [6]. In particular, the design process is the root cause of many project life-cycle problems, such as quality and cost misalignments and low productivity in construction [10]. Scholars suggest the construction industry has been caught itself in a "mirror trap", where knowledge is trapped tightly with the task dependencies themselves [11]. Thus, the industry resists attempts to innovate. In order to overcome this resistance "disruptive paradigms" are in need [12]. The use of new approaches such as digital fabrication provides the opportunity for integration and systemic innovation that can be key for such a change [13].

In order to bring digital fabrication from theory into practice, scholars suggest digital system-based management approaches can provide better integration [1, 6]. Hall et al. [13] identified digital systems integration as a firm-based "mirror-breaking" approach to adopt digital fabrication. This involves web-based configuration platforms for flexible kits-of-parts to integrate supply chain for design to enable digital production. García de Soto et al. [14] also propose the use of cloud-based platforms and platform-based integration as a project-based approach to implement digital fabrication from design to construction. Such platform-based management requires new roles and new tasks in both design and construction processes. Platform-based integration supports operational and management-related technical requirements for BIM-based collaboration platform. It facilitates the adoption of technologies and intelligent and automated collaboration in design and construction, supply-chain management and systems integration [15]. This includes BIM-based collaboration platforms that allow stakeholders to engage, co-create, communicate, coordinate and collaborate design in a common virtual environment for design modelling in 2D and 3D, design review and project management. Such platform facilitates information exchange and knowledge sharing for design review, progress monitoring and optimisation of cost and constructability, as well as immersive environments for collaboration and the adoption of automation and innovation in design process [7, 16]. BIM-based platforms provide measurable data for progress tracking, risk management, trust-building and benchmark of deliverables for quality control and trade tendering, and supports design integration and integrated management [4, 17].

3 Research Design

To investigate and analyse the industry requirements for BIM-based collaboration platforms and platform-based integrated management for design for digital fabrication, the authors conduct (i) content analysis of literature review, (ii) an online survey with a multiple-choice questionnaire, and (iii) analyses and visualisations of the results.

Firstly, this work involves a content analysis of literature review to identify, condense and categorise the requirements for collaboration platforms in the design process of digital fabrication in construction projects [18]. The authors conduct two rounds of keywords search to screen and review literature published in the past ten years. In the first round of literature search, the keywords used are "digital fabrication", "design process", "collaboration" and "parametric". In another round, the keywords used for literature search are "collaboration", "design process", "platform" and "BIM". Amongst all, the authors filter irrelevant contents to identify the operational and management requirements [15]. The authors group the requirements into five categories, namely technical, technological, organisational, contractual and business-related requirements.

Secondly, based on the content analysis, the authors compose 18 questions in a multiple-choice questionnaire to undertake an anonymous online survey of the industry stakeholders with digital fabrication design and/or construction experience. Each question is composed of seven to twelve multiple choice answers. For most of the questions, participants could choose a minimum one and maximum of three choices. The goal of this survey is to understand the industry needs for collaboration and integration

country	Switzerland	United Kingdom	Italy	U.S.A.	Japan	Singapore
Terms in this survey	**SIA Leistungsmodell**	**RIBA Plan of work 2020**	**ITA Procurement**	**AIA Phases of Design**	**TAAF 設計から完成までの流れ**	**BCA Stages**
Strategic Definition	1. Strategische Planung	0. Strategic Definition	progetto di fattibilità tecnico-economica	Project Brief	企画 (kikaku)	Project Brief
Feasibility Study	2. Vorstudien	1. Preparation & Brief		Pre-design/ Concept	基本設計 (kihonsekkei)	Concept Design
Schematic Design	3.1 Vorprojekt	2. Concept Design	progetto preliminare	Schematic Design		
Detailed Design	3.2 Bauprojekt	3. Spatial Coordination	progetto definitivo	Design Development	実施設計 (jisshisekkei)	Detailed Design
Technical Design	4. Ausschreibung	4. Technical Design	progetto esecutivo			Pre-Construction
Documentation				Construction Documentation		
Construction	5. Ausführung	5. Manufacturing & Construction	costruzione	Construction	工事監理 (koujikanri)	Construction
Handover	5.3 Inbetriebnahme	6. Handover	collaudo e consegna	Commission	完了検査 (kanryokensa)	Post-Completion
Operation	6. Bewirtschaftung	7. Use	uso e manutenzione	Occupancy	建物使用 (tatemonoshiyo)	

Table 1. Design stages terminology in this work in reference to the plans of work in Switzerland, U.K., Italy, U.S.A., Japan and Singapore

platform for the design process of digital fabrication in construction.

To assist stakeholders in their survey participation, the authors summarise a comparison of the design stage terminology in existing plans of work in six countries as shown in Table 1. To promote comparative international responses, the definitions are summarised in accordance with the plans of work from Swiss Society of Engineers and Architects (SIA) in Switzerland, the Royal Institute of British Architects (RIBA) in the U.K., Italian (ITA) Procurement Law in Italy, the American Institute of Architects (AIA) in the U.S.A., Tokyo Association of Architectural Firms (TAAF) in Japan and the Building and Construction Authority (BCA) in Singapore, as well as the authors' first-hand work experience in projects in these six countries. The definitions of the design stage terminology might vary project by project, company by company. Thus, Table 1 merely serves as a reference to the terminology for the survey participants.

Thirdly, this work visualises and analyses the results of the industry needs analysis based on the survey [15]. Fourthly, based on the survey results, the authors propose a conceptual management framework for platform-based integration to manage BIM-based design process of digital fabrication in construction projects, and propose future research areas.

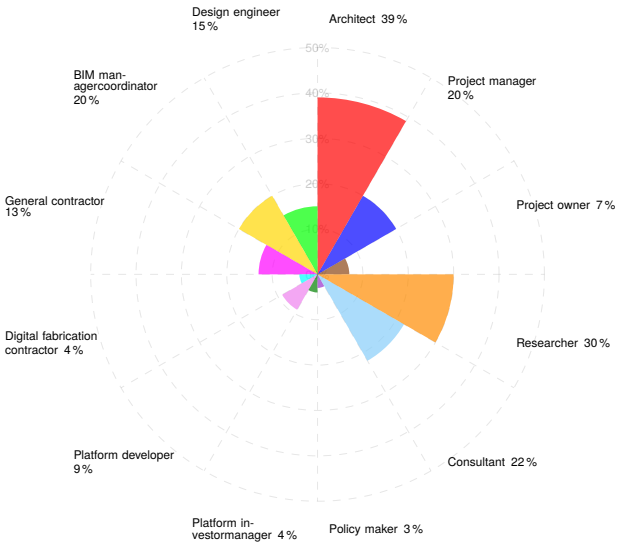

Figure 1. Summary of professions of the online survey participants

4 Findings

Based on the content analysis, the authors elaborated 18 questions in five categories. (1) *Technical requirements* are digital fabrication specific. During the design process, fabrication information and machine code are often required from downstream to upstream decision-making [2]. Moreover, tools such as sensors are used to keep track on the motions of the fabrication machines to ensure consistency between the digital design model and the digital fabrication performance [4]. (2) *Technological requirements* are platforms specific. The authors identify the current trends in cloud-based collaboration platforms for BIM-based design process. Such platform supports multidisciplinary information exchange and constant feedback loops between design and fabrication, and facilitates co-creation and BIM data management for project integration [14, 15, 17]. (3) *Organisational requirements* are digital fabrication design project specific. Implementation of digital fabrication restructures a project's organisation and supply-chain [6, 13]. New roles such as digital fabrication (DFAB) manager and DFAB design coordinator, are evolved in projects. This is similar to the new roles derived due to BIM implementation in projects [7]. While several existing downstream roles such as DFAB programmer are required to participate in the upstream decision-making [14, 19]. (4) *Contractual* and (5) *business-related requirements* are platforms specific. Platform-based integrated management derives new contractual and business strategies to ensure such novel design management approach for process integration, organisational integration and information integration [5, 13, 17]. These two categories are not analysed and presented in this work.

In May 2020, the authors undertook an anonymous online survey of the industry experts who have experience

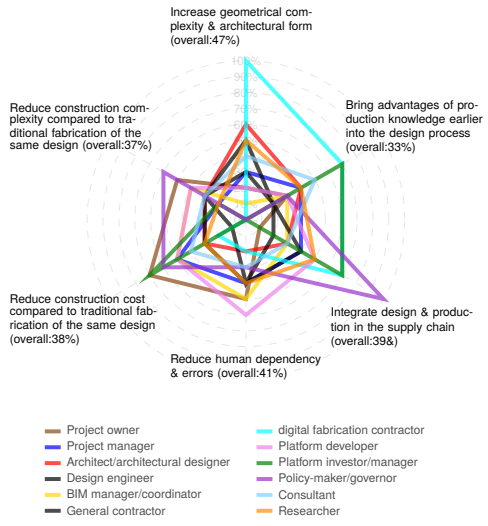

Figure 2. Primary motivations from project stakeholders

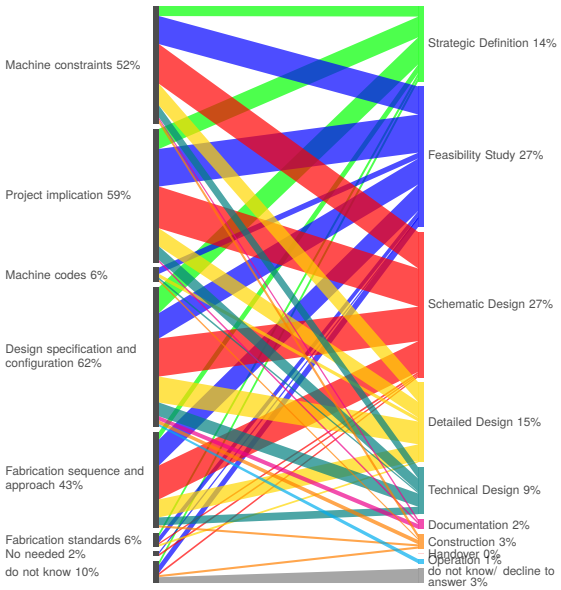

Figure 3. Most needed fabrication-related information at each design stage

Figure 4. Most needed aspects in design modelling for digital fabrication

in digital fabrication in design and/or construction. The survey received 144 responses. Figure 1 shows a summary of the professions of the survey participants. Amongst all, one-third of the participants and one-forth have more than five years of digital fabrication experience in design and in construction respectively.

The following paragraphs describe the fabrication specific *technical requirements* in BIM-based design process of digital fabrication. Figure 2 illustrates in a spider-web diagram the primary motivations of the project stakeholders for design for digital fabrication over traditional construction processes. The overall percentages of each answer are listed. It also shows that the primary motivations of different professions are not the same. The answers exclude the option of construction quality, which is commonly seen as the most popular motivation [1, 2, 3, 5, 14].

Figure 3 differentiates and illustrates in a bipartite-sankey diagram the most needed fabrication-related information at each design stage in the design process of digital fabrication as per the terminology defined in Table 1 is the fabrication-related information first needed. The overall percentages of each most needed information and the overall percentages of each design stage are listed. Figure 3 reveals that various different types of fabrication-related information are in fact needed since the early design stages.

Figures 4, 5 and 6 illustrate the most needed aspects in design modelling, design reviews and design documentation respectively in the design process of digital fabrication in construction projects. Regarding design modelling, Figure 4 shows that the answers are quite evenly distributed among all the multiple choices answers. 4% of the participants provided other answers such as fabrication machines and process constraints are also needed for design modelling to meet fabrication tolerances; interactions between design modelling and fabrication tools such as robotic arms and collaborative mindsets among multidisciplinary stakeholders are also needed in terms of fabrication-related information in design modelling. Regarding design review, the survey results as illustrated in Figure 5 reveal that over half of all the participants expressed their needs in process visualisation and simulation and collaboration in a common virtual environment. 4% of the participants provided other answers such as options such as optimisation, design status scheduling and tracking and information to connect to the factory floor are also needed for design review. Regarding design documentation, Figure 6 shows that the stakeholders needs are also quite evenly distributed amongst all answers. 2% of the participants provided other answers such as configuration

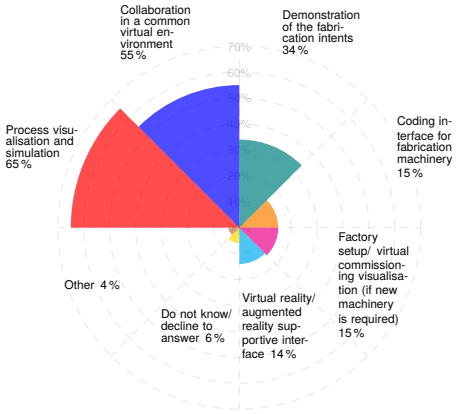

Figure 5. Most needed aspects in design review for digital fabrication

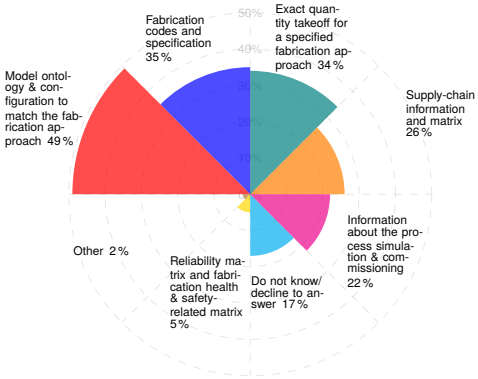

Figure 6. Most needed aspects in design documentation for digital fabrication

management is also needed for design documentation.

Figure 7 illustrates the most needed digital twin strategies for design for digital fabrication. Only 3% of the participants required neither digital twin nor virtual commissioning for design for digital fabrication. 4% of the participants expressed that the digital twin strategies depend on the complexity and delivery models of the projects.

The following paragraphs describe the platforms specific *technological requirements* in BIM-based design process of digital fabrication. Figure 8 illustrates the background information of the platforms and programming languages being used in the current practice. 3% of the participants provided other answers such as solidworks, cadwork and Robot Operating System.

Figure 9 differentiates and illustrates in a bipartite-sankey diagram the most needed ways to support machine code on the collaboration platforms for project stakeholders to edit at each design stage in the design process of digital fabrication as per Table 1. The overall percentages of each most needed ways of support and the overall percentages of each design stage where such support is first needed are listed. 5% of the participants provided other

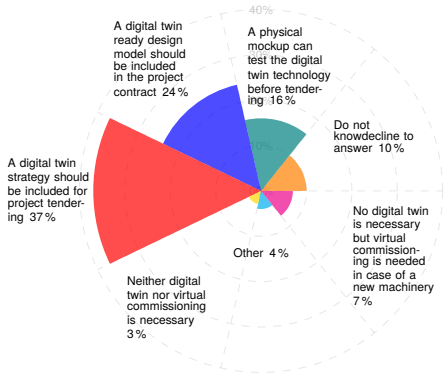

Figure 7. Most needed digital twin strategy for design for digital fabrication

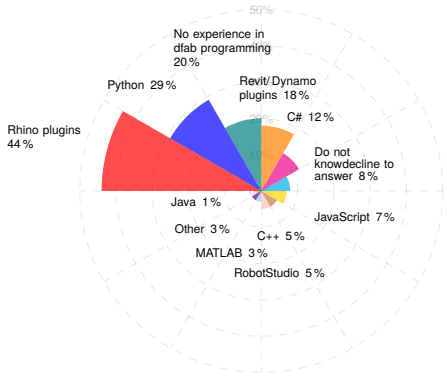

Figure 8. Most used platforms and programming languages for design for digital fabrication in the current practice

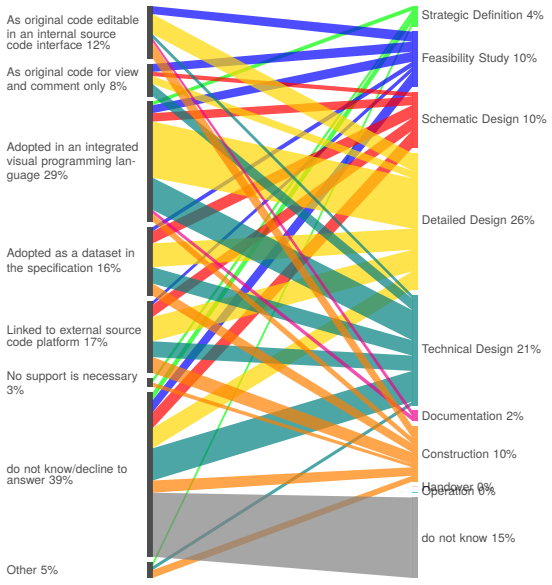

Figure 9. Most needed ways to support machine-code on cloud-based platforms at each design stage

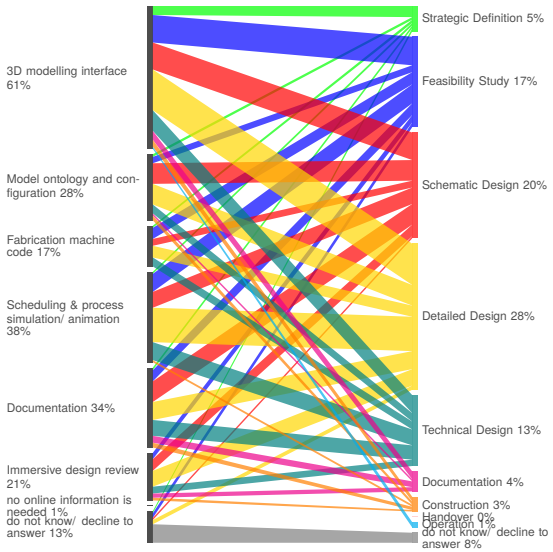

Figure 10. Most needed fabrication information shared on cloud-based platforms at each design stage

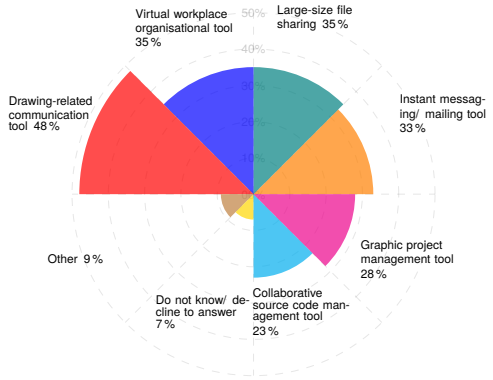

Figure 11. Most needed supporting functions for communication and knowledge sharing on collaboration platforms

answers such as machine code should only be accessible by the fabrication contractor instead of being editable by all project teams on the platforms; another answer is that the ways of support depend on the vary project by project, depending on the project stakeholders' preference. Moreover, only 1% of the participants required no machine-code support on the platforms.

Figure 10 differentiates and illustrates in a bipartite-sankey diagram the most needed digital fabrication information to be shared on cloud-based collaboration platforms at each design stage as per Table 1. The overall percentages of the most needed information to be shared online and the overall percentages of each design stage where such cloud-based sharing is most needed are listed. Only 1% of the participants required no online sharing of digital fabrication. 2% indicated that information sharing on such platforms require a common data environment.

The most needed supporting functions for communication and knowledge sharing on collaboration platforms are illustrated in Figure 11. The answers are quite evenly distributed. The authors especially did not include modelling-related tool because this is by default a must on such platforms. 9% of the participants provided other answers such as issue trackers are needed. They also indicated that the functions require a common data environment for data management.

The following paragraphs describe the digital fabrication design project specific *organisational requirements* in BIM-based design process of digital fabrication. Scholars identified that new roles and new responsibilities are cre-

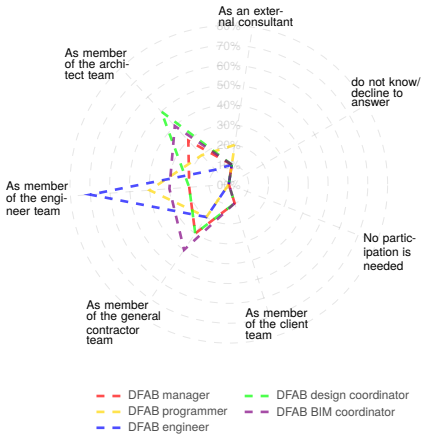

Figure 12. Most needed ways of the new digital fabrication roles' involvements in a multidisciplinary project

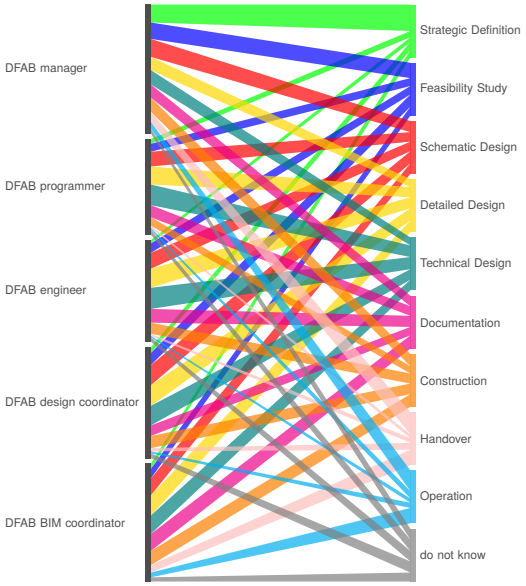

Figure 13. Most needed involvement of the new digital fabrication roles at each design stage in a construction project

Figure 14. A conceptual management framework for platform-based integration in BIM-based design process of digital fabrication in construction projects

ated in particular for digital fabrication projects [19, 14]. The new roles include digital fabrication (DFAB) manager, digital fabrication (DFAB) programmers, digital fabrication (DFAB) engineers, digital fabrication (DFAB) design coordinator and digital fabrication (DFAB) BIM coordinator. Figure 12 illustrates in a spider-web diagram the most needed ways of the five new roles' involvements in projects. In average only 1% of the survey participants required no new roles in projects. The required ways of involvements are different for each role. All in all, the results show that the new roles should be integrated within the existing project team structure.

Figure 13 illustrates in a bipartite-sankey diagram the answers of the question about when the new roles are needed. The percentages of the roles required in each stage are shown in proportion on the left-hand side. It can be seen that new roles for digital fabrication are not isolated to a single design stage but are needed across multiple phases of design and many of the new roles are required to join the project team since early design stages.

5 Discussion and future research

From the industry needs analysis conducted in this work, implementation of digital fabrication significantly impacts the design process with respect to information exchange, workflow and organisational structure in construction projects. The design process of digital fabrication requires new approaches to design management. The industry has specific requirements for the design process of digital fabrication. These requirements enable platform-based integration and integrated project management for design for digital fabrication to integrate process, information and organisation for construction projects [5, 17]. Moreover, such collaboration platforms should connect a BIM-based design process with digital fabrication through a common data environment. This can enable integrated data management and common virtual environments for project stakeholders to visualise, simulate and coordinate design for digital fabrication.

Based on the survey results, the authors propose a conceptual platform-based management framework to manage a BIM-based design process of digital fabrication (see Figure 14). This framework considers four categories of tasks, namely design, digital fabrication (DFAB), BIM and project management. The framework illustrates how tasks of research, planning, preparation, development and provision at each design stage match with the requirements identified in the survey. The proposed deliverables of the tasks are also indicated in red.

The goal of this framework is to assist project managers and stakeholders to manage the BIM-based design process of digital fabrication in construction projects. Furthermore, in order to facilitate BIM-platform-based integration and integrated project management for design for digital fabrication, the authors propose that emerging design management approaches such as Set-Based Design (SBD) and Target Value Design (TVD) could be considered to manage the design process of digital fabrication.

Future research on how to integrate and manage the complexities of design for digital fabrication could include:

1. An in-depth industry needs analysis to investigate how each aspect of the requirements inter-relate and impact on each other;
2. More detailed statistical analysis of the data such as a paired-means test to determine if answers differ by discipline and /or experience level of the participants;
3. An in-depth research on such platform-based management framework for design for digital fabrication;
4. Further investigation and application of lean design management strategies such as SBD and TVD.

6 Conclusion

One potential reason for the slow adoption of digital fabrication in AEC is the lack of a developed management model to integrate project stakeholders. Existing research identifies that BIM-based collaboration platforms and platform-based integration can help to break through the socio-technical barriers and facilitate the implementation of digital fabrication in the design process in projects. To investigate such platforms and their management approaches, this work conducts an industry needs analysis through an online survey of 144 project stakeholders in current practice. The preliminary analysis finds: (i) fabrication-related information such as specification and project implication is needed since early design stage, (ii) collaboration in a common virtual environment and process simulation are needed in the design process, (iii) model ontology to follow the fabrication approach is required in design documentation, preparation for digital twin in digital fabrication is required before tendering, (iv) digital fabrication information is required to be shared and edit among project stakeholders to different extents at different design stages in a common data environment and (v) new roles such as DFAB manager and DFAB BIM coordinators are required since early design stages and continuing throughout the design process. This work further elaborates a conceptual platform-based management framework to manage such complex BIM-based design process of digital fabrication in construction projects.

References

[1] T. Bock and T. Linner. Robotic Industrialization. *Robotic Industrialization*, 2015.

[2] K. Graser et al. DFAB HOUSE: A Comprehensive Demonstrator of Digital Fabrication in Architecture. In *Fabricate 2020: Making Resilient Architecture*, pages 130–139, 2020.

[3] G. Carra et al. Robotics in the construction industry: State of the art and future opportunities. *ISARC 2018 - 35th ISARC and Intl. AEC/FM Hackathon: The Future of Building Things*, (Isarc), 2018.

[4] T. Svilans et al. New Workflows for Digital Timber. In F. Bianconi and M. Filippucci, editors, *Digital Wood Design: Innovative Techniques of Representation in Architectural Design*, pages 93–134. Springer, 2019.

[5] M.S. Ng and D.M. Hall. Toward Lean Management for Digital Fabrication: a Review of the Shared Practices of Lean, DfMA and dfab. *27th Intl. Group for Lean Construction Conf.*, pages 725–736, 2019.

[6] D.M. Hall et al. Identifying the Role of Supply Chain Integration Practices in the Adoption of Systemic Innovations. *J. of Mgmt. in Eng.*, 34(6), 2018.

[7] M.M. Bonanomi et al. The impact of digital transformation on formal and informal organizational structures of large architecture and engineering firms. *Eng., Construction and Arch. Mgmt.*, ahead-of-p (ahead-of-print), 2019.

[8] F. Barbosa et al. Reinventing Construction: A Route To Higher Productivity. Technical Report February, McKinsey, 2017.

[9] R. Agarwal et al. Imagining construction's digital future. Technical report, 2016.

[10] P.A. Tilley. Lean design management - A new paradigm for managing the design and documentation process to improve quality? *13th Int. Group for Lean Construction Conf.: Proceedings*, (2002): 283–295, 2005.

[11] L.J. Colfer and C.Y. Baldwin. The mirroring hypothesis: Theory, evidence, and exceptions. *Industrial and Corporate Change*, 25(5):709–738, 2016.

[12] R.E. Levitt. CEM Research for the Next 50 Years: Maximizing Economic, Environmental, and Societal Value of the Built Environment. *J. of Const. Eng. and Mgmt.*, 133(9), 2007.

[13] D.M. Hall et al. Mirror-breaking strategies to enable digital manufacturing in Silicon Valley construction firms: a comparative case study. *Const. Mgmt. and Economics*, 0(0):1–18, 2019.

[14] B. García de Soto et al. Implications of Construction 4.0 to the workforce and organizational structures. *Int. J. of Const. Mgmt.*, pages 1–13, 2019.

[15] V. Singh et al. A theoretical framework of a BIM-based multi-disciplinary collaboration platform. *Automation in Construction*, 20(2):134–144, 2011.

[16] M.S. Ng and D.M. Hall. VR/AR in Design Management: Use-cases and Future Research. In *24th Industriebauseminar 2019 Proc.. Vienna, Austria*, pages 55–57, 2019.

[17] M. Fischer et al. A simple framework for integrated project delivery. *22nd Int. Group for Lean Construction Conf.: Understanding and Improving Project Based Production*, pages 1319–1330, 2014.

[18] H.F. Hsieh and S.E. Shannon. Three approaches to qualitative content analysis. *Qualitative Health Research*, 15(9):1277–1288, 2005.

[19] K. Graser et al. Social Network Analysis of DFAB House: a Demonstrator of Digital Fabrication in Construction. In *Eng. Project Organization Conf.*, pages 1–21, Vail, CO, 2019.

A BIM-Based Approach for Optimizing HVAC Design and Air Distribution System Layouts in Panelized Houses

P.B Noveiri [a], M. Zaheeruddin[a] and S. Han[a]

[a]Department of Building, Civil and Environmental Engineering, Concordia University, Canada

E-mail: pouya.noveiri@dal.ca, sanghyeok.han@concordia.ca, zaheer@encs.concordia.ca

Abstract –

In a centralized air distribution system, the designed ductwork layout impacts the system performance and the construction time and cost. Engineers face various challenges, including spatial limitations, leading them to use assumption-based design methods to balance their design with construction requirements. As a result of this shortcoming, insufficient design details for construction and improper coordination between designers and trade workers will occur, increasing the project duration and risk for conflicts. As the construction industry shifts towards off-site and fast-paced construction methods, the design processes must comply with construction requirements to ensure a smooth transition from conventional methods to off-site construction. This research provides a scientific and systematic method for design and optimization of the HVAC air distribution system in terms of the ductwork layouts, and sizes and types of ducts to standardize the construction processes for time and cost reduction in the off-site environment. The proposed methodology utilizes Building Information Modeling for coordination of the air distribution system using a 3D database. Furthermore, a trained genetic algorithm processes the data and identifies alternative solutions. As the final step, the algorithm generates the optimal air distribution system in the BIM 3D environment for a visual assessment and detailing. The results are verified based on existing case studies in the Canadian prefabricated, panelized construction company. The potential benefits include 23% savings in duct material, whilst providing an integrated design solution with 32% less conflicts comparing to traditional design methods.

Keywords –

HVAC; Air Distribution System Layout; BIM; MEP Coordination; Constructability Analysis; off-site Construction, Optimization; Genetic Algorithm

1 Introduction

1.1 Overview

In an HVAC project, the engineer is responsible for determining the required size of the ducts and the capacity of the HVAC equipment. This design process does not consider the detailed layout of the air distribution system for construction. This leads the contractor to use past experience to determine the exact location of supply and return air terminals as well as the routing paths for the installation of floor and wall ducts. In turn, skilled trade workers are then responsible for identifying missing details in the design and resolve the conflicts based on their experience. Lack of coordination between the contractors and designers will cause conflicts during the construction, resulting in increased construction time, cost, and material waste. Uncalculated decisions and assumptions decrease building performance by creating conflicts between the building systems (e.g., plumbing) and/or structural members. This lack of information is a primary barrier to taking the leap between conventional and modular construction. Off-site construction requires extensive planning for the mechanical, electrical, and plumbing (MEP) elements to be installed on the assembly line in parallel with the construction of the panelized walls, floors, and roofs in a closed environment. The design must meet the needs of modular construction to eliminate rework and allow the construction tasks to be synchronized. The duct system must align perfectly with the structural design and other MEP elements to ensure installation is not interrupted by conflicts. If the plumbing system and ductwork overlap, the construction process of the two systems cannot take place in parallel, and there will be idle time for the trade workers.

Furthermore, the traditional experience-based HVAC design and construction do not satisfy the requirements of modular construction, which are standardized designs and sequential tasks aimed at reducing variance in the processing time of tasks on the manufacturing line. In order to address these limitations and industrialize the HVAC system in modular construction, this research integrates modular construction and design requirements when planning the air distribution system layout. This

paper presents an applied approach for designing the air distribution layout, featuring an optimization algorithm that eliminates conflicts and reduces overall cost. The proposed algorithm utilizes BIM data in a tailored GA framework to determine the optimum layout for a given project. The proposed methodology was tested on various housing projects, reducing overall material waste, and eliminating design conflicts for every scenario.

1.2 Background

The MEP systems are complex and variable in terms of design and layout configurations. Improper design and integration at the planning and design stage can negatively influence the entire project. MEP construction can consist of 25%-45% of the total project cost [1]. The HVAC system is generally the most time-consuming and expensive system. One of the most challenging and time-consuming processes during the design of an HVAC system is designing the air distribution layout. The air distribution system is constructed from multi-levels of ductwork, which imposes challenges for the contractors in the decision-making process. The challenges related to the ductwork undertaken in this research are (1) determining the location of the air terminals and (2) selecting the optimum paths for connecting the duct through the floor and wall panels. The location of the air terminals and the duct paths must consider system performance and ease of constructability. During the design and planning stage, the engineer confronts parametric variations, including space occupancy and spatial constraints. The current methods for designing the ductwork focus exclusively on the size of the ducts and the fans, and the layout is not explicitly defined [2].

Space limitations and coordination between different trades are crucial factors affecting the construction time of a proposed design. The architectural design defines most of the spatial constraints and the preliminary limitations in the design and construction of an HVAC project [3]. The constraints of the air distribution system design can vary by the level of significance. They can be directly or indirectly related to system performance, e.g., occupant comfort, construction cost, and life cycle cost (LCC) [4]. Previous research suggests that because ducting system designers are forced to balance constraints and requirements with layout decisions, they often make decisions based on rules of thumb, which can come at a cost to the life cycle of the system [4].

Many HVAC design challenges are optimization problems. Researchers often focus on the most energy-efficient designs and life-cycle costs. According to [4], GA is an effective optimization technique in HVAC applications. However, in the published research projects regarding HVAC optimization, construction challenges, which include a significant portion of the cost, are not considered. The air distribution layout directly influences the construction processes and effects not only the performance of the system but the entire cost and duration of the project. The Air distribution performance index (ADPI) is a standard method for assessing how well the designed air distribution layout performs in terms of the occupant's comfort and the uniform supply of air within the building enclosure [7]. ADPI will assist the designers in the process of selecting the correct diffusers and positioning them in each space. It is a guideline for selecting supply air terminals according to the manufacturer's specifications. The application of the ADPI in the selection of commonly used diffusers for heating and low cooling modes is assessed by [9] and [10], respectively. ADPI is considered a guideline when specifying the location of diffusers prior to construction.

After the locations of the air terminals are identified, the remaining challenge is determining the optimum duct layout that will connect the air terminals to complete the design of the air distribution system layout. 3D tools are proven to be effective in facilitating an integrated design for the layout of the MEP systems. BIM is an industry-standard platform that allows all the project designers, architects, construction managers, and trade workers to seamlessly monitor project progress and exchange information in a 7-D database. BIM integrated design is an effective approach supported by a significant amount of published research. [3, 5, 6]. Utilizing a 3D collaborative database, the designers can compare their plans with the plans of other trades in order to check for interferences and to solve conflicts prior to construction. According to [5], time and cost savings are amongst the multiple benefits of BIM-based coordination as compared to conventional construction methods.

2 Methodology

2.1 Problem Structure

The objective of optimizing an air distribution layout is to generate alternative design solutions to assist the designer in achieving the most efficient performance and cost-effective results. The focus of the proposed framework is on the location of the air terminals and the designed ductwork layout required to create the HVAC system network. There are several requirements to be satisfied to create a high-performance and cost-efficient air distribution system design. (1) The location of the supply and return air terminals must follow ASHRAE guidelines [8]. (2) The duct layout must be easy to install in accordance with the building structure and other plumbing and electrical system configurations. (3) The duct layout must consist of efficient use of duct material

to reduce material waste and construction time.

The scope of this research is to propose a systematic approach for determining the optimal location for the installation of the air terminals and ductwork layout. This research will use BIM for analyzing project information and GA to identify the optimal solution. The final step is to validate the result in a 3D environment. The proposed methodology is illustrated in Figure 1 below.

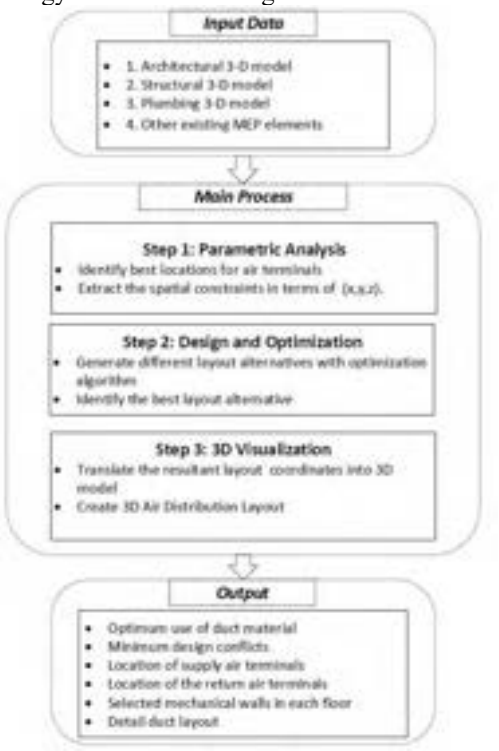

Figure 1. The proposed methodology

In order to apply the proposed methodology, manual input is required from the user, consisting of the project physical model. The 3D architectural model, 3D structural model, other existing MEP elements and a material database must be created in the BIM environment before the implementation of this methodology. The three-step processing modules are created to address the challenges in regards with the design and construction of an air distribution system layout.

The first step in the main process is the parametric analysis. In this module, the architectural boundaries required for the design of the air distribution layout are identified and extracted from the BIM model. Other physical constraints are the location of structural members and MEP elements that co-exist along with the ductwork, which may interfere with the chosen path for the ducts. The spatial constraints from BIM will be used to calculate the suitable locations for installing the supply air terminals based on the ADPI calculations and the relative location for the return air terminals based on ventilation requirements. From the parametric computation module, the extracted parameters are fed into the design and optimization algorithm. This process will assign a single position for each air terminal and asses the routes that are suitable for connecting the air terminals and creating the ductwork layout. The optimization algorithm will then generate different solutions for the layout and verify feasibilities. The layout solution, which is identified as the optimal solution, will satisfy all conditions to the highest degree and will be the resultant design solution.

The result of the design and optimization algorithm is a set of x, y, and z coordinates. The output includes the location of the air terminals and the ductwork layout relative to the chosen floor and wall panels for installation. The final step is to transfer this information back into the BIM model. The final output will be a complete air distribution layout in the BIM environment that is correlated with the project's physical model and is cost-effective. This methodology will assist the designer with the preliminary design of the air distribution network layout. Implementing this framework will automatically generate a duct network layout for any given project with optimized system performance and construction parameters. The proposed design will allow for efficient use of duct material and minimum conflicts with the building structure and MEP systems for improving constructability.

2.2 Parametric Analysis

To factor in all the data required for designing the air distribution system layout, it is crucial to follow a detailed decision-making process throughout the design. This section describes the step-by-step process of the parametric model. Just like a human designer, the proposed algorithm is trained to make decisions at each step. This section will review the process of populating the air terminals, including the supply air outlets and return air inlets, highlighting the design parameters followed by the spatial limitation and constraints.

2.2.1 Floor Mounted Supply Registers

Floor registers with a vertical discharge of supply air are identified as the preferred method of providing heat, especially in the residential houses. For selecting the optimal position of a floor register, the floor area in each space must be considered in accordance with the physical constraints as well as the occupancy requirements. The room perimeter is the ideal location for a floor register with the jet flow direction aiming towards the length of the room. [7]. Each space varies in terms of the architectural layout as well as the occupancy usage. The proposed algorithm identifies the most suitable location for the floor register in each space through a process of elimination. In this subsection, an example of a floor

layout is used to demonstrate the intelligent process of selecting possible locations for supply air floor-mounted registers.

In the initial stage, each space that requires supplied air must be identified (Step 1). In the selection process, the floor space is automatically populated with a series of points (Step 2). Each point represents a possible location for the installation of floor-mounted registers. In this process, each point is eliminated, if it does not meet the design criteria. In Step 3, the points that are adjacent to the walls are eliminated because a clearance distance of 6 inches is required for construction. A floor register should not interfere with the occupancy path. Step 4 removes the points that take away from the living space. Step 5 identifies the points in front of doors and windows and eliminates them accordingly. Step 6 removes the points adjacent to external walls, and finally, Step 7 eliminates the points in each corner, which are constrained by two walls. This process is illustrated in Figure 2 below.

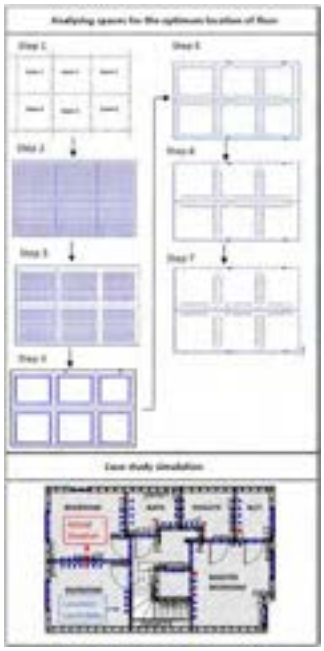

Figure 2. Identifying the best locations for installing floor mounted supply registers.

The algorithm is implemented in Dynamo and verified using the BIM simulation model created in Revit Autodesk. The blue points remaining are a set of locations suitable for the installation of the floor-mounted supply registers. The actual position where the registers are installed by the contractor exists amongst the candidate points in simulation (identified by red points). The similarity of the simulation result and the actual projects confirms the accuracy of the results. However, the final solution must only contain a single point for each space. In order to identify the optimal locations automatically, the optimization algorithm finds alternative routes for connecting the points and creating the air distribution layout. The final layout will be demonstrated in the case study section of this paper.

2.2.2 Ceiling Mounted Supply Diffusers

A ceiling-mounted diffuser is designed to diffuse the airflow in four directions instead of aiming downward. The optimum location to place a ceiling-mounted diffuser is in the middle of a room. However, each space is not perfectly symmetrical, and one side of the room boundary may be closer to the middle than the other. There are different methods for selecting the optimal location for a diffuser in each space; the position of a diffuser always depends on the room geometry, the total number of diffusers, and the required capacity. In this paper, the ADPI will be the primary design method for selecting the position of the diffusers in the designated spaces.

ADPI is a measure that indicates how well the supplied air is mixed with the existing air in the space before ventilation. It is directly related to occupant comfort, designed system performance, and energy efficiency [7]. The location for each diffuser is calculated by finding the isothermal throw distance for the selected outlet type. The throw is the farthest distance a diffuser can project the supplied air before the air stream starts losing velocity. The distance to the closest wall from the diffuser is referred to as the characteristic length. The throw to characteristic length ratio that will result in the maximum ADPI for a selected diffuser will be provided in the manufacturing guide. Table 11-1 of the ASHRAE Handbook Fundamentals Volume 1997 provides the required data for calculating the throw distance of commonly used supply air diffusers [8]. Diffuser manufacturers each have their own specifications for their products. The following equation demonstrates the calculation of the throw distance for a selected diffuser, and according to the result, the optimal position for that diffuser can be determined based on the room boundaries.

$$Maximium\ ADPI = \frac{X_{50}}{L_{Characteristic}} \quad (1)$$

Where:

X_{50} = throw distance with 50 ft/min velocity,
$L_{characteristic}$ = room characteristic length from BIM
Maximum ADPI = from Table 11-1 [8] or manufacturers catalogue

The throw distance provides a relationship between the diffuser's performance and the room boundaries. The throw distance is used to identify suitable locations for installing the supply air diffusers by ensuring that the areal range of diffusion fits inside the space and covers at

least 80% of the area. Each room has a different characteristic length, and the information obtained from BIM will allow the calculation of the diffuser's performance in accordance with the designated spaces. The following region [X_{max}-X_{min}, Y_{max}-Y_{min}] is adequate for installing the diffuser with respect to the throw distance and the room boundaries. Within this region, the characteristic length does not change. Anywhere inside the identified region, the diffuser can be installed while maintaining the areal range of diffusion inside the room boundaries. With this logic, the maximum ADPI remains the same.

Figure 3. Identified boundary suitable for installing a diffuser

Each space has a different required flow rate, which will determine the type and the total number of diffusers required. Based on the selected diffusers and their capacities, the algorithm will determine how many diffusers need to be installed in each space. According to [7], if space requires more than one diffuser, the distance between each diffuser must be 2x the throw distance. The following figure demonstrates each diffuser's specific throw requirement in the simulation model.

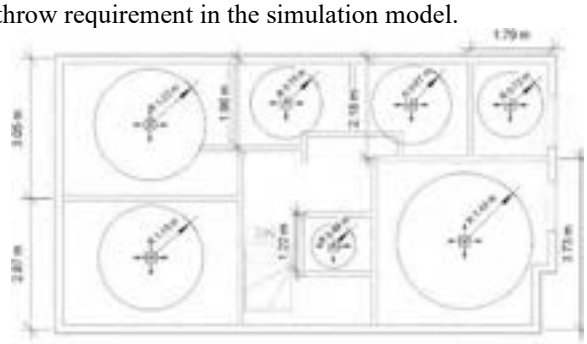

Figure 4. The range of diffusion for each diffuser

The location for each diffuser is identified, and the range of flexibility for the region of installation is determined. Each diffuser can be placed inside a box calculated based on the areal range of diffusion demonstrated in Figure 3. In order to determine the final position, the ductwork layout and accessibility for construction must be considered. The duct layout will create an air distribution network by connecting all the diffusers together. The remaining challenge is to determine the optimal layout for the system, which will be covered in the design and optimization section of this paper.

2.2.3 Return Air and Ventilation

In practice, the return air inlets are positioned as far as possible from the supply air outlets to avoid short-circuiting the conditioned air. Distancing the inlet and outlet air terminals will provide adequate time for the supplied energy to be distributed in the building before it is captured and returned to the central air handling unit. Two modes of ventilation commonly used in residential buildings are demonstrated in this research:

1. Mixing Ventilation
2. Displacement Ventilation

According to [11], mixing ventilation is suitable for heating and cooling applications. To create a network consisting of displacement ventilation, the supply air outlet, and the return air inlets must be installed in the ceilings. Displacement ventilation is a buoyancy-driven, stratified flow with high ventilation effectiveness. Based on the displacement ventilation requirements, the supply system will consist of floor-mounted registers, and the return inlets will be positioned on high walls. This design will allow the supplied air mass to gradually distribute the energy in each space as it rises toward the ceiling and exits through the vents. The figure below demonstrates displacement ventilation in a 3D model.

Figure 5. 3D rendering of a floor register and a side wall return vent in Revit (displacement ventilation)

Based on the mixing ventilation requirements, the supply system will consist of ceiling-mounted diffusers. The return inlets will be positioned relative to the position of the supply air outlets. The return vent must be placed in the farthest location away from all supply diffusers. The path that the supplied air travels must be far enough to allow adequate circulation and mixing of air within the space before the air stream reaches the return inlets and exits the zone.

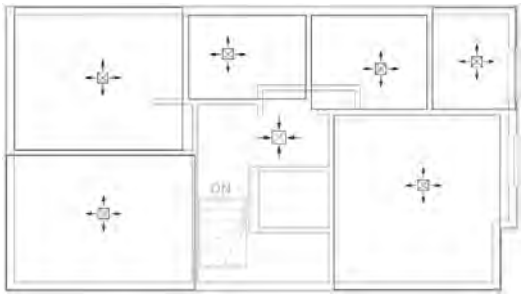

Figure 6. The position of supply and return air terminals for mixing ventilation in Revit

Depending on space flow requirements, the flow in must be equal to the flow out of each zone to provide a net-zero pressure inside the building enclosure. The supplied air must be distributed and cover the entire floor area. Therefore, the total number of supply outlets is more than the return air inlets. The building enclosure must maintain balanced pressure, and all the supplied air must eventually be ventilated. For a residential building, centralizing the return air system within the corridors of the buildings will allow the supply airflow to circulate in each room and gradually travel towards the central corridors prior to ventilation. The return air system will be designed after the supply system is set in place accordingly.

2.2.4 Spatial Constraints

Building construction is an interdisciplinary project that requires extensive planning and correspondence between all trades to ensure timely and cost-effective project delivery. Overlapping MEP elements can lead to congestion, which will increase construction time. For example, the plumbing crew will have to wait for the sheet metal crew to install the ducts and then proceed with the installation of the pipes. With the use of BIM and GA optimization, the proposed solution for the air distribution layout will comply with all spatial constraints of the project without conflicting with any other trades, ultimately reducing the cost and the total construction time.

Building structure dictates the space limitation for installing MEP elements. When the ductwork layout is interfering with structural framing, the workers need to puncture holes in the beams for routing the ducts through the framing. The rough-in work required for fitting the ducts inside the beams will increase construction time and create more construction material waste. Also, the structural integrity may be damaged in the process. Therefore, the designed air distribution system must align with the building structure. The proposed framework integrates the design parameters during the planning stage, using spatial constraints from BIM to automatically assess the number of conflicts in the alternative air distribution layout designs.

2.3 Design and Optimization

2.3.1 Problem Formulation

Once the location for all the air terminals is identified, the remaining challenge is connecting each air terminal to create the final air distribution system layout. The entire system will be constructed from two main parts.

1. Main ducts:
   - The largest duct carrying the highest flow rate from the central air handling unit to each floor
   - The horizontal segment of the main duct is centralized in each floor to reach both sides of the building
   - The vertical segment of the main duct connects each floor and exists in the mechanical walls
2. Branch ducts:
   - Smaller in cross-section
   - Deliver the flow required from the main duct to the diffusers in each space

When considering a duct network, the appropriate route for the main duct carrying the highest flow rate must be considered first. The main duct is often placed along the building corridors or the centreline of the building to have almost equal distance from the furthest air terminals in both directions; this creates a more balanced system in terms of pressure drops due to the friction losses in the duct channel. The branch ducts can be constructed partially from flexible duct material. The branch ducts are required to carry the supply air from the main duct to the location of each air terminal.

The length of the designed system is calculated using a set of coordinates extracted from the project model. These points will be categorized into two groups: endpoints — the location of the air terminals, and the starting points —the connection with the main duct. The distance between the two points will be equal to the length of that duct section. The total length is calculated by the sum of all the branch ducts plus the length of the main duct.

2.3.2 Genetic Algorithm Optimization (GA)

i. Multi-objective Optimization:

The application of GA is used in modern construction problems with multi-objective targets to achieve optimal results that satisfy each parameter requirement. The random generation and nature of this algorithm create a flexible approach to a problem with multiple interacting variables. Each generation will be assessed using a defined fitness function to evaluate the level of satisfaction for each parameter based on a weighted distribution. In this research, GA considers the following objectives:

- Reduction of total duct length
- Space air diffusion (positioning the air outlets in the most effective location in each room)
- Compliance with space availability (routing the ducts through the most accessible spaces for ease of construction and minimum interference with other building components).
- Selection of the most suitable mechanical walls to install vertical duct segments

ii. Fitness Function:

The fitness function is used to evaluate the different solutions generated by the tailored GA algorithm. The defined fitness function measures the total length of the duct system. The solution consisting of the shortest total length, is the most desirable. The two other objectives are the intersection of the ductwork with the structure and MEP elements. The fitness function evaluates the total system interferences for each solution, the system with the least intersection with the structural elements, and MEP congestion is the most favorable choice.

The fitness function is a weighted sum, which means each of the measurable objectives has a different weight on the result. The total length of the system is not as significant as the duct path intersection with the structure; therefore, more weight is assigned to the latter objective. The user can decide which objective is more important and assign the weights accordingly. Each variable is assigned a negative value because the target is reducing these parameters.

$$\text{Fitness Value} = -(W_1)\ \text{Length} + -(W_2)\ \text{MEP Congestion} + -(W_3)\ \text{Structural Interference}$$

iii. Generation vs. Improvement:

The GA starts with generating random solutions and improves the results over each generation. The graph below demonstrates the applied GA on a sample case study with a system of supply air ceiling mounted diffusers. The tabulated results display the total length of the system, the total intersection with the structural members, and the total congestion with MEP members reducing over the evolution process. The result is an air distribution layout solution that satisfies all the conditions as much as possible. Table 1 demonstrates the improvement of the solution over generations. The fitness value is the weighted sum of the total duct length, the number of intersections between the duct and the structural lumbers, and the number of overlapping with the plumbing system.

Table 1. Improvement of the fitness value over the process of evolution (Fitness Value vs Generation)

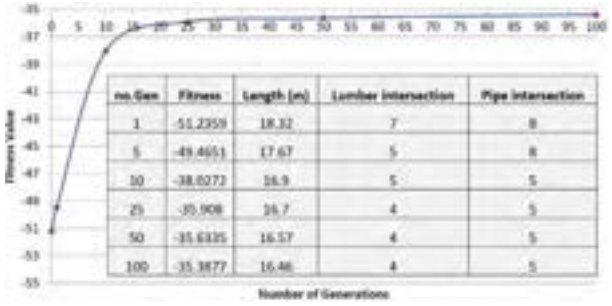

no.Gen	Fitness	Length (m)	Lumber intersection	Pipe intersection
1	-51.2359	18.32	7	8
5	-49.4651	17.67	5	8
10	-38.0273	16.9	5	5
25	-35.908	16.7	4	5
50	-35.6335	16.57	4	5
100	-35.3877	16.46	4	5

3 Case Study

This section presents a review of the real-world case study where HVAC system construction was identified to be overly time-consuming in panelized construction. The proposed methodology has been implemented, and the highlighted finding validates the given framework. A new and improved design for the air distribution system layout, providing time and cost savings by improving constructability, is proposed in this section. This approach was implemented on four multi-level houses with different layouts. Off-site construction is used for manufacturing these houses. The purpose of off-site construction is to enforce fast-paced construction. During construction the installation of the duct system took a long time due to the following reasons: First, the plumbing and the ductwork were installed in the same planum spaces, which prevented the simultaneous installation of the two trades; and second, the selected ductwork layout required excessive rough-in work, which required many holes to be made in the beams for routing the ductwork.

The following example includes the 3D model of a 3-storey single-family home with an area of 1200 ft^2. Following the framework presented in this paper, the 3D BIM model will be the primary source of data for generating the air distribution system layout. Figure 7 outlines the process for implementing the proposed methodology. This process is applied to four different cases, and the consistent results validate the accuracy of the methodology. Figure 8 demonstrates the three optimization objectives that have improved in comparison with the original design used by the company. The results presented highlight the total savings in terms of the duct length, which is approximately 10 meters (23%). Five intersections with TJI Joists were eliminated, representing a 25% reduction in drill-through holes in the structure. Furthermore, the plumbing and the ductwork did not overlap, thereby eliminating conflicts. Another significant benefit is that the design and drafting time will be reduced because the process of designing the layout and modeling it in a 3D environment is done automatically by applying the proposed algorithm.

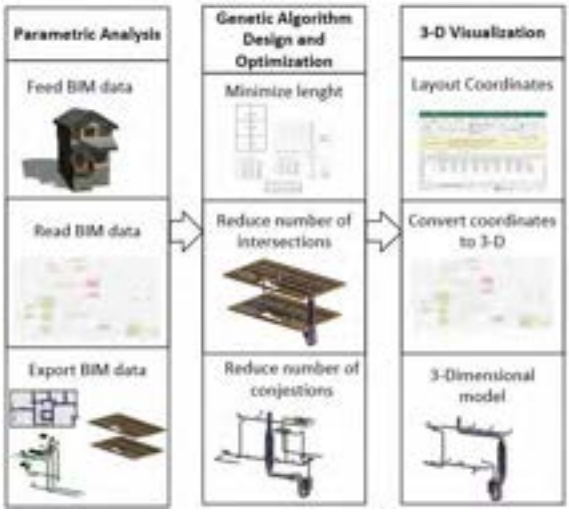

Figure 7. Framework for applying the methodology on the case study

Figure 8. Benefits of the result with comparison

4 Conclusion and Future Work

HVAC systems play a significant role not only in the final performance of the project but also in the initial investment cost and the total construction duration. Assessing alternative solutions during the planning stage will allow the construction process to be applied with more certainty in the outcome, meaning fewer change orders and less waste in the time for the contractors solving conflicts and making assumptions for the missing details. Experienced contractors often produce the best results, but it is proven in this research that this knowledge can be programmed artificially with effective results. The final results include 23% savings in duct material, whilst providing an integrated design solution with 32% less conflicts comparing to traditional design methods. For future work, it is recommended that this framework be applied in compliance with Industry Foundation Classes (IFC). Energy simulation and Computational Fluid Dynamics (CFD) can also be integrated into the process to evaluate the energy efficiency of the results. This framework can be expanded for larger and industrial projects.

Acknowledgments

The author would like to acknowledge the support of ACQBUILT Inc. for providing the necessary data for implementing this research as well as sharing the challenges in the manufacturing line regarding the industrialization of the HVAC system.

References

[1] Jang S. and Lee G. Process, productivity, and economic analyses of BIM–based multi-trade prefabrication—A case study. *Automation in Construction*, vol. 89, pp. 86–98, 2018.

[2] Jorens S., Verhaert I. and Sörensen K. Design optimization of air distribution systems in non-residential buildings. *Energy and Buildings*, vol. 175, pp. 48–56, 2018.

[3] Lv X. B. and. Liang Z. J. Case Study of Three-Dimensional Optimization Design on Architectural MEP Based on BIM. *AMM*, vol. 507, pp. 177–181, 2014.

[4] Asiedu Y., Besant R., and Gu P. HVAC Duct System Design Using Genetic Algorithms. *HVAC&R Res*., vol. 6, no. 2, pp. 149–173, 2000.

[5] Wang J. Wang X. Shou W. Chong H.-Y. and Guo, J. Building information modeling-based integration of MEP layout designs and constructability. *Automation in Construction*, 61, 134–146, 2016.

[6] Korman T. M. and Lu N. Innovation and Improvements of Mechanical, Electrical, and Plumbing Systems for Modular Construction Using Building Information Modeling. In *AEI*, pages 448–455, Oakland, United States, 2011.

[7] McQuiston, F. C., Parker J. D. and Spitler J. D. Heating, ventilation, and air conditioning: analysis and design, Sixth edition. New York: Wiley. 2000.

[8] American Society of Heating, Refrigerating and Air-Conditioning Engineers. ASHRAE handbook fundamentals, Atlanta, 1997.

[9] Liu S. and Novoselac A. Air Diffusion Performance Index (ADPI) of diffusers for heating mode. *Building and Environment*, vol. 87, pp. 215–223, 2015.

[10] Liu, S. Clark J. and Novoselac A. Air diffusion performance index (ADPI) of overhead-air-distribution at low cooling loads. *Energy and Buildings*, 134, 271–284, 2017.

[11] Awbi H. B. Ventilation and Air Distribution Systems in Buildings. *Front. Mech. Eng.,* vol. 1, 2015.

Synthetic Data Generation for Indoor Scene Understanding using BIM

Yeji Hong[a] , Somin Park[a], and Hyoungkwan Kim[a]

[a]Department of Civil and Environmental Engineering, Yonsei University, South Korea
E-mail: hongyeji@yonsei.ac.kr, somin109@yonsei.ac.kr, hyoungkwan@yonsei.ac.kr

Abstract –

Visual facility inspections performed manually are tasks that can be automated. Segmentation of facility image data is one of the automated methods of identifying problems in facilities. However, the machine learning methodology that is mainly used to train the segmentation model requires a large amount of training dataset. Preparing training dataset accompanies laborious manual labeling. To address this issue, we present a new method for generating synthetic data that do not require manual labeling. The method is to create photograph-style images from the BIM images; a generative adversarial network called CycleGAN is used to enable style transfer between the two different domains.

Keywords –

BIM; Cycle-Consistent Adversarial Networks (CycleGAN); Facility Management; Scene Understanding; Synthetic Data

1 Introduction

Facility management aims to effectively operate the facility for a long period of time. Whether the facility is functioning can be understood by comparing the ideal state and the current state. Recent advances in imaging devices have caused image data to be widely used to monitor the current state of facilities. Images show the appearance of the facilities so that people can understand their condition. However, in a large-scale infrastructure, it takes time for a person to check images or videos. Therefore, it is necessary to automatically extract valuable information that provides the current state from the image. Segmentation extracts information such as spatial context [[1], [2]] and structure installation [3] from the image, enabling the identification of the current state of the facility on behalf of the human.

There is a difficulty when carrying out the segmentation. The difficulty is that large-scale training dataset is needed to train machine-learning models for segmentation (such as supervised-learning). Preparing a training dataset involves collecting and annotating multiple images. While image acquisition is effortless, annotating operation requires a lot of time and effort [4]. To deal with this, we propose a novel method for generating synthetic data similar to photograph using Building Information Model (BIM) designed during infrastructure construction.

BIM is the digital twin of the infrastructure, representing geometry, material and time information of the construction entities, in electronic form. Therefore, the images captured from BIM are similar to the photograph, but not completely identical. It is our proposal to create synthetic data that can be used as training data in segmentation models by applying the style of the photograph to the image captured in the BIM. Style transfer between real-world domain and BIM domain is performed using Cycle-consistent adversary networks (CycleGAN[5]). An evaluation of whether the generated virtual data is suitable for scene understanding will be conducted in further research. The framework of the research is shown in Figure 1.

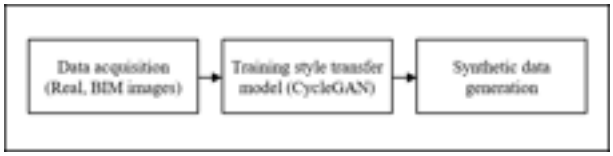

Figure 1. Research framework

2 Related work

In the field of construction, vision-based analysis has been used as an important instrument for understanding the situation. In particular, vision-based analysis using deep learning has recently been actively conducted due to the performance enhancement of computer (CPU and GPU). Among the 2D image-based analysis techniques using deep learning are classification, detection, and segmentation. Among them, segmentation, the technology that classifies the class of each pixel and includes the two preceding methods, are widely used in the latest research in the construction sector. It was used for various construction management purposes including

worker safety enhancement [3], progress monitoring [6], defect identification [[7], [8], [9]], and to update the status of the building [[10], [11]].

The aforementioned deep leaning-based method has limitation that requires a lot of training data to train the model. Preparation for the training dataset includes a labeling task, which is labour-intensive. In an effort to overcome this limitation, the previous studies created databases (ImageNet[12], SUN[13], COCO[14], Cityscape[4]). However, infrastructure facility classes such as HVAC system, plumbing system, structural element and construction materials often do not exist in the mentioned databases. Therefore, it is necessary to create training datasets that can be labelled easily on the desired objects.

To address the above issue, research have been conducted to generate training data using a 3D model [[15], [16]]. In the field of construction, Soltani et al. generated a synthetic image by adding background images and images captured from various angles on the 3D expansion model for visual reconstruction services [17]. Kim et al. took photographs of the concrete mixer trucks with a UAV camera, then created a 3D point cloud with a structure from motion technique, and created 2D synchronous images by projecting the point cloud on the plane [18].

Recently, research has also been conducted to generate synthetic data using BIM, the digital twin of infrastructure. Jong Won Ma et al. generated synthetic point clouds using 3D BIM to train the semantic segmentation model based on deep learning [19]. Although the synthetic point clouds are analogous to real point clouds, the differences in detail and volumetric information of some objects were cited as limitations. It is also difficult to train the model with the 2D synthetic images generated with unprocessed BIM. Inhae Ha et al. showed that differences exist in the feature map of the BIM images and the photographs for the same scene [20]. As such, the gap between real world and BIM is a factor that makes it difficult to use BIM image as training data. In order to reduce this gap, we create synthetic datasets that is transferred with CycleGAN so that the image obtained from BIM has a style similar to photographs.

CycleGAN [5] is a network that transfers images of different domain by learning the two mapping functions. To achieve the objective, the adversarial loss as defined in the Generative Adversarial Networks (GAN [21]) and the cycle consistency loss are used.

3 Methodology

The proposed methodology consists of a step of training CycleGAN and a step of generating synthetic data utilizing the trained network. Details are explained in the following paragraphs.

3.1 Training CycleGAN

CycleGAN [5] is a network that trains mapping function between two different domains. The network include two generators, G_{AB} mapping A to B and G_{BA} mapping B to A and two adversarial discriminators D_A and D_B, which enable mapping between source domain A and target domain B. In the adversarial loss $\mathcal{L}_{GAN}(G_{AB}, D_B, A, B)$, G_{AB} tries to make $G_{AB}(A)$ similar to B, and D_B tries to distinguish B from $G_{AB}(A)$. $\mathcal{L}_{GAN}(G_{BA}, D_A, B, A)$ also works the same. The additional loss due to the possibility that the correct mappings are not achieved with adversarial loss alone is a cycle consistency loss ($\mathcal{L}_{cyc}$). In $\mathcal{L}_{cyc}(G_{AB}, G_{BA})$, $G_{BA}(G_{AB}(A))$ is encouraged to have the same value as A, and $G_{AB}(G_{BA}(B))$ is encouraged to have the same value as B. As a result, the network operates to find G_{AB}^* and G_{BA}^* that satisfy the following expressions:

$$G_{AB}^*, G_{BA}^* = \min_{G_{AB}, G_{BA}} \max_{D_A, D_B} \mathcal{L}(G_{AB}, G_{BA}, D_A, D_B) \quad (1)$$

where,

$$\mathcal{L}(G_{AB}, G_{BA}, D_A, D_B) = \mathcal{L}_{GAN}(G_{AB}, D_B, A, B) + \mathcal{L}_{GAN}(G_{BA}, D_A, B, A) + \lambda \mathcal{L}_{cyc}(G_{AB}, G_{BA}) \quad (2)$$

In this study, real world is the source domain and BIM is the target domain. The structure of CycleGAN is illustrated in Figure 2. The generator G_{AB} receives the real world image (photograph) A_1 as an input and generates $G_{AB}(A_1)$ similar to the BIM image as an output. G_{BA} that receives $G_{AB}(A_1)$ as an input generates $G_{BA}(G_{AB}(A_1))$ similar to the original image A_1. L1-norm between A_1 and $G_{BA}(G_{AB}(A_1))$ is calculated in cycle consistency loss. Conversely, G_{BA} generates $G_{BA}(B_1)$ that is similar to the photograph from BIM image B_1, and the discriminator D_A discriminates whether the input image is from domain A or B.

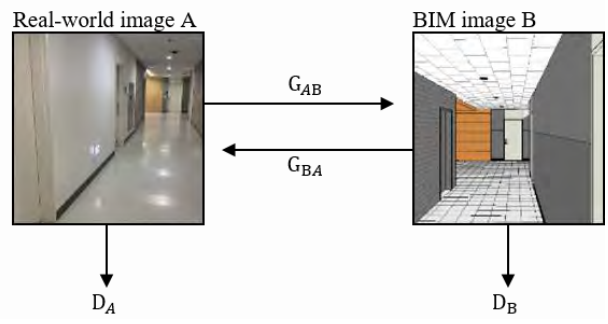

Figure 2. The structure of CycleGAN

3.2 Generating synthetic data

In this study, CycleGAN is set to train for 200 epochs. We used two learning rate settings. One sets the learning

rate to 0.0002 for 200 epochs. The other one sets the same learning rate during the first 100 epochs, and linearly decreases the learning rate from 0.0002 to 0 for the remaining 100 epochs. Then every 40 of the 200 epochs, G_{BA} takes the BIM images as the input and generates the synthetic datasets. Figure 3 shows the process in which synthetic datasets are generated from each generator. We call the generator by concatenating the generator name with the number of epochs and adding the suffix "d" if the learning rate decays.

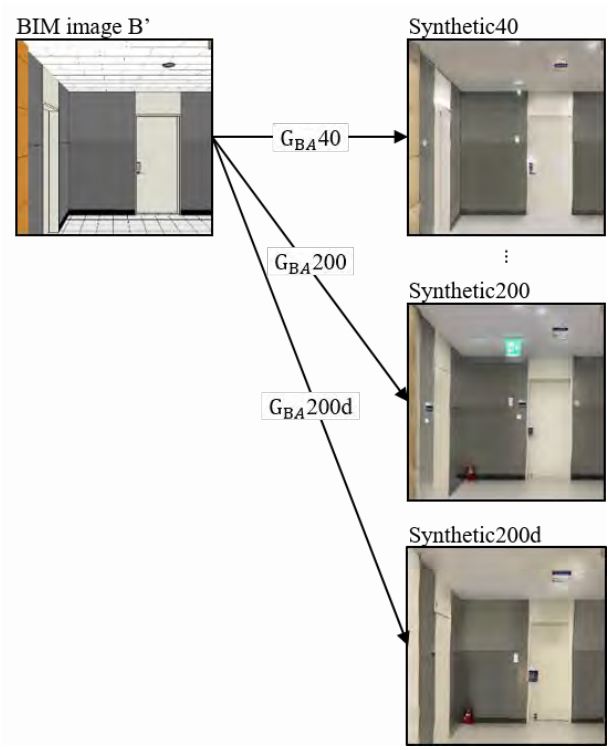

Figure 3. The process of synthetic data generation

4 Experimental Study

4.1 Dataset

The real-world domain training dataset was taken in the corridor of the north wing on the fifth floor of Yonsei University's first engineering building. 550 images were scaled from 3024 × 3024 to 512 × 512 pixels. Another training dataset, BIM domain, was extracted from Yonsei University's first engineering building BIM, which was implemented in Revit software. This BIM is the same as that used in Inhae Ha et al. [20]. 564 images with image size 512 × 512 were obtained by creating 3D views and extracting views as image files. The 3D views were also constructed in the north wing on the fifth floor of BIM.

The dataset, used as an input of generator G_{BA} to generate synthetic datasets, is a set of 100 512 × 512-sized images that do not overlap with training dataset.

4.2 Implementation

CycleGAN was trained with λ of 10 in Equation (2) and a batch size of 1. As mentioned in section 3.2, two settings of the learning rate were used: (1) non-decay setting and (2) decay setting.

4.3 Results and Discussion

This section compares one BIM dataset and eight synthetic datasets. The notation for the synthetic dataset is the same as for the generator. Figure 4 shows the image examples of BIM and synthetic datasets.

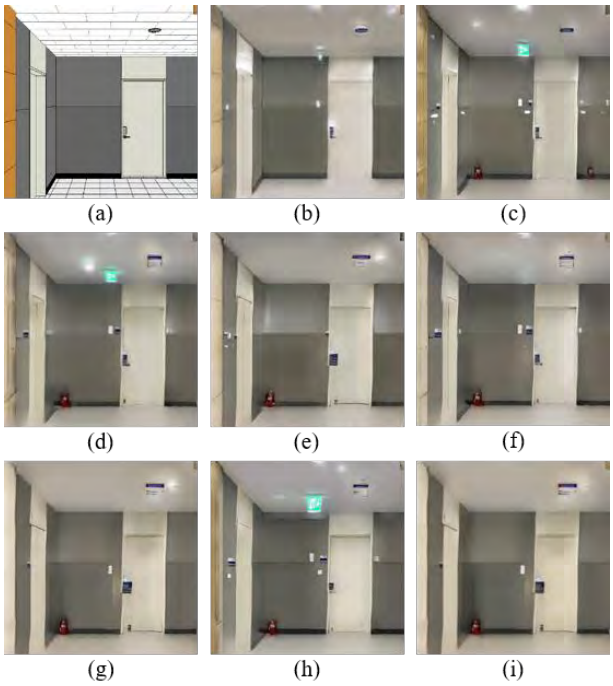

Figure 4. Examples of results from different datasets; (a) BIM, (b) Synthetic40, (c) Synthetic80, (d) Synthetic120, (e) Synthetic120d, (f) Synthetic160, (g) Synthetic160d, (h) Synthetic200, (i) Synthetic200d

As shown in Figure 4(b), synthetic40 looks similar to BIM. The color changed similar to the photograph, and the light shape and part of the exit marking in the BIM were generated. Some noise generated patterns of doorplates that appeared in the photograph. The grid patterns of floor and ceiling in the BIM have not yet disappeared. Synthetic80 shows the disappearance of a number of doorplate patterns in Figure 4(c). The position of the light is similar to the photograph, and the reflection of the light on the walls looks realistic in synthetic80. As shown in Figure 4(h), BIM's floor pattern and repetitive

patterns (especially in wood and brick area) are almost eliminated in synthetic200.

As a result of the style transfer, it was found that the network produced small objects such as the fire extinguisher and exit marker, and caused color changes to produce values similar to those of photograph. In that process, small patterns such as exit marker appeared and disappeared, depending on the number of epochs. It is assumed that the synthetic200 and synthetic200d, the models trained with the 200 epochs, did not converge.

Cosine similarity was used as an indicator of evaluating synthetic datasets. Cosine similarity is a measure of the similarity of two vectors. The cosine similarity was calculated between the photographs having the same scene and generated synthetic datasets. Table 1 shows the average and standard deviation of cosine similarity. All the synthetic datasets have cosine similarity greater than BIM dataset.

Table 1. Average and standard deviation of cosine similarity with same scene real dataset

Dataset	Cosine Similarity Avg.	Cosine Similarity Std.
BIM	.9145	.0220
Synthetic40	.9488	.0198
Synthetic80	.9495	.0193
Synthetic120	.9497	.0204
Synthetic120d	.9479	.0211
Synthetic160	.9492	.0217
Synthetic160d	.9454	.0232
Synthetic200	.9500	.0209
Synthetic200d	.9442	.0237

The synthetic datasets with photograph style and BIM content were created. The datasets, whose label can be easily obtained from BIM, are valuable as the training datasets of the segmentation model. In further research, the segmentation model will be trained with synthetic datasets and the performance of the model will be evaluated to assess whether the datasets are adequate for scene understanding.

5 Conclusion

This study proposed a method for generating synthetic image data that can be used as a training set for scene understanding in the field of facility management. In the proposed method, CycleGAN is used to train a mapping function such that transfer between BIM images and their corresponding real-world images is performed. The generator of the proposed model produces synthetic data similar to real images using the BIM images. Cosine similarity values calculated using corresponding scene-photographs showed that the synthetic data are more realistic than BIM images. The label of synthetic data is the same as that of the corresponding BIM image, so labelled data can be obtained without any annotating works. This method could be highly beneficial for collecting data to train deep learning models in that the models usually require a large amount of data. In the experiment, noise patterns on the synthetic data appeared and disappeared repeatedly as the training of CycleGAN progressed. The noise patterns are expected to adversely affect the training of deep learning models when synthetic data, including the patterns, are used as training data for the models. To tackle this problem, further research should be conducted to improve the stability of training. In a future study, synthetic datasets generated in consideration of the aforementioned problem will be used as training sets for scene understanding.

Acknowledgement

This work was supported by the National Research Foundation of Korea (NRF) grant funded by the Ministry of Science and ICT (No. 2018R1A2B2008600) and the Korea Agency for Infrastructure Technology Advancement (KAIA) grant funded by the Ministry of Land, Infrastructure and Transport (Grant 20SMIP-A156488-01).

References

[1] Asadi, K., Ramshankar, H., Pullagurla, H., Bhandare, A., Shanbhag, S., Mehta, P., … and Wu, T. Vision-based integrated mobile robotic system for real-time applications in construction. *Automation in Construction*, 96: 470-482, 2018.

[2] Atkinson, G. A., Zhang, W., Hansen, M. F., Holloway, M. L. and Napier, A. A. (2020). Image segmentation of underfloor scenes using a mask regions convolutional neural network with two-stage transfer learning. *Automation in Construction*, 113: 103118, 2020.

[3] Fang, W., Zhong, B., Zhao, N., Love, P. E., Luo, H., Xue J., and Xu, S. A deep learning-based approach for mitigating falls from height with computer vision: Convolutional neural network. *Advanced Engineering Informatics*, 39: 170-177, 2019.

[4] Cordts, M., Omran, M., Ramos, S., Rehfeld, T., Enzweiler, M., Benenson, R., … and Schiele B. The cityscapes dataset for semantic urban scene understanding. In *Proceedings of the IEEE conference on computer vision and pattern recognition*, pages 3213-3223, Las Vegas, USA, 2016.

[5] Zhu, J. Y., Park, T., Isola, P., and Efros, A. A. Unpaired image-to-image translation using cycle-consistent adversarial networks. In *Proceedings of the IEEE international conference on computer*

vision, pages 2223-2232, Venice, Italy, 2017.

[6] Rahimian, F. P., Seyedzadeh, S., Oliver, S., Rodriguez, S., and Dawood, N. On-demand monitoring of construction projects through a game-like hybrid application of BIM and machine learning. *Automation in Construction*, 110: 103012, 2020.

[7] Dung, C. V. Autonomous concrete crack detection using deep fully convolutional neural network. *Automation in Construction*, 99: 52-58, 2019.

[8] Bang, S., Park, S., Kim, H., and Kim, H. Encoder–decoder network for pixel-level road crack detection in black-box images. *Computer-Aided Civil and Infrastructure Engineering*, 34(8): 713-727, 2019.

[9] Zou, Q., Zhang, Z., Li, Q., Qi, X., Wang, Q., and Wang, S. DeepCrack: Learning hierarchical convolutional features for crack detection. *IEEE Transactions on Image Processing*, 28(3): 1498-1512, 2018.

[10] Ferguson, M., Jeong, S., and Law, K. H. Worksite Object Characterization for Automatically Updating Building Information Models. In *Computing in Civil Engineering 2019: Visualization, Information Modeling, and Simulation*, pages 303-311, Atlanta, USA, 2019.

[11] Ying, H. Q. and Lee, S. A Mask R-CNN Based Approach to Automatically Construct As-is IFC BIM Objects from Digital Images. In *ISARC. Proceedings of the International Symposium on Automation and Robotics in Construction*, pages 764-771, Banff, Canada, 2019.

[12] Deng, J., Dong, W., Socher, R., Li, L. J., Li, K., and Fei-Fei, L. Imagenet: A large-scale hierarchical image database. In *2009 IEEE conference on computer vision and pattern recognition*, pages 248-255, Miami, USA, 2009.

[13] Xiao, J., Hays, J., Ehinger, K. A., Oliva, A., and Torralba, A. Sun database: Large-scale scene recognition from abbey to zoo. In *2010 IEEE Computer Society Conference on Computer Vision and Pattern Recognition*, pages 3485-3492, San Francisco, USA, 2010.

[14] Lin, T. Y., Maire, M., Belongie, S., Hays, J., Perona, P., Ramanan, D., … and Zitnick, C. L. Microsoft coco: Common objects in context. In *European conference on computer vision*, pages 740-755, Zurich, Switzerland, 2014.

[15] Peng, X., Sun, B., Ali, K., and Saenko, K. Learning deep object detectors from 3d models. In *Proceedings of the IEEE International Conference on Computer Vision*, pages 1278-1286, Santiago, Chile, 2015.

[16] Handa, A., Patraucean, V., Badrinarayanan, V., Stent, S., and Cipolla, R. Understanding real world indoor scenes with synthetic data. In *Proceedings of the IEEE Conference on Computer Vision and Pattern Recognition*, pages 4077-4085, Las Vegas, USA, 2016.

[17] Soltani, M. M., Zhu, Z., and Hammad, A. Automated annotation for visual recognition of construction resources using synthetic images. *Automation in Construction*, 62: 14-23, 2016.

[18] Kim, H. and Kim, H. 3D reconstruction of a concrete mixer truck for training object detectors. *Automation in Construction*, 88: 23-30, 2018.

[19] Ma, J. W., Czerniawski, T., and Leite, F. Semantic segmentation of point clouds of building interiors with deep learning: Augmenting training datasets with synthetic BIM-based point clouds. *Automation in Construction*, 113: 103144, 2020.

[20] Ha, I., Kim, H., Park, S., and Kim, H. Image retrieval using BIM and features from pretrained VGG network for indoor localization. *Building and Environment*, 140: 23-31, 2018.

[21] Goodfellow, I., Pouget-Abadie, J., Mirza, M., Xu, B., Warde-Farley, D., Ozair, S., … and Bengio, Y. Generative adversarial nets. In *Advances in neural information processing systems*, pages 2672-2680, Montreal, Canada, 2014.

Cyber-physical System for Diagnosing and Predicting Technical Condition of Servo-drives of Mechatronic Sliding Complex during Construction of High-rise Monolithic Buildings

Alexey Bulgakov[a], Thomas Bock[b], Tatiana Kruglova[a]

[a]Department of Mechatronic, Platov South-Russia State Polytechnic University, Novocherkassk, Russia
[b]Department of Building Realisation and Robotics, Technical University of Munich, Germany
E-mail: agi.bulgakov@mail.ru, thomas.bock@br2.ar.tum.de, tatyana.kruglova.02@mail.ru

Abstract –

The article is devoted to the problem of improving the reliability and efficiency of the operation of mechatronic sliding complexes. To solve this problem, a cyber-physical system is proposed that implements the diagnosis and prediction of the technical condition of servo drives. Methods for calculating the current and additional loads on servo drives are proposed. Recommendations are given on changing the lifting mode of the sliding formwork de-pending on the technical condition of the servos.

Keywords –

slip form; servo drive; approximate envelope straight line; Morlet wavelet; fuzzy logic; neural network

1 Introduction

Construction is one of the main actively developing sectors of the national economy of any country. Every year the number of high-rise buildings is growing steadily. Constantly changing requirements for the quality and speed of construction of the building. It leads to the emergence of new construction technologies using robotic and mechatronic systems, allowing high-precision performance and good quality of construction. To solve this problem, it is necessary to ensure the reliable functioning of all the machines and mechanisms of the complex that operate in tight relationship with each other. Analysis of the construction of high-rise buildings technology showed that the main actuating elements of the buildings mechatronic complex are DC or AC servo motors. Their proper work determines the buildings and structures quality. Failure or malfunction of one of the drives can lead to disruption of the entire complex, damage to building materials and to the construction of inadequate quality. Therefore, the urgent task is to ensure the reliable functioning of all the servos included in the mechatronic complex. This problem can be solved by cyber-physical system synthesis that implements monitoring of each servo motors technical condition and optimizing the technological process at the construction site, taking into account the current and predicted state of building robotic and mechatronic complex servo motors.

2 Mechatronic sliding formwork complex structure

The most common method of high-rise buildings and structures is monolithic construction [1]. Technology this method provides a continuous supply and laying of concrete, installation of rebar, formwork hoist, regulation of project sizes and control settings of the building [2]. The modern method of automation of monolithic construction is the use of mechatronic sliding formwork complex (Fig.1), which is a spatial form installed on the perimeter of the structures and moved up by lifting jacks (LJ) [3].

The position of the formwork panels is fixed by Jack frames that accept the loads of the laid concrete. Lifting of the formwork is carried out by Electromechanical lifting jacks based on DC or AC servo motors. Jacks should provide high load capacity, synchronous movement of the formwork, lifting speed regulation and ease of maintenance [4]. It also includes adjustment mechanisms, dynamic properties, design and technological features that determine the structure of control algorithms and the choice of control laws. For example, for structures of conical and hyperbolic shape, these are radial movement mechanisms (RMM), which are located along the radius with a uniform step (Fig.1,a). Their task is to move the formwork panels in the process of lifting it. Changing the position of the boards should be synchronized with the LJ. To do this, the number of RMM mechanisms (m) is chosen as a multiple of the number of LJ (n). This will allow the platform radial beams to be distributed evenly with angular pitch $2\pi/m$ and used for the RMM installation. Important conditions for the quality of construction work are the con-

tinuity of the technological process and maintaining a constant movement speed of the formwork not less than 1 cm/min, as well as the need to strictly horizontal platform. To implement these requirements, it is necessary to ensure consistent operation of all servo motors included in the complex. This problem can be solved by using methods and tools for predictive diagnosis of LJ and RMM servo motor with its operation mode subsequent optimization. For this purpose, it is necessary to provide the technical condition control of all servo motors which are a part of the MSFC, information exchange between drives and decision-making for MSFC operation mode changing.

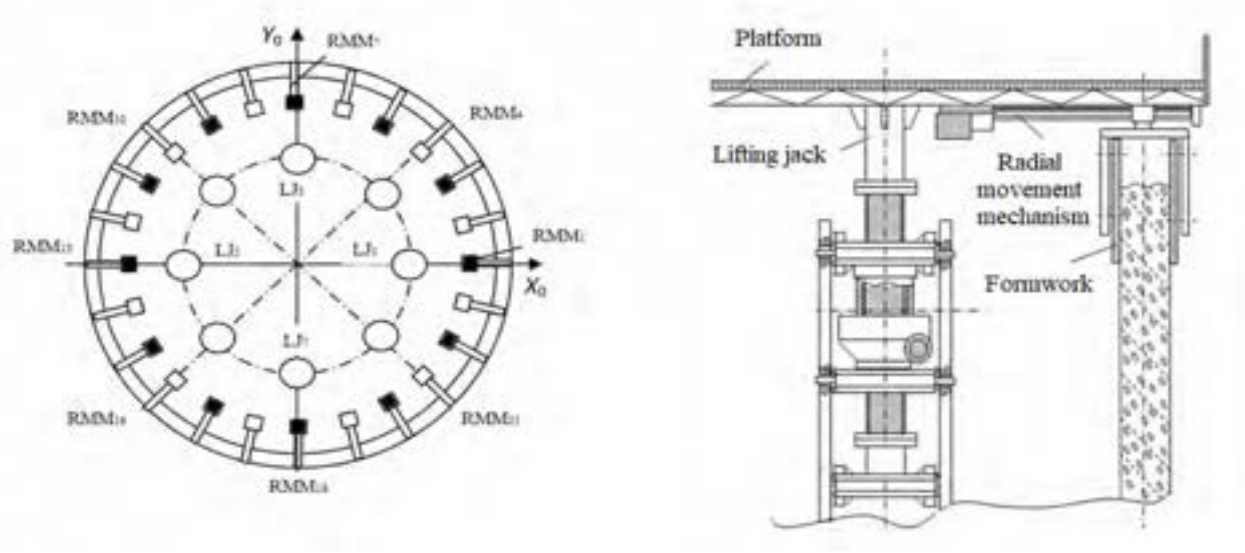

a) b)

Figure 1. Mechatronic sliding formwork complex (MSFC): a) longitudinal and vertical section of the MSFC; b) the distribution of lifting jacks (LJ) and radial movement mechanisms (RMM) in the plane of the complex platform.

The implementation of this approach involves the integration of computational resources into physical processes using a cyber-physical system. In such a system, sensors, equipment and information systems interact throughout the life cycle of the MFSC and information exchange is carried out using standard Internet protocols. This allows performing self-tuning and MSFC adaptation to changing operating conditions and technical condition of the equipment. Therefore, the development the analysis methods and optimal synthesis of cyber-physical systems for technical condition diagnosis the of MSFC servo motors to improve the operation efficiency and their operational safety ensure is very important.

3 The cyber-physical system structure

The cyber-physical system should implement the collection of diagnostic information, its processing, storage and analysis to determine the current technical conditions, defects development forecasting and the servo failure time determination, MSFC operation mode optimization depending on the its servos technical condition. The cyber-physical system includes the cyber and physical parts (Fig. 2), and the main functions are transferred to the software part. The physical part of the system is represented by the "Hardware" block, which includes MSFC servo-drives functioning in a given technological process. The cyber part is represented by the “Data” and “Internal Software” blocks.

The “Data” block provides diagnostic information from the sensors of the facility, as well as storing the diagnostic results for previous periods of operation of the MSFC in a database used for the technical condition forecasting.

The “Internal software” block analyzes the current and predicted technical condition of all servo drives of the MSFC followed by a decision to change the mode of its operation. The “Internal software” block analyzes the current and predicted technical condition of all MSFC servo drives followed by a decision to change the mode of its operation. In this structure, the technical condition predictive diagnosis is implemented for each servo motor and decision-making is performed for the entire MSFC as a whole.

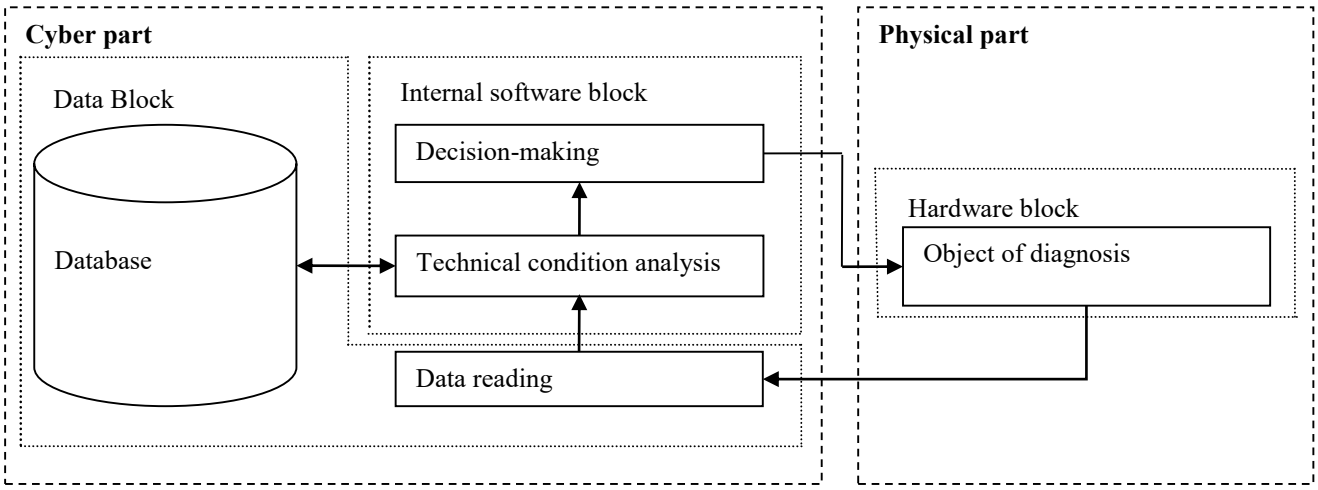

Figure 2. The structure of the information processing in cyber-physical system MSFC predictive diagnosis

Based on this, the architecture of the cyber-physical system has two levels. The main computing function of the system is performed by the lower level associated with the object of diagnosis. At the same time, a higher level of the system will receive information exclusively on the results of diagnostics and prediction of the status of servos and make a decision on reconfiguring the system and changing the operating mode of the mechatronic sliding complex

4 The lower level of the cyber-physical system

4.1 Servo motors diagnosis method

At the lower level of the cyber-physical system, the tasks of determining the current and predicted technical condition of each MSFC servo drive are solved.

For its implementation, it is necessary to develop methods that satisfy the following requirements:

- ability to assess the technical condition in real time;
- minimum composition of measured parameters;
- lack of complex bulky measuring equipment installed on the body of the servo drive, affecting the operation of the MSFC;
- ability to use on a moving object in conditions of high humidity and dustiness of the working environment;
- applicability for AC and DC servo motors;
- ability to automatically analyze the measured parameters in real time;
- ability to record and store diagnostic results on a cloud server and provide the user with an Internet protocol.

Analysis of existing methods and diagnostic tools showed that the only method that satisfies most of the above requirements is the analysis of current consumption. To synthesize a method for analyzing temporary servo signals using wavelet transform, a number of experimental studies have been carried out to diagnose servo motors at different loads. The measured time signals of the servo current were decomposed using a Morlet wavelet in a selected range of scales and a comparative analysis of the results was performed. The results of the analysis of the current signals of the servo drive at various rotational speeds and loading modes made it possible to establish a regularity between the type of wavelet-coefficient graph and the technical state of the servo motors [5]. The established graph types of wavelet coefficients can be classified into three groups: decaying, linear, increasing. Damped oscillations are characteristic of a healthy servo motor, linear - for a faulty unloaded motor, and increasing - for a faulty loaded motor.

To formalize the derived regularity, it is advisable to use the Hilbert transform, which allows for the function of the continuous wavelet transform $\psi_{ab}(t)$, calculated for each characteristic scale to calculate the analytically conjugate function $\hat{\psi}_{ab}(t)$, the mathematical form of which has the following form:

$\hat{\psi}_{ab}(t) = \int_{-\infty}^{\infty} \frac{\psi_{ab}(\tau)}{t-\tau} d\tau = I\left[\psi_{ab}(t)\right]$,

Based on these two functions, an analytical signal is generated.

$$s(t) = \psi_{ab}(t) + j \cdot \hat{\psi}_{ab}(t)$$

from which it is possible to find the instantaneous amplitude (envelope of the signal):

$$A(t) = |s(t)| = \sqrt{{\psi_{ab}}^2(t) + {\hat{\psi}_{ab}}^2(t)}$$

As a result, pairs of points $t(t_1, t_2, \ldots . t_n)$ and ψ_{ab} $(\psi_{ab1}, \psi_{ab2}, \ldots . . \psi_{abn})$ between which there is some dependence $\psi_{ab_i} = f(t_i)$ are obtained.

To search for the analytical dependence, the least squares method was used, according to which the arguments of the function $f(t, c_1, c_2, \ldots c_k)$ must be chosen so that the sum of the squares of the deviations of the measured values

$Y = f(t, c_1, c_2, \ldots c_k)$ minimal

$$S(c_1, c_2, \dots c_k) = \sum_{i=1}^{n} (Y_i - \psi_{ab_i})^2 \to min$$

For a formal description of the envelope obtained as a result of experimental researches, it is advisable to choose a polynomial of degree m, the generalized formula of which has the following form:

$$\psi_{ab}(t) = c_0 + c_1 t + c_2 t^2 + \dots + c_m \mathrm{t}^{\mathrm{m}}$$

The goal of the envelope description being performed is the mathematical formalization of its shape, which allows us to unambiguously describe the process taking place on a given scale. Since the envelope graph has three characteristic features: it is downward, linear, or upward, the change in the amplitude of the wavelet coefficients in time can be unambiguously described using the linear law. Therefore, to formalize the shape of the envelope of the signals, it suffices to choose a polynomial of the first degree.

$$\psi_{ab}(t) = c_1 t + c_0$$

Thus, the problem of approximating the shape of the envelope of the wavelet coefficients can be reduced to obtaining a straight line equation of the type $y = kx + b$, (where $c_1 = k, c_0 = b$), the coefficients of which allow us to describe the main changes in the wavelet coefficients on the selected scale. An analysis of the coefficients k and b of the approximating straight envelope of the wavelet coefficients at characteristic scales showed that a working servo corresponds to a coefficient $k < 0$, and the approximating straight line descends to the abscissa axis, $k \geq 0$ is typical for a faulty state of the servomotor. Coefficient b is always positive, however, with an increase in load on a serviceable drive, coefficient b increases and k decreases.

For a faulty servo motor, an increase in load will lead to an increase in all the parameters of the approximation line. Thus, the sign of the coefficient k of the approximating direct envelope at the characteristic scales of the wavelet coefficients will determine the current state of the servo motor.

4.2 Current servo motor load determination

To determine the current load of the servo motor, it is necessary to calculate the coefficients of the approximating straight envelopes at characteristic scales for a known-good unloaded servo drive ($k_0,\ b_0$) and at maximum load (k_{max}, b_{max}).

The passport data of any servo contains the overload capacity of the servo current K_T, which is calculated by the following formula:

$$K_T = \frac{I_{max}}{I_{nom}}, \text{ then } I_{max} = K_T I_{nom}$$

where I_{max}, I_{nom} - maximum permissible and rated currents of the servo drive.

If the coefficients k_0, b_0 correspond to the rated current, then k_{max}, b_{max} will correspond to the maximum permissible current. Then

$$k_{max} = \frac{k_0 \cdot I_{max}}{I_{nom}} = \frac{k_0 \cdot I_{nom} \cdot K_T}{I_{nom}} = k_0 \cdot K_T;$$
$$b_{max} = \frac{b_0 \cdot I_{max}}{I_{nom}} = \frac{b_0 \cdot I_{nom} \cdot K_T}{I_{nom}} = b_0 \cdot K_T.$$

The coefficients of the approximation straight line k and b of a healthy servo motor are in the following range:

$$k_{max} \leq k \leq k_0 \qquad b_{max} \leq b \leq b_0$$

If the coefficients go beyond the specified limits, it is urgent to stop the operation of the servo drive.

Relative coefficients showing the load on the servo drive can be calculated from the following relationships:

$$\Delta k = \frac{k - k_0}{k_{max} - k_0}; \qquad \Delta b = \frac{b - b_0}{b_{max} - b_0}$$

If $k = k_0$ and $b = b_0$, then $\Delta k = 0, \Delta b = 0$, which indicates the absence of load on the drive. If $k = k_{max}$ and $b = b_{max}$, then $\Delta k = 1$, $\Delta b = 1$, which shows the maximum load on the servo drive. If $k \in [k_0, k_{max}]$, $b \in [b_0, b_{max}]$,, then $\Delta k \in [0,1], \Delta b \in [0,1]$. If $\Delta k < 0$, then the servomotor is faulty and must be turned off. If $\Delta k > 1, \Delta b > 1$ then the load level is higher than the maximum permissible value and it is necessary to change the operating mode of the servo motor.

If both factors are within the specified limits, then you can determine the level of load on the servo motor.

A fuzzy logical model has been developed, the inputs of which are the relative coefficients Δk and Δb, and the output is the level of load on the servo as a percentage of the maximum permissible. To describe such a model, a *Sugeno*-type fuzzy logic inference system with two inputs and one output is used. For each input parameter on the interval [0; 1] the corresponding membership functions are set (Fig. 3). The output parameter *Load* is the corresponding coefficient on the interval [0; 100], showing the percentage of engine load. If this parameter is equal to zero, then the servo drive operates in the nominal mode without load. If it is 100%, then the engine has a maximum load and it is necessary to change its operation mode.

The relationship between the introduced sets is described by the following fuzzy rules:

R_1: *If* k *is* k_0 *and* b *is* b_0, *then* $Load = l_1$;
R_2: *If* k *is* k_{max} *and* b *is* b_{max}, *then* $Load = l_2$;

To convert clear input values to clear output, n is used - the *Takagi – Sugeno* algorithm [6].

The resulting model allows us to determine the degree of loading of the servo motors as a percentage of the maximum permissible value from the analysis of the coefficients of the approximation direct envelope.

This will allow you to choose the operating mode of each specific drive and optimize the operating mode of construction robotic and mechatronic complexes in order to increase their reliability and efficiency.

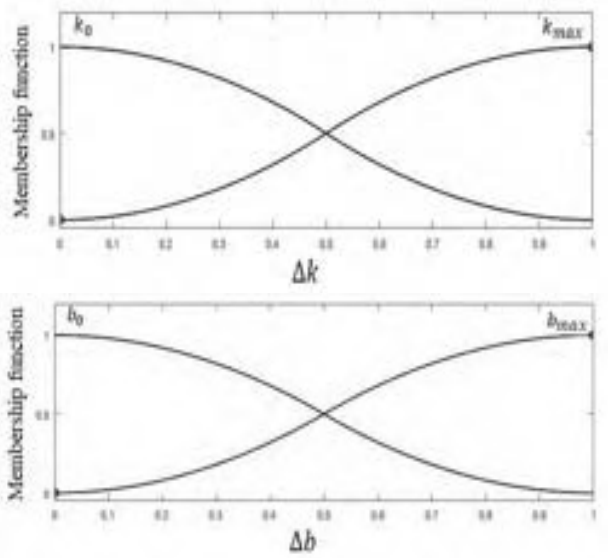

Figure.3. Input data of a fuzzy model for servomotor load determination

4.3 Prediction of technical condition

A method for servo motor technical condition prediction using neural networks is proposed. The forecasting initial data are the trend of the coefficients *k* of the approximating direct envelope of the wavelet coefficients of the current signals at characteristic scales for previous periods of operation, distributed over equal time intervals. The forecasting process includes three levels. At the first level, the values of the coefficients *k* of the approximation direct envelope of the wavelet coefficients for each characteristic wavelet scales are predicted. A direct signal transmission network with three inputs and one output is simulated.

The input vector of the neural network

$$P = [k(t_1),...k(t_{N-3}); k(t_2),...k(t_{N-2}); k(t_3),...k(t_{N-1})]$$

The target vector *H*, the values of the determining parameter are set, which should be obtained at the output

$$H = [k(t_4),...k(t_N)].$$

For a given input *P*, the neural network calculates the output value of the predicted parameter *C*

$$C = [k(t_{N-2});\ k(t_{N-1});\ k(t_N)],$$

corresponding to a given target vector *H*.

To train the neural network, the back propagation algorithm is used.

Similar calculations are performed for each scale of wavelet coefficients. If during the calculation all the coefficients are negative, then the servomotor will remain operational in the next period of operation. If at least one is zero or positive, then in the next period of operation the object will fail.

The forecast at the next levels is an approximation of the values obtained at the previous level. To predict the time of the onset of faults, network outputs are needed that predict the values of the corresponding coefficients of the approximation straight envelope of the wavelet coefficients, apply to the input of the radial basis network. Since the output of the first level consists of values of the coefficients k, negative values of which indicate a working condition, and zero or positive ones indicate a faulty state of the servo, the result of the next level of forecasting can be obtained by maximizing the previous level. The determination of the development coefficients of the motor malfunction K_{MOTOR} ·

$$K_{FAULT_j} = \max(\exp(-(\sum(K_i \cdot IW^{1.1} + b))^2);$$

$$K_{MOTOR} = \max(\exp(-(\sum(K_{FAULT\,i} \cdot IW^{1.2} + b))^2),$$

where $IW^{1.1}$ $IW^{1.2}$ - weights vector of the first (development of a malfunction) and second (forecast of the state of the servo motors) of the approximation steps.

To determine the servo motor failure time, it is necessary to add the predicted values of the coefficients of the approximation direct envelope of the wavelet coefficients in the training set and repeat the entire forecasting process until the coefficient determining the state of the servo motor becomes $K_{MOTOR} \geq 0$. The number of iterations passed will be equal to the number of time intervals *T* during which the servomotor remains operational. The implementation structure of the above method is shown in Fig. 4

The proposed method for forecasting the technical condition will allow short-term and long-term forecasting of defects of each MSFC servo motor. The results will be used for subsequent optimization of the operating mode of MSFC.

The proposed method for forecasting the technical condition will allow short-term and long-term forecasting of defects of each MSFC servo motor. The results will be used for subsequent optimization of the operating mode of MSFC.

5 Cyber-physical system upper level

According to the developed architecture, the upper level collects information about the current state, load and the forecast period of maintaining operability from all MSFC drives and makes a decision on its further operation.

Let be *m* - number of radial movement mechanisms; *n* - is the number of lifting jacks of the MSFC. An important condition for the operation of the system is the identity of the RMM and LJ drives, as well as the uniformity of their loading

If $Load_{RMM}$ and $Load_{LJ}$ corresponding load on each servomotor RMM and LJ, then the total load on all drives of the system will be calculated as follows:

$$\sum Load_{RMM} = m \cdot Load_{RMM};$$
$$\sum Load_{LJ} = n \cdot Load_{LJ}.$$

If the number of simultaneously operating drives RMM as m^*, where $m^* = 1 \ldots . m$ and LJ as n^*, where n^*, then the total load on simultaneously working drives can be determined from the relations

$$\sum Load^*_{RMM} = \frac{m}{m'} \cdot \sum Load_{RMM};$$
$$\sum Load^*_{LJ} = \frac{n}{n'} \cdot \sum Load_{LJ}.$$

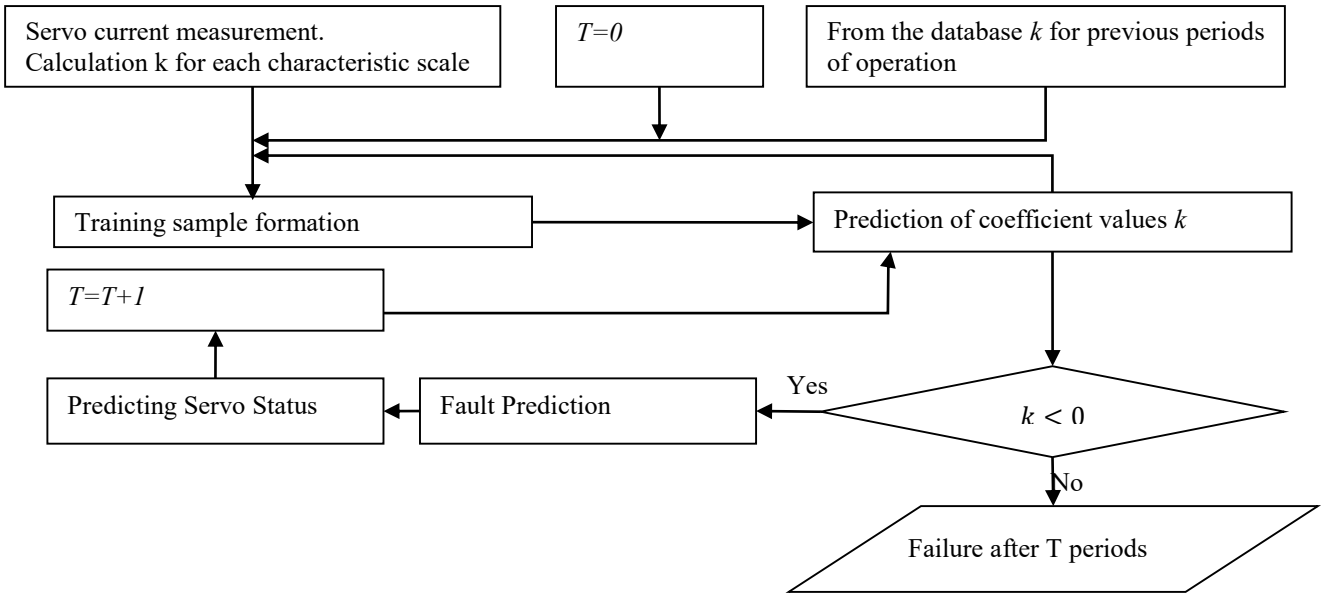

Figure. 4 Structure of the implementation of the method for predicting the technical condition of MSFC servo motors

The additional load on each drive can be found from the ratio

$$\Delta Load_{RMM} = \sum Load^*_{RMM} - Load_{RMM};$$
$$\Delta Load_{LJ} = \sum Load^*_{LJ} - Load_{LJ}.$$

Thus, a ratio is obtained that, knowing the total number of RMM and LJ drives and the number of currently motors operation determines the required load increment for each motor.

The average ($Load$) and average additional ($\Delta Load$) load on the servos of the RMM or LJ group are determined from the relations:

$$Load = \sum Load_{i(j)} / n^*(m^*)$$
$$\Delta Load = \sum \Delta Load_{i(j)} / n^*(m^*),$$

where $Load_i,\ i \in [1, n^*]$; $Load_j,\ j \in [1, m^*]$ - load for each motor RMM and LJ; $\Delta Load_i,\ i \in [1, n^*]$; $\Delta Load_j,\ j \in [1, m^*]$ -additional load for each motor RMM and LJ.

The average predicted period of good operation of the servos group RMM and LJ

$$T_g = \sum T_{i(j)} / n^*(m^*)$$

where $T_i,\ i \in [1, n^*]$; $T_j,\ j \in [1, m^*]$ - the predicted period of good operation of each servo RMM and LJ calculated according to the forecasting model.

The simulated fuzzy logical decision-making system will have three inputs and one output. To convert clear input values into clear output, the *Mamdani* fuzzy logic algorithm is used [7-12]. The fuzzy knowledge base that describes the relationship between the input term sets and the output sets is presented in Table 1. The result of the decision-making model is the value of the decision $D \in [-1, 1]$.

Table 1. The truth table of the fuzzy decision-making model

Current motor load	**Change motor load, %**		
	Less 20	**25**	**More 30**
Forecasted period of service 1 month			
Less 30	+1	+1	-1
50	-1	-1	-1
More 60	-1	-1	-1
Forecasted period of service 3 month			
Less 30	+1	+1	+1
50	+1	+1	0
More 60	-1	-1	-1
Forecasted period of service more 6 month			
Less 30	+1	+1	+1
50	+1	+1	+1
More 60	0	0	0

If $D > 0$, then it is necessary to change the load on serviceable servos of the group by the value $\Delta Load$. If $D=0$, then the operating mode must be left unchanged. If $D<0$, then the condition of the drives of the group is unsatisfactory and it is necessary to stop the process. Based on this model, an intelligent decision-making method has been developed on the operation mode of each of the MSFC servo groups based on the technical condition of its servos, the implementation structure of which is shown in Fig. 5.

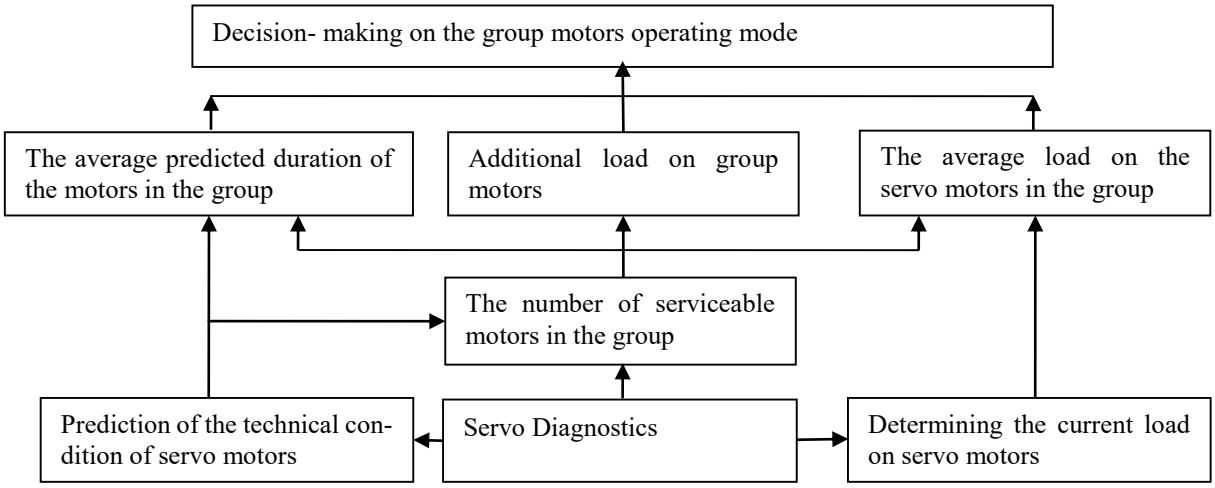

Figure 5. The structure of the implementation of the intellectual decision-making method for managing building mechatronic and robotic complexes according to the results of diagnosing their servos

6 Experimental research

A study of the prediction diagnosis methods of MSFC has been performed. For servo motor KY110AS0415-15B-D2-2000 was carried out according to the measurement of the current signal from January 2008 to January 2015. The obtained records of the supply current signals were processed using the proposed diagnostic method. The coefficients of the approximation straight envelope are found for each scale. According to the data obtained, it is clear that in January 2015 this servo motor was in the boundary state, since the approximation coefficient k for the rolling bearing malfunction is close to 0. According to the record in the equipment maintenance journal, the KY110AS0415 - 15B - D2 - 2000 servo drive failed on 27.02.2015 due to wear of the bearings, which confirms the accuracy of the proposed diagnostic method. According to the values of the coefficients *k* for the period from 2008 to 2012, the values of these coefficients are predicted for 2013-2015. A comparison of the results of diagnosis and forecasting (Fig. 7). It can be seen from this graph that, according to the forecast, the failure of the servo drive occurred earlier than in fact, which will prevent a sudden failure of the equipment. The analysis of the effectiveness and reliability of the proposed methods of predictive diagnosis.

It is established that the use of these methods will increase the coefficient of technical use by 16%. The reliability of the diagnosis is 93%. The accuracy of short-term forecasting is 1.7%, long-term forecasting does not exceed 10%. Prediction accuracy can be increased by increasing the volume of the training sample, as well as adding it to the current values of the diagnostic parameters.

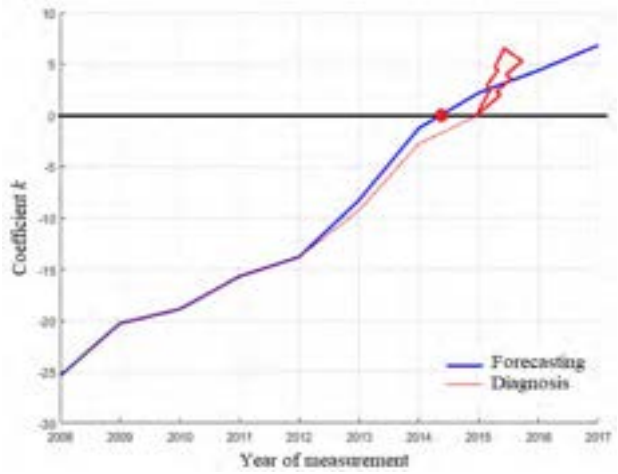

Figure 7. Comparative analysis of the diagnosis and forecasting results

A study of the prediction diagnosis methods of MSFC has been performed. The experimental stand was a fragment of a sliding formwork of four lifting jacks interconnected by formwork panels suspended on crossbars. This stand was put into step-by-step motion at a speed of 1 cm / min. For each scale of wavelet coefficients, the relative coefficients of the approximation straight envelope were calculated, which were substituted into the model for calculating the load. As a result of the calculation, it was found that the average load on the drive is approximately the same and amounts to 29.52% of the maximum, which corresponds to the average statistical load on the formwork drives during operation. The health checks of the models for calculating the load change and the decision on

the control of servo drives were carried out with the KY110AS0415-15B-D2-2010 formwork drive turned off. The objective of the experiment was to calculate the necessary change in the load on the three remaining drives and to study the behavior of the system when working on three servos. To compensate for the failure of one of the drive jacks, it is necessary to increase the load on each of the three remaining drives by 9.84%. As a result of the calculation using a fuzzy decision-making model, it was found that the current load on the group drives can be increased by $\Delta Load = 9{,}84$ %.

For the three switched-on drives, the load on the calculated percentage was increased and the speed of the fragment of the sliding formwork was measured. The results of the study showed that the control system allows for uniform constant movement of formwork panels with a given speed of 1 cm / min with four drives with a load of 29.52% each, and with three motors with a load of 39.36%.

The nature of the movement of the mechanism remains almost unchanged when the load is redistributed within the motors group. This makes it possible to carry out repair work on replacing a faulty drive without stopping the process, reducing complex performance and losing quality of the monolithic structure being constructed.

7 Conclusions

The article presents the structure of the cyber-physical system for predictive diagnosis of the technical condition of MSFC servo motors. This system contains two levels. The first level is connected to the servos and provides their predictive diagnosis. At the second level, decision making and changing the operating mode of the servo drive are implemented. The innovative methods of diagnosing and predicting the technical condition are described. Methods of calculating the current and additional load are presented, as well as a decision-making model on the advisability of changing the load on the servos depending on the current state of operable motors.

References

[1] Bulgakov, A., Parshin, O., Gudikov, G. Automation of sliding formwork for the construction of industrial structures- Overview. M.: VNIINTPI, 2000. Ser. Technology and mechanization of construction. - Issue 1. 64 p.

[2] Bulgakov, A., Parshin, D., Gudikov, G. Management of sliding formwork during the construction of monolithic buildings and stiffness cores. Mechanization of construction, 1987, No. 12, 15-16.

[3] Construction and reconstruction of buildings and structures of urban infrastructure. Volume 1. Organization and construction technology / Under the total. ed. V.I. Telichenko. Moskov, 2009 520 p.

[4] Bulgakov, A., Kruglova, T. Intelligent method of Electric drive diagnostic with due Account for its operation mode. Journal of Applied Engineering Science - 2017. - Vol. 15, № 4. - Art. 465. - P. 426-432.

[5] Bulgakov, A., Kruglova, T., Bock, T. Synthesis of the AC and DC Drives Fault Diagnosis Method for the Cyber-physical Systems of Building Robots-MATEC Web of Conferences - 2018. - Vol. 251 : : № 03060

[6] Kruglova, T., Bulgakov, A., Vlasov, A., Shmelev, I. Artificial Intelligence Method for Electric Drives Mode Operating and Technical Condition Determination MATEC Web of Conferences - 2017.- Vol. 132 : Dynamic of Technical Systems (DTS-2017) : XIII International Scientific-Technical Conference, Rostov-on-Don, 2017. № 04012.

[7] Bulgakov, A., Kruglova, T., Bock, T. Formulation of the Optimization Problem of the Cyber-physical Diagnosis System Configuration Level for Construction Mobile Robots // In *Proceedings of the 36th International Symposium on Automation and Robotics in Construction (ISARC 2019).* – Alberta: 2019, pp. 704-708.

DOI: https://doi.org/10.22260/ISARC2019/0094

[8] Parshin, D., Bulgakov, A., Buzalo, N. Robotization of slip form for monolithic construction of tall buildings // In *Proceedings of the International Construction Specialty Conference*, Vancouver, June 7 - 10, 2015, pp. 1445-1454.

[9] Bulgakov, A., Emelianov, S., Buzalo, N., Parshin, O. A mechatronic slip complex control when erecting monolith objects // Procedia Engineering 164 (2016) pp. 115-120.
DOI: 10.1016/j.proeng.2016.11.599 Reference: PROENG392340

[10] Zayed, T., Reza Sharifi, M., Baciu, S. and Amer, M. Slip-Form Application to Concrete Structures// Journal of construction engineering and management, March 2008, pp. 157-168. DOI:10.1061/(ASCE)0733-9364(2008)134:3(157).

[11] Hyejin Yoon, H., Won Jong Chin, W.J., Kim, H.S. andJin Kim, Y.j. A Study on the Quality Control of Concrete during the Slip Form Erection of Pylon // Engineering, 2013, 5, 647-655. DOI: 10.4236/eng.2013.58078

[12] Fossa, K.T., Kreiner, A. and Moksnes, J. Slipforming of advanced concrete structures. - Tailor Made Concrete Structures – Walraven&Stoelhorst (eds), 2008 Taylor & Francis Group, London, pp. 831-836.

Proposal for Automation System Diagram and Automation Levels for Earthmoving Machinery

Takeshi Hashimoto[a], Mitsuru Yamada[a], Genki Yamauchi[a], Yasushi Nitta[b] and Shinichi Yuta[c]

[a] Public Works Research Institute, 1-6, Minamihara, Tsykuba-shi, Ibaraki-ken, 305-8516, Japan
[b] Ministry of Land, Infrastructure, Transport and Tourism, 2-1-3 Kasumigaseki, Chiyoda-ku, Tokyo, Japan
[c] Shibaura Institute of Technology, 3-7-5, Toyosu, Koutou-ku, Tokyo, Japan
E-mail: t-hashimoto@pwri.go.jp, m-yamada@pwri.go.jp, yamauchi-g573bs@pwri.go.jp, nitta-y92qx@mlit.go.jp, yuta@ieee.org

Abstract –

In Japan, earthmoving workers are aging rapidly, and more than one million skilled workers will retire at once in the near future. Thus, the mass retirement of these skilled technicians could bring a significant drop in production capabilities throughout the earthmoving industry. To solve this problem, it is expected that automatic construction systems using robotics technology will improve productivity at earthmoving field. To efficiently promote further advancements in earthmoving automation research, it is necessary to systematize the entire earthmoving construction and classify automation levels.

In this paper, we formed a team in collaboration with project owners, civil engineers, engineers of construction machinery manufacturers, and robotics researchers, and others. Then, with them, we attempted to formulate a "automation system diagram for earthmoving work" to systematize the entire earthmoving construction, and "automation levels for earthmoving machinery" to grasp the achievement of current technologies. It is anticipated that these will make it possible to give concrete shape to research aims and plans, and that automation research will proceed as a result.

Keywords –

Earthmoving machine; Automation; system diagram; level

1 Introduction

The aging of workers in Japan's construction industry has been progressing rapidly in recent years. The percentage of construction workers aged 55 years or older, which stood at 24.2% in 1998, rose to 34.1% in 2017. Meanwhile, the percentage of workers aged 29 or younger, which was 21.6% in 1998, fell to 11.0% in 2017 (Figure.1, [1]). Moreover, looking at the number of construction workers by age group in 2015 (Figure.2, [2]), a reverse pyramid is created whereby the number is largest in the elderly group and becomes smaller with each descending age group. This problem is more serious in the earthwork field than in the building field.

From this, it is estimated that at least one million skilled technicians will retire in the near future. The production capabilities of skilled technicians (having at least 15 years of experience) is roughly 1.8 times that of less-skilled technicians (having experience of less than

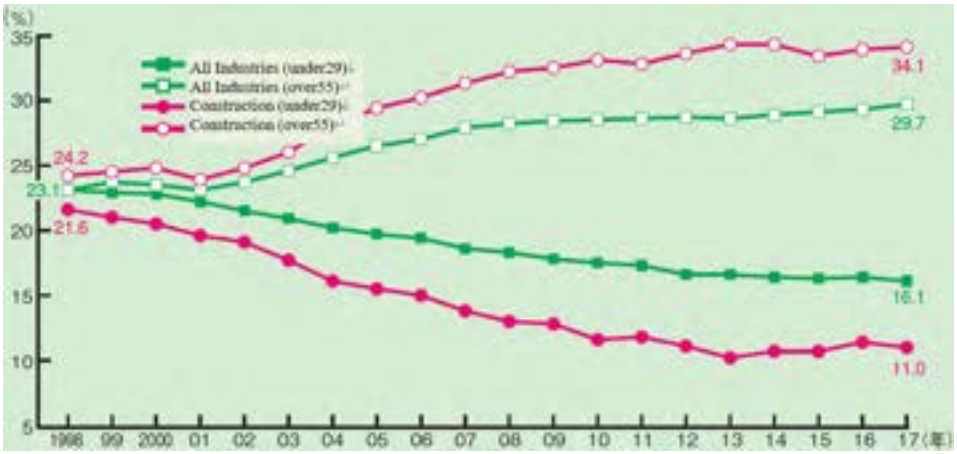

Figure 1. Number of workers [1]

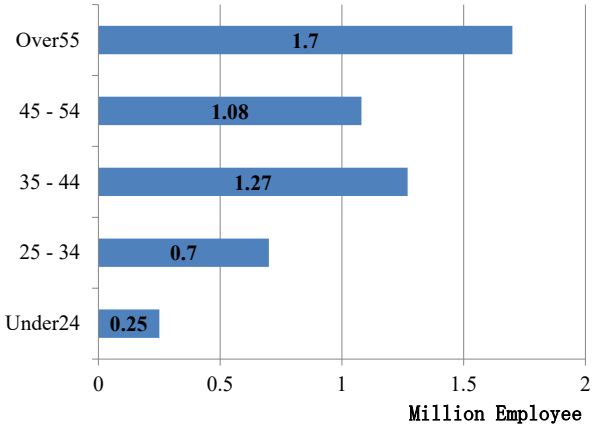

Figure 2. Number of construction workers (2014) [2]

ten years) [3]. Thus, the mass retirement of these skilled technicians could bring a significant drop in production capabilities throughout the earthmoving industry.

It is expected that one way of resolving this problem is to improve productivity by applying robotics technologies in earthmoving work. Specifically, it is anticipated that automating earthmoving work with robotics technologies will raise the production capabilities of less-skilled technicians and achieve manpower savings at earthmoving sites. A number of such automation technologies have already been studied and some are being put to practical use [4] – [11].

However, most of the research conducted so far has been limited to the automation of individual earthmoving machinery, and is far from the automation of the entire earthmoving work.

To efficiently promote further advancements in earthmoving automation research, it is necessary to clarify the research goal to be carried out next by understanding the scope that the current research occupies in the entire earthmoving work and the degree of achievement of the research. For that purpose, it is necessary to systematize the entire earthmoving construction and classify automation levels. There are some examples of these studies in the earthwork field [12] – [14]. However, these are discussed on limited conditions only, and overall examination by many category researchers (for example, owner, contractor, robotics engineer, etc..) is insufficient.

In view of this, we, the authors, formed a team in collaboration with project owners, civil engineers, engineers of construction machinery manufacturers, and robotics researchers, and others. Then, with them, we attempted to formulate (1) a "automation system diagram for earthmoving work" to systematize the entire earthmoving construction, and (2) "automation levels for earthmoving machinery" to grasp the achievement of current technologies. It is anticipated that these will make it possible to give concrete shape to research aims and plans, and that automation research will proceed as a result.

This paper presents one such proposal that we studied toward this end.

2 Study of a vision and an automation system diagram for earthmoving work

Earthmoving work involves various types of work, for example embankment work, cutting work, slope work, and soil improvement. earthmoving sites are comprised of the some types of work that are required there. For example, if a site is for road construction, it will be comprised by embankment work, cutting work, culvert work, and pavement work, etc..

Additionally, types of work are largely divided into components termed "construction," "construction planning," and "inspection." "Construction" is the execution of actual work by earthmoving machinery and people; "construction planning" includes the ordering, arrangement, and scheduling of personnel, machinery, and materials; and "inspection" is the task of inspecting daily operations and final products to determine if they meet specifications.

Furthermore, there are elements that comprise each of the components of "construction," "construction planning," and "inspection." For example, "construction" in embankment work that is part of road construction is mainly comprised of the four operations using various types of earthmoving machinery shown in Table 1. In the case of "construction planning", it is comprising elements include "effective arrangement of machinery, workers, materials, etc." "appropriate ordering" and "coordination of various types of machinery". While in the case of "inspection," it is comprising elements include "measurements of layer thickness, as-built form, density, etc." and "pass/fail judgments."

Figure 3 provides an outline of the study detailed above. It is an "automation system diagram for earthmoving work."

We presented "road construction" and "embankment work" as examples for this diagram. However, it is possible to prepare diagrams for various types of work by changing necessary components and elements.

3 Study of automation levels for earthmoving machines

Next, we conducted our study with the goal of proposing "automation levels for earthmoving machines" necessary to grasp the performance of current technologies.

Here, we studied with the following approach, referring to the previous research [12] – [14].

- "Construction" and "construction planning" are considered to be separate. This is because, as mentioned in the previous chapter, they are separate in the system diagram.
- Remote control is not included as an intermediate step to autonomous. This is because, remote operation is the

same as boarding operation, except that only the operation location is different.

Then, we decided to use the levels for motor vehicles, for which similar automation levels already exist, as a reference.

It should be noted that, in order to simplify our study, we narrowed it to the work of "excavating and loading by hydraulic excavator" in embankment work within road construction.

Table 1. Elements of construction (ex. embankment work)

Operations	Image
Excavation and Loading (Hydraulic Excavator)	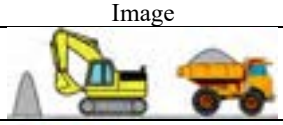
Transportation and Dropping (Dump Truck)	
Spreading (bulldozing) (Bulldozer)	
Compaction (Compactor)	

3.1 Study of levels of driving automation for motor vehicles

The Society of Automotive Engineers (SAE) of the United States has issued a standard for levels of driving automation vehicle called SAE J3016 that has become the international mainstream. On this SAE J3016, the level is divided by whether "(1) vehicle motion control," "(2) object and event detection and response (ODER)," and "(3) dynamic driving task fallback (DDT fallback)" is handled by a person (driver) or by a car (system), and whether "(4) operational design domain (ODD = conditions)" is limited or not (Table.2, [15]).

Using these levels as a reference, we first decided to substitute items (1) to (4) above to achieve compatibility with earthmoving machinery.

3.2 Item substitution

(1) "Vehicle motion control" → "earthmoving machine control"

Here, we focus on earthmoving machine control. In the case of a hydraulic excavator used in embankment work, for example, this refers to commanding the excavator to move, excavate, rotate, drop soil, etc.

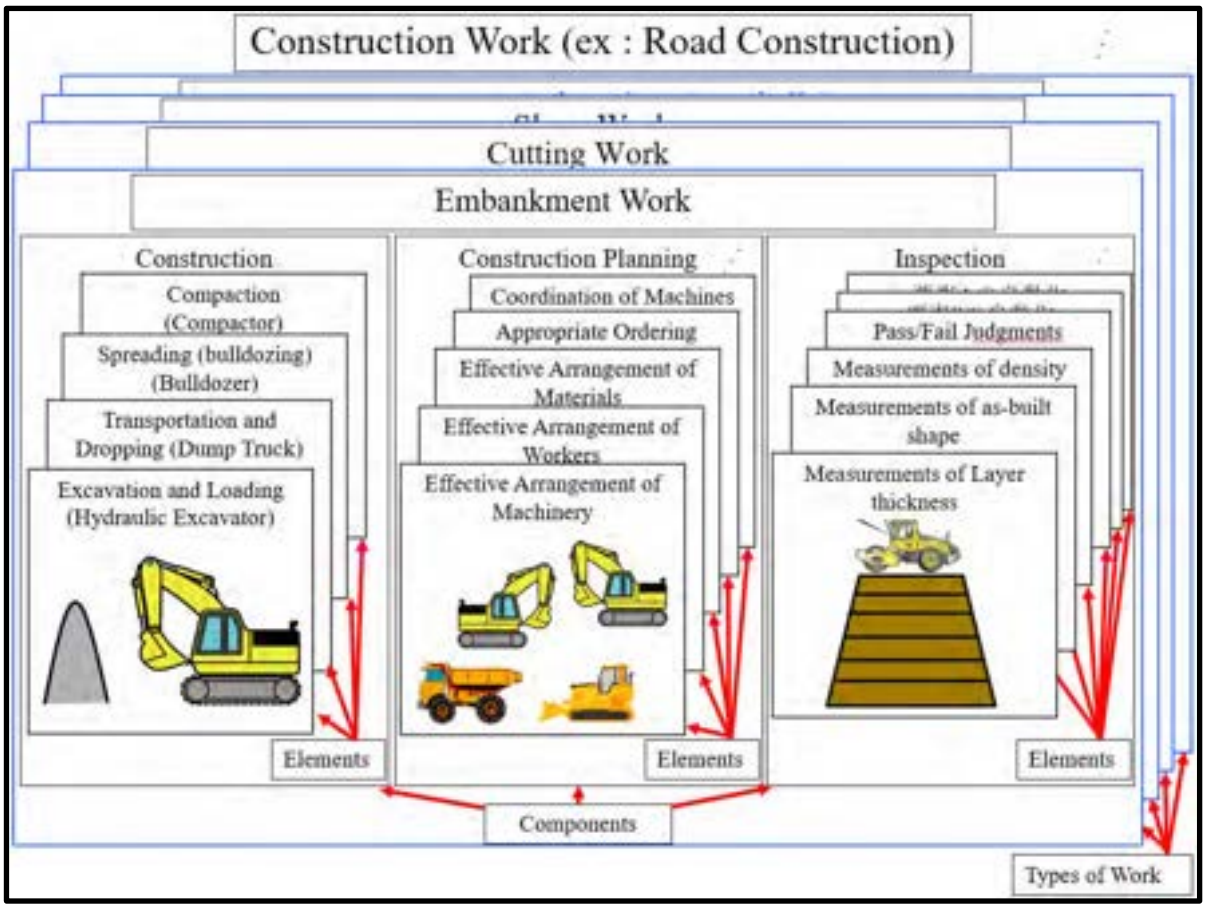

Figure 3. Automation system diagram for earthmoving work

(2) "Object and event detection and response" → "detection and judgment for high-efficiency construction"

This is the conscious (or unconscious) detection of surrounding information and judgment by the operator to improve construction efficiency. For example, in the case of a hydraulic excavator used in embankment work, this refers the detection and decision of optimal machine position, optimal excavation operation, optimal soil drop position, etc., based on conditions around the machine (e.g., locations of other machines, condition of materials).

(3) **"Dynamic driving task fall back" → "Response when autonomous operation is difficult to continue"**

This refers to response to unexpected events that make continuous automated driving difficult. In the case of a hydraulic excavator used in embankment work, for example, such events include obstacles within excavated materials, load spillage from the bucket, obstacles encountered while moving, deviation from course, etc.

(4) **"Operational design domain" → "site condition limitations"**

This refers to whether or not to limit the conditions of the construction site. Examples include topography (e.g., size or slope of worksite, etc.), ground (firmness, surface conditions, etc.), targeted material (type [such as sand or clay], moisture content, etc.), and weather.

Table 2. Levels of Driving Automation [15]

Level	Name	Narrative definition	DDT		DDT fallback	ODD
			Sustained lateral and longitudinal vehicle motion control	OEDR		
Driver performs part or all of the *DDT*						
0	No Driving Automation	The performance by the *driver* of the entire *DDT*, even when enhanced by *active safety systems*	*Driver*	*Driver*	*Driver*	n/a
1	Driver Assistance	The *sustained* and *ODD*-specific execution by a *driving automation system* of either the *lateral* or the *longitudinal vehicle motion control* subtask of the DDT (but not both simultaneously) with the expectation that the *driver* performs the remainder of the *DDT*	*Driver* and *System*	*Driver*	*Driver*	Limited
2	Partial Driving Automation	The *sustained* and *ODD*-specific execution by a *driving automation system* of both the *lateral* and *longitudinal vehicle motion control* subtasks of the *DDT* with the expectation that the *driver* completes the *OEDR* subtask and *supervises* the *driving automation system*	**System**	*Driver*	*Driver*	Limited
ADS ("*System*") performs the entire *DDT* (while engaged)						
3	Conditional Driving Automation	The *sustained* and *ODD*-specific performance by an *ADS* of the entire DDT with the expectation that the *DDT fallback-ready user* is *receptive* to *ADS*-issued *requests to intervene*, as well as to *DDT performance-relevant system failures* in other *vehicle* systems, and will respond appropriately	*System*	**System**	*Fallback-ready user (becomes the driver during fallback)*	Limited
4	High Driving Automation	The *sustained* and *ODD*-specific performance by an *ADS* of the entire *DDT* and *DDT fallback* without any expectation that a *user* will respond to a *request to intervene*	*System*	*System*	**System**	Limited
5	Full Driving Automation	The *sustained* and unconditional (i.e., not *ODD*-specific) performance by an *ADS* of the entire *DDT* and *DDT fallback* without any expectation that a *user* will respond to a *request to intervene*	*System*	*System*	*System*	**Unlimited**

DDT : DYNAMIC DRIVING TASK
ODER : OBJECT AND EVENT DETECTION AND RESPONSE
ODD : OPERATIONAL DESIGN DOMAIN

3.3 Study of automation levels

Table.3 shows the results of our study of automation levels for the work of "excavating and loading by hydraulic excavator" based on the items presented in the previous section are shown.

In this levels, we focused solely on the element of "excavating and loading by hydraulic excavator." However, it is possible to propose automation levels for other element and other machines by changing the details of the work, the specifics of problems, limiting conditions, and other factors.

It should be noted that remote operation is not considered in these levels, as mentioned above. Although the operator will get off the earthmoving machine at one of the levels, we decided not to specify that level. In other words, the operator can engage in either onboard operation or remote operation at levels 1 to 5. SAE J3016 is the same in this regard.

4 Conclusion

In this study, we discussed with many category researchers, project owners, civil engineers, engineers of construction machinery manufacturers, and robotics researchers, and others. And through this study, we successfully proposed draft versions of an "automation system diagram for earthmoving work (Figure 3)" and "automation levels for earthmoving machines (Table 3)." We believe that referencing these outcomes will make it possible for all researchers to understand the scope that the current research occupies in the entire earthmoving work and the degree of achievement of the research. And it will be possible to clarify the research goal to be carried out next.

For example, based on the outcomes of this paper, "Autonomous Hydraulic Excavator", which is researched recently [10][11], are autonomous research only for a "Hydraulic Excavator" element in "construction" component (Figure 3). And it corresponds to "automation level 1 (Table 3)". Thus, as future research and development policies, it is possible to propose an advancing the automation level or an automatization other elements or components (Figure 4). It can be expected that this will effectively promote further advancements in earthmoving automation research.

Additionally, no single correct definitions exist for the diagram and levels mentioned here, and interpretations will vary depending on the viewpoint. It is therefore inappropriate

Table 3. Levels of Automation for Construction Machines

Level	Name / Definition Example：Hydraulic shovel in embankment work 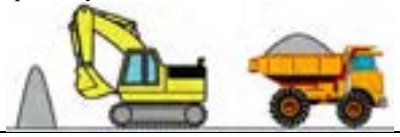	Construction Machine Control	Detection and Judgment for High-efficiency Construction	Response when Autonomous Operation is Difficult to Continue	Site condition limitations
0	No automation	Human Operator	Human Operator	Human Operator	Limited
1	Automation of individual behavior Automation of locomotion / excavation / turning / releasing (Automation of each operation can be individual) Excavation position, bucket point, release point, each optimal operation, completion judgment, etc. can be instructed by a human operator.	Human Operator and System	Human Operator	Human Operator	Limited
2	Automation of series operation Automation of series operation. Move→Excavate→Turn→Release Excavation position, bucket point, release point, each optimal operation, completion judgment, etc. can be instructed by a human operator.	System	Human Operator	Human Operator	Limited
3	Automation of detection and judgment for high efficiency work The system determines and executes the optimum excavation position, optimum bucket point, optimum release point, optimum operations, completion judgment, etc. for high efficiency construction.	System	System	Human Operator	Limited
4	Trouble shooting Example : Load collapse, sudden obstacle, etc.	System	System	System	Limited
5	Open the limited scenario	System	System	System	Unlimited

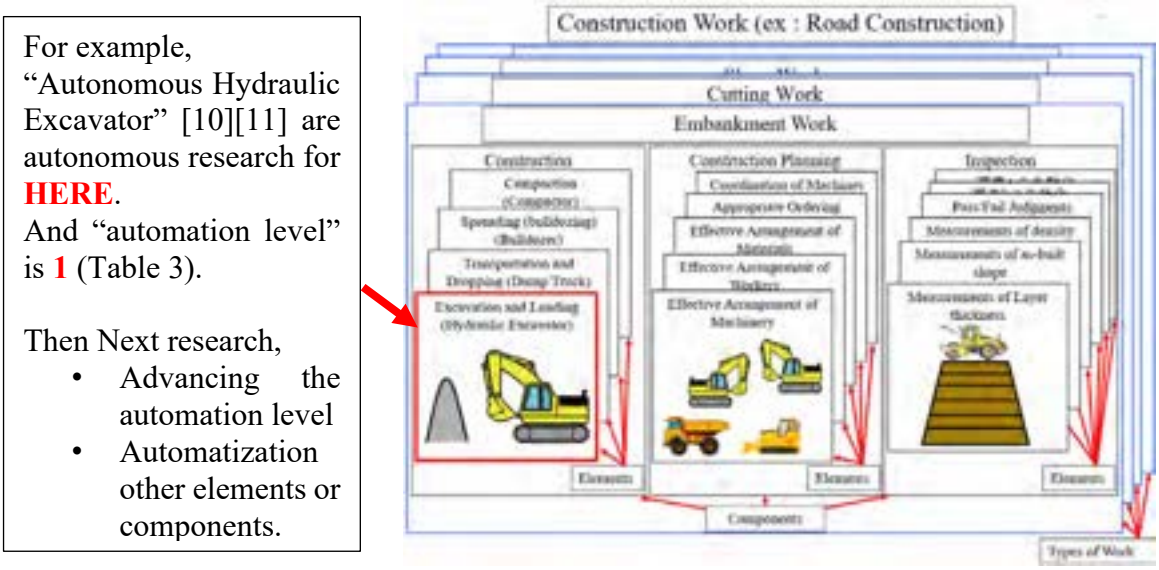

Figure 4. An example of understanding the position and level of current technology and setting the next goal

to immediately view them as universal standards. However, we believe that concretely conceptualizing the performance of current technologies and R&D aims by illustrating proposals and stimulating discussion by presenting studied processes are extremely meaningful endeavors. We would like to see the outcomes described herein be at the forefront of discussions among researchers.

We hope that the outcomes presented in this paper will be of assistance to researchers and engineer who aim to autonomous earthmoving construction.

References

[1] Japan Federation of Construction Contractors. Handbook of Construction Industry 2018. p.18, 2018.

[2] Japan Federation of Construction Contractors. Handbook of Construction Industry 2015. p.19, 2015.

[3] Takeshi Hashimoto, Kenichi Fujino: Comparative Study of Experienced and Inexperienced Operators of Construction Machine, ISARC2019, pp658-664, 2019.

[4] E. Halbach, A. Kolu, and R. Ghabcheloo: Automated Pile Transfer Work Cycles with a Robotic Wheel Loader, 17th International Conference on Computing in Civil and Building Engineering, 2018.

[5] S. Dadhich, U. Bodin, and U. Andersson: Key challenges in automation of earth-moving machines, Automation in Construction, vol. 68, pp. 212–222, 2016.

[6] T. Makkonen, K. Nevala, and R. Heikkilä: A 3D model based control of an excavator, Automation in Construction, vol. 15, no. 5, pp. 571–577, 2006.

[7] A. Stentz, J. Bares, S. Singh, and P. Rowe: A robotic excavator for autonomous truck loading, Autonomous Robots, vol. 7, no. 2, pp. 175–186, 1999.

[8] TOPCON. Machine control system. On-line: https://www.topcon.co.jp/en/positioning/products/product/mc/ , Accessed: 26/05/2020.

[9] KAJIMA Corporation: KAJIMA A4CSEL, Kajima Integrated Report 2019, p41, 2020.

[10] Taisei Corporation. Autonomous Hydraulic Excavator. On-line: https://www.taisei.co.jp/about_us/wn/2019/190426_4636.html , Accessed: 26/05/2020.

[11] Obayashi Corporation. Autonomous Hydraulic Excavator. On-line: https://www.obayashi.co.jp/news/detail/news20190718_1.html , Accessed: 26/05/2020.

[12] R. Heikkilä, T. Makkonen, I. Niskanen, M. Immonen, M. Hiltunen, T. Kollo, and P. Tyni: Development of an Earthmoving Machinery Autonomous Excavator Development Platform, 36th International Symposium on Automation and Robotics in Construction, 2019.

[13] E. Azar, V. Kamat: Earthmoving equipment automation: a review of technical advances and future outlook, Journal of Information Technology in Construction, vol.22, pp. 247–265, 2016.

[14] S. Kim, J. Russell: Framework for an intelligent earthwork system Part I. System architecture, Automation in Construction, vol. 12, pp. 1–13, 2003.

[15] SAE International: Taxonomy and Definitions for Terms Related to Driving Automation Systems for On-Road Motor Vehicles J3016_201806, p.19, 2018.

Applications of LiDAR for Productivity Improvement on Construction Projects: Case Studies from Active Sites

F.A. Westling[a], R. Abbas[a], C. Skinner[a], M. Hanus-Smith[a], A. Harris[a] and N. Kirchner[b]

[a]Engineering Excellence Group, Laing O'Rourke, Australia
[b]Presien, Australia
E-mail: fwestling@laingorourke.com.au, rabbas@laingorourke.com.au, cskinner@laingorourke.com.au

Abstract -

The McKinsey Global Institute's digitisation index ranks construction amongst the least digitised sectors globally. This translates to a relatively slow rate of labour-productivity growth which, according to McKinsey, costs the global economy US$1.6 trillion per year. One area ripe for improvement is validation of final components on construction sites. This is a critical step in the quality assurance process, but also one that consumes significant resources when performed manually. Digitisation, using reality capture technology, can enable rapid component analysis through automation. However, traditional survey tools, which focus on individual points or fixed locations, tend to provide limited coverage, are difficult to operate and hard to interpret. More recently, developments in Light Detection and Ranging (LiDAR) has enabled rapid digital representation of geometry. The resulting point clouds can then be processed using modern computing techniques, including the proprietary BuiltView platform used here, to perform automatic checks that are faster and more accurate than manual measurement and achieve greater coverage than traditional surveying technologies. As the technology develops to become cheaper and more readily available, potential on-site applications should be fully explored. To improve the understanding of options, applications and productivity benefits, we present case studies performed on active construction sites in which an aspect of the built environment was scanned with LiDAR and the data analysed to estimate value accretion for the builder. In floor flatness analysis and site visualisation we demonstrate results that are prohibitively difficult to perform manually. In LiDAR-based precast scanning and formwork analysis we show promise for detecting defects before they cause delays and costs further down the value chain. We present the context and methodology for each case study, along with the benefits and difficulties encountered with LiDAR use. Finally, we calculate the approximate value added compared with traditional approaches to quantify the relative merit of point cloud data. Findings from our case studies suggest LiDAR has the potential to significantly improve construction productivity, quality of works, documentation and client engagement.

Keywords -

LiDAR; Construction; Productivity; Case studies

1 Introduction

Due to a variety of factors including underinvestment in digitisation and innovation, the construction industry is losing $1.6 trillion globally each year [1]. As project and site complexities increase, the industry can leverage technological advancements to increase productivity through automation and quality improvements. In this study, we focus on one such technology - Light Detection and Ranging, or LiDAR - and investigate its potential for adoption through the BuiltView platform to complete a variety of tasks on active sites. LiDAR, like that shown in Figure 1 is commonly used by surveyors to take accurate measurements of spaces, particularly where traditional manual measurement is prohibitively difficult or slow.

Figure 1. Survey grade tripod LiDAR scanning piles during excavation works.

Here we present case studies of five applications of LiDAR that were conducted to address issues site engineers were facing during a particular phase of construction, with a high-level overview of the technical approach taken in each case.

Our main objective for each case study is to estimate the potential for productivity, financial o r r isk management improvements provided by the LiDAR application.

2 Background

The construction industry is worth roughly US$10 trillion (2017), accounting for roughly 13% of world GDP. According to the McKinsey Global Institute [1], this number could grow by US$1.6 trillion if productivity enhancements, such as digitisation and advanced automation, were more widespread. These productivity improvements can come from a variety of sources, including additive manufacturing [2], increase prefabrication [3], or by automating progress monitoring [4, 5] inspection [6] or as-built modelling [7], to name a few.

One of the major issues facing construction is the cost of rework, defined as "activities in the field that have to be done more than once, or activities which remove work previously installed as part of the project" [8]. A 6-year study of nearly 20,000 rework events across 346 projects concluded that the mean yearly profit reduction was 28%[9]. As much as 52% of total cost growth is due to rework, which also increases schedule overrun by 22%[10, 8]. As such, any preventative methods to reduce rework, for instance by increasing quality checks [11, 12, 13], have the potential to drive considerable productivity improvements.

Technological advancements in laser scanning using Light Detection and Ranging (LiDAR) have enabled several notable high-accuracy inspection processes with the potential for automation, primarily focused on 3D model reconstruction and geometric quality inspection [12]. LiDAR produces an output commonly referred to as a "point cloud", which is a collection of thousands to millions of positions in 3D space representing solid matter and derived from high accuracy distance measurements from the sensor. A lot of work has gone into converting these point clouds into Building Information Models (BIMs) which are more common in the industry and easier to work with. This can take the form of generating as-built models of site [14, 15] or precast units [7], quickly generating models of existing structures for heritage, renovation or integration purposes [16], or updating progress through comparison with 4D BIM [4].

Another common use for point clouds is high-fidelity quality inspection. In some cases, this involves directly measuring particular built elements like railway power lines [6] or concrete rebar positions [13]. Another case is floor flatness measurement, typically performed using manual straightedge methods which can be automated with tripod-based LiDAR or aerial scanning [17]. Laser scanning is capable of great accuracy, with some scanners detecting 1mm flatness defects from 20m away [18].

Recent advances in algorithm development have enabled a trend towards mobile LiDAR, which enables rapid surveying, whether handheld [16, 14], vehicle-mounted [6] or aerial [19, 20]. With handheld LiDAR, for example, a single operator can scan entire floors of buildings in a few minutes using a backpack-sized device. Similar scanning using static (tripod mounted) equipment can take hours. The downside however, is mobile LiDAR lacks the accuracy of static sensors. The need for programmatic stitching, and a proclivity towards cheaper laser scanners, means handheld sensors typically achieve 5-30mm accuracy, depending on the object being scanned [14]. Despite this impediment, mobile LiDAR has several site applications due to its ease of use. For example, colourised mobile LiDAR enables rapid detailed capture of site conditions which can be used for communication or documentation purposes [21].

Our study employed a combination of mobile and static LiDAR, while also varying static LiDAR between high density (1M points per scan) and low density (1K points per scan) capture.

2.1 Sites

This study was undertaken on a number of active construction sites operated by Laing O'Rourke in various stages of development which have different contexts and priorities.

Project 1 was a newly developed Health Precinct consisting of an 8-story building. The building comprised mainly teaching and learning areas including lecture theatres, labs, hospital simulation studios, X-Ray and CT rooms and other work spaces.

Project 2 was a 10 story building composed mainly of engineering laboratories. This was further complicated by revitalisation and integration with an existing engineering building which was still largely operational for classes and research.

Project 3, located in Western Australia's Pilbara region, required replacement of 7 active railway bridges with precast concrete culverts. The project complexities included high desert temperatures over 40°C and short time windows to replace each bridge to ensure the rail line remained operational.

Finally, Project 4 was not a construction site but rather a Design for Manufacture and Assembly (DfMA) facility in London, England, operated by Laing O'Rourke which produces high-volume and bespoke components for sites around the country. For quality assurance purposes, laser scanning is used to validate precast components and formwork. However, technical constraints limit the rate at which such analyses can be performed, so automation can add significant value.

3 Methodology

In this section we provide an overview of our five case studies, the data capture and method used, and processed data visualisations.

Throughout these case studies, we utilise the BuiltView platform for data capture and processing. BuiltView is a software platform developed in house which comprises robust data handling methods and innovative point cloud handling tools. The technical details of this platform are out of scope for this report.

3.1 Precast verification

As described in Section 2.1, Project 3 involved assembling a railway bridge using large precast concrete culverts. Due to the site conditions and time constraints, there was interest in verification of the culverts before attempting assembly. Of particular interest were any twists in the uprights which would affect the fit of adjoining culverts.

To enable the analysis, site engineers scanned two precast culverts using static LiDAR, compiling scans from multiple directions into one point cloud shown in Figure 2. The point clouds were then split into individual culverts and registered to their respective design models by performing optimised alignment using the Iterative Closest Point (ICP) algorithm.

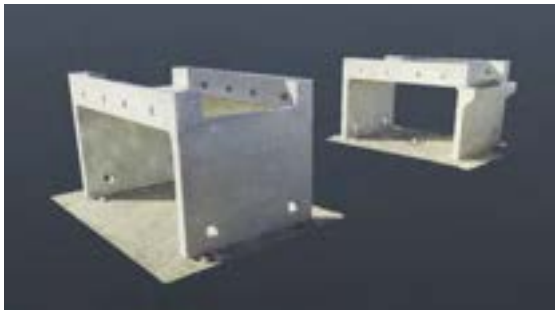

Figure 2. Point cloud scans of precast culverts at Project 3. The culverts are approximately 4m tall.

After the scan was aligned with the design model, a pointwise distance metric was computed by finding the distance between each point in the scan and the nearest point on the model. This metric allowed identification of specific points that were significantly deviated from design, in addition to geometric differences like scale and twist. For improved understanding, we displayed this information as a heatmap by projecting the distance metric of each point on a colour scale from blue to red.

3.2 Floor flatness

At Project 1, site engineers requested an analysis of floor flatness on several levels of the building. Due to changeover of subcontractors, a short timeframe was required, as any defects discovered after several weeks would cause program delays. Consequently, manual checking was infeasible, and LiDAR was trialled as a potential solution.

In previous collaborations with Project 1, we found static LiDAR scanning prohibitively slow. This was primarily due to increased processing (registration) time, caused by internal walls that limited the visibility from individual locations. Knowing this, we opted to use a handheld mobile LiDAR for this capture - a Paracosm PX-80, shown in Figure 3 - that enabled rapid scanning of the building.

(a) Scanning

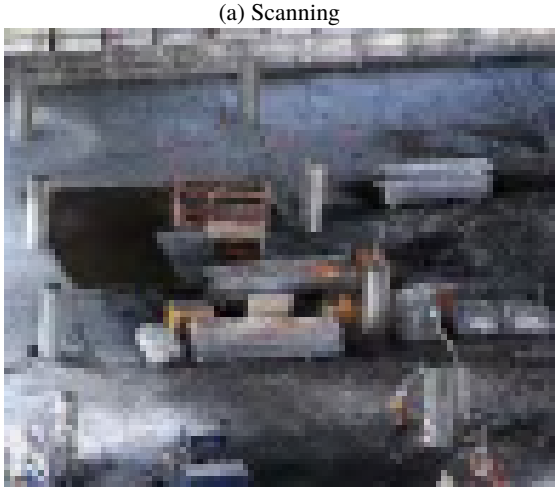

(b) Raw scan output

Figure 3. Capture process and output from Paracosm PX-80 handheld LiDAR scan.

When processing the data, we considered registering the point cloud to the BIM to compare points with their exact location on the ground plane. However, this approach would demonstrate global deviation (the entire slab being slightly too low or high), when the desired insight for flooring compliance was relative deviation. Therefore, we extracted the points representing the ground from the raw point cloud data and computed a best-fit p lane. We then computed the point-to-plane distance from each point to this best fit plane and displayed this data using a heat map

visualisation.

3.3 Formwork

Prevention is always preferable to reparation on site, as rework is costly in both time and money. With this being the case, we investigated the possibility of validating concrete pours at the formwork stage rather than after the pour as in the other case studies. Also taking place on

(a) Scanner on site

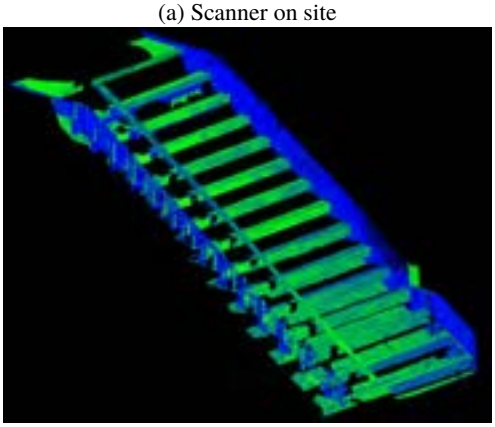

(b) A section of the point cloud scan

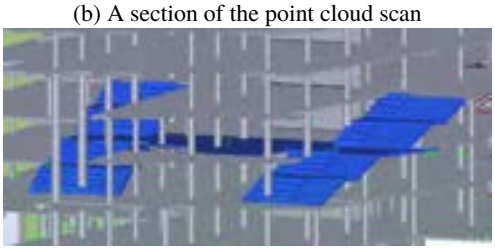

(c) Building Information Model

Figure 4. Context of staircase formwork at Project 1. Four sensor locations captured using a Leica BLK360 were registered to generate a scan which was then compared to the BIM shown.

Project 1, this case related to a set of multilevel staircases undergoing rework due to an error in the original design. Due to this context, we had an opportunity to scan the formwork of the stairs before the pour, and compare it to a correct BIM as well as an incorrect BIM to investigate preventative analysis.

We scanned the formwork using a Leica BLK360 static LiDAR as shown in Figure 4. Since a static LiDAR was used, occlusion was a significant concern so we scanned the formwork at several positions along the staircase and then registered the scans using common points. We then aligned the completed scan to the BIM, using the inner faces of the formwork to align to the outer faces of the concrete model. This process was repeated for the correct and incorrect model, at which point computing the shortest distance metric allowed us to analyse the formwork scan to determine if it was correctly built.

3.4 Reinforcement scanning

Correct placement of rebar in concrete is critical to the long-term survival of the construction project. Inspecting the size, number and spacing of rebar can be difficult and time-consuming. Enabling easier inspections is of particular interest at Project 4's manufacturing facility, where components are prepared for use on construction sites. Furthermore, there is value and interest in having detailed information about the internal structure of a slab for future works including penetrations and proof of completion to specifications in the case of disputes.

Figure 5. LiDAR scan of rebar at Project 4

By scanning the reinforcement before the concrete is poured, the structure can be inspected digitally using the point cloud and future works can be performed using a 3D map of the internal structure of the component. Rebar is difficult to scan with LiDAR due to the reflective properties of the steel, so the scanner used by Project 4 is a low-density high-accuracy scanner which captures point clouds in the order of thousands of points rather than millions. An example of this scan is shown in Figure 5.

Our primary aims in this case were identifying bars by diameter and detecting relative spacing between bars. To achieve both aims, we perform cylinder fitting on the point clouds. This generates a collection of 3D shapes from which the diameter and spacing can be derived.

3.5 Visualisation and Documentation

Documentation and communication between parties involved can be difficult, particularly between agents in different industries. Project 4 faced challenges in this domain communicating a planning error with the client relating to shared access to a teaching lab which was intended to be used while construction was being undertaken. The issue faced was caused by a design element whose size dictated an overlap into the teaching space which would cause logistical issues, but communicating and proving this using 2D resources proved difficult. By using LiDAR to capture the contested space in 3D, dimensions and clashes could be made more visible and easier to communicate.

Again, we used the Leica BLK360 static LiDAR to create a highly detailed colourised scan of the space. Use of this LiDAR also allowed capture of panoramic photography during scanning which could also be used for visualisation. Due to the cluttered nature of the scene caused by internal walls and furniture, many scans were required to generate a clear and complete scan of the area. All individual scans were then registered together using shared points and vision targets to create a cohesive scan, which was then further registered to the building model to allow the scan and model to be overlaid to demonstrate any clashes.

4 Results

4.1 Precast verification

We validated precast components on Project 3 using nearest-point heatmap analysis, comparing the point cloud scans as built to the design model. An example of the result for this analysis is shown in Figure 6.

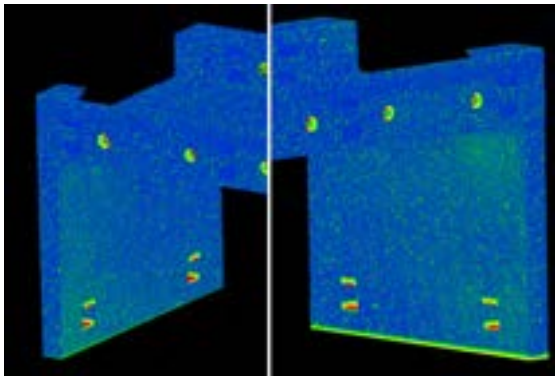

Figure 6. Heatmap analysis of Project 3's precast culverts. Colour scale represents distance from each point to the design model, from blue at 0mm to red at 100mm.

In general, the distances measured are blue, implying little difference between the scan and the model. However, the green gradients towards particular corners of the culvert imply a subtle twist in the uprights which are designed to be planar, which was a very useful insight for the site team as it is a difficult thing to measure manually but could cause gaps between installed culverts which could have flow-on effects. The other features of note were the interfacing holes at the bottom of the uprights. The red points around these reveal that they are not in the correct location, rather they are approximately 11cm out of place vertically.

There is good potential here for process improvements here, specifically in the area of risk mitigation. The LiDAR scan can analyse the entire culvert at once, and potential catch geometrical deformations that a human inspector would not notice. Project 3 required many of these culverts to be cast, so early detection of any issues would prevent inordinate amounts of rework.

4.2 Floor flatness

Our results for floor flatness analysis are similarly presented in heatmap form, though the distances in this case are computed as normal distance to an artificial plane. The results for one floor are shown in Figure 7. Around the starting position of the scan, circular "ridges" in the point cloud can be seen which likely are artefacts caused by the initialisation procedure of the mobile sensor and can be safely ignored. The rest of the scan shows minor variations in the height of the floor, where green points are level with the computed best-fit plane, blue points are lower and red points are higher. The pattern of points shows areas which are of concern, in particular near the edges of the scan where some areas demonstrate a rapid shift from green to red. Besides gradient changes, the other area of interest is local inconsistencies which could cause problems for flooring, and small red and blue areas can be seen in the scan which also merit manual inspection.

Another consideration here is that the operator was able to scan 5 floors in only a few hours, despite significant internal occlusions.

As mentioned, the floor flatness inspection at Project 1 took place before a changeover of subcontractors. Typically, the surveyors used have a turnaround time of approximately 2 weeks, which would delay the identification of faults until after the relevant workforce had vacated the site. These sorts of delays to rectification works can easily cause cost increases of 5 to 10 times, due to the additional logistics of bringing back subcontractors to perform the works. Rapid detection of issues would enable the project to keep the relevant workforce in place and siginificantly reduce the cost of rectification.

4.3 Formwork

Analysis of the Project 1 formwork is a slightly different case, since the object of interest is the concrete

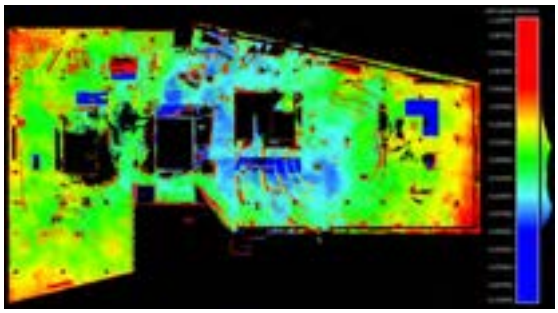

Figure 7. Point-to-plane distance heatmap analysis for the floor slab of a single level of Project 1.

pour which does not yet exist, so the analysis has to be of the shapes surrounding it. As mentioned earlier, we performed a heatmap analysis after aligning the inner faces of the formwork structure with the outer faces of the correct and incorrect building models, then compared the results. This comparison can be seen in Figure 8.

The result for the incorrect model demonstrates some notable characteristics. Several steps are mostly blue and green, representing the part of the scan which has aligned best to the model. However, further along the scan the shortest distances get higher, with significantly more orange and red points visible.

The result for the correct model, however, is far more uniform, with most steps an even blend of blue and green. In this context, the green points represent the sections of formwork which are not close to the final concrete product, while the blue points represent the faces which will directly contact the concrete.

Comparing the two, it is easy to distinguish a correct model from an incorrect model when measured against the as-built formwork, implying the possibility of a method to assess the correctness of formwork prior to the pour and enabling pre-emptive rectification works.

This could potentially reduce costly rework. In particular, this case involved a demolishing and reconstructing a four-story concrete staircase due to design errors. The rework required to complete this took several weeks, increasing both budget and schedule blowout. Through formwork assessment, many situations like this can be avoided.

4.4 Reinforcement scanning

Due to the difficulty in scanning steel rebar and the low-density scanner used, the cylinder fitting must be able to distinguish between individual bars in the point cloud. Figure 9 shows a section of the rebar scan with each point assigned a unique colour according to the cylinder to which it was fit.

The resulting colours demonstrate that the analysis is able to correctly distinguish between the bars using cylinder fitting. The derived cylinders also have specific geometric properties which can be used to analyse the rebar as needed. Firstly, each cylinder has a diameter, which is important during inspection since certain numbers of bars need to be installed to fulfil design specifications. Furthermore, since the cylinders are roughly parallel, the distance between them can be derived, which is another important consideration for as-built verification.

Errors in reinforcement and a lack of asbuilt information can significantly affect project risk, from increased danger during slab penetrations to short- or long-term deterioration of structural components. At Project 4, one engineer with expensive LiDAR equipment is able to inspect 5-10 elements before casting per day on the manufacturing line, which is approximately 10% of the project throughput. By automating the data processing and limiting manual activities to data capture, this productivity can be easily improved by 2 to 5 times, enabling a much higher coverage rate and significantly reducing risk.

4.5 Visualisation and Documentation

A high-density visualisation of the contested space on Project 2 was completed using colourised LiDAR scans. A snapshot of the results is presented in Figure 10.

The visualisation allowed for better communication with the client since two dimensional plans can be harder to understand for people outside construction, and furthermore the scan is correctly scaled such that the building model can be overlaid to illustrate conflicts. Improvements in communications can have signficant effects on productivity and avoiding rework by ensuring a cohesive understanding of the works to be undertaken. In this case specifically, the improved ability to convey information ensured that the project did not impact, and was not impacted by, client operations in the same space. This avoided damaging relationships with stakeholders as well as preventing rework due to a misunderstanding.

5 Discussion and Future Work

The case studies presented here represented just a few use cases for LiDAR on construction sites. Even with the scanning infrastructure used here, many more applications could be implemented. For example, the floor scans of Project 1 were used for floor flatness analysis, but the data captured also included construction equipment which could be used to infer utilisation, service installations which could update progress, and incomplete elements which could be analysed for impending clashes. The adoption of scanning as a frequent operation in the industry would enable more value-add propositions in this vein, though several considerations are involved.

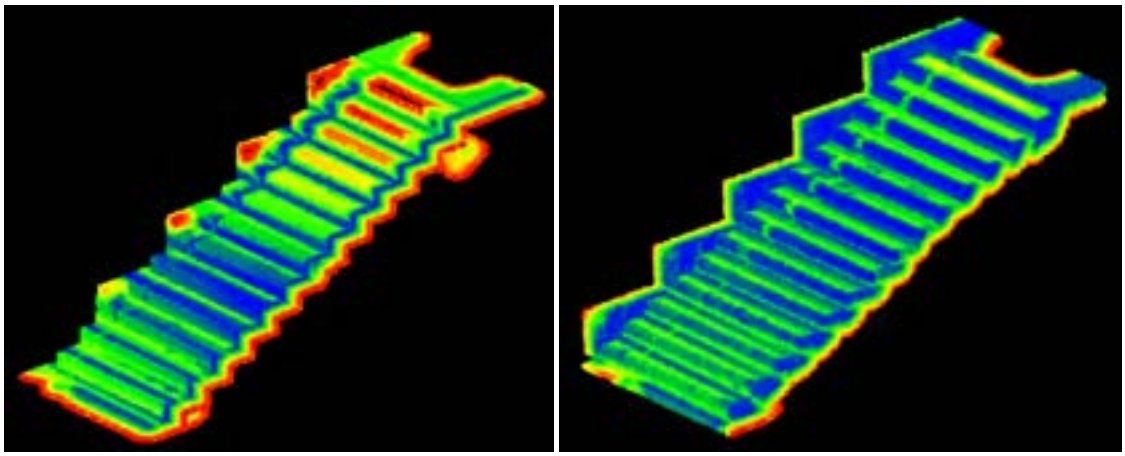

(a) Incorrect BIM (b) Correct BIM

Figure 8. Heatmaps for the same point cloud compared to two different versions of the BIM. The first version was revised due to stair spacing and the scanned formwork was built to the specifications of the second.

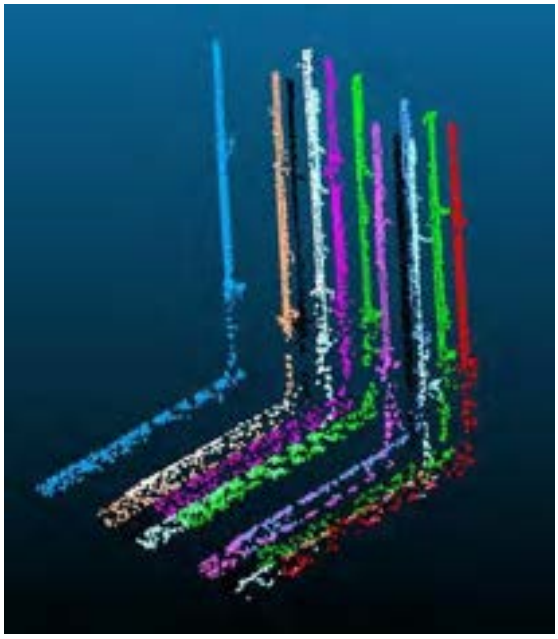

Figure 9. Analysis of rebar using LiDAR scans. Each bar has been identified as separate using cylinder fitting.

Static LiDAR is currently used commonly in surveying but requires significant processing and trained operators. Furthermore, scanning can take a long time when features like internal walls are involved and causing occlusions. The rise of mobile LiDAR enable scanning of large-scale infrastructure projects (using vehicle-mounted scanners), scanning of difficult-to-reach areas (using aerial LiDAR) and rapid scanning for applications requiring frequent updates (using handheld LiDAR). Many handheld sensors are also very simple to use, requiring minimal training or

Figure 10: Snapshot of visualisation of contested space at Project 2

processing time. However, the accuracy of mobile LiDAR is not as good as that of static scanners, due to error introduced by motion. Because of this, the application of the different technologies depends on tolerance requirements and liability. Operations like progress updates, communication and visualisation can easily be performed using mobile scanners, while small-tolerance deviation analysis requires more accurate static ones.

A major advantage of the processes presented here is the potential for significant automation. If sensors can be operated autonomously, as is already the case with certain aerial or robotic scanners[20], certain aspects of processing may also be automated. This can enable high quality inspection and verification works with far less human intervention and allow the industry to operate with more confidence than it currently does with less effort.

There is also a push in the construction industry for greater progressive documentation of the build. Such documentation can be helpful for future works on completed sites, and also reduce difficulties during conflict resolution. LiDAR is a powerful way to capture this data, since the results are relatively simple to collate and analyse and contain high quality measurements of all surfaces. Whereas

traditional point-and-line survey can verify locations of key components, LiDAR measures the entire visible area, so defects or deformations are more likely to be discovered early.

6 Conclusion

In this study we have presented several applications of LiDAR on active construction sites to provide value using relatively simple algorithmic techniques and user-friendly outputs. As the technology develops and becomes more usable and affordable, we hope to see widespread adoption to help the industry close the digitisation and productivity gap which is currently in evidence.

References

[1] Filipe Barbosa, Jonathan Woetzel, Jan Mischke, Maria João Ribeirinho, Mukund Sridhar, Matthew Parsons, Nick Bertram, and Stephanie Brown. Reinventing construction: a route to higher productivity. McKinsey Global Institute, 2017.

[2] Daniel Delgado Camacho, Patricia Clayton, William O'Brien, Raissa Ferron, Maria Juenger, Salvatore Salamone, and Carolyn Seepersad. Applications of additive manufacturing in the construction industry–a prospective review. In ISARC. Proceedings of the International Symposium on Automation and Robotics in Construction, volume 34. IAARC Publications, 2017.

[3] Bon-Gang Hwang, Ming Shan, and Kit-Ying Looi. Key constraints and mitigation strategies for prefabricated prefinished volumetric construction. Journal of Cleaner Production, 183:183–193, 2018.

[4] Nisha Puri and Yelda Turkan. Bridge construction progress monitoring using lidar and 4d design models. Automation in Construction, 109:102961, 2020.

[5] Changmin Kim, Hyojoo Son, and Changwan Kim. Automated construction progress measurement using a 4d building information model and 3d data. Automation in Construction, 31:75–82, 2013.

[6] Ana Sánchez-Rodríguez, Mario Soilán, Manuel Cabaleiro, and Pedro Arias. Automated inspection of railway tunnels' power line using lidar point clouds. Remote Sensing, 11(21):2567, 2019.

[7] Qian Wang, Hoon Sohn, and Jack CP Cheng. Automatic as-built bim creation of precast concrete bridge deck panels using laser scan data. Journal of Computing in Civil Engineering, 32(3):04018011, 2018.

[8] JM Dougherty, N Hughes, and JG Zack Jr. The impact of rework on construction and some practical remedies. In Navigant Construction Forum, 2012.

[9] Peter ED Love, Jim Smith, Fran Ackermann, Zahir Irani, and Pauline Teo. The costs of rework: insights from construction and opportunities for learning. Production Planning & Control, 29(13):1082–1095, 2018.

[10] Nuria Forcada, Marta Gangolells, Miquel Casals, and Marcel Macarulla. Factors affecting rework costs in construction. Journal of Construction Engineering and Management, 143(8):04017032, 2017.

[11] Min-Koo Kim, Qian Wang, Joon-Woo Park, Jack CP Cheng, Hoon Sohn, and Chih-Chen Chang. Automated dimensional quality assurance of full-scale precast concrete elements using laser scanning and bim. Automation in Construction, 72:102–114, 2016.

[12] Qian Wang and Min-Koo Kim. Applications of 3d point cloud data in the construction industry: A fifteen-year review from 2004 to 2018. Advanced Engineering Informatics, 39:306–319, 2019.

[13] Qian Wang, Jack CP Cheng, and Hoon Sohn. Automated estimation of reinforced precast concrete rebar positions using colored laser scan data. Computer-Aided Civil and Infrastructure Engineering, 32(9):787–802, 2017.

[14] Samad ME Sepasgozar, Samsung Lim, and Sara Shirowzhan. Implementation of rapid as-built building information modeling using mobile lidar. In Construction Research Congress 2014: Construction in a Global Network, pages 209–218, 2014.

[15] M Cabaleiro, B Riveiro, P Arias, JC Caamaño, and JA Vilán. Automatic 3d modelling of metal frame connections from lidar data for structural engineering purposes. ISPRS journal of photogrammetry and remote sensing, 96:47–56, 2014.

[16] Dimitrios-Ioannis Psaltakis, Katerina Kalentzi, Athena-Panagiota Mariettaki, and Antonios Antonopoulos. 3d survey of a neoclassical building using a handheld laser scanner as basis for the development of a bim-ready model. In International Conference on Transdisciplinary Multispectral Modeling and Cooperation for the Preservation of Cultural Heritage, pages 119–127. Springer, 2018.

[17] Frédéric Bosché and Emeline Guenet. Automating surface flatness control using terrestrial laser scanning and building information models. Automation in construction, 44:212–226, 2014.

[18] Pingbo Tang, Daniel Huber, and Burcu Akinci. Characterization of laser scanners and algorithms for detecting flatness defects on concrete surfaces. Journal of Computing in Civil Engineering, 25(1):31–42, 2011.

[19] N Puri and Y Turkan. A comparison of tls-based and als-based techniques for concrete floor waviness assessment. In ISARC. Proceedings of the International Symposium on Automation and Robotics in Construction, volume 36, pages 1142–1148. IAARC Publications, 2019.

[20] E Jones, J Sofonia, C Canales, S Hrabar, and F Kendoul. Applications for the hovermap autonomous drone system in underground mining operations. Journal of the Southern African Institute of Mining and Metallurgy, 120(1):49–56, 2020.

[21] Dino Bouchlaghem, Huiping Shang, Jennifer Whyte, and Abdulkadir Ganah. Visualisation in architecture, engineering and construction (aec). Automation in construction, 14(3):287–295, 2005.

Design and Construction of Shell-shaped Bench using a 3D Printer for Construction

Hajime Sakagami [a], Haruna Okawa [a], Masaya Nakamura [a],

Takuya Anabuki [a], Yoshikazu Ishizeki [a], and Tomoya Kaneko [a]

[a] Technical Research Institute, OBAYASHI Corporation
E-mail: sakagami.hajime@obayashi.co.jp, haruna.okawa@obayashi.co.jp, masaya.nakamura@obayashi.co.jp, takuya.anabuki@obayashi.co.jp, yoshikazu.ishizeki@obayashi.co.jp, tomoya.kaneko@obayashi.co.jp

Abstract –

One of the problems in the practical use of 3D printers using cement-based materials is how to withstand the tensile force. In general, cement-based materials can withstand compressive forces. Therefore, reinforced concrete structures are applied as composite structures with steel materials such as reinforcing bars that can withstand tensile force.

In this study, we developed a composite structure, in which the outer part was laminated with mortar exclusively for 3D printers, and the inner part was filled with ultra-high strength fiber-reinforced concrete as a substitute of reinforcing bars. When the test piece was manufactured and its mechanical properties were tested by experiments, it was concluded that the desired strength had been obtained. Then, a large shell-shaped bench, whose outer dimensions comprised a width of 7 m, depth of 5 m, and height of 2.5 m, was manufactured. The design used topology optimization that derived a shape with high structural rationality; the total weight was reduced by approximately 60%. The shape derived by topology optimization would have been difficult to construct with a formwork, and we were able to exploit the advantages of using a 3D printer.

Keywords –

3D Printer; Automation; Laborsaving

1 Introduction

A 3D printer using cement-based materials (hereinafter called "3D printer") ejects special mortar (hereinafter called "3D mortar") from a nozzle attached to a mobile mechanism, such as a robot arm, and laminates the mortar to construct a structure. We have developing a 3D printer, which we refer to as a 3D printer for construction. Since the structures could be constructed automatically without using a formwork, freedom in design and laborsaving ways of construction could be realized.

One of the problems in the practical use of 3D printers is how to withstand the tensile force generated in the structure. In general, cement-based materials can withstand compressive forces. Therefore, reinforced concrete structures are applied as composite structures with steel materials such as reinforcing bars that can withstand tensile force. To solve this problem, the following methods have been devised: a) inserting a steel material such as a reinforcing bar during the 3D printing process [1], b) manufacturing a piece with a hollow using a 3D printer, and inserting a PC steel bar into the hollow to introduce a prestressed force [2], and c) using a cement-based material capable of withstanding the tensile force such as ultra-high strength fiber-reinforced concrete (hereinafter called "UFC") [3].

Therefore, we developed a composite structure in which the outer part was laminated with 3D mortar and the inner part was filled with UFC as a substitute to reinforcing bars. In this study, basic structural experiments were conducted to confirm that an actual structure could be constructed using this composite structure. And, we designed and constructed a large shell-shaped bench with outer dimensions comprised a width of 7 m, depth of 5 m, and height of 2.5 m; this experiment demonstrated the use of the composite structure.

2 Development of Composite Structure

2.1 Composition of Composite Structure

We developed a composite structure by using 3D mortar and UFC. In order to construct the composite structure, first, the outer portion of the structure was laminated with 3D mortar so that the portion that was to be reinforced by a reinforcing bar became hollow. Then, the UFC was placed into the hollow. The filled UFC could withstand the tensile force generated in the structure.

2.2 3D Mortar and UFC

For the 3D mortar, mortar premixed with a hardening accelerator was used, and the hardening speed was adjusted by setting up a retarder. In addition, polyvinyl alcohol (PVA) fiber was mixed to increase the bending strength. It had a compressive strength of 60 N/mm^2 and a bending strength of 3.5 N/mm^2.

UFC [4] is a room-temperature-hardening-type mortar, developed by the Obayashi Corporation that can achieve a compressive strength of 180 N/mm^2, tensile strength of 8.8 N/mm^2, and bending strength of 32.6 N/mm^2. This material has a high tensile strength, bending strength, and tensile toughness; thus it can function as a structure in itself. This slump flow was approximately 600 mm and had a self-filling property. Therefore, the placement work was easy, and the automation and mechanization will be easy as well, compared to the manual arrangement of reinforcing bars.

2.3 Verification of Mechanical Performance

2.3.1 Outline of Experiment

Figure 1 shows the cross section of the test piece. The width and thickness are 500 mm and 120 mm, respectively, and the UFC parts with a width of 50 mm and a thickness of 70 mm, are evenly arranged in five different positions.

Photo 1 shows the manufacturing status of the test piece. First, the 3D mortar was laminated with a 3D printer until the height was 1 m. Next, as shown in Photo 2, the UFC was placed in the hollow. The UFC, which was placed in the hollow, was constructed without being spliced.

A three-point bending test was conducted to confirm the bending properties of the test piece (No. 1) manufactured with the composite structure. For comparison, a bending test was also conducted on a test piece (No. 2), which was not filled with UFC, as shown in the cross-section of Figure 1.

2.3.2 Methods of Loading and Measuring

Photo 3 shows the device loading for the bending test. The left end of the test piece was supported by a pin, the right end was supported by a pin roller, and the distance between the supporting points was 800 mm. In order to maximize the bending moment at the center of the test piece, a hydraulic jack and ball seat were attached to the upper center part of the span, and the load was applied vertically downward. Since the width of the test piece was as large as 500 mm, a vertical load was applied through a beam with a height of 200 mm. The applied force was a monotonic load that was pushed in one direction. The vertical load at the center of the test piece was measured with a load cell. The displacement in the vertical direction at the center of the test piece was

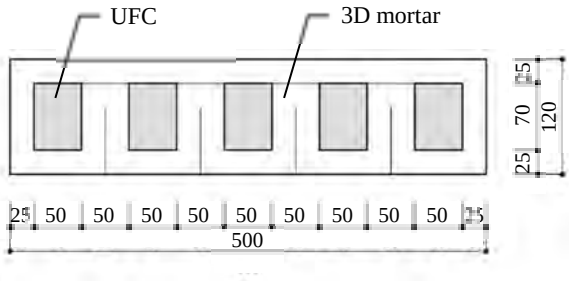

Figure 1. Cross section of the composite structure

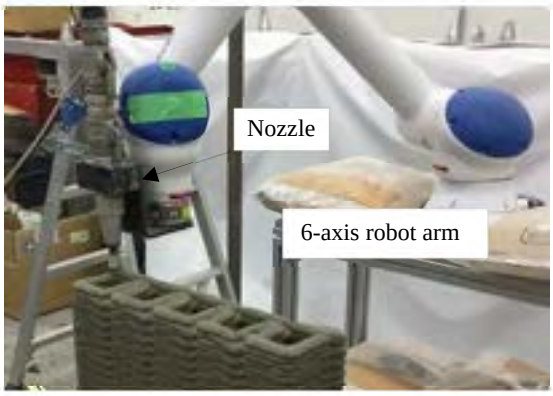

Photo 1. Printing of test piece

Photo 2. Placing UFC

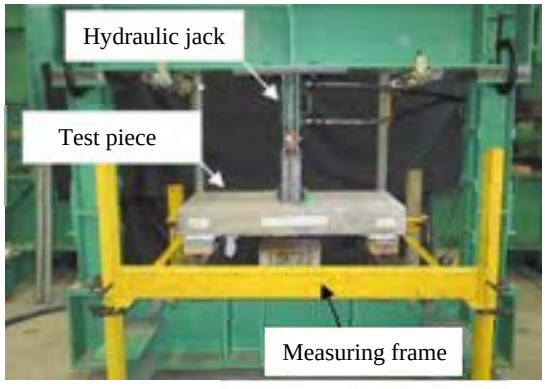

Photo 3. Loading device

measured with a displacement meter, and the downward direction reflected the positive values. The displacement was the average of the values measured at the front and at the back of the test piece.

2.3.3 Result of Experiment

Photos 4 and 5 show the final destruction status. Photo 4 shows the final fracture of No. 1. Photo 5 is an enlarged photograph of the fractured surface of No. 1. In both No. 1 and No. 2, cracks were found near the lower end of the center of the test piece, and finally a fracture surface was formed almost in the center of the test piece. Many steel fibers protruded from the portion of the UFC on the fracture surface of No. 1. It was also confirmed that the hollow was filled with the UFC without any gaps. In both the test pieces, there were no evidences that the mortar at the compression edge had undergone compression failure.

Figure 2 shows the relationship between the vertical load and the center deflection. The maximum load of No. 1 was 47.4 kN. On the other hand, the maximum load of No. 2, which was not filled with the UFC, was 22.5 kN. No. 1 shows a maximum load of more than twice the maximum load of No. 2, because the UFC withstood the tensile force. Moreover, in No. 2, brittle fracture occurred after the maximum load was applied, and the yield strength decreased sharply. However, in No. 1, due to the tensile toughness of the UFC, the yield strength gradually decreased.

From the above, it was found that the developed composite structure improved both the maximum load and the toughness performance, because the UFC was placed in the hollow and could withstand the tensile force.

3 Design of Shell-shaped Bench

3.1 Outline of Design

To verify the practicality of the developed composite structure, the shell-shaped bench, which is shown in Figure. 3, was manufactured. The design included a cantilever shape that produced a large tensile force and incorporated a curved surface that 3D printers were good at.

The outer shape was manufactured by laminating the 3D mortar, but if the entire interior was filled with the UFC, as shown in Figure 4, the weight increased and the structural rationality decreased. Therefore, the internal structure of the shell-shaped bench had a hollow part, as shown in Figure 5, to reduce the weight. Therefore, in order to determine the morphology of the internal structure, we applied topological optimization that gradually removed the stress and derived the optimum morphology by Finite Element Method (FEM) analysis. Figure 6 shows the design flow of the internal structure.

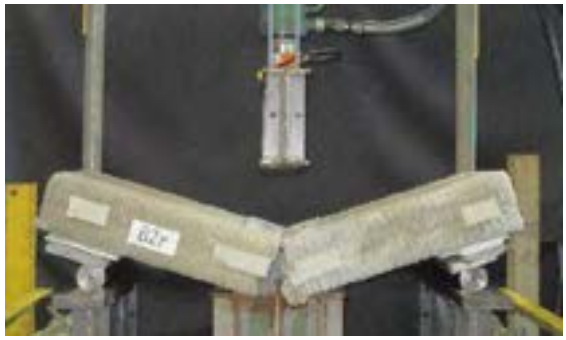

Photo 4. Final fracture (No.1)

Photo 5. Detail of the fracture surface (No.1)

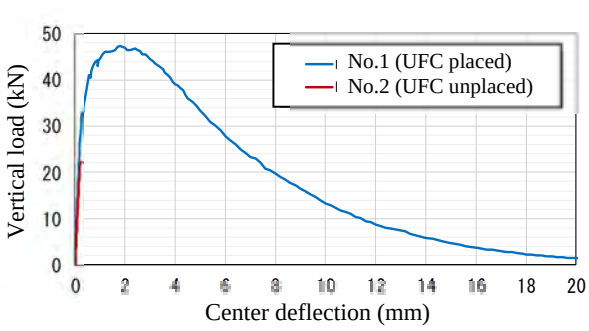

(1) Entirety

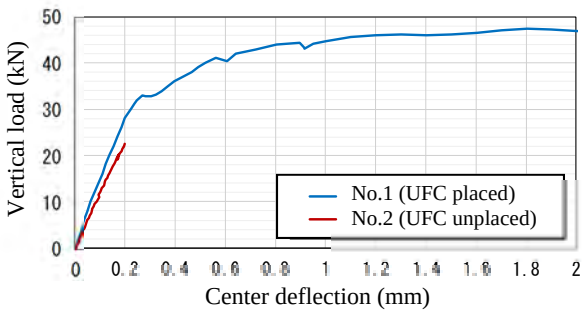

(2) Initial loading

Figure 2. (Relationship between) vertical load and center deflection

Since a 3D printer could manufacture pieces without using the formwork, it was suitable for manufacturing complex shapes that had hollow internal structures derived by topology optimization.

3.2 Topology Optimization

In topology optimization, the ratio of the reduced weight to the initial weight was set as the target value. Then, a form in which the stress was minimized in a range satisfying this target value was derived. The target value for weight reduction was set at 65% of the initial weight. Only the long-term load (self-weight) was used as the load condition in the FEM analysis, and the short-term load (horizontal force) generated during use was not considered. The reason for this is that shell-shaped benches have a cantilever shape and are easily affected by their own weight. As shown in Figure 7, topology optimization was performed by assuming a thin plate with a width of 30 mm in the cross-sectional shape of the center position of each piece obtained by dividing the total bench width of 7 m into 1 m intervals. For fixing the conditions, both the ends of the bottom of each piece were fixed.

Figure 8 shows an example of the result of topology optimization. The result of topology optimization of each piece divided into seven parts was truss-shaped, similar to that shown in Figure 8. The truss-shaped portion derived by topology optimization was made visible as a shell-shaped bench design. Therefore, as a design adjustment, the position of the bundle was adjusted finely so that the positions of the holes could be seen continuously from one end to the other.

3.3 Checking Allowable Stress

Topology optimization does not check whether the stress calculated in the morphology derivation process is within the allowable stress level of the material used. Therefore, the static stress analysis was performed on the design adjusted form, and the allowable stress level was checked. At that time, in addition to the long-term load, the horizontal force (0.2 G) was also considered as a short-term load that was generated during the use. The structural designer manually corrected the cross-sectional shape till the allowable stress level was cleared. Structural experiments have suggested that in the composite structure, 3D mortar and UFC behave as a unit. However, since the mechanism is still unclear, we used a design so that it could be established only for the cross section of the UFC.

3.4 Final Design

Figure 9 shows the final design of the shell-shaped bench. The shell-shaped bench was divided into 12 parts.

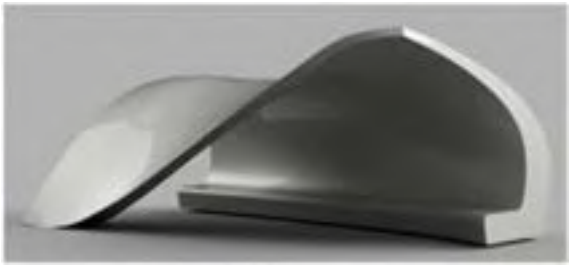

Figure 3. External design of shell-shaped bench

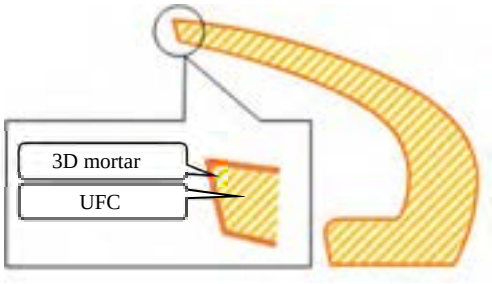

Figure 4. Layout of 3D mortar and UFC (Fully filled)

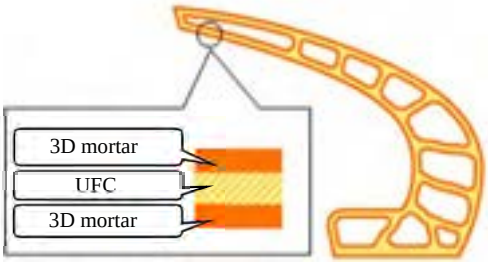

Figure 5. Layout of 3D mortar and UFC (Structurally rational)

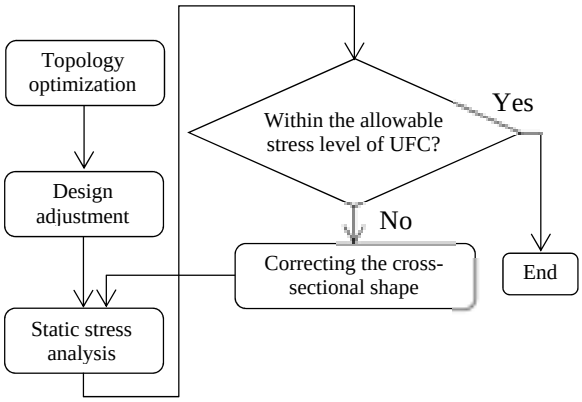

Figure 6. Design flow

The reason for this was that the time required for printing 3D mortar (working time per day) was limited, and transportation and erection after manufacturing became safe and smooth. The divided width of the 12 pieces was 500 mm at both ends and 600 mm at the other parts. Each piece was installed by a crane, with a joint width of 10 mm from the adjacent piece, and then sealed without connecting to the adjacent piece. The final design was approximately 60% lighter than the structure fully filled with the UFC.

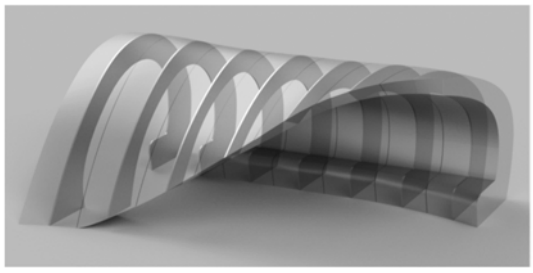

Figure 7. Sections to apply topology optimization

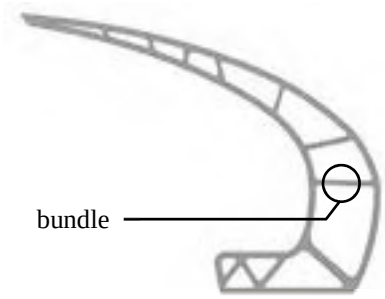

Figure 8. Example of applying topology optimization

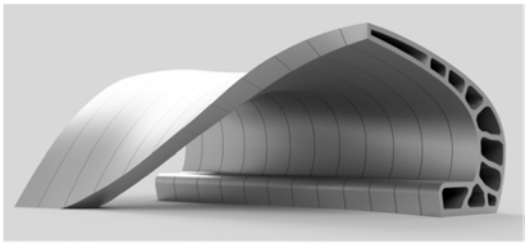

Figure 9. Final design

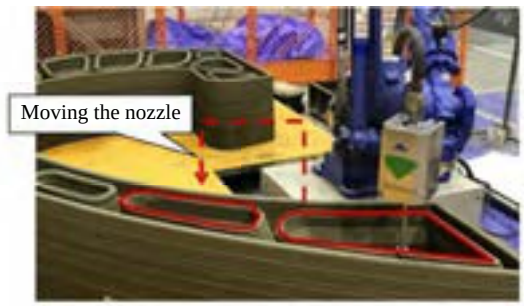

Photo 6. Example of jump in the print path

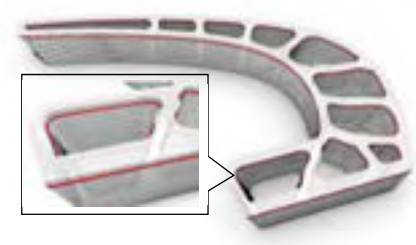

Figure 10. Automatic generation of the print path

4 Development of Elemental Technology for Printing 3D Mortar

4.1 Development of Valve

If the material ejection cannot be stopped in the printing 3D mortar, the print path must be a one-stroke and a non-intersecting path. Since the shell-shaped bench had a hollow, it was necessary to print the outer and the inner peripheries separately. Therefore, as shown in Photo 6, it was necessary to intermittently move the nozzle from the outer periphery to the inner periphery and from the inner periphery to the other inner peripheries. Therefore, we developed a valve that worked with the pump so that the ejection of the mortar could be stopped temporarily.

4.2 Automatic Generation of Print Path

We developed a software that automatically generated print path data from a 3D model. The 3D model was prepared in a format that represented a solid with a triangular mesh called the stereolithography (STL) format. In 3D modeling software, the STL format is a standard output format. Figure 10 shows an example of automatic generation. The 3D model was cut with the laminated thickness of the mortar, and the coordinates of the obtained intersections were classified into "outer periphery" and "inner periphery ". A print path was generated from the classified intersections and converted into a robot language used to control the robot arm.

5 Construction of Shell-shaped Bench

5.1 Outline of Construction

The 3D printer was installed in the building for experiments using concrete. Figure 11 shows the manufacturing process of the shell-shaped bench pieces. Manufacturing is a 5-day process. On the first day, the outer shape of the composite structure was manufactured using a 3D printer. The second day was a curing day and was used for developing the strength of the 3D mortar. The third day was the placement day of the UFC. The

fourth day was also a curing day for developing the strength of the UFC. On the fifth day, the piece was moved from the 3D printer to the installation location.

5.2 State of Construction

5.2.1 Printing 3D Mortar

Photos 7 and 8 show the condition of the printing 3D mortar. The width and thickness of the 3D mortar lamination could be controlled to a designated size by adjusting the ejected amount of the 3D mortar and the moving speed of the nozzle. These were adjusted in advance to obtain a mortar width of 30 mm and a mortar thickness of 5 mm.

The piece was printed, laid down, and was divided into three layers in the direction of the height. The net time required for printing the 3D mortar was approximately 5 h. To lift the piece during construction and connect it to the foundation, a hole with a diameter of 24 mm was drilled, and an insert with an inner diameter of 20 mm was attached before the 3D mortar hardened. After printing the 3D mortar, it was covered with a wet curing mat. Water was sprayed till evening before the day of placing the UFC.

5.2.2 Placing UFC

UFC was placed at once without any jointing, using a concrete bucket with a capacity of 0.3 m^3. Photo 9 shows the UFC condition. The UFC is self-filling. Therefore, the UFC could be placed without any problem even if a 3D printer complicated the shape. In addition, because it has the characteristic of being hardened at room temperature, special curing methods such as heat curing was not required. However, after the placement was completed, a sheet curing was performed, after spraying a surface curing material, in order to prevent the dry shrinkage cracks on the top surface.

5.2.3 Moving Pieces

After the curing day of the UFC, the piece was moved from the 3D printer to the installation location. Lifting was performed under balanced conditions based on the position of the center of gravity calculated from the 3D model of the piece. After moving the piece, the 3D printing yard was cleaned to prepare for the next piece.

5.2.4 Erection and Installation of Pieces

First, the laid-down piece was raised. Gradually the roof side of the piece was lifted with a crane. When the piece was raised, the level was adjusted using the level gauge. Next, the piece was moved to the installation position, as shown in Photo 10. Support was installed to the bottom side of the roof to temporarily receive the piece. Then, the piece was anchored to the foundation with an insert attached to the bottom of the bench seat.

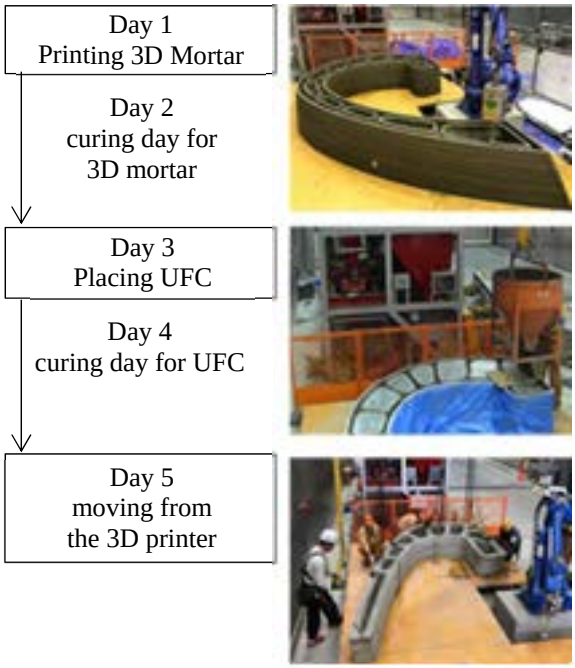

Figure 11. Manufacturing process of shell-shaped bench

Photo 7. Printing of 3D mortar (at the start)

Photo 8. Printing of 3D mortar (at the finish)

This support was removed after the foundation was established.

5.2.5 Finishing Work

A modified silicone sealing material for construction was applied to the joints between the pieces. In order to perform an exposure test on the coating performance on the 3D mortar surface, an aqueous fluororesin-based paint and a weak solvent-type two-component silicone-based paint were applied half by half. Photo 11 shows the completion of the shell-shaped bench.

6 Conclusion

We developed a composite structure in which the outer part was laminated with 3D mortar and the inner part was filled with UFC, as a substitute for reinforcing bars. In this study, basic structural experiments were conducted to confirm that a structure could be actually constructed with this composite structure. In this paper, we have described the design and the construction of a large shell-shaped bench with outer dimensions comprised a width of 7 m, depth of 5 m, and height of 2.5 m, respectively, which were conducted as a demonstration experiment for this composite structure. The findings obtained are as follows:

1. In the developed composite structure, the UFC withstood the tensile force and the maximum load, and toughness performance improved. Using this composite structure, it was possible to manufacture a shell-shaped bench having a complicated shape that generated tensile force.
2. By topology optimization, the overall weight of the shell-shaped bench was reduced by approximately 60%. In addition, the hollow part consisting of curved surfaces, generated by topology optimization, had a shape that was difficult to construct with a formwork, and we were able to exploit the advantages of manufacturing with a 3D printer.
3. Since UFC has a self-filling property, it was possible to place it into a complicated shape manufactured by the 3D printer without any gaps.

Photo 9. Placing UFC

Photo 10. Erection and installation of the pieces

Photo 11. Completion of the shell-shaped bench

Acknowledgments

In this research, we cooperated with Denka Company Limited for the design and the supply of 3D mortar.

References

[1] apis cor. The biggest 3d printed building. On-line: https://www.apis-cor.com/gallary, Accessed:18/8/2020.

[2] bam. A World First: the first fully 3D printed, structurally pre-stressed concrete cycle bridge in the world. On-line: https://www.bam.co.uk/media-centre/news-details/a-world-first-the-first-fully-3d-printed-structurally-pre-stressed-concrete-cycle-bridge-in-the-world, Accessed:18/8/2020.

[3] Nadja G., Romain D., Charles B., Alban M., Philippe R., Mahriz Z., and Justin D. Large-scale 3D printing of ultra-high performance concrete – a new processing route for architects and builders, *Materials and Design*, Vol. 100, pp. 102-109, 2016.

[4] Takayoshi H. "SLIM-CRETE": DEVELOPMENT OF UFC FROM WHICH HIGH STRENGTH IS OBTAINED AT AN EARLY AGE IN NORMAL TEMPERATURE ENVIRONMENT (in Japanese). *CEMENT and CONCRETE*, JAPAN CEMENT ASSOCIATION, Vol.782:24–28, 2012.

Requirements for Safe Operation and Facility Maintenance of Construction Robots

Alexey Bulgakov[a], Thomas Bock[b], Jens Otto[c], Natalia Buzalo[d] and Thomas Linner[b]

[a]Department of Mechatronic, South Russian State Polytechnic University, Russia
[b]Department of Building Realisation and Robotics, Technical University of Munich, Germany
[c]Department of Construction Management, Technical University of Dresden, Germany
[d]Department of Information Management, Chaoyang university of technology, Taiwan
E-mail: agi.bulgakov@mail.ru, thomas.bock@br2.ar.tum.de, jens.otto@tu-dresden.de, n.s.buzalo@mail.ru

Abstract –

Construction robots are devices of increased danger and, under certain conditions, can become a source of injuries to maintenance personnel, as well as lead to the failure of technological equipment. Most of the accidents are associated with the presence of maintenance personnel in the working area during programming, configuration, training, repair and maintenance of robots. The article describes measures to ensure safety during the maintenance of robots and manipulators. The stages of preparing the construction industry for the use of manipulators, robots and robotic complexes are presented. A system of measures for preparing equipment for use and its maintenance during operation is proposed.

Keywords –

Construction Manipulators and Robots; Maintenance of Robotic Systems; Operation; Service; Safety

1 Introduction

Under certain conditions, construction robots can become a source of injuries for maintenance personnel, as well as lead to the failure of technological equipment. The main causes of emergency situations during the operation of robots and robotic complexes are mechanical damage, disruption of the drives, failure of control systems, increased positioning error, programming and tuning errors, exceeding permissible load values, occurrence of super-permissible dynamic modes, loss of the manipulated object, malfunction of safety equipment, violation service personnel operating conditions. Most of the accidents are associated with the presence of maintenance personnel in the working area during programming, tuning, training, repair and maintenance of robots [1-10].

Important in achieving the safe operation of robots and manipulators is their rational installation. Placement of robots and robotic systems (RS) should provide free, convenient and safe access for maintenance personnel to equipment and controls. The layout of the RS should take into account the shape, size and characteristics of the technological equipment, the location of the working areas, the level of automation and the degree of information support. When organizing the RS, it is necessary to have special devices that provide for the safety of staff. Enhancing safety is facilitated by safety enclosures, blocking and signaling devices, as well as the development of an information support system about the state of equipment and the environment. Protection devices must turn off the equipment when a person is in the danger zone of the workspace. The signal can only be taken by an operator who is setting up and maintaining equipment. The safety fence of the working areas of robots should not impede visual control over its work and the associated technological equipment. Safety fence is installed at a distance of at least 0.8 m from the boundaries of the working area of the robot and can be performed not only mechanically, but also on the basis of special devices: contact, power, ultrasonic, capacitive, induction, optical, etc. Automatic and automated lines and sections at enterprises manufacturing construction products should be equipped with emergency shutdown facilities equipment placed along the line with an interval of not more than 4 m.

During the operation of robots in the RS and in conditions of limited space, their working bodies are necessarily equipped with tactile sensors that are triggered by the contact of the working body with an obstacle.

The operation of robots and robotic systems imposes high requirements on the training of staff. Only persons who have undergone special training should be allowed to work on commissioning and operating robots. In addition to safety issues during the training of personnel, the device and features of the work of robots, the

procedure for controlling them, and actions of operators in emergency situations should be considered. Training in practical skills in working with building robots is preferably carried out on special simulators equipped with an automatic training system. Each operator should be given a safety note and instructions for controlling manipulators and robots. The industrial safety service of the construction firm should periodically monitor compliance by personnel with safety requirements, equipment status, and check the serviceability of safety equipment.

It is very important to have a choice of a rational mode of work and rest for staff, as fatigue can become a source of emergency situations caused by wrong actions.

2 Preparation of construction production for the use of manipulators, robots and robotic systems

The installation of robots by the construction projects and plants of the construction industry is preceded by a set of preparatory work, including a number of stages. The economic and social efficiency of robotization depends on the composition, volume, sequence and completeness of the implementation of the complex of works [11-14].

Preparation of building production for the use of manipulators and robots has its own distinctive features, characterized by the specificity of technological processes and the need to use new methodological foundations for their design concept. In addition, the content and scope of preparation of processes at construction sites differs significantly from the preparation of technological processes at construction plants, which are more similar in character to technological processes in mechanical engineering. The process of preparing for the introduction of robots is determined by the character of the re-equipment of production. In the case of capital reconstruction, the construction of new manufacturing divisions and plant floors in the construction industry, the basic technical solutions for process automation should be underprin at the stage of preparation of technical documentation and comprehensively linked to the design and technological features of robotics objects. With the technical re-equipment of individual production lines and plant floors and in the case of robotization of individual operations at existing plants, preparation for the introduction of robotics should begin with an analysis of the process features and the effectiveness of the existing technology, the degree of use of equipment and the identification of tight spots when performing certain operations. A variety of technologies for work on construction sites and technological operations at construction industry plants requires a systematic approach to assessing the volume of implementation of manipulators and robots, choosing the objects of robotization and drawing up a work plan. In preparing the construction industry for the introduction of manipulators, robots and RSs, special attention should be paid to the issues of specialization, typification, unification, conveyorization and improvement of technology. The system of preparation for the robotization of production processes in construction should be based on rational organization, mechanization and automation. When solving robotization issues, it is necessary to achieve the optimal technology option based on the economically feasible choice of equipment, manipulators and robots, devices and tools that provide the necessary level of mechanization and automation of production processes.

In connection with the peculiarities of the introduction of robotics in the construction industry, let us consider in more detail the volume and composition of organizational and technical measures for the preparation of technological processes for the use of manipulators and robots.

At the plants of the construction industry, robotization of technological processes can be carried out both comprehensively on the production line, site, in the workshop, and locally in individual operations. Currently, manipulators and robots are mainly introduced in separate operations with the aim of eliminating tight spots in the process and eliminating monotonous and heavy physical labor. However, due to the large capital costs, this method is ineffective. This greatly inhibits the widespread adoption of robots in the construction industry. It is possible to increase the economic efficiency of using robotics tools only by preparing the conditions for their use in the complex solution of automation and robotization of production lines and plant floors on the basis of improving technology and product design. Therefore, the robotization of technological processes in the construction industry must be carried out on the basis of comprehensive scientifically based plans for technical re-equipment, which provides for a phased transition from the robotics of individual operations to complex automation and robotization of lines and sections. With this approach, individual local control systems of operations are gradually combined into systems for controlling lines, sections, and workshops with simultaneous solutions to the issues of automation and robotization of transport-auxiliary operations. In this regard, the process of introducing robots in the construction industry is preceded by a series of preparation stages associated with the formation of plans for technical re-equipment and reconstruction of production facilities.

In order to prepare a comprehensive production robotics program, which is an integral part of these plans,

the existing production processes (Fig. 1), technologies, equipment, products and transportation relations are

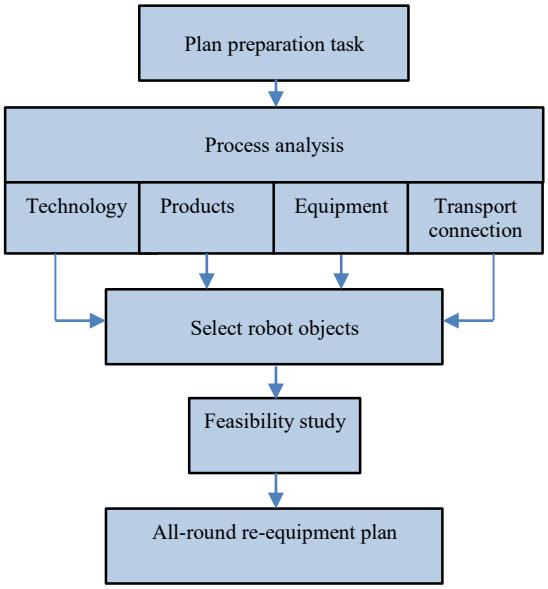

Figure 1. Scheme for a comprehensive plan for the technical re-equipment of production processes in the construction industry

analyzed. Depending on the scope of tasks for the reconstruction of production, it is necessary to analyze the entire production process, as well as its components or individual operations. The analysis reveals all the features of production, unused reserves, bottlenecks, the level of technological and design solutions, the level of mechanization and automation of individual operations, the composition and characteristics of technological equipment, organization methods and means for performing transport and auxiliary operations, transportation and storage of finished products.

As a result of the analysis, ways to improve the production process are developed, recommendations are given for the modernization of technological equipment or its replacement, ways to change the organizational structure and increase the efficiency of the process are outlined, measures are proposed to increase labor productivity, reduce the complexity of operations and employment of workers, improve working conditions.

In the course of a comprehensive assessment of technical, technological, organizational and social factors, proposals are formed for comprehensive mechanization, automation and robotization of production processes. An important stage of this work is the preliminary selection of objects of robotization, the purpose of which is to determine the feasibility of robotization of a particular technological operation. A number of factors are used as evaluation criteria. The use of manipulators and robots in the production process can be aimed at increasing production productivity, improving product quality, improving working conditions for workers, improving labor safety, reducing the complexity of auxiliary and transport operations, ensuring a high degree of equipment load. When introducing robotic means in existing plants, the volumes of redevelopment of production facilities, modernization of installed equipment and additional costs should also be taken into account.

Preliminary selection of robot objects is usually carried out by expert experts. At the stage of preliminary selection, a group of experts determines the significance of factors for a comprehensive assessment of production and, depending on its conditions and the resulting estimates, carries out an adjustment of the composition of factors. Further, each expert gives an assessment of the measure of influence of each factor on the decision in favor of robotization, and an average and relative assessment of the significance of each factor is established. The priority of production robotization is determined by the results of a comprehensive assessment in accordance with the preference rank identified during the expert assessment. Preliminary selection of operations is completed by compiling a list of objects of robotization.

The next step is the feasibility study of the selected facilities. The feasibility study ends with the exclusion from the list of robotic objects that do not give an economic effect. In the presence of dangerous and harmful conditions for the performance of production operations, the decision on the need for robotics is made regardless of the results of economic calculations.

Based on the results of the feasibility study, in accordance with the rank of preference assigned to each object of robotization, a comprehensive robotization program is compiled. In this case, it is necessary to provide for the phased introduction of RS and automation of processes. At the first stage, the tasks of creating separate robotic positions and combining them in the RS are solved. At this stage, priority is given to automatic and semi-automatic equipment. The second stage envisages further improvements to systems for servicing RTKs and combining individual RTKs into robotic production lines. At the third stage, the issues of robotization of all auxiliary operations, operations to remove production waste and create an automated process control system are solved.

Preparation of production for the introduction of manipulators and RSs, included in the plans for its technical re-equipment, contains a set of technological, technical and design works (Fig. 2). At the enterprises of the construction industry, the implementation process begins with a detailed analysis of the object of robotization and compiling a group of technical requirements. In the process of its comprehensive critical examination, all the constituent elements of the robotic part of the production process are exposed. In robotic

workplaces, the manufacturability of product designs, its compliance with robotization requirements is additionally investigated, technical and technological documentation is studied, the sequence of operations and the movement of workers is analyzed. The cyclograms of completed operations are built, their temporal and technical indicators are determined. In addition, the nomenclature and product release program in selected areas for robotization are studied. Objects of robotization are analyzed using methods of qualitative and quantitative assessment of possible options for the construction of RS.

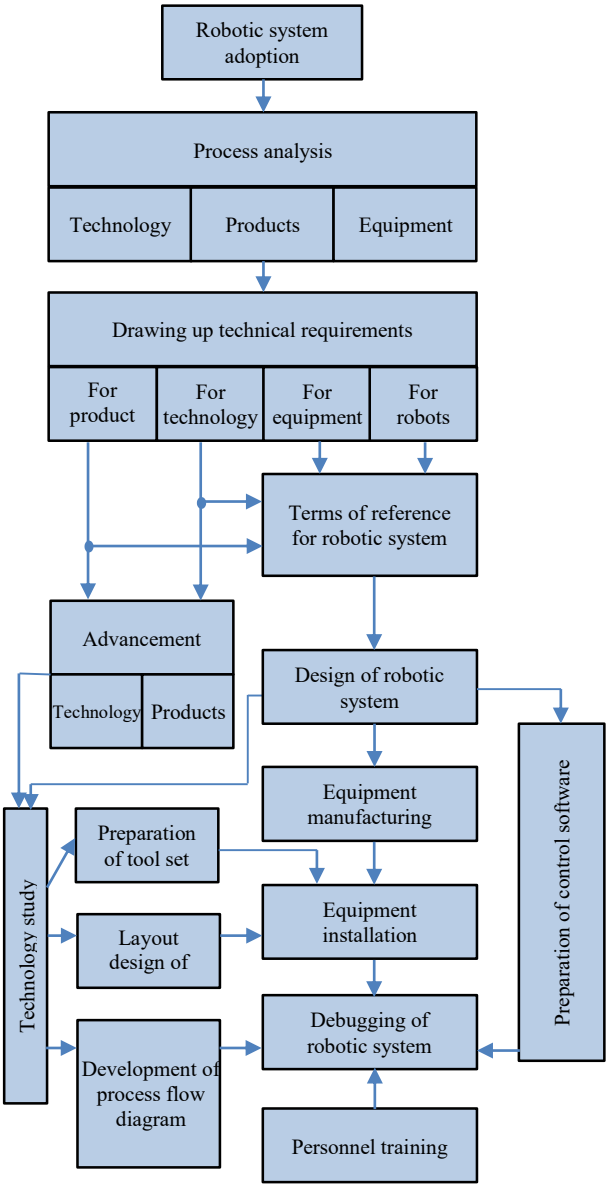

Figure 2. A set of works on the introduction of RS in the construction industry

Based on the analysis, technical requirements are formed for the technology, the main and auxiliary equipment, manipulators, tooling, control systems. The main requirements for the developed RS are set by technological, operational and economic indicators. The first determine the functional characteristics of the robot necessary for its inclusion in the RS, the second determine the ease of maintenance, maintainability, and other operational indicators, and the third establish the capital and operating costs that provide the necessary economic effect.

The formulated requirements serve as initial data for the preparation of technical specifications for the development of the RS and the implementation of works to perfecting the designs of products and their manufacturing technology. On the basis of the technical specifications, RSs are designed, preliminary they are developing a new technology and layout of the complex. When developing a project, when choosing technical means, it is necessary to take into account the productivity of each unit of equipment included in the complex, its mutual coordination with respect to constructive and technical performance. Particular attention should be paid to increasing technical productivity, which takes into account technical interruptions in the operation of the equipment. During the design process, a robot, additional equipment and working bodies are selected. The model of the manipulator or robot is selected based on a comparison of economic indicators for specific operating conditions. In the absence of robots that satisfy the task, it is being maid up the terms of reference for the development of a special design.

Particular attention in the design is given to transport-technological schemes and means of delivery of components and materials. At the design stage of the RS, safety and security equipment, magazine devices, special containers and facilities for the disposal of industrial waste are developed. Based on the results of a preliminary study of the operating technology of the PC, technological equipment is developed and manufactured that meets the basic requirements for the operation of the complex.

An important stage of preparation for implementation is the layout of the RS. When compiling it, much attention is paid to the optimal location of the main and auxiliary equipment, taking into account the technology of work, the safety of maintenance of this equipment and the possibility of its repair.

The final stages of preparation are the manufacture and installation of the RS, the development of process maps, the preparation of control programs, the debugging of individual equipment and the entire complex. Maps are drawn up in accordance with the general rules for the technological preparation of enterprises in the construction industry, determined by the Building Norms and Rules (BNaR).

Installation and debugging of the RS includes the development of an installation plan, the execution of work, the manufacture of an experimental batch of products and acceptance tests. Technological maps are developed after the final selection of the main and auxiliary equipment, means of its automation and tooling design. During production robotization, simultaneously with the design, manufacture and installation of the RS, the issues of personnel training for their maintenance should be addressed. Persons who have undergone special training are allowed to work on servicing robots and RS.

Based on a detailed review of the stages of preparation for production at the enterprises of the construction industry, it should be noted its features in the robotization of processes at construction sites. The main feature of the robotization of operations at the construction site is the non-stationary nature of the performed works, the temporary nature of the installation of equipment, possible changes in the layout and technology when changing construction. In this regard, it is advisable to implement robots and RSs at construction sites based on the use of standard projects for the robotization of certain types of work. Such projects are developed by a specialized organization for the construction of mass buildings based on an analysis of typical technologies for the construction process (Fig. 3).

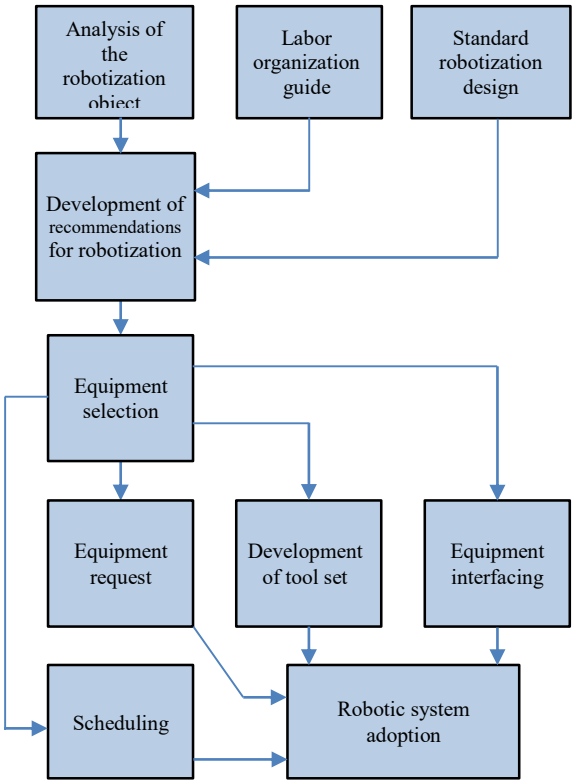

Figure 3. Scheme for the development of standard projects for the robotization of construction works

Typical projects include diagrams of the robotoization process, the composition of the recommended equipment, operation cyclograms of equipment, standard technological maps and basic labor protection measures when working with robots and RS.

The development of standard projects is preceded by a comprehensive analysis of the existing technologies of the robotic type of work and the organization of the construction process. Based on the results of the analysis, recommendations are made for improving the technology. Based on these recommendations and the results of the analysis, the objects of robotization are pre-selected and their feasibility study is carried out, technological schemes of operations are developed, the recommended equipment is selected, typical layout schemes, cyclograms and routings are drawn up. Based on the results of this work, a typical robotization project for this type of work is drawn up. To provide technical assistance to construction organizations on the implementation of manipulators, robots and RSs, it is advisable to prepare labor management guidelines for builders on the basis of standard designs when using robotics.

The process of preparing the construction for the implementation of manipulators, robots and RS during the construction, restoration, repair and reconstruction of buildings and structures begins with an analysis of the construction and technological characteristics of the robot object (Fig. 4). On the basis of this analysis, as well

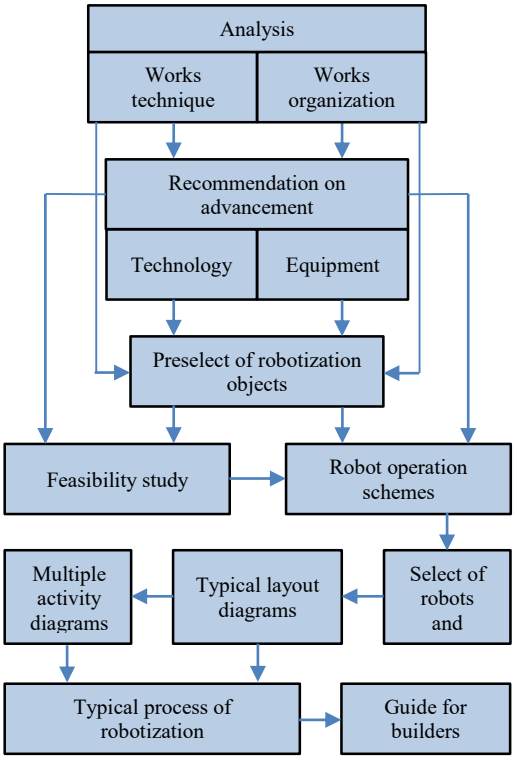

Figure 4. Scheme of works on the robotization of construction processes based on standard projects

as typical projects of robotoization of this type of works, recommendations are developed to improve the technology of robotic operations and modernize the equipment used with the goal of being able to interface with robotic mechanisms. At the next stage of work, it are selected the main and auxiliary equipment, automation tools; it are developed applications for their supply; it are prepared technical tasks for the design of technological equipment; it are developed equipment, devices and means of pairing old equipment with new one. After the completion of design work, equipment is manufactured and adjusted. The final stage of preparation is the development of a project for the production of works. Technological maps for the robotic operations that are part of the project are developed on the basis of standard ones with specific reference to the construction site and local construction conditions. Particular attention should be paid to the development of labor protection measures [15-20].

3 Maintenance of robotic systems

Manipulators, robots and RSs are complex technical devices, the effectiveness and reliability of which largely depends on the organization of maintenance. The low level of this service leads to a significant decrease in the efficiency of the use of automation and robotic means for construction and production processes, and in some cases it can even nullify the effect of their use. The correct construction of a maintenance system for manipulators, robots and RSs and their precise organization lead to an increase in the operating time, reduction of downtime, enhance reliability and, as a result, contribute to the growth of their operation in the production process.

Construction robots and RS as objects of maintenance have a number of characteristic features. They are distinguished by increased complexity, the presence of mechanical, electromechanical, hydraulic, measuring, electronic and other components and devices, which increases the risk of working with them. Therefore, high demands are placed on the labor protection of service personnel. The introduction of robots and manipulators requires not only appropriate technological preparation of production, but also changes in the activities of the technical and technological services of the enterprise, professional and psychological training of workers and engineering personnel.

The use of robots and RЬI at construction sites sets the task of creating a special repair and maintenance service that can provide maintenance of complex equipment directly at the site of construction vn work.

In the general case, maintenance of robotic devices includes a system of measures for preparing equipment for use and its maintenance during operation. In accordance with this, the following main stages of maintenance of robots and RTKs can be distinguished:

- the period of preparation of equipment and control systems for operation,
- preventive maintenance of devices during operation,
- restoration of the operability of devices in the event of failures.

The block diagram of the maintenance of robots, reflecting the listed stages of maintenance, is shown in Fig. 5. It can be seen from it that each stage includes a

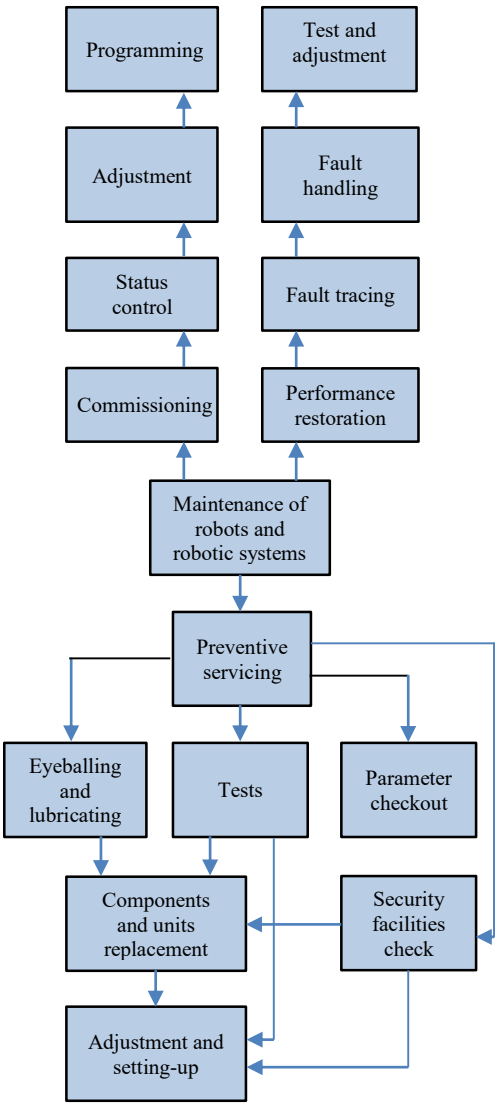

Figure 5. Block diagram of robots and RSs technical maintenance

group of measures necessary to ensure operability, the required reliability and durability of the equipment. So, the period of preparation of robotic facilities for use includes monitoring the status and performance of devices, their configuration and programming. Preventive maintenance includes periodic inspections of

individual devices, components and units of equipment, tests, verification of basic parameters and characteristics, replacement of elements and components, as well as verification of safety equipment. In the process of preventive maintenance, lubrication and adjustment of both individual elements and the equipment as a whole are performed. Faults and failures in the operation of nodes and blocks arising during the operation of robots are eliminated by carrying out restoration work, including troubleshooting, their elimination, as well as the verification and adjustment of devices.

Important indicators of robots and RS as service objects are maintainability, recovery efficiency and time spent on troubleshooting.

Maintainability characterizes the degree of adaptability of robots and manipulators to the prevention and detection of causes of failures in work and the elimination of failures. This characteristic determines the readiness of the equipment for work and is taken into account at the design and development stages. From the point of view of maintainability, robots and systems created on their basis should have handling devices, control systems, information support tools and technological equipment that meet the requirements of convenient access to elements, units and modules when troubleshooting and eliminating failures. The maintainability of robots and RSs depends on unification, interchangeability, availability of troubleshooting systems, as well as the level of preparation of diagnostic tests.

For robots servicing, determining the category of complexity of their repair, as well as evaluating the length of the overhaul period, is of particular importance. These indicators are determined depending on the design characteristics of robots, load capacity, degrees of mobility, complexity of control systems, type of drives, positioning accuracy and other indicators. A major role in robotic servicing is played by troubleshooting time. It is determined by a group of components and includes the time intervals necessary for detecting a failure, preparing a tool, finding a faulty unit and element, troubleshooting, after-sales adjustment and tuning. The time spent on troubleshooting depends on both technical and organizational factors, and primarily on the degree of maintainability, the level of organization of maintenance, training of maintenance personnel and the availability of diagnostic tests.

Carrying out repair work is also characterized by the efficiency of the restoration of failed nodes and systems of robots and technological equipment that is part of the RS. This indicator depends on the quality and reliability of the restoration, its cost, labor costs of maintenance personnel, as well as losses associated with untimely equipment repair.

When using robots in the construction industry, much attention is paid to the preparation period. This maintenance phase is especially important for robots used on construction sites where there are no special conditions for repair service and maintenance. In this case, it is advisable before sending the equipment to a new construction site under stationary conditions of the repair and maintenance service to monitor its condition and operability, to carry out the necessary adjustment and configuration of units and blocks, as well as programming based on the technological maps of the work at this object.

A prerequisite for the performance and reliability of construction robots is the organization of their preventive maintenance. It includes a system of preventive measures that reduce the likelihood of failures. Preventive measures are planned based on an analysis of the particular features of the functioning of all devices and systems of the robot. The choice of the timing, volume and sequence of these measures depends on the nature of the failures, the amount of restoration work, the requirements for reliability and operability of both individual components of the work, and the entire equipment complex. When planning work on preventive maintenance of robots, it is necessary to take into account the nature of failures of individual nodes and elements. Their planned replacement is carried out in case of failures due to wear and tear and for elements subjected to aging. For elements, blocks and devices having a specified service life, a plan for their replacement is drawn up in accordance with the achievement of the maximum operating time. Elements for which the service lives are unknown are replaced by the results of periodic control tests, during which the technical parameters are checked. If limit values are reached, the elements unsuitable for further operation are replaced. Parts subject to rare occasional failures must be replaced if they fail. Their planned replacement is non-forest-like, since it can lead not to an increase, but to a decrease in the reliability of the equipment. Their planned replacement is impractical, since it can lead not to increase, but to reduce the reliability of the equipment.

4 Conclusion

To ensure safe working conditions for construction robots and manipulators, a set of measures is provided that is implemented at the design, installation and operation stages.

The complication of production associated with the introduction of robots, raises the need to address in the process of preparing a set of issues on the organization and operation of robotic systems. In this case, special attention should be paid to ensuring labor safety during the operation of manipulators and robots.

For the selection of objects of robotization in each case, the priority of the set goals is established. First of all, during robotization, attention is drawn to labor-intensive, traumatic and harmful to human health operations, and secondly, to low-prestige, auxiliary, etc.

The main tasks of the maintenance of robotics tools are periodic monitoring of the technical condition of the equipment as a whole and its individual parts, timely detection of precautionary conditions, troubleshooting and restoration of equipment performance.

The effectiveness of the use of robots and RTK in construction largely depends on a clear organization of repair services. At the same time, planning and calculating the nomenclature and the number of spare parts is of paramount importance. During operation, robots and RTK are equipped with spare elements, blocks, replaceable modules. Repair service is provided with the necessary set of tools and devices. The troubleshooting process involves several steps. It begins with finding the failure by external signs and compiling, on the basis of logical analysis, a list of faults that can cause the observed set of failure. After that, the optimal sequence of checks is determined, allowing to find the faulty module, block, functional unit. Then a faulty element is searched. Diagnostic tests allow to simplify the troubleshooting task and quickly find a failed item.

References

[1] Cousineau L. and Miura N. Construction robots: the search for new building technology in Japan. – ASCE Press, 1998. ISBN 0-7844-0317-1

[2] Bock T. and Linner T. Robot-Oriented Design, Design and Management Tools for the Depolment of Automation and Robotics in Construction; Published since May 2015.

[3] Bock T. and Linner T. Robotic Industrialization. Automation and Robotic Technologies for Customized Component, Module, and Building Prefabrication; Published since August 2015.

[4] Bock T. and Linner T. Automated/Robotic On-Site Factories; Published since October 2015.

[5] Bock T. and Linner T. Construction Robots. Elementary Technologies and Single-Task-Construction Robots; Available February 2016.

[6] Bock T. and Linner T. Robotic Ambience. Automation and Robotic Technologies for Maintenance, Assistance, and Service, Available 2017

[7] Delgado J.M. D. et al. Robotics and automated systems in construction: Understanding industry specific challenges for adoption. Journal of Building Engineering Volume 26, November 2019, 100868 doi.org/10.1016/j.jobe.2019.100868

[8] ISO 13482:2014(en) Robots and robotic devices — Safety requirements for personal care robots.

[9] ISO 10218-1:2011, Robots and robotic devices — Safety requirements for industrial robots — Part 1: Robots.

[10] ISO 10218-2:2011, Robots and robotic devices — Safety requirements for industrial robots — Part 2: Robot systems and integration.

[11] Seward D. and Zied K. Graphical Programming and Development of Construction Robots. Journal of Construction Engineering and Management (2004), ASCE. 65.

[12] Everret, J.G. Automation and Robotics Opportunities Construction Versus Manufacture. Journal of Construction Engineering and Management (1994), ASCE. 120(2), pp. 443- 452.

[13] Balaguer C. and Abderrahim M. A Trends in Robotics and Automation in Construction. University Carlos III of Madrid, 2008.

[14] Bock T. Special Issue on Construction Robotics. Autonomous Robots. Volume 22. Number

[15] Cousineau L. and Miura N. Construction Robots: The Search for New Building Technology in Japan. American Society of Civil Engineers. 1998.

[16] Taylor M. and Wamuziri S.Automated Construction in Japan". Proceedings of ICE. 2005.

[17] Giretti A., Carbonari A., Naticchia B., DeGrassi M. Design and first development of an automated real-time safety management system for construction sites. Journal of Civil Engineering and Management. Volume 15. Issue 4. 2009.

[18] Bock T. CAR: Construction Automation Robotics. - In: 22nd International Symposium on Automation and Robotics in Construction (ISARC), Ferrara, 11.-14.09.2005.

[19] Bock T. Affordable and Adaptive Housing for Socio-technical Innovation by Construction Automation and Robotics. Journal of Industrial and Civil Enginnering, Russian Engineering Academy of the Russian Society of Civil Engineers, ISSN:0869-7019, pp. 5-10, Vol.10, 2014.

[20] Linner T. and Bock T. Automation, robotics, services evolution of large-scale mass customization in the Japanese building industry. In: Mass Customisation and Personalisation in Architecture and Construction: A Compendium of Customer-centric Strategies for the Built Environment , Edited by P. A.E. Piroozfar & F. T. Piller, London & New York: Routledge/ Taylor & Francis Group, June 2013, pp. 154-163.

Safety Concept and Architecture for Autonomous Haulage System in Mining

H. Ishimoto and T. Hamada

Mining Solutions Div., Client Solutions Group, Hitachi Construction Machinery Co. Ltd, Japan
E-mail: h.ishimoto.gl@hitachi-kenki.com, t.hamada.at@hitachi-kenki.com

Abstract –

In recent years, automation of mining equipment has been required to improve productivity, predictability, and safety of mining operations. Some major mining companies have begun efforts to automate dump trucks that transport overburden and minerals, eliminating the need for human operators, aiming for reducing labor costs, increasing operating hours, and improving efficiency of vehicle assignment. It is called an autonomous haulage system.

The introduction of an autonomous haulage system requires significant changes in operations management. Particularly, safety needs to be carefully considered.

Conventionally, in manned mining operations, ensuring the safety while at work has largely been the responsibility of site managers, fleet controllers, machine operators, and field workers.

However, when making the machine unmanned, it is necessary that the system bears a part of the function for ensuring safety, which has been conventionally carried out by humans, and that the user appropriately understand and operates the system.

This paper describes the concept of ensuring safety when applying an autonomous haulage system using unmanned dump trucks to mining operations, and a system architecture based on it.

First, we proposed the basic structure of the autonomous haulage system, conducted a risk assessment assuming mine operation using the system, and identified possible protection measures.

Next, we examined the architecture of an autonomous haulage system with a safety function that enables more deterministic performance evaluation while considering the complexity of the system.

This system was installed in an actual mine site, tested and operated, and it was confirmed that the safety functions worked properly. When introducing the system, the safety concept and architecture of the system have been explained to the site safety manager and governmental regulators and have been validated.

Keywords –

Autonomous haulage; Dump truck; Unmanned Control; Safety; Mining

1 Introduction

1.1 Background

1.1.1 Industry Trends

Prices of resources such as coal, iron ore and copper have risen sharply since around 2005 due to economic growth in China and emerging countries. During this period, there was a shortage of workers due to the booming mining industry, and so the rise in personnel costs was a problem. In response, major Australian resource development companies have expanded their investment, especially for machine automation, with the aim of unmanned mining in the future.

Due to the subsequent slowdown of the Chinese economy, which caused the global economic downturn, resource prices peaked, and mining companies were required to improve the efficiency of mine operations and reduce operating costs. This change in circumstances, together with the recent development of IoT and AI technology, has become the driving force for accelerating the shift to unmanned mining and machine automation, rather than stopping it.

1.1.2 Demand for Autonomy

In the mining industry, ensuring the safety of workers has been an issue for a long time. Particularly, there is a need to improve the safety and comfort of the operators of machinery operating on the site. In addition, the ESG concept has spread as a method of corporate evaluation in investment activities, and the mining industry is in a situation where improvement of environmental impact and working environment is required.

1.2 Autonomous Haulage System (AHS)

One of the efforts for unmanned or automated mining equipment is the autonomous driving system (AHS: Autonomous Haulage System) of dump trucks. AHS is a system that allows the dump truck to be unmanned and to be centrally managed from the control system in the office to carry out hauling and dumping products. Unmanned dump trucks not only reduce labour costs for operators, but also increase economic benefits, such as extended operating hours by eliminating breaks and shift changes, reduced fuel consumption by an efficient and appropriate driving by computer-controlled operations, and an extended machine life by driving control with less damage to the vehicle body. In addition, safety is expected to be improved by reducing human error during dump truck operation. Furthermore, it is expected that the mine operation itself can be made more efficient by linking the hauling process with the production management system.

The introduction of AHS to actual operation began around 2008, and in recent years the number of deployment cases has gradually increased, especially in iron ore mines in Western Australia. [1][2]

1.3 Safety of AHS

AHS will change dump trucks in a conventional mining haulage operation to unattended. Therefore, many of the roles played by the dump truck operator, including ensuring safety, are replaced by the functions of various systems that are components of AHS.

The operator is not present in the driver's cab of an autonomous haulage truck (AHT) during AHS operation, but a mixed situation of AHT and other manned vehicles in the AHS operation area can occur at any time. In addition, operations involving human intervention such as AHT start/end operations, maintenance/conditioning work, and manual operation for moving inside parking areas and workshops will continue to be performed. Thus, given the actual mining operation and site environment, it is difficult to take intrinsically safe measures such as physically isolating AHT, which is a major hazard source, from humans and manned vehicles. Therefore, it is essential that the system functions play a certain role to ensure safety.

Based on the above, this paper aims to show the AHS safety concept and architecture for safe operation of the mine.

2 AHS architecture

2.1 Overview

Various architectures can be applied to the system configuration that realizes AHS. It is possible to have a completely centralized implementation in which even the actuator control of the dump truck is performed on the cloud server side, and conversely, there may be an autonomous decentralized configuration in which each vehicle determines its own target position and route.

A centralized system has the advantage of reducing the number of in-vehicle devices for dump trucks and facilitating software updates. On the other hand, since the responsiveness of each vehicle control strongly depends on the communication performance with the central control system, there is a problem that the system scale and operation are limited when the wireless communication infrastructure is not sufficient.

The autonomous decentralized system can reduce the dependency on wireless communication, but the dispersion of autonomous operation of each vehicle becomes large. As a result, multiple vehicles may not be properly controlled, and efficient operation may not be realized as the entire system.

As an alternative to these, an intermediate approach is applied to the AHS we have developed (hereinafter simply referred to as AHS). In other words, this is an approach that achieves overall efficiency while suppressing the dependence on wireless communication by giving each vehicle a certain degree of autonomy.

Figure 1 shows the architecture of AHS.

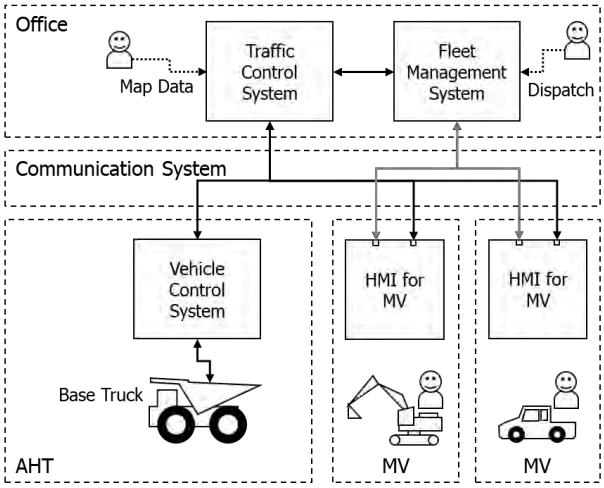

Figure 1. Architecture of AHS

The AHS consists of Fleet Management System and Traffic Control System located in Office, Vehicle Control System installed in AHT, and Communication

System that connects them. The manned vehicle (MV) used in the AHS operation site is equipped with a Human Machine Interface (HMI) that can monitor the operation status of the AHS and the status of AHTs.

The role of each subsystem that constitutes AHS is explained in the following sections.

2.2 Fleet Management System (FMS)

The role of the Fleet Management System (FMS) is to give a dispatch instruction to each AHT. That is, a destination such as a loading place or a dumping place to which the AHT should head is designated according to the current position of each AHT or the loading state. This dispatch instruction includes a method of directly setting a destination by an Office operator and a method of automatically issuing a repeat dispatch instruction based on a preset destination. The dispatch instruction is once passed to the Traffic Control System, converted into smaller driving instructions by the Traffic Control System, and sent to AHTs.

The FMS also displays the operating status of AHTs and the production volume estimated from them.

2.3 Traffic Control System (TCS)

In addition to multiple AHTs, MVs such as excavators, dozers, and light vehicles that are driven by humans also operate on the AHS operation site. The Traffic Control System (TCS) wirelessly communicates with AHTs and MVs, adjusts vehicle traffic throughout the site so that the interference between AHTs or between AHTs and MVs does not occur. The travel route of the AHT is divided into multiple sections, and by allowing the travel of each section exclusively to one AHT, interference between the AHTs is prevented. When the permitted section of AHT and the buffer area set in the traveling direction of MV overlap, the MV operator is guided by the HMI mounted on the MV so as not to enter the permitted section of AHT. At the same time, the TCS issues a deceleration/stop instruction to the AHT to avoid interference. [3]

2.4 Vehicle Control System (VCS)

The Vehicle Control System (VCS) controls the dump truck to move along the route to the destination specified by the FMS based on the TCS-controlled travel-permitted section. The AHT performs route-following traveling while comparing the route map information received from the TCS in advance with the self-position estimation results from the GNSS and IMU. In addition, the AHT detects obstacles with an environment recognition sensor and performs deceleration/stop behaviour as necessary.

2.5 Communication System (CMS)

Communication System (CMS) is responsible for information transmission between FMS, TCS, VCS, and HMI for MV. The CMS also has a function of monitoring the communication status including wireless communication.

3 Safety Concept

3.1 Principle

In the conventional hauling operation, the responsibility for ensuring safety during work has been delegated to appropriate actions and communication between people, such as operation managers, dispatchers, dump truck operators and other vehicle operators. On the other hand, in the AHS operation, it is necessary for the system to take over many of the roles for ensuring the safety, which was performed by the dump truck operator in the conventional operation.

However, it is hard to say that the concept of safety is established in the industry because AHS is still used only in some mines and is not widely used in many mines of the world. In addition, AHS is not a product with standardized structure and function like earthmoving machinery, and system configurations and functions are not common among manufacturers. Therefore, no common understanding has been established regarding the specific methodologies on which safety design is based or the performance target values for safety functions.

Therefore, we considered securing AHS safety based on the following basic policy:

- Compliance with safety requirements based on related international standards.
- Conduct risk assessments based on the operating environment and system architecture.
- Clarification of safety design requirements for protection measures derived from risk assessment.

3.2 International Standards

In 2017, ISO issued ISO 17757 “Earth-moving machinery and mining – Autonomous and semi-autonomous machine system safety”. The revised version was published in 2019. The standard covers systems in general that provide for autonomy in earth-moving machinery, primarily mining equipment and dump trucks in particular, and specifies the requirements that the system must have in its design, the information that the system integrator (which may be the same as the machine manufacturer) must disclose to the user, and the operating conditions that the user must control.

Regarding the safety of the system, it is required to carry out risk assessment according to the principles shown in ISO 12100. What constitutes a safety function in a specific system, and the required safety performance level thereof, cannot be uniformly determined because they largely depend on the operating conditions of the mine. Therefore, ISO 17757 does not provide a common target specification, and system integrators should make decisions based on the results of risk assessment. It is suggested to refer to ISO 13849, IEC 62061 or IEC 61508 for requirements in designing safety related control systems.

We have referred to this ISO 17757 as the basis for our AHS safety concept development and safety design.[4][5][6][7]

However, ISO 17757 does not mention specific procedures for risk analysis of autonomous systems and determination of required performance levels of safety functions. Therefore, we referred to the method proposed in the process industry that applies IEC 61508 or IEC 61511 to plant design.[8][9]

3.3 Layers of Protection

ISO 17757 describes risk management requirements for both AHS system integrators and users. Based on this, it was decided to secure safety based on the concept of hierarchical protection layers which combines system functions and operation management. The concept is shown in Table 1.

Table 1. Protection Layers of AHS

PL#	Protection Layer Category	Provided by
PL4	AHS Safety Functions	System Integrator (OEM)
PL3	AHS Control Functions	
PL2	Physical Barricades / Signage	User
PL1	Site Rules / Education	

At the first layer, user protection measures require AHS operation rules, provision of appropriate procedures, and education/training for workers involved in AHS operation [PL1 Rules/Education]. In the next layer, facilities to prevent human-AHT interference, such as signage and physical barriers that indicate the boundary between the AHT operation area and the manned area (parking area, workshop, etc.), are required. [PL2 Barricades/Signage].

As a protection measure by the system integrator (manufacturer), two layers of AHS control function [PL3 Control Functions] and safety function [PL4 Safety Functions] are provided.

PL3 is a layer for measures devised based on the AHS use cases assumed at present and the system architecture (shown in previous chapter) and comprises a variety of functionalities for realizing the main operation of the system. Each subsystem that constitutes the AHS has functions such as map management, traffic control, route tracking, and environment recognition, and these have the effect as protective measures in addition to realizing efficient operation.

PL4 is a layer of functions intended exclusively to ensure safety regardless of the action of the various functions of PL3 or the occurrence of a failure of the PL3 layer functions. In other words, it is a more universal and primitive protection measure that is less dependent on the functional specification of the system.

In ISO 12100 and ISO 13849, “safety function” is defined as “function of a machine whose failure can result in an immediate increase of the risk(s)”. PL4 is based on this definition. On the other hand, PL3 is regarded as a control function rather than a safety function. This means that a single failure of the PL3 function does not immediately increase the risk. In other words, even if one function of PL3 fails, as long as the function classified in PL4 is effective, the risk is still reduced to an acceptable level and it does not result in an immediate increase in risk.

The protection measures for PL4 or PL3 provided as AHS are designed on the assumption that the protection measures for PL2 and PL1 by the user are functioning properly. Safety cannot be ensured only by the protection measures by the function of AHS.

3.4 Risk Assessment

To extract the requirements that the system and the user should support for ensuring AHS operation safety, a risk assessment has been conducted according to the following procedure based on ISO 12100.

1. Assumed hazardous events due to system malfunction or human error.
2. Devised protective measures that can reduce the probability of occurrence of harm or the severity of harm.
3. Categorized to which layer of the hierarchical protection layers the devised protective measures should be placed.

Table 2 shows examples of hazardous events extracted by the risk assessment. In the actual development process, the probability of occurrence of harm and the severity of harm are estimated for each dangerous event, but they are omitted here.

Table 2. Examples of hazardous events

Origin	Hazardous Scenario	Target of Harm
AHT fault	Unexpected movement of AHT causes a collision with personnel.	Bys
AHT/TCS /CMS fault	AHT deviates from its travel route due to any abnormality in VCS/TCS/CMS, which causes a collision with personnel/MV.	Bys /MV Op
MV Op human error	The MV operator inadvertently enters MV into the AHT travel route, which causes a collision with the AHT.	MV Op
Bys human error	Personnel accidentally approaches the AHT, which causes collides with the AHT.	Bys

MV Op: Manned Vehicle Operator
Bys: Bystander (Field Operator, Maintenance Personnel)

Table 3 shows examples of the major protective measures (PRM: Protective Measure) devised corresponding to hazardous events extracted in the risk assessment. Each PRM is classified into one of layers PL1 to PL4. By applying a combination of a plurality of these PRM to each of the previously assumed hazardous events, the probability of occurrence of harm or the severity of harm can be reduced. PL1 and PL2 are user-controlled measures, and PL3 and PL4 are measures provided by the system integrator.

Table 3. Examples of Protective Measures

PRM type	Description	PL#
Rules / Education	Restrict personnel and MVs from entering the AHS area and AHT traveling routes.	PL1
Rules / Education	AHT start/stop procedure.	PL1
Barricades	Install a protective barrier between the AHS area and the manned area.	PL2
Barricades / Signage	Install AHS area entrance/exit gates.	PL2
AHT mode switching device	Proper placement of AHT start and mode switching devices.	PL3
AHT anomaly detection	AHT stops when it detects a system malfunction.	PL3
AHT deviation detection	AHT stops when it detects a deviation from the given route.	PL3
AHT obstacle detection	AHT stops when it detects an obstacle with the onboard sensor.	PL3
AHT permission control	AHT will stop within the given permit section if the next permit is not obtained.	PL3
AHT indicator	Notify the surroundings of the operating status of the AHT using indicators etc.	PL3
AHT audible warning	External notification of AHT start/start via horn, etc.	PL3
Site info provision	Provision of AHS area map information to MV operator.	PL3
Approach notification	Notify MV operator when MV and AHT approach each other.	PL3
AHT status info provision	Notify MV operator of moving/stopping status of AHT.	PL3
AHT Remote Stop	MV operator or personnel on site remotely stops AHT.	PL4
AHT approach speed limit	Limit the speed of the AHT when the MV and the AHT are close to each other.	PL4
AHT control system shutdown	Shut off the AHT vehicle control system during non-AHS operation.	PL4

The procedure for selecting PL4 safety functions from PRMs provided by the system integrator is described in the next section.

3.5 Selection of Safety Functions and PLr Determination

Figure 2 shows the safety function selection procedure.

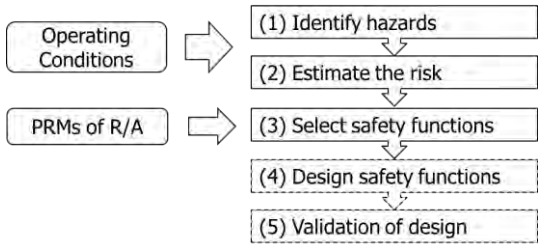

Figure 2. Safety functions selection process

3.5.1 Identify hazards

Accident scenarios due to AHT operation failure are identified as hazards. AHT operation failure means that the AHT does not operate as instructed, or that it operates unexpectedly. The cause of AHT operation failure is not necessarily limited to the failure of the hardware/software that controls the AHT base truck. AHS is a system that operates a dump truck by FMS, TCS, CMS and VCS triggered by human operation input. Therefore, the failure of any of the components that make up the AHS and the error of the person who operates the AHS can ultimately cause the operation

failure of the AHT. (For example, improper destination setting to FMS by a person, input error of map data, error of instruction to AHT due to TCS software bug, loss of operation instruction to AHT due to communication error, etc.)

AHS has a large system scale, and the number of hardware and software that constitutes it is also large. There are also various combinations of operations between subsystems. Therefore, it is not practical to perform failure mode and effect analysis (FMEA) on all system components and consequently analyse all possible hazards in the entire system.

Therefore, we decided to conduct HAZOP for the behaviour of AHT, which finally becomes a hazard to humans, and identify the hazard. First, the movement of the dump truck was classified into acceleration, deceleration, steering, stop, and body lifting. Next, based on the HAZOP guide word for each movement, we assumed deviations such as "NO OR NOT", "MORE", "LESS", "REVERSE", and identified the resulting hazards.[8]

3.5.2 Estimate the risk

For all identified hazards, the risk estimation was performed and the required performance level (PLr) for the safety function to reduce the risk of hazard was determined.

For risk estimation, the analysis method using the risk graph (Figure 3) shown in ISO 13849-1, Annex A was applied.

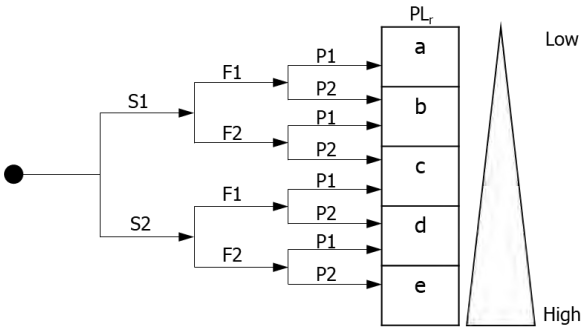

S Severity of injury
S1 Slight
S2 Serious
F Frequency and/or exposure to hazard
F1 Seldom-to-less-often and/or exposure time is short
F2 Frequent-to-continuous and/or exposure time is long
P Possibility of avoiding hazard or limiting harm
P1 Possible under specific conditions
P2 Scarcely possible

Figure 3. Graph for determinating PLr for safety function

The procedure for determining the PLr based on the risk graph is described below.

1 Assume the situation before setting the intended safety function.
2 Estimate the risks caused by the failure of the safety function (in other words, the lack of the safety function). Consider the following parameters:
  2.1 Severity of injury
  2.2 Frequency and/or duration of exposure times to hazards
  2.3 Possibility of avoiding the hazard and probability of occurrence of a hazardous event
3 By selecting the above parameters, PLr to be assigned to the intended safety function is determined.

3.5.3 Select safety functions

Select a specific protective measure that can reduce the risk against the identified hazard from the results of the risk assessment. The selected protection measure is placed as the safety function of PL4, and PLr determined in the previous section is applied.

As a method of actual system design, safety functions are selected from the following viewpoints:

- To enable common risk reduction for more hazards with fewer safety functions.
- Safety functions can be placed independently of control functions.
- Safety-related part of the control system (SRP/CS) that performs the safety function can be downsized and the number of components can be reduced.

Table 4 shows examples of safety functions for each AHT operation scene selected in the above procedure.

Table 4 Examples of Safety Functions

AHT Operation Scene	Safety Function
Unmanned /Autonomous Mode	ASL: Approach Speed Limit
	R-Stop: Remote Stop
Manned /Manual Mode	AHT Control System Shutdown

During AHS operation is being conducted, AHT is in unmanned/autonomous mode. In this case, the situation where the AHT approaches a MV is a major hazard. As a protective measure, when the MV is close to the AHT within a certain range, the traveling speed of

the AHT is limited to reduce the kinetic energy of the AHT and lower the severity of harm. In addition, if the AHT is in low speed, the possibility that the MV operator can avoid the collision with the AHT increases, so that the risk can be reduced. Moreover, the possibility of avoiding a collision is further enhanced by equipping the MV with a device capable of remotely stopping the AHT.

During non-AHS operation, AHT may be used in manned/manual mode. In that case, there is a risk that the AHS function is activated unintentionally and obstruct human operations, resulting in a hazardous event. As a protection measure, the circuit is configured so that the AHT autonomous/manual mode switching device shuts off the power of the AHT control system during manual operation. This will prevent unexpected behaviour of the AHT in manual mode and reduce risk.

For each safety function, PLr based on the risk estimation under the assumption that the safety function is not provided is applied. This determines the target performance of the safety function and enables deterministic evaluation.

Note: The purpose of this chapter is to show the process of developing the AHS safety concept and determining the target performance of the safety function. It is out of scope to assert the need for a specific safety function and show a unified value of PLr for general automation systems for mining machinery. As described above, what kind of safety function is set and how the value of PLr should be are depending on the conditions under which the system is operated and the system architecture, and there is no general specification. Therefore, PLr value of each safety function is not described here.

3.6 AHS architecture with safety functions

Figure 4 shows the architecture in which the safety function components selected in the previous section are added to the AHS main function system shown in the previous chapter.

To provide the ASL function, the MV is equipped with means for measuring its own position and means for wirelessly transmitting the position. The AHT is equipped with means for measuring its own position and means for receiving position information from the MV. The received MV position and the AHT's own position are compared, and if it is determined that they are close to each other, the speed limit control of the base track is activated.

Similarly, to provide the R-Stop function, the MV comprises a wireless transmission means with a stop switch. When the AHT receives the stop signal from the MV, the control for activating the brake and stopping the base truck is activated. The MV transmitter and AHT receiver are shared by both ASL and R-Stop functions.

The communication system that transmits ASL/R-Stop signals is provided independently of the AHS main function communication system (CMS) and is used only for safety functions.

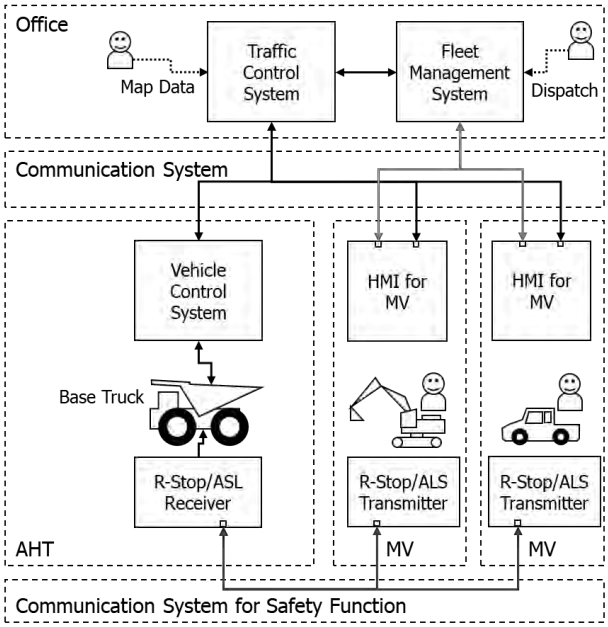

Figure 4. AHS architecture with safety functions

Implementing the system that provides the PL4 safety function independently of the system that provides the PL3 control function as described above has the following advantages:

- The safety function can always be activated as required without being affected by the operating status or malfunction of the main control function.
- The design of the separated SRP/CS becomes relatively easy and its performance can be evaluated deterministically.
- Since the safety function is not easily affected by the specification change of the main control function, it is possible to expand the functionality of the entire system without modifying the safety function.

4 Deployment and Evaluation

4.1 Deployment

With the cooperation of Stanwell Corp, an electric power company in Queensland, Australia, a trial of the AHS of the configuration introduced in this paper is being conducted within the Meandu coal mine owned by the company.[11]

As a result, commercial deployments of the AHS have commenced at the Maules Creek mine owned by Whitehaven Coal, a major coal producer in New South Wales, Australia. [12]

4.2 Evaluation

Mining companies that introduce and operate autonomous/unmanned systems are required to report their safety management plans and/or safety measures to the mining inspector in their state. In that case, the system integrator who provides AHS may also be required to submit the AHS system configuration, safety concept, and functional safety study report. If the information is insufficient, AHS operation in the mine may not be approved.

In preparation for the AHS operational test mentioned above, the safety of the AHS system and operation was reported based on the approach described in this paper and was validated by the mining companies' safety managers and state regulators.

5 Conclusions

We have developed a safety concept for introducing an autonomous haulage system (AHS) for dump trucks in mining operations. This concept is in line with the safety policy of earthmoving machinery and autonomous machine system, which is indicated by international standards.

Specifically, we conducted a risk assessment based on the AHS operating environment and system characteristics, and proposed protection measures for both the user side and the manufacturer side based on the concept of hierarchical protection layers. Hazard analysis was carried out to select the protection measures placed as safety functions, and the method to determine the required performance level of the safety function was established. An AHS architecture was formulated in which the selected safety function is provided independently of the main control function.

AHS based on this safety concept was introduced to an actual mining site. At that time, our approach to system safety was accepted by mining companies and officials, and the effectiveness of this approach was confirmed.

References

[1] Cecilia J. Rio Tinto autonomous trucks now hauling a quarter of Pilbara material. Online: https://www.mining.com/rio-tinto-autonomous-trucks-now-hauling-quarter-pilbara-material/, Accessed: 15/06/2020

[2] Daniel G. Why the Pilbara leads the way in haul truck automation. Online: https://im-mining.com/2019/08/06/pilbara-leads-way-haul-truck-automation/, Accessed: 15/06/2020

[3] Hamada T. and Saito S. "Autonomous Haulage System for Mining Rationalization". Hitachi Review, 67(1): 87-92, 2018.

[4] ISO 17757, "Earth-moving machinery and mining – Autonomous and semi-autonomous machine system safety". 2019.

[5] IEC 61508, "Functional safety of electric/electronic/programmable electronic safety related systems". 2010.

[6] IEC 62061, "Safety of machinery – Functional safety of safety-related electrical, electronic and programmable electronic control systems". 2005

[7] ISO 13849, "Safety of machinery – Safety-related parts of control systems"., 2015.

[8] IEC 61511, "Functional safety – safety instrumented systems for the process industry sector". 2003.

[9] Sakuma A. and Yoneki S. and Kushibiki T. "Risk Analysis and Safety Integrity Level Analysis Services for Plants, Machinery, and Equipment". Toshiba Review, 61(11):40-43, 2006.

[10] IEC 61882, "Hazard and operability studies (HAZOP studies) – Appication guide"., 2016

[11] PRESS RELEASE. Successful trial of Hitachi autonomous system. Online: https://www.miningmagazine.com/innovation/news/1331994/successful-trial-of-hitachi-autonomous-system, Accessed: 15/06/2020

[12] Daniel G, Whitehaven Coal hits automation milestone at Maules Creek mine. Online: https://im-mining.com/2020/04/16/whitehaven-coal-hits-automation-milestone-maules-creek-mine/, Accessed: 15/07/2020

On-site Autonomous Construction Robots: A review of Research Areas, Technologies, and Suggestions for Advancement

X. Xu[a] and B. García de Soto[a]

[a] S.M.A.R.T. Construction Research Group, Division of Engineering, New York University Abu Dhabi (NYUAD), Experimental Research Building, Saadiyat Island, P.O. Box 129188, Abu Dhabi, United Arab Emirates
E-mail: xx927@nyu.edu, garcia.de.soto@nyu.edu

Abstract –

The use of robotic systems on construction sites can efficiently reduce construction time and increase safety by replacing construction workers in monotonous or dangerous operations. Robots for on-site construction applications are challenging and difficult to implement because of the evolving and unstructured nature of construction sites, the inherent complexity of construction tasks, the uniqueness of products, and labor-intensive modeling and commanding, which require significant human effort and expertise. With the development of data-driven techniques such as machine learning and computer vision, more advanced frameworks and algorithms can be developed to increase the level of adoption in the automation of construction robots. To better understand existing challenges and figure out the best strategies to implement high-level autonomous robotic systems for on-site construction, this study (1) summarizes technologies and algorithms used in construction robots and robotic applications in other industries, (2) discusses potential best usage and development of computer vision and machine learning techniques used in related areas to implement higher-level autonomous construction robotic systems, and (3) suggests a preliminary framework that integrates different technologies, such as vision-based data sensing to collect information, advanced algorithm to detect objects and reconstruct models of the built environment, and reinforcement learning to train robots to self-generate execution plans. This will allow construction robots to navigate and localize on construction sites, recognize and fetch materials, and assemble structures per a simulated plan. The proposed conceptual framework could help with the definition of future research areas utilizing complex robotic systems.

Keywords – Automation; Construction robots; Computer vision; Reinforcement learning

1 Introduction

Construction robots refer to robotic systems designed for construction operations, which typically take place in dynamic environments [1, 2]. Construction automation and robotics have been generating much interest in the construction community for the last decades as a way to improve productivity and reduce injuries or fatalities [3, 4]. Repetitive and labor-intense tasks, such as bricklaying, painting, loading, and bulldozing, are good candidates for automation, and the use of robots can assist in reducing labor force, and create safer work environments. However, compared to the robotic systems used in factories/manufacturing, construction robots have more complicated situations. They are exposed to dynamic and unconstructed environments, which means that predefined actions may not be suitable for all circumstances as construction sites and workspaces are always changing. Therefore, robots need to perceive the environment and understand how to react to the changes [5]. Besides, construction tasks comprise many variables, include different materials [6], and have different sequencing and requirements for assembling. This means that the control of construction robots requires a lot of manual effort to preprogram the motion and trajectory of the robotic system [7]. These challenges make it difficult to implement a high-level autonomous construction robotic system. Considering these challenges, to be able to have an autonomous robotic system to execute specific tasks, other technologies such as data sensing techniques and machine learning can be used to deliver unprecedented levels of data-driven support to substitute human efforts and instructions.

This paper presents an objective review of the use of computer vision techniques (CV) and machine learning (ML) technologies that could be used to achieve a high level of autonomy in robotic construction systems. Based on that, suggestions on a possible framework to implement a high-level autonomous construction robotic

system are provided. The rest of this paper is organized as follows. Section 2 summarizes construction robotic applications, discusses challenges currently faced, and provides an overview of CV and ML techniques developed and used in relevant areas that could advance robotic systems applied to construction. Section 3 proposes a possible framework in which CV and ML are used to create an integrated system to achieve autonomous localization, material recognition, and task execution planning. Section 4 summarizes the work presented and provides directions for future research.

2 Application of Construction Robots

In general, construction robots can be classified into four categories: (1) Off-site prefabrication systems, (2) On-site automated robotic systems, (3) Drones and autonomous vehicles (AV), and (4) Exoskeleton wearable devices. For each of these categories, there are several applications. Some examples are summarized in Table 1.

Table 1. Example of construction robot applications

Category	Reference
Off-site prefabrication	[8], [9], [10], [11], [12]
On-site automated and robotic systems	[13], [14], [15], [16], [17]
Drones and AV	[18], [19], [20], [21], [22]
Exoskeletons	[23], [24], [25]

Considering the adoption of each category in the construction industry, off-site prefabrication can significantly help with the advancement of building materials, which follows the same logic and principles of the manufacturing industry. Several building components and structures have already been constructed successfully in this way. Drones and AV applications have already been used widely on construction sites to help with the monitoring process and materials delivery. Exoskeletons pushed the limits of human-robot interaction (HRI). These systems can assist and protect workers performing heavy and dangerous tasks such as lifting heavy loads and are useful to reduce fatigue and facilitate the use of other tools and equipment in awkward positions [26].

However, applications for on-site construction robots have many limitations when compared to other categories. Current on-site construction robots mostly rely on preprogrammed processes to perform single repetitive tasks, such as bricklaying, steel-truss assembly, steel welding, façade installation, wall painting, concrete laying, etc., which do not involve multi-task or multi-robot construction. Current on-site robotic systems assist the construction work but could not take the place of workers and need supervision or assistance from an operator. Having the possibility of on-site construction robots being able to adapt to construction environments and perform multiple tasks without humans' hardcoding or programmed orders is not trivial, and further research is needed to create a high level autonomous on-site construction robot to unleash the great potential and opportunities of such systems. The focus of this paper is in that area.

2.1 Data-driven techniques

The advancement of data-driven techniques such as computer vision and machining learning has dramatically improved the efficiency and accuracy of robotic systems in multiple areas. Different applications in manufacturing, surgery, self-driving vehicles, structure inspection, and maintenance, have benefited from this and experienced improved productivity and accuracy.

Considering how a construction robot should work on a construction site, previous researches focused on the following elements to fulfill the automation of construction robot: (1) localization of the robot, (2) materials (i.e., workpiece) recognition and selection, (3) optimized control and task execution, and (4) monitor and maintenance, the following subsections provide a review of the technologies that could be used in each step (Tables 2 and Table 3).

2.2 Localization

Construction sites are characterized by being unstructured and dynamic. This creates extraordinary challenges for robots to localize and navigate in such environments. On-site robots should be able to avoid obstacles to reach a specific location to execute a given task. That requires extra sensing strategies or modalities to help robots perform work adaptively.

Table 2. CV techniques used in construction robots

Step	Computer Vision Techniques		
Localization	GPS	Camera markers	SLAM (mapping and reconstruction)
Material recognition	Point clouds segmentation	Stereo image (reconstruction)	Edge detection
Task plan execution		VR models simulation	VR, HRI
Monitor control	Point cloud	SLAM	VR

An excellent way to make sure robots find the right position while guaranteeing accuracy is by using cameras and markers. For example, [5] showed that a robot could use a camera and fiducial markers to find the position to execute a construction activity. While that provided reliable position reference for the robot to navigate, it did not consider obstacles. Robots cannot react to the

dynamic changes of the construction site, and the position of the markers needs to be manually modified, which requires a lot of manual efforts.

Table 3. ML techniques used in construction robots

Step	Machine Learning
Localization	Reinforcement learning for path planning and tracking (A*, LQR)
Material recognition	Deep learning or machine learning for Object Detection
Task plan execution	Reinforcement learning for simple task simulation such as bricklaying.

Currently, the most effective way to solve this problem is by using Simultaneous Localization and Mapping (SLAM). For example, [27] used V-SLAM with RGBD camera on an autonomous Unmanned Aerial Vehicle (UAV) platform for asset tracking in an outdoor construction site. [28] proposed a mobile indoor robotic monitoring and data collection framework using RGB sensors and fiducial markers. [29] proposed an autonomous robot equipped with different sensors to collect data used to conduct an automatic assessment of the state of construction. Autonomous navigation was achieved using an Adaptive Monte Carlo Localization (AMCL) algorithm. SLAM provides mapping and localization in an unknown environment and gives feedback for robots to understand the environment as well as estimating their current pose. Other applications based on SLAM include research focused on the modeling and reconstruction of the built environment using point cloud segmentation. For example, [30] proposed an integrated system that automatically provides detailed as-is semantic 3D models of buildings through raw data of point clouds. This system can better deliver environment information into digital models, provide a more reliable platform for robotic execution planning and simulation.

Based on this, reinforcement learning (RL) and optimal control could be used to provide a more robust trajectory planning result to deal with complex and dynamic problems. [31] utilized an A* algorithm to find an optimal sequence of biped robots' feet and hand contacts to cross a complicated terrain. [32] presented a quadrotor controller using iterative linear-quadratic regulator (LQR) algorithm to pass a window with slung load without the need for manual manipulation of the system dynamics, heuristic simplifications, or manual trajectory generation. RL can easily apply the navigation and collision avoidance mechanisms by learning from scratch, via a continuous, self-supervised learning process with less human effort involved and provide much more reliable simulation for more complicated non-linear dynamic systems. RL allows for further advancement of the mobility functionalities of robots.

2.3 Workpiece recognition and selection

The robot needs to go to its workpiece instead of having the workpiece brought to it, which produces a reversed spatial conveyance between the robot and the product [33]. Construction materials (i.e., workpiece) tend to exhibit considerable geometric variation. Due to their substantial size and properties, materials are often susceptible to large deflections and geometric irregularities [34]. Thus, the methods used to sense and identify the material on specific parts of the structure would be crucial for the robot to navigate around the site and find the right place to start the construction work. Previous research has investigated the ability of construction robots to adapt to the actual pose and geometry of their workpiece to perform their work. The following subsections address some of the key elements required.

2.3.1 Model registration techniques

Some approaches in manufacturing register complete 3D CAD models to determine the relative pose of the workpiece to be carried out [35]. However, such approaches are not expected to work well for construction tasks because the geometry of an individual workpiece can deviate substantially from its as-designed shape [36]. Previous studies utilized model registration techniques by matching the corresponding data and information of the workpiece with the registered models to figure out the relative pose between the as-designed object and the actual object. [7] proposed a framework to sense the data of complicated and irregular materials by producing a correlation score between the sensor data and the model to conduct dexterous tasks. These tasks require acquiring enormous and high-quality information from the environment, which requests an advanced integrated sensing system to describe the real world. Besides, the matching process also relies on human efforts or advanced algorithms to provide quick and reliable feedback. There is still great potential for the advancement of techniques and integrated frameworks to generate reliable feedback to on-site robotic systems.

2.3.2 Vision-based techniques

To get precise information and sensor data of the pose and the geometry of the workpiece, many studies used vision-based techniques such as fiducial markers to target desired objects for on-site construction robots. [37] proposed a framework using fiducial markers for robots to set specific waypoints to navigate around the building to gather information. However, the approach required the environment to be fitted with fiducial markers, which may not be ideal for real-world construction applications.

Other computer vision techniques (e.g., stereo images, edge detection, and laser scanning) have been used to find the best algorithm and strategy to identify the

workpiece. Some examples are summarized next.

1. *Stereo images*

[38] showed the rudimentary ability of a robot to identify and pick up tiles using stereo cameras and a suction gripper in a robotic tile installation operation. Stereo images can help with the 3D reconstruction of specific objects; however, the efficiency and accuracy of the learning algorithm significantly limited the shape and categories of the materials.

2. *Edge detection*

[39] and [40] used edge detection to identify simple shape wires; however, their applications might not work well for a wide range of object geometries. The edge detection approach and algorithm are widely developed and greatly used in related areas, such as self-driving vehicles using supervised learning, or a weakly supervised learning framework. For example, [41] proposed a segmentation-detection collaborative network (SDCN) for more precise object detection under weak supervision with less dataset required. With these advancements in object detection techniques, on-site construction robotic system could be further developed to recognize more complicated and specific materials.

3. *Laser scanning*

Another method to get the geometry and pose of the objects is using laser scanning techniques to get the point-cloud data of the object and then clarify the object into different classes. [42] demonstrated that a robotic excavator could use laser rangefinders to adapt its plan to the topology of nearby soil and the pose of a nearby truck for a digging and dumping operation. Similarly, [43] showed that a robot could construct a dry block wall in an adaptive manner by sensing the wall's top course with a 2D laser rangefinder and modifying the installation poses of subsequent blocks accordingly. However, point clouds are massive and do not have specific classifications.

2.4 Task execution and planning

Once the materials are prepared, the next stage is to generate the execution plan. Instead of manually hardcoding the plan and trajectory to execute specific tasks, machine learning techniques can be used to train the robot so that the best trajectories and motions can be autonomously generated. Among multiple varieties of machine learning technologies, RL is the most relevant techniques to the robotic motion and control. RL is a subfield of machine learning where an agent learns by interacting with its environment, observing the results of these interactions, and receiving a reward accordingly [44]. RL enables a robot to autonomously discover an optimal behavior through trial-and-error interactions with its environment.

2.4.1 RL applications

Many studies have contributed to the applications of RL in robotics, included locomotion [45], manipulation [46], and autonomous vehicle control [47]. However, there are very few reinforcement learning-based applications for construction robots. Most of them are in the areas of simple tasks such as grasping objects, in-hand object manipulation, door opening, and simple structures construction. For example, [48] described an iterative decentralized planning and learning method, to generate construction and motion strategies to build different types of three-dimensional structures using multiple quadrotors. [49] presented a framework using an actor-critic algorithm consisting of small autonomous mobile robots and block sources, which allows robots to gather blocks from the sources to build a user-specified structure.

2.4.2 From Single-Agent to Multi-Agent

In early 2016, [50] proposed a novel multi-agent framework along with deep reinforcement learning to learn a single-agent policy.

For large-scale control systems and communication networks, multi-agent reinforcement learning allows collaboration among different agents. The system's behavior is influenced by the whole team of simultaneously and independently acting agents in a common environment. For example, [51, 52] investigated a network which optimally divides the tasks for indoor building environment navigation among a group of robots to determine optimal routes to visit multiple locations. This is crucial for large-scale work, especially construction activities, which allows multiple robots to work simultaneously and can either give feedback to other agents or speed up construction work.

3 Discussion and proposed system

Construction robots have the potential to conduct specific construction tasks autonomously. A possible direction for the evolution of on-site robots is to train them to construct like human beings without humans' hardcoding or preprogrammed orders. This means that after getting the models and instructions from the engineers and designers, robotic systems can automatically make their own decisions and select different materials among various parts of the structure to accomplish complicated tasks. With that in mind, we proposed a high-level (conceptual) on-site autonomous construction robotic framework that combines CV and ML techniques (Figure 1).

3.1 Localization

We propose to fulfill the autonomous localization function by using SLAM algorithms, such as V-SLAM (RGB-sensor, Inertial Measurement Unit), and Laser-SLAM (Kinect) and point cloud segmentation to map and reconstruct the dynamic environment into virtual models. This allows to set up the position of execution by using augmented markers or manual selection.

For path planning in real-world on-site construction, robots should be able to work on large construction sites to fulfill different functionalities such as climbing, getting across holes, and balancing on uneven surfaces. The controllers for that involve complex analytical manipulation of the dynamics, which requires lots of extra effort to program. Reinforcement algorithms seem to be a good fit for more complex robotic applications that allow real-time environment feedback with less error while providing robust control for localization.

3.2 Workpiece recognition and selection

The proposed framework uses a combination of model registration techniques and sensing techniques to find the right materials to use and the installation position of the workpiece. BIM and CAD models are used by previous research to conduct the matching between a pre-designed plan to the material in use. With relation to the virtual models created in the localization subsection, the reconstructed VR models of the environment can also help with the matching of the real-world materials with desired models and provide feedback on the construction process. In general, the next step to recognize and select materials is set up manually with much effort of commanding. In the conceptual framework, with a predefined dataset of materials to use in the designed structure (i.e., stereo images, edge detection, laser scanning), the robots could automatically recognize the materials required through deep neural networks. Even though they are in different shapes or different locations, the robots could tell them apart in different classes. The matching process can provide state and action feedback for robots to generate the execution plan in order to get the required materials when constructing a complicated structure composed of different materials.

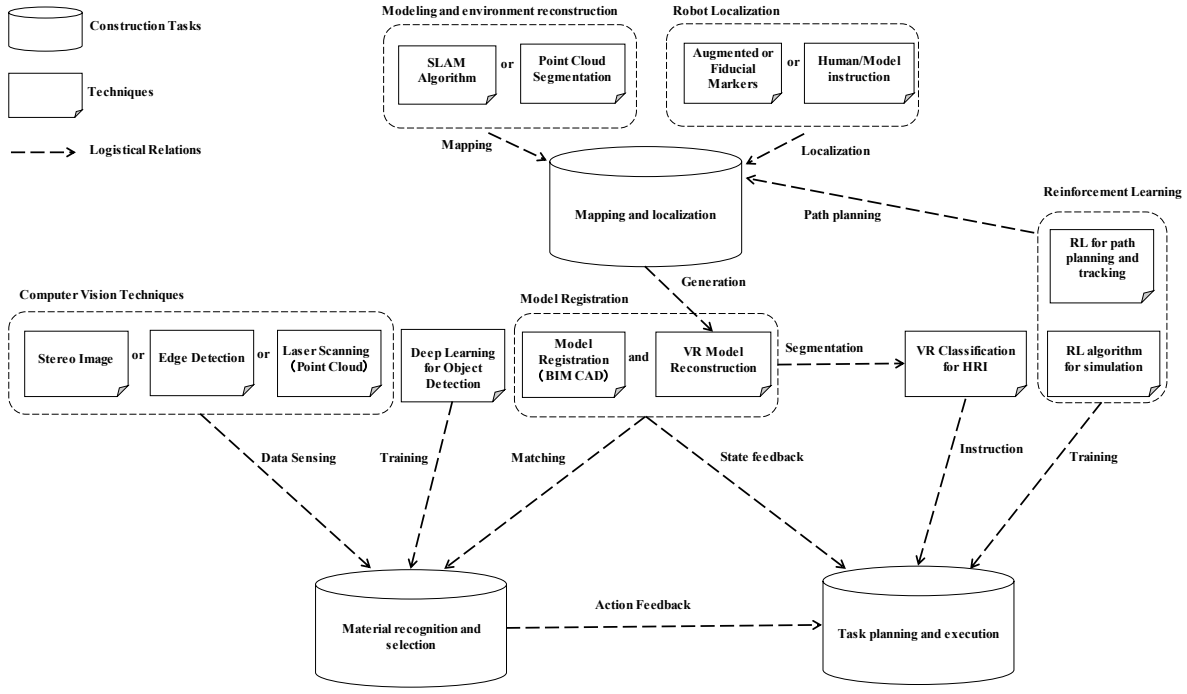

Figure 1. Conceptual on-site autonomous construction robotic system

3.3 Task execution and planning

For the autonomous execution and planning of tasks, there is no doubt that a combination of robotics and reinforcement learning will be very relevant. Some simple tasks (e.g., laying bricks, tying rebar, installing doors), could be done by current computation capacity and frameworks developed. With the information of the environment extracted from the previous step of mapping and information of material, we can describe the state of the robot and task. Then algorithms can be developed with a predefined reward policy to tell the robot what the

demanded motion or execution is. Commonly used is the deep neural network-reinforcement learning framework or inversed reinforcement learning, which can teach the robot to search for the right policy when the environment and state evolve. This can greatly decrease the human interaction with the robot(s) during construction. Besides, the proposed framework allows for the advancement of multiple robots to do the construction at the same time on the same tasks with future development.

4 Conclusions and outlook

Robotic systems have the potential to provide numerous advantages to the construction industry. This paper summarizes and discusses some of the techniques and algorithms that could be used to develop autonomous on-site construction robots further. Based on that, we propose a generic conceptual framework that can fulfill the whole construction process with minimal human interaction. We suggest using computer vision techniques and point clouds with an advanced algorithm to detect, identify, and reconstruct components in the construction environment. The framework aims to train the robot to understand the environment and identify the task and allocated materials in construction sites. Besides, the framework involves virtual reality models to extract and deliver information to robots for simulation and training, which not only guarantees the best solution for construction tasks but also allows the monitoring and controlling process to ensure that the motion and execution of the robots are executed as planned. At the same time, we propose reinforcement learning to train robots to learn like humans so that they can learn from previous errors and the results from previous iterations conducted during the simulation.

However, there are still some big challenges in the implementation of the proposed framework. First, the complexity of the construction site could produce noise to the robotic system, which will greatly influence the efficiency and accuracy. Second, the calculation capacity of the algorithm is not advanced enough to finish a complicated task. Techniques and algorithms are still in development and require extra effort to test and improve. Third, the implementation from the virtual world to the real environment could result in unexpected differences. To solve this problem, more advanced sensing techniques and more accurate models need to be generated in order to make sure the accuracy of the simulation process.

Future work includes testing the efficiency of the proposed framework using a robotic arm to build-up specific applications with computer vision techniques and reinforcement learning algorithms. We will develop and test schemes on mapping and reconstruction of real-world construction environments into virtual models. Tests will be conducted on construction materials from simple shape to irregular shape, as well as from single category to multi-categories. Based on this, we will train the robot to generate its own execution plan, from a single task to complex works that involve multiple tasks. To account for scalability, a multi-agent-based framework that allows several robots to collaborate will be considered.

References

[1] S. Lee, “Glazed Panel Construction with Human-Robot Cooperation,” New York, NY, USA*: Springer, vol. 8,* 2011. DOI: https://doi.org/10.1007/978-1-4614-1418-6

[2] B.R.K. Mantha, B. García de Soto, C.C. Menassa, and V.R. Kamat, “Robots in indoor and outdoor environments,” Chapter 16. In A. Sawhney, M. Riley & J. Irizarry (Eds.). *Construction 4.0: An Innovation Platform for the Built Environment* (pp. 307-325). 1st Edition. London: Routledge, 2020. DOI: https://doi.org/10.1201/9780429398100-16

[3] E. Rojas, P. Aramvareekul, “Is construction labor productivity really declining?” *J. Constr. Eng. Manag.* 129 (1), 41-46, 2003. DOI: http://dx.doi.org/10.1061/(ASCE)0733-9364(2003)129:1(41)

[4] B. García de Soto and M.J. Skibniewski, “Future of robotics and automation in construction,” Chapter 15. In A. Sawhney, M. Riley & J. Irizarry (Eds.). *Construction 4.0: An Innovation Platform for the Built Environment* (pp. 289-306). 1st Edition. London: Routledge, 2020. DOI: https://doi.org/10.1201/9780429398100-15

[5] C. Feng, Y. Xiao, A. Willette, W. McGee, V.R. Kamat, “Vision guided autonomous robotic assembly and as-built scanning on unstructured construction sites,” *Autom. Constr.*, Volume 59, 128–138, 2015. DOI: https://doi.org/10.1016/j.autcon.2015.06.002

[6] C.J. Liang, K. M. Lundeen, W. McGee, C. C. Menassa, S.H. Lee, V. R. Kamat, “A vision-based marker-less pose estimation system for articulated construction robots,” *Autom. Constr.,* Volume 104, pp. 80-94, 2019. DOI: https://doi.org/10.1016/j.autcon.2019.04.004

[7] K.M. Lundeen, V. R. Kamat, C. C. Menassa, W. McGee, “Autonomous motion planning and task execution in geometrically adaptive robotized construction work,” *Autom. Constr.,* Volume 100, pp. 24-45, ISSN 0926-5805, 2019. DOI: https://doi.org/10.1016/j.autcon.2018.12.020

[8] T. Bock, T. Linner, “Robotic Industrialization: Automation and Robotic Technologies for Customized Component, Module, and Building Prefabrication,” *Cambridge University Press,*

2016.
[9] L. Jaillon, C.S. Poon, "The evolution of prefabricated residential building systems in Hong Kong: a review of the public and the private sector," *Autom. Constr.*, 18, pp. 239-248, 2009. DOI: https://doi.org/10.1016/J.AUTCON.2008.09.002
[10] S. Lim, R.A. Buswell, T.T. Le, S.A. Austin, A.G.F. Gibb, T. Thorpe, "Developments in construction-scale additive manufacturing processes," *Autom. Constr.*, 21, pp. 262-268, 2012. DOI: https://doi.org/10.1016/J.AUTCON.2011.06.010
[11] I. Perkins, M. Skitmore, "Three-dimensional printing in the construction industry: a review," *Int. J. Constr. Manag.*, 15, pp. 1-9, 2015. DOI: https://doi.org/10.1080/15623599.2015.1012136
[12] P. Wu, J. Wang, X. Wang, "A critical review of the use of 3-D printing in the construction industry," *Autom. Constr.*, 68, pp. 21-31, 2016. DOI: https://doi.org/10.1016/J.AUTCON.2016.04.005
[13] A. Jayaraj, H.N. Divakar, "Robotics in construction industry," *IOP Conf. Ser. Mater. Sci. Eng.*, 376, p. 012114, 2018. DOI: https://doi.org/10.1088/1757-899X/376/1/012114
[14] S. Dritsas, G.S. Soh, "Building robotics design for construction," *Constr. Robot.*, pp. 1-10, 2018.
[15] A. Więckowski, "JA-WA - a wall construction system using unilateral material application with a mobile robot," *Autom. Constr.*, 83, pp. 19-28. 2017. DOI: https://doi.org/10.1016/j.autcon.2017.02.005
[16] T. Bock, T. Linner, "Site Automation: Automated/Robotic On-Site Factories," *Cambridge University Press,* 2016.
[17] C. Kasperzyk, M.-K. Kim, I. Brilakis, "Automated re-prefabrication system for buildings using robotics," *Autom. Constr.*, 83, pp. 184-195, 2017. DOI: https://doi.org/10.1016/j.autcon.2017.08.002
[18] K. Asadi, H. Ramshankar, H. Pullagurla, A. Bhandare, S. Shanbhag, P. Mehta, S. Kundu, K. Han, E. Lobaton, T. Wu, "Vision-based integrated mobile robotic system for real-time applications in construction," *Autom. Constr.*, Volume 96, pp. 470-482, 2018. DOI: https://doi.org/10.1016/j.autcon.2018.10.009
[19] H. Peel, S. Luo, A.G. Cohn, R. Fuentes, "Localisation of a mobile robot for bridge bearing inspection," *Autom. Constr.*, 94, pp. 244-256, 2018. DOI: https://doi.org/10.1016/J.AUTCON.2018.07.003
[20] C. Brown, "Autonomous vehicle technology in mining," *Eng. Min. J.*, 213 (2012)
[21] S. Dadhich, U. Bodin, U. Andersson, "Key challenges in automation of earth-moving machines," *Autom. Constr.*, 68, pp. 212-222, 2016. DOI: https://doi.org/10.1016/J.AUTCON.2016.05.009
[22] N. Koyachi, S. Sarata, "Unmanned loading operation by autonomous wheel loader," *ICCAS-SICE, Fukuoka, 2009, pp. 2221-2225,* 2009.
[23] T. Bock, T. Linner, W. Ikeda, "Exoskeleton and humanoid robotic technology in construction and built environment," *The Future of Humanoid Robots-Research and Applications, InTech,* 2012.
[24] M.P. de Looze, T. Bosch, F. Krause, K.S. Stadler, L.W. O'Sullivan, "Exoskeletons for industrial application and their potential effects on physical workload," *Ergonomics*, 59, pp. 671-681, 2016. DOI: https://doi.org/10.1080/00140139.2015.1081988
[25] A. Alwasel, K. Elrayes, E. Abdel-Rahman, C. Haas, "Reducing shoulder injuries among construction workers," *ISARC*, pp. 1–5, 2012.
[26] J.M. Davila Delgado, L. Oyedele, A. Ajayi, L. Akanbi, O. Akinade, M. Bilal, H. Owolabi, "Robotics and automated systems in construction: Understanding industry-specific challenges for adoption," *Journal of Building Engineering*, Volume 26, 100868, ISSN 2352-7102, 2019. DOI: https://doi.org/10.1016/j.jobe.2019.100868
[27] Z. Shang, Z. Shen, "Real-time 3D Reconstruction on Construction Site using Visual SLAM and UAV," *Construction Research Congress 2018*, American Society of Civil Engineers, 2018. DOI: http://dx.doi.org/10.1061/9780784481264.030
[28] B.R.K. Mantha, C.C. Menassa, V.R. Kamat, "Robotic data collection and simulation for evaluation of building retrofit performance," *Autom. Constr.*, Volume 92, Pages 88-102, 2018. DOI: https://doi.org/10.1016/j.autcon.2018.03.026
[29] S.A. Prieto, B. García de Soto, A. Adán, "A Methodology to Monitor Construction Progress Using Autonomous Robots," *ISARC*, 2020.
[30] A. Adán, B. Quintana, S.A. Prieto, F. Bosché, "An autonomous robotic platform for automatic extraction of detailed semantic models of buildings," *Autom. Constr.*, Volume 109, 102963, 2020. DOI: https://doi.org/10.1016/j.autcon.2019.102963
[31] Y.-C. Lin, B. Ponton, L. Righetti, and D. Berenson, "Efficient Humanoid Contact Planning using Learned Centroidal Dynamics Prediction," in 2019 *IEEE International Conference on Robotics and Automation (ICRA)*, Montreal, 2019.
[32] C. de Crousaz, F. Farshidian, M. Neunert, and J. Buchli, "Unified motion control for dynamic quadrotor maneuvers demonstrated on slung load and rotor failure tasks," 2015 *IEEE International*

Conference on Robotics and Automation (ICRA), Seattle, WA, pp. 2223-2229, 2015. DOI: https://doi.org/10.1109/ICRA.2015.7139493

[33] C. Feng, Y. Xiao, A. Willette, W. McGee, V.R. Kamat, "Towards autonomous robotic in-situ assembly on unstructured construction sites using monocular vision," *ISARC*, pp. 163–170, 2014. DOI: https://doi.org/10.22260/ISARC2014/0022

[34] D.T. Koenig, "Process Control Engineering and Quality Control in Job Shops: In Manufacturing Engineering: Principles for Optimization, *ASME Press*, New York, pp. 279–284, 2007. DOI: https://doi.org/10.1115/1.802493.ch10

[35] M. Rodrigues, M. Kormann, C. Schuhler, P. Tomek, "An intelligent real time 3D vision system for robotic welding tasks," *IEEE 2013 9th International Symposium on Mechatronics and its Applications (ISMA)*, pp. 1–6, 2013. DOI: https://doi.org/10.1109/ISMA.2013.6547393

[36] J. Willmann, M. Knauss, T. Bonwetsch, A.A. Apolinarska, F. Gramazio, M. Kohler, "Robotic timber construction—expanding additive fabrication to new dimensions," *Autom. Constr.*, Volume 61, pp. 16–23, 2016. DOI: https://doi.org/10.1016/j.autcon.2015.09.011

[37] B.R.K. Mantha and B. García de Soto, "Designing a Reliable Fiducial Marker Network for Autonomous Indoor Robot Navigation" *ISARC*, pp. 74–81, 2019. DOI: https://doi.org/10.22260/ISARC2019/0011

[38] D.H. Jung, J. Park, M. Schwartz, "Towards on-site autonomous robotic floor tiling of mosaics," *IEEE 14th International Conference on Control, Automation, and Systems (ICCAS)*, pp. 59–63, 2014. DOI: https://doi.org/10.1109/ICCAS.2014.6987959

[39] M. Giftthaler, T. Sandy, K. Dörfler, I. Brooks, M. Buckingham, G. Rey, M. Kohler, F. Gramazio, J. Buchli, "Mobile robotic fabrication at 1:1 scale: the in situ fabricator," *Constr. Robot.* 3–14, 2017. DOI: https://doi.org/10.1007/s41693-017-0003-5

[40] M. Lussi, T. Sandy, K. Doerfler, N. Hack, F. Gramazio, M. Kohler, J. Buchli, "Accurate and adaptive in situ fabrication of an undulated wall using an on-board visual sensing system," *IEEE International Conference on Robotics and Automation (ICRA)*, 2018. DOI: https://doi.org/10.3929/ethz-b-000227968

[41] X. Li, M. Kan, S. Shan, X. Chen, "Weakly Supervised Object Detection with Segmentation Collaboration," *IEEE International Conference on Computer Vision (ICCV)*, pages 1440–1448, 2015.

[42] A. Stentz, J. Bares, S. Singh, P. Rowe, "A robotic excavator for autonomous truck loading," *Auton. Robot.* 7 (2) 175–186, 1997. DOI: https://doi.org/10.1023/A:1008914201877

[43] V. Helm, S. Ercan, F. Gramazio, M. Kohler, "Mobile robotic fabrication on construction sites: DimRob," *IEEE/RSJ International Conference on Intelligent Robots and Systems (IROS)*, pp. 4335–4341, 2012.

[44] J. Kober, J. Andrew (Drew) Bagnell, and J. Peters, "Reinforcement Learning in Robotics: A Survey," *International Journal of Robotics Research*, July 2013.

[45] N. Kohl and P. Stone, "Policy gradient reinforcement learning for fast quadrupedal locomotion," *International Conference on Robotics and Automation (IROS)*, 2004.

[46] E. Theodorou, J. Buchli, and S. Schaal, "Reinforcement learning of motor skills in high dimensions," *International Conference on Robotics and Automation (ICRA)*, 2010.

[47] P. Abbeel, A. Coates, M. Quigley, and A. Ng, "An application of reinforcement learning to aerobatic helicopter flight," *Advances in Neural Information Processing Systems (NIPS)*, 2006.

[48] S. R. Barros dos Santos, S. Givigi, C. L. Nascimento, *Intelligent Robot System*, 90: 217, 2018. DOI: https://doi.org/10.1007/s10846-017-0659-6

[49] G. Sartoretti, Y. Wu, W. Paivine, T. K. S. Kumar, S. Koenig, H. Choset, "Distributed Reinforcement Learning for Multi-Robot Decentralized Collective Construction," In: Correll N., Schwager M., Otte M. (eds) Distributed Autonomous Robotic Systems. *Springer Proceedings in Advanced Robotics*, vol 9. pp. 35-49, Springer, Cham, 2019. DOI: https://doi.org/10.1007/978-3-030-05816-6_3

[50] V. Mnih, A.P. Badia, M. Mirza, A. Graves, T. Lillicrap, T. Harley, "Asynchronous methods for deep reinforcement learning," *In Proceedings of the International Conference on Machine Learning*, pp. 1928-1937, 2016.

[51] B.R.K. Mantha and B. García de Soto, "Task Allocation and Route Planning for Robotic Service Networks with Multiple Depots in Indoor Environments," *ASCE International Conference on Computing in Civil Engineering (i3CE2019)*, June 2019. DOI: https://doi.org/10.1061/9780784482438.030

[52] B.R.K. Mantha, M.K. Jung, B. García de Soto, C.C. Menassa, V.R. Kamat, "Generalized Task Allocation and Route Planning for Robots with Multiple Depots in Indoor Building Environments," *Autom. Constr.*, Volume 119, 2020. DOI: https://doi.org/10.1016/j.autcon.2020.103359

Curtain Wall Installation for High-Rise Buildings: Critical Review of Current Automation Solutions and Opportunities

B. Johns[a], M. Arashpour[b] and E. Abdi[a]

[a]Department of Mechanical and Aerospace Engineering, Monash University, Australia
[b]Department of Civil Engineering, Monash University, Australia
E-mail: brandon.johns@monash.edu, mehrdad.arashpour@monash.edu, elahe.abdi@monash.edu

Abstract –

In the construction of high-rise buildings, the conventional methods for the on-site installation of prefabricated facade modules require considerable manual handling. This unsafe and inefficient practice can be solved through automation.

This paper critically reviews automated Unitized Curtain Wall (UCW) installation and discusses opportunities for future development, as found in adjacent fields. A generalized solution to the installation of UCW modules is applied to analyze the conventional method in safety, economic efficiency, and logistic viability.

Recent automation solutions control wall module vertical transport trajectories with guide rails or redundant parallel cables. Both approaches specialize in capability, leaving many installation scenarios unautomated. Opportunities for improvement exist in efforts to automate crane operations by development of robotic crane end effectors. Localization in uncertain conditions for automated feature detection can be improved by dynamically changing the operator interface. Directions to improve safety and efficiency of UCW on-site installation are identified and recommendations are presented.

Keywords –

Assembly; Automation; Construction; Control systems; Curtain wall; Facade; High-rise building; Installation; Robotics; Tower crane

1 Introduction

The method chosen to construct the exterior wall of a high-rise building can significantly affect the entire construction process [1, 2]. Consideration of worker safety, economic efficiency, and logistic viability is of high importance in choosing the optimal solution. Potential for construction delays is increased with reliance on shared workspace [1–3] and equipment [1, 2, 4].

The unitized curtain wall (UCW) is a non-structural facade that is potentially compatible with these considerations. UCWs are comprised of prefabricated modules, hence complex designs can be manufactured in low cost, high precision factory environments [5]. The on-site installation procedure is also faster compared to other wall types [5].

High-rise building facades commonly incorporate UCWs, but the conventional method for on-site installation is unsafe and inefficient [1]. During installation, curtain wall modules (CWMs) are lifted by crane, hoist, or telescopic handler to the attachment location and then fixed to brackets which are preinstalled on the building [6]. The conventional installation method requires considerable manual handling to guide the large, heavy, suspended wall modules into position [6]. This presents risk of collision which can cause human injury or damage to the CWM [3].

Automation of the on-site UCW installation procedure is a solution to these issues. However, the current automation solutions are limited in addressing only a small part of the installation procedure [7], or in scope of application [2, 8]. For example, many automation solutions are limited to handling only common types of CWM [2, 7, 8], hence they do not apply to custom designs as in [9].

Automation of high-rise construction, including curtain wall installation, was reviewed by Cai et al. [10, 11]. To increase interdisciplinary communication, it was suggested to review the advancement of basic technologies that can be utilized in high-rise construction [11]. Iturralde et al. explored the task of lifting CWMs from the ground to the attachment location for an optimal automation solution [12]. However, the scope of their research did not include informational tasks.

This paper critically reviews the state of the art in UCW installation methods and discusses the potential incorporation of related mechanical and informational technologies. A generalized solution to CWM vertical transportation from the ground to the installation point and precision alignment with the attachment location is presented. The relations among components of the solution are then discussed and flaws in the conventional

installation methods are identified. Venues for further improvement are then determined through analysis of automation technologies in adjacent fields with respect to the generalized solution.

Section 2 describes the scope and methodology of this review. Section 3 then presents the generalized solution for vertical transport and precision alignment of CWMs, then discusses limitations in the conventional solution. In section 4, venues for improvement are suggested in the mechanical design as well as in the informational processes of sensing, analysis, operator feedback, and operator control. Conclusions and future research directions are then presented in section 5.

2 Research Scope and Methodology

The UCW installation procedure is described by Taghavi et al. [6] and Yu et al. [7]. The procedure comprises of designing the curtain wall, manufacturing CWMs, delivery to the construction site, vertical transportation to the installation point, alignment with the attachment location, and attachment of CWMs to the building. Within this procedure, the attachment interface on the building side can be prepared before, or at the point of, module attachment [6]. The scope of this paper is limited to the tasks of CWM vertical transportation and alignment with the attachment location. These tasks are particularly dangerous in the conventional procedure, while there is potential to significantly improve both safety and economic efficiency through mechanization and automation [1–4, 13].

This review includes literature directly related to UCW installation as well as literature from other fields where the mechanisms and processes are relevant to UCW installation. The reviewed mechanisms and processes are categorized in Figure 1.

The literature search mostly utilized the search engine ‘Google Scholar’ as a means to reduce bias towards specific research fields, conferences, or journals. Search keywords that were identified by Cai et al. [11] were utilized. The most relevant were ‘curtain wall’, or ‘facade’, with ‘installation’, ‘assembly’, ‘automation’, or ‘robot’. Other keywords were identified through relating mechanisms and processes utilized during UCW installation. For example, ‘crane’ was combined with ‘vision’, ‘mapping’, ‘localization’, ‘skew control’, and ‘operator assistance’. Results were filtered by title and then abstract, based on relevance. Further literature was found with the snowball methodology; by following the citations found in highly relevant literature.

Where large volumes of similar literature were found, only representative samples were selected to be discussed in this review. This increases the breadth of the review, as the review is intended to broadly survey the applicable technologies rather than focus on the individual implementation of each. The selection criteria weighed year of publication, number of citations, and relevance to UWC installation.

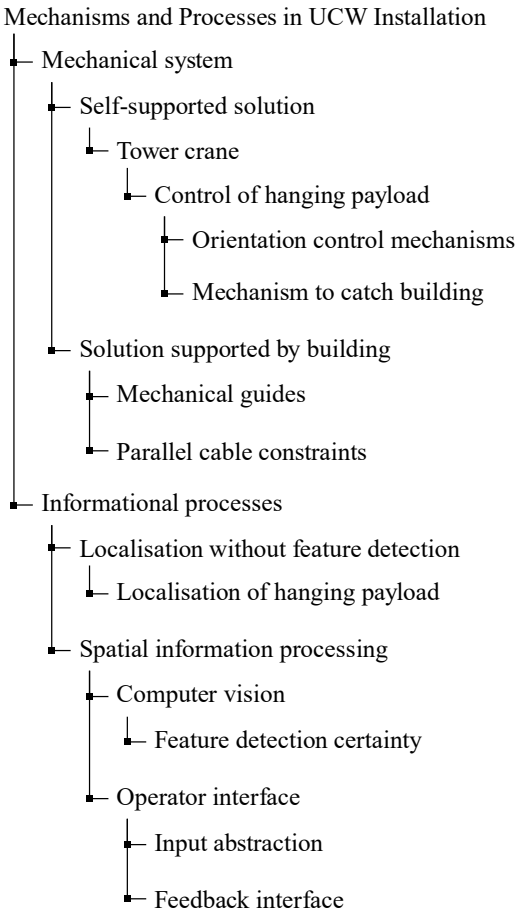

Figure 1. Reviewed mechanisms and processes

3 The UWC Installation Method

A generalized solution to CWM vertical transportation and precision alignment is presented in Figure 2. The desired state of the system has the CWM aligned to the attachment location. To achieve this, the decision-maker commands the hardware controller, which actuates the mechanical system toward the desired state. The state of the system is sensed, and the sensed information is pre-processed by the analysis unit before being fed back to the decision-maker. Information may also be sent directly from the sensors or analysis unit to the controller, creating an inner feedback loop to stabilize the system state by suppressing deviations from the command signal.

There are two main conventional UCW installation methods: direct and staged. Figure 3 presents the direct method. In this approach, CWMs are lifted directly from

the ground to the attachment location with a crane or hoist. This method is used as a basis for comparison, rather than the staging methods described in [1, 3, 6, 7], as it is more similar to the most recent automation solutions [1, 2, 4, 6, 9]. The direct method is most appropriate for large and heavy CWMs. It is faster to install UCWs that are comprised of larger modules [2, 3, 14]. Additionally, by not requiring on-floor staging, the impact on other construction operations can be reduced [1, 2]. This follows the lean construction methodology of decoupling operations.

In the direct conventional method, the operator of the crane or hoist performs analysis and decision-making. Their role is to send commands to the hardware controller based on feedback from the sensors. The hardware controller actuates the mechanical system based on the operator's input. Feedback from crane pose measurement sensors allows tracking of the command and deployment of anti-sway technologies [15]. These sensors also feedback to the operator's user interface.

The crane 'dogman' is situated at the installation point. They perform sensing and analysis of spatial information for localization, and feedback this information to the operator [16]. In the case of a 'blind lift', where the crane operator cannot see the CWM directly, the operator is entirely dependent on the dogman. The dogman also performs decision-making and actuates the system to control the orientation and position of the CWM during the alignment phase. With their interdependent responsibilities, the crane operator and dogman must operate in unison. Hence the installation speed is limited by the speed of communication between the crane operator and dogman [17].

This indicates that the safety and efficiency of UCW installation can be improved through automation of the work conventionally performed by the dogman. The effectiveness of removing the dogman is supported by the results of research to automate crane operations, as applied in adjacent fields. Crane operator performance can be improved in safety and efficiency through utilization of automated systems to sense, analyze and feedback spatial information [13]. Mechanization of payload orientation control with an active rotary crane hook is economically beneficial and greatly increases safety [18]. Combining an active rotary crane hook with automated alignment sensing and analysis unit can increase the speed of alignment operations [19].

The solution to safe and efficient CWM vertical transportation and precision alignment requires unison in communication between the systems that perform decision-making, control, actuation, sensing, and analysis. The utilization of a dogman impedes effective communication. The minimum requirements to remove the dogman are automation of sensing and analysis, and mechanization of precision positioning.

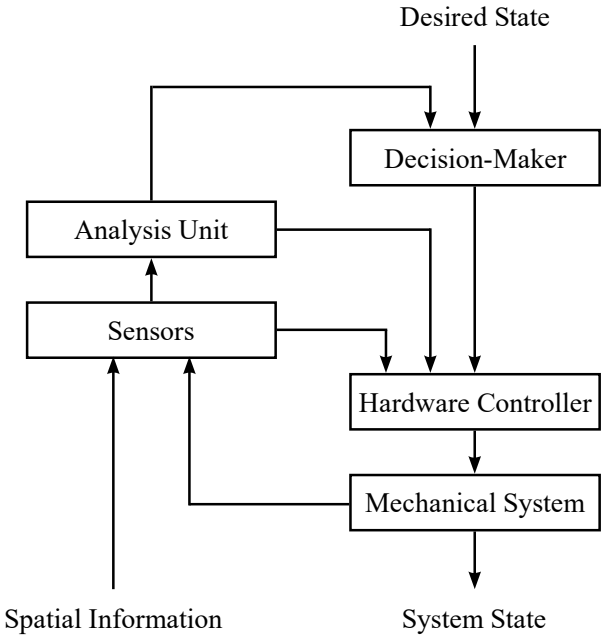

Figure 2. Generalized solution to UCW assembly

Figure 3. Direct conventional UCW installation method: Transitioning from the vertical transport task to the alignment task (photo by B. Johns, 2019)

4 Discussion of Technologies Relevant to UCW Installation

This section explores opportunities for improvement in each UCW installation mechanism and process, with the objective to eliminate the requirement of a dogman in CWM vertical transportation and precision alignment. It is assumed that an operator will be required, hence fully autonomous path planning and logistics is not explored.

4.1 Mechanical System

Mechanical requirements of the solution are CWM loadbearing, vertical transport to the attachment location, and precise position and orientation control with 1mm tolerance [8, 20].

To better interface CWMs with robotic tools, many automation solutions require specific or custom UCW designs [1, 2, 12]. This also simplifies the automation of processes that vary significantly with variation in curtain wall design, such as the automated fixing of an aligned CWM to the building. However, limiting the application of the solution to compatible designs of curtain wall could cause long term problems. For example, the solution by Friblick et al. [1] does not allow for CWMs to be installed with any procedure other than the intended procedure. Hence, repairs to and disassembly of the proprietary mechanism may require special parts and tools that have ceased being produced during the lifespan of the UCW. Thus, we mainly highlight solutions that are compatible with existing designs of curtain wall.

The most appropriate class of robot for performing high-rise UCW installation without on-floor staging, has previously been assessed as the hanging robot [12]. A challenge for hanging systems is to control all degrees of freedom (DOF) with the precision required for the alignment operation. In the conventional solution, a single vertical hoist cable usually supports the CWM. This system is highly underactuated and susceptible to wind induced oscillations [21], hence the need for a dogman to perform fine position and orientation control.

Two approaches to control a hanging system are to either suppress oscillations with control systems or to introduce additional kinematic constraints. Given the large workspace, the only practical available stationary reference for constraint is the building that is under construction [12]. For example, an effective strategy is to attach guide rails to the building and hoist CWMs along the single remaining DOF [1, 2]. In constrained systems, it is often required for the building to support the load of the installation system and CWM. This increases potential to significant cost reduction [1–3]. Conversely, this may not be practical if the geometry of the building is not suitable or if higher floors are not yet completed. The following discussion is divided into solutions that require the load of the CWM to be supported by the building, and solutions that can independently support the load.

4.1.1 Self-Supported Solutions

Tower cranes are, to the best of our knowledge, the only independent load support structure deployed in high-rise UCW installation. The lack of utilization of other types of support body in high-rise construction indicates that no other independent support structure is practical, backed by the analysis by Iturralde et al. [12]. In the crane supported installation method, any geometry of CWM can be lifted to any attachment location that is not below overhanging building geometry. Hence, this method can be deployed to almost any application. The requirement of situating a tower crane on-site is typically satisfied due to the requirements of other on-site construction operations, and the crane can be shared amongst these operations [1].

To achieve the positional accuracy required for UCW installation, all vibrational modes of the suspended CWM should be suppressed. For a load supported by a single vertical cable, such as a crane suspended load, while allowing for elasticity of the cable, there are 6 DOF of vibrational modes. They are sway (pendulum swinging of the hook with 2 DOF), roll (payload tilting about the hook with 2 DOF), skew (rotation about the cable axis with 1 DOF), and heave (linear oscillation along the cable axis with 1 DOF) [22]. Based on a 2017 review of crane control systems [21], most research considers only the sway modes with a few considering the roll modes. Very little research considers skew [23] or heave [21].

Heave, roll, and sway oscillations can be controlled with regular tower crane motions; however, control is underactuated. Furthermore, the rotational motion of the jib about the tower (slewing), has highly coupled non-linear dynamics, making control of the payload very difficult [21]. Hence, to achieve the positional accuracy needed to install a CWM, an additional mechanism is required.

With the assumption that the alignment roll orientation is consistent for each application and does not need to be changed often, the roll orientation can be manually set to the aligned orientation before the lift operation by adjusting the rigging configuration. In this case, pre-setting the roll orientation and passively or actively suppressing roll oscillations does not limit the system capabilities. If this assumption is not valid, then a mechanism that translates the center of mass relative to the hook can adjust roll orientation by small angles [24].

Active skew control is necessary to perform alignment with complex building geometry or when using slewing cranes [25]. Several devices have been developed which utilize heavy flywheels to exert skew torque through conservation of angular momentum [19, 26]. These devices can become saturated and must

be heavy to be effective. Another method of skew control is seen on harbor cranes. For slewing harbor cranes, skew control is achieved with an active rotary crane hook (also known as a 'Rotator' or 'Power Swivel') [23, 25, 27, 28]. For system stability, at least two separated cables must connect the trolley and hook block. Full scale outdoor experiments show that very small skew error is achievable [25], likely to a degree that is sufficient for UWC installation.

To aid in vibration suppression when the CWM is near to the building, the building and the previously installed CWMs can act as reactionaries. A manipulator can take hold of the building and drive the CWM into position by utilizing the sway degrees of freedom [29] or an extendable hook attachment [30]. For the gripper type, inspiration can be taken from harbor crane operations, where the spreader is mechanically aligned to the target container with 'flippers'. The flippers are driven closed onto the edges of the container from all directions, mechanically forcing the parts into alignment.

For the swaying manipulator to catch the reactionary, an impulsive load will be generated. Thus, to prevent damage to the building or CWM, dampening of the collision is required. This problem has been investigated in research to assemble suspended large steel beams, where a pre-acting control strategy has been proposed [29]. An adaptation would need to be made for the swaying crane end-effector to catch the building instead of the other way around.

4.1.2 Load Supported by the Building

Rather than lifting CWMs to the attachment location and then catching the building for stability, CWMs can be guided through a constrained path throughout the entire lift. As risk of damage by collision with the building is eliminated, the lift path can stay close to the building for the entire lift [1–3]. This allows for performing the lift with a hoist that is mounted on the building, thus eliminating dependence on the expensive tower crane. The building can also support any constraining fixtures.

Kinematic constraints in current UCW installation methods include guide cables [3] or guide rails [1, 2]. These constraints limit application to geometrically prismatic buildings that can support the mass of the hoist and CWM from the location of the hoist. Furthermore, the guide rails themselves must be installed without the aid of guide rails, requiring dangerous manual labor. An alternative approach is to constrain the orientation with tensioned cables, terminated at, and attaching each corner of the CWM to the ground [31]. However, guide cables may not be feasible for automated alignment due to interference with the already installed CWMs.

In another approach, a redundantly cable-driven parallel robot for UCW installation is currently in development [6]. Tensioned cables connect the robot to the corners of the building face, over-constraining the floating robot. Even with this design, to achieve 1mm precision with the end effector, a secondary robot arm is attached to the cable suspended base through a passive damper [8, 32]. Hence this robot has many DOF, which is not ideal for cost or maintenance. Another limitation of the design is that for flat faced buildings, the constraint cables will be closely in-plane, which leaves the design sensitive to out-of-plane disturbances [33]. Additionally, the cable tension must increase as the angle of the cable from vertical increases [33]. Very large cable tension would then be required to install the top row of CWMs which the building may not be designed to withstand.

The main challenges for the mechanical system to vertically transport and precisely align CWMs are to achieve high positional accuracy and suppress vibration. Supporting the load of the system with the building has many advantages but is not suitable for every application. Supporting the CWM with a tower crane can be deployed to almost any application, but vibration suppression is more difficult. A specialized crane end effector is a potential solution to this problem.

4.2 Informational Processes

The hardware controller requires feedback of the system state to perform command tracking, and the decision-maker requires feedback of spatial information to perform path planning (Figure 2). The state of a crane system is typically characterized with pose and load measurements [27, 34], while the spatial information to feedback is dependent on the required input.

4.2.1 Localization Without Feature Detection

Measurement of the system state is a requirement of setpoint command tracking and oscillation suppression. The positional tolerance requirement of the alignment task is 1mm [8, 20]. Hence the position of the CWM relative to the attachment location needs to be measured to this tolerance. If a map of the workspace is acquired, then accurate measurement of the pose of the system is sufficient for localization.

The state of the art techniques in crane pose measurement to estimate the payload location are insufficient in accuracy and reliability for application to CWM alignment [34]. However, the nature of UCW installation separately requires both large payload displacement and accurate positioning. Hence it may be practical to utilize separate measurement systems for each task. Pose measurement can be utilized during vertical transport, as well as to deploy anti-sway technologies.

A challenge in pose measurement is determining the location of the hanging payload. The sway angle of the cable can be measured by aiming a camera horizontally

at the top segment of the cable [35]. Robustness to changes in background light levels can be achieved by utilizing an infrared camera and emitter [36]. Sway and skew can be measured together by fusing the data from an inertial measurement unit (IMU) placed on the hook block, with feed from a camera pointing down from the top of the hoist [34]. However, the reliability of computer vision techniques to identify the payload with a downward pointing camera is subject to lighting conditions, hoist length, and similarity between the colors in the background to the payload.

4.2.2 Measurement, Analysis, and Feedback of Spatial Information

Measurement of spatial information can supplement the low accuracy of crane pose measurement. CWM alignment can be measured relative to a fiducial feature of the target, by utilizing a camera or laser scanner mounted on the crane hook block. For example, a camera mounted on a crane spreader can reliability detect and locate the lock holes of shipping containers [37]. Relative alignment to adjacent CWMs can be measured accurately with computer vision utilizing structured lasers by analyzing the gaps between CWMs [38]. Error accumulation from relative measurements can be corrected by aligning measurements taken at a known location to a CAD model of the building [9].

In case of low certainty in feature detection, the operator can assist in analysis. For example, the operator can select the locations of bolt holes from a camera feed to provide a region of convergence to the feature detection algorithm [39]. After the alignment target has been identified, the controller can then perform path planning and complete the alignment semi-autonomously. This requires abstracting the operator input into higher level actions and programming the controller to decompose the task into actuator inputs [40]. This separates their decision from the action generated by internal feedback. This separation is beneficial, as absence of separation creates conflict between the operator and internal feedback anti-sway systems [15].

Another source of conflict in the operator interface is feedback. Depending on the operators perception of a tasks difficulty, feedback may be interpreted as either helpful or distracting [13]. To keep feedback relevant to the current task, it may be appropriate to use separate interfaces for large payload displacement and accurate positioning. Since these tasks are completed separately, the interfaces will not interfere with each other.

Only the required feedback should be provided to the operator [13]. Providing too much feedback increases the operator's mental workload in performing analysis, which increases their reaction time. Pre-processing and analysis of camera feed to draw attention to the relevant information is common solution in research. A map can be generated by piecing together images captured by an overhead camera at different crane orientations [41]. The height of obstacles can be highlighted by thresholding rangefinder data [42]. However, trials of an operator feedback system indicated that a raw camera view should still be provided [43], which may increase operator trust in the system and also provide a fallback in case of poor operating conditions for automated analysis.

Lee et al. fused sensor data with the CAD model of the construction site [43]. The simulated camera views were feed back to the operators display. It was concluded that split 2D top and side views are easier to interpret than a 3D view. Additionally, the interface for altering the feedback display should be simple and preferably hands free. In a similar approach, Chen et al. pre-processed sensor data with a game engine to create a 3D workspace visualization [34]. This is presented to the operator through a similar interface which is manipulated with voice control.

The main challenges in automating the informational processes required for UCW installation are precise localization of CWMs and managing the information feedback to the operator. Sensing of the system pose is inadequate in accuracy for alignment, but relative localization with computer vision is viable. Dynamically changing the control and feedback interface is a potential solution to keep the user interface relevant to the current task.

5 Conclusions

The UCW installation automation solutions currently deployed and under development are limited in scope of application. Limitations include requirement for the building to support the transport mechanism, requirement of custom designs of curtain wall, incompatibility with complex building geometries and existing designs of curtain wall, and solution complexity.

Research to automate large steel beam assembly provides potential solutions to better constrain a CWM. Compared to construction operations, a high level of precision and automation is achieved in harbor crane operations to move shipping containers. The requirement of a dogman is removed by introducing an active rotary crane hook, and high positional accuracy is achievable through control systems.

Measurement of the pose of a crane to estimate the payload location is insufficiently accurate for CWM alignment. Computer vision can be used instead. Operator input can be combined with automated analysis to improve feature detection. The operator is a feedback controller, and hence their interface is an essential part of the system. Removing the lag caused by the slow communication between the dogman and the operator can improve both safety and installation speed. Pre-

processing of feedback and careful choice of the relevant information to feedback is required.

Further research is recommended to develop an automated UCW installation solution that is widely applicable to different types of curtain wall, building geometry, and building load capacity; addressing situations where the more specialized solutions do not apply, for example, in refurbishing projects or when installing unusually shaped CWMs. The solution should primarily aim to mechanize and automate the tasks that are conventionally completed by the dogman. This will result in a safer and more economically efficient installation methodology.

Acknowledgements

This research was supported by an Australian Government Research Training Program (RTP) Scholarship.

References

[1] Friblick F., Tommelein I. D., Mueller E., and Falk J. H. Development of an Integrated Facade System to Improve the High-Rise Building Process. In *17th Annual Conference of the International Group for Lean Construction*, pages 359–370, 2009.

[2] Falk H., Andersson H., Friblick F., and Mul M. J. A Novel Facade System to Improve the Whole High-Rise Building Process. In *CTBUH 2016*, pages 1077–1086, 2016.

[3] Tommelein I. D. and Beeche G. De-Coupling Cladding Installation From Other High-Rise Building Trades: A Case Study. In *Proceedings of the 9th Annual Conference International Group for Lean Construction, Singapore*, 2001.

[4] Pan W., Bock T., Linner T., and Iturralde K. Development of a fast and effective solution for on-site building envelope installation. In *Proceedings of the 33rd International Symposium on Automation and Robotics in Construction (ISARC2016)*, 2016.

[5] Vigener N. P. and Brown M. A. Building Envelope Design Guide - Curtain Walls. National Institute of Building Sciences, 2016.

[6] Taghavi M., Iturralde K., and Bock T. Cable-driven parallel robot for curtain wall modules automatic installation. In *Proceedings of the 35th International Symposium on Automation and Robotics in Construction (ISARC2018)*, pages 396–403, 2018.

[7] Yu S. N., Lee S. Y., Han C. S., Lee K. Y., and Lee S. H. Development of the curtain wall installation robot: Performance and efficiency tests at a construction site. *Autonomous Robots*, 22(3):281–291, 2007.

[8] Taghavi M., Kinoshita T., and Bock T. Design, Modelling and Simulation of Novel Hexapod-Shaped Passive Damping System for Coupling Cable Robot and End Effector in Curtain Wall Module Installation Application. In *Proceedings of the 36th International Symposium on Automation and Robotics in Construction (ISARC)*, pages 665–671, volume 36, 2019.

[9] Liang Y., Che Z., Chen X., and Liu C. Total Assembly Construction Technology of Ultra-long Variable Cross-section Spiral Aluminum Plate Unit of Qingdao Citizen Fitness Center Sports Stadium. *Engineering and Applied Sciences*, 4(5):98, 2019.

[10] Cai S., Ma Z., Skibniewski M., Guo J., and Yun L. Application of automation and robotics technology in high-rise building construction: an overview. In *Proceedings of the 35th International Symposium on Automation and Robotics in Construction (ISARC2018)*, pages 1–8, 2018.

[11] Cai S., Ma Z., Skibniewski M. J., and Bao S. Construction automation and robotics for high-rise buildings over the past decades: A comprehensive review. *Advanced Engineering Informatics*, 42:100989, 2019.

[12] Iturralde K., Linner T., and Bock T. Comparison of Automated and Robotic Support Bodies for Building Facade Upgrading. In *Proceedings of the 32nd International Symposium on Automation and Robotics in Construction and Mining (ISARC2015)*, 2015.

[13] Fang Y., Cho Y. K., Durso F., and Seo J. Assessment of operator's situation awareness for smart operation of mobile cranes. *Automation in Construction*, 85:65–75, 2018.

[14] Iturralde K., Linner T., and Bock T. Development and preliminary Evaluation of a concept for a Modular End-Effector for automated/robotic Facade Panel Installation in Building Renovation. In *Proceedings of the 10th Conference on Advanced Building Skins*, 2015.

[15] Vaughan J., Karajgikar A., and Singhose W. A study of crane operator performance comparing PD-control and input shaping. In *Proceedings of the 2011 American Control Conference*, pages 545–550, 2011.

[16] Workplace Health and Safety Queensland. A Guide for doggers. 2010.

[17] Shapira A., Rosenfeld Y., and Mizrahi I. Vision System for Tower Cranes. *Journal of Construction Engineering and Management*, 134(5):320–332, 2008.

[18] Lee C. and Lee G. Feasibility of beam erection with a motorized hook-block. *Automation in Construction*, 41:25–32, 2014.

[19] Liang C.-J., Kang S.-C., and Lee M.-H. RAS: a

robotic assembly system for steel structure erection and assembly. *International Journal of Intelligent Robotics and Applications*, 1(4):459–476, 2017.

[20] Han C. S., Lee S. Y., Lee K. Y., and Park B. S. A multidegree-of-freedom manipulator for curtain-wall installation. *Journal of Field Robotics*, 23(5):347–360, 2006.

[21] Ramli L., Mohamed Z., Abdullahi A. M., Jaafar H. I., and Lazim I. M. Control strategies for crane systems: A comprehensive review. *Mechanical Systems and Signal Processing*, 95:1–23, 2017.

[22] Arena A., Casalotti A., Lacarbonara W., and Cartmell M. P. Dynamics of container cranes: three-dimensional modeling, full-scale experiments, and identification. *International Journal of Mechanical Sciences*, 93:8–21, 2015.

[23] Ho T., Suzuki K., Tsume M., Tasaki R., Miyoshi T., and Terashima K. A switched optimal control approach to reduce transferring time, energy consumption, and residual vibration of payload's skew rotation in crane systems. *Control Engineering Practice*, 84:247–260, 2019.

[24] Wehrli R. F. and Gallione J. Method and Apparatus for Vertically Orienting Precast Concrete Wall Panels. U.S. Patent WO2011028879A12011.

[25] Schaper U., Dittrich C., Arnold E., Schneider K., and Sawodny O. 2-DOF skew control of boom cranes including state estimation and reference trajectory generation. *Control Engineering Practice*, 33:63–75, 2014.

[26] Inoue F., Wiuanabe K., Ikeda Y., Wakisaka T., Wakabayashi A., and Nekomoto Y. A Practical Development of the Suspender Device that Controls Load Rotation by Gyroscopic Moments. In *Proceedings of the 14th International Symposium on Automation and Robotics in Construction (ISARC)*, pages 486–495, 1997.

[27] Liebherr. Liebherr Port Cranes FCC and TCC. 2011.

[28] Cibicik A., Myhre T. A., and Egeland O. Modeling and Control of a Bifilar Crane Payload. In *2018 Annual American Control Conference (ACC)*, pages 1305–1312, 2018.

[29] Kyungmo J., Dongnam K., Kihyun B., Daehie H., Shinsuk P., and Myo-Taeg L. Pre-acting manipulator for shock isolation in steel construction. In *2007 International Conference on Control, Automation and Systems*, pages 1203–1208, 2007.

[30] Hatton I. G. M. Fly jib for a crane and method of use. U.S. Patent US8979148B12015.

[31] Seung-Kyou L., Nakju Lett D., Gwi-Tae P., Kyung-In K., Myo-Taek L., Dae-Hie H., Shin-Suk P., Ung-Kyun L., and Tae-Koo K. Robotic technologies for the automatic assemble of massive beams in high-rise building. In *2007 International Conference on Control, Automation and Systems*, pages 1209–1212, 2007.

[32] Taghavi M., Heredia H., Iturralde K., Halvorsen H., and Bock T. Development of a Modular End Effector for the installation of Curtain Walls with cable-robots. *Journal of Facade Design and Engineering*, 6(2):1–8, 2018.

[33] Jung K., Chu B., and Hong D. Robot-based construction automation: An application to steel beam assembly (Part II). *Automation in Construction*, 32:62–79, 2013.

[34] Fang Y., Chen J., Cho Y. K., Kim K., Zhang S., and Perez E. Vision-based load sway monitoring to improve crane safety in blind lifts. *Journal of Structural Integrity and Maintenance*, 3(4):233–242, 2018.

[35] Smoczek J., Szpytko J., and Hyla P. The anti-sway crane control system with using dynamic vision system. In *Solid State Phenomena*, pages 589–593, volume 198, 2013.

[36] Hyla P. Night vision applicability in anti-sway vision-based solutions. In *2015 20th International Conference on Methods and Models in Automation and Robotics (MMAR)*, pages 358–363, 2015.

[37] Diao Y., Cheng W., Du R., Wang Y., and Zhang J. Vision-based detection of container lock holes using a modified local sliding window method. *EURASIP Journal on Image and Video Processing*, 2019(1):69, 2019.

[38] Li H., Duan X., Zhan Y., and Gao L. A Handle Inspection Device for Curtain Wall Installation based on Structured Laser. In *2016 IEEE International Conference on Mechatronics and Automation*, pages 1623–1628, 2016.

[39] Chu B., Jung K., Lim M.-T., and Hong D. Robot-based construction automation: An application to steel beam assembly (Part I). *Automation in Construction*, 32:46–61, 2013.

[40] Lytle A. M. and Saidi K. S. NIST research in autonomous construction. *Autonomous Robots*, 22(3):211–221, 2007.

[41] Wang Y., Suzuki H., Ohtake Y., Kosaka T., and Noguchi S. Generating a visual map of the crane workspace using top-view cameras for assisting operation. In *Proceedings of the Creative Construction Conference (CCC2018)*, 2018.

[42] Domingue B. and Vaughan J. Crane Workspace Mapping via a Scanning Laser Rangefinder. In *ASME 2015 International Mechanical Engineering Congress and Exposition*, volume 4A, 2015.

[43] Lee G., Cho J., Ham S., Lee T., Lee G., Yun S.-H., and Yang H.-J. A BIM- and sensor-based tower crane navigation system for blind lifts. *Automation in Construction*, 26:1–10, 2012.

Rationalization of Free-form Surface Construction Method using Wooden Formwork

Sei Hayashi and Tomoyuki Gondo
Department of Architecture, School of Engineering, The University of Tokyo, Japan
E-mail: sei@arch1.t.u-tokyo.ac.jp, gondo@arch1.t.u-tokyo.ac.jp

Abstract –

In Japan's construction industry, techniques of producing complex three-dimensional (3D) formwork at construction sites are conventionally developed using the sophisticated skills of carpenters. Inspie of the development of digital technologies, the production of free-form shapes faces considerable cost and time management risks that require pragmatic solutions. In the efficient building of free-form shapes, the continuous surface should be divided into portable elements for formulating production plans and for making products in the factory. The products should then be installed and assembled at the construction site. Hence, new methods with computational design are assumed to require an approach different from the traditional processes of designing and constructing with two-dimensional (2D) drawings.

This research aims to analyze the productivity of these conventional means and propose a New Method of constructing free-form formwork for real-scale buildings.

First, we focused on how the designed geometric coordinate information is translated for construction on complex wooden formwork. We revealed how these shapes were realized by carpenters, and organize cases from 1991 to 2020 to see how the existing Japanese wooden formwork technology can realize double-curved surfaces.

Second, we focused on a completed project that has a 5,100 m^2 free-form RC roof constructed using the nonuniform rational B-spline (NURBs) curve and conventional production methods. Additionally, we analyzed the project's production time and cost from the construction records and revealed that the methods heavily depended on on-site labor.

Finally, based on the analysis results, we propose a production method in which curved surfaces are divided into portable units to reduce on-site labor and ensure high accuracy. We also analyzed its productivity through some assembly experiments. The labor cost of the New Method is lower by 93% than that of the existing method.

Keywords –

free-form structures; 3D CAD; wooden formwork; labor productivity

1 Introduction

1.1 Background and purpose of the study

In Japan's construction industry, techniques of producing complex three-dimensional (3D) formwork at construction sites are conventionally developed using the sophisticated skills of carpenters [1]. The development of digital technologies, especially 3D computer-aided design (CAD) and 3D structural analysis, has recently facilitated the design of even free-form shapes. However, the production of such free-form shapes still has considerable risks in cost and time management. In addition, in recent years, it has become difficult to maintain these skills due to Japan's aging population and shortage in carpenters. These problems require pragmatic solutions. To build free-form shapes efficiently, one should divide the continuous surface into portable elements for formulating production plans and for making products in the factory. The products should then be installed and assembled at the construction site. Hence, new methods with computational design are assumed to require an approach different from the traditional processes of designing and constructing with two-dimensional (2D) drawings. Creating complex and continuous shapes on the architectural scale requires considerable time and money, given the need to adjust the details of each part and assemble them at the construction site.

This study aims to develop a construction method that optimizes productivity throughout the building process—from design to on-site-assembly—by combining digital fabrication with conventional wooden construction techniques on the actual building scale. This study focuses on methods in the Japanese construction industry and assumes the proficiency and costs of labor to be those in Japan.

1.2 Methodology

First, we analyze and organize cases after the emergence of CAD to see how the existing Japanese wooden formwork technology can realize double-curved surfaces, which are difficult to reproduce with wooden formwork. Second, we examine the current situation of free-form shape production by surveying an example of a free-form reinforced-concrete (RC) roof construction project that was realized using conventional construction methods in Japan and nonuniform rational B-spline (NURBs) surfaces, which have become a mainstream method for describing 3D geometries since the 2010s. And we analyzed the time and cost of its construction process. Third, we developed a production method in which curved surfaces are divided into portable units to reduce on-site labor and ensure high accuracy. Fourth, by analyzing and comparing the time, cost, and shape reproducibility of the new method with those of the conventional construction method, we offer an ideal method of constructing free-form buildings.

2 Classification of construction methods of wooden formwork with double-curved surfaces

2.1 Classification of construction methods

In the classification in the graphic science, curved surfaces can be divided into two typologies: ruled and double-curved surfaces [2]. A ruled surface, such as a cylinder or hyperbolic paraboloid surface, can be defined as a linear trajectory that moves smoothly with a one-degree-of-freedom parameter. This type can be further classified into single-curved surfaces, such as columnar and conical surfaces, and warped surfaces, such as bipolar parabolas and spirals with torsion. Because these curved surfaces can be considered an accumulation of straight lines, they have been used in architectural design since the 1960s before the advent of CAD. By contrast, a double-curved surface does not have such a linear element and is thus difficult to regard as an accumulation of linear elements. In particular, free-form and double-curved swept surface shapes are difficult to accurately define in two-dimensional drawings. Around 1990, CAD began to penetrate the field of architectural design and has since made it possible to construct such surfaces.

In this study, buildings with double-curved surface RC elements constructed using wooden formwork were selected from issues of the most widely read monthly architectural design magazine in Japan, Shinkenchiku, published between January 1991 and May 2020. The number of buildings extracted was 72. Formwork methods for double-curved surfaces described in the magazine and other materials can be categorized into the following (Table 1).

(1) Small unit
(2) Radial unit
(3) Rectangle unit
(4) On-site construction: beams and joists
(5) 3D grid

(1), (2), and (3) are supposed to be made in the factory and assembled or joined on-site to make a larger surface. (4) and (5) are based on on-site production, and the use

Table 1. Classification of construction methods for double-surface formwork

	Figure	Method	Structure	Characteristics of the method	Sheathing board	Cases	Number
1		Small unit	Wooden ribs/foam	-Method for small objects, columns or slab edges	Narrow cedar boards	OMOTESANDO KEYAKI bldg.	1-c
2		Radial unit	CNC cut wooden ribs	-Method for surfaces close to the rotating shape -Often be made as fabricated unit	Veneers lamination	Kawaguchi city "Meguri-no-mori Crematorium in Kakamigahara	2-a
					Narrow boards	Yasko Kawagoe Museum	2-c
3		Rectangle unit	CNC cut wooden ribs	-Method to make large curved surfaces by joining factory-produced square units in the construction site	Veneers lamination	Kawaguchi city "Meguri-no-mori Hokkaido-Daikannon	3-a
					Hot pressed board	Inumori Hall, Kagoshima Univ.	3-b
					Flexible plywood	Gokayama Seikatsukan Science Hills Konatsu	3-d
4	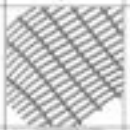	On-site construction: beams and joists	Beams:CNC cut boards, Square timbers	-Method based on on-site assembly of beams, joists and sheathing board	Narrow boards	Crematorium in Kakamigahara Kawaguchi city "Meguri-no-mori	4-c
			Joists:Narrow boards		Flexible plywood	Island City Central Park "GRIN GRIN" Ginan Town Hall	4-d
5		3D grid	Square timbers	-Method to assemble bending wood or bamboo on a grid with rotatable joints	Fabric	Uchiho Community Center Naiju Community Center Kumamoto Ashikita Youth Center	5-e

of digital fabrication at factories is limited to the cutting of parts according to CAD data or on-site positioning.

According to how the sheathing plates are generated, construction method are further classified into the following categories.

(a) Thin veneer lamination
Three or four layers of thin and narrow veneer (3 mm) strips are laminated and glued to create a cylindrical shape with a large curvature.
(b) Hot press
Multiple laminated veneers with adhesive are heated and pressed against the male and female molds. Since the structure is made from a single plate, a seamless surface can be made with high accuracy.
(c) Use of narrow boards
Cedar or plywood strips with a width of 100–300 mm are fastened to joists (method (4)) on-site. Although the surface that can be reproduced is not as large as those in (a) and (b), it is easy to work on and can be assembled at the construction site.
(d) Use of flexible plywood
This is mainly employed in conjunction with (3) and (4). Flexible plywood is used and can be applied according to the shape of the small curvature surface.
(e) Use of fabric material
Fabric is used as a sheathing plate that needs to be followed by the movement in accordance with method (5).

Next, we explain the characteristics of each method (1)–(5) combined with the sheathing board method (a)–(e) with several case studies. Explains of These cases are based on construction plans prepared at the construction phase, or construction reports published in magazines.

2.2 Small unit

Small-scale units are used for the formwork of specially shaped elements, such as columns and slab edges. In ”OMOTESANDO KEYAKI bldg.”, designed by Norihiko Dan, each outer pillar is inclined and twisted, so the cedar board for finishing was glued to the foam that was hollowed out along the column’s outlines (1-c) [3].

2.3 Radial unit

For curved surfaces whose shape is close to rotating or convex shapes, the frame of the formwork is assembled radially. Radial structures are difficult to assemble at construction sites, so smaller ones are often made into units. In “Kawaguchi City Meguri-no-Mori” designed by Toyo Ito, the radial units were applied in a 2.6 m x 2.6 m area of the large curved column section. Sheathing plates consisting of four layers of 3 mm-thick veneer strips were affixed to the rib structures (2-a). Since the bottoms of the pillars gradually thin, the veneer was applied by twisting to follow the narrow cylindrical shape. Since the columns are 3–5 m high, they were divided into three sections and assembled at the site [4].

2.4 Rectangle unit

Large curved surfaces are made by joining factory-produced square units side by side on a grid to shorten the work at the construction site and ensure shape accuracy. In Japan, 1820 mm × 910 mm plywood board is common; the units are often made in a size of about 1.8 m × 0.9 m or 0.9 m × 0.9 m, with ribs lined up at a pitch of about 300 mm or 450 mm to create a guide for the shape. In the construction of the Gokayama Seikatsukan roof, designed by Elias Torres, the formwork was divided into 1,700 mm × 850 mm units (3-d) [5]. In the construction of Hokkaido’s Daikannon, a large RC Buddha sculpture designed by Ishimoto Architectural & Engineering, a scale model created by a sculptor was used to measure coordinates by physical contact, and a ring-cut model was made in the height direction. Based on these coordinate data, the shape between the contour lines was reproduced by carpenters by bending cedar and veneer boards (3-c) [6].

2.5 On-site construction: beams and joists

This method is based on the on-site assembly of the formwork, wherein beams, joists, and sheathing plates are placed on support pipes. For the roof of Building for Island City Central Park “GRIN GRIN”, designed by Toyo Ito, square timbers were used as beams for the small curvature of the roof; they were poured over the supports and then attached with plywood.

Square timber beams were pulled from the bottom with a turnbuckle to recreate the shape of the model at the site (4-d) [7]. However, this method was not able to achieve the expected level of shape accuracy. Based on this experience, steep and precise formwork was realized at the Crematorium in Kakamigahara (designed by Toyo Ito) by using CNC (computer numerical control)-cutting beams and layering a few layers of 12 mm-thin cedar boards on them to make flexible and strong joists (4-c) [8].

2.6 3D grid

This method was used in the 1990s to assemble bending wood or bamboo on a grid with rotatable joints. At the Naiju Community, designed by Shoei Yo, bamboo cage-like surface materials were assembled on a flat ground, and the roof’s shape was created by adjusting the shape of the cage over props. The sheathing board is made of fabric material; the shape can be adjusted on-site.

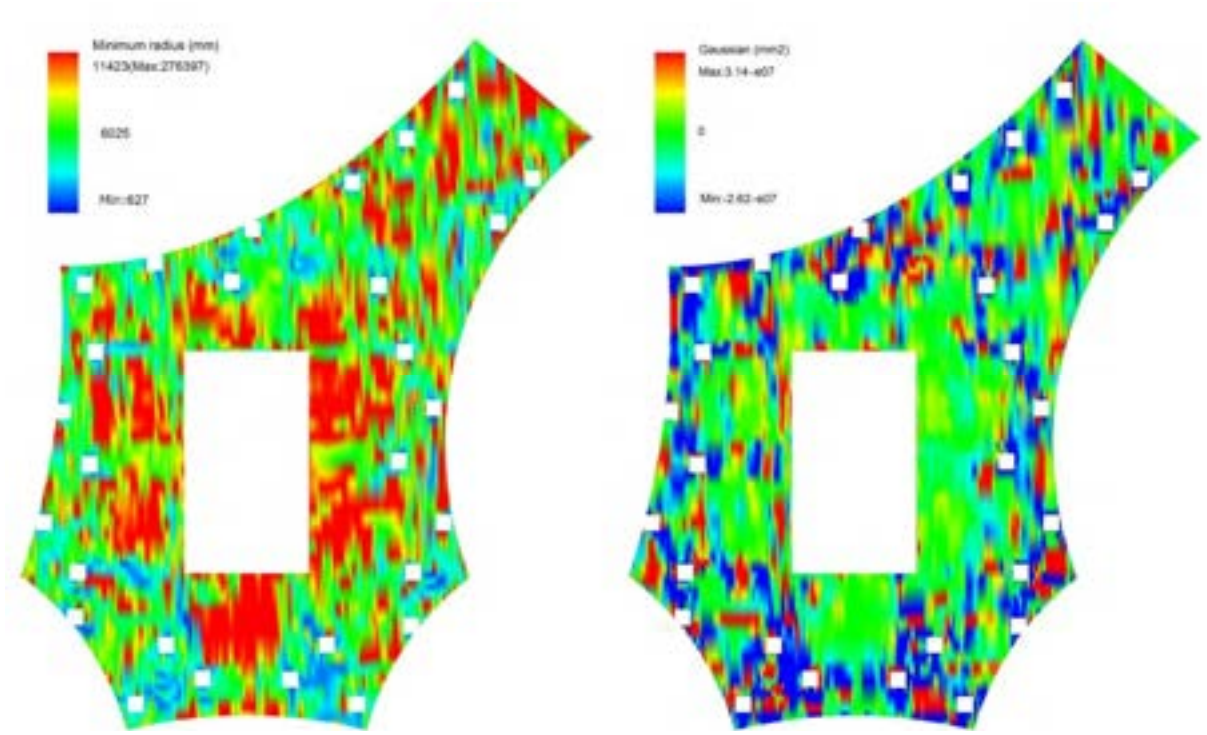

Figure 1. Minimal curvature and Gaussian curvature distributions on roof surface of Kawaguchi project

The fabric and bamboo were left behind after the concrete was poured to become the finishing material [9].

2.7 Summary

In Chapter 2, we classified construction methods for frames and sheathing plates for double-surface formwork. Each method is employed according to the shape of the curved surface, and all of these methods depend on-site work and the skills of formwork carpenters. The choice and combination of methods depend largely on the experience of formwork fabricators and carpenters. There are no previous studies comparing the productivity, shape accuracy, and price of these techniques or optimizing these methods.

3 Analysis of productivity of conventional construction methods

3.1 Outline of example of free-form RC roof formwork constructed with conventional methods

We focused on a completed project which has 5,100 m^2 free-form roof made from a 200 mm-thick RC slab using a conventional formwork construction method. We analyzed the production time and cost of the method from the construction records of the general contractor and found that the method heavily depend on on-site labor. The target is "Kawaguchi City Meguri-no-Mori" (hereafter the "Kawaguchi project"), designed by Toyo Ito & Associates, Architects and Sasaki Structural Consultants. The curved roof is supported by concrete-covered steel columns, and the shell structure was designed with computational morphogenesis (Fig. 1).

For constructing the main part of the roof, a method was adopted to build a curved formwork, with hand-bent joists and sheathing built on-site and installed with machine-cut beams. These beams were bridged on telescopic steel props placed on a Japanese traditional module grid measuring 915 mm. Each joist on the beams comprised four layers of 12 mm-thick pine strips (100 mm wide), and sheathing (also made from 12 mm-thick pine strips) was bent and installed manually at the construction site (hereafter the "Kawaguchi method," 4-c, Fig. 2) Box forms (2-a, 3-a, 3-c) were adopted for the areas where the curvature changes abruptly (columns and roof edge) [4]. This chapter retrieves and analyzes productivity and shape accuracy data from the construction records of the Kawaguchi project's general contractor.

3.2 Analysis of production time

In this project, on-site formwork production lasted from November 2016 to May 2017. A total of 1,883 man-days over 136 working days, excluding holidays, were needed for producing the curved roof formwork. On average, 13.8 people were working each working day,

Figure 2. Work procedure of formwork for Kawaguchi project's free-form roof

with a maximum of 33 man-days. The man-hours at each stage of the formwork's installation in the main part of the roof are shown below.

1. Placing temporary supports: 408 man-days
2. Installing beams: 192 man-days
3. Installing joists: 320 man-days
4. Installing sheathing panels: 320 man-days
5. Adjusting levels and fixing: 288 man-days

Each laborer in this set of data worked eight hours a day, and the areas analyzed included the curved roof, the columns, and the joints between the roof and the wall, totaling 5,112 m^2. The total working hours of these stages were 1,528 man-days, and the average working time per construction area was 2.39 man-hours/m^2.

3.3 Shape accuracy analysis

In this construction project, before the concrete's placement, the general contractor measured the height coordinates of each point on the formwork's surface just above the prop with a light wave rangefinder. The prop's height was adjusted whenever there was a difference of more than 20 mm between the height of the formwork and that of the 3D model.

Because the top of the glass curtain wall's mullion was in direct contact with the concrete slab, the construction manager had to carefully manage the height of each contact point. Therefore, every month following the removal of the formwork, the roof slab's height was measured at each of the 153 mullion locations, and these data were fed back to the mullions' production length. Creep or deformation of the concrete slab was expected in the long-spanning area. Thus, the heights of several points in the middle of the span were also measured, and height displacement was checked to prevent any sudden transformation.

The data showing the height of these points immediately after the formwork's removal can be used as a data sample that shows the shape accuracy of the formwork at arbitral points on the surface. Fig. 3 shows the distribution of the height error for each measurement point.

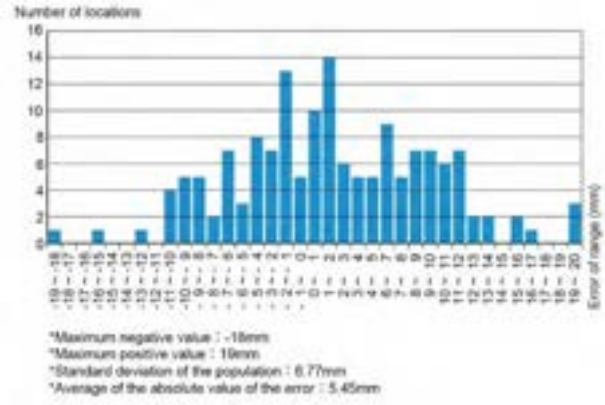

Figure 3. Distribution of height error of form

Table 2. Details of calculation of construction costs for Kawaguchi method's formwork

	Specification	Unit	Unite price(JPY)	Units per square meter	JPY/㎡	Calculation basis of unite price
material cost						
Machine-cut beam	h=100mm・double side / 915mm pitch	m	1,000	1.092 pieces/㎡	1,092	interviewes
Joist	75mm×t13mm×300mm pitch×4layers（4m length）	pieaces	500	3.3 pieces/㎡	1,650	interviewes
Sheeting panel	75mm×t13mm（4m length）	pieaces	500	2.79 pieces/㎡	1,666	interviewes
Telescopic steel props		pieaces	2,000	1.31pieces/㎡	2,620	the construction estimation standard [10]
Beam setting material		pieaces	170	1.31pieces/㎡	222	the construction estimation standard [10]
Square timber for bottom		㎡	33,000	0.032㎡/㎡	1,069	the construction estimation standard [10]
Prop joint connector		pieaces	1,890	0.76 pieces/㎡	1,436	the construction estimation standard [10]
Fixing clamp tool	150 days rental	pieaces	600	2.621pieces/㎡	1,575	interviewes
Fixing chain	150 days rental	㎡	400	1	400	interviewes
labor cost	2.39 man-hour/㎡	man-hour	3,075	2.39 man-hour/㎡	7,349	the construction estimation standard[10]
Total					19,079	(JPY/㎡)

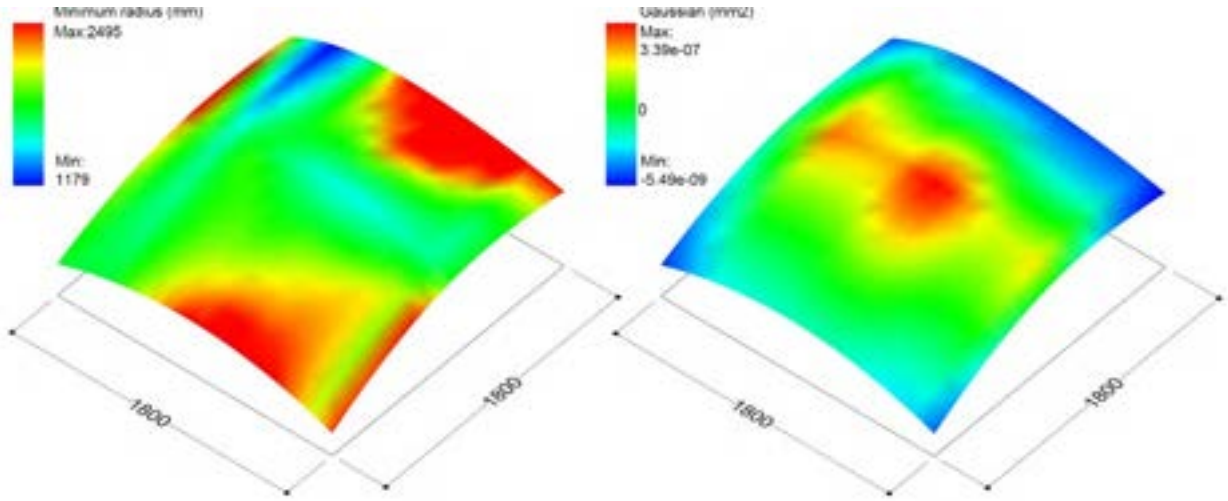

Figure 4. Minimal curvature and Gauss curvature distribution of target shape of new method's experiment

3.4 Cost analysis

We also calculated the cost per square meter of constructing the Kawaguchi project's formwork. The amount of material required to produce the formwork was calculated based on the project's construction plan papers.

We consulted periodically published standard construction estimation books [10] to find unit prices for each material, and asked contractors to fill in the missing data. The labor cost per square meter was calculated from the man-hours calculated in 3.1. The sum of the material and labor costs was regarded as the construction cost. Table 2 shows the process of calculating the total construction cost, which was 19,079 JPY/m^2.

4 Development of new unit construction method

4.1 Outline of new method

The cost analysis in Chapter 3 shows that labor costs account for 39% of the total construction costs, while the time taken to place temporary supports accounts for 27% of the total on-site assembly time. The time taken on-site to laminate five layers of a 100 mm-thick narrow board (joists and sheathing plates) accounts for 42% of the total construction time.

Therefore, in this chapter, we develop a new formwork method (hereafter "New Method") that uses factory-manufactured units to minimize on-site labor and reduce total costs. New Method proposes a way to use factory-manufactured 900 mm × 900 mm units instead of bending and assembling wooden boards at the construction site. It uses a rigid unit to reproduce surfaces with various curvatures (3-c). This system makes it possible to select a method for generating curved surfaces by matching the curvature of each part by dividing the surface into units. The overall cost and time required to construct the whole formwork are also optimized.

The experimental formwork units comprise a folding support system and a bent wooden sheathing panel that is reinforced by curved beams cut by CNC machines. Both the support unit and the sheathing panel can be manually operated by two laborers. Each part is manufactured in a factory and then assembled and fixed at the construction site to create an architectural-sized formwork with a free-form roof surface.

4.2 Outline of analysis subject

4.2.1 Sample shape

We extracted a sample shape measuring 1,800 mm × 1,800 mm from Kawaguchi's free-form roof to compare New Method with the Kawaguchi method. The sample area had the highest amount of curvature on the Kawaguchi project's roof (except for the column area, where the box form method was adopted). The minimal radius was 1,179 mm, and the maximum Gaussian radius was 3.39e-07 (Fig. 4).

In this experiment, we made a free curved surface using four 900 mm × 900 mm units fabricated in the factory to compare the assembly times and costs of New Method and the Kawaguchi method.

4.2.2 Fabrication of test specimen

The test specimen was fabricated at a wood machining factory, which is good at compregnating and bending such sawn veneer. Each unit comprised two parts: one for the support system and another for the sheathing panel (Fig. 5).

Figure 5. New Method's formwork unit

Part 1. Support system

The supporting part was formed of a bottom plate and two sideboards. These were connected by two hinges at each end of the boards, meaning that the support unit could immediately be extended from a flat folded state. The adjacent units were rotated by 90° alternately and placed side by side. The tops of the sideboards were connected to an adjacent unit with screws at the edges.

Part 2. Sheathing panel

The sheathing panel was made of narrow boards (100 mm wide and 12 mm-thick) that were bent along a 300 mm grid of CNC-cut walls. The gap between each board was filled with a coating putty to ensure they were watertight. The sheathing panel was fixed onto the sideboards of the support system and screwed with a joint board.

The total cost of producing each unit was 20,000 JPY, and the working hours of each stage of the production process in the factory are shown below.

1. CNC-machine cutting: 0.5 man-hours
2. Assembling and setting the sheathing panel and the support: 6 man-hours

4.3 Analysis of workability and cost

In this section, we analyze the assembly process of New Method by dividing it into five sub-processes and measure each process's working time and compare the experimental results with the assembly time of the Kawaguchi project's on-site formwork.

4.3.1 Analysis of production time

The time taken to assemble the four formwork units was measured and analyzed in a factory's woodworking laboratory. Two unskilled workers conducted the construction experiment. All parts were folded at the beginning of the assembly process. At the end of the assembly process, all parts were assembled and joined in their designated positions. Table 3 shows the measured time for each sub-process.

According to the experimental results, New Method's assembly process takes 0.283 man-hours/m^2, which is approximately 12% of the working time of the Kawaguchi method's on-site process.

Table 3. Time for each assembly process in New Method

Process	Time (s)	Time per area(s/m2)
Transport and placement of support parts	410	126.5
Joinning of support parts	120	37.0
Transport and placement of sheeting panel parts	260	80.2
Joinning of sheeting panel parts	750	231.5
Others(preparation,transport)	110	34.0
Total	1650	509.3
Man-hour per square meter for total assembly process (man-hour/m2)		**0.283**

4.3.2 Analysis of shape accuracy

The 3D coordinates of the assembled formwork surface's shape were measured at a pitch of 100 mm using a 3D laser distance-measuring machine. We used a fixed-type surveying instrument that can calculate the 3D coordinates and angles of any point on the measurement

object's surface through laser irradiation. The laser measures with an accuracy of ±1 mm at a distance of 10 m.

The distance error between each point on the specimen and the 3D model's surface was then measured, and the accuracy of the sample's shape was analyzed. Total Number of measurement points is 360.

Maximum negative error value: −7.4 mm
Maximum positive error value: +6.3 mm
Standard deviation of the population: 1.96 mm
Average of the absolute value of error: 1.86 mm

The surface error of New Method was much smaller than the construction error of the Kawaguchi method. The Architectural Institute of Japan recommends that such formwork's form accuracy error be maintained within ±20 mm [11] ; therefore, New Method has sufficient shape accuracy for this formwork's construction.

4.3.3 Cost analysis

The cost of constructing the formwork of New Method is detailed below.

1. Material cost: 24,600 JPY/m^2
2. Labor cost: 481 JPY/m^2 *1
3. Total direct cost: 25,081 JPY/m^2

*1: Non-professional labor cost:
1,700 JPY/man-hour[10]

The overall cost of formwork construction of New Method is higher by 31% than that of the Kawaguchi method.

5 Conclusion and discussion

In this study, we explained the conventional Japanese construction method of double-curved surface formwork. Based on examples of curved surface structures from the past 30 years, we classified and organized these methods by the structure and sheathing plate.

We then focused on a case study of a completed project with a 5,100 m^2 free-form RC roof built with conventional construction methods. We also analyzed these methods' time and cost of production based on the general contractor's construction records. The study results revealed that these methods depend heavily on on-site labor.

We then developed a new production method for reproducing curved surfaces with high shape accuracy without relying on existing advanced carpentry skills and field labor on-site works. We analyzed its productivity by performing assembly experiments. The proposed method reduced the project's on-site labor costs by 93% compared with those of the existing method.

In future studies, a more systematic and cost-optimized formwork program should be created by developing a cost- and time-efficient construction method that delivers a product with the accuracy required for the curvature of the area.

Acknowledgements

We are grateful to Horie Seikan.Co.,Ltd for their help with experiments. And we would like to thank Toa Corporation and Kiyama Corporation also for providing us with valuable materials.

References

[1] A. Forty, *Concrete and Culture: A Material History*, Reaktion Books,United Kingdom, 2012
[2] T. Tachi, Double curved surface/Single curved surface/Wrapped surface, *Journal of Graphic Science of Japan*, 51(2017): 81–83, 2017 (in Japanese)
[3] N. Dan, Omotesando Keyaki bldg., *Shinkenchiku*, 89 (1): 136-139, 2014 (in Japanese)
[4] S. Hayashi, K. Yamazaki, T. Kimura, T. Gondo, Construction process and rationalization of reinforced concrete roof with free-form surface using NURBS model, *AIJ Journal of Technology and Design*, 25 (2019): 941–946, 2019 (in Japanese)
[5] K. Kushita, E. Horiuchi, Construction of GOKAYAMA-SEIKATSUKAN, *Kawada Technical Report*, 19: 53-58, 2000 (in Japanese)
[6] R. Hamade, M. Mukouyama, K. Hashimoto, S. Yuhara, Construction method for reinforced concrete multi-curved surface structure and rationalization of construction work by using of CAD-Hokkaido Dai-Kannon Projects, *Concrete Journal*, 28 (5): 49–58, 1990 (in Japanese)
[7] H. Shinozaki, Construction process of Building for Island City Central Park "GRIN GRIN," *Shinkenchiku*, 80 (9): 99, 2005 (in Japanese)
[8] S. Ito, The method of curved formwork for Crematorium in Kakamigahara, *Kenchiku Gijyutu*, 709: 174–175, 2018 (in Japanese)
[9] S. Yoh, 12 Calisthenics for Architecture, *Space design*, 388: 30–33, 2005
[10] Construction Research Institute, *Monthly "Kensetsu Bukka,"* 1201, Construction Research Institute, Japan, 2017 (in Japanese)
[11] Architectural Institute of Japan, *Recommendation for Design and Construction Practice of Formwork*, Architectural Institute of Japan, Japan, 2014 (in Japanese)

Comparison of Shortest Path Finding Algorithms for Cable Networks on Industrial Construction Projects

F. Alsakka[a], S. Khalife[a], M. Nomir[a], Y. Mohamed[a], and R. Hermann[b]

[a] Department of Civil and Environmental Engineering, University of Alberta, Canada
[b] *PCL Industrial*, Canada
E-mail: falsakka@ualberta.ca, khalife@ualberta.ca, nomir@ualberta.ca, Yasser.Mohamed@ualberta.ca, rhhermann@pcl.com

Abstract –

Cable path optimization is a commonly encountered problem in industrial construction projects. Numerous designs are technically feasible but are associated with varying construction costs and effort. Hence, selecting the right network is deemed a critical decision. Multiple shortest path algorithms could be deployed to identify the optimal solution. Although they could potentially identify solutions of equal values, there could be differences among their performance which become more significant as the project size increases. Thus, this study compares the results of applying three shortest path algorithms, Dijkstra, A* and Bellman-Ford, in finding the shortest paths for power and instrument cables in an industrial facility project. Moreover, it presents an integrated methodology that combines different software to help practitioners experiment with different scenarios in a fast and systematic manner and make decisions accordingly: (1) Build a 3D model of the project under study, (2) Design a database for data retrieval and management, (3) Import data from the model into the database, (4) Develop a code that reads from the database, finds the optimal paths for the planned cables in the facility, and writes the results back into the database, and (5) Import the obtained results into NavisWorks for visualization and validation purposes. The results have shown that the three algorithms identified the same paths for six cables. Yet the optimal path found using Dijkstra and A* for the seventh cable was one node longer than that identified using Bellman-Ford, but the three paths were of equal weights. Generally, Dijkstra and A* exhibited a close performance. Meanwhile, the main difference between Dijkstra and A*, on one hand, and Bellman-Ford, on the other hand, lied in fact in the time needed to solve the optimization problem. The percent difference between Dijkstra and Bellman-Ford's runtimes for one of the cables reached 4,800% making Dijkstra superior with respect to runtime. Even though the impact of the runtime difference is considered insignificant within the scope of this study as it is in the range of milliseconds, its criticality would increase as the size of the network increases. Therefore, a proper selection of the optimization algorithm would support a rapid and efficient decision-making process.

Keywords –

Cable Network; Shortest path algorithms; Optimal path; Nodes; Edges

1 Introduction

Construction projects entail critical decisions in connection with planning, developing and executing major engineering elements, which would have a severe impact on cost and time savings if not dealt with in a responsible manner. In particular, the issue of planning and designing cable networks on industrial projects is of great concern for construction managers and owners, specifically with respect to cost implications. The main problem encountered in such networks is their complexity as deciding on the optimal solution with respect to different considerations is not a straightforward decision. Cable network optimization is, thus, one of the several optimization problems in construction that need supportive methods, such as mathematical techniques, to help in identifying the most feasible solutions [1]. Examples of similar optimization problems comprise time-cost trade-off [2], resource levelling [3], site layout optimization [4,5], planning and allocating equipment [6], among others.

Mathematical algorithms have a great potential in solving complex problems, specifically those including a large number of alternative solutions given the numerous possible permutations [2]. For cable network problems, specific algorithms are found that deal with identifying the optimal path for a given connection. Three of the most

prevalent algorithms used to determine the shortest path between two nodes are Dijkstra, A* (A-star) and Bellman-Ford [7]. Similar algorithms prove to be highly useful for various applications given their ability to account for factors other than distance when identifying the optimal path [8]. For instance, the Dijkstra and A*, along with other algorithms, were evaluated for their performance and accuracy in finding the optimal path on construction sites considering multi criteria requirements, including travel distance, safety and visibility [8]. Such studies offer a detailed comparison between the different algorithms to help specify what type of problems best fit each algorithm.

While the literature offers a plenty of studies comparing shortest path algorithms in different contexts, the construction industry literature remains in shortage for research discussing opportunities for the application of shortest path algorithms in a systematic manner specifically for cable networks. Given the potential cost and performance impact of cable network design on construction projects, this paper aims at presenting an application of the shortest path method to find optimal paths for a set of pairs of start and destination nodes for power and instrument cables in an industrial facility. The optimal path in the context of this paper represents the shortest path for connecting the cables in the facility while achieving minimum costs that are dictated by the type of trays that cables pass through. The paper achieves this by utilizing the commonly used algorithms: Dijkstra, Bellman-Ford and A* algorithms. The performance of these algorithms is also compared based on the number of connection nodes in the identified shortest paths, the total weight of the paths, and the computation duration (i.e. runtime) to recommend the most suitable algorithm for this type of problem.

The main contribution lies in presenting a convenient approach for solving a critical practical problem on industrial projects while analysing some key points of departure whenever considering similar problems on different projects.

2 Literature Review

2.1 Overview of the Selected Algorithms

Although various algorithms could yield similar results, they exhibit distinct properties such as speed, efficiency, and computation method. This section provides a brief and general overview of the three algorithms employed in this study.

2.1.1 Dijkstra Algorithm

Theoretically, Dijkstra is considered the most common algorithm for finding the shortest path in network problems having a single-source (i.e. one source node) [7]. It is a straightforward and simple algorithm which has gained popularity in network optimization field [9]. In Dijkstra, the number of nodes is specified, and the node which represents the source is just one specific vertex while the destination could include several vertices [10]. Thus, this algorithm is beneficial when the destination is unknown [11]. The function of this algorithm f(n) is equal to g(n), where g(n) is the cost of the path from the source node to the destination node, n [11].

Dijkstra's time complexity is computed by O(n2), where n is the total number of nodes [9], [12]. Hence, in case of problems that are relatively large, Dijkstra is successful as it has a time complexity of an order of n^2. However, the algorithm is generally considered to take a long time and waste resources due to the blind search it performs [11], [13]. Dijkstra adopts the "Greedy Best First Search" approach, and it takes a big search area prior to reaching the destination [11]. It works by going equally in all directions [11] and terminates after visiting all the nodes [14].

2.1.2 A* (A-Star) Algorithm

Another common algorithm for solving the shortest path problem is A*. A* comprises the summation of two functions; a function, g(n), that constitutes the exact cost of the path extending from the start node to node n, and a heuristic function, h(n), that represents an acceptable estimated cost to reach the destination node [12]. The heuristic function provides an estimate of the best path from any node to the destination node, where the order of this estimate defines how the nodes will be visited [11]. A* uses the "Best First Search" approach in which the node with the best heuristic value is chosen to be visited first [15]. The algorithm focuses only on the region in the direction of the goal [12]. However, there is no assurance that optimal solutions will be obtained with the use of heuristics [16].

The performance of A* is significantly impacted by the choice of the heuristic function. In fact, heuristics are used as guidance to improve performance, and they affect the time complexity of the algorithm [12]. If h(n) is exactly equal to the cost required to move from node n to the destination node, the algorithm will only follow the optimal path, without expanding into anything else, resulting in a high search speed. The path to the goal node can be discovered even faster if h(n) overestimates the cost required to reach the destination node from node n. Yet the cost of the identified path might not be the most favorable one in this case [12]. The time complexity is O(n log n), where n is the number of nodes [11]. A* is usually efficient when both the start node and the target node are known [11].

Overall, it can be said that the main difference between Dijkstra and A* algorithms is the heuristic

function h(n) used in A*. In fact, if the value of h(n) is set to zero, A* will give the same outcomes as Dijkstra [12]. Since A* uses the "Best First Search", it is considered faster than Dijkstra which adopts the "Greedy Best First Search" approach [11].

2.1.3 Bellman-Ford Algorithm

Similar to Dijkstra algorithm, Bellman-Ford is a traditional algorithm used for solving shortest path problems from a single-source node [17]. However, Bellman-Ford algorithm can run in a distributed manner unlike the Dijkstra algorithm which is a global algorithm and cannot run easily in a distributed manner [18]. In this sense, distributed algorithms, being subtypes of parallel algorithms, are characterized by the ability of the nodes to keep track of the shortest distances between themselves and the other nodes, while communicating with its neighbour nodes by transmitting messages over the links [19]. Thus, unlike Dijkstra, parallelization takes place in Bellman-Ford easily [20], [21]. Additionally, Bellman-Ford has a looping behaviour, where iterations occur over all edge connections in order to continuously update the nodes until the final distances are reached. However, this reduces Bellman-Ford's efficiency in comparison to Dijkstra's [20], and this is considered a major drawback of the distributed Bellman-Ford algorithm [19]. As for the runtime of Bellman-Ford algorithm, it is O(nm), where n is the number of nodes and m is the number of edges [22]. Bellman-Ford is also dominant in solving the majority of routing problems which have various constraints and occur in a flat network found in an autonomous system, where the primary objective function is the minimum node count [23].

2.2 Some Applications of Shortest Path Algorithms in Construction

Various optimization problems that require the use of shortest path algorithms are found in the construction industry. Material flow on construction sites is an example of similar problems. Optimizing material flow and reducing travel time are valuable as cost and time are impacted by the path that the materials go through [8]. Moreover, optimizing site layout to minimize travel distances can boost production rate as wastage and working time are reduced [8].

Shortest path algorithms are also used in transportation applications. Related examples include in-vehicle route guidance systems that require an immediate response upon request for information and identify vehicle routing and scheduling. Accordingly, a rapid identification of the shortest paths is needed [24]. Moreover, with the use of intelligent robots in construction, there is a need for planning their movement path on site. The focus is on finding an effective and short path that is also collision-free from the initial position to the final position, by avoiding both stationary and movable obstacles [25].

Other applications are focused on optimizing some more important aspects of construction operations while trying to minimize the travel distance. Lei et al. [26] developed a generic algorithm to manage the movement of large mobile cranes used to lift prefabricated units on site while taking into account the site constraints including the congestion of different site areas, the geometry of lifted items and the configuration of cranes. This aims at saving time, satisfying safety and efficiency requirements as well as minimizing the risks of failure and accidents' occurrence on site.

3 Problem Description and Modelling

Designing paths for power and instrument cables within a project requires identifying the shortest feasible paths in order to minimize costs accompanied with their installation. The project presented in this paper deals with this problem of finding the optimal solution for connecting five power cables and two instrument cables between pre-specified source and destination points. The project under study is an industrial facility of which the network consists of a total of 6,155 nodes. These nodes are connected via different types of trays which are modelled as edges. Edges are grouped into three different categories based on their type:

- Category 1: It accommodates the extension of power cables only and is, thus, designated as "CTP".
- Category 2: It accommodates the extension of instrument cables only and is, thus, designated as "CTI".
- Category 3: It accommodates the extension of both types of cables and is, thus, designated as "All".

The nodes and edges of the network are modelled as shown in Figure 1 below. In the 3D model, a CTP is represented by a red line, a CTI is represented by a blue line, and the "All" type is represented with an orange line. The total number of edges is 9,711.

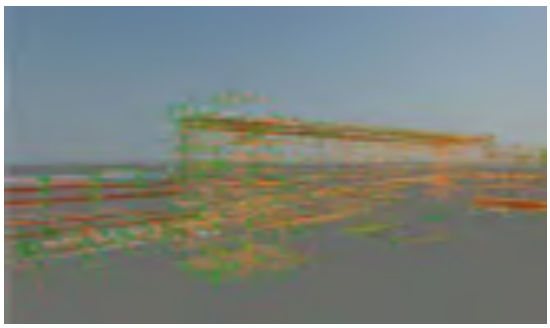

Figure 1. Network Model

Given equal lengths, different types of trays/edges differently impact the final cost. Thus, the type of each edge must be considered when finding the optimal path. This is achieved by factoring a cost-related weight into the total weight. Accordingly, for each tray type, a weight multiplier is computed to reflect its cost. This multiplier is used to adjust the distances between the nodes reflecting cost considerations for each edge type. Different edge types and their corresponding multipliers are summarized in Table 1 below.

Table 1. Weight Multipliers for Weight Groups

Weight Group	**Multi-plier**	**Weight Group**	**Multi-plier**
Cable Tray	1	Field Run to Tag	25
Cable Tray Angled 3D or Rotated	1.5	Ignore	1000
Cable Tray Angled East Vertical	1.5	Jumper Manual	15
Cable Tray Angled Horizontal	1.5	Steel Jumper	15
Cable Tray Angled North Vertical	1.5	Steel Tray Connect	1.1
Cable Tray East	1	Structural Steel	10
Cable Tray Elbow	1.5	Structural Steel Angled East Vertical	15
Cable Tray North	1	Structural Steel Angled North Vertical	15
Cable Tray Vertical	2	Structural Steel East	10
Cable Tray Jumper	1.5	Structural Steel North	10
Cable Tray Steel Jumper	1.5	Structural Steel Vertical	20

4 Methodology

The study presents a structured methodology that integrates multiple software to help decision makers find optimal network solutions quickly and efficiently. The methodology has been devised based on the following steps:

1. Build a 3D model of the cable network under study.
2. Design a database to store relevant data and identify the properties of nodes and edges. Microsoft Access database is used in this study. The database comprises five different tables as summarized in Table 2.

Table 2. Access Tables and Attributes

Table	Attributes
Nodes	ID, x, y, and z coordinates
Edges	ID, start node, end node, edge length (i.e. distance between nodes), edge type, edge category
Weight Groups	Edge type, weight multiplier
End Points	Source node, destination node
Shortest Paths	Tag (i.e. cable), start node, end node, sequence number (i.e. the position of the connection edge (node1, node2) in the path)

2.1 Extract the (x, y, z) coordinates of nodes from the 3D model of the facility and import them into the database.

2.2 Compile data on the edges which are represented by the nodes they connect. Identify and record the types of different edges as well as their lengths. The lengths of edges are computed using the Euclidean distance (Equation 1). Note that this distance is to be multiplied by the weight multiplier to obtain the total weight used for path optimization.

$$d = \sqrt{(x_2 - x_1)^2 + (y_2 - y_1)^2 + (z_2 - z_1)^2} \quad (1)$$

2.3 Identify the source node and destination node for each cable of the seven cables.

3. Develop a program that retrieves data from the database, identifies the shortest path, and exports the optimal path back into the database. Python programming language is used in this study; Python is widely used in numeric computation and includes libraries that help in data analysis and modelling of data [27]. The problem presented in this paper benefits from the built-in libraries, mainly NetworkX and pyodbc. NetworkX is a package used for the creation and the study of complex networks and includes standard shortest path algorithms [28]. pyodbc is an open-source Python module that allows accessing ODBC databases [29] and is used to establish a direct connection to the Access database. For each cable, the developed program performs the following tasks:

3.1 Retrieve relevant information from the database using SQL queries. Based on the cable type (power vs. instrument), the queries select the edges belonging to the categories that are compatible with the cable type. They also select a total weight column calculated by multiplying the distance by the weight multiplier.

3.2 Build a weighted graph from the nodes and the

available weighted edges.

3.3 Identify the shortest path using Dijkstra, A*[1], and Bellman-Ford algorithms from Networkx library.

3.4 Compute the total weight of the identified paths using the three algorithms.

3.5 Compute the time taken by each algorithm to identify the shortest path (i.e. runtime). The runtime is computed to compare the performance of the algorithms.

3.6 Select the path with the lower total weight if there is a difference between the weights.

4. Store the nodes of the identified shortest path back into the database.

5. Store the shortest path nodes in XML structure format that is readable by NavisWorks to visualize and verify the shortest path.

The presented methodology is illustrated in Figure 2.

5 Results and Comparison

The three algorithms found the same shortest paths for six sets of source and destination nodes out of the seven sets. Nevertheless, the shortest path identified for one set using Bellman-Ford passes through 100 nodes while those found using Dijkstra and A* require 101 nodes. However, the three of the identified paths have the same total weight indicating that both solutions are equally favourable given the imposed optimization criterion (i.e. minimal total weight).

The identified shortest path nodes for each set were imported into NavisWorks and highlighted. Figure 3 illustrates the shortest paths for three of the cables. The paths are highlighted in blue. It could be noted that the optimum path between the source and destination nodes is not necessarily the path with the shortest distance between them. As illustrated, the first path bypasses the location of the destination point before it returns back to it. This is a result of factoring costs of different types of edges in the total weight of edges.

The results of the three algorithms for each set are summarized in Table 3. Dijkstra and A* algorithms generally showed close performances with respect to runtime. Meanwhile, Bellman-Ford exhibited a lower performance in terms of computation speed as compared to the other two algorithms. The percentage difference between Dijkstra and Bellman-Ford's runtimes for the first cable reached 4,800% as it took 0.0980 and 0.00200 seconds to identify the optimal path using Bellman-Ford and Dijkstra, respectively.

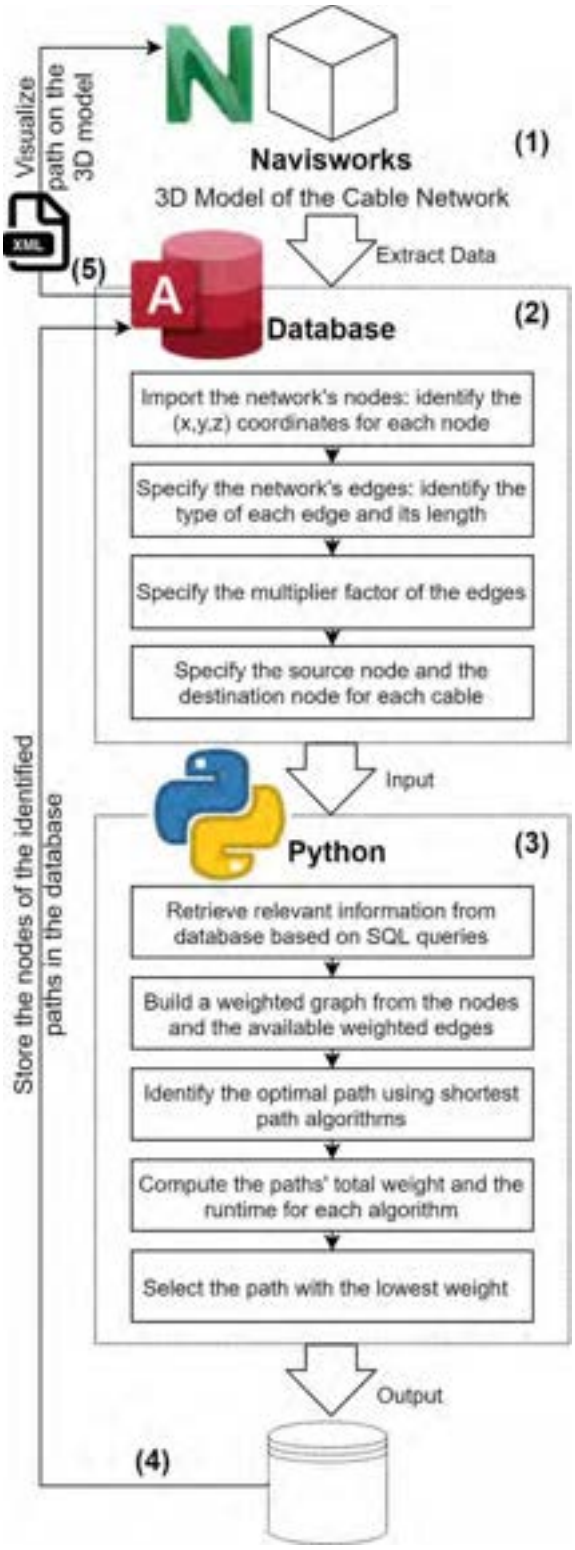

Figure 2. Methodology

[1] The Euclidean distance is used as the heuristic function for A* algorithm

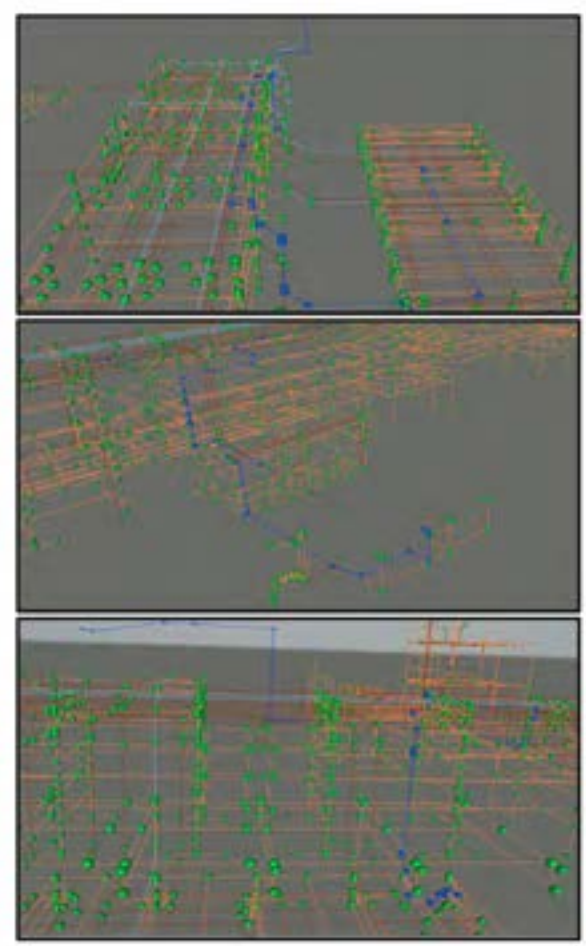

Figure 3. Shortest Paths in NavisWorks

The obtained results have shown that there is no significant difference between Dijkstra and A* algorithms. This could be attributed to the fact that the heuristic estimates (the Euclidean distance) of the A* algorithm are lower than the actual cost (the weighted distance) of moving from the nodes to the destination nodes. Consequently, the algorithm expands more nodes and, hence, takes a longer computation time. On the other hand, Bellman-Ford's underperformance in terms of speed was anticipated as a result of its looping behaviour. Although the difference between their performances is in the order of milliseconds, it becomes more significant as the size of the problem increases (i.e. as the number of nodes and edges increase). As the algorithm runtime is considered a major determinant in selecting the most convenient algorithm for a specific application [30], it could be concluded that Dijkstra and A* algorithms are deemed more suitable for solving a similar type of problems.

Table 3. Shortest Paths Results

Dijkstra			
Cable	Number of Nodes	Runtime	Weight
Test 1	45	0.00200	611.929
Test 2	78	0.0150	467.658
Test 3	101	0.0240	654.499
Test 4	41	0.00400	317.676
Test 5	55	0.00800	564.203
Test 6	84	0.0220	435.403
Test 7	78	0.0220	502.488
A*			
Cable	Number of Nodes	Runtime	Weight
Test 1	45	0.00400	611.929
Test 2	78	0.0300	467.658
Test 3	101	0.0480	654.499
Test 4	41	0.00400	317.676
Test 5	55	0.00900	564.203
Test 6	84	0.0270	435.403
Test 7	78	0.0350	502.488
Bellman-Ford			
Cable	Number of Nodes	Runtime	Weight
Test 1	45	0.0980	611.929
Test 2	78	0.0510	467.658
Test 3	100	0.114	654.499
Test 4	41	0.0620	317.676
Test 5	55	0.0670	564.203
Test 6	84	0.0720	435.403
Test 7	78	0.0480	502.488

6 Conclusion

Shortest path algorithms have been proven effective in providing support for decision makers when solving complex path-defining problems. On construction projects, these algorithms were used for diverse problems to attain optimal solutions. This paper considers the problem of selecting the shortest path for power and instruments cables in an industrial facility. The Dijkstra, Bellman-Ford, and A* algorithms were adopted to find the shortest path while considering the total weight of the edges. The total weight for this problem is dependent on both the distance and the cost subject to the type of each edge/tray.

Using the developed Python program to identify the shortest paths, results showed that all algorithms gave the same paths for six cables out of the seven cables. Additionally, the total weight is found to be the same across all tests indicating that these methods were equally efficient in finding the optimal solution given the optimization criteria. However, the results showed that the Dijkstra and A* algorithms had a better performance than that of Bellman-Ford with respect to runtime in all of the cases. Specifically, the difference between

Dijkstra's and Bellman-Ford's runtime reached 1,524% in one of the cases. Although for this case the difference is only in milliseconds, the difference between their performance becomes more significant in larger scale problems.

The paper also presented an integrated approach that combined different software platforms to automate the process of inputting data, computing the shortest path and then plotting this path in 3D format for visualization. The problem represented a case on the importance of using the shortest path method when dealing with decisions that are complicated by nature. Construction projects could benefit from using such algorithms and integrated approach for helping in various decision-making processes.

The methodology presented in this study could be extended to address the previously mentioned applications of shortest-path algorithms in construction. Today, with the continuously increasing level of automation in construction, the problem of finding the collision-free shortest paths for mobile robots on construction sites is of a particular importance. Hence, a case study on mobile construction robots shall be addressed in a future study. Efforts shall be devoted to select a case study of a larger size to demonstrate the impact of the performance of the different algorithms on the efficiency of solving the problem.

7 Acknowledgement

The authors wish to acknowledge the technical support and assistance of Nehme Roumani in this study.

8 References

[1] Al-Tabtabai H. and Alex AP. Using genetic algorithms to solve optimization problems in construction. *Engineering Construction and Architectural Management*, 6(2):121-32, 1999.

[2] Hegazy T. Optimization of construction time-cost trade-off analysis using genetic algorithms. *Canadian Journal of Civil Engineering*; 26(6):685-97, 1999.

[3] Damci A., Arditi D. and Polat G. Multiresource leveling in line-of-balance scheduling. *Journal of Construction Engineering and Management*, 139(9):1108-16, 2013.

[4] Lien LC. and Cheng MY. A hybrid swarm intelligence based particle-bee algorithm for construction site layout optimization. *Expert Systems with Applications*, 39(10):9642-50, 2012.

[5] Wong CK., Fung IW. and Tam CM. Comparison of using mixed-integer programming and genetic algorithms for construction site facility layout planning. *Journal of construction engineering and management*, 136(10):1116-28, 2010.

[6] Al Hattab M., Zankoul E. and Hamzeh FR. Near-real-time optimization of overlapping tower crane operations: a model and case study. *Journal of Computing in Civil Engineering*, 31(4):05017001, 2017.

[7] Yin C. and Wang H. Developed Dijkstra shortest path search algorithm and simulation. In *Proceedings of the 2010 International Conference on Computer Design and Applications,* pages V1-116, Qinhuangdao, China, 2010.

[8] Soltani AR., Tawfik H., Goulermas JY. and Fernando T. Path planning in construction sites: performance evaluation of the Dijkstra, A∗, and GA search algorithms. *Advanced engineering informatics*, 16(4):291-303, 2002.

[9] Magzhan K. and Jani HM. A review and evaluations of shortest path algorithms. *International journal of scientific & technology research*, 2(6):99-104, 2013.

[10] Zhang Z. and Zhao Z. A multiple mobile robots path planning algorithm based on A-star and Dijkstra algorithm. *International Journal of Smart Home*, 8(3):75-86, 2014.

[11] Chen JC. Dijkstra's shortest path algorithm. *Journal of Formalized Mathematics*, 15(9):237-47, 2003.

[12] Goyal A., Mogha P., Luthra R. and Sangwan N. Path finding: A* or Dijkstra's?. *International Journal in IT & Engineering*, 2(1):1-5, 2014.

[13] Ramadani E., Halili F. and Idrizi F. Tailored Dijkstra and Astar Algorithms for Shortest Path Softbot Roadmap in 2D Grid in a Sequence of Tuples. *International Journal of Science and Engineering Investigations*, 8(92), 2019.

[14] Gogoncea V., Murariu G. and Georgescu L. The use of Dijkstra's algorithm in waste management problem. *The Journal The Annals of "Dunarea de Jos" University of Galati, Fascicle IX. Metallurgy and Materials Science*, 28(2):125-127, 2010.

[15] Singh G. and Chopra V. An analysis of various techniques to solve travelling salesman problem: A Review. *International Journal of Advanced Research in Computer Science*, 3(5), 2012.

[16] Goldberg A. and Radzik T. *A heuristic improvement of the Bellman-Ford algorithm*. Computer Science Department, Stanford University, Stanford, CA 94305, 1993.

[17] Zou B., Hu J., Wang Q. and Ke G. A distributed shortest-path routing algorithm for transportation systems. In *Proceedings of the Seventh International Conference on Traffic and Transportation Studies*, pages 494-500, Kunming, China, 2010.

[18] Humblet PA. Another adaptive distributed shortest path algorithm. *IEEE transactions on communications*, 39(6):995-1003, 1991.

[19] Busato F. and Bombieri N. An efficient implementation of the Bellman-Ford algorithm for Kepler GPU architectures. *IEEE Transactions on Parallel and Distributed Systems*, 27(8):2222-33, 2015.

[20] Weber A., Kreuzer M. and Knoll A. A generalized Bellman-Ford algorithm for application in symbolic optimal control. In *Proceedings of the European Control Conference*, 2001.06231, Saint Petersburg, Russia, 2020.

[21] Bannister, M.J. and Eppstein, D. Randomized speedup of the Bellman–Ford algorithm. In *Proceedings of the Ninth Workshop on Analytic Algorithmics and Combinatorics (ANALCO)*, pages 41–47, Kyoto, Japan, 2012.

[22] Dinitz, Y. and Itzhak, R. Hybrid Bellman–Ford–Dijkstra algorithm. *Journal of Discrete Algorithms*, 42:35–44, 2017.

[23] Cavendish, D. and Gerla, M. Internet QoS routing using the Bellman-Ford algorithm. In *Proceedings of the International Conference on High Performance Networking*, pages 627–646, 1998.

[24] Fu, L., Sun, D. and Rilett, L.R. Heuristic shortest path algorithms for transportation applications: state of the art. *Computer and Operations Research*, 33(11): 3324–3343, 2006.

[25] Kim, S.K., Russell, J.S. and Koo, K.J. Construction robot path-planning for earthwork operations. *Journal of Computing in Civil Engineering*, 17(2):97–104, 2003.

[26] Lei, Z., Han, S., Bouferguène, A., Taghaddos, H., Hermann, U. and Al-Hussein, M. Algorithm for mobile crane walking path planning in congested industrial plants. *Journal of Construction Engineering and Management*, 141(2):5014016, 2015.

[27] Python.org. Applications for Python. On-line: https://www.python.org/about/apps/, Accessed: 03/06/2020.

[28] PyPI.org. Network X. On-line: https://pypi.org/project/networkx/, Accessed: 03/06/2020.

[29] PyPI.org. pyodbc. On-line: https://pypi.org/project/pyodbc/, Accessed: 03/06/2020.

[30] Zhan, F.B. and Noon, C.E. Shortest path algorithms: an evaluation using real road networks. *Transportation Science*, 32(1): 65–73, 1998.

Constructability: The Prime Target in Value Engineering for Design Optimization

Arun Sekhar [a] and Uma Maheswari [b]

[a]Research Scholar,Department of Civil Engg, IIT Delhi, India
[b]Associate Professor, Department of Civil Engg, IIT Delhi, India
E-mail: Arun.Sekhar@civil.iitd.ac.in, J.Uma.Maheswari@civil.iitd.ac.in

Abstract –

An ideal Design-Construction Interface is assumed in the decision making process of initiation and planning. The uniqueness, site conditions and contingencies cannot be envisaged and incorporated in its entirety in all projects. Constructability in resonance to the appropriate technology becomes paramount in deciding the material, structural forms and construction methodology. The construction industry is gradually evolving to a manufacturing and product delivery process where design for Manufacturability and Assembly takes precedence. Optimization of targeted values viz logistics, manufacturability, assembly, maintenance, lifecycle cost and ergonomics becomes critical to ensure smooth execution of the Project. The data collected from a pre cast construction project is analysed to map the degree of ease in Design-Construction interface and compared with a framed structure to draw parallels with respect to constructability as a target in value engineering. The objective of the study is to examine the components of constructability in Design Process to optimize effort and resources. Target Value Design gives the stakeholders more rationale inputs for monitoring and decision making. The study attempts to predict the future of manufacturability and constructability in construction where smooth assembly with minimum labour is essential for value addition. The bottom up approach of new policy initiatives and better communication between stakeholders promise more refined designs in future where technology will be pushed to achieve design optimization.

Keywords –

Constructability; Design Optimization; Value Engineering; Design-Build; Target Value Design; Manufacturability; Assembly

1 Introduction

It is an intriguing task for designers across the globe to take a foolproof final print of the drawings and precedence diagrams incorporating all possible changes during execution of a Project. Unfortunately we do not have the ability to speculate and predict the future. But we do have the ability to learn from the past and adopt better practices in the next project. An ideal condition is assumed by the planners while formulating the conceptual design. Building construction industry suffers greatly from cost and time overrun due to oversights in planning and design inaccuracies. The success of a project is decided by the Value it provides to the user. To provide 'Value' to the client, the concept and its execution has to be well coordinated to provide the best performance. The term Design encompasses all activities in the design studio including concept, schematic, design development, preparation of tender documents and entering into a legally valid contract for construction. According to Jergeas et al. [1] and Cleland [2], efficient management of the relationship between the project and its stakeholders is an important key to project success. Conceiving the plan in a broader framework and executing it with minutest detail with optimization of all resources is possible only when the details are constructible. For this to happen, communication between stakeholders is must. In their study of critical success factors across the project's life cycle, Pinto and Slevin [3] emphasize the importance of interaction with the clients throughout the duration of the project. Almost 40% of the change orders or deviation orders are rooted in the design phase [4] and 30% cost escalation is attributed to poor communication during design phase [5]. This amply highlights the importance of reducing the change orders during execution phase and targeting constructability from the planning stage. Constructability translates to be the ability to construct something with appropriate technology within a specified budget and schedule producing intended value. Value Engineering has to be an integral part of constructability as its prime aim is to increase value than to reduce cost [6]. The design table is very much a place where the fate of the project lies and decides the value it will generate. The constructability and value generation is critically analysed in adopting an emerging technology like pre cast construction to draw lessons in design optimization along with procurement management challenges.

2 Constructability and Value

Right from the very first house human beings constructed, the intended purpose was his concern. 50,000years ago the concern was only to provide shelter from weather and safety from wild animals. The need to design a product was felt when he realized that the final outcome was not matching the imagined one. As we evolved the scope got expanded towards gaining more utility from the same effort. The difficulties faced during execution were traced back to the plan and it was realized that the lessons learned should be incorporated in the next design. Target Value Design gives the stakeholders more rationale inputs for monitoring and decision making. Target Values have to be identified to incorporate in the design process which might vary for each stakeholder. The study aim to define values in a design process for optimization of resources. Forensic Schedule Analysis of a pre-cast housing project is carried out to study the Design-Construction interface fault lines which cause hiccups in achieving intended values. The study examines the various constructability factors influencing the smooth interface from design to construction and critically examine the bottlenecks. For this purpose the concept of Value needs to be addressed in a more objective way.

2.1 Value in Design

Value is a set of concerns with respect to cost and function. It has a futuristic component which is based on a various inputs and assumptions. It can be expressed as ratio of design function to cost. It is quite obvious that in order to increase value, the cost has to be reduced or the design functions have to be increased. But while preparing a tender document, in the process of procurement, the price is the only readily available factor. A correlation between price, cost and value need to be established to define the target values in design. Table 1 illustrates the comparison of price, cost and value with respect to various functions as obtained from focus group discussions with stakeholders in construction projects. It can be seen that value is a user's utility perspective through opinion. This opinion could be based on a single factor or a combination of factors. The comparison illustrates that price is related to past tense, cost to present tense and value in future tense when we evaluate a facility or a project at planning. The price comes from the market and documented in the schedule of prices by various agencies and the cost is budget at completion of the project. The value is an opinion which goes back to market as set of benchmarks with respect to utility of the product or service**.** Figure 1 gives the flow chart of value generation in a typical construction project.

Table 1. Comparison of Price, Cost and Value

Price	Cost	Value
Amount paid for acquisition	Amount incurred in production	Utility of a product or service
Ascertained from consumers perspective	From producers perspective	From users perspective
Estimates through policy	Through fact	Through opinion

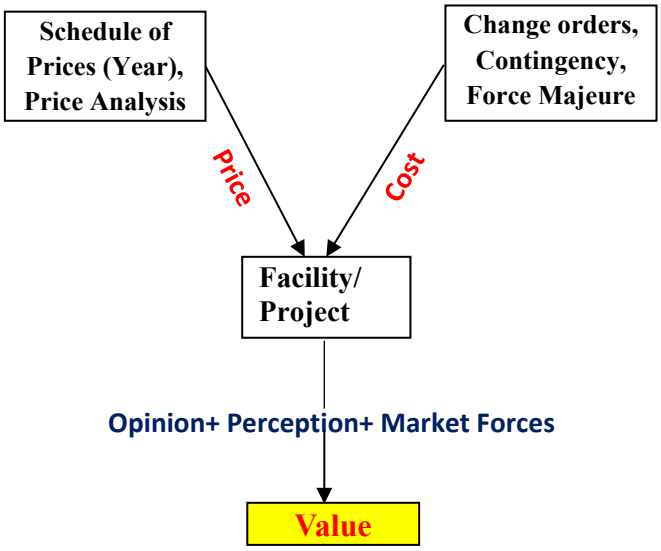

Figure 1. Interaction of Price, Cost and Value

Price is a fixed factor compared to cost and value. It is obtained from schedule of prices which is periodically updated by regulatory bodies. In a Project it makes sense to plan cost cutting, but not price reduction. Price of materials are fixed with respect to time and location. These are 'fait accompli' and we can only opt for the most suitable in terms of economy, quality and availability. Cost is what the client pays to own a facility [7]. Once the BOQ is prepared the price factor has been considered. But the cost factor eludes the designer as that is depended on change orders, contingency and force majeure. Value is a promise in future which is based on opinion, perception and market forces. In order to optimize the value what should we aim for? The answer probably lies in the way we produce an automobile or an aircraft. Though a civil engineering project cannot be templated into a product manufacturing process, many

lessons can be drawn from the evolution of assembly line manufacturing process which revolutionized the industrial production of construction materials.

2.2 Constructability in QFD

Quality Function Deployment in construction industry is not often practiced due to its invisibility compared to other manufactured products. A direct translation of QFD concept from an automobile production unit may not suit a building contractor. Customer's aspirations from a car varies greatly from a building or an apartment. Constructability is the synthesized end product after analyzing all QFD inputs. Table 2 illustrates the conflicting yet complementing requirements of users and designers while planning a pre-cast apartment building. Customers are often smitten by the cost not by the value. At the same time cost eludes the designers as they are indulged in price. These conflicting demands in constructability makes it more challenging to set specific targets for planning the project.

Table 2. QFD requirements of Customers and Designers for a Pre-Cast facility

Customer	Designer
Should be Earth Quake proof	Monolithicity of connections
Smooth finish	Vibro Compaction
Low maintenance cost	Easy access to MEP lines
No disputes	EPC Contract
Affordability	Break even quantity
Fast delivery	Steam curing of RCC members
Quick assembly	Cranes part of inventory

2.3 Genesis of Pre-Cast Technology

The pre-cast construction technology was emerged as a natural evolutionary process by improving on the lacunas of cast-in-situ construction. The advancements in reinforced concrete technology and feasibility of slender sections made designers to take a bold step towards treating the concrete members like steel. From the table 1, it is very evident that the industry has adopted pre-cast technology for achieving value by taking advantage of certain unique features of the new technology.

Table 3. Comparison of Pre-Cast vs. Cast-in-Situ

Pre-Cast	Cast-in-Situ
Cast and cured in manufacturing plant	Members are cast at construction site
Accelerated curing required	Normal curing time
Faster Construction	Slow Construction
Greater control on quality	Less control on Quality
Not hampered by adverse weather	Severely hampered by weather
Assembly based	Activity based
Minimum waste	Considerable Waste

From construction activity, the entire process got converted to a manufacturing process to add value. In an evolutionary curve we can see that steel overtook cement concrete as a preferred material for fast track construction. Though the shift towards steel for many high rise buildings in mid-20th century happened intuitively, a closer look will show that it was a natural option for the rapid rebuild of post war Europe. True to the old adage, necessity was the mother of invention and a solution emerged with less labour, time and superior finish. It is interesting to note that though the technology is not based on any new theory, the adoption happened by default, not by design. The reason is more value generation through manufacturing and assembly. Pre cast system is widely used now in many repetitive structures and claddings due to its versatility to act both as architectural and structural material.

2.4 Cost Benefit Analysis and Break Even Quantity

The actual value of pre-cast is often misunderstood as the direct cost of structural components will be high compared to the cast-in-situ framed system [8]. The components have to be manufactured in a pre-cast plant and transported to the site. Huge initial investment of casting plant and steam curing facility can be justified only with a minimum assured order of repetitive nature. This technology is ideally suited for housing sector as the layout is similar and slabs are spanning less than 5m. The Cost Benefit Analysis in figure 2 shows that minimum number of 800 units have to be constructed to make the rate comparable to the conventional cast-in-situ technology.

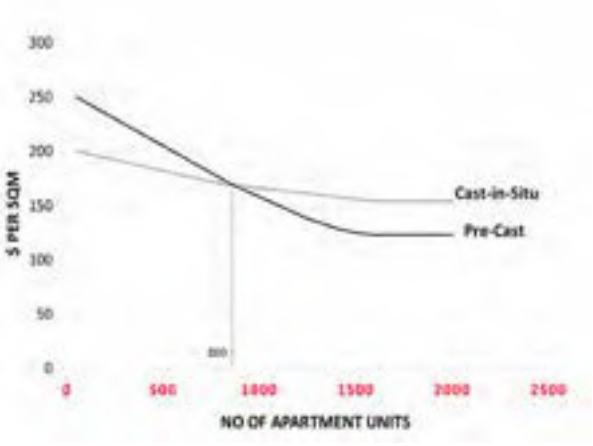

Figure 2. Break Even Quantity for Pre-Cast feasibility

This break even quantity is specific to a turnaround distance as the distance of plant increases from the construction site, the cost changes. Figure 2 shows the data collected from Delhi, India. The construction firm which invested almost $7 million on the plant definitely had a look at the national policy on the housing sector which pledged 1.5 % of GDP towards the cause.

3 The Design Targets

Having defined the relation between Price, Cost and Value; it's time to fix the design targets specific to the intended value. They could be Assembly, Modularity, Manufacturability, Maintainability or Logistics (AND/OR). These target values may be required in varied quantities as per the design optimization which should fit in the cost and time framework. The present study is focusing on Precast Technology and obviously the targets have to be assembly, manufacturability and logistics.

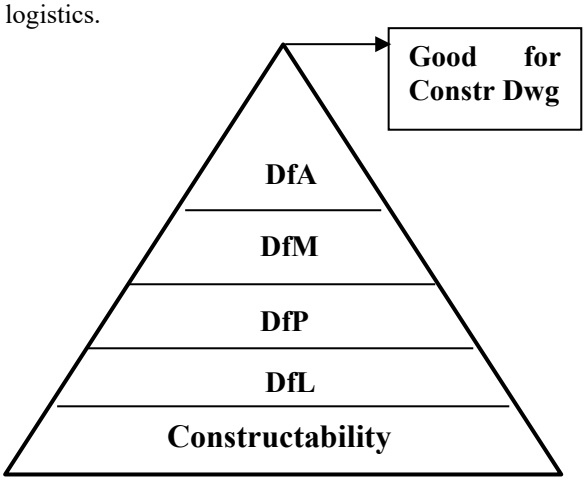

Figure 3. Target Value Triangle

A close examination will show that the relative importance of Assembly and Manufacturability is more predominant than logistics or transportability. Location of a manufacturing plant can be selected as per the logistical requirement but if the components are not fit for assembly, there is no scope to perform any repair on site. Taking them back to the plant for changes will incur huge financial burden which may derail the whole financial plan. The target value triangle for the pre cast construction project is shown in figure 3. As time progresses, the influence of design aspects of logistics starts reducing and manufacturability increases. The iterative design process zoom in on to design for Assembly as the prime target to achieve in the design process and constructability remains the superset of Logistics, Manufacturability and Assembly.

3.1 Design for Logistics (DfL)

The Pre-Cast components have to be manufactured in a location which makes the turnaround time logistically feasible and economically viable. The location of the plant has to be decided based on the availability of the raw material and resources. The logistical challenges involves setting up the Pre-Cast plant, Transportation of raw materials and Transportation of manufactured components to the construction site. The dimension of vehicles for the above purpose will be governed by the size of the building components and their weight. The maximum height clearance permissible under the rail bridges and fly overs on the way plays an important role in this logistical planning. Once the location of manufacturing plant is fixed, rest of the parameters will be dependent on this aspect of logistical baseline. Figure 4 shows the map of three sites A, B, C and the location of the pre-cast plant, P. The location of plant is so selected that the time to reach each site is almost same. The plant is sited based on the logistical feasibility which has a direct bearing on the overall cost and thereby being a value deciding factor.

3.2 Design for Manufacturability (DfM)

The components have to be pre cast in the plant and assembled at the site. This assembly operation will be requiring cranes. That infers to the correct size and shape of components which will make the assembly easy. Assembly will govern manufacturability. The beams, columns, floors and walls have to be cast in the casting yard. The dimensions of structural components have to be fixed and ready mix concrete is poured using automated systems. How can compaction be achieved? A normal vibrator cannot be used as it will consume more time and will result in non-uniform compaction. The casting bed has to act as a vibrator to save time and effort. This important criteria for casting bed design and the cost

involved is a governing factor in manufacturability. The components have to be cured for required period to attain full strength and this for fasten the process, a steam curing facility has to be set up. All members should be hoistable using cranes as they will be moved several times once removed from casting bed. The location of these lifting hooks will have to be decided on the drawing table as they are part of structural analysis process. Table 4 lists the criterion considered for manufacturability of pre-cast technology.

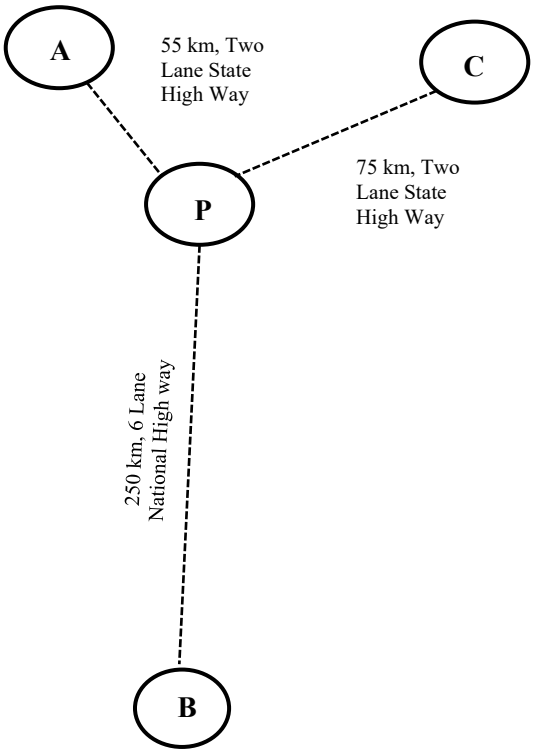

Figure 4. The Location of Plant P, with respect to sites A,B and C

Table 4. The Manufacturability criterion

Criterion	Manufacturability
Concreting	Automated Concrete Pouring Facility
Compaction	Vibro Compaction of Casting Bed
Curing	Steam Curing Facility
Mobility of Components	Overhead Crane in the Plant
Execution at Site	Limiting the weight of each components to the crane capacity at site

3.3 Design for Assembly (DfA)

Assembly of various structural components at site has to be in perfect sequence to ensure a smooth execution. Unlike the cast-in-situ method, the pre-cast members lack monolithic connection. The structural analysis is carried out based on certain rigidity of connection and these design assumptions have to match with the site conditions. In reality, the DfA is the most important factor in a pre-cast design process. If the connections are not strong enough, catastrophic failures might happen. After the structural analysis and design, a scaled model may be tested in lab condition to ensure that the assumptions are correct. The cost for these tests has to be borne part of the Research and Development effort rather than in the estimates of the design at hand. These are part of the initial investments as it is practically impossible to carry a destructive shake table test every time. The results of the initial test can be interpolated or extrapolated in subsequent designs as the case may be.

After taking into account of logistics and manufacturability, the ease of assembly takes precedence. The aspect of assembly is so important that the structural design has to be carried out by taking these assembly into consideration. The design of floor slabs will illustrate this aspect in detail. Unlike a cast-in-situ slab, the pre cast slab has many functions to perform. It should have shear connectors to ensure connection between next slabs, it has to give a smooth floor finish and it should be easily liftable by crane. These functions are possible only when the design is robust, flexible and innovative. A lattice girder reinforcement is specifically manufactured for the purpose and this girder serves many purpose. Figure 5 shows the manufacturing process and figure 6 [9] shows slabs stacked after curing process which are ready to be transported to the site.

Figure 5. Lattice Girder Manufacturing (Courtesy: BG Shirke Group of Companies)

Figure 6. Shear key as Lifting Hook in Lattice Girder

4 Monitoring and Control

The traditional monitoring and control process is designed to keep the budget always on track and effect minimum change orders. The stakeholders involved are reacting to the precedence diagram actual unravelling on site. In pre-cast system, the construction activity has been converted to an assembly process. So the monitoring process almost reduces to an assembly supervision as there are very few decisions to be taken during construction. The scope is fixed in pre-cast the moment construction drawings are issued to the casting plant and no change order with respect to architectural or structural is feasible. This lack of flexibility is accounted for by numerous design iterations after repeated interactions with stakeholders.

5 Procurement Management

PMBOK has covered forty nine processes in ten knowledge areas and five process groups in its 6th edition [10]. The processes involved in procurement management is limited to plan, conduct and control. In conventional construction management, the procurement is a reaction to what is designed. But when we plan to adopt an assembly based technology, the procurement management cannot be independent of the design process. The Design-Build format suits procuring the pre-cast systems as the bid preparation is challenging when it comes to design and estimation. In an open competition to bid for a specific design, the purpose of providing equal opportunity and level playing field is not achieved. Moreover the DfA challenges will make the design favour a particular firm who has adopted a specific dimension for their projects in hand. Using design-build procurement format, the owner saves time and effort by executing only one contract with a design–builder, who takes responsibility for completing both the design and construction of the project [11]. The Engineer, procure and Construct (EPC) model is often considered synonymous with Design-Build one in function as both shift the design and build responsibility and a bigger portion of risk to the contractor [12]. In EPC mode the contractor is often entrusted with the desired output in the case of a production facility. In a construction project like precast mass housing, design-build provides more value. The evolution of any technology has taken considerable settling time before the rest of the world catches up with a universally accepted price for procurement. A market survey will show that construction firms which innovated to adopt faster and durable construction technology are faring better than those who continued with older ones. From clients perspective, (s)he may opt for any technology or procurement format which gives a better return. In the Design-Build system, the designer, the builder and the consultant, all could be rolled into one due to uniqueness of technology and there may be very less control by the client over the Project once the design has been finalized. But the designer has to ensure assembly, manufacturability and logistical feasibility by taking the client on board. Keeping the architectural, structural and MEP changes out of purview, the Work Breakdown Structure and the activity precedence diagram can now be fixed. This facilitates the designer to provide exact quantities for the QS team which makes their task of estimation much effortless and almost accurate.

5.1 Design for Procurement (DfP)

Design for Procurement (DfP) is also an important parameter in construction when it comes to innovative and emerging technologies. Every exotic design cannot be constructed and every technological feasibilities are not buildable on ground. There is a fine line between building a design and design something buildable. In the former case, the procurement team is searching for solutions which were not considered by the design team. In the latter, design office is involved in the procurement decisions. In the pre cast example, the activities are designed to be repetitive so that once the components are manufactured, transporting and assembling completes the construction process. The design is tailor made for procurement to suit a Design-Build system so that the facility is built by the firm which designs it, thereby eliminating communication hiccups between a consultant and contractor. But is this killing fair competition and leading to monopoly of business? This question lingers on with all new innovations where very few people are experts initially. Any technology can compete for design parameters like minimum waste generation, faster construction and minimum cost per unit plinth area. The fittest and adaptable will survive and probably the theory of evolution is applicable to construction industry too.

6 Modularity: The Modern Solution for Constructability

Modularity has emerged as a modern day solution to ease the construction complexity. The design complexity of assembly can be smartly eliminated in the modular approach. Similar to the pre cast technology, on a larger scale modularity reduces the project cost [13]. The concept of modularity was borrowed from the shipping transportation containers which offered quick loading and unloading of cargo from ships. The uniformity of the containers and cranes made the cargo handling very smooth saving billions of dollars in demurrage. This path breaking idea can be simulated in construction too where the rooms are relatively small in dimension. The design for modularity assumes complexity as the height of the building increases due to higher seismic design requirements. Unlike a pre cast building, a modular building is 100% reusable and relocatable having few beam-column-slab connections. In modular system, rather than member strength, the geometry is holding the structure together.

7 Constructability in Design Optimization

It is quite evident that constructability is a function of many parameters like assembly, manufacturability, logistics, procurement, cost and time. In order to take the best out of technology, we have to move away from the traditional network crashing mindset to dynamic parameters mentioned above. The time saving techniques employed by the defense forces may not fit for a building project. The forces may not be worried about the budget but in construction projects, the client is worried about the cost. It is imperative that constructability has to be considered as the benchmark for value generation. The figure 7 depicts the relative importance of various design targets to mix and match the optimum one. The most suitable targets can be given more weightage and design optimized according to the technology involved.

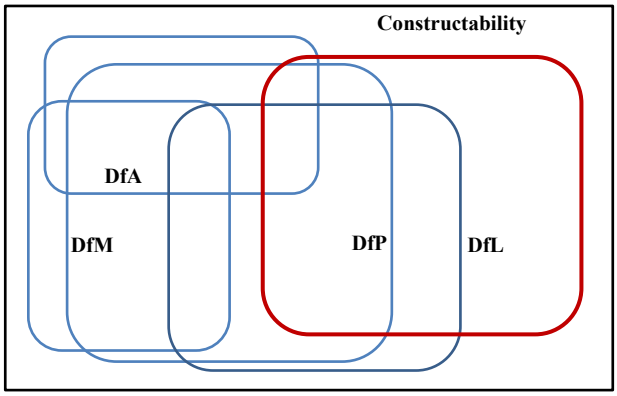

Figure 7. Design Targets in Constructability

Constructability is pitched as the superset in which various other design target sub sets are accommodated as per the requirement. It is more of a tailor made solution rather than pre fixed one. The study reveals the relevance and influence of procurement management on constructability and importance of value generation in construction industry.

8 Stakeholder Synergy and Design Optimization

Better communication between stakeholders is a pre requisite for optimizing the effort and resources. This can be achieved by clash detection at an early stage. Design is a cocktail of disciplines and technologies which often lack the similar wavelength of people and ideas. The diverse opinions and assumptions need to fit in to the design parameters suitable for the project in hand. Communication between stakeholders is highly influenced by the structural system and procurement methodology. The constructability components like DfA, DfL, DfM and DfP is examined for a specific technology ie Pre-Cast. Similar analysis of design targets might have to be carried out for other construction methodologies too. It is pertinent to mention that in the example of Pre-Cast the procurement mode was Design-Build as the builder was responsible for the architectural, structural and MEP design. Better stakeholder synergy is achieved in this case as one stakeholder viz consultant has been eliminated. Previous studies have established that 40% of the change orders are rooted in the design phase and 30% cost escalation is attributed to poor communication during design. At the same time it has to be noted that each facility is unique and a tailor-made approach have to be adopted for different scenarios. The design team has to work out the best cocktail of design targets to achieve maximum value for the project not compromising on stakeholder synergy.

9 Conclusion

The human race has travelled a long journey from Pyramids to Burj Khalifa. As the theory of evolution has proved, only the ergonomic design will be passed on and imbibed by the next generation. Economic viability with desired value will remain the sole criteria for the project's success in the modern world. Only constructible designs will be executed and a trade-off will be arrived between design and construction which could be an iterative process to reach at minimum financial burden, carbon foot print and maximum value for money. The monitoring and control techniques like EVM will be helpful only when Design-Construction interface is hitch free. Construction is a nation building exercise where each activity is contributing towards the GDP. The study validates ample reasons to predict a symbiotic relation

between various procurement options and technologies to achieve targeted values. Design and Construction will remain complimentary activities with the constructability deciding the success and client satisfaction. The study predicts that constructability coupled with smooth assembly using minimum labour is essential for value addition. The bottom up approach of new policy initiatives and better communication between stakeholders promise more refined designs in future where technology will be pushed to achieve design optimization.

References

[1] Jergeas, George F., Erin Williamson, Gregory J. Skulmoski, and Janice Thomas, 'Stakeholder Management on Construction Projects', *AACE International Transaction*, pp. P12.1-P12.6, 2000.

[2] Cleland, David I., 'Project Stakeholder Management,' *Project Management Journal*, 17:4, pp. 36-44, 1986.

[3] Pinto, Jeffrey K. and Dennis P. Slevin, 'Critical Success Factors across the Project Life Cycle', *Project Management Journal*, 19:3, pp. 59-66, 1988.

[4] Chen, Q., Reichard, G. & Beliveau, Y., 'Interface Management - A Facilitator of Lean Construction and Agile Project Management', 15th Annual Conference of the International Group for Lean Construction. East Lansing, Michigan, USA, 18-20 Jul 2007. pp 57-66

[5] Forbes,L.H and Ahmed, *S.M. Modern Construction: Lean Project Delivery and Integrated Practices*, CRC Press, 2010.

[6] Lawrence D. Miles, *Techniques of Value Analysis and Engineering,* MCGraw-Hill Book Company, 1972.

[7] A Nain. Valuation Principles and Procedures, volume 1. Dew Drops Education Pvt Ltd, Kolkata, 2009.

[8] V. N. Nanyam, A. Sawhney, R. Basu and H. Vikram, 'Implementation of Precast Technology in India; Opportunities and Challenges," *Creative Construction Conference* 2017, CCC 2017, 19-22 June 2017, Primosten, Croatia.

[9] Keegan Precast Ltd Filigree (Omnia) floor plate system,http://www.keeganprecast.com/products/precast-floors-stairs/omnia-floor-slab, Accessed: 03/04/2020.

[10] Project Management Institute. A guide to the project management body of knowledge (PMBOK guide). Newton Square,Pa: Project Management Institute, 2004.

[11] Suzanne H. Harness, AIA, J.D. 'Construction and Design Risk (C&DR) Briefing Design Build Contracting', LLC & Harness Projects, LLC, 2014.

[12] Patrick T Jordan, Difference between EPC and Design-Build delivery. Online: https://www.lexology.com/library/detail, Accessed: 05/04/2020.

[13] Generalova, Elena & Generalov, Viktor & Kuznetsova, Anna. Modular Buildings in Modern Construction. Procedia Engineering. 153. 167-172. 10.1016/j.proeng.2016.08.098.

Blockchain based Framework for Verifying the Adequacy of Scaffolding Installation

Chan-woo Baek[a] , Do-Yeop Lee[a] and Chan-Sik Park[a]

[a]School of Architecture and Building Science, Chung-Ang University, Republic of Korea
E-mail: ba9899@gmail.com, doyeop@cau.ac.kr, cpark@cau.ac.kr

Abstract –

Falls are the leading cause of construction site accidents and made up more than 60 percent of all construction-related deaths in 2018, according to the Korea Occupational Health and Safety Administration (KOSHA). Accordingly, the government conducts intensive management and supervision of scaffolding and scaffolding installation at small sites while inducing safe working environments through support for system scaffolding installation. However, the timing of scaffolding installation for external work varies by site, and visiting inspections of more than 400,000 sites annually are practically limited. In particular, in the case of small sites, the work is often carried out with a high risk of falling accidents due to installation or defects that do not comply with KOSHA rule and the occurrence of accidents is frequently reported. To solve these limitations, information on whether the right amount of scaffolding has been purchased and installed at the right time according to the size and shape of each site needs to be managed by a systematic method.

In this paper, we propose a framework for verifying the adequacy of the installation of scaffolding needed at the individual construction site using blockchain technology. The system provide Dapp, an application that runs on the block chain server, so that General contract (GC) and Supplier can enter information related to ordering and procurement of scaffolding. The core information required to determine the adequacy of scaffolding installation is stored in a non-modifiable form using the distributed ledger storage technology of the block chain. As a result, scaffolding installation adequacy can be automatically verified through the algorithms that can compare the installation schedule and quantity calculation with the actually purchased quantity.

It is anticipated that using the proposed framework, government agencies can identify the safety levels of individual sites without on-site visits.

Keywords –

Scaffolding; Blockchain; Framework

1 Introduction

The death rate of domestic industrial accidents has been the highest among Organization for Economic Cooperation and Development (OECD) countries for decades. In addition, half of the domestic casualties occur in the construction industry. Particularly, the fall accident occurred from temporary structure shows high rate especially in a small site where facilities such as scaffolding are not installed [1].

Besides, according to the analysis data of major disasters in the construction industry over the past five years, 448 people died during scaffolding-related work, accounting for 23 percent of the total (2,134). Accidents occurred 63 percent at small and medium-sized sites (with a construction amount of less than 2 million USD), 44 percent due to the use of conventional steel pipe scaffolding, and 38 percent in housing-amenities construction [2]. Therefore, to prevent the risk of falling at the construction site, it is necessary to manage the appropriateness of scaffolding for more than 400,000 small and medium-sized sites annually [3]. However, at the construction site in Korea, the importance of scaffolding is still not recognized, and it is neglected for several reasons such as shortening the period and reducing costs.

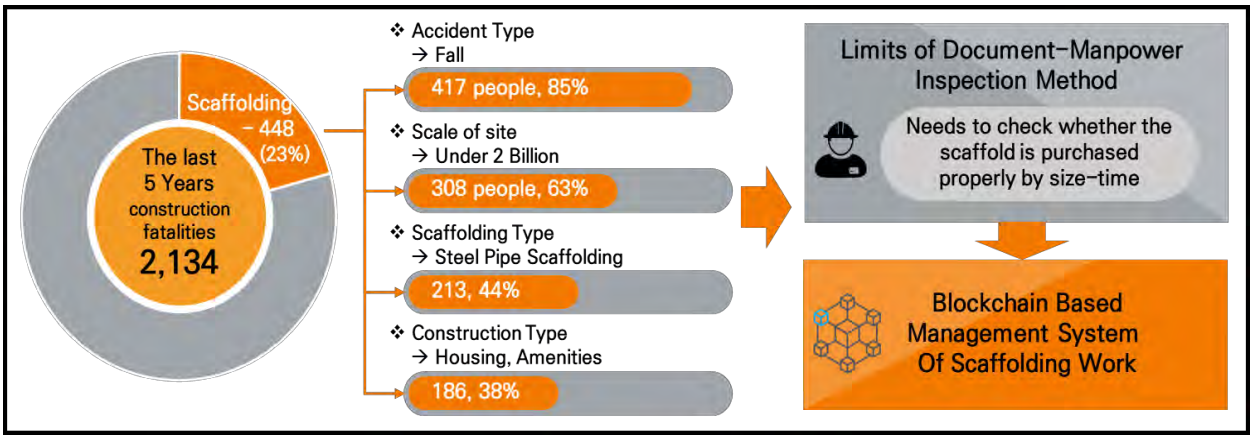

Figure 1. Construction Disaster Statistics by KOSHA (2015~2019)

Accordingly, the government induced on-site safety through a scaffold installation support system such as a clean project, and conducted inspections mainly on small and medium-sized construction sites that are vulnerable to safety accidents, but there are limitations in conducting inspections due to manpower based checking and document-oriented records. Therefore, for efficient management, it is necessary to manage information on whether the appropriate amount of scaffold is purchased and installed at the right period according to the size and shape of each site. For these reasons, this study intends to propose a blockchain-based framework for verifying the adequacy of scaffold that can automatically discriminate the information generated in the process of scaffolding work by a system other than a person and simultaneously secure the reliability of the generated information.

2 Literature Review

2.1 Scaffolding-Safety

Scaffolding is a temporary structure that is assembled and installed around a structure in order to install a construction passageway or work plate to facilitate high-rise work [2]. Due to the development of construction technology, the number of high-rise works has increased compared to the previous one, as the buildings are gradually becoming taller and larger. Therefore, as the importance and utilization of scaffolding in the field has expanded, the importance of safety issues related to scaffolding work has been emphasized.

As for the main research related to scaffolding, studies on accident analysis and countermeasures related to scaffold-safety, scaffold modeling using BIM, and risk identification are in progress. First, as research related to scaffolding and safety, Hola [4] analyzed accidents involving falls from scaffolding, which took place in Poland in the years 2008-2015. In addition, this study deduced that the biggest influence on the formation of accidents came from a lack of or inadequate equipment that secures work posts on scaffolding, and also improper collective protection measures e.g. roofing or protective nets, poor stability of scaffolding or its components and also an inadequate spatial structure of scaffolding. Kim [5] analyzed accidents that were caused by scaffolding during a fall disaster occurring at a domestic construction site. Besides, a variety of key factors affecting the fall was drawn from four aspects: worker, manager, material and construction, and design. Sakhakarmi [6] proposes a method that can be used during operation to make an automated safety prediction for scaffolds. It implements a divide-and-conquer technique with deep learning. This study emphasized that implementation will enhance the reliability of automated safety assessment systems on construction sites. Pienco [7] presented the results of analysis of 100 full-scale scaffolding structures in terms of compliance with legal acts and safety of use. He examined scaffolds in Poland located at buildings which were at construction or renovation stage from 2016~2017. Based on the analyzed scaffoldings, the most common errors concerning assembly process and use of scaffolding were collected.

Also, diverse researches are conducted related to scaffolding using BIM include automatic scaffolding design, risk identification through scaffold modeling, and safety planning. Kim [8] presented a framework and algorithms to integrate temporary structures to the automated safety analysis. Focusing on scaffolds, this research integrates temporary structures into an automated safety checking approach using BIM. Also a safety planning platform was created to simulate and visualize spatial movements of workers using scaffolding. Computational algorithms in the platform

automatically identify safety hazards related to activities working on scaffolding and preventive measures can be prepared before the construction begins. Kim [9] developed a rule-based system that automatically plans scaffolding systems for pro-active management in Building Information Modeling (BIM). Their computational algorithms automatically recognize geometric and non-geometric conditions in building models and produce a scaffolding system design that a practitioner can use in the field. We implemented our automated scaffolding system for commercially-available BIM software and tested it in a case study. project.

2.2 Blockchain Technology

Blockchain as a Distributed Ledger Technology (DLT) is a distributed data logging and maintenance system that depends on and is ensured by the consensus mechanism implemented by the agents. The autonomy and updating of the information contained in the blocks are subject to verification and authorization by all participants [12]. All participants with transaction data and management authority form a peer-to-peer (P2P)-type network to verify the previously centrally managed data by all participants within the network to ensure data integrity and reliability. The types of blockchains classified according to their characteristics include public blockchain that anyone can participate in, private blockchain that can only participate with permission, and consortium blockchain [10]

Table 1. Classification of Blockchain

	Participant	Anonymity	Usecase
Public Blockchain	Anyone	o	Bitcoin
Private Blockchain	Optional	x	Nasdag's Linq
Consortium Blockchain	Optional	x	Hyperledger Fabric

A representative function of blockchain is smart contract. A smart contract is a system that automatically fulfills a contract when all programmed conditions are met. Previously, a lot of documents were required until the contract was concluded and executed, but smart contract is a technology in which the terms of the contract are specified in computer code, and the contract is made when the terms are met.

Although the applying blockchain technology and smart contracts in the construction industry has not yet been conducted, many researches have been done to apply to the construction industry in recognition of the advantages and necessities of each technology. Major research areas related to construction include procurement, payment, and data reliability through connection with BIM.

Wang [11] proposed a blochchain-based information management model. The study suggests that proposed model can enhance real-time information communications among the different stakeholders and improve the efficiency of supply chain management. Besides, they also mentioned that through an adjustment in the smart contract, the model can also be applied to tackle issues in other traditional supply chains. Kim [12] proposed a procurement management system that applied Block Chain and Big Data technology within the construction industry. Through this, he emphasized that information generated as the project progresses can be applied to Block Chain to secure the immutable information and records, and that distributed network interworking can contribute to minimizing conflicts between project management and project entities by contributing to increased connection and reliability of information. Giuda [13] emphasizes that the progressive introduction of BIM based on the blockchain technology can provide a trustworthy infrastructure for information management during the design, tender, and construction phases. Luo [14] proposed a blockchain-based smart construction contract framework for semiautomatic execution of construction contracts for interim payments. They developed a smart contract implementation framework that satisfies the sequential approval process requirements in a distributed environment such as the construction industry by utilizing blockchain technology. Kang [15] emphasized that through smart contracts, transactions between interested parties can be managed in a decentralized manner, reducing the risk of contract changes and inducing reasonable transactions with transparent transaction terms. Besides, he also proposed that an Ethereum-based smart contract could be solved, which is difficult to solve with the centralized control method of the current construction industry. Lanko [16] referred that almost none of the fields of human activity can do without supply chain management. Therefore, in this study, the necessity and limitations of blockchain technology application were presented by taking the manufacturing process and delivery process of ready-mixed concrete as an example. Turk [17] emphasised that blockchain has the potential to address some issues that discourage the industry to use BIM such as confidentiality, provenance tracking, disintermediation, non-repudiation, multiparty aggregation, traceability inter-organizational recordkeeping, change tracing, data ownership, etc. Moreover, they also mentioned that on the construction site, blockchain could improve the reliability and reliability of construction logbooks, works performed and material quantities recorded. San

[18] referred that the application of blockchain technology can improve the construction process that shows the limitations of centralized technology in the current construction project lifecycle. In addition, Dakhli [19] emphasized that block chain technology can improve the limitations of the design and construction process and reduce costs.

2.3 The necessity of Blockchain Framework

Recently, interest in the smart contract technology, which is automatically traded when the reliability and security of data and conditions are met through the distributed ledger, a representative characteristic of blockchain, is growing in all industries. In particular, the construction industry expects that the problem of chronic distrust in the construction industry will be resolved if transparency and completeness of transactions can be secured in subcontracting, material delivery, and real estate transactions. For this reason, various blockchain platforms and functions are developed and continued research is conducted according to the purpose of utilization. However, there is no research on safety management related to scaffolding construction based on blockchain technology. In this regard, the blockchain-based framework that determines the adequacy of scaffolding installations presented in this study is needed.

Furthermore, the framework to be proposed in this paper is expected to improve the limitations of the existing construction management process by using reliable data and the decentralization of information through distributed storage, a typical characteristic of blockchain technology.

3 Proposing Framework

3.1 Framework Overview

The framework proposed in this study is focused on preventing falls during scaffolding operations that are severe in the construction industry. To this end, the framework will be designed as a system process that manages the suitability of scaffolding installation by discriminate the purchase of scaffolding quantities.

1) The proposed framework utilizes a Hyperledger fabric, a kind of Consortium blockchain, so that only designated users can have access to data. Through this, we will give authority only to construction participants such as GC, suppliers, and inspection agency. Then we will configure the scope of data access differently according to the characteristics of each participant.

2) As a technical method for automatically verifying scaffolding-related power generation information, a structure will be designed that automatically calculates the time and quantity of scaffolding installation based on design information such as 4D-BIM, compares them with the order-procurement information entered through the app, and stores the results in the block chain system.

3) Blockchain technology utilizes core composition technologies such as channel composition for authority setting by participating parties, consensus algorithm for ledger records and viewing, and guarantee policy. We will set up Membership Service Providers (MSP) for channel configuration and form a system for data access and verification in conjunction with the blockchain network. We will also design a separate system structure of the On-Chain, Off-Chain network to prevent overload of the blockchain network.

4) The key demand for this framework is the Government Inspection Agency, which conducts on-site inspections. It is intended to design a system structure that can store information that needs to be verified when checking the appropriateness of scaffolding at individual sites of this system in a blockchain manner and provide the information needed for verification from the inspector's point of view.

3.2 Key functions of Blockchain Framework

This section describes the core functions of the framework proposed. The framework utilizes various key technologies in the blockchain to identify the entered data and store the identified data as reliable data. Key functions are as channeling, smart contract, text mining, consensus algorithm and on/off chain.

- *Channeling*

Channeling defines participants who participate in scaffolding-related activities of construction projects and sets different access authority to information by subject. Channel composition can be divided into groups that generate information through scaffolding-related activities and groups that view them. The first group that generates information is a supplier that procures scaffolding and a contractor that orders scaffolding. The supplier grants authority only to the relevant field channel, so that information from other sites cannot be viewed, preventing sensitive information such as order history and cost from being shared with other suppliers. The contractor grants authority to all managed sites so that data can be provided and viewed for scaffolding. The inspection agency is designed to allow access to all data, such as ordering-procurement data and discrimination results so that it can be determined whether appropriate scaffolding is installed.

- *Smart Contract*

Smart contract is one of the key functions of the

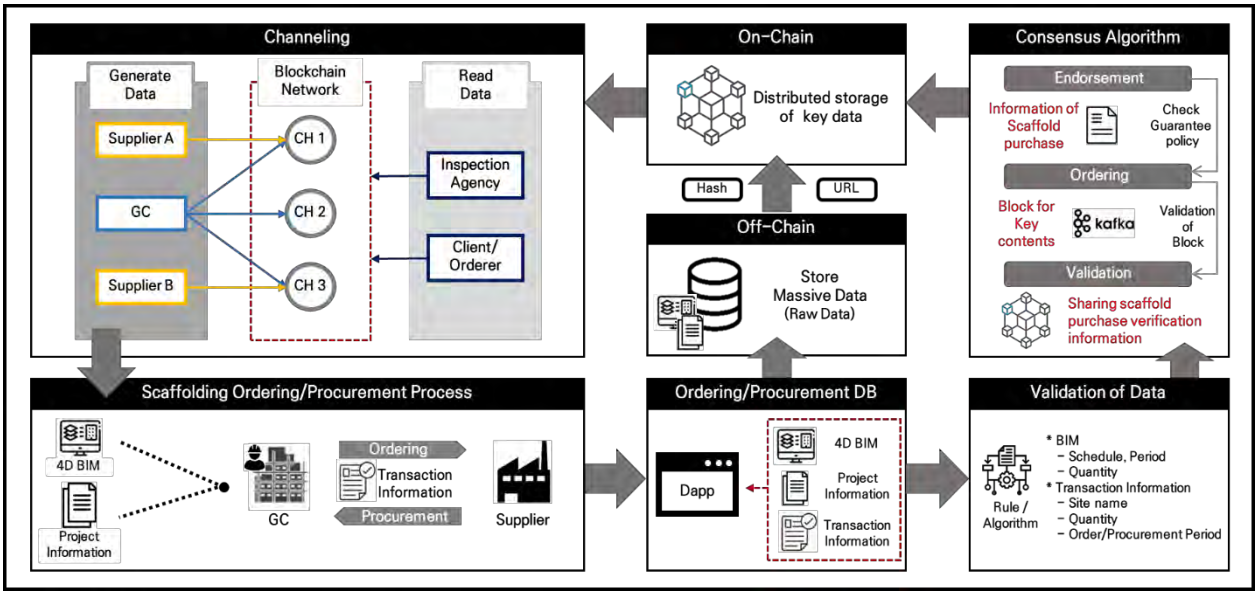

Figure 2. Blockchain-based scaffolding management process and key features

blockchain. It implements functions such as reading and storing data from the blockchain server so that the algorithm on the application can compare the data entered in the order-procurement process with the key data such as area, time, and installation quantity identified in the 4D BIM data.

- *Dapp*

Dapp is an application that works on distributed ledger systems. It is used by the transaction participant to input information generated during the ordering and procurement process and basic information of construction. In addition, Inspection agency can view the scaffold installation suitability and related data derived through data verification.

- *Consensus Algorithm*

This algorithm automatically uploads discriminative data from verification of proper scaffold purchase to On-Chain to prevent forgery of data due to third-party intervention that may occur before being recorded in distributed ledger. In addition, by checking the authority of the viewer, it is possible to prevent ledger access by unauthorized users to the corresponding blockchain network or channel.

- *On-Chain / DLT*

This technology is a function to store verified data on the blockchain. Every participant in the channel maintains a copy of the ledger on its own and the copy goes through a consensus process to keep it consistent with the copies of all other peers. Through this, it is possible to prevent forgery and falsification of all scaffolding-related data input to the ledger and ensure data reliability.

- *Off-Chain*

Off-chain is a method of recording data outside the blockchain. If large capacity data is stored in the on-chain, processing speed may be reduced and overload may occur. To prevent this, massive data (photo, BIM, etc.) is stored in a single DB outside the block chain and the hash and URL of the data are recorded in the distributed ledger.

4 Scenario of proposed framework

In this section, we would like to present a sample scenario of the proposed framework to demonstrate the process of the entire framework.

Based on the basic information of the project and the 4D-BIM, the GC calculates the amount of scaffolding installed by construction period. Then, order the materials from the supplier and receive them. Through the ordering-procurement process, information about the transaction between GC and supplier is generated, such as ordering and procurement quantity and ordering time. The generated transaction information is uploaded by the participant through the dapp. Then uploaded data is verified through the data comparison algorithm to discriminate whether the proper scaffolding purchase and installation.

For verification, key information of each original

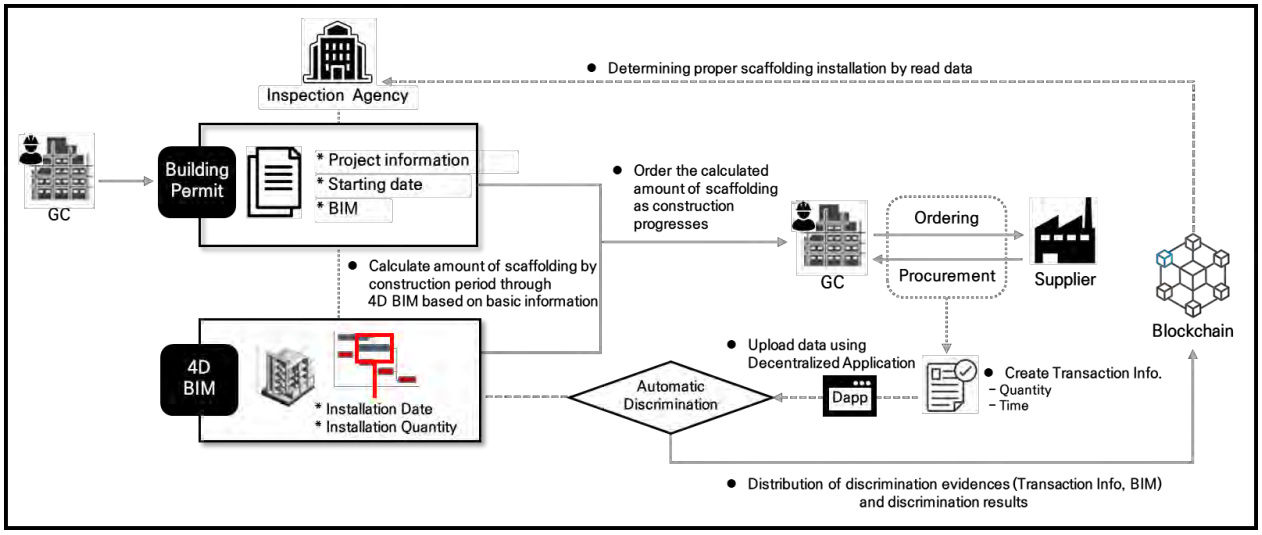

Figure 3. Example scenario of Framework

data is used (shown in figure 4). First, information about the scaffolding quantity required according to the progress of the construction is collected through the area, the scaffolding quantity calculated, and the construction schedule data from 4D-BIM. This data is compared with major data among transaction information such as order quantity and procurement time uploaded through dapp to determine whether the necessary scaffolding is prepared on site at the appropriate time. After that, the results of the verification will be distributed and stored in the blockchain network through a consensus process along with key information such as transaction information and 4D-BIM. At the same time, massive data such as 4D-BIM data is stored separately in off-chain to prevent overload of the blockchain system, and only hash or URL of the data is stored on-chain together. Finally, the inspection agency checks whether the proper amount of scaffolding has been purchased by viewing the stored data and checks whether the proper scaffolding is installed or not. And it will determine whether an on-site inspection is necessary. Moreover, if such data were accumulated later to form big data, it could be used to calculate and verify the necessary scaffolding quantities depending on site characteristics, even without BIM. And it is expected that this could be reflected as a big advantage in small sites where BIM is

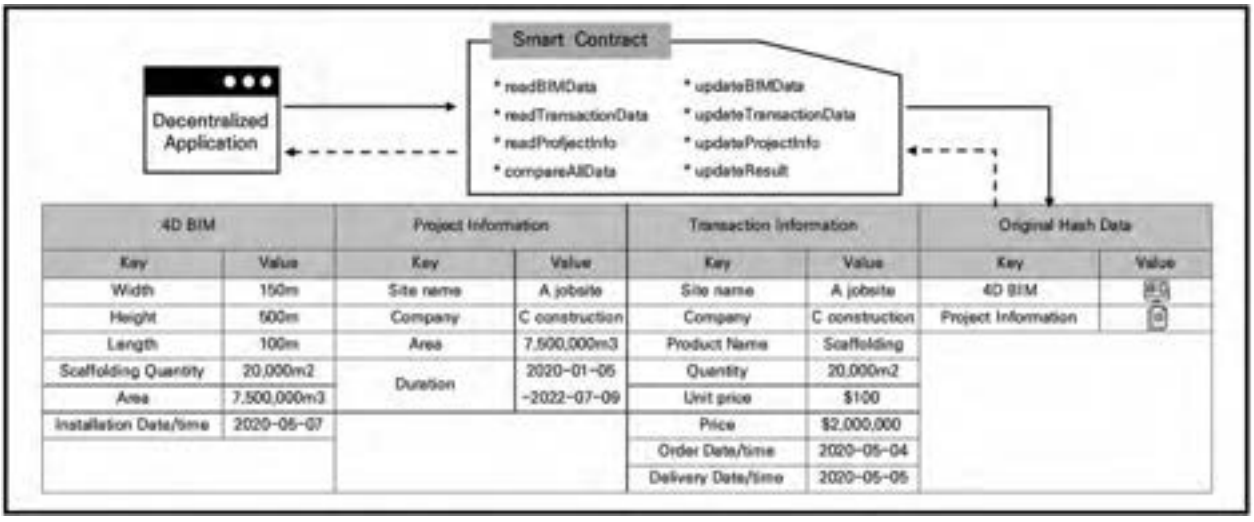

4D BIM		Project Information		Transaction Information		Original Hash Data	
Key	Value	Key	Value	Key	Value	Key	Value
Width	150m	Site name	A jobsite	Site name	A jobsite	4D BIM	
Height	500m	Company	C construction	Company	C construction	Project Information	
Length	100m	Area	7,500,000m3	Product Name	Scaffolding		
Scaffolding Quantity	20,000m2	Duration	2020-01-05	Quantity	20,000m2		
Area	7,500,000m3		-2022-07-09	Unit price	$100		
Installation Date/time	2020-05-07			Price	$2,000,000		
				Order Date/time	2020-05-04		
				Delivery Date/time	2020-05-05		

Figure 4. Type and flow of Key information

not available in the field due to costs and other issues.

In addition, this framework can be applied not only to the scaffolding proposed in the study, but also to various supplies. For example, ready-mixed concrete is also worked through the process of 'Quantity calculation-Order&Procurement-Installation'. Although there are differences in several processes such as quality verification in the intermediate process, it is expected that it can be applied as similar processes are being conducted in a large framework. As such, it is expected that the proposed framework can be applied to various supplies of construction work to improve the current construction process.

5 Conclusion

The construction industry is becoming increasingly high-rise, large-scale and complex due to the development of technology. As a result, the proportion of dangerous work and complaint work is increasing, and the frequency of 'falling' is increasing. However, at the construction site, there are still many small construction sites do not recognize the importance of the scaffolding that should be basically installed to prevent fall accidents and do not properly install it even if it is omitted or installed. Recognizing this situation, the government has proposed counterplan such as increasing the number of on-site inspections. However, they still has difficulties due to lack of manpower.

For this reason, this paper proposed a blockchain framework to determine whether the proper scaffolding is installed according to the characteristics of the construction site and to ensure the reliability of the information. The proposed framework secures the reliability of data such as project information, scaffold purchase information and BIM through distributed ledger technology. In addition, it also can verify the suitability of scaffolding installation automatically by compare and determine scaffolding-related information

By using the proposed framework, the inspection agency can check the results of the adequacy of scaffolding installation utilizing blockchain network without the need to visit the site, which requires a lot of manpower. Ultimately, it is anticipated that efficient management will reduce the occurrence of accidents at the construction site.

If a method to acquire the state of the scaffold installed in the actual site is devised, it will be possible to more effectively verify the suitability of installing the scaffold. For example, on-site manager uploads and confirms the installation status of a scaffold on the site as a photo, or a method of confirming the installation status of a site scaffold through CCTV installed on the site. As an available technology, it is expected that scaffolding can be identified and confirmed through images acquired in the field using image recognition technology.

Acknowledgement

This study was financially supported by the National Research Foundation of Korea (NRF) grant funded by the Korea government Ministry of Science and ICT (MSIP) [No.NRF-2019R1A2B5B02070721] and [No. NRF-2020R1I1A1A01073167].

References

[1] *Korea Occupational Safety & Health Agency*, Analysis of Industrial Accident Status, 2018

[2] *Korea Occupational Safety & Health Agency*, Safety Guide for Scaffolding Work at Construction Sites, 2019

[3] *Safety journal*, Ministry of Employment and Labor, Differential Management according to Construction Scale, on-line: http://www.anjunj.com/news/articleView.html?idxno=22726

[4] Hoła, A., B. Hoła, and Mariusz Szóstak. Analysis of the causes and consequences of falls from scaffolding using the Polish construction industry as an example. IOP Conference Series: Materials Science and Engineering, 251(1), IOP Publishing, 2017.

[5] Kim and Boo.' A Study on the Falling Risk Factors about Construction Scaffolding Work." *Journal of Korean Architectural Institute of Korea's Academic Presentation Conference*, 39(2): 710-711, 2019

[6] Sakhakarmi, Sayan, and Jee Woong Park. "Multi-level-phase deep learning using divide-and-conquer for scaffolding safety." *International journal of environmental research and public health* 17.7 (2020): 2391.

[7] Pieńko, M., et al. "Safety Conditions Analysis of Scaffolding on Construction Sites." *International Journal of Civil and Environmental Engineering* 12.2 (2018): 93-98.

[8] Kim, Cho, and Zhang. Integrating work sequences and temporary structures into safety planning: Automated scaffolding-related safety hazard identification and prevention in BIM. *Automation in Construction*, 70: 128-142, 2016.

[9] Kim, Kyungki, and Jochen Teizer. Automatic design and planning of scaffolding systems using building information modeling. *Advanced Engineering Informatics*, 28(1) : 66-80, 2014.

[10] Kang, Kim, and Hong. "Study for IoT-based secure blockchain system." *Journal of the Korean Institute of Communication Sciences*, 66-67, 2017
[11] Wang, Zhaojing, et al. Blockchain-based framework for improving supply chain traceability and information sharing in precast construction. *Automation in Construction,* 111: 103063, 2020
[12] Giuda, Martino, et al. The Construction Contract Execution Through the Integration of Blockchain Technology. *Digital Transformation of the Design, Construction and Management Processes of the Built Environmen,* Springer, Cham, 27-36, 2020
[13] Wang, Jun, et al. "The outlook of blockchain technology for construction engineering management." *Frontiers of engineering management* (2017): 67-75.
[14] Luo, Das, Wang and Cheng. Construction payment automation through smart contract-based blockchain framework. *ISARC 2019: Proceedings of the 36th International Symposium on Automation and Robotics in Construction,* Pages 1254-1260, International Association for Automation and Robotics in Construction (IAARC), 2019
[15] Kang. Smart Contracts, Blockchain and BIM. *Communications of the Korean Institute of Information Scientists and Engineers*, 36(5): 21-27, 2018
[16] Lanko, A., N. Vatin, and A. Kaklauskas. "Application of RFID combined with blockchain technology in logistics of construction materials." *Matec Web of conferences*. Vol. 170. EDP Sciences, 2018.
[17] Turk, Žiga, and Robert. Potentials of blockchain technology for construction management. *Procedia engineering*, 196: 638-645, 2017.
[18] San, Kiu Mee, Chia Fah Choy, and Wong Phui Fung. "The Potentials and Impacts of Blockchain Technology in Construction Industry: A Literature Review." *IOP Conference Series: Materials Science and Engineering.* Vol. 495. No. 1. IOP Publishing, 2019.
[19] Dakhli, Zakaria, Zoubeir Lafhaj, and Alan Mossman. "The potential of blockchain in building construction." *Buildings* 9.4 (2019): 77.

Towards a Comprehensive Façade Inspection Process: An NLP based Analysis of Historical Façade Inspection Reports for Knowledge Discovery

Zhuoya Shi, Keundeok Park, and Semiha Ergan

Tandon School of Engineering, New York University, the USA
E-mail: zs1110@nyu.edu, kp2393@nyu.edu, semiha@nyu.edu

Abstract –

Façade condition assessment for buildings is essential to public safety in cities. Currently, twelve major cities across the U.S. ensure the building façade safety with mandatory façade inspection programs. Even in major cities with the façade inspection programs, there have been seventeen falling debris accidents reported in 2019, three of which were fatal. These accidents indicate a need to improve the current façade inspection practice. Shadowing work conducted by the research team with expert inspectors on three buildings, and analysis of façade inspection programs and guidelines show that inspectors check façades based on defect types or on façade components, whereas existing documentation to guide inspectors are based on major material types. This mismatch results in inspectors checking façade components based on their experience, which might not align well with the expectations of agencies. Systematic and detailed assessment guidance is necessary to get a comprehensive and consistent façade inspection. Towards such systematic guidance and to understand the underlying reasons for continuing accidents, this paper provides the details of an approach to identify generic vocabularies and the relationships between major entities that play a role in the inspection domain for systematic inspection processes. To identify these, we developed a data-driven approach that analyzed around 100 façade inspection reports that were filed to the NYC Department of Buildings (DOB) during the past inspection cycle (2014-2019). Among the twelve major cities, New York City (NYC) has the longest history of façade inspection, and most buildings (14,000) enrolled in the façade inspection program. We believe that study about NYC buildings can provide a general understanding of inspection requirements in other cities where similar problems exist. The developed mechanism is based on natural language processing and unsupervised machine learning techniques and is used to extract the vocabularies of façade elements, defect types, associated defect attributes, and mapping between them. The results also provide the mapping relationship of façade components and defect types for a specific façade type (e.g., stone/limestone). This work provides the foundation for an ontology to be used to systematically guide façade inspection for any given building.

Keywords –

Façade inspection, Report analysis; Natural Language Processing (NLP); Unsupervised learning.

1 Introduction

Twelve major cities in the U.S. have a façade inspection program to ensure the safety of buildings. Accidents and incidents caused by debris falling from building façades, however, are still happening in cities. For example, in the past year (2019), 17 accidents due to debris falling occurred in the U.S., causing deaths and injuries. The past decade has shown that more than 700 complaints about façade safety were received annually by the department of buildings (DOB) in the city of New York (NYC) [1]. These accidents and complaints indicate a need to improve the current façade inspection practice.

Shadowing of façade inspectors by the authors resulted in the identification of several challenges in the current façade inspection practice [2]. One of these challenges is the lack of a comprehensive and detailed checklist that can serve as a guideline to a systematic inspection that is based on defect and façade component types instead of material types. Current façade inspection regulations in different cities and international guide for standard periodic façade inspections published by the standards organization [3] cover information on conditions of buildings that need an inspection, length of inspection cycles, general and close visual inspection of façade, and reports formulation and submission. Information about what defect types need to be checked and what associated attributes are essential for façade safety assessment, however, is missing from the

regulations and practice standard documents. Aside from the regulations and practice standards, a few glossaries formulated by industry professionals aim to provide descriptions and illustrations of defect types for different façade materials [4-6]. The glossaries are only for educational purposes and are not integrated into any guideline for defect identification in the façade inspection practice. Façade inspection is still a practice that relies solely on the personal experience of each inspector and company-specific templates. Figure 1 shows an example of different inspection results in two inspection reports for the same brick masonry building and its roof.

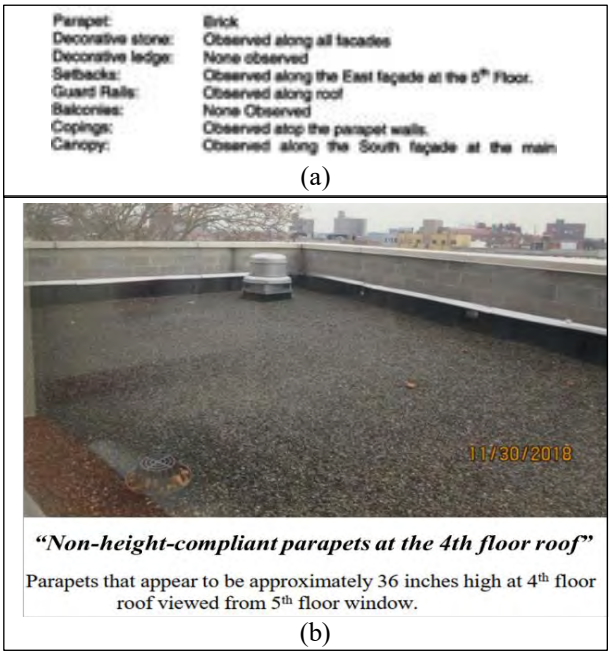

Figure 1. Examples of different inspection results for the same roof. (a) Previous inspector (Cycle 7) only mentioned the existence of a parapet. (b) The current inspector (Cycle 8) checked the height of the parapet with respect to the code compliance.

For safety concerns, the height of parapets should comply with the construction code that was applicable when the building was constructed. The inspector, who conducted the inspection work in the prior cycle, only mentioned the existence of a parapet at the roof (Figure 1a) and its material type as the information collected for the parapet. The inspector we shadowed, however, also checked the height of the parapet, compared it to the requirements in the code, and identified that the height of the parapet is not compliant with the applicable building code (Figure 1b). Such differences of what components to check, what specific parameters to check for each façade component are common, and show a need for a checklist that the inspectors can follow to conduct an in-depth and comprehensive inspection regardless of their experience.

Shadowing work and the review of submitted reports showed that the inspection is conducted per façade component and is not based on material types. For example, when an inspector is checking a balcony, he/she will check the concrete panels for cracks, the railings for connection stability, and compliance of spacing between railings and their heights to the code altogether, instead of checking cracks in all concrete components at once. One example of this component-based practice is provided in Figure 2. The inspector, who submitted the report, grouped the observed conditions based on the façade components (i.e., openings). The current façade condition glossaries, however, summarize the defect types based on façade materials (e.g., concrete, metal) and there is a need to know which defects are applicable to which façade components for a comprehensive and consistent façade inspection.

Masonry Openings *a.* ***Window Frames*** *Description: The windows are constructed of aluminum. Condition: The windows were observed to be in satisfactory condition during the critical examination (see photo #13).Classification: SAFE b.* ***Window Sills*** *Description: The windowsills are constructed of brick masonry. Condition: The windowsills were observed to be in satisfactory condition during the critical examination. Classification: SAFE*

Figure 2. Façade inspection report grouping the conditions based on façade components.

Towards a comprehensive façade inspection guidance, what is needed is the knowledge of how defect types (and defect-related attributes) map to façade component types, and the comprehensive vocabularies for these defect types, defect attributes, and façade component types. The objective this paper is to identify this mapping and the vocabularies of the defect, attribute, and façade component types. With this objective, we developed an approach using bidirectional long short-term memory (bi-LSTM) model to automatically analyze around 100 façade inspection reports that were submitted in the past inspection cycle (2014-2019) for buildings in NYC. Here, the assumption is that inspectors' practice is reflected on the inspection reports they submit and can be leveraged for investigating the relationships between façade components and defects, and expanding the available material-specific vocabularies towards component-specific vocabularies. This paper provides an overview of the developed bi-LSTM model and the results of this mapping and resulting vocabularies of façade components, defect types, and defect attributes. These findings also lay the foundation for an ontology for systematic and comprehensive façade inspection.

2 Literature Review

Here we present a synthesis of previous researches on urban façade inspection, structural health monitoring, and the application of natural language processing (NLP) in the civil engineering domain.

Previous researches on façade inspection and structural health monitoring were mainly focused on automatic defect detection using digital data, particularly point clouds and images. Researchers developed algorithms to detect cracks [7-9], moisture [10], spalling [8, 9], vegetation [8], and efflorescence [9] on concrete, masonry, and steel surfaces. Several algorithms are able to quantify the defects, such as the area of spalling [11] and the width of cracks [7] automatically or manually on 3D models [12]. Although these studies provide a handful of defect types/attributes on a select type of materials, their focus is not aligned with this study that aims to define the vocabularies of defects, component types, and the mapping between them for improvement of the façade inspection practice.

Previous NLP applications in the civil engineering domain aim to extract essential information such as condition assessment information from bridge inspection reports, or project relevant information from unstructured construction documents, or regulatory information from building codes with different machine learning models [13-15]. Although there are NLP applications in the domain, the analyzed documents are semi-structured or structured with logical-connected words (e.g., "*equal to*" and "*less than*" represent quantification compliance in the building codes) or with known defect types (e.g., crack, spall, efflorescence, etc.) and rating categories (e.g., minor, moderate, severe) [16], which can be analyzed with rule-based information pattern matching. Different from previously studied document types, façade inspection reports are personal narrative descriptions written without guidance or specific templates. Thus, this unstructured nature of the inspection reports requires unsupervised learning to find relevant words (e.g., parapet, crack, diagonal), label them correctly (e.g., façade component, defect type, defect attribute) within the context of a report, and maintain the relationships between these labels. We implemented a natural language processing (NLP) algorithm to identify the vocabularies for façade components, defect types, defect attributes, and the hidden relationships between façade components and defect types. Long short term memory network (LSTM) is one of the Recurrent Neural Network (RNN) architectures and is known to be suitable for processing sequence data (e.g., time-series, speech sequence, and text) because LSTM preserves information about the data that the model sees earlier in a sequence. Unlike general sequential data processing, NLP has a feature that the context in a sentence is defined by the interrelationships among words in both backward and forward directions. Since the unidirectional LSTM passes input information forward only, bidirectional LSTM is more proper for automated understanding of natural language. In addition, the conditional random field (CRF) is a statistical modeling method that is widely known for its high performance in predicting a label for sequence data. Adding CRF as an output layer in the bi-LSTM model (i.e., bi-LSTM-CRF model) is proved to outperform previous state-of-the-art models in the information labeling tasks [17]. It has been utilized in the approach presented in this paper. To further improve the performance of NLP models, skip-gram models, which are unsupervised learning models and can precisely capture the semantic (i.e., meaning) and syntactic (i.e., grammatical structure) relationships between words [18]in a context. Previous research studies trained skip-gram models with general English text and used them to improve the performance of machine learning models on extracting information from documents (e.g., [13]). In this study, we trained a skip-gram model with domain-specific text (i.e., façade inspection reports text). We used it to generate the dependency information that was included in the input of the machine learning model to boost the performance of the model.

3 Research Method

To obtain comprehensive vocabularies for façade components, defect types, and their attributes together with the mapping relationship among those, we developed an algorithm that is capable of extracting key information in unstructured inspection reports. In a nutshell, this algorithm includes a trained bi-directional long short term memory (bi-LSTM) model, boosted with outputs of an unsupervised skip-gram model developed by the research team to capture semantic and syntactic relationships between words (as detailed in section 4).

For the training of the bi-LSTM models that we enhanced with domain-specific skip-gram models, first, we needed to generate initial vocabularies of façade components, defect types, and defect attributes. For this purpose, we reviewed current façade inspection practice standards [3], local laws/regulations [19], and façade condition glossaries [4-6] to generate defect types and attributes vocabularies. Similarly, we reviewed building component libraries of 3D modeling tools (e.g., Revit libraries) and building classification models (e.g., Uniformat) to prepare the façade components vocabulary. We defined four labels, which are ***façade-component***, ***defect-type***, ***defect-attribute***, and ***others*** (i.e., information that is irrelevant to façade conditions), to automatically label worlds in reports. The details of this approach are provided in the next section.

4 Boosted Bi-LSTM model for mining of inspection reports

Figure 3 provides an overview of our approach. Data preprocessing (step 1) and labeling (step 2) steps are provided in section 4.1, dependency information provided by the skip-gram model (step 3) is presented in section 4.2, and the utilization of the model to identify vocabularies and mapping relationships (step 4) is discussed in section 4.3.

4.1 Preprocessing and labeling of the text

We obtained around 3,000 façade inspection reports that cover all the seven façade types in document format from the NYC DOB database. For this study, we analyzed 100 inspection reports for only stone limestone façade buildings. Preprocessing starts with using a parser to extract the raw text from the sections where inspectors describe their findings and splitting the raw text into indexed sentences with the sentence tokenizer. The indexed sentences were tokenized into words (i.e., separating a given sentence into the list of its words), then lemmatized (i.e., returning to the root form of the words) to eliminate the influence of different tenses, plural forms, verb/noun differences. The part-of-speech (POS) information of each token (e.g., noun, verb, adverb, adjective, etc.) was used to achieve a more accurate lemmatization. For instance, the word "*rose*" can be the past tense of "*rise*" or the flower. Depending on the POS of the word, the result of lemmatization differs. These lemmatized sentences were temporarily used in the labeling process to eliminate labeling errors due to the different formats of the words in the text and the identified vocabulary list. Next, we labeled the preprocessed and lemmatized text using the Inside-outside-beginning (IOB) tagging mechanism. With this tagging mechanism, we are able to label compound words that are consisted of multiple words with the beginning token (i.e., a word in this context) and inside tokens. The "**I-**" tag stands for "inside" of a label, referring to the subsequent word in a compound word (e.g., "*escape*" in "*fire escape*"). The "**O**" tag stands for "outside" of a label, referring to the irrelevant word. The "**B-**" tag stands for "beginning" of a label, referring to the first word in a compound word (e.g., "*fire*" in "*fire escape*"). For example, in the term "the window lintel", "window lintel" should be labeled as a single ***façade-component***. Using IOB tagging mechanism, the word "*the*" is labeled as "**O**", and "*window lintel*" will be automatically labeled as [window (B: façade-component) lintel (I: façade-component)]. The label categories we used are façade components, defect types, defect attributes (i.e., length, width/depth, direction, location, material, number of floors, and façade sections), and others.

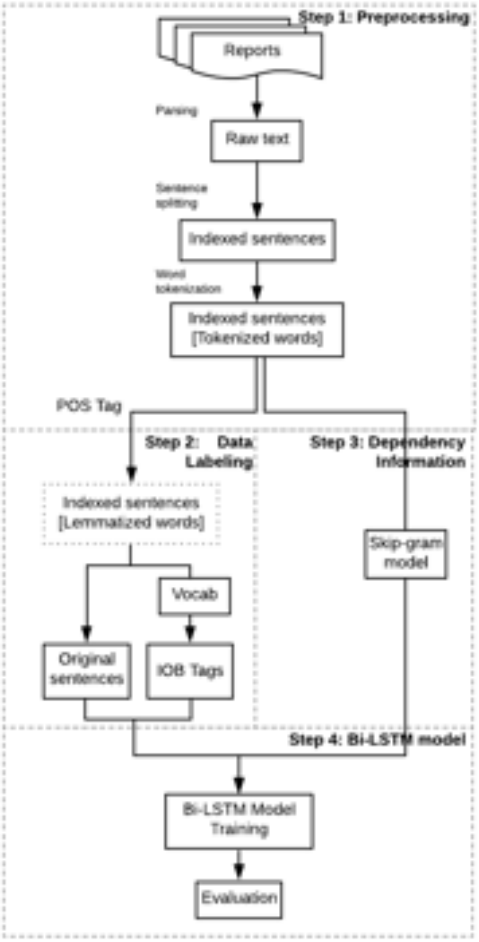

Figure 3. Overview of the developed approach.

Figure 4 provides an example of a sentence from the reports and its labeling result. If there are no compound words, each identified word that corresponds to one of the four label categories will be labeled with "**B**". All the other words that are not of interest in this labeling process are to be labeled as "**O**" (i.e., others).

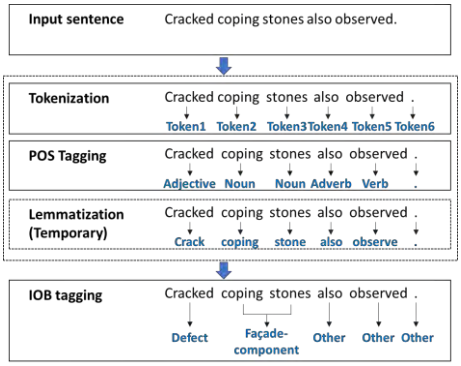

Figure 4. An example of a sentence preprocessed and labeled with the IOB tagging mechanism.

4.2 Obtaining dependency information through the domain-specific skip-gram model

Word embedding is the process of vectorization of words to convert natural language into a computer-readable format based on the extracted features of the language. Word embedding approach takes a large input of tokens, projects them to a vector space, and assigns each unique token a corresponding vector for the representation in the vector space. In this study, we used two word embedding approaches to compare the results of the bi-LSTM model with and without dependency information. These two embedding approaches are the one-hot encoding, which does not provide dependency information between words, and the skip-gram model, which includes the dependency information in the word embedding process. One-hot encoding is a vector representation of word in binary vector format (e.g., *crack = [1,0,0], window = [0,1,0], maintenance = [0,0,1]*). Since the vectors represent words in binary value, one-hot encoding cannot provide the similarity/distance between words. On the other hand, the skip-gram model is an unsupervised learning method for word embedding that uses vector space to capture and represent the semantic and syntactic relationships between words efficiently. Semantic refers to the word meanings and relations, and syntactic refers to the rules of a language and grammatical arrangement of words in sentences. For example, sentences like "*window identifies crack*" ("subject"+ "verb" + "adjective") is a syntactically correct sentence, but it is not semantically correct. After the word embedding, all the input words are mapped into the N-dimensional vector space ($word_1 = [v_1, v_2, v_3, v_4, \ldots, v_n]$). Since the mapped words are using vector representation (e.g., word "*crack*" is represented as [-0.478, 0.917, 0.196, -0.443, -0.978, …, -0.207]) with respect to the other words in the same context, the skip-gram model can perform analogical reasoning precisely. In other words, if two words are placed at similar locations in two different sentences, and the meaning of the terms are similar, then the distance between those two words is relatively small in the vector space if the same pattern is observed often by the skip-gram model. For example, given the following two sentences from a report: (1) "*We recommend repairs to be made to correct these deficiencies by February*." (2) "*We recommend timely maintenance to repair the SWAMP condition observed our inspection*." In vector space, the distance between "*repairs*" and "*maintenance*" is relatively small. Figure 5 presents an example for a simplified 2D projection of the vector space showing the distance between "*repairs*" and "*maintenance*".

Previous studies indicate that the skip-gram model trained with general English text improves the information labeling model performance [13]. In this study, we trained a skip-gram model with the façade inspection reports and included the dependency information, which is represented by vectors generated from the skip-gram model, as part of the input for the bi-LSTM model.

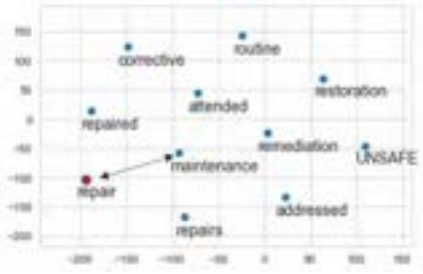

Figure 5. An example of the tokens "repair" and "maintenance" in projected vector space.

4.3 Identifying vocabularies with the boosted bi-LSTM-CRF model

In this study, we built and trained a bi-LSTM-CRF model boosted with skip-gram model outputs. The input for the bi-LSTM-CRF model is the labeled sentences (i.e., the output of step 2 in Figure 3) and the dependency information (i.e., the output of step 3 in Figure 3). Figure 6 provides an illustration of the boosted bi-LSTM-CRF model with a short sentence as an example. The model has an input layer, where the preprocessed sentence "*Exterior wall has crack*." is converted into vector representation by word embedding as input into the bi-LSTM layers. Then, the LSTM model learns from the input data in both forward and backward propagations to update the parameters. The output of bi-LSTM is then inputted to the CRF layer to refine the relational information between tags. The CRF layer works as a classifier to predict the label of each token and improves the performance of the model because it can learn the constraints of labels based on their positions. Constraints such as "inside labels (i.e., I) cannot exist without beginning labels (i.e., B)", and "I of one label cannot appear after B of another label (e.g., 'I-defect' cannot appear after 'B-component')" are learned by this layer. After the CRF layer, the final output of this bi-LSTM-CRF model is the labels for each token in the sentence.

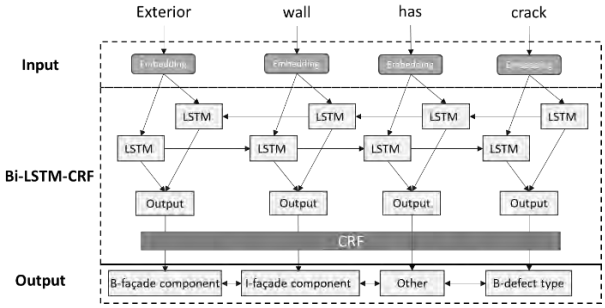

Figure 6. Illustration of bi-LSTM-CRF models with an example sentence.

4.4 Model development

The sentences extracted from the reports were randomly separated into training (i.e., data that is used to build the models), validation (i.e., data that is used to prevent overfitting problem in the training process), and testing (i.e., data that is used to test the performance of the models) sets with 7:2:1 ratio. We trained two bi-LSTM models with one of them included the dependency information provided by the skip-gram model and the other one using one-hot code input. We trained the models with the training set, and the validation set was used to fine-tune the models and avoid the overfitting problem. The testing set remains unseen by the model and is used for model performance evaluation. After we trained and optimized the models, the sentences in the testing set are labeled by the model. The output labels are compared with the labels provided by the IOB tagging mechanism. We calculated the F_1 score, precision, and recall for model performance evaluation using Equations 1-3, where TP represents true positive (i.e., the number of tokens that were correctly labeled), FP represents false positive (i.e., the number of tokens that were mislabeled), and FN represents false negative (i.e., the number of tokens that should be labeled but were missed). The evaluation metrics can be calculated with the following rules. Precision is the ratio of correctly labeled tokens to all the tokens that are labeled in the testing set for each label (Equation 1). The recall is the ratio of the correctly labeled tokens to the total number of correct labels expected to be labeled in the testing set for that label (Equation 2). F_1 score is the weighted average of precision and recall (Equation 3). The performances of both models are evaluated using stone/limestone façades.

$$Precision = \frac{TP}{TP + FP} \quad \text{Equation(1)}$$

$$Recall = \frac{TP}{TP + FN} \quad \text{Equation(2)}$$

$$F_1\ score = 2 \times \frac{Precision \times Recall}{Precision + Recall} \quad \text{Equation(3)}$$

5 Preliminary results and discussions

This section provides the results of the labeling process using the developed boosted bi-LSTM-CRF model. The results are provided for reports analysis of stone/limestone façades.

5.1 Preliminary results of vocabulary identification in stone/limestone façade inspection reports

For stone/limestone façade buildings, 100 façade inspection reports were available, and 1771 sentences were extracted from the reports. The training, validation, and testing sets had 1272, 319, and 180 sentences, respectively. After preprocessing and IOB tagging, there were 3446 tokens labeled as façade components, 190 tokens labeled as defect types, and 256 tokens as defect attributes in the training set. Table 1 shows the precision, recall, and F_1 score for each label category identified by the developed approach. As shown in Table 1, the left columns with normal text show the model performance when the input data does not include dependency information. The right columns with bold text show the model performance when we include the dependency information as part of the input. The model performs well in the vocabulary labeling for façade components, defect types, and defect attributes given their consistently high scores in precision and recall. The labeling performance for both façade components and defect types has been improved approximately by 10% by including the dependency information, while the labeling performance for defect attributes did not change much by including the dependency information. Resulting vocabularies after the trained model is finalized for stone/limestone façade are discussed with respect to their categories.

Vocabulary for façade component types: For façade component types, a total of 38 component types (e.g., cornice, storefront, column, mortar joint, coping stone, etc.) were identified for stone/limestone façades as a result of this automated report analysis. All the identified façade component types were covered by our initial vocabulary, and no additional façade components were expected to be identified.

Table 1. Precision, recall, and F-1 score for labeling (with/without dependency information).

Label category	Precision		Recall		F-1 score	
Dependency information	w/	**w**	w/	**w**	w/	**w**
Façade component	0.78	**0.88**	0.85	**0.91**	0.82	**0.90**
Defect type	0.62	**0.76**	0.59	**0.74**	0.61	**0.75**
Defect attributes	0.91	**0.91**	0.74	**0.77**	0.82	**0.83**

Bold w: model performance with word embedding information. **w**: with; w/: without.

Vocabulary for defect types: There were 12 defect

types identified by the automated report analysis of stone/limestone façade inspection reports. These include cracking, peeling, missing, hazardous condition, removed, spalling, corrosion, displacement, bulging, delamination, chipping, and hollow. Certain defects such as deformation, misalignment, and loose that are important to the safety condition assessment were not mentioned in the reports.

Vocabulary for defect attributes: The defect attributes included in the inspection reports of stone limestone buildings are location (e.g., corner, roofline, floor line, joint, etc.), direction (e.g., horizontal, vertical, inward, etc.), material (e.g., paint, rust, etc.), section (i.e., east/west/north/south façade), area (e.g., square feet), and related deterioration (e.g., chalking, staining, discoloration, etc.). Among all the defect attributes, related deteriorations, and façade section information was not identified correctly by the approach.

5.2 Mapping relationship between defect types and façade components for stone/limestone façades

An important outcome of the trained models is the discovery of the unknown mapping relationships between façade components and defect types, which are required for a systematic component-based façade inspection guidance. The mapping relationships identified for the stone limestone façades are provided in Figure 7. Numbers in each cell indicate the frequency of the "façade component-defect type" pairs that appeared in the façade inspection reports. The frequency of identified pairs is normalized over the defect types to show the most frequent defect types on each façade component. The density of color in each cell represents the normalized results. The underlying assumption here is that the vocabularies appeared in the same sentence is describing one defect observed on a façade component by the inspector. For stone/limestone façades, 38 building elements and 12 defect types are identified from the façade inspection reports. When the figure is analyzed vertically, it is possible to identify the relations discovered between façade elements and a given defect type. Crack is the defect type that relates to most of the façade elements to be inspected for stone/limestone façades and is related with 30 out of 38 façade elements. Hazardous condition (associated with 15 façade elements), spalling (associated with 14 façade elements), and peeling (associated with 10 façade elements), are defect types that rank high in mapping to façade components. Delamination and chipping, both associated with 6 façade elements, are defect types that rank low in mapping to façade components. Hollowness, which is only associated with coping, is the defect type that relates to the least number of façade components.

When Figure 7 is analyzed horizontally, it is possible to observe what types of defects are applicable to a given façade component. Among all 38 façade elements, brick pieces (that require inspection for 11 different defect types), copings (that require inspection for 10 different defect types), parapets (that require inspection for 9 different defect types), and lintels (that require inspection for 8 different defect types) are the façade components that have the highest number of defect types associated with them. On the other hand, glass panels, columns, window panels, ladders, entrance doors, and fascia are the façade elements that only have crack associated with them.

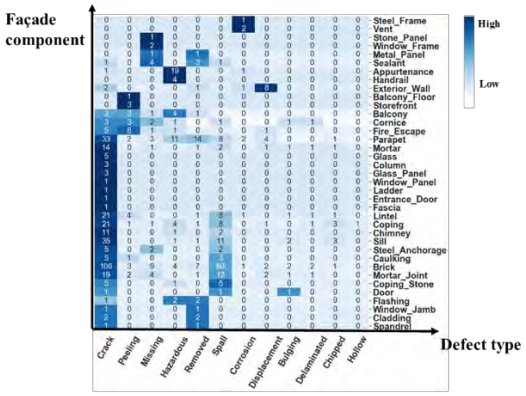

Figure 7. Mapping of façade components and defect types for stone/limestone façades

6 Conclusions

In this study, the authors proposed an automated approach for analyzing façade inspection reports to extract vocabularies for critical façade inspection information (e.g., defect type, façade component types) and discover the undocumented but critical information on how defect types map to façade component types. This information is needed to streamline the façade inspection process by providing the flexibility for inspectors to organize their inspection findings per façade component type or per defect type. A natural language processing approach, combined with an unsupervised skip-gram model, was developed and trained using NYC façade inspection reports. By comparing the labeling results, we proved that including the dependency information can improve the performance of bi-LSTM-CRF in information identification and labeling. NYC has the longest history of the façade inspection program and the largest number of buildings that need inspection regularly-hence it has been used as a test site. The analysis conducted in this study can shed light on other cities where an in-depth understanding of the façade inspection practice is needed. As an immediately following work, the authors will analyze the façade inspection reports of buildings with other façade types

(e.g., brick masonry, metal panel) and include a larger set of reports to improve the performance of the approach. The vocabularies developed and the mappings identified in this study can be helpful for future research that aims to provide a model-based comprehensive guide for the façade inspection practice.

References

[1] NYC OpenData. DOB Complaints Received. Online: https://data.cityofnewyork.us/Housing-Development/DOB-Complaints-Received/eabe-havv, Accessed: 06/05/2020

[2] Shi Z. and Ergan S. Towards point cloud and model-based urban façade inspection: challenges in the urban façade inspection process. In *Proceedings of the ASCE Construction Research Congress*, Tempe, Arizona, 2020.

[3] ASTM International. Standard guide for conducting inspections of building facades for unsafe conditions. Online: https://compass.astm.org/EDIT/html_annot.cgi?E2841+19, Accessed: 06/05/2020.

[4] Eschenasy D. Façade conditions: an illustrated glossary of visual symptoms. Online: https://standardwaterproofing.com/wp-content/uploads/2016/09/FacadePresentation.pdf, Accessed: 06/05/2020.

[5] Vergès-Belmin V. ICOMOS-ISCS: illustrated glossary on stone deterioration patterns. Online: https://www.icomos.org/publications/monuments_and_sites/15/pdf/Monuments_and_Sites_15_ISCS_Glossary_Stone.pdf, Accessed: 06/05/2020.

[6] Kopelson E. Conditions glossary. Online: https://vertical-access.com/resources/conditions-glossary/, Accessed: 06/05/2020.

[7] Anil, E. B., Akinci, B., Garrett, J. H., and Kurc, O. Characterization of laser scanners for detecting cracks for post-earthquake damage inspection. In *Proceedings of the International Symposium on Automation and Robotics in Construction*, Montreal, Canada, 2013.

[8] Brackenbury, D., Brilakis, I., and DeJong, M. (2019). Automated Defect Detection For Masonry Arch Bridges. In *International Conference on Smart Infrastructure and Construction 2019 (ICSIC) Driving data-informed decision-making*, pages: 3-9, Cambridge, UK, 2019.

[9] Wang, N., Zhao, Q., Li, S., Zhao, X., and Zhao, P. Damage classification for masonry historic structures using convolutional neural networks based on still images. *Computer‐Aided Civil and Infrastructure Engineering*, 33(12): 1073-1089, 2018.

[10] Feng, C., Liu, M. Y., Kao, C. C., and Lee, T. Y. Deep active learning for civil infrastructure defect detection and classification. In *Computing in civil engineering 2017*, pages: 298-306, Seattle, Washington, 2017.

[11] Kim, M. K., Sohn, H., and Chang, C. C. Localization and quantification of concrete spalling defects using terrestrial laser scanning. *Journal of Computing in Civil Engineering*, 29(6): 04014086, 2015.

[12] Russo, M., Carnevali, L., Russo, V., Savastano, D., and Taddia, Y. Modeling and deterioration mapping of façades in historical urban context by close-range ultra-lightweight UAVs photogrammetry. *International Journal of Architectural Heritage*, 13(4): 549-568, 2019.

[13] Li, T., and Harris, D. Automated construction of bridge condition inventory using natural language processing and historical inspection reports. In *SPIE Smart Structures + Nondestructive Evaluation*, Denver, Colorado, 2019.

[14] Fan, H., Xue, F., and Li, H. Project-based as-needed information retrieval from unstructured AEC documents. *Journal of Management in Engineering*, 31(1): A4014012, 2015.

[15] Zhang, J., and El-Gohary, N. M. Semantic NLP-based information extraction from construction regulatory documents for automated compliance checking. *Journal of Computing in Civil Engineering*, 30(2): 04015014, 2016.

[16] Hartle, R. A., Ryan, T. W., Mann, E., Danovich, L. J., Sosko, W. B., Bouscher, J. W., and Baker Jr, M. Bridge Inspector's Reference Manual: Volume 1 and Volume 2 (No. DTFH61-97-D-00025). United States, Federal Highway Administration, 2002.

[17] Huang, Z., Xu, W., and Yu, K. Bidirectional LSTM-CRF models for sequence tagging. arXiv preprint arXiv:1508.01991, 2015.

[18] Mikolov, T., Sutskever, I., Chen, K., Corrado, G. S., and Dean, J. Distributed representations of words and phrases and their compositionality. In *Advances in neural information processing systems*, pages: 3111-3119, Lake Tahoe, Nevada, 2013.

[19] NYC DOB. NYC Construction Codes §28-302.1. Online: https://www1.nyc.gov/assets/buildings/building_code/2008_cc_ac_combined.pdf, Accessed: 06/05/2020.

Scheduling Simulator by Ensemble Forecasting of Construction Duration

[a]Shigeomi Nishigaki, [b]Katsutoshi Saibara, [c]Takashi Ootsuki, [d]Hirokuni Morikawa
[a] CEO, Mazaran, Co., Ltd. and kick, Co, Ltd., Japan
[b] Senior reseach engineer, Kick, Co., Ltd., Japan
[c]Senior Researcher, Advanced Construction Technology Div.,Research Center for Infrastructure Management, NILIM, MLIT, Japam
[d]Head, Advanced Construction Technology Div.,Research Center for Infrastructure Management, NILIM, MLIT, Japan
E-mail: sleepingbear@c2mp.com, saibara@c2mp.com, ohtsuki-t2sh@mlit.go.jp, morikawa-h573ck@pwri.go.jp

Abstract –

As is well known, resident engineers on site might plan a heuristically deterministic construction schedule by PERT/CPM program. Since it is boring and time-consuming to gather, edit and input field data into the PERT/CPM program, however, there are very few opportunities to revise the construction schedule on daily works. This paper proposed an easy-to-use and -learning method to plan and revise construction schedule and to do ensemble forecasting construction schedule. First, this paper outlines this study and analysis methods to calculate daily real operational hour and rate based on 3-axis acceleration excited by machine operation. The 3-axis acceleration response values could be collected by sensor built in on-board smartphone for construction machine. In addition, the paper explains methods applied to the machine hour data and rate, to determine shape parameters of Beta distribution, to execute bagging based on samples from the Beta distribution, and to conduct ensemble forecasting of construction schedule. Finally, this paper discusses lesson learned from the empirical study and discussion of predictability of the ensemble forecasting of construction schedule.

Keywords –

Real operational hour and rate; LOESS; Hampel filter; Beta distribution; Ensemble forecasting

1 Introduction

As is well known, resident engineers on site plan heuristically deterministic construction schedule by PERT/CPM program. However, since it is boring and time-consuming to gather and edit field data into the PERT/CPM program, there are very few opportunities to revise construction schedule on day-to-day works.

Largely, scheduling construction schedule for mechanized earthworks are grouped into the following three types:

Type 1: Push works such as dozer operation, which means "make-to-stock process" in which the earthworks are not constructed based on actual demand,

Type 2: Pull works, which means "make-to-order process" in which the earthworks are cyclic distributions based on actual demand, for examples, LHD (Loading, Haulage, Dumping), concrete placement, etc., and

Type 3: Labour-intensive works such as reinforcement bar processing assembly, formwork assembly and disassembly, constructing slope frame, etc.

Due to limitation of space, our inquiring minds in this paper focuses on the Type 1 “dozer operation,” and proposals of easy-to-use and -learning methods to analyse and revise construction schedule and to do ensemble forecasting of the construction schedule. As for study on the type 2 and type 3, we intend to report at the ISARC 2021.

Here, we focus on automation as follows:

- Gathering and calculating data as to daily machine operational hours and rates,
- Repetitively calculating and learning on real operational rate sequence and pitch times for each of work-in days,
- Doing ensemble forecasting of construction schedule, and
- Generating infographics such as time series graph of real operational hour and rate sequence, and diagram of comparison between as-planned and as-built productions in order to grasp the current situations and evaluate the productivity.

This paper unfolds as follows:

First, this paper outlines this study on ensemble forecasting of construction schedule of mechanized earthworks. Secondly, this paper describes analysis methods being applied in this study, for example, LOESS (locally weighted scatter plot smooth) to capture time-series features, and Hampel filter to finding abnormal observations latent in daily real operational hour and rate sequence. In addition, the following methods are described:

- To determine shape parameters (alpha, beta) of Beta distribution, and

- To conduct bagging by samples from the Beta distribution, and do ensemble forecasting of construction schedule.

Thirdly, this paper provides empirical study on the above methods. Finally, this paper discusses lesson learned from the empirical study and discusses about possibility to detect features and abnormality latent in time-series of real operational hour and rate, and predictability of the ensemble forecasting of construction schedule.

2 Outline of this study

2.1 Overview of this Study

Image of dozer operation supposed in this study is shown in Figure 2.1.1.

Figure 2.1.1. Image of dozer operation supposed in this study

In the dozer operation in Figure 2.1.1, readings of 3-axix acceleration, 3-axix angular velocity, and GPS position (latitude, longitude) are automatically gathered from on-board smartphone for dozer. And then, daily machine hour and rate could be automatically calculated from triaxial composite value of the 3-axix acceleration, Besides, as shown in top right of Figure 2.2.1, dozing trajectory and area could be visualized based on GPS data.

Generally speaking, M/M/c queueing theory might be applied to cyclic LHD operation. For simplicity and efficiency of discussion in this study, it is supposed that daily dumping volume is heuristically determined by the initial plan. Needless to say, dividing the day-to-day dumping volume by the dozing area on that day could give us the value of the thickness of embankment on that day.

2.2 Analysis Methods being Applied

This study supposes the workflow as shown in Figure 2.2.1 to analyse daily operational hour and rate and do bagging based on the Beta distribution, which is one of ensemble methods in machine learning, and to do ensemble forecasting of construction schedule.

Finishing ensemble forecasting of each of work types leads to PERT/CPM program. However, our inquiring minds focus on one dozer operation for embankment in this paper.

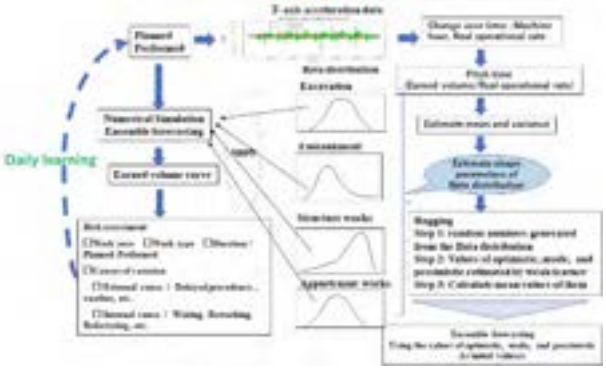

Figure 2.2.1 Workflow to analyse the dozer operation

Data collection and analysis methods applied in this study are described below.

1. Points on Construction(PoC)

The PoC takes sensor-based event detection approach to track a fleet, which is complement of construction machines, dump trucks and workers which are working together on site, and to automatically and real-timely gather a set of readings related to events occurred by the fleet activities as shown in Figure 2.2.2 [1],[2].

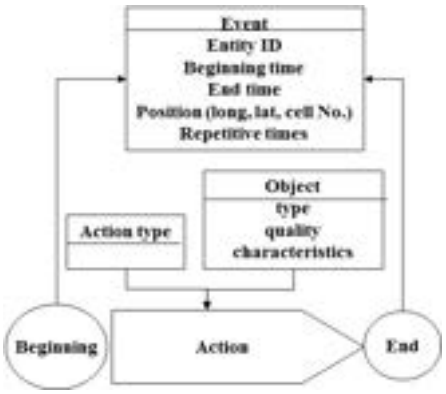

Figure 2.2.2. Image of sensor-based event detection approach

In this approach, construction machine behaviour from beginning to end could be automatically observed by sensors built in smart phone (e.g., 3-axial accelerometer, 3-axial angular velocity meter, GPS receiver, and communication module), and otherwise recognized by a button pressed event, that is, pushing predetermined function key on the smart phone by the operator. Construction machine has on-board smart phone whenever it is being operated. And then, the smart phone automatically sends the data set of readings via the Internet to store them into the database. Readings captured by the PoC consist of time, longitude, latitude,

direction, speed, 3-axis acceleration, 3-axis angular velocity, and son.

2. Calculation of real operational hour and rate

Composition value of 3-axis acceleration is gained by

$$force = \sqrt{ax^2 + ay^2 + az^2} \quad (1)$$

,

where force: composition value, ax: lateral acceleration, ay: longitudinal acceleration, and az: vertical acceleration.

Figure 2.2.3 shows images of variance values of the forces by each of the dozer operations.

Figure 2.2.3 Images of variance values of the forces by each of the dozer operations

It is assumed here that variance values of force generated by idling and driving might be smaller than ones by pushing, spreading and compacting material. Therefore, events with time stamps, which have variance values of forces larger than the predetermined threshold, are extracted and then the operation hour could be calculated. In addition, dividing the daily operation hour sequence by the work hour on that day gives us the corresponding real operation rate sequence.

3. Bagging method

Bagging method is one of the ensemble methods in machine learning. The bagging often considers homogeneous weak learners, and learns them independently from each other in parallel and combines them following some kind of deterministic averaging process [3], [4].

Mean and variance of the averaged real operational hour and rate sequence determine shape parameter (alpha, beta) of Beta distribution**,** and then bagging by samples at random sampling with replacement from the Beta distribution would be executed

4. LOESS (locally weighted scatterplot smoothing model) [5]

The LOESS is a non-parametric approach that uses a weighted, sliding window and coverage to fit multiple regression in local neighbourhood. A weight is Tukey's tri-weight function as follows:

$$W(u) = \begin{cases} (1-|u|^3)^3 & |u| < 1 \\ 0 & |u| > 1 \end{cases}. \quad (2)$$

The weight sequence is defined by

$$w_i(x_0) = W\left(\frac{x_i - x_0}{h(x)}\right), \quad (3)$$

Incidentally, f(x) is approximated by a polynomial, that is, a quadratic approximation shown by

$$f(x) \approx \beta_0 + \beta_1(x - x_0) + \frac{1}{2}\beta_2(x - x_0)^2 \quad (4)$$
$$for\ x \in [x_0 - h(x_0), x_0 + h(x_0)]$$

To estimate $f(x_i)$, find the $\beta = (\beta_0, \beta_1, \beta_2)^T$ that minimizes

$$\hat{\beta} = \arg\min_{\beta \in R^3} \sum_{i=1}^{n} w_i(x_0)\left[Y_i - \left\{\beta_0 + \beta_1(x - x_0) + \frac{1}{2}\beta_2(x - x_0)^2\right\}\right]^2 \quad (5)$$

5. Beta distribution

As is well known, the mean of Beta distribution is given by:

$$\mu = \frac{\alpha}{\alpha + \beta} \quad (6)$$

If α > 1, β > 1, the mode by

$$m = \frac{\alpha - 1}{\alpha + \beta - 2}, \quad (7)$$

where m is the mode, and the variance by

$$\sigma^2 = \frac{\alpha\beta}{(\alpha + \beta)^2(\alpha + \beta + 1)}. \quad (8)$$

In addition, relationships among mean and variance of data sequence, and shape parameters (α, β) of Beta distribution are represented as follows:

$$\alpha = \mu\left(\frac{\mu(1-\mu)}{\sigma^2} - 1\right) \text{ and} \quad (9)$$

$$\beta = (1-\mu)\left(\frac{\mu(1-\mu)}{\sigma^2} - 1\right). \quad (10)$$

6. Ensemble forecasting of dozer operation schedule

Procedure of conducting ensemble forecasting of dozer operation schedule is shown below.

Step 1: When number of days elapsed becomes one third of process days of dozer operation, let put the day the 1st milestone, and the two third one the 2nd milestone. Calculate mean and variance of the real operation rate sequence at each of the milestones, and then specify the corresponding Beta distribution.

Step 2: Repeat n times to generate random number sequences with replacement from the Beta distribution.

Step 3: As for each of the random number sequences, calculate summary statistics that includes mean, standard deviation, variance, min, max, median, mode. and quantile.

Step 4: Average the summary statistics and then let put the 1st quantile be equal to optimistic, the mode be equal to most likely and the 3rd quantile be equal to pessimistic.
Step 5: To do ensemble forecasting, we would utilize the LOESS model, where each of the values such as optimistic, most likely and pessimistic are used as the initial value. And then ensemble forecasting should be executed from the 1st mile stone to the 2nd mile stone, and from the latter to the end of schedule
7. Quantitative performance indexes as to performance evaluation

The Performance index (PI) is depicted by coefficient of concordance, which is a ratio of the precedent rate to the successive one in each of work cells. The PI is given by:

$$PI = \frac{S}{P}, \qquad (11)$$

where S is successive rate; P is precedent rate.
8. Detecting probably abnormal events

Probably abnormal events could be found by median absolute deviation (MAD). The absolute deviations from the median is absolute deviation around the median, which means a robust measure of central tendency, and is not sensitive to the presence of outliers. Besides, given a vector of data, find peaks in ranges of data that exceeds a set threshold. Hampel filter is utilized in this study [6]

3 Empirical Study

3.1 Outline of materials handled in this Empirical Study

Materials handled in this empirical study are dozer operation on river embankment construction, which outlines [7]:
1. The crown width is equal to 7m, the high-water level is equal to 10m, the free board of levee is equal to HWL+2m,
2. The front and back slope gradient is equal to 1:2 and 1:3, respectively, and the embankment length is equal to 877m,
3. The material of dike is sandy soil, and process days is equal to 91 days.
4. The dozer operation in the embankment works as follows:

- The earthmoving volume: 81,600 m3,
- The volume of dozer operation: 80,400 m3,
- The dozer class is 15 ton (D6),
- Number of dozers is equal to 3, and so Dozer volume per one dozer becomes equal to 2,800 m3.

3.2 Work Suppositions

Below are some more details on the work suppositions in this empirical study.

1. Let the embankment area be partitioned into the three work cells and focus on one dozer operation in one of the work cells.
2. Let rainy day, day off, etc. occur based on Poisson arrival

Let work out days be random number sequence generated by rpois (91, 0.28), and then we could gain number of work-in days “74” and umber of work-out days”17”.
Therefore,

- The compacted volume per one dozer for a day is almost equal to 362 m3 (80,400/74/3), and
- The earthmoving volume by one dozer per a day is almost equal to 368 m3 (81,600/74/3).

3. Setting two milestones

Let set the 1st milestone at the point where one third of the process days intersects with 25% of the as-planned production volume and the 2nd milestone at the point where two third point of process days with 75% of the as-planned production volume. Here, we get the baseline curve, which goes along theses milestones, shall be utilized as reference line to compare with as-built production volume.
4. Handling work out days

Values at work-out day in pseudo-random number sequence of real operation rates are replaced by almost equal to zero, that is, sqrt(.Machine$double.eps)= 1.490116e-08;
5. Pseudo-real operation rate sequence

Let pseudo-real operation rate sequence be generated as follows:

- From beginning until the 1st milestone: the mean 0.3 plus rnorm(26,0,3)/100
- From the 1st milestone until the 2nd milestone: the mean 0.46 plus rnorm(27,0,2.5)/100, and
- From the milestone 2 to the end: the mean 0.4 plus rnorm(38,0,2)/100.

Let the pseudo real operational rate be regarded as hand-on real operational rate on site.

3.3 Pseudo-real operation rate sequence

Figure 3.3.1 shows pseudo-real operation rate sequence with the LOESS smoothing line and red cross marks detected by the Hampel filter as mentioned above.

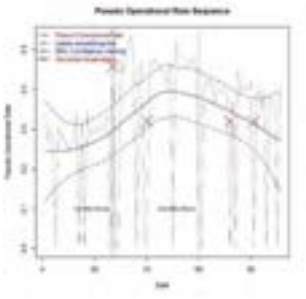

Figure 3.3.1 Pseudo-real operation rate sequence with LOESS smoothing line and red cross marks

Although the LOESS smoothing line shows time series feature very well, values at work-out day incline to push it down as a whole. Here, the sliding window width is 7.5. The smaller its value becomes, the more the predicted curve finely engraved along the original line graph. The red cross marks in Figure 3.3.1 means abnormal observations deviated from the median, which could be found by Hampel filter, where values on work-out days are replaced by the mean value of data sequence in order to avoid detection of ones on work-out days.

Figure 3.3.2 shows performance indexes as to the pseudo-real operation rate sequence. Similarly, the red cross marks in Figure 3.3.2 means abnormal observations deviated from the median.

As for the abnormal observations in both of Figure 3.3.1 and Figure 3.3.2, run length is not seen. Considering work suppositions here, probably, the causes of abnormal observations might be holiday, rain, machine failure, or something like that at the day before.

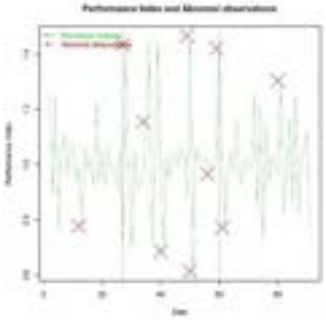

Figure 3.3.2. Performance indexes with probably abnormal observations

In daily construction control, the pseudo-real operation rate sequence with the LOESS smoothing line and observed abnormal ones might be drawn by each of work cells, leads to field inspection to explore the potential causes.

3.4 Productivity assessment

From our long experience in construction field, productivity by dozer operation is gained by the following equation.

$$Q=60*q*f*E/Cm \quad \#(m3/hr) \text{ and} \qquad (12)$$

$$Cm=0.027*L+0.55, \qquad (13)$$

where Q： hourly production quantity(m3/hr), q： bank quantity per one cycle of dozing, f： soil conversion factor, E： work efficiency, and Cm：one cycle time.

Table 3.4.1 shows hourly production quantity by dozing (m3/hr).

Here, let put q=44 m3, f=0.9, E=0.8, L=50m, Cm=1.9 min, work hour per day=8 hr, and then t
Cm =1.9 and Q=1000.421 m3/hr are gained.

Applying the LOESS model as mentioned above to the data in Table 3.4.1 gives us productivity curves in Figure 3.4.1. Comparing actual productivity with the productivity curves in Figure 3.4.1 enables us to evaluate productivities for each the work sells.

Table 3.4.1 Hourly production quantity by dozing

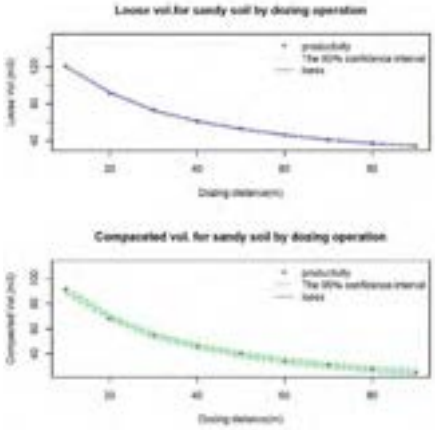

Figure 3.4.1 Productivity curves by the LOESS model

Multiplying the pseudo-real operation rate sequence in Figure 3.3.1 by the Q value gives the accumulative production sequence in Figure 3.4.2, which could be utilized as a reference line to compare with ensemble forecasting lines. Also, the accumulative production curve in Figure 3.4.2 shows speed of construction.

There are two important evaluation points of productivity, which are the 1st milestone and the 2nd milestone. It is very important to seriously grasp the actual states in each of work cells at the 1st milestone and to project work process toward to the 2nd one. In our bitter experience, problems latent in work progress incline to break out at the 2nd evaluation point, and then it might often compel us to rush-works.

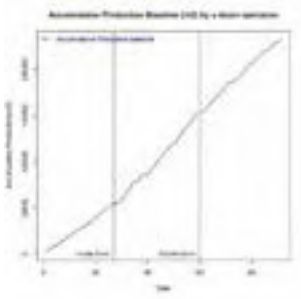

Figure 3.4.2 Accumulative production curve

3.5 Ensemble forecasting

Although doing the pessimistic, optimistic and most likely ensemble forecasting, respectively, this section reports the infographics on just the most likely one. That's why space did not permit us to insert the infographics on the pessimistic and optimistic ones.

3.5.1 Ensemble forecasting at 1st milestone

1. Shape parameters (alpha, beta) of Beta distribution

The equations (9) and (10) determine shape parameters (alpha, beta) of Beta distribution. From the descriptive statistics at the 1st milestone in Table 3.3.1, the mean "0.257" and the variance "0.014" give us B(13.382, 38.68).

2. Bagging method

At the 1st milestone, let repeat five times to extract 10,000 samples from B(13.382, 38.68) by random sampling with replacement, it leads to values at each of the five times the weak learner as shown in Table 3.5.1.1.

As described before, in the bagging method values at the weak learners are averaged. Table 3.5.1.2 shows the average of Table 3.5.1.1. Here, Let put

- 1st Qu=pessimistic,
- mode=most likely, and
- 3rd Qu=optimistic.

Table 3.5.1.1 Values at each of the five times the weak learner at the 1st milestone

	1st-	2nd-	3rd-	froth-	fifth-
Min.	0.00088	0.003006	0.00088	0.00088	0.001775
1st Qu.	0.161531	0.16108	0.163922	0.16458	0.160241
Median	0.262068	0.26198	0.262268	0.264431	0.264399
Mean	0.254653	0.254057	0.255458	0.256171	0.255417
3rd Qu.	0.353164	0.351715	0.352772	0.355252	0.354979
Max.	0.45866	0.458455	0.458458	0.458458	0.458458
Variance	0.013989	0.013904	0.0137	0.013822	0.01403
Mode	0.070389	0.416551	0.136546	0.334552	0.138386

Table 3.5.1.2 Average of Table 3.5.1.1

Min.	0.001059
1st Qu.	0.163119
Median	0.262625
Mean	0.255609
3rd Qu.	0.353726
Max.	0.458514
variance	0.013796
mode	0.207936

The most likely ensemble forecasting from the 1st milestone to the 2nd milestone are shown below.

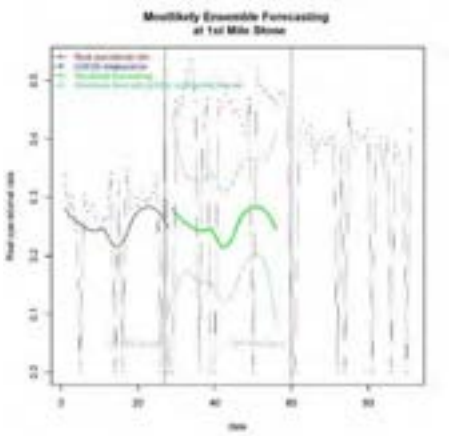

Figure 3.5.1.1 Most likely ensemble forecasting from the 1st milestone to the 2nd milestone

3.5.2 Ensemble forecasting at 2nd milestone

In the same way as mentioned above, let repeat five times to extract 10,000 samples from B(13.382, 38.68) by random sampling with replacement, it leads to values at each of the five times the weak learner at the 2nd milestone, and then average them. Similarly, the descriptive statistics at the 2nd milestone gives the mean "0.319" and the variance "0.03", and so the Beta distribution ~ B (6.9223, 14.7777)

The most likely ensemble forecasting from the 2nd milestone toward the completion are shown in Figure 3.5.2.1. The ensemble forecasting value is a bit larger than the determined production at the completion.

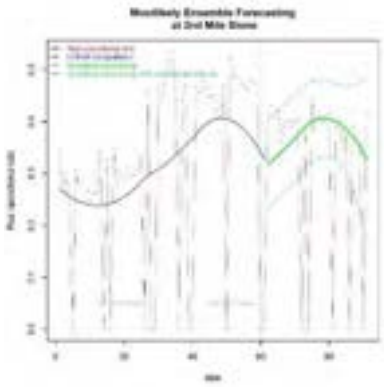

Figure 3.5.2.1 Most likely ensemble forecasting from the 2nd milestone to the completion

3.5.3 Comparison between Accumulative Production Baseline and Most Likely Ensemble Forecasting Line of Production

Figure 3.5.3.1 shows comparison between the accumulative production baseline in Figure 3.4.2 and the most likely ensemble forecasting line of production to the completion.

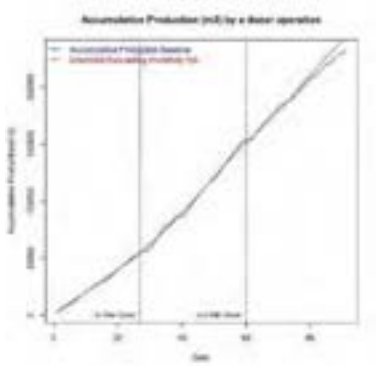

Figure 3.5.3.1 Accumulative production baseline and most likely ensemble forecasting line of production to the completion

4 Lesson Learned from Empirical Study

In this chapter, lesson learned from the empirical study is described and discussed.

As is well known, smoothing line method, for examples, simple exponential smoothing (SES), LOESS, and beta regression model, could show time-series features very well. The SES and the LOESS are non-parametric methods and could be easily handled without specific distribution. The LOESS could be easily used for extrapolate prediction. Whereas, the SES is not easily handled for extrapolate prediction. Beta regression model literally assumes Beta distribution. In many situations, scheduling problems assumes Beta distribution, and so the Beta regression model looks like to be more consistent than others. Concretely, GLM (generalize linear model) with logit function are used to the calculation of the Beta regression model. Incidentally it is prediction based on the logit transformed scale [7],[8]. However, relationship between logit distribution and Beta distribution is unclear.

Originally, interpolated prediction could be easier handled than extrapolated one. Therefore, with ensemble learning with the LOESS model, in other words, simulation-based ensemble forecasting in long term, is utilized in this study.

Although data analysis is generally expensive and time-consuming, the automatic analysis methods proposed in this study is easy-to-use and -learning and cost-effective for daily repetitive learning and automatically execute to find probable causes of unacceptable performance.

On-site usage of the ensemble forecasting method proposed in this paper forks two folds. The first is daily ensemble forecasting in short term, for example, ten-days productivity. The second is periodic ensemble forecasting in long term, for example, forecasting from the 1st milestone to the 2nd milestone, and from the 2nd milestone to the end. The second one is illustrated in the chapter three.

Figure 4.1 shows image of the ensemble forecasting for ten-days productivity. Work hack here is shown as below. As mention before, the hourly productivity "Q" by dozer operation is gained by the equation (12) and (13). During the first ten days from the dozer operation start, multiplying daily real operation rate in-suite gained from the PoC by the value "Q" could give the daily productivity by dozer operation, and then do ensemble forecasting for the first ten-days productivity.

Figure 4.1 Ensemble forecasting for ten-days productivity

In the meantime, both of average of pushing distance for spreading fill material and dumping volume of fill material by the number of arrivals of dump trucks could be calculated by GPS data, and also the real operation rate in-suite could be gained from the PoC each day. And then the "Q" values could be gained on that day. Similarly, ensemble forecasting in the coming ten-days productivity could be executed. Moreover, these data could give us the dozer operation area, the thickness of spreading earth on the ground, and the progress rate to the target volume each day.

The above procedure enables us to repetitively do ensemble learning regarding scheduling of dozer operation, as considering environmental and ground condition.

It can be seen from the empirical study that show predictability of the ensemble forecasting of construction schedule. When watching transition of real operational rate sequence and finding abnormal observations as shown in Figure 3.3.2, the following matter shall be examined:

1. Appearance of new phenomena
2. Disappearance of existing phenomena
3. Sift change in mean and variance
4. Trend of increase or decrease

Looking around performance chart summary in each work cells and works backward from the 2nd to 1st milestones enables us to understand should-can-will-did works and to improve the working practices required

from now on. On the other hand, looking ahead the ensemble forecasting at the 2nd milestones could inform us what the prospects are until the completion.

In practice, watching hand-on real operational rate sequences in each of work cells could give us information on which activities are most fragile and opportunities to examine resource allocation and reduction of lead time in each of work cells. Here, Infographics with early precautions (refer to ANSI 2535.5) such as charts, tables, and ensemble forecasting of construction schedule could provide a snapshot of work in progress over daily, weekly, bi-weekly or monthly.

These infographics would be automatically displayed on the dashboard of the remote real-time monitoring system [10]. These infographics would play a role in:

1. Thinking and decision-making support to:
- Provide workers with opportunities to recognize potential hazards, develop proactive countermeasures and start monitoring; and
- Pick a set of building block of information at the right level of abstraction and at the right time, and
- Stimulate or guide worker's creative thinking, i.e., indication or hint; and
2. Communication support to:
- Save or share information and mail back and forth to each other; and
- Help workers structure conversation and keep track of tasks.

The further development and research on this study are listed below:

1. Conducting hand-on verification and validation of the methods proposed in this study, and then we intend to report the results of this filed test at the ISARC 2021,
2. Applying M/M/c queueing theory to cyclic works such as LHD, concrete placement works, etc., and
3. Developing algorithm ensemble forecasting for each of work types including LHD and labour-intensive works, and integrated with PERT/CPM programs.
4. Cyber-agent, that is, computerized agent who work for ensemble forecasting of construction schedule. The cyber-agent here is a virtual engineer or line-manager who inhabit within a cyberspace composed of computer systems. The cyber-agent will passively or actively walk through the cyberspace to help workers explore and capture critical factors latent in a large amount of information that may go into making decisions [11].

In closing, we would like to say that any help and suggestions on this study would be heartedly appreciated.

References

[1] Shigeomi Nishigaki, Katsutoshi Saibara, et al. Points on construction, 25th ISARC 2008, pp.796-803, 2008.

[2] Shigeomi Nishigakia and Katsutoshi Saibarab. Infographics on Unmanned Dozer Operation,36th International Symposium on Automation and Robotics in Construction (ISARC 2019).

[3] Nura Kawa. Bagging an ensemble method for variance reduction in unstable models. On line: https://rpubs.com/nurakawa/bagging

[4] Joseph Rocca. Ensemble methods: bagging, boosting and stacking. On line: https://towardsdatascience.com/ensemble-methods-bagging-boosting-and-stacking-c9214a10a205。

[5] Rafael Irizarry. Applied Nonparametric and Modern Statistics. On line: http://rafalab.github.io/pages/754/

[6] Willie Wheeler. Clean up your time series data with a Hampel filter. On line: https://medium.com/wwblog/clean-up-your-time-series-data-with-a-hampel-filter-58b0bb3ebb04

[7] Hiroshi Hagihara edited. Examples and methods of scheduling network for resident engineers on site for civil engineering, Kindai Tosho,2003, in Japanese.

[8] Silvia L.P. Ferrari, Francisco Cribari Neto. Reta regression for modeling rates and proportions. On line: https://www.tandfonline.com/doi/abs/10.1080/026647604200021450l

[9] Jacob C. Doumai, James T. Weedon. Analysing continuous proportion in ecology and evolution: A practical introduction to beta and Dirichlet regression, Vl. 10, Issue 9, Methods in Ecology and Evolution. On line: https://besjournals.onlinelibrary.wiley.com/doi/full/10.1111/2041-210X.13234

[10] Shigeomi Nishigaki, Katsutoshi Saibara. Infographics on Unmanned Dozer Operation, 36th International Symposium on Automation and Robotics in Construction (ISARC 2019)

[11] Shigeomi Nishigaki, Masanori Kaku, Yoshio Maruyama, Kinya Tamaki. Current Challenges in the Application of Agent Theory to Construction Management in Innovative, Intelligent Field Factory, pages 148-153, Proceedings of the 14th ISARC, 1997 On line: http://www.iaarc.org/publications/fulltext/Current_challenges_in_the_application_of_agent_theory_to_construction_management_in_innovative,_i.PDF

A Technology Platform for a Successful Implementation of Integrated Project Delivery for Medium Size Projects

Luke Psomas[a] and Hani Alzraiee[b]

[a]Undergraduate in Civil Engineering, California Polytechnic State University San Luis Obispo, USA
[b]Department of Civil Engineering, California Polytechnic State University San Luis Obispo, USA
E-mail: lpsomas@calpoly.edu, halzraie@calpoly.edu

Abstract –

Traditional project delivery methods are inflexible for projects that require a high level of collaboration among project teams as well as present challenges to innovative design and construction approaches. In today's era, projects are executed at a faster pace at the early stages of scope definition. This causes a high cycle of requests for information (RFI), change orders, and disputes. To address this issue, a framework for implementing IPD to a medium-size energy project from the engineering phase to the commissioning phase was developed. The framework consists of 1) project stakeholders classification; 2) disciplines identification; 3) relationships, responsibilities; and objectives matrix, and 4) monitoring, control, and feedback. The framework was implemented using Building Information Modelling (BIM) platform and project Document Management System. Synchronizing everyone's objectives in the framework and ensuring these objectives are achieved is a strategy for the success of the project's delivery. The framework was implemented using actual project and was able to enhance design and construction coordination and reduce project cost by 20% and cut project duration by 25%. However, stakeholder coordination and availability of technologies pose a challenge for the successful implementation of the framework.

Keywords –

Integrated Project Delivery; Building Information Modeling; Construction Information System; Construction

1 Introduction

Increased collaboration in the architecture, engineering, and construction (AEC) industry is integral in responding to construction deficiencies within complex projects. These deficiencies are common among nearly all projects and, within traditional delivery methods, responses to them include late, disconnected decision making that results in more rework, schedule overrun, and a high number of requests for information (RFI). The American Institute of Architects defines integrated project delivery as "a project delivery method by a contractual agreement between a minimum of the owner, design professional, and builder, where risk and reward are shared and project team's success is dependent on project success" [1]. Since its introduction to the industry about 15 years ago, professionals have had a high level of optimism for Integrated Project Delivery (IPD) becoming a reliable and accepted delivery method [2].

Construction projects are complex, dynamic in nature and subjected to cost, time, and scope deviations. When these deviations inevitably occur, workers investigate and often submit an RFI to the architect. IPD has provided an approach to communication problems that results in ongoing collaboration and quick responses to deviations. In general, the latest uses of IPD on projects have mainly produced fewer change orders, decreased project timeline, fewer costs, and incidentally fewer requests for information [2]. However, the limitations of IPD still exist. The current research on IPD has dealt with its performance, potential collaboration techniques, pairing with BIM, contractual implications, and adoption into the industry. There is a knowledge gap on the structure of implementation, the mechanism of interactions among the project players (design and construction), and required supporting technology. We claim these are three elements responsible for the failure associated with IPD implementation.

Building Information Modeling (BIM) is a powerful technological tool that provides a rich 3D model with digital information of the project to stakeholders. Furthermore, and more importantly, BIM acts as a "shared knowledge resource for information about a facility (physical and functional) forming a reliable basis for decisions during its lifecycle from inception onward" [3]. BIM has closed many gaps on the issue of interoperability and is most efficiently used in conjunction with a document management system and a common information exchange software, such as

Industry Foundation Classes (IFC) or BIM Cloud, that tackles the difficulty of diversity between software [4]. Future research efforts need to focus on a sophisticated and diverse implementation of BIM and the associated technologies to support the smooth adoption and implantation of the IPD [5], additionally the socio technical implications in the flow of production within a given project [6].

IPD is an emerging method of delivering complex projects and projects that require a higher overlap between design and construction. This method is an efficient tool to apply when integrated collaboration, cost, and schedule are major constraints for the successful delivery of the projects. However, implementing this method successfully in the AEC industry continues to be a challenge, especially for medium size projects or inexperienced project stakeholders with IPD. Other challenges are also observed in selecting the right technology for implementation (BIM, cloud based-data management system for design and as-build data, and the implementation infrastructure).

This paper proposes a framework to assist owners to implement IPD to medium-sized projects and allow them to measure project performance based on several metrics. These metrics include customer satisfaction, safety, quality, cost, and schedule. The framework is made possible by IPD and BIM implementation and describes the relationships and responsibilities of stakeholders within each phase of the project lifecycle.

2 Literature Review

2.1 Why IPD Should Be Implemented

The AEC industry has struggled for a long time with low productivity, cost overrun, schedule delay, and a high number of change orders and rework. One of the main reasons for these issues is impeded in the rigid mechanism of delivering projects. In comparing IPD with other delivery methods, IPD produces fewer change orders, cost savings, and a shorter schedule [2]. Additionally, traditional project delivery methods contain ten RFI per one million dollars and a 2-week processing time, compared to an IPD project, which contains two RFI per one million dollars and 1-week processing time [7]. IPD represents a hope to overcome many of the problems that the AEC industry faced for decades without a rigorous solution. Many studies have shown that the AEC industry is the only industry that did not show signs of productivity improvement for a long time and still this issue continues to be the main cause for high waste in the construction industry. IPD has proven its ability to increase efficiency and save resources in construction projects. However, successful implementation of the method represents the main hurdle in current practices.

2.2 Basic Strategies for Implementing IPD

There are 2 basic strategies for implementing IPD in the AEC industry: heavy collaboration among project stakeholders and adopting an advanced design and data management system.

To achieve collaboration, it is helpful to use a platform that allows for shared knowledge between major parties. The “big room” in design refers to the physical shared space for early design development that includes all necessary parties. For medium-sized projects, the big room can be tricky to maintain because many of the employees might have several projects at once and may not be in the same geographic area [8]. This obstacle was carefully weighed in our implementation of a virtual big room with many participants, similar in principle to past research [8][9].

Along with collaboration, the right technology must be used. BIM provides an integrated platform for live feedback and collaboration. BIM gives foresight to the different proposed possibilities of the project beforehand and visualizes necessary changes during for clarity of the project managers [10]. In the Autodesk HQ construction case study, a BIM execution plan was established and moved forward with at-risk subcontractors having been BIM-enabled [11]. This allowed for constant feedback during the design phase from the builders who knew construction processes well.

IPD allowed for scope changes totaling 30% in this project [11]. Furthermore, when a hefty design change was requested from the owner, the design firm acted quickly to provide a virtual walkthrough using BIM of the proposed change within a week of the request, allowing the owner to make an informed decision on the change [11]. The integration capabilities of BIM make it appealing to any construction project because of its time and cost estimation capabilities [12]. BIM is most useful in an IPD project because of its allowance for multi-user access and contributions to the model [4]. The following is an excellent descriptor of how BIM can aid in IPD:

“The project team can deal and interact with a unified model when a composite model is built from an amalgam of various disciplines’ models. Having this capability, and through the different phases of a construction project, BIM can coordinate the design, analysis, and construction activities on a project and, therefore, results in integrity of projects.” [13]

2.3 Gaps in prior research

It is crucial that we identify the basic components of IPD which include a multi-stakeholder contract, rigorous collaboration and coordination, and technology usage.

However, we also identified a knowledge gap with a few implementation factors. We are defining this necessary knowledge gap as:

The methods of collaboration between stakeholders and their subsequent responsibilities during each phase of construction in IPD.

This gap demands a system to define the methods of collaboration, which includes classifying the stakeholders, defining the relationships, responsibilities, and objectives between stakeholders, and monitoring the construction through constant feedback. If chosen to perform, stakeholder analysis and classification are usually done by the project manager [14], but in our IPD framework, the responsibilities will be distributed among the major stakeholders based on the accepted framework. This is supported by the conclusion that an iterative process that includes cooperation between major stakeholders on their classification is more effective than considering it a desk task by one individual [14]. A simple classification of stakeholders includes key members, key supporting participants, tertiary stakeholders, and extended stakeholders [15]. An IPD framework has been defined in the past with macro and micro aspects, but we are more interested in one of the micro aspects: information design [16]. In IPD, information must be the common basis of understanding for all stakeholders, and information must be accessible, available, and reliable [16]. Due to the lack of research linking information design to collaboration, we are interested in the relationships shared between stakeholders as they utilize our information framework.

3 Integrated Project Framework

IPD is set apart from other delivery methods in the unique early stages of project planning and communication, wherein every player in the project, regardless of their role, must be incorporated into planning and development before the design is finalized to optimize the usage of IPD. This enhanced collaboration is hard to achieve and requires shared project planning goals and a rigid strategy for communication. For us, this meant putting a system in place so that the implementation of the technology is smooth. The following system is a step by step procedure through the entirety of the project that can be agreed upon by the major stakeholders. The system has been divided into 5 stages: qualification, bidding, pre-construction,

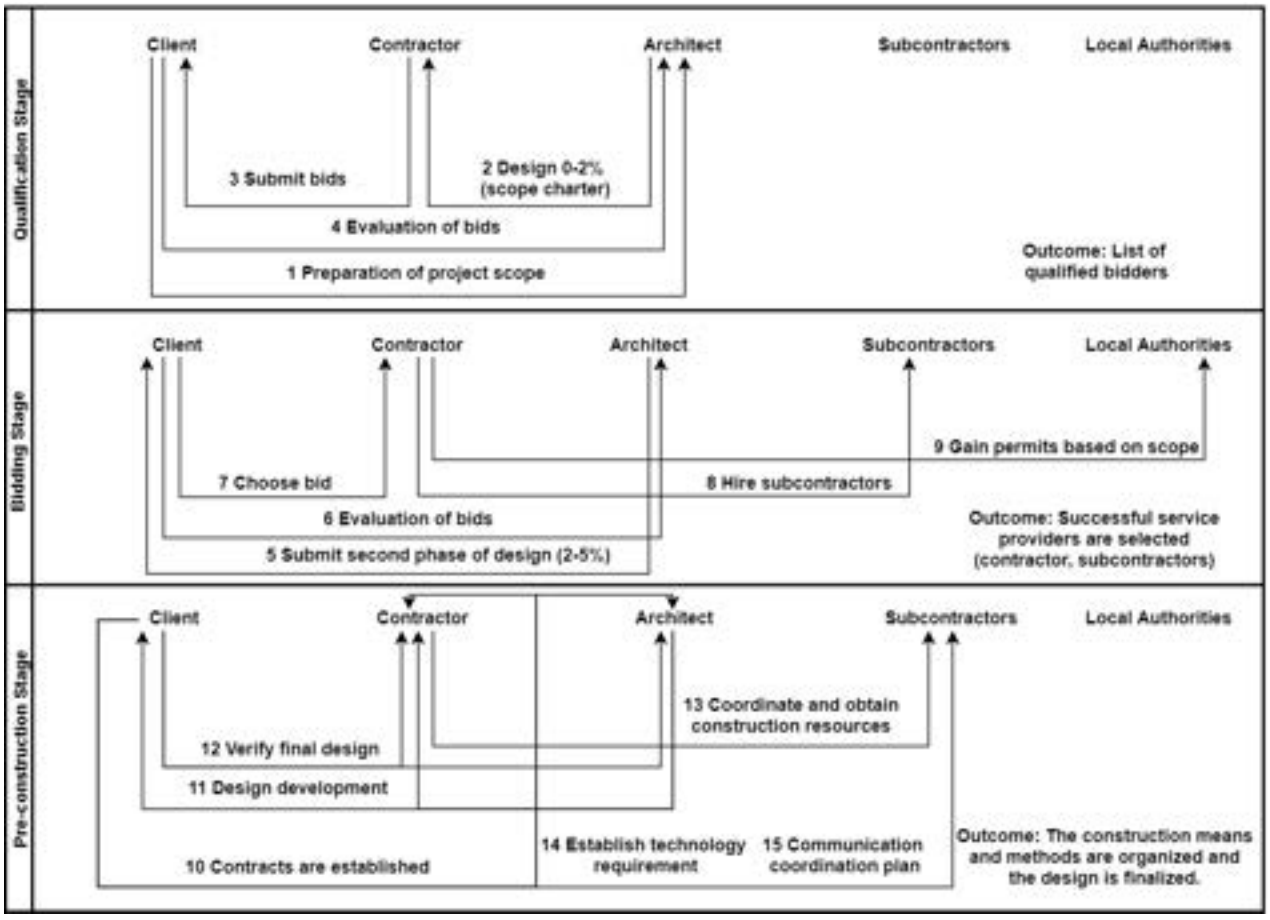

Figure 1. First 3 Stages of the IPD Implementation Framework

construction, and closeout as illustrated in Figure 1 and Figure 2. Each step is organized chronologically, and the final step of each stage is followed closely by the first step of the next stage. The most important phase in our research, the construction stage, contains many moving parts and will be organized in a different way than the other stages.

3.1 Qualification Stage

The first stage is named the qualification stage because the main outcome of this stage is the client having a list of qualified bidders, as shown in Figure 1. This stage is an early stage in the project and should involve the client and the architect only. This is because there is a need to create the project framework and the scope charter. The project's goals and expectations come from the client and are communicated to the architect for better refinement. This stage begins with the client preparing the project scope and delivering it to the architect, who reviews the scope and develops a high-level schematic design. The high abstract of the project's scope lays out the project's goals and necessary design and construction work, and a clearly defined scope main framework necessary in avoiding design delays and cost overruns [17]. Then, the architect will begin the design based on the initial scope of work and the schematic designs. Up to 2% of the Front End Engineering Design (FEED) put together by the architect along with Request for Qualification (RFQ) is shared with the client so the client in collaboration with the architect solicits interested prime contractors in executing the project within the IPD environment. The interested contractors will then submit the qualification to the client for evaluation. In IPD, this step includes the architect evaluating the bids with the client because of the architect's knowledge of the design. The qualification stage results in the client having a list of qualified service providers, which allows the team to move into the bidding stage.

3.2 Bidding Stage

In the bidding stage, there are a variety of steps required which involves every party, as shown in Figure 1. The outcome of this stage is that the service providers are selected, which includes the contractor and subcontractors. This stage begins with the architect submitting the second phase of design (2-5%) to the client, followed by the bidding for the project by the selected list in the first stage, then the successful bidder will be selected. All submitted bids must include the major subcontractors and their qualifications for the successful implementation of the IPD. This step is very essential to ensure every stakeholder is going to function in an integrative type of design and construction environment. Contractual obligations and terms are stated in this stage among all parties. Clear expectations of schedule, tasks, deliverables, coordination, cost, frequency of data update, and meetings are stated at this stage. From the authors' experience, the mechanism of implementation can be overwhelming to many subcontractors due to the unfamiliarity with the IPD. Equality important, the implementation technology platform for all parties involved should be created at this stage through the Technology Execution Plan (TEP). Subcontractors should be involved in creating the TEP and should have access and be familiar with the implementation infrastructure.

3.3 IPD Technology Requirement

Technology infrastructure is the most important aspect of IPD implementation. There is no doubt that IPD became a choice for many owners due to the development of design approaches such as BIM and project data management. Incorporating BIM approach into the IPD process allows project team to utilize the information in an integrative environment. For example, information from design, procurement, construction, quality, and other areas is being received and processed in a way it allows everyone to be informed. This high level of information management is essential for the fast pace of the IPD. To achieve this, however, a technology infrastructure must be accessible to those who are involved. BIM is the main platform to use for design, construction, and commission for the proposed method. The issue that can create problems in using BIM in IPD environment is the interoperability of the project 3D files.

The next part of the technology infrastructure for the IPD is having a system that handles the information receiving, using, and transferring. Many cloud-based tools available such as Procure and Aconex that can be utilized for managing the project information. The strength of the cloud-based tool in the multi-organizations project collaboration, where data can be stored and accessed efficiently. Tasks that include document and correspondence management, workflow automation, request for information, change orders, BIM file management, and more can be reviewed and addressed.

3.4 Pre-Construction Stage

The pre-construction stage contains many vital responsibilities that must be performed effectively for construction to even be possible, as shown in Figure 1. In this stage, the implementation of the technology infrastructure is tested. Flaws in the IPD technology system should be captured in this stage to modify the TEP. Flaws represented through subcontractors include not having the proper technology or the lack of required

subcontractors' crew training. For instance, a mechanical subcontractor might be using an IFC complying tool to model the mechanical design part, but files generated from this tool are not properly interoperable with another parametric model generated by the electrical subcontractor. The outcome of this stage is to define the major construction means and methods. After ensuring all project parties are familiar with the project scope and technology, contracts between the contractor and the major stakeholders are established. This includes defining many details, such as the level to which risk and reward are shared, the possible incentives for quality construction, and more. The level of integration of the project, or level to which IPD is implemented, must be defined in the contract and must be agreed upon by all major stakeholders. Following this, an intensive collaboration between the client, architect, and contractor ensues with the goal of developing the design further. IPD is unique in that it brings these 3 major stakeholders into the "big room" before construction is initiated so that any inconsistencies between the design and construction can be worked out. Developing the design among these stakeholders carries through the construction stage but is initiated in the pre-construction stage. The client will verify or request changes to the in-progress design with the architect and the contractor. After verification, the contractor will organize the obtaining of construction resources alongside the subcontractors. Finally, the client will clarify to the architect, contractor, and subcontractors the plan of communication between the stakeholders, which includes the updating of BIM, a communication software, and regular "big room" meetings, and the client will distribute access to the agreed upon technology which will be utilized throughout the project.

3.5 Construction Stage

The construction stage must be closely monitored throughout because there are many actions and cycles working all at once. The outcome of this stage is that the design and construction of the project are finished. The technology platform holds IPD together, as displayed in Figure 2. BIM is the technology that collects and analyses data from every important member during construction. This stage works in a cyclic process and casual feedbacks fashion. For example, if a major stakeholder (architect, contractor, client, or subcontractor) encounters a design or construction issue, they report the issue using the proper technology tools so all other stakeholders can receive the information about the issue. The responsible stakeholder will then update the project data management system (BIM tool) with the necessary answer and information to move forward, whether that be a slight change in design or major change order. Since the subcontractor has continual access to BIM, this process takes the least amount of time in an IPD setting. Processes like these can start on the construction site or from the desk of the client and flow through BIM quickly and efficiently. Useful information that can be accessed in BIM in the construction stage includes equipment, construction processes, materials, quality, subcontractors' contributions, RFIs, change orders, safety guidelines, and environmental compliances. This information is inputted into BIM and used by stakeholders to perform project status tracking, information management, and activity scheduling. These three functions of BIM are optimized by stakeholders through heavy collaboration and on-site monitoring. Project status tracking demands accurate reporting and documentation on design changes which limits contractual issues and cost overruns. Information management of BIM data helps to limit the number of inconsistencies between design and construction. Activity scheduling requires ongoing communication on-site so that stakeholders can plan accordingly to minimize the project's timeline. Through the construction stage, the design is constantly being changed and approved in BIM. The construction project is finished in this stage.

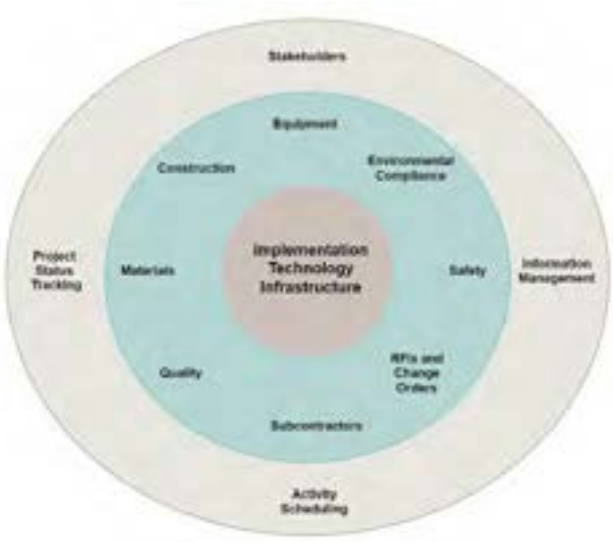

Figure 2. Construction Stage

3.6 Closeout Stage

The closeout stage is an often-overlooked part of the project but must be carried out to ensure success. The client will start by making sure that the design changes inputted into BIM were fulfilled in construction. Then, the client and contractor will evaluate the success of the project based on 5 metrics in Figure 4: customer satisfaction, safety, quality, cost, and schedule. Finally,

the client will fulfill the obligations laid out by the contract to the contractor, architect, and subcontractors. Risk and reward sharing are important parts of the contract and are based on the accurate success evaluation of the project. The outcome of this stage is that the final project is evaluated based on 5 metrics and the contractual obligations are fulfilled.

4 Project Success Metrics

There are a variety of factors to consider when determining the success of a project delivery. Some of the main performance metrics considered are execution schedule, project cost, client satisfaction, changes, quality, and safety. Similarly, the success of the project delivery can be measured by interactive processes, contractual arrangements, and project characteristics and participants [18]. Table 1 contains the project success criteria that the authors used to measure the satisfaction of the project stakeholder of using IPD.

4.1 Customer Satisfaction

We measure customer satisfaction by the number of legal claims made by the client and the potential for future business with the other stakeholders. The claims refer to if a mistake in construction is large enough the client will submit a legal claim against the contractor, which adds more time to the closeout stage. The potential for future business refers to the level of project satisfaction of the client based on the specific work of each stakeholder and if the client would do business with them again. A low number of legal claims and a high level of potential for future business results in good customer satisfaction.

4.2 Safety

We measure safety by the number of incidents in construction that occurred and the lost-time due to injuries. The number of incidents is the number of construction accidents by the workers; a high number of incidents reflect poorly on the project's safety. The lost-time due to injuries refers to the time delays after an incident has occurred. A low number of incidents and a small amount of lost time due to injuries results in good project safety.

4.3 Quality

We measure quality by the number of non-conformance reports, the punch list, the number of RFIs, and construction rework. Non-conformance reports refer to those reports that list the failures of adherence to construction and environmental regulations of the final project. The punch list is the report made by the contractor that contains the deviations between the contractual specifications and the final construction product. RFIs, or requests for information, refer to the requests made by the contractor or subcontractors for more information if there is a gap in knowledge of a part of the design. Construction rework is the amount of rework done on the project because of structural or design failures. A low number of non-conformance reports, a small amount of deviations on the punch list, a low number of RFIs, and a low amount of construction rework results in good project quality.

4.4 Cost

We measure cost by cost overrun, change order cost percent, RFIs per unit price, and markups percent. Cost overrun refers to the extra cost to finalize the project based on the original cost laid out by stakeholders. Cost overrun percent is the difference between the actual project cost and the award price over the award price (1).

$$Cost\ Overrun\ \% = \frac{Actual\ Cost - Baseline\ Budget}{Baseline\ Budget}\ x\ 100 \quad (1)$$

Change orders are the requests to add or delete certain parts of the design when in construction. The change order cost percent is the total cost of all the change orders submitted over the actual total project cost (2).

$$Change\ Order\ Cost\ \% = \frac{\sum Change\ Orders\ \ Cost}{Baseline\ Budgte}\ x\ 100 \quad (2)$$

The percentage of the cost impact of the RFIs is the total cost of the add work due to the RFI answers over the project budges cost (3).

Table 1. Project Success Metrics

Customer Satisfaction	Safety	Quality	Cost	Schedule
Claims	# of Incidents	Non-Conformance Reports	Cost Overrun	Schedule Overrun
Future Business	Lost-Time-Injuries	Punch List	Change Order Cost %	Constructability
		# of RFIs	Markups %	
		Rework		

$$RFIs\ Cost\ \% = \frac{cost\ of\ added\ scope\ due\ to\ RFIs}{Baseline\ Budget} \text{x}100 \quad (3)$$

The markup percent is the profits for each stakeholder based on the final product. A low cost overrun, a low change order cost percent, a low RFIs per unit price, and a high markup percent result in good project cost.

4.5 Schedule

We measure schedule by schedule overrun and constructability. Schedule overrun is how much construction deviated from the project timeline and is most easily measured by schedule delays, which are defined as the difference between the actual duration and the baseline duration over the baseline duration of the project (4). The actual duration is how long the project took and the baseline duration is the construction time reported by the planned timeline.

$$Schedule\ delays\ \% = \frac{Actual\ Duration - Baseline\ Duration}{Baseline\ Duration} \text{ x } 100 \quad (4)$$

To evaluate the added time to execute the scope described in the RFIs, the RFIs Time % is calculated by finding the total extra time needed to execute the RFIs scope over the baseline duration (5).

$$RFIs\ Time\ \% = \frac{Total\ time\ added\ due\ to\ RFIs}{Baseline\ Duration} \text{ x } 100 \quad (5)$$

The constructability is how easily the project was constructed and kept close to the timeline. A low number of schedule delays and a high level of constructability results in a good project schedule.

5 Preliminary Results and Analysis

The presented framework was developed and implemented for a medium-size gas plant of 120-million-cubic-foot-per-day capacity. The project owner's objective was to complete the design, construction, and commissioning of the project in less than 2 years. The project contract was a Guaranteed Maximum Price (GMP) of 263 million dollars. The IPD implemented was described in the previous sections. The project was completed in 20 months with an actual budget of $220 million dollars. The framework reduced the project cost by 20% and cut project duration by 25%. There was zero Lost Time Injury (LTI). The changes in the project scope were minimal and were easily accommodated. The execution design and construction team established design and construction gates (milestones), which meant if a milestone stage in the design was completed, reviewed, and approved, then there was no need to go back for changes. This was because the next stage involved major equipment sizing and manufacturing. The required equipment usually is of long-lead items and needed to be procured early enough to get manufactured by vendors. Similarly, other critical design gates involved major pipes sizing and power load determination. However, the implementation of the proposed framework involved tedious coordination and high caliber management and engineering skills. The team selected to work on this project was very experienced and of different years of experience. Another major challenge was ensuring the functionality and interoperability of infrastructure technology. Furthermore, some of the vendors on the project were from overseas and ensuring their attendance in the coordination meetings was a difficult task to achieve all the time. The next phase of this IPD framework is to track and analyze the project's performance indicators and then refine the framework for a wide-scale implementation.

6 Conclusions

Integrated project delivery is groundbreaking for the construction industry, but still new and challenging to implement. Forming the right project team that is committed to the main aspects of IPD is essential to the project's success. Consistent collaboration and usage of the right technology must be considered when delivering an IPD project.

The framework we have laid out focuses on the relationships between stakeholders and their responsibilities during each stage of an IPD project. By adhering to this system, the client can keep the project delivery organized and maintain the efficiency of the contributions from each team member. Our project success criteria are based on the framework and on the researched effects of IPD projects.

We acknowledge the many moving parts of a construction project and advise any clients who want to use our system to plan accordingly because IPD takes a large amount of work to efficiently implement. There are still gaps of knowledge, mainly in the construction stage, due to the increasing capabilities and benefits of construction monitoring in IPD. Similarly, the technology used in the construction stage demands much organization and coordination between stakeholders. IPD linked with BIM has the potential to change the construction industry through increased planning and further research into the relationships between the two.

References

[1] AIA California Council, "Integrated Project Delivery: A Guide," *Am. Inst. Archit.*, pp. 1–62, 2007, doi: 10.1016/j.autcon.2010.09.002.

[2] D. C. Kent and B. Becerik-Gerber, "Understanding construction industry experience and attitudes toward integrated project delivery," *J. Constr. Eng. Manag.*, vol. 136, no. 8, pp. 815–825, 2010, doi: 10.1061/(ASCE)CO.1943-7862.0000188.

[3] NIMBS Committe, "National Building Information Modeling Standard," *Nbim*, p. 180, 2007, doi: 10.1017/CBO9781107415324.004.

[4] N. Azhar, Y. Kang, and I. U. Ahmad, "Factors influencing integrated project delivery in publicly owned construction projects: An information modelling perspective," in *Procedia Engineering*, 2014, doi: 10.1016/j.proeng.2014.07.019.

[5] R. Ghassemi and B. Becerik-Gerber, "Transitioning to integrated project delivery: Potential barriers and lessons learned," *Lean Constr. J.*, vol. 2011, pp. 32–52, 2011.

[6] R. E. Smith, A. Mossman, and S. Emmitt, "Editorial: Lean and integrated project delivery," *Lean Constr. J.*, vol. 2011, pp. 1–16, 2011.

[7] M. El Asmar, A. S. Hanna, and W. Y. Loh, "Quantifying performance for the integrated project delivery system as compared to established delivery systems," *J. Constr. Eng. Manag.*, vol. 139, no. 11, pp. 1–14, 2013, doi: 10.1061/(ASCE)CO.1943-7862.0000744.

[8] B. Dave, E. Pikas, H. Kerosuo, and T. Mäki, "ViBR – Conceptualising a Virtual Big Room through the Framework of People, Processes and Technology," *Procedia Econ. Financ.*, vol. 21, no. 15, pp. 586–593, 2015, doi: 10.1016/s2212-5671(15)00216-6.

[9] Z. Ma, D. Zhang, and J. Li, "A dedicated collaboration platform for Integrated Project Delivery," *Autom. Constr.*, 2018, doi: 10.1016/j.autcon.2017.10.024.

[10] S. Qiu, H. Xu, J. Jin, H. Zhang, and K. Sun, "Application of BIM Technology in Construction Engineering," *IOP Conf. Ser. Earth Environ. Sci.*, vol. 371, no. 2, pp. 107–115, 2019, doi: 10.1088/1755-1315/371/2/022073.

[11] J. Cohen, "Integrated Project Experiences in Collaboration : On the Path to IPD Delivery : Case," no. January, p. 59, 2010.

[12] R. Lahdou and D. Zetterman, "BIM for Project Managers," *Bim-Pm*, pp. 1–46, 2011.

[13] S. Rokooei, "Building Information Modeling in Project Management: Necessities, Challenges and Outcomes," *Procedia - Soc. Behav. Sci.*, vol. 210, pp. 87–95, 2015, doi: 10.1016/j.sbspro.2015.11.332.

[14] A. L. Jepsen and P. Eskerod, "Stakeholder analysis in projects: Challenges in using current guidelines in the real world," *Int. J. Proj. Manag.*, 2009, doi: 10.1016/j.ijproman.2008.04.002.

[15] A. Aapaoja and H. Haapasalo, "A Framework for Stakeholder Identification and Classification in Construction Projects," *Open J. Bus. Manag.*, vol. 02, no. 01, pp. 43–55, 2014, doi: 10.4236/ojbm.2014.21007.

[16] H. Ashcraft, "The IPD Framework (26 pages)," 2012, [Online]. Available: http://www.hansonbridgett.com/Publications/~/media/Files/Publications/IPD_Framework.pdf.

[17] H. A. Mesa, K. R. Molenaar, and L. F. Alarcón, "Exploring performance of the integrated project delivery process on complex building projects," *Int. J. Proj. Manag.*, 2016, doi: 10.1016/j.ijproman.2016.05.007.

[18] B. C. Hollings and A. Centre, "C Ritical S Uccess F Actors for," *Engineering*, vol. 125, no. June, pp. 142–150, 1999.

Simulation-based Reinforcement Learning Approach towards Construction Machine Automation

K. Matsumoto[a], A. Yamaguchi[a], T. Oka[a], M. Yasumoto[a], S. Hara[b], M. Iida[b] and M. Teichmann[c]

[a]Araya inc., Japan
[b]Information Services International-Dentsu, Ltd., Japan
[c]CM Labs Simulations, Canada
E-mail: matsumoto_k@araya.org, atsusysw@araya.org, t.oka@araya.org, yasumoto@araya.org, shara@isid.co.jp, iida.michitaka@isid.co.jp, marek@cm-labs.com

Abstract –

Research towards automation of heavy construction machines for efficient and safe construction processes that are robust to various environments and disturbances has been conducted for many years. In this paper, we show two contributions towards this objective. Firstly, we explore the use of reinforcement learning to automate construction machines. Secondly, we evaluate the effectiveness of three methods to reduce learning time of reinforcement learning: designing reward function, pre-training with BC, and changing frame-skip rate. The reinforcement learning approach is expected to gain robustness against disturbances through learning. We run experiments on two different realistic tasks. The first task is to reduce sway of a load suspended from a mobile boom crane, behaving as a single pendulum. The second task is to load an excavator bucket with soil with a hydraulic excavator. We demonstrate the effectiveness of algorithms using the reinforcement learning approach on the commercial simulator, Vortex Studio developed by CM Labs Simulations.

Keywords –

Reinforcement Learning; Imitation Learning; Automation; Autonomous; Simulation

Figure 1. A construction machine that performs tasks in a simulator. Anti-sway crane (left). Load the soil with excavator (right).

1 Introduction

For many years, automation of heavy construction machines has been studied to improve safety, work productivity, and construction quality. However, it has been pointed out that even recent studies lacks consideration of model uncertainties [1], parameter variations, and disturbances [2].

Reinforcement learning combined with neural networks has been shown to be an effective framework for solving complex problems. In reinforcement learning, an agent interacts with the environment through trial and error and learns the optimal control method based on signals from the reward function. Various problems in robotics are naturally expressed as reinforcement learning problems [3]. Using reinforcement learning, robots can autonomously find optimal movements and gain robust movement by gaining experience in dealing with various disturbances.

Reinforcement learning has had a great success in the game field [4], but is more difficult to apply in robotics [5]. Since reinforcement learning improves the controlling policy in an incremental manner, an initial movement is almost like a random movement, which can be sometime dangerous in the real-world tasks. Furthermore, agents need to learn in a wide variety of environments in order to prevent over-fitting to the specific environment and improve the robustness against the environment changes. However, this type of learning requires a lot of time and cost to prepare such environment in the real world.

A simple way to solve the above problem is to use a simulator [6][7]. One can easily create a wide variety of environments and simulation is completely safe i.e. the virtual construction machine will never be damaged even if it accidentally crashes in the learning phase. We chose to use Vortex Studio as a simulator which is specialized in construction machine models and can perform high-precision physical simulations quickly.

The biggest problem we face when using

reinforcement learning is sample efficiency. Generally, more than millions trial and error iterations are required to achieve human-level performance. Although simulators can generally run tasks much faster than real time, it still needs a couple of weeks to complete learning which hinders the efficiency of experiments.

Various reinforcement learning algorithms have been proposed to improve sampling efficiency such as distributed learning [8][9][10], transforming or adding reward functions such as reward shaping[11] and intrinsically motivated function[12], mixing imitation learning and reinforcement learning [13] and changing frame-skip, the number of frames an action is repeated before a new action is selected [14].

In this paper, we define two tasks for the construction machines and apply reinforcement learning for these tasks. We also introduce and evaluate some of the techniques for improving sample efficiency. In order to implement these techniques, we made some modification to the Vortex Studio simulator, which was originally not intended for reinforcement learning use and convert it to a "Reinforcement learning ready" simulator. In this paper, our contributions are:

- We introduce reinforcement learning for the following two tasks as shown in Figure 1: The first task is to reduce sway of a load suspended from a mobile boom crane, behaving as a single pendulum. The second task is to load an excavator bucket with soil with a hydraulic excavator. We show that reinforcement learning is one of the effective methods that can perform as well as humans in the automation of construction machine.
- We evaluate the effectiveness of the three methods to improve sample efficiency for reinforcement learning: designing reward function, pre-training, and changing frame-skip rate.
- We provide examples of practical methods on how to parallelize learning when applying reinforcement learning algorithms to domain-specific simulators that are not for reinforcement learning.

The paper has been organized as follows. Section 2 describes the fundamental concept of reinforcement learning. Section 3 describes the methods applied to improve sample efficiency. In Section 4, we describe the detail setup of the experiments. In Sections 5, we mention some considerations and ideas for performing high-speed learning with a simulator that is not built for reinforcement learning. In Section 6, we describe the experimental results performed on crane or excavator tasks. Section 7 presents the summary and conclusions of this paper and discusses future work.

2 Preliminary

2.1 Reinforcement learning

In this section, we provide a definition used in reinforcement learning [15] focusing on the case the environment E as a finite-state Markov decision processes (MDP). An agent maximizes cumulative rewards by selecting an optimal action from all actions $A = \{a^1, \dots, a^k\}$ an agent can select, in discretized timesteps in some state $s \in S$ of an environment E,where k is the number of actions the agent has. Rewards are the criteria by which an agent learns good or bad behavior. At every timestep t, an agent takes an action $a_t \in A$ when in state s_t. After that, an environment transitions to next state s_{t+1} by transition function $s_{t+1} = T(s_t, a_t)$ and the agent gets a reward $r_t = R(s_t, s_{t+1})$ where T gives the state transition and R gives the reward. To evaluate how much the action performed in a certain time step has contributed to the total cumulative reward, we consider the estimated reward

$$G_t = r_{t+1} + \gamma r_{t+2} + \cdots + \gamma^{T-t-1} r_{\mathrm{T}} = r_{t+1} + \gamma G_t \quad (1)$$

, where $\gamma \in (0, 1]$ is the discount factor, and T is the time when the episode ends. An agent learns a policy $\pi(s_t)$ that maximize cumulative expected rewards until the end of episode. In reinforcement learning, an optimal policy $\pi^*$is obtained by interacting with the environment until the action-value function

$$Q_\pi(s_t, a_t) = \sum_{s_{t+1}} T(s_t, a_t)\,(R(s_t, s_{t+1}) + \gamma G_{t+1}) \quad (2)$$

converges.

Generally, it is difficult to model real transition functions T. The use of model-free algorithms to approximate action-value function

$$Q_\pi(s_t, a_t) \approx R(s_t, s_{t+1}) + \gamma \max_{a_{t+1}} E[Q_\pi(s_{t+1}, a_{t+1})] \quad (3)$$

is now mainstream [16].

In this paper, we use the PPO algorithm[9], which is well known as the stable model-free algorithm and support distributed learning. Distributed learning is the way to learn effectively by replicating the agent and the environment, having the agents act in each environment and gaining a lot of experience. With distributed learning we can speed up the learning. The algorithms in [9] is composed of Actor-Critic network architecture. Actor-Critic is common methodology for Critic to encourage Actor to update the policy, and there are various implementations such as making the Actor and the Critic in different networks or sharing a part of the network.

2.2 Imitation learning

Imitation learning is another approach to create an agent. It learns an optimal policy from demonstrations of expert human by imitating. A simple approach to imitation learning is behavior cloning (BC) [17], which learns a policy from demonstrations of successful behavior through supervised learning.

Pure imitation learning methods cannot exceed the capabilities of the demonstrations. In addition, a huge number of demonstrations is required when applying it to actual tasks because it is not possible to respond to scenes that are not in the demonstration.

Imitation learning can also be used to boost the learning efficiency of reinforcement learning by using the learned policy of BC as an initial policy of reinforcement learning.

3 Method

In this section, we describe three methods to improve the sample efficiency of reinforcement learning in detail. All of these methods are ways to simplify the state space that the agent explores. Figure 2 shows how the state space is simplified by each method. Even if the state space is continuous, the reachable state space is discretized by time, so we represent the state space by grid world.

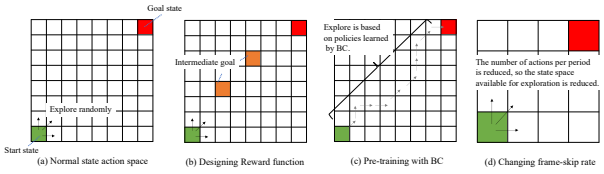

Figure 2. State space is how simplified by each method.

3.1 Designing Reward function

The simplest form of reward is a binary reward, that is, an agent gets a positive reward when an agent achieves the desired state at the end of an episode, otherwise a negative reward. This form of reward leads an agent to get desired policy. The problem with this reward is that the agent is essentially exploring by random actions at first, and therefore cannot learn good behavior at all until the agent is able to earn the reward. This is especially problematic when the state space or action space is large, as it takes longer to explore and the possibility that the agent gets a reward is lower.

To avoid this problem, there is a way to give a reward at each action or state that will lead to the final goal. This type of reward is called as a dense reward. While this can improve learning speed, you need to design dense reward function carefully otherwise the learned behavior may be different from what we actually want.

In this paper, we presented two results for each task: sparse reward and dense reward.

3.2 Pre-training with BC

In general, RL uses random behavior as an initial policy, which is one of the reasons for low sample efficiency of the RL algorithms. As mentioned in 2.2, exploration can be performed efficiently by properly initializing the policy using imitation learning[13].

In this paper, we combine BC [17] with the PPO algorithms[9]. Unlike [13], we use the model trained in BC as the initial value of the model for reinforcement learning.

3.3 Changing frame-skip rate

Another way to speed up learning is to change the frame-skip rate[14]. Frame skipping is the technique to repeat the same action for several frames. Increasing the frame-skip rate has the effect of coarsening the granularity of action. The coarsening of the granularity of the action reduces the state that can be reached within a certain time step. As a result, the combination of state and action spaces is reduced, which simplifies the task.

Increasing the frame-skip rate will also be very important when applying reinforcement learning to real construction machines because it allows the granularity of a single action choice to be changed and the overall action to be smoother. Increasing the frame-skip rate reduce not only productivity but also fuel efficiency and machine fouling and wear. However, simply increasing the frame-skipping rate does not allow for fine-grained action, and thus does not explore the state space that makes the task successful and may prevent agents from achieving their goals. Trade-offs between fineness of action and learning time should be considered, depending on the task and state in order to decide the appropriate number of frame skips. In this paper we tried two patterns about frame-skip rate, no frame skip and 19 frame skips.

4 Experiments

In our experiments we aim at answering the following questions:

1. Does reinforcement learning work to solve realistic construction machine tasks?
2. Which is the most effective method to reduce learning time?

We evaluate our approach on two different realistic construction tasks, anti-sway crane and loading the soil with an excavator. We used the stable baselines framework [18] as the basis for our implementation in

this experiment. The network architecture of our system is depicted in Figure 3. Both policy network and value network have 3 fully connected layers, and each network are independent.

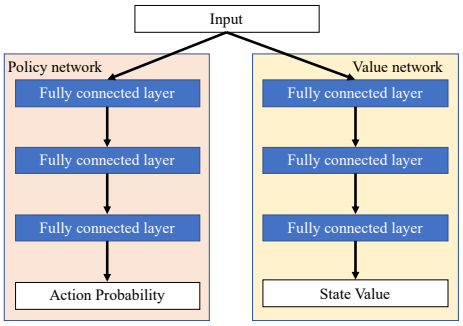

Figure 3. The network architecture of our system.

The Learning is performed on a single machine with an Intel Core i7-8700 and GeForce GTX 1070.

The hyperparameters we used, are same as the default values defined in [18].

4.1 Simulators

CM Labs' Vortex Studio provides a virtual environment for real-time simulation of complex multibody systems. In Vortex, each rigid body is formulated using six degrees of freedom, and these bodies can be connected with several constraint types with varying numbers of linear and/or angular degrees of freedom. The toolkit supports equality as well as inequality constraints, e.g., contacts, which can be holonomic or nonholonomic. Vortex employs the method of Lagrange multipliers together with a direct solver and a semi-implicit integration scheme for stable and fast multi-body simulation. With its optimized core for fast and real-time simulation and its advanced graphical capabilities, Vortex has various applications including operator training, mission planning and design. Furthermore, there are some modules provided in Vortex for particular applications. We used the Cable system module and the Earthwork system module for this study which differentiates Vortex Studio from other real-time simulations [19].

4.1.1 Vortex Cable system simulation

Vortex Studio's Cable Systems provides a realistic simulation of heavy-equipment cables. These extended capabilities ensure real-time behavior by allowing cables to adjust to bends while distributing mass and forces correctly. It can predict cable behavior with minimum number of segments to simulate, which the number of segments changes depending on the curvature of the cable using Adaptive Cable method. This allows Vortex to consider all bending/axial/torsion stiffness and damping to simulate the real cable behavior without falling behind the time step as required by real-time simulation.

4.1.2 Vortex Earthworks system simulation

The Vortex Earthwork Systems module is tailored to the needs of high-fidelity, real-time earth-moving simulations, and employs physically based soil deformation algorithms. Terrain deformations, caused by earth-moving tools such as buckets, and the corresponding terrain reaction forces, are captured in real-time and full two-way force coupling with other simulation entities is modelled. The interactions between machine and soil are fully simulated, allowing soil to be cut, compressed and spilled, all inside an interactive environment by using a hybrid particle-based and mesh-based soil simulation method [20].

4.2 Task 1: Crane

In this task, the goal is to control the relative position shift and speed of the suspended load (the rotation of the load is not taken into account in this experiment) as shown in Figure 4, so this crane is regarded as a single pendulum.

Figure 4. At first, the load suspended by the crane is intentionally shaken a certain amount. After a certain time, the operational agent reduces sway of a load suspended from a mobile boom crane.

4.2.1 Experimental setup

We model the components of the crane task as shown in Figure 5. In this figure, x_{diff} and y_{diff} are distance between boom tip coordinate to load center coordinate, $|v|$ is absolute value of speed of the load, $|a|$ is acceleration of the load. We stack these 4-dimensional data for 3 timesteps and use them as input for reinforcement learning model.

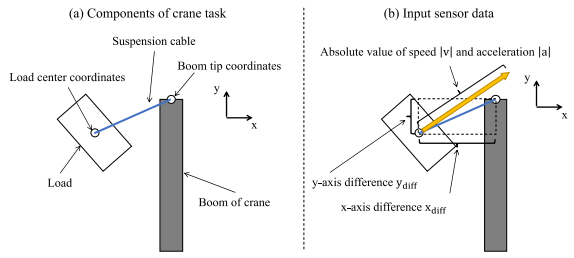

Figure 5. (a) Components of crane task (b) Input

sensor data.

We define the agent actions as elevation and boom as shown in the Figure 6. While PPO [9] can handle both continuous and discrete action spaces, we use the discretized elevation action out of 3 and the discretized boom action out of 5. The reason to use the discretized action is to speed up the learning.

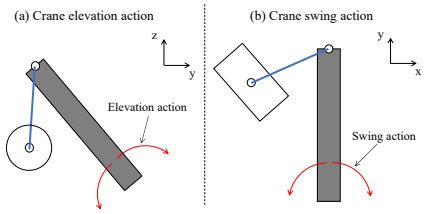

Figure 6. (a) Crane elevation action (b) Crane swing action.

We set one episode to consist of a maximum of 600 steps to use the framework of reinforcement learning. We define the episode success condition as maintaining $|x_{diff}|$ and $|y_{diff}|$ below 1.5 m and speed $|v|$ below 1.5 m/s for 60 steps. We define the episode failure conditions as follows:

- The acceleration of the suspended load exceeds a certain threshold
- The suspended load collides with another object (ground or crane body)
- 600 timesteps elapse without reaching episode success condition

4.2.2 Method detail

Details of each method to be compared in the crane task are presented below.

Base condition: We define the base method as follows:

- $+1.0$ reward when episode reaches success condition, and -1.0 reward when episode reaches failure condition (sparse reward)
- Learning starts from scratch (random actions)
- No frame-skip

Designing reward function: We design the dense reward function as follows:

- For every step, reward is given according to the following function

$$r_t = \frac{1.0}{\max\left(1, \sqrt{x_{diff}^2 + y_{diff}^2}\right)} \quad (3)$$

- $+(960 - current\ step)$ reward when episode success condition
- -1.0 reward when episode failure condition

Pre-training with BC: We do not attempt pre-training with BC because the algorithm in [18] doesn't support BC with multi-discrete actions.

Changing frame-skip rate: We change frame-skip rate to 19.

4.3 Task 2: Excavator

In this task, the goal is to load more soil in a single excavation with a hydraulic excavator as shown in Figure 7.

Figure 7.The agent operates only the bucket part. The agent scoops as much soil as possible in accordance with the movement of the excavator that follows a certain trajectory.

4.3.1 Experimental setup

We model the components of the excavator task as shown in Figure 8. In this figure, y_{diff} and z_{diff} are distance between the excavator body to the bucket, v_y and v_z are value of speed of the bucket, n is an actuator force of the bucket cylinder, θ is a bucket angle, w is the Weight of the soil in the bucket. We stack this 7-dimensional data for 3 timesteps and use them as input for reinforcement learning model.

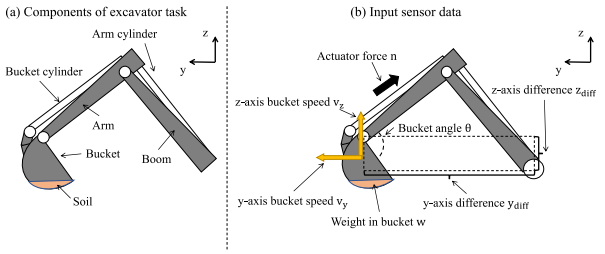

Figure 8. (a) Components of excavator task (b) Input sensor data.

We define the agent bucket action as shown in Figure 9. We discretize the bucket action into 11 values.

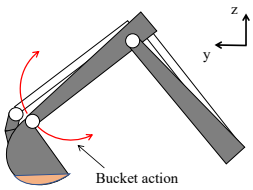

Figure 9. Excavator action.

We set one episode to consist of up to 460 steps to use the framework of reinforcement learning. We define the episode success condition to be $w \geq 1800$ after 460 steps have elapsed. We define the episode failure condition to be the lack of satisfaction of the success condition after 460 steps have elapsed.

4.3.2 Method detail

Details of each method to be compared in the excavator task are presented below.
Base condition: We define base method as follows:

- $+w/1800$ reward when episode reaches success condition, and -1.0 reward when episode reaches failure condition (sparse reward)
- Learning starts from scratch (random actions)
- No frame-skip

Designing reward function: We design the dense reward function as follows:

- Every step, $+1.0$ reward is given when $w \geq 1800$
- $+w/1800$ reward when episode success condition is satisfied
- -1.0 reward when episode failure condition is satisfied

Pre-training with BC: To perform pre-training with BC, we collected 120 expert demonstration data on the simulator.
Changing frame-skip rate: We change frame-skip rate to 19.

5 Implementation

In order to implement distributed learning with Vortex simulator, we consider three options, as shown in the Figure 10.

Figure 10. (a) Launching multiple processes on a single machine. (b) Creating multiple environments on a single physical simulator process. (c) Provide multiple machines on which the physical simulator process can run.

There are cases that GUI operation is the only way to advance the time of the simulator. In this case, Method 1 take much time due to the interaction with the GUI, but this can be resolved by using the Vortex python language scripting API to run the simulation. However, each process of the multiple simulators needs memory and CPU which requires a high-performance computer.

Method 2 needs only one process, so it is efficient in terms of memory and CPU. However, if the simulator is unable to reset each separate environment in the process to its initial state individually (synchronous parallel environment) as in Vortex, one needs to develop a new function module to summarize the environment state in the process because it is a requirement of the OpenAI gym interface, which is de facto interface and is assumed by many reinforcement learning frameworks. Moreover, as shown in the Figure 10, in the case of synchronous parallel environments, unlike asynchronous parallel environments, all environments need to reach the end of the episode. This may lead to a deterioration of the sample efficiency.

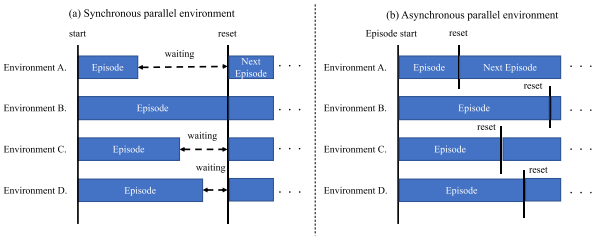

Figure 11. Progress of episodes in synchronous and asynchronous parallel environments

Method 3 is very simple but requires multiple computers.

Method 1 or 2 and Method 3 can be used together, and faster learning is expected. In our experiment, we adopt Method 2, which requires the lowest machine cost and is expected to achieve better performance than Method 1.

Note that Vortex simulator plan to develop an asynchronous parallel environment, so it will resolve the problem of sample efficiency in the future.

6 Results

In this section, we evaluate how each method contributes to each task success rate and learning speed. The results are showed in the Figure 12. The success rate is measured through 100 trials. We also show the task

success rate using the best performance model after learning. Table 1 shows the best success rate for each method on the simulator.

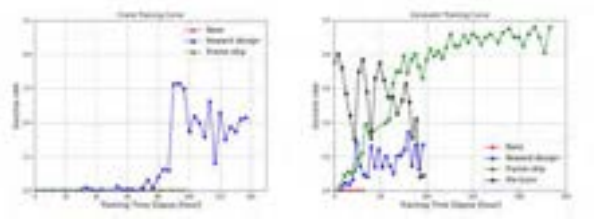

Figure 12. Learning efficiency for each method (left) crane (right) excavator

Table 1. Task success rate

Task	Success rate by methods, %			
	Base	Designing Reward function	Pre-training with BC	Changing Frame-skip
Crane	0	63	-	0
Excavator	0	34	80	96

6.1 Base condition

In both tasks, the base condition had no success, while other methods are starting to succeed at the same point in learning time. This indicates that the base condition needs more learning time and the other methods make learning more efficient.

6.2 Designing the reward function

In the crane task (see Figure 12 left), this method was the only one that worked. It reached about 60% success rate, and then the success rate dropped off. And also, in the excavator task (see Figure 12 right), this method had about 30% success rate. This indicates that the designed reward function is not directly related to the success of the task.

6.3 Pre-training with BC

Pre-training with BC took almost 1 hour wall-clock time to converge. In the early stages of learning, BC gave a high performance, but as the learning progressed, the performance gradually decreased. We believe that it is because the form of reward is different between BC and PPO.

6.4 Changing Frame-skip

The frame skip method achieved 96% success rate in the excavator task, whereas the crane task did not succeed at all. This indicates that the exploration for a good frame skip rate for each task or scene will yield good results.

7 Conclusion & Future work

In this paper, we demonstrated through simulations that reinforcement learning works effectively for two tasks: reducing sway of a load suspended from a mobile boom crane and loading an excavator bucket with soil with a hydraulic excavator. In addition, we confirmed the effectiveness of three methods to reduce learning time of reinforcement learning: designing the reward function, pre-training, and changing frame-skip rate. Finally, we provided examples of practical methods on how to parallelize learning when applying reinforcement learning algorithms to domain-specific simulators that were not originally designed for reinforcement learning.

In future work, we intend to compare our reinforcement learning algorithms with an existing control method on simulation. We also consider that the current learning on simulation is not tolerant to transfer to the real world. In recent years, methods to close the reality gap has been widely studied [21][22][23]. It is necessary to apply these methods to smoothly transfer learning result of simulation to real world operation.

References

[1] S. Dadhich, U. Bodin, and U. Andersson, Key challenges in automation of earth-moving machines. Automation in Construction, 68:212-222, 2016.

[2] L. Ramli, Z.Mohamed, A. M. Abdullahi, H. I. Jaafar, and I. M. Lazio, Control strategies for crane systems: A comprehensive review. Mechanical Syst-ems and Signal Processing, 95:1-23, 2017.

[3] J. Kober, J. A. Bagnell, J. Peters, Reinforcement Learning in Robotics: A Survey, The International Journal of Robotics Research, 32.11: 1238-1274, 2013.

[4] V. Mnih, K. Kavukcuoglu, D. Silver, A. Graves, L. Antonoglou, D. Wierstra, and M. Riedmiller, Playing Atari with Deep Reinforcement Learning, arX-iv preprint arXiv: 1312.5602, 2013.

[5] L. Tai, J. Zhang, M. Liu, J. Boedecker, and W. Burgard, A Survey of Deep Network Solutions for Learning Control in Robotics: From Reinforcement to Imitation, arXiv preprint arXiv: 1612.07139v4, 2018.

[6] J. García, and F. Fernández, A Comprehensive Survey on Safe Reinforcement Learning, Journal of Machine Learning Research 16.1: 1437-1480, 2015.

[7] D. Amodei, C. Olah, J. Schulman, J. Steinhardt, P. Christiano, D. Mané, Concrete Problems in AI

Safety. arXiv preprint arXiv:1606.06565v2, 2016.

[8] V. Mnih, A. P. Badia, M. Mirza, A.Graves, T. Harley, T. P. Lillicrap, D. Silver, and K. Kavukcauoglu, Asynchronous Methods for Deep Reinforcement Learning. International conference on machine learning:1928-1937, 2016.

[9] J. Schulman, F. Wolski, P. Dhariwal, A. Radford, and O. Klimov, Proximal Policy Optimization Algorithms. arXiv preprint arXiv:1707.06347, 2017.

[10] S. Kapturowski, G. Ostrovski, W. Dabney, J. Quan, and R. Munos. Recurrent experience replay in distributed reinforcement learning. In International Conference on Learning Representations, Louisiana, United States, 2019.

[11] A. Y. Ng, D. Harada, and S. Russell, Policy invariance under reward transformations: Theory and application to reward shaping. *ICML*. Vol. 99:278-287, 1999.

[12] S. P. Singh, A. G. Barto, and N. Chentanez. Intrinsically motivated reinforcement learning. In Advances in neural information processing systems: pages 1281–1288, 2005.

[13] T. Hester, M. Vecerik, O. Pietquin, M. Lanctot, T. Schaul, B. Piot, D. Horgan, J. Quan, A. Sendonaris, G. Dulac-Arnold, L. Osband, J. Agapiou, J. Z. Leibo, A. Gruslys, Deep Q-learning from Demonstrations. arXiv preprint arXiv:1704.03732, 2018.

[14] A. Braylan, M. Hollenbeck, E. Meyerson and R. MiikkulainenFrame Skip Is a Powerful Parameter for Learning to Play Atari. Workshops at the Twenty-Ninth AAAI Conference on Artificial Intelligence, 2015.

[15] R. S. Sutton, and G. B. Andrew, Introduction to reinforcement learning. Vol. 135. Cambridge: MIT press, 1998.

[16] R. S. Sutton, D. A. McAllester, S. P. Singh, and Y. Mansour, Policy gradient methods for reinforcement learning with function approximation. In Advances in neural information processing systems:1057-1063, 2000.

[17] D. A. Pomerleau, Efficient training of artificial neural networks for autonomous navigation. Neural Computation, 3(1):88–97, 1991.

[18] H. Asheley, R. Antonin, E. Maximilian, G. Adam, K. Anssi, T. Rene, D. Prafulla, H. Christopher, K. Oleg, N. Alex, P. Matthias, R. Alec, S. John, S. Szymon, and W. Yuhuai, Stable Baselines. Online: https://github.com/hill-a/stable-baselines, Accessed: 04/03/2020.

[19] Daniel Holz, Ali Azimi, and Marek Teichmann,Virtual Reality Simulation of Vehicles and Tools Interacting with Deformable Terrain, CM-Labs Simulations Inc.,2012

[20] CM-Labs Simulations Inc., Vortex Studio 2018a Product Capability Specifications, Online: https://cmlabsnew.kamacom.com/vortexstudiodocumentation/Vortex_User_Documentation/Content/Resources/Vortex_Studio_2018a_Product_Specifications.pdf, 06/05/2020.

[21] J. Tobin, R. Fong, A. Ray, J. Schneider, W. Zaremba, P. Abbeel, Domain Randomization for Transferring Deep Neural Networks from Simulation to the Real World. arXiv preprint arXiv:1703.06907, 2017.

[22] X. B. Peng, M. Andrychowicz, W. Zaremba, and P. Abbeel, Sim-to-Real Transfer of Robotic Control with Dynamics Randomization. arXiv preprint arXiv:1804.10332, 2018.

[23] I. Clavera, D. Held and P. Abbeel, Policy Transfer via Modularity. in IROS. IEEE, 2017.

Optimization of Trajectories for Cable Robots on Automated Construction Sites

Roland Boumann, Patrik Lemmen, Robin Heidel and Tobias Bruckmann

University of Duisburg-Essen, Germany
E-mail: {roland.boumann, patrik.lemmen, robin.heidel, tobias.bruckmann}@uni-due.de

Abstract -

In contrast to conventional serial robot arms, a cable robot offers special characteristics which make it predestined for usage in automated construction: Cable robots use a robust and simple mechanical layout, including a frame, motor-driven winches, pulleys and cables connected to the end effector in a parallel kinematic structure. Derived from BIM data, suitable trajectories need to be generated for every payload, e.g. as set values for the robot control. This paper focuses on the generation and optimization of such trajectories, considering several requirements and optimization criteria, using a hybrid particle swarm algorithm for global optimization. The optimization costs include transportation time, cable forces, collision avoidance, stiffness and movements of the pulleys. Some of these criteria are in conflict of aims, e.g. a short transportation time and low cable forces, which is resolved by weights in the cost function.

Keywords -

Cable Robot; Optimization; Path Planning; Construction

1 Introduction and State of Art

Over the last decades, repeatedly, the automation of bricking was considered. Projects in the 1990s, such as ROCCO, with a payload of around 500 kg and a range of up to 8.5 m [1], and BRONCO [2], use modern and economic approaches, using conventional industrial robots, partly on mobile platforms.

At ETH Zurich, mobile platforms have also been equipped with robot arms to investigate automated construction processes, initiated by Gramazio and Kohler in 2011. Different sensor concepts and tools were tested in installations such as “Endless Wall”, “Stratifications” and “Fragile Structure” [3, 4].

Currently, the Australian company Fastbrick Robotics is developing large manipulators called Hadrian and HadrianX , which are designed to bring building blocks along a large manipulator arm via belt conveyors to a desired position on the building site, using special bricks.

In parallel, the American company Construction Robotics LLC offers the SAM (Semi-Automated Mason). SAM employs a conventional serial robot on a movable platform or mounted on a large manipulator to achieve all the necessary poses on the construction site. According to Brehm [5], SAM is designed as a semi-automated system that is able to increase the productivity of a bricklayer by a factor of five, whereby the bricklayer is still responsible for creating the calibrating layer, the joints and setting the corners. SAM works with small-format bricks with grouted butt joints, which are applied using the dipping method.

2 Concepts for Bricking using Cable Robots

To construct a building by a robot, the size of the required workspace is supposed to be one of the dominant technical challenges. Here, cable robots offer outstanding advantages in terms of workspace size, stiffness, modularity and mobility [6, 7, 8]. Currently, first feasibility studies on cable robots for application in bricking have been done in lab scale. To extend this to practical full scale experiments, recently projects have been initiated that face specific technical challenges for the prototype, which are discussed here in short.

To allow for fast assembly and dismantling, and easy adaption to variable dimensions of the building to be constructed, the frame of the cable robot providing suspension of the end effector must consist of lightweight modular elements. Still, stiffness and constructive accuracy should not be less than with a fabricated steel construction. Here, good calibration procedures for setting up the geometric parameters (e.g. pulley positions) are needed in the future. Furthermore, the lower cable deflection pulleys – see Figure 1 – must be vertically movable in order to avoid collisions between cable and building during the construction process with a growing building structure. For good model accuracy – and thus for good positioning accuracy of the system – the guides of the deflection pulleys must be correspondingly precise.

Furthermore, the robot’s end effector – realized as a platform connected to the cables, carrying the brick gripper and a set of sensors – needs a home position, e.g. for revision purposes. As the ground is blocked by the building, it is necessary to construct a set-down position on the upper frame structure.

Another component specifically to be developed for this application is the brick gripper. For the exact positioning

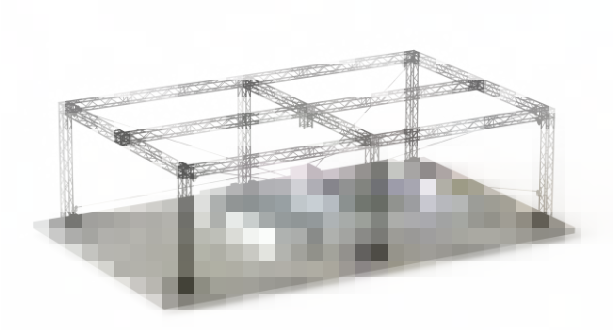

Figure 1. Principal CAD drawing of a cable robot for automated construction sites

of the brick, the brick must be gripped in a precisely defined way in order to guarantee a defined brick placing process. A sophisticated sensor concept for detecting both the stone to be gripped, as well as the objects and bricks already placed, is essential. In addition, the stone gripper must generate the gripping force passively to avoid the brick falling down in the event of power loss. Still, a form-fit gripping of the stone is not possible when using conventional bricks and mortar to be applied to the brick.

The use of a cable robot on a site also places special demands on the protection class of any components. The robot must be designed to be protected against dust and dirt and the influence of different weather conditions. The safety concept for working on a construction site must also be reviewed, which may require the design of new functions, such as the self-locking gripper.

3 Methodology

While the realization of the prototype components is a complex mechatronic task, another open issue is the model-based optimization of the robot and its behaviour. In this work and as a first step, the motion of the end-effector as well as the motion of the lower four cable deflection pulleys is optimized for the bricking process. This is resolved by a comprehensive physical model discussed in this work, and the careful formulation of a numerical optimization problem.

4 Numerical Optimization Approach

To be able to optimize the cable robot behaviour for bricking, its physics and properties will be modeled in the next sections.

The numerical optimizers to be used base on defining a vector of scalar parameters to be optimized, their boundaries and a scalar cost function. Thus, the properties to be optimized need to be modeled and evaluated resulting in a scalar cost function for each property. The formulation of those scalar cost functions will be given in the following.

Noteworthy, the different cost functions, each representing a property to be optimized, need to be merged. In this work, the multiobjective optimization is resolved by simply adding the single cost values $\mathcal{V}_\chi$ using weights $\mathcal{W}_\chi$ where all properties changing along a robot motion are discretized in n_s time steps, see section 5.

Some properties are subject to physical limits. As some of them are not parameters but result of the models to be developed, the question of considering those boundaries arises. Thus, this work uses penalty terms $\mathcal{P}_\chi$.

Accordingly, the total cost $\mathcal{V}_{\text{total}}$ is computed by summarizing the costs and penalties for all properties χ over all n_s time steps .

5 Trajectory Modeling

The trajectory describes the motion of the robot as a path defined over time. Accordingly, it covers information on pose, velocity and acceleration. Hence, a model for the description of these quantities must be found that allows a parametrization by the numerical optimizer. Here, splines – i.e. a composition of interconnected polynomials – are a popular choice. Within this work, only the platform position $\boldsymbol{r_P}$ with three degrees-of-freedom (DOF) as well as the lower four pulley positions $\boldsymbol{s}$ may change over time and thus are described by splines. As shown in table 1, for the platform position, six parameters per DOF are added to the optimization variables, resulting in 18 parameters for the description of the translational movement in three DOF. Note, rotations are not performed. Additionally, per segment a time duration $t_k, k = 1, 2, 3$, is defined as an optimization parameter, which adds three parameters. Resulting, the vector of optimization parameters contains 18 + 3 = 21 elements subject to numerical optimization.

Four parameters per pulley are added to the optimization variables, resulting in 16 parameters for the description of the movement of the four lower pulleys. The segment times are copied from the platform motion. Summarizing, 21 + 16 = 37 parameters are used in the numerical optimizer.

To evaluate the properties of the robot along a motion described by these splines, each spline needs to be discretized. Let $\dot{s}_i(q), i \in \{1, 2, 5, 6\}$, be the velocity of the lower pulleys along the linear axis at the q^{th} discretization step of one spline segment, n_{s_k} be the number of discretization points along one spline segment and n_k the number of spline segments.

While $\boldsymbol{r}_P$ and $\boldsymbol{s}$ as well as their temporal derivatives can be efficiently bound at the knots by limits (see table 3), they need to be bound along the whole trajectory as well. Thus, they are checked on each step and penalty terms $\mathcal{P}_{\text{traj}}$ and $\mathcal{P}_{\text{pulleys}}$, respectively, are associated. Noteworthy, as high robot dynamics per se are desirable, but already reflected by time, $\mathcal{V}_{\text{traj}} = \mathcal{W}_{\text{traj}} = 0$.

Table 1. Description of spline and optimizer parameters.

	Start (1st knot)	2nd knot	3rd knot	Goal (4th knot)
Spline segment	1	2	3	
Platform position; one spline per DOF; i.e. three splines in total				
Spline order	7	7	7	
Constraints	$\boldsymbol{r}_P$ is given; $\dot{\boldsymbol{r}}_P, \ddot{\boldsymbol{r}}_P, \dddot{\boldsymbol{r}}_P$ are set to zero	$\boldsymbol{r}_P, \dot{\boldsymbol{r}}_P, \ddot{\boldsymbol{r}}_P$ are parameters, $\dddot{\boldsymbol{r}}_P$ is set to zero	$\boldsymbol{r}_P, \dot{\boldsymbol{r}}_P, \ddot{\boldsymbol{r}}_P$ are parameters, $\dddot{\boldsymbol{r}}_P$ is set to zero	$\boldsymbol{r}_P$ is given; $\dot{\boldsymbol{r}}_P, \ddot{\boldsymbol{r}}_P, \dddot{\boldsymbol{r}}_P$ are set to zero
$\sum$ of constraints per DOF	4	4	4	4
$\sum$ of optimization parameters in total	0	3×3	3×3	0
Pulley position; one spline per pulley; four splines in total				
Spline order	3	5	3	
Constraints	$\boldsymbol{s}$ is a parameter; $\dot{\boldsymbol{s}}, \ddot{\boldsymbol{s}}$ are set to zero	$\boldsymbol{s}$ is a parameter; $\dot{\boldsymbol{s}}, \ddot{\boldsymbol{s}}$ are computed from first segment	$\boldsymbol{s}$ is a parameter; $\dot{\boldsymbol{s}}, \ddot{\boldsymbol{s}}$ are computed from last segment	$\boldsymbol{s}$ is a parameter; $\dot{\boldsymbol{s}}, \ddot{\boldsymbol{s}}$ are set to zero
$\sum$ of constraints per pulley	3	1 (1st segment); 3 (2nd segment)	1 (last segment); 3 (2nd segment)	3
$\sum$ of optimization parameters in total	4×1	4×1	4×1	4×1

To avoid collisions (see section 6.3), a reconfiguration of the cables might be necessary. Yet, in terms of power consumption, all movements of the pulleys require energy and are thus associated with costs. A detailed dynamic modeling of the pulley movement is neglected in this paper. For simplicity, viscous friction with a friction constant μ_f is assumed and results in costs for movement of the pulleys, scaled down to one pulley.

$$\mathcal{V}_{\text{pulleys}} = \frac{1}{4} \sum_{k=1}^{n_k} \sum_{q=1}^{n_{s_k}} \left(\|\dot{s}_1\| + \|\dot{s}_2\| + \|\dot{s}_5\| + \|\dot{s}_6\| \right) \mu_f \quad (1)$$

As the robot motion should be completed as fast as possible, the segment durations t_k can be simply summarized to the total time t_{total}. The cost function $\mathcal{V}_{\text{time}} = \left(t_{\text{total}} - n_k\, t_{\min}\right) \frac{1}{n_k\, t_{\min}}$ computes a value with respect to the smallest possible time. Furthermore, it puts this difference in relation to the smallest possible time, which allows an interpretation. The minimum reachable cost value is zero. As all t_k are directly defined as optimization parameters, their limits (see table 3) can be directly considered by the optimizer avoiding penalty terms, i.e. $\mathcal{P}_{\text{time}} = 0$.

6 Modeling

6.1 Kinematics and Dynamics

The cable robot, as shown in Figure 2, is referenced in the inertial coordinate system $\mathcal{B}$. The end-effector carries the platform-fixed coordinate-system $\mathcal{P}$. The

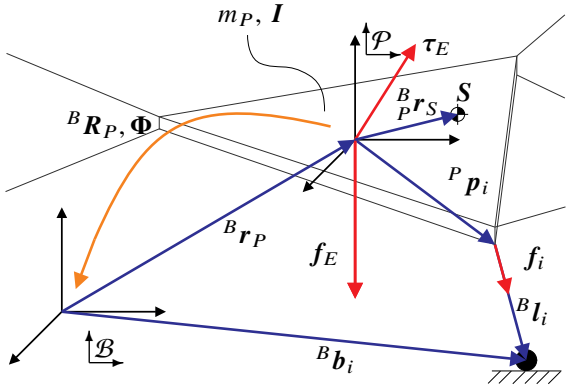

Figure 2. Cable-robot model parameters

robot is driven by m cables and has n degrees-of-freedom and therefore a redundancy of $r = m - n$. The posture in the inertial coordinate-system, consisting of position ${}^B\boldsymbol{r}_P$ and orientation $\boldsymbol{\phi}$ of the platform, is ${}^B\boldsymbol{x}_P = [{}^B\boldsymbol{r}_P\ \boldsymbol{\phi}]^{\mathrm{T}}$. The rotation matrix ${}^B\boldsymbol{R}_P$ describes the orientation of the platform with respect to $\mathcal{B}$, in the means of roll-pitch-yaw angles. ${}^B\boldsymbol{l}_i$ are the cable vectors, obtained by the inverse kinematic.

$${}^B\boldsymbol{l}_i = {}^B\boldsymbol{b}_i - \underbrace{({}^B\boldsymbol{r}_P + {}^B\boldsymbol{R}_P\, {}^P\boldsymbol{p}_i)}_{{}^B\boldsymbol{p}_{B_i}}, \quad 1 \le i \le m \quad (2)$$

The cables enter the workspace at the end of the base vectors ${}^B\boldsymbol{b}_i$, which are derived by using inverse pulley kinematics, see [9]. As introduced, the system can be

reconfigured by moving the pulleys along a straight line in vertical direction. The attachment points of the cables at the platform are ${}^{P}\boldsymbol{p}_i$. The cable force vector $\boldsymbol{f} \in \mathbb{R}^{m\times 1}$ contains all cable forces f_i in direction $\boldsymbol{v}_i$ of each cable i. Every i^{th} cable exerts the tension $\boldsymbol{f}_i$ on the platform.

$$\boldsymbol{f}_i = f_i \cdot \frac{\boldsymbol{l}_i}{\|\boldsymbol{l}_i\|_2} = f_i \cdot \boldsymbol{v}_i, \quad 1 \le i \le m \tag{3}$$

The static force equilibrium at the platform is given by

$$-\boldsymbol{w}_E = \begin{bmatrix} -\boldsymbol{f}_E \\ -\boldsymbol{\tau}_E \end{bmatrix} = \begin{bmatrix} \boldsymbol{v}_1 & \dots & \boldsymbol{v}_m \\ \boldsymbol{p}_1 \times \boldsymbol{v}_1 & \dots & \boldsymbol{p}_m \times \boldsymbol{v}_m \end{bmatrix} \begin{bmatrix} f_1 \\ \vdots \\ f_m \end{bmatrix} = \boldsymbol{A}^{\mathrm{T}} \boldsymbol{f}. \tag{4}$$

Herein, $\boldsymbol{A}^{\mathrm{T}}$ is the structure matrix of the robot and the forces and torques at the platform are included in $\boldsymbol{w}$. Setting up Newton-Euler equations [10] in $\mathcal{B}$, one obtains

$$\underbrace{\begin{bmatrix} m_P \boldsymbol{E}_3 & -m_P {}^{B}_{P}\boldsymbol{R}_S \boldsymbol{\mathcal{H}} \\ m_P {}^{B}_{P}\boldsymbol{R}_S & {}^{B}\boldsymbol{\theta}_P \boldsymbol{\mathcal{H}} \end{bmatrix}}_{\boldsymbol{M}(\boldsymbol{x}_P)} \underbrace{\begin{bmatrix} {}^{B}\ddot{\boldsymbol{r}}_P \\ \ddot{\boldsymbol{\phi}} \end{bmatrix}}_{\ddot{\boldsymbol{x}}_P} + \dots$$
$$+ \underbrace{\begin{bmatrix} m_P \left[(\dot{\boldsymbol{\mathcal{H}}}\dot{\boldsymbol{\phi}}) \times {}^{B}_{P}\boldsymbol{r}_S + (\boldsymbol{\mathcal{H}}\dot{\boldsymbol{\phi}}) \times ((\boldsymbol{\mathcal{H}}\dot{\boldsymbol{\phi}}) \times {}^{B}_{P}\boldsymbol{r}_S) \right] \\ {}^{B}\boldsymbol{\theta}_P \dot{\boldsymbol{\mathcal{H}}}\dot{\boldsymbol{\phi}} + (\boldsymbol{\mathcal{H}}\dot{\boldsymbol{\phi}}) \times ({}^{B}\boldsymbol{\theta}_P \boldsymbol{\mathcal{H}}\dot{\boldsymbol{\phi}}) \end{bmatrix}}_{\boldsymbol{K}(\boldsymbol{x}_P, \dot{\boldsymbol{x}}_P)} \dots$$
$$\dots + \underbrace{-{}^{B}\boldsymbol{w}_E}_{\boldsymbol{Q}(\boldsymbol{x}_P, \dot{\boldsymbol{x}}_P)} = {}^{B}\boldsymbol{A}^{\mathrm{T}} \boldsymbol{f}. \tag{5}$$

The mass of the platform is m_p and its inertia tensor is ${}^{B}\boldsymbol{\theta}_P$. $\boldsymbol{E}_3$ is a 3×3 identity matrix. Matrix $\boldsymbol{\mathcal{H}}$ and its time derivative $\dot{\boldsymbol{\mathcal{H}}}$ can be obtained from the kinematic Kardan equations [11]. Matrix ${}^{B}_{P}\boldsymbol{R}_S$ is a transformation matrix between the center of gravity and origin of the platform coordinate system. $\dot{\boldsymbol{x}}_P$ and $\ddot{\boldsymbol{x}}_P$ are the first and second time derivative of the end-effector pose $\boldsymbol{x}_P$. The vector from the platform coordinate system to its center of gravity is ${}^{B}_{P}\boldsymbol{r}_S$. $\boldsymbol{M}(\boldsymbol{x})$ is the mass matrix of the platform, $\boldsymbol{K}(\boldsymbol{x}_P, \dot{\boldsymbol{x}}_P)$ contains Coriolis and centrifugal forces and torques and $\boldsymbol{Q}(\boldsymbol{x}_P, \dot{\boldsymbol{x}}_P)$ holds all remaining forces and torques including gravitational forces, friction and disturbances.

To obtain set point cable forces for the control, based on a desired trajectory, eq. (5) needs to be solved for $\boldsymbol{f}$ with a given $\boldsymbol{w}$. As the cable can only pull put never push, a minimum tension $f_{\min}$ in the cables is necessary. To avoid cable breaks, the cable forces must not exceed a maximum tension $f_{\max}$. Several well-known methods exist to solve this problem [12], which differ e.g. in real-time capability or the resulting force level.

As cable forces correspond to the power usage of the system, low cable forces are desired in terms of costs. Let $\boldsymbol{f}(q)$ be the cable force distribution at the q^{th} discretization point of one spline. Per spline, the magnitude of the cable forces along each spline segment is summarized and then weighted using the time per spline t_k.

$$f_w(k) = \frac{t_k}{t_{\text{total}}} * \frac{1}{n_k} * \sum_{q=1}^{n_{s_k}} \sum_{i=1}^{m} f_i(q) \tag{6}$$

Based on the weighted forces f_w, the average cable force with respect to one cable throughout the whole trajectory is calculated using the total number of discretization points n_s and the number of cables m. Further on, the value gets normalized with respect to $f_{\min}$ to allow for zero costs when the optimal value is reached. The resulting costs for cable forces are

$$\mathcal{V}_{\text{force}} = \Big(\sum_{k=1}^{n_k} f_w(k) * \frac{1}{n_s} * \frac{1}{m} - f_{\min} \Big) * \frac{1}{f_{\min}}. \tag{7}$$

To cope with invalid cable force distributions in the optimization process, a penalty term is added to $\mathcal{P}_{\text{force}}$ as soon as at one time step, the cable forces are beyond the force limits (see table 3) and thus invalid. To allow the optimizer to iteratively resolve disadvantageous trajectories, each additional time step with invalid forces adds another increment to $\mathcal{P}_{\text{force}}$.

6.2 Stiffness

Stiffness is a critical issue for large and elastic manipulators such as cable robots. Assuming a linear behavior, the stiffness can be described by a spring equation such as

$$\delta \boldsymbol{w} = \boldsymbol{K}(\boldsymbol{x}_P) \delta \boldsymbol{x}_P, \tag{8}$$

where $\delta \boldsymbol{w}$ is the reaction force caused by a displacement $\delta \boldsymbol{x}_P$ that occurs due to a stiffness defined in a diagonal matrix $\boldsymbol{K}$, where the latter is determined for a platform position $\boldsymbol{x}_P$. $\boldsymbol{K}(\boldsymbol{x}_P)$ is computed according to [13, 14] as

$$\boldsymbol{K}(\boldsymbol{x}_P) = \underbrace{-\frac{\partial \boldsymbol{A}^{\mathrm{T}}}{\partial \boldsymbol{x}_P} \boldsymbol{f}}_{\boldsymbol{K}_g} + \underbrace{\boldsymbol{A}^{\mathrm{T}} \boldsymbol{K}_l \boldsymbol{A}}_{\boldsymbol{K}_c}, \tag{9}$$

which includes two matrices $\boldsymbol{K}_c$ and $\boldsymbol{K}_g$. $\boldsymbol{K}_c$ denotes the so-called passive stiffness which simply describes the elastic behaviour of the cable and might also include the stiffness of the winch position controller. $\boldsymbol{K}_g$ is the active stiffness of the system. Contrarily to the passive stiffness, it does not depend on elasticity effects such as compliance of a material. Instead, it reflects the attempts of the system to return to its force and torque equilibrium position once the platform is subject to a position disturbance. This behaviour only depends on the geometry and pose of the system, condensed in $\boldsymbol{A}^T$.

Now compliance matrix $\boldsymbol{C}$ allows to compute the displacement for a given disturbance wrench.

$$\delta \boldsymbol{x}_P = \boldsymbol{K}^{-1} \delta \boldsymbol{w} = \boldsymbol{C} \delta \boldsymbol{w} \tag{10}$$

As this includes both translational and rotational motions, a diagonal homogenization matrix $\boldsymbol{J}_v$ according to [15, 16] can be employed, i.e. $\boldsymbol{A}_h^{\mathrm{T}} = \boldsymbol{J}_v^{-1} \boldsymbol{A}^{\mathrm{T}}$, which can be used instead of $\boldsymbol{A}^{\mathrm{T}}$ in eq. (9), allowing to apply eq. (10) to get a homogenized displacement $\Delta \boldsymbol{x}_{Ph}$. The magnitude of this displacement $\kappa = \|\Delta \boldsymbol{x}_{Ph}\|_2$ gives a scalar measure for the stiffness which can be used as part of a cost function. Within this paper, the disturbance force $\boldsymbol{w}$ includes two wrenches: First, the gravity is included as it leads to relevant position deviations, espcially in upper parts of the workspace, see Figure 3 and Figure 4. Second, it includes the influence of constant cross wind of $7 \frac{m}{s}$ (4 Bft), modeled by the drag equation. Cross wind might lead to hardly predictable oscillations of the platform. For both wrenches, a high stiffness is desirable for the generated trajectories to minimize their effects.

Let $\kappa(q)$ be the displacement criterion at the q^{th} discretization step of one spline. The sum of $\kappa(q)$ over one spline segment is weighted using the time per segment.

$$\kappa_w(k) = \frac{t_k}{t_{\text{total}}} * \frac{1}{n_k} * \sum_{q=1}^{n_{s_k}} \kappa(q) \tag{11}$$

Following, the total cost for stiffness throughout the whole trajectory is calculated based on the weighted sum $\kappa_w(k)$.

$$\mathcal{V}_{\text{stiff}} = \sum_{k=1}^{n_k} \kappa_w(k) * \frac{1}{n_s} \tag{12}$$

As there is no bound defined for stiffness is this work, $\mathcal{P}_{\text{stiff}} = 0$. In future work, requiring a minimum stiffness could be easily considered.

6.3 Collision Detection

As cable robots might use a high number of cables, collisions and their avoidance are crucial. The methods in this section were derived from [17, 18]. Within this work, only collisions between the lower cables and obstacles as well as between platform and objects are considered. In this simulation, the only obstacles on the site are the bricks which might be either on a pallet delivered by the supply chain, or already placed as part of the building. Accordingly, the poses of all objects on this simplified site are known. Generally, also collisions between the cables with each other and between cables and platform can be taken into account, but as the application at hand avoids platform rotations and uses a simple geometry – where the corners of the platform are connected to the corresponding corners of the frame, avoiding interference – those cases are neglected.

The employed approach bases on the Separated Axis Theorem as presented by [18]. Here, obstacle bounding volume and end-effector bounding volume are calculated by axis-aligned bounding boxes (AABB).

Using the AABB approach, intersection tests in all axes are simple. Furthermore, the Euclidean distance d between two objects can be determined. Noteworthy, in this work, the distance is measured using two approaches: For measurements between end-effector and obstacles, face-to-face distances $d_{ee}(q)$ are computed. Face-to-center distances are applied for measurements $d_{c_i}(q)$ between each i^{th} cable and obstacles. In case of multiple obstacles, the smallest distance to the nearest obstacle in each discretization step is taken into account for the cost function. If any of the distances falls below the minimum distance $d_{\min}$ or $w_{\min}$ (see table 3), respectively, costs are applied to avoid collisions within the trajectory. To calculate the cost in each discretization step q, the distances d are fed to an arbitrarily chosen nonlinear function

$$\mathcal{D}_{\text{EEOB}}(q) = \left(3(1 - \frac{d_{ee}(q)}{d_{\min}})\right)^3 \tag{13}$$

which avoids the objects getting close to each other. The total costs for collisions between end effector and objects are given by the sum

$$\mathcal{V}_{\text{EEOB}} = \frac{1}{n_s} \sum_{k=1}^{n_k} \sum_{q=1}^{n_{s_k}} \mathcal{D}_{\text{EEOB}}(q). \tag{14}$$

Similarly, the cost for collisions between cables and objects are calculated by an arbitrarily chosen nonlinear function that basically multiplies a weight to eq. (13)

$$\mathcal{D}_{\text{CAOB}}(q) = \sum_{i=1}^{m} \left(3(1 - \frac{d_{c_i}(q)}{w_{\min}}\right)^3 * \frac{1}{10} \tag{15}$$

and summarized as

$$\mathcal{V}_{\text{CAOB}} = \frac{1}{n_s} \sum_{k=1}^{n_k} \sum_{q=1}^{n_{s_k}} \mathcal{D}_{\text{CAOB}}(q). \tag{16}$$

Whenever a step q along the path leads to a collision, penalties $\mathcal{P}_{\text{EEOB}}$ and $\mathcal{P}_{\text{CAOB}}$, respectively, are added each time. This holds for collisions between cables and objects as well as the end effector and objects. To save computation times, all bricks of a completed layer in the building are represented by a common box.

7 Discussion of Results

The models employed and the optimizer were set up using an installation plan for a small building. Table 3 lists

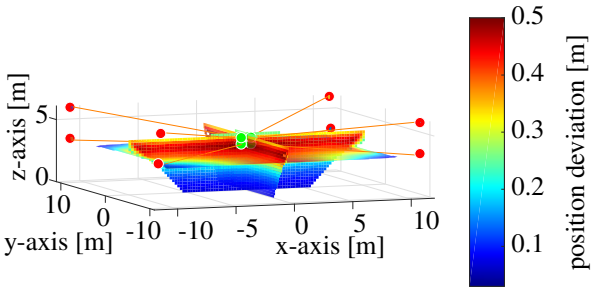

Figure 3. Stiffness in the workspace with lower pulleys upwards. The applied wrench $\delta \boldsymbol{w}$ includes crosswind of $7\frac{m}{s}$ (4 Bft) and platform weight of 100 kg, but no brick.

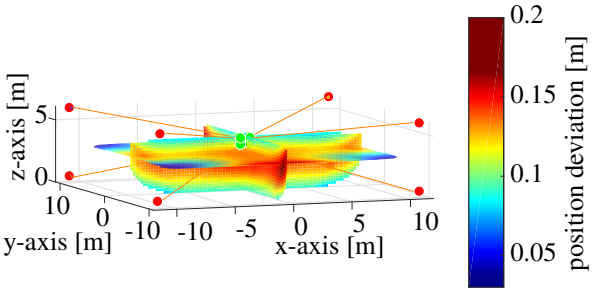

Figure 4. Stiffness in the workspace with lower pulleys downwards. The applied wrench $\delta \boldsymbol{w}$ includes crosswind of $7\frac{m}{s}$ (4 Bft) and platform weight of 100 kg, but no brick.

Table 2. Costs $\mathcal{V}$ and weights $\mathcal{W}$. *a) without stiffness optimization. *b) with stiffness optimization. *c) save overhead trajectory

$\mathcal{V}$	*a	*b	*c	$\mathcal{W}$
$\mathcal{V}_{\text{time}}$	11.8732	11.2863	39.0000	0.5
$\mathcal{V}_{\text{force}}$	2.8247	3.0550	6.0302	1
$\mathcal{V}_{\text{EEOB}}$	0.0001	0.0021	0.0000	1
$\mathcal{V}_{\text{CAOB}}$	0.0000	0.0000	0.0000	1
$\mathcal{V}_{\text{pulleys}}$	0.0338	0.1100	0.0000	1
$\mathcal{V}_{\text{stiff}}$	(0.1234)	0.1205	(0.2237)	50
$\mathcal{V}_{\text{total}}$	8.7952	14.8369	25.5302	
$\begin{bmatrix} t_1 \\ t_2 \\ t_3 \end{bmatrix} =$	$\begin{bmatrix} 0.5894 \\ 0.8683 \\ 2.4043 \end{bmatrix}$ s	$\begin{bmatrix} 0.4747 \\ 1.3457 \\ 1.8655 \end{bmatrix}$ s	$\begin{bmatrix} 3.0000 \\ 6.0000 \\ 3.0000 \end{bmatrix}$ s	

the applied parameters. For computational efficiency during the optimization, only few time steps were used within the prime calculation of the optimizer, see table 3. Noteworthy, for higher accuracy, a final computation including a penalty check was carried out with a increased resolution of $[n_{s_1}, n_{s_2}, n_{s_3}] = [30, 29, 29]$. For the numerical optimization, MATLAB's particleswarm() with a hybrid setting – which basically appends a gradient decent using fmincon() – was chosen. These methods support parallel computing to speed up the simulation. The swarm population size was set to 60 and the maximum iterations to 1000.

Noteworthy, the moving masses of the platform change if a brick is picked. In optimization procedure, mass and inertia of both platform and brick are considered in the dynamics model, transformed with respect to $\boldsymbol{x}_P$ located at the bottom of the brick. The results reflect the compromise found as a consequence of the – partly contrary – cost functions. Under the influence of platform and payload mass in gravity, the lower parts of the workspace are favorable as they provide an advantageous angle of attack for the cables and thus lower cable forces.

A trajectory not considering stiffness is shown in Figure 5. Here, brick no. 300 was arbitrarily chosen, starting its motion at $r_{\text{start}} = [-5.747, -0.876, 0.748]^{\text{T}}$ and placing the brick at $r_{\text{goal}} = [0.0875, 6.922, 0.748]^{\text{T}}$ after a motion time of 3.8619 s.

As introduced in section 4, the total cost function chosen in this work is

$$\mathcal{V}_{\text{total}} = \sum_{\chi} \mathcal{W}_{\chi} \times \mathcal{V}_{\chi} + \mathcal{P}_{\chi} \tag{17}$$

where $\chi \in \{\text{time, traj, force, EEOB, CAOB, pulleys}\}$.

On the other hand, stiffness influences the result of the optimizer, both regarding platform trajectory and lower pulley motion. This is illustrated in Figure 3 and Figure 4. Obviously, the stiffness massively varies within the workspace, and the pulley position has a major impact. As a rule of thumb, the lower pulleys down configuration shown in Figure 4 has clear advantages over the lower pulleys up configuration shown in Figure 3. Noteworthy, the active stiffness term $\boldsymbol{K}_g$ takes advantage from high cable forces which on one hand, contradicts $\mathcal{V}_{\text{force}}$, see eq. (7), and on the other hand increases stiffness at the workspace boundaries. Still, eq. (17) applies where now $\chi \in \{\text{time, traj, force, EEOB, CAOB, pulleys, stiff}\}$. Accordingly, including $\mathcal{V}_{\text{stiff}}$ in $\mathcal{V}_{\text{total}}$, the motion of platform and pulley for brick no. 300 changes, as shown in Figure 5. Table 2 shows the resulting cost functions in comparison. An interesting finding is, that for the chosen parameters settings, the trajectory optimized for stiffness as well is even faster requiring 3.6859 s, but at the price of generally higher forces and faster pulley motions. Collisions were totally avoided in both cases along all trajectory steps. All penalty terms were zero upon convergence of the optimizing process.

While the spline-based approach provides maximum flexibility for optimization, the resulting motions might be

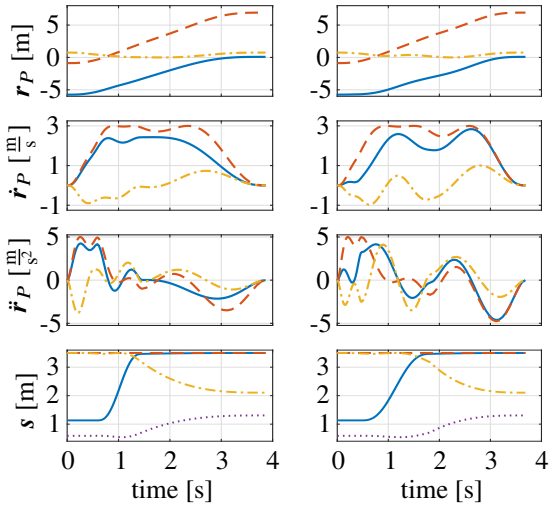

Figure 5. Optimized trajectories and pulley motion. Left: without stiffness optimization. Right: with stiffness optimization. Top three plots: Solid blue line: x-component of the vector. Dashed red line: y-component of the vector. Dash-dotted orange line: z-component of the vector. Bottom plots: Pulleys $[1, 2, 5, 6]$: Solid blue line, dashed red line, dash-dotted orange line, dotted magenta line.

unintuitive for any potential personnel on the site. Thus, in parallel, a slow simplified, unoptimized straight line trajectory over head level with fixed time was performed that is collision-free: It vertically lifts the brick to a height of 2 m above current wall height, horizontally moves to the goal position and vertically moves down to place the brick. The pulleys remain at the current wall height plus $s_{\min}$. For completeness, the results are given in table 2 as well. Clearly, since this trajectory is fully predefined at low dynamics, it is not optimal in comparison.

8 Conclusion and Outlook

This contribution introduced the models, the optimization problem and the solution approach to optimize the trajectories of a cable robot for automated bricking. The results indicate that the choice of the cost functions and their weights have a major impact on the trajectory and allow a tuning regarding preferences like transport time, stiffness and cable tension level. Collisions and paths outside the workspace could be effectively avoided.

This work will be extended by additional spline formulations and more effective parallelization in the future. The generated trajectories will be tested on real prototypes.

Acknowledgment

This research received funding by the Federal Ministry for Economic Affairs and Energy based on a resolution of the German Bundestag. This funding is within the project “Entwicklung von Seilrobotern für die Erstellung von Kalksandstein-Mauerwerk auf der Baustelle” (IGF Vorhaben Nr.: 20061 BG), supported by the German Federation of Industrial Research Associations (AiF).

References

[1] Jürgen Andres, Thomas Bock, Friedrich Gebhart, and Werner Steck. First results of the development of the masonry robot system rocco: A fault tolerant assembly tool. In The 11th International Symposium on Automation and Robotics in Construction (ISARC), pages 87–93. The International Association for Automation and Robotics in Construction (IAARC), 1994.

[2] Günther Pritschow, Michael Dalacker, J. Kurz, and Jörg Zeiher. A mobile robot for on-site construction of masonry. In Proceedings of IEEE/RSJ International Conference on Intelligent Robots and Systems (IROS’94), volume 3, pages 1701–1707. IEEE, 1994. ISBN 0-7803-1933-8. doi:10.1109/IROS.1994.407628.

[3] Volker Helm, Selen Ercan, Fabio Gramazio, and Matthias Kohler. In-situ robotic construction: Extending the digital fabrication chain in architecture. In Synthetic Digital Ecologies: Proceedings of the 32nd Annual Conference of the Association for Computer Aided Design in Architecture (ACADIA), pages 169–176. CUMINCAD, 2012.

[4] Tobias Bonwetsch. Robotically assembled brickwork – Manipulating assembly processes of discrete elements. PhD thesis, ETH Zürich, 2015.

[5] Eric Brehm. Robots for masonry construction – status quo and thoughts for the german market. Mauerwerk, 23(2):87–94, 2019. doi:10.1002/dama.201900004.

[6] Tobias Bruckmann, Hannah Mattern, Arnim Spengler, Christopher Reichert, Alexander Malkwitz, and Markus König. Automated construction of masonry buildings using cable-driven parallel robots. In Proceedings of the 33rd International Symposium on Automation and Robotics in Construction, volume 33, pages 332–340. The International Association for Automation and Robotics in Construction (IAARC), 2016. doi:10.22260/ISARC2016/0041.

[7] José Pedro Sousa, Cristina Palop, Eduardo Moreira, Andry Maykol Pinto, José Lima, Paulo Costa, Pedro Costa, Germano Veiga, and A. Paulo Moreira. The SPIDERobot: A Cable-Robot System for

Table 3. Values of the simulation parameters.

$\boldsymbol{P} = [{}^P\boldsymbol{p}_1 \dots {}^P\boldsymbol{p}_8] = \begin{bmatrix} 0.415 & -0.415 & 0.415 & -0.415 & 0.415 & -0.415 & 0.415 & -0.415 \\ -0.24 & -0.24 & -0.24 & -0.24 & 0.24 & 0.24 & 0.24 & 0.24 \\ 0.7 & 0.7 & 1.21 & 1.21 & 0.7 & 0.7 & 1.21 & 1.21 \end{bmatrix}$ m							
$\boldsymbol{B} = \left[{}^B\boldsymbol{b}_1 \dots {}^B\boldsymbol{b}_8\right] = \begin{bmatrix} 11.1 & -11.1 & 11.1 & -11.1 & 11.01 & -11.1 & 11.1 & -11.1 \\ -10.185 & -9.6375 & -10.185 & -10.185 & 9.6375 & 10.185 & 10.185 & 10.185 \\ 0 & 0 & 6.0 & 6.0 & 0 & 0 & 6.0 & 6.0 \end{bmatrix}$ m							
$\boldsymbol{J}_v = \text{diag}\,(1, 1, 1, 0.415, 0.24, 0.955)$		$\begin{matrix} {}^B_P\boldsymbol{r}_S = [0 \quad 0 \quad 0.576]^{\mathrm{T}}\ \text{m} \end{matrix}$		$m_P = 121.5264$ kg		$\mu_f = 0.1$	
$[n_{s_1}, n_{s_2}, n_{s_3}] = [10, 9, 9]$		$f_{\min} = 150$ N		$f_{\max} = 9000$ N		$d_{\min}, w_{\min} = 0.1$ m	
${}^B\boldsymbol{\theta}_P = \begin{bmatrix} 57.405 & 49.331 & 49.331 \\ 49.331 & 53.639 & 49.331 \\ 49.331 & 49.331 & 7.8261 \end{bmatrix}$ kgm^2		$[t_{\min}, t_{\max}] = [0.1, 15]$ s		$[s_{\min}, s_{\max}] = [0.5, 3.5]$ m			
$[\boldsymbol{r}_{P_{\min}}, \boldsymbol{r}_{P_{\max}}] = \begin{bmatrix} -11.100, 11.100 \\ -10.185, 10.185 \\ 0, 6 \end{bmatrix}$ m		$[\dot{\boldsymbol{r}}_{P_{\min}}, \dot{\boldsymbol{r}}_{P_{\max}}] = \begin{bmatrix} -3, 3 \\ -3, 3 \\ -3, 3 \end{bmatrix} \frac{\text{m}}{\text{s}}$		$[\ddot{\boldsymbol{r}}_{P_{\min}}, \ddot{\boldsymbol{r}}_{P_{\max}}] = \begin{bmatrix} -5, 5 \\ -5, 5 \\ -5, 5 \end{bmatrix} \frac{\text{m}}{\text{s}^2}$			

On-site Construction in Architecture, pages 230–239. Springer International Publishing, 02 2016. ISBN 978-3-319-26376-2. doi:10.1007/978-3-319-26378-6_17.

[8] Andry Maykol Pinto, Eduardo Moreira, José Lima, José Pedro Sousa, and Pedro Costa. A cable-driven robot for architectural constructions: A visual-guided approach for motion control and path-planning. Autonomous Robots, 41(7):1487–1499, 10 2017. ISSN 1573-7527. doi:10.1007/s10514-016-9609-6.

[9] Tobias Bruckmann, Lars Mikelsons, Thorsten Brandt, Manfred Hiller, and Dieter Schramm. Wire robots part I - kinematics, analysis & design. In Jee-Hwan Ryu, editor, Parallel Manipulators - New Developments, ARS Robotic Books, pages 109–132. IntechOpen Limited, London, 4 2008. doi:10.5772/5365.

[10] Hubert Hahn. Rigid Body Dynamics of Mechanisms: 1 Theoretical Basis. Springer, 1 edition, 2002. doi:10.1007/978-3-662-04831-3.

[11] Dieter Schramm, Manfred Hiller, and Roberto Bardini. Modellbildung und Simulation der Dynamik von Kraftfahrzeugen. Springer Vieweg, 3 edition, 2018. ISBN 978-3-662-54481-5. doi:10.1007/978-3-662-54481-5.

[12] Katharina Müller, Christopher Reichert, and Tobias Bruckmann. Analysis of geometrical force calculation algorithms for cable-driven parallel robots with a threefold redundancy. In Jadran Lenarčič and Oussama Khatib, editors, Advances in Robot Kinematics, pages 203–211, Cham, 2014. Springer International Publishing. ISBN 978-3-319-06698-1. doi:10.1007/978-3-319-06698-1_22.

[13] Christopher Reichert, Paul Glogowski, and Tobias Bruckmann. Dynamische Rekonfiguration eines seilbasierten Manipulators zur Verbesserung der mechanischen Steifigkeit. In Torsten Bertram, Burkhard Corves, and Klaus Janschek, editors, Fachtagung Mechatronik 2015: Dortmund (12.03.-13.03.2015), Tagungsband, pages 91–96, Aachen, 2015. Institut für Getriebetechnik und Maschinendynamik. ISBN 978-3-00-048814-6. doi:10.17877/DE290R-7388.

[14] Teun Hoevenaars. Parallel manipulators with two end-effectors: Getting a grip on Jacobian-based stiffness analysis. PhD thesis, Delft University of Technology, 2016.

[15] Leo Stocco, S.E. Salcudean, and Farrokh Sassani. Matrix normalization for optimal robot design. In 1998 IEEE International Conference on Robotics and Automation (Cat. No.98CH36146), volume 2, pages 1346–1351, 06 1998. ISBN 0-7803-4300-X. doi:10.1109/ROBOT.1998.677292.

[16] Dinh Quan Nguyen and Marc Gouttefarde. Stiffness matrix of 6-dof cable-driven parallel robots and its homogenization. In Jadran Lenarčič and Oussama Khatib, editors, Advances in Robot Kinematics, pages 181–191, Cham, 2014. Springer International Publishing. ISBN 978-3-319-06698-1. doi:10.1007/978-3-319-06698-1_20.

[17] Mario Lehmann. Bahnplanung für Seilroboter unter Berücksichtigung von Kollisionen. Bachelor thesis, University of Duisburg-Essen, 2019.

[18] Christer Ericson. Real-Time Collision Detection. CRC Press, 2004. ISBN 978-1558607323.

A Robust Framework for Identifying Automated Construction Operations

Aparna Harichandran[a,b], Benny Raphael[a] and Abhijit Mukherjee[b]

[a] Department of Civil Engineering, Indian Institute of Technology Madras, India
[b]School of Civil and Mechanical Engineering, Curtin University, Perth, WA 6102, Australia
E-mail: aparnaharichandran@gmail.com, benny@iitm.ac.in, abhijit.mukherjee@curtin.edu.au

Abstract –

Machine learning techniques have been successfully implemented for the identification of various construction activities using sensor data. However, there are very few studies on activity recognition in the automated construction of low-rise residential buildings. Automated construction is faster than conventional construction, with minimal human involvement. This requires high accuracy of identification for monitoring its operations. This paper discusses the development and testing of machine learning classifiers to identify normal automated construction operations with high precision. The framework developed in this work involves decomposing the activity recognition problem into a hierarchy of learning tasks in which activities at the lower levels have more details. The top recognition level divides the equipment states into two classes: 'Idle' and 'Operations'. The second recognition level divides the 'operations' into major classes depending on the top-level activities performed by the equipment. The third recognition level further divides the activities into subclasses and so on. Since the number of classes and the similarity between them increase with the recognition level, identification becomes extremely difficult. The identification framework developed in this study classifies operations belonging to the parent class at each level in the hierarchy. The efficacy of this framework is demonstrated with a case study of a top-down modular construction system. In this construction system, the modules of a structural frame are assembled and lifted starting with the top floor followed by the ones below. The accelerometer data collected during top-down construction is used to identify the construction operations. The proposed framework shows superior performance over conventional identification using a flat list of classes.

Keywords –

Automated Construction; Construction Monitoring; Machine Learning; Accelerometer

1 Introduction

Construction operations are monitored for several purposes like the determination of cycle time, productivity, fuel consumption, quality of work and possible failure conditions [1]–[3]. Identifying the activity with reasonable accuracy is sufficient for these purposes. However, for the development of a monitoring system to ensure safety, high accuracy of identification is necessary.

Automated construction is faster than conventional construction, with minimal human involvement. In a fast automated construction system, an undetected faulty operation might cause catastrophic accidents [4], [5]. Besides, the level of detail required in this activity recognition problem is also higher. If an operation is detected as faulty in ongoing automated construction, the details like which operation, the stage of construction in which it happens and its location, have to be identified to take appropriate corrective actions. Hence, the operation identification problem has to be carefully formulated to develop a monitoring system.

Existing studies on equipment activity recognition aim to improve the identification results by exploring advanced machine learning techniques, training options, hyperparameters, features extracted and also by carefully selecting the data [6]–[9]. The current study examines the significance of problem formulation in activity recognition.

The main objective of this study is to identify automated construction operations with high accuracy. A hierarchical operation recognition framework has been developed in this study which involves decomposing the activity recognition problem into a hierarchy of learning tasks. At the top level, equipment states, 'idle' and 'operations' are identified. The activities at lower levels have more details. The performance of this framework is compared with that of the conventional approach to operation recognition which involves a flat list of classes to be separated. The two approaches were evaluated using data from an automated construction system (ACS)

prototype. Acceleration data collected from the structure is used for operation identification. Both approaches use artificial neural networks (ANN) as the learning algorithm.

2 Equipment activity recognition methods

Advancements in computing technology have opened a wide range of possibilities for automated activity recognition. There are mainly three methods for automated activity recognition: sensor-based methods, computer vision-based methods and audio-based methods [3]. In some cases, a combination of these methods is also adopted.

Sensor-based methods capture the characteristic signals associated with operations [10]. Accelerometers, gyroscopes, inertial measurement unit (IMU) and Global Positioning System (GPS) are some of the widely used sensors for activity recognition [6], [8], [11]. Sensor-based methods can be reliably applied to chaotic construction sites where equipment is often beyond the line of sight. A broad range of studies explored various supervised learning methods, starting from simple ANN, K-nearest neighbour (KNN), logistic regression, Support vector machine (SVM) to deep learning methods in recent times [7], [8], [12], [13].

Vision-based methods have the potential to identify any type of equipment if ambient conditions are favourable. Images or videos of the construction equipment are used for activity recognition. Initial studies used SVM and 2D motion descriptors for activity recognition from spatiotemporal data [14], [15]. More recent studies explore deep learning methods for automated labelling of activities in video data [2], [16]. Major limitations associated with the vision-based methods include high sensitivity to ambient conditions, obstructions, cost of implementation and need for large storage space.

Audio-based methods can be used to identify any equipment that generates sound. Numerous machine learning classifiers were implemented for sound classification. Some of the most popular classifiers are KNN, SVM, ANN, Hidden Markov model (HMM) and deep neural networks [17]–[20]. Microphones can capture the data from all directions without getting affected by visual obstructions [3]. This data is not biased by the skill level of the operator. However, not all equipment can be identified by this method. Data collecting for these methods can be challenging for noisy construction sites.

The current study attempts to identify operations of an ACS prototype for low-rise buildings. Acceleration data is used for activity recognition. ANN is one of the best performing machine learning classifiers for equipment activity recognition. Hence, ANN with a simple architecture (single hidden layer) is selected for the current study.

3 Methodology

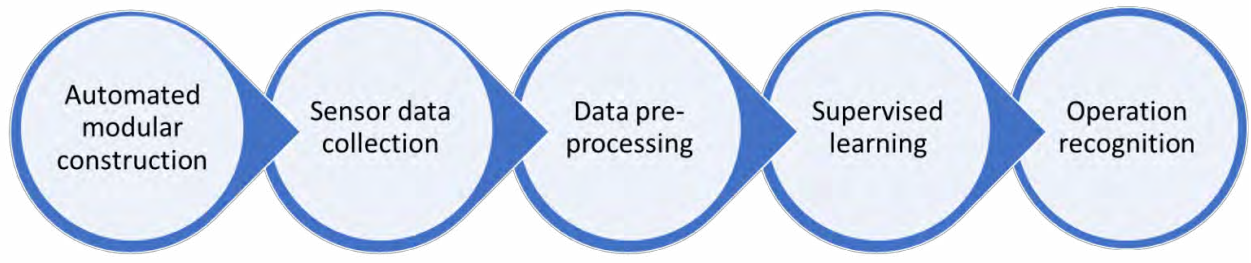

Figure 1. Methodology for operation recognition

Figure 1 shows the methodology adopted for this study. Acceleration data is collected during the modular construction of a structural frame using an Automated Construction System (ACS) prototype. After pre-processing, the data is supplied to the operation recognition framework. This machine learning-based framework identifies the operations that are organized hierarchically into 4 recognition levels (RL). Two approaches are compared: a) Conventional approach using a flat list of classes to be identified, and b) Hierarchical operation recognition framework. Each step of the research methodology is described in detail in the following sections.

3.1 Automated modular construction

The automated top-down construction method is adopted for the construction of the structural frame in this study [4], [5], [21], [22]. This method is mainly developed for the modular construction of low-rise buildings. For automated top-down construction, the main load-bearing parts of a structure are divided into smaller components. The modules of the beam and column are assembled sequentially, starting from the topmost parts of the structural frame. After the assembly of the first set of components, the completed structure is lifted to a certain height. The modules of the column are

added to the existing structure and lifted it again in the next operation cycle. Since the structure is completed from top to bottom using an ACS, this method is called automated top-down construction.

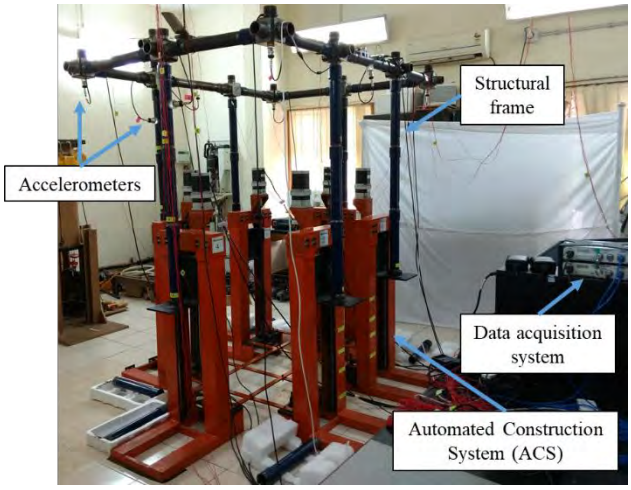

Figure 2. Data collection during automated modular construction

Figure 2 shows the laboratory prototype of the ACS and the structural frame developed for this study. The ACS consists of 6 lifting machines. Each of these machines is capable of operating individually for lifting or lowering of specific support and as a group for simultaneous lifting or lowering of all supports (coordinated lifting or coordinated lowering). The structural frame modules are made of standard steel pipe sections with external threading on both edges. They are connected by couplers and universal joints with internal threading. The structure has redundant columns to ensure stability during top-down construction. Each column of the structure is supported by a lifting platform of the ACS.

At the beginning of the top-down construction, the top most beam and column modules are connected and supported by these lifting platforms. This idle condition before the beginning of the operation cycle is termed as 'Idle_CS0' where CS0 refers to Construction Stage 0. This is followed by the first operation cycle of top-down construction. The operations involved in one cycle are given below [21].

1. Coordinated lifting
2. Lowering support 1
3. Assembling module of column 1
4. Lifting support 1 till the load is transferred from column 1
5. Repeat steps (2) to (4) for other supports (support 2 to support 6)

One cycle of the top-down construction finishes one stage of construction (CS). Two cycles of operations were carried out for one set of experiments. Totally 6 sets of experiments were conducted for the study.

3.2 Data collection

Acceleration data was collected from 8 different locations on the structure during automated construction (Figure 2). Monoaxial piezoelectric accelerometers (measurement range: -5g to +5g, sensitivity: 1000 mv/g) were installed on the topmost beam-column assembly for this purpose. The data is acquired through HBM universal measuring amplifier (model: QuantumX MX840B) at 200 Hz sampling frequency. The timestamps of all operations were manually recorded in a time tracking excel sheet. These sheets were compared with the timestamps of the acquired data for generating operation labels required for supervised learning.

3.3 Data pre-processing

The acceleration data collected using HBM data acquisition software is exported to Microsoft Excel and MATLAB files for analysis. Based on the studies of equipment activity recognition, 5 time-domain features and 5 frequency domain features were extracted from the raw data [6], [11], [23]. The time-domain features include mean, variance, interquartile range, peak and root mean square error. The period of the signal and signal energy were extracted through autocorrelation of the signal. The other frequency domain features include the three prominent frequencies from the Fast Fourier Transform (FFT) of the signal. Totally 80 features (10 features x 8 sensor locations) were extracted from the raw acceleration data.

3.4 Supervised learning and operation recognition

In previous studies, supervised learning techniques have demonstrated superior performance compared to unsupervised learning techniques for unbalanced datasets [6], [14]. The current study adopts Artificial Neural Networks (ANN) for the classification of automated construction operations.

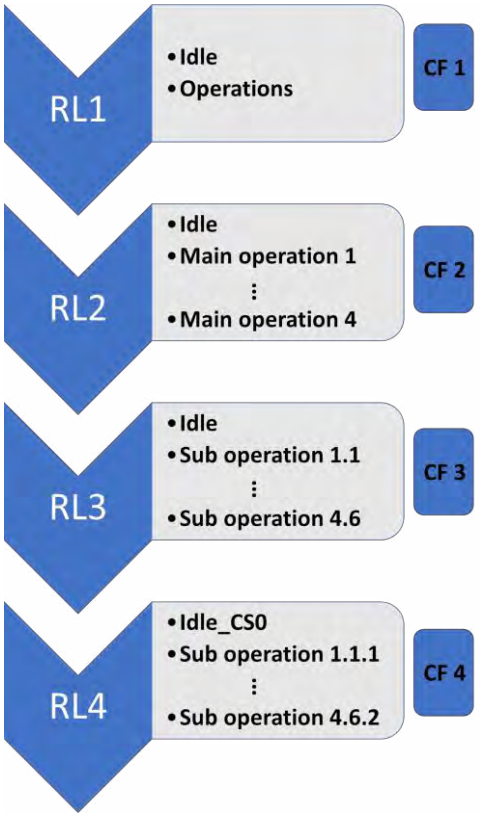

Figure 3. Conventional approach for operation recognition

The identification problem has 4 recognition levels (RL) as follows.

- RL1: Recognizes whether the ACS is 'idle' or 'operating'
- RL2: Recognizes the major operation categories
- RL3: Recognizes the sub-operation categories
- RL4: Recognizes stage of construction

The conventional approach for operation recognition uses a flat list of classes to be separated. However, in order to test the performance of this approach at different recognition levels, the identification problem is divided into 4 different identification tasks, one task per RL (Figure 3). An ANN classifier is assigned to each identification task. The classifiers are named as CF 1, CF 2, ..., CF 4, represented by blue boxes in figure 3. The operation categories identified are given as a list next to it. The actual operation categories identified by the classifiers are given in Table 1. The complexity of the identification problem seems to increase from RL1 to RL4 in this approach.

Hierarchical operation recognition framework is developed by considering the hierarchical relationship among the operations (Figure 4). If the major category of an operation is identified with high accuracy, the further identification task can be simplified by exploring the subcategories of that operation. This idea is the basis of the hierarchical operation recognition framework. The main

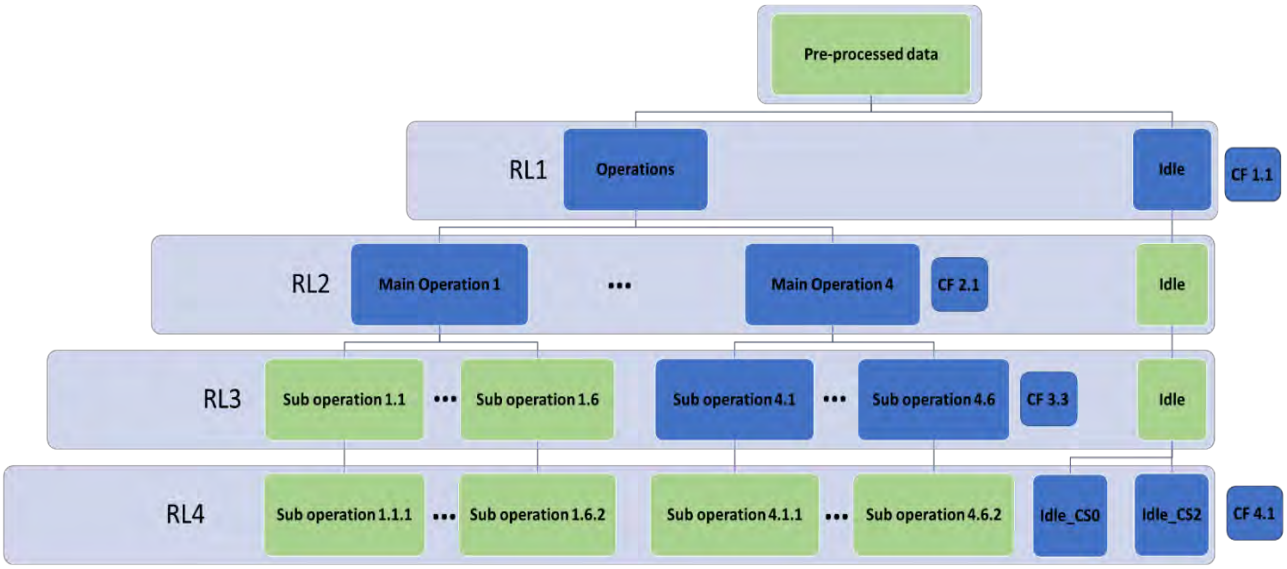

Figure 4. Hierarchical operation recognition framework

Table 1. Classifiers in operation recognition frameworks

Recognition Level	Classifiers in conventional approach	Classifiers in hierarchical operation recognition framework	Name of Classes
1	CF 1	CF 1.1	Idle
			Operations
2	CF 2	CF 2.1	Idle
			Coordinated Lifting
			Lowering Support
			Assembling Column Module
			Lifting Support
3	CF 3	CF 3.1	Idle
			Coordinated Lifting
			Lowering Support 1 ... Lowering Support 6
		CF 3.2	Assembling Column Module Step 1 … Assembling Column Module Step 6
		CF 3.3	Lifting Support 1 … Lifting Support 6
4	CF 4	CF 4.1	Idle_CS0
			Idle_CS2
		CF 4.2	Coordinated Lifting_CS0
			Coordinated Lifting_CS1
			Coordinated Lifting_CS2
		CF 4.3	Lowering Support 1_CS1 Lowering Support 1_CS2
		…	…
		CF 4.8	Lowering Support 6_CS1 Lowering Support 6_CS2
		CF 4.9	Assembling Column Module Step 1_CS1 Assembling Column Module Step 1_CS2
			…
		CF 4.14	Assembling Column Module Step 6_CS1 Assembling Column Module Step 6_CS2
		CF 4.15	Lifting Support 1_CS1 Lifting Support 1_CS2
			…
		CF 4.20	Lifting Support 6_CS1 Lifting Support 6_CS2

the identification problem is divided into a hierarchy of simple identification tasks across the RLs. Hence, there can be more than one identification task per RL. The classifiers are named as 'CF RL.n' where the first index RL represents recognition level and n denotes the number of the classifier in that RL. For clarity, only one classifier is shown per RL in figure 4 The classifier and the operations classified are shown in blue boxes. This figure is also for the representation of the concept of hierarchical operation recognition framework. The actual details of the framework are given in Table 1.

The performance of all classifiers is assessed through k-fold cross-validation. This avoids the problem of overfitting to the given data. The classifiers in RL1 to RL3 are 10-fold cross-validated and those in RL4 are 5-fold cross-validated for both identification frameworks. The predicted class labels were compared with the digital

record of actual class labels to estimate the accuracy of identification. The accuracy is computed as given in equation 1.

$$Accuracy = \frac{Number\ of\ samples\ correctly\ identified}{Total\ number\ of\ samples}\ x\ 100\ \% \quad (1)$$

4 Results and discussion

Table 2. Summary of operation recognition results

Recognition level (RL)	Conventional approach for operation recognition		Hierarchical operation recognition framework	
	Classifiers	Overall accuracy per RL (%)	Classifiers	Overall accuracy per RL (%)
1	CF 1	99.58	CF 1.1	99.58
2	CF 2	99.18	CF 2.1	100.00
3	CF 3	95.92	CF 3.1 - CF 3.3	99.07
4	CF 4	84.56	CF 4.1 - CF 4.20	99.19

The operation recognition results are summarized in Table 2. For comparing the performance of the two approaches, the prediction accuracy of all classifiers in the hierarchical framework is combined to estimate the overall accuracy per RL. The classifier CF 1 and CF 1.1 are assigned with the same identification task: classifying 'idle' and 'operations'. Hence the accuracy of identification is also equal. At RL 2, the hierarchical framework performs slightly better than the conventional approach with 100% accuracy. Meaning all main operations were identified correctly. CF 2.1 removes the 'idle' from the classes. This is the reason for improved accuracy.

RL 3 onwards there is a significant difference in the problem formulation. The hierarchical framework has focused classifiers for the identification of sub-operations at RL3. Hence the operations were better identified in this framework. At RL 4 where the construction stage is to be identified, there is a significant difference in performance between two recognition frameworks.

While the hierarchical framework consistently delivers accuracy close to 100%, the performance of the conventional approach continuously declines with the increase in the recognition level. Even though both approaches use the same machine learning algorithm, their performances are different. The results emphasize the importance of problem formulation in activity identification.

5 Conclusions

This study proposes a robust framework for identifying automated construction operations with high accuracy. The hierarchical operation recognition framework formulates the identification problem into a hierarchy of learning tasks. The performance of this framework is compared with the conventional approach to operation recognition using a flat list of classes representing activities.

Both approaches use ANN as the learning algorithm. Even though their performances are comparable at the top level, the hierarchical framework outperforms the conventional approach while identifying operations with minute levels of details. Most previous activity recognition studies have attempted to improve the performance by carefully selecting data, and exploring learning algorithms, training options, parameter selection and features extracted. This study shows that the problem formulation can make a tremendous difference in the performance.

Acknowledgement

The project is funded by the Department of Science and Technology (DST), India through the grant DST/TSG/AMT/2015/234.

References

[1] J. Kim, S. Chi, and J. Seo, "Interaction analysis for vision-based activity identification of earthmoving excavators and dump trucks," *Autom. Constr.*, vol. 87, pp. 297–308, Mar. 2018, doi: 10.1016/j.autcon.2017.12.016.

[2] A. Khosrowpour, J. C. Niebles, and M. Golparvar-Fard, "Vision-based workface assessment using depth images for activity analysis of interior construction operations," *Autom. Constr.*, vol. 48, pp. 74–87, 2014, doi: 10.1016/j.autcon.2014.08.003.

[3] B. Sherafat *et al.*, "Automated Methods for Activity Recognition of Construction Workers and Equipment: State-of-the-Art Review," *J. Constr. Eng. Manag.*, vol. 146, no. 6, 2020, doi: 10.1061/(ASCE)CO.1943-7862.0001843.

[4] A. Harichandran, B. Raphael, and A. Mukherjee, "Identification of the Structural State in Automated Modular Construction," in *36th International Symposium on Automation and Robotics in Construction (ISARC 2019)*, 2019, pp. 187–193, doi: https://doi.org/10.22260/ISARC2019/0026.

[5] A. Harichandran, B. Raphael, and A. Mukherjee, "Determination of Automated Construction Operations from Sensor Data Using Machine Learning," in *Proceedings of the 4th International Conference on Civil and Building Engineering Informatics*, 2019, pp. 77–84.

[6] R. Akhavian and A. H. Behzadan, "Construction equipment activity recognition for simulation input modeling using mobile sensors and machine learning classifiers," *Adv. Eng. Informatics*, vol. 29, pp. 867–877, 2015, doi: 10.1016/j.aei.2015.03.001.

[7] T. Slaton, C. Hernandez, and R. Akhavian, "Construction activity recognition with convolutional recurrent networks," *Autom. Constr.*, vol. 113, no. August 2019, p. 103138, 2020, doi: 10.1016/j.autcon.2020.103138.

[8] K. M. Rashid and J. Louis, "Times-series data augmentation and deep learning for construction equipment activity recognition," *Adv. Eng. Informatics*, vol. 42, p. 100944, Oct. 2019, doi: 10.1016/j.aei.2019.100944.

[9] C. Chen, Z. Zhu, and A. Hammad, "Automated excavators activity recognition and productivity analysis from construction site surveillance videos," *Autom. Constr.*, vol. 110, p. 103045, Feb. 2020, doi: 10.1016/j.autcon.2019.103045.

[10] C. R. Ahn, S. Lee, F. Peña, and P. Peña-Mora, "Application of Low-Cost Accelerometers for Measuring the Operational Efficiency of a Construction Equipment Fleet," *J. Comput. Civ. Eng.*, vol. 29, no. 2, p. 04014042, 2015, doi: 10.1061/(ASCE)CP.1943.

[11] L. Joshua and K. Varghese, "Accelerometer-Based Activity Recognition in Construction," *J. Comput. Civ. Eng.*, vol. 25, no. 5, pp. 370–379, Sep. 2011, doi: 10.1061/(ASCE)CP.1943-5487.0000097.

[12] A. Harichandran, B. Raphael, and K. Varghese, "Inferring Construction Activities from Structural Responses Using Support Vector Machines," in *35th International Symposium on Automation and Robotics in Construction (ISARC 2018)*, 2018, pp. 332–339, doi: https://doi.org/10.22260/ISARC2018/0047.

[13] L. Joshua and K. Varghese, "Automated recognition of construction labour activity using accelerometers in field situations," *Int. J. Product. Perform. Manag.*, vol. 63, no. 7, pp. 841–862, 2014, doi: 10.1108/IJPPM-05-2013-0099.

[14] M. Golparvar-Fard, A. Heydarian, and J. C. Niebles, "Vision-based action recognition of earthmoving equipment using spatio-temporal features and support vector machine classifiers," *Adv. Eng. Informatics*, vol. 27, no. 4, pp. 652–663, Oct. 2013, doi: 10.1016/J.AEI.2013.09.001.

[15] E. Rezazadeh Azar, S. Dickinson, and B. McCabe, "Server-Customer Interaction Tracker: Computer Vision–Based System to Estimate Dirt-Loading Cycles," *J. Constr. Eng. Manag.*, vol. 139, no. 7, pp. 785–794, Jul. 2013, doi: 10.1061/(ASCE)CO.1943-7862.0000652.

[16] D. Roberts and M. Golparvar-Fard, "End-to-end vision-based detection, tracking and activity analysis of earthmoving equipment filmed at ground level," *Autom. Constr.*, vol. 105, Sep. 2019, doi: 10.1016/j.autcon.2019.04.006.

[17] C.-F. Cheng, A. Rashidi, M. A. Davenport, and D. V. Anderson, "Activity analysis of construction equipment using audio signals and support vector machines," *Autom. Constr.*, vol. 81, no. March, pp. 240–253, Sep. 2017, doi: 10.1016/J.AUTCON.2017.06.005.

[18] J. Cao, W. Wang, J. Wang, and R. Wang, "Excavation Equipment Recognition Based on Novel Acoustic Statistical Features," *IEEE Trans. Cybern.*, vol. 47, no. 12, pp. 4392–4404, Dec. 2017, doi: 10.1109/TCYB.2016.2609999.

[19] J. Cao, W. Huang, T. Zhao, J. Wang, and R. Wang, "An enhance excavation equipments classification algorithm based on acoustic spectrum dynamic feature," *Multidimens. Syst. Signal Process.*, vol. 28, no. 3, pp. 921–943, Jul. 2017, doi: 10.1007/s11045-015-0374-z.

[20] J. Cao, T. Zhao, J. Wang, R. Wang, and Y. Chen,

"Excavation equipment classification based on improved MFCC features and ELM," *Neurocomputing*, vol. 261, pp. 231–241, Oct. 2017, doi: 10.1016/j.neucom.2016.03.113.

[21] A. Harichandran, B. Raphael, and A. Mukherjee, "Development of Automated Top-Down Construction System for Low-rise Building Structures," *Int. J. Ind. Constr.*, vol. 1, no. 1, pp. 22–33, 2020, doi: doi.org/10.29173/ijic217.

[22] B. Raphael, K. S. C. Rao, and K. Varghese, "Automation of modular assembly of structural frames for buildings," in *Proceedings of the 33rd International Symposium on Automation and Robotics in Construction (ISARC 2016)*, 2016, pp. 412–420, doi: https://doi.org/10.22260/ISARC2016/0050.

[23] D. Figo, P. C. Diniz, D. R. Ferreira, and J. M. P. Cardoso, "Preprocessing techniques for context recognition from accelerometer data," *Pers. Ubiquitous Comput.*, vol. 14, no. 7, pp. 645–662, Oct. 2010, doi: 10.1007/s00779-010-0293-9.

Analysis of Excavation Methods for a Small-scale Mining Robot

M. Berner[a] and N.A. Sifferlinger[b]

[a]Senior Researcher, Department of Mineral Resources Engineering - Conveying Technology and Design Methods, University of Leoben, Austria

[b]Professor for Excavation and Conveying Technology and Design of Mining Machinery, Department of Mineral Resources Engineering, University of Leoben, Austria

michael.berner@unileoben.ac.at, nikolaus-august.sifferlinger@unileoben.ac.at

Abstract -

The following paper is discussing the potential excavation systems and development of the production tool system of a small-scale mining robot. The limitations of power and weight increase the complexity of the design of the production tools immensely. Each excavation method's efficiency is depending on the material to be excavated, the available power and the machine's capability of handling the reaction forces. In this paper, different, individual excavation methods will be compared and analysed for their applicability. This includes conventional, alternative and combined excavation tools. The individual technologies are assessed in terms of their efficiency and feasibility by surveying existing technologies and analytical studies. The contribution of this paper is a summary of viable excavation methods for small-scale robotic miners.

Keywords -

Excavation; Production Tools; Robotics; Small-scale Mining

1 Introduction

Upcoming challenges in mining due to sustainability and ecological aspects require additional efforts in research and development. The trend towards zero personnel in underground mining demands full mechanization and automation of the mining process up to the use of fully autonomously operating robots. To reduce the residue risk to a minimum for workers in harsh conditions, it is indispensable to develop automated mining machines, which can take over the hazardous parts of the mining operation. Some of the work is already done entirely by independently working machines, but there is still personnel needed for many different tasks (e.g. maintenance). Possible tasks for robots in mining are the maintenance of machinery, exploration (e.g. abandoned mines) and selective mining (especially in difficult to access areas). [1, 2]

Today we see early research and development in robot technology [2], which are expected to replace the human workforce in underground mining within the next 30 years, see figure 1.

Figure 1. Robotics in mining - Prospect

The progress during this timeline can be divided in 3 parts, which will all develop consequently. Ongoing researches focus on the development of new mining and perception systems and also on sustainable mining ecosystems. The goal of the next 10 years is to create first industrial pilots, which can operate semi-autonomously in "small deposit scenarios". Eventually, the vision for 2050 is to have completely autonomous systems, which are able to work in ultra-depth scenarios.

In this paper, excavation methods are assessed in terms of their applicability for a small-scale mining robot.

Scope of this robot are exploration and selective mining underground, under water and in slurries. One of the key components of this robot is the production tool system, capable of mining hard and abrasive rock. Considerably low weight and power are challenges to be overcome in this project.

2 Excavation methods

In mining, the excavation of material can be performed by many different methods. For the subsequent analysis, the excavation methods are classified in four main categories: drilling and blasting, mechanical excavation, alternative excavation and combined excavation (figure 2).

Figure 2. Classification - Excavation methods

2.1 Drilling and blasting

The drilling and blasting method is one of the most used excavation methods for extracting large amounts of hard rock [3]. Drilling the boreholes is usually done by automated drill rigs, equipped with specifically selected drills. Standardized drilling methods are electro-hydraulically, rotary or rotary-percussive drilling (explained in section 2.2.1). Applications of drilling and blasting can be found in rock excavation and tunneling. [3, 4, 5]

Drilling and blasting is known for its generic applicability, the high production rate and the high grade of fragmentation. Especially when mechanical excavation reaches its limits, drilling and blasting proves its effectiveness. On the other side, drilling and blasting requires a series of individual tools, the blasting process is accompanied by some side effects (noise, vibration and toxic fumes) and represents generally a discontinuous excavation process. [3]

The low reaction forces of the drilling process and the capability of excavating very hard material are beneficial f or t he r ealization o f t he m ining r obot and therefore, the applicability to a robotic-miner will be assessed in more detail in section 3

2.2 Mechanical excavation

Mechanical excavation is next to drilling and blasting the second main excavation technique in mining [3, 5]. Compared to drilling and blasting, mechanical excavation has some benefits [3]:

- Safer operation
- Potential for selective mining
- Continuous excavation

In this section conventional mechanical excavation methods are described and analysed in terms of their applicability to a robotic miner.

2.2.1 Drilling

Drilling is mainly used as one link in the chain of an excavation process (e.g. drilling and blasting) or as an auxiliary tool, but not as a standalone excavation method due to the low production rate. Further applications are drilling well holes and material collection by sample drilling [6].

Drilling is a comparatively easy technology and is able to excavate small amounts of both soft and hard rock with the suitable technology. State-of-the-art drilling methods used, are:

- Tophammer drilling
- Down-the-hole-hammer drilling
- Rotary drilling
- Core drilling

In section 3 drilling will be analysed in more detail in connection with the applicability assessment of drilling and blasting.

2.2.2 Partial-face cutting

Partial-face cutting machines are excavating only a part of the rock face at a time and are known for their mobility and flexibility. The cutting head is a rotating drum, equipped with picks and mounted on a boom. During the cutting process, only a number of the entire amount of picks is in contact with the rock to be excavated. [3]

With a partial-face cutting head, large volumes of soft to medium hard rock can be excavated, curves be cut and tunnels be created. [3, 7]

In the mining industry, partial-face cutting machines (e.g. roadheaders) are mining machines with usually high mass

and weight to be able to penetrate the rock. The machine needs to withstand the high reaction forces resulting from the cutting process.

Small-scale cutting heads exist [8, 9], but are very limited in terms of rock strength. A robotic-miner equipped with a cutting head would possess very restricted capabilities, although the advantages of the system could be beneficial for certain scenarios.
Hence, partial-face cutting systems are considered in more detail in section 3.

2.2.3 Full-face cutting

The fellow of the partial-face cutting machine is the full-face cutting machine. As the name indicates, a full-face cutting machines' cutting head is constantly in contact with the rock face. The cutting head is a rotating part, equipped with pick or disc cutting tools and pushed against the rock face to excavate the material. [3, 10]
In reality, full-face cutting machines, e.g tunnel boring machines (TBM) [11, 12, 13], pipe-jacking machines (PJM) or boxhole boring machines (BBM) [14], are available in various designs from rather small to large diameters and mainly taken for boring tunnels, pipelines or shafts.

The cutting technology of full-face machines makes them capable of excavating very hard and abrasive rock. This requires, compared to the other methods, very high performance for the generation of the cutting and reaction forces. The demanded amount of power and traction lead to comparatively long and heavy machines, which make them much less flexible and mobile. [3, 7, 10]

Due to the existence of micro-tunneling machines or pipe-jacking machines with diameters below 1 m, it is worth checking the feasibility of the implementation in a mining robot (section 3).

2.2.4 Impact hammer

Impact hammers are rock excavation tools, especially used for breaking or scaling operations. A piston produces high frequent impulses and transmits it to the impact tool on the front end. [3]

The method is simple and an impact hammer can be mounted on different types of machines. Typical applications are breaking oversized boulders, quarrying or scaling operations. Impact hammers are mainly taken as an auxiliary tool to the main excavation machine. [3]
Excavation of soft rock or soil is not feasible. Further on, the reaction forces of an impact hammer are considerably high and the production rate is low. Hence, this technology is not further investigated.

2.2.5 Saw cutting

Rock cutting chainsaws are characteristically used in quarrying operations for extraction of dimensional blocks. The capabilities are limited to cutting of soft to medium hard rock. Rock cutting saws are not considered as a production tool for a robotic miner. [3]

2.2.6 Grinding

Characteristically for a grinding process are the high frequency and low amplitude of the process. Due to the fact, that grinding is not used for excavation and tools tend to wear off easily, it will not be analysed any further in this paper.

2.2.7 Auger drilling

Auger drilling combines both excavation and conveying in one method. Often used in coal seam operations, drill rigs with a rotating auger and a drill head on the front tool end require high thrust forces and torque. Continuous excavation of rock and tunneling are not viable with this certain method. [3, 15]

2.2.8 Dredging

Transshipping or excavation of very soft material can be managed by dredging. Excavation of greater amounts of hard rock and tunnels are not viable with a dredging technology.

2.2.9 Bucket wheel excavation

Bucket wheel excavators are employed for soft coal mining in open pit scenarios. The buckets dig into a layer of material and drop it onto a conveyor belt. [16] presents a mining robot with a bucket wheel excavation technology for lunar soil. This excavation method is not feasible for an underground, hard rock mining scenario. [17]

2.3 Alternative excavation systems

Alternative excavation systems cover non-conventional excavation methods apart from mechanical excavation and drilling and blasting.

2.3.1 High-pressure water cutting

Water jet cutting technology is a method for shattering and cutting material from very close distance. [18] The pressure of the water jet is increased by a high-pressure pump, pushed through a nozzle pointing towards the material to be cut. Often employed for precise cuts, high-pressure water jets have their reason for being utilized in

the mining industry. Various forms of water jets can be applied for individual operations. [18, 19]

[18] defines following appearances of high-pressure water jets:

- Continuous plain water jets
- Pulsating and modulated water jets
- Abrasive water jets

Cutting rock reasonably well requires a minimum water pressure around 100 MPa. A comparatively high specific energy leads to a prerequisite of large volumes of water and decreases the potential as a production tool in a robotic miner. A combination of high-pressure water jets with conventional mining methods seems to be more practical and will be discussed in section 2.4.1 and 2.4.2.

2.3.2 Hydrofracturing

Hydrofracturing, or hydraulic fracturing, is the employment of pressurized liquid (mostly mixed with additives) into a borehole to fracture rock formations. If the present pressure exceeds the rock's tensile strength, crack formations are induced. [20] Mainly used in oil and gas production, hydrofracturing is currently not used for rock excavation and is considered to be not important for detailed investigations.

2.3.3 Laser cutting

Laser cutting technology exhibits high specific energy levels and is typically used for precise cuts of blocks with rather small thickness. [21] Excavation of big volumes is not feasible, therefore not considered for further analyses.

2.3.4 Chemical excavation

Chemical excavation is a very restricted technology, only used in very special scenarios and therefore not discussed in detail. [22]

2.4 Combined excavation systems

Combined excavation systems combine the advantages of mechanical excavation systems with alternative, auxiliary methods.

2.4.1 High-pressure water assisted to drilling

As pointed out in section 2.2, mechanical excavation has some benefits over drilling and blasting. Though, the operating field of mechanical excavation is limited by geotechnical conditions. Many activities involve overcoming those limitations by improving the conventional technologies or developing new excavation systems.
A number of researches and studies [18, 19, 23, 24] investigate the improvement of the overall drilling time and efficiency of rotary-percussive drills.
Assisting water jets enter the cracks in the crushed zone and, due to the water wedge effect, increase the crushing effect.[24]

If the water pressure exceeds the critical stress of the rock, cracks will be induced and result is a reduction of the required drilling performance. In order to decrease drilling time and increase lifetime of the drill bit, high-pressure water jet assisted to drilling seem to be a practical solution. [24] In this specific case, only drilling will be used, if for the excavation method of the mining robot drilling and blasting is chosen. A trade-off between complexity respectively costs and efficiency has to be made.

2.4.2 High-pressure water assisted to cutting

Besides from drilling, cutting can also be assisted by high-pressure water jets. The purpose of assisting water jets are the reduction of the cutting force and decrease of the tool wear. [23]
The greatest disadvantage of currently used, mobile and flexible excavators (e.g. roadheaders) is the limitation of cutting rock with UCS above 150 MPa [7]. Joy Mining [25] has introduced a new disc cutting technology with assisted water jets, the Dynacut^{TM}. Aim of this research project is combining mechanical excavation technology for hard rock cutting with high-pressure water jets. Until now, no test results could be found. [7, 25]

The importance of assisting high-pressure water jets arises, when conventional cutting method reach their limits. Scope of the robotic miner is the excavation of hard rocks. An implementation of a common cutting drum with pick tools will not even be capable of excavating medium hard rock, and therefore, cutting technology with assisting high-pressure water jets will not be discussed further in this paper.

2.4.3 Microwaves assisted to cutting

The basic idea of using microwaves is the same as of using high-pressure water jets: Implementation as an auxiliary tool to a main excavation process for decreasing the rock quality. [26]
One method is the use of microwave irradiation to reduce the rock strength by inducing cracks. Cracks pre-weaken the rock and lower the cutting resistance. Researches show, that the net cutting force can be reduced by approximately 10 %. [26]

The operating fields of the mining robot are wet or submerged underground scenarios. Microwaves are

absorbed by water and as a consequence, the applicability of microwaves is not given.

2.4.4 Ultrasonic drilling

As mentioned in section 2.2.1, drilling is i.e. used for exploration, shaft drilling and extracting samples. Shortcoming of common rotary-percussive drills, while drilling hard and abrasive rock, is maintenance due to tool wear. Purpose of ultrasound drilling is the reduction of operating costs by increasing the penetration rate. A piezoelectric transducer converts the electric energy to mechanical vibration. This oscillation is superposed with the rotation of the drill and provides the penetration. [27]

Compared to conventional drilling, ultrasonic drilling is an elaborate technology and no applications in wet or completely submerged conditions have been found. A comparatively minimal increase of the penetration rate is not the most important point, hence, ultrasonic drilling is not investigated further in this paper.

3 Analysis

In this chapter, the most promising excavation methods, assessed in the previous section, are analyzed in more detail. The applicability of the production tool system is depending on some properties:

- Production rate
- Penetration rate (Advance rate)
- Specific energy
- Limitations

Following parameters are assumed for the calculations in this chapter:

- Input power: 40 kW
- Tunnel cross sectional area: 1 m^2

3.1 Drilling and blasting

The advantages of drilling and blasting already have been discussed in the previous section. The most important feature, for this study, is the capability of excavating larger amounts of very hard rock with one blast. Furthermore, a complete mechanization is state-of the art, however, a full automation of the loading process is a complex challenge to be mastered.

Drilling is the most time consuming step in drilling and blasting. To keep the blasting cycle to a minimum, the penetration rate of the drill to be used is crucial. The penetration rate reflects the drilled length per hour. In this case, a rotary-percussive drill is chosen with a bit diameter of 60 mm. The penetration rate is calculated after [28] (figure 3).

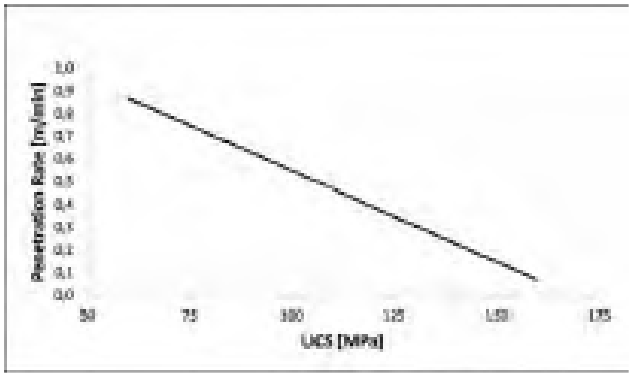

Figure 3. Rotary-percussive drilling - Penetration rate

The formula used for estimating the penetration rate results of a linear regression model of measurement data. The penetration rate is decreasing linearly with the rock strength. [28]
If a bore hole with 300 mm depth is assumed, the time for drilling varies between 20 seconds and 4.5 minutes. Depending on the employed explosives, excavating a tunnel with the assumed cross sectional area requires between 5 and 10 blast holes. Following from this, the total time for one blast (including loading the boreholes with explosives) is estimated between 1-2 hours. For simplicity, the time between drilling the individual holes, for crushing and for conveying is neglected. The precise analysis of the blasting cycle will be done in future investigations.

The specific energy is the amount of energy to excavate one unit volume of rock [3]. A drilling process exhibits, compared to other mechanical excavation systems, a high specific energy (calculated after [3]), see figure 4. However, this peculiarity is extensively decreased by the subsequent blasting operation.

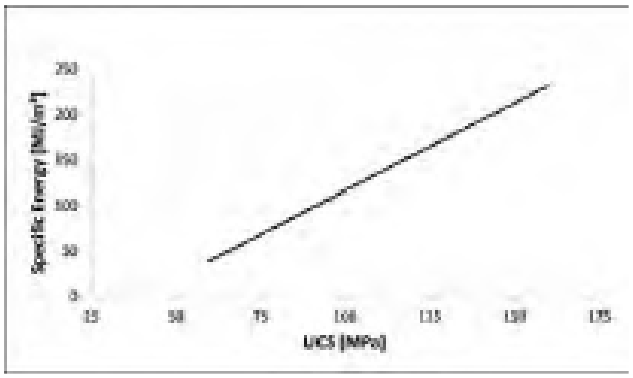

Figure 4. Rotary-percussive drilling - Specific energy

The specific energy of the drilling process is approximated by a linear regression model of [28]. This model provides satisfactory results according to the measurements.

3.2 Partial-face cutting

Partial-face cutting machines distinguish their self by their flexibility and mobility. Excavation of tunnels, cutting curves or limited selective mining are characteristic capabilities. Shortcomings are the severe restrictions by the rock properties. Standard partial-face cutting machines' cutting abilities fatigue at rocks with UCS around 150 MPa [3, 7]. In this paper, a cutting head with a considerably less lower amount of power is investigated, which will limit the mining robot's abilities to excavating soft rocks only. The instantaneous breaking rate, the rock volume excavated per hour, is calculated after [3] (figure 5) and is provided by a prediction model, which is based on full-scale linear cutting tests.

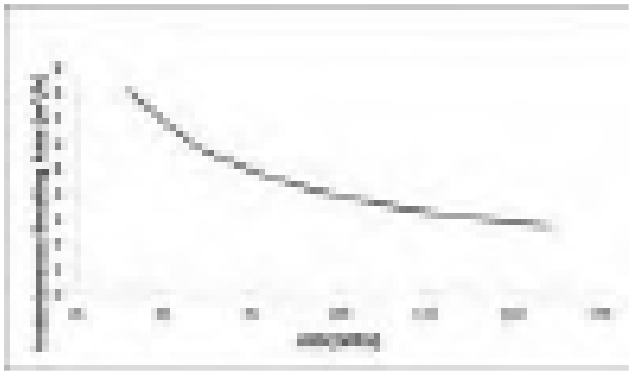

Figure 5. Partial face cutting - Instantaneous breaking rate

In practice, the mining machine would not be able to withstand the reaction forces, resulting from cutting, due to the little weight and traction. In this order of magnitude, the ability of cutting rock above 60 MPa is believed to be very unlikely.

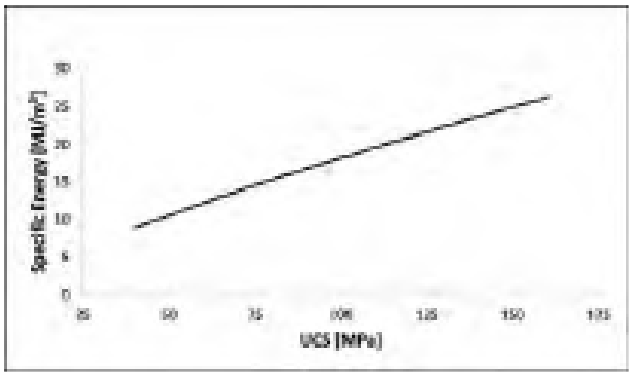

Figure 6. Partial face cutting - Specific energy

After [3], specific energies above 20 MJ/m^3 are not economical and lead to damage of the cutting tools. The estimated specific energy can be derived from the instantaneous breaking rate and the provided input power. [3]
However, for the chosen scope of application, the specific energy levels are bearable (figure 6).

The advance rate is the excavated length of the tunnel (with the determined cross sectional area) per hour. Again, for the advance rate, only the region below 60 MPa is important (figure 7). The estimation of the advance rate presupposes an ideal and continuous cutting operation and is calculated for the fictitious cross sectional area of 1 m^2.

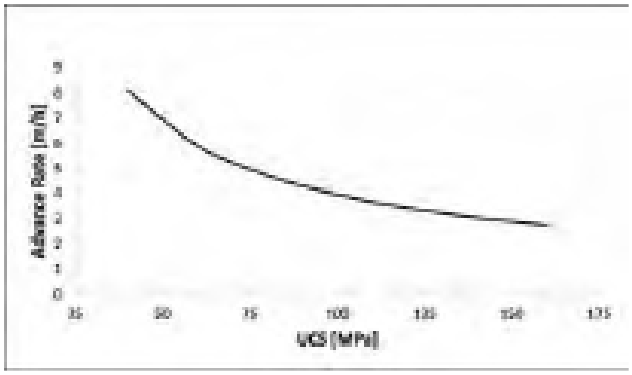

Figure 7. Partial face cutting - Advance rate

3.3 Full-face cutting

In practice, a number of reputable companies have developed small-scale full-face cutting machines. [11, 12, 13, 14] Exemplary machines are: Micro-tunneling machine (MTBM), pipejacking machine and boxhole boring machine.

Those machines already exist with diameters within the range of 1 m. Biggest advantage over the partial-face cutting machines is the ability of excavating hard rock. Despite the size, such machines are capable of excavating rock up to 180 MPa [11, 12, 13, 14].

The net production rate shows the volume of rock excavated per hour (figure 8), calculated after [3] and again based on full-scale laboratory cutting experiments.

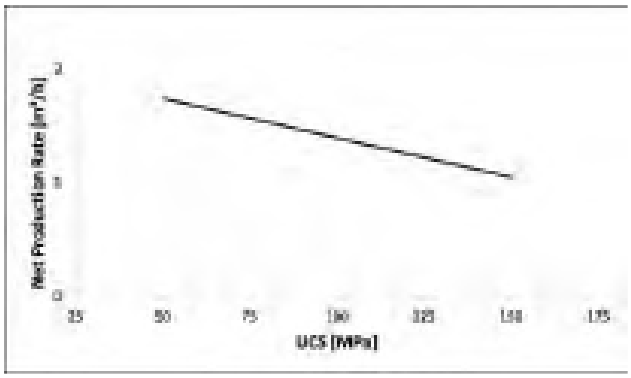

Figure 8. Full face cutting - Net production rate

Theoretically, an average net production rate of 1.5 m^3 per hour is feasible.

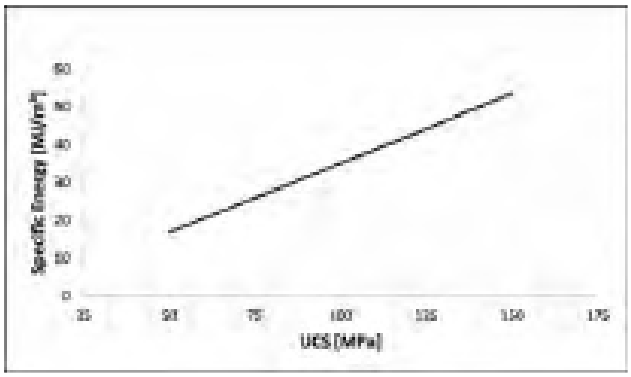

Figure 9. Full face cutting - Specific energy

Compared to the partial-face cutting machines, full-face cutting machines have relatively high specific energies, see figure 9 . Due to the higher power, full-face cutting machines are operating more efficiently in "high specific energy-regions". Specific energy levels are calculated by estimation formula of [3], obtained from full-scale cutting experiments.

The advance rate for the determined tunnel size is shown in figure 10. Ideal and continuous cutting operation is assumed and the fictitious cross sectional area of 1 m^2 is chosen for estimating the advance rate. In contrast to the partial-face cutting machines, the full-face cutting machines' advance generally slower, but does not slow down that much with increasing UCS.

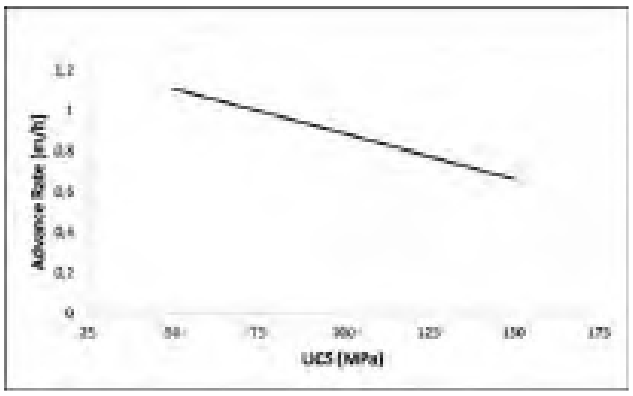

Figure 10. Full face cutting - Advance rate

Eventually, the cutting rate of full-face cutting machines is a crucial parameter to be investigated. The tendencially high cutting forces represent an omnipresent problem of mechanical excavators [3, 7]. [29] has introduced regression models for estimating disc cutting forces. In this certain case, the extraordinarily high cutting forces (calculated after [29]), seen in figure 11, can not be withstood by the robotic miner.

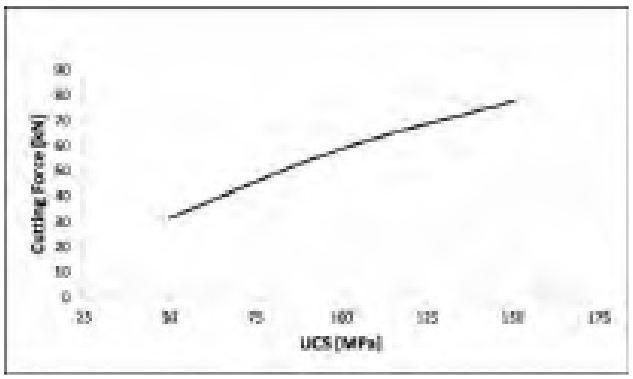

Figure 11. Full face cutting - Cutting force

4 Discussion

From the literature survey and analytical studies following conclusions can be made:

- Advantages of the partial-face cutting systems are the continuous material excavation, the high production rate, the flexibility and the possibility of selective mining. But they are limited by the rock's strength (UCS) and abrasivity (CAI). The excavation process requires very high cutting forces and frequent maintenance of the cutting tool. The cutting forces for excavation hard rock cannot be provided by the given power and weight. Partial-face cutting is only a viable option for small amounts of soft rock. For these special cases, a partial-face cutting robot seems to be a practical solution.
- The capabilities of full-face cutting machines (MTBMs or BBMs) theoretically exceed those of the partial-face cutting machines, but the cutting forces are generally even higher. Furthermore, the less flexibility and higher specific weight are additional limitations and counteract the applicability.
- Drilling and blasting is a very complex process. Multiple, individual tools and working steps increase the efforts of rock excavation and need to be adjusted precisely. Advantages are the comparatively low reaction forces acting on the robot and the excavation of hard rock. To excavate justifiable amounts of hard rock with the given boundary conditions, it is worth to focus on further investigations of drilling and blasting.

In the following chapter, a concept for the implementation of drilling and blasting process is introduced.

5 Conclusion

As explained previously, drilling and blasting requires a minimum of three individual steps:

1. Drilling: Drilling of the borehole
2. Loading: Charging of the boreholes with explosives
3. Hauling/Transporting: Transportation of the fragmented rock

The tool set which is required for excavation process only, consists of a drill, a tool for clearing the blastholes from the drilling debris and an arm for charging the blastholes with the explosives. In figure 12, the implementation of the main operations of the excavation process is visualized. The autonomous work of the mining robot demands a fully mechanized and automated production tool system,

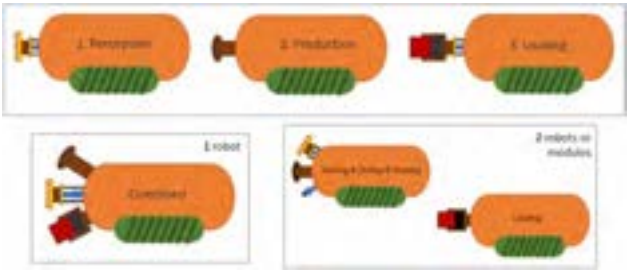

Figure 12. Implementation of drilling and blasting

including drilling, removing residues (debris or small rock grains), loading the blast holes and blasting.

Following the boundary conditions (limited size, weight and power) impede the development of an universally operating robot. Therefore, it is beneficial splitting up the tools into a reasonable number of robots. At least, one drilling and one blasting robot. Due to safety reasons and potential shortage of space inside the robot, the loading setup is completely isolated from the other equipment. In return, other instruments (e.g. perception and navigation instruments) can be installed in the drilling robot.

Aim is to develop a fully mechanized and automated robotic miner, which is capable of detecting the ore, excavating the material and transporting. For a better understanding of the complexity of the drilling and blasting method, a few important points need to be discussed: In addition to the excavation tools, a number of other instruments and equipment are necessary. Navigation and perception shall be executed completely autonomously and demand corresponding technology. If the robot has detected a potential ore vein, a decision of further proceeding has to be made. Samples of the material decide if it is worth mining. A sample can be extracted with the drill and then be assessed in terms of quality by chemical analysis. The fragmented rock is rarely evenly distributed in terms of grain size. Therefore, an on-board crusher is mandatory. After crushing the rock, the material has to be conveyed to a desired area. A feasible, mobile way of transporting material in an underground mining scenario is the slurrification of the excavated rock. Eventually, a couple of side tasks accompany the main excavation process. The mined tunnel possibly requires stabilization and mechanical parts typically tend to wear out. General utility and maintenance are tasks not to be underestimated.

The above mentioned tasks describe an entire mining ecosystem. To turn this ecosystem into a fully autonomously operating operation, it is not avoidable to define a robotic family with complete division of labor. A universal robot body creates the base for the individual robots. The tasks to be executed define the instruments

and tools implemented in every single robot. In this specific case at least six individual modules need to be built. A combination of specific modules can reduce the amount of robots. In figure 13 it is visualized, if every main task is done by an individual robotic vehicle.

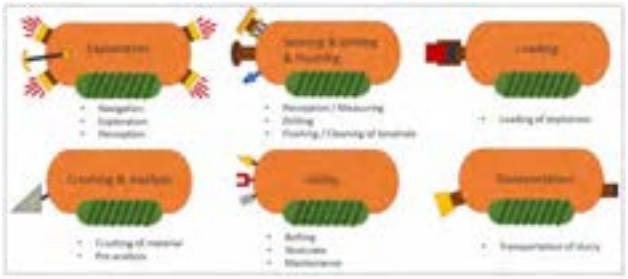

Figure 13. Robot family

The figure shows an exemplary robot family with the following tools implemented:

1. Exploration: Navigation, exploration and perception
2. Sensing, drilling and flushing: Perception / measuring, drilling and clearing of blastholes
3. Loading: Charging of the blastholes with explosives
4. Crushing and analysis: Crushing the fragmented material to evenly distributed size and analyse the excavated material
5. Utility: Stabilization of structures and maintenance
6. Transportation: Transportation of the crushed ore/slurry

Funding

This project has received funding from the European Union's Horizon2020 research and innovation programme under grant agreement No. 820971.

References

[1] Joshua A. Marshall et al. "Robotics in Mining". In: *Springer Handbook of Robotics*. Ed. by Bruno Siciliano and Oussama Khatib. Cham: Springer International Publishing, 2016, pp. 1549–1576. ISBN: 978-3-319-32550-7. DOI: 10.1007/978-3-319-32552-1{\textunderscore}59.

[2] Robert Hiltz. *Taking a step into the robotic future*. 2020. URL: https://www.miningmagazine.com/innovation/news/1387411/taking-step-into-the-robotic-future.

[3] Nuh Bilgin, Hanifi Copur, and Cemal Balci. *Mechanical Excavation in Mining and Civil Industries*. Hoboken: Taylor and Francis, 2013. ISBN: 978-1-4665-8475-4. URL: http://gbv.eblib.com/patron/FullRecord.aspx?p=1408037.

[4] Alex Spathis. *Tunneling in Rock by Drilling and Blasting*. Hoboken: CRC Press, 2012. ISBN: 9780415621410. URL: http://search.ebscohost.com/login.aspx?direct=true&scope=site&db=nlebk&db=nlabk&AN=573100.

[5] Bartłomiej Skawina et al. "Mechanical Excavation and Drilling and Blasting – A Comparison Using Discrete Event Simulation". In: *Mine Planning and Equipment Selection*. Ed. by Carsten Drebenstedt and Raj Singhal. Vol. 62. Cham: Springer International Publishing, 2014, pp. 367–377. ISBN: 978-3-319-02677-0. DOI: 10.1007/978-3-319-02678-7{\textunderscore}36.

[6] *Drilling and excavation technologies for the future*. Washington, D.C: National Academy Press Washington D.C, 2010. ISBN: 978-0-309-05076-0. URL: http://search.ebscohost.com/login.aspx?direct=true&scope=site&db=nlebk&db=nlabk&AN=752.

[7] Nikolaus August Sifferlinger, Philipp Hartlieb, and Peter Moser. "The Importance of Research on Alternative and Hybrid Rock Extraction Methods". In: *BHM Berg- und Hüttenmännische Monatshefte* 162.2 (2017), pp. 58–66. ISSN: 0005-8912. DOI: 10.1007/s00501-017-0574-y.

[8] Epiroc. *Anbaufräsen - Epiroc*. 2020-06-16T06:48:17.000Z. URL: https://www.epiroc.com/de-at/products/excavator-attachments/drum-cutters.

[9] Simex. *TF - Cutter Heads*. 2020-06-16T06:49:15.000Z. URL: https://www.simex.it/en-gb/products/tf-cutter-heads.

[10] D. Festa, W. Broere, and J. W. Bosch. "An investigation into the forces acting on a TBM during driving – Mining the TBM logged data". In: *Tunnelling and Underground Space Technology* 32 (2012), pp. 143–157. ISSN: 08867798. DOI: 10.1016/j.tust.2012.06.006.

[11] The Robbins Company. *Microtunneling Machines | The Robbins Company*. 2017-06-08T06:52:00+00:00. URL: https://www.therobbinscompany.com/products/microtunneling-machines/.

[12] The Robbins Company. *Small Boring Machines | The Robbins Company*. 2020-01-07T23:44:42+00:00. URL: https://www.therobbinscompany.com/products/small-boring-machines/.

[13] Herrenknecht AG. *Boxhole Boring Machine (BBM) - Herrenknecht AG*. 2020-06-16T06:45:12.000Z. URL: https://www.herrenknecht.com/de/produkte/productdetail/boxhole-boring-machine-bbm/.

[14] Herrenknecht AG. *AVN-Maschine - Herrenknecht AG*. 2020-06-16T06:46:00.000Z. URL: https://www.herrenknecht.com/de/produkte/productdetail/avn-maschine/.

[15] Yang Daolong et al. "Research on vibration and deflection for drilling tools of coal auger". In: *Journal of Vibroengineering* 19.7 (2017), pp. 4882–4897. ISSN: 1392-8716. DOI: 10.21595/jve.2017.18581.

[16] Robert P. Mueller et al. "Regolith advanced surface systems operations robot (RASSOR)". In: *2013 IEEE Aerospace Conference*. 2013, pp. 1–12.

[17] V. I. Seroshtan. "Determining the productivity of a bucket-wheel excavator". In: *Soviet Mining Science* 7.3 (1971), pp. 313–316. ISSN: 0038-5581. DOI: 10.1007/BF02501631.

[18] R. Ciccu. "WATER JET IN ROCK AND MINERAL ENGINEERING". In: ().

[19] Paul Hagan. "The cuttability of rock using a high pressure water jet". In: 1992.

[20] Luca Gandossi. *An overview of hydraulic fracturing and other formation stimulation technologies for shale gas production*. Vol. 26347. EUR, Scientific and technical research series. Luxembourg: Publications Office, 2013. ISBN: 9279347292.

[21] Sadao Nakai, Lloyd A. Hackel, and Wayne C. Solomon, eds. *High-Power Lasers in Civil Engineering and Architecture*. SPIE Proceedings. SPIE, 2000.

[22] Constro Facilitator. *Chemical Demolition of Rock and Soil Excavation*. 2019. URL: https://www.constrofacilitator.com/chemical-demolition-of-rock-and-soil-excavation/.

[23] R. Ciccu et al. "Rock disintegration using water jet-assisted diamond tools". In:

[24] Songyong Liu, Hongsheng Li, and Huanhuan Chang. "Drilling Performance of Rock Drill by High-Pressure Water Jet under Different Configuration Modes". In: *Shock and Vibration* 2017.3 (2017), pp. 1–14. ISSN: 1070-9622. DOI: 10.1155/2017/5413823.

[25] Carly Leonida. *Making hard-rock history*. 2016. URL: https://www.miningmagazine.com/innovation/news/1263406/hard-rock-history.

[26] Philipp Hartlieb and Bruno Grafe. "Experimental Study on Microwave Assisted Hard Rock Cutting of Granite". In: *BHM Berg- und Hüttenmännische Monatshefte* 162.2 (2017), pp. 77–81. ISSN: 0005-8912. DOI: 10.1007/s00501-016-0569-0.

[27] PKSC Fernando, Meng Zhang, and Zhijian Pei. "Rotary ultrasonic machining of rocks: An experimental investigation". In: *Advances in Mechanical Engineering* 10.3 (2018), p. 168781401876317. ISSN: 1687-8140. DOI: 10.1177/1687814018763178.

[28] M. Z. Abu Bakar, I. A. Butt, and Y. Majeed. "Penetration Rate and Specific Energy Prediction of Rotary–Percussive Drills Using Drill Cuttings and Engineering Properties of Selected Rock Units". In: *Journal of Mining Science* 54.2 (2018), pp. 270–284. ISSN: 1062-7391. DOI: 10.1134/S106273911802363X.

[29] Jamal Rostami. "DEVELOPMENT OF A FORCE ESTIMATION MODEL FOR ROCK FRAGMENTATION WITH DISC CUTTERS THROUGH THEORETICAL MODELING AND PHYSICAL MEASUREMENT OF CRUSHED ZONE PRESSURE". PhD thesis. May 1997.

Robotic Insertion of Timber Joints using Visual Detection of Fiducial Markers

N. Rogeau[a], V. Tiberghien[a], P. Latteur[b] and Y. Weinand[a]

[a]Laboratory for Timber Constructions, Ecole Polytechnique Fédérale de Lausanne, Switzerland
[b]Louvain School of Engineering, Université Catholique de Louvain, Belgium
E-mail: nicolas.rogeau@epfl.ch

Abstract –

Timber building industry is facing a major transformation with digitalization and automation being more broadly adopted. Prefabricated timber frame structures can be mass-produced on large robotic assembly lines, increasing the productivity and competitiveness of wood over standard inorganic materials such as steel or concrete. While standardization is likely to limit creativity, new digital tools, on the contrary, give the possibility to design and build complex and unique geometries. Recent research in bespoke digital prefabrication notably led to the development of Integrally Attached Timber Plate Structures (IATPS). This system consists in assembling wooden panels connected only with timber joints inspired by traditional Japanese carpentry. The elements are digitally prefabricated and inserted into one-another to form bespoke architectural structures. In order to propose a fully automated process for IATPS, from design to construction, this paper investigates a method for assembling the panels with a 6-axis robotic arm. Preliminary studies have shown that significant discrepancies can occur between virtual models and physical prototypes due to joint tolerances, hygrometric variations, and self-weight deformations. To address this challenge and to adapt the robot position to the actual location of the elements, a visual feedback loop was developed using fiducial markers. Several tests were performed with structural wood panels to assess the accuracy of the method for different configurations and adapt the geometry of the joints in consequence. Finally, the insertion of a panel with two through-tenon joints was achieved by taking pictures of the target with a camera mounted on the end-effector of the robot.

Keywords –

Robotic assembly; Timber joints; Fiducial markers; Insertion

1 Introduction

The construction sector is recognized as one of the main players in the current ecological crisis, as the production of new construction materials is responsible for a significant share of CO_2 emissions and plays a major role in the generation of landfill waste. In order to reach the Sustainable Development Goals set by the United Nations for 2030 [1], it is necessary to reconsider the whole construction process and take material life cycles into account upstream in the design phase.

Engineered wood products have been identified as an alternative to commonly used concrete and steel components, which could lead to more sustainable construction systems by lowering the embodied carbon energy of the structure [2]. In addition, connections between timber panels can be integrated into the element geometry taking inspiration from traditional timber joinery techniques and benefiting from recent advances in digital fabrication to generate the toolpath [3]. This construction system, also referred to as Integrally-Attached Timber Plate Structures (IATPS), reduces the number of steel fasteners and improve the structural performance. Since additional connectors are not required, the amount of time allowed to the construction phase can also be reduced.

Previous research has both demonstrated the architectural and structural interest of IATPS, leading to the realization of large-scale projects such as the theater of Vidy [4], the BUGA wood pavilion [5], and the Annen head office [6]. Different workflows have been set up for each of those projects in order to integrate fabrication constraints in the design and automate the cutting of the different pieces using a CNC machine or a 6-axis robotic arm. For the BUGA wood pavilion, collaborative robots have also been used to glue the construction components. However, for each of the three projects, the assembly of the different modules remained a manual process.

First investigations about the robotic assembly of IATPS have highlighted two main challenges for automating the insertion of timber joints [7]. First, friction forces are growing with the number of connections and can hinder the insertion. Second, the robotic insertion has to be performed with enough precision to avoid the introduction of gaps, which would decrease the rigidity of the connections. This paper focuses on the development of a method combining different strategies to automate the insertion of the panels.

2 State of the art of robotic insertion

Pick and place operations are usual tasks, which can be handled by industrial robotic arms. If the initial and final positions of the objects relative to the robot are known, the trajectory can be easily computed and the precision of the insertion will only depend on the accuracy of the robot from point to point. However, for large and heavy construction elements, significant discrepancies can occur between virtual models and reality. Timber panels are typically subject to slight dimensional changes over time and are very sensitive to hygrometric variations. Even for standardized elements, fabrication tolerances are usually around 1 mm. Besides, wood-wood connections are not ideally rigid and gaps in the joints can add up through the structure causing large deviations and preventing the robot from assembling the pieces. Three strategies, which can be combined to ensure a precise insertion, have been identified in the literature and presented here.

2.1 Self-centering connections

A first method consists in adapting the design of the connections to enhance the tolerance and progressively guide the pieces to the final position. Usually the modification consists in chamfering one or both pieces or adding a separated guide.

Conic joints with a tolerance about 4 cm have for example been used in the FutureHome Project [8] in order to compensate for the swing of the automated crane, which was used to assemble the large modules. The slope of the cone was related to the friction forces between the different parts. In the extreme case of structures assembled by drones were precision is an even bigger challenge, specific joints have also been developed for masonry and timber elements [9]. Chamfering through-tenon joints is a commonly used technique in traditional woodworking. Such joints have notably been optimized for the insertion of the panels of the double-layered timber plate structure of the Vidy Theater [4].

A potential downside effect of self-centering connections is the diminution of the rigidity of the joint as the induced slopes are leading to smaller bending resistance.

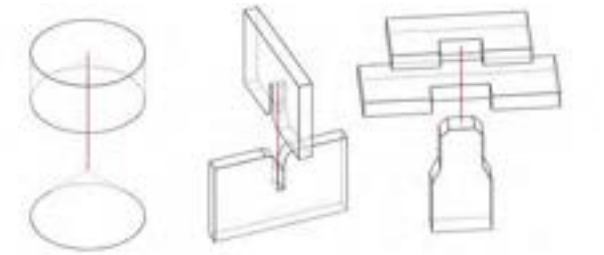

Figure 1. Three types of self-centering connections: conic joint (left), drone-compatible joint for interlocked timber beams (middle), and chamfered through-tenon joint (right).

2.2 Force sensitive end effectors

As manual insertion relies mostly on haptic feedback, another strategy is to use torque sensors to adapt the robot position according to the measured forces. A classic example consists in trying to insert a peg in a hole using integrated force sensors to align the robot position [10]. The need to manage material tolerances by developing robot sensitivity has also been illustrated in the DIANA project [11] where a robotic arm was interactively taught how to insert wooden rods to shape a ruled surface.

Impedance control has also been used for the insertion of gear-shaft mechanisms with a precision around 5 μm for applications in medical fields or aeronautics [12]. More complex feedback loops using behavior-based or machine learning approaches have also been used to develop optimal strategies for inserting pieces into one another [13].

However, the interpretation of the measured force is always dependent of the shape and weight of the piece to insert and the above-mentioned techniques are established for standards symmetrical elements. Developing an adaptive strategy for the case of timber joinery is challenging as elements come in different sizes and the number and type of connections can also vary.

2.3 Visual feedback

Different position tracking systems based on visual feedback loops have been already developed for on-site applications and could also be applied off-site.

A total station can be used to track selected points and deduce the robot position by triangulation while another possibility is to rely on cameras and image recognition. A comparative study has highlighted the performance of fiducial markers for reducing deviation with a clear advantage regarding the execution speed [14]. Fiducial markers have also been used to guide the In situ Fabricator developed at ETH Zurich [15].

Other applications of visual detection includes precisely laying mortar on a brick wall [13] and assembling large modular frames [16] using a combination of cameras and lasers to guide the insertion.

Photogrammetry and laser scanning technologies have also been combined with robotic arms to gather data on-site for indoor and outdoor localization [17][18][19]. However, image reconstruction, point cloud acquisition, and mesh post processing are all computationally intensive and data interpretation requires complex machine-learning algorithms in order to work with different geometries.

3 Methodology

3.1 Integrated design framework

Our approach consists in linking project design and technical constraints by means of computational geometry. Instead of locally solving the insertion problem, the goal is to inform the designer with fabrication and assembly constraints by developing a cross-platform workflow. Custom scripts are used to convey the geometric information between software.

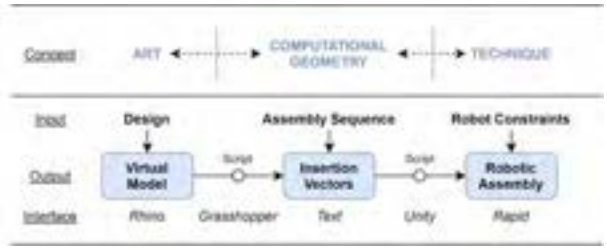

Figure 2. Integrated design framework linking design to robotics constraints.

The assembly is driven by three major inputs: design, assembly sequence, and robot constraints. In a traditional workflow each input is integrated one at a time in the construction process. Digitalization allows for more agility since parameters can be modified and information can flow back and forth.

It was decided to rely on existing specialized software for each part of the workflow instead of building a single custom program from scratch. *Rhinoceros 6* (Robert McNeel & Associates) was chosen as the design interface and the plugin *Grasshopper* as a tool to extract and manipulate data from the model. To simulate and execute the robot trajectory, the research benefitted from a collaboration with a specialized industrial partner, Imax Pro S.A. A custom application was developed, for the purpose of the research project, on the game engine *Unity* (Unity Technologies) to convert geometric data from text file to robot instructions.

Splitting the workflow between different software avoided making compromises between design possibilities and robotic performance. Meanwhile custom scripts ensured a smooth transition between the different interfaces allowing almost instantaneous feedback and testing of multiple design iterations.

3.2 Insertion vectors

Insertion vectors are an essential parameter for IATPS as the geometry of the joints is tightly connected to the assembly sequence. In fact, it is not possible to design the shape of the connectors without knowing the trajectory of the insertion beforehand. The integration of fabrication and assembly constraints follows an iterative process and is inherent to the design of IATPS.

A parametric script was thus coded inside the Grasshopper interface to deduce insertion vectors from a geometric input and a specific assembly sequence. Contact zones are identified by computing intersections between the panels while the type of joints that is generated depends on which faces are connected (e.g. through-tenon joints are created for a connection between the side of a panel and the face of its neighbor).

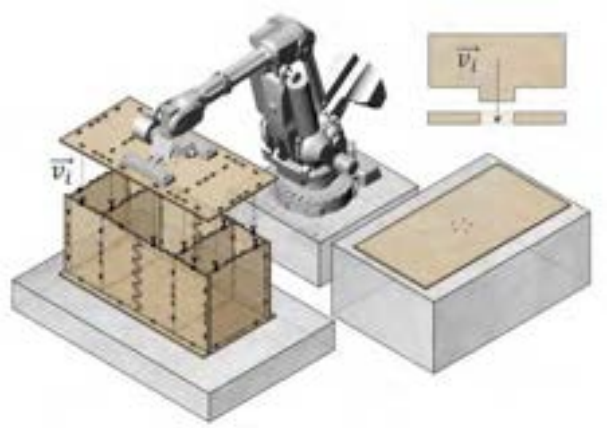

Figure 3. Insertion vectors are inducing the shape of the connections as well as the robot trajectory.

Once the 3D model is created, the contour of the panel can be extracted and the panels can be cut using a CNC. Then insertion vectors are used a second time to generate the robot trajectory, as further described in section 3.5.

3.3 Position detection using fiducial markers

Given the variety of possible configurations for IATPS, the use of fiducial markers was found to be the most efficient method to keep track of the position of the different timber panels. The open-source library OpenCV [20] provides a robust solution for estimating the position of fiducial markers (ArUco) from different sizes. A custom python executable was, therefore, developed to assess the performance of the detection before being integrated to the global workflow.

The algorithm consists in taking one picture from a targeted marker on a panel, computing its orientation and position coordinates and saving those results in a text file. This information is later accessed by the robot controller to update the trajectory.

The image is processed by applying perspective transformation and thresholding to get potential markers from the pixels. Analyzing the color of the 36 cells composing the ArUco provides the unique identification number of the marker. The position and the orientation are obtained by finding the tridimensional transformation from the coordinate system of the camera to the coordinate system of the marker. Rotations are obtained in Euler angles but converted to quaternions to ease the conversion to Unity software, which is using another axes convention.

Figure 4. Image processing of an ArUco Marker using OpenCV library to get the position and orientation of a timber panel.

A key feature of the developed application is that the position of the different targets constituting the robot trajectory are expressed relatively to different coordinate systems. The position of some targets is associated to the coordinate system of the starting location while the position of some other targets is expressed relatively to the position and orientation of an ArUco marker. Hence, updating the position of this marker will automatically update the absolute coordinates of all associated targets while others will remain unchanged.

A unique marker has to be assigned to each panel and positioned at the center of gravity of the panel. Although the point of reference can be set arbitrarily, making it coincide with the point from which the tool would lift the panel, seems the most logical. Potential bending of the panel is minimized by picking it from its center of gravity.

Before proceeding to the robotic assembly, the position of the stack of panels is precisely referenced. Hence applying the visual feedback loop to adjust the starting location of the panels was not considered as necessary and only the end point of each trajectory is updated using fiducial markers. Prior to each pick and place operation, pictures of a marker, placed on the panels on which the insertion will occur, are taken with a camera mounted on the robotic arm (technical specifications are given in 4.1).

3.4 Fail-safe process

One drawback of working in relative with a feedback loop is that detection errors can potentially lead to unexpected trajectories, different from the simulation. Indeed, under certain circumstances, such as in case of insufficient luminosity or when the marker is too far or in the periphery of the angle of view of the camera, the precision of the detection significantly decreases.

In order to prevent updating the position of the marker with inaccurate coordinates, it was decided to take three pictures of each marker at different angles and set two tolerance parameters. If the dispersion of the results or the deviation from the model is too high, new pictures are taken and the updated values are again compared.

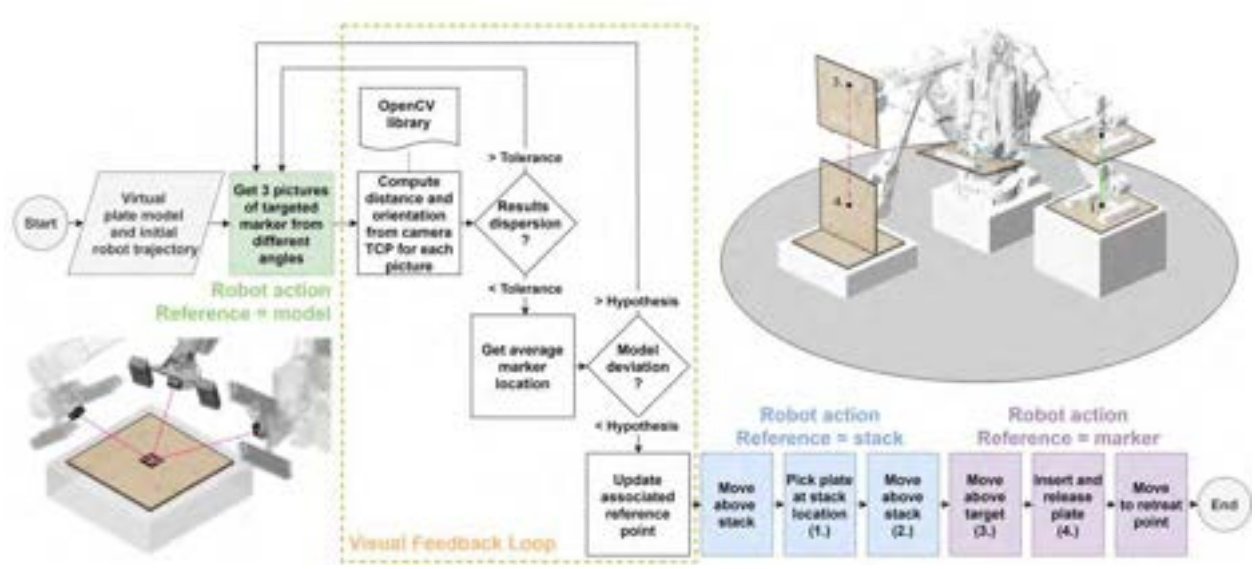

Figure 5. Robotic workflow: camera shooting with robot moving according to model (green), image processing (orange), picking phase with robot moving according to the stack of panels (blue), insertion phase with robot moving according to marker (purple).

3.5 Robotic Workflow

Putting together the initial information given by the insertion vectors with the visual feedback loop, a complete workflow was established to insert the timber panels with a robotic arm (Figure 5). No path planning algorithm was used for the robot trajectory. Instead a strategic approach was preferred.

After the first panel of the sequence is placed, the robot positions itself above the marker using the information of the model as reference. The visual feedback loop is executed and pictures are taken from different angles at a distance of about 50 cm. Then the position of the marker in the virtual model is updated through image processing.

The second step consists in picking the next panel at the stack location. As the position of the stack as well as the dimensions of the panels are known, the robot uses that information to move right above the stack and lift the panel from its center of gravity.

For the third step, the updated position of the fiducial marker is used as the new system of reference and a target is generated above the place of assembly. As a linear move is not always possible between those two position, a joint move is then preferred for this part of the trajectory. In order to constrain the interpolation additional targets can eventually be created in between.

For the last step, the insertion of the panel is finally performed (Figure 7). The robot reaches a target located a few centimeters away from the final position, in the opposite direction of the vector of insertion associated to the panel. Then it follows that vector until the panel is inserted. The panel is released by the vacuum gripper and the robot moves away along the normal to the panel surface before going back above the assembly. A structure is gradually assembled by repeating the process with the next panels.

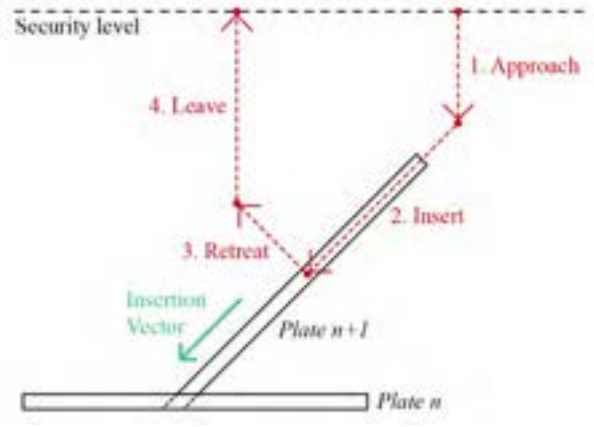

Figure 6. 2D representation of the assembly strategy based on the vector of insertion associated to the panel.

3.6 Intermediate robot language

Once established, the workflow was converted to robot instructions. Target positions and special actions such as taking a picture or activating the vacuum gripper were interpreted from a text file, which was manually typed or automatically generated by script (e.g. in the case of complex assemblies or when a high number of elements needs to be inserted). An intermediate programming language with a high level of abstraction was therefore developed in order to integrate custom commands.

Two examples of instructions are given in Figure 7. The number of parameters on each line depends on the first keyword: *Camera* will start the visual feedback loop and requires 4 additional parameters while *JointMove* requires up to 12 parameters including the coordinates of the targeted position to execute an unconstrained motion between the actual position of the robot and the specified point.

Other typical commands include *LinearMove,* which takes the same parameters as *JointMove*, *Vacuum* followed by *On/Off,* which is used to activate the suction of the gripper, and *Wait* followed by a number to pause the execution of the code during a certain amount of time.

Finally, each line of the code is parsed by our application in Unity for simulation, and converted to the specific programming language of the robot for execution. On a side note, the additional layer of abstraction added by this intermediate language proved to significantly enrich the user-experience by providing an explicit workflow.

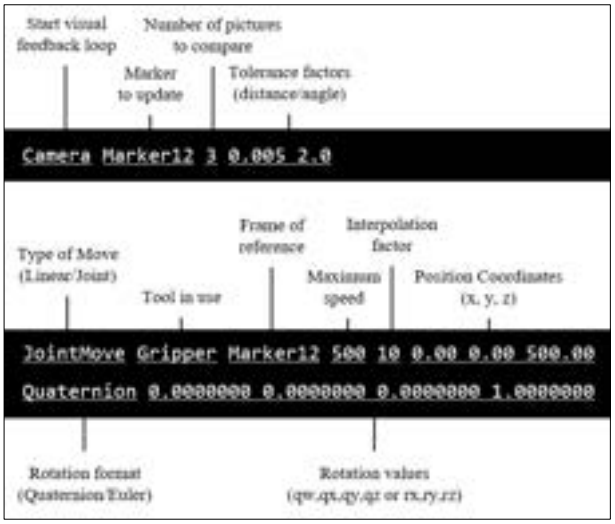

Figure 7. Samples of a text file interpreted by our custom application in Unity to send instructions to the robot controller: Activation of the visual feedback loop (top) and joint move above a marker (bottom).

4 Tests and results

4.1 Experimental set up

Experiments were led with a 6-axis robotic arm (ABB IRB 6400R) with a reach of 2.5 m. The end effector was equipped with two vacuum grippers, which can lift panels up to 80 kg. In addition, a standard webcam (Logitech C270) with a resolution of 1 megapixel was mounted on top of the robot effector and connected by USB cable in order to take pictures of the ArUco markers. Calibration was carried out by taking a series of 20 pictures of an ArUco board from different angles to get the intrinsic parameters of the camera such as the focal distances and the center of the camera. Fiducial markers were then printed as 10 cm square and precisely fixed to the center of the panels following guiding lines previously engraved with a CNC.

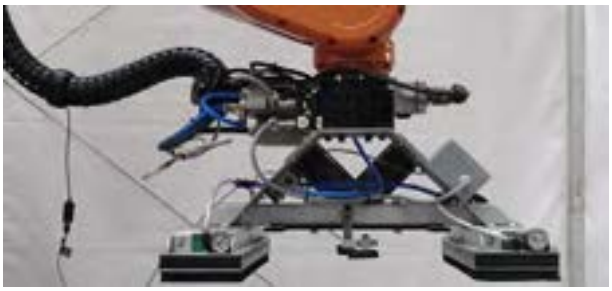

Figure 8. End-effector of the robot equipped with a vacuum gripper and camera for visual feedback.

4.2 Insertion without visual feedback loop

A first test was led without the visual feedback loop to evaluate the difficulty of inserting panels with a robotic arm. The objective was to automate the assembly of 3 non-orthogonal timber boxes composed of 13 panels of 45 mm thick cross laminated timber (CLT). The gap between the tenon and the mortise was set to 0.5 mm to reduce friction forces and reached up to 0.7 mm in some cases due to slight material deformations in addition to the tolerance of fabrication.

Figure 9. Assembly of 13 non-orthogonal timber panels without using the visual feedback loop.

The accumulation of small discrepancies due to the tolerance in the joints and the dimensional variation of the panels caused large deviations between the virtual model and the physical prototype. When inserting the last panel, a difference of about 1 cm was measured at the top of structure. This could be explained by the fact that only the first panel was anchored while the rigidity of the connections for the other panels was not enough to prevent them from slightly rotating. This led to the impossibility of assembling the pieces without a manual intervention. In conclusion, as inaccuracy increases with the number and the size of the elements in the structure, a visual feedback loop was found to be necessary.

4.3 Precision of the visual feedback loop

Prior to testing the insertion of panels, the accuracy of the visual feedback was evaluated. The position of the camera in relation to the end effector of the robotic arm was found by manually referencing the position of 4 markers (Figure 10) and matching the values obtained by taking a picture. It is assumed that both the calibration of the sharp tool and the manual referencing of the markers was achieved with a precision of about 0.5 mm.

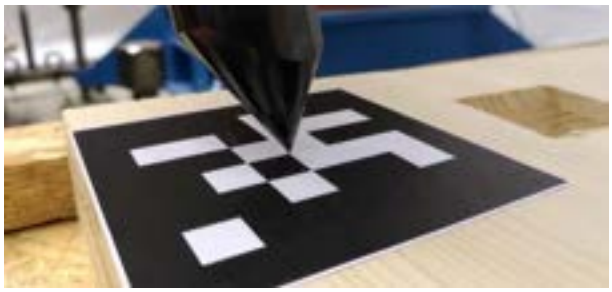

Figure 10. Finding relative camera position by comparing manually referenced coordinates with computed values from the visual feedback.

Once the position of the camera was properly set up, new pictures were taken with multiple camera orientations and distances and the acquired data was compared with the coordinates of the manually referenced markers. Three pictures were taken at each location to assess the consistency of the results.

Extreme values for distances of 30, 50 and 80 cm between the camera and the fiducial marker are reported in Figure 11. Both precision and accuracy were affected by the distance from which the picture was taken. However, below 30 cm, the dispersion of the results stayed below 1 mm, which stays in the range of precision of the manual measurements. Further than 50 cm, the accuracy of the visual detection was decreasing considerably reaching several millimeters at 80 cm. In addition, a loss of precision was also observed as the dispersion of the results which were obtained from the same camera position raised to 2 mm at 80 cm.

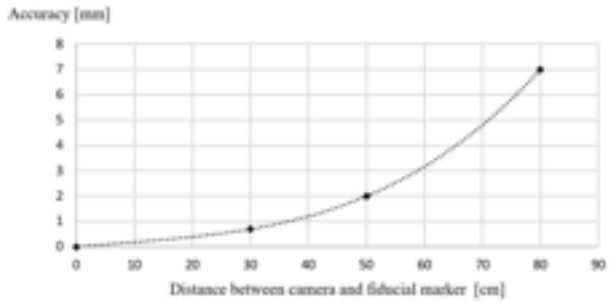

Figure 11. Maximum distance between target position and the results obtained with the visual feedback loop.

Additional tests were performed with different orientations of the robot end-effector and also produced slight deviations from the referenced point. Targets on the edge of the field of view of the camera were particularly misinterpreted by the algorithm and reported position errors up to 2 cm. On one hand, the calibration of the camera was found to be a key parameter to reach more accurate results but was, at the same time, limited by the precision of the manual measurements. On the other hand, the precision of the detection was also limited by the algorithm itself and the exactitude of the spatial transformation.

4.4 Insertion with visual feedback loop

Based on the previous results, a tolerance threshold was established. It was shown that all pictures taken at a distance below 50 cm, with the camera parallel to the marker, were interpreted with a maximum error of 3 mm. The design of the timber joints was therefore adapted in consequence to match that tolerance threshold as shown in Figure 12.

A test of insertion was conducted using two panels with 1 square meter each connected by two trough-tenon joints. Following the principles of auto-centering connections, a chamfer of 4 mm was applied to tenons and mortises. As the fabrication process excluded cutting the panel from below, the chamfer was doubled on top of the tenon instead of being equally distributed. Using the visual feedback loop, the two panels could finally be inserted into one another (Figure 13).

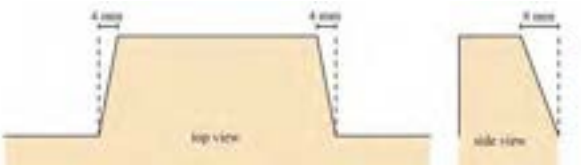

Figure 12. Chamfered tenon based on the measured precision of the visual feedback loop.

Figure 13. Insertion of a laminated veneer lumber (LVL) panel with the visual feedback loop.

5 Conclusion and outlook

A complete workflow was established to assemble prefabricated timber panels connected by wood-wood connections with a robotic arm. The study included the development of a strategy of insertion using different software and linking design and assembly constraints by the means of computational geometry. In addition, an explicit programming language was introduced to ease the interactions between designer and machine.

A particular focus was set on performing a precise insertion despite the large deviations that might occur between physical prototypes and virtual models. The visual detection of fiducial markers, which can easily be placed on top of timber plates, was found to be a cheap and effective solution for updating the position of the panels through a feedback loop.

The evaluation of the method performance showed satisfying results at distances up to 50 cm. For larger distances, the precision of the detection of the markers showed some limitations but could probably be enhanced by refining camera calibration. Eventually, increasing the camera resolution or the size of the ArUco markers could improve the quality of image processing and lead to better outcomes.

Finally, applying the visual feedback loop to the assembly of two timber plates demonstrated the potential of the concept and the feasibility of the proposed workflow in order to automate the assembly of Integrally Attached Timber Plate Structures. The method presented in this paper could have applications on-site. However, further research is still required to extend the workflow to the architectural scale such as solving issues related to friction when inserting multiple joints at the same time.

Acknowledgement

This research was supported by the NCCR Digital Fabrication, funded by the Swiss National Science Foundation (NCCR Digital Fabrication Agreement #51NF40-141853). In addition, the authors would also like to acknowledge Imax Pro S.A. for the technical support regarding the integration of the robotic system.

References

[1] United Nations. Sustainable Development Goals. Online: https://sustainabledevelopment.un.org/, Accessed: 18/05/2020.

[2] Churkina G. Organschi A. Reyer C. Ruff A. Vinke K. Liu Z. Reck B. Graedel T.E. Schellnhuber H.J. Buildings as a global carbon sink. *Nature Sustainability*, 3, 269-276, 2020.

[3] Robeller C. Integral Mechanical Attachment for Timber Folded Plate Structures. EPFL, 2015.

[4] Robeller C. Gamerro J. Weinand Y. Théâtre Vidy Lausanne - A double-layered timber folded plate structure. Journal of the International Association for Shell and Spatial Structures, 58(4):295–314, 2017.

[5] Alvarez M. Wagner H.J. Groenewolt A. Krieg O.D. Kyjanek O. Sonntag D. Bechert S. Aldinger L. Menges A. and Knippers J. Integrative interdisciplinary advancements of digital timber architecture - The BUGA Wood Pavilion. In *Proceedings of the Association for Computer Aided Design in Architecture, Austin, United States, 2019.*

[6] Nguyen A.C. Vestartas P. Weinand Y. Design framework for the structural analysis of free-form timber plate structures using wood-wood connections. *Automation in Construction*, 107, 2019.

[7] Robeller C. Weinand Y. Helm V. Thoma A. Gramazio F. Kolher H. Robotic Integral Attachment. *Fabricate*, 2017.

[8] Balaguer C. Abderrahim M. Navarro J.M. Boudjabeur S. Aromaa P. Kahkonen K. Slavenburg S. Seward D. Bock T. Wing R. and Atkin B. FutureHome: An integrated construction automation approach. *Robotics and Automation Magazine*, 9(1):55–66, 2002.

[9] Goessens S. Rogeau N. De Beusscher G. Mueller C. Latteur P. Parametric Design of Drone-Compatible Architectural Timber Structures. In *Proceedings of the International Association for Shell and Spatial Structures (IASS)*, Boston, United States, 2018.

[10] Strip D.R. Technology for Robotic Mechanical Assembly: Force - Directed Insertions. *AT&T Technical Journal,* 67(2):23-34, 1988.

[11] Odehnal B. Hornung P. Santorso K. Ambrosz B. Sampl G. Golob E. Brell-Cokçan S. Braumann J. Cokçan B. Robotic Woodcraft - Towards The Craftmanship Of The Future. University of Applied Arts Vienna, 2019.

[12] Guo P. Zhang Z. Liu Y. Sun W. Li Z. Precision assembly method based on coaxial alignment and force control. *Journal of Physics: Conference Series*, 1303, 2019.

[13] Elashry K. Glynn R. An Approach to Automated Construction Using Adaptive Programing. In *Proceedings* of *Robotic Fabrication in Architecture*, *Art and Design*, pages: 51–66, 2014.

[14] Iturralde K. Kinoshita T. Bock T. Grasped Element Position Recognition and Robot Pose Adjustment during Assembly. In *Proceedings of 36th International Symposium on Automation and Robotics in Construction*, pages: 461-468, Banff, Canada, 2019.

[15] Giftthaler M. Sandy T. Dörfler K. Brooks I. Buckingham M. Rey G. Kohler M. Gramazio F. Buchli J. Mobile robotic fabrication at 1:1 scale: the In situ Fabricator System, experiences and current developments. Construction Robotics, 1:3–14, 2017.

[16] Qin Z. Wang P. Sun J. Lu J. Qiao H. Precise Robotic Assembly for Large-Scale Objects Based on Automatic Guidance and Alignment. *IEEE Transactions on Instrumentation and Measurement*, 65:1398–1411, 2016.

[17] Vincke S. Bassier M. Vergauwen M. Image Recording Challenges for Photogrammetric Construction Site Monitoring. *ISPRS Annals of the Photogrammetry*, *Remote Sensing and Spatial Information Sciences*, pages: 747–753, 2019.

[18] Kim P. Chen J. Cho Y.K. Autonomous mobile robot localization and mapping for unknown construction environments. *Construction Research Congress*, pages: 147-156, 2018

[19] Gawel A. Blum H. Pankert J. Krämer K. Bartolomei L. Ercan S. Farshidian F. Chli M. Gramazio F. Siegwart R. Hutter M. Sandy T. A Fully-Integrated Sensing and Control System for High-Accuracy Mobile Robotic Building Construction. *International Conference on Intelligent Robots and Systems (IROS)*, 2019.

[20] Garrido-Jurado S. Muñoz-Salinas R. Madrid-Cuevas F.J. Marín-Jiménez M.J. Automatic generation and detection of highly reliable fiducial markers under occlusion, *Pattern Recognition,* 47:2280–2292, 2014.

Constraint Control of a Boom Crane System

Michele Ambrosino[a], Arnaud Dawans[b], Emanuele Garone[a]

[a]Service d'Automatique et d'Analyse des Systèmes, Universitè libre de Bruxelles, Brussels, Belgium
[b]Entreprises Jacques Delens S.A., Brussels, Belgium

Michele.Ambrosino@ulb.ac.be, adawans@jacquesdelens.be, egarone@ulb.ac.be

Abstract -

Boom cranes are among the most used cranes to lift heavy loads. Although fairly simple mechanically, from the control viewpoint this kind of crane is a nonlinear underactuated system which presents several challenges, especially when controlled in the presence of constraints. To solve this problem, we propose an approach based on the Explicit Reference Governor (ERG), which does not require any online optimization, thus making it computationally inexpensive. The proposed control scheme is able to steer the crane to a desired position ensuring the respect of limited joint ranges, maximum oscillation angle, and the avoidance of static obstacles.

Keywords -

Boom crane; Constrain control; Obstacle avoidance; Explicit reference governor; underactuated system.

1 Introduction

Cranes are one of the most commonly used devices to hoist heavy equipment and/or materials. Due to benefits such as high maneuverability and low costs, boom cranes are particularly common. Compared with gantry cranes and tower cranes, boom cranes are much more flexible and can be easily transported and deployed. Currently, this kind of cranes are operated manually. The piece is moved in proximity of its final position, then, a worker uses his hands to finish the positioning. Considering the potentials dangers and uncertain factors of manual operations, it is essential to design efficient control methods to improve the control performance of boom cranes and restrict the payload swing amplitudes.

Compared with gantry cranes, that are simpler and have been extensively studied in the literature, boom cranes have much more coupled and nonlinear dynamics [1]-[2]. In particular, boom cranes involve pitching and rotational movements, which generate complicated centrifugal forces, and consequently, make the equations of motion highly nonlinear. Furthermore, as all cranes, boom cranes are underactuated [3], having fewer independent actuators than the system degrees of freedom (DoFs). Accordingly, it is fairly challenging to control boom cranes effectively.

In the literature, some interesting and meaningful solution have been proposed for the control of boom cranes[4]. Open loop control schemes have been widely used because they are easy to implement. Input shaping is one of the most used open loop techniques based on a linear system. [5] discusses three types of input shapers including positive and modified specified negative amplitude, positive zero vibration, and positive zero-vibration-derivative input shapers, which can reduce the sway angle during rotation. [6] proposes a combination of input shaping and feedback control to counteract the effect of the wind. Open-loop trajectory planning methods [7]-[8] such as the S-curve trajectory and the straight transfer transformation model, are proposed and demonstrated to be effective for boom crane systems. The main drawback of open loop control schemes is that they are sensitive to external disturbances and to model mismatch.

Recently some research focused on the development of closed-loop control schemes for boom cranes. Closed-loop control methods allow for increased robustness and can usually lead to better control performance in the presence of perturbations. A Linear Quadratic Regulator (LQR) is used in [9] with a cameras system to move the crane to the desired position and reduce the payload swing angles. To reduce the payload oscillation of boom cranes, [10] proposes a delayed position feedback antiswing control strategy. In [11] the authors present a partial-state feedback control method with an integrator to achive accurate rotary positioning and swing suppression. A Model Predictive Control (MPC) for an industrial boom crane is shown in [12]. A second-order sliding mode control law is proposed in [13] for trajectory tracking and anti-sway control. In addition to model-based controllers, a series of intelligent algorithms, such as neural networks [14] and fuzzy logic control [15], are also introduced for boom cranes to improve the overall control performances.

Note that almost all existing control approaches focus on stabilization objectives, i.e., boom positioning and payload swing suppression. However, from the practical perspective, the payload swing's transient responses also need to be ensured, e.g., swing angles should be restricted within prescribed safety ranges to ensure stable transportation. Furthermore, it must also be guaranteed that the trajectories avoid obstacles (e.g. walls).

On the basis of this analysis it is possible to point out two open problems in the control of boom cranes:

- Existing closed-loop control laws focus on reducing residual oscillations only when the system reaches the desired position. Instead, a good control strategy should take into account of oscillations throughout the movement in order to reduce the energy stored by the system and avoid potentially dangerous situations;
- There are only few results for the trajectory planning (and for obstacle avoidance) for this kind of crane (see e.g. [16]). These solutions are almost always very complicated, based on the specific nonlinear trajectory planning process and focus on kinematics aspects, not taking into account the dynamics of the crane.

Recently a novel approach for the control of nonlinear systems subject to constraints called Explicit Reference Governor (ERG) has been introduced in [17]-[18]. The ERG is an add-on control unit to be used on a pre-stabilized system and is based on the general Reference Governor (RG) philosophy (see [19] for a survey on RG schemes) which ensures constraint satisfaction by manipulating the reference of a pre-stabilized system so that the transient response does not violate the constraints. An interesting feature of the ERG is that it can enforce both state and input constraints of nonlinear systems without having to solve an online optimization problem.

This paper *aims* at designing a novel control framework, the ERG, for boom crane subject to limited joint ranges and static obstacle avoidance constraints.

2 Dynamic Model and Problem Statement

The dynamic model of a 3-D boom crane (see Fig. 1), with fixed cable length, can be described by the following equations [7]:

Figure 1. Model of an underactuated boom crane system. [20]

$$
\begin{aligned}
&ml^2(1+\theta_1^2)\ddot{\theta}_1 + ml^2\theta_1\theta_2\ddot{\theta}_2 + mlL(-\theta_1 sin\theta_3 + cos\theta_3)\ddot{\theta}_3 \\
&-ml^2\theta_2\ddot{\theta}_4 + ml^2\theta_1(\dot{\theta}_1^2\dot{\theta}_2^2) - mlL(sin\theta_3 + \theta_1 cos\theta_3)\dot{\theta}_3^2 \\
&-ml(l\theta_1 + Lsin\theta_3)\dot{\theta}_4^2 - 2ml^2\dot{\theta}_2\dot{\theta}_4 + mgl\theta_1 = 0,
\end{aligned} \tag{1}
$$

$$
\begin{aligned}
&ml^2\theta_1\theta_2\ddot{\theta}_1 + ml^2(1+\theta_2^2)\ddot{\theta}_2 - mlL\theta_2 sin\theta_3\ddot{\theta}_3 \\
&+(ml^2\theta_1 + mlLsin\theta_3)\ddot{\theta}_4 + ml^2\theta_2(\dot{\theta}_1^2 + \dot{\theta}_2^2) \\
&-mlL\theta_2 cos\theta_3\dot{\theta}_3^2 - ml^2\theta_2\dot{\theta}_4^2 + 2ml^2\dot{\theta}_1\dot{\theta}_4 + 2ml^2\dot{\theta}_1\dot{\theta}_4 \\
&+2mlL\dot{\theta}_3\dot{\theta}_4 cos\theta_3 + mgl\theta_2 = 0,
\end{aligned} \tag{2}
$$

$$
\begin{aligned}
&mlL(cos\theta_3 - \theta_1 sin\theta_3)\ddot{\theta}_1 - mlL\theta_2 sin\theta_3\ddot{\theta}_2 \\
&+(mL^2 + J_y)\ddot{\theta}_3 - mlL\theta_2 cos\theta_3\ddot{\theta}_4 - mlLsin\theta_3(\dot{\theta}_1^2 + \dot{\theta}_2^2) \\
&-[\tfrac{1}{2}(J_x - Jz)sin(2\theta_3) + mlL\theta_1 cos\theta_3 + \tfrac{1}{2}mL^2 sin(2\theta_3)]\dot{\theta}_4^2 \\
&-2mlL\dot{\theta}_2\dot{\theta}_4 cos\theta_3 - g(\tfrac{1}{2}ML + mL - \tfrac{1}{2}M_1L_1)sin\theta_3 = u_3,
\end{aligned} \tag{3}
$$

$$
\begin{aligned}
&-ml^2\theta_2\ddot{\theta}_1 + (ml^2\theta_1 + mlLsin\theta_3)\ddot{\theta}_2 - mlL\theta_2 cos\theta_3\ddot{\theta}_3 \\
&+[mL^2(sin\theta_3)^2 + ml^2(\theta_1^2 + \theta_2^2) + 2mL\theta_1 sin\theta_3 + I_b \\
&+J_x(sin\theta_3)^2 + Jz(cos\theta_3)^2]\ddot{\theta}_4 + [mL^2 dot\theta_3 sin(2\theta_3) \\
&+2ml^2(\theta_1\dot{\theta}_1 + \theta_2\dot{\theta}_2) + 2mL(\dot{\theta}_1 sin\theta_3 + \theta_1\dot{\theta}_3 cos\theta_3) \\
&+(J_x - J_z)\dot{\theta}_3 sin(2\theta_3)]\dot{\theta}_4 + mlL\theta_2\dot{\theta}_3^2 sin\theta_3 = u_4.
\end{aligned} \tag{4}
$$

The system parameters are reported in Tab. 1. The system can be compactly rewrite as

$$
M(q)\ddot{q} + C(q,\dot{q})\dot{q} + g(q) = \begin{bmatrix} 0_{2x2} \\ I_{2x2} \end{bmatrix} u, \tag{5}
$$

where q = $[\theta_1, \theta_2, \theta_3, \theta_4]^T \in \mathbb{R}^4$ represents the state vector, and u = $[u_3, u_4]^T \in \mathbb{R}^2$ represents the control input vector. The matrices M(q) $\in \mathbb{R}^{4x4}$, $C(q,\dot{q}) \in \mathbb{R}^{4x4}$, and g(q) $\in \mathbb{R}^4$ represent the inertia, centripetal-Coriolis, and gravity.

2.1 Control objective

The control objective is to move the boom to a desired position and dampen the load swing at the same time. This can be described mathematically as follows:

$$
\begin{aligned}
&\lim_{t\to\infty}\theta_1(t) = 0, \quad \lim_{t\to\infty}\theta_2(t) = 0, \\
&\lim_{t\to\infty}\theta_3(t) = \theta_{3d}, \quad \lim_{t\to\infty}\theta_4(t) = \theta_{4d},
\end{aligned} \tag{6}
$$

where θ_{3d} and θ_{4d} are the boom's desired angles.

Typically in this kind of applications we have three main types of constraints: constraints concerning the maximum

range of the joints, safety constraints related to the suspended load, and constraints modelling the collision avoidance with objects and structures (e.g. walls).

In this paper for the joint range constraints we will assume that the boom pitch angle (i.e., $\theta_3(t)$) is constrained within the range $(\frac{8\pi}{9}, \frac{-\pi}{18})$. Thus

$$\theta_3 \leq \frac{8\pi}{9}, \tag{7}$$

$$-\theta_3 \leq -\frac{\pi}{18}. \tag{8}$$

For what concerns safety constraints linked to the swinging load, a number of different constraints can be defined. A simple form of safety constraints is to impose that θ_i never violates a maximum swing angle. In this paper we will consider the constraint $|\theta_i| \leq \theta_{mi}$, with i =1,2, where $\theta_{mi} = \frac{\pi}{36}$. Thus

$$\theta_1 \leq \frac{\pi}{36}, \tag{9}$$

$$-\theta_1 \leq \frac{\pi}{36}, \tag{10}$$

$$\theta_2 \leq \frac{\pi}{36}, \tag{11}$$

$$-\theta_2 \leq \frac{\pi}{36}, \tag{12}$$

Collision avoidance constraints are constraints where we want to avoid that the load collides with some object/structure. We consider a wall construction scenario where the mason waits for a new brick to bring it to its final position (Fig. 2). In this paper we assume that we want to avoid the collision of the swinging load with three obstacles that are present during this activity: the mason, the brick already placed and the wall.

Since the cable length is fixed and since constraints (9)-(12) will be enforced, we embed the obstacles into boxes taking into account a safety margin equal to the maximum displacement between the rest condition of the load and the maximum swing compatible with constraints (9)-(12). A schematic view of these three boxes is shown in the Fig. 3.

Table 1. Parameters of the boom crane system

Parameters	Physical	Units
$\theta_1(t)$	Payload radial swing angle	rad
$\theta_2(t)$	Payload tangential swing angle	rad
$\theta_3(t)$	Boom pitch angle	rad
$\theta_4(t)$	Boom yaw angle	rad
M	Boom mass	kg
m	Payload mass	kg
M_1	Ballast mass	kg
L	Boom length	m
l	Rope length	m
L_1	Ballast length	m
J_x, J_y, J_z	Moments of inertia of the boom	$kg \cdot m^2$
I_b	Ballast inertia moment	$kg \cdot m^2$
$u_3(t), u_4(t)$	Control inputs	$N \cdot m$

Figure 2. Mason activity

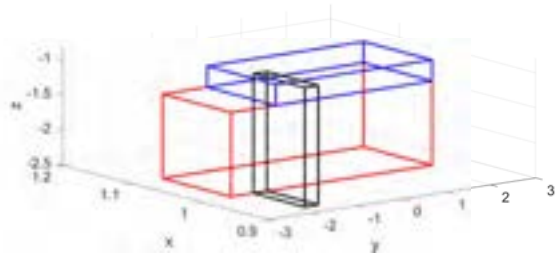

Figure 3. Obstacle constraints. Blue line: Bricks. Red line: Wall. Black line: Mason .

To write these three constraints in the operational space, the direct kinematics of the crane is used [16]:

$$x = Lsin(\theta_3)cos(\theta_4) + l\theta_1 cos(\theta_4) - l\theta_2 sin(\theta_4), \tag{13}$$

$$y = Lsin(\theta_3)sin(\theta_4) + l\theta_1 sin(\theta_4) + l\theta_2 cos(\theta_4), \tag{14}$$

$$z = Lcos(\theta_3) - l\theta_2 cos(\sqrt{\theta_1^2 + \theta_2^2}). \tag{15}$$

Thanks to (13)-(15) we can translate the constrains of each obstacles (e.g. mason, brick and wall) into the joint space. Since the boxes considering the constraints are robust for any swing satisfying (9)-(12), we can consider $\theta_1 = \theta_2 = 0$, and write the constraints only in terms of θ_3 and θ_4 as follows

$$W_i = \{h_i(\theta_3, \theta_4) \geq 0\}, \quad i = 1...3, \tag{16}$$

where h_i is a nonlinear function. These three nonlinear constraints mapped in the joint space are reported in Fig. 4. Note that in the joint space each of these constraints is easily embeddable as a union of linear constraints. This fact can be exploited for the control law following the same lines proposed in [21].

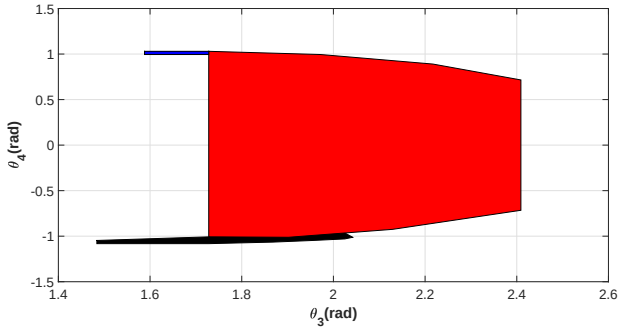

Figure 4. The constraints in the joint space. Blue: Bricks. Red: Wall. Black: Mason.

In conclusion, constraints (7)-(12) are linear constraints, while the constraints obtained by (16) are non linear constraints.

The main goal of this paper is to build a control law able to stabilize the system around each desired point of equilibrium ensuring good dynamic performances while, at the same time, ensuring the satisfaction of constraints (7)-(12), and (16).

3 Control Desing

The control architecture proposed in this paper consists of two cascade control loops as shown in Fig. 5. The first loop pre-stabilizes the system, whereas the second loop manipulates the reference of the pre-stabilized system to ensure constraint satisfaction and reference tracking. In this paper a Linear Quadratic Regulator is used in the inner loop to ensure stability and fast dynamics. For what concerns the constraints management, the external loop consists of an Explicit Reference Governor.

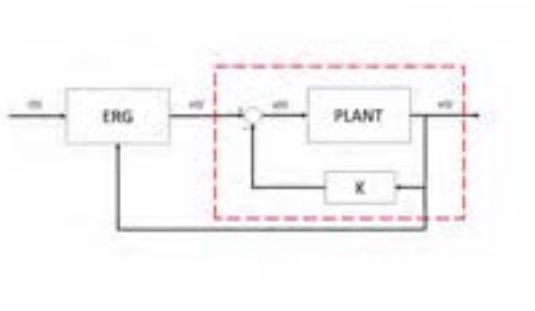

Figure 5. ERG based feedback control scheme.

3.1 LQR Synthesis

Let us define $x = [q \quad \dot{q}]^T$ as state of our system.
In order to design a control law for the system at hand we proceeded with the linearization of the nonlinear equations (5) around the point of equilibrium $x_v = [0, 0, \frac{\pi}{3}, 0, 0, 0, 0, 0]^T$, and considering as equilibrium input u_{eq}:

$$u_{eq} = \begin{bmatrix} -g(\frac{1}{2}ML + mL - \frac{1}{2}M_1L_1)sin(x_{v,3}), \\ 0 \end{bmatrix} \tag{17}$$

which represents the so-called "desired gravity compensation".
The resulting linearized system

$$\delta\dot{x}(t) = A\delta x(t) + B\delta u(t), \tag{18}$$

is then used to compute an LQR control law $\delta u(t) = -K\delta x$ for the linear system (18).

Using this gain matrix K the following control law is obtained

$$u = -K(x - x_v) + u_{eq}, \tag{19}$$

It is worth noticing that the matrix A in (18) depends on the value of the equilibrium angle θ_3. However, it has been numerically verified that, for the choices of weight used in this paper and in the operative ranges prescribed by the system constraints, the control law (19) is able to stabilize the system regardless of the initial condition.

3.2 ERG Synthesis

The idea behind the Explicit Reference Governor [22] is to generate the applied reference signal v (see Fig. 5) so that, if v was to be frozen at any time instant, the transient dynamics of the pre-stabilized system would not violate the constraints. This is achieved by manipulating the derivative of the applied reference in continuous time using the nonlinear control law.

$$\dot{v}(t) = \Delta(x(t), v(t))\rho(r(t), v(t)), \tag{20}$$

with

$$\Delta(x(t), v(t)) = k \min_i(\Gamma_i(v(t)) - V_i(q(t), v(t))), \tag{21}$$

where $k > 0$ in a tuning parameter, and i=1...n_c, with n_c is the number of the constraits. $\Delta(x(t), v(t))$ and $\rho(r(t), v(t))$ are the two fundamental components of the ERG scheme, called the Dynamic Safety Margin (DSM) and the Navigation Field (NF), respectively. The scheme is proven to ensure recursive feasibility and asymptotic convergence to a constant reference [22].
The definition of the DSM differs for the linear constraints and non linear constraints.
For the linear constraint, the first step is to write the (7)-(12) in the form $\beta_{x,i}x \leq d_i, i = 1...6$. For the i^{th} linear constraints (7)-(12), $\Gamma(v(t))$ is

$$\Gamma_i(v) = \frac{(\beta_{x,i}^T x_v + \beta_{v,i}^T v - d_i)^2}{\beta_{x,i}^T P_i^{-1} \beta_{x,i}}, \tag{22}$$

where accordingly to [17], the matrix $Pi > 0$ can be found by solving the offline LMI optimization problem:

$$\begin{aligned} &P_i = \min_P \, logdet(P) \\ &s.t. \\ &(A - BK)^T P + P^T (A - BK) < 0 \\ &P > \frac{\beta_{x,i}^T \beta_{x,i}}{||\beta_{x,i}||^2} \end{aligned} \tag{23}$$

For the nonlinear constraints (16), to be able to evaluate the DSM, we propose the following procedure.
These constraints are well embedded as a union of linear constraints. Fig.6 shows the embedding for the mason constraint. The same approach is used for the other two constraints. In this way, for each obstacle, we obtain a set of linear constraints that we can exploit in the design of the control law. Accordingly, we can rewrite each new set as the union of sets described by linear constraints in the form $\beta_{t,i,j} x \leq d_{i,j}, i = 1...n_{t,j}, \quad j = 1...3$, where $n_{t,j}$ is the number of tangent used for each of the embeddings.

Accordingly to [21] the DSM of the union of $n_{t,j}$ sets defined by linear constraints can be evaluated as

$$\Delta_{t,j}(q(t), v(t)) = \max_{l=1,\ldots,n_t} (\Delta_{t,l,j}(q(t), v(t)), \tag{24}$$

where

$$\Delta_{t,l,j}(q, v) = \Gamma_{t,l,j}(v) - V_{t,l,j}(q, v), \tag{25}$$

whit $1 = 1,...,n_{t,j}, \quad j = 1...3$, where $\Gamma_{t,l,j}$ and $V_{t,l,j}$ can be evaluated by solving the (22)-(23) for each tangent constraint.

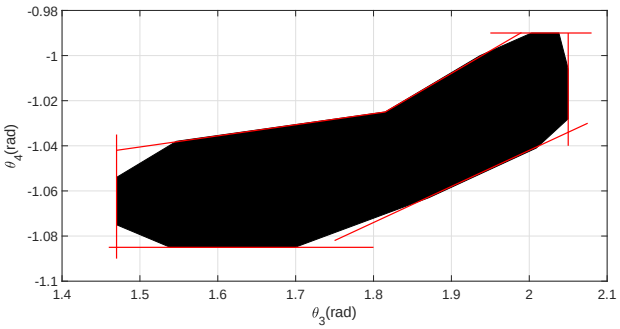

Figure 6. Embedding mason constraint

For what regards the NF, it can be designed by decoupling into an attraction and a repulsion term as [23]

$$\rho(r(t), v(t)) = \rho_a(r(t), v(t)) + \rho_r(r(t), v(t)), \tag{26}$$

where $\rho_a(r(t), v(t))$ is a vector field which points towards the desired position, and $\rho_r(r(t), v(t))$is a vector field which points away from the constraints. For the attraction term $\rho_a(r(t), v(t))$, the most intuitive choice is

$$\rho_a(r(t), v(t)) = \frac{r(t) - v(t)}{\max\{||r(t) - v(t)||, \eta\}}, \tag{27}$$

where $\eta > 0$ is a smoothing factor. Repulsion terms can be split into two terms as:

$$\rho_r(r(t), v(t)) = \rho_{r,1}(r(t), v(t)) + \rho_{r,2}(r(t), v(t)), \tag{28}$$

where

$$\rho_{r,1}(r(t), v(t)) = \sum_{i=1}^{6} \max\left\{\frac{\zeta - \beta_{x,i} x(t) - d_i}{\zeta - \delta}, 0\right\} \frac{\beta_{x,i}}{||\beta_{x,i}||}, \tag{29}$$

$$\rho_{r,2}(r(t), v(t)) = \sum_{j=1}^{3} \max\left\{\frac{\zeta - \beta_{l(t)_j^\star} x(t) - d_{l(t)_j^\star}}{\zeta - \delta}, 0\right\} \frac{\beta_{l(t)_j^\star}}{||\beta_{l(t)_j^\star}||}, \tag{30}$$

where $\zeta > \delta > 0$ and $(t)^\star$ is the index such that $\Delta_{t,j}(q(t), v(t)) = \Delta_{t,l(t)^\star,j}(q(t), v(t))$ in 24.

In this paper, we will use a discrete-time implementation of the ERG. Note that, one could use the Euler approximation of (20), such as

$$v(k+1) = v(k) + kT_s \Delta(q, v) \rho(r(k), v(k)), \tag{31}$$

where T_s is the sampling time of the system. However, as it is, this approximation might not ensure recursive feasibility if T_s is not sufficiently small with respect to the dynamics of the system. For this reason in this paper we will use the scheme introduced in ([18]), which verifies that the candidate reference $\hat{v}(k)$ ensures recursive feasibility one step ahead. To do so, it predicts the evolution of the close loop states $\hat{x}_{cl}(k+1)$, given this candidate reference $\hat{v}(k)$, and evaluates if the dynamic safety margin is positive when maintaining the candidate reference one step ahead, i.e., $\Delta(\hat{x}_{cl}(k+1), \hat{v}(k))$. If the candidate reference holds feasibility, it is applied as the reference at the current step, i.e. v(k) = $\hat{v}(k)$.

4 Simulation Results

To demonstrate the effectiveness of the proposed ERG strategy, in this section we simulate the boom crane shown in Fig. 1.The physical parameters are shown in Tab. 2

The parameters of the control architecture of Fig. 5, are as follows.
For the inner feedback loop:

$$K = \begin{bmatrix} -106.1665, 0, 89.6362, 0, -11.28, 0, 68.877, 0 \\ 0, -91.3357, 0, 31.6228, 0, -7.8488, 0, 52.3688 \end{bmatrix} \tag{32}$$

For the ERG loop, $k = 30$, $\eta = 10e^{-4}$, $\omega = 0.6$,$\zeta = 10$, $\delta = 0.09$.

To validate the proposed scheme experimentally, we consider the following case scenario. Starting from the initial position $x_0 = [0, 0, \frac{105\pi}{180}, \frac{\pi}{2}, 0, 0, 0, 0]^T$. Similar to what happens in reality, we decided to first apply the first desired reference $[\theta_{3,r1}, \theta_{4,r1}] = [\frac{59\pi}{180}, \frac{-48\pi}{180}]$ to move the crane over the mason. Later on, we apply the second desired reference $[\theta_{3,r2}, \theta_{4,r2}] = [\frac{88\pi}{180}, \frac{-58\pi}{180}]$ to move the payload in front of the mason.
Figg. 9- 10 show that the boom pitch and yaw angle follows the desired reference.
As one can see, in Fig. 7 the system follows the desired reference and the control law is able to avoid collisions with the wall. In Fig. 8 it is shown the same trajectory but in the space of end-effector.
Figg. 11-12 show that, during the desired trajectory, the payload swing angles do not violate the constraints (9)-(12).
It is worth noting that in this paper no constraints have been imposed on the actuation limits (see Figg. 13- 14)). However, as one can seen from Figg. 13- 14, they do not represent a problem as the inputs profile and values are reasonable and well within the typical limits of the crane actuators.

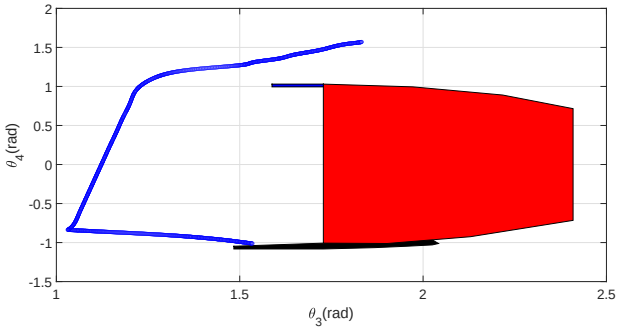

Figure 7. Trajectory in the joint space

Figg. 15- 16 show the comparison between the proposed control strategy and the control reported in [20]. As one can see, our controller is able to drive the crane to the desired position while the payload swings have a smaller amplitude.

Table 2. Physical Parameters

Parameters	Value	Units
M	2.5	kg
m	3.5	kg
M_1	6	kg
L	2	m
l	1	m
L_1	0.5	m

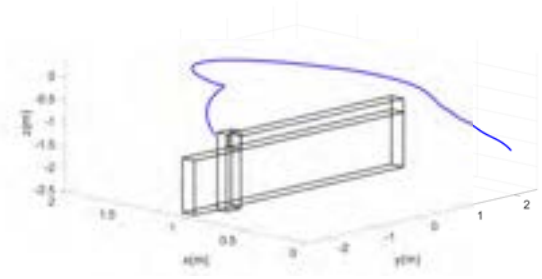

Figure 8. Trajectory in the operational space

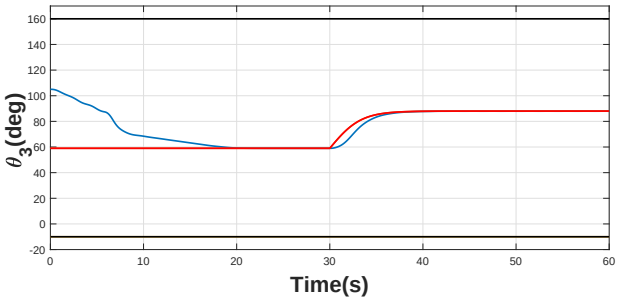

Figure 9. Boom pitch angle θ_3. Red line: Desired reference. Blue line: Real value. Black line: Constraints

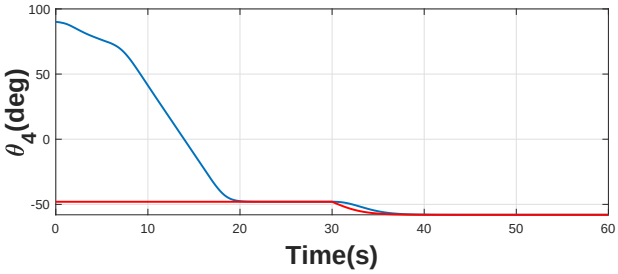

Figure 10. Yaw pitch angle θ_4. Red line: Desired reference. Blue line: Real value.

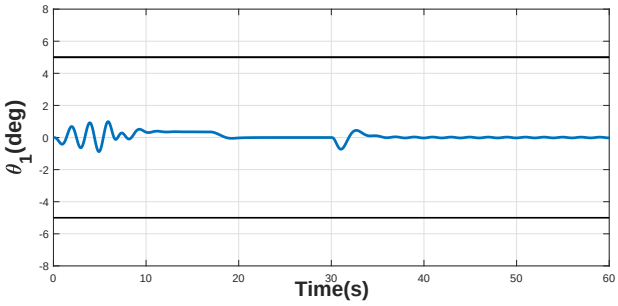

Figure 11. Payload angle θ_1. Blue line: Real value. Black line: Constraints

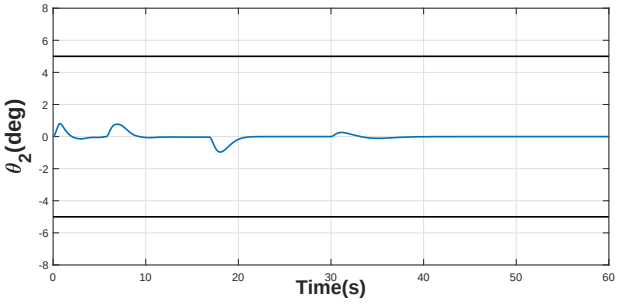

Figure 12. Payload angle θ_2. Blue line: Real value. Black line: Constraints

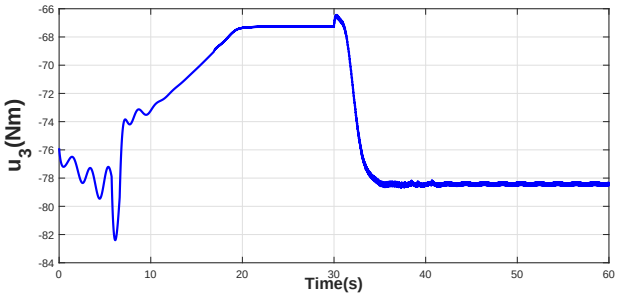

Figure 13. Input u_3

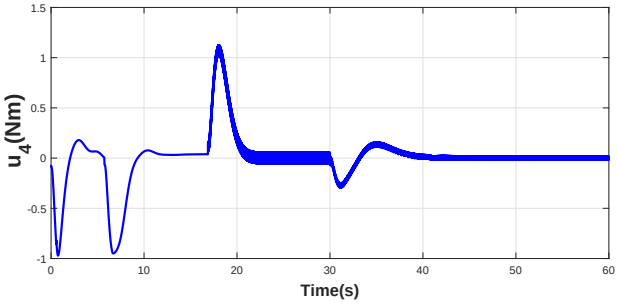

Figure 14. Input u_4

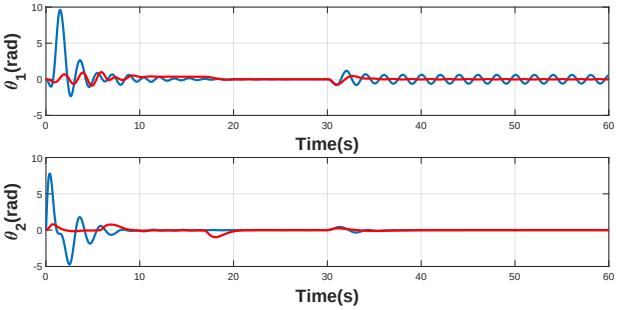

Figure 15. Payload swing angles. Red line: ERG. Blue line: Controller [20]

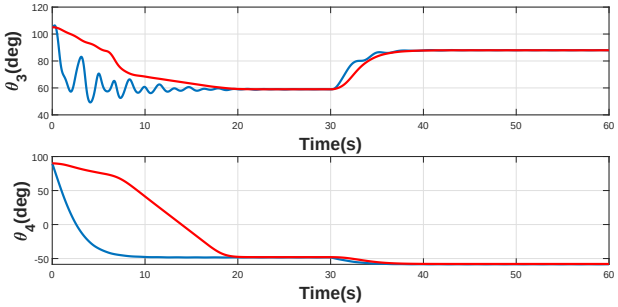

Figure 16. Boom angles. Red line: ERG. Blue line: Controller [20]

5 Conclusion

This paper proposed a constrained control scheme based on the ERG framework for the control of boom cranes. The main contribution of this paper w.r.t. existing closed-loop control methods for boom cranes is that the proposed solution is able to guide the crane towards a desired reference, avoiding collisions with the wall and ensuring that the non-actuated variables (i.e.,θ_1 and θ_2) do not exceed a pre-defined maximum value. It is worth noting that no off-line trajectory has been calculated that it is the control law itself that decides how to move the reference to avoid the obstacle.

References

[1] M. Ambrosino, M. Berneman, G. Carbone, A. Dawans, and E. Garone. Modeling and control of a 5-dof boom crane. In *ISARC. Proceedings of the International Symposium on Automation and Robotics in Construction*, 2020.

[2] M. Ambrosino, B. Thierens, A. Dawans, and E. Garone. Oscillation reduction for knuckle cranes. In *ISARC. Proceedings of the International Symposium on Automation and Robotics in Construction*, 2020.

[3] Javier Moreno-Valenzuela and Carlos Aguilar-Avelar. *Motion Control of Underactuated Mechanical Systems*, volume 88. 01 2018. ISBN 978-3-319-58318-1. doi:10.1007/978-3-319-58319-8.

[4] Liyana Ramli, Zaharuddin Mohamed, Auwalu Abdullahi, Hazriq Izzuan Jaafar, and Izzuddin M. Lazim. Control strategies for crane systems: A comprehensive review. *Mechanical Systems and Signal Processing*, 95C:1–23, 10 2017. doi:10.1016/j.ymssp.2017.03.015.

[5] R. E. Samin, Z. Mohamed, J. Jalani, and R. Ghazali. Input shaping techniques for anti-sway control of a 3-

dof rotary crane system. pages 184–189, Dec 2013. doi:10.1109/AIMS.2013.36.

[6] Jie Huang, Ehsan Maleki, and W.E. Singhose. Dynamics and swing control of mobile boom cranes subject to wind disturbances. *Control Theory & Applications, IET*, 7:1187–1195, 06 2013. doi:10.1049/iet-cta.2012.0957.

[7] Naoki Uchiyama, Huimin Ouyang, and Shigenori Sano. Simple rotary crane dynamics modeling and open-loop control for residual load sway suppression by only horizontal boom motion. *Mechatronics*, 23 (8):1223 – 1236, 2013. ISSN 0957-4158.

[8] Kazuhiko Terashima, Ying Shen, and Ken'ichi Yano. Modeling and optimal control of a rotary crane using the straight transfer transformation method. *Control Engineering Practice*, 15(9):1179 – 1192, 2007.

[9] T. Inukai and Y. Yoshida. Control of a boom crane using installed stereo vision. pages 189–194, Dec 2012. ISSN 2156-8073. doi:10.1109/ICSensT.2012.6461668.

[10] Ziyad Masoud, Ali Nayfeh, and Amjed Almousa. Delayed position-feedback controller for the reduction of payload pendulations of rotary cranes. *Journal of Vibration and Control - J VIB CONTROL*, 9: 257–277, 08 2003. doi:10.1177/107754603030750.

[11] Naoki Uchiyama. Robust control of rotary crane by partial-state feedback with integrator. *Mechatronics*, 19:1294–1302, 12 2009. doi:10.1016/j.mechatronics.2009.08.007.

[12] Eckhard Arnold, Oliver Sawodny, J. Neupert, and Klaus Schneider. Anti-sway system for boom cranes based on a model predictive control approach. *IEEE International Conference Mechatronics and Automation, 2005*, 3:1533–1538 Vol. 3, 2005.

[13] R. M. T. R. Ismail and Q. P. Ha. Trajectory tracking and anti-sway control of three-dimensional offshore boom cranes using second-order sliding modes. pages 996–1001, Aug 2013. ISSN 2161-8089. doi:10.1109/CoASE.2013.6654071.

[14] Kunihiko Nakazono, Kouhei Ohnishi, Hiroshi Kinjo, and Tetsuhiko Yamamoto. Vibration control of load for rotary crane system using neural network with ga-based training. *Artificial Life and Robotics*, 13 (1):98–101, Dec 2008.

[15] M. A. Ahmad, M. S. Saealal, M. A. Zawawi, and R. M. T. Raja Ismail. Classical angular tracking and intelligent anti-sway control for rotary crane system. pages 82–87, 2011.

[16] Tong Yang, Ning Sun, He Chen, and Yongchun Fang. Motion trajectory-based transportation control for 3-d boom cranes: Analysis, design, and experiments. *IEEE Transactions on Industrial Electronics*, PP:1–1, 07 2018. doi:10.1109/TIE.2018.2853604.

[17] M. M. Nicotra and E. Garone. Explicit reference governor for continuous time nonlinear systems subject to convex constraints. pages 4561–4566, 2015.

[18] Emanuele Garone, Marco Nicotra, and Lorenzo Ntogramatzidis. Explicit reference governor for linear systems. *International Journal of Control*, 91: 1–28, 04 2017.

[19] Emanuele Garone, Stefano Di Cairano, and Ilya Kolmanovsky. Reference and command governors for systems with constraints: A survey on theory and applications. *Automatica*, 75:306 – 328, 2017.

[20] N. Sun, T. Yang, Y. Fang, B. Lu, and Y. Qian. Nonlinear motion control of underactuated three-dimensional boom cranes with hardware experiments. *IEEE Transactions on Industrial Informatics*, 14(3):887–897, March 2018. doi:10.1109/TII.2017.2754540.

[21] R. Romagnoli, L. D. Couto, M. M. Nicotra, M. Kinnaert, and E. Garone. Computationally-efficient constrained control of the state-of-charge of a li-ion battery cell. pages 1433–1439, 2017.

[22] E. Garone and M. M. Nicotra. Explicit reference governor for constrained nonlinear systems. *IEEE Transactions on Automatic Control*, 61(5):1379–1384, 2016.

[23] E. Hermand, T. W. Nguyen, M. Hosseinzadeh, and E. Garone. Constrained control of uavs in geofencing applications. pages 217–222, 2018.

Optimal Travel Routes of On-road Vehicles Considering Sustainability

N. Mehrvarz[a], Z. Ye[a], K. Barati[a], and X. Shen[a]

[a]School of Civil and Environmental Engineering, University of New South Wales, Australia
E-mail: n.merhvarz@unsw.edu.au , zhilin.ye@student.unsw.edu.au, Khalegh.barati@unsw.edu.au, X.shen@unsw.edu.au

Abstract –

Transportation is one of the major contributors in global energy consumption and greenhouse gas emissions. Currently, there are approximately 1.32 billion on-road vehicles around the world, which is expected to be doubled by 2040. This increase has triggered deep concerns over the global issues of climate change and sustainable development. Current GPS navigation systems determine the best travel route in terms of time or distance. However, there are significant challenges to determine an optimal travel route considering sustainability. This paper aims to develop an automated system in order to evaluate different travel routes and suggest the most sustainable one. In this paper, a mathematical model is proposed to estimate the travel time and fuel consumption given different travel route options. Five operational and engine variables of acceleration rate, speed, road slope, engine load, and fuel consumption rate are incorporated in the quantitative analysis. Remote data acquisition was conducted using a GPS-aided inertial navigation system (GPS-INS) and an engine data logger for seven days. The results indicate that the fastest route selected by the current navigation system may not be the most sustainable option. It was also found in the field experiments that the most sustainable route could potentially save on average 5% fuel consumption compared to the fastest route.

Keywords –

Sustainability; Route Selection; Vehicle; Fuel Consumption; GPS-INS

1 Introduction

The transportation field has been widely regarded as one of the major sections of energy consumption, which has produced a significant amount of greenhouse gases (GHGs) worldwide, leading to negative impacts on the environment as well as the climate. There are more than 1.3 billion vehicles in operation throughout the world, which can consume approximately five trillion liters of petroleum annually [1]. The rate related to which petroleum is being consumed and the external costs that result from its use are incredibly unsustainable [2].

Family vehicles play an important role in the total use of global fossil fuels in the transportation field. There is still a rapid increase in the number of family vehicles in the current situation. It is predicted that the number of global on-road vehicles and cars will reach two billion by 2050 [3]. Therefore, it is of great importance to provide quantitative models with high accuracy to estimate the amount of fuel use and emissions caused by on-road vehicles.

There are several GPS navigation systems for vehicles such as Google Maps, which can show the best route in terms of time to users; however, this selected route may not be the best way in terms of sustainability. For this reason, how to measure the best route in terms of sustainability requires to be taken into critical consideration.

The main purpose of this study is to provide a comprehensive model to compare the sustainability of each travel path quantitatively. Furthermore, this research will confirm that the best route offered by current navigation systems may not be the most sustainable route, as well as to potentially develop an updated concept of GPS navigation systems. A comprehensive framework of methodology has been developed to model the fuel use of vehicles as well as evaluate the sustainability of route choice. Three experimental parameters including speed, acceleration, and road slope have been identified and investigated in this study. Two main instruments called GPS-based inertial navigation system (GPS-INS) device and on-board diagnostics (OBD) engine data logger have been employed to collect real-world data. At the end of this study, research limitations as well as recommendations for the future studies are provided.

2 Literature Review

This section focuses on the parameters which can affect the traffic modeling and the fuel use modeling of on-road vehicles.

The value of speed can be used to measure the service level of traffic. As is known, the on-road vehicles can keep the speed around a relatively high value without interruption, e.g. running on a freeway, which means that the traffic condition is on the highly satisfying level [4]. In addition, flow is a relatively macroscopic parameter in traffic modeling, which can help controlling the traffic condition under a macroscopic view. California Department of Transportation (Caltrans) Freeway Performance Measurement System (PeMS), a widely used traffic modeling, can offer 30 seconds or 5 minutes per-loop averages of lane occupancy, flow, speed, and delay for various links in the roadway network [5].

Ahn and Lee developed the operation efficiency parameter to consider idling and non-idling emission coefficients [6]. Besides, Barati and Shen chose both engine attributes (size and load) and operational parameters (operation efficiency, cycle time, and operator skill) as affecting parameters on fuel use [7]. Lewis and Hajji presented a model to estimate the total fuel use, unit cost, activity duration, and emissions of vehicles. Using multiple linear regression (MLR) method, the impact of different affecting parameters including distance and speed was modeled on the fuel use and cost [8].

3 Methodology

This section introduces a comprehensive framework which has been developed to model the fuel use of vehicles as well as evaluate the sustainability of available routes. This methodology can be applied to estimate the fuel consumption of vehicles at the operation level and to appraise the routes sustainability. It can help drivers to identify the best route in their daily trips in terms of sustainability rather than the time.

The fuel use model in this study can be developed in three steps. As the first step, instantaneous engine load value is estimated based on collected operational and environmental parameters. Then, the fuel use in each second can be predicted considering the engine attributes. The fuel use for each trip is eventually measured having instantaneous fuel consumption (IFC) and travel time.

As Figure 1 presents, five steps should be followed to develop the model. Instrumentation and data collection phases are to obtain real data from the field. Raw data should be synchronised and filtered to remove potential errors. The processed data must be finally analysed to estimate the fuel consumption and evaluate the available routes in terms of time and sustainability.

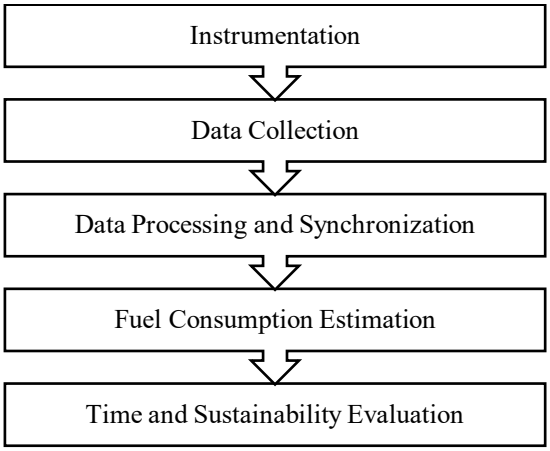

Figure 1. Research framework for selecting most sustainable route

3.1 Parameters Identification

The parameters related to engine size and engine load have been widely regarded as two essential attributes affecting fuel consumption and consequently emissions. The engine load can be defined as the ratio of the used power in different working conditions comparing to the maximum power as a percentage [9]. As for engine size, the greater capacity of the engine generally means more fuel use and emissions. The operational parameters which can influence engine load are acceleration and speed. In addition, the vehicle may use more power of engine at an upward slope than a levelled route. Therefore, the effect of road slope, as an environmental variable, cannot be ignored on engine load estimation. Further, gross vehicles' weight (GVW) is a major variable impacting the effect of other operational parameters on engine load.

The fuel use of a vehicle has a direct relationship with its engine load and size. Having the values of engine load and engine size, the instantaneous fuel use of vehicles can be estimated.

3.2 Instrumentation

There are two main instruments called GPS-INS device and OBD engine data logger employed to collect real-world data of identified parameters. The V-gate iCar Pro OBD2 Scanner is an OBD instrument used to collect field data of engine attributes in this research. It can satisfy almost all the required parameters except acceleration and road slope. JY-GPSIMU is a three-axis inertial navigation GPS-INS device, which can collect, measure, and record the accurate position, speed, acceleration by using an attitude and heading reference system (AHRS). This GPS-INS instrument is installed

inside the cabin of vehicle on a leveled surface, and it should be fixed on a surface with minimum vibration and without any lateral movement to increase the accuracy of data collection. In order to collect data of higher accuracy as well as keep better satellite signal connection, the antenna of GPS-INS is installed on the roof of the vehicle cabin and connected to the main unit via a wire. Finally, all the data collected by OBD engine data logger and GPS-INS device will be stored, synchronised, and analysed in a Toughpad.

3.3 Data Collection

In this research, the data collection has been completed in two preliminary testing and field experimentation parts. The preliminary tests in this study were completed by three selected family vehicles to check and evaluate the performance of instruments. Completion of the whole preliminary experiments took around six hours, and more than 20000 data points have been collected. The field experimentation was conducted by the same vehicles used in the preliminary experiments. The total field experimentation took about 20 hours with more than 80000 collected data points. In order to collect more reliable data during experimentation, several deliberate arrangements have been applied to make the location and time of each experiment different. Moreover, there were significant differences among different routes in each experiment. For example, some had longer distances and fewer traffic lights, some had shorter distances and more traffic lights, and some routes included part of highways.

Table 1 summarises four conducted experimentations. Table 2 demonstrates the samples of the operational parameters collected by instruments. Photos of instrumentation and experimentation, as well as an operation interface version of master computer software are shown in Figure 2a-d. There are five parameters identified to be used for measuring the experiments in this research. Three of them, i.e. acceleration, speed, and road slope, are collected by the GPS-INS device. The other two parameters, i.e. engine load and fuel use rate, are recorded by the OBD engine data logger.

Table 1. A summary of conducted experimentation

Experiment	Vehicle Model	Experiment Location	Experiment Time	Model Year	Engine Size (kW)	Empty/Total Weight (kg)	Number of Data Points
1	Honda Civic	Suburban	Evening Peak	2016	104	1255/1505	15832
2	Honda Civic	Suburban	Midnight	2016	104	1255/1505	17251
3	Toyota Corolla	City	Midnight	2010	81	1060/1210	17449
4	Honda Sylphy	City	Evening Peak	2012	86	1220/1445	20558

Table 2. Samples of field data collected by instruments

Time	Angle X (deg)	GPS V (km/h)	Acceleration (m/s^2)	Calculated Engine Load (%)	Fuel Use (L/100km)
12:54:32 AM	8.09	19.083	0.6508	60.4	8.4
12:54:33 AM	7.40	21.518	0.6764	59.9	7.9
12:54:34 AM	7.34	23.174	0.4600	54.7	6.2
12:54:36 AM	6.39	26.626	0.4408	55.5	6.5

Figure 2. Sample photos of instrumentation and experimentation, (a) the GPS-INS device, (b) external antenna of the GPS-INS device, (c) the OBD engine data logger, and (d) the operation interface version of OBD Auto Doctor.

4 Result Analysis

The aim of this section is to develop a model to estimate fuel consumption as well as the most sustainable route selection of on-road family vehicles by the analysis of operational parameters collected in the experimentation. As one of the essential sections of this research, this section presents the estimation of fuel use among different routes and the results of model validation.

4.1 Model Development

This section examines how to estimate the total fuel use of a trip. As mentioned in section 3.1, engine load can be described as a function of acceleration, speed, road slope, and vehicle load factor (LF). As for LF, it is the ratio of current vehicle weight to its GVW. The LF of the three selected vehicles, Honda Civic, Toyota Corolla, and Honda Sylphy, are 0.67, 0.4, and 0.6, respectively, and their engine size are 104kW, 81kW, and 86kW, respectively. The highest speed of these vehicles during the experiment are 64.35 km/h, 70.29 km/h, and 49.18 km/h, respectively. The acceleration fluctuation range of these vehicles in the experimentation are between -2.37 m/s^2 and 3.15 m/s^2 (-8.52 km/h.s to 11.3 km/h.s), -3.08 m/s^2 and 3.22 m/s^2 (-11.1 km/h.s to 11.6 km/h.s), -3.08 m/s^2 and 3.22 m/s^2 (-11.1 km/h.s to 11.6 km/h.s), respectively. The parameter of road slope in the selected routes varied from -17.9° to +16.7° (-19.9% to 18.5%).

4.1.1 Engine Load Estimation

Barati and Shen developed a model based on the real-world data to estimate of engine load by acceleration, slope, speed, and the LF. In addition, they also offered the relationship among these coefficients and LF (Equation (1)) [7]. Table 3 presents LF and three experimental coefficients of vehicle acceleration (C_{AC}), slope of road (C_{SL}), and vehicle speed (C_{SP}). Using linear interpolation technique, a relationship between C_{AC}, C_{SL}, C_{SL}, and LF can be developed (Equations (2-4)).

$$EL = (C_{AC} * AC) + (C_{SL} * SL) + (C_{SP} * SP) + C \quad (1)$$

where:

EL Engine load of vehicle (%)
AC Acceleration of vehicle (m/s^2)
SL Slope of road (degree)
SP Speed of vehicle (km/h)
C Engine load of vehicle in idle mode which is around 20%.

Table 3. The coefficients of parameters in the engine load estimation model

Model	Coefficients			
Load Factor	0	0.33	0.67	1
C_{AC}	15.65	16.36	24.8	27.37
C_{SL}	1.12	1.29	1.67	1.86
C_{SP}	0.41	0.52	0.57	0.64

$$C_{AC} = 12.163\ LF + 15.713 \quad , R^2 = 0.985 \quad (2)$$

$$C_{SL} = 0.749\ LF + 1.096 \quad , R^2 = 0.0.986 \quad (3)$$

$$C_{SP} = 0.221\ LF + 0.424 \quad , R^2 = 0.973 \quad (4)$$

4.1.2 IFC Estimation by Engine Load

According to the field data provided by Klein et al. there is an exponential relation between IFC and engine load (Equation (5)). In other words, a small increase in engine load may result in a significant growth of IFC [9]. Figure 3 shows all the results of IFC estimation and engine load of experimented vehicles in this study.

$$IFC = 0.126 * e^{0.036*EL} \quad (5)$$

where:

IFC Instantaneous fuel consumption (L/sec)
EL Engine load of vehicle (%)

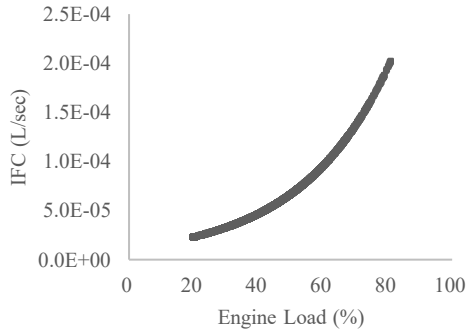

Figure 3. IFC results based on engine load

4.1.3 Total Fuel Consumption Estimation by IFC

The last step of fuel consumption estimation is the calculation of the total amount of fuel used in one trip. The total fuel consumption in a small unit of time can be regarded as the product of IFC and one unit of time. The amount of total fuel consumption in one route is the sum of IFC (Equation (6)).

$$TFC = \sum(IFC) \quad (6)$$

where:

TFC Total fuel consumption (L)
IFC Instantaneous fuel consumption (L/sec)

4.2 Time and Sustainability Evaluation

A vehicle navigation system equipped with GPS-INS can use a significant amount of real-time information for route planning. On the one hand, this GPS-INS system first searched the origin and destination of the trip and used positioning information and internal program algorithms to find several alternative routes. On the other hand, the real-time mega data will be used to simulate the running condition of each route and make an evaluation, which can finally select the best route in terms of time. The GPS-INS system can provide drivers with the best route in terms of time; however, this route might not be the best choice in terms of sustainability. Figure 4 makes a comparison of time and sustainability evaluation.

As an example, in experiment 3, route 1 took the least time but with the most fuel consumption, which means that this route is the most unsustainable one in all three routes. Although the route 3 took a relatively long time to arrive at the destination, it is the best route selection in terms of sustainability. In addition, in experiment 5, route 2 seems to spend almost the longest time; however, the

fuel consumption of this route is significantly lower than the other two paths. The experimental results also confirmed three rules, which can be regarded as the principle of sustainable traveling. First and foremost, it is more sustainable to travel during off-peak hours rather than peak hours in both urban and suburban areas. Secondly, it is more sustainable to travel in suburban areas rather than urban areas. Thirdly, it is more sustainable to select the route which has less road slope fluctuation as well as traffic signals.

In conclusion, according to the results of this experimentation, the best route in terms of time provided by the GPS-INS system is not the best route in terms of sustainability sometimes. For the concept of reaching a higher level of sustainability, it is essential to develop another algorithm in the GPS-INS system, which can make simulation and calculation to choose the best route in terms of sustainability.

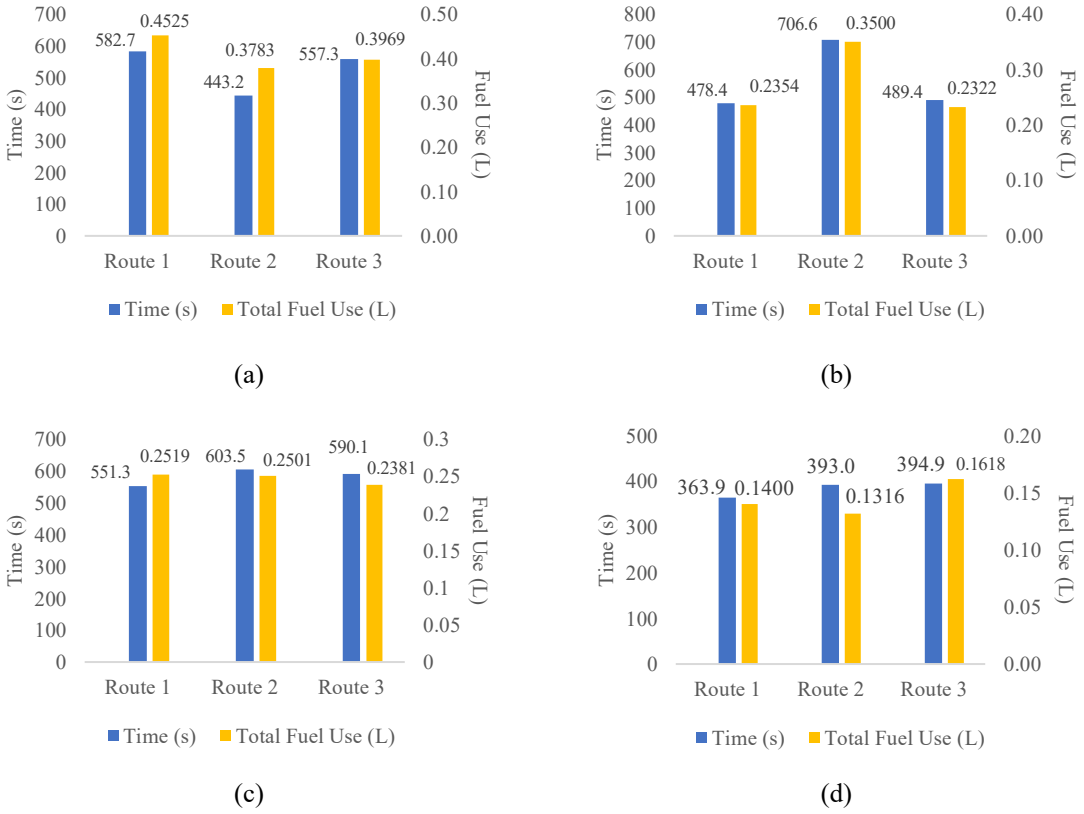

Figure 4. Time and sustainability evaluation of the four conducted experiments, (a) experiment 1, (b) experiment 2, (c) experiment 3, and (d) experiment 4.

5 Conclusion

The transportation field has been widely considered as one of the major sections of energy consumption, such as the use of fossil fuels by vehicle engines. The widespread use of fossil fuels has also produced a significant amount of air pollutants worldwide. It requires a quantified model to estimate family vehicle fuel consumption and select the best route. An assumption has been presented that the best route offered by current navigation systems, which cost the shortest time may not be the most sustainable route. This paper mainly concentrates on confirming the validity of this assumption as well as developing a comprehensive methodology to quantify the total fuel consumption in alternative routes.

The model used in this study can be divided into three steps: engine load estimation by operating parameters, instantaneous fuel consumption estimation by engine load, and total fuel consumption estimation by instantaneous fuel consumption. The concept of this modelling can be applied to all on-road family vehicles. The GPS system can be updated to provide the best route selection in terms of sustainability based on the model in this study.

The experimentation and the results of this research confirmed that the total fuel consumption of each alternative route can be calculated by the identified parameters. Due to the fact that the GPS navigation systems can make simulation and calculation with the support of GPS real-time mega data, it can make the modelling reach a more practical level and be widely applied. It is strongly recommended that the GPS navigation systems should perform the normal route selection as well as the best route selection in terms of sustainability based on the model concept in this study at the same time. Moreover, the GPS navigation systems can present both these two plans of route selection to the user interface for operators to determine. Furthermore, the GPS navigation systems can even simulate the travel of a short period of time in the future to provide better travel recommendations. For example, the evening peak will last for half an hour, and then the updated GPS navigation system can present the total fuel consumption of the current travel and the deferred travel after the simulation and calculation. The simulation may show that a 30 min deferral in a travel can save significant time and fuel. The core concept of this research is to make the traditional navigation systems combine with sustainability and make operators take sustainability into consideration in their daily life.

References

[1] Dargay J., Gately D. and Sommer M. Vehicle Ownership and Income Growth. *The Energy Journal*, 143-170, 2007.

[2] Khan, M.A., Khan, M.Z., Zaman, K., and Naz, L. Global estimates of energy consumption and greenhouse gas emissions, *Renewable and Sustainable Energy Reviews,* (29): 336-344, 2014.

[3] Sperling D. and Gordon D. *Two billion cars: driving toward sustainability*. Oxford University Press, 2014.

[4] Transportation Research Laboratory (TRL). A Review of Instantaneous Emission Models for Road Vehicles. *Project Report PPR*, 267, 2007.

[5] Boriboonsomsin K., and M. Barth. Modeling the Effectiveness of HOV Lanes at Improving Air Quality. Draft Final Report. *California Department of Transportation*, 2006.

[6] Ahn C.R. and Lee S.H. Importance of Operational Efficiency to Achieve Energy Efficiency and Exhaust Emission Reduction of Construction Operations. *Journal of Construction Engineering and Management*, 139(4), 404-413, 2013.

[7] Barati K. and Shen X. Operational level emission modelling of on-road construction equipment through field data analysis, *Journal of Automation in Construction*, (72): 338-346, 2016.

[8] Lewis M.P. and Hajji A. Estimating the Economic, Energy, and Environmental Impact of Earthwork Activities, In *Proceedings of Construction Research Congress*, pages 1770-1779, Indiana, USA, 2012.

[9] Klein, J., Shen, X., and Barati, K., Optimum driving pattern for minimizing fuel consumption of on-road vehicles, Proceedings of the 33rd International Symposium on Automation and Robotics in Construction and Mining (ISARC 2016), Auburn, USA, 2016.

Modeling and Control of 5-DoF Boom Crane

Michele Ambrosino[a], Marc Berneman[b], Gianluca Carbone[a], Rémi Crépin[a], Arnaud Dawans[c], and Emanuele Garone[a]

[a]Service d'Automatique et d'Analyse des Systèmes, Université Libre de Bruxelles, Brussels, Belgium
[b] Vrije Universiteit Brussel,[c]Entreprises Jacques Delens S.A., Brussels, Belgium

Michele.Ambrosino@ulb.ac.be, marc.berneman@vub.be, Gianluca.Carbone@ulb.ac.be, Remi.Crepin@ulb.ac.be, adawans@jacquesdelens.be, egarone@ulb.ac.be

Abstract -

Automation of cranes can have a direct impact on the productivity of construction projects. In this paper, we focus on the control of one of the most used cranes, the boom crane. Tower cranes and overhead cranes have been widely studied in the literature, whereas the control of boom cranes has been investigated only by a few works. Typically, these works make use of simple models making use of a large number of simplifying assumptions (e.g. fixed length cable, assuming certain dynamics are uncoupled, etc.) A first result of this paper is to present a fairly complete nonlinear dynamic model of a boom crane taking into account all coupling dynamics and where the only simplifying assumption is that the cable is considered as rigid. The boom crane involves pitching and rotational movements, which generate complicated centrifugal forces, and consequently, equations of motion highly nonlinear. On the basis of this model, a control law has been developed able to perform position control of the crane while actively damping the oscillations of the load. The effectiveness of the approach has been tested in simulation with realistic physical parameters and tested in the presence of wind disturbances.

Keywords -

Boom cranes; Robotics; Motion control; Underactuated systems; Nonlinear control.

1 Introduction

A crane is a type of machine, generally equipped with a hoist rope, that is used to move materials. Cranes can be classified in overhead cranes [1]-[2], offshore cranes [3]–[4], and rotary cranes [5]-[6]. Currently, the automation of cranes is still in a relatively early phase. To improve the efficiency and safety of cranes some control approaches have be proposed using sliding-mode control [7]-[8], optimal control [9], adaptive control [10], prediction control [11], intelligent control [12].

In this paper we focus on the modeling and control of a very common type of rotary crane, know as 'boom crane'. Compared with other cranes, boom cranes have higher flexibility and lower energy consumption. Therefore, boom cranes have been widely used in the maintenance of buildings and to handle masonry in urban streets and construction sites. There the cranes have a boom that can rotate in two directions (e.g. pitch and yaw motions) and the load swing can be split into two dimensions. Consequently, the nonlinear dynamic models of boom cranes are more complex than those of other types of cranes.

In recent years, a number of studies have been carried out to solve the control problems of such complex systems. [13]-[14] proposed the use of S-curve trajectories as an open-loop control approaches to achieve anti-sway control for the payload. Moreover, input shaping has been widely applied to control boom cranes [15]. However, the open-loop control strategies are sensitive to external disturbances and to model mismatch. Motivated by these reasons, closed-loop control approaches have been proposed. In [16] the combination of command shaping and feedback control was proposed which can reduce payload oscillation. In [17], a state feedback control law based on linearized model is used to achieve the control objectives. In [18]-[19] the authors proposed a Proportional-Derivative (PD) controller with gravity compensation based on the nonlinear model of the boom crane. In [20] the authors present constrained control for boom cranes.

Most of the existing closed-loop control laws for boom cranes have two main drawbacks:

1. The dynamic of the hoisting mechanism is neglected (e.g. the length of the cable is considered as constant).
2. In the design of the control law, the possibility of measuring the oscillations of the payload (e.g. angular positions and speeds) is usually ignored.

In order to address these problems, we propose a control law that exploits all states of the system to control it. The proposed control scheme is based on a detailed mathematical model in which we takes into account all the degrees of freedom (DoFs) that characterize this type of system (i.e. the two rotations, the length of the rope, and

the payload swing angles). Realistic physical parameters of an existing boom crane are used in simulation tests to show the effectiveness of the proposed approach.

2 Dynamic Model

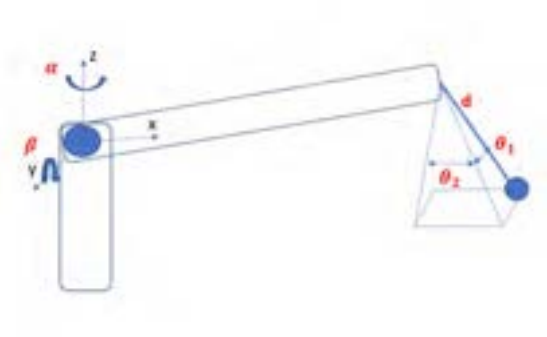

Figure 1. Model of a boom crane

The type of crane considered in this paper (see Fig.1) is represented by five generalized coordinates: α is the slew angle of the tower, β is the luff angle of the boom, d is the length of the rope, θ_1 is the tangential pendulation due to the motion of the tower, and θ_2 is the radial sway due to the motion of the boom.
The equations of the motion obtained using the Euler-Lagrange approach are

$$\begin{aligned}
&I_t\ddot{\alpha} + d^2\ddot{\alpha}m + \ddot{\alpha}l_B^2mC_\beta^2 + (\ddot{\alpha}l_B^2m_BC_\beta^2)/4 - d^2\ddot{\theta}_2mS_{\theta_3}\\
&+2\dot{d}\dot{d}\dot{\alpha}m - 2d^2\dot{\theta}_1\dot{\theta}_2mC_{\theta_1} - d^2\ddot{\alpha}mC_{\theta_1}^2C_{\theta_4}^2 - \dot{\alpha}\dot{\beta}l_B^2mS_{2\beta}\\
&-(\dot{\alpha}\dot{\beta}l_B^2m_BS_{2\beta})/4 - 2\dot{d}d\dot{\theta}_2mS_{\theta_3} + \ddot{d}l_BmC_\beta C_{\theta_4}S_{\theta_3}\\
&-2\dot{d}d\dot{\alpha}mC_{\theta_1}^2C_{\theta_4}^2 + 2d^2\dot{\theta}_1\dot{\theta}_2mC_{\theta_1}C_{\theta_4}^2 + d^2\ddot{\theta}_1mC_{\theta_1}C_{\theta_4}S_{\theta_4}\\
&+2d\ddot{\alpha}l_BmC_\beta S_{\theta_4} + 2\dot{d}\dot{\alpha}l_BmC_\beta S_{\theta_4} - d^2{\dot{\theta}_1}^2mC_{\theta_4}S_{\theta_3}S_{\theta_4}\\
&+2d\dot{\alpha}\dot{\theta}_2l_BmC_\beta C_{\theta_4} - 2d\dot{\alpha}\dot{\beta}l_BmS_\beta S_{\theta_4}\\
&+2d^2\dot{\alpha}\dot{\theta}_2mC_{\theta_1}^2C_{\theta_4}S_{\theta_4} + d\ddot{\theta}_1l_BmC_\beta C_{\theta_1}C_{\theta_4}\\
&+2\dot{d}\dot{\theta}_1l_BmC_\beta C_{\theta_1}C_{\theta_4} + 2\dot{d}d\dot{\theta}_1mC_{\theta_1}C_{\theta_4}S_{\theta_4}\\
&+d\ddot{\beta}l_BmC_{\theta_4}S_\beta S_{\theta_3} - d\ddot{\theta}_2l_BmC_\beta S_{\theta_3}S_{\theta_4}\\
&-2\dot{d}\dot{\theta}_2l_BmC_\beta S_{\theta_3}S_{\theta_4} + d\dot{\beta}^2l_BmC_\beta C_{\theta_4}S_{\theta_3}\\
&-d{\dot{\theta}_1}^2l_BmC_\beta C_{\theta_4}S_{\theta_3} + 2d^2\dot{\alpha}\dot{\theta}_1mC_{\theta_1}C_{\theta_4}^2S_{\theta_3}\\
&-d{\dot{\theta}_2}^2l_BmC_\beta C_{\theta_4}S_{\theta_3} - 2d\dot{\theta}_1\dot{\theta}_2l_BmC_\beta C_{\theta_1}S_{\theta_4} = u_1,
\end{aligned} \tag{1}$$

$$\begin{aligned}
&I_B\ddot{\beta} + \ddot{\beta}l_B^2m + (\ddot{\beta}l_B^2m_B)/4 + gl_BmC_\beta + (gl_Bm_BC_\beta)/2\\
&+(\dot{\alpha}^2l_B^2mS_{2\beta})/2 + (\dot{\alpha}^2l_B^2m_BS_{2\beta})/8 - \ddot{d}l_BmS_\beta S_{\theta_2}\\
&-\ddot{d}l_BmC_\beta C_{\theta_1}C_{\theta_2} + d\dot{\alpha}^2l_BmS_\beta S_{\theta_2} + d{\dot{\theta}_2}^2l_BmS_\beta S_{\theta_2}\\
&-d\ddot{\theta}_2l_BmC_{\theta_2}S_\beta - 2\dot{d}\dot{\theta}_2l_BmC_{\theta_2}S_\beta + d\ddot{\theta}_1l_BmC_\beta C_{\theta_2}S_{\theta_1}\\
&+d\ddot{\theta}_2l_BmC_\beta C_{\theta_1}S_{\theta_2} + 2\dot{d}\dot{\theta}_1l_BmC_\beta C_{\theta_2}S_{\theta_1}\\
&+2\dot{d}\dot{\theta}_2l_BmC_\beta C_{\theta_1}S_{\theta_2} + d\ddot{\alpha}l_BmC_{\theta_2}S_\beta S_{\theta_1}\\
&+2\dot{d}\dot{\alpha}l_BmC_{\theta_2}S_\beta S_{\theta_1} + d{\dot{\theta}_1}^2l_BmC_\beta C_{\theta_1}C_{\theta_2}\\
&+d{\dot{\theta}_2}^2l_BmC_\beta C_{\theta_1}C_{\theta_2} - 2d\dot{\theta}_1\dot{\theta}_2l_BmC_\beta S_{\theta_1}S_{\theta_2}\\
&-2d\dot{\alpha}\dot{\theta}_2l_BmS_\beta S_{\theta_1}S_{\theta_2} + 2d\dot{\alpha}\dot{\theta}_1l_BmC_{\theta_1}C_{\theta_2}S_\beta = u_2,
\end{aligned} \tag{2}$$

$$\begin{aligned}
&\ddot{d}m - d\dot{\alpha}^2m - d{\dot{\theta}_2}^2m - d{\dot{\theta}_1}^2mC_{\theta_2}^2 - gmC_{\theta_1}C_{\theta_2}\\
&+d\dot{\alpha}^2mC_{\theta_1}^2C_{\theta_2}^2 - \ddot{\beta}l_BmS_\beta S_{\theta_2} - \dot{\alpha}^2l_BmC_\beta S_{\theta_2}\\
&-\dot{\beta}^2l_BmC_\beta S_{\theta_2} + 2d\dot{\alpha}\dot{\theta}_2mS_{\theta_1} - \ddot{\beta}l_BmC_\beta C_{\theta_1}C_{\theta_2}\\
&+\ddot{\alpha}l_BmC_\beta C_{\theta_2}S_{\theta_1} + \dot{\beta}^2l_BmC_{\theta_1}C_{\theta_2}S_\beta\\
&-2d\dot{\alpha}\dot{\theta}_1mC_{\theta_1}C_{\theta_2}S_{\theta_2} - 2\dot{\alpha}\dot{\beta}l_BmC_{\theta_2}S_\beta S_{\theta_1} = u_3,
\end{aligned} \tag{3}$$

$$\begin{aligned}
&dmC_{\theta_2}(gS_{\theta_1} + 2\dot{d}\dot{\theta}_1C_{\theta_2} + d\ddot{\theta}_1C_{\theta_2} - \dot{\beta}^2l_BS_\beta S_{\theta_1}\\
&-2d\dot{\theta}_1\dot{\theta}_2S_{\theta_2} + \ddot{\alpha}l_BC_\beta C_{\theta_1} + d\ddot{\alpha}C_{\theta_1}S_{\theta_2} + 2\dot{d}\dot{\alpha}C_{\theta_1}S_{\theta_2}\\
&+\ddot{\beta}l_BC_\beta S_{\theta_1} - d\dot{\alpha}^2C_{\theta_1}C_{\theta_2}S_{\theta_1} + 2d\dot{\alpha}\dot{\theta}_2C_{\theta_1}C_{\theta_2}\\
&-2\dot{\alpha}\dot{\beta}l_BC_{\theta_1}S_\beta) = 0,
\end{aligned} \tag{4}$$

$$\begin{aligned}
&-dm(d\ddot{\alpha}S_{\theta_1} - 2\dot{d}\dot{\theta}_2 - d\ddot{\theta}_2 + 2\dot{d}\dot{\alpha}S_{\theta_1} - gC_{\theta_1}S_{\theta_2}\\
&-(d{\dot{\theta}_1}^2S_{2\theta_2})/2 + \dot{\alpha}^2l_BC_\beta C_{\theta_2} + \dot{\beta}^2l_BC_\beta C_{\theta_2}\\
&+\ddot{\beta}l_BC_{\theta_2}S_\beta + \dot{\beta}^2l_BC_{\theta_1}S_\beta S_{\theta_2} + d\dot{\alpha}^2C_{\theta_1}^2C_{\theta_2}S_{\theta_2}\\
&+2d\dot{\alpha}\dot{\theta}_1C_{\theta_1}C_{\theta_2}^2 - \ddot{\beta}l_BC_\beta C_{\theta_1}S_{\theta_2} + \ddot{\alpha}l_BC_\beta S_{\theta_1}S_{\theta_2}\\
&-2\dot{\alpha}\dot{\beta}l_BS_\beta S_{\theta_1}S_{\theta_2}) = 0.
\end{aligned} \tag{5}$$

where m, m_b denote the load mass, and the boom mass, respectively, l_b is the boom length, I_t is the inertia moment of the tower, and I_b is the inertia moment of the boom. Moreover, the following abbreviations are used:
$S_\alpha \triangleq sin(\alpha)$, $S_\beta \triangleq sin(\beta)$, $S_{\theta_1} \triangleq sin(\theta_1)$, $S_{\theta_2} \triangleq sin(\theta_2)$, $C_\alpha \triangleq cos(\alpha)$, $C_\beta \triangleq cos(\beta)$, $C_{\theta_1} \triangleq cos(\theta_1)$, $C_{\theta_2} \triangleq cos(\theta_2)$.

The system dynamics (1)-(5) can be rewritten in matrix form as

$$M(q)\ddot{q} + C(q,\dot{q})\dot{q} + G(q) = \begin{bmatrix} I_{3x3} \\ 0_{2x2} \end{bmatrix} u, \tag{6}$$

where $q = [\alpha, \beta, d, \theta_1, \theta_2]^T \in \mathbb{R}^5$ represents the state vector, and $u = [u_1, u_2, u_3]^T \in \mathbb{R}^3$ is the control input

vector. The matrices M(q) $\in \mathbb{R}^{5x5}$, $C(q,\dot{q}) \in \mathbb{R}^{5x5}$, and G(q) $\in \mathbb{R}^5$ represent the inertia matrix, centripetal-Coriolis forces, and gravity term, respectively.

As one can seen from (6), the boom crane is an under-actuated system, having fewer independent actuators than system degrees of freedom (DoFs). Thus, we can rewrite its model as

$$\begin{aligned} M_{11}(q)\ddot{q}_1 + M_{12}(q)\ddot{q}_2 \\ +C_{11}(q,\dot{q})\dot{q}_1 + C_{12}(q,\dot{q})\dot{q}_2 + G_1(q) = U, \end{aligned} \tag{7}$$

$$\begin{aligned} M_{21}(q)\ddot{q}_1 + M_{22}(q)\ddot{q}_2 + C_{21}(q,\dot{q})\dot{q}_1 \\ +C_{22}(q,\dot{q})\dot{q}_2 + G_2(q) = 0, \end{aligned} \tag{8}$$

where $q_1 = [\alpha \quad \beta \quad d]^T$ is the vector of actuated states and $q_2 = [\theta_1 \quad \theta_2]^T$ of non-actuated states and

$$M_{11}(q) = \begin{bmatrix} m_{11} & m_{12} & m_{13} \\ m_{21} & m_{22} & m_{23} \\ m_{31} & m_{32} & m_{33} \end{bmatrix}, M_{12}(q) = \begin{bmatrix} m_{14} & m_{15} \\ m_{24} & m_{25} \end{bmatrix},$$

$$M_{21}(q) = \begin{bmatrix} m_{41} & m_{42} & m_{43} \\ m_{51} & m_{52} & m_{53} \end{bmatrix}, M_{22}(q) = \begin{bmatrix} m_{44} & 0 \\ 0 & m_{55} \end{bmatrix},$$

$$C_{11}(q,\dot{q}) = \begin{bmatrix} c_{11} & c_{12} & c_{13} \\ c_{21} & c_{22} & c_{23} \\ c_{31} & c_{32} & c_{33} \end{bmatrix}, C_{12}(q,\dot{q}) = \begin{bmatrix} c_{14} & c_{15} \\ c_{24} & c_{25} \end{bmatrix},$$

$$C_{21}(q,\dot{q}) = \begin{bmatrix} c_{41} & c_{42} & c_{43} \\ c_{51} & c_{52} & c_{53} \end{bmatrix}, C_{22}(q,\dot{q}) = \begin{bmatrix} c_{44} & 0 \\ 0 & c_{55} \end{bmatrix},$$

$$G_1(q) = \begin{bmatrix} 0 \\ g_2 \\ g_3 \end{bmatrix}, G_2(q) = \begin{bmatrix} g_4 \\ g_5 \end{bmatrix}, U = \begin{bmatrix} u_1 \\ u_2 \\ u_3 \end{bmatrix}.$$

3 Control Design

The aim of the control is to move the crane to the desired position and to dampen the swing angles of the load. In our development we will consider the following reasonable assumptions.

Assumption 1 *The payload swing are such that* $|\theta_{1,2}| < \frac{\pi}{2}$.

Assumption 2 *The cable length is always greater than zero to avoid singularity in the model (6), i.e.* $d(t) > 0, \forall t \geq 0$.

As one can see, (8) can be rewritten as

$$\begin{aligned} \ddot{q}_2 = -M_{22}^{-1}(q)(M_{21}(q)\ddot{q}_1 + C_{21}(q,\dot{q})\dot{q}_1 \\ +C_{22}(q,\dot{q})\dot{q}_2 + G_2(q)). \end{aligned} \tag{9}$$

It is worth noticing that in (9) the $M_{22}(q)$ is a positive definite matrix due to Assumptions (1)-(2).

Substituting (9) into (7), one obtains

$$\bar{M}(q)\ddot{q}_1 + \bar{C}_1(q,\dot{q})\dot{q}_1 + \bar{C}_2(q,\dot{q})\dot{q}_2 + \bar{G}(q) = U, \tag{10}$$

where

$$\begin{aligned} \bar{M}(q) &= M_{11}(q) - M_{12}(q)M_{22}^{-1}(q)M_{21}(q), \\ \bar{C}_1(q,\dot{q}) &= C_{11}(q,\dot{q}) - M_{12}(q)M_{22}^{-1}(q)C_{12}(q,\dot{q}), \\ \bar{C}_2(q,\dot{q}) &= C_{12}(q,\dot{q}) - M_{12}(q)M_{22}^{-1}(q)C_{22}(q,\dot{q}), \\ \bar{G}(q) &= G_1(q) - M_{12}(q)M_{22}^{-1}(q)G_2(q). \end{aligned}$$

According to Assumptions (1)-(2), the matrix $\bar{M}$ is positive definite. Then, (10) can be rewritten as

$$\ddot{q}_1 = \bar{M}^{-1}(q)(U - \bar{C}_1(q,\dot{q})\dot{q}_1 - \bar{C}_2(q,\dot{q})\dot{q}_2 - \bar{G}(q)) \tag{11}$$

Substituting (11) into (9) yields

$$\begin{aligned} \ddot{q}_2 = -M_{22}^{-1}(q)(M_{21}(q)\bar{M}^{-1}(q)(-\bar{C}_1(q,\dot{q})\dot{q}_1 - \bar{C}_2(q,\dot{q})\dot{q}_2 \\ -\bar{G}(q) + U) + C_{21}(q,\dot{q})\dot{q}_1 + C_{22}(q,\dot{q})\dot{q}_2 + G_2(q)). \end{aligned} \tag{12}$$

Following the classical approach of a feedback linearization technique, (11) can be "linearized" by using the control law

$$U = \bar{M}(q)v + \bar{C}_1(q,\dot{q})\dot{q}_1 + \bar{C}_2(q,\dot{q})\dot{q}_2 + \bar{G}(q). \tag{13}$$

Thus, (11) becomes

$$\ddot{q}_1 = v, \tag{14}$$

where $v \in \mathbb{R}^3$ as additional control inputs.

To move the crane to the desired position, the additional control inputs (14) can be chosen as

$$v = \ddot{q}_{1d} - K_{ad}(\dot{q}_1 - \dot{q}_{1d}) - K_{ap}(q_1 + q_{1d}), \tag{15}$$

where $K_{ad} = diag(K_{ad1}, K_{ad2}, K_{ad3})$, $K_{ap} = diag(K_{ap1}, K_{ap2}, K_{ap3})$ are positive diagonal matrices. Substituting (15) into (14), we obtain

$$\ddot{\tilde{q}}_1 + K_{ad}\dot{\tilde{q}}_1 + K_{ap}\tilde{q}_1 = 0, \tag{16}$$

where $\tilde{q} = q_1 - q_{1d}$ is the tracking error vector of the actuated states. (16) is exponentially stable for every $K_{ad} > 0$ and $K_{ap} > 0$.

To stabilize the non-actuated states q_2, following what is proposed in [21], we define a second additional inputs as

$$v_u = -K_{ud}\dot{q}_2 - K_{up}q_2, \tag{17}$$

where $v_u \in \mathbb{R}^2$ are additional inputs which take into account the non-actuated states, $K_{ad} = diag(K_{ud1}, K_{ud2})$, $K_{ap} = diag(K_{up1}, K_{up2})$ are positive diagonal matrices.

Considering $q_{1d} = const$, the overall additional inputs are proposed by linearly combining (15) and (17)

$$v = -K_{ad}\dot{q}_1 - K_{ap}(q_1 - q_{1d}) - \alpha(K_{ud}\dot{q}_2 - K_{up}q_2), \tag{18}$$

where

$$\alpha = \begin{bmatrix} \alpha_1 & 0 \\ 0 & \alpha_2 \\ 0 & 0 \end{bmatrix} \tag{19}$$

is a weighting matrix.

Substituting the (18) into (13) the overall control law is obtained as

$$U = (\bar{C}_1(q,\dot{q}) - \bar{M}(q)K_{ad})\dot{q}_1 + (\bar{C}_2(q,\dot{q}) - \bar{M}(q)\alpha K_{ud})\dot{q}_2 - \bar{M}(q)K_{ap}(q_1 - q_{1d}) - \bar{M}(q)\alpha K_{up}q_2 + \bar{G}(q). \tag{20}$$

Replacing (20) into (12), we obtain

$$\ddot{q}_2 = -M_{22}^{-1}(q)(-M_{21}(q)(K_{ad}\dot{q}_1 + K_{ap}q_1 + \alpha(K_{ud}\dot{q}_2 + K_{up}q_2)) + C_{21}(q,\dot{q})\dot{q}_1 + C_{22}(q,\dot{q})\dot{q}_2 + G_2(q)). \tag{21}$$

Considering Assumption 1, in the rest of this Section we have to demonstrate that (21) converges to the equilibrium point expressed by: $q_2 = \dot{q}_2 = 0$ to achieve the control goal.

Setting $q_1 = q_{1d}$ in (21), one achieves

$$\ddot{q}_2 = -M_{22}^{-1}(q)(-M_{21}(q)(\alpha(K_{ud}\dot{q}_2 + K_{up}q_2)) + C_{22}(q,\dot{q})\dot{q}_2 + G_2(q)). \tag{22}$$

The stability analysis of (22) is analyzed by linearizing (22) around the equilibrium point $q_2 = \dot{q}_2 = 0$.
We can rewrite (22) as

$$z_1 = \theta_1, \quad z_2 = \dot{\theta}_1, \quad z_3 = \theta_2, \quad z_4 = \dot{\theta}_2.$$

Then, we obtain the following state-space forms:

$$\dot{z}_1 = z_2, \tag{23}$$

$$\dot{z}_2 = h_1(z), \tag{24}$$

$$\dot{z}_3 = z_4, \tag{25}$$

$$\dot{z}_4 = h_2(z), \tag{26}$$

with $z = [z_1 \quad z_2 \quad z_3 \quad z_4]^T$ as a state vector. Linearizing (23)-(26) around $z = 0$, we obtain

$$\dot{z} = Az, \tag{27}$$

where

$$A = \begin{bmatrix} 0 & 1 & 0 & 0 \\ \frac{\partial h_1}{\partial z_1} & \frac{\partial h_1}{\partial z_2} & \frac{\partial h_1}{\partial z_3} & \frac{\partial h_1}{\partial z_4} \\ 0 & 0 & 0 & 1 \\ \frac{\partial h_2}{\partial z_1} & \frac{\partial h_2}{\partial z_2} & \frac{\partial h_2}{\partial z_3} & \frac{\partial h_2}{\partial z_4} \end{bmatrix}_{z=0} = \begin{bmatrix} 0 & 1 & 0 & 0 \\ a_{11} & a_{12} & 0 & 0 \\ 0 & 0 & 0 & 1 \\ 0 & 0 & a_{21} & a_{22} \end{bmatrix}. \tag{28}$$

The non-zero elements in (28) are the flowwing:

$$a_{11} = -\frac{(g - a_1 K_{pu1} l_B cos\beta)}{d}, \tag{29}$$

$$a_{12} = \frac{a_1 K_{du1} l_B cos\beta}{d}, \tag{30}$$

$$a_{21} = -\frac{(g + a_2 K_{pu2} l_B sin\beta)}{d}, \tag{31}$$

$$a_{22} = -\frac{a_2 K_{du2} l_B sin\beta}{d}. \tag{32}$$

The linearized system (27) is stable around the equilibrium point $z = 0$, if the A matrix (28) is a Hurwiz matrix. Therefore, it is necessary to properly choose the control parameters that appear in (29)-(32). In this way, (27) is stable around equilibrium point z = 0, which leads to the local stability of (21). In the Section 4 the values for each of the control parameters are listed.

4 Simulation Results

In this section, three different simulation scenarios will be shown to demonstrate the proposed control scheme. In each of them the goal is to move the crane to a desired position and to reduce the swings of the payload as much as possible. In the second and third simulation, the effects of a gust of wind for the payload will be shown.

To get realistic values for the simulation tests, we consider a small boom crane: the NK 1000 Mini Crane from NEMAASKO [22]. Some parameters are taken directly from the datasheets. Others, like the boom dimensions were estimated by CAD simulations.
The crane system parameters are selected as follows:

$$I_t = 207.13kgm^2, \quad l_B = 6.2m, \quad m_B = 312.2kg,$$
$$I_B = 2068kgm^2, \quad g = 9.81ms^{-2}, \quad m = 50kg.$$

The control parameters for controller (18) are set as $K_{ad} = diag(100, 100, 150)$, $K_{ap} = diag(10, 20, 50)$, $K_{ud} = diag(120, 120)$, $K_{up} = diag(10, 10)$, $a_1 = -1$, $a_2 = sign(\beta)$.

Scenario 1. In this simulation scenario, we show the performance of the proposed control law described in the Section 3. The goal is to move the crane to a desired configuration while damping the payload swing angles as much as possible. In this first scenario no external disturbances to the crane will be considered. The simulation results are shown in Figg.2-6. We can see that the boom arrives at the desired positions in around 30 seconds, Additionally, the maximum payload swing amplitudes in the two directions are confined in $-2.5°$ and $1°$, respectively. In Fig.7 the input controls are shown. For the boom actuator following the [22], the limit of the working range of the crane is of 210kg for the payload mass with a boom length of 8.9m then the maximal torque should be around $u_{2max} = 18.2kNm$. The values of the other two inputs do not represent a problem as the inputs values are reasonable and well within the typical limits of the crane actuators.

Scenario 2. In this simulation scenario, we consider a gust of wind as external disturbance for the crane. The desired configuration for the crane is the same of the previous scenario. In this case the controller must be able to counteract the effect of wind during the whole movement of the crane. The perturbation seen by the system will be characterized by a duration and a time dependent amplitude. Concerning the first one, a study from a meteorological center of the Netherlands reported that wind gusts have periods of 2 to 7 seconds with average speeds comprised between 4 and 20 m/s [23]. The force applied on the payload can be seen as distributed force $F = \frac{1}{2}\rho V^2 A_w C_D$, where V is the wind average gust speeds, and A_w is the surface exposed to the wind. According to [24], $C_D = 1.05$ will be chosen. Assuming ISA conditions at sea level, $\rho = 1.225[kg/m^3]$.
In this Scenario, we consider a force that acts laterally to the load (e.g. increases the swing angle θ_1). In this scenario, only one gust of wind will occur when the simulation is at 20s. In our simulations, the wind speed will have a trapezoidal shape (e.g. increase linearly from zero, constant for a time window and finally linearly decrease to zero).
As one can see in Figg. 11-12, due to the wind gust, the swing angle θ_1 increases and consequently also the angle θ_2 oscillates. To counteract this effect, the controller modifies the tower angle α (Fig.8 and Fig.13) and the boom angle β (Fig.9 and Fig.13) to reduce the swing angles as fast as possible. The small effects on the length of the cable can be seen in Fig.13, where one can see that the force on the cable changes a little.

Scenario 3. In this Simulation scenario, the main effect of the wind is on the angle θ_2. In this case, the swing radial angle increases (see Fig.18) and consequentially the controller modifies the value of the luff angle (Fig.15) and the length of the cable (Fig.16) to reduce the oscillations as much as possible. There are no significant effects on the angle θ_1, therefore no changes are required for the slew angle α. As one can see in Fig.19, to quickly counteract the effect of the wind, the control input u_2 reaches its limit value and then decreases.

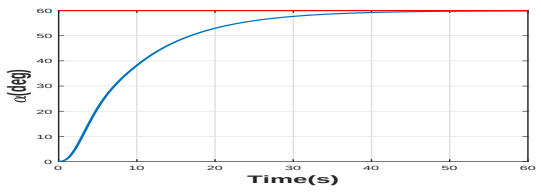

Figure 2. Scenario 1. Tower angle α. Red line: Desired reference. Blue line: Simulation result.

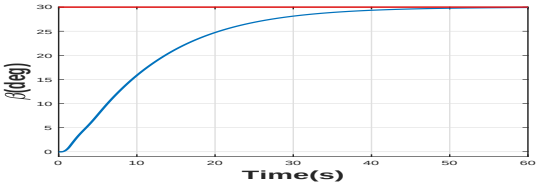

Figure 3. Scenario 1. Boom angle β. Red line: Desired reference. Blue line: Simulation result.

5 Conclusion

The paper proposed a detailed mathematical model of a boom crane which takes into account all of the degrees of

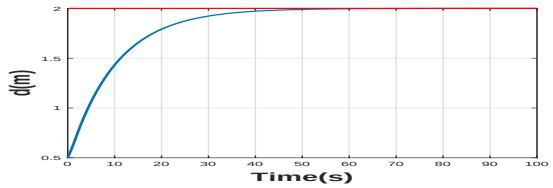

Figure 4. Scenario 1. Cable length. Red line: Desired reference. Blue line: Simulation result.

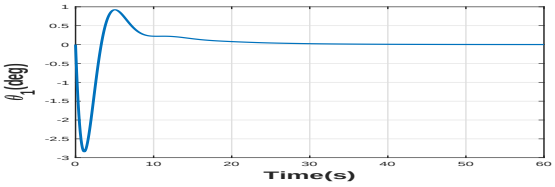

Figure 5. Scenario 1. Payload angle θ_1.

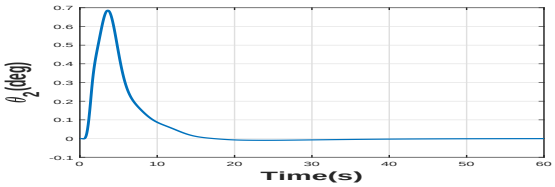

Figure 6. Scenario 1. Payload angle θ_2.

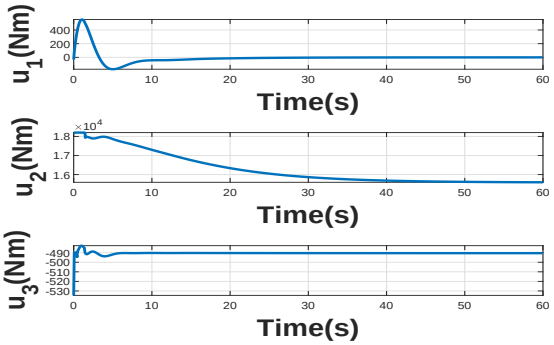

Figure 7. Scenario 1. Control inputs

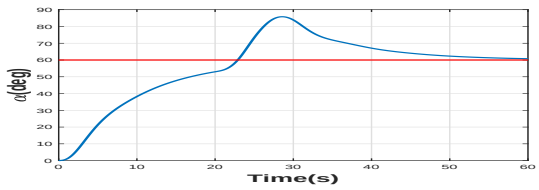

Figure 8. Scenario 2. Tower angle α. Red line: Desired reference. Blue line: Simulation result.

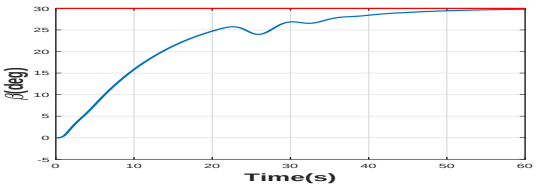

Figure 9. Scenario 2. Boom angle β. Red line: Desired reference. Blue line: Simulation result.

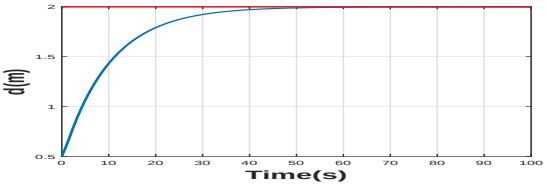

Figure 10. Scenario 2. Cable length. Red line: Desired reference. Blue line: Simulation result.

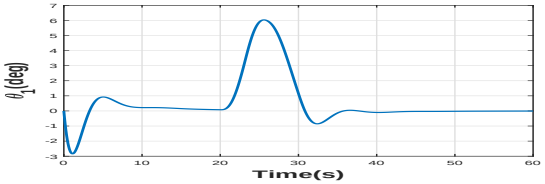

Figure 11. Scenario 2. Payload angle θ_1.

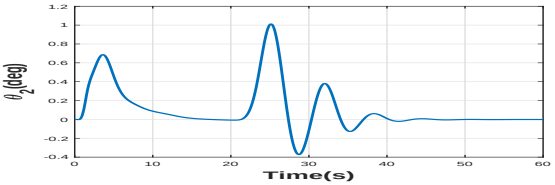

Figure 12. Scenario 2. Payload angle θ_2.

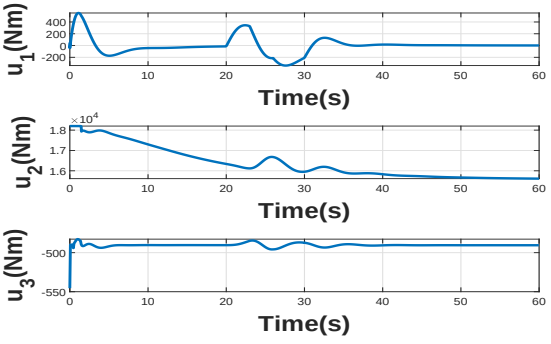

Figure 13. Scenario 2. Control inputs

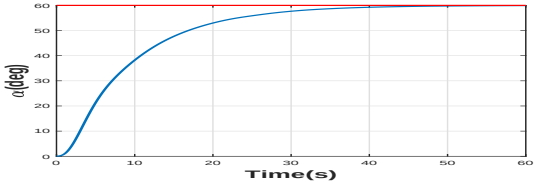

Figure 14. Scenario 3. Tower angle α. Red line: Desired reference. Blue line: Simulation result.

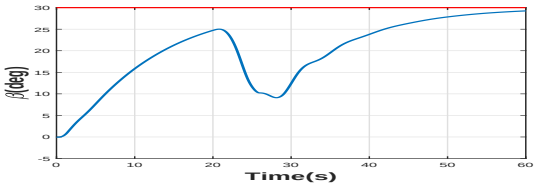

Figure 15. Scenario 3. Boom angle β. Red line: Desired reference. Blue line: Simulation result.

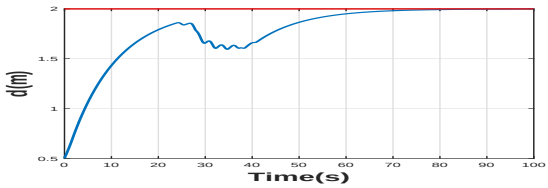

Figure 16. Scenario 3. Cable length. Red line: Desired reference. Blue line: Simulation result.

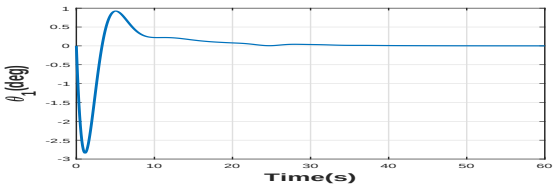

Figure 17. Scenario 3. Payload angle θ_1.

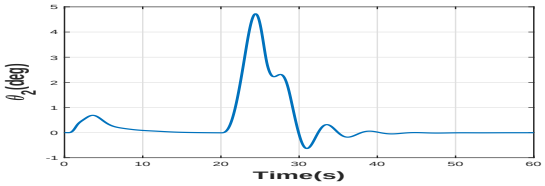

Figure 18. Scenario 3. Payload angle θ_2.

freedom (DoFs) that characterize this type of system (i.e. the two rotations, the length of the rope and the payload swing angles). Despite the complexity of the model, we design a nonlinear control law that exploits all the states of the model to guide the crane towards a desired reference

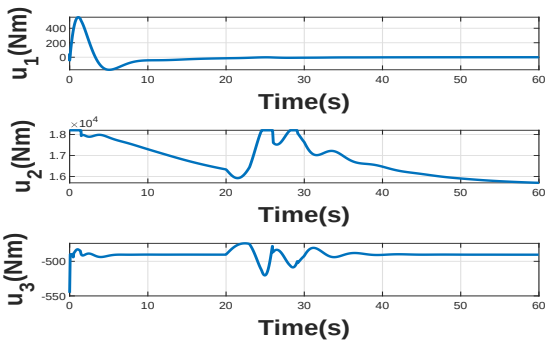

Figure 19. Scenario 3. Control inputs

and ensuring that the non-actuated variables (i.e., θ_1 and θ_2) go to zero in a fast way. The simulation results with realistic physical parameters show the efficiency of the proposed control scheme even in the presence of wind disturbance.

References

[1] L. A. Tuan, G. Kim, and S. Lee. Partial feedback linearization control of the three dimensional overhead crane. pages 1198–1203, 2012. doi:10.1109/CoASE.2012.6386314.

[2] N. Sun, Y. Fang, H. Chen, and B. Lu. Amplitude-saturated nonlinear output feedback antiswing control for underactuated cranes with double-pendulum cargo dynamics. *IEEE Transactions on Industrial Electronics*, 64(3):2135–2146, 2017. doi:10.1109/TIE.2016.2623258.

[3] Le Tuan, Hoang Cuong, Soon-Geul Lee, Nho Cong, and Kee Moon. Nonlinear feedback control of container crane mounted on elastic foundation with the flexibility of suspended cable. *Journal of Vibration and Control*, 22, 11 2014. doi:10.1177/1077546314558499.

[4] Ning Sun, Yongchun Fang, He Chen, Yiming Wu, and Biao lu. Nonlinear antiswing control of offshore cranes with unknown parameters and persistent ship-induced perturbations: Theoretical design and hardware experiments. *IEEE Transactions on Industrial Electronics*, PP:1–1, 10 2017. doi:10.1109/TIE.2017.2767523.

[5] Naoki Uchiyama, Huimin Ouyang, and Shigenori Sano. Simple rotary crane dynamics modeling and open-loop control for residual load sway suppression by only horizontal boom motion. *Mechatronics*, 23:1223–1236, 12 2013. doi:10.1016/j.mechatronics.2013.09.001.

[6] M. Ambrosino, B. Thierens, A. Dawans, and E. Garone. Oscillation reduction for knuckle cranes. In *ISARC. Proceedings of the International Symposium on Automation and Robotics in Construction*, 2020.

[7] Zhiyu Xi and Tim Hesketh. Discrete time integral sliding mode control for overhead crane with uncertainties. *Control Theory & Applications, IET*, 4:2071 – 2081, 11 2010. doi:10.1049/iet-cta.2009.0558.

[8] Raja Mohd Taufika Raja Ismail and Quang Ha. Trajectory tracking and anti-sway control of three-dimensional offshore boom cranes using second-order sliding modes. pages 996–1001, 08 2013. doi:10.1109/CoASE.2013.6654071.

[9] Aurelio Piazzi and Antonio Visioli. Optimal dynamic-inversion-based control of an overhead crane. *Control Theory and Applications, IEE Proceedings* -, 149:405 – 411, 10 2002. doi:10.1049/ip-cta:20020587.

[10] Ning Sun, Yiming Wu, Yongchun Fang, and He Chen. Nonlinear antiswing control for crane systems with double-pendulum swing effects and uncertain parameters: Design and experiments. *IEEE Transactions on Automation Science and Engineering*, PP:1–10, 07 2017. doi:10.1109/TASE.2017.2723539.

[11] Eckhard Arnold, Oliver Sawodny, J. Neupert, and Klaus Schneider. Anti-sway system for boom cranes based on a model predictive control approach. *IEEE International Conference Mechatronics and Automation, 2005*, 3:1533–1538 Vol. 3, 2005.

[12] Kunihiko Nakazono, Kouhei Ohnishi, Hiroshi Kinjo, and Tetsuhiko Yamamoto. Vibration control of load for rotary crane system using neural network with ga-based training. *Artificial Life and Robotics*, 13 (1):98–101, Dec 2008.

[13] N. Uchiyama, H. Ouyang, and S. Sano. Residual load sway suppression for rotary cranes using only s-curve boom horizontal motion. pages 6258–6263, 2012. doi:10.1109/ACC.2012.6315369.

[14] Shigenori Sano, Huimin Ouyang, and Naoki Uchiyama. Residual load sway suppression for rotary cranes using simple dynamics model and s-curve trajectory. *IEEE International Conference on Emerging Technologies and Factory Automation, ETFA*, 128181071281512035281381512815101231268513336741221 35: 1–5, 09 2012. doi:10.1109/ETFA.2012.6489665.

[15] Reza Ezuan Samin, Zaharuddin Mohamed, Jamaludin Jalani, and Rozaimi Ghazali. Input shaping techniques for anti-sway control of a 3-dof rotary crane system. *Proceedings - 1st International Conference on Artificial Intelligence, Modelling and Simulation, AIMS 2013*, pages 184–189, 11 2014. doi:10.1109/AIMS.2013.36.

[16] Jie Huang, Ehsan Maleki, and W.E. Singhose. Dynamics and swing control of mobile boom cranes subject to wind disturbances. *Control Theory & Applications, IET*, 7:1187–1195, 06 2013. doi:10.1049/iet-cta.2012.0957.

[17] R. Kondo and S. Shimahara. Anti-sway control of a rotary crane via switching feedback control. 1:748 – 752 Vol.1, 10 2004. doi:10.1109/CCA.2004.1387303.

[18] Tong Yang, Ning Sun, Yuzhe Qian, and Yongchun Fang. An antiswing positioning controller for rotary cranes. pages 1586–1590, 07 2017. doi:10.1109/CYBER.2017.8446568.

[19] Ning Sun, Tong Yang, Yongchun Fang, Biao lu, and Yuzhe Qian. Nonlinear motion control of underactuated 3-dimensional boom cranes with hardware experiments. *IEEE Transactions on Industrial Informatics*, PP:1–1, 09 2017. doi:10.1109/TII.2017.2754540.

[20] M. Ambrosino, A. Dawans, and E. Garone. Constraint control of a boom crane system. In *ISARC. Proceedings of the International Symposium on Automation and Robotics in Construction*, 2020.

[21] L. A. Tuan, G. Kim, and S. Lee. Partial feedback linearization control of the three dimensional overhead crane. pages 1198–1203, 2012. ISSN 2161-8089. doi:10.1109/CoASE.2012.6386314.

[22] NEBOMAT. *NK 1000 User Manual*. NEBOMAT, 2005.

[23] F. J. Verheij, J. W. Cleijne, and J. A. Leene. Gust modelling for wind loading. *Journal of Wind Engineering and Industrial Aerodynamics*, 42:947–958, October 1992. ISSN 0167-6105. URL `http://www.sciencedirect.com/science/article/pii/016761059290101F`.

[24] Liebherr. Wind influence on crane operations, 2017. 4th Edition.

Automating Crane Lift Path through Integration of BIM and Path Finding Algorithm

Songbo Hu[a] and Yihai Fang[a]

[a]Department of Civil Engineering, Monash University, Australia
E-mail: Songbo.Hu@monash.edu, YihaiFang@monash.edu

Abstract -

Path planning, as a primary mission in crane lift planning, has a profound and direct impact on the safe and efficient execution of lift jobs on construction sites. Typically, the main objective of path planning is to find the shortest (or a relatively short) and collision-free path from the load supply point to the demand point in a finite 3D space with the presence of obstacles, while considering the mechanical constraints of the crane. Despite collision-free being a primary criterion in path planning, other critical safety issues have not been adequately addressed in existing methods. For example, blind lifts and reduced visibility of crane operators are prevalent in construction and have been recognized as major safety concerns in crane lifts. Furthermore, complex coordination of crane motions and frequent changes of moving direction potentially lead to human errors. To address this gap in the knowledge, this paper proposes a semi-automated planning approach by using Building Information Modeling (BIM) and an intelligent path finding algorithm. First, dimension and weight data of building components to be lifted are retrieved from the BIM model. Then, a modified RRT* algorithm is used to generate a short and collision-free path that satisfies the desired level of path smoothness, visibility, and motion coordination. Finally, paths for all lifts are stored and associated with corresponding elements in BIM for easy analysis and visualization. Preliminary results show that the proposed method can effectively reduce the occurrence of blind lifts while ensuring a practical path for execution. In the future, the proposed method is expected to enable a BIM-based risk analysis tool for the safety of crane operation and its impact on other adjacent construction activities.

Keywords -

Building Information Modeling (BIM); Path planning Algorithm; Tower Cranes; Practicality; Construction Safety; Lift Planning

1 Introduction

A crane is a piece of indispensable equipment on construction sites, undertaking both vertical and horizontal transportation [1]. However, it is also one of the main contributors to the construction fatality [2]. According to various accident analysis research, these fatal accidents related to cranes were primarily caused by inappropriate positioning of the lift load, which either violates the maximum reach or has spatial conflicts with workers, machinery, existing structures, and prohibited area [3]. Therefore, planning the load position during the lift, which is also known as path planning, is an essential procedure to avert safety hazards. In conventional practice, path planning is manual and based on experience, usually leading to a time-consuming process and error-prone outcomes [4].

In recent decades, researchers have made significant efforts to optimize and automate the path planning process. Multiple pieces of literature utilized the robotic path finding algorithms to generate the shortest and collision-free path abide by the load chart [5]. This method is able to shorten the planning time and eliminate multiple safety hazards, such as crane tipping-over and collisions between the load and static obstacles [6]. However, using robotic path finding algorithms is subjected to a number of strong assumptions, leading to incomplete considerations of safety hazards. For example, it is assumed that the operator has the ability to precisely execute the planned path. In reality, however, it is impractical for a human operator to carry out over-complicated maneuvers such as blind lifts [7] or complex coordination of swinging, luffing, and hoisting [8]. Meanwhile, most algorithms assume that the obstacles are static [9]. This assumption is inconsistent with the dynamic nature of construction sites and ignores the risk of spatial conflicts between the lift load and dynamic obstacles. Although in recent years, several novel frameworks enabled the path re-planning based on real-time monitoring of moving objects [10], these works sorely rely on the crane operators to alter the path on the spot and cannot coordinate with the affected objects and workspaces to avoid spatial conflicts.

To mitigate the spatial conflicts between the crane and other workspaces, one strategy is to visualize the crane workspace in the planning stage based on crane parameters [11]. It helps the construction stakeholders to understand the spatial relationships between the crane and dynamic/static obstacles and to identify potential safety hazards proactively. This strategy usually involves data visualization and analysis, on an effective information management platform. Building Information Modelling (BIM) has been exploited as a core data generator for risk management tools to demonstrate geometric information, analyze spatial conflicts, and communicate safety risks [12]. In such an approach, the parametric crane workspace is usually over-estimated and unable to explicitly reflect the location of the lift load [13]. There is a demand for a realistic path finding algorithm that guides and predicts the trajectory of lift loads. The algorithm-planned results for each building component need to be stored in BIM for further risk analysis.

Therefore, this paper proposes a novel approach that integrates a modified RRT* path finding algorithm and BIM to create a decision support tool for proactive path planning. Firstly, the original RRT* algorithm is improved to incorporate common practicality considerations. These practicality considerations determine the operational complexity for a crane operator and profoundly impact the crane lift safety, including avoiding frequent turning, minimizing blind lifts, and limiting the coordination of crane motions. Secondly, BIM is utilized to interoperate with the modified RRT* algorithm bi-directionally, which provides information to the algorithm and visualizes its output.

In the rest of this paper, Section 2 introduces the background information about the practicality considerations in path finding algorithms with respect to crane safety, as well as the potential application of BIM in this paper. Section 3 introduces the proposed methods, including the overall framework and the development of a prototype system. The proposed methods are validated and demonstrated in a case study in Section 4. Section 5 concludes the paper and indicates future directions.

2 Background

2.1 Path Finding Algorithm

Planning the lift path is a critical task in the lift planning process. In reality, an experienced human path planner not only avoids collisions between the lift load and obstacles but balances the operational complexity and path length [14]. A number of studies have been proposed to automate this task with path finding algorithms, including A* [15], Genetic Algorithm (GA) [16], Probability Roadmap [7], and Rapid Random-exploring Tree algorithm (RRT) [17]. These algorithms were designed to find a collision-free path within its kinematic ranges and comply with capacity limits. However, rather than applying these algorithms directly, these studies had to scrutinize the characteristics of crane lifting and modified the algorithms accordingly to generate a practical path with acceptable operational complexity. These unique considerations are referred to as practicality considerations in this study.

Three practicality considerations have been discussed in the related work, including the smoothness of a path, the blind lifts, and the motion coordination. First, a smooth path benefits construction safety since it requires gentle maneuvers and reduces the likelihood of human errors [18]. However, “smoothness” is a vague description and researchers have divergent opinions on what it embodies. For example, Ali et al. [5] defined a roughness index, which accumulated the angular displacements for each point on the paths. Together with the path length, the roughness index was integrated into the objective function for optimization. The description of operability using path roughness was later adopted by Zhang and Hammad in an RRT-based path planning method [18]. This interpretation of smoothness yields a continuous path and prevents abrupt changes in moving direction. Similar efforts can be found in [17], which employs a spline function to remove acute angles in the path. These efforts smoothen a path to prevent abrupt turnings, but it requires constant and complicated adjustment of moving directions. To address this issue, other researchers defined a smooth path as a path with fewer motion switches and consequentially fewer way-points. To remove redundant way-points, two strategies have been applied, which either adds operation switching cost to the objective function [19] or post-process a candidate path via the “straight-line strategy” [20]. These two strategies have both strengths and weaknesses. Using an operation switching cost can guide the path searching process to find a smooth path, but the definition of cost is subjective [20]. Also, the “straight-line strategy” is effective but it cannot compare the “smoothened” path with other alternatives generated during the planning process.

Motion coordination is another factor determining the operational complexity and thus researchers attempted to limit the number of coordinated motions in path planning. For example, Olearczyk et al. [21] avoided the coupling of crane rotation (i.e., swinging) and translation (i.e., luffing, hoisting, or both) to decrease the operational complexity. Chi et al. [7]assumed that crane operators can at most coordinate two motions simultaneously and applied this assumption to the generation of the roadmap using the probabilistic roadmap (PRM) algorithm. Cai et al. [16] adopted similar measures of prohibiting three simultaneous motions out of four degrees of freedom (i.e.,

swinging, luffing, hoisting and load rotation) and eliminated the complex motion coordination in post-processing. While these pieces of research followed an overwhelmingly stringent restriction on motion coordination, Hung et al. [22] allowed the combination of all crane motions and designed a user-defined parameter to limit the maximum number of coordinated motions.

In addition to being smooth and with a minimum level of motion coordination, a practical path should avoid blind lifts and ensures clear visibility to the load. Good visibility is essential for the crane operator to gain acute situational awareness, which helps to recognize and mitigate the severe safety risks [23]. In addition to safety concerns, blind lifts often compromise efficiency as the operator has to maneuver slowly with extra caution while communicating with the signal person [24]. To account for the extra time due to lifts in blind areas, researchers often estimate the total lift time using a mathematical model where poor visibility incurs a time penalty [25]. Abundant studies were devoted to enhancing the vision of crane operators [4]. However, there still lacks precaution against blind lifts in the planning stage [26]. Among the literature reviewed, only Chi et al. [7]examined the visibility of the path generated by a PRM algorithm. If the candidate path has any invisible segment, they execute PRM for an extra iteration until the path is fully visible. Although this method ensures the result to be visible, it did not modify the mechanism of PRM itself. Thus, the computational efficiency and success rate are subject to randomness due to the nature of PRM.

To accommodate these three practicality considerations, the RRT* algorithm is selected as the base for further modifications. RRT*, which is a variant of the classic RRT algorithm, is designed to efficiently search a high-dimensional space and converges towards the shortest collision-free path [27]. The optimality in the path length comes from two searching procedures, “Choose Parent” and “Rewire”. These two procedures dynamically reduce redundancy in the path set and remove unnecessary movements along every alternative path, which not only shorten the path length but smoothen the path. Additionally, the searching mechanism of the RRT* algorithm is highly adaptable, which allows modifications to consider visibility and motion coordination.

2.2 Building Information Modelling (BIM)

BIM is an emerging research focus in construction risk management [12]. In this task, BIM serves as two fundamental roles: the core data reservoir which provide baseline data to BIM-based risk management tools; and a visualization platform that enhances the identification, communication, and prevention of safety hazards [28]. Specific to the crane, BIM can both provide component information for automated lift planning [13], and visualize the paths and workspace of the crane to help stakeholders identify potential spatial conflicts [29]. For example, Ji and Leite [13] proposed an automatic rule-based checking system for reviewing a lift plan by using a 4D BIM model as the information source to reduce tedious manual input. Wang et al. [30] used BIM as an information source for a location optimization algorithm (i.e., firefly algorithm) and further visualized the algorithm-planned crane locations.

Despite some attempts, path planning, as a critical planning task, has not leveraged full benefit of BIM yet. Integrating BIM and the path finding algorithms is expected to not only eliminate tedious manual inputs, but explicitly predict the risks of cranes by analyzing the spatial relationship between an algorithm-planned path and existing structures in the pre-construction phase.

3 Methodology

3.1 Framework

This paper proposes a novel approach to improve the safety of lifting activities in the pre-construction phase via the integration of a practicality-and-safety-aware RRT* algorithm (PSRRT*), and BIM. Figure 1 presents the overall structure of the framework, which has three components: information retrieval, path generation, and path visualization. This framework starts with a query in the BIM model to retrieve information relevant to the building components to be lifted, the site area, existing structures, and the crane specifications. The retrieved information formulates the search space for PSRRT* who generates a path that satisfies the practicality considerations specified. The geometry of the path is then stored and visualized in the BIM model with invisible parts highlighted.

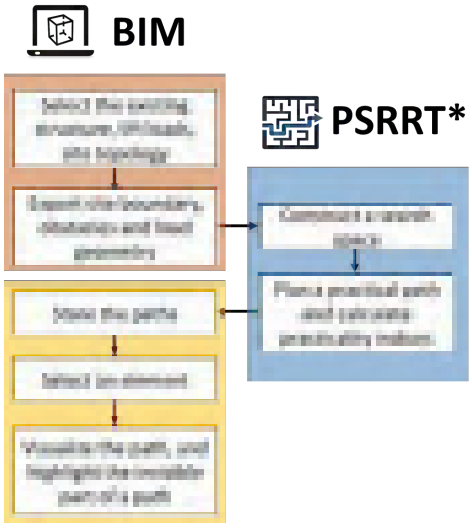

Figure 1. Research framework

3.2 Prototype Development

To validate the proposed framework, a prototype system was developed using Autodesk Revit, Dynamo Studio, and Python programming language. Python was employed to realize the PSRRT* algorithm while Revit and Dynamo were used to enable the data exchange between the BIM model and PSRRT*.

3.2.1 Information Retrieval

The first step in the prototype system involves the search for and retrieve of lift-related information from a Revit model using Dynamo. The information to be retrieved includes (1) the geometry and location of existing structures; (2) the ID, geometry, location, and weight of the lift load; and (3) the geometry of site topology. In addition to the building information, crane specifications are also required. In some cases, there exist detailed crane information models, which include the crane specifications such as the capacity, the boom length, and location of the crane and its cabin. However, more often, the crane information has a source other than the BIM model, such as a spreadsheet from crane manufacturers. Therefore, this step focuses on general cases and retrieves building information only.

Based on the retrieved information, the search space of PSRRT* can be constructed, with the location and dimension of obstacles and the space boundary. First, building structures existing prior to the lift are given axis-aligned minimum bounding boxes (AABB), which are further buffered with the length and height of the lift load. The buffered boxes are used to represent obstacles in the search space. To minimise computational complexity, existing structures with a top constraint lower than the base constraint of the lifted load in the BIM model are consolidated to be one single obstacle. Then, the search space boundary is determined by the site topology, which is presented by toposurface in Revit. Figure 2 shows the Dynamo code overview for retrieving necessary information from Revit models to construct the search space for PSRRT*. As a result, three .csv files are exported, which contain information on obstacles, the lift load, and the site boundary.

3.2.2 Path Generation

As an integral component in this framework, PSRRT* is devised to find a practical path given the search space, obstacles, and load supply and demand points. Although the algorithm can easily adapt to other types of cranes, in this study, PSRRT* is designed for cranes with three DoFs (i.e., swinging, luffing, and hoisting), such as the luffing tower crane or the truck mobile crane. As discussed in Section 2.1, a practical path is defined as a smooth and visible path with an acceptable level of motion coordination. As the original RRT* algorithm can produce a smooth path, PSRRT* mainly aims to improve the outcomes' practicality in visibility and motion coordination.

The flowchart in Figure 3 illustrates how PSRRT* explores the search space and makes adjustments to reflect the practicality considerations. The searching mechanism relies on a "tree" with the "root" at the initial point of the lift load. The tree is defined as vertices and edges that connect the parent vertices and its child vertices. Since one child vertex only has one parent vertex, a path connecting the initial point to the goal point is found when the tree grows to reach the goal. To expand the tree, PSRRT* randomly samples a node (q_{rand}) in the search space and attempts to connect q_{rand} to the nearest node ($q_{nearest}$) on the existing tree rooted in the initial node ($q_{initial}$). If the distance between $q_{nearest}$ and q_{rand} is longer than a given resolution for tree expansion (Δq), a new node q_{new} is created Δq away from $q_{nearest}$ in the direction towards q_{rand}.

If q_{new} is visible and collision-free, the nearby nodes (q_{near}) are found. For each q_{near}, if the edge between q_{new} and q_{near} is visible and collision-free, the cumulate distance from $q_{initial}$ to q_{new} via q_{near} and the distance between q_{near} to q_{goal} are calculated. These two distances are summed up as a total distance to reach q_{new}. The q_{near} with the smallest total distance is considered as the parent of q_{new}. This procedure is known as "Choose Parent". It is followed by the "Rewire", which measures the cumulative distance from $q_{initial}$ to q_{near} via q_{new} if the in-between edge is visible and collision-free, and changes the parent of q_{near} to q_{new}. This loop iterates until any tree

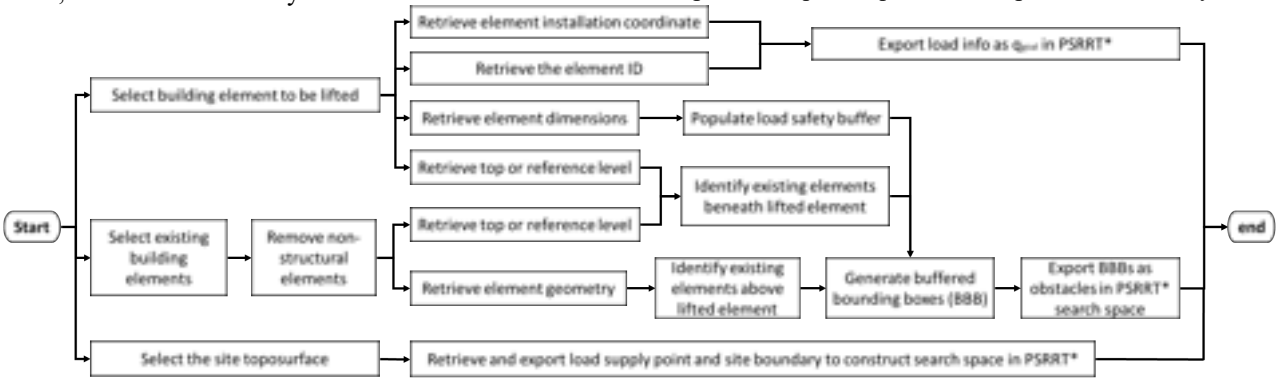

Figure 2. Flowchart for information retrieval from BIM model to PSRRT*

node can be connected to q_{goal} with a collision-free and visible edge.

In this process, the motion coordination is limited by redefining distance in the algorithm. Usually, distance is defined as the Euclidean distance, which neglects the complex coordination of motions in the configuration space (C-space). As a result, PSRRT* uses a weighted Manhattan distance to model the cost between any two configurations:

$$\text{Cost} = w_1 \Delta \alpha + w_2 \Delta \theta + w_3 \Delta \text{L}$$

Where α indicates the swing angle, θ indicates the luffing angle, L indicates the length of the hoist line, which connects the tip of the crane boom and the lift load; weights (i.e., w_1, w_2, w_3) are determined according to the operating speed of each crane motion.

On the other hand, blind lifts are avoided via visibility checks. The visibility check uses the AABB collision detection technique to examine the spatial relationship between the points along the vision line and the physical obstacles. The vision lines are straight lines in the Cartesian space, starting from the crane cabin. It is worth noting that a search space usually has two representations: a Cartesian space and a C-space, and these two representations are transformable. In this algorithm, tree expansion is conducted in the C-space since it is convenient to identify motion coordination, while the collision detections and visibility checks are implemented in the Cartesian space.

Once a valid path is found, PSRRT* executes a post-processing procedure, to further eliminate redundant motion coordination by restricting the first and last segments of the path to be vertical (i.e., only hoisting is allowed) to reflects the real practice. If they are collision-free, the algorithm returns a new path that is exported to Revit for visualization.

3.2.3 Path Visualization

Although the algorithm-planned path has already incorporated most practicality considerations, there still exist various safety concerns in path planning, depending on the site condition and the characteristics of lift loads. Therefore, it is necessary for construction stakeholders to review the algorithm-planned path in a context-rich manner. Figure 4 shows an overview of the dynamo code for path visualization. By selecting the building component to be reviewed, this component automatically reads the path from an excel and presents the path geometry with the invisible parts highlighted.

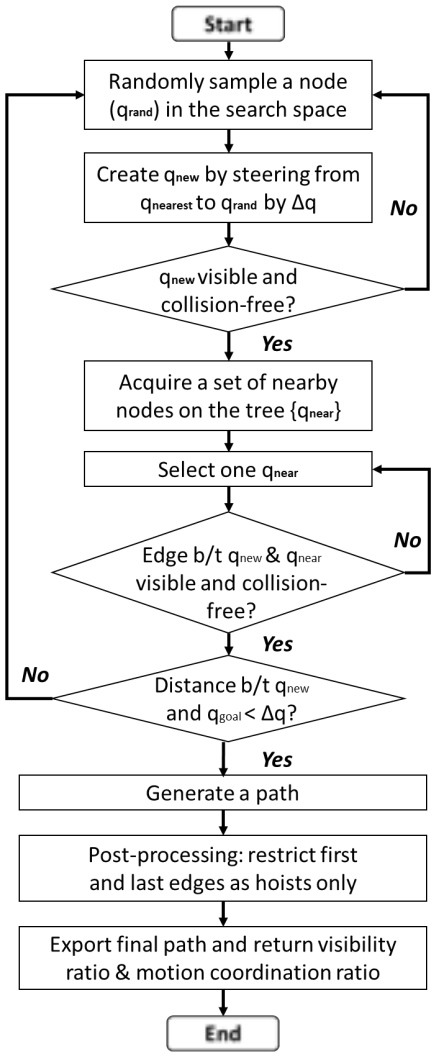

Figure 3. PSRRT* path generation mechanism

4 Case Study

The performance of the prototype system was assessed in a case study on a building project at Monash University, Melbourne, Australia. The building project consisted of a 5-story steel structure errected by three 28m-high luffing boom tower cranes with a 40m boom. The model of these tower cranes is FAVCO M390D and the deployment locations for each crane is indicated in Figure 5(a). According to the schedule, Tower Crane 3 (TC3) was required to lift three beams to level 1 in one working day, as shown in Figure 5(b). These lifting activities are selected as the test scenario in this case study. The building information was stored in a Revit model. Meanwhile, since there was no available Revit family for this particular crane model, the crane specifications and location of the supply area were stored in a .csv file.

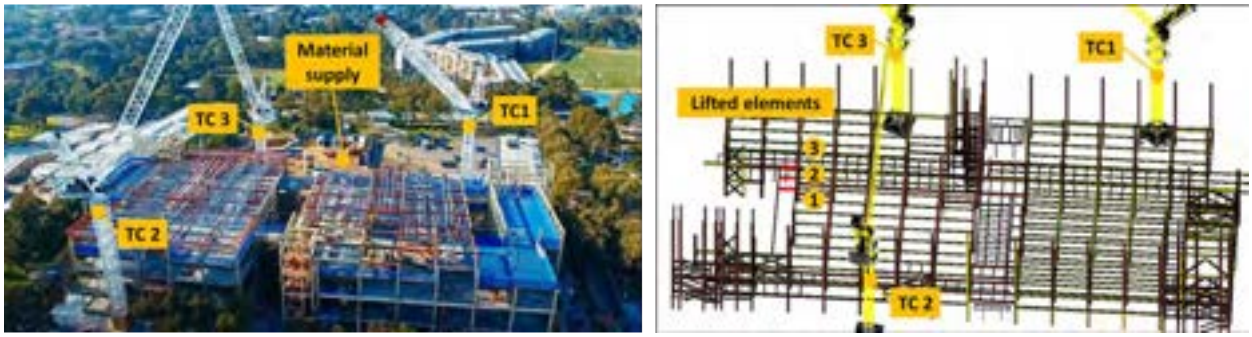

Figure 4. Overview of the project (left) and building elements to be lifted in the BIM model (right)

Firstly, the prototype system retrieved information from the Revit model. In this process, there were 1390 elements retrieved as structures existing prior to the lifts. These elements were exported as 503 obstacles in a 150m x 140m area. Based on this information, PSRRT* calculated the paths for the three lift tasks, as shown in Figure 6(a-c). All three paths have similar trajectories, where the load is vertically lifted from the material supply area, then moved to above the demand points through a combination of swinging and luffing, and finally lower the loads to the target elevation for installation. As illustrated in Figure 6(d), although the number of obstacles is high, the computing times of PSRRT* are relatively low. The average computing time is 0.0523s for the paths. For a project with 3000 elements to be installed, the proposed method is anticipated to finish the planning task within 3 minutes. This prediction requires further verification since RRT* is stochastic and its computing time is influenced by random sampling. Meanwhile, to quantitively evaluate the improvement of the proposed path finding algorithm in smoothness, visibility, and motion coordination, Figure 6(d) also tabulated the number of way-points, the ratio of the visible path to the entire path, and the ratio of the path with three coordinated motions to the entire path. It is observed that the average visibility ratio is 91.5%, and the invisible parts for each path are visible to the beam connector (i.e., the last segment). Furthermore, the coordination ratio for these three paths is zero, indicating an optimal complexity of operations.

Despite the encouraging outcome from the proposed approach, several limitations of the proposed methods are also identified. For example, the proposed method assumes the structures below the lift load as a rectangular

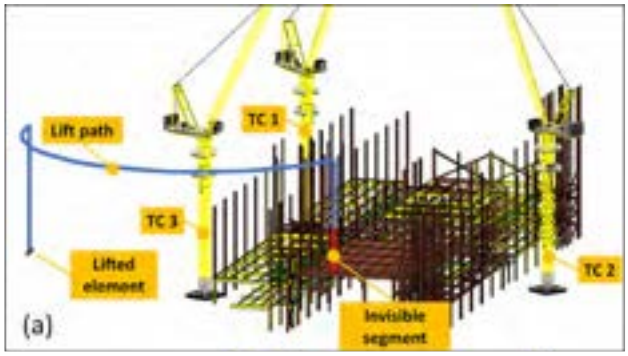

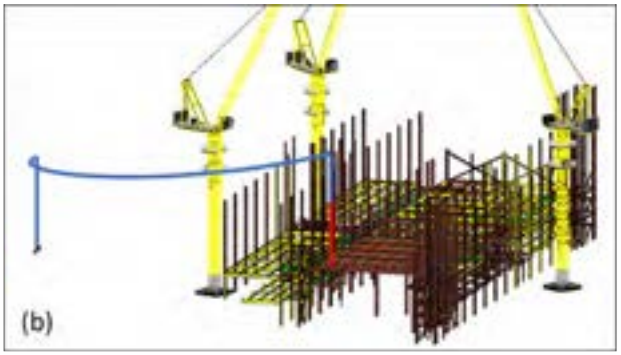

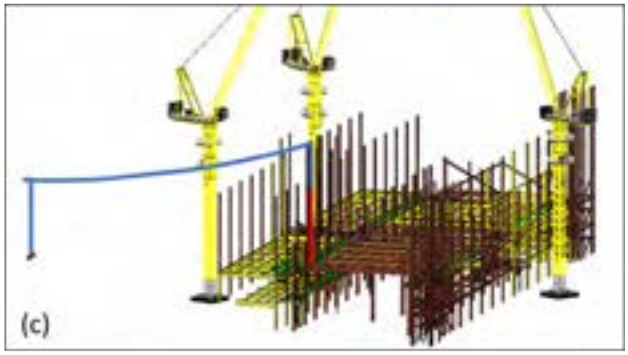

Lifted Element	1	2	3	Average
Computing time (second)	0.063	0.053	0.041	0.0523
Number of way-points	4	4	4	4
Path Length (meter)	142.398	131.425	123.364	132.396
Visibility ratio	93.5%	92.1%	88.6%	91.5%
Coordination ratio (3 motions)	0	0	0	0

Figure 5. Planned paths for the lifted elements (1) to (3) in (a) to (c), respectively, and results for computing time, path length, visibility ratio and coordination ratio for each path

obstacle to decrease computing complexity, which is only valid for building projects with a rectangular geometry. This limitation can be overcome by using advanced collision detection algorithms (e.g., OBB) or voxelizing the search space. Furthermore, the proposed approach requires a comprehensive BIM model, which is not always available. Essential information for path planning, including lift sequences and the crane specifications are usually stored in other software, causing difficulty in interoperability. Therefore, there is a demand to create and standardize customized parameters and family types to store the necessary information for lift planning. Thirdly, the proposed approach focuses on the BIM model and may ignores environmental obstacles (e.g., adjacent buildings). In congested environments, the BIM model is expected to fuse with reality capturing technologies, such as laser scanning, to acquire information on site conditions.

5 Conclusion and Future Research

This paper proposes an approach to automatically plan and visualize a safety and practical lifting path using a novel path finding algorithm and BIM. Two main contributions can be highlighted: (1) the modified RRT* algorithm successfully incorporates the practicality considerations to generate a feasible and realistic path. (2) the proposed approach exploited the BIM model to visualize the planning results to facilitate coordination between stakeholders.

Furthermore, this paper demonstrated the potential of the proposed approach as a 4D risk management system where engineers can proactively plan the activities and workspaces under the impact of crane lift activities. In the future, the proposed method is expected to automatically plan paths for the entire building project for lifting experts to review and adjust. By analyzing adjusted paths, the hazardous zone of crane swing-over is generated to support safety-related decisions, such as coordinating active workspace and crane operations.

References

[1] R. Li, Y. Fu, G. Liu, C. Mao, P. Xu, An algorithm for optimizing the location of attached tower crane and material supply point with BIM, in: ISARC 2018 - 35th International Symposium on Automation and Robotics in Construction and International AEC/FM Hackathon: The Future of Building Things, 2018. https://doi.org/10.22260/isarc2018/0057.

[2] E. Gharaie, H. Lingard, T. Cooke, Causes of fatal accidents involving cranes in the australian construction industry, Construction Economics and Building. 15 (2015) 1–12. https://doi.org/10.5130/AJCEB.v15i2.4244.

[3] J.E. Beavers, J.R. Moore, W.R. Schriver, R. Rinehart, Crane-Related Fatalities in the Construction Industry, Journal of Construction Engineering and Management. 132 (2006) 901–910.

[4] Y. Fang, Y.K. Cho, J. Chen, A framework for real-time pro-active safety assistance for mobile crane lifting operations, Automation in Construction. (2016). https://doi.org/10.1016/j.autcon.2016.08.025.

[5] M.S.A.D. Ali, N.R. Babu, K. Varghese, Collision Free Path Planning of Cooperative Crane Manipulators Using Genetic Algorithm, (2005) 182–193.

[6] J. An, M. Wu, J. She, T. Terano, Re-optimization strategy for truck crane lift-path planning, (2018). https://doi.org/10.1016/j.autcon.2018.02.029.

[7] H.L. Chi, S.C. Kang, S.H. Hsieh, X. Wang, Optimization and evaluation of automatic rigging path guidance for tele-operated construction crane, in: 31st International Symposium on Automation and Robotics in Construction and Mining, ISARC 2014 - Proceedings, 2014: pp. 738–745.

[8] W.H. Hung, C.W. Liu, C.J. Liang, S.C. Kang, Strategies to accelerate the computation of erection paths for construction cranes, Automation in Construction. 62 (2016) 1–13. https://doi.org/10.1016/j.autcon.2015.10.008.

[9] X. Wang, Y.Y. Zhang, D. Wu, S. De Gao, Collision-Free Path Planning for Mobile Cranes Based on Ant Colony Algorithm, Key Engineering Materials. 467–469 (2011) 1108–1115. https://doi.org/10.4028/www.scientific.net/KEM.467-469.1108.

[10] J. Zhang, F. Yu, D. Li, Z. Hu, Development and implementation of an industry foundation classes-based graphic information model for virtual construction, Computer-Aided Civil and Infrastructure Engineering. (2014). https://doi.org/10.1111/j.1467-8667.2012.00800.x.

[11] J.K.W. Yeoh, J.H. Wong, L. Peng, Integrating crane information models in BIM for checking the compliance of lifting plan requirements, in: ISARC 2016 - 33rd International Symposium on Automation and Robotics in Construction,

2016. https://doi.org/10.22260/isarc2016/0116.

[12] Y. Zou, A. Kiviniemi, S.W. Jones, A review of risk management through BIM and BIM-related technologies, Safety Science. 97 (2017) 88–98. https://doi.org/10.1016/j.ssci.2015.12.027.

[13] Y. Ji, F. Leite, Automated tower crane planning: leveraging 4-dimensional BIM and rule-based checking, Automation in Construction. 93 (2018) 78–90. https://doi.org/10.1016/j.autcon.2018.05.003.

[14] J. Olearczyk, A. Bouferguène, M. Al-Hussein, U. Hermann, Automating motion trajectory of crane-lifted loads, Automation in Construction. 45 (2014) 178–186. https://doi.org/10.1016/j.autcon.2014.06.001.

[15] H.R. Reddy, K. Varghese, Automated Path Planning for Mobile Crane Lifts, Computer-Aided Civil and Infrastructure Engineering. 17 (2002) 439–448. https://doi.org/10.1111/0885-9507.00005.

[16] P. Cai, Y. Cai, I. Chandrasekaran, J. Zheng, Parallel genetic algorithm based automatic path planning for crane lifting in complex environments, Automation in Construction. 62 (2016) 133–147. https://doi.org/10.1016/j.autcon.2015.09.007.

[17] D. Wu, Y. Sun, X. Wang, X. Wang, An improved RRT algorithm for crane path planning, International Journal of Robotics and Automation. (2016). https://doi.org/10.2316/Journal.206.2016.2.206-4180.

[18] C. Zhang, A. Hammad, Improving lifting motion planning and re-planning of cranes with consideration for safety and efficiency, Advanced Engineering Informatics. 26 (2012) 396–410.

[19] X. Wang, Y.Y. Zhang, D. Wu, S. De Gao, Collision-free path planning for mobile cranes based on ant colony algorithm, Key Engineering Materials. 467–469 (2011) 1108–1115. https://doi.org/10.4028/www.scientific.net/KEM.467-469.1108.

[20] J. An, M. Wu, J. She, T. Terano, Re-optimization strategy for truck crane lift-path planning, Automation in Construction. 90 (2018) 146–155. https://doi.org/10.1016/j.autcon.2018.02.029.

[21] J. Olearczyk, A. Bouferguène, M. Al-Hussein, U. Hermann, Automating motion trajectory of crane-lifted loads, Automation in Construction. 45 (2014) 178–186. https://doi.org/10.1016/j.autcon.2014.06.001.

[22] W.-H. Hung, C.-W. Liu, C.-J. Liang, S.-C. Kang, Strategies to accelerate the computation of erection paths for construction cranes, Automation in Construction. 62 (2016) 1–13. https://doi.org/10.1016/j.autcon.2015.10.008.

[23] Y. Fang, Y.K. Cho, F. Druso, J. Seo, Assessment of operator's situation awareness for smart operation of mobile cranes, Automation in Construction. (2018). https://doi.org/10.1016/j.autcon.2017.10.007.

[24] Y. Fang, J. Chen, Y.K. Cho, K. Kim, S. Zhang, E. Perez, Vision-based load sway monitoring to improve crane safety in blind lifts, Journal of Structural Integrity and Maintenance. (2018). https://doi.org/10.1080/24705314.2018.1531348

[25] C. Huang, C.K. Wong, C.M. Tam, Optimization of tower crane and material supply locations in a high-rise building site by mixed-integer linear programming, Automation in Construction. 20 (2011) 571–580. https://doi.org/10.1016/j.autcon.2010.11.023.

[26] H. Guo, Y. Yu, M. Skitmore, Visualization technology-based construction safety management: A review, Automation in Construction. 73 (2016) 135–144. https://doi.org/10.1016/j.autcon.2016.10.004.

[27] S. Karaman, E. Frazzoli, Sampling-based algorithms for optimal motion planning, in: International Journal of Robotics Research, 2011. https://doi.org/10.1177/0278364911406761.

[28] R. Sacks, C. Eastman, G. Lee, P. Teicholz, BIM Handbook: A Guide to Building Information Modeling for Owners, Managers, Designers, Engineers and Contractors. 2018. https://doi.org/10.1002/9781119287568.

[29] L. Peng, D.K.H. Chua, Decision Support for Mobile Crane Lifting Plan with Building Information Modelling (BIM), in: Procedia Engineering, Elsevier, 2017: pp. 563–570. https://doi.org/10.1016/j.proeng.2017.03.154.

[30] J. Wang, X. Zhang, W. Shou, X. Wang, B. Xu, M.J. Kim, P. Wu, A BIM-based approach for automated tower crane layout planning, Automation in Construction. 59 (2015) 168–178. https://doi.org/10.1016/j.autcon.2015.05.006.

A study on an Autonomous Crawler Carrier System with AI based Transportation Control

H. Hatamoto[a], K. Fujimoto[b], T. Asuma[a], Y. Takeshita[a], T. Amagai[a], A. Furukawa[a], and S. Kitahara[a]

[a]Kumagai Gumi Co.,Ltd., Japan
[b] SOINN Inc., Japan
E-mail: hironobu.hatamoto@ku.kumagaigumi.co.jp, kazuya.fujimoto@soinn.com

Abstract – This paper proposes an autonomous crawler carrier system to improve productivity of earth and sand transportation work. In general, multiple crawler carriers on the transportation work repeatedly move on almost the same route between loading and unloading locations. There is a risk that the crawler carrier deviates from the transport path due to the driver's fatigue and reduced concentration since the transportation work is a monotonous and repetitive operation. The proposed system enables multiple crawler carriers to automatically move on the same route without collision using an artificial intelligence (AI) based control. There are four steps in the AI control flow. First, the driver performs the teaching operation while checking the route from the camera image. Then, teaching route data for an autonomous crawler carrier is created. Second, the AI on the personal computer selects several routes that can maintain safe crawler carrier positions for all routes of multiple carriers. Third, AI generates an efficient operation plan that minimizes the working cost and time from all positional relationships. Finally, when the operator presses the start switch on the control panel, AI controlled multiple crawler carriers move efficiently without collision. This smart control was introduced for the construction of earth and sand transportation in the Aso-Ohashi area, and efficient operation was confirmed.

Keywords –
Autonomous crawler carrier system; Artificial intelligence; Productivity improvement

1 Introduction

In recent years, information and communication technology (ICT) [1] has made great progress with the development of signal processing technology [2], computer technology [3], wireless communication technology [4], and so on. As a future society, "Society 5.0" has been proposed by the Cabinet Office, which is a Japanese administrative agency [5]. Although life has become more convenient in Japan with the progress of ICT, an aging society causes labor shortages and increasing energy consumption. Society 5.0 tries to incorporate robot technology [6], artificial intelligence (AI) technology [7, 8], etc. into society in order to solve such social issues. To realize Society 5.0 in Japan construction industry, a big project called "i-Construction" is underway to improve the productivity of the entire construction production system.

This i-Construction, which is managed by the Ministry of Land, Infrastructure, Transport and Tourism, includes the development of an unmanned system for construction machinery [9-11]. In the automatic control of this construction machine, the personal computer (PC) in the control device drives the crawler carrier instead of human operators. The application of the automatic control reduces the needs of skilled operators, solves the shortage of human resources, and can be expected to improve productivity.

In this paper, we noticed that the earth and sand transportation work is a monotonous repetitive work of reciprocating the route. This cyclical work causes physical and mental fatigue of the operator. Therefore, we are developing an automatic driving technology for crawler carriers to reduce accidents by operators during the transportation work using the AI technology [12].

The remainder of this paper is organized as follows. Section II introduces the details of automatic driving system in the earth and sand transportation field. In Section III, we explain the proposed autonomous crawler carrier system with AI based transportation control. Moreover, in Section IV, we verifies the effectiveness of our proposed scheme by the computer simulation. In addition, experimental results of Aso-Ohashi area are briefly explained in Section V. Finally, the conclusion and future works are presented in Section VI.

2 Automatic driving system in the soil and sand transportation field

2.1 System configuration

The automated driving system uses a network-compatible crawler carrier that enables human-less construction. Figure1 shows two crawler carriers which are used for transporting earth and sand. The specifications of this crawler carrier, which is manufactured by KATO WORKS, are as follows. It has a payload of 11,000 kg, a machine mass of 14.100 kg, a length of 6.05 m, a width of 2.84 m and a height of 2.91 m.

Figure 1. Two Crawler carriers for transporting earth and sand.

Figure 2 shows system configuration for the automated driving system. In this construction, the crawler carriers are controlled using the internet protocol (IP) network. The automatic driving system is composed of the following devices.

- Global Navigation Satellite System (GNSS) / IMU(Inertial Measurement Unit) device that measures the position information of the moved route, where this device includes GNSS reference station
- PC for automatic driving control (1 vehicle side, 1 remote control side)
- Vehicle camera to watch the surrounding conditions during remote control

IP addresses are assigned to these devices, and they can be controlled by packet transmissions using a wired local area network (LAN) system or a wireless LAN system. GNSS / IMU is a combined inertial measurement device for GNSS and IMU. In addition to the position information from the G

GNSS device, the position and direction of the vehicle can be combined with the IMU device to measure the position of the vehicle with high accuracy.

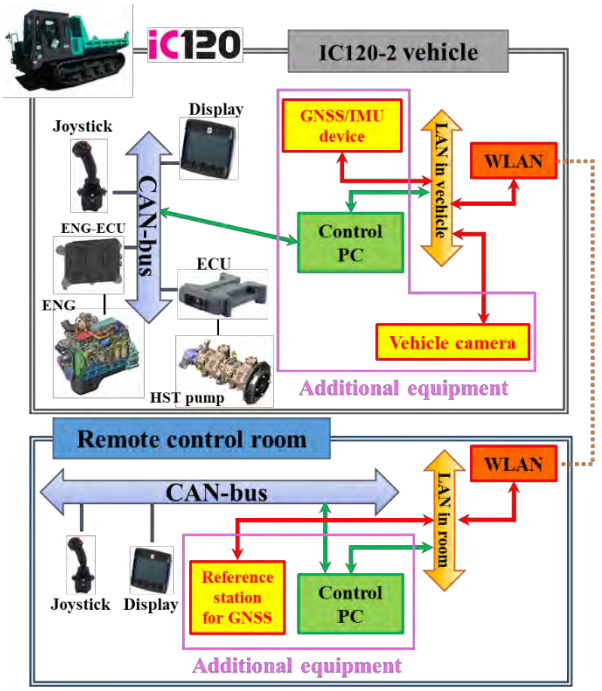

Figure 2. System configuration for the automated driving system where wireless communication is conducted between the remote control room and crawler carriers.

2.2 System control flow

Figure 3 shows a framework related to the important devices for teaching and automatic driving operations. In this figure, there are two modes, which are teaching mode and auto-driving mode. As shown in this figure, a remote and automatic operation panel including the PC is set in the remote control room which has monitors, PCs, and wireless communication devices. If the operator would like to control the crawler carrier, command signals are transmitted to the PC which is set in the crawler carrier via the WLAN packets. On the other hand, the crawler carrier's information is transmitted to the remote control room via the WLAN packets.

There are three flows: teaching operation, preparation of automatic driving, and automatic driving mode. These flows are explained as follows in detail.

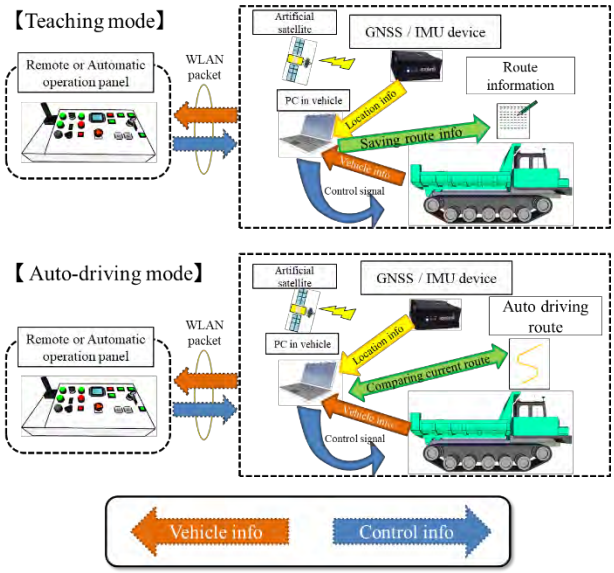

Figure 3. The framework related to the important devices for teaching and automatic driving operations.

2.2.1 Teaching operation

A start signal for the teaching operation is transmitted from the remote control room to the PC in the crawler carrier, and the operator moves it remotely. When the crawler carrier is running, the position and speed information from the GNSS / IMU device are stored in the in-vehicle PC as a teaching path. This information is used in the automatic driving mode.

2.2.2 Preparation of automatic driving

First, a control packet for switching the remote driving mode to the automatic driving mode is transmitted from the remote control room to the crawler carrier. Secondly, the control signal to start the automatic operation is transmitted. Third, the teaching data for the automatic driving is saved in the in-vehicle PC inside the crawler carrier. Thirdly, the teaching data for automatic driving is saved in the hard disk of the PC stored inside the crawler carrier.

2.2.3 Automatic driving mode

The in-vehicle PC automatically drives the crawler carrier while comparing the teaching data with the current position from the vehicle's GNSS / IMU device. In addition, the movement of the crawler carrier is automatically stopped when the teaching path and the current position greatly deviate from each other.

3 AI based automatic driving technique

3.1 Necessity of AI-based autonomous driving

In the automatic driving system described in the previous section, a stop operation by a worker in the remote control room is required in order to halt the crawler carrier during the automatic moving from the start point to the end point. Therefore, at least two operators are needed in the working field. One remotely controls the excavator and loads the crawler carrier with sand, and the other manages and watches the movement of the crawler carrier. If the number of autonomous crawler carriers increases, operation management by one worker becomes much difficult, and there is a possibility of collision among crawler carriers. In order to prevent collisions, a system that manages the operation of multiple crawler carriers on behalf of the worker is required. Therefore, in this paper, we propose an AI-based autonomous driving technique.

The developed AI-based automated driving technology does not require human operation management, and single worker can perform a series of operations from loading and unloading sediment. Figure 4 shows the configuration of the AI-controlled automatic driving system. As shown in this figure, the PC in the remote control room (PC-r) controls two remote and automatic operation panels via and two in-vehicle PCs (PC-v). The PC-r transmits the AI start signal to the PC-v via the operation panel. Moreover, the PC-r directly transmits the stop signal to the PC-v. On the other hand, the PC-v transmits the vehicle information to the PC-r via the operation panel, but it directly transmits the position information to the PC-r. There are two information flows among the control PC in the remote control room and two crawler carriers.

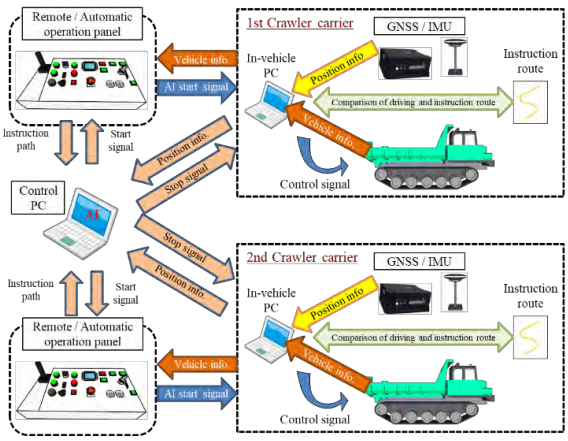

Figure 4. Configuration of the AI-controlled automatic driving system.

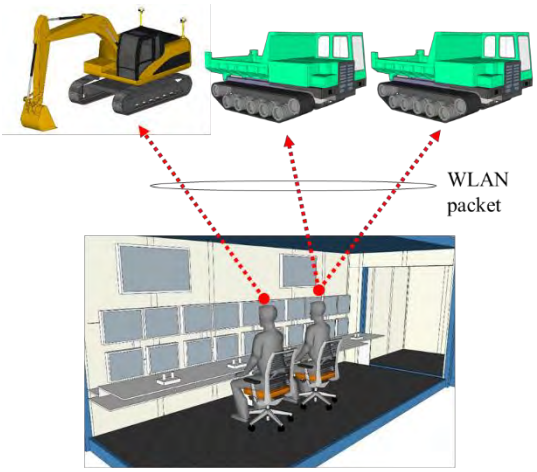

The number of construction machineries is three.
The number of operators is two.

(a) Before AI based remote control room

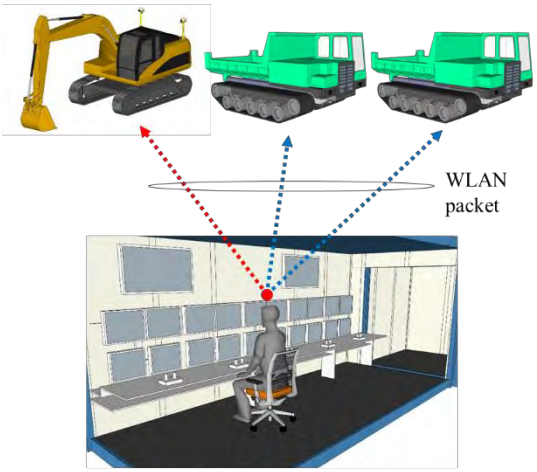

The number of construction machineries is three.
The number of operators is one.

(b) After AI based remote control room

Figure 5. Control of multiple vehicles by one operator.

Figure 5 shows the control of multiple vehicles by one operator. As shown in this figure, the number of operator is two, when the number of construction machineries is three before AI based remote control room. On the other hand, the number of operator is only one after the AI based remote control room. This means that our proposed system is one of the best solutions for the shortage of human resources in Japanese construction field.

3.2 AI control flow

Figure 6 shows our proposed AI control flow in which there are four steps: instruction, analysis, plan, and command. These steps are explained as follows.

- First, the operator remotely moves the crawler carrier, and the route information for teaching process is generated.
- Second, based on the obtained route data and crawler carrier size conditions, the AI on the PC-r finds safety positions between crawler carriers and positional relationships in possible. Then, several candidate routes that allow safe operation are selected.
- Third, the operation pattern that minimizes the cost and time is selected from the candidate routes in the previous step, considering the productivity of earth and sand transportation work. At this time, the start and end positions of the instruction route are also taken into consideration. For example, the unloading and loading operations are conducted in the start and end points. Optimal operation pattern of vehicles is calculated from the candidate routes and other conditions. The operation pattern satisfies spatial limitation to avoid interference between vehicles while minimizing expected time necessary to complete load and unload of sediment. In this phase, algorithms to solve multi agent path finding problem are used with original expansions to increase flexibility and efficiency [13].
- Finally, the PC-r remotely controls the two crawler carriers on the most efficient operation pattern. The GNSS position information from the each carrier is sent to the remote control room, and the start and stop of moving can be determined by the AI monitoring in constant. Moreover, the second and third processes are re-conducted in our proposed scheme if the variation of the environmental condition, for example a muddy road and an increase of loading time, changes the position relationship between two crawler carriers.

As a result, the number of operators for monitoring the crawler carriers can be reduced. When the number of vehicles is only one, the difference of driving efficiency between the automatic driving with and without the AI is none. However, in the case of more than two vehicles, the AI based automatic control considers the collision avoidance on the driving route. On the other hand, in the case of the automatic control without the AI, if a forward vehicle and a return vehicle meet on a narrow road, either one vehicle needs to return to the back wide road, which incident wastes operation time. Therefore, the AI control will enable efficient transportation in the construction field.

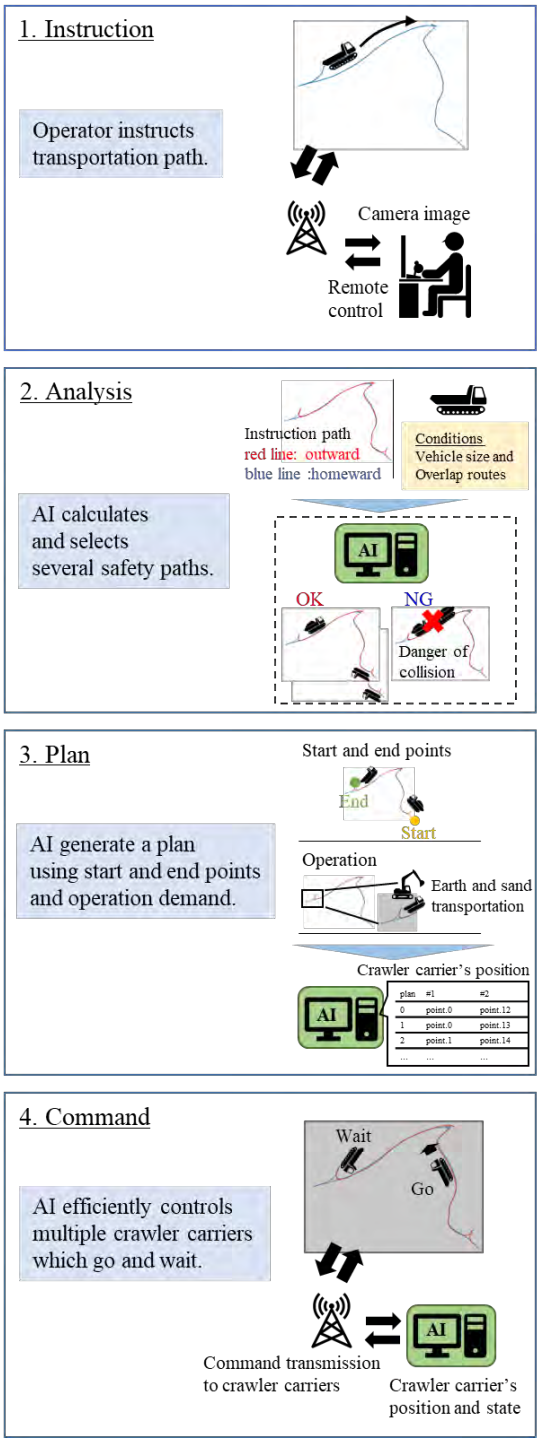

Figure 6. Configuration of the AI-controlled automatic driving system including instruction, analysis, plan, and command processes.

4 Computer simulation

4.1 Simulation parameters

Performances of our proposed AI-controlled automatic driving system are evaluated by the computer simulation. There are three fields in this simulation, where the first field is in the Aso-Ohashi area, the second and third fields are in Tsukuba area.

In this simulation, the sand loading time to the crawler carrier using the excavator was not considered. The maximum number of crawler carriers (maximum N_t) is two. In addition, the start point for moving the crawler carrier is the unloading point. There are two routes. One is an outbound route from the unloading point to the loading point. The other is a homeward route from the loading point to the unloading point. Overlap of forward and return routes is allowed. Even if there is no overlap between the forward and return paths, it is not possible to pass each other within 6 m. We set the waiting and separating points in the driving route. These points increase the driving efficiency and they are determined by the operator's empirical knowledge.

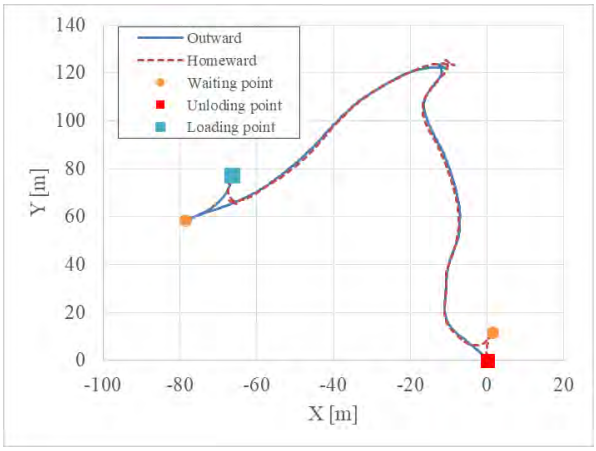

Figure 7. Driving route in the Aso-Ohashi operation area in which the number of waiting points is two.

Figure 7 shows driving route in the Aso-Ohashi operation area which size is 80m by 120m. There are two separating points. When one crawler carrier is in the loading point, the excavator loads its crawler carrier with earth and sand. The other crawler carrier waits until the loading work is completed at the waiting point which is near the loading point. Similarly, when one crawler carrier is unloaded, the other crawler carrier waits until the unloaded operation is completed at the waiting point which is near the unloading point.

Figure 8 shows driving route in the 1st Tsukuba area which is inside Technical research & Development institute on Kumagai Gumi. The area size is 40m by 30m. There are two waiting point.

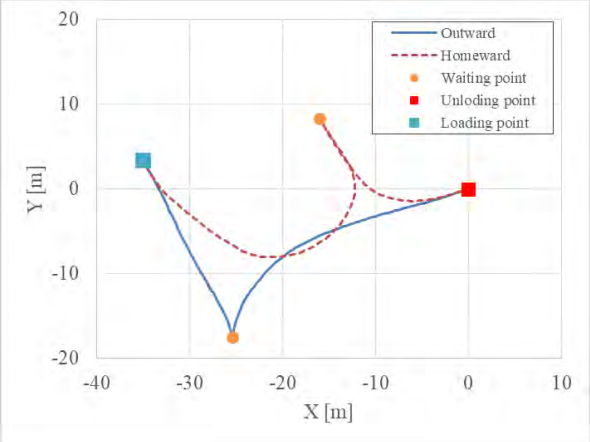

Figure 8. Driving route in the 1st Tsukuba area in which the number of waiting points is two.

Figure 9 shows driving route in the 2nd Tsukuba area which is inside Technical research & Development institute on Kumagai Gumi. The area size is 40m by 30m. There are two waiting points in order to increase work efficiency for more than two crawler carriers. Moreover, two separating points(SPs) are added to this filed. If there are no waiting points, either of crawler carriers frequently stops the movement on the outward and homeward path because the AI based control selects the extremely safe operation plan. Therefore, it is expected that two waiting points improve work efficiency in the case of $N_t = 2$.

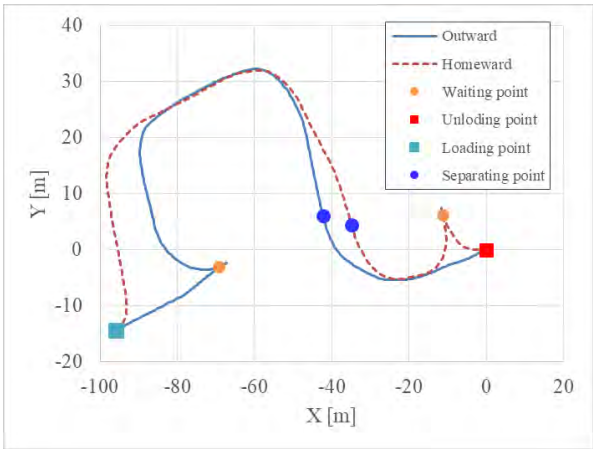

Figure 9. Driving route in the 2nd Tsukuba area in which there are two waiting points and two separating points in order to increase work efficiency for more than two crawler carriers.

4.2 Simulation results

Table 1 shows work efficiency in Aso-Ohashi and Tsukuba area in the simulation. As shown in this table, at first, work efficiencies for the case of $N_t = 1$ and $N_t = 2$ are 16.2 and 31.1 cycle/hour in the Aso-Ohashi area. In this area, work efficiency for the case of $N_t = 2$ is improved by 72% compared to the case of $N_t = 1$.

Secondly, work efficiencies for the case of $N_t = 1$ and $N_t = 2$ are 66.1 and 105 cycle/hour in the 1st Tsukuba area. In this area, work efficiency for the case of $N_t = 2$ is improved by 59% compared to the case of $N_t = 1$.

Thirdly, work efficiencies for the case of $N_t = 1$ and $N_t = 2$ are 24.5 and 42.2 cycle/hour in the 2nd Tsukuba area without two separating points. In this area, work efficiency for the case of $N_t = 2$ is improved by 72% compared to the case of $N_t = 1$. On the other hand, work efficiency for the case of $N_t = 2$ is 46.4 cycle/hour in the 2nd Tsukuba area with two separating points. Work efficiency for the case of $N_t = 2$ is improved by 89% compared to the case of $N_t = 1$.

By determining two separating points and planning the automatic driving routes, the unnecessary waiting time of the two crawler carriers due to the overlap of the outward and homeward routes is reduced. Efficiency ratio for the case of $N_t = 2$ with separating points is 17% higher than that for the case of $N_t = 2$ without waiting points. Therefore, if our proposed automated driving is applied in an area where the travel paths are complicated, it is important to provide some separating points when making the driving plan.

Table 1. Work efficiency in Aso-Ohashi and Tsukuba area in the simulation.

Area	Work efficiency [cycle/h]		Efficiency ratio
	1 vehicle	2 vehicles	
Aso-Ohashi	16.2	31.1	1.72
1st Tsukuba	66.1	105	1.59
2nd Tsukuba (w/o SP)	24.5	42.2	1.72
2nd Tsukuba (w/ SP)		46.4	1.89

5 Experimental results

In this section, experimental results of the construction in Aso-Ohashi area are briefly described.

Table 2 shows construction outline in this area. As shown in this table, verification period of this construction was in September 2018. The verification place was a collapse slope area at the top of the soil retaining embankment. One way distance was about 300m. Path width and maximum path gradient were about 5m and 20%. The path gradient was able to

decrease the moving speed of crawler carrier. The number of construction machines was three including one excavator and two crawler carriers.

Table 2. Construction outline in Aso-Ohashi area.

Construction name	Slope countermeasure work in Aso-Ohashi area	
Verification period	September 2018	
Verification place	Collapse slope area at the top of the earth retaining embankment	
Path condition	Distance (one way)	about 300m
	Width	about 5m
	Gradient (maximum)	20%
Num. of construction machines	Excavator	1
	Crawler carrier	2

Figure 10. External remote control room in Aso-Ohashi area in which the number of operators is only one.

Figure 10 shows an external remote control room in Aso-Ohashi area. There were two remote control panels including the PC-r. Multiple monitors were set on the table in order to check movements of crawler carriers and their surrounding area. The excavator loaded earth and sand to the crawler carrier which was controlled by the AI when the operator remotely moved the excavator.

Figure 11 shows the snapshot of the verification in Aso-Ohashi area, which is a partial area of -80 to -60 m on the X axis and 55 to 80 m on the Y axis in Fig. 7. The crawler carrier (green) had waited at the waiting point while the earth and sand loading operation for the other carrier (magenta) had been conducted. After its operation was finished, the crawler carrier (magenta) with earth and sand went to the unloading point and the crawler carrier (green) approached the loading point as shown in Fig. 11. If the waiting point was not set on this path, the incident may happen where one of the crawler carriers turned back the way which it came from.

Figure 11.Snapshot of the verification in Aso-Ohashi area where one crawler carrier (magenta) moves to the unloading point and the other (green) moves to the loading point near the excavator.

Table 3 shows work efficiency in Aso-Ohashi and Tsukuba area in the simulation and real environment. As shown in this table, the simulation result is same as Table. 1. Work efficiencies for the case of $N_t = 1$ and $N_t = 2$ are 7.47 and 13.1 cycle/hour in the real field. In this case, work efficiency for the case of $N_t = 2$ is improved by 75% compared to the case of $N_t = 1$.

The results of work efficiency for the real environment are low compared to the simulation results, because time durations of earth and sand loading and discarding are not assumed in the simulation environment. In addition, we consider that the influence of mud and gradient in the real field can decrease the speed of crawler carriers. Moreover, the maximum speed of the crawler carrier is adopted in the simulation. On the other hand, the difference of efficiency ratio between the real and simulation environments is almost the same value. The simulation analysis enables us to search the semi-optimal waiting points and separating points in the driving route. Therefore, its analysis is important before the verification of our proposed scheme in the real environment.

Table 3. Work efficiency in Aso-Ohashi area in the simulation and real environments.

Area	Work efficiency [cycle/h]		Efficiency ratio
	1 vehicle	2 vehicles	
Aso-Ohashi (simulation)	16.2	31.1	1.72
Aso-Ohashi (real)	7.47	13.1	1.75

6 Conclusions

This paper proposes an autonomous crawler carrier system with the AI based transportation control. In the proposed scheme, the AI based operation management eliminates the need for the safety confirmation between two crawler carriers. Moreover, it reduces the number of operation monitoring workers, which means that the proposed system is one of the best solutions for the shortage of construction workers in Japan.

The AI makes the movement plan for crawler carriers in the earth and sand transportation. This plan is produced by the major flow consisting of instruction, analysis, plan, and command processes. In the simulation results, when two crawler carriers in the Aso-Ohashi area are automatically controlled by the AI, work efficiency improves 72% compared to the case of one crawler carrier. In addition, when the same AI controls the automatic driving in the 1st Tsukuba area, work efficiency improves 59% compared to the case of one crawler carrier. Moreover, work efficiency improves 72% compared to the case of one crawler carrier in the 2nd Tsukuba area which is larger than the 1st area when there are no separating points. On the other hand, work efficiency improves 89% compared to the case of one crawler carrier in the 2nd Tsukuba area with setting two separating points.

Moreover, results of efficiency ratio for real and simulation environments are almost the same value. Therefore, we aggressively use the simulation analysis before the verification of the AI based auto driving system in the real construction field.

As a future study, it is possible to further improve work efficiency of the earth and sand transportation by efficiently arranging the waiting and separating points in the driving routes. Furthermore, determination of waiting and separating points using AI control will be conducted.

References

[1] Y. Mehmood, F. Ahmad, I. Yaqoob, A. Adnane, M. Imran and S. Guizani, “Internet-of-Things-Based Smart Cities: Recent Advances and Challenges,” in IEEE Communications Magazine, vol. 55, no. 9, pp. 16-24, Sept. 2017.

[2] Q. Mao, F. Hu and Q. Hao, “Deep Learning for Intelligent Wireless Networks: A Comprehensive Survey,” in IEEE Communications Surveys & Tutorials, vol. 20, no. 4, pp. 2595-2621, Fourthquarter 2018.

[3] Y. Mao, C. You, J. Zhang, K. Huang and K. B. Letaief, “A Survey on Mobile Edge Computing: The Communication Perspective,” in IEEE Communications Surveys & Tutorials, vol. 19, no. 4, pp. 2322-2358, Fourthquarter 2017.

[4] S. A. A. Shah, E. Ahmed, M. Imran and S. Zeadally, “5G for Vehicular Communications,” in IEEE Communications Magazine, vol. 56, no. 1, pp. 111-117, Jan. 2018.

[5] https://www8.cao.go.jp/cstp/english/society5_0/index.html

[6] E. Jung, J. H. Lee, B. Yi, J. Park, S. Yuta and S. Noh, “Development of a Laser-Range-Finder-Based Human Tracking and Control Algorithm for a Marathoner Service Robot,” in IEEE/ASME Transactions on Mechatronics, vol. 19, no. 6, pp. 1963-1976, Dec. 2014.

[7] H. Yao, M. Li, J. Du, P. Zhang, C. Jiang and Z. Han, “Artificial Intelligence for Information-Centric Networks,” in IEEE Communications Magazine, vol. 57, no. 6, pp. 47-53, June 2019.

[8] M. Elsayed and M. Erol-Kantarci, “AI-Enabled Future Wireless Networks: Challenges, Opportunities, and Open Issues,” in IEEE Vehicular Technology Magazine, vol. 14, no. 3, pp. 70-77, Sept. 2019.

[9] K. Chayama, A. Fujioka, K. Kawashima, H.Yamamoto, Y.Nitta, C. Ueki, A. Yamashita, and H.Asama, “Technology of Unmanned Construction System in Japan,” Journal of Robotics and Mechatronics, vol. 26, no. 4, July 2019.

[10] S. Kitahara, Y. Nitta, and S. Nishigaki, “Study on Ultra-long-distance Unmanned Construction and Pilot Study at Aso Bridge District,” Proceedings of 36th International Symposium on Automation and Robotics in Construction (ISARC 2019), May 2019.

[11] H. Aoki, S. Katayama, H. Sindou, and S. Nakashima, “Field Verification of Autonomous Driving System for Career Dump Truck Based on Next Generation Cellular Communication Standards (5G),” Proceeding of 19th Symposium on Construction Robotics in Japan, Oct. 2019. (in Japanese)

[12] T. Asuma， S. Kitahara， K. Miyagawa， A. Furukawa，and K. Fujimoto, “Development of the Automatic Traveling Technology of Crawler Carriers with Artificial Intelligence (AI) Control,” Proceeding of 19th Symposium on Construction Robotics in Japan, Oct. 2019. (in Japanese)

[13] A. Felner, S. E. Shimony, R. Stern, E. Boyarski, G. Sharon, G. Wagner, M. Glodenberg, N. Sturtevant, and P. Surynek, “Search-based Optimal Solvers for the Multi-agent Pathfinding Problem: Summary and Challenges”, Tenth Annual Symposium on Combinational Search, June 2017.

Accuracy and Generality of Trained Models for Lift Planning Using Deep Reinforcement Learning

- Optimization of the Crane Hook Movement Between Two Points -

A. Tarutani[a] and K. Ishida[b]

[a]Department of Architecture, Graduate School of Creative Science and Engineering, University of Waseda, Japan
[b]Department of Architecture, Assistant Professor, Doctor of Engineering, Waseda University, Tokyo, Japan
E-mail: taru4boo@fuji.waseda.jp, k_ishida@waseda.jp

Abstract –

An optimization system of a lifting plan must have generality to manage different design conditions and real-time changes at a construction site. Furthermore, it must optimize the construction planning and scheduling. In a previous study, we trained a two-point locomotion model for crane hook movement using deep reinforcement learning to generate and optimize lifting plans automatically. However, we did not test the accuracy and generality of the model. In this study, we test (1) the accuracy and (2) the generality of the trained model using a new environment. To evaluate the accuracy of the optimal solution, we examined the locus of the movement of each frame between two points. To verify the generality of the trained model, we solved an optimization problem of the crane hook movement under different conditions of the crane's learning environment using the trained model. From the results, we found that the movement path was 3.6 times the shortest path and the crane hook initially moved vertical. Furthermore, the agent solved the optimization problem of the crane hook movement when the size of the crane changed. Therefore, the corresponding range increased with increasing size of the crane. However, the agent did not solve the problem when the slewing angle in the target position was larger than the slewing angle in training. Based on these results, we believe that the limited vertical movement range and rotation range of the crane reduces the accuracy and generality of the trained model.

Keywords –

Deep Reinforcement Learning; Crane Lifting Plan; Optimization; Generality; Virtual Space; Trained Model

1 Introduction

Improving efficiency in building construction is a principal research topic in the construction field, where the shortage of skilled workers is increasing. Therefore, optimization and automation of construction planning and scheduling is important to improve construction [1]. However, optimization of construction planning and scheduling is a complicated task. Therefore, it is generally prudent to optimize each task [2].

The following two aspects are considered necessary to optimize construction planning and scheduling: (1) solving complex combinatorial optimization problems and (2) providing general versatility to manage design and real-time situation changes during construction. Considering (1), problems such as those concerning work interference, route planning, placement planning, and quantity planning can be replaced with typical problems, and optimization research has been conducted [2]. In case of (2), solving problems can be difficult or impossible when changes not existing in the optimization simulation, such as work delay and obstacle interference, occur in the real space. Furthermore, adding all necessary factors in the optimization simulation to provide generality is challenging.

Therefore, we focused on using deep reinforcement learning (RL) to ensure generality. In a previous study, we developed a crane lifting plan using deep RL. Reasons for optimizing lifting tasks are as follows:

1. lifting task is a cooperative task involving several sub-tasks, and
2. lifting task is a complex optimization problem because it includes factors such as the lifting route, layout, model, quantity, and building order.

In Section 2, we review some related work on lifting planning and deep RL.

In Section 3, we first explain the trained model for two-point movement developed in the previous study, and then we present the methods to test the accuracy and generality of the trained model of the previous study.

In Section 4, we discuss the results of the verifications, and in Section 5, we propose a method for creating the environment.

2 Related Work

2.1 Previous Research on the Construction Planning Optimization Problem

In general, construction planning and scheduling can be considered as an optimization problem. Therefore, research is conducted from optimization perspectives in work interference, construction equipment arrangements, and route planning. The construction planning optimization problem considers factors, such as safety, environment, cost, time, and work cooperation.

Wo et al. indicated that a lifting plan requires a planning scheme that considers the numbers, layouts, models, and operating times of cranes. They established a mathematical model for the spatio-temporal planning of tower cranes that reduces the total cost compared to the initial solution, indicating that it provided the optimal solution for all construction projects [2].

2.2 Previous Research on Deep RL

We focused on RL to ensure the generality of the optimization and/or automation system. RL is a machine learning method; it is different from supervised learning because it acts by itself and collects environmental information regardless of the existence of accurate or ground truth data. Therefore, it responds to unknown events for which the correct answer is unknown.

RL is mainly used for autonomous control of machines and problems with no accumulated data. When creating an autonomous control system for a robot, it is difficult to establish rules for sensor systems, control values, etc. Therefore, the robot learns the surrounding situation through RL and controls itself [3]. In addition, RL is used to generate data when there is no accumulated training data, such as building vibration control, to derive optimal vibration control values [4].

There are several phenomena where the correct answers are unknown because data are not accumulated. Construction planning and scheduling are among them.

Moreover, we can perform complex information processing by combining deep learning and RL (called deep RL). This combination aids in generating an optimal solution. The solution is used to generate long-term strategies, such as artificial intelligence for gaming.

This study combines the aforementioned features to develop a crane lifting plan.

The crane lifting plan optimization problem (based on the features of deep RL) is classified as follows.

1. A path creation function for lifting a target object by controlling movements such as slewing, derricking, and lifting and lowering.
2. A function to provide a strategy for deciding the order of construction that is the most efficient.

By developing a model with these functions, we aim to automatically develop a lifting plan for an unknown condition in a simulation. We partially performed this task in a previous study and developed a trained model. This outline is presented in Section 3.

In addition, research is being conducted to investigate methods to generalize trained models developed using RL. According to Miyashita et al., a trained model for car collision prevention using deep RL prevented collisions with cars not learned during training [4].

When training a lifting task, a construction site with several factors, is difficult to reproduce. However, if the inference model can be provided with a general versatility as described earlier, the need to describe each element in the field can be minimized. In this study, the versatility is verified using a trained model [5] for moving a crane hook between two points, as developed in the previous study. Furthermore, we propose a method for creating a learning environment for general purposes based on the inference result.

3 Method

3.1 Research Aim

In this study, we perform a simulation to investigate the following.

- Accuracy of the trained model.
- Generality of the trained model.
- Creation of a learning environment to improve the accuracy and versatility of the trained model at the learning stage.

3.2 Outline of the Research Method

In this section, we present the development environment for deep RL and the structure of the study using deep RL.

We use Unity ML-Agents [6] for deep RL. Unity ML-Agents is a framework for building "environment" for RL on Unity and for "training" and "inference" agents. The proximal policy optimization algorithm [7] is used for the RL algorithm.

As shown in Figure 1, deep RL is categorized into

two processes: learning and inference. In the learning stage, an agent learns an action to maximize the cumulative reward in some environment (learning environment). A model (a formula/method of calculation) developed by this process is called a trained model. In inference, a trained model is applied to an unknown data to provide an answer. At the inference stage, we create an unknown environment for 4D construction simulation and scheduling with several changes.

In Section 3.3, we first explain the trained model developed in the previous study. In Section 3.4, we describe the methods to test the accuracy and generality of the trained model developed in the previous study.

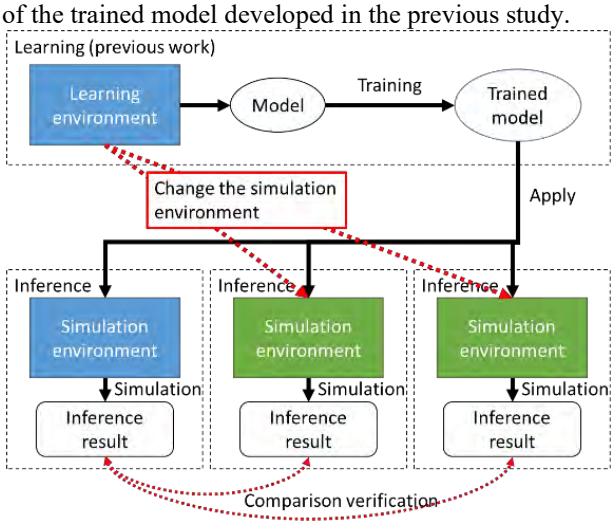

Figure 1. Verification of inference results with changed simulation environment

3.3 Training Environment

3.3.1 Simplification of Learning Content

The optimization problem of the crane lifting plan using deep RL based on the features of deep RL is categorized into the following problems.

- Optimizing hook route: lifting a target object by controlling movements such as slewing, derricking, and lifting and lowering.
- Optimizing assembly order: providing efficiency order to assemble building components.

By developing a model with these functions, we aim to automatically create a lifting plan for an unknown site in a simulation. To learn these functions, we divide the route creation function into moving between two points and collision prevention, as shown in Figure 2. This approach simplifies the environmental information and aims to converge learning.

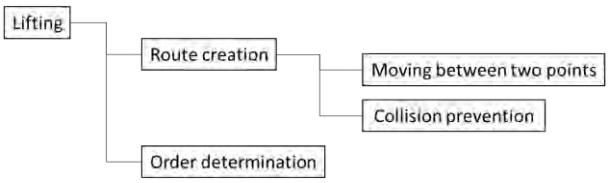

Figure 2. Simplification of learning content

3.3.2 Environment

This section presents an overview of RL, the environment, and inference results under the same conditions as during training.

RL is a machine learning algorithm that learns from the interaction between agents and the environment. Agents are learners and decision-makers. The environment is a non-agent factor on which the agent operates. As shown in Figure 3, the agent refers to the crane; the environment refers to the target, floor, coordinate space, reward, status, and other information. The agent (crane) operates on the environment and receives information such as coordinates, vector, and speed from the environment to determine new actions.

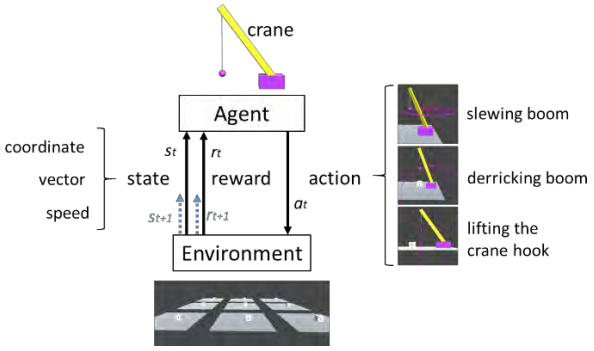

Figure 3. Interaction between agent and environment in reinforcement learning

Figure 4 (a) shows the start and end points when the crane moves between two points. Figure 4 (b) depicts the installation range of the target (box). The center coordinate of this box is the end point. During training, a target (end point) randomly appears in this range (on the horizontal plane). Figure 5 presents the inference result from the trained model for movement between the two points. The crane instantly moves between the two points, and when the end point is reached, the end-point position is initialized.

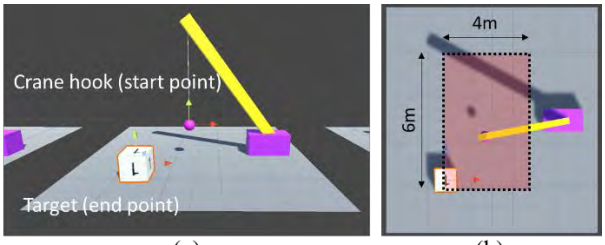

Figure 4. Start and end points (a); target (end point) installation range (b)

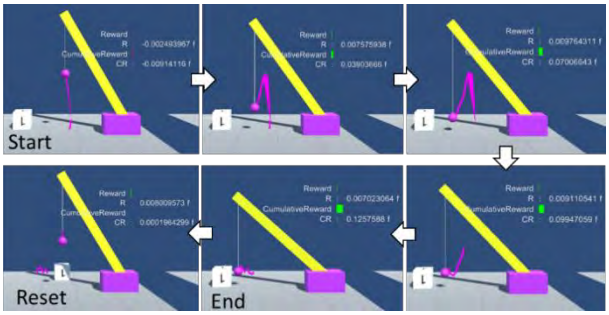

Figure 5. Trained model for moving between two points

3.3.3 Agent Action and Crane Models

In this section, we explain the operations of agents (crane) on environments in deep RL.

As shown in Figure 6, we developed a crane with three operations: slewing the boom, derricking the boom, and lifting and lowering the crane hook. The agent learns these control values by training, without limiting the rotation angle of the slewing and derricking. When lifting the crane hook, the vertical direction is restricted such that it does not exceed the boom tip. By simplifying the model in the initial stages of training, unnecessary information is deleted from the search, and the search converges easily, as shown in Figure 7.

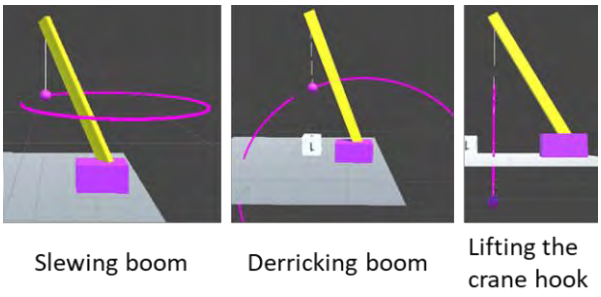

Figure 6. Movement of the crane

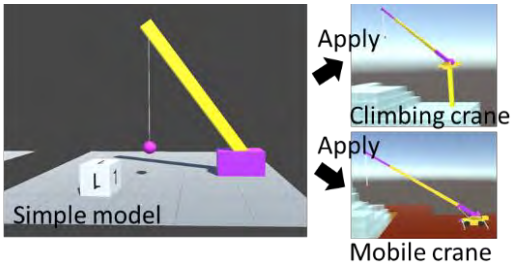

Figure 7. Simplified crane model

3.3.4 Training Method

Figure 8 shows the situation during training. The model training time was reduced by 87% by parallelizing and training nine models simultaneously. The number of iterations was 500,000.

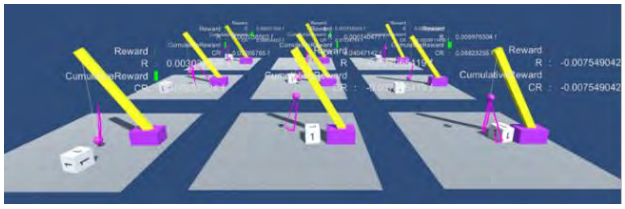

Figure 8. Parallel training of nine models

3.3.5 State and Reward

In this section, we detail a remarkable method to develop a route for a crane hook to move between two points. In deep RL, the environment rewards agents based on their behavior; agents learn behaviors that maximize their cumulative rewards. We created an environment to reward the agents as follows.

- Reward when the crane hook reaches the end point.
- Reward the movement of the crane hook towards the end point.

For a route search between two points in the horizontal direction, we can create a movement route between two points by only giving a reward when the crane hook reaches the end point. However, the optimization of the crane hook route is a path search in a three-dimensional space; hence, we created an environment to reward the operation of the crane hook approaching the end point. We used the inner product to reward the action of the crane hook approaching the end point. We multiply the inner product of the two vectors by the reward and assign it as the reward. As shown in Figure 9, the two vectors are crane hook to target direction vector and crane hook speed vector. If the angle between these two vectors is small (i.e., the inner product is close to 1), the reward is close to 1×reward.

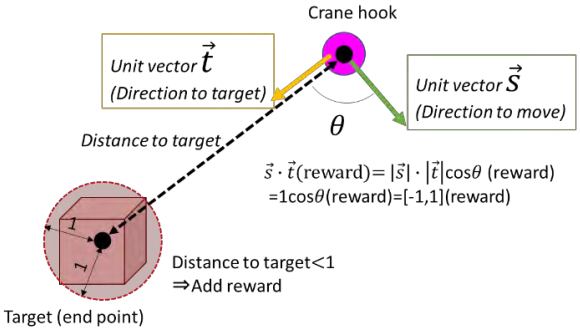

Figure 9. Simplification of rewards

3.4 Method of Verification

3.4.1 Verification of the Optimal Solution

This section presents a method investigate the accuracy of the optimal solution of the trained model.

We verify the accuracy of the optimization of the movement between two points by comparing "the length of the trajectory of the crane hook" and "the length of the shortest path between the two points."

To obtain the length of the crane hook trajectory and the shortest path between the two points, we record the coordinates of the crane hook and the start point for each frame, as listed in Table 1, and track the length and the shortest distance between the two points.

Furthermore, to visualize the crane hook's trajectory, we draw the trajectory of the crane hook, as shown in Figure 10.

Table 1. Recorded coordinates for each frame

start			end			now			last			len
0.00	-6.17	0.00	-1.50	0.50	-2.70	-1.90E-7	-6.54	7.19E-9	0.00	-6.17	0.00	0.00
0.00	-6.17	0.00	-1.50	0.50	-2.70	6.85E-7	-7.66	1.55E-8	-1.90E-7	-6.54	7.19E-9	0.36
0.00	-6.17	0.00	-1.50	0.50	-2.70	1.59E-6	-9.26	1.35E-8	6.85E-7	-7.66	1.55E-8	1.49
0.00	-6.17	0.00	-1.50	0.50	-2.70	1.29E-6	-10.9	1.06E-8	1.59E-6	-9.26	1.35E-8	3.08
0.00	-6.17	0.00	-1.50	0.50	-2.70	2.35E-6	-12.2	-2.91E-8	1.29E-6	-10.9	1.06E-8	4.70
0.00	-6.17	0.00	-1.50	0.50	-2.70	3.22E-6	-13.7	-1.12E-7	2.35E-6	-12.2	-2.91E-8	6.02
0.00	-6.17	0.00	-1.50	0.50	-2.70	3.40E-6	-14.8	-2.01E-7	3.22E-6	-13.7	-1.12E-7	7.52
0.00	-6.17	0.00	-1.50	0.50	-2.70	4.40E-6	-16.2	-2.22E-7	3.40E-6	-14.8	-2.01E-7	8.64
0.00	-6.17	0.00	-1.50	0.50	-2.70	5.35E-6	-17.2	-2.57E-7	4.40E-6	-16.2	-2.22E-7	10.07
0.00	-6.17	0.00	-1.50	0.50	-2.70	4.74E-6	-18.4	-2.62E-7	5.35E-6	-17.2	-2.57E-7	10.98

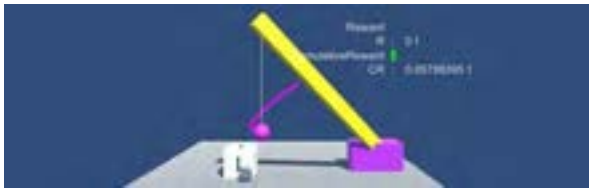

Figure 10. Visualization of the crane trajectory

3.4.2 Verification of the Generality of the Trained Model

This section presents methods to investigate the generality when altering the environment in which the trained model is adapted.

As discussed in Section 2.2, the models trained by deep RL can perform in situations different from the learning environment. However, its adaptability is unknown. Therefore, we make the following changes to the simulation environment during inference.

- Placement: Change the positional relationship between the crane and the end point. We set the end points inside and outside the "installation range of the end point during training." As shown in Figure 11, we examine the inference results while installing the end points in sequence on the horizontal plane. We do not change the position of the crane and the position of the start point.
- Type: We use a default crane for training and a large crane with a different boom length and vertical height (Figure 12).

From the inference results, we examine the generality of the inference model and propose a method to create a learning environment to improve generality.

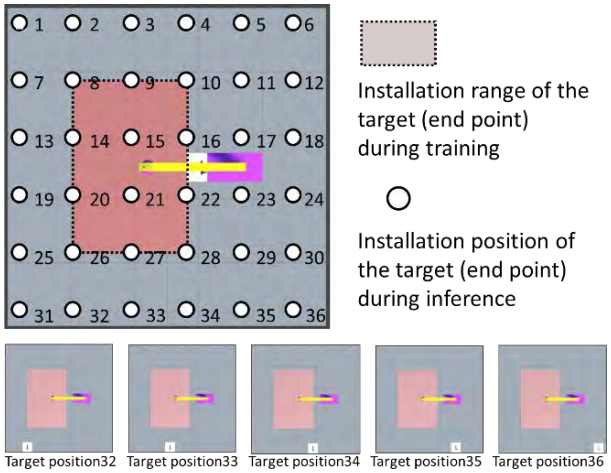

Figure 11. Change in the installation position of the end point

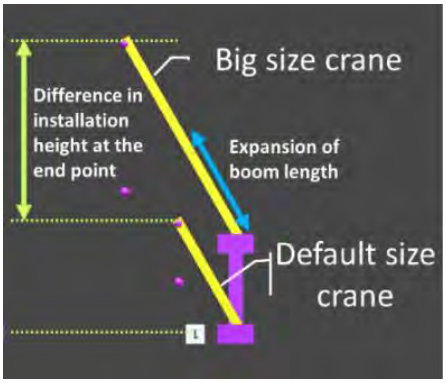

Figure 12. Change in crane type

4 Results and Discussion

4.1 Verification of the Accuracy of the Trained Model

In this section, we present the results of the accuracy verification of movement between two points using deep RL and propose a method for creating an environment to improve the accuracy of this movement.

Based on the coordinates of the start and end points, trajectory length, and the visualization of the crane hook trajectory, the following were observed.

- The movement path was 3.6 times the shortest path
- The trajectory length was almost constant, regardless of the change in the distance between the two points.
- Vertical movement was rapid, whereas horizontal movement was slow.

Figure 13 shows the transition of the locus length for each frame, i.e., the locus of movement between the two points for six iterations, with different lengths between the two points. In addition, as shown in Figures 13 and 14, the length of the trajectory is constant regardless of the distance between the two points. Figure 14 compares the shortest distance between the two points and the actual trajectory length. The length of the trajectory is approximately 3.6 times longer.

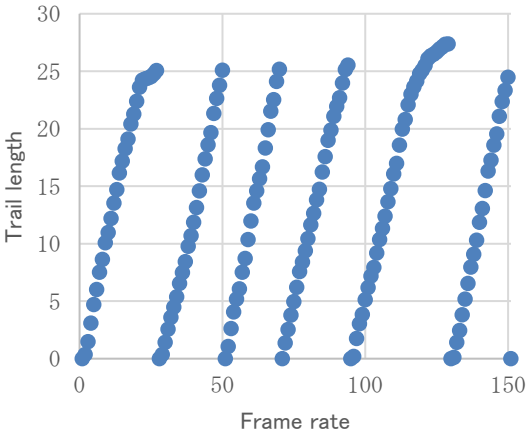

Figure 13. Change in the crane hook trail length for each frame

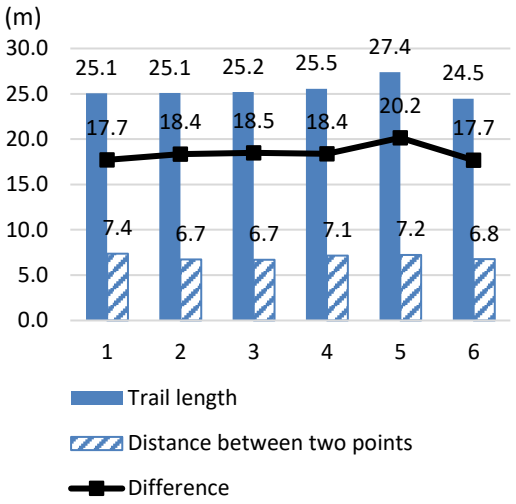

Figure 14. Comparison of shortest path length and crane hook movement path length

As shown in Figure 15, the crane hooks initially moves in the vertical direction and then in the x and z horizontal directions. This occurs because although the position of the end point is rearranged in the horizontal direction during training, it does not move in the vertical direction. Therefore, it is essential to lower the crane hook, and a reward can be obtained based on the movement toward the target direction. Therefore, when the end point is set on the plane, as shown in Figure 16 (a), the agent learns to move the crane hook and then move in the horizontal direction.

To prevent the agent from moving excessively by prioritizing the movement of the lowering of the crane hook, we propose to create an environment, as shown in Figure 16 (b). We randomly set the installation position of the end point in the vertical direction such that the crane hook lifts in the vertical direction above the start point.

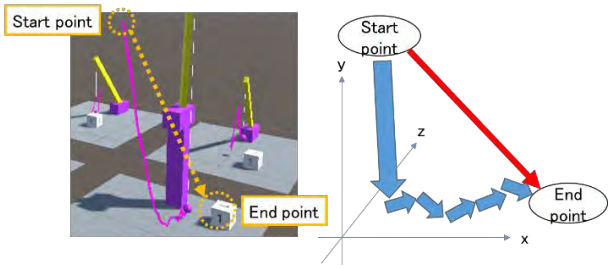

Figure 15. Trail of movement between the two points of the crane hook

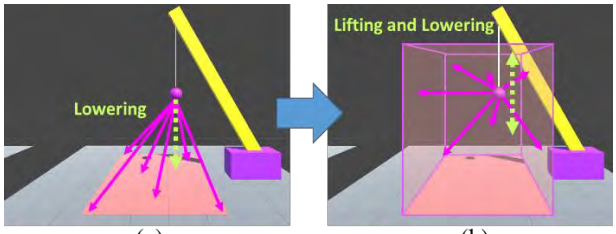

(a) (b)

Figure 16. Environment that causes wasted movement of lowering the crane hook (a); environment for preventing wasted movement (b)

4.2 Verification of the Generality of the Trained Model

In this section, we describe the inference results that were examined based on the method discussed in Section 3.4.2 and propose a method to create an environment that improves the generality from inference results.

For the simulation environment, in inference, we set the end points inside and outside the "installation range of the end point during training" and let the agent infer. Consequently, as shown in Figure 17, the inference result is classified into three cases: reaching the end point, reaching the end point and performing unnecessary movements, and not reaching the end point. Figures 18 (a) and 19 (a) show the inference results corresponding to the location of the end point. Figures 18 (b) and 19 (b) depict the list of images of each inference result with the end-point position changed. Figure 18 shows the inference results using the default size crane. The inference result of installing the end point on the front of the crane includes the result that the boom is not sufficiently long. Figure 19 illustrates the inference result from the movement between two points using the larger crane with different boom lengths and crane heights.

These results show that changing the crane size does not affect the agent performance. When the size of the crane is changed, the positional relationship with the end point changes vertically. However, we confirmed that the agent can perform the movement between two points even if the positional relationship between the crane and the end point is changed. In addition, the range of movement between two points is expanded according to the size of the crane.

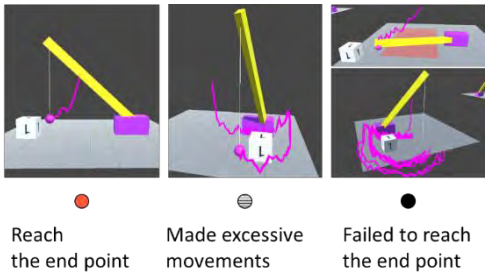

Figure 17. Three types of inference results

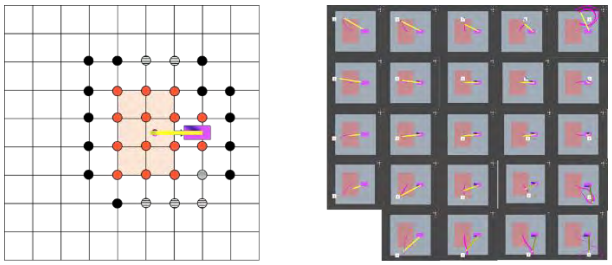

(a) (b)

Figure 18. Result of reaching the end point by the default size crane (a); simulation of movement between two points with the end point placed at each point (b)

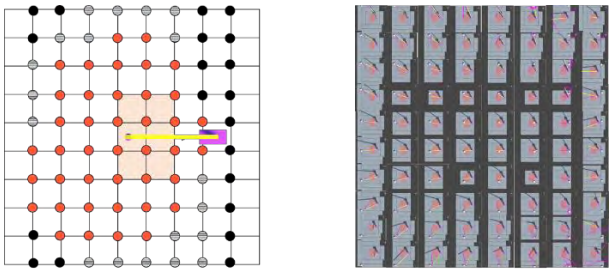

(a) (b)

Figure 19. Result of reaching the end point by the big size crane (a); simulation of movement between two points with the end point placed at each point (b)

Based on Figures 18 (a) and 19 (a), we hypothesized that the range of end-point positions where the agent can perform a movement between two points is proportional to the size of the crane. Therefore, we expanded the mapping of the default size crane (Figure 18 (a)) and verified the similarity of the range of movement between two points by superimposing it on the mapping of the big crane (Figure 19 (a)), as shown in Figure 20 (a). Consequently, the range of movement between the two points was the same.

Furthermore, as shown in Figure 20 (b), the agent did not perform the movement between two points when the slewing angle of the crane increased. The slewing

angle remains within the range to reach the installation position of the end point during learning. This is probably because the slewing angle of the crane is narrow with respect to the installation range at the end point during training. Therefore, to obtain a trained model that moves in a wide range in the horizontal direction, we propose setting the end-point position such that the slewing angle becomes large, as shown in Figure 21. Additionally, when training with a small crane in a small range during training, the process can be adapted to a large crane by inference.

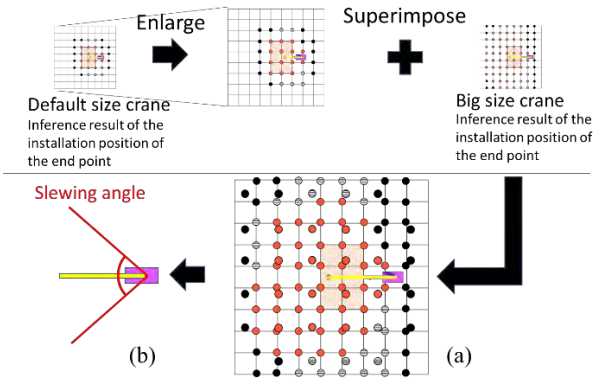

Figure 20. Similarity of the two ranges (a); limit of slewing angle for trained model (b)

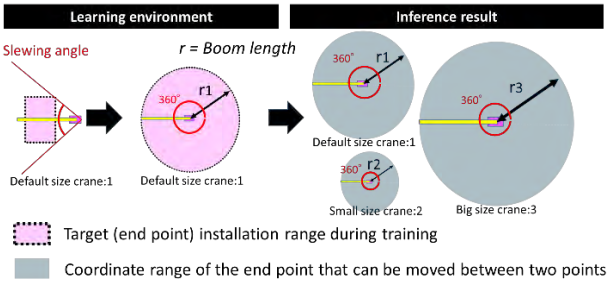

Figure 21. Environment that improves model slewing

5 Conclusion

In this study, we evaluated the accuracy of the trained model and the generality of an environment using a trained model that learned the route creation for a crane hook in a lifting task using deep RL.

We observed the following.

- The trained model's movement between two points did not traverse the shortest path. Although, it was not the optimum solution, it was inferred that the accuracy of movement between two points can be improved by creating an environment in which the crane hook is vertically lifted and lowered.
- Changing the crane size does not affect the model performance.
- The agent did not perform the movement between two points when the turning angle of the crane increased. To obtain a trained model that traverses a wide range in the horizontal direction, it is necessary to position the end points for large slewing angles.

Therefore, we conclude that the method for improving the accuracy and generality of the model for moving the crane hook between two points involves the creation of an environment that moves the crane hook vertically and horizontally (Figure 22).

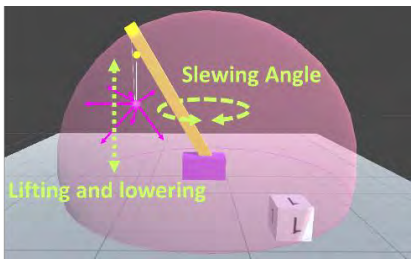

Figure 22. Environment that improves model accuracy and generality

References

[1] Zhiqian Z. and Wei P., Lift planning and optimization in construction: A thirty-year review, In *Automation in Construction,* Volume 118, 2020.10

[2] Keyi W., Borja G S. and Feilian Z., Spatio-temporal planning for tower cranes in construction projects with simulated annealing, In *Automation in Construction,* Volume 111, 2020.3

[3] Megumi M., Shirou M. Yasuhiro F., Mitsuru K., Tobias P., Eiichi M., Ryosuke O. and Daisuke O. Toward onboard control system for mobile robots via deep RL. In *32nd Conference on Neural Information Processing Systems (NIPS 2018)*, 1–12, 2018.

[4] Mikio S., Masateru H., Daisuke C and Keisuke W. Development of Active Response Control System Using AI (Part1. Outline of System). In *Summaries of technical papers of annual meeting (Tohoku Chapter, Architectural Institute of Japan)*,397-298, 2018.9

[5] Aoi T. and Kosei I., Crane Lifting Simulation Using Reinforcement Learning. In *Proceeding of the architectural research meetings II (Kanto Chapter, Architectural Institute of Japan)*, 455-458,

2020.3
[6] Arthur J., Vincent P.B., Ervin T., Andrew C., Jonathan H., Chris E., Chris G., Yuan G., Hunter H., Marwan M. and Danny L. Unity: A General Platform for Intelligent Agents. On-line: https://arxiv.org/pdf/1809.02627.pdf, Accessed: 15/06/2020.
[7] John S., Filip W., Prafulla D., Alec R. and Oleg K., Proximal Policy Optimization Algorithms. On-line: https://arxiv.org/pdf/1707.06347.pdf, Accessed: 15/06/2020.

Reaching Difficulty Model of Swinging Operations of a Hydraulic Excavator Considering the First-Order Delay

K. Matsumura[a], M. Ito[b], C. Raima[b], S. Saiki[c], Y. Yamazaki[c], and Y. Kurita[b]

[a]Graduate School of Engineering, Hiroshima University, Japan
[b]Graduate School of Advanced Science and Engineering, Hiroshima University, Japan
[c]Kobelco Construction Machinery Co., Ltd., Japan
E-mail: itoma@hiroshima-u.ac.jp, raima@hiroshima-u.ac.jp, ykurita@hiroshima-u.ac.jp

Abstract –

Hydraulic excavators are used for various purposes, such as excavation, dismantling, and leveling. The accurate positioning of the excavator is particularly important in loading operations, such as positioning a bucket immediately above a target. The positioning of a bucket via the swinging operation can also be regarded as a kind of pointing operation. There are the dynamic characteristics of hydraulic excavators. However, a pointing motion model that considers dynamic characteristics, such as delay, has not been proposed. In this study, the swinging operation of a hydraulic excavator was simulated and experiments were performed to clarify the relation between the dynamic characteristics of hydraulic excavators and their work efficiency. The dynamic characteristics of the swinging operation of the hydraulic excavator were assumed as a first-order system with dead time. Based on this result, a new difficulty model considering dead time and the time constant was proposed, and it was compared with the original Fitts' model based on the coefficient of determination. It was confirmed that the proposed model represented difficulty more accurately compared to the original Fitts' model.

Keywords –

Hydraulic excavator; Pointing; User Interface

1 Introduction

Hydraulic excavators (Figure 1), which are a type of construction machinery, are used for various purposes, such as excavation, dismantling, and leveling, because of many degrees of mechanical freedom and a variety of attachments. In recent years, teleoperated hydraulic excavators have been used at multiple disaster sites. These excavators are highly versatile. However, there are design problems based on ergonomics, such as the lack of feedback information and low visibility, and these problems reduce the work efficiency of excavators [1].

The operation of a hydraulic excavator in general civil engineering works is broadly divided into three operations, i.e., swinging, running, and excavation. Operators control hydraulic excavators using joysticks that are located close to their hands. When the swinging operation is carried out, according to the International Organization for Standardization, the swinging direction and swinging speed of a hydraulic excavator are determined by moving the left lever to the right or left. The accurate positioning of the excavator is particularly important in loading operations, such as positioning a bucket immediately above a target. Conventionally, the pointing operation involves pointing and selecting a target using a mouse or touchpad on a graphical user interface. However, the positioning of a bucket via the swinging operation can also be regarded as a kind of pointing operation. Hayashi and Tamura [2] experimentally investigated the pointing operation using a bucket to verify the effectiveness of the vibration of a joystick in a teleoperated hydraulic excavator system.

In our previous study [3], we developed a difficulty model that extends Fitts' law for the relationship between the range of view and work efficiency. The field of view affects the work efficiency of a hydraulic excavator when it performs the swinging operation. There is a boom on the right side of the driver's seat of the hydraulic excavator, and the field of view on the right side is narrower than that on the left side. Particularly in the case

Figure 1. Hydraulic excavator components

of teleoperation, the field of view is limited by the display range of the monitor. In addition, the dynamic characteristics of hydraulic excavators, such as dead time and inertia, cannot be neglected. The purpose of this study was to investigate the relationship between the dynamic characteristics and work efficiency of a hydraulic excavator. However, as it is difficult to change the dynamic characteristics of an actual hydraulic excavator, the swinging operation of a hydraulic excavator was simulated and experiments were performed. The dynamic characteristics of the swinging operation were assumed as a first-order system with dead time, and the time until turning to the target angle was measured for different dead times and time constants. Additionally, a difficulty model for estimating task time was proposed. By using this model, we can evaluate and increase the rotate work efficiency of the excavator.

2 Previous Studies on Pointing Motion Models

Numerous studies have attempted to model the difficulty of pointing motion. One of the existing models is Fitts' law, which models the relationship between the index of difficulty, ID, and the pointing time, MT, of a pointing task. According to Fitts' law, MT increases as the distance from the starting position to a target increases and the target size decreases. MacKenzie [4] improved Fitts' model and expressed the ID as follows:

$$ID = \log_2\left(\frac{D}{W} + 1\right) \quad (1)$$

where D is the pointing distance and W is the pointing size. MT tends to increase linearly with ID. This relationship can be expressed using experimentally obtained constants a and b, as follows:

$$MT = a + bID \quad (2)$$

Fitts' law was originally proposed as a simple motor response model with one dimension. MacKenzie [5] extended this model to consider two-dimensional pointing operations. Subsequently, Murata and Hirose [6] extended it to consider three-dimensional pointing operations. Various studies have extended Fitts' law to consider factors other than distance and size. Jax et al. [7] proposed the following equation to predict pointing time when pointing motion was performed on a curved line, OI, assuming that an obstacle existed:

$$MT = a + bID + cOI \quad (3)$$

where a, b, and c are experimentally obtained constants. Accot and Zhai [8] proposed an index of difficulty for the steering operation required by a vehicle passing an elongated path, such that the vehicle does not extend beyond the path's width.

Figure 2. Swinging operation simulator

$$ID = \frac{D}{W} \quad (4)$$

MacKenzie and Buxton [9] proposed the following equation for extending Fitts' law to two dimensions. The equation incorporated the target width W and the target height H.

$$ID = \log_2\left(\frac{D}{\min(W,H)} + 1\right) \quad (5)$$

Bi et al. [10] conducted a pointing test using a smartphone-sized display and proposed a more accurate difficulty model for small displays. It is possible to evaluate the operability of pointing devices and environments using appropriately designed pointing difficulty models.

In our previous study [3], we attempted to model pointing motion considering the effect of the field of view. We created a simulation environment for swinging pointing operations and examined the relationship between the range of the field of view and pointing difficulty. Based on the results, the following equation, which incorporated the size, V, of the field of view, was proposed:

$$ID = \log_2\left(\frac{D}{W} \cdot \frac{D}{V} + 1\right) \quad (6)$$

To the best of our knowledge, a pointing motion model that considers dynamic characteristics, such as delay, has not been proposed. In this study, the swinging pointing operation with delay was simulated and the relationship between the delay parameter and pointing difficulty was investigated.

3 Approximation of Dynamic Characteristics of Hydraulic Excavator

A hydraulic excavator is operated using joysticks, and the angular velocity of the operated object changes according to the angle of the joysticks. The input from

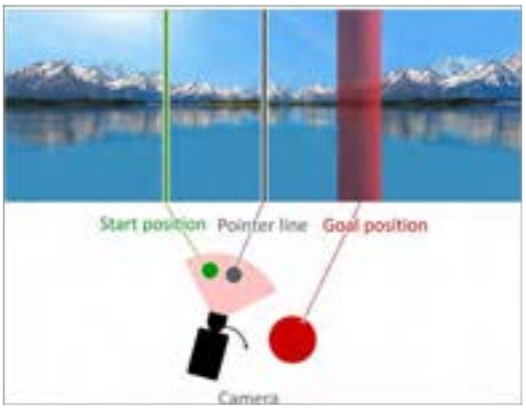

Figure 3. Display image of Simulator

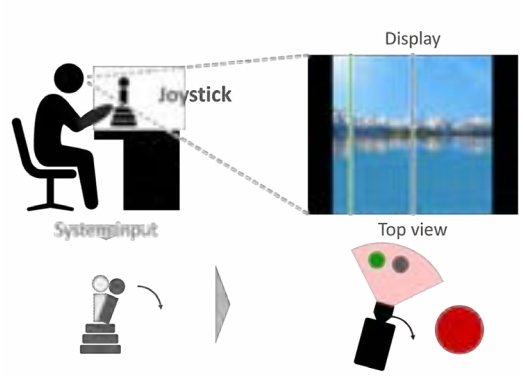

Figure 4. Task of simulation experiment

the joysticks causes attachments to move and swing through a hydraulic circuit and a hydraulic cylinder. Therefore, there is response delay. In this study, the dynamic characteristics, $G(s)$, of the swinging operation of the hydraulic excavator were assumed as a first-order system with dead time, as follows:

$$G(s) = \frac{K}{1+Ts} e^{-Ls} \quad (7)$$

where K is system gain, T is the time constant, and L is dead time. Dead time is the time elapsed from application of the input to the observation of the output, and the time constant is the constant about the rise time. We constructed a difficulty model that incorporated these parameters.

4 Experiments Using Swinging Pointing Simulator

4.1 Simulator Configuration

We created a system to simulate the swinging operation of hydraulic excavators to clarify the effect of dynamic characteristics. The system is shown in Figure

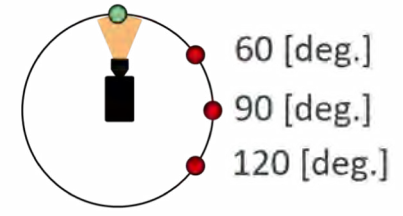

Figure 5. Target position

Table 1. Parameters of transfer function in simulation experiment

	Dead time (s)		Time constant (s)	
Condition	L_{acc}	L_{dec}	T_{acc}	T_{dec}
1	0	0	0	0
2	0.16	0.08	0.6	0.35
3	0.16	0.08	1.2	0.69
4	0.32	0.16	0.6	0.35
5	0.32	0.16	1.2	0.69
6	0.32	0.16	2.4	1.40
7	0.64	0.32	1.2	0.69
8	0.64	0.32	2.40	1.40

2; it consisted of a personal computer, a monitor, and an input joystick. The experimental system was created using Unity, which is a three-dimensional game engine. The start point, pointer line, and target area were displayed on the monitor, as shown in Figure 3. When the joystick was tilted, the camera in the Unity environment rotated according to the tilt direction and the angle of the joystick.

4.2 Experimental Protocol and Conditions

Experiments were performed with four participants (Sub. A to D). We recruited the participants from the students at Hiroshima University. Informed consent based on the Declaration of Helsinki was obtained from all participants prior to the experiments. The participants performed a swinging pointing task by viewing the image projected by the camera in the Unity environment (Figure 4). First, the camera pointed to the start point, which is indicated by the green line. The camera turned according to the operation of the joystick by the participants. The pointer line, which is indicated by the black line, existed at the center of the camera. The task was finished when the pointer was stopped in the target area, which is indicated in red. Prior to the task, the participants were informed that the target area exists in the right direction and that they must finish the task as quickly as possible. When one task was completed, it was displayed on the monitor that the task has been completed, and the next task was started after 1 (s).

The distance to the target, D, was defined as 60° ,

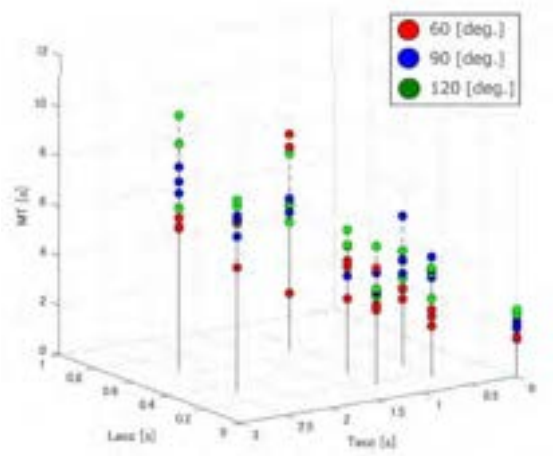

Figure 6. Experiment result (Sub. A)

90° , and 120° (Figure 5). The values of the time constant, T, and dead time L are shown in Table 1. In the swinging of the hydraulic excavator, these parameters are different for acceleration and deceleration. The time constant and dead time were T_{acc} and L_{acc} for acceleration and T_{dec} and L_{dec} for deceleration, respectively. The target size, W, was 0.5 (m) and the range of the field of view was constant.

There were 24 experimental conditions, which were obtained based on the combination of three conditions of the distance to the target, D, and eight conditions of the dynamic characteristics. The order of the conditions was random for each participant. Each participant performed the task three times under each condition, and pointing time was measured. Participants practiced three times when conditions changed. The average pointing time calculated using the three measurements was considered as the pointing time under a particular condition.

4.3 Results

The experimental results for Sub. A are shown in Figure 6. This figure shows the pointing time, MT (s), under the target distance conditions of 60° , 90° , and 120° for the dead time, L_{acc} (s), and time constant, T_{acc} (s). It can be seen that the pointing time tends to increase as the distance to the target, D, increases, as in the original Fitts' law. Furthermore, it was confirmed that the pointing time increased with the time constant and dead time.

5 Modeling of Swinging Pointing Operations

5.1 Proposed Model

A new difficulty model is proposed based on the above results. The difficulty model incorporates dead time and the time constant for Fitts' model considering that pointing time increases with dead time and the time constant and difficulty increases with pointing time. The equation for the model is as follows:

$$ID^{\mathrm{new}} = \log_2\left\{\frac{D}{W}(L_{\mathrm{acc}} + L_{\mathrm{dec}} + T_{\mathrm{acc}} + T_{\mathrm{dec}}) + 1\right\} \quad (8)$$

In this work, the coefficient of determination is used as an evaluation index, and the proposed model is compared with the original Fitts' model.

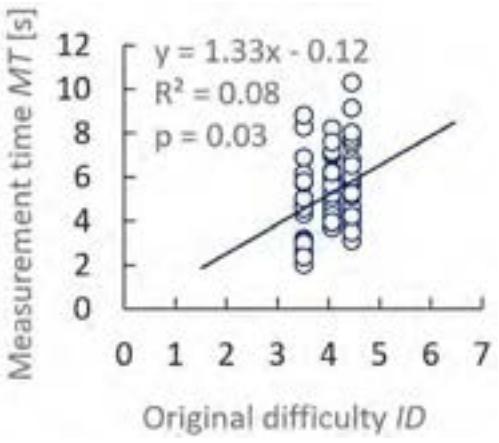

Figure 7. Correlation between index of difficulty ID and pointing time MT for original model

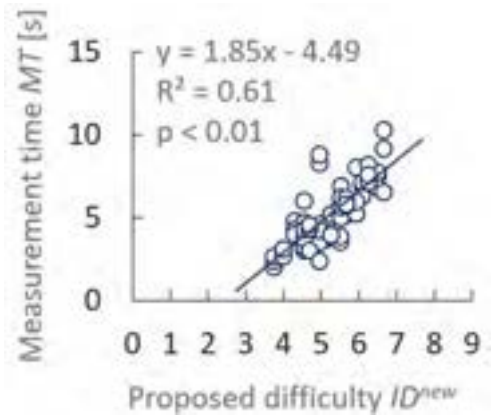

Figure 8. Correlation between index of difficulty ID^{new} and pointing time MT for proposed model

5.2 Evaluation of Proposed Model

Figures 7 and 8 show the relationship between the index of difficulty (horizontal axis) and pointing time (vertical axis) for Sub. A. The regression line and the coefficient of determination are shown. Figures 7 and 8 show are for the original and proposed models, respectively. The coefficient of determination for the

Table 2. Coefficient of determination (all subjects)

	Sub.A	Sub.B	Sub.C	Sub.D	Mean
for ID	0.076	0.078	0.073	0.063	0.073
for ID^{new}	0.61	0.45	0.34	0.35	0.44

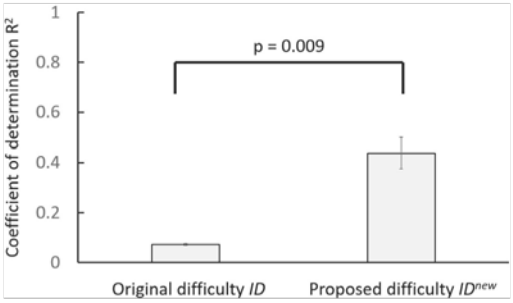

Figure 9. Comparison of coefficient of determination between original and proposed models

proposed model is R^2=0.61, which is higher than the coefficient of determination for the original model (R^2=0.08). Table 2 and Figure 9 show the coefficients of determination for all subjects and their mean values. The coefficient of determination for the proposed model is higher than that for the original model for all subjects. In addition, the average values of the coefficient of determination for the original and proposed models are compared using Student's t-test, and a statistically significant difference is observed (p=0.009).

6 Discussion and Conclusions

In this study, the swinging operation of a hydraulic excavator was simulated and experiments were performed to clarify the relation between the dynamic characteristics of hydraulic excavators and their work efficiency. The dynamic characteristics of the swinging operation were approximated as a first-order system with dead time, and the time until swinging to the target area was measured for different dead times and time constants. It was confirmed that pointing time increased with dead time and the time constant. Based on this result, a new difficulty model considering dead time and the time constant was proposed, and it was compared with the original Fitts' model based on the coefficient of determination. It was confirmed that the proposed model represented difficulty more accurately compared to the original Fitts' model. The original Fitts' model may not be applicable to the swinging operation of a hydraulic excavator because it does not consider response delay. The proposed model can be used to evaluate the performance of hydraulic excavators, and it is expected to improve their work efficiency. However, the size of the field of view is not considered in this study. It is necessary to develop and evaluate a model that considers the size of the field of view. In addition, the suitability of the proposed model must be confirmed in actual environments where hydraulic excavators are used.

References

[1] J. Akyeampong, S. Udoka, G. Caruso, and M. Bordegoni. Evaluation of hydraulic excavator human-machine interface concepts using NASA TLX. *International Journal of Industrial Ergonomics*, 44(3): 374–382, 2014. doi:10.1016/j.ergon.2013.12.002.

[2] K. Hayashi and T. Tamura. Teleoperation performance using excavator with tactile feedback. In *International Conference on Mechatronics and Automation*, pages 2759–2764, Changchun, China, 2009.

[3] K. Matsumura, M. Ito, S. Saiki, Y. Yamazaki, and Y. Kurita. Influence of restrictions on range of view from cockpit in operation of hydraulic excavator. *IEEE Access*, 8:90520–90527, 2020. doi:10.1109/ACCESS.2020.2994202.

[4] I. S. MacKenzie. Fitts' law as a research and design tool in human-computer interaction. *Human-Computer Interaction*, 7(1):91–139, 1992. doi:10.1207/s15327051hci0701_3.

[5] I. S. MacKenzie. A note on the information-theoretic basis for Fitts' law. *Journal of Motor Behavior*, 21(3):323–330, 1989. doi:10.1080/00222895.1989.10735486.

[6] A. Murata and H. Iwase. Extending Fitts' law to a three-dimensional pointing task. *Human Movement Science*, 20(6):791–805, 2001. doi:10.1016/S0167-9457(01)00058-6.

[7] S. A. Jax, D. A. Rosenbaum, and J. Vaughan. Extending Fitts' law to manual obstacle avoidance. *Experimental Brain Research*, 180(4):775–779, 2007. doi:10.1007/s00221-007-0996-y.

[8] J. Accot and S. Zhai. Beyond Fitts' law: Models for trajectory-based HCI tasks. In *Proceedings of ACM Human Factors in Computing Systems*, pages 295–302, Atlanta GA, USA, 1997. doi:10.1145/258549.258760.

[9] I. S. MacKenzie and W. Buxton. Extending Fitts' law to two-dimensional tasks. In *Proceedings of the SIGCHI Conference on Human Factors in Computing Systems*, pages 219–226, Monterey CA, USA, 1992. doi:10.1145/142750.142794.

[10] X. Bi, Y. Li, and S. Zhai. FFitts law: Modeling finger touch with Fitts' law. In *Proceedings of the SIGCHI Conference on Human Factors in Computing Systems*, pages 1363–1372, Paris, France, 2013. doi:10.1145/2470654.2466180.

Mechatronic Control System for Leveling of Bulldozer Blade

Alexey Bulgakov[a], Thomas Bock[b], Georgii Tokmakov[a]

[a]South-Russian State Polytechnic University (NPI), Russian Federation
[b]Technical University of Munich, Germany
E-mail: agi.bulgakov@mail.ru, thomas.bock@br@br2.arch.tum, tokmakov.tun@gmail.com

Abstract – Recently, it began the spread of bulldozers using information technology during controlling the machine to increase the efficiency of the entire execution of work, including avoiding the usually necessary final surface treatment. Blade control mechatronic system for leveling work of bulldozer blade enables the bulldozer to effectively perform a ground leveling work or a grading work with high accuracy in a minimum amount of time. The system compensates for pitching of a tractor portion of the bulldozer, and for variations in the amount of earth to be moved by a blade of the bulldozer.

The biggest feature of this mechatronic system is automation of digging and soil carrying work by optimally controlling a load applied to the work equipment even if there is digging depth to some extent up to the finishing surface, while the work application range of conventional bulldozers was limited mainly to finishing leveling work under light load. Seamless automatic execution without concern for damage to a finishing surface has been enabled by automatically switching from digging control to leveling control as the work progresses and approaches the finishing surface.

This will reduce operator fatigue during operation, and will also allow even an inexperienced operator to perform work equivalent to the work of a qualified operator.

Keywords – Mechatronic system; Bulldozer blade; Leveling control; Design surface

1 Introduction

Industries such as mining and construction in which earthmoving plays a fundamental role are constantly under pressure to improve productivity (amount of work done), efficiency (cost of work done in terms of labor and machinery), and, safety (injury sustained by workers). Mechatronics and robotics offers the possibility of contributing to each metric but has been slow in being accepted. Until recently, it has been possible to make gains using traditional means— over the last four decades earthmovers have become progressively larger and their mechanisms more efficient. Also, automation of fieldworthy earthmovers is a difficult problem.

These machines must operate in unstructured, dynamic, outdoor environments, often in poor visibility conditions and inclement weather. However, after decades of increases in size and power, practical limits have been reached and now automation is being sought for further improvements. At about the same time, several enabling technologies relevant to earthmovers, particularly in the area of environmental perception, are becoming reliable and affordable. Computing technology has also reached the stage where fast, compact and rugged components can match the bandwidth of sensory data.

The cycle of operation for a mechatronics machine is: sense, plan, and execute. First, a machine must sense its own state and the world around it. Next it must use this information along with a description of a goal to be achieved to plan the next action to be taken. In some cases the mapping from sensing to action is direct, and, can take the form of a pre-determined control law. In other cases, deliberation, or the use of models (sensors, mechanisms, and, actions) is necessary. Finally, the action must be executed via the mechanism. Since, relatively few systems are fully autonomous, depending on human input or control to achieve some of their function, this article examines various aspects of the enabling technologies used by partially automated systems [1].

The cycle of operation for a fully autonomous machine is: sense, plan, and execute. First, an automated machine must sense its own state and the world around it. Next it must use this information along with a description of a goal to be achieved to plan the next action to be taken. In some cases the mapping from sensing to action is direct, and, can take the form of a pre-determined control law. In other cases, deliberation, or the use of models (sensors, mechanisms, and, actions) is necessary. Finally, the action must be executed via the mechanism [2].

Bulldozers equipped with modern navigation and information systems are mobile mechatronic objects, and they can be integrated into general process of intellectual construction [3]. The integration will provide optimal efficiency of the construction cycle and will ensure lean

production process [4,5].

Application of regulators based on classical control theory is difficult due to the frequent changes in workflow conditions. Thus, it is necessary to develop adapted control systems to eliminate the difficulties described. The system includes both the bulldozer's dynamics modeling and bulldozer's workflow control method to take into consideration the complex non-linear dependencies between workflow parameters and incomplete information on its working conditions changes.

Having reviewed adaptive and intellectual control methods [6, 7], we propose to create an adaptive control system for technological processes to increase efficiency of bulldozer's control in comparison with traditional control methods.

2 Bulldozer - mathematical description as mobile mechatronic object

When researching a dozer's working process usually a number of design schemes are considered – straight line, thread milling, wedge and exponential cutting. Meanwhile, a dozer moves along the surface that is formed by its blade. Therefore, when driving onto any surface roughness resulting from the dozer blade control or the change in its position due to any reason, causes position changes of the machine frame and along with the cutting edge that is any face deviation from a straight line in some extent is copied by the dozer.

Observations [8] show that quite often while designing a face its roughness is progressing, reaching a size at which the control over the workflow is lost. In this case, the operator has to align the face deliberately, trying to ensure its "tranquil" profile that allows doing excavation works smoothly, without frequent control system switching and reducing the dozer's operating speed that causes a slowdown and shows inferiorities of the blade control system. Obviously, if the control system operates in the antiphase towards deviations of the tractor frame with sufficient accuracy, the initial face roughness will not evolve and will be gradually cut. One of the most likely causes of the opposite phenomenon observed in practice, is the disparity between the velocity of the dozer V_p and actual conveying speed of the working body V_{ot} required in certain areas S_i of the digging operating cycle, where *i* – is the number of the speed change V_{ot}. Speed ratio depends on the dozer's geometrical dimensions (Figure 1) and its control system.

Mathematical model of the dozer's movement on a straight line tracking (frame alignment) is built using the Lagrange equations of the 2nd kind, under the assumption that the contribution to the dynamics of the drive gears and a track is small, compared with the contribution of the remaining parts of the dozer.

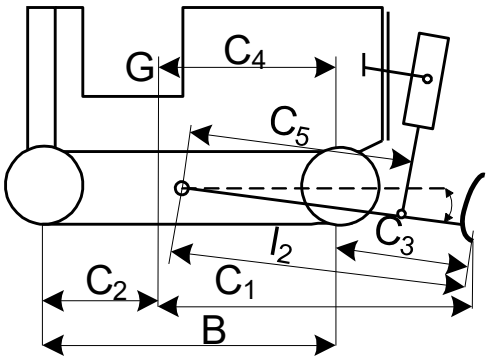

Figure 1. Dozer's geometrical dimensions

$$\begin{cases} \frac{d}{dt}\left(\frac{\partial T}{\partial \dot{x}}\right) - \frac{\partial T}{\partial x} = Q_x, \\ \frac{d}{dt}\left(\frac{\partial T}{\partial \dot{\varphi}}\right) - \frac{\partial T}{\partial \varphi} = Q_\varphi. \end{cases} \quad (1)$$

where kinetic energy:

$$T = \frac{1}{2}m_1\dot{x}^2 + \frac{1}{2}m_2\left(\dot{x}^2 + (l_2 l_{c2}\dot{\varphi})^2 + 2\dot{x}l_2 l_{c2}\dot{\varphi}\sin(\varphi)\right) + \frac{1}{2}J_{c2}\dot{\varphi}^2 + \frac{1}{2}\sigma hx\left(\dot{x}^2 + (l_2\dot{\varphi})^2 + 2\dot{x}l_2\dot{\varphi}\sin(\varphi)\right) + \frac{1}{2}\sigma hx i_{rz}^2\dot{\varphi}^2, \quad (2)$$

generalized forces acting on a dozer:

$$Q_x = -\sigma hgl_2\sin\varphi + F_т - F_s, \quad Q_\varphi = -(m_2 l_{c2} + \sigma xh)gl_2\cos\varphi + M. \quad (3)$$

m_1 – tractor mass; m_2 – blade frame mass; σ – soil surface density; $F_т$ machine pulling power; F_s ground cutting resistance; h – depth of the soil cutting; l_{c2} – center of the blade mass; i_{rz} - gyration radius of the dumping soil.

$$m_1\ddot{x} + m_2\ddot{x} + m_2 l_2 l_{c2}\ddot{\varphi}\sin\varphi + m_2 l_2\, l_{c2}\dot{\varphi}^2\cos\varphi + \sigma h\dot{x}^2 + \sigma hx\ddot{x} + \sigma h\dot{x}l_2\dot{\varphi}\sin\varphi + \sigma hxl_2\ddot{\varphi}\sin\varphi + \sigma hxl_2\dot{\varphi}^2\cos\varphi - \frac{1}{2}\sigma h\dot{x}^2 - \frac{1}{2}\sigma hi_{rz}^2\dot{\varphi}^2 - \frac{1}{2}\sigma h(\dot{x}^2 + l_2^2\dot{\varphi}^2 + 2\dot{x}l_2\dot{\varphi}\sin\varphi) = -\sigma hgl_2\sin\varphi + F_т - F_{сопр}. \quad (4)$$

$$m_2 l_2^2 l_{c2}^2\ddot{\varphi} + m_2\ddot{x}l_2 l_{c2}\sin\varphi + m_2\dot{x}l_2 l_{c2}\cos\varphi\dot{\varphi} + J_{c2}\ddot{\varphi} + \sigma h\dot{x}l_2^2\dot{\varphi} + \sigma hxl_2^2\ddot{\varphi} + \sigma h\dot{x}l_2\sin\varphi + \sigma hxl_2\cos\varphi\dot{\varphi} + \sigma h\dot{x}i_{rz}^2\dot{\varphi} + \sigma hxi_{rz}^2\ddot{\varphi} - m_2\dot{x}l_2 l_{c2}\dot{\varphi}\cos\varphi - \sigma hx\dot{x}l_2\dot{\varphi}\cos\varphi = -(m_2 l_{c2} + \sigma xh)gl_2\cos\varphi - (m_2 l_{c2} + \sigma xh)gl_2\cos\varphi + M. \quad (5)$$

The system (1) solution allows getting the differential equations (4) and (5) that describe the dozer's movement on a straight line track, and determining control actions through the parameters of the machine in areas S_i of the digging operating cycle as the coefficients a_i in the dependence $V_{ot} = a_i V_p$. Such a dependence is typical for dozers with a single-motor drive with a hard pump hydraulic drive connection to the motor shaft.

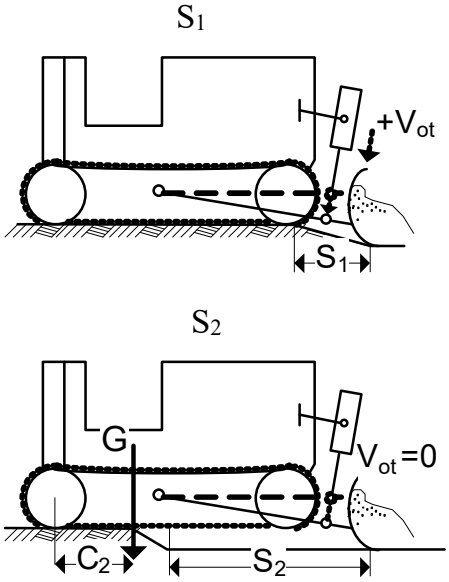

Figure 2. The movement of the tractor frame the beginning of digging.

At the beginning of digging (Figure 2), the frame of the tractor makes a strictly forward movement over a distance of S_1+S_2 without hesitation relatively its mass center. The blade cutting edge in the area S_1 dives into the soil to a depth equal to a predetermined cutting thickness h. Thus, the control action a_1 may be determined by the formula:

$$a_1 = \frac{30 i_{tr} m l_2}{\pi r_k F_z i_{pr} C_5 n}, \quad (6)$$

where i_{tr}, i_{pr} - tractor transmission and hydraulic pump ratios; n - number of hydraulic cylinders; m - fluid mass in the hydraulic cylinders;

In the area S_2 the movement is made with $a_2=0$ until the mass center of the tractor won't move to the buttonhole edge.

On further movement the dozer "dives" in the drawn buttonhole (Figure 3), so in the area S_3 it is necessary to lift the blade at a rate of V_{ot}, determined by the coefficient a_3:

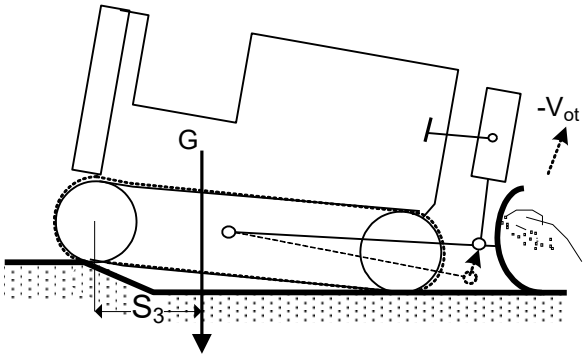

Figure 3. The movement the dozer "dives" in the drawn buttonhole

$$a_3 = \operatorname{tg}\beta \left[e^{\frac{a V_п t}{C_1 + V_п t}} \left(1 + \frac{a C_1}{C_1 + V_п t}\right) - 1 \right]. \quad (7)$$

The area S_3 ends after the dozer's back gear hits the edge of the face and reverse alignment of tractor frame starts. Length of the alignment area is $S_4 \approx S_1$. Obviously, during this period it is necessary to start dropping the blade. The a_4 determines the rate of dropping the blade in the given area:

$$a_4 = \frac{C_3 S_1}{(C_4 + S_3 + V_п t)^2}. \quad (8)$$

To implement control actions $a_i = f(S_i, t, h)$ the dozer must be equipped with a vertical blade control system.

3 Adaptive control principles for a mechatronic bulldozer blade control system

The article proposes the bulldozer workflow neural network model adaptive learning algorithm based on the recurrent least square method (exponential forgetfulness method) and on the algorithm of Forward Perturbation or dynamic back propagation.

The autoregressive model structure with external inputs (Figure 4) is a dynamic two-layer recurrent neural network. It is found from the autocorrelation signal functions that the autocorrelation coefficient is greater than 0.8 in the time interval 0.1 sec. for speed $\vartheta(t)$ of 0.5 sec. for digging depth $h(t)$ and 0.2 sec for the resistance force $P(t)$. Length of delay lines TDL taking into account the sampling frequency of 10 Hz are up to 1, 5 and 2 accordingly (Figure 4).

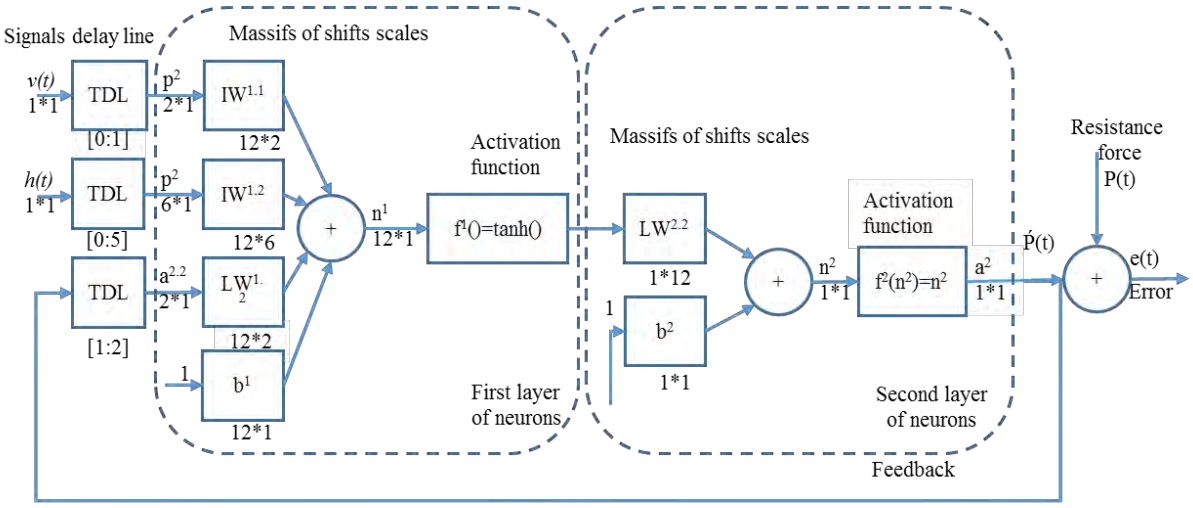

Figure 4. Autoregressive model structure

In the process of learning the neural network accumulates information on workflow dynamics, new tendencies of process development prevail on the earlier ones at that.

It is a method of random search with elements of adaptation, which is based on principles similar to the Darwin's evolution process of biological organisms. In this case, three types of operations are performed: crossing, mutation, selection. The fitness degree (how the population corresponds to the given task) is defined through the fitness function that can also include penalty functions for violation of additional restrictions on variable variables. There are various forms of crossing [8]. They make a selection of the fittest specimen, which constitute a parental pair and the crisscrossing of the chromosomal chains takes place, i.e. the descendant line code inherits fragments of codes of parental chromosomes. The mutation operator produces a local change in the line code of chromosomes with a given probability, which is one of the configurable parameters of the genetic algorithm [9, 10].

The selection operator allows creating a new population from a set of specimen, generated and modified descendants of specimen after mutation. The genetic algorithm is used to adjust the membership functions that are defined within the accuracy of a few changeable parameters, such as triangular, trapezoidal, radial functions. When simultaneously configuring several membership functions, the parameters of each of them are coded by their own segment of the chromosome, so that during the process of crossing the code sharing occurs only between chromosome segments of the same type. To configure a rule base to a specific chromosome fragment, some variant of the rule base is corresponded and in accordance with the accepted coding the choice of the genetic operators' type is performed.

Conclusions and Results

Adaptive neural network model of digging allows you to simulate and predict the dependence of the resistance strain of gauge bogie displacement depending on the dig depth and trolley speed in dynamics. The accuracy of the prediction $P(t)$ being estimated, the average relative error after learning the network is 4.5 %[11-13].

A neural network model of bulldozer workflow has been developed, allowing modeling the dependence of pulling power from the blade penetration.

Input model signal, used for training, simulation and verification is presented in Figure 5a. Adaptive learning for the model is stopped at time t = 9,5 sec. Receiving at this moment a neural network model parameter values, modeled digging resistance force and speed of the machine (Figure 5b, 5d) are accomplished, as well as the forecast for another 0.5 seconds is developed.

Figure 5c shows the output of neural network models-pulling power of the bulldozer. In modeling and prediction of the neural network output is close to the experimental data only in the time interval of 7-10 sec. This is due to a change in unmeasurable chip thickness, as well as the rapidly changing conditions of the mover clutch with the ground. Therefore, the parameters of the adaptive neural network model must be adjusted in real time. The accuracy of prediction of pulling power $N(t)$ has been estimated; the average relative error being 14.7 % on an interval from 7 to 10 s [14]. Identification Technique of bulldozer workflows and models obtained on its basis, are designed for use in the development of adaptive systems of automatic workflow management of bulldozer [15-16].

The development methodology of the adaptive control systems of bulldozer workflows is based on the application of neural network technology [17].

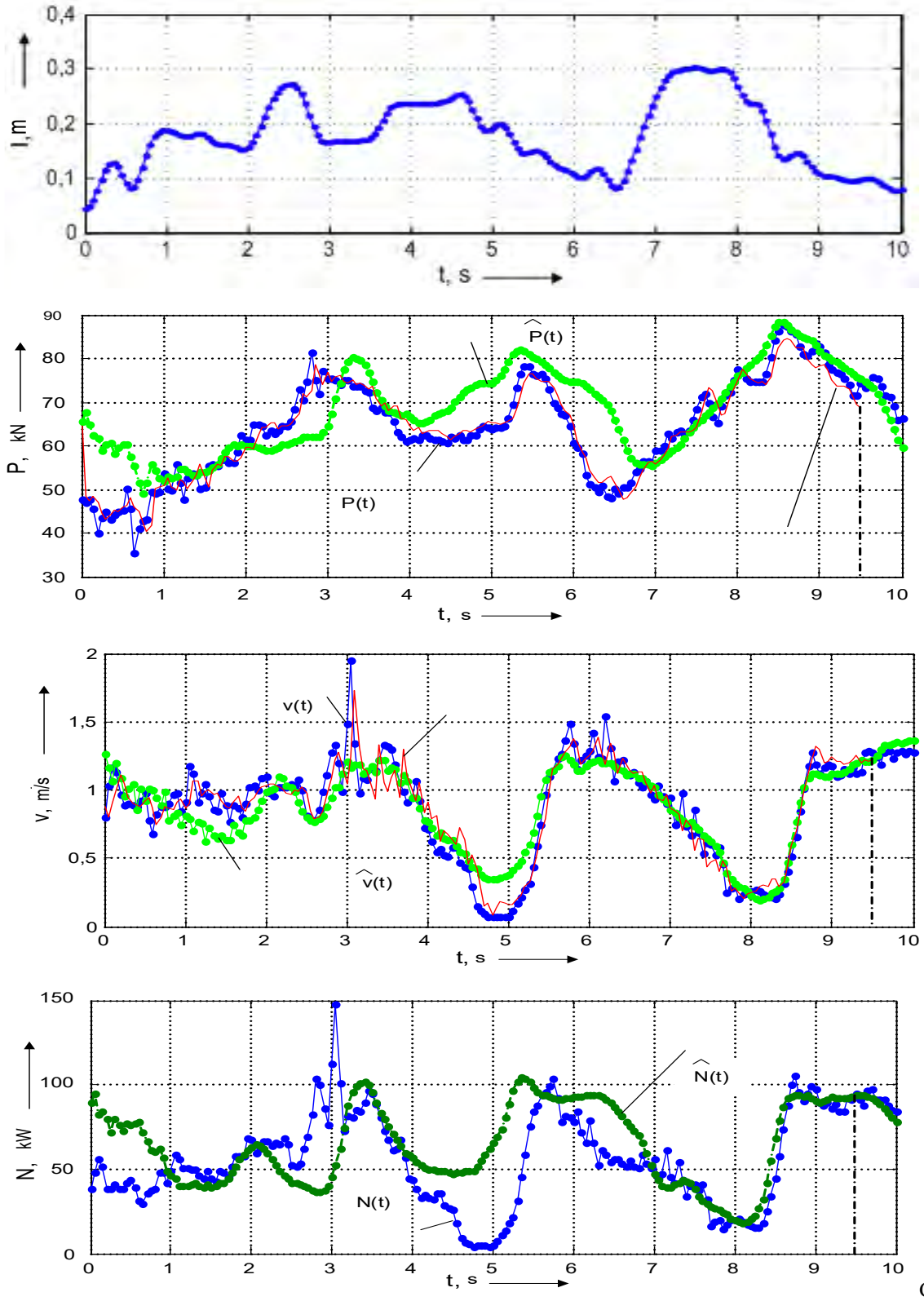

Figure 5. Comparison of Bulldozer operational parameters obtained with the Model and actual operational parameters: A) Deepening Dozer Blade; B) Digging Resistance Force; D) Bulldozer Current Velocity; C) Bulldozer Pulling Power.

For the formation of the control actions influencing the bulldozer, particularly electrical signals actuating control valves of hydraulic cylinders lifting and lowering the working organ, the structure and algorithms of adaptive neural network controller have been designed. Based on the obtained results of practical measurements and the simulation carried out on their basis, the team set the following goal as the practical testing of the machine in real working conditions.

References

[1] https://www.cat.com/en_US/products/new/technology/grade.html

[2] Singh S. The State of the Art in Automation of Earthmoving. *ASCE Journal of Aerospace Engineering*, Vol 10, Nr. 4, October 1997.

[3] Shestopalov K. Hoisting-and-transport, building and road machines and equipment. Moscow, Academy, 2009. – pp. 67-72.

[4] Bulgakov A., Jehle P., Tokmakov G. SCM-logistic and mechatronics systems for ensuring the smooth construction process // Innovation in Mechanical Engineering – Shaping the Future: 56-th International Scientific Colloquium (12–16 September 2011: Conference Proceedings / Ilmenau University of Technology).Ilmenau, 2011.

[5] Hughes S., Tippett D., Thomas W.K. Measuring project success in the construction industry // EMJ – Engineering Management Journal. 2004. 16(3), pp. 31–37.

[6] Cheng M-Y., Tsai H-C., Sudjono E. Evolutionary fuzzy hybrid neural network for construction industry. Automation in Construction 21 (2012), pp. 46-51.

[7] Meshcheryakov V. Identification of earth-moving machines as a dynamic objects based on neural network technology // Problems of development and operation of vehicles, special machinery and technology in Siberia and the Far North. Proceedings 43td International Scientific Conference of the Association of Automotive Engineers. - Omsk: Publishing House of the "LEO", 2004, p. 176.

[8] Krapivin D., Nefedov V., Tokmakov E. Mathematical model for the movement of mechatronischen devices for the intelligent building site, Mechatronik, Lik, Nowotscherkassk, 2010, pp. 50-54.

[9] Georgy M., Chang L., Zhang L. Prediction of engineering performance: a neurofuzzy approach, Journal of Construction Engineering and Management 131 (5) (2005), pp. 548–557

[10] Cheng T., Feng, C., Hsu, M. An integrated modeling mechanism for optimizing the simulation model of construction operation, Automation in Construction. 15 (2006), pp. 327–340.

[11] Bulgakov A., Tokmakov G. ERP-systems, logistics and mechatronics systems for ensuring the smooth construction process // Journal of Applied Engineering Science Volume 16, Issue 1, 2018, pp. 1-4. ISSN: 14514117 DOI: 10.5937/jaes16-14653

[12] Bulgakov A., Tokmakov G., Otto J. and Langosch K. Evaluation of the construction project success with use of neural networks // Proceedings of the Creative Construction Conference (2018), 30 June - 3 July 2018, Ljubljana, Slovenia, pp. 46-50. ISBN 978-615-5270-45-1 DOI: 10.3311/CCC2018-007

[13] Bulgakov A., Emelianov S., Bock T., Tokmakov G. Adaptive control of bulldozer's workflows // Collaboration between ACADEMIA + INDUSTRY: proceedings of the 33rd International Symposium on Automation and Robotics in Construction (ISARC 2016). – Auburn: 2016, pp. 90-97. ISBN: 9781510829923

[14] Bulgakov A., Bock T., Tokmakov G. Adaptive control of bulldozer's workflows // 5th International Construction Specialty Conference, Vancouver, June 7 - 10, 2015, pp. 434-442.

[15] Jehle P., Bulgakov A., Tokmakov G. Mechatronics Systems and Logistic Service for Ensuring the Smooth Construction Process. // Creative Construction Conference 2014 June 21–24, 2014 Prague, Czech Republic. – Budapest, Szent István University, Proceedings CCC 2014, pp. 242-247.

[16] Bulgakov A., Bock T., Tokmakov G. Bulldozer as a mechatronics system with the intelligent control. // Automation, construction and environment: proceedings of the 31st International Symposium on Automation and Robotics in Construction and Mining, 9-11 July 2014, Australia. – Sydney: University of Technology, 2014, pp. 768-777. ISBN 978-0-646-54610-0.

[17] Bulgakov A., Bock T., Tokmakov G. Neural network model of bulldozer workflow. // International scientific conference Construction Technology and Management, 9-11 September 2014. – Bratislava, Slovenska Technika Univerzita, 2014, pp. 45-52.

Multiple Tower Crane Selection methodology utilizing Genetic Algorithm

P.D. Lodaya[a], A.R. Singh[b] and V.S.K. Delhi[c]

[a]Undergraduate Student, Department of Civil Engineering, Indian Institute of Technology Bombay, India
[b]PhD Candidate, Department of Civil Engineering, Indian Institute of Technology Bombay, India
[c]Assistant Professor, Department of Civil Engineering, Indian Institute of Technology Bombay, India
E-mail: 160040014@iitb.ac.in, arsingh@iitb.ac.in, venkatad@iitb.ac.in

Abstract –

Equipment selection for a construction project is a complex decision making task that impacts the project cost significantly. The literature highlights the increasing focus of recent studies on tower crane (TC) optimization, largely due to the shift from horizontal to vertical construction. Many studies tend to select a single TC model to be used throughout the site and assume the number of cranes to be used as a priori knowledge or is calculated using heuristics and schedule demands. Selection of a combination of TC models is relatively unexplored. Existing literature focuses on finding a single most optimum solution to a multimodal problem. Need to look for multiple optimums arises from the uncertainties of an integral but disjoint simulation process and the local and specific nature of un-modelled constraints. Thus to address this gap the study presents a selection approach, aiming to leverage the long reach of TC, formulated as a function of the rental cost and lifting requirements. The selection of the equipment is of prime focus in this research with implicit consideration for the positioning of the TC. A Bi-level optimization problem is formulated involving task allocation to different TC models and minimization of required crane count for each model. Genetic Algorithm (GA) has been employed to work with non-differentiable multimodal function and obtain the preferable TC combinations from the available model variations. The results derived from the proposed model included optimal yet dissimilar TC combination options, task allocation to the utilized TCs and feasible regions for crane placement. The major limitations were parameter setting for the adopted algorithm and the inability of the distance metric to robustly capture phenotypic differences.

Keywords–
Genetic Algorithm; Tower Crane selection; Bi-level optimization; Multimodal optimization.

1 Introduction

Site Layout Planning (SLP) involves optimum space utilization for the resources required to aid construction. The equipment and machinery form an integral part of these required resources. Construction activities involve tasks like shifting of materials, lifting and hoisting along with holding up of loads in place for processing. Cranes being better suited for such tasks have gained the interest of site practitioners. Crane selection is one of the many critical decisions that construction managers have to make. As highlighted by Shawney and Mund [1], time, cost and safety pertaining to construction operations are significantly hinged to the selection of a suitable crane. Deployment of tower cranes typically demands the biggest investment for construction equipment on a site. On an average, major equipments amount to nearly 36% of the total procurement cost [2].

Crane selection consists of two components i.e. type selection and model selection. The former pertains to the selection of the crane type from the range of options available like Tower Cranes, Derricks, Wheel or Crawler mounted Cranes etc. This is highly dependent on the nature of work, geotechnical conditions of a particular construction site and limitations of crane type. Crane model selection is the next step which involves choosing the best combination of cranes of certain type. This choice is governed by a multitude of criteria like rental and operation costs, safety etc. Another challenge faced by construction practitioners is related to positioning of this heavy lifting machinery. This study is an attempt of TC model selection addressing certain limitations of present literature.

2 Crane Selection and Location Optimization Research

Extensive research has been undertaken on the topic of crane type selection in the existing studies. Alkass et al.[3] proposed a methodology utilizing object oriented programming providing solutions to the crane selection

problem using Rule-based and Case-based reasoning with project specific user inputs. Another Fuzzy logic approach to the problem was proposed by Hanna and Lotfallah[4] to incorporate qualitative factors like soil conditions, access road requirements etc. Sawhney and Mund[1] used Artificial Neural Networks in Intellicranes selection tool to tackle the subjectivity involved in decision making regarding the aforementioned factors. These studies laid down the drivers of crane type selection decision using codified expert knowledge. Simulation was relied upon in [3] & [1] for ensuring that the geometric constraints and productivity demands were met at possible crane locations for the suggested solutions. However no guided search algorithm was used in these efforts.

Many TC location optimization models have been developed. Tam et al.[5] used genetic algorithm to minimize the hook travel time by varying the TC and supply point locations around fixed demand points for sites using a single TC. Abdelmegid et al.[6] contributed in improving the travel time minimization model by incorporating the vertical velocity of the hook. Wang et al.[7] further linked this model to BIM and simulation modules to detect schedule conformance and clash detection. However these studies either considered a single TC ([5] and [6]) or assumed a single TC model by largest lift weight and task distances and number of TCs decided by heuristically derived crane efficiency ([7]). Shapira et al.[8] quantified a safety index for any construction site with TC. Safety related to the wind, operator proficiency, shift length, positioning of the cranes with respect to surrounding facilities etc. was captured.

Selection and location of group of TCs has garnered only limited attention. While the primary hard constraint for TC model selection is to ensure the ability of the TC group to lift the prescribed material weights, divergent approaches have been used for location determination. Zhang et al.[9] optimized the safety and efficient operation by minimizing the number and extent of jib clashes and balancing workloads of cranes respectively. A major limitation included pre-determination of number and model of TC to be used. Irizarry and Karan [10] built on this work and displayed the selection of minimum number of TCs when a particular model was specified while claiming that the model being capable of finding the best combination with multiple models at disposal. Minimization of overlapping area of cranes among themselves and with facilities was used to reduce conflicts. Marzouk and Abubakr[11] used maximum site coverage for the same. Y. Ji and Leite[12] minimized the hook travel time and demonstrated the importance of doing so for the crane group as a whole rather than for each TC individually. However all these TC selection and location studies only find a singular most optimal solution to a multimodal problem. The potential value addition in looking for the local optimums is described below.

TC location finalization is subject to it being free from spatial clashes and the arrangement possessing the ability to adhere to the schedule. Simulations have been widely proposed to test for such requirements. As pointed out in [11], the processes of location optimization and simulation in most research efforts have been disjoint, i.e. visualization for clash detection is done in a separate module by using outputs of the optimization module. Thus, the study reported, that a wide range of feasible solutions must be tested in simulation runs to find the near optimum. In case of a discovery of any issue through simulation, the knowledge of a favorable yet dissimilar solution to the one under consideration would add great value. Models integrating the optimization and visualization processes can be a viable option to tackle the issue. However, the gains, as stated by Einbu[13], of greater reusability, concealment of data and operations and higher adaptability that modularization provides to the software manufacturers and the service providers cannot be ignored. Moreover, Sepasgozar and Forsythe[14] highlighted how the studies up till now have focused on project specific factors while the organization based factors have remained largely unattended. The difficulty of factoring the complexity of maintenance and local availability of after sales services demands greater alternatives for decision makers to compare and choose from.

Thus to counter the unforeseen hindrances in simulations and the inability to model an exhaustive list of constraints in an optimization problem a TC selection model capable of giving multiple and varied sub-optimal solutions from a multitude of feasible options can provide flexibility. This study borrows from the framework adopted in [10] of a rental cost based TC selection model while the subsequent location determining objective not focused upon. The model uses Genetic Algorithm (GA) to minimize the rental cost of the group of TCs with an attempt to find local optimums has also been demonstrated. The scope of this study is TC selection and the aim is to supplement the currently proposed TC location methodologies by providing varied alternative solutions.

3 Optimization Model Description

This section contains a detailed description of the underlying logic used in the model. For a crane to successfully perform a task, i.e. shift a weight w from supply point (S) to demand point (D), it must be able to lift the prescribed weight at both the locations. Every crane can be characterized by their jib length (R) and

the maximum lifting capacity (W_m). The lifting capacity of a crane varies along its jib, decreasing towards the tip, and is obtained from the load-radius curve provided by the manufacturer. Thus, for each weight $w \leq W_m$, a circular area of radius „r" (obtained from the curve) exists for a particular crane inside which it can lift that weight. To perform a task, the crane must lie within the intersection area of the buffer zones centered about S and D points. This intersected region is called the feasible task area. No intersection implies the task cannot be performed by the crane. The size of the area is related to the distance between S and D, the weight of the load, and crane capacity. Larger the feasible area, more easily the task can be handled. A tower crane can handle two or more tasks, if it is located within the feasible areas of all those tasks (Fig. 1(a)), which is essentially the intersection of feasible areas of those individual tasks. If no common overlap exists, then a single TC is inadequate to handle all of those tasks (Fig. 1(b)).

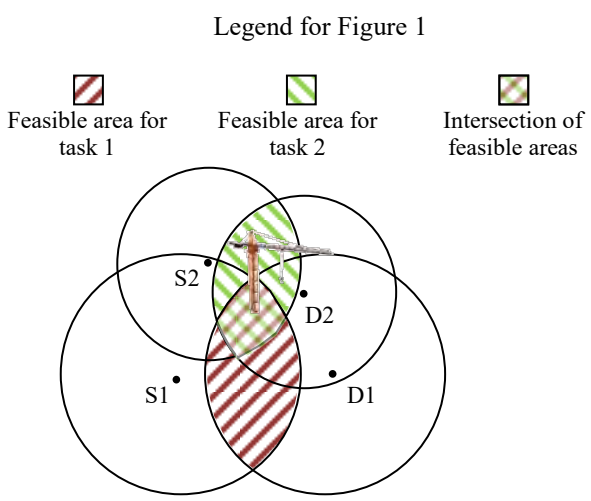

Figure 1(a). Single TC sufficient for two tasks if placed in the common feasible region

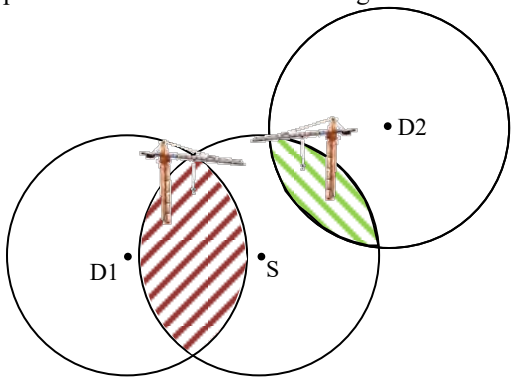

Figure 1(b). At least two TCs required for the tasks, one in each feasible region.

Assumptions of this study:-

1. Geometric Layout of all the S and D points is known along with the module weights for each S-D pair (task).
2. Only one TC is designated to perform any task.
3. For every task, there exists at least one crane in the database which is capable of performing it.

3.1 Bi-Level optimization

Two decisions are involved in finalizing the TC selection for a group of tasks - TC model that will be used to do certain tasks and the number of cranes of that model required to perform the allocated tasks. Thus for every task allocation, a minimization operation is required for each utilized TC model to find the respective number of cranes.

A bi-level optimization problem is a hierarchy of two optimization problems (upper-level or leader, and lower-level or follower). Although different objective is optimized at each level independent of each other, the decisions of each level have effects on one another [15]. The decision of the upper level (TC model allocation to tasks) determines the search space of the lower level (tasks for which minimum TC count is to be determined). The result of the follower contributes in the objective function evaluation of the leader.

3.1.1 Upper Level :- Crane Allocation to Tasks

Ability of a crane to perform amy task i depends on the distance between S and D points ($Dist_i$) and the module weight to be carried (W_i). Subject to them, the potential TC models for each task can be finalized. The constraint has been handled through a combination of two measures - appropriate structuring of population initialization and mutation operators and through exterior static penalty functions as summarized by Smith and Coit[16]. Initially, TC models capable of doing a task are filtered by comparing jib lengths and $Dist_i$ and if they are rendered incapable for that task due to reduced reach owing to load-radius curves, a penalty is added. In addition, the aggregate feasible region after considering all the allocated tasks for a single TC of any model must be greater than a typical threshold value.

Let m be the number of tasks to be undertaken and n be the different TC models available for selection, an identification label is attached to each model. Number of optimization variables is equal to m. The variable x_i assumes the label value of the crane model being used for i^{th} task. Thus, the variables are of categorical type. Ordinal encoding has been preferred over one hot encoding to keep the dimensionality of the problem low, which in turn obviated handling of the constraint- every task must be allocated one and only one crane model.

$$Minimize \quad \sum_{TC=1}^{n} N_{TC}(x) R_{TC} \qquad (1)$$

Subject to constraints

1. $x_i = y,\ y \in \{z \mid 2*(\text{reduced radius})_z \geq \text{Dist}_i\} \forall\ i,$
2. $(\text{aggregate feasible area})_y \geq (\text{Threshold area})_y,$

where denotations are as follows
i = i^{th} task, z = label given to the TC model, R_{TC}= rental cost of the TC model, $N_{TC}(x)$=minimum number of cranes of a model required according to the allocation x, obtained from lower level of optimization. Threshold area is set as the base area of crane.

A widely utilized fitness sharing method for multimodal optimization has been used. It is based on evolution of different species in separated niches of nature. The search space is divided into niches and search for local optimums in them occurs in parallel. Fitness of closely resembling chromosomes is decreased to maintain diversity in population. Thus convergence to single optimum is prevented since the presence of a high number of similar individuals is discouraged. In this study, similarity between two chromosomes has been measured using genotypic distance which is the number of string positions by which they differ. Greater the distance, lesser is the similarity. As outlined by Deb and Goldberg[17], setting the dissimilarity threshold (the minimum distance between two chromosomes above which they don"t affect each others" fitness) must be done carefully. Method proposed by them for calculating the parameter for binary string is as follows

$$\frac{2^l}{q} \leq \sum_{i=0}^{k} {}^{l}_{i}$$

where l stands for the string length, q for the number of optimal/suboptimal solutions and the lowest integer value of k for which the inequality holds gives the parameter value. The parameter is denoted as $_{share}$.

The LHS denotes the average volume of search space occupied by each niche and the RHS denotes the number of possible different strings if at most k bit differences are allowed. Same logic was applied to get the value of dissimilarity threshold although with modification to the expression since the categorical variables of proposed model are not necessarily binary but can take multiple values. The q is an input from the user to be decided arbitrarily when no prior information is known about the problem.

Following is a summary of how the fitness of individuals is altered according to the fitness sharing method as described by Deb[18]. The value of sharing function is defined for a pair of individuals with d as the distance between them.

$$Sh(d) = \begin{cases} 1 - (\frac{d}{\text{share}}), & d < \text{share} \\ 0, & otherwise \end{cases}$$

The summation of sharing function values for an individual paired with every other individual gives the scaling factor (m_i") for that particular individual.

$$m_i" = \sum_{j=1}^{N} \text{Sh}(d_{ij})$$

The fitness value is divided by the scaling factor to get the shared fitness value.

$$f_i' = \frac{f_i}{\text{mi'}}$$

Greater the population density in a certain search space area, greater is the scaling of fitness of those individuals. .

3.1.2 Lower Level :- Minimum Crane Count

Once the crane model has been allocated to each task, determination of the minimum number of cranes of each model required to perform them remains, i.e. finding the values of $N_{TC}(x)$ for evaluating function (1).

Let m_1 number of tasks from the total m be allocated to TC model with label 1. The variable encoding is similar to the upper level with the exception that all the cranes here are exactly identical. Earlier, two variables assuming different label values of TC models implied they had been allocated to different models of TC whereas at this level, two variables assuming different label values implies that they will be performed by two physically different cranes of the same model. Thus a maximum number of cranes of each model must be fixed to limit the search space. Let this number be n_1.

The objective function value is the number of cranes used which is equal to the number of unique label values taken by the variables. The task variables with the same label value are said to be grouped together. Feasibility of these grouped tasks to be performed by a single TC is tested. For every such infeasible task group, a constant penalty equal to n_1 is added. The objective function is minimized and its value, representing the number of cranes is fed into the upper level as N_{TC}.

Derivation of n_1 is empirical. Lower level optimization model is run for each TC model separately assuming all the tasks satisfying the constraint (1) and (2) of upper level are allocated to that TC model. A large n_1 translates to a huge search space for the algorithm which might result in inability to find the least sufficient crane count. Initially, n_1 is kept large and its value updated after every algorithm run, changed to the output of the previous run until there"s no difference in the value of n_1 and result. Hence n1 is the minimum number of cranes of model 1 required if it gets assigned all the tasks it can perform.

The presented case in this research targets selection of TC from a pool of options available to the construction practitioner to choose from. This underlying assumption of availability of multiple options of TC represents the market scenario and thus providing a single solution will make the decision making task stringent. Also, the fitness function is highly sensitive to the underlying decision variable values. Due to traditional optimization algorithms‟ reliance on derivative or slope information and their ability to reach a single optimum solution only, they are not suitable for this problem. Therefore a nature inspired algorithm capable of providing a set of optimal solutions is adopted in this study. Moreover , the ability of GAs to move from highly fit lower order schemata to higher order ones [19] is of particular interest as it translates to grouping of geometrically closer tasks in the phenotypic space. Fig.2 explains the flow process of the adopted algorithm. At every fitness evaluation step, lower optimization function is called for each TC model used.

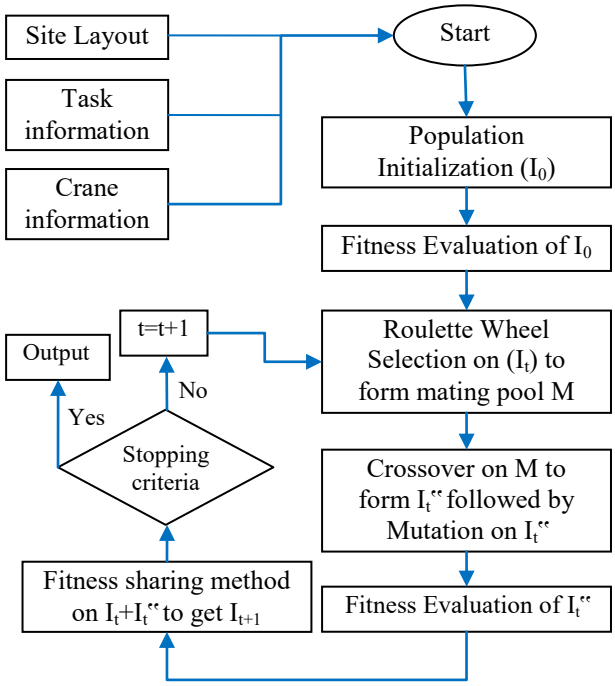

Figure 2. Flow process of the GA fitness sharing model

4 Case Study

A hypothetical site layout was used to test the proposed selection model. The boundaries of both temporary and permanent facilities in the layout are considered to be enclosing the areas not allowed for TC placement. These boundaries also include the minimum clearance from entities required for placing a TC. The inputs to the model include geometric information of temporary site facilities and the details for coordinates and module weights for each task, as highlighted in Table 2. Load charts and rents of available TC models are uploaded. As mentioned in Table 3, four models of varying jib lengths and lifting capacity were used. Table 1 summarizes the input parameters used for the upper level problem.

Table 1. Algorithm parameters

Parameter	Value
Population Size	100
Maximum Generation	150
Number of Variables	17
Crossover Rate	0.8
Mutation Rate	0.06
q (Number of peaks)	3
$_{\text{share}}$	12

Setting of GA parameters for the lower level problem like population size and n_1 as discussed before is empirical and requires fine tuning with multiple runs to ensure correct answers and also to keep run time in check.

The final population of chromosomes produced by the algorithm contained different optimal solutions with varying task allocation to different crane models and hence varying combination of crane requirements. The results display a combination of TCs of dissimilar jib lengths and lifting capacity can result in lower rental costs as against the common practice of a common TC model usage across the site. Table 4 gives the total rental cost for the solutions and the number of tasks performed by each utilized crane. The feasible areas for TC combinations for the obtained solutions along with the temporary and permanent facilities of the site have

Table 2. Task information:-S&D coordinates, lift weight

ID	Supply (in m)		Demand (in m)		W_i (t)
	Abscissa	Ordinate	Abscissa	Ordinate	
1	46.25	116.25	41.25	141.71	2.25
2	46.25	116.25	25	100	2
3	15	30	25.25	60.71	2.25
17	91.84	90.62	25.25	127.71	1

Table 3. Tower Crane Model information

Label	1	2	3	4
Rent ($\times 10^3$/day)	15	20	27	35
Jib Length	25m	40m	50m	60m
Max. lift capacity(t)	3.5	8	9	12

Legend for Figure 3

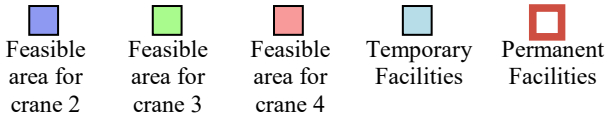

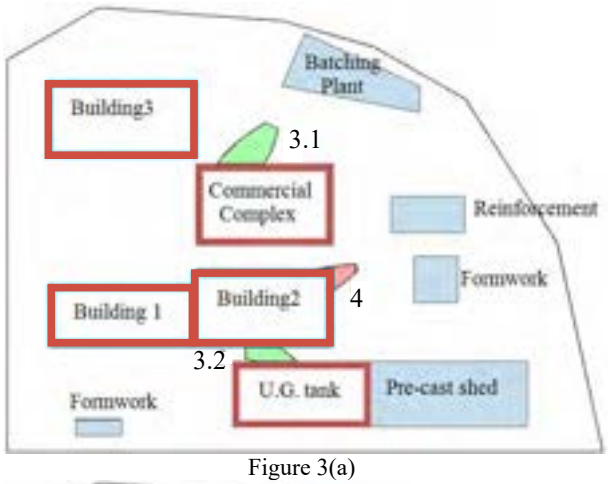

Figure 3(a)

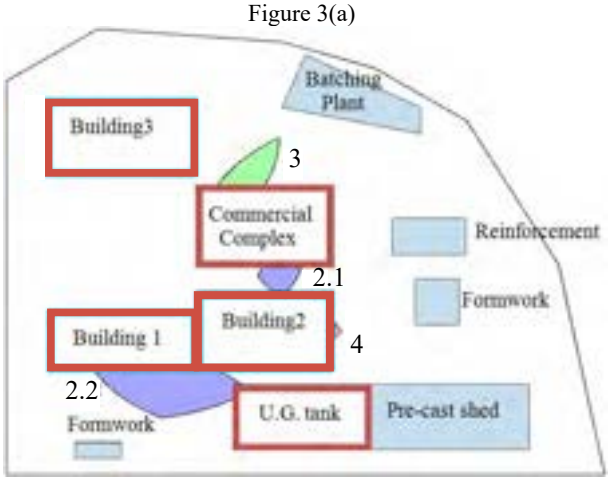

Figure 3(b)

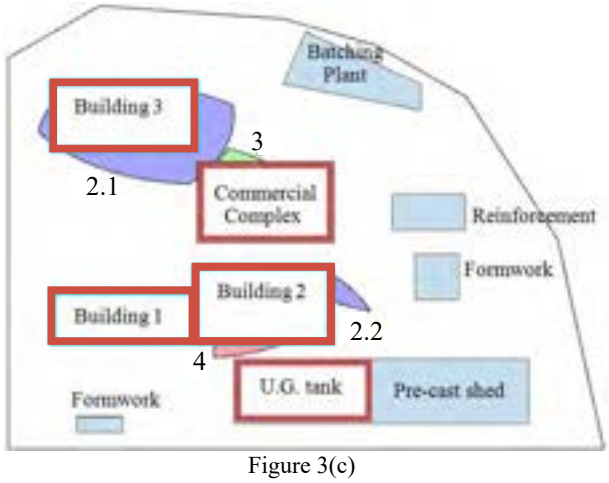

Figure 3(c)

been shown in Figure 3. Legend indicates what the shaded regions represent. One TC model of the indicated type is required to be placed in each of the shaded feasible region. The neighboring number to the shaded region points to the corresponding entry in Table 4 to get the number of tasks it handles. For example two TCs of model 3 are required in solution of Figure 3(a) with the crane placed in the region corresponding to 3.1 performs four tasks.

Table 4. Total rental cost and number of tasks performed by each crane

Solution	Rental cost per day	TC model 2		TC model 3		TC model 4
		2.1	2.2	3.1	3.2	
Fig. 3(a)	89000	-		4	5	8
Fig. 3(b)	102000	3	3	3		8
Fig. 3(c)	102000	3	5	3		6

The algorithm was successful in maintaining sub-optimal solutions through the generations. Also, the feasible regions produced by them showcase a certain degree of variety in terms of the potential TC locations. Such provision can endow the decision makers with flexibility while making decisions about TC model selection and location. Difficult to encode constraints like soil conditions or to account for intangibles like TC maintenance, availability of options can prove helpful. Moreover, the flexibility of multiple solutions can provide options if clashes are detected in simulations. It must be noted that for a certain ownership cost, more than one Task Distributions can be possible. The ones shown above have been chosen from the solution set based on more equitable task distribution among TCs.

5 Limitations and Future Scope

K-means clustering was used to separate the final population into 3 clusters, equal to the set value of q. Relatively low silhouette values suggest weak clustering in the population. The genotypic distance between the optimal solutions from different clusters was lesser than the value of $_{share}$ used which points towards a revision to a lower value. A smaller $_{share}$ implies sustenance of more number of solutions which demands higher population levels leading to impractical processing times. Moreover, the existence of individuals in a niche with fitness values lower than the local optimum indicates a highly rugged landscape which leads to survival of less fit but different individuals even within

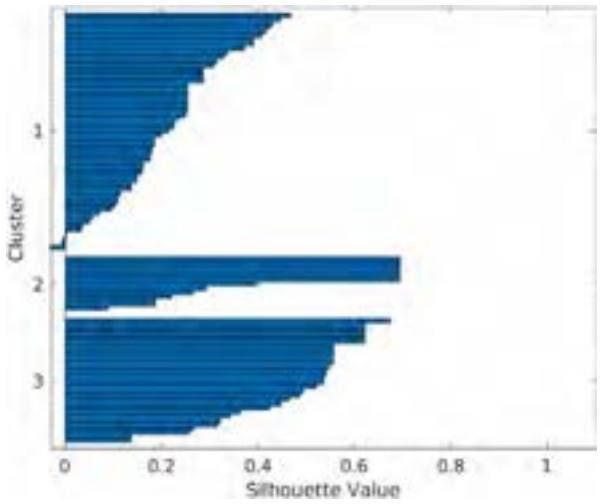

Figure 4. Silhouette plot for k-means clustering

a niche.

The root cause of this limitation of the study lies in the distance metric. As outlined in [17], phenotypic distance can perform better than genotypic distance in certain problems. The problem with this approach is the limited translation of genotypic distance to the physical space. Consider two instances of task distribution for 5 tasks using the scheme described above

X= [4 4 4 3 3]
Y= [4 4 4 2 2]
Z= [4 4 4 1 1]

The genotypic distance between X&Y and X&Z is equal to 2. But if a single TC of model 2 and 3 is sufficient in X and Y, it is plausible two TCs of model 1 are required in Z. Thus a measure to capture phenotypic information i.e. the feasible area for each task, for distance calculations between two individuals can result in better results. The presented approach in this study is part of an ongoing project and the developed code to select TC is yet to be validated on a real construction project. The code will be made available in public interest but only after validation. Till then any request in this regard can be made directly to the authors.

6 Conclusion

Fitness sharing method for Genetic Algorithms was used for multimodal optimization problem of TC selection. The proposed methodology in the study was particularly aimed at finding cost effective combinations of TC from the available models without restricting to finalization of a single model based on aggregate site demands or heuristics. The results produced alternative solutions for TC selections, which provided varied feasible solutions for the user to choose for location optimization and subsequent simulations. The process of planning site utilization involves intertwined tasks. This calls for addressing interdependencies between these tasks. Therefore as part of an ongoing project, the presented approach is sought to be integrated with site layout planning problem where positioning of temporary facilities would be dealt. These positions would be taken up as input for the demonstrated approach in this study and is expected to result in a much robust solution.

References

[1] A. Sawhney and A. Mund, “Adaptive probabilistic neural network-based crane type selection system,” *J. Constr. Eng. Manag.*, vol. 128(3), pp. 265–273, 2002.

[2] K. T. Yeo and J. H. Ning, “Managing uncertainty in major equipment procurement in engineering projects,” *Eur. J. Oper. Res.*, vol. 171(1), pp. 123–134, 2006.

[3] S. Alkass, M. Al-Hussein, and O. Moselhi, “Computerized Crane Selection For Construction Projects,” in Proceedings of the *13th Annual ARCOM Conference*, pp. 427–436, Cambridge, U.K., 1997.

[4] A. S. Hanna and W. B. Lotfallah, “A Fuzzy logic approach to selection of cranes,” *Autom. Constr.*, vol. 8(5), pp. 597–608, 2004.

[5] B. C. M. Tam, T. K. L. Tong, and W. K. W. Chan, “Genetic Algorithm for optimizing supply locations around Tower Crane,” vol. 127(4), pp. 315–321, 2002.

[6] M. A. Abdelmegid, K. M. Shawki, and H. Abdel-Khalek, “GA optimization model for solving tower crane location problem in construction site s,” *Alexandria Eng. J.*, vol. 54(3), pp. 519–526, 2015.

[7] J. Wang *et al.*, “A BIM-based approach for automated tower crane layout planning,” *Autom. Constr.*, vol. 59, pp. 168–178, 2015.

[8] A. Shapira, M. Simcha, and M. Goldenberg, “Integrative model for quantitative evaluation of safety on construction sites with tower cranes,” *J. Constr. Eng. Manag.*, vol. 138(11), pp. 1281–1293, 2012.

[9] P. Zhang, F. C. Harris, P. O. Olomolaiye, and G. D. Holt, “Location Optimization for a Group of Tower Cranes,” *J. Constr. Eng. Manag.*, vol. 125(2), pp. 115–122, 1999.

[10] J. Irizarry and E. P. Karan, “Optimizing location of tower cranes on construction sites through GIS and BIM integration,” *Electron. J. Inf. Technol. Constr.*, vol. 17, pp. 351–366, 2012.

[11] M. Marzouk and A. Abubakr, “Decision support

for tower crane selection with building information models and genetic algorithms," *Autom. Constr.*, vol. 61, pp. 1–15, 2016.

[12] Y. Ji and F. Leite, "Optimized Planning Approach for Multiple Tower Cranes and Material Supply Points Using Mixed-Integer Programming," *J. Constr. Eng. Manag.*, vol. 146(3), pp. 1–11, 2020.

[13] J. Einbu, *A program architecture for improved maintainability in software engineering*, Longman Higher Education, London, England, 1989.

[14] S. M. Sepasgozar and P. Forsythe, "Lifting and Handling Equipment: From Selection To Adoption Process," in *Proceedings of the 40th Australasian Universities Building Education Association (AUBEA) 2016 Conference*, pp. 829–838, Queensland, Australia, 2016.

[15] J. Lu, C. Shi, and G. Zhang, "On bilevel multi-follower decision making: General framework and solutions," *Inf. Sci. (Ny).*, vol. 176(11), pp. 1607–1627, 2006.

[16] A. E. Smith and D. W. Coit, "Constraint-Handling Techniques - Penalty Functions," in *Handbook of Evolutionary Computation*, Oxford University Press and Institute of Physics Publishing, Bristol,U.K., 1996.

[17] K. Deb and D. E. Goldberg, "An investigation of niche and species formation in genetic function optimization," in *Proceedings of the third International Conference on Genetic algorithms*, pp. 42–50, Fairfax, USA, 1989.

[18] K. Deb, *Multi-objective optimization using evolutionary algorithms*. John Wiley & Sons, New Jersey, USA, 2001.

[19] D. E. Goldberg, *Genetic Algorithms in Search, Optimization, and Machine Learning,* Addison-Wesley Longman Publishing Co., Boston, USA, 1989.

Fuzzy Controller Algorithm for Automated HVAC Control

M. Chae[a], K. Kang [b], D. Koo [b], and S. Oh [c], Jae Youl Chun [d]

[a]Construction Management, Central Connecticut State Univ., USA
[b]Department of Engineering Technology, Indiana University Purdue University Indianapolis, USA
[c]Mechanical & Biomedical Engineering, Boise State University, Boise, ID, USA
[d]Department of Architectural Engineering, Dankook University, South Korea
E-mails: chae@ccsu.edu, kyukang@iu.edu, dankoo@iupui.edu, sukjoonoh@boisestate.edu, jaeyoul@dankook.ac.kr

Abstract –

This research presents the design framework of the artificial intelligent algorithm for an automated building management system. The AI system uses wireless sensor data or IoT (Internet of Things) and user's feedback together. The wireless sensors collect data such as temperature (indoor and outdoor), humidity, light, user occupancy of the facility, and Volatile Organic Compounds (VOC) which is known as the source of the Sick Building Syndrome (SBS) or New Building Syndrome because VOC are often found in new buildings or old buildings with new interior improvement and they can be controlled and reduced by appropriate ventilation efforts. The collected data using wireless sensors are post-processed to be used in the neural network, which is trained in accordance with the collected data pattern. When the users of the facility have the control of the building's ventilation system and the AI system is fully trained using the user input, it will mimic the user's pattern and control the building system automatically just as the user wants. In this research, data were collected from 4 different buildings: university library, university cafeteria, a local coffee shop, and a residential house. Fuzzy logic controller is also developed for better performance of the HVAC. Indoor air quality, temperature (indoor and outdoor), HVAC fan speed and heater power are used for fuzzified output. As a result, the framework and simulation model for the energy efficient AI controller has been developed using fuzzy logic controller and the neural network-based energy usage prediction model.

Keywords – IOT; AI; Neural Network; Fuzzy Controller; Smart Building

1 Introduction

The energy efficiency has become an urgent issue for sustainability of our society under global warming and it is closely related to infrastructure design such as buildings and the usage patterns of residents. Energy efficient buildings have evolved over decades, and intelligent control systems have been adopted for efficient operations of the buildings. Next generation buildings will be smart buildings equipped with various sensors and autonomous control systems that interact with the users.

This research paper suggests an innovative and systematic approach in smart building management system for energy saving and sustainable development of society. Smart building means automated control of building systems such as lighting, heating and cooling, ventilation, security, etc. to provide the users productive and comfortable environment. Lighting, power meters, pumps, heating, and fire alarms are all connected and monitored as part of the building management system.

The authors of this paper have been working on developing wireless sensor network (WSN) to monitor indoor air quality and energy profiles, and this current paper aims at testing the WSN at real community facilities and developing a method for objectively evaluating the energy consumption patterns of the participating community organizations. This research suggests the preliminary investigation and study of feedback from the community participants regarding the deployment of the wireless sensor network and the integration of the feedback into the design of smart building management system. The smart buildings system will automatically control building functions such as lighting, heating, cooling, ventilation, security, etc. to provide occupants with more productivity and comfort.

2 Smart Building Technologies for Public Facility

2.1 Smart Facilities and the Community

In this project, the wireless sensors collected data from the buildings that are used in the community. Installed sensors are temperature, humidity, light, Volatile Organic Compounds (VOC) level, and movement sensors. The collected sensory data along with the user input will be fed to the Artificial Intelligent (AI) system, which learns the usage patterns and produces

similar outputs just like users control the air-conditioning and heating units. In addition to copying the usage pattern, the researchers will look for the way to improve energy efficiency by optimized control of building management system.

Artificial intelligent system using neural network and fuzzy logic algorithms is used to analyze the IoT data and controls the smart building systems. Volatile Organic Compounds (VOC) which is known as the source of the Sick Building Syndrome (SBC) is also monitored. The control of VOC can be done by controlling HVAC system. The authors have developed the pilot model of automated HVAC system as the proof-of-concept for the smart building system.

The authors of this research have been developing collaborative relations with several community partners for energy efficiency improvement in their public facilities. The testing facilities are (1) New Britain Police Station, (2) New Britain Public Library, (3) Hospital of Central Connecticut, and (4) YWCA at New Britain. The four different community partners have very unique characteristics in size, number of users, and the form of ownership as follows:

(1) New Britain Police Station. The HVAC system is 20 years old and the system is very energy inefficient.
(2) Public Library is management by the New Britain Foundation that is non-government, non-profit organization.
(3) The Hospital of Central Connecticut (New Britain General) is very large facility with the daily float population is 80,000~100,000. Residents like doctors and nurses stay most of time in the building while visitors like patients and helpers are float population. User pattern analysis and customer feedback will be very beneficial to the development of adaptive smart building.
(4) YWCA building in New Britain, CT has been renovated and expanded. The adaptive smart building system will be tested and compared on existing building and new expansion.

2.2 Energy Peak Demand Control

The authors of this papers have been with the local energy company in the state of Connecticut and New England area. The energy company can provide energy consumption of the buildings in real time monitoring the peak usage as well as low usage time. The peak power use is critical because more than maximum peak power usage may cause catastrophic power outage. The smart building helps alleviate the peak use and reduce the risk of the power loss. The researchers of this paper have designed artificial intelligent system for smart building management, and the community partners' energy usage data to be collected in this research will verify the effectiveness of the developed system.

3 Methods

Smart building systems are beneficial for both the owner and the users working within. These benefits range from energy savings to productivity gains to sustainability. They reduce energy consumption, increase the productivity of the users, improve building operations, support sustainability efforts and enhance decision-making across the organization for efficient use of optimal start/stop of HVAC system.

3.1 Artificial Intelligence in Building Management

Artificial Intelligent (AI), first introduced in the Dartmouth Conference in 1961, is a flexible rational system that perceives its input data and produces outputs that maximizes the goal. For example, if the energy cost saving while maintaining the user's comfort level is the goal, AI would provide the optimum heating/cooling operation scenarios.

3.2 Sensors and IoT

Smart sensors collect environmental information that can be processed to manage the facilities better for effective heating, cooling and electricity saving. Temperature, motion, vibration, light, and indoor air quality sensors such as VOC sensor are installed. They monitor occupancy and floating population to recognize the usage patterns, which are analyzed by artificial neural networks.

3.3 Interpretation of Sensor Data using Neural Network

The sensor data are collected, preprocessed and fed to the neural network to determine the usage patterns of the facility, which are recognized to produce the optimized operations of the smart buildings. Elevators, HVAC, lightings, security systems, and electrical usage of the buildings can be analyzed and optimized for the most energy efficient operation.

3.4 Fuzzy Logic Systems and Fuzzy Controller

User's inputs are verbal values or although it is in numerical scale, they are not exact number but they can be considered as fuzzy numbers or fuzzy membership functions which can have error tolerance. Fuzzy membership and membership functions is a simple and easy to use tool to convert verbal expressions in numerical values. For example, if user answers "very satisfied", "satisfied", "moderate", and "not satisfied" in the customer experience in new automated heating and cooling system, user's response can be converted into certain numerical representation in order to be used in

computer system.

4 The Development of Neuro-Fuzzy Controller for Smart Building

4.1 IOT Data Collection and Post Processing

The indoor sensors utilized in this research are (1) Temperature, (2) Humidity, and (3) Volatile Organic Compounds (VOC) that is considered as the main cause of the bad indoor air quality. Any materials that have chemical compounds such as new paints and new carpets can result in high VOC readings. VOC is also known as a cause of the Sick Building Syndrome (SBS). VOC can be monitored by IoT sensors and can be controlled automatically in the smart building systems.

In this research, data were collected in the Elihu Burritt Library and Devil's Den (Student Cafeteria) at Central Connecticut State University (CCSU). In addition to the indoor temperature and VOC, outside temperature and the number of people using the facility were monitored. The number of people in the facility was indirectly estimated by the wireless motion sensors. Persons sit still and not moving will not be detected. However, simple motion sensors provide an effective indirect way of measuring how the facility is used. The result of collected data are shown in the figures below.

The wireless sensors were tested and successfully utilized. The collected data are analyzed using neural network which is the machine learning algorithm for artificial intelligence systems. In order to complete the machine learning training and develop the robust smart HVAC system, the automated HVAC controller needs to be developed.

The researchers have tested the wireless sensors on the community facilities and the result is processed and fed to the feedforward neural network. The authors of the paper used simulated HVAC control data to develop the energy usage pattern analysis. The controlling system of HVAC is designed using fuzzy controller system.

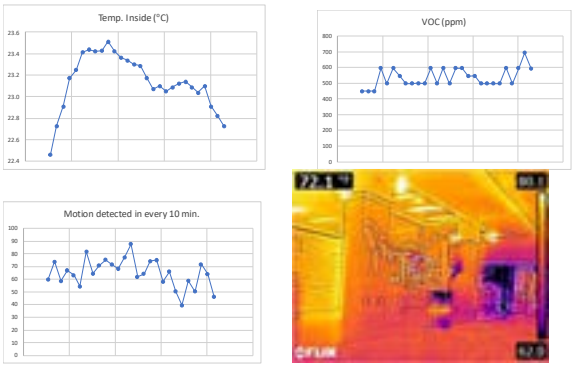

Figure 1. Wireless sensor data and infrared images at the library

The neural network model for the energy usage pattern utilizes the variables such as: Outdoor-Temperature, Number-of-occupancy, Time, Date, and Day. The variables such as Time, Date, and Day have been converted into 2-digit codes for the neural network pattern training purpose. The neural network for energy usage pattern recognition and energy usage prediction model has been developed and it is continuously being compared with the real energy consumption data. The more data are collected the better prediction model can be developed.

4.2 Fuzzy Controller

There are some research findings that compares traditional Proportional-Integral-Differential (PID) controller and fuzzy logic controller for heating and cooling system (Gouda et al. 2000, Attia et al. 2015). PID controller is considered reasonable and efficient alternative to the manual or simple on/off controllers of HVAC systems. However, recent studies showed that fuzzy logic controllers perform better than PID controllers when the users satisfaction level is considered. PID controller uses simple mathematical formulas of integration and differentiation of temperature changes over time, while fuzzy logic controller converts users' linguistic expressions into mathematical functions, and calculates the fuzzy if-then rules using fuzzy inferences.

Conventional PID controller can be shown as following equation,

$$u(t) = K_P e(t) + K_P K_I \int_{t=0}^{t} e(t)\,dt + K_P K_D \frac{de(t)}{dt} + u(0) \quad \text{eq. 1}$$

where K_P is the controller gain representing a proportionally constant between error and controller output, K_I is the reset constant relating the rate to the error in units of [%/(%-sec)], K_D is the rate constant in units of [(%-sec)/%], and u(0) is the controller output at t = 0 (Tsoukalas 1997).

Once the fuzzy variables are defined, the fuzzy logic controller is simply shown as,

$$u(k) - u(k\text{-}1) = \Delta u^*(k) \quad \text{eq.2}$$

where $u(k)$ and $u(k\text{-}1)$ are temperature readings at time k and $k\text{-}1$ and Δu is the extent of change of the control variable u at time $t = k$ that is change in action and the defuzzified output is $\Delta u^*(k)$.

In this research, authors developed the fuzzy membership functions and inference rules to control the heater and indoor air quality. Defined fuzzy membership functions are: (1) Current Temperature and Humidity (indoor and outdoor) and forecast temperature and humidity; (2) Time, Day, Date, and holiday information; (3) Number of people; and (4) VOC (Volatile Organic

Compounds). The simulation model shown in this research, only the temperatures and VOC are fuzzified. The fuzzy controller was developed only the heating and indoor air quality control. The fuzzy membership functions are defined such as VH for very high and L for low, etc.

The outputs of the fuzzy controller are: HVAC fan speed and heater power. So, the fuzzy membership functions for HVAC fan speed are *VH, H, and OFF*, and fuzzy membership functions for heating power are *VH, H, and OFF*. The fuzzy controller inputs variables are crisp values such as: Temperature reading, temperature setting, and temperature differences (*D_Temp*) between temperature setting and temperature reading. Indoor air quality read by VOC sensor is also used as input variable. Figure 2 shows input, output variables and if-then rules.

The fuzzy controller for heating/cooling system has been created. Variables are the differences between the target VOC and current VOC level. If fuzzy variable *D_VOC* (differences of VOC level) can be defined as *Very_High, High, and Zero*. According to the fuzzy values of *D_VOC,* the HVAC control can be *High, Low, and Off*. In the same way, fuzzy variable *D_Temp* can be driven from the Temperature and Target-Temperature. The fuzzy controller delivers accurate control of the heating/cooling system for optimum temperature and VOC levels.

Fifteen sample fuzzy if-then rules were developed. Rules are very simple. If the temperature difference is high, turn the heater high, if the indoor air quality is low turn the fan high, and so on. Fuzzy if-then rules are defined as followings:

- R_1: If *D_Temp* is *VL* and *VOC* is *H* then *HEAT* is *VH* and *FAN* is *VH* *ELSE*
- R_2: If *D_Temp L* and *VOC* is *VH* then *HEAT* is *H* and *FAN* is *VH* *ELSE*
- …..

By using the Mamdani-min for fuzzy implication, defuzzification results are shown as Figure 2. As an example, when *D-Temp* is 5^{O}F and VOC is 600ppm, the controller settings will be 2.65 for heater and 3.65 for fan speed.

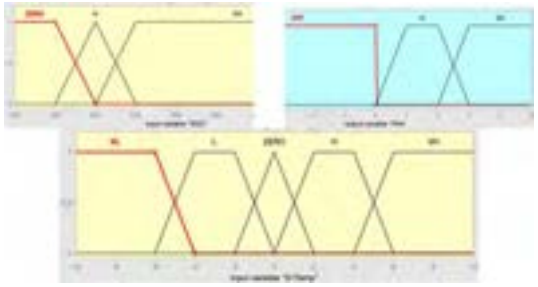

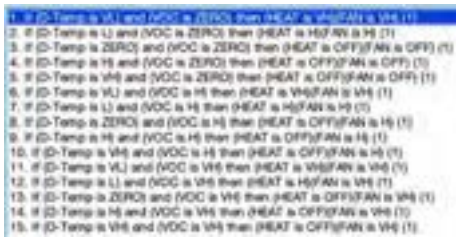

Figure 2. Input/Output Variables and Fuzzy If-then Rules

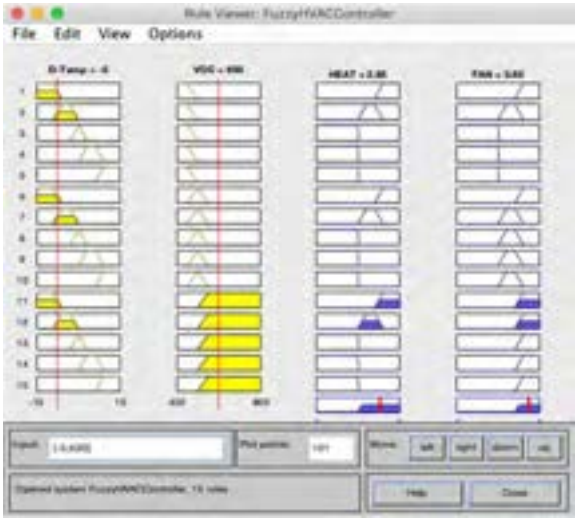

Figure 3. Fuzzy implication and defuzzification result for HVAC controller

5 Conclusions

The main advantage of the developed neural network prediction system and fuzzy logic controller is that it will deliver precise control of the heating/cooling system as well as energy consumption prediction models for different temperature and VOC target levels. The predictive system operates the HVAC pre-emptively saving energy cost and more efficient use of the heating/cooling system. Fuzzy logic controller makes precise control of HVAC improving comfort of the users.

In this research, fuzzy logic controller algorithm is developed only for the heater and indoor air quality control. Neural network prediction model was developed for HVAC usage prediction but the energy saving results and analysis are still under development.

ACKNOWLEDGEMENT

This research was partially supported by the Connecticut State University AAUP University Research Grant.

References

[1] Attia, A., Rezeka, S. F., and Saleh, A. M (2015) "Fuzzy logic control of air-conditioning system in residential buildings", Alexandria Engineering Journal, Vol. 54, Issue 3, pp 395-403 https://doi.org/10.1016/j.aej.2015.03.023

[2] Chae, M., and Abraham, D. M. (2001) "Neuro-Fuzzy Approaches for Sanitary Sewer Pipeline Condition Assessment," Journal of Computing in Civil Engineering, Vol. 15, No. 1, ASCE, pp. 4–14

[3] Chae, M., Yoo, H., Kim, J., and Cho, M. (2012) "Development of Wireless Sensor Network System for Suspension Bridge Health Monitoring," Journal of Automation in Construction, Jan. 2012, Vol. 21, pp. 237-252

[4] Gouda, M.M., Danaher, S. and Underwood, C.P. (2000) "Fuzzy Logic Control Versus Conventional PID Control for Controlling Indoor Temperature of a Building Space", IFAC Proceedings Volumes 33, Issue 24, pp 249-254

[5] Schiavon, S. Hoyt, T., and Piccioli, A. (2014) "Web application for thermal comfort visualization and calculation according to ASHRAE Standard 55 Building Simulation", Volume 7, Issue 4, 321-334. http://dx.doi.org/10.1007/s12273-013-0162-3

[6] Sheridan, T. B., and Verplank, W. L. (1978) Human and computer control of undersea Teleoperators. Cambridge, Mass: Massachusetts Institute of Technology, Man-Machine Systems Laboratory

[7] Tsoukalas, L. H., and Uhrig, R. E. (1997) Fuzzy and neural approaches in engineering, Wiley, New York.

[8] Wong, J., Li, H., Lai, J. (2008) "Evaluating the system intelligence of the intelligent building systems Part 1: Development of key intelligent indicators and conceptual analytical framework", Automation in Construction, Vol. 17, Issue 3, March 2008, pp 284-302.

[9] Zadeh, L.A. (1965) "Fuzzy Sets" Journal of Information and Control, Elsevier, Vol 8, No. 3., pp 338-353

A Probabilistic Motion Control Approach for Teleoperated Construction Machinery

Hyung Joo Lee[a] and Sigrid Brell-Cokcan[a]

[a]Chair of Individualized Production (IP), RWTH Aachen University, Schinkelstr. 1 52062 Aachen Germany
E-mail: lee@ip.rwth-aacehen.de, brell-cokcan@ip.rwth-aacehen.de

Abstract –

Automation of construction machinery has the potential to improve efficiency and safety during the construction process. However, most construction machinery is directly teleoperated limiting the control to a single paradigm. Moreover, the abundance of non-linearities due to the design of pumps, valves and the interaction of different actuators complicates planning precise movements. Complicated motion planning optimization can be applied to program the movement in the desired manner which often requires a model representing the system dynamics. Whereas this approach is promising, modeling the system dynamics is a formidable task. In this work, we present a framework that uses a probabilistic approach to learn movements from expert demonstrations. In this way, efficient movements can be learned without explicitly estimating system dynamics. Here, efficiency is defined by the experiences of the human operator which makes the programming able to benefit from existing knowledge of operators. The performance of the proposed scheme is evaluated with a real demolition machine BROKK 170.

Keywords –

On-site robotics; construction robotics; robot motion programming; automation in construction

1 Introduction

Currently, remote-controlled hydraulically driven construction machinery is of great importance and mainly used on construction sites. However, local accuracy is often limited in remote-controlled systems due to the interface (for example 2D camera feedback). Moreover, it is challenging for the operator to generate optimized motions with a remote controller since the operator can only see the appropriateness of the motion only when it is already executed. As a result, manual work is still mostly preferred on construction sites. Sequentially, automating construction machinery has already drawn much attentions over the last years [1–5]. The common goal in automating construction machinery is to generate accurate motions in an automated way under various conditions (outdoor conditions, dirty and dynamic environments) to fulfill given tasks.

In particular, the automation of machinery can be regarded as controlling the end-effector in the desired manner. In automated machines, a precise movement is a key part, however, there are several difficulties in automating hydraulic construction machinery arising from the abundance of non-linearities due to the design of pumps, valves and fluid flow [6]. A common approach is the design of dynamics-based control, which typically uses a model for the system to be controlled to predict system states and develop a controller minimizing the discrepancy between the predicted and measured system states. Although this model-based control shows promising results in many researches [7, 8], modeling system dynamics can be often challenging due to its nonlinear characteristics. Moreover, force sensors required for force control are not standard components of construction machinery, since the system is designed to be directly controlled by human operators [9]. Hutter et al. [10] achieved joint torque control based on feedback from pressure sensors integrated into servo valve. However, it is common that pressure sensors are not installed in each valves but only in the main valve due to economic reasons [11].

On the other hand, with the advent of research advances in robotics, robotic systems with a large number of degrees of freedom were developed [12, 13]. Subsequently, Programming by Demonstration (PbD) has drawn the attention of many researchers [14–15], since it allows to program a robot just by showing the desired manner of performing tasks. In contrast to traditional motion planning methodologies, this approach offers an intuitive and less time consuming alternative for non-experts to teach a robot skill [16-18]. Popular approaches for encoding the demonstrations in a way that can be used for motion planning include Dynamic Movement Primitives (DMPs) and Gaussian Mixture Regression (GMR).

Our work concentrates on mitigating the aforementioned issues in automating construction machinery by utilizing the recent methodology from robotics. More precisely, we aim at replacing the time-consuming model-based motion programming of hydraulic construction machinery by an automatic programming process: Programming by Demonstration. In this paper, we present a framework that learns a direct

joint motion mapping from expert demonstrations. This learned mapping so-called policy allows to reproduce joint space motions under different environmental conditions while non-linearities in the hydraulic system are handled by utilizing experiences of the human expert in operating the system.

2 Previous work and challenges

In our previous work [19], we presented a teleoperated demolition machine BROKK 170 that has been retrofitted with controllers, so that one can also program its motion with high-level commands. Although the experiments from our previous work showed the feasibility that proven construction machinery can be adapted and accept advances from robotic to extend its capability, we identified that a Cartesian controller solely based on encoders is not sufficient to enable accurate arm control. As depicted in Figure 1, the machine was not able to follow the given trajectory without any error. The main error source is the unstable system pressure. The hydraulic machine BROKK 170 used in our work consists of one main pump supplying volumetric flow for the whole system. This flow is used in each control valves to move actuators and returned into the tank. During this circulation, flow losses are raised by partially closed or opened valves, bent pipes, expansions or contractions. A generic joint position level controller such as an Inverse Kinematics (IK) solver rapidly reaches its limits, since it typically takes the desired (x, y, z) values as input and outputs the corresponding joint configuration without considering the non-linearities in a hydraulic system.

We aim at overcoming the aforementioned issue by demonstrating basic movements to the machine. Using prior experience and trainings, expert human operators can create more controlled motion with the hydraulic system than IK-based motion controller. By capturing the operator's behavior to overcome the non-linearities of the system, we aim at improving the accuracy in planning of the motion.

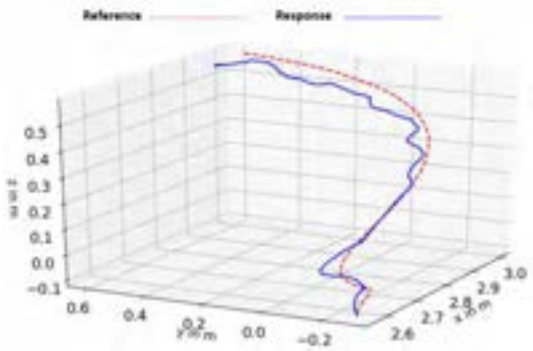

Figure 1. Tracking result using an IK solver based framework

3 Manipulator Control

The manipulator control can be formulated as finding proper joint space configurations $\boldsymbol{q} \in \mathbb{R}^N$ given an operational space description $\boldsymbol{x} \in \mathbb{R}^M$,where N is the number of degree-of-freedoms (DoF) of the machine and M is the operation dimension. As depicted in Figure 2, the operational space $\boldsymbol{x}$ and joint configuration $\boldsymbol{q}$ of the demolition machine can be described as:

$$\boldsymbol{x} = [x \quad y \quad z \quad \theta]^T \in \mathbb{R}^4 \tag{1}$$

$$\boldsymbol{q} = [q_1 \quad q_2 \quad q_3 \quad q_4 \quad q_5]^T \in \mathbb{R}^5 \tag{2}$$

The mapping problem can be formulated as:

$$\dot{\boldsymbol{x}} = \boldsymbol{J}(\boldsymbol{q})\dot{\boldsymbol{q}} \tag{3}$$

where $\boldsymbol{J} \in \mathbb{R}^{M \times N}$is the Jacobian matrix. To obtain the $\dot{\boldsymbol{q}}$ out of the relation in (10), we use the closed loop inverse kinematic (CLIK) approach introduced in [20]. However, as described in the previous section 2, this analytical method does not consider non-linearities in a hydraulic system causing a discrepancy between the estimated and real motion. To address this problem, we employ a probabilistic approach based on Gaussian Process Regression (GPR) first to learn policies from expert demonstrations and program the manipulator by reproducing the learned policies under different environmental conditions.

3.1 Closed-loop inverse kinematic controller

For manipulators with N > M, the inverted Jacobian matrix can be obtained as follow:

$$\boldsymbol{J}^+ = \boldsymbol{J}^T(\boldsymbol{J}\boldsymbol{J}^T)^{-1} \tag{4}$$

The pseudo-inverse has the property to provide the best possible solution according to the equation $\boldsymbol{J}\dot{\boldsymbol{q}} = \dot{\boldsymbol{x}}$. If $\dot{\boldsymbol{x}}$ is not in the range of $\boldsymbol{J}$, an exact value of $\dot{\boldsymbol{q}}$ is not available. However, the provided $\dot{\boldsymbol{q}}$ still minimizes the magnitude difference of $\boldsymbol{J}\dot{\boldsymbol{q}} = \dot{\boldsymbol{x}}$ [21]. By using this property and closed-loop behavior in CLIK, the convergence to the desired $\dot{\boldsymbol{x}}$ can be ensured. The equation from (3) can be formulated as follows:

$$\dot{\boldsymbol{q}} = \boldsymbol{J}^+(\dot{\boldsymbol{x}} + \boldsymbol{K}\boldsymbol{e}) \tag{5}$$

where $\boldsymbol{K} \in \mathbb{R}^{M \times M}$ is a positive definite gain matrix and $\boldsymbol{e} \in \mathbb{R}^{M \times 1}$ is the remained difference between the desired and actual motion. The CLIK controller is further extended with damped-least squares for achieving robustness in the vicinity of singularities [21] and with weighted least norms for joint limits [22].

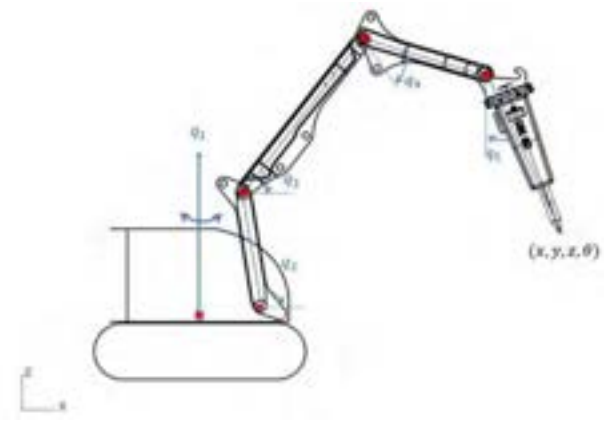

Figure 2. Joint geometric representation of the 5 degree of freedom BROKK 170. The joint space coordinates are noted in blue, whereas the operational space coordinates are in black. The joint positions are noted in red.

3.2 Gaussian Process Models

GPR is a non-parametric method for regression that models a joint distribution of the observed data without directly modeling a regression function[23]. By assuming the existence of m demonstration, each demonstration can be described as $D = \{\xi_i, y_i\}_{i=1}^{n}$. Here, ξ denotes the environmental information, such as the temporal value, y refers to the observations such as the trajectories in the joint space that ξ should be mapped to and n denotes the length of the demonstration.

In GPR, the distribution of observations can be modeled as follows:

$$\begin{bmatrix} y \\ y^* \end{bmatrix} \sim \mathcal{N}\left(0, \begin{bmatrix} K(X,X) & K(X,X^*) \\ K(X^*,X) & K(X^*,X^*) \end{bmatrix}\right) \quad (6)$$

where K is the kernel matrix defined as follows:

$$\begin{aligned} K(X,X) &\in \mathbb{R}^{M\times M}, & K_{i,j} &= k(\xi_i,\xi_j) \\ K(X^*,X) &\in \mathbb{R}^{1\times M}, & K_{1,j} &= k(\xi^*,\xi_j) \\ K(X,X^*) &\in \mathbb{R}^{M\times 1}, & K_{i,1} &= k(\xi_i,\xi^*) \\ K(X^*,X^*) &\in \mathbb{R}, & K &= k(\xi^*,\xi^*) \end{aligned} \quad (7)$$

A key parameter in GPR is the kernel function denoted as $k(\cdot,\cdot)$ in (2). It encodes the structure of functions in the space of distributions. In this work, the squared exponential kernel function is employed:

$$k(x_1,x_2) = \sigma_f^2 \, exp\left(-\frac{1}{2l^2}(x_1-x_2)^T(x_1-x_2)\right) \quad (8)$$

The goal of GPR is to predict the joint motion y^* conditioned on the new environmental information $\boldsymbol{\xi}^*$ and the observed information from the demonstrations. It is assumed that noises σ_n from process and measurement are identically distributed within demonstrations. In this case, the joint distribution of y^* can be described as:

$$y^*|y, D \sim \mathcal{N}\,(\mu^*, \Sigma^*) \quad (9)$$

where

$$\mu^* = K(X^*,X)(K(X,X) + \sigma_n^2 I)^{-1} y \quad (10)$$

$$\Sigma^* = K(X^*,X^*) + \sigma_n^2 I - K(X^*,X)(K(X,X) + \sigma_n^2 I)^{-1} K(X,X^*) \quad (11)$$

The performance of GPR depends on so-called hyper parameters [σ_n, σ_n, l] which can be defined by maximizing the marginal log likelihood [23]. We use GPflow to model GPR and also to estimate the parameters [24].

Using these equations, the proposed controller generates joint trajectories based on expert human demonstrations which indicate the operator maneuvers we would like to apply to the manipulator.

3.3 Programming by Demonstration Framework

During demonstrations of different lengths, the sensor information is collected and stored as training input-output pairs. The mapping from the input to the output is called a policy and is modeled from equations (6) - (11), so that the model can predict a new output based under different input conditions based on the learned policy. In our work, multiple demonstrations of different lengths are used to model the policy. Accordingly, the time alignments of the demonstrated trajectories are normalized using Dynamic Time Warping (DTW) method [25].

Suppose we have m demonstrations with BROKK 170, then the demonstrations are normalized to the length T. The data set D for the GP will be of length $n = mT$. Thus, the data set can be formulated as $D = \{\xi_i, y_i \} \mid i = 0, \ldots, mT$.

In our training phase, policies are created with respect to the initial joint states q and the temporal value. In our experiments, we use simple timestamp t as the temporal value. More precisely, joint angle values are collected and stored during an expert demonstration, where the expert controls each joint to move the end-effector tip straight forward. Policies are created with respect to these collected values so that new trajectories in the joint space can be generated for the new initial joint angle values and the timestamps.

In the reproduction phase, a new initial starting point is defined with joint angle values. Together with the timestamps, the initial joint angle values are used as input for the trained Gaussian process models.

In the evaluation phase, the predicted trajectories are directly tracked with a fixed maximum joint speed. The

resulting end-effector trajectory is obtained by computing the forward kinematics relationship and compared with the end-effector trajectory generated by the CLIK solver.

4 Experiment

We demonstrate our framework on a hydraulic demolition machine BROKK 170. Originally, the BROKK 170 demolition machine is designed to be controlled with a remote controller in a strict master-slave relationship limiting the control to a single paradigm. To control the machine with computation algorithms and integrate computational capabilities in the machine control, we follow the approach introduced in [19].

Our host PC interacts with the main control unit (MCU) of the machine through a bus controller MCP2515 and an embedded controller Mega2560. The communication takes place via the Controller Area Network (CAN) bus system. The bus protocol containing information about bus messages is obtained from the manufacturer. The script is developed in C++ on the host PC and then compiled and deployed to the embedded controller via Arduino IDE.

In this work, the kinematics of the machine and the shape of each axes are assumed to be known, so that the joint angles are enough to describe the full configuration of the machine, in particular the end-effector pose. Like most other construction machines, BROKK 170 used in this work is not equipped with any sensors. We use wire-type encoders (BCG05, SICK) to measure the joint angle values q_2, q_3, q_4, q_5 and a rotary encoder (A3M60, SICK) to measure q_1. The joint angle values are separately measured and sent to the host PC via Wi-Fi-Modules ESP8266 at a rate of 20 Hz. UDP packets are used for data exchange between the Arduino IDE and the proposed controller developed in Python.

The experiment consists on moving the manipulator straight forward from the initial point which requires structured joints movement. Moreover, the non-linearities of the hydraulic system complicate the task, so that trajectories generated by a conventional IK solver result in poor quality, as depicted in Figure 4. Throughout the experiments, the base q_1 is not used, since the trajectories for the given task lie within the xz-plane. The second axis q_2 is also not utilized in our experiment, since it cannot be simultaneously moved with other axes in the current setup.

Figure 3. The task considered in this work: By moving the joints q_3, q_4 and q_5 with joysticks the operator tries to end-effector tip straight forward.

For the given task, the environment conditions are the initial joint positions and the timestamp, $\boldsymbol{\xi} = \{(q_{3\_o}, q_{4\_o}, q_{5\_o}, t_i) | i = 0, \dots, T\}$. The joint trajectories are used as observations, $y = \{(q_{3\_i}, q_{4\_i}, q_{5\_i}) | i = 0, \dots, T\}$. Three demonstrations are performed under various initial positions, as shown in Figure 4. Since the execution time for demonstrations slightly differs The demonstrations are of different lengths. We order these demonstrations according to their length:

$$D_{m-1} < D_m < D_{m+1} \tag{7}$$

Using the median length sequence $\overline{D} = D_{[2]}$ as a reference demonstration, the rest of the demonstrations are aligned in the time domain using DTW. The result of the DTW is illustrated in Figure 5. The thick trajectories represent the reference trajectories estimated as described above. It can be clearly seen that the temporal variations in the demonstrations are synchronized after the DTW process.

We perform trajectory planning with a new initial joint values $[q_{3\_o}, q_{4\_o}, q_{5\_o}] = [-0.547, 1.107, 1.016]$. The reproduction of the expert's demonstrations with respect to the new condition is visualized in Figure 6. It is worth noting that the step size for each joint trajectory is empirically estimated. The resulting end-effector trajectory is visualized in Figure 5. Since the effect from the non-linearities in the hydraulic system increases with the joint angle speed, we evaluate the developed system with two different joint angle speed: $\dot{q}_{max} = 0.11\ rad/s$ and $\dot{q}_{max} = 0.07\ rad/s$.

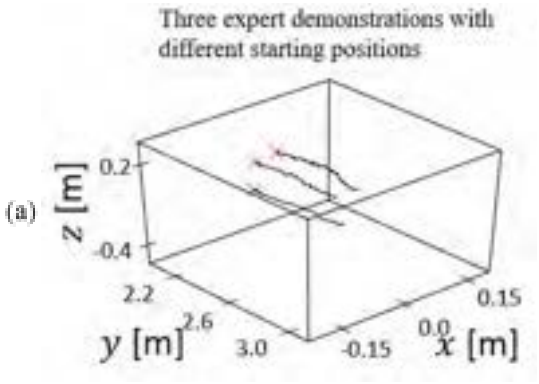

.

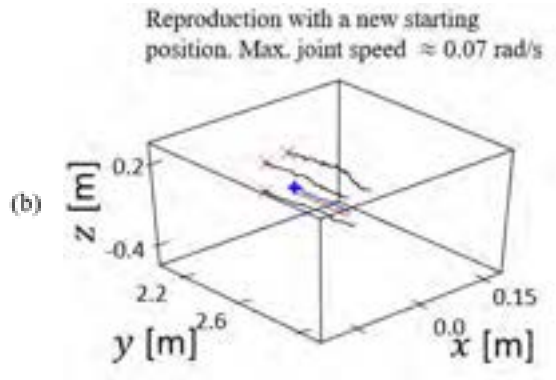

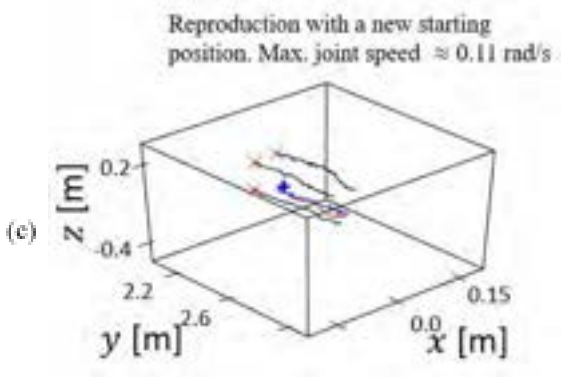

Figure 4. Three demonstrations for the given task in 3D Cartesian space (a). During the demonstrations different initial joints angles are considered. The resulting end-effector tip positions are visualized with 'x' signs. The demonstrations are reproduced for the new initial joints angles (blue '+' signs). The corresponding end-effector tip trajectories are visualized in (b) and (c) by computing the forward kinematic relationship (blue). The red trajectories are generated using the CLIK solver.

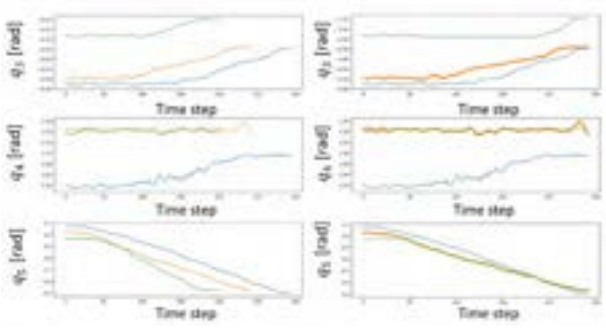

Figure 5. Results of collected trajectories in the joint space before (left) and after (right) the DTW process. The thick lines in the right plots represent the reference trajectories.

To quantify the correctness, first, the end-effector position is computed using the forward kinematic solution with the reproduced joint trajectories. Then, the desired end-effector trajectory (i.e. from the given initial position straight forward) is uniformly resampled with the total number of data points on the computed end-effector trajectory. Finally, the RMS error between the computed and planned end-effector trajectories in the operational space is computed.

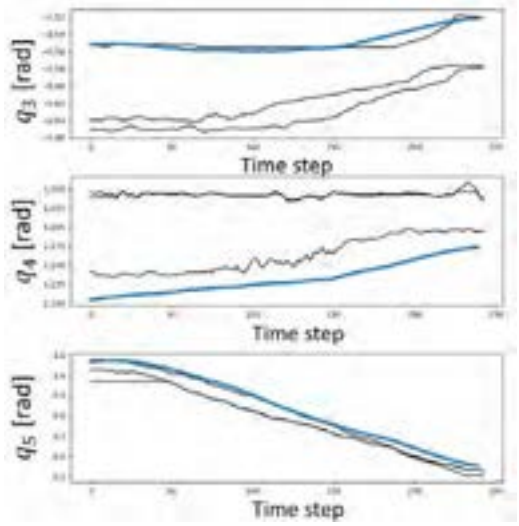

Figure 6. The black trajectories show the collected values from the demonstrations. The blue trajectories show the reproduction attempt by considering the new condition $[q_{3\_o},\ q_{4\_o},\ q_{5\_o}] = [-0.547,\ 1.107,\ 1.016]$. It can be clearly seen that the joint 5 q_5 is mainly used in the demonstration and this policy is preserved in the reproduced trajectories.

The same task is executed using the CLIK solver and the results are compared with the tracking results from the developed GPR based system. For the given task, the RMS errors of the CLIK solver are 0.027 m at the maximum joint angle speed of 0.07 rad/s and 0.039 m at

the maximum speed of 0.11 rad/s, respectively. Whereas the reproduced trajectories result in 0.016 m and 0.025 m, respectively.

Table 1. RMS error comparison in tracking task

	Max. Speed	RMSE
CLIK	0.07 rad/s	0.027 m
GPR	0.07 rad/s	0.016 m
CLIK	0.11 rad/s	0.039 m
GPR	0.11 rad/s	0.025 m

The end-effector tip trajectories generated by both the CLIK solver and the proposed system are visualized in Figure 7. We see that the trajectory from the CLIK solver deviates from the desired trajectory, whereas the deviation is smaller by the trajectory that is generated from expert demonstrations.

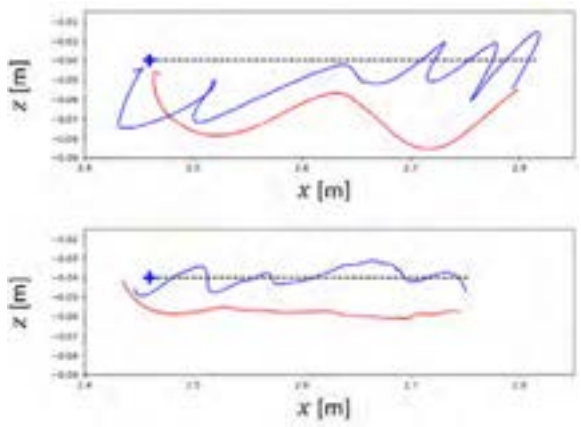

Figure 7. Results with both the reproduction from expert demonstration (blue) and from the CLIK solver (red). The desired trajectory is visualized with dashed line.

5 Discussion

In the experiments, the dimension of environmental conditions was set to four. Because of the low dimensionality, the policy of controlling a nonlinear hydraulic system could be modeled and reused to generate an appropriate end-effector trajectory using a relatively small number of expert demonstrations.

The proposed approach presents advantages by directly providing reference trajectories in the joint space. Compared to the inverse kinematic approach which typically generates joint motion without considering the non-linearities in a hydraulic system. As a result, the discrepancy in Figure 7 occurred which is increased according to the increased joint angle speed. During the demonstrations the expert corrects the joint motions according to the effect generated by the non-linearities in the hydraulic system. More precisely, the expert takes into account that he cannot perfectly move multiple axes at the same time and adapt the axes motion according to the resulting non-linear motion. By reproducing trajectories in the joint space considering this policy we slightly improve the tracking result. The captured policy that the joint 5 q_5 should be mainly utilized for the given task is valid for the faster joint angle speed, thus improving the tracking result as shown in Table 1.

However, as the GPR models the joint distribution of the observed data, the learned policy is only valid in the range of given demonstrations. Although the expert can demonstrate to cover the great area of workspace to reduce the uncertainty in the prediction caused by unforeseen environmental conditions. An efficient approach which can apply the existing demonstrations for the unforeseen conditions should be studied.

6 Conclusion

This study presented a framework for generating trajectories based on expert demonstrations. This work showed an alternative to programming a teleoperated construction machinery without a dynamical model. The experiment showed the preliminary performance of the proposed scheme. The expert demonstrations were normalized in the time domain using DTW and the mapping between the environmental conditions and the joint trajectories was modeled using GPR. By learning the mapping between the exact joint trajectories and the initial joint positions, the policy from a human expert could be learned so that a specific joint can be mainly utilized to perform the given task. The proposed scheme was implemented in a teleoperated deconstruction machinery, and the performance of the developed system was tested through preliminary experiments showing improved results compared to the inverse kinematic approach. Experimental results indicate the feasibility of construction machinery automation using generalizing the human demonstrations.

Future work will consider the use of Reinforcement Learning to equip the machine with self-improvement abilities. As shown in Figure 4, it was even for an experienced operator a challenging task to move the tip of the end-effector straight forward, since the operator can only see the appropriateness of its joystick manipulation after the machine has moved. We also aim at extending our framework to dynamic environmental conditions, since in this work only static conditions such as the initial joint angle values are considered.

Acknowledgements

This work is partially supported by the BROKK DA GmbH.

7 References

[1] D. Jud, G. Hottiger, P. Leemann, and M. Hutter, "Planning and Control for Autonomous Excavation," *IEEE Robot. Autom. Lett.*, vol. 2, no. 4, pp. 2151–2158, 2017.

[2] S. J. Keating, J. C. Leland, L. Cai, and N. Oxman, "Toward site-specific and self-sufficient robotic fabrication on architectural scales," *Sci. Robot.*, vol. 2, no. 5, eaam8986, 2017.

[3] A. Montazeri and J. Ekotuyo, "Development of dynamic model of a 7DOF hydraulically actuated tele-operated robot for decommissioning applications," in *2016 (ACC)*, Boston, MA, USA, pp. 1209–1214.

[4] S. Tafazoli, S. E. Salcudean, K. Hashtrudi-Zaad, and P. D. Lawrence, "Impedance control of a teleoperated excavator," *IEEE Trans. Contr. Syst. Technol.*, vol. 10, no. 3, pp. 355–367, 2002.

[5] D. Schmidt, M. Proetzsch, and K. Berns, "Simulation and control of an autonomous bucket excavator for landscaping tasks," in *2010 IEEE ICRA,* Anchorage, AK, pp. 5108–5113.

[6] S.-U. Lee and P. H. Chang, "Control of a heavy-duty robotic excavator using time delay control with switching action with integral sliding surface," in *Proceedings 200 IEEE ICRA*, Seoul, South Korea, pp. 3955–3960.

[7] M. M. Bech, T. O. Andersen, H. C. Pedersen, and L. Schmidt, "Experimental evaluation of control strategies for hydraulic servo robot," in *2013 IEEE International Conference on Mechatronics and Automation*, Kagawa, Japan, pp. 342–347.

[8] A. Bonchis, P. I. Corke, and D. C. Rye, "Experimental evaluation of position control methods for hydraulic systems," *IEEE Trans. Contr. Syst. Technol.*, vol. 10, no. 6, pp. 876–882, 2002.

[9] J. Mattila, J. Koivumaki, D. G. Caldwell, and C. Semini, "A Survey on Control of Hydraulic Robotic Manipulators With Projection to Future Trends," *IEEE/ASME Trans. Mechatron.*, vol. 22, no. 2, pp. 669–680, 2017.

[10] M. Hutter *et al.,* "Towards optimal force distribution for walking excavators," in *2015 (ICAR)*, Istanbul, Turkey,pp. 295–301.

[11] BROKK AB, "Brokk Troubleshooting Guide | Repair Maintain Troubleshoot Guide Brokk Demoltion Equipment,"

[12] M. Keppler, D. Lakatos, C. Ott, and A. Albu-Schaffer, "A passivity-based approach for trajectory tracking and link-side damping of compliantly actuated robots," in *2016 (ICRA)*, Stockholm, Sweden, pp. 1079–1086.

[13] B. Bauml *et al.,* "Catching flying balls and preparing coffee: Humanoid Rollin'Justin performs dynamic and sensitive tasks," in *2011 IEEE ICRA*, Shanghai, China, pp. 3443–3444.

[14] P. Abbeel, A. Coates, and A. Y. Ng, "Autonomous Helicopter Aerobatics through Apprenticeship Learning," *IJRR*, vol. 29, no. 13, pp. 1608–1639, 2010.

[15] T. Osa, J. Pajarinen, G. Neumann, J. A. Bagnell, P. Abbeel, and J. Peters, "An Algorithmic Perspective on Imitation Learning," *FNT in Robotics*, vol. 7, 1-2, pp. 1–179, 2018.

[16] T. Osa, N. Sugita, and M. Mitsuishi, "Online Trajectory Planning in Dynamic Environments for Surgical Task Automation," in *RSS X*, Jul. 2014.

[17] S. Schaal, "Is imitation learning the route to humanoid robots?," *Trends in Cognitive Sciences*, vol. 3, no. 6, pp. 233–242, 1999.

[18] A. J. Ijspeert, J. Nakanishi, H. Hoffmann, P. Pastor, and S. Schaal, "Dynamical movement primitives: learning attractor models for motor behaviors," *Neural computation*, vol. 25, no. 2, pp. 328–373, 2013.

[19] H.J. Lee, S. Brell-Cokcan, K. Schmitz," A General Approach for Automating Teleoperated Construction Machines", *in 2019 Advances in Service and Industrial Robotics*, vol.980, pp.210-219.

[20] B. Dariush, M. Gienger, B. Jian, C. Goerick, and K. Fujimura, "Whole body humanoid control from human motion descriptors," in *2008 IEEE ICRA*, Pasadena, CA, USA, pp. 2677–2684.

[21] Y. Nakamura and H. Hanafusa, "Inverse Kinematic Solutions With Singularity Robustness for Robot Manipulator Control," *Journal of Dynamic Systems, Measurement, and Control*, vol. 108, no. 3, pp. 163–171, 1986.

[22] T. F. Chan and R. V. Dubey, "A weighted least-norm solution based scheme for avoiding joint limits for redundant joint manipulators," *IEEE Trans. Robot. Automat.*, vol. 11, no. 2, pp. 286–292, 1995.

[23] C. M. Bishop, *Pattern recognition and machine learning,* 8th ed. New York, NY: Springer, 2009.

[24] M. van der Wilk, V. Dutordoir, S. T. John, A. Artemev, V. Adam, and J. Hensman, "A Framework for Interdomain and Multioutput Gaussian Processes," Mar. 2020. [Online]. Available: http://arxiv.org/pdf/2003.01115v1

[25] H. Sakoe and S. Chiba, "Dynamic programming algorithm optimization for spoken word recognition," *IEEE Trans. Acoust., Speech, Signal Process.*, vol. 26, no. 1, pp. 43–49, 1978.

[26] J. Lee, N. Mansard, and J. Park, "Intermediate Desired Value Approach for Task Transition of Robots in Kinematic Control," *IEEE Trans. Robot.*, vol. 28, no. 6, pp. 1260–1277, 2012.

Excavation Path Generation for Autonomous Excavator Considering Bulking Factor of Soil

Shinya Katsuma[a], Ryosuke Yajima[a], Shunsuke Hamasaki[a], Pang-Jo Chun[a], Keiji Nagatani[a] Genki Yamauchi[b], Takeshi Hashimoto[b], Atsushi Yamashita[a] and Hajime Asama[a]

[a]The University of Tokyo, Japan
[b]Public Works Research Institute, Japan

E-mail: katsuma@robot.t.u-tokyo.ac.jp, yajima@i-con.t.u-tokyo.ac.jp, hamasaki@i-con.t.u-tokyo.ac.jp
chun@i-con.t.u-tokyo.ac.jp, keiji@i-con.u-tokyo.ac.jp, yamauchi-g573bs@pwri.go.jp
t-hashimoto@pwri.go.jp yamashita@robot.t.u-tokyo.ac.jp, asama@robot.t.u-tokyo.ac.jp

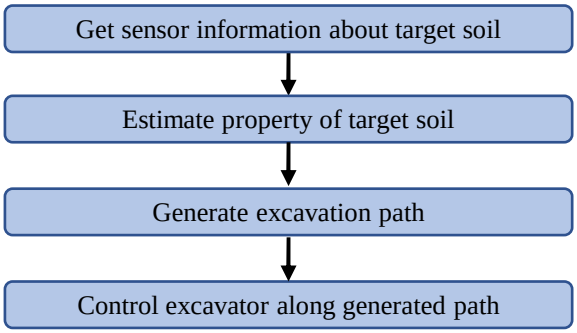

Figure 1. Overall process of autonomous excavation

does not consider the interaction between the excavator tools and the soil. Therefore, it is unclear whether this method will even work in an actual excavation process.

Yamamoto et al. developed a prototype of an autonomous hydraulic excavator using 3-D information of the construction model and successfully demonstrated the autonomous operation of hydraulic excavators[2]. However, while this method does not require any orders from human operators during the excavation process, the users must manually specify the excavation path in advance according to the target soil ' s properties. Therefore, the efficiency of the excavation process might degrade in a situation where the soil properties are unknown.

To address the above-mentioned problems, this study aims to establish an excavation path generation method that guarantees high efficiency based on the soil type. For this purpose, the excavator must automatically generate an excavation path itself according to the property of the target soil. Therefore, we focus on the bulking factor of soil, which is a soil property frequently used in construction sites, as an indicator of soil type. By considering the bulking factor of the target soil, we realize an efficient excavation for different soil types.

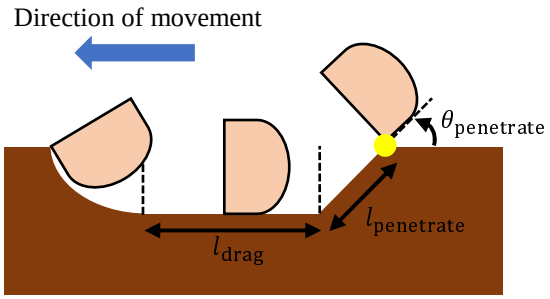

Figure 3. Modeled excavation path

we find a set of appropriate parameters $[\theta_{\text{boom}}, \theta_{\text{arm}}, \theta_{\text{bucket}}]$ for the entire excavation process.

2.3 Excavation Model

In this study, the excavation process is modeled using three parameters: $[\theta_{\text{penetrate}}, l_{\text{penetrate}}, and l_{\text{drag}}]$. In this modeling, we refer to the excavation motion performed by experienced operators as a reference. In general, the excavation motion can be classified into three phases: penetrate, drag, and scoop [5]. In the penetration phase, the operators pierce the surface of the target soil using the bucket edge and move the bucket until it reaches the bottom line. Then, the bucket is dragged horizontally along the bottom line. Finally, to collect the accumulated soil into the bucket, the scooping motion is executed. To model this excavation motion, the three above-mentioned parameters have been used; the excavation path represented by them is illustrated in Fig. 3. Here, $\theta_{\text{penetrate}}$ indicates the angle between the soil surface and the penetrating line, $l_{\text{penetrate}}$ indicates the length of the penetrating line, and l_{drag} indicates the length of the dragging line. In the scooping phase, only the bucket part is rotated by 90°, with the tip of the arm part fixed in position. Once these parameters are determined, the position of the bucket tip and the rotation of the bucket over the whole excavation process can be determined. By using this position and rotation of the bucket, the parameters $[\theta_{\text{boom}}, \theta_{\text{arm}}, and \theta_{\text{bucket}}]$, explained in section 2.2, can be calculated using inverse kinematics.

2.4 Bulking Factor of Soil

As discussed in Section 2.3, three parameters have been used to specify the excavation model. The values of these parameters need to be defined. In this respect, the soil property is accounted for so that the generated path can guarantee its efficiency for different soil types. For this purpose, this study considers the bulking factor of soil, which is a soil property based on the phenomenon observed in the excavation process [6]. In general, the exca-

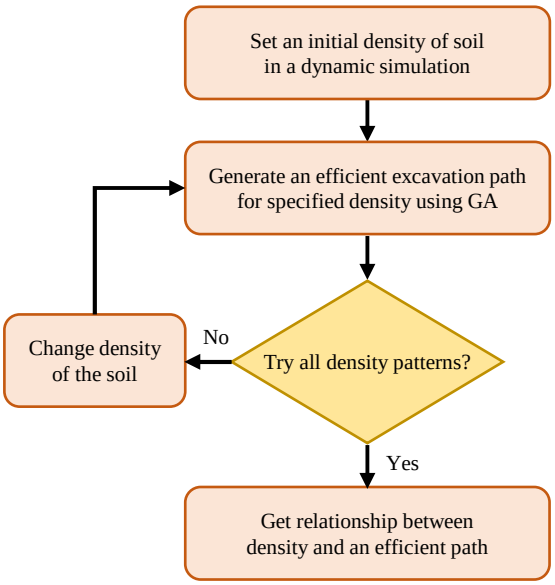

Figure 4. Excavation path generation process

vated soil particles do not fit together as they did before excavation, which increases the void space among these particles. Thus, the soil volume increases after excavation, and the bulking factor of soil is used to quantify this volume increase. Qualitatively, soil with a large bulking factor means the soil is hard. Conversely, soil with a small bulking factor means the soil is soft. Assuming k to be a bulking factor of soil, it can be defined as follows:

$$k = \frac{V_{\text{after}}}{V_{\text{before}}}, \tag{1}$$

where V_{after} and V_{before} denote the volumes after and before excavation, respectively. In related works, there are other properties of soil such as soil density used in [7]. However, this study focuses on the bulking factor of soil because of its simplicity of measurement. Compared to the other properties of soil, the bulking factor can be easily calculated, by simply measuring the volumes before and after excavation with an RGB-D sensor.

2.5 Path Generation with Dynamic Simulator

In this section, the excavation path generation method using a dynamic simulator has been explained. As discussed in Section 2.4, the proposed method generates an efficient excavation path based on the soil properties, to guarantee efficient excavation for any soil type. To enable this, the proposed method learns the relation between the soil property and an efficient excavation path using a dynamic simulator before executing the actual excavation. The use of a dynamic simulator allows us to replicate the interaction between the excavator and soil during the excavation process. In addition, the properties of the target soil can be changed by specifying the simulator parameters.

The process of excavation path generation using a dynamic simulator is shown in Fig. 4. To understand the relation between soil property and an efficient excavation path, efficient excavation paths for different soil properties were determined in advance. Specifically, an efficient excavation path is generated while changing the initial density of soil in the simulation. In terms of the method for finding an efficient excavation path for each condition, a genetic algorithm (GA) is used, where the excavation model parameters $[\theta_{\text{penetrate}}, l_{\text{penetrate}}, and l_{\text{drag}}]$ are regarded as the genes of each individual. Based on this setting, the fitness of each individual is defined as follows:

$$f = \frac{V_d}{E}, \tag{2}$$

where f denotes the fitness of each individual, V_d denotes the volume of soil accumulated in the bucket during one excavation motion, and E denotes the total energy consumed by the excavator joints during the excavation motion. According to this formalization, an efficient excavation path is ideally assigned high fitness. Thus, an efficient excavation path can be obtained as the final output of GA. This operation is repeated until an efficient excavation path for all density patterns is obtained. Furthermore, the relation between the density and efficient excavation path is obtained, which will be used for path selection during the actual excavation process.

2.6 Path Selection via Bulking Factor

In this section, the path selection method based on the bulking factor has been explained. As discussed in Section 2.5, the proposed method has already analyzed the relation between the soil density and an efficient excavation path through a dynamic simulator. These findings are used in the process of path selection. However, it is not easy to measure the density of the target soil directly. Therefore, the bulking factor of soil is used to estimate the soil density because measuring the bulking factor is not difficult. In terms of the density estimation method, empirical knowledge is used. According to the model described in [8], higher the soil density, larger is the bulking factor. In this way, the soil density is estimated via the bulking factor calculated using the measurement data. After we obtain information about the density of the target soil, we select an efficient excavation path using the knowledge gained via the dynamic simulator.

Table 1. Conditions of the genetic algorithm

Parameters	Value
Number of generations	10
Number of individuals	15
Probability of crossover	0.8

Table 3. Three conditions of soil

Conditions	Density [%]
Soft soil	20
Medium soil	50
Hard soil	80

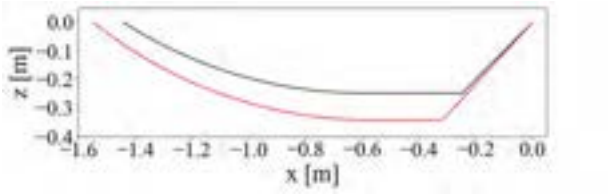

(a) Soft soil

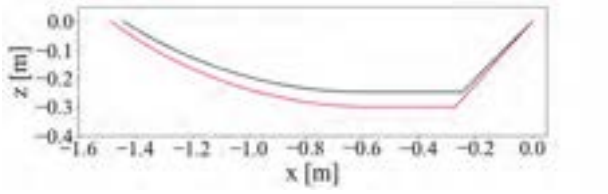

(b) Medium soil

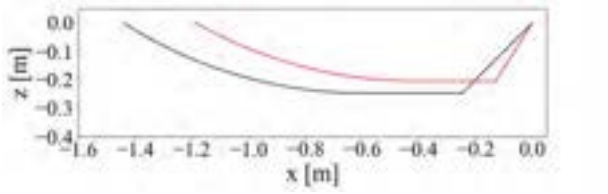

(c) Hard soil

Figure 5. Calculation results for each condition

$[\theta_{\text{penetrate}}, l_{\text{penetrate}}, and l_{\text{drag}}]$ were set to $[\pi/6, 0.35, 0.35]$, respectively.

3.2 Experimental Result

Figure 5 shows the calculation results for each condition. In Fig. 5, (a) shows the result for soft soil, (b) shows the result for medium soil and (c) shows the result for hard soil. In each graph, the red line shows the trajectory of bucket tip in case of using the proposed method, while the black line shows the trajectory of bucket tip in case of not using the proposed method. Here, the origin [x, z] = [0, 0] is defined as a position where an excavator starts penetrating. As shown in Fig. 5, the proposed method changed the excavation path according to the soil condition. Figures 6 and 7 show the results of the simulation experiment. Figure 6 shows the efficiency of soft and medium soil and Figure 7 shows the efficiency of hard soil. In each graph, the left light-blue bar shows the excavation efficiency in case of not using the proposed method, while the right dark-blue bar shows the excavation efficiency generated by the proposed method. As shown in Figs. 6 and 7, the

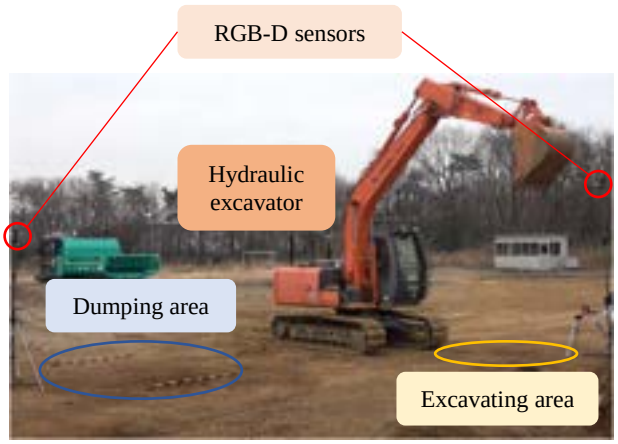

Figure 8. Field experiment setting

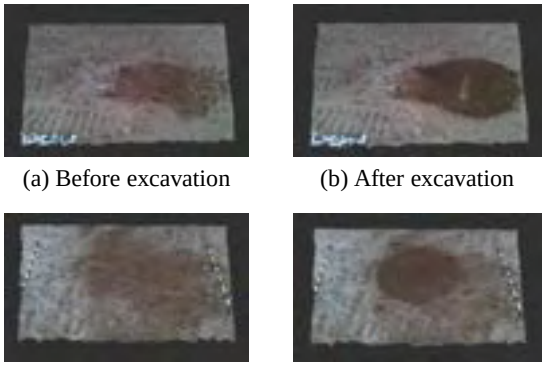

(a) Before excavation (b) After excavation

(c) Before dumping (d) After dumping

Figure 9. 3-D point cloud data (First trial)

of soil was calculated by considering the differences between the soil volume before and after dumping. Based on the above volume changes, the soil volumes before and after excavation were calculated, and its bulking factor was calculated based on these data.

In this experiment, the bulking factor was calculated under two conditions. For the first trial, compacted soil was excavated. For the second trial, the soil we filled back after the first trial was excavated. Thus, the soil for the second trial was loosened than that in the first trial. This enabled us to confirm the possibility of calculating the bulking factor of soil, which has a different density.

4.2 Experimental Result

The 3-D point cloud data obtained in this experiment are shown in Figs. 9 and 10. Figures 9 and 10 show the data of the first and second trials, respectively. In both these figures, (a) shows the area before excavation, (b) shows the area after excavation, (c) shows the area before dumping, and (d) shows the area after dumping. Table 4 lists the soil

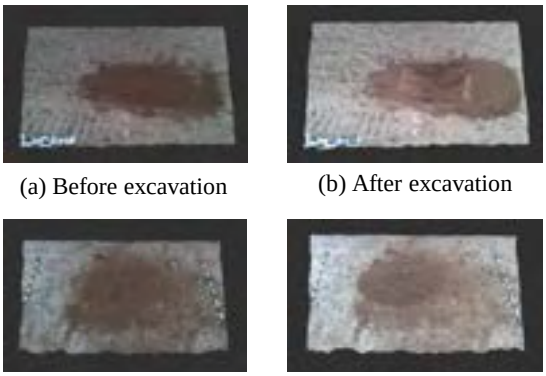

(a) Before excavation (b) After excavation

(c) Before dumping (d) After dumping

Figure 10. 3-D point cloud data (Second trial)

Table 4. Bulking factor k of soil

	$V_{\text{before}}[m^3]$	$V_{\text{after}}[m^3]$	k
First	0.4552	0.6619	1.4540
Second	0.5081	0.5926	1.1663

volume before excavation, V_{before}; that after excavation, V_{after}; and the bulking factor of soil, k, calculated using 3-D point cloud data. As discussed in Table 4, the value of the bulking factor of soil in the first trial is larger than that in the second trial. This indicates the difference in density between the first and second trials. Therefore, the bulking factor of soil can be calculated based on the 3-D measurement data.

5 Conclusion

This paper proposes an excavation path generation method for an autonomous excavator. The proposed method considers the bulking factor of soil as a soil property during the excavation process, which enables the generation of an efficient excavation path for different soil types. A GA was used to determine an efficient excavation path for a specific soil. Additionally, a simulation and a field experiment were conducted to validate the proposed method. For future work, it is necessary to complete the implementation of the entire system on an actual hydraulic excavator and perform full-scale field experiments to validate the proposed method.

Acknowledgement

This work was partly supported by the Construction Technology R&D Grant by MLIT (Ministry of Land, Infrastructure, Transport, and Tourism) in Japan and JSPS (Japan Society for the Promotion of Science) KAKENHI Grant Number 20H02109.

References

[1] S. Yoo, C-G. Park, S-H. You, and B. Lim. A dynamics-based optimal trajectory generation for controlling an automated excavator. Proceedings of the Institution of Mechanical Engineers, Part C: Journal of Mechanical Engineering Science, 224(10):2109–2119, 2010. doi:10.1243/09544062JMES2032.

[2] H. Yamamoto, M. Moteki, H. Shao, K. Ootuki, Y. Yanagisawa, Y. Sakaida, A. Nozue, T. Yamaguchi, and S. Yuta. Development of the autonomous hydraulic excavator prototype using 3-d information for motion planning and control. In Proceedings of the 2010 IEEE/SICE International Symposium on System Integration, pages 49–54, Sendai, Japan, 2010. doi:10.1109/SII.2010.5708300.

[3] J. Park, B. Lee, S. Kang, P. Y. Kim, and H. J. Kim. Online learning control of hydraulic excavators based on echo state networks. IEEE Transactions on Automation Science and Engineering, 14(1):249–259, 2017. doi:110.1109/TASE.2016.2582213.

[4] D. Wang, L. Zheng, H. Yu, W. Zhoua, and L. Shao. Robotic excavator motion control using a nonlinear proportional integral controller and cross coupled pre compensation. Automation in Construction, 64:1–6, 2016. doi:10.1016/j.autcon.2015.12.024.

[5] F. E.. Sotiropoulos and H. H. Asada. A model free extremum seeking approach to autonomous excavator control based on output power maximization. IEEE Robotics and Automation Letters, 4(2):1005–1012, 2019. doi:10.1109/LRA.2019.2893690.

[6] A. Nelson. Dictionary of Mining. Philosophical Library, 1965.

[7] P. Gyorgy, H. Attila, G. Zoltan, and K. Peter. Determination of soil density by cone index data. Journal of Terramechanics, 77:69–74, 2018. doi:10.1016/j.jterra.2018.03.003.

[8] M. F. O'Sullivan and E. A. G. Robertson. Critical state parameters from intact samples of two agricultural topsoils. Soil and Tillage Research, 39:161–173, 1996. doi:10.1016/S0167-1987(96)01068-9.

Development of an Algorithm for Crane Sway Suppression

Yasuhiro Yamamoto[a] , Chunnan Wu[a], Hisashi Osumi [b] , Masayuki Yano [c] and Yusuke Hara [b]

[a]Sumitomo Heavy Industries, LTD, Technology Research Center
[b]Chuo University, Faculty of Science and Engineering
[c]Chuo University, Graduate School of Science and Engineering
E-mail: yasuhiro.yamamoto@shi-g.com, chunnan.wu@shi-g.com, osumi@mech.chuo-u.ac.jp

Abstract –

In this research, a sway suppression algorithm was developed for a crane operator support system. To evaluate the effect of sway suppression, a crane experiment testbed was manufactured. The crane testbed is designed by the crane dynamic model, and the swing motion, boom motion and load hoisting are driven by the electric motors. The validity of the dynamic model for a crane was verified by the testbed experiment. The algorithm for sway suppression is consisted of the open loop control based on the phase plane theory, and was implemented in the testbed. The effect of sway suppression was verified by the testbed, and the effectiveness of algorithm was confirmed.

Keywords –

Crane; Sway Suppression; Phase Plane; Model

1 Introduction

In recent years, the number of skilled operator has decreased and many demands for safety work in construction site has increased. Therefore, the automation and improving safety function of construction machinery has become an important subject. Especially, there are many danger in rotary crane operation because of many reasons such as its fall down, load's sway, and so on.

There are many researches about sway suppression control of the translation crane[1][2][3]. Because the translation crane moves two axis independently, the load's sway in two dimensional plane can be suppressed easily.

But considering about the rotary crane, since it controls the load by swing and boom motion, it is difficult to move like the translation crane and the centrifugal force works to the load, so the load's sway is difficult to suppress.

For sway suppression for the rotary crane, there are some researches[4][5][6]. However, implementing feedback system or complex control system in real machine has many problems in ensuring safety.

To solve these problems, we had proposed a simple algorithm based on open loop control for crane sway suppression only using swing motion, and also developed a crane experiment testbed to evaluate the effect of the algorithm. This crane testbed has three electric motors for swing motion, boom motion and load hoisting, and we confirmed the effect of the algorithm by using the crane testbed.

2 Sway suppression algorithm

2.1 Principal of the algorithm

There are many researches of translation crane with using open loop control based on a phase plane which describes state of vibration[7][8]. The concept of the phase plane is shown in Figure 1, where l is the wire length, g gravitational acceleration, and θ deflection angle.

The equation of motion is described as Equation (1). From solving Equation (1), the deflection angle and angular velocity are described as Equation (2) and (3), where A is a constant.

$$\theta'' = -\frac{g}{l}\theta = -\omega^2\theta \quad (1)$$

$$\theta = A\cos(\omega t) \quad (2)$$

$$\theta'/\omega = -A\cos(\omega t) \quad (3)$$

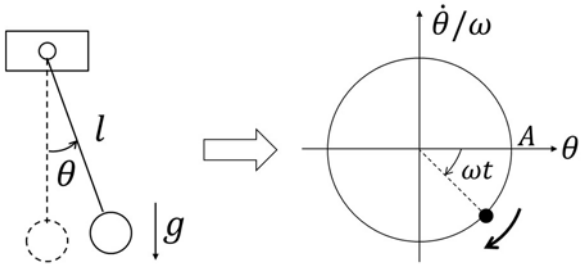

Figure 1. Concept of the phase plane

Based on Equation (2) and (3), the phase plane is described using the deflection angle as the horizontal axis, and the angular velocity, which normalized by natural

frequency ω, as the vertical axis.

The motion of pendulum is translated as rotation motion in the phase plane, and the time required for one round is pendulum period T ($=2\pi/\omega$).

As shown in Figure 2, considering when the acceleration a is applied to the crane, the equation of motion changes to Equation (4). Transforming this equation into Equation (5), it can be seen the rotary motion on the phase plane is switched into the rotation which its center is $-a/g$.

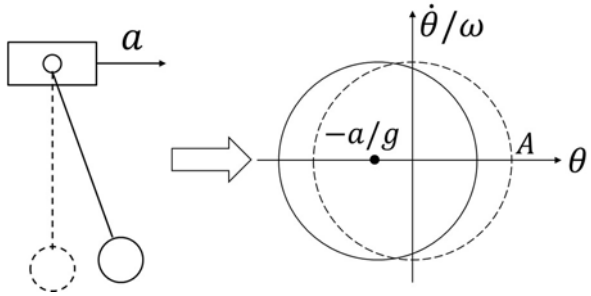

Figure 2. Effect of acceleration in the phase plane

$$\theta'' = -\frac{g}{l}\theta - \frac{1}{l}a \quad (4)$$

$$\left(\theta + \frac{a}{g}\right)'' = -\frac{g}{l}\left(\theta + \frac{a}{g}\right) \quad (5)$$

Hence, by giving the required acceleration at appropriate timing, the rotation motion can be directed to the origin. Shown in Figure 3, make the acceleration zero when the motion is reached to the origin, the vibration can be converged.

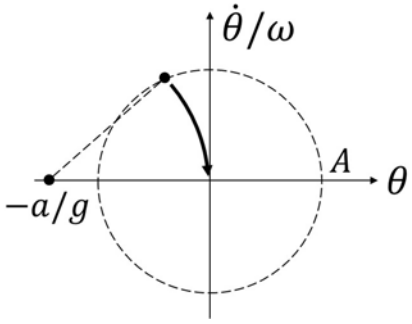

Figure 3. Convergence of the vibration

Based on the above theory, the acceleration pattern shown in Figure 4 is proposed as the sway suppression algorithm. According to this pattern, the acceleration a is first applied to the stopped crane for a time Δt. Next, the acceleration is set to zero for a time $T/2$-Δt, where the crane moves as uniform motion. Finally, setting the acceleration to a for a time Δt, the crane can accelerate without swaying. And then, after transporting the crane for arbitrary time, the crane can be stopped without swaying by applying the deceleration pattern, which the sign of the acceleration pattern is reversed.

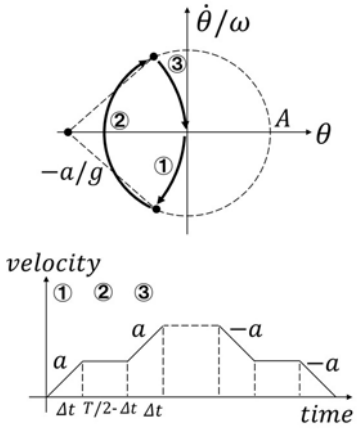

Figure 4. Sway suppression algorithm pattern

2.2 Pendulum model in crane's 3D motion

In order to apply the sway suppression pattern, which described in previous section, the dynamic model of the crane is expressed in this section. Figure 5 shows the model of the crane. By taking the coordinate system as shown in Figure 5, the position of boom tip (x, y, z) is expressed by Equation (4)~(6), where l is the wire length, g gravitational acceleration, B boom length, p swing angle, q boom angle, and ψ, φ sway angle.

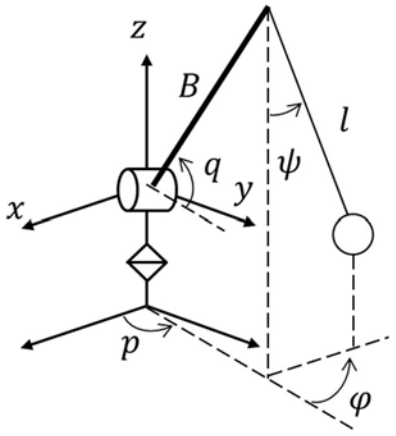

Figure 5. Crane dynamic model

$$x = B\cos q\cos p \quad (6)$$

$$y = B\cos q\sin p \quad (7)$$

$$z = B\sin q \quad (8)$$

Hence, the acceleration at the boom tip is described as Equation (9)~(11).

$$x'' = -Bq''\sin q\cos p - Bp''\cos q\sin p - B(q'^2 + p'^2)\cos q\cos p + 2Bq'p'\sin q\sin p \quad (9)$$

$$y'' = -Bq''\sin q\sin p + Bp''\cos q\cos p - B(q'^2 + p'^2)\cos q\sin p - 2Bq'p'\sin q\cos p \quad (10)$$

$$z'' = Bq''\cos q - Bq'^2\sin q \quad (11)$$

Then the position of load's centroid (x_p,y_p,z_p) can be described as Equation (12)~(14), where the origin of load's coordinate system is the boom tip.

$$x_p = lsin\psi cos\varphi \quad (12)$$

$$y_p = lsin\psi sin\varphi \quad (13)$$

$$z_p = -lcos\psi \quad (14)$$

According to Equation (12)~(14), the equations of rotary motion about ψ, φ are described as Equation (15), (16), where x'', y'', z'' is the acceleration at the boom tip described in Equation (9)~(11).

$$\psi'' = -\frac{1}{l}(2l'\psi' - l\varphi'^2 sin\psi cos\psi + gsin\psi + cos\psi cos\phi x'' + cos\psi sin\phi y'' + sin\psi z'') \quad (15)$$

$$\varphi'' = -\frac{1}{lsin\psi}(2l'\varphi' sin\psi + 2l\varphi'\psi' cos\psi - sin\varphi x'' + cos\varphi y'') \quad (16)$$

3 Simulation with crane testbed

3.1 Configuration of crane testbed

In the previous chapters, the sway suppression algorithm and the crane dynamic model were described.

In order to confirm these above, a crane experiment testbed has been made as shown in Figure 6.

Table 1 shows the specifications. The crane testbed has three electric motors for swing, boom and hoisting, and these motors has the encoder for measuring a motor angle and angular velocity. For holding the posture, the boom and hoisting motors are connected to the winches driven by the worm wheels.

Table 1. Specification of a crane experiment testbed

	Specification
Boom	length 1.0 m (parallel link)
Load	400.0 g (30.0*50.0*80.0mm)
Swing Motor	Max angular velocity 135.0 deg/s
Boom Motor	Max angular velocity 6.8 deg/s
Hoist Motor	Max angular velocity 32.6 deg/s
Camera	DFK Z30GP031 (30 fps)

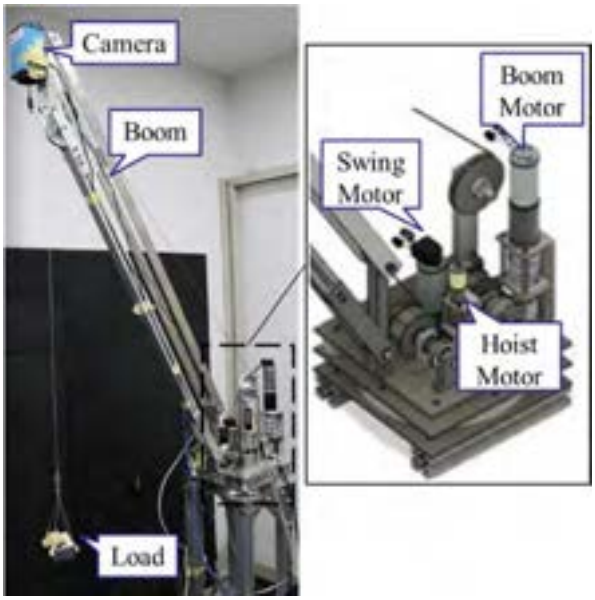

Figure 6. Crane experiment testbed

Here, a camera is mounted on the boom tip to measure the centroid of the load. The boom is composed of the parallel link so that the camera faces perpendicular downward regardless of the boom angle. Figure 7 shows the relationship of the coordinate of system between crane and camera. The xy coordinates of the camera (x_{cam}, y_{cam}) are expressed as a state, which they are rotated by $-\pi/2$ [rad] about z axis of the coordinate of crane and further by swing angle p.

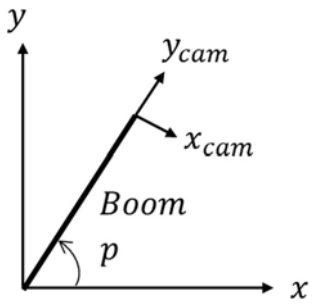

Figure 7. Camera coordinates

3.2 Configuration of control system

The control system configuration of the crane testbed is shown in Figure 8. This system has the crane testbed, a motor driver, an image processing PC for camera, a rapid controller which includes the crane dynamic model, and host PC for the rapid controller. These components are coupled and make one simulation system. The dynamic model in the rapid controller has been modelled as mathematical equations and implemented in MATLAB & SIMULINK models. The crane testbed is

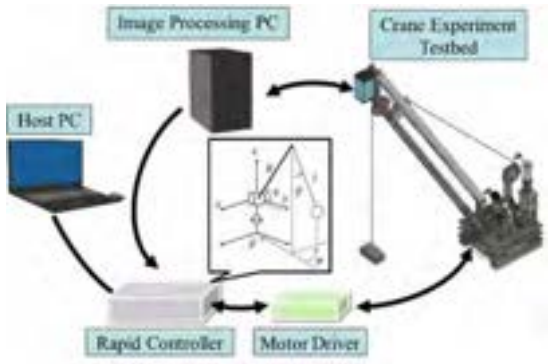

Figure 8. System Configuration

driven by the control signal, which outputted from the host PC via the rapid controller and the motor driver. In addition, the image acquired by the camera is sent to the image processing PC, and the *xy* coordinates of the load's centroid are calculated.

The *xy* coordinates are sent to the rapid controller for recording. The frame rate of the camera is 30 fps, and it is possible to calculate and output the coordinates of each frame in real time.

3.3 Verification of sway suppression

The sway suppression algorithm is verified in the crane testbed by applying the algorithm to the swing motor. The simulation conditions are shown in Table 2.

Table 2. Simulation conditions

	Specification
Wire	1 m fixed
Boom Angle	60 deg fixed
Swing Angle	90 deg swing
Transport time	5 s

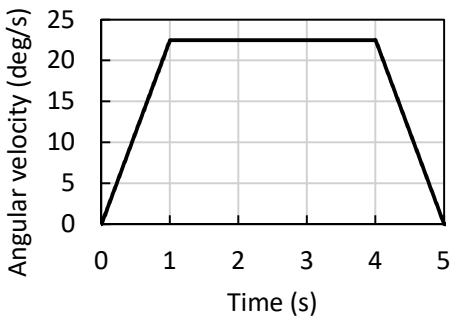

(a) Velocity Pattern

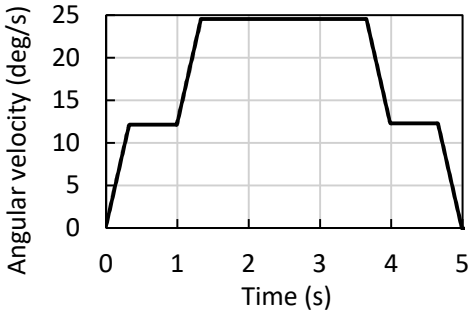

(a) Velocity Pattern

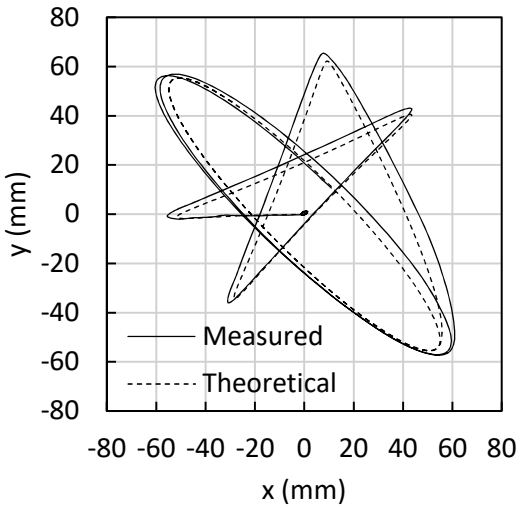

(b) Locus of load's centroid

Figure 9. Experiment results

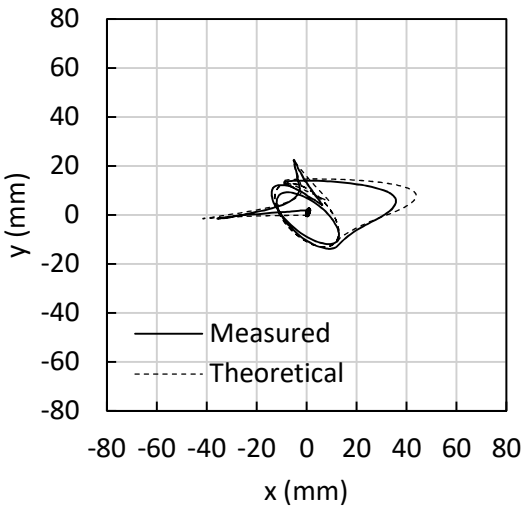

(b) Locus of load's centroid

Figure 10. Experiment results

First, it is confirmed whether the behaviour of the load of the crane testbed follows the crane dynamic model. The results of the experiment are shown in Figure 9. The velocity pattern described in Figure 9 (a) is inputted to the swing motor, and then the locus of the load's centroid is observed, as shown in Figure 9 (b), by the camera on the boom tip.

Since this input pattern is not match the sway suppression algorithm pattern, it can be seen from the locus that the amplitude of the residual vibration ±60mm in the *x* direction and ±60mm in the *y* direction.

By comparing the locus calculated by the equation of motion with the measured locus of the load, the crane dynamic model is considered to be sufficient, though there are slight error in the locus. This error is considered to be occurred since there are many parameters not included in the equation of motion such as the vibration, expansion and contraction of the wire.

Next, the results of the experiment are shown in Figure 10 with inputting the sway suppression algorithm. The input pattern described in Figure 10(a) is inputted to the swing motor of the crane testbed, and then the locus of the load's centroid is observed, as shown in Figure 10(b).

Comparing with the result in Figure 9 (b), the amplitude of the residual vibration in Figure 10(b) is suppressed well, where the amplitudes are ±13mm in the *x* direction and ±13mm in the *y* direction. This residual vibration is mainly caused by the centrifugal force.

According to this experiment, the algorithm is also effective when it is applied only to the swing axis, if the posture change of crane is small during the acceleration and deceleration period.

Future work will aim the development of the sway suppression algorithm which includes the compensation of the centrifugal force, using this simulation system.

4 Conclusion

In this research, an algorithm for the crane sway suppression was proposed, which based on the phase plane theory, and confirmed its effectiveness by applying to a crane experiment testbed, which composed of the electrical motors and the link mechanism. And also, the validity of the crane dynamic model was verified.

According to the experimental results, it is confirmed that applying the algorithm only to the swing axis is effective, when the posture change of crane is small during the acceleration and deceleration period.

In future work, the new sway suppression algorithm needs to be proposed, which includes the compensation of the centrifugal force by the swing motion, and verified by applying to the crane testbed.

References

[1] Sun, You-Gang, et al. "The nonlinear dynamics and anti-sway tracking control for offshore container crane on a mobile harbor." Journal of Marine Science and Technology-Taiwan 25.6 (2017): 656-665.

[2] Chwa, Dongkyoung. "Sliding-mode-control-based robust finite-time antisway tracking control of 3-D overhead cranes." IEEE Transactions on Industrial Electronics 64.8 (2017): 6775-6784.

[3] Ahmad, Mohd Ashraf, and Zaharuddin Mohamed. "Hybrid Fuzzy Logic Control with Input Shaping for Input Tracking and Sway Suppression of a Gantry Crane System 1." (2009).

[4] Shen, Ying, and Kazuhiko Terashima. "Optimal control of rotary crane using the straight transfer transformation method to eliminate residual vibration." *Transactions of the Society of Instrument and Control Engineers* 39.9 (2003): 817-826.

[5] Ouyang, Huimin, Naoki Uchiyama, and Shigenori Sano. "S-curve trajectory generation for residual load sway suppression in a rotary crane system using only horizontal boom motion." *Journal of System Design and Dynamics* 5.7 (2011): 1418-1432.

[6] Ichise, Kenji, Shigeto Ouchi, and Kang Zhi Liu. "ANTI-SWAY CONTROL SYSTEM OF A ROTATIONAL CRANE USING A NON-LINEAR CONTROLLER." *The Proceedings of the International Conference on Motion and Vibration Control 6.2*. The Japan Society of Mechanical Engineers, 2002.

[7] Kobayashi, K., Y. Kato, and S. Nakano. "Development of an Automatic Operation System of Overhead Travelling Cranes in Steel Coil Warehouse." *IFAC Proceedings Volumes* 22.11 (1989): 311-315.

[8] Yamagishi, T. "Optimal control of load swing of crane." *IFAC Proceedings Volumes* 7.2 (1974): 345-355.

Analysis of Energy Efficiency of a Backhoe during Digging Operation

Yusuke Sano[c], Chunnan Wu[c], Hisashi Osumi[a], Yuki Kawashima[b] and Tomoaki Tsuda[d]

[a]Chuo University, Faculty of Science and Engineering
[b]Chuo University, Graduate School of Science and Engineering
[c]Sumitomo Heavy Industries, LTD, Technology Research Center
[d]SUMITOMO CONSTRUCTION MACHINERY CO., LTD.
E-mail: yusuke.sano@shi-g.com, chunnan.wu@shi-g.com, osumi@mech.chuo-u.ac.jp

Abstract –

The energy consumption of a backhoe during digging operation is the sum of the energy due to earth pressure and backhoe motion. The authors' previous studies have revealed the earth pressure model on the arc trajectory, but not on the horizontal trajectory, which is often used in normal digging operation. Moreover, in order to optimize energy efficiency, a comparative experiment of energy consumption was carried out for the multiple excavation trajectories involving horizontal direction. However, since the theoretical model of earth pressure has not been completed, the experimental data obtained from the testbed is used as a reaction force. If it can be confirmed that the reaction force of the horizontal trajectory can be calculated with a theoretical value, the energy efficiency can be calculated from the excavation trajectory without experiment. In this study, the earth pressure model for the horizontal trajectory was confirmed, and the method for the evaluation of energy efficiency was verified using the theoretical values.

Keywords –

Backhoe; Digging force; Coulomb's earth pressure

1 Introduction

In recent years, autonomous construction machines have been developed due to the decrease in the working population and the deterioration of infrastructure. The automatic construction system for construction machinery is complicated by three-dimensional measurement, operation planning, electronic hydraulic control, etc. [1]. In the case of a construction machine that excavates sediment like a backhoe, automatic control is difficult because the reaction force affects the operation and the energy consumption of the machine. We have formulated the reaction force during digging operation based on Coulomb's earth pressure theory by observing the behavior of sediment in the bucket when the backhoe scoops sediment on the arc trajectories [2]. The energy consumption of a backhoe during digging operation is the sum of the energy due to earth pressure and backhoe motion, and the excavation efficiency was evaluated [3]. However, although the earth pressure model for the arc trajectory has been clarified, but not on the horizontal trajectory which is often used in normal digging operation. The earth pressure model for horizontal trajectories depends on the amount of sediment deposited on the upper side of the bucket. Therefore, it is necessary to consider the amount of sediment. In addition, in order to optimize energy efficiency, a comparative experiment of energy consumption was carried out for the multiple excavation trajectories involving horizontal direction [3]. However, since the theoretical model of earth pressure has not been completed, the experimental data obtained from the testbed is used as a reaction force. If it can be confirmed that the reaction force of the horizontal trajectory can be calculated with a theoretical value, the energy efficiency can be calculated from the excavation trajectory without experiment. In this study, we verified the earth pressure model for the horizontal trajectory and applied it to the calculation of the excavation energy. Using the sum of the energy due to earth pressure and backhoe motion, we evaluated the energy efficiency without any experiment.

2 Overview of experiment system

Figure 1 shows an excavation testbed used in this study. The mechanism consists of three axes: an X axis that moves horizontally, a Y axis that moves vertically, and an R axis that rotates the bucket. The backhoe excavation motion can be simulated by giving displacement and velocity to each axis. The sediment container installed at the bottom of the equipment is the same size as the drive range, and the wall on one side of the container is made of polycarbonate. This makes it

possible to observe sediment behavior during digging. The bucket made of stainless steel is designed on the 1/14 scale of the actual machine, and a removable side plate is attached. Only the side plates are made of polycarbonate, and the behavior of the sediment in the bucket can be observed in the same way. Table 1 shows the parameters of the sediment used in this experiment.

The dynamic friction angle between the sand and the bucket and the angle of repose were determined to be 23 degree and 32 degree from the results of the basic experiment.

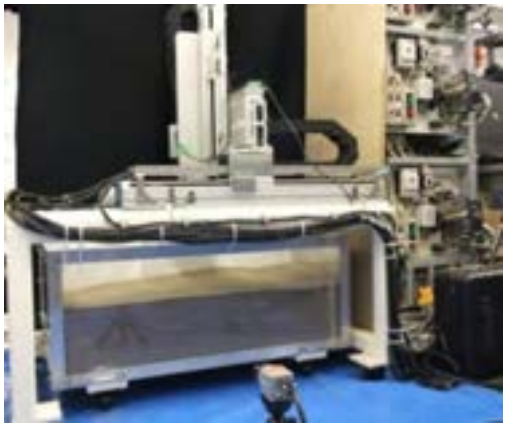

Figure 1. Overview of excavation testbed

Table 1. Parameters of sand

	Max.	Middle	Min.
density of sand [g/cm^3]	1.731	-	1.433
internal frictional angle [deg]	38.3	36.0	33.6

3 Modeling Reaction Force

3.1 Behavior during digging

Figure 2 shows the excavation trajectory using an excavation testbed. The trajectory is arc penetrating and horizontally sweep. At the end, scoop with the arc trajectory.

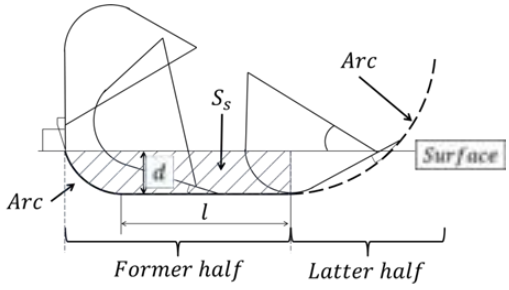

Figure 2 Digging trajectory for modeling

The behavior of the sediment in the bucket was observed from the video that reproduced a series of excavation motions of the backhoe. From the result, it was found that it is necessary to divide the process as follows for formulation (Figure 3).

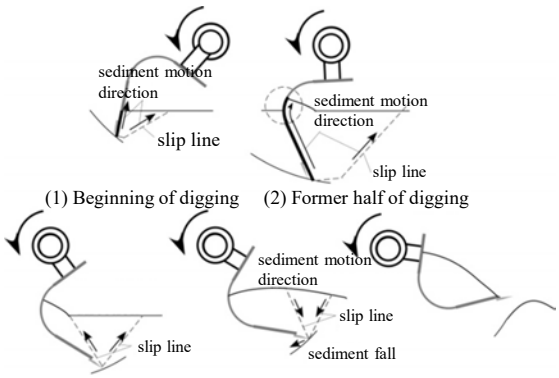

Figure 3. Divided digging phases based on sediment behaviour

1. Beginning of digging
2. Former half of digging
3. Latter half of digging
4. Soil fall phase
5. Lifting of sediment

The reaction force was formulated in each phase, and its validity was verified by comparison with the experiment result.

3.2 Reaction Force Model

It is known that the reaction force can be calculated with high accuracy by using a model of multiple triangles based on the Coulomb's passive earth pressure [4]. Based on this, the theoretical value of the reaction force was calculated using Coulomb's passive earth pressure.

First, assuming the slip on the bucket surface, the passive earth pressure is calculated. Next, the passive earth pressure assuming slippage in the sediment is calculated until the trajectory of the bucket teeth reaches the angle of repose. The phenomenon that actually occurs in this section is the one where the value of the passive earth pressure is small. In addition, the amount of sediment deposited on the upper side of the bucket is required to determine the passive earth pressure. The calculation of passive earth pressure is greatly affected by the accumulated sediment. From the observation results and the reaction force measurement results, it was assumed that sediment did not accumulate during the intrusion and 0.7 times the swept volume by the bucket accumulated after reaching the horizontal

trajectory. Furthermore, the shape of the deposited sediment was calculated from the slip line shape in the sediment. This assumption makes it possible to calculate the increase in the reaction force when sweeping horizontally. When the trajectory of the tooth tip exceeds the angle of repose, sand collapses in the space below the tooth, and the sediment above the tooth begins to flow downward. At this time, active earth pressure is generated. And the reaction force becomes even smaller than the active earth pressure. When the tip of the tooth comes to the ground, the horizontal component of the reaction force disappears and the vertical component becomes the weight of sand in the bucket. However, since the amount of sediment in the bucket is unknown, it is set to zero in this model.

4 Excavation reaction force measurement experiment and simulation

4.1 Reaction force measurement

In order to evaluate the validity of the reaction force model during digging, the measurements were carried out using an excavation testbed. The reaction force of the trajectory shown in Figure 2 was measured and a video was recorded. An analysis was performed based on the behavior of the sediment at this time. A 6-axis force sensor attached to the bucket root was used to measure the excavation reaction force. At this time, the weight of the bucket etc. is corrected. Figure 4 shows the horizontal and vertical components F_h and F_v in absolute coordinates of the measured reaction force, and the coordinate system of F_{hr} and F_{vr} based on the bucket bottom. These transformations are calculated using the rotation matrix.

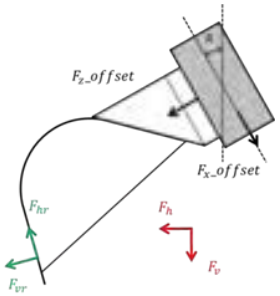

Figure 4. Coordinate system of reaction force

4.2 Comparison of excavation reaction force

For verification of the reaction force model, the difference between the theoretical value and the measurement result was compared. Figure 5 shows the horizontal component of the measurement result and theoretical value of the excavation reaction force, and Figure 6 shows the vertical component.

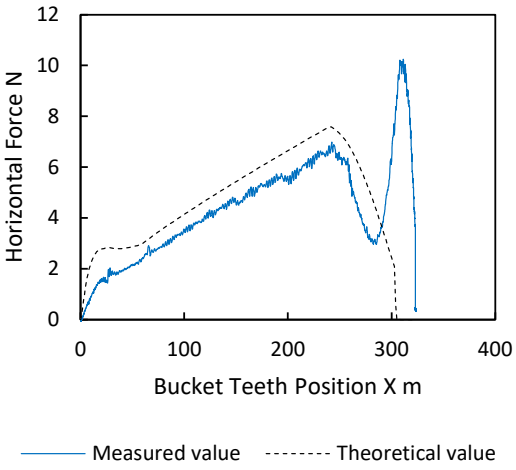

Figure 5 Reaction force comparison of horizontal direction

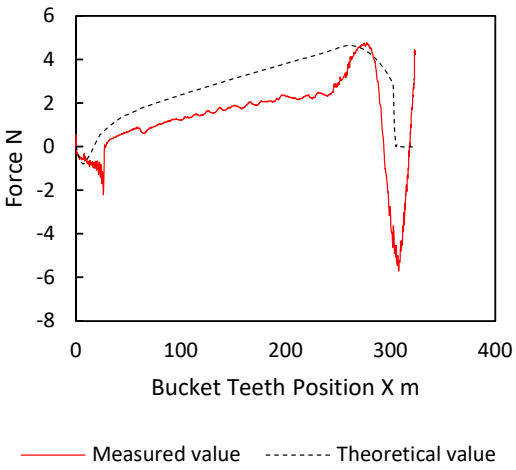

Figure 6 Reaction force comparison of vertical direction

From this result, it can be seen that the passive earth pressures until the tip of the tooth reaches 240 mm are approximately the same. The reaction force increase after 200 mm occurs in the phase of lifting the sediment. This is caused by contact between the sediment and the outside of the bucket. Since the trajectory does not contact the earth and sediment with the outside of the bucket, it is considered that the sediment that fell from the surroundings come into contact with the bucket. Ideally, there is no sediment on the trajectory, so the model does not consider this effect. Active earth pressure occurs at the tip of the tooth between 280 mm and 290 mm. The value of active earth pressure is very

small and is mostly controlled by the weight of sediment in the bucket. Approximately 300 mm, the tip pf the tooth reach the ground. The vertical component of the reaction force is adjusted by the weight of the passive earth pressure inside the slip line. However, it can be seen that the theoretical value is larger than the measurement result because the weight inside the slip line is large.

5 Backhoe energy consumption

5.1 Backhoe modeling

The backhoe attachment consists of three axes: boom, arm, and bucket, and is driven by a hydraulic system. Since each joint rotates as the hydraulic cylinder expands and contracts, it can be treated as a 3-link manipulator. Figure 7 shows the model when the boom drive is used as the origin. However, L_3 is the distance from the bucket joint to the point of action of the reaction force. In this research, the trajectory is generated so that the bucket attitude is uniquely determined for the excavation trajectory. By determining the angle of the third joint of the bucket, the remaining joint angles are derived by inverse kinematics.

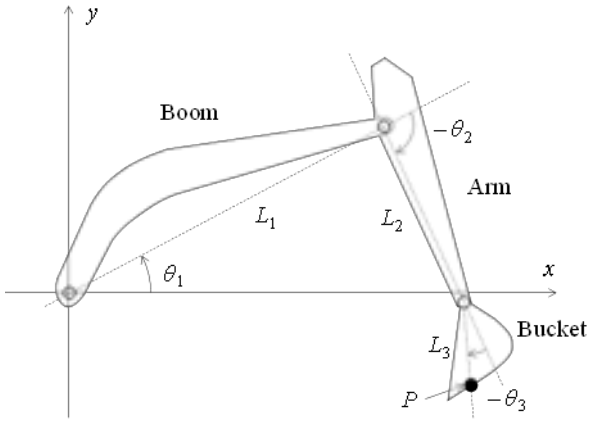

Figure 7. Kinematic model of backhoe

5.2 Energy consumption calculation

The work performed by each joint is represented by the product of joint displacement and torque. Energy is output when the rotation direction of the joint and the direction of receiving torque are different, but in the same direction, energy is received from the outside. However, in reality, torque is generated to keep the joint at the target angle. For this reason, the joint outputs the torque to oppose even if it receives a torque so as to receive energy. It is output as energy and consumes the energy that it should have received. This is called negative energy [5]. Therefore, in order to obtain the work, it is necessary to integrate the absolute value of the product of joint displacement and torque.

Since, the work required for the link to operate is represented by the sum of earth pressure and backhoe motion, the work required in the link model is expressed by Equation (1).

$$|\Delta\theta^T\tau_{ext}| = \sum_{k=1}^{3}|\Delta\theta_k||\tau_{ext\,k}| + |\Delta\theta_k||\tau_{mech\,k}| \qquad (1)$$

Negative energy is generated depending on the posture of the link, the direction of travel, and the direction of external force. Therefore, the excavation starting point where negative energy is not generated as much as possible can maximize energy efficiency.

5.3 Excavation simulation

The factors that affect the reaction force are the attitude of the bucket and the excavation depth. Therefore, in order to reduce the reaction force during excavation and increase energy efficiency, it is known that the excavation depth should be as small as possible and the bucket during digging should be tilted. In the past research [3], excavation trajectories with these characteristics were generated, but since the theoretical model of reaction force was not completed, the experimental data obtained from the testbed was used as reaction force. In this research, the excavation efficiency was evaluated from the simulation results using the earth pressure model with horizontal trajectory described in Chapter 4.2.

The excavation trajectory applied for the simulation is shown in Figure 2, and the trajectory conditions are shown in Table 2. In order to excavate a certain amount of sediment, the volume to be excavated before lifting must be greater than the bucket volume. For this reason, the ratio of the excavation volume S_s and the bucket volume S_b was used as the trajectory parameter. Two patterns of excavation trajectories were created by combining excavation depth and excavation volume.

This is the same trajectory as when the experimental data was used as a reaction force in the past research [3]. Therefore, the experimental results are shown in Table 3 for comparison with the simulation. This is the result of a partial revision of past research. According to the experimental result, the energy consumption of Test case 1 and Test case 2 is almost the same. This result is the energy consumption generated by the testbed when the excavation trajectory is applied, and is not the result converted to the actual scale shown in Chapter 5.2.

Simulations were performed for each trajectory to confirm the effectiveness of the method that consumes less energy. The simulation was carried out with the

value converted to the actual backhoe scale. The simulation results are shown in Table 4. Test case 1 is a "long and shallow" orbit, and test case 2 is a "deep and short" excavation trajectory.

Table 2. Trajectory conditions

Test case	S_s / S_b	l mm	d mm	Scooping velocity mm/s
1	2	208	23.5	20
2	1	47.5	33.5	20

Table 3. Experimental results of scooping [3]

Test case	Scooped soil [g]	Works [J]	Energy efficiency [g/J]
1	486	2.97	164
2	450	2.99	151

Table 4. Simulation results

Test case	Work ratio	Works ratio by earth pressure	Work ratio with gravity
1	1	1	1
2	0.486	1.099	0.408

From the simulation results, it is found that the backhoe consumes less energy under the condition 2 where the excavation depth is deep and the horizontal distance is short. The energy consumption at the tooth tip position during excavation is shown in Figure 8. The integral of this value becomes the energy consumption during excavation. It can be seen that Test1 consumes less energy at the same position than Test2, but the total energy is larger. This is because the excavated distance is long. It is considered that the influence of negative energy became large due to the long excavation distance. The energy consumption due to earth pressure has almost the same result. The experimental results in Table 3 show the energy consumption only by earth pressure, but both trajectories have the same energy consumption, and the simulation results and the experimental results show the same tendency. From this result, it can be said that it is possible to compare the energy efficiency with theoretical values.

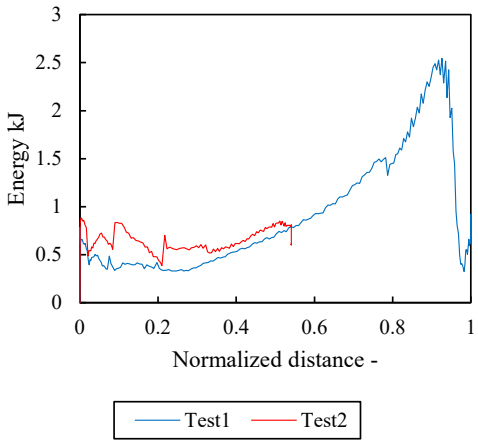

Figure 8. Energy consumption simulation result

The energy consumption due to the earth pressure is shown in Figure 9. As for the energy consumption due to the earth pressure, the maximum value of Test case 2, which is deep in the excavation trajectory, is large. It was also confirmed that the negative energy generation condition changes depending on the excavation start position, and the energy consumption changes. However, the energy consumption is about the same. The energy consumption due to the mechanism of the backhoe is shown in Figure 10. The energy due to the backhoe mechanism is more than twice as large in Test case 1 as in Test case 2. Under the condition that the distance to sweep horizontally is long, it is found that the energy consumption increases due to the negative energy.

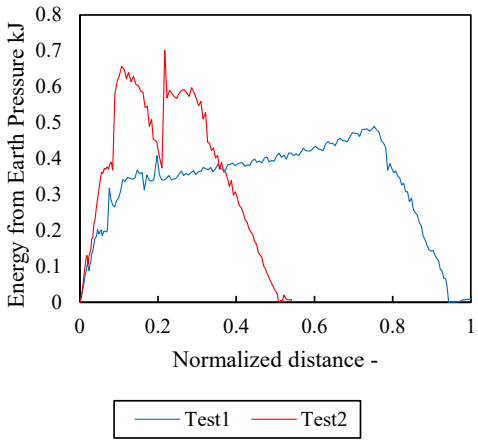

Figure 9. Energy consumption from earth pressure

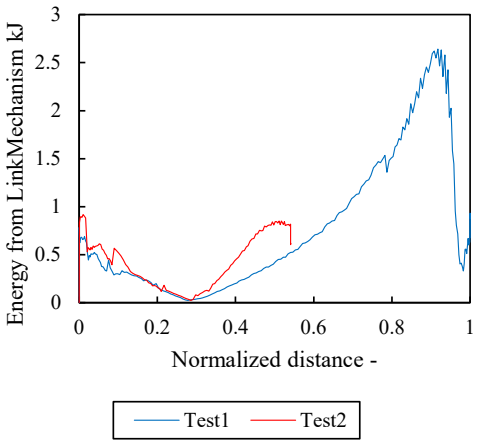

Figure 10. Energy consumption from link mechanism

6 Conclusion

From the analysis results of the reaction force using the testbed, the excavation reaction force in the horizontal trajectory, which is often used in digging operation, was formulated. It was confirmed that the theoretical values of the formulated model and the experimental results were almost the same. The energy efficiency in two patterns of excavation trajectories was evaluated using the newly derived earth pressure model. Regarding the energy consumption due to earth pressure, the results of simulation and experiment showed the same tendency. From this result, it was shown that the energy efficiency of the excavation trajectory can be evaluated by using the theoretical value. In the evaluation results of the excavation efficiency based on the theoretical value, the energy efficiency of the short excavation trajectory was good because of the energy consumption by the mechanism.

References

[1] H. Yamamoto, M. Moteki, T.Ootuki, Y. Yanagisawa, A. Nozue, T. Yamaguchi, and S.Yuta Development of the Autonomous Hydraulic Excavator Prototype Using 3-D Information for Motion Planning and Control. Transactions of the Society of Instrument and Control Engineers, 48(8):488–497, 2012(in Japanese)

[2] H. Osumi et al., Analysis of soil behavior in a bucket during digging operation by a backhoe, The 17th Symposium on Construction Robotics in Japan, 2017.(in Japanese)

[3] H. Osumi at al., Design of efficient scooping trajectory for a backhoe, The 18th Symposium on Construction Robotics in Japan, 2018.(in Japanese)

[4] H. Iwase at al., Analysis of soil excavation reaction force acting on backhoe, The 15th Symposium on Construction Robotics in Japan, 2015.(in Japanese)

[5] S. Hirose, and Y, Umetani, The Basic Consideration on Energetic Efficiencies of Walking Vehicle, 15(7):928–933, 1979(in Japanese)

Action Recognition of Construction Machinery from Simulated Training Data Using Video Filters

Jinhyeok Sim[a], Jun Younes Louhi Kasahara[a], Shota Chikushi[a], Hiroshi Yamakawa[a], Yusuke Tamura[b], Keiji Nagatani[a], Takumi Chiba[c], Shingo Yamamoto[c], Kazuhiro Chayama[c], Atsushi Yamashita[a], and Hajime Asama[a]

[a]The University of Tokyo, Japan
[b]Tohoku University, Japan
[c]Fujita Corporation, Japan
E-mail: sim@robot.t.u-tokyo.ac.jp, louhi@robot.t.u-tokyo.ac.jp, chikushi@robot.t.u-tokyo.ac.jp
yamakawa@susdesign.t.u-tokyo.ac.jp, y.tamura@srd.mech.tohoku.ac.jp, keiji@i-con.t.u-tokyo.ac.jp
takumi.chiba@fujita.co.jp, syamamoto@fujita.co.jp, chayama@eae.co.jp
yamashita@robot.t.u-tokyo.ac.jp, asama@robot.t.u-tokyo.ac.jp

Abstract –

In the construction industry, continuous monitoring of actions performed by construction machinery is a critical task in order to achieve improved productivity and efficiency. However, measuring and recording each individual construction machinery's actions is both time consuming and expensive if conducted manually by humans. Therefore, automatic action recognition of construction machinery is highly desirable. Inspired by the success of Deep Learning approaches for human action recognition, there has been an increased number of studies dealing with action recognition of construction machinery using Deep Learning. However, those approaches require large amounts of training data, which is difficult to obtain since construction machinery are usually located in the field. Therefore, this paper proposes a method for action recognition of construction machinery using only training data generated from a simulator, which is much easier to obtain than actual training data. In order to bridge the feature domain gap between simulator-generated data and actual field data, a video filter was used. Experiments using a model of an excavator, one of the most commonly used construction machinery, showed the potential of our proposed method.

Keywords –

Action recognition; Deep learning; Video filter;

1 Introduction

In the construction industry, expenses related to heavy equipment, such as construction machinery, occupy large portions of the overall budget. Improving productivity and efficiency at construction sites is an important issue, and therefore, particular care has been attributed to the monitoring of such construction machinery. By obtaining and maintaining the time and costs required to complete a task, a more efficient construction plan can be made [1]. Traditionally, monitoring, consisting of recognizing and recording the actions performed by construction machinery, was conducted manually by the site manager's observations at the construction site [3]. This involved high costs and time. Therefore, automatic action recognition of construction machinery is highly desirable.

Figure 1. Simulator environment used in our proposed method (Vortex Studio [2])

Previous works dealing with the action recognition of construction machinery either employed added sensors onboard the machinery, such as GPS [4], or employed sensors positioned on the construction sites, such as cameras [5]. Approaches using cameras, which consist in placing several cameras in the construction site and recording the machinery at work, are especially appealing since they do not require modifications on the

construction machinery. Furthermore, inspired by the success of Deep Learning methods for Computer Vision-based approaches to human action recognition [6][7], several works have also managed remarkable results for the action recognition of construction machinery using Computer Vision and Deep Learning [8][9].

However, one of the major practical drawback of Deep Learning approaches is that a large amount of training data is required. Obtaining large amounts of training data is a tedious task. This was alleviated in some part for human action recognition thanks to the advent of the Internet and open-access data but it is not the case regarding specific targets such as construction machinery, which comes in a plethora of shapes and forms. High costs, in logistics, in manpower and in time, can be reasonably expected in order to obtain the training data appropriate for action recognition of construction machinery.

On the other hand, generating such training data using a simulator, illustrated in Figure 1, is comparatively easier: only a human operator to control the virtual construction machinery and a computer to run the simulator is needed. Therefore, the objective of the present paper is to conduct action recognition of construction machinery using Deep Learning based on training data obtained from a simulator.

Since the simulator differs too much from real construction sites to allow directly learning the features required for action recognition, a video filter is introduced in order to force a common ground between the data generated in the simulator and the data collected in actual construction sites.

2 Action Recognition of Construction Machinery based on Simulated Training Data

2.1 Concept

Training a model using training data generated from a simulator is not effective for action recognition of construction machinery at actual construction sites. This is because the training data would not be appropriate for the task at hand. This would be akin to train a model to distinguish pictures of dogs and cats and then testing it on pictures of cows. More generally, the features that could be extracted by the model from the feature space defined by the training data generated from the simulator do not match the features contained in the data collected at actual construction sites. Simply put, the construction machinery in the simulator does not *look like* real construction machinery.

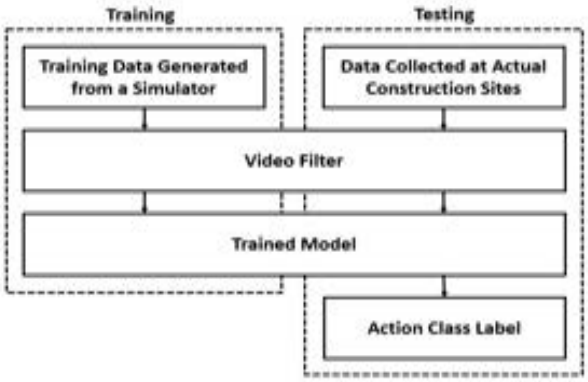

Figure 2. Overview of proposed method.

In such situation, a couple of options can be considered. Increasing the amount of training data, in a Big Data fashion, or a Data Augmentation approach could be considered. This would allow to expand the area of the feature space covered by the training data and hopefully encompass the desired portion of the feature space. However, in our case, this would have little hope to succeed since no matter the amount of additional training data generated from the simulator, the training data would still differ from the data collected at actual construction sites. Another option would be to attempt to bias the training data towards data collected at actual construction sites. To do so, domain adaption methods, i.e., using unlabeled data collected at actual construction sites in the training, or improvements to the simulator to match more closely actual construction sites can be considered. However, the former usually involves strong priors and expensive field data collection and the latter involves tedious software development.

The concept of the proposed method in this paper is a different approach: since the learning is hindered by a mismatch between the training data and the data collected at actual construction sites, the idea is to transform both of them into a third feature domain, which would be neither the feature domain of the simulator-generated training data nor of the data collected at actual construction sites. The introduction of a third feature domain would allow to bypass the previously mentioned issues related to trying to skew one domain towards another since the destination domain would be set independently of the available data.

An overview of the proposed method is shown in Figure 2. First, training data for action recognition of construction machinery is generated using a simulator. Then, both the training data generated from a simulator and the are transformed using a video filter. After this, the model for action recognition is trained on the transformed simulator training data and finally tested on the transformed data collected at construction sites.

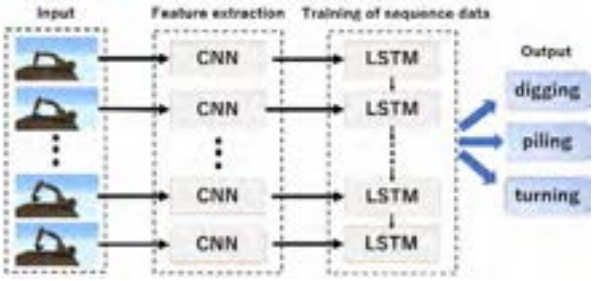

Figure 3. Learning model used in our proposed method consisting of a CNN coupled with LSTM.

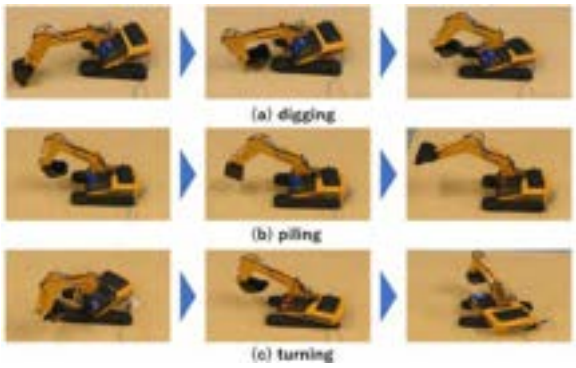

Figure 4. Examples of excavator action classes: (a) Digging; (b) Piling; (c) Turning

2.2 Training Data Generating using a Simulator

The most ideal training data for construction machinery action recognition is the data collected at actual construction sites, i.e., labeled data of the construction machinery working at the actual construction site. However, it is practically difficult to collect and label a large amount of data at the actual construction site. Therefore, in this study, Vortex Studio [2], which is a real-time simulator for mechanical system operation, is used to generate training data. A model of an excavator, one of the most commonly used construction machinery, is considered as shown in Figure 1.

In this study, RGB video data is used as input data, i.e., video of the construction machinery working. However, it is known that RGB data is easily affected by the background and camera viewpoint. Therefore, a background was created with only soil around the excavator. Moreover, the training data was generated from multiple camera viewpoints.

Concretely, to generate the training data, the camera viewpoint was first fixed while the excavator was moving in Vortex Studio and the excavator operation was conducted by human using a controller. The process was repeated several times with different camera viewpoints and different actions to generate training data.

2.3 Transformation to third Feature Domain using a Filter

In this study, the training data, generated from a simulator, differs from the data collected at actual construction sites. There is therefore a domain gap between the data used to train the model and the data used to test the model: the model trained in one domain cannot accurately conduct inference on the other domain. The concept of the proposed method is to match those two data on an independent third domain, where both would be similar.

The most obvious disparity between the data generated from a simulator and the data collected at construction sites is their appearance: they simply do not look alike and are easily differentiable. The differences mainly lie in color and texture: the simulator environment noticeably lacks the color modulations and textured appearance of surfaces compared to the real world. In order to erase those differences and basically make both the data generated from a simulator and the data collected at construction sites similar, an edge video filter is used. This edge filter is applied to both the training data generated from a simulator and the data collected at construction sites.

2.4 Action Recognition Learning Model

For action recognition, Deep Learning approaches such as using Convolutional Neural Network (CNN) and Long Short Term Memory (LSTM) [10] or a method using 3D CNN [11] has been recently used, and these methods using deep learning have higher accuracy of action recognition than other methods.

In this study, CNN and LSTM are used as network framework. CNN is a network which middle layer is composed of convolutional layer and pooling layer and extracts a feature map containing spatial information. LSTM is a network suitable for time sequence data and capable of learning long-term dependency. Therefore, by using CNN and LSTM, it becomes possible to recognize the motion of the construction machinery that considers spatial information and temporal information at the same time.

The proposed network architecture is shown in Figure 3. First, from each training data video sample, recorded at 30 fps, each frame of RGB data is extracted. Next, the extracted RGB data is resized to a size of 298×298×3. Resized RGB data is inputted to the CNN and features are extracted. The CNN network used in this study uses a trained model called Inception V3 [12] pre-trained on over 1 million images. After that, the result of feature extraction from Inception V3 is inputted into LSTM. LSTM consists of three layers and classifies action labels in the softmax layer.

3 Experiments

In experiments, an excavator was selected as target for action recognition since it is one of the most commonly used construction machinery. Furthermore, action recognition was narrowed down to 3 action classes: digging, piling, and turning.

Training data was generated from four viewpoints using Vortex Studio simulator according to the procedure in Section 2.2. As a result, about 60 videos segments at 1920×1080 resolution and 30fps were generated for each action class. The average video duration is 7s, with the shortest being 4s and the longest being 13s.

The CNN and LSTM network in this study for action recognition was trained for 150 epochs using a batch size of 32 with the Adam optimizer.

Two test datasets were considered. The first test dataset was generated from the simulator with the same procedure as for the training data for the purpose of providing a baseline in ideal learning conditions. We generated about 20 video segments for each action class. The second test dataset corresponds to actual data collected at construction sites, i.e., real world test data. However, since we were unfortunately not able to gain access to actual construction sites, we opted instead to use a remotely controlled scale model excavator. At that time, we created a background environment similar to the simulation environment, then filmed the excavator work from four different angles and generated about 20 video segments for each action class.

Regarding the edge video filter, the sketch filter of the open source video editing software Shotcut [13] was used.

The following experiments were conducted:

• (A1) CNN+LSTM trained on simulator-generated training data and tested on simulator-generated test data.

• (B1) The proposed method trained on simulator-generated training data and tested on simulator-generated test data.

• (A2) CNN+LSTM trained on simulator-generated training data and tested on real world test data.

• (B2) The proposed method trained on simulator-generated training data and tested on real world test data.

The performance was evaluated by calculating the classification accuracy defined as the ratio of the number of correctly classified samples n_{correct} over the total number of samples in the test dataset N_{samples}.

$$\text{accuracy} = \frac{n_{\text{correct}}}{N_{\text{samples}}} * 100 \quad (1)$$

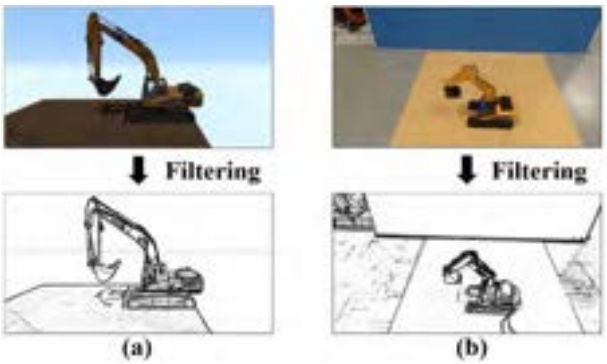

Figure 5. Effects of applying a video filter: both the data generated from a simulator (a) and real world data (b) have their differences suppressed.

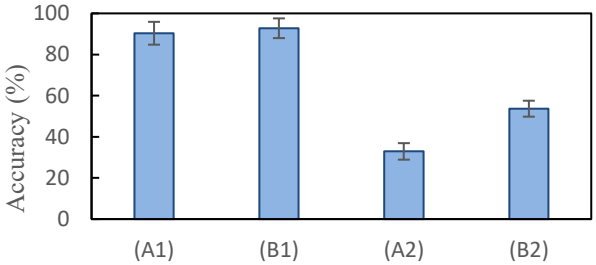

Figure 6. Average testing performance over 3 training runs of (A1) CNN+LSTM on simulator testing data, (B1) proposed method on simulator testing data, (A2) CNN+LSTM on real world test data and (B2) proposed method on real world test data. 3 action classes were considered. Error bars correspond to one standard deviation.

4 Results and Discussions

Figure 5 shows the simulator-generated data and the real world data along with the output after applying the filter. It can be noticed that most apparent features enabling differentiation have been successfully suppressed and that both data look very similar.

Results regarding action recognition performance are reported on Figure 6.

In experiments (A1) and (B1), when the training data and the test data are both generated from the simulator, it can be seen that both the proposed method and CNN+LSTM have high performance, exceeding 90%. This indicates that learning was successful. The proposed method achieved a slightly better performance at 92.3% accuracy. This is due to the fact that in our proposed method, the model learns on the training data on which the video filter was applied: this is simpler than learning directly from RGB.

In experiments (A2) and (B2), both CNN+LSTM and the proposed method were trained on the simulator-generated training data but testing was conducted with real world test data. It can be first noticed that both suffer

drop in performance. CNN+LSTM's accuracy dropped from 90.3% to 32.8%. Since 3 action classes were considered in our experiments, this is equivalent to random classification and it can be concluded that learning an appropriate model has failed. This illustrates the previously mentioned need for training data matching test data for successful learning of classification features in Section 2.1. On the other hand, the proposed method obtained an average performance of 53.7%. While there is still a performance drop, the proposed method managed to significantly perform better than a random classifier. This indicates that the introduction of a video filter allowed a performance gain of over 20%. This likely points out that the filter was successful in matching the simulator training data and real world data onto a similar domain.

5 Conclusion

A method to conduct action recognition of construction machinery from simulator-generated training data using a video filter was proposed. The differences between simulator data and real world data which prevented learning a successful model were suppressed by the use of a filter and allowed an accuracy increase of over 20%, effectively allowing the model to learn features for classification and not fail into a random classifier.

Experiments reported in this paper are still preliminary and served to demonstrate the potential of shifting the learning problem into a third domain. In the future, we plan investigate the effects of training data size and search for more suited filters for action recognition in order to improve performance. Incorporating the filter into the learning process, to learn a filter optimized for action recognition in parallel to the action recognition itself, is also considered.

References

[1] Jinwoo Kim, Seokho Chi, and Jongwon Seo: "Interaction Analysis for Vision-Based Activity Identification of Earthmoving Excavators and Dump Trucks," Automation in Construction, Vol. 87, pp. 297-308, 2018.

[2] Vortex Studio, accessed 2020.06.27. https://www.cm-labs.com/vortex-studio/

[3] Hyunsoo Kim, Changbum R.Ahn, David Engelhaupt, and Sanghyun Lee: "Application of Dynamic Time Warping to the Recognition of Mixed Equipment Activities in Cycle Time Measurement," Automation in Construction, Vol. 87, pp. 225-234, 2018.

[4] Nipesh Pradhananga, and JochenTeizer: "Automatic Spatio-Temporal Analysis of Construction Site Equipment Operations Using GPS Data," Automation in Construction, Vol. 29, pp. 107-122, 2013.

[5] Reza Akhavian, and Amir H.Behzadan: "Construction Equipment Activity Recognition for Simulation Input Modeling Using Mobile Sensors and Machine Learning Classifiers," Advanced Engineering Informatics, Vol.29, pp. 867–877, 2015.

[6] Quoc V Le, Will Y Zou, Serena Y Yeung, and Andrew Y Ng: "Learning Hierarchical Invariant Spatio-Temporal Features for Action Recognition with Independent Subspace Analysis," In Proceedings of the IEEE Conference on Computer Vision and Pattern Recognition (CVPR 2011), pp. 3361-3368, 2011.

[7] Samitha Herath, Mehrtash Harandi, and Fatih Porikli: "Going Deeper into Action Recognition: A Survey," In Image and vision computing, Vol 60, pp. 4-21, 2017.

[8] Jinwoo Kim, Seokho Chi: "Action Recognition of Earthmoving Excavators based on Sequential Pattern Analysis of Visual Features and Operation Cycles," Automation in Construction, Vol. 104, pp. 255-264, 2019.

[9] Chen Chen, Zhenhua Zhu, and Amin Hammad: "Automated Excavators Activity Recognition and Productivity Analysis from Construction Site Surveillance Videos," Automation in Construction, Vol. 110, 103045, 2020.

[10] Jeffrey Donahue, Lisa Anne Hendricks, Sergio Guadarrama, Marcus Rohrbach, Subhashini Venugopalan, Kate Saenko, and Trevor Darrell: "Long-term Recurrent Convolutional Networks for Visual Recognition and Description," In Proceedings of the IEEE Conference on Computer Vision and Pattern Recognition (CVPR 2015), pp. 2625-2634, 2015.

[11] Du Tran, Lubomir Bourdev, Rob Fergus, Lorenzo Tor-resani, and Manohar Paluri: "Learning Spatiotemporal Features with 3D Convolutional Networks," In Proceedings of the IEEE International Conference on Computer Vision (ICCV 2015), pp. 4489-4497, 2015.

[12] Christian Szegedy, Vincent Vanhoucke, Sergey Ioffe, Jon Shlens, and Zbigniew Wojna: "Rethinking the Inception Architecture for Computer Vision," In Proceedings of the IEEE Conference on Computer Vision and Pattern Recognition (CVPR 2016), pp. 2818–2826, 2016.

[13] Shotcut, accessed 2020.06.27. https://shotcut.org/

Real-time Aarly Warning of Clogging Risk in Slurry Shield Tunneling: A Self-updating Machine Learning Approach

Qiang Wang[a], Xiongyao Xie [a], and Yu Huang [a]

[a]Department of geotechnical engineering, Tongji University
E-mail: wangqiang_tju@qq.com, xiexiongyao@tongji.edu.cn, yhuang@tongji.edu.cn

Abstract –

Clogging is one of the main risks when slurry shield tunneling in the mixed ground condition containing clayey soils. Severe consequences, such as instability in the excavation face and high cutter wear, may occur if the shield machine operators don't take specific measures to eliminate clogging. Therefore, early warning of clogging during one ring excavation becomes essential for the safety of tunneling. The currently available methods to judge the clogging risks focus mainly on field engineer experience, which seems arbitrary sometimes. In this paper, an automatic self-updating machine learning approach is proposed to realize the real-time early warning of clogging. More specifically, the random forest is employed with several minutes (e.g. 2 min at the beginning of one ring excavation) of tunneling parameters as input. When one ring has been finished, it will become a new training sample to update the model via randomized parameter optimization. With the case study of Nanning metro line 1, it's found that the self-updating mechanism is beneficial for better judgment of clogging, and 4 minutes tunneling parameters (24 samples) are suitable for early warning. The model can achieve an accuracy of 95% in the mixed ground condition. Meanwhile, in comparison with the other machine learning approaches is also discussed. With the training data set updating mechanism, the RF model can use less tunneling data to realized the clogging prediction. According to the feature importance result, the variation of cutterhead torque is essential for clogging prediction.

Keywords –

Shield tunneling; Clogging; Early warning; Random forest; Self-updating

1 Introduction

Shield tunneling in clayey soils is frequently obstructed by clogging problems, both for earth pressure balanced (EPB) tunnel boring machine (TBM) and slurry pressure balanced (SPB) tunnel boring machine [1,2]. The clogging problem will trigger risks during tunneling construction, such as slower tunneling efficiency[3], instability of tunnel face[4], higher wear of cutterhead[5], etc. As a typical kind of clayey soil, mudstone has a high potential to result in a clogging problem[4]. Several projects in China have been encountered with clogging problems in mudstone rich area, for example, Wuhan Sanyang cross-river road tunnel[6], the metro tunnel line 1&2 in Nanning city[7], Nanchang metro line 1[8], Nanjing Yangze river tunnel[9]. The filed experience indicates that it's difficult to maintain the normal tunneling state in mudstone rich area, especially for the mixed ground containing mudstone.

Clogging is induced by the stickiness of the excavated clayey soil, which can be influenced both by the clay mineralogy and the slurry flow behavior [2,10]. There are several laboratory tests have been presented for evaluating the clogging potential of one certain kind of soil and slurry flow behavior [2,10–12], which brings out some directly or indirectly methodologies for clogging judgment. These clogging elevation methods rely on the soil properties and most of them focused on either sand or clayey soils, which has a limitation in mixed ground conditions[2,13]. Moreover, there is still a lack of early warning methods for clogging during the tunneling process.

The criteria to evaluate clogging potential mainly focused on the soil properties but pay little attention to the slurry or foam properties well as shield driver operations in shield tunneling process[14]. When SPB shield tunneling in the mixed ground containing mudstone, it is difficult to determine whether clogging occurs only rely on the geological conditions. Therefore it is crucial to develop an early warning approach for clogging both based on the geological conditions and tunneling parameters. The data-driven approach, such as the random forest (RF) method, seems appropriate in the tunneling process. The clogging state can be regarded as an abnormal tunneling situation, thus it can be considered as a binary classification problem. RF algorithm for the development of descriptive and predictive data-mining models has become widely accepted in engineering

applications, promising powerful new tools for practicing engineers [15].

Kohestani et al.[16] presented an RF-based model for prediction of seismic liquefaction potential of soil based on the cone penetration test data, and the proposed RF models provide more accurate results than the artificial neural network (ANN) and the support vector machine (SVM) models. Zhou et al.[17] employed eleven algorithms to predict the rockburst classification and found the RF achieved the best result. The above-mentioned applications of the RF-based classification model are all static models. They employed well-trained RF models for all test data sets, which is not suitable for the shield tunneling process. As a real-time early warning model for clogging, the proposed model should be trained via as few rings as possible and is supposed to realize self-updating as new rings have been finished. As a result, a training data set updating mechnism will be designed in this paper to realize the real-time early warning of clogging risk in SPB shield tunneling.

The remainder of the paper is organized as follows: In section 2, we introduce the real-time early warning model based on RF. In section 3, the case study in Nanning metro will be presented. The impact of training data set updating mechanism will be discussed in section 4 before presenting the conclusions.

2 Real-time early warning of clogging risks based on RF

Figure 1 shows the process for real-time early warning of clogging risks with training data updating during shield tunneling construction. Suppose there are L rings in total for a tunnel section, and the shield machine is going to tunneling at the ring #i ($i \quad L$). Firstly, we select N minutes tunneling data at the beginning of each i-1 rings as the early warning input feature ($N = 0.5,1,2,3\ldots$) and take the i-1 rings clogging state as output, which will be composed as the training data set. Secondly, the ith clogging prediction model is trained with the above training data set, whose hyper-parameters are determined by the 5-fold cross-validation and randomized search[18]. Then, the proposed prediction model is used to predict the clogging state of ring #i via the N minutes tunneling data at the beginning of the ith ring. Finally, when the ring #i has been finished, we will determine the real clogging state for the ith ring based on the above mentioned three criteria. Moreover, the training data set will be updated by adding the input feature and clogging state of ring #i. This process will continue until the tunneling section has been finished.

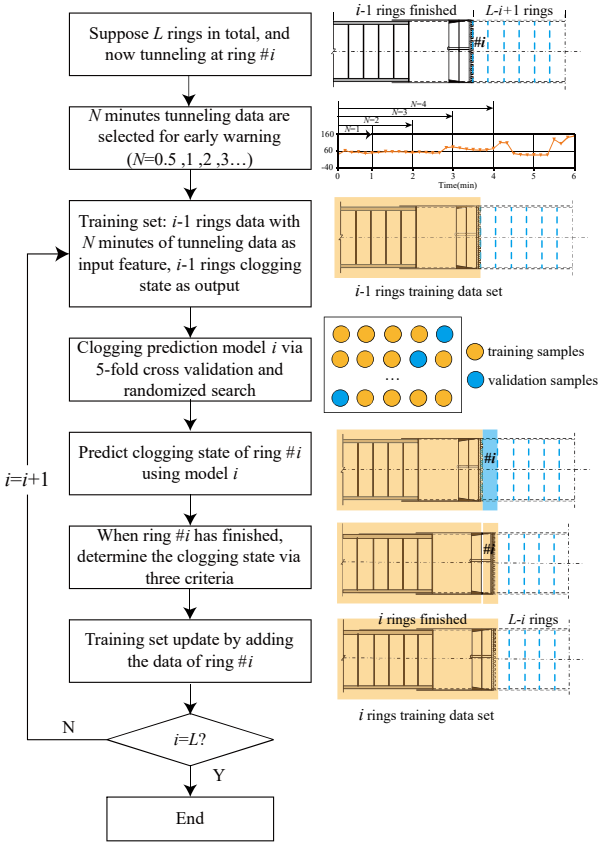

Figure 1. Flow chart for real-time early warning of clogging with training data updating

Random forest (RF) is an ensemble learning method for classification that operates by constructing a large number of decision trees at training time and outputting the class that is the mode of the classes of the individual trees[19]. As illustrated in Figure 2, samples and features are randomly selected from the data set using the bootstrap aggregating method. Therefore, many sub-samples are created by choosing random features with replacement. Then each decision tree will be trained on the sub-sample and the final class (clogging or normal) will be determined by averaging the probabilistic prediction of all the trees. Several hyper-parameters in the RF will be determined by cross-validation, such as the number of trees in the forest ($n\_estimators$), the maximum depth of the tree ($\max\_depth$), etc. To improve the training efficiency during shield tunneling construction, the randomized search strategy is employed instead of the traditional grid search method. This strategy implements a randomized search over the hyper-parameters, where each setting is sampled from a distribution over possible hyper-parameter values.

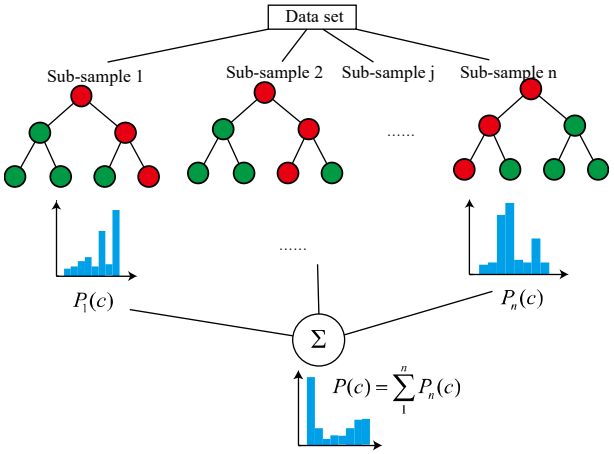

Figure 2. Schematic diagram of random forest classifier

3 Case study in Nanning metro

3.1 Project Overview

Nanning metro line 1 is the first metro line with twin tunnels in Guangxi province. The section of left line in Nanning Metro Line 1 between Bai Cang Ling Station and Railway Station (BR section) is 1209 m (806 rings in total with segment width of 1.5 m), which is encountered with the mixed ground condition of mudstone and round gravel and is thus selected as a case study. As a massive of sensitive adjacent buildings along the tunnel section, shown in Figure 3 (a), the BR section was excavated with a Herrenknecht SPB shield machine with a diameter of 6.28 m.

The tunnel in the BR section is surrounded by complex geological and hydrological conditions. The tunnel passing through geological profiles (illustrated in Figure 3 (b)) are mainly round gravel, mudstone, and sand, which are shown in different colors in Figure 3 (b). The mixed ground containing mudstone locates around ring # 120 to ring # 220, and ring # 283 to ring # 470. A total of 36 boreholes have been drilled to obtain the geotechnical characteristics of the soils found along the BR section (refer to Table 1). The distance between the ground to the tunnel crown ranges from 14 m to 22 m, while the distance between the underground water table to the tunnel crown is about 1.5m to 9m. The round gravel is saturated in the BR section, which mainly consists of gravel with a small number of pebbles (Figure 4 (a)). The average content of particles with a grain size of 2-20mm is 52.8%, and the average content of particles with a grain size greater than 20mm is 25.3%. The inter-particle filling is mainly medium and coarse sand. The round gravel has a very strong permeability coefficient of 90 m/d. In contrast, the mudstone (Figure 4 (b)) has a small permeability coefficient of 0.01 m/d, as listed in Table 1. Figure 4 (c) illustrates the grain size distribution of mudstone samples obtained in the BR section. It can be found that the grain size of mudstone is almost smaller than 0.1 mm and there are about 64% of particles with a grain size smaller than 0.005 mm.

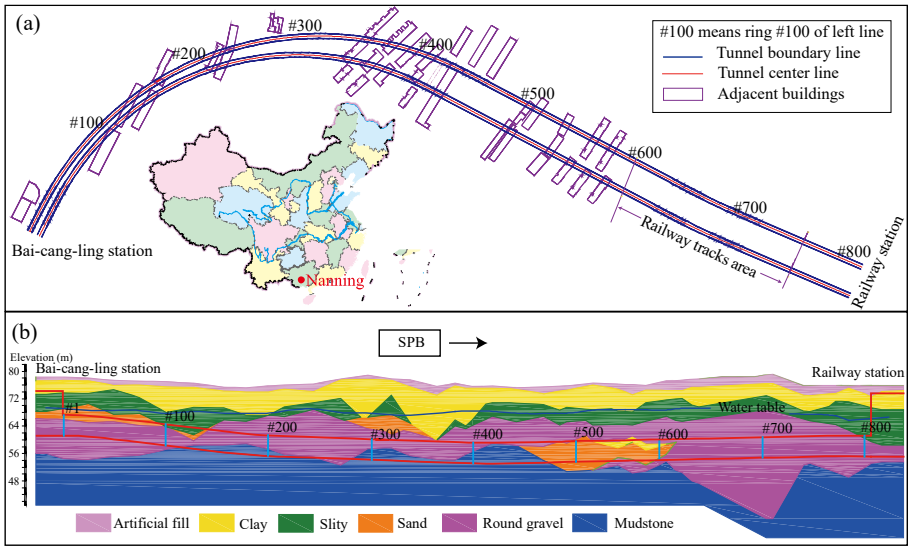

Figure 3. Schematic illustration of BR section of Nanning metro line 1, (a) plan view and parts of adjacent buildings, and (b) cross-section view. # 100 means ring # 100 in the left line

Table 1. Geotechnical characteristics of round gravel and mudstone in the BR section

Soil			c		K
	g/cm^3		kPa	°	m/d
Round gravel	2.05	0.27	0.0	35.0	90
Mudstone	2.15	0.20	90.0	21.0	0.01

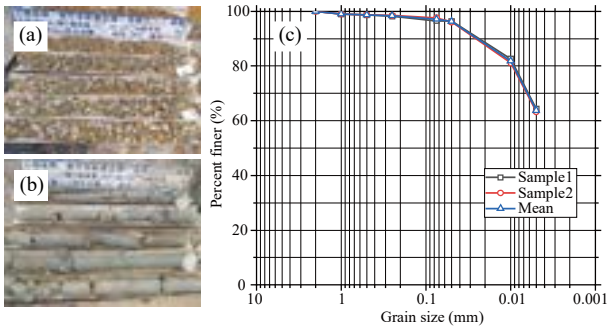

Figure 4. Borehole results of (a) round gravel and (b) mudstone, and (c) grain size distribution curve of mudstone in the BR section

According to the classification diagram raised by F. S. Hollmann and Thewes[1], the mudstone in the BR section is in the form of lumps, this may cause massive clogging because large lumps of this clay could form blockages in critical flow paths of an SPB shield machine. What's worse, to keep tunnel face stability of the water-rich round gravel, the marsh funnel viscosity of the slurry used in the SPB ranges from 24s to 32s, which has made the excavated material more easily clog at the opening of the submerged wall between the excavation chamber and the working chamber, as demonstrated in Figure 5.

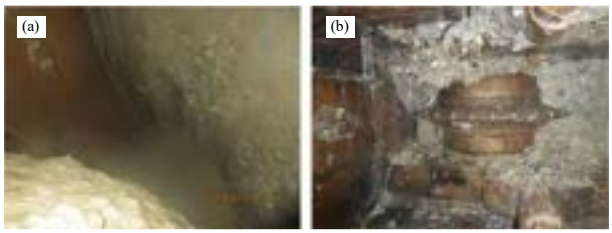

Figure 5. (a) clogging situation observed by opening the excavation chamber and (b) high wear of cutters

3.2 Data Description

The tunneling parameters in the BR section are recorded via the programmable logic controller (PLC) every 10 seconds. There is a total of 666 complete ring data that will be analyzed in this study. Four kinds of tunneling parameters are selected for clogging prediction, which are the difference (ΔSP) between slurry pressure in the excavation chamber (SPE) and slurry pressure in the working chamber (SPW), the cutterhead torque (TOR), total thrust (THR), penetration rate (PR). The SPE and SPW are measured by pressure sensors locating at the spring line of both chambers. To elevate the influence of mudstone, a mixed ratio λ [4] is defined as Eq. (2).

$$\Delta SP = SPW \quad SPE \tag{1}$$

$$\lambda = H_m / D \tag{2}$$

where H_m is the mudstone thickness in the tunnel excavation face and is determined by the geological report. D is the SPB cutterhead diameter.

Here we pay more attention to the instantaneous values of ΔSP, so we define a slurry pressure fluctuation index (SPFI) θ, as illustrated in Figure 6(a) and in E.q.(3). In normal conditions, the values of ΔSP are in the range of 0 to 20 kPa (Figure 6(d)). However, when clogging occurs, the values of ΔSP may range from -50 kPa to -150 kPa (Figure 6(b)). We plot 10 minutes of instantaneous values of ΔSP and their SPFIs in Figure 6 considering different ground conditions.

$$S_{positive} = \frac{1}{2}\left(\Delta SP dt + |\Delta SP| dt \right)$$

$$S_{negative} = \frac{1}{2}\left(\Delta SP dt - |\Delta SP| dt \right) \tag{3}$$

$$\theta = \frac{abs(S_{negative})}{S_{positive} + abs(S_{negative})}$$

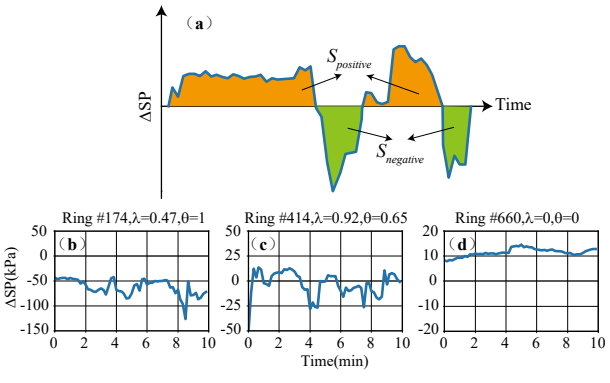

Figure 6. Definition of slurry pressure fluctuation index and typical examples in different ground conditions (10 minutes data), (a)schematic diagram of θ, (b) ring #174, $\theta = 1$ in half mudstone and half round gravel condition, (c) ring

#414, $\theta = 0.65$ in mudstone condition, and (d) ring #660, $\theta = 0$ in round gravel condition.

According to field observation, we plot the clogging rings distribution, as well as the SPFI θ and mixed ratio λ, as shown in Figure 7. It can be found that there are dramatic fluctuations of SPE in most clogging rings as the values of θ are all near one when clogging occurs. Also, the distribution of the mixed ratio is not always consistent with the clogging state, which may be caused by the uncertainty of the mudstone distribution in the geological survey as well as the mudstone that stuck to the cutterhead.

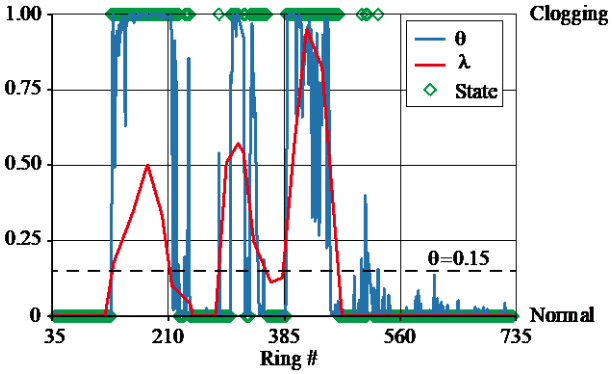

Figure 7. Distribution of mixed ratio, SPFI, and clogging state in the BR section

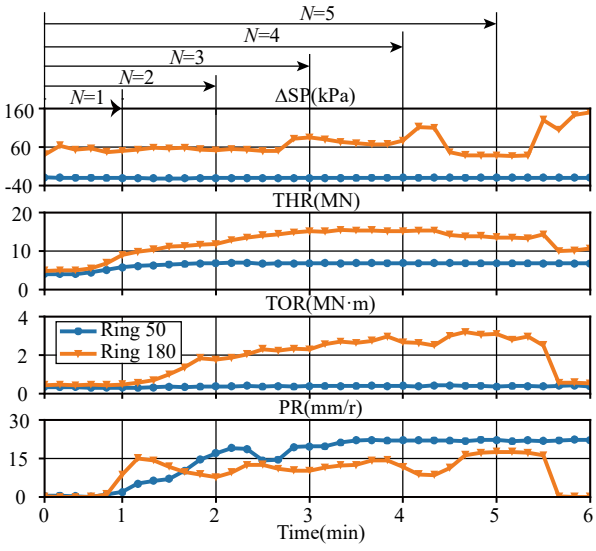

Figure 8. Demonstration of six minutes of tunneling data of clogging ring (ring #180) and normal ring (ring #50) at the beginning of each ring

Figure 8 demonstrates an example of the six minutes tunneling data that will be used as the input feature for clogging prediction.We employ 17 kinds of features as the input, including the statistical indexes (mean values, standard deviations, maximum values, and range values) of the ΔSP, THR, TOR, PR, as well as the SPFI (θ). We will explore the influence of parameter length N because the smaller of N value, the better for real-time early warning.

3.3 Clogging Prediction Results in the BR Section

We define the confusion matrix for clogging prediction in Table 2, where the P=Positive, that means the clogging state; the N=Negative, that means the normal state; TP=True Positive, that means the actual state of one ring is clogging and the predicted state is also clogging; FP=False Positive, that means the actual state of one ring is normal but the predicted state is clogging; TN=True Negative, that means the actual state of one ring is clogging but the predicted state is normal; FN=False Negative, that means the actual state of one ring is normal and the predicted state is also normal. We conduct the error rate, precision, recall, and F1 to evaluate the prediction model performance, as shown in E.q. (4). The high precision relates to a low false positive (FP) rate, and high recall relates to a low false negative (FN) rate. High scores for both show that the classifier is returning accurate results (high precision), as well as returning a majority of all positive (clogging) results (high recall).

$$
\begin{aligned}
error\ rate &= \frac{FP+FN}{TP+TN+FP+FN}\times 100\% \\
precision &= \frac{TP}{TP+FP}\times 100\% \\
reacall &= \frac{TP}{TP+FN}\times 100\% \\
F1 &= \frac{2\times precision\times reacall}{precision+reacall}
\end{aligned}
\tag{4}
$$

Table 2. Confusion matrix for clogging prediction

		Actual class	
		P: Clogging	N: Normal
Predicted class	P: Clogging	TP	FP
	N: Normal	FN	TN

As mentioned before, there are 666 rings for analysis in the BR section, and 229 rings are regarded as clogging state (Figure 7). We choose the first 90 rings as the initial training data set and then examine the different tunneling data length ($N = 0.5, 1, 2, 3, 4, 5, 6, 8$). The hyper-parameters ($n\_estimators$ and max_depth)

distribution for the RF model is the random number between 0 to 1000. To compare different model performances, we also employ the *K*-nearest neighbor (KNN) model[20], the support vector classification (SVC) model[21], and the multi-layer perceptron (MLP) model[22]. The hyper-parameters (*n_neighbors*) distribution for the KNN model is the random number between 0 to 10. The RBF function is adopted as the kernel function in the SVC model, which has a logarithmically spaced *C* values range from 1 to 1000 with a vector length of 20, a logarithmically spaced *gamma* values range from 0.001 to 1000 with a vector length of 7. The MLP model has one hidden layer with different neurons from 5 to 25 with an increase of 25. The learning rate of the MLP model is set as a logarithmically spaced values range from 1 to 1000 with a vector length of 4.

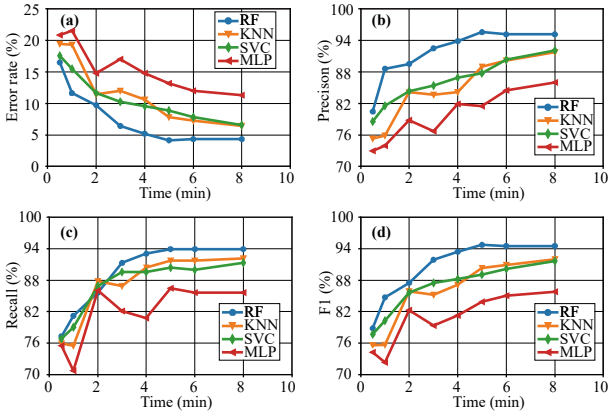

Figure 9. Clogging prediction model performances with different tunneling data length, (a) error rate, (b) precision, (c) recall, and (d) F1

After the simulation of 666 rings in the BR section, Figure 9 illustrates the metrics of the four clogging prediction models with different tunneling data length. The model performance becomes better as the tunneling data length increases, and the RF model performs best among these four models considering all the metrics. The KNN model performance is similar to the SVC model while the MLP model performs worst with a very high error rate. From Figure 9 (a), it can be found that when we use four minutes of tunneling data to predict the clogging state, the RF model error rate is 5%, which seems well enough for tunneling construction. What's more, the four minutes tunneling data makes the RF model yield a high precision (Figure 9 (b)), recall (Figure 9 (c)) and F1 score (Figure 9 (d)), which are about 94%. With the increase of tunneling data length, the RF model performance increases slightly. Therefore, we believe the data length of four minutes at the beginning of one ring tunneling period is a good choice for clogging state prediction.

3.4 Discussion on Model Performance

3.4.1 Model Performance without Training Data Updating

Table 3 lists the metrics of the RF clogging prediction model considering different training strategies. One strategy uses the updating training data set and the other one just employs the initial training data set without updating. We can see that the model with updating the training data set achieves a better prediction accuracy than the model with the static training data set. We can realize the early warning of clogging with the four minutes of tunneling data with an error rate of 5.2% in the proposed model. However, we need five to eight minutes of tunneling data to realize the same goal when the training data remains unchanged. One possible reason for this difference is that the RF model learns more patterns about clogging when the training data set is updated as shield machine advances.

Table 3. Metrics comparison of RF clogging prediction model considering different training strategies

Tunneling data length (minutes)	Error rate (%)		Precision (%)		Recall (%)		F1 (%)	
	Updating	No updating	Updating	No updating	Updating	No updating	Updating	No updating
0.5	16.5	20.7	80.5	80.2	77.3	62.8	78.9	70.4
1	11.6	18.6	88.6	77.5	81.2	75.2	84.7	76.3
2	9.7	24.5	89.5	64.3	85.6	84.5	87.5	73.0
3	6.4	12.5	82.5	80.1	91.3	91.2	86.7	85.3
4	5.2	9.7	93.8	84.6	93.4	92.7	93.6	88.5
5	4.2	5.4	95.6	94.1	93.9	92.8	94.7	93.4
6	4.3	5.5	95.1	95.2	93.9	92.6	94.5	93.9
8	4.3	5.2	95.1	94.2	94.0	92.8	94.6	93.5

3.4.2 Influence of Input Features on Clogging Prediction

In section 3.2, we employ 17 kinds of features as the clogging prediction model input. For better guidance for shield tunneling construction, here we carry out feature importance to investigate which kind of features has a crucial impact on clogging prediction. The permutation feature importance technology [23] is adopted with four minutes of tunneling data in the RF model. Figure 10 shows the feature importance result with the metric of error rate in different states. Firstly, we consider the whole tunnel section, and there are two kinds of input feature that has feature importance larger than 10%, which are the mean and maximum values of the TOR. Also, the maximum and range values of the PR should be considered. Then, if we just consider the normal state rings, the influence of PR seems quite important as the feature importances of maximum values, range values, and standard deviations of PR are larger than 10%. Finally, when we consider the clogging rings, it can be found that the feature importances of the mean and maximum values of the TOR are larger than 15%, which means the variation of TOR should be taken as the priority to make the judgment of clogging.

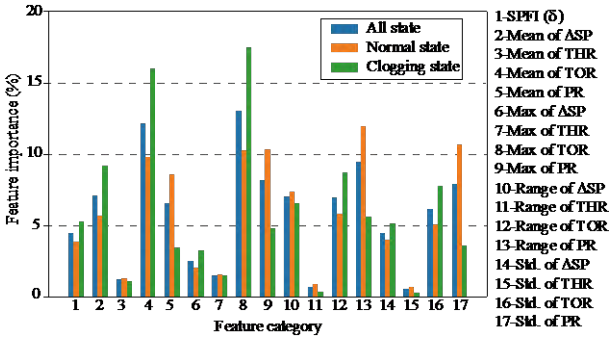

Figure 10. Feature importance of the RF model considering different states

4 Conclusion

This paper proposed a real-time early warning strategy of clogging risks based on RF. The clogging early warning model performance was evaluated. Results of conducted analyses show that:

(1) The RF model can realize the real-time early warning of clogging with four minutes of tunneling data at the beginning of one ring, which achieves an error rate of 5%. Compared with the KNN model, the SVC model, and the MLP model, the RF model gives the best performances.

(2) The statistical indexes of TOR are essential for clogging judgment while the PR is crucial for normal state identification based on the importance of the explanatory features. Without updating the training data set, the RF model needs more tunneling data to make a good prediction of clogging.

Although we have realized some achievements in the analysis and prediction of the clogging risks based on the tunneling parameters, we still pay more attention to the control measures to mitigate the clogging problem. For example, more appropriate slurry properties design for mixed ground containing mudstone is vital, which can keep the tunnel face stability and convey the excavated material more smoothly. Besides, it's significant to carry out the intelligent models that can have good control of tunneling parameters in high clogging risk areas instead of the trial-error process based on field experience.

References

[1] F.S. Hollmann, M. Thewes, Assessment method for clay clogging and disintegration of fines in mechanised tunnelling, Tunn. Undergr. Sp. Technol. 37 (2013) 96–106.

[2] D.G.G. de Oliveira, M. Thewes, M.S. Diederichs, Clogging and flow assessment of cohesive soils for EPB tunnelling: Proposed laboratory tests for soil characterisation, Tunn. Undergr. Sp. Technol. 94 (2019) 103110.

[3] N. Tokgöz, I. Serkan Binen, E. Avunduk, An evaluation of fine grained sedimentary materials in terms of geotechnical parameters which define and control excavation performance of EPB TBM's, Tunn. Undergr. Sp. Technol. 47 (2015) 211–221.

[4] X. Xie, Q. Wang, Z. Huang, Y. Qi, Parametric analysis of mixshield tunnelling in mixed ground containing mudstone and protection of adjacent buildings: case study in Nanning metro, Eur. J. Environ. Civ. Eng. 22 (2018) s130–s148.

[5] J. Zhao, Q.M. Gong, Z. Eisensten, Tunnelling through a frequently changing and mixed ground: A case history in Singapore, Tunn. Undergr. Sp. Technol. 22 (2007) 388–400.

[6] L. Bo, B. Qin, Key Techniques for Construction of Sanyang Road Cross-river Tunnel of Wuhan Rail Transit Line 7, Tunn. Constr. 39 (2019) 820–831.

[7] Q. Wang, X. Xie, Z. Huang, Y. Qi, Protection of adjacent buildings due to mixshield tunnelling in mixed ground with round gravel and mudstone, in: Proc. World Tunn. Congr. 2017 – Surf. Challenges – Undergr. Solut., Bergen, Norway, 2017: pp. 14635-1–10.

[8] X. Ye, S. Wang, J. Yang, D. Sheng, C. Xiao, Soil conditioning for EPB shield tunneling in argillaceous siltstone with high content of clay

minerals: Case study, Int. J. Geomech. 17 (2017) 1–8.
[9] F. Min, W. Zhu, C. Lin, X. Guo, Opening the excavation chamber of the large-diameter size slurry shield: A case study in Nanjing Yangtze River Tunnel in China, Tunn. Undergr. Sp. Technol. 46 (2015) 18–27..
[10] R. Zumsteg, A.M. Puzrin, G. Anagnostou, Effects of slurry on stickiness of excavated clays and clogging of equipment in fluid supported excavations, Tunn. Undergr. Sp. Technol. 58 (2016) 197–208.
[11] F.S. Hollmann, M. Thewes, Assessment method for clay clogging and disintegration of fines in mechanised tunnelling, Tunn. Undergr. Sp. Technol. Inc. Trenchless Technol. Res. 37 (2013) 96–106.
[12] N. Tokgöz, I. Serkan Binen, E. Avunduk, An evaluation of fine grained sedimentary materials in terms of geotechnical parameters which define and control excavation performance of EPB TBM's, Tunn. Undergr. Sp. Technol. 47 (2015) 211–221.
[13] J.N. Shirlaw, Pressurised TBM tunnelling in mixed face conditions resulting from tropical weathering of igneous rock, Tunn. Undergr. Sp. Technol. 57 (2016) 225–240.
[14] C. Budach, D. Placzek, E. Kleen, Quantitative Bestimmung des Verklebungspotenzials feinkörniger Böden auf Basis von Adhäsionsspannung: Aktuelle Untersuchungen und neue Erkenntnisse, Geotechnik. 42 (2019) 2–10.
[15] S.E. Seker, I. Ocak, Performance prediction of roadheaders using ensemble machine learning techniques, Neural Comput. Appl. 31 (2019) 1103–1116.
[16] V.R. Kohestani, M. Hassanlourad, A. Ardakani, Evaluation of liquefaction potential based on CPT data using random forest, Nat. Hazards. 79 (2015) 1079–1089.
[17] J. Zhou, X. Li, H.S. Mitri, Classification of rockburst in underground projects: Comparison of ten supervised learning methods, J. Comput. Civ. Eng. 30 (2016) 1–19.
[18] J. Bergstra, Y. Bengio, Random search for hyper-parameter optimization, J. Mach. Learn. Res. 13 (2012) 281–305.
[19] L. Breiman, Random forests, Mach. Learn. 45 (2001) 5–32.
[20] R. Akhavian, A.H. Behzadan, Smartphone-based construction workers' activity recognition and classification, Autom. Constr. 71 (2016) 198–209.
[21] Q. Zhang, Z. Liu, J. Tan, Prediction of geological conditions for a tunnel boring machine using big operational data, Autom. Constr. 100 (2019) 73–83.
[22] C.O. Sakar, S.O. Polat, M. Katircioglu, Y. Kastro, Real-time prediction of online shoppers' purchasing intention using multilayer perceptron and LSTM recurrent neural networks, Neural Comput. Appl. 31 (2019) 6893–6908.
[23] A. Fisher, C. Rudin, F. Dominici, All models are wrong, but many are useful: Learning a variable's importance by studying an entire class of prediction models simultaneously, J. Mach. Learn. Res. 20 (2019) 1–81.

Efficient Numerical Methods for Accurate Modeling of Soil Cutting Operations

A. Haeri[a], D. Tremblay[a], K. Skonieczny[a]
D. Holz[b], M. Teichmann[b]

[a]Department of Electrical and Computer Engineering, Concordia University, Canada
[b]CM Labs Simulations, Canada

[a]{a_hae, kskoniec}@encs.concordia.ca, dominique.tremblay@concordia.ca, [b]{danielh, marek}@cm-labs.com

Abstract -

This research investigates the development and validation of state-of-the-art high-fidelity models of soil cutting operations. The accurate and efficient modeling of complex tool-soil interactions is an open problem in the literature. Modeling options that provide more flexibility in trading off accuracy and computational efficiency than current state-of-the-art continuum or discrete element methods are sought. In this work, two modern numerical methods, the material point method (MPM) and a hybrid approach, are presented with the goal to simulate excavation maneuvers efficiently and with high accuracy. MPM, as an accurate, continuum-based and meshfree method, uses a constitutive model (here, nonlocal granular fluidity model) for computing internal forces to update particle velocities and positions. The hybrid approach, a combination of particle and grid-based methods, avoids explicit integration scheme difficulties and unnecessary computations in the static regime. Visual and quantitative data, including forces on the excavation tool, are collected experimentally to evaluate these two simulation methods with respect to geometry of the soil deformation as well as interaction forces, both as a function of time.

Keywords -

Granular Flow; Physics-Based Simulation; Physically-Based Modeling; Terramechanics; Soil Mechanics; Computer Graphics; Experiment

1 Introduction

On Earth, construction, mining, and agricultural vehicles are extensively in contact with soil as a granular material. In space, exploration rovers are as well, as will robots for in situ resource utilization. However, granular flows and their interactions with rigid bodies are still poorly understood. In fact, their modeling is complex since they can experience various solid-like, fluid-like and gas-like deformations in time. Besides experiments, simulations can hugely contribute to this end. Nevertheless, the accurate and efficient modeling of complex tool-soil interactions is still an open research problem. In terms of accuracy, one current direction of this research is the discrete element method (DEM), which simulates contact mechanics for millions of individual particles [1]. This state-of-the-art approach demonstrates promise in modeling but it is so computationally intensive as to be infeasible for real-time applications, and for large physical domains can be untenably expensive even in offline industrial applications [2]. On the other end of the complexity spectrum, several researchers highlight the insufficient predictive power of classical terramechanics models [3, 4], and their limitations to specific flow geometries [5], though they are computationally efficient.

In order to maintain a desired accuracy while enhancing computational efficiency, one possible direction is using methods from continuum mechanics. In continuum methods, there are two main aspects to make them appropriate for a specific modeling problem. One aspect is the constitutive model; it should be specific to the material being used to capture most of the static and/or flow regimes. For granular materials, they should generally cover elastic (solid-like), viscoplastic (fluid-like), and free (gas-like) behaviors. For the two extremes, elastic and free models have been developed based on soil mechanics (e.g. Drucker-Prager) and kinetic theory of gases, respectively. However, the middle regime of (visco) plastic deformation is more challenging. Plastic models can suffer from rate-independency [6] and in some cases, they may have issues with modeling strain hardening [7]. Whereas, viscoplastic models eliminate some numerical difficulties associated with plastic models, such as hardening [8]. In viscoplastic models, although local models [9] lack robustness in their ability to predict all flow phenomena, nonlocal models are accepted as highly predictive in different flow regimes [10]. The other aspect in continuum modeling is the numerical solver. Among the several continuum-based numerical solvers, finite difference (FD) for viscoplastic deformation, and finite element (FE) for elastic deformation, are the most common methods [11]. Both can yield good results in certain cases. However, the FD method has difficulties with extensional disconnection and static regime, while the FE method has issues when mesh dis-

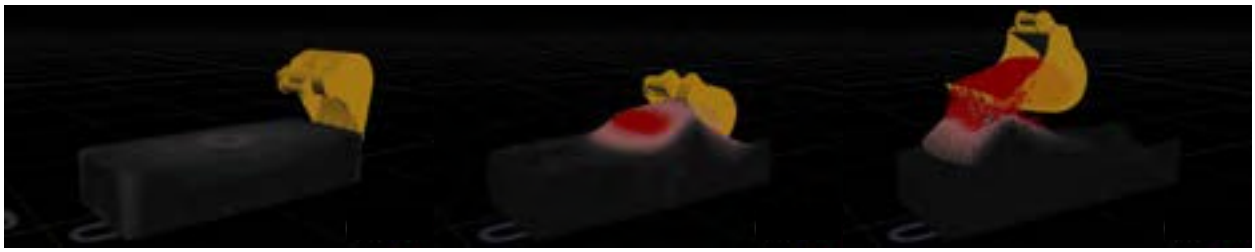

Figure 1. Industrial excavator modeling. Soil colors represent velocity magnitude.

tortion becomes large. Alternatively, the material point method (MPM) is a modern approach that combines the advantages of both FD and FE methods [12].

On the other hand, some novel techniques can be applied to terramechanics models to simultaneously maintain their efficiency and refine their accuracy and flexibility (i.e. extending to complex geometries). In fact, some intensive computations can be ignored in the physical domains that are in the static regime [13]. For the domains in the quasi-static regime which have less deformation, terramechanics models seem to be good candidates. With that, a classical terramechanics model is introduced by McKyes [14] as a method of trial wedges for 2-dimensional soil cutting (known as McKyes model). It is later generalized for 3-dimensional applications such as bucket of excavators and backhoes by Holz et al. [15]. In that, soil cutting forces are formulated based on the fundamental equation of earth-moving (FEE) [16]. Also, Skonieczny [17] replaces the generic surcharge force term in McKyes model with an explicit model of how cutting forces change due to accumulating soil. Thus, this model (McKyes) with all of its modifications can be employed for calculating forces on the cutting tool when the flow is quasi-static. Moreover, more flexible and advanced approaches can be applied to the domains in the intermediate regime specifically with (visco) plastic deformations. Particle-based methods are good candidates due to the nature of the granular flows. However, they often come with prohibitive computational cost, as in traditional DEM. An efficient granular material simulation method, based on Position Based Dynamics (PBD) Muller et al. [18], was introduced by Holz [19] as a faster variation of the traditional DEM. This method showed promising results and was experimentally verified in [20] for a wheel-on-soil configuration. Therefore, this parallel position based approach can be utilized to model the (visco) plastic granular flows when required, and even be used in combination with the modified McKyes model.

With the two aforementioned areas in mind, in this paper, two modern numerical methods are proposed for modeling of soil cutting. First, for the sake of accuracy, while being reasonably efficient, an efficient MPM (Moving Least Squares MPM) solver is utilized with an accurate constitutive model (nonlocal granular fluidity) developed specifically for 3D MPM in a thermodynamically consistent manner and written in C++. Second, a real-time capable and relatively accurate hybrid simulation approach, combining particle and grid-based methods, is presented. This approach was previously introduced by Holz et al. [15] and is here extended with a dynamic soil failure angle calculation for soil cutting operations. Furthermore, the numerical results are compared and evaluated by the experimental data collected by innovative robotic equipment, designed for this type of operation.

2 Methodology

2.1 Numerical Methods

MPM with Nonlocal Granular Fluidity. As discussed, MPM is similar to the FE method but also takes the advantage of FD method by keeping an undeformed Cartesian background grid appropriate for large-deformation problems as well. In addition to the grid, MPM consists of particles that carry information (mass and momentum) during the simulation. The particles can freely deform and, at the end of each time step, transfer the information to the grid nodes and vice versa. The procedure of MPM with the nonlocal model is shown in algorithm 1.

The momentum equation ($\phi\rho\dot{v} = \phi\rho G + \mathrm{div}T$) as the governing equation in the weak form

$$\frac{1}{\Delta t}\int_\Omega \phi\rho\Delta v q\, dV = \int_\Omega \phi\rho G q\, dV - \int_\Omega T\nabla q\, dV \qquad (1)$$

is solved on grid nodes. Where v is velocity, T is Cauchy

Algorithm 1: MPM-NGF

1. Initialization
repeat
   2. Articulate rigid bodies
   3. Calculate contact forces
   4. Affect gravity, internal and contact forces on particle
   5. Transfer momentum from particles to grid
   6. Solve momentum equation on grid nodes
   7. Calculate Laplacian term in NGF on grid
   8. Transfer momentum from grid to particles
   9. Advect particles and rigid bodies
   10. Calculate particle internal forces via NGF

until *Simulation ends*;

stress tensor, G is gravity acceleration, ϕ is volume fraction, q is test function, ρ is density, and V is volume. The angular momentum and energy conservations are satisfied due to the symmetric stress tensor and the implementation of hyperelasticity framework, respectively. To discretize the spatial terms, the Moving Least Squares (MLS) shape function [21] is used. It can speed up MPM by eliminating the need for explicitly calculating the weighting function derivative. Furthermore, it is consistent with the APIC (affine particle-in-cell [22]) particle-grid transfer scheme in the sense that MLS-MPM uses the $\frac{\partial v}{\partial x}$ quantity from APIC, required in the deformation gradient update, to enhance efficiency.

One novel advance in this research is the accurate calculation of internal forces via the unsteady form of Nonlocal Granular Fluidity (NGF) model [23] with hyperelasticity. In fact, this is a thermodynamically consistent version of the nonlocal theory for three-dimensional MPM [24, 25]. Hyperelasticity requires keeping track of the deformation gradient, which is multiplicatively decomposed into elastic and plastic parts. The total deformation gradient is updated via $\dot{F} = \frac{\partial v}{\partial x} F$, and the elastic deformation gradient is calculated via $F^e = F(F^p)^{-1}$. The nonlocal constitutive model is hence utilized to calculate F^p. By assuming that the viscosity ($1/g$ where g is granular fluidity) is time-dependent, the unsteady PDE of the model

$$t_0 \frac{\partial g}{\partial t} = A^2 d^2 \nabla^2 g - (\mu_s - \mu) g - b \sqrt{\frac{\rho_s d^2}{p}} \mu g^2 \quad (2)$$

should be solved for granular fluidity g. Where t_0 is a constant time-scale, A is a dimensionless material parameter called nonlocal amplitude, and d, p, and ρ_s are grain diameter, mean normal stress and grain density, respectively. Also, b is a local rheology parameter, the friction coefficient μ, and static friction coefficient μ_s cause flow to happen. Then the equivalent plastic shear strain rate can be obtained via $\dot{\gamma^p} = g\mu$.

Since in MPM granular materials can be separated, the open-state particles should also be modeled. While kinetic theory of gases is capable of this modeling, in most cases it is accurate enough to handle granular gas via pure kinematics (stress-free). To detect this regime, pressure (mean normal stress) should be tracked for every individual particle. Figure 2 shows four possible states that can occur for a particle in the next time step.

The algorithm used to calculate the internal forces with the nonlocal model is inspired from [25] for the implementation of the hyperelasticity framework. It is well adapted for use in MPM with the techniques used to handle stress-free particles, and to solve the unsteady nonlocal equation explicitly (and uncoupled with the momentum equation). In this, the particle nonlocal Laplacian term is obtained via a second-order FD scheme on the centre grid node in the kernel support of the particle, via equation (3) and the particle internal force can be obtained given the calculated Cauchy stress tensor.

$$\nabla^2 g_{i,j,k} = \frac{1}{\Delta x^2}(g_{i+1,j,k} + g_{i,j+1,k} + g_{i,j,k+1} - 6g_{i,j,k} + g_{i-1,j,k} + g_{i,j-1,k} + g_{i,j,k-1}). \quad (3)$$

The MPM code used is from Hu et al. [21] with an unsteady nonlocal model extension developed by authors of this paper, and written in C++. Also, two issues addressed as corner and penetration issues in [21] are fixed here. From a high performance computing (HPC) viewpoint, multithreading (via Intel TBB) and vectorization (via explicit SIMD) are utilized in the code, in addition to some algorithmic improvements. These techniques make the current MPM 2x faster than a traditional MPM [21].

Hybrid Approach. The hybrid approach presented in this work extends on the hybrid, particle- and grid-based simulation method introduced by Holz et al. [15], which is included in the dynamics simulation toolkit Vortex Studio, created by CM Labs Simulations Inc. In this simulation model, the static soil state is efficiently represented by a grid (a height field in this case). Soil portions in the grid that transition into a dynamic, moving state are replaced by particles. These so-called soil particles are simulated using the Parallel Particles solver (P^2) which ensures efficiency and unconditional stability [19]. The organization of soil in particles and grid is illustrated on the left side of Figure 3.

The motivation behind the described approach is to provide a computationally efficient and stable, yet accurate model, which, by modifying select discretization parameters such as particle count or simulation frequency, can achieve real-time or faster than real-time performance. By using only a limited number of particles at a time,

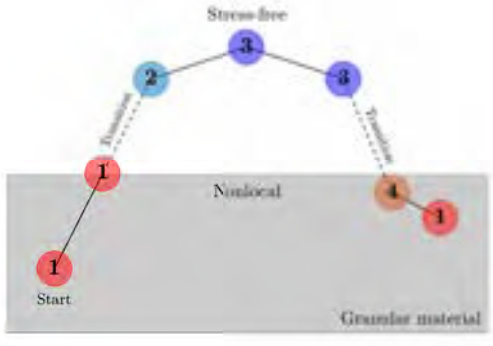

Figure 2. Possible states for a particle: under compression (red) and stress-free (blue). Gray area represents granular material.

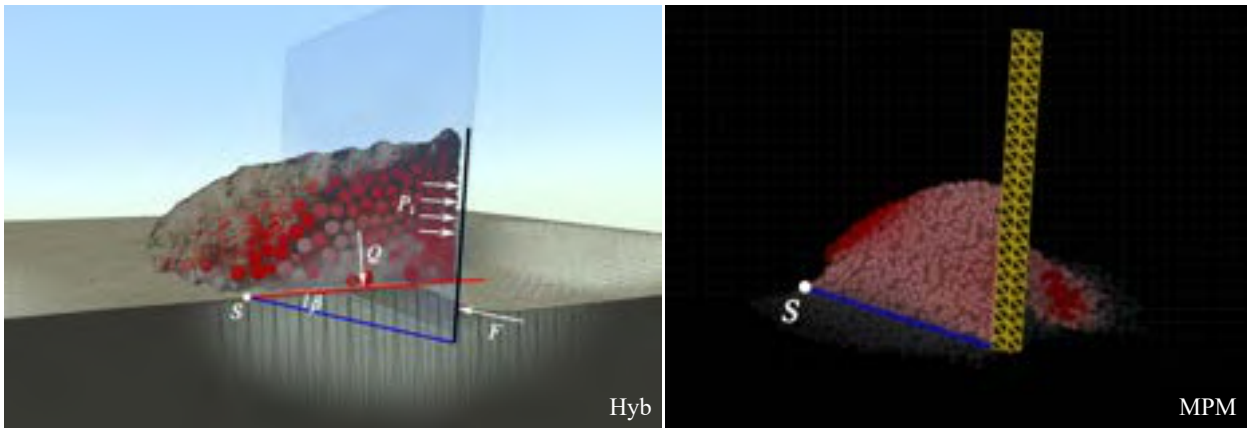

Figure 3. Left: Separation of simulated soil in particles and grid in the Hybrid method and force sources. Particle/blade contact forces, P_i, surcharge force, Q, applied to soil wedge, and McKyes cutting force, F, are indicated. Point S and angle β denote the soil failure point and the soil failure angle, respectively.
Right: Soil deformation pattern in MPM method shows soil failure point S and linear soil failure surface.

cies, i.e., fewer steps per second, can be used without significantly reducing the solution accuracy or causing instabilities. This measure is a great tool for speeding up the proposed method up to real-time running times, as will be shown in Section 3.2.

In the aforementioned setting, soil reaction forces applied to the cutting blade are produced by two sources, the soil mass represented by particles, and the soil mass represented by the grid. Soil particles, which model the surcharge in front of the blade, directly exert contact forces to the contacting blade surface. And the soil grid applies force via a semi-empirical terramechanics model developed by McKyes [14]. This separation of forces is depicted in Figure 3. With increasing surcharge, i.e., increasing amount of soil particles, the soil reaction forces also increase. This is modeled by injecting a surcharge force into the McKyes model as described by Holz et al. [15] and explained in the following sections.

In the McKyes model, soil surface and blade are both assumed to be linear. A non-cohesive soil in front of a moving blade can then be assumed to fail along a straight line. This results in a triangular soil wedge formed by the surface of the terrain, the failure line and the blade. The forces acting on the soil wedge are depicted in Figure 4. In this configuration, the cutting force F per tool width required to induce soil failure and deform the soil can be computed as

$$F = \gamma g d^2 N_\gamma + c d N_c + Q N_Q + c_a d N_a \tag{4}$$

where

$$N_\gamma = \frac{(\cot\rho+\cot\beta)\sin(\alpha+\phi+\beta)}{2\sin(\delta+\rho+\phi+\beta)}, \quad N_Q = \frac{\sin(\phi+\beta)}{\sin(\delta+\rho+\phi+\beta)}, \tag{5a}$$

$$N_c = \frac{\cos\phi}{\sin\beta\sin(\delta+\rho+\phi+\beta)}, \quad N_a = \frac{-\cos(\rho+\phi+\beta)}{\sin\rho\sin(\delta+\rho+\phi+\beta)} \tag{5b}$$

with gravity g, soil slope inclination angle α, tool/soil angle ρ, tool penetration depth d, soil failure angle β, soil internal friction angle ϕ, soil cohesion c, specific weight of the soil γ, tool/soil friction angle δ, tool/soil adhesion c_a and surcharge force per tool width Q.

In the original hybrid model [15], it was assumed that soil failure occurred in the passive Rankine state, leading to a constant soil failure angle β. However, it has been shown that the soil failure angle does not remain constant during a cutting operation and therefore must be dynamically updated [17]. We assume that for non-cohesive soils the point of failure (which is the intersection between soil surface and failure line) roughly occurs at the far end of the accumulating pile of soil that is being pushed by the blade. We verified this assumption in the context of our experiments based on visual inspection of soil failure patterns occurring in the experiments themselves, as well as by inspecting the particle flow in simulations obtained by MPM (cf. right side of Fig. 3). We make use of this assumption by walking across the particle skeleton in front of the blade and in the general blade's forward direction until no more particles can be visited. The position of the

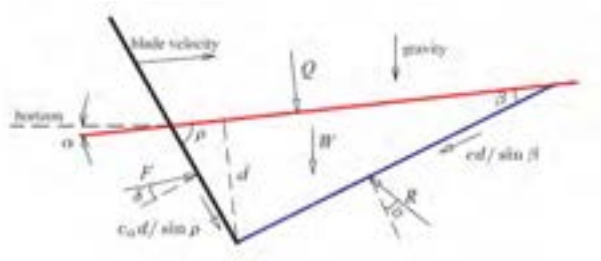

Figure 4. Forces acting on the soil wedge.

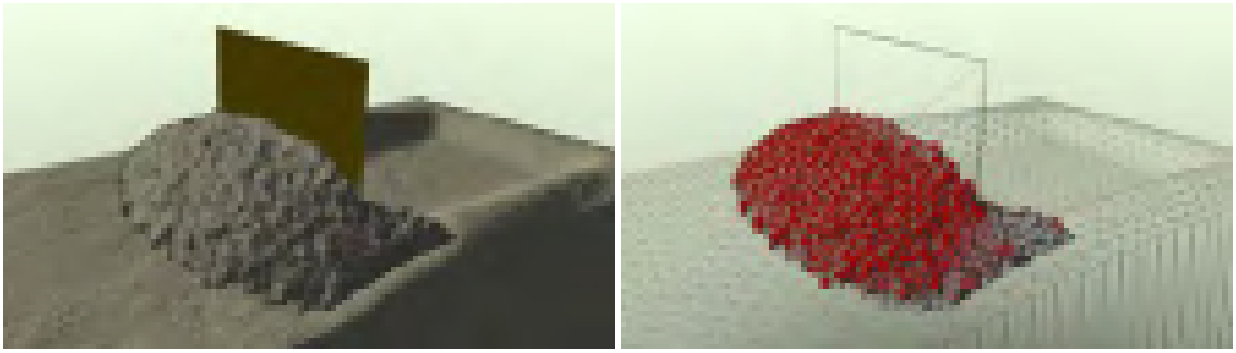

Figure 5. Hybrid method using real-time, screen-space visualization from [26] (left), and display of particles and grid (right), for experiment with 5-cm depth.

last visited particle indicates the location of the soil failure point and is used to compute the soil failure angle used in the McKyes model.

Once the soil failure point is found, the length of the soil wedge ahead of the blade can be determined. All particles sitting on top of this soil wedge contribute to the surcharge force Q from Equation 4, which is measured by summing up all contact forces of the particles colliding with the soil grid and sitting on top of the soil wedge. We experienced that introducing the full surcharge force into the McKyes model leads to too high a soil reaction force computed by the model. Consequently, we suggest a convenient force tuning parameter, denoted as *surcharge contribution factor* $s_q \in [0, 1]$, with which the surcharge force submitted to the McKyes model can be weighted, leading to the following modified version of Equation 4.

$$F = \gamma g d^2 N_\gamma + c d N_c + s_q Q N_Q + c_a d N_a \qquad (6)$$

As will be shown in Section 3, the s_q-factor can be used to calibrate the hybrid method in order to match the simulated soil reaction forces to the forces that are observed in experiments.

2.2 Experimental Method

In this research, an excavation experiment (identical to the simulations) was set up to validate the numerical methods. It consists of a sandbox positioned under a 3-degree-of-freedom motorized unit to which an excavation accessory is attached. For this experiment and for the numerical simulation presented here, the excavation accessory is a flat plate (blade) as depicted in Figure 6 (top). The rake angle of the blade can be set manually and it remains constant during the run. The excavator can be moved horizontally and vertically independently. The motors are controlled such that the impulses from the soil flow do not affect the trajectory of the excavator. The excavator is installed on a force-torque sensor Delta IP60 (ATI Industrial Automation Inc.) that measures the forces and torques on the blade along each direction. The blade trajectory is composed of three segments: first, a downward ramped motion at the start to dive into the soil with a specific depth, then a long-duration horizontal motion, and finally an upward ramp in the end to resemble the motion of an industrial excavator. Two tests were done based on this trajectory but at different (2-cm and 5-cm) depths.

The soil in the experiment is a NASA Glenn Research Center lunar soil simulant (GRC-1). The relative density used is 44.6 +/- 7.2%. This is calculated based on the cone index gradient of 5.30 +/- 0.6 kPa/mm using the correlation in [27]. Thus, the corresponding internal friction angle can be obtained as 35 deg. The grain diameter and density are 0.3 mm and 2583 kg/m^3. Using the triaxial test performed by Oraveca et al. [27] the estimated Young's and shear moduli are 150 and 60 kPa, respectively. Also, the measured external friction angle between the blade and soil is ~30 deg. The setup of the experiment is shown in Figure 6.

3 Results

3.1 Experimental Verification

The tool-soil interactions in the simulations here are evaluated by the forces measured in the experiments (torque comparison is left). Figure 7 compares all the forces from the experiment, MPM and Hybrid method. The quantitative force values are in good agreement with the experimental forces in the three (forward, vertical and lateral) directions. A quantitative assessment of the simulation accuracy in terms of mean percentage error (MPE) is provided in Table 1. Due to the fast technique used to calculate the nonlocal Laplacian term in MPM, the MPM results seem to be slightly more oscillatory than the experimental results. However, in addition to the overall trend, MPM is able to capture drops and rises in force at various time steps of the two experiments. This can highlight the unsteady form of the MPM solver as well as the nonlocal constitutive model. Also, as a real-time method,

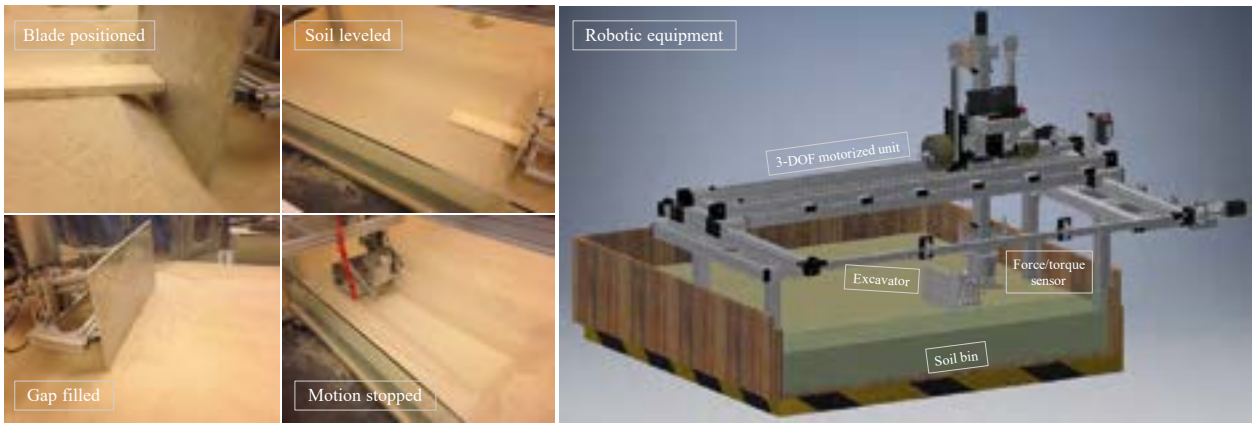

Figure 6. Robotic equipment and experiment setup.

Hybrid has the ability to predict forces as deformations increase. In fact, this time-dependent prediction is made possible by the introduction of the dynamic soil failure angle in the McKyes model, and modeling of the accumulating soil surcharge by particles. Note, that the surcharge contribution factor $s_q = 0.1$ was found to produce the best match between the Hybrid method and the experimental results. All other simulation parameters are set based on the physical properties of the soil used in the experiment.

A qualitative and visual comparison of the simulations and the experiment is shown in Figure 8. This illustration shows the soil geometry at the end of the second trajectory segment in the 5-cm experiment for both MPM and Hybrid method. Also, a real-time soil visualization for the 5-cm experiment simulated with the hybrid method is provided in Figure 5. In general, the soil behavior in MPM and Hybrid are predicted similar to the one in the experiment. The particle velocities visualized in colors clearly depict the static (gray) and dynamic (red) parts; while static parts in Hybrid are visualized as grid consistent with its methodology. The MPM velocity field is more compatible with the experiment. It can be due to either the nature of MPM as a continuum-based method or the higher number of particles used. However, even with a lower number of particles and with real-time running times, the Hybrid velocity field is still in good agreement with the experiment, as can also be seen in Figure 5.

3.2 Run-Time Measurements

We measured the computational time spent in both MPM and Hybrid method with 20 seconds of simulated time in the 5-cm depth excavating experiment. The measurements were performed on an Intel(R) Core(TM) i7-6700 CPU @ 3.40GHz with 4 physical cores for MPM, and on an Intel(R) Core(TM) i7-8700 CPU @ 3.20GHz with 6 physical cores for the Hybrid method. The results are provided in Table 1.

Run-time as well as accuracy of both methods can be influenced by modifying the simulation discretization parameters, e.g. particle count and simulation frequency. In order to demonstrate this fact, the mean percentage error (MPE) of the forward cutting force in the simulation relative to the experiment was calculated for different discretization settings.

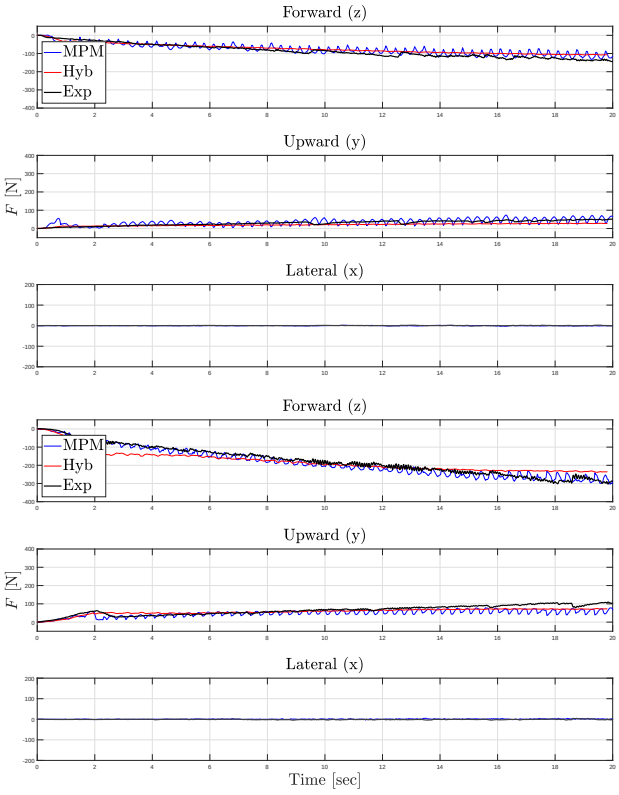

Figure 7. Interaction forces from MPM, Hybrid, and experiment for 2-cm (top) and 5-cm (bottom) depths.

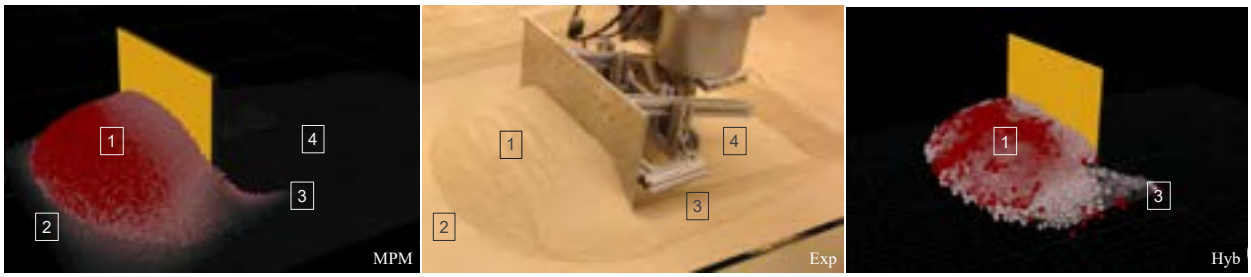

Figure 8. Geometries of soil deformations in MPM, Hybrid, and experiment for 5-cm depth. Four visual criteria are emphasized for comparison.

As can be seen in the results, MPM runs slower than real-time on the target hardware but can be substantially sped up by reducing the number of particles per cell (ppc) and/or increasing the grid spacing (Δx), both of which results in a lower particle count. Using a lower simulation frequency, i.e., a larger time step (Δt), would also lead to a simulation speed-up, but since in MPM equations are solved explicitly, the stability condition could become violated as a consequence. An implicit MPM solver could rectify this issue and would be future work.

The Hybrid method can run at real-time or faster than real-time by reducing particle radius and simulation frequency. Due to its implicit nature, the hybrid method remains stable regardless of the chosen simulation frequency. However, as can be seen in the results, the MPE increases significantly for simulation runs with lower simulation frequencies. This situation can be remedied by also choosing larger particle radii at which point the error reduces. This effect is likely due to excessive particle collisions or tunneling artifacts caused by particles being too small compared to the distances they travel between steps at low simulation frequencies. Thus, by choosing appropriate discretization settings, the error in the Hybrid method can be reduced to a level that rivals with the precision achieved in the MPM simulations with faster run-time settings.

4 Conclusion

Two efficient simulation methods for soil cutting operations have been presented and compared with experimental results. Both methods show good agreement with the experiments, with the MPM method yielding more accurate results than the Hybrid method. While the MPM method runs consistently slower than real-time, the Hybrid method can produce results at real-time and even faster than real-time without significant loss in accuracy. This ability makes the Hybrid method well-suited for use in virtual prototyping contexts such as the development of a real-time excavation automation control system. Accurate and efficient simulation methods are specifically useful in the training of machine-learning algorithms since faster simulation allows accelerating the training procedure. For an example application in which a precursor of the presented Hybrid method has been used for design of an excavator automation system the reader is referred to [28].

References

[1] C. Osullivan and J. Bray. Selecting a suitable time step for discrete element simulations that use the central difference time integration scheme. *Engineering Computations*, 2004.

[2] S. Dunatunga and K. Kamrin. Continuum modeling of projectile impact and penetration in dry granular media. *J. Mech. Phys. Solids*, 100:45–60, 2017.

[3] L. Ding, Z. Deng, H. Gao, J. Tao, K. Iagnemma, and G. Liu. Interaction mechanics model for rigid driving wheels of planetary rovers moving on sandy terrain with consideration of multiple physical effects. *Journal of Field Robotics. In press.*, 2014.

[4] C. Senatore and K. Iagnemma. Analysis of stress distributions under lightweight wheeled vehicles. *Journal of Terramechanics*, 51:1–17, 2014.

[5] J. Shen and R. Kushwaha. *Soil-machine interactions: a finite element perspective*. Books in soils, plants, and the environment, 1998.

[6] W. Chen and G. Baladi. Soil plasticity: Theory and implementation. 1985.

[7] G. Klar, T. Gast, A. Pradhana, C. Fu, C. Schroeder, C. Jiang, and J. Teran. Drucker-prager elastoplasticity for sand animation. *ACM Transactions on Graphics*, 2018.

[8] W. Abdullah. Viscoplastic finite element analysis of complex geotechnical problems. *Journal of Civil Engineering*, 5, 2011.

[9] P. Jop, Y. Forterre, and O. Pouliquen. A constitutive law for dense granular flows. *Letters*, 441, 2006.

Table 1. Method comparison for 20-sec simulation of 5-cm depth experiment. Number of steps as well as average run-time per simulated second of the experiment are provided. The *-symbol in the *Method* column indicates real-time or faster than real-time performance. The column *Discretization* provides grid spacing and particle radius values utilized in simulations by the MPM and the Hybrid method, respectively. Mean percentage error (MPE) in forward force is specified relative to the experiment.

Method	# Steps/sec	Discretization	Particle # (ppc)	Total Run-Time	Avg Run-Time/sec	Error (MPE)
MPM	10K	0.0033 m	230K (8)	8.0K sec	400 sec	-9.9%
MPM	10K	0.0033 m	32K (1)	1.5K sec	75 sec	-14.8%
MPM	3K	0.0040 m	15K (1)	220 sec	11 sec	15.8%
Hybrid	480	0.0066 m	6883 (-)	134.3 sec	6.7 sec	-18.6%
Hybrid	240	0.0066 m	6681 (-)	67.5 sec	3.4 sec	-19.0%
Hybrid	120	0.0066 m	6391 (-)	40.3 sec	2.0 sec	-28.7%
Hybrid*	120	0.0090 m	3079 (-)	20.3 sec	1.0 sec	-22.8%
Hybrid*	60	0.0090 m	2548 (-)	12.0 sec	0.6 sec	-31.2%
Hybrid*	60	0.0120 m	1582 (-)	8.0 sec	0.4 sec	-21.7%

[10] K. Kamrin. Non-locality in granular flow: phenomenology and modeling approaches. *Front. Phys.*, 7, 2019.

[11] C. Coetzee. Discrete and continuum modelling of soil cutting. *Comp. Part. Mech.*, 2014.

[12] S. Dunatunga and K. Kamrin. Continuum modeling and simulation of granular flows through their many phases. *J. Fluid Mech*, 2015.

[13] G. Tardos, S. McNamara, and I. Talu. Slow and intermediate flow of a frictional bulk powder in the couette geometry. *Powder Technology*, 131:23–39, 2003.

[14] E. McKyes. Soil cutting and tillage. 1985.

[15] D. Holz, A. Azimi, M. Teichmann, and S. Mercier. Real-time simulation of mining and earthmoving operations: a level set-based model for tool-induced terrain deformations. *30th International Symposium on Automation and Robotics in Construction and Mining (ISARC)*, 2013.

[16] A. Reece. The fundamental equation of earth-moving mechanics. *Proceedings of the Institution of Mechanical Engineers*, 1964.

[17] K. Skonieczny. Modeling the effects of surcharge accumulation on terrestrial and planetary wide-blade soil–tillage tool interactions. *Soil and Tillage Research*, 2018.

[18] M. Muller, B. Heidelberger, M. Hennix, and Ratcliff J. Position based dynamics. *Journal of Engineering Mechanics*, 2006.

[19] D. Holz. Parallel particles: a parallel position based approach for fast and stable simulation of granular materials. *Workshop on Virtual Reality Interaction and Physical Simulation VRIPHYS*, 2014.

[20] E. Karpman, D. Holz, J. Kovecses, P. Niksirat, and K. Skonieczny. Particle-based modelling for wheel-soil interaction and analysis of effects of gravity. *International Conference On Particle-Based Methods. Fundamentals and Applications*, 2019.

[21] Y. Hu, Y. Fang, Z. Ge, Z. Qu, Y. Zhu, A. Pradhana, and C. Jiang. A moving least squares material point method with displacement discontinuity and two-way rigid body coupling. *ACM Transactions on Graphics (TOG)*, 37(4):150, 2018.

[22] C. Jiang, C. Schroeder, A. Selle, J. Teran, and A. Stomakhin. The affine particle-in-cell method. *ACM Transactions on Graphics*, 34(51), 2015.

[23] David L. Henann and Ken Kamrin. Continuum thermomechanics of the nonlocal granular rheology. *International Journal of Plasticity*, 60:145–162, 2014.

[24] S. Dunatunga. *A framework for continuum simulation of granular flow*. PhD dissertation, Massachusetts Institute of Technology, 2017.

[25] D. Henann and K. Kamrin. A finite element implementation of the nonlocal granular rheology. *International Journal for Numerical Methods in Engineering*, 60, 2016.

[26] D. Holz and A. Galarneau. Real-time mud simulation for virtual environments. In *ACM SIGGRAPH Symposium on Interactive 3D Graphics and Games (i3D)*, 2018.

[27] H. Oraveca, X. Zenga, and V. Asnanib. Design and characterization of grc-1: A soil for lunar terramechanics testing in earth-ambient conditions. *Journal of Terramechanics*, 2010.

[28] D. Jud, G. Hottiger, P. Leemann, and M. Hutter. Planning and control for autonomous excavation. *IEEE Robotics and Automation Letters*, 2(4):2151–2158, 2017.

IoT-enabled Dependable Co-located Low-cost Sensing for Construction Site Monitoring

Huynh A.D. Nguyen, Lanh V. Nguyen, and Quang P. Ha

Faculty of Engineering and Information Technology,
University of Technology Sydney, Australia
Email: huynhanhduy.nguyen@uts.edu.au, vanlanh.nguyen@uts.edu.au, quang.ha@uts.edu.au

Abstract –

This paper proposes an IoT-enabled network of low-cost sensors that are co-located for construction site monitoring. The network performance enhancement is achieved via its system dependability in terms of improved availability, integrity, reliability, maintainability, security and safety in real-time monitoring of environment parameters. The sensor motes of various sensing modules form a reliable wireless in-situ cluster for gathering on-site information of air temperature, soil moisture, air pressure, humidity, particulate matters (PM), emissions and weather variables. They are useful for the site management, improving safety and effective operation of construction equipment. The components for the development include inexpensive microcontrollers ESP32 embedded with wireless gateway function and energy-efficient motes featuring cost-effective sensors. Here, the adoption of the dependability concept for collocated sensor motes aims to introduce a level of redundancy to allow for improving fault-tolerance and reliability. Extensive field tests have been conducted in different environments. Experimental results as well as statistical analysis are provided to verify the merits of the proposed approach.

Keywords –

Site monitoring; Volatile environment; Wireless sensor motes; Dependability; Reliability

1 Introduction

The Internet of Things (IoT) has been applied into various pieces of equipment which are called smart devices, incorporating digital intelligence. However, most of the IoT devices operate indoors with optimized temperatures, relative humidity (RH), dust filter or in well-controlled conditions, that may incur extra budget and resources. The rapid innovation of electronic platforms offers to mitigate these constraints from the availability of commercially low-cost devices. Nevertheless, the quality and performance of these inexpensive components need to be verified and standardized in practical conditions where unpredictable variations or imperfect conditions are unavoidable. The low-cost wireless sensor networks (WSN) adopted for environment-monitoring is an example for addressing this concern. The promising use of IoT-enabled systems operating in the harsh environment has recently attracted researchers in many areas including construction automation. A low-cost sensing system named AIRQino [1] was designed and developed to be as the auxiliary observatory point combining with high-quality reference stations in the Arctic. Cost-effective WSN are also being implemented for military, agriculture, transportation, on land and in marine environment [2], in which instruments may be easily prone to damage. In the construction sector, the IoT-based low-cost WSN technology is still in its infancy [3]. On a construction site, most of the studies focus on critical themes of safety, construction progress monitoring, BIM-related technology, project management, machine and resource management [4], which often consider normal operations with less concern to difficult conditions on a jobsite that may be subject to uncertainty and unpredictability.

Volatility in a jobsite is referred to as varying, unpredictable conditions, such as with varying weather, which may involve drastic changes in construction activities, and cause serious impacts. For example, earthworks usually take place under difficult conditions that have been widely referred to as 3D's, namely Dull, Dirty and Dangerous. In addition being vulnerable to a volatile environment, a construction process may also encounter abnormal disadvantages known as 3H's, i.e. Harsh, Hostile and Hazardous, such as in military or some mining and earthmoving missions [5]. Harsh conditions may degrade the quality of collected data and performance of controllers and the whole system. For reliable and resilient performance in construction processes against environmental variations, disturbances, imperfect conditions or ambient changes, the wireless sensing system should improve system dependability to allow for increased robust, safe and fault tolerant monitoring performance in real time.

The dependability of an IoT system is recently considered and explained as the ability of system proving justifiably trusted services [6]. A dependable system has typical characteristics such as availability, integrity, reliability, maintainability, security and safety. In cost-saving wireless sensing systems, reliability and availability are most critical in order to guarantee the continuous communication, data completeness and power consistency [7]. To increase reliability and availability of the system, and hence, resilience of construction or any industrial process, the downtime from the permanent failure of core controllers should be avoided [8]. In this regard, fault tolerance schemes have been developed in both hardware and software to improve dependability of a management system for solar energy consumption in a smart building [9].

This paper presents the design and development of low-cost wireless sensor systems that are collocated and controlled by our proposed dependable scheme. The availability of power supply is discussed by the combination of Dynamic Energy Conservation (DEC) scheme and the low-power network (ESP-NOW) from low-cost platform ESP32 in Section 2. The developed prototype is validated in laboratory before conducting field tests. Onsite collected data are analyzed by using statistic tools, whereby stochastic regression will be used to impute missing data during online operation. Sections 3 and 4 present the field test results for monitoring construction sites in different environments. Finally, a conclusion for the paper is drawn in Section 5.

2 Development of low-cost wireless sensor system

2.1 Hardware system

Figure 1 shows the proposed diagram of the dependable sensing system, developed for the low-cost WSN, which comprises two subsystems. The first subsystem is called *sensor mote* which constitutes four identical sensing modules of which one is operating while the others are in a stand-by status. Each IoT device operates as an autonomous sensor module (ASM) that consists of components such as micro-control unit (MCU), environmental sensors (soil moisture, soil temperature, RH, pressure, particulate matter - PM2.5 and PM10), two battery cells – Panasonic Lithium-Ion 18650 (3.7V-3400mAh/cell), one mini solar PV panel, real-time reading module, boost-buck converter and battery charging modules, all at a low cost, as shown in Table 1.

The second subsystem is called *gateway mote* or *router mote*. This device is assigned as the role of an intermediate transceiving point between sensor motes and the server when there is no cloud network in a construction site. The gateway mote is assembled by two redundant ESP-32s connecting each other by the serial communication protocol. One MCU communicates regularly with sensor motes in the local network (ESP-NOW) and the other connects to the cloud with Wi-Fi standard 802.11b/g/n. Data packets are sent to the Thingspeak server (https://thingspeak.com) by the hyper transfer text protocol (HTTP).

The printed circuit board (PCB) and main components are protected in a waterproof box (IP68 standard) from the intrusive water and dust at construction sites. Although each sensor module is designed separately, four modules are collocated on the same spots, ensuring redundancy of the sensor mote. Figure 2 shows the prototype with electronic components in a sensor module.

Table 1. Main components of the sensor mote

Components	Features
Sensor SDS011	PM2.5 and PM10
BME280	Air RH, air pressure and temperature
Soil Moisture	Corrosion resistance
Kit ESP32-dev	IoT Microcontroller
TP4506	Charging battery
HT016	DC-to-DC converter
Solar panel	Harvesting solar energy
Battery	Supply voltage (2 cells)

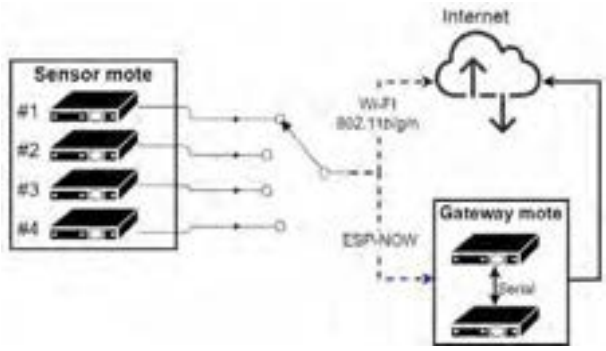

Figure 1. Diagram of the dependable IoT system

2.2 The microcontroller ESP32 and ESP-NOW communication protocol

The MCU ESP32, manufactured by Espressif System company, is a low-power System on Chip (SoC) with wireless communication features in both Wi-Fi and Bluetooth Low Energy (BLE) protocols. This low-cost platform provides multiple peripherals and various communication types (e.g. PWM, I2C, SPI, RS232, etc.). Thanks to the energy-saving architecture with different power modes and 2-core processing capacity at frequency up to 240MHz, the ESP32 MCU is suitable for cost-saving and real-time solutions [10]. The Wi-Fi protocol in ESP32 offers two IoT functions: *Station (ST)*

and *Access point (AP)*, from which the controller can be a member of an available network (e.g. cloud network) or can set up its own local network as a gateway respectively.

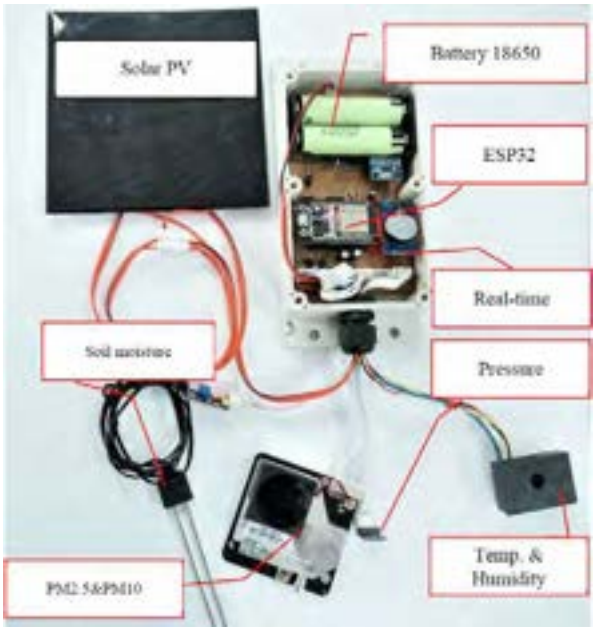

Figure 2. Low-cost sensor mote

Figure 3. Vendor-specific Action Frame and Vendor-specific Content [10]

For the machine-to-machine protocol, the Esprissef wireless ESP-NOW is used, featuring low-power 2.4GHz-radio communication that can connect up to 20 devices without handshake. As shown in the diagram of Figure 3, the data frame of this protocol is encapsulated by a vendor-specific action frame transmitted at the default bit rate of 1 Mbps. Moreover, data transceived by ESP-NOW are secured by the cryptography method (CCMP) defined in IEEE 802.11-2012. This method reduces the risk of interference from other devices or networks to assure the dependable feature of the proposed system in terms of network security.

The body of Vendor-specific Content allows the maximum data packet up to 250 bytes which are more than the requirement in this study because the total sensing data are 112 bytes in the proposed system. In order to validate the efficiency of ESP-NOW protocol, the experiment was conducted in the laboratory with the Virtual Bench NI VB-8012 All-in-one instrument, which could capture signals up to 100 MHz to measure and compare the energy consumption and duration for different wireless communication protocols (ESP-NOW vs. Wi-Fi standard).

In the first experiment with ESP-NOW, the current draining for transceiving a 112-byte packet is 324 mA in 1.6 ms, i.e. a small capacity $C_{ESP\text{-}NOW} = 0.144\times10^{-3}$ mAh. In comparison with sending directly the same packet by Wi-Fi protocol in the second experiment, the expensed capacity is 173 mA in 1285 ms, equivalent to $C_{Wi\text{-}Fi} = 61.751\times10^{-3}$ mAh. To this end, ESP-NOW communication is selected as the local network connecting with gateway motes due to its energy efficiency in radio communication. Besides, the real discharge current were measured without connecting to network ($I_{measure}$ = 162 mA) and during the deep-sleep mode ($I_{deep\text{-}sleep}$ = 10 mA) of the module for the later evaluation of power cost in each working cycle of WSN.

2.3 Dynamic Energy Conservation (DEC) scheme

We apply the Dynamic Energy Conservation (DEC) scheme based on the saving-energy features of ESP32 platform, which varies the duration of the active-sleep cycle dynamically. Here, the active-sleep cycle of the when sensor module includes (1) the active period counted from the "wake-up" and data collection time; (2) period for connecting the local network and transmitting data successfully; (3) the stand-by (sleep) period from triggering the deep-sleep mode until the next wake-up time.

In environmental monitoring application, the ambient parameters are measured as discrete variables with slow variation (e.g. temperature) to reduce constraints of power resource. Here, the regulation sampling frequency depends on the construction activities in dayshifts or nightshifts to flexibly increase the availability of the system. Next, we will consider the various active-sleep cycles from DEC to optimize the power consumption of this system.

The average discharge current in one cycle is:

$$I_{cycle} = \frac{\sum_{i=1}^{3} m_i I_i}{\sum_{i=1}^{3} m_i}, \quad (1)$$

where m_i and I_i (i=1,2,3) is the period and discharge current according to the mode i^{th} as listed in Table 3. In this study, the time to initiate sensors and wireless connection is at least 30 seconds prior to data measurement and transmission, we choose time for active mode m_1 = 30s, whereas the ESP-NOW transmission period for a data packet is very small (m_2 = 1.6 ms) that could be neglected. Hence, the dynamic operation cycles

will be determined by the sleeping time (m_3). We designed a switching mechanism for alternating the battery usage. One battery is charged by solar energy and the other is responsible for supplying power for the whole module.

Table 3. The active-sleep cycle of the sensor module with discharge current measured in each mode

Mode	Action	Period	Discharge current
Active	Measure data	Flexible	162 mA
Active	Communication	1.6 ms	324 mA
Deep-sleep	Stand-by	Flexible	10 mA

Due to the back-up design, this mechanism remains the power supply over the whole working duration, whereas it reduces the aging problem of the battery by intermittent charge and discharge. Therefore, the energy-discharged calculation will be considered for one battery cell. The expected working time of a battery cell in the sensor module is determined by the average discharge current in one cycle (1) and the battery time calculated as

$$T_{bat} = \frac{C_{bat}}{I_{cycle} . n_{cycles}}, \qquad (2)$$

where T_{bat} (in hours) is the average service-time of the battery being fully charged; I_{cycle} is the average discharge current in one cycle; n_{cycles} is the number of cycles per hour according to sleeping time, and C_{bat} is the capacitance discharge current. In our application, C_{bat} = 3000 mA from fully-charged to cut-off point (from 4.2V to 3.0V respectively) with Lithium-Ion NCR18650B battery [11].

From the estimated time listed in Table 4, the larger sleeping period the longer the battery service time. However, the over-extending idle time will reduce the temporal resolution of data, which may cause unreliable analysis results and decisions. This requires further improvement from dependable algorithms [12].

Table 4. The estimated battery service-time with fixed value of active mode (m_1+m_2 ≈ 30s; T_{total} = m_1+m_2+m_3)

Sleeping period	Cycle time (T_{total} - ms)	n_{cycles}	I_{cycle} (mA)	T_{bat} (hour)
30	60	60	91.5	0.6
60	90	40	64.3	1.2
120	150	24	42.6	3.1
300	330	10.9	24.8	11.5
600	660	5.5	17.7	31.6
900	930	3.9	15.3	51.6

3. Field test and results: on-campus construction site

3.1 Field testing and data validation

The first field test was conducted at a construction site in at coordinates 10.0323^{0}N, 105.7682^{0}E. Due to the safety policy from the contractor, the on-site testing period was conducted in a short period from 26th to 29th October 2019 and the sampling interval is 15 min/cycle.

The proposed IoT-enabled dependable scheme illustrated in Figure 1 was implemented with four modules (MD1-MD4), and installed at the site as shown in Figure 4. It will control the communication switch to connect gateways or the server to each sensor module consecutively. Hence, data samples increase four times compared to the single wireless sensor as conventional WSN. As a result, the spatial and temporal distributions of environmental parameters on the construction site have been significantly improved.

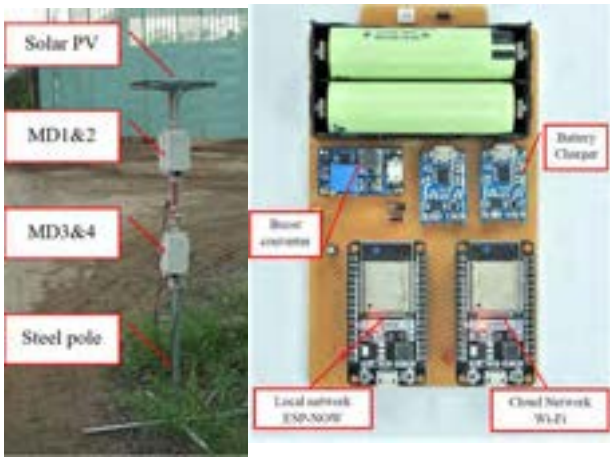

Figure 4. On-site sensor mote (left) and the gateways mote PCB board (right).

The temporal distributions of temperature, RH, PM2.5 and PM10 are illustrated in Figure 5. The profiles of all data show similar trends between collocated modules with small variations. Although some points are affected by noises, they could be removed by filtering out.

To investigate the correlation and linear relationship between the data collected from the low-cost sensor modules, Pearson's correlation coefficient is used

$$r = \frac{\sum_{i=1}^{n}(x_i - \bar{x})(y_i - \bar{y})}{\sqrt{\sum_{i=1}^{n}(x_i - \bar{x})^2}\ \sqrt{\sum_{i=1}^{n}(y_i - \bar{y})^2}}, \qquad (3)$$

where r is the Pearson's correlation coefficient; x and y are the measured values of two sensors; $\bar{x}$ and $\bar{y}$ are means of two datasets and n is the total samples. To evaluate on the deviation between measurements collected from the sensor modules, we use the Mean

Absolute Error (MAE) and Root Mean Square Error (RMSE) calculated as [13],

$$MAE = \frac{1}{n}\sum_{i=1}^{n}|x_i - y_i|\,, \quad (4)$$

$$RMSE = \sqrt{\frac{\sum_{i=1}^{n}(x_i - y_i)^2}{n}}\,. \quad (5)$$

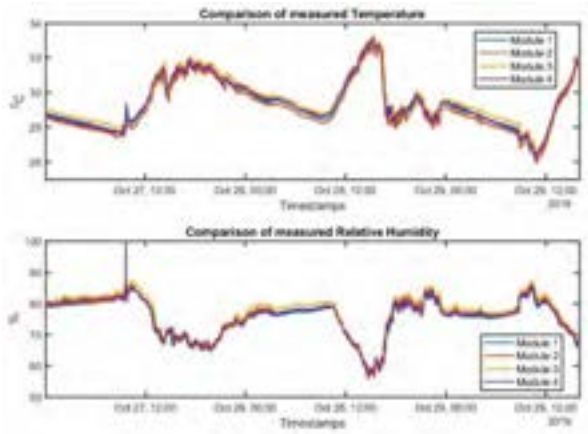

(a) Temperature and relative humidity

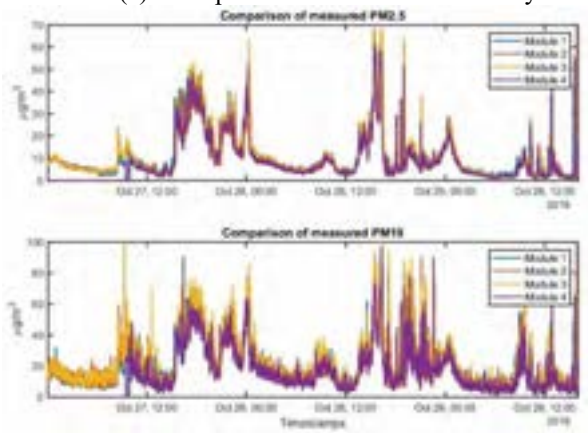

(b) Particulate matters (PM2.5 and PM10)

Figure 5. Profiles of environmental variables measured from the low-cost sensor mote

The correlations from the collocated sensors are depicted for temperature in Figure 6 typically for three modules MD1, MD2 and MD3. The results show that sensors are highly linearly-correlated with Pearson's coefficient r >0.9. From this analysis, we could also identify a sensor module which might have some issues during measuring data. Such a problem may be caused by inappropriate calibrations, misreading of the MCU, being located close to a noise source, or weather volatility.

Table 5 shows deviations in terms of MAE and RMSE of the inexpensive sensors collocated in the same spot. Therein, the highest MAE and RMSE can be observed for PM records, which remain an important component in monitoring of construction sites, particularly subject to a difficult environment. The dissimilarity could stem from calibrated issues that would require some benchmarking with authority stations for comparison and verification.

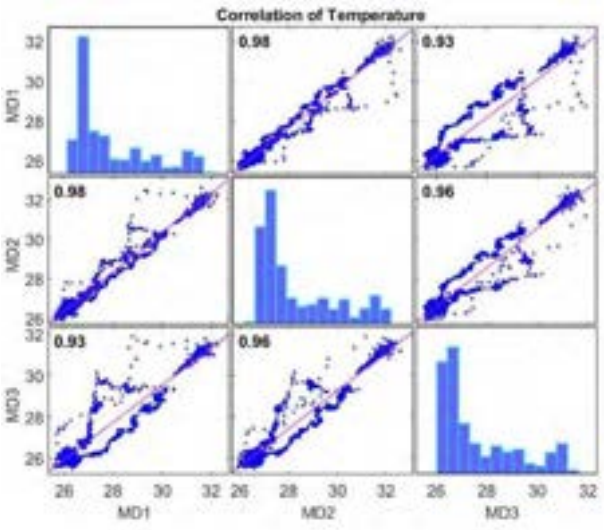

Figure 6. Correlations of temperature by three modules

Table 5. Calculated RMSE and MAE of the sensors

Types of sensors	Ranges of RMSE	Ranges of MAE
Temperature (°C)	0.48 – 0.72	0.37 – 0.69
RH (%)	1.72 – 3.20	1.23 – 2.1
PM2.5 (µg/m^3)	8.37 – 11.2	5.22 – 7.22
PM10 (µg/m^3)	12.57 – 15.34	8.38 - 9.14
Soil moisture (%)	6.13 – 6.55	4.60 – 8.83
Pressure (mbar)	0.51 – 0.99	0.36 – 1.12

3.2 Imputation for missing data

Missing data remain an issue that may cause misinterpretation or bias upon using low-cost WSN. Unlike other studies where missing values are imputed in the offline processing phases, here we propose the stochastic regression scheme that can be integrated in the embedded program to predict the lost data by considering the correlation of the previous data collected from all co-located sensors. The gateway motes could estimate online after receiving data from the sensor motes. The benefit from a co-located sensing system is that the data from well-operated modules can be used as the references without concerning the temporal and spatial distribution of other sensor motes as in [14].

Let P_{k+1}^{j} be the imputed value from module j^{th} (j = 1, 2, 3 or 4) missing information at the index (k+1). During the operation, if device j^{th} sends no data to the gateway, the gateway will poll d previous values received from all four sensors (assuming all previous d values are valid). Given known values of redundant data (P_{k+1}^{i}), the imputation is given by

$$P_{k+1}^{j} = \sum_{k-d}^{k} (w_{ij}.P_{k+1}^{i}) + rand(std^{j}), \quad (6)$$

where the weights w_{ij} are calculated by

$$w_{ij} = \frac{r_{ij}}{\sum r_{ij}}, \quad (7)$$

in which r_{ij} are the correlation coefficients of module i^{th} and module j^{th} ($i \neq j$, e.g. if j = 3 then i = 1, 2, 4), obtained in the range of indices from ($k-d$) to k. A random number, *rand*(.), in dependence of the standard deviation of sensor j^{th} (std^{j}), is added to ensure the estimated data being close to the actual measured data but not overfitting.

To validate the imputation method, we assume 1000 datapoints of temperature and RH in module MD3 are missed during the service time, while the others (modules 1, 2 and 4) still operate well with full transceiving of data packets. The selected polling threshold is d = 20 (i.e. 20 previous samples of the missing point are used to identify coefficients and weights). Figure 7 shows the imputation results for missing values of temperature and RH. The estimated and the actual data relatively fit with small residuals. The RMSE of those data are 0.684 (Celsius degree) for temperature and 2.84 for RH. Therefore, the proposed technique is promising in improving reliability of the monitoring system for the construction site.

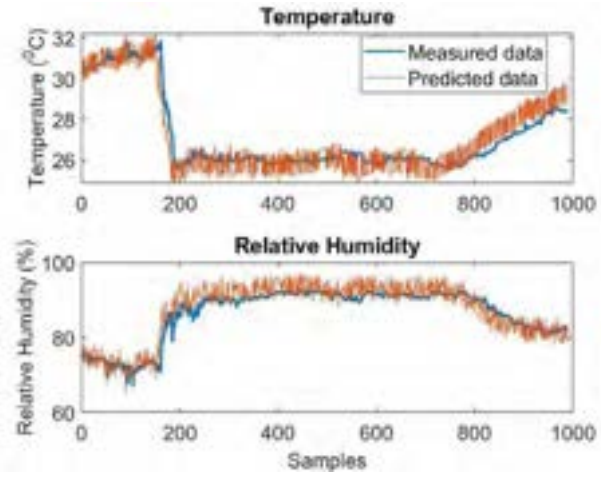

Figure 7. Estimated missing data of temperature and RH sensors from imputation.

4. Field test and results: residential construction site

The proposed dependable scheme is now adopted for monitoring the emissions of a construction site at coordinates 33°49′11″S, 151°4′38″E. The low-cost sensor motes are fixed on the electrical poles at the height of 3 meters above the ground to assure a proper coverage without damage risk from construction activities.

There were 15 devices denoted as T1 to T15 installed over the whole area of approximately 1 km^2. The construction site was monitored by co-located sensor motes T1 to T8, while the surrounding residential zones were monitored by T9 to T15, as depicted in Figure 8.

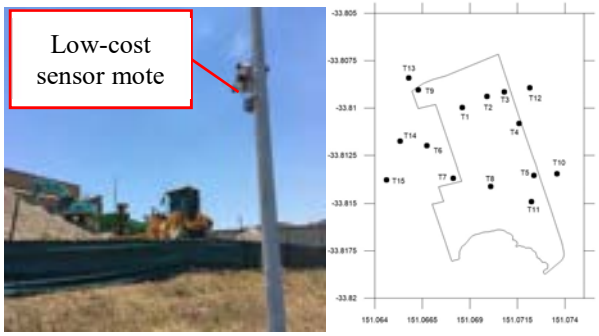

Figure 8. Low-cost sensing devices installed over the monitoring area

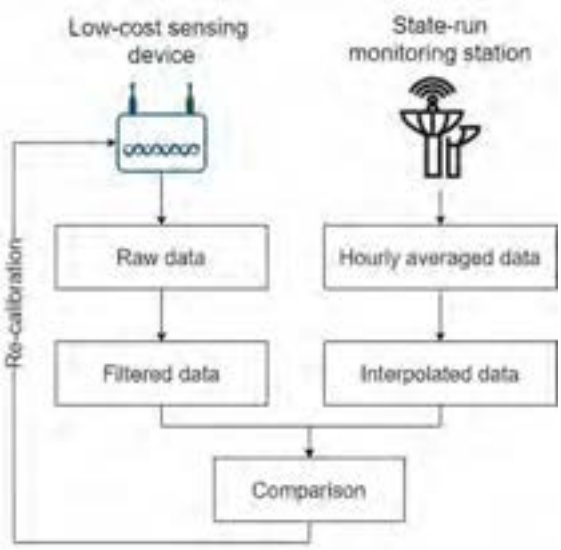

Figure 9. The iterative process of data processing of low-cost IoT-enabled monitoring system

Figure 9 presents the process of data interpolation and for long-term monitoring operations. Therein, two streams are considered: (1) data from a nearby state-run monitoring station, extracted for referencing; (2) data

measured by the developed system on the construction site. Both data are processed prior to comparison, and the differences will be analyzed and fed back to the devices for re-calibrating to reduce any issues in association (e.g. time drift, gain and bias, etc.).

4.1 Processing measured data

The raw data are collected from the devices wirelessly through the Thingspeak server. The surveying period covered 65 days (from 15th November 2019 to 19th January 2020), with 6161 samples/device for each sensor (temperature, RH, PM2.5, PM10 and battery voltage). For the scope of this paper, only data of fine particle concentrations (PM2.5) are used for evaluating the performance of the wireless sensing system. The low-cost sensors collected data continuously 24 hours per day with a sampling period of 15 minutes to ensure stable operation, network connection, and battery lifetime. The raw data were affected by multiple noises causing imperfect recording of monitored parameters, for which anomalous values were treated by a moving average filter. Figure 10 presents the graphs before and after processing. It can be observed of the contribution from construction emissions to the rise of PM2.5 level when resuming the onsite work after the New Year break, while the high concentration of the fine particle dust reflected the impact of bushfires at the time.

4.2 Interpolating reference data

For validation of information gathered by low-cost devices, the measured data are compared with the data recorded by state monitoring stations, managed by the Department of Planning, Industry and Environments (DPIE) of the NSW Government [15]. Here, the closest state-run monitoring station is about 7 km to the site. In order to match with the time scale of the measured data, the DPIE records are resampled, with a cubic interpolation method, from 1920 to 6161 samples over the studied period.

Figure 11 shows the comparison between the two datasets after processing, which display a good fit with a high correlation as presented in Figure 12 despite some small phase shifts between two temporal profiles. This could be due to the spatial difference between the two locations with a systemic delay in DPIE reporting as well as the effects from other meteorological parameters.

The collected data from all 15 low-cost sensor motes are visualized in 3D for the spatial distribution by Surfer® v.11 and MATLAB® v.2020a software for further evaluation the influence of construction activities to the air pollution over the surrounding residential area, as depicted in Figure 13, with data being obtained on Jan 8th 2020. Therein, it can be observed of some higher concentration of PM2.5 (over 90 µg/m^3) at the construction site, whereas the lower levels were in the residential area albeit still above the national threshold of 25 µg/m^3 [16]. The reason was attributed to the prolonged impact of bushfires in the state [17].

5. Conclusion

This paper has presented the development of effective wireless sensing networks for reliable monitoring of construction sites using IoT-enabled dependable co-located low-cost sensor motes. The availability and resilience of the proposed system is assured by the saving-energy modes of hardware architecture, DEC framework and the redundancy of stand-by co-located sensing modules. Extensive field tests have been conducted on construction sites at different environments to validate and verify the advantages of the system implementation and its meritorious attributes. The proposed monitoring systems, coupled with various data processing techniques and the developed imputation algorithm, have resulted in significant improvement of the monitoring performance in terms of accuracy and dependability. Our future work will focus on the incorporation of learning schemes in order to cope with site monitoring in challenging conditions of abrupt changes in a volatile environment for accurate assessment of micro-climate conditions.

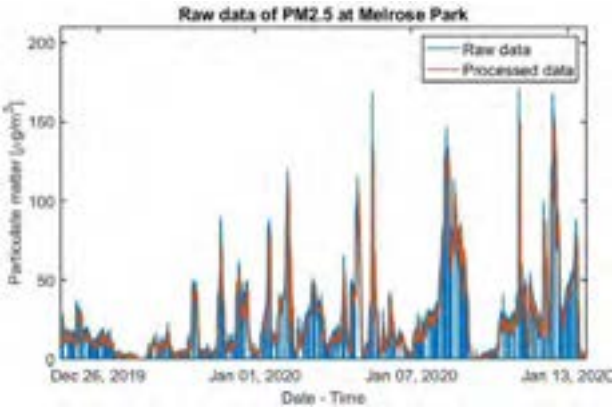

Figure 10. Raw and processed data from a low-cost sensor mote for PM2.5

Acknowledgement

This work is supported by Project 1032959 PRO19-7375 at University of Technology Sydney, and by the Vingroup Science and Technology Scholarship (VSTS) Program for Overseas Study for Master's and Doctoral Degrees. The VSTS Program is managed by VinUniversity and sponsored by Vingroup.

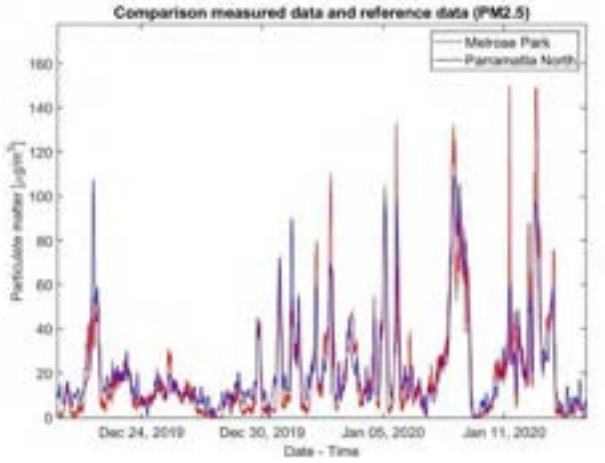

Figure 11. Comparison of measured (red) and reference data (blue)

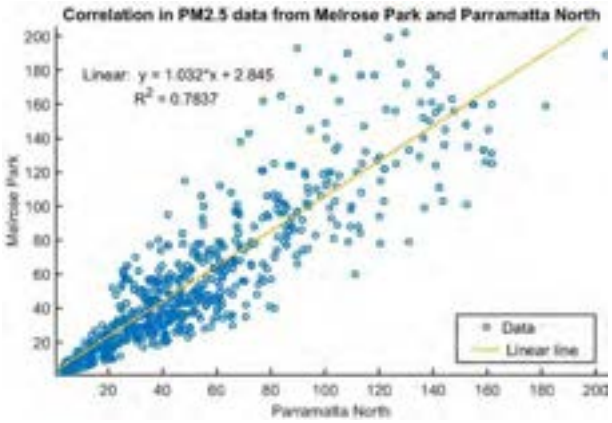

Figure 12. Correlation of two datasets by a sensor mote and by a state-run monitoring station

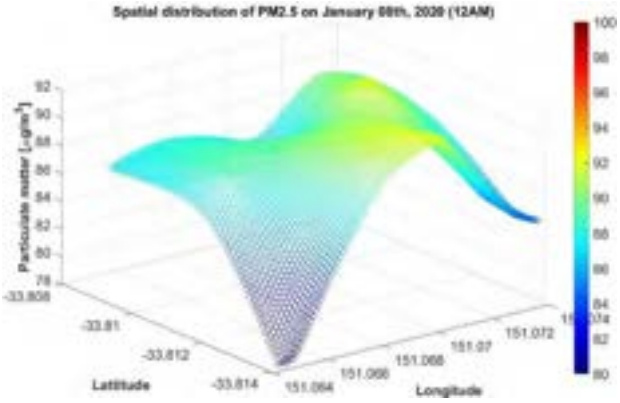

Figure 13. Spatial distribution of 15 sensor motes over the whole studied area for PM2.5

References

[1] Carotenuto F., Brilli L., Gioli B., Gualtieri G., Vagnoli C., Mazzola M., and Zaldei A. Long-Term Performance Assessment of Low-Cost Atmospheric Sensors in the Arctic Environment. *Sensors*, 20(7), 2020. DOI: 10.3390/s20071919.

[2] Xu G., Shen W., and Wang X. Applications of wireless sensor networks in marine environment monitoring: a survey. *Sensors*, 14(9), 16932–16954, 2014. DOI: https://doi.org/10.3390/s140916932.

[3] Reja V.K. and Varghese K. Impact of 5G Technology on IoT Applications in Construction Project Management. In *Proceedings of the 36th ISARC*, Banff, Alberta, Canada, pp. 209-217, 2019. DOI: https://doi.org/10.22260/ISARC2019/0029.

[4] Tagliabue L. C. and Ciribini A. L. C. A BIM-Based IoT Approach to the Construction Site Management. *Journal of Structural Integrity and Maintenance, 3*(4), 254-261, 2018. DOI: https://doi.org/10.6092/issn.2036-1602/8827

[5] Ha Q.P., Yen L. and Balaguer C. Robotic Autonomous Systems for Earthmoving in Military Applications. *Automation in Construction*, 107, 2019. DOI: 10.1016/j.autcon.2019.102934.

[6] Andrade E. and Nogueira B. Dependability evaluation of a disaster recovery solution for IoT infrastructures. *J. of Supercomputing*, 76(3), 1828-1849, 2020. DOI: 10.1007/s11227-018-2290-0.

[7] Bruneo D., Puliafito A. and Scarpa M. Dependability evaluation of Wireless Sensor Networks: Redundancy and topological aspects. *IEEE Sensors*, 1827–1831, 2010. DOI: https://doi.org/10.1109/ICSENS.2010.5690005.

[8] Silva I. Leandro R., Macedo D. and Guedes L. A dependability evaluation tool for the Internet of Things. *Computers and Electrical Engineering*, 39(7), 2005–2018, 2013. DOI: https://doi.org/10.1016/j.compeleceng.2013.04.021.

[9] Ha Q.P. and Phung M.D. IoT-enabled dependable control for solar energy harvesting in smart buildings. *IET Smart Cities*, vol. 1, no. 2, pp. 61-70, 2019. DOI: 10.1049/iet-smc.2019.0052.

[10] Espressif Systems. ESP32 Series the Datasheet, version 3.4, 2020. Online: https://www.espressif.com/sites/default/files/documentation/esp32_datasheet_en.pdf, Accessed: 12/05/2020.

[11] Panasonic. Datasheet of Lithium Ion NCR18650B. Online: https://www.batteryspace.com/prod-specs/NCR18650B.pdf. Accessed: 01/05/2020.

[12] Tran T., Ha Q.P. and Hunjet R. "Reliability Enhancement with Dependable Model Predictive Control," *ISA Transactions*, https://doi.org/10.1016/j.isatra.2020.06.027, online 6 July 2020.

[13] Heumann C., Schomaker M. and Shalabh S. *Introduction to Statistics and Data Analysis With Exercises, Solutions and Applications in R*, Springer, Cham, ISBN 978-3-319-46162-5, 2017. DOI: https://doi.org/10.1007/978-3-319-46162-5.

[14] Li Y. and Parker L. A spatial-temporal imputation technique for classification with missing data in a wireless sensor network. In *Proceeding of IEEE/RSJ International Conference on Intelligent Robots and Systems*, 3272–3279, 2008. DOI: https://doi.org/10.1109/IROS.2008.4650774.

[15] New South Wale Government – Planning Industry and Environment. Online: https://www.dpie.nsw.gov.au/air-quality/search-for-and-download-air-quality-data, Accessed: 24/04/2020.

[16] Australia - State of the Environment. National Air Quality Standard. Online: https://soe.environment.gov.au/theme/ambient-air-quality/topic/2016/national-air-quality-standards, Accessed: 21/04/2020.

[17] Ha Q.P., Nguyen H.A.D., and Metia S. Construction Site Impact on Urban Air Quality using Low-cost Sensing Networks. In *Melrose Park: Smart Planning for Climate Responsive Neighbourhoods*, Report PRO19-7375.

Threat Modeling in Construction: An Example of a 3D Concrete Printing System

M.U.R. Mohamed Shibly [a] and B. Garcia de Soto [a]

[a] S.M.A.R.T. Construction Research Group, Division of Engineering, New York University Abu Dhabi (NYUAD), Experimental Research Building, Saadiyat Island, P.O. Box 129188, Abu Dhabi, United Arab Emirates
E-mail: maahirur@nyu.edu, garcia.de.soto@nyu.edu

Abstract –

Cybersecurity threats related to new technologies get little attention until an incident occurs, and vulnerabilities are highlighted. In the case of construction projects, any cyber breach, either malicious or incidental, has the potential to cause significant damage. This varies from unauthorized access of sensitive project information to hijacking construction equipment to cause structural damage to the site or harm to personnel. Given the potential implications of threats in cyber-physical systems, and the potential for physical damage to products and personnel, serious consideration from a research perspective is needed. The risk of such attacks occurring is exacerbated in regions such as the UAE, where new technologies, such as 3D printing, are trending.

With that in mind, the objective of this study is twofold. First, to raise awareness about the cybersecurity implications of the new technologies adopted by the AEC industry. Second, to understand the core cybersecurity aspect of threat modeling concerning cyber-physical systems applied to construction projects. Several threat modeling methods such as STRIDE, OCTAVE, PASTA, and VAST have been developed. However, they are not easy to adopt by construction professionals who generally have limited knowledge of the cybersecurity domain. To address that, this study aims to develop a preliminary threat modeling approach that is relevant to the construction industry and can be quickly adopted to investigate the current technology being implemented. To demonstrate the practical feasibility of the proposed threat model, we consider an industrial-grade robotic arm system to 3D print construction elements offsite. This threat model will provide insights into a range of different threats that these systems are vulnerable to, allowing us to secure these systems against such threats, and raising awareness about the cybersecurity implications of implementing such technologies in the AEC industry.

Keywords –

3D Concrete Printing; Construction4.0; Cyber-Physical Systems; Cybersecurity; Cyberattack; CVSS; Risk Propagation; Smart Construction Sites; STRIDE; Threat model; Vulnerability Assessment

1 Introduction

The notion of having a digital model and a machine able to build it with a high degree of accuracy, with little human intervention, and in a timely fashion is very attractive and appealing. In the construction sector, that notion has been materialized with the development of 3D printing technology along with the use of contour crafting in which successive layers of cementitious material are placed to generate building elements. Although there are still many challenges to overcome (e.g., scalability, mobility, materials), there are already construction projects that have benefited from the use of 3D printing [1]. Some recent examples include the Apis Cor's two-story building in Dubai, UAE [2], Winsun China's villa [3], concrete bridges in Spain [4] and China [5], portions of the DFAB HOUSE [6] and the Concrete Choreography project [7] in Switzerland, single-family houses in Denmark [8] and France [9], and military barracks in the US [10].

A lot of efforts have been made in the research community regarding the technical aspects of 3D printing in the construction sector; however, the aspect of cybersecurity has been disregarded. The use of 3D printing in construction opens the door to new risks and vulnerabilities. Researchers are starting to consider the cybersecurity challenges and vulnerabilities caused by the digital transformation taking place in the construction industry [11, 12] and quantifying the cyber vulnerability of construction participants [13]. The ability to maliciously access to remote devices has already been documented. For example, [14] found that the radio signals typically used for crane controllers are not encrypted and can be easily intercepted and spoofed using off-the-shelf equipment and basic knowledge of electronics and radio engineering.

Similarly, regarding cybersecurity implications of 3D printing in other industries, [15] investigated how sabotage attacks could compromise the quality of 3D printed parts. Their study showed an attack against a desktop 3D printer used to manufacture propellers for an unmanned aerial vehicle (UAV). The sabotaged part experienced structural decay and caused the UAV to crash during flight.

As with other cyber-physical and connected systems, the connectivity requirements of 3D printing systems (e.g., controllers and manipulators, network connectivity, and peripherals, such as pumps or mixers), raises the potential for cyber-attacks. Considering the sensitive nature of construction projects, the introduction of the 3D concrete printing system as a cyber-physical system (CPS) that can be accessed by third parties with malicious intents poses several problems that need to be addressed.

The rest of the paper is organized as follows. In Section 2, we provide an overview of threat modeling, including existing methods and an evaluation of appropriate methods applicable to the construction industry. Section 3 discusses our efforts in the development of a threat modeling method (TMM), along with a high-level description of the overall procedure. In Section 4, we show the application of the TMM using a generic 3D Concrete Printing (3DcP) System. Also, we explain the specifics of each stage in the proposed TMM. Section 5 contains a discussion of the application and an identification of where the TMM succeeds and where it does not. Finally, we summarize key findings and suggest areas for future work in Section 6.

2 Threat Modeling

Threat modeling can be defined as the process of identifying potential threats, vulnerabilities, attackers, and targeted assets, with the goal to define countermeasures and plan risk mitigation strategies. The objective is to get a clear picture of the attack map, that is, how, where, why, and by whom an attack might occur. It consists of analyzing the security of an application or system by systematically cataloging and inspecting vulnerabilities present in a variety of contexts in the system under consideration [16]. The threat modeling process, as viewed by [17], can loosely be seen to consist of three high-level stages: (1) system characterization, (2) asset and access point identification, and (3) threat enumeration. Based on these principles, threat modeling requires a fundamental understanding of the underlying architecture, its design and implementation in order to prepare a thorough review and security analysis that can then be used to provide countermeasures that would prevent, or mitigate, the effects of any threats to the system. We proceed to identify two primary threat targets, Information Technology (IT) and Operational Technology (OT). The former relates to threats concerning the network infrastructure governing the system under consideration, while the latter relates to matters of physical security concerning the hardware operating in the system and potential damages to surrounding areas and people.

As with [18], in which a new threat modeling method was developed to fit a unique case, there is a need in the construction industry to investigate and consider the risks of cyberattacks due to the integration of new technology. With this in mind, we develop a threat modeling method that suits the small-scale but heavily interconnected nature of a 3D printing system used in construction.

2.1 Threat Modeling Methods (TMMs)

We place a heavy emphasis on understanding the nuances of existing TMMs, and what makes these methods suitable for specific systems. Our review of [19], [20], and [21] provided an understanding of a broad range of methodologies, from commonly used systems such as STRIDE and PASTA to uncommon ones such as CORAS and TRIKE. A summary of all the TMMs considered is shown in Table 1. This information will allow us to gauge the strengths and weaknesses of a range of TMMs along with which of their characteristics might come into use based on a variety of situations. There are a variety of characteristics to consider, from the range of threats, the existence of a built-in empirical component, to the availability of documentation.

2.2 Shortlisting Candidates

Considering the range of TMMs evaluated (Table 1), the following criteria were used to narrow down the selection of the TMMs to be used.

1. Threat Range (Low, Medium, High): Refers to the variety of threats captured.
2. Empiricism (Yes, No): Whether the TMM has an empirical component to gauge threats.
3. Consistency (Yes, No): Whether repeated use of the TMM yields the same results.
4. Risk-Mitigation (Yes, No): Whether the TMM contains some in-built component for mitigating the threats captured.
5. Suitability (Yes, No): Whether the TMM has not been explicitly developed for some specific system.
6. Documentation (Low, Medium, High): The amount of documentation available.

These characteristics are chosen based on our perspective on what would a generic situation be in which our TMM is used, with regards to the participants involved, the resources available, and the system under consideration. We chose the characteristics to capture a

broad range of threats, output an empirical result to gauge the magnitude of the risk of each threat, produce the same results consistently, contain in-built prioritization of risk mitigation and management that can be applied to a generic context while having proper documentation to aid during the threat modeling process.

Table 1. Summary of TMMs and characteristics used for selection in this study

Method	Threat Range	Empiricism	Consistency	Risk - Mitigation	Suitability	Documentation
OCTAVE	Medium	Yes	Yes	Yes	No	Medium
Trike	High	Yes	No	Yes	Yes	Low
PASTA	Medium	Yes	Yes	Yes	No	High
STRIDE	High	No	No	Yes	Yes	High
CORAS	Medium	Yes	Yes	Yes	No	Low
VAST	Medium	No	Yes	Yes	No	High
LINDDUN	High	No	No	Yes	Yes	Medium
hTMM	High	No	Yes	Yes (4)	Yes	N/A (3)
QuantitativeTMM	High	Yes	Yes	Yes (4)	Yes	N/A (3)
CAPEC (1)	Medium	No	N/A	No	No	N/A
ATT&CK (1)	Medium	No	N/A	Yes	No	N/A
IIDIL / ATC	High	No	Yes	Yes	Yes	Low
Security Cards + PnG (2)	Medium	No	Yes (SC) – No (PnG)	No	No	High (SC) – Low (PnG)

(1) CAPEC and ATT&CK are considered threat libraries and do not necessarily provide information as to modeling threats in a system
(2) Security Cards + PnG are essentially a gamification of the threat modeling process and should be used for training and brainstorming purposes only
(3) hTMM and QuantitativeTMM use STRIDE, and therefore we use the STRIDE documentation as a baseline for these TMMs; however, the methods themselves are not as mature as STRIDE
(4) Risk Mitigation based on STRIDE

Based on the selection characteristics previously described, Table 1 yields a few clear winners, with STRIDE and its derivatives meeting most of our criteria at their highest standards. Therefore, we have chosen the QuantitativeTMM as the basis for the modeling method for threat modeling in the rest of the paper.

3 Framework of proposed TMM – QuantitativeTMM

The framework of the QuantitativeTMM (QTMM) described in this section is a combination of the QTMM proposed in [22] along with parts of [23]. The high-level steps are shown in Figure 1 and described as follows.

Step 1: Define use case / problem statement
We begin by delineating our system; this includes an explanation of the system goals, the system components, information flows within our system, as well as users of our system [24].

Step 2: Define Data Flow Diagram (DFD)
Data Flow Diagrams are a method of breaking down the system into single components in the form of *Entities, Data Flows, Data Stores,* and *Processes. Trust Boundaries* are another component used to delineate the border between trusted and untrusted components in the DFD. The DFD acts as a graphical representation of these components in order to present the user with a high-level overview of the interactions between separate components in the system [23]. For a given use case or problem statement, the user creates a DFD with the required granularity. A finer granularity will produce a more refined overview that, at later stages, will yield a higher number of threats related to specific component interactions.

Step 3: Map STRIDE Elements into DFD
Once the DFD is created, we use the STRIDE classification of threats to 'map' individual components of the DFD to the respective threat classes. Table 2, adapted from [24], delineates the threat classes associated with each component. Once this is done, the user may begin to internalize the form of threats that may appear.

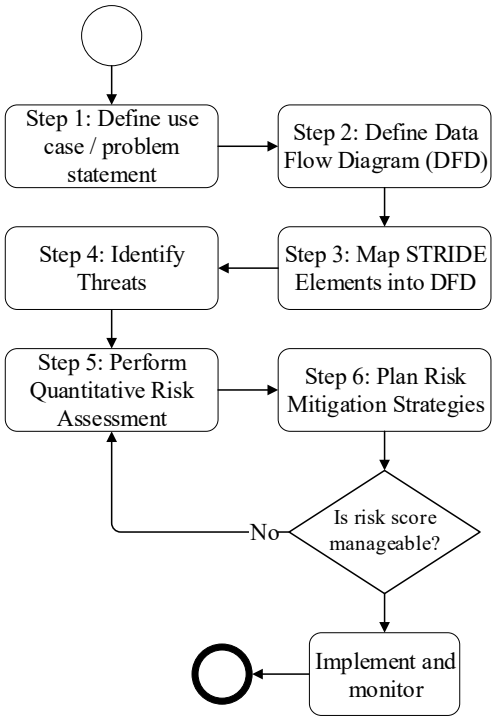

Figure 1. Main steps of the QTMM

Table 2. DFD Component Vulnerabilities as per STRIDE Threat Classes

Component	S	T	R	I	D	E
Data Flow		✓		✓	✓	
Data Store		✓		✓	✓	
Entity	✓		✓			
Process	✓	✓	✓	✓	✓	✓

A brief description of the different threat classes as per the STRIDE threat classification is summarized in Table 3. The purpose of this step is to identify the threat classes that are most prevalent to each component and prioritize the threat identification procedure for those classes.

Step 4: Identify Threats
Iterate over each component in the DFD and begin considering potential threats starting from generic attacks to more process-specific ones. If necessary, once threats are enumerated and cataloged, create short misuse case scenarios [25] for each attack. Due to space limitations, we forgo creating misuse case scenarios in this study.

Step 5: Perform Quantitative Risk Assessment
For each component in the DFD, and the relevant STRIDE threat classes, we generate attack trees using the information collected from the previous step. These component-based attack trees are then scored using a combination of the Common Vulnerability Scoring System (CVSS) and a risk propagation technique in order to gauge the final risk value of the threats [22].

Table 3. Threats classes per STRIDE

Threat	Description
Spoofing	An attacker attempts to mislead users or systems by falsifying either a process or an identity.
Tampering	An attacker modifies the system to cause harm.
Repudiation	An attacker rejects a transaction in the system.
Information Disclosure	An attacker obtains access to sensitive data concerning the system.
Denial of Service	An attacker makes the system unavailable to users.
Elevation of Privilege	An attacker manages to obtain administrator privileges.

Step 6: Plan Risk Mitigation Strategies
Considering the attack trees and their relevant scores, as well as the earlier generated misuse-case scenarios, the user can continue to ideate on potential actions to mitigate these threats. After mitigation strategies have been developed, a user may re-evaluate the previously defined attack trees to update the risk score for a threat class. Steps 5 and 6 are repeated until the user is satisfied with the level of threat mitigation. Once an acceptable risk score is obtained, the mitigations are implemented, and the system is monitored and updated as needed.

4 Example: TMM for 3DcP application

To illustrate the implementation of the proposed framework, we use a generic Robotic 3D Concrete Printing System as an example.

4.1 Define use case / problem statement

The system under consideration was chosen based on the review of existing literature and information obtained from industry experts to ensure a realistic case. The specification in question is based on ABB's IRB 6620 6-axis robot arm, with additional interfaces provided by the IRC5 industrial robot controller [26].

A schematic representation of the different elements for the 3DcP system used in this example is shown in Figure 2. The different elements identified in Figure 2 are described below.

1. **System Command:** The System Command refers to whichever device is used to relay instructions to the robot controller. This can be an Arduino microcontroller.

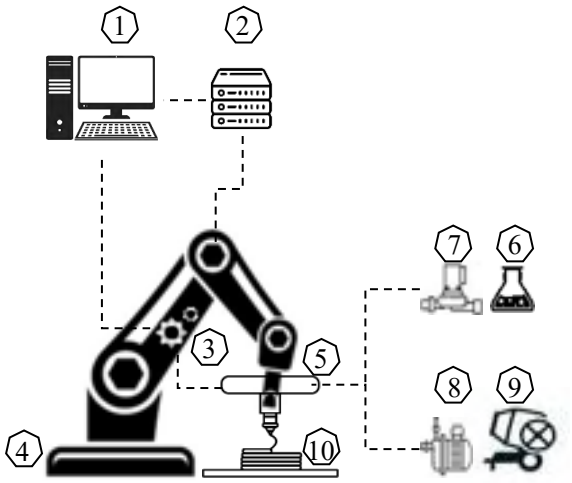

Figure 2. Schematic of the 3DcP system

2. **Robot Controller:** The Robot Controller is responsible for converting and relaying high-level commands passed through the system command onto the robotic arm itself. The IRC5 is an industrial standard for robot controllers.
3. **Printing Controller:** Based on the dimensions of what is being printed, the printing controller has several axes of movements that it can operate in to facilitate printing over a large surface area.
4. **Robotic Arm:** The Robotic arm is responsible for receiving instructions from the system command and passing on instructions to the precise part of the printing controller.
5. **Printhead:** The printhead is responsible for extruding the concrete mixture.
6. **Accelerating Agent:** A deposit containing the accelerating agent used in speeding up the concrete formation chemical reaction.
7. **Pump for Accelerating Agent:** Responsible for pumping the accelerating agent into the mixture, controls factors such as speed and throughput.
8. **Pump for Premix:** Responsible for pumping the premix into the printhead, controls factors such as speed and throughput.
9. **Premix Mixer:** A deposit containing the concrete premix used in the concrete printing process.
10. **3D Printed Object:** The designated 3D printed object as specified by the user.

4.2 Define the Data Flow Diagram (DFD)

Using the Legend defined in Microsoft's STRIDE Application article [24], we have defined the Data Flow Diagram, as shown in Figure 3, for our use case of the generic 3DcP application in Figure 2. Each of the data flows represent the flow of instructions in some digital format necessary in the 3DcP process.

A. 3D Specification Loaded into the System Command
B. Printed Item Specifications
C. Pump Control Information
D. Robotic Arm Printing Instructions
E. Robotic Arm Movement Instructions
F. Printhead Positioning Instructions
G. Printhead Extrusion Information

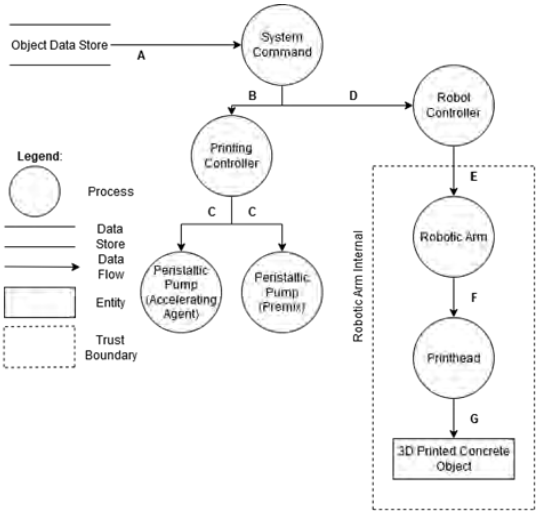

Figure 3. Data Flow Diagram

The trust boundary is a subjective measure of different levels of security that are present within the same system. The trust boundary in this example has been defined at the robotic arm and printhead, assuming that those elements would be less susceptible to direct access.

4.3 Map STRIDE to Elements into DFD

There are multiple 'process' components in the DFD. These components are, by nature, susceptible to all threat classes introduced by the STRIDE threat classification. Considering the data flows between these components, we realize that the information moved across the system is related to one another and, at times, are subsets of the preceding data flow. Threats that target one such data flow can potentially be replicated on another as per the goals of the attacker. However, the risk evaluation is dependent on the component in question. If we were to consider the "Robot Controller" component, it is unlikely that *Spoofing* or *Elevation of Privilege* threats are prevalent; *Tampering* threats, however, pose a serious concern.

4.4 Identify Threats

Consider the "Robot Controller" component. As a 'process,' it is susceptible to any of the STRIDE classes of attacks, but as mentioned previously, certain threats classes pose a greater risk than others. If we were to

deliberate on the potential threats that fall under the threat class of 'Tampering,' we would see threats like those delineated in Figure 4. As previously mentioned, these generic threats could take place in another DFD component, considering the nature of the data flow. To understand these threats in greater detail, the user may choose to generate misuse-case scenarios that dive into the context-aware specifics of these threats while providing a basis upon which risk-mitigation strategies are developed. The ideation performed at this step is fundamental to the remainder of the threat modeling process as it deepens the users' understanding of the system while providing a foundation upon which the Quantitative Risk Assessment may be carried out.

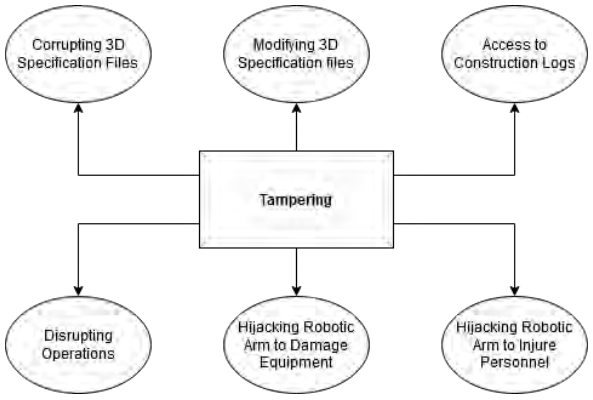

Figure 4. Potential Tampering Threats

4.5 Perform Quantitative Risk Assessment

An understanding of the variety of threats associated with the 'Tampering' threat class for the Robotic Controller aids us in developing the attack trees for this scenario. Using [22] as a guideline, we create Component Attack Trees (CAT) for a STRIDE threat class. This system uses four nodes, the *root node* (red), *intermediary node* (black), *leaf node* (gold), *class node* (white), and *mitigation node* (blue). The *class node* is designed to help systematically divide up threats. Each of the leaf and mitigation nodes are assigned a value reflecting the probability of success. This value is propagated upwards to the root node to determine the odds of success. To read the CAT, a user would begin at a leaf node and follow the path until the root node, at which point the attack has 'succeeded' [22].

Figure 5a is the high-level attack tree we generate for the Tampering threat class, and Figure 5b the risk propagation using CVSS. Unless otherwise specified, all leaf nodes are related by an 'OR'. Once we have created the attack tree, we use the CVSS to attribute a risk score to the leaf (gold) nodes. We then propagated these risks upwards as per the operations listed in [22] and summarized here.

"OR" operation between two nodes (x,y): P(x)+P(y)-P(x)P(y)
"AND" operation between two nodes (x,y): P(x)P(y)
"MITIGATION" of node (x), with mitigation P(m): P(x) = P(x)*(1-P(m))

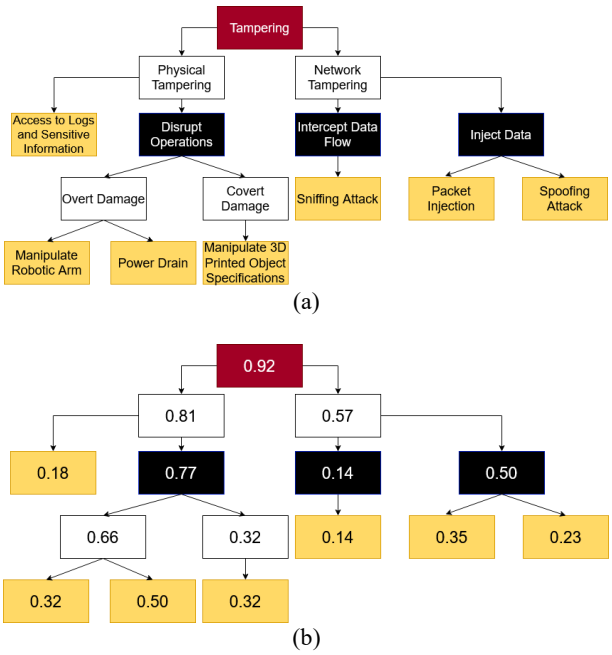

Figure 5. (a) Attack tree and (b) risk propagation and assessment for the Tampering Threat Class

Using the CVSS score [27] for the leaf nodes of this attack tree and the operations above to calculate the remaining risk scores for the various nodes, the overall risk score for the tampering threat class can be determined. This is showcased in Figure 5b. To illustrate the calculation of the score, consider the "Overt Damage" class, the 'manipulate robotic arm' threat has a lower risk value than 'power drain' because it is harder to accomplish while disconnecting the system from a power source is much easier to accomplish. However, they both present a threat, and together their risk score is calculated as follows:

$$0.50 + 0.32 - (0.5 * 0.32) = 0.66$$

Following the same approach, the overall risk score for the Tampering Threat Class is calculated to be 0.93 (9.3/10 in the CVSS scale), which is classified as a critical threat.

4.6 Plan Risk Mitigation Strategies

As a process, risk mitigation begins with the generation of the attack trees. Once a user has identified the different attack vectors, their understanding of the system will allow them to intuit strategies to counteract

threats at the lowest levels. The more detailed the DFDs and, consequently, the attack trees, the more nuanced simplified components will be available for a user to ideate mitigation strategies. Usage of attack libraries such as CAPEC and ATT&CK may help this brainstorming process. Figure 5 displays a scenario where there are no mitigation strategies. The user may update the attack tree with mitigation nodes (Figure 6) that would reduce the risk score of the corresponding leaf node (the "*" in Figure 6b indicates the pre-mitigation risk score). For illustration purposes, a subjective mitigation score was assigned to the mitigation (blue) nodes. Once the mitigations are considered, the overall risk score of the threat class can be recalculated. In this example, the mitigation nodes considered reduce the overall risk from 0.93 to 0.83, or a reduction of the risk of the tampering threat class from a critical risk threat, to a high-risk threat. This feedback loop can continue until the user is satisfied with the risk level, as well as the quality of the risk mitigation strategies in place.

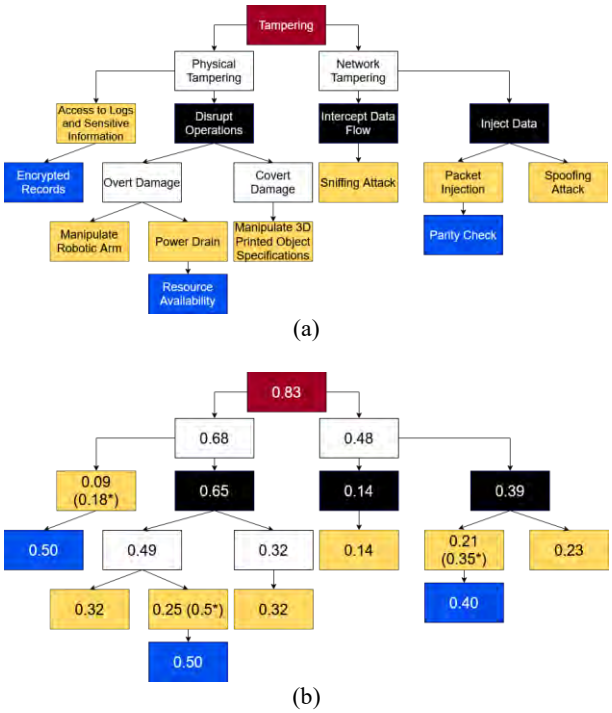

Figure 6. (a) Attack tree and (b) risk propagation and assessment for the Tampering Threat Class with countermeasures (mitigation nodes)

5 Discussion

The nature of this paper hinges on providing an example of applying a TMM in the field of 3D printing in construction. Section 4 shows an example that can be used as a guide for users when tackling similar systems.

Although the length of this paper imposes limitations on the extent of details shown in the example, enough information is provided to allow the reader to get a general idea of the different steps required in the threat modeling analysis. The DFD and attack trees are simplistic in nature to convey the idea of the threat modeling process as opposed to providing a thorough threat model of this system specification.

The threat class we chose for this application was the STRIDE threat class of 'Tampering' applied onto the DFD's 'Robot Controller' process component. Considering the nature of the data flows in our system, many of the attack trees generated are likely to contain the same threats in relation to those components that are either inside the trust boundary or outside of it. However, the threats delineated in these attack trees would be scored differently, and ultimately the same threat could have different risk levels based on the component in question. We consider the Robot Controller component, a rather central piece in the 3DcP process, and one that is highly susceptible to Tampering threats.

For our example, we modeled both physical and network threats as two separate classes. While there is a degree of overlap between the two, we realized it would be more beneficial from a practical standpoint to illustrate a wider scope of threats. The threats related to network tampering are a generic class of threats that involve exploiting known vulnerabilities in any network system. On the other hand, the physical tampering threats are process-aware and are attacks that are carried out respective to the system in question.

The methodology presented is effective in detailing and visualizing the extent of the threats posed to a system with minimal effort, that is, once the attack trees have been generated and the CVSS scores for the lead nodes calculated, the risk propagation is straightforward. The most significant obstacle to a TMM is in its ability to capture a substantial proportion of potential threats. To succeed in this endeavor, a great deal of emphasis must be placed into developing the DFD; this aspect of the TMM is core to all subsequent steps.

6 Conclusion and Future Work

As 3D printing technologies emerge and their use in construction projects become more common, it is of utmost importance to develop methods and frameworks to identify vulnerabilities and address them before full implementation or integration with other systems is done.

This endeavor is heavily based on understanding the nuances of a threat modeling method in relation to cyber-physical systems and developing a threat modeling method with a specific application in mind, in this case, the use of 3D printers in construction. A large part of this involves an understanding of both the existing threat modeling methods as well as contemporary 3D printing

technology in construction that would allow the creation of an applicable threat modeling method.

Our ongoing work includes improving the current threat modeling method to better suit a more extensive scope of 3D printing specifications and configurations that involve supplementary machinery that would complicate the threat landscape. Such improvements will be complemented with research into specific attacks allowing us to gauge their viability. Attacks that involve physical externalities can be conducted over a simulated environment, whereas more traditional IT-related attacks can be attempted directly with the appropriate equipment on hand.

Once a thorough modeling methodology to scope threats is in place, our focus will shift into techniques for securing the systems investigated. This process is two-pronged, considering both proactive and reactive measures. Proactive measures will aim to patch security flaws in the system that can be easily avoided. Reactive measures will seek to provide guidance to 'worst-case' scenarios.

The culmination of this research will be a holistic guide to identifying and securing 3D printing specifications in construction against any manner of threats for both OT and IT scenarios.

Acknowledgment: *The authors would like to thank the support from the Center for Cyber Security at New York University Abu Dhabi (CCS-AD).*

References

[1] P. Raitis and B. García de Soto, "Preliminary Productivity Analysis of Conventional, Precast and 3D Printing Production Techniques for Concrete Columns with Simple Geometry," In: Bos F., Lucas S., Wolfs R., Salet T. (eds) *Second RILEM International Conference on Concrete and Digital Fabrication*. DC 2020. RILEM Bookseries, vol 28. Springer, Cham. https://doi.org/10.1007/978-3-030-49916-7_100.

[2] N. Webster, "Dubai unveils world's largest 3D printed two-storey building," 2019. Online: https://www.thenational.ae/uae/government/dubai-unveils-world-s-largest-3d-printed-two-storey-building-1.927590 (accessed April 18, 2020).

[3] Y. Ma and Y. Che, "A brief introduction to 3D printing technology," *GRC 2015 Dubai*, p. 4, 2015.

[4] IAAC, "3D printed bridge," *IAAC*, 2016. Online: https://iaac.net/project/3d-printed-bridge/ (accessed April 18, 2020).

[5] Z. Yu, "3D-printed 'ancient bridge' put to use in Tianjin - Chinadaily.com.cn," 2019. Online: https://www.chinadaily.com.cn/a/201910/17/WS5da7d747a310cf3e35571065.html (accessed April 18, 2020).

[6] Empa, "Empa - NEST - Digital Fabrication," 2017. Online: https://www.empa.ch/web/nest/digital-fabrication (accessed April 18, 2020).

[7] A. Anton, P. Bedarf, A. Yoo, B. Dillenburger, L. Reiter, T. Wangler, J.R., Flatt, "Concrete choreography: prefabrication of 3D printed columns," In: Burry, J., Sabin, J.E., Sheil, B., Skavara, M. (eds.) *FABRICATE 2020*, 2020, pp. 286-293, 2020.

[8] The BOD, "The BOD - The first 3D printed building in Europe," 2019. Online: https://cobod.com/the-bod/ (accessed April 18, 2020).

[9] T. Vialva, "A French family is the first to move into a 3D printed house - 3D Printing Industry," 2018. Online: https://3dprintingindustry.com/news/a-french-family-is-the-first-to-move-into-a-3d-printed-house-135881/ (accessed April 18, 2020).

[10] K. Kelly, "MCSC teams with Marines to build world's first continuous 3D-printed concrete barracks," *The Official United States Marine Corps Public Website*, 2018. Online: https://www.marines.mil/News/News-Display/Article/1611532/mcsc-teams-with-marines-to-build-worlds-first-continuous-3d-printed-concrete-ba/ (accessed April 18, 2020).

[11] B.R.K. Mantha and B. García de Soto, "Cyber security challenges and vulnerability assessment in the construction industry," pp. 29–37, 2019, doi: 10.3311/ccc2019-005.

[12] E.A. Pärn and B. García de Soto, "Cyber threats and actors confronting the Construction 4.0," in *Construction 4.0*, Routledge, pp. 441–459, 2020, doi: 10.1201/9780429398100-22.

[13] B.R.K. Mantha, Y. Jung, and B. García de Soto, "Implementation of the Common Vulnerability Scoring System to Assess the Cyber Vulnerability in Construction Projects," *In Proceedings of the Eight Creative Construction Conference*, pp. 117-124, 2020, doi: 10.3311/CCC2020-030.

[14] J. Andersson, M. Balduzzi, S. Hilt, P. Lin, F. Maggi, A. Urano, and R. Vosseler, "A Security Analysis of Radio Remote Controllers for Industrial Applications," 2019, Technical Report, Trend Micro, Inc.

[15] S. Belikovetsky, M. Yampolskiy, J. Toh, J. Gatlin, and Y. Elovici, "Dr0wned – Cyber-physical attack with additive manufacturing," in *11th USENIX Workshop on Offensive Technologies, WOOT 2017, co-located with USENIX Security 2017*, Sep. 2017.

[16] A. V. Uzunov and E. B. Fernandez, "An extensible pattern-based library and taxonomy of security threats for distributed systems," *Comput. Stand. Interfaces*, vol. 36, no. 4, pp. 734–747, Jun. 2014, doi: 10.1016/j.csi.2013.12.008.

[17] S. Myagmar, A. J. Lee, and W. Yurcik, "Threat Modeling as a Basis for Security Requirements," *StorageSS '05 Proc. 2005 ACM Work. Storage Secur. Surviv.*, pp. 94–102, 2005.

[18] K. Singh and A. K. Verma, "Threat modeling for multi-UAV Adhoc networks," in *IEEE Region 10 Annual International Conference, Proceedings/TENCON*, Dec. 2017, vol. 2017-Decem, pp. 1544–1549, doi: 10.1109/TENCON.2017.8228102.

[19] N. Shevchenko, T. A. Chick, P. O. Riordan, T. P. Scanlon, and C. Woody, "Threat Modeling : a Summary of Available Methods," 2018.

[20] S. Hussain, A. Kamal, S. Ahmad, G. Rasool, and S. Iqbal, "Threat Modelling Methodologies: a Survey," *Sci.Int.(Lahore)*, vol. 26, no. 4, pp. 1607–1609, 2014.

[21] J. Selin, "Evaluation of Threat Modeling Methodologies A Case Study," *Sch. Technol. Inf. Commun. Technol.*, MSc Thesis. May, 2019.

[22] B. Potteiger, G. Martins, and X. Koutsoukos, "Software and attack centric integrated threat modeling for quantitative risk assessment," HotSoS '16. pp. 99–108, 2016, doi: 10.1145/2898375.2898390.

[23] J. Luna, N. Suri, and I. Krontiris, "Privacy-by-design based on quantitative threat modeling," *7th International Conference on Risks and Security of Internet and Systems (CRiSIS)*, Cork, 2012, pp. 1-8, doi: 10.1109/CRISIS.2012.6378941.

[24] S. Hernan, S. Lambert, T. Ostwald, and A. Shostack, "Uncover Security Design Flaws Using The STRIDE Approach," Microsoft Docs. Online: https://docs.microsoft.com/en-us/archive/msdn-magazine/2006/november/uncover-security-design-flaws-using-the-stride-approach (accessed June 01, 2020).

[25] G. Sindre and A. L. Opdahl, "Eliciting security requirements by misuse cases," *Proc. Conf. Technol. Object-Oriented Lang. Syst. TOOLS*, no. TOOLS-PACIFIC2000, pp. 120–131, 2000, doi: 10.1109/tools.2000.891363.

[26] ABB, "IRB 6620 - Industrial Robots from ABB Robotics." Online: https://new.abb.com/products/robotics/industrial-robots/irb-6620 (accessed Jun. 01, 2020).

[27] FIRST, "Common Vulnerability Scoring System Version 3.0 Calculator," Forum of Incident Response and Security Teams. Online: https://www.first.org/cvss/calculator/3.0 (accessed June 06, 2020).

Measuring Adhesion Strength of Wall Tile to Concrete by Non-Contact Inspection Using Electromagnetic Waves

Hussain Alsalem [a], Takayuki Tanaka[b], Takumi Honda[c], Satoru Doi [d], Shigeru Uchida[e]
[a]Department of Information Science, University of Hokkaido, Japan
[b]Department of Information Science, University of Hokkaido, Japan
[c]Central Research Institute of Electric Power Industry, 2-6-1, Kanagawa, Japan
[d]Obayashi Corporation, Tokyo, Japan
E-mail: hussain@hce.ist.hokudai.ac.jp, ttanaka@ssi.ist.hokudai.ac.jp, honda3793@criepi.denken.or.jp, {doi.satoru, uchida.shigeru }@obayashi.co.jp

Abstract **–** The separation of exterior tiles from buildings diminishes the visual appeal of cities and can injure pedestrians when they are struck by falling tiles. Therefore, tiles should be inspected periodically. However, completion of the inspection process has hurdles, including high cost and the need for qualified human inspectors. This study describes a non-destructive inspection method for detecting voids that match those seen in tile separation in a concrete specimen using electromagnetic waves, specifically microwaves. The method can be performed using devices that are simpler, smaller, and easier to use than those required by conventional methods. In addition, this method can be used to measure the adhesion strength of tiles.

Keywords **– Non-contact inspection; Electromagnetic wave; Adhesion strength; Multi-layered scanning.**

1 Introduction

The separation of exterior tiles from buildings reduces the visual attractiveness of cities and falling tiles can injure pedestrians below, especially during earthquakes. Therefore, tiles should be checked periodically. However, high cost and the need for a qualified human inspector hinders the completion of inspections. In this study, voids that match those seen in tile separation were detected in a tiled concrete specimen using non-destructive inspection (NDI) with electromagnetic waves (EMWs), specifically microwaves. Several methods based on NDI techniques using EMWs have been developed and reported. These methods include ground-penetrating radar [1], microwave tomography [2], microwave non-destructive testing, and other evaluation methods [3] [4] that use a network analyser in the time/frequency domain to calculate the position of foreign bodies in the object; such methods are very complex and costly.

Our proposed method uses EMW reflection intensity data for analysis, and the measuring device required is simpler, smaller, and easier to use than that required for the above-mentioned methods. Our method can also use the reflection data to estimate the adhesion strength of the tiles. An antenna that transmits and receives microwaves was used to obtain the reflection intensity from the concrete specimen, and the distribution of reflection intensity was determined using a multi-layered scanning (MLS) method. This reflection intensity was compared with normal concrete data (trend data) to predict the integral of the difference, which indicates the size of the void [5] [6]. In our experiments, first, a tiled concrete specimen with voids was evaluated by MLS to calculate the strength distribution. Second, tensile strength testing of the tiled concrete was performed, and the strength to failure was measured. Third, the correlation between the tensile strength and the reflection intensity by MLS was examined to evaluate the possibility for practical use.

2 Microwave NDI

2.1 Inspection apparatus

The inspection apparatus for detecting voids consists of a linear actuator and a flaw detection device. The flaw

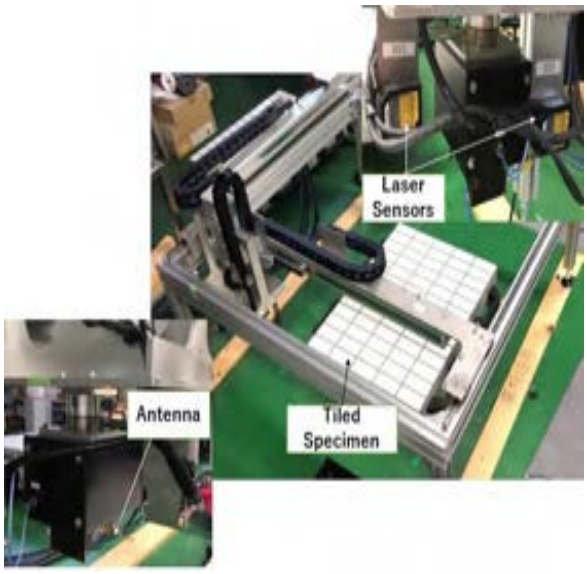

Figure 1. Inspection apparatus.

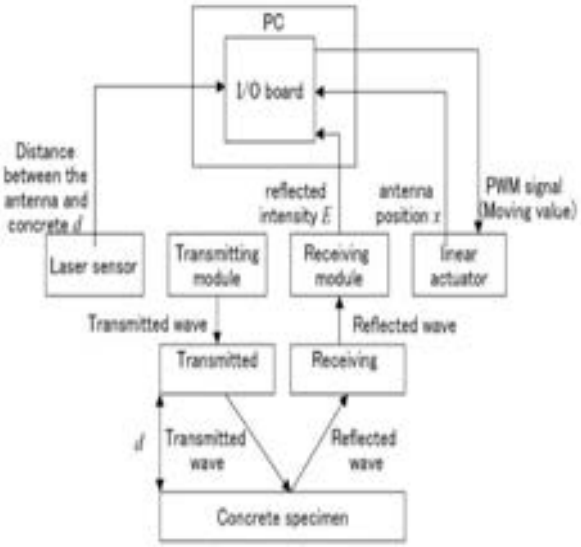

Figure 2. Measurement system.

detection device consists of a lifter, an antenna, and a laser sensor, as shown in Figure 1. An overview of the signal processing system is shown in Figure 2. The linear actuator is used to move the flaw detection device over the concrete surface, and the device scans the surface to detect voids.

2.2 Tiled concrete specimen

Figure 3 shows the tiled concrete specimen, which comprises tiles, adhesive mortar, and concrete. Figure 4(a) shows the dimensions of the tiled concrete and the positions and widths of the voids, Figure 4(b) shows the design of the tiled concrete specimen from the side, and Figure 4(c) shows the positions of the voids as seen from the side. The experiments demonstrate the effectiveness of the proposed void detection method by applying NDI using EMWs to an actual tiled concrete specimen. In addition, the system used the void sizes to indicate the tile adhesion strength.

2.3 MLS method

This section describes the MLS method [5-6], which is used to acquire the reflected intensity and to estimate and remove interference and noise caused by EMWs.

The detection void algorithm is shown in Figure 5. First, the total reflection intensity, E_r, is measured by MLS. In abnormal areas, the received intensity is the effective value of the sum of the direct wave, surface wave, and air gap reflected wave. Next, the trend reflection intensity, E_t, is measured by MLS. This shows the reception intensity of normal (void less) areas, which is the effective value of the sum of the direct wave and

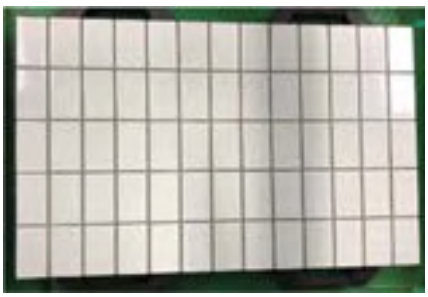

Figure 3. Tiled concrete specimen.

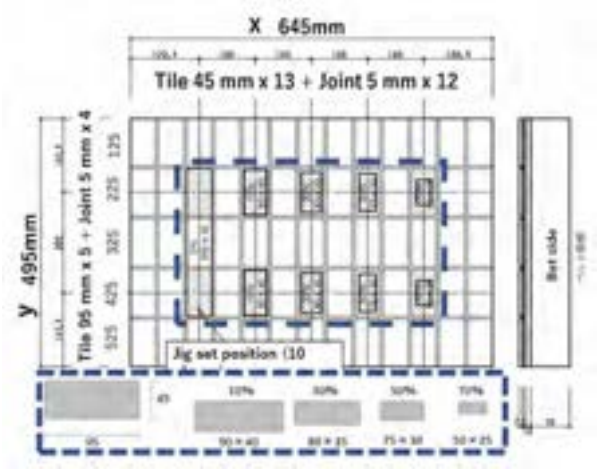

(a) Concrete dimensions and void positions and widths.

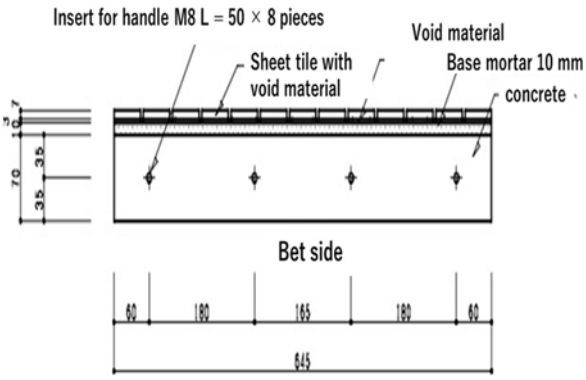

(b) Side view of concrete specimen design.

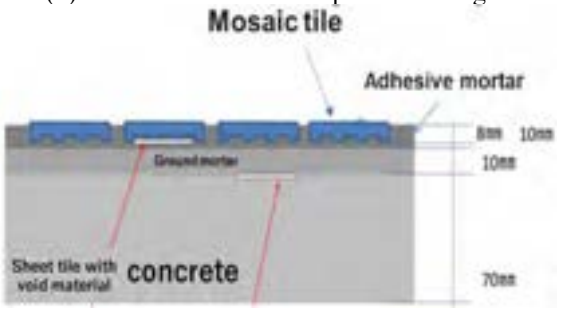

(c) Side view of void positions

Figure 4. Experimental setup.

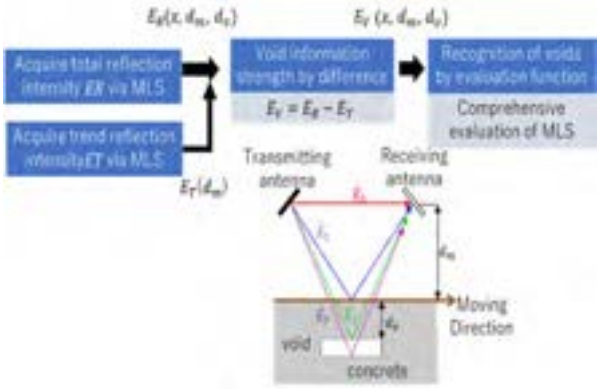

Figure 5. Algorithm for void detection.

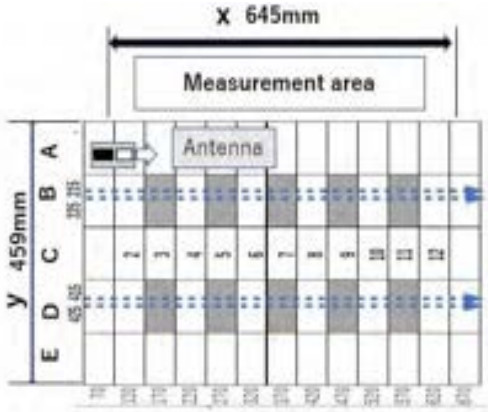

Figure 6. Overview of tiled specimen scanning.

the surface wave. Then, void reflection intensity E_v is obtained by taking the difference between the total reflection intensity and the trend intensity strength. The last step recognizes voids by a comprehensive evaluation of MLS.

2.3.1 Detecting voids

This section shows how an evaluation function $P(x)$ can quantitatively detect voids from the measured reflected intensity. $P(x)$ can detect voids from $\hat{E}_v(x,d)$ which is the void information is obtained by taking the difference between$E_t(d)$and$E_t(x,d)$. This compensation makes the scanning more robust against the noise caused by small variations in d. Hence, this procedure should be useful for scanning a real tiled wall. And is defined as

$$P(x) = \frac{1}{N}\sum_i^n |\hat{E}_v(x,d_i)| \quad (1)$$

where N is the number of data points along the d-axis at each value of x. Because $\hat{E}_v(x,d)$ is obtained from the difference between reflected intensities, it can be negative. By removing the variation of d, scanning collects only the reflected intensity from the voids and the concrete, allowing the voids to be detected and distinguished more easily.

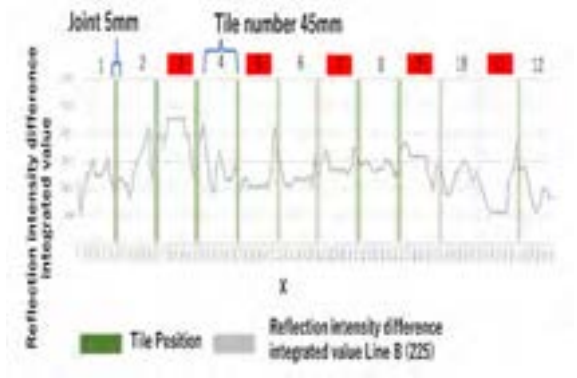

(a) $y = 215$ mm (Line B 225).

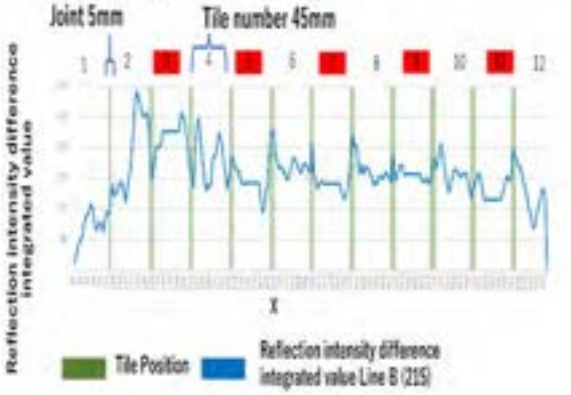

(b) $y = 225$ mm (Line B 215).

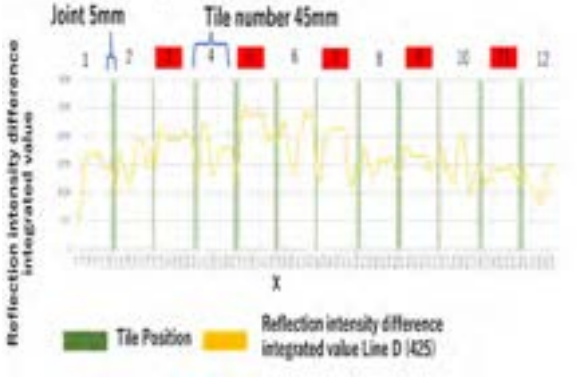

(c) $y = 415$ mm (Line D 425).

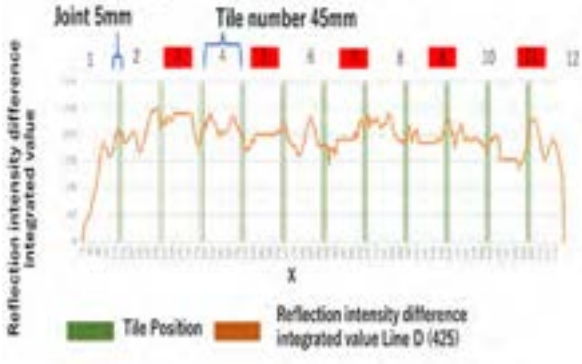

(d) $y = 425$ mm (Line D 415).

Figure. 7. Distribution of $P(x)$ at various tile locations.

2.3.2 MLS measurement results

Experiments were conducted using real tiled concrete to demonstrate the effectiveness of the proposed method for inspecting actual tiled walls. The concrete specimen shown in Figure 3 comprises the tile, its adhesive mortar, and concrete. MLS was performed at $y = 215, 225, 415, \text{and } 425$ mm, with a measurement area as shown in Figure 6. Intensity $E_R(x, d)$ was obtained by scanning along the x-axis in each scanning area several times at intervals of $60 \text{ mm} < d < 90 \text{ mm}$. through changing y-axis, we can set up the Anita in position of Line. The evaluation function $P(x)$ using this result is shown in Figure 7. The vertical axis shows the variation of the integrated reflection intensity, which varies according to whether voids are present. The average integrated reflection intensity was taken at a distance ± 10 mm from joints. The horizontal axis is the tile position. Red tiles have voids ranging from 30% to 100% of the tile size. Other tiles are normal tiles without voids. In most scanning lines, the integrated reflection intensity is high at large voids and low at small voids.

Figure 8. Manual Pull-off adhesion tester.

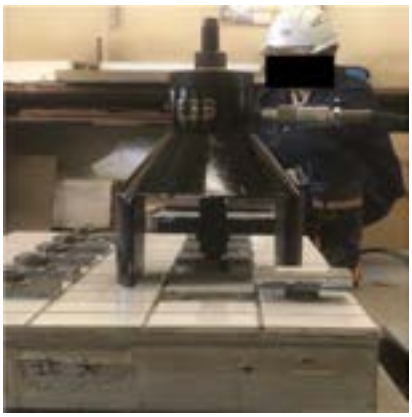

Figure 9. Tile removal operation. Nuts are installed on the tiles to be removed.

3 Tile pulling test

3.1 Inspection Apparatus

Measurement of the adhesion strength was demonstrated using a pull-off adhesion tester (LPT-3000, Ox Jack Co., Ltd.). Before using the adhesion tester, a hammering test was performed to determine whether a void was present. Figure 8 shows the tester, which

Table 1. Adhesion test results

Tile position	Void size (%)	Load (kN)	Load (N/mm^2)	Integrated reflection intensity V
Line D 425, No. 3	100	0.2	0.047	$1{,}995 \le V \le 2{,}091$
Line D 415, No. 3	100	0.2	0.047	$2{,}213 \le V \le 2{,}748$
Line B 225, No. 3	100	0.2	0.047	$2{,}072 \le V \le 2{,}542$
Line B 215, No. 3	100	0.2	0.047	$1{,}962 \le V \le 2{,}526$
Line D 425, No. 5	90	0.2	0.047	$1{,}883 \le V \le 2{,}011$
Line D 415, No. 5	90	0.2	0.047	$2{,}213 \le V \le 2{,}748$
Line B 225, No. 5	90	0.5	0.12	$978 \le V \le 1{,}255$
Line B 215, No. 5	90	0.5	0.12	$1{,}962 \le V \le 2{,}526$
Line D 425, No. 7	70	1.8	0.42	$1{,}080 \le V \le 1{,}262$
Line D 415, No. 7	70	1.8	0.42	$1{,}611 \le V \le 2{,}260$
Line B 225, No. 7	70	2.5	0.58	$1{,}155 \le V \le 1{,}364$
Line B 215, No. 7	70	2.5	0.58	$1{,}310 \le V \le 1{,}448$
Line D 425, No. 9	50	2.3	0.54	$1{,}403 \le V \le 1{,}577$
Line D 415, No. 9	50	2.3	0.54	$1{,}727 \le V \le 2{,}026$
Line B 225, No. 9	50	1.5	0.35	$1{,}532 \le V \le 1{,}744$
Line B 215, No. 9	50	1.5	0.35	$1{,}402 \le V \le 1{,}674$
Line D 425, No. 11	30	1.8	0.42	$1{,}244 \le V \le 1{,}533$
Line D 415, No. 11	30	1.8	0.42	$1{,}403 \le V \le 1{,}755$
Line B 225, No. 11	30	4.5	1.05	$379 \le V \le 739$
Line B 215, No. 11	30	4.5	1.05	$964 \le V \le 1{,}316$

consists of an analogue load cell, a pump handle, and an attachment. When the pump handle is turned clockwise, the attachment rises and pulls the tile until it separates from the concrete, as shown in Figure 9. At the moment of tile removal, the strength is measured by the load cell and recorded. The recorded load data are shown in Table 1, columns 3 and 4.

3.2 Results of adhesive strength measurements and MLS analysis

Figure 10(a) and (b) show the values of exact value of P(x) of all lines at locations of each tile for which adhesion strength was tested. The six points of P(x) was taken over a total distance of 20 mm and ± 10 mm from joints to avoid effects from the joints themselves [6]. The points were distributed on Lines B 215, B 225, D 415, and D 425. Data recorded from the tile pulling tests and MLS analysis are shown in Table 1. Column 1 shows the location of each tile for which adhesion strength was tested and MLS was performed. Column 2 is the void size, which varied from 30% to 100% of the tile size in 20% increments. Column 3 shows the recorded pull strength data in kilonewtons, which is the power required to remove the tile and is directly analogous to load cell results. In column 4, the power is converted to newtons per square millimetre. MLS results are shown in column 5. Based on the adhesive strength and MLS data from Figure 10(a) and (b), Table 1, the scatter plot in Figure 11 was created. This plot shows the adhesive strength of all lines on the horizontal axis and integrated reflection intensity on the vertical axis. The intersection of the two values is shown by colours indicating the tile and scanning position.

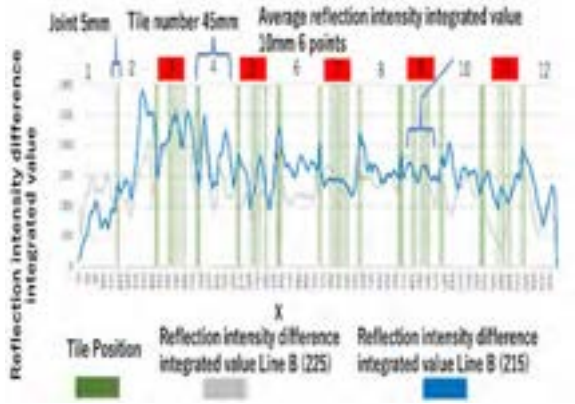

(a) $y = 225$ mm (Line B 225) and$y = 215$ mm (Line B 215).

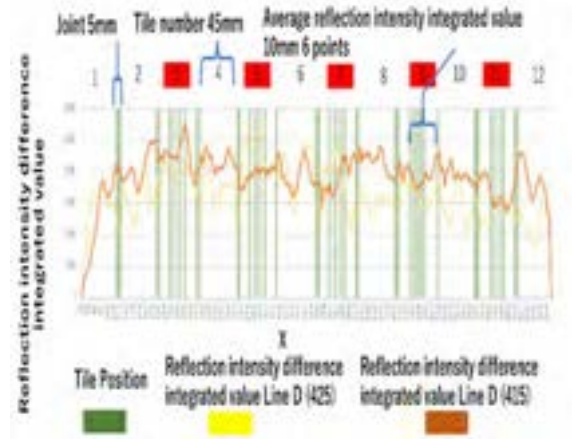

(b) $y = 425$ mm (Line D 425) and$y = 415$ mm (Line D 215).

Figure 10. Distribution of tensile bond strength.

3.3 Analysis of adhesive strength measurements and MLS results

The results of adhesive strength measurements plotted against MLS values in Figure 11 indicate that there is a negative correlation between adhesive strength and the value of the tensile strength. Also, there appears to be a linear relationship between the two variables. Testing of the significance of the correlation coefficient confirmed a strong negative correlation, meaning that a decreased tensile bond strength is correlated with increased integrated reflection intensity, with $R = -0.622$ at $p < 0.001$. Furthermore, regression analysis provided the result $R^2 = 0.382$ at $p < 0.001$.

3.4 Discussion

The results show that this method can estimate the adhesion strength, but with a large error. The regression analysis R-squared result is significantly low. This low value might be caused by the experimental procedure, or it might indicate that there was a problem in how voids were implanted under the tile to make the specimen. As

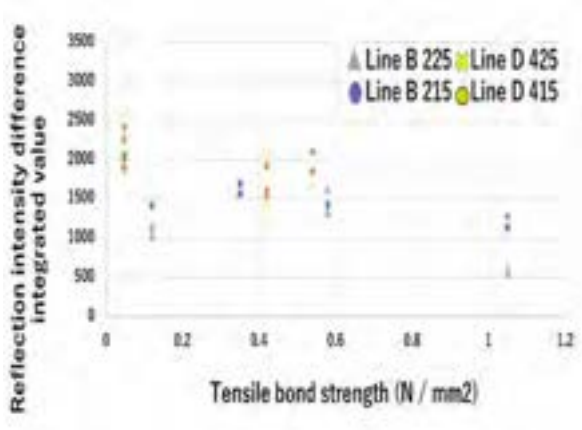

Figure 11. Reflection intensity integrated value versus tensile bond strength

seen in Figure 10(a), in Line D 425, tile No. 3 has a void size bigger than that of No. 5. Therefore, it should have a higher intensity value. However, the integrated value for reflection intensity difference is lower. In Line B, tile Nos. 7 and 8 have the same issue. These issues might have occurred because the tiled concrete specimen was not cured. Environmental effects on sheet strength due to the time that elapsed between performing MLS and measuring the tensile strength needs to be taken into consideration. To improve the accuracy of the estimation, more data are needed by analysing tiles of different sizes. In addition, the experimental procedure would be improved if the MLS scanning data and the adhesive strength were obtained at the same time. Furthermore, a more accurate adhesive strength measurement device should be used.

4 Concluding Remarks

This paper describes ability of the MLS method in determining tile adhesive strength. This method will increase the accuracy of the safety tests required for wall tiles used in building exterior finishes. In particular, the MLS method does not require an expert to implement it. Therefore, it has the potential to reduce the cost and time required for tile safety examinations.

References

[1] Xu. X, Xia. T, Venkatachalam. A, and Huston. D, "Development of high-speed ultrawideband ground-penetrating radar for rebar detection," Journal of Engineering Mechanics, Vol.139, No.3, pp.272-285, 2012.

[2] Kim. Y. J. Jofre. L, De Flaviis. F, and Feng. M. Q, "Microwave reflection tomographic array for damage detection of civil structures," IEEE Transactions on Antennas and Propagation, Vol.51, No.11, pp.3022-3032, 2003.

[3] Arunachalam. K, Melapudi. V. R, Udpa. L, and Udpa. S. S, "Microwave NDT of cement-based materials using far-field reflection coefficients," NDT and E International, Vol.39, No.7, pp.585-593, 2006

[4] Zoughi. R, and Bakhtiari. S, "Microwave nondestructive detection and evaluation of voids in layered dielectric slabs," Research in Nondestructive Evaluation, Vol.2, No.4, pp.195-205,1990.

[5] Kawataki. S, Tanaka. T, Doi. S, Uchida. S, and Feng. M. Q, "Nondestructive In-spection of Voids in Concrete by Multi-layered Scanning Method with Electro-magnetic Waves," Proc. of the IEEE International Conference on MECHA-TRONICS (IEEE-ICM2017), pp. 336-341,2017.

[6] T. Honda, T. Tanaka, S. Doi, S. Uchida, and M. Feng, “Visualization of Voids Between Tile and Concrete by Multi-Layered Scanning Method with Electromagnetic Waves,” J. Robot. Mechatron., Vol.31, No.6(2019) 863-870

Construction Method of Super Flat Concrete Slab using High Precision Height Measurement

Y. Fukase[a], R. Saito[a] , Y. Takemoto[a] and Y. Muramatsu[b]

[a]Institute of Technology, Shimizu Corporation, Japan
[b]Construction Technology Division, Shimizu Corporation, Japan
E-mail: fukase@shimz.co.jp, ryosuke.saito@shimz.co.jp, y.takemoto@shimz.co.jp, yoshiki@shimz.co.jp,

Abstract -

The new Hachinohe indoor skating rink required an extremely flat concrete slab. ±2mm precision concrete surface was expected across 6,350 m^2 concrete slab. It is impossible to construct such a large super flat slab with a conventional construction method to maintain the height of the concrete surface at intervals of few meters using human hands and eyes. Therefore, we have developed a construction method using high precision height measurement which maintains the height of the concrete surface in the levelling and the finishing processes with high density and precision.

In the levelling process, a 18m long truss screed was used. Such a long truss screed is easily deformed and the deformation of the truss screed during the process directly leads to the deterioration of surface accuracy. Therefore, we developed a mechanism to measure and correct the deformation of the truss screed with high accuracy.

In the finishing process we precisely scanned the levelled concrete surface with a 3D laser scanner. An unevenness distribution map was calculated from the scanned point-cloud data and projected onto the concrete surface using a projector to remove the concrete on the convex part.

Finally, all the finished concrete surface was measured with a 3D laser scanner and confirmed that it had extremely high flatness.

Keywords -

Flatness of Concrete; 3D Laser Scanner; Projection Mapping; Truss Screed

1 Introduction

The Hachinohe Nagene indoor speed skating oval rink, equipped with 400m double tracks, is the third indoor speed skating facility that is in conformity with international standards in Japan. The construction of this skating rink involved various efforts to build a high-quality, indoor skating rink meeting international standards, one of which is the construction of the concrete slab beneath the ice.

The cross-sectional structure of the skating rink is shown in Figure 1. Refrigerate pipes were installed in the ice-making concrete slab, and the ice layer will be formed over the slab via cooling. The surface precision of the ice-making concrete slab affects the thickness of the ice layer, thereby affecting the hardness of the ice layer. Building a high-quality skating rink with an even level of ice layer requires ice-making concrete slab with high surface precision; in this construction, the goal surface precision was set within ±2mm.

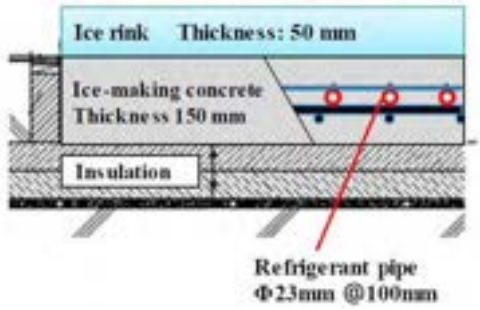

Figure 1. The cross-sectional structure of the rink

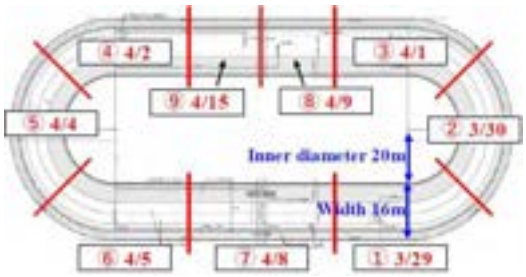

Figure 2. Construction sections of the ice-making concrete slab

The ice-making concrete slab is comprised of a straight section with a width and length of 16m and 110m, respectively, and a curved part with inner and outer diameters of 20m and 30m, respectively. The total area of the skating rink is about 6,350 m^2.

The conventional construction method of concrete

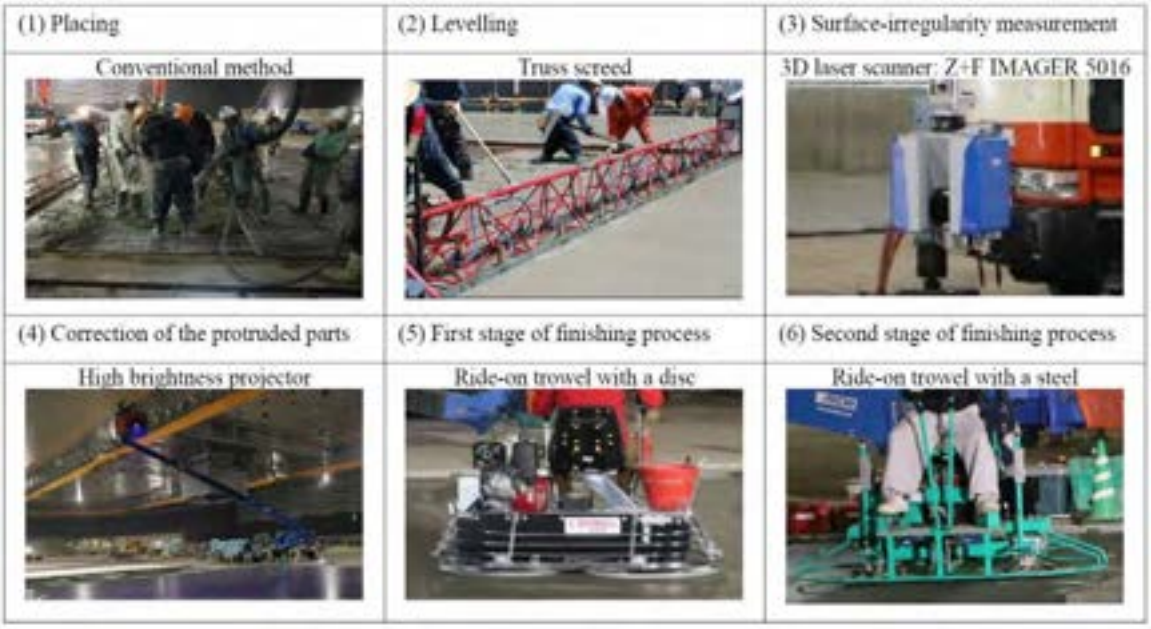

Figure 3. Construction processes of concrete slab

slab involves human hands and eyes to maintain the height of the concrete surface at intervals of few meters, thereby rendering the ±2mm precision across this large area practically inconceivable. Therefore, we assumed a mechanized construction method that maintains the surface height in the levelling and finishing processes with high density and precision. As shown in Figure2, the 400m circumference was divided into nine sections, and each section was constructed within one day. Figure 3 shows the construction flow and the machines used in the ice-making concrete slab. After the hardening of the concrete, 3D Laser Scanner was used to evaluate the flatness [1],[2].

2 Construction of Super Flat Concrete Slab

We have developed a construction method using high precision height measurement which maintains the height of the concrete surface in the levelling and the finishing processes with high density and precision.

2.1 Levelling Process

A truss screed, which was composed of an iron truss frame and a blade, was used to level the concrete. Units, each with a width of 3.5m, can be linked to make the maximum width of 20m. The portion that meets the concrete is an L-shaped blade with multiple oscillators driven by compressed air. Both ends of the truss screed are placed on rails installed outside the cast concrete area., and the concrete surface is levelled by moving the truss screed along these rails while providing vibration. Truss screed is deformed because of the loosening of the joints which is caused by vibration and of the force from the placed concrete. Because the shape of the truss screed directly affects the surface precision of the ice-making concrete slab, we attempted to improve the surface precision during the levelling process using a high-precision level monitoring system for managing the levelling. The method of level monitoring is described below.

At each joint, we measured the top height of the blade and adjusted it by tightening the joint every 2 m in the driving direction. As shown in Figure 4, we installed rotating laser receivers at five locations on the truss screed and used a level monitoring system which displayed the heights with 0.1mm resolution on a tablet PC in real-time. Using a rotating laser level, we can detect relative changes in height with high accuracy and in real time, but we cannot measure absolute height accurately. On the other hand, using a digital level, we cannot measure the height change in real time, but can measure the absolute height accurately. Therefore, we decided to measure the absolute height at each location using a digital level and monitor the changes from the measured values with a monitoring system using a rotation laser level. By using this system and adjusting the height of the blade to within ±1mm from the standard level, a precise levelling process could be performed.

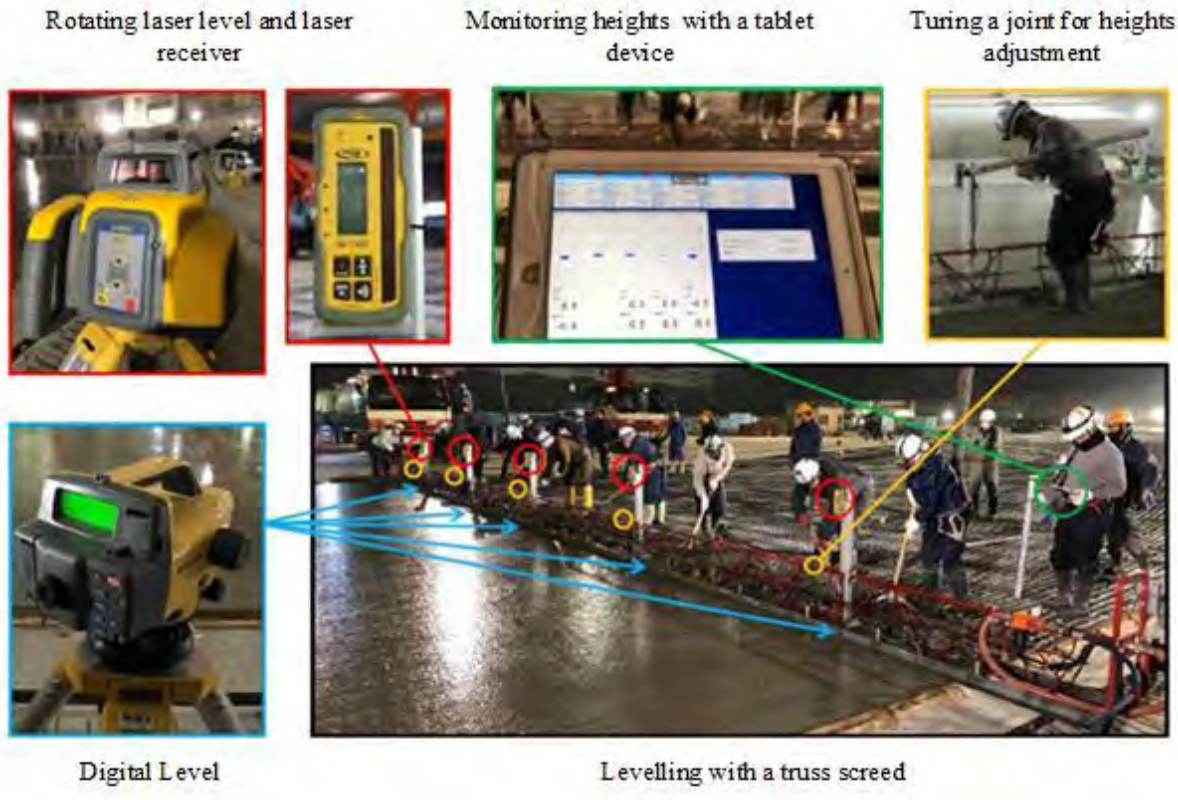

Figure 4. Monitoring for the levelling blade using a display system for level change

2.2 Measurement of Surface Irregularities immediately after Levelling

We used a 3D laser scanner to measure the surface irregularities immediately after levelling. Figure 5 is a picture of the situation of this measurement. The concrete surface, immediately after levelling, has a gloss that bends the laser light, so a small incident angle to the measured surface is preferred. Therefore, the scanner was attached at a boom of a crawler crane and scanned the concrete surface from a height of approximately 9 m. Each measurement was performed over a 16 m × 12.5 m area, 1/4 of the total placement area for a day, and it took 43 seconds for an irregularity measurement with a maximum 10mm pitch. Using this measurement method, the boom oscillation in the crawler crane and the boom drop were suspected to affect the measurement of surface irregularities. Therefore, we obtained the data on the boom oscillation and the boom drop in advance and verified that they would not affect the measurement results if the time of scanning was 43 seconds.

Figure 6 shows an example of point-cloud data for the concrete surface obtained by the 3D laser scanner. The point-cloud data are obtained in the coordinate system of the 3D laser scanner. Hence, if the coordinate axis in the height direction is not vertical, we cannot accurately evaluate the irregularities on the concrete surface against the design height. Thus, we evaluated the surface irregularities using the following method.

1) We placed four 700mm × 700mm reference plates around the target concrete surface.
2) The surface of each reference plate was levelled with a high-precision inclinometer, and the heights of the four reference plates were adjusted to be the same.
3) From point-cloud data obtained by the 3D laser scanner, we extracted the clouds corresponding to the reference plates and from that clouds, computed one virtual reference plane.
4) As shown in Figure 7, the reference surface is horizontal and its height (H) is known, so it was used to calculate the irregularity (h) compared to the design height based on the distance of each point cloud (d) from the virtual reference plane.

Figure 5. 3D scanning a concrete just after levelling process

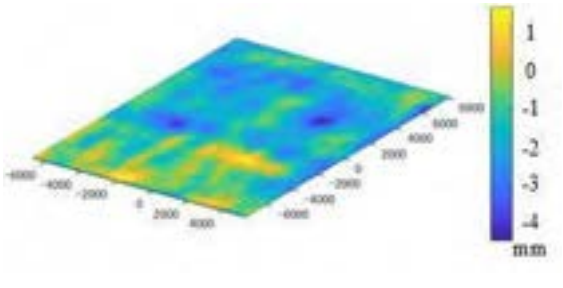

Figure 6. Example of a point-cloud data

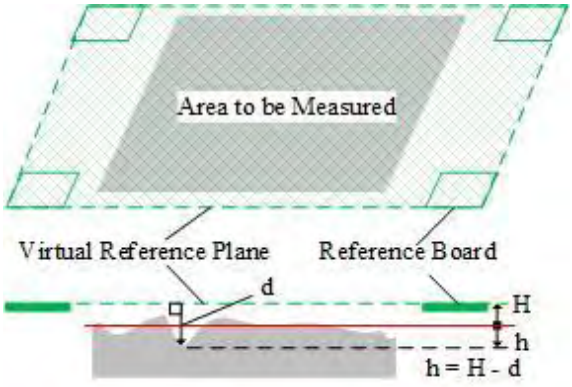

Figure 7. Calculate irregularity of surface

2.3 Correction of Irregular Portions

To further improve the surface precision of the concrete, which was levelled by the truss screed, we conducted a process of scraping the protruded concrete. When the craftsman with the plasterer's boots can stand on the concrete without deforming the concrete surface, the correction process can be started. From the previous setting test, we found that this condition was met when the penetration-resistance value exceeded 0.5 N/mm^2, thus, we began the correction process when the penetration-resistance value became 0.5 N/mm^2.

In the point cloud data of surface unevenness acquired after leveling, the part where the surface height is higher than the design height (= +0 mm) was set as a correction target. Moreover, we generated a 2D image (image for correction) of the point-cloud data with the target and other areas indicated by red and blue colors, respectively. Figure 8 shows an example of such a correction image. The scraping depth on the concrete was set 2 mm from the surface. Furthermore, to allow the operators to accurately view the operation areas, we directly projected and visualized the correction image on the concrete surface. For the projection, a large projector was installed on an elevating work platform approximately 10 m above the ground. Figure 9 shows a picture of the correction process. The concrete surface became rough after the scraping. Hence, a disc was installed on a trowel and the surface of corrected portions were smoothed.

Figure 10 shows an example of the comparison between the surface irregularities measured immediately after levelling and after the finishing process. The standard deviation of the surface irregularities decreased

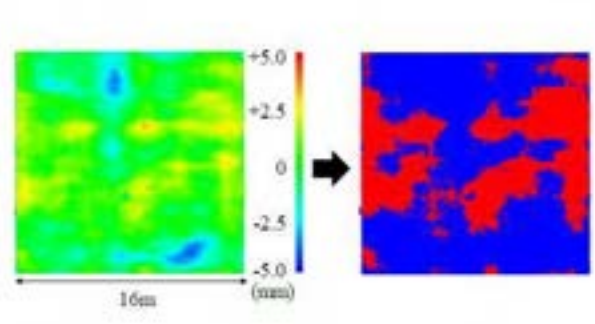

Figure 8. Example of a correction image

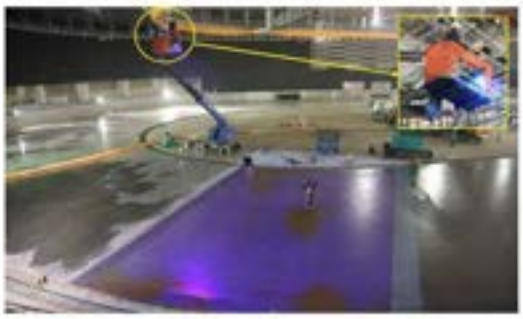

Figure 9. Projection of the correction image

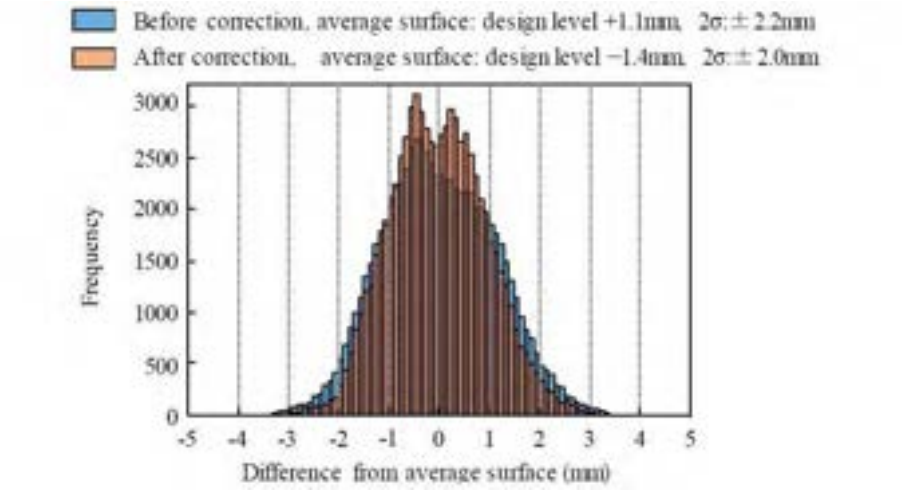

Figure 10. Comparison of the surface irregularities after the levelling and after the correction process

from 1.1 to 1.0 mm, and the frequency of the mean value ±1 mm increased by 14.4%, indicating an improvement of the surface precision. Here the median value is not the design height but the average height of the concrete surface. The average height of the concrete surface shifted from +1.1 to −1.4 mm, because of the rise in bleeding water and the compaction on the surface from the finishing process.

3 Flatness of the Completed Ice-Rink

3.1 Measurement using 3D Laser Scanner

In general, the 3DLS is not able to be set strictly horizontal and the level of the scanner is unknown. The scanner coordinate system is based on different height and attitude from a base coordinate system. To measure the height of the concrete slab, we must match the height and attitude between the scanner coordinate system and the base coordinate system. Around the scanning area, we put three reference boards and measure each height of the boards. We translate the scanned point-cloud in order to match each height of levelled boards in the point-cloud to the measured height of them in the real world. The detailed procedure is shown below.

1) Putting 3 boards, which size is 700mm x 700mm, around the scanning area. Adjusting lengths of the three support legs to level the boards.
2) Using a digital level, measuring Z_{DL1}, Z_{DL2} and Z_{DL3} which are the board surface heights.
3) Using 3DLS, scanning the area which includes the 3 reference boards.
4) From the scanned point-cloud, detecting Z_{ave1}, Z_{ave2} and Z_{ave3} which are heights of center of the 3 reference boards.
5) Deriving a rigid body translation T from an equation below.

$$\begin{pmatrix} x_1 & x_2 & x_3 \\ y_1 & y_2 & y_3 \\ z_{DL1} & z_{DL2} & z_{DL3} \end{pmatrix} = T \begin{pmatrix} x_1 & x_2 & x_3 \\ y_1 & y_2 & y_3 \\ z_{ave1} & z_{ave2} & z_{ave3} \end{pmatrix} \quad (1)$$

x_i, y_i, i = 1, 2, 3 are x-y positions of each center of the

Figure 11. Conventional measurement method

Figure 12. Proposed measurement method

reference boards in the scanner coordinate system.

6) Translating the scanned point-cloud with the rigid body translation T and getting a point-cloud in which, each height of board equals the height measured using a digital level.

3.2 Confirming Measurement Method

In order to confirm our proposed method, we measured a part of the rink (14m x 15m) using the proposed measurement method and a conventional measurement method. And we compared the data which was acquired with the two methods.

3.2.1 Conventional measurement method

We used a digital level for conventional measurement method. At first, we draw measured points on the floor in a grid of 0.5m. We divided the measurement area (14m x 15m) into 3 parts. 6 people, 3 pairs, measured each part. In the pair, one set a staff and the other collimated it and recorded the measured height (Figure 11). It took more than 4 hours to measure 899 points.

3.2.2 Proposed measurement method

3 people worked in the proposed measurement method. We set 4 reference boards and measured the height of each board. Since the circle with a radius of about 1.0 m just below the scanner cannot be scanned, we scanned the target area at two different points. It took less than 10 minutes and measured about 10,000 points height in grid of less than 10mm.

3.2.3 Comparing the two measured data

Figure 13 shows the measurement result using conventional method and proposed method. Visualization processing was performed so that irregularities with 100 mm grid spacing were displayed for comparison. According to this figure, the height distributions in each calculation result are almost the same in two dimensions. The height distribution is shown as a histogram in figure 14. Both have same standard deviations of 1mm. Although the number of samples is different, the height distribution tendencies are the same. Therefore, the measurement results of the proposed method are highly reliable.

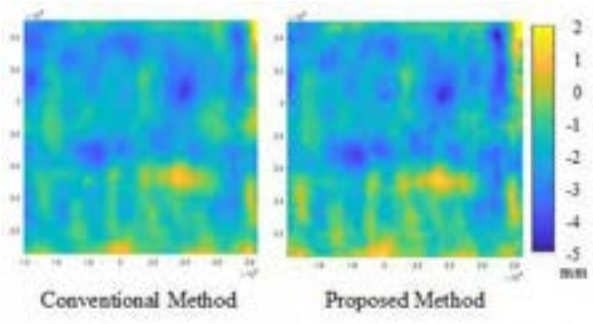

Figure 13. Comparison of two methods

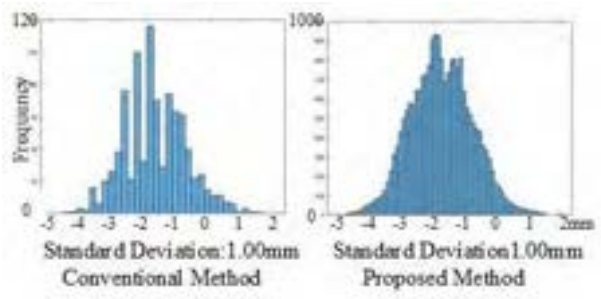

Figure 14. Comparison of two methods

3.3 Measurement Result of the Ice-Rink

Figure 15 shows that the ice-making concrete slab divided into 84 sections and the 3D laser scanner set at the centre of each section. Figures 16 and 17 show the measurement results. The standard deviation of the height is 1.22 mm, and 90.3% of the whole area is within ±2-mm precision. The curved portions in sections tend to be low. The reason is considered that the operation of the truss screed is difficult compared to the straight part of the rink owing to the difference in speed between the inner and outer portions.

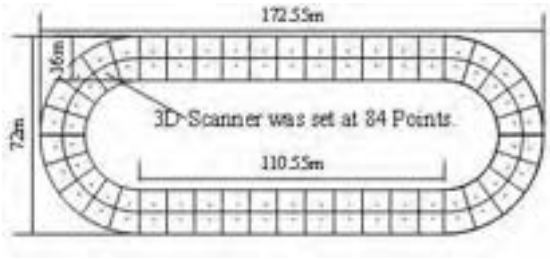

Figure 15. Scanned area was divided into 84 parts.

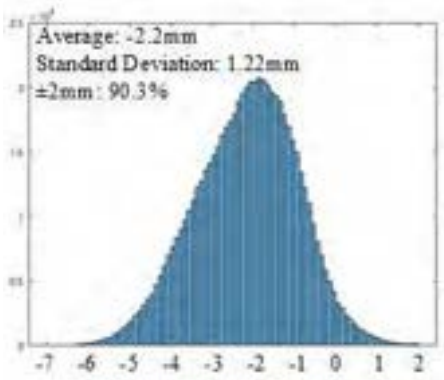

Figure 16. Height Deviation of the ice-rink

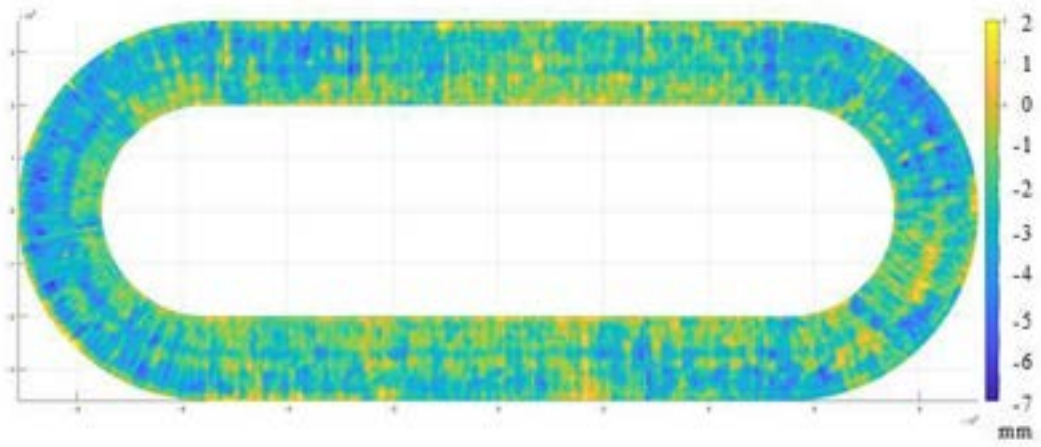

Figure 17. Height Map of the ice-rink

4 Conclusion

For the construction of super flat concrete slabs using a truss screed, we developed a method for obtaining the real-time level of the truss screed and achieved high precision levelling. After levelling, we measured the surface irregularities using the 3D laser scanner and applied the results to correct the protruding portions visualized with a large projector, thereby improving the surface precision of the concrete. Using the above methods, we achieved ±2mm precision for 90.3% of the entire area of approximately 6,350 m^2.

References

[1] E. Valero and F. Boshe: Automatic Surface Flatness Control using Terrestrial Laser Scanning Data and the 2D Continuous Wavelet Transform, In *Proceedings of the 33rd ISARC2016*, Auburn, US, 2016.

[2] T. Funtik, J.Erdelyi, M. Dubek and J. Gasparik: Innovative Assessment of Selected Properties of Industrial Floors, In *Proceedings of the 33rd ISARC2016*, Auburn, US, 2016.

Method for Estimating Subgrade Reaction Modulus by Measuring Wheel-terrain Interactions

Yasushi Wada[a] and Taizo Kobayashi[b]

[a] Graduate School of Science and Engineering, University of Ritsumeikan, Japan
[b] Department of Civil and Environmental Engineering, University of Ritsumeikan, Japan
E-mail: rd0059rx@ed.titsumei.ac.jp, kobat@fc.ritsumei.ac.jp

Abstract –

For several years, the compaction quality of embankments has been controlled by the dry bulk density and water content. However, the quality assessment is time consuming and merely a point measurement. We are developing a method that measures the mechanical properties of soil by observing the soil - wheel interaction behavior. In this study, we have proposed a method for estimating the subgrade reaction modulus of the soil by towing a wheel on the ground surface. This paper describes the theoretical basic concept of this method and discusses its validity with the results obtained from a laboratory model experiment.

Keywords –

Soil compaction; Quality control; Subgrade reaction modulus

1 Introduction

For several years, the quality control of soil compaction has been assessed by measuring soil density and water content. However, the measurement is time consuming and is only a point measurement. Recently, a new technique called "intelligent compaction [1]" has become widespread; this is because the quality is controlled by the number of roller passes required to achieve the desired compaction. Intelligent compaction using a GNSS-mounted roller enables real-time continuous measurements. In contrast, the number of roller passes is only considered to be an index without a physical meaning.

In this study, we have proposed a soil testing method that allows us to continuously evaluate the rigidity of soil (subgrade reaction modulus) by towing a wheel on the surface of the ground. Figure. 1 depicts an illustrative example of the possible future applications of this technique. One possible application is a mobile measurement in which a wheel-type testing tool is equipped in a construction vehicle. The other application is also a mobile measurement using a wheeled roller. The

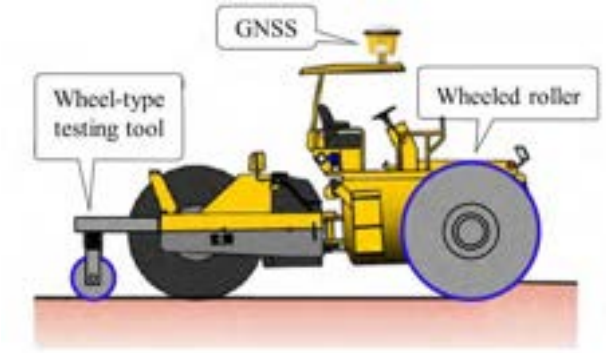

Figure 1. Possible future applications of the wheel testing tool

proposed method has the following two advantages:

- Direct measurements for assessing the mechanical properties of soil: As mentioned above, the existing methods for examining the quality control of soil compaction assess the physical properties of soil (e.g., soil density and water content) or calibrated index. This is based on the premise that as far as the compacted soil satisfies the desired control value, the quality also satisfies the requirements for mechanically stabilizing the soil structure. The proposed method directly provides the subgrade reaction modulus, which is an important mechanical parameter that is commonly used in pavement designs, foundation designs, and for predicting the behaviors of other soil-structures. We consider that the proposed method allows direct assessment to determine whether the compaction quality meets the requirements of the design.
- Continuous real-time measurements: As for in-situ soil investigation techniques for assessing the stiffness/rigidity of soil surface, the plate load test, California Bearing Ratio (CBR) test, and Falling Weight Deflectometer (FWD) are commonly used in practice [2]. The existing methods evaluate the point measurement of soil rigidity whereas the proposed method evaluates the continuous spatial distribution of soil rigidity.

At present, we have not implemented mobile

measurement using a vehicle-mounted device under actual situations; therefore, we cannot evaluate the practicality of the proposed method. As a feasibility study, this paper describes the theoretical basic concept of the method for estimating the subgrade reaction modulus and discusses its validity with the results obtained from a laboratory model experiment.

2 Method for estimating subgrade reaction modulus

The mechanism of wheel-soil interaction is complicated, as depicted in Figure. 2. When a rigid wheel travels on soft soil, a rut occurs on the soil surface. In addition to the soil compression that generates the rut, plastic soil flows of a soil bed occur at the front, rear, and sides of the wheel. Considering that the rate of energy input to the wheel is consumed by the soil-wheel interaction, we obtain the following energy conservation equation:

$$\dot{E}_t + \dot{E}_d = \dot{D}_c + \dot{D}_p + \dot{D}_e + \dot{D}_l \tag{1}$$

where $\dot{E}_t$ and $\dot{E}_d$ are the external rate of work performed by the drawbar pull and driving force, respectively; $\dot{D}_c$ and $\dot{D}_p$ are the rate of internal energy dissipation due to soil compression and plastic soil flows, respectively; $\dot{D}_e$ is the rate of potential energy variation of the wheel; $\dot{D}_l$ is the rate of mechanical energy transformation loss due to friction inside the wheel.

In this study, we have postulated a condition in which a rigid wheel is towed on a soil surface without a driving torque. In this situation, the wheel slip does not occur. In addition, plastic soil flows do not occur when the wheel sinkage is small. This suggests that the rate of internal energy dissipation due to plastic soil flows can be ignored. Furthermore, assuming a condition in which the mechanical energy transformation loss and variations in the wheel elevation are also negligible, Eq. (1) can be rewritten as

$$\dot{E}_t = \dot{D}_c \tag{2}$$

Eq. (2) suggests that the input energy rate is consumed by the soil compaction for generating the rut. Denoting the towing speed and drawbar pull as V and F, respectively, the input energy rate can be written as

$$\dot{E}_t = FV \tag{3}$$

In contrast, assuming that the load–settlement relationship of the surface soil can be approximated as $p = k_w z$, where k_w is the subgrade reaction modulus and z is the wheel sinkage, then the rate of internal energy dissipation due to soil compression can be expressed as

$$\dot{D}_c = \frac{1}{2} k_w z^2 BV \tag{4}$$

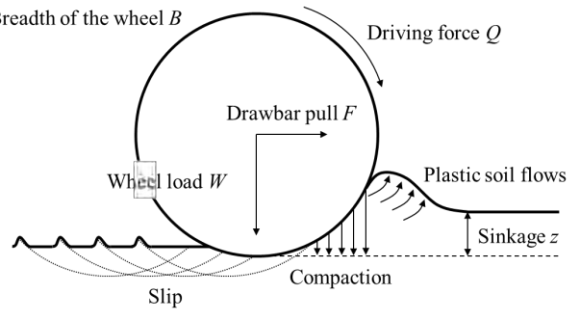

Figure 2. Soil-wheel interaction

where B is the breadth of the wheel.

By substituting Eq. (3) and Eq. (4) into Eq. (2), the subgrade reaction modulus can be obtained as follows:

$$k_w = \frac{2F}{z^2 B} \tag{5}$$

Eq. (5) suggests that it is possible to continuously estimate the variation in k_w as the wheel rotates by measuring F and z. Note that although the wheel load (W) is not explicitly included in Eq. (5), it will certainly influence both F and z.

Although we ignored $\dot{D}_e$ in Eq. (2), it could be taken into account by considering the following equation:

$$\dot{D}_e = W\Delta h \tag{6}$$

where Δh is the increment in the wheel elevation.

$\dot{D}_l$ can also be experimentally obtained by measuring the drawbar pull (F_0) of the wheel traveling on a horizontal rigid surface (this situation does not cause any energy dissipation except $\dot{D}_l$).

$$\dot{D}_l = F_0 V \tag{7}$$

3 Verification by laboratory model experiment

3.1 Experimental setup

In this study, a laboratory model experiment was performed to validate the theoretical concept of our proposed method. Figure. 3 depicts the experimental setup used in this study. An aluminum wheel with a diameter of 200 mm and breadth of 100 mm was used. As mentioned above, we used a wheel that spins freely in this experiment. A sheet that was made of rough sandpaper was attached onto the wheel surface to avoid slipping. The wheel could move freely in the vertical direction, and the wheel load (W) was adjusted using counterweights. The wheel was towed using a feed screw that was further controlled by an electric motor. A load cell was installed between the wheel and support jig to

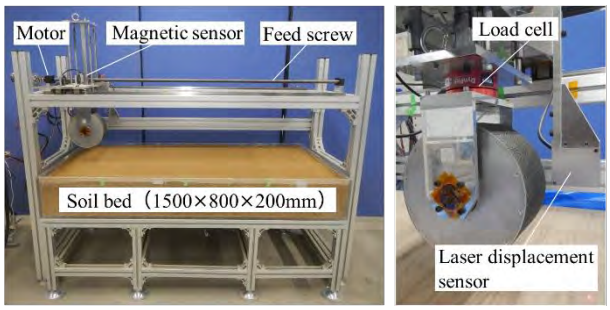

Figure 3. Experiment setup

measure the drawbar pull, F. The wheel elevation (h) was detected using a magnetic scale sensor attached to a support shaft that vertically moves in response to the soil surface topography and/or wheel sinkage. The wheel sinkage (z) was determined as the difference in the soil surface elevations at an arbitrary point between the wheel passes, and these were measured using a non-contact laser displacement sensor that was attached in front of the wheel and magnetic scale sensor as mentioned above.

In this experiment, the towing speed (V) was permanently set as 10 mm/s, and the wheel load (W) was changed to 68.6, 98.0, 127.4, and 156.8 N. Two types of decomposed granite soil were used for the model ground, namely, soil A: fine-grained sand with an average water content of 12.1%, and soil B: gravel-grained sand with an average water content of 14.9%. The soil bed was 1500 mm in length, 800 mm in width, and 200 mm in depth. The model ground was prepared to have three zones with different degrees of compaction: D_c = 65%, 70%, and 75% in the direction of travel, further indicating the varying rigidity of the soil surface with respect to the travel distance in one pass.

3.2 Small-diameter plate load test

In this study, the subgrade reaction modulus was independently measured using a small-diameter plate load test equipment (Figure. 4) to verify the estimate of k_w obtained by measuring the wheel-terrain interaction. A rigid circular plate with a diameter of 50 mm (same size as that of the CBR test), was set on the soil surface, and the plate was vertically pushed into the soil at a constant rate of 0.1 mm/s. The load-settlement behaviors (p-z relationship) were observed at various points on the model ground.

Figure. 5 depicts examples of the p-z relationship obtained from the test for the model ground of soil A. From the figure, it could be observed that the p-z relationship has an inflection point after a certain settlement. The inflection is usually regarded as a point at which the material fails. In this study, the subgrade reaction modulus, hereinafter referred to as k_p, is determined as the initial slope that appears prior to the inflection point.

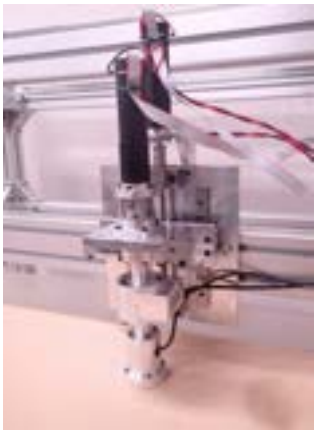

Figure 4. Small-diameter plate load test equipment

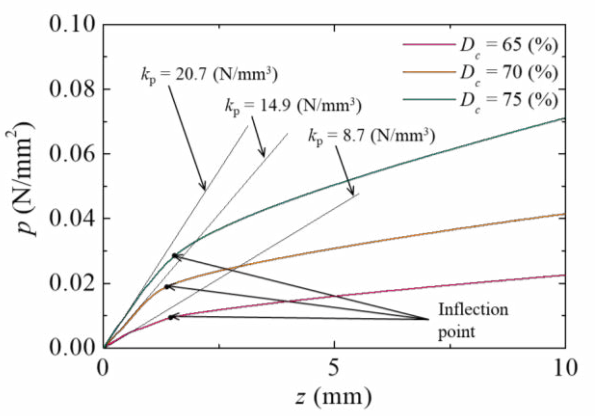

Figure 5. Typical examples of p-z relationship

3.3 Results and discussion

Figure. 6 depicts typical examples of the drawbar pull (F), sinkage (z), and the estimated subgrade reaction modulus (k_w) obtained from the laboratory model experiment. k_p obtained from the plate-load tests were also plotted as ◇ in this figure. It can be observed from the figures that both F and z increase with an increase in W for each soil. With some exceptions, it also appears that both F and z tend to decrease with an increase in D_c. In Figure. 6 (a), k_w obtained for each W is consistent regardless of W in the zone when D_c = 65%, where the degree of compaction is relatively small. This provides evidence to support the hypothesis that k_w does not explicitly depend on W in Eq. (5). However, when the degree of compaction increases (in the zone when D_c = 65% and 75%), the differences in k_w due to W becomes remarkable. In particular, when W is small, as in W = 68.6 and 98.0 N, the estimates of k_w show random fluctuations further resulting in huge gaps between k_w and k_p. From Eq. (5), it can be noted that k_w is inversely proportional

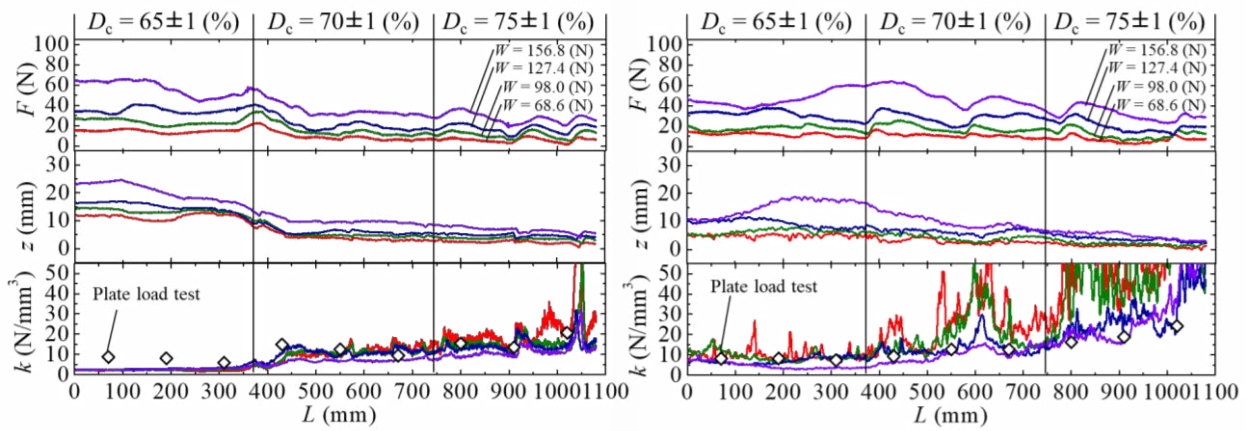

(a) Soil A: fine-grained sand (b) Soil B: gravel-grained sand

Figure 6. Experiment results and estimated subgrade reaction modulus

to z^2, and thus, k_w drastically increases when z decreases by one order of magnitude. The gaps can be attributed to the fact that the wheel with a smaller wheel load travels on a zone with a higher degree of compaction, thus resulting in a considerably small sinkage.

Figure. 7 depicts the comparison between k_w and k_p. The plots of k_w are the extracted data corresponding to the points at which k_p was measured using the plate load test equipment. It can be noted that k_w has an approximately positive correlation with k_p, and many of them are consistent with each other. However, it could be seen that k_w tends to underestimate k_p when subgrade reaction modulus is relatively small. In addition, k_w tends to overestimate k_p when W is relatively small. Possible reasons for this inconsistency are as follows. The underestimation occurred when the soil rigidity was small, further implying that the plastic soil flows occurred owing to the excessive sinkage under the soft soil. In this study, we ignored the internal energy dissipation due to the plastic soil flows, and the energy conservation equation was simplified as in Eq. (2). This assumption may yield an underestimation. Conversely, the reason for the overestimation may be due to the small sinkage that was used to calculate k_w, as mentioned earlier. Although Eq. (5) may be simple to estimate, a positive correlation between k_w and k_p could be observed. Even though there is still room for improvement and experimental verification, we conclude that the feasibility of the proposed method was confirmed from the laboratory model experiment.

4 Conclusion

In this study, we have proposed a method for estimating the subgrade reaction modulus of soils from wheel-terrain interaction measurements. The experimental results demonstrated the potential of the proposed method for estimation of subgrade reaction

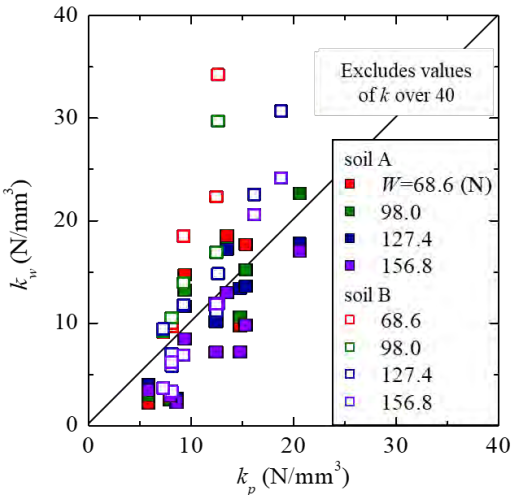

Figure 7. Comparison between k_w and k_p

modulus. However, it was revealed that the estimation equation had some limitations. We plan to proceed with the study for its practical use by improving the estimation equation.

References

[1] Japanese Geotechnical Society: Soil compaction, Chapter 3: Testing method for compaction and concept of construction management, pp. 16~56, 2012 (in Japanese).

[2] Japanese Geotechnical Society: Geotechnical investigation Methods and Explanations-Part 2 Volume 2- Chapter 8: Loading Tests, pp.661~761, 2013 (in Japanese).

Report on the Measurement of the Form of SHOTCRETE GRID BEAM-FREE FRAME Using Point Cloud Data

Takayuki Kojima[a] and Yori Nomoto[b]

[a,b]East Nippon Expressway Company Limited Yuzawa Management Office, Japan
E-mail: t.kojima.ad@e-nexco.co.jp, y.nomoto.aa@e-nexco.co.jp

Abstract –

We conducted a measurement accuracy and laborsaving in the spraying slope frame work by appli-cation of ICT earth works using UAV was verified by using field of actual work.

In the UAV survey, it was possible to apply the Ministry of Land, Infrastructure, Transport and Tour-ism (MLIT) standards to the UAV survey by facing front of a slope.

The measurement accuracy of the cross-sectional measurement of the frame was ensured by setting the frame cross-section at 5 mm/pixel and 90% wrapping, and In the area measurement, a difference of -1% to +2% could be calculated.

The introduction of UAV is expected to significantly reduce the time required to work in the field on steep slopes.

The measurement of a 1500m2 of a field was completed with about 50% less labor than the con-ventional method.

Keywords –

i-Construction; UAV; Spraying Slope Frame Construction Method; Form measurement

1 Introduction

The Ministry of Land, Infrastructure, Transport and Tourism (MLIT) says it will promote "i-Construction" with the aim of improving productivity and making construction sites more attractive.

The Ministry of Land, Infrastructure, Transport and Tourism (MLIT) has established various standards for ICT construction in order to promote "i-Construction".

At present, the guidelines for ICT earthworks and ICT paving have been established, and in March 2020, the glue surface construction was added.

In this report, we report on the measurement of the construction status of the slope surface by aerial photogrammetry using an unmanned aerial vehicle (UAV), which was carried out in 2019.

The results of the survey were used to confirm the accuracy of the measurements and to verify labor-saving measures.

2 Contents of the survey

The test was conducted at the Echigo-Kawaguchi Service Area on the Kanetsu Expressway, as shown in Figure 1.

Figure 1. Map of Kanetsu Expressway Area

The glue surface here had collapsed due to heavy rainfall in July 2017,to restore the disaster, we planned and commissioned the reinforcement using sprayed method frames and Tests were conducted as part of this work (test area was about 50 meters high and 30 meters wide).

Figure 2. Test Area (50m×30m)

The verification items were selected from the "Earthwork Construction Management Guidelines" of the East Nippon Expressway Co. It has been done.

The four items selected were (1) measurement of length, (2) measurement of cross section width and height, (3) measurement of extension, and (4) measurement of the area.

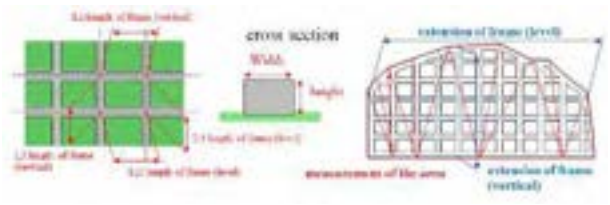

Figure 3. Verification items of sprayed frames

2.1 Measurement method

For the measurement of the profile of the spraying slope frame by UAV survey, the point cloud data obtained by field surveying with the 3D reconstruction data created by the method described in the previous section, the position of the workpiece was confirmed by tape surveying, and the shape dimensions and the extension was measured.

However, considering the differences in slope, complicated undulations and structural details, the issues to be addressed in the application of the slope work were discussed and some of the specifications were modified as shown in Table 1.

Table 1. Summary of Improvement Measures

item	ICT earth works standards (MLIT) : March 2018	Try and compare
photo shoot	downward direction	⇒facing front of a slope
measurement performance	pixel size 10mm/pix	pixel size ⇒5mm/pix
LAP rate	next to 80% lap course 60% lap	⇒next to 90% lap ⇒course 90% lap
reference point	outside of shooting area (outer edge)	⇒inside of shooting area

3 Inspection

3.1 Comparison with actual measurements (frame shape)

This presents the results of the comparison of measurements from 3D data and tape surveying of the frame profiles, i.e. (1) length of frame, (2) width and height of frame, (3) extension of frame area.

3.1.1 Length of the frame and section of the frame

The difference between the frame length and the reference value, which is the actual measurement, was less than ±1 cm. As for the cross-sectional width (W), an error of a few millimeters from the reference value was observed, but it was found that the NEXCO standard is not applied to the cross-sectional area. values. A maximum height (H) error of -55 mm was confirmed. When the comparison was carried out with the modified plan (5mm/pixel, 90% lap), the maximum margin of error was 9 mm. They converged.

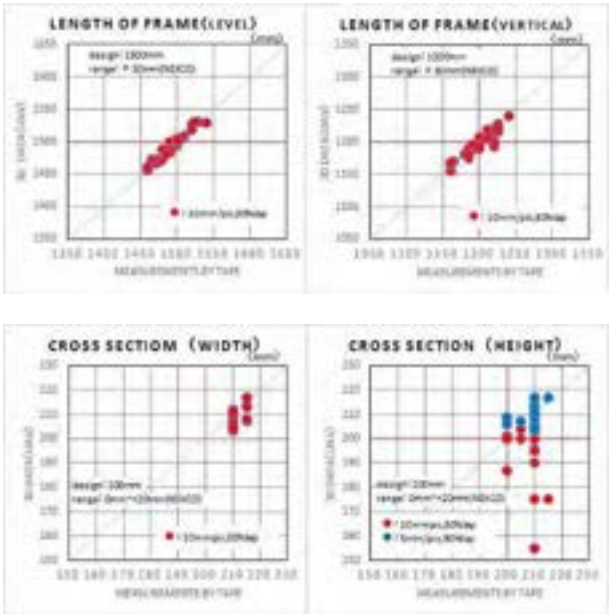

Figure 4. measurement of length, width and height

3.1.2 Length of the entire framework

The results of the comparison of the length of the entire framework with the actual measurement showed that the extension of the frame was a few centimeters (less than ±1%) in both vertical and horizontal directions.

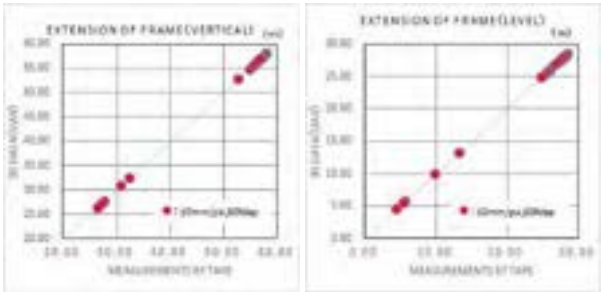

Figure 5. measurement of extension

3.2 Comparison and verification of actual measurement results (area)

The area was verified by comparing the results of the UAV survey with the development of the tape survey (triclinic method).

The difference between UAV survey and actual measurement is less than -1% in the calculation of area by actual measurement and co-located measurement as shown in Table 2. The total area of each frame increased by a little less than 2% compared to the actual measurement, indicating that the total unevenness was measured.

Table 2. Area Comparison

	Tape Surveying	3D data(UAV)	3D data(UAV) (in detail)
AREA	1522.67m²	1510.52m²	1548.16m²
difference		-12.15m² (-0.8%)	+25.49m² (+1.7%)
development view	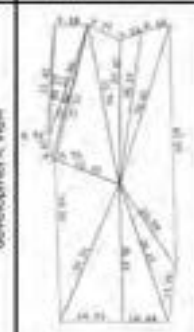	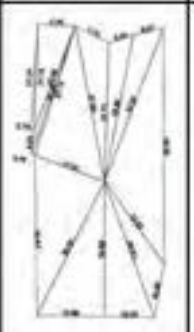	

3.3 Verification of efficiency through the use of ICT

Surveying by UAV of the workpiece (per 1500m2) requires more off-site work than actual measurement (tape surveying). The reduction is about a quarter. However, the total reduction effect is about half due to the increase in internal work such as analysis work. As shown in Table. 3, the work was performed on a steep slope, and the use of the UAV made the work site safer. In addition, we have improved in the following areas.

Figure 6. Status of surveying works

Table 3. Improving Efficiency through ICT (UAV)

per 1500m2

reference point	2 workers × 0.5 days	3D modeling	1 worker × 1.0 days
TS survey	2 workers × 0.5 days	development view	1 worker × 0.5 days
UAV survey	2 workers × 1.0 days	Frame measurement	1 worker × 1.5 days
		Cross-section	1 worker × 1.5 days
fieldwork total	4.0	deskwork total	4.5

※Not including the time the PC calculates.

UAV survey	total:	8.5	4.0	4.5
Tape survey	total:	17.0	16.0	1.0

50% OFF

Area measurement	6 workers × 1.0 days	development view	1 worker × 0.5 days
Frame measurement	6 workers × 1.0 days	compilation	1 worker × 0.5 days
Cross-sectional	2 workers × 2.0 days		
total	16.0	deskwork total	1.0

4 Summary

The UAV surveying method for measuring the workmanship of the sprayed-on slope is the same as the UAV method. It is considered possible to apply the "as-is" rule to the case. As for the cross-section of the frame, 5mm/pixel, 90% wrapping is considered to be sufficient. However, the restriction of flight zones by trees and other factors needs to be considered. The area is affected by the subdivision of the triclinic method, but can be calculated with a difference of about -1 to +2%. In addition, safety has been improved and workloads have been reduced by about 50% compared to the conventional measurement method.

Single Camera Worker Detection, Tracking and Action Recognition in Construction Site

Hiroaki Ishioka[a], Xinshuo Weng[b], Yunze Man[b], and Kris Kitani[b]
[a] Institute of Technology, Shimizu Corporation, Japan
[b] Robotics Institute, Carnegie Mellon University, United States
E-mail: h.ishioka@shimz.co.jp, xinshuow@cs.cmu.edu, yman@andrew.cmu.edu, kkitani@cs.cmu.edu

Abstract –

In Japan, the construction industry strongly be needed productivity improvement and increasing the number of new hires due to improvement of working environment. Site manager needs to grasp whether the daily progress is as planned and updates the schedule appropriately for improve site's productivity and safety. In image-based data acquisition approach in japan, there is a problem that learning is insufficient with only global public data, since construction worker in Japan has originality in image feature compare with other countries. In this study, we make original dataset for additional learning firstly. Then we proposed domain-specific algorithms specific to the Japan construction site, including a worker detection and tracking algorithm and a worker action recognition algorithm. As a result, our worker detection showed 87.9% accuracy in same-site evaluation and 77.5% accuracy in cross-site evaluation. Our worker action recognition showed 60.2% mean accuracy. Finally, the method of translation into activity element based on the output value of worker detection was indicated.

Keywords –

Construction Process; Worker Detection and Tracking; Action Recognition

1 Introduction

In construction management study area, many researchers try to improve productivity and safety by acquiring various data from construction work in construction site. Tarak et al [1] reviewed various paper and classified these research technologies into 3 types; Enhanced IT technologies, Geospatial technologies, and Imaging technologies. Amin et al [2] also reviewed various papers focusing on BIM and Computer Vision (CV) and describe the development.

In Japan, decreasing the number of construction workers is pointed out based on annual statistical data changes [3]. Therefore, the construction industry strongly be needed productivity improvement and increasing the number of new hires due to improvement of working environment. In construction management in Japan, site manager who belongs to general contractor company is assigned to the construction site to manage the progress of construction. Site manager needs to grasp whether the daily progress is as planned and updates the schedule appropriately. In the case of typical Japanese construction sites, site manager saves the construction time by subdividing the work space so that multiple contractors can perform their work on the same day. In order to appropriately update the schedule, it is necessary to understand the daily construction process. In data capturing, site manager wants to reduce management effort by reducing the number of capturing devices. It is better to use a camera that can sense the area with one unit than wearable sensors that be required the same number of workers.

In image-based approach in japan, there is a problem that learning is insufficient with only global public data, since construction worker in Japan has originality in image feature compare with other countries. From the safety awareness of Japanese construction workers, it is common in the construction industry to wear long-sleeve workwear that has both resistance and protectiveness. It also has color-variation. Due to the protective properties of workwear, safety vests in vivid color common on construction sites around the world are not usually worn on construction sites in Japan. The rules for wearing hard hat and safety belts have been generalized, and there are various product variations for tool bags attached to safety belts. In order to build image-based data acquisition technology for images with these unique characteristics of Japan, it is necessary to build a unique Japanese dataset.

In this study, we make original dataset for additional learning firstly. Then we proposed domain-specific algorithms specific to the Japan construction site, including a worker detection and tracking algorithm and a worker action recognition algorithm. Additionally, the method of translation into activity element which has effect to grasp whether the daily progress is as planned and updates the schedule appropriately based on the output value from the algorithms.

2 Literature review

2.1 Dataset in construction site

In study about image-based data acquisition technologies, there are many example of dataset for each case study. Jun et al [4] made 11 actions' movie clips for action recognition. Kaijian and Mani [5] described comparison of efficiency on various annotation task condition for out sourcing. Mohammad et al [6] made dataset of Excavator, Loader, and Truck for comparison of accuracy using various CV technologies. Recently, Mingzhu et al [7] made dataset of construction equipment and workers. Each of them, the images included dataset made from each country's construction site. These are not Japan. Still, Japanese construction site datasets need to be uniquely constructed.

2.2 Object Detection and Tracking

Object detection. There has been tremendous advancement in object detection in the last decades. Before the era of the deep learning, methods with hand-crafted feature descriptors for detecting specific types of objects were dominating in the literature. For example, various feature descriptors such as HoG (Histogram of Gradient) [10], SIFT (Scale-Invariant Feature Transform) [11] and DPM (Deformable Part Model) [12] have been proposed, which were customized for detecting pedestrians. While these methods made significant improvement in object detection, manual engineering of these feature descriptors requires significant efforts from the researchers for each individual type of object, making it difficult to generalize to other object types.

With deep learning technique becomes favorable in recent years, many modern data-driven object detectors have been proposed which can learn universal feature descriptor for many object types jointly from the data, removing the need of feature engineering. Among different approaches, region proposal-based object detectors [13, 14, 15, 16, 17, 18] are most popular. These approaches first define a set of anchors with different scales and size and covering the entire image, and then a box regression and classification network is applied to classify object class and meanwhile refine the box position and size. In this work, we choose one popular universal object detector, Faster-RCNN [15], and adapt it to specifically work on the construction workers in the Japan construction site, in order to achieve the best possible performance.

Multi-Object Tracking. Beyond classifying the object class and detecting the object location in the image, multi-object tracking aims to associate the detected objects in video and output movement of objects. To that end, recent multi-object tracking methods often employ a tracking-by-detection pipeline. Specifically, given detected objects in all frames, the tracker assigns the identity to each object where the same object receives the same identity. For example, SORT [19] proposed to use the motion information and used the Kalman filter with constant velocity as the motion model in the tracking-by-detection pipeline. To leverage the appearance cue in addition to the motion cue, deep learning-based methods such as Deep-SORT [20] and MOTS [21] incorporated an object re-identification branch to learn the object appearance feature for discriminative feature learning. While these data-driven methods with deep learning technique often achieves better performance than Kalman filter-based methods when the appearance information is sufficient, data-driven methods lack the ability to run in the real-time speed. In this work, we employ the Kalman-filter based tracking methods due to their favorable speed and the lack of appearance differences in construction workers who often wear similar uniforms and helmets.

2.3 Action recognition

Different from learning the location, orientation and trajectory of the object, action recognition aims to learn the internal logic of the object motions and its interaction with the environment. With the development of deep convolution networks in the computer vision area, a large number of CNN based methods have significantly improve the performance of traditional action recognition methods [25, 26]. We broadly categorize video action recognition methods into two genres: 2D and 3D CNN approaches. Methods of the first type make use of the recent advances in 2D single image CNNs by applying a CNN to each individual video frame and aggregating the prediction along the time axis [27]. In order to further consider the temporal dynamics of a motion rather than treat them individually, two-stream method [28, 29] are proposed to model appearance and dynamics separately and allow their interaction by early or late fusion. Among these methods, Simonyan et al. [30] first proposed the two-stream ConvNet architecture by introducing the temporal stream which takes optical flow frames as input. Wang et al. [31] proposed Temporal Segment Networks – a sparse temporal sampling strategy for the two-stream structure and fused the two streams by a weighted average. Other methods have taken different approaches to help better incorporate temporal information into single-frame feature extraction backbones such as CRF and LSTM [32, 33].

The other genre seeks to learn spatiotemporal features from videos directly with 3D CNN [34, 35, 36, 37]. Among them, C3D [34] is the first to leverage 3D

kernel on video data to learn spatiotemporal features, making it able to capture long range temporal information. Following C3D, Joao Carreira et al. [35] proposed i3D, in which they inflated the ImageNet pre-trained 2D kernel into 3D and take advantage of optical flow information with a two-stream architecture. They also proposed a new large-scale action recognition dataset named Kinetics and achieved competitive performance in other benchmark datasets. STCNet [36] inserted its STC block into 3D ResNet to capture the channel-wise correlation of both spatial and temporal features. Slowfast [37] proposed a slow-path to capture spatial semantics and a fast path the capture motion at fine temporal resolution.

Other than CNN, there is also method that model action recognition as a graph-based problem and use graph neural network to solve this problem [38]. In this work, we leverage two-stream 3D-ConvNet as our backbone [35] due to its stability and its strong feature extraction ability in complex scenario. We adapt the method to work in the Japan construction site scenario which contains high occlusion and complex actions and achieve the best possible performance.

2.4 Data usage

Output data from various data acquisition technologies reshape and use for each purpose. For example, Eirini and Ioannis [8] got the time when the worker stopping at workspace as production time from 4D trajectory data. Ye et al [9] showed time-space heatmap from workers' location data from BLE beacon for grasp usability of workspace. The former lack the method to grasp works on moving time, and the latter has difficulty to understand the meaning of location.

3 Method

3.1 Dataset creation

Dataset creation will be done by process below.

1. Selection of sites
2. Negotiation about permission
3. Capture movies and pickup movies
4. Annotate worker location and parameter

In annotation, we define three data; bounding box for worker detection, workers' ID for worker tracking, and tag of action categories for worker action recognition, into each frame. Action categories should be defined on common words for easily understand by annotator who not familiar with construction work and image of inside of construction site. In this study, we defined action as 6 actions; Walk, Crouch, Stand-up, Carry, Place, and Pick-up. Table 1 shows work definition for annotator and Figure 1 shows additional category definition about stable action Standing and Crouching which were needed because "other" tag was too large amount.

Table 1. Work definition for annotator

[Human Bounding Boxes]
●Description: A minimum enclosing box for a person
●Start: When all parts above shoulder (include face/head) is visible or when more than half of the person's body is visible
●End: When the above conditions no longer hold
●Notes:
○Must cover all the visible parts of the person, occluded parts do not need to be covered in the bounding box
○If the person is interacting with an object, all the contact points between the person and the object must be included in the bounding box, but it is not necessary to cover the whole object
○The bounding box should be as tight as possible. Small misalignment due to Imperfect interpolation is allowed, but it should be reasonable and calibrated at least every 10 frames.
[Actions]
Notes for all actions:
·There are 6 actions. All of them are single human actions. Walk, Crouch, Stand-up are atomic actions that do not have any object interactions. Pick-up, Place, Carry are interactive actions that depend on object interactions.
·One person can belong to one of the above 6 actions or none of them at a time.
·The 6 actions are not complete. A person can be doing "other" action, which does not need to be labeled.
·Only need to label when visually satisfies the definitions. For example, a man might start crouching when he is 90% occluded. We don't need to label this action. Another example, a man might pick-up something while the contact points between his hands and the object are totally occluded, we don't need to label this action.
[Action Definitions:]
●Walk
○Description: A person walking without carrying any object.
○Start: When the person starts moving and his first foot leaves the ground
○End: When the person stops walking.
○Note: Walking must be obvious and at least two steps. If a person is just changing the position by a little bit or moving just one step, that is not walking
●Crouch
○Description: A person starts to bend, sit, squat, crouch, knee down, etc. from a non-crouching status.
○Start: When the person's knees, waist, or back starts to bend
○End: When the person's knees, waist, or back stops moving or is fully bent
○Note: The actions must be obvious, for example a person looking down and bending only a little bit doesn't belong to crouch.
●Pick-up
○Description: A person makes contact, lifts, and starts to support an object against gravity.
○Start: When the person starts to lift the object up and begins supporting its gravity.
○End: When the person finishes lifting the object and reaches a stable gesture.
●Carry
○Description: A person starts walking/moving with a wide, long, large, or heavy object.
○Start: When the person starts walking/moving with the object
○End: When the person stops moving, or stops supporting the object's gravity
○Note: The object should be wide, long, large, or heavy. Carrying a small bag or backpack doesn't belong to carry.
●Place
○Description: A person lose contact, putting down, and stops supporting an object against gravity.
○Start: When the person starts lowering the object or starts to put it down
○End: When the person lose contact with the object, no longer supports its gravity, or body stops moving.
●Stand-up
○Description: A person stands up from a crouching or other non-standing status.
○Start: When the person's knees, waist, or back starts to recover from bent status
○End: When the person's knees, waist, or back is fully recovered from bent status

Figure 1. Additional category definition

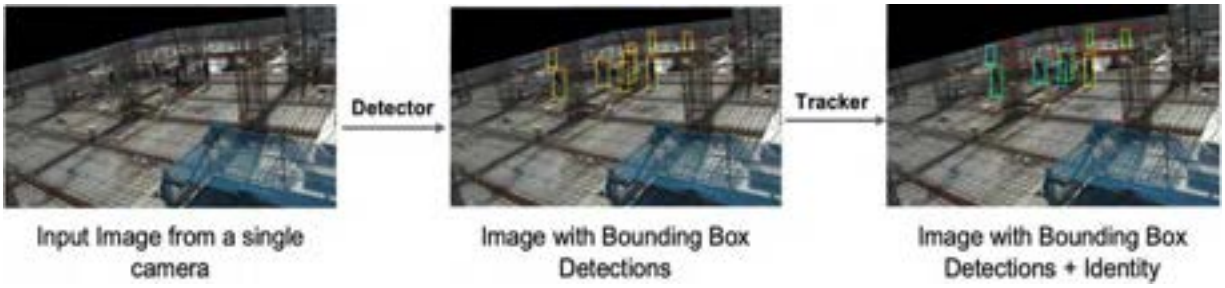

Figure 2. Illustration of our worker detection and tracking pipeline

3.2 Worker detection and tracking

We show the pipeline of our worker detection and tracking algorithm in Figure 2 Given a single image from video, we first run our worker detector to obtain a list of bounding boxes representing detected workers. Every worker bounding box has the same yellow color as we have not assigned an identity to each worker yet. Then, the outputs of the worker detector will be fed to the worker tracker, where we assign the identity to each worker based on temporal information. In the tracking outputs, each box is painted with a different color in the image as we know their identities now.

As we have mentioned in the related work, we use FasterRCNN [15] network as our worker detector, which was originally designed for universal object detection. To adapt the network for our task, which is to differentiate foreground workers and background, we change the dimension and parameters in the last few layers of the FasterRCNN so that the network only outputs for two classes instead of near 100 classes defined in COCO [22]. Also, to output more accurate worker detection, we change the size and aspect ratio of the default anchors so that the anchors are more aligned with the size and aspect ratio of our workers. To achieve the best possibly performance, we first train the original network on ImageNet [23] and COCO to learn universal features, and then we fine-tune the network on our own datasets with construction workers. We will show in the experiments that our pre-training help improve the performance and generalization to new videos compared to directly train on our dataset from scratch.

Besides customizing our worker detector, we also track the detected workers over time. Specifically, we use Kalman filter-based tracking method SORT [19] as our worker tracker. In this way, we remove the need of training for tracking algorithm and can also achieve real time worker safety monitoring. Beyond tracking in the images, we also develop a 2.5D tracking method by using homography transformation technique. As a result, we can visualize the resulting worker motion trajectory in the top down view so that it is helpful to site manager for better understanding the worker's activities. The final output worker trajectories from our tracker will be used as inputs to our action recognition system to obtain detailed action category information for each worker.

3.3 Worker action recognition

Following detection and tracking of the objects in the video, we further conduct action recognition with a two-stream 3D-ConvNet architecture. Our architecture follows i3D with an RGB appearance stream and an optical flow dynamics stream. As stated in the previous section, our tracker will aggregate bounding boxes in continuous frames of the same person as video clips, these videos are treated as input of our RGB stream. We use an off-the-shelf optical flow extraction algorithm from OpenCV toolbox. In order to ignore the background shift caused by bounding box shift, we calculate the flow directly from the video, and clip the patch from the generated flow videos.

We use 3D Inception-v1 as our backbone for feature extraction as used in i3D [35]. The image stream takes RGB frames as input, and flow stream takes optical flow frames as input. Each video clip is stacked by 60 continuous frames. After backbone network extracts appearance and dynamic feature maps, we leverage the late fusion strategy by averaging the two feature maps. Finally, a classification head is used to get the final the prediction. Horizontal flip and random translation of bounding box is used as data augmentation, and the same augmentation is conducted on all frames of a video sample.

3.4 Data usage

Site manager needs to grasp whether the daily prog-

Table 2. Method to get activity element

Element	Data type	Method
When	Datetime	Read from video metadata
Who	WorkerID	Use output from worker tracking
Where	XYZ in real	Calculate from 2D coordination in image and camera parameter
What	Work name	Search from worklist by When and Where
How	Process of action	Use output from worker action recognition

ress is as planned and updates the schedule appropriately. Daily progress can be grasped from some elements; when the work has done, who done the work, where is the worker done the work, what is the work, how the worker has progressed the work, as shown in Table 2.

4 Result and Discussion

4.1 Dataset creation

Selection of sites. We selected 6 sites in Japan managed by Shimizu Corporation which were under construction of main structures. Example image of 6 sites are shown in Figure 3.

Negotiation about permission. By promising that the image of worker not to link the workers' personal data (i.e. name), the legal department of Shimizu Corp and CMU permitted this study. Then we got permission about capturing movie from onsite manager and the owner of the building which the site construct. Then we displayed notification of movie capturing and its purpose for the workers in the site.

Capture movies and pickup movies. We set 2 cameras (Sony-FDRX3000, JVC-GZRY980) onto outer scaffolding frame using metal clip on little look-down direction. After capturing, we checked all movies and selected or cut into 52 movies on 17 scenes. As shown in Figure 3, site 1 was concrete placing work on sunny day, site2 was placing rebar of floor work in sunny day, site3 was formwork carrying in sunny day, site4 and site5 were formwork related work in cloudy day, site6 was formwork and scaffolding work in rainy day. Table 3 shows total length of movies. Total frame count was about 270k, and total length was about 2.5h.

Annotate worker location and parameter. Annotation was done by over 10 annotators hired by outsourcing company and spent over 2 months. The total count of data is shown in Figure 4. Since site1 and site4 had over 10 workers in each frame, total data count was be huge. Figure 4 colored by size category of height of bounding box (i.e. count of pixel), by this, we can understand the workers image size almost in Easy (>=40pixel) category. Action category ratio is shown in Figure 5. It can be seen "other" category occupied more then half of all and can be seen basic 6 categories has mis-balanced.

In the future data set creation, it will be necessary to set the video length according to the number of workers included in the video, and to define the action category as avoiding a mismatch in the number of tags.

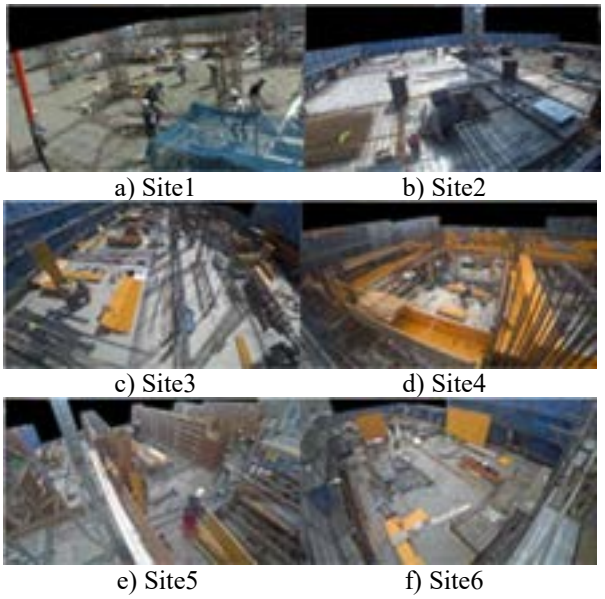

a) Site1 b) Site2

c) Site3 d) Site4

e) Site5 f) Site6

Figure 3. Example of each 6 sites' image

Table 3. Total length of movies each 6 sites

Name	Weather	Movie Count	Frame Count	FPS	Total length
Site1	Sunny	9	50535	29.97	28'06"
Site2	Sunny	5	30591	29.97	17'01"
Site3	Sunny	7	61695	29.97	34'19"
Site4	Cloudy	9	64637	29.97	35'57"
Site5	Cloudy	4	24825	29.97	13'48"
Site6	Rainy	18	38565	29.97	21'27"
Total	-	52	270848	-	150'37"

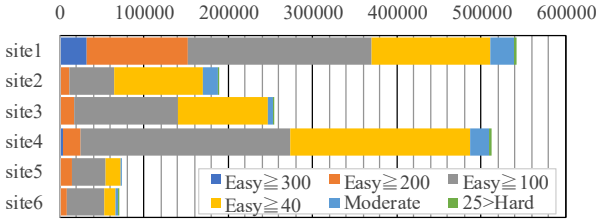

Figure 4. Data amount and size ratio

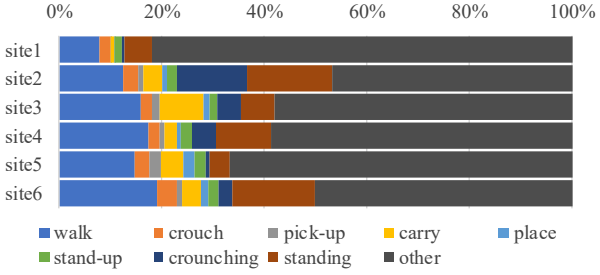

Figure 5. Action category ratio

4.2 Worker detection evaluation

We evaluate our worker detector on our dataset collected from the Shimizu Corp. construction site. We use the standard metric of average precision (AP) defined with an IoU (intersection of union) threshold of 0.5 for worker detection evaluation. Also, we use three difficulty levels for evaluation (easy, moderate and hard) where each difficulty level has a different threshold on the number of pixels (40, 25, 1 respectively) in the ground truth worker's bounding box height. For example, for the easy case, we filter out ground truth workers that have height less than 40 pixels and only evaluate the rest of workers which are relatively closer to the camera and easy to be detected. We compare our customized worker detector trained on our Shimizu data with generic detectors such as Faster RCNN [15] and Mask RCNN [24] pre-trained on the COCO dataset.

We use two types of data split during evaluation: (1) same site evaluation; (2) cross-site evaluation. For each construction video in the same site evaluation, we use first 70% frames for training, middle 15% for validation and the last 15% for testing. We summarize our results for same site evaluation in Table 4. We can see that, without any customization, the generic object detectors do not perform well on our construction dataset, and have lower performance than our customized detector, e.g., 33.5 AP of the Mask RCNN v.s. 66.8 AP of our detector in the easy case. Also, when we pretrain our customized detector on the COCO dataset before fine-tuning on our construction data, the final performance can be even higher, e.g., 87.9 AP v.s. 66.8 AP in the easy case. This proves that pretraining on the COCO dataset with many generic objects does help improve final detection performance on our construction dataset.

In addition to same site evaluation, we also perform the cross-site evaluation, i.e., evaluation across different construction site videos. This means that we select one site (e.g., 5 videos from the site 2) as the testing data, while using the rest of other data from other sites for training and validation. In this way, the detection is more difficult than in the same-site evaluation as the data in the testing set is not seen during training. We summarize the results in Table 5. We can see that our customized detector still achieves reasonable performance when evaluating on the construction sites that are not seen during training. This can be useful to construction manager as our customized detector can be potentially applied to other new site videos collected in the future. Also, same as the same site evaluation, our customized detector works better than the generic object detector Faster RCNN in the cross-site evaluation (e.g., 77.5 AP of our customized detector v.s. 50.7 AP of the generic detector in the easy case).

Table 4. Quantitative performance of worker detection in same-site evaluation

Method / AP	Easy (>=40)	Moderate (>=25)	Hard (>=1)
Mask RCNN (COCO)	31.7	31.3	31.3
Faster RCNN (COCO)	33.5	32.1	31.9
Our Detector (Shimizu)	66.8	66.5	66.4
Our Detector (COCO+Shimizu)	**87.9**	**87.4**	**86.2**

Table 5. Quantitative performance of worker detection in cross-site evaluation

Method / AP	Easy (>=40)	Moderate (>=25)	Hard (>=1)
Faster RCNN (COCO)	50.7	48.7	48.3
Our Detector (COCO+Shimizu)	**77.5**	**72.8**	**72.7**

4.3 Worker action recognition

Similar to detection and tracking task, we evaluate our action recognition model on our dataset collected from the Shimizu Corp. construction site. Specifically, we first pre-train the model on Kinetics and fine-tune on our dataset. The dataset is randomly split into 80% training set and 20% validation set. We evaluate the performance of each class by their recall rate, and the overall performance is measured by mean class accuracy. In order to get more information about surrounding environment, we expand the bounding box from detector by 10%. The learning rate for our model is set to 0.0005 with a weight decay 0.0001. Batch size is set to 4. We show some qualitative results of our model in figure 6. Note that the real data is in video format, and we show a representative frame of each video clip.

We summarize our quantitative results in Table 6. We can see that our method performs better than generic ST-GCN [38] and i3D [35]. Note that ST-GCN was trained on an early labelling strategy where standing and crouching are not specifically labeled, making the dataset simpler. As we can see, even with a simpler task, generic ST-GCN performs worse than our method. And generic i3D only performs marginally better on walk and carry class. We can see that for Other class, out method performs the worst, this is because we are using recall as our metric. A high recall of un-defined class is usually the result of many false positive samples in other classes. Also, we notice that the performance on Place class is very low. This is because of the internal imbalance of our dataset in number and

difficulty of each class. In real-world construction site, “Place” happens far less frequent than other classes of actions like walk or standing. Moreover, it usually lasts very short, sometimes less than 1 second. These results in the high relative difficulty of class “Place”.

Figure 6. Qualitative performance of our worker action recognition model

Table 6. Quantitative performance of worker action recognition

Method	Mean Class Accuracy	Walk	Crouch	Stand-Up	Pick-Up	Carry	Place	Standing	Crouching	Other
ST-GCN	33.1	34.7	49.2	49.5	14.7	8.1	**18.7**	-	-	**57.2**
i3D	54.0	**80.7**	37.2	85.9	38.2	**79.6**	5.6	73.8	30.3	55.0
Our Method	**60.2**	75.5	**84.1**	**90.5**	**59.0**	61.1	6.1	**82.2**	**34.3**	50.0

Table 7. Ablation study on our worker action recognition model

Method	Mean Class Accuracy	Walk	Crouch	Stand-Up	Pick-Up	Carry	Place	Standing	Crouching	Other
RGB	51.6	44.0	82.0	86.0	56.0	77.0	0.0	71.0	16.0	28.0
Flow	56.2	68.0	82.0	83.0	49.0	40.0	**18.0**	77.0	**39.0**	48.0
RGB + Flow	**60.2**	**75.5**	**84.1**	**90.5**	**59.0**	**61.1**	6.1	**82.2**	34.3	**50.0**

We also conduct ablation study as shown in Table 7. The first two rows are using only RGB stream or optical flow stream without late fusion. We see that using only one stream will result in a performance drop in mean class accuracy and most classes. This experiment also proves that RGB is better at extracting appearance feature like “Pick-up” and “Carry” which involves interaction with other objects that might not be visible in optical flow. On the other hand, optical flow steam helps the model by providing better dynamic feature, and thus improves classes like “Walk” and “Place”.

4.4 Data usage

The data acquisition technology was implemented except for the "How" element. A result of data acquisition using our method is shown in Figure 7. The rectangle frame was output from detector and the “id001” was output from tracker. The line in bounding box indicated a vertical line calculated from 2D coordination of bounding box output from worker detector and camera parameter. The XYZ and height of worker were calculated by regarding the center of the frame as the midpoint of the worker's height. It also can be seen the work name was successfully searched from list by datetime and XYZ coordination. The activity elements were acquired as planned.

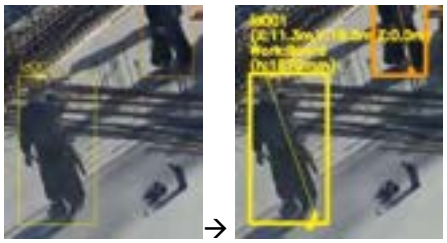

Figure 7. Translation to activity element

5 Conclusion

We first built a dataset for a Japanese construction site. Then, the domain specific algorithms of worker detection, tracking, and worker action recognition were customized. As a result, our worker detection showed 87.9% accuracy in same-site evaluation and 77.5% accuracy in cross-site evaluation. Our worker action recognition showed 60.2% mean accuracy. Finally, the method of translation into activity element based on the output value of worker detection was indicated. Whether these accuracies are actually sufficient needs to be verified in the future.

As a limitation, this method cannot deal with occlusion because it uses a single camera. It is possible to deal with this by installing multiple units on site so that occlusion is reduced.

As future work, it is essential to improve accuracy by increasing the data set, and it will be necessary to build technology to ensure data consistency when multiple cameras are installed.

6 Reference

[1] Tarek O. and Moncef N., Data acquisition technologies for construction progress tracking, Automation in Construction 70 (2016) 143-155

[2] Amin A. et al., Sensor-based safety management, Automation in Construction 113 (2020) 103128

[3] Construction industry handbook 2019 [in Japan ese], Japan federation of construction contractors, https://www.nikkenren.com/publication/pdf/handbook/2019/2019_04.pdf, Accessed: Jun./06/2020

[4] Jun Y. et al, Automatic Recognition of Construction Worker Activities Using Dense Traj ectories, 2015 Proc. of the 32nd ISARC, Pages 1-7

[5] Kaijian L. and Mani G., Crowdsourcing Video-based Workface Assessment for Construction Activity Analysis, 2015 Proc. of the 32nd ISARC

[6] Mohammad S. et al, Evaluating the Performance of Convolutional Neural Network for Classifying Equipment on Construction Sites, 2017 Proc. of the 34rd ISARC, pages 509-516

[7] Mingzhu W. et al, Predicting Safety Hazards Among Construction Workers and Equipment Using Computer Vision and Deep Learning Techniques, 2019 Proceedings of the 36th ISARC, Pages 399-406

[8] Eirini K. and Ioannis B., Trajectory-Based Worker Task Productivity Monitoring, 2018 Proc. of the 35th ISARC, Pages 1145-1151

[9] Ye H. et al, A Visualization System for Improving Managerial Capacity of Construction Site, 2017 Proceedings of the 34rd ISARC, Pages 388-395

[10] N. Dalal and B. Triggs. Histograms of oriented gradients for human detection. In CVPR, 2005.

[11] D. Lowe. Distinctive image features from scale-invariant keypoints. IJCV, 2004.

[12] Felzenszwalb et al. A Discriminatively Trained, Multiscaled, Deformable Part Model. CVPR 2008.

[13] R. Girshick, J. Donahue, T. Darrell, and J. Malik. Rich feature hierarchies for accurate object dete ction and semantic segmentation. In CVPR 2014

[14] R. Girshick. Fast R-CNN. In ICCV, 2015.

[15] S. Ren, K. He, R. Girshick, and J. Sun. Faster R-CNN: To- wards real-time object detection with region proposal net- works. In NIPS, 2015.

[16] T.-Y. Lin, P. Doll´ar, R. Girshick, K. He, B. Hariharan, and S. Belongie. Feature pyramid networks for object detection. In CVPR, 2017.

[17] J. R. Uijlings, K. E. van de Sande, T. Gevers, and A. W. Smeulders. Selective search for object recognition. IJCV, 2013.

[18] J. Dai, Y. Li, K. He, and J. Sun. R-FCN: Object detection via region-based fully convolutional networks. In NIPS, 2016.

[19] A. Bewley, G. Zongyuan, F. Ramos, and B. Upcroft, Simple online and realtime tracking. in ICIP, 2016.

[20] N. Wojke, A. Bewley, D. Paulus. Simple Online and Realtime Tracking with a Deep Association Metric. ICIP 2017.

[21] Paul Voigtlaender, Michael Krause, Aljosa Osep, Jonathon Luiten, Berin Balachandar Gnana Sekar, Andreas Geiger, and Bastian Leibe. MOTS: Multi-Object Tracking and Segmentation. CVPR, 2019.

[22] T.-Y. Lin, M. Maire, S. Belongie, J. Hays, P. Perona, D. Ra- manan, P. Doll´ar, and C. Zitnick. Microsoft COCO: Com- mon objects in context. In ECCV 2014.

[23] J. Deng, W. Dong, R. Socher, L.-J. Li, K. Li, and L. Fei-Fei. ImageNet: A Large-Scale Hierarchical Image Database. In CVPR 2009.

[24] K. He, G. Gkioxari, P. Doll´ar, and R. Girshick. Mask RCNN. In ICCV 2017.

[25] Wang, Heng, et al. "Action recognition by dense trajectories." CVPR 2011.

[26] Wang, Heng, et al. "Action recognition with improved trajectories." In ICCV 2013.

[27] Karpathy, Andrej, et al. "Large-scale video classifyation with convolutional neural networks." In CVPR 2014.

[28] Feichtenhofer, Christoph, Axel Pinz, and Andrew Zisserman. "Convolutional two-stream network fu sion for video action recognition." In CVPR 2016.

[29] Chen, Yunpeng, et al. "A^ 2-nets: Double attention networks." Advances in Neural Information Processing Systems. 2018.

[30] Simonyan, Karen, and Andrew Zisserman. "Two-stream convolutional networks for action recognition in videos." Advances in neural information processing systems. 2014.

[31] Wang, Limin, et al. "Temporal segment networks: Towards good practices for deep action recognition." In ECCV 2016.

[32] Sigurdsson, Gunnar A., et al. "Asynchronous tem poral fields for action recognition." In CVPR 2017.

[33] Donahue, Jeffrey, et al. "Long-term recurrent convolutional networks for visual recognition and description." In ICCV 2015.

[34] Tran, Du, et al. "Learning spatiotemporal features with 3d convolutional networks." In ICCV 2015.

[35] Carreira, Joao, and Andrew Zisserman. "Quo vadis, action recognition? a new model and the kinetics dataset." In CVPR 2017.

[36] Diba, Ali, et al. "Spatio-temporal channel correlation networks for action classification." In ECCV 2018.

[37] Feichtenhofer, Christoph, et al. "Slowfast networks for video recognition." In ICCV 2019.

[38] Yan, Sijie, Yuanjun X., and Dahua Lin. "Spatial temporal graph convolutional networks for skeleton-based action recognition." In AAAI 2018.

MR-based Equipment Remote Control and 3D Digital Working Guidance for Field-oriented Maintenance

J.W. Song[a], K.H Lee[b], M. K Jeong[c], S.J. Lee[d], and S.W. Kwon[e]

[a]Department of Convergence Engineering for Future City, SungKyunKwan University, Republic of Korea
[b]Department of Convergence Engineering for Future City, SungKyunKwan University, Republic of Korea
[c]Department of Convergence Engineering for Future City, SungKyunKwan University, Republic of Korea
[d]Department of Convergence Engineering for Future City, SungKyunKwan University, Republic of Korea
[e] School of Civil, Architectural Engineering and Landscape Architecture, Sungkyunkwan University, Republic of Korea
E-mail: wls171@skku.edu, uksktk@gmail.com, dufguf147@gmail.com, sjlee3003@skku.edu, swkwon@skku.edu,

Abstract –

Recently, as technologies combine, AR (Augmen ted Reality)/VR(Virtual Reality)/MR(Mixed Reality) and advanced sensing equipment are being developed. The possibilities of their application to construction fields is likewise increasing. Research into applying these techniques to facility maintenance, manager training, and safety/evacuation training is being actively conducted. In the case of the existing facility maintenance process, it is difficult to identify the exact management matters and departments that have problems during facility inspection or history management. In the case of complex equipment, it is necessary to respond to equipment maintenance needs through real-time support technology with on-site workers due to the difficulty of promptly dispatching related advanced equipment experts. In addition, digitization of the maintenance manual is required for time, cost and losses to be minimized due to equipment downtime; to improve understanding, thus proper utilization, of non-specialist facilities maintenance and work safety through realistic work guidance based on 3D content. Therefore, in this study, we propose MR-based remotely controlled technology, real-time worker decision-making and work performance support technology for process improvement, preventing quality problems in the field manager-centered equipment inspection maintenance.

Keywords –

Augmented Reality; Mixed Reality; BIM; Working Guidance

1 Introduction

1.1 Research Background and Purpose

Research into application of AR/VR/MR technologies in various ways are also being actively conducted in the construction field. In particular, studies are being conducted to apply such technology in semiconductor and battery factories, where demand continues to increase due to the rapidly accelerating technological development and the fourth industrial revolution.

Plant construction projects are large and involve complex maintenance activities. Therefore, they have a higher project cost than other construction projects and require efficiency in maintenance.

In the construction of battery and semiconductor plants, a huge amount of data is produced at various stages of operation due to complicated internal design, pipe installation, electricity, and other facilities; with many studies being conducted to efficiently maintain them.

As major research for enhancing the work efficiency of plant workers, research on information management systems using QR codes, barcodes, radio frequency identification (RFID), and cloud system technologies is actively being conducted.

However, these technologies make it difficult to provide visually intuitive information to workers, which increases the incidence of human errors. These problems extend the working time at the plant site and cause task revisions.

This study develops a suitable MR-based 3D digital working guidance system through analysis of the maintenance work process at the plant site based on the opinions of practitioners and presents a worker-oriented maintenance work process.

At the existing plant site, workers have performed inefficient operation management tasks due to lack of intuitive work information visualization systems and lack of interoperability due to the dualization of construction sites and offices. In addition, the worker had difficulties in communication with the manager due to the complex plant design. In order to solve this problem, this study draws a plant field maintenance plan for effective equipment location and installation by using a Mixed Reality-based smart device for general equipment maintenance work of the plant.

1.2 The Scope and Methods of Research

This study proposes a 3D digital working guidance system for workers using AR-based smart devices at the plant site. At the plant site, workers have performed maintenance work based on past information and manuals. Currently, due to extensive and complex plant field work, difficulties arise in actual work. The typical maintenance tasks of unskilled worker include difficulties in figuring out the route due to the wide range of plant sites, and human error occurs when replacing equipment. Therefore, in the case of maintenance work, it needs an information exchange system that can intuitively communicate the exact plant site situation between the worker and the manager. Therefore, this study intended to solve such problem through an AR-based smart device.

The method and process of this research is:
(1) Preceding Research Analysis
- Existing review of literature
- Analysis of management characteristic of plant maintenance and process
(2) Requirement Analysis and Function Derivation
- Figuring out smart device applicability in the plant field
- Requirement analysis to solve problems
(3) Establishing MR-based 3D digital working guidance for optimal plant maintenance
- Process Analysis of Plant maintenance
- Analysis of maintenance Work at Plant Site
- MR-Based Equipment Assembly Management Process
(4) MR-based 3D digital Technology at Plant Site.

2 Research Trend

2.1 Literature Review

From the mid-2000s, much research has been carried out in order to derive improvements to general interests in the construction industry such as shortening the construction period, cost reduction, flawless construction, accident-free planning, predictability improvement, waste factor elimination, productivity improvement, and maintenance cost reduction through the use of various IT technologies.

The table below shows some of the existing research pertaining to the subject of smart, IT-based construction. This research focused on the exchange and maintenance of construction information for smooth installation of facility equipment among participants in the project in relation to the plant maintenance process. The process is illustrated in Figure 1.

Table 1. Existing research

Area of management	Research subjects
Construction	Ontology-based BIM modeling; AR-based system framework
Site condition	4D tools for greater efficiency in site management
	Use of smart phone to improve management process; visualization of project information using real-time data sharing and management, wireless communication; and augmented reality
Safety	New 4D safety management and monitoring system ‘C-RTICS2’ for more efficient construction and communication among work partners
	Behavior-based preventive safety system, visualized management with VCS (Virtual Construction Simulation System)
	Note
Construction	Marker-based AR: Research on identification of objects, selection of marker type, marker detection, and marker-less AR technology
Site condition	Wearable device for real-time work coordination
	Wearable device; Cloud system for massive data management
Safety	Set apart in terms of device and visualization method, while similar in technology for communication between office and construction site
	Partly applicable to safety management in terms of carrying out preventive safety management in visualized form

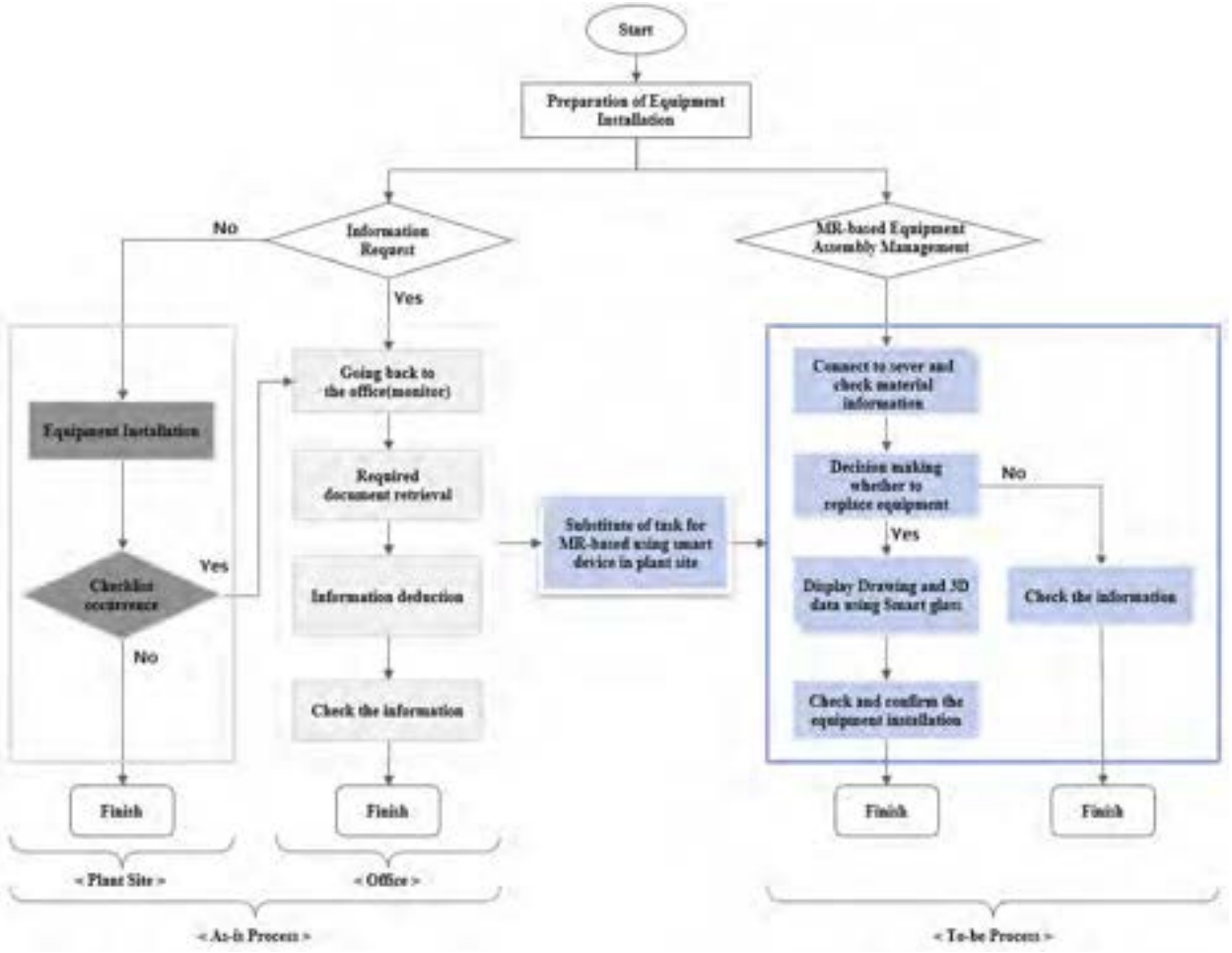

Figure 1. Improved Plant Site Management Process

2.2 Plant Maintenance Management

The equipment replacement procedure at the existing plant site differs depending on the method of obtaining equipment replacement work information. When the worker no longer needs to obtain work information, the worker goes to the site to proceed and finish the work. However, in the event of an unusual occurrence in the middle of the work or when the manager orders the work in the middle, the worker needs a means to receive information. In this case, if the information is complicated, face-to-face communication between workers and managers is needed, or a visualization information sharing system for work orders is required.

In the improved process based on the Mixed Reality, it is possible to intuitively figure out information through 3D digital working guidance during the process of equipment replacement work, and even unskilled worker can more easily understand the work to reduce the occurrence of human error.

3 Analysis of plant workers' needs

According to Moon (2015)[1], as a result of conducting site surveys and interviews with major construction company in Korea, "S", the Construction Assistance App, Data confirmation and check App, Guideline App, and especially Communication support App and Progress Management App at the plant site were found to be required. These territories are tabularized below. This shows that the MR-based smart device system for workers is required to share information at the plant site.

Table 2. Applicable work territories

Direction	Contents
1	Construction Assistance App.
2	Data confirmation and check App.
3	Data input App.
4	Guideline App.
5	Communication support App.

6	Progress management App.

During the materials management and product installation process at the plant site, workers need drawings and related information data. At this time, the information provided exists in various forms and is visualized in various ways and delivered to the worker. When one data is converted, new conversion information is generated by deriving from other data in real time. Various applications of smart devices must be provided to support this.

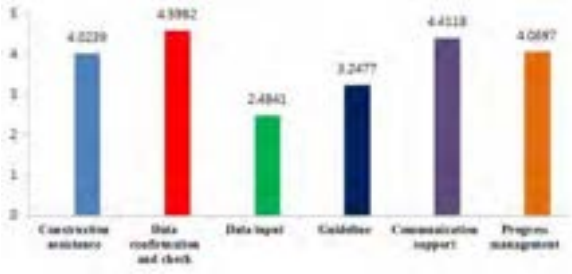

Figure 2. Overall result

4 MR-based 3D Digital Working Guidance

4.1 Worker Equipment Replacement Process Analysis in Plant Site

Through an interview with the Battery Plant Equipment Management Team at the battery plant site in Korea, a detailed work process of the worker was derived from the Mixed Reality-based to-be process.

Workers are assigned to equipment management tasks, identify the location of the target equipment, and move to the site. In addition, the state of the equipment is determined through visual inspection and it is determined whether the equipment is replaced. If it is necessary to replace the equipment, he/she selects a replacement and records the reason. Subsequently, a procedure for applying for replacement equipment is carried out, and another colleague carries the replacement equipment and delivers it to the work site. In the field, the operation of existing equipment will be stopped, and the equipment disassembled. The disassembled equipment is returned according to the return procedure, and new equipment is installed by determining the presence of abnormalities. When the installation of new equipment is completed, the test operation will be performed, and the test operation will be made for diagnosing the normal operation.

Figure 3. Worker Equipment Replacement Process

4.2 Usage of AR Data in the plant site

The data types that can be used in the detailed equipment management process based on the mixed reality derived above are classified into four types: 1) modeling data, 2) attribute information data, 3) AR data, and 4) job reporting data.

Modeling data and attribute information data can be extracted from BIM data. BIM data was converted to 3D model-based neutral file format (fbx, ojb) and then mapped to be usable in the AR environment. Also, the modeling data can be used to check the optimal path for operator's navigator and equipment transportation at the plant site, and to check interference between members. The attribute information data can identify the performance of the installed equipment or the cost information, replacement cycle, and the like.

AR data in the form of 3D model can be used to guide the on-the-spot movement route based on a digital map, work sequence guide, and to understand the current state of the equipment. The worker can always record the work contents in the work report data to check the past records of the activities in the field and to understand the operation information of how it is currently operating.

Table 3. Applicable work territories

	① Modeling Data
Image	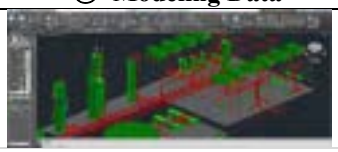
Type	3D Model
Utilization	1. Use as a digital map on site 2. Equipment type can be checked 3. Check the optimal path for equipment transportation 4. Interference check between members
	② Attribute Information Data
Image	
Type	Object Specification
Utilization	1. Identify the performance of equipment 2. Identify the replacement cycle of equipment 3. Equipment unit price information
	③ AR Data
Image	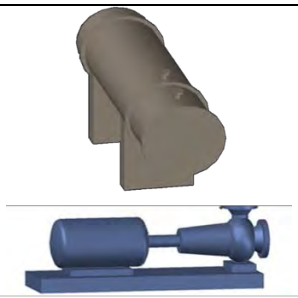
Type	3D Model
Utilization	1. Identify the current position of the operator(Based on Device's GPS data) 2. Guidance on the on-site route 3. Guide to the sequence 4. Guidance on current status of equipment
	④ Task Reporting Data
Image	
Type	Work Sheet
Utilization	1. Confirmation of historical information 2. Records of workers' work activities 3. Checking factory operation information

4.3 AR Data-based workspace and equipment replacement procedure

The four types of data classified above can be divided to data available for each step in the worker equipment replacement process analyzed above. Each worker equipment maintenance procedure is divided into three groups as shown in Figure 4. : 'Decision to replace equipment', 'Procedure for returning existing equipment, and 'New equipment replacement procedure', and AR data has high utilization in 'Decision of equipment replacement' and 'New equipment replacement procedure' respectively.

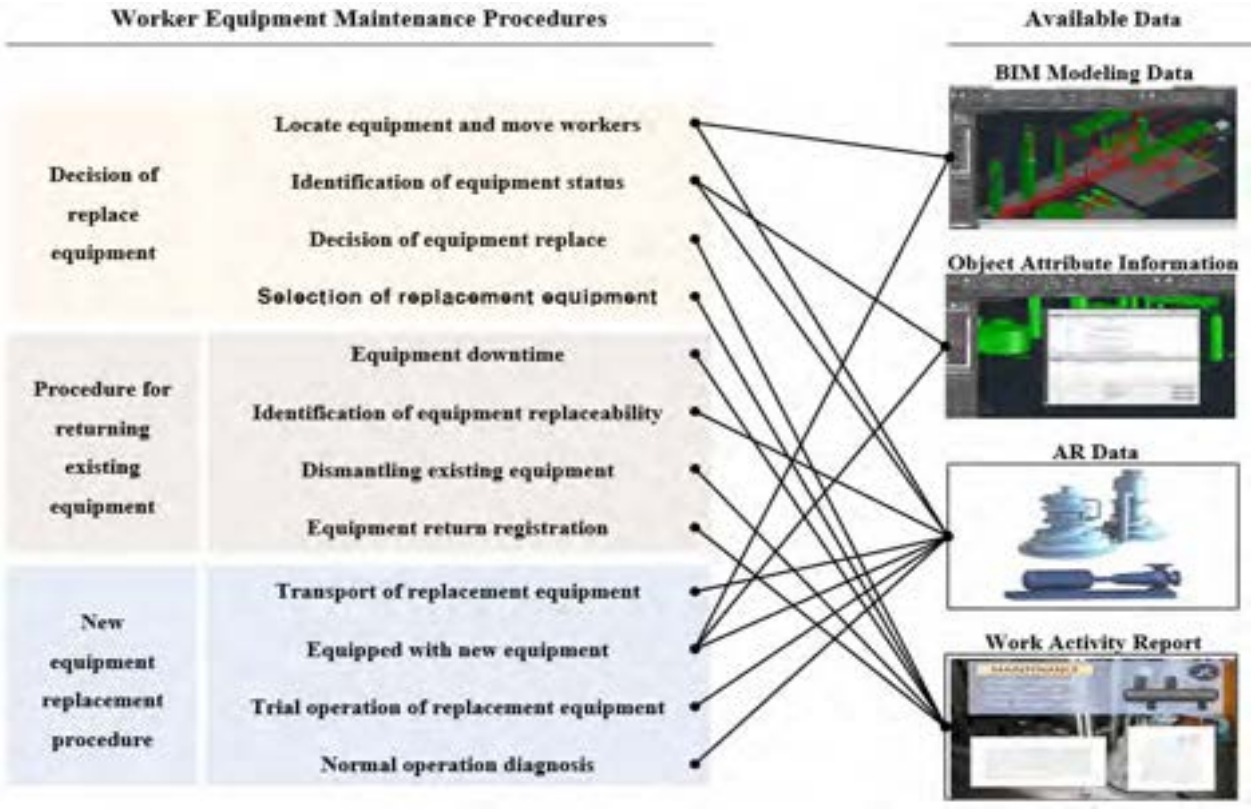

Figure 4. Matching of available data and equipment replacement procedure

When the work activity report is visualized as an AR image, the utilization of AR data is also increased in the 'Procedure for returning existing equipment' stage, and the AR visualization data is used in the overall worker equipment replacement process.

Therefore, BIM Modeling Data and Object Attribute Information can be used as data to implement AR Data. AR Data and Work Activity Report Data implemented based on this can be visualized in AR and used in 3D digital working guidance, as the example in Figure 5. illustrates.

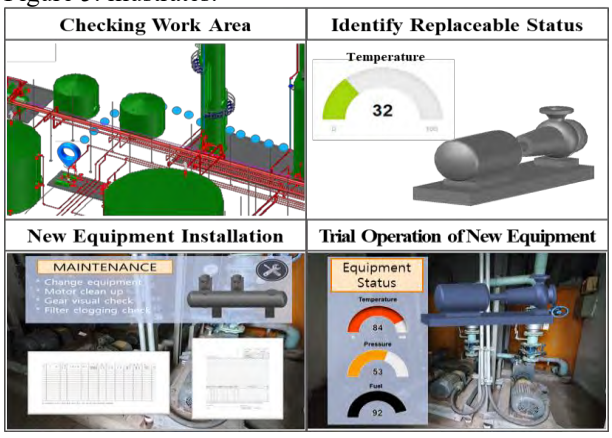

Figure 5. Main application methods of MR-based 3D digital working guidance

5 3D Digital Working Guidance in Plant Site

A 3D digital working guidance test-bed system was implemented in accordance with the Worker Equipment Replacement Process Analysis previously analyzed, and the MR-based work environment was tested based on the equipment replacement work generally performed by workers.

The test-bed environment (Figure 6.) was tested in the following six steps. 1) Work selection, 2) Checking work area and moving workers, 3) Worker Navigator, 4) Check work objects and work contents, 5) Check equipment status, 6) Dismantling existing equipment. The role of each stage is as follows:

1. Work selection: Confirms the work assigned to the worker with AR and selects the work to be performed.
2. Checking work area and moving workers: Figure outs the position of the selected work and the current position of the worker.
3. Worker Navigator: Guides the way for the worker to move from the field to the work location.
4. Checking work objects and work contents: Figures out the contents of the work to be performed by the current worker.

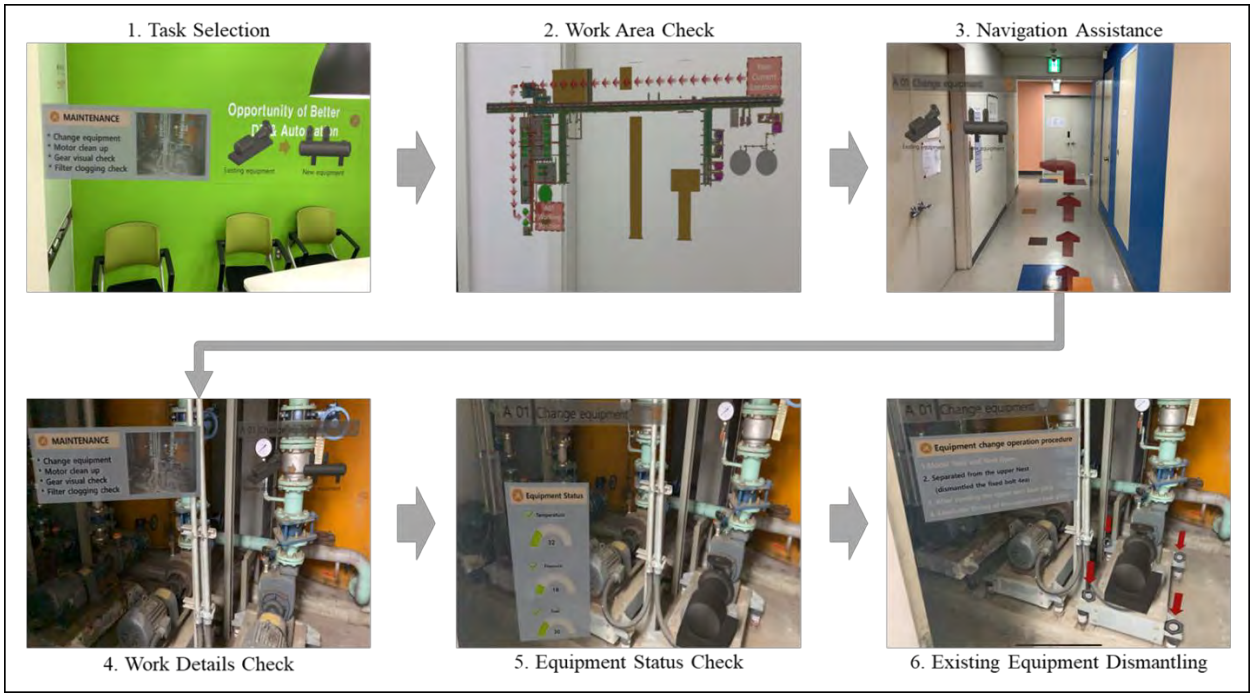

Figure 6. MR-based 3D Digital Working Guidance Test - Worker Perspectives

5. Checking equipment status: Figures out the status of currently installed equipment before the operator performs the equipment replacement work.

6. Dismantling existing equipment: Intuitively guides the operator to the dismantling order of the existing equipment.

In this study, the above 6 steps were experimentally implemented to test the 3D digital working guidance environment for the unskilled or alternative workers to accurately understand the work. If such a system is applied in the field, it is judged that human error can be reduced.

6 Conclusions

This study analyzed the process of the existing plant work, identified problems in the plant site through worker interviews, and analyzed the Worker Equipment Replacement Process. Based on this, detailed work process was derived based on the Mixed Reality-based to-be process, and the applicable data was classified into 4 types (BIM Modeling Data, Object Attribute Information, AR Data, Work Activity Report).

In addition, the purpose of using the data was identified by matching the operator's equipment maintenance procedures with data classified in four types. Among them, four main methods of using MR-based 3D digital working guidance include 'Checking work area and moving workers', 'Identify replaceable status', 'New equipment installation and check', and 'Trial operation of replacement equipment'. Working Guidance environment was built and tested according to Worker Equipment Replacement Process.

This study visualized AR information for workers using MR-based work information data. For visualization information, four types of data were set according to business procedures. Based on this, equipment maintenance workers can increase understanding of their services through AR visualization information. Furthermore, if CPS (Cyber Physical Systems) in which a virtual model and a physical model are connected is introduced, information exchange between managers and workers will be facilitated in real time. In future studies, this study will be used as basic data to conduct digital interface & physical object linkage research on a small number of objects.

Acknowledgment

"This work is financially supported by Korea Ministry of Land, Infrastructure and Transport(MOLIT) as 「Innovative Talent Education Program for Smart City」".

"This work was supported by the National Research Foundation of Korea(NRF) grant funded by the Korea government(MSIP) (No. NRF-2019R1A2C2005540) ".

References

[1] Moon D. Y, Improved Method for Increasing Maintenance Efficiency of Construction Structure Using Augmented Reality by Marker-Less Method, Journal of the Korean Society of Civil Engineers Vol. 35, No. 4: 961-968

[2] Hyojoon Bae, and Mani Golparvar-Fard. High-precision and infrastructure-independent mobile augmented reality system for context-aware construction and facility management applications. In Proc., 2013 ASCE Int. Workshop on Computing in Civil Eng, pp. 637-644, 2013.

[3] WANG, Junfeng, et al. An augmented reality based system for remote collaborative maintenance instruction of complex products. In: 2014 IEEE International Conference on Automation Science and Engineering (CASE). IEEE, 2014. p. 309-314.

[4] Koch C. Matthias N. Markus K. and Michael A. Natural markers for augmented reality-based indoor navigation and facility maintenance. Automation in Construction 48: 18-30, 2014.

[5] FIORENTINO, Michele, et al. Augmented reality on large screen for interactive maintenance instructions. Computers in Industry, 2014, 65.2: 270-278.

[6] R. Akhavian, A.H. Behzadan, Construction equipment activity recognition for simulation input modeling using mobile sensors and machine learning classifiers, Adv.Eng. Inform. 29 (4) (2015) 867–877

[7] SANNA, Andrea, et al. Using handheld devices to sup port augmented reality-based maintenance and assembly tasks. In: 2015 IEEE international conference on consumer electronics (ICCE). IEEE, 2015. p. 178-179.

[8] R.Palmarii, J.A Erkoyuncu, R. Roy, An innovative process to select augmeneted reality(AR) technology for maintenance, Procedia CIRP 59(2017) 23-28 no. TESCpmf 2016

[9] Agarwal S., Review on Application of Augmented Reality in Civil Engineering, International Conference on Inter Disciplinary Research in Engineering and Technology 2016 [ICIDRET 2016]

[10] Hongling Guo, Yantao Yua, Martin Skitmore, Visualization technology-based construction safety management: A review, Automation in Construction 73 (2017) 135 – 144

[11] Kevin K. Han, Potential of big visual data and building information modeling for construction performance analytics: An exploratory study, Automation in Construction 73 (2017) 184-198

[12] J.A Erkoyuncu, I. Fernandez, M, Dalle Mura, R. Roy, G. Dini, Improving efficiency of industrial maintenance with context aware adaptive authoring in augmented reality, CIRP Annals Manuf. Technol. (2017) Accepted, January.

[13] Zhou Y., Lou H., Yang Y., Implementation of augmented reality for segment displacement inspection during tunneling construction, Automation in Construction 82 (2017) 112-121

[14] Li X., Yi W., Chi H.L., Wang X., Chan A.P.C., A critical review of virtual and augmented reality (AR/VR) applications in construction safety, Automation in Construction 86 (2018) 150-162

[15] Fazel A., Izadi A., An interactive augmented reality tool for constructing free-form modular surfaces, Automation in Construction 85 (2018) 135-145

[16] Pei-Huang D, and Naai-Jung Shih. BIM-Based AR Maintenance System (BARMS) as an Intelligent Instruction Platform for Complex Plumbing Facilities Applied Sciences Journal Article. (2019) 1592 -1604

[17] Ruide Li, Guohua Gao, Yingjie Liang, Xin Zhang, and Yongqiang Liao. 2019. An AR Based Edge Maintenance Architecture and Maintenance Knowledge Push Algorithm for Communication Networks. In Proceedings of the 2019 4th International Conference on Big Data and Computing (ICBDC 2019). Association for Computing Machinery, New York, NY, USA, 165–168.

[18] WANG, Ting-Kwei; PIAO, Yanmei. Development of BIM-AR-Based Facility Risk Assessment and Maintenance System. Journal of Performance of Constructed Facilities, 2019, 33.6: 04019068.

Use of Laser scanning, Remote Sensors & Traffic Data Collection, Drones & Mobile Application. MoEI Federal Highways network case study.

Eng. Khamis Al Shehyari, Eng. Habiba Noor Aflatoon and Ph.D. R. Civil Eng. Daniel Llort Mac Donald

Ministry of Energy and Infrastructure, United Arab Emirates
E-mail: khamis.alshehyari@moid.gov.ae, habiba.aflatoon@moid.gov.ae, daniel.llort@moid.gov.ae

Abstract –

Application of technologies as laser scanning, remote sensors, drones or mobile applications are playing a major role in changing the management procedures of maintenance and operation activities in the roads. Without scarifying the quality of the data, tasks can be performed in less time while maintaining the same level of accuracy of the outcomes and results.

Keywords –

Laser scanning; remote sensors and traffic data collection sensors; UAV (Unmanned Aerial Vehicles or drones) inspection; mobile application; assets management.

1 Introduction

The Ministry of Energy and Infrastructure (MoEI) is the arm of the Federal Government in the United Arab Emirates to plan, design, execute, operate and maintain the Federal roads Network in the five Northern Emirates (800Km center line, 1600Km carriageway and 3700Km lane of highways), *(figure 1)*

Figure 1. Federal Roads Configuration

Operation and maintenance of the roads is a cycle of various interconnected fields and specialties, being all of them interconnected and affecting each other.

By nature, that interconnection happens around numerous variables, and as a road network having hundreds or thousands of kilometers big amount of inputs for those variables are required, thus generating a big database.

UAE MoEIhas detected the need of a comprehensive system to manage and operate the maintenance activities with the highest efficiency. Developing an own assets management customized system to obtain, collect and process the related data of roads elements, intending to enlarge their life span and keep the level of service of some parameters within the suitable range.

The level of service for those established parameters are related to the sustainability aspects from which the MoEI is responsible for. [1]

These systems use the historical information contained in the database as a self-learning tool to enhance any analysis. Therefore, a good quality database will provide as well a good quality results through the modification and enhancement of the algorithms behind the calculations ensuring that self-learning process will also be improved.

The technologies that recently the MoEI has implemented within the assets management system are mentioned below as well as the reason of why were they chosen. [2]

1.1 Laser scanning (LiDAR)

The inventory of the elements within the right of way of the federal road is a requirement to perform the proper maintenance (it is impossible to asses a right maintenance either predictive or corrective if the elements to be maintained are unknown for the road owner). This knowledge is not only referred to “know” that the element exists; it is necessary to have some basic information which will allow the decision maker to choose the most appropriate method for intervention in order to preserve the assets, taking into consideration the reduction in time and effort reduction, and most importantly, ensure safety for the road users as well as the rest of the sustainability parameters. [3]

In the case of MoEI these pictures have been obtained since 2012 using a high-performance vehicle in which the pictures are taken and assembled every 2 meters composing frames of 10 meters length. The data collection can be achieved by using different cameras arrangement combined with a series of devices, which will relate the pictures with geographic positions (GPS, distanciometers and correlation of that information with the typical used road milestones used in the country,

which in MoEI's case are the light-pole number (sequential numbers placed in each light-poles). [4]

Within those 10-meter images, those elements constituting the road assets will be assigned to the system through their corresponding position and type through a file where their information can be stored after collecting it to create the full roads environment (dimensions, properties, condition, camber, slope, radius of curvature, etc.).

Implementation of *LiDAR* (*Light Detection and Ranging*) will combine all the previously mentioned parameters by generating a cloud of points then creating a 3D environment. This cloud of points creates a 3D attributes for each point, therefore we can obtain the geometric characteristics, relating them to 360 degrees pictures and describe the elements contained in the network, one by one.

LiDAR used to collect this information is a TRIMBLE MX9 equipment with capacity of 1 million points per second acquired with an average vehicle speed of 80Km/h and a mesh density of 1,000 points per square meter, *(figure 2).*

Figure 2. LiDAR vehicle used for data collection

Data acquisition from this device will provide the following described information .

As mentioned previously, within the information related to the inventory is very important to have the type, location and properties of the elements contained within the road network, *(figure 3).*

Figure 3. Data Inventory tables correlated with the Cloud of points and images

The typical data collection for the road network using the conventional methods took around 4 weeks of continuous work, and is compelled to be done during the daytime (considering as well the position of the sun to ensure the quality of the images). The data collection for the same length using LiDAR took only 14 days (saving therefore approximately 50% of the time required before).

The use of the cloud of points, allow to obtain cross sections of different segments of the road as well as distances between two or more points, areas and volumes. The benefit of that will be described after.

1.1.1 3D model creation

Both technologies mentioned previously, have been able to inventory more than 30,000 elements. And the creation of the continuous 3D model for the roads network can be integrated with other applications, systems and models in a near future as the usage in BIM *(Building Information Models)* or modeling base mesh for future growths or expansion of the roads, *(figure 4).* [5]

Figure 4. Bridge 3D model from LiDAR data collection

1.2 Remote sensors

Within the Bridge Management System (BMS), the main objective of these system is to store information of the bridge that can identify it as a singular and unique unit and to relate to that unit the condition of the structure, assessed by an assestment condition index developed by the MoEI and the University of Sharjah [6], [7], [8]

That index, indicates the condition of the structure according with a scale, depends on any defect affecting durability, structural behavior or operation of the bridge *(figure 5).*

Figure 5. Bridge Assessment Condition Index within the Bridge Management System

These defects in each structure can be detected through *principal inspections* that are performed in a period of 3 years by specialized engineers. This period can however vary, depending on the severity of the structure's condition. shortened if the needs of the bridge advise to do that. These conditions can be determined by:

- Unpredicted events (as for example, a flood or high tide stream, or any other extraordinary climate event)

- Hit by a vehicle or any other external element which can compromise the safety of the structure
- To follow special conditions of defects found (for example follow up the evolution of any mechanic or chemical phenomenon)

Sensors will be assigned to some found defects minimizing the need of site inspections, especially when their behavior can affect the assessment condition index of the bridge.

Below, the descriptions of the technologies used in the bridge assessment condition are described, divided into 2 main categories: Mechanical and Chemical sensors.

The main advantage of the mentioned sensors is the continuous data collection without the need of physical inspections to measure the values for some important parameters. The values measured on site, will represent the evolution of the parameter in a specific time. Using sensors for data registry, will provide not only that date during sequential shorts periods of time, but also the historical information of that parameter. The connection between the sensors is achieved by using an interface at the MoEI.

1.2.1 Mechanical sensors

Some bridges have special mechanical conditions to be monitored. These conditions can appear because of the combination of the loads, materials properties, excess of stress or/and strain, or similar, *(figure 6).*

In some bridges of the network, there are some required mechanical aspects to be followed as described below.

- Crack monitoring in beams
- Bi-directional tilting in piers
- Stress and strain in beams and piers
- Temperature in the elements

The defects found in a bridge might disturb some of the mechanical responses of the structure. The measurement of the defect response will help not only to know the behavior of the element of the bridge where that defect is located, but as well, to understand why that happened, and to predict what will happen to similar elements under similar circumstances.

The monitored parameters can be measured not only individually during the analyzed period of time but as well, all can be co-related to find existing interconnections. The analysis of that behavior along the time can help as well to predict and perform some preventive actions and maintenance. [9]

Figure 6. Mechanical remote sensors for bridge data collection

2.2.2 Chemical sensors

In the particular case of the highways located in the northern emirates of UAE, the majority representing 97% of the bridges are made of concrete (as well pre-casted in situ or prestressed, or casted in situ), *(figure 7).*

Figure 7. Chemical remote sensors for bridge data collection

Some of those locations are adequate to develop corrosion (because of the presence of chlorides or carbonation), creating the worst scenario for the structure's durability. Affection can be accelerated by high temperatures and humidity, presence of salt in the soil in some locations and chlorides due to sea tides in others. [9], [10]

The main parameters reported by the sensors, installed within the concrete of elements of bridges in service are:

- pH evolution
- Temperature
- Humidity
- Chlorides content

The way to prevent and control this situation is to monitor the progress of the parameters creating and propagating corrosion and create the preventive measurements according to each bridge affected.

2.2.3 Traffic sensors

The third category for sensors installed in the network, are the Traffic Sensors, collection traffic data. These sensors are registering the number of vehicles, speed, type and some of them weight.

nother significant aspects are traffic characterization and users' driving behavior. As roads operator, knowing these aspects are crucial in order to help to prevent and attend accidents, moreover, try to predict them in the best possible way. This information also helps to understands the effect of traffic on bridges and pavements, thus do the proper design as new and rehabilitated assets. Moreover, these analysis helps other stakeholders in their fields such as Ministry of interior in procedures related to traffic and security, Ministry of Justice to improve or create laws

related to traffic and Ministry of Health to prevent the resources dedicated to traffic accidents.

The traffic sensors are divided in two types, the Radars, which are utilized to measure the following group of parameters per lane and per direction in each road (22 out of 27), *(figure 8)*:

- Number of vehicles
- Type of the vehicles based on the length
- Speed

The remaining five (radars combined with piezo electric) in addition to the above parameters do register, *(figure 9)*:

- Gross weight of the vehicle
- Number of axles
- Weight per axle

Creation of enquiries about the traffic database will happen in special dashboards, which will provide in fast time the possibility to combine the information of different lanes and directions in a determined period of time, [11]. The enquiries parameters that can be calculated are:

- Average daily traffic
- Accumulated traffic
- Speed
- Intensity
- Occupancy
- Peak times (morning, mid-day and evening, time)
- Classification by length
- Classification by number of axels (using Federal Highway Administration criteria) (include here reference)
- Distribution on weight per axle per type
- Real time traffic conditions

Figure 8. Electromagnetic loops for traffic data collection

Figure 9. Radar traffic data collection

1.3 Unmanned Aerial Vehicles (Drones) inspection

Within the Bridge Management System MoEI included the bridge inspection by using UAV(drones), *(figure 10)*.

The inspection helps to enhance the inspection time by:

- Inspection components which are difficult to reach by conventional resources
- Creation of 3D cloud of points
- Creation of 3D model

Drones to do the inspection are equipped by different devices such as camera, LiDAR and GPS.

Figure 10. Drone for LiDAR data collection

The inspection outcome is a report showing the pictures and defect detected. These reports include the location, evidence and the quantity of the damage registered. Once the defect is reported, it can be transferred to the BMS carrying along the possibility to modify the assessment condition index.

The data collected offer as well the possibility of creating a 3D model of the bridge using photogrammetry tools combined with the cloud of points.

1.4 Mobile application

One of the most important aspects in MoEI Roads Department is to keep active tasks related to the daily maintenance. The daily found incidents can't be predicted and need to be attended as fast as possible, therefore the MoEI has implemented a Performnace Based Maintenance Contract based on KPI, (basically related to time response and quality). *(figure 11)*.

Since this type of contracts are controlled by penalties applied to the main contractor if the deficiencies or incidents are not attended on time, it is necessary to improve the registration, control and monitoring of all the road elements. [12]

An inspectors' fleet checking continuously the roads, can register any defect allocated in the road through a mobile application, relating that report automatically to the location of the mobile device live.

Fig 11. Mobile application for incidents management

The report will be uploaded in the database of the Assets Management System. In this way, MoEI as well is aware of the events pending to be finished and the available time before penalizing them, at the same time, allowing the contractor to register the closure of the report.

After, the inspectors are able to check and verify if the event was effectively closed and the quality level of service is achieved.

The mobile application shows the information contained in each report created by the road inspectors. And assuming that the reports can't have an "open" status for a longer period of 30 consecutive days without closing it by applying the corresponding maintenance, the reports for the last 30 days can be viewed in a list and in a map.

This mobile application as well allows to do the inspection of any other inventoried element in the road, including the bridges. The inspections will determine the assessment condition index of the elements that are in the same spot the inspector is.

2 Interrelation of all these technologies applied and benefit for the asset management in the Roads Department

All the previous described technologies can seem interesting from a technical point of view, individually.

However, a very important aspect is, how these technologies are interconnected amongst them and what benefit provide to the asset management of MoEI and how this benefit is can be noticed.

These properties and capabilities which are the base for the interrelation between them and the assets management, constitute significant aspects that will feed the specialized fields in the assets management tasks.

2.1 LiDAR (inventory and 3D model)

The inventory with LiDAR will feed the database of the mobile application and the inventory database for the main system for the Roads Department. The Road elements will be reflected in both and all the information as well as the assessment condition index can be modified and corrected by the user.

Moreover, the 3D models created during the process can merge with those 3D representations created by the *drones.*

3D models open possibilities to do a better analysis for specific road elements. For instance, if a structural/durability issue needs to be studied in a bridge, it will be easy to define the grid of this bridge and its elements, isolating it from the general cloud of points and exporting it to an 3D structural analysis software, *(figure 12).*

Figure 12. Cloud of points for post use in other applications

The importation of the cloud of points as a mesh to a conceptual design software for roads, used in widening or modification projects can provide with an initial high accuracy database for that project, without the need to collect more information with other methodologies, *(fig 13).*

Fig 13. 3D model from LiDAR data. Creation of cross sections for post analysis in structural analysis

A very important use of this tool will be to define the contour conditions for an *Autonomous Driving Car* simulation (of different road parameters and their current condition to calibrate the possibility of autonomous vehicles to circulate within the network).

As well, this model will be very useful for the creation of High Definition Maps, which will be used by this type of technology which constitutes one of the main pillars on the development of the transportation sector in the coming 20 years in UAE, *(figure 14),* [13]

Figure 14. Autonomous vehicles simulation

2.2 Mechanical and chemical sensors

They provide a real valuable information related to problems (mechanical or chemical) which can influence the response of the bridge in different ways.

The inputs these sensors can have in order to modify the condition assessment index of the bridge are evident (is not the same case to have a "dead" shearing crack in a beam that notice that it is progressing, *(figure 15).*

Figure 15. Bridge sensor's platform (location of sensors)

However, monitoring the same crack, and correlating this information with the traffic passing over the element can show if there is any need to restrict the traffic or make any urgent amendments to the element before the limits are reached (vehicles are calculated by the technologies mentioned in this paper as well).

Furthermore, the proper correlation between the crack and the registered stresses and strains can give an idea of the materials condition and characteristics, *(figure 16).*

Figure 16. Correlation between parameters in remote bridge sensors

Chemical sensors can provide information about the presence of carbonation and therefore some corroded steel bars which are not well appeared in some of the inspections performed, *(figure 17).*

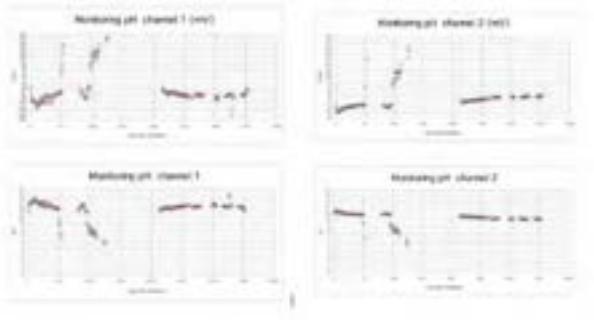

Figure 17. Chemical parameters correlated from bridge sensors

These actions will enhance the rehabilitation project and will make it to be adjusted to the real conditions that need to be corrected, *(figure 18)*

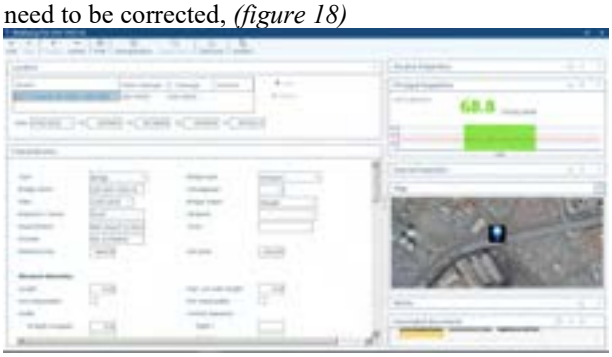

Figure 18. Modification of the Bridge Assessment Condition Index using the information from the remote sensors information

The proper rehabilitation project will be designed according with the traffic supported by the element and (as mentioned in this paper). The best solution will be the one therefore providing the best life cycle solution.

The possibility of having a 3D mesh from LiDAR representing the bridge and the possibility of overlapping pictures with the defects and parameters determining their behavior, allow to model and predict different scenarios as well as create maintenance programs for clusters of similar bridges.

The strategic knowledge of live traffic behavior makes possible to analyze some parameters as the growth factor, which will influence directly, not only the geometry of the roads and the elements within them to be built and maintain, but as well the development of urban or industrial areas, *(figure 19).*

Figure 19. Road live traffic conditions map

Instant conditions of the traffic are basic to operate the traffic management procedures in the correct way for the road user's safety, using those parameters as well as information of any anomaly in the road that can be attended by the maintenance contractor (accelerating the response time in those events, which can be register in the mobile application), *(figure 20)*.

Figure 20. Traffic incidents detection from traffic live monitoring

Knowing the traffic flow and conditions can help to apply restrictions and ban times for some vehicles in a more precise way, *(figure 21)*.

Figure 21. Traffic data integration. Parameters analysis

Integration of the traffic database allow to check the efficiency of some operational aspects, as better level of service usually implies a better the operation of the highway.

A good and accurate traffic data will provide better models (in 3D integrating the models created by LiDAR) to predict and model the traffic according to the corresponding economic, social and environmental conditions (see point 2.4).

2.3 Unmanned Aerial Vehicles (Drones) inspection

The inspections performed with drones will help to the creation of 3D models that can be merged into the cloud of points obtained by LiDAR along with photogrammetry technologies with inputs from the images taken during the inspection, (*figure 22)*.

Figure 22. Defects detection from Drone bridge inspection

Damages acquisition by drone can be as well overlapped on the 3D mesh of the bridge and analyze their influence into the context of the element or the bridge.

Information obtained in this inspection can be used as well in traffic modeling programs for example in the case of intersections and junctions. In some of our highways these points constitute "hot spots" and need to be simulated under special conditions. Counting with a 3D model of the bridge will make the microsimulation easier and more realistic, *(figure 23)*.

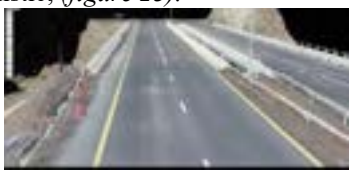

Figure 23. 3D model for traffic simulation implementation

2.4 Mobile application

The mobile application as smart tool allows to manage information of assets in the spot, live, *(figure 24)*.

This is an important aspect, considering the synchronization performed between both data bases which representing the reality of the road elements.

Figure 24. Mobile application for road maintenance incidences

Any new incidence registered by the mobile application will be automatically synchronized with the general database, which allows to manage the assets condition and the traffic management and maintenance actions.

If any incident is urgent an alarm is launched then immediate actions and monitoring with the traffic devices can be performed, *(figure 25)*.

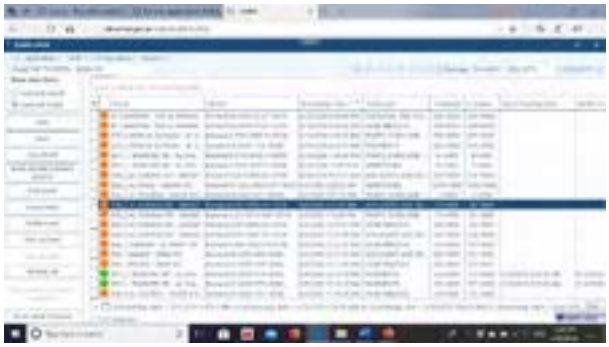

Figure 25. Data base synchronized with the mobile application

Then the MoEI is able to predict the consequences on traffic and road safety meanwhile having any repair or rehabilitation. Discussion with the corresponding police department can be started and all the possibilities to implement the best road safety action according with the urgency of the incidence and the traffic conditions can be done.

A fast update of this inventory data base using the mobile application, will allow as well, to do faster calculations involved in the asset management, maintenance plan and valuation of the assets.

3 Conclusions

The intense work at MoEI during the past 8 years, arose in the creation of a Roads Assets Management that has been continuously developing and improving.

Nowadays, the integration of the tools the MoEI already implemented to do a proper roads management leads to the implementation and integration of the following recent technologies:

- Data collected with LiDAR to create 3d models and cloud of points during the inventory of the road elements
- Remote sensors in bridges to monitor their mechanical and chemical conditions
- Traffic data collection with remote sensors to calculate the traffic parameters
- Drones to perform LiDAR and inspection in bridges to enhance the inspection result in less time and create 3D models for the bridge
- Mobile application to report and register the incidences in the roads live

Continuous feedback of the received information to different specialists in the Ministry allow to increase the service level to the road users and reduce the time response in different situations. All the technologies as mentioned before are interrelated and the outcome can benefit different aspects of the road management.

4 References

[1] UNITED ARAB EMIRATES CABINET. National Agenda. https://uaecabinet.ae/en/national-agenda

[2] PIARC. World Road Association. Asset Management Manual. A guide for practitioners. Case Study 1. *SUCESSFUL IMPLEMENTATION OF A ROAD ASSETS MANAGEMENT TOOL FOR THE FEDERAL ROADS OF UNITED ARAB EMIRATES.* https://road-asset.piarc.org/en/applications-asset-management-tools-case-studies/case-study-1

[3] PIARC. World Road Association. Asset Management Manual. A guide for practitioners. 2.1.3.2 METHOD AND TECHNOLOGY OPTIONS FOR DATA COLLECTION. https://road-asset.piarc.org/en/data-and-modeling-inventory-and-condition-process/method-and-technology-options-data-collection

[4] PIARC. World Road Association. Asset Management Manual. A guide for practitioners. https://road-asset.piarc.org/en/management/asset-management-implementation
QUEENSLAND, AUSTRALIA. Building Information Modelling (BIM) for Transport and Main Roads. A guide to enabling BIM on Road Infrastructure Projects. Queensland Australia. May 2017

[5] ABU DABOUS, AL-KHAYYAT, LLORT, ALKHEYAILI. A New Bridge Condition Index Considering Potential of Evolution and Extension of the Deterioration Process. 2nd IRF Asia Regional Congress & Exhibition October 16-20, 2016 – Kuala Lumpur, Malaysia

[6] ELLIS, REED and THOMPSON. Bridge Asset Valuation and the Role of the Bridge Management System. 2007 Annual Conference and Exhibition of the Transportation Association of Canada: Transportation-An Economic Enabler (Les Transports: Un Levier Economique). 2007.

[7] NYSDOT (New York State Department of Transport). Bridge inspection manual, New York State Department of Transportation, New York. 1997

[8] ROBERTS, JAMES AND SHEPARD. "Bridge management for the 21st century." Transportation Research Record: Journal of the Transportation Research Board 1696 (2000): 197-203.

[9] MULONE. Chlorides Concentration and Ph Measurements of concrete structure through immersed sensors (proceedings in the conference *X Convegno Nazionale INSTM sulla Scienza e Tecnologia dei Materiali).* Favignana, Italy. 28/June/205 to 01/July/2015

[10] TRANSPORT RESEARCH BOARD. Highway Capacity Manual. 6th edition. A Guide for Multimodal Mobility Analysis. 2016. ISBN 978-0-309-36997-8

[11] UNITED ARAB EMIRATES, MINISTRY OF INFRASTRUCTURE DEVELOPMENT.
Tender & contract documents. Volume 3. Project Service Terms & Conditions.

[13] DUBAI FUTURE FOUNDATION.
Dubai's Autonomous Transportation Strategy. https://www.dubaifuture.gov.ae/our-initiatives/dubais-autonomous-transportation-strategy/

Safety Monitoring of Construction Equipment based on Multi-sensor Technology

Zi-qing Yang [a] , Jian Yang [a,b,c] and Enliu Yuan [d]

[a] School of Naval Architecture, Ocean and Civil Engineering, Shanghai Jiao Tong University, China;
[b] State Key Laboratory of Ocean Engineering, Shanghai Jiao Tong University, China;
[c]Shanghai Key Laboratory for Digital Maintenance of Buildings and Infrastructure, China
[d] Department of engineering, Lancaster, United Kingdom

E-mail: yangzq@sjtu.edu.cn, j.yang.1@sjtu.edu.cn

Abstract –

The growth in the size and the level of complexity of construction equipment imposes tremendous hazards in construction sites. Any breakdown or failure of such systems may not only cause the delay in construction but also lead to the loss of life and properties. To address these issues, this paper proposes an intelligent monitoring system based on multi-sensor technology, which consists of multiple sensor clusters, signal transmission and data acquisition systems, condition evaluation, identification and alerting systems, assisted by Wifi or Zigbee wireless transmission technology to obtain the real-time state data from various parts of construction equipment. The center computer can manage and analyze the relevant parameters to reveal the safety reserve of the tower crane, scaffolds, self-climbing platform and other construction equipment in a visual image. In addition, the alerting alerts can be sent directly to security officers and operators to respond to and avoid accidents. Lastly, the intelligent multi-sensor monitoring system is simulated tested in 6013 flat crane, which is shown the workflow of whole technology and demonstrates this technology is fast, accurate and valid for the safety management of construction.

Keywords –

Construction equipment; High-rise buildings; Intelligent safety monitoring system; Multi-sensor technology.

1 Introduction

Because of the high casualty rate, site safety is one of the most concerned issues in the construction industry. Statistics data from Ministry of Construction suggests that, in china, there have been 637 safety accidents and 736 deaths in the first ten months of 2018, with 6.52% and 4.69% increased, respectively, compared to 2017.

Although the construction technology is constantly updated and upgraded, the management of construction site safety still primarily relies on the manual approaches, such as the daily patrol and regular inspections by the safety officers. With the gradual introduction of Industry 4.0 technology[1] into the construction industry, some construction robots and large-scale integrated construction platforms have emerged[2], which enhance the size and the level of complexity of construction equipment. Traditional safety monitoring methods may not be applicable to such complex construction environments and many unexpected causes of risks may render faults or failure, even with the tight security control measures[3]. For instance, the long-term environmental exposition, the inappropriate use and maintenance, the installation tolerances and their growth may all give rise to the unpredictable risks, which may eventually cause the bucking or collapse of scaffolds and the toppling of the tower cranes.

This safety matter is especially challenging in the construction industry and requires intelligent methods to monitor the stiffness, strength and stability of these complex construction equipment and temporary structures, such as scaffolds, in order to eliminate potential hazards. Literature review suggests that a wide range of studies have looked at the intelligent monitoring system or technology used for construction sites. Moon[4] studied an automated data acquisition system and appliance based on the Ubiquitous Sensor Network (USN) technology to collect structural responses. Zhu and Roh[5-6] introduced a method based on multi-sensors, visualization technology and computer vision technology for updating 3D equipment movements in order to prevent the collision between equipment, workers and other objects on the construction site. Son[7] proposes an efficient, automated 3D structural component recognition and modeling method that employs color and 3D data acquired from a stereo vision system for use in

construction progress monitoring.

To address these issues, this paper proposes an intelligent monitoring system based on multi-sensor technology, consisting of multiple sensor clusters, signal transmission and data management systems, condition evaluation, identification and alerting systems. Assisted by Wifi or Zigbee wireless transmission technology[8], the structural parameters of key parts of construction equipment are received by the central server, which are used to monitor the working status of equipment structure in the real time. For instance, taking the data from the wind speed meter to measure wind velocity, inclination and displacement sensors to monitor deformation and movements, strain sensors to capture the stress/strain conditions and accelerometers to understand the dynamic properties, the data processing center can collect and analyze the relevant parameters to reveal the safety reserve of the tower crane, scaffolds, self-climbing platform and other construction equipment.

Safety monitoring of construction equipment technology is an intelligent and automated technology that the original data collected by multiple sensor clusters are automatically processed and converted to structural parameters in accordance with a predetermined programme and the damage degree of the equipment is shown by visualization. This paper mainly introduces the working principle and integration mechanism of systems, with the key focus on how to integrate, transmit and process data in each system.

2 Safety monitoring system

The intelligent monitoring system can automatically transform the original data collected by multiple sensors and feed to the evaluation modules[9] revealing and monitoring the structural health state of construction equipment in real time seen in Figure 1. The process entails the following steps: 1) data collection and acquisition by utilizing different types of sensors or multiple sensor clusters; 2) data analysis and modelling; 3) damage identification and health evaluation. The final step can be revealed by visual representation together with some alerting systems[10].

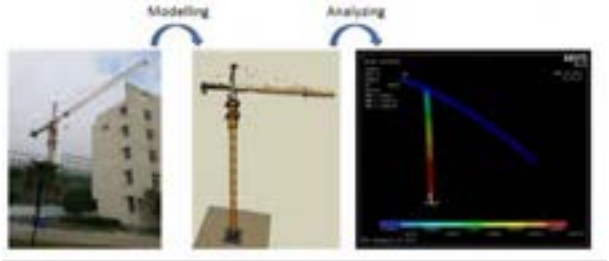

Figure 1. Data-driven modelling of tower cranes

The above process can be presented in the workflow as shown in Figure 2, which can be generally divided into four subsystems, namely multiple sensor clusters, signal transmission and data management subsystems, condition evaluation and identification an alerting subsystem. The data from various sensors, often in differing formats and output signals, are integrated so that the data, resources and process states can be shared across the system. Pre-alerting of impeding faults or failure of those construction equipment structures can be alerted. The key of this type of system is the stability and timeliness of wireless transmission[11] and the optimization of data processing[12]. The massive data will be accumulated in the data center and the big data analysis technology can be employed so that the minimal size of them should be stored and feed into the structural modelling.

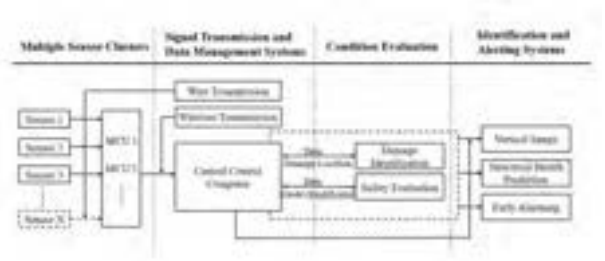

Figure 2. Workflow of safety monitoring system

2.1 Multiple sensor clusters

Multiple sensor clusters are the first tier in the intelligent monitoring system[13]. The common sensors used include the wind speed sensor to measure wind velocity, inclination and displacement sensor to record the movements, strain sensor to acquire the strain condition and accelerators to capture the dynamic properties. The locations of sensors are properly designed and selected, so are the acquisition frequencies.

In order to reduce the amount of data for transmission and storage, the initial processing of the original data is required so that the unimportant or redundant data are filtered out in the first instance. Kalman filter is usually used to preprocess the original data, which is an algorithm to extract the real value of the dynamic system in a series of measure data with noise. And then, feature selection of the initial preprocessed array is carried out to manifest the principal and precise characteristics in one set period. Common feature extraction methods are principal component analysis (PCA), linear singular analysis (LDA)[14], independent component analysis (ICA)[15], neural network, etc. The method of feature selection is properly selected on the basis of structural characteristics and monitoring requirements. In general, the application of feature selection is beneficial to reduce the amount of calculation and improve the accuracy of

structural analysis in the process of condition evaluation.

In the collection process, it is assumed that cycle of the sensor data collection is 2s and the cycle of central computer operation is 30s. So, within 30 seconds, the sensor-1 will gain 15 pieces of data: $[X]_1 = [X_1, X_2, X_3, \dots, X_{15}]$. Before feature selection, simple preprocessing should be carried out on the original data to delete the data with large errors. In the end, the eigenvalue X_1 will be calculated by single-chip microcomputer (MCU) and transmitted to the central control computer.

2.2 Signal transmission and data management systems

Signal and data transmission can be regarded as the logistics support for the whole system[16]. Only with stable transmission technology can the whole system be sampled synchronously and the structural data of each part at the same time point can be obtained. Otherwise, if data in different cycles arrive at the central computer and be processed simultaneously, it will yield data chaos[17].

In this present system, there are two transmission modes, wired transmission and wireless transmission. Wired transmission is used to transmit data from sensors to microcomputers, which is the front-end data transmission of the whole system. Due to the space limitation of wired transmission, the locations of both sensors and microcomputers need to be considered and a single-chip microcomputer (MCU) can process data up to 8 sensors at the same time. Wireless transmission, such as Wifi or Zigbee wireless transmission technology, transfers the data preprocessed from MCU to the central computer for the further data analysis. In the construction environment, due to the signal reception blocking of the concrete or metal, the wireless transmission signal is usually weak. In order to establish a wireless network for real-time data acquisition, the system uses ZigBee technology to receive data by using radio frequency (RF) signal transmission, which can connect up to 65,000 sensor nodes and transmit data at 250 kbps[18].

Data collection from multiple sensors is usually synchronized. In the real applications, such synchronization can be compromised due the delay in the data transmission (see Figure 3). To address this problem, step by step filtering (SSF) fusion algorithm is adopted. Compared with centralized fusion algorithm (CFA), SSF (see Figure 4) has fewer requirements for calculation efforts and the number of central processors and network bandwidth, but stronger system survivability[19-20].

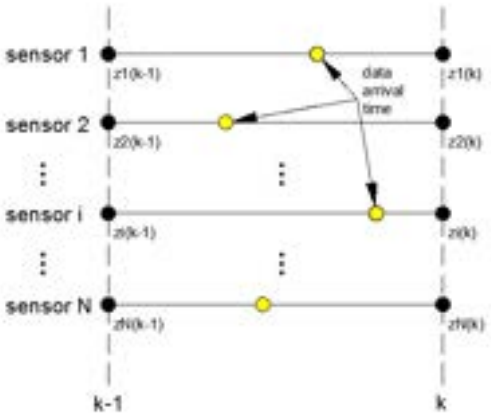

Figure 3. Simultaneous sampling with transmission delay[17]

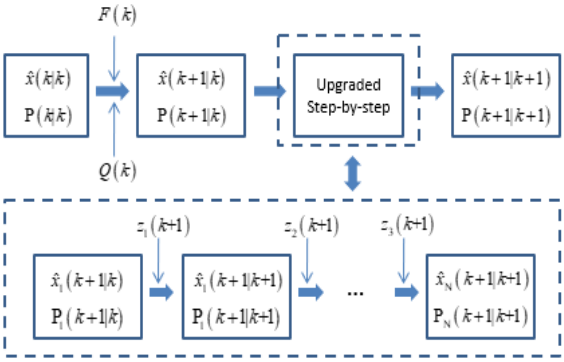

Figure 4. SSF Fusion Algorithms[20]

Table 1. Definition of mathematical expression

No.	Mathematical Expressions	Definition
1	k	A certain moment
2	$k+1$	The moment of one cycle after k moment
3	$x(k)$	State function
4	$x(k+1)$	State function in k+1 moment. $x(k+1) = F(x)x(k) + v(k)$
5	$\hat{x}(k\|k)$	The global estimated value
6	$\hat{x}(k+1\|k+1)$	The global information-based estimated value
7	$P(k\|k)$	The corresponding estimated error covariance
8	$P(k+1\|k+1)$	The corresponding error covariance
9	$z_1^k(i)$	The set of measurement sequences of the i-th (i =1,2, ⋯ ,N) sensor at

		1,2, ⋯ ,k moments. $Z_1^k(i) = [z_i(1)^T, z_i(1)^T, \dots, z_i(k)^T]$
10	Z_1^k	The set of measurement sequences of all N sensor at time 1,2,⋯,k moments.$Z_1^k = [Z_1^k(1), Z_2^k(2), \dots, Z_2^k(k)\ ]$
11	$F(k)$	Distribution function of X,X is random variable and k is any real. $F(k) = P\ (x < k)$
12	$Q(k)$	Covariance function. $Q(k) = E[v(k)v(k)^T]$
13	$v(k)$	White noise sequence of zero mean gauss process

In the actual monitoring process, due to the instability of data transmission, it is difficult to ensure that all sensor data can reach the computing platform synchronously. To solve this problem, the database store method is adopted. If a value X_n fails to reach the computing platform synchronously, the X_{n-1} of the previous array is retrieved. And if the value fails to reach the computing platform for three processing cycles, the warning system would started to report the error.

The subsystem involves both hardware and software. The hardware includes transmission cables, optical cables, RF transmitters, RF receivers, digital-to-analog conversion cards (A/D), etc. The software is used to store and manage the digital signals, using a common software platform such as C++.

In a real-time monitoring system, even in the case of data pre-processing, there are thousands of data collected every day, which requires a robust data management system and program. The data management system is not only responsible for managing the preprocessed data, but also managing all information in each subsystem, including materials, geometric information, and structural analysis results of devices. Should any accident strike, this type of data can be traced for the forensic analysis purpose.

2.3 Condition Evaluation

In this subsystem, the structural software is used to model the system based on the collected real-time data so that the health condition of the equipment can be assessed.

To this end, the first step is to transform the preprocessed data from multi-sensors clusters into physical data [Vm], such as strain or movements, and then check with the specified threshold value [Vd] to identify the any damages. If there's a big difference between the value [Vm] and value [Vd], the structure must be secure and there is no point to expand extra unnecessary computations. Once any damage is identified, a reliability analysis can be conducted to evaluate the severity of damage, based on which due alerting is released for the management purpose.

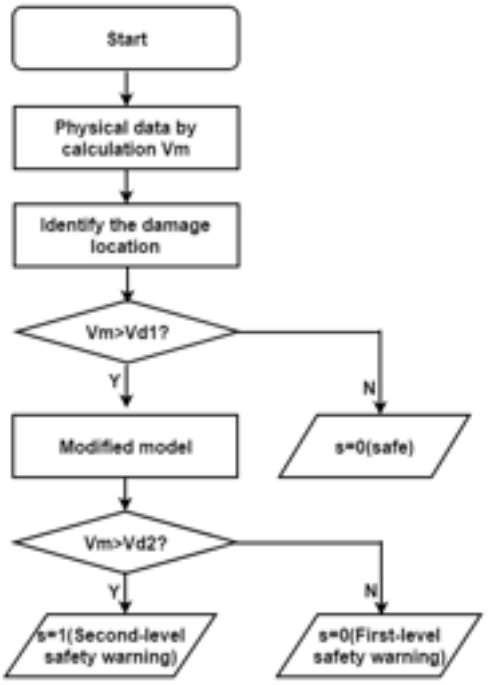

Figure 5. Workflow of condition evaluation

1. Safety assessment

Safety assessment consists of serviceability limit state assessment and ultimate limit states assessment. The evaluation indicators of serviceability limit state are the deformation of structure, cracking growth acceleration, etc. And the ultimate limit states can be assessed by structural analysis software. The simplest method of evaluation is to analyze the development trends shown by the measured stress, deflection, acceleration and other indicators.

2. Damage identification

At present, an increasing number of damage identification methods have been applied in engineering projects, such as structural modal parameter identification based on wavelet transform[21], damage sensitivity analysis based on structural modal parameters[22], structural damage detection based on neural network, structural damage detection based on improved genetic algorithm[23], etc. These methods mainly perform modal analysis of structural dynamic response, and then calculate the damage indicators with different damage identification methods.

2.4 Identification and alerting systems

Through data processing and mining, the system will eventually be able to obtain real-time visualized structural health monitoring images, structural health predictions and early warnings.

1. Visual monitoring image

The final structural health state can be showed by a visual image. Construction workers and manager can quickly and accurately monitor the structural health status of the equipment remotely, and then find problems in time and take measures.

2. Structural health predictions

Through sufficient data mining, state estimation and prediction of the structural state of the construction equipment can be performed. A large amount of data collected and the simulated force model can be used to detect the weak places of the equipment structure for focal monitoring. the weak points can be predicted by well-rounded algorithm, including linear regression method, nonlinear model method, unsupervised supervised learning method and other methods, so as to prevent risks in advance.

3. Early warming

The identified damages with its location and size are systemized for formulating the alerting information, which can be circulated via mobile electronically devices or other type overall alerting system. Due measures can be taken to respond to such alerting information.

3 Case Study

The intelligent monitoring system is employed for the real-time supervision of the construction equipment and temporary structures used in the construction site. Four subsystems are instrumented to collect, transmit and process the data. A visualization program is to reveal the data and work status of the monitored systems.

The system is mounted into a tower crane, which is presented below to show the entire process of coordinated work and data processing of each subsystem. In the simulated test, 6013-flat-head tower crane is selected as the experimental tower crane with 800KN*m load moment, 46 meters maximum free height, 60 meters maximum radius of revolution and lifting 6 tons materials at most

According to the specifications for tower crane design, there are five key performance indicators for the overall structure safety operation, namely, temperature $[T]$, the bending strength $[\sigma_1]$ and deflection $[v_1]$ of crane jib, the vibrational frequency $[f]$,the deformation of crane column$[v_2]$. For each indicator, one or more sensors are placed to obtain the corresponding structural parameters directly or indirectly. By data fusion, calculation and estimation, the large amount of original data are processed to the structural parameters to realize the visual monitoring of the loading state of the tower crane.

It is worth noting that the working stress of crane tower is constantly changing due to the moving load during the lifting operation. Under different loading scenarios, the maximum stress points change, and, therefore, the sensors need to be placed in some crucial places. According to the "Tower crane design specification (GBT 13752-2017)", the layout of the sensors should follow the following principles:

a) The places with significant stress changes or large stress, which can be calculated by the finite element analysis;

b) Important component of the structure, such as structural cross-middle rod parts and suspension rod parts, etc;

c) Representative and regular places, such as fatigue-prone and corrosion-prone positions, etc.

3.1 Multiple sensor clusters

In this simulated case, five types of sensors are mounted in selected locations, i.e. temperature sensors, wind speed sensors, accelerometers, displacement and strain sensors. Ten sensors were placed in the simulated experiment (shown in Figure 6)and the original data obtained were named as $[A_1]$, $[A_2]$, $[B]$, $[C]$, $[D_1]$, $[D_2]$, $[D_3]$, $[E_1]$, $[E_2]$, $[E_3]$, $[F_1]$, $[F_2]$, $[F_3]$, $[F_4]$, as shown in Table. Among them, the displacement sensor consists of a transmitter and a receiver. It can simultaneously collect the displacement in X, Y, Z directions, and the data are all collected by the receiver.

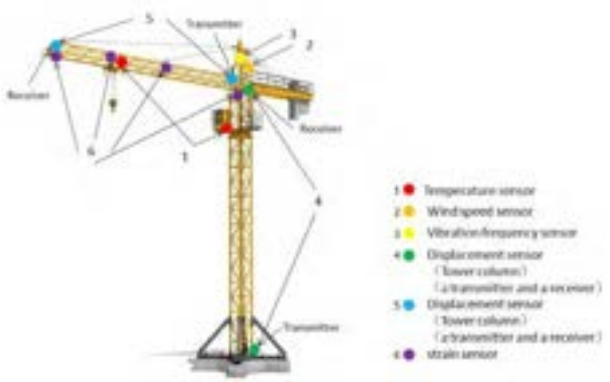

Figure 6. Diagram of the location of multiple sensor clusters

Table 2. Types of sensors and corresponding dataset

No	Sensors	Data Set	Note
1	Temperature sensor	$[A_1]$, $[A_2]$	Environment temperature $[A_1]$ and engine

			temperatur e $[A_2]$
2	Wind speed sensor	$[B]$	Wind velocity
3	Accelerom eters	$[C]$	
4	Displacem ent sensor （Tower column）	$[D_1]$-X Direction $[D_2]$-Y Direction $[D_3]$-Z Direction	A transmitter and a receiver
5	Displacem ent sensor （Tower jib）	$[E_1]$-X Direction $[E_2]$-Y Direction $[E_3]$-Z Direction	A transmitter and a receiver
6	Strain sensor	$[F_1], [F_2], [F_3], [F_4]$	Key position

3.2 Signal transmission and data management systems

Through wired transmission, the original data will be transmitted to MCU for initial processing, and then the mathematical sets$[A_1]$, $[A_2]$, $[B]$, ⋯, $[F_4]$ acquired by multiple sensor clusters will gain the corresponding values A_{1i}, A_{2i} , B_i ⋯, F_{4i}.Since the wired transmission is limited by space, an MCU connected up to 8 sensors is to process data at the same time. In installing MCU, the quantity and locations of MCU shall be determined by the relationship between the sensor clusters and MCU.

In this case, three single-chip microcomputers are placed in the tower crane (Figure 7). The first one is on the top of tower column, which is used to collect the engine temperature $[A_2]$, the displacement of tower column $[D_1]$, $[D_2]$, $[D_3]$, the stain of tower column $[F_1]$; the second one is at the junction of tower column and jib, which is used to collect wind velocity $[B]$, vibration frequency $[C]$ and stain of tower jib $[F_2]$; the third one is at the end of tower jib, which is used to collect the environment temperature $[A_2]$, the displacement $[E_1]$, $[E_2]$, $[E_3]$ and the stain of tower jib $[F_3]$, $[F_4]$.

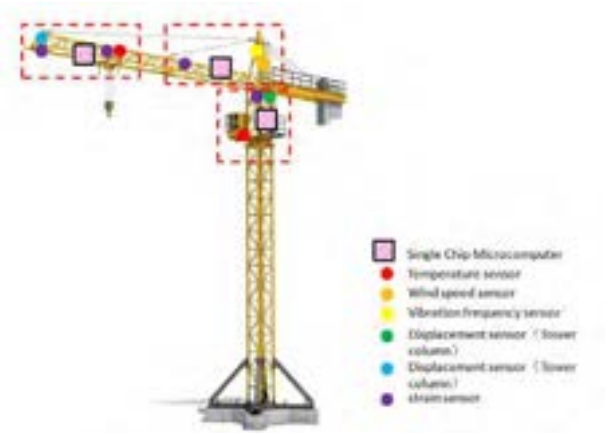

Figure 7. Diagram of the location of MCU

The preprocessed data (A_{1i}, A_{2i} , B_i ⋯, F_{4i}.) are transmitted wirelessly to the central control computer, using the robust and fast wireless transmission technology, Zigbee. The central control computers not only are responsible for data processing, but also for date management and storage. Date management subsystem is responsible for storing the pre-processed data, the modelled structural parameters, and the structural images at certain intervals, which is used for continuous system inspection and identification and analyzing the cause of failure if the tower crane collapses.

3.3 Risk assessment

The obtained values are analyzed by using MATLAB software to determine the presence, the location and size estimation of damages. Furthermore, the safety evaluation can be conducted and reported.

3.4 Identification and alerting systems

ANSYS software is used to simulate the component response of tower crane based on the collected data. The displacement of x-component, y-component and z-component, the rotation of x-component, y-component and z-component, elastic strain and plastic strain can be calculated for the entire structure (Fig. 8).

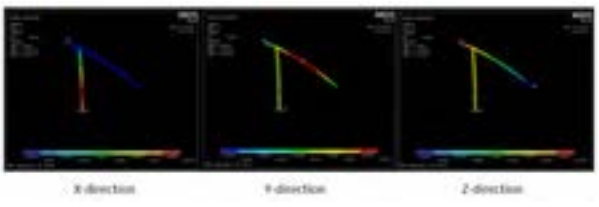

Figure 8. Diagram of modelled deformation

4 Conclusion

The safety monitoring system can intelligently monitor the working status of construction equipment in real time, establish visual model for the strength and deflection of the entire structure, and inform the safety state of construction site in the visualized way. By means of data collection of sensors and step-by-step processing of computers, security officers can obtain real-time structural state of construction equipment or temporary structures to avoid accidents, especially in severe environment. Such system possesses the following features:

1. **Fully automation.** Except installation and regular system inspections, the system can archive data collection, multi-software interactive data processing, and identification of the location and size of damage, visual representation and producing alerting messages to the related personnel.
2. **High timeliness**. The sensor collects data in the real time, and the data is processed by program in automatic way, so the final structural state can be obtained in a nearly synchronized manner.
3. **Visualization.** The displacement and stress of the structure can be visualized.
4. **Other applications**. A large number of environmental and structural parameters collected in the data management subsystem can provide detailed experimental data for equipment structural design, from which the correlation relationship between the environmental action and vibration frequency can be established.

The safety monitor system can replace the traditional methods of maintaining construction equipment, such as tower crane, which provides improved accuracy and enhanced safety level.

Acknowledgement This work was supported by the Scientific Research Project of Shanghai Science and Technology Commission [Grant No. 18DZ1205603].

References

[1] Schmidt R, Möhring M, Härting R C, et al. Industry 4.0-potentials for creating smart products: empirical research results[C]//*International Conference on Business Information Systems.* Springer, Cham: Poznan University of Economics, 2015: 16-27.

[2] Jung Y, Ryu J, Kim K-m, et al. Automatic construction of a large-scale situation ontology by mining how-to instructions from the web[J]. *Web Semantics: Science, Services and Agents on the World Wide Web*. 2010, **8**(2):110-24.

[3] Yuan X, Anumba CJ, Parfitt MK. Cyber-physical systems for temporary structure monitoring [J]. *Automation in Construction*. 2016, **66**:1-14.

[4] Moon S, Choi B, Yang B. USN-Based Data Acquisition for Increasing Safety in the Concrete Formwork Operation[J]. *Journal of Computing in Civil Engineering*. 2012, **26**(3):271-81.

[5] Roh S, Aziz Z, Peña-Mora F. An object-based 3D walk-through model for interior construction progress monitoring[J]. *Automation in Construction*. 2011, **20**(1):66-75.

[6] Zhu Z, Ren X, Chen Z. Integrated detection and tracking of workforce and equipment from construction jobsite videos[J]. *Automation in Construction*. 2017, **81**:161-71.

[7] Son H, Kim C. 3D structural component recognition and modeling method using color and 3D data for construction progress monitoring[J]. *Automation in Construction*. 2010, **19**(7):844-54.

[8] Figueiredo CP, Gama ÓS, Pereira CM, et al. Autonomy Suitability of Wireless Modules for Ambient Assisted Living Applications: WiFi, Zigbee, and Proprietary Devices[C] //*2010 Fourth International Conference on Sensor Technologies and Applications*; Washington, DC, USA: IEEE Computer Society, 2010:169-172.

[9] Li H, Zhou W, Ou J, Yang Y. A study on system integration technique of intelligent monitoring systems for soundness of long-span bridges[J]. *China Civil Engineering Journal*, 2006, **39**:46-52.

[10] Popescu D, Dobrescu R, Nicolae M, et al. Communication and processing consideration for alerting systems implemented through mobile sensor networks[J]. *WSEAS TRANSACTIONS on COMMUNICATIONS*, 2009; **8**(3):363-372.

[11] Jiang S, Georgakopoulos SV. Optimum wireless power transmission through reinforced concrete structure[C] //*2011 IEEE International Conference on RFID*; Orlando, FL, USA: Institute of Electrical and Electronics Engineers, 2011:50-56.

[12] Curry R M, Smith J C. A survey of optimization algorithms for wireless sensor network lifetime maximization[J]. *Computers & Industrial Engineering*, 2016, 101: 145-166.

[13] Tam N T, Hai D T. Improving lifetime and network connections of 3D wireless sensor networks based on fuzzy clustering and particle swarm optimization[J]. *Wireless Networks*, 2018, **24**(5): 1477-1490.

[14] Boukas EK, Liu ZK. Delay-dependent stability analysis of singular linear continuous-time system[J]. *Control Theory and Applications,* 2003, **150**(4):325-30.

[15] Ding N, Sadeghi P, Smith D, et al. Distributed Data Compression in Sensor Clusters: A Maximum

Independent Flow Approach[C]//*2018 IEEE International Symposium on Information Theory (ISIT)*. IEEE, 2018: 2221-2225.

[16] Smith J. The Joint Optimization of Transmitted Signal and Receiving Filter for Data Transmission Systems[J]. *Bell System Technical Journal*. 1965, **44**(10):2363-2392.

[17] Abrar M. Performance Comparison of Routing Protocol by Deploying ZIBGEE as Wireless Sensor Network[J]. *Bahria University Journal of Information & Communication Technologies (BUJICT)*, 2018, **11**(1): 45-50.

[18] Zahurul S, Mariun N, Grozescu I V, et al. Future strategic plan analysis for integrating distributed renewable generation to smart grid through wireless sensor network: Malaysia prospect[J]. *Renewable and Sustainable Energy Reviews*, 2016, **53**: 978-992.

[19] Vaidehi V, Kalavidya K, Gandhi S. Cluster-based centralized data fusion for tracking maneuvering targets using interacting multiple model algorithm[J]. *Sadhana*. 2004;**29**(2):205-216.

[20] Xing Z, Xia Y. Comparison of centralised scaled unscented Kalman filter and extended Kalman filter for multisensor data fusion architectures[J]. *IET Signal Processing*, 2016, **10**(4): 359-365.

[21] . Laier JE, Villalba JD. Ensuring reliable damage detection based on the computation of the optimal quantity of required modal data[J]. *Computers & Structures*. 2015, 147:117-125.

[22] Baker J W. Efficient analytical fragility function fitting using dynamic structural analysis[J]. *Earthquake Spectra,* 2015, **31**(1): 579-599.

[23] Sehgal S, Kumar H. Structural dynamic model updating techniques: A state of the art review[J]. *Archives of Computational Methods in Engineering*, 2016, **23**(3): 515-533.

Autonomous UAV flight using the Total Station Navigation System in Non-GNSS Environments

A.Ishii[a], T.Yasuno[a], M.Amakata[a], H.Sugawara[a], J.Fujii[a], and K.Ozasa[a]

[a]Yachiyo Engineering Co., Ltd., Research Institute for Infrastructure Paradigm Shift
E-mail: akri-ishii@yachiyo-eng.co.jp, tk-yasuno@yachiyo-eng.co.jp, amakata@yachiyo-eng.co.jp, sugawara@yachiyo-eng.co.jp, jn-fujii@yachiyo-eng.co.jp, kh-ozasa@yachiyo-eng.co.jp,

Abstract –

In this study, we propose autonomous UAV flight using the total station to estimate self-localization at a dam in a non-global navigation satellite system (GNSS) environment and suggest a flight path planning method for the UAV's flight position. As a result of the UAV's stable autonomous flight, a certain distance from the dam body's surface can be maintained by flying accurately along the planned path, allowing for uniform quality and high-resolution images to be captured. Moreover, geotags can be added to the image by measuring the flight position of the captured images; this is achieved via the total station, which can track the UAV even in a non-GNSS environment. Resultantly, the accuracy of the three-dimensional reconstruction model using photogrammetry technology can be improved.

We further implement a field study to demonstrate the utility of the proposed approach. Moreover, we propose aging detection using AI analysis.

Keywords –

Autonomous UAV flight; Non-GNSS; Total station navigation system; Flight path planning; Dam

1 Introduction

An unmanned aerial vehicle (UAV) can fly autonomously via self-localization and flight attitude stabilization technologies, including global navigation satellite systems (GNSSs) and various sensors; e.g., gyroscopes, an accelerometer, a barometric sensor, and inertial measurement unit (IMU). Therefore, UAVs have recently seen increasing use in various inspections [1,2,3,4] owing to their high functionality and practicality. Conversely, autonomous UAV flight in outdoor environments, where GNSSs are unavailable, is a challenge.

In Japan, many social infrastructures are aging and inspections are necessary for maintenance. As shown in Figure 1, it is necessary to efficiently capture the dam body's surface image for an inspection or survey, via a digital camera mounted on the UAV. However, GNSSs cannot normally be used because the radio waves from global positioning system (GPS) satellites do not reach mountainous areas; i.e., a dam's location cannot be determined, or a multipath caused by interference and phase shift of the radio waves occurs around a dam body.

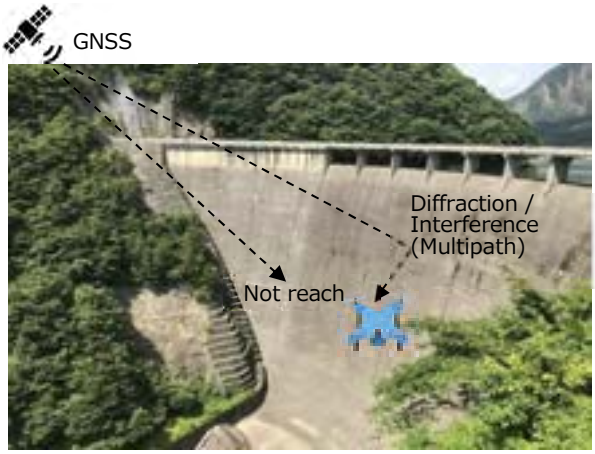

Figure 1. Depiction of the GNSS environment at the dam. The GNSS is likely to be unavailable or unreliable due to sky occlusion in mountainous areas and multipath around the large structures.

Therefore, the UAV needs to be manually controlled by a pilot, which increases the UAV operator workload and makes it difficult to: 1) Obtain high-resolution images with uniform quality for inspection and management, or 2) prevent human errors, such as lapses in capturing the image. Hence, the realization of autonomous UAV flight in a non-GNSS environment is required.

The remainder of this paper is organized as follows. Section 2 introduces the related works. Section 3 presents the proposed system applied to autonomous UAV flight at the dam in a non-GNSS environment. Section 4

validates the proposed system in a field study. Section 5 proposes the flight opportunity. Finally, the conclusions and future work are discussed in Section 6.

2 Related Works

There are three important technologies for obtaining clear and high-resolution images of uniform quality to inspect and manage the dam's body via a digital camera mounted on a UAV: the flight path planning method, self-localization for autonomous UAV navigation, and photogrammetry technology. An overview of each method is presented below, with an application of this research.

2.1 Flight Path Planning Method

A flight path is planned by successively creating way points (WPs) and arranging and connecting them continuously. The WPs contain the latitude, longitude, and altitude of the UAV and action information, such as the change in nose and flight speed direction at that time. There are three approaches for setting WPs: manual creation, simulation-based, and pilot flight trajectory.

2.1.1 Manual Creation Method

This method requires the pilots to manually and sequentially set all the WPs using the general autopilot software function.

However, it is difficult to accurately set the WPs near the reservoir on the upstream side of the dam body or in the complicated shape of the dam body and its surroundings as the terrain information available to pilots and software is only approximate.

2.1.2 Simulation-Based Method

If there is a three-dimensional point cloud data of the dam, it is possible and useful to accurately set the WPs to maintain a certain distance from the dam body surface via coordinate calculation.

However, many dams do not have three-dimensional point cloud data as they are time-consuming and costly. Therefore, an inexpensive, highly accurate flight path planning method for dams that do not have three-dimensional point cloud data is required.

2.1.3 Using Pilot Flight Trajectory Method

Some commercial autopilot software attached to general consumer UAVs, such as DJI, possess a function for recording the flight trajectory of the pilot [5], allowing for flight path planning. In addition, there is a method that collects and analyzes many pilot's flight paths and analytically plans a path from them [6].

There are many artificial errors in the flight trajectory via manual UAV operation as the position of the UAV does not work in a non-GNSS environment. In addition, the GNSS flight trajectory coordinate is noisy and inaccurate. Therefore, this low-precision GNSS flight trajectory coordinate is not suitable for inspecting flight paths. However, it is a useful method if the flight trajectory can be accurately measured, even in a non-GNSS environment.

2.2 Self-localization Technology for UAV Autonomous Navigation

For the UAV to automatically navigate along the flight path, it needs to estimate its flight position. The general basic structure of the UAV is shown in Figure 2. The autonomous navigation of a UAV can be classified according to the difference in the self-localization estimation method shown in Figure 2. An overview of each method is presented below.

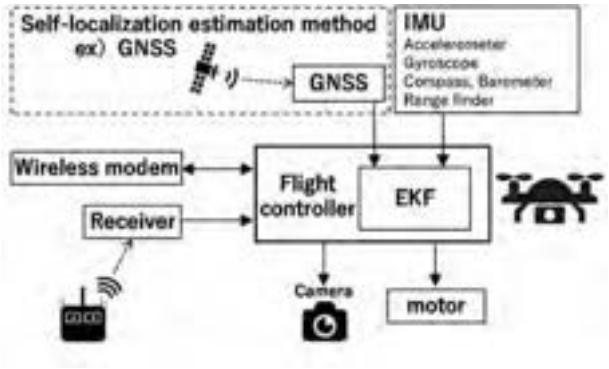

Figure 2. The general basic UAV structure

2.2.1 GNSS Navigation

GNSS positioning information is used as a self-localization estimation method and can be received by a small and inexpensive sensor mounted on the UAV. Therefore, this is the most popular method of autonomous UAV navigation using widespread communication technology.

However, as GNSSs cannot normally be received at a dam, this navigation system cannot be adopted. Even if GNSSs can be received normally, the positioning error is in the order of several meters or more, which is not suitable for inspection flights that require high accuracy.

2.2.2 SLAM Navigation

Simultaneous localization and mapping (SLAM) technology consists of front-end processing that focuses on sensor signal processing and back-end processing that focuses on optimizing the pose graph and performs simultaneous self-localization estimation of a moving body and constructs a three-dimensional spatial map. In addition, SLAM is approximately classified into visual SLAM and light detection and ranging (LiDAR) SLAM,

according to the front-end processing. As feature points, visual SLAM uses the color and light/dark information of each pixel of the camera or image sensor image, and LiDAR SLAM uses the point cloud coordinates measured by the laser sensor (distance sensor). In both SLAMs, the three-dimensional spatial map is recognized by matching the feature points, the movement is estimated sequentially, and the self-localization is estimated via accumulation.

Although this is a self-localization technique that does not depend on GNSS, some problems do exist:

- The position estimation errors accumulate and are not cleared; hence, the estimated position does not return to a true value.
- The self-position is lost if the feature point extraction fails.
- A high calculation cost for processing and optimization is required.
- The flight safety and image efficiency are reduced because the UAV flies close to the target object so as not to lose the feature points.

2.2.3 Total Station Navigation (TS Navigation)

The total station is a surveying instrument comprising a light wave rangefinder, which measures distance, and a theodolite, which measures angles. In this method, a prism is attached to the UAV; the prism's position is measured as the flight location via the total station. The UAV recognizes the self-location by feeding back the measurement result to the UAV. Originally, as a method of enabling autonomous flight even in a non-GNSS environment, this technology was predominantly developed for indoor flight using a consumer UAV [7].

We also attempted to apply it to autonomous UAV flight for dam body surface inspection. However, the flight control of the consumer UAV is a black box, and the fail-safe function cannot be completely canceled. Thus, the UAV did not fly autonomously owing to limited flight control and altitude.

It is a useful technique if flight control is possible as the position information accuracy is higher than that of other methods.

2.2.4 Cooperative Navigation

Two UAVs fly at the same time and communicate with each other. The first UAV flies where GNSS can be received normally, and the second UAV flies in a non-GNSS environment. The second UAV receives the position information estimated via the first UAV's optical tracking in real-time and can recognize the self-location by processing this information with low latency [8,9].

Advanced and complicated control technology for two UAVs is also required. Moreover, large-scale structures, such as dams, cannot be shot over the course of one flight as the flight time is limited by the battery. Thus, it is very difficult to maintain two UAVs simultaneously, and several operational issues exist.

2.2.5 Marker Recognition Navigation

The AR markers, or QR codes, placed on the flight route are successively read via the camera mounted on the UAV, and flight control can be enabled via recognition of the respective information on the marker; e.g., flight position, flight direction, travel, and distance.

Thus, this method enables autonomous flight, even in a non-GNSS environment; it is easy to prepare for indoor use, by placing a paper with a marker printed on the wall, but is difficult to install, manage, and maintain for outdoor use in large-scale infrastructure, such as a dam.

2.3 Photogrammetry technology

In recent years, the development of a scale-invariant feature transformation (SIFT) algorithm has automated the extraction and matching of image feature points and camera lens calibration. Therefore, it has become possible to easily reconstruct the three-dimensional model via SfM (structure from motion) and MVS (multi-view stereo).

As GNSSs cannot normally be received at the dam, it is not possible to add geotags to images captured using the digital camera mounted on the UAV. Therefore, three-dimensional reconstruction relies only on the feature points of the image. However, a problem is presented as the shape of the dam is distorted and approximate, even if the three-dimensional reconstruction model is corrected via GCPs (ground control points), as GCPs exist only in a limited flat space, such as the dam's top.

3 Proposed System Overview

This paper proposes a self-localization technique by using the total station applied to an autonomous UAV flight at a dam in a non-GNSS environment. In addition, UAV tracking by the total station is enabled to plan a highly accurate flight path for inspection and to add geotags to images. Therefore, it is possible to properly inspect and manage the entire dam body by analyzing the clear high-resolution images of uniform quality captured using a digital camera mounted on a UAV.

3.1 TS Navigation System Configuration

Figure 3 shows the proposed UAV autonomous navigation system at the dam using the total station. First, the coordinates of the installation position, the direction of the lens, and the vertical angle are set to the total station. Next, a prism is attached to the UAV, allowing flight position measurement by automatically tracking

the total station; the measurement result is sent to the UAV. Finally, the flight position is automatically adjusted while the error between the estimated position and the WPs is checked.

The equipment used in this system is shown in Table 1. The image of the prism attached to the UAV is shown in Figure 4.

Figure 3. Image of the proposed UAV navigation system using the total station.

Table 1. System specification

UAV	
Product name	QC730 produced by ENROUTE
Size [mm]	D1100×W1100×H310
Flight controller	Pix hawk
Sensor	Accelerometer (3 axes), Gyroscope (3 axes), Compass, Barometer, Light ware LW20
Total Station	
Product name	TOPCON GT-1005
Prism	Leica Geosystems GRZ101
Camera	
Product name	Sony α6300
Lens	SEL35F28Z
Recording pixels	6000×4000

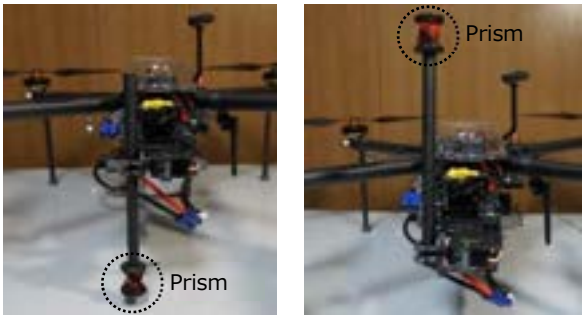

Figure 4. The image of the prism attached to the UAV. The prism is attached to the lower side of the UAV when tracking from below (left) and to the upper side of the UAV when tracking from above (right).

3.2 Flight Path Planning with Pilot Flight Trajectory

It is necessary to plan the flight path to confirm the resolution required by the AI analysis and to accurately set the WPs that are a certain distance away from the dam body surface, considering the performance of the digital camera.

In this study, if three-dimensional point cloud data of the dam exist, the flight path for inspection, which maintains a certain distance from the surface of the dam body, is planned by coordinate calculation. Conversely, if there is no three-dimensional point cloud data of the dam, the flight trajectory of the pilot's manual operation is used to plan an inexpensive, efficient, and highly accurate flight path. The UAV tracked at the total station uses the position information to control its attitude, even by manual operation in a non-GNSS environment, resulting in a stable flight path. This stable flight enables accurate flight path planning by using the self-position estimated by the UAV as the WPs while measuring the distance to the dam body surface with the range finder sensor mounted on the UAV.

3.3 Improved Accuracy of Photogrammetry Technology

In this study, geotags can be added to the image by measuring the flight position at which the image is taken and using the total station, which even tracks the UAV in a non-GNSS environment. Therefore, it is possible to accurately reconstruct a three-dimensional model using the captured image's geotags, as shown in Figure 5.

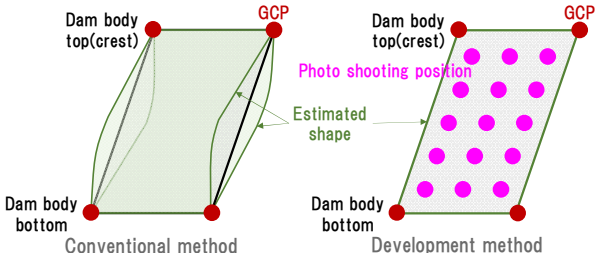

Figure 5. Improving the accuracy of the three-dimensional modeling

4 Field Study

In this paper, we implement a field study to demonstrate the utility of this proposed system for two types of concrete dams in Japan, as shown in Table 2. In a field study, uniform quality and high-resolution images of 2.0 mm/pixel are required for the dam body's inspection by AI analysis.

Table 2. Dam structure specifications

Classification ID	Dam-1	Dam-2
Dam type	Gravity	Arch
Dam height[m]	156.0	94.5
Dam top length[m]	375.0	215.0
Three-dimensional point cloud data	No-exist	Exist

4.1 Flight Path Planning

The flight path has to be planned approximately 18.0 m from the dam body's surface as per the AI analysis request. Since the horizontal flight exerts a lower battery load and involves more flight time than those of vertical flight, the flight path has to be essentially horizontal.

The flight path is planned by the pilot flight trajectory because there is no three-dimensional point cloud data at Dam-1 as shown in Table 2. Figure 6 shows the UAV flying and tracking by the total station at Dam-1. This flying UAV is manually operated while being tracked by the total station. Figure 7 shows an example of the WP results and the planned flight path using the manual flight trajectory of the UAV, via tracking using the total station; thus verifying that an accurate flight path can be created.

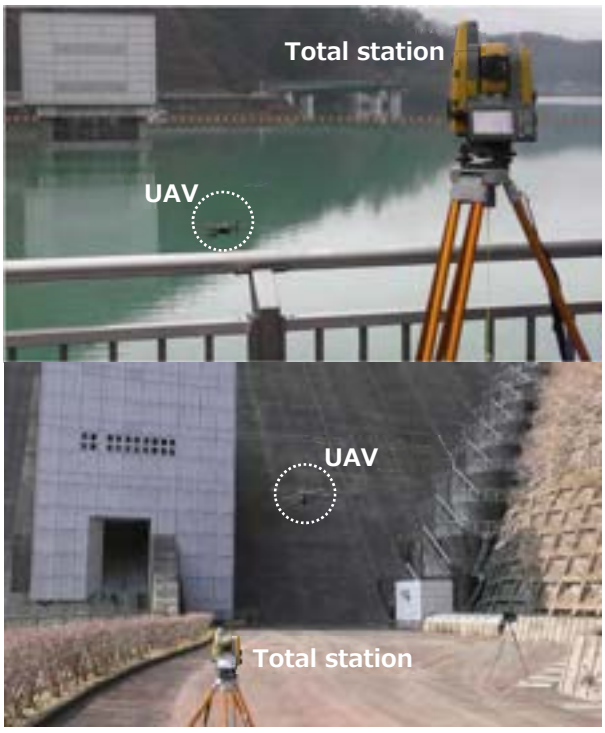

Figure 6. The flying UAV and tracking by the total station (Dam-1). The above image shows the tracking from above and the image below shows tracking from below.

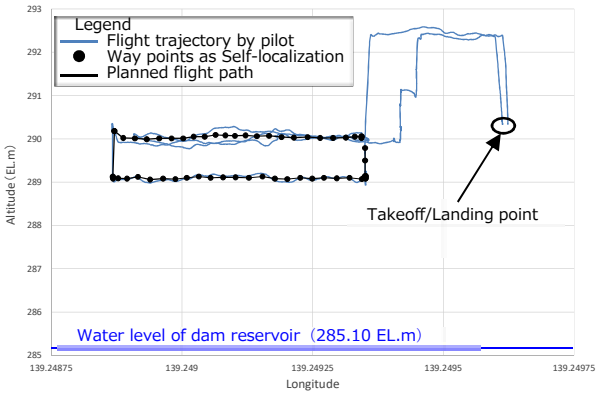

Figure 7. The WP results and the planned flight path using the manual flight trajectory (upstream side of the dam body at Dam-1). The blue line shows the manual flight trajectory of the UAV by tracking using the total station. The black marker indicates the self-estimated position as a WP and the black line shows the planned flight path for inspection.

4.2 Autonomous Flight Accuracy

Figure 9 shows a comparison of the WPs and flight trajectory for autonomous UAV flight. It can be verified that autonomous UAV flight is conducted with high accuracy, even if the vertical direction of the levee gradually thickens from top to bottom and has a complicated shape with horizontally curved lines.

In addition, the difference in distance between 228 WPs and autonomous flight coordinates is summarized in Figure 8. The maximum deviation distance was 0.90 m, the minimum was 0.03 m, and the median was 0.29 m; 90 % of the distance was covered within a deviation of 0.50 m. This flight accuracy is impossible with manual operation.

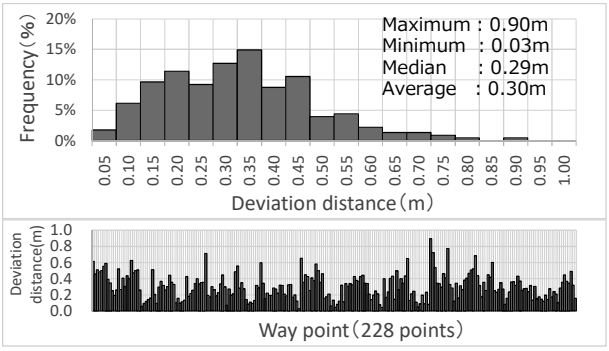

Figure 8. The distance difference frequency distribution between 228 waypoints and autonomous flight coordinates (Dam-2).

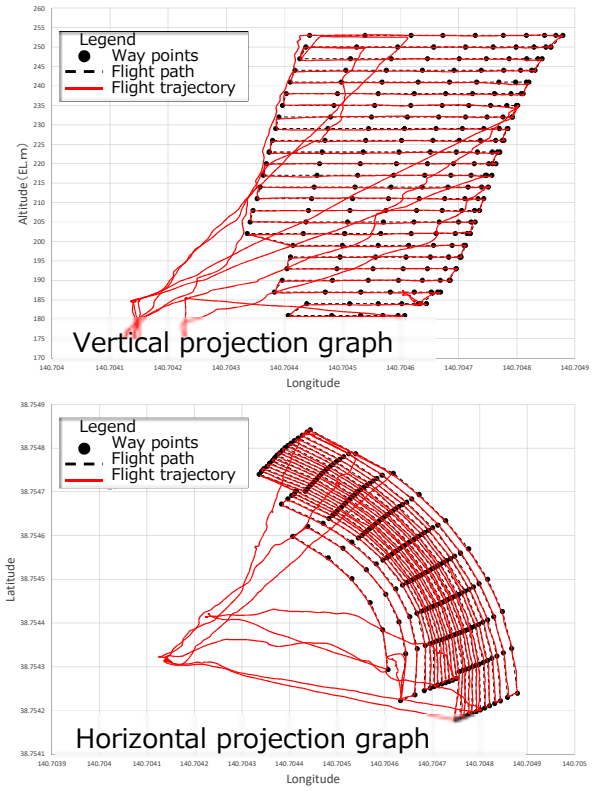

Figure 9. Comparison of WPs and flight trajectory for autonomous UAV flight (Dam-2). The black marker indicates the WPs. The black line shows the planned flight path for inspection. The red line shows the flight trajectory of the autonomous UAV flight.

4.3 Image Quality and Three-Dimensional Reconstruction Accuracy

Figure 10 shows an example of a dam body surface image taken via autonomous UAV flight. Although the absolute width and length could not be measured from the images obtained, it was possible to capture images with a resolution of approximately 1.75 mm/pixel as the vertical joint spacing of the dam is 2,000 mm.

In addition, a three-dimensional model is reconstructed using the SfM software Metashape, as shown in Figure 11. The difference between the three-dimensional point cloud data created by the two different flights was 0.255 mm in the horizontal direction and 0.203 m in the vertical direction; the shape of the dam body was not significantly distorted. As shown in Figure 12, it is confirmed that the use of geotags measured at the total station improved the photograph's alignment. Moreover, this stable and autonomous flight enabled the capture of clear and uniform images; furthermore, the feature point matching between the images taken from two different points is dense and good, as shown in Figure 13.

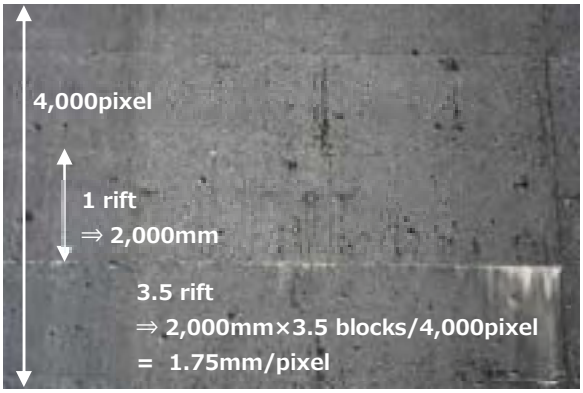

Figure 10. Accuracy verification of image (Dam-1)

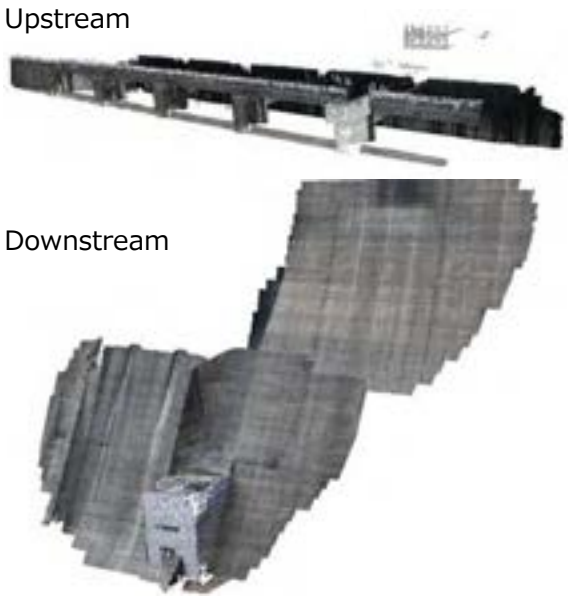

Figure 11. The result of the three-dimensional reconstruction model (Dam-2). The above image shows the view from upstream of the dam body. The image below shows the view from downstream of the dam body.

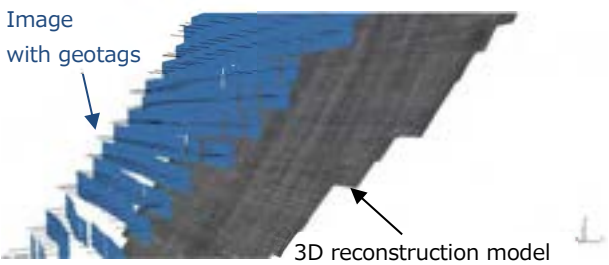

Figure 12. An example of the photograph's alignment (Dam-2).

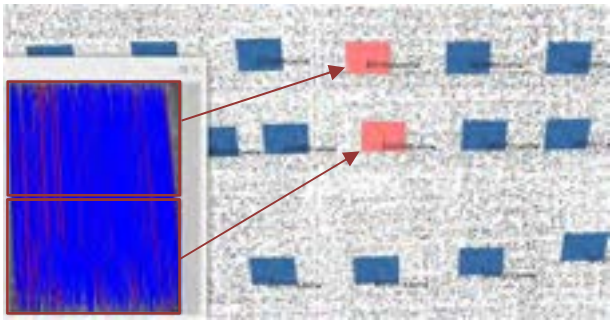

Figure 13. An example of feature point matching between images taken from two different points. The blue lines are a valid match. The red lines are an invalid match (Dam-2).

5 Proposed Flight Opportunity for Aging Detection Using AI Analysis

There are two methods for detecting dam surface aging via AI analysis: supervised and unsupervised learning.

Supervised learning is a method that enables AI to detect even unknown images by learning the teacher information with aging information annotations. Thus, this method is useful only if the observed aging target is obvious as only the annotated teacher information can be detected.

Conversely, unsupervised learning is a method in which AI learns the concept of a normal state and detects information when changes or abnormalities appear. As shown in Figure 14, it is possible to reconstruct a healthy image from a real damaged image and extract the damage from the difference.

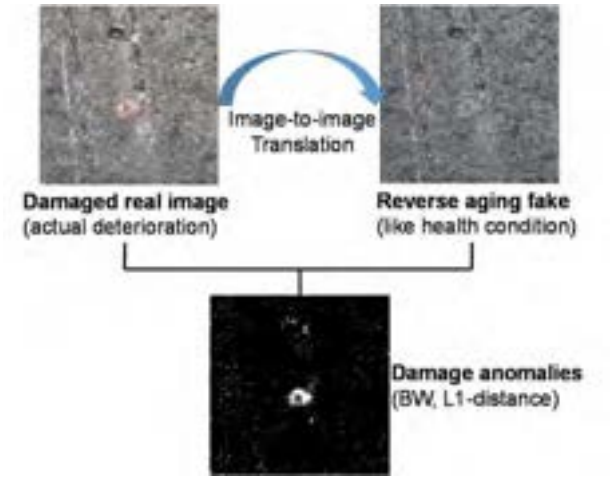

Figure 14. The unsupervised learning image (Dam-2)

There are few abnormal data points on the dam body and it is necessary to extract the various abnormal aging information from a wide range of dam bodies. Thus, unsupervised learning is suitable for the aging detection of dams. Therefore, it is necessary to accumulate images of the dam body during normal times, with uniform quality and accuracy. However, flight opportunities are limited because the dam inspection cycle is very long, i.e., once every few decades. Therefore, using the system proposed in this paper facilitates effective flight and imager accumulation.

6 Conclusion and Future Work

This paper proposes autonomous UAV flight using the dam's total station in non-GNSS environments. In addition, a flight path planning method based on the UAV's flight position, using a total station and geotags that can be added to the image by measuring the flight position at which the image is taken using the total station, which tracks the UAV, is proposed to obtain uniform quality and clear high-resolution images for inspection and management of the dam's body via a digital camera mounted on the UAV.

We implemented a field study and demonstrated the utility of the proposed approach. As a result, we could achieve a high flight accuracy, which is impossible via manual operation. Furthermore, we proposed flight opportunities for aging detection using AI analysis.

Future work is summarized as follows:

- Many field demonstrations will be conducted to verify its practicality.
- To sufficiently reduce the error in three-dimensional reconstruction accuracy, it is necessary to verify the accuracy by changing the lap ratio of the image and correcting it with GCP.
- It is necessary to accumulate images of the dam body surface during normal times.

References

[1] Cheng-Hsuan Yang, Ming-Chang Wen, Yi-Chu Chen, Shih-Chung Kang. An Optimized Unmanned Aerial System for Bridge Inspection. In *Proceedings of the 32nd ISARC*, pages 1–8, Oulu, Finland, 2015.

[2] Manh Duong Phung, Van Truong Hoang, Tran Hiep Dinh, Quang Ha. Automatic Crack Detection in Built Infrastructure Using Unmanned Aerial Vehicles. In *Proceedings of the 34rd ISARC*, pages 823–829, Taipei, Taiwan, 2017.

[3] Henk Freimuth, Jan Müller, Markus König. Simulating and Executing UAV-Assisted Inspections on Construction Sites. In *Proceedings of the 34rd ISARC*, pages 647–654, Taipei, Taiwan,

2017.

[4] Takato Yasuno, Junichiro Fujii, Masazumi Amakata. Pop-outs Segmentation for Concrete Prognosis Indices using UAV Monitoring and Dense Dilated Convolutions, In *Proceedings of 12th International Workshop on Structure Health Monitering*, pages 3175, California, USA, 2019.

[5] DJI. DJI GS PRO. On-line: https://www.dji.com/jp/ground-station-pro, Accessed: 15/6/2020.

[6] Jeonghoon Kwak and Yunsick Sung. Autonomous UAV Flight Control for GPS-Based Navigation. *IEEE Access*, 6:37947–37955, 2018.

[7] jitsuta. Drone navigation system (TS drone). On-line: https://www.jitsuta.co.jp/pickup/drone, Accessed: 15/6/2020.

[8] Alexis Stoven-Dubois, Laurent Jospin, Davide A. Cucci. Cooperative Navigation for an UAV Tandem in GNSS Denied Environments. In *Proceedings of 31st International Technical Meeting of the Satellite Division of the Institute of Navigation*, pages 2334–2339, Florida, USA, 2018.

[9] Cledat, E. and Cucci, D.A. Mapping GNSS Restricted Environments with a Drone Tandem and Indirect Position Control. *ISPRS Annals of the Photogrammetry, Remote Sensing and Spatial Information Sciences*, IV-2/W3:1–7, 2017.

Depth-Camera-Based In-line Evaluation of Surface Geometry and Material Classification For Robotic Spraying

V. Frangez, D. Salido-Monzú, and A. Wieser

Institute of Geodesy and Photogrammetry (IGP), ETH Zürich, Switzerland

valens.frangez@geod.baug.ethz.ch, david.salido@geod.baug.ethz.ch, andreas.wieser@geod.baug.ethz.ch

Abstract -

This paper presents a feasibility study of surface geometry (SG) evaluation and material classification (MC) for robotic spraying. We propose two complementary approaches using point clouds and intensity data provided by a state-of-the-art industrial time-of-flight (ToF) depth camera. The SG evaluation is based on geometric feature computation within local neighbourhoods, which are then used within a supervised classification. The results of this approach are SG classes according to the level of geometric variability of the surface, displayed as SG maps. For MC, active reflectance estimation is investigated and exploited to derive features related to the reflectance and diffusive properties of each material for classification. The result of both approaches can be prospectively used as feedback in digital fabrication for in-line adaptation of the process to improve control of relevant geometrical and material properties.

Keywords -

Surface Geometry; Material Classification; Digital Fabrication; Depth Camera; Machine Learning

1 Introduction

Assuring the required geometric quality of digitally fabricated structures is of high importance not only after but also during the construction process. Recent rapid growth of interest in robotically assisted construction [1] has also boosted the use of sensing technologies to acquire process-relevant information. These works showcased the potential of various sensors in digital fabrication processes and demonstrated ways in which accurately measured 3D information and object parameters extracted from such information can be used for in-line process improvement via feedback control [2, 3]. In order to extract the relevant information for construction processes, appropriate processing algorithms and interpretation of the 3D data need to be employed.

In this contribution we focus on the concept development and feasibility study of algorithms for surface geometry (SG) evaluation and material classification (MC) for robotic spraying applications. The goal is to address the possibility of replacing the manual and subjective SG evaluation and MC processes, currently relying on experts, with novel sensing technology and data analysis. A state-of-the-art industrial depth camera was chosen for data acquisition within this investigation. This sensor technology offers a good trade-off between in-line process acquisition capacity, sufficiently high accuracy and resolution, and areal coverage on the object of interest. It provides not only geometric information of the acquired scene in the form of 3D point clouds (PCs), but also the underlying raw data related to the measured distances and intensities. These data types have potential for extracting various relevant parameters of the observed object by employing a single sensor solution.

SG of structures produced with spraying is important not only for visual and design considerations, but also from a structural viewpoint. The acquired PC data follows the SG of the captured object and implicitly contains its geometric properties. To exploit these geometric properties, i.e. features, it is necessary to carry out a 3D analysis within local neighbourhoods. To achieve this, a processing scheme of four main steps is proposed in this paper: (i) separation of the acquired SG to spatial frequency components, (ii) neighbourhood selection, (iii) feature computation, and (iv) supervised classification. The outcome of this approach are geometry classes according to the level of geometric variability of the surface for different spatial frequencies, displayed as SG maps.

Obtaining adequate information of the early hydration state or local coverage and volume of each sprayed material (e.g. concrete, plaster finish, or paint) requires classifying the materials within the observed scene. This is critical for closed-loop control of the spraying process, such that complete coverage of the surface per material can be ensured. In this context we explore MC exploiting the observations provided by a time-of-flight (ToF) depth camera related to material-specific reflectance properties. The observed differences on repeatable features for the materials used in this initial investigation (i.e. wood, cardboard, metal, and plastic) are then used for developing a simple classifier based on a k-nearest neighbour (kNN) algorithm.

The contributions of this study are twofold. On the one hand, the SG evaluation algorithm can be used within the geometric feedback system of the fabrication in order to

adapt the process accordingly. Chosen SG class ought to be considered as a goal SG, while others indicate areas that need further surface treatment, i.e. either adding additional geometry variation or applying more material to smooth out the dominant SG features. On the other hand, the MC approach can be used within a process of early concrete hydration by distinguishing different states of the concrete and their associated reflectances to automatically regulate the time-window between consecutively sprayed layers.

To introduce this study, a brief overview of the working principle of ToF depth cameras and a basic performance assessment of the one used within this work is given in Section 2. The specific SG evaluation (Section 3) and MC (Section 4) approach is then detailed, including an overview of processing steps, used experimental setups, and datasets. The results of the two discussed concepts are then given and interpreted in Section 5, and the general conclusion and outlook of the investigation are summarized in Section 6.

2 ToF camera

2.1 Measurement Principle

Depth cameras produce 2D depth images of a scene relying on various measurement principles, such as stereo triangulation, structured light, or ToF approaches [4]. With the increase in sensor resolution, the latter have gained attention in recent years for being able to operate over larger ranges with accuracy levels more independent of the scene geometry and background illumination. The most established technique to implement ToF cameras is based on measuring the accumulated phase of an intensity modulated optical signal illuminating the scene and detected independently on each pixel. The illumination is typically produced by one or several near-infrared LEDs driven by a radio-frequency (RF) carrier. The detected signal on each pixel, associated to the illumination signal back-reflected on the corresponding patch of the scene, is demodulated at device level by a dedicated 2D array that computes the correlation of the received signal with an internal reference derived directly from the driver of the emitted modulation. Simplifying the modulation to one sinusoidal component, this correlation $c(\tau)$ can be written as

$$c(\tau) = a \cdot \cos(\tau + \phi) + b, \tag{1}$$

where τ is the correlation lag, a the optical intensity at the modulation frequency, ϕ the phase shift proportional to the propagation delay—and therefore to the range of interest—and b the illumination bias. This correlation is typically computed for four lags regularly spaced with $\frac{\pi}{2}$ rad, so that the obtained correlation samples A_i are

$$A_i = c\left(i \cdot \frac{\pi}{2}\right), \quad \text{with } i = 0, \cdots, 3. \tag{2}$$

The distance-dependent phase can be directly calculated from this correlation samples as

$$\phi = \arctan\left(\frac{A_3 - A_1}{A_0 - A_2}\right) \tag{3}$$

which, considering a sufficiently well-known value of the modulation frequency f_m and assuming a sufficiently accurate approximation for the propagation speed c of the optical signal under typical operation meteorological conditions, can be used to estimate the distance of interest for the given pixel as

$$\hat{d} = \frac{c}{4\pi f_m}(\phi - \phi_0) \tag{4}$$

where ϕ_0 accounts for the systematic delay offset in the correlation process with respect to the mechanical zero of the camera, which should be compensated by calibration. As any phase-based measurement system, these observations are ambiguous beyond one modulation wavelength. This ambiguity is practically solved by performing quasi-simultaneous measurements at several f_m and combining them to resolve a larger unambiguous range. Once computed for each pixel of the depth image, the estimated distances can be used to generate a 3D PC by means of perspective projection [5].

In addition to the accumulated phase, the optical intensity a can also be computed from the correlation samples as

$$a = \frac{1}{2}\sqrt{(A_3 - A_1)^2 + (A_0 - A_2)^2}, \tag{5}$$

being typically used to augment the generated PCs with intensity values. These intensities are proportional to the amplitude of the detected modulated signal, hence independent of the ambient illumination. Given a sufficiently stable illumination and detection efficiency, the measured intensities can be processed considering the spatial distribution of the illumination signal and radiometric attenuation with distance and viewing angle, what enables deriving observations proportional to the material reflectance independently on its position on the scene. By including a prior calibration of scale using a known reflectance standard, these compensated intensities can be in turn extended to absolute reflectance estimations for each point on the scene. Note that such estimations would correspond to the reflectance of the illuminated patch of surface associated to each pixel at the specific angle of incidence (AOI) defined by its relative orientation with respect to the camera.

2.2 Performance Evaluation

An evaluation of the performance using a state-of-the-art ToF camera Helios Lucid [6], has been carried out. The

camera operates based on the measurement principle described in Section 2.1, and its most relevant specifications are given in 2.2. This camera provides both raw correlation samples as directly computed on each pixel according to (2), and on-device pre-processed PC data after averaging multiple frames, correcting of systematic errors, and spatial data smoothing to reduce noise. The ToF sensor used in the camera allows users to access raw data for four modulation frequencies f_M (25 MHz, 50 MHz, 75 MHz, and 100 MHz), however for the processed PC dataset, only 75 MHz and 100 MHz are employed as indicated in Table 2.2.

Table 1. Selected relevant properties of Helios Lucid depth camera, see [6] for more.

Property	Value
Resolution	640 pix x 480 pix
FoV	59° x 45°
Mode	1.5 m (75 MHz and 100 MHz) 6 m (100 MHz)
Precision	<1.6 mm @ 1 m
Accuracy	± 5 mm (1.5 m mode) ± 10 mm (6 m mode)
Illumination	850 nm (VCSEL laser diodes)

Practical limitations on the achievable accuracy of ToF depth cameras are mainly related to sources of variability for the systematic deviations, such as changes of the operating conditions, namely environment temperature, or multipath effects on the scene [5]. Performance assessment procedures of commercial depth cameras primarily addressing those limitations are presented in [7, 4]. Some of these error sources can be mitigated to a large degree by calibration and others further reduced by a careful design of the acquisition conditions and geometry when allowed by the application. Additionally, depth precision is dominated by the signal quality at the sensor level, proportional to the detected optical power and therefore defined mostly by the distance and relative orientation between the sensor and the scene patch, and the reflectance properties of the latter. Precision can only be improved under certain acquisition conditions at the expense of dynamic performance for the given application, by averaging over several measurements of an unchanged scene.

Before using our camera for the data acquisition of our proposed application, We have performed a basic performance assessment to gain a better understanding of the expected data quality and practical limitations. This assessment has specifically addressed stability and noise figure, warm-up effect, and intensity-related depth errors.

The stability and noise characteristics of the raw data were evaluated by computing the Allan deviation of the phases calculated according to (3). This computation was based on a time-series of 8000 samples acquired over two hours on a static scene composed of a flat white plane at a distance of about 1 m using the 1.5 m operating mode. Phase stability was analysed for each of the f_M, using values for a single pixel and is shown in Figure 1. The results indicate a high long term stability on the evaluated time scale without significant low-frequency drifts. A linear fit based on the Allan deviation yields a slope very close to -1, indicating that the noise background is mostly uncorrelated and flat over the evaluated bandwidth—the expected improve by averaging over several acquisitions is therefore approximately proportional to the square root of the number of acquisitions. Computing the distance corresponding to each phase according to 4, the measured precision (2σ) for a single acquisition on each frequency on the evaluated conditions are 5.5 mm (25 MHz), 3.3 mm (50 MHz), 2.9 mm (75 MHz) and 2.3 mm (100 MHz). Precision is expected to increase proportionally to the modulation frequency due to the reduction of distance sensitivity to phase errors. This increase is, however, partly limited by a slight reduction of detected power on faster modulations more attenuated by the sensor bandwidth.

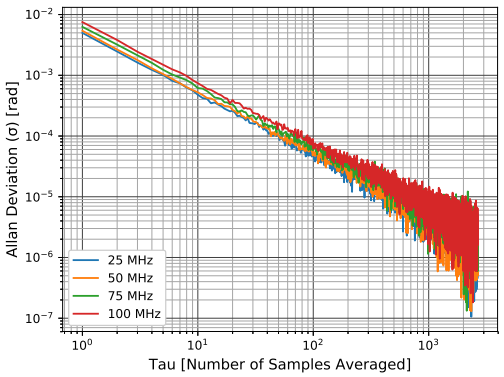

Figure 1. Allan deviation of phase observations for each f_M, using a sample of 8000 measurements for a single pixel.

The internal warm-up of the camera and its impact on accuracy due to temperature-dependent scale errors was evaluated to determine empirically the required warm-up time until reaching optimal performance. Static measurements under similar conditions as described above for precision were carried out acquiring PCs on a flat white plane. This process was initiated immediately after the device was turned on and carried out over three hours with measurements triggered every 20 s. Each PC was used to fit a plane, based on which the maximum and average deviations between the points and the fitted plane were

computed. To reduce the impact of outliers in the analysis, the maximum deviations were computed as the median of the largest 20 deviations. Initial maximum and average deviations were 14 mm and 6 mm, respectively. The results indicate the camera performance stabilizes at about 45 minutes after the camera was turned on, i.e. when the internal camera temperature reaches 36°C. The maximum and average deviations then drop and remain constant at 8 mm and 2 mm, respectively.

The evaluation of intensity-related depth errors due to the spatial inhomogeneity of the illumination pattern were assessed by acquiring PCs using the 6 m operating mode on a white flat surface at distances between 30 cm and 120 cm on 10 cm steps. Deviations to a plane fitted to each PC were computed for each distance. The deviations were grouped in three categories: deviations up to 2 mm, deviations from 2 mm to 4 mm, and deviations larger than 4 mm. These values were chosen to approximate the empirically computed precision discussed in the previous section and its double. The results can be seen in the Figure 2 (left). The figure also shows the area covered by the camera at selected distances. An oscillation patter can be seen within the deviation groups. This pattern agrees with oscillations observed in the distances computed using the raw phase data at 100 MHz (not shown), which suggest a residual uncalibrated cyclic error. Based on the obtained results, it is advised to acquire data at either 40 cm or 80 cm, where the deviations are minimum. Figure 2 (right) shows PCs colored according to the previously defined deviation categories. The most and least optimal PCs were chosen for this representation, being 40 cm and 60 cm respectively. The observed errors could be further mitigated by applying an online compensation taking into account the measured intensity and distance. As a simple approach for the data acquisition during the presented investigation, we have designed our experiment setup geometry and correspondingly cropped the acquired data to exclude the areas with highest deviations.

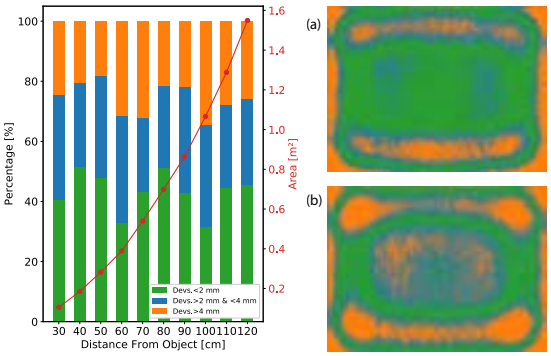

Figure 2. Deviations grouped in three categories, displayed in proportions. Red line represents the area covered by the camera as a function of distance (left). PCs acquired at 40 cm (a) and 60 cm (b) colored according to deviation category (right).

3 Surface Geometry Evaluation

SG captured within the PC can be exploited by local geometric feature analysis. A proposed scheme of assigning points a class of geometry according to the power of change is depicted in Figure 3. The input point cloud is first pre-processed. Then the data is partitioned to three spatial frequency components, and based on a selected neighbourhood, features are computed for each point within the dataset. Next a supervised classification is carried out, outputting the classes for each point which are then spatially filtered. The outcome of this six step processing are SG classes displayed as SG maps.

In general, the presented approach relies on the input data used for model training in the classification step. The observed geometry in the investigated samples is not referenced to a certain absolute definition, but grouped together according to distinctive SG variations.

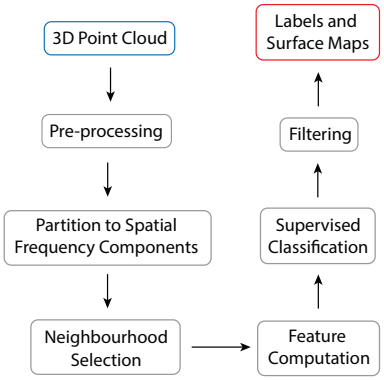

Figure 3. Proposed processing pipeline for SG evaluation.

For the purpose of concept development and evaluation, concrete samples of various geometries were produced using mould casting. Six out of seven sample geometries are shown in Figure 4. These types of geometry were chosen such that they resemble the sprayed surface, since the actual sprayed surface samples were not yet available for this investigation. The chosen dataset is however not completely representative of the sprayed surface and as mentioned, changing the input dataset would lead to different class definitions. Variations in height components (based on Reckli GmBh specifications) are from 11 mm up to 60 mm, therefore covering a wide range of geometric diversity.

The first step after acquiring the data is to pre-process it, which includes two operations: data detrending and crop-

ping. The first operation removes the global linear trend from the whole PC using principal component analysis and reorients it according to the first and second greatest variance of the coordinates. The measured surface might be oriented and at certain angle with respect to the camera, leading to wrong assumptions about a certain geometry. The second operation is to crop the PC and to keep only the central part, which is less affected by intensity related errors compared to the edge parts and therefore displaying higher accuracy (see Section 2.2).

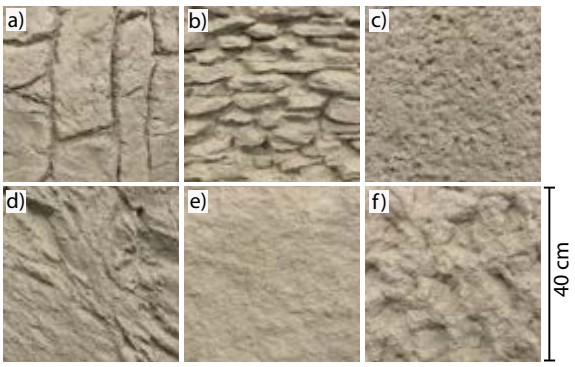

Figure 4. Concrete samples used within the SG evaluation investigation.

3.1 Partition to Spatial Frequency Components

A systematic approach for SG evaluation is adopted based on an existing method for inspection in surface metrology [8], which separates the surface into form, waviness, and roughness components. Typical values for these three components are within a range from microns to a few mm. We have adapted this concept within our SG evaluation and made it representative of the level of geometric variations present in our samples that is both relevant for digital fabrication and observable with the proposed technology, covering a range from a few mm to several cm. We established relative terms, which cover the complete geometric range of the used sample data, namely low- (LSFG), medium- (MSFG), and high-spatial frequency geometry (HSFG).

Two approaches of partitioning the SG to components were employed, making use of either discreet Fourier (FT) or discreet wavelet transform (WT). Since the PC structure is a grid, the transformation can be directly applied to columns and rows of the dataset without any need for interpolation of points. A spatial profile is treated as a time series signal where, instead of time, X- or Y-coordinates are used for rows and columns, respectively. In the first approach, the frequency threshold values between the components of the spectrum were determined empirically based on the observed spectrum in the frequency domain after using the FT. Then Butterworth low-, band-, and high-pass filters were used to partition the signal into three components. An empirically optimized order of the filter was used, which led to more optimal results. In the second approach, using the WT, a selection of a wavelet family and a decomposition level had to be made. Coiflet wavelets and level 5 were empirically selected, since they showed the most optimal results, after trying out different parameter options. The first parameter defines the signal that will be used to convolute the spatial profile, while the second sets the number of levels (i.e. components) that the signal gets partitioned to. In our case LSFG corresponds to level 1, MSFG to levels 2 and 3, and HSFG to levels 4 and 5.

The results of the two approaches applied to a randomly selected spatial profile from surface sample c) are shown in Figure 5. The tree SG components, the original SG, and the reassembled SG are shown. It can be noticed that the results based on the FT approach cannot be reassembled to the original SG profile, while this is successfully achieved for the WT. This confirms that Wavelets perform better on natural signals, i.e. non-stationary signals, as demonstrated in [9]. The FT approach using Butterworth filters does not, on the other hand, perform well on sharp changes in the signal and it tends to smooth over those features.

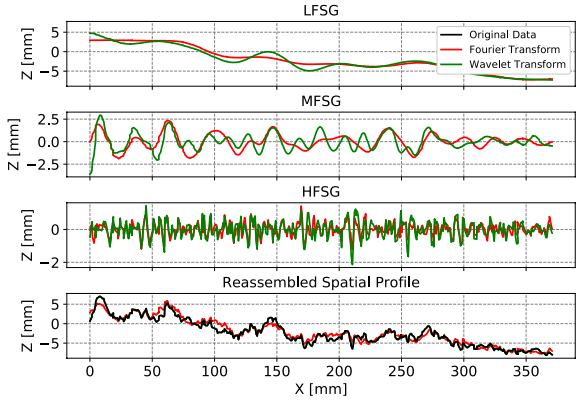

Figure 5. Profiles for each of the three surface components for surface sample c).

The whole PC can be partitioned to components, once this approach is applied to the complete dataset, i.e. all rows and columns. Both approaches are used in this processing, namely WT for partitioning to SG components (see example in Figure 7), and FT for generation of spectrograms. Spectrograms are a visual representation of the spectrum of frequencies of the signal in the time domain, however here shown for spatial domain. A visualization for surface sample b) is shown in Figure 6. The visible information in the spectrograms differs for the dataset ob-

tained from geometries as shown in Figure 4. It can serve to provide additional information of the spatial frequency content of the surface to the user.

The intensity image is obtained by using the same WT approach partitioned to a high- (HFI) and low-frequency intensity (LFI). The LFI component is dominated by the contribution of the camera illumination pattern and is discarded from further analysis. The HFI component, on the other hand, is influenced by small scale features in the observed surface, and can be therefore used to extract small scale features.

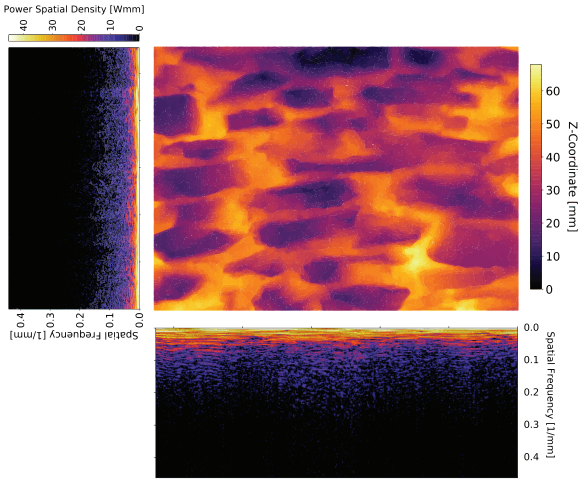

Figure 6. Spectrograms generated for surface sample b) in direction of columns and rows.

Only WT results were used in the end for this investigation, since the results were more optimal compared to the FT. The FT and its results were only used for generation of the SG spectrograms.

3.2 Geometric and Intensity Feature Computation

Each surface component dataset is used for extraction of local geometric features, with features being different for each of the three components. The selected features were handpicked in order to capture the information within the SG components as good as possible. The selection is shown in Figure 7. More information on geometric features that were taken as a starting point in this investigation and on their properties can be found in [10].

The computation of features is carried out for each point within the dataset, using its neighbourhood. Within the implemented algorithm, points are included within a certain neighbourhood based on either the list of indices of the kNN of the anchor point or a query of all points with distances to the anchor point smaller than a given radius. The results shown in this paper were produced based on a chosen radius, being 7 cm, 3 cm, and 1 cm, for LSFG, MSFG, and HSFG, respectively. This makes the classification results independent on the distance from which the acquisition was done.

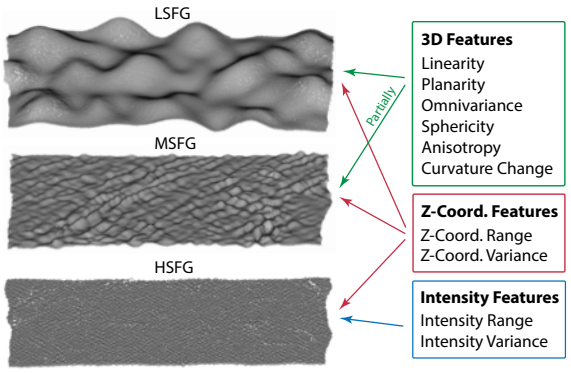

Figure 7. Three SG components (left). A list of features used for computation (right).

The intensity features play a relevant role when analyzing the HSFG component. The goal is to exploit small scale (i.e. sub-mm) features that cannot be captured by the geometry of the PC, due to the accuracy limitation of the used technology. However, the input intensity images of highly reflecting and absorbing local areas could cause intensity variations, in this case the intensity variations would not be related to the geometric but rather to radiometric features.

3.3 Supervised Classification

Once the features for all points are computed, they are normalized per feature to a range of [0, 1], such that none of the feature values dominate on the further processing. Those values are then used within a process of clustering to form groups of points that share similar geometric properties. For this purpose, an agglomerative hierarchical clustering approach was chosen. The algorithm requires a user specified number of clusters. This can be chosen based on a dendrogram, a tree diagram that displays an arrangement of clusters and the similarity between them. The number of clusters was selected as 3 for all components. Only a random subset of about 10% of points with their features was used for model training. It is assumed that the sub-set is sufficiently representative for the whole dataset, which was validated by the result repeatability after selecting different random subsets. The rest of the points is used later on for the evaluation of the model.

Next, the segmentation approach is extended to supervised classification using kNN. The algorithm learns the relationship between the feature value list of each point and assigned cluster indices. The number of clusters from the clustering process and the classification process is there-

fore the same. This classifier can then be applied to another dataset, to predict the closest class label using kNN.

To derive labeling of points with higher spatial regularity, a median filter is applied to the initial class label image. This results into smooth labels and surface maps. Additionally, it is possible to omit patches of areas smaller than the chosen threshold to decrease granularity, however this is not implemented in the proposed approach.

Furthermore, an assessment of each of the features was carried out to understand which have the highest impact on the label outcome. For this the analysis of variance (ANOVA) statistical test was employed, usually used within similar classification tasks. Based on the features and assigned labels, ANOVA assesses how much a class label is dependent on each particular feature and assigns each feature a score of relevance. It then ranks the features based on the calculated score. The most important features were intensity range and Z-coordinate range for HSFG and MSFG, respectively. For LSFG the most important features were change of curvature, omnivariance, and sphericity. The results of the labeling are shown in Section 5.1.

The process of feature computation and classification is computationally intensive, since a set of feature values has to be computed for each point. This makes it unsuitable for a quasi-real-time application. However, this can be overcome by computing features for a subset of points, e.g. every 10th point, classifying them, and then using interpolation of classes on the rest of the points to produce fully classified maps.

4 Material Classification

We have investigated the MC potential of ToF cameras in the context of our targeted applications by developing a MC strategy exploiting active reflectance estimations derived from the raw correlation data. The goal is to propose a processing pipeline to derive information of the reflectance and diffusiveness of the materials in the scene and use it for in-line classification, and to provide a simple demonstration of the feasibility of such approach.

4.1 Experiments and Datasets

An experimental setup for material-related data acquisition was designed making use of the horizontal comparator bench on our calibration laboratory. The ToF camera was mounted on a steel pole in front of the bench and the material samples were placed on a motorized trolley that moves automatically between selected positions measured with a linear Doppler interferometer. This allowed for accurate control of the relative distance changes between samples and camera, which were extended to absolute distances by independently measuring the distance between the camera and the sample at the starting position of the trolley using a laser tracker.

Two experiments were carried out on the described setup using four material samples, namely wood, plastic, metal, and cardboard, chosen arbitrarily as a simple subset of common materials. In the first experiment, each of the four material samples was placed on the trolley and displaced from 0.57 m to 1.6 m on steps of 3 cm. The scene on each position was acquired 10 times sequentially to enable an approximate quantification of measurement dispersion. The complete procedure was repeated for three orientations of the samples (5°, 25°, and 35°) by controlling the orientation with a highly repeatable rotation stage. The values for the distance range and sample orientations were selected to cover the expected working regions of the camera for the envisioned applications, providing sufficient resolution while keeping the effort for the experiments low. In the second experiment, all four material samples were placed on the trolley. The scene containing all materials was then captured for distances between 0.57 m and 1.07 m on steps of 0.1 m, repeating the process for the three aforementioned orientations.

4.2 Active reflectance estimation

Our proposal for reflectance-based MC relies on distinguishing materials based on their reflectance pattern. This approach is based on the estimation of a simple model of the material absolute reflectance as a function of AOI, obtained from calibrated intensity observations of the same surface patch from different points of view. The features extracted from such estimation can potentially provide differentiation for a large number of materials as long as they do not showcase both similar absolute reflectance and diffusive behaviour.

Defining in the simplest case a two-parameter reflectance model R as a generalized Lambertian scatterer

$$R\,(\mathrm{AOI}) = R_0 \cdot \cos^n(\mathrm{AOI}), \tag{6}$$

where R_0 is the material absolute reflectance on normal incidence and n defines the patter directivity; materials can be characterized based on their features R_0 and n. These are obtained from a minimum but sufficient number of two observations of the same surface patch from different perspectives, each observation providing estimations of both the absolute reflectance and the AOI. The AOI can be estimated from the depth map by analyzing the local region of the pixel of interest. The absolute reflectance, on the other hand, can be derived from the intensities calculated from the correlation raw data by applying adequate distance and instrumental corrections. The intensity a measured at pixel px for certain distance d, considering the dominant sources of variability, can be modeled as

$$a\,(d, px) = K_{ill}\,(d, px) \cdot K_{det}\,(px) \cdot G\,(d) \cdot R\,(\mathrm{AOI}), \tag{7}$$

where K_{ill} accounts for the spatial distribution of the illumination signal, K_{det} represents the detection efficiency of the corresponding pixel, and $G(d)$ the overall radiometric attenuation of detected power with distance. These three components can be compensated online using fitted functions or lookup tables obtained by a single calibration process based on acquisitions of a known geometry (e.g. a planar target) with homogeneous reflectance properties over several distances within the range of interest. By additionally including measurements on a material with known reflectance such as a calibrated reflectance standard, the overall scale of the amplitudes can be corrected. The final compensated amplitude provides an estimation of the material reflectance $\hat{R}$ of the surface patch covered by each pixel independently of distance and viewing angle from the camera, thus enabling the generation of absolute reflectance images. Combining these images with the estimated AOI per pixel for pairs of acquisitions allows deriving and mapping the reflectance features R_0 and n for any part of the surface covered on both acquisitions. These features can be then used to classify the materials in the scene by direct comparison with a pre-collected material database.

We have used the data from the two experiments described in Section 4.1 to provide a simple validation of this approach. The correlation data from the first experiment was used to compute the optical intensities per modulation wavelength according to (5). Figure 8 shows an extract of the computed intensities as a function of the interferometric reference distance across all the evaluated materials for the fastest modulation wavelength, with solid lines representing the average of 10 acquisitions per position while shaded areas correspond to the dispersion of those acquisitions in $\pm 1\ \sigma$. These results are good representatives of the overall behaviour of the other three f_M. The analysis of the intensity values indicates unreliable intensity observations due to saturation for some materials at close range. This is specially critical on the metal sample that showcases much higher specular reflectance. This makes the received intensity very high for the 5° orientation, which saturates the sensor for any distance smaller than approximately 1.1 m as confirmed by inspection of the underlying correlation samples. Conversely, the more specular behaviour produces very low intensities for the AOIs on the 25° and 35° orientations. The data derived from saturated observations was excluded from subsequent analyses.

The intensities obtained in the first experiment have been used to generate reference data for the classification. To avoid the need of introducing a reflectance standard, the classification is carried out using relative reflectance values normalized to the average amplitude of wood at 5°. The computed relative reflectances are depicted in Figure 9 for the three evaluated AOIs, where solid and shaded areas represent the average and standard deviation ($\pm 1\ \sigma$) between all wavelengths. The results show that, excluding the regions when the sensor is close to saturation due to high material reflectance and short range, the computed values per material are consistent within a 10% of variability independently from distance. This indicates that features derived from these values hold potential to provide robust classification of the evaluated materials.

Figure 8. Measured intensity at 100 MHz as a function of reference distance for all materials and AOIs.

Figure 9. Normalized intensities at all f_M as a function of reference distance for all materials and AOIs.

The relative reflectances per AOI computed for each material, f_M, and distance have been used to estimate the two parameters R_0 and n of the simple reflectance model in (6), which are to be used as reference features for the classification. Figure 10 shows the resulting features for all frequencies and distances with their associated material class. As seen in the figure, the computed features provide good separability for the evaluated materials.

The data from the first experiment has been additionally used to derive the distance correction $G(d)$, and an additional independent experiment on a planar target at several distances has been used to compute the illumination distribution $K_{ill}(d, px)$. These corrections are used on a scene containing all materials from the second experiment to test

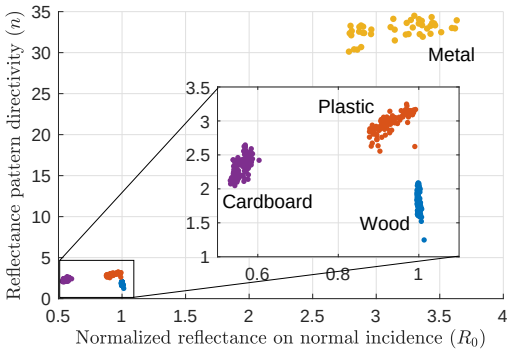

Figure 10. Normalized reflectance features extracted for four materials for all frequencies and distances.

the MC performance against the reference data. The intermediate steps for these corrections and the classification results are shown and discussed next in Section 5.2.

5 Results

5.1 Surface Geometry

The results of the SG evaluation are maps colored according to the assigned classes. Each class signifies the level of geometric variability for each of the spatial frequency components LSFG, MSFG, and HSFG (Figure 11).

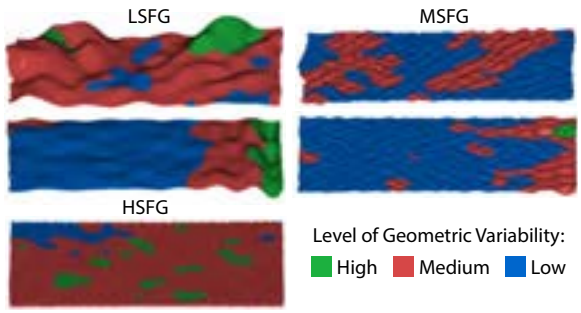

Figure 11. Resulting classified SG map for LSFG, MSFG, and HSFG components.

The results indicate that the proposed evaluation approach works well, with clearly classifying the most similar geometric parts of the datasets in the same class. The differences between classes are obvious and very distinctive. The level of in-class variation is directly related to how many classes were chosen in the classification step. For the given dataset this value has been optimized, to allow only for minor variations within the classes. The selection of the number of the classes should thus be a data driven decision. Due to the unavailability of ground truth data, a plausibility check of the obtained results was done based on subjective evaluation. This resembles standard practice, where SG is evaluated by human inspection.

The results are useful within the process of robotic spraying, where certain classes indicate areas requiring further surface treatment. If the target SG would be a class of medium geometric variability, regions showing high variability imply the need of being filled with more material around it or removed, while regions showing low variability require additional texture.

5.2 Material Classification

A scene containing all four materials seen from two different perspectives (5° and 25° with respect to the camera axis) has been used to assess the MC performance. The intensities as directly computed from the correlation samples are shown in Figure 12.a, for wood (W.), cardboard (C.), plastic (P.), and metal (M.). These intensities were compensated for the impact of distance and illumination spatial distribution with the corrections calculated as described in Section 4.2. The illumination distribution can be seen in Figure 12.c, and the resulting distance- and illumination-corrected intensities are shown in Figure 12.b. The AOI across the scene was calculated geometrically, and the need for calibrating the detection efficiency and overall scale was overcome by computing reflectances normalized to a patch of the scene known to correspond to wood on the 5° acquisition. The two reflectance features were then derived from the computed relative reflectances and compared to the reference data using a kNN classifier. The final results of the classification per pixel after applying a median filter can be seen in Figure 12.d. The results demonstrate high accuracy on the classification of pixels corresponding to metal, cardboard, and wood. Pixels corresponding to plastic get wrongly classified as wood on certain areas. This is caused by wood and plastic being relatively close to each other in the feature space as shown in Figure 11, and suggests the need for a more complex reflection model—thus requiring additional viewpoints—to distinguish materials with similar reflectance properties.

6 Conclusion and Outlook

An exploratory investigation and concept development for SG evaluation and MC using PCs and optical intensity values acquired with a state-of-the-art depth camera was carried out. The results for SG evaluation show that it is possible to classify geometry based on the level of geometric variability that it exhibits, by 3D feature analysis and supervised classification. The generated SG maps are easy to interpret, by both human and computer-aided analysis. Furthermore, the evaluation of the presented MC approach on a reduced subset of materials shows successful classification based on an approximated model of their

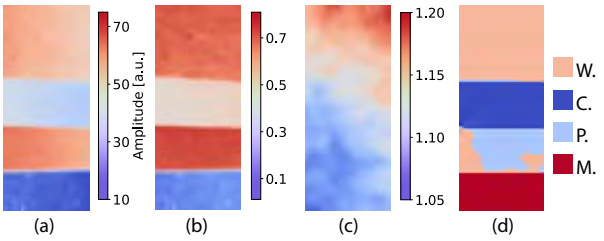

Figure 12. Result and intermediate steps for reflectance-based MC using 100 MHz data at distance of 1.5 m: a) measured intensities, b) corrected intensities, c) illumination distribution, and d) classified pixels, with material initials used for label names.

diffuse reflectance properties estimated from two viewpoints. The proposed method does not require in-situ calibration and can be easily extended to more complex reflectance models—hence potentially increasing classification robustness—by adding measurements from additional viewpoints.

The ultimate goal of the two proposed approaches is their in-line application within the robotic spraying process, providing feedback regarding geometric and material properties to adapt the process accordingly. On the one hand, the SG classes indicate whether further surface treatment in the fabrication process is needed or if the desired SG is met. On the other hand MC results can provide information on local coverage and volume of each sprayed material and also indicate early hydration states of the concrete to automatically regulate the time-window between consecutively sprayed layers.

As a continuation two main further investigations will be addressed. Firstly, the performance of the SG evaluation and MC approaches should be assessed on surfaces actually produced within the spraying process. Secondly, the combination of both approaches for enhanced performance should be explored. The latter means that geometry information (i.e. distances, orientation of the sample, etc.) should be used directly within the MC process where necessary, and vice-versa. Having MC results as one of the features within the SG evaluation, the material within the scene might contain information relevant for the SG classification.

Acknowledgments

This research was supported by the NCCR Digital Fabrication, funded by the Swiss National Science Foundation (NCCR Digital Fabrication Agreement #51NF40-182887).

The authors would like to thank Reckli GmBh for providing the moulds for concrete samples and to Andreas Reusser (NCCR dfab) for the help with concrete casting.

References

[1] Freek P Bos, Zeeshan Y Ahmed, Rob JM Wolfs, and Theo AM Salet. 3d printing concrete with reinforcement. In *High Tech Concrete: Where Technology and Engineering Meet*, pages 2484–2493. Springer, 2018.

[2] Rob Wolfs. *Experimental characterization and numerical modelling of 3D printed concrete: controlling structural behaviour in the fresh and hardened state*. PhD thesis, Technische Universiteit Eindhoven, Netherlands, 2019.

[3] Pablo Rodríguez-Gonzálvez and Gabriele Guidi. Rgb-d sensors data quality assessment and improvement for advanced applications. In *RGB-D Image Analysis and Processing*, pages 67–86. Springer, 2019.

[4] Benjamin Langmann, Klaus Hartmann, and Otmar Loffeld. Depth camera technology comparison and performance evaluation. In *ICPRAM (2)*, pages 438–444. Citeseer, 2012.

[5] Radu Horaud, Miles Hansard, Georgios Evangelidis, and Clément Ménier. An overview of depth cameras and range scanners based on time-of-flight technologies. *Machine vision and applications*, 27(7):1005–1020, 2016.

[6] *Time-of-flight forged ahead: design tips to boost 3D performance and cut integration time and cost*. Lucid Vision Labs, 2019. Manual, v.1.3, 18.10.2019.

[7] Monica Carfagni, Rocco Furferi, Lapo Governi, Michaela Servi, Francesca Uccheddu, and Yary Volpe. On the performance of the intel sr300 depth camera: metrological and critical characterization. *IEEE Sensors Journal*, 17(14):4508–4519, 2017.

[8] J Raja, B Muralikrishnan, and Shengyu Fu. Recent advances in separation of roughness, waviness and form. *Precision Engineering*, 26(2):222–235, 2002.

[9] Ali N Akansu, Wouter A Serdijn, and Ivan W Selesnick. Emerging applications of wavelets: A review. *Physical communication*, 3(1):1–18, 2010.

[10] Martin Weinmann, Boris Jutzi, Stefan Hinz, and Clément Mallet. Semantic point cloud interpretation based on optimal neighborhoods, relevant features and efficient classifiers. *ISPRS Journal of Photogrammetry and Remote Sensing*, 105:286–304, 2015.

Combining Reality Capture and Augmented Reality to Visualise Subsurface Utilities in the Field

L.H. Hansen[a], S.S. Wyke[a] and E. Kjems[a]

[a]Department of the Built Environment, Aalborg University, Denmark

lhha@build.aau.dk, ssw@build.aau.dk, kjems@build.aau.dk

Abstract -

In this paper, Reality Capture technologies are used to reconstruct 3D models of utility excavation holes which can later be visualised in the field, allowing for a more reliable, comprehensive and perceptible documentation and viewing of utilities before excavating to potentially reduce subsurface utility damages. An Augmented Reality (AR) prototype solution was developed and demonstrated for a group of respondents, concluding that visualising reality capturing models in AR would benefit fieldwork before, during and after excavation.

Keywords -

Augmented Reality; Reality Capture; Point Clouds; Underground Infrastructure; Subsurface utilities; Damage Prevention; Utility strike;

1 Introduction

Most streets in industrial countries are filled with hidden infrastructure beneath ground creating risk of striking underground utilities during excavation work. In the UK the direct cost is estimated at £3600 per utility strike which led to a total cost of approx. £7 Million in 2017-2018 [1]. However, this does not take the indirect cost of strike damages into account, which include project overrun, downtime and social cost such as traffic delays and loss of productivity in businesses. By adding these indirect costs the total cost is significantly higher and has an estimated average ratio between direct and indirect cost of 1:29 [2], thereby increasing cost of each utility strike to approx. £100,000. Similarly, in Denmark it is estimated that the Danish society has lost 2.8 billion DKK over a 10-year period due to underground utilities being damage during excavating [3]. Clearly there is a need for new tools and work processes, preventing underground utility damage.

Poor documentation in terms of quality, accuracy, and access to utility data is often the cause of utility strikes [4] [3]. In best case scenarios utility data is documented in GIS as straight poly-lines with attributes such as elevation and thickness, allowing qualified estimation of where utilities are located. In worst case scenarios the documentation is missing, incomplete or out-of-date and often represent as-planned data instead of as-built data [5]. This form of documentation is, therefore, more a schematic representation of where the utility is placed rather than a representation of its accurate shape where twists and turns can occur along the path [6]. As a consequence, issues often arise when trying to locate utilities before and during excavation. In Al-Bayati and Panzer's survey, (2019) [5], completed by 477 contractors, the most contributing cause for hitting underground utilities was a) the lack of depth information, b) painted markings placed to far from the utilities either because of inaccurate data or the surveyor being rushed or untrained, and c) the temporary state of the marking, i.e. the marking disappears when the top-layer surface is removed or is washed away by weathering. Locating equipment to measure the depth of utilities is, nonetheless available, such as Ground Penetrating Radar, which is often rejected because of the added cost for the utility owner and the limited benefits it provides [5]. Using locating equipment and following good-practice Subsurface Utility Engineering (SUE) is another solution that can be applied to prevent utility strikes [7], it can, however, be very expensive and time consuming. Often this solution does not harmonize with the contractor and utility owner being on a tight schedule and budget [5]. It is clear that more complete and accurate utility data are needed in today's construction industry and also, if not just as important, a more reliable way to display utility information before and during excavation work.

In this paper we showcase a potential solution to reduce utility damage that combines two emerging technologies to deliver a more informed, comprehensible and perceptible visualisation for utility professionals by combining Augmented Reality and Reality Capture. The aim is to visualise point cloud models of previous captured utility excavation holes informing the next person in the field to come.

1.1 AR visualisation of underground infrastructure

One popular solution used to display underground utility information in the field is Augmented Reality (AR). The method was first demonstrated by Roberts et al. (2002) [8] who visualised a 2D projection of underground utility

lines on the surface area. The AR prototype was a rather clumsy setup, compared with today's standards, consisting of a backpack powering a wired and handheld binocular-formed viewing device. Later Schall et al. (2009) [9] improved the concept with a smaller handheld device resembling nowadays handheld mobile devices in form factor. Besides visualising utility lines on the surface the handheld device could generate a geospatial 3D model from GIS utility data and display it at a given elevation value. To aid the users depth perception of the underground placed 3D model, the AR system used a cut-away visualisation technique resembling a virtual excavation. The 3D model was then only visible inside the virtual excavation cut-away volume. According to the authors in later studies this visualisation technique as well as the ability to change between other "x-ray" visualisation techniques, like Ghosting [10] and Shadow Projecting onto the surface, was very useful [11]. The studies further recommended to use comprehensible visualisation techniques to avoid depth perception issues instead of having the user trying to imagining the depth distance between utility pipe and surface [12]. A user study done by Eren Balcisoy (2018) [13] evaluated the vertical depth judgement performance on different x-ray visualisation techniques. It showed that users were performing better in estimating depth of 3D pipelines when using a cut-away excavation box technique compared to a careless overlay and edge-based ghosting technique. A survey by Ortega et al. (2019) [14] similarly showed that the virtual cut-away excavation technique also performed best when compared to other visualisation techniques for viewing of underground infrastructure in virtual environments.

As previously mentioned, other scientific work has primarily focused on visualising 2D GIS data superimposed to the surface or 3D models generated from the existing GIS data and occasionally as-planned 3D models. The latter being more common for large infrastructure projects, such as highway projects [15]. However, not much focus has been directed at using 3D models generated from Reality Capture. In fact to the best of our knowledge this has not before been attempted as a way of visualising underground utility information in the field.

1.2 Documentation of utility assets with Reality Capture

Reality capture is a technology that is used in a wide range of industries and is often used by surveyors to 3D scan constructions such as cultural heritage sites [16], bridges [17] and underground utilities [18].

One popular Reality Capture technique is Close-range Photogrammetry because of the widely available hardware in form of mobile cameras in smartphones and amateur drones as well as a wide range of reliable software. The 3D data output of Reality Capture is most often represented as either point clouds or 3D textured meshes. In this paper we use dense point clouds of underground utilities as our reality capturing data. The point clouds are provided by a Danish utility company and originates from an on-going pilot test made in cooperation with another Danish surveying company to use their Reality Capture technology for documenting underground utilities [19]. Using a smartphone app, workers in the field video-recorded the exposed utilities located in the excavation holes. A dense point cloud was then generated using close-range photogrammetry of the captured video recording. The point clouds were also geo-referenced, ensuring that location and scale were aligned with the existing surroundings. The point clouds serves as improved documentation and can be revisited by the utility company if needed in future activities. The interface view of how point clouds are managed by the utility company is shown in figure 1.

In this paper the mentioned Danish utility company provided access to point clouds from a water distribution renovation project from 2019, in which 14 utility excavations were captured and documented with Reality Capture.

1.3 Research goals

This paper is a preliminary attempt to utilise Augmented Reality as a planning tool allowing both surveyors, inspection engineers and contractors to attain a perceptible visualisations of where utilities are located below ground, based on documentation of previous excavations registered using Reality Capture.

The research presented in this paper consist of the development of an AR prototype and a showcase session for the utility owners and the surveying company, participating in the study. The study demonstrate how captured point clouds can be visualised to inform workers in the field before a new utility excavation project is carried out in the area of a previously captured location.

The aim is to highlight the usefulness of visualising point cloud captures in AR for field workers to prevent damage when excavating as well as assist in other general asset managing tasks in the utility industry. Using Reality Capture in combination with AR has yet to be studied in-depth with regards to obtaining better interaction and visualisations techniques for underground infrastructure in this study.

This paper additionally presents incentives for utility companies to document utility assets with Reality Capture technologies as well as share these 3D captures with other utility owners in the industry.

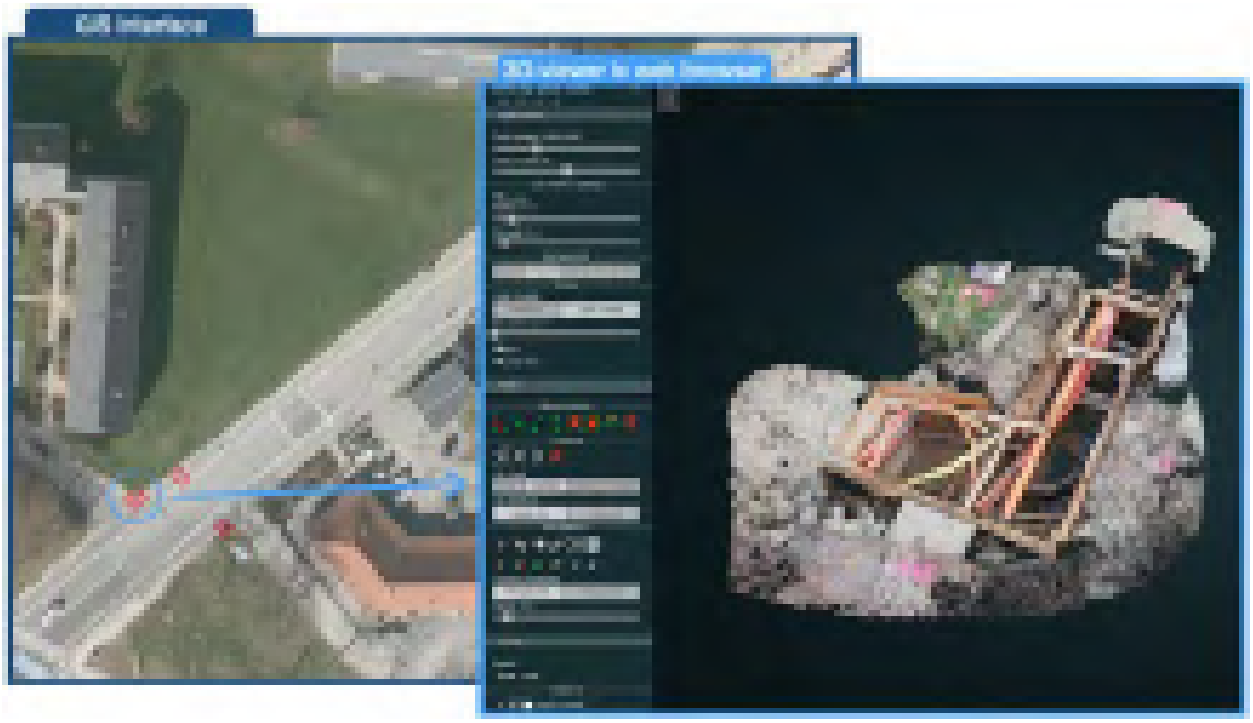

Figure 1. Right: Polygons boundaries in a GIS interface indicating the location of utility excavation point clouds. Left: A dense point cloud capture of an utility excavation displayed in an interactive 3D web-viewer using Potree

2 Methodology

2.1 Empirical method

Empirical data was acquired through a series of informal interviews with stakeholders from the utility industry over the span of six months.

Interviews were conducted in two parts. The first part included phone-calls with two stakeholders to attain background information with respect to current practises and experiences with excavation, strike-damages and planning of underground utility work. The second interview partly consisted of a demonstration of the AR prototype developed as part of this research, and partly of an informal group interview evaluating said AR prototype demonstration. The participating respondents were all employees in the already mentioned utility company and surveying company. In all, seven respondents participated, five male and two female with various years of experience in the utility industry.

Empirical data acquisition was based on semi-structured interviews, as described by Brinkman and Tangaard (2015) [20], documented through sound-recordings. A selection of predefined questions were directed to the respondents guiding the interview session whilst follow-up questions were added to the discussion by the interviewer in reaction to the comments given by the respondents, allowing elaboration on comments as well as getting spontaneously occurring questions relevant to the prototype demonstration answered. The questions guiding the interviews were divided into two categories, 1) AR for informed decision-making in the field and 2) AR to prevent utility excavation damage.

Data collected in the interview-session additionally include comments from the respondents from conversations happening during the demonstration of the AR prototype. After empirical data were collected it was analysed and structured through a brainstorming process harmonizing the interview-data gathered with the scope of this paper.

2.2 Prototype development

The AR prototype was developed using Unity3D and ARKit as AR framework running on a 2nd Gen. 12,9" iPad Pro. The dense point cloud models of the utility excavations were managed using Potree created by Schuetz (2016) [21]. By leveraging the octree structure implemented in Potree the rendering process was made efficient to visualise the relative large point clouds (avg. 1-2 million points), for the prototype hardware to handle with a satisfying frame-rate while shown in the AR view. The implementation of Potree in Unity3D was made possible by using a Unity-package developed by Fraiss (2017) [22].

Prior to the demonstration of the prototype tool, markers

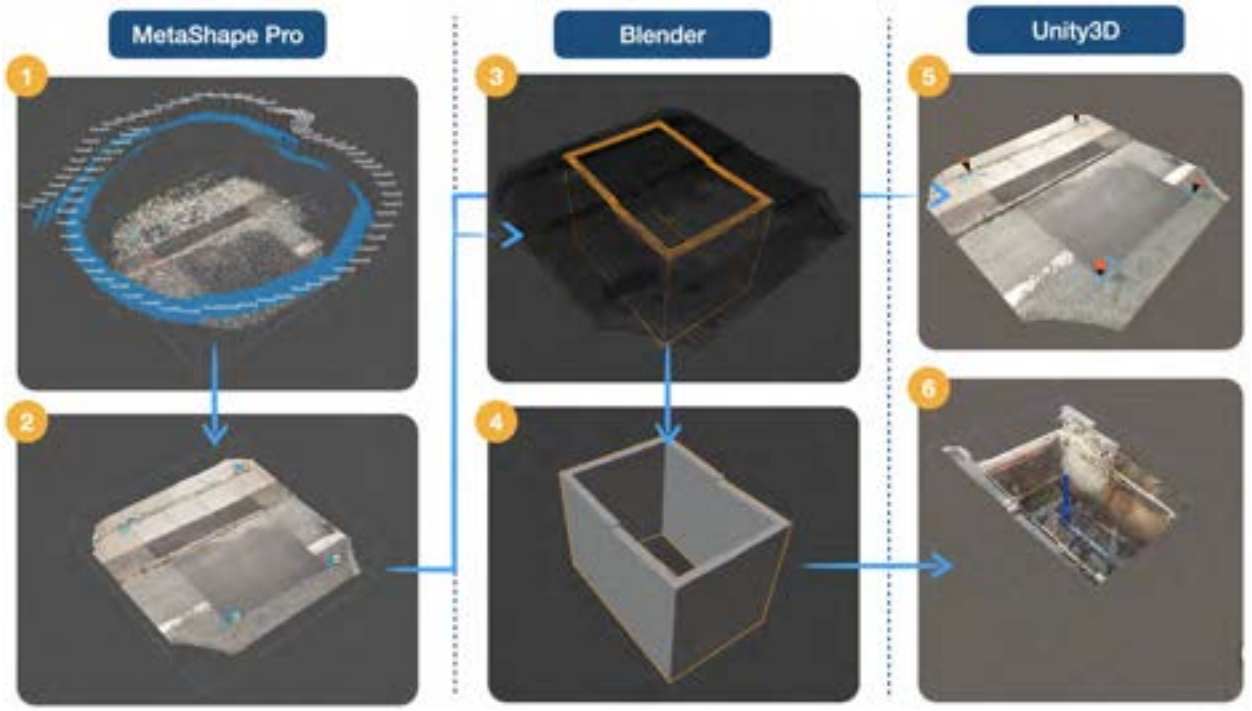

Figure 2. The overall workflow for creating occlusion box

was painted around the ground surface of the previously reality captured utility excavations. By video recording the surface area and surveying the painted markers on the test-site a 3D mesh was generated by using close-range photogrammetry in Metashape Pro. This process is illustrated in figure 2 in step 1 and 2. The surface mesh was aligned with its corresponding utility excavation point cloud. This was done for two reasons.

Firstly, to create an occlusion box around the utility excavation point cloud to keep the illusion of how a physical utility excavation hole would look, i.e. it is not possible to see the outer sidewalls of the excavation as the ground surface occludes it. This was done by modelling a box-shaped 3D model around the utility excavation point cloud using Blender as illustrated in step 3 and 4 in figure 2. The 3D model box was then imported to Unity3D and an occlusion shader was applied as illustrated in the last steps (5 and 6) in figure 2.

Secondly, to manually positioning and orientating the utility excavation point clouds at the correct geo-position in AR. By manually place the point clouds on top of the known markers by utilising ARKits horizontal plane detection and model-free tracking capabilities a stable and robust Six Degrees of Freedom (6DoF) tracking was achieved. This approach was used to obtain a simple and yet reliable AR geo-positioning and tracking solution, satisfying for demonstration purposes.

3 Results

The seven employees from the Utility Company (UC) and the Surveying Company (SC) participating in the demonstration as respondents were given a hands-on demonstration of the AR prototype, as seen in figure 3, before the semi-structured interview was conducted. The participant's roles in the company were primarily team leaders and department managers, all responsible for people with field work, such as planning, inspection and management on site as well as collaborating with contractors responsible for excavation.

In the following section the results from the demonstration and interview are presented, following the structure of the questioning categories presented in section 2. An important aspect to have in mind is that the use of Reality Capture for documentation of utility assets is, a new work process for the UC, as mentioned in section 1, and therefore they are still exploring what value-creation Reality Capture can add to their work routines.

To start the interview the UC first described what current value-gain they have achieved from using Reality Capture. Besides being an additional form of documentation that can be accessed through GIS, as seen in figure 1, the UC also use the point clouds to quality inspect the utility installation work done by the contractors. At the moment only larger water distribution construction projects are documented with Reality Capture, but the UC is confident that

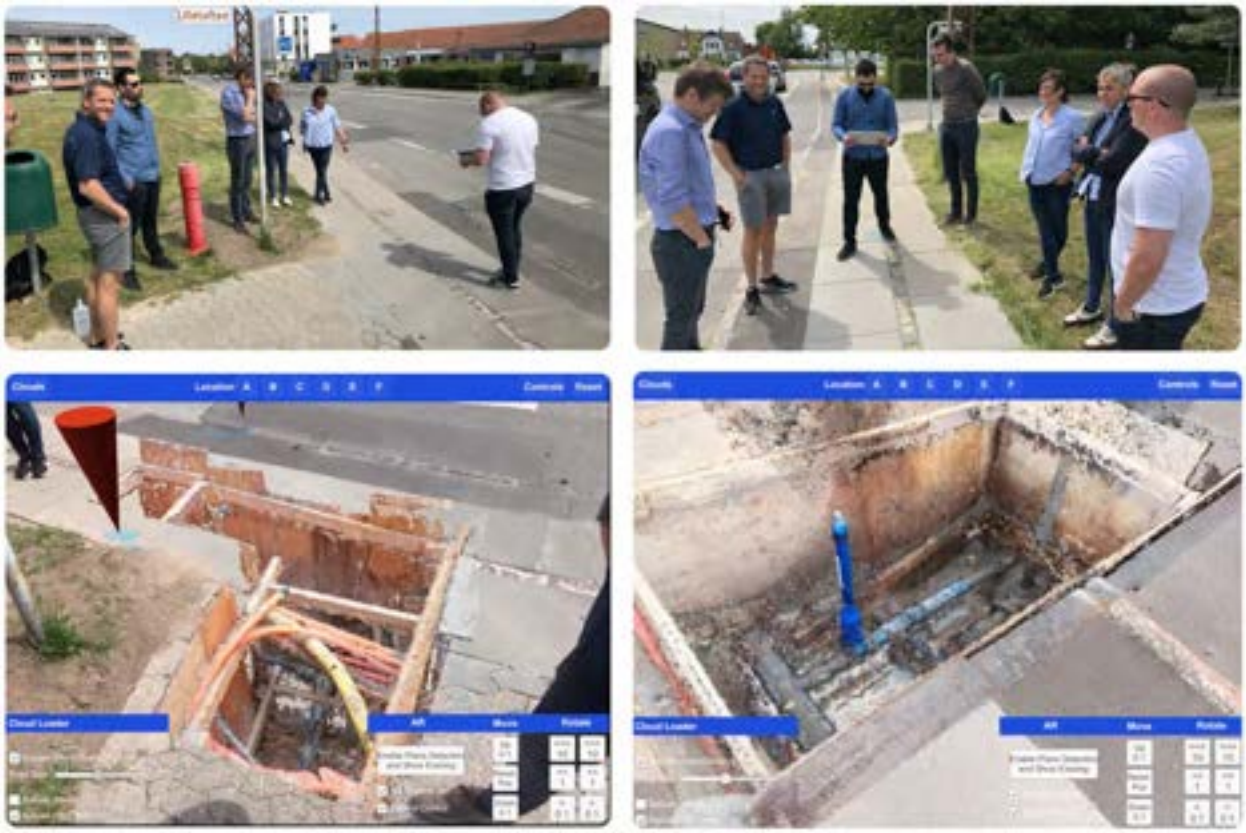

Figure 3. AR prototype in use during the hands-on demonstration seen from AR device view (bottom) and 3rd-person view (top).

it is to be utilised in other types of excavation projects, such as district heating, waste and storm water, in the future. Looking further ahead they believe these point clouds can be useful in the planning phase of new excavation projects near locations of previously reality captured utility assets. In fact, this was one the reasons why the UC was interested to see what their 3D point cloud models would look like when visualised in the field using AR.

3.1 AR for informed decision-making in the field

None of the respondents from the UC has experience working with AR solutions for displaying GIS data to aid fieldwork. The SC, however, is a seller of professional industry AR solutions (currently AugView and Trimble SiteVision) but has not seen Reality Capture 3D models visualised with these systems.

The respondents were asked to discuss what kind of value-creation it would add to their work routines based on their hands-on experience with the AR prototype. All respondents agreed that the ability to view the point cloud models in AR during fieldwork would greatly help planning and coordination with other professionals and non-professionals e.g. in communicating with citizens. The most impressive aspect for the respondents was how perceptibly and comprehensible the virtual utility excavation was visualised in the AR prototype, making it suitable for communicating technical details. For example, to help visualise where a water supply utility is located in relation to cadastre boundary for a house-owner. Another example, could be in case of a water leakage. In such case the UC might have a rough estimation of where the leakage is located based on sensor data. However, entering the field with the ability to look through the surface and see the underground utility pipes with high visual detail, and in context with the physical surroundings, might lead to a faster localisation of the leakage. Ultimately the respondents felt motivated to include the AR prototype in their fieldwork as they agreed it would support a more informed decision-making.

During and after the demonstration the respondents from the UC got so inspired when interacting with the AR prototype that they started to suggest new functionalities. The most requested functionality was distance measuring in the two primary directions: 1) vertical depth from util-

ity to surface level and 2) horizontal distance from utility pipe snapping to horizontal road cross-section features such as center line, drive lane, curbs, bicycle-path, sidewalk, shoulder and road boundary limit. They also would like to have their own 2D GIS utility data visible together with the utility excavation point cloud. When asked about visualising 2D GIS utility data from other utility owners like tele-com and power, they where more hesitant.

3.2 AR to prevent utility excavation damage

When asked if the demonstrated AR prototype could help prevent utility damage during excavation work, all respondents agreed that it would be helpful for the contractor. Again, the main reason is the ability for the contractor to get a perceptible view of what underground utility assets are hidden beneath the surface. This information can then easily be understood by the contractor to plan the digging activity before breaking ground, and reassess during excavation. A particular useful scenario is when multiple underground utilities are buried in the same place, as shown in the utility excavation seen in the bottom left picture in figure 3. In the utility excavation, the flexible and smaller orange and yellow cables are clearly visible, even though the purpose of Reality Capture was only to document the blue water supply pipe laying below. When experiences with utility damages occurring during excavation work was discussed further the respondents agreed that the main cause for utility damages are inaccurate and out-of-date utility data - especially data from tele-com companies. Technical drawings of tele-com cables are often only schematic representation. This can lead to a lot of guesswork for the contractor, when locations of underground cables on the drawings does not correspond to locations in reality. The presented AR prototype solution has great potential to reduce utility strikes, however, as commented by the respondents, this is only useful if previous captured point clouds located beneath or close around the excavation site exist and can be accessed.

4 Discussion

4.1 Reality Capture and AR to incentivise data sharing

The presented AR solution in this paper uses point cloud models of previous reality captured utility excavation to deliver a more informed, comprehensible and perceptible visualisation for utility professionals in the field. Using Reality Capture models as the only data source of visualisation, however, creates the obvious limitation, that the coverage is only as adequate as the number of utility excavations which have been excavated, reality captured and transferred into the AR device. Even though this approach has a weakness in terms of coverage area, it ensures that only accurate utility information is presented for the user. Compared to other AR solutions that use traditionally 2D GIS utility data which are prone to be inaccurate as told by the respondents and others [5]. One could argue that the approach, presented in this paper, is actually a strength by only visualising utility information that are accurate and thus trustworthy for the professionals in the field. Nevertheless, it is clear that the more point clouds the UC can capture, the more relevant the AR solution will become, as the likelihood of revisiting a previous reality captured location increases.

In the future the UC hopes that its neighbouring utility owners will also begin documenting utility assets with Reality Capture. This, they hope, will lead to data sharing between them, which they can all leverage from. For example it is clearly visible from figure 3 that other types of utilities are present in the excavated hole. It is certainly possible that other utility owners have plans to revisit these utilities before the utility owner that originally captured it. It seams only logical to share Reality Capture models. This type of sharing is already a known practice in Denmark as it is mandatory to ask for underground utility information before a contractor starts excavating. However, the utility data is at best only regular 2D GIS utility data and is prone to be inaccurate for some utility types. When documenting utility assets with Reality Capture it automatically documents other utilities appearing in the excavation. This could lead to updating out-of-date data of utilities and cables, benefiting the next contractor to excavate at a previously captured location. Especially if the contractor is able to visualise these virtual utility excavations in the field as demonstrated in the AR prototype presented in this paper. Such sharing of utility data through an AR platform has been proven as an attractive solution for utility owners to engage in as demonstrated by Fenais et al. (2019), although the AR platform was only using regular 2D GIS utility data [23].

4.2 Visualisation of Reality Capture models in AR

The AR prototype used dense point cloud models of utility excavations provided from the utility company. The reason was to demonstrate for the utility company what is possible to visualise in AR with data they already possess. However, that is not to say the point clouds were the optimal Reality Capture model datatype to visualise in AR. In fact it might be more suitable to use 3D textured mesh representations. One of the benefits 3D meshes is that it consist of triangulated faces and therefor occludes the surrounding background when viewed in AR. Contrary, when using point clouds it is possible to see-through where the points are not dense enough which can sometimes break the illusion of AR. In either case, it is interesting to have both point clouds and 3D meshes being optimized for AR

visualisation to be suitable for as many Reality Capture techniques as possible.

5 Conclusion

The aim of this paper was to identify potential value-creation using Reality Capture models of utility excavations, visualised in Augmented Reality for utility professionals in the field. Based on the responses collected in a prototype demonstration and interviews with respondents from a Utility Company and a Surveying Company, it is possible to conclude that visualising Reality Capture models in AR can be useful for field workers for planning of subsurface work, and also during excavations. All participating respondents, furthermore, noted that they wanted to implement a finished version of the prototype-tool demonstrated in this study, in the future.

Many of the respondents had not previously tried AR in an outdoor professional context and was quite overwhelmed with how much sense and value it added. Although visualising Reality Capture models in AR was concluded useful the respondents further noted that more interaction features in the AR prototype, with respect to specific fieldwork tasks and needs. Future work will investigating and develop prototypes to study what value-creation such interaction features can facilitate for utility construction professionals in planning and executing excavation work.

6 Disclaimer

The interview results presented in this paper was collected with participation of the surveying company that provided point cloud models of the utility excavations to the utility company using the survey company's own developed Reality Capture app. The solution and the conclusion of advocating the use of Reality Capture as a way of documentation could therefore be in the surveying company's own interest.

References

[1] USAG. Utility Strike Damages Report 2017-2018. (January), 2019.

[2] Lewis Makana, Nicole Metje, Ian Jefferson, and Chris Rogers. What Do Utility Strikes Really Cost? Technical Report January, University of Birmingham - School of Civil Engineerin, 2016. URL https://www.researchgate.net/publication/321110173.

[3] Energy Danish Ministry of Climate and Utilities. Udveksling af data om nedgravet infrastruktur. On-line: https://kefm.dk/data-og-kort/udveksling-af-data-om-nedgravet-infrastruktur/, Accessed: 01/06/2020.

[4] Lewis O Makana, Nicole Metje, Ian Jefferson, Margaret Sackey, and Chris DF Rogers. Cost Estimation of Utility Strikes: Towards Proactive Management of Street Works. *Infrastructure Asset Management*, pages 1–34, 2018. ISSN 2053-0242. doi:10.1680/jinam.17.00033.

[5] Ahmed Jalil Al-Bayati and Louis Panzer. Reducing Damage to Underground Utilities: Lessons Learned from Damage Data and Excavators in North Carolina. *Journal of Construction Engineering and Management*, 145(12):1–8, 2019. ISSN 07339364. doi:10.1061/(ASCE)CO.1943-7862.0001724.

[6] Paul Goodrum, Adam Smith, Ben Slaughter, and Fady Kari. Case study and statistical analysis of utility conflicts on construction roadway projects and best practices in their avoidance. *Journal of Urban Planning and Development*, 134(2):63–70, 2008. ISSN 07339488. doi:10.1061/(ASCE)0733-9488(2008)134:2(63).

[7] Kevin Vine. Subsurface Utility Engineering (SUE): Avoiding 4 Potential Pitfalls to Ensure a Successful Program. In *Transportation 2014: Past, Present, Future-2014 Conference and Exhibition of the Transportation Association of Canada*, pages 1–16, 2014.

[8] Gethin W Roberts, Andrew Ewans, Alan Dodson, Bryan Denby, Simon Cooper, and Robin Hollands. The use of augmented reality, GPS and INS for subsurface data visualization. *FIG XXII International Congress*, 4:1–12, 2002.

[9] Gerhard Schall, Erick Mendez, Ernst Kruijff, Eduardo Veas, Sebastian Junghanns, Bernhard Reitinger, and Dieter Schmalstieg. Handheld Augmented Reality for underground infrastructure visualization. *Personal and Ubiquitous Computing*, 13(4):281–291, 2008. ISSN 1617-4917. doi:10.1007/s00779-008-0204-5. URL http://dx.doi.org/10.1007/s00779-008-0204-5.

[10] Stefanie Zollmann, Denis Kalkofen, Erick Mendez, and Gerhard Reitmayr. Image-based ghostings for single layer occlusions in augmented reality. In *9th IEEE International Symposium on Mixed and Augmented Reality 2010: Science and Technology, ISMAR 2010 - Proceedings*, pages 19–26. IEEE, 2010. ISBN 9781424493449. doi:10.1109/ISMAR.2010.5643546.

[11] Gerhard Schall, Stefanie Zollmann, and Gerhard Reitmayr. Smart Vidente: Advances in mobile

augmented reality for interactive visualization of underground infrastructure. *Personal and Ubiquitous Computing*, 17(7):1533–1549, 2012. ISSN 16174909. doi:10.1007/s00779-012-0599-x.

[12] Stefanie Zollmann, Gerhard Schall, Sebastian Junghanns, and Gerhard Reitmayr. Comprehensible and Interactive Visualizations of GIS Data in Augmented Reality. In *Advances in Visual Computing. ISVC 2012*. Springer. ISBN 978-3-642-33178-7. doi:10.1007/978-3-642-33179-4_64.

[13] Mustafa Tolga Eren and Selim Balcisoy. Evaluation of X-ray visualization techniques for vertical depth judgments in underground exploration. *Visual Computer*, 34(3):405–416, 2018. ISSN 01782789. doi:10.1007/s00371-016-1346-5.

[14] Sebastián Ortega, Jochen Wendel, José Miguel Santana, Syed Monjur Murshed, Isaac Boates, Agustín Trujillo, Alexandru Nichersu, and José Pablo Suárez. Making the invisible visible—strategies for visualizing underground infrastructures in immersive environments. *ISPRS International Journal of Geo-Information*, 8(3), 2019. ISSN 22209964. doi:10.3390/ijgi8030152.

[15] Lasse Hedegaard Hansen and Erik Kjems. Augmented Reality for Infrastructure Information: Challenges with information flow and interactions in outdoor environments especially on construction sites. In *37th eCAADe Conf. Proceedings*, volume 2, pages 473–482, 2019.

[16] H. M. Yilmaz, M. Yakar, S. A. Gulec, and O. N. Dulgerler. Importance of digital close-range photogrammetry in documentation of cultural heritage. *Journal of Cultural Heritage*, 8(4):428–433, 2007. ISSN 12962074. doi:10.1016/j.culher.2007.07.004.

[17] Ruinian Jiang, David V. Jáuregui, and Kenneth R. White. Close-range photogrammetry applications in bridge measurement: Literature review. *Measurement: Journal of the International Measurement Confederation*, 41(8):823–834, 2008. ISSN 02632241. doi:10.1016/j.measurement.2007.12.005.

[18] Jingya Yan, Siow Wei Jaw, Kean Huat Soon, Andreas Wieser, and Gerhard Schrotter. Towards an underground utilities 3D data model for land administration. *Remote Sensing*, 11(17):1–21, 2019. ISSN 20724292. doi:10.3390/rs11171957.

[19] Michela Bloch Eiris. Videoindmåling - en ny teknologi til dokumentation af aktiver, GeoForum. Technical Report Oktober. URL `https://issuu.com/geoforum5/docs/geoforum_207_issue`.

[20] Lene Tanggaard and Svend Brinkmann. *Interviewet: Samtalen som forskningsmetode*, pages 29–53. Hans Reitzels Forlag, Danmark, 2. edition, 2015. ISBN 9788741252551.

[21] Markus Schuetz. *Potree: Rendering Large Point Clouds in Web Browsers*. PhD thesis, Vienna University of Technology, 2016. URL `https://publik.tuwien.ac.at/files/publik{_}252607.pdf`.

[22] Simon Maximilian Fraiss and Michael Wimmer. *Rendering Large Point Clouds in Unity*. PhD thesis, Vienna University of Technology, 2017. URL `https://www.cg.tuwien.ac.at/research/publications/2017/FRAISS-2017-PCU/`.

[23] Amr Fenais, Samuel T. Ariaratnam, Steven K. Ayer, and Nikolas Smilovsky. Integrating geographic information systems and augmented reality for mapping underground utilities. *Infrastructures*, 4(4), 2019. ISSN 24123811. doi:10.3390/infrastructures4040060.

Condition Prediction of Highway Assets Based on Spatial Proximity and Interrelations of Asset Classes: A Case Study

A. Karimzadeh[a], S. Sabeti[a], H. Tabkhi[b] and O. Shoghli[a]

[a] Department of Engineering Technology and Construction Management, University of North Carolina at Charlotte, USA

[b] Department of Electrical and Computer Engineering, University of North Carolina at Charlotte, USA

E-mail: akarimza@uncc.edu, ssabeti@ieee.org, htabkhiv@uncc.edu, oshoghli@uncc.edu

Abstract – Deterioration models significantly contribute to increasing the efficiency of life-cycle planning for highway assets. Therefore, asset managers strive to maximize the accuracy of such models and intensify the efficacy of the life-cycle plan. Even though nearby assets have been thought to have an impact on each other's conditions, usually, such interrelations have not been considered in previous deterioration models. To this end, in this paper, we focused on investigating the impact of considering nearby assets interrelations on the accuracy of prediction models. Our results show that this consideration resulted in more accurate prediction models in comparison to considering each asset individually.

Keywords – Highway Asset Management; Condition Prediction; Logistic Regression; Nearby Assets

1 Introduction

The optimization of budget allocation in highway asset management programs is gaining more attention due to the massive maintenance needs of the existing aged roadways. Furthermore, in recent years, the constrained budget has resulted in an ever-growing backlog of funding. As an example, the amount of budget shortage for preserving the U.S. roadways in a good state of repair was estimated $836 billion in 2017. As a result, this budget deficit emphasizes the need for optimal and smart investments in highway asset management programs [1]. Therefore, in the pursuit of optimal allocation of the available funds, highway decision makers look for procedures that maximize the level of service with minimal expenditure. To this end, information modeling and management are the keys in establishing optimized Life Cycle Plans (LCPs) and maintenance works [2; 3; 4; 5]. In the meantime, the accuracy of deterioration prediction models highly affects the efficiency of LCPs and, in turn, highway asset management programs. Therefore, decision makers strive to increase the accuracy of data-driven deterioration prediction models given the limited extent of available data so that they could better predict possible future deficiencies in roadways.

In a highway system, several asset classes can be found next to each other. According to the first law of geography that specifies there is a relation between everything with nearby elements being more related, it can be hypothesized that the conditions of neighboring assets are correlated [6]. For instance, the condition of neighboring pavements, shoulders, and slopes might be correlated because of the similar impact of the identical temperature variations and precipitation rates that happen in their vicinity. Also, defects in adjacent asset items could be affected by possible interrelations between the degradation of neighboring elements. For example, the deformation of a slope next to a shoulder might cause the shoulder's subsidence.

However, the majority of previous studies developed their condition prediction models when each asset was considered individually [7, 8, 9, 10, 11]. For this reason, the possible interrelations of nearby asset classes have not been fairly considered in previous deterioration models. To address this challenge, the main motivation of this study is to examine the impact of incorporating the condition of neighboring asset classes into condition prediction models on the accuracy of condition forecasts. To this end, we selected flexible pavement, paved shoulder, and slope to perform the analysis. We selected these assets because: (i) they are made of similar materials, (ii) they are located in close proximity, and (iii) similar factors affect their degradation rates. Then, we developed deterioration models for the selected asset types in a case study. We then performed a comparative study to measure the impact of including the conditions of neighboring assets in the developed prediction frameworks for the selected asset items. The following section moves on to the review of the literature in deterioration prediction models of the selected asset items.

2 Background

Several studies targeted developing deterioration models for pavements and bridges. However, other roadway assets have received less attention. In addition, agencies have focused more on measuring the performance of pavements and bridges in comparison to the other assets [12]. Therefore, sometimes agencies do not own enough performance data of other assets such as slopes and shoulders. Yet, in a roadway asset management system, all asset types are required to be considered together under a framework wherein their performance prediction models specify their maintenance investment needs. Consequently, adding the information of assets with abundant data (e.g. pavement) in condition prediction of other assets with less available data could mitigate uncertainties and contribute toward a better budget allocation.

We identified two main shortcomings in previous works. The first found gap is that the majority of prediction models were developed based on the data of a single asset type, where each asset was modeled individually. For instance, [7], [13], and [14] developed prediction models for the condition of pavements only based on the historical data of pavement segments. Another identified shortcoming in the literature is that even though the condition of nearby assets might be dependent, this dependency was not considered in developing prediction models. For example, in spite of the probable impacts of underlying pavements on the condition of pavement markings, the majority of studies investigated their conditions separately [15, 16]. In addition, several studies performed individual investigations of degradations for other asset types, such as signs, barriers, and culverts [17, 18, 9]. Therefore, the possible interrelations between neighboring assets have not been fairly considered in previous studies. However, a few of the past studies partially investigated the mutual impacts of some of the neighboring assets on each other. For example, the impact of drained and undrained base and subbase layers on the condition of pavement were examined in some works, where the outcomes unveiled that the presence of water in the subsurface layer and its surroundings can significantly influence the pavement's stiffness [19, 20]. In addition, [21] studied the role of routine maintenance of paved shoulders on the condition of adjacent flexible pavement. In another study, [22] investigated the influences of shoulders' rumble strip on the pavement condition. Finally, [23] performed a correlational study between the condition of nearby flexible pavements, paved ditches, and paved shoulders. They identified some interrelations that mutually impact the condition of the selected asset items. However, they did not study the possible impacts of these correlations in the condition prediction models of each asset.

To fill the identified gaps in the body of knowledge, the main objective of this study is to examine how including the condition of nearby assets as a predictor in the condition prediction of a particular asset improves the accuracy compared to single asset modeling where the deteriorations are predicted based on the information of each asset individually. The next section moves on to the step-by-step methodology proposed in this study and explains each step in more detail.

3 Methodology

In this study, we selected three asset classes for our analysis: flexible pavement, shoulder, and slope. We used a wide range of contributing factors to degradation in our analysis under three main categories: weather, traffic, and historical asset's condition due to their importance and data availability. We developed the prediction model of each asset in two different scenarios: when the conditions of its adjacent assets were considered (i.e. nearby-asset modeling) and ignored (i.e. single asset modeling). Prior to developing prediction models, we performed a feature reduction step to ensure there was no multicollinearity in the input dataset. Next, we used logistic regression to predict the existence of pothole defects in flexible pavement and shoulder, and erosion and erosion patterns in slope under the scenarios as mentioned earlier.

To measure the capability of the proposed framework, we applied it on 321.4 kilometers of I-81, I-77, and I-381 highways in Virginia as our case study. Selected roadways were split into 84 segments, each of which has a length of 3.2 kilometers (2 miles). The utilized datasets in this study recorded the corresponding values of weather, traffic, and historical conditions between 2015 and 2019. Fig. 1 shows the framework of the proposed methodology. The following sections provide a detailed description of each step.

3.1 Data Collection and Preparation

The utilized data in this study were categorized into three groups: weather, traffic, and condition. First, we collected data from available resources and then audited the data to detect and correct possible errors, abnormalities, and irregularities.

3.1.1 Traffic

The traffic dataset was extracted from a public portal [24]. We performed a cleaning step to identify missing information and inaccuracies in the dataset. Next, in order to prevent the occurrence of bias in the results, we used the min-max scaling in our analysis to linearly map the features between 0 and 1 [25]. We applied this scaler on each feature of the cleaned traffic dataset separately. The summary of the utilized traffic features, as well as

their descriptive statistics, including minimum, maximum, 25th percentile, median, and 75th percentile before scaling are provided in Table 1 and Figure 2, respectively.

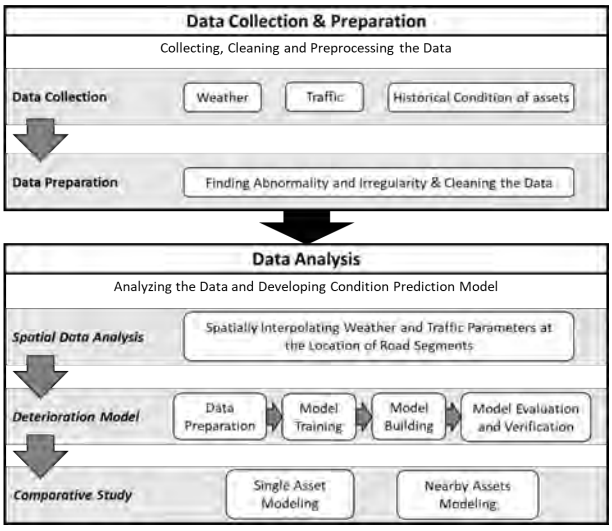

Figure 1. Proposed methodology framework

Table 1. Traffic features

Parameter	Definition
ADT	average daily traffic
AAWDT	average annual weekday traffic
ADT_4	average daily traffic of 4-tire vehicles
ADT_BU	average daily traffic of buses
ADT_TR	average daily traffic of trucks with 1 trailer
ADT_1	average daily traffic of trucks with 2 axles
ADT_2	average daily traffic of trucks with 2 trailers
ADT_3	average daily traffic of trucks with 3 axles

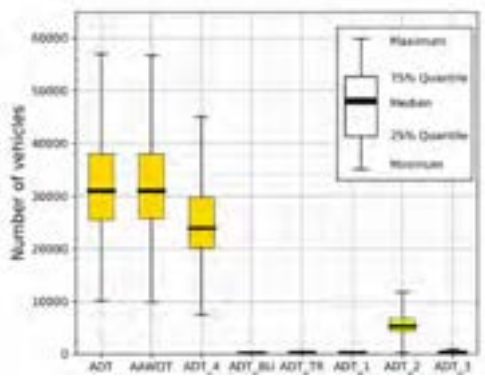

Figure 2. Traffic feature statistical description

3.1.2 Weather

We extracted the weather data from the National Oceanic Atmospheric Administration (NOAA) database. We collected the data from 24 weather stations to cover our case study. Figure 3 shows the selected weather stations and their location with respect to the case study.

Figure 3. Selected weather stations and the case study

We cleaned the dataset to minimize inaccuracies and missing information. We filtered the stations to the ones with more than 250 days of recorded data, which reduced the number of remaining stations to 20. Table 2 provides a summary of the weather features used in our analysis.

We used the ordinary kriging to interpolate the extracted weather features onto each segment. We used this technique due to its acceptable accuracy for weather-related features [26, 27, 28]. In addition to the common weather features, we devised and considered more attributes to incorporate temperature variations. For instance, the average daily maximum-minimum temperature difference in a year, TMAXTMIN, is one of the attributes that we used to take into account the daily fluctuation of the temperature. TMAXTMIN ranges between two extremums: the upper bound, which takes place in desert-like regions, and the lower bound being observed in low-lying humid areas.

Table 2. Weather features

Parameter	Definition
TMAX	annual maximum daily temperature (° C)
TMIN	annual minimum daily temperature (° C)
TMAXMIN	annual average of daily max_min temperature difference (° C)
DWT32	number of days with minimum temperature<0° C (32° F) in a year
DWT80	number of days with maximum temperature>26.7° C (80° F) in a year
DWTMXN30	number of days with Tmax-Tmin>16.7° C (30° F) in a year
DSNW	number of days with snow depth > 2.54 cm (1 inch) in a year
EMSD	maximum annual daily snow depth (cm)
EMXP	maximum annual daily precipitation depth (cm)
PRCP	total annual precipitation (cm)
SNOW	total annual snow depth (cm)

We additionally added another feature to our analysis to include the number of days with maximum-minimum temperature difference greater than 16.7 degrees Celsius (30 degrees Fahrenheit), called DWTMXN30. Then, like traffic data, we used min-max scaling to map the weather data as well. Figure 4 provides the statistical descriptions of the extracted weather features through a set of boxplots prior to scaling.

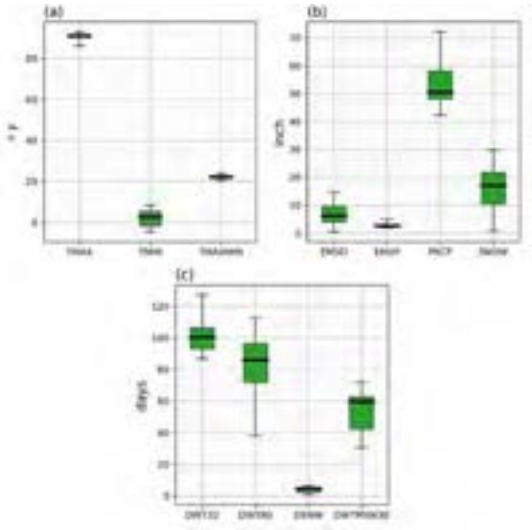

Figure 4. Weather features' statistical description

3.1.3 Condition

The condition of each asset corresponds to its physical characteristics that affect its performance at the time of inspection [29]. We extracted the condition data from a Maintenance Quality Assurance Program (MQAP) that inspected and recorded the condition of the selected assets (i.e. flexible pavement, paved shoulder, and slope) in our case study between 2015 and 2019. The MQAP recorded pothole defects on flexible pavement and shoulder in each segment of roadways, and erosion and erosion patterns in slopes. Being a common defect on flexible pavements and shoulders, potholes pose extreme dangers to vehicles and drivers. Driving over potholes can harm different parts of vehicles and could force drivers to show dangerous maneuvers for avoiding driving over them. Like potholes in flexible pavements and shoulders, erosion and erosion patterns are major probable defects in slopes that endanger their stability. They could cause dangerous failures in slopes. Therefore, we considered these defects in our analysis. The utilized MQAP rated the recorded conditions in 4 classes: very poor, poor, good, and very good. The definitions of all classes of recorded conditions for each asset are provided in Table 3 to Table 6.

Table 3. Condition descriptions for flexible pavement - pothole

Condition	Description
Very Poor	More than one pothole present
Poor	One pothole present
Good	No pothole
Very Good	No pothole or any sign of distressed asphalt such as rutting, heaving, or troughing

Table 4. Condition descriptions for shoulder - pothole

Condition	Description
Very Poor	More than one pothole present
Poor	One pothole present
Good	No pothole
Very Good	No pothole or any sign of distressed asphalt such as rutting, heaving, or troughing

Table 5. Condition descriptions for slope - erosion

Condition	Description
Very Poor	Multiple erosion along slope greater than 8 inches deep
Poor	Erosion along slope greater than 8 inches deep
Good	Less than or equal to 8 inches deep erosion.
Very Good	No slope erosion.

Table 6. Condition descriptions for slope - erosion pattern

Condition	Description
Very Poor	Pattern of erosion that endangers the stability of at least 25% of the slope.
Poor	Pattern of erosion that endangers the stability of less than 25% of the slope.
Good	No pattern of erosion that endangers the stability of the slope.
Very Good	N/A

3.2 Prediction Model

We used logistic regression to develop prediction models and to predict the future condition of selected assets. In developing prediction models, we aggregated the defects into pass or fail classes. This new classification is aligned with trigger levels in maintenance decision making systems that highlights the necessity of repairs for very poor and poor classes. Therefore, in each asset, very poor and poor conditions were merged into the fail class while good and very good into the pass class. As a result, the output of the model would be a binary value (pass/fail), which corresponds to the predicted condition of each asset in the considered segment.

Prediction models in this study were developed in two different scenarios so that the interrelations of neighboring assets could be investigated. In the first scenario, we only considered weather, traffic, and the condition of each individual asset in the modeling (single

asset modeling). The condition feature only contains the recorded condition in the prior year of the targeted prediction time. For example, to forecast the condition of the flexible pavement in 2017, the single asset prediction model uses only the condition of flexible pavement in 2016 as a predictor, as well as other weather and traffic features. Figure 5 schematically shows the single asset prediction modeling used in this study.

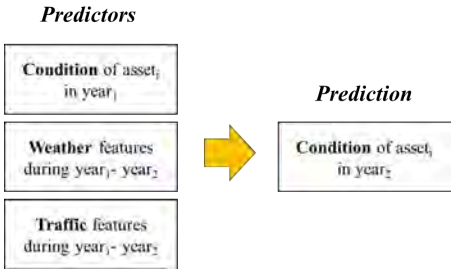

Figure 5. Single asset prediction modeling procedure

In the other scenario, we added the historical condition of the nearby assets in both the prior and the prediction years into the feature space as well (nearby-asset prediction modeling). For instance, for predicting the recorded condition of slope (i.e. slope erosion) in 2017, in addition to weather, traffic, and conditions of the slope (slope erosion and erosion patterns) in 2016, the condition of nearby flexible pavement, shoulder, and the condition of the slope under erosion pattern in 2017 were also included in the modeling. In this way, the interrelations between the condition of neighboring assets in the past and also in the year of prediction are taken into account. Figure 6 schematically describes the modeling process used in this study.

In both scenarios, we first performed a feature reduction step to ensure that the considered features are not highly correlated.

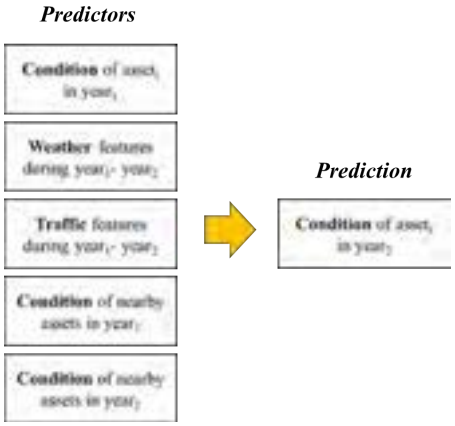

Figure 6. Nearby-asset modeling procedure

3.2.1 Feature Reduction

The efficiency of a multivariable analysis could be highly impacted by multicollinearity among features. Multicollinearity corresponds to the existence of high correlations among some attributes in a dataset, which can bias the result toward correlated attributes [30]. Therefore, we used a correlational investigation to find high correlations between features and to remove multicollinearity.

Given the essence of the considered inputs, we performed the feature reduction in two steps. First, we ensured that there was not any high correlation among continuous features, i.e. weather and traffic, using Pearson correlation coefficients. As a rule of thumb, features whose pairwise absolute Pearson correlation coefficients are more than 0.9 are considered highly correlated [31, 30]. Therefore, we clustered such features and chose only one of them as the only representative of the group.

In the next step, we measured the correlation between the remaining continuous and categorical features, i.e. condition classes, utilizing absolute point-biserial correlation coefficients. Any group of attributes with a more significant correlation than 0.9 were considered as highly correlated and represented with only one of the considered features.

3.2.2 Logistic Regression

After feature reduction, we used logistic regression to develop the condition prediction model, which predicts the probability of each condition category, i.e. pass or fail, for each asset based on multiple independent variables that were available in the dataset, i.e. weather, traffic, and condition. Maximum likelihood estimation was used to evaluate the probability of categorical membership in the binary logistic regression [32, 33]. For example, if y_i is the dependent variable with two categories (0/1), the probability of being in category 1 could be denoted by $\pi_i^{(1)} = \Pr(y_i = 1)$ with the chosen reference category, $\pi_i^{(0)}$. If only one independent variable x_i existed, a logistic regression model would be written as Equation 1:

$$Log\left(\frac{\pi_i^{(1)}}{\pi_i^{(0)}}\right) = \beta_0^{(1)} + \beta_1^{(1)} x_i \quad (1)$$

Wherein $\beta_0^{(1)}$ is the intercept and $\beta_1^{(1)}$ is the regression coefficient. In addition, the probability of being y_i in the reference category (0) is written in Equation 2.

$$\pi_i^{(0)} = 1 - \pi_i^{(1)} = \frac{1}{1 + e^{(\beta_0^{(1)} + \beta_1^{(1)} x_i)}} \quad (2)$$

Therefore, $\pi_i^{(1)}$ can be calculated using Equation 3.

$$\pi_i^{(1)} = \frac{e^{(\beta_0^{(1)}+\beta_1^{(1)}x_i)}}{1+e^{(\beta_0^{(1)}+\beta_1^{(1)}x_i)}} \quad (3)$$

3.2.3 Validation of Prediction Models

After developing prediction models, we validated them using k-fold cross-validation that evaluates and controls the performance of the models over unseen data. We utilized five folds for this purpose.

4 Results and Discussion

This section provides the results that we obtained after applying the proposed methodology to our case study. Figure 7 shows the correlation matrix and corresponding pairwise absolute Pearson correlation coefficients among continuous features i.e. weather and traffic. As it can be observed, traffic features are highly correlated. In addition, TMAXTMIN and DWTMXN30 are highly correlated as well. Therefore, we only considered ADT as the representative of the traffic features, as well as all of the weather features except for TMAXTMIN in the final dataset.

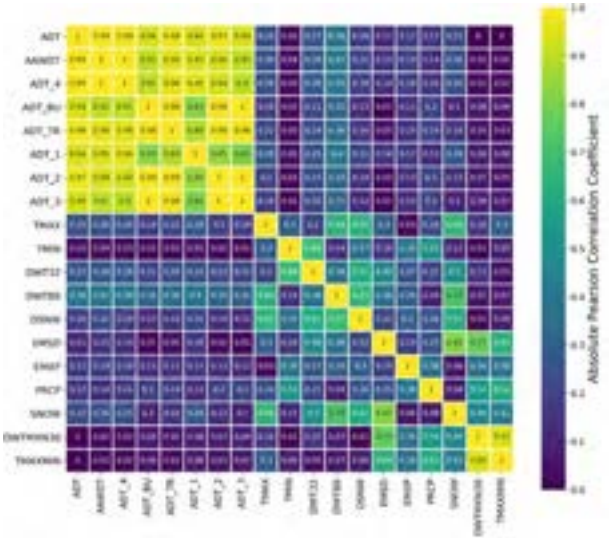

Figure 7. Correlation matrix of continuous features

In the next step, we measured the correlation between the remaining continuous and categorical features (i.e. conditions). The corresponding correlation matrix, using absolute point-biserial correlation, is provided in Figure 8.

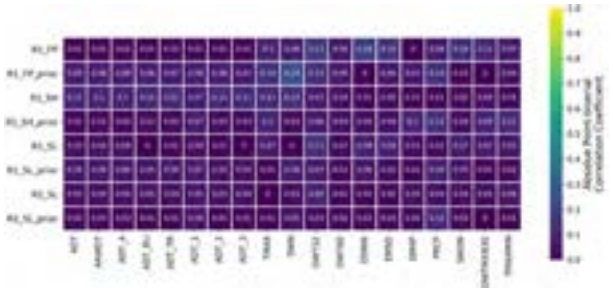

Figure 8. Correlation matrix of mixed features

As Figure 8 suggests, there is not any high correlation in the mixed feature, and we proceeded with the remaining features ensuring that the multicollinearity has been removed.

Next, we fed the reduced dataset into the logistic regression to develop the condition prediction models. We developed the models for each asset in both single asset and nearby-asset modeling scenarios and reported the obtained confusion matrices in Figure 9 and 10, respectively. In addition, the results of the average accuracy of the final validated prediction models for the two considered scenarios are summarized in Table 7. It can be observed that in all cases when the conditions of the nearby asset items were considered in developing the condition prediction model, the accuracy of predictions increased in comparison to single asset prediction models.

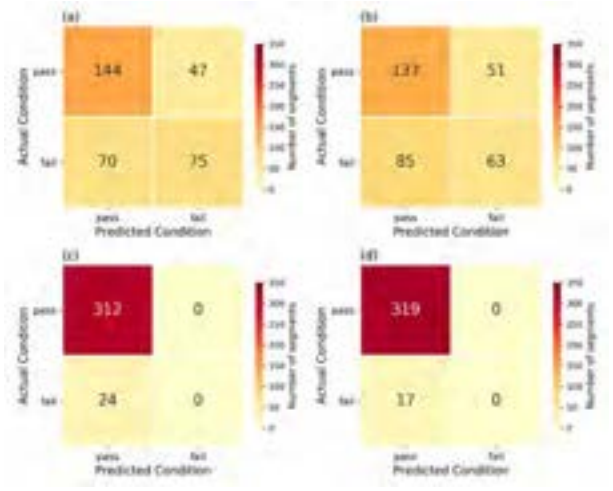

Figure 9. Confusion matrix of single asset modeling: (a) Flexible Pavement-Pothole, (b) Shoulder-Pothole, (c) Slope-erosion, (d) Slope-erosion pattern

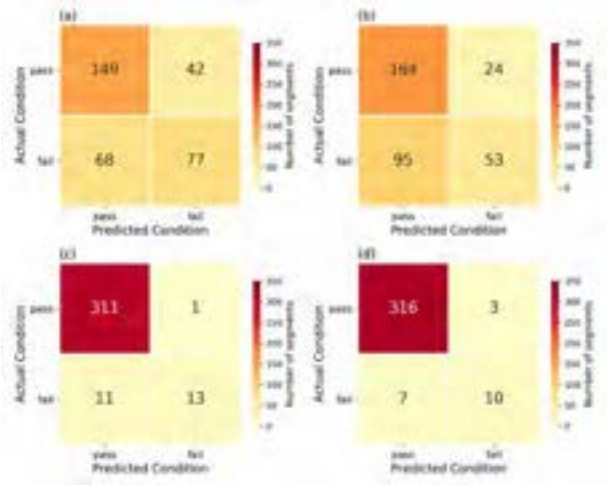

Figure 10. Confusion matrix of nearby-assets modeling: (a) Flexible Pavement-Pothole, (b) Shoulder-Pothole, (c) Slope-erosion, (d) Slope-erosion pattern

Table 7. Summary of the obtained accuracies

Asset/Defect	Accuracy		Improvement
	Single asset	Nearby-asset	
Flexible Pavement-Pothole	65.2%	67.3%	3.22%
Shoulder-Pothole	59.5%	64.6%	8.57%
Slope-Erosion	92.9%	96.4%	3.77%
Slope-Erosion Pattern	94.9%	97.0%	2.21%

5 Conclusion

In this study, we examined the impact of interrelations between nearby assets in the accuracy of their condition predictions. We selected three assets (flexible pavement, shoulder, and slope) to investigate how considering the condition of nearby assets into the condition prediction of each one improves the accuracy of predictions. To this end, we developed prediction models in two different scenarios: when the conditions of nearby assets were and were not considered as a predictor. We then implemented the proposed methodology on a case study in the state of Virginia. The results show that in all of the selected asset items, when the conditions of nearby assets were included in the modeling, the accuracy of condition predictions increased. This highlights the interrelation between nearby assets and its impact on the condition of individual asset items. With potentially increasing the accuracy of deterioration models, the results of this study could benefit the optimization and scheduling of maintenance activities and facilitate planning for an optimum and effective Life Cycle Plan (LCP). In this study, we applied the methodology on three assets. Similarly, the idea could be applied to the other highway asset items with more possible interrelations. Furthermore, we considered weather, traffic, and maintenance as major contributing factors to the degradation of the selected assets. However, other factors such as construction quality potentially impact the condition and could be taken into account in future studies. Another limitation of this study is that we performed the feature reduction using a traditional approach (correlation matrix). It is suggested that future studies utilize other techniques as well.

References

[1] ASCE. *Infrastructure Report Card*, ASCE, Reston, VA. 2017.

[2] Cooksey, S. R., Jeong, D. H. S., & Chae, M. J. Asset management assessment model for state departments of transportation. *Journal of Management in Engineering*, 27(3), 159-169. 2011.

[3] Guevara, J., Garvin, M. J., & Ghaffarzadegan, N. Capability trap of the US highway system: Policy and management implications. *Journal of Management in Engineering*, 33(4), 04017004. 2017.

[4] Le, T., Le, C., & David Jeong, H. Lifecycle data modeling to support transferring project-oriented data to asset-oriented systems in transportation projects. *Journal of Management in Engineering*, 34(4), 04018024. 2018.

[5] *National Commitment to the Interstate Highway System: A Foundation for the Future*. National Academies Press. Washington DC.

[6] Zhu, A. X., Lu, G., Liu, J., Qin, C. Z., & Zhou, C. Spatial prediction based on Third Law of Geography. *Annals of GIS*, 24(4), 225-240. 2018.

[7] Abaza, K. A. Empirical Markovian-based models for rehabilitated pavement performance used in a life cycle analysis approach. *Structure and Infrastructure Engineering*, 13(5), 625-636. 2017.

[8] Anyala, M., Odoki, J., & Baker, C. Hierarchical asphalt pavement deterioration model for climate impact studies. *International Journal of Pavement Engineering*, 15(3), 251-266. 2014.

[9] Halmen, C., Trejo, D., & Folliard, K. Service Life of Corroding Galvanized Culverts Embedded in Controlled Low-Strength Materials. *Journal of Materials in Civil Engineering*, 20(5), 366-374. doi: 10.1061/ (ASCE) 0899-1561 (2008) 20:5 (366). 2008.

[10] Rasdorf, W. J., Hummer, J. E., Harris, E. A., Immaneni, V. P. K., & Yeom, C. *Designing an efficient nighttime sign inspection procedure to ensure motorist safety* (No. FHWA/NC/2006-08). NCDOT, Raleigh, N.C. 2006.

[11] Sun, L., Hudson, W. R., & Zhang, Z. Empirical-mechanistic method based stochastic modeling of

fatigue damage to predict flexible pavement cracking for transportation infrastructure management. *Journal of Transportation Engineering*, 129 (2), 109-117. doi: 10.1061 / (ASCE) 0733-947X (2003)129: 2 (109). 2003.

[12] Falls, L. C., Haas, R., & Tighe, S. Asset service index as integration mechanism for civil infrastructure. *Transportation research record*, 1957(1), 1-7. 2006.

[13] Chopra, T., Parida, M., Kwatra, N., & Chopra, P. Development of Pavement Distress Deterioration Prediction Models for Urban Road Network Using Genetic Programming. *Advances in Civil Engineering*. 2018.

[14] Gao, L., Aguiar-Moya, J. P., & Zhang, Z. Bayesian analysis of heterogeneity in modeling of pavement fatigue cracking. *Journal of computing in civil engineering*, 26(1), 37-43. doi: 10.1061/ (ASCE) CP.1943-5487.0000114. 2012.

[15] Sitzabee, W. E., White, E. D., & Dowling, A. W. Degradation modeling of polyurea pavement markings. *Public works management & policy*, 18(2), 185-199. 2012.

[16] Malyuta, D. A. *Analysis of Factors Affecting Pavement Markings and Pavement Marking Retroreflectivity in Tennessee Highways*. University of Tennessee at Chattanooga. 2015.

[17] Immaneni, V. P., Hummer, J. E., Rasdorf, W. J., Harris, E. A., & Yeom, C. Synthesis of sign deterioration rates across the United States. *Journal of Transportation Engineering*, 135(3), 94-103. doi: 10.1061 /(ASCE)0733-947X (2009)135:3(94). 2009.

[18] Chimba, D., Emaasit, D., Allen, S., Hurst, B., & Nelson, M. Factors affecting median cable barrier crash frequency: new insights. *Journal of Transportation Safety & Security*, 6(1), 62-77. 2014.

[19] Forsyth, R. A., Wells, G. K., & Woodstrom, J. H. *Economic impact of pavement subsurface drainage* (No. 1121). 1987.

[20] Ghabchi, R., Zaman, M., Khoury, N., Kazmee, H., & Solanki, P. Effect of gradation and source properties on stability and drainability of aggregate bases: a laboratory and field study. International *Journal of Pavement Engineering*, 14(3), 274-290. 2013.

[21] Al-Mansour, A. I., Sinha, K. C., & Kuczek, T. Effects of routine maintenance on flexible pavement condition. *Journal of Transportation Engineering*, 120(1), 65-73. 1994.

[22] Coffey, S., & Park, S. Observational study on the pavement performance effects of shoulder rumble strip on shoulders. International *Journal of Pavement Research and Technology*, 9(4), 255-263. 2016.

[23] Karimzadeh, A., Sabeti, S., Burde, A., Tabkhi, H., and Shoghli, O. Spatial-Temporal Deterioration of Multiple Highway Assets: A Correlational Study, *ASCE Construction Research Congress (CRC-2020)*, Tempe, Arizona. 2020.

[24] Virginia Department of Transportation (VDOT). *Virginia Roads*. https://www.virginiaroads.org/. 2019.

[25] Aksoy, S., & Haralick, R. M. Feature normalization and likelihood-based similarity measures for image retrieval. *Pattern recognition letters*, *22*(5), 563-582. 2001

[26] Da Silva, A. S. A., Stosic, B., Menezes, R. S. C., & Singh, V. P. Comparison of interpolation methods for spatial distribution of monthly precipitation in the state of Pernambuco, Brazil. *Journal of Hydrologic Engineering*, 24(3), 04018068. 2018.

[27] Frazier, A. G., Giambelluca, T. W., Diaz, H. F., & Needham, H. L. Comparison of geostatistical approaches to spatially interpolate month-year rainfall for the Hawaiian Islands. *International Journal of Climatology*. *36*(3), 1459-1470. 2016.

[28] Plouffe, C. C., Robertson, C., & Chandrapala, L. Comparing interpolation techniques for monthly rainfall mapping using multiple evaluation criteria and auxiliary data sources: A case study of Sri Lanka. *Environmental Modeling & Software*. 67, 57-71. 2015.

[29] Karimzadeh, A., & Shoghli, O. Predictive Analytics for Roadway Maintenance: A Review of Current Models, Challenges, and Opportunities. *Civil Engineering Journal*, *6*(3), 602-625. 2020.

[30] Yoo, W., Mayberry, R., Bae, S., Singh, K., He, Q. P., & Lillard Jr, J. W. A study of effects of multicollinearity in the multivariable analysis. *International Journal of Applied Science and Technology*, 4(5), 9. 2014.

[31] Bujang, M. A., Sa'at, N., & Bakar, T. M. I. T. A. Determination of minimum sample size requirement for multiple linear regression and analysis of covariance based on experimental and non-experimental studies. *Epidemiology, Biostatistics and Public Health*, 14(3). 2017.

[32] Friedman, J., Hastie, T., & Tibshirani, R. *The elements of statistical learning (Vol. 1)*: Springer series in statistics, New York. 2001.

[33] Wang, Y. A multinomial logistic regression modeling approach for anomaly intrusion detection. *Computers & Security*, 24(8), 662-674. 2005.

A Simulation Approach to Optimize Concrete Delivery using UAV Photogrammetry and Traffic Data

Robert Sprotte[a] and Hani Alzraiee[b]

[a]California Polytechnic State University, San Luis Obispo, United States
[b]California Polytechnic State University, San Luis Obispo, United States
E-mail: rsprotte@calpoly.edu, halzraiee@calpoly.edu

Abstract –

Unmanned Aerial Vehicles (UAVs) are an emerging technology that serve a range of applications for construction purposes including the creation of site survey maps, jobsite monitoring for routine progress reports, and structural inspections. Though while promising, drones have not yet been widely utilized by the construction industry to their fullest potential and there are still many areas to explore. One such activity is utilizing drones to optimize concrete delivery to a jobsite. Ready-mix concrete is an essential part of many projects, but its quick setting time makes proper delivery planning essential. The purpose of this paper is to investigate the application of UAVs and traffic data in scheduling a concrete delivery and develop an overall framework to optimize this activity. The proposed Automated Construction Data Acquisition and Simulation (ACDAS) framework is comprised of three main steps: collection, simulation, and reporting. To implement the concept, traffic data of a construction site in San Luis Obispo, California was collected and EZStrobe discrete event simulation modelling was used to model three potential routes from a local concrete batch plant to the specified job site. The model was able to predict the most efficient route for concrete delivery in a congested traffic area.

Keywords – Unmanned Aerial Vehicles; UAVs; optimization; ready mix concrete; construction planning, delivery

1 Introduction

A large amount of information is involved in the planning of construction projects and the interdependency among information imposes a heavy burden on planners [1]. Construction projects often involve huge operations, with activities taking place over large areas so one of the major issues that construction practitioners struggle with is having real-time control of the project. This is simply because real-time control requires a high volume of real-time data. Without a comprehensive set of real-time data about all parameters that impact the project, it will be difficult to reach the optimum productivity of construction activities. The most common tools used for recording visual data on construction sites include digital cameras, smart phones, tablets, laser scanning devices, and terrestrial and aerial unmanned vehicles [2,3]. Information that is collected manually generally is not comprehensive and does not relate the data to other parameters that impact the project. In recent years, Unmanned Aerial Vehicles (UAVs) have gained popularity thanks to their demonstrated superiority over traditional methods in various construction tasks by offering an opportunity to capture information for visualizing site layout, planning, and organization in real-time [4]. Drones are currently used in construction to examine terrain at future construction sites, track progress at existing construction sites, inventory the assets, and provide routine facility maintenance [5]. They achieve this by using LiDAR (a detection method utilizing lasers) or a technique called Photogrammetry which uses photography to extract measurements of the environment. Overlapping imagery provides multiple perspectives of the same feature and allows for distance and volume measurements to be taken and provides outputs in the form of "point clouds", 3D images used to render the observed environment in a virtual setting [6]. While drones are a proven powerful tool, they have not yet been widely utilized by the construction industry. This has been partly due to low familiarity and autonomy of project teams with the use of the visual data technologies [7]. Because of this, many aspects of the construction process could still incorporate drones to improve efficiency.

One integral activity that could benefit from UAV incorporation is scheduling concrete deliveries to a construction site. Delivering concrete to a jobsite is an essential step in many construction projects and must be completed with precision. Procuring, delivering, and pouring concrete is a major milestone in many projects as concrete is often the foundation. Propper planning is essential as conflicts between delivery and production

will arise during the execution of plans which can cause chaos in operations management [8]. Planning is especially important for the ready-mix concrete (RMC) industry as it has more potential transport barriers than any other manufacturing industry since RMC has a low value-to-weight ratio and is highly perishable as it must be laid on site before it solidifies [9]. Per ASTM C94, concrete discharge should occur within 90 minutes after the introduction of the mixing water to the cement and aggregates [10]. Going over this threshold can result in the batch being sent back to the plant and essentially wasted. Therefore, optimizing the travel time and distance the concrete travels in the truck is extremely important to ensure the concrete is poured within the 90-minute window.

Unfortunately, this time constraint can pose a problem since transportation of RMC is heavily influenced by current traffic conditions such as traffic congestions [11]. Understanding the access routes available for travel to the construction site and their potentials for congestion. While the traffic impact caused by isolated incidents such as car accidents cannot be predicted, understanding overall traffic patterns can be an important tool in concrete delivery planning. The time chosen for a concrete delivery can have a significant impact on the success of the delivery as the travel time between concrete batching plants and construction sites can significantly fluctuate at different hours of the day and on different days of the week [12]. Therefore, barring the unexpected, historical traffic data is a useful resource in selecting the optimal time to leave. In addition to traffic delays, pedestrian and bicycle traffic can also impact concrete dispatch by increasing the amount of time the concrete is in transport. This issue can be assumed to be especially pertinent to college campuses and city centres, locations often undergoing construction activities. All these hurdles pose the question: how can concrete be delivered efficiently?

This constraint can be referred to as the Concrete Delivery Problem (CDP). The CDP aims to find efficient routes for a fleet of (heterogeneous) vehicles, alternating between concrete production centres and construction sites, adhering to strict scheduling and routing constraints. Procuring and coordinating a fleet is especially important since the amount of concrete requested by a single customer typically exceeds the capacity of a single truck [13]. When multiple deliveries are needed, the temporal spacings between the consecutive deliveries may not exceed certain limits (time lags) to prevent the concrete already poured from partially hardening before the rest of the supply arrives at the site [14]. Therefore, with multiple deliveries (variables) required, optimizing the concrete delivery path is essential to avoid time-induced failure.

2 Background

With such a high level of uncertainty in concrete operations travel times, traditional practices for scheduling concrete production and delivery are largely based on trial and error and depend on the dispatcher's experience [15]. Transitioning from this reliance on human intuition to sophisticated data collection and modelling techniques can help to optimize concrete delivery time. This paper seeks to utilize data collected by UAV, Google Maps, and local transportation departments to model and simulate concrete delivery to a construction site. The model output is expected to impact the construction schedule and provide more reliable dates and times to pour the concrete.

2.1 Traffic Impacts on RMC Delivery

Concrete delivery is an integral part of the construction process. RMC delivery planning is mainly determined by skilled batch plant managers that schedule truck assignments to single deliveries and estimate the vehicles needed such that the total demand can be satisfied. The goal is to plan the whole process optimally to ensure utilization of machinery and workers of the batch plant and construction site [11,16]. A major variable in concrete delivery is traffic. Because of this, traffic patterns and their effects on construction activities have been investigated. Carr 2000 created a Construction Congestion Cost system for the Michigan Department of Transportation to balance construction productivity and traffic delay using 5 excel sheets to produce an output of daily user cost, total user cost, and project cost [17]. Naso et al. 2007 determined that on-time delivery of RMC can be significantly affected by peak-hour and non-peak-hour traffic [18]. Hadiuzzaman et al. 2014 directly utilized traffic information by creating a construction-traffic interdisciplinary simulation (CTISIM) framework based on high level architecture [19]. After determining the optimal arrangement of truck-mixers, their deviation between simulated and requested arrival of truck mixers was reduced by 68.7%, compared to the deviation for the arrangement as in the off-peak hour. In addition, their requested and optimized arrival intervals were all below 5.0 min, showing the feasibility of their integrated simulation model. These studies highlight that any useful simulation model for concrete delivery must consider traffic factors and conditions.

2.2 Simulation Modeling

The construction industry has embraced the power of simulation in recent years. Construction Simulation can be defined as the science of developing and experimenting with computer-based representations of construction systems to understand their underlying

behaviour [20]. Various researchers have utilized this to solve problems related to construction planning and activities.

Simulation modelling has been investigated as a means for optimizing scheduling of various construction-related activities. Maghrebi et al. 2015 investigated six machine learning algorithms tailored to RMC dispatching and compared them to observed human decision data that was employed for a specific case study [21]. While some models worked faster than others, they all were more successful than the human-decision control. Torjai and Kruzslicz 2016 sought to optimize the delivery of biomass from satellite storage locations to a central biorefinery and found that the mean trip duration is a good estimation of the minimal number of required trucks and a schedule without truck idle time was always found even when the number of trucks had been locked at its minimum [22]. Razavialavi and AbouRizk 2017 outline a framework to enable planners to anticipate site layout variables (temporary facilities size, location, orientation) and construction plan variables (resources and delivery plans) to simultaneously optimize them in an integrated model [23]. Khan et al. 2017 describes the implementation of a failure mode, effects, and criticality analysis (FMECA) tool and discrete event simulation to assess supply chain risks, identify vulnerabilities, and measure the impact of disruptions of a ready-mix concrete supply chain [24]. Kim et al. 2020 proposes a dynamic model for precast concrete production scheduling by using discrete-time simulation method to respond to due date changes in real time and by using a new dispatching rule that considers the uncertainty of the due dates to minimize tardiness [25]. The results of these studies indicate that simulation modelling is a viable method for planning and optimizing activities and should be investigated for applying to ready mix concrete delivery.

Although these studies indicate that simulation modelling is a proven tool that can be used to charter the optimal path from a concrete batch plant to a job site, they all share a limitation in that they do not account for the impacts smaller scale factors, mainly pedestrians and bicyclists, can have on deliveries to populated areas and many do not explicitly use data collected by drones, which could prove a beneficial addition.

While there are many studies on the impact construction activities have on pedestrians, no previous studies have been found that investigate how pedestrians and bicyclists impact the construction schedule. While this may not seem like an issue at first glance, underestimating the impacts of non-vehicles on construction can have just as much impact when trying to prevent delays. Take, for example, a model that perfectly simulates the local traffic data in San Luis Obispo, California and schedules the optimal concrete delivery to Cal Poly to arrive at 8:05 AM on a Tuesday. This falls during a passing period where thousands of students will be entering and leaving campus on foot and on bike. This severely compromises the simulation model and what was originally thought to be the best choice based solely on vehicular traffic can end up being the worst when pedestrian and bicycle data is included. Therefore, data should be collected on pedestrian and bicycle patterns around populated job sites; this can be accomplished with unmanned aerial vehicles (UAVs).

3 Methodology

The literature review conducted by the authors revealed both drones and simulation modeling are effective tools for construction practitioners, but they have not been combined for concrete delivery applications. The following is a contribution to bridge this gap. Traffic data and drones can be used to provide data to model the optimal delivery scenarios. The proposed framework is named Automated Construction Data Acquisition and Simulation (ACDAS) and consists of three modules.

3.1 Simulation Model

The following sections detail the framework modules created. The steps in sequence are Collect, Simulate, and Report. Fig. 1 summarizes the steps of this framework.

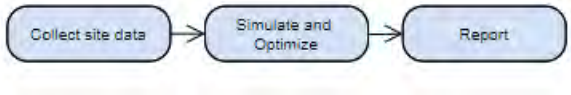

Figure 1. Main Steps of ACDAS Framework

3.1.1 Data Collection

The first step of this framework is to capture relevant traffic data for the potential concrete delivery routes. For this proposal, the data collected is two-fold: traffic data for the roads leading to the site and traffic data immediately on and around the site. Historical traffic data for the roads leading from the concrete batch plant to the job site will be collected from Google Maps, a common GPS system used by drivers (Fig. 2). Google Maps not only provides data for how long a trip will take at the given time; it can also predict the duration of a trip planned in the future based on historical precedents. This allows the eventual model to compare the durations of different paths and different departure times. In addition to Google Maps data, local databases can be utilized to determine information about the roads relevant to the planned delivery. For our experimental study in San Luis Obispo, the County of San Luis Obispo provides Traffic

Counts can provide valuable information to our model [26]. This site lists the peak hour (the time and traffic volume for the highest AM and PM peak hour for the duration of the count) and peak day volume (the day of the week and the traffic volume on the highest day for the duration of the count) for all county maintained roads. This information is compiled for every day of the year from 2015 to present and thus can provide good estimations of historical precedents.

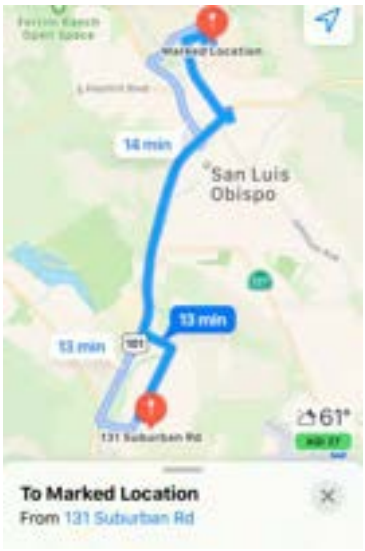

Figure 2. Sample Google Maps routes between a concrete batch plant and construction site.

While traffic data can predict the impact vehicles will have on deliveries, other site-specific factors such as pedestrian traffic and bicycles should be incorporated into the analysis. Drones can be utilized on construction sites to survey conditions around the site to determine when any pedestrian- or bicycle-induced traffic could occur. Drone data collected daily can be fed into the model to determine if there are any patterns in small-scale traffic at specific times in the day to allow the model to account for and avoid these bottlenecks. The following case study is the first iteration of this framework so data from drones was not included but will be the focus of future expansions.

If the collected data is not sufficient, the collection process can be expanded to fill in any gaps. Once all required data is captured and complied, the next step is to input that data into a simulation model.

3.1.2 Discrete Event Simulation Model

The modelling steps of the concrete delivery process are shown in Fig. 3. The first step involved is developing a discrete simulation that depicts the real-world scenario of the concrete delivery process. The model for this study was built using EZStrobe simulation software [27]. EZStrobe is used in the construction industry as a general-purpose simulation system designed for modelling construction processes. However, it is also utilized to model other types of systems because it is domain independent. EZStrobe takes multi-step activities, such as concrete delivery, and models them as just one activity and provides a duration that represents the time it takes to perform all n steps. After the simulation model is generated, it can be run for each of the route alternatives. The model results for each scenario are then analysed and summarized to highlight the most efficient route.

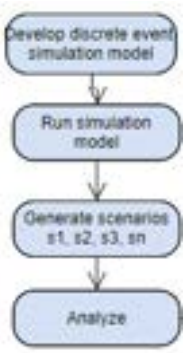

Figure 3. Development of the discrete event simulation model.

3.1.3 Reports

The purpose of this framework is to generate a report that accurately outlines the most efficient delivery path for a truck to take from a concrete batch plant to a job site. The report outputs include: the optimal route to take to the job site, the total delivery duration, the optimal time to start the delivery, the forecasted arrival time, and the number of trucks required. This report will aid Project Managers in planning the concrete pour activities months in advance and will allow the activity to proceed as efficiently as possible when the time comes.

3.2 Experimental Study

The proposed framework was implemented to verify its applicability. The implementation was specifically tried to verify how collected traffic data can help in developing an optimum schedule for the concrete delivery to the construction site. The site investigated in this study is a four-level 102,000 square foot construction project at the California Polytechnic State University campus in San Luis Obispo, California (Fig. 4). This site was selected because it can only be accessed by a limited

Figure 4. An image of the construction site investigated for this study.

number of heavy traffic routes. The goal is to utilize simulation modeling to determine the best route to deliver the concrete to the site to assist the project team in planning this activity efficiently. The preliminary implementation collected traffic data on three routes that started at a local batch plant and ended at the job site; these routes are denoted as R1, R2, and R3 (Fig. 5).

Figure 5. Project site layout before construction with potential delivery routes (Google Maps).

The traffic data collected was sourced using a combination of Google Maps data and local data. This data was fed into a developed simulation model that held the number of trucks available, number of mixing stations, and total amount of concrete required constant for each route (Table 1).

Table 1. Constants used in the simulation model.

nTrucks	Number of Mixer trucks	6
nStations	Number of loading Stati	1
AmtOfConc	Amount of Concrete in CY	720

Three simulations were run to account for each of the three routes. Each analysis follows the life cycle of a single truck and uses statistical modelling to determine the total durations of each step in the concrete pour activity and the total duration of the concrete pour event. The flowchart in Fig 6. summarizes the simulation model created in EZStrobe for Route 1. The circles represent the

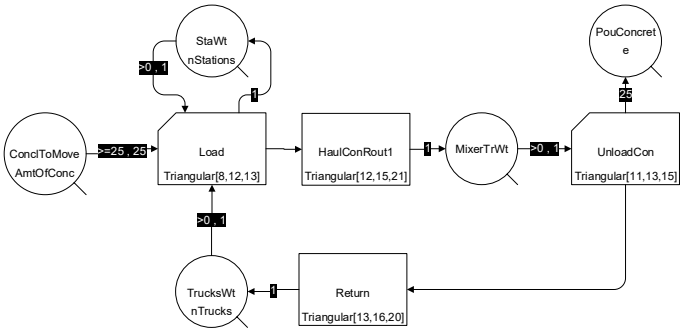

Figure 6. EZStrobe simulation model flow for Route 1.

queuing systems the trucks encounter such as loading and pouring while the rectangles represent the truck entity. When the entity (truck) and its resource (concrete) are two units (i.e. the truck cannot leave until all concrete is loaded or poured) the rectangle has a corner missing and when the entity and resource are one unit (i.e. the truck and concrete traveling together to the job site) the rectangle is intact. The model assumes each truck has a capacity of 25 CY and estimates of the minimum, mean, and maximum durations for each segment in the event (values denoted in brackets in each rectangle). A triangular distribution is used based on these values to determine the overall duration of each 25 CY delivered to the site; this process is repeated until all 720 CY of concrete have been delivered. At the end of the simulation a total activity duration is outputted. The process is repeated for Routes 2 and 3. A summary of the preliminary results for each of the three routes is highlighted in Table 2.

Table 2. Preliminary Results of the Simulation Model

Model Parameters	**S01**	**S02**	**S03**
Number of Mixer trucks	6	6	6
Number of loading Stations	1	1	1
Amount of Concrete in CY	720	720	720
Factory Loading Station Utilization	0.87	0.87	0.85
Mixer Truck utilization	1	1	1
Time of operation in hours	5.9	3.1	5.95
Production rate in CY/hr	133	131	135

The results of this experiment highlight the complex relationship between route selection and delivery time.

Immediately, it is noted from Table 2 that S01 and S03 (R1 and R3) are very similar with total operation times of 5.9 and 5.95 hours, respectively. Conversely, the results for S02 (R2) yield a duration of 3.1 hours, almost three hours faster than the previous two options. Looking at the results for all three routes shows the impact route selection has on the overall duration of a large concrete pour activity. The conclusion that can be drawn from this is R2 should be chosen over R1 or R3 for the concrete delivery in this specific task.

It is important to note that this analysis held the number of trucks present at the jobsite constant at 6 and only compared the different routes. If the number of trucks available were to change this model can quickly show how, if at all, that would impact the optimal route selection. Determining the number of trucks present is another key part of project optimization and is a function of the cycle time of each truck. Because the cycle time is in part determined by how long the trucks are driving from location to location, changing the selected route may (in some cases) allow for additional trucks to be added in the system if their cycle times are reduced substantially. This may be beneficial for projects prioritizing saving time over the incurred costs of expanding the truck fleet. If the number of available trucks is not subject to change under any circumstances this model will still optimize the trucks in their present condition.

Currently, we are working on including UAV data into the simulation model to account for small-scale factors such as bicycle and pedestrian traffic around the job site. Once the university population is back to normal, UAVs will collect data around the job site to determine time frames of peak-traffic. These times are hypothesised to occur in the morning and at passing periods throughout the day when students and faculty are going to and from classes. Our future analysis will reveal the magnitude of influence of these small-scale factors and if they should be considered in future simulation models. Through data collection, simulation, and analysis of multiple scenarios, better construction productivity can be achieved.

3.3 Conclusion

This paper proposes a framework for simulation modeling and drone integration in planning the delivery of a concrete pour activity. This framework is known as Automated Construction Data Acquisition and Simulation (ACDAS) and is achieved through a three-step process. First, the site conditions are quantified using vehicular traffic data and pedestrian and bicycle traffic data, with vehicular data sourced from Google Maps and local databases and pedestrian and bicycle data sourced from on-site UAVs. Second, a simulation model is developed using the collected information to investigate the many possible scenarios the delivery could take. Third, the model determines the most efficient option and outputs the optimal delivery path and delivery time the trucks will take from the batch plant to the construction site. This study will contribute to the construction industry in two major ways. Firstly, utilization of the ACDAS framework in concrete delivery will improve project performance by increasing the efficiency of concrete deliveries to a job site. This will minimize waste and maximize productivity which will lead to lower costs, fewer delays, and less wasted concrete in concrete activities. Secondly, the easy-to-follow nature of the ACDAS steps busts one of the major myths involving using drones (and other advanced technologies) in the construction industry, implementation is too difficult. With this ACDAS path laid out, it will be much easier for interested parties to invest in the new technologies described and utilize their benefits to improve concrete pour deliveries in their projects. Gaining experience in these technologies could also lead to improvements in other aspects of their projects as simulation modeling and drones have proven to be useful for other construction applications.

Our preliminary experiment proved the efficacy of using vehicular traffic data in a simulation model to determine the optimal route for trucks to take while delivering concrete to the jobsite. These findings are not exclusive to just concrete delivery. The constants in our model (Number of trucks, distance of R1, distance of R2, etc.) can be adjusted to fit other activities and routes relevant to the construction process and a similar analysis can be performed to find the optimal course of action.

A limitation of this framework is the lack of a major case study utilizing the ACDAS process in a large-scale construction project. Because of this, while optimization of individual activities has been tested and proven to work, the theorized effects of this framework have yet to be confirmed. Further research is already under way on expanding this topic to include UAV data and future publications will seek to qualitatively measure the efficacy and results of the ACDAS framework.

References

[1] V.K. Bansal, Potential Application Areas of GIS in Preconstruction Planning, J. Prof. Issues Eng. Educ. Pract. (2016). https://doi.org/10.1061/(ASCE)EI.1943-5541.0000257.

[2] K.K. Han, M. Golparvar-Fard, Potential of big visual data and building information modeling for construction performance analytics: An exploratory study, Autom. Constr. (2017). https://doi.org/10.1016/j.autcon.2016.11.004.

[3] K. Han, J. Degol, M. Golparvar-Fard, Geometry-

and Appearance-Based Reasoning of Construction Progress Monitoring, J. Constr. Eng. Manag. (2018). https://doi.org/10.1061/(ASCE)CO.1943-7862.0001428.

[4] M.H.S. et Al., Potential Application of GIS to Layout of Construction Temporary Facilities, Int. J. Civ. Eng. (2008).

[5] A. Otto, N. Agatz, J. Campbell, B. Golden, E. Pesch, Optimization approaches for civil applications of unmanned aerial vehicles (UAVs) or aerial drones: A survey, Networks. (2018). https://doi.org/10.1002/net.21818.

[6] C. Snow, The Truth About Drones in Construction and Infrastructure Inspection, Skylogic Res. LLC. (2016).

[7] J.S. Álvares, D.B. Costa, Construction progress monitoring using unmanned aerial system and 4D BIM, in: 27th Annu. Conf. Int. Gr. Lean Constr. IGLC 2019, 2019. https://doi.org/10.24928/2019/0165.

[8] Z. Liu, Y. Zhang, M. Li, Integrated scheduling of ready-mixed concrete production and delivery, Autom. Constr. (2014). https://doi.org/10.1016/j.autcon.2014.08.004.

[9] M. Lu, H.C. Lam, Optimized concrete delivery scheduling using combined simulation and genetic algorithms, in: Proc. - Winter Simul. Conf., 2005. https://doi.org/10.1109/WSC.2005.1574553.

[10] ASTM C94, Ready-Mixed Concrete 1, Stand. Specif. Ready-Mixed Concr. (2004).

[11] M. Weiszer, G. Fedorko, V. Molnár, Z. Tučková, M. Poliak, Dispatching policy evaluation for transport of ready mixed concrete, Open Eng. (2020). https://doi.org/10.1515/eng-2020-0030.

[12] M. Durbin, K. Hoffman, The dance of the thirty-ton trucks: Dispatching and scheduling in a dynamic environment, Oper. Res. (2008). https://doi.org/10.1287/opre.1070.0459.

[13] J. Kinable, T. Wauters, G. Vanden Berghe, The concrete delivery problem, Comput. Oper. Res. (2014). https://doi.org/10.1016/j.cor.2014.02.008.

[14] L. Asbach, U. Dorndorf, E. Pesch, Analysis, modeling and solution of the concrete delivery problem, Eur. J. Oper. Res. (2009). https://doi.org/10.1016/j.ejor.2007.11.011.

[15] P.C. Lin, J. Wang, S.H. Huang, Y.T. Wang, Dispatching ready mixed concrete trucks under demand postponement and weight limit regulation, Autom. Constr. 19 (2010) 798–807. https://doi.org/10.1016/j.autcon.2010.05.002.

[16] V. Schmid, K.F. Doerner, R.F. Hartl, J.J. Salazar-González, Hybridization of very large neighborhood search for ready-mixed concrete delivery problems, Comput. Oper. Res. (2010). https://doi.org/10.1016/j.cor.2008.07.010.

[17] R.I. Carr, Construction congestion cost (CO3) basic model, J. Constr. Eng. Manag. (2000). https://doi.org/10.1061/(ASCE)0733-9364(2000)126:2(105).

[18] D. Naso, M. Surico, B. Turchiano, U. Kaymak, Genetic algorithms for supply-chain scheduling: A case study in the distribution of ready-mixed concrete, Eur. J. Oper. Res. (2007). https://doi.org/10.1016/j.ejor.2005.12.019.

[19] M. Hadiuzzaman, Y. Zhang, T.Z. Qiu, M. Lu, S. AbouRizk, Modeling the impact of work-zone traffic flows upon concrete construction: a high level architecture based simulation framework, (2014).

[20] S. Abourizk, Role of simulation in construction engineering and management, J. Constr. Eng. Manag. (2010). https://doi.org/10.1061/(ASCE)CO.1943-7862.0000220.

[21] M. Maghrebi, C. Sammut, S.T. Waller, Feasibility study of automatically performing the concrete delivery dispatching through machine learning techniques, Eng. Constr. Archit. Manag. (2015). https://doi.org/10.1108/ECAM-06-2014-0081.

[22] L. Torjai, F. Kruzslicz, Mixed integer programming formulations for the Biomass Truck Scheduling problem, Cent. Eur. J. Oper. Res. (2016). https://doi.org/10.1007/s10100-015-0395-6.

[23] S. Razavialavi, S. AbouRizk, Site Layout and Construction Plan Optimization Using an Integrated Genetic Algorithm Simulation Framework, J. Comput. Civ. Eng. (2017). https://doi.org/10.1061/(ASCE)CP.1943-5487.0000653.

[24] M.A. Khan, S. Deep, M. Asim, Z.R. Khan, Quantization of risks involved in supply of ready mix concrete in construction industry in Indian scenario, Int. J. Civ. Eng. Technol. (2017).

[25] T. Kim, Y. woo Kim, H. Cho, Dynamic

production scheduling model under due date uncertainty in precast concrete construction, J. Clean. Prod. (2020). https://doi.org/10.1016/j.jclepro.2020.120527.

[26] County of San Luis Obispo Traffic Counts, (n.d.). https://www.slocounty.ca.gov/Departments/Public-Works/Services/Traffic-Counts.aspx, Accessed: 07/15/2020.

[27] P.A. Ioannou, EZStrobe Description, (2019). http://www.ioannou.org/stroboscope/ezstrobe, Accessed: 07/29/2020.

Quality Control for Concrete Steel Embed Plates using LiDAR and Point Cloud Mapping

Hani Alzraiee[a], Robert Sprotte[a], Andrea Leal Ruiz[a]

[a]Department of Civil and Environmental Engineering, California Polytechnic State University, USA

E-mail: halzraie@calpoly.edu, rsprotte@calpoly.edu, alealrui@calpoly.edu

Abstract –

Steel embed plates are a vital component in connecting steel to concrete members. They are most often used in the construction of tilt-wall concrete buildings, but can be used anytime there is a need to attach steel to a concrete panel or slab. Proper anchorage and connection to concrete should follow the ACI standards. Inspections need to verify the correct location (x, y, z) of steel embeds until concrete placements are finished. Typically, embeds should not affect the positioning of reinforcement, unless specifically allowed in the specifications. Currently, the process of ensuring the position of embeds is completed manually, which is costly, time consuming, and involves errors in complex construction. This paper proposes an approach to ensure embeds are positioned as per the design and within the tolerance limits stated in ACI 117. The proposed approach maps the BIM model geometry into a 3D point cloud of the as-built construction. The mapping process uses different computing platforms that eventually result in a position deviation report in the x, y, and z directions. An experiment was developed and conducted in the laboratory to show the applicability of the method. The results showed high accuracy in capturing the steel plates' deviations from the original position and generated a meaningful report for improving quality control and quick rework.

Keywords –

Concrete Embeds; Building Information Modeling; Quality; 3D Point Cloud; LIDAR

1 Introduction

1.1 Overview

Steel embeds are an element of precast concrete construction that take the form of pipes, ducts, sleeves, and conduits [1, 2]. Embeds, also known as headed studs, serve as connectors of concrete and steel as modelled in Figure 1. These elements in embedded steel plates connect to structural steel framing, MEP components, and other elements of construction [3]. Embeds are utilized for purposes of ventilation, passing cables, and wherever proper connection to concrete is necessary [3]. Proper implementation results in cleaner and safer construction practices, whereas oversight in the manufacturing process can lead to system failures and construction delays [2, 3].

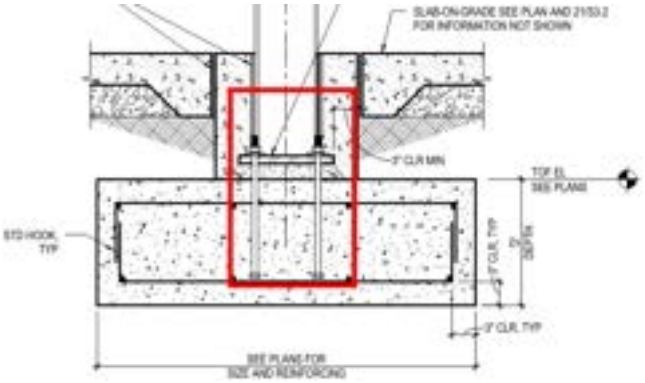

Figure 1. Model of beams connecting to girder at steel embeds.

Per ACI 318, embedment can be manufactured using any material that is not harmful to concrete, and that which is approved by a licensed design professional. Embeds made using aluminium must be coated to prevent corrosive reactions between aluminium and steel. Thus, they are typically manufactured using different materials as designed [1].

1.2 Design

The placement of steel embed plates should follow ACI 318 standards and cannot be implemented where concrete strength is decreased significantly. Proper positioning directly impacts RC strength, such as in the

reinforced concrete beam in a CMU wall shown in Figure 2, and thus guidelines set by ACI 318 and ACI 117 must be followed. Embed placement is permitted where (1) strength of concrete is not significantly decreased, (2) total embedment within a column does not surpass 4% of the area of the cross-section, (3) outside dimensions do not exceed 1/3 of the structure where embedded for pipes and conduits, (4) designed to resist effects of associated materials, temperature, and pressure, (5) not spaced less than three diameters on center, and (6) other limitations in Code 3.6 are maintained [5].

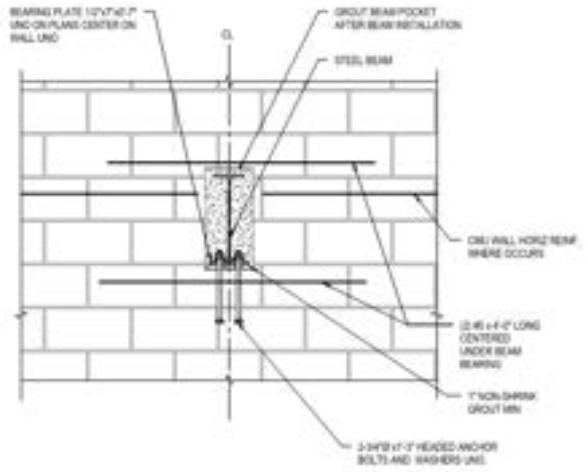

Figure 2. Bearing steel embeds on Concrete Masonry Wall.

Per ACI 117-23, embedment should meet outlined tolerances such that (1) horizontal and vertical deviation from the centreline of the assembly is ±1 in (25 mm), (2) the surface of an assembly from the specified plane for an assembly 12 in. (305 mm) or smaller is ±1/2 in per 12 in (40 mm per m), otherwise, it is ±1/2 in., and (3) anchor bolts and other elements follow through standards outlined [6].

1.3 Coordination and Construction

A careful review of formwork, embed, reinforcing bar, and structural steel drawings should be conducted to regulate work packages from multiple subcontractors [3]. Coordination should run through embed changes guidelines, shipping, on-site operations management, and construction procedures, as well as cover possible conflicts that may arise in any of these fields. Planning should be conducted to reduce potential damage to formwork panels and other structures in the installation of embeds [3]. Clear communication and coordination between parties responsible for design and construction should be the main goal.

Embeds should be placed as per the design. Proper layout reduces discrepancies in as-designed and as-built work. Quality in the field can be preserved by (1) providing sufficient control lines in order to provide accuracy and consistency in layout, (2) checking control lines back to primary control on ground, (3) revising dimensions prior to layout, (4) locating centerline, edges and sizes of embeds, and noting where placement is critical, to name a few [3]. Procedures for layout are outlined by the contractor, but coordination prior to construction is essential to reduce the need for rework in the long run. Installation of concrete should be conducted after all embeds are set, and supervision should be maintained to prevent movement or displacement of embeds as much as possible. Placement of steel embeds in concrete walls or foundations present a great challenge to contractors. The misalignment of these small supports, in addition to non-compliance with code requirements, can result in costly rework and design changes. Hence, it is imperative for contractors to have a tool that allows for a comparison between as-designed and as-built embed locations to capture misplacement or out-of-tolerance variation.

In the past years, smart sensing technologies have gained great interest in the construction sector. Laser scanning and photogrammetry are being used in many aspects of construction. One of them is capturing reinforcement layout and quality of the formwork geometry [4, 7-9]. However, none of these studies address the proper position of concrete embeds prior to concrete casting. Consequently, the objective of this study is to develop an approach to identify the tolerance of the concrete embeds in the three directions (x, y, z).

2 Background

Traditional methods of ensuring embeds are properly placed involve manual inspection performed by quality personnel which is time consuming and costly [10]. Three-dimensional models that capture precise details can be used for planning and coordination of systems like earth retention, safety perimeters, shoring and formwork, post-tensioning, mild reinforcing, embeds, and equipment such as screen walls, tower cranes, and material hoists. Team members at the jobsite can capture value from Building Information Modelling (BIM) by using apps on tablets and smartphones, and workers can transfer coordinates and linework from 3-D models to total stations for concrete layout. The visual nature and the enormous information provided by BIM models help crews understand exactly what they are building and when, while in the field [11]. The approach of directly identifying an object with a laser scanner and comparing it to a uniquely placed object within a BIM model is known as the “Scan-vs-BIM” approach [12]. This allows for a quick and efficient comparison of the as-built state

to the design model to determine if there are any unacceptable discrepancies. This is a common approach used in the relevant research discussed.

2.1 Dimension and position estimation for cast-in-place concrete and other applications

Various studies have been conducted using BIM technologies for quality assurance of concrete structures. Kim et al. describe a holistic approach for dimensional and surface quality assessment of precast concrete elements based on BIM and 3D laser scanning technology. They created a framework consisting of four cores: inspection checklists, inspection procedure, selecting an optimal scanner and scan parameters, and the inspection storage and delivery method. Their BIM and laser scanner quality assessment system were successful in estimating precast panel dimensions with an average error of 2.5 mm and detecting spalling defects with an accuracy of 86.9%. However, their results are limited to precast elements that are rectangular and uniform in thickness and their system did not fully automate the process of comparing the as-built data to the design model [2]. Wang et al. completed a similar study and estimated the dimensions of precast concrete elements with a direct scanning error of 1.7 mm [8]. Kim et al. achieved full automation by developing a non-contact Dimensional Quality Assurance (DQA) technique that automatically and precisely assesses the key quality criteria of full-scale precast concrete elements. They achieved this by developing a new coordinate transformation algorithm to account for the scales and complexities of precast slabs to fully automate the DQA. Precise dimension estimations of the actual precast slab were determined using a geometry matching method based on the Principal Component Analysis (PCA), which relates the as-built model constructed from the point cloud data to the corresponding as-designed BIM model. Lastly, a BIM-assisted storage and delivery approach for the obtained DQA data was proposed so that all relevant project stakeholders can share and update DQA data through the manufacture and assembly stages of the project [4]. Tan et al. used LiDAR and BIM to inspect the geometric quality of individual structural, mechanical, and MEP elements of prefabricated housing units. Their results showed the technique provides inspection results with 0.7 mm and 0.9 mm accuracy for structural and MEP elements [13].

2.2 Related studies on Concrete Embeds inspection

While there are not many studies specifically tailored towards concrete embeds, there has been work done on a similar topic: automated dimensional quality assessment for formwork and rebar of reinforced components. DQA of formwork and rebar is relevant to concrete embeds inspection because embed plate sizes or locations may force altering of formwork tie locations and all embeds should be set before concrete placement — just like the formwork and rebar [3]. Figure 3 demonstrates the interconnectedness of formwork, rebar, and steel embeds as they are all present in the stage of construction that precedes concrete pouring. Because of this, any demonstrated successes in using laser scanners to inspect formwork and rebar can be assumed to have the capacity to inspect steel embeds as well.

Figure 3. Formwork, rebar, and embeds positioned prior to concrete pour.

Kim et al. conducted a study focusing on DQA of formwork and rebar during the fabrication stage. The authors describe a TLS-based automated DQA technique that measures the dimensions of formwork and rebar of RC elements to assess dimensional conformity with design specifications. The proposed method resulted in small average discrepancies in the items measured: rebar spacing (2.15 mm), formwork dimension (2.52 mm), concrete cover (2.18mm), and side cover (3.12 mm). The experimental results demonstrate that the proposed technique yields accurate solutions for the formwork and rebar DQA during fabrication before concrete is poured [10]. Wang et al. developed a system to automatically estimates positions of precast concrete rebar using colored laser scan data. Their technique was successful with the vast majority of differences between the rebar positions estimated by the developed technique and those measured by the manual inspection under 1.5 mm (137 out of 142) and an average difference of 0.9 mm [7]. Gikas combined high accuracy total station and laser scanning surveys to check 3D geometric documentation of the formwork for a highway tunnel in full expansion and compared against the design drawings. The laser

scanner method arc radius of both sides of the formwork deviate from their nominal values by less than 2.0 cm [14]. Turkan et al. used two methods based on extensions of the discussed "Scan vs. BIM" object recognition framework to detect and track temporary structures (formwork, scaffolding, and shoring) and secondary components (rebar). Their experimental results showed it is feasible to recognize secondary and temporary objects in TLS point clouds with good accuracy using their two novel techniques [12].

While the various studies investigated in this literature review are not specifically targeted towards steel embeds in concrete, their demonstrated successes in the areas of rebar and formwork indicate that the technology for high-quality dimensional quality assurance using laser scanners currently exists.

3 Methodology

The proposed components of the approach used to identify the concrete embedded steel plates is shown in Fig. 4. In the following subsections, details are provided on each stage.

3.1 Data Collection

The data of the concrete embed is acquired using FARO Focus 350 [15]. Proper planning of the scan position, resolution, and quality should be completed before conducting the actual scan. A resolution of 1/4 or 1/5 and quality of 4x are reasonable for outdoors in sunny condition scans. The engineer should ensure enough data is collected to ensure enough scans are completed to achieve proper registration with high accuracy.

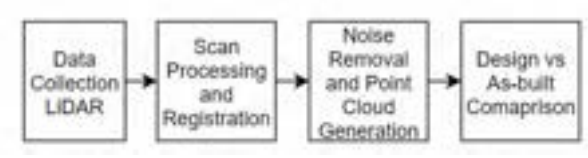

Figure 4. Workflow of identifying concrete embedded steel plates

3.2 Scan Processing and Registration

FARO SCENE software is used to process, register, and generate the point cloud data [16]. Processing the scans is a stage where the captured data is handled to improve the scan quality; this ensures the best results in 3D data. This step is followed by scan registration, which involves aligning multiple scans in a parent coordinate system using reference positions common between scans. These references can be natural or artificial that help in completing the registration.

3.3 Noise Removal and Point Cloud

During the data collection, the required scan parameters are identified. These parameters determine if the scan is acceptable or not. Based on these parameters the scan limit can be defined. Scan points outside of the acceptable parameters are considered "noise." Different filters such as Outlier, Dark Scan Points, and Smooth are available in SCENE software and can be applied to minimize the noise in the data. Once the scan nose is removed from the registered scans, the final step involves generating and exporting the point cloud model that will be used in the analysis and the as-built comparison.

3.4 Design Vs As-Built Comparison

The comparison of the BIM model to the as-built model to determine the deviation can be done in different ways. This step can be completed by comparing the BIM model to an as-built point cloud or comparing old as-built to new as-built. The latter is most widely used in quality control. The analysis of different as-builts is completed using CloudCompare vs2.11.0 [17].

4 Experiment and Results Analysis

The proposed approach involved testing in the lab by building a formwork of a square concrete footing with rebar and steel embed plates. Then, the footing was scanned to generate the as-built point cloud. In the next stage, the steel plate position was modified, and another round of scanning was completed to generate a second as-built point cloud model. In the following sections, more details are provided about the experiment and testing procedures.

4.1 Experiment

The designed BIM model of a concrete footing is shown in Fig. 5a. This plan view shows the dimensions of the footing and distances in relation to the steel plates. The footing itself was designed to be 1.17 m wide by 1.22 m long. The distances from the edge of the steel plates to the short inner edge of the footing are 0.21 m and 0.20 m. The distance between the steel plates is 0.40 m. The distances from the outer edges of the steel plates to the longer inner sides of the footing are 0.48 m and 0.45 m. The footing formwork has a depth of 2 ft and #4 rebar used in both directions. Fig 5b shows an image of the constructed formwork of the footing, steel plates and rebar. Fig 5c shows the point cloud of the scanned footing. This 3D point cloud informs on the dimensions of the actual structure, and the deviations from the intended design. By comparing the constructed footing measurements with measurements obtained from the point cloud model, the results show that a deviation of

0.7 mm is captured for one side and a 0.3 mm deviation between Fig 5a and 5e. The scanner registration accuracy is 0.7 mm as shown in Fig 5d. In conclusion, the scanner achieved high accuracy and can be used to verify the measurement and conduct quality control in construction.

5a) with the as-built point cloud model of the footing (Fig 5c) or, Method 2: compare as-built point cloud model (Fig 5b) to a modified as-built model (Fig 6). In this experiment, we used Method 2. After constructing the footing as per the BIM model, the footing was scanned to

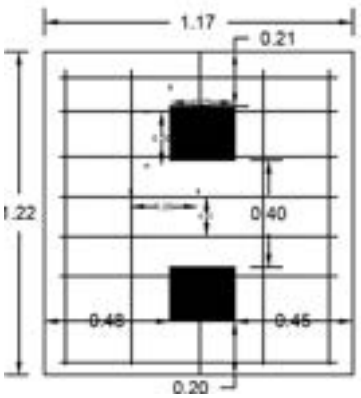

a) BIM model

b) Constructed footing

c) 3D Poind Cloud of the footing (as-built 1)

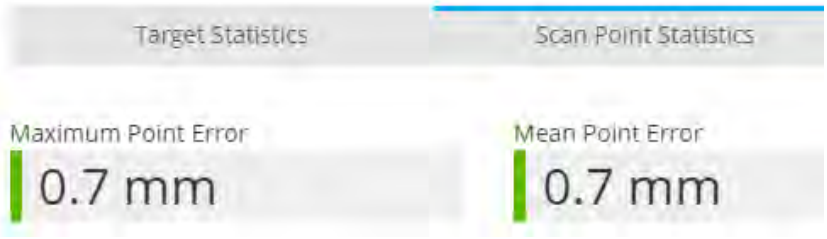

d) Scan registration results.

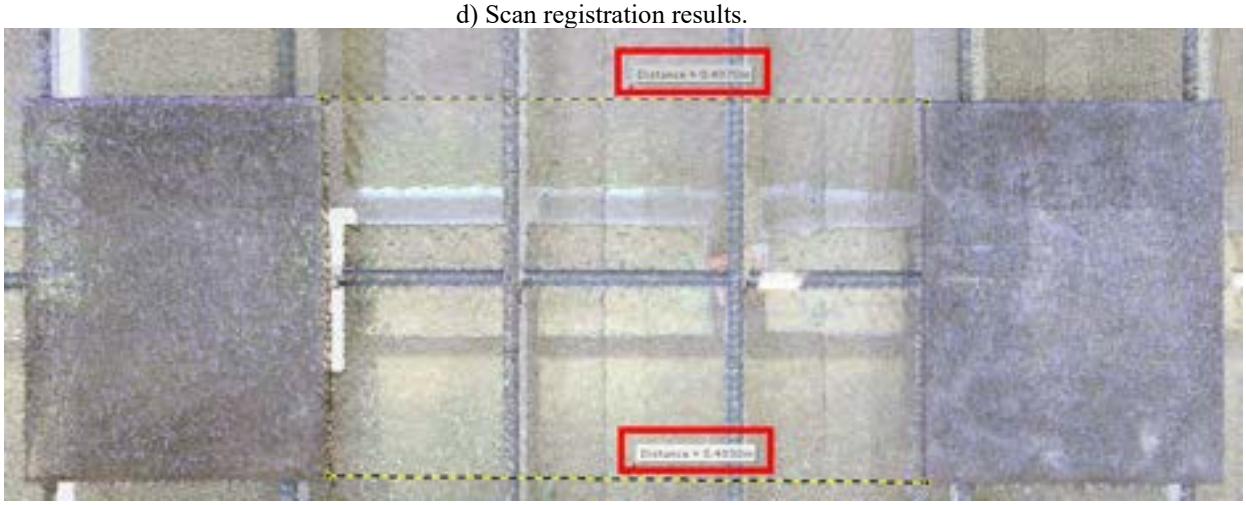

e) Steel Embed Plates Spacing and Position

Figure 5. Experiment Design and Components

4.2 Results and Analysis

The proposed approach can be verified in two different ways. Method 1: compare the BIM model (Fig

create an as-built model (as-built 1). In the next stage, we modified the steel plates' location, as shown in Fig. 6, and then rescanned to generate another point cloud model (as-built 2). The embed placements were changed from

the layout in Figure 5c to the layout in Figure 6. Each layout was scanned using the FARO 350 laser scanner, and the new layout was compared to the original. Figure 7 shows the two layouts with embeds 1 and 3 denoting the original placements and embeds 2 and 4 being the final positions.

Figure 6. New layout with steel embed plates shifted to the left (as-built 2).

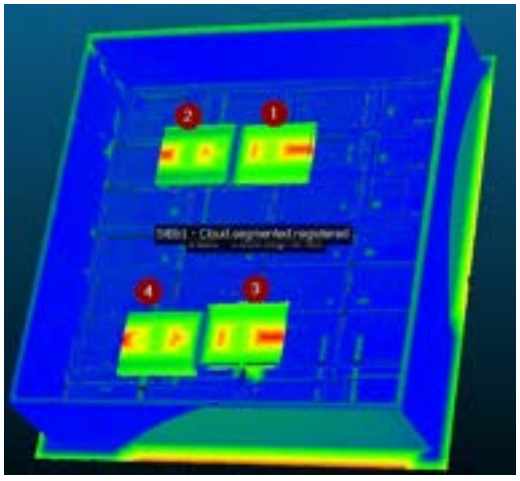

Figure 7. Original embed locations (1 and 3) and moved locations (2 and 4).

Figure 8 shows the heat map that was generated in the model analysis comparing the moved embeds (embeds 2 and 4) to the original layout (embeds 1 and 3). The heat map essentially detects and informs engineers if the embeds are in the correct position by overlaying the as-designed model with the as-built model. For this experiment, the heat map highlights areas in blue to denote negligible change (less than 0.5 mm) between the two scans, which is correct because no adjustments were made there. However, the location where the embeds were moved to is in stark contrast with the surrounding rebar with deviations ranging from 3 cm to 8 cm. This is because the model expected this location to have rebar, but instead it has embeds. Note that the largest deltas, marked with red and orange, occur at the areas that should have open space but now have embed plates. The regions where the embed is on top of rebar still have a difference but the heat map shows a smaller delta because the difference in elevations between the rebar and embed plate is smaller than the elevation changes between the bottom of the formwork and the embed plates.

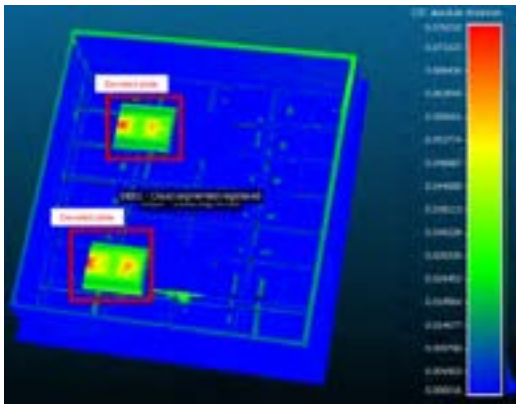

Figure 8. Heat map identifying out of compliance regions.

In addition to identifying which areas are out of compliance, it is also helpful to know how far the items have moved to assist in adjusting the layout to its correct position. Comparing the original and moved layouts provides distance values for how far out of tolerance each embed is. The delta of the left corner of each embed is measured by the software as shown in Figure 9. The shift of the top embeds from location 1 to 2 was 0.262 m horizontally. The shift of the bottom embeds from location 3 to 4 was 0.269 m in magnitude with components in the x, y, and z directions identified. Note that the model can capture differences in a three-dimensional coordinate system which provides precise direction on how far out of tolerance the items are.

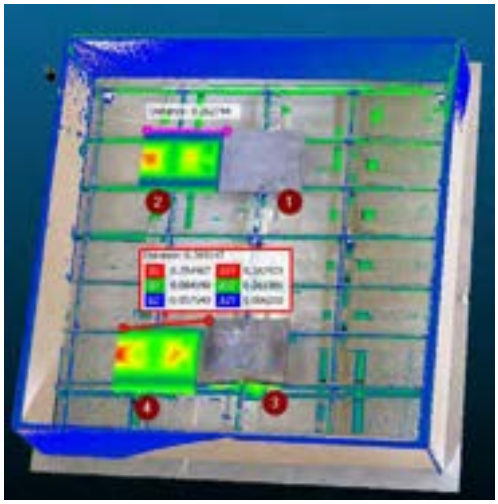

Figure 9. Determination of how far the embeds moved.

This experimental study showed a successful application of LiDAR technology to inspect the as-built conditions of formwork with steel embed plates. The scan created an accurate point cloud model of the formwork and extracted dimensions. CloudCompare vs2.11.0 compared the two scans and generated a heat map that showed the differences between the two. This application can significantly improve rebar and embed inspections, especially for large sites, by linking all the deviations to surveying data to quickly identify what items are out of compliance and where they are.

5 Conclusion

Rework and quality control of steel embed plates installation in construction are difficult tasks for construction professionals. Even small deviations in embeds position can be costly to correct, especially after the concrete hardens. This paper proposed a method to enhance the quality control of steel embed plates installed in concrete and verifies the geometry of the formwork. The method uses a high-quality LiDAR system (laser scanner) and multiple analysis platforms. A 3D point cloud model that is generated from the laser scanner allows for better analysis and reduction of costly rework compared to traditional methods.

The developed method was implemented using a FARO Focus 350 laser scanner. A custom-built 1.17m x 1.22m formwork was built with rebar and steel embed plates placed as per the BIM design that was created. The constructed formwork was scanned to generate an as-built model of the formwork (as-built 1). Then, the position of the steel embed plates was modified and another round of scanning and registration was completed to generate as-built 2. Cloud to Cloud comparison was conducted to capture the deviation the two as-built models in three directions (x, y, z). The experiment showed high accuracy in the results (0.3 mm). This methodology will be especially helpful for capturing the deviation of complex steel embed plates layout so construction practitioners can quickly inspect concrete formwork and embeds. Using LiDAR for concrete embeds inspection will result in increased time and labor savings and can be extremely helpful to construction practitioners.

Future research will focus on developing a tool that automatically captures the deviations once the design and point cloud model are loaded. Currently, the process follow many steps to generate the deviation report. Thus, eliminating steps that require user input will speed up the process and make the framework more user-friendly.

Data Availability

All data generated from this study is available upon request from the first author.

Acknowledgment

This research is supported by Research, Scholarly, and Creative Activities grant program from California Polytechnic State University, San Luis Obispo.

References

[1] Hamakareem, M. I. (2018). “Embedments in Concrete and When it is Used in Reinforced Concrete.” *The Constructor*, <https://theconstructor.org/concrete/embedments-reinforced-concrete/21700/> (Jun. 28, 2020).

[2] Kim, M.-K., Cheng, J. C., Sohn, H., and Chang, C.-C. (2015). “A framework for dimensional and surface quality assessment of precast concrete elements using BIM and 3D laser scanning.” *Automation in Construction*, 49, 225–238.

[3] Klinger, J., Salzano, F., Manherz, T., and Suprenant, B. A. (2018). “Constructability of Embedded Steel Plates in Cast-in-Place ...” *CECO Concrete Construction*, Concrete International, <https://www.cecoconcrete.com/wp-content/uploads/2018/10/Constructability-of-Embedded-Steel-Plates-in-CIP-Concrete.pdf> (Jun. 28, 2020).

[4] Kim, M.-K., Wang, Q., Park, J.-W., Cheng, J. C., Sohn, H., and Chang, C.-C. (2016). “Automated dimensional quality assurance of full-scale precast concrete elements using laser scanning and BIM.” *Automation in Construction*, 72, 102–114.

[5] ACI Committee 318, “Building Code Requirements for Structural Concrete (ACI 318-14) and Commentary (ACI 318R-14),” American Concrete

Institute, Farmington Hills, MI, 2014, 519 pp.
[6] ACI Committee 117, "Standard Specification for Tolerances for Concrete Construction and Materials (ACI 117-10) and Commentary (ACI 117R-10) (Reapproved 2015)," American Concrete Institute, Farmington Hills, MI, 2010, 76 pp.
[7] Q. Wang, J.C.P. Cheng, H. Sohn, Automated estimation of reinforced precast concrete rebar positions using colored laser scan data, Comput. Aided Civ. Inf. Eng. 32 (9) (2017) 787–802, https://doi.org/10.1111/mice.12293.
[8] Q. Wang, M.-K. Kim, J.C. Cheng, H. Sohn, Automated quality assessment of precast concrete elements with geometry irregularities using terrestrial laser scanning, Autom. Constr. 68 (2016) 170–182, https://doi.org/10.1016/j.autcon.2016.03.014.
[9] S. Yoon, Q. Wang, H. Sohn, Optimal placement of precast bridge deck slabs with respect to precast girders using 3D laser scanning, Autom. Constr. 86 (2018) 81–98, https://doi.org/10.1016/j.autcon.2017.11.004.
[10] Kim, M.-K., Thedja, J. P. P., and Wang, Q. (2020). "Automated dimensional quality assessment for formwork and rebar of reinforced concrete components using 3D point cloud data." Automation in Construction, 112, 103077.
[11] Erickson, K. (2020). Emerging technologies in concrete construction. Concrete International, 42(1), 26-29.
[12] Turkan, Y., Bosché, F., Haas, C. T., and Haas, R. (2014). "Tracking of secondary and temporary objects in structural concrete work." Construction Innovation, 14(2), 145–167.
[13] Y. Tan, S. Li, Q. Wang, Automated Geometric Quality Inspection of Prefabricated Housing Units Using BIM and LiDAR, Remote Sens. (2020). https://doi.org/10.3390/rs12152492.
[14] Gikas, V. (2012). "Three-Dimensional Laser Scanning for Geometry Documentation and Construction Management of Highway Tunnels during Excavation." Sensors, 12(8), 11249–11270.
[15] FARO. FARO Focus Laser Scanners. On-line: https://www.faro.com/products/construction-bim/faro-focus, Accessed: 15/05/2020.
[16] FARO. FARO Focus SCENE Software. On-line: https://www.faro.com/products/construction-bim/faro-scene/, Accessed: 15/05/2020.
[17] CloudCompare. 3D point cloud and mesh processing software. On-line: https://www.danielgm.net/cc/, Accessed: 15/08/2020.

Exploring Gerontechnology for Aging-Related Diseases in Design Education: An Interdisciplinary Perspective

R. Hu[a], T. Linner[a], M. Schmailzl[a], J. Güttler[a], Y. Lu[b], and T. Bock[a]

[a]Chair of Building Realization and Robotics, Technical University of Munich, Germany
[b]Department of Industrial Design, Eindhoven University of Technology, Netherlands
E-mail: rongbo.hu@br2.ar.tum.de, thomas.linner@br2.ar.tum.de, marc.schmailzl@tum.de, joerg.guettler@br2.ar.tum.de, y.lu@tue.nl, thomas.bock@br2.ar.tum.de

Abstract –

Aging society is not only a crisis in the developed world but also a severe challenge in some emerging economies. However, the awareness of population aging and gerontechnology is far from sufficiently addressed in the architectural design education in universities. Therefore, an interdisciplinary approach in design education is urgently needed to raise the awareness of the aging crisis among the future architects, interior designers, and beyond. This article introduces a novel model of a design seminar offered by a German University, addressing population aging issues in the architecture department. The syllabus, formality, and the expected results of the seminar are revealed in detail. The participants are encouraged to apply interdisciplinary knowledge such as barrier-free architecture, mechanical engineering, electrical engineering, robotics, medicine, psychology, and business to achieve the goals of the seminar. Based on the originality and degree of completion, several students' works are selected and reported, targeting a variety of diseases or syndromes related to aging, such as dementia, immobility, and tremors. Overall, participants of this seminar are motivated and have positive feedback on this seminar, oftentimes claiming that they have seldom studied similar topics in previous architecture education. This enables students from architecture as well as other fields to be better prepared to tackle the upcoming challenges such as labor shortages and infectious diseases in a rapidly aging world. Furthermore, the seminar creates novel concepts that serve as a win-win "honeypot" for both students and their instructors, potentially sparking research topics and start-ups with concepts fostered in this seminar.

Keywords –

Aging-related diseases; Bauhaus 2.0; COVID-19; Dementia; Design education; Gerontechnology; Interdisciplinary

1 Introduction

The worldwide crisis of population aging has drawn the attention of more and more countries. According to the United Nations, the percentage of global older population 60 years or over is expected to rise to 21% by 2050 compared to 13% in 2017 [1]. Many studies pointed out that as the average life expectancy of the world's population increases, the number of people suffering from aging-related diseases increase as well. Therefore, the significance of gerontechnology became prominent in recent years. The terminology of gerontechnology was officially proposed at the 1st International Congress on Gerontechnology, Eindhoven, Netherlands in 1991 [2]. It is a broad interdisciplinary domain that includes subjects such as gerontology, assistive technology (e.g., medical devices, home automation, companion robots, etc.), and inclusive design. Ever since its establishment, researchers and developers around the world continuously made contribution in this field. In architectural design education, however, population aging and gerontechnology does not seem to draw sufficient attention. Furthermore, it is predictable that the ongoing coronavirus pandemic will fundamentally reshape architectural design, challenging doctrines formed since the Modernist Movement such as open plan and shared spaces in order to assist and protect habitants especially the vulnerable elderly [3]. As a result, gerontechnology naturally becomes a powerful tool in this transition. Therefore, future architects and interior designers need to be prepared to respond to the challenges that aging society brings. In conjunction, architecture educators need to provide them with opportunities to study in the related fields.

2 Research aim

This paper reveals an innovative method of teaching interior design seminars in the context of aging society,

mimicking the environment of a business incubator, which distinguishes itself from traditional interior design studios. It involves cross-disciplinary knowledge in inclusive design, mechanical engineering, electrical engineering, robotics, medicine, psychology, and business, based on the key concepts and methods of a large European research project. The results of selected student projects addressing several commonly seen aging-related diseases or syndromes will be presented. Last but not least, the effectiveness and key learnings of this teaching process will be discussed.

3 Methods

Oftentimes, in an interior design or architecture studio, after reviewing exemplary designs, a certain design task is given to the students. Next, students and instructors work together, pushing their sketches iteratively into final plans and renderings. In the end, the design is presented in the form of posters and architecture models.

The seminar presented in this paper entitled "Incubator" is offered to the master level students primarily from an architecture background, also among other fields. Incubators are used in the innovation science and industry to specifically generate innovations or to systemize the innovation process. The aim of the seminar is to let the student study and develop their projects using interdisciplinary knowledge in a simulated environment of an incubator. The key concepts and methods of this seminar are based on the REACH project, a large European interdisciplinary research project aiming at developing customized healthcare systems to promote the elderly's activity level and independence [4]. In REACH, a special type of smart furniture named Personalized Intelligent Interior Unit (PI^{2}U) was developed, which seamlessly integrates the required functions (e.g., unobtrusive sensing and monitoring, training/gaming, nutrition, AI assistant, etc.) into the different living environments. The development process of the PI^{2}Us (including but not limited to PI^{2}U-SilverArc, PI^{2}U-MiniArc, PI^{2}U-SilverBed, PI^{2}U-ActivLife) follows iterative design principles on both hardware and software levels, which allows the project team to optimize the products through prototyping, testing, analyzing, and refining (see Figure 1).

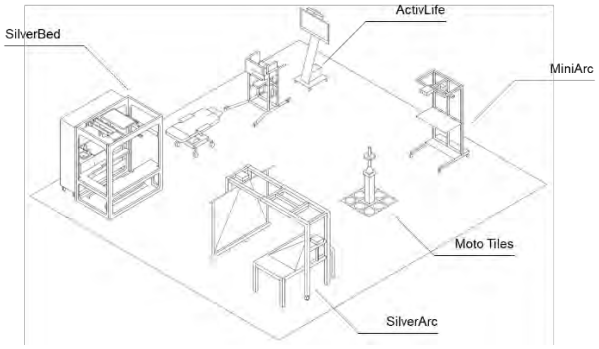

Figure 1. Various PI^{2}Us developed in the REACH project

Based on a variety of PI^{2}Us, the project team proposed a modularized smart home solution, namely the Total Room Assistive Care Kit (TRACK) concept (see Figure 2), which integrates PI^{2}Us and key technologies in REACH to create a complete interior living and care environment for elderly users in different living environments such as home, hospital, and community [5].

Figure 2. TRACK concept including real-life testing of the PI^{2}Us

At the beginning of the seminar, the instructors provide an overview of the key concepts and methods in the REACH project and give various lectures on topics such as the phenomenon of population aging, aging-related diseases, gerontechnology with a special focus on the field of Ambient Assisted Living (AAL), and previous examples from both selected student projects and other relevant research projects such as USA² [6] and LISA "Habitec" [7]. After, specific tasks are defined for all groups with expectations to develop their own approaches and strategies of the solutions based on the abovementioned concepts and methods. The proposed solutions must be interdisciplinary approaches, combining knowledge in barrier-free architecture, mechanical engineering, electrical engineering, robotics, medicine, psychology, and business. Seminar and demonstration sessions are held in the chair's laboratory. By supervising the students' work and evaluating their intermediate presentations, the progress is ensured, and relevant questions are discussed. This process fosters students' awareness of subject-specific problems, and furthermore, uncovers their personal weaknesses and strengths. Through this problem-oriented approach, the course participants are motivated and thus maximize their knowledge gain. The teaching process is highly student-oriented. Work groups are intentionally formed, comprising students from various backgrounds. The instructors actively assist them with both problem solving as well as developing and improving the student's concepts within the project task.

The expected results from the group work are supposed to include 1) an overall study of a specific target disease (or in some cases a series of diseases with certain similarities) related to aging, 2) a systematic and interdisciplinary design solution to assist the target elderly patients to independently perform their activities of daily living (ADLs) in the form of design drawings, mock-ups or prototypes, and/or experiment setups, and 3) business aspects of the proposed solution (e.g., business model generation, a simplified cost-benefit analysis, etc.). At the end of the seminar, students are to present their project solutions in front of the whole class and the course instructors in order to finalize the whole semester's progress and outcomes.

4 Results

As mentioned above, at the end of the semester, student groups are to present their projects in front of the seminar participants and instructors, targeting various diseases or syndromes associated with aging, such as dementia, mobility impairments, and tremors. Several selected works representing a variety of perspectives of diseases are reported as follows.

4.1 Dementia

The word "dementia" comes from Latin, literally meaning "without mind". According to the World Health Organization, dementia is "a syndrome in which there is deterioration in memory, thinking, behaviour and the ability to perform everyday activities" [8]. A large number of the world population is suffering from dementia, and Alzheimer disease is estimated to contribute to 60-70% of the cases. By 2015, roughly 47 million people suffer from dementia and the number is expected to reach 132 million in 2050 [9]. In Germany, for example, more than 1.6 million people were affected by dementia [10]. With no effective treatment currently available to cure it or reverse its progression, the dementia epidemic has a significant negative impact in terms of physical, psychological, economic, and social aspects, not only on the patients themselves, but also on their caregivers, families, and society. Therefore, innovative solutions are needed to mitigate the impact of this disease. In the following sections, three assistive systems, MAK, METIS, and Dooropener are proposed by the course participants to address the severe challenges brought by dementia.

4.1.1 Kitchen for dementia sufferers: Project MAK

The aim of the Modular Adaptive Kitchen (MAK) is to create an Ambient Assisted Living (AAL) concept for a kitchen that supports people who suffer from dementia. Although many ideas that have been implemented to support people with this condition, few holistic concepts fully meet the physical and mental demands of a dementia patient. This project explores an approach that addresses critical challenges by utilizing advanced technologies, such as assistive technology and automation. Eating and drinking are two of the most basic human needs. As a result, daily nourishment is one of the strongest driving fields of human behavior. Due to increased life expectancy, the number of those who suffer from dementia worldwide is also increasing. Among other aspects, this disease is associated with the inability to accomplish everyday tasks. People who suffer from dementia also lose the normal urge to take in nourishment over time. The patients can no longer assess the importance of adequate nutrition and fluids, nor understand the dangers related to malnutrition. In addition to the physical meaning of eating and drinking, food can also influence feelings, evoke memories, stimulate contacts and relationships, and ultimately influence the well-being and quality of the patients' life in a positive way.

Figure 3 depicts the kitchen system, composed of functional modules, a sliding system, and a guidance system. The functional modules ensure high customizability and flexibility for the individual users.

The sliding system not only offers height adjustment and accessibility for both standing patients and users of wheelchairs, but also prevents patients from reaching possibly hazardous products as the disease advances. The guidance system includes symbol stickers to remind the users of the right locations of items meanwhile keeping the integrity and elegance of the kitchen, and a combination of a projector and a motion sensing device (e.g., Microsoft Kinect) which projects a gesture-operable user interface to guide patients' cooking step by step. The advantages of this kitchen system benefit all members of society, especially people with dementia [11].

Figure 3. Modular Adaptive Kitchen for dementia patients (Image: A. T. Braun and M. Zanchetta)

4.1.2 Assistive home system for dementia sufferers: Project METIS

The Multifaceted Equipment to Independence System (METIS) for dementia sufferers (METIS) comprises an assistive home system for people suffering from dementia. After a comprehensive analysis on dementia, including its general specifics, forms, courses, and treatments, a research on caregivers was conducted. The research revealed an increasing number of elderly people affected by the disease within care of informal caregivers and living alone because of a highly important correlation between home and identity. Therefore, a special emphasis was placed on prolonging the independence of seniors and their preferred stay at home on the backdrop of architectural guidelines for physical and cognitive support. The various needs of a person with dementia have to be met in order to ensure their individual comfort. This requires a flexible and modular system, which can adapt to said needs. This system is specifically designed for seniors who live independently or are in home care. Different concepts for health, database, orientation, safety, and process guide yield METIS. One of the key components of the project is the multifunctional floor tiling system. The system features embedded microchips that ensure the interconnectivity, integrated pressure-powered energy generators and storage units that provide electricity for the whole floor titling system, and an embedded RGB LED lighting system that creates an illuminated path to remind the user of his or her daily routes. In addition, the embedded pressure sensors can be integrated with a gaming system to perform various productive games (see Figure 4).

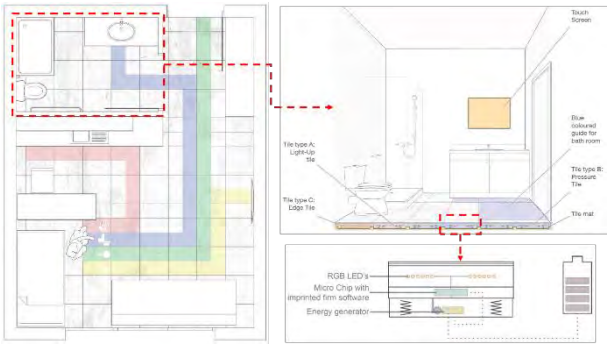

Figure 4. The assistive smart floor tile system (Image: J. Bielski and L. Alsammak)

4.1.3 Smart door handle for people living with dementia

Demographic change is one of the most impactful challenges for our aging population facing new socio-economic, technical and health challenges. We therefore need to find new design solutions to assist older people to stay independently, safe and keep them in a good mood to prevent social isolation. The design of the smart door handle can provide a solution to help older adults to improve their quality of life.

The design responds to the progressive condition of dementia with a modular, as well as adaptive system for three different dementia stages. The three focus aspects of the design configuration variants are mood (for early stage of dementia), independence (for mid stage of dementia) and safety (for late stage of dementia). The system consists of the door, door handle, speaker, passive infrared (PIR) sensor for silent alarm, light module, intelligent switch, security switch and interface (see Figure 5).

Based on the term anticipation, the intent of the project was to design a door system which prevents people suffering from dementia at home and in nursing home from leaving a designated area or building when doing so could otherwise endanger themselves or others. People living with dementia exhibit behavioral disturbances such as mood disorders or wandering,

which can lead to serious safety issues. That is why the system has a few security features such as the security switch, intelligent switch, and speaker to prevent wandering. Additionally, the system keeps them in a good mood through mood nudging with a light module, as well as guarantee their independence through the progressive condition of dementia. The project seeks to combine intuitive technology with a minimalistic form to create a design that can be universally implemented.

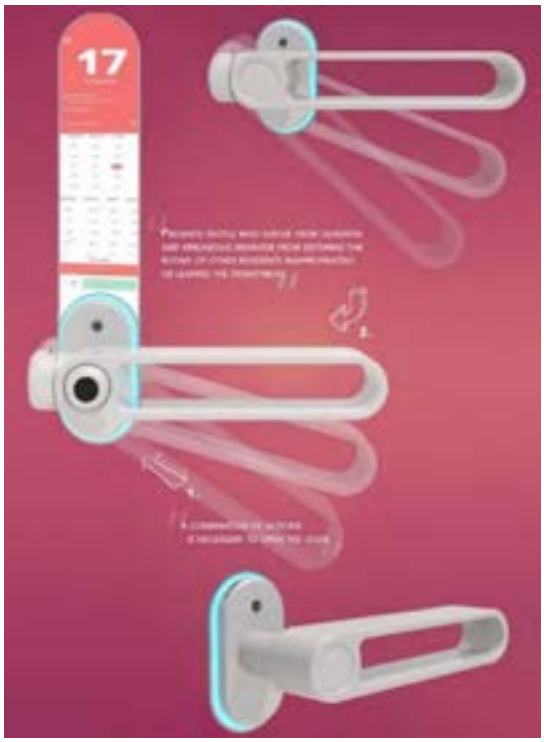

Figure 5. Three configurations for three stages of dementia (Image: M. Schmailzl)

4.2 Mobility impairment

Mobility impairment generally refers to the lack of ability of a person to use one or more limbs in order to move. In general, there are two types of mobility impairments: orthopedic and neurological, both of which have a negative impact on patients' quality of life as well as the healthcare system. Research suggests that among the elderly people aged between 60 to 69 years old, the epidemic of disability in mobility as well as basic and instrumental ADLs is growing at a significant rate [12]. Rosenberg et al. summarized that increasing physical activity has strong benefits on physical, cognitive, and mental health for all age groups, let alone the older adults [13]. Therefore, developing systems that assist patients with limited mobility to move independently meanwhile promoting their activity level is substantially beneficial. In the following sections, such kind of a proposal developed by the course participants will be reviewed.

4.2.1 Interior mobility assistance: Project 3D Movement

Individuals without mobility are exposed to a list of physical and mental problems that affect many of their organs. The 3D Movement system slows the progressive decline of a patient's functions, allowing the users to take care of themselves. Considering the patient's age and physical condition, consistent and intelligent physical activity could reduce or even prevent the degeneration of the patient's state. Researchers have proved that muscular stem cells will decrease with time, but with training, these cells continually regenerate, counteracting the process of aging. The proposed system is designed to support the patient by making movement possible and preventing falls. Assuming the system will be used by people who can stand up on their own, but have difficulties moving independently, the machine allows the patient to regain autonomy in basic daily tasks (e.g., going to the bathroom, cooking, or walking around the living space). Through the integration of a mechatronic system with an appropriate guide-and-support "vest", the system will keep the user in a steady position while preventing the user from falling. When the user intends to move, the force sensor will detect the direction and strength of the movement and move in a safe velocity accordingly. Therefore, the user will be able to move independently while being safe and feeling secure (see Figure 6). As a result, the physical and mental conditions of the patient will improve. The objective of the 3D Movement system is to help people with reduced mobility of all ages, by creating a system that eliminates the use of a wheelchair within confined space. The system can be fitted in hospital rooms and particular types of homes, further benefiting a variety of members of society [14].

Figure 6. Visualization of 3D Movement interior mobility assistance (Image: F. Martini and C. Guernier)

4.3 Parkinson's disease

Being the second most common neurodegenerative disorder, Parkinson's disease (PD) is a progressive nervous system disorder specially affecting the elderly community. It affects about 6 million people around the world, and the number of patients is expected to double over the next generation [15,16]. Without a known cure as of today, PD oftentimes leads to tremors, rigidity, disability, long-term care (LTC), deteriorated quality of life, and eventually premature death, which put increasing burdens on the caregivers and affect the patients and their families both financially and emotionally [17].

Therefore, it is important to create environments that can assist PD patients' activities of daily living (ADL) while minimizing the need for constant care. Therefore, one course participant proposed Project PATRICK ("Parkinson's and Tremor Rehabilitation Interior Care Kit") to empower the PD patients to enhance their ADL through architecture, industrial design, and mechatronics techniques.

4.3.1 Parkinson's and tremor rehabilitation interior care kit: Project PATRICK

This project begins with research into the diseases prevailing in the elderly community. The primary focus is on PD; hence the project is named PATRICK. The research revealed issues with mobility for a large majority of patients, drawing focus on independent movement through the project. The project aims to integrate multiple systems within the architecture of the home, concealing "assistance" and encouraging independence.

Developed through the project focusing on the primary tasks of daily living, there are four systems: the walking assistance, sleeping assistance, fall assistance, and dining assistance. The project creates a secured circulation handrail system for patients within the wall that can extend out when the embedded touch sensors are triggered. The handrail system (walking assistance) is ubiquitous for the entire circulation of the apartment, connected to the sleeping station and eating station. The bed structure (sleeping assistance), maneuvered by a pulley system hidden in the ceiling, can assist the patients to change positions (e.g., lying, sitting, etc.). Meanwhile, the floor and ceiling work together to detect falls and assist the patients with a descending handle. In addition, the dining assistance integrated within the walking assistance features an integrated exoskeleton arm to offset tremors of the user's arm while eating (see Figure 7). In this sense, the entire interior space of the home becomes an assistive robot for the PD patients. The minimalist design ensures that PATRICK can be easily installed and operated within any space, creating a plug-and-play system. Through the research of the disease, understanding its symptoms, investigating current assistive systems on the market, PATRICK make independence possible for PD patients.

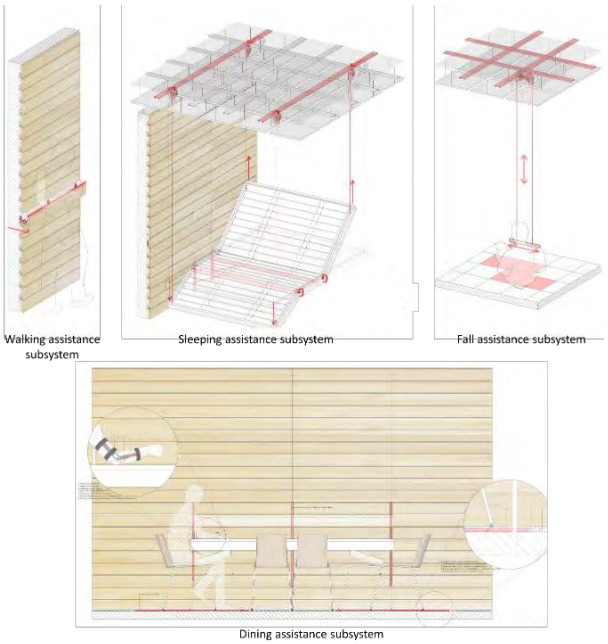

Figure 7. Four subsystems proposed in project PATRICK (Image: H. Bavishi)

5 Discussion

In this paper, the authors presented an interdisciplinary approach in design education to raise awareness of the aging crisis among the future architects and interior designers. Several exemplary results from the participants of this course are revealed in detail.

Experts in related fields already predicted that emerging technologies will have a substantial impact on society, such as replacing a large amount of human jobs [18,19]. Moreover, there is no doubt that emerging technologies will also significantly influence higher education in many aspects in terms of admission, curricula, and organization. Ma and Siau suggested that advanced technologies should be introduced in the curricula of all faculties, not just in STEM majors (i.e., science, technology, engineering, and mathematics), in order to enhance students' ability to adapt to the rapid development in technology [20].

It is widely known that Germany's Bauhaus Movement revolutionarily transformed our world as well as the design education system since its establishment in 1919 [21]. As its founder, Gropius, famously said in the Bauhaus Manifesto [22], the goal of the movement is to "create a new guild of craftsmen, free of the divisive class pretensions that endeavored to

raise a prideful barrier between craftsmen and artists". 100 years have passed since the initiation of the Bauhaus, and facing the severe challenges caused by population aging and emerging technologies today, a "Bauhaus 2.0" Movement, which refers to applying cutting-edge emerging technologies to the education approach of the Bauhaus, is needed to tackle these challenges. To summarize, the key features of both movements can be seen in the following formulas (Figure 8).

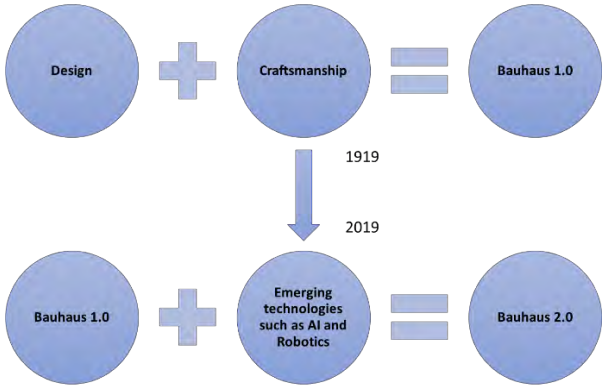

Figure 8. Equations of the Bauhaus 1.0 and the Bauhaus 2.0

As a result, the seminar reported in this paper created a win-win "honeypot" for both students and academic researchers. On the one hand, most students were motivated in the beginning and satisfied in the end of the course because as many claimed they have never experienced such kind of course in architectural education before. The benefits they gain is manifold: the participants obtained a deeper understanding of the impact of population aging through studying various aging-related diseases; they reinforced their design skills in the context of ongoing aging society; they also cultivated an interdisciplinary and flexible mentality in order to better embrace the upcoming age of AI and robotics; more importantly, they learned to collaborate with peers in a simulated business incubator environment. On the other hand, researchers can potentially foster the students to further co-develop their project results into scientific research projects, innovative products, and business startups.

In addition, this approach will inspire educators in the design field to experiment with novel curricula in their teaching practices. Furthermore, the COVID-19 pandemic started in late 2019 has fundamentally changed our society in many aspects. It forces us to rethink the status quo in elderly care today. A trend of applying advanced technologies such as robotics and AI in disease prevention, screening, diagnosis, and operation has already been observed, which especially protects and benefits the elderly individuals who are among the most vulnerable population to the novel coronavirus [23]. Apparently, gerontechnology introduced in the above-mentioned course goes in line with this trend and beyond, making the students better prepared to develop intelligent living environments that promote independent living and well-being of the elderly in the future. The methods and proposals from the past design seminars presented in this paper are by no means an exhaustive range of possibilities. The opportunities for new architectural and technological innovations for aging society are endless, especially with the ever-increasing demand for the young yet promising research field of gerontechnology integrated in the built environment.

Acknowledgements

The research has received funding from *the European Union's Horizon 2020 research and innovation programme* under grant agreement No 690425. In addition, the authors would like to express their gratitude to all participants of the course over the years, especially to A. T. Braun, M. Zanchetta, J. Bielski, L. Alsammak, F. Martini, C. Guernier, and H. Bavishi who share valuable contents to make this paper possible.

References

[1] United Nations. World Population Prospects: The 2017 Revision, Key Findings and Advance Tables. On-line: https://population.un.org/wpp/Publications/Files/WPP2017_KeyFindings.pdf, Accessed: 07/08/2020.

[2] Bouma, H. Gerontechnology: making technology relevant for the elderly. In H. Bouma, & J. A. M. Graafmans (Eds.), *Gerontechnology* (pp. 1-5). (Studies in health technology and informatics; Vol. 3). Amsterdam: IOS Press, 1992.

[3] Chayka, K. How the Coronavirus Will Reshape Architecture. *The New Yorker*, 2020. On-line: https://www.newyorker.com/culture/dept-of-design/how-the-coronavirus-will-reshape-architecture, Accessed: 07/08/2020.

[4] Linner, T., Seeliger, A., Vogt, L., Schäpers, B., Steinböck, M., Krewer, C., & Bock, T. REACH: Solutions for Technology-Based Prevention and Empowerment for Older People and their Caregivers. *Journal of Population Ageing*, 13(2): 131–137, 2020. https://doi.org/10.1007/s12062-020-09268-5

[5] Hu, R., Linner, T., Trummer, J., Güttler, J.,

Kabouteh, A., Langosch, K., and Bock, T. Developing a Smart Home Solution Based on Personalized Intelligent Interior Units to Promote Activity and Customized Healthcare for Aging Society. *Journal of Population Ageing*, 13(2): 257–280, 2020. https://doi.org/10.1007/s12062-020-09267-6

[6] Linner, T., Güttler, J., Georgoulas, C., Zirk, A., Schulze, E., and Bock, T. Development and Evaluation of an Assistive Workstation for Cloud Manufacturing in an Aging Society. In R. Wichert & H. Klausing (Eds.), *Ambient Assisted Living: Advanced Technologies and Societal Change*, pages 71–82, Cham: Springer International Publishing, 2016. https://doi.org/10.1007/978-3-319-26345-8_7

[7] Güttler, J., Linner, T., Bittner, A., Engler, A., Schulze, E., and Bock, T. Development and Evaluation of Assistive Terminals for the Improvement of Functional Performance of the Elderly in a Variety of Life Centers. In *Proceedings of the first international symposium on applied abstraction and integrated design (AAID)*, Yokohama, Japan, 2017.

[8] World Health Organization. Dementia. On-line: https://www.who.int/news-room/fact-sheets/detail/dementia, Accessed: 07/08/2020.

[9] World Health Organization. Global action plan on the public health response to dementia, 2017-2025. On-line: https://apps.who.int/iris/bitstream/handle/10665/259615/9789241513487-eng.pdf;jsessionid=93778462CBE241FDE2B7DE43580442F3?sequence=1, Accessed: 07/08/2020.

[10] Michalowsky, B., Flessa, S., Hertel, J., Goetz, O., Hoffmann, W., Teipel, S., and Kilimann, I. Cost of diagnosing dementia in a German memory clinic. Alzheimer's Research and Therapy, 9(1), 2017. https://doi.org/10.1186/s13195-017-0290-6

[11] Braun, A. T., Zanchetta, M., Hu, R., and Pawlitza, K. MAK– Modular Assisted Kitchen for Dementia Sufferers. In Proceedings of International Conference on Smart, Sustainable and Sensuous Settlements Transformation (3SSettlements), page 55–62, Munich, Germany, 2018.

[12] Seeman, T. E., Merkin, S. S., Crimmins, E. M., and Karlamangla, A. S. Disability Trends Among Older Americans: National Health and Nutrition Examination Surveys, 1988–1994 and 1999–2004. *American Journal of Public Health*, 100(1): 100–107, 2010. https://doi.org/10.2105/AJPH.2008.157388

[13] Rosenberg, D. E., Bombardier, C. H., Hoffman, J. M., and Belza, B. Physical activity among persons aging with mobility disabilities: shaping a research agenda. *Journal of Aging Research*, 708510, 2011. https://doi.org/10.4061/2011/708510

[14] Martini, F., Guernier, C., Hu, R., and Pawlitza, K. 3D Movement – Assistive System for People with Reduced Mobility. In *Proceedings of International Conference on Smart, Sustainable and Sensuous Settlements Transformation (3SSettlements)*, page 70-76, Munich, Germany, 2018.

[15] De Lau, L. M. L., and Breteler, M. M. B. Epidemiology of Parkinson's disease. *The Lancet Neurology*, 5(6): 525–535, 2006. https://doi.org/10.1016/S1474-4422(06)70471-9

[16] Poewe, W., Seppi, K., Marini, K., & Mahlknecht, P. New hopes for disease modification in Parkinson's Disease. *Neuropharmacology*, 171, 108085, 2020. https://doi.org/https://doi.org/10.1016/j.neuropharm.2020.108085

[17] Heinzel, S., Berg, D., Binder, S., Ebersbach, G., Hickstein, L., Herbst, H., … Amelung, V. Do We Need to Rethink the Epidemiology and Healthcare Utilization of Parkinson's Disease in Germany? *Frontiers in Neurology*, 9, 500, 2018. https://doi.org/10.3389/fneur.2018.00500

[18] West, D. What happens if robots take the jobs? The impact of emerging technologies on employment and public policy. Centre for Technology Innovation at Brookings. On-line: https://www.brookings.edu/wp-content/uploads/2016/06/robotwork.pdf, Accessed: 07/08/2020.

[19] Oxford Economics. How robots change the world: what automation really means for jobs and productivity. On-line: https://www.automation.com/pdf_articles/oxford/RiseOfTheRobotsFinal240619_Digital.pdf, Accessed: 07/08/2020.

[20] Ma, Y., and Siau, K. Higher Education in the AI Age. In *Proceedings of the 25th Americas Conference on Information Systems*. Cancun, Mexico, 2019

[21] Droste, M. *Bauhaus*. TASCHEN, 2019.

[22] Gropius, W. Manifesto of the Staatliches Bauhaus. On-line: https://bauhausmanifesto.com/, Accessed: 07/08/2020.

[23] Yang, G.-Z., J. Nelson, B., Murphy, R. R., Choset, H., Christensen, H., H. Collins, S., … McNutt, M. Combating COVID-19—The role of robotics in managing public health and infectious diseases. *Science Robotics*, 5(40), eabb5589, 2020. https://doi.org/10.1126/scirobotics.abb5589

Changing Paradigm: a Pedagogical Method of Robotic Tectonics into Architectural Curriculum

Xinyu Shi[a, b], Xue Fang[a, b], Zhoufan Chen[c], Tyson Keen Phillips[d] and Hiroatsu Fukuda[a]

[a]Faculty of Environmental Engineering, The University of Kitakyushu, Fukuoka, Japan
[b]iSMART, Qingdao University of Technology, Qingdao, China
[c]Perkins and Will, Los Angeles, United States
[d]Robotics Lab, IDEAS Campus, A.UD UCLA, Los Angeles, United States
E-mail: sxy@qut.edu.cn, fangxue@qut.edu.cn

Abstract –

With the rapid spreading of digital technology and automated construction applications in architecture, engineering and construction (AEC) society, the current trend is becoming clearer, that automation will change the way we design and build. Robotic Tectonics, as a part of automatic construction methods aiming to achieve the integration workflow from architectural design to finial construction products, emerged from architectural profession for a decade. Avant-garde architects explored the possibility of this new design paradigm through creating the integration of digital design software within the simulation and controlling of robotic construction, and only recently, this completed digital workflow pushes architectural design to re-control the process from initial design conception to finial physical construction, guiding the AEC industry towards a precise, efficient, thus more sustainable development.

However, a success technology innovation is based on the widespread acceptance, where education plays an important role, but in the current architectural education, there is barely no professional courses focused on this. The need to find a framework to integrate the robotic tectonics workflow with architectural curriculum is increasing. Therefore, it became mandatory to integrating and testing of the complete robotic tectonics workflow into architectural curriculum.

In this paper, a pedagogical method of robotic tectonics is defined through a linear scenarios of four stages, based on experiences gleaned from 'Robotic Tectonics' workshops and various other teaching practices. Then this pedagogical method is tested into an architectural curriculum with 135 undergraduate students, for each student, the complete participation of the overall process and questionnaires is required. Results shows this pedagogical method introduces multi-layered interdisciplinary knowledge to architecture students and enables them to using related technologies of robotic arms for automated construction practices, changing the paradigm of architectural curriculum for new design and build processes that will redefine architecture in the near future.

Keywords –

Robotic Tectonics; Architectural Education; Pedagogical Method; Digital Workflow; Architectural Curriculum

1 Introduction

As the industrial revolution replaces manpower with machines to produce large-scale production, it will gradually change our production and lifestyle. Automation technology becomes the key to accelerate transitions of the manufacturing industry from traditional inefficient and labor-intensive mode to present an opportunity to do things more efficiently, accurately, and creatively. As the most representative tool to promote the wave of automation technology, robots have been widely used, especially in the automotive industry. However, like every technological upgrade process, the field of architecture, engineering, and construction (AEC) industry is still in an exploring period of shifting the conventional technology to the advanced technology.

Nevertheless, a bunch of advanced technology applied into AEC industry has enlightened a digital future for the architectural design field, the combination of parametric design tools, design and multi-data simulation, automated construction and robotics. The most advanced technologies start shifting the conventional design methods to the next efficient design workflows. This brings the opportunity to fully realize MacLeamy's curve which advocates shifting design effort forward in the project, frontloading it, in order to archive high-efficiency design process and high-performance architecture eventually (Figure 1). Following the

pavement contributed from the avant-garde architects, like Fabio Gramazio and Matthias Kohler in Zurich, and the demonstration of developing a workflow that challenged the current limitations of computational digital fabrication in design and construction, we believe the relevance of Advanced Architectural Design method with Robotic Tectonics is growing, and it may have the potential to serve as the catalyst for the automation of construction across the diverse architectural field [1,2].

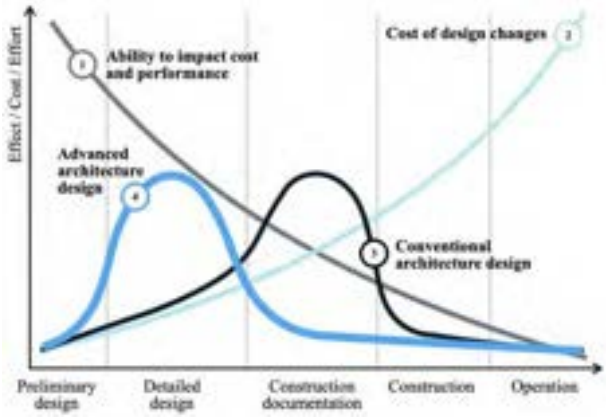

Figure 1. MacLeamy's curve which advocate shifting design effort forward in the project, frontloading it, in order to archive high efficiency design [3].

Therefore, it is necessary to provide future architects in advance with training in new technical techniques and methods suitable for the development of the industry at the educational stage. We believe that successful technology innovation is based on widespread acceptance, where education plays an important role. In recent years, a few of the world's top universities have begun to combine robot manufacturing technology with curriculum design in various forms, such as the representative Harvard University, Carnegie Mellon University, University of Michigan and Princeton University in the United States, University of Stuttgart, ETH Zurich and Delft University in Europe, and Tsinghua University and Tongji University in China, etc. Those are successfully revealed the potential of combining the most frontier advanced robotic technology with the pursuit of humanities and art into the architectural design method under the core concept of architectural tectonics though still at the practice stage. Moreover, we could witness that the ability of robotic tectonics is growing, are advancing in such an efficient and incomparably unstructured environments, as well as has the potential to serve as the necessitated trigger for construction automation in a numerous and diverse field in the future.

From 2015 to the present, we have been eagerly making efforts to find a framework to integrate the robotic tectonics workflow with the architectural curriculum and make it became mandatory to integrating and testing of the complete robotic tectonics' workflow into the architectural curriculum. Thankfully, the feedbacks and opinions collected from students proved that our teaching practice is effective and worthwhile.

2 Pedagogical approach of Robotic Tectonics workflow

with the interdisciplinary requirements and technical difficulty of robotic tectonics, how can we integrate it into architectural education in a simple and understandable way that could allow students to master the necessary skillset while addressing the critical challenge of sustainable development in architecture? As a response to this challenge, we are pushing to establish a novel workflow that can act as a model for a digitally-focused pedagogy and define it within a sustainable framework that combines advanced robotic technology and architectural tectonics. We intend to focus on construction techniques driven by robotics in order to significantly improve material, structural, energetic, and procedural efficiency, all while promoting the aesthetic innovation emblematic of an architectural education. In this linear model, we aim to test the integration of a variety of interdisciplinary techniques in the early design stages, which we believe will aid in the advancement of sustainable development, that changing the paradigm of architectural education. [4-7].

Since its induction in 2016, DAMlab (digital architecture & manufacturing laboratory) has established an experimental teaching platform exploring a myriad of digital tools including 3 KUKA robots (KR120R2700, KR60R2100, KR9R1100) and various CNC machines. Since then, we have hosted several workshops focused on the topic of robotic tectonics. From these last three years of teaching practices, a prominent didactic pedagogical approach has emerged. This new pedagogy is a fully comprehensive robotic tectonic workflow, but it is more easily understood through its four stages – **Parametric Design**: A parametric model-based design conception, **Multi-data Simulation:** robot-oriented multi integral data virtual simulation, **Robotics Application:** Construction-aimed robot end effector development, and **Robotic Construction:** Robotic tectonics represented through automated construction. Within the confines of these individual stages, students can easily break down this overly complex and technically difficult workflow into successive phased steps which each contribute to the learning objectives of this new pedagogy, while simultaneously experience the integrated design to construction workflow which attempting to realize the frontloading concept of

MacLeamy's curve for high efficiency design. (Figure. 2)

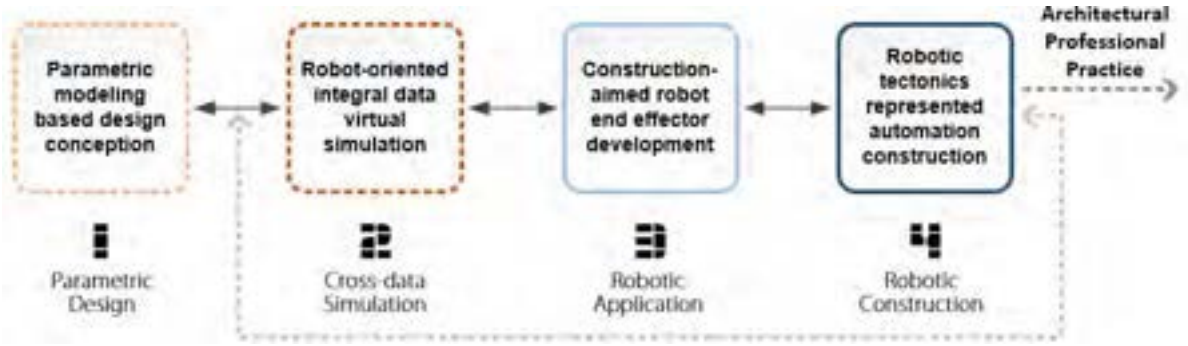

Figure 2. Workflow of the Robotic Tectonics [8]

This pedagogical approach explores the entirety of the typical design and construction cycle, providing the necessary technical skills required to make automated construction into a reality. It expresses a global initiative for students to understand and apply contemporary technology to critical thinking in order to pursue design innovations towards a more sustainable future. Leaders in automated construction practices must be proficient not only in traditional computational and technical skills, but also in a new form of digital materialization which includes a critical understanding of constantly changing manufacturing processes [8].

3 Bricklaying experiment for Robotic Tectonic curriculum courses

The pedagogical method is tested into an architectural curriculum with 135 undergraduate students, for each student, the complete participation of the overall process and questionnaires is required. Our experimental course is conducted in groups. The task of course is to build a columnar brick structure within the range of 0.9m*0.9m*2m, using the standard bricks (200mm*100mm*50mm). The 6-axis KUKA KR30HA robot is applied in this experiment. The robotic arm vertical range of activity is from +35° to -135° with a large turning range of 185°in both directions.

3.1 Pedagogical purpose for bricklaying experiment

The purpose of this course setting is to let students to fully experience the entire robotic tectonic process to systematic understand:

- The theoretical concepts and workflows of "Robotic Tectonic" from design to construction.
- The "Robotic Tectonic" is a combination of Interaction between material and construction, clear and logic structure, and performative architecture.
- The current trends in architectural design and construction technology.
- The modeling and programing techniques, as well as the basic robot working logic and operation skills.

3.2 Experimental content

The four stages of the workflow contents virous works of different levels of interaction, such as information interaction between parametric design and virtual simulation, the parametric design provide geometry generation, program definition, etc. to the virtual simulation process, and get feedbacks as multi-data information, visual configuration, etc. to change design decisions. All these contents are opened reachable for students to experiment with, the whole workflow of experiment contents is illustrated on figure 3.

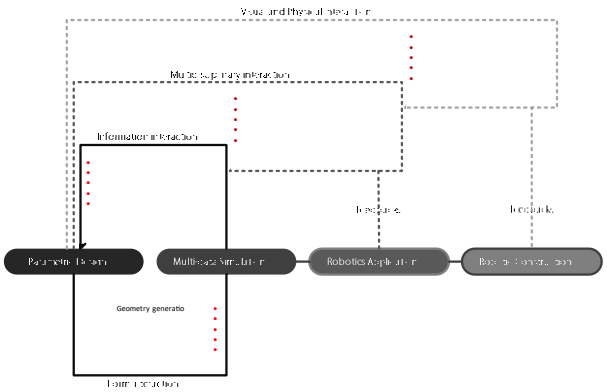

Figure 3. experiment content of Robotic Tectonics workflow

3.3 Bricklaying experiment

3.3.1 Concept and overlapping logic

The priority of a brick structure is to design the overlapping bricks pattern. By deconstructing conventional brick masonry structures, students can learn

the brick overlap logic and its mechanical behaviour, then try to break through the inherent impression of the physical properties of the material itself and further expand the possibilities of the material in design. With the help of digital modelling technology, datum points of curved shapes are generated in Rhino software. After that, a reasonable curve shape is obtained through the algorithm and a curved surface is generated to obtain a basic shape. Then import this basic surface into the parameterized software grasshopper to analyse and arrange the bricks, further optimize the interaction between bricks and bricks by adding functional mapping, object interference and other methods to generate new overlapping logic of the brick structure.

3.3.2 Parametric design for brick structure

The priority of a brick structure design is the overlapping form between bricks. By extracting the logic of brick overlap from the traditional brick structure masonry form, and then by adding function mapping, object interference and other methods to change the interactive relationship between bricks to explore a new spatial logic for the parametric design of brick structure.

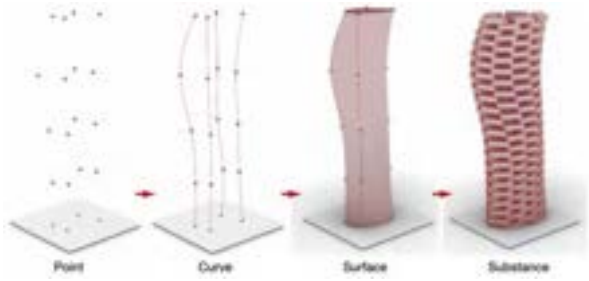

Figure 4. Parametric Design process

3.3.3 Multi-data simulation for brick assembly

The sequences of picking up each brick, reposition it, gluing at certain area on it, locate into a precise spot, and configure the overall processes for the whole structure's building sequence, are fully considered in this stage. (figure 5) Therefore, not only design factors, but also procedure factor, material information, robot operation data, signals, etc. are all integrated and simulated here.

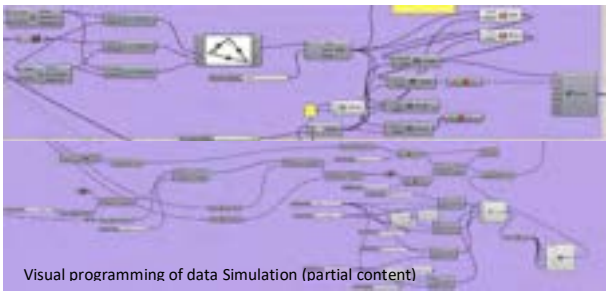

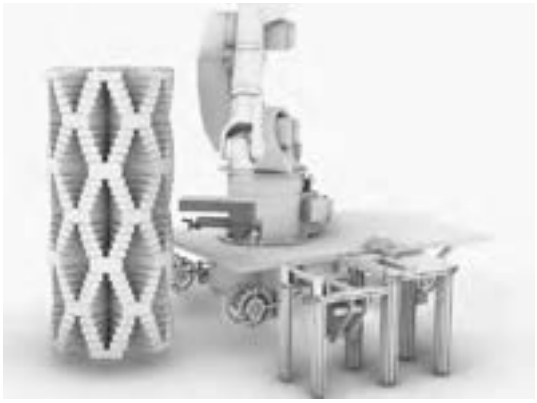

Figure 5. Process of multi-data virtual simulation

3.3.4 Robotics application for bricklaying

Robotics technology of gripper tools, sensing devices, plc components are applied to form a complete end-effector and building environment for the bricklaying.

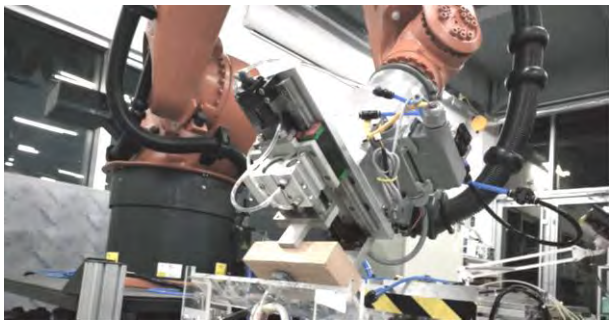

Figure 6. End-effector of robotics application for bricklaying experiment

3.3.5 Robotic bricklaying practice

After setting up the parametric design, multi-data simulation, and robotics application procedures, the final building experiment could be operated (figure 7). During this physical building process, feedbacks could also directly deliver to the previous stages, and manipulate accordingly to the current building situation.

Figure 7. Physical building process

3.4 Experiments results

During the courses, 8 groups of bricklaying experiments are completed, students participate all processes from parametric design to robotic construction. For each stage of the Robotic Tectonics workflow, students have fully experienced through building experiments. Each group of bricklaying project explored virous configurations of robotic bricklaying tectonic, the experiments achievements are fruitful. (figure 8)

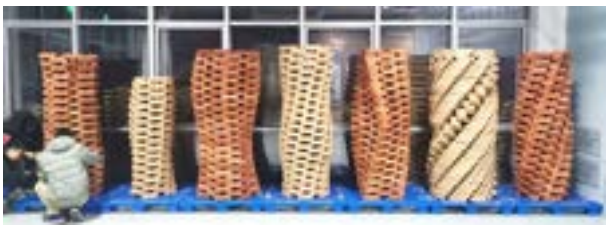

Figure 8. Experiments achievements for courses

4 Teaching questionnaire survey and analysis

To explore the students' perceptions of the proposed pedagogical approach of robotic tectonics and obtain their feedback on teaching effectiveness, we conducted a questionnaire survey of 135 students in the third grade of architecture major who participated in our course. According to the survey, all students' existing relevant knowledge and skill experience of "Robotic Tectonics" has little difference before attending the course. That indicates the feedback information of the questionnaire, which could not be affected by the factor of personal experience, is valid and reliable.

4.1 Comparative analysis between before and after attending the course

The comparative analysis of the results of the questionnaire before and after the course shows in Table 1 that the students have obvious views on the impact of the "Robotic Tectonics" in the AEC industry, the position in the future architectural design and the necessity as the content of the architectural design course. Among them, the proportion of students who believe that "Robotic Tectonics has a great positive influence or plays a dominant approach" has increased from 24.44%, 45.19% (before attending the course) and 42.22% to 68.89%, 75.56% and 54.81% (after attending the course). Similarly, the proportion of students who believe that "Robotic Tectonics has a revolutionary influence or plays an essential decisive approach" has increased from 2.22%, 3.70% and 8.89% to 17.78%, 20.74% and 42.23%, respectively. Then, from the results of internal consistency analysis, the grand mean values of the above set of questions changed a lot from 2.44 to 3.20 and the values Cronbach's alpha increased from 0.442 to 0.791. It means that after experiencing the course learning, the students recognized with more uniform consistency. Most students' opinions have changed from "Robotic Tectonics has a small influence or plays an auxiliary approach" to "that has a great positive influence or plays a dominant approach" on the relevant dimensions of industry, architectural design or professional curriculum.

Table 1. Comparative analysis between before and after attending the course

	Before attending the course		
Questions / Options	Impact on future AEC industry	Role in future architectural design	Role in future architectural design courses
1: No influence / An optional approach	7 (5.19%)	3 (2.22%)	2 (1.48%)
2: Small influence / An auxiliary approach	92 (68.15%)	66 (48.89%)	64 (47.41%)
3: Great positive influence / A dominant approach	33 (24.44%)	61 (45.19%)	57 (42.22%)
4: Revolutionary influence / A necessary approach	3 (2.22%)	5 (3.70%)	12 (8.89%)
Summary of internal consistency	Grand mean	Cronbach's alpha	Sig.
	2.44	0.442	0.000

	After attending the course		
Questions / Options	Impact on future AEC industry	Role in future architectural design	Role in future architectural design courses
1: No influence / An optional approach	1 (0.74%)	1 (0.74%)	0 (0.00%)
2: Small influence / An auxiliary approach	17 (12.59%)	4 (2.96%)	4 (2.96%)

3: Great positive influence / A dominant approach	93 (68.89%)	102 (75.56%)	74 (54.81%)
4: Revolutionary influence / A necessary approach	24 (17.78%)	28 (20.74%)	57 (42.23%)
Summary of internal consistency	Grand mean	Cronbach's alpha	Sig.
	3.198	0.791	0.000

4.2 Improvement of students' design capacity

The analysis of multiple-choice question (Figure 9) finds that the majority of students of (132 people) indicated that the concept of robotic tectonics will continue affecting the architectural design. There are 90 students who reported that their logical thinking improved through the simulation process. There are 86 students considered "human-machine collaboration improves our efficiency". 79 students thought that "robotic tectonics improve the quality of our construction work". 65 students think that their innovative ability improved by using the parametric design method. Few students (29 people) have the view of "It has a positive impact in other areas that are not clear", while only one student thought "it has no help."

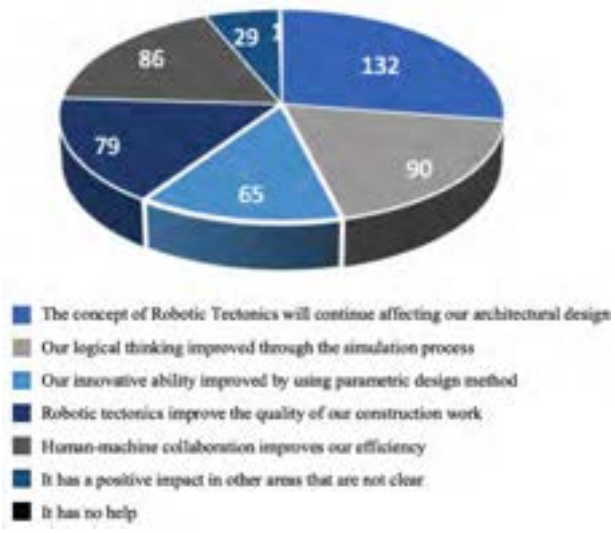

Figure 9. The questionnaire analysis of the improvement of students' design capacity

4.3 Open-ended responses

The students' open-ended responses to the survey questions overwhelmingly provided meaningful improved suggestions and personal reflections about the proposed course. Some specific comments include:

"This is the first time I have manipulated a robot. It is highly professional and requires more systematic learning. I suggest adding related auxiliary courses."

"Compared with the previous manual construction model, the accuracy of the robot construction is particularly high, and it can save labor time."

"For me, it is a magical and surprising experience to compile the design into the program and then let the robot build it into the real thing. I hope to have more opportunities in the future."

"We young people in the contemporary age should actively learn and master this new knowledge and new technology and prepare for the future in advance."

5 Conclusion

Applying the pedagogical method of robotic tectonics into architectural curriculum has significant efforts for the future participants in the AEC industry. It can be considered that the conventional architectural design concept is necessary, but it will allow students to form an inherent thinking, which has a negative effect on the acceptance of new technologies and concepts. Curriculum theory and practical education through reasonable process arrangements are effective for developing students' thinking and perceiving to adapt to the advanced architectural design concepts of the future era. The proposed pedagogical approach and its workflows are reasonable, which can make students fully understand the whole process from architectural design to construction through step-by-step teaching practices and effectively imparted advanced architectural design concepts. All analysis of the questionnaire results quantifies the beneficial effects of this course even are highly recognized and supported by students. The paradigm of architectural education is changing with the integration of emerging robotics technology.

This study reveals a pedagogical approach for future architectural education towards interdisciplinary vision of future sustainable automated construction. All new technologies need widespread for fully acceptance and manipulation, where education always plays an important way. With the digitalization transforming of every field of our lives and societies, students as the future professional participates have somehow generated consciousness for creating brand new ideas of architectural design and construction methods, which could be read through the positive attitude towards future challenges, therefore, adapting to the trends of digitalization and interdisciplinary developing for

architecture, engineering and construction industry is crucial. Searching for the proper pedagogical methods for this changing paradigm are necessary, also, creative and attractive approaches for both students and other participates are indispensable, which always be the future works for our further research.

References

[1] Picon, A. Futurism and nostalgia aside : Digital design and fabrication according to Archi-Union", préface à Philip F. Yuan. In Collaborative laboratory Works of Archi-Union and Fab-Union, Oscar Riera Publishers: Hong Kong, 2018; pp. 12-17.

[2] Ursprung, P. Matter and Memory: Archi-Union's Surfaces. Yuan, P.F., Ed. Oscar Riera Ojeda Publishers: 2018; p. 219.

[3] MacLeamy, P.J.C., Integrated Information,; Design, t.P.L.i.B.; Construction; Operation. MacLeamy curve. 2004.

[4] Mavromatidis, L. Constructal Macroscale Thermodynamic Model of Spherical Urban Greenhouse Form with Double Thermal Envelope within Heat Currents. Sustainability 2019, 11, doi:10.3390/su11143897.

[5] Mavromatidis, L. Linking Wide-ranging Geometrical and Non-geometrical Glazing Options for Daylight Effectiveness Estimation at an Early Design Stage. Energy Procedia 2015, 78, 711-716, doi:10.1016/j.egypro.2015.11.077.

[6] Mavromatidis, L. Coupling architectural synthesis to applied thermal engineering, constructal thermodynamics and fractal analysis: An original pedagogic method to incorporate "sustainability" into architectural education during the initial conceptual stages. Sustainable Cities and Society 2018, 39, 689-707, doi:10.1016/j.scs.2018.01.015.

[7] Bejan, A. Sustainability: The Water and Energy Problem, and the Natural Design Solution. European Review 2015, 23, 481-488, doi:10.1017/s1062798715000216.

[8] Shi, X.; Fang, X.; Chen, Z.; Phillips, T.K.; Fukuda, H. A Didactic Pedagogical Approach toward Sustainable Architectural Education through Robotic Tectonics. Sustainability 2020, 12(5), 1757; doi:10.3390/su12051757

Augmented Reality Sandboxes for Civil and Construction Engineering Education

Joseph Louis [a] and Jennifer Lather [b]

[a] School of Civil and Construction Engineering, Oregon State University, USA
[b] Durham School of Architectural Engineering and Construction, University of Nebraska – Lincoln, USA
E-mail: joseph.louis@oregonstate.edu, lather@unl.edu

Abstract –

Civil and Construction Engineering (CCE) is a discipline that seeks to engineer the physical world, yet students in classrooms are limited to studying and applying concepts predominantly on paper or computer screens. This paper proposes a framework for the use of augmented reality (AR) sandboxes to bring the vastness of the physical environment that characterizes the problem domains of civil and construction engineering and the students will eventually be working in, into the classroom. Because the surface of the sandbox can be intuitively fashioned to represent a scaled-down version of the wide range of terrain found in the physical world, this tool can demonstrate not just the application of classroom concepts, but even their development from first principles. A description of the AR Sandbox is provided along with the software architecture that is created to enable course delivery to meet the related learning objectives for earthwork planning. This paper presents learning CCE design and analysis concepts that are traditionally presented through diagrams to be delivered through an AR Sandbox. A framework for evaluating the effectiveness of this new mode of instruction is proposed which can inform guidelines on the implementation of novel visualization and interaction technologies in the CCE classroom. Implications of this work include use by earthwork construction teams and professional engineers where AR sandboxes can aid planning and managing large scale construction projects.

Keywords –

Augmented Reality; Sandbox; Heavy Civil; Construction Education; Mass Haul Diagram

1 Introduction

Civil and Construction Engineering (CCE) is a discipline that seeks to engineer and transform the physical world around us, yet students in classrooms are limited to studying and applying concepts predominantly on paper or computer screens. While the technology available in education have increased to many interactive media, CCE as well as many engineering disciplines are slow to implement new modes of learning into modern curricula [1]. The traditional modes and media of instruction, e.g., paper and screens, create a disconnect between the concepts learned in class and their application in the field, e.g., spatial reasoning and broad concept understanding, which is usually bridged only after considerable work-experience in industry. A similar disconnect exists between the designers and builders of civil infrastructure, who necessarily work in two different environments (the office vs. the field).

This paper seeks to bring the vastness of the physical environment that students will be working in, into the classroom, with a tangible interface known as an augmented reality (AR) sandbox. The AR sandbox will serve as an interactive media through which civil infrastructure design and construction concepts will be demonstrated in the classroom. This platform will augment traditional learning tools such as CAD and spreadsheet programs by providing a much needed and appropriate kinesthetic aspect to student learning and engagement. This paper focuses on the development of the physical sandbox and software applications that enable the teaching of various CCE concepts through the AR sandbox. The methodology that will be used to evaluate the effectiveness of the sandbox as a media for education is also discussed in this paper. The concept of mass haul diagraming for earthwork planning and analysis is used as a case study to explore the use of the sandbox in civil and construction education.

A literature review of existing implementations of AR sandboxes for education is first provided to set the context for this research, which is followed by a description of the hardware and software architecture necessary for the working of the sandbox. This is followed by a description of the experimental methods to evaluate the effectiveness of the sandbox for teaching and learning, followed by conclusions of the research.

2 Literature Review

A review of current literature in the field of mixed virtual reality and augmented reality sandboxes is provided to set the context for the research. Following that, a discussion of diverse learning styles is provided to highlight the need for incorporating spatial reasoning into the CCE curriculum, which is provided by the AR sandbox. This sets the stage for presenting the point of departure of this paper from the current state of CCE education and AR sandbox research.

2.1 Augmented and Virtual Reality

Within the commonly used Mixed Reality continuum (Fig. 1), there are two poles, the real world (reality) and the virtual world (virtual reality), where either can be augmented by the other [2]. The augmented reality (AR) is the part of the spectrum where virtual objects are augmented on reality. The augmented virtuality (AV) is the part of the spectrum where real objects are augmented on the virtual environment. In the AR Sandbox, both of these augmentations can occur, sometimes where the virtual representation of the sand is used to generate a virtual topographical map (AR) and sometimes where the sand is meant to augment the understanding of data through exploring how changes in the sand impact a simulation of roadway construction (AV), for example in a cut and fill diagram. These theoretical differences have implications for AR sandbox design and implementation in educational settings. Through understanding the types of tasks to be performed in the mixed reality sandbox environment, the software specifications for AR and AV tasks can be identified. These can aid identification of technology for investigation, design, and analysis tasks associated with spatial reasoning in the civil and construction engineering domain.

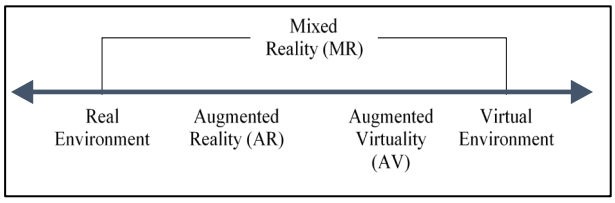

Figure 1. Mixed Reality Continuum

2.2 Augmented Reality Sandbox

The augmented reality (AR) sandbox is a device consisting of a depth sensor, projects, and a physical box filled with sand. It was initially developed at UC Davis to enable a tangible means of manipulating and visualizing spatial data [3]. This device represents a novel application of AR wherein the virtual information is dependent on the physical shape of the real-world sand. Its primary applications thus far have been in providing students with an intuitive understanding of geographic concepts [4] such as topographic maps, and hydrology [5]. Apart from concepts in these fields, other educational and visualization experiences have been created in the areas of natural sciences [6], mathematics [7], and disaster response [8]. The common theme regarding all of the AR experiences implemented in an AR sandbox thus far has been the presence of a strong spatial component relating to vast areas of physical terrain. Furthermore, all of the above experiences only allow one primary means of interacting with the underlying model and visualization, through physically manipulating the sand. For the above applications, the primary concepts under study is the natural terrain, which is can be represented and interacted with adequately by the sand alone.

However, civil and construction engineering concepts involve additional built infrastructure to be considered along with the surrounding terrain. Therefore, this paper builds upon the current capabilities of the AR sandbox interface to provide a more general platform for the sandbox that enables multiple modes of interactivity with the underlying terrain and physical infrastructure under consideration.

2.3 Engineering Education for Diversity

Many researchers have investigated how learning style impacts learning in the STEM fields [9], as well as gender differences in learning style for engineering students [10], suggesting that engineering education be approached with a mixed method approach to incorporate more Active, Sensing, Visual and Global components.

In addition, spatial reasoning has been shown to be a key indicator of engineering education success especially for female engineering students [11]. New trends in VR and AR have added new tools for educators across engineering topics and grade levels [12], [13]. With a large number of new tools, the need for evaluation is expanding into understanding specific interactions, including human-computer interaction (HCI), team interaction, and conventional communication. Previous work has begun to develop metrics to aid researchers in understanding different factors associated with interactive media and teams [14]. Additional tools are needed to understand how both media and interaction play a role in the use of mixed reality in engineering education and how they can assist different learners to succeed in their engineering education. To aid research in this area, research is needed in a new method of incorporating spatial reasoning for engineering education, particularly in the area of civil and construction engineering, where spatial concepts are of critical importance.

It is anticipated that the use of the AR sandbox will provide the spatial component to learning that will enable core concepts in civil and construction engineering to be appeal to a more diverse audience.

2.4 Point of Departure

The point of departure of this paper from current work lies at the intersection of current state of the art in AR sandboxes and the need for enhanced means of incorporating spatial reasoning in engineering educations, especially for civil and construction engineering. Current implementations of the AR sandbox do not consider the interaction of built infrastructure with the terrain, and rather focus on the terrain itself, thereby limiting its application to areas of study relating to geology and hydrology. Therefore the overarching goal of this paper enhance the capabilities to the AR sandbox to enable users to create, visualize, and interact with digital representations of the built environment and infrastructure in addition to the physical terrain that is represented by the sand. Towards this end, the paper describes the development of the sandbox and a case study of developing an application for a specific construction engineering concept taught in the classroom. Furthermore, a discussion of the experimental method for evaluating the effectiveness of the sandbox for education is also provided.

3 Development of AR Sandbox

The AR sandbox used in this research was built from commonly available materials and implemented by the authors and a team of students at Oregon State University. This section describes the hardware and software architecture that comprises the AR sandbox.

3.1 Hardware Design of AR Sandbox

Figure 2 shows a schematic representation of the AR sandbox along with its three primary hardware components: depth sensor, projector, and computer terminal. As can be seen in the figure, the depth sensor and projector are mounted side-by-side on a metal bracket that extends over a box of sand. Both the depth sensor and the projector are connected to the computer terminal.

For portability, the sandbox was mounted on a wheeled double shelf cart, wherein the sand was placed on the top shelf along with the computer terminal. Half inch (1.27 cm) thick clear acrylic board walls were affixed to the sides of the top shelf to accommodate the volume of sand. The picture of the finished sandbox is shown in Figure 3.

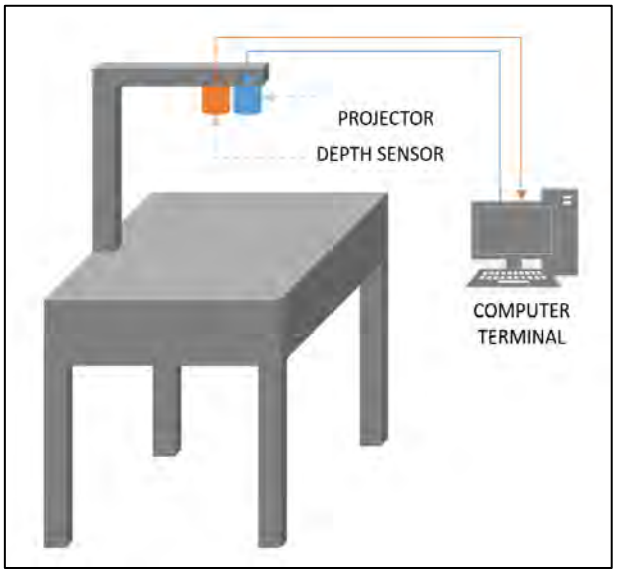

Figure 2. Schematic diagram of AR sandbox

Figure 3. AR sandbox mounted on wheeled cart

The role of the three primary components are the depth sensor, projector, and computer terminal, described below:

3.1.1 Depth Sensor

The depth sensor that was used is a Kinect Sensor by Microsoft. The Kinect is equipped with a 1280x960p full-color camera, and an infrared (IR) emitter and sensor along with an array of microphones and a tilt motor. For this project's purposes, the Kinect's IR sensor and emitter are primarily used and allow us to capture a depth image. This IR system offers a workable range of 0.8m to 3.5m from the target with a data precision of 1cm [15]. When choosing the Kinect, the

most important factors for considerations were the accuracy the sensor and the usability of its application programming interface (API). The Kinect is one of the most accurate depth sensors on the common market and the API created by Microsoft has been created specifically for developers to use when utilizing the sensor for their applications.

3.1.2 Projector

The projector that was used for this sandbox is an AAXA M5 Mini Portable Business Projector. This projector occupies of a volume of 1.5cm x 1.5cm x 4.6cm (6in x 6in x 1.8in) and only weighs 0.86kg (1.9 pounds), while offering a 1280x800p picture at 900 lumens. Allowing for a screen up to 3.81m (150in), this projector allows for a very bright and clear image for its size. The most important factors of the projector are its size, weight, and brightness. Because of the way the projector is mounted above the box, a smaller and light projector was necessary to ensure its stability. With the majority of projectors at this size providing a brightness of 50-100 lumens, the 900 lumens make this projector highly suitable for its intended purpose.

3.1.3 Computer Terminal

To power the AR sandbox, a HP Z240 full tower desktop computer was used which had 16 GB of RAM, a 1TB spinning disk, and an Intel core i7 processor with a base speed of 4.2 GHz. Furthermore, a Nvidia GTX 10XX series graphics card was implemented in the terminal to handle rendering. In regard to the computer terminal, it is necessary to use a full tower desktop since a majority of graphics cards are too big to fit in a small form factor machine. Using a Nvidia GTX graphics card provides the best results for rendering real time graphics at the lowest cost when compared to a similar workstation graphics card. A mouse and keyboard are connected to the computer terminal to enable additional interaction capabilities to the AR sandbox. The output of the terminal is projected on to the sandbox and thus there is no additional monitor that is provided with the sandbox, although one can be easily added for development and debugging purposes.

3.2 Software Architecture of the AR Sandbox

The software architecture of the AR sandbox was developed to provide future developers the opportunity to develop applications relating to core concepts in CCE that could be deployed through the AR sandbox interface without the need to interface with low-level details of the hardware components. Thus, the fundamental functionality that was enabled involved obtaining a depth image information from the depth sensor using Kinect's API and storing that as a heightmap to provides heights on the sandbox at any given x and y location in the sensor region. Also, a geometry interpreter was implemented to convert heightmap data from the depth sensor into a three-dimensional mesh. Apart from dealing with the depth sensor, calibration is required to ensure that the sensor and projector are correctly aligned with each other as well as with the surface of the sand. These settings include adjustments to the area exposed to the depth sensor and to the area covered by the projection. This module continually interacts with the user interface (UI) as it prompts the user with the setting to be adjusted and then stores these settings in the Calibration Settings.

In order to ensure satisfactory graphical performance of the system, this architecture utilizes two pairs of vertex and fragment shaders written in the OpenGL Shader Language (GLSL). The first is responsible for coloring the terrain mesh in order to visually represent height information. The second is used to color road segments to represent cut and fill data. The visual appearance of these shaders will change depending on the current display mode. The rendering subsystem is handled by the Unity game engine and is accessed indirectly through shaders and Unity's UI system.

Finally, a basic application that is enabled to ensure that the system is working correctly is the display of real-time depth information. Display depth is used to visualize the height or altitude of an area. If a part of the sand is above a certain height, then it's displayed using a shade of red. If the sand is below a certain height, then is displayed using a shade of blue. The intensity of the color depends on how far the height of the sand is from a predetermined height. A close up of this display of depth is shown in Figure 4 along with contour lines along sections of equal height.

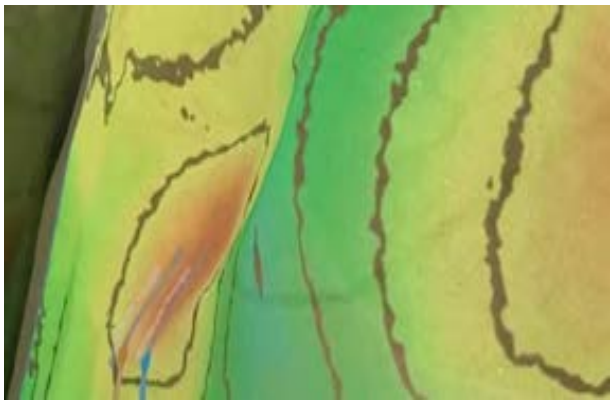

Figure 4. Height map display with contour lines

4 Case Study for Mass Haul Diagrams

Mass haul diagrams are an analytical tool that is used in the planning of horizontal construction projects

like the building of roadways and trenching for pipelines [16]. Mass haul diagrams provide a visualization of the quantities of earth that need to be cut, filled, and moved, along the centerline of the horizontal project. This information is used by project managers to plan for earthmoving equipment fleets and enables them to determine the schedule and cost of the project. Traditional mass haul diagrams are taught to students using a spreadsheet interface which takes as input the elevation profile of the existing ground and proposed pavement and the cross sections of the roadway (or trench) to be built. The output of the analysis is a two-dimensional visualization of cut and fill volumes on the y-axis plotted against the distance along centerline on the x-axis. An example mass haul diagram is shown in Figure 5.

As can be observed from the figure, the information in the mass haul diagram is not intuitive to grasp, especially given its similarity to the input elevation profiles. Another key aspect of the earthmoving that is missing in the current visualization is that it does not show indicate the three-dimensional nature of the volume of soil to be moved. Furthermore, there is no indication of the surrounding terrain as the information is only plotted along a one-dimensional centerline of the road. This can lead to potential misunderstanding of the entire concept.

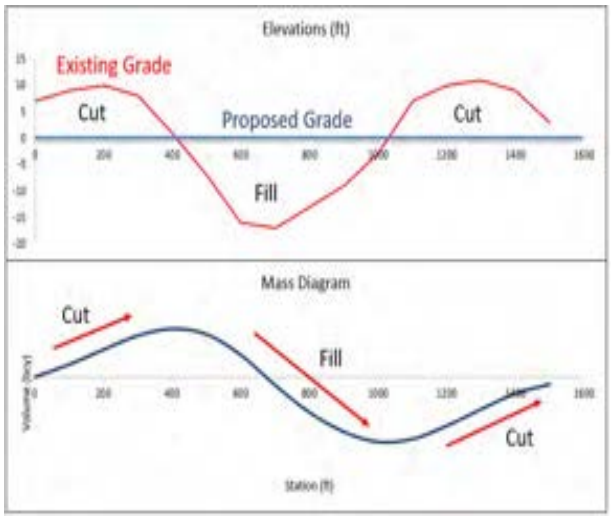

Figure 5. Mass haul diagram for earthmoving

These limitations of the traditional method of instruction of mass haul diagrams present a barrier to the understanding of the core concepts of the method, which essentially relate to the volumes of earth to be moved. Thus, an application was created upon the foundational AR sandbox software architecture described previously for visualizing an interactive mass haul diagram. This application could be run in two modes: Design and Cut & Fill modes.

4.1.1 Design Mode

In the design mode, the user designs the road segment location. The design mode is used to enable the user to create the shape of the roadway segment for mass haul analysis. Specifically, the user can design the horizontal and vertical alignment of the roadway using Bezier control points that provide smooth curves to the shape of the roadways segment. Figure 6 shows an example of the control points (represented as yellow squares) on the alignment of the roadway. This figure also shows the cut and fill representation which will be explained in the following subsection.

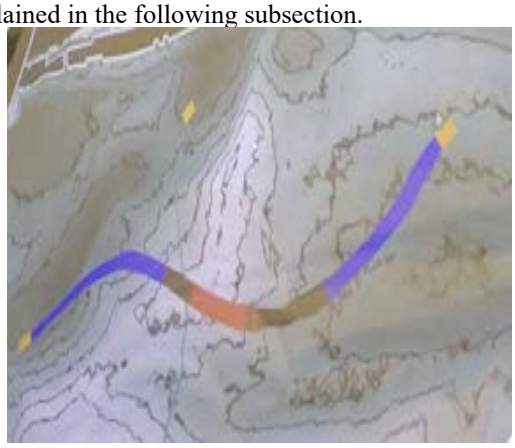

Figure 6. Control points on virtual roadway projected on the sandbox

The user can edit the horizontal alignment of the road by using a mouse to select and move a specific control point. The user can change the vertical alignment of the roadway by selecting and moving a control point and pressing down on the shift key on the provided keyboard. The user can also add and delete control points using UI buttons that are available. Adding a control point enables the user to greater length and curvature to the road segment.

4.1.2 Cut & Fill Mode

Cut and Fill mode is used to visualize the volumes of material that must be added or removed in order to achieve the desired road path. This mode is the default mode and differs from the design mode only in terms of not showing the control points that determine the alignment of the roadway. The cut or fill of a road will be calculated by determining the height of a part of the sand where the road should be, then displaying a colored view of the road. As can be observed in Figure 6, the cut and fill of soil that is required to bring the existing grade of the terrain to the proposed grade of the roadway is displayed visually along the roadway.

Specifically, cut is represented in red and fill in blue. If the elevation of the terrain along the roadway of the proposed roadway, that portion is represented in black color. Apart from providing students with the spatial

context of where the cut and fill areas on the roadway are, moving sand out of cut and into fill portions along the roadway enables them to obtain tactile sensory feedback in obtaining an understanding of the quantity of soil needed to be moved to build a roadway.

Also, the effect of change in terrain on cut-fill sections of the roadway are represented immediately to due to the real-time nature of the depth sensor. This provides students with immediate visual feedback on the effect of physically moving soil from one part of the roadway to another. Quantities are also presented along with the visualization.

4.2 Evaluation of Tasks in AR Sandbox

There has not been a substantial amount of research on the effectiveness of learning using AR sandboxes for CCE. Most evaluation has been on the use of AR Sandboxes in understanding hydrology and topography concepts in Environmental Engineering, with mixed results [4], [17], [18]. The main findings from these studies have found that user experience was positive while statistical differences between learning pre- and post- task have been minimal [19]. Rigorous evaluation of user learning and experience are needed in a variety of task types to understand the value of AR Sandboxes in education. Since previous studies have focused on learning concepts, we propose expanding evaluation to include both unstructured and structured tasks to help understand the use of this technology in both broad understanding of CEE and learning spatial concepts.

The two tasks of the AR Sandbox for CEE, design and cut & fill modes, represent the key tasks for evaluation. As mentioned earlier, spatial understanding has been identified as an indicator for engineering success [4], and this concept is especially important for people with a variety of cognitive styles. In order to understand the benefit of AR Sandboxes in CEE, we propose the collection of data across different task types (design and analysis type tasks), the collection of data on cognitive style, understanding of broad concepts through pre and post-tests, class performance, measures of user perception of the media interaction and potential team interaction during the activity, and comparison with traditional teaching and learning methodologies. For evaluation of AR sandboxes in the CCE education to be valuable, many more studies are needed with enough sample size to produce enough power to have statistical evidence of the value of these systems. Value can be in many forms, including performance, future success, confidence in abilities as an engineer, and enjoyment in education. Additional valuable parameters are expected to arise as researchers evaluate more types of tasks beyond concept understanding, such as unstructured design tasks and cut and fill analysis tasks.

5 Conclusions and Future Work

There exists an inherent dichotomy between the education and practice of civil and construction engineering because the former necessarily happens inside the classroom while the latter is mostly performed out in the real and physical world. This disconnect is usually bridged only after the student has spent sufficient time out in the field and is struck by the inevitable, but much delayed “a-ha” moment - a congruence achieved when abstract concepts are finally placed within their rightful physical context. The AR sandbox, through its seamless blending of virtual content within a tangible interface, has immense potential to deliver concepts to students in an intuitive and engaging manner to assist in alleviating that disconnect. Because the surface of the sandbox can be intuitively fashioned to represent a scaled-down version of the wide range of terrain found in the physical world, this tool can demonstrate not just the application of classroom concepts, but even their development from first principles, through interaction with design and analysis tasks in earthwork planning.

This project specifically provides an alternative means of teaching mass haul diagrams for earthwork planning. Whereas current lessons utilize static two-dimensional profile and plan views of three-dimensional terrain and roadways, this tool enables students to use their own hands to both construct roadways and modify surrounding terrain. The tool then displays the results of the mass haul analysis directly on the physical roadway itself in real-time, to provide an intuitive, interactive, and ultimately effective learning experience for students. The following specific advancements in interactive learning are enabled by the tool. The use of actual sand in the sandbox is anticipated to increase student learning and retention of concepts such as bank, loose, and compacted volumes; and which volumes are to be used during quantity calculations. The provision of a physical terrain and roadway model combined with a dynamically updated mass haul diagram in this project can demonstrate the utility of abovementioned tools for earthwork volumes calculation. The sandbox will serve as a physical medium to aid students in interpreting the design drawings that are provided from an authentic real-world project. The real-time nature of the proposed tool will also enable students to experiment with the terrain to see how it changes the cost and schedule of the operation. The provision of a modifiable scale model of the terrain will enable the testing of different alternatives and scenarios at no expense to the students or instructors.

While the effectiveness of the tools in imparting the lesson has not been evaluated yet, this paper details the experimental process that will be followed for assessment across a series of novel AR sandbox task

types: design and analysis tasks. The results of this assessment can inform educators on the utility of the sandbox and other such novel methods of teaching and guide their plan for implementation.

Future work can also focus on integrating the presented approach of visualizing heavy civil operations with existing means of using virtual reality [20] and augmented reality [21] for visualizing simulated construction operations.

References

[1] M. Borrego, J. E. Froyd, and T. S. Hall, "Diffusion of engineering education innovations: A survey of awareness and adoption rates in US engineering departments," *J. Eng. Educ.*, vol. 99, no. 3, pp. 185–207, 2010.

[2] P. Milgram and F. Kishino, "A taxonomy of mixed reality visual displays," *IEICE Trans. Inf. Syst.*, vol. 77, no. 12, pp. 1321–1329, 1994.

[3] "Augmented Reality Sandbox." https://arsandbox.ucdavis.edu/ (accessed Jun. 14, 2020).

[4] T. L. Woods, S. Reed, S. Hsi, J. A. Woods, and M. R. Woods, "Pilot study using the augmented reality sandbox to teach topographic maps and surficial processes in introductory geology labs," *J. Geosci. Educ.*, vol. 64, no. 3, pp. 199–214, 2016.

[5] G. Zhang *et al.*, "An efficient flood dynamic visualization approach based on 3D printing and augmented reality," *Int. J. Digit. Earth*, pp. 1–19, 2020.

[6] A. Ables, "Augmented and virtual reality: Discovering their uses in natural science classrooms and beyond," in *Proceedings of the 2017 ACM SIGUCCS Annual Conference*, 2017, pp. 61–65.

[7] S. Á. Sánchez, L. D. Martín, M. Á. Gimeno-González, T. Martín-Garcia, F. Almaraz-Menéndez, and C. Ruiz, "Augmented reality sandbox: a platform for educative experiences," in *Proceedings of the Fourth International Conference on Technological Ecosystems for Enhancing Multiculturality*, 2016, pp. 599–602.

[8] D. Savova, "AR Sandbox In Educational Programs For Disaster," in *6th International Conference on Cartography and GIS*, 2016, p. 847.

[9] P. Pallapu, "Effects of visual and verbal learning styles on learning," *Inst. Learn. Styles J.*, vol. 1, no. 1, pp. 34–41, 2007.

[10] P. A. Rosati, "Gender differences in the learning preferences of engineering students," *age*, vol. 2, p. 1, 1997.

[11] S. Hsi, M. C. Linn, and J. E. Bell, "The role of spatial reasoning in engineering and the design of spatial instruction," *J. Eng. Educ.*, vol. 86, no. 2, pp. 151–158, 1997.

[12] A.-H. G. Abulrub, A. N. Attridge, and M. A. Williams, "Virtual reality in engineering education: The future of creative learning," in *2011 IEEE global engineering education conference (EDUCON)*, 2011, pp. 751–757.

[13] F. Castronovo, D. Nikolic, S. E. Zappe, R. M. Leicht, and J. I. Messner, "Enhancement of learning objectives in construction engineering education: a step toward simulation assessment," in *Construction Research Congress 2014: Construction in a Global Network*, 2014, pp. 339–348.

[14] J. I. Lather, G. A. Macht, R. M. Leicht, and J. I. Messner, "Development of indices for user perceptions of interactive technologies in construction engineering," in *Proceedings of the 33rd International Conference of CIB W78*, 2016, pp. 1–10.

[15] M. R. Andersen *et al.*, "Kinect depth sensor evaluation for computer vision applications," *Aarhus Univ.*, pp. 1–37, 2012.

[16] R. L. Peurifoy and W. B. Ledbetter, "Construction planning, equipment, and methods," 1985.

[17] S. Giorgis, N. Mahlen, and K. Anne, "Instructor-led approach to integrating an augmented reality sandbox into a large-enrollment introductory geoscience course for nonmajors produces no gains," *J. Geosci. Educ.*, vol. 65, no. 3, pp. 283–291, 2017.

[18] N. Theodossiou, D. Karakatsanis, and E. Fotopoulou, "The Augmented Reality Sandbox as a tool for the education of Hydrology to Civil Engineering students."

[19] S. K. Kim, S.-J. Kang, Y.-J. Choi, M.-H. Choi, and M. Hong, "Augmented-Reality Survey: from Concept to Application.," *KSII Trans. Internet Inf. Syst.*, vol. 11, no. 2, 2017.

[20] J. Louis, P. Dunston, and J. Martinez, "Simulating and visualizing construction operations using robot simulators and discrete event simulation," in *Computing in Civil and Building Engineering (2014)*, 2014, pp. 355–363.

[21] J. Louis and J. Martinez, "Rendering stereoscopic augmented reality scenes with occlusions using depth from stereo and texture mapping," in *Construction Research Congress 2012: Construction Challenges in a Flat World*, 2012, pp. 1370–1380.

Education of Open Infra BIM based Automation and Robotics

T. Kolli[a] and R. Heikkilä[a]

[a] University of Oulu, Faculty of Technology. Structures and Construction Technology, P.O Box 4200, FI-90014 University of Oulu, Finland
E-mail: tanja.kolli@oulu.fi, rauno.heikkila@oulu.fi

Abstract –

This paper presents the learning outcomes of the Open InfraBIM and Construction Automation workshop in OuluZone motorsport Center, Finland, during October 2019. Totally of 45 students from the University of Oulu, the Oulu University of Applied Sciences, and the Oulu Vocational College were challenged to build the Speedway track by using the latest tools, such as real-time cloud service, work machines with automated 3D control systems, and drones. Furthermore, an autonomous excavator was demonstrated to the participants during the workshop. The students were divided into six groups. Each group had six different interesting tasks of a typical construction site guided by teachers and technology company experts. The idea was to practice real construction site work and problem solving. The feedback from the students, teachers and technology company experts were positive. The practical learning has found to be an excellent way to educate open infraBIM based automation and robotics.

Keywords –

Automation; Education; Infra Built Environmental Information Model (infraBIM); Robotics

1 Introduction

During last decade, Building Information Modelling (BIM) digitalized the entire construction sector from designing to the implementation and site logistic. Infra BIM is an acronym for Infra Built Environment Information Model, which includes the infrastructure information model and related structures and environment information [1]. According to Costin et al. [2] literature review, many publications have been published since 2002 to 2017 where BIM has studied various infrastructures related to the transport sector, such as bridges, roads, and mass transit. BIM has found to have unlimited potential for improving infrastructure, but there is still challenges interoperation and data exchange.

In Finland, a lot of trial project works have been done to obtain general guidelines and requirements for infrastructure construction since 2010. Building SMART Finland has been published Common infraBIM requirements (YIV2015, now second edition YIV2019), together with the infraBIM Classification and information transferring format [3] that are recommended to use in projects. Instead in Norway, the use of BIM become mandatory in large public infrastructure projects in 2016 [4]. The German Ministry of Transport and Digital Infrastructure (BMVI) aims at establishing the mandatory usage of BIM from 2020 for all building projects in its range of authority. For this reason, many pilot projects have been made [5]. In Sweden, government has assigned in 2012 to the Transport Admiration the task to the implement of BIM throughout of the construction industry. [6] These types of infraBIM piloting, guidelines and exploitations experiences have also been reported in other countries, such as in Spain ROAD-BIM EU-project [7]. As the benefits of BIM in the infrastructure pilots, demonstrations and projects have been found to be significant, it is important to be aware of the need for infraBIM training and education both for professionals and for construction students.

Currently, BIM education in higher education or technical training institutions has been reported providing globally in 17 countries, most in Architecture Engineering Construction (AEC) sector. In the report of NATSPEC 2019 [8], Infrastructure education has been provided only in Finland and Switzerland. History in Finnish infraBIM education was that technology companies involved in the infraBIM projects started to train employees in specific training content. Since 2014 YIV2015 become one of the lecture topics in courses organized for example in Metropolia University of Applied Science, Tampere University of Applied Science and University of Oulu. Since 2015, machine operators have also been trained model-based workflow i.e. infraBIM. Specific infraBIM coordinators training courses, including lectures, learning tasks, e-learning and development task, has been given in university of applied

science level with a collaboration of construction industry started in 2020. [9] Tallinn University of Applied Sciences, Estonia, BIM for Infrastructure course has been developed more for active learning using Moodle for sharing, assessments, and the forum of questions and answers. Students learn by watching, listening, reading and doing step-by-step materials. During the course a number of different software design, construction and visualization tools are utilized in teaching. [10] HSR University of Applied Science Rapperwill, Switzerland, offers the BIM basic education three-day course. The content of the lectures is e.g. Industry Foundation Classes (IFC) and openBIM, and virtual project room (Common Data Environment, CDE) [11] Politecnico di Torino, Italy, has presented their experiences to train professionals to be qualified as infraBIM Managers expert both in the building process and in the parametric digital modelling. During the lectures, individual internship, and the project work students learned that the procedures and processes can be work properly no matter the BIM platform or tool used, the importance of teamwork and the importance of openBIM by presenting previous projects. [12]

In this paper, we present the findings and lessons learning from the practical workshop in Ouluzone 2019. The goal of the workshop was to challenge students to learn open infraBIM and automation by building Speedway track. For example, real-time cloud service, 3D measuring machines, and drones were used as modern tools.

2 Development of the Open infra BIM Workshop

OuluZone workshops were kept in OuluZone, which is a motorsport center owned by the city of Oulu, Finland. OuluZone is located in a place called Arkala, which is around 35 km northeast from the city center of Oulu. One goal of OuluZone is to enlarge its activities and develop it as research, development, and education centre. Currently many research activities have already going on related to drones, robotics, and autonomous excavators. In addition, different workshops have be done for infrastructure technology professionals. The collaboration education week is so called OuluZone – Open Infra BIM and Automation workshop. In the years 2017 [13], 2018 [14], and 2019 workshops were concentrated on educating open infra BIM automation and robotics for students. The objective of the workshop is to provide the latest knowhow, challenges and the future needs in the open infraBIM based automation and robotics to the students. The other goals were to develop teaching and collaboration between organizations. The learning outcomes of OuluZone workshop have been to understand the conceptional and practical knowledge relating to infraBIM technologies, workflows and protocols in the infrastructure construction sites. Each year the teachers met several times to plan the content of the workshop. Depending on the year, the OuluZone workshop week has been contained 2-3 lecture days from teachers and technology company partners, 2-3 practical days in the OuluZone motor center, and finally 0,5-1 feedback day. In the year 2019, the program for the OuluZone workshop week is presented in Table 1.

Table 1. The program of the OuluZone – Open Infra BIM and Automation workshop week 44, 2019 (28.10.-1.11.2019).

Day	Content	Example of the topics
1.	Lectures by teachers and technology company experts	Common InfraBIM Requirements 2019, Infra information modelling, foundations of cloud service system, and automation construction site. Questionnaire
2.	Lectures by teachers and technology company experts	Typical work tasks in construction site such as foreman and designer. Occupational safety, MVR-form
3.	Practical training	Tasks in Ouluzone motor center: training
4.	Practical training	Tasks in Ouluzone motor center: problems solving. Construction site audit. Autonomous excavator show
5.	Summary of the workshop	Results from occupational safety, feedback collection from participants. Questionnaire

2.1 Participants in OuluZone workshop

The Finnish educational system consists of nine-year compulsory comprehensive school, three-year upper secondary education and four to five-year higher education. In OuluZone workshop, the participants came from secondary education provided by vocational college (Education consortium OSAO), and from higher education by the University of Oulu and the Oulu University of Applied Sciences (Oamk). The curriculum of these schools includes infrastructure construction and automation as one field of the study program. For a Masters' Degree students of Technology there is a five-credit course called "Information modelling and automation building construction and maintenance", at the Department of Structures and the Construction

Technology Research Unit at the University of Oulu. For engineering students at the Oulu University of Applied Sciences (OAMK) there is a five- credit course entitled "Infra BIM modeling and building a construction project". The Oulu Vocational College (OSAO) provides three years teaching for construction machinery and lorry drivers as well as logistics instructors. Each workshop had the different number of the participants depending of the year. In Table 2 is presented the number of participants from University of Oulu, Oamk, OSAO and industry in the year 2019. The others are presenting the visitors who were interested to follow and visiting the workshop.

Table 2. The total number of participants was 82 from University of Oulu, Oulu University of Applied Sciences (Oamk), OSAO, and technology company organization as well as visitors.

Organization	Students	Teachers	Visitor
University of Oulu	7	10	3
Oamk	19	3	
OSAO	19	3	
Company		11	7
Total	45	27	10

Before Ouluzone workshop week, each school was preparing their students by different ways. The master's degree students of the University of Oulu had lectures and trainings by teachers and visitor lectors from technology companies in the autumn 2019. In the lectures, students learn how to make a road plan over a measured terrain model using a Novapoint program. Trimble R10 GNSS System was used to produce a terrain model. The measurement guide of Finnish Transport Infrastructure Agency Machine was followed during producing the terrain model [15]. Machine control model for each layer was made by using the 3D-win program. Machine control model is a continuous (3D) surface and/or line model needed for the automation control systems of machines [1]. Inframodel (IM) is Finnish national XML-based application specification which is based on the international LandXML schema [1]. In addition, the students visited to OSAO Haukipudas campus to learn the machine control system is working, and to test the excavator simulator (Tenstar) integrated Leica's 3D machine control system.

Oamk students are either engineering, builders or multiform level. Their lectures were already completed during spring 2019. The topics of the lectures were e.g. infrastructure in society, infrastructure project constructions and contracts, the cost planning of the infrastructure project in a project owners' perspective, construction tasks and good practices ensuring the safety of the constructions projects, and finally general terms and conditions of the construction contract, i.e YSE 1998. After lectures, students had the training period in the construction site.

The third-year students of OSAO practice their earth moving machinery such as excavator and loaders' operator skills and how to actually use 3D-machine control systems first in simulators mention above and then in practice. In Ouluzone OSAO construction driver students were doing their skill tests. The institutes each measured their own students' learning outcomes using appropriate methods.

2.2 Workshop tools during OuluZone

During the OuluZone week, the students continued to build with a help of teachers and technology experts a new Speedway track and its cutting operation in real-world conditions. The Speedway track geometry was designed first in 2D drawings and then in 3D model in open file formats (.dxf and Inframodel). The geometry was designed by using the 3D-Win program presented in Figure 1. The total length of the Speedway track is 437m in with the straight line of 65m. It was calculated that the cutting mass is 7848 m^3, filling mass 7727 m^3, and surplus mass 100 m^3.

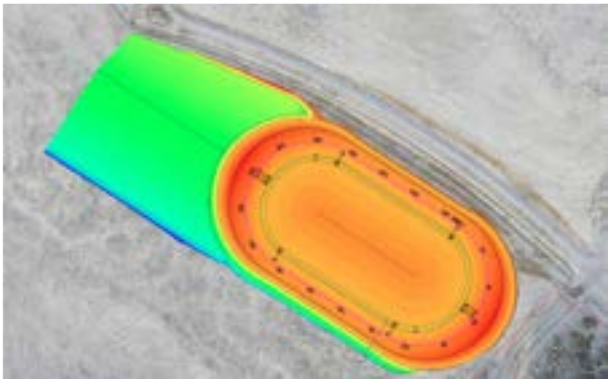

Figure 1. Speedway track geometry designed by using 3D-Win program (Mitta Oy).

The unmanned aerial vehicle (UAV) field measurements were carried out in August 2019.The Speedway track area was photographed using photometry technique to produce the digital surface model (Figure 2). First, the reference points were made by RTK-GNSS Base Station around 50 to 100 meters each other for the area to be photographed. The reference points are searched for in the 200 photos to get coordinates and the margin of error. Similar type of UAV measurements procedure than in Ouluzone were also done in sub-Arctic Mining Site [16]. In Figure 2 is presented the accurate georeferenced dense point cloud based on the targeted photos and reference points. Before workshop 2019, around 30-40% of Speedway track cutting was already made in previous workshops. The cutting operation in workshop 2019 was decided to

continue in the centre of the speedway track.

Figure 2. UAV field measurements made in photometry technique to get Speedway track cutting situation in OuluZone motor center August 2019.

The students were using the latest technology tools at Speedway track construction site. Infrakit cloud service (provided by Infrakit Group Oy) was used as the open infra BIM tool to monitor real-time the Speedway track building progress. Infrakit was selected as cloud service tool based on past experience of its easy of use, and that it can be combined with several devices from different manufactures [17]. In Figure 3 shows the Speedway project view in Infrakit cloud service. For example, during the project, the construction site can be monitored in real-time. The excavator operators are measured the values of the as build point every 20 meters. These as build points are used for the quality control of the dimensional accuracy of structures during work and for monitoring the progress of the work.

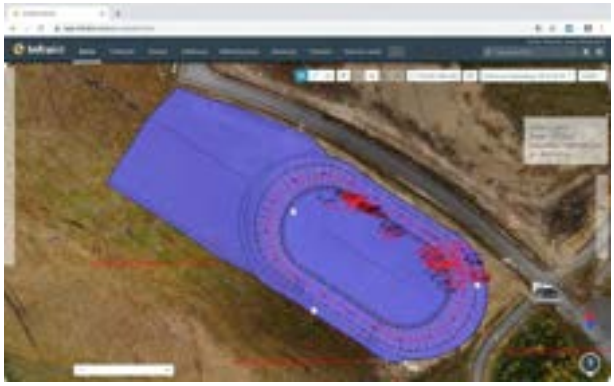

Figure 3. Speedway project in Infrakit cloud service. The combination model is a combination of Speedway track geometry integrated the drone picture.

To build the Speedway track, two excavators and wheel loader with the automatic Leica-3D control system, and two trucks and a dumper with Infrakit-android application were used, too. The other necessary equipment needed in Speedway-track construction site were RTK-GNSS- base station, three to four pieces' reference points around the Speedway track. The coordinates of the reference points were measured using the static GNSS measuring method in ETRS-GK26 map coordinates and N2000 height system [18].

2.3 Tasks in OuluZone

For the Ouluzone practical training, the students were divided into six teams. The number of students in the team was from 5 to 6. The same number of different tasks of a typical site organization were developed where students could practice practicing the work tasks involved. The teachers also organized various change and problem situations in the workshop, which students had to deal with in their various roles. The practical training tasks were:

1. Road designer
2. Speedway -project owner and surveyor
3. Construction' head manager
4. BIM Coordinator
5. Excavators, trucks, and wheel loader drivers
6. Drone-monitoring

Figure 4 shows the time schedule of for each teams 1 to 6. In the Figure Z, numbers 1 to 6 presents task mention above. Both on Wednesday and Thursday at the Ouluzone motor center, the teams followed the same time schedule.

Time	Team 1	Team 2	Team 3	Team 4	Team 5	Team 6
8:30	Arrival, registration and grouping, morning coffee					
9:00	1	2	3	4	5	6
9:50	2	3	1	5	6	4
10:40	3	1	2	6	4	5
11:30	Lunch - cafe			free time		
12:00	free time			Lunch - cafe		
12:30	4	5	6	1	2	3
13:20	5	6	4	2	3	1
14:10	6	4	5	3	1	2
15:00	COFFEE and return of helmets and vests etc					
15:30	Departure					

Figure 4. The time Schedule of Wednesday and Thursday in OuluZone workshop for each team 1 to 6. The number in colored area is the practical tasks: 1) road designer, 2) speedway project owner and surveyor, 3) construction' head manager. 4) BIM foreman, 5) excavators, trucks, and wheel loader drivers, and 6) drone-monitoring.

Occupational safety was monitored by using MVR-form. MVR is used at civil engineering as a method of assessing working conditions and safety and for carrying out statutory weekly inspections. Throughout the

workshop, the safety manager counseled students on if any problems or issues appeared. In addition, the students had the Infrakit app in their mobile phones and a possibility to use Infrakit-support during the workshop. Finally, the students had a possibility to follow the autonomous excavator [19] show provided by the University of Oulu. The tasks were located in Ouluzone in several different places e.g. judge tower and construction site.

3 OuluZone workshop

The Ouluzone workshop 2019 was contained 2 lecture days, 2 practical days in OuluZone and finally the feedback and evaluation day. In this chapter, the results and discussion about the findings and lesson learned about this workshop is presented.

3.1 Lectures

The purpose of the lectures was to go through the various stages of the construction site from the planning to handling over the Speedway track to the project owner. Here is presented few examples of the content of the lectures. Teachers and experts from technology companies prepared their presentation with slides including videos and they explained many real-life examples in their presentations. First, it was explained to students the objectives, organization and general things related to the Ouluzone workshop week. During the lectures was mentioned, Finnish legislation and requirements of the road construction that must be taken into account. Cooperation forum BuildingSMART Finland and its work to disseminate information on infraBIM and to support those in the implementation was presented. In addition, the use of the right documents for example to safety and construction site technical quality requirements (based on InfraRYL) was presented

An integral part of infra information modelling is various geographic dataset such as ground (level) model, and environmental information which can be visualised also in 3D models. Survey control is an essential element in the design and construction survey data. The using correct coordinates and high system is very important and using the correct unit of measure (meter).

Students learned the principles of road construction design and model-based quality assurance. The designer is responsible for the correctness of the initial or source data model. Therefore, it is important that all the term such as lines are defined correctly. The final planning model has gone many rounds from designer to the project owner to ensure quality. The importance of occupational safety issues was emphasized during the lectures before the practical training in Ouluzone. The principle of the MVR-form as a tool for following the safety was gone through.

A simple Kahoot-play questionnaire was conducted to found what student was learned before the workshop. The questionnaire contained 10 questions and there were four answer options in each question. The result of Kahoot-play questionnaire is presented in Figure 5. Based on the correct answers, it can be said that the students had moderate starting knowledge for the workshop.

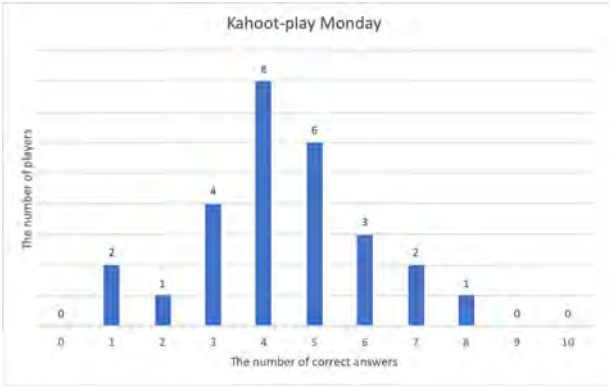

Figure 5. The Kahoot-play questionnaire in the begin of the workshop. The number of answers were 28. The average degree was 4.25 by the standard deviation 1.85.

3.2 Practical training in Ouluzone

The goals of two day practical training in the Ouluzone workshop was to learn open infraBIM-based automation and robotics in practice and problem solving. The construction site of Speedway track contained human resources, digital models, machines and devices, materials and time. It was important that everybody knows their role and responsible to optimize the high quality result. The location of the base station was vital to achieve the best connection to all machines, automation systems and Infrakit cloud service. The learning tools during the tasks were slides, videos, real-life examples, discussions, exercises and demonstrations. In each task, the main responsivities were discussed and how Infrakit cloud service was used. The learning outcomes of students for each practical task can be summarised as following:

1. Road designer: Understanding about model-based road construction work accordance to design and modelling instructions. Describe the documentation procedure to ensure the compatibility of models and absence of conflicts.
2. Speedway-project owner and surveyor: Understanding about decisions and purchase procedures for the preparation and implementation of the project. At each stage of the life cycle, the acceptance the final outcome into maintenance systems is compliant.

3. Construction' head manager: Describe the overall operations (e.g. scheduling, control, implementation, and quality assurance) of the model-based construction site responsibilities.
4. BIM Coordinator: Describe how to use and apply up-to-date information management from the construction site such as ensuring the quantity calculations, a model-based quality assurance procedure, the survey control and preparation of digital handover material.
5. Excavators, trucks, and wheel loader drivers: Understanding about the machine control equipment operation. Describe the model-based quality control procedure in accordance with as build surveys and mappings performance.
6. Drone-monitoring: Understanding about the UAV field measurements procedure to receive the digital surface model, or to follow construction site progress.

The second day at OuluZone was problem solving, and therefore construction site audit was arranged. There were two reasons: 1) the location of the construction site was suspected to be in a wrong place, and 2) the size of the rock found on the construction site. All the participants gathered at the construction site to evaluate and solve the situation.

During the Ouluzone practical days the students were requested to monitor both the positive and negative things at the construction site by using MVR-form. The MVR- form included considerations such as working and machine operation, equipment, electricity and lighting, protection and safety areas, driveways and traffic routes, and ordering and storage.

One possibility for future construction sites is autonomous machinery for example dangerous environments. All the Ouluzone workshop participants were demonstrated, how the automated control of the movements of the excavator (the Smart Bobcat E85 Excavator 6) is working.

3.3 Final day of the workshop week

The final day of the workshop was for receiving the feedback survey both from students and from teachers. The questions were about the successes and development ideas. In addition, the best practical test was evaluated. The participants mentioned time scheduling and getting industry partners as teachers involved as positive things during the OuluZone week. Each group presented their MVR-findings. It was interesting to notice that if the group had any construction site experience, the findings were more accurate. In addition, the debate on the importance of occupational safety was lively.

One of the development ideas was MVR-form as a new practical task was desired, since the discussions with the expert give the new off reinforces perspective. The construction site audit was surprise to students and therefore the problem-solving situation went unclear for some. Thus, the instructions at the beginning of the week should be more exact. This means that there could be even more communication between teachers before workshop week. The best practical tasks were evaluated to be the drone and designer, since teachers were prepared their materials properly.

Finally, Kahoot-play questionnaire was conducted to found what student was learned during the workshop. The questionnaire contained 10 questions and there were four answer options in each question. The results of Kahoot-play questionnaire are presented in Figure 6, in where can be seen that the participants received more correct answers than on Monday Kahoot-play. Therefore, it can be said that the students had good knowledge after the workshop.

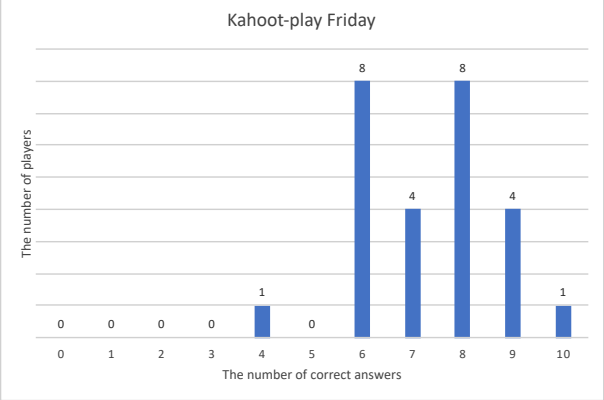

Figure 6. Tue Kahoot-play questionnaire in the final day of the OuluZone workshop. The number of answers were 26. The average degree was 7.31 by the standard deviation 2.32.

4 Summary

The results and findings from the education collaboration workshop week between the University of Oulu, the Oulu University of Applied Sciences (OAMK), and Oulu Vocational College (OSAO) is reported. The goal of the workshop week was to educate Open InfraBIM and construction Automation and robotics to students. During the week students learned from lectures and practical training in OuluZone motor center what are the typical tasks of the responsible person in the constructions site and how they are using modern tools such as automation and cloud service (Infrakit). Practical learning was found to be motivating way to educate students. Technology companies reported that they have received new ideas from the Ouluzone workshop for further product and application development. Based on

good learning experience and the feedback from the participants, the development of Ouluzone workshop will be continued.

Acknowledgements

The authors would like to acknowledgement all the students and teachers from University of Oulu, Oulu University of Applied Science (OAMK), and Oulu Vocational College (OSAO) that took the courses and participating to OuluZone workshop week 2019. Authors are grateful to the experts from construction industry Mitta Oy, Destia Oy, Infrakit Oy, Welado Oy, Ni-Ro Oy, Pointscene Oy, and Novatron Oy for provided the feedback on their experiences and for brought their technology. BusinessOulu is also acknowledged for their great support on this workshop. This OuluZone+ project was financed by European Regional Development Fund (A71660).

References

[1] Sarén K., *InfraBIM-Sanasto*. Eurostep Oy, 2014 Online: https://buildingsmart.fi/wpcontent/uploads/2013/10/InfraBIM_Sanasto_0-7.pdf, doi: 42625EB1C630 Accessed: 26/05/2020.

[2] Costin A., Adibfar A., Hu H. and Chen SC. Building Information Modelling (BIM) for transportation infrastructure – Literature review, applications, challenges, and recommendations. *Automation in Construction*, 94:257-281, 2018. https://doi.org/10.1016/j.autcon.2018.07.001

[3] BuildingSMART Finland, Infra infrastructure business group. *Common InfrabIM requirements YIV 2019*. On-line: https://buildingsmart.fi/wp-content/uploads/2019/08/YIV_main_document_ENG_DRAFT1.pdf, Accessed: 26/05/2020.

[4] B. Dongmo-Engeland, C. Merschbrock. *A research review on Building Information Modelling in Infrastructure projects. Life-Cycle of Engineering Systems: Emphasis on Sustainable Civil Infrastructure* – Bakker, Frangopol & van Breugel (Eds). 2017, Taylor& Francis Group, London. ISBN 978-1-138-02847-0. p. 601-607.

[5] Borrmann A., König M., Hochmuth M., Liebich T., and Elixmann R. Die INFRABIM-Reifegradmetrik. *Bautechnik* 94:215-219, 2017. https://doi.org/10.1002/bate.201700004

[6] Anderson K. Implementation of BIM in design, procurement and construction of the Stockholm bypass NETLIPSE 25.10.2016. On-line: http://netlipse.eu/media/88731/5_karin-anderson-bim.pdf, Accessed: 26/05/2020.

[7] TYPSAgroup. ROAD-BIM. On-line: https://www.typsa.com/en/roadbim/, Accessed: 26/05/2020.

[8] NATSPEC. BIM education - Global – 2019 update report. International Construction Information Society. 2019 On-line: https://www.icis.org/wp-content/uploads/2019/05/BIM_Education_Global_2019_Update_Report_V6.0.pdf, Accessed: 26/05/2020.

[9] Kostamo M. Implementation Open InfraBIM to Finnish construction education system. On-line: https://infrabimopen2020.exordo.com/files/papers/51/presentation_files/1/Implementing_Open_InfraBIM_to_Finnish_construction_education_system_Miika_Kostamo_InfraBIM_Open_2020.pdf, Accessed: 26/05/2020.

[10] Puust R. Skills development in infraBIM topics by using active learning method. On-line: https://infrabimopen2019.exordo.com/files/papers/6/presentation_files/1/InfraBIM_Open_2019_-_RaidoPuust.pdf. Accessed: 04/06/2020.

[11] Hochschule für Technik Rapperswil. BIM Bassic Education. On-line: https://www.hsr.ch/de/weiterbildung/bau-und-planung/module-kurse-und-seminare/#c15112. Accessed: 26/05/2020.

[12] Osello A., and Fonsati A. The experience of the second level master to be qualified as InfraBIManager. On-line: https://infrabimopen2020.exordo.com/files/papers/94/presentation_files/1/The_experience_of_the_Second_Level_Master_to_be_qualified_as_InfraBIManager_Osello_Fonsati.pdf. Accessed: 26/05/2020.

[13] Kolli T., Heikkilä R., Röning J., Sipilä T., Erho J., Hyyryläinen M., and Lammassaari P. Development of the education of open Infra BIM based construction automation. In *Proceedings of the International Symposium on Automation and Robotics in Construction and Mining (ISARC)*, 35:791-797, 2018. https://doi.org/10.22260/ISARC2018/0110

[14] Heikkilä R. And Kolli T. OuluZone – Infrastructure Building Information Modelling and Automation workshop 29.10.-2.11.2018. On-line: http://www.bim4placement.eu/wp-content/uploads/2018/12/BIM-TRAINING_OULUZONE-REPORT_EN.pdf, Accessed: 26/05/2020.

[15] *Liikenneviraston ohjeita. Tie- ja ratahankkeiden maastotiedot. Mittausohje*. On-line: https://julkaisut.vayla.fi/pdf8/lo_2017-18_maastotiedot_mittausohje_web.pdf, ISBN 978-952-317-392-7 Accessed: 26/05/2020.

[16] Rauhala A., Tuomela A., Davids C, and Rossi P.M. UAV Remote Sensing Surveillance of a Mine Tailing Impoundments in Sub-Arctic Conditions. *Remote Sensing* 9:1318, 2017. doi:10.3390/rs9121318

[17] Kivimäki T. and Heikkilä R. Infra BIM based Real-

time Quality Control of Infrastructure Construction Projects. In *Proceedings of the International Symposium on Automation and Robotics in Construction and Mining (ISARC),* 32:1-6, 2015. https://doi.org/10.22260/ISARC2015/0117

[18] Heikkilä R., Vermeer M., Makkonen T., Tyni P. and Mikkonen, M. Accurary assessment for 5 commercial RTK-GNSS systems using a new roadlaying automation test center calibration track. In *Proceedings of the International Symposium on Automation and Robotics in Construction and Mining (ISARC),* 33:812-817, 2016. https://doi.org/10.22260/ISARC2016/0098

[19] Heikkilä R., Makkonen T., Niskanen I., Immonen M., Hiltunen M., Kolli T. and Tyni P. Development of an Earthmoving Machinery Autonomous Excavator Development Platform. In *Proceedings of the International Symposium on Automation and Robotics in Construction and Mining (ISARC),* 32:1-6, 2019. https://doi.org/10.22260/ISARC2019/0134

Automated Data Acquisition for Indoor Localization and Tracking of Materials Onsite

H. Bardareh[a] and O. Moselhi[b]

[a]Department of Building, Civil and Environmental Engineering, Concordia University, Montréal, Canada
[b]Centre for Innovation in Construction and Infrastructure Engineering and Management (CICIEM), Department of Building, Civil and Environmental Engineering, Concordia University, Montréal, Canada
E-mail: hassan.bardareh@mail.concordia.ca, moselhi@encs.concordia.ca

Abstract –

Considerable body of literature exits on automated site data acquisition for tracking and progress reporting of construction operations. While GPS-based solutions have been widely investigated in many studies for outdoor tracking of these operations, indoor tracking proved to be more challenging. This paper focuses on indoor material localization and investigates the use of two remote sensing (RS) technologies including ultra-wideband (UWB) and radio frequency identification device (RFID) in order to support automated tracking of indoor operations. The integrated use of these two technologies is proposed to benefit from the capabilities of each technology and to have a cost-effective and practical solution for location identification of the materials on site. The proposed methodology includes two steps. First, tracking of the items located above floor level such as plumbing and HVAC installations. This was performed using accurate identification and 3D-location information generated by an UWB system. A set of experiments were carried out using various filters to improve the localization information. The results indicate that an increase in range distance between UWB tags and receivers increases the mean ranging error from around 20 centimeters to over 50 centimeters. In the second step, an UWB tag is attached to a hand-held RFID reader and accordingly the accurate location of that reader is stored. Then, by using algorithms such as boundary condition trilateration (BConTri) and received signal strength (RSS), the objects that are labelled by RFID tags are localized. Accordingly, this integrated configuration of the sensors eliminates the need for using a large number of RFID reference tags onsite for indoor material localization. The data fusion embedded in the proposed configuration is expected to enhance automated progress reporting. Besides, it is likely to enable identification and measurement of deviations from as-planned models in a timely manner. The experimental data captured in the lab will be analyzed and presented, highlighting the advantages of the proposed method.

Keywords –

Automated progress tracking; RFID system; UWB system; Data fusion

1 Introduction

Progress reporting is a critical part of the project control in which a large amount of as-built information related to a variety of tasks onsite are provided. However, it is not a simple task due to challenges associated with data acquisition and handling a large amount of information for a variety of functions such as scheduling, construction methods, and cost management. Object tracking is an important part of a progress reporting system in which the identification and localization information of the various objects onsite are needed.

The literature reveals a wide range of studies for identification and localization of the objects, as the main parameters of a tracking system. These two types of information can enable us to track an activity in a desired time span. Tracking materials and accessing onsite information can be challenging due to dynamic nature of onsite operations including material delivery and utilization. In fact, material management was identified as one of the areas that has a great potential for improvement on sites [1].

Many researchers have proposed the application of various Remote Sensing (RS) technologies such as GPS, Radio Frequency Identification Device (RFID) and Ultra-wideband (UWB) in tracking of various objects onsite [2]. However, applications associated with outdoor tracking of the materials are mostly based on GPS-based technologies [3-9]. But, this technology is not suited for indoor environment. Besides, due to a wide range of materials and structural objects in an indoor environment, there is a need for a system in which a large number of items can be tracked efficiently.

RFID technology has been used in this respect with

great capability in automatic identification and tracking of tagged objects onsite. It is applicable for both built facilities and during construction due to its non-line-of-sight capability, wireless communication and on-board data storage capacities [10]. Besides identification capability, RFID technology is also used for localization of the tagged objects onsite. There are three main methods to localize an object using RFID sensors including triangulation, proximity, and scene analysis. Range-based localization is usually based on trilateration and triangulation techniques in which the received signal strength index (RSSI), phase-based indicator and time-of-arrival (TOA) are used to measure the range distance from a tagged object. Proximity technique is based on using some reference points with known locations in order to investigate whether a tagged object is close to those reference points or no. Scene analysis uses some algorithms (e.g. k-nearest-neighbor (KNN) or probabilistic methods) to localize tagged objects based on the similarity of received signal with a prior location fingerprints collected from the environment. In the range-based techniques mentioned above, the distance value between a hand-held RFID reader and a tagged object can be measured by converting the RSSI to an experimental range value. Having said that, these received signal strength (RSS) values are unreliable since they are highly dependent on various factors in different environments. However, proximity and scene analysis techniques are not based on the range value between tag-reader, but they still rely on RSS value for localization which makes the localization not reliable enough. Besides, they face additional barriers in terms of system configuration with extra cost and deployment, computing complexity and calibration difficulties [1]. In [1], application of the RFID technology for indoor location identification of the materials was investigated. However, the individual use of RFID sensors faces some difficulties since a high density of reference tags are needed [1,11].

UWB technology is a Real-time Location System (RTLS) which has a performance almost similar to an active RFID system, however, it uses very narrow pulses of radio frequency energy which are occupied in a wide bandwidth for communication between tags and receivers. Various types of UWB sensors use different positioning techniques for localization, including: time of arrival (ToA) or time of flight, angle of arrival (AoA), time difference of arrival (TDoA), and received signal strength (RSS). AoA has some advantages over TDoA as it does not require synchronization of the sensors nor an accurate timing reference. While TDoA is less sensitive to changes in setup calibration, it still requires more cabling to have an accurate timing reference. Several researchers have investigated the possibility of using this technology for location identification of objects to track construction operations. Most of their efforts were focused on evaluating real-time tracking of workers, equipment and materials in indoor and outdoor environments [2,12-15]. Besides, some studies have investigated the effect of the UWB sensors geometry, employment of some filters (e.g. Kalman Filter, particle filters and etc.) and the possibility of using static reference tags in order to enhance the localization accuracy of these sensors [12-13,16-21].Studies have been conducted on integrated use of the RS technologies to overcome their individual limitations in order to achieve a more reliable and economical system in which a large number of objects can be tracked and localized. Examples of these integrated systems for outdoor tracking of objects include systems in which a RTLS such as GPS is integrated with Barcode and RFID to benefit the positioning and identification capability of these two technologies. In [22], a low-cost integrated system of GPS-Barcode was designed for tracking of materials on a storage yard. Furthermore, an integrated use of GPS with RFID technologies could provide better performance for tracking of the resources onsite [2,3,23-25]. For instance, in [23], a system consists of spatially distributed mobile RFID readers equipped with GPS technology was used to track a set of mobile RFID tags. Besides, boundary constraints were introduced to facilitate RFID-based localization applications to overcome the challenge associated with unknown tag-reader distance.

Applications of indoor location identification of objects in construction industry include the real-time progress reporting, safety, materials management, and productivity analysis [26]. This paper aims to introduce a new technique in which an integrated use of the UWB and RFID technologies helps to efficiently track the materials in an indoor environment. Besides, a large number of objects are localized in a more economical way which can enable us to recognize and measure deviations from planned models by having both time and location of the available objects associated with each activity. This can result in a more enhanced and timely progress reporting onsite, which is essential for an accurate earned value analysis (EVA) and project estimating.

2 Experimental Performance of the UWB System

In a set of experiments in the Construction Automation Lab. (CAL) in Concordia University, performance of the Trek1000 UWB Evaluation Kit which is an off-the-shelve product is investigated. These sensors utilizes an atomic timer embedded in their PCB board that provides a high positioning accuracy in the range of a few decimeter. This product is almost eight times less expensive than the available commercialized

sensors, however, it is still not a final product with a protected enclosure.

The initial setup of the experiment includes a system of four receivers and one tag. The data rate of this setup is fixed on 110 kb/s and in Channel 2. This is the standard setting defined by the manufacturer for maximum range measurements. For calibration and measuring the accuracy of this system, a grid on the floor with tiles in size of 90 cm × 90 cm was marked in order to define the 65 ground-truth test points which covers both Line-of-Sight (LOS) and None-Line-of-Sight (NLOS) scenarios. The anchors were put at height of 1.65 m except one of them at the height of 2.15 m, and a moving tag at height of 1.35 m. The experimentation consists of moving one mobile node to 65 different ground-truth locations. For each tie point, a time interval of 30 seconds was considered, so each tests lasted 32.5 minutes (i.e. 65X30 s=1950 s). However, 10 seconds before and after each displacement was rejected in order to guarantee a good ground-truth data. Figure 1 shows the good performance of this system. As we expected, all data points are above diagonal line which indicates the positive aspect of error due to the NLOS dispersion since there should never be range measurements shorter than the real straight path.

2.1 Range Measurement Accuracy of the UWB System

Range measurement is important since the location of the tagged objects are achieved based on their values. One way to improve ranging measurement is to remove the clearer outlier measurements from our estimation. A comparison of the methods to mitigate localization error associated with NLOS situation and the situations in which they can be employed are discussed in reference [26]. For the case of this research, there are technically two groups of objects which need to be tracked and localized by the UWB system. The first group is stationary objects which are tagged by UWB sensors. The second one is a moving RFID reader. For the first application, since the objects are stationary (or semi-stationary such as plumbing and mechanical facilities) a tailed UWB-ranging measurement model is used which is fitted to a histogram of the ranges error in NLOS situation (Figure 2). For simplicity, the same particle filter was used for the moving RFID reader.

In this experiment, first any outlier reading ranges in NLOS situation with the error value more than 0.8 m are removed from the initial data. Then, the testing ranges are split into three intervals with step of five meter (0-5,5-10,10-15). Finally, the remained reading ranges in middle of 10-second out of 30-second stop in each tie point are averaged to calculate the tag's location in each time step. Figure 3 illustrates the mean range error and standard deviation for each ranging interval with and without omitting initial outliers.

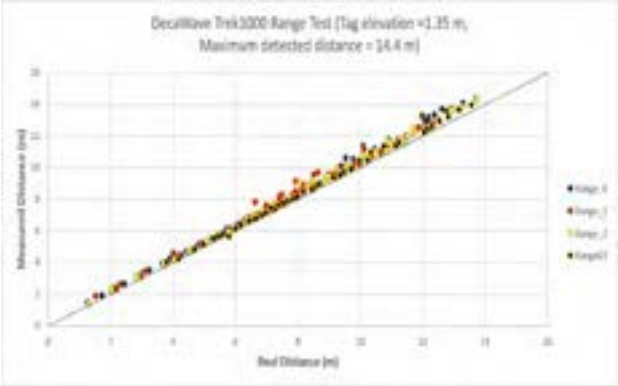

Figure 1. Real versus measured ranges.

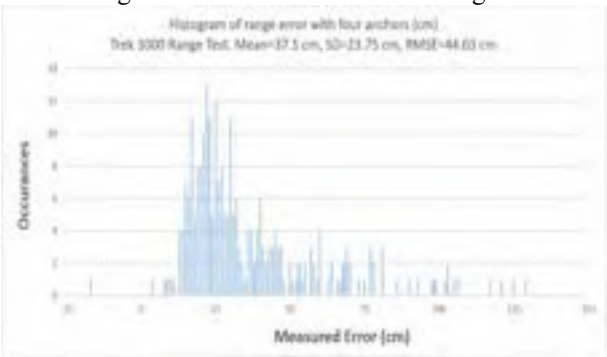

Figure 2. Error histogram in NLOS.

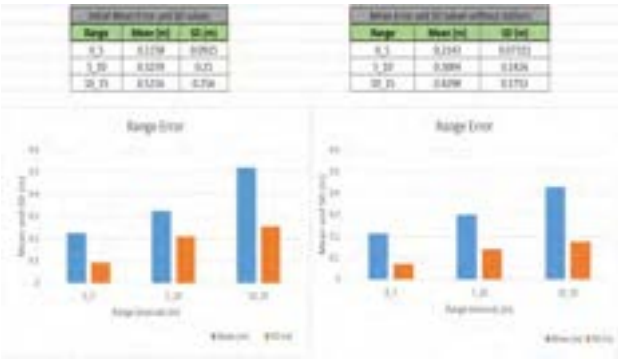

Figure 3. Mean and SD error values with outliers (left) and without outliers (right).

2.2 Localization Accuracy of the UWB system

In this research experiment the 3D location of the critical elements in elevation are tracked by UWB tags attached to these elements such as installations and critical spools in plumbing system. Besides, it is possible to localize and track the items which are tagged by RFID tags. For that, the real-time location of the hand-held RFID reader is acquired by the UWB tag attached to it (section 3.1).

From various techniques to mitigate the localization error [16,26], for tracking stationary (or semi-stationary) objects tagged by UWB sensors, a tailed UWB ranging measurement model is fitted to the experimental

measurements presented in the last section. In fact, this model combines a Gaussian distribution (for the LOS measurements), a Gamma distribution (for the NLOS cases) and a constant value to cope with additional uncertainty and spurious measurements. By creating a measurement model using the error histogram in NLOS situation (Figure 2), it is possible to alleviate in-excess range measurements. Then, a particle filter with three states (i.e. X, Y and Z) is used to change the weight of each particle. Finally, the location of the moving object is obtained by computing the weighted mean location of all particles [16].

3 Proposed Methodology

There are various techniques for localization of the objects by using a RFID system. Since in this experiment a roving RFID reader (s) with known location is used, the application of a range-based technique is investigated to localize stationary tagged objects. Here an integrated system of both RFID and UWB sensors is designed. In fact, it is not economically practical to use only UWB tags for tracking objects onsite. While, the reasonable price for RFID tags make them a good choice for object identification and localization. However, the calibration of the system in this approach is problematic since the RSSI varies over time and it is highly dependent on the site environment. Plus, there is no direct relationship between this RSS value and a conventional ranging formula which results in low positioning accuracy [27].

In another approach, the tagged objects are localized by using a boundary condition-based algorithm in which the maximum reading range of a hand-held RFID reader helps to localize those objects which can satisfy the condition of appear in-out in that range limit [24,28].

Using only RFID tags for localization of the objects in an indoor environment needs to employ a large number of RFID reference tags [23]. Saying that, for outdoor tracking of materials, an integrated system of RFID and GPS-based sensors was proposed in previous literatures which eliminated the need for reference tags [23,25]. It was basically based on finding the location of the RFID reader (s) by a GPS receiver and then finding the tags location through trilateration technique. Unfortunately, in an indoor environment the performance of the GPS sensors are highly degraded since they need a direct access to the sky to receive signals from satellites. In this way, the UWB system can be replaced with GPS system to localize RFID reader in each time span.

3.1 Integrated UWB and RFID Technologies

An integrated system of the UWB and RFID sensors helps to benefit from positioning capability of UWB sensors for localization of RFID reader (s) in an indoor environment. In fact, by knowing the location of the RFID reader (s), it would be possible to localize RFID tags by using a Boundary-condition Trilateration (BConTri) algorithm or a received -based technique. In the boundary condition-based algorithm, a tag location is measured by solving three (four) lateration equations (Equation 1) in which the intersection of three circles (four spheres) for 2D (3D) localization is needed. While, the RSS-based algorithms estimate the tag location as an average weighted over received RSSI of the three (four) corresponding reader locations under the boundary condition (Equation 2) [23].

$$(x - X_{i,t})^2 + (y - Y_{i,t})^2 = r^2 \quad (1)$$

$$(x,y) = \left[\frac{\sum_{i=0}^{2} X_{i,t^*}\, rs_i}{\sum_{i=0}^{2} rs_i} + \frac{\sum_{i=0}^{2} Y_{i,t^*}\, rs_i}{\sum_{i=0}^{2} rs_i}\right] \quad (2)$$

Where (x,y) are unknown target tag coordinates, $(X_{i,t}, Y_{i,t})$ are the RFID reader location at time t which are measured by UWB sensor (i=0, 1, 2 for three different RFID reader locations), r is the range distance between tag and reader and rs_i is received signal strength indicator of reader i.

In BConTri technique, the initial value for r is set to the nominal range value of the RFID device (r_0). However, this value needs to be corrected until achieving an acceptable area of intersection between three circles for 2D localization. In this way, an even virtual distribution of points in all three circles is considered. If there is no common intersection area between these circles (number of the virtual points are less than a defined value), then this radius should be increased. In contrary, if the intersection area is more than a defined value, the radius should be decreased. Finally, the estimated location for each tag is calculated by averaging the points available in the intersection area.

It is worth mentioning that since here the tagged objects are static, a few number of readers would be fine for location identification of the items. However, in case of tracking moving objects, a large number of RFID readers would be required. To localize a tag, a set of acceptable boundary reader points (BRPs) should be identified. Around 10 points would be enough for an experimental assessment to localize a tag. Then, three (four) out of ten points are selected to solve the trilateration equations for 2D (3D) localization. Since selection of these three (four) points combination can affect the location accuracy, the combination with the highest value of dilution of precision (DoP) is preferred. In fact, in a GPS system the localization accuracy will increase when visible satellites are far apart which results in a higher DoP and geometry is stronger. Saying that, unlike GPS system, RFID system is not working based on clock offset (using the time difference to measure distance). In this way, a new approach to consider the effect of the RFID reader locations on the localization

accuracy is needed. In fact, besides measuring the accuracy of the system to localize the RFID tag (s), a calibration model for distribution of the RFID reader (s) is also needed. Similar to the DOP factor in GPS system, this model can enable us to measure the variance for various three (four) combination of the BRPs. Each of these variances are corresponding to an average error value in localization of the tag. In this way, each combination of the BRPs is equivalent to a specific accuracy in measurement which can be used as a standard for selection of the reader (s) distribution.

3.2 Schematic Design of the RFID and UWB Data Fusion Model

Below shows a schematic diagram of the methodology to integrate the UWB and RFID systems in order to achieve a more practical and cost effective technique for indoor location identification of the materials onsite (Figure 4). This information can be used for automated progress reporting and a more timely earned value analysis.

The first part of the tracking system is based on using UWB tags to track objects above floor level. For this type of objects, the UWB tags are used to provide 3D identification-location information of the objects. However, due to high cost of UWB tags it would not be reasonable to tag all objects for tracking each activity. This issue can be addressed by tagging critical objects to track critical activities.

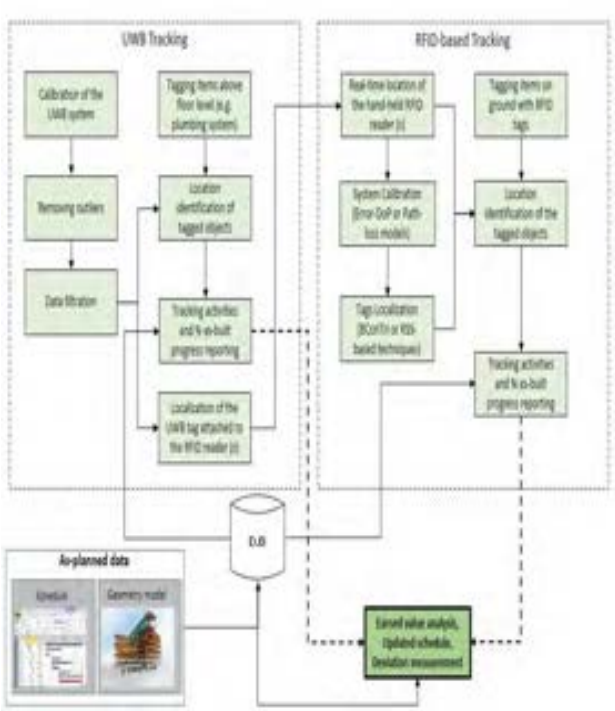

Figure 4. Conceptual overview of the location identification material tracking system.

In the second part of the tracking system, the integrated use of RFID and UWB systems is proposed to track a larger number of objects but in a cost effective manner. In fact, by attaching an UWB tag to the hand-haled RFID reader (s), it would be possible to localize the RFID reader by using the data acquired by the UWB system. By knowing location of the mobile RFID reader (s) and using a localization technique (e.g. BConTri or RSS-based technique), it is possible to localize objects with the attached RFID tags. As mentioned, system calibration should be conducted before tags localization. In the following subsections, after a brief review on some protocols for data acquisition, the calibration and localization modules are elaborated.

3.2.1 Data Acquisition protocol

The data acquired by integrated RFID-UWB sensors should be time-stamped. Saying that, the UWB system have a timer with ms accuracy, while the timer accuracy for RFID system is in second.

a) Data acquisition for system calibration: to achieve the path-loss model required for the RSS-based range measurement, the RSSI received from 10 RFID reference tags on the ground are recorded. Since the exact position of all the tie points and the 10 reference tags are known, it would be possible to measure the range distance between the reader and each reference tag. The RFID reference tags are located at the height of 1 m, while the hand-held RFID reader output is set to 22 dbm (with an approximate reading range of 3.5m). Here we move forward on the 35 tie points (the same tie points for UWB system calibration) every 30 seconds. After deducing the first and last five seconds in each step, the data read by the RFID reader are analysed. In another scenario, the real-time location of the hand-held RFID reader is estimated by the UWB tag attached on it. In this way, there is no need to move on any tie-points, however, a time-step (such as one second) should be considered for matching RFID and UWB data. To enhance the accuracy of the UWB tag in localizing the RFID reader, we should ask the surveyor to stop moving when triggering the hand-held reader.

b) Data acquisition for the RFID tags localization: in order to meet the condition required for localization based on the BConTri algorithm, some protocols for data acquisition need to be respected by the surveyor. In fact, an acceptable reading for a tag in this algorithm is based on a roving RFID reader moving to different directions in each time step. For that, we should ask the surveyor to not stop moving when pushing the trigger of the hand-held RFID reader. Plus, for better performance of the hand-held reader, it is needed to put it in rest mode every minute in which the surveyor should stop moving.

3.2.2 Calibration Module

To calibrate the system for localization of the tags by the hand-held RFID reader, first a set of acceptable readings for localization need to be selected. The acceptable reading data can be varied depending on the algorithm we use for localization. Here, both BConTri and RSS-based algorithms are tested to evaluate the accuracy of each of them for localization. For instance, in BConTri algorithm the acceptable readings are those in which the event appear in-out happens for each tie point. For the RSS-based algorithms, on the other hand, there are some factors that may affect the accuracy of the localization measurements. This includes factors associated with the RFID devices such as operating frequency, the hand-held RFID device power and distance between the tag (s) and reader. The results of an experiment showed that if the distance of the reference tags from each other is half of the device reading range (0.5RR) then a better detection rate is resulted [28]. The factors associated with indoor environment also influence the RSSI signal such as free space loss factor, multipath reflection, and interference effects [29]. As mentioned above, by putting some reference tags with known locations, it would be possible to evaluate the accuracy of the measurements. Figure 5 illustrates the various steps for the system calibration.

a) In BConTri-based technique: for this method, the combination of RFID reader locations with the highest value of Spatial Dilution (SD) is preferred in order to achieve better localization accuracy. Saying that, the SD value refers to the distribution of a number of objects in space and their geometric configuration, mostly used as an indicator of the locating accuracy for systems which are working based on the ToA and AoA positioning techniques. In fact, it is equivalent to the mathematical variance and DoP in GPS-based systems. In this case, for each combination the SD factor for hand-held RFID locations and the corresponding error in identified reference tags location are calculated. Then, the SD can be normalized into a ratio of the SD (RSD) by diving its value to the highest tag-reader distance to omit the effect of range distance in estimation. The details of the mathematical calculations are provided in [25].

After repeating the steps above for all possible combinations of the RFID locations geometry, a linear regression is assigned to the points achieved in a graph in which the error value (m) and RSD are the variables in vertical and horizontal axis respectively. This graph can be used as a standard for standard value of DoP and the corresponding accuracy. The standard value is used as a threshold for selection of the data in localization of other tagged objects. In fact, only the RFID reader location combinations with SD value more than the standard SD value are accepted.

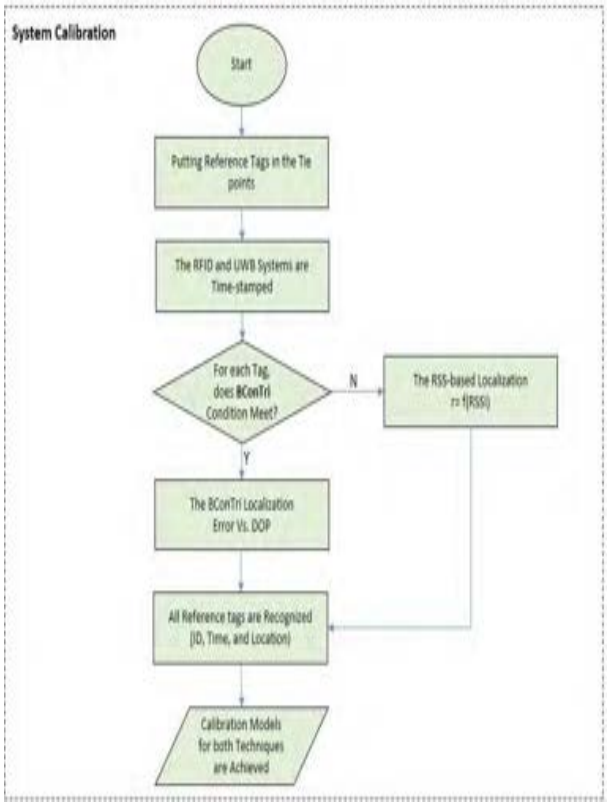

Figure 5. System calibration diagram.

b) In RSS-based technique: to use this technique for tags localization, a path-loss model is needed. In fact, based on the RSSI recorded for each reference tag and the corresponding distance range value (DRV), the model would be achieved (Equation 3). Then, by knowing the location of the RFID reader recorded by UWB sensor attached, the location of the each RFID tag is calculated by solving three distance equations (Equation 4).

$$DRV = - 0.5617\ RSSI - 39.9337 \quad (3)$$

$$DRV = [(x_{r\_uwb} - x_i)^2 + (y_{r_{uwb}} - y_i)^2]^{1/2} \quad (4)$$

In which (x_{r_uwb}, y_{r_uwb}) are the location of the hand-held RFID reader (s) which are acquired by UWB device attached to it. And (x_i, y_i) are the coordinates of the identified RFID reference tags with known locations. For each identified tag, an average of the RSSI values and the calculated range value are recorded.

The result of the system calibration to achieve the path-loss model is shown in Figure 6. It depicts the RSSI versus the distance between the reference tags and the reader in each tie point. In fact, the average of the RSSI for each tag identified in each tie point is calculated. Then, for assigning a regression model to the data acquired, the data are again averaged for every 5 cm increments. Details of the best regression model and their accuracy can be found in [26].

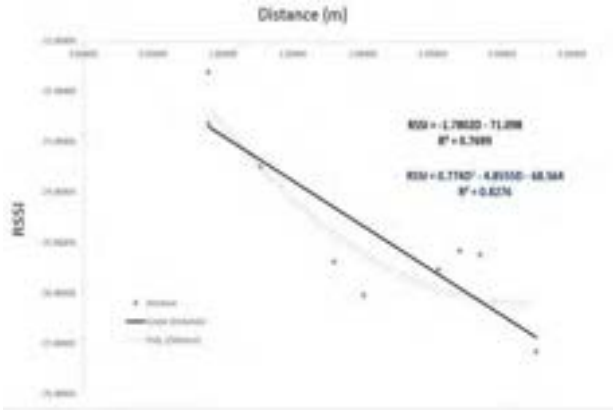

Figure 6. RFID system path-loss model.

3.2.3 Localization Module

After conducting the calibration, it is time to localize the tags location by using the standard spatial dilution (SD_{st}) or the path-loss model to localize tags in BconTri and RSS-based techniques respectively.

a) Localization through BConTri technique: to localize a tagged object, the location data achieved from the selected combinations of SD (SD> SD_{st}) for each identified tagged object are averaged.

b) Localization through RSS-based technique: to localize a tagged object, first the location of the hand-held RFID device in each time span is achieved from the UWB tag attached to it. Then, by using the path-loss model achieved in the calibration step, the range of the tagged object from the hand-held RFID is calculated. The results for the sample RSSI received from 10 target tags indicated an absolute average error of 0.94 m.

4 Summery and Concluding Remarks

This paper investigates the possibility of tracking objects in an indoor environment by doing both identification and localization of a set of tagged objects onsite. For objects in elevation, the performance of the UWB tags were investigated. However, to track a larger number of objects, the integrated use of UWB and RFID technologies was proposed. For that, a hand-held RFID reader was tagged with an UWB sensor in which the location of the RFID reader was acquired by the UWB system. A two-step algorithm developed including calibration and localization modules. In fact, the calibration was based on using some tie points with known locations in order to provide calibration models. After achieving the calibration models for both BConTri and RSS-based techniques, the tagged objects were localized in plane surface. However, the efficiency of this algorithm for 3D localization of the tagged objects need to be investigated more in future.

4.1 The Methodology Contributions

The tracking system proposed can provide identification and localization information for a set of objects in an indoor environment. The use of low cost RFID tags made it possible to track and localize a larger number of objects in comparison with systems in which the individual use of UWB tags were proposed in previous studies. The two-step algorithm developed for localization of the RFID tags would make it possible to have less missing data of the tagged objects in cases that the tagged objects cannot meet the BConTri required condition. In these cases, the object will be localized by the RSS-based technique. Besides, the integrated use of UWB-RFID technologies solved the problem of using a large number of reference tags for localization of the hand-held RFID reader that was proposed in previous studies.

4.2 The Methodology limitations

The localization algorithm provided in this experiment has some limitations. First, to localize a tag in BConTri algorithm, it is needed that at least three (four) readings happens for that tag in which the tag should appear and disappear to be considered as an acceptable reading. This condition may not be possible especially for 3D localization in an indoor environment with a cluttered distribution of the objects. To mitigate this problem, the tags were localized by RSS-based techniques in case that the BConTri requirement is not met. However, the accuracy of the RSS-based localization is still less than the BConTri algorithm.

Another limitation is the difference in reading rang of the RFID sensors in which considering a circular (spherical) profile for reading range may get biased if the direction of the hand-held RFID reader to the tag differs. Finally, the accuracy of this localization method is highly dependent on the calibration of the system in each environment. For that, an accurate positioning of the reference tags (tie points) is required.

References

[1] Montaser A. and Moselhi O. RFID indoor location identification for construction projects. *Automation in Construction*, 39:167-179, 2014.

[2] Moselhi O. and Bardareh H. Automated data acquisition in construction with remote sensing technologies. *Applied Sciences*, 10(8):2846, 2020.

[3] Li H. and Chan G. Integrating real time positioning systems to improve blind lifting and loading crane operations. *Construction Management and Economics*, 31:596–605, 2013.

[4] Langley R.B. RTK GPS. GPSWorld 9. Online: https://www.gpsworld.com, Accessed: 1/9/1998.

[5] Labant S. and Gergel'ová M. Analysis of the use of GNSS systems in road construction. *In Proceedings of the IEEE Geodetic Congress*, pages 22–25, Gdansk, Poland, 2017.
[6] Magdy I. and Moselhi O. Automated productivity assessment of earthmoving operations. Journal of Information Technology in Construction (ITcon), 19:169–184, 2014.
[7] Seo W. and Hwang S. Precise outdoor localization with a GPS–INS integration system. *Robotica*, 31:371–379, 2013.
[8] Jo K. and Lee M. Road slope aided vehicle position estimation system based on sensor fusion of GPS and automotive on board sensors. *IEEE Transactions on Intelligent Transportation Systems*, 17:250–263, 2016.
[9] Akhavian R. and Behzadan A.H. Construction equipment activity recognition for simulation input modeling using mobile sensors and machine learning classifiers. *Advanced Engineering Informatics*, 29(4):867–877, 2015.
[10] Li N. and Gerber B.B. Performance-based evaluation of RFID-based indoor location sensing solutions for the built environment. *Advanced Engineering Informatics*, 25(3):535–546, 2011.
[11] Maneesilp J. and Wang C. RFID support for accurate 3D localization. *IEEE Transactions on Computers*, 62(7):1447–1459.
[12] Cheng T. and Venugopal M. Performance evaluation of ultra wideband technology for construction resource location tracking in harsh environments. *Automation in Construction*, 20(8): 1173-1184, 2011.
[13] Siddiqui H. UWB RTLS for construction equipment localization: experimental performance analysis and fusion with video data. Master's Thesis, Department of Information Systems Engineering, Concordia University, Montréal, QC, Canada, 2014.
[14] Park J. and Cho Y.K. A BIM and UWB integrated mobile robot navigation system for indoor position tracking applications. *Journal of Construction Engineering and Project Management*, 6(2):30–39, 2016.
[15] Masiero A. and Fissore F. A low cost UWB based solution for direct georeferencing UAV photogrammetry. *Remote Sensing*, 9:414, 2017.
[16] Jimenez A. and Seco F. Comparing decawave and bespoon UWB location systems: Indoor/outdoor performance analysis. *In Proceeding of the 6th International Conference of Indoor Positioning Indoor Navigation* (IPIN), pages 4–7, Alcal´a de Henares, Spain, 2016.
[17] Xu Y. and Shmaliy Y.S. Robust and accurate UWB-based indoor robot localization using integrated EKF/EFIR filtering. *IET Radar Sonar Navigation*.12:750–756, 2018.
[18] Nurminen H. and Ardeshiri T. A NLOS-robust TOA positioning filter based on a skew-t measurement noise model. *In 2015 International Conference on Indoor Positioning and Indoor Navigation (IPIN),* pages1-7, Alberta, Canada, 2015.
[19] Sun M. and Wang Y. Indoor positioning integrating pdr/geomagnetic positioning based on the genetic-particle filter. *Applied Sciences*, 10(2):668, 2020.
[20] Almeida A. and Almeida J. Real-time tracking of moving objects using particle filters. *In Proceedings of the IEEE International Symposium on Industrial Electronics*, pages1327-1332, Dubrovnik, Croatia, 2005.
[21] Zhu Z. and Ren X. Visual tracking of construction jobsite workforce and equipment with particle filtering. *Journal of Computing in Civil Engineering*, 30(6):04016023, 2016.
[22] Song L. and Tanvir M. A cost effective material tracking and locating solution for material laydown yard. *Procedia Engineering*, 123:538–545, 2015.
[23] Cai H. and Andoh A. A boundary condition based algorithm for locating construction site objects using RFID and GPS. *Advanced Engineering Informatics*, 28(4):455-468, 2014.
[24] Andoh A.R. and Xing S. A framework of RFID and GPS for tracking construction site dynamics. *Construction Research Congress*, West Lafayette, Indiana, 2012.
[25] Su X. and Li, S. Enhanced boundary condition–based approach for construction location sensing using RFID and RTK GPS. *Journal of Construction Engineering and Management*, 140(10): 04014048, 2014.
[26] Razavi S.R., Montaser A. and Moselhi O. RFID deployment protocols for indoor construction. *Construction Innovation*, Vol. 12 Iss 2 pp. 239 – 258, 2012.
[27] Ruiz A. R. J. and Granja F. S. Comparing ubisense, bespoon, and decawave uwb location systems: Indoor performance analysis. *IEEE Transactions on instrumentation and Measurement*, 66(8):2106-2117, 2017.
[28] Shahi A. and Safa M. Data fusion process management for automated construction progress estimation. *Journal of Computing in Civil Engineering,* 29(6):04014098, 2015.
[29] Omer, M., Ran, Y., & Tian, G. Y. (2019). Indoor Localization Systems for Passive UHF RFID Tag Based on RSSI Radio Map Database. Progress in Electromagnetics Research, 77, 51-60.

Laser Scanning with Industrial Robot Arm for Raw-wood Fabrication

P. Vestartas [a] and Y. Weinand[a]

[a] Laboratory for Timber Constructions, IBOIS, EPFL, Switzerland

petras.vestartas@epfl.ch, yves.weinand@epfl.ch

Abstract -

This paper presents an integrated raw-wood fabrication workflow using an industrial robot arm and a laser scanner. The research is situated in a Swiss mountain forestry context where timber in its natural form could be applied locally without relying on large centralized timber industries. While local saw-mills relies on the standard processing tools to transform raw-wood into regular beams and boards, an automated robotic application could exploit timber in its natural form directly for construction. The research proposes a digital fabrication workflow that links industrial robot arm and laser scanning to adapt timber joinery tool-paths to irregular raw-wood such as straight, bent and forked tree trunks. The application employs ABB IRB6400 robot and Faro Focus S150 laser scanner. Several methods are developed for the point-cloud processing including flat-cut sectioning, mesh reconstruction and cylinder fitting. The methodology is tested in two stages: a) scanning a set of tree trunks b) continuous integration within robotic fabrication. The findings compare the scanning method in regards to calibration, pointcloud processing, time needed to communicate between the robot controller, the accuracy of the application. The results show that is possible to perform robotic cutting and scanning interchangeably and the speed of the scanning application is proportionally fast (3-4 min) considering the overall robotic cutting time (60-90 min) depending on the study case.

Keywords -

Laser Scanning; Industrial Robot; Robotic Fabrication; Unprocessed Timber; Raw-wood; Round-wood

1 Introduction

Timber as a construction material is commonly unified into engineered timber products such as panels, boards and beams of regular sections [1, 2]. However, these techniques could be avoided by employing machining tools that help to transform raw-wood into a building material with a minimal processing time. CNC and robotic arms can have a computer-vision, cutting and assembly techniques to adapt to the irregularity of the tree shapes [3, 4, 5].

The scanning methods of timber are applied in sawmills, ranging from fast laser scanners [6, 7] to volumetric CT scans [8, 9, 10]. In the industrial context, the geometry acquisition is used to optimize the cutting pattern of trees into boards, identify timber knots and disregard crooked timber. The process is often well structured using a digital data-base to track the maximum use of material, its age, species, and location where the wood is harvested from [11]. This data is applied only at the scale of the saw-mill companies and is not transferred for a design use.

The introduction of industrial robots arms in the architectural research environments helped to change the notion of a standardized-timber and apply its original form for construction. There is a series of scanning methods that gives a vision to the industrial fabrication methods and informs design decisions such as manual measurement, markers and tracking devices, photogrammetry, camera sensors, laser scanning, virtual reality applications, and volumetric scanning.

1.1 Manual Measurement

Trees are primarily inspected using manual measurement tools and selected based on physical dimensions needed [5, 12, 3, 4]. The selection criteria depends on a geometrical data: length, radial parameters i.e. axis and diameter, curvature, and topology i.e. straight, bent, bifurcated tree trunks. The fabrication process could also be assisted by a visual measurement employing a teach-pendant when coordinates are transferred to a digital model [13]. For example, 3 points could be taken to visualize an end of a beam in a form of circle fitting.

1.2 Markers and Tracking

The marker-tracking system is a lightweight geometric method that allows a fast positioning of an irregular tree trunk. Markers or positioning points could ease the fabrication process if a 3d scan has already been performed. There are several possible solutions to position a log within a fabrication setup: (i) aligning two point-clouds by targets captured during a design stage (ii) pre-drilling dowel holes that match a machining setup [4] (iii) employing point tracking system i.e. (OptiTrack) [11]. The reference of markers is determined by probing and matching reference features both found in a digital data-set and the actual raw-woods.

1.3 Photogrammetry

Digital models of raw-trees could also be obtained by taking multiple photos with a low-cost camera [5]. The process requires a slow post-processing technique to translate the photos'pixel-data to a point-cloud or mesh repre-

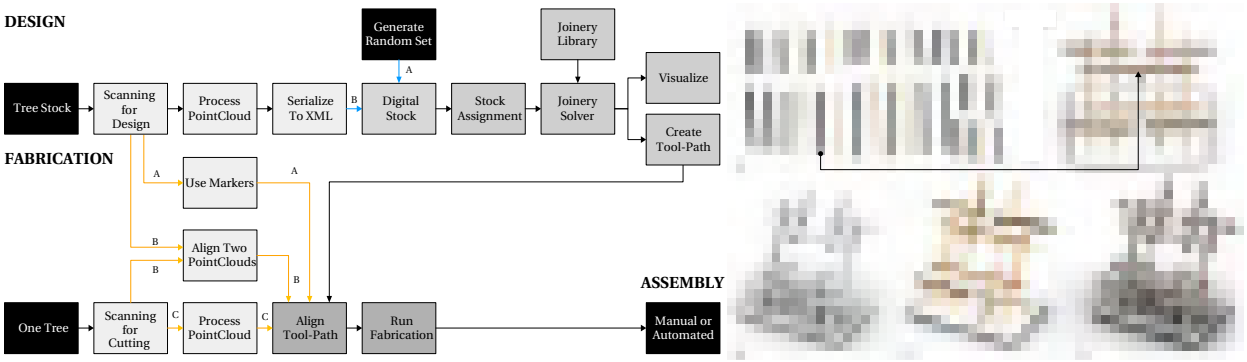

Figure 1. The workflow focusing on design-to-fabrication methods (left). Design method (right) of raw-wood assignment (A) to a digital model (B) that is adjusted for fabrication considering trees radial parameters (C-D).

sentation. The scanning could be combined with a photographic selection and 2D post-processing technique [14] for a large set of forks and only scanning trees that are chosen for a fabrication [4]. When a scanned object is relatively small i.e. tree branches, a rotary table, cylindrical supports, camera, and AR markers could be employed [13, 15]. This is an inverse application when a camera is stationary and the object is rotated in small increments to get a 3d representation.

1.4 Camera Sensors

Camera sensors often employ structured light techniques by projecting a known light pattern to an object [16]. The deformation of the pattern relates to a calculation of depth and surface information in a scene. In a raw-wood context, the most common application is a Kinect sensor [12, 17, 18] due to low-cost and open-source SDK. The technique is subject to light conditions and may require scanning to be performed indoors [12] for a better registration process.

1.5 Laser Scanning

The method combines controlled steering of laser beams with a laser range-finder. Due to the high speed of light, this technique is not appropriate for high precision sub-millimeter measurements, where triangulation and other techniques are often used. This technology has already been successfully applied to scan parcels of forest in Kielder Water and Forest Park (UK) by ScanLAB [19] and a forest in Each Sussex by Universal Assembly Unit. Also, laser scanning could be used for analyzing tree biomass regardless of noise data added by small tree branches [20, 21, 22]. There are several raw-wood applications employing the laser-scanning method for fabrication as well. The method is used with a motion tracking system to guide the raw-wood manufacturing process [11].

1.6 Point-cloud Processing

After the scanning process is finished a skeleton extraction has to be performed to change a high-resolution model to a minimal 3d representation. The tree central-axis and radial-parameters are key elements both for visualization and fabrication. These parameters could be obtained by sectioning a closed mesh [4], 2D projection method following local radii [13], contouring [15], point-cloud sectioning [11]. Then the centers of the sections of the scan are connected to form a central-axis. The axis is used for orientation transformation in design-to-fabrication workflows Figure 1 by analyzing the curvature or topology of a tree trunk. When the geometrical data is collected, a tree database could be constructed containing 3D models and a spreadsheet of tapering diameters, changing curvature, best sawing positions, and markers for positioning.

2 Context and Objective

2.1 Contribution of the Study

While automation in scanning applications and robotic controllers is a well studied field and there are readily available commercial products that could collect the scanning data in real-time i.e MetraScan, Artec RoboticScan, Hexagon, Sick, there is a lack of integration in the raw-wood fabrication and timber design. In the research applications (sections 1.1 - 1.6) the process is based on manual point-cloud processing and the scanning is separated from the robotic control. Commercial practices in raw-wood construction make use of the standardized fabrication that requires a minimal skilled labour to complete the projects by local workers such as Unilog / TTT (New Zealand) and FEEL (Japan). Crooked timber is applied in practice as well i.e. WholeTrees with manual carpentry and stationary scanning i.e. Faro Focus. Moreover, raw-wood could be machined using robot cells i.e. Balmer Systems (Canada) along with scanning Mobic SA (Belgium). A

collaboration is built with the later enterprise to employ a scanning application with a robot controller[23] that could gather pointclouds within 4-5 min. using linear movements of a robot for a tree in 5 - 10 m length and diameter of 40-70 cm. The hardware could be optimized further using high-precision and long-range stationary scanners i.e. Faro Focus S 150 and applying a faster communication between a robot controller and the scanner. However, there is a lack of reliable point-cloud processing tools for crooked wood because the current practices do not consider such timber as a valuable resource. Consequently, there is a minimal development of the machining tool-path integration. Small radius straight, tapered, bent and forked beams has a strong structural advantage and could be exploited while developing and automating the workflow between architectural design, digital fabrication and tree harvesting.

2.2 Mountain Forestry

The tree harvesting process is assisted by a collaboration with a mountain forestry in Rossiniere and Lausanne. The Spruce trees are harvested in the Swiss Alps using a cable system due to a high terrain, then brought to a temporary processing site where trees are cut to 5 meters length for the transportation and saw-mill processing Figure 2. In the Swiss forestry context, the raw-wood economic value no longer covers the harvesting costs. Therefore, there is a need to exploit timber in a closed circular economy where wood is not sold to large sawmills but applied locally. Currently, the sawmills rely on the traditional cutting tools and the digital fabrication workflow is absent.

Figure 2. Scans showing a local mountain forestry context: a high and steep terrain where large Spruce trees are cut to fit to a small truck size for transportation to neighbour sawmills.

2.3 Raw-wood Workflow

The research employs ABB IRB6400 industrial robot arm and Faro Focus S150 stationary laser scanner. The scanning of whole-timber is part of a design-to-fabrication system including a laser-scanning, joinery solver, and fabrication techniques for the assembly of irregular timber elements in circular sections Figure 1. The objective is to scan the raw-wood for a design and fabrication using an automatic tool-changer that enables to perform different tasks interchangeably such as scanning, vacuum-grip, and cutting (mill, saw-blade) Figure 3. The scanning is needed because the orientation and position of the work-piece is not known in relation to machining-space. Also, the geometry acquisition is needed for a design scope when a group of selected trees are scanned to create a digital stock. The stock informs the design target - a structural roof system when central-axes of the tree trunks are assigned to a digital model. Afterwards, the timber joints are created depending on a curvature of a beam axis-and radii. Consequently, the fabrication tool-paths are oriented to machining space.

Figure 3. A laser scanner is mounted on a robot vacuum gripper and the $TCP_{Scanner}$ is not known.

3 Methods

The methodology focuses on a scanning application to automate a stationary laser scanner that can be used both for scanning parcels of forest and employed in a digital fabrication. The data acquisition is composed of following parts: physical setup of a scanner mounted on the robot, calibration of the scanner to know the relative position to the robot end-axis, standalone application of the Faro LS 150 SDK (software development kit), its integration within the robot control software (Rhino, Unity), point-cloud processing to obtain radial parameters of harvested timber, serializing data for further design and tool-path alignment for cutting Figure 1.

3.1 Setup of Industrial Robot Arm

The scanner is mounted on a vacuum gripper Figure 4 for safety reasons. The communication between the scanner and computer is enabled by a wi-fi. Then the SDK is applied and .NET application is made to send and retrieve signals from a scanner. The application could trigger following methods: connection, synchronization of scanning parameters, start, pause and stop scanning, send and read data. The power is supplied by 5 hour lasting batteries or a 19 V cable. The files are stored inside SD card that could be sent to computer via the robot-controller. The field-of-view of the scanner is 0◦ × 360◦ in the horizontal and -150◦ × 150◦ in a vertical rotation.

Figure 4. Laser scanner is positioned on a vacuum gripper. When the scan is finished the tool is automatically changed to the spindle

The raw-wood mounting setup is built as a rail-system that has three reference points. The rails are made from L-shape profiles that are fixed to stands to hold a tree trunk. Four steel Y-beams ensures the stability of the setup. Two parallel stands are used for a straight beam fixation and a third one is employed for forks. A beam is fixed to the setup by straps and pre-drilled holes helps to reduce a rotation during the fixation Figure 4.

Figure 5. Cutting process using spindle and milling while the scanner and gripper is removed.

3.2 Control of Robot and Laser Scanner

The robot control is based on a software interoperability between the CAD/CAM application (Rhinoceros) and the cross-platform game engine (Unity). One software is utilized for geometry processing algorithms that could be applied to define the robot tool-path while the other is used to simulate the robot‘s movements physically and digitally. Each software has different coordinate systems that has to be matched to get an exact representation. The notation of rotation (Quaternion) and position (XYZ) is translated as following R_{ABCD} to R_{BDC-A} and T_{XYZ} to T_{XZY}. The match between two coordinate systems is found by computing all possible permutations for rotations and positions. The text interface with a robot controller enables to move robot in absolute and linear movements, change tools and tool-holders, perform scans, retrieve and process pointclouds. The cutting process is connected within a design-scanning workflow where a series of fabrication tool-paths are generated considering saw-blade cutting, milling and drilling. Each scan is triggered when the robot reaches a target and then the next pose is taken when the scan is finished.

3.3 Calibration of Laser Scanner

The laser scanner has to be calibrated in relation to the end-axis of the robot to know a pointcloud location at each scan. This process helps to avoid point-cloud processing and registration because the position of the scanner is already known in the robot world space Figure 6. The unknown (1) is a transformation matrix X of a scanner TCP_S that is relative to the end of the robot 6th axis TCP_R.

$$TCP_S = TCP_R + X \tag{1}$$

When a scanner is calibrated, a list of scan points P_i in a world-space is found by multiplying the rotation matrix XR_R^W and the translation matrix XT_R^W of the robot in the world space with points p_i that are positioned relative to the scanner rotation XR_S^R and position XT_S^R that is mounted on the robot arm (2).

$$P_i = XR_R^W * (XR_S^R * p_i + XT_S^R) + XT_R^W \tag{2}$$

While the robot and laser scanner is fixed, a calibration accuracy limits the alignment of scans (3). Several calibration methods were applied including: (a) the multi-scan registration on a sphere, (b) alignment to a robot base, (c) employing an external scanner device and (d) sharp tool manual reference, (e) 4TCP method for the scanner holder measurement. The precision T of the scanning technique depends on a scanner tolerance T_S (±0.1-0.5), marker detection precision T_M, robot accuracy T_R (±0.5-1.0), a calibration method precision T_C (3).

$$T = T_S + T_M + T_R + T_C \quad (3)$$

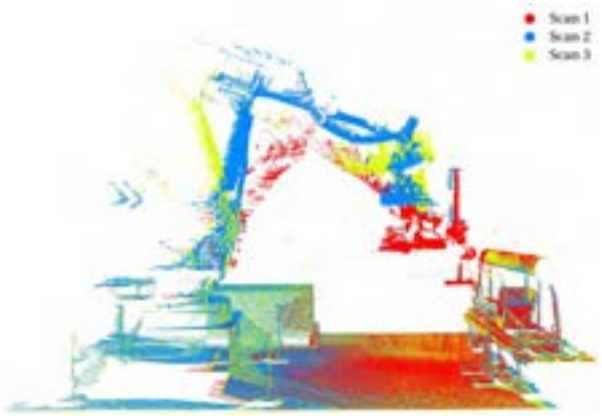

Figure 6. Result of the calibration using Faro Focus S 150 laser scanner.

3.3.1 External Scanner Device

First calibration test was made by employing Faro Arm Figure 7 D to measure the end-flange of the robot and laser-scanner. The result was inaccurate and only gave an approximate position of the scanner. The imprecision varied between ±1.0-2.0 cm in translation and ±1.0∘ in an arbitrary rotation. While the Faro Arm is a precise measurement tool, the reflective surfaces and possible laser-scanner tilt in relation to the tool-holder could have resulted in such a high inaccuracy.

Figure 7. Calibration methods. A - 4TCP Toolfolder, B - Robot-base scan, C - Multiple scans on a sphere, D - Faro Arm

3.3.2 Reference Points

A reference point calibration using an engraver tool and checkerboard markers proved to gain a sufficient tolerance. Robot is moved manually using the Teach Pendant to the centre of each target within several tries. The tolerance of manual measurement ranges between ±0.25-0.75 mm. Then the robot is moved to the highest reachable position and the scan signal is triggered from the robot controller. When the scan is finished, the data is sent to computer where it is processed to detect the positions of the markers. The scan position is oriented by a plane-to-plane transformation. The plane of the measured points is defined from 4 points and the target plane is retrieved from the detected markers. Four planes are created from the points, that are averaged by planes‘ origins and axes to obtain a better fit. The same procedure was tested using 12 targets to increase the tolerance. The resulting precision is between ±1.5-2.0 mm which is good enough for detecting the raw-wood trunk position for the manufacturing of timber joints.

Figure 8. Targets are measured by a sharp-tool and captured by the laser-scanner.

3.4 Point-cloud Processing

When multiple scans are taken and sent to computer, they are processed to obtain the radial parameters and central-axis of the tree. The duration of scanning depends on point-cloud density, measurement accuracy, connection type, the file transfer and geometry processing. The geometry survey could be divided in two parts: (i) creating a tree stock for a design and (ii) a tool-path alignment within the fabrication setup. Three methods were developed to obtain the radial parameters including (i) Flat-cut Sectioning, (ii) Mesh-skeletonization, (iii) Cylinder-fitting.

3.4.1 Flat-cut Sectioning

The method for calculating central-axis and radial-parameters from straight or curved logs is based on a point-cloud sectioning and assumption that every beam has two flat-circular ends Figure 9. The workflow is divided into following parts: get minimal bounding-box of a

point-cloud using PCA (Principal-Component-Analysis), get two smallest planes of the bounding-box, find the closest-points within the two planes, perform RANSAC (RANdom-SAmple-Consensus) algorithm to identify the flat-cuts of the beam [24], interpolate planes from the RANSAC, cut the point-cloud by a closest-plane method, fit sections to circles, draw axis between circle centers, serialize the data to XML file. The method will fail if the robot cannot move far enough to obtain he flat cut or the beam is not cut flat on the both ends.

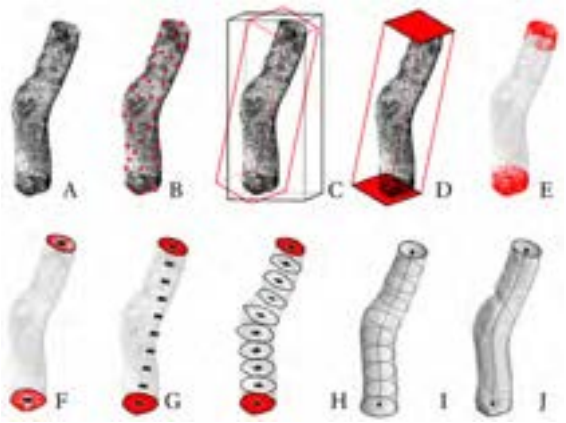

Figure 9. Flat-cut Sectioning method: A - Point-Cloud, B - Sub-sampling, C - PCA, D - two smallest faces, E - closest points, F - RANSAC plane, G - interpolation, H - 2D Convex-hull, I - circle-fit, J - surface representation.

3.4.2 Mesh Reconstruction

The method is based on a surface reconstruction from a point-cloud [25] and the closed mesh skeletonization [26]. Unlike the Flat-cut Sectioning method, it can be applied to the tree forks as well as bent or straight trees. Poisson surface reconstruction is chosen to retrieve a closed mesh from point coordinates and normals. The normals are approximated by fitting points to a plane using a least-square method. Structured point array simplifies the normal estimation because the orientation point (scanner position) is already known. The local radii of a log is found by sectioning the mesh by planes that are tangent to the skeleton-axis. The method is implemented as part of the robotic framework and tested within a series of bifurcated trees Figure 10 G-H.

3.4.3 Cylinder Fitting

The third method employs a cylinder fitting of the point-cloud. The list of points is projected to a 2D plane to approximate an outline of the point-cloud using the Marching Squares algorithm. Afterwards, the axis is extracted from

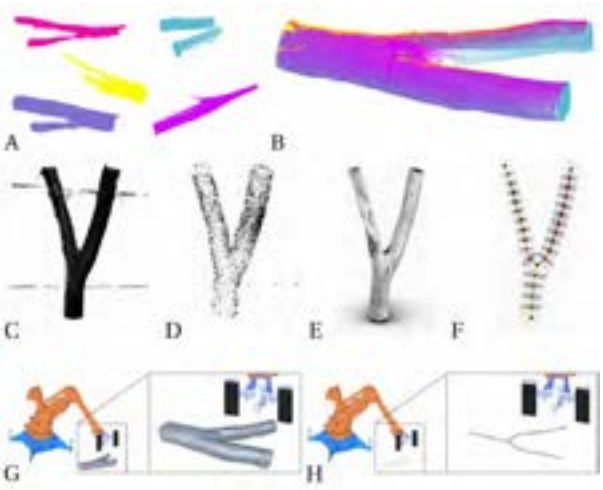

Figure 10. A - Individual Scans, B - Aligned Point-clouds. Mesh Skeletonization method: C - Point-Cloud, D - Normals Estimation, E - Poisson Mesh Reconstruction, F - Mesh-Skeletonization, and implementation in the robotic workflow G - mesh, H - skeleton.

a 2D curve using Zhang-Suen thinning algorithm. Then the axis is projected to the initial list of points by measuring the local radii of axial points. Consequently, cylinders are fit along each line of axis. The method was tested for both bent and bifurcated beams that contained noise from scanning and external objects such as straps of the fabrication setup and robot parts Figure 11.

Figure 11. A - PointCloud, B - Projection, C - 2D Thinning, D - Cylinder-fit, E - Radial parameters, F - Application in straight, curved and forked trees.

3.4.4 Fabrication Tool-path Alignment

When the point-cloud is processed, it is serialized for a digital timber stock and machining alignment. While the setup seems almost equal between beams Figure 12, each position changes up to 3-5 cm because of manual positioning, beam properties and rotation during the fixation

within an already small radii beam. The minimal model of a scan allows to position the timber joinery following the radius and tangent direction of the axis. There are several ways to reference a digital and analog model such as: a) alignment of a beam to the scanned object before the machining starts Figure 5 b) employing markers that have a distinctive reflective color that are captured during the scanning process.

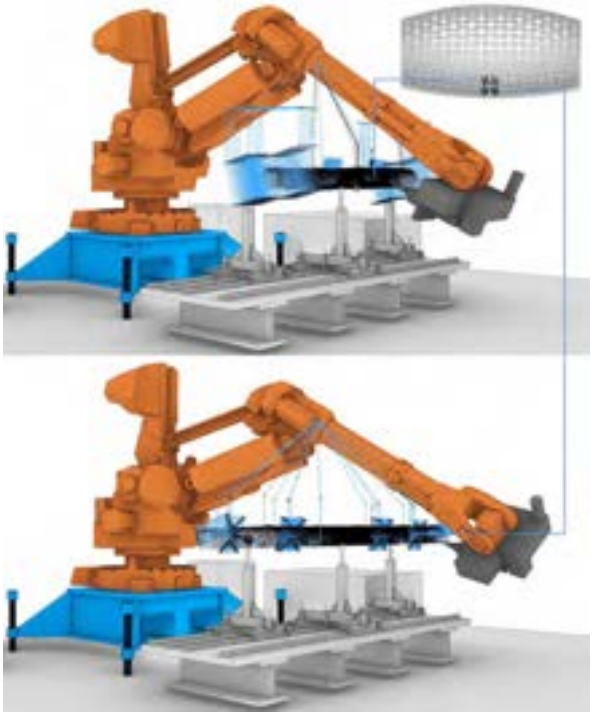

Figure 12. The tool-path is oriented from the design model to the machining space.

3.4.5 Validation Process of Results and Outcomes

The proposed methodology was applied in the realization of a first prototype made from 13-16 cm diameter logs Figure 13. A second one is planned as a tree fork truss to validate other tree topologies. The first model is composed 24 elements. The cylinder-fitting was applied repeatedly before cutting each beam and resulted in the successful model realization even if beams were small, crooked and bent. The scanning application itself is relatively fast in comparison with the milling and saw-blade cutting (60-90 min). Nevertheless the application could be optimized further by controlling the scanner via the automation adapter to send CAM messages and connecting the device with the robot controller to avoid latency in w-lan communication. Furthermore, the helical-scan could be connected with the robot movements to capture the point-cloud data in one step instead of two separate stages.

Figure 13. First prototype in small radius round-wood made using the applied methodology.

4 Discussion

The SDK of the Scanner, software of the robot control and tool-changer allowed to automate the scanning and fabrication workflow. The scanning precision was expected to be higher considering the specifications of the scanner due to the manual calibration, target detection and robot tolerance. Nevertheless, the precision needed to machine the raw-wood is sufficient enough because the imperfection of wood such as branches, chain-saw cuts, cracks is discarded. Multiple point-cloud processing algorithms were tested and the cylinder-fitting method was proved to be the most successful because it works when a point-cloud is incomplete and if there are outliers within the fewer scan taken per one tree. The challenge of the raw-wood integrated workflow is to speed the cutting process which takes the longest time comparing to the scanning and standardized timber products.

5 Conclusions

The laser-scanner and the industrial robot arm made the geometry acquisition of irregular timber faster from 45 min manual process to the 3 min automated solution, including robot movement, scanning and point-cloud processing. 24 beams were scanned without additional manual processing that directly guided the machining process. The scanning method was necessary to get a position of a tree trunk that helped to position cutting tool-paths within ±1.5-2.0 mm tolerance. The prototyping demonstrated the feasibility of the proposed workflow for low value tree trunks harvested from the local forests.

References

[1] Aurimas Bukauskas, Paul Mayencourt, Paul Shepherd, and et al. Whole timber construction: A state of the art review. *Construction and Building Materials*, 2019.

[2] Aryan Rezaei Rad, Henry Burton, and Yves Weinand. Macroscopic Model for Spatial Timber Plate Structures with Integral Mechanical Attachments. *Journal of Structural Engineering*, 146(10), 2020.

[3] Zachary Mollica Martin Self. Tree Fork Truss. *Advances in Architectural Geometry 2016*, 2016.

[4] Zachary Mollica and M Self. Tree Fork Truss: An Architecture of Inherent Forms. *Design and Make*, 2016.

[5] Peter von Buelow. The combination of SQL database queries and stochastic search methods used to explore generative design solutions. *IASS Annual Symposium 2019*, pages 1163–1170, 2019.

[6] Piotr Siekański, Krzysztof Magda, Krzysztof Malowany, and et al. On-line laser triangulation scanner for wood logs surface geometry measurement. *Sensors (Switzerland)*, 2019.

[7] Liya Thomas, Lamine Mili, Edward Thomas, and Cliffod Shaffer. Defect detection on hardwood logs using laser scanning. *Wood and Fiber Science*, 38 (4):682–695, 2006.

[8] Yuntao An and Gary Schajer. Geometry-based CT scanner for measuring logs in sawmills. *Computers and Electronics in Agriculture*, 105:66–73, 2014.

[9] Alfred Rinnhofer, Alexander Petutschnigg, and Jean Philippe Andreu. Internal log scanning for optimizing breakdown. *Computers and Electronics in Agriculture*, 41(1-3):7–21, 2003.

[10] Anders Berglund, Olof Broman, Anders Gronlund, and Magnus Fredriksson. Improved log rotation using information from a computed tomography scanner. *Computers and Electronics in Agriculture*, 2013.

[11] Niels Martin Larsen and Anders Kruse Aagaard. Exploring Natural Wood. *Acadia*, pages 500–509, 2019.

[12] Yingzi Wang. Hooke park biomass boiler house. *Advancing Wood Architecture: A Computational Approach*, pages 169–181, 2016.

[13] Maria Larsson, Hironori Yoshida, and Takeo Igarashi. Human-in-the-loop fabrication of 3D surfaces with natural tree branches. *Proceedings of ACM Symposium on Computational Fabrication*, 2019.

[14] Yung Sheng Chen and Wen Hsing Hsu. A modified fast parallel algorithm for thinning digital patterns. *Pattern Recognition Letters*, 7(2):99–106, 1988.

[15] Fabio Bianconi and Marco Filippucci. Digital Wood Design: Innovative Techniques of Representation in Architectural Design. *Springer*, 24:1524, 2019.

[16] Lukas Allner, Daniela Kroehnert, and Andrea Rossi. Mediating Irregularity: Towards a Design Method for Spatial Structures Utilizing Naturally Grown Forked Branches. In *Impact: Design With All Senses*. Springer, 2020.

[17] Axel Kilian Kaicong Wu. *Robotic Fabrication in Architecture, Art and Design 2018*. Springer International Publishing, 2019.

[18] Ryan Luke Johns and Nicholas Foley. Bandsawn Bands. *Robotic Fabrication in Architecture, Art and Design 2014*, pages 17–33, 2014.

[19] Bob Sheil. *High definition : zero tolerance in design and production*. AD, 2014.

[20] Wen Fang Ye, Chuang Qian, Jian Tang, and et al. Improved 3D stem mapping method and elliptic hypothesis-based DBH estimation from terrestrial laser scanning data. *Remote Sensing*, 12(3):1–19, 2020.

[21] Tiago de Conto. Performance of tree stem isolation algorithms for terrestrial laser scanning point clouds. *Swedish University of Agricultural Sciences Master Thesis no. 262*, page 34, 2016.

[22] Pasi Raumonen, Mikko Kaasalainen, Markku Akerblom, and et al. Fast automatic precision tree models from terrestrial laser scanner data. *Remote Sensing*, 5(2):491–520, 2013.

[23] Boleslaw Jodkowski Vitalii Kutia. Design of robotic 3d scanning system. *Integrated Intellectual Robotechnical Complexes*, 2017.

[24] Martin Fischler and Robert Bolles. RANSAC. *Graphics and Image Processing*, 24(6):381–395, 1981.

[25] Andrea Tagliasacchi, Ibraheem Alhashim, Matt Olson, and et al. Mean curvature skeletons. *Computer Graphics Forum*, 2012.

[26] Matthew Bolitho Michael Kazhdan and Hugues Hoppe. Poisson surface reconstruction. *Eurographics Symposium on Geometry Processing*, 2006.

Workspace Modeling: Visualization and Pose Estimation of Teleoperated Construction Equipment from Point Clouds

Jingdao Chen[a] , Pileun Kim[b], Dong-Ik Sun[c], Chang-Soo Han[c], Yong Han Ahn[d], Jun Ueda[e], and Yong K. Cho[b*]

[a]Institute for Robotics and Intelligent Machines, Georgia Institute of Technology, U.S.A
[b]School of Civil and Environmental Engineering, Georgia Institute of Technology, U.S.A
[c]Department of Mechatronics Engineering, Hanyang University ERICA, South Korea
[d]Department of Architectural Engineering, Hanyang University ERICA, South Korea
[e]School of Civil and Environmental Engineering, Georgia Institute of Technology, U.S.A
E-mail: jchen490@gatech.edu, pkim45@gatech.edu, jeniussdi@naver.com, cshan@hanyang.ac.kr, yhahn@hanyang.ac.kr, jun.ueda@me.gatech.edu, yong.cho@ce.gatech.edu (*corresponding author)

Abstract –

In order to teleoperate excavators remotely, human operators need accurate information of the robot workspace to carry out manipulation tasks accurately and efficiently. Current visualization methods only allow for limited depth perception and situational awareness for the human operator, leading to high cognitive load when operating the robot in confined spaces or cluttered environments. This research proposes an advanced 3D workspace modeling method for remotely operated construction equipment where the environment is captured in real-time by laser scanning. A real-time 3D workspace state, which contains information such as the pose of end effectors, pose of salient objects, and distances between them, is used to provide feedback to the remote operator concerning the progress of manipulation tasks. The proposed method was validated at a mock urban disaster site where two excavators were teleoperated to pick up and move various debris. A 3D workspace model was constructed by laser scanning which was able to estimate the positions of the excavator and target assets within 0.1 - 0.2m accuracy.

Keywords –

Pose estimation; laser scanning; excavator

1 Introduction

Robotic agents have enormous potential to be used to perform manipulation tasks for excavation, sample collection and repair work in remote areas. In hazardous environments such as nuclear power plants or post-earthquake disaster sites, it is common for these robots to be teleoperated by human operators from a remote location [1,2]. Such challenging conditions require a high level of situational awareness from the operator. It is difficult for human operators to efficiently and accurately carry out manipulation tasks through a teleoperation medium without clearly perceiving the pose of the robot and objects around it.

Research and field studies at major disaster relief operations such as the World Trade Center collapse showed that when mobile robots were deployed in confined spaces, the lack of perceptive data processing capability reduced the robotic skill set and added to the operator's cognitive responsibilities [2]. Armed with only a raw video feed with noisy and blurry images, operators and rescuers were unable to keep track of where the robots searched and the conditions during the deployment [2]. This problem of deficient perceptive information is amplified in the case of grasping tasks. Conventional teleoperation systems [1,3,4] make use of only a video camera that provides 2D images to the operator and the lack of depth perception makes it difficult for the operator to estimate the size and distances of unknown objects. Moreover, visual cameras do not work well at night or in adverse weather conditions. As a result, operators require a significant amount of trial and error to correctly control the robot to complete a grasping task.

An integral part of intelligent perception is transforming sensor data into knowledge and expressing that knowledge as information for use by other members in a human-robot team [5]. The idea of workspace modeling is to create a 3D representation of the robot and its surrounding environment [6–8] containing both semantic and geometric information that can be shared among all human and robotic agents in the operational team. The workspace model is constructed in real-time by processing the raw sensor data, organizing it, and labelling relevant objects [9]. Then the workspace model is used to provide visual feedback to the operator on the

task progress.

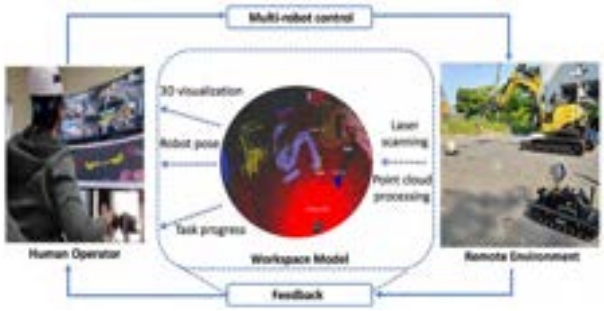

Figure 1. Feedback loop for teleoperation with 3D workspace modeling

This research proposes a context-aware 3D workspace modeling of remote equipment to improve perception and situational awareness for efficient teleoperation (Figure 1). In contrast to contemporary methods [1,4] which only provide views of the environment from the camera viewpoint to the remote operator, this research proposes a third-person viewpoint with automated state estimation and visualization of the relative pose between the end effector and salient objects. In addition, this research was validated at a large-scale outdoor environment with real construction equipment, compared to existing methods which were more focused on small to medium scale indoor environments [10,11]. To summarize, the contributions of the proposed work are as follows:

- designed a 3D workspace modeling and visualization scheme for teleoperated construction equipment
- developed an accurate algorithm for pose estimation of articulated equipment without prior dynamic models
- demonstrated the effectiveness of the 3D workspace modeling system with field trials using a multi-excavator system teleoperated in real-time

2 Literature Review

2.1 Remote Excavator System

Demand has recently been increasing for unmanned robotic excavator systems to carry out dangerous construction operations or disaster relief work. In such hazardous environments, direct human operation of excavators is unsafe due to the threat of rollover accidents, collisions, or radioactivity in the case of nuclear disaster sites. If the excavator could be robotized and teleoperated from a remote location, this would lead to a safer work environment for the human operators involved.

There are several teleoperation systems for excavators that have been studied in the literature. For example, [12] developed a excavator teleoperation system using the human arm, where sensors are attached to the operator's arm in order to detect movements so that command signals from sensors can be transmitted to the excavator. It is also possible to perform motion control with the teleoperation system by using posture sensor devices for receiving the kinematic information [13,14]. In these existing teleoperation systems, operators receive feedback either in the form of visual feedback [15,16] or force feedback [17] to monitor the interaction between the machine and the environment. More advanced excavator teleoperation systems [18,19] make use of a modular system such that a single operator can control multiple excavators with multiple end effectors at once to carry out more complex manipulation tasks. In such cases, effective feedback for teleoperation becomes even more important due to the higher risk of collision and other confounding factors such as occlusion and requirement for a larger field of view.

2.2 Workspace Visualization Systems

In a general teleoperation scenario, there are multiple ways to provide feedback to the remote operator including video feeds [3], laser scans [7], and haptic feedback [13]. In spite of these options, conventional teleoperated robots [1,4] mostly rely on a single video camera due to its simplicity and ease of use. Even when additional sensors are installed on the robot, they are poorly utilized due to the lack of information processing [2]. This causes the remote operator to have a limited field of view of surrounding objects and have limited depth perception.

There are several strategies in the literature to improve the visualization system for robot operation. [3] used a separate robot arm for visualization to overcome occlusions while performing visual servoing. However, being a primarily visual system, it still had limitations in terms of field of view and depth perception. [10] and [11] used RGBD-cameras paired with interactive visualizations to allow the operator to customize the 3D view. However, these works only considered the case of a single robot on an indoor, tabletop environment without any base displacement. [6] used 3D laser scanning to track the motion of construction equipment, but only modeled the construction equipment itself without visualizing the surrounding objects. [20] employed a multi-sensor system using four fisheye cameras and a 360◦ laser scanner to continuously reconstruct a 3D model of the surroundings with Simultaneous Localization and Mapping (SLAM). However, the method was only tested in static, indoor environments. Moreover, these methods have no automated object recognition or annotation of task-relevant entities,

leading to difficulty in identifying objects in cluttered or confined spaces. For the case of construction equipment, there exist algorithms for recognition [21,22] and pose estimation [23–25], but they still lack integration into a complete workspace visualization system.

3 Methodology

This research proposes a workspace modeling framework for teleoperation of remote construction equipment. As shown in Figure 1, the workspace model enables a feedback loop where the remote operator is able to simultaneously observe the effect of control inputs and interpret the remote environment from a 3D visualization interface, thus improving the situational awareness and efficiency for performing complex manipulation tasks. The workspace modeling procedure is designed to be independent from the equipment control such that the visualization and pose estimation process can remain the same regardless of any control configuration changes. The following subsections will provide details for each component of the proposed framework.

3.1 GHOST teleoperation system

This research makes use of the GHOST teleoperation system [19], which retrofits construction equipment such as excavators to be operated remotely. The manipulators are controlled wirelessly from a remote operation room equipped with monitors, joysticks and pedals. In general, each excavator can receive six different types of control signals which are assigned to the boom, arm, bucket, cabin, left track and right track respectively. Since the combination of one set of joystick and pedals is sufficient to transmit six control signals, the complete system allows a single operator to control two excavators at the same time.

However, teleoperating multiple excavators at once using conventional visualization methods is challenging even for experienced operators. Besides problems with the limited field of view and limited depth perception, the remote operator has to continuously monitor for multiple events including coordination between the excavators, occlusions, risk of collisions and risk of rollovers. This leads to a high cognitive burden for the operator, potentially causing lower efficiency and higher risk of accidents. To overcome this problem, this study implements a remote laser scanning system to provide 3D visualization of the environment surrounding the excavators, which will be described in the following sections.

3.2 Remote laser scanning system

Figure 2 shows the remote laser scanning system used to acquire a 3D reconstructed model of the excavator workspace. The VLP-16 LiDAR was mounted on a small teleoperated tracked mobile robot and utilized to acquire real-time laser scans of the site. The VLP-16 has a range of up to 100 meters with ± 15° vertical field of view. This means that the vertical angular resolution is only 2° because the VLP-16 has only 16 scan lines (channels) in the vertical direction. Thus, the scanned point cloud will be overly sparse for regions far away from the scan origin. For this reason, this study implemented an improved scanning system by installing the VLP-16 at 90° sideways and spinning it continuously with a stepper motor (refer Figure 2). In this way, the limited vertical resolution (now horizontal resolution) can be mitigated by rotating the scans horizontally, thus creating a higher resolution point cloud.

The effectiveness of 3D workspace modeling depends heavily on the point cloud update rate and resolution, which can impact the subsequent object recognition and pose estimation [26]. From the rotation mechanism discussed previously, the LiDAR scanner can generate a 360° point cloud of the surrounding environment after spinning about the vertical axis for half a revolution [27,28]. The update interval, between which the point cloud is updated to capture changes in the environment, is thus determined by the time it takes for the LiDAR scanner to spin for half a revolution. There exists a tradeoff between the rotation speed and resulting point cloud resolution due to this rotation mechanism of the laser scanner. When the rotation speed of the laser scanner is increased, the update rate increases but the point cloud resolution degrades because of the larger distance covered between consecutive scans. In contrast, when the rotation speed of the laser scanner is decreased, the point cloud resolution improves but the update rate decreases.

To find the best rotation speed, a simulation was carried out to determine the generated non-overlapping vertical scan lines when rotating the scanner. Based on this simulation, the average angle between the vertical scan lines as well as the maximum angle between the two adjacent vertical scan lines were calculated as shown in Table 1. From these results, the rotation speed corresponding to a 2.4s update interval was selected to minimize the update interval while maintaining a high horizontal resolution. This means that it is difficult for the scanner to capture rapid motions in the environment, but the higher resolution is necessary for object recognition.

Using this rotation setting, the resulting laser scanning system has a 0.25° resolution in the horizontal direction and a 0.4° resolution in the vertical direction, generating 324,000 points per update. The individual scans within each update are registered by multiplying by a rotation matrix, calculated from the rotation angle of the stepper motor. The laser scan data is published

wirelessly to the operation room as a ROS (Robot Operating System) message.

Table 1. Relationship between update interval and horizontal angular resolution

Update Interval	1.2s	1.4s	2.1s	2.4s	2.5s	2.9s
# vertical lines	374	447	641	720	523	927
avg. horiz. resolution (°)	0.48	0.40	0.28	0.25	0.34	0.19
max. horiz. resolution (°)	0.50	0.43	0.29	0.25	0.40	0.28

Figure 2. Remote laser scanning system

3.3 Point cloud pre-processing and segmentation

Processing the point clouds in real-time is challenging due to noisy sensor data, limited resolution of the laser scanner (refer Section 3.2), limited data bandwidth, and motion blurring of objects. Moreover, the point cloud is dynamically changing due to the movement of equipment and in the scene, meaning that it has to be processed incrementally.

A voxel grid filter is first used to equalize the point cloud resolution to 0.1m throughout the scene. This serves a dual purpose of allowing more consistent segmentation as well as speeding up the processing time by downsampling the point cloud. Next, the point cloud scene is segmented into smaller units corresponding to individual objects to enhance visualization of the scene. To meet the real-time constraint, the fast segmentation method of [29] is used. The ground plane is first segmented using the RANSAC algorithm [30] to estimate the 3D plane parameters. Alternatively, for the case of non-flat ground, the ground segmentation algorithm from [21] can be used. From the remaining points, Euclidean clustering is used to form clusters consisting of points that neighbor each other within a margin of 0.15m. As new scan points are acquired, they are matched to the closest existing clusters and each cluster is then updated. New scan points also cause new clusters to be initiated if no neighboring clusters are found. This allows the segmentation process to occur incrementally, similar to the method used in [31].

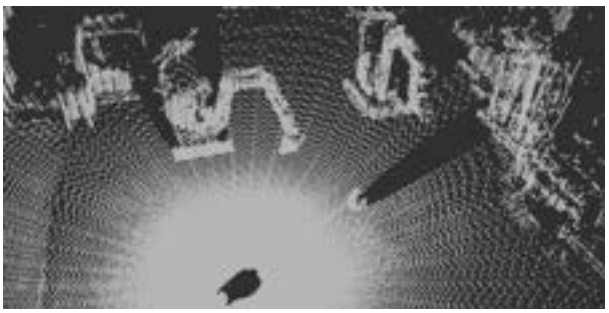

(a) Raw point cloud acquired by laser scanning

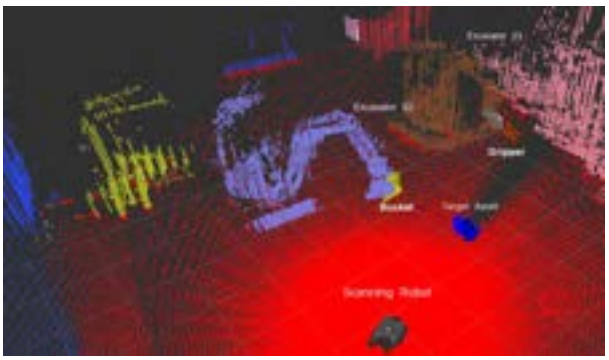

(b) Segmented point cloud showing relevant entities

Figure 3. Point cloud segmentation results for a scene with two excavators and a single target asset

Next, the following relevant entities are automatically labeled in the scene: (i) laser-scanning robot, (ii) construction equipment, and (iii) target assets for manipulation tasks. The position of the laser-scanning robot can be easily determined as the origin of the point cloud scan. On the other hand, the positions of various construction equipment can be determined by using the method in [21], where a feature descriptor is computed for each point cloud cluster and classified with a pre-trained classifier. Finally, the point cloud clusters for objects lying on the ground close to the construction equipment are labelled as potential targets for manipulation.

Figure 3 shows an example of the segmentation results for a scene with two excavators and a single target asset. The segmentation results are additionally overlaid with CAD models of the end effectors (bucket or gripper) and other relevant entities (e.g. target asset and scanning robot) to enhance the visualization. From Figure 3, the

raw point cloud data is extremely blurry, and it is difficult to keep track of the movement of objects in the robot workspace. However, with automated segmentation and annotation of the point cloud data, the remote operator is able to better perceive the robot workspace.

3.4 Point cloud-based pose estimation

(a) Model parameters for excavator joint configuration

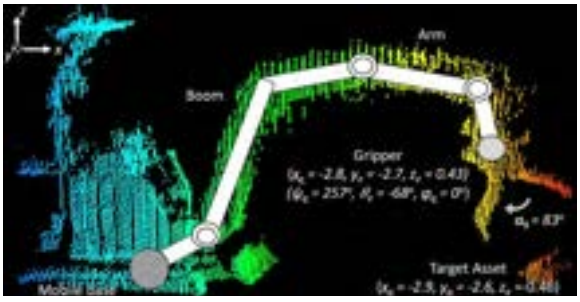

(b) Pose estimation result for a gripper and a target asset

Figure 4. Excavator pose estimation

Figure 4a shows the model of the excavator joint configuration used in this study. For each excavator, the robot pose can be described in terms of the following variables: (x_b, y_b, z_b), position of the mobile base; α_1, rotation of the mobile base with respect to the z-axis; α_2, rotation of the boom relative to the mobile base; α_3, rotation of the arm relative to the boom; α_4, rotation of the end effector relative to the arm. Similarly, the pose of the end effector can be described in terms of the following variables: (x_e, y_e, z_e), the position of the end effector and (ψ_e, θ_e, φ_e), yaw, pitch, roll angles of the end effector with respect to the world frame. In addition, the variable α_5 is used to describe the opening angle of the end effector if a gripper is used.

To perform pose estimation on articulated equipment such as excavators, the strategy used is to approximate each joint as a line segment and use line detection algorithms to extract corresponding segments from the point cloud. Due to the noisy nature of the point cloud, robust parameter estimation methods such as RANSAC [30] and PCA [32] are used. Then the tangent direction of each line segment is used to estimate the joint rotation angles α. Empirically, using RANSAC for detecting the boom and PCA for detecting the arm gives the best results. Next, the end effector points are segmented by taking the rightmost points of the excavator after correcting for rotation. (x_e, y_e, z_e) is calculated by taking the centroid of this segment whereas (ψ_e, θ_e, φ_e) can be inferred from the internal joint angles. The gripper opening angle, α_5, is estimated by taking the width of the end effector segment after correcting for rotation. On the other hand, to perform pose estimation of a target asset for manipulation, the position, (x_a, y_a, z_a), is first estimated by taking the centroid of the corresponding point cloud segment. Then the orientation, α_a is estimated by extracting the convex hull and solving for the minimum bounding box [33]. Each step of the pose estimation process also employs error correction using the smooth motion constraint. That is, if a new prediction differs from the previous prediction by more than a predetermined threshold (e.g. due to outlier data), the new prediction is discarded.

Figure 4b shows an example of the point-cloud based pose estimation result for an excavator equipped with a gripper. The segmentation can be computed in 0.05 - 0.1s whereas the pose estimation can be computed in 0.02 - 0.03s. The delay in showing the 3D visualization depends on network latency, but is usually within 1s. The final 3D workspace model is displayed through an interactive user interface. The remote operator is allowed to select the target asset of interest for manipulation. The user interface will then display task progress in terms of grasping the target asset.

4 Results

4.1 Experimental setup

Figure 5. Experimental setup of two excavators at a mock urban disaster site.

The experimental setup consists of two robotic unmanned excavators deployed at a mock urban disaster site (Figure 5). The operator has two options to remotely

monitor the test environment: (i) 2D images from cameras mounted on the excavator roof and (ii) 3D visualization obtained from the mobile laser scanning system. One excavator is equipped with a gripper as the end effector whereas the other excavator is equipped with a bucket. Using one or both of the excavators, the operator is tasked with carrying out various manipulation tasks such as picking up miscellaneous wreckage and moving them to a specified location. The accuracy and effectiveness of the proposed workspace modeling and visualization system is then validated using the pose estimation accuracy.

4.2 Pose estimation accuracy

The pose estimation results are visualized as shown in Figure 6. Note that this evaluation only considers a single excavator, but the proposed system is able to estimate the poses of multiple excavators simultaneously. The left 4 columns show results for a propane tank as the target object whereas the rightmost column show results for a plastic container as the target object. From the 2D images of the operator view, it is difficult to perceive whether the gripper is in line with the target object and the distance of the gripper to the target object. On the other hand, the 3D visualization provides helpful information in terms of physical distances and poses that can assist the remote operator in decision making.

As shown in Table 2, the pose estimation accuracy is measured using three metrics: (i) error in estimating the distance from the center of the end effector to the center of the target asset, d_1, (ii) error in estimating the distance from the center of the end effector to the ground, d_2, (iii) error in estimating the distance from the center of the end effector to the center of the excavator body, d_3. The accuracy of the proposed method is compared against two baselines methods: (i) simple line-fitting with linear least-squares regression [34] and (ii) Iterative Closest Point (ICP) [35] to fit the end effector model to the scanned point cloud. Results show that the proposed method achieved lower pose estimation errors compared to the two baseline methods. This is because the scanned point cloud is too noisy and has low resolution for simple line-fitting or ICP to work, whereas the proposed method is able to estimate the pose parameters from point clouds more robustly.

Table 2. End effector pose estimation error

Method	d_1 error (m)	d_2 error (m)	d_3 error (m)
Simple line-fitting [34]	0.93±1.06	0.39±0.50	0.15±0.07
ICP [35]	0.15±0.11	0.10±0.07	0.24±0.26
Our method	**0.13±0.07**	**0.09±0.09**	**0.10±0.08**

5 Conclusions

In summary, this research proposed a workspace modeling system for teleoperated construction equipment based on laser scanning. Through field tests at a mock urban disaster site, the constructed 3D workspace model was demonstrated to be able to estimate the positions of the excavator and target assets accurately and improve the performance of human operators on manipulation tasks. This represents an important step towards achieving the goal of improving the efficacy of remote robot operation, reducing human operator needs, and reducing the operator's cognitive burden during teleoperation. For future work, the method will be extended to more types of heavy equipment such as

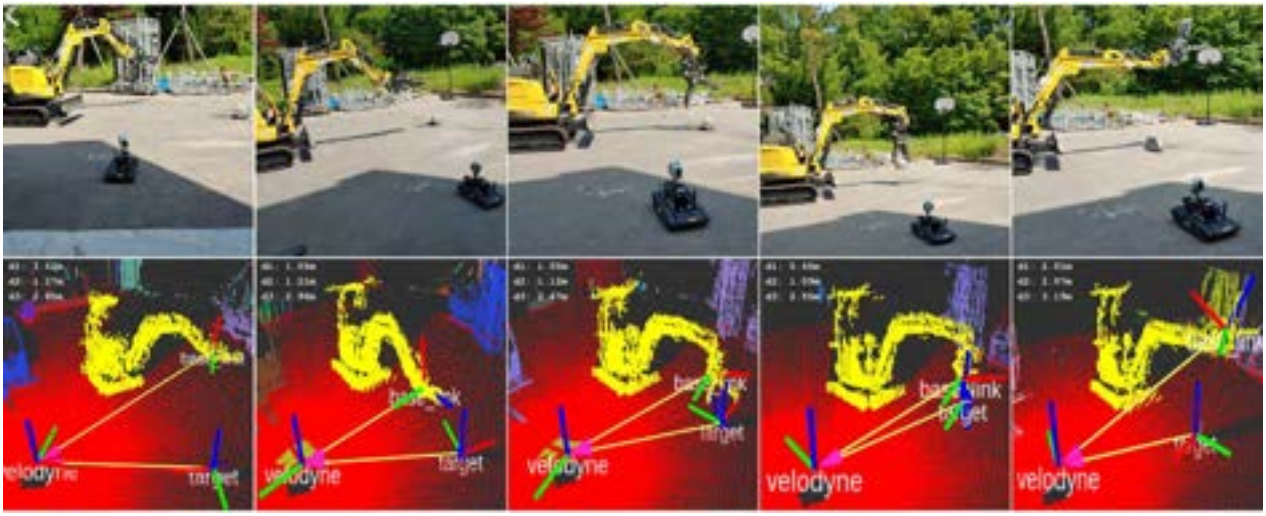

Figure 6: Visualization and pose estimation of excavator workspace. The top row shows 2D images of the scene whereas the bottom row shows the corresponding 3D visualization

loaders and dump trucks and further evaluated in more challenging manipulation scenarios.

Acknowledgements

This material is based upon work supported by the Air Force Office of Scientific Research (Award No. FA2386-17-1-4655) and by the Technology Innovation Program (No. 2017-10069072) funded by the Ministry of Trade, Industry & Energy (MOTIE, Korea). Any opinions, findings, and conclusions or recommendations expressed in this material are those of the authors and do not necessarily reflect the views of the United States Air Force or MOTIE.

References

[1] T. Sakaue, S. Yoshino, K. Nishizawa, K. Takeda, Survey in Fukushima Daiichi NPS by Combination of Human and Remotely-Controlled Robot, in: IEEE International Symposium on Safety, Security and Rescue Robotics (SSRR), 2017.

[2] J. Casper, R.R. Murphy, Human – Robot Interactions During the Robot-Assisted Urban Search and Rescue Response at the World Trade Center, IEEE Transactions on Systems, Man and Cybernetics. 33 (2003) 367–385. doi:10.1109/TSMCB.2003.811794.

[3] D. Nicolis, M. Palumbo, A.M. Zanchettin, P. Rocco, Occlusion-Free Visual Servoing for the Shared Autonomy Teleoperation of Dual-Arm Robots, IEEE Robotics and Automation Letters. 3 (2018) 796–803. doi:10.1109/LRA.2018.2792143.

[4] G. Beraldo, M. Antonello, A. Cimolato, E. Menegatti, L. Tonin, Brain-Computer Interface Meets ROS: A Robotic Approach to Mentally Drive Telepresence Robots, in: 2018 IEEE International Conference on Robotics and Automation (ICRA), 2018: pages 1–6. doi:10.1109/ICRA.2018.8460578.

[5] R.R. Murphy, Human-robot interaction in rescue robotics, IEEE Transactions on Systems, Man, and Cybernetics, Part C (Applications and Reviews). 34 (2004) 138–153. doi:10.1109/TSMCC.2004.826267.

[6] C. Wang, Y.K. Cho, Smart scanning and near real-time 3D surface modeling of dynamic construction equipment from a point cloud, Automation in Construction. 49 (2015) 239–249. doi:10.1016/j.autcon.2014.06.003.

[7] Y.K. Cho, C. Wang, P. Tang, C.T. Haas, Target-Focused Local Workspace Modeling for Construction Automation Applications, Journal of Computing in Civil Engineering. 26 (2012) 661–670.

[8] J. Chen, Y. Fang, Y.K. Cho, Real-Time 3D Crane Workspace Update Using a Hybrid Visualization Approach, Journal of Computing in Civil Engineering. 5 (2017). doi:10.1061/(ASCE)CP.1943- 5487.0000698.

[9] J. Chen, Y.K. Cho, J. Ueda, Sampled-Point Network for Classification of Deformed Building Element Point Clouds, in: Proceedings of the 2018 IEEE Conference on Robotics and Automation (ICRA), 2018.

[10] T. Zhang, Z. McCarthy, O. Jow, D. Lee, X. Chen, K. Goldberg, P. Abbeel, Deep Imitation Learning for Complex Manipulation Tasks from Virtual Reality Teleoperation, in: 2018 IEEE International Conference on Robotics and Automation (ICRA), 2018: pages 1–8. doi:10.1109/ICRA.2018.8461249.

[11] D. Kent, C. Saldanha, S. Chernova, A Comparison of Remote Robot Teleoperation Interfaces for General Object Manipulation, in: ACM/IEEE International Conference on Human-Robot Interaction (HRI), 2017: pages 1–8. http://www.rail.gatech.edu/wp-content/uploads/2017/06/hri2017-kent-saldanha-chernova.pdf.

[12] D. Kim, J. Kim, K. Lee, C. Park, J. Song, D. Kang, Excavator tele-operation system using a human arm, Automation in Construction. 18 (2009) 173–182. doi:https://doi.org/10.1016/j.autcon.2008.07.002.

[13] T. Hirabayashi, J. Akizono, T. Yamamoto, H. Sakai, H. Yano, Teleoperation of construction machines with haptic information for underwater applications, Automation in Construction. 15 (2006) 563–570. doi:https://doi.org/10.1016/j.autcon.2005.07.008.

[14] Soon-Young Yang, Sung-Min Jin, Soon-Kwang Kwon, Remote control system of industrial field robot, in: 2008 6th IEEE International Conference on Industrial Informatics, 2008: pages 442–447. doi:10.1109/INDIN.2008.4618140.

[15] K. Yoshihiro, A remotely controlled robot operates construction machines, Industrial Robot: An International Journal. 30 (2003) 422–425. doi:10.1108/01439910310492185.

[16] T. Sasaki, K. Kawashima, Remote control of backhoe at construction site with a pneumatic robot system, Automation in Construction. 17 (2008) 907–914. doi:https://doi.org/10.1016/j.autcon.2008.02.004.

[17] J. Hou, D. Zhao, A new force feedback algorithm for hydraulic teleoperation robot, in: 2010

International Conference on Computer Application and System Modeling (ICCASM 2010), 2010: pages V15-15-V15-18. doi:10.1109/ICCASM.2010.5622490.

[18] E. Rohmer, K. Yoshida, E. Nakano, A Novel Distributed Telerobotic System for Construction Machines Based on Modules Synchronization, in: 2006 IEEE/RSJ International Conference on Intelligent Robots and Systems, 2006: pages 4199–4204. doi:10.1109/IROS.2006.281913.

[19] D. Sun, S. Lee, Y. Lee, S. Kim, J. Ueda, Y.K. Cho, Y. Ahn, C. Han, Assessments of Intuition and Efficiency: Remote Control of the End Point of Excavator in Operational Space by Using One Wrist, ASCE International Conference on Computing in Civil Engineering 2019. (2019) 273–280. doi:10.1061/9780784482438.035.

[20] S.-H. Kim, C. Jung, J. Park, Three-Dimensional Visualization System with Spatial Information for Navigation of Tele-Operated Robots, Sensors. 19 (2019). doi:10.3390/s19030746.

[21] J. Chen, Y. Fang, Y.K. Cho, C. Kim, Principal Axes Descriptor for Automated Construction-Equipment Classification from Point Clouds, Journal of Computing in Civil Engineering. (2016) 1–12. doi:10.1061/(ASCE)CP.1943-5487.0000628.

[22] J. Chen, Y. Fang, Y.K. Cho, Performance evaluation of 3D descriptors for object recognition in construction applications, Automation in Construction. 86 (2018) 44–52. doi:10.1016/j.autcon.2017.10.033.

[23] C.-J. Liang, K.M. Lundeen, W. McGee, C.C. Menassa, S. Lee, V.R. Kamat, Fast Dataset Collection Approach for Articulated Equipment Pose Estimation, in: Computing in Civil Engineering 2019, n.d.: pages 146–152. doi:10.1061/9780784482438.019.

[24] C. Chen, Z. Zhu, A. Hammad, W. Ahmed, Vision-Based Excavator Activity Recognition and Productivity Analysis in Construction, in: Computing in Civil Engineering 2019, n.d.: pages 241–248. doi:10.1061/9780784482438.031.

[25] J. Kim, S. Chi, M. Choi, Sequential Pattern Learning of Visual Features and Operation Cycles for Vision-Based Action Recognition of Earthmoving Excavators, in: Computing in Civil Engineering 2019, n.d.: pages 298–304. doi:10.1061/9780784482438.038.

[26] J. Park, P. Kim, Y.K. Cho, J. Kang, Framework for automated registration of UAV and UGV point clouds using local features in images, Automation in Construction. 98 (2019) 175–182. doi:https://doi.org/10.1016/j.autcon.2018.11.024.

[27] P. Kim, J. Chen, Y.K. Cho, Automated Point Cloud Registration Using Visual and Planar Features for Construction Environments, ASCE Journal of Computing in Civil Engineering. 32 (2018) 1–13. doi:10.1061/(ASCE)CP.1943-5487.0000720.

[28] P. Kim, Y.K. Cho, J. Chen, Target-Free Automatic Registration of Point Clouds, ISARC. Proceedings of the International Symposium on Automation and Robotics in Construction. 33 (2016) 1–7.

[29] M. Himmelsbach, F. v. Hundelshausen, H.-. Wuensche, Fast segmentation of 3D point clouds for ground vehicles, in: 2010 IEEE Intelligent Vehicles Symposium, 2010: pages 560–565. doi:10.1109/IVS.2010.5548059.

[30] M. a Fischler, R.C. Bolles, Random Sample Consensus: A Paradigm for Model Fitting with Apphcatlons to Image Analysis and Automated Cartography, Communications of the ACM. 24 (1981) 381–395. doi:10.1145/358669.358692.

[31] R. Dubé, M.G. Gollub, H. Sommer, I. Gilitschenski, R. Siegwart, C. Cadena, J. Nieto, Incremental-Segment-Based Localization in 3-D Point Clouds, IEEE Robotics and Automation Letters. 3 (2018) 1832–1839. doi:10.1109/LRA.2018.2803213.

[32] R.B. Rusu, Semantic 3D Object Maps for Everyday Manipulation in Human Living Environments, KI - Künstliche Intelligenz. 24 (2010) 345–348.

[33] J. O'Rourke, Finding minimal enclosing boxes, International Journal of Computer & Information Sciences. 14 (1985) 183–199. doi:10.1007/BF00991005.

[34] I.-K. Lee, Curve reconstruction from unorganized points, Computer Aided Geometric Design. 17 (2000) 161–177. doi:https://doi.org/10.1016/S0167-8396(99)00044-8.

[35] S. Kwon, M. Lee, M. Lee, S. Lee, J. Lee, Development of optimized point cloud merging algorithms for accurate processing to create earthwork site models, Automation in Construction. 35 (2013) 618–624. doi:https://doi.org/10.1016/j.autcon.2013.01.004.

A Critical Review of Machine Vision Applications in Construction

Saeed Ansari Rad[a] and Mehrdad Arashpour[a]

[a]Department of Civil Engineering, Monash University, Melbourne, Australia
E-mail: saeedansari71@ut.ac.ir, mehrdad.arashpour@monash.edu

Abstract -

Automation for retrieving relevant contents without human interventions has been considered as an essential task in the construction industry. Computer vision has grasped attention to be employed for providing rich data from the surrounding environment and automation of such critical tasks. Nonetheless, various challenges, including the detection of complicated and changing interactions and processing large-scale data remain unresolved. Deep learning methods have led to satisfactory achievement in providing progress monitoring systems, especially with detecting complex human motions and activities in construction scenes. However, further research contributions for vision-based safety monitoring are required to determine existing limitations and gaps in the construction and infrastructure field. In this paper, through some bibliographics and scientometrics analyses, more research backgrounds are suggested for application of computer vision and especially, deep learning, in construction robotics. Moreover, the accuracy of various computer vision methods is analyzed and compared by considering publishing year, countries, institutes. This demonstrates that Deep Learning application is still premature in the construction context, and current researches lack robust and swift image processing techniques.

Keywords -

Automation; Computer Vision; Construction; Deep Learning

1 Introduction

Automated methods have been considered as a vital task intended to retrieve relevant contents and features without any human interventions in the construction robotics [1]. In this regard, machine vision has drawn attention since several critical tasks, including continuous object recognition, monitoring of motion behaviour [2], productivity analysis [3], health and safety monitoring [4], require automation in their procedure [5] . It is worth noting that a major prerequisite for applying computer vision methods is data collection. Despite their importance, current methods of on-site data collection are still time-consuming, costly, and error-prone [6]. In addition, having large-scale database for most of industrial projects is another challenge for computer vision methods. In the recent years, several studies have been carried out in the construction field to evaluate unsafe conditions and acts. Despite the relative success of the research conducted by [7], some unresolved gaps and challenges remain in construction and infrastructure Civil Engineering, including the recognition of activities in complicated and varying conditions, multi-subject interactions and group activities.

Computer vision has achieved satisfactory performance in providing progress and quality monitoring systems and identifying unsafe conditions and actions in ongoing works, especially by detecting human motions and activities in construction sites [8, 9] In fact, color-based techniques such as the detection of workers, equipment, and materials in the construction sites are commonly used in various object detection [10] A behaviour based safety approach can be used to observe and identify people's unsafe actions in order to modify their future behaviour [11, 12] The advent of deep learning in machine learning field provides solution to the problems of manual observation of unsafe actions. The Convolutional Neural Network, CNN, based methods have been widely applied to a variety of problems that are encountered in construction [13, 14]. Object detection using deep learning algorithm can be employed for identifying construction components, counting objects, and objects size determination [15]. Furthermore, motion detection can be deployed in cameras via deep learning computer vision methods for surveillance purposes. In [16], a deep CNN is developed by integrating optical flow and gray stream CNNs to automatically recognize motion on construction sites.

By searching through the database of publications, 11 review articles are found which have put their effort on this area of interest, among which, from 2017, four papers have been published. This is important since what has developed from 2017 changes in data science interaction with construction and civil infrastructure fields. In Table 1, the information of the published review papers in this field has been demonstrated. From 2015 to 2016, five review articles have focused on this field of research, trying to provide bibliographic information,possible solutions and gaps on computer vision with share keys including progress monitoring, condition assessment, image-based 3D reconstruction, computer vision, and building information modeling;

Table 1. Analysis of published review papers on application of computer vision in the construction field.

Review Papers	Analyzing Date	Review Style	Reviewed Papered
[10]	2009-2019	bibliometric	97
[5]	1999-2019	scientometric	375
[19]	2000-2018	scientometric	216
[20]	1990-2018	bibliometric	235
[21]	2005-2016	scientometric	614
[22]	2010-2015	bibliometric	40
[6]	2000-2015	bibliometric	101
[23]	1995-2015	bibliometric	96
[24]	1995-2015	bibliometric	121
[25]	2005-2015	bibliometric	104
[26]	2000-2015	bibliometric	139

the most published articles belong to the journal of Advanced Engineering Informatics. Nonetheless, what has been considered has chiefly changed in recent years. As a case, one of the gaps in review papers was referred to the lack of suitable tool for processing and interpreting of high value of images and videos which was addressed in several articles, including [17, 18], by introducing deep learning methods in civil and infrastructure construction fields. It is worth mentioning that the relation between ontology and deep learning application in Civil Engineering has been analyzed in [19] which leads to suggestions for analyzing background detail and employing ontology in order to improve the accuracy of computer vision methods in monitoring and safety. Nonetheless, what has totally been off the topic in the scientometric analysis is the role of accuracy of different computer vision methods in the future of the construction field. None of the review papers has scrutinized and demonstrated the possible reasons and trends in the accuracy of computer vision methods from sceintometrical view point.

Therefore, further studies are required to find out existing limitations in order to boost the adoption of the advanced techniques. Several practical challenges could be identified in studies including a lack of robust and swift image processing techniques in industrial settings, considering the varying and dynamic conditions which are demonstrated in construction and civil infrastructure sites. Moreover, the review papers neglected the recent improvements and achievements in the general computer vision and machine vision. Hence, more researches are required for computer vision that involve the state-of-the-art deep learning findings in the construction field in order to provide the practitioners with more accuracy in identifying conditions resulting in inferior quality, productivity and safety performance. In this regard, using of a computational light convolutional network such as MobileNets [27], ShuffleNets [28], ResNets [29] seems necessary.

This research has tried to analyze this topic from different view point, that is more or less related to the data science field. In this paper, different methods of computer vision have been analyzed considering their application in the construction field. In Section 2, the way of acquiring bibliographical records of articles in the fields of machine vision and construction is explained. Thereafter, in Section 3 the recent achievements in the aforementioned fields are categorized and the most leading and cutting-edge articles in the field of application of computer vision in construction are extracted. Section 4 is devoted to the more detailed scientometrics analysis of the selected articles. Finally, discussions and future trends are included in Section 5.

2 Data acquisition

In this section, the method of acquiring bibliographical data is explained. In this research, the Dimension platform is employed as the basic search platform which offers more advantages[30, 31], such as proving plentiful research options, easily extracting research results, access to profiles at author and journal level, awarded grants and patents. In this regard, journals and conference papers are selected as the research option, since several highly cited documents have been published in both publication types. Moreover, the surveyed date has been set to 2000-2020 which contains the most published papers in the field of construction and machine vision. A suitable research keyword for application of machine vision in the construction and Civil Engineering might be as follows: ("Computer vision*" OR "Machine vision*" OR "Vision systems*") AND ("building*" OR "construction*"). Based upon the aforementioned settings for carrying out search in the platform, 2515 documents have been found for the rest of the research.

3 Bibliographical Analysis

In this section, the literature of computer vision application in construction is analyzed from bibliographical point of view. In this regard, VOSviewer software [32] possesses useful features in the text mining and bibliometrics analyses, which provides researchers with graphical way of literature data-set presentation. Considering the bibliographical results, demonstrated in Figure 1, four main clusters have been identified in the graph. The graph contains top 160 documents by total link strength. The first cluster, which has been demonstrated with yellow color, is mostly related to the articles belonging to implementation of conventional computer vision methods in construction. The leaders of the cluster [33, 9, 34, 16] share similar keywords, i.e., Support Vector Machine (SVM), computer vi-

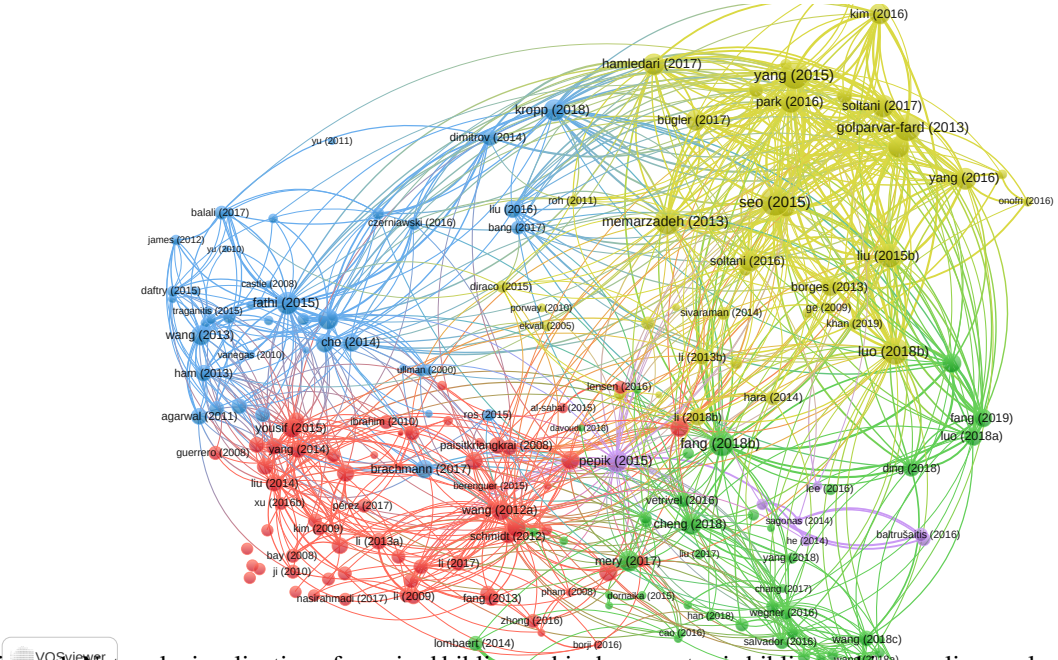

Figure 1. Network visualization of acquired bibliographic documents via bibliographic coupling analysis method.

sion and monitoring. The similar cluster with gree
#2, represents articles which has been published
2017 in the application of deep learning in constr
The leaders of the cluster [35, 36, 37] share simil
words, deep learning, computer vision, construct
the scientometrics analysis, the articles of the clu
and #2 are employed in order to analyze the con
between the keywords of those articles which form
understanding of computer vision application const
and Civil Science. Therefore, the articles from clus
and #2, with the number of 110, have been analyze
scientometrics section, from different aspects of s
metrics, especially accuracy of computer vision m
data base, and co-occurrence. Nonetheless, there are two other main clusters that have been found in the bibliographical results in Dimensions search platform. One of these two clusters with red color, #3, has focused on the general computer science field with shared keywords, computer vision, classification, and object recognition, while the another with blue color, #4, has put the attention on Civil Engineer, 3D reconstruction, and building model. As a results, excluding these articles from main articles based on the titles and abstract in the bibliographics is impossible; only by employing methods such as the bibliographical coupling analysis, these clusters are separable. In the Scientometrics section, these two clusters are not analyzed since those are relatively far from the main topic of this research.

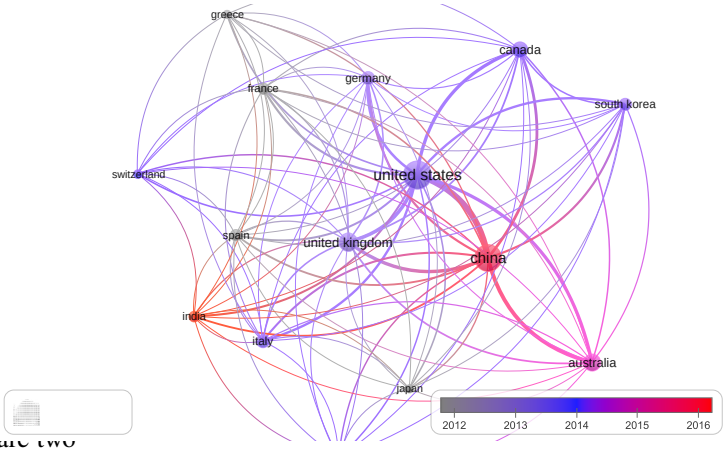

Figure 2. Overlay visualization of countries of published documents respecting to average publishing year via bibliographic coupling analysis.

Based on the bibliographical data from Figure 2, the United States, China, United Kingdom, South Korea, Australia, and Canada have mainly attempted to contribute in construction and vision fields of researches. The graph nodes are scaled by total link strength in which minimum number of documents of a country is set as 20, minimum number of citation of a country is chosen as 10, and top 15 countries are visualized considering total link strength. Moreover, the graph demonstrates that from 2016 till now, China, Australia, and India have attempted to extend the application of computer vision in Civil Engineering. On the other hand, the focus of researchers in the United States and United kingdom is mostly respected to the span of 2012 to 2014 on average, and predicated upon the citation records, their researchers had received enormous attention

and citation.

4 Scientometrics Analysis

In this section, the aforementioned extracted articles from clusters #1 and #2 of Figure 1 are analyzed through varied points of view. From 2015, a brand new way of literature review, namely, scientometrics analysis, , has been introduced [38] which detects the correlation between keywords and the most repetitive words through co-occurrence analysis. Consequently, by combining the bibliographical information of the selected articles with the extracted data such as accuracy, source of database, abstract and so forth, the scientometrics analysis has been carried out in this section in order to focus on surveying the published articles in the field of computer vision and construction. Employing corpus and scores files, composed by integrating abstract and keywords of the selected articles, the demonstrated graph in Figure 3 is obtained. The graph shows top 20 of most relevant and important terms scaled weight by Occurrence, with minimum number of occurrence of a term as 10. Based on the graph, Deep Learning as a representation for complex image processing methods and SVM as one for conventional image classification toolbox have been mentioned more than other methods.

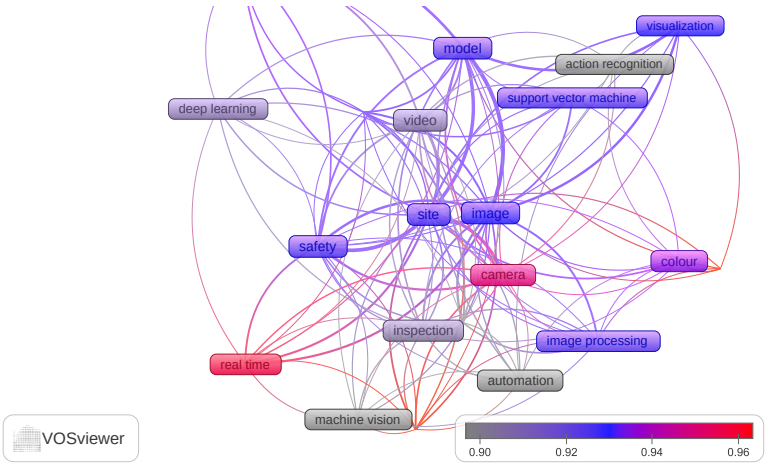

Figure 3. Overlay visualization of occurrence analysis of abstract and keywords of selected articles with respect to average accuracy timeline.

In the clusters #1 and #2 of Figure 1, representing fields of construction and machine vision, 3 publication journals have mostly contributed from volume of published papers point of view. In Table 2, several information have been presented on the publication resources, namely Automation in Construction, Advanced Informatics, Computing in Civil Engineering, and Computer-Aided Civil and Infrastructure Engineering and the corresponding details.

Table 2. Scientometrics analysis of the publication sources of selected articles.

Publication Journal	Percentage	Average Published Year	Average Citation	Dominant Method
Automation in Construction	37.04%	2016	91	Deep Learning
Advanced Engineering Informatics	14.81%	2013	92	Deep Learning
Journal of Computing in Civil Engineering	13.89%	2012	117	Edge Detection
Computer-Aided Civil and Infrastructure Engineering	8.35%	2012	193	Edge Detection

Table 3. Scientometrics analysis of the first author countries of selected articles.

Institution	Percentage	Average Published Year	Average Accuracy	Dominant Method
Huazhong University of Science and Technology	10.19%	2018	0.895	Deep Learning
Georgia Institute of Technology	12.04%	2012	0.938	Tracking Method
Yonsei University	6.48%	2014	0.967	Edge Detection
University of Illinois	9.26%	2011	0.982	Motion Detection

The focus of Automation in Construction and Advanced Informatics has been shifted toward applying deep learning methods in the construction field from 2016 [17, 35]. Nonetheless, the journal of Computing in Civil Engineering and Computer-Aided Civil and Infrastructure Engineering have published the articles, mostly employing edge detection methods, in the construction and civil engineering [39, 40].

From the countries point of view, the United States, China, Canada, the United Kingdom, and Australia are pioneers in applying computer vision in the construction field. In Table 3, it is shown that 4 institutions have had more contributions in publishing their results in the relevant journals. The average publishing year for Georgia Institution [8] and the University of Illinois [9] is around 2012; tracing methods and motion detection, respectively, are employed which have led to highly cited articles, but their focus has been shifted away from this field since

2014. On the other hand, several papers such as [41, 42] have been published from Huazhong University that contributes in this field by applying CNN and deep learning in the object and human recognition. These papers have been specialized in such a narrow topic that limits the citation while the average accuracy of the deep learning methods is less than the aforementioned institutions in the United States.

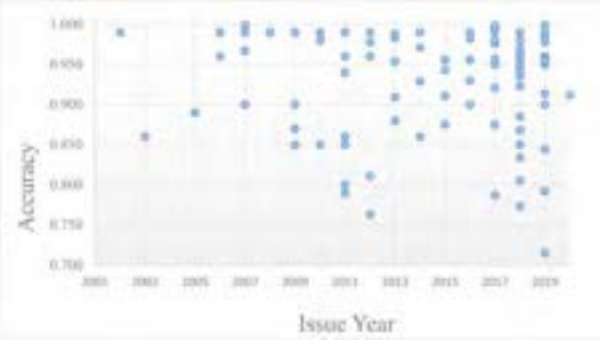

Figure 4. Scatter plot of the issue year of selected articles versus the accuracy of computer vision methods.

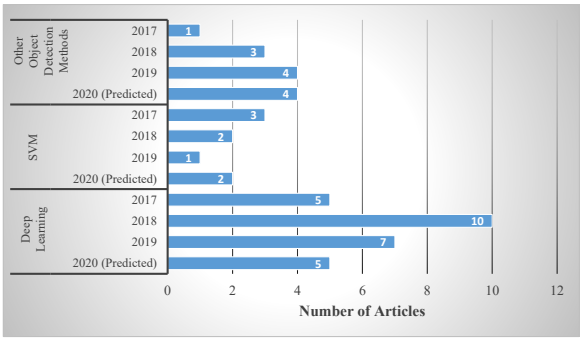

Figure 5. Comparing the applied dominant machine vision and classification methods in selected articles respecting to the issue year of articles.

Since 2008, by deployment of computer vision in the construction industry, the number of published papers in this field rouse by gaining appropriate accuracy of the object and edge detection methods. For instance, in Figure 4, one can observe that from 2008, more articles have achieved high accuracy in vision methods of construction mostly due to the advancement in face recognition and object detection methods. However, it is worth mentioning that one can find several articles including [41, 43] that cannot achieve expected accuracy, that is above 95 % on average, since the volume of processing data has increased as well. Consequently, in this field, the span of accuracy

Table 4. Scientometrics analysis of the dominant machine vision and classification methods in selected articles.

Method	Percentage	Average Published Year	Average Accuracy	Average Citation
Deep Learning	20.37%	2018	0.908	68
SVM	14.81%	2015	0.905	2120
Other Object Detection methods	12.04%	2015	0.955	49
Other Edge Detection methods	9.26%	2010	0.887	136

that publications in the construction field has gotten bigger whilst the bold part of this span is still on the highest possible accuracy of computer vision. Most importantly, the rate of published research paper in this field has accelerated since 2017. This has happened mostly due to attention that deep learning methods have received. Based on what has been demonstrated in Figure 5, since 2018, more research articles such as [44, 14] have put the base of their concentration on Deep Learning and big data science field. Face recognition, object detection, and huge amount of data classification methods are eventually possible to be carried out by deep learning methods. This trend decreased in 2019 which might be respected to the existing gaps of deep learning in the construction and safety field which will be discussed later in Section 5. Meanwhile, SVM method, which represents fast classification of data, fails to receive more credit in comparison to what has happened in 2015 [45, 46], according to Table 4. This shows that the focus of automation in construction has been shifted from speed toward the accuracy and processing of huge database information.

5 Discussion and Future Trends

In the recent years, the vision-based tasks have improved due to the need for automation in the construction field. Some of the researchers have tried to extend the volume of image processing, from motion and object detection tasks towards activity recognition. This has led to increasing complexity of the space of data regressors while the conventional methods lack the ability to conform to big data process. As a result, more complicated and powerful tools in learning patterns and data are required to solve the problem. However, based on what has been illustrated in Table 4, it is clear that deep learning methods could not achieved the accuracy that has been achieved in the

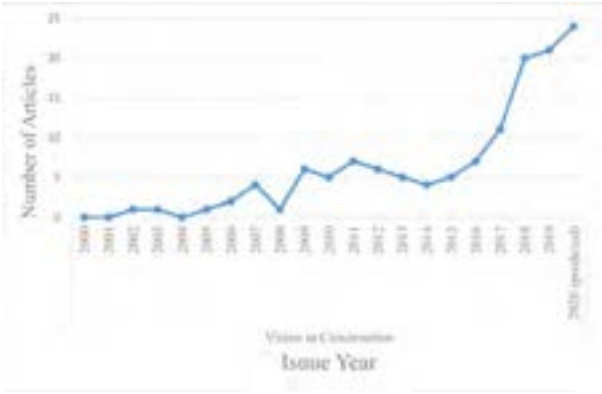

Figure 6. Number of published articles on the application of machine vision in construction respecting to the issue year.

vision field [18], that is approximately 95 %. Moreover, it is demonstrated that the achievement of conventional vision methods in the object detection, motion detection, classification reveals better accuracy in comparison to the deep learning methods [47]. The existing gap among the capabilities of deep learning in the construction field, employing pre-trained networks in non-similar contexts and lack of experience and background researches, decrease the possible success in obtaining successful results in the vision methods. In fact, setting AI field techniques such as MobileNets [27], ShuffleNets [28], ResNets [29] in construction and infrastructure civil field are demanding and time-consuming. Therefore, the upcoming articles must be inclined to increase the accuracy and efficiency of deep learning methods. By doing so, the predicted number of published articles on application of machine vision in construction, demonstrated in Figure 6, will be realizable.

Another important topic is the way of acquiring database for application of vision in construction industry. Most of researchers in this field have employed specific database. Based on the scientometrics data, the majority of the analyzed published documents in this field possess their own construction images database. Some of review papers, especially [19], believed that considering the copyright rules and respecting the privacy of workers in construction site often lead to the fact that most researchers do not publish their researches database in the publications. In this regard, there is rare published well-known database of construction images and the authors are obliged to put more of their effort and resources on acquiring images from a construction site. This may be the key point why researchers have put less effort and attention on improving the efficiency of computer vision methods, especially in deep learning-based recognition method, in the recent years. Furthermore, lacking general image databases in the construction field makes validation of the results in this field even harder. In other word, the precise comparison between application of varied machine learning methods in construction and infrastructure Civil Engineering is not mainly feasible since each articles applied the method on a specific database which is not accessible for other researchers and authors [17, 42]. In this regard, the average accuracy has been employed in this paper in spite of applying machine learning methods on each case study of construction field. As a future trend, a general database of construction sites must be formed respecting the privacy of involved people and the copyright rules, which surely involves more researchers in the applications of machine learning in the construction field.

References

[1] Min Chen, Shiwen Mao, and Yunhao Liu. Big data: A survey. Mobile networks and applications, 19(2): 171–209, 2014.

[2] Man-Woo Park and Ioannis Brilakis. Continuous localization of construction workers via integration of detection and tracking. Automation in Construction, 72:129–142, 2016.

[3] Jie Gong and Carlos H Caldas. Computer vision-based video interpretation model for automated productivity analysis of construction operations. Journal of Computing in Civil Engineering, 24(3):252–263, 2010.

[4] Bahaa Eddine Mneymneh, Mohamad Abbas, and Hiam Khoury. Evaluation of computer vision techniques for automated hardhat detection in indoor construction safety applications. Frontiers of Engineering Management, 5(2):227–239, 2018.

[5] Pablo Martinez, Mohamed Al-Hussein, and Rafiq Ahmad. A scientometric analysis and critical review of computer vision applications for construction. Automation in Construction, 107:102947, 2019.

[6] Jun Yang, Man-Woo Park, Patricio A Vela, and Mani Golparvar-Fard. Construction performance monitoring via still images, time-lapse photos, and video streams: Now, tomorrow, and the future. Advanced Engineering Informatics, 29(2):211–224, 2015.

[7] Jun Yang, Zhongke Shi, and Ziyan Wu. Vision-based action recognition of construction workers using dense trajectories. Advanced Engineering Informatics, 30(3):327–336, 2016.

[8] Man-Woo Park and Ioannis Brilakis. Construction worker detection in video frames for initializing vision trackers. Automation in Construction, 28:15–25, 2012.

[9] Milad Memarzadeh, Mani Golparvar-Fard, and Juan Carlos Niebles. Automated 2d detection of construction equipment and workers from site video streams using histograms of oriented gradients and colors. Automation in Construction, 32:24–37, 2013.

[10] Weili Fang, Peter ED Love, Hanbin Luo, and Lieyun Ding. Computer vision for behaviour-based safety in construction: A review and future directions. Advanced Engineering Informatics, 43: 100980, 2020.

[11] Shengyu Guo, Lieyun Ding, Yongcheng Zhang, Miroslaw J Skibniewski, and Kongzheng Liang. Hybrid recommendation approach for behavior modification in the chinese construction industry. Journal of construction engineering and management, 145 (6):04019035, 2019.

[12] Hongling Guo, Yantao Yu, Qinghua Ding, and Martin Skitmore. Image-and-skeleton-based parameterized approach to real-time identification of construction workersâĂŹ unsafe behaviors. Journal of Construction Engineering and Management, 144(6): 04018042, 2018.

[13] Young-Jin Cha, Wooram Choi, and Oral Büyüköztürk. Deep learning-based crack damage detection using convolutional neural networks. Computer-Aided Civil and Infrastructure Engineering, 32(5):361–378, 2017.

[14] Lieyun Ding, Weili Fang, Hanbin Luo, Peter ED Love, Botao Zhong, and Xi Ouyang. A deep hybrid learning model to detect unsafe behavior: Integrating convolution neural networks and long short-term memory. Automation in construction, 86:118–124, 2018.

[15] June Tay, Patrick Shi, Yihong He, and Tushar Nath. Application of computer vision in the construction industry. Available at SSRN 3487394, 2019.

[16] Hanbin Luo, Chaohua Xiong, Weili Fang, Peter ED Love, Bowen Zhang, and Xi Ouyang. Convolutional neural networks: Computer vision-based workforce activity assessment in construction. Automation in Construction, 94:282–289, 2018.

[17] Daeho Kim, Meiyin Liu, SangHyun Lee, and Vineet R Kamat. Remote proximity monitoring between mobile construction resources using camera-mounted uavs. Automation in Construction, 99:168–182, 2019.

[18] Jiuwen Cao, Min Cao, Jianzhong Wang, Chun Yin, Danping Wang, and Pierre-Paul Vidal. Urban noise recognition with convolutional neural network. Multimedia Tools and Applications, 78(20):29021–29041, 2019.

[19] Botao Zhong, Haitao Wu, Lieyun Ding, Peter ED Love, Heng Li, Hanbin Luo, and Li Jiao. Mapping computer vision research in construction: Developments, knowledge gaps and implications for research. Automation in Construction, 107:102919, 2019.

[20] Billie F Spencer Jr, Vedhus Hoskere, and Yasutaka Narazaki. Advances in computer vision-based civil infrastructure inspection and monitoring. Engineering, 2019.

[21] Xianbo Zhao. A scientometric review of global bim research: Analysis and visualization. Automation in Construction, 80:37–47, 2017.

[22] Youngjib Ham, Kevin K Han, Jacob J Lin, and Mani Golparvar-Fard. Visual monitoring of civil infrastructure systems via camera-equipped unmanned aerial vehicles (uavs): a review of related works. Visualization in Engineering, 4(1):1, 2016.

[23] JoonOh Seo, SangUk Han, SangHyun Lee, and Hyoungkwan Kim. Computer vision techniques for construction safety and health monitoring. Advanced Engineering Informatics, 29(2):239–251, 2015.

[24] Christian Koch, Kristina Georgieva, Varun Kasireddy, Burcu Akinci, and Paul Fieguth. A review on computer vision based defect detection and condition assessment of concrete and asphalt civil infrastructure. Advanced Engineering Informatics, 29(2):196–210, 2015.

[25] Jochen Teizer. Status quo and open challenges in vision-based sensing and tracking of temporary resources on infrastructure construction sites. Advanced Engineering Informatics, 29(2):225–238, 2015.

[26] Habib Fathi, Fei Dai, and Manolis Lourakis. Automated as-built 3d reconstruction of civil infrastructure using computer vision: Achievements, opportunities, and challenges. Advanced Engineering Informatics, 29(2):149–161, 2015.

[27] Andrew G Howard, Menglong Zhu, Bo Chen, Dmitry Kalenichenko, Weijun Wang, Tobias Weyand, Marco Andreetto, and Hartwig Adam. Mobilenets: Efficient convolutional neural networks for mobile vision applications. arXiv preprint arXiv:1704.04861, 2017.

[28] Xiangyu Zhang, Xinyu Zhou, Mengxiao Lin, and Jian Sun. Shufflenet: An extremely efficient convolutional neural network for mobile devices. In Proceedings of the IEEE conference on computer vision and pattern recognition, pages 6848–6856, 2018.

[29] Kaiming He, Xiangyu Zhang, Shaoqing Ren, and Jian Sun. Deep residual learning for image recognition. In Proceedings of the IEEE conference on computer vision and pattern recognition, pages 770–778, 2016.

[30] Daniel W Hook, Simon J Porter, and Christian Herzog. Dimensions: building context for search and evaluation. Frontiers in Research Metrics and Analytics, 3:23, 2018.

[31] Enrique Orduña-Malea and Emilio Delgado López-Cózar. Dimensions: Re-discovering the ecosystem of scientific information. arXiv preprint arXiv:1804.05365, 2018.

[32] Nees Van Eck and Ludo Waltman. Software survey: Vosviewer, a computer program for bibliometric mapping. scientometrics, 84(2):523–538, 2010.

[33] JoonOh Seo, Kaiqi Yin, and SangHyun Lee. Automated postural ergonomic assessment using a computer vision-based posture classification. In Construction Research Congress 2016, pages 809–818, 2016.

[34] Mani Golparvar-Fard, Arsalan Heydarian, and Juan Carlos Niebles. Vision-based action recognition of earthmoving equipment using spatio-temporal features and support vector machine classifiers. Advanced Engineering Informatics, 27(4):652–663, 2013.

[35] Qi Fang, Heng Li, Xiaochun Luo, Lieyun Ding, Hanbin Luo, Timothy M Rose, and Wangpeng An. Detecting non-hardhat-use by a deep learning method from far-field surveillance videos. Automation in Construction, 85:1–9, 2018.

[36] Jack CP Cheng and Mingzhu Wang. Automated detection of sewer pipe defects in closed-circuit television images using deep learning techniques. Automation in Construction, 95:155–171, 2018.

[37] Domingo Mery and Carlos Arteta. Automatic defect recognition in x-ray testing using computer vision. In 2017 IEEE Winter Conference on Applications of Computer Vision (WACV), pages 1026–1035. IEEE, 2017.

[38] Mehmet Yalcinkaya and Vishal Singh. Patterns and trends in building information modeling (bim) research: A latent semantic analysis. Automation in construction, 59:68–80, 2015.

[39] Yuhong Wu, Hyoungkwan Kim, Changyoon Kim, and Seung H Han. Object recognition in construction-site images using 3d cad-based filtering. Journal of Computing in Civil Engineering, 24 (1):56–64, 2010.

[40] Jorge Abeid Neto, David Arditi, and Martha W Evens. Using colors to detect structural components in digital pictures. Computer-Aided Civil and Infrastructure Engineering, 17(1):61–67, 2002.

[41] Xiaochun Luo, Heng Li, Hao Wang, Zezhou Wu, Fei Dai, and Dongping Cao. Vision-based detection and visualization of dynamic workspaces. Automation in Construction, 104:1–13, 2019.

[42] Zeli Wang, Heng Li, and Xiaoling Zhang. Construction waste recycling robot for nails and screws: Computer vision technology and neural network approach. Automation in Construction, 97:220–228, 2019.

[43] Ran Wei, Peter ED Love, Weili Fang, Hanbin Luo, and Shuangjie Xu. Recognizing peopleâĂŹs identity in construction sites with computer vision: A spatial and temporal attention pooling network. Advanced Engineering Informatics, 42:100981, 2019.

[44] Qi Fang, Heng Li, Xiaochun Luo, Lieyun Ding, Hanbin Luo, and Chengqian Li. Computer vision aided inspection on falling prevention measures for steeplejacks in an aerial environment. Automation in Construction, 93:148–164, 2018.

[45] Mani Golparvar-Fard, Feniosky Pena-Mora, and Silvio Savarese. Automated progress monitoring using unordered daily construction photographs and ifc-based building information models. Journal of Computing in Civil Engineering, 29(1):04014025, 2015.

[46] Andrey Dimitrov and Mani Golparvar-Fard. Vision-based material recognition for automated monitoring of construction progress and generating building information modeling from unordered site image collections. Advanced Engineering Informatics, 28(1): 37–49, 2014.

[47] Bahaa Eddine Mneymneh, Mohamad Abbas, and Hiam Khoury. Vision-based framework for intelligent monitoring of hardhat wearing on construction sites. Journal of Computing in Civil Engineering, 33 (2):04018066, 2019.

An Agent-based Approach for Modeling Human-robot Collaboration in Bricklaying

Ming-Hui Wu[a] and Jia-Rui Lin[a,*]

[a]Department of Civil Engineering, Tsinghua University, China
E-mail: wmh17@mails.tsinghua.edu.cn, lin611@tsinghua.edu.cn

Abstract -

Construction robots have drawn attention in research and practice for decades. Considering most of the construction robots are not fully automated and humans are always involved in the construction process, how humans and robots collaborate has a great impact on the total productivity. Unlike collaboration systems between human-human, human-device and robot-robot, human-robot collaboration process has its complexity and uniqueness. Thus, this paper starts with analysis of human-robot collaboration system in construction, then provides an agent-based approach to simulate the process in bricklaying with emphasis on its complexity. A real project in Beijing is utilized to validate the feasibility of the proposed method. Besides, managerial insights useful for the workers to better utilize construction robots can be drawn from the results, which shows the effectiveness of the proposed model. This research contributes to the body of knowledge an agent-based approach to modeling, simulating, and analyzing the human-robot collaboration process in construction sites. This research serves as a foundation for further in-depth investigation in this area.

Keywords –

Construction robots; human-robot collaboration; agent-based simulation; communication mode; human factor

1 Introduction

Construction robots have drawn attention in research and practice these years to cover the shortage of conventional construction. In terms of the entire industry, its productivity has been declining in recent years and the conventional construction paradigm has reached the technological performance limit[1]. In terms of workers in this industry, construction tasks are usually of high physical demand, and sometimes are harmful to their health[2]. Therefore, construction robots have aroused increasing interest in the last 15-20 years because it can improve the productivity while replace workers from doing heavy duties and dangerous tasks[3]. The application of robots involves nearly every construction-related tasks, including glazing[4], beam assembly[5], earthmoving[6], concrete wall fabrication[7], etc.

However, construction industry cannot be fully automated currently even with the aid from robots[3]. As a result, various operations and tasks still need to be fulfilled by human workers. In other words, human-robot collaboration is a critical part of the construction process.

Agent-based (AB) modeling, a simulation approach to model systems by using virtual agents to imitate the behaviors and interactions of participated individuals[8] is commonly used to simulate construction scenarios to understand and further optimize the process. Multiple collaboration systems between human-human[9], human-device[10] and robot-robot[11] in construction have been studied. However, human-robot collaboration system has its specific complexity and uniqueness comparing to other collaboration systems, which calls for further investigation.

This research starts with analysis of human-robot collaboration system in construction, then chooses bricklaying process as a typical application in the construction domain, and adopts an agent-based (AB) modeling approach to simulate human-robot collaboration process with emphasis on its characteristics. Managerial insights are drawn to show the applicability and benefits of the proposed model. The remainder of the article is organized as follows. Section 2 introduces the methodology used in the research. Section 3 provides the analysis for human-robot collaboration systems in construction. Section 4 proposes the development of the AB simulation model. Section 5 presents case studies and draws managerial insights. Section 6 summarizes the research and discusses possible future investigations.

2 Methodology

The objective of this research is to model human-robot collaboration in bricklaying with an AB modeling approach. To achieve the objective, AnyLogic© (version 8.5.0) is used as a simulation platform. A six-step

methodology is utilized (Figure 1), which contains system analysis, model scope determination, simulation environment determination, agent property definition, data collection and scenario application.

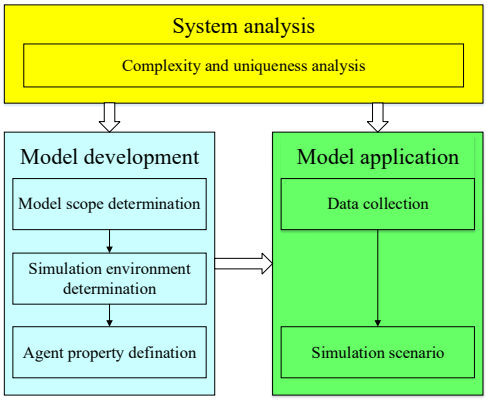

Figure 1. Overview of the research methodology

At the very beginning, the human-robot collaboration system in construction is analysed. Its complexity and uniqueness comparing to other collaboration systems are further stressed, which is the foundation of all the rest steps. In model development, model scope is first determined. Robot agents, worker agents, brick agents, and recorder agents are incorporated. A real project in Beijing is used as the simulation environment. Acting behaviors are captured to define the agents' property. Then, agents can act spontaneously in the experiments. The model is further applied to a case study to test its applicability and draw managerial insights. Data collection should be done at first to determine parameters in the model. Considering the practical applications of bricklaying robots are still limited, the parameters cannot directly be acquired from real bricklaying robots. To address this, the parameters are based on theoretical and empirical evidence, including previous papers and video records. However, it is important to mention that the parameters can be easily adjusted to other values when needed. Considering the randomness in experiments, the simulation scenario is simulated three times and outputs are set to the average value.

3 Analysis for human-robot collaboration systems in construction

3.1 Collaboration system

Collaboration systems are classified by participants. In construction, collaboration systems between human-human, human-device, robot-robot and human-robot are common (Figure 2). Human-human and robot-robot collaboration refers to the collaboration among workers and machines respectively. The difference between human-device collaboration and human-robot collaboration is that human conducts a mission by manipulating a device (i.e. infrared cameras in bridge inspection[12]) while human and robots can work on different tasks side by side[13].

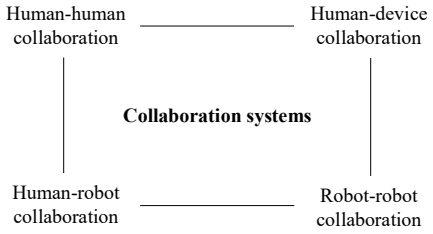

Figure 2. Classification of collaboration systems

Several communication modes are involved in collaboration systems[13] (Table 1). These modes are originally used in human-robot collaboration, but they can be generalized to other collaboration systems as well. Therefore, agents are used to represent the participants, corresponding to the AB approach.

3.2 Complexity and uniqueness of human-robot collaboration system

3.2.1 Traditional collaboration system

Traditional collaboration systems between human-human, robot-robot and human-device are involved in simulation scenarios of previous papers. Table 2 summarized the scenario, collaboration type, communication mode of representative works. For example, in bridge inspection process[12], on one hand, preparation and inspection are conducted in sequence by technicians. Technicians use voice to communicate, which is considered a form of RCI. On the other hand, technicians move with the devices in the inspection process, and since technicians need to set or program the devices first, the communication mode is ME.

It can be concluded that traditional collaboration systems only involves a simple communication mode, either RCI or ME. This is reasonable since humans only need to communicate by voice; robot-robot system as a fully automated system only needs electronic signals to send messages; while device as a passive object only need to be programed.

3.2.2 Human-robot collaboration system

Comparing to traditional collaboration systems, human-robot collaboration is complex and unique in the following three aspects. All three aspects will be further illustrated in Section 4. (1)Simultaneously involving

multiple communication modes: since many robots in construction is not fully automated, they still need to be installed, programmed or manipulated (ME, TL) like devices; however, robots have much higher autonomy and independence as a collaborator rather than a passive tool, which provide possibility for more communication modes (RCI, DPI). (2)Safety requirement: for extremely complicated and distributed environment like construction site, it will be very hard to set up fence to separate workers and robots. Since human workers are exposed to robots, human-robot collaboration system needs some safety requirements such as safety distance[14]. Safety issue is seldom considered in traditional collaboration systems. (3) Different characteristics between participants: the two participants, human and robot, have different characteristics. For example, human workers will forget or feel tired, but robots will not. This is unique as well. For human-device collaboration, when humans are tired, the efficiency of device will also be effected as it is manipulated by humans.

Table 1. Communication modes in collaboration systems[13]

Communication mode	Description
Direct physical interaction (DPI)	One agent's body contact with another in order to perform a task
Remote contactless interaction (RCI)	Agents contact by interfaces (e.g. voice, camera)
Teleoperation(TL)	Workers directly drive a machine with interface
Message exchange(ME)	Information is exchange using digital signals transmitted through physical button

Table 2. Traditional collaboration systems in previous work

Paper	Scenario	Collaboration type	Communication mode
Seo et al.[9]	Bricklaying	Human-human	RCI
Abdelkhalek et al.[12]	Bridge inspection	Human-human	RCI
Zhe et al.[15]	Pump maintenance	Human-human	RCI
Jabri et al. [11]	Earthmoving	Robot-robot	RCI
Yassin et al. [16]	3D printing reinforced concrete	Robot-robot	RCI
Abdelkhalek et al.[12]	Bridge inspection	Human-device	ME
Jung et al.[10]	Lift system	Human-device	ME

4 AB model development for human-robot collaboration

After having an understanding of the complexity and uniqueness of human-robot collaboration system, this section provides an AB model to simulate this process.

4.1 Model scope

Model scope determines the content of agents. Four kinds of agents are involved in this model, robot agents, worker agents, brick agents and recorder agents. The first two agents will work together to fulfil masonry tasks. Four agent states are introduced to capture the working condition of both robots and workers: (1) working state refers to an agent working on a given mission; (2) idle state refers to agent being in idle without missions; (3) moving state refers to workers moving robots or robots being moved; (4) operating state refers to workers and robots doing preparatory works. Bricks are considered as passive agents for robots and workers to manipulate. Besides, in order to record the agent state at any time, a kind of dummy agent, recorder, is introduced to the model. Each recorder agent has one corresponding robot agent or worker agent. It will record the state and the corresponding time when the state has changed.

4.2 Simulation environment

The simulation environment is the construction site where agents are acting and interacting with each other. In this research, a typical residential project in Beijing is used to provide references to the design of the simulation environment. Several assumptions are made to simplify the original layout of the construction site without losing generalization. One of the buildings in the layout is picked as the construction object. The corner of the site is assumed to be Long-term Store Place to deposit construction materials, such as bricks. A small place near

the building is considered as Temporary Store Place for workers' convenience. A rectangle area that envelopes the building is assumed to be Work Zone. Besides, a small rectangle place near Temporary Store Place is set to be Robot Store Place. The simplified layout of the simulation environment is shown in Figure 3. It is then imported to the simulation model in Anylogic© using real-world plotting scale to ensure the reliability.

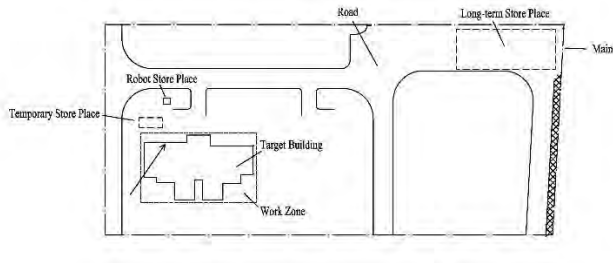

Figure 3. The simulation environment of the model

At the beginning, all bricks are deposited in the Long-term Store Place. The robot is placed in the Robot Store Place, while all the workers are randomly placed in Work Zone. In this research, we mainly focus on the situation with one robot. It is assumed that three workers are needed to move the robot. Therefore, the simulation environment contains 3 worker agents and 1 robot agent.

4.3 Agent properties

In AB models, agents have two types of properties, attributes and variables, to regulate their performance[17]. Attributes are fixed properties, while variables may change in the process.

4.3.1 Robot agent

The main job for robot agents is to construct brick walls. Conventionally, brick walls function as infilled walls that locate between columns. Two dummy nodes, start node and end node, are extracted to represent the endpoints of each wall. The set of all nodes, Node Set (NS), is introduced to record all the start nodes and end nodes. It represents all the construction tasks for the bricklaying robot. One attribute, Number of Nodes (NN) and one variable, Number of Completed Nodes (NCN), are applied correspondingly to capture the number of all nodes and completed nodes in NS. Another attribute, Number of Layers (NL), is introduced to determine the number of layers in each wall.

The robot agent will pass through four stages during the whole construction process. (1): Robot agents start waiting for workers at Robot Store Place, so it is classified as idle state. (2): After moved and installed by workers, the robot is working in Work Zone, and is classified as working state. Although there are several types of bricklaying robot existing in industry or academic [2, 18-23], most robots share the same process of laying one brick. Therefore, SAM100 is chosen as an example to model the laying process. For SAM100[24, 25], the whole process can be summarized into the iteration of two procedures, moving to target position and bricklaying. Bricklaying is a generalized process that contains plastering on the surface, grabbing one brick and laying it on the mortar. Two attributes, Moving Velocity in Working (MVW) and Brick Laying Duration (BLD) are critical in this stage. The first attribute captures the velocity as robots moving to the target position, and the second attribute captures the duration for the bricklaying process. When one layer is finished, the robot will return to the start node. For safety reason, it is assumed that the robot will not start the next layer until the worker responsible for extra mortar removing (introduced in the next section) finishes this layer. (3): After all layers are finished, the robot will automatically move back to the start node and stop operating. It is classified as idle state. Meanwhile, the start node and the end node for this wall will be labeled as "Complete" and NCN will increase by two. (4): Because several bricklaying robots has a pipe to deliver mortar[25], it is assumed that the mortar is always sufficient. However, robots probably will still run out of bricks that are stored inside. When this happens, the robot will pass to Stage 4 and stop operating, therefore the state will change into idle state. The attribute, Robot Storage Capacity (RSC), is applied to determine the maximum number of bricks that can be stored inside the robot. When the bricks are supplemented, the robot will start operating again and continue the previous task.

4.3.2 Worker agent

In this model, workers are responsible for three kinds of tasks in the whole process. First, workers need to carry the robot to target locations, called Robot Moving and Installing (RMI). Second, considering when robots squeeze a brick on the mortar, the robot arm will also push some mortar beyond the below brick's edges[23], this extra mortar is supposed to be removed by one human worker. This task is called extra mortar removing (EMR). Third, when robots run out of bricks in their storage, one worker is responsible to supplement bricks[26]. This task is called Brick Supplement (BS). For the three worker agents in the model, one is responsible for BS and RMI (called the BS worker), one is responsible for EMR and RMI (called the EMR worker), and the last one only need to participates in RMI (called the RMI worker).

RMI task can be divided into two parts. (1): At the very beginning, workers first move to Robot Store Place. Their moving speed is determined by the parameter Walking Velocity (WV). Some preparation works need

to be done before they move the robot. Then, workers will carry the robot to Node 1. Another attribute, Robot Moving Velocity (RMV), is introduced to capture this moving speed when carrying loads. Then, workers need to install it on the work site. These two processes, determined by Preparation Duration (PD) and Installation Duration (ID), belong to operating state. (2): When the robot finishes the bricklaying work for one wall, workers will judge whether there are other unconstructed walls. If so, they will move the robot to the next unfinished node in NS. Otherwise, workers will move the robot back to Robot Store Place.

EMR task is the iteration of moving to target brick and removing extra mortar on the brick. Since the worker is not carrying loads, it is assumed that the moving speed is WV as well. An attribute, Mortar Removing Duration (MRD), is introduced to determine the time for the worker to remove mortar on one brick. To ensure that the EMR worker has a safe distance with the robot, it is assumed an at least 10 bricks length separation distance.

Since the EMR worker is beside the robot, he will inform the BS worker when the robot runs out of bricks and stops operating. Then, the worker will go to Temporary Store Place or Long-term Store Place to supplement bricks, depending on the number of bricks at Temporary Store Place. If it is larger than RSC, he will grab, move and add these bricks to the robot. Otherwise, the BS worker will first transport five times RSC bricks from Long-term Storage Place and drop them to the Temporary Storage Place. Three time-related attributes, Grabbing Duration (GD), Dropping Duration (DD), and Supplement Duration (SD) are introduced to determine the duration the BS worker needs to grab, drop and supplement RSC number of bricks. Besides, Carrying Velocity (CV) is introduced to decide the moving velocity for the BS worker when transporting bricks. Besides just waiting for the information from the EMR worker, it is assumed the BS worker will check the number of remaining bricks periodically. If the BS worker finds that bricks in the robot are less than Supplement Limit (SL), he will start the supplement process directly. Check Interval (CI) is introduced to determine the checking frequency.

Two ergonomic behaviors are incorporated.

(1) Forgetting: Because the BS worker may repeat checking many times a day, he is very possible to forget some checks. To capture the forgetting behavior, the variable Forgetting Possibility (FP) is introduced. FP is determined by the following equation[15]:

$$FP = e^{-0.01CI} \quad (1)$$

(2) Muscle fatigue: In bricklaying process, several tasks have physical work load on masons [27], which leads to muscle fatigue. To address this, we reference a dynamic fatigue model proposed by Seo et al. [9]. A worker will take a voluntary rest when his current level of muscle strength is lower than the physical demand in the following work element, and will not perform the task until the former is at least 10%MVC higher than the latter. MVC refers to the maximum muscle strength. Relation of current muscle strength and work load is shown in equation (2), and muscle strength in the recovery process can be explained in equation (3).

$$\frac{F_{cem}(t)}{MVC} = e^{-\frac{F_{load}}{MVC}d} \quad (2)$$

$$F_{cem}(t_b) = [1 + r \times (b - a)]F_{cem}(t_a) \quad (3)$$

$F_{cem}(t)$ represents the currently available maximum force at time t. d refers to the duration of the task, and F_{cem} refers to the average physical demand of a work element. Only four work elements that have physical demand are considered based on Seo et al. [9]. The physical demand for extra mortar removing is 0.1%MVC; while the physical demand for grabbing bricks, dropping bricks, and adding bricks to the robot are 0.4%MVC. Besides, r equals 5%MVC per 1 min when F_{cem} is lower than 90%MVC, and equals 0.3%MVC per 1 min otherwise.

4.4 Characteristics of human-robot collaboration in the AB model

This section introduces how the characteristics of human-robot collaboration mentioned in Section 3.2.2 is embedded in the AB model.

Table 3 shows the communication modes related to the bricklaying process. It shows that the human-robot collaboration simultaneously involves three communication modes except TL. These there modes are successfully captured by the proposed model.

Table 3. Involved communication modes in AB model

Communication mode	Scenario
DPI	BS supplements bricks for the robot Workers move the robot
RCI	Communication among workers The Robot waits EMR for next layer
TL	/
ME	Workers install the robot

As mentioned before, the robot will not start laying the next layer until the EMR worker finish the layer; the minimum distance between the robot and the EMR worker is required. These two rules represent the safety requirements. Other requirements can be embedded to the model as well in the same way. Besides, the different characteristics of human and robot are modelled by considering two human factors.

5 Model application and demonstration

5.1 Data collecting

The simulation model is set up based on a range of parameters, including attributes and variables. Attributes are given default values, and variables can be calculated from attributes. Attributes in the model are classified into four types. (1): NS, NN, NL are defined by the construction tasks; (2): PD, ID, MVW, BLD, RSC are related to the robot type; (3): RMV, WV, MRD, GD, DD, SD, CV are determined by the workers' capacity; (4): SL, CI represents the inspection policy. This research aims at providing a modeling approach, without focusing on specific robots, workers or policies. Therefore, the attributes are decided in Table 4 based on theoretical evidence, empirical evidence and necessary assumptions[18, 24, 28]. Triangular distributions with a 20% variance are applied to PD, ID, MRD, GD, DD and SD to capture workers' random performance[29].

Table 4. Default value of attributes

Robot agent		Worker agent	
Attribute	Value	Attribute	Value
PD	10min	RMV	0.33m/s
ID	10min	WV	0.75m/s
MVW	0.2m/s	MRD	5s
BLD	8s	SL	100 bricks
RSC	300 bricks	CI	15min
		GD	30s
		DD	30s
		SD	10s
		CV	0.67m/s

5.2 Case study

This scenario gives a demonstration of the output in order to shed light on a better understanding of the proposed model, while draw useful managerial insights from the output. The construction task for this scenario is the first wall with ten layers, which is labeled with an arrow in Figure 2. Therefore, NS contains two nodes, NN equals two and NL equals ten. Other attributes equal default values.

5.2.1 Recording duration data

The model is capable of recording total and classified construction duration for both robot agents and worker agents. Based on the duration data, the proportion of working time and idle time can be calculated. Duration data for robot agents are shown in Table 5. The construction duration, together with proportion of working time and idle time can serve as an indicator of the productivity of the construction process.

Table 5. Duration data for robot agents

	1	2	3	average
Construction time (h)	5.07	5.10	5.04	5.07
Working time(h)	2.78	2.77	2.77	2.77
Idle time (h)	1.58	1.57	1.54	1.56
Moving time (h)	0.06	0.06	0.06	0.06
Operating time (h)	0.66	1.57	1.54	0.67
Working proportion		/		54.6%
Idle proportion		/		30.8%

5.2.2 Generation of state-to-time variation

Based on the data recorded by recorder agents, figures that show state-to-time variation can be generated. In the figures, different states are labeled with different numbers (2 refers to working state, 1 refers to idle state, 0 refers to operating state, -1 refers to moving state). This grading approach can capture the divergence of states from working state. The state-to-time variation of primary agents, including the robot agent, the BS worker agent and the EMR worker agent are showed in Figure 4.

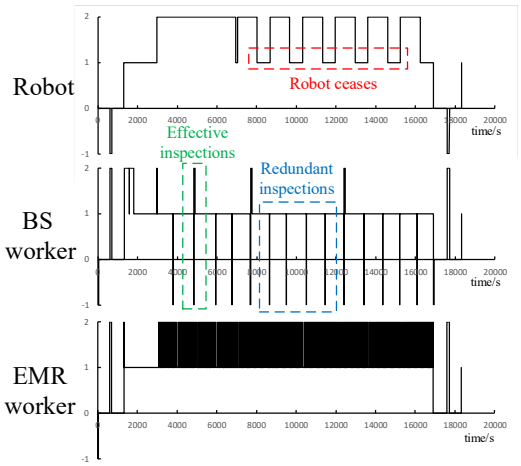

Figure 4. State-to-time variation of main agents

The state-to-time variation clearly shows the working condition of each agent, therefore it is considered to be a good tool to examine the productivity of the process. For example, it stresses the impact of inspection policy on total productivity. Beside effective inspections labeled with the green rectangle, the BS worker has several redundant inspections labeled with the blue rectangle, which infers CI should be adjusted longer than the default value to achieve better effectiveness. Besides, the robot still ceases several times labeled with the red rectangle due to the fatigue of the EMR worker. It is clearly shown in Figure 6 that all the pauses happen after the F_{cem} of the EMR worker reached 0.11, 10%MVC higher than the physical demand of his tasks. Another important managerial insight can be drawn to address this. At the

early stage, workers' strengths match well with the robot. However, when the construction is carried forward, workers become incompetent due to muscle fatigue. At this time, some managerial actions (i.e. shifts) should be taken to regain the balance between workers and robots. The proposed model can indicate the best time to shift the EMR worker, which is labeled by red line in Figure 5.

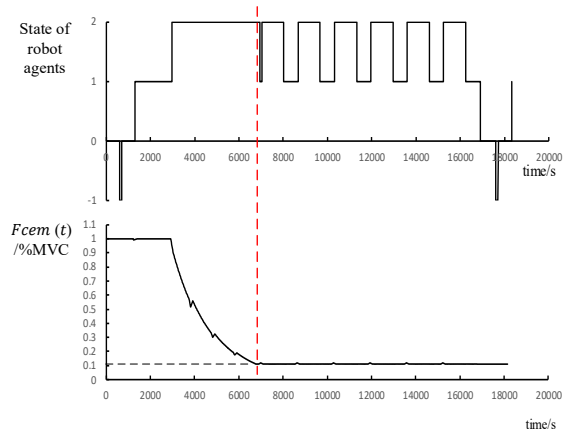

Figure 5. Impact of fatigue on productivity

6 Conclusion

Comparing to collaboration systems between human-human, human-device and robot-robot, human-robot collaboration is complex and unique because it involves multiple communication at the same time; it has special safety requirements; its participants, human and robot, have different characteristics. In this research, an agent-based approach is applied to simulate human-robot collaboration process in typical bricklaying scenarios, in order to provide a bottom-up approach to help understand and further optimize this complicated process.

The proposed model fully integrates the behaviors of both workers, robots and their interaction. The effect of muscle fatigue and forgetting is incorporated as human factors to further emphasize the differences between robots and workers. The AB model is capable of recording total and four types of classified construction duration corresponding to the four states, and is able to capture state-to-time variation. Development of the simulation model is based on a range of parameters to capture the quality of both workers and robots, which is further based on theoretical and empirical evidence, including previous papers and video records. The result confirms the potential of AB modeling for analyzing human-robot collaboration process in construction. The results also draw some managerial insights: (1) inspection policy can be adjusted to achieve a higher effectiveness; (2) shifts in workers are highly recommended to retain the strength balance between workers and robots to maximize the productivity, since muscle fatigue will greatly hamper workers' capacity.

Further research can be conducted to improve and utilize the proposed model. Although the proposed model reflects the coexistence of different communication modes, it will be very meaningful to abstractly model the four communication modes, which can guide the establishment of future simulation models related to human-robot collaboration. Besides, currently only forgetting and muscle fatigue are considered in the model. However, other human factors (i.e. communication errors etc.) and ergonomic behaviors (i.e. muscle fatigue increases the forgetting possibility etc.) can be incorporated. Furthermore, many parameter values in this research are not based on actual robots due to the limited practical application. As construction robots become more prevalent, parameters can be adjusted to actual values.

7 Acknowledgement

The research is supported by the National Key R&D Program of China (No. 2018YFD1100900), the National Natural Science Foundation of China (No. 51908323), the Tsinghua University Initiative Scientific Research Program (No. 2019Z02UOT) and Tsinghua University Students Research Training Program.

References

[1] T. Bock. The future of construction automation: Technological disruption and the upcoming ubiquity of robotics. *Automation in Construction,* 59: 113-121, 2015.

[2] T. Bock, Robotic Assembly System for Computer Integrated Construction, In *Proceedings of the 13th International Symposium on Automation and Robotics in Construction*, Tokyo, Japan, 1996

[3] G. Carra, A. Argiolas, A. Bellissima *et al.*, Robotics in the Construction Industry: State of the Art and Future Opportunities, In *Proceedings of the 35th International Symposium on Automation and Robotics in Construction (ISARC)*, Berlin, Germany, 2018

[4] S. Lee, and J. Ⅱ. Moon. Case Studies on Glazing Robot Technology on Construction Sites. *Proceedings of the 32nd International Symposium on Automation and Robotics in Construction (ISARC)*: 978-983, Oulu, Finland, 2015.

[5] K. Jung, B. Chu, S. Park *et al.* An implementation of a teleoperation system for robotic beam assembly in construction. *International Journal of Precision Engineering and Manufacturing,* 14 (3): 351-358, 2013.

[6] T. Groll, S. Hemer, T. Ropertz *et al.*, A Behaviour

Based Architecture for Excavation Tasks, In *Proceedings of the 34th International Symposium on Automation and Robotics in Construction (ISARC)*, Taipei, Taiwan, 2017

[7] B. García de Soto, I. Agustí-Juan, J. Hunhevicz *et al.* Productivity of digital fabrication in construction: Cost and time analysis of a robotically built wall. *Automation in Construction,* 92: 297-311, 2018.

[8] P. Twomey, and R. Cadman. Agent‐based modelling of customer behaviour in the telecoms and media markets. *info,* 4 (1): 56-63, 2002.

[9] J. Seo, S. Lee, and J. Seo. Simulation-Based Assessment of Workers' Muscle Fatigue and Its Impact on Construction Operations. *Journal of Construction Engineering and Management,* 142 (11), 2016.

[10] M. Jung, M. Park, H.-S. Lee *et al.* Agent-Based Lift System Simulation Model for High-Rise Building Construction Projects. *Journal of Computing in Civil Engineering,* 31 (6), 2017.

[11] A. Jabri, and T. Zayed. Agent-based modeling and simulation of earthmoving operations. *Automation in Construction,* 81: 210-223, 2017.

[12] S. Abdelkhalek, and T. Zayed. Simulation-based planning of concrete bridge deck inspection with non-destructive technologies. *Automation in Construction,* 119, 2020.

[13] S. E. Hashemi-Petroodi, S. Thevenin, S. Kovalev *et al.* Operations management issues in design and control of hybrid human-robot collaborative manufacturing systems: a survey. *Annual Reviews in Control,* 49: 264-276, 2020.

[14] V. Villani, F. Pini, F. Leali *et al.* Survey on human–robot collaboration in industrial settings: Safety, intuitive interfaces and applications. *Mechatronics,* 55: 248-266, 2018.

[15] Z. Sun, C. Zhang, and P. Tang. Modeling and simulating the impact of forgetting and communication errors on delays in civil infrastructure shutdowns. *Frontiers of Engineering Management*, 2020.

[16] A. Abou Yassin, F. Hamzeh, and F. Al Sakka. Agent based modeling to optimize workflow of robotic steel and concrete 3D printers. *Automation in Construction,* 110, 2020.

[17] S. AbouRizk, D. Halpin, Y. Mohamed *et al.* Research in Modeling and Simulation for Improving Construction Engineering Operations. *Journal of Construction Engineering and Management,* 137 (10): 843-852, 2011.

[18] Z. Dakhli, Z. Lafhaj, and S. K. Shukla. Robotic mechanical design for brick-laying automation. *Cogent Engineering,* 4 (1), 2017.

[19] M. L. Aguair, and K. Behdinan. Design, Prototyping, and Programming of a Bricklaying Robot. *Journal of Student Science and Technology,* 8 (3), 2015.

[20] G. Pritschow, M. Dalacker, J. Kurz *et al.* Technological aspects in the development of a mobile bricklaying robot. *Automation in Construction,* 5 (1): 3-13, 1996.

[21] A. V. Malakhov, D. V. Shutin, and S. G. Popov. Bricklaying robot moving algorithms at a construction site. *IOP Conference Series: Materials Science and Engineering,* 734, 2020.

[22] A. V. Malakhov, and D. V. Shutin. The analysis of factors influencing on efficiency of applying mobile bricklaying robots and tools for such analysis. *Journal of Physics: Conference Series,* 1399, 2019.

[23] S.-N. Yu, B.-G. Ryu, S.-J. Lim *et al.* Feasibility verification of brick-laying robot using manipulation trajectory and the laying pattern optimization. *Automation in Construction,* 18 (5): 644-655, 2009.

[24] C. Robotics. How Robots Are Changing the Construction Industry,On-line: https://www.construction-robotics.com/6275/2019/25/, Accessed: 01/29/2020.

[25] R. Bogue. What are the prospects for robots in the construction industry? *Industrial Robot: An International Journal,* 45 (1): 1-6, 2018.

[26] S. Moon, B. Becerik-Gerber, and L. Soibelman, "Virtual Learning for Workers in Robot Deployed Construction Sites," *Advances in Informatics and Computing in Civil and Construction Engineering*, pp. 889-895, 2019.

[27] H. F. Van Der Molen, P. P. Kuijer, P. P. Hopmans *et al.* Effect of block weight on work demands and physical workload during masonry work. *Ergonomics,* 51 (3): 355-66, 2008.

[28] C. Robotics. https://www.construction-robotics.com/video/, Accessed: 16/05/2020.

[29] M. Goh, and Y. M. Goh. Lean production theory-based simulation of modular construction processes. *Automation in Construction,* 101: 227-244, 2019.

A Vision for Evaluations of Responsive Environments in Future Medical Facilities

D. B. Lu[a], S. Ergan[a], D. Mann[b], K. Lawrence[b]

[a]Department of Civil and Urban Engineering, New York University, United States
[b]Medical Center Information Technology, New York University Langone Health, United States
E-mail: dbl299@nyu.edu, semiha@nyu.edu, Devin.Mann@nyulangone.org, Katharine.Lawrence@nyulangone.org

Abstract –

Medical facilities in the United States (US) are facing growing demands due to shifts in patient demographics, healthcare policies, costs of care, and medical technologies. An emerging trend is the growing importance of outpatient and ambulatory care relative to inpatient care. Whereas the term "inpatient" involves a patient needing admission into a hospital over an extended period of time, ambulatory care (i.e., outpatient clinics, dialysis clinics, ambulatory surgical centers, etc.) generally involves medical and surgical services performed outside a hospital environment, with the overall patient visit duration typically lasting less than a few hours. Changes in healthcare policy and advances in medical technologies are driving the need for ambulatory facilities to be more flexible in terms of functionalities and environmental qualities (e.g., light, acoustics, etc.). Responsive environments, as a design approach focusing on how spaces can change in response to user and environmental input (e.g., user interfaces, sensors), can uniquely address these changing and contemporary needs of medical practices. Architectural robotics, a key element of responsive environments, can facilitate rapid changes in building component configurations, such as interior wall, display screen, and furnishing layout, enabling spatial flexibility for medical staff. In this paper, we envision a novel application of responsive environments in the context of outpatient clinics and ambulatory care facilities. We present two ambulatory practice scenarios demonstrating architectural robotics use cases, based on preliminary observations of six ambulatory care medical staff and their patterns of interactions with existing technologies, building spaces, and navigation between spaces. Virtual environments, modeling those two scenarios, have been scripted and tested with an initial group of nine medical professionals activating architectural robotic transformations and experiencing the changes in configurations, with feedback collected through a follow-up questionnaire. Collected data on participants' feedback on the scenarios' applicability to healthcare practice and usability are presented in this paper. We expect to develop subsequent responsive environments to serve specialized medical practices as we identify them by shadowing a larger cohort of medical staff. Outcomes will be helpful for design practitioners as our findings suggest updates to the typical medical building layouts given digital technology advancements in healthcare practice. This work serves as an initial proof of concept for how responsive environments and architectural robotics can improve the spatial flexibility of future ambulatory care settings in particular and medical facilities overall, and how these are positively perceived by medical staff.

Keywords –

responsive environments; immersive virtual environments; healthcare; architectural robotics

1 Introduction

Medical facilities in the United States (US) face numerous challenges amidst a changing landscape of policy, demographics, and technology. An emerging trend is the growing importance of outpatient and ambulatory care relative to inpatient care. Inpatient care typically refers to hospitals, where a patient stays for an extended period of time under significant levels of monitoring and treatment. Outpatient and ambulatory care (i.e., outpatient clinics, dialysis clinics, ambulatory surgical centers, etc.) generally involves medical and surgical services performed outside a hospital environment, with the overall patient visit duration typically lasting less than a few hours. Within the last fifteen years, the number of outpatient facilities in the US has increased 51% due to numerous factors including an aging population, changes in US healthcare policy, and rising costs of inpatient care [1] [2]. These trends motivate us to specifically focus within the context of healthcare on improving the built environment of outpatient and ambulatory care facilities. While the terms "outpatient" and "ambulatory" have nuanced definitions in medical research, for the purposes of simplicity, this

paper use "outpatient clinics" to refer to both terms.

Outpatient clinics are starting to involve new digital technologies, raising questions of how the existing and future facilities can be better designed. For example, the predominant use of electronic health records (EHR) has created a challenge for physicians to balance their attention to EHR computer screens while making sure the patient still feels a sense of connection [3]. This has led to various investigations in how the built environment can be better designed with optimal positioning of furniture and EHR screens within an exam room [4]. EHRs are also getting integrated with wearable health technologies to capture more data on patients and streamline medical staff workflows [5]. Telemedicine has changed the relationship between people and the built environment, allowing patients to check in with their doctors without having to visit an outpatient care facility [6] [7]. Driven by these changes in technology, expectations of patients, and medical staff workflows, outpatient practices need flexibility in terms of the amount of space, variations in environmental qualities (e.g. lighting, acoustics, temperature), and ability to use the same space for multiple purposes [2]. The need for flexibility in outpatient clinics compels us to re-evaluate what medical staff and patients currently require from their environments.

Updating medical staff and patient requirements on the usage of facilities will inform the design of outpatient clinic environments that work in conjunction with the information technologies being used. In fact, those same technologies that reduce the number of in-person visits also present an opportunity for improving outpatient clinic environments for situations when an in-person visit is necessary. As technologies become more interconnected, more ubiquitous computing ecosystems and cyber-physical systems may become possible to incorporate into the design of outpatient clinic environments. We anticipate that these new technologies can enable the spatial and environmental flexibility desired by current outpatient practices through a responsive environment design approach.

Specifically, we see potential for architectural robotics to be involved in medical staff workflows, allowing for greater functionality within a given floor area. We present in this paper preliminary demonstrations of architectural robotics in virtual environments of outpatient clinic spaces, use cases of space transformations that were identified through field observations in medical facilities, and evaluate the feedback we received from medical professionals who navigated within those VEs. Overall, these VEs provide a means for evaluating whether the needs of outpatient medical staff are well identified and addressed.

For this study, we performed preliminary ethnographic studies observing medical staff working in current outpatient care facilities. Based on those observations, we developed two scenarios of how architectural robotics can transform clinic spaces. We then present feedback from nine medical professionals after they walk through virtual environments demonstrating those two scenarios. While the focus of this paper is on outpatient and ambulatory care facilities, we expect that the findings are applicable to medical facilities in general.

2 Related Work

2.1 Responsive Environments

While the term "responsive environments" has varied over time and different contexts, it generally refers to elements of a built environment that react to a stimulus of social (e.g., a person) or environmental (e.g., air temperature) nature [8]. Within these responsive environments, a range of explicit (e.g., a person turning on an air conditioner) and implicit (e.g., a thermostat determining space cooling needs) interactions providing that stimuli are possible [9]. A more specific definition of interest to our research is a responsive environment that can perceive people's changing needs through a system of sensors [10] [11] [12]. Past research in responsive environments has developed means of modulating visual and auditory stimuli in office environments [13].

At the same time, forward thinking designs of outpatient clinics has focused attention on the static placements of digital screens and medical devices in the patient-centered experience [14] [15]. While much research has focused attention on optimal environmental features (e.g., lighting, noise levels, color, optimal room layouts, etc.), not much has been investigated on how those features could change in response to changes in people's needs [3] [16] [17]. Similarly, past research has investigated flexibility strategies for inpatient medical facilities, presenting a gap in how responsive environment design approaches can improve outpatient clinic environments [2] [18]. Our work seeks to develop responsive features that enable dynamic interactions between users of outpatient clinics (e.g., medical staff and patients) and their surrounding environment. This approach will integrate clinics' emerging technologies and ultimately enable more flexibility in how spaces can serve users' needs.

2.2 Architectural Robotics

We consider responsive environments as an overall design approach. Architectural robotics, a term referring to intelligent machines at the scale of built physical environments, can be considered a cornerstone of

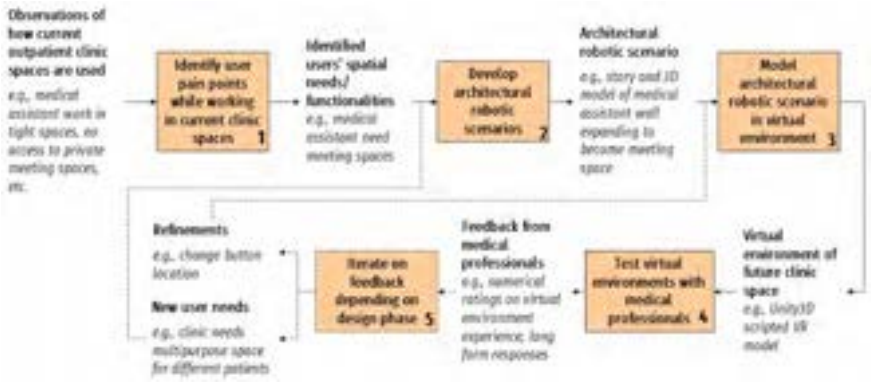

Figure 1. General process followed to identify architectural robotics use case scenarios for future outpatient clinics. Dashed lines indicate steps that lie beyond the scope of this paper to be pursued in future work.

responsive environments [12] [19] [20]. Architectural robotics, as a concept, proposes a connection between conventionally analog building features, such as interior wall partitions, and technologies typically categorized as building control systems (BCS). Two notable works serve as a point of departure for our vision in this paper. Houayek, et al. developed physical architectural robotic prototypes for novel work environments for designers in response to emerging technologies within the architectural design and office work domains [21]. In the context of healthcare, Threatt et al. envisioned an ecosystem of architectural robotics for a rehabilitation inpatient setting [22]. In contrast, our study focuses more on the needs of outpatient clinic spaces and developed architectural robotic use cases in response to emerging technologies in the healthcare domain.

It is important to emphasize that this paper concerns the role robotics can play beyond anthropomorphic (i.e., human-like) forms and outside of heavy surgery and intensive care applications in healthcare. Numerous research work has been done on how human-like robots can assist with healthcare, both as standalone assistants and arms for robotic surgery [23]. The term "architectural robotics" is used here to refer to autonomous and ubiquitous computing available for transforming the built environment [24]. Our study focuses on understanding the unique requirements of outpatient healthcare settings and how robotics at the scale of the built environment can satisfy them.

2.3 Virtual Environments

One major barrier to the implementation of architectural robotics is the cost of prototyping and mockups. While early/rapid prototyping is deemed essential for iterating on design options, designers are limited by the time and costs to produce high fidelity prototypes and mockups. Virtual reality (VR) is aptly suited for creating game-like environments for stakeholders to preview how to interact with architectural robotics in outpatient care facilities. Early virtual environment (VE) walkthroughs by medical staff can clarify their workflow requirements and point to better use cases for architectural robotics in outpatient care. Later in the design process, these virtual environments can inform specific usability and interface decisions (e.g., should a button be placed on a wall?) (Figure 1).

Notable among virtual environments research in healthcare is the study by Dunston et al., which used a cave automatic virtual environment (CAVE) set up to preview mockups of a hospital patient room [25]. Previous studies have used virtual environments for developing robotic prototypes both for healthcare and outside that domain [26] [27]. Our study utilizes virtual environments for testing architectural robotics and responsive environments, beyond the physical scale of human-like robot forms. Virtual environments afford designers the opportunity to test room-scale interactions, rather than passively previewing an architectural design.

3 Methodology

Steps taken to identify how architectural robotics could improve outpatient clinics are summarized in Figure 1. First, we set out to understand how current outpatient clinic spaces are used through firsthand observations of medical staff. These observations focused on how people interacted with the built environment (e.g., space usage patterns, sequence of navigations between spaces, etc.). Based on these observations, key workflow pain points were pinpointed using the identified patterns of interactions with existing technologies, clinic spaces, and space-to-space navigations (Figure 1, box 1). If multiple pain points all indicated a particular subset of clinic spaces, a scenario would be developed outlining how the architectural robotic transformations could resolve those pain points

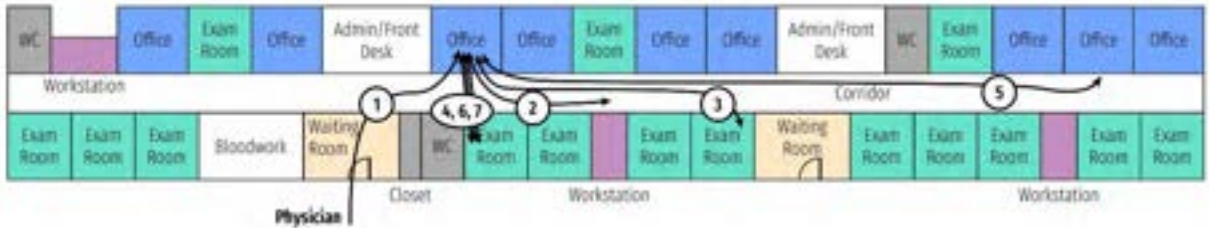

Figure 2. Navigation pattern mapping of physician in primary care clinic.

by changing a room's layout from one space type to the other (Figure 1, box 2). Two scenarios developed from this process are presented in this paper: *Scenario 1:* a physician's private office transforming into a patient exam room; and *Scenario 2:* a medical assistant work area transforming into a larger meeting space. Virtual environments demonstrating these scenarios were then built in a game engine platform, showing the transformations and user interactions needed to trigger them (Figure 1, box 3). Finally, an initial group of nine medical professionals were invited to test the scenarios in the virtual environments and provide feedback on the transformations enabled, its potential value to healthcare practices, and specific usability issues (Figure 1, box 4). This study utilizes virtual environments to test two specific architectural robotic use case scenarios in outpatient clinic spaces. Future studies will refine those designs to be more practical and usable while also identifying additional use cases, based on medical professionals' feedback (Figure 1, box 5).

Regarding the first step of observations, the research team conducted in-person observation of a primary care physician and his medical team over the course of an afternoon at an outpatient clinic. Field notes were taken recording the physician's actions and general notes about how the space was used by all medical staff. Observations focused on tracking the navigation patterns between spaces in anticipation that future spaces could minimize the time medical staff need to spend walking between spaces and improve their work efficiency. The physician's walking patterns within the outpatient clinic were recorded as shown in Figure 2 on the floor plan of the medical facility. Each line in Figure 2 shows an approximate walk path direction, labeled in the chronological order taken during the workday. Paths 3, 4, 6, and 7 show the physician walking between exam rooms to see patients. Path 2 occurred when the physician needed to check on a patient's status with a medical assistant at their workstation. Path 5 occurred when the physician's colleague needed help finding an empty office for a private meeting. These trends illustrate how the physician needs to primarily walk to exam rooms but also other areas for impromptu tasks. Field notes obtained from a different research study examining computer screen and equipment usage in an obstetrics and gynecology (OBGYN) clinic were also analyzed for identifying the patterns of how spaces were used. The walking paths of various staff (physician, physician assistant, etc.) were plotted onto the clinic floorplan (Figure 3). Similar to Figure 2, it was also observed that the physician primarily walks between exam room and office spaces as shown with red colored paths. Unlike the primary care physician, however, the OBGYN physician also occasionally sees patients in their office. Figure 3 also examined the walk path of other clinic staff. Physician assistants (Figure 3 in purple) and medical assistants (Figure 3 in blue) tended to also converge at the exam rooms, while surgical coordinators (Figure 3 in pink) remained in their office during the observed period.

These observations and navigation pattern mappings directly informed the development of architectural robotic scenarios for user testing. *Scenario 1: Office to Exam Room* was developed in response to alleviate the physician's need to walk between office and exam room, as illustrated in both Figures 2 and 3. By combining office and exam room into a single reconfigurable space, physicians can potentially save time walking. In *Scenario 1*, with a press of a button on the physician's desk, a sliding partition opens to reveal an exam table, consult desk, and display screen. The exam table reclines into a seated position and the display screen turn on automatically, providing an area for the physician to consult the patient while viewing electronic health records. Pressing the button again returns the room to the original office layout. *Scenario 2: Workstation to Meeting Space* was developed from observations in the primary care physician's clinic, where medical assistants

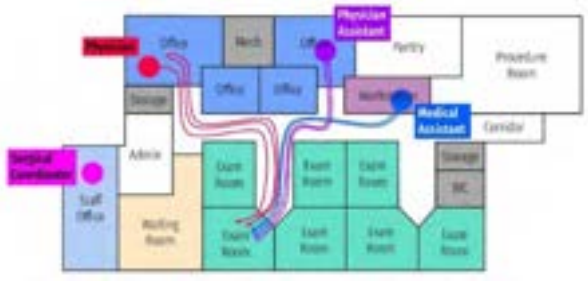

Figure 3. Navigation pattern mapping of medical staff in OBGYN clinic.

use the empty offices for privacy during lunch breaks and individual staff meetings. These pain points collectively suggested a need for medical assistants to have spaces to meet, especially given the smaller spaces given to medical assistant workstations (Figure 2). In *Scenario 2*, the medical assistant can press a button to activate a sliding partition wall, expanding their small workstation area into a larger meeting space. The expansion necessitates the adjacent office space to be compressed, requiring the office desk to fold up and chairs to be clear of the sliding partition wall before the transformation can be completed. The user is expected to press the button twice: once to begin the overall transformation, and again after confirming the office space area is clear and ready to be compressed. The same logic applies to returning the rooms to their initial layout but in reverse. Table 1 summarizes the details of these transformation sequences Both scenarios were developed from related paint points involving a pair of spaces (office/exam room, workstation/meeting space), which indicated the potential to be combined into a single reconfigurable space using architectural robotics. Scenarios were developed initially as stories defining a premise (i.e., when do medical staff need spatial transformations to occur) and a transformation sequence (e.g., "desk folds up, chair moves, etc.") (Table 1). The scenarios were then modeled in a 3D modeling software, where the exact sequence of transformations was planned to fit within spatial constraints (e.g., chairs fit through door, desk folds to provide more space, etc.). Both scenarios were modeled to occur within the same general area of a hypothetical outpatient clinic, with room sizes based on the floor plan of an existing outpatient clinic familiar to the research team. The 3D models were then imported into a game engine software, where the exact movements of the architectural robotic elements and interactions were scripted.

Nine medical professionals (8 physicians, 1 nurse informaticist), were invited to walk through the VEs demonstrating the two scenarios in individual testing sessions. During the testing sessions, participants ran the application on their own personal computer while sharing their screen to a researcher over web conference. Participants went through a training scene before the two

Table 1. Scenarios demonstrating future clinic spaces utilizing architectural robotics.

Scenario Name and Description	***Transformations***
Scenario 1: Office-to-Exam Room ***Premise:*** Participants were asked to imagine themselves as a *physician* in their private office. With all exam rooms full, the physician can transform their private office space into an exam room to consult patient. ***Transformations:*** (1) User presses button, office desk folds up. (2) Hidden partition wall slides up. (3) Exam table, consultation table, and large display screen comes out of hidden wall partition. (4) Exam table reclines upwards for patient to sit while facing display screen. (5) Display screen turns on showing health information and teleconference consult.	***Plan View*** *Initial* *Intermediate* *Final*  ***First Person Point-of-View (POV)*** *Initial* *Intermediate* *Final* 
Scenario 2: Workstation-to-Meeting Room ***Premise:*** Participants were asked to imagine themselves as a *medical assistant* at their workstation. With conference and meeting rooms all occupied, they must convert their space to a small group meeting room. ***Transformations:*** (1) User presses button, office desk folds up. (2) Office chairs move automatically towards the wall. (3) User presses button again, workstation-office wall partition moves. (4) Office chairs move automatically into place, grouped with medical assistant chairs. (5) Large display screen automatically turns on.	***Plan View*** *Initial* *Intermediate* *Final*  ***First Person Point-of-View (POV)*** *Initial* *Intermediate* *Final* 

scenarios to get acquainted with the VE interface (e.g., arrow keys for movement, how to press buttons, etc.). On screen instructions indicated possible actions to the participants while the researcher guided them through the transformations. Participants could stand, walk around, or sit in chairs to get a sense of space in as much time as they wanted before moving on to the next scenario. Afterwards, participants filled out a standard questionnaire to provide feedback on the robotic transformations, their potential value to healthcare practices, and point to possible scenarios to explore in the future. Initial findings are provided in this paper. Overall, the study focused on evaluating whether the architectural transformations met the needs of medical staff. Future studies may refine specific robotic features in each scenario, such as button interactions and self-moving furniture, to determine which are needed and practical for medical professionals to use.

4 Results and Discussion

Nine medical professionals gave feedback on the two scenarios. A majority (N=6) of the participants were primary care physicians. Two participants considered themselves specialist physicians (e.g., pulmonary medicine, etc.), one listed themselves as a nurse informaticist. Most participants (N=6) have more than 15 years of professional experience beyond medical school, while the rest had less. The questionnaire asked them to also specify the percentage of their time spent in various clinic space types (e.g., exam room, private office). An aggregated percentage of time spent by all the participants is presented in Figure 4. Participants spent a majority of their time (81%) in an exam room, private office (i.e., a room used only by the participant), or shared office (i.e., a room used by multiple people simultaneously or different times over a workweek). Only 2% of the clinic workday was spent by all participants at an auxiliary workstation like the starting space for *Scenario 2*. When asked on their experience with 3D modeling/game applications, most participants stated having some experience (N=6) while the rest stated no experience (N=3).

When asked to rate the statement "I find the transformations presented in both scenes to be a necessity, given limited space within current clinics and trends in medical practice," 55% of participants strongly or somewhat agreed (N=5), and 44% neither agreed or disagreed (N=4). When asked specific questions about each scene's transformations' potential value to healthcare practices, participants had consistent responses as seen in Figure 5. A majority of participants agreed (strongly/somewhat) the premise of *Scenario 1* (N=7) and *Scenario 2* (N=6) were commonly observed in

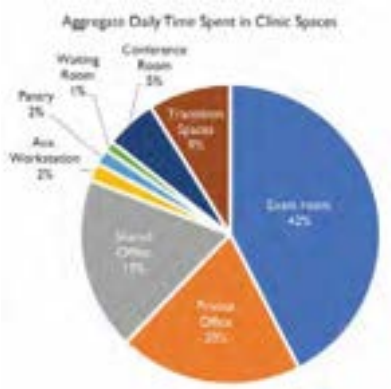

Figure 4. Percentage of time spent in clinic spaces by all VR user test participants.

their clinics. A majority (N=8) of participants agreed that *Scenario 1*'s transformations could provide a better experience for patients, but some (N=3) questioned whether the scenario would help physicians work more efficiently. Six of the respondents felt that *Scenario 2*'s transformations would help staff with finding meeting space and work together, and hence improve work efficiency (Figure 5).

Long form questions asked participants to elaborate on their ratings of overall experience and applicability to healthcare and their responses were generally positive. One participant especially liked *Scenario 1*'s concept, noting from their experience that patients tend to feel more comfortable speaking to their physician in a private office. Those who disagreed that *Scenario 1: Office to Exam Room* (N=2) would help physicians work efficiently stated concerns that the folding desk would have to be clear of items before the transformations began, and exam table surfaces would need to be sanitized after patient visit, per common health safety practices. While they noted that they see an increasing prevalence of "multiuse spaces" over private offices, some questioned the relevance of these scenarios given COVID19 and the prevalence of telemedicine. Though some participants saw *Scenario 2: Workstation to Meeting Space* as potentially helpful to nurses and medical assistants, others raised concerns regarding how the transformations could be used for natural ad hoc meetings and maintaining privacy. These responses conveyed that while participants found the general idea of space transformations valuable and applicable, they questioned the two specific scenarios presented in the virtual environments.

Overall, the virtual environment experiences spurred participants to point to other clinic use cases to consider at larger scales, such as how these transformations could assist the rest of the patient experience beyond the exam room and the entire clinic floor space. These suggestions indicate while there is a general positive interest among medical professionals in responsive environments, there

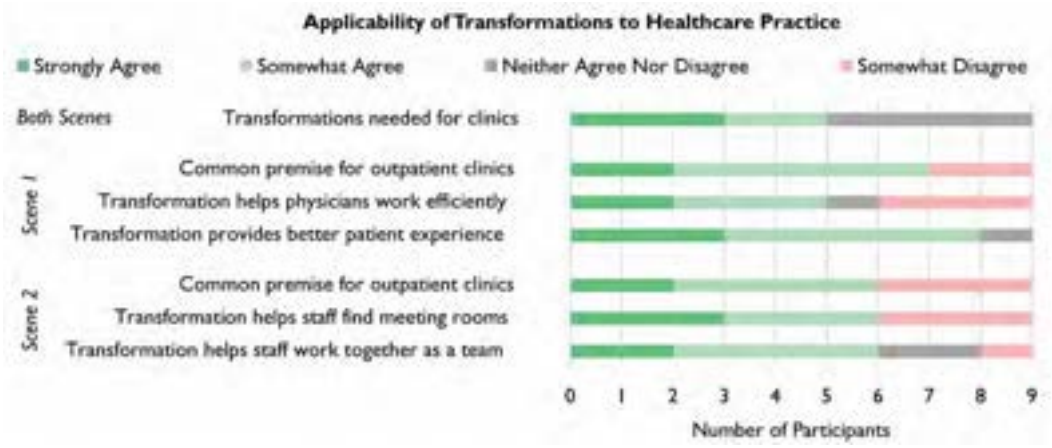

Figure 5. Participant responses on how applicable architectural robotic transformations are to healthcare.

are potentially other architectural robotic use cases that can better address the needs of outpatient medical staff. Additionally, scenarios demonstrated here are examples of explicit interaction between users and environments, where changes in layout are activated by button presses. New use cases in outpatient clinics and implicit interaction mechanisms for changing environment layouts will be developed and presented in future publications.

5 Conclusion

Responsive environments and architectural robotics have a potential to address the need for greater flexibility in medical facility spaces, especially in outpatient and ambulatory care settings. Our preliminary study showed a positive interest among medical professionals for the applicability of responsive environments and architectural robotics in medical settings. Their feedback provided specific concerns and suggestions, which prompt us to investigate other potential use cases in clinic spaces in future studies, beyond the two scenarios presented here.

References

[1] A. Kacik, "Number of outpatient facilities surges as industry values more convenient, affordable care," Dec. 2018. [Online]. Available: https://-www.modernhealthcare.com/article/20181220/NEWS/-181229992/number-of-outpatient-facilities-surges-as-industry-values-more-convenient-affordable-care

[2] U. Nanda, M. Hoelting, J. Essary, W. Fuessel, G. Park, Z. Overschmidt, M. Ossmann, and S. Starner, "Flexx: a study of flexibility in outpatient settings," Tech. Rep., 2019. [Online]. Available: https://-cadreresearch.squarespace.com/flexx

[3] G. B. Gulwadi, A. Joseph, and A. B. Keller, "Exploring the impact of the physical environment on patient outcomes in ambulatory care settings," *Health Environments Research & Design Journal*, vol. 2, no. 2, pp. 21–41, Jan. 2009. [Online]. Available: http://-journals.sagepub.com/doi/10.1177/-193758670900200203

[4] Z. Zamani and E. C. Harper, "Exploring the effects of clinical exam room design on communication, technology interaction, and satisfaction," *Health Environments Research & Design Journal*, vol. 12, no. 4, pp. 99–115, Oct. 2019. [Online]. Available: http://-journals.sagepub.com/doi/10.1177/1937586719826055

[5] C. Dinh-Le, R. Chuang, S. Chokshi, and D. Mann, "Wearable health technology and electronic health record integration: scoping review and future directions," *JMIR mHealth and uHealth*, vol. 7, no. 9, p. e12861, Sep. 2019. [Online]. Available: https://-mhealth.jmir.org/2019/9/e12861/

[6] D. M. Mann, J. Chen, R. Chunara, P. A. Testa, and O. Nov, "COVID-19 transforms health care through telemedicine: Evidence from the field," *Journal of the American Medical Informatics Association*, p. ocaa072, May 2020. [Online]. Available: https://-academic.oup.com/jamia/advance-article/doi/10.1093/-jamia/ocaa072/5824298

[7] "Telehealth index: 2019 consumer survey." [Online]. Available: https://static.americanwell.com/-app/uploads/2019/07/American-Well-Telehealth-Index-2019-Consumer-Survey-eBook2.pdf

[8] J. D. Lee, "Adaptable, kinetic, responsive, and transformable architecture : an alternative approach to sustainable design," thesis, Aug. 2012. [Online]. Available: https://repositories.lib.utexas.edu/handle/-2152/ETD-UT-2012-08-6244

[9] W. Ju, B. A. Lee, and S. R. Klemmer, "Range: exploring implicit interaction through electronic whiteboard design," in *Proceedings of the ACM 2008 conference on Computer supported cooperative work -*

CSCW '08. San Diego, CA, USA: ACM Press, 2008, p. 17. [Online]. Available: http://portal.acm.org/-citation.cfm?doid=1460563.1460569

[10] M. W. Krueger, "Responsive environments," in *Proceedings of the June 13-16, 1977, national computer conference on - AFIPS '77*. Dallas, Texas: ACM Press, 1977, p. 423. [Online]. Available: http://portal.acm.org/-citation.cfm?doid=1499402.1499476

[11] K. Eng, A. Babler, U. Bernardet, M. Blanchard, M. Costa, T. Delbruck, R. Douglas, K. Hepp, D. Klein, J. Manzolli, M. Mintz, F. Roth, U. Rutishauser, K. Wassermann, A. Whatley, A. Wittmann, R. Wyss, and P. Verschure, "Ada - intelligent space: an artificial creature for the SwissExpo.02," in *2003 IEEE International Conference on Robotics and Automation (Cat. No.03CH37422)*, vol. 3. Taipei, Taiwan: IEEE, 2003, pp. 4154–4159. [Online]. Available: http://-ieeexplore.ieee.org/document/1242236/

[12] H. Bier, T. Nacafi, and E. Zanetti, "Developing responsive environments based on design-to-robotic-production and-operation principles," in *36th International Symposium on Automation and Robotics in Construction and Mining (ISARC 2019)*, vol. 36, 2019, pp. 870–875.

[13] N. Zhao, A. Azaria, and J. A. Paradiso, "Mediated atmospheres: a multimodal mediated work environment," *Proceedings of the ACM on Interactive, Mobile, Wearable and Ubiquitous Technologies*, vol. 1, no. 2, pp. 1–23, Jun. 2017. [Online]. Available: https://-dl.acm.org/doi/10.1145/3090096

[14] "Forward, a $149 per month medical startup, aims to be the Apple Store of doctor's offices." [Online]. Available: https://social.techcrunch.com/2017/01/17/-anappleaday/

[15] "LAB100." [Online]. Available: https://-www.cactus.is/lab100

[16] R. Gunn, M. M. Davis, J. Hall, J. Heintzman, J. Muench, B. Smeds, B. F. Miller, W. L. Miller, E. Gilchrist, S. Brown Levey, J. Brown, P. Wise Romero, and D. J. Cohen, "Designing clinical space for the delivery of integrated behavioral health and primary care," *The Journal of the American Board of Family Medicine*, vol. 28, no. Supplement 1, pp. S52–S62, Sep. 2015. [Online]. Available: http://www.jabfm.org/cgi/doi/-10.3122/jabfm.2015.S1.150053

[17] D. Wingler and R. Hector, "Demonstrating the effect of the built environment on staff health-related quality of life in ambulatory care environments," *Health Environments Research & Design Journal*, vol. 8, no. 4, pp. 25–40, Jul. 2015. [Online]. Available: http://-journals.sagepub.com/doi/10.1177/1937586715573745

[18] P. Astley, S. Capolongo, M. Gola, and A. Tartaglia, "Operative and design adaptability in healthcare facilities," *TECHNE - Journal of Technology for Architecture and Environment*, pp. 162–170, Apr. 2015. [Online]. Available: https://oaj.fupress.net/-index.php/techne/article/view/4433

[19] K. E. Green, "Dispositions and Design Patterns for Architectural Robotics," in *Robotic Building*, H. Bier, Ed. Cham: Springer International Publishing, 2018, pp. 121–138. [Online]. Available: http://link.springer.com/-10.1007/978-3-319-70866-9_6

[20] K. Green, *Architectural Robotics: Ecosystems of Bits, Bytes, and Biology*, ser. The MIT Press. MIT Press, 2016. [Online]. Available: https://-books.google.com/books?id=lUGNCwAAQBAJ

[21] H. Houayek, K. E. Green, L. Gugerty, I. D. Walker, and J. Witte, "AWE: an animated work environment for working with physical and digital tools and artifacts," *Personal and Ubiquitous Computing*, vol. 18, no. 5, pp. 1227–1241, Jun. 2014. [Online]. Available: http://link.springer.com/10.1007/s00779-013-0731-6

[22] A. L. Threatt, J. Merino, K. E. Green, I. Walker, J. O. Brooks, and S. Healy, "An assistive robotic table for older and post-stroke adults: results from participatory design and evaluation activities with clinical staff," in *Proceedings of the 32nd annual ACM conference on Human factors in computing systems - CHI '14*. Toronto, Ontario, Canada: ACM Press, 2014, pp. 673–682. [Online]. Available: http://dl.acm.org/-citation.cfm?doid=2556288.2557333

[23] L. D. Riek, "Healthcare robotics," *arXiv:1704.03931 [cs]*, Apr. 2017, arXiv: 1704.03931. [Online]. Available: http://arxiv.org/abs/1704.03931

[24] K. E. Green, "Why Make the World Move?" *SPOOL*, vol. 4, no. 1, pp. 27–36, Dec. 2017. [Online]. Available: https://journals.open.tudelft.nl/spool/article/-view/1912

[25] P. S. Dunston, L. L. Arns, J. D. Mcglothlin, G. C. Lasker, and A. G. Kushner, "An immersive virtual reality mock-up for design review of hospital patient rooms," in *Collaborative Design in Virtual Environments*, X. Wang and J. J.-H. Tsai, Eds. Dordrecht: Springer Netherlands, 2011, pp. 167–176. [Online]. Available: http://link.springer.com/10.1007/978-94-007-0605-7_15

[26] J. Kim, C. Koo, and S. H. Cha, "Immersive virtual environment as a promising tool for the elderly-friendly assistive robot design," in *ISARC. Proceedings of the International Symposium on Automation and Robotics in Construction*, vol. 34. IAARC Publications, 2017.

[27] V. Weistroffer, A. Paljic, L. Callebert, and P. Fuchs, "A methodology to assess the acceptability of human-robot collaboration using virtual reality," in *Proceedings of the 19th ACM Symposium on Virtual Reality Software and Technology*, ser. VRST '13. Singapore: Association for Computing Machinery, Oct. 2013, pp. 39–48. [Online]. Available: https://doi.org/-10.1145/2503713.2503726

Toolbox Spotter: A Computer Vision System for Real World Situational Awareness in Heavy Industries

Stuart Eiffert, Alexander Wendel, Peter Colborne-Veel, Nicholas Leong, John Gardenier, and Nathan Kirchner

Presien

{stuart.eiffert, alexander.wendel, peter.colborne-veel, nicholas.leong, john.gardenier, nathan}@presien.com

Abstract -

The majority of fatalities and traumatic injuries in heavy industries involve mobile plant and vehicles, often resulting from a lapse of attention or communication. Existing approaches to hazard identification include the use of human spotters, passive reversing cameras, non-differentiating proximity sensors and tag based systems. These approaches either suffer from problems of worker attention or require the use of additional devices on all workers and obstacles. Whilst computer vision detection systems have previously been deployed in structured applications such as manufacturing and on-road vehicles, there does not yet exist a robust and portable solution for use in unstructured environments like construction that effectively communicates risks to relevant workers. To address these limitations, our solution, the Toolbox Spotter (TBS), acts to improve worker safety and reduce preventable incidents by employing an embedded robotic perception and distributed HMI alert system to augment both detection and communication of hazards in safety critical environments. In this paper we outline the TBS safety system and evaluate it's performance based on data from real world implementations, demonstrating the suitability of the Toolbox Spotter for applications in heavy industries.

Keywords -

Workplace Health and Safety; Hazard Detection; Computer Vision; Human Machine Interface (HMI)

1 Introduction

In 2018 there were 99 fatalities in the heavy industries of Transportation, Agriculture, and Construction alone in Australia, accounting for 69% of all workplace fatalities across all industries [1]. The vast majority of these (71%) were directly related to vehicle collisions and impacts with other moving machinery.

ToolBox Spotter (TBS) is an embedded robotic perception and distributed alert system for use in heavy industries that works to supplement existing safety procedures in these critical environments. It addresses both the detection of hazards that may result in a collision or injury, as well as the effective communication of these hazards to vehicle operators and nearby pedestrians. The TBS is a modular system consisting of local sensor nodes, a central processing node (CPN), and distributed alert devices. This forms an intelligent detection system and alert network for use on vehicles, mobile plant and machinery, and on infrastructure as a safety control measure.

Figure 1. *The Toolbox Spotter (TBS) hazard awareness system in use on heavy machinery at a construction site. The sensor node (highlighted in blue) is alerting the operator to the presence of the two people standing in the vehicle's blind spot.*

Existing approaches to safety include the use of a hierarchy of controls which aim to eliminate and mitigate risks where possible through the use of standard policies such as task isolation and the use of personal protective equipment (PPE). Whilst these procedures can be effective when correctly employed, it is not always practical to completely remove a risk during normal operations. Additionally, worker distractions and lapses of attention can greatly reduce the effectiveness of these approaches. Recently, proximity based collision detection devices combined with wearable RFID tags have been used in safety systems in construction [2]. However, these systems cannot always differentiate between objects when RFID tags are not worn and crucially rely on human behaviour and supervision to ensure this.

In this work we describe our solution to the problem

of safety around moving vehicles and plant in heavy industries, the ToolBox Spotter. Section 3.1 provides an overview of the components of the TBS system.

We also evaluate our proposed system in Section 5 on three diverse datasets of real world video clips, chosen to reflect current implementations of the TBS on construction sites. We outline the performance of the system as well as addressing usage of the system with consideration of its application as a human in the loop safety system.

2 Background

2.1 Safety in Heavy Industries

A comprehensive study of occupational safety in the construction industry [3] detailed that the primary conditions influencing safety performance in a workplace were not just the organisational procedures and policies in place, but the individual attitudes towards safety, including personal engagement, the taking of responsibility, and prioritisation of safety. Whilst the proper use of control procedures are critical in the elimination of avoidable risks, there will always be situations in which a degree of inherent risk is unavoidable. In these cases there is a clear need for safety controls that are not dependent on individual behaviours, such as the use of PPE.

Previous approaches to reducing vehicle collisions in heavy industry have made use of proximity sensors, including RADAR and ultrasonic based systems [4, 5]. These devices have less capability of differentiating between different types of objects, and so have been used alongside body tags, using RFID or magnetic fields [2]. Whilst these systems can work effectively to reduce the risk of collisions they again depend on individual behaviours, requiring each worker to wear the tag as additional PPE. These signals are also significantly impacted by conductive materials and can be obstructed by nearby vehicles and human bodies [6].

2.2 Computer Vision based Safety Systems

The use of computer vision object detection in safety systems is well established in areas including automotives and manufacturing, where these systems are integrated into the vehicles or fixed infrastructure [7, 8]. Similar systems have also seen recent application in mining vehicles, where they are used for both personnel and vehicle detection in less structured environments [9]. These systems have been shown to effectively detect hazards in heavy industries, but are generally used within a completely automated process, rather than forming a human in the loop system that communicates these hazards to relevant workers. Additionally, these safety systems are often built in to the hardware in which they are used, minimising their capability to be retro-fitted to existing vehicles and infrastructure or be used in a portable manner. Other applications include the use of computer vision technologies for safety management, in which the detection of workers' locations, activities and behaviours from surveillance cameras is used to inform management strategies for mitigation of future risks [10]. Whilst these approaches can help decrease incidents over a longer time period, they do not communicate immediate hazards to vehicle operators or workers.

Human in the loop safety systems require a thorough understanding of the interaction between humans and automation [11]. The system's behaviour should be intuitive to the human and not cause extra cognitive load. An example of intuitive behaviour is to only alert an operator of the presence of a distant person when the person is approaching the operator, not when the person is moving away. This example only holds for distant objects, as all close objects should result in an alert to the operator. Behaviour of a human operator will be influenced to be more positive and safe in a well-designed human in the loop safety system.

Our TBS system can communicate with human operators via haptic, visual, and audio alerts. Additionally, a halo-light can be placed on top of a vehicle to alert people approaching the vehicle to the detection of their presence. This acts to enhance 'positive communications', a procedure where a person walking behind or alongside a construction vehicle must establish that the operator is aware of their presence.

3 System Details

3.1 Overview

The TBS is composed of a network of connected devices, including a single Central Processing Node (CPN), multiple camera sensing nodes, and a Human Machine Interface (HMI) consisting of distributed AlertWear alert devices and a user interface (UI) tablet device. Each sensing node passes 2D images to the CPN where the Alert Pipeline, outlined in Figure 2, is used to determine when to send an alert to the distributed AlertWear devices. The behaviour of the Alert Pipeline is configurable by the operator using the UI device, allowing the setting of which types of hazards to be alerted to, including people, light vehicles, heavy vehicles, and demarcations such as traffic cones and bollards. Additionally, the operator is able to configure exclusion zones within each sensing node's field of view, in order to define alerts to a region of interest.

3.2 Alert Pipeline

The main components of the alert pipeline are outlined in Figure 2. Input images are first preprocessed, including

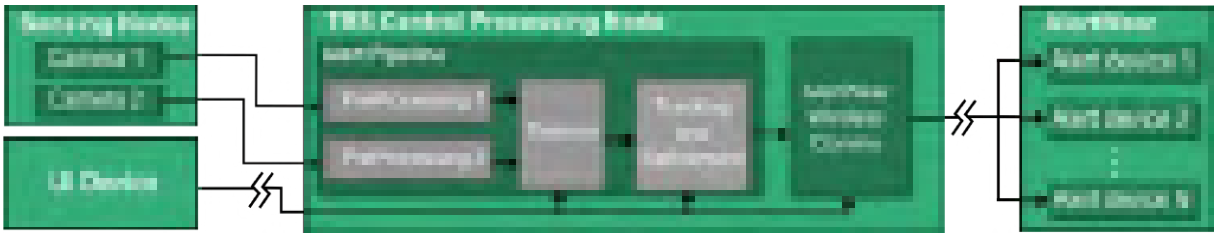

Figure 2. *Network architecture of the TBS system, illustrating communication between sensing nodes, central processing node (CPN), UI device, and distributed AlertWear devices. Alert Pipeline is detailed in Section 3.2*

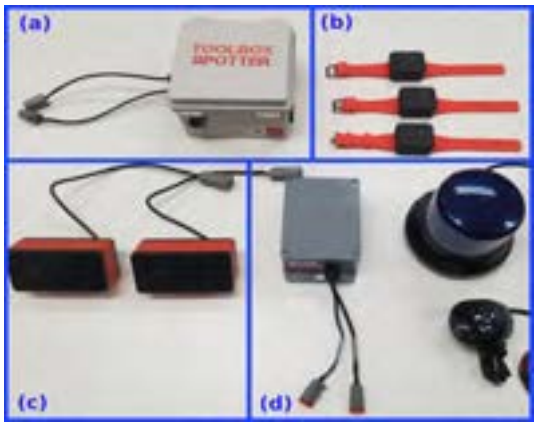

Figure 3. *The physical TBS system, showing the Central Processing Node (CPN) (a), Alertbands (b), Sensing Nodes (c) and additional AlertWear devices (d) including the Alertbeacon (top right), halo-light (bottom right) and expansion node (left) which allows connection to external devices.*

a check of image quality used to advise operators if the quality is outside operating conditions via the UI device.

Object detection in the camera frame is performed using convolutional neural networks (CNNs) [12, 13, 14], which have been pretrained as per Section 3.3. In order to minimise duplicates and false detections, improve detection localisation accuracy, smooth alerts, and to determine the final confidence of each detection, the output is further processed before alerts are communicated to the operator. Objects are tracked between frames and if an object's confidence exceeds the user defined threshold, an alert is issued to each connected AlertWear device. Tracked objects are finally filtered based on selected class types in the UI, and by region of interest, if an exclusion zone is being used (see Section 3.4).

3.3 Application Specific Training

We make use of a proprietary dataset of 15870 labelled construction specific scenes to fine-tune our models after pre-training on publicly available datasets, e.g. [15]. To evaluate detection performance, the dataset is split randomly into a train and a test set. Dataset balance and labelling quality is critical to the trained model performance. Data augmentation is performed during training, allowing the model to generalise better to new unseen data. When our system is implemented in new environments, images from the new environment are added to the train and test dataset. Semi-automatic human-in-the-loop labelling is performed using the existing model to provide labels.

3.4 HMI

AlertWear

The purpose of the AlertWear system is to communicate detected hazards and risks to all relevant workers in a clear and non-intrusive manner. This system involves a wireless mesh network (IEEE 802.15.4 std) of devices which can expand to accommodate user selected devices.

The main means of communication is an Alertband, worn by workers which vibrates to communicate various alerts. This interface was chosen based on initial pilot studies conducted of the system on a major construction company's operational sites, in which users deemed visual and audible warnings either too distracting or not noticeable enough, leading to the misuse and non-use of the system. From these studies it was found that a two second pulsed vibration was the most effective means of communicating an alert. The AlertWear system also supports visual and audible warnings through the use of the halo-light, which can be mounted on vehicle to illuminate exclusion areas, and the Alertbeacon which can provide area wide alerts, as shown in Figure 3.

Operator Interface

A UI app has been developed to allow configuration of each device, including checking sensor field of view, selection of detection classes, setting of any exclusion zone and the changing of Alert Pipeline settings. Alert Pipeline settings are input by using sliders which allow configuration of the detection and tracking thresholds. Changing these values will alter the false positive and false negative rate.

In this work we have tested three different alert modes based on different configurations of these sliders: (1) *Default*; (2) *Reactive*; and (3) *Certain*, where *Reactive* aims

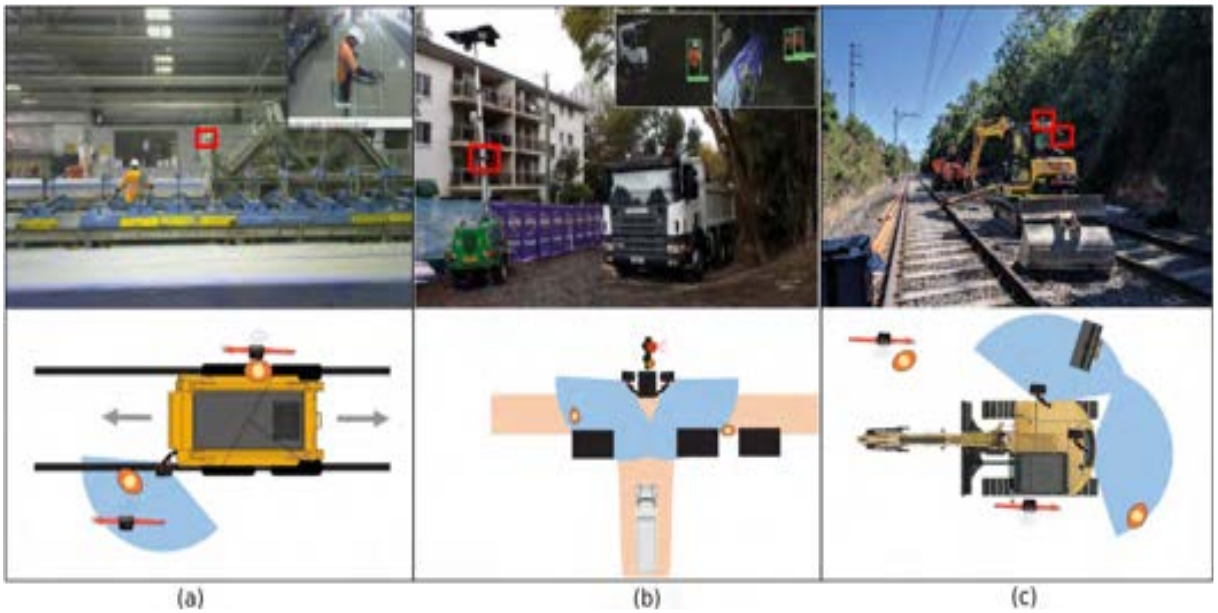

Figure 4. *Real world use cases of the TBS are shown in the top row, with the location of sensing nodes highlighted in red and camera views as inset if available. The bottom row is a top down illustration of the setup, showing the location of sensing nodes, AlertWear, and objects, as well as the field of view of each sensing node in blue, and people as orange ellipses . Example (a) demonstrates a single sensing node on a manufacturing line covering a blind spot of the mobile machinery from the operator's viewpoint. (b) shows two nodes and an Alertbeacon installed on infrastructure at intersection alerting oncoming traffic to the presence of hazards around a blind corner. (c) shows two nodes covering a rail vehicle's blind spots.*

to minimise alert delay, *Certain* minimises false positives, and *Default* aims to strike a balance between the two other modes. This UI also allows the setting of user defined exclusion zone, which can be used to limit alerts to detections that intersect with an area of interest in the camera frame. An example of an exclusion zone is shown in Figure 5 (c).

4 Empirical Evaluation

Evaluation of the overall TBS system has been conducted in order to determine performance across a variety of real world scenarios and visual variations. This evaluation has been done specifically with the class type of people, rather than other hazards and vehicles in the images for the sake of clarity and to to provide an indicative example of performance on the highest priority class.

4.1 Datasets

The TBS is currently implemented across a number of real world heavy industry sites, including construction, mining, agriculture and manufacturing. Within these implementations the TBS is being used on vehicle, on infrastructure or buildings, and within manufacturing lines.

Figure 4 provides examples from each implementation, showing both the system in use and a top down diagram of installation. The datasets used in this work have been chosen to reflect these real world use-cases, and include:

1. **Vehicle**: On vehicles in an off-road environment
2. **Indoor**: On mobile machinery for indoor use.
3. **Infra**: On infrastructure in a road environment

The Vehicle dataset contains a total of 17 clips, Indoor dataset 10 clips, and Infra dataset 7 clips. Each clip contains approximately 20 seconds of video. Example images from each dataset are shown in Figure 5. These clips cover the following range of visual variations, encountered during real world implementations of the TBS:

- Overexposure and glare
- Varying target obstruction
- Image degradation (blur and dust)
- Varying target distance
- Varying clutter in image

Additionally, a second subset of clips has been created for supplementary testing, which we refer to as 'Outlier Clips'. This subset was compiled based on a subjective measure of how difficult it was for a human labeller to initially identify the person in the clip and includes examples

Figure 5. *Example TBS viewpoint images from each of the test datasets as outlined in Section 4.1, illustrating the visual variance tested. (a) is mounted on a vehicle in an outdoor environment, (b) on moving machinery indoors, and (c) on stationary infrastructure on road. Example (c) illustrates how a user defined exclusion zone (shown in red) is displayed in the UI, as described in Section 3.4.*

that the average user would not be expected to see within a reasonable length of time.

These examples are a result of:

- The sensing node being set up without a clear view of the area of interest
- The person of interest being very heavily occluded or located very far from the sensor
- The person of interest appearing in an unexpected area of the frame
- Extreme visual aberrations including glare or usage at night

Testing on the 'Outlier Clips' subset is detailed further in Section 6. Figure 7 provides two typical examples of images from this data subset.

4.2 Metrics

Performance of the TBS system has been measured on the following metrics for all datasets:

- **Precision** - True positives over all detections
- **Recall** - True positives over ground truth occurrences
- **Alert %** - Proportion of people resulting in an alert
- **Alert Delay** - Time from first appearance to initial alert for each person

Precision and recall have both been calculated on a frame-wise basis. Alert % is calculated based on the number of completely missed alerts. For instance, a clip containing a single person walking through the scene would score 100% if an alert was sent whilst the person was in frame, or 0% otherwise. Alert Delay is calculated based on the time between a person entering the frame and the an alert being sent. Testing has been repeated for each of the three detection modes outlined in Section 3.4 determined by the system configurable parameters, including: (1) *Default*; (2) *Reactive*; and (3) *Certain*. Testing has then been repeated 5 times for each dataset.

4.3 Implementation

During testing each recorded dataset has been played by an external host computer over an ethernet network. This has been done using the ROS framework, duplicating the logged video over two separate streams to replicate usage of two sensing nodes. The output of the TBS has then been taken prior to the TBS CPN passing the alerts to the AlertWear wireless comms module. Alerts were then streamed back to the host using the same network.

Measured round trip network latency between host computer and TBS (83.0ms) has been deducted from all alert delay calculations and replaced with the measured real world sensing latency of the used cameras (67.0ms). Additionally, the time taken to send an alert over the AlertWear network has not been included in measures of alert delay. As this network uses IEEE 802.15.4 standard, we instead refer to previous testing which has shown a round-trip latency of 18ms for a 'single hop' less than 100m line of sight and 100ms for 4 hops. [16].

5 Results

Both *Default* mode and *Reactive* mode were able to correctly detect all people present in each clip, whilst *Certain* mode achieved an average accuracy of only 96.67%. The *Reactive* mode was also able to increase recall compared to *Default*, meaning that more frames containing a person were correctly identified as such. However this came at a cost to precision, meaning that false positives grew significantly. Conversely, *Certain* mode was able to increase precision at a cost to recall.

Figure 6 illustrates the distribution of delays for each tested mode across all datasets. Both *Default* and *Reactive* modes achieve significantly less delay than *Certain* mode, with peaks of 200ms compared to 1000ms. This equates to over 50% of all alerts occurring with a delay of

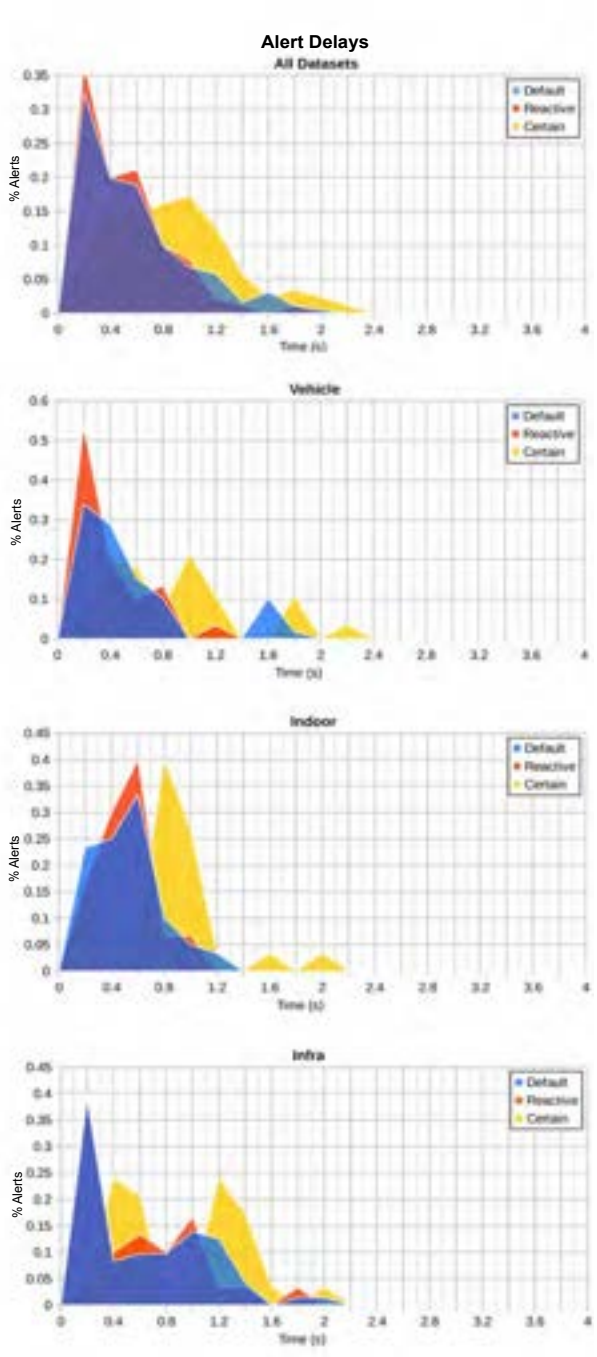

Figure 6. *Delays for each tested mode across all datasets. Delay refers to time between an object becoming present in the camera frame until the time at which an alert is passed to the TBS AlertWear. Combined result for all datasets is shown on top.*

less than 600ms for *Default* and *Reactive*, and 1000ms for *Certain*. This delayed response is due to the increased requirement that *Certain* mode has with regards to detection confidence. An alert will only be sent when the system has gained increased confidence in the likelihood that there is a person present. Whilst this does lead to slower reaction times, it also greatly reduces the number of unnecessary alerts, as reflected by the increased precision in *Certain* mode. It should be noted that the Infra dataset yielded a large number of delayed alerts for all modes. As the Infra dataset is significantly smaller than either the Vehicle or Indoor datasets (see Section 4.1), it is likely that some significantly harder clips have a greater detrimental influence on the resulting metrics. This can also be seen to a lesser extent in the Vehicle and Infra datasets in which minor second peaks occurs.

	Dataset	Mode		
		Default	*Reactive*	*Certain*
Precision	*Vehicle*	0.845	0.826	**0.891**
	Infra.	0.751	0.547	**0.863**
	Indoor	0.925	0.868	**0.955**
	AVG	0.841	0.747	**0.903**
Recall	*Vehicle*	0.771	**0.961**	0.660
	Infra.	0.829	**0.849**	0.726
	Indoor	0.872	**0.925**	0.796
	AVG	0.824	**0.912**	0.727
Alert %	*Vehicle*	**100.00%**	**100.00%**	93.33%
	Infra.	**100.00%**	**100.00%**	96.67%
	Indoor	**100.00%**	**100.00%**	**100.00%**
	AVG	**100.00%**	**100.00%**	96.67%

Table 1. *Performance of TBS on all datasets. Alert % refers to the number of correctly alerted people per clip. Both the Default and Reactive mode are able to correctly detect all occurrences. Certain mode significantly increases precision, resulting in fewer false positive alerts, at a cost of Alert %. Consideration of the cost of false alarms versus missed alerts is required in real world usage.*

5.1 Difficult Scenarios and Failure Cases

Performance on the 'Outlier Clips' set (described in Section 4.1) is shown in Table 2 and Figure 8. As expected, the performance is significantly lower than that on the three main datasets, however the system still detects the majority of occurrences in *Default* and *Reactive*, with the majority of these alerts having a delay of <1s. This performance would still be beneficial when used to augment existing safety measures, especially considering the difficulty that a human has in perceiving a detection in these examples. Additionally, these results highlight the importance of correct installation, as situations where the camera's field of view does not line up well with the actual area of interest can result in similar cases to Figure 7.

6 Discussion

The TBS was able to successfully detect and alert the user to the presence of all people in the test dataset in both *Default* and *Reactive* modes. However, there is a clear trade off between alert delay and frequency of false

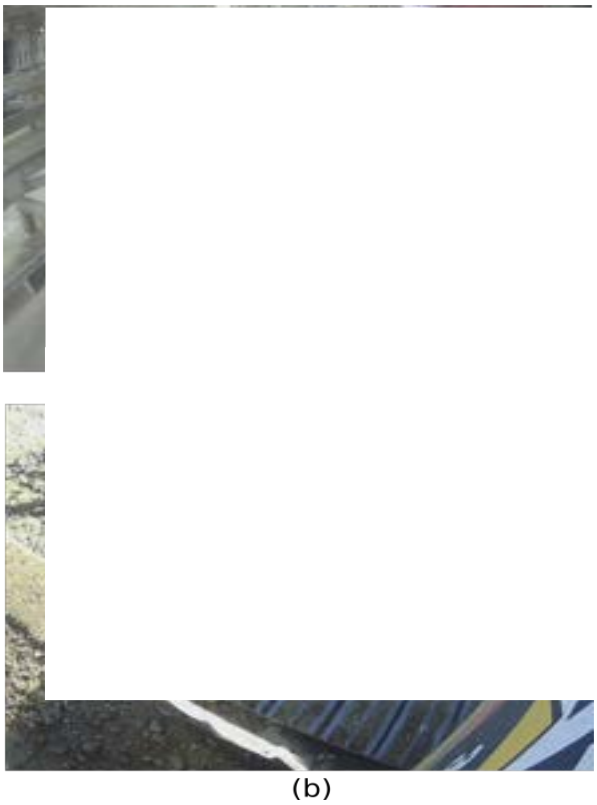

Figure 7. *Example frames from videos in 'Outlier Clips' set with the person highlighted in each frame. Both (a) and (b) are the frame selected by a human labeller as being the easiest frame in each respective clip to identify the person.*

positives that must take into account the actual usage of the system in the real world. The TBS is a human in the loop safety system that does not operate in isolation, but instead augments the existing perception of workers with regards to their ability to detect hazards in their working environment. Human reaction time to a visual stimulus in perfect conditions has been shown to be between 200-250ms [17, 18]. This time grows significantly in the presence of distractions, with the addition of just two coloured images alongside the target image of a stop sign increasing reaction time to over 550ms [19]. In the presence of tasks requiring significant mental focus, such as those carried out in all heavy industries, workers can even experience inattentional blindness, resulting in the complete missing of hazards altogether [20]. The *Alert Delays* reported in this work are comparable to those of a human applying their entire focus on the task of detecting a hazard without any distractions. The results from this work are taken from real world use cases in which the system is currently being applied, and involve cluttered and distracting environments in which human reaction time has been shown to greatly deteriorate. The TBS can achieve these results whilst not suffering from fatigue of lapses of attention.

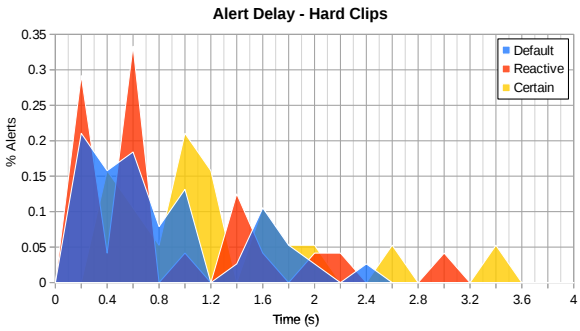

Figure 8. *Delays when testing on the 'Outlier Clips' data subset, displaying noisier alerts as expected.*

Outlier Clips	**Mode**		
	Default	*Reactive*	*Certain*
Precision	**0.915**	0.771	0.884
Recall	0.463	**0.482**	0.378
Alert %	**53.3%**	**53.3%**	46.7%

Table 2. *Performance of TBS on 'Outlier clips' (detailed in Section 4.1) which have been chosen by a human labeller as being difficult to identify any person in the video.*

An understanding of how the system is used is required when considering the importance of each metric reported in this work. Recall, a measure of how many frames were correctly classified for each person, is not as important in pratice as the metrics of alert % and delay due to how the alerts are interpreted by a human user. As each alert sent across the AlertWear network results in a two second window of notification, as described in Section 3.4, any incorrect classifications during this time are filtered out and not noticed by the user.

The results of this work additionally highlight how different modes are appropriate for different use cases. *Default* and *Reactive* both suit safety critical situations where delayed response to hazards is the crucial factor, while *Certain* would be more useful for less time pertinent uses, such as security or site access control in which false positives would want to be minimised. Whilst a number of alerts were missed in the 'Outlier Clip' set, these examples were based on videos in which a human labeller operating in perfect conditions struggled to identify the hazard, and so would likely have also been missed by a worker.

7 Conclusion

We have evaluated the performance of the TBS system for the detection of people in safety critical environments, validating its use as a tool for improving situational awareness in heavy industries. Evaluating the TBS system as

'fit for purpose' cannot be achieved by simply comparing Detection % on the test datasets to a given acceptable threshold. Instead, as the system is intended to augment a human's perception in real world use, it should be evaluated based on it's ability to improve this perception. It is clear when we compare the performance of TBS to human workers operating in similarly demanding environments, as discussed in Section 6, that the TBS provides a significant benefit with regards to the detection and communication of hazards in safety critical environments, and is able to do so without being subject to issues of fatigue and attention.

With the benchmark set in this paper, future work in testing the complete TBS will involve evaluation of additional detection classes and validation of additional sensing nodes, and will be conducted on a larger and more diverse dataset.

Acknowledgments

The authors would like to thank Laing O'Rourke and the Engineering Excellence Group for their support and contributions, as well as everyone involved at Presien, except for Jason.

References

[1] SafeWork Australia. Work-related traumatic injury fatalities report. *Online Version*, 2018.

[2] B. Jo, Y. Lee, R. Khan, J. Kim, and D. Kim. Robust construction safety system for collision accidents prevention on construction sites. *Sensors*, 2019.

[3] M. Törner and A. Pousette. Safety in construction – a comprehensive description of the characteristics of high safety standards in construction work, from the combined perspective of supervisors and experienced workers. *Journal of Safety Research*, 40(6): 399–409, 2009.

[4] V. Sabniveesu, A. Kavuri, R. Kavi, V. Kulathumani, V. Kecojevic, and A. Nimbarte. Use of wireless, ad-hoc networks for proximity warning and collision avoidance in surface mines. *Int. J. Min. Reclam. Environ*, (29):331–346, 2015.

[5] U. Lee, J. Kim, H. Cho, and K. Kang. Development of a mobile safety monitoring system for construction sites. *Autom. Constr*, (18):258–264, 2009.

[6] H. Rajagopalan and Y. Rahmat-Samii. On-body rfid tag design for human monitoring applications. In *2010 IEEE Antennas and Propagation Society International Symposium*, 2010.

[7] P. Koopman and M. Wagner. Autonomous vehicle safety: An interdisciplinary challenge. *IEEE Intelligent Transportation Systems Magazine*.

[8] Z. Liua, X. Wanga, Y. Caic, W. Xua, Q. Liua, Z. Zhoua, and D. Phamd. Dynamic risk assessment and active response strategy for industrial human-robot collaboration. *Computers and Industrial Engineering*, 141, 2020.

[9] A. Bewley and B. Upcroft. From imagenet to mining: Adapting visual object detection with minimal supervision. *Field and Service Robotics; Springer Tracts Adv Robot*, 113:501–514, 2016.

[10] A. Asadzadeha, M. Arashpour, H. Lib, T. Ngoc, A. Bab-Hadiashard, and A. Rashidi. Sensor-based safety management. *Autom. Constr*, (113), 2020.

[11] N. Kirchner and A. Alempijevic. A Robot Centric Perspective on the HRI Paradigm. *J. Hum.-Robot Interact.*, 1(2):135–157, January 2013.

[12] J. Redmon and A. Farhadi. Yolov3: An incremental improvement. *arXiv:1804.02767*, 2018.

[13] W. Liu, D. Anguelov, D. Erhan, C. Szegedy, S. Reed, C. Y. Fu, and Z. C. Berg. SSD: Single shot multibox detector. In *ECCV*, 2016.

[14] S. Ren, K. He, R. Girshick, and J. Sun. Faster R-CNN: Towards real-time object detection with region proposal networks. In *Advances in neural information processing systems*, 2015.

[15] J. Deng, W. Dong, R. Socher, L.-J. Li, K. Li, and L. Fei-Fei. ImageNet: A Large-Scale Hierarchical Image Database. In *CVPR*, 2009.

[16] *AN1138: Zigbee Mesh Network Performance*. Silicon Laboratories Inc., 4 2020. Rev. 0.2.

[17] A. Jain, R. Bansal, and K. Singh. A comparative study of visual and auditory reaction times on the basis of gender and physical activity levels of medical first year students. *International Journal of Applied and Basic Medical Research*, 5(2):124–127, 2015.

[18] E. Martinez-Martin and A. Pobil. Object detection and recognition for assistive robots: Experimentation and implementation. *IEEE Robotics Automation Magazine*, 24(3):173–183, 2017.

[19] C.J. Holahan, R.E. Culler, and B.L. Wilcox. Effects of visual distraction on reaction time in a simulated traffic environment. *The Journal of the Human Factors and Ergonomics Society*, 20:409–413, 1978.

[20] J. Chen, X. Song, and Z. Lin. Revealing the "invisible gorilla" in construction: Estimating construction safety through mental workload assessment. *Autom. Constr*, 63:173–183, 2016.

Evaluating SLAM 2D and 3D Mappings of Indoor Structures

Y.Nitta[a], D.Y.Bogale[b], Y.Kuba[c] and Z.Tian[a]

[a]Division of Architecture and Civil Engineering, Ashikaga University, JAPAN
[b]Department of Civil Engineering, Debre Berhan University, Ethiopia
[c]Division of Systems and Information Engineering, Ashikaga University, JAPAN
E-mail: yonitta@aoni.waseda.jp, derbewyenet@yahoo.com, quba.yorimasa@v90.ashitech.ac.jp, zhangtian04@gmail.com

Abstract –

This paper introduces a navigation algorithm of mobile indoor unmanned ground vehicle (UGV). The navigation methodology with AR markers is presented and demonstrated in detail. In the navigation algorithm, the mobile indoor UGV can make 2D or 3D map inside the structure. From the driving test, it has seen that the navigation algorithm with AR marker is essential to control the attitude of the UGV and drive autonomously. The proposed navigation algorithm is very important to drive UGV autonomously inside building.

Lastly, for investigating the capability of Simultaneous Localization and Mapping (SLAM) data, the 2D and 3D maps are evaluated by comparing to traditional survey and structure from motion (SfM). In conducting the map, slowing the speed of UGV affects the 2D map negatively, while it has positive impact in 3D mapping. Using visual SLAM with LiDAR makes 3D map very easily and rapidly as compared to SfM.

From these results, the proposed navigation algorithm and manufactured prototype UGV with the mapping device for 2D and 3D are useful for studying the inside buildings even in the developing countries.

Keywords –

SLAM; Visual SLAM; LiDAR; UGV; AR Marker

1 Introduction

Many research topical issues, about technologies in specific, which related to construction industry have only been discussed to some extent in the context of industrialized nations. Usually it is considered that these technologies do not matter the developing countries. This research paper addresses some of the issues about construction technologies from the perspective of developing countries in basic and industrialized countries as well. It starts with some construction and maintenance problems which usually seen as a concern of only developing countries, but also relevant to industrialized nations. It then proceeds to discuss the navigation of unmanned ground vehicle (UGV) and data collection for making 2D and 3D.

Construction problems can be discussed according to the existing situations. In general consideration some construction problems can be financial problems, lack of skilled man power, construction time delay, project management problems, human resource problems, technological problems etc.

The use of technologies has been limited only to the manufacturing industry. Recently the interest of using these technologies in construction industry growing. But this interest is limited to big companies which can afford these technology easily in any cost. Since construction industry is labor-intensive by nature, it is profitable to use technologies like robots [1]-[12].

Similar to the construction problems, there are also common maintenance problems of buildings. Some of these problems include: Lack of proper management, financial problems, lack of engineers or specialists, lack of human resource, lack of technologies etc. These problems can be defined in the same manner of construction problems. Many kinds of building maintenance has been discussed by researchers. This paper is more related to making 2D and 3D for maintenance which consists of elementary tasks (data collection, inspection, surveying, etc.) that needs brief training. So, these tasks can be held by ordinary people in the support of some technologies. Especially historical structures may not have proper design plan and it needs to collect data for preparing 2D or 3D plan.

In an effort to address the need for surveying and data collection, this paper introduces a navigation algorithm of mobile indoor UGV. The navigation methodology with AR markers is also presented and demonstrated. With the navigation algorithm, the mobile indoor UGV can make 2D or 3D map inside the structure. Lastly, for investigating the capability of SLAM data, the 2D and 3D maps will be evaluated by comparing to traditional survey and structure from motion (SfM).

2 Devices for 2D and 3D Mapping

In this research, two types of the mapping device sets shown in Figure 1 are used. Each mapping device set consists of three elements: light detection and ranging (LiDAR), IMU and the depth camera. LiDAR is used for measuring the scale of the structure component and making the map. The IMU device provides the 3-axis accelerations, roll, pith, yaw and 3D orientations form the 3-axis accelerometer, gyro and magnetometer. To use these information, the ROS package estimates the 3D pose of the depth camera and the LiDAR. The mapping device with Slamtec mapper shown in Figure 1(a) utilizes IMU inside Slamtec Mapper [13], [14]. Using URG-04LX shown in Figure 1(b) employs 9DOF Razor IMU. The depth camera is used to obtain 3D information, which are image, distance and point could data. Both devices employ the RealSense Depth Camera D435i. Properties of D435i is shown in Table 1. LiDARs used in this research are Hokuyo URG-04LX UG01 and Slamtec mapper. The characteristics of LiDARs are shown in Table 2.

For making 2D map, Simultaneous Localization and Mapping (SLAM) algorithm is utilized. Many kinds of SLAM algorithms are developed by many robotics researchers. Many of these SLAM algorithms need the wheel odometry information, which means the velocity of wheel, the motor speed and so on. Inside of the building, there are various friction and load conditions on the floor surface. So, it is difficult to implement the wheel odometry information to the SLAM algorithm. Based on this fact, SLAM algorithms which do not require wheel odometry information to conduct map are used in this research paper. For mapping device with Slamtec mapper shown in Figure 1 (a), the 2D SLAM algorithm produced by Slamtec is employed. SLAM algorithm of Slamtec mapper uses IMU information inside the device and not need the wheel odometry. For the other device with URG-04LX, the Hector slam [15], [16] is used with the 9DoF Razor IMU. For conducting map by using Hector slam, the Odometry information is not necessary.

To conduct 3D map of the point cloud data, Rtabmap [17]-[19], which is one of the visual SLAM, is employed for both devices. To make the point cloud data, Rtabmap uses the 3D pose information of the depth camera calculated by 2D SLAM using Slamtec mapper or URG-04LX. For estimating the accuracy and the usefulness, SfM using Agisoft Metashape is also used. For SfM, the photographs are taken with Cannon camera. Its properties are shown in Table 3.

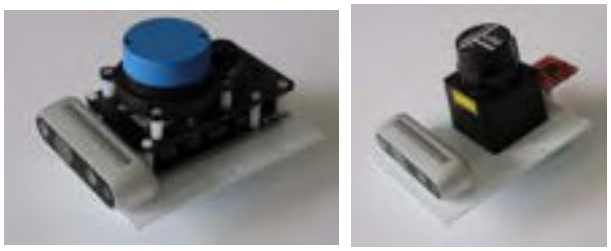

(a) With Slamtec Mapper (b) With URG-04LX

Figure 1. Mapping Devices

Table 1. Properties of Depth Camera

Left/Right Imager Type	Wide
Depth FOV HD (degrees)	H:87±3 / V:58±1 / D:95±3
Depth FOV VGA (degrees)	H:75±3 / V:62±1 / D:89±3
IR Projector	Wide
IR Projector FOV	H:90 /V:63 / D:99
Color Camera FOV	H:69±1 / V:42±1 / D:77±3
IMU	6DoF

Table 2. Characteristics of LiDARs

	Slamtec Mapper	URG-04LX-UG01
Distance Range	20m	4m
Smaple Rate	7k Hz	10Hz
Resolution	5cm	1mm
IMU	9DoF	-
Max Mapping Area	300m×300m	-
Re-localization Accuracy	< 0.02m	-

Table. 3

Image quality	Image size in pixel	ISO sensitivity
NEF(RAW) JPGE normal	6000x4000	100

3 Results of 2D and 3D Mapping

To measure and determine the scale and layout of the structural components and openings, demonstration for

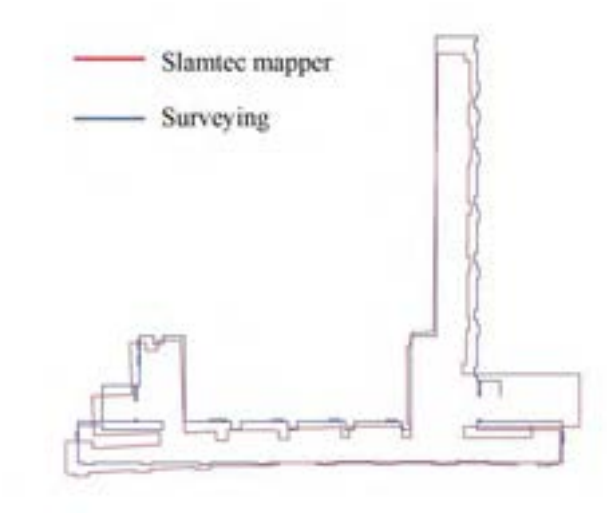

(a) Slamtec Mapper

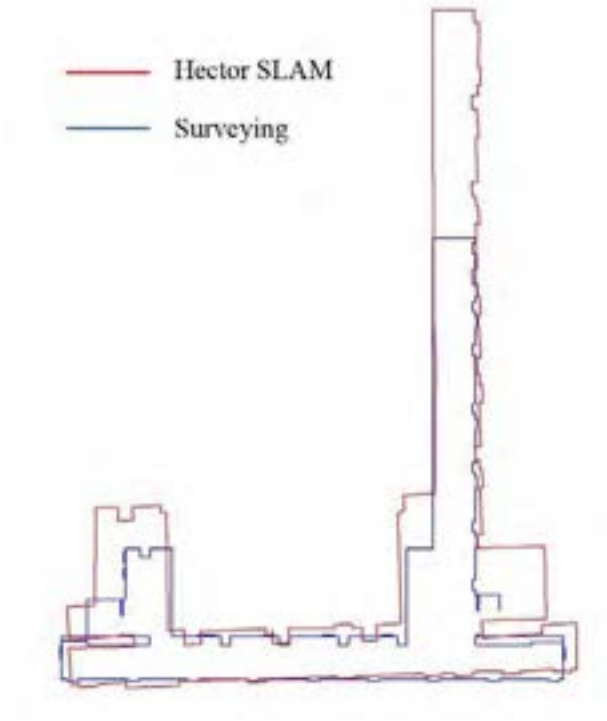

(b) Hcetor SLAM with IMU

Figure 2. 2D Mapping made by SLAM

2D and 3D mapping were carried out within the buildings of Ashikaga University. The mappings were performed in passer-free environments.

Firstly, 2D maps utilized SLAM are evaluated by comparing to traditional survey results for investigating the accuracy of the 2D mapping. The compared results for Slamtec mapper is shown in Figure 2 (a) and Hector SLAM with URG-04LX and IMU is shown Figure 2(b). Figure 3 shows the result of Slamtec mapper with different moving speeds. From Figure 3 it is clear that the

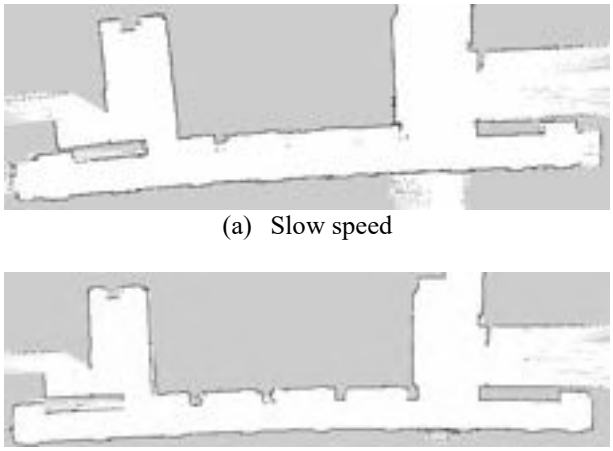

(a) Slow speed

(b) Suitable Speed

Figure 3. Slamtec Mapper with different speed

Slamtec mapper with slow speed can not specify the location and shape of columns. Throughout the experiment results, the accuracy of 2D mapping depends on moving speed of mapping device. Slow speeds are not good for creating 2D map, but 3D mapping needs slow speed. And the length of the corridor is difficult to measure, because the corridor generally has few features. From Figure 2, Slamtec mapper can estimate the length of corridor and gives more accuracy on 2D mapping compared with Hector SLAM. The length using Slamtec mapper is about 0.96 times of actual, and using Hector SLAM is about 1.51 times.

Next, 3D mappings utilized by Rtabmap, which is one of the visual SLAM, are evaluated. The 3D results of Rtabmap are shown in Figure 4. And Figure 5 shows the projection maps of Rtabmap. In Figure 5, the projection maps using Hector SLAM and using the depth camera only estimated the length of corridor in lateral direction longer than actual length. The estimated length using Slamtec mapper is almost same as actual length. From these facts, 3D mapping using SLAM data are more accurate compared with the result using the depth camera only. And scale of 3D mappings using Slamtec mapper creates more accurate than using Hector SLAM. From these results, the pose information of UGV from 2D SLAM is important in making 3D mappings. Comparing to SfM, Rtabmap makes it easy to create an entire 3D layout inside building. But, SfM can provide more detailed 3D mapping.

From these results, SLAM and visual SLAM with mapping devices easily makes 2D and 3D mapping compared with traditional methodologies.

4 Navigation Algorithm

Inside the building, the navigation algorithm can not use the GPS signal. Even it is difficult to use the navigation tool of SLAM as the layout of the building is

(a) RealSense Depth Camera D435i only

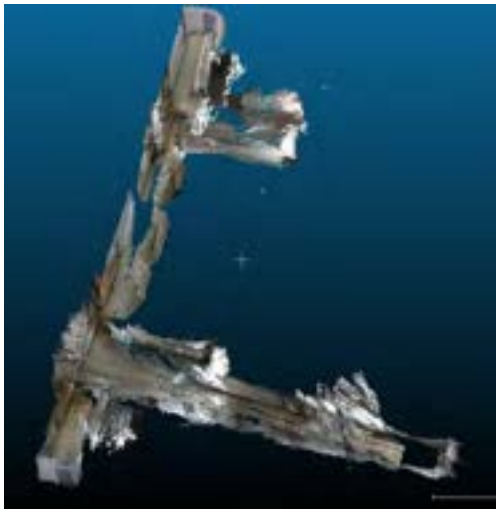

(b) D435i with Slamtec mapper

(c) D435i with Hector SLAM

Figure 4. 3D Mapping conducted by Rtabmap

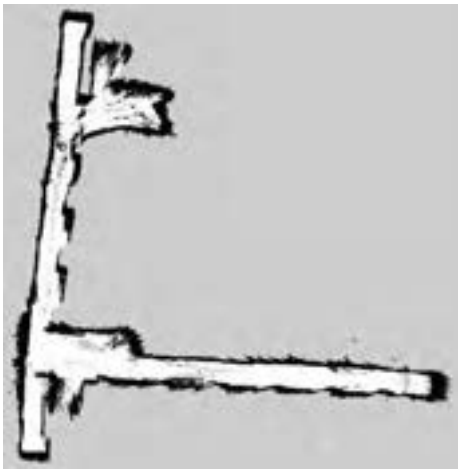

(a) RealSense Depth Camera D435i only

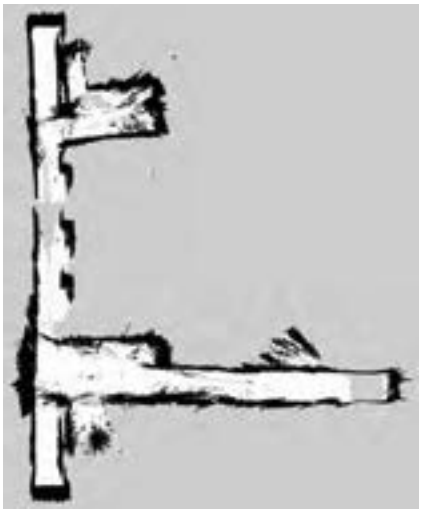

(b) D435i with Slamtec mapper

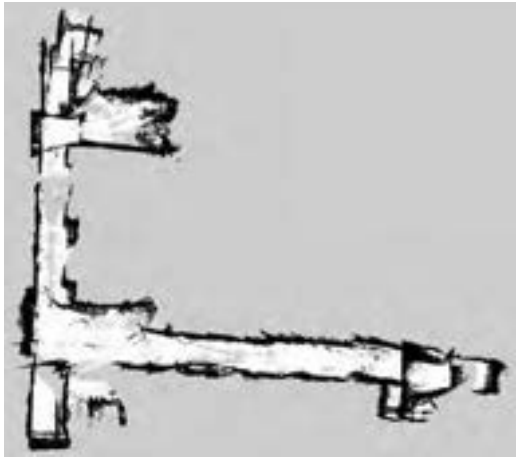

(c) D435i with Hector SLAM

Figure 5. Projection Mapping of Rtabmap

Figure 6. Result of SfM

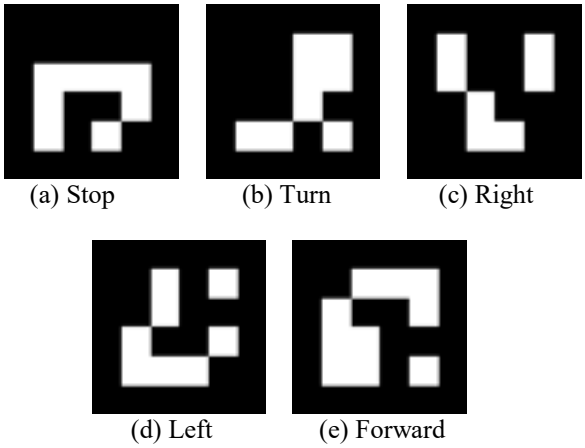

(a) Stop (b) Turn (c) Right

(d) Left (e) Forward

Figure 7. AR Marker

changing frequently. Hence, it can be understood that developing navigation algorithm without the use GPS and the navigation tool of the SLAM is needed [20]-[23]. This paper propose the navigation algorithm that utilizes AR markers on the floor. AR markers are used for two purposes. One is attitude control of UGV and the other is command to the robot, which are "turn" and "stop". The used AR markers are shown in Figure 7. The schematic figure of navigation algorithm with AR markers is shown in Figure 8. In this proposed navigation algorithm, the size of x axis coordinate and angle of AR marker in the image are important for attitude control and command. The size of AR marker in the image is measured by using Eq.(1).

$$L = 0.5 \times (x_2 - x_1 + x_3 - x_4) \quad (1)$$

in which (x_1, y_1) = coordinates of upper left corner; (x_2, y_2) = coordinates of upper right corner; (x_3, y_3) = coordinates of lower right corner; (x_4, y_4) = coordinates of lower left corner. And the x axis coordinate, x_M, and angle, y_{dif}, of AR maker is detected from Eq.(2).

$$x_M = 0.25 \times (x_1 + x_2 + x_3 + x_4) \quad (2)$$

$$y_{dif} = 0.5 \times (y_1 + y_4) - 0.5 \times (y_2 + y_3) \quad (3)$$

The need of controlling the attitude of the UGV is to keep AR marker at the middle of the camera view and parallel to the X-axis. The concept of the attitude control of UGV is shown schematically in Figure 9 and 10. When Eq.(4) is satisfied,UGV will firstly move in horizontal direction to satisfy Eq.(5). Eq.(4) indicates the range of the control.

$$L > \gamma \quad (4)$$

$$|x_c - x_M| \leq \alpha \quad (5)$$

in which x_c = center X-axis coordinate in the image; γ=threshold value of AR marker size; α = threshold value. If $x_c - x_M$ is the positive value, UGV moves to

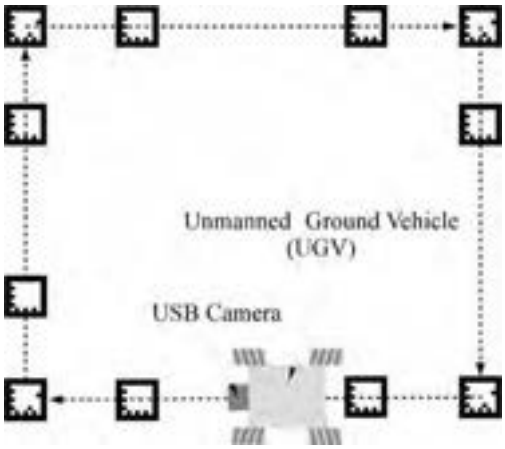

Figure 8. Navigation Algorithm using AR Marker

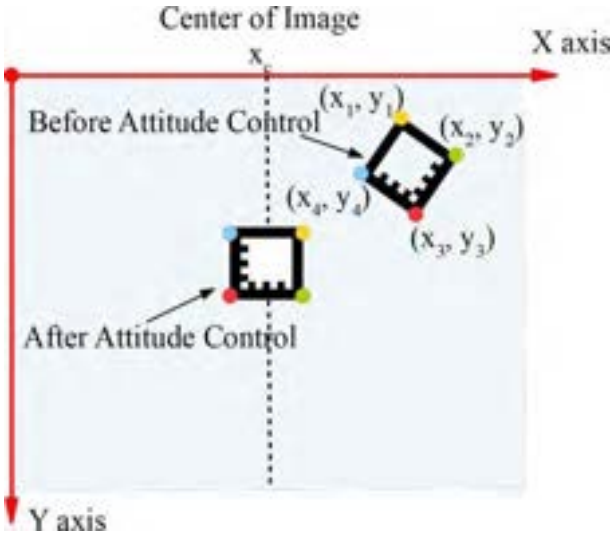

Figure 9. Schematic Figure for Attitude Control

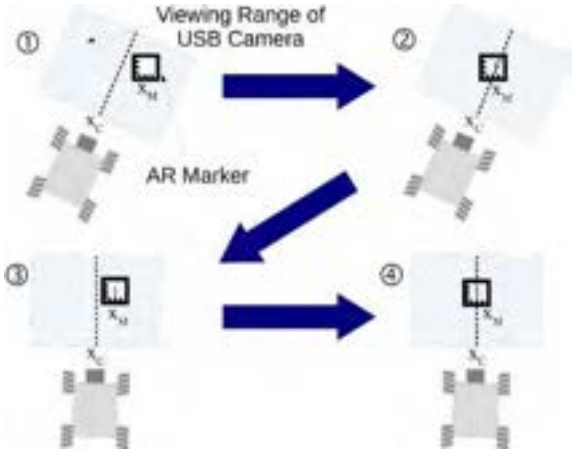

Figure 10. Attitude Control Utilizing AR Marker

the right direction. If $x_c - x_M$ is the negative value, UGV moves to the left direction. Next, when Eq.(4) is satisfied, UGV will rotates so as to satisfy Eq. (6).

$$|y_{dif}| < \beta \quad (6)$$

in which β = threshold value. If y_{dif} is the negative value, UGV turns to counter clockwise. If y_{dif} is the positive value, UGV turns to clockwise.

For command control, four different AR markers are used for ordering "Stop", "Right Turn", "Left Turn" and "Turning with 180 degrees". In this control, UGV is commanded when Eq.(4) is satisfied.

To investigate the capability of the proposed navigation algorithm, AR maker detecting tests are conducted. In Figure 11, UGV detects the AR marker and controls the attitude of UGV. After the attitude control, UGV is ordered to move "Forward". In Figure 12, AR maker commands UGV to turn the "Right".

5 Prototype of UGV for Mapping

From the results of Section 2 and 3, two prototypes of the small UGV with SLAM function is manufactured for measuring and determining the scale and layout of the inside building components. Manufactured UGVs are shown in Figure 13. The main components of the prototype UGVs are: UP board, Arduino board, the mecanum wheels, Intel Realsense camera D435i, which is depth camera and LCDpanel. UGV shown in Figure 13(a) employs the Slamtec Mapper as LiDAR and IMU device. In Figure 13(b), URG-04LX is used as LiDAR while as 9DOF Razor IMU is used for measuring the pose of the UGV. The UP board with the Intel x86 processor has the higher performance of the calculation than the Raspberry pi, which is one of the famous small Linux computers. The UP board is installed "ROS", that is useful robot OS. On the "ROS", two kinds of program

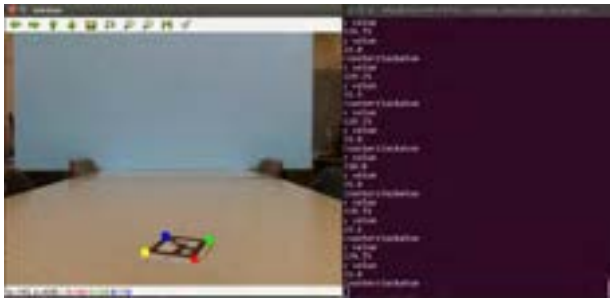

(a) Turning in attitude control

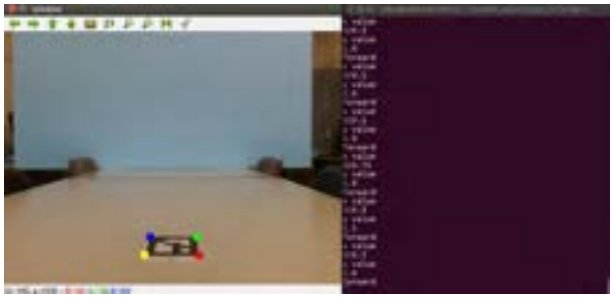

(b) Forward moving

Figure 11. Detecting AR Marker in Attitude Control

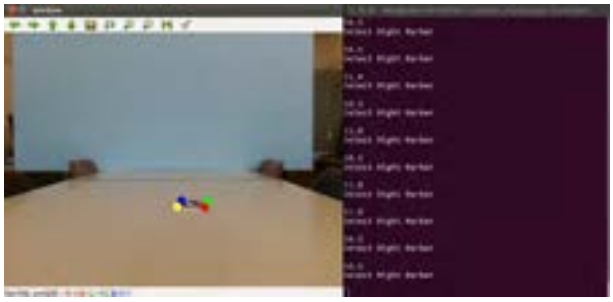

(a) Out of Range

(b) Right Turn

Figure 12. Command Control

are running. The first one is the proposed navigation algorithm to detect and follow AR markers. The second one is 2D and 3D SLAM algorithm for measuring the scale of the structure components. Arduino board controls the motors of UGV depending on the control signal from the UP board. For moving in any direction,

(a) With Slamtec Mapper (b) With URG-04LX

Figure 13. Two Prototypes of UGV for Mapping

the UGV uses the mecanum wheel. Although, mecanum wheel is better to adjust the attitude of the UGV easily for setting the measured location. The total cost of the UGV components is about $2,500, which can be reasonable for developing countries to afford.

6 Conclusion

To measure and determine the scale and layout of the inside buildings, this paper introduces a navigation algorithm of UGV and manufactures the prototypes UGV for 2D and 3D mapping.

Firstly, to evaluate the accuracy and usefulness of the 2D and 3D mapping conducted by two type of the mapping device, the 2D and 3D mapping results of the mapping devices are compared with traditional surveying and SfM. In conducting the maps, the speed of UGV has significant influence in making 2D and 3D maps. Slamtec mapper can estimate the length of corridor and create more accurate 2D and 3D maps as compared with Hector SLAM. Using Rtabmap with LiDAR is easy way to make 3D map as compared to SfM method.

Secondly, the navigation algorithm utilizing AR markers is proposed. From the demonstration tests, AR markers in the navigation algorithm are used to control the attitude of the UGV and drive autonomously. The proposed navigation algorithm is very useful to drive the UGV autonomously inside the buildings.

Finally, the prototype of UGVs with two kinds of mapping devices are manufactured for measuring and determining the scale and layout of the inside buildings. The approximate cost of the UGV components is around $2,500, which is reasonable cost for developing countries

From the discussion of the research results, it can be conclude that the proposed navigation algorithm and manufactured UGV prototype with the mapping device can be used for studying inside buildings in the developing countries as well.

Acknowledgement

This work was supported by JSPS KAKENHI Grant Number JP18K04439.

References

[1] Tsuruta T., Miura K., and Miyaguchi M., Improvement of Automated Mobile Marking Robot System Using Refectorless Three-Dimensional Measuring Instrument, *Proceedings of the 35th International Symposium on Automation and Robotics in Construction*, pages 756-763, 2019

[2] Kim P., Park J., and Cho Y.K. As-is geometric data collection and 3D visualization through the collaboration between UAV and UGV, *Proceedings of the 35th International Symposium on Automation and Robotics in Construction*, pages 544-551, 2019

[3] Oh B., Kim M., Lee C., Cho H., and Kang K.-I. 3D modeling approach of building construction based on point cloud data using LiDAR, *Proceedings of the 35th International Symposium on Automation and Robotics in Construction*, pages 906-912, 2019

[4] Jung J., Yoon S., Ju S. and Heo J. Development of kinematic 3D laser scanning system for indoor mapping and as-built BIM using constrained SLAM. *Sensors*, 15:26430-26456, 2015

[5] Chen S., Laefer D. F., Mangina E., Zolanvari S. M. I., and Byrne J. UAV bridge inspection through evaluated 3D reconstructions, *Journal of Bridge Engineering*, 24(4):05019001, 2019

[6] Phillips S. and Narasimhan S. Automating Data Collection for Robotic Bridge Inspection, *Journal of Bridge Engineering*, 24(4):04019075, 2019

[7] Cha G., Park S. and Oh T. Terrestrial LiDAR-based detection of shape deformation for maintenance of bridge structures, *Journal of construction Engineering and Management*, 145(12): 04019075, 2019

[8] Valero E., Adan A. and Bosche F. Semantic 3D reconstruction of furnished interiors using laser scanning and RFID Technology, *Journal of Computing in Civil Engineering*, 30(4):04015053, 2016

[9] Kim P., Jingdao C. and Cho Y. K. Automated point cloud registration using visual and planar features for construction environments, *Journal of Computing in Civil Engineering*, 32(2):04017076, 2018

[10] Peel H., Luo S., Cohn A.G. and Fuentes R. Localisation of a mobile robot for bridge bearing inspection, *Automation in Construction*, 94:244-256, 2018

[11] Xu L., Feng C., Kamat V. R., and Menassa C. C. An occupancy grid mapping enhanced visual SLAM for real-time locating applications in indoor GPS-denied environments, *Automation in Construction*, 104:230-245, 2019

[12] Khaloo A. and Lattanzi D. Hierarchical dense structure-from-motion reconstructions for

infrastructure condition assessment, *Journal of Computing in Civil Engineering*, 31(1):04016047, 2017
[13] SLAMTEC MAPPER On-line: https://slamtec.com /en/Lidar/Mapper, Accessed: 25/05/2020
[14] Welcome to Slamware ROS SDK, On-line: https:// Developers.slamtec.com/docs/slamware/ros-sdk-en /2.6.0_rtm/, Accessed: 25/05/2020
[15] Kohlbrecher S., Meyer J., Graber T., Petersen K., Kingauf U., and Stryk O., Hector open source modules for autonomous mapping and navigation with rescue robots, *RoboCup 2013*, pages 624-631, 2014
[16] hector_slam, On-line:http://wiki.ros.org/hector_ slam, Accessed: 25/05/2020
[17] Labbe M. and Michand F. Online global loop closure detection for large-scale multi-session graph-based SLAM. *International Conference on Intelligent Robots and Systems*, IEEE, pages 2661-2666, 2014
[18] Labbe M. and Michand F. Long-term online multi-session graph-based SPLAM with memory management, *Autonomous Robot*, 42:1133-1150, 2018
[19] Rtabmap_ros/Tutorials, On-line:http://wiki.ros.org/ Rtabmap_ros/Tutorials, Accessed: 25/05/2020
[20] Mantha B. R. K., Menassa C. C. and Kamat V. R. Robotic data collection and simulation for evaluation of building retrofit performance, *Automation in Construction*, 92:88-102, 2018
[21] Mantha B.R.K. and Garcia de Soto B. Designing a reliable fiducial marker network for autonomous indoor robot navigation, *Proceedings of the 35th International Symposium on Automation and Robotics in Construction*, pages 75-81, 2019
[22] Kayhani N., Heins A., Nahangi M., McCabe B., and Schoelig A.P. Improved tag-based indoor localization of UAVs using extended Kalman filter, *Proceedings of the 35th International Symposium on Automation and Robotics in Construction*, pages 624-631, 2019
[23] Hoskere V., Park J.-W., Yoon H. and Spencer Jr. B. F., Vision-based modal survey of civil infrastructure using unmanned aerial vehicles, *Journal of Structural Engineering*, 145(7): 04019062, 2019

A Novel Audio-Based Machine Learning Model for Automated Detection of Collision Hazards at Construction Sites

Khang Dang[a] and Tuyen Le[b]

[a]Glenn Department of Civil Engineering, College of Engineering, Computing and Applied Sciences, Clemson University, United States
[b]Glenn Department of Civil Engineering, College of Engineering, Computing and Applied Sciences, Clemson University, United States
E-mail: kdangho@g.clemson.edu, tuyenl@clemson.edu

Abstract –

Collisions between workers and operating vehicles are the leading source of fatal incidents in the construction industry. One of the most prevalent factors causing contact hazards is the decline in construction workers' auditory situational awareness due to the hearing loss and the complicated nature of construction noises. Thus, a computational technique that can augment the audible sense of a worker can significantly improve safety performance. Since construction machines often generate distinct sound patterns while operating at the construction sites, audio signal processing could be an innovative solution to achieve the goal. Unfortunately, the current body of knowledge regarding automated surveillance in construction still lacks such advanced methods. This paper presents a newly developed auditory surveillance framework using convolutional neural networks (CNNs) that can detect collision hazards by processing acoustic signals in construction sites. The study specifically has two primary contributions: (1) a new labeled dataset of normal and abnormal sound events relating to collision hazards in the construction site, and (2) a novel audio-based machine learning model for automated detection of collision hazards. The model was trained with different network architectures, and its performance was evaluated using various measures, including accuracy, recall, precision, and combined F-measure. The research is expected to help increase the auditory situational awareness of construction workers and consequently enhance construction safety.

Keywords –

Machine Learning; Sound Surveillance; Hazard Detection; Construction Safety

1 Introduction

According to the Occupational Safety and Health Administration (OSHA), the annual fatality rate in the construction industry in the United States is relatively high compared to that in other industrial sectors [1]. Most of these fatalities occurred when workers being struck by a construction vehicle. This is because the nature of construction sites often includes potential hazards during the situation that construction workers and heavy mobile equipment are in proximity [2]. The critical factor leading to collision hazard was reported as the decline in auditory situational awareness of construction workers due to the hearing loss [3] and the complicated nature of construction noises [4]. Therefore, a novel audio-based technique that can augment the audible sense of a worker needs to be developed to improve safety performance.

The use of advanced computational techniques in auditory signal processing for hazard detection is motivated by strong acoustic emissions coming from hazardous situations. Hence, it is possible to extract much useful information from sounds at job sites. For example, construction machines often produce unique sound patterns while performing certain activities [5], [6]. Moreover, the detection of acoustic events is further complicated by the heterogeneous sound types of construction equipment operations generated from diverse working environments [7], [8]. In this case, the detection tends to fall under the categorization of construction equipment-related activities. Therefore, abnormal acoustic events that can cause collision hazards are classified as mobile equipment, and normal acoustic events are identified as stationary equipment. This is especially the case when one of the most common causes of construction accidents was "struck by moving vehicles" [9]. Thus, such auditory

surveillance of potential accidents would significantly improve construction safety.

However, sound sensing in the construction field for safety has received little attention from the academic community in the past decade. A majority number of related studies were only focused on tracking various activities of construction equipment to reduce operating costs and the identification of working and operation activities [5], [6], [10], [11]. To address these existing issues, we propose a novel audio-based machine learning model for automated detection of collision hazards at construction sites. The study specifically has two primary contributions: (1) a new labeled dataset of normal and abnormal sound events relating to collision hazards in the construction site, and (2) a CNN model for automated detection of collision hazards.

The remainder of this paper is organized as follows: Section 2 surveys recent related work on the applications of auditor surveillance, and the use of CNN for the detection of abnormal events; Section 3 describes the novel audio-based machine learning model for automated detection of collision hazards; Section 4 describes the setup of an experiment in which we compare the performance of CNN across various datasets; Section 5 discusses the results of this experiment; and, finally, Section 6 summarizes the paper and proposes directions for future work.

2 Related Work

Auditory surveillance technologies in the construction industry help support the construction industry's safety performance since lack of excellent visibility was the principle factor leading to fatalities [1]. However, there is still a lack of such research in the field. Most of the sound-based surveillance technologies were only focused on monitoring construction work activities and equipment operations. For instance, a hybrid system for recognizing multiple construction equipment activities was proposed [11], and a supervised machine learning-based sound identification algorithm was implemented to enhance construction site activity monitoring and performance evaluation [12]. A few studies attempted to develop new approaches for conducting an audio-based event detection system for safety, but some limitations still existed. Experimental trials were designed to deploy sensing technology to provide alerts to proximity detection when heavy construction equipment and workers are in close proximity [2]. Nonetheless, the devices were installed on construction equipment only, not equipped on construction workers. Another approach using a machine learning algorithm can categorize sound events and make construction workers aware of possible safety risks and hazards [7]. Still, the sound data relating to collision hazard was only collected from a particular worksite. Such an approach is restrained because the sounds emitted by the equipment from various construction sites may differ. To address the gap, there is a need to investigate the surveillance approach to detect collision hazards from the perspective of construction workers using the sound collected from multiple construction sites.

Auditory surveillance has been extensively applied for the detection of abnormal events in various contexts and achieved promising results even in environments with complicated noises. For instance, some researchers developed a technique for detecting shouting events in a real-life railway environment [13]. Additionally, efforts have been made focusing on the detection of crimes in elevators [14], and the detection of human emotions based on verbal sounds during hazardous situations in public spaces [15], [16]. Other researchers also implemented signal processing for the surveillance of healthcare facilities, including a system for medical telesurvey [17], and a framework that detects older adults' falls [18].

Previous machine learning approaches to recognize and classify the auditory events typically used conventional machine learning models such as Gaussian Mixture Models (GMM) [19], [20], Hidden Markov Models (HMM) [12], [21], [22], and Support Vector Machine [11], [18], [23]. However, those techniques have been proved to underperform deep learning methods, such as Deep Neural Networks (DNN), in a variety of tasks for sound classification [24]-[26]. Recently, several studies have used a more complex architecture of DNN, such as Convolutional Neural Networks (CNN), for audio classification [27]–[30]. In sound processing, CNN can learn filters that are shifted in both time and frequency so that it can cover numerous input fields [29]. It was also found that the performance of CNN networks for signal classification is highly regulated by the optimum number of convolutional layers [28], [30]. CNN models can also be trained with a back-propagation mechanism that consists of two processes, including the pattern creation process and the testing process [31]. Motivated by these recent impressive performances in auditory surveillance, we applied CNN to the detection of hazard collisions in raw audio.

3 Novel Audio-Based Machine Learning Model for Automated Detection of Collision Hazards

Hereby, we present an innovative framework using supervised deep learning for sound detection associated with the recognition of mobile equipment. This framework is based on processing audio signals

generated at construction jobsites. The overall process, including three main steps, is illustrated in Figure 1. First, audio files are collected and labelled as abnormal and normal types. Then, acoustic features are extracted using the Fast Fourier Transform (FFT) function. Those features are the input of the CNN model, which is trained on the labelled data to detect acoustic events.

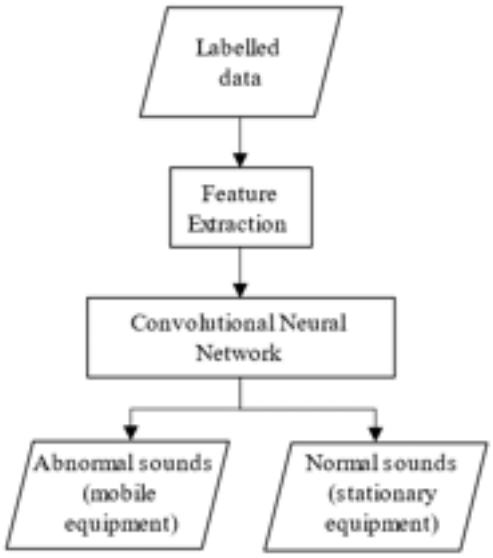

Figure 1. Overall flowchart for automated detection of collision hazards

3.1 Labelled Data

Given the goal of creating an audio event detection of collision hazards, we need to define the set of events the system should recognize. Thus, the sound sources originated from construction equipment-related activities need to be classified as a set of classes. This set of classes will allow us to collect labelled data for training and evaluation. Since the occurrence of abnormal sounds is an essential indicator of dangerous situations requiring quick safety responses, collected sound events are labelled into normal and abnormal types.

3.2 Feature Extraction

This step aims to extract the acoustic features in both time and frequency domains from audio signals by using different extraction functions. In this work, the most commonly used Mel-Frequency Cepstral Coefficients (MFCCs) are extracted by the FFT. They are mainly used to depict the spectral envelope in a significant number of audio processing applications. Through feature extraction, the components of the sound signals that are good for identifying the sound contents are recognized. In other words, the feature extraction process transforms the raw signals into feature vectors in which specific properties of audio signals are emphasized.

To obtain MFCCs from a discrete audio signal, the audio signal undergoes a pre-emphasis process, where the extraction function FFT is employed to convert the signal to the frequency domain. Then, the spectrum of the frequency domain is fed into mel-filter banks. Each filter has a center frequency called the filter bank energies. This compression operation makes the acoustic features match more closely to what humans hear. In the following step, the Discrete Cosine Transform (DCT) is applied to filter bank energies. The output coefficients of DCT are called Mel Frequency Cepstral Coefficients (MFCCs). It is worth noting that only 13 MFCC coefficients are extracted in our work, as recommended in several studies in sound classification [32]–[34]. This is because the higher MFCC coefficients represent fast changes in the filter bank energies, and it turns out that these fast changes actually degrade sound classification performance. The MFCCs extracted from the sound signal are stored as an array of values. The vertical axis represents the number of MFCCs calculated in order and the horizontal axis represents the number of frames available.

3.3 Convolutional Neural Network

After the feature extraction is completed, the CNN model is developed for sound detection with the array of the MFCC values as the input. The deep CNN architecture proposed in this study is comprised of four convolutional layers, as depicted in Figure 2, followed by a max-pooling layer, a dropout layer, a flatten layer, and two fully connected layers to get the output. The activation function used for convolutional layers and dense layers is the Rectified Linear Unit, which is most commonly used in deep learning models. The function returns zero if it receives any negative input, but for any positive value, it returns the same amount back. The Softmax activation function is applied to the output layer. The output is a prediction of which class an audio belongs to.

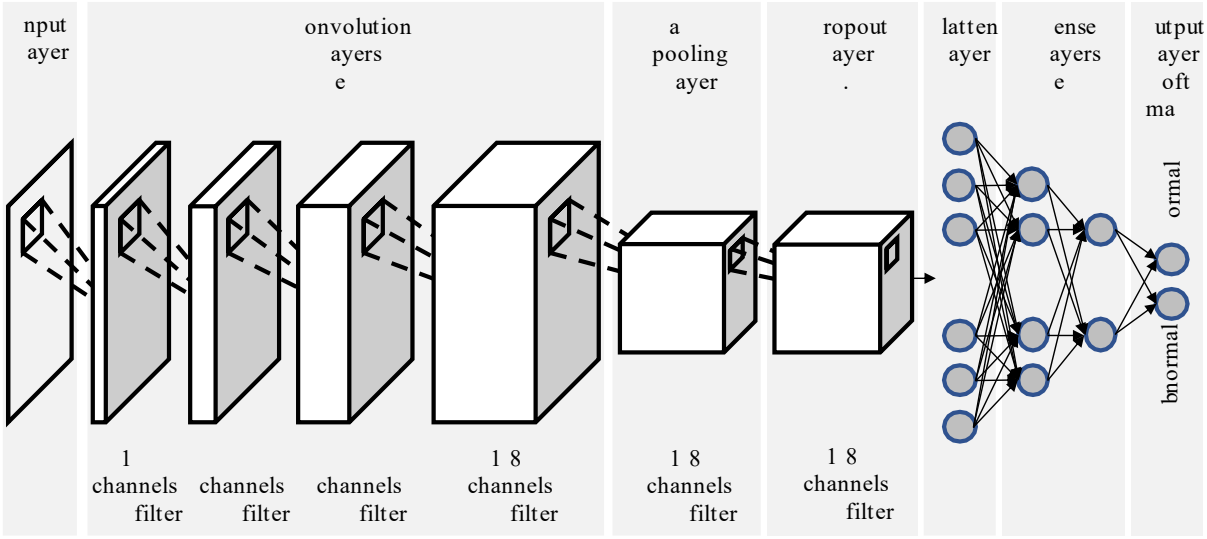

Figure 2. Detailed architecture of the convolutional neural network

The prediction is achieved through several steps in training the neural network. The first step is convolution, which is a process of taking a small matrix of numbers, called filter, then passing it over our input and transform it based on the values from the filter. Subsequent feature map values throughout convolution layers are calculated. The following steps are achieved through Max-pooling and Dropout layers. While the Max-pooling layer selects a maximum value from each region and put it in the corresponding place in the output, Dropout works by randomly setting the outgoing values to 0 at each update of the training phase to prevent overfitting. Then the shape of the data is changed from a two-dimensional matrix to a one-column vector, which is the correct format for dense layers to interpret in the last step. Each dense layer consists of neurons represented by nodes. Each node of the previous layer is connected to all nodes of the next layer. This connection is defined as a scalar value called weights. The model adjusts its weights by a training process called backpropagation. The backpropagation process can be separated into four distinct steps: the feedforward pass, the loss function, the backward pass, and the weight update. At first, the weights are randomized, and the feedforward pass is implemented. Then, the backpropagation is processed with a loss function. In this work, a loss function is represented as categorical cross-entropy, which is a great measure to distinguish two discrete probability distributions. To achieve the correct prediction, the amount of loss needs to be reduced. Therefore, the model finds out which weights most directly contributed to the network's loss and adjusts the weights so that the loss decreases. Finally, all the weights are taken and updated.

4 Experimental Setup

4.1 Datasets

Since the videos on YouTube, which is the most popular video sharing website, have become a treasure of data, the audio files of the dataset prepared for this research were extracted from this abundant source. To extract high-quality sounds from the videos, the authors avoid noisy backgrounds by using only videos that enable a broad view of recordings to ensure that no other irrelevant sound sources affect the sound quality. The audio files were then converted into wav format at 44.1 kHz sampling rate, 16-bit depth, and mono channel. An extensive set of acoustic signals in the construction site were finalized, as shown in Table 1. This dataset consists of two classes: the abnormal class includes sound excerpts from nine mobile equipment, and the normal class includes sound excerpts from seven stationary equipment. The original audio files extracted from YouTube videos were segmented into smaller frames with an equal length of 3 seconds and 2/3 overlapping. The total duration in seconds of audio files in each subset of the abnormal class, the normal class is summarized in Table 1. At this stage, the total number of the whole dataset is 3,629 audio files.

Table 1. Number of original examples in each subset of data

Abnormal class		Normal class	
Type	Total duration (s)	Type	Total duration (s)
Excavator	522	Pneumatic tamper	459

Bulldozer	387	Concrete pumper	180
Grader	1185	Pile driver	174
Front end loader	558	Pneumatic breaker	312
Forklift	123	Steel welding	1533
Compactor roller	855	Hammer	291
Scraper	2712	Saw	807
Water truck	147		
Crane	642		

The audio files were artificially mixed with background audio from two backgrounds, the wind noise, and the street noise. The mixture has the purpose of evaluating the CNN model performance to see if the model is more difficult to detect in one environment than the other. A noisy training dataset was created to enable the model the ability to detect acoustic events among noisy background. Specifically, the audio files were mi e d at different "signal-to-noise" ratios s (-15dB, -5dB, 5dB, 15dB). As a result, two different datasets with wind-noise background and street-noise background were created. Each dataset has a total number of 14,516 samples.

4.2 Model Training

The authors trained the CNN model on each dataset. 64% of the samples in each dataset were used for training, and the remaining 16% and 20% of the samples were used for validation and testing, respectively. With each dataset, the training procedure was stopped after 15 epochs when the good performance was achieved on the validation set. Various measures, specifically accuracy, recall, precision, and F1-score, are used to evaluate the sound detection performance. Accuracy is the number of correct predictions divided by the total number of predictions. While precision quantifies the number of positive class predictions that actually belong to the positive class, recall quantifies the number of positive class predictions made out of all positive examples in the dataset. F1-score is the weighted average of Precision and Recall. Therefore, this score takes both false positives and false negatives into account.

5 Results

The system correctly classified almost all audio files. The performance of the proposed CNN model on the two datasets is shown in Table 2. We found that the CNN model performed good predictions on both datasets, with "wind" and "street" backgrounds. Besides, the results show that the ability of the model to detect collision hazards is affected by different acoustic environments. As can be seen that the accuracy of the model slightly varies across the different acoustic scenarios, with 98. % and 97. 9% in the "wind" and "street" scenarios, respectively. This concludes that the model detects the abnormal sounds relating to collision hazards better in the wind-noisy background with no missed "abnormal" detection the precision of "normal" detection = 1.00).

Table 2. Measures for the performance of the proposed CNN model on each dataset

Dataset	Wind background		Street background	
Class	Ab-normal	Normal	Ab-normal	Normal
Precision	0.98	1.00	0.97	0.99
Recall	1.00	0.96	1.00	0.93
F1-score	0.99	0.98	0.98	0.96
Accuracy	98.52%		97.49%	

6 Conclusion and Future Work

In this paper, the authors applied a machine learning technique for automated detection of collision hazards. The presented framework was tested using multiple audio files collected from YouTube videos, and the results are profound. As the first stage of this research project, we found that the proposed CNN model trained on two datasets accurately recognizes sound patterns of sounds from mobile equipment.

The limitation of this research is that the model was not developed to work on more sorts of background noises provided that a construction site is considered as noisy workplace. Besides, the system could not capture the localization of mobile equipment provided that a mobile vehicle moving toward a worker is a risk and a mobile vehicle moving away the worker is considered as safety. As the plan for future research, the authors intend to develop a model that can operate across different noise backgrounds, such as rain and ocean wave sounds or the noise from people talking, and consider the factor of localizing the sound source. This work is a great start to build more realistic models that can work on detecting collision hazards under the complicated nature of construction noises.

7 Acknowledgments

This research was funded by the National Science Foundation (NSF) through the Award # 1928550. The authors gratefully acknowledge 's support. ny opinions, findings, conclusions, and recommendations expressed in this paper are those of the authors and do

not necessarily reflect the views of NSF.

References

[1] J. W. Hinze and J. Teizer, "Visibility-related fatalities related to construction equipment," a f. Sci., vol. 49, no. 5, pp. 709–718, Jun. 2011, doi: 10.1016/j.ssci.2011.01.007.

[2] E. . arks and J. Teizer, " eth od for testing proximity detection and alert technology for safe construction equipment operation," onstr. anag. Econ., vol. 31, no. 6, pp. 636–646, Jun. 2013, doi: 10.1080/01446193.2013.783705.

[3] T. C. Morata, C. L. Themann, R. F. Randolph, B. L. Verbsky, D. C. Byrne, and E. R. Reeves, "Working in noise with a hearing loss: perceptions from workers, supervisors, and hearing conservation program managers," Ear Hear., vol. 26, no. 6, pp. 529–545, Dec. 2005, doi: 10.1097/01.aud.0000188148.97046.b8.

[4] E. Vinnik, P. M. Itskov, and E. Balaban, " ndividual differences in sound-in-noise perception are related to the strength of short-latency neural responses to noise," P o ne, vol. 6, no. 2, pp. 1–8, 2011, doi: 10.1371/journal.pone.0017266.

[5] C. F. Cheng, A. Rashidi, M. A. Davenport, and D. V. nderson, " cti vity analysis of construction equipment using audio signals and support vector machines," utom. o nstr., vol. 81, pp. –253, Sep. 2017, doi: 10.1016/j.autcon.2017.06.005.

[6] C. F. Cheng, A. Rashidi, M. A. Davenport, and D. nde rson, " udio signal processing for activity recognition of construction heavy equipment," in ISARC 2016 - 33rd International Symposium on Automation and Robotics in Construction, 2016, pp. 642–650, doi: 10.22260/isarc2016/0078.

[7] Y. C. Lee, M. Shariatfar, A. Rashidi, and H. W. ee, "Evidence-driven sound detection for prenotification and identification of construction safety hazards and accidents," utom. onstr., vol. 113, p. 103127, May 2020, doi: 10.1016/j.autcon.2020.103127.

[8] Y. Xie et al., "Historical ccide nt and njury Database-Driven Audio-Based Autonomous on struction afety urv eillance."

[9] . Perlman, . ac ks, and . Barak, "Hazard recognition and risk perception in construction," Saf. Sci., vol. 64, pp. 13–21, Apr. 2014, doi: 10.1016/j.ssci.2013.11.019.

[10] C. A. Sabillon, A. Rashidi, B. Samanta, C. F. hen g, . . av enport, and . V. nderson, " productivity forecasting system for construction cyclic operations using audio signals and a Bayesian approach," in Construction Research Congress 2018: Construction Information Technology - Selected Papers from the Construction Research Congress 2018, 2018, vol. 2018-April, pp. 295–304, doi: 10.1061/9780784481264.029.

[11] h erafat, a shidi, ee , and hn, " Hybrid Kinematic-Acoustic System for Automated cti vity ete ction of o nstruction Equipment," Sensors, vol. 19, no. 19, p. 4286, Oct. 2019, doi: 10.3390/s19194286.

[12] T. Zhang, Y. C. Lee, M. Scarpiniti, and A. Uncini, " supervised machine learning-based sound identification for construction activity monitoring and performance evaluation," in o nstruction Research Congress 2018: Construction Information Technology - Selected Papers from the Construction Research Congress 2018, 2018, vol. 2018-April, pp. 358–366, doi: 10.1061/9780784481264.035.

[13] J.-L. Rouas, J. Louradour, and S. Ambellouis, " udio Events etect ion in Public Transport Vehicle," in EEE ntelligent Transportation Systems Conference, 2006, pp. 733–738, doi: 10.1109/ITSC.2006.1706829.

[14] . a dhakrishnan and . i vakaran, " y stematic acquisition of audio classes for elevator surveillance," in mage and Video Communications and Processing 2005, 2005, vol. 5685, p. 64, doi: 10.1117/12.587814.

[15] C. Clavel, I. Vasilescu, L. Devillers, and T. Ehrette, " ic tion database for emotion detection in abnormal situations," in 8th nternational Conference on Spoken Language Processing, ICSLP 2004, 2004.

[16] C. Clavel, I. Vasilescu, L. Devillers, G. Richard, and T. Ehrette, " ear -type emotion recognition for future audio-based surveillance systems," p eech Commun., vol. 50, no. 6, pp. 487–503, Jun. 2008, doi: 10.1016/j.specom.2008.03.012.

[17] M. Vacher, D. Istrate, L. Besacier, J.-F. Serignat, E. a stelli, and . Besacier, " ound etect ion and l assification for e dical Telesurvey," .

[18] S. M. Adnan, A. Irtaza, S. Aziz, M. O. Ullah, A. Javed, and . T. ahmood, " al l detection through acoustic ocal Ternary Patterns," ppl. Acoust., vol. 140, pp. 296–300, Nov. 2018, doi: 10.1016/j.apacoust.2018.06.013.

[19] W. hoi, J. ho, . K. Han, and H. Ko, " elective background adaptation based abnormal acoustic event recognition for audio surveillance," in Proceedings - 2012 IEEE 9th International Conference on Advanced Video and Signal-Based Surveillance, AVSS 2012, 2012, pp. 118–123, doi: 10.1109/AVSS.2012.65.

[20] Y. Lee, D. K. Han, and H. Ko, " c oustic signal

based abnormal event detection in indoor environment using multiclass adaboost," EEE Trans. Consum. Electron., vol. 59, no. 3, pp. 615–622, 2013, doi: 10.1109/TCE.2013.6626247.

[21] " n abnormal sound detection and classification system for surveillance applications - IEEE onfere nce Publication." [n line]. vailable: https://ieeexplore.ieee.org/document/7096526. [Accessed: 19-Nov-2019].

[22] . V. ott on and . P. W. Ellis, " pectr al vs. spectro-temporal features for acoustic event detection," in EEE Workshop on pplic ations of Signal Processing to Audio and Acoustics, 2011, pp. 69–72, doi: 10.1109/ASPAA.2011.6082331.

[23] Y. ls ouda, . Pllana, and . Kurti, " a chine Learning Driven IoT Solution for Noise Classification in Smart Cities," arXiv Prepr. arXiv1809.00238, Sep. 2018.

[24] M. Asgari, I. Shafran, and A. Bayestehtashk, " nferring social conte ts from audio recordings using deep neural networks," in EEE nternational Workshop on Machine Learning for Signal Processing, MLSP, 2014, doi: 10.1109/MLSP.2014.6958853.

[25] M. Ravanelli, B. Elizalde, K. Ni, and G. Friedland, " udio concept classification with Hierarchical eep eural et works," in European ig nal Processing Conference, 2014.

[26] O. Gencoglu, T. Virtanen, and H. Huttunen, " ecognition of acoustic events using deep neural networks," in European ig nal Processing Conference, 2014.

[27] J. ala mon and J. P. Bello, " eep onvolutional Neural Networks and Data Augmentation for Environmental ound l assification," EEE ig nal Process. Lett., vol. 24, no. 3, pp. 279–283, Mar. 2017, doi: 10.1109/LSP.2017.2657381.

[28] K. J. Piczak, "Environmental sound classification with convolutional neural networks," in 1 IEEE 25th International Workshop on Machine Learning for Signal Processing (MLSP), 2015, vol. 2015-Novem, pp. 1–6, doi: 10.1109/MLSP.2015.7324337.

[29] A. Salekin, S. Ghaffarzadegan, Z. Feng, and J. tanko vic, " e al-Time Audio Monitoring Framework with Limited Data for Constrained ev ices," 19, pp. 98–105, doi: 10.1109/dcoss.2019.00036.

[30] J. Salamon, J. P. Bello, A. Farnsworth, and S. Kelling, " u sing shallow and deep learning for bioacoustic bird species classification," in P , IEEE International Conference on Acoustics, Speech and Signal Processing - Proceedings, 2017, pp. 141–145, doi: 10.1109/ICASSP.2017.7952134.

[31] . Glowacz, " cousti c based fault diagnosis of three-phase induction motor," ppl. c oust., vol. 137, pp. 82–89, Aug. 2018, doi: 10.1016/j.apacoust.2018.03.010.

[32] B. Kim and B. Pardo, " human-in-the-loop system for sound event detection and annotation," ACM Trans. Interact. Intell. Syst., vol. 8, no. 2, Jul. 2018, doi: 10.1145/3214366.

[33] Z. H. Janjua, M. Vecchio, M. Antonini, and F. n tonelli, " E E: n intelligent rare-event detection system using unsupervised learning on the oT edge," Eng. Appl. Artif. Intell., vol. 84, pp. 41–50, Sep. 2019, doi: 10.1016/j.engappai.2019.05.011.

[34] D. Carmel, A. Yeshurun, and Y. Moshe, " etec tion of alarm sounds in noisy environments," in Signal Processing Conference (EUSIPCO), 2017 25th European, 2017, vol. 2017-Janua, pp. 1839–1843, doi: 10.23919/EUSIPCO.2017.8081527.

Training of YOLO Neural Network for the Detection of Fire Emergency Assets

A. Corneli[a*], B. Naticchia[a], M. Vaccarini[a], F. Bosché[b] and A. Carbonari[a]

[a]Polytechnic University of Marche, DICEA, Ancona, Italy
[b]Institute for Infrastructure and Environment, University of Edinburgh, Edinburgh, UK

a.corneli@staff.univpm.it, b.naticchia@univpm.it, m.vaccarini@staff.univpm.it, f.bosche@ed.ac.uk,a.carbonari@staff.univpm.it.

Abstract -

Building assets surveys are cost and time demanding and the majority of current methods still rely on manual procedures. New technologies could be used to support this task. The exploitation of Artificial Intelligence (AI) for the automatic interpretation of data is spreading throughout various application fields. However, a challenge with AI is the very large number of training images required for robustly detect and classify each object class.

This paper details the procedure and parameters used for the training of a custom YOLO neural network for the recognition of fire emergency assets.

The minimum number of pictures for obtaining good recognition performances and the image augmentation process have been investigated. In the end, it was found that fire extinguishers and emergency signs are reasonably detected and their position inside the pictures accurately evaluated.

The use case proposed in this paper for the use of custom YOLO is the retrieval of as-is information for existing buildings. The trained neural networks are part of a system that makes use of Augmented Reality devices for capturing pictures and for visualizing the results directly on site.

Keywords -

YOLO; Neural Network; Asset inventory

1 Introduction

Facility Management (FM) is the most costly phase of the building lifecycle, accounting for up to 80/90% of total costs [1]. For this reason, improving efficiency of FM processes can lead to significant savings. To establish an asset management system, component inventory has first to be conducted [2][3]. But, this process still relies on manual procedures that make it time-consuming, expensive and prone to errors and omissions. Construction industry is increasingly moving through digitization, consequently is growing the awareness about the value of integration of new technologies such as AI, in process automation. Component inventory is an area that could certainly benefit from this. The automatic acquisition of geometric and semantic data of built assets has been pursued, principally through point cloud collecting technologies, photogrammetry and image processing. But computer vision, especially object detection using artificial intelligence (AI) has seen limited exploitation in that field, despite being aggressively pursued in others engineering fields: from autonomous driving to automated fruit picking. AI systems, and more specifically Deep Learning frameworks, generally require large datasets for training [4][5]. A challenge about this is that it is never obvious what the minimum number of pictures is for developing a well-performing neural network. You Only Look Once (YOLO) networks [6][7][8] are state-of-the-art real-time object detection and classification systems, demonstrating to be fast and accurate. The aim of this research is to investigate and detail the training process for customized YOLO Convolutional Neural Networks (CNNs).

This first development of a customized NN is part of an on-site application project which allows to automate surveys using mixed reality. NNs are exploited for automation of object detection while localization is performed by means of sensors and algorithms embedded in the augmented reality device. On site collected data can be immediately verified through the use MR device that shows information overlapped to real world and the possibility of adding semantic data directly on site avoiding long post processes phases.

2 Scientific Background

There is an increasing need to have structured and semantically enriched "as-is" 3D digital models of buildings in order to handle, more efficiently, maintenance, restoration, conservation or modification. Especially, as far as existing buildings are concerned, it is necessary to develop an efficient approach to generate a semantically enriched digital model. Various digital tools for building capture and auditing are available, such as 2D/3D geometrical drawings, tachometry, laser scanning or photogrammetry, but they need increased modelling and planning efforts of skilful personnel. Approaches that

process point clouds are beginning to appear for the semi-automatic identification of objects [3][9].
There are also systems like the one by [10] that exploit images rather than point clouds. However, these methods consist of complex processing operations that not only require long processing time and therefore high costs, but they are also pursued not on site with major difficulties in comparing collected data and real conditions. This leads to an error prone process and difficulties in the interpretation of gathered data.
Machine learning techniques have been widely applied in a variety of areas such as pattern recognition, natural language processing and computational learning [11]. Particularly, the field of image recognition, and object detection especially, has seen an increase in development in the recent years. In the automotive industry, for example, the use of deep learning algorithms has allowed self-driving cars to recognize lanes and obstacles without the need for more expensive and complex tools [12]. Object detection is a problem of importance in computer vision. Similarly to image classification tasks, deeper networks have shown better performance in detection. At present, the accuracy of these techniques is excellent. Hence, they are used in many, diverse applications, touching all engineering fields [13]. [14] studied an application of machine learning for the construction industry to categorize images of building designs. [15] proposed a similar approach towards the recognition of 3D BIM environments. [16] used NN for the automatic recognition of house spaces. Some interesting applications of ML regard diagnostic issues such as in [17] where semantic segmentation networks are used to recognize wall cracks on both stone and plastered walls. [18] proposed a system for the automatic detection of formworks in construction site images acquired with a Unmanned Aerial Vehicle (UAV).
Despite their huge potential NNs have not been wholly exploited in the AECO sector, partly due to the challenge of developing specific domain labelled datasets. In this paper the use of YOLO CNN for is considered along with the creation of a dataset for fire protection system components. In particular, an investigation is reported on the sufficient number of images for YOLO customization. Two objects classes have been implemented: fire extinguishers and emergency signs. This research work starts from the retrieval of specific images for the creation of multiple datasets with different number of pictures, then the setup of the whole training system has been specified. Finally, the trainings results are exposed and commented.

3 Methods

3.1 Training environment settings

In order to train the network, it is necessary to have a training environment. Since this project involves the use of YOLO neural network it has been decided to use the training platform advised by the developer of the network itself: Darknet-19 [13]. Darknet is an open source neural network framework written in C and CUDA. It supports CPU and GPU computation [8]. In order to install Darknet it is necessary to set the proper environment. The following ones are all the necessary requirements [7][19]:

- Windows or Linux;
- CMake >= 3.8 for modern CUDA support;
- CUDA;
- OpenCV >= 2.4;
- cuDNN >= 7.0;
- GPU with CC >= 3.0;
- on Linux GCC or Clang, on Windows MSVC 2015/2017/2019.

The development system is Visual Studio installed with its default options. The dependencies are CUDA, cuDNN and OpenCV. Starting from CUDA, the version installed is the 9.1. This installation requires also the installation of the NVIDIA Graphics Drivers if not yet on the pc. The second installation to be done is cuDNN version 7.0. Finally, it follows the installation of OpenCV 3.4.0. After having done all these installations, Darknet needs to be compiled with the following procedure:

1. Start Microsoft Visual Studio
2. Open the darknet.sln
3. set x64 and Release
4. Include cudnn.lib in your Visual Studio project
5. Build > Build darknet.

At this moment the darknet.exe is generated inside the folder. Finally, darknet needs to be prepared for using OpenCV, CUDA and cuDNN. The bin file has to be placed in the same folder of darknet.exe. Bin and include folders have to be inserted also in CUDA folder if they are not already there. Finally, a new Windows variable cudnn has to be created.

3.2 Dataset creation

The dataset to train the network to recognize a specific object must have specific features. Shape of the object, lighting conditions and varying viewpoints are aspects to take into consideration when gathering the images. According to the COCO dataset approach, choosing images with the object in context improves the recognition of it in real scenarios [20]. The presence of multiple objects in the same pictures is another parameter that improves the

performance of the network. For this reason, pictures with the objects in their common context have been preferred in this research.
The network capability of recognizing the object at first sight and with a high level of confidence depends, among other factors, upon the quantity of pictures in the dataset, although a minimum number is not suggested in the literature.
Collecting original images is always a time consuming task. Pictures can be gathered using various methods, including:

1. crowdsourcing;
2. web scraping.

Generally speaking, crowdsourcing regards all the possible processes to obtain information or input into a particular task or project by enlisting the services of a large number of people, either paid or unpaid, typically via the Internet. Unlike datasets shot in controlled environments crowdsourcing brings in diversity which is essential for generalization [21]. In this case, the task was not conducted using internet sources, but was spread among people in the department and acquaintances outside the university. In the case of web scraping three popular sites have been exploited: 1. Google; 2. Flickr (already used in other research like [22]); 3. Instagram. In this research, the three sources were exploited. Using keywords, images were manually searched and downloaded from Flickr and Instagram. For Google, a python script has been used for web scraping images through keywords as well [23]. To further increase the size of the dataset at low cost, a common technique consists in the usage of both original pictures, from real buildings in this case, and graphically reedited photos; a process called Data Augmentation. Data augmentation introduces additional variety during training, producing robustness in the model to various inputs. The percentage of original images and modified images has been studied in order to obtain a trained network with good performances [24]. In this work the augmentation involves the modification of pictures with the help of a custom MatLab script, to automatically modify the photos, choosing what transformations must be performed, the starting dataset and the number of images to be created. The custom script applies the following transformations: resize, shifting, additive noise, rotate, zoom, crop. The creation of the dataset involves also labelling all the images. Creating the label involves both the design of the bounding box around the object to recognize and attaching the correct label to it. This operation is performed in this thesis using VoTT, a tool that supports the manual drawing of the bounding box [25]. This tool gives the possibility to choose the right output format according to the kind of network chosen. The output for the YOLO network is a .txt file, with the coordinates of the boxes and the label attached to them. The final task to complete the dataset is the definition of the training and testing sets of images. We allocate 80% of the images to training, and 20% to testing. Anyway in this study the same testing dataset has been used so as to can better compare the data. Specifications about the testing process can be find in Section 5.

3.3 Training process settings

After having created the dataset there are some files to set before starting the training: the .cfg file of the network chosen; the .data file; the .names file; the .weights file. The parameters to customize in the cfg file are: batch = 64, this means we will be using 64 images for every training step; subdivision = 8, the batch will be divided by 8 to decrease GPU VRAM requirements. If one has a powerful GPU with loads of VRAM, this number can be decreased, or batch could be increased. The other parameters to change are classes = 1, the number of categories we want to detect; filters = (classes + 5)*5 [19][26].
The .data contains all the paths to the other necessary files for the training process. The .names file is the file that contains the name of the tag inside the images of the dataset.
The weights have to been chosen according to the network that one wants to train. Choosing the weight file means that the network used is a pre-trained network with a general dataset (CoCo, PascalVoc or others). It would be possible also not to choose any weights file and in that case the network will be trained from scratch and it will not profit from transfer learning, which is valuable particularly for low level feature learning.
The output of the training process is:

- the chart with the Mean Average Precision (mAP) progress and the Aerage loss progress;
- the log file with all the operations executed to train the network. It contains the report of all the epoch, with the avg and mAP values;
- the backup folder which contains the weights of the trained network saved at predefined stages.

The question "when the average loss is low enough?" does not find its answer in existing literature. As a rule of thumb, according to what is stated in other customizing network processes, when the first decimal digit reaches 0 it is low enough (e.g. 0.02).

3.4 Validation metrics

To compute the mAP, the Precision and Recall are required. Precision is the ratio of correctly predicted positive observations to the total predicted positive observations. Recall is the ratio of correctly predicted

positive observations to all the observations in actual class. (Equation 2) [27][28][29][30][22].

$$Precision = TP/(TP + FP) \quad (1)$$

$$Recall = TP/(TP + FN) \quad (2)$$

Figure 1. From left to right: emergency sign door, emergency sign man, emergency sign.

True Positives (TP) and False Positives (FP) are the number of objects correctly and incorrectly predicted, respectively, as the object of interest. Similarly, True Negatives (TN) and False Negatives (FN) are the number of objects correctly and incorrectly recognized as background. Because the precision and recall rates cannot be reported for scenes without any actual positives, the images taken into consideration contain at least one instance of the objects of interest [28].
For each class, a Precision/Recall curve is obtained by varying the threshold parameter from 0 to 1. The average precision is defined as the area under the curve. The mAP is computed by averaging the AP value for all classes. This process is applied to obtain the AP for each class [24]. Besides the calculation of Precision and Recall also the F1 parameter has been measured. This metrics is frequently used in pattern recognition performance assessment [30]. F1-measure is a measure that combines Precision and Recall, using a sort of weighted average (Equation 3).

$$F1 = 2 * ((Precision * Recall)/(Precision + Recall)) \quad (3)$$

4 YOLO trainings

Training a customized neural network starts from the creation of the dataset which has been achieved through the method explain in 3.2. In this research two objects have been introduced into the datasets: fire extinguisher and emergency signal. Among the pictures referring to emergency signals there was a distinction between different types 1: Emergency sign; Emergency sign door and Emergency sign man. In 1 the original pictures have been reported.

The network chosen for the training sessions has been the tiny YOLOv2. This choice depends upon the further uses of the customized network, which has to be compatible with other components. The chosen network came from a training with CoCo dataset and thus pre-trained weights have been used. In 2 all the training sessions for fire extinguisher category have been detailed. In this table, TRAINING 2 uses the same dataset as TRAINING 1 but a network that is not pre-trained. 3 reports the list of all the training session for emergency signs.
Finally, a training (TRAINING 17) with a combined dataset has been done using 500 original pictures of fire extinguishers and 581 images of emergency signs. In this case, the mAP = 71,98%.

5 Testing the networks

The testing process of all the trainings has been pursued through the calculation of the metrics exposed in 3.4. This process has been done using the same test dataset, composed by 100 original pictures, so as to make the tests comparable. 2 shows the output of the tests and the evaluation about the result for the calculation of precision and recall. The third column shows the confidence score for every single object detected marked by its bounding box. At test time YOLO defines the confidence score as P(object) * (intersection/union) between the predicted box and the ground truth which provides class-specific confidence scores for each box. These The confidence score threshold for the testing process has been set equal to 60%.
Since the trainings produced a new weights file every 1000 iterations for every test it has been selected the weights closer to the number of iteration that had obtained the higher mAP. The test has been performed for the most relevant networks as shown in 4.
On the other hand, Figure 4 displays the values of precision, recall and F1 in a graph. Following these calculations it is possible to express some observations:

- it can be seen that all the F1 values are acceptable since they are higher than 80%;
- a high percentage of image augmentation deeply worsen the performances of the network, as can be seen in TRAINING 13;
- moderate percentage of image augmentation are still acceptable as suggested by TRAINING 15.

Moreover, from these tests it is evident that the higher the number of pictures the better the performances is not true, with or without augmentation.

Table 1. Dataset composed by original images.

Object	Dataset	Number and origin of images
FIRE EXTINGUISHERS	Dataset 1	175 from Polytechnic University of Marche and Flickr
	Dataset 2	118 original images from University of Edinburgh
	Dataset 3	286 images from Google
	Dataset 4	127 images from Google
	Dataset 5	270 images from Google
	Dataset 6	24 images from Instagram
EMERGENCY SIGNS	Dataset 7	45 images from Polytechnic University of Marche
	Dataset 8	536 images from Google

Table 2. Fire extinguishers training sessions.

Training	Dataset	mAP
TRAINING 1	1000 original pictures using all fire extinguisher images	89%
TRAINING 2	1000 original picture using all fire extinguisher images	90,80%
TRAINING 3	100 original pictures taken from Dataset 1	89,11%
TRAINING 4	200 original pictures taken from Dataset 1, 6 and 2	92,86%
TRAINING 5	300 original pictures taken from Dataset 1, 6 and 2	98,91%
TRAINING 6	400 original pictures taken from Dataset 1, 6, 2 and 3	99,30%
TRAINING 7	500 original pictures taken from Dataset 1, 6, 2 and 3	73,43%
TRAINING 8	600 original pictures taken from Dataset 1, 6, 2 and 3	82,73%
TRAINING 9	700 original pictures taken from Dataset 1, 6, 2, 3 and 4	82,73%
TRAINING 10	800 original pictures taken from Dataset 1, 6, 2, 3, 4 and 5	76,68%
TRAINING 11	900 original pictures taken from Dataset 1, 6, 2, 3, 4 and 5	78,13%
TRAINING 12	175 original pictures from Dataset 1 and 175 pictures coming from augmentation	94,95%
TRAINING 13	4000 pictures, only 175 original	16,43%

Table 3. Emergency signs training sessions.

Training	Dataset	mAP
TRAINING 14	1373 pictures, 539 original and 834 from re-edited photos	86,40%
TRAINING 15	581 original photos	80,98%.
TRAINING 16	310 original photos, 155original and 155 from augmentation	84,46%.

Table 4. Training testing results.

Training	Precision	Recall	F1
TRAINING 1	97,83%	97,83%	97,83%
TRAINING 2	97,08%	96,03%	96,55%
TRAINING 3	89,51%	98,56%	93,81%
TRAINING 6	97,08%	96,03%	96,55%
TRAINING 7	97,09%	96,39%	96,74%
TRAINING 14	86,57%	93,98%	90,12%
TRAINING 15	84,80%	91,77%	88,15%
TRAINING 16	81,97%	89,29%	85,47%
TRAINING 17	83,19%	89,31%	86,14%

With the aim of testing the network in real world conditions it has been performed a test inside the Polytechnic University of Marche premises. The customized network was the one able to detect fire extinguishers only. The chosen building is a three-floor construction and the fire extinguisher were 32, 15 at the ground floor, 11 at the first floor and 6 at the basement floor. Performances with real and unfortunate light condition have been test in this case, especially using the Hololens for taking the pictures while in the aforementioned tests the pictures had been taken with phone camera. This real world test has been done with an embedded system composed by the Hololens for taking the pictures, a raspberry and a neural compute stick to run the network locally. In this case the network has been always able to recognize the object although with different level of confidence. Less than 10% of the object have obtained a value of level of confidence lower than 60%. In 9 cases the recognition did not worked at the first attempt. This was due not to light condition but to the chosen point of view. When the white label usually on top of fire extinguisher was not visible the network struggled in recognize the object at the first attempt.

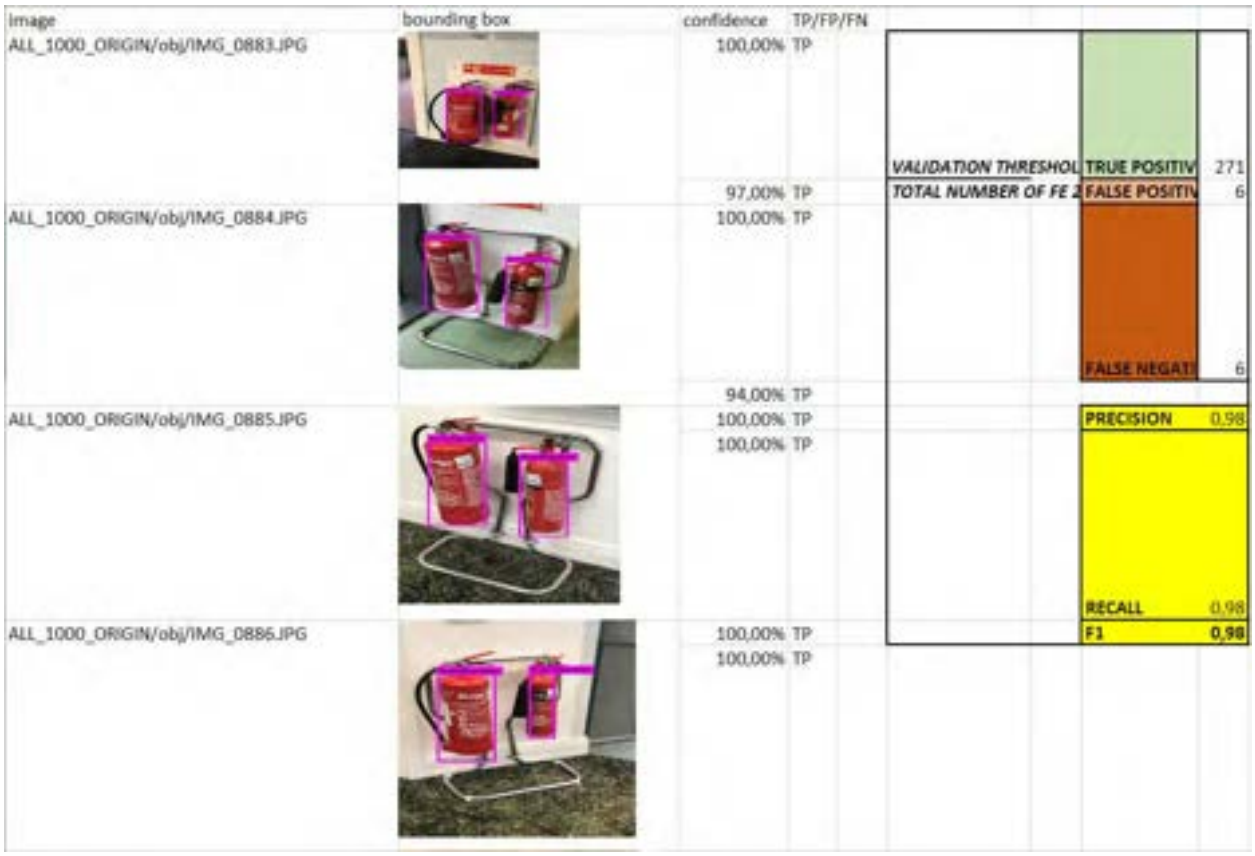

Figure 2. Testing sheet reporting the obtained bounding box, true positive, false positive, false negative and calculating performance indexes.

6 Conclusion

In this paper a study about the creation of a customized YOLO CNN for fire safety system object recognition has been proposed. Details about the training processes and indications on the right number of images for good performances have been provided. The results show that there is not a minimum number for all the purposes and categories. Furthermore, this research tried to investigate the role of augmentation for creating datasets that provide good trainings which result in good performances. A deeper analysis can be carry out exploring different proportion between original and re-edited pictures.
This application of CNN represents a part of an automated method for system components inventory exploiting AI and augmented reality so as to perform data collection and interpretation directly on site.

References

[1] FMLink. Reducing the total cost of ownership through a lifecycle approach. https://fmlink.com/articles/reducing-the-total-cost-of-ownership-through-a-lifecycle-approach/, Accessed: 09/06/2020.

[2] M. Kong, H. Lee, H. Shin, and M. Park. Study on Standardization and Construction of Inventory Database for Asset Management in Water Supply System. *International Journal of Database Theory and Application*, 9(9):11–24, 2016. doi:10.14257/ijdta.2016.9.9.02.

[3] L. Díaz-Vilariño, H. González-Jorge, J. Martínez-Sánchez, and H. Lorenzo. Automatic LiDAR-based lighting inventory in buildings. *Measurement: Journal of the International Measurement Confederation*, 73:544–550, 2015. doi:10.1016/j.measurement.2015.06.009.

[4] H. J. Jeong, K. S. Park, and Y. G. Ha. Image Preprocessing for Efficient Training of YOLO Deep Learning Networks. *Proceedings - 2018 IEEE International Conference on Big Data and Smart Computing, BigComp 2018*, pages 635–637, 2018. doi:10.1109/BigComp.2018.00113.

[5] S.D. Kulik and A.N. Shtanko. Experiments with neural net object detection system yolo on small training datasets for intelligent robotics. In *Advanced Technologies in Robotics and Intelligent Systems*, pages 157–162. Springer, 2020.

[6] J. Redmon, R. Girshick, A. Farhadi, and A. Dataset. You Only Look Once : Unified , Real-Time Object Detection. 2016.

[7] J. Redmon and A. Farhadi. YOLO9000: Better, faster, stronger. In *Proceedings - 30th IEEE Conference on Computer Vision and Pattern Recognition, CVPR 2017*, volume 2017-Janua, pages 6517–6525, 2017. ISBN 9781538604571. doi:10.1109/CVPR.2017.690.

[8] J. Redmon and A. Farhadi. YOLOv3: An Incremental Improvement. Accessed: 09/06/2020. URL http://arxiv.org/abs/1804.02767.

[9] E. Valero, F. Bosché, and A. Forster. Automation in Construction Automatic segmentation of 3D point clouds of rubble masonry walls , and its application to building surveying , repair and maintenance. *Automation in Construction*, 96(August):29–39, 2018. ISSN 0926-5805. doi:10.1016/j.autcon.2018.08.018. URL https://doi.org/10.1016/j.autcon.2018.08.018.

[10] Q. Lu, S. Lee, and L. Chen. Image-driven fuzzy-based system to construct as-is IFC BIM objects. *Automation in Construction*, 92(March):68–87, 2018. ISSN 09265805. doi:10.1016/j.autcon.2018.03.034. URL http://linkinghub.elsevier.com/retrieve/pii/S0926580517306118.

[11] W. Liu, Z. Wang, X. Liu, N. Zeng, Y. Liu, and F. E. Alsaadi. A survey of deep neural network architectures and their applications. *Neurocomputing*, 234 (December 2016):11–26, 2017. ISSN 18728286. doi:10.1016/j.neucom.2016.12.038. URL http://dx.doi.org/10.1016/j.neucom.2016.12.038.

[12] B. Huval, T. Wang, S. Tandon, J. Kiske, W. Song, J. Pazhayampallil, M. Andriluka, P. Rajpurkar, T. Migimatsu, R. Cheng-Yue, F. Mujica, A. Coates, and A. Y. Ng. An Empirical Evaluation of Deep Learning on Highway Driving. pages 1–7, 2015. URL http://arxiv.org/abs/1504.01716.

[13] S. Shinde, A. Kothari, and V. Gupta. YOLO based Human Action Recognition and Localization. *Procedia Computer Science*, 133 (2018):831–838, 2018. ISSN 18770509. doi:10.1016/j.procs.2018.07.112. URL https://doi.org/10.1016/j.procs.2018.07.112.

[14] F. Lamio, R. Farinha, M. Laasonen, and H. Huttunen. Classification of Building Information Model (BIM) Structures with Deep Learning. *Proceedings - European Workshop on Visual Information Processing, EUVIP*, 2018-November, 2019. ISSN 24718963. doi:10.1109/EUVIP.2018.8611701.

[15] Z. K. Zhao, L. Wang, and N. Xu. Deep belief network based 3D models classification in building information modeling. *International Journal of Online Engineering*, 11(5):57–63, 2015. ISSN 18612121. doi:10.3991/ijoe.v11i5.4953.

[16] T. Bloch and R. Sacks. Comparing machine learning and rule-based inferencing for semantic enrichment of BIM models. *Automation in Construction*, 91(July 2017):256–272, 2018. ISSN 09265805. doi:10.1016/j.autcon.2018.03.018. URL https://doi.org/10.1016/j.autcon.2018.03.018.

[17] E. Cosenza, A. Salzano, C. Menna, D. Asprone, and M. Serra. Digitalizzazione del danno sismico di edifici su piattaforma BIM attraverso tecniche di intelligenza artificiale. *Ingenio*, 2:1–17, 2018.

[18] A. Braun, K. Jahr, and A. Borrmann. Formwork detection in UAV pictures of construction sites. *eWork and eBusiness in Architecture, Engineering and Construction*, pages 265–271, 2019. doi:10.1201/9780429506215-33.

[19] AlexeyAB. https://github.com/AlexeyAB/darknet, Accessed: 09/06/2020.

[20] T. Lin, M. Maire, S. Belongie, L. Bourdev, R. Girshick, J. Hays, P. Perona, D. Ramanan, C. L. Zitnick, and P. Dollár. Microsoft COCO: Common Objects in Context. pages 1–15, may 2014. URL http://arxiv.org/abs/1405.0312.

[21] I. Laptev and A. Gupta. Hollywood in Homes : Crowdsourcing Data. 1:510–526, 2016. doi:10.1007/978-3-319-46448-0.

[22] M. Everingham, S. M. A. Eslami, L. Van Gool, C. K. I. Williams, J. Winn, and A. Zisserman. The pascal visual object classes challenge: A retrospective. *International Journal of Computer Vision*, 111(1):98–136, Jan 2015. ISSN 1573-1405. doi:10.1007/s11263-014-0733-5. URL https://doi.org/10.1007/s11263-014-0733-5.

[23] Github. Darknet: yolov3workflow. https://github.com/reigngt09/yolov3workflow/tree/master/1_WebImage_Scraping, Accessed: 09/06/2020.

[24] D. M. Montserrat, Q. Lin, J. Allebach, and E. J. Delp. Training object detection and recognition CNN models using data augmentation. *IS and T International Symposium on Electronic Imaging Science and Technology*, pages 27–36, 2017. ISSN 24701173. doi:10.2352/ISSN.2470-1173.2017.10.IMAWM-163.

[25] Github VoTT. Labelling tool. https://github.com/microsoft/VoTT, Accessed: 09/06/2020.

[26] Nils T. Customizing yolo. https://timebutt.github.io/static/how-to-train-yolov2-to-detect-custom-objects/, Accessed: 09/06/2020.

[27] G. Li, Z. Song, and Q. Fu. A new method of image detection for small datasets under the framework of yolo network. In *2018 IEEE 3rd Advanced Information Technology, Electronic and Automation Control Conference (IAEAC)*, pages 1031–1035, 2018.

[28] H. Hamledari, B. Mccabe, and S. Davari. Automated computer vision-based detection of components of under-construction indoor partitions. *Automation in Construction*, 74:78–94, 2017. ISSN 0926-5805. doi:10.1016/j.autcon.2016.11.009. URL http://dx.doi.org/10.1016/j.autcon.2016.11.009.

[29] J. Deng, W. Dong, R. Socher, L. Li, K. Li, and L. Fei-fei. ImageNet : A Large-Scale Hierarchical Image Database. *2009 IEEE Conference on Computer Vision and Pattern Recognition*, pages 2–9, 2009. URL 10.1109/CVPR.2009.5206848.

[30] B. Quintana, S. A. Prieto, A. Adán, and F. Bosché. Door detection in 3D coloured point clouds of indoor environments. *Automation in Construction*, 85 (October 2016):146–166, 2018. ISSN 0926-5805. doi:10.1016/j.autcon.2017.10.016. URL https://doi.org/10.1016/j.autcon.2017.10.016.

Improvement of 3D Modeling Efficiency and Accuracy of Earthwork Site by Noise Processing Using Deep Learning and Structure from Motion

N. Yabuki[a], Y. Sakamoto[a] and T. Fukuda[a]

[a]Division of Sustainable Energy and Environmental Engineering, Osaka University, Japan
E-mail: yabuki@see.eng.osaka-u.ac.jp, fukuda@see.eng.osaka-u.ac.jp

Abstract –

Nowadays, we can relatively easily create 3D models of earthwork construction sites by taking many pictures from multiple viewpoints using Unmanned Aerial Vehicles (UAV) and by applying Structure from Motion (SfM) technique to the pictures. However, since many construction machines are moving at the construction site, they become noise or disturb the model when generating a 3D model. Thus, it is necessary to take measures such as removing the noise, i.e., construction machinery after surveying, stopping construction work during the survey, or surveying on weekends when all machines are parked at proper places, which can result in reduced efficiency and productivity. On the other hand, object detection technology using deep learning is making great progress. Therefore, this research proposes an efficient and accurate UAV photogrammetry system that generates high-precision 3D models by detecting and removing construction machinery from UAV aerial images in advance. First, the object detection method by deep learning is used to detect the construction machinery. Next, the parts of the construction machines are removed from the images, and the removed parts are completed by image interpolation or compensation. Finally, a 3D model is created using SfM. We developed a system based on the proposed methodology and applied it to an actual earthwork construction site. The result showed that accuracy and efficiency have been enhanced by using this system.

Keywords –

Photogrammetry; Unmanned Aerial Vehicle; Structure from Motion, Deep Learning, Object Detection

1 Introduction

It has become easy to take multi-viewpoint images thanks to the Unmanned Aerial Vehicle (UAV) technology. In addition, photogrammetry technology that combines aerial images taken by UAV and the Structure from Motion (SfM) that generates a 3D model from multi-viewpoint images was developed. These technologies have been used in various fields, such as forest management, situational assessment at the time of disasters and construction field. Application to progress management and soil volume management using 3D models is expected to contribute greatly to productivity improvement. However, many construction machines are working at the construction site. When photogrammetry is performed by UAV and a 3D model is generated in such a situation, the working construction machine causes errors and noise. Therefore, it is necessary to take measures such as surveying with construction work stopped, surveying during weekends, or removing noise manually after surveying, resulting in low efficiency. Also, surveying with UAV takes several hours, so it is difficult to do it frequently.

On the other hand, object detection technology using deep learning is making great progress. While various high-accuracy methods have been proposed, many studies have been conducted to apply the detection results to various systems.

In this study, the object detection method using deep learning is adapted to the construction site by fine tuning, and the construction machinery is automatically detected, removed, and complemented from UAV aerial images in advance. As a result, we propose a system that can generate 3D models with high accuracy even under construction work. Also, verify the detection accuracy of construction machinery.

2 Literature Review

2.1 Research on Utilization of 3D Modeling of Construction Sites

Many methods using 3D models for construction site

management and surveying have been proposed. In recent years, with the spread of SfM technology, it has become possible to easily generate a 3D model by taking a large number of pictures with a digital camera. The use of 3D models is expected to improve productivity at construction sites.

Omari et al. [1] proposed an efficient method to generate a 3D model of a construction site by combining a 3D laser scanning and photogrammetry. In surveying using a laser scanner, it is necessary to measure at many points. Efficient surveying was made possible by reducing the number of surveying points and making up for the lack of scanning by using photogrammetry. The proposed method succeeded in reducing 75% of the time required for surveying the construction site.

Gore et al. [2] proposed a photo-based 3D modeling method for space planning to improve construction site safety and productivity. With the conventional visual inspection and space planning method that relies on 2D drawings, the construction site is usually very complicated and difficult to capture, therefore we proposed a method for generating 3D models from multi-view photographs.

Yamaguchi et al. [3] proposed a system for efficient photogrammetry using UAV. The system automatically detects and removes construction machinery from UAV aerial images, and generates a highly accurate 3D model using SfM. An object detection method based on the features in the image was used to detect construction machinery. Detection was performed for each construction machinery using the Joint-HOG feature value generated by Real AdaBoost in two steps from the HOG feature value, which is a co-occurrence table of the feature value histograms of the gradient direction of the brightness of the local region. Construction machinery was classified into six classes: backhoe, wheel roller, heavy dump, hydraulic breaker, bulldozer, dump truck, and learning was conducted, accuracy was verified, the average detection rate by object class was 54.5%, which was low.

2.2 Object Detection Method

In recent years, various high-precision object detection methods have been proposed and are expected to be used in a wide range of fields such as application to automatic driving technology of automobiles. Many object detection methods using classifiers based on convolutional neural networks such as SSD [4] and YOLO [5] have been proposed, and each has high detection accuracy. The feature of SSD is that it is designed to be able to detect multi-scale from various output layers. However, at the stage of prediction at the low layer, there is a disadvantage that the accuracy is lowered because the feature quantity obtained in the subsequent layers cannot be captured. YOLO is a fast object detection algorithm. Since the object can be detected by looking at the entire image, the possibility of misrecognizing the background as an object has decreased, but it is difficult to detect when many small objects are included.

In the construction field, to improve productivity, attempts are being made to detect construction machinery using these evolving object detection algorithms and to develop systems that utilize the detection results.

Yabuki et al. [6] proposed a system for improving the efficiency of managing many photos taken at construction sites and disaster areas. The system detects various construction machines, workers, and signboards in photographs and automatically classifies them into folders. By using SSD for object detection and transfer learning, we obtained high accuracy from a few learning data sets.

Kim et al. [7] detected objects of construction machinery from photos to improve the accuracy of the vision-based construction site monitoring method to capture the situation at the construction site in real-time. R-FCN was used as the construction machinery detection method, and high accuracy was obtained from a few data sets by performing transfer learning.

While object detection based on deep learning from UAV aerial images has also been attempted. Matija et al. detected an airplane from UAV aerial images using the object detection method YOLO of a convolutional neural network. The detection accuracy is 97.5%, and the object detection method based on deep learning is useful for detecting objects from aerial images.

In this paper, an object detection method based on a convolutional neural network is used for construction machinery detection from UAV aerial images, aiming to enable more accurate detection and removal than when using Joint-HOG.

3 Proposed System

3.1 Overview of the Proposed System

The flow of the system proposed in this study is shown in Fig. 1. First, UAV is used to photograph the construction site under construction work. Next, construction machinery is detected from all photos. Next, the detected construction machinery part is masked and image complementation is performed. Finally, the goal is to create a highly accurate 3D model efficiently by creating a 3D model using SfM.

3.2 Detection of Construction Machinery

In this paper, You Only Look Once v3 (YOLOv3)

[8], which is an object detection method based on a convolutional neural network, is used to detect construction machinery. YOLOv3 has high precision and detecting small objects in images with high accuracy. In addition, YOLOv3 uses Feature Pyramid Network (FPN) to cope with the detection of different scales and aims to improve accuracy by capturing more features. For example, SSD does not use FPN, and the feature obtained in subsequent layers cannot be used in lower layers, but YOLOv3 overcomes this problem.

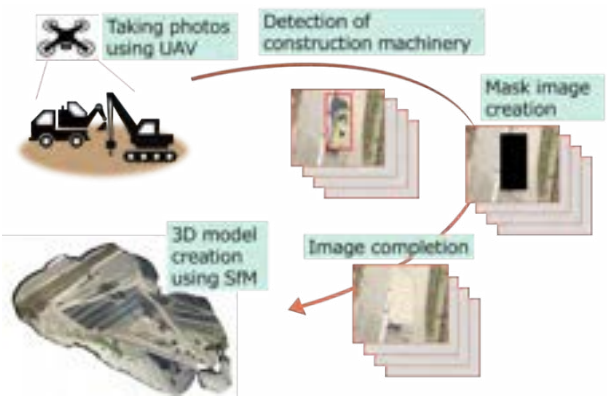

Figure 1. The Flow of the Proposed System

From the study of Matija et al. that YOLO is useful for detecting objects from UAV aerial images, it is expected that high detection accuracy can be obtained even in the detection of construction machinery by using YOLOv3, which was developed from YOLO. Also, because photogrammetry using UAV aerial photography is performed from a high altitude, the construction machinery that is the detection targets of this study often appear small. Therefore, YOLOv3, which is good at detecting small objects and has high detection accuracy, is considered an appropriate detection method.

In YOLOv3, learned models of general objects such as people and dogs are released. In this study, detection is performed by creating and fine-tuning construction machinery data set using the publicly learned model.

3.3 Detecting Object Types and Creating a Dataset

In this paper, 6 types of construction machinery are detected. We defined six classes: backhoe, bulldozer, road roller, dump truck, mixer truck, and car (Fig. 2). The class of 'car' was defined as passenger cars or light trucks moving in the construction site. By visual identification from UAV aerial images, 6 types of construction machinery were classified as shown in Table 1.

Based on the classification, a dataset was created from the UAV aerial images. There were 2,182 images included in a training dataset and 219 images included in a test dataset.

(a) backhoe (b) bulldozer (c) road roller (d) concrete mixer truck (e) dump truck (f) car

Figure 2. Examples of construction machinery to be detected (a) backhoe (b) bulldozer (c) road roller (d) concrete mixer truck (e) dump truck (f) car

Table 1. The numbers of classified objects

Object class	Number of objects
backhoe	213
bulldozer	19
road roller	24
dump truck	185
mixer truck	18
car	350

3.4 Fine Tuning of YOLOv3

YOLOv3 was fine-tuned using the data-set described in Section 3.3. By using this result, the construction machinery is detected from the aerial image from UAV.

4 Validation

4.1 Detection accuracy verification method

An index called mean Average Precision (mAP) was used for verification. The mAP is an average value for the entire class, calculated from Average Precision (AP), which calculates the precision for each defined class. When evaluating using mAP, it is necessary to obtain Intersection over Union (IoU). IoU is the index that shows how accurately an object is detected. It can be calculated that the common part of the ground truth and the prediction area divided by the area of sum (Fig. 3).

$$IoU = \frac{area(B_p \cap B_{gt})}{area(B_p \cup B_{gt})} \quad (1)$$

where

B_p: Predicted bounding box

B_{gt}: Ground truth bounding box

In order to calculate the mAP, the relationship between the ground truth area and the prediction area is important. These two relationships can be divided into four types True Positive (TP), True Negative (TN), False Positive (FP), and False Negative (FN) (Fig. 3). TP indicates a state in which an object existing in the image is correctly detected. FP indicates a state in which an object that does not exist in the image is detected (false detection). TN recognizes that the object does not exist and indicates a state in which it does not actually exist. FN indicates a state in which an object actually exists in the image but is not detected.

In this paper, when IoU $\geqq$ 0.5, it is defined as TP, and AP and mAP are calculated. First, the precision AP for each class is calculated. Then, mAP which is the average value of the whole is calculated.

$$AP = TP/(FP + TP) \quad (2)$$

$$mAP = \frac{1}{M}\sum_{i=1}^{M} AP \quad (3)$$

where

M : The number of classes

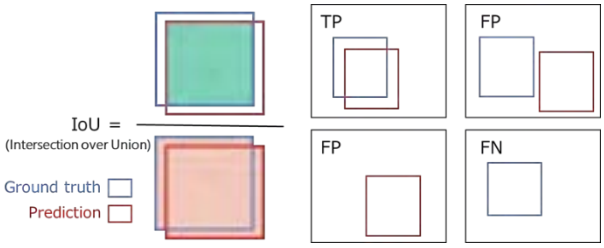

Figure 3. Image of IoU and the relationship between ground truth area and prediction area

4.2 Verification of Construction Machinery Detection Accuracy by YOLOv3

The accuracy of fine tuning was verified using mAP. The test data set created. Which is described in Section 3.3 was used for verification (Table. 2).

The mAP was 92.20%. For the five classes of the backhoe, bulldozer, road roller, dump truck, and car, high accuracy of over 90% was obtained, but for concrete mixer truck, the accuracy was relatively low at 71.43%. The road roller with the same number of objects in the data set has a detection rate of 100%. Therefore, the cause of the decrease in accuracy is considered to be due to the characteristics of the image. Many images included the road roller has a clear hue difference from the background and are considered easy to detect. On the other hand, compared to the road roller image, many of the concrete mixer trucks are not clearly different in hue from the surroundings, which may have led to a decrease in the detection rate. Fig. 4 shows examples of test data sets including concrete mixer truck and road roller. Fig. 5 shows examples of construction machinery detection based on the obtained learning results

The test data set is images that are not used for learning of YOLOv3, but it can be confirmed that construction machinery has been detected. In addition, even if the construction machinery in the image is small because of UAV aerial images, they can be detected.

Table 2. YOLOv3 construction machinery detection accuracy

Object class	Number of objects	Average Precision (%)
backhoe	187	98.40
bulldozer	16	92.73
road roller	22	100.0
dump truck	180	97.12
mixer truck	21	71.43
car	299	93.51
mAP		92.20

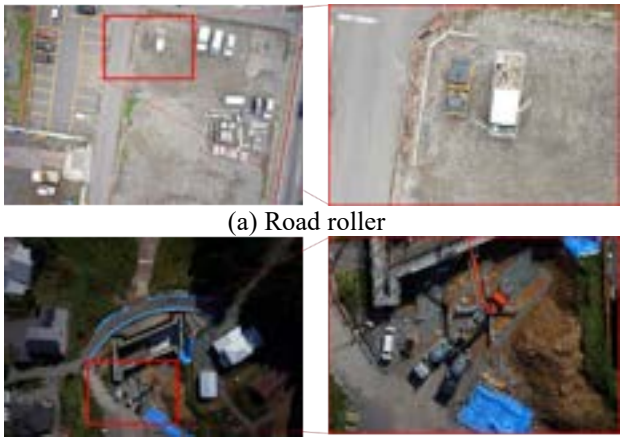

(a) Road roller

(b) Concrete mixer truck

Figure 4. Examples of test datasets

Figure 5. Example of construction machinery detection by YOLOv3

5 Conclusion

In order to perform photogrammetry with UAV, it is necessary to stop construction work or to remove noise manually after creating a 3D model. We proposed a system for efficient UAV photogrammetry by detecting construction machinery by deep learning method and removing them that causes noise.

For the detection of construction machinery from UAV aerial images, YOLOv3, which is an object detection method based on convolutional neural networks, is used. 2182 training data sets are created for the construction machinery to be removed and performed detection and accuracy evaluation using 219 test data sets. As a result, it was found that the detection of construction machinery with a high accuracy of 92.2% compared with previous studies. Since the construction machines shown in the UAV aerial images handled in this study are often small, the usefulness of using YOLOv3, which is good at detecting small scales, were confirmed. On the other hand, the detection rate of mixer truck was relatively low among the classes we tried to detect in this paper. This is thought to be due to the characteristics of the images used for training. Increasing the detection rate is expected by adding various mixer track images to the training data set.

As future work, the construction machinery part detected by YOLOv3 should be masked and complemented, and a 3D model should be generated by SfM, aiming at completion of a system that enables high-precision UAV photogrammetry even under construction work. We will examine an image completion method suitable for this study and verify the accuracy of noise removal after generating the 3D model. Further, the robustness of the system against environmental changes of sites should be evaluated.

References

[1] Omari S. E. and Moselhi O. Integrating 3D laser scanning and photogrammetry for progress measurement of construction work, *Automation in construction*, 18.1, 1-9, 2008.

[2] Gore S. Song L. and Eldin N. Photo-modeling for construction site space planning, In *Construction Research Congress 2012: Construction Challenges in a Flat World*, 1350-1359, 2012.

[3] Yamaguchi R. Yabuki N. and Fukuda T. Accuracy Improvement of 3D Models Generated by Structure from Motion (SfM) Using Joint Histogram of Oriented Gradients (Joint-HOG), *Internet Journal of Society for Social Management Systems*, Vol. 11, Issue 1 sms17-4917, 2017.

[4] Liu W. Anguelov D. Erhan D. Szegedy C. Reed S. Fu C. Y. and Berg A. C. Ssd: Single shot multibox detector, In *European conference on computer vision*, Springer, Cham, 21-37, 2016.

[5] Redmon J. Divvala S. Girshick R. and Farhadi A. You only look once: Unified, real-time object detection, In *Proceedings of the IEEE conference on computer vision and pattern recognition*, 779-788, 2016.

[6] Yabuki N. Nishimura N. and Fukuda T. Automatic Object Detection from Digital Images by Deep Learning with Transfer Learning, In *Workshop of the European Group for Intelligent Computing in Engineering*, Springer, Cham, 3-15, 2018.

[7] Kim H. Kim H. Hong Y. W. and Byun H. Detecting construction equipment using a region-based fully convolutional network and transfer learning, *Journal of Computing in Civil Engineering*, 32.2, 04017082, 2017.

[8] Redmon J. and Farhadi A. Yolov3: An incremental improvement. arXiv preprint arXiv:1804.02767, 2018.

Real-time Judgment of Workload using Heart Rate and Physical Activity

Nobuki Hashiguchi[a], Yeongjoo Lim[b], Cyo Sya[c], Shinichi Kuroishi[c], Shigeo Miyazaki[c], Shigeo Kitahara[c], Taizo Kobayashi[d], Kazuyoshi Tateyama[d] and Kota Kodama[a]

[a]Graduate School of Technology Management, Ritsumeikan University, Japan;
[b]Faculty of Business Administration, Ritsumeikan University, Japan
[c]Kumagai Gumi Co.,Ltd., Japan
[d]College of Science and Engineering, Department of Environmental Systems, Ritsumeikan University, Japan
[d]College of Science and Engineering, Department of Civil Engineering, Ritsumeikan University, Japan
E-mail: gr0325kr@ed.ritsumei.ac.jp, kkodama@fc.ritsumei.ac.jp,

Abstract –

Workers in a construction site may be exposed various hazards and risks and may work with excessive demands beyond their physical abilities. It is important for construction companies to sustain a workforce in the work environment that does not sacrifice worker safety and health and maintains the required productivity. The purpose of this study was to develop a method for real-time estimation of the workload risk of individual workers at a construction site. Based on previous studies, we developed a workload model that includes behavioral information and physical characteristics of workers in addition to heart rate reserve (%HRR). Recent wearable devices have sufficient performance for measuring biological and physical load data without interfering from their work. In this case study, heart rate and physical activity were measured using smart wear equipped with a biosensor, an acceleration sensor and IoT system developed in our research. Using a logistic regression analysis as the statistical methods and SPSS as the analysis tool, we analyzed the risk caused by the workload. As a result, it became clear that the physical activity and the heart rate will be the important parameters for estimating workload risk in construction works. However, worker age and body mass index (BMI) did not have a significant effect on estimating workload risk. In the construction site, types of works and skills of workers will change according to the progress of the project. In order to ensure a stable workforce and productivity, it is necessary for construction industry to manage workers' health and safety. In conclusion of this paper, we propose that the real-time monitoring of heart rate and physical activity during construction work can be used for human resource management (HRM). With the development of this study, it will be possible to determine how the workers' workload affects productivity. It is believed that this research will be useful as an element of the integrated management technology of the entire construction site using ICT tools.

Keywords –

Workload estimation; Heart rate reserve; Wet bulb globe temperature; Construction hazards; Worker safety

1 Introduction

The construction industry serves as the base for several other industries in every country and contributes significantly to the national economy. In order to maintain the industry's productivity, it is essential to ensure the safety and health of its workers [1,2]. Characterized by poor working environments, such as poor scaffolding, aerial work platforms, high humidity at high temperatures, and a worksite adjacent to heavy construction equipment, construction sites often contribute toward increasing the physical workload of construction workers [3,4]. A high-temperature or highly humid work environment and long-term physical workload expose workers to chronic fatigue, injury, illness, and health risk, and thereby reduce a site's productivity [5].

This study uses heart rate to understand the impact of the physical load of a job as well as that of the personal and environmental factors [6,7]. Since it is difficult to identify the important factors affecting workers' health in every situation, an analysis based on workers' heart rate can be useful for understanding their work capacity. As an indicator, the heart rate reserve (%HRR) has been reported to be a major predictor for estimating an individual's workload capacity [8,9]. This method assumes resting HR resting (i.e., minimum HR

during resting) as a level with no physical load, and calculates a percentage of the difference between working and resting HRs among HR reserve (i.e., HR reserve indicates the difference between HR max and HR resting) [8-10]. Considering the health risks of workers, workers with more than 40% HRR should not undertake any heavy workload exceeding 30 minutes [9,10]. In this study, workers with more than 40% HRR were considered to be at health risk. Although %HRR is a useful determination method, most studies often identify HRR based on certain activities such as walking, jogging, or treadmill. Given the frequent inflow and outflow of workers at construction sites, it often becomes difficult to use specific activities to measure the HR max and HR resting for each worker precisely. Hence, it is difficult to use %HRR as an indicator of workload at construction sites.

It uses a model composed of workers' movement acceleration, age, body mass index, and the wet bulb globe temperature (WBGT), which take into account temperature, humidity, and radiant heat. By using the model, the impact of workload risk is estimated through the worker's %HRR. In order to formulate strategies to manage workers and improve their productivity, it is important to determine the impact of workload on their health using simple and accurate methods.

2 Materials and Methods

2.1. Measurement system

In order to evaluate the type of work environment, the study measured the air temperature, relative humidity, and WBGT; HRR and acceleration (ACC) detected from the respiratory rate (R-R) interval in ECG were measured in order to determine the workload.

We measured the heart rate and the physical activity of workers on the basis of the ECG signals captured using the smart clothing worn by construction workers, as shown in Figure 1., a is heart rate and acceleration sampling sensor (WHS-2), b is smart clothing (COCOMI) and c is Data acquisition device (CC2650).

The smart clothing is an underwear-type shirt integrated with biometric information sensor (detection of heart rate) [11-13] and a 3-axis acceleration sensor. Since the smart clothing is made of stretchable fabric, stretchable ECG electrodes were integrated with the hardware for measuring the heart rate [14]. The heart rate was detected by detecting the R-R intervals in the ECG signals. HRRs during load and rest were obtained by converting the detected R-R intervals. We attached a small heartbeat sensor device (WHS-2) to the smart clothing; we monitored the heart rate and the amount of physical activity by taking the 3-axis acceleration showing the spacing between the R-R waves of and the physical activity the subjects [15]. Using a Bluetooth low energy device, the heart rate and 3-axis acceleration data were sent to the data acquisition device used by the workers (Texas Instruments, Inc. CS2650). Subsequently, data from the data acquisition device were transmitted to and stored on the server installed on network using the established wireless access point (data transfer device) in the work area.

Based on the data provided by workers on their height, weight, and age, we calculated their BMI; the WBGT was calculated based on their labor time. In order to grasp the temperature and the relative humidity of the work environment, the WBGT was measured at 5-minute intervals.

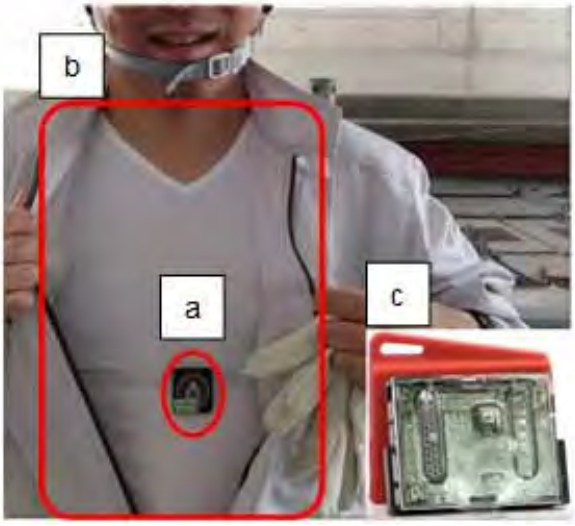

Figure 1. Picture of measurement equipment.

2.2. Measurement method

Table 1 shows the measurement parameters and techniques used in this study. The participants were expected to be aware of their body measurements as they worked in construction companies that conducted these measurements on a regular basis. We asked questions related to age, height, and body weight of the subject and, subsequently, used the responses to determine the BMI. As per a study [16] on an East Asian cohort, people with a BMI between 22.6 and 27.5 had the lowest death risk, whereas people in a higher BMI range were at a higher risk of deaths from cancer, cardiovascular diseases, and other causes. The BMI was added to this study's explanatory variables to examine worker health risk.

Heart rate during work ($HR_{working}$) was determined by the average value of the heart rate measured every 5 minutes for each worker. Thus, the heart rate during work denotes the average of the data collected every 5

minutes; this data has been corrected by deleting null data or outliers [17,18]. An accurate measurement of the HR_{max} is not suitable for construction workers who are often in flux. Therefore, the HR_{max} was predicted using the equation of Tanaka [19]. In order to confirm the stability of the heart rate at rest time, the subject's heart rate at rest time was measured more than thrice at 5-minute intervals; the lowest average heart rate was used to determine the $HR_{resting}$.

Table 1. Measurement parameters.

Measurement parameters [unit]
$BMI = weight / (height)^2$ $[kg/m^2]$
$HR_{working}$ = average heart rate in 5 minutes during working hours [bpm]
$HR_{resting}$ = average heart rate in 5 minutes during the rest hours [bpm]
$HR_{max} = 208 - 0.7 \times age$ [bpm]
$\%HRR = \frac{HR\ working - HR\ resting}{HR\ max. - HR\ resting} \times 100$ [%]
$ACC\ [mG] = \sqrt{(A_{X_n} - A_{X_{n-1}})^2 + (A_{Y_n} - A_{Y_{n-1}})^2 + (A_{Z_n} - A_{Z_{n-1}})^2}$

By using the 3-axis acceleration sensor for continuous monitoring, the physical activity level of the subject was evaluated to get ACC [20] of the three axes (the longitudinal axis: X, the lateral axis: Y, and the vertical axis: Z); the resulting ACC, which is physical activity, was calculated by an average value generated during the 5-minute intervals. The intensity level of the physical activity is shown to be a predictor of good health [21]. The 3-axis acceleration method observed the strength of each worker's overall movement during the working hours. Unlike office workers, construction workers can provide a more detailed operating data than those derived from the measured parameters; this data may include data on their capacity to lift load up the stairs. In other words, the method captures the intensity of the workers' movement between the work activities (for example, walking, standing, and crouching) performed during the working hours.

2.3. Participants

The data were collected at the water injection pump construction sites of a construction company in the following dates of the year 2018: May 25th, June 29th, and November 16th (Kumagai Gumi Co., Ltd.). The participants were tasked with the dismantling of the steel scaffolding. Specifically, eight steeplejack workers performed repetitive tasks (of those involved in the demolition) and four assistant workers carried out indirect work such as equipment installation. These 12 participants were notified of their selection as subjects in the experiment.

2.5. Data collection

Table 2 shows the dates of data collection, ages of the subjects, work tasks, and body measurements each subject. The data were measured from 8:30 am to 5:00 pm, and the data were collected during the entire period or at any of the 5-minute interval in the time zone of half of the period of the working day. All the subjects were men; they were asked about their age, job title, and the provision of information about their body and weight. Since the cardiopulmonary function aims to eliminate the unhealthy subjects from the measurement, the subjects were also asked about the presence or absence of the history of cardiovascular disease and their current health condition (for example, whether they suffer from chronic cardiovascular disease). Among the 13 workers who expressed a desire to participate, 1 subject with arrhythmia did not participate in the experiment. Except for the preparation time for data collection, 5 minutes were given to each of the 882 datasets collected from 12 subjects.

When measuring the subject, we checked for the Hawthorne effect [22]. In this experiment, we did not monitor the activity of the subject; we waited a little farther from the work area and recorded and photographed the work with the help of two cameras installed in the work area. In general, manual laborers performing high-load work have their own health concerns; they also focus on the physical workload resulting from their daily operations. Hence, before starting the measurements, we instructed the subjects not to depart from the usual work patterns; they were also informed that the study did not intend to measure their productivity but their physical workload.

Table 2. The Collected Data on the Subjects.

ID#	Age (years)	Main job task	Height (cm)	Weight (kg)
S1	20	Scaffolder	159.0	57.0
S2	39	Scaffolder	179.0	74.0
S3	32	Scaffolder	177.0	93.0
S4	25	Scaffolder	182.0	82.0
S5	41	Scaffolder	176.0	70.0
S6	40	Scaffolder	176.0	75.0
S7	36	Scaffolder	170.0	68.0
S8	22	Scaffolder	165.0	55.0
L1	43	Worker	168.0	70.0
L2	50	Worker	174.5	87.5
L3	27	Worker	170.5	62.5
L4	59	Worker	169.0	76.0

2.6. Model development and statistical analysis

The independent variables comprised subjects' ages, BMI, the amount of physical activity during labor, and the WBGT in the field environment. The binomial logistic regression was used to analyze the health risks determined by the level of %HRR. Logistic regression assessed the value of new medical treatments. It is one of the regression analysis methods evaluating the factors affecting a problem surrounded by controversies [23]. Logistic regression modeling is not limited to the study of physiological medicine, but it is also used in biology, engineering, ecology, health policy, linguistics, and business and finance [24]. Regression analysis has become an integral element of data analysis for describing the relationship between the independent variables and one or more of the explanatory variables.

A prediction model considering the parameters of these independent variables improves the accuracy of risk detection; in this study, we observe a strong correlation between risk factors. Therefore, it is necessary to consider the possibility of multicollinearity while conducting the statistical analysis. When developing the statistical model, the Pearson's correlation coefficient and variance inflation factors (VIF) were calculated for determining the physical activity ACC, AGE, and BMI of the subjects and WBGT in the work environment.

Table 3. Correlation matrix for workers' risk.

	ACC	BMI	AGE	WBGT	VIF
ACC	1.00				1.17
BMI	0.02	1.00			1.48
AGE	0.33^{***}	0.42^{***}	1.00		1.43
WBGT	-0.07^{*}	0.39^{***}	0.05^{*}	1.00	1.20

Table 3 shows the results obtained with respect to the correlation coefficient and the VIF between independent variables. A p-value less than 0.05 (typically $\leq$ 0.05) is statistically significant, *** indicates $p \leq 0.001$ and * indicates $p \leq 0.05$. A weak negative correlation coefficient (-0.33) was observed between physical activity ACC and the AGE of the subjects, while there was no correlation against the BMI and WBGT. The BMI of the subjects was slightly positively correlated (0.42) with the AGE and weakly correlated with the WBGT (-0.39). Furthermore, it was observed that the AGE of subjects was hardly correlated with the WBGT. The VIF serves as a reference for checking multicollinearity; the values of all the independent variables were the extent of the value 1-2, indicating a low likelihood of multicollinearity [25].

3. Results

3.1 The relationship between ACC and %HRR

Figure 2 shows the results of the %HRR for the ACC measured in each subject. The relationship between the ACC and the %HRR is shown in linear approximation; Table 5 describes the correlation coefficient $r_{L1\text{-}L4}$ of L1-L4 and the correlation coefficient $r_{S1\text{-}S8}$ of S1-S8. In all the subjects, the %HRR increased according to the increase in the ACC, and the correlation coefficient r of the ACC and the %HRR was at about 0.7–0.9. When compared to assistant workers, the higher heart trend of the scaffold workers shows their exposure to a high physical workload. During the break time, the workers' ACC and %HRR were relatively low and their physical activity and heart rate at rest time were stable.

Figure 2 also shows that, despite an increase in ACC from S5 to S8, the %HRR tends to be relatively large. S1 recorded the highest ACC among all subjects because S1 not only placed the dismantled steel materials under the scaffold stairs but also carried them to the collection location. It is presumed that there was an increase in the transportation task between the unloading location of the scaffold stairs and the collection location, which led to an increase in both %HRR and ACC. S1 is the youngest among the subjects; as HR_{max} increased by the calculation based on age, there is a possibility that even same $HR_{working}$ is no longer conspicuous when compared to the other subjects. Conversely, although relatively high-age assistant members, such as L3, had a relatively low ACC without a big movement behavior, S1's %HRR was seen to be higher than the other assistant workers. This can be attributed to the fact that HR_{max} obtained for L1's age is lower than that for the other subjects.

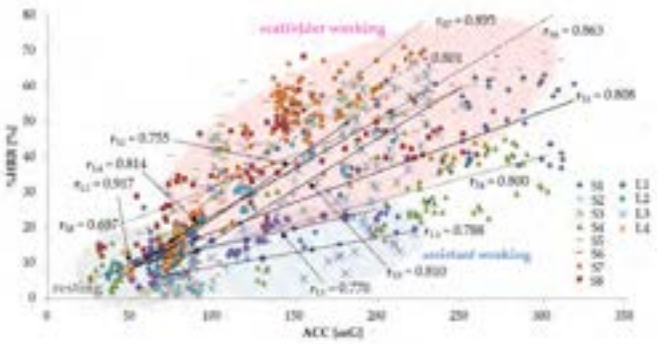

Figure 2. Relationship between ACC and %HRR (Scaffolder $_{S1\text{-}S8}$, Assistant worker $_{L1\text{-}L4}$). $\mathbf{r}_{S1\text{-}S8}$ denotes the correlation coefficient of the relationship between ACC and %HRR for S1-S8, and $\mathbf{r}_{L1\text{-}L4}$ is the correlation coefficient of the relationship between ACC and %HRR for L1-L4.

3.2. Logistic regression model

Logistic regression analysis was performed using the statistically significant ($p < 0.05$) independent variables in Table 4. The logistic model formula used in this study is shown below.

Workers' health risk (≥%40 HRR: 1, <%40 HRR: 0)
= f（ACC、AGE、BMI、WBGT）

where the objective variable is 1 for the worker's health risk (≥40% HRR), and it is 0 for no health risk (<40%HRR).

The independent variables are physical activity ACC, AGE of subjects, BMI calculated from height and weight, and WBGT in the work environment. Using the HR max and HR resting of each subject and calculating their %HRR, the independent variable was estimated by whether HRR ≥40%.

Table 4 shows the estimation results of the model on the health risks of workers examined in this study. In the Model 1, ACC, AGE, BMI, and WBGT were independent variables. By p-value, the ACC, AGE, and WBGT of the subjects of the work environment were statistically significant, but the BMI of workers was not significant. Wald χ^2 shows the contribution of each variable to the model, and it indicates that the larger the value, the higher is its importance [26]. In the Model 1, compared to AGE and WBGT, the contribution of the ACC was relatively high. To determine the influence of the dependent variable, we use the odds ratio in the logistic regression. It is indicated that independent variable increases due to an increase in the odds when OR>1; hence, the odds ratio can be a measure of a likelihood of a decline in independent variable with an increase in the odds when OR <1 [23,24,27].

Table 4. Estimation by logistic regression model.

Model	Variables	Coeff.	*p*-value	95% CI for Odds
Model 1	Constant	-25.6	< 0.001	–
	ACC	0.041	< 0.001	1.04 – 1.05
	AGE	0.074	< 0.001	1.04 – 1.12
	BMI	-0.035	0.548	0.86 – 1.08
	WBGT	0.705	< 0.001	1.67 – 2.44
Model 2	Constant	-28.1	< 0.001	–
	ACC	0.041	< 0.001	1.04 – 1.05
	AGE	0.066	< 0.001	1.04 – 1.10
	WBGT	0.742	< 0.001	1.82 – 2.43

When the odds ratio is larger than 1, while the lower limit of the confidence interval (CI) is not less than 1, the ACC, AGE of workers, and WBGT in the work environment are independent variables. However, the BMI of workers is the independent variable whose odds ratio is less than 1—the lower limit does not exceed 1. By the results, without BMI, the Model 2 examined a model based on independent variables ACC, AGE, and WBGT. It is indicated the statistical significance of the three independent variables; AGE, ACC, and WBGT may be high to show the health risks of workers, which is important for the Model. Furthermore, according to the odds ratio, the influence of the WBGT on the health of workers was the largest.

Concerning the estimation results of the model, Table 5-1 shows predicted results by model and Table 5-2 show the suitability index of the model due to its goodness of fit (GoF). The positive discrimination rate by the estimation of Model 1 was 88.9%; the positive discrimination rate by the estimation of Model 2, except the BMI that did not have statistically significant results, increased to 89.2%. Three indicators were determined to test the significance of the model by GoF. Akaike's information criteria (AIC) = -2logL + 2k were defined, and AIC were considered as indicative of the model fit [28,29]. Here, k denotes the number of parameters in the model; the first term model represents the true goodness of AIC, and the second term represents the penalty due to an increase in the variable. The values of the AIC are small. According to the obtained AIC, the adaptation of Model 2 was slightly better than the Model 1. The Cox-Snell R2 corresponds to determining coefficients of a linear regression analysis R2, referred to as pseudo-R2. The fit of the model becomes better as the Cox-Snell R2 becomes larger; the Cox-Snell R2s of Model 1 and Model 2 are 0.4-0.5, while the fit of the independent variable for the dependent variable was not very high [30,31]. However, when Nagelkerke R2 approaches from 0.5 to 1, the fit becomes higher [32-34]. The fit of the independent variable for the dependent variable of Model 1 is 0.590 and the one of Model 2 is 0.589. Both of them were high. Both the fit of Model 1 and Model 2 were good by these results.

Table 5-1. Estimation of subjects' physical load.

Model (independent variables)	Observed		Predicted Risk 0	Predicted Risk 1	Percentage (%)
Model 1 (ACC, AGE, BMI, WBGT)	Risk	0	487	53	90.2
		1	45	297	86.8
	Overall				88.9
Model 2 (ACC, AGE, WBGT)	Risk	0	486	54	90.0
		1	41	301	88.0
	Overall				89.2

Table 5-2. GoF of Estimation.

Model (independent variables)	GoF		
	AIC	Cox-Snell R^2	Nagelkerke R^2
Model 1 (ACC, AGE, BMI, WBGT)	57.5	0.435	0.590
Model 2 (ACC, AGE, WBGT)	59.5	0.434	0.589

4. Discussion

This study shows that a continuous measurement of the physical load of construction workers can change work conditions and increase an understanding of their health conditions. It measures the load fluctuation of the workers by using data collected from the smart clothing; this fluctuation corresponds to workers' age, the temperature of the working environment, and working conditions (e.g. foreman and the real workers and the difference between the assistants and the scaffold workers). In line with the results of previous studies, this study shows that the physical demands differs in case of each worker; hence, results seen in previous studies on wearable devices (wristband-type devices) correspond [4,34] to this study.

Based on the work patterns (dismantling, transportation task, and the percentage of work activities, including preparation work), the physical demands of the workers vary even in the same construction site. In order to understand the health risks of workers, there is a need for continuously measuring a work in progress.

When measuring the subjects, we observed that the physical demands should not be sustained for a longtime. Concerning the workplace and physical demands, specific guidelines were created. (i.e., the work activities that increase the %HRR beyond 40% should be limited to 30-60 minutes [10].) Based on these guidelines, as shown in the subjects S5 and S7 (Table 5 and Figure 2), there were several workers with more than 40%HRR who continued to work throughout the day. Therefore, in order to reduce the high physical demands of these workers, some intervention must be implemented. This study provides insights on the appropriate interventions required for managing excessive physical requirements.

Most studies determine %HRR based on typical activity patterns and experimental environments, and there are very few cases that consider an actual construction site. Concerning the application of methods for determining %HRR of construction workers, it is difficult to measure HR max and HR resting [35] in advance for workers, and it is likely that %HRR will interfere with actual use as the indicators.

The important finding of this study is that it proved its hypothesis on the impact of physical workload on the %HRR of workers, by using the covariates in logistic regression. The relationship among these covariates influence the heart rate of workers [36]. WBGT has the largest odds ratio among all the covariates and the impact on workers' %HRR was significant [16]. To the best of our knowledge, this is the first study to report how the physical activity, workers' age, and WBGT could be used to determine workers'physical workload without calculating their %HRR. Concerning ≥40%HRR, the accuracy rate is about 89.2%, based on the estimation of the judgement model of the health risks of workers. Thus, in an environment where HR max and HR resting cannot be measured, it was indicated that the health risk could be judged by %HRR.

We have several limitations in our study. First, the sampled Japanese construction company had only 12 workers in total. Due to this limited number of subjects, the dataset used the average of the physical activity and heart rate collected at 5-minute intervals. We recognized that the observation period is sufficient for analyzing workers because previous studies have used data on heart rate and physical activity collected at about 30-minute and 5-minute intervals, respectively [8-10,18,37]. However, since the measured values are averaged, rapid changes in the worker's condition could not be observed. Second, some physical activity and heart rate data were missing, which might have led to measurement errors. However, almost the same results were obtained even when these outliers were included in the analyses (data not shown in table). These outliers may slightly affect the heart rate mean or standard variance. To avoid these technical errors, there is a need to monitor more accurately the heart rate and physical activity. Third, the study used a self-reporting method that could result in differences between workers' information on their height and weight. Future research should seek to include observable data to better understand the potential impacts of the physical workload on workers. Finally, this study provides an insight into the degree of contribution of the physical activity and other variables for estimating workload. Workers' health is very fragile, and it is affected by their physical workload, mental state, and lifestyle. Hence, it is necessary to carry out further study in this regard. Further studies in other working conditions are required to accumulate more evidence and assure the accuracy of the models.

5. Conclusions

In this study, the heart rate and physical activity, the age, BMI, and WBGT of the working environment were measured for workers of a Japanese construction company. Given the high workforce mobility in the construction industry, this study developed a new judgement model of workers' health risks as an alternative to %HRR. By using workers' physical activity, age, BMI, and WBGT of the work environment as independent variables, it can be easily observed the physical load of worker without preparation such as HR max and HR resting. It measured the heart rate and physical activity of construction workers by using a smart clothing equipped with biological and acceleration sensors. By logistic regression analysis, the risk to health by physical workload was analyzed. The results showed that physical activity, age and WBGT are important parameters of workload estimation. However, BMI of workers was not statistically significant, and hence it did not have a significant impact on the estimation of the health risks posed by the workload.

This study aimed to develop a method to facilitate a practical estimation of the workload risk of individual workers at a construction site in real-time. The use of a lightweight wearable device in this study has important theoretical implications in that it presents a real-time monitoring mechanism for examining workers' health condition. This monitoring mechanism is very easy, without special preparation. It can also be adopted by firms to minimize the workers' health damage.

In managing the health and safety of workers, it is useful to assess workers' workload and health state quantitatively. Although there are several studies on workforce management [38-40], few studies focus on using workers' individual heart rate, physical activity, and body measurements. Further research on the use of these attributes can improve the identification of the health risks of workers quantitatively and promote the productivity of workers at construction sites.

Acknowledgments

This study was conducted with financial support from the Ministry of Land, Infrastructure, Transport and Tourism of Japan. The authors would like to thank all the construction workers who completed the questionnaires.

References

[1] Choudhry R. M. Achieving safety and productivity in construction projects. *J. Civ. Eng. Manag,* 23(1):311–318, 2017.

[2] Chen Y., McCabe B. and Hyatt D. Impact of individual resilience and safety climate on safety performance and psychological stress of construction workers: A case study of the Ontario construction industry. *J Safety Res*, 61:167–176, 2017.

[3] Leung M.Y., Chan I.Y.S. and Cooper C.L. *Stress Management in the Construction Industry*; John Wiley & Sons: West Sussex, UK, 1-27, 2014.

[4] Hwanga S. and Lee S. Wristband-type wearable health devices to measure construction workers' physical demands. *Automation in Construction,* 83:330–340, 2017.

[5] Yoon S. J., Lin H. K., Shinjea G.C, Coi Y.J. and Rui Z. Effect of occupational health and safety management system on work-related accident rate and differences of occupational health and safety management system awareness between managers in South Korea's construction industry. *Saf Heal Work*, 4(4):201–209, 2013.

[6] Achten J. and Jeukendrup A. E. Heart rate monitoring, *Sports Med*, 33(7):517–538, 2003.

[7] Nelesen R., Dar Y., Thomas K. and Dimsdale J. E. The relationship between fatigue and cardiac functioning, *Arch. Intern. Med,* 168(9):943–949, 2008.

[8] Borg G. *Borg's Perceived Exertion and Pain Scales*, Human Kinetics, Champaign, IL, 54-62, 1998.

[9] Wu H. C.; Wang M.J. Relationship between maximum acceptable work time and physical workload. Ergonomics, 45(4):280–289, 2002.

[10] Norton K., Norton L, Sadgrove, D. Position statement on physical activity and exercise intensity terminology. *J Sci Med Sport*, 13(5):496-502, 2010.

[11] Lin C. C.; Yang C. Y. and Zhou Z. and Wu S. Intelligent health monitoring system based on smart clothing. *Int J Distrib Sens N,* 14, 2018.

[12] Axisa F., Schmitt P. M., Gehin C, Deklhomme G., McAdams E. and Dittmar A. Flexible Technologies and Smart Clothing for Citizen Medicine, Home Healthcare, and Disease Prevention. *IEEE Trans Inf Technol Biomed,* 9(3):325–336, 2005.

[13] Lee K. and Ji Y. G. Standardization for Smart Clothing Technology. *International Conference on Human-Computer Interaction* HCI: Human-Computer Interaction. Ambient, Ubiquitous and Intelligent Interaction 768–777, 2009.

[14] TOYOBO Co., ltd., Discover TOYOBO's New Materials. Online: https://www.toyobo-global.com/discover/materials/cocomi/index.html, Accessed: 7/April/2020.

[15] Shiozawa N., Lee J., Okuno A. and Makikawa M. Novel Under Weare "Smart-Wear" with Stretchable and Flexible Electrodes Enables

Insensible Monitoring Electrocardiograph, World Engineering conference and Convention 2015, OS7-6-3, 1-2, 2015.

[16] Zeng W., et al. Association between Body-Mass Index and Risk of Death in More Than 1 Million Asians. *N Engl J Med Overseas Ed.,* 364(8):719–729, 2011.

[17] Porges S. and Byrne E. Research methods for measurement of heart rate and respiration. *Journal of biological physics* 34(2-3):93–130, 1992.

[18] Caballero Y., Ando T. J., Nakae S.; Usui C., Aoyama T., Nakanishi M., Nagayoshi S., Fujiwara Y. and Tanaka S. Simple Prediction of Metabolic Equivalents of Daily Activities Using Heart Rate Monitor without Calibration of Individuals. *IJERPH*, 17(1):216, 2019.

[19] Tanaka H., Monahan K.D. and Seals D.R. Age-predicted maximal heart rate revisited. *J Am Coll Cardiol*., 37(1):153–156, 2001.

[20] Bruin E. D., najafi B., Murer K, Uebellhart, D. and Animian K. Quantification of everyday motor function in a geriatric population. *J Rehabil Res Dev*, 44(3):417–428, 2007.

[21] Menai M., Hees V.T., Elbaz A., Kivimaki, M. and Singh-manoux A. Accelerometer assessed moderate-to-vigorous physical activity and successful ageing: results from the Whitehall II study. *Scientific Reports*, 8:45772, 2017.

[22] Adair J. G. The Hawthorne effect: A reconsideration of the methodological artifact. *J Appl Psychol*, 69(2):334–345, 1984.

[23] Agresti, A. *An Introduction to categorical data analysis;* John Wiley and Sons: New Jersey, NJ, 99-136, 2007.

[24] Hosmer D. W. and Lemeshow S. *Applied logistic regression*. New York, NY: John Wiley and Sons, 2000.

[25] Daoud J. Multicollinearity and Regression Analysis. *J. Phys. Conf. Ser.*, 949(1):012009, 2017.

[26] Onder S., Mutle M. Analyses of non-fatal accidents in an opencast mine by logistic regression model – a case study *Int J Inj Contr Saf Promot.,* 24(3):328–337, 2017.

[27] Onder M., Onder S. and Adiguzel E. Applying hierarchical loglinear models to nonfatal underground coal mine accidents for safety management. *Int J Occup Saf Ergon.*, 20(2):239–248, 2014.

[28] Uh HW, Mertens B.J., Wijk JH., Houwelingen HC, Houwing-Duistermaat J. Model selection based on logistic regression in a highly correlated candidate gene region. *BMC Proceedings*, 1(1):S114, 2007.

[29] Hastie T., Tibshirani R. and Friedman J. The Elements of Statistical Learning: Data Mining, Inference, and Prediction New York, Springer, 2001.

[30] Smith T. J. and McKenna, C. M. A Comparison of Logistic Regression Pseudo R Indices. Mathematics, 39(2):17-26, 2013.

[31] Bewick V., Cheek L. and Ball J. Statistics review 14: Logistic regression. Critical Care, *9(1):*112–118, 2005.

[32] Mbachu H. I.; Nduka E. C. and Nja M. E. Designing a Pseudo R-Squared Goodness-of-Fit Measure in Generalized Linear Models. *J. Math. Res.*, 4(2):148–154, 2012.

[33] Hammert G. A. J., Schons L. M., Wieseke J. and Schimmelpfennig H. Log-likelihood-based Pseudo-R2 in Logistic Regression: Deriving Sample-sensitive Benchmarks. *Sociol Methods Res*, 47(3), 507–531, 2016.

[34] Guo H., Yu Y., Xiang T., Li H. and Zhang D.; The availability of wearable-device-based physical data for the measurement of construction workers' psychological status on site: From the perspective of safety management. *Automation in Construction*, 82:207–217, 2017.

[35] She J., Nakamura H., Makino K., Ohyama Y. and Hashimoto H. Selection of Suitable Maximum-heart-rate Formulas for Use with Karvonen Formula to Calculate Exercise Intensity. *IJAC*, 12(1):62–69, 2015.

[36] Buller M. J., Latzka W. A., Yokota, M., Tharion W. J. and Moran, D. S. A real-time heat strain risk classifier using heart rate and skin temperature. *Physiol Meas*, 29(12):79–85, 2008.

[37] Nakanishi M., Izumi S., Nagayoshi1 S., Kawaguchi H., Yoshimoto M., Shiga T., Ando T., Nakae S., Usui C., Aoyama T. and Tanaka S. Estimating metabolic equivalents for activities in daily life using acceleration and heart rate in wearable devices. *Biomed Eng Online,* 17(1):100, 2018.

[38] Brandenburg S. G., Haas C. and Byrom K. Strategic Management of Human Resources in Construction. Journal of Management in Engineering, 22-2(89):471–480, 2009.

[39] Siew R. Human Resource Management in the Construction-Industry Sustainability Competencies. *AJCEB*, 14(2):87–103, 2014.

[40] Hashiguchi N., Cao J., Lim Y,, Kubota Y., Kitahara S., Ishida S. and Kodama K.; The Effects of Psychological Factors on Perceptions of Productivity in Construction Sites in Japan by Worker Age, *IJERPH*, 17,:3517, 2020.

An Integrated Sensor Network Method for Safety Management of Construction Workers

Tingsong Chen[a], Nobuyoshi Yabuki[b] and Tomohiro Fukuda[c]

[a,b,c]Graduate School of Engineering, Osaka University, Japan
E-mail: chen.tingsong@it.see.eng.osaka-u.ac.jp, yabuki@see.eng.osaka-u.ac.jp, fukuda@see.eng.osaka-u.ac.jp

Abstract –

With the development of the construction industry, many problems such as human safety are remaining unsolved. The construction holds the worst safety record compared to other industrial sectors, approximately 88% of accidents are related to workers' safety. The high complexity of the construction site compare to the ordinary living environment is also a major factor that cannot effectively protect the safety of workers. In this paper, an integrated sensor network method is proposed for the safety management of construction workers. The main signals collected in this paper are visual signals and electronic signals. The compatibility issues caused by cooperation between different types of signals will also be discussed in this paper. At the same time, a multi-signal automatic correction method is used to improve the accuracy and efficiency of our proposed method.

Keywords –

sensor fusion; motion recognition; safety management; IMU; depth camera.

1 Introduction

"Smart City" concept is widely known by people around the world for many years, the main purpose of it is using information technology to help to improve city service. Currently, Smart City is applied in transportation, citizen management, urban resource allocation and so on, they all perform well compare to traditional methods. Along with the rising of Smart City, the concept of "Smart Construction" is also proposed recently, many well applied methods from other fields are poured into construction area. But due to the differences in management mode and implementation, those methods perform not so well. There is a lot of room for development of Smart Construction.

Speaking of which, construction industry field still holds a worst record in safety compare to others. In Japan, death number in construction accidents is twice that of Germany and 3 times that of UK from data since 2003 to 2005 [1], and haven't improve well during the last 20 years [2]. Comparing to other developed countries, accident monitoring efficiency is the main reason that workers cannot be found and rescue in time.

The main causes of workers' injuries and deaths are heat stroke, hitting by heavy objects, felling from a height and so on. Some of the injuries are caused by accident, some of them happened because of the unsupervised unsafe acts of workers' own due to cost, time pressure and other reasons. Normal monitoring system such as web camera requires manual operation, it is inefficient because of human neglect, obstacle and other factors. A more efficient and accurate safety management and monitoring method is needed.

Camera-based monitoring method is widely used and researched around the world, it has a lot of benefits, such as low cost, easy to be assembled, and so on. Yet more disadvantages are unavoidable, such as unable to solve occlusion problem, low accuracy in weak light or dark environment. Other methods concentrate on changing RGB frame to RGB-D frame by adding depth into the picture, such as Kinect and Realsense. RGB-D is more accurate to detect human and object comparing to RGB's pixel crop, it also works well even in weak light environment. However, due to the limit of working distance, reflective surfaces and relative surface angles, depth maps in RGB-D frame always contain significant holes and serve noise, as shown in Figure 1, these errors limit the practical usage of RGB-D frame in real applications, thus depth maps restoration in hole filling and noise removing becomes a necessary step in depth-camera-based monitoring system.

Monitoring method based on Inertial Measurement Unit (IMU) sensors is also a hot topic in recent years, because of its undoubtable benefits compare to other methods such as visual camera. IMU sensors are nonintrusive, lightweight and portable measuring devices, they can overcome the sensor viewpoint and occlusion issues, once they were attached on subject, the activities can be detected in a non-hindering manner [4], [5], [6]. After pre-processing of the motion for activity

Figure 1. Depth map (top) and infrared frame

recognition, discriminative features are then derived from time and/or frequency domain representation of the motion signals [7] and used for activity classification [8]. Although there are a lot of benefits of IMU sensors, there are also some disadvantages, first, it is not intuitive, not easy for manual recheck, second, model complexity is hard to control especially when precise motion capture is needed.

In order to fix injuries problems in construction field, we propose a safety management method based on multiple sensor network. This method aims at using data of workers from different kinds of sensors to detect human motion and movement more accurately, sensors such as depth camera and IMU sensor will be used, and by cooperating them to decrease the error rate and improve efficiency in accident alert and injury rescue.

The main contributions of this paper are as below:

1. Improve the accuracy of multi-type sensor fusion based motion recognition in specific motions in construction site environment;
2. Multi-type sensor fusion based motion recognition correction method.

The remaining sections are organized as follows. Related works are reviewed in Section 2, including camera-based, depth camera-based and IMUs-based methods. The proposed methodology is introduced in Section 3, visual sensor-based human recognition, IMU s-based human recognition and sensor fusion method will be introduced. The simulation and experiment details and hardware parameters will be introduced in Section 4. The conclusion is drawn in Section 5.

2 Related works

2.1 Camera-based human modeling

Commercial camera-based human detection method requires subjects wear markers and depend on multiple calibrated cameras mounted in the environment. [9], it is inconvenient, to overcome these constraints, other researchers focus on developing marker-less approaches from multiple cameras, yet some of these methods require offline processing to achieve high quality results [10], [11]. But some other real-time approaches have been proposed [12], these approaches typically fit a skeletal model to image data. Other approaches to real-time performance include combining discriminative and generative approaches [13]. However, multi-view approaches assume stationary and well calibrated cameras, therefore they are not suitable in mobile scenarios.

2.2 Depth camera-based depth map restoration and human modeling

As for regular camera, RGB-based depth prediction normally uses large body of literature, training exclusively using ground truth metric depth, [14,15,16,17,18]. As for depth camera, many methods have been proposed for restoring depth maps by Kinect, these methods can be classified into two types: filtering-based and reconstruction-based. Filtering-based methods use different filters to restore captured depth maps. Lai et al. [19] applied a median filter in RGB space to fill holes in depth map recursively, however this method will blur sharp edges obviously. To preserve sharp edges, Camprani et al. [20] applied a joint bilateral filter in depth map iteratively. Matyunin et al. [21] considered using temporal information to restore depth map, but this method occurs delay because it uses multiple consecutive frames to restore target depth map. Reconstruction-based methods use image inpainting techniques to fix missing values in depth maps. Telea [22] proposed FMM (Fast Marching Method) for image inpainting. Miao et al. [23] proposed a texture-assisted method in which the texture edge information is extracted for assisting depth restoration. These methods can remove noise and fill small holes in depth maps, however when it comes to large holes exist in depth map, such as holes in Figure 1, the results are unsatisfactory.

About human modeling, Anguelov et al. [24] introduced SCAPE, a data-driven method for building a human 3D model than spans variation in both shape and pose. It shows that given a high-resolution range image from a single view, the SCAPE model can be used to observe data. Based on SCAPE parameterized model, Weiss et al. [25] combined multiple views of person and several low-resolution scans to obtain an accurate human 3D model. Liao et al. [26] introduced prior of human body pose and shape, then proposed a human 3D modeling method based on a monocular depth camera.

2.3 IMUs-based human modeling

Roetenberg et al. [27] used 17 IMUs equipped with 3D accelerometers, gyroscopes and magnetometers, fused together using a Kalman Filter. Assuming the measurement are noise-free and contain no drift, the 17 IMU orientations completely define the full pose of the subject (using standard skeletal models). However, 17 IMUs are very intrusive for the subject, long setup times are required, errors such as placing a sensor on the wrong limb are common, which makes it difficult to reproduce. Marcard et al. [28] compute accurate 3D poses using only 6 IMUs. They take a generative approach and place synthetic IMUs on Skinned Multi-Person Linear Model (SMPL) body model [29]. They solve for the sequence of SMPL poses that match the observed sequence of real measurements by optimizing over the entire sequence. But this method relies on computationally expensive offline optimization, which is also hard to reproduce. Therefore, a smaller number of IMU sensors and less computation complexity is the key of future IMUs-based human modeling and motion detection.

3 Methodology

In this paper, we propose an integrated sensor network method for safety management of construction workers. This method mainly uses depth camera, IMU sensor, and environment sensor to collect data from workers and construct human model to analyze human motion, gesture and some physical index such as temperature and air pressure. This method concentrates on multiple sensor cooperation, by using different kinds of sensor to decrease the errors caused by sensor defects, to increase the accuracy of detecting and improve efficiency.

3.1 Depth camera-based human recognition

Yin et al. [3] proposed a two-stage stacked hourglass network based on Varol et al. [30] to get high-quality result of human depth prediction. Instead of using RGB image directly, this method uses RGB image and human part-segmentation together to predict human depth. It consists of convolution layer, part-segmentation module, and depth prediction module. First, RGB image input goes through the convolution layer and turns into heat maps, then enter the part-segmentation module, after then, heat maps turn into human part-segmentation results, these heat maps are summed as the input of the following depth prediction module with previous layers features, finally human depth prediction results are outputted.

Algorithm 1 GradientFMM

1. **Procedure** GradientFMM (*depthmap*)
2. *Known* ← all pixels with known values in *depthmap*
3. *Unknown* ← all unknown pixels adjacent to *Known* in *depthmap*
4. insert all pixels in *Unknown* into min-heap
5. **while** *Unknown* not empty **do**
6. p ← root of min-heap
7. calculate p's value using *depth value equation*
8. add p to *Known*
9. remove p from *Unknown*
10. perform down heap
11. **for** each neighbor q of A **do**
12. **if** q not in *Known* and *Unknown* **then**
13. add q to *Unknown*
14. perform up heap
15. **end if**
16. **end for**
17. **end while**
18. return *Known*
19. **end procedure**

The algorithm above is called GradientFMM [3], it propagates depth from known pixels to unknown pixels. After the process, every pixel in depth map in the unknown region has a depth value. In order to mark useful pixels in depth maps to predict possible human skeleton, we use GradientFMM as our pre-treatment method in human depth prediction.

The resolution of collected image from depth camera is 848x480 and 30 frames per second. In our method, firstly we apply GradientFMM algorithm to analyze each frame and get data of human depth maps, next, we consider frame platform and depth direction as a 3D coordinate, and collect all coordinate data of each pixel inside depth map. At the same time, well-trained image processing algorithm will be used to identify skeleton based on depth map, in this research, we use OpenPose or Intel skeleton tracking SDK. After human skeleton is detected, the 3D coordinate changes of specific parts of human (head, hand, foot) and required parts (arm, waist) will be recorded, and compare with collected database, to find out the best match and output. Frames with skeleton will be used as input for further image processing to improve accuracy of skeleton mapping.

3.2 IMUs-based human recognition

This part introduces IMUs-based human motion detection, IMUs can measure triaxial (3D) accelerations and triaxial angular velocities. It is also easy to obtain information directly without numerous restrictions.

In our proposal, we mainly consider the motion capture while workers are working, so the upper body will be observation focus. 3 IMU sensors will be used to detect movement changes, two will be attached on outer arms, another one will be attached on front waist.

Not only can IMU sensors collect movement data, but also, they are able to collect workers' surrounding environmental factors such as temperature, height, air pressure and so on, by doing data exchange with environment sensors, to ensure that workers are in proper working environment.

IMU motion recognition is based on Dehzangi et al. [31], this paper introduced a human activity recognition method in normal environment, the activities they considered are walking, walking upstairs, walking downstairs, sitting, standing and sleeping. In our proposal, due to the difference of subjects, new motions are added: uplift (one or two arms up), pick up heavy object (the swing amplitude of both arms is reduced and stiff), hold up heavy object (the arms are partially angled and stiff), arms raised (arms at right angles to body), regular cyclical movement (arms turn the roulette), bend over (lean forward or backward).

The framework of IMU-based human activity recognition system is: first, collecting relevant data through users; then, in the learning phase, relevant features are extracted from the time-series raw data. Model complexity is reduced by applying Feature selection/ Dimension reduction technique. Recognition model is created from the dataset of selected features. Then, in the testing phase, this model is used to evaluate raw signal and create an activity label. Finally, raw data will be outputted as labeled motion.

IMU sensors attached in 3 parts will continuously record data, and using motion recognition method to analyze amplitude changes. At the same time, when there is a dramatic change during the process, the differences between triaxial accelerations and angular velocities before and after the change will be counted and recorded as change graphs. Finally, the differences will be compared with motion database and find out the best match.

3.3 Multi-type sensor fusion and analysis

Normally, visual signal and IMU electronic signal are quite different, it is hard to make a comparison between them. In our proposal, both visual camera-based method and IMU sensor-based method can perform results individually, but when it comes to some special occasion such as partly occlusion, using only one kind of signal will cause high error and effect the whole system.

In this research, we try to cooperate two kinds of signal, by educe the advantages and disadvantages of them to further improve accuracy of this method. We consider the whole area as a huge 3D coordinate system, as shown in Figure 3, depth camera is placed on one side of the system, IMU sensors are also calibrated before loading to make sure they are consistent at time 0.

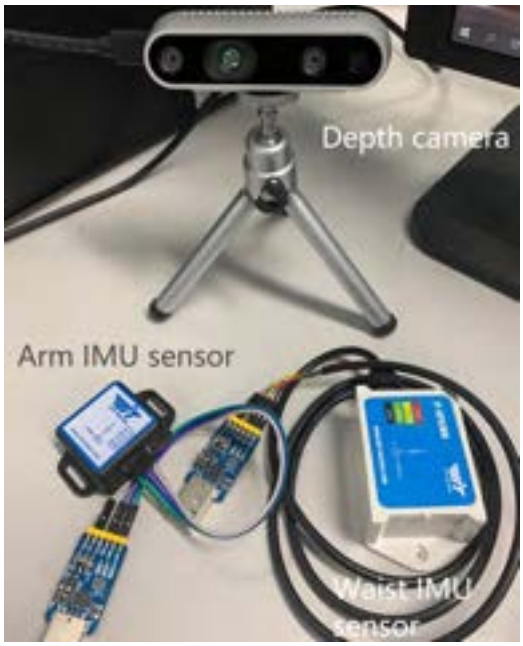

Figure 2. Depth camera and IMU sensors

As introduced in previous sections, when record starts, both camera and IMU sides will generate constant 3D coordinate changes. As for depth camera side, the variation and value of specific point can get from the coordinate made by depth map and frame platform. As for IMU sensor side, during the movement, three axes will change in different accelerations, based on the origin set at time 0, the path changes and distance can be calculated by double integral:

$$\vec{S} = \int(\int(\vec{a})\mathrm{dt})\mathrm{dt} \quad (1)$$

where $\vec{S}$ represent directional distance, $\vec{a}$ represent average acceleration during time period t.

Although the unit, distance and size are quite different between depth map coordinate and IMU sensor coordinate, we can describe the change amplitude curve between specified coordinate points (in this case, points of two arms and waist), by considering the weight of each kind of sensor, we can get a more accurate result to make comparison with database, and gaining a higher reliability on human motion recognition.

The equation of final degree of change is:

$$\Delta P = (\Delta P_v / P_v^0 \cdot \alpha + \Delta P_I / P_I^0 \cdot \beta)/2 \quad (2)$$

where ΔP_v is the change of motion from visual side, ΔP_I is the change of motion from IMU sensor side, P_v^0 and P_I^0 are the initial states of the current time segment, α and β are weight coefficients for visual and IMU sides.

The directional distance of each axes in each sensor can be calculated by Equation (1), and the degree of change in each sensor can be evaluated by Equation (2).

4 Experiment

This section makes experiment to validate the feasibility of our proposal. It includes the following aspects:

(1) Using depth camera to detect human skeleton and motion based on our visual recognition method, and record the 3D coordinates of depth maps;
(2) Using attached IMU sensors to detect human upper body skeleton and motion based on our applied motion recognition method, and record the coordinate differences of each sensor;
(3) Using our multi-type signal fusion correction method based on weight to generate coordinate differences from each frame and frequency. And output final accuracy.

In order to get the depth maps of subjects, an Intel Realsense D435i camera is settled, and shooting from one side of our experiment area. The picture of camera is shown in Figure 2, it can achieve a smooth video streaming with 848x480 resolution and 30 frames per second. Possible detecting range is from 0.3 m to 16 m.

In order to get the 3D motion data of subjects, 3 Witmotion IMU sensors are attached on subjects' two outer arms, and front waist. The arm sensor model is BWT901CL, the detectable parameters are acceleration, angle, velocity, magnitude, temperature. The waist sensor model is WTAHRS2, the detectable parameters include above and air pressure, height, which can make sure the surrounding environment of workers is stable and comfortable.

The experiment area is settled as Figure 3, depth camera is placed in front of the whole area, IMU sensors are attached on worker's outer arms and front waist, the worker will continue making different gestures in front of the depth camera.

Before the beginning of experiment, the database of actions to be tested which also is the control group will be prepared. In this experiment, several motions will be considered, including normal motions such as stand, sit, and sleep (lie down), other specific motions in construction site such as uplift, pick up heavy object, hold up heavy object, arms raised, regular cyclical movement and bend over will also be included.

The experiment process will be introduced as follows:

First, experiment subject (worker) will be attached with sensors, and stand in the proper position inside experiment area;

Next, experiment subject will make corresponding actions in order, there will be a break between each two motions;

Then, depth camera-based method will generate depth map, all pixels' coordinate information will be recorded, human skeleton will be generated based on image processing, human parts will be labeled and

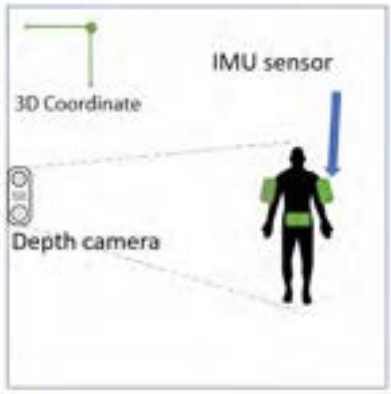

Figure 3. experiment area layout

corresponding to pixels, the coordinate amplitude of these parts will be recorded as well;

Next, IMUs-based method will collect data changes from 3 sensors, during the process, a low pass filter will be settled to eliminate redundant noise;

Then, the acceleration changes of each sensors will be used to calculate path changes by double integral;

Next, the changes of points of three human parts from visual side and IMUs side will be calculated separately to obtain degree of change within a certain period of time;

Then, degree of change from visual and IMUs side will be used to calculate the weight average, the result will be compared with database to find the best match;

Meanwhile, origin degree of change from visual and IMUs side will be compared with database separately;

Finally, the similarity from visual side, IMUs side and sensor fusion side will be compared, to prove if the sensor fusion method shows the best result.

As for the degree of change for IMUs, we set experimental steps as follows:

1. Calibration procedure: remove the output offset component of the acceleration sensor because of the presence of static acceleration (gravity). The method is to average the acceleration when there is no motion in accelerometer. (the more samples we collect, the more accurate the calibration result will be)
2. Low pass filtering: eliminate signal noise in accelerometers (both mechanical and electronic), to decrease the error while integrating the signal.
3. Mechanical filtering: when in a stationary state, small errors in acceleration will be treated as constant speeds, it indicates a continuous movement and unstable position, which will affect the actual motion detection. A mechanical filtering window will help to distinguish the small errors.
4. Positioning: the acceleration of each time period is known, we use double integral to obtain distance

information. The first integral gains speed and the second gains position.

In our simulation, we suppose 9 motions have their own perfect degree of change, includes vector changes from left arm, right arm and front waist:

$$M_n = \begin{bmatrix} \overrightarrow{L_n} \\ \overrightarrow{R_n} \\ \overrightarrow{W_n} \end{bmatrix}, n \in [1,9] \quad (3)$$

$$\overrightarrow{L_n} = \left(\Delta x_n^L, \Delta y_n^L, \Delta z_n^L\right) \quad (4)$$

$$\overrightarrow{R_n} = \left(\Delta x_n^R, \Delta y_n^R, \Delta z_n^R\right) \quad (5)$$

$$\overrightarrow{W_n} = \left(\Delta x_n^W, \Delta y_n^W, \Delta z_n^W\right) \quad (6)$$

where $\vec{L}, \vec{R}, \vec{W}$ represent the change of motion from left arm, right arm and front waist.

Generated data are divided into 2 groups, on visual side, the vector changes will be found by pixels and depth, on IMUs side, through the acceleration of three axes and time, Equation (1) will be used to obtain the distance in all directions, thereby obtaining the vector change. Then, assign a weighting coefficient to vision and IMU part through standard normal distribution, next, we will use Equation (2) to calculate the integrated vector change:

$$F = \begin{bmatrix} (L_v/L_v^0 \cdot \alpha + L_I/L_I^0 \cdot \beta)/2 \\ (R_v/R_v^0 \cdot \alpha + R_I/R_I^0 \cdot \beta)/2 \\ (W_v/W_v^0 \cdot \alpha + W_I/W_I^0 \cdot \beta)/2 \end{bmatrix} \quad (7)$$

where L_v is the left arm vector change on visual side, L_I is the left arm vector change on IMU side. F will be compared with M_1 to M_9 in Equation (3) to find out the best match.

100 pairs of sample data for each motion are generated based on our database by adding random interferences and white noise, to simulate deviations caused by the effects of real data collection. Weight coefficients obey standard normal distribution. By comparing our modified data with real motion data, the result of accuracy is shown on Figure 4. We can see that some similar motions such as standing and pick up heavy object, hold up heavy object and arm raised, sometimes are indistinguishable, this may become a more serious problem in real world sampling. Our simulation on 900 pairs of motion samples in total shows that averagely the accuracy of motion recognition by multi-type sensor fusion is about 97%, although the number of samples is not large, but this result shows that multi-type sensor fusion is possible to improve the accuracy of specific motion recognition in construction site condition. In real world experiment, due to other unexpected interferences and noises, the result may

real motion / detected motion	stand	sit	sleep	uplift	pick up heavy	hold up heavy	arm raised	regular cyclical	bend over	total
stand	95	3			2					
sit		96			1					
sleeping			100							
uplift				98			1			
pick up heavy	5	1			96					
hold up heavy						92	5			
arm raised				2	1	8	94			
regular cyclical								100		
bend over									100	
accuracy	95%	96%	100%	98%	96%	92%	94%	100%	100%	97%

Figure 4. simulation result.

change a bit, but due to the large number of samples, we expect the result to be as good as our simulation result.

5 Conclusion

In this paper, a new method is proposed for motion recognition and safety management of construction workers by using integrated sensor network, in order to effectively ensure the safety of workers in complex environment of construction site. We improve the motion recognition with depth maps, we also proposed several new motions that are usually shown in construction site and generate the database of each new motions' degree of change in relative 3D coordinate system. We proved that using multi-type sensor fusion to recognize human motion is possible, and our simulation shows that the accuracy is quite high compare to some related works.

We also noticed several problems during our research, such as distinction of similar motions. In the future, we will consider to add more special motions to expand recognition range, we will also improve the accuracy of skeleton interest point movement to decrease detection error from similar motions. IMUs-based motion recognition method is considered to be improved as well, meanwhile, a remote VR-based motion recognition system is included in our consideration.

References

[1] ACCESS, Comparison of Japan with other developed countries, Online: http://www.kasetsuanzen.or.jp/industrial_accident/compare.html, Accessed: 08/06/2020.

[2] JCOSHA, Occurrence of labor disaster in construction, Online: https://www.kensaibou.or.jp/safe_tech/statistics/occupational_accidents.html, Accessed: 08/06/2020.

[3] J. F. Yin, et al., Depth Maps Restoration for Human Using RealSense. IEEE Access, Vol. 7, pages 112544-112553, 2019.

[4] O. C. Ann, et al., Human activity recognition: A

review, IEEE International Conference on Control System, Computing and Engineering (ICCSCE 2014), pages 389–393, Batu Ferringhi, Malaysia, Nov. 2014.

[5] O. Dehzangi, et al., "IMU-based gait recognition using convolutional neural networks and multi-sensor fusion, Sensors, vol. 17, no. 12, page 2735, 2017.

[6] A. Cismas, et al., Crash detection using imu sensors, 21st International Conference on Control Systems and Computer Science (CSCS), pages 672–676, Bucharest, Romania, May 2017.

[7] S. J. Preece, et al., A comparison of feature extraction methods for the classification of dynamic activities from accelerometer data, IEEE Transactions on Biomedical Engineering, vol. 56, no. 3, pages 871–879, March 2009.

[8] S. J. Preece, et al., Activity identification using body mounted sensors a review of classification techniques, Physiological Measurement, vol. 30, no. 4, page R1, 2009.

[9] N. Sarafianos, et al., 3d human pose estimation: A review of the literature and analysis of covariates. Computer Vision and Image Understanding, 152, pages 1–20, 2016.

[10] L. Ballan, et al., Motion capture of hands in action using discriminative salient points. Computer Vision–ECCV 2012, pages 640–653, 2012.

[11] Y. H. Huang, et al., Towards Accurate Markerless Human Shape and Pose Estimation over Time. International Conference on 3D Vision (3DV), pages 421–430, 2017.

[12] H. Rhodin, et al., A versatile scene model with differentiable visibility applied to generative pose estimation. In Proceedings of the IEEE International Conference on Computer Vision, pages 765–773,2015.

[13] A. Aguia, et al., MARCOnI-ConvNet-Based MARker-Less Motion Capture in Outdoor and Indoor Scenes. IEEE transactions on pattern analysis and machine intelligence 39, 3, pages 501–514, 2017.

[14] D. Eigen, et al., Predicting depth, surface normal and semantic labels with a common multi-scale convolutional architecture, In Proc. IEEE Int. Conf. Comput. Vis., pages 2650-2658, Dec. 2015.

[15] B. Li, et al., Depth and surface normal estimation from monocular images using regression on deep features and hierarchical CRFs, in Proc. IEEE Conf. Comput. Vis. Pattern Recognit., Jun. 2015, pages 1119-1127.

[16] F. Liu, et al., Deep convolutional neural fields for depth estimation from a single image, in Proc. IEEE Conf. Comput. Vis. Pattern Recognit., pages 5162-5170, Jun. 2015.

[17] Z. Zhang, et al., Monocular object instance segmentation and depth ordering with CNNs, arXiv:1505.03159, Dec. 2015.

[18] X. Zhou, et al., Towards 3D human pose estimation in the wild: A weakly-supervised approach, In Proc. IEEE Int. Conf. Comput. Vis., pages 398-407, Oct. 2017.

[19] K. Lai, et al., A large-scale hierarchical multiview RGB-D object dataset, In Proc. IEEE Int. Conf. Robot. Automat., pages 1817-1824, May 2011.

[20] M. Camplani, et al., Efficient spatio-temporal hole filling strategy for Kinect depth maps, Proc. SPIE, vol. 8290, Art. no. 82900E, Jan. 2012.

[21] S. Matyunin, et al., Temporal filtering for depth maps generated by Kinect depth camera, In Proc. 3DTV Conf., True Vis.-Capture, Transmiss. Display 3D Video, May 2011, pages 1-4.

[22] A. Telea, An image inpainting technique based on the fast marching method, J. Graph. Tools, vol. 9, no. 1, pages 23-34, 2004.

[23] D. Miao, et al., Texture-assisted Kinect depth inpainting, In Proc. IEEE Int. Symp. Circuits Syst., pages 604-607, May 2012.

[24] D. Anguelov, et al., SCAPE: Shape completion and animation of people, ACM Trans. Graph., vol. 24, no. 3, pages 408-416, Jul. 2005.

[25] A. Weiss, et al., Home 3D body scans from noisy image and range data, in Proc. Int. Conf. Comput. Vis., pages 1951-1958, Nov. 2011.

[26] L. Liao, et al., Individual 3D model estimation for realtime human motion capture, in Proc. Int. Conf. Virtual Reality Vis., pages 235-240, Oct. 2017.

[27] D. Roetenberg, et al., Moven: Full 6dof human motion tracking using miniature inertial sensors. Xsen Technologies, December 2007.

[28] T. Marcard, et al., Sparse inertial poser: Automatic 3D human pose estimation from sparse IMUs. In Computer Graphics Forum, Vol. 36. Wiley Online Library, pages 349–360, 2017.

[29] M. Loper, et al., SMPL: A skinned multi-person linear model. ACM Transactions on Graphics (TOG) Vol.34, no.6, page 248, 2015.

[30] G. Varol, et al., Learning from synthetic humans, In Proc. IEEE Conf. Comput. Vis. Pattern Recognit., pages 109-117, Jul. 2017.

[31] O. Dehzangi, et al., "IMU-Based Robust Human Activity Recognition using Feature Analysis, Extraction, and Reduction", ICPR 2018, pages 1402-1408, Beijing, China, 2018.

Data-Driven Worker Detection from Load-View Crane Camera

Tanittha Sutjaritvorakul, Axel Vierling and Karsten Berns

Department of Computer Science, Technische Universität Kaiserslautern, Germany
E-mail: {tanittha,vierling,berns}@cs.uni-kl.de

Abstract -

Cranes as an essential part of the construction machinery, are one of the prominent sources of fatalities in the construction sites. The camera assistant system can contribute significantly to the safety of the crane operation particularly in blind lifts tasks, where the operator highly relies on the load-view camera. In this paper, we address the worker detection from an off-the-shelf load-view crane camera using a data-driven approach. Due to the difficulties in collecting data, we generate five training datasets via a simulation platform to build up the synthetic samples to improve the state-of-the-art detector. Despite the fact that only the simulation data is used as training datasets, the trained network demonstrates the average precision of up to 66.84% in two real-world scenarios.

Keywords -

Construction safety; Crane simulation; Worker detection; Visibility assistance

1 Introduction

The number of crane accidents caused by visibility remains high. The load-view crane camera is essentially used to widen the operator's field of v iew. However, it is hard for operators to keep observing hazards from merely a seven-inch monitor with no semantic information such as the position of the worker with respect to the crane or load. This work presents an analysis of a data-driven worker detection from a load-view camera using solely synthetic data in the learning procedure. The large volume of synthetic data is created by the simulation platform.

According to visibility-related fatalities, struck-by accidents contribute to 87.7% of all construction equipment accidents [8]. Cranes, which are the main machines in the construction, carry out the major activities in the building construction industry. Falling loads or struck-by loads are the most common and most dangerous crane-related hazards. The workers can be struck or hit by any moving load while they are working in close proximity to the crane. The poor visibility or blindspot causes the operator has difficulties to identify any personnel or objects in the work zone. Unlike in the street environment, the construction site is complex and unstructured. Workers and machines work side by side. The operator simultaneously monitors many things e.g., load radius, workers-on-foot, and spotter. Automated localizing workers or objects surrounding the load allows operators to understand the situation, and make decisions and actions accordingly.

Figure 1. Crane load-view camera circled in red.

Not all sensor types are suitable to monitor objects from the load. Numerous crane safety assistance methods are presented in previous studies. The proximity warning is prevalent. Many sensor-based technologies have been adopted for construction safety assistance. These sensors can be installed on the site, workers or machines themselves to recognize objects. To increase spatial awareness of the operator, the load sway monitor can be observed using IMU or a camera [4, 5]. Similarly, hook motion tracking can measure the working radius in order to avoid collision [28, 12, 17]. Wearable devices such as bluetooth, RFID, and ultra-wideband (UWB) tag on safety helmet which provides the position can be irritating and privacy-intrusive to the workers [25, 29]. The operator mainly depends on the load-view camera during lifting tasks. It allows the operator to inspect the distance between the load and obstruction without occlusion among other objects. The view provides the top perspective from the camera mounted at the boom head pointing down to the ground. Information from any sensors installed on-site or on the cabin itself can be insufficient for the operator

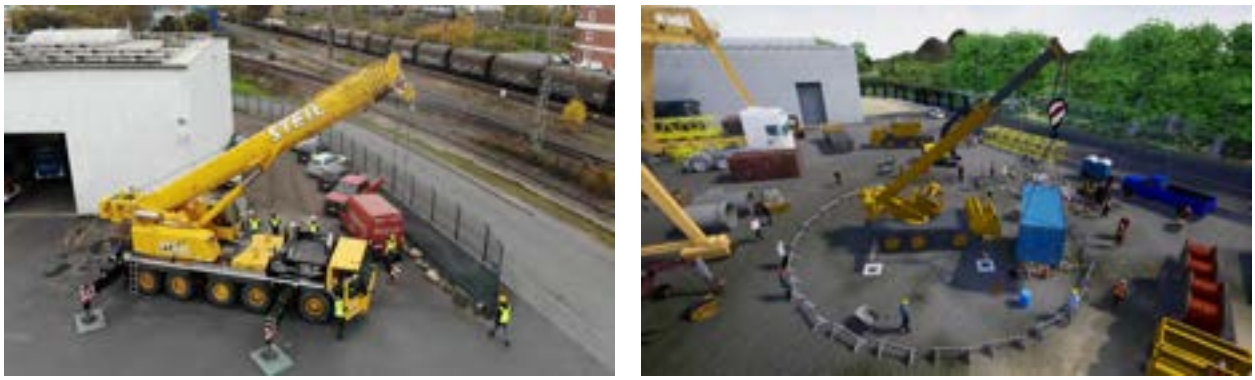

Figure 2. Comparison of real (left) and virtual (right) view at the experimental site in Trier, Germany.

during lifting materials over or into the building. The operator is unable to directly observe any adjacent objects due to the obstruction.

Detecting workers from the load-view is challenging. There is a lack of research on this topic. Traditional worker detection methods are based on simple features like helmet and color of high visibility vest [18, 26, 24]. In fact, most workers do not regularly wear protective clothes. The average of 87 percent of construction workers is reported as Personal Protective Equipment (PPE) noncompliance [20]. Thus using PPE information, the high-visibility color of helmet or vest, as a feature to detect workers may not be adequate. In general, it is very hard for a human to notice the small-sized workers from the top view, see Figure 3(f) which explains the high fatality rate in crane operation and necessitates the application of load-view worker detection. The construction area is cluttered and dynamically changing over time.

With the outstanding results, the construction domain also employs the data-hungry learning methods into worker recognition. The following studies of detecting workers from load-view camera or similar use deep learning approaches. Yang et al. [34] use Mask R-CNN to detect workers from a tower crane and identify if the workers are in the safety distance. Hu et al. [9] use YOLOv3 to detect non-complaint worker without a helmet. Vierling et al. [30] propose an automatic zoom load-view camera based on the working zone and load occlusion. The authors train the convolutional neural network with the load-view image and current zoom level, then result the optimal zoom level for the operator.

There is an intensive shortage of training data in the construction domain. The performance of deep learning methods is highly dependent on the existence of ample training samples. The self-driving car datasets publicly exist in great amount [11]. However, these datasets are not applicable to load-view object detection due to the frontal viewpoint. In addition, Unmanned Aerial Vehicle (UAV) datasets [23, 33, 1] could not be used as an alternative because of an uncluttered and static background, unlike the construction area. The pose or activity of the worker and the pedestrian are not identical, which can lead to different image features.

Data collection is crucial. Gathering data consists of two main steps, namely data recording, and annotation. Recording data from a car is relatively straightforward as opposed to a huge construction machine. The sensors can be easily mounted and adjusted. The driver does not require any additional specific skills. Image annotation techniques can be manual, semi-automatic, and automatic. Manual annotating data is tedious. The annotator required the knowledge to fulfill the task e.g., occlusion constraints, object representation, and boundary [2]. For a very large scale dataset, there exist crowd-sourcing platforms, such as Amazon Mechanical Turk (MTurk), to gather image annotation possible. Regardless of the verified annotated data, Zhang et al. [35] show the localization errors of original annotation in Caltech dataset.

Besides the benefits of using simulation as a construction robot test platform or vocational training, simulation also helps to augment data while reducing localization error and time from the manual labeling. Vierling et al. [31] develop the automated data generation tool in a game engine. Soltani et al. [27] propose automated annotation using synthetic images of construction resources is able to reduce the annotating time while improving the detection accuracy. The synthetic data can be used as an additional option to generate the training samples. Several studies [19, 32] demonstrate the synthetic data, which is generated from a game engine, can be used in a real-life scenario. With the rendering capability, the game engines like Unreal Engine[1] can generate the photorealistic environment and human characters. The virtual characters

[1]A game engine developed by Epic Games (www.unrealengine.com)

should behave naturally. Jan et al. [7] modelled and validated the usage of virtual characters in Unreal Engine for pedestrian-vehicle interaction system for an autonomous vehicle.

This paper aims to detect workers from a load-view crane camera using a data-driven detection approach. Worker detector can semantically provide information about what is happening nearby the load for the operators. With promising performance of DNN, RetinaNet architecture [14] is selected as a worker detector for our experiment. In order to cope with the absence of data, we generated the synthetic training data from virtual environment which is similar to the real experimental site. Special attention is given to construct the worker appearance, clothing and movements.

2 Methodology

Our approach consists of two main parts, data collection, and worker detection. First, the data collection describes how we gather the dataset from the real scenario and simulated platform. The second part explains the choice of detection algorithm and training strategy. The test crane used in this work is a telescopic crane (Liebherr LTM1130) while the testing took place in Trier, Germany. The standard crane load-view camera (Motec MC5200) is used in detecting workers. It is mounted at the boom end via pendulum bracket, looking downward, see Figure 1. The hardware used in detection experiments is NVIDIA GeForce GTX 1060, 3GB GDDR5.

(a) UT0 (b) UT1 (c) UT2 (d) UT4 (e) R1 (f) R2

Figure 3. Sample datasets for worker detection.

2.1 Data Collection

All collected data is listed in Table 1. The sequence name with a prefix of *R* is collected from the real mobile crane at the experimental site while the one with prefix *UT* is data generated by Unreal Engine. Examples of the data can be found in Figure 3. In a real-world scenario, the data is taken from the crane using 3-7 participants in the scene. The estimated distance of the camera to the ground (D_{cam}) is 25-35 meters, which refers to a 6- to 8-floor building. The crane performs basic lifting task—hoisting, extending, retracting boom, etc. In sequence R2, the test load is a wooden pallet. The annotation is done by hand which took about 14-20 seconds per frame.

For the synthetic data, we use a simulation system that developed in [32, 6]. The platform exploits the game engine features which allow us to create alike environment as the experimental site, see Figure 2. It provides large, diverse data with accurate annotation in an instant. The datasets contain workers, with and without PPE on diverse appearances and activities e.g., talking on the phone, standing upright, driving in the truck, carrying, pushing the wheelbarrow, or working with the device. Similar to the real world, construction machines, equipment, and material are present. Within the same scenario, different weather conditions can be rendered. The load-view camera setup is installed in the same manner as the real hardware. We generated 5 virtual image sequences, UT0-UT4 under daylight conditions. The sequence number of the synthetic data defines the level of boom arm extension e.g., UT0 means no boom extension and UT4 means the crane extends the boom up to 4th section. The main boom angle to the ground of all synthetic sequences is 60 degrees. In each sequence, the images are randomly captured while the turret is rotating from 0 to 360 degrees.

2.2 Worker Detection

Choosing network architecture is a difficult task because of speed–accuracy trade-offs [10]. With the great achievement of the deep neural network (DNN), it has been widely used and takes over the traditional image recognition methods. Regarding the requirement of visibility assistance, the operator should be alarmed about any surrounding

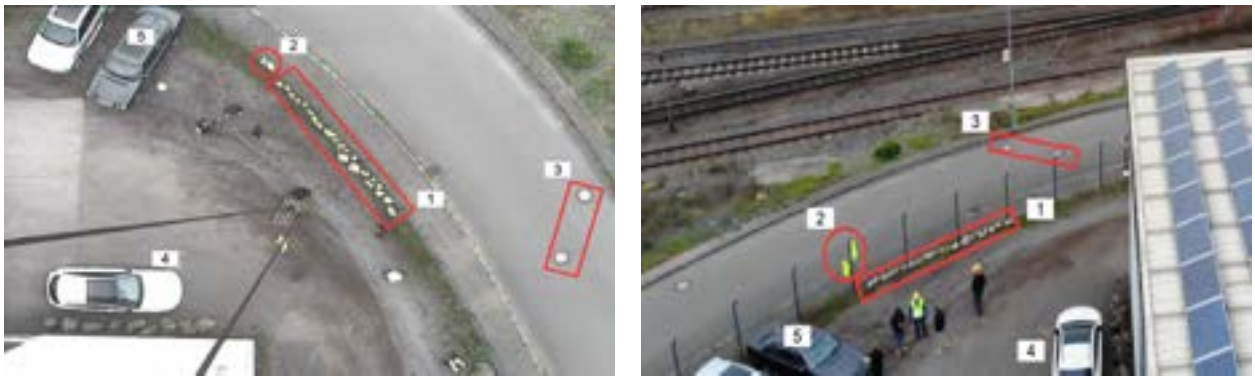

Figure 4. Comparison of the top view perspective between load-view camera (left) and drone camera (right). The identity of each object in both images is defined by the same number tag in the scenario. Number 1 is a rock border next to the fence. Number 2 is two green emergency vests hanging on the fence. Number 3 is two road manholes. Number 4-5 are cars.

Table 1. Dataset Summary.

Seq name	Frames	Resolution	D_{cam}(m)	Average object instances per frame	Total object instances
UT0	120	1600x1200	12	2	283
UT1	300	1600x1200	19	3	753
UT2	303	1600x1200	26	5	1636
UT3	501	1600x1200	33	9	4463
UT4	1110	1600x1200	39	8	8448
R1	713	720x480	25	3	2139
R2	400	720x480	35	7	2795

workers-on-foot in order to be aware of the hazards in (near) real-time.

Object detectors based on the DNN can be mainly categorized into two groups, two-stage detector, and single-stage detector. Two-stage detectors, such as all R-CNN model series [22], are mainly based on regional proposal network (RPN). In the first stage, the model proposes a set of sparse regions of interest by RPN or selective search. The candidates are later classified in the second stage. The accuracy of these models results relatively high but is typically slower. On the other hand, one-stage detectors, SSD [16], YOLO family models [21], and RetinaNet [14], propose the candidates from the input image directly without region proposal step. This leads to simpler and faster model architecture while lessening the performance slightly.

In this paper, we select the object detector based on RetinaNet for our experiments. It is introduced to handle objects in different scales and accurately localize dense objects. The focal loss in RetinaNet tackles an extreme imbalance between background which contains no object and foreground which has objects of interest. In other words, there are a very large number of negative samples and only a few positive samples. Therefore, RetinaNet works well in detecting small targets and high density such as the view from the UAV or load-view crane camera. The backbone network of RetinaNet is the featurized image pyramids which allow detecting object in multiscale [13].

To create the synthetic data closely resembling the target dataset (i.e., R1 and R2), the synthetic data are pre-processed by image filtering. We notice that the target images have more motion blur than the training samples because they tend to come from the swing movement of the camera, the vibration of the machine, or video interlace. For this reason, the motion blur is added to the synthetic data. In practice, the averaging filter with the kernel size of 10x10 applies to all simulated data in order to blur the images. The original synthetic datasets are denoted as UT0-UT4 and the blurred datasets are denoted $\overline{\text{UT0}}$-$\overline{\text{UT4}}$.

The ResNet-50 model is used as a backbone network. We initialize our weights from a pre-trained checkpoint of the COCO dataset [15]. All synthetic data, $\overline{\text{UT0}}$-$\overline{\text{UT4}}$ are combined and randomly shuffled into training and validation sets. The train set and the validation set consist of

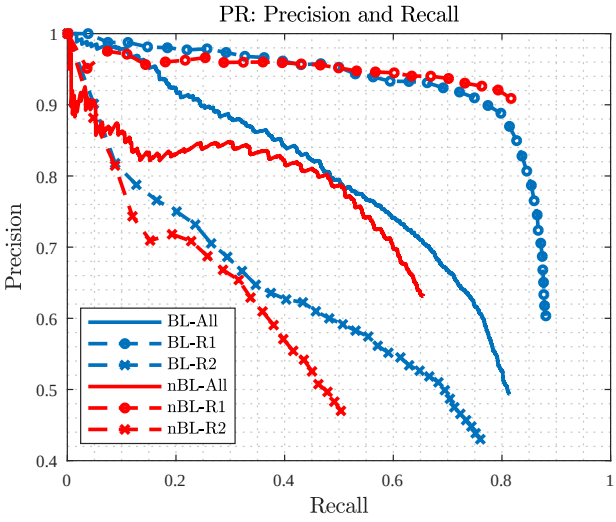

Figure 5. Precision-Recall curves of the experiments. AP in Table 2 can be achieved by the approximation of area under PR curve.

10907 and 4675 objects respectively. The test set with 4934 objects are from R1 and R2. The network is trained until the optimal point with a learning rate of $1e-7$. The sizes of anchors are set to {32, 64, 128, 256, 512} and the strides to {8, 16, 32, 64, 128}.

3 Results and Analysis

We conducted two main trials. In the first trial (BL), we trained the network with the blurred images ($\overline{\text{UT0}}$-$\overline{\text{UT4}}$) and for the second trial (nBL) the non-blurred images, UT0-UT4, are used for training. In each trial, we validate the network with two test sets, R1 and R2. Our detection evaluation metric is adopted from PASCAL Challenge [3] with Intersection over Union (IoU) threshold of 0.5.

$$IoU = \frac{B_p \cap B_{gt}}{B_p \cup B_{gt}} \quad (1)$$

B_p is predicted bounding box and B_{gt} is ground truth bounding box. Average Precision (AP) is widely used in measuring the accuracy among object detectors. The metric is based on the precision-recall (PR) curve. Figure 6 presents several predicted frames from both test sets. APs of the trials are listed in Table 2. The AP is obtained by the approximation of areas under PR curve.

First, we evaluate the networks, which are trained with blurred and non-blurred images on the test sequence R1. Both of them, $BL-R1$ and $nBL-R1$, yield nearly the same results (AP≈78%). The workers in the sequence most often can be recognized by both networks. Despite the low-light condition, the workers were wearing the high-visibility color vest and hard helmet which can be visible

Table 2. Results of AP on each dataset.

Trial	Test seq name	AP@0.5 (%)	Average inference time (ms per frame)
$BL-All$	R1,R2	**66.84**	-
$BL-R1$	R1	78.10	150.0
$BL-R2$	R2	**50.10**	152.7
$nBL-All$	R1,R2	53.13	-
$nBL-R1$	R1	**78.20**	155.6
$nBL-R2$	R2	38.26	151.7

to the networks. Afterward, we assessed the second test sequence R2 for the trial $BL-R2$ and $nBL-R2$. The detector trained with blurred images, $BL-R2$, shows a positive outcome. As a result, the overall AP of the network is higher when trained with the blurred datasets ($\overline{\text{UT0}}$-$\overline{\text{UT4}}$), compared to the non-blurred ones (UT0-UT4), check the AP values for trial $BL-All$ and $nBL-All$ in Table 2. The difference in the average predicting times among trails is minor.

In fact, R2 is a difficult sequence. It is recorded in higher elevation and thus it is hard to recognize the worker. Figure 4 shows the comparison of the same objects from two different camera angles. Apparently, the white rocks (number 1) and manholes (number 3) are almost identical to the person wearing the safety helmet. The workers' appearance form a similar color and shape view as of the ground. For the green emergency vest, we notice that the load-view camera is unable to reproduce the same color as shown in the drone camera or being visible to the human eye. Instead, it displays as white pixels, see Figure 4. This could be caused by the variant brightness, low image resolution, etc. In addition to the issue of the traditional detectors using only PPE color features mentioned in Section 1, color inaccuracy shown in the load-view camera can worsen these detectors because those color feature ranges are normally predefined. These negative samples can likely lure the human to misjudge as well as the detector.

Furthermore, we had prior experience in training the load-view worker detector with UAV data whose detail is not included in this work. The data are initially expected to be used as an alternative to augment the training dataset for load-view worker detection. However, the prediction results were unsatisfactory. Evidently, the workers in the drone camera in Figure 4 can be seen fully while only the heads and shoulders of the workers in the load-view camera are visible. Consequently, using artificial data to train a DNN model is beneficial. The model acquires the image features and is able to yield good performance without seeing none of the real-world data.

Figure 6. Predicted results of trial *BL* on the test sequence R1 in the first row (frame 30, 219, 632) and R2 in the second row (frame 40, 297, 348). The blue bounding box is the detected target with confidence score label while the green box is groundtruth.

4 Conclusion

In this paper, we demonstrate the worker detector from a load-view camera using RetinaNet. This one-stage detector is able to localize and classify small-sized objects in dense areas. Two test image sequences are collected from the real crane. Regarding data shortage and complexity in data collection, we created the five image sequences from different altitudes by the simulated platform in Unreal Engine. The platform allows us to generate plenty of data in an accurate and fast manner. The datasets are synthesized with the motion blur and later fed into the learning procedure. There are two networks trained for evaluation. The first network is trained with preprocessed images and the second is trained with the primitive images. Finally, the detector ran on the two test sequences were taken from the real crane. Blurred virtual data appears to make data more realistic to the learning algorithm.

For future study, worker tracking and activity recognition could be added to reduce misinterpretation between non-object and object. Different synthesized techniques can possibly experiment on the images for training, such as video interlace and synthetic image refiner. Using synthetic data still requires more effort to study because the synthetic data sometimes looks realistic to a person but it can appear to be unrealistic to the learning algorithms.

In conclusion, the worker detector can be used as additional information for risk assessment for each worker. Visualization of workers nearby in 2D or 3D with respect to the crane including the risk level of each worker can be useful for the situational awareness of the operators. This can provide support to the crane operators to identify hazards during operation.

5 Acknowledgement

This work is funded from the Federal Ministry of Education and Research (BMBF) under grant agreement number 01|16SV7738 and named SAFEGUARD.

References

[1] Mohammadamin Barekatain, Miquel Martí, Hsueh-Fu Shih, Samuel Murray, Kotaro Nakayama, Yutaka Matsuo, and Helmut Prendinger. Okutama-action: An aerial view video dataset for concurrent human action detection. In Proceedings of the IEEE Conference on Computer Vision and Pattern Recognition Workshops, pages 28–35, 2017.

[2] Adela Barriuso and Antonio Torralba. Notes on image annotation. arXiv preprint arXiv:1210.3448, 2012.

[3] M. Everingham, L. Van Gool, C. K. I. Williams, J. Winn, and A. Zisserman. The PASCAL Visual Object Classes Challenge 2007 (VOC2007) Results.

[4] Yihai Fang, Jingdao Chen, Yong K Cho, Kinam Kim, Sijie Zhang, and Esau Perez. Vision-based load sway monitoring to improve crane safety in blind lifts. Journal of Structural Integrity and Maintenance, 3(4):233–242, 2018.

[5] Yihai Fang and Yong K Cho. Crane load positioning and sway monitoring using an inertial measurement unit. In Computing in Civil Engineering 2015, pages 700–707. 2015.

[6] Jan Qazi Hamza, Kleen Jan, and Karsten Berns. Self-aware pedestrians modeling for testing autonomous vehicles in simulation. In Proceedings of the 6th International Conference on Vehicle Technology and Intelligent Transport Systems (VEHITS 2020), 2020.

[7] Jan Qazi Hamza, Klein Sascha, and Berns Karsten. Safe and efficient navigation of an autonomous shuttle in a pedestrian zone. In International Conference on Robotics in Alpe-Adria Danube Region, pages 267–274. Springer, 2019.

[8] Jimmie W Hinze and Jochen Teizer. Visibility-related fatalities related to construction equipment. Safety science, 49(5):709–718, 2011.

[9] J. Hu, X. Gao, H. Wu, and S. Gao. Detection of workers without the helments in videos based on yolo v3. In 2019 12th International Congress on Image and Signal Processing, BioMedical Engineering and Informatics (CISP-BMEI), pages 1–4, 2019.

[10] Jonathan Huang, Vivek Rathod, Chen Sun, Menglong Zhu, Anoop Korattikara, Alireza Fathi, Ian Fischer, Zbigniew Wojna, Yang Song, Sergio Guadarrama, et al. Speed/accuracy trade-offs for modern convolutional object detectors. In Proceedings of the IEEE conference on computer vision and pattern recognition, pages 7310–7311, 2017.

[11] Charles-Éric Noël Laflamme, François Pomerleau, and Philippe Giguère. Driving datasets literature review. arXiv preprint arXiv:1910.11968, 2019.

[12] Yanming Li, Shuangyuan Wang, and Bingchu Li. Improved visual hook capturing and tracking for precision hoisting of tower crane. Advances in Mechanical Engineering, 5:426810, 2013.

[13] Tsung-Yi Lin, Piotr Dollar, Ross Girshick, Kaiming He, Bharath Hariharan, and Serge Belongie. Feature pyramid networks for object detection. In The IEEE Conference on Computer Vision and Pattern Recognition (CVPR), July 2017.

[14] Tsung-Yi Lin, Priya Goyal, Ross Girshick, Kaiming He, and Piotr Dollár. Focal loss for dense object detection. In Proceedings of the IEEE international conference on computer vision, pages 2980–2988, 2017.

[15] Tsung-Yi Lin, Michael Maire, Serge Belongie, James Hays, Pietro Perona, Deva Ramanan, Piotr Dollár, and C Lawrence Zitnick. Microsoft coco: Common objects in context. In European conference on computer vision, pages 740–755. Springer, 2014.

[16] Wei Liu, Dragomir Anguelov, Dumitru Erhan, Christian Szegedy, Scott Reed, Cheng-Yang Fu, and Alexander C Berg. Ssd: Single shot multibox detector. In European conference on computer vision, pages 21–37. Springer, 2016.

[17] Shunsuke Nara, Daisuke Miyamoto, and Satoru Takahashi. Position measurement of crane hook by vision and laser. In IECON 2006-32nd Annual Conference on IEEE Industrial Electronics, pages 184–189. IEEE, 2006.

[18] M Neuhausen, J Teizer, and M König. Construction worker detection and tracking in bird's-eye view camera images. In Proceedings of the 35th ISARC, Berlin, Germany, 2018.

[19] Marcel Neuhausen, Patrick Herbers, and Markus König. Synthetic data for evaluating the visual tracking of construction workers. In Construction Research Congress 2020, 2020.

[20] Occupational Health and Safety. Survey Finds High Rate of PPE Non–Compliance —Occupational Health and Safety, November 2008. [Online; accessed 18-06-2019].

[21] Joseph Redmon and Ali Farhadi. YOLOv3: An incremental improvement. CoRR, abs/1804.02767, 2018.

[22] Shaoqing Ren, Kaiming He, Ross Girshick, and Jian Sun. Faster r-cnn: Towards real-time object detection with region proposal networks. In C. Cortes, N. D. Lawrence, D. D. Lee, M. Sugiyama, and R. Garnett, editors, Advances in Neural Information Processing Systems 28, pages 91–99. Curran Associates, Inc., 2015.

[23] Alexandre Robicquet, Amir Sadeghian, Alexandre Alahi, and Silvio Savarese. Learning social etiquette: Human trajectory understanding in crowded scenes. In European conference on computer vision, pages 549–565. Springer, 2016. Stanford Drone Dataset.

[24] A. H. M. Rubaiyat, T. T. Toma, M. Kalantari-Khandani, S. A. Rahman, L. Chen, Y. Ye, and C. S. Pan. Automatic detection of helmet uses for construction safety. In 2016 IEEE/WIC/ACM International Conference on Web Intelligence Workshops (WIW), pages 135–142, 2016.

[25] Suranga Seneviratne, Yining Hu, Tham Nguyen, Guohao Lan, Sara Khalifa, Kanchana Thilakarathna, Mahbub Hassan, and Aruna Seneviratne. A survey of wearable devices and challenges. IEEE Communications Surveys & Tutorials, 19(4):2573–2620, 2017.

[26] H Seong, H Choi, H Cho, S Lee, H Son, and C Kim. Vision-based safety vest detection in a construction scene. In ISARC. Proceedings of the International Symposium on Automation and Robotics in Construction, volume 34. IAARC Publications, 2017.

[27] Mohammad Mostafa Soltani, Zhenhua Zhu, and Amin Hammad. Automated annotation for visual recognition of construction resources using synthetic images. Automation in Construction, 62:14–23, 2016.

[28] Satoru Takahashi and Shun'ichi Kaneko. Motion tracking of crane hook based on optical flow and orientation code matching. In 2008 10th IEEE International Workshop on Advanced Motion Control, pages 149–152. IEEE, 2008.

[29] D Triantafyllou, S Krinidis, D Ioannidis, IN Metaxa, C Ziazios, and D Tzovaras. A real-time fall detection system for maintenance activities in indoor environments. IFAC-PapersOnLine, 49(28):286–290, 2016.

[30] A Vierling, T Sutjaritvorakul, and K Berns. Crane safety system with monocular and controlled zoom cameras. In ISARC. Proceedings of the International Symposium on Automation and Robotics in Construction, volume 35, pages 1–7. IAARC Publications, 2018.

[31] Axel Vierling, Tanittha Sutjaritvorakul, and Karsten Berns. Dataset generation using a simulated world. In International Conference on Robotics in Alpe-Adria Danube Region, pages 505–513. Springer, 2019.

[32] Sutjaritvorakul T. Vierling A., Pawlak J. and Berns K. Simulation platform for crane visibility safety assistance. In Proceedings of the 29th Conference on Robotics in Alpe-Adria-Danube Region (RAAD 2020), volume 84 of Mechanisms and Machine Science. Springer, Cham, 2020.

[33] Dongfang Yang, Linhui Li, Keith Redmill, and Ümit Özgüner. Top-view trajectories: A pedestrian dataset of vehicle-crowd interaction from controlled experiments and crowded campus. arXiv preprint arXiv:1902.00487, 2019.

[34] Zhen Yang, Yongbo Yuan, Mingyuan Zhang, Xuefeng Zhao, Yang Zhang, and Boquan Tian. Safety distance identification for crane drivers based on mask r-cnn. Sensors, 19(12):2789, 2019.

[35] Shanshan Zhang, Rodrigo Benenson, Mohamed Omran, Jan Hosang, and Bernt Schiele. How far are we from solving pedestrian detection? In Proceedings of the IEEE Conference on Computer Vision and Pattern Recognition, pages 1259–1267, 2016.

Using Deep Learning for Assessment of Workers' Stress and Overload

S. Eskandar[a] and S. Razavi[b]

[a] Ph.D. Candidate, Department of Civil Engineering, McMaster University, Canada
[b]Associate Professor, Department of Civil Engineering, McMaster University, Canada
E-mail: eskandah@mcmaster.ca, razavi@mcmaster.ca

Abstract –

Spotting indications of unsafe human behaviour, a leading cause of an accident, is critical in providing a safe workspace. Among factors affecting human behaviour, stress and overload are the most significant ones, where limited knowledge exists on their underlying causes. Tracing physiological signs caused by stress and overload might be a feasible approach in detecting a specific neurological status leading to unsafe human behaviours, such as disobeying safety rules, standards, and instructions. In this paper, we present a deep learning technique to recognize distinctive neurological status by assessing physiological signals such as temperature and heart rate. An open database of non-EEG physiological signals was used to train and test the model. The database includes electrodermal activity, temperature, acceleration, heart rate, and arterial oxygen level signals of 20 healthy subjects through relaxation, physical, emotional and cognitive activities. A robust automated pattern recognition method, using deep learning, was used to predict and identify stress and overload. The experimental results indicate that the model can detect neurological status with higher accuracy than the traditional classification-based methods.

Keywords –

Deep Learning; Pattern Recognition; Stress; Overload; Safety

1 Introduction

Despite the ongoing safety studies and policy recommendations in construction, the extent of injuries is still significant. Based on the Canada Work Injury, Disease, and Fatality Statistics from Association of Workers' Compensation Boards of Canada (AWCBC/ACATC 2018)[1], each year, around 200 people die in construction sites. There are about 28000 time-loss injuries in construction-related accidents. The number of Canada's fatalities in 2018 shows that the construction industry has the highest number of fatalities among all sectors and accounts for almost 20 percent of the reported fatalities. So, improving safety and discovering the leading causes of accidents are still considered significant contributions to the construction industry.

In Eskandar et al. 2019 [2], three major categories of social, physiological, and cognitive human factors that influence the safe behaviour in construction were studied to guide future research around improving safety in construction. From a physiological perspective, stress and overload presented to have a high-level association with unsafe behaviour among construction workers, which motivated many researchers to detect stress in the work setting.

Stress can be described as the response of the body to the pressures on the human nervous system [3], which have been measured through subjective tests and questionnaires to collect individual responses [4], [5] . Moreover, stress can be measured through variations in human physiological features such as heartbeats, body temperature, and respiration [6]–[8]. With the advances in wearable biosensors and real-time data collection, many researchers focused on the physiological effects of stress on the human body to build a stress detection model. Several supervised learning algorithms were employed to detect stress and overload by detecting patterns of stored physiological signals during experiments.

Below, we first look at the stress and overload of construction workers and relevant physiological information that could guide their identification. Then a deep supervised learning model is proposed to classify different stress-inducing neurological states by processing physiological signals.

2 Stress and Overload

Stress (including physical and psychological) is among the contributing factors that lead to unsafe behaviour [9], [10]. Examples of stress factors in construction setting

were presented as (1) physical stressors like noise, vibration, lighting, boredom, fatigue, cold or heat, and (2) social psychological stressors like fear, uncertainty, anxiety, mental overload, and time pressure [10]–[13]. Overload as an essential stressor that affects human behaviour was selected to focus on due to the nature of manual work in a construction environment that causes workers to exceed their capacity of handling the job.

Tracking symptoms of stress and high mental overload with multiple physiological features give us insight into a human's neurological state. Most physiological measurements come from a network of sensors in which become easier to collect in an unobtrusive real-time manner. Currently, the human body's vital signs can simply be recorded through wearable biosensors and health gadgets (e.g., smartwatch, earbuds, headset). Many researchers used sensors to measure specific physiological conditions to study factors that affect individual neurological statuses such as stress [14], sleep deprivation [15], fatigue [16], and social aspects [17].

Among different measuring methods that could reflect stress and mental overload, Electroencephalogram (EEG) sensors have been commonly applied in many studies [18]–[20]. EEG is a valuable source in identifying brain activities to measure electrical activities of the brain by electrodes positioned on the scalp, and they capture neurons in the brain by electric potentials. However, there are limitations in applications during physical activities as these signals are sensitive to face and body movements (e.g. eye blinks), which makes them impractical for application in construction safety [20]–[22]. Considering the EEG limitations, viable biosensors that could detect and reflect the stress in construction were presented in [14] as; Photoplethysmography (PPG), Electrodermal Activity (EDA), and peripheral skin temperature (ST), that are sensitive to extrinsic and intrinsic artifacts which require extensive filtering.
In addition to the feasibility of data collection in construction, data should reflect the sign of stress and overload. In an open-source database from a Birjandtalab et al. [23], that was conducted on subjects while confronted by stress and overload; seven different non-EEG physiological signals were collected during the experiment. In the current study, the above-noted database (Non-EEG dataset) was used as a source of information to study and train a stress and overload detection model. This database provides us with useful insights over the physiological features of individuals while confronted with overload and stress. This paper is distinct from previous studies by focusing on the physiological impact of mental stress and protecting the model against biases other than the ultimate goal, such as; not including 3-axis acceleration, which leads the model to movement recognition.

3 Non-EEG dataset

A non-EEG physiological signal from [23] includes acceleration (Ax, Ay, Az), electrodermal activity (EDA), temperature, heart rate, and arterial oxygen level (SpO2) signals of 20 healthy subjects during relaxation, physical, emotional and cognitive activities. This dataset includes individual responses while facing different stress-inducing activities. The experimental procedure includes: (1) Five minutes of relaxation, (2) Physical stress by walking on a treadmill at 1 mile/hr. For two minutes and jogging at 3 miles/hr for two minutes, (3) Relaxation, (4) Cognitive stress by counting backwards by sevens from 4285, and then performing Stroop test while alerted by a buzzer, (5) Relaxation, (6) Emotional stress by watching clips from a horror movie, (7) Relaxation.

Figure 4 displays a time-series for the Subject1 during the experiment collected by wrist-worn biosensors. The data file was in the WFDB (WaveForm DataBase) format, which can be read using its associated software package [24]. Records were labelled through ".atr" annotations file format (i.e. red stars on the a_x signal), which indicate a change in the activity of a human subject (i.e., moving from one step to another in the experiment steps).

The data files contain two records per person; one is recorded 3D acceleration, temperature, and electrodermal activity (EDA) with a frequency equal to eight (Figure 1). Another measurement technology recorded heart rate (HR) and arterial oxygen level (SpO2) with a frequency of one reading per second (Figure 2) [23].

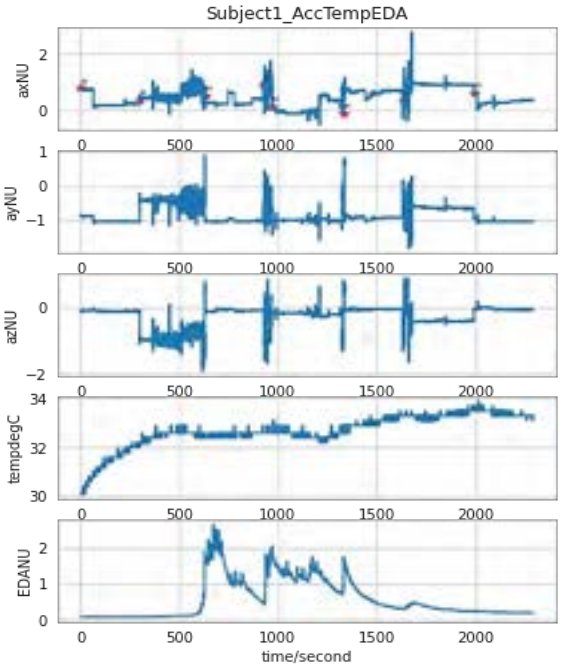

Figure 1. Acceleration (Ax, Ay, Ax), Temperature, and EDA recorded time-series for Subject1.

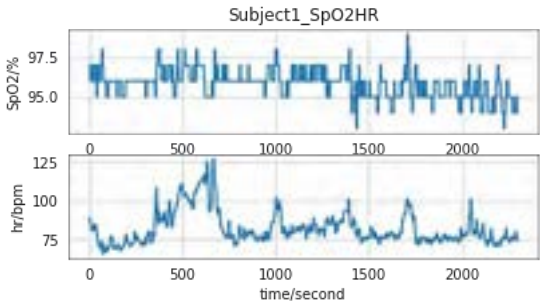

Figure 2. SpO2 and Heart rate recorded time-series for Subject1

3.1 Preprocessing

3.1.1 Aligning

Before analyzing and preprocessing the recorded data, we need to align data of different frequencies from different devices. There are two strategies for resampling and aligning: (1) Upsampling the lower frequency by repeating or interpolating data between reading samples, (2) Downsampling the higher frequency data by replacing extra readings with mean or median. The following graph (Figure 3) shows the difference between Downsampling (with median) and original reading for an accelerometer-x signal. Whether we need to maintain a precision of the higher frequency or not, we can align data of different frequencies. Downsampling signals might result in loss of data, and upsampling the lower frequency reading was chosen to align readings from two separate measuring devices (Figure 4).

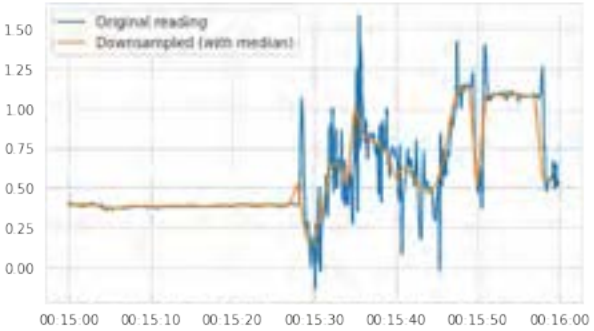

Figure 3. Accelerometer-x down sampled (with median) side-by-side to the original high-frequency

3.1.2 Feature scaling

As it is visible in Figure 4, recorded signals are from different range and amounts. So it is essential to scale all data and perform feature scaling before any processing. Mainly, in classification problems, the majority of algorithms perform based on the distances, scaling the features before processing is necessary.

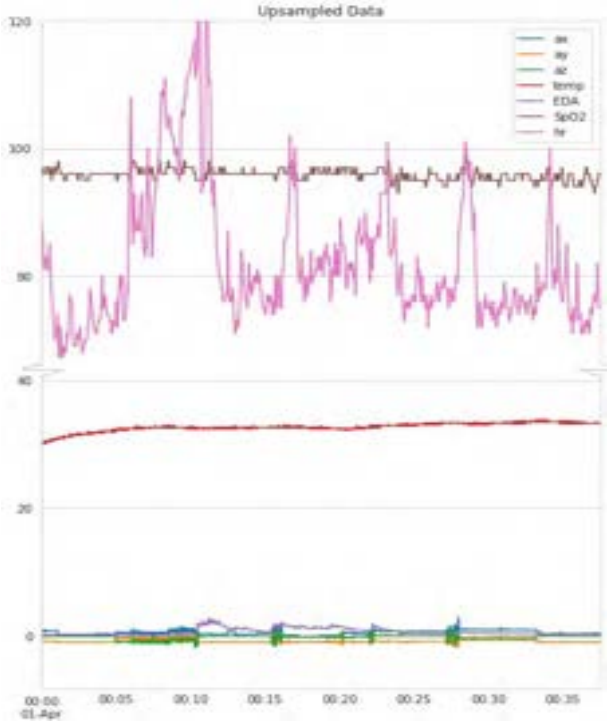

Figure 4. Aligned signals using the upsampling method (with interpolation) for SpO2 and Heart rate

3.1.3 Feature selection

In the preprocessing stage, it is essential to study correlations between different features. In Figure 5, the Pearson r correlations coefficient matrix has been shown to measure the degree of the relationship between linearly related variables to indicate whether two variables are strongly dependent or independent as a part of preprocessing. Based on the Pearson correlation coefficient and Cohen's standard, there is a significant association between acceleration signals (Ax, Ay, and Az). However, temperature and electrodermal activities (EDA) are independent.

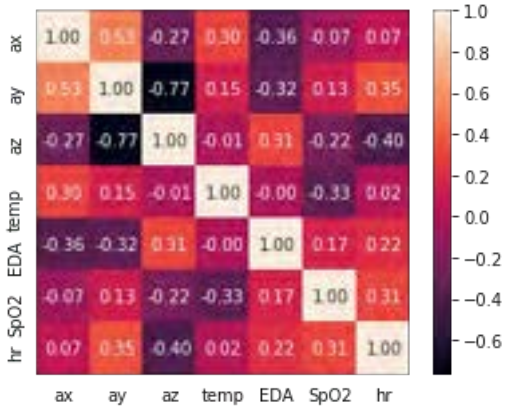

Figure 5. Correlation matrix calculated using the Pearson method

Processing the correlation between features and eliminating those attributes that are unrelated enables a robust feature selection. Feature selection is a critical part of any machine learning pipeline, which leads to the accuracy in the models. Also, having perfectly correlated features increase a chance that the model performance obstructed by Multicollinearity (i.e. when one part can linearly be predicted from the others with a high degree of accuracy, in this case, Ay and Az are negatively correlated). High accuracy cannot be achieved without applying different methods of feature selection, such as Pearson or Spearman correlation matrix, Chi-squared, or Recursive feature elimination. Here, based on the Pearson correlation, features that are highly correlated decrease the performance of the model.

In the current research, in addition to the highly correlated features, it is required to remove three signals of accelerators. Acceleration in different directions is beneficial for activity and movement detection, not the stress and mental overload, which is the focus of this study. Especially in a construction setting due to the physically demanding nature of work, eliminating data regarding movement and activities protects the model to biases, and it focuses on the ultimate goal of stress and mental overload detection.

Since the recorded signals are continuous reading over time, slices of data during a window of time were selected as a separate entry to the model. The optimal window size was detected by calculating the accuracy of the model for different window sizes. Moreover, in classification models, it is essential to have balanced classes for training a model. So, a similar number of windows representing each class were selected as the input to the model.

3.1.4 Feature extraction

After the feature selection stage, a feature extraction tool is needed to provide the training stage with more information regarding data distribution. For this matter, a convolutional neural network (CNN) layer was added at the beginning of the model pipeline.

4 Model

For time-series pattern recognition and classifying different neurological statuses (i.e., relaxation, physical, emotional and cognitive stress), long short-term memory (LSTM) algorithm was selected for training purposes. Long short-term memory (LSTM) is a form of recurrent neural network (RNN) in the field of deep learning. LSTM has feedback connections in addition to the standard feedforward processing. These features enable LSTM to process entire sequences of data and make it accessible in time series data. At the beginning of the model pipeline, convolutional neural network CNN extracts features from signals, and it prepares input for the pattern recognition stage, which was conducted through sequential LSTM layers. Three different LSTM layers were added to the model to give more depth into the calculation, which provides a model with a better chance of prediction. Then, two fully connected layers at the final stage of training prepared the processed data for classification. Different classifiers can be applied to the final stage, namely: Bayes classifier, Hidden Markov Models, Random Forest Classifier, and Ensemble algorithm classifier (meta-algorithms that combine several methods into one model to decrease bias and variance and improve predictions). Adam classifier was chosen for the proposed model as the best fit.

There are multiple hyperparameters (e.g., number of units in each layer, number of dense layers, type of classifier, and number of epochs) in the proposed model, which requires a hyperparameter tuning for selecting the best match for the model. By defining a search area and training a model for several combinations, the best combination was chosen for training a model. For instance, by applying different window sizes, a window of 20 continuous reading of the signal was selected as an optimum number for the proposed model.

For training and testing processes, twenty percent of data were kept unseen for testing and from remaining samples, twenty percent was allocated to the cross-validation for backward propagation.

Figure 6 depicts the categorical accuracy and validation loss during the training session.

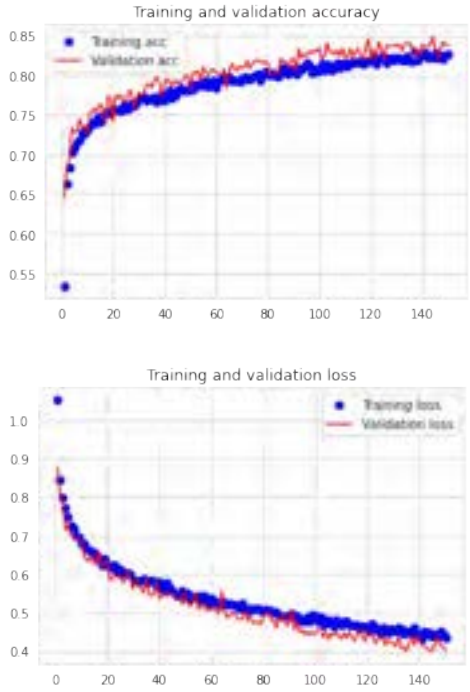

Figure 6. Training and validation accuracy and loss

Figure 7 presents the proposed model classification results that achieved an overall 85 percent accuracy for the test data set. Based on the f1-score (i.e. is a balanced amount of precision and recall) in the following report, we can conclude that the trained model is robust toward detecting physical stress and has more limitations in cognitive stress detection.

Classification Report

	precision	recall	f1-score	support
CognitiveStress	0.71	0.90	0.79	487
EmotionalStress	0.89	0.81	0.85	510
PhysicalStress	0.94	0.94	0.94	506
Relax	0.89	0.75	0.81	481
accuracy			0.85	1984
macro avg	0.86	0.85	0.85	1984
weighted avg	0.86	0.85	0.85	1984

Figure 7. Model classification report

In Figure 8, the confusion matrix for four different classes represents the actual classes in vertical and predicted classes in a horizontal direction.

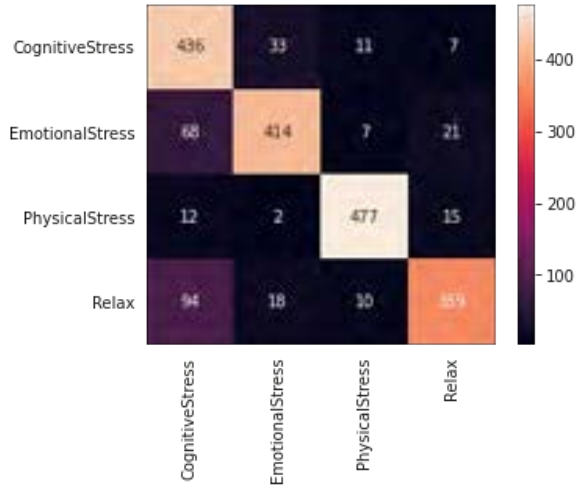

Figure 8. Confusion matrix

5 Results discussion and conclusions

In this research, efforts were taken to detect stress and mental overload, not only by employing deep learning techniques but by knowing the inputs of the model and removing preconceptions of the experimental study. The presented trained model in this study achieved 85 percent accuracy over unseen samples, which is a distinct improvement compared to using traditional methods of manual feature extraction (e.g., calculating the median, range, and standard deviation over the time series), combined with classifier algorithms.

Based on the confusion matrix, the trained model has difficulty recalling the Relax state, which needs more improvement in the data-gathering stage for future studies. Inputs to the proposed model were heart rates, temperatures, electrodermal activities, and arterial oxygen levels of subjects during an experiment, in which Ax, Ay, and Az accelerations were removed to enable the model to detect mental overload and stress instead of activities and movement detection. In addition to the importance of input to the model, the level of personal capacity while confronted with stressors has to be considered as individuals have different capacities under pressure.

Furthermore, for detecting stress and overload, multiple sub-classes should be considered to represent different levels of neurological status. For this matter, the severity of the neurological state uncovers, and only the higher level of stress in each category is considered hazardous.

References

[1] AWCBC/ACATC, "Association of Workers' Compensation Boards of Canada. 2016-2018 National Work Injury, Disease and Fatality Statistics," 2018. Accessed: Apr. 29, 2020. [Online]. Available: http://awcbc.org/?page_id=14#fatalities.

[2] S. Eskandar, J. Wang, and S. Razavi, "A review of social, physiological, and cognitive factors affecting construction safety," *Proc. 36th Int. Symp. Autom. Robot. Constr. ISARC 2019*, no. Isarc, pp. 317–323, 2019, doi: 10.22260/isarc2019/0043.

[3] S. Cohen, R. Kessler, and L. Gordon, *Measuring stress: A guide for health and social scientists*. 1997.

[4] H. Wittchen, P. B.-T. B. J. of Psychiatry, and undefined 1998, "Screening for anxiety disorders: Sensitivity and specificity of the Anxiety Screening Questionnaire (ASQ–15)," *cambridge.org*, Accessed: Jun. 26, 2020. [Online]. Available: https://www.cambridge.org/core/journals/the-british-journal-of-psychiatry/article/screening-for-anxiety-disorders/E786FEDE4C5C6EE0C2BD7DAE1754CC52.

[5] S. Reiss, R. A. Peterson, D. M. Gursky, and R. J. McNally, "Anxiety sensitivity, anxiety frequency and the prediction of fearfulness," *Behav. Res. Ther.*, vol. 24, no. 1, pp. 1–8, Jan. 1986, doi: 10.1016/0005-7967(86)90143-9.

[6] O. D. Kothgassner *et al.*, "Salivary cortisol and cardiovascular reactivity to a public speaking task in a virtual and real-life environment," *Comput. Human Behav.*, vol. 62, pp. 124–135,

Sep. 2016, doi: 10.1016/j.chb.2016.03.081.

[7] G. M. Harari, N. D. Lane, R. Wang, B. S. Crosier, A. T. Campbell, and S. D. Gosling, "Using Smartphones to Collect Behavioral Data in Psychological Science: Opportunities, Practical Considerations, and Challenges.," *Perspect. Psychol. Sci.*, vol. 11, no. 6, pp. 838–854, Nov. 2016, doi: 10.1177/1745691616650285.

[8] T. G. M. Vrijkotte, L. J. P. Van Doornen, and E. J. C. De Geus, "Effects of work stress on ambulatory blood pressure, heart rate, and heart rate variability," *Hypertension*, vol. 35, no. 4, pp. 880–886, 2000, doi: 10.1161/01.HYP.35.4.880.

[9] M. Y. Leung, Y. S. Chan, and K. W. Yuen, "Impacts of stressors and stress on the injury incidents of construction workers in Hong Kong," *J. Constr. Eng. Manag.*, vol. 136, no. 10, pp. 1093–1103, 2010, doi: 10.1061/(ASCE)CO.1943-7862.0000216.

[10] M. Y. Leung, Q. Liang, and P. Olomolaiye, "Impact of Job Stressors and Stress on the Safety Behavior and Accidents of Construction Workers," *J. Manag. Eng.*, vol. 32, no. 1, pp. 1–10, 2016, doi: 10.1061/(ASCE)ME.1943-5479.0000373.

[11] R. M. Choudhry, D. Fang, and S. Mohamed, "The nature of safety culture: A survey of the state-of-the-art," *Saf. Sci.*, vol. 45, no. 10, pp. 993–1012, 2007, doi: 10.1016/j.ssci.2006.09.003.

[12] R. R. Langdon and S. Sawang, "Construction Workers' Well-Being: What Leads to Depression, Anxiety, and Stress?," *J. Constr. Eng. Manag.*, vol. 144, no. 2, pp. 1–15, 2018, doi: 10.1061/(ASCE)CO.1943-7862.0001406.

[13] L. M. Goldenhar, L. J. Williams, and N. G. Swanson, "Modelling relationships between job stressors and injury and near-miss outcomes for construction labourers," *Work Stress*, vol. 17, no. 3, pp. 218–240, 2003, doi: 10.1080/02678370310001616144.

[14] H. Jebelli, B. Choi, and S. H. Lee, "Application of Wearable Biosensors to Construction Sites. I: Assessing Workers' Stress," *J. Constr. Eng. Manag.*, vol. 145, no. 12, 2019, doi: 10.1061/(ASCE)CO.1943-7862.0001729.

[15] R. Powell and A. Copping, "Sleep deprivation and its consequences in construction workers," *J. Constr. Eng. Manag.*, vol. 136, no. 10, pp. 1086–1092, 2010, doi: 10.1061/(ASCE)CO.1943-7862.0000211.

[16] T. S. Abdelhamid and J. G. Everett, "Ironworkers: Physiological demands during construction work," *Proc. Constr. Congr. VI Build. Together a Better Tomorrow an Increasingly Complex World*, vol. 278, no. October, pp. 631–639, 2000, doi: 10.1061/40475(278)68.

[17] R. M. Choudhry, D. Fang, and H. Lingard, "Measuring safety climate of a construction company," *J. Constr. Eng. Manag.*, vol. 135, no. 9, pp. 890–899, 2009, doi: 10.1061/(ASCE)CO.1943-7862.0000063.

[18] H. Jebelli, S. Hwang, and S. Lee, "EEG-based workers' stress recognition at construction sites," *Autom. Constr.*, vol. 93, pp. 315–324, Sep. 2018, doi: 10.1016/j.autcon.2018.05.027.

[19] J. Chen, J. E. Taylor, and S. Comu, "Assessing Task Mental Workload in Construction Projects: A Novel Electroencephalography Approach," *J. Constr. Eng. Manag.*, vol. 143, no. 8, p. 04017053, Aug. 2017, doi: 10.1061/(ASCE)CO.1943-7862.0001345.

[20] D. Wang, J. Chen, D. Zhao, F. Dai, C. Zheng, and X. Wu, "Monitoring workers' attention and vigilance in construction activities through a wireless and wearable electroencephalography system," *Autom. Constr.*, vol. 82, pp. 122–137, Oct. 2017, doi: 10.1016/j.autcon.2017.02.001.

[21] E. Lew, R. Chavarriaga, S. Silvoni, and J. del R. Millán, "Detection of self-paced reaching movement intention from EEG signals," *Front. Neuroeng.*, no. JULY, Jul. 2012, doi: 10.3389/fneng.2012.00013.

[22] M. Teplan, "Fundamentals of EEG measurement," *Meas. Sci. Rev.*, vol. 2, no. 2, pp. 1–11, 2002, Accessed: May 20, 2020. [Online]. Available: http://www.edumed.org.br/cursos/neurociencia/MethodsEEGMeasurement.pdf.

[23] J. Birjandtalab, D. Cogan, M. B. Pouyan, and M. Nourani, "A non-EEG biosignals dataset for assessment and visualization of neurological status," in *IEEE Workshop on Signal Processing Systems, SiPS: Design and Implementation*, Oct. 2016, pp. 110–114, doi: 10.1109/SiPS.2016.27.

[24] A. L. Goldberger *et al.*, "PhysioBank, PhysioToolkit, and PhysioNet: components of a new research resource for complex physiologic signals.," *Circulation*, vol. 101, no. 23, Jun. 2000, doi: 10.1161/01.cir.101.23.e215.

Development of a Workers' Behavior Estimation System Using Sensing Data and Machine Learning

R. Tanaka[a], N. Yabuki[a], and T. Fukuda[a]

[a]Department of Sustainable Energy and Environmental Engineering, Osaka University, Japan
E-mail: rikuto.tanaka@it.see.eng.osaka-u.ac.jp, yabuki@see.eng.osaka-u.ac.jp, fukuda@see.eng.osaka-u.ac.jp

Abstract –

Accurate information on workers' behavior is important for safety and productivity management on construction sites. In recent years, some methods for estimating construction workers' behavior using sensing data have been proposed to collect the data based on scientific evidence. Due to the limitations of previously proposed methods that usually relied on expensive devices such as motion capture systems, the huge amount of investment on the system installation and human resource costs are required. This paper proposes a method for estimating workers' posture with Long Short-Term Memory (LSTM) by using terminals that have already been introduced to construction sites, taking into consideration the operational cost and issues in the previous studies. Moreover, we also propose and evaluate a data augmentation method for utilizing limited training data sets. The experiment results for a reinforcing bar worker indicated that the proposed method could estimate not only the forward-leaning and squatting postures with 79% or more F-measure but also the number of rebar binding points by the acceleration data. Besides, we confirmed that the data augmentation method improved the accuracy of posture estimation by 5%.

Keywords –

Construction worker; Sensing data analysis; Machine Learning; Behavior estimation

1 Introduction

While the number of labor accidents at construction sites in Japan is decreasing, the number of serious accidents continues to be higher than in other industries [1]. Therefore, it is necessary to take improvement measures in consideration of both the organization and the technology through a meeting among construction-related people. Moreover, as construction demand is expected to be stabilized in recent years, there is a concern that the labor force will be insufficient due to a decrease in the number of young employees and the aging of skilled technicians. Thus, regarding labor productivity as well, it is necessary to formulate efficient construction plans by saving labor costs while also considering the safety of workers [2].

In recent years, for managing construction plans that consider safety and efficiency at construction sites, the introduction of construction support systems that have the function of visualizing the situation of workers and equipment on the site from past accumulated data has been promoted [3]. At such time, it is important to collect the condition data of the workers by using informative equipment such as sensors and cameras and convert them into information that is practical for site management such as the behavior history of the workers.

Video data acquired by RGB cameras and sensing data from wearable terminals are used to gather behavior data of construction workers. In this study, we employ a method using sensing data that enables data acquisition in consideration of the obstructions on the site and personal privacy and estimates the workers' behavior [4]. Also, it has been reported that supervised learning can be used for behavioral estimation based on individual characteristics.[5]. By applying these methods to workers at construction sites, the estimation of tools used by workers [6] and the work estimation of reinforcing bar workers [7] have been performed. Furthermore, smartphones with built-in inertial sensors or motion capture systems that attached multiple inertial sensors to the joints of the workers were also proposed to estimate their behavior [8]. However, these equipment costs are not easily achievable and besides, it is also essential to prepare the human resources for security and maintenance of these devices. Therefore, it is necessary to consider constraints such as project size and budget when applying it to the field.

In this study, thus, we propose a construction worker behavior estimation system that considers the limitations when introducing it to a construction site by using monitoring devices that have already been used at the construction sites. Our method considers constraints such as sampling frequency when collecting data by adopting a model corresponding to time series data as a behavior estimation algorithm. Besides, we propose a data

augmentation method because it is labor-intensive and costly in order to prepare a high amount of training data for the behavior estimation model. Finally, we verify the posture estimation accuracy of the proposed system by conducting a verification experiment using the sensing data of the workers acquired at the actual construction site.

2 Literature review

Human behavior estimation technology has gained attention in recent years such as in medicine and engineering scopes [9]. Data collection for human behavior estimation can be separated into two types: a vision-based method, in which video devices are used to collect data from a target person at a distance, and a sensor-based method, which utilizes a device with a built-in sensor directly attached to the target person. In this section, we summarize the applications of each method that have been implemented on construction sites.

2.1 Vision-based methods

Video data is used in various fields because it is easy for humans to intuitively understand and obtain useful information from the images by looking at them directly [10]. In recent years, due to cost reduction, downsizing, and high resolution of video equipment, it has been introduced to the construction sites as well, and research on data collection of worker status and construction machines' positions have been conducted [11]. In particular, recent research has been carried out to apply computer vision technology using deep learning. Some of the studies were to automatically identify which task a worker is engaged in [12] and to verify the appropriate utilization of safety devices such as safety belts [13]. In those studies [12-13], the practitioners use cameras to track the workers. However, hiring extra staff to work on these tasks increases the cost of the project. A fixed-point camera-based method [14] has also been proposed. However, on the construction sites where workers and equipment are densely packed, the target workers may be hidden behind the equipment and the data cannot be continuously collected.

In recent years, a method using a depth camera for behavior estimation[15] has also been reported. Depth information makes it possible to correctly reproduce the human posture that occurs in the real space. However, the depth camera cannot accurately obtain depth information of distant objects and may face some difficulties when some objects are exposed to sunlight.

2.2 Sensor-based methods

The sensor-based method is proposed to eliminate the weaknesses of behavior estimation using video data. The posture and motion can be estimated by attaching a terminal with built-in inertial or biometric sensors to the human body and performing the calculation on the sensing data. This method can compensate for the shortcomings of vision-based method because it can continuously collect data without being affected by surrounding obstacles, light sources, and sight distance [4]. Also, sensor-based method can collect data in consideration of the privacy of the subject [4]. Behavior estimation using sensing data has been applied in a variety of fields, as the recent spread of micro-electro-mechanical-systems (MEMS) technology made it possible to easily develop behavior estimation systems [9]. In the construction sector, a motion capture system using multiple inertial sensors attached to human body to prevent Work-Related Musculoskeletal Disorders (WRMDs) was proposed at a construction site, and verification experiments have shown the effectiveness of the warning function [8]. However, the motion capture systems are hardly affordable and attaching many sensors to the human body is intrusive. With respect to productivity management, smartphone-based methods have been proposed to estimate tools handled by workers [6] and work estimation for rebar workers [7]. It is cost-effective to use personal smartphones for data collection which are ubiquitous these days. Nevertheless, the recent diversification of smartphone models and specifications leads to an increase in the burden for system administrators. Thus low-cost, nonintrusive and uniform equipment is suitable for installation to construction sites.

2.3 Objective of this research

Considering the constraint for installing the equipment as shown through the literature review, we adopt the monitoring devices for the workers that have already been installed to construction sites. The devices meet the requirements of low-cost, nonintrusive and uniform. Then, we propose a system for estimating workers' posture using a machine learning-based estimation algorithm and a data augmentation method corresponding to the sensing devices.

3 Proposed method

3.1 Overview of the proposed method

In this study, we propose a behavior estimation method for construction workers that uses a helmet-mounted terminal, which has already been installed on actual construction sites. Figure 1 shows an overview of the proposed system. The terminal with a built-in composite sensor provides sensing data including acceleration and positional information obtained by positioning system every second. These data are stored in

the terminal's memory. The stored data are transferred to the database in the laptop by connecting the terminals to the equipment installed at the site. Then, we construct a system to estimate the postural state of construction workers from the stored sensing data by utilizing a neural network model that is trained using past behavior data of workers.

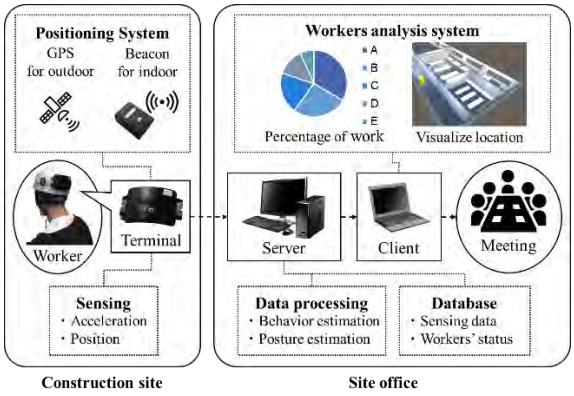

Figure 1. Overview of the proposed system

3.2 Data Acquisition by terminals

We use the "Construction Site Operation Monitoring System [16]" developed by Hitachi, Ltd. as a terminal for acquiring sensing data. The positional information is provided by Beacon or Global Positioning System (GPS) and sensing data, including triaxial acceleration, barometric pressure, and temperature are stored in the terminal's internal memory every second. The stored data are transferred to a server PC by connecting to the cradle installed on the site at the end of workday. The collected data are used to confirm the walking path of each worker verifying whether or not there are dangerous movements through the aforementioned system.

The monitoring system has functions such as detection of approaching the dangerous area and falling, and calculation of worker's posture based on the triaxial acceleration values obtained every second, but it does not have a function to estimate worker's behavior considering the change of worker's condition over time. Therefore, it is not possible to use the results obtained from the estimation of worker's behavior for productivity analysis or safety management measures.

3.3 Behavior estimation using sensing data

3.3.1 Data processing flow

Focusing on the fact that the workers' behavior estimation function is not implemented in the monitoring system, the proposed system employs a posture estimation method based on acceleration data and its time-series. Figure 2 shows the flow of the behavior estimation process in the proposed system. After the processing starts, input data for estimation are read from workers lists and sensing data registered in the database. In the preprocessing phase, acceleration data are extracted and formatted to suit the input of estimation model. Then the posture state of the target worker is estimated and processed as the posture data of the worker at that time by inputting the extracted data into the estimation model inside the system.

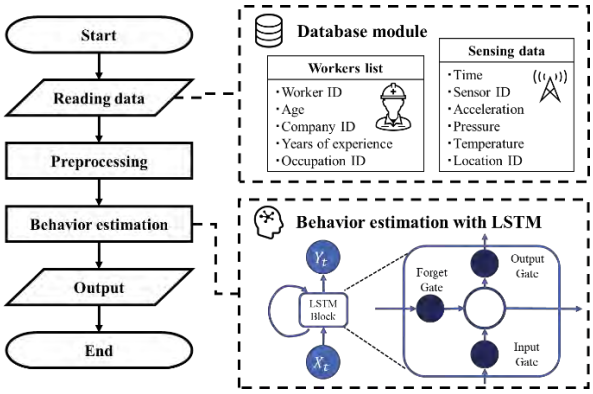

Figure 2. Data processing flow in the proposed system

3.3.2 Reading data and prerprocessing

The structure of the dataset used in this method for posture estimation and training of the estimation model is shown in equation (1). After reading sensing data from the database module, the time-series data is converted to the right side of the matrix in the equation (1). We assume that the worker's condition at time t is determined from the worker's condition before time t and the acceleration values around time t. Then, we define the dataset as a mapping between the posture label P_t at time t and the acceleration values around time t.

$$P_t \leftrightarrow \begin{bmatrix} x_{t-n} & y_{t-n} & z_{t-n} \\ \vdots & \vdots & \vdots \\ x_t & y_t & z_t \\ \vdots & \vdots & \vdots \\ x_{t+n} & y_{t+n} & z_{t+n} \end{bmatrix} \quad (1)$$

where

P_t: Posture label at time t
x_t, y_t, z_t: Acceleration value of each axis at time t
$2n+1$: Time window width

3.3.3 Posture estimation with LSTM

In the posture estimation phase, a feature and classification algorithm should be selected in consideration of the terminals used for sensing and the

behavior characteristics of individuals [4]. We implement a neural network model that automatically extracts and learns features from the input training data to perform posture estimation for various occupations and individual differences in this study. We also use Long Short-Term Memory (LSTM), which has been reported to have a high performance in predicting time series data among neural network models [17]. The structure of the LSTM employed in the system is shown in Figure 3. LSTM is a kind of recurrent neural network, which replaces the hidden layer in the recurrent neural network (RNN) with a module called LSTM blocks. LSTM addresses the gradient vanishing problem, where the value of the hidden layer is decayed and lost, which is inherited by the next time layer by adopting the LSTM block. It is known that LSTM performs better than RNN for the problem of predicting time series data with long-term dependency [18].

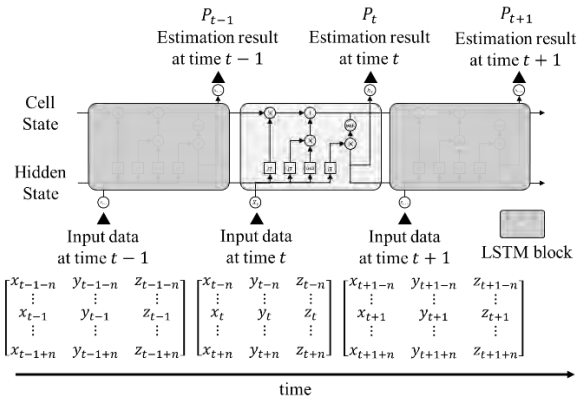

Figure 3. The structure of LSTM network for behavior estimation

3.3.4 Data augmentation

The data labeling should be done referring to data other than sensing data, such as video data, as shown in Figure 4, in creating datasets for behavior estimation. In the labeling of time-series behavior data, video data are commonly used to label behavior conditions [19]. On the other hand, this method is costly and labor-intensive, and inadvertent mislabeling may occur. In order to eliminate these tasks, previous works sharing human behavior data focusing on basic actions in daily life have been done [20]. Nevertheless, studies providing behavior data on specific workers such as construction workers have yet not been made. Therefore, we implement a data augmentation method for sensing data and propose a method to utilize limited data collected in the field as training data.

The conceptual diagram of the data augmentation proposed in this study is shown in Figure 5. While most of the studies on action recognition using inertial sensors use a sampling frequency of 25 Hz or higher, the terminals used in the proposed system have a low sampling frequency of 1 Hz. Taking this condition into consideration, the proposed method restores the acceleration waveform using the interpolation formula for the data discretized by sensing. After that, the number of data sets is artificially increased by cutting out data from the interpolated acceleration waveform at equal intervals. By using this method, it is possible to add diversity to the training data while maintaining the correspondence between time-series information and posture labels, which can be used to generate models with high generalization performance. Indeed, our low-frequency sampling system and this method are inappropriate for instantaneous motion classification problems such as gesture recognition. However, we adopt this method because of the postures targeted in this study record more stable data in the long term than gestures.

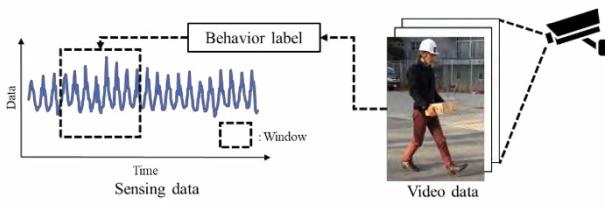

Figure 4. Conceptual diagram of data labeling

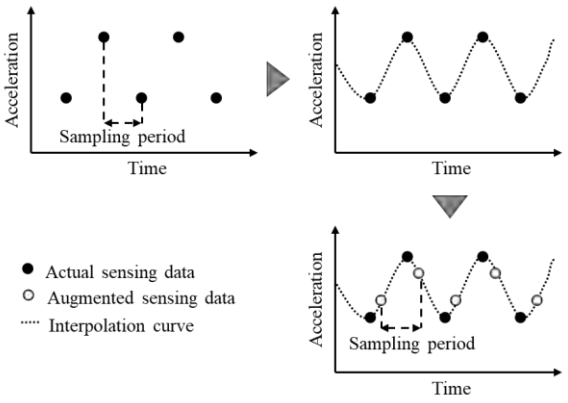

Figure 5. Conceptual diagram of data augmentation for sensing data

4 Verification of the proposed system

We evaluated the accuracy of posture estimation, verified the effectiveness of data augmentation, and estimated the number of binding points of rebar using acceleration data for a rebar worker at an actual construction site.

4.1 Experiment

4.1.1 Target work setting and data collection

A reinforcing bar worker (male, in his 50s, 37 years of experience) who works on binding rebars of floor slabs was asked to wear a terminal and recorded the working state together with the sensing by the terminal. In the work of binding the reinforcing bars of the floor slab, because the transition from the standing state to the forward-leaning posture and the squatting posture occurred repeatedly, the burden on the lumbar region of the worker was large, which caused a disorder of the musculoskeletal system. Because our system can be used for planning preventive measures against musculoskeletal disorders by quantifying and estimating the posture state. This criterion was also utilized for verification.

The rebar binding work is a typical repetitive work of moving to the rebar binding point, preparing a binding wire at a hand, transitioning to the forward-leaning or squatting posture, binding rebar, and moving to the next binding point. Figure 6 shows the flow of the work for binding the reinforcing bars of the floor slab. Unevenness and excessive reduction in repetitive work times are important information for ensuring an appropriate working environment for workers.

In this experiment, forward-leaning and squatting postures for a long time would be counted as rebar binding. The relationship between the posture and the rebar binding work of the floor slab is defined as shown in Figure 7. The number of rebar binding points is estimated based on that. Subsequently, by counting the number of binding points visually based on the actual video data and comparing the estimation results with the actual number, we consider the possibility of applying the proposed system to estimate the number of binding points of the reinforcing bars.

4.1.2 Datasets preparation

After acquiring the terminal record, the correct posture labels (hereinafter called ground truth label) were extracted from the video in every second. Then, the sensing data and correct labels were associated with each other to create data sets. Typically, the time window width is set to have a 50% overlap with respect to the sampling frequency [6], but in this experiment, given the low sampling frequency, we set it to 5 seconds with an 80% overlap. Then, the acceleration data for 5 seconds before and after was associated with the posture label P_t at time t. Three types of postures, standing, leaning-forward, and squatting, were extracted as the static state from "The Nagamachi Work Posture Classification [21]", which defines postures from the ergonomics point of view based on the magnitude of the load applied to the lumbar region of the human body in each work posture.

For dynamic states, we set two categories: transitioning of posture states such as forward-leaning posture from standing posture and walking. Table 1 summarizes the aforementioned posture categories and their definitions in this experiment.

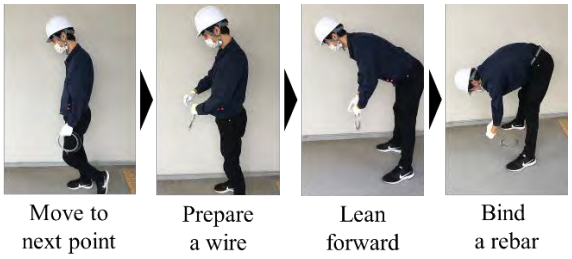

Figure 6. The workflow for binding the reinforcing bars of the floor slab

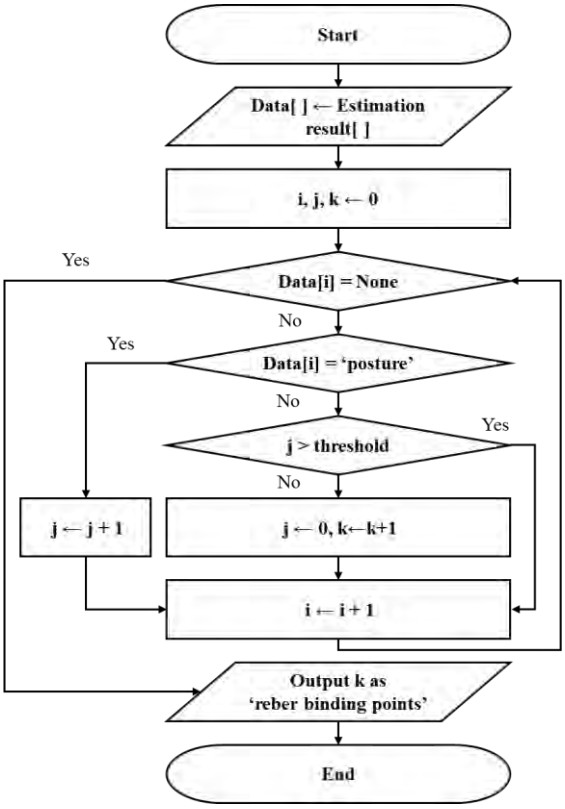

Figure 7. The flow of the estimation for the number of rebar binding points

Table 1. Posture classification of workers in the verification experiment

State	Posture	Definition
Static state	Standing	Upright posture with knees extended
	Forward-leaning	Posture with the waist bent by 30° or more with knees extended
	Squatting	Sitting on the heels posture
Dynamic state	Transitioning	State during changing posture
	Walking	State of advancing step by step

4.1.3 Estimation of accuracy indicators

After the data sets were created, they were divided into training data and test data. The estimation model was trained based on the training data, and the estimation accuracy was calculated based on the test data. Table 2 shows the breakdown of these data in the verification experiments. We allocated the correct labels and estimation results to the confusion matrix shown in Table 3 and calculated the precision, recall, F-measure, and accuracy from Equation (2) to Equation (5) to evaluate the accuracy of the posture estimation.

Table 2. The breakdown of datasets used for accuracy verification

Posture	Training data	Test data
Standing	160	16
Forward-leaning	607	40
Squatting	502	46
Transitioning	344	53
Walking	106	6
Total	**1719**	**161**

Table 3. Confusion matrix in two-class classification

		Estimation result	
		Positive	Negative
Ground truth	Positive	True Positive (TP)	False Negative (FN)
	Negative	False Positive (FP)	True Negative (TN)

$$Precision = \frac{TP}{TP + FP} \quad (2)$$

$$Recall = \frac{TP}{TP + FN} \quad (3)$$

$$F - measure = \frac{2 \times Precision \times Recall}{Precision + Recall} \quad (4)$$

$$Accuracy = \frac{TP + TN}{TP + FP + TN + FN} \quad (5)$$

4.2 Results

4.2.1 Evaluation of data augmentation

Table 4 shows the estimation results with the data augmentation ratio as a comparison when generating the estimation model. For the data augmentation ratio, 1x (without data augmentation), 2x, 4x, and 8x values were used, while linear interpolation was also implemented with the waveforms for the augmentation. The results in Table 4 indicated that the F-measures in each posture, increased and decreased as the ratio of the data augmentation was increased, while the accuracy tended to increase as the ratio was increased. It was confirmed that forward-leaning and squatting postures could be estimated with the F-measure of 79% or higher for all data augmentation ratios.

Table 4. The estimation accuracy at each data augmentation ratio

	Posture	Data augmentation ratio			
		1x	2x	4x	8x
F-measure	Standing	0.73	0.60	0.62	0.60
	Forward-leaning	0.82	0.88	0.85	0.87
	Squatting	0.80	0.79	0.82	0.83
	Transitioning	0.41	0.51	0.60	0.65
	Walking	0.40	0.14	0.33	0.22
	Accuracy	**0.68**	**0.70**	**0.73**	**0.73**

4.2.2 Evaluation in time-series

Figure 8 shows a time-series evaluation of the ground truth labels and the estimation results at the data augmentation ratio of 8x, which recorded the highest accuracy in the estimation results as shown in Table 4. It was confirmed that the accuracy increased when the same posture continued for a long time. On the other hand, the accuracy tended to be lower if the posture changed frequently in a short period.

Figure 8. Time series evaluation of posture estimation

4.2.3 Evaluation of rebar binding points estimation

Table 5 shows the results of the estimation of the rebar binding points based on the results of the estimation flow of the binding points shown in Figure 7. The results of the posture estimation are shown in Figure 8. The condition that the rebar is bound while the forward-leaning or squatting posture was continued for more than 5 seconds was set. The number of binding points, the total time required for rebar binding, and the time spent on binding each point were also calculated.

Table 5. Evaluation of rebar binding points estimation

Input data for estimation	Posture estimation	Ground truth posture
The number of binding points	6	8
Total binding time (sec)	72.0	83.0
Binding time per point (sec)	12.0	10.4

4.3 Discussions

The results in Table 4 show that the proposed system can estimate the worker's posture correctly up to 73% accuracy based on the triaxial acceleration. The accuracy of the proposed system was increased from 68% to 73% by using the data augmentation method. It was also confirmed that the F-measure of 79% or more was able to be achieved for the forward-leaning and squatting postures. Their accuracies are higher than the other gestures in every data augmentation ratio. This is because the LSTM network learned the change in direction of the gravitational acceleration caused by the tilt of the worker's head as effective feature for posture estimation. In the posture classification based on the influence on the musculoskeletal system [21], forward-leaning and squatting postures are set as the level of 5th and 6th out of 10th respectively. Therefore, calculating the cumulative frequency of these levels enable improvement of working environment using quantitative indicators. For further improvement of accuracy, we need to use positional information that was not used in this experiment and add small devices that consider intrusiveness of wearing. According to the results shown in Table 5, the number of rebar binding points were estimated, and six of the eight points were correctly estimated from the posture estimation results. By comparing these estimated results with the quantities of components extracted from product models such as Building Information Modeling (BIM), site stakeholders will be able to understand the progress quantitatively.

5 Conclusions

This paper proposed a system for estimating workers' posture using a helmet-mounted terminal, which is already in use at a construction site to collect worker's behavior data. From the results of posture estimation using triaxial acceleration data acquired at the terminal, it was confirmed that five different postures could be estimated with an accuracy of up to 73% by using LSTM and the data augmentation method. In particular, the system was able to detect forward-leaning and squatting postures with high accuracy, which indicates the system can be used to improve the ergonomic work environment, such as quantifying the load on the body, by calculating the cumulative time of those postures. It was also confirmed that the results of the posture estimation can be used to predict the number of rebar binding points.

Future work includes collecting data to expand the range of jobs and postures to be estimated and improving the accuracy of posture estimation by linking with other types of sensing data such as positional information. We also aim to develop a management system that links behavior estimation with geometric and attribute information of the BIM model.

References

[1] Labour Standards Bureau, Ministry of Health, Labour and Welfare: Survey on Industrial Accidents, On-line: https://www.mhlw.go.jp/bunya/roudoukijun/anzeneisei11/rousai-hassei/dl/b19-16.pdf, Accessed: 6/6/2020.

[2] Ministry of Land, Infrastructure, Transport and Tourism: White Paper on Land, Infrastructure, Transport and Tourism in Japan 2019, On-line: https://www.mlit.go.jp/common/001325161.pdf, Accessed: 6/6/2020.

[3] Park, C. and Kim, H.: A framework for construction safety management and visualization system,

Automation in Construction, Vol.33, pp.95-103, 2013.

[4] Yang, X., Wang, F., Li, H., Yu, Y., Luo, X. and Zhai, X.: A Low-Cost and Smart IMU Tool for Tracking Construction Activities, In 2019 *Proceedings of the 36th ISARC*, Banff, Alberta, Canada, pp.35-41.

[5] Bao, L. and Intille, S.S.: Activity Recognition from User-Annotated Acceleration Data, *Pervasive Computing*, pp.1-17, 2004.

[6] Akhavian, R. and Behzadan, A.H.: Smartphone-based construction workers' activity recognition and classification, *Automation in Construction*, Vol.71, pp.198-209, 2016.

[7] Zhang, M., Chen, S., Zhao, X. and Yang, Z.: Research on Construction Workers' Activity Recognition Based on Smartphone, *Sensors*, Vol.18, 2667, 2018.

[8] Yan, X., Li, H., Li, A. and Zhang, H.: Wearable IMU-based real-time motion warning system for construction workers' musculoskeletal disorders prevention, *Automation in Construction*, Vol.74, pp.2-11, 2017.

[9] Chen, L., Hoey, J., Nuget, C. D., Cook, D.J. and Yu, Z.: Sensor-Based Activity Recognition, *IEEE Transactions on Systems, Man, and Cybernetics, Part C (Applications and Reviews)*, Vol.42, No.6, pp.790-808, Nov. 2012.

[10] Nakamura, Y. and Kanade, T.: Semantic Analysis for Video Contents Extraction – Spotting by Association in News Video, In *Proceedings of the fifth ACM international conference on Multimedia*, pp.393-401, 1997.

[11] Yang, J., Arif, O., Vela, P.A., Teizer, J. and Shi, Z.: Tracking multiple workers on construction sites using video cameras, *Advanced Engineering Informatics*, Vol.24, No.4, pp.428-434, 2010.

[12] Luo, H., Xiong, C., Fang, W., Love, P.E.D., Zhang, B. and Ouyang, X.: Convolutional neural networks: Computer vision-based workforce activity assessment in construction, *Automation in Construction*, Vol.94, pp.282-289, 2018.

[13] Fang, W., Ding, L., Luo, H. and Love, P.E.D.: Falls from heights: A computer vision-based approach for safety harness detection, *Automation in Construction*, Vol.91, pp.53-61, 2018.

[14] Park, M. and Brilakis, I.: Construction worker detection in video frames for initializing vision trackers, *Automation in Construction*, Vol.28, pp.15-25, 2012.

[15] Ray, S.J. and Teizer, J.: Real-time construction worker posture analysis for ergonomics training, *Advanced Engineering Informatics*, Vol.26, No.2, pp.439-455, 2012.

[16] Hitachi, Ltd.: Hitachi Develops Systems to Increase Productivity and Safety at Construction Sites Using IoT Technologies, On-line: http://www.hitachi.com/New/cnews/month/2018/03/180327.pdf, Accessed: 6/6/2020.

[17] Hochreiter, S. and Schmidhuber, J.: Long short-term memory, *Neural Computation*, Vol.9, No.8, pp.1735-1780, 1997.

[18] Graves, A., Fernández, S. and Schmidhuber, J.: Bidirectional LSTM networks for improved phoneme classification and recognition, In *Proceedings of the 15th International Conference on Artificial Neural Networks: Formal Models and Their Applications - Volume Part II*, pp.799–804, Sep. 2005.

[19] Anguita, D., Ghio, A., Cneto, L., Parra, X. and Reyes-Ortiz, J.L.: A Public Domain Dataset for Human Activity Recognition Using Smartphones, ESANN 2013 proceedings, European Symposium on Artificial Neural Networks, Computational Intelligence and Machine Learning, pp.437-442.

[20] Ramanan, D. and Forsyth, D.A.: Automatic Annotation of Everyday Movements, In *Proceedings of Neural Info. Proc. Systems (NIPS)*, Vancouver, Canada, Dec. 2003.

[21] Nagamachi, A.: Requisite and practices of participatory ergonomics, *International Journal of Industrial Ergonomics*, Vol.15, pp.371-377, 1995.

Incident Detection at Construction Sites via Heart-Rate and EMG Signal of Facial Muscle

Mizuki Sugimoto[a], Shunsuke Hamasaki[a], Ryosuke Yajima[a], Hiroshi Yamakawa[a]
Kaoru Takakusaki[b], Keiji Nagatani[a], Atsushi Yamashita[a], and Hajime Asama[a]

[a]The University of Tokyo, Japan
[b]Asahikawa Medical University, Japan

E-mail: m-sugimoto@robot.t.u-tokyo.ac.jp, hamasaki@robot.t.u-tokyo.ac.jp, yajima@robot.t.u-tokyo.ac.jp, yamakawa@robot.t.u-tokyo.ac.jp, kusaki@asahikawa-med.ac.jp, keiji@i-con.u-tokyo.ac.jp, yamashita@robot.t.u-tokyo.ac.jp, asama@robot.t.u-tokyo.ac.jp

Abstract -

Fatal accidents occur at construction sites. Incidents involving dangerous situations but not reaching the category of fatal accidents also take place. When an incident occurs, workers typically generate an on-site physiological reaction. In this paper, an automatic detection system is proposed to automatically identify incidents by measuring biological signals related to emotions of on-site workers, such as heart rate and the masseter muscle. In the first stage of this study, some virtual reality (VR) video-based experiments were conducted with some wearable sensors to confirm whether the aforementioned biological signals are suitable to detect incidents. While watching the VR videos, biological signals of the subjects were measured using different wearable sensors. The experimental results corroborated that the proposed sensing method is suitable to detect construction-site incidents.

Keywords -

Construction site; Safety; Biological signals; Incident detection

1 Introduction

According to a survey by the Ministry of Health, Labour and Welfare, there has been a slight increase in the number of occupational accidents in Japan. In particular, more fatal workplace accidents occur in the construction industry than in other industries [1]. The reasons for this are the shortage of workers caused by the decline in the population due to the low birth rate, and the aging of the on-site workers. Therefore, the need to establish a safer working environment is becoming urgent. To this end, we need to detect an "incident", i.e., a situation in which there is a risk of an accident or other danger, and conduct an analysis of the cause of the problem.

There are two main methods for detecting incidents, as shown in Figure 1: detection from the external environment through devices such as a camera, and detection of hazards perceived by field workers. For the latter method, biological signals related to physiological responses are often used to detect and register dangerous situations perceived by the workers at the site. In this study, this method was used because we finally would visualize the hazards perceived by the field workers not only for incident detection but also for removing the mental burden of the workers in the future.

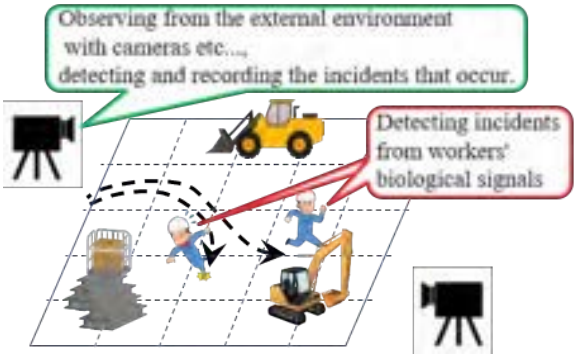

Figure 1. Two main methods for detecting incidents.

Previous studies related to ours reported a construction-site incident detection method based on the heart rate [2]. In this study, the subjects' heart rate was measured using a chest-belt smartwatch, and incidents were detected using the measured heart-rate variability. There are also previous studies for traffic incidents, where the heart rate of drivers is used to detect incidents[3][4]. The heart rate varies according to the activity of sympathetic and parasympathetic nerves [5]. This is related to a person's mental state. Remarkably, the sympathetic nervous system is dominant during tension, resulting in a higher heart rate. In other words, the heart rate is higher when the user feels in danger. However, it is generally known that the heart rate increases not only during mental tension but also during exercise[6]. At construction sites, workers often carry heavy materials and perform other tasks that require strenuous exercises. Therefore, the problem of uncertainty about whether an elevated heart rate is caused by exercise or worker ' s unsafety feelings is expected to occur.

In this study, to solve the aforementioned problems, we aimed to detect incidents at construction sites by using various biological signals related to physiological responses in addition to heart rate. To achieve this, we created virtual reality (VR) videos that simulated incidents that can occur at construction sites. We also conducted experiments using the VR videos. Subjects were asked to watch the VR videos while their physiological responses were measured in terms of heart rate and electromyography (EMG) of the masseter muscle. The detectability of construction-site incidents using these biological signals was verified.

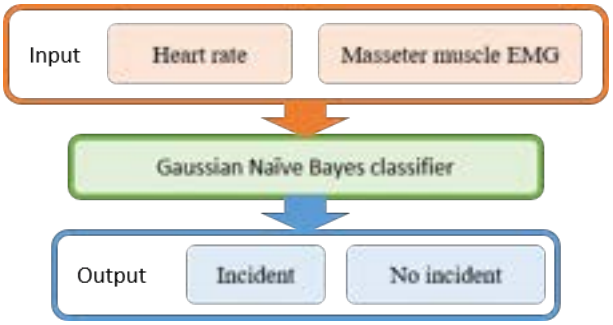

Figure 2. Outline of the proposed method.

2 Proposed Method

2.1 Biological Signals Used

The final goal of this study was to detect situations where workers feel in danger in the field through a wearable sensor. The sensor measures their biological responses and correlates them with the work content. To achieve this, it is necessary to select the biological signals for detecting the scene where a worker feels in danger. Typical biological signals related to human emotions include the heart rate and the masseter muscle.

The heart rate fluctuates according to sympathetic and parasympathetic, i.e., autonomous, nervous activity [5]. This activity is related to the human psyche and is associated with a higher heart rate owing to the dominance of sympathetic nerves during tension. In other words, it is believed that the heart rate increases when the worker is in a tense state due to potential danger to himself.

Facial muscles, such as the masseter muscle, are known to be related to human emotions [7]. Therefore, it is possible to estimate workers' emotions toward danger by measuring the activity of the masseter muscle.

Overall, heart rate and EMG of the masseter muscle can constitute physiological indicators to detect situations where a worker feels danger. In this study, we used these indicators as candidates for the biological response. We conducted indoor VR experiments to test whether these candidate biological signals can be used to detect construction-site incidents.

2.2 Detection Method

In this study, heart rate and EMG of the masseter muscle were used as features, and a Gaussian naive Bayes classifier was used to detect construction-site incidents, as shown in Figure 2.

As in previous studies, we used the average heart rate h at a given time t as a feature of heart rate [2]. Given that the maximum amplitude is generally used for the evaluation of EMG, the masseter EMG feature in our study was the maximum amplitude f at a given time t. The feature vector $\mathbf{x}$ used in this study is expressed as follows:

$$\mathbf{x} = (h, f)^{\mathrm{T}}. \tag{1}$$

Using this $\mathbf{x}$ as inputs, a Gaussian naive Bayes classifier, which is often employed to classify time series data such as those generated in this study, was used to determine whether an incident occurs at a construction site or not. A Gaussian naive Bayes classifier assumes the independence of each feature and simultaneously estimates the probability from each feature. The label with the highest probability constitutes the output. The classifier is expressed according to the following formula:

$$\hat{y} = \mathrm{argmax}[p(y|\mathbf{x})], \tag{2}$$

$$= \mathrm{argmax}[p(y)\prod_{d=1}^{D} p(x_d|y)], \tag{3}$$

where $\hat{y}$ is the output label, $p(y|\mathbf{x})$ is the posterior probability of correct label y given the input vector $\mathbf{x}$, $p(y)$ is the prior probability of correct label y, $p(x_d|y)$ is the likelihood, x_d is the feature in the d-th dimension, and D is the dimension of $\mathbf{x}$.

To use the classifier, we need a unique parameter for each probability distribution. The optimal value of the eigen-parameters is found by maximum likelihood estimation, with the feature matrix of the training data as $\mathbf{X}$ and the corresponding correct label vector as $\mathbf{y}$. The maximum likelihood function $L(\mathbf{X}, \mathbf{y})$ is expressed as follows:

$$L(\mathbf{X}, \mathbf{y}) = \prod_{n=1}^{N} p(y_n)p(\mathbf{x}_n|y_n), \tag{4}$$

$$= \prod_{n=1}^{N}[p(y_n)\prod_{d=1}^{D} p(x_{nd}|y_n)], \tag{5}$$

where N is the number of training data, y_n is the correct label in the n-th training data, $\mathbf{x}_n$ is the feature vector in the n-th training data, and x_{nd} is the feature in the d-th dimension of the n-th data.

A Gaussian naive Bayes classifier assumes that the likelihood $p(x|y)$ follows a Gaussian distribution and finds the optimal value of the intrinsic parameters such that the likelihood function $L(\mathbf{X}, \mathbf{y})$ is maximized for each event. The Gaussian distribution is represented by the following equation:

$$p(x|y) = \frac{1}{\sqrt{2\pi\sigma^2}}\exp(-\frac{x-\mu}{2\sigma^2}), \quad (6)$$

where σ^2 is the distribution of the feature x when the correct label is y and μ is the mean of the feature x when the correct label is y. A Gaussian naive Bayes classifier estimates the correct label from the input features by computing the above equation.

In this study, the aforementioned methods were used to classify whether incidents occur at a construction site.

3 VR Experience

3.1 Outline of Experience

In this study, we conducted experiments in which subjects watched a simulated environment of a construction site through VR videos and simultaneously obtained biological signals from a wearable sensor. Subjects sat in a designated position in the laboratory, wore a wearable sensor for biometric measurements, and watched a VR video. To understand which scenes subjects felt as dangerous, we gave them a controller and instructed them to press the button on the controller when they felt a situation as dangerous; we recorded the time when they pressed the button. This experiment was conducted with the approval of the Ethics Committee of the University of Tokyo.

3.2 VR videos

In the construction industry, personal injuries involving contact between workers and construction equipment or machines such as automobiles are very common [8]. Therefore, in this study, we prepared VR videos of incident scenes where a subject and an excavator are likely to come into contact. Specifically, we prepared the following eight videos.

- Two types of incident scenes in which a hydraulic excavator moves backwards unaware of the presence of a worker and almost comes into contact with the worker, changing the stopping position (long-distance backward and short-distance backward)
- Two types of incident scenes where a hydraulic excavator turns unaware of the presence of a worker and the tip of the bucket almost comes into contact with the worker at different distances (long-distance turning and short-distance turning)

Figure 3. Example of VR image.

- One type of non-accident scene where a hydraulic excavator waits at a long enough distance from a worker (standby)
- One type of non-accident scene where a hydraulic excavator turns in the opposite direction with respect to a worker (non-accidental turning)
- One type of non-accident scene where a hydraulic excavator moves forward and away from a worker (forward)
- One type of non-accident scene where a hydraulic excavator crosses at a long enough distance from a worker (crossing)

In addition, we prepared videos so that the subject could see papers near the subject's hand, simulating that the subject is working at a site while looking at papers such as instructions. The subjects were instructed in advance to look at the papers before them and to pay attention to the construction machines in front of them, as if they were in a construction site. An example of such prepared VR images is shown in Figure 3. These VR images were filmed at the Public Works Research Institute using Ricoh Theta V, operated by Hitachi Construction Machinery ZAXIS120.

3.3 Devices

The wearable sensors used in this experiment are shown in Figure 4. The S&ME DL-310 was used to measure the heart rate, as shown in Figure 4a, and the S&M DL-140 was used to obtain the EMG, as shown in Figure 4b. The S&ME's DL-310 amplifies the R wave of the cardiac signal detected by the sensor with a filter amplifier, and outputs this pulse. EMG of the masseter muscle was measured by the S&M's DL-140 with electrodes attached to the temporal area of the face. The biological signals acquired

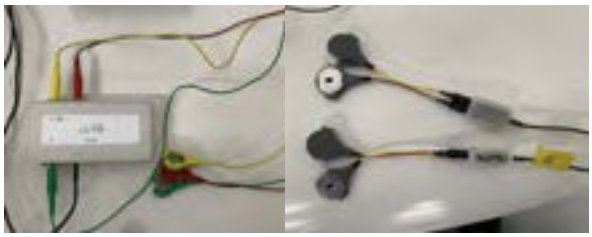

(a) S&ME DL-310 (b) S&ME DL-140

(c) S&ME DL-3100

Figure 4. Sensors employed in the experiments.

from these sensors were recorded in an S&ME data logger (DL-3100), as shown in Figure 4c. This S&ME DL-3100 has a sampling frequency of 1000 Hz and 16-bit A/D conversion resolution and can store measurement data in its on-board memory.

Vive Cosmos was used to present the VR videos. This head-mounted display is also equipped with headphones; thus, subjects could hear the sound recorded at the time of filming and watch the video.

3.4 Biological Signals Processing

After applying a bandpass filter in the frequency range from 0.16 to 500 Hz to the cardiac telegraphic signal in the amplifier section, the biometric information was transmitted to the receiver and recorded in the device. Simultaneously, a pulse waveform synchronized with the R wave was generated in the amplifier section and was recorded in the biometric device concurrently with the cardiac signal. Given that the synchronized pulse rises at the time position of the R wave, the R-R interval was calculated from the time position of the rise of the pulse, and the heart rate was calculated from the inverse of the pulse. The time at the midpoint between consecutive R waves was used to record the heart rate.

In this study, the root mean square (RMS) method was used, which is commonly used for analyzing an EMG of the masseter muscle. Considering the frequency range of EMGs in previous studies, a 5-Hz high-pass filter was used to process the EMGs [9]. Given that humans usually chew in a range from 0.1 seconds to several seconds when they chew, the frame length in this study was set to 100 ms and the interval between frames was set to 1 ms. Denoting the value of RMS at sample point n as $S(n)$, we obtain the

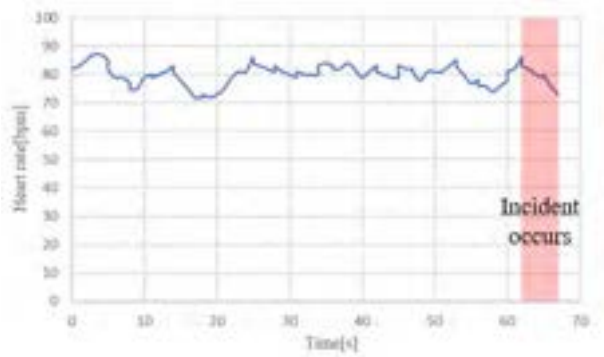

(a) Heart-rate variability in subject A.

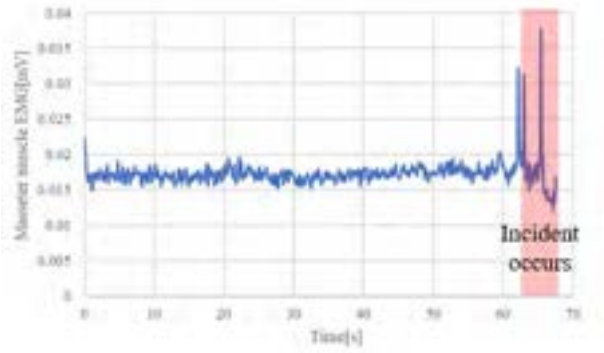

(b) EMG of the masseter muscle in subject A.

Figure 5. Biological signals of subject A.

following equation:

$$S(n) = \sqrt{\frac{1}{N}\sum_{i=0}^{N} f^2(n+i)}, \tag{7}$$

where N is the frame length and f(n+i) is the signal of the masseter muscle at sample point n+i.

3.5 Result

Three male students in their twenties were the subjects of this study.

As an example of experimental results, the variations of heart rate and EMG of the masseter muscle for subject A while he was watching the short-distance turning VR video are shown in Figure5. Figure5a shows the heart rate of subject A. The horizontal axis represents the time of the VR video and the vertical axis represents the heart rate. Figure5b shows the variation of the EMG of the masseter muscle for subject A. The horizontal axis shows the time of the VR video and the vertical axis shows the amplitude variation of the EMG of the masseter muscle. The area in red in both Figure5a and Figure5b is the interval of the incident. Figure5 shows that the heart rate ranged from 73 to 86 bpm during the incident, and there was only a slight

difference from the time before the incident occurred. In contrast, the amplitude of the EMG of the masseter muscle reached up to 0.38 mV, which is approximately twice as large as before the incident occurred. This suggests the possibility of detecting incidents from the EMG of the masseter muscle.

In this study, among the experimental data of 3 subjects watching 8 VR videos, 3 subjects watching 4 VR videos (short-distance backward, short-distance turning, standby, and crossing) were used as training data, and 3 subjects watching the remaining 4 videos (long-distance backward, long-distance turning, forward, and no-accident turning) were used as evaluation data. Correct labels were assigned for the experimental data as incidents at the time of the simulated incident in the VR video and no incidents otherwise.

The detection of construction-site incidents by the proposed method was evaluated using accuracy and recall. Accuracy was calculated by comparing the estimation results of the proposed method with the correct labels of the test data and dividing the number of correct answers by the total number of test data. Thus, it provides the percentage of correct estimation results. Recall is calculated by dividing the number of test data correctly detected as incidents by the proposed method by the number of test data actually labeled as incidents. Thus, it indicates the completeness of the incident detection. The equations for accuracy A and recall R are as follows:

$$A = \frac{D^C}{D^T}, \tag{8}$$

$$R = \frac{D_I^C}{D_I^T}, \tag{9}$$

where D^C is the total number of correct data, D^T is the total number of evaluated data, D_I^C is the number of correct data detected as incidents, and D_I^T is the number of data labeled as incidents.

The accuracy and recall of the proposed method are shown in Table 1. In addition, for comparison, the accuracy and recall obtained by the method of estimating only the heart rate as a feature are also shown in Table 1. Accuracy was 0.48 for the proposed method and 0.87 for the heart-rate-only method. Therefore, the accuracy of the heart-rate-only method was higher. By contrast, recall was 0.57 for the proposed method and 0 for the heart-rate-only method. Therefore, the recall of the proposed method was higher. The purpose of this study was to detect incidents, and it is important to detect incidents comprehensively for achieving a safe construction-site environment. Therefore, it is desirable to have a method with high recall and accuracy. Given that the recall of the heart-rate-only method is 0, it is assumed, according to such method, that no incidents were detected at all. The proposed method is more effective than the heart-rate-only method because the recall is higher and more comprehensive, even though the accuracy of the proposed method is lower than that of the heart-rate-only method. The reason why we could not detect an incident using the heart-rate-only method in these environments may be because heart rate responds after a short period of time after an incident occurs. Generally, the heart rate is known to respond about 10 to 20 seconds after an incident occurs, but in the VR video used in these experiments, the video ended within 10 seconds after the incident occurred. It is thought that we could not detect incidents using the heart-rate-only method. In the future, we will consider creating a VR movie with more than 20 seconds left after an incident and using it for experiments.

Table 1. Accuracy and recall of the proposed method and heart-rate-only method

Method	Accuracy	Recall
Proposed Method	0.48	0.57
Heart-Rate-Only	0.87	0

4 Conclusion

In this study, a method for detecting construction-site incidents through a Gaussian naive Bayesian classifier using heart rate and masseter EMG as features was developed. Indoor experiments in which subjects experienced the simulated environment of a construction site through VR videos were conducted to obtain biological signals. The performance of the proposed method was evaluated using the data obtained from the experiments. A comparison between the proposed method and a heart-rate-only method confirmed that the proposed method was more effective in detecting incidents comprehensively. In the future, we will aim to establish a method for detecting incidents in which workers and construction machines are close to come into contact with each other through verification of experiments using VR videos.

References

[1] Ministry of Health, Labour and Welfare: "Fiscal Year 2017 Workers' Accident Situation", https://www.mhlw.go.jp/stf/houdou/0000209118.html (Access: 7th July, 2019).

[2] Ryuichi Imai, Daisuke Kamiya, Haruka Inoue, Shigenori Tanaka, Jun Sakurai, Takuya Fujii Nobuya Honda and Makoto Ito: "Research for Experimenting Various Possibilities Grapsing Near Miss Incidents and Physical Fatigue Using Smart Watch in Construction Fields", Journal of Japan Society of Civil Engineers F3, Vol. 74, No. 2, pp. 167-177, 2018.

[3] Masayasu Tanaka, Fumiaki Obayashi, Toshiya Arakawa, Shinji Kondo and Kazuhiro Kozuka: "Detection of Driver's Surprised State Based on Blood Pressure and Consideration about Sensitivity of Surprised State", Proceeding of the 2nd International Conference on Intelligent Systems and Image Processing 2014, pp. 56-60, 2014.

[4] Toshiya Arakawa, Masayasu Tanaka, Fumiaki Obayashi, Shinji Kondo and Kazuhiro Kozuka: "Probability of Driver's State Detection Based on Systolic Blood Pressure", Proceeding of 2015 IEEE International Conference on Mechatronics and Automation (ICMA), pp. 2106-2111, 2015.

[5] Julian F. Thayera, Fredrik Åhs, Mats Fredrikson, John J. Sollers III and Tor D. Wager: "A Meta-Analysis of Heart Rate Variability and Neuroimaging Studies: Implications for Heart Rate Variability as a Marker of Stress and Health", Nueroscience and Biobehavioral Reviews, Vol. 36, No. 2, pp. 747-756, 2012.

[6] Tasuku Sato, Toshihiro Ishiko, Junichiro Aoki, Tatsuo Shimisu and Takashi Maejima: "Exercise Change of Heart Rate, Blood Pressure and Respiatory Rate in Relation to Sex and Age", Japanese Journal of Physical Fitness and Sports Medicine, Vol. 26 No. 4 pp. 165-176 1977.

[7] John T. Cacioppo, Richard E. Petty, Mary E. Losch and Hai Sook Kim: "Electromyographic Activity Over Facial Muscle Regions CanDifferentiate the Valence and Intensity of Affective Reactions", Journal of Psrsonality and Social Psychology, Vol. 50, No. 2, pp. 260-268, 1986.

[8] Japan Construction Occupational Safety and Health Association: "Fatal Construction Accidents by Type of Construction Work and Type of Accident, 2018", https://www.kensaibou.or.jp/safe_tech/statistics/construction/h30.html (Access: 19th Februally 2020).

[9] Roberto Merletti and Politecnico di Torino: "Standards for Reporting EMG Data", J Electromyogr Kinesiol, Vol. 9, No. 1, pp. 3-4, 1999.

Scenario-Based Construction Safety Training Platform Using Virtual Reality

Ankit Gupta[a] and Koshy Varghese[b]

[a]Post Graduate Student, Department of civil engineering, Indian Institute of Technology Madras, India
[b]Professor, Department of civil engineering, Indian Institute of Technology Madras, India

E-mail: ankitgupta1008@gmail.com, koshy@iitm.ac.in

Abstract –

Learning by doing creates a marked impact on a trainee's cognitive ability. Technologies such as Virtual Reality (VR), Augmented Reality (AR) etc. aid in developing platforms to enhance the learning experience of users. These technologies can be particularly effective in construction sites which are complex and contain hazards difficult to foresee. These technologies can enable the formulation of robust safety training procedures that will enhance awareness among workers about workplace risks and help to mitigate the same. Currently, the customized development and expense in execution of these digital platforms are major deterrents in its practical deployment and optimum utilization.

In this study, a framework is proposed for the design and development of a VR platform for safety training. The proposed framework classified as Decision-Making Accident Scenario (DMAS) - produces an information skeleton which is derived out of an assessment of potential accidental situations emerging out of a functioning construction site. This skeleton works as a design document to conceptualize the accident scenario as per the identified accidental situation. In each scenario, trainees need to analyze simulated situations, identify risks, and make informed decisions about the mitigation measures which create alternate outcomes. Immersive VR experience of the scenario is built with the help of a gaming engine Unity and Google VR SDK. Smartphone-based VR platform is suggested for user interaction as it is economical to deploy. A pilot study to evaluate this proposed framework was experimentally executed by developing cases related to an ongoing project and synthesizing the different scenarios and storylines into the VR platform. This was tested on three users, and preliminary findings empirically indicated that that safety training using the aforementioned digital platform was significantly more effective in creating better understanding of safety practices on-site.

Keywords –

Virtual Reality (VR); Unity; Decision Making Scenario; Construction Safety Training

1 Introduction

The advancements made in the field of construction have facilitated the implementation of more complex projects in the sector. However, the complexity of a construction project also resulted in making the workplace more prone to accidents and injuries. Despite the industry's sustained efforts to train and educate its workforce about safety practices in the workplace, the construction industry continues to record the highest number of work-related accidents and injury. The USA Occupational Safety & Health Administration (OSHA), reports "out of every 5000 private-industry worker fatalities, 20% are in the construction industry, which means that one out of every five workers deaths is construction related" [1]. This data is based solely on officially reported injuries, and it is widely known that a majority of the workplace injuries go unreported [2]. Such statistics reveal how dangerous and potentially unsafe the construction industry is.

From the perspective of project performance, any on-site accident or injury can cause substantial project delay and cost overrun [3]. To avoid such uncalled for circumstances, the industry follows various protocols, standards, and systems established by the concerned regulatory body of the respective government of the country. The industry also ensures that basic safety training is given to its workforce and generally employs conventional methods for the same which are based on videos, presentations, lectures, and apprenticeship programs [4]. Though this approach gives an insight to the construction practitioners about risk identification and mitigation measures, its effectiveness is limited as it does not prepare them for anticipating and appropriately addressing hazard scenarios [5].

Research has shown that Virtual Reality (VR) has the potential to serve as a training platform, especially

in applications that require visualization. It combines 3D vision and sound; and allows active participation by evoking a sense of the presence of the user [6]. Based on the capabilities of VR, it is proposed to develop a detailed framework to identify and analyze experiences of various accidental situations of a construction site. A platform to implement the framework that enables interactive scenario-based safety training VR application for a smartphone is also proposed. It is expected that the immersive experience of accident scenarios derived from the analysis of the accidental situation will enhance the trainee's ability of risk identification and enable suitable precaution selection.

This paper is organized into seven sections. The following section discusses the existing literature, related work and current gaps in VR based safety training. Sections 3 and 4, present the proposed solution: DMAS based VR training platform and the methodology to develop it. A pilot study to develop and apply the prototype is presented in Section 5. Section 6 shows the analysis of the results obtained after testing the prototype on users, and Section 7 presents the conclusions of the study along with the future work.

2 Related work

This section presents the methods of conventional safety training followed on-site and their limitations. It also discusses the existing VR based safety platforms along with potential and current limitations.

2.1 Conventional Training Method

Safety awareness gets imbibed in workers primarily through field experience and safety training exercise among others. The construction industry has well-established systems for imparting safety training by using methods and platforms like videos, PowerPoint presentations, lectures, or safety toolbox meetings [4]. A survey was conducted on 121 construction practitioners who completed an OSHA 10-hours construction safety training course to check their perception about the efficacy of existing training programs [7]. The survey shows that most of the participants were dissatisfied with the way the training was given. Another study shows that trainees faced problems in being able to visualize construction tasks and activities. In a way, though the videos enabled visualization, the passive role of the trainee in the training procedure renders this method tedious and insufficiently engaging [8]. Thus, these conventional training platforms failed to give the desired results and time and again resurfaces and reinforces the need for a better and effective training program. The inclusion of digital advancements like VR in safety training, can go a long way in devising the potential solution to this problem.

2.2 VR Based Construction Safety Training

The use of VR in the training and education field is widespread. Its first implementation was to train the aircraft pilots by using a flight simulator. In recent years, VR has also become popular in the construction field. Many researchers have tried different ways of using VR for safety training purposes and found largely satisfactory results.

The main advantage of VR lies in the fact that it enables visualization. One study tried to verify this aspect by comparing hazard recognition and risk perception skills of two sets of test subjects: one, who worked with photographs and documents and the other who visualized the situation using VR [9]. Results show clearly that the test subjects from the VR set were able to identify most hazards correctly.

Another study tried to solve the visualization problem faced by the safety management team in risk identification [5]. In this, gaming technology was used to develop the Virtual Safety Assessment System (VSAS). This system simulated high-risk activities and asked complicated multiple-choice questions related to the activity, where the trainee had to think and observe before opting for any option. Such platforms managed to cover various aspects of general safety training. However, VR is not limited to just this. Researchers tried to train a group of students and workers about general safety training as well as task-specific safety training like safety in cast-in-situ concrete and stone cladding work [10]. Task-specific training simulation consisted of various accident scenarios that could arise because of the possible mistakes committed by the trainee while performing the assigned task. The results from the study suggests that the VR platform had a clear advantage in task-specific training, while no significant improvement was seen in the case of general safety training. It also verifies that VR training is indeed very effective as it required the trainees to maintain a high level of alertness and engagement for the entire period.

A social/collaborative VR-based framework was developed to make the workers aware of the critical elements in a collaborative task on-site. Here the students were given an opportunity to learn about construction safety measures by doing experiments on 3D virtual world space [8]. The prototype allowed the student to play an active role while collaborating with other students. The results clearly indicate that it improved the students' involvement, ability to collaborate with other students.

Although research in the field of VR has grown rapidly in the last decade; most of the existing VR platforms for construction safety training still have certain limitations. Some of these are as follows:

Currently, existing VR platforms, while proving useful, lack a well-defined framework and

methodology, which tends to generalize the process of VR based construction safety training platform development.

Most VR simulations teach about risk identification but seldom provide scenarios on how to mitigate the risk.

The cost associated with any VR based safety training platform is very high as a result of which deployment across construction sites gets limited.

3 Proposed DMAS Based VR Training Platform

Based on the above limitations, a Decision-Making Accident Scenario (DMAS) based VR android application platform was proposed which was economical and didn't require high-end VR devices. This platform was prompted by a requirement to focus on improving trainee's ability of risk identification as well as identifying suitable mitigation techniques. It would consist of various accident scenarios, which would be the modified replica of identified accidental situations in a real construction site.

The trainee would be introduced to these scenarios in a virtual environment. Based on observations and assessment, the trainee would need to identify the correct risks associated with the scenarios and try to mitigate those risks by suggesting appropriate precautions. After making those decisions, the trainee would need to verify the safety of that scenario's location by testing it. Identifying risks correctly and suggesting corresponding precautions accurately would be the parameters for evaluation. While testing, it might result in an incident/accident, if the trainee make errors in taking all necessary and correct precautions. These simulated accident outcomes would create a significant and much needed impact on the trainees in raising awareness about how a wrong judgment on site could lead to severe danger.

4 Methodology

To develop a DMAS based VR training platform, a detailed methodology, as shown in Figure 1, was designed and developed. The first step was to develop a detailed Risk Identification Framework (RIF) having the same structure as shown in the first part of Figure 1. This framework was used to classify general types of accidents that could occur on-site into standard categories (A), along with its root causes (R) and precautions (P) to mitigate it. For developing the RIF, safety manuals and accident case studies were referred.

After RIF preparation, the second step was to assess the specifics of the site and identify where training is required. The site visit was intended to identify and analyze various Accidental Situations (As), which might lead to an accident in case of negligence. The Possible Accidents (PA) in those situations were classified as per pre-classified accident categories (A), as shown in the second part of Figure 1.

The third step was to form a DMAS information skeleton. This skeleton was a design document that conceptualized the VR visualization of DMAS. As sketched out in the third part of Figure 1, there were two variables: what accidents should be framed and what corresponding precautions should be suggested for that Framed Accident (FA). The analysis of the accidental situation (As), as shown in the second part of Figure 1, would become the base for deciding the first variable as well as a storyboard (S) and surrounding environment in VR world space. The list of both the correct and incorrect precautions (CP/IP) for the other variable could be derived from RIF, as shown in Figure 1.

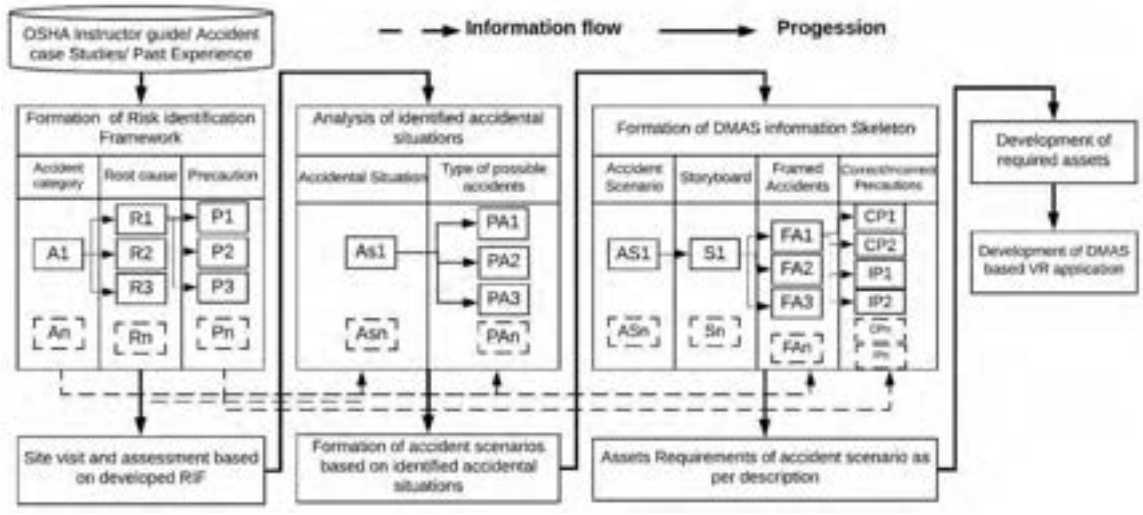

Figure 1. Framework for development of DMAS based VR safety training platform

In the fourth step, the DMAS information skeleton had specified a list of required assets (3D models, etc.). Later, these 3D models were developed with the help of modeling software. Then these all developed models were brought together on a single platform to create VR experience of DMAS where the trainee could experience the outcome of the Framed Accidents (FA).

5 Pilot Study

5.1 Risk Identification Framework (RIF)

This pilot study was executed in the sequence described in the Figure 1. This RIF was based on OSHA's four instructor guides (Construction focus four) for construction safety training [11]–[14]. The RIF output is depicted in Table 1.

The first column classified all possible types of accidents which could occur in any construction site into five general accidents categories (A) (fall from height, struck-by, caught-in or between, electrocution and scaffold collapse) along with its minimum basic requirements to occur.

The second column had root cause analysis (R) for each accident category with the possible reasons which might cause that particular accident. The third column had a set of common suitable precautions (P) suggested and recommended by OSHA, which could eliminate the cause as well as the risk. This given RIF in Table 1 is limited to including only those accident categories which were identified on-site and further used in VR simulation development. Shaded cells in Table 1 highlight the used elements of RIF.

5.2 RIF Based Site Assessment

The site selected for assessment was a commercial office building project. The project consisted of multiple towers which were in different stages of construction. Activities like wall cladding installation and concreting on the top floors were in progress. RIF was used to identify hypothetical accidental situations based on ongoing work.

Table 1. Risk Identification Framework (RIF)

Accidents category (A)	Root Causes (R)	Precaution (P)
Fall from height (Location's elevation higher than 6fts)	Unprotected roof edges, roof, scaffolds, and floor openings, and leading edges, etc.	Provide guardrail systems
		Provide safety net
		Wear Personal Fall Arrest Systems (harness or lanyard)
	Improper scaffold construction	Check for proper access, full planking, and guard railing.
	Unsafe portable ladders	Check for stable footing and the proper angle.
		Choose the correct ladder in good condition for the task Check for surrounding hazards,
Electrocution (Location has any electrical equipment or power lines under or above it)	Contact with overhead power lines (in case of Cranes, other high reaching equipment, Mobile heavy equipment, Ladders, and Material storage)	Maintain a safe distance from overhead power lines
		De-energize the Utility company and visibly grounded the power lines or installed insulated sleeves on power lines
		Check for Flagged warning lines installed to mark horizontal and vertical power line clearance distances
	Contact with underground power lines (in case of excavation)	Check for the markings from underground line location service before digging
		Hand dig within three feet of cable location.
		Use ground-fault circuit interrupters (GFCI)
	Contact with energized sources (live parts, damaged or bare wires, defective equipment)	Use gloves and appropriate footwear
	Improper use of extension and flexible cords	Inspect portable tools and extension cords
		Use power tools and equipment as designed
Scaffold collapse (Location has scaffold)	Improper construction	Check for safety tag (Scaffold Identification Tag)
	Use of parts manufactured in different organizations	Use same manufactured part from one organization
	Instability	Check for unsupported overall height to length of the shortest side of the base
		Check for the firmness of soil under the scaffold
		Check for weather conditions (Wind & Rain)

Figure 2. Accidental situation (As)

Even though four hypothetical accidental situations were identified, this paper focuses on the observation, illustration, and analysis of one of such accidental situations. The situation formulated is based on a new scaffold that was erected for the installation of the formwork, as shown by red arrows in Figure 2. However, the scaffold installation was incomplete and didn't have a suitable platform to work. Also, it wasn't verified by the safety engineer and hence had a red safety tag. Table 2 depicts the performed analysis of Accidental Situation (As) based on RIF. Furthermore, these observations and analysis of Accidental Situation (As) were utilized for creating Accident Scenario (AS).

Table 2. Analysis of Accidental Situation (As)

Possible Accident (PA)	Possible Worker's Negligence
Fall from Height	Workers could perform a task on that platform without any fall protection.
Scaffold collapse	Worker could perform a task on the improperly erected scaffold.

5.3 DMAS Information Skeleton

The Accident Scenario (AS) was a modified VR replica of the identified Accidental Situation (As). The analysis of the identified accident situation resulted in two possible accident types. Since there are many cases of electrocution while working on the scaffold platform, this accident type was also included in the skeleton. A list of correct and incorrect precautions was also prepared for each framed accident with the help of RIF. This was mapped into a detailed storyboard. The prepared DMAS information skeleton for this scenario is shown in Table 3.

5.4 DMAS Based VR Application Development

Figure 3 shows the followed system architecture and its information flow for VR application development. As shown in Figure 3, the first step for developing a VR application representing DMAS was to create all required 3D models, shown in Table 3.

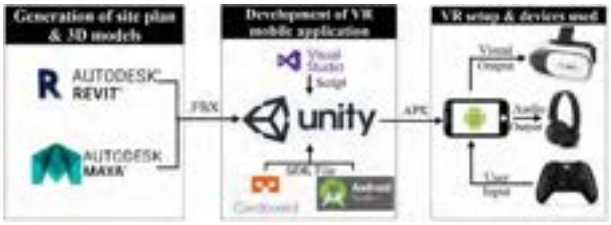

Figure 3. System architecture and technical integration

Autodesk Revit was used for creating models such as under-construction building, transmission tower etc. However, models like a safety net, harness etc., required more flexibility in modeling their shapes. Since Revit was not a non-uniform rational B-spline (NURBS) modeler, which generally helped in manipulating 3D curves and surfaces of any object, it couldn't be used for creating these models. For these models, Autodesk Maya (a NURBS modeling software) was used. After creation, these models were exported into .fbx format

Figure 4. Visual representation MainScene of DMAS

As shown in the second step of Figure 3, these 3D models were imported into Unity where it was navigable. In the Unity environment, all models were located as on-site, so that the overall view of the GameScene (MainScene - Figure 4) could present the prepared Accident Scenario (AS). Animation and user-controlled movement of the character were added to make the static GameScene functional. The dynamics of these models were customized, and conditions were levied on the models, by adding scripts created in Visual Studio using C#. Multiple outcomes for the framed accidents (fall from height, Electrocution, Scaffold Collapse), were also developed in a similar way in various GameScenes. Physics engine, visual effects in the form of Particle System Prefab, and audio effect in the form 3D sound were added to augment the reality quotient of these Outcome GameScenes. The options of correct/incorrect risks and precautions, were empanelled in the form of buttons inside User Interface (UI).

The MainScene was then interlinked with the Outcome GameScene, so that the trainee could be directed to the respective Outcome GameScene based on his responses in MainScene. The Plain visual output of the MainScene was converted in stereo screen format by using Unity Package - Google VR SDK. It was decided to use a smartphone-based VR platform as this is economical to deploy. Android SDK was utilized to process the Unity output for a smartphone-compatible application in .apk format.

Table 3. DMAS Information Skeleton of the accident scenario

Description	A scaffold having a platform higher than 24 feet will be erected. It will be having red safety identification tags with some unprotected platform openings without any fall protection system. A power cable from the transmission tower will be going just above the scaffold platform in proximity to the workplace.
Storyboard (S)	A workforce is going to start work on the newly erected steel scaffold platform. Its tasks include welding and reinforcement fixing. Look carefully and identify the possible accidents and suggest suitable precautions.

Framed Accident (FA)	Correct Precaution (CP)	Incorrect Precaution (IP)	3D Model Required
Fall from Height	Provide edge protection Provide safety net Cover scaffold's opening Wear harness	Do nothing Clean the area Wear safety shoes Wear eyeglasses Wear safety gloves Deny to work	Wooden plank to cover scaffold openings Edge protection Safety nets Harness Under-construction building
Scaffold Collapse	Check for safety-identification tag Call the supervisor	Wear harness Wear safety gloves Work and walk slowly	Scaffold with openings Safety tags
Electrocution	De-energize the cable Wear safety gloves Wear safety shoes	Wear eyeglasses Clean the area	Transmission tower Power cables Safety Gloves Safety Shoes

As shown in the third part of Figure 3, the visual output and audio output of the application were received by Google Cardboard and headphones, respectively, and a gaming pad was used to give user input for controlling the character's movement in 3D world space.

5.5 System Evaluation

Feedback from users was obtained on the basis of their experience of using the platform in order to enable an evaluation of the application. For the evaluation, the user was first introduced in the form of an avatar at a predefined location in virtual space. Within this space, the user explored the site with the aid of navigation options and made informed decisions regarding potential hazards and ways to mitigate it as per options available in UI. The scenario got modified depending on the user response. Figure 5 showed how users could mitigate fall from height risk by selecting the options such as provide edge protection, provide safety net, and provide cover for scaffold openings in UI of the MainScene.

After the user had taken all the precautions to secure the situation, he/she was asked to verify the efficacy of the selected precautions. If all correct precautions were taken for the identified potential risks, then work should progress as planned, with minimal chances of any untoward incident occurring in the virtual space. However, if the user happened to miss one or more of the recommended precautions for a risk in hand, then the user would have faced the accident outcome linked to the missed precautions. The VR accident experience-of typical framed accident (scaffold collapse) is shown in Figure 6.

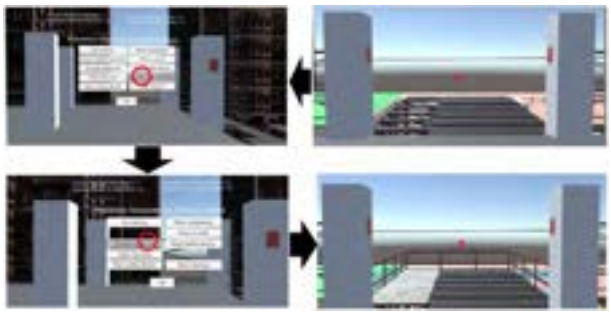

Figure 5. Modification of scenario as per the options selected by the trainee

The scenario presented to the three users had a total of 3 correct, 2 incorrect risk situations, and 9 correct and 11 incorrect precautions. The user responses to the scenario experience is recorded in the four outcomes:

Number of correct risks identified
Number of incorrect risks identified
Number of correct precautions taken
Number of incorrect precautions taken

This prototype application was evaluated based on feedback collected from three students of the civil engineering department. Each of these students had already worked in a construction site before and had taken a course on construction safety thereby having an introductory understanding of the safety practices to be

adhered to on-site.

Figure 6. VR experience of scaffold collapse accident

6 Results & Discussions

The results of the training test and the feedback survey are presented in Table 4 and Table 5.

Table 4. User response records of training test

User no	Risk Identified		Precautions Taken	
	Correct	Incorrect	Correct	Incorrect
1	2 of 3	0 of 2	4 of 9	1 of 11
2	2 of 3	1 of 2	3 of 9	4 of 11
3	3 of 3	0 of 2	6 of 9	4 of 11

Observations of Table 4 show that only user 3 was able to identify all risks. User 1 and 2 were not able to identify all the risks, specifically electrocution. The conversation after the training test revealed that these users neglected the electrical hazard near the scaffold as they were not anticipating this. This confirms that though VR could definitely help in visualization it doesn't necessarily improve risk identification ability, as this ability requires site experience as well.

Table 4 also shows that there were many events where even after identifying the correct risks, users had failed to identify the appropriate precautions recommended for the same. An analysis of two similar events post their occurrence are discussed further. User 1 and 2 failed to take two precautions from the list of recommended precautions to mitigate fall from height as listed in Table 3. They missed covering the scaffold openings because they thought wearing the harness and providing edge protection with safety net would be sufficient to ensure safety. In the event of electrocution, two potential sources of this risk were framed. The first one was emanated from the power cable coming from the transmission tower, the second from the welding task assigned to the trainee as per the storyboard of the scenario. User 3 verified the effectiveness of the selected precaution just after de-energizing the power cable, but he forgot to wear safety shoes and gloves which were essential for the welding task.

In the risk scenario of scaffold collapse wearing harness was one of the incorrect precautions chosen by the users. Similarly, for fall from height - safety shoes and gloves were incorrectly identified as a precaution. Committing such mistakes however made the user reflect on his knowledge gaps and raised awareness about chances of negligent behavior in such situations.

The feedback survey in Table 5 evinces that DMAS based VR training significantly enhanced responsible behavior and improved decision-making ability of the user. This is largely because the simulation of the vivid accident scenario gave the user an opportunity to experience the accidents and hence take cognizance of negligent behavior that causes the same in a graphically visual form. Besides this, the experientiality of these virtual scenarios helped to create a deep and long-lasting impression on the user, thereby enhancing their decision-making ability in the face of such situations at the site in future.

Further, the survey evinces that the VR training boosted the user's confidence and significantly enhanced their safety knowledge and awareness. This can be attributed to the real-time scenario that the platform was capable of simulating, which was crucial to reinforcing the importance of applying the correct precaution and gave the user a chance to witness and realize immediately why his selection of precautions were incapable of mitigating the risk completely. Thus, this platform helped to identify and bridge the gaps in the user's knowledge thus enabling him to make more informed and confident decisions.

The main limitation of the smart-based VR platform was its unpleasant experience as the user felt VR sickness during the test. Despite this limitation, all users agreed that this training would go a long way in helping them to avoid accidents on site and strongly recommended the importance of such training in the future also.

7 Conclusion and Future Work

It was found that of all the steps in the proposed methodology, RIF preparation was the most crucial and time-consuming step. The high level of detail involved in developing RIF enhances its efficacy to identify a sizeable range of accidental situations on-site and also ensures that a high quality of training is maintained. The RIF used in this study is limited to general safety training, but it can be extended to develop site-specific or task-specific training.

Site assessment or analyzing the identified accidental situation is also another vital step. The analysis of the accidental situation should be done rigorously, and all possible outcomes need to be identified and taken into account as it formulates the scope of DMAS information skeleton.

Table 5. Feedback of the users

Questions	User 1	User 2	User 3	Avg
To what extent this training affected your knowledge about safety?	8	9	9	8.7
To what extent will you remember what you've learned a year from now?	9	7	9	8.3
To what extent will training affect your behavior on a construction site?	9	8	9	8.7
To what extent was learning a pleasant experience?	4	3	1	2.7
To what extent, this training improved your confidence in identifying risks on the construction site?	9	9	10	9.3
To what extent, this training improved your decision-making ability?	10	8	10	9.3
Will the training help you avoid accidents on the site?	Yes	Yes	Yes	*
Do you want to have similar training in the future?	Yes	Yes	Yes	*

The skeleton of this study is based on only one accidental situation, but it can be expanded and made more informative by merging various accidental situations of multiple sites thus opening up significant scope for a wider range of training.

The study concludes that the proposed framework made the development process of VR application-based training platform more intuitive, perspicuous, and pragmatic. Moreover, unlike the existing literature on the safety training using VR, the proposed framework isn't limited to this presented scenario, but the same can be further utilized to develop various other scenarios covering all broader aspects of general safety training.

Furthermore, the final product architecture and the prototype VR platform performed well in terms of giving a virtual experience of accidents, identifying gaps in existing knowledge, teaching the immediate applicability and thereby reinforcing the significance of the precautions recommended, and enhancing the confidence of users. However, extended usage may cause VR sickness, and this may be addressed by sophisticated technological improvements.

The DMAS based VR training platform is presently limited to general safety training. This study could be extended to encompass and develop a safety training module for task-specific and site-specific training as well. Further, these DMAS related to task-specific training can be prepared for multi-user environments also. Such environments will enable the participants to play collaborative roles on site and bring the virtual experience even closer to the real scenarios.

References

[1] Commonly Used Statistics | Occupational Safety and Health Administration. Online : www.osha.gov/data/commonstats , Accessed: 01/04/2020.

[2] Fagan K. M. and Hodgson M. J. "Under-recording of work-related injuries and illnesses: An OSHA priority," *J. Safety Res.*, vol. 60, pp. 79–83, 2017.

[3] Asanka W. A. and Ranasinghe M. "Study on the Impact of Accidents on Construction," in *ICSECM*, Kandy, Sri Lanka, 2015.

[4] Toole T. M. "Increasing engineers' role in construction safety: Opportunities and barriers," *J. Prof. Issues Eng. Educ. Pract.*, vol. 131, no. 3, pp. 199–207, 2005.

[5] Li H., Chan G. and Skitmore M. "Visualizing safety assessment by integrating the use of game technology," *Autom. Constr.*, vol. 22, pp. 498–505, 2012.

[6] Pantelidis V. S. "Reasons to Use Virtual Reality in Education and Training Courses and a Model to Determine When to Use Virtual Reality," *Themes Sci. Technol. Educ.*, vol. 2, no. 1–2, pp. 59–70, 2010.

[7] Wilkins J. R. "Construction workers' perceptions of health and safety training programmes," *Constr. Manag. Econ.*, vol. 29, no. 10, pp. 1017–1026, 2011.

[8] Le Q. T., Pedro A. and Park C. S. "A Social Virtual Reality Based Construction Safety Education System for Experiential Learning," *J. Intell. Robot. Syst. Theory Appl.*, vol. 79, no. 3–4, pp. 487–506, 2015.

[9] Perlman A., Sacks R. and Barak R. "Hazard recognition and risk perception in construction," *Saf. Sci.*, vol. 64, pp. 13–21, 2014.

[10] Sacks R., Perlman A. and Barak R. "Construction safety training using immersive virtual reality," *Constr. Manag. Econ.*, vol. 31, no. 9, pp. 1005–1017, 2013.

[11] *Construction Focus Four : Fall Hazards*, vol. 1, no. September. OSHA Training Institute, 2011.

[12] *Construction Focus Four : Caught - In or - Between Hazards*, vol. 2, no. April. OSHA Training Institute, 2011.

[13] *Construction Focus Four : Struck - By Hazards*, vol. 3, no. April. OSHA Training Institute, 2011.

[14] *Construction Focus Four : Electrocution Hazards*, vol. 4, no. April. OSHA Training Institute, 2011.

Generation of Orthomosaic Model for Construction Site using Unmanned Aerial Vehicle

Alexey Bulgakov[a], Daher Sayfeddine[a], Thomas Bock[b], Awny Fares[c]

[a]Department of Mechatronic, South Russian State Polytechnic University, Russia
[b]Department of Building Realisation and Robotics, Technical University of Munich, Germany
[c]Khatib Alami and Partners, Muscat, Oman
E-mail: agi.bulgakov@mail.ru, daher@live.ru, thomas.bock@br2.ar.tum.de, awny.fares@gmail.com

Abstract –

Researches on the combined platform of unmanned vehicles, especially aerial, and artificial intelligence can be executed on hobbyists' level with a low budget along with inside multi-billion-dollars technological laboratories. This flexibility has allowed UAV to attract financial potentials and even to migrate them from another technological field. Nowadays, UAVs are used in many industrial fields such as photogrammetry, cinematography, monitoring, cloud seeding. In this paper, we present our work on using UAV to generate a 3D model for a construction site. The purpose of the 3D model is to analyze day-by-day the development and progress on-site, to reconfirm the construction planning, discover opportunities and eliminate potential risks.

Keywords –

Construction site; Unmanned Aerial Vehicle; Artificial intelligence; 3D model

1 Introduction

There are different methodologies to generate 3D models. Mostly are based on Odometry and Photogrammetry algorithms [1-6]. The latter consists of obtaining information on a certain object by using recorded videos or pictures. The sources of the visual information vary depending on the purpose of the 3D model. For instance, it is possible to superimpose LIDAR scanning data [7-13] on infra-red and thermal pictures to detect cracks on the building and identify which construction material (type) has been exposed to damage. The value of photographic interpretation is well-founded in other medical and technical fields such as the Roentgen Stereo Photogrammetry. The application of this method in the construction field is called a computer stereo vision. It allows comparing information about a scene from two vantage points, for instance, obtained by satellite scanning and actual UAV recording.

The advantage of such an approach is to extract 3D information by examining the relative positions of the objects in two different panels. Often this method is used to assess a shore suffered previously by a damaging cyclone [6]. The hidden risk of micro motion displacement can only be identified many years later. Using the Stereo Photogrammetry on a frequent basis will allow the identification of such risks and mitigate them prior to their occurrence.

On the other hand, the inconvenience of using such a method is the embedded high cost and a huge amount of data to be stored and processed. Researchers in photogrammetry field are proposing a different solution for data compaction, however, most frequently the same is leading to decrease pictures quality, hence the generated model, or introducing additional processing noise due to combination of multiple algorithms and working desks.

For a construction field with a limited budget, the generation of a 3D photogrammetric model using UAV is cost-effective and serves the purpose of monitoring, activity planning, and progress control. In this paper, we present our work in generating a rendered 3D model based on orthomosaic and mesh model.

2 Mathematical foundation

In space, the unmanned aerial vehicle has six degrees of freedom, and its motion is described by six differential equations of motion (Euler equations). The solution of these equations in the general case would make it possible to determine the nature of the spatial motion of the UAV at any moment of time, and, in particular, defining the operator's influence on the controls, and would also make it possible to judge the stability of this flight.

However, the direct solution of these equations presents certain difficulties even when using modern computing machines. If we use a straight-line steady flight without sliding for the initial flight mode and consider the deviations of the motion parameters from the initial values to be sufficiently small, then due to the

symmetry of the UAV, the system of six equations of motion can be divided into two independent systems of equations that describe the motion of the UAV with an unknown degree of accuracy longitudinally and laterally.

It should be noted that for the photogrammetry task, the mathematical model will have three different referential axis systems (fig. 1): The Fixed-Earth system, the UAV or body-axis system, and the Camera system.

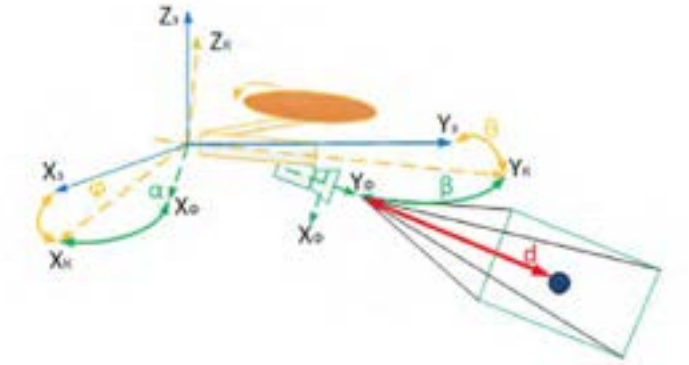

Figure 1. Representation of different systems for photogrammetry task

It is possible to establish mathematical equations for the transition between camera reference system and body-axis system. This is done using the following equations:

$$X_{\text{п}} = \frac{x}{\Pi x}.\cos\left(\arctan\left(\frac{H_B}{H_{\text{г}}}\right)\right); \qquad (1)$$

$$Y_{\text{п}} = \frac{y}{\Pi y}.\sin\left(\arctan\left(\frac{H_B}{H_{\text{г}}}\right)\right),$$

$$\rho_x = \sqrt[2]{{X_{\text{п}}}^2 + {Y_{\text{п}}}^2} * cos(arctan\left(\frac{H_B}{H_{\text{г}}}\right)); \qquad (2)$$

$$\rho_y = \sqrt[2]{{X_{\text{п}}}^2 + {Y_{\text{п}}}^2} * sin(arctan\left(\frac{H_B}{H_{\text{г}}}\right)).$$

Where, $X_{\text{п}}$ and $Y_{\text{п}} -$ are the pixel coordinates corresponding to linear motion, x and $y -$ are the Earth-Fixed axis coordinates; Πx and $\Pi y -$ are the scale coefficients, ρ_x and $\rho_y -$ are the pixel coordinates representing the rotational motion (roll and pitch angles); $H_{\text{г}}$ and $H_{\text{B}} -$ are the horizontal and vertical distance to Earth-axis coordinate in 2D mode.

3 Application of Photogrammetry

The following initial data were taken into consideration prior to launching the photogrammetry task. The construction plot is 416 Km^2, the average ground sampling distance or the distance between two consecutive pixel centers measured on the ground is 3.39 cm. The bigger the value of the image Ground Sampling Distance (GSD), the lower the spatial resolution of the image and the less visible details. The GSD is related to the flight height: the higher the altitude of the flight, the bigger the GSD value. The median of key points per image or the key points that are characteristic and can be detected on the images are 38981 key points per image. In total 1542 images were taken.

Based on equations (1) and (2), it could be retrieved that 1536 out of 1542 pictures could be processed considering the 60-degree angle introduced to install the camera on the UAV-axis. As such 0.94% relative difference between initial and optimized internal camera parameters can be computed (fig. 2).

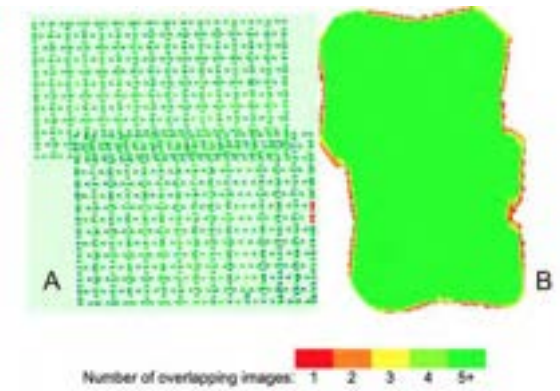

Figure 2. Offset results

Fig. 2 (A) shows the offset between initial (blue dots) and computed (green dots) image positions as well as the offset between the Ground Control Points (GCPs) initial positions (blue crosses) and their computed positions (green crosses) in the top-view (XY plane), front-view (XZ plane), and side-view (YZ plane). Red dots indicate disabled or uncalibrated images. Dark green ellipses indicate the absolute position uncertainty of the bundle block adjustment result. (B) shows the number of overlapping images computed for each pixel of the orthomosaic. Red and yellow areas indicate low overlap for which poor results may be generated. Green areas indicate an overlap of over 5 images for every pixel. Good quality results will be generated as long as the number of key point matches is also sufficient for these areas.

Fig. 3 shows the computed image positions with links between matched images. The darkness of the links indicates the number of matched 2D key points between the images. Bright links indicate weak links and require manual tie points or more images. The absolute geolocation variance shows the following:

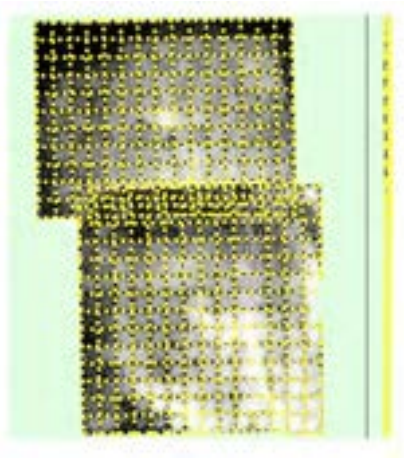

Figure 3. Links between matched images

Table 1. Absolute Geolocation Variance

Min Error [m]	**Max Error [m]**	**Geolocation Error x [%]**	**Geolocation Error y [%]**	**Geolocation Error z [%]**
-15	-12	0	0	0
-12	-9	0	0	0
-9	-6	0	0	0
-6	-3	0	0	0
-3	0	0.39	0	1.24
0	3	47.79	54.62	50.26
3	6	51.17	44.79	46.94
6	9	0.65	0.59	1.56
9	12	0	0	0
12	15	0	0	0
15	-	0	0	0
Mean [m]		**0**	**0**	**0**
Sigma [m]		**1.2513**	**1.2472**	**1.324**
RMS Error [m]		**1.2513**	**1.2472**	**1.324**

Where, Sigma is The standard deviation of the error in each direction (X,Y,Z) and RMS is the Root Mean Square error in each direction (X,Y,Z).

As the geolocation error is the difference between the initial and computed image positions, it should be stated that the image geolocation errors do not correspond to the accuracy of the observed 3D points. Min Error and Max Error represent geolocation error intervals between -1.5 and 1.5 times the maximum accuracy of all the images. Columns X, Y, Z show the percentage of images with geolocation errors within the predefined error intervals.

Table 2. Geolocation RMS Error

Geological Orientational Variance	RMS [degree]
Omega (roll)	2.006
Phi (Pitch)	1.901
Kappa (Yaw)	4.575

The geological orientational variance can be computed to define the Root Mean Square (RMS) in terms of degrees for the roll, pitch and yaw angles. Geolocation RMS error of the orientation angles identifies the difference between the initial and computed image orientation angles.

Figure 4. Orthomosaic Model of Construction Plot

4 Conlusion

The translating results from 2D orthomosaic to 3D Mesh shows several results. Firstly, as the proposed capturing angle is 60 degree and it is not assisted with any other capturing devices such as NADIR, the calibration of the images will be limited to the rendering algorithm. The first step is to produce mesh points obtained in Fig. 2 and Fig. 3 respectively. The result is shown in Fig. 5 along with the mesh textures.

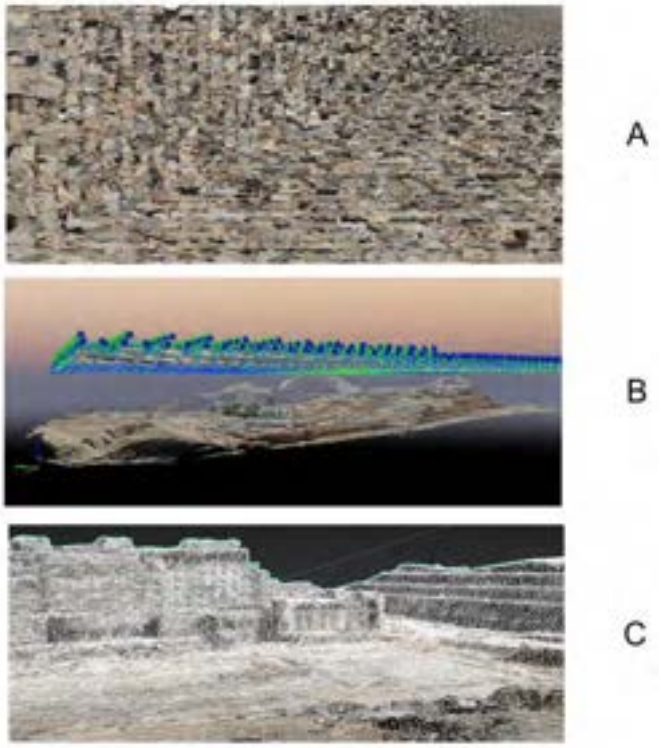

Figure 5. 3D Mesh and Texturing

The latter will be used to skin the mesh geometries, so the façades of the orthomosaic will reflect the actual status of the construction site. Lastly, the 3D model is rendered and illustrated in fig. 6.

Figure 6. Rendered 3D model

References

[1] Wierzbicki, D. Multi-Camera Imaging System for UAV Photogrammetry. 2018 Aug; 18(8): 2433.

[2] Guiseppina Vacca et al. The Use of Nadir and Oblique UAV Images for Building Knowledge. ISPRS Int. J. Geo-Inf. 2017, 6(12), 393

[3] Samad, A.M., Kamarulzaman, N., Hamdani, M.A., Mastor, T.A., Hashim, K.A. The potential of Unmanned Aerial Vehicle (UAV) for civilian and mapping application. In Proceedings of the IEEE 3rd International Conference on System Engineering and Technology (ICSET), Shah Alam, Malaysia, 19–20 August 2013; pp. 313–318

[4] Wang, C., Liu, X., Zhao, X., Wang, Y. An Effective Correction Method for Seriously Oblique Remote Sensing Images Based on Multi-View Simulation and a Piecewise Model. Sensors. 2016;16:1725. Doi: 10.3390/s16101725

[5] Hastedt H., Ekkela T., Luhmann T. Evaluation of the Quality of Action Cameras with Wide-Angle Lenses in UAV Photogrammetry. ISPRS-Int. Arch. Photogram. Remote Sens. Spat. Inf. Sci. 2016;XLI-B1:851–859.
Doi: 10.5194/isprsarchives-XLI-B1-851-2016

[6] Gonçalves, J.A., Henriques, R. UAV photogrammetry for topographic monitoring of coastal areas. ISPRS J. Photogramm. Remote Sens. 2015;104:101–111.
Doi: 10.1016/j.isprsjprs.2015.02.009

[7] Emelianov, S., Bulgakow, A., Sayfeddine, D. Aerial laser inspection of buildings facades using quadrotor. // Procedia Engineering, 85 (2014), pp. 140-146.

[8] Karabork, H., Sari, F. Generation of 3d city models from terrestrial laser scanning and aerial photography: A case study. 6 pages.

[9] Bulgakov, A., Evgenov, A., Weller, C. Automation high-rise structures inspection using quadrotor // Procedia Engineering, 123 (2015), pp. 101-109.

[10] Bulgakov, A., Sayfeddine, D., Otto, J., Emelianov, S. Dispersed cyber-physical coordination and path planning using unmanned aerial vehicle // Proceedings of the 36th International Symposium on Automation and Robotics in Construction (ISARC 2019). – Alberta: 2019, pp. 730-734.
DOI: https://doi.org/10.22260/ISARC2019/0098

[11] Kemper M. and Fatikow S. “Impact of center of gravity in quadrotor helicopter controller design,” in Proc. 4th IFAC-Symposium on Mechatronic Systems, (Heidelberg, Germany), 2006.

[12] Upadhay A. et al. UAV-Robot relationship for coordination of robots on a collision free path. International conference on robotics and smart manufacturing (RoSMa2018), pp. 424-431.

[13] Bertram, T., Bock, T., Bulgakov, A., Evgenov, A. Generation the 3D Model Building by Using the Quadcopter // 31st International Symposium on Automation and Robotics in Construction and Mining, 9-11 July 2014, Australia. – Sydney, University of Technology, 2014, pp. 778-783.

Field Application of Tunnel Half Section Inspection System

Nobukazu Kamimura[a] , Satoru Nakamura[a], Daisuke Inoue[a] and Takao Ueno[a]

[a]Institute of Technology, Tokyu Construction Co.,Ltd.
E-mail: Kamimura.Nobukazu@tokyu-cnst.co.jp

Abstract –

To inspect Road Tunnels every five-years is obliged in Japan, because for managing base the LCC (Life cycle cost). However, there are serious issues that not enough of engineer and budget to maintenance, so new technology for growing inspect efficiency is desired.

To solve these issues, we developed Tunnel full section inspection system within Crack measurement unit, Hammering unit and Protective frame. Our target tunnel of this system was one-lane on one side road tunnel, so especially protective Frame was designed for this kind of section. On the other hand, it needs to huge modify the frame to apply for another shaped section tunnel for example two-lane on one side road or train tunnel.

Therefore to expand application these inspection system, we developed the tunnel inspection system to apply varied tunnel section with mounted on aerial work vehicle. In this paper, we report the result of field application at two different shaped section tunnel with this system.

Keywords –

Inspection; Tunnel; Field application

1 Introduction

In Japan, many infrastructure face ageing issue. Especially half of road tunnels will over 50 age in 2033. Now in Japan, road tunnel must be inspected every five-years based on the road laws, because for managing base the LCC (Life cycle cost) [1]. However, there are serious issues that there are not enough of engineer and budget to maintenance, so new technology for growing inspect efficiency is desired.

From these background, we developed Tunnel full section inspection system (hereinafter, referred to as Full-Section-System) within Crack measurement unit, Hammering unit and Protective frame as in Figure 1 [2] [3]. Our target tunnel of Full-Section-System, especially the shape and size of Protective frame was designed for one-lane on one side road tunnel, because this size of road tunnels are major type at country areas in Japan.

Full-Section-System has advantages as follows.

- Protective frame secured space through which the vehicle can pass.
- To inspect full section of tunnel at one time.
- To avoid accident with falling concrete piece or another material under inspection by Protective frame.

On the other hand, Full-Section-System was designed for one-lane on one side road tunnel, therefore it needs huge modify to apply another shaped section tunnel for example two-lane on one side road. Add another thing, component parts of Full-Section-System are huge, so high transport cost and long preparing time at inspection site are taken.

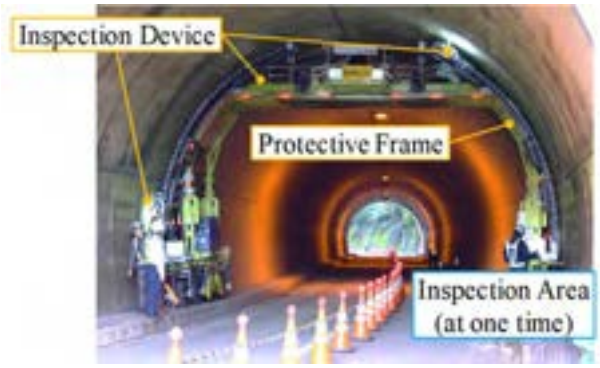

Figure 1. Full-Section-System

Figure 2. Half-Section-System

We thought these are the weak points of expansion of application. So to apply this system to many shaped section tunnel, we started to develop another type of frame as second generation system. The concept of development for second generation are as follows.

- To design flexible rail that easy to adjust for many section types of tunnel.
- Decrease component parts for easy to transport.
- Reduce preparation time at inspection site.
- To increase mobility, use truck based vehicle, instead of Protective frame.

The Gen2 of tunnel inspection system (hereinafter, referred to as Half-Section-System) as in Figure 2.

2 Outline of System

Functions of Half-Section-System are as follows, specifications of Half-Section-System are as in Table 1.

2.1 Flexible Rail

A number of curved rail are connected, top of rail is flexible and rail angle can be adjust by jack mechanism to fit tunnel shape as in Figure 3. Flexible rail and base frame need be compatible to stiffness and lightweight, so there were designed with FEM analysis as Figure 4.

2.2 Transferring Mechanism

Inspection devices are mounted on the tram, and the tram can move up and down by winch as in Figure 5. The caster of tram rolls on inner of lip channel steel, transferring condition is smooth, silent and stable.

2.3 Inspection Device

Crack measurement unit and Hammering unit are mounted on the tram as in Figure 5. We can obtain information of cracks and efflorescence by Crack measurement unit, and we can obtain information of spalling concrete by Hammering unit, these information are detected automatically.

2.4 Base Vehicle

The frame of Half-Section-System mounts on base vehicle with boom and roller type outrigger, it can be easy to set and adjust inspection device to tunnel surface and can drive without storing the outrigger and boom.

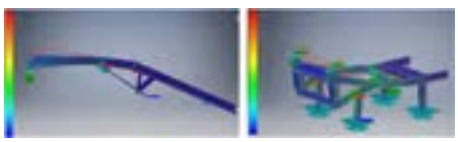

Figure 4. FEM analysis for Rail and Base Frame

Table 1. Specifications of Half-Section-System

Item	Specification
Rail Length	10.2m *1
Applicable Tunnel Inner Radius	R3.5~6.5m *1
Weight	Total 800kg *2 Device 50kg *3
Inspection Speed	9.0m^2/min *4
Inspection Width	600mm/scan
Resolution of Crack Width	0.2mm
Width of Hammering Interval	150mm *5

*1 Rail length and radius are adjustable if needed.
*2 Frame, inspection devices, control board are included, without aerial work vehicle.
*3 Transportable device weight by Tram.
*4 Set up time is excluded.
*5 Hammering interval can be adjustable.

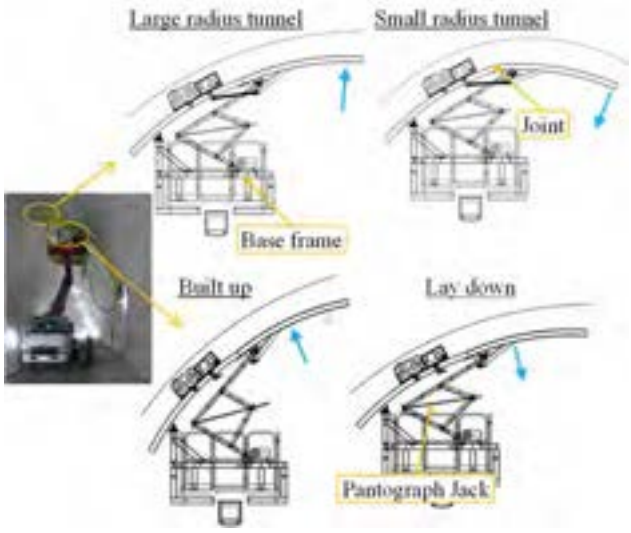

Figure 3. Function of Flexible Rail

Figure 5. Mechanism of Inspection Device Transfer

3 Outline of Inspection

We applied Half-Section-System to two types of tunnels. Type A is wide section for road tunnel, Type B is tall section for train tunnel. To compare the inspection results, conventional methods inspection by engineer was conducted at same time. Both of them were inspected as completion inspection. These tunnel's specifications are as in Figure 6, 7 and Table 2, 3.

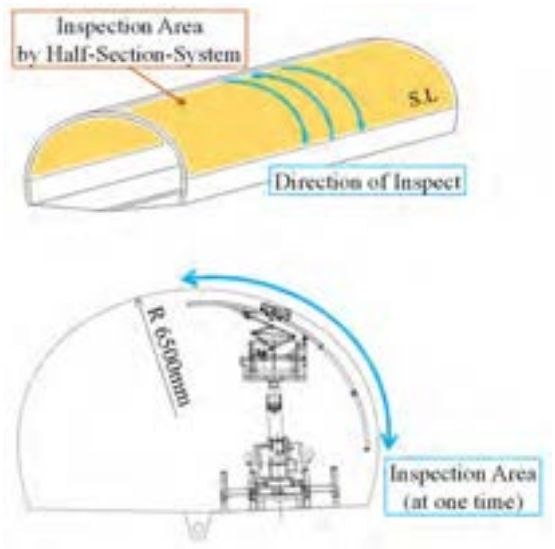

Figure 6. [Type A] Inspect area and Appearance

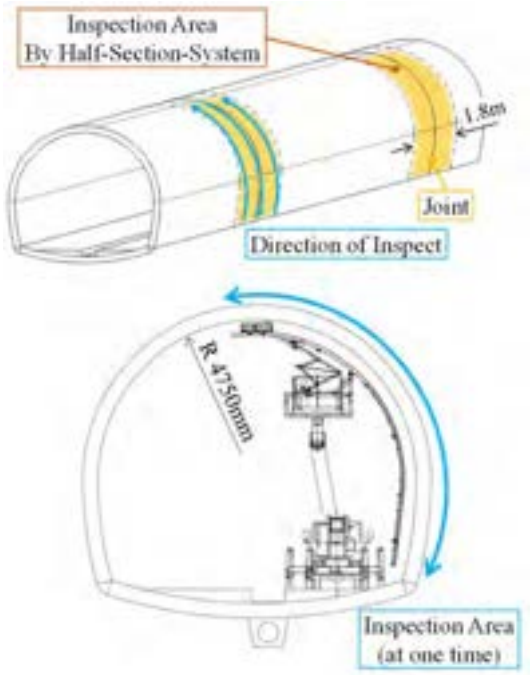

Figure 7. [Type B] Inspect area and Appearance

Table 2. Specifications of Tunnel [Type A]

Item	Specification
Length	397m
Section	H6.9m×W11.0m
Application	Road
Construction Method	NATM
Condition	New construction
Road condition	Non pavement surface
Inspect area by Half-Section-System	All of Surface except under the Spring Line *1

*1 Under the Spring Line area was inspected by another methods.

Table 3. Specifications of Tunnel [Type B]

Item	Specification
Length	1,450m
Section	H8.4m×W9.5m
Application	Train
Construction Method	NATM
Condition	New construction
Road condition	Pavement surface
Inspect area by Half-Section-System	Around the Joint of Lining Concrete *1

*1 the other area was inspected by another methods.

4 Results of Field Application

We inspected two types of Tunnel by Half-Section-System, and we evaluated the results about flexibility, mobility, inspection results comparison between system and engineer and work efficiency (Field work, office work) as follows.

4.1 Flexibility and Mobility

One of concept of Half-Section-System is general versatility, so we designed the frame and flexible rail could be mounted on base vehicle. Then we could inspect two different types of tunnel by one type rail with adjustable mechanism.

Frame, rail and control box of Half-Section-System are compact, so we could transport and assemble by one truck with crane. And another thing, lower section of rails are foldable without crane or another heavy machine. Half-Section-System was able to fold rail and U-turn in the tunnel, so we confirmed that Half-Section-System has high mobility. System transport, assemble and foldable rail are as Figure 8. Results from field applications, we make evaluation that flexibility, stiffness and mobility of Half-Section-System is generally well.

Figure 8. System Transport, Assemble and Foldable Rail of Half-Section-System

4.2 Inspection Results Comparison

We made an inspection results report inspected by Half-Section-System example of tunnel type A as Figure 9. There was no defect, so we reported as no cracks and no defected area.

Tunnel type B, there were few defects, so we compared results by Half-Section-System and by conventional methods (visual inspection and hammering by inspection engineer) as Figure 10.

For comparison, inspection result by Full-Section-System in 2018y is shown as Figure 11. This inspected tunnel is different from type A and type B.

By the comparison, cracks and spalling concrete were detected at same area in both inspection. In report of Half-Section-System, three cracks were detected. It was assumed that crack I and II were connected at out of inspect area and were same as crack A by conventional methods. We assumed that maximum width of crack A was out of inspect area of Half-Section-System, this was the reason that width had difference in between crack I, II and A, we thought.

It was assumed that spalling concrete Ⅳ and spalling concrete B were the same. However the detected length of both were difference (Ⅳ: 0.6m, B: 2.8m). In this case, the detection of spalling concrete was judged by hammering inspect. However, hammering point of Half-Section-System was approx.65mm near the edge of joint. So, if the spalling concrete was located on less 65mm area from edge of joint, it had possibility to be undetected by Half-Section-System. We thought this is the reason detected area of Half-Section-System was shorter than detected by inspector.

We assumed that crack 3 and spalling concrete C were same defect, though both of them were detected another category. In fact, this defect had step and ditch near the joint, so Crack measurement unit could find this spalling concrete as crack. However, Hammering unit could not detect this defect, because spalling concrete was too near to the joint to hammering.

There are some difference in inspected results between system and engineer, however accuracy of inspection results by Half-Section-System are enough to judge the soundness of tunnel.

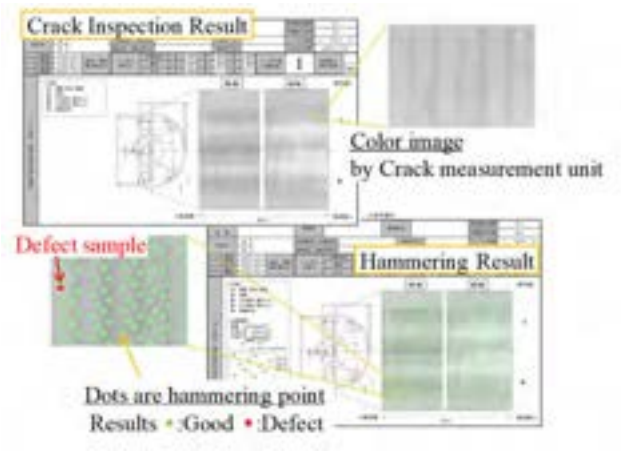

Figure 9. [Type A] Example of Inspection report

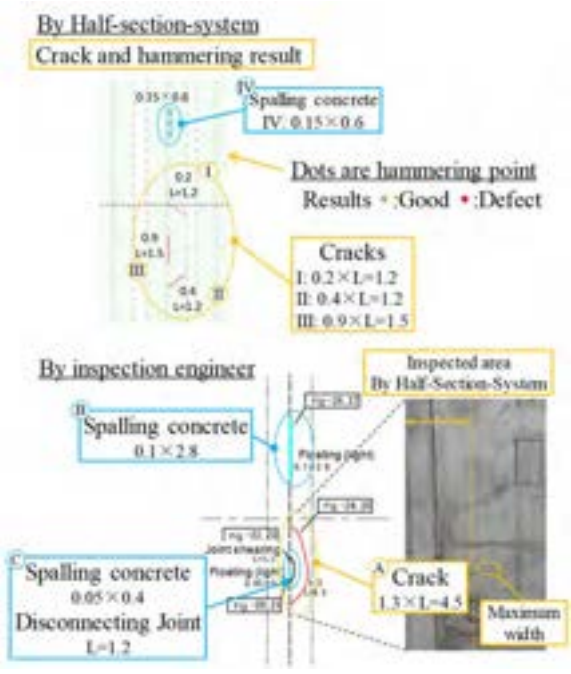

Figure 10. [Type B] Comparison results between by Half-Section-System and by Inspection Engineer

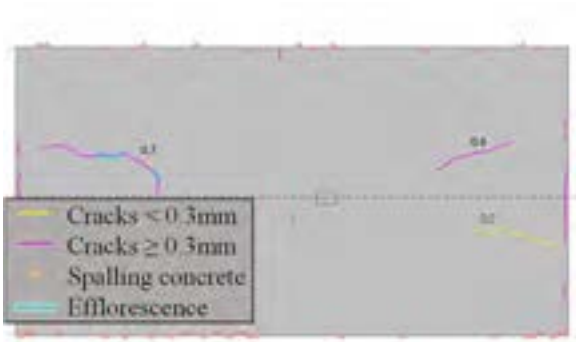

Figure 11. Example results by Full-Section-System in 2018y

From comparison results between Half-Section-System and Full-Section-System, the minimum detected crack width are 0.2mm, so we assume the preciseness of inspection are almost equal between two types of systems.

4.3 Work efficiency (Field work)

We evaluated work efficiency of field work by comparison with estimate and actual work time as Table 4. In table 5, we compared about assemble/disassemble time with Full-section-system and Half-section-system, and compared about inspection time with conventional methods at type B tunnel and Half-section-system.

Especially "Reduce preparation time" was one of the target of Half-Section-System. Working time of assemble and disassemble were shorter than Full-section-system, it means almost satisfied with our target, however actual inspection time were longer than conventional methods.

So we analyzed inspection time of Half-section-system about two types of tunnel as Figure 12. In this chart, "Inspection" means inspection time only. "Drive/Positioning" includes time to drive the vehicle and to position to prepare to inspect next line. "Adjust/Preparing" includes preparation before start working, warming up the system, maintenance the system and daily cleanup. "Fixing" includes repair the system or replace to spare parts if trouble.

"Drive/Positioning" time of Type B is longer than type A, because total drive distance of type B is longer than type A. However, we think "Drive/Positioning" time is too long, Type A is almost 15% of total inspection time and Type B is over 40%, and this process has room for improvement.

" Fixing" time of type B took long, because hammering unit had a breakdown about inner connection trouble of control unit in large part. So it is necessary to improve reliability about these trouble.

Table 4. Detail of work time (Half-section-system)

	Item	Working hours (Hrs.) Estimate	Actual
Type A	Assemble	4.0	5.8
	Inspection (Total)	56.0	99.1
	Inspection	-	48.0
	Drive/Positioning	-	13.8
	Adjust/Preparing	-	31.8
	Fixing	-	5.5
	Disassemble	4.0	3.5
Type B	Assemble	4.0	4.0
	Inspection(Total)	80.0	120.9
	Inspection	-	20.9
	Drive/Positioning	-	51.7
	Adjust/Preparing	-	19.4
	Fixing	-	28.9
	Disassemble	4.0	3.0

Table 5. Working time comparison

For comparison	Working hours (Hrs.)
Assemble	
Full-section-system in 2018y	7.6
Half-section-system [Type B]	4.0 (-47%)
Inspection	
Conventional methods [Type B]	96.0 *1
Half-section-system [Type B]	120.9 (+26%)
Disassemble	
Full-section-system in 2018y	4.8
Half-section-system [type B]	3.0 (-38%)

*1 3teams × 4days (8Hrs/day)

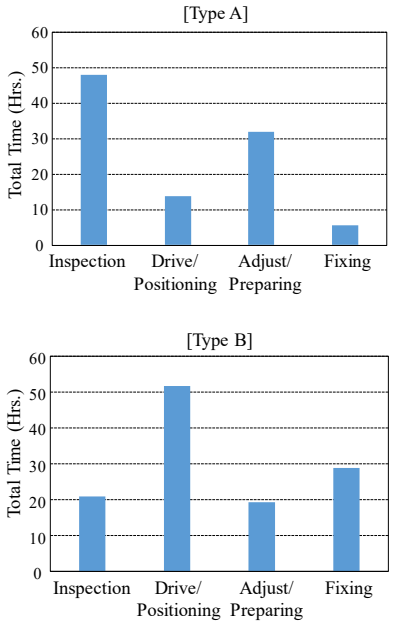

Figure 12. Breakdown of Inspection Time

There are some points need to improve to reduce "Drive/Positioning" time, especially positioning process, as follows and Figure 13.

- Add the target by laser marker line, to help positioning at tunnel lining wall.
- Add angle-meter to notice tilt of rail to operator in control monitor by value.
- Add distance value to inspected data measured by road measure, to help to prepare inspection report by automatically.

Figure 13. Improvement Plan for Reducing Work Time

4.4 Work efficiency (Office work)

We obtained defect information, cracks by Crack inspection device and peel at surface layer by Hammering inspection device, by Half-Section-System automatically. However the office work for preparing inspection report is almost manually, so there is few merit for office work at this time.

We think that automation of inspection report creation is essential for social implementation. So we will plan to prepare inspection report automatically.

5 Conclusion

In this paper, we evaluated Half-Section-System at two types of tunnel and concluded as follows.

- Working time of assemble/disassemble at field was approx. 40% shorter than Full-section-system of it.
- Confirmed general versatility, flexibility and mobility of Half-Section-System.
- Obtained inspection results enough to judge the soundness of tunnel, and preciseness of inspection is almost equal as Full-Section-System.
- Working time of inspection was approx. 26% longer than conventional methods (inspect by engineer). So especially positioning process needs to improve to reduce work time at field.
- Automation of inspection report creation is essential for social implementation.

In the future, we will develop work efficiency at field and at office.

On field work, our plan is to add sensor and target to frame, our target time of positioning process is half than current process. By this improvement, the working time of Half-section-system will be shorter than conventional methods.

On office work, our plan is to make software, our target is automatic process of making inspection report. That means, first input to software the data inspected by device, then picture and defect data are arranged automatically by software, finally inspector analyses and determines the soundness of tunnel by arranged data.

Our goal from these improvement is, total inspection cost of Half-section-system will be competitive than standard cost of conventional methods, so Half-section-system will solve the tunnel inspection issues that not enough of engineer and budget of inspection.

This result is part of accomplishment supported by Council for Science, Technology and innovation, "Cross-ministerial Strategic Innovation Promotion program (SIP), Infrastructure maintenance Renovation, and Management" in 2014-2018. (Funding agency: NEDO)

References

[1] Road Bureau, Ministry of Land, Infrastructure, Transport and Tourism. *Annual Report of Road Maintains*, MLIT, Japan, 2019.

[2] Nakamura.S Yamashita.A. Inoue.F Inoue.D Takahashi.Y Kamimura.N Ueno.T *Journal of Robotics and Mechatronics vol.31 No.6 2019*, pages762-771, 2019.

[3] Kamimura.N Nakamura.S Ueno.T Inoue.D and Takahashi.U. Demonstration experiment at road tunnel with Tunnel Overall Inspection System. *The 19th Symposium on Construction Robotics in Japan*, O2-3, 2019.

Challenges in Capturing and Processing UAV based Photographic Data From Construction Sites

Saurabh Gupta[a] and Syam Nair[b]

[a,b] Department of Civil Engineering, Indian Institute of Technology Kanpur, India
E-mail: saurabg@iitk.ac.in, syamnair@iitk.ac.in

Abstract– Construction industry is going through a paradigm shift where remote data collection approaches are replacing manual processes that are presently being followed in construction related activities. Unmanned Aerial Vehicles (UAV) are being engaged in various construction applications, like real-time supervision, progress evaluation, surveys, mapping, safety evaluations etc. The paper discusses some of the typical challenges related to operations, data acquisition, and post-processing of data collected using UAV when used in civil engineering applications. Issues related to obstructions, reflection, illuminations, lighting condition, blurred image data, inaccuracies in georeferenced image data etc. are discussed and possible solutions suggested based on a field study. A DJI Phantom 4 Pro V2.0 was used in data collection and the solutions for various issues identified from literature were evaluated and discussed based on collected field data. Feasible solutions for the above mentioned problems are also discussed and presented.

Keywords– Image Recordings; Recording Challenges; Construction Site Monitoring; Photogrammetry; UAV data processing challenges

1 Introduction

Over the last decade, use of Unmanned Arial Vehicles (UAV) in civilian activities have increased rapidly which ranges from infrastructure development to surveillance, goods delivery, agricultural, mining and many more [1]. Infrastructure development sector has started using UAVs in construction related activities like progress monitoring, surveying, aerial photography and surveillance, visual inspections, safety inspections, quantity take-off and estimation, defect and damage detection etc. [2]. Visual monitoring using camera equipped UAV is being used in earthwork measurement, damage assessment on structure, archeological site survey, safety planning and monitoring in high rise building construction, pavement distress detection, bridge inspections etc. [3, 4, 5, 6, 7, 8]. Utility of UAV data is not limited to construction monitoring at large, but can be extended for use in ortho-mapping, model development (digital elevation model, digital surface model), augmented reality models, 3D plans for structure, mesh model etc., using point cloud data generated from digital images [9, 10]. Use of UAV based photogrammetric data has now become the preferred option for civil engineers due to the diverse utility, accuracy, cost effectiveness and pace of data collection when compared to manual survey options used earlier. Efforts to adopt new and innovative technologies often encounter issues related to implementation, processing and data extraction which needs to be identified and solved in order to inculcate these approaches in construction activities. The objective of this study is to enumerate operational, data collection and post processing challenges while working with UAV data and to identify and evaluate feasible solutions from literature using field data.

2 Methodology

Challenges while working with UAV can broadly be classified into three categories (Figure 1). Section 3 of the paper addresses operational challenges which primarily include challenges in flight planning, like trajectory planning for cost minimization, avoiding data redundancy, occlusions, etc. [4]. Trajectory decisions often depend on the chosen flying height and required image overlay, details of which are included in section 3. Section 4 discusses the data collection issues related to occlusion, reflection, shadows etc. Issues encountered while working with blind spots, poor lighting conditions, similarity in object texture etc. during image processing is also discussed. Post-processing issues like blurred image, coordinate errors etc. are discussed briefly in section 5 of this paper.

3 Operational Issues

Flight planning for data collection involves trajectory planning, selection of data collection mode (manual or auto), deciding coverage area, selecting required image overlap etc., while accounting for logistical issues like, flight time, clearances, climatic issues etc. Trajectory is the path followed in data collection which often is the shortest route that can capture all required details along the project location. Selection of trajectory is often based

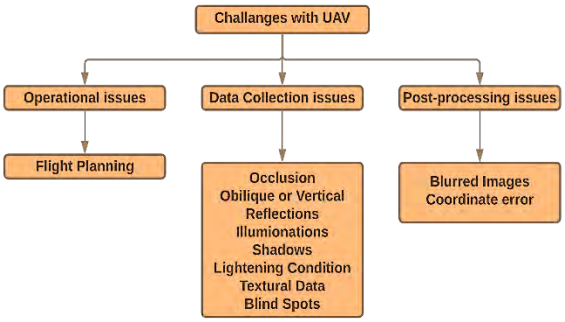

Figure 1. Classification of Challenges on working with UAV [4][5].

on optimizing coverage with minimal occlusions at the site. Even though trajectory is meant to cover maximum feature points of components falling in field of view (FOV) of UAV, pertinent details sometimes gets occluded as observed in schematic diagram (Figure 2). Semsch et al. (2009) in their study using multiple UAVs tried to identify the shortest trajectory that covers maximum feature points. After determining the starting points of UAVs, a surveillance algorithm which runs independently was used without any further coordination between the two trajectories. The occlusion-aware control mechanism developed during the study can be effective in trajectory planning for UAV-based data collection [11].

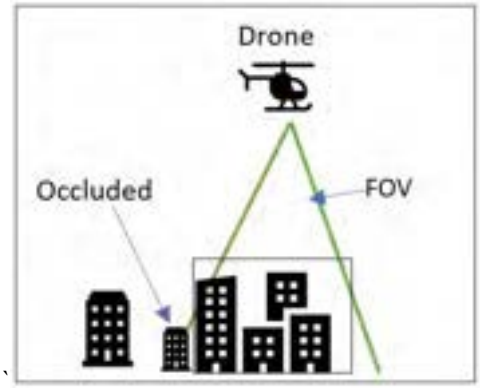

Figure 2. Graphical representation of occlusion in the FOV.

Parameters like shortest trajectory, battery constraints are also variables that need to be considered during trajectory planning which are often equipment specific due to variations in pay load capacity, flying time etc. Factors like lighting conditions, speed and shutter timing, and relative location of light source etc. need to be accounted for before actual data collection. Logistics issues like obtaining flying clearances, permissions based on the size and weight of different UAVs, etc. often varies across countries, details of which are explained and compared by Shrivastava et al. (2019). Information/details required while seeking permission for aerial survey from concerned authorities are also addressed by the authors [1].

4 Data Collection Issues

Issue related to data collection is discussed below with probable solutions.

4.1 Occlusions: Clutter, Auxiliary equipment's

Construction sites are often congested and cluttered with equipments which can lead to occlusions while collecting data remotely. Occlusions can be of two types (a) static occlusions and (b) dynamic occlusion [12, 13]. Static occlusions include missing data points due to stationary objects like formwork, scaffolding etc. whereas missing data points due to movement of workers, moving construction equipment's etc. can be considered as dynamic occlusions as illustrated in figure 2 and 3 [6] [7].

Construction sites are dynamic in nature which can lead to poor registration of dataset during progressive data collection. Given in Figure 3, is an issue related to dynamic occlusion while capturing data for foundation work at a construction site. While calculating quantity of earthwork from day 1 and day 2, occlusion due to auxiliary equipment in captured data set can lead to errors in estimated quantities. The data is also difficult to register with previously collected data set.

Figure 3. Example of dynamic occlusion

Images presented in Figure 4 explains issues related to dynamic occlusion in data collected for construction monitoring at site. Some of the ground control points (GCPs) is covered with construction materials, while few are occluded by clutters. Randomness, prompted by ease of construction, in positioning and arrangement of materials at construction site can lead to dynamic occlusions and difficulties in registration. Manual data processing techniques can address these errors to certain extent by eliminating identical objects with variable data sets from captured images or by registering only common points in both the data sets. However, issues may arise

especially while using automated or unsupervised data processing algorithms.

Figure 4. (a) Marked GCP at construction site and (b) GCP occluded due to site activities.

Solution: Researchers presented different solutions to address dynamic occlusions ranging from 2D image processing to 3D photogrammetric techniques. The data collected for generating meshes and point cloud may have disturbances due to similarity in colors of objects at site, say, scaffoldings vs other structural components. Xu et al. [8] presented a solution for eliminating similar issues using fast point feature histogram (FPFH) and random forest classification algorithms. Point cloud data were classified with linear fitting algorithm and by using the signature of histograms of orientations (SHOT) algorithm to detect the shape to make the results more accurate. Golparvar-Fard et al. used an alternate approach where instead of the fixed camera location, photographs were captured in a random/unordered manner from nearby locations to avoid occlusion. Using structure from motion (SfM) technique thereafter helps removing small occlusion automatically, and the generated point clouds will not require any post-processing [9].

Tuttas et al. (2014) used construction logics and precedence charts, which assume completion of severely occluded construction elements based on the completion of dependent elements [10]. Another option in addressing dynamic occlusion is through point picking method where the selected points can be easily recognized and registered when executed manually. The approach works around locating common points in different images and use them as tie point for creating dense point cloud. Photogrammetric software's that can automate point picking approach are also available which saves time and can register more feature points. This method is further modified by Kim et al. (2013) using machine learning (ML) approach for comparing as-built vs. as-planned data sets. They used supervised learning Lalonde feature (which is a 3-dimensional vector that can be used to detect linearity, surface uniformity, and scatter of a 3D data set) and extracted structural components out from the data set. The assessment is based on the extracting data set of structural components only and neglecting feature points related to an auxiliary equipment causing occlusion [11].

Since construction sites and too complex and dynamic to handle, researchers have attempted many pre-processing and post-processing strategies to overcome clutter and dynamic occlusions while processing captured data. A simplified approach followed during data collection is to alter the time of data collection, subject to construction schedule, so that dynamic occlusion such as moving personnel and equipment can be avoided [6]. Another approach is to consider dynamic occlusion as a static if they are stationary in multiple data sets. A good example would be a welding machinery for steel construction held in one location for many days while working personal uses it for nearby locations. Approaches mentioned below to remove static occlusions can be applicable in this case.

Static occlusion on the other hand can be solved by adopting proper flight planning techniques and recording strategy. Trial and error approach are also being followed in many cases, where trial trajectories are used to identify areas where potential static occlusions may affect the registration. Trajectories are then modified to cover maximum details pertaining to objects relevant for assessment. A simulation study by Semsch et al. (2009) shows possibilities of managing occlusion, by testing trajectory even before flying. A good example would be AgentFly UAV simulation testbed which can be used to model a real world to create a framework for flight planning and collision avoidance [4]. Figure 5 shows a similar issue related to static occlusion in field which was overcome by using multiple trajectories.

Another approach in reducing registration inaccuracies is to ensure a large overlap between two data set, which helps increases the number of feature points. The feature point are higher in figure 6(b) as the number of occlusions reduced by changing the trajectory of the UAV [5].

Figure 5. (a) Occlusion due to structural component, (b) occlusion avoided using different UAV trajectory.

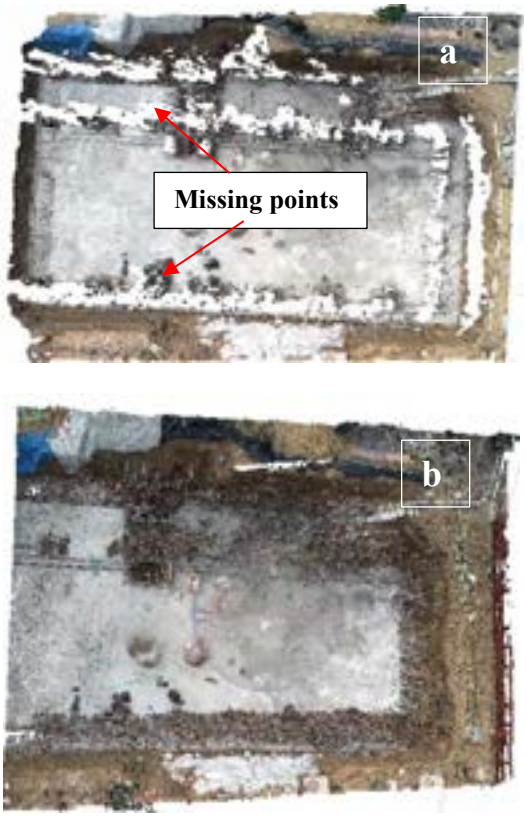

Figure 6. showing (a) missing cloud points due to occlusion (b) missing point filled up using images from modified trajectory.

4.2 Issues related to camera positioning

Aerial photographs captured using UAV can either be vertical or oblique. A vertical photograph can be taken by keeping the camera's optical axis in a direction perpendicular to the ground surface, whereas in oblique photography the camera's optical axis carries a depression angle (angle at which the optical axis is depressed below the imaginary horizontal line drawn along the camera axis) between 0º and 45º [12] [13]. Figure 7 shows a schematic representation for vertical and oblique photography.

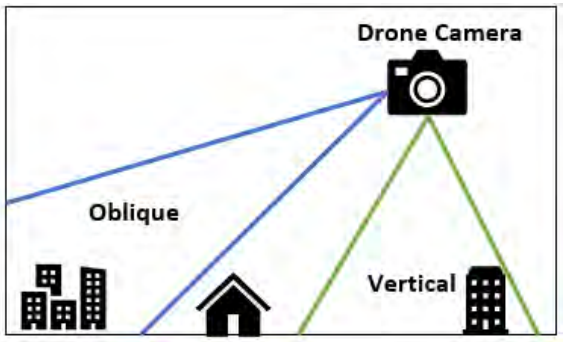

Figure 7. Representation of vertical and oblique coverage.**Solutions:** Vertical photography is beneficial in creating ortho-images that can be superimposed on the digital plan of structure for comparison. Oblique image is useful in capturing facades of structure. For vertical photography, the scale always remains a constant whereas oblique photography can have a variable coverage depending on the inclination angle of camera. If GPS or RTK option is available in UAV, images can be geotagged which eliminates scaling issues in oblique images. Rao et. al. (2018) observed 3D model reconstructed from oblique photography to be more precise and less noisy when compared to models based on vertical photogrammetry [14]. Table 1: Comparison between points generated by oblique and vertical images.

Parameters	Vertical images	Oblique images
No. of images	4	4
Processing time	49 sec	60Sec
Accuracy	Medium	Medium
No. of points	1531286	1648910

Table 1. above shows details of parameters used in capturing images using a stationary UAV to develop point cloud showing differences in data set generated due to camera positioning. Point cloud data shown in figure 8 was generated using oblique and vertical images captured using a DJI Phantom 4 Pro V2.0 with 3-axis (pitch, roll, yaw) gimbal flying at a height of 30 m.

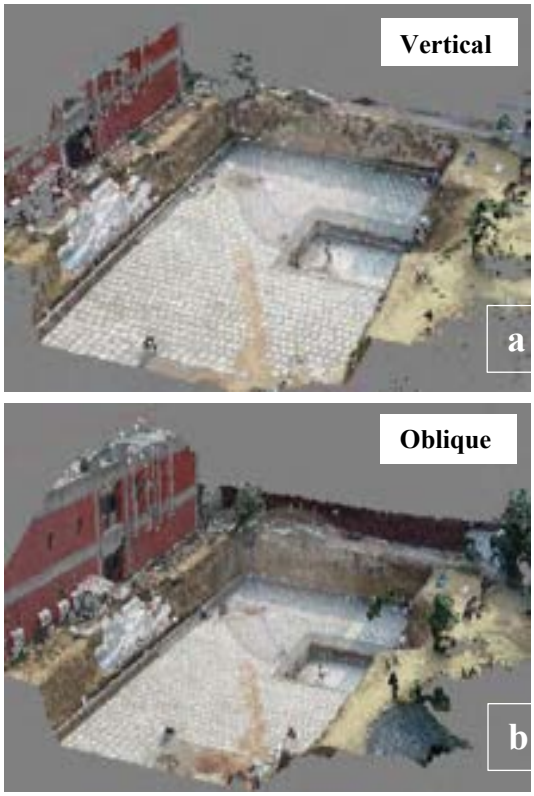

Figure 8. 3D point cloud model of the vertical and oblique images.3D point cloud model shown in Figure 8 suggest models developed using oblique images to have more coverage and feature points. The number of data points generated were also high in case of oblique images as shown in table 1. The results are in agreement with observations by previous researchers where the angle between ground and the camera was found to significantly affects the density of point cloud generated [21, 22]. Aicardi et al. (2016) and Chen et al. (2017) recommend using an inclination angle of 0° to 30° for obtaining dense data clouds as the points density start decreasing for angles above 30°.

4.3 Illumination, Reflections & Shadows

Processing reflections and shadows in photographic images poses another challenge while working with these datasets. Illumination and reflections may arise due to light scattering, textural properties of materials, or differences in site conditions. These can affect the final data at the time of processing, due to pixel value changes on similar objects leading to inaccurate point cloud generation. Shadows generated due to location of light source can also influence the accuracy of final data set.

Solutions: There are no literature available, to the best of our knowledge, towards addressing issues related to reflections and shadows in captured images. Since reflections are primarily dependent on the position of light source, use of SfM approach can be a feasible option to address this issue (figure 9 [a, b]). Selection of vertical image capturing option instead of oblique photography can also be effective in certain cases. However, the final solution is very much site dependent and the choice has to be made on a case by case manner.

However, Partama et al. (2018) suggested an alternate post processing approach to eliminate reflections and shadows, where videography was chosen over photographs, and ideal frames were extracted for processing. Since the UAV was moving continuously, the frames obtained from the video had different extrinsic properties where pixel values of objects at a given location keep changing in extracted frames. The discrepancy was adjusted using a temporal minimum filter algorithm to extract data points with smaller RGB pixel values, thereby eliminating the effect of reflection leading to an increase in RGB value [15].

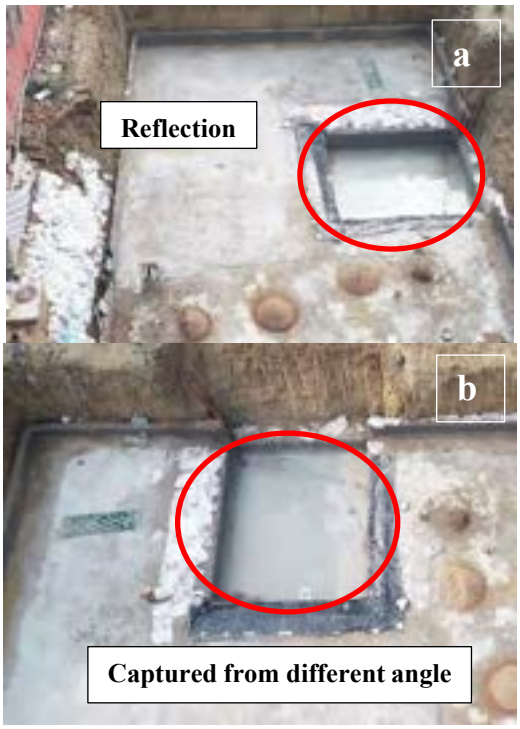

Figure 9. (a) reflection due to water (b) reflection avoided by trajectory modification

Since there are limited options available to address the issue related to shadows, two simplified approaches are generally followed during data capturing where trajectory modifications or camera positioning are altered to minimize the effect of shadows on the data set. A comparison of images collected using trajectory modification approach is included in figure 9 [a,b]. Even though selective post-processing strategies are being used to eliminate the effect of shadows, the process is time consuming and computationally heavy [16]. In summary, since the efficacy of strategies adopted to address reflection, shadows and illuminations can vary depending on site conditions, suggesting a unique

solution to address the problem may not be possible.

4.4 Lightening condition:

Difference in lighting condition can arise locally due to weather conditions or due to local features restricting light availability. Wierzbicki et al. (2015) observed a 25 percent reduction in point cloud density on using data from ortho-images collected during poor weather conditions [17].

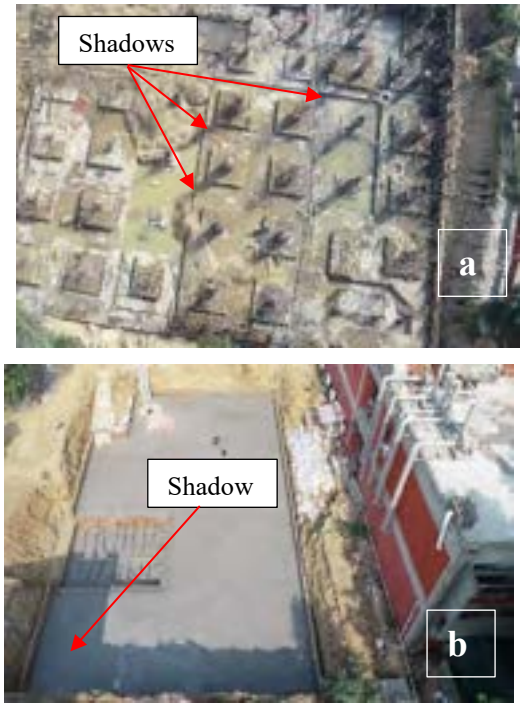

Figure 10. (a) Multiple shadows due to structural elements (b) Shadows due to adjacent structures

Since lighting issues can affect quality of the collected data, a common approach followed is to increase ISO values of photographs. This approach may not be feasible for UAVs as the proportionate increase in image capturing time can result in noise generation or motion blur due to stability issues in UAVs. Differences in lighting condition can also result in over/under exposure of images from FOV resulting in quality issues on point clouds generated.

Solutions: Even though artificial lightning can be a solution, the idea may not be feasible for all locations and often not cost effective (Perfetti et al., 2017). Efficacy of vehicle mounted lighting will also depend on power/battery/payload constraints of the UAV used. Improving quality using artificial lighting can have range limitations, as it can give a better quality image of elements in the foreground as against a noisy image for background elements. Other option is to increase ISO sensitivity and slowing down the shutter speed. ISO sensitivity represent the camera's ability of capturing light. The captured light is then converted into electrical signals, and by amplifying the signals the ISO sensitivity can be increased. Even though ISO changes allow us to capture images with many feature points, a reduced shutter speed slow down the data collection process (due to the additional time taken by cameras to adjust to the changes). Increase ISO can also lead to noise, grains, and blur which also get amplified with the signals. Method of changing ISO may not always be beneficial while aligning images for processing as the available feature points vary significantly with luminosity factor due to differences in captured pixel properties [18]. Use of High Dynamic Range (HDR) techniques can result in motion blur due to the longer exposure time required for capturing images. Hence the option may work reasonably only in cases were vehicle movements can be controlled manually.

4.5 Textural data

Properties of pixels in raster image captured from UAVs is dependent on texture of the object. Processing images of objects with quasi-uniform color, say concrete, is often challenging as distinctive feature point are hard to obtain. Hence feature points are often identified along edges and corner of the element which has different pixel values from the rest of the surface. The mesh generation and reconstruction from these data are often less accurate due to decrease in point cloud density.

Figure 11. 3D point cloud model of the under-construction foundation work.

Solutions: During field experiments, the authors came across issues due to reduced point density while performing dense reconstruction of objects with poor texture properties. Textural issues were also found to be dependent on lighting conditions as the quality of images reduces with deterioration in lighting as observed in point cloud data given in figure 11.

4.6 Blind Spots

Accessibility issues can create problems during data collection. Data collection on open construction sites like pavements are easier in comparison with data collection

on complex residential structure due to accessibility issues. The field of view (FOV) for UAV is limited and typically lies between 70° to 95° [19]. The coverage of an area also depends on the inclination angle of camera used during data collection. Figure 12 shows an example of a blind spot encountered by the author during field study.

Figure 12. Blind spot encountered during the field experiment.

Solutions Perfetti et al. (2017) suggested the use of wide angle lenses such as fisheye to enhance the FOV during data accusation [18]. However, the level of details achievable using this approach is often less than what is required for generating a dense point cloud. Use of vertical camera positioning instead of oblique positioning may help getting more feature points than by using a wide-angle lens.

5 Post-processing issues

5.1 Blurred Images

Since UAVs fly at a height of more than 30m to capture images, the captured data is often affected by wind, vibration and stability issues of UAV. In Blurred images, pixels get distorted; the RGB values and vectors of the image changes, which can all affect the quality of point cloud generated.

Solutions: Haar algorithm (HAAR), intentional blurring pixel difference algorithm (IBD), SIEDS (saturation image edge difference standard-deviation) are some of the available techniques to detect and remove blur from the images. Nobert et al. (2011) evaluated the effectiveness of SIEDS algorithm on two data sets collected using UAV and found the algorithm to be reliable in detecting blurred images [20][21].

5.2 Coordinate errors

Modern UAVs often have on board GPS that can create geotagged images and thereby generate geo tagged cloud points. However, problems can arise due to differences in latitude or longitude data for a given location in the dataset collected during multiple runs as the GPS may link with different set of satellites during individual runs.

Solutions: Use of real-time kinematics (RTK) in post-processing of data or use of local coordinate system instead of the global coordinate system can help overcome this issue [20].

6 Conclusion

Construction sites pose several challenges during collection and photogrammetric processing of images collected using UAVs. Use of occlusion-aware control mechanism developed by Semsch E. et al. (2009) may be an effective option for flight planning operations. Issues related to static and dynamic occlusions during data collection can be addressed in part by changing trajectory and angle of capturing data or by using machine learning approaches during post processing to remove irrelevant data points. Cloud density was observed to be higher when oblique images were used in point cloud generation when compared to vertical images. Even though density of point cloud may be compromised, mesh generation and reconstruction using edge and corner based feature points appears to be the only available option to segregate objects with similar textural properties. Discrepancies arising from differences in GPS coordinates may be addressed either by using RTK or a local coordinates system.

7 References

[1] S. Srivastava, S. Gupta, O. Dikshit, and S. Nair, “A review of UAV regulations and policies in India,” in *Lecture Notes in Civil Engineering*, vol. 51, Springer, 2020, pp. 315–325.

[2] I. Mosly, “Applications and Issues of Unmanned Aerial Systems in the Construction Industry,” *Int. J. Constr. Eng. Manag.*, vol. 6, no. 6, pp. 235–239, 2017, doi: 10.5923/j.ijcem.20170606.02.

[3] N. Metni and T. Hamel, “A UAV for bridge inspection: Visual servoing control law with orientation limits,” *Autom. Constr.*, vol. 17, no. 1, pp. 3–10, 2007, doi: 10.1016/j.autcon.2006.12.010.

[4] E. Semsch, M. Jakob, D. Pavlíček, and M. Pěchouček, “Autonomous UAV surveillance in complex urban environments,” *Proc. - 2009 IEEE/WIC/ACM Int. Conf. Intell. Agent Technol. IAT 2009*, vol. 2, pp. 82–85, 2009, doi: 10.1109/WI-IAT.2009.132.

[5] S. Vincke, M. Bassier, and M. Vergauwen, “Image recording challenges for photogrammetric construction site monitoring,” *ISPRS Ann. Photogramm. Remote Sens. Spat. Inf.*

Sci., vol. 42, no. 2/W9, pp. 747–753, 2019, doi: 10.5194/isprs-archives-XLII-2-W9-747-2019.

[6] H. Omar, L. Mahdjoubi, and G. Kheder, "Towards an automated photogrammetry-based approach for monitoring and controlling construction site activities," *Comput. Ind.*, vol. 98, pp. 172–182, 2018, doi: 10.1016/j.compind.2018.03.012.

[7] K. K. Han and M. Golparvar-Fard, "Appearance-based material classification for monitoring of operation-level construction progress using 4D BIM and site photologs," *Autom. Constr.*, vol. 53, pp. 44–57, 2015, doi: 10.1016/j.autcon.2015.02.007.

[8] Y. Xu, J. He, S. Tuttas, and U. Stilla, "Reconstruction of scaffolding components from photogrammetric point clouds of a construction site," *ISPRS Ann. Photogramm. Remote Sens. Spat. Inf. Sci.*, vol. 2, no. 3W5, pp. 401–408, 2015, doi: 10.5194/isprsannals-II-3-W5-401-2015.

[9] M. Golparvar-Fard, F. Peña-Mora, and S. Savarese, "Automated Progress Monitoring Using Unordered Daily Construction Photographs and IFC-Based Building Information Models," *J. Comput. Civ. Eng.*, vol. 29, no. 1, p. 04014025, 2012, doi: 10.1061/(asce)cp.1943-5487.0000205.

[10] S. Tuttas, A. Braun, A. Borrmann, and U. Stilla, "Comparision of photogrammetric point clouds with BIM building elements for construction progress monitoring," *Int. Arch. Photogramm. Remote Sens. Spat. Inf. Sci. - ISPRS Arch.*, vol. 40, no. 3, pp. 341–345, 2014, doi: 10.5194/isprsarchives-XL-3-341-2014.

[11] C. Kim, C. Kim, and H. Son, "Automated construction progress measurement using a 4D building information model and 3D data," *Autom. Constr.*, vol. 31, pp. 75–82, 2013, doi: 10.1016/j.autcon.2012.11.041.

[12] B. M. Evans and L. Mata, "Acquisition of 35-mm Oblique Photographs for Stereoscopic Analysis and Measurement," no. Figure 2, 1984.

[13] "Vertical and Oblique Aerial Photography | NCAP - National Collection of Aerial Photography." [Online]. Available: https://ncap.org.uk/feature/vertical-and-oblique-aerial-photography. [Accessed: 02-Jun-2020].

[14] C. C. Rao, Z. H. Xu, and R. C. Liao, "Comparative Analysis of Image Shooting Methods Based on UAV Photogrammetry," *IOP Conf. Ser. Earth Environ. Sci.*, vol. 199, no. 3, 2018, doi: 10.1088/1755-1315/199/3/032095.

[15] I. G. Y. Partama *et al.*, "Removal of water-surface reflection effects with a temporal minimum filter for UAV-based shallow-water photogrammetry," *Earth Surf. Process. Landforms*, vol. 43, no. 12, pp. 2673–2682, 2018, doi: 10.1002/esp.4399.

[16] Y. Li, P. Gong, and T. Sasagawa, "Integrated shadow removal based on photogrammetry and image analysis," *Int. J. Remote Sens.*, vol. 26, no. 18, pp. 3911–3929, 2005, doi: 10.1080/01431160500159347.

[17] D. Wierzbicki, M. Kedzierski, and A. Fryskowska, "Assesment of the influence of UAV image quality on the orthophoto production," *Int. Arch. Photogramm. Remote Sens. Spat. Inf. Sci. - ISPRS Arch.*, vol. 40, no. 1W4, pp. 1–8, 2015, doi: 10.5194/isprsarchives-XL-1-W4-1-2015.

[18] L. Perfetti, C. Polari, and F. Fassi, "Fisheye photogrammetry: Tests and methodologies for the survey of narrow spaces," *Int. Arch. Photogramm. Remote Sens. Spat. Inf. Sci. - ISPRS Arch.*, vol. 42, no. 2W3, pp. 573–580, 2017, doi: 10.5194/isprs-archives-XLII-2-W3-573-2017.

[19] DJI, "Phantom 4 Pro / Pro+ User Manual," *2020.01, User Man.*, 2020.

[20] N. Haala, M. Cramer, F. Weimer, and M. Trittler, "Performance Test on Uav-Based Photogrammetric Data Collection," *ISPRS - Int. Arch. Photogramm. Remote Sens. Spat. Inf. Sci.*, vol. XXXVIII-1/, no. September, pp. 7–12, 2012, doi: 10.5194/isprsarchives-xxxviii-1-c22-7-2011.

[21] T. Sieberth, R. Wackrow, and J. H. Chandler, "Automatic detection of blurred images in UAV image sets," *ISPRS J. Photogramm. Remote Sens.*, vol. 122, pp. 1–16, 2016, doi: 10.1016/j.isprsjprs.2016.09.010.

Research and Development on Inspection Technology for Safety Verification of Small-Scale Bridges using Three-Dimensional Model

Kazuhiko Seki[a] , Koichi Iwasa[b] , Satoshi Kubota[c] , Yoshinori Tsukada[d] , Yoshinori Yasumuro[c] and Ryuichi Imai[e]

[a]EYESAY Co., LTD, Japan, Graduate School of Kansai University, Japan
[b]EYESAY Co., LTD, Japan
[c]Faculty of Environmental and Urban Engineering, Kansai University, Japan
[d]Faculy of Business Administration, Setsunan University, Japan
[e]Faculty of Engineering and Design, Hosei University, Japan

E-mail: seki-k@eyesay.co.jp, iwasa-k@eyesay.co.jp, skubota@kansai-u.ac.jp, yoshinori.tsukada@kjo.setsunan.ac.jp, yasumuro@kansai-u.ac.jp, ryuichi.imai.73@hosei.ac.jp

Abstract –

In 2014, a regular inspection of public infrastructure facilities (bridges, etc.) once every five years be-came a legal system. Of the approximately 730,000 bridges nationwide, 530,000 are small-scale bridges with a bridge length of 2-15m. These bridges are often not easily accessible by inspection engineers. Therefore, in this study, for the purpose of studying inspection methods as an alternative to visual inspection for small-scale bridges, development of inspection robots, examination of efficient methods for creating 3D CAD data, inspection using 3D models. We examined the results from four viewpoints, the management system of results and the extraction of damaged parts from photographs by AI. As a result of the research, we conducted demonstration experiments several times, arranged the scope of technology application according to the usage scene, and clarified the definition of functional requirements. This can be expected to contribute to the development of more efficient inspection, improvement of productivity, safety, etc. in future small-scale bridges, as a material for development for actual operation.

Keywords –

Bridge Inspection; Structure from Motion; 3D Damage Figure; AI Damage Detection

1 Introduction

In 2014, the Japanese Ministry of Land, Infrastructure, Transport and Tourism (MLIT) put in place regulations requiring periodic inspections of public infrastructure facilities (e.g., bridges) once every 5years [1]. This meant that municipally managed bridges that were not previously subject to regular inspections, were inspected all at once. Many of these bridges are relatively small and difficult to inspect. Provisions were often made for sites that could not be approached without risk to inspectors, such as use of various inspection equipment or adjustments of inspection timing, but even this was insufficient for some sites, resulting in “inspection impossible” categorization.

There are about 730,000 bridges in Japan, of which around 530,000 are small structures measuring 2–15 m in length. Many such small bridges are not easily accessible to inspectors, making visual inspections according to the designated procedure impossible. In 2019, the MLIT revised the inspection procedures, allowing them to be based primarily on close-up visual inspections, and permitting the use of new technologies for complementing or replacing close-up visual inspections by inspectors [2]. These revisions allowed conditional use of drones or robots for inspecting conditions at sites that are otherwise difficult to approach. Further, there are plans to develop guidelines on the use of new technologies, which requires the development of efficient inspection technologies and investigation into their scope of application.

2 Objectives and Methodologies

In this study, we conducted proof-of-concept experiments targeting various issues and risks for small bridges with the aim of investigating the scope of application of technologies according to usage scenarios, clarifying functional requirement definitions, and providing material for developments toward actual

operations.

We develop a robot for use in place of human visual inspections at sites that cannot be entered, or where entry is possible, but space is insufficient for inspections. Such a robot would likely be effective for application to various civil engineering structures, but in this study, we focus on its application to small bridges.

The implementation plan and focus of this study are as follows. To investigate and extract various issues and the scope of application, we conducted proof-of-concept experiments such as robot operation tests, data acquisition via mounted equipment, and post-processing tasks using the acquired data, and provided comments regarding their implementation.

2.1 Development of an inspection robot

Concerns surrounding safety, labor shortages in the construction industry due to low birthrates and the aging population, and a shortage of engineers in local governments have prompted active research and development of inspection robots for the purpose of more economical inspections. The MLIT has published materials on inspection support technologies [3], but most are related to the use of drones and target relatively large bridges. In this study, we developed a robot capable of entering beneath bride girders in place of a human.

2.1.1 Conditions

Based on our knowledge accumulated over 20 years of experience in bridge inspections and surveying tasks, we set the primary specifications for the robot as follows. A height of 70 cm is sufficient to allow human inspectors to enter the space beneath bridge girders but make it difficult to look up at the girders (slabs) that are the target of inspections. Figure 1 shows the state of inspection tasks for a bridge of the same scale as the bridges targeted in this study.

- The robot must be capable of entering and exiting a 70 cm space beneath bridge girders.
- It must be possible to mount cameras or other devices capable of recording damage.
- The robot must be capable of traversing over small rocks, mud, and other surface irregularities of up to several centimeters in size.

2.1.2 Implementation plan and focus

In developing the robot, we first selected usage scenarios for various issues such as expected operational environments, communication environments, and robot operations under low visibility situations. We next investigated what equipment should be installed. In proof-of-concept experiments, we first verified factors such as the operational performance of the robot, wireless communication quality between it and its controller, and the mounting position of the mounted devices, and then we varied and investigated types of mounted devices, their mounting positions, and settings for data acquisition methods. Figure 2 shows the robot developed in this study, and Table 1 lists its primary specifications.

Figure 1. Status of inspection work on small bridges

Figure 2. Developed robot and 3D CAD

Table 1. Primary specifications of the robot developed in this study

Specification	Value
Size	Width: 498mm/Depth: 592mm /Height: 375mm
Weight	4.0kg
Transmitter device	Futaba 14SG
Receiving device	COOLTECH R7008HV
Tire	140mm Off-road tires
Athletic performance	4WS

2.2 Efficient method for 3D model data creation

The MLIT has been carrying out common information model (CIM) tasks since 2012 and has confirmed information sharing and safety improvement effects among stakeholders using three-dimensional (3D) models during infrastructure design and at construction sites. Based on the CIM model creation specifications, Yamaoka et al. [4] , [5] verified usage methods in maintenance management using precise CIMs created at the design stage. Further, Shimizu et al. [6] developed a system for managing photographs taken during inspections in a 3D model. They also proposed a method for constructing 3D models by parametric modeling, and this method is highly effective for newly creating 3D models of existing bridges that are undergoing

maintenance and for which models do not exist. However, humans or drones generally take photographs in these cases, and there are no examples of creating 3D models from photographs taken beneath the girders of small bridges using an autonomous robot.

In this study, we therefore investigated methods by which data obtained from a robot entering the space beneath bridge girders can be easily and efficiently applied to creation of 3D model data. In bridge inspections as well, there are increasing opportunities for converting 2D image data into 3D point group data through "structure from motion" (SfM) processing, allowing creation of 3D model data. Specifically, a fixed laser scanner is used to interpolate complex forms that could not otherwise be acquired. These are conditions like those of the small bridges targeted in this study.

2.2.1 Conditions

Bridges are built in various forms, but we limit our focus to girder bridges with reinforced concrete slabs and box culvert bridges, which account for the majority of small bridges.

2.2.2 Implementation policy and focus

As an initial point of interest, it is important to acquire still images with sufficient overlap for performing SfM processing. We performed proof-of-concept experiments to investigate how such images can be acquired not by humans, but by robots. Specifically, we established photo acquisition methods (for still images and video), photo resolutions, overlap ratios, distances to the target structure, view angles, and the presence or absence of feature points, and evaluated accuracy for point cloud data generated through SfM processing under various environments.

For our second point of interest, we created 3D modeling data from the generated point cloud data. Currently, computer-aided design (CAD) engineers must select (click) arbitrary points among point cloud data to create line segments and surfaces based on their experience and knowledge of bridge construction and combine these to create 3D model data. This is a bottleneck because the process requires huge amounts of time and labor. We therefore investigated methods for performing this task more efficiently and with less effort.

2.3 Inspection results management using 3D models

We constructed a prototype support system for 3D damage map creation as a management method for accurate and reliable sharing of structural lifecycle information among facility managers, inspectors, and repair workers, and investigated its necessary functional requirements. As the development environment, we used Unity [7], an integrated game development environment by Unity Technologies that can handle 3D models.

Table 2 shows the performance requirements. It is important to confirm the system's use as a platform that allows information sharing between stakeholders in different positions.

Table 2. System function Lists

No	Function
1	Bridge Specific Data Registration
2	Specifications Data of bridge Registration/Browse/Editing
3	Data Search
4	View and Operation of 3D model of bridge
5	Damage Data of bridge Registration/Browse/Editing
6	Narrowed-down display of damage information (Part of Member/Damage Kind/Damage Rank level)

2.4 Application of AI to detection of damage in photographs

We investigated conditions for application and operation of artificial intelligence (machine learning) to extract training data for automatically discovering damage from among the huge amounts of image data acquired by robots that are unable to distinguish between soundness and abnormalities.

Inspectors apply machine learning using as training data photographs of damage taken as in conventional inspection methods from near the structure, thereby creating a discriminator. This discriminator is used to identify damage in photographs taken by the robot and consider the results.

3 Implementation

3.1 Development of the inspection robot

3.1.1 Mounted equipment

Primary mounted equipment consists of a camera for robot operations, a camera for photographing damage (we compared two models, a Panasonic GH5S and a GoPro Hero7), and LiDAR (Velodyne VLP-16 Hi-Res) for position tracking.

3.1.2 Robot dimensions, maneuverability, and operability

Table 1 shows robot data, such as its dimensional specifications. The requirements call for an ability to enter beneath a bridge girder of height 70 cm and to acquire images of its underside, so as to ensure a constant view angle; the design is for a 15 cm distance from the

tire contact surface to the baseplate on which the equipment is mounted. We must also consider possible obstacles to the robot's undercarriage as it advances beneath small bridges, such as sediment (mud and sand), gravel, pebbles, dead leaves, and vegetation. Therefore, to improve its operability and obstacle avoidance performance, we adopted four-wheel steering (4WS), a steering method that allows independent setting of steering angles for each wheel of the robot. Further, we set the tire diameters to 140 mm to allow operation in small amounts of water. We attempted use of continuous track propulsion in preliminary experiments but leaves and twigs frequently became caught in the treads, immobilizing the wheels, so we adopted tires instead. For the battery, we used a small, lightweight, high-power lithium polymer battery, and allocated sufficient space in the robot's middle for mounting a battery with capacity for 1 hour of continuous operation. In terms of image transmission between the operator and the robot that has entered a narrow space, we confirmed that transmissions were not interrupted from beneath the target bridges with which we conducted our experiments. We further confirmed that image transmissions were uninterrupted during gradual movement of the operator's position about 20 m upstream and downstream from the center of the road surface and beneath the bridge. We did not conduct tests from farther distances because 20 m was considered sufficient for the small bridges targeted in this study.

3.1.3 Proof-of-concept experiment I

We performed this experiment with a bridge of length 2.0 m, width 4.5 m, and 80 cm clearance beneath girders. We confirmed positioning of onboard devices, the quality of SfM processing results using acquired images, and the possibility of position tracking by the LiDAR. Tables 3 and 4 list parameters investigated in each proof-of-concept experiment.

When investigating parameters related to SfM processing, we used two camera models to confirm differences in camera image quality and view angle. We also confirmed differences arising due to turning the high dynamic range (HDR) setting on or off in each installation direction and when using or not using wide-angle mode. To investigate whether substitution of the equipment used for normal inspections as a photocontrol point improves the results of SfM processing, we also used the presence or absence of photocontrol points as a parameter.

When setting LiDAR-related parameters, to verify any differences due to the incident angle of the laser on the structure and the reference object, we investigated three horizontal installation angles, using the presence or absence of a reference object as a parameter.

Table 5 shows primary specifications for the bridge used in this proof-of-concept experiment, and Figure 3 shows a photograph of the proof-of-concept experiment being carried out. Figure 4 shows the installation angles. Figure 5 shows conditions for camera installation directions.

Panoramic view (bridge1/ bridge2/ bridge3)

Side view (bridge1/ bridge2/ bridge3)

Material installation status
(aluminium staff/ white line/ eslon tape)

Figure 3. Demonstration work status

Horizontal direction Vertical direction

Figure 4. LiDAR installation angle

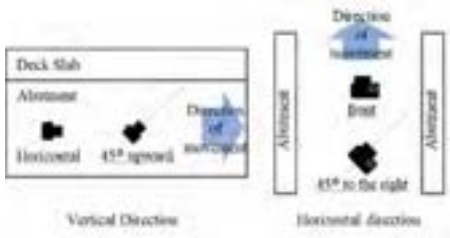

Figure 5. Camera installation directions

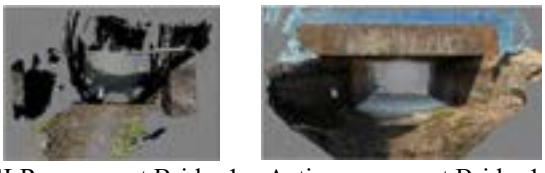

SLR camera at Bridge1 Action camera at Bridge1

Figure 6. SfM processing results

The results of this experiment showed that when performing position tracking using the LiDAR, the bridge form was not reproduced in any case where the reference object was not installed on a side face of the bridge. Also, form replication tended to improve when the LiDAR was installed horizontally. This is likely because the ability of a laser to capture the installed reference well is more effective for shape reproduction than for capturing the bottom surface of slabs.

However, installing plates for use as reference objects during inspections would be labor intensive and time-consuming, making inspections highly inefficient. Further, wind could blow plates over, which is a potential task hazard.

We next confirmed generation of 3D forms through SfM processing using robot-acquired image data. Figure 6 shows the results of SfM processing using image data for the same bridge as acquired by a single-lens reflex (SLR) camera and an action camera. The SLR camera could partially capture forms before entering beneath girders but capturing structures beneath the girders was nearly impossible. In contrast, the action camera could capture the entire form, including beneath girders. Due to this difference, there were many omissions in point cloud data created using the SLR camera. One effect likely influencing this is the difference in brightness when entering the dark environment beneath the bridge compared with the bright environment outside. Figure 7 compares still images captured by the SLR and action cameras. The action camera automatically and immediately changes brightness settings when entering beneath the girder, allowing capture of clear images while operating there. It is of course possible to change brightness settings for an SLR camera, but considering operability during inspections, the ease-of-use of an action camera likely makes it better suited to inspection tasks. Such cameras are also superior in terms of their small size and low weight.

Table 3. Study parameters (SfM)

	Value	Note
Camera Type	Single-Lens Reflex (SLR) camera Action camera	
Installation direction	Vertical / Horizontal	
Shooting method	Still Image / Video	Shooting interval 3 Cases
Control point	With or Without	Eslon tape paste on Deck slab bottom
Camera Settings	Wide angle mode: On / Off HDR mode: On / Off	

SLR camera Action camera

Figure 7. Comparison of still images from single-lens reflex cameras and action cameras

Table 4. Study parameters (LiDAR)

	Value	Note
Installation direction	Horizontal/15°/45°	
Reference object (Board)	With or Without	change distance
Reference object (White Line)	With or Without	
Reference object Shape/Size	Aluminium staff/board/man	change distance

Table 5. Bridge Specification

No	Length	Width	Height of under the girder	Structure type
1	2.0 m	4.5 m	85 cm	RC Deck Slab bridge
2	2.2 m	4.0 m	70 cm	RC Deck Slab bridge
3	13.0 m	1.8 m	85 cm (Inner)	Concrete Box Girder bridge

3.1.4 Proof-of-concept experiment II

Based on the results of proof-of-concept experiment I that concerned LiDAR-based position tracking, in proof-of-concept experiment II we verified whether equipment used in conventional inspection tasks or inspectors themselves could substitute for the reference object. To confirm any influences of surface shape or size of the

reference object, we investigated cases where an aluminum staff and an inspector were used as reference objects. Figure 8 shows a photograph of the installed reference object.

In proof-of-concept experiment II, we set investigated parameters with a focus on photography conditions for the action camera, and we considered what effects these might have on the generation of 3D forms.

To confirm the conditions inferred from the results of proof-of-concept experiment I, we set investigated parameters in consideration of improved operability, efficiency, and safety of inspections, confirmed whether similar trends were reproduced in experiments performed on two bridges of similar type, and investigated the validity of the inferred conditions.

The results suggested that parameters minimizing defects in the 3D form were a fisheye lens mode, horizontal installation direction, and illumination turned on. No differences were seen between still images and video capture. Because video capture has improved on-site operability, and clipping intervals can be adjusted for still image extraction in post-processing, video capture is likely most appropriate.

Board Man Aluminium staff

Figure 8. Installed reference object

3.2 Efficient methods for 3D model data creation

In LiDAR-based form measurements beneath a bridge girder was possible to capture the form of bridge1 and bridge2, but not bridge3. This was likely because it was impossible to maintain continuous recognition of the installed reference object.

We constructed an algorithm for generating 3D model data from 3D point cloud data. Table 6 describes an overview of processing, investigation content, and processing content in each step. First, we prune the point cloud data to improve processing speed. We next perform clustering to estimate planar regions in the target object. The existence of point cloud data other than those belonging to the modeled bridge lowers modeling precision, so we remove such data and perform 3D labeling before processing for planar-surface fitting. When planar surfaces are formed, their intersections with other planes are taken as edges. We created an algorithm that creates a surface model from the vertices generated up to this point, and then a triangulated irregular network (TIN), finally converting data into a specified CAD format.

Table 6. Process overview and examination/process details of each process

No.	Process	Overview	Investigation/Processing
1	Point cloud data pruning	Reduce point cloud data acquired by SfM	Pruning processing is sped up by using an octree data structure.
2	Normal vector clustering	Group the resulting point cloud data for each generated plane	Generate planes from points in a given space by the least squares method and perform clustering by the K-means method using the angle formed by the Z-axis and the normal vector for each plane.
3	3D labeling	Remove point cloud data not subject to modeling	For all spaces in the space octree, merge connectable grids (labeling by distance), leaving only spaces containing point cloud data, and remove labels that do not correspond to some minimal volume.
4	Planar fitting	Generate fitted planes for each label	Use the least squares method for fitting. Planes determine the outer region within the range including the projected points.
5	Edge extraction	Generate surface model vertices	Search for intersections between a given plane and other planes; where intersections are found, update boundary as edges.
6	Surface modeling	Generate surface model from generated vertices	Generate a TIN using Delaunay triangulation. Convert the TIN into a specified CAD format and output.

To confirm the utility of the algorithm, we performed trials using highly accurate point cloud data as verification data and confirmed that the 3D model data were generated as expected. We used a ground-based laser scanner (Focus S350; FARO Technologies, Inc.) to generate ideal point cloud data for verification. Further, we performed SfM processing using image data acquired by the robot, performed verification using the generated data, and were thereby able to construct a model. By calculating root mean square values for planes in the

generated 3D model data and the point cloud data, we confirmed that accuracy was within the LiDAR catalog value of ±0.030 m. This can be considered as sufficient accuracy for 3D model data applied to the maintenance management that is the objective of this study.

No method for quantitatively evaluating SfM-generated point cloud data has been established. Therefore, there is need for performing various verifications in the future to establish evaluation methods and confirm robustness in actual operations.

3.3 3D model-based inspection results management system

We constructed a prototype support system for 3D damage map creation to allow stakeholders to intuitively and accurately grasp and share locations and states of damage and identified and organized application ranges and issues for various parties.

The Windows application maintains a database of bridge specification data, damage information, and damage site ID numbers. The Unity application displays 3D model data on a screen. This system has functions for superimposing damage data on model data and for confirming and editing damage information.

The system is designed to maintain minimal information on bridge specifications, assuming there are components such as a ledger system already managed by the local government. Similarly, for inspection information, we prepared a database table using a damage location identifier as its key to represent damage locations, assuming a connection with an existing system.

Table 7 lists the main issues as indicated by persons responding to a survey that involved 200 visitors to an exhibition. Figure 9 shows the main screen of the constructed prototype system and the damage data input screen. In future work, we will develop a mechanism or device that allows efficient association of damage sites on the 3D model data.

. Many small bridges in Japan have a low maintenance cost per bridge. Therefore, the current situation is that there is almost no cost to newly create 3D model data. How to efficiently create 3D model data is important.

In this study, it was found that the structure and shape of a small bridge is simple, and it is difficult to understand the damage situation if a damage map is expressed by a 3D model.

In such a case, the use of CAD data as 3D model data, rather than using CAD data with colored point cloud data or textures attached, improves the grasp of damage conditions.

In future R&D, it is necessary to add a function that can read such data to the system.

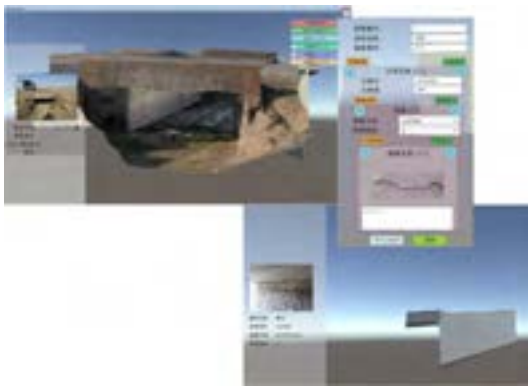

Figure 9. System screen and damage data registration/browse screen.

Table 7. Main issues as indicated by persons

Role of each persons	Main issues
Facility manager	Support function to make an optimal maintenance plan. Interoperability with the existing road management system (ledger system).
Bridge Inspectors	Output function for inspection reports. Automatic registration of damage location.
Repair workers	Optimal repair method and construction planning support. Automatic calculation of construction quantity.

3.4 AI application to identification of damage sites from photographs

We investigated algorithms and prepared an environment for introduction of AI methods. For training data, we used photographs previously taken by the authors or other inspectors judged as indicating damage.

For damage photograph labeling, we compared cases of labeling performed by inspectors and those by inexperienced persons provided with samples.

The results of discrimination in robot-acquired images included misidentification of cracks, peeling, and rebar exposure, an overall lack of recognition of peeling, and differences in scopes of occurrence. The results thus included many misidentifications of locations, scopes, and types of damage to be extracted. However, we obtained knowledge about constructing a learning environment and learning data, which enabled identification of requirements for condition setting. The following are items we identified as being particularly important development policies:

- Ensure consistent labeling of training data and prepare learning data that are high-quality (annotated) as well as abundant. Document how inspectors think for conversion from tacit to formal knowledge and identify what should be learned and how.
- Clarify relations between the required learning data scale and classification performance for each target damage class (e.g., damage type and degree) to be identified.
- Develop and formulate tools, interfaces, and operation processes that are linked with tasks so that learning data can be collected without placing burdens on primary tasks.
- Manage training data not as individual image files but matched with bridge specifications and other related information.

4 Conclusion

In this study, we summarized the requirements for robot development that can enter the girders of small bridges and acquire necessary and sufficient data for post-process work from the viewpoints of technological trends, development and maintenance costs, and versatility.

We have developed a robot that enters and exits under the girder of a small bridge with a space below the girder height of 70 cm or less. In addition, we performed a comparative verification of the conditions and installation methods of the equipment mounted on the robot and proposed an efficient method for 3D model data.

Regarding the 3D damage map creation support system, the system requirements and issues were organized from the perspective of the relevant parties (facility managers, inspection operators, repair work operators, etc.). In addition, it is also important to propose activities to replace the current 2D drawing management method with the proposed method.

Regarding damage extraction by AI, the requirements for a series of maintenance up to the introduction of AI have been arranged.

In the future, further verification in various bridge types and under girder environments will be required for actual operation.

Acknowledgements

This work was supported by JKA and its promotion funds from KEIRIN RACE, which was entrusted by the New Media Development Association.

References

[1] National Road and Disaster Prevention Division, Road Bureau, Ministry of Land, Infrastructure, Transport and Tourism: Guidelines for Bridge Regular Inspection, 2014.

[2] National Road and Disaster Prevention Division, Road Bureau, Ministry of Land, Infrastructure, Transport and Tourism: Guidelines for Bridge Regular Inspection, 2019.

[3] Ministry of Land, Infrastructure, Transport and Tourism: Inspection support technology Performance catalog (draft), 2019.

[4] Yamaoka, D., Aoyama, N., Taniguchi, H., Fujita, R., Shigetaka, K. Development of the three-dimensional data model standard of the bridge which assumed the use by the maintenance. In *Journal of Japan Society of Civil Engineers, Ser. F3 (Civil Engineering Informatics)*, Vol.71(2), I_204-I_211, 2015 (in Japanese).

[5] Yamaoka, D., Aoyama, N., Kawano, K., Shigetaka, K., Sekiya, H. Verification of how to create the CIM model of the bridge which assumed the use by the maintenance. In *Journal of Japan Society of Civil Engineers, Ser. F3 (Civil Engineering Informatics)*, Vol.72(2), I_21-I_28, 2016 (in Japanese).

[6] Shimizu, T., Yoshikawa, S., Takinami, H., Misaki, N., Takahashi, T., Nakayama, T., Uchida, O., Kondo, K. Development of bridge management system using three-dimensional model. In *Journal of Japan Society of Civil Engineers, Ser. F3 (Civil Engineering Informatics)*, Vol.69(2), I_45-I_53, 2013 (in Japanese).

[7] 2019 Unity Technologies: Unity-Game Engine, On-line: http://japan.unity3d.com, Accessed: 17/06/2019.

Development of Cloud Computing System for Concrete Structure Inspection by Deep Learning Based Infrared Thermography Method

Shogo Hayashi [a] and Koichi Kawanishi [b] and Isao Ujike [c] and Pang-Jo Chun [d]

[a] [b] West Nippon Expressway Engineering Shikoku Company Limited, Takamatsu, Japan
[c] Ehime University, Matsuyama, Japan
[d] The University of Tokyo, Tokyo, Japan

E-mail: shogo.hayashi@w-e-shikoku.co.jp, koichi.kawanishi@w-e-shikoku.co.jp, iujike@cee.ehime-u.ac.jp, iujike@cee.ehime-u.ac.jp, chun@g.ecc.u-tokyo.ac.jp

Abstract –

In recent years, deterioration of concrete structures such as floating and delamination has occurred. These damages can lead to the falling of concrete pieces. It may cause damage to third parties such as vehicles or pedestrians passing under the bridge. Therefore, the concrete damages need to be detected and repaired early.

Japanese highway companies conduct hammering tests on concrete structures once every five years to detect damages such as floating and flaking. However, the inspector must be near the bridge to perform the hammering sound inspection, which requires work at a high place and a lot of time and cost. Also, when using aerial work vehicles, traffic regulation under the bridge is required which may cause traffic congestion and accidents.

Infrared thermography is a non-destructive inspection technique that detects areas of floating or delamination by imaging a unique temperature distribution on the concrete surface using an infrared camera. The inspection cost of infrared thermography is significantly lower than that of hammering test. Since it is a long-distance non-destructive inspection, work at heights and traffic restrictions are not required. However, it is difficult to ensure the accuracy of damage detection because the peculiar temperature distribution acquired by infrared thermography includes an abnormal temperature distribution caused by something other than damages.

In this study, by using deep learning, we improved the accuracy of the unique temperature distribution imaged by infrared thermography and ensured detection accuracy that can be used practically. We also report on the construction of an automatic discrimination system that implements the deep learning discrimination algorithm on a cloud server.

Keywords –

Deep Learning；Infrared Thermography；Cloud Computing System

1 Introduction

Aging of concrete structures has been escalating recently, and there have been several reports of concrete piece falling accidents due to fractures of PC reinforcement rods and PC stranded wire in prestressed concrete, or corrosion of reinforcement steel rods. For instance, On April 3, 2009, the cover concrete with a length of 1 m, a width of 100 mm, a thickness of 260 mm, and a weight of 6 kg fell due to the corrosion of the rebar installed in the drainage unit of Tooridani bridge in Shikokuchuo-city. If flaky concrete hits a passer-by, it can cause a secondary disaster, so such accidents should be prevented as much as possible.

Several nondestructive inspection (NDI) techniques are available for the task [1][2]. In our project, we have decided to establish a detection technique of areas with floating and delamination based on the passive infrared thermography method, which would not limit the target bridges and should be able to inspect the target remotely and entirely.

The infrared thermography method has already been applied in the detection of floating of building tiles, but currently, it has not been applied to the inspection of floating and delamination of the concrete structures that have been put to practical use[4][5]. That's because the detection rate is significantly lower than conventional hammering tests. To enhance the detection rate, we first

examined infrared cameras by comparing their performances. As a result, the most suitable type was a cooling type camera, which has a shorter measurement wavelength range. We also developed a method to analyze the acquired thermal images and detect damages thoroughly. Specifically, it enables the machine to detect damages through machine learning, which has learned both anomalous forms in the areas of temperature alteration and the texture within the target areas.

2 2 EQUIPMENT AND METHOD OF INSPECTION

2.1 Equipment

ASTM D 4788 (Standard Test Method for Detecting Delaminations in Bridge Decks Using Infrared Thermography) requires the following conditions in thermal imaging [3].

1) Targets that are in constant contact with water, ice, or snow should not be applicable for shooting; they must be dried at least for 24 hours.
2) The condition with over 25 km/h wind velocity should not be applicable for shooting.
3) Thermal imaging at night should be taken in fine weather.

It also requires specific weather criteria for shooting as shown in the following table.

Table 1. The weather criteria for thermal imaging.

The weather condition of two hours before the test start	Determination
Fair	Possible
Fair with occasional clouds	Possible
Cloudy with occasional fine weather	Possible
Cloudy with temporary fine weather	Impossible
Cloudy	Impossible
Rain	Impossible

It is also critical to select the right infrared camera to get accurate detection results. Some of the essential specifications for an infrared camera should be its pixel resolution, detecting element, measurement wavelength, noise equivalent temperature difference (NETD), or frame rates, in which NETD is the most important. Regarding NERD, the infrared camera candidates we evaluated for our investigation were roughly classified into two groups; 0.02℃-NETD and 0.06℃-NETD. To determine the selection criteria for the thermal camera, we need to confirm the temperature difference in the target floating/delamination areas. Considering the fact that the typical cover of the bridge's upper structure is 40mm, it is essential to select the camera capable of detecting cracks and voids 40mm below the surface. We built some model structures to investigate thermal cameras' detection capability and weather conditions and selected one that could detect the cracks and the voids 40 mm below.

2.1.1 Building Model Structures and Photographing Conditions

We built cubic concrete model structures. Each model has a void with the size of 100mm x 100mm (t=10mm) in a different depth from the surface; 20mm, 30mm, 40mm, and 60mm, respectively (Fig. 1). In order to avoid the influence of daytime sunshine, a model was installed in the shade under the bridge on the Takamatsu Expressway and photographed at night (23:00) under weather conditions with a daily difference of 10°C or more.

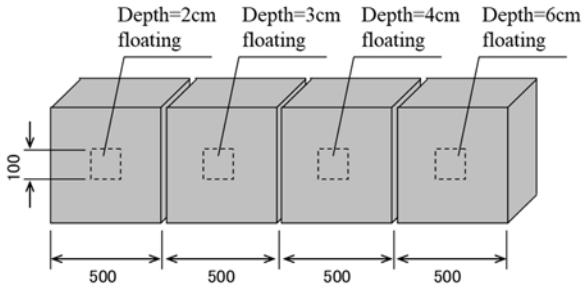

Figure 1. Concrete model structures and locations of voids.

2.1.2 Thermal Images of Each Infrared Camera

We used three cameras with different measurement wavelength and NTED in photographing model structures. We set two cameras of different NTED in line and photographed model structures simultaneously. Photographing with the camera of the minimum thermal sensitivity below 0.06℃ could not detect the void. The thermal images of the camera with minimum thermal sensitivity of 0.025℃ or less succeeded in detecting the void up to the depth of 40mm. We also learned that even the camera with below 0.025℃ minimum thermal sensitivity could not detect the void in 60mm deep, due to signal-to-noise ratio (SNR) of the camera. The result suggests that the camera with minimum thermal sensitivity below 0.025℃ is applicable for inspection of the upper structure, but not for lower structures with much thicker covers.

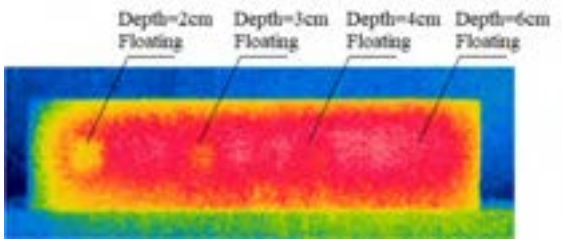

(a) Thermal sensitivity below 0.06℃

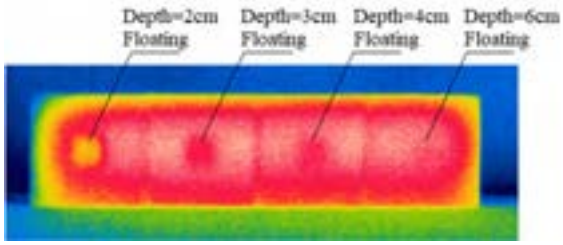

(b) Thermal sensitivity below 0.025℃

Figure 2. Thermal images of concrete model structure

2.2 Thermal Environment Suitable for Infrared Thermography Method

The infrared thermography method requires the generation and the retention of heat flow inside the target object for several hours. Usually, Equation 1 should calculate the required time for the operation. However, due to heat transmission from the area around the target, it takes longer than the time derived from Equation 1 before the surface temperature of the floating/delamination area changes. In our experiment, the temperature change appeared in the condition with 2℃ difference continuously for an hour between object and air temperatures.

$$d = 2\sqrt{\frac{\lambda t}{\rho c}} \quad (1)$$

where

d: Heat transmission depth (m)

λ: Heat conductivity (W/mk)

t: Time of appearance (sec)

ρ: Density (kg/m^3)

c: Specific heat (J/kg K)

3 3 EXAMINATION OF THERMAL IMAGE ANALYSIS METHOD

3.1 Necessity and outline of the thermal image analysis method

Some of the problems with infrared thermography measurements are the risk of overlooking and false detection of floating and delaminations by inspection personnel. Therefore, we have built an automatic detection system for floating and delamination based on machine learning.

However, the analysis requires preprocessing of the target images. Due to the different thickness of components in concrete structures, external influences such as solar radiation cause temperature differences in the components depending on the component thickness (Figure 3).

Figure 4 is a model showing a unique temperature distribution under different thermal conditions, that is, detection in uniform temperature and detection with temperature gradient. If the temperature of the target structure is uniform, not only the amount of temperature change but also the size of the damage can be easily detected. However, in reality, the surface temperature of the target concrete structure has a significant temperature gradient due to the difference in component thickness, which makes it harder to detect damages than in stable temperature conditions.

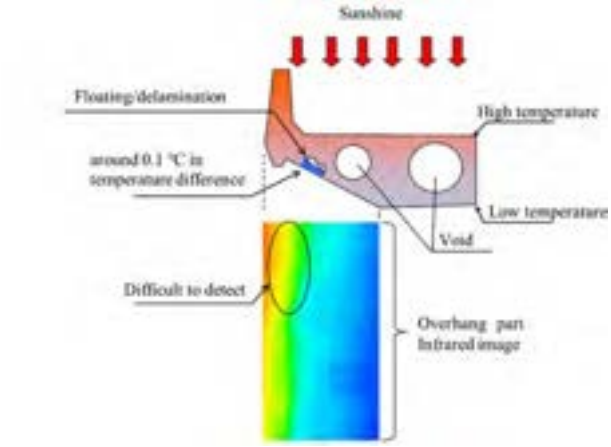

Figure 3. Thermal image example of RC hollow bridge with temperature difference

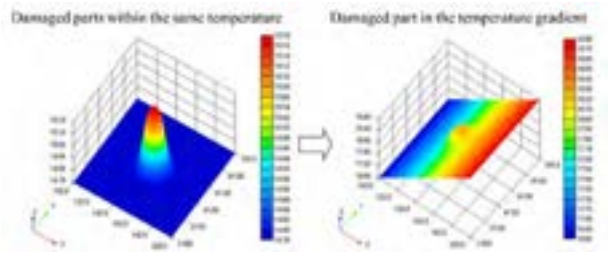

Figure 4. Concept of thermal change in the damaged area

In our study, to eliminate the influence of temperature gradient in concrete structures, we calculate the moving average of temperature distribution and subtract the target pixel temperature. It enables damage detection in concrete structures under the influence of temperature gradient; the detection result should be free from the temperature gradient in the target structures.

After the abovementioned preprocessing, we have constructed a system by machine learning to detect floating/delamination from thermal images. Machine learning requires training data, for which we collected through infrared thermography measurement, as well as the full-scale hammering tests on RC, steel and box-girder bridges that has been in service for 5 to 38 years. As for the infrared thermography, we conducted the measurement at night on the day when the diurnal range exceeded 10°C. Detecting singular temperature distribution with infrared thermography does not always mean the detection of floating/delamination. For instance, there are several factors that affect the temperature distribution of the target, such as free limes piled up by rainwater infiltration and roughness of the target surface itself. The following Table 2 shows the list of factors that cause temperature irregularity. Each is described in the following sections.

Table 2 Factors of temperature irregularity

Floating area
Delamination area
Adhered slag
Foreign substances
Repair marks
Free limes
Color irregularity

3.2 Factors of temperature irregularity

3.2.1 Floating area

The floating area, in this case, is an area where noise is generated in the hammering test, but the concrete surface is still intact. Comparing with the thermal image of the healthy area where a foreign object attached, the temperature distribution image on the floating area is not distinct.

3.2.2 Delamination area

The delaminating area, in this case, is an area where concrete flakes should fall when the hammering tests are conducted. Compared to the thermal image of the floating area, the image of this area distinctively shows a singular temperature distribution.

3.2.3 Adhered slag

The delaminating area, in this case, is an area where Slags remain on the joint form marks after the initial concrete placement turned to a thickness of 2-5 mm; thus, they are detected distinctively as thin linear singular temperature distributions that run along with the joint form marks by infrared thermography.

3.2.4 Foreign substances

If foreign materials such as wood chips are mixed in the concrete of the covered components, they are detected as temperature irregularities by infrared thermography. Because the mortar plastered on top conceals the wood chips, it is impossible to detect from the visual image whether the foreign materials are mixed in it.

3.2.5 Repair marks

The standard repair procedure of the floating/de-lamination of concrete due to rebar corrosion is to remove that areas and fill the damaged sections with materials such as shrinkage-compensating mortar. If the thermal conductivity of the materials used for repair is different from that of concrete, they appear as singular temperature irregularities.

3.2.6 Free limes

Free limes adhering to the concrete surface appear as singular temperature irregularities in thermal detection. The difference in reflectance or thermal conductivity between free limes and healthy concrete surface or the existence of gaps in between free limes and concrete surface would be the cause of the detection.

3.2.7 Color irregularity

The color irregularity causes a singular temperature irregularity detection in the thermal image.

3.3 Full-Scale Hammering Test Results Summary

Figure 5 shows thermal images organized according to characteristics in detection shapes. We collated organized images with hammering test results to confirm significant characteristics in the shape of areas with singular temperature irregularity in the following five types; 1) delamination, 2) floating, 3) slag, 4) foreign substances, and 5) healthy area. Table 3 shows each characteristic. If we can calculate the value expressing the shape of the temperature irregularity area (shape features), we determined that it is possible to classify using these five types of machine learning.

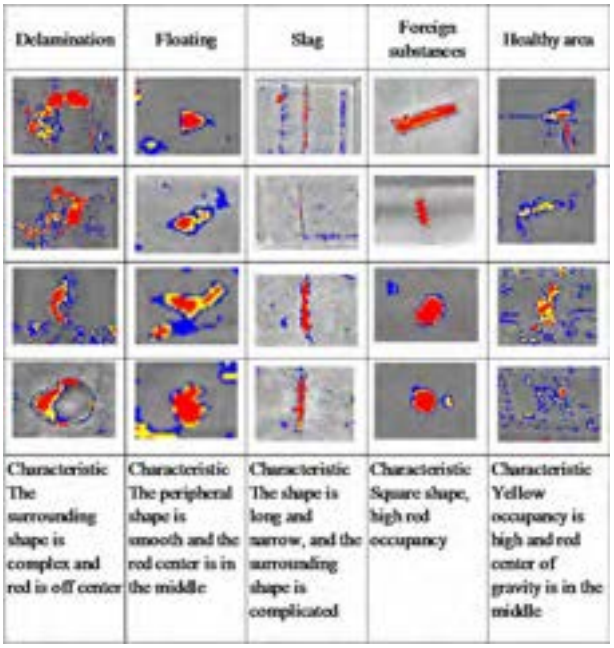

Figure 5. Relationship between hammering test results and image processing

Table 3 Relationship between hammering test results and detection image shape characteristics

Sounding result	Unique temperature area shape characteristic	note
delamination	The red area is off the center of the whole area	Knock down
Abnormal sound only	The red area is at the center of the whole area	floating
foreign substances	Square shape, high red occupancy	False positive
slag(t=2～5mm)	The occupancy rate of red is high and the shape is square, but the periphery is more complicated than foreign substances	False positive
healthy area（Reflection）	High yellow area occupancy	False positive

3.4 Discrimination Index Using Geometrical Features in Thermal Images

In this study, we have examined the image filtering process that ternarizes the thermal images. Based on the emphasized index, we set the threshold values of ternarized red, yellow, and blue as follows; over 0.11 as red, over 0.08 and less than 0.11 as yellow, and over 0.04 and less than 0.08 as blue, respectively.

Considering the results in the previous section, the positional relationship between the red, yellow, and blue areas is important. If the red area appears near the center of the blue area, the detected image is probably a floating area with abnormal sound alone. On the other hand, if the red area appears at the location apart from the center of the blue area, the detected area could be a delamination area. Thus, the distance between the centers of each area should be calculated as a feature for the discrimination index.

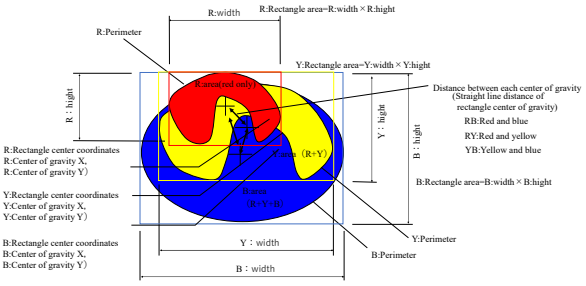

Figure 6. Concept of shape feature calculation of ternarized thermal images

The Shapes of red, yellow, and blue areas are also significant. In the thermal images of false detection, if its edge is smooth, it could be a floating area. Therefore, we examined shape features of red, yellow, and blue areas. The number of pixels represents circumference and dimension of the area. Occupancy rate, degree of shape complexity, and circularity level of each shape are calculated by the following equaitons, where L is the circumference and S is the area.

$$\text{Occupation rate (O)} = \frac{S}{R(height) \times R(width)}$$

$$\text{Degree of shape complexity (C)} = \frac{L}{S} \qquad (2)$$

$$\text{Circularity level (CL)} = \frac{4\pi A}{L^2}$$

In addition to the above values, we use the co-occurrence matrix[6][7][8], which is an image texture analysis method that can quantify changes in image contrast. The co-occurrence matrix firstly derives the matrix that uses the P-value of the target contrast in a specific position δ = (r, θ) away from the point i should be the contrast j, Pδ = (i, j), as its element (hereinafter referred to as stochastic matrix) to calculate several features by the matrix as shown in Figure 7. Values of the stochastic matrix represent frequency to each sample image, but practically we normalized them so that all numbers should be 1.

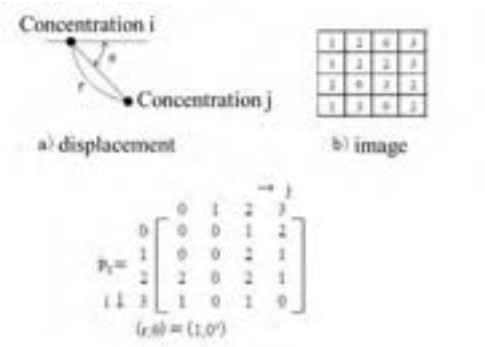

Figure 7. Co-occurrence matrix sample

We calculated following 14 features in total by the co-occurrence matrix mentioned above; Angular second moment, Contrast, Correlation, Sum of square variance, Inverse difference moment, Sum average, Sum variance, Sum entropy, Entropy, Difference variance, Difference entropy, Information measure of correlation 1, Information measure of correlation 2, Maximal correlation coefficient. We also set the position value δ as r = 1, 2 and the angle value θ as 0, 45, 90, 135, 180, 225, and 270. As for the contrast, we set it in 32 levels of gray, and we generated the co-occurrence matrix.

3.5 Deep neural network

We used hammering test results as the training data for the deep neural network[9][10][11] developed in this study based on shape features obtained from analyzed images in the previous section. The shape features are ternarized areas, their positional relations, and those obtained by co-occurrence matrix. The data amount was 2,353 cases (hammering test results from 2008 to 2010).

In this study, a deep neural network with one input layer, six hidden layers, and one output layer was developed. The number of nodes in hidden layers are 453, 500, 600, 400, 300, and 100. The drop-out layer is also sandwiched between these layers. In this paper, the number of layers of the hidden layer for high accuracy is investigated by grid search. It is probably not the optimum value, but it is almost the optimum value and there is no problem in practical use.

4 RESULTS AND CONCLUSION

4.1 Results

Table 4 shows the accuracy of the deep neural network model. The overall accuracy was 88.7 % (2,086/2,353). In addition, 800 data which were not used for the learning were prepared, and the analysis by this method was carried out. As a result, Over 97% of the hammering results are in the top two of the prediction results, which proves that this system is highly accurate.

Table 4 Analysis results of training dataset

sounding results / analysis results	Delamination	Floating	Slag	Healthy area	Foreign substances	total
Delamination	**111**	2	0	32	2	147
Floating	2	**116**	2	12	0	132
Slag	1	0	**34**	6	0	41
Healthy area	64	71	17	**1,732**	42	1926
Foreign substances	3	0	0	11	**93**	107
total	181	189	53	1793	137	**2353**

4.2 Conclusion

It has been confirmed that the temperature gradient generated in the structure is removed by the image filtering process of the thermal image taken by the infrared camera, and the damage detection rate is improved. In addition, the image filtering process should be sufficient to deal with the influence of temperature differences around bridge appendages.

We also succeeded in building a deep neural network model that evaluates the presence and type of damage due to temperature changes. As inputs of deep neural network model, 14 feature quantities obtained from co-occurrence matrix, etc. were used. As a result, the accuracy of 88.7% was realized. Furthermore, the high accuracy was obtained even in the data set which was not used for the training. As a result of this study, floating/delamination can be remotely evaluated, which is considered to contribute to drastic improvement in efficiency of present inspection that depends on hammering sound.

5 Automatic detect system using a cloud server

5.1 Introduction of the system

Statistical analysis software is required to perform the damage detection described above, but such software can only be used by a limited number of users. Therefore, we have built a cloud server that can automate the damage detection for many users, and are currently conducting trial operations as shown in Fig. 8. This system is based on the machine learning system described above and can automatically detect damages based on infrared measurement and hammering test result data. Figure 9 shows an example of the use of an automatic detect system using a cloud server.

1. The thermal image (Figure 9(a)) is loaded into the analysis software “J-system” and ternarized areas, and their positional relations, and those obtained by

co-occurrence matrix are automatically output.
2. Upload the output to the cloud server.
3. Users download the results of the damage detection by the cloud server (Figure 9b).

The results of the infrared measurement are summarized in the above procedure. Figure 12c shows an example of delamination in a hammering test. This was the damage the proposed system determined to have a high probability of damage.

Figure 8. Automatic detect system using a cloud server

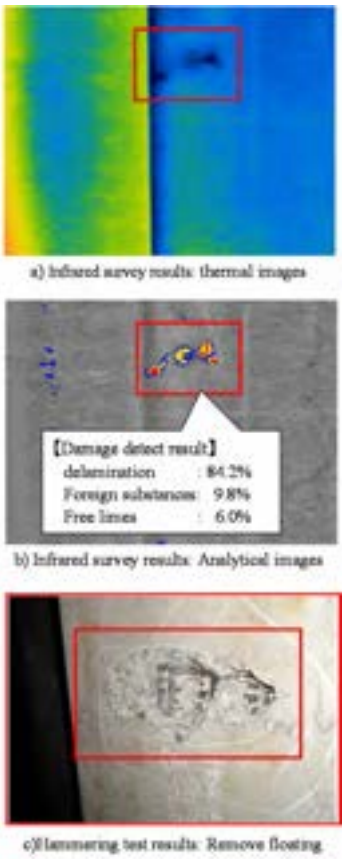

Figure 12. Example of Automatic detect Results from a Cloud Server

Utilizing a highly accurate system that automatically detects damages from infrared measurement results, the individual differences of surveyors are eliminated. The more data this system has, the more accurate the system will be at determining damages. When users of J-system perform the infrared survey and use the cloud server, the survey data will be stored on the cloud server, and as a result, the accuracy of the automatic detect system will be improved.

5.2 Introduction result

The J-system has been evaluated as a "non-destructive inspection technology that can detect floating and delamination of concrete structures" by the Bridge Maintenance Subcommittee of the Committee for Verification of Robots for Next Generation Infrastructure.

In addition, the J-system has been installed in the Shikoku branch of NEXCO West Japan since 2008 as a hammering sound screening system for periodic bridge inspections. It has also been used by NEXCO Central Japan, NEXCO East Japan, and Honshu-Shikoku Bridge Expressway, and has been introduced on a trial basis on bridges owned by the national government since fiscal 2015. The total survey area that West Nippon Expressway Engineering Shikoku Co., Ltd. received an order for is 2.55 million square meters (as of the end of FY2017). We will continue to develop a high-precision infrared measurement system so that it can be widely used for bridge inspection and surveys, including prevention of damage to third parties.

References

[1] Cheng, L., & Tian, G. Y. 2012. Comparison of nondestructive testing methods on detection of delaminations in composites. *Journal of sensors*, *2012*.

[2] Oh, T., Kee, S. H., Arndt, R. W., Popovics, J. S., & Zhu, J. 2012. Comparison of NDT methods for assessment of a concrete bridge deck. *Journal of Engineering Mechanics*, *139*(3), 305-314.

[3] ASTM. 2007. Standard test method for detecting delaminations in bridge decks using infrared thermography. *ASTM D 4788*.

[4] Kimura, T., Zhang, T., & Fukuda, H. 2019. A Proposal for the Development of a Building Management System for Extending the Lifespan of Housing Complexes in Japan. *Sustainability*, *11*-(20), 5622.

[5] Plesu, R., Teodoriu, G., & Taranu, G. 2012. Infrared thermography applications for building investigation. *Buletinul Institutului Politehnic Din Lasi. Sectia Constructii, Arhitectura*, *58*(1), 157.

[6] Chun, P., Funatani, K., Furukawa, S., & Ohga, M.

2013. Grade classification of corrosion damage on the surface of weathering steel members by digital image processing, In *Proceedings of the Thirteenth East Asia-Pacific Conference on Structural Engineering and Construction (EASEC-13)* (pp. G-4). The Thirteenth East Asia-Pacific Conference on Structural Engineering and Construction (EASEC-13).

[7] Partio, M., Cramariuc, B., Gabbouj, M., & Visa, A. 2002. Rock texture retrieval using gray level co-occurrence matrix. In *Proc. of 5th Nordic Signal Processing Symposium* (Vol. 75).

[8] Pathak, B., & Barooah, D. (2013). Texture analysis based on the gray-level co-occurrence matrix considering possible orientations. *International Journal of Advanced Research in Electrical, Electronics and Instrumentation Engineering*, *2*(9), 4206-4212.

[9] LeCun, Y., Bengio, Y., & Hinton, G. 2015. Deep learning. *nature*, *521*(7553), 436-444.

[10] Sainath, T. N., Mohamed, A. R., Kingsbury, B., & Ramabhadran, B. 2013. Deep convolutional neural networks for LVCSR. In *2013 IEEE international conference on acoustics, speech and signal processing* (pp. 8614-8618). IEEE.

[11] Simões, N., Simões, I., Tadeu, A., & Serra, C. 2012. Evaluation of adhesive bonding of ceramic tiles using active thermography. In *Proceedings of 11th Quantitative InfraRed Thermography conference, paper QIRT2012-362, Naples (Italy)*.

Stereo Vision based Hazardous Area Detection for Construction Worker's Safety

Doyeop Lee[a], Numan Khan[a] and Chansik Park[a]

[a]Department of Architectural Engineering, Chung-Ang University, Seoul, South Korea

E-mail: doyeop@cau.ac.kr, numanpe@gmail.com, cpark@cau.ac.kr

Abstract –

In order to ensure the safety of construction workers during the construction process, supervision of violations of safety regulations and control of hazardous situations not recognized by the workers are continuously required. However, due to the dynamic nature of the construction site, the hazardous situation is always changing and there is a limit to managing all these risk situations in a manual manner by the supervisor. To address these limitations, various computer vision-based researches are being conducted that can automatically identify and manage risk factors. The aim of this study is to propose a system for detecting potential horizontal and vertical risks of moving or static objects around workers by measuring distance between objects using Stereo Vision. Proposed system consists of motion detection, object detection and distance measurement between objects using depth image from stereo camera. It synthesizes images from multiple cameras into one and uses motion-detection and object-detection to identify the movement of objects in a vertical or horizontal position. Then, based on the depth information of the stereo camera, the distance is calculated to identify whether a worker is in the hazardous zone. The proposed system was implemented in the lab environment to verify the proposed functionality. The lab test results indicate that the proposed system can detect vertical and horizontal hazards. It is expected to contribute to the prevention of possible accidents by detecting and controlling the dangers around the workers in real time.

Keywords –

Construction Safety; Depth Measurement; Distance Calculation; Risk Area; Stereo Camera

1 Introduction

Despite various efforts to reduce the number of accidents and fatality in construction sites, construction Safety accidents are occurring continuously. Safety in construction remains a critical issue. Among various types of accidents, this study aims to focus on ways to manage risk situations that are not recognized by workers.

Based on the KOSHA database, the accident cases that happened during 2016-2018 have reported 1345 fatalities in construction. The reported three years of data have been analyzed to find the proximity and collision-related accident cases. As a result, 222 cases are identified related to proximity risks, either horizontally or vertically, that account for 12% of the total fatalities that happened during that interval of time.

For instance, the accident that happened during vertical simultaneous work is a case in which a worker hit by fallen rebar lifted by a crane, hitting by the fallen pipe from the upper floor while working near the window, and hitting by the falling temporary structure while working at the basement. The accident happened during horizontal simultaneous work is a collision happened with a moving car while cleaning up the site, falling into an opening during the site inspection.

These fatal accidents may occur because the worker is not aware of the dangerous situation, but in some cases, the accident is caused by the worker ignoring the dangerous situation. The main purpose of this study is to propose a stereo-vision based system that can determine in real time whether a worker is exposed to a dangerous situation by measuring the distance between the worker and the risk factors. Through this, it is possible not only to control the dangerous situation, but also to identify how often workers are exposed to the danger at the site, and to provide information that can be reflected in future safety management plans.

2 Related Work

2.1 Sensor-based Proximity Risk Detection Systems

The complex nature of the construction site and dynamic movements of construction entities tend to produce many struck-by hazards. To avoid collisions

between the objects, the proximity warning system (PWS) is widely used [1]. The PWS operates based on the spatial relationships between the interested entities, and their performance depends on the type of object's tracking technology, for instance: radio frequency (RF) sensing, ultrasonic, radar, global position system (GPS), and magnetic field [2]. To determine the proximity between the objects, the radiofrequency sensing technology emits the electromagnetic signals from a mounted device on objects [3]. This technology uses predefined rules to generate an alert based on signal strengths between the device and objects with the attached tags. Based on the power source in the tags, RF technology can be grouped into three classes:(1) active RF technology and (2) passive RF technology [4]. The active technology needs a power-source for long-range detection. For instance, a type of active RF technology, Ultra-Wideband (UWB) robustly transmits the signals using comparatively low power for tracking the objects, with the errors of centimeter-level [5]. However, passive RF technology requires a power source for the RF device in the shorter-range detection. Passive tags are less expensive, powered by the radio waves from the reader, and have a range of up to 30 feet [4]. Since the RF-based PWS only requires signals strength adjustments and data processing step, thus, it can be easily implemented in the construction site [5]. However, RF technology requires additional work of putting tags on every interested object. Moreover, their signals could be interfered and disturbed by the multipath fading effect [1].

On the contrary, the Global Positioning System (GPS) is employed to recognize the absolute location of objects [3,6]. The GPS sensor identifies the latitudinal and longitudinal coordinates of the objects which required to be monitor. To detect the proximity risk of the entities, the heading direction and speed also need to be considered and extracted [1]. GPS can be used to cover large scale area; thus, many researchers have extensively studied this technology for the practical implementation in the large construction sites [2,7]. However, previous efforts revealed various limitations such as manual input from the supervisor to limit the access to a hazard zone by using risk zone information [8], and accuracies dependent cost ranges of the GPS sensors. Moreover, the additional significant limitation is the strength of the signals, which could be blocked by buildings or other objects.

2.2 Vision-based Proximity Risk Detection Systems

To detect the proximity risks in construction, previous studies have used object tracking techniques for monitoring the trajectories of the localized objects in a series of images [7,9,10]. The primary step for object tracking and action recognition includes the detection of objects. Once the entities of interest are successfully recognized, the location of the bounding boxes in a frame with respect to time could be traced by utilizing the object tracking algorithm [11]. The localization of objects takes place based on their pixel information, changes in brightness, intensity, and other local features. Detection of the sudden slope failure is possible based on the change in pixel intensity [12]. The extracted location information is then used to identify unsafe actions and conditions.

Compared to sensor-based tracking techniques such as RFID tags, UWB, and GPS, Computer vision as a technique has the capability to identify multiple object's information form construction worksites using images only, without human involvement or any additional devices for instance, tags or sensors. Furthermore, the camera can cover large area, thus, multiple objects can be simultaneously captured and easily tracked. Location and detailed information such as types and velocity of the objects can also be acquired. However, the performance of the vision-based systems may vary under poor light conditions, snow, rain, or dusty storms.

3 Proposed Methodology

The purpose of this study is to propose a stereo vision-based risk detection system that can identify how close a worker is to vertical and horizontal hazards and determine whether they are dangerous. Figure 1. illustrates the operating process of the proposed system.

The system consists of motion detection, object detection, and object depth and distance measurement technology using Stereo vision. This system is designed to use the stereo camera's depth calculation in a way that works only under certain conditions, so that it can be used in real time even on low computing resources. First, motion detection and object detection algorithms are applied to the stereo video information to determine the movement and presence of objects in the air and on the ground, and to check the possibility of a dangerous situation. After that, the distance between objects is measured based on the depth information of the stereo camera to determine whether the distance between objects located on the ground is a dangerous situation horizontally and whether an object located in the air poses a danger to objects on the ground.

This system is applied Motion Detection technology that detects motion compared to the current frame and previous frames, YOLO V4 Object Detection algorithm that enables stable real-time detection, and the depth measurement technology of the object using INTEL RealSense Stereo Camera. This stereo camera measures the depth of a specific pixel value through operation using video taken from two or more different angles and additional infrared or RGB color image sensors. When

using a general camera, more computation is required at the same resolution, which increases the consumption of computing resources. Thus, the proposed method is designed to minimize depth calculation by utilizing the stereo camera (Intel RealSense) so that it can operate in real time even with low computing resources. For this purpose, motion detection and object detection are designed to operate sequentially in one video information, which identifies the movement and presence of objects in the air and on the ground, and identifies the possibility of dangerous situations. Then, after calculating the distance based on the depth information of the stereo camera, it is determined whether a specific object is in a dangerous situation.

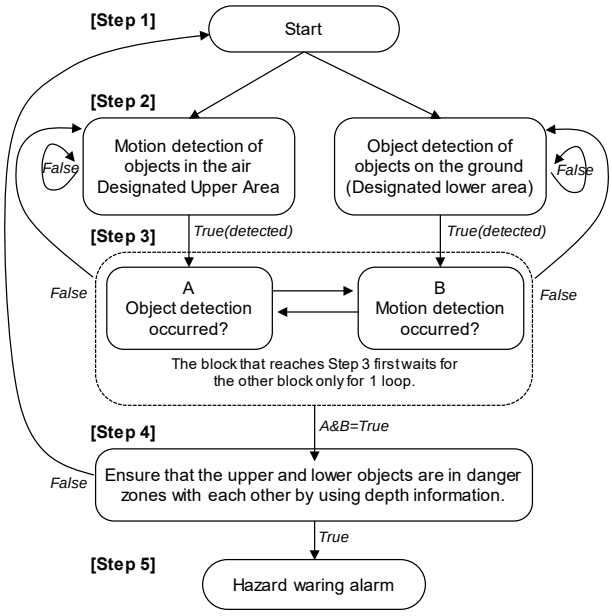

Figure 1. Overview of the proposed process

4 Lab Test and Results

4.1 Lab Test Process

Lab test was conducted on two conditions for determining vertical and horizontal hazards (Figure 2). In the case of horizontal hazards, the distance between a worker working on the ground and a dump truck was measured, and in the case of vertical hazards, the distance between a worker working on the upper area and a worker working on the ground was measured. The risk level was set to be dangerous when the distance between vertically and horizontally located objects is within 2 m, caution when 2 to 4 m, and safe when 6 m or more. For the lab test, a 1/20 scale model was used.

Depth estimation using stereo vision from two images (taken from two cameras separated by a baseline distance) involves three steps: First, establish correspondences between the two images. Then, calculate the relative displacements (called "disparity") between the features in each image. Finally, determine the 3-d depth of the feature relative to the cameras, using knowledge of the camera geometry [13]. The typical stereo vision geometry for depth measurement is illustrated in Figure 3. The stereo depth camera used in this study, RealSense 435i, uses two infrared sensors to measure the depth value.

The procedure for measuring the distance between two objects by utilizing the measured depth values is as follows. (1) The full width of the camera Field of View (FOV) at a specific distance from the camera to the object is applied at an absolute value. (2) The total horizontal length of the camera FOV is calculated from the position of the object in front of the objects to be measured in proportion to the previously applied value. (3) Obtain the depth value of the object in front through Object Detection (Set to X). (4) Set the difference between depth values between objects to Y. The distance R between objects is calculated by following equation [R^2 = X^2 + Y^2].

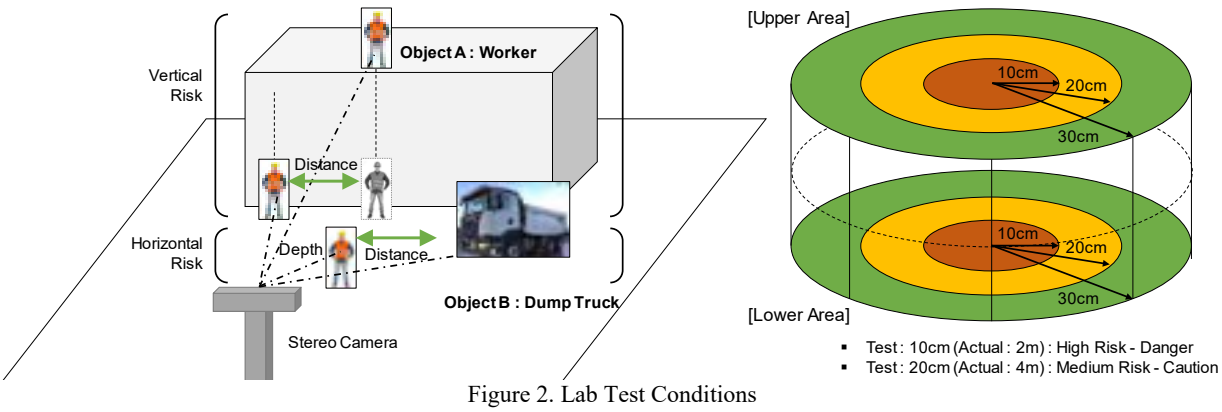

Figure 2. Lab Test Conditions

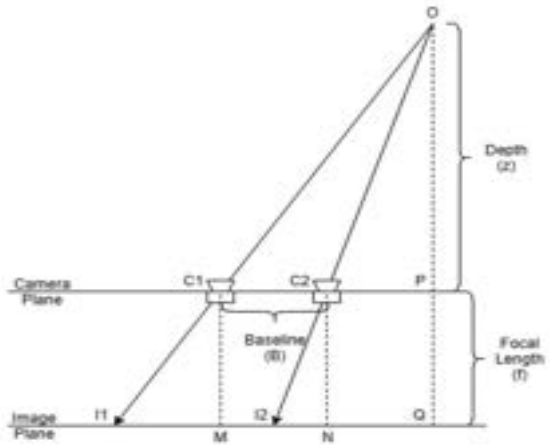

Figure 3. The Stereo Vision Geometry for Depth Measurement [14]

4.2 Lab Test Results

Lab test was performed on the laptop system with specifications as follows; Intel Core i7 8700K, 16 GB RAM, GTX1080TI VGA, Intel RealSense435i, Ubuntu 18.04, and Tensorflow 2.1.0.

As shown in Figure 4, the horizontal risk level (danger, caution, and safe) was determined in real time according to the set risk area as the worker approaches the dump truck.

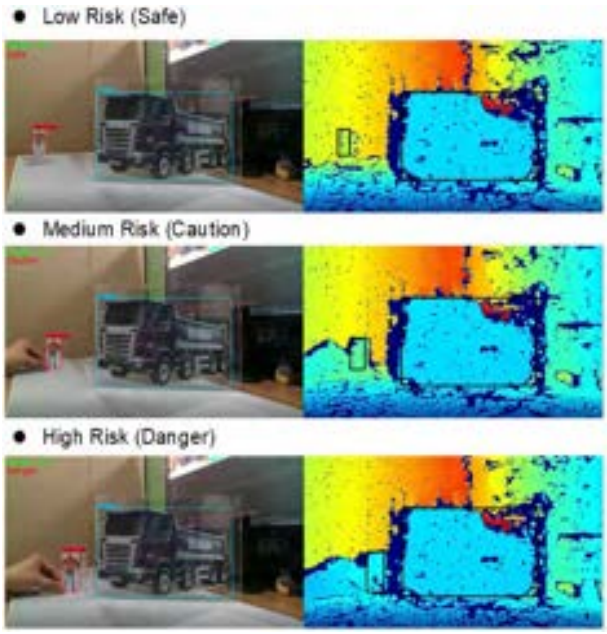

Figure 4. Example of Real-time Horizontal Risk Checking

As shown in Figure 5, motion detection determines the motion by comparing pixel changes between the current frame and a certain number of previous frames.

Figure 5. Example case of a motion detection

As described in the system process, when an object that moves at the top of the video frame is detected, the object detection algorithm is applied to determine the risk based on the distance between objects. In this test, the position of the lower worker was fixed and the upper worker was approached toward the lower worker. The difference between the X-axis value of the left pixel of the upper worker and the right pixel X-axis value of the lower worker was calculated as the horizontal distance.

As shown in Figure 6, the vertical risk level (danger, caution, and safety) was determined in real time according to the set risk area as the upper worker approaches the lower worker.

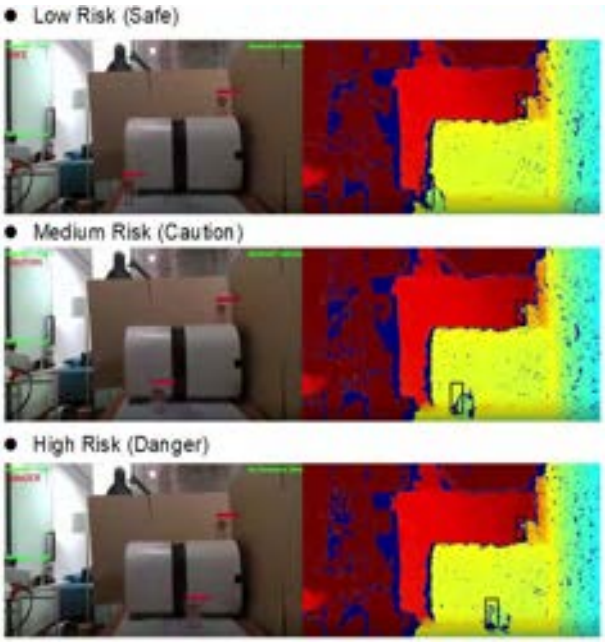

Figure 6. Example of Real-time Vertical Risk Checking

Table 1 and 2 show the results of vertical and horizontal risk level measurement. Tests were performed by measuring the depth and distance values by placing objects on the basis of the risk level (10 cm, 20 cm, 30 cm).

In the horizontal hazard test, when the distance between the worker and the dump truck was placed at 30cm, the measured distance was 31.6cm, with an error of 5.3%, but when placed at 10cm, the measured distance

was 8.81cm, with a slightly larger error of 11.9%. The size of the 1/20 scale model used for the test was small, so close-up shots were taken, which caused the infrared sensors to be unstable.

Table 1. Results of Horizontal Risk

Actual Distance (Risk Level)	Depth Measurement		Distance between Objects	Error
	Worker	Dump truck		
10cm (Danger)	30cm	25cm	8.81cm	11.9%
20cm (Caution)	40cm	25cm	18.5cm	7.5%
30cm (Safe)	55cm	25cm	31.6cm	5.3%

In the horizontal hazard test, when the distance between the workers was placed at 30cm, the measured distance was 29.7cm, with an error of 1%, but when placed at 10cm, the measured distance was 9.8cm, with an error of 2%. In the case of vertical hazard determination, the error was relatively low because the distance was measured using the RGB image-based pixel information, not the infrared sensor-based depth measurement method.

Table 2. Results of Vertical Risk

Actual Distance (Risk Level)	Depth Measurement		Distance between Objects	Error
	Worker (Lower Area)	Worker (Upper Area)		
10cm (Danger)	45cm	57.4cm	9.8cm	2%
20cm (Caution)	45cm	52.8cm	20.5cm	2.5%
30cm (Safe)	45cm	50cm	29.7cm	1%

5 Conclusions

This study proposed horizontal and vertical risks detecting system around workers by measuring distance between objects using stereo vision technology, with the goal of preventing accidents caused by unrecognized hazards such as material drop during lifting and collision with construction vehicle. In this paper, motion detection and object detection are designed to operate sequentially in one video information to minimize computing resources.

The proposed system is tested in the lab environment. Test results showed that objects moving horizontally and vertically were detected in real time, and hazard levels were also determined in real time. However, the accuracy of the measured distance was low due to the size of the scale model utilized in the lap test and the narrow distance between the infrared lenses of the camera used.

In the future research, in order to increase the accuracy and applicable range of distance measurement between objects, we intend to test the measurable distance and viewing angle by using various stereo depth cameras on the actual field.

Acknowledgement

This work is supported by the Korea Agency for Infrastructure Technology Advancement(KAIA) grant funded by the Ministry of Land, Infrastructure and Transport (Grant 20SMIP-A158708-01).

References

[1] Wang, J.; Asce, S.M.; Razavi, S.N.; Asce, M. Low False Alarm Rate Model for Unsafe-Proximity Detection in Construction.

[2] Kim, K.; Kim, H.; Kim, H. Image-based construction hazard avoidance system using augmented reality in wearable device. *Autom. Constr.* **2017**, *83*, 390–403.

[3] Lee, H.-S.; Lee, K.-P.; Park, M.; Baek, Y.; Lee, S. RFID-Based Real-Time Locating System for Construction Safety Management. *J. Comput. Civ. Eng.* **2012**, *26*, 366–377.

[4] Rock, L. BIM and RFID integration : A pilot study. *Adv. Integr. Constr. Educ. Res. Pract.* **2002**, 570–578.

[5] Lu, Q.; Lee, S. Image-Based Technologies for Constructing As-Is Building Information Models for Existing Buildings. *J. Comput. Civ. Eng.* **2017**, *31*, 04017005.

[6] Ju, Y.; Kim, C.; Kim, H. RFID and CCTV-Based Material Delivery Monitoring for Cable-Stayed Bridge Construction. **2012**.

[7] Brilakis, I.; Park, M.-W.; Jog, G. Automated vision tracking of project related entities. *Adv. Eng. Informatics* **2011**, *25*, 713–724.

[8] Teizer, J.; Cheng, T. Proximity hazard indicator for workers-on-foot near miss interactions with construction equipment and geo-referenced hazard areas. *Autom. Constr.* **2015**, *60*, 58–73.

[9] Teizer, J.; Vela, P.A. Personnel tracking on

construction sites using video cameras. *Adv. Eng. Informatics* **2009**, *23*, 452–462.

[10] Park, M.W.; Makhmalbaf, A.; Brilakis, I. Comparative study of vision tracking methods for tracking of construction site resources. *Autom. Constr.* **2011**, *20*, 905–915.

[11] Seo, J.; Han, S.; Lee, S.; Kim, H. Computer vision techniques for construction safety and health monitoring. *Adv. Eng. Informatics* **2015**, *29*, 239–251.

[12] Mchugh, E.L. VIDEO MOTION DETECTION FOR REAL-TIME HAZARD WARNINGS IN SURFACE MINES Edward L. McHugh Spokane Research Laboratory, National Institute for Occupational Safety and Health, Spokane, Washington, USA.

[13] Saxena, A.; Schulte, J.; Ng, A.Y. *Depth Estimation using Monocular and Stereo Cues*;

[14] Praveen, S. Efficient Depth Estimation Using Sparse Stereo-Vision with Other Perception Techniques. In *Coding Theory*; IntechOpen, 2020.

Artificial Intelligence and Blockchain-based Inspection Data Recording System for Portable Firefighting Equipment

Numan Khan [a], Doyeop Lee [a], Ahmed Khairadeen Ali[a], and Chansik Park [a*]

[a] School of Architecture and Building Sciences, Chung-Ang University, Seoul 06974, Republic of Korea
E-mail: numape@gmail.com, doyeop@cau.ac.kr, ahmedshingaly@gmail.com, cpark@cau.ac.kr

Abstract

Fire poses an enormous threat to human safety; many people get injured or die due to fire accidents each year. As permanent firefighting equipment usually available in a build building, they do not exist in many construction job sites, so they merely depend upon the portable firefighting equipment (PFE) to keep the fire damage limited and minimum. To ensure the proper functionality of the PFE in the case of fire, perfectly located and in-good order are the two vital factors for the PFE. According to standards specified by safety regulations, PFE inspection and maintenance are required to ensure the perfect location and good order of the PFE. Currently, the PFE inspection and maintenance includes the safety auditor from the government and safety manager from the concerned companies. Moreover, the PFE inspection and maintenance process depends on the paper-based manual reporting and recording system, which is time-consuming, cumbersome, and can be easily manipulated. To automate the process of PFE inspection and maintenance, this study will propose optical character recognition (OCR) and Blockchain-based reporting and recording system. A mobile application is developed to validate the proof of concept. One of the artificial intelligence techniques, the optical character recognition (OCR) is adopted in the mobile application, which automatically converts the image tag or report of the PFE inspection and maintenance to the text. The text data is encrypted in a hash using encryption scheme SHA 256 of online service with open API, named as truetimestamp. The generated hash will signify the date inside of the file, which will be immutable and incorruptible. Moreover, the coordinates of the captured image will be extracted from the device to ensure the location of the PFE. It is expected that the proposed system will decrease the paperwork, reduce the burden of the safety manager, with increased efficiency and reliability of the PFE inspection records. The collected inspection record data could also be used to evaluate the safety performance of the concerned contractors.

Keywords –

Artificial Intelligence; Blockchain; Inspection Data Records: Portable Firefighting Equipment

1 Introduction

The construction industry includes many unhealthy activities that are perceived as the causes of workers discouragement, project progress delay, additional cost, low project productivity, damage to reputation, and ultimately human fatalities and injuries [1]. The inherited features of the construction industry itself have potential threats of accidents since its unique nature, open space, working at height, fire risks, exposure to severe weather, confined spaces, unskilled labor involvement, working with toxic and explosive materials, physical and psychologically vulnerable working conditions, and occasionally tight project duration with high productivity demand [2]. Academic researchers and industry professionals have been devoted vital attention to enhance construction safety for many decades. Despite much efforts, construction job sites are still known to be hazardous worksites with high accidents rate, thus, safety in construction remains a vital issue in many countries.

Many people become seriously injured or die due to fire accidents each year [3]. Fire incidents came into existence after its discovery and are intimately proportional to the progress and development of human civilization [4]. World Health Organization (WHO) report for fire-induced burns revealed more than 300,000 deaths annually. Unfortunately, annoying statistics are that 95 percent of these deaths are happening in low-income and middle-income countries [3]. The report from the U.S Bureau of Labor Statistics in 2018 divulge the death of 66 construction workers each year due to fires and explosion [5]. The five years (2010-2014) study by National Fire Protection Association (NFPA) revealed $280 million in direct damage to the property annually in renovation or under construction residential projects (discounting one- and two-units projects) [6].

The quantity of industrial and civil construction projects are swiftly growing due to socio-economic

development policies in many countries [7]. The growing challenges for fire safety with respect to economic progress have significantly supported the evolution of fire science and technology [4]. Initially, fire science and technology's primary intention was to save large factories, properties and evade sweeping fires conflagration [8]. Extensive research has been carried out in the domain of fire safety monitoring and early detection. Many studies have focused on the detection of smoke and heat by using various tools and techniques such as Dual infrared (IR/IR) spectral band flam detection, very early smoke detection apparatus (VESDA), linear infrared flammable gas detection, and fiber optic attached to distributed temperature sensing (DTS) [4,9,10]. Apart from fire safety monitoring and fire detection, several studies have also focused on fire safety and evacuation planning for existing as well as under-construction buildings and tunnels [11–14].

Fire safety management is a significant issue for every business; however, it is notably vital in construction due to several reasons that engender grim fire risks frequently. Firstly, workers are exposed to combustible substances in many construction job sites, and the presence of wind around the unfinished buildings can immediately cause a fire. Secondly, as under-construction sites do not possess permanent and adequate fire protection system, so, PFE or sometimes water tanks are the only preventive measures which they can adopt. With this regard, the Occupational Safety and Health Administration (OSHA) stipulates that a site-specific safety plan should include a fire protection plan for every construction project. Since many construction job sites depend on the PPE as a preventive measure, the vital factors which need to be considered are two: (1) perfect location of PFE, and (2) good working order of PFE [15]. The former is addressed in the previous study using a visual programming approach [16], while the latter is considered in this study. To ensure the maintenance of the fire extinguisher and overcome fraud or modifications in inspection records, this research work proposed an android app that uses optical character recognition (OCR) and blockchain technology for inspection data recording system PFE for maintaining the right order of the equipment.

2 Current Issues in Recording Safety Inspection of PFE

In the past, people typically have to depend on themselves or rely on their nearby vicinity for rescue operations in case of fire [17]. However, based on the necessities, new tools and techniques are developed over time. Many buildings, tunnels, or any other workplaces are currently using fire extinguishers (portable firefighting equipment). To maintain the PFE, frequent interval inspection and maintenance are required. In the past, the essential inspection information about these types of equipment was often dispersed between the stakeholders, which sometimes could lead to data loss [18]. Another significant issue is filling the documents or tags of PFE falsely with the same pen and the same pattern of dates [19]. To sort out the issue, a BIM-based approach has been introduced, which could store the necessary information about these devices such as device name, manufacturer name, maintenance staff, type, equipment warranty, last repair/inspection time, exterior features, and other specifications, as well as the location of fire-fighting equipment, equipment status [15]. However, to take the inspection data recording system to the next level, a much reliable and transparent system is inevitable to make the PFE in order and ultimately use it as a performance evaluation metric in the bidding process.

3 Blockchain and optical character recognition technologies applications

The rapid evolution in the internet of things (IoT), artificial intelligence (AI), and blockchain technologies have witnessed unprecedented contributions to the current world. This has resulted in many automated devices, time-saving, cost reduction, and a paradigm shift from the real world to the digitized world. Blockchain technology offers encrypted, distributed, and secure logging of digital transactions that could revolutionize many areas, mainly where transparency and privacy are essential [20]. As the name indicates, the blockchain can be regarded as a series of blocks (virtual cubes) in a vertical structure, aligned linearly, where each block contains a specific amount of data in the form of ciphers and codes [21]. Once the block's data is completed and validated, the said block is then permanently locked, which cannot be modified. This technology has the potential to address some problems that discourage the construction industry from using new technologies such as BIM, for instance, confidentiality, disintermediation, provenance tracking, non-repudiation, inter-organizational recordkeeping, change tracing, and data ownership [20]. Considering optical character recognition (OCR) with blockchain, previous efforts depict extensive research on recognizing characters through optic vision. OCR intends to convert handwritten or typed texts in the image to encoded texts [22]. Compared to typed or printed texts, recognition of handwritten text is challenging. Generally, an individual's handwriting style varies from others; thus, handling these variations is vital in OCR [23]. The OCR techniques include image acquisition, pre-processing, segmentation, feature extraction, classification, and recognition [22–24]. Previous efforts witnessed of OCR and blockchain technologies in construction safety

inspection and record keeping. Therefore, the innovative and useful approach for the construction safety inspection data recording system pertaining to PFE is presented in this research work.

4 System Development

This study proposed an android app for the inspection data recording system pertaining to PFE. The research was initiated with the analysis of fire-related accidents in the construction industry. Since PFE was determined as a significant measure for the first quick response to the fire emergency in the construction job site, therefore, pivotal attention is inevitable to make sure the good location and good order of PFE. Traditional inspection of PFE and its manual recording process were studied. The roles responsible for the safety inspection data recording and conformance were identified. Optical Character Recognition (OCR) and Blockchain technology were adopted to develop the proposed approach. This android app was developed in android studio using Java and Extensible Markup Language (XML). Streaming API for XML (StaX), which is considered dominant to Simple API for XML (SAX) and Document Object Model (DOM), was used in Java 6.0 for parsing XML documents. Java was used for backend business logic, while XML was used for the front end design. An objected-oriented language, Java, is user-friendly, which is platform-independent to operate; however, it is compiled in bytecode with the support of Dalvik Virtual Machine. To extract the ID of PFE and other relevant information from the tag, this system integrated the open-source google OCR library, named as, Vision API that extracts and detects text from images. The Vision API executes feature detection on an image file through sending the contents as abase64 encoded text. The database was designed in MySQL for storing the user's information and record saving. To make the server and Android App layers separate from each other, REpresentation State Transfer (REST) API was utilized to interact with the reside database and share information between them in JavaScript Object Notation (JSON). REST API was developed in PHP to make communication between the app and the server. An open-source blockchain service TrueTimeStamp (truetimestamp.org), is used as a proof of existence for each transaction. When an image of PFE's tag is submitted, the complex mathematical formula converts the file into a string of numbers and characters. Two different submissions, even with a slight variance, would generate a different hash. The system then uploads that hash, not the image, to the TrueTimeStamp Service, where it is then stored in the database. The transaction can then be verified by going to the TrueTimestamp website and putting the same hash in the verify box. The confirmation of time and date when it was initially being updated can then be seen. Moreover, the network-based location service API from google was also integrated into the app, which determines the location based on Wi-Fi access point or cell tower available in the area.

5 Process description of inspection data recording system for PFE

In this study, an application for reliable and transparent recording of PFE's inspection is developed that runs on the Android device. The entire system can be delineated in Figure 1. The developed application process includes two major stages, such as OCR and blockchain time stamping, as portrayed in Figure 1.

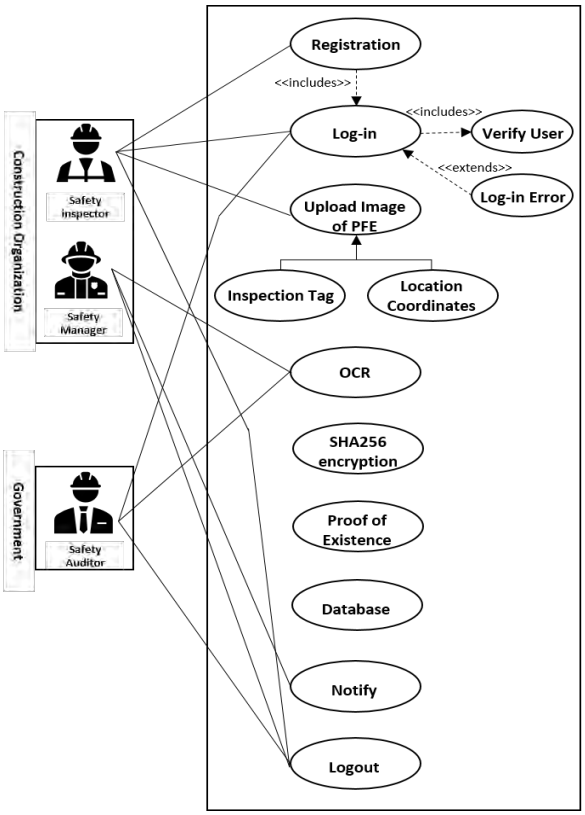

Figure 1. A use case diagram for the developed application

Figure 2 explains the process for users to register and access the functions and database of the application. The associated stakeholders must be registered in the system before they need to use this application. In the OCR process, image taken by built-in camera of the smartphone will go across three phases, including localization (region of test is located), segmentation (extraction of each symbol), and recognition

(reconstruction of words and numbers using contextual information). Next, the system will extract the ID of the focused PFE and will match it with the corresponding input ID for submission to the database. Matching extracted ID and input ID will ensure the exact tag image of the given PFE, which will reduce false reporting. The submission process would be smoothly done if both the IDs are identical, and a hash value would be allocated to the uploaded image using the Secure Hashing Algorithm (SHA-256). This hash value is a digital signature that provides cryptographic proof to avoid any modification or reproduction. As Figure 1 depicts, the uploaded image will be store in the database, and the generated hash value will be recorded on a server using truetimestamp service. All the associated stakeholders, particularly the safety auditor from the government agency can see the stored records and verify any transaction from the server.

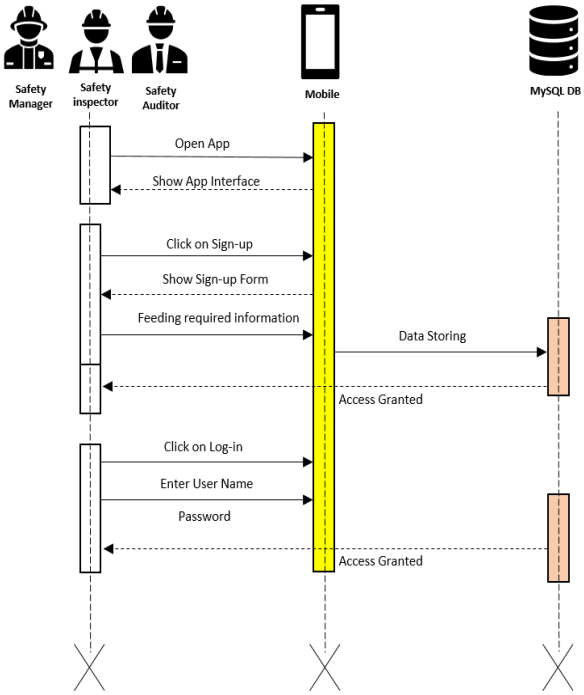

Figure 2. The sequence of users registration

6 Case testing of developed application

This section presents a case study for the Optical Character Recognition and Blockchain-based inspection data recording system pertaining to PFEs. This case study intended to validate the concept; therefore, the second-floor corridor in the Department of architecture engineering building (208) was selected for the experiment (see Figure 3).

Figure 3. Location of a case study for the developed application testing

The app users consist of three major participants, such as a safety auditor from the government agency, a safety manager, and a safety inspector from the given company. Figure 4. explains the registered roles using the sign-up process for the developed app and database. Following the exhibited procedure in Figure 2., three emails have been registered against the corresponding roles (see Figure 4). A new project named "Construction Technology Innovation Lab (ConTIL)" is registered in the project list (see Figure 4-(b).) using the safety inspector account (see Figure 4-(a).). Tags after inspections were assigned to each PFEs, and images of those tags were captured and uploaded to the database with the ID of each PFE, as shown in Figure 4-(b). The embedded OCR technology in the app extracts the ID from the image and matches it with the manually entered ID. Next, the blockchain-based proof of existence service allocates a unique hash value (a digital signature) to each record and will store that on the server using the procedure discussed in the previous section. In our case, several images have been uploaded to the server, however, one of the tag's image is exemplified in Figure 4-(b) and the hash value generated for this specific inspection can be seen in Figure-(c-2)., which is "b5f4687aff73ba6418d15ecb2f2eb3bc3a3ea90d358a0b036d67f9e9105764b6". As depicted in Figure 5-c, the safety auditor from the government agency or safety officer from the company can remotely check and verify

the inspection done by a safety inspector through logging-in to their concerned accounts. The respective transaction of each PFE's inspection associated with the enlisted projects can be verified by clicking on the "VERIFY TIMESTAMP" button in their corresponding interval is inevitable to ensure the good order and location of PFE. Currently, the PFE inspection process depends on the paper-based manual reporting and recording system. So, during the government agency's scheduled visits of safety auditors, the manual and paper-

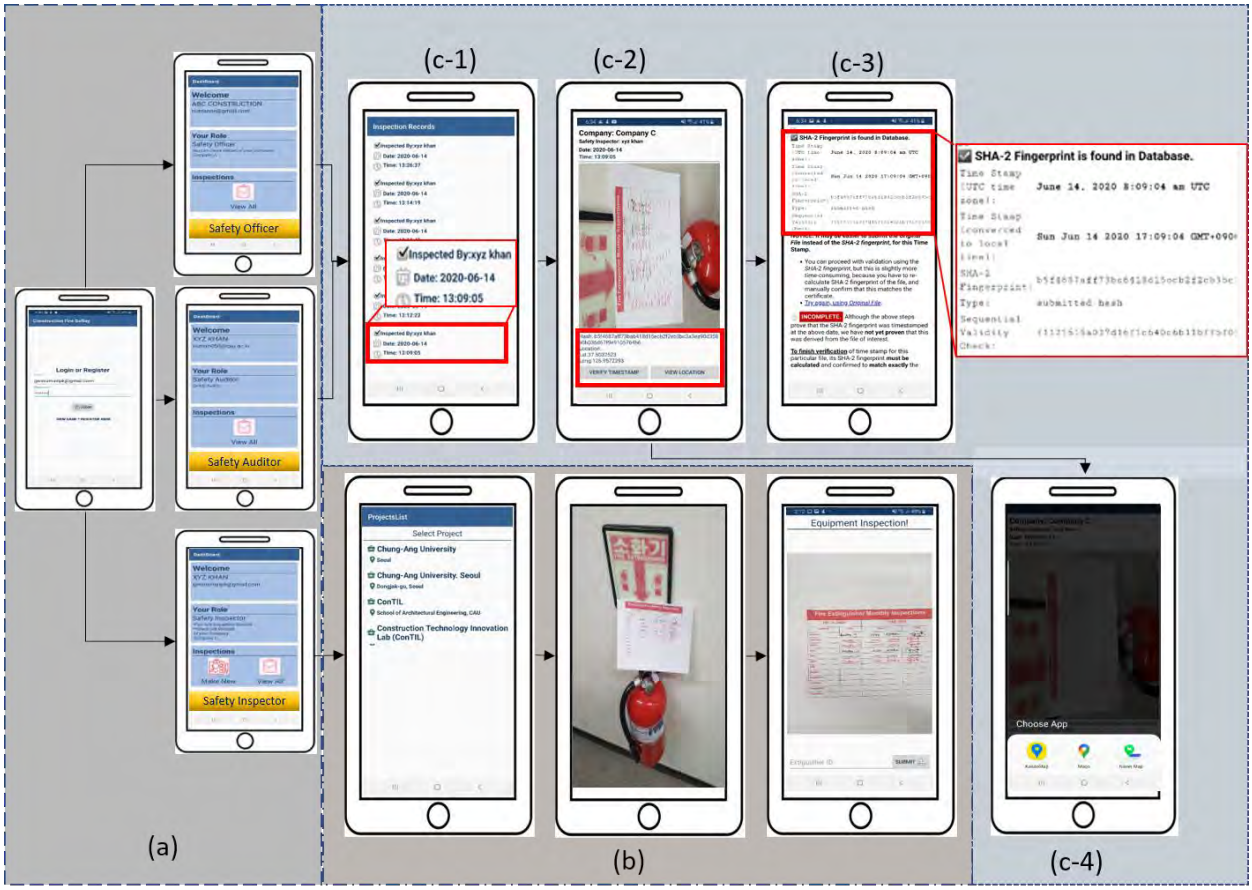

Figure 4. Screen shots of the andriod application depicting data flow and functions

dashboards. For instance, in our case, the inspection done by xyz khan on dated 2020-06-14 at 13:09:05 is verified, and the results regarding the record are visualized in Figure 4-(c-3)., which shows that SHA-2 Fingerprint is found in the database", with the same hash, date and time. In addition to verifying the transaction, the location can also be traced using different maps such as kakao, Naver, or google.

7 Conclusion

In construction, numerous workers get injured or died due to fire accidents each year. To keep the fire damage limited and minimum, many construction sites solely depend on PFE due to the absence of permanent firefighting equipment during the construction stage. Therefore, appropriate inspection with an identified based records can be easily manipulated. To address this issue, this study has developed an android mobile app that utilizes OCR and Blockchain technology for reporting and recording data. The OCR intends to automatically detect the ID from the captured tag image and the blockchain assigns a digital signature to the image.

A simple case study within the campus has been carried out to validate the concept that confirms the functionality of the developed app. It is anticipated that this app will enhance transparency, minimize the usage of paper, decrease the burden of the concerned stakeholders, and reduce the physical visits of safety auditor and safety manger, which is significantly required in the current situation of COVID-19 pandemic.

In the future, a comprehensive system will be designed to collect PFE inspection records and other

inspections or reported unsafe behavior data for the safety performance evaluation of the concerned contractors in the bidding process.

Acknowledgement

This study was financially supported by the National Research Foundation of Korea (NRF) grant funded by the Korea government Ministry of Science and ICT (MSIP) [No.NRF-2019R1A2B5B02070721].

References

[1] S. Kumar, V.K. Bansal, Construction Safety Knowledge for Practitioners in the Construction Industry, 2 (2013) 34–42.

[2] C. Vigneshkumar, Nature of Fall Accidents in Construction Industry : An Indian Scenario, (2014) 144–146.

[3] M. Shokouhi, K. Nasiriani, Z. Cheraghi, A. Ardalan, H. Khankeh, H. Fallahzadeh, Preventive measures for fire-related injuries and their risk factors in residential buildings: a systematic review, J. Inj. Violence Res. 11 (2019) 1–14. https://doi.org/10.5249/jivr.v11i1.1057.

[4] T.N. Guo, Z.M. Fu, The fire situation and progress in fire safety science and technology in China, Fire Saf. J. 42 (2007) 171–182. https://doi.org/10.1016/j.firesaf.2006.10.005.

[5] Bureau of Labor Statistics, Census of Fatal Occupational Injuries (CFOI) - Current and Revised Data, (n.d.). https://www.bls.gov/iif/oshcfoi1.htm (accessed October 3, 2018).

[6] R. Campbell, Fires in Structures Under Construction, Undergoing Major Renovation or Being Demolished Fact Sheet, NFPA Res. Data Anal. (2017).

[7] H. Liu, Y. Wang, S. Sun, B. Sun, Study on safety assessment of fire hazard for the construction site, Procedia Eng. 43 (2012) 369–373. https://doi.org/10.1016/j.proeng.2012.08.064.

[8] J. Gehandler, The theoretical framework of fire safety design: Reflections and alternatives, Fire Saf. J. 91 (2017) 973–981. https://doi.org/10.1016/j.firesaf.2017.03.034.

[9] P. Johnson, C. Beyler, P. Croce, C. Dubay, M. McNamee, Very Early Smoke Detection Apparatus (VESDA), David Packham, John Petersen, Martin Cole: 2017 DiNenno Prize, Fire Sci. Rev. 6 (2017). https://doi.org/10.1186/s40038-017-0019-4.

[10] D. Cram, C.E. Hatch, S. Tyler, C. Ochoa, Use of distributed temperature sensing technology to characterize fire behavior, Sensors (Switzerland). 16 (2016). https://doi.org/10.3390/s16101712.

[11] Y.Y. Chen, Y.J. Chuang, C.H. Huang, C.Y. Lin, S.W. Chien, The adoption of fire safety management for upgrading the fire safety level of existing hotel buildings, Build. Environ. 51 (2012) 311–319. https://doi.org/10.1016/j.buildenv.2011.12.001.

[12] K. M, B. A, Fire and Rescue Operations during Construction of Tunnels, Proc. from Fourth Int. Symp. Tunn. Saf. Secur. (2010) 383–394. http://www.diva-portal.org/smash/record.jsf?pid=diva2%3A318344&dswid=6732.

[13] P. Yang, C. Shi, Z. Gong, X. Tan, Numerical study on water curtain system for fire evacuation in a long and narrow tunnel under construction, Tunn. Undergr. Sp. Technol. 83 (2019) 195–219. https://doi.org/10.1016/j.tust.2018.10.005.

[14] M.Y. Cheng, K.C. Chiu, Y.M. Hsieh, I.T. Yang, J.S. Chou, Development of BIM-based real-time evacuation and rescue system for complex buildings, ISARC 2016 - 33rd Int. Symp. Autom. Robot. Constr. (2016) 999–1008. https://doi.org/10.22260/isarc2016/0120.

[15] S.H. Wang, W.C. Wang, K.C. Wang, S.Y. Shih, Applying building information modeling to support fire safety management, Autom. Constr. 59 (2015) 158–167. https://doi.org/10.1016/j.autcon.2015.02.001.

[16] N. Khan, A.K. Ali, S.V.T. Tran, D. Lee, C. Park, Visual language-aided construction fire safety planning approach in building information modeling, Appl. Sci. 10 (2020). https://doi.org/10.3390/app10051704.

[17] M. Kobes, I. Helsloot, B. de Vries, J.G. Post, Building safety and human behaviour in fire: A literature review, Fire Saf. J. 45 (2010) 1–11. https://doi.org/10.1016/j.firesaf.2009.08.005.

[18] K.C. Wang, S.Y. Shih, W.S. Chan, W.C. Wang, S.H. Wang, A.A. Gansonre, J.J. Liu, M.T. Lee, Y.Y. Cheng, M.F. Yeh, Application of building information modeling in designing fire evacuation-a case study, 31st Int. Symp. Autom. Robot. Constr. Mining, ISARC 2014 - Proc. (2014) 593–601. https://doi.org/10.22260/isarc2014/0079.

[19] en-Gauge, Fire extinguisher Fire extinguisher, (n.d.). https://www.engaugeinc.net/fire-extinguisher-fraud-challgenes (accessed May 29, 2020).

[20] Z. Turk, K. Robert, Potentials of Blockchain Technology for Construction Management, in: Creat. Constr. Conf. 2017, 2017: pp. 638–645.

[21] BIM World Munich, BIM and Blockchain (Part 1): Basics of Blockchain, 11 (2019) 26–27.

[22] Q. Lu, L. Chen, S. Li, M. Pitt, Semi-automatic geometric digital twinning for existing buildings based on images and CAD drawings, Autom.

Constr. 115 (2020) 103183. https://doi.org/10.1016/j.autcon.2020.103183.

[23] N.S. Rani, T. Vasudev, M. Chandrajith, N. Manohar, 2D Morphable Feature Space for Handwritten Character Recognition, Procedia Comput. Sci. 167 (2020) 2276–2285. https://doi.org/10.1016/j.procs.2020.03.280.

[24] A.F. Mollah, N. Majumder, S. Basu, M. Nasipuri, Design of an Optical Character Recognition System for Camera-based Handheld Devices, (2011). http://arxiv.org/abs/1109.3317 (accessed June 1, 2020).

Development of Field View Monitor 2

-An assisting function for safety check around a hydraulic excavator using real-time image recognition with monocular cameras

Yoshihisa Kiyota[a] , Shunsuke Otsuki[a], Susumu Aizawa[a] , Danting Li[a]

[a]Information & Communication Technology Dept, Technology Research Center, Sumitomo Heavy Industries, Ltd.
E-mail: yoshihisa.kiyota@shi-g.com, shunsuke.otsuki@shi-g.com,
susumu.aizawa@shi-g.com, danting.li@shi-g.com

Abstract –

We have developed a function to process the images of three monocular cameras mounted on a hydraulic excavator in real time, and to notify the user of any human-like images on the monitor and by sound. This function is composed of the following four functions. (1) Detection of the human head by random forest, (2) Normalization of the region of interest, (3)Evaluation of human presence based on luminance gradient features, and (4) Tracking based on the human and the excavator motion model. The algorithm is implemented in a FPGA unit, and the 3-camera images are input into the FPGA unit and processed by time-division manner to achieve both high-speed processing and low-cost.

Keywords –

Excavator; Image recognition; Human detection; Electronic Control Unit

1 Introduction

Hydraulic excavators are large, heavy, and fast-moving, and they do not only run but also turn. Operators are required to check the surrounding area reliably and over a wide area in order to ensure safety at sites where workers and obstacles are mixed in. However, there are many blind spots in the rear and right side of the vehicle that are not directly visible to the operator, because the engine hood and counterweight block the view from the operator's cabin at the front left of the vehicle. Therefore, it is necessary to make it possible to check the surroundings with mirrors and cameras. We developed a function to process the images of three monocular cameras mounted on the hydraulic excavator in real time. After processing the images, the function notifies the operator of any human-like images with a monitor display and sound. An image of the function is shown in Figure 1.

Figure 1. An example of the image recognition function.

The conventional function developed by us [1] [2] consists of three monocular cameras with wide angle, high sensitivity and wide dynamic range at the rear, right and left sides of the hydraulic excavator, which are combined in real time and displayed on a monitor in the operator's cabin. This function allows the operator to see 270 degrees view behind the excavator at a glance while

sitting on the operator's seat. An example of the camera arrangement and a composite image is shown in Figure 2. The pipeline processing using FPGA allows for the composite display of images without frame rate degradation. In 2011, this function was first sold as an option for hydraulic excavators and later it becomes standard equipment.

Figure 2. An example of a three-camera arrangement and image composition

However, the timing of when operators check the monitor is different depending on the operators. For example, it is assumed that workers in the vicinity may approach the hydraulic excavator while you are concentrating on your work and taking your eyes off the monitor. We developed a function to recognize camera images and notify the operator of the presence of human-like images with a monitor display and sound so that, the operator checks the area. The development's goal was to achieve a low-cost system configuration with only a monocular camera and to process the composite image that covered the entire 270-degree rearward area. In this paper, we introduce the technical issues and solutions to realize these problems, as well as examples of actual operations.

2 Targets and issues

The development goals were set as follows. This chapter describes the technical challenges for achieving the goals.

Target 1: Evaluation of the human presence using only monocular image recognition

Target 2: Processing of camera images with three different directions at least 10 times per second.

Target 3: Development compact and inexpensive in-vehicle equipment

2.1 Apparent change of a person in an image

The apparent appearance of the person in the image changes in a variety of ways, such as the color contrast of the background and the clothing, clothing with different colors for the upper and lower body, personal belongings, position and orientation to the camera, and pose. In addition, since the camera is mounted on the top of the hydraulic excavator body, which is taller than the person's height, the ratio of the image of the head to the body changes when the person approaches the camera and when he or she moves away from the camera. An example of this image is shown in Fig. 3. Although we assumed that only pedestrians appear in the images in this development, it is still difficult to manually design an algorithm to quantify human-like appearance by assuming all kinds of apparent changes of pedestrians.

Figure 3. Examples of changes in the appearance of a person on an image

2.2 Distortion of the wide-angle camera image

A wide-angle camera is used to capture the boundary between the rear camera and the side camera without any gaps, and it is installed at an angle downward to cover the entire distance from the very near to the far side of the excavator. As a result, the image of an object may be tilted at the left and right ends of the field of view, while the image of the excavator may be reflected at the lower end of the field of view. An example of the image is shown in Figure 4. When we set the region of interest to evaluate the human presence if there is a human in the area, a part of the attention region might be outside the image or covered by the excavator. This means that image information is missing.

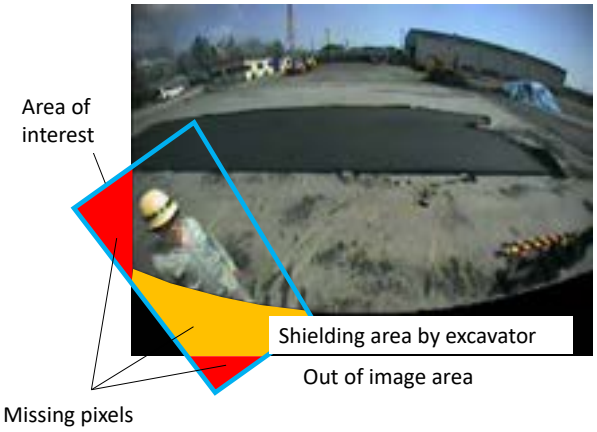

Figure 4. The missing pixels at the edge of the field of view

2.3 Faster and more stable image recognition processing cycle

It is necessary to keep executing image recognition processing, which requires a large number of computations, at a stable time cycle; FPGA can be used for stable processing time, but low-cost FPGA is limited by resources such as multipliers and internal memory.

2.4 Dense placement of the attention area

Even if the area of image for the human detection is limited to reduce the computations, thousands of regions of attention are still needed for each camera to evaluate human presence. But if we evaluate the human presence for all of regions, it is too computationally intensive to achieve the target processing cycle.

2.5 Reduction of substrate area

If the FPGA or CPU that implements image synthesis and image recognition processing is mounted separately, the board area becomes larger and more expensive, and the external appearance of the device becomes larger and more difficult to install in the excavators.

3 Evaluation of the human presence by Monocular Image Recognition

We adopts an evaluation model based on machine learning technique for the technical issues from 2.1 to 2.2 in this development. However, publicly available databases and evaluation image cropping methods [3] are not configured to address the issues described in 2.1 and 2.2, especially when a person comes directly under the camera.

In order to obtain the evaluation model for human presence in machine learning technique, a large number of supervised images are required. To collect the supervised images, we assumed a simulated environment where there is a hydraulic excavator equipping a laser sensor and a camera. The camera images were collected while the laser sensor measured the position of a person. Thousands of images were collected in the simulated environment, varying the background, weather, people's clothing, time of day, season. Then, based on the measurement results of the position of the person, a region of interest was set on the camera image, and the image was cropped and stored in the database. The position of the person in relation to the camera, the date and time of shooting, the background images and the weather, the region of interest outside the image range or the image of the car, and the original camera image were also stored in the database.

We divided the database into two categories. Category one is for the data taken very close distance from the camera, and category two is for the data taken away from the camera. We randomly selected samples from the data of the two categories. The supervised images for human detection were obtained by excluding pixels of outside the image range from the sample images or removing sample images with a large proportion of pixels of the excavator. This is to prevent the learning of pixels outside of the image range or the image of an excavator body as a characteristic of human. It is also possible to generate and use separate training models for the vicinity of the camera and for other areas to accommodate differences in the way people are reflected. The non-personal images are randomly selected by setting an arbitrary region of interest in the image without a person.

We tried to increase the number of combinations of clothing and backgrounds for supervised images, but there was a limitation. Therefore, as a preprocessing method for machine learning, we performed a feature vector transformation based on the distribution of the luminance gradient direction and normalized it for each 84-segmented partial feature vector to make it less susceptible to effects such as the contrast between background and clothing and clothing with different colors in the upper and lower body. Machine learning is ensemble learning in which the normalized sub-feature vectors are selected for a maximum of 99 logistic regressions.

4 Image recognition processing and overall structure

For the technical issues 1.3 to 1.4, we have adopted the overall structure shown in Figure 5.

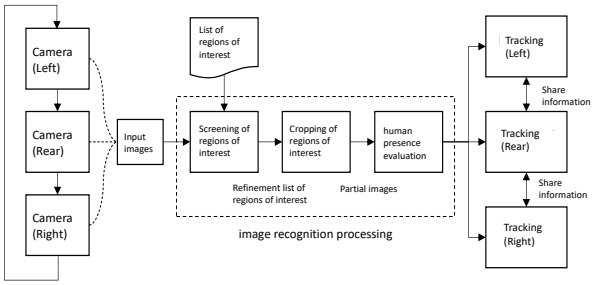

Figure 5. Overall structure of the image recognition process

The region of interest is the rectangle that surrounds the person in the image. The position of rectangles are calculated in advance for each position of the person in relation to the camera.

The image recognition process is the FPGA module that inputs grayscale images extracted from the camera images and outputs information on the area of interest that is judged to be human-like. It includes the processing of area of interest screening, the area of interest cropping, and the human presence evaluation.

In the screening of regions of interest process, all the region of interest in the field of view are input and the candidates are narrowed down by simple image recognition without trimming the area. In this case, we assume that there is a human-like image in the region of interest and transform the feature vectors of the region corresponding to the human head based on the luminance distribution. After that, we evaluate the image recognition with a machine learning model. The machine learning model is a lightweight random forest.

The region of interest extraction process extracts the pixels in the region of interest narrowed down by the region of interest screening process and normalizes them to a partial image with a uniform size.

The human presence evaluation process applies the human presence evaluation model described in Chapter 3 to the partial image generated by the region of interest cropping process, and judges whether the image is humanness or not by comparing it with the threshold value.

The tracking process obtains the location, time and camera ID of the region of interest that is determined to be humanness. The position of the region of interest is determined to be within the range of a human movement by comparing it with the results of the judgement made up to the previous time. This movable range is calculated from the relative speeds of the man and the excavator. If the judgment is positive, the positional information of the region of interest is output. This positional information is a rectangle that surrounds the object in the image and is fine-tuned to take into account the deformation of the edge of the field of view and the speed of movement. It can be done. In addition, as the person may move between cameras, a function to share location information between adjacent cameras is provided. The system is equipped with a function to select a person in the same field of view in order of near distance from the camera if more than one person is detected in the same field of view. When two or more persons are detected in the same field of view, a function to select them in the order of their distance from the camera is provided. This set of processes is a lightweight algorithm that applies a histogram filter [4] and does not affect the speed of overall image recognition cycle.

5 System Configuration and Hardware

In this development, the structure shown in Figure 6 was adopted to solve the technical problem of 2.5. The outline specifications of the configuration are shown in Table 1.

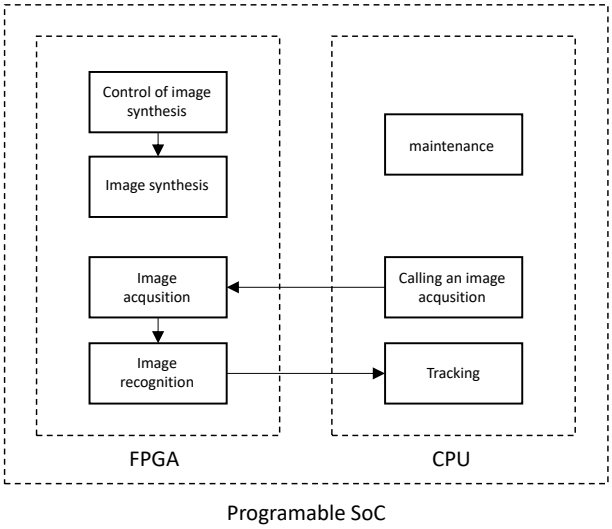

Figure 6. Overall configuration using a programmable SoC

Table 1. System specifications

In-vehicle unit	Specification	
Image Signal form	NTSC	
CPU	800	MHz
RAM	DDR3L SDRAM 2048	MB
Image synthesis memory	SDR-SDRAM 64	Mbit
Dimensions	Width 215	mm
	Length 128	mm
	Height 36	mm

The programmable SoC consists of the FPGA part, a CPU and a microcomputer part with various peripheral interfaces in the same chip.

In the FPGA part, an image synthesis module, a control module, an image recognition module, and an image acquisition module that supplies grayscale images to the module are integrated. In the microcomputer, a software that calls the image acquisition module, tracking software, and maintenance software for setting and adjusting each FPGA module and software were installed.

The evaluation of various scenes was based on the part of the database described in Chapter 3. Scenes in which people were present in the vicinity of 2 m from the camera and should be correctly detected were selected as the dataset for human detection evaluation. In addition, scenes that did not contain people were selected as a dataset for false alarm evaluation. While analyzing the processing results of these data sets, we adjusted the balance between the sensitivity to detect people and the false alarm rate. As shown in Figure 10, we were able to detect people with simple backgrounds with almost no misses. On the other hand, as shown in Figure 11, when the background contains high contrast and complex edges, the number of missed images and false alarms increases. Specifically, this includes the shadows of the excavated ground, plants and trees, other work equipment, cars, and man-made objects such as drums and benches.

Figure 7. Dataset for human detection and evaluation

Figure 8. Dataset for false alarm evaluation

6 Examples of system operation

Figure 9 is an example of a monitor display of the recognition results for various orientations and distances of people from the camera, and for various types of clothing and backgrounds. If there is a human-like image, we can see that the image can be displayed on the monitor regardless of the change in appearance on the image.

Figure 9. Perceptional results of people with diverse appearances

Figure 10 is an example of a monitor display of the recognition result when a person is approached by walking along the boundary between adjacent cameras. Even if the image appears to be tilted near the edge of the field of view, if there is a human-like image, it can be displayed on the monitor because of the image distortion of the wide-angle camera.

Figure 10. Recognition results at the edge of the field of view

Figure 11 is an example of the conventional function of displaying recognition results on a composite image. The system not only allows the operator to check the rear 270 degrees of the excavator at a glance, but also notifies the operator of any human-like images on the monitor display, and at the same time the system notifies the operator by sound, etc., which can be a trigger for the operator to check the area around the excavator.

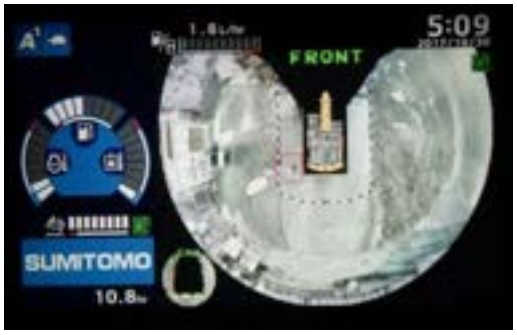

Figure 11. Display of recognition results on the composite image

Figure 12 is an example of the monitor display of the recognition result when a non-human object is judged as a human.

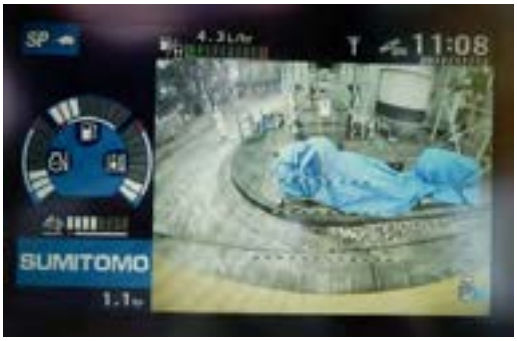

Figure 12. Examples of not being a person, but recognizing a person as a person

7 Conclusion

We have developed and put into practical use a function that recognizes images from a monocular camera mounted on a hydraulic excavator and notifies the operator of any human-like images with a monitor display and sound, giving the operator the opportunity to check the surroundings. The system was also approved for registration in the New Technology Information System (NETIS) [5].

References

[1] Yoshihisa Kiyota. and Masato Indo. and Hidehiko Kato. Development of a Field View Monitor System - A Support System for Confirming the Surroundings of Hydraulic Excavators by Video Synthesis. *SUMITOMO HEAVY INDUSTRIES TECHNICAL REVIEW*, No.179 Aug.2012, pages 5-8.

[2] New Technology Information System：NETIS，https://www.netis.mlit.go.jp/netis/pubsearch/details?regNo=KT-110057%20, 2018

[3] Yuan Li, Masaya Itoh, Masanori Miyoshi, Hironobu Fujiyoshi. Human Detection using Smart Window Transform and Edge-based Classifier. *The Japan Society for Precision Engineering Fall Conference*, Sep.2011, pages920-921.

[4] Sebastian Thrun, Wolfram Burgard, Dieter Fox, Probabilistic Robotics, The MIT Press. simulated environment

[5] New Technology Information System：NETIS，https://www.netis.mlit.go.jp/netis/pubsearch/details?regNo=KT-190106%20, 2020

Development of ROV for Visual Inspection of Concrete Pier Superstructure

Toshinari Tanaka, Shuji Nogami, Ema Kato and Tsukasa Kita

Port and Airport Research Institute, National Institute of Maritime, Port and Aviation Technology, Japan
E-mail: tanaka_t@p.mpat.go.jp, nogami-s852a@p.mpat.go.jp, katoh-e@p.mpat.go.jp, kita-t@p.mpat.go.jp

Abstract –

Visual inspections of underside of concrete superstructures of piled piers are usually carried out by inspectors on small boat or divers. it is not easy to ensure work safety in such a narrow space because of affection by waves and tides during inspection work. And, in-service facilities require to carry out the inspection work efficiently within a limited amount time and period. Therefore, the authors developed a ROV type inspection device with various support functions that takes images of the underside of the pier superstructure for improving the safety and efficiency of the inspection work. Moreover, we also developed a software to support documentation of the inspection and diagnosis of pier superstructures.

In this paper, a developed ROV for visual inspection of concrete pier superstructure and cooperation between various support functions are described.

Keywords –

Visual inspection; Concrete pier superstructure; ROV; Work support functions

1 Introduction

In typical periodic inspections, visual inspections of underside of concrete superstructures of piled piers are usually carried out by inspectors on small boat. If there is insufficient clearance to access the underside by boats, divers carry out the inspection work. However, it is not easy to ensure work safety in such a narrow space because it is affected by tidal and wave conditions during work. In addition, inspection work should be carried out efficiently so that it does not interfere with the mooring or cargo works.

For the purpose of improving the safety and efficiency of such inspection work, our R&D group has been developed a ROV (Remotely Operated Vehicle) type inspection device that takes images for diagnosis of the underside of the pier superstructure by remote control from land since 2014. We have been conducting the ROV demonstration tests since 2017, and the ROV was equipped with various work support functions at each development phase in order to reliably navigate and operate the ROV in the environments described above. Typical support functions are a positioning under the pier superstructure without using GNSS (Global Navigation Satellite System), shooting position management, a collision avoidance for obstacles, and a shooting history presentation for preventing shooting omissions. Moreover, we also developed a software for documentation of inspection and diagnosis to support in-house work.

In this paper, a developed ROV for visual inspection of concrete pier superstructure and cooperation between various support functions are described in detail by citing references of each development report.

2 ROV for Visual Inspection of Concrete Pier Superstructure

The ROV for visual inspection of concrete pier superstructure, named ROV-PARI, consists of an underwater vehicle platform and the camera system intended for concreate superstructure shooting. This is a semi-submersible ROV with a camera mounted on the top of the underwater vehicle platform and floats on the side. With this configuration, the distance from the center of buoyancy to the center of gravity can be extended, and so the ROV ensured stability against hull fluctuation.

The underwater vehicle platform is a movable body with payload part and a device extension function. It is equipped with an underwater camera and six underwater propulsor units, and can be also used as a general ROV that can dive up to 200m by itself. The underwater camera of the underwater vehicle platform and the two aerial cameras in front and behind make a wide field of view when operating as ROV-PARI.

The camera system intended for the superstructure shooting is equipped with one GigE camera for preview and image processing and one digital single-lens reflex camera (DSLR) for inspection images facing upward. It is as tolerant to low-light and deposits as humans.

In addition, ROV-PARI is equipped with LRF (Laser Range Finder) in order to grasp the situation of obstacles around itself, and a directional gyro is installed for the

ROV's own heading estimation. The scanning results obtained from the two LRFs are combined to form the omnidirectional scanning result and be imaged, and pier piles are detected by image processing, and its position information are used. The positions of these detected piles and the piles in the map database are collated, the collated piles are regarded as landmarks, and the ROV's own position and heading seen from the position of the landmarks are estimated by inverse calculation. In the case that the number of collated piles is less than two, the ROV's own heading is estimated by the directional gyro. Moreover, the ROV's own position and direction are measured using a GPS compass on the sea outside piers.

Therefore, attaching the position information to the obtained pictures, it is possible to manage the inspection position. Figure 1 shows ROV-PARI, and Table 1 shows the specifications.

a) ROV-PARI

b) Camera system with glass surface cleaning function

Figure 1. The ROV for visual inspection of concrete pier superstructure

Table 1. Specifications of ROV-PARI (2019)

Items	Specifications
Cameras	<u>For navigation</u> GigE* camera with pan, tilt, AF and zoom×1 in-water (forward) GigE* cameras with pan, tilt, AF and zoom×2 in-air (forward and backward)
	<u>For inspection</u> GigE* camera×1 (f=3.5) for preview and image processing Full-size DSLR** camera (f=14mm)×1
Lights	Forward Dimmable LED 1W×12 Upward LED with 80deg diffuser×8
Sensors	<u>On ROV platform</u> Pressure gauge×1 Direction sensor×1 (magnetic compass + MEMS gyroscope)
	<u>On upward camera system</u> Laser Distance meter×1 Laser marker×1 (2pts, W=250mm) LRF***×2 (270deg) Directional gyroscope (FOG****)×1 GPS compass×1
Thrusters	Forward and side thrusters 200W×4 Vertical thrusters 200W×2
Performance	Maximum speed: about 1.5kts
Other functions	Direction keeping, Depth keeping (ROV platform only) Power outlet×8 (selected from DC5V50W, 12V100W, 24V400W) Universal I/O port×8 (selected from LAN 1000BASE-T, RS232C) Autonomous collision avoidance Positioning under slabs using LRFs
Dimension	L1200×W800×H925 except lugs
Mass	About 100kg without ballasts and optional devices

*GigE; Gigabit Ethernet
**DSLR; Digital Single-lens Reflex
***LRF; Laser Range Finder
****FOG; Fiber Optic Gyro

Figure 2 shows usage situations of the ROV equipped with tele-operation assistance functions. a) shows lifting recovery of the ROV using cage without rigging, and b) shows situation of the ROV operation by onshore equipment.

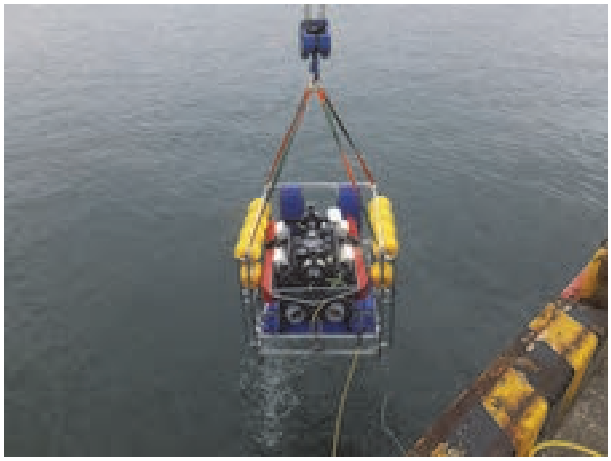

a) Lifting recovery of ROV-PARI using cage without rigging

b) Situation of ROV-PARI operation by onshore equipment

c) Automatic shooting underside of pier superstructure

Figure 2. Usage situations of ROV-PARI

3 Work Support Functions

3.1 Software for In-situ the ROV-PARI Operation

The ROV is remotely operated while confirming the shooting position on the software for in-situ ROV-PARI operation onshore. Figure 3 shows the screenshot of the software used by operators.

In order to support the operation and navigation of the ROV by the operator, the software presents the ROV position information and surrounding obstacles information in real time. This figure is a screenshot while actual operation in the field verification test. Operation panels are prepared on the left side of the window, and various support functions can be used by checking the necessary functions. The main functions are described below:

- CamConPanel: Shooting interval setting. Checking “HIGH” is 1 second, and “MIDDLE” is 2 seconds.
- INSTRUMENTS: Power control of each of the following devices: “CAMERA (all upward cameras)”, “O-GYRO (optical-gyro)”, “LRF (Lase Range Finder)”, “DISTANCE (distance meter)”. LRFs and distance meter are indispensable devices for making after-mentioned “COLLISION AVOIDANCE” and “FOOT PRINT” work.
- GPS COMPASS: Checking “GPS”, it is possible to measure the position and heading of the ROV on the sea outside piers. Mainly used for initial position setting before approaching under pier.
- A-CAS: Autonomous Collision Avoidance System. Measuring positional relationship with obstacles detected by LRFs, the ROV avoids collision with obstacles autonomously. The avoidance action is added to human operation. Checking “UP LINK”, onshore equipment and the ROV are connected. Checking “COLLISION AVOIDANCE”, the function is working.
- REC: Recording logs. Checking “REC LOG”, log recording and interval shooting are started.
- SHOOTIN: Shooting functions. Blue line rectangle is shooting area calculated by shooting distance and optical system of camera, and fill the shoot area. Checking “FOOT PRINT”, shooting history is presented. On “ERASE EP” button down, shooting history is reset. On “ONE SHOT” button down, one picture is shoot manually.

On the lower left side of the screen, an image of the underside of the pier superstructure taken by the GigE camera for preview described in Chapter 2 among the two upper cameras installed is constantly displayed. This shooting area is slightly narrower than the area of DSLR for inspection images.

On the lower right side of the screen, the all-around scanning image obtained by LRFs is displayed. Namely, measuring the relative positional relationship with surrounding objects and obstacles obtained by all-around scanning is calculated, and the result is always displayed in heading-up. Using the relative position information of the closest and second closet piles, shown in Figure 3 as pink and orange piles respectively, the position of the ROV is estimated from the relative position with the closest pile, and the heading is estimated from the angle between the line segment of the closest-the second closet piles and the ROV itself. The positioning function is described in Section 3.2.

In addition, since the all-around scanning result using LRFs are obtained while the positioning process, not only the piles but also the surrounding obstacles are observed. The collision avoidance direction and the level are presented by measuring the relative positional relationship with surrounding objects, and the autonomous collision avoidance behaviour is performed based on this information. The autonomous collision avoidance function is described in Section 3.3.

On the top of the screen is a map created from the prepared pile placement information. By displaying the ROV on this map based on the previous positioning result, the operator can grasp the current position of the ROV under the pier superstructure, and the reliable operation of the ROV along the pre-planned inspection route is possible. Blue line rectangle is shooting area, and filled it is presented as shooting history. In the figure, the filled area in light grey is the captured area. It is possible to easily distinguish captured area and the uncaptured area underside of the pier superstructure in real time, and toto present the omission of shooting. The shooting history presentation is described in Section 3.4.

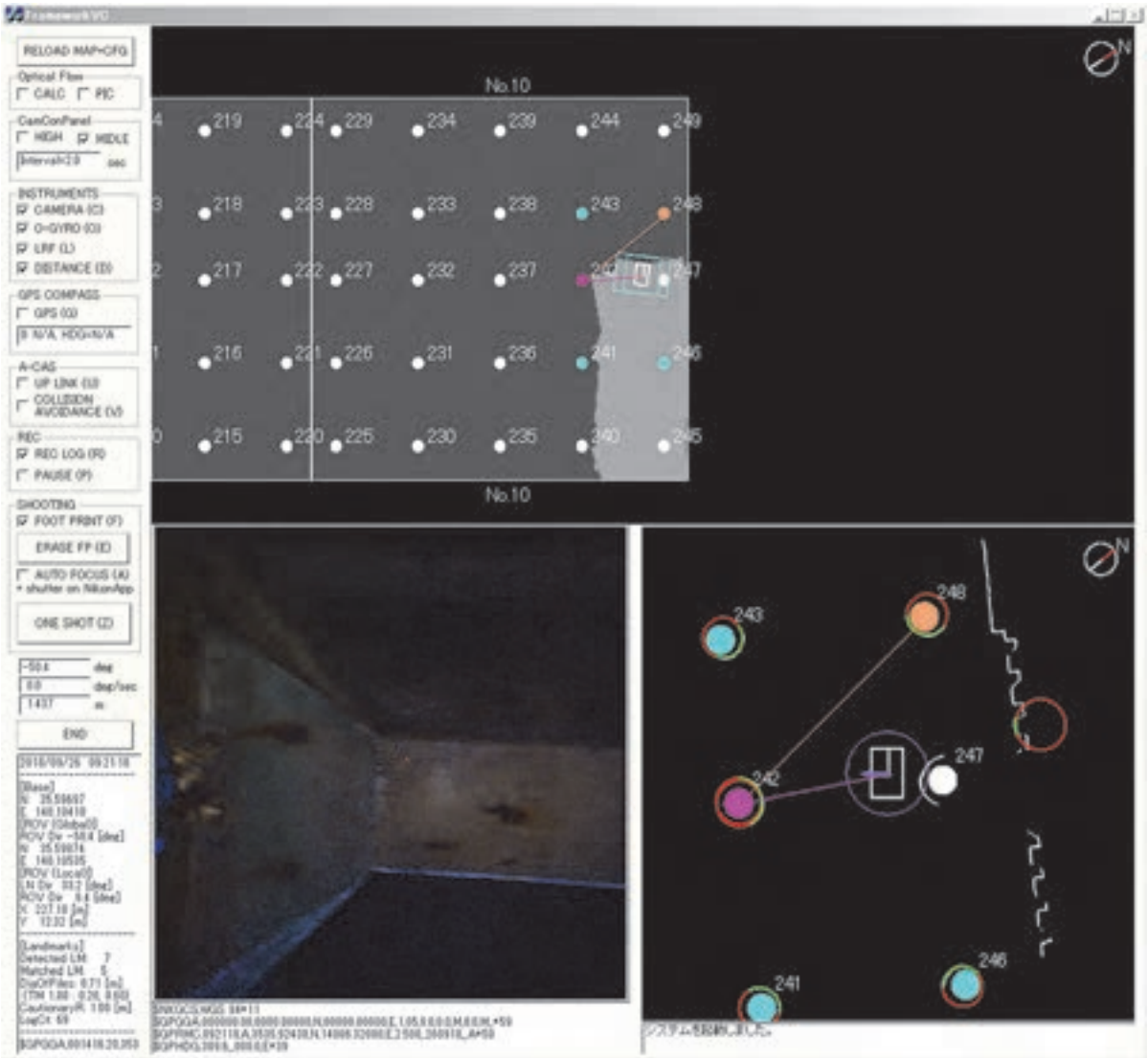

Figure 3. Screenshot of software for in-situ ROV-PARI operation

3.2 Positioning under Pier Superstructures

First, the scanning results obtained by the two LRFs are combined to make an all-around scanning result and is imaged. Next, the piles are detected from the image by image processing, and the position information are used. In fact, the positions of these detected piles and the piles in the map database are collated, the collated piles are regarded as landmarks, and the ROV's own position and heading seen from the position of the landmarks are estimated by inverse calculation.

When there are two or more Matched piles that succeeded in matching the position of the "detected objects" of circular cross-sectional shape by image processing from the scanning image with the position of the piles in the map database, the matched pile proximate to the ROV is "reference point for positioning" (Pink circle in Figure 3) and positioning of the ROV's own position is conducted relative to the point (Pink line in Figure 3). Next, the matched pile secondly proximate to the ROV is the "auxiliary point for azimuth estimation"(Orange circle in Figure 3.), and the heading of the ROV is estimated from the angle between the baseline connecting the positioning reference point and the azimuth estimation auxiliary point (Orange line in Figure 3) and the ROV. In case that the number of matched piles is less than one, the heading estimation is switched to the gyro-base. In case that there is no matched pile, the position estimation of the ROV is allowed to be switched to inertial navigation.

The mathematical presentations of the positioning are shown in the following sections. The first and second axes of the ROV coordinate system are the Roll and Pitch axes on the horizontal plane, and the third axis is the vertically downward Yaw axis, respectively.

The first and second axes of the local map coordinate system are the axis parallel to the face line of the wharf and the orthogonal axis that land side is positive on the horizontal plane, and the third axis is vertically upward, respectively. The first and second axes of the world coordinate system are north latitude and east longitude, and the third axis is vertically downward, respectively. However, all coordinate systems are positive-oriented.

3.2.1 Position on a Local Map Coordinate System

Each positional vector of the piles is defined in Equation (1). Here, the left-superscripts of the variables represent the coordinate systems, and the right-subscripts of the variables represent the objects. Bolds represent vectors or matrices.

$$
\begin{aligned}
&{}^{\mathrm{ROV}}\boldsymbol{P}_{\mathrm{MAP}_k},\ {}^{\mathrm{MAP}}\boldsymbol{P}_{\mathrm{MAP}_k} &&: \text{Piles positions}\\
&{}^{\mathrm{ROV}}\boldsymbol{P}_{\mathrm{RES}_j},\ {}^{\mathrm{MAP}}\boldsymbol{P}_{\mathrm{RES}_j} &&: \text{DP positions}\\
&{}^{\mathrm{ROV}}\boldsymbol{P}_{\mathrm{RES}_{P_i}},\ {}^{\mathrm{MAP}}\boldsymbol{P}_{\mathrm{RES}_{P_i}} &&: \text{MP positions}\\
&{}^{\mathrm{ROV}}\boldsymbol{P}_{\mathrm{MAP}_{Q_i}},\ {}^{\mathrm{MAP}}\boldsymbol{P}_{\mathrm{MAP}_{Q_i}} &&: \text{MP positoin on the local map}
\end{aligned}
\tag{1}
$$

Here, the position of the detected pile j is compared with that of the pile k on the map database, and if the norm between them is less than or equal to a threshold, the detected pile j is regarded as the pile k, and is becomes the matched pile i. In addition, P_i is an index which sorted i in near order to the ROV, and Q_i is the index corresponding to P_i on the map database. After that, P_1 and Q_1 are the index of the proximate matching piles to the ROV, and regarded as positioning reference points, then P_2 and Q_2 are the index of the secondly proximate matching pile to the ROV, and are regarded as auxiliary points for azimuth estimation. The heading and positional vectors of the ROV are defined in Equation (2).

$$
\begin{aligned}
&{}^{\mathrm{ROV}}\theta_{\mathrm{MAP}}: \text{Angle btween first axes of ROV and MAP}\\
&{}^{\mathrm{MAP}}\theta_{\mathrm{ROV}}: \text{Angle between first axes of MAP and ROV}\\
&{}^{\mathrm{ROV}}\theta_{\mathrm{RES}_{P_1\to P_2}}: \text{Angle between ROV and segment RES}_{P_1\to P_2}\\
&{}^{\mathrm{MAP}}\theta_{\mathrm{MAP}_{Q_1\to Q_2}}: \text{Angle between MAP and segment MAP}_{Q_1\to Q_2}\\
&{}^{\mathrm{ROV}}\boldsymbol{P}_{\mathrm{ROV}},\ {}^{\mathrm{MAP}}\boldsymbol{P}_{\mathrm{ROV}}: \text{Positioal vectors of the ROV}\\
&\boldsymbol{R}_1(\theta): \text{Rotation matrix. The subscript is rotational axis}\\
&\qquad \text{, and the argument is rotational angle.}\\
&\text{where,}\quad {}^{\mathrm{ROV}}\boldsymbol{P}_{\mathrm{ROV}} \equiv \boldsymbol{O}
\end{aligned}
\tag{2}
$$

From the above definition, if there are two or more matching piles, heading of the ROV ${}^{\mathrm{MAP}}\theta_{\mathrm{ROV}}$ in the local map coordinate system can be estimated by using the positioning reference point and the auxiliary point for azimuth estimation from Equation (3) [1].

$$
\begin{aligned}
{}^{\mathrm{ROV}}\theta_{\mathrm{RES}_{P_1\to P_2}} &= \operatorname{atan2}\left(\frac{{}^{\mathrm{ROV}}y_{\mathrm{RES}_{P_2}} - {}^{\mathrm{ROV}}y_{\mathrm{RES}_{P_1}}}{{}^{\mathrm{ROV}}x_{\mathrm{RES}_{P_2}} - {}^{\mathrm{ROV}}x_{\mathrm{RES}_{P_1}}}\right)\\
{}^{\mathrm{MAP}}\theta_{\mathrm{MAP}_{Q_1\to Q_2}} &= \operatorname{atan2}\left(\frac{{}^{\mathrm{MAP}}y_{\mathrm{MAP}_{Q_2}} - {}^{\mathrm{MAP}}y_{\mathrm{MAP}_{Q_1}}}{{}^{\mathrm{MAP}}x_{\mathrm{MAP}_{Q_2}} - {}^{\mathrm{MAP}}x_{\mathrm{MAP}_{Q_1}}}\right)\\
{}^{\mathrm{ROV}}\theta_{\mathrm{MAP}} &= {}^{\mathrm{ROV}}\theta_{\mathrm{RES}_{P_1\to P_2}} - {}^{\mathrm{MAP}}\theta_{\mathrm{MAP}_{Q_1\to Q_2}}\\
{}^{\mathrm{MAP}}\theta_{\mathrm{ROV}} &= {}^{\mathrm{MAP}}\theta_{\mathrm{ROV}_{inc}} = -{}^{\mathrm{ROV}}\theta_{\mathrm{MAP}}
\end{aligned}
\tag{3}
$$

If Equation (3) cannot be used because the number of matched piles is less than 1, it is possible to seamlessly switch the heading source from Equation (3) to ${}^{\mathrm{MAP}}\theta_{\mathrm{ROV}_{inc}}$ and to estimate ${}^{\mathrm{MAP}}\theta_{\mathrm{ROV}}$ by initializing the heading ${}^{\mathrm{MAP}}\theta_{\mathrm{ROV}_{inc}}$ by the directional gyro with ${}^{\mathrm{ROV}}\theta_{\mathrm{MAP}}$ while the heading ${}^{\mathrm{ROV}}\theta_{\mathrm{MAP}}$ can be estimated by Equation (3).

Next, the relative positioning method of the ROV position in the local map coordinate system is described. Here, the ROV position vector ${}^{\mathrm{MAP}}\boldsymbol{P}_{\mathrm{ROV}}$ in the local map coordinate system is calculated by Equation (4) using the estimated heading and the positional vector of the positioning reference point.

$$
\begin{aligned}
\begin{pmatrix} {}^{\mathrm{MAP}}\boldsymbol{P}_{\mathrm{ROV}} \\ 1 \end{pmatrix} &= \begin{pmatrix} \boldsymbol{R}_3\left({}^{\mathrm{MAP}}\theta_{\mathrm{ROV}}\right) & {}^{\mathrm{MAP}}\boldsymbol{P}_{\mathrm{MAP}_{Q_1}} \\ \boldsymbol{O}^T & 1 \end{pmatrix} \begin{pmatrix} -{}^{\mathrm{ROV}}\boldsymbol{P}_{\mathrm{RES}_{P_1}} \\ 1 \end{pmatrix}\\
{}^{\mathrm{MAP}}\boldsymbol{P}_{\mathrm{ROV}} &= \boldsymbol{R}_3\left({}^{\mathrm{MAP}}\theta_{\mathrm{ROV}}\right)\left(-{}^{\mathrm{ROV}}\boldsymbol{P}_{\mathrm{RES}_{P_1}}\right) + {}^{\mathrm{MAP}}\boldsymbol{P}_{\mathrm{MAP}_{Q_1}}
\end{aligned}
\tag{4}
$$

If the number of matched piles is less than one, the heading estimation is switched to the gyro-base. If there are no matched piles, the positional estimation is allowable to be switched to inertial navigation and so on.

Finally, using the positional vectors and heading of the ROV estimated, the positional vectors of piles on the map database in the ROV coordinate system is updated by Equation (5). As a result, the new detected piles and the new map database can be collated even in the next positioning step, and positioning can be continued.

$$^{\mathrm{ROV}}\boldsymbol{P}_{\mathrm{MAP}_k} = \boldsymbol{R}_3(^{\mathrm{ROV}}\theta_{\mathrm{MAP}})(^{\mathrm{MAP}}\boldsymbol{P}_{\mathrm{MAP}_k} - ^{\mathrm{MAP}}\boldsymbol{P}_{\mathrm{ROV}}) \quad (5)$$

3.2.2 Transform to the World Coordinate System

Positional vector of the origin of the local map coordinate system $^{\mathrm{MAP}}\boldsymbol{P}_{\mathrm{MAP}} \equiv \boldsymbol{O}$ is $^{\mathrm{W}}\boldsymbol{P}_{\mathrm{MAP}}$ in world coordinate system, and the inclination of the local map coordinate system with respect to the world coordinate system is direction of face line of the wharf $^{\mathrm{W}}\theta_{\mathrm{MAP}}$. Transformation to world coordinate system of $^{\mathrm{MAP}}\boldsymbol{P}_{\mathrm{ROV}}$ estimated by Equation (4) is represented by rotation trough $^{\mathrm{W}}\theta_{\mathrm{MAP}}$ about third axis, multiplying by meter-lat/long transformation matrix $\boldsymbol{L}$, and parallel translation $^{\mathrm{W}}\boldsymbol{P}_{\mathrm{MAP}}$ [1].

The equation for conversion the positional vector of the ROV $^{\mathrm{MAP}}\boldsymbol{P}_{\mathrm{ROV}}$ in the local map coordinate system to world coordinate system is shown in Equation (6).

$$\begin{pmatrix} ^{\mathrm{W}}\boldsymbol{P}_{\mathrm{ROV}} \\ 1 \end{pmatrix} = \begin{pmatrix} \boldsymbol{L} & \boldsymbol{O} \\ \boldsymbol{O}^T & 1 \end{pmatrix} \begin{pmatrix} \boldsymbol{R}_3(^{\mathrm{W}}\theta_{\mathrm{MAP}}) & ^{\mathrm{W}}\boldsymbol{P}_{\mathrm{MAP}} \\ \boldsymbol{O}^T & 1 \end{pmatrix} \begin{pmatrix} \boldsymbol{R}_1(\pi) \cdot ^{\mathrm{MAP}}\boldsymbol{P}_{\mathrm{ROV}} \\ 1 \end{pmatrix} \quad (6)$$
$$^{\mathrm{W}}\boldsymbol{P}_{\mathrm{ROV}} = \boldsymbol{L} \cdot \boldsymbol{R}_3(^{\mathrm{W}}\theta_{\mathrm{MAP}})(\boldsymbol{R}_1(\pi) \cdot ^{\mathrm{MAP}}\boldsymbol{P}_{\mathrm{ROV}}) + ^{\mathrm{W}}\boldsymbol{P}_{\mathrm{MAP}}$$

According to the Chronological Scientific Tables (NAOJ), the length $\Delta l_{\mathrm{LAT}}[\mathrm{m/deg}]$ corresponding to a latitude of 1deg depending on the geographical latitude φ and the length $\Delta l_{\mathrm{LON}}[\mathrm{m/deg}]$ corresponding to a longitude of 1deg are approximately expressed by the Equation (7).

Therefore, the meter-lat/long transformation matrix $\boldsymbol{L}$ around geographical latitude φ and in the vicinity of $^{\mathrm{W}}\boldsymbol{P}_{\mathrm{MAP}}$ is given by Equation (8). If GRS 80 is applied as an earth ellipsoid model, the equatorial radius a is 6 378 137m, and the ellipticity f is 1/298.257 222 101. Moreover, the eccentricity of the earth ellipsoid e is $\sqrt{f(2-f)}$, and e^2 is an approximate value of 0.006 694 380 022 900 788.

$$\Delta l_{\mathrm{LAT}} \approx {}^{\pi}/_{180} \cdot {}^{a(1-e^2)}/_{(1-e^2\sin^2\varphi)^{3/2}}$$
$$\Delta l_{\mathrm{LON}} \approx {}^{\pi}/_{180} \cdot {}^{a\cos\varphi}/_{\sqrt{1-e^2\sin^2\varphi}} \quad (7)$$

$$\boldsymbol{L} = \begin{pmatrix} 1/\Delta l_{\mathrm{LAT}} & 0 & 0 \\ 0 & 1/\Delta l_{\mathrm{LON}} & 0 \\ 0 & 0 & 1 \end{pmatrix} \quad (8)$$

3.2.3 Correspondence between Shooting Position Information and Obtained Pictures

Two methods are prepared regarding the correspondence between the obtained pictures and the shooting-attribute information such as shooting position. One is directly attaching to the picture data on real-time and another one is recording in a log file synchronized with the shooting time.

The first method is to convert the latitude and longitude position information in world coordinate system calculated by Equation (6) into NMEA0183-compliant packet information and pass it directly to the camera at the same time as shooting. The shooting date and time, shooting direction, shooting position, and so on are directly written in the Exif GPS IFD tag in the picture data, then it is possible integrally to manage and to utilize the obtained pictures in conjunction with shooting position on a map-linked photo viewer or GIS application.

The second method is to prepare a log file synchronized with the shooting, and record the shooting date and time, shooting direction, shooting position, and so on at the same time of shooting in the file. Here, in addition to the latitude and longitude position information in world coordinate system recorded of the first method, the position information in the local map coordinate system with higher resolution calculated by Equation (4) is also recorded. it is possible to utilize highly accurate position information on the local map coordinate system, and it makes easy to secondary use of obtained pictures using shooting position such as making development view using the obtained pictures.

3.3 Avoidance Direction and Autonomous Collision Avoidance Function

Collision avoidance direction is presented on the operation screen in order to support remote control of the ROV. First, the distance L_{LRF_θ} from the ROV to the first reflection points all-around direction observed by two LRFs are obtained. Next, as shown in Figure 4, an alert circle (broken line) with radius R_{margin} is set around the ROV, the weight w_θ in each direction is calculated by Equation (9) according to the magnitude relationship of L_{LRF_θ} and R_{margin}.

As a result, the avoidance direction vector $^{\mathrm{ROV}}\boldsymbol{A}_{\mathrm{LRF}}$ in the ROV coordinate system is calculated by the Equation (9) according to multiply the unit vector $\boldsymbol{e}_\theta$ of each direction by the weight w_θ and taking the sum [1].

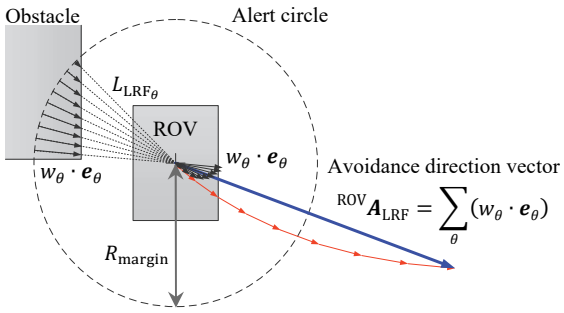

Figure 4. Calculation of collision avoidance direction based on the LRFs

$$
{}^{\mathrm{ROV}}\boldsymbol{A}_{\mathrm{LRF}} = \sum_{\theta}(w_{\theta} \cdot \boldsymbol{e}_{\theta})
$$
$$
\text{where,}\quad w_{\theta} = \begin{cases} -\frac{R_{\mathrm{margin}} - L_{\mathrm{LRF}_{\theta}}}{R_{\mathrm{margin}}} & \left(\text{if } L_{\mathrm{LRF}_{\theta}} \le R_{\mathrm{margin}}\right) \\ 0 & \left(\text{if } L_{\mathrm{LRF}_{\theta}} > R_{\mathrm{margin}}\right) \end{cases} \tag{9}
$$

Here, since the collision avoidance direction is indicated by ${}^{\mathrm{ROV}}\boldsymbol{A}_{\mathrm{LRF}}$, the collision avoidance behaviour vector ${}^{\mathrm{ROV}}\boldsymbol{B}_{\mathrm{LRF}}$ is multiplied by the gain G, and expressed by Equation (10).

$$
{}^{\mathrm{ROV}}\boldsymbol{B}_{\mathrm{LRF}} = G \cdot {}^{\mathrm{ROV}}\boldsymbol{A}_{\mathrm{LRF}} \tag{10}
$$

In addition, the ROV always receives the normalized navigation vector ${}^{\mathrm{ROV}}\boldsymbol{B}_{\mathrm{JOY}}$ by the joystick operation. Therefore, the total navigation vector ${}^{\mathrm{ROV}}\boldsymbol{B}_{\mathrm{TOTAL}}$ of the ROV is expressed by Equation (11) with saturation condition according that the collision avoidance behaviour vector ${}^{\mathrm{ROV}}\boldsymbol{B}_{\mathrm{LRF}}$ is added to the navigation vector ${}^{\mathrm{ROV}}\boldsymbol{B}_{\mathrm{JOY}}$ [2].

$$
{}^{\mathrm{ROV}}\boldsymbol{B}_{\mathrm{TOTAL}} = \begin{cases} {}^{\mathrm{ROV}}\boldsymbol{B}_{\mathrm{JOY}} + {}^{\mathrm{ROV}}\boldsymbol{B}_{\mathrm{LRF}} & \left(\text{if } \left|{}^{\mathrm{ROV}}\boldsymbol{B}_{\mathrm{JOY}} + {}^{\mathrm{ROV}}\boldsymbol{B}_{\mathrm{LRF}}\right| \le 1\right) \\ \frac{{}^{\mathrm{ROV}}\boldsymbol{B}_{\mathrm{JOY}} + {}^{\mathrm{ROV}}\boldsymbol{B}_{\mathrm{LRF}}}{\left|{}^{\mathrm{ROV}}\boldsymbol{B}_{\mathrm{JOY}} + {}^{\mathrm{ROV}}\boldsymbol{B}_{\mathrm{LRF}}\right|} & \left(\text{if } \left|{}^{\mathrm{ROV}}\boldsymbol{B}_{\mathrm{JOY}} + {}^{\mathrm{ROV}}\boldsymbol{B}_{\mathrm{LRF}}\right| > 1\right) \end{cases} \tag{11}
$$

However, the upper limit of the collision avoidance behaviour vector ${}^{\mathrm{ROV}}\boldsymbol{B}_{\mathrm{LRF}}$ is set to 50% of the total navigation vector in order to avoid out of control while collision avoidance (Equation 12).

$$
{}^{\mathrm{ROV}}\boldsymbol{B}_{\mathrm{LRF}} = \begin{cases} G \cdot {}^{\mathrm{ROV}}\boldsymbol{A}_{\mathrm{LRF}} & \left(\text{if } \left|G \cdot {}^{\mathrm{ROV}}\boldsymbol{A}_{\mathrm{LRF}}\right| \le 0.5\right) \\ 0.5 \cdot \frac{{}^{\mathrm{ROV}}\boldsymbol{A}_{\mathrm{LRF}}}{\left|{}^{\mathrm{ROV}}\boldsymbol{A}_{\mathrm{LRF}}\right|} & \left(\text{if } \left|G \cdot {}^{\mathrm{ROV}}\boldsymbol{A}_{\mathrm{LRF}}\right| > 0.5\right) \end{cases} \tag{12}
$$

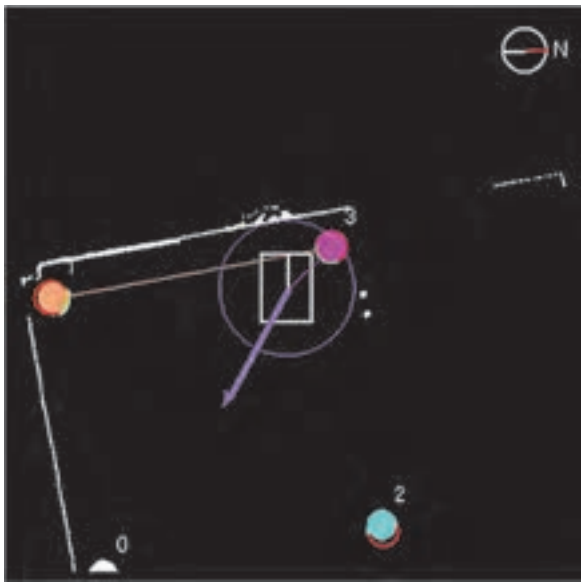

Figure 5. Autonomous collision avoidance behaviour of the ROV

The autonomous collision avoidance behaviour of the ROV is shown in Figure 5. In this figure, the collision avoidance direction has been calculated in response to penetration of the proximate pink pile into the alert-circle-area, and the ROV avoids collision with the pile autonomously.

3.4 Presentation of Shooting History

The picture displayed in the upper part of the in-situ operation application in Figure 3 is the navigation window that displays the ROV on the map database of the piles layout. The operator grasps the current position of the ROV from the information on this window and operates the ROV along the planned inspection route.
The blue line rectangular surrounding the ROV indicates the shooting area of the inspection camera, and the shooting history is presented by leaving the filled shooting area as footprints. In the figure, the filled area in light gray is the captured area. With this function, it is possible to easily distinguish the captured area and the uncaptured area on the underside of the pier superstructure in real time, and it is possible to prevent shooting omissions.

Here, in case of angle of view θ, φ[deg] (horizontal, vertical), shooting distance D[mm], focal length F[mm], sensor size W_s, H_s[mm] (horizontal, vertical), the filled-in area W, H[mm] (horizontal, vertical) as the shooting history in one shooting is expressed multiplying the shooting area of the camera by the safety factor R by Equation (13) [3].

$$
W = 2D \cdot R\tan\theta/2\,,\quad H = 2D \cdot R\tan\varphi/2
$$
$$
\text{where,}\quad \tan\theta/2 = 0.5W_s/F\,,\quad \tan\varphi/2 = 0.5H_s/F \tag{13}
$$

An example of the presentation of the shooting history in field experiment to verify the effect is shown in Figure 6. On the other hand, Figure 7 shows a 3-D model of the pier superstructure constructed by SfM-MVS software from the obtained pictures corresponding to the shooting history.

Both pictures are perspective view looking down the pier superstructure vertically. Comparing shooting history in Figure 6 and the 3-D model in Figure 7, each uncaptured area is the same.

3.5 Effectiveness of Introducing the Developed Technologies

Authors have conducted several field tests for the verification of the developed technologies to date. The proposed method using the technologies is secure and safety because there are no inspectors on the sea.

The proposed method performed well in every test although obtained information were increased. And, one of results showed more than fourfold efficiency on site work to the conventional method by inspectors [4].

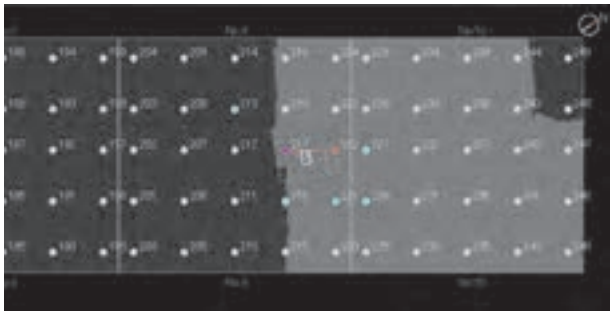

Figure 6. Foot-print of the shooting history

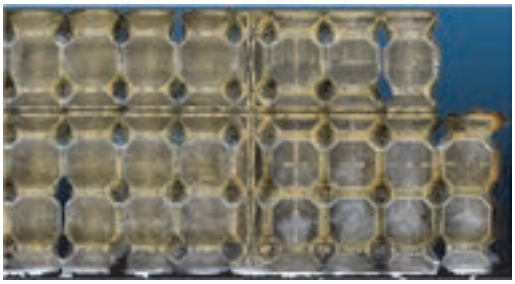

Figure 7. 3-D model concrete pier superstructure constructed by SfM-MVS photogrammetry

4 Inspection and Diagnosis Support System

An inspection and diagnosis support system was also developed for supporting the work to make inspection reports because of obtaining an enormous inspection picture by introduction of the ROV to field work [4][5].

First, 3-D model of the underside of the pier superstructure is composite from obtained pictures using commercially SfM-MVS (Structure from Motion-Multi View Stereo) software. The SfM-MVS technology is a general-purpose technology recently applied to drone photogrammetry and shape measurement of structures.

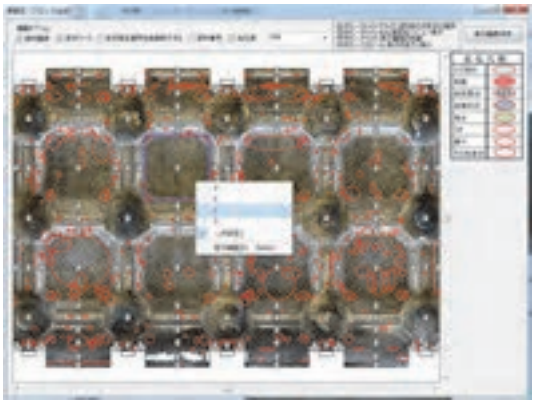

Figure 8. 2-D development view and candidates of suspected deterioration on the support system

2-D development view for each member is automatically created from 3-D model by the inspection and diagnosis support system, and the location that have the possibility of deterioration are automatically detected from the development view in Figure 8. The user distinguishes the position and deterioration type from the detected objects, and classifies the deterioration of the target member as grades a, b, c or d. The inspection report is automatically created based on the distinguished deterioration.

5 Conclusions

This paper reported the ROV for visual inspection of concrete pier superstructure, work support functions for ROV operation, and the inspection and diagnosis support system to save the related work. These are considered to have largely reached a practical level technically

These results promise a certain level of contribution to the improvement of safety and efficiency of the work. Development of linking tool with BIM/CIM is current in progress in order to further improve convenience of them.

Acknowledgements

This work was supported by the Infrastructure Maintenance, Renovation, and Management program of the Cross-Ministerial Strategic Innovation Promotion Program (SIP), which is sponsored by the Council for Science, Technology and Innovation, and funded by the Japan Science & Technology Agency (JST).

References

[1] Tanaka T. et al. Field experiments of positioning and shooting system equipped in inspection vehicle for concrete superstructure of piled pier. In *Proc. the 17th SCR*, O-54, 2017 (in Japanese, USB).

[2] Tanaka T. et al. Enhancement of tele-operation assistance functions of inspection vehicle for concrete superstructure of piled pier. In *Proc. the 18th SCR*, O4-2, 2018 (in Japanese, USB).

[3] Tanaka T. et al. Field test of ROV equipped with tele-operation assistance functions for inspection of concrete pier superstructure. In *Proc. the 19th SCR*, O2-5, 2019 (in Japanese, USB).

[4] Nogami S. et al. Improvement of inspection and diagnosis of concrete pier superstructure by Remotely Operated Vehicle and diagnosis support software. In *Proc. the 74th annual conference of the JSCE*. VI-770, 2019 (in Japanese, DVD-R).

[5] Kato E. et al. Demonstration test for improvement of inspection and diagnosis of concrete pier superstructure by remotely operated vehicle. In *Proc. the 3rd ACF symposium*, S5-3-1, 2019 (USB).

An automated Approach to Digitise Railway Bridges

M. Al-Adhami[a], S. Rooble[b], S. Wu[c], C. Osuna-Yevenes[b], V. Ruby-Lewis[b], M. Greatrix[b], Y. Cartagena[a], and S. Talebi

[a]School of Art, Design and Architecture, University of Huddersfield, UK
[b]Waldeck consulting, UK
[c]School of Architecture and Built Environment, Nottingham Trent University
E-mail: mus.adhami@hud.ac.uk, sagal.rooble@waldeckconsulting.com, song.wu@ntu.ac.uk, clara.osuna-yevenes@waldeckconsulting.com, veronica.ruby-lewis@waldeckconsulting.com, mark.greatrix@waldeckconsulting.com, yreilyn.cartagenadelgado@hud.ac.uk , S.Talebi@hud.ac.uk

Abstract –

In the UK, the railing sector has a large number of ageing masonry bridges that need to be examined every year. The traditional inspection regime consists of visual observation with manually recording the defect information observed on the structure. Previous studies have shown that this method of inspection is not reliable, time-consuming, depends on the inspector's judgment and result in further costs to the inspection process. Thus, there is a need to revolutionise the current inspection regime and improve the efficiency and reliability of the acquired data.

The development of digital surveying technology such as terrestrial laser scanning (TLS) and progressions in innovative software techniques will support the production of accurate representation of any asset, this automation, which results in achieving a tangible survey of a physical asset in a digital environment. In this paper, a strategic approach for an effective solution to automating the traditional process of surveying and processing point cloud data is presented, with further automation of implementing an automated bridge generation approach to large and complex cloud data sets. The presented digital method will generate a digital asset from the point cloud, and this will support surveyors and engineers to identify defects through various digital means. The presented approach has been tested on real-life projects which have demonstrated time-saving workflow on generating digital assets. This research will demonstrate the effective automation of point cloud to producing a physical asset of a structure with the ability to produce BIM model.

Keywords –

Bridge automation; Inspection; Masonry bridge; Terrestrial scanning; Point clouds; Scan to BIM

1 Introduction

In the UK, infrastructure management is facing significant challenges due to ageing assets and increasing demand. In the railway sector, it is estimated that there are approximately 29000 bridges, 22000 retaining walls, 21000 culverts, 200 miles of coastal defence and 600 tunnels, which require regular examination. The current visual examination process involves deploying a large workforce onto unsafe sites to inspect and report upon the status of each bridge on the network. There is increasing demand to replace the current cumbersome process (resource-intensive, unsafe conditions, sub-optimal process) with a faster, safer, digitally-enabled process using digital operators for mostly off-site inspection, automatic defects detection supported by an automated process, such as machine learning.

Due to the ageing nature of the assets, the original design information is often not readily available. The immediate challenge of implementing the digital process is to reconstruct the 3D BIM model from the captured data on-site. This paper aims to address this challenge by proposing a practical solution to rapid reconstruct the 3D BIM model from the point cloud data captured by reality capture technology. A real-life project is presented to demonstrate the effectiveness of the solution.

2 Literature review

2.1 Reality capture technology

Reality capture technology for recording the state of the existing structure has been a focus of many studies [1, 2]. Several technologies have been used for digital surveying such as terrestrial laser scanning (TLS), Terrestrial video and photogrammetry technology, and Unmanned Aerial Vehicle (UAV). The precision of these technologies is varied, which make some of them better than others on different surveying scenarios. For example,

UAV is useful in post-disaster assessment, such as post-earthquake evaluation [3], tornado and hurricanes damage assessment [4], that could give a general damage identification of a structure as a whole [5].

TLS can provide detailed information about the structure with higher accuracy than photogrammetry and UAVs [6]. Zeibak-Shini et al. [6] claimed that the TLS was applicable for damage assessment on building element with better quality than the UAV scanning. In Spain, different digital surveying technologies were used to document the as-is state of heritage masonry arch bridge, static and mobile TLS integrated with a digital camera were able to provide high accuracy 3d digital model [7]. In the US, a study used pre- and post-event approach for damage assessment of buildings after a tornado, both aerial and TLS surveying technology were used to document the state of each building before and after the event to evaluate the damage caused to buildings [8]. In the same study, they have also estimated wind speed and path direction of the tornado using the same digital data.

TLS, terrestrial video, photogrammetry, and UAV can generate point clouds model of a scene, and other low-cost approaches have also been studied to generate the similar dataset such as digital photogrammetry technique called Structure-from-Motion (SfM) [9], Multi-View Stereopsis (MVS) [10], and the combination of both [11]. Even though the above techniques are able to reconstruct the surveyed structure in a 3D environment, none of them can automatically produce and recognise the structure at the component level that is required for a BIM model.

2.2 Scan to BIM – 3D reconstruction of BIM model

Scan to BIM is also known as Point cloud to BIM, the process aims to use point cloud data to generate BIM model [12]. Typically, the point cloud data is obtained by TLS, and the data is transferred to BIM tools such as Revit, Bentley, Graphisoft, to reconstruct a BIM model. The problem of reconstruction of the as-as infrastructure/building assets is not a new area of research [1, 2]. Currently, the scan to BIM process remains largely a manual process which is time-consuming and error-prone [3]. In recent years, researchers around the world have been investigating ways to automate the process, including automatic identification of objects from the geometric features [13].

Roberts et al. [14] developed a technique to digitally capture a physical space from various points using the data to create an intelligent 3D model. The process provides a vital starting point for design teams that use BIM to iterate their designs and then manage, coordinate, and share all of the project information.

In buildings, the reconstruction of interiors and exteriors using the laser scanner was the case of many studies [4-6]. Although many algorithms presented for model reconstruction, most of them emphasise on model creation for visualisation rather than the accuracy of the geometries. Furthermore, the algorithms do not recognise the identity of components such as floors, walls, and ceilings [7]. Macher et al. [3] presented a semi-automatic approach, and segmentation was performed, so that point clouds corresponding to grounds, ceilings, and walls can be established. The output of building components can then be integrated into BIM software using IFC format. In the outdoor environment, Bassier et al. [8] used random forests classifier to automatically identify structural elements such as floors, ceilings, roofs, walls, and beams.

In the infrastructure management sector, several algorithms for 3D data processing and modelling have been developed to achieve surveying goals [9]. One of the significant studies was presented by Sacks et al. [10], they developed a 3D engine to create a geometric model of the assets associated with the point cloud model. The engine was based on surface primitive extraction algorithm, component detection, and classification algorithm for detection and classification. A set of training data was also presented to establish the relationships between surface primitives and the integrated component. However, the BIM reconstruction process is still at its infancy in geometrical creation, particularly for non-standard components with complex geometry.

3 Bridge Scan to BIM approach

In recent years, many algorithms have been developed to extract planar patches from point data or to recognise and identify the components of a structure such as walls, ceilings, and floors [15]. However, very few studies have successfully demonstrated the practicality of rapid reconstructing bridges from point cloud data in a large scale. In this paper, the authors propose a component library based approach especially developed for masonry railway bridges.

The result of the approach is a rich BIM model generation tool that is capable of producing Autodesk Revit BIM model with all the required information about each component constituent of a bridge structure. Furthermore, the proposed system follows the end-user requirements for condition assessment of railway bridge structure to ensure the resulting BIM model is semantically rich and suitable for condition assessment.

In this paper, three key aspects have been considered during the development of the system.

1. From a practical point of view, it is essential to have both data from the survey and BIM in the same development environment, not only for BIM model

creation but also for component check and validation.
2. Clear definition of the relationships between the elements [16], i.e. bridge elementsneed to be connected in a logical format.
3. The output BIM model must comply with the international standard such as IFC schema.

The railway bridges have a wide variety of components in their geometrical shape, parameters, and position. For example, each bridge component from the same type could have different geometries, parameters, and positions within the overall structure, see Table 1.

Table 1. Different type of wing wall and connection to abutment

Image	Point cloud	BIM
		
		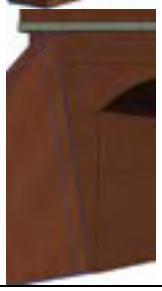

During the development, the authors recognise the relationships exists between the components in terms of the geometries, parameters and composition. As a result, a unique bridge component library is proposed to include all components and structural elements for bridges in order to reconstruct a bridge from point cloud data. A typical bridge can consist of several major components, such as Deck (DK), End Support (ES), and Intermediate supports (IS). Each major component is formed by several elements, such as Abutment, Wing wall, etc.

The bridge components and elements in the library are modelled based on the following protocols a) a logic of component reconstruction sequence, b) a number of required parameters for flexible geometries c) and relationships between components and elements. Figure 1 provides a high-level overview of the approach, which breaks the BIM reconstruction process into four stages.

In the first stage, a bridge component library is developed, and the bridge components and elements are categorised based on bridge condition marking index (BCMI) guideline. The BCMI helps develop a robust and flexible bridge component from a geometrical perspective that can be used in most bridges with a similar structure. The component library can be developed in standard BIM tools such as Autodesk Revit.

The second stage is to identify the component from the point cloud scene. It will examine if there is a new element, feature with the element, that is missing and/or not included in the library. This step is essential to maintain the library and keep it up to date with all components.

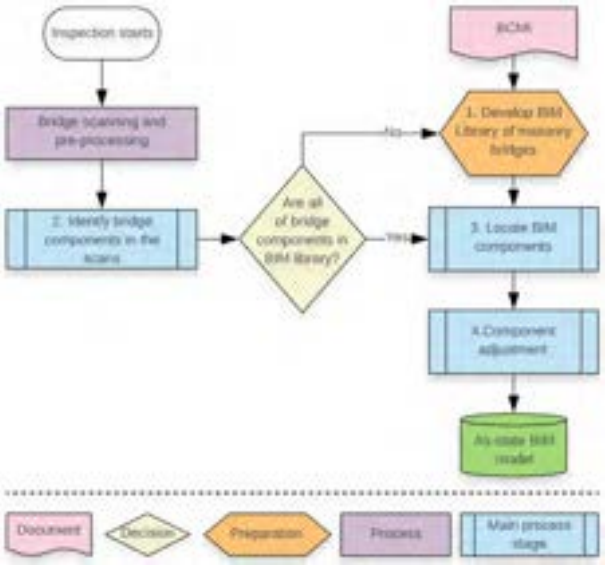

Figure 1. system overview

The third stage is to establish the position and orientation of individual components and elements of the bridge. The scanning provides a point cloud scene registered within a local coordinate system. The point cloud is then used to identify the spatial location of each bridge component. Moreover, the component's connection to other components in the whole structure can also be established based on the relationship rules in the library.

In the fourth stage, the bridge components are being reconstructed from elements in the library based on the information for previous stages. The parametric nature of each component and element gives the flexibility to adjust the geometries of the components based on the point cloud data. The algorithm will extract the required parameters of the individual components from the point cloud data. For the actual implementation, a set of algorithms is developed to connect all stages and interact with point cloud data and the component library.

The proposed approach has been tested on thirty railway bridges in the UK. In the following section, a brief description of the implementation on a single-span arch bridge is presented.

4 Implementation

The single-span arch bridge consists of three major components, Deck (DK), End Support (ES), and Intermediate supports (IS). Figure 2 shows the structural system of the single-span masonry arch bridge. Major and minor elements, names, and codes are explained in Table 2.

The process of data acquisition, BIM reconstruction, and the validation of the produced model are explained in the following sections.

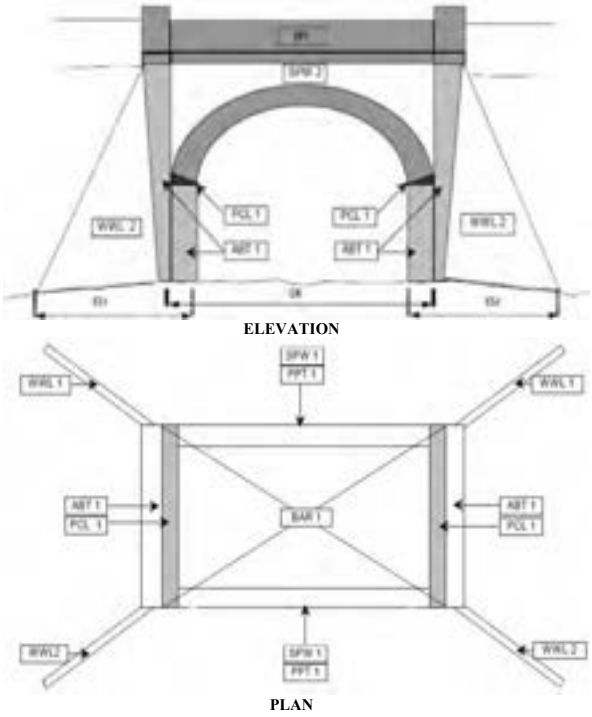

Figure 2. Single-span masonry arch bridge drawing

Table 2 elements in the single-span masonry arch bridge

Elements	Code
Abutment	ABT
Wing wall	WWL
Barrel arch	BAR
Spandrel wall	SPW
Parapet	PPT
Padstone	PCL

4.1 Data acquisition

For the single-span masonry arch bridge as shown in Figure 3, TLS is used for data acquisition. The site condition, weather condition, and other environmental conditions such as site access, traffic situation, vegetation, flooding, etc, are assessed before the scan. The scanning set-points are also planned in order to cover the entire structure.

Figure 3. Single-span masonry arch bridge

On-site, the survey team sets up a ground control point (GCP) for the project. A Global Navigation Satellite System (GNSS) is used to record the GCP in the Ordnance Survey National Grid (OSGB) reference system, and the resulting coordinates will be used in the processing of TLS data sets. The TLS scan is performed at every pre-planned set-point to capture 3D point cloud. The individual scans are then registered to each other using automated software to produce a dense point cloud model of the bridge.

4.2 BIM Reconstruction

In the proposed system, the BIM reconstruction algorithm process the point cloud data and generate a BIM model almost automatically. Moreover, the proposed system does not require a clean point cloud model (noise points such as people, trees in the scene, are not removed). However, a clean model can save processing time and produce better results. In the single-span masonry arch bridge, the scan by TLS has around 440million points (Figure 4).

Figure 4. The point cloud model of the bridge

The resulting 3D BIM model as shown in Figure 5 is a digital representation of the bridge which is formed by the components and the corresponding structural elements of a masonry arch bridge listed in Table 2.

The algorithm is able to identify the structural elements from the bridge point cloud scene. It assembles

bridge components of the elements associated with the point cloud of the structure from the component library. It also fetches the required parameters of each component to finetune the BIM component geometry to fit the point cloud.

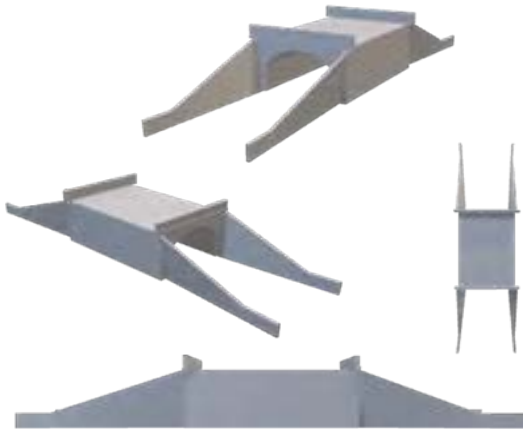

Figure 5. BIM model of the single-span arch bridge.

The algorithm would also position the bridge components following the density of the point cloud data and the relationships between components as shown in Figure 6

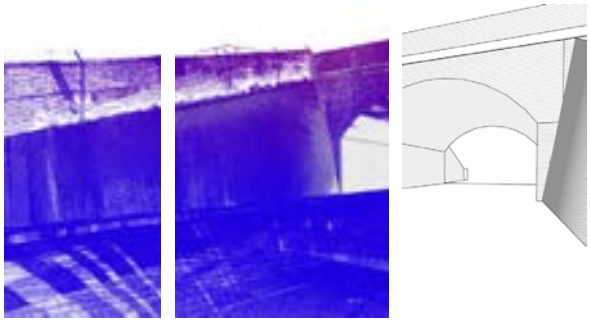

Figure 6. bridge reconstruction

4.3 Validation process

The output BIM model is in Autodesk Revit format that can be exported in IFC. The BIM model is validated in Verity, a construction verification software. Verity would check the point cloud against each bridge component. The visual verification reports show if the structural components are generated correctly within the required 50mm tolerance.

Figure 8 shows the BIM model of a Wing Wall (WWL) that is compared to the surveyed point cloud data under 50 mm tolerance. The colours in the model represent the distance of the points to the BIM component; green shows the perfect match while red is out of tolerance.

Figure 7 shows the results of bridge spandrel (SPW) to 50 mm tolerance. Although the SPW component passed the verification process, the result shows the point cloud does not fully match the BIM components. This could be because the BIM component is not flexible enough to fit the geometry of the bridge, or the point cloud model has too many noises that affect the verification process or both.

As previously mentioned, the system was validated with thirty bridges. Majority of the BIM models could meet the tolerance requirement. On occasion, the component would not line up with point cloud perfectly, and further adjustments are made to improve the accuracy of the bridge model.

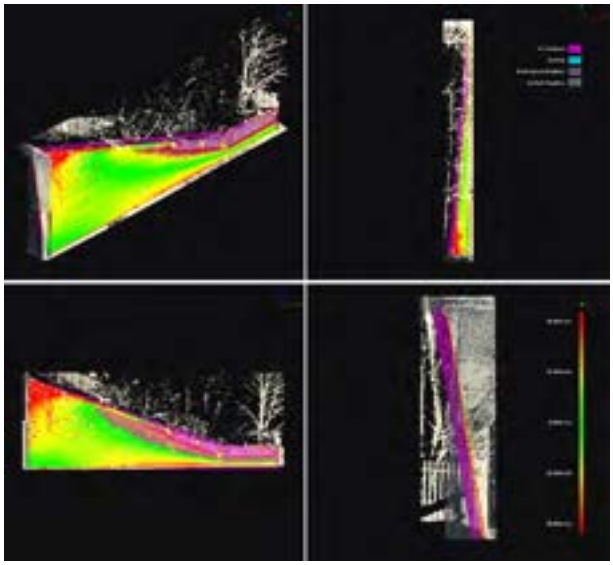

Figure 7. Verification results of the WWL

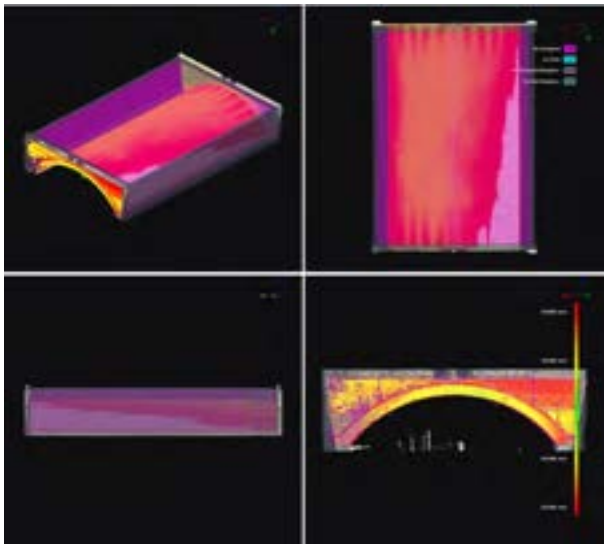

Figure 8. Verification results of SPW

5 Conclusion

Reality capture technology is a promising solution for bridge condition assessment. However, the data acquired from scanning tools can not be directly used to establish a digital information system. Furthermore, the conventional process of creating a BIM model from point cloud data is a time-consuming manual process.

Due to the increasing demand for digitising UK infrastructure, there is a need to develop a workflow to rapid scan the asset and generate a BIM model for condition assessment. This paper proposed a new approach to automate the reconstruction of a BIM model of railway bridge from point cloud data, which can also be applied to other physical assets. The approach is demonstrated on an industry project of thirty bridges of different types, shapes, and spans.

The process includes capturing the masonry structure using TLS and producing a point cloud representation of the bridge and further generating a 3D BIM model. The output result of each bridge component is validated against the point cloud under 50 mm tolerance. The new process has reduced the traditional modelling times from days/weeks to hours for the thirty bridges. The project also identified several advantages and limitations of the proposed approach.

Advantages

- The system can process a complex structure of masonry bridges.
- The digital representation is sufficiently accurate for condition assessment.
- The algorithms work well with an uncleaned point cloud data and are still able to to generate an accurate BIM model.
- The system is very efficient compared to the manual process. (average 15min processing time as opposed to hours in the manual process).

Limitations

- In some cases, it might require manual adjustment of the output in order to achieve 50 mm tolerance level.
- Further development of the library is required when dealing with a new type of bridge.
- The additional parameters of the components/element might be needed to accommodate a certain type of bridge.

Overall, this paper presented a new component library based scan to BIM approach for bridges. It has been tested on a real-life project with a significant number of bridges. Although the current library is limited to railway bridges, it is possible in the future to expand into other infrastructure assets, such as tunnels, culverts and retaining walls.

References

[1] Abu Dabous, S. and S. Feroz, *Condition monitoring of bridges with non-contact testing technologies.* Automation in Construction, 2020. **116**: p. 103224.

[2] Koch, C., et al., *Machine vision techniques for condition assessment of civil infrastructure*, in *Advances in Computer Vision and Pattern Recognition*. 2015, Springer-Verlag London Ltd. p. 351-375.

[3] Liu, W., et al., *Evaluation of three-dimensional shape signatures for automated assessment of post-earthquake building damage.* Earthquake Spectra, 2013. **29**(3): p. 897-910.

[4] Mao, Z., et al. *Towards Automated Post-Disaster Damage Assessment of Critical Infrastructure with Small Unmanned Aircraft Systems*. 2018. Institute of Electrical and Electronics Engineers Inc.

[5] Dong, P. and H. Guo, *A framework for automated assessment of post-earthquake building damage using geospatial data.* International Journal of Remote Sensing, 2012. **33**(1): p. 81-100.

[6] Zeibak-Shini, R., et al., *Towards generation of as-damaged BIM models using laser-scanning and as-built BIM: First estimate of as-damaged locations of reinforced concrete frame members in masonry infill structures.* Advanced Engineering Informatics, 2016. **30**(3): p. 312-326.

[7] Puente, I., et al., *NDT documentation and evaluation of the roman bridge of lugo using GPR and mobile and static LiDAR.* Journal of Performance of Constructed Facilities, 2015. **29**(1).

[8] Kashani, A.G., et al., *Automated tornado damage assessment and wind speed estimation based on terrestrial laser scanning.* Journal of Computing in Civil Engineering, 2015. **29**(3).

[9] Westoby, M.J., et al., *'Structure-from-Motion' photogrammetry: A low-cost, effective tool for geoscience applications.* Geomorphology, 2012. **179**: p. 300-314.

[10] Furukawa, Y. and J. Ponce, *Accurate, Dense, and Robust Multiview Stereopsis.* IEEE Transactions on Pattern Analysis and Machine Intelligence, 2010. **32**(8): p. 1362-1376.

[11] James, M.R. and S. Robson, *Straightforward reconstruction of 3D surfaces and topography with a camera: Accuracy and geoscience application.* Journal of Geophysical Research: Earth Surface, 2012. **117**(F3).

[12] Bosché, F., et al., *The value of integrating Scan-to-*

BIM and Scan-vs-BIM techniques for construction monitoring using laser scanning and BIM: The case of cylindrical MEP components. Automation in Construction, 2015. **49**: p. 201-213.

[13] Wang, Q., J. Guo, and M.-k. Kim, *An Application Oriented Scan-to-BIM Framework.* Remote Sensing, 2019. **11**: p. 365.

[14] Roberts, C., et al., *Digitalising asset management: concomitant benefits and persistent challenges.* International Journal of Building Pathology and Adaptation, 2018. **36**: p. 152-173.

[15] Xiong, X., et al., *Automatic creation of semantically rich 3D building models from laser scanner data.* Automation in Construction, 2013. **31**: p. 325-337.

[16] Borin, P. and F. Cavazzini, *CONDITION ASSESSMENT OF RC BRIDGES. INTEGRATING MACHINE LEARNING, PHOTOGRAMMETRY AND BIM.* ISPRS - International Archives of the Photogrammetry, Remote Sensing and Spatial Information Sciences, 2019. **XLII-2/W15**: p. 201-208.

Mirror-aided Approach for Surface Flatness Inspection using Laser Scanning

Fangxin Li[a] and Min-Koo Kim[b*]

[a] Department of Building and Real Estate, Hong Kong Polytechnic University, Hong Kong SAR
[b]Department of Architectural Engineeringe, Chungbuk National University, Korea
E-mail: fangxin.li@connect.polyu.hk, joekim@cbnu.ac.kr

Abstract –

Surface flatness is an essential indicator for quality assessment of concrete surfaces in the construction industry. Terrestrial laser scanning (TLS) has been popularly applied for surface flatness inspection due to its speed and accuracy. However, scanning area far away from the TLS usually suffers from inaccurate surface flatness measurement and physical barriers such as interior walls are likely to cause occlusion for the surface flatness inspection. To address these limitations, this study proposes a mirror-aided technique for surface flatness inspection. There are two concepts proposed from the mirror-aided technique. First, the mirror-aided approach can address the low accuracy of surface flatness inspection caused by long scanning range and high incident angle, which enlarge the scanning area and increase the surface flatness inspection efficiency. Second, the mirror-aided approach can measure the flatness of the concrete surfaces occluded by barriers based on the mirror reflection principle with one single scan, resulting in efficient surface flatness inspection. To validate the proposed two concepts, a series of tests on laboratory-scale specimens are conducted. The results show that the proposed method provide accurate surface flatness estimation results with an accuracy of more than 85% for the scanning area far away from the TLS and concrete surfaces with occlusion problem, demonstrating the great potential for the application of mirror-aided surface flatness inspection in the construction industry.

Keywords –

Surface flatness; quality inspection; terrestrial laser scanner (TLS); mirror-aided laser scanning

1 Introduction

Surface flatness is an essential checklist for dimensional quality inspection of construction elements and construction floors after manufacturing and construction in the construction industry [1,2,3]. This is because concrete surfaces which have unacceptable deviation from specific tolerance can seriously effect both aesthetic and functional performance of target structures [3,4,5]. Furthermore, the serious non-flatness concrete surfaces are likely to influence subsequent construction and cause poor connection between adjacent elements, resulting in deteriorated structural problem in long term [3,6]. Therefore, it is necessary to implement surface flatness inspection after production to evaluate the flatness quality of the target structure. Currently, surface flatness of concrete surfaces is commonly inspected manually using straightedges in the construction industry [10]. As for straightedge approach, inspectors use a long straightedge to assess surface flatness based on certain measurement patterns, such as grid, to define the gap between the surface and straightedge [1,10]. However, the existing flatness assessment methods have limitations in terms of time consumption, labor intensity and low measurement accuracy.

3D laser scanning has been widely used as a promising data acquisition technology for the purpose of surface flatness inspection of concrete surfaces [11-14]. This is because 3D laser scanning could provide accurate and dense 3D scan points efficiently for surface flatness inspection [15,16]. However, scanning area far away from the TLS usually has large scanning distance and high incident angle, which decrease the accuracy of the surface flatness inspection. Furthermore, construction components are likely to cause occlusion of the floor, which limits the scanning area of the floor. To address these limitations, this study aims to 1) propose a mirror-aided technique for surface flatness inspection to address the low accuracy of the scanning area far away from the TLS and occlusion problems caused by barriers 2) validate the applicability of the mirror-aided flatness inspection technique. The organization of the paper is as follow. The two concepts of the proposed mirror-aided techniques are described in Section 2, followed by validation tests and experiment results in Section 3 and Section 4. Finally, this paper

ends with a brief summary and suggestions for further work in Section 5.

2 Overall concept of mirror-aided approach for surface flatness inspection using laser scanning

Figure 1 shows the overall concepts of mirror-aided approach. Figure 1(a) illustrates the concept of the mirror-aided technique to increase the accuracy of the scanning area far away from the TLS. Here, the scanning area far away from the TLS has large scanning distance and high incident angle (θ). Therefore, the accuracy of the surface flatness inspection for the scanning area far away from the TLS is low, which limits the scanning area of the floor. As for the mirror-aided approach, the flat mirror is located at the backward of the target area far away from the TLS with a certain angle to the ground. The laser beam emitted from the TLS is first reflected by the mirror and then reaches on the scanning area, resulting in a lower incident angle (β). In this way, the mirror-aided approach can increase accuracy of surface flatness inspection caused by large scanning distance and high incident angle, which enlarge the scanning area and increase the surface flatness inspection efficiency. Also, there are rectangular patches attached on the surfaces of flat mirrors to obtain scan points falling onto the patches. Based on the mirror reflection principle [11], the scan points of actual surface obtained from the mirror will be located on the virtual surface. Also, note that the virtual surface and actual surface on the floor are symmetric with respect to the mirror. Figure 1(b) illustrates the concept of the mirror-aided technique to address the occlusion problems caused by barriers. The structural components such as the interior wall are likely to cause occlusion of the floor, which limits the scanning area of the TLS. Therefore, it requires multiple scans to perform the data collection, which deteriorates the surface flatness inspection efficiency. To address the limitation, the mirror is applied to adjust the direction of the laser beam, enabling the scanning of the occlusion area of the floor. In this way, the mirror-aided approach can measure the flatness of the floors based on mirror reflection principle with one single scan, resulting in efficient surface flatness inspection.

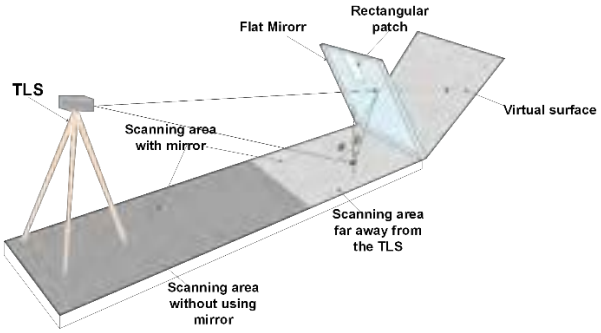

(a)

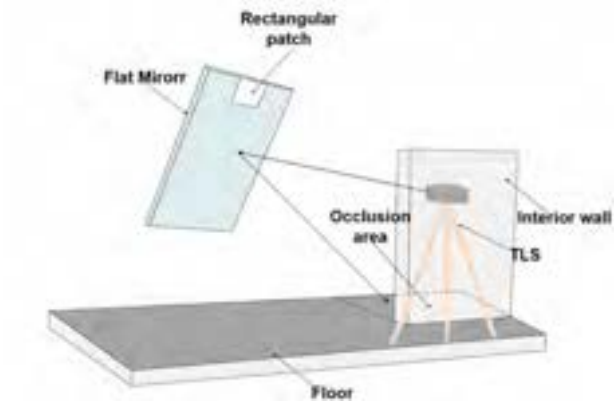

(b)

Figure 1. Overall concepts of mirror-aided approach: (a) the concept of the mirror-aided technique to increase the accuracy of the scanning area far away from the TLS and (b) the concept of the mirror-aided technique to address the occlusion problems

3 Materials and test setup

In order validate the two concepts of the mirror aided approach for surface flatness inspection, two experiments named as 'Experiment I' and 'Experiment II' of laboratory-tests were conducted on two specimens. The specific objectives of 'Experiment I' and 'Experiment II' are : 1) to validate that the mirror-aided approach can increase surface flatness inspection accuracy of the area with large scanning distance and high incident angle, 2) to validate the mirror-aided approach can address the occlusion problem caused by construction components for surface flatness inspection, respectively. Figure 2 shows the two specimens named as 'Specimen I' and 'Specimen II' for the validation experiments. The two specimens were manufactured by a ZRAPID iSLA880 3D printer [17] with the material of photopolymer resin. Table 1 shows the dimensions and F_F numbers of the specimens. Specimen I was manufactured with a size of 400 mm (length) × 400 mm (width)× 10-23 mm (height) and has an F_F number of 10.28. Specimen II, which is flatter than the Specimen I, was sized at 400 mm × 400 mm× 20-38 mm and has an F_F number of 21.23. Note that the size of the mirrors is 1000 mm (length) × 1000 mm (height). In this study, a phase-shift TLS, FARO M70 [18], with an accuracy of ±3 mm at 20 m, was used to acquire scan points of the specimen.

Table 1. Dimensions and F_F numbers of the specimens

Items	Size (length × width × height)	F_F number
Specimen I	400 mm×400 mm×10-23 mm	10.28
Specimen II	400 mm×400 mm×20-38 mm	21.23

(a) (b)

Figure 2. Test specimens for the validation experiments: (a) Specimen I and (b) Specimen II

3.1 Experiment I

3.1.1 Experiment set-up

Figure 3 shows the experimental configuration of Experiment I. The height distance of the TLS was set to 1.5 m and scanning distance was adjusted from 2.5 m to 12.5 m with an interval of 2.5 m. Besides, the mirror was rotated based on the bottom line with an angle of 75° to the ground and there was a gap of 0.35 m between the mirror bottom line and the specimen. On the other hand, two rectangular patches of 100 mm × 100 mm in size were attached to the upper-side region of the mirrors. In addition, three different angular resolutions of 0.036°, 0.072°, and 0.144° were used to investigate the effect of angular resolution. Note that the estimation error of F_F number is defined as the difference between the estimated F_F number of the proposed technique and the designed F_F number of the specimen. Also, note that scan points of the surface which are directly falling on the specimen are called 'actual scan points' and the scan points obtained on the virtual surface through the mirror are called 'virtual scan points' hereafter.

Figure 3. Test configuration of experiment I

3.1.2 Data processing

There are four procedures for the proposed mirror-aided surface flatness inspection technique after data acquisition, which are (1) data pre-processing, (2) virtual scan points transformation, (3) coordinate transformation and (4) surface flatness estimation. First, background noise is removed to extract the scan points corresponding to the specimen and the rectangular patch. Next, using the estimated mirror plane estimated from the scan points of the rectangular patch, the virtual scan points of the specimen surface are transformed to the position of actual scan points. Finally, surface flatness is estimated based on F_F number method [10]. Figure 4 shows the determination of F_F number of a test surface. The detailed procedure of determining the F_F number of a test surface according to ASTM E 1155 (ASTM 2008) [10] is illustrated as the following 5 steps.

Step 1: Determination of the sample measurement lines on the test surface. The orientations of the lines should all be parallel, perpendicular or 45° to the longest boundary. In addition, equal number of lines should be placed in two perpendicular directions. Furthermore, the lengths of lines should not be smaller than 3,300 mm and the distance between two parallel lines should not be smaller than 1,200 mm. Step 2: Subdivision of the sample measurement lines. Each sample measurement is divided into 300 mm long intervals and the points marking the ends of these intervals are named 'sample reading points'. Step 3: Measurement of the elevations of the sample reading points (or the elevation difference between all adjacent sample reading points). For sample measurement line j, denote all sample reading points along it as P_0 and P_1, and P_2 and P_3, ... P_{i-1} and P_i, etc. Then, the evaluations between the corresponding reading points are designated as h_0 and h_1, and h_2 and h_3, ... h_{i-1} and h_i accordingly. Step 4: Calculate the F_F number of each sample measurement line. For sample measurement line j, calculate the profile curvatures, q_i, between all sample reading points separated by 600 mm as $h_i - 2h_{i-1} + h_{i-2}$, where i = 2, 3, 4 … n. Subsequently, the F_F number of sample measurement line j, denoted as F_j, is estimated by Eq. (1).

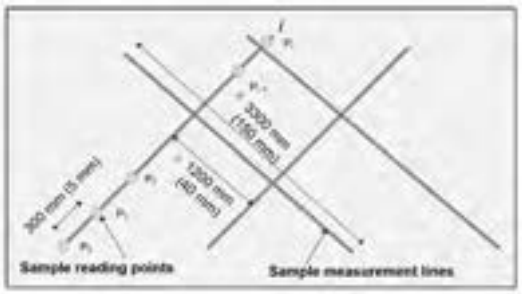

Figure 4. Determination of the F_F number of a test surface

$$F_j = \frac{115.8454}{3S_{qi} + |q_i|} \quad (1)$$

where S_{qi} and $|q_i|$ denote the standard deviation and the absolute value of the mean of all $(n-1)$ q_i values, respectively. Step 5: Calculate the F_F number of the test surface by combining all of the F_F numbers of individual sample measurement lines within the test surface. Considering the limitation of the size of the test specimen, the length of measurement lines and the distance between two parallel measurement lines in this study are selected as 150 mm and 40 mm respectively. In addition, the intervals which separate the sampling reading points is set as 5 mm and the profile curvatures, q_i, is calculated between all sample reading points separated by 10 mm. Since the F_F number is calculated based on the collected scan points, the elevation of each sample reading point will be obtained with the nearest laser scan point. Then, in order to improve the reliability of the results, F_F number is calculated as the average value of the results that is calculated iteratively in 1000 times. For each time, the number of the sample measurement lines and the relative locations between each measurement line are unchanged. As for the distances from the sample measurement lines to the surface boundaries, these values vary in every iteration and is determined by a random number.

3.2 Experiment II

3.2.1 Experiment set-up

In order to validate the concept 2, the height distance of the TLS was set to 2.5 m and scanning distance from the TLS to the mirror and the specimen were 2 m and 1.5 m respectively. Figure 5 shows the test configuration of Experiment II. Besides, barriers were located between the TLS and specimen to make the specimen invisible from the TLS. In addition, a mirror with the size of 1000 mm × 1000 mm was located behind the specimen with a gap of 0.2 m. Here, the center point of the mirror is the pivot point of the rotation and the mirror was aided by a goniometer to achieve rotation in the horizontal and vertical direction. In this experiment, the vertical mirror rotation angle and horizontal mirror radiation angle were set as 20° and 30° respectively. On the other hand, two rectangular patches of 100 mm × 100 mm in size were attached to the upper-side region of the mirrors for mirror plane estimation. In addition, three different angular resolutions of 0.036°, 0.072°, and 0.144° were used to investigate the effect of angular resolution.

Figure 5. Test configuration of Experiment II

3.2.2 Data processing

The data processing process is similar to the experiment I and the only difference is that noise removal. In experiment II, there is no need to extract the virtual scan points of specimen because it cannot be scanned from the TLS.

4 Result and discussion

4.1 Experiment I result and discussion

Table 2 shows the estimation errors of F_F number under varying angular resolutions with different scanning distances. There are three distinctive observations from the results.

First, the estimation errors of F_F number from the scan points are decreased as the scan density increases. Note that the data density is presented as the number of scan points captured each square centimetre. Here, the estimation errors of F_F number under different scan densities from virtual can points are taken as an example to illustrate the effects of scan density on estimation errors. As the scan density increases from 0.3 pts/ cm^2 to 87.7 pts/ cm^2, the estimation error in percentage is decreased from 318.8% to 3.9%. It is also observed that the F_F number cannot be estimated when the scan density is less than 0.2 / cm^2 since the measurement lines are not able to be sampled in sparse scan points for F_F number estimation. In addition, it is also noticed that scan density which excess 5.5 pts /cm^2 are likely to result in accurate F_F number estimation, resulting in error in percentage of less than 20%. However, the actual scan points directly acquired from the TLS usually has low scan density caused by the large scanning distance and high incident angle, which cause low estimation accuracy for surface flatness inspection.

Second, the mirror-aided method can achieve the improvement of 81.5% in accuracy for surface flatness inspection compared to actual scan points under scanning distance of 10 m, addressing the low accuracy of surface flatness inspection caused by large scanning distance and high incident angle. This is because the proposed mirror-aided approach can adjust the incident

Table 2. Estimation errors for F_F number under varying angular resolutions with different scanning distances

Object	Scanning distance (incident angle)	Estimation error of F_F number for Specimen I in percentage (Data density: pts/cm^2)			Estimation error of F_F number for Specimen II in percentage (Data density: pts/cm^2)		
		Angular resolution			Angular resolution		
		0.036°	0.072°	0.144°	0.036°	0.072°	0.144°
Virtual scan points	2.5m (51°)	9.5% (87.7)	13.8% (21.9)	17.1% (5.6)	3.9% (87.2)	8.4% (21.9)	19.9% (5.5)
	5m (43°)	9.6% (27.0)	11.1% (6.7)	91.6% (1.7)	4.0% (27.1)	19.1% (6.7)	29.1% (1.7)
	7.5m (40°)	18.6% (12.7)	37.1% (3.2)	71.2% (0.8)	8.9% (12.9)	11.7% (3.2)	24.1% (0.8)
	10m (38°)	15.1% (7.3)	49.0% (1.8)	183.5% (0.5)	19.8% (7.3)	23.3% (1.8)	48.1% (0.5)
	12.5m (37°)	31.1% (4.9)	49.1% (1.2)	318.8% (0.3)	20.9% (4.8)	37.0% (1.2)	69.6% (0.3)
Actual scan points	2.5m (70°)	19.9% (67.3)	36.1% (16.6)	65.2% (4.5)	4.4% (64.9)	27.0% (16.6)	23.8% (4.2)
	5m (79°)	82.5% (10.6)	83.1% (2.7)	152.9% (0.6)	19.8% (10.6)	19.5% (2.5)	64.1% (0.6)
	7.5m (82°)	161.4% (3.6)	140.5% (0.9)	- (0.2)	58.7% (3.3)	88.4% (0.8)	- (0.2)
	10m (84°)	211.1% (1.5)	278.8% (0.4)	- (<0. 1)	107.3% (1.4)	143.0% (0.3)	- (<0. 1)
	12.5m (86°)	210.3% (0.7)	- (0. 2)	- (<0. 1)	155.6% (0.6)	-(0.2)	- (<0. 1)

angle of laser beam and address the low-density scan points caused by the long scanning range and high incident angle. Due to the long scanning range and high incident angle, the actual scan points which are directly acquired from the specimen are not able to provide accurate results (with error in percentage of less than 20%) when the scanning distance is larger than 5 m. However, the scan density of virtual scan points are around 2 to 4 times that of actual scan points in the same circumstance. Therefore, the mirror-aided approach can acquire accurate result with the scanning distance of 10 m, which enlarge scanning area and increase the efficiency for surface flatness inspection.

Third, Specimen II achieves more accurate F_F number estimation results than Specimen I in most cases, indicating that the mirror-aided approach is more robust for flatness inspection of flatter surfaces. This phenomenon is caused by that the Specimen I with non-flatter surface as shown in Figure 2 is more likely to suffer from the effect of the high incident angle compared to Specimen II with relative flatter surface. Hence, the proposed mirror-aided approach can be effectively applied for floor surface flatness inspection since the concrete floor normally has relative flatter surface.

In summary, the mirror-aided approach can adjust the incident angle of laser beam to address the low measurement caused by the large scanning distance and high incident angle. Therefore, the mirror-aided approach is able to acquire accurate F_F number estimation for surface flatness inspection within a large scanning distance, which enlarge scanning area and increase data collection efficiency.

4.2 Experiment II result and discussion

Table 3 shows the mirror-aided F_F number estimation errors under varying angular resolutions for specimens with occlusion problem. The average errors for Specimen I and Specimen II in percentage are 22.4% and 11.6% respectively, which indicates the applicability of the proposed mirror-aided method for concept 1. This is because that the mirror-aided method adjusts the laser beam direction, enabling the scanning of the specimen occluded by barriers. Moreover, Specimen II achieves more accurate F_F number estimations than Specimen I in most cases since flatter surface of Specimen II is more robust to incident angle

Table 3. Mirror-aided F_F number estimation errors under varying angular resolutions with different scanning distances with occlusion

Object	F_F number estimation error of Specimen I (mm)				F_F number estimation error of Specimen II (mm)			
	Angular resolution				Angular resolution			
	0.036°	0.072°	0.144°	Ave.	0.036°	0.072°	0.144°	Ave.
Discrepancy	1.10	2.84	3.97	2.30	2.21	2.51	2.69	2.47
Discrepancy in percentage	10.7%	27.6%	38.6%	22.4%	10.4%	11.8%	12.6%	11.6%

influence compared to non-flatter surface of Specimen I.

5 Conclusion

This study presents a mirror-aided technique for surface flatness inspection to address low accuracy of the scanning area far from TLS and occlusion problems caused by barriers. First, the mirror-aided approach can increase the low accuracy of surface flatness inspection caused by large scanning distance and high incident angle, which enlarge the scanning area and increase the surface flatness inspection efficiency. The validation results showed that the mirror aided approach can improve the surface flatness inspection accuracy in 81.5%, which address the low accuracy caused by large scanning distance and high incident angle. Second, the mirror-aided approach can measure the flatness of the floors occluded by structural components based on mirror reflection principle with one single scan, resulting in efficient surface flatness inspection. Based on the proposed two concepts, the validation experiments are conducted on two laboratory-scale specimens. From the validation results, the proposed mirror-aided approach achieves an accuracy of more than 85% for Experiment II, indicating the applicability of the proposed mirror-aided approach to address occlusion problems.

However, there are limitations which are left for further study in the near future. First, the test specimens used in this study are lab-scale, so further study is necessary in order to investigate the applicability of the proposed technique to large-scale or full-scale elements. Second, the large-scale mirrors are fragile and take large space which may not be available for extremely large-scale environment.

Acknowledgement

This work is supported by the Korea Agency for Infrastructure Technology Advancement (KAIA) grant funded by the Ministry of Land, Infrastructure and Transport (Grant 20SMIP-A157453-01).

References

[1] British Standards Institution (BSI). BS 8204 — Screeds, Bases and In Situ Flooring (2009)

[2] American Concrete Institute (ACI). ACI 302.1R-96 — Guide for Concrete Floor and Slab Construction (1997)

[3] Park, H. S., Lee, H. M., Hojjat, A., and Lee, I. A new approach for health monitoring of structures: Terrestrial laser scanning. *Computer-aided Civil and Infrastructure Engineering*, 22(1), 19–30, 2007.

[4] Shih, N. J., and Wang, P. H. Using point cloud to inspect the construction quality of wall finish. In *Proceedings of the 22nd eCAADe Conference, pages* 573-578, 2004.

[5] Li, D., Liu, J., Feng, L., Zhou, Y., Liu, P., and Chen, Y. F. Terrestrial Laser Scanning Assisted Flatness Quality Assessment for Two Different Types of Concrete Surfaces. *Measurement*, 107436, 2020.

[6] Wacker, J.M., Eberhard, M.O. and Stanton, J.F. State-of-the-art Report on Precast Concrete Systems for Rapid Construction of Bridges (No. WA-RD 594.1). Washington State Department of Transportation, 2005.

[7] Wang, Q., Kim, M. K., Sohn, H., and Cheng, J. C. Surface flatness and distortion inspection of precast concrete elements using laser scanning technology. *Smart Structures and Systems*, 18(3), 601-623, 2016.

[8] Bosché, F., and Guenet, E. Automating surface flatness control using terrestrial laser scanning and building information models. *Automation in construction*, 44, 212-226, 2014.

[9] Hieber, D. G., Wacker, J. M., Eberhard, M. O., and Stanton, J. F. State-of-the-art report on precast concrete systems for rapid construction of bridges (No. WA-RD 594.1). *Washington State Transportation Center*,2015.

[10] ASTM, ASTM E 1155-96 —Standard Test Method for Determining FF Floor Flatness and FL Floor Levelness Numbers, 2008.

[11] Kim, M. K., Wang, Q., Yoon, S., and Sohn, H., A mirror-aided laser scanning system for geometric quality inspection of side surfaces of precast concrete elements. *Measurement*, 141, 420-428, 2019.

[12] Kim, M. K., Thedja, J. P. P., and Wang, Q., Automated dimensional quality assessment for formwork and rebar of reinforced concrete components using 3D point cloud dat. *Automation in Construction*, 112, 103077, 2020.

[13] Kim, M. K., Wang, Q., and Li, H., Non-contact sensing based geometric quality assessment of buildings and civil structures: A review. *Automation in Construction*, 100, 163-179, 2019.

[14] Wang, Q., and Kim, M. K., Applications of 3D point cloud data in the construction industry: A fifteen-year review from 2004 to 2018. *Advanced Engineering Informatics*, 39, 306-319, 2019.

[15] Wang, Q., Tan, Y., and Mei, Z., Computational methods of acquisition and processing of 3D point cloud data for construction applications. *Archives of Computational Methods in Engineering*, 27(2), 479-499, 2020.

[16] Josephson, P. E., and Hammarlund, Y., The causes and costs of defects in construction: A study of seven building projects. *Automation in Construction*, 8(6): 681-687, 1999.
[17] ZRAPID SLA 3D Printer. Available from: http://www.zero-tek.com/en/sla880.html.
[18] FARO. FARO® LASER SCANNER FOCUS. Available from: https://www.faro.com/en-sg/products/construction-bim/faro-laser-scanner-focus/.

A Predictive Model for Scaffolding Man-hours in Heavy Industrial Construction Projects

W. Chu[a] , S.H. Han[a] , L. Zhen[b] , U. Hermann[c] ,and D. Hu[c]

[a]Department of Building, Civil and Environmental Engineering, Concordia University, Canada
[b]Department of Civil Engineering, University of New Brunswick, Canada
[c]PCL Industrial Management Inc., Edmonton, Canada

monian0627@gmail.com, sanghyeok.han@concordia.ca, zlei@ualberta.ca, RHHermann@pcl.com, dhu@pcl.com

Abstract –

In typical heavy industrial construction projects, scaffolding can account for 30% to 40% of the total direct man-hours. However, most industrial contractors estimate scaffolding man power based on a certain percentage of the direct work, which leads to cost increase and schedule delay due to inaccurate estimation. In order to aid industrial companies to plan and allocate the resources for scaffolding activities before construction, this paper proposes a methodology which combines the classification tree and multiple linear regression to estimate scaffolding manhours based on available project features. The evaluation matrix involves R Squared value (R^2), Adjusted R Squared value (Adj. R^2), mean absolute error (MAE), root mean squared error (RMSE), and relative absolute error (RAE). The proposed methodology has been tested on the historical scaffolding data in a heavy industrial project and the results showed its effectiveness.

Keywords –

Scaffolding Man-hours; Linear regression; Classification tree; Heavy Industrial Constructions

1 Introduction

Occupational safety and health services [1] defines scaffolding as any structure (suspended structure) which is built for temporary purposes, used for the support and/or protection of the construction workers by providing easy access to work areas horizontally and vertically, and also helps in material transferring. Due to these functions, heavy industrial construction projects usually involve various types and a large amount of scaffoldings to feed the need for different disciplines (e.g., civil, mechanical, and electrical), leading to increased project costs. In the construction site, the scaffolding should be installed, modified and/or dismantled in accordance with the requirements of various disciplines on their demand times in order to prevent project schedule delays. Due to the demand-based scaffolding operation, the construction domain has difficulty to plan scaffolding operation in the early phases of the project.

In practice, planning of scaffolding activities is completely subjective and differs from company to company [2]. The scaffolding tends to be planned and operated as an ad hoc way which leading to schedule delays and cost overrun due to the inefficient utilization of resources. As an effort to develop a scientific and practical planning method for the scaffolding activities, the previous research [2] claims that most construction companies regard scaffolding as a part of indirect expense and calculated as a percentage of the total man-hours of direct work . In this respect, previous study [3] has identified that scaffolding works accounts for up to 30%-40% of the total direct man-hours in the heavy industrial project.

Scaffolding has potential for significant productivity improvement with respect to project cost reduction in construction, especially industrial construction. However, planning and estimating of scaffolding works have received little attention in academia and practice. In its infancy, research on scaffolding mainly focused on structural performance [4]. With safety gaining prominence in scaffolding research, the factors contributing to scaffolding collapse have been studied more recently [5]. In terms of planning of scaffolding works as a temporary structure on-site, there are several research efforts that have investigated the application of artificial intelligence (AI) algorithms (e.g., fuzzy logic and genetic algorithm) and geometries of 3D models for temporary structure or facility planning [8]. However, these studies have not fully directed their efforts to developing methods or systems to improve efficiency of planning and estimating of scaffolding activities for productivity improvement based on the project time progress.

Thus, this paper proposes an integrated method that

combines the classification tree with the multiple linear regression model in order to estimate the scaffolding man-hours efficiently and accurately in the heavy industrial construction projects. The proposed methodology mainly consists of five steps: (*i*) collecting data from construction site through cloud-based computer systems; (*ii*) identifying and cleaning potential outliers from the dataset; (*iii*) selecting and/or transforming the most important independent variables which affect the scaffolding man-hours through statistical diagnosis, (*iv*) developing classification tree based on selected text variables in the dataset, and at each tree node, the multiple linear regression performed to obtain a predictive model for man-hour estimation, and (*v*) evaluating the performance using the tenfold repeated cross-validation.

The proposed methodology has been implemented in Python 3.7 environment. It was tested with the historical scaffolding data in a heavy industrial project in Alberta, Canada, provided by an industrial collaborator.

2 Scaffolding Related Research

Based on the investigation of the previous studies done by authors in planning the scaffolding-related resources in construction domain, previous research has mainly focused on structural performance and safety management. Peng et al. [4] introduced a scaffolding design system in terms of the performance of steel and bamboo scaffolding. Yue et al. [5] studied the effect of wind load on scaffolding in order to promote safety in the design of integral-lift scaffolds. Based on optimization of the scaffolding schedule, which can help in coordinated safety management and control efforts, Hou et al. [6] introduced an operational framework by integrating mathematical models with virtual simulation to optimize scaffolding erections. According to the introduction of advanced technologies, Kim et al. [7] have actively integrated building information modelling (BIM), image processing or wireless sensors with optimization algorithms, to not only identify and mitigate the safety risks but also plan the scaffolding schedules to eliminate potential hazards. Furthermore, Cho et al. [10] have used machine learning algorithms (support vector machine) to assess real-time safety and unsafety status of the scaffolds based on different conditions of scaffolds (safe, overturning, overloading or uneven settlement), which adopts actual strain data of scaffolding members obtained by wireless sensors.

Construction Owners Association of Alberta (COAA) reports that scaffolding plan must provide the estimated scaffolding types, location, duration and quantity requirements including materials and labours [11]. Based on the result of planning and estimating the scaffolding activities, previous studies [12] have suggested that the effective management of the scaffolding in construction projects can improve productivity by: (i) preventing the delays of crews due to absence of scaffolding materials or even man-power; and (ii) understanding the resource requirements to avoid work space conflicts. However, in practice, industrial company plans and estimates the scaffold activities subjectively, which can be up to 40% of total direct man power of an industrial project, based on the regulations of company and engineer's experience which may cause excessive use of man-power, schedule delays and resource shortage.

As scaffolds and their supporting structures being a temporary work platform, there are several research efforts to investigate the applications of artificial intelligence (AI) algorithms and geometries of 3D models for temporary structure or facility planning [9]. However, these studies have not discovered the field of improving efficiency and accuracy of planning and estimating scaffolding man powers. Therefore, several studies [2-3] made an effort to analyse the factors affecting industrial scaffolding estimation based on historical data provided by a construction company. A simulation tool and linear regression models have been developed to predict a range of man-hour values for only scaffold erection on site in their works. However, since the lack of available scaffolding data, the analysis merely regarding scaffolding erection is insufficient. The authors also suggested that further analysis is required with more historical data from other industrial projects and other optimization algorithms in order to generalize a general methodology for estimation and planning of scaffolding works. As a recent study, Moon et al. [13] have investigated the effect on productivity of resource configurations measured during scaffolding operation as part of the construction of an actual liquefied natural gas (LNG) plant. Hou et al. [14] have proposed a feasible multi-object discrete firefly algorithm for optimizing scaffolding project resources and scheduling. However, this model needs to not only be improved in terms of accuracy for scheduling the scaffolding resources, but also be made generically applicable to other projects by incorporating various types of scaffolding constraint. In addition, these previous studies have had difficulty for further analysis or better models to plan and/or schedule the scaffolding activities due to the insufficient scaffolding data since it has not been attention and tends to be ignored in practice. As a result, the development of scientific and systematic methods is still required in the planning and estimating of scaffolding activities due to the lack of accuracy, efficiency, and applicability in the existing systems for various types of construction projects, especially heavy industrial projects.

3 Research Methodology

In order to predict the required man-hours for scaffolds accurately in the early planning phase of the project, this paper proposes an integrated method that combines the classification tree with the multiple linear regression model. As shown in Figure 1, there are in total five steps in the proposed methodology, which are data collection, data cleaning, input data determination, development of classification tree structure, and the final model evaluation with all the outputs from the previous steps.

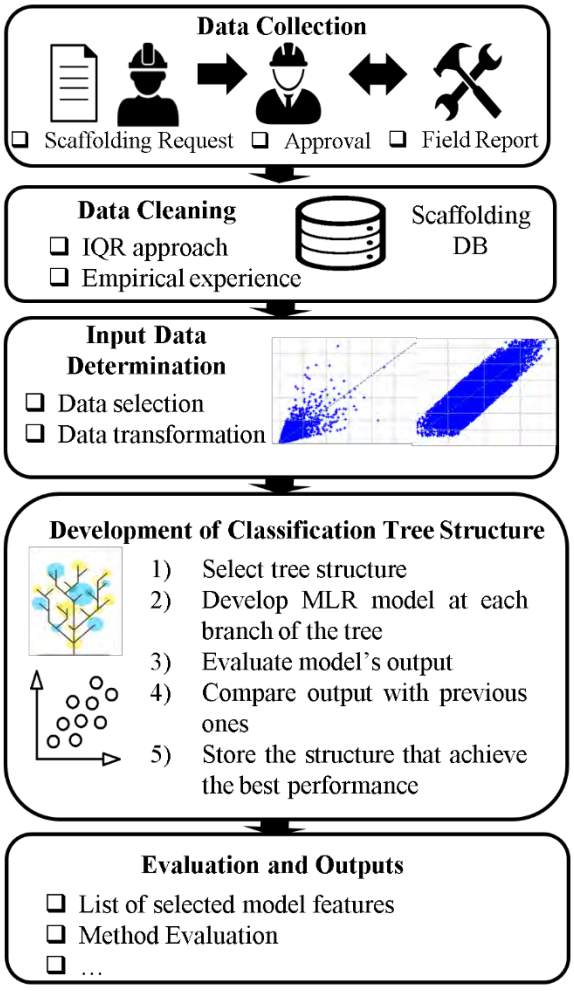

Figure 1. Flowchart of proposed methodology

3.1 Data Collection

As mentioned in Figure 1, the data collection process can be simplified as: scaffolding requests generated for approval along with detailed scope of work, and once the requests are approved and completed, the actual man-hours and work details are recorded. Individual scaffold component details are documented, and the weights summed up for each request by date. The information that can be tracked in the scaffolding activities may vary, but by nature, the key ones are work classification (i.e. erection, modification, and dismantle), scaffolding type (i.e. platform deck, tower, barricade, etc.), actual man-hours, total scaffolding weights. Meanwhile, other project related data that maybe likely to affect the manhour prediction should be extracted from other sources and consolidated for analysis, such as the average temperature during each scaffolding task, the elevation of the scaffold built according to the ground level, and the average aluminum percentage of the scaffolding.

3.2 Data Cleaning

The objective of data cleaning is to remove the outliers in the collected dataset. Outliers are extreme observations in the dataset that are not consistent with the trend of correlation in the data. In data collection process, the outliers may result from errors in data entry. There are generally, two ways of filtering outliers: (i) using statistical approaches to identify outliers mathematically regardless of the nature of data; and (ii) using user experience-based approaches to identify outliers based on users' logics. Often, the statistical approaches take less efforts than the user experience-based approaches due to the experience-based approach do not have a certain criterion but based on understanding, experience and trail-and-error tests. In this paper, an integrated data cleaning process has been adopted using both statistical and experience-based methods.

At first, the interquartile range (IQR), one of the statistical approaches, is used to identify the outliers. IQR is a measure of the location of middle 50% data in the dataset, and it is calculated by subtracting the first quartile (Q1) from the third quartile of the dataset (Q3). Potential outliers are defined as observations that fall below Q1 – 1.5* IQR or above Q3 + 1.5 * IQR. Moreover, under the guidance of the scaffolding experts, the following experience-based rules should be applied to further filter out the outliers: (*i*) value of man-hours is null or less than 5 hours; (*ii*) value of scaffolding weights is null or less than 20 lbs; and (*iii*) productivity (i.e. weight per man hour) is less than 6 lbs/hr, or greater than 125 lbs/hr. These experience-based rules may vary in different project scenario. However, the core concept is to remove data observations that are not physically feasible in scaffolding work, normally reflected by manhours, weight of scaffolding, and scaffolding weight divided by manhours (productivity).

3.3 Input Data Determination

In order to ensure the effectiveness of results from multiple linear regression model, there are five

assumptions need to be fulfilled before the analysis [15]. The assumptions are (*i*) the relationship between dependent variables and independent variable should be approximately linear; (*ii*) the error term ε has zero mean; (*iii*) the error term ε has constant variance σ2; (*iv*) the independent variables are uncorrelated; and (*v*) the errors are normally distributed. Among these assumptions, the linearity between the dependent variables and independent variable and the independence among the independent variables are of the utmost importance. The zero mean of error term can be fulfilled by involving the intercept term in the regression equation and the normally distributed error generally is not a must-have check. The following model feature selection section and model feature transformation section are responsible for check independence and linearity among the dataset, separately.

3.3.1 Model Feature Selection

The model feature selection is one of the most important part in the field of machine learning since (i) the irrelevant input features can induce greater computational cost; (ii) the irrelevant input features may lead to overfitting, which in turn leads to poor results on the validation datasets. Feature selection methods can also adapt the dataset to better suit the selected machine learning algorithm, given that different algorithm may have various requirement for the features. In terms of multiple linear regression, a reliable set of features contains independent variables that are highly correlated to a dependent variable (i.e., scaffolding manhour), also called as a predicted variable, but uncorrelated with each other.

The condition that some of the independent variables are highly correlated is called collinearity [16]. Collinearity can lead to imprecise coefficient estimates during the development of the predictive model since it inflates the standard errors of the coefficients of collinear variables. In this respect, this paper uses correlation matrix which supports users to identify the collinearity problem. The correlation matrix for all the independent variables should be developed at each classification tree node. The Spearman method [17] has been adopted here to perform the correlation analysis since (*i*) it is a non-parametric procedure in which the observations are replaced by their ranks in the calculation of the correlation coefficient so that it can deal with data with outliers; (*ii*) it does not carry any assumptions about the distribution of the data (e.g. Pearson method requires both variables to be normally distributed) [18]. In the correlation matrix M, it is easy to identify that which two variables are highly correlated (> 0.5) [19] and which one of them should be removed to avoid collinearity.

While collinearity means the correlation between only two independent variables are high, multicollinearity can exist between one variable and linear combination of more than two variables [16]. As another indicator of model feature selection for linear regression, multicollinearity can cause regression coefficients to change dramatically in response to small changes in the model or the data. Thus, it may cause serious difficulty with the reliability of regression coefficients. In order to detect whether a regression model exists multicollinearity, Variance Inflation Factor (VIF) [20] of each independent variable need to be checked in the model. VIF is a traditional measure to detect the presence of multicollinearity in multi-linear regression model. It shows how much the variance of the estimator is inflated due to the linear relation between the regressors. Typically, a VIF, which is larger than ten, has been used as a rule of thumb to indicate serious multicollinearity.

3.3.2 Model Feature Transformation

Given a selected feature set, the quality of data can be enhanced by feature transformation. It is common that the real-world data may not show strong linearity between independent variables and predicted variable. However, there are several data transformation methods, such as logarithm, square root, reciprocal, cube root and square, can be applied to enhance the linear trend in data. There are also some guidelines for the selection of transformation method, such as if the standard deviation is proportional to the mean, the distribution can be positively skewed and logarithmic transformation can be performed, or if the variance is proportional to the mean, squared root transformation may be preferred etc. [21].

Among various transformation methods, logarithmic transformation is the most popular one. Using natural logs for variables on both sides of the linear regression equation can be called log-log model. Theoretically, any log transformation can be used in the transformation and all of them tend to generate similar results. However, using the natural log can be seen as the convention since the interpretation of the regression coefficients is obvious using the natural log. The coefficient in the natural log-log model represents the estimated percent change in the dependent variable for a percent change in the correspondent independent variable [22] .

3.4 Model Development

The classification tree structure determines the way how the overall dataset can be divided into several groups in which the regression model can be separately developed. The function of the classification tree is to cluster the similar observations together to obtain more accurate regression sub-models instead of messing all

the data together and get only one model. The proper classification may largely alleviate the effort to achieve the required model efficiency and accuracy. To efficiently build the classification tree, the key categorical variables used to split the tree are of the utmost importance. There are several available categorical variables such as work classification, scaffold type and discipline. The repeated tenfold cross-validation can be used to compare the effectiveness of different classification tree structures developed using various combinations of categorical variables.

The classification tree needs to be utilized with multiple linear regression model. After developing the classification tree structure based on selected key categorical variables, multiple linear regression can be implemented at each tree end node, as long as there are sufficient number of records at the tree node. Previous researchers discovered that when the number of observations n >= 15 * k where k represents the number of independent variables, the model parameter estimation tends to achieve a prescribed level of accuracy [23]. On the other hand, if the number of records at certain nodes cannot meet this requirement, the upper level model should be used to complement the miss of model under certain classification category. Normally, the multiple linear regression model at each classification tree node can be denoted as Eq. (1).

$$y = \beta + \sum \alpha_i x_i \quad (1)$$

Where: y is the predicted variable (i.e. scaffolding manhour) for the *ith* record at current classification tree node; β is the intercept value; α_i is the coefficient for independent variable x_i.

3.5 Model evaluation

Repeated tenfold cross validation has been selected to evaluate the regression models. Kim has found that the repeated cross-validation estimator is recommended for general use regardless of the sample size [24]. Moreover, Witten et al. have conducted extensive tests with different machine learning techniques, and the results have shown that, by repeating the tenfold cross validation 10 times, the results can reliably estimate errors [25]. Tenfold cross validation means to split the whole dataset into ten stratified subsets of equal size ten times, and each subset can be used for testing once and the combination of the rest can be used for training. The final error estimates are averages across each of the fold. Repeat the tenfold cross validation ten times and the mean value would be the final validation result. The evaluation matrix has five parameters in all, including R Square (R^2), Adjusted R Square (Adj.R^2), Mean Absolute Error (MAE), Root Mean-Squared Error (RMSE) and Relative Absolute Error (RAE). All the calculation equations can be found in a book [25] .

4 Case study

The proposed methodology has been implemented in the Python 3.7 environment and the case study is based on a heavy industrial project with data provided by a construction company. The scaffolding related data has been collected onsite through cloud-based data systems, as well as company's internal systems (e.g. project control systems, payroll systems, etc). There are in total three categorical variables and twelve numerical variables have been collected. The categorical variables are work classification, scaffolding type, discipline of trade that scaffolding is built/modified for.

The numerical variables are: average temperature, apprenticeship ratio (the ratio of work carried out by apprentices), night-time ratio, overtime ratio, aluminium percentage of the scaffolding, percentage of completed project, scaffolding weight, workable area (available space for building scaffolds), average scaffolding employee time on site, elevation of the scaffolds, major pieces and minor pieces (number of large/small pieces of scaffolding materials). After data consolidation and cleaning, the dataset contains 12,087 valid observations in total. Figure. 2 compares the manhour distribution of the raw dataset and the dataset after data cleaning.

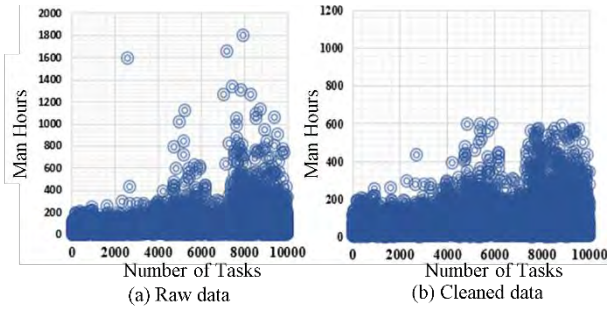

Figure 2. Manhour distribution comparison

After the data collection and data cleaning, the independence in the dataset should be checked. Table 1 illustrates a part of the sample correlation matrix of a classification tree branch (classification: Erection). The independent variables that have much lower correlation with others have been trimmed in the table due to the space limitation; only the most correlated variables were kept: workable area, scaffolding weight, major pieces, and minor pieces. It can be seen that almost all the values in Table 1 are larger than 0.5, which means the four variables are all highly correlated to each other. It should also be noted that all these variables are also highly correlated to the scaffolding manhours which is the predicted variable. According to the previous research, the collinearity can be simply addressed by keeping only one highly correlated independent variable but removing the others [26]. From the industrial view,

these four variables describe the scaffolding work from a similar perspective. To determine which variable is of the most importance, the multi-linear regression models have been developed based on one of these four variables in turn with the rest un-collinear eight variables. The sample results using classification as key variable can be found in Table 2.

Table 1. Sample correlation matrix

	Workable Area	Weight	Major Pieces	Minor Pieces
Workable Area	1.00	0.66	0.63	0.49
Weight	0.66	1.00	0.87	0.62
Major Pieces	0.63	0.87	1.00	0.67
Minor Pieces	0.49	0.62	0.67	1.00
Manhour	0.51	0.60	0.61	0.59

Table 2. Result using different variables

Index	Workable Area	Weight	Major Pieces	Minor Pieces
R^2	0.54	0.73	0.69	0.58
Adj.R^2	0.54	0.73	0.68	0.58
MAE	70.69	51.51	52.18	61.82
RMSE	134.65	107.56	115.32	145.36
RAE	1.30	0.69	0.72	1.01

It can be clearly seen from Table 2 that R^2, Adj.R^2 are the highest while MAE, RMSE, and RAE are the lowest when selecting the scaffolding weight variable. Since the weight variable can give less error and better predicted results, it has been kept in the model feature set but the other three have been excluded to prevent the collinearity.

Moreover, Table 3 shows VIF of all the numerical independent variables in the model at the branch of Erection-Tower as an example. The result shows that there are four variables with VIF factor value larger than 10, which are night-time ratio, project complete percentage, employee time on site, and apprenticeship ratio. Thus, these four variables have been excluded from the analysis to address the multicollinearity problem. Table 4 has been created to detect multicollinearity one more time after the adjustments. It can be seen that the multicollinearity has been solved since all the VIF values are lower than 10 when regress the model using the selected variables.

Table 3. VIF of each numerical variable

VIF Factor	Features
3.61	Temperature
3.52	Aluminum percentage
1.58	Weights
2.69	Elevation meters
1.07	Night-time ratio
28.00	Overtime ratio
70.06	Project complete percentage
223.20	Employee time on site
76.84	Apprenticeship ratio

Table 4. VIF of modified variable

VIF Factor	Features
1.13	Temperature
1.22	Aluminum percentage
2.03	Weights
1.04	Elevation meters
2.04	Night-time ratio

The regression model has been built using the selected five variables which are temperature, aluminum percentage, weight, scaffolding elevation, and night-time ratio. However, some negative manhours are predicted by the model. This phenomenon prompts the discovery of the exact contribution of each explanatory variable. According to the summary of previous work [27], the Standardized Regression Coefficients (SRC) method is suitable to conduct the sensitivity analysis for the linear model. Table 5 shows the result of sensitivity analysis for the classification tree built upon work classification and scaffolding type. It should be noted that the average value of night-time is negative, which indicates that with the increase of night-time working, the required manhours decreases. Thus, the night-time ratio has been removed not only due to its minimum contribution to predict manhours, it is also counter-intuitive to industry experts.

Table 5. Average result of sensitivity analysis

	Temp	Weight	Elevation	Night time	Aluminum percentage
Avg	-0.05	0.83	0.05	-0.02	0.07

Thus, there are four independent variables have been selected at the end. Next, the linearity between the independent variables and predicted variable should be checked. From the sensitivity analysis, it is obvious that in the linear regression model, the scaffolding weight is far more important than other variables. As the most prominent variable, the relationship between weight and manhour has been discovered and some sample scattered figures have been plotted in Figure 3. It can be seen that the dots in the upper left figure are scattered. The original manhour do not show strong linear trend with original scaffold weights. However, after taking the natural logarithm of both manhour and weights, there exists clear linearity between log(weight) and log(manhour). Other data transformation ways have been tried out as well, such as reciprocal transformation (weights versus reciprocal of manhour) shown in the lower left figure, and single logarithmic transformation

which means only transforming one side of variable (log(weight) versus manhour) as shown in the lower right figure. Nevertheless, the log-log model is obviously the best to generate linearity.

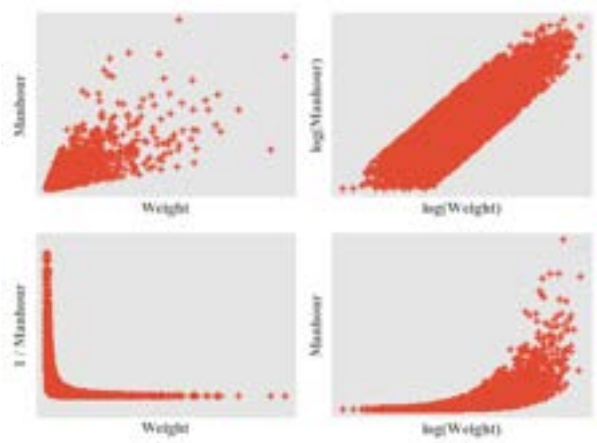

Figure 3. Comparison of data transformation

Furthermore, the log-log model should be applied to all the independent variables instead of only scaffolding weights. It is worth mentioning that since the log-log model can only be applied to positive variables, the temperature variable has been normalized in the range [0°, 10°]. In addition, to deal with the zeros in the dataset, a constant λ has been added to the log-log transformation equation as shown in Eq. (2).

$$\log(y) = \beta + \sum \alpha_i * \log(x_i + \lambda) \quad (2)$$

where λ can be one half of the smallest value in the dataset . In this study, $\lambda = 0.001$ has been adopted.

As for the classification tree structure, the trail-and-error method has been used to determine the best classification method. The repeated tenfold cross-validation results for various classification structures can be found in Table 6. Overall, the work classification works as the best classification tool since it gives the highest Adj. R2, way more than 0.7 which is the criterion to check whether a linear model is a good fit. Also, it produces less error than using other classification methods. After the regression models have been built at each tree node in the classification tree, the correspondent coefficient tables are stored for the future use.

Table 6. Cross-validation results

CT	R^2	Adj.R^2	MAE	RMSE	RAE%
WC	0.81	0.8	38.24	82.53	37.93
DIS	0.78	0.78	48.17	101.93	42.54
ST	0.76	0.76	47.49	87.94	41.09
WC+DIS	0.79	0.79	41.52	94.33	38.84
WC+ST	0.82	0.82	44.5	94.06	36.02
DIS+ST	0.79	0.78	48.04	99.36	40.5

5 Conclusion

As one of the largest temporary works, scaffolding is indispensable, but difficult to manage. Over decades, its requirement has been generally determined based on a percentage factor of the direct work in that project and the expert's opinion. It may result in an ineffective management of scaffolding-related resources and project cost. To address this practical issue, this paper proposes an integrated methodology to predict the required man-hours in the planning stage of the project. There are five main steps in the proposed methodology, which are the data collection, data cleaning, input data determination, development of classification tree structure, and model evaluation.

A case study has been implemented to validate the methodology. From the methodology, four independent variables have been selected at the end. Moreover, it has been found that when use the log-log transformation in the model, the linearity can be built between independent variables and dependent variable. After that, the results show that when using the work classification to build up the classification tree, the performance can be maximized. The best model produces R^2= 0.81, Adj. R^2=0.8, MAE=38.24, RMSE=82.53, and RAE=37.93%.

The current work has been proven to be effective to predict the manhours based on four independent variables which should be available in the early stage of scaffolding construction. However, with the increase of the amount of the available and reliable scaffolding data, the model can be further fine-tuned and trained. Moreover, the non-linear regression such as neural network is still a further research direction and needs to be discovered and compared with the proposed methodology in this research.

6 Acknowledgements

The authors would like to thank the support from our industry partner, PCL Industrial Management Inc. The research funding support from NSERC (Natural Sciences and Engineering Research Council) CRD grant (CRDPJ-536164-18) is also acknowledged.

References

[1] Occupational Safety and Health Services (OSHA) (1994), Safe Erection and use of Scaffolding, Department of Labour, Wellington, New Zealand.

[2] Kumar, C., S. M. AbouRizk, Y. Mohamed, H. Taghaddos, and U. Hermann (2013), Estimation and planning tool for industrial construction scaffolding, Proc., 30th ISARC, International Association for Automation and Robotics in Construction, Bratislava, Slovakia, 634–642.

[3] Wu, L., Y. Mohamed, H. Taghaddos, and R. Hermann (2014), Analyzing scaffolding needs for industrial construction sites using historical data, ASCE Construction Research Congress (CRC), 1596–1605.
[4] Peng, J. L., A. D. Pan, D. V. Rosowsky, W. F. Chen, T. Yen, and S. L. Chan (1996), High clearance scaffold system during construction II, Structural analysis and development of design guidelines, Engineering Structure, 18(3), 258–267.
[5] Yue, F., Y. Yuan, G. Li, K. Ye, Z. Chen, and Z. Wang (2005), Wind load on integral-lift scaffolds for tall building construction, Journal of Structural Engineering, 131(5).
[6] Hou, L., C. Wu, X. Wang, and J. Wang (2014), A framework design for optimizing scaffolding erection by applying mathematical models and virtual simulation, Proc., International Conference on Computing in Civil and Building Engineering, 323–330.
[7] Kim, K., Y. K. Cho, and Y. H. Kwak (2016), BIM-based optimization of scaffolding plans for safety, ASCE Construction Research Congress (CRC), 2709–2718.
[8] Sulankivi, K., T. Mäkelä, and M. Kiviniemi (2009), BIM-based site layout and safety planning, 1st Int. Conf. on Improving Construction and Use through Integrated Design Solution CIB, Espoo, Finland.
[9] Kim, J., M. Fischer, J. Kunz, and R. Levitt (2015), Semiautomated scaffolding planning: Development of the feature lexicon for computer application, Journal of Computing in Civil Engineering, 29(5).
[10] Cho, C., J.W. Park, K. Kim, and S. Sakhakarmi (2018), Machine Learning for Assessing Real-Time Safety Conditions of Scaffolds, Proc., 35th ISARC, International Symposium on Automation in Construction.
[11] Construction Owners Association of Alberta (COAA) (2013), Workforce Planning Subcommittee, Construction Work Packages Best Practice, Construction Owners Association of Alberta (COAA), Document Number: COP-WFP-SPD-16-2013-v1.
[12] Guo, S. J., (2002), Identification and resolution of work space conflicts in building construction, Journal of Construction Engineering and Management, 128(4), 287-295.
[13] Moon, S., J. Forlani, X. Wang, and V. Tam (2016), Productivity study of the scaffolding operations in liquefied natural gas plant construction: Ichthys project in Darwin, Northern Territory, Australia, Journal of Professional Issues in Engineering Education and Practice, 142(4).
[14] Hou, L., C. Zhao, C. Wu, S. Moon, and X. Wang (2017), Discrete firefly algorithm for scaffolding construction scheduling, Journal Computing in Civil Engineering 31(3).
[15] Lucko, G., Anderson-Cook, C. M., & Vorster, M. C. (2006). Statistical considerations for predicting residual value of heavy equipment. Journal of construction engineering and management, 132(7), 723-732.
[16] A. Alin, Multicollinearity, Wiley Interdiscip. Rev. Comput. Stat. 2 (2010) 370–374.
[17] Zar, J. H. (1972). Significance testing of the Spearman rank correlation coefficient. Journal of the American Statistical Association, 67(339), 578-580.
[18] D.G. Bonett, T.A. Wright, Sample size requirements for estimating Pearson, Kendall and Spearman correlations, Psychometrika. 65 (2000) 23–28. doi:10.1007/BF02294183.
[19] A. Hall, Mark, Correlation-based feature selection for machine learning, Diss. Univ. Waikato. (1999) 1–5. doi:10.1.1.149.3848
[20] Salmerón, R., García, C. B., & García, J. (2018). Variance Inflation Factor and Condition Number in. Journal of Statistical Computation and Simulation, 88(12), 2365-2384.
[21] Bland JM, Altman DG. Transforming data. BMJ 1996, 312:770
[22] Bland JM, Altman DG. The use of transformation when comparing two means. BMJ 1996, 312:1153.
[23] Stevens, J. P. 1995. Applied multivariate statistics for the social sciences. 3rd Ed., Lawrence Erlbaum Associates, Hillsdale, N.J
[24] J.H. Kim, Estimating classification error rate: Repeated cross-validation, repeated hold-out and bootstrap, Computer. Stat. Data Anal. 53 (2009) 3735–3745.
[25] Witten, I. H., Frank, E., Hall, M. A. & Pal, C. J. (2016). Data Mining: Practical Machine Learning Tools and Techniques (4th Ed), Elsevier Science.
[26] S.B. Kotsiantis, D. Kanellopoulos, Data preprocessing for supervised leaning, Int. J. (2007) 1–7.
[27] Brevault, L., Balesdent, M., Bérend, N., & Le Riche, R. (2013). Comparison of different global sensitivity analysis methods for aerospace vehicle optimal design. 10th World Congress on Structural and Multidisciplinary Optimization.
[28] Osborne, J. (2010). Improving your data transformations: Applying the Box-Cox transformation. Practical Assessment, Research, and Evaluation, 15(1), 12.

Ontological Base for Concrete Bridge Rehabilitation Projects

Chengke Wu[a], Rui Jiang[a], Jun Wang[b], Jizhuo Huang[c], Xiangyu Wang[c,d*]

[a]School of Design and Built Environment, Curtin University, Australia
[b]School of Architecture and Built Environment, Deakin University, Australia
[c]College of Civil Engineering, Fuzhou University, China
[d]Australasian Joint Research Centre for Building Information Modelling, Curtin University, Australia
*Corresponding author: Xiangyu Wang
E-mail: chengke.wu@postgrad.curtin.edu.au, rui.jiang2@postgrad.curtin.edu.au, jun.wang1@deakin.edu.au, jzhuang_fj@163.com, xiangyu.wuang@curtin.edu.au

Abstract –

Concrete bridges are important infrastructures, which thus need effective rehabilitation to maintain good condition. Bridge rehabilitation projects often have tight schedules, multiple participants and constraints, and scattered project information. Thus, improving information integration in these projects can be critical. This research develops a concrete bridge rehabilitation project management ontology (CBRPMO) to integrate various project information, e.g. information of constraints, tasks, procedures, project participants, and relations between these project entities. The CBRPMO was built based on domain knowledge collected from various documents and was refined in a focus group. The development followed standard procedures. The CBRPMO was also validated in a case study. It turns out the CBRPMO can effectively integrate information and support effective querying, which can save time to manually search for information from scattered sources. The CBRPMO contributes to industry because it expands the boundary and application of ontologies for bridge maintenance by covering the rehabilitation stage.

Keywords –

bridge rehabilitation; project management; semantic web; ontology

1 Introduction

Bridge rehabilitation projects often have a tight schedule and complex tasks with various constraints, e.g. labour, materials, and equipment [1]. Information of these constraints should be timely integrated to assist constraint removal [2]. Moreover, rehabilitation projects involve participants of different backgrounds, who often have isolated databases. Thus, information for managing the project, e.g. constraints and tasks/procedures, are often scattered in project documents or systems [3]. As such, it is essential to improve information integration and exchange in bridge rehabilitation projects so that information can be timely delivered to the right person, e.g. project managers, to support informed decisions.

Ontology is an emerging semantic web technique (SWT), which is built in a standard format while can link heterogeneous information sources. Ontologies have been increasingly applied in construction projects to enhance information integration and sharing [4]. Compared to traditional relational databases, ontologies are more effective to integrate domain-specific and unstructured information, such as constraints related information [5]. Therefore, this study develops the concrete bridge rehabilitation project management ontology (CBRPMO) to integrate information in bridge rehabilitation projects and address challenges of integrating and exchanging information.

2 Related Work

Concrete bridge maintenance includes four stages: inspection, condition evaluation, maintenance decision-making, and rehabilitation. Rehabilitation can include hazard treating, reinforcement, and replacement. Hazard treating fixes damages. Reinforcement increases the structure load-carrying capacity by adding components or materials. Replacement substitutes severely damaged bridge components. In the digital era, many modern information technologies have been applied to collect, analyse, and store bridge data for bridge inspection, monitoring, and decision-making [6, 7].

However, at the rehabilitation stage, studies focus on engineering techniques (e.g. the confinement technique [8], and grouted splice sleeve [9]) and materials (e.g. ultra-high-performance fibre reinforced concrete [10]). Compared to other stages, the rehabilitation stage is also complex and requires extensive information exchange. Rehabilitation projects have a tight schedule, multiple participants, and complex constraints that need to be removed [11]. Constraints are things that prevent work from being smoothly executed (e.g. delay of materials),

and work should not start until all constraints are removed. Constraint removal means required entities of a certain amount and quality are in place on time. The importance of removing constraints is highlighted in other complex projects [12]. Constraint removal relies on identifying constraints based on domain knowledge and sharing constraints related information so that the management attention can be properly directed [11]. However, it can be difficult to access such information in bridge rehabilitation projects because they are often scattered in isolated systems and documents [13]. As such, more efforts are needed to improve information integration in these projects. Bridge management systems (BMSs) and bridge information modelling (BrIM) have been applied for bridge inspection and evaluation and can be used to integrate rehabilitation information as well. However, BMSs are restricted to pre-rehabilitation stages, and they often suffer from the data island problem as they do not adequately consider integration of data of different formats and managed by different parties [14]. Besides, due to features of the industry foundation class (IFC) schema, BrIM tools are good at modelling geometry information rather than semantic information. In this case, SWT-based methods, e.g. ontologies, can be applied.

An ontology is a graphical method for describing domain information and knowledge, which consists of nodes (i.e. classes and instances of classes) and relations (i.e. edges between nodes). Studies of ontologies for information integration focus on building semantic relations between information sources and applying semantic query (e.g. SPARQL) to search for relevant information. Thus, one can not only find contents that match key words textually, but contents semantically related. For instance, a bridge beam can be semantically related to its design drawings. Hence, when searching for the beam, information of the drawing can also be easily explored by navigating the relation between the two ontological instances.

Ontologies can be object or process oriented. The former is based on taxonomies of objects, such as building objects like walls and windows; the latter is based on sequences and constraints of tasks [15]. The object-oriented ontologies are the dominant form, which often stores information that is relatively static, such as material and geometry, defects, quantity and cost, risk, and structure condition from project documents and systems (e.g. BIM and BMS) [16]. Some studies have also built process-oriented ontologies (or as a part of their work) to record information of project progress [15].

However, studies of ontologies in the construction sector focus on vertical buildings and bridge inspection and evaluation. Besides, most ontologies are objects oriented. Therefore, the industry still lacks an ontology especially designed for bridge rehabilitation projects to integrate information specific in such projects, e.g. tasks and procedures, constraints, and participants.

3 Development of the CBRPMO

The ontology development 101 published by the Stanford University was adopted to build the CBRPMO. The document is a general and mature guideline to develop different ontologies and has been applied in several projects in the construction sector[17-19]. The key steps are shown in Figure 1.

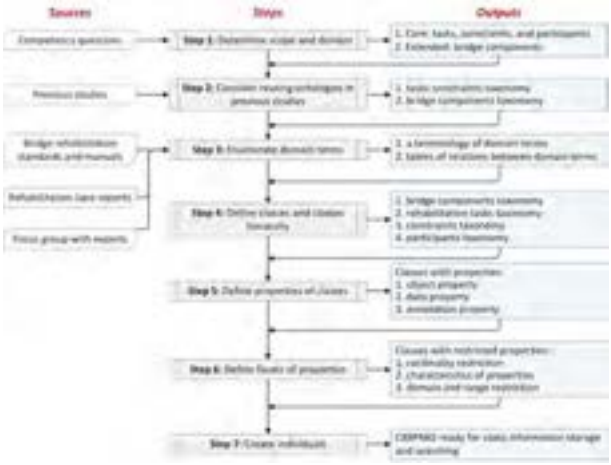

Figure 1. Development process of CBRPMO

3.1 Determine domain and scope

The first step is to define the domain and scope of the ontology. This step can be achieved by answering the following fundamental questions:

Q1: What domain will the CBRPMO cover?

A1: The domain is concrete bridge rehabilitation project management; therefore, the ontological model will cover rehabilitation tasks and procedures, constraints, and project participants.

Q2: For what purpose will the CBRPMO be used?

A2: The CBRPMO aims to improve current project management in bridge rehabilitation projects by integrating project-related information.

Q3: Who will use and maintain the ontology?

A3: The main user is the management team of rehabilitation projects, but other stakeholders, e.g. the bridge owner, can also have access.

Q4: What are the sources for the ontology?

A4: Concrete bridge rehabilitation standards and manuals, case reports, project documents (e.g. work plans and project meeting records), and experts' opinions are the main sources.

Q5: For what types of questions will the CBRPMO provide answers?

A5: The CBRPMO will answers questions that a rehabilitation project manager can ask, e.g. procedures, constraints, detailed activities, precautions of tasks, and methods to address constraints not timely removed.

3.2 Consider reusing existing ontologies

Reusing existing ontologies can save time taken to build the ontology from scratch. Several online ontology libraries were searched, such as the Ontolingua, DAML, and DMOZ; however, no relevant ontologies were found. Current bridge maintenance ontologies focus on the static information of bridge components rather than the rehabilitation project process, and therefore, such ontologies were not adopted [1, 10]. Nevertheless, there are some ontologies including common taxonomies of construction task and constraints [5, 6, 11, 27] which fit the scope of CBRPMO and thus were adopted as reference for the following steps.

3.3 Collecting domain terms

Critical terms of concrete bridge rehabilitation were identified in this step, including project entities, e.g. tasks/procedures, constraints, and project participants, their attributes (e.g. the finish date of a task), and relations between entities. Five types of relations were identified: 1) between tasks and procedures; 2) between procedures and constraints; 3) between constraints, i.e. if one constraint is not removed timely, the removal of its related constraints related may also be delayed; for instance, if design drawings are not provided, working plans depending on the drawings can be delayed; 4) between tasks/procedures and participants supervising the task/procedures; and 5) between constraints and participants responsible for constraint removal.

Table 1. Profiles of focus group participants

Expert No.	Years of experience	Area of expertise
1	8	Application of ICTs in infrastructure projects
2	8	Construction management
3	10	Bridge design and construction
4	11	Bridge maintenance and rehabilitation
5	13	
6	15	

Reviewing related documents is a common approach to realise this step [9, 17, 19]. This study reviewed 11 manuals and 52 cases reports in China, North America, and Australia, because of the large volume and rich experience of bridge maintenance in these regions [1, 13]. A focus group was organised to refine the findings. Six experts from both academia and industry were invited, who were selected based on experience and expertise of bridge maintenance [20] (see Table 1). This is necessary because the initial findings can be biased to the authors' knowledge and thus need to be modified by experts. Moreover, the documents do not adequately reflect the third to fifth relations which are complex to model. For instance, some material constraints can affect removal of equipment constraints, whereas the opposite scenario can occur for other constraints pairs. The relations of supervision and constrains removal also vary among projects. In addition, the documents do not consider the strength of the second and third relation, i.e. a procedure or constraint is more likely to be affected by some constraints if their removal is delayed, which is important to identify critical constraints.

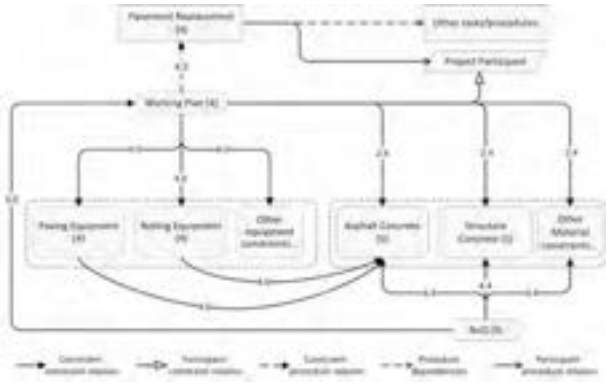

Figure 2. Partial view of the obtained relations (the numbers in this figure indicate the level of the class in the constraint hierarchy in Figure 5)

The results of this step include a terminology and knowledge of relations. The terminology maps tasks and procedures to constraints, and participants while records attributes of these entities. The obtained relations are shown in Figure 2. It should be noted that: 1) constraints are divided into groups (Figure 5) to facilitate relations setting-up; 2) only direct relations are considered; for instance, the bill of quantities directly affects material delivery, but it can also indirectly affect equipment supply by affecting working plans that determine the equipment, but such relation is addressed by the work plan; 3) relation strength ranges from 1 to 5, and larger numbers indicate higher strength; 4) Strength is rated at the most specific sub-classes of the constraint hierarchy under which, according to the experts, constraints have similar impact on others and thus can share the strength (see Figure 2); 5) because of the reliance on project conditions, experts only provide common practices for the fourth and fifth relations; for instance, sub-contractors often provide labour. Thus, such relations can be setup in specific projects.

3.4 Define Classes and Classes Hierarchy

In this step, classes are extracted from domain terms, using a mixed extraction approach where the most salient classes are extracted first, which are generalised and specialised. For instance, the term 'Deck System Replacement' is extracted, and then, 'Replacement' is extracted as its super-class, while terms like 'Pavement Replacement' and 'Auxiliary System Replacement' are extracted as its sub-classes. The classes are divided into four groups: rehabilitation task, constraint, project participant, and procedure. Each group forms a taxonomy and can be expanded up to the fifth level (as shown in the white boxes in Figures 4-6). A high-level overview of the CBRPMO is shown in Figure 3.

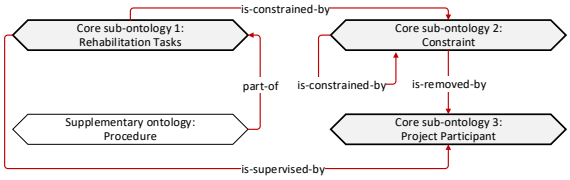

Figure 3. High-level overview of the CBRPMO

The taxonomy of rehabilitation tasks is shown in Figure 4. It should be noted that a task is often formed by procedures so that some procedures can proceed without removing all constraints. Thus, a taxonomy of procedures is built, with four basic classes: preparation, inspection, execution, and acceptance. A task can have some or all of these procedures, and a procedure can be detailed and expanded.

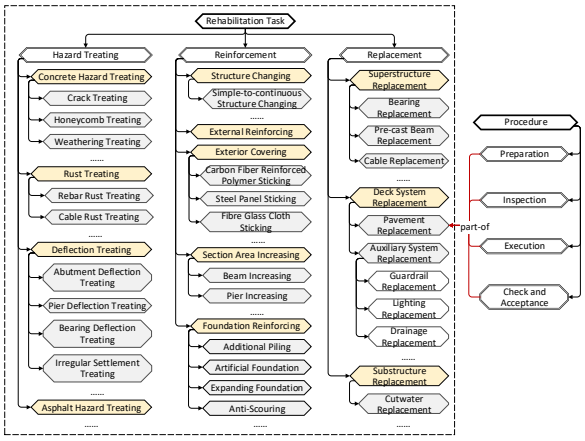

Figure 4. Overview of the tasks' taxonomy

The constraints taxonomy is shown in Figure 5. The engineering constraints refer to the absence of drawings and approvals, supply chain constraints include late delivery of materials and equipment, and site constraints hinder work of on-site crews [2].

The project participant taxonomy is shown in Figure 6. This taxonomy is mainly divided by responsibilities of participants, while project-level participants are first divided by project phases.

Figure 5. Overview of the constraints' taxonomy

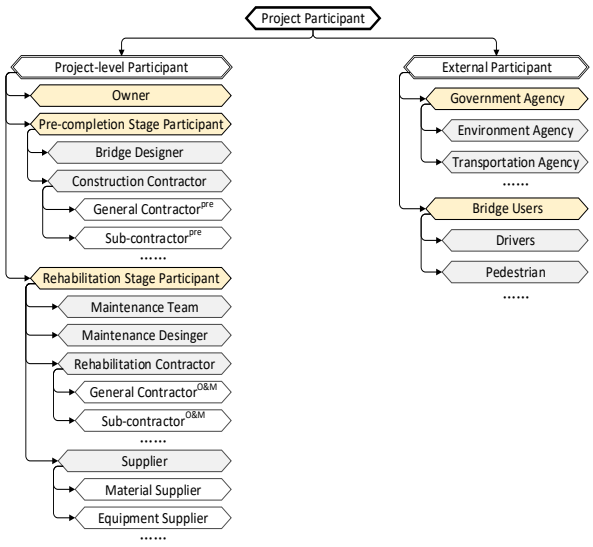

Figure 6. Overview of the taxonomy of project participants

3.5 Define Properties

Properties are relations that connect two classes or a class and its attributes, forming a subject-property-object triple [21]. There are three types of properties, i.e. object, datatype, and annotation properties. Object properties

describe relations among classes and instances of classes (Step 7), e.g. the 'is-constrained-by' relation between procedures and constraints and between two constraints. Datatype properties describe quantitative or qualitative attributes of classes and their instances. For instance, the 'Constraint' class has a 'has-planned-removal date' property linking the constraint to its expected date of removal. Annotation properties add explanations of classes, instances, and other properties. They can be applied to set relation strength between constraints and between procedures and constraints. Figure 7 shows examples of object properties while Figure 8 shows examples of datatype and annotation properties.

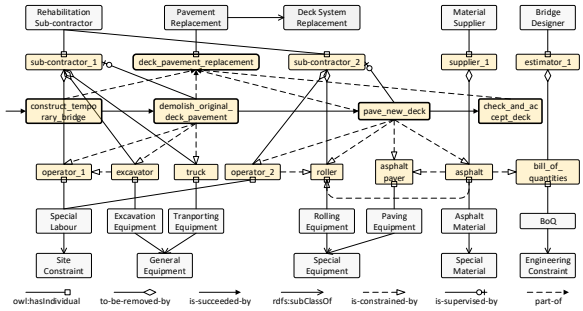

Figure 7. Properties in the CBRPMO

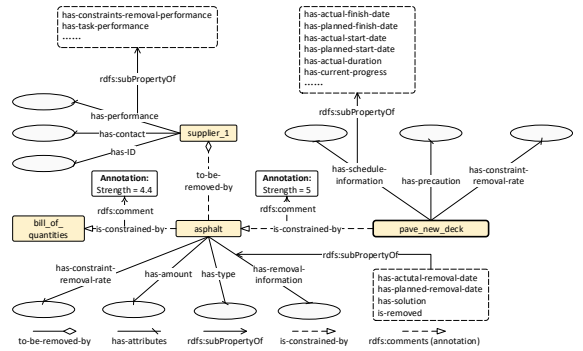

Figure 8. Properties in the CBRPMO

3.6 Define facets of properties

Facets can enrich semantics of properties, including cardinality restrictions, characteristic settings, and domain and range restrictions. Cardinality restrictions specify the number of values that a property can have, for instance, the 'has-actual-finish-date' property has a single cardinality because a task has only one actual finish date. For characteristics, object properties in the CBRPMO can be normal (no characteristics), transitive, symmetric, asymmetric, and invertible. A detailed introduction of characteristics can be found in [22]. Domain and range restrictions specify the type of the subject and object of a property, respectively. The type can be either datatypes or classes. For instance, the domain of 'has-actual-finish-date' and 'is-constrained-by' should be 'Date' datatype and 'Constraint' class, respectively. Properties and their facets are defined at the class level, which are inherited by instances of the class. For instance, during instance creation (Step 7), a task instance cannot be connected to a constraint instance through the 'is-supervised-by' because the property's range, i.e. object, is restricted to 'Project Participant'.

3.7 Create Instances

Instances represent specific and physical entities of abstract classes. For instance. the 'asphalt paver' and 'roller' in Figure 7 are instances of the class 'Special Equipment'. Instances creation is project dependent and should be performed during ontology implementation. The number of instances depends on the complexity and scale of the project whereas the names of instances can be flexible as long as they are consistent. Finally, as mentioned, properties of instances should comply with definitions of their classes.

4 Case Study

For a new ontology, its semantic and syntactical correctness must be verified. Semantic validation should be completed before implementing CBRPMO in real projects. This can be realised by asking competency questions, consulting experts, and ontology alignment. CBRPMO is a new ontology and there are no similar ontologies for cross comparison. Hence, the first two methods were adopted. Asking competency questions is a simple way to check semantics of CBRPMO[23]. Such questions should echo questions in A5 of Step 1 and cover both classes and instances, such as: 1) how many sub-classes do certain constraint classes have; 2) what are the constraints of certain constraints and procedures; 2) what are the planned/actual finished date of certain procedures; and 4) who are the participants responsible for removing certain constraints? Artificial instances (created by the authors for validation) can be created, and the CBRPMO is checked if it contains enough information to answer the questions.

Above self-checking was performed by the authors periodically during ontology development, which to some extent ensured semantic correctness of CBRPMO. In addition, the initial CBRPMO (i.e. without instances which should be created during implementation in practice) was sent to experts of the focus group mentioned before. The authors explained each class and property, e.g. the definition of the class and reasons to setup the property, to the experts to further validate semantic correctness and modify the ontology.

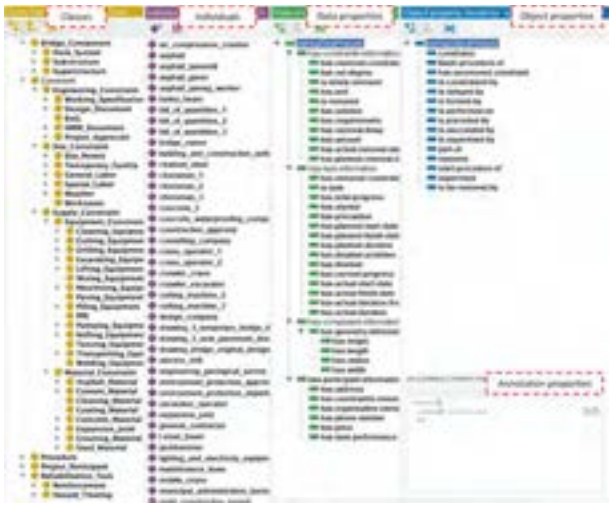

Figure 9. Partial review of the CBRPMO in the Protégé

On the other hand, syntactical validation checks the CBRPMO against ontology syntax, e.g. subsumption, equivalence, and consistency. Syntactical validation should be performed in both ontology creation and implementation phases. The validation can be realised by the Pellet reasoner which can detect syntactic errors in ontologies automatically. Whenever the CBRPMO was modified because of either self-checking or specific project conditions, the reasoner was ran to ensure the CBRPMO can pass syntactical validation [23].

The CBRPMO was implemented in a real project to demonstrate its usefulness for information management. This requires three components. 1) The ontological base. 2) A tool that can edit the ontology, where Protégé 5.50 was adopted. 3) A reasoner, i.e. Pallet, which interacts with the ontology by sending and interpret queries.

A rehabilitation project performed on the Jinghu bridge in Zhejiang, China, was selected to validate the CBRPMO. The bridge is a suspension bridge which is 415-m long. The rehabilitation took about five months (May to October 2018). The CBRPMO was implemented by creating instances and setting up and modifying properties between the instances by combing domain knowledge previously obtained and project specific information, such as information provided by the project team and information in project documents, e.g. work plans and equipment and material inventories. The resultant ontology in Protégé is shown in Figure 9.

The case focused on the deck pavement replacement task because it was the most time-consuming (more than 4 months) and labour-intensive task and it required more constraints than other tasks. It was assumed that the project manager wanted to search for information of the task. Instead of looking for information scattered in project documents or systems manually, the CBRPMO encoded relevant information to support efficient queries using SPARQL, which is demonstrated in Figure 10. To reflect the traditional method of searching information, the same information was manually searched by the authors in project documents and management systems. Then, the searching time was cross compared to show capability of the ontology.

Figure 10. SPARQL queries and results

Query 1 (Figure 10 (a)) not only shows constraints of a procedure (e.g. steel materials for temporary bridge construction) but also requirements (e.g. type and amount) of constraints, so that the manager can arrange constraint removal more easily.

Query 2 (Figure 10 (b)) can rapidly retrieve related information (e.g. contact information) of project participants (e.g. asphalt supplier), which can facilitate communication between the participants.

Query 3 (Figure 10 (c)) can show detailed activities and precautions of a procedure (e.g. new deck pavement). Such information can be generally required by onsite foreman and supervisors to supervise work sequences and quality.

Query 4 (Figure 10 (d)) can answer questions related to solutions to unremoved constraints (e.g. rain), serving as remedial actions when delay occurs.

The information of query 1, 2 and 3-4 was scattered in a project meeting record, an address book, and a work plan, respectively. A few information (e.g. certain steel materials to construct the temporary bridge) needed consulting the project team, which further increased the searching time. Table 2 compares the searching time through the CBRPMO and manual approach. It turns out searching time can be reduced significantly when the information from scattered sources is integrated.

Table 2. Comparison of searching time

Query	CBRPMO	Manual searching

1	0.13s	562s
2	0.08s	116s
3	0.09s	77s
4	0.11s	108s

In addition, the CBRPMO can also identify critical constraints of procedures and tasks. Specifically, the ontology forms a network with classes and instances as nodes and properties (i.e. relations) as edges. Hence, network measures (i.e. in-degree and out-degree) can be computed for every constraint instance, where the former reflects vulnerability (i.e. how many constraints can affect it), while the latter reflects its impact (i.e. how many other entities it can affect). The in- and out-degree of a constraint instance is computed by counting the number of inward and outward properties, weighted by the relation strength stored in annotation properties. Constraints with high degree are regarded as critical.

Figure 11 illustrates critical constraints at different levels. Figure 11(a) shows results at the procedure (i.e. new deck pavement) level. The vulnerable constraints include workspace, approvals, and equipment. Thus, more attention should be given to their constraints and responsible participants to minimise delay. Figure 11(b) shows constraints with greater impact on others at task (i.e. deck replacement) level, including engineering drawings, approvals, permits, and temporary facilities. Thus, they should be closely monitored, additional buffer should be assigned to procedures constrained by them, and remedial solutions should be proposed to mitigate impact when their removal is delayed.

Figure 11. Identification of critical constraints

5 Discussion and Conclusion

Successful rehabilitation projects are important for bridge maintenance. Such projects require effective integration of project information. The challenge is that such information is often buried and scattered in project documents and systems. However, studies on bridge rehabilitation are limited to engineering techniques and methods, which do not cover information management. In addition, although ontologies are effective tools to manage heterogenous and unstructured information, previous ontologies in the construction sector focus on integrating information of static objects of vertical building and bridge inspection and evaluation [4, 16]. However, bridge rehabilitation projects have specific information, e.g. specific constraints and tasks. Thus, existing ontologies cannot be directly applied. The proposed CBRPMO focuses on the rehabilitation stage therefore can bridge the gap. The CBRPMO was built by reviewing rehabilitation knowledge in case reports, manuals, standards, and related studies, which was refined through a focus group. As such, the CBRPMO covers sufficient knowledge in the bridge rehabilitation domain and can integrate scattered information of constraints, tasks and procedures, and participants in a software neutral environment.

The CBRPMO is an effective tool to integrate and search for various information in scattered sources, such as constraints of procedures, information of participants, solutions of unremoved constraints, as well as critical constraints. Moreover, extensibility and flexibility are important for ontologies. The CBRPMO can be merged with existing ontologies without major modifications. For example, the 'Procedure' class can be linked to bridge components in ontologies developed by [16, 17] through an object property 'is-performed-on'. However, currently, the CBRPMO was built manually, which can be time-consuming and inefficient. Therefore, the future studies will focus on automating development of the CBRPMO. For instance, information extraction methods can be employed to extract information from source documents for ontology development (e.g. manuals and standards) then automatically identify relevant classes and properties. Nevertheless, this study still lays a basis (e.g. the basic framework of the ontology) to implement those advanced techniques.

To this end, it can be argued that the CBRPMO has made a contribution by expanding ontologies in the bridge sector to cover the rehabilitation stage while it is also compatible with previously developed ontologies. As demonstrated in the case study, when the CBRPMO was implemented in projects, the project teams can access critical information for project management quickly rather than manually searching the scattered documents. Thus, enormous time can be saved, and the efficient exchange of information can also facilitate informed management decision-making.

References

[1] Frangopol, D.M. and P. Bocchini, Bridge network performance, maintenance and optimisation under uncertainty: accomplishments and challenges. *Structure and Infrastructure Engineering*, 8(4): p. 341-356, 2012.

[2] Wang, J., et al., Developing and evaluating a framework of total constraint management for improving workflow in liquefied natural gas construction. *Construction Management and*

Economics, 34(12): p. 859-874, 2016.

[3] Park, C.S., et al., A framework for proactive construction defect management using BIM, augmented reality and ontology-based data collection template. *Automation in Construction*, **33**: p. 61-71, 2013.

[4] Zhou, Z.P., Y.M. Goh, and L.J. Shen, Overview and Analysis of Ontology Studies Supporting Development of the Construction Industry. J*ournal of Computing in Civil Engineering*, **30**(6), 2016.

[5] Xu, X. and H. Cai, Semantic approach to compliance checking of underground utilities. *Automation in Construction*, **109**: p. 103006, 2020.

[6] Riveiro, B., M.J. DeJong, and B. Conde, Automated processing of large point clouds for structural health monitoring of masonry arch bridges. *Automation in Construction*, **72**: p. 258-268, 2016.

[7] Carrion, F.J., J.A. Quintana, and S.E. Crespo, SHM of a stayed bridge during a structural failure, case study: the Rio Papaloapan Bridge. *Journal of Civil Structural Health Monitoring*, **7**(2): p. 139-151, 2017.

[8] Ma, C.K., et al., Repair and rehabilitation of concrete structures using confinement: A review. *Construction and Building Materials*, **133**: p. 502-515, 2017.

[9] Parks, J.E., et al., Seismic Repair of Severely Damaged Precast Reinforced Concrete Bridge Columns Connected with Grouted Splice Sleeves. *Aci Structural Journal*, **113**(3): p. 615-626, 2016.

[10] Bastien-Masse, M. and E. Bruhwiler, Ultra high performance fiber reinforced concrete for strengthening and protecting bridge deck slabs. *Bridge Maintenance, Safety, Management and Life Extension*, p. 2176-2182, 2014.

[11] Hamdi, O., Advanced work packaging from project definition through site execution: driving successful implementation of WorkFace planning. *The University of Texas at Austin*, 2013.

[12] Li, X., et al., SWP-enabled constraints modeling for on-site assembly process of prefabrication housing production. *Journal of Cleaner Production*, **239**, 2019.

[13] Woldesenbet, A.K., Highway Infrastructure Data and Information Integration & Assessment Framework: A DataDriven Decision-Making Approach, *Iowa State University*: Iowa, USA, 2014.

[14] Liu, H.X., M. Lu, and M. Al-Hussein, Ontology-based semantic approach for construction-oriented quantity take-off from BIM models in the light-frame building industry. *Advanced Engineering Informatics*, **30**(2): p. 190-207, 2016.

[15] Dong, H., F.K. Hussain, and E. Chang, ORPMS: An Ontology-based Real-time Project Monitoring System in the Cloud. *Journal of Universal Computer Science*, **17**(8): p. 1161-1182, 2011.

[16] Liu, K.J. and N. El-Gohary, Ontology-based semi-supervised conditional random fields for automated information extraction from bridge inspection reports. *Automation in Construction*, **81**: p. 313-327, 2017.

[17] Ren, G.Q., R. Ding, and H.J. Li, Building an ontological knowledgebase for bridge maintenance, *Advances in Engineering Software*, **130**: p. 24-40, 2019.

[18] El-Diraby, T.E., Domain Ontology for Construction Knowledge. *Journal of Construction Engineering and Management*, **139**(7): p. 768-784, 2013.

[19] El-Gohary, N.M. and T.E. El-Diraby, Domain Ontology for Processes in Infrastructure and Construction. *Journal of Construction Engineering and Management*, **136**(7): p. 730-744, 2010.

[20] El-Diraby, T.E. and H. Osman, A domain ontology for construction concepts in urban infrastructure products. *Automation in Construction*, **20**(8): p. 1120-1132, 2011.

[21] Niknam, M. and S. Karshenas, A shared ontology approach to semantic representation of BIM data. *Automation in Construction*, **80**: p. 22-36, 2017.

[22] Hitzler, P., M. Krotzsch, and S. Rudolph, Foundations of semantic web technologies. Chapman and Hall/CRC, 2009.

[23] Stanford University. Ontology Development 101: A Guide to Creating Your First Ontology. Stanford University, San Francisco, USA, 2002.

IoT Enabled Framework for Real-time Management of Power-Tools at Construction Projects

Ashish Kumar Saxena[a], Varun Kumar Reja[a], and Koshy Varghese[a]

[a]Department of Civil Engineering, IIT Madras, India
E-mail: ashishsaxena816@gmail.com, varunreja7@gmail.com, koshy@iitm.ac.in

Abstract-

Real-time monitoring of the condition of equipment enhances effective decision-making in terms of machine maintenance and operational efficiency. This study presents a multi-layered system architecture to monitor the real-time health of a sensor-integrated hand-tool. The architecture is designed based on specific components, features, and requirements of each layer. The study discusses the flow of information in the system and addresses compatibility issues. The selection of required hardware and software was made based on the applicability and compatibility of various available alternatives. The selected modules were a sensor unit, an open-source IoT Platform, and a Wi-Fi Module. A prototype of the sensing unit was developed and was integrated with the tool for conducting the experiments to acquire the vibration data. The experimental setup was designed, and the free-run mode and drilling-mode acceleration data were generated. The obtained real-time acceleration plots indicate that the overall IoT system performed as intended. The quality of the data was verified using the Western Electric rules. The study extends the framework to a warning system using a freeware web-service, which operates sequentially. Upon arriving at the threshold value of acceleration, the web-service automatically sends a warning message to the maintenance team for on-time maintenance.

Keywords –

Smart Maintenance; Internet of Things (IoT); Predictive Maintenance; Construction 4.0; Construction Tools Management

1 Introduction

"*Global Construction 2030*" estimates the construction output to grow by 85% worldwide by 2030 [1]. As per the empirical data and prediction of this study, this growth will be accompanied by the increasing use of small power tools that are essential to improve the productivity of the workforce. As practical experience and productivity logic demonstrates, timely and continuous availability of the tools ensures uninterrupted work at the sites. The relevance of smooth-functioning machines in operational sites may be derived from the survey conducted by one of the leading asset manufacturers Hilti Corp., which clearly quotes that "*On average of 90 hours a month are spent searching for assets across construction sites*." [2]. Apart from theoretical study and predictions, industry professionals also equate the loss in productivity with mismanagement of power tools, which results in tools going unaccounted and undocumented or noticed only when there is a requirement of the machine, thus furthering machine-attrition, waste, and loss of time. These seemingly minor losses can cumulatively result in overall delays in the project, causing heavy monetary and reputation loss. Addressing such loss is thus imperative from an academic as well as industry point of view. The mismanagement can be due to inconsistent implementation and monitoring.

Tools that are not maintained properly can perform below par or disrupt work through breakdowns, adversely affecting, not just their own functions but also of the interconnected tasks. As evident from most of the studies, most construction sites lack a systematic surveillance and maintenance strategy [3]. Currently, the best practices in tool maintenance rely on periodic maintenance either as specified by the manufacturer or when there is an apparent malfunction. However, technological advancements have made it possible to monitor and calibrate the characteristics of a tool in operation in more reliable, robust, and consistently cumulative manner. Based on the pattern changes in functioning tool characteristics; proactive and pre-emptive maintenance measures may be taken to resist machine attrition. Such measures can minimize operational interruptions and ensure the optimal performance of tools and workforce.

The objective of the study is to develop and test a framework for an IoT Enabled predictive maintenance schedule using real-time data. This will also facilitate remote monitoring of assets, making decision-making more efficient and rational. Most importantly, it will

aspire to offer a model that may be mapped on to complex situational systems, ensuring optimal machine productivity and safety with multiple monitoring frames.

As per a survey on power tools, drilling machines are among the most widely used hand tools in the construction industry [4]. As drills are constantly utilised on demanding tasks, they tend to require constant monitoring and maintenance to ensure the best performance. The scope of the current study is limited to the monitoring of hand-held drilling machines.

In terms of structure, this paper is broadly divided into four sections. The first section reviews the current practices in the field of equipment health maintenance. The second section explains the system architecture and design. This section explains the individual layers and their components and the flow of data across them. The third section studies the various parameters that affect the health of the machine. This section also describes the experimental setup and documents the results obtained. The final section discusses the results and intends the integration of the proposed framework with MathWorks' '*Predictive Maintenance Toolbox*' and its use in Machine prognostics. This section concludes the study with discussion on the future research scope in the domain of maintenance studies.

2 Review of Maintenance Planning

This section presents a brief review of maintenance planning and discusses the potential of IoT technologies for construction management.

2.1 Maintenance Planning

Equipment require maintenance due to various factors, ranging from systemic to situational. Usage patterns and ageing of the machine are key factors causing a decrease in reliability and functional ability of an equipment over time [5]. Most construction sites follow a time-based maintenance schedule for pragmatic purposes and in compliance to conventional industry requirements. Figure 1 shows a comparison of the three broad types of maintenance strategies in the industry [6].

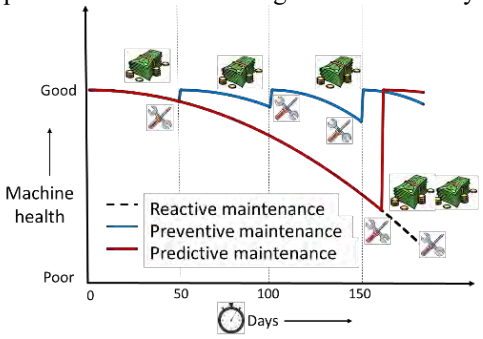

Figure 1. Maintenance Strategies based on MathWorks

The figure shows a trade-off between the usable life of the machine and the potential cost incurred in the maintenance. It clearly states that the predictive maintenance strategy is the most suitable among the three strategies, considering the improvement in the useful life in a more cost-efficient manner. This ensures pre-emptive measures and utilization of the machine and its components apropos of the designed life. This also confirms a method most suited to address unforeseeable interruptions based on its immediate condition.

Predictive Maintenance or Condition Based Maintenance (CBM) is based on monitoring of the visible performance parameters that indicate the deterioration of the machine. Some of these parameters for a drilling machine include vibration threshold, Rate of penetration (ROP), and temperature rise. Vibration-based condition monitoring can facilitate early detection of the problem, improve maintenance procedure, and avoid catastrophic failures which will ensure fullest functionality and uninterrupted usage of the machine [7]. CBM ensures that each component receives customized care, which also addresses the overall health and smooth functionality of the machine.

2.2 Potential of IoT technologies

Recent studies have shown the potential of sensor integrated automated systems to address abrupt impediments and perform customized micro-management of machines. The systems find a variety of applications in the field of personnel management, prefabrication, material management, and enhancing safety and quality at construction sites [8]–[10]. These systems allow detecting, analysing, measuring, and processing various changes like change in position of resources, the dimension of a facility, and textural appearance that occur in construction sites. Practitioners have appreciated the contribution of IoT based systems for batching plant monitoring, diesel generator utilization, and asset tracking systems for heavy machinery such as tower cranes, transit mixers, and trucks. Moreover, applications such as early flood detection (warning) system, predicting the location of workers in construction sites are thought-provoking ideas that can be utilised for efficient construction management. As most of the work in the field of IoT is focussed in monitoring the heavy machinery, workforce management, inventory management, and progress forecasting, power tools have been almost kept out of the scope of the IoT implementation. Hilti Corp., Trackinno, Qubes, and BOSCH are some of the pioneers in the field of automated power tool management system but most of the innovations in this field serve administrative purposes. These include maintaining a database of the tool, automatic utilization reports, and warnings about the pre-loaded maintenance schedule [11]–[13].

In Construction 4.0, an automated CBM framework can facilitate real-time health monitoring of the machine without any human intervention. This will reduce the chances of errors due to human involvement, such as delayed, misinterpreted, and manipulated information. IoT enabled system frameworks can enable real-time data transmission from the machine to the managers. The use of appropriate sensors is a crucial aspect of any IoT system for customized control and overall functionality. Understanding the behaviour of Micro-Electro-Mechanical Systems (MEMS) and the characteristics of an accelerometer or gyroscope allows designers to design more efficient and low-cost products for high-volume applications [14]. Various types of sensors, like RFID sensors, sound, and vibration sensors can discover the changes in the patterns of the data and can be part of an effective warning system, connecting each machine component to the overall machinery.

The selection of suitable sensors is a vital part of an IoT system, which integrates information and pre-emptive action through triggers and warning signals. There are various types of sensors ranging from a simple temperature and pressure sensor to a very sophisticated MEMS sensor such as MPU6050 and ADXL345, which can be selected based on specific situational requirements. Studies show that MEMS sensor-based systems have the potential to transfer the data over a network to an IoT platform using micro-controllers and Wi-Fi connectors [15]. The current study tries to create a warning system based on the real-time vibration values from the tool.

The literature on various IoT based frameworks shows that some of the major challenges in the implementation of IoT based system are privacy, security, and power consumption requirements of the system. The dynamic, complex, and often unpredictable nature of the environment at a construction site is also considered to be one of the major challenges along with the interoperability of different data formats, extendibility, and middleware challenges such as reliability and usability [16]. Some of the researchers have identified and argued that the failure of the IoT implementation could be attributed to scalability, adaptability, connectivity, maintainability, and inter-compatibility of the IoT components [17]. The current study averts the compatibility issue by identifying the resources that are fulfilling the requirements of the layers of a typical IoT system architecture. In the process, it aims to offer a reliable and elegant model where the practical impediments can be addressed and redressed at low cost.

3 System Architecture & Design

The overall system architecture and component-based design is a key part of this work. Figure 2 shows the layered architecture, the specific components, features, and requirements for each layer. These requirements of the layers are based on literature, on-line forums, and discussions held with the industry practitioners. Enabling the implementation in a constrained and complex environment requires a well-defined and robust IoT architecture [17]. Resource constraints such as low memory, bandwidth, and processing can pose challenges to practical implementation of IoT. This section discusses the details of each layer and the components required to implement this architecture for monitoring hand-held drilling equipment. The resources identified are found the best to serve the purpose of the study while fulfilling the specific layer requirements with their unique conditions. The resources are selected based on a comparative study of their counterparts, considering the future scope, cost and spatial benefits. As the MPU6050 sensor is a 6DOF with an integrated accelerometer, gyroscope, and a thermal sensing unit, it is expected to serve a wider range of applications at a reasonable cost. This also solves the issue of space constraint, by using single sensor that has multiple sensing units.

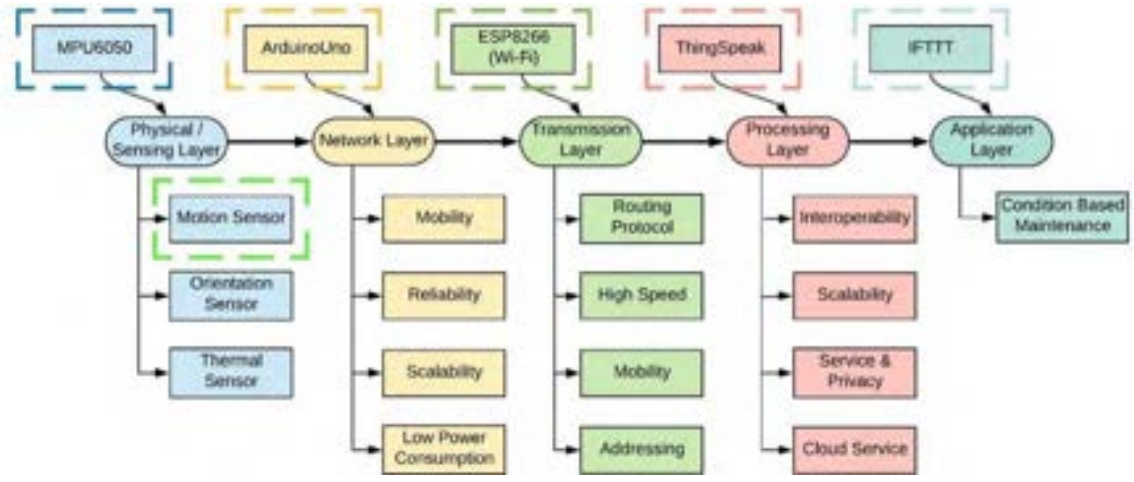

Figure 2. Resource identification in the IoT architecture layers

3.1 Multi-layered Architecture

A brief description of the architecture is as follows:

3.1.1 Physical / Sensing Layer

This layer senses the data through various sensors. It uses MPU6050, an MEMS sensor that measures acceleration, velocity, orientation, displacement in addition to the temperature sensing. This study uses the acceleration readings only, however angular and thermal sensing can add to the value and space utilization of the sensor over others. The "InvenSense document for the specification of MPU6000 and MPU6050" provides information about the connections and the key pin-values. The sensitivity of the accelerometer can be adjusted between ±2g to ±16g, to customize the requirement.

3.1.2 Network Layer

This layer acts as a communicator and transfers the data to the network through the Wi-Fi module. It uses ArduinoUNO, an open-source microcontroller which is equipped with pins for digital and analog input/output data. The sensor and the Wi-Fi module are connected to the Arduino by jumper wires. Arduino collects and transmits the data as per the code written in the IDE (Integrated Development Environment) [18]. The IDE is a cross-platform application that supports coding in most of the computer languages such as java, python, MATLAB, C, or C++. The necessary codes are available on github.com, which can be modified and be uploaded in the editor. The system should meet the minimum requirements to use the Arduino editor smoothly [19].

3.1.3 Transmission Layer

This layer comprises of a Wi-Fi module that transfers the data over the network without the use of any cable or direct communication material. In the current study, ESP8266, an economic Wi-Fi module is used that transmits the data to the IoT platform. The major impediments to the effective functioning of the module is poor network connectivity and volume of data being transferred. The quality network connectivity can affect the time in transferring the data and thus affect the overall functioning of the entire unit.

3.1.4 Processing Layer

This layer contains an IoT platform that is designed to enable a symbiotic relationship between the functioning machines and the maintenance personnel. ThingSpeak is chosen as the IoT platform here, which is an open-source platform and allows a more flexible and interactive interface. Real-time data collection, data analysis, data processing, data visualization, and message transmission are some of the key features of this platform. It is an intuitive, interactive, and inclusive operating system accommodating a wide range of user interfaces enabling a reliable monitoring environments such as C, Node.js, Python, and MATLAB.

3.1.5 Application Layer

This layer facilitates actuation from mobile or web-application for the end-users. IFTTT is a freeware web-based service that triggers the notification as soon as a certain condition is met. It uses real-time APIs (Automated Program Interface) to trigger the event and execute the action [20]. It can thus on auto-pilot mode and generate unique and relevant responses addressing complex and fast-changing situations. It also minimizes human intervention and the errors that can emerge from the same during dysfunctional moments that can potentially create disasters and hazards at workplace.

3.2 Flow of data

After identifying the resources for the study, a framework for the flow of data is necessary. Figure 3 shows a schematic diagram for the flow of data from the point of sensing to the point of notification. The diagram also considers the function that is to be performed in conjunction with each IoT ecosystem layers. This subsection explains interactions and interconnectedness among the various resources and the unique roles they play in the proposed framework.

MPU6050 sensor senses the three directional motion

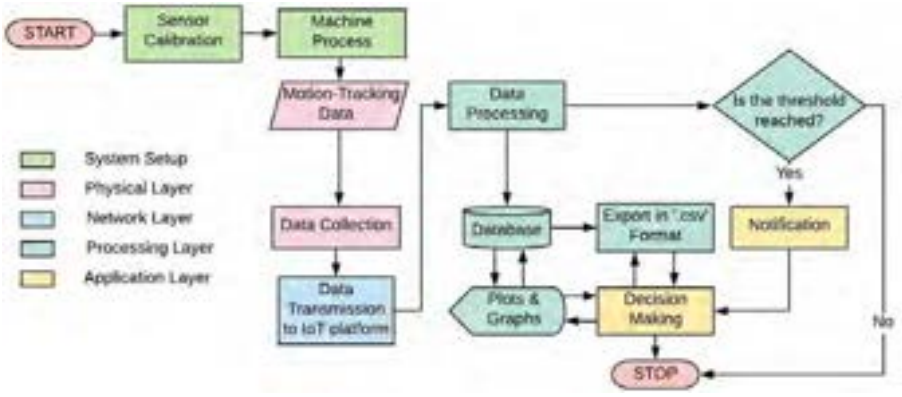

Figure 3. Flow Proposed system

of the machine. ArduinoUNO acts as a communicator for storing and transferring the data to 'ThingSpeak' through Wi-Fi module ESP8266 and data customization as per the application. The ArduinoUNO coding uses I2C library for transmission and easy functioning. ThingSpeak allows us to create channels to visualize the data. The data is transferred to the channels using the respective APIs, which ensures that correct data is used for analysis.

Moreover, ThingSpeak has an integrated 'Predictive Maintenance Toolbox' that facilitates the deployment of an analytical algorithm. A suitable algorithm can be used for estimating the Remaining Useful Life (RUL) of the machine. Another web-based freeware service IFTTT enables to create an event in order to run the system in real-time. The event includes the HTTP link of the ThingSpeak channel, threshold value, and the message that is to be displayed while notifying. The notification can be sent through Email or SMS. As soon as the threshold condition is met based on the data analytics, IFTTT triggers the alarm to the O&M team for timely intervention and maintenance.

4 Experimental Methodology

Having set up framework for the study, an experiment is designed to check the functionality of the proposed system. As already discussed, many performance parameters can be visible and reliable indicators of the machine's health. Figure 4 shows the cause and effect of the parameters that affect the performance indicators of a machine. A drilling operation includes multiple changes in the working environment of the machine. It can be understood from the literature and discussions held with the practitioners that one of the most explicit and easily recognisable indicators of the health of a machine is the amount of vibration produced. The amount of vibration largely depends on the age and size of the machine and drill-bits, the pressure applied while drilling, type of material drilled, and continuous usage of the machine. Process instabilities and wearing out of the cutting tool can be easily recognised by the changes in vibration patterns.

The interdependency of the indicators, as shown in Figure 4, allows us to explore further the effect of these input parameters on the performance indicators. Based on the discussions, the scope of the current study is limited to the accelerometer readings only, but the framework presented is theoretically applicable to all sensor-based systems with a suitable selection of sensors.

The experimental runs were conducted for various combinations of varying drill bit diameter (D: 5mm, 6mm, and 8mm) and plywood thickness (T: 12mm and 19mm) to check the variations in the acceleration produced in the machine, Rate of Penetration (ROP), and Time of Penetration. Figure 5 shows a schematic diagram for the proposed experimental setup.

The sensor-system comprising of MPU6050, ArduinoUNO, and ESP8266 is attached to the drilling machine. The material to be drilled is fixed in a firm place to prevent its movement. The sensor-system transmits the data to the ThingSpeak platform, which plots graphs, displaying the real-time acceleration produced in the three directions. Once the acceleration crosses the threshold (pre-fixed value), a warning is sent to the maintenance engineer for action. The data can also be downloaded in '*.csv*' format for records and further analysis. Thus, this model allows innovative intervention as well as archiving of data for production of templates that may be drawn on for future references.

4.1 Data Processing

Statistical Process Control (SPC) suggests the minimum number of data points to check the appropriateness of the experiment in Eq. (1):

$$ARL = \frac{1}{p} \quad (1)$$

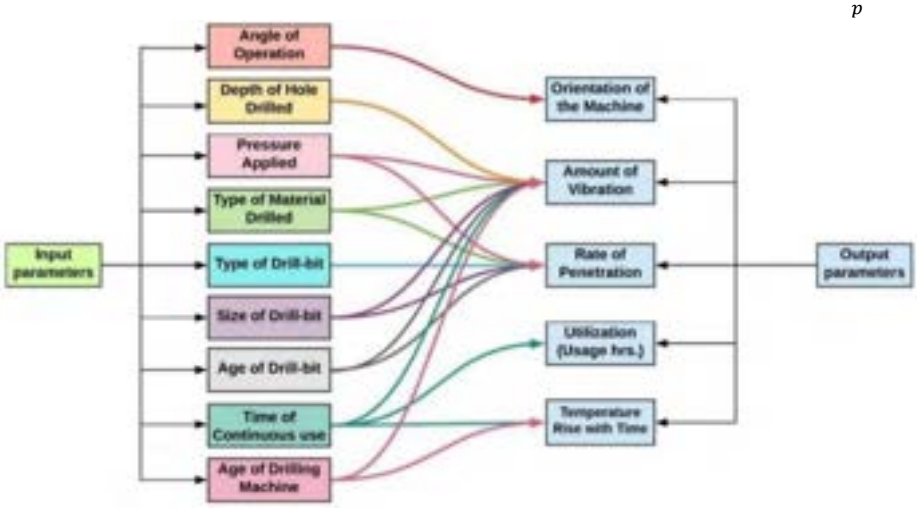

Figure 4. Factors affecting the performance

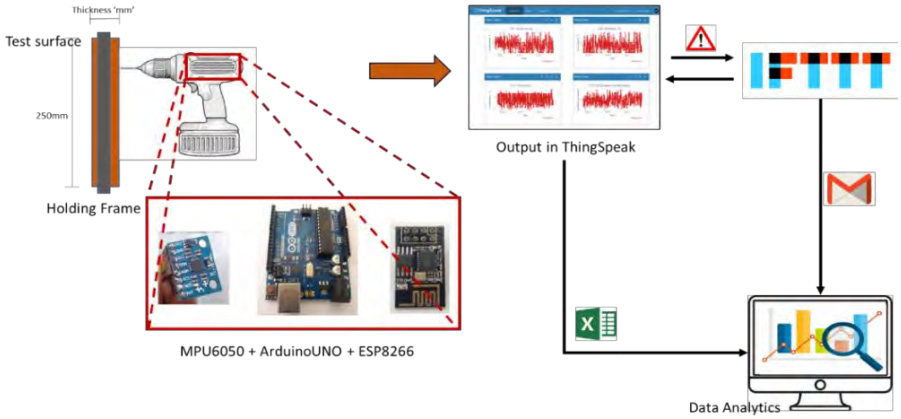

Figure 5. Schematic Diagram for Experimental Setup

For ±3σ control limits, p = 0.0027. Substituting value of 'p' in in Eq. (1) we get, ARL = 370 data points [21].

The trial runs were conducted for different D-T combinations to estimate an average penetration time for each combination. The code (ArduinoIDE) is adjusted so that the number of points is not less than 370. A drilling run is continued until the hole is perfectly penetrated.

As the individual resultants in the three directions may not justify showing the real motion produced in the machine, the Resultant (R) of the three accelerations is calculated using Eq (2) :

$$R = \sqrt{A_x^2 + A_y^2 + A_z^2} \quad (2)$$

The threshold value or the control limit (±3σ) for a D-T combination is determined from the RMS value of acceleration. For the scope of this study, the '+3σ value' is fixed as the threshold value to trigger the warning for maintenance. The trigger request is completed with a ThingHTTP, which initiates the predefined HTTP requests with an API key. Additionally, a GET request from the web when the threshold is reached and triggers the Webhooks at IFTTT which sends an Email with a customized message prompting immediate action.

Similarly, runs were conducted for the various D-T combinations and the free run condition. The results are discussed in the next section.

5 Results

The experiments were performed for various D-T combinations, and the results are shown in Figure 6 and Figure 7. Figure 6 shows the RMS Acceleration for a free run condition that gives a reliable idea about the inherent vibration in the machine when in operation. Figure 7 depicts a comparison of the ranges in which the value of RMS acceleration lies for the different D-T combinations.

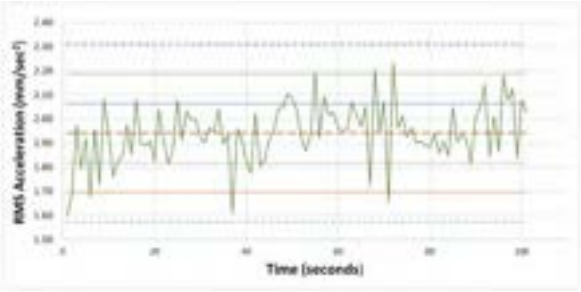

Figure 6. Observation for Free-run condition

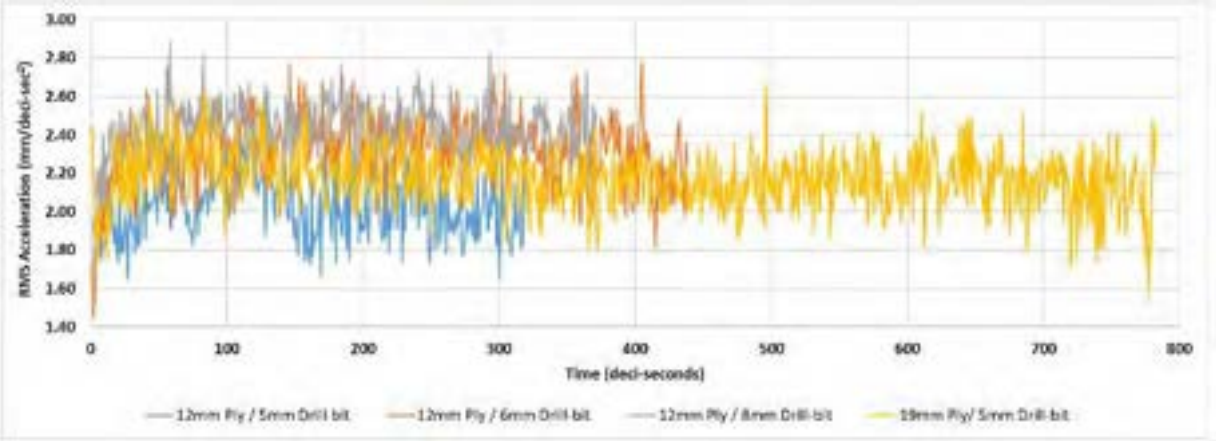

Figure 7. RMS acceleration for 12mm plywood and 5mm, 6mm and 8mm drill-bit diameter.; 19mm plywood and 5mm drill-bit diameter

The receipt of data on the IoT platform and the triggering of the Webhooks event named "Threshold Reached!" confirms that the proposed framework performed as expected. Figure 8 shows screenshots of the creation of ThingHTTP and warning received.

Figure 8. Setting up Threshold in ThingSpeak & receiving a warning from IFTTT

The quality of the data is checked using the 'Western Electric Rule', the results of which are summarized in Table 1. These rules are in accordance with the statistical norms and suggest that the quality of data is controlled under experimental as well as industrial conditions [21]. As there are no outliers in the plots, this explains the potential of the system to be used in sophisticated and controlled experiments across various situational frames.

Table 1. Western Electric Rules to check process control

S. No.	Decision Making Rules	Free-run	12P-8B	12P-6B	12P-5B	19P-5B
1	One or more points outside of the control limits	No	No	No	No	No
2	Two of three consecutive points outside the two-sigma warning limits but still inside the control limits.	No	No	No	No	No
3	Four of five consecutive points beyond the one-sigma limits.	No	No	No	No	No
4	A run of eight consecutive points on one side of the center line	Yes (1)	Yes (1)	Yes (1)	Yes (2)	Yes (3)

6 Discussion and Conclusion

The smooth functioning of the proposed system architecture and components validate the functionality of the system for the current scenario. This study facilitates the implementation of an effective IoT system for real-time health monitoring of a hand-held drilling machine. Testing the acquired data against the Western Electric Rules suggest that the quality of the experiment was controlled, and the exhibited framework can be used for a variety of applications in accordance with the selection of appropriate sensors. The successful functioning of the framework ensures that the tools can be monitored continuously and remotely through an inexpensive system, which is also practically easy to maintain.

The experimental setup plots the real-time acceleration data from the machine while in operation on an IoT platform. Vibration is one of the visible performance indicators of the machine's health, and can be used in the study of Machine Prognostics. This involves the estimation of RUL of the machine, which is a well-framed four-staged procedure. The process includes Data Acquisition, Health indicators (HI) construction, Health Stage (HS) division, and finally the RUL prediction. Various approaches, such as the statistical model-based (Random co-efficient, AR models, etc.), AI approach, Physics model-based approach, have been developed to display various strategies to predict the RUL [22]. The selection of an approach for RUL estimation is based on the type of application. For the scope of the current study, the RMS value of the resultant acceleration is considered as the threshold value for triggering the warning system.

Furthermore, the ThingSpeak platform has an integrated Toolbox for Predictive Maintenance supported by MathWorks. An appropriate algorithm can be deployed on the cloud using ThingSpeak and MATLAB prediction server to estimate the real-time RUL. This will monitor the health of the machine and warns once the threshold is achieved. These thresholds can be specific to the type and make of the machine. The presented framework facilitates keeping track of the used life of a machine, which is useful during the inter-site transfer of the machine. This can also enable the site management to have stricter surveillance over the hand tools and make more informed and intelligent procurement strategies.

Preliminary analysis should be conducted to decide the position of the sensor on the equipment, as the vibration data obtained will be sensitive to it. In this study, the sensor was attached based on the driller's convenience, at a place where it was assumed that the vibration is maximum. In some cases, the limited connectivity at construction sites due to the remote location is a challenge for the proposed architecture as it may result in delayed information due to the restricted transfer of data across the interconnected layers.

The predictive approach showcased here is expected to save a considerable amount of time, cost, and effort than what is conventionally required in the reactive or preventive approach. It will also allow end-users to utilize the machine up-to its design life. The system can be an appropriate tool for the manufacturing industry to design the components having similar operational lives.

The potential of advances in Machine Learning and Artificial Intelligence in conjunction with more

sophisticated sensors such as Hall sensor and tip-pressure sensor can make the system more robust and extensive. Furthermore, the system is expected to flourish with a substantial amount of data coming from the industry and using more advanced degradation models of ML learning integrated with AI. This study can be a robust and elegant template for future research on maintenance strategies.

Acknowledgement

The first author is supported by Build India Scholarship (BIS) program by L&T Construction Ltd. All the authors are thankful for their support.

References

[1] G. Robinson, "Global construction market to grow $ 8 trillion by 2030 : driven by China , US and India," *Glob. Constr. 2030*, vol. 44, no. 0, pp. 8–10, 2015.

[2] Hilti India, "Smart Tools are Changing Construction." https://www.hilti.group/content/hilti/CP/XX/en/services/tool-services/internet-of-things/smart-tools.html.

[3] Constructible, "The Top 5 Features of a Construction Asset Management Software Solution." https://constructible.trimble.com/construction-industry/the-top-5-features-of-a-construction-asset-management-software-solution.

[4] Contractor, "Power tool survey: the most used power tools by contractors." https://www.contractormag.com/tools/cordless-tools/article/20880440/power-tool-survey-the-most-used-power-tools-by-contractors.

[5] A. Krontiris and G. Balzer, "Condition assessment of power system equipment the impact of ageing and deterioration," in *16th Power Systems Computation Conference, PSCC, January* 2008.

[6] MATLAB, "*Predictive Maintenance, Part 1- Introduction*.". https://www.youtube.com/watch?v=RmVWKLbLq2Y

[7] A. Gillespie, "Condition Based Maintenance : Theory , Methodology , & Application", *Reliability and Maintainability Symposium, At Tarpon Springs, FL*, January, 2015.

[8] R. Indira, G. Bhavya, D. D. S, and R. Devaraj, "IOT Asset Tracking System," *SSRG International Journal of Computer Science and Engineering - Special Issue ICFTESH Feb 2019*, ISSN: 2348 - 8387 pp. 45–50, 2019.

[9] M. A. Thomas Bock, "Construction Automation and Robotics", *Robotics and Automation in Construction*, October, 2012, doi: 10.5772/5861.

[10] S. Vara Kumari, O. Sailaja, N. V S Rama Krishna, and C. Thrinisha, "Early Flood Monitoring System using IoT Applications," *International Journal of Engineering and Advanced Technology (IJEAT), ISSN: 2249-8958, Vol. 8 Issue-5,* June, 2019.

[11] Hilti India, "Asset Tracking Software - Construction Equipment Tracking Software - Hilti India." https://www.hilti.in/content/hilti/A2/IN/en/services/tool-services/on-track.html.

[12] Trackinno, "Trackinno Assets.", https://trackinno.com/asset-management/.

[13] BOSCH, "Asset management system," *Public Works*, 2002. https://bluehound.boschtools.com/.

[14] M. Dadafshar, "Accelerometer and gyroscopes sensors: operation, sensing, and applications," *Maxim Integr.*, pp. 1–11, 2014.

[15] M. R. Kumar, S. A. . Jilani, S. J. Hussain, and P. R. R. Raju.K, "An Automated ThingSpeak System representing MPU6050 Sensor data using Raspberry PI," *Int. J. Eng. Trends Technol.*, vol. 29, no. 1, pp. 29–34, 2015, doi: 10.14445/22315381/ijett-v29p206.

[16] K. Ed, "IoT - Applications, Merits, Demerits & Challenges," no. March, 2018, doi: 10.15680/IJIRCCE.2018.0602037.

[17] V. K. Reja and K. Varghese, "Impact of 5G technology on IoT applications in construction project management," in *Proceedings of the 36th International Symposium on Automation and Robotics in Construction, ISARC 2019*, 2019, no. July, pp. 209–217, doi: 10.22260/isarc2019/0029.

[18] L. Louis, "Working Principle of Arduino and using it as a Tool For Study And Research," *Int. J. Control*, vol. 1, no. 2, 2016, doi: 10.5121/ijcacs.2016.1203.

[19] Programino, "Download Programino IDE for Arduino." https://www.programino.com/download-programino-ide-for-arduino.html.

[20] X. Mi, Y. Zhang, F. Qian, and X. Wang, "An empirical characterization of IFTTT: Ecosystem, usage, and performance," *Proc. ACM SIGCOMM Internet Meas. Conf. IMC*, vol. Part F1319, pp. 398–404, 2017, doi: 10.1145/3131365.3131369.

[21] D. C. Montgomery, *Introduction To Statistical Quality Control.*, 6th Edition, 2009.

[22] Y. Lei, N. Li, L. Guo, N. Li, T. Yan, and J. Lin, "Machinery health prognostics: A systematic review from data acquisition to RUL prediction," *Mechanical Systems and Signal Processing*, vol. 104, no. December 2017. Elsevier Ltd, pp. 799–834, 2018, doi: 10.1016/j.ymssp.2017.11.016.

Web-Based Communication Platform for Decision Making in Early Design Phases

Z. Meng[a], A. Zahedi[b], and F. Petzold[b]

[a]Chair of Construction Management & Economics, University of Wuppertal, Germany
[b]Department of Architecture, Technical University of Munich, Germany
E-mail: meng@uni-wuppertal.de, ata.zahedi@tum.de, petzold@tum.de

Abstract –

During the early phases of building design, the architects create many variants and make important decisions about different design aspects and details mostly based on their own experience and know-how. In order to reduce the risks brought by arbitrary decisions, a lot of effort was put into developing simulation tools. However, most of these simulation tools require more elaborate details as what is available during these early phases, or they will provide some cumbersome results via oversimplification. Therefore, it is equally important to develop a communication tool enabling the earlier integration of suggestions given by diverse domain experts. Hence, a research based on the concept of adaptive detailing has been made by Zahedi and Petzold since 2018, according to which those suggestions and feedback provided by multiple domain-experts could be documented using a minimized machine-readable communication protocol based on BIM [1]. Consequently, an online platform for supporting the collaborative work through adaptive detailing at early stage of design is developed in this paper. This paper focuses on the Optimization of workflow and effectiveness of user interface in this platform. As evaluation of this platform, a user-study was carried out among students and practitioners in AEC industry. The result of user-study not only practically verifies the usefulness of this tool, but also implies the difficulty in transforming the daily communication mode into digital platform.

Keywords –

Building Information Modeling; Early Design Phases; Adaptive Detailing Strategies; Computer Supported Collaborative Work

1 Introduction

The integration of Building Information Modeling (BIM) applications at early stage of design have great impact on the final design and overall cost, while the additional costs resulting from design changes in early phases are also significantly lower [1]. Furthermore, the main idea of BIM is about the exchange of information including 3D-models with semantics among the participated domains [2]. For the reasons above, early collaborative work is of great importance to improve efficiency of design in a project.

However, according to our online survey 31.5% of the students or practitioners from the Architecture, Engineering and Construction (AEC) industry have tried BIM software as communication tool before at early stage of design, whereas 78.9% of them use BIM products for 3D modeling in design phase. Those statistics prove that more attention should be put on developing BIM tools for communication in design phase, so that diverse domain-experts could better help the architects by providing suggestions from their point of view.

This work aims to develop an online communication platform with optimized workflow and user interface, based on literature review on computer supported communication and collaboration, as well as on other BIM based communication tools on the market. The effectiveness of this platform would be validated during a user-study at the end of this paper.

2 State of the Art

2.1 Adaptive Detailing Strategies, Multi-LOD, and Building Development Level

Although many model-based planning tools are currently available, they require extensive input data and detailed model construction even in the early design phase. However, a model that is too precise and reliable can lead to incorrect assumptions and evaluations, such as in energy calculations or structural analyses, which affect planning decisions in all planning phases [2][3]. In order to close this gap, the research unit FOR2363 from German Research Foundation (DFG) is developing methods for the evaluation of architectural design

variants in the early stages of their development by means of adaptive detailing strategies that allow the detailing and evaluation of alternative, partially incomplete and vague building models [4]. This research project is also called Early BIM. To allow the explicit expression of potential information vagueness in the design phase, the research group develop a multi-LOD meta-model. Under the case of that, it is possible to define the uncertainty of information as well as building components at different LODs in a design variant [3]. A new concept called Building Development Level (BDL) is therefore introduced to describe the maturity of building models at difference design stages [3]. The BDL concept is also used in this project as milestone for new requirement of decision making.

2.2 Computer Supported Communication and Collaboration

To further promote communication and cooperation in the BIM field, the introduction of a research area called Computer Supported Cooperative Work (CSCW) is unavoidable. CSCW investigates on an interdisciplinary basis how individuals cooperate in working groups and how they can be supported by information and communication technology [5]. In this section mainly the socially acquired phenomena of CSCW research are described, whereas the technological aspects are explained afterwards in section 2.3.

Communication between the cooperating partners is the prerequisite for cooperation. The goal of cooperation is to coordinate the work processes and technical interfaces of the project participants as optimally as possible and to ensure a consistently efficient use of information [6].

2.3 File Formats for BIM Based Communication

The best-known collaboration format is the BIM Collaboration Format (BCF) from buildingSMART, which supports workflow communication in BIM processes. Project participants can use it to create various topics, such as problems, proposals and change requests. The BCF also allows the structured description of model conflicts or defects. Among other things, the camera position and the viewing direction are transmitted for the representation in the 3D model.

Since version 2.0, the BCF format also offers schematized files and machine-readable topics. However, this format is mainly used as comment based and human readable [4]. Therefore, based on the concept of adaptive detailing, and for better documenting suggestions and feedback provided by multiple domain-experts, a minimized machine-readable communication protocol based on BIM was developed by Zahedi and Pezold [6].

Using this protocol, a Feedback package contains information about:

- missing details in a design variant that are essential for a certain simulation to be performed
- suggested options to fulfill those missing details.

Further details about this minimized BIM-based communication protocol is discussed via demonstrative examples by Zahedi and Petzold [4][7]. Using this computer-interpretable protocol in communication tools can largely reduce the misunderstanding incidences in the whole progress.

2.4 BIM Based Communication Tools

With the development of software in AEC industry, many solutions which were mostly used for IT companies are now also integrated in BIM applications. For example, the ticket system, mainly used for tracing every request from the start until its completion, was firstly used in IT companies where a huge number of requests are produced in daily basis, is now widely embedded in BIM communication tools. Those tickets are normally shown in a dashboard and named “issues” or “tasks” in BIM based communication tools. Other frequently implemented functions are, for instance, presentation of the up-to-date overall information about the project, message notification, 3D visualization, marking and commenting on models, merging the partial models, preview of interim document, etc. The most popular BIM based applications such as Autodesk BIM 360, BIM Plus from Allplan, thinkproject, etc. have included all of these functions. However, the visualization mode of different types of data is seldom discussed. To fill this gap, various types of viewing mode or graphics will be provided in this project and tested via user evaluation.

3 Concept and Methodology

Practitioners in AEC industry are long used to conventional communication media such as face-to-face meetings, telephone, fax and email. However, for better decision making and more efficient information exchange in early design phases, it is reasonable to integrate BIM common data environment into the communication tool. In this way, the function for file exchange, preview of design variant and intuitive comparison of simulation results can be feasibly embedded (Figure 1).

As Lubich in Figure 2 suggested, the proper way to develop a CSCW tool starts from representing the working environment. In this case it means to explain how communication between project participants actually works, or what the conventional working environment in the construction industry is. Turk

explains that the most important activity in the construction industry is not "processing", such as problem solving or decision making, but maintaining a network of conversations in which requests and commitments lead to a successful completion of the work [8].

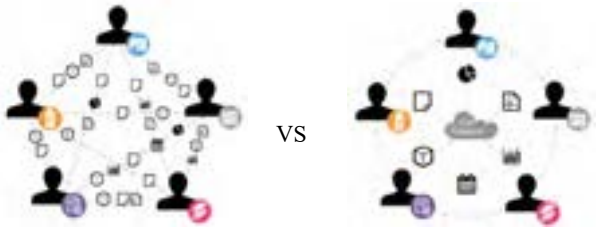

Figure 1. Compared to conventional communication, different communication methods are integrated into the new web-based platform.

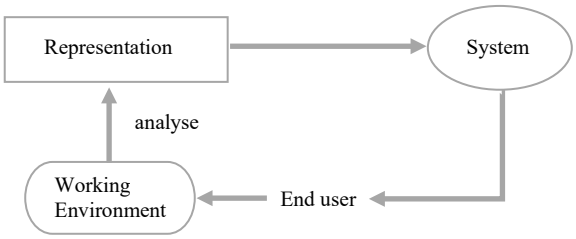

Figure 2. Development cycle of computer-aided collaboration software [9] (first orally presented by J.E.Dobson in 1991)

As we can observe in real working environment, it might possibly happen that an architect asks a civil engineer to check about the load-bearing structure, and the engineer accepts the request. Several days later the architect asks the engineer about whether the simulation result is generated or not. And finally, the engineer informs the architect that the task is finished. Of course, in most cases this process doesn't run smoothly, and there are normally special occasions happening during the process. Winograd and Flores have named such an interaction "conversations for action – those in which an interplay of requests and commissives are directed towards explicit cooperative action" and have therefore mapped the possible answers at each point in a conversation in an example model (see Figure 3) [10][11].

In this model, for example, one party (A) asks a question to another party (B). The request is interpreted by each party to meet certain conditions. After the initial statement (the request), B can accept (thus commit to meet the conditions), reject (to end the conversation), or make a counteroffer with alternative conditions. Each further confirmation has its own possible continuation (e.g. A can either accept, reject, or offer again the counteroffer from B). This diagram is not a model of the mental state of a speaker or listener but shows the conversation as a "dance" in which the actions create the structure or termination of the conversation.

To further use this model in the implementation part, it is translated into a graphical specification language, the Business Process Model and Notation (also known as BPMN) (see Figure 4).

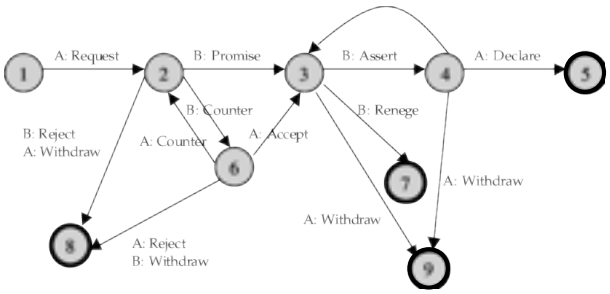

Figure 3. The basic conversation for action process model [10]

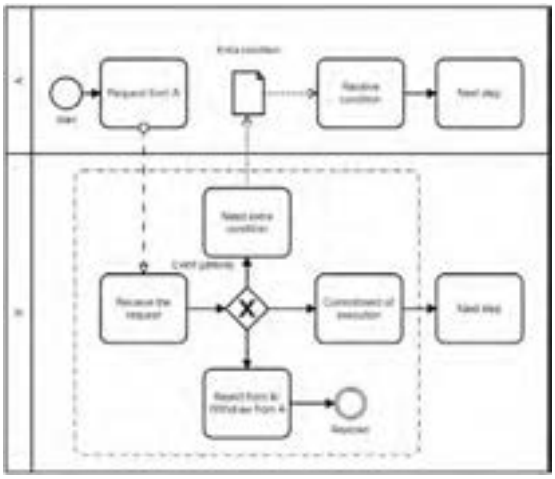

Figure 4. Simplified BPMN of the "conversation for action" model adapted to Maaß, 1991 [11]

4 Implementation

The implementation of optimized communication tool is carried out in two steps: 1. Definition of proper workflow of communication (corresponding to "Representation" in Figure 2); 2. Developing the tool (same as "System" in Figure 2).

4.1 Definition of optimized communication workflow in the platform

In the beginning of this step, a few concepts which are very often used in the workflow must be clarified:

- VARIANTS are the different versions of the design, which architects offer as a proposed solution.
- OPTIONS refer to the suggestions for the missing parts in variant which are provided by domain experts. The architects then may choose one of these options to fulfill the requirements for simulations.
- REQUEST contains the information of an action that the architects ask domain experts to execute, for instance, the request of simulation or request of options for missing parts. It is a kind of "Request for Information" (RFI), which is often used in business processes for collection of information and making decisions.
- FEEDBACK is the message that domain experts give to the architects including their reaction on the request, such as rejection, agreement, as well as further information. There could be three types of feedbacks: 1. Interim report on missing values which are necessary for the analysis or simulation; 2. Interim report with options; 3. Final report on simulation results and evaluations of various variants. Since a file format "feedback package" especially for the case of communication is invented [4][7][13], it will be used later for accurate expression of the feedback.

The workflow of this whole communication system is divided into three scenarios (Figure 5):

1. Request for analysis
   At a certain point, the architect needs simulation results and evaluations from other specialist planners. Therefore, he sends the planner a request for analysis by ticket. Using the ticket system, the whole process can be monitored and managed. General Information such as actor, deadline of the request and the processing status of each request/ticket can be displayed. According to the conversation to act model [11][12], there can be three possible types of reaction to any request for an action [4][7][13]: accept, reject or counteroffer with alternative conditions. If some geometric details or semantic information, which are necessary for further analysis, is missing, the specialist planner will give a feedback to the architects.

2. Request for options and update the variant
   In this case, after step 1, the architect receives a feedback with a message containing the missing values. Then he precedes to ask for options to continue the process. Although in the normal working environment, mostly an architect makes decisions based on his knowhow, but using adaptive detailing he could ask for experts' opinion via request for options.
   After the request, options for missing components, their consequences on analysis results, as well as a comparison between options will be packed up and sent back to the architect as feedback. The Architect would then evaluate the properties of each option, make a choice, and complete the variant model. The variant is therefore updated during the process.

3. Execution of simulation and optimize the variant
   The execution of the simulation can only be

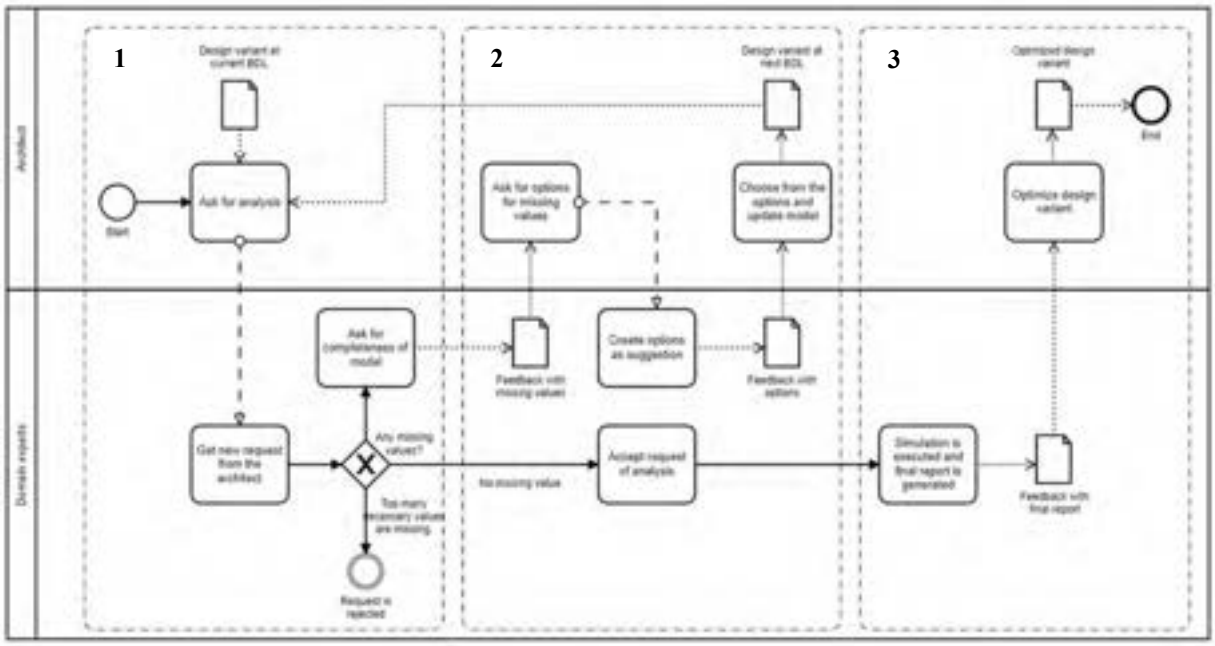

Figure 5. BPMN of the conversation for action Process between architects and specialist planners

achieved if the coordination model has already been checked by all the domain experts and has no more missing values. After the simulation, each domain expert submits a report with simulation result of the variant and their suggestions for optimization. The architect then collects all reports and accordingly improves the variant.

The objective of this whole workflow is to let domain experts give suggestions from their point of view as early as possible. It consequently prevents the case of endless revising on design model and reduces the potential problems which can become big issues in later phases.

4.2 Building the web-based communication tool with ideal user interface

4.2.1 Design of user interface

After the communication process is created, the functions in optimized workflow are first summarized in Table 1, so that the required items and their file format as well as possible visualization forms are categorized.

To visualize the core function of this communication system, which includes sending request and receiving feedback, a dialogue panel is created. On the dialogue panel, notification of new message, basic information in request or feedback, and project profile will be presented. Also, a block for free discussion between group members is available on the dialogue panel. In order to spare extra place for presenting content in details, the dialogue panel is designed as foldable (see Figure 6).

According to Gadelhak, Lang and Petzold [14], it is recommended to use a dashboard to display the attached information of the conversation. On one hand, several options can be displayed on different panels of a dashboard. On the other hand, the dashboard gives an overview of all relevant performance aspects of the building and can provide detailed information at the same time if required. The dashboard is therefore in this case particularly applicable for presenting and comparing various options or variants contained in feedback (see Figure 6).

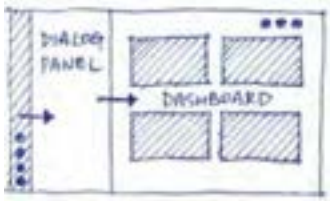

Figure 6. Layout and navigation of platform

4.2.2 Frontend development

In this project the frontend of the web-based application is implemented. There are two types of files to be visualized: the IFC files such as the coordination model and partial model, and the CSV/ JSON files that

Table 1. Information to be visualized, corresponding file format and possible visualization form in platform

Role	Function lists according to workflow in Figure 5	Required items	Data/ File format	Visualization form
General	Show variant at current BDL / at next BDL	Participating projects of the user	JPG / TXT	List / Images
		Information about the user	JPG / TXT	Text / Images
		Participants in a project	JPG / TXT	List / Images
		Process log	CSV	Graphic
		Project status	CSV	Graphic
		Fixed meeting	JSON	Dialogue
Architect	Request for analysis by ticket	Message of the request	JSON	Dialogue
		Coordination model	IFC	3D / Images
	Request for options	Message of the request	JSON	Dialogue
	Update variant	Coordination model	IFC	3D / Images
Domain experts	Feedback with rejection	Message of the feedback	JSON	Dialogue
	Feedback with missing values	Message of the feedback	JSON	Dialogue
		Partial model	IFC	3D / Images
	Feedback with approval	Message of the feedback	JSON	Dialogue
	Feedback with options	Message of the feedback	JSON	Dialogue
		Performance of the options	CSV	List/ Graphics
		Partial model	IFC	3D / Images
	Optimize variant	Coordination model	IFC	3D / Images
	Feedback with final report	Message of the feedback	JSON	Dialogue
		Partial model	IFC	3D / Images
		Annexes	DOC / PDF / JPG / IFC	List/ Images
		Final report	CSV	List/ Graphics

Figure 7. Various visualization mode for options

Figure 8. Different graphical representations of simulation results

capture the log and problems in the process or final report. The IFC file should first be transferred to the Obj file by data preprocessing such as ifc OpenShell or xbim toolkit. After that it is visualized by ObjLoader.js (provided by three.js) on the web page. Another important file type is the CSV file, which can record the process log, project status, option performance and final report. To visualize the data in several display modes, the libraries of ZingChart and Dygraphs are used specifically. To validate the specific process of implementation we take a three-storey office building of Ferdinand Tausandpfund GmbH & Co. KG [15] in Regensburg, Germany as an example. After the functions are organized and implemented, a web-based application could be developed.

Because all the information of requests and feedbacks is collected on the side of architect, it is meaningful to show the user interface from this view. As Figure 7 and 8 present, various graphical representations are provided. For comparing the options, user can choose floor plan view, bird eye view or inner perspective view (see Figure 7). And for identification of issues in simulation results, user can define a visualization mode from tree chart, pie chart or list (see Figure 8). As mentioned before in 2.4, one important objective of this project is to provide different visualization forms so as to test which one is more preferable for the user and gives the architect more intuitive criteria in decision making [13].

5 Evaluation

Since the implementation of the web-based communication tool is completed, 19 students or practitioners from the AEC industry were invited to participate a user experience study. After experiencing the whole process, more than 60% of the participants consider the platform to be usable in most cases.

It is worth mentioning that in the answer to the question "Which tool do you think is irreplaceable through this platform?" more than a half of users (almost 58%) still consider the face-to-face meeting as irreplaceable. It is very interesting for us because in hypothesis we considered the face-to-face meeting as the most likely replaced media. Some of the reasons given by respondents are:

- The personal meeting is always the most dynamic one and gives the quickest results.
- It can help solving complex problems.
- It is a quick and direct communication way.
- It is real time communication. Whenever you put up a question, there would be an answer immediately.

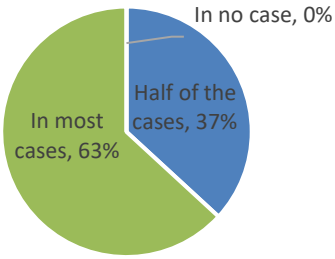

Figure 9. Answer to the question "In how many cases do you think this platform is applicable?"

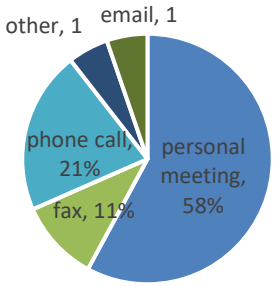

Figure 10. Answer to the question "Which of the following means of communication is irreplaceable by this platform?"

According to the user study, the communication system is helpful especially in illustrating the feedback, and the display of the simulation results. More specifically, most respondents chose bird eye view as best visualization mode for options (50%), and the list as most efficient graphical presentation for issues during simulation (50%) (see Figure 11 & Figure 12). These results for favorite graphical representation can be used later in other corresponding products.

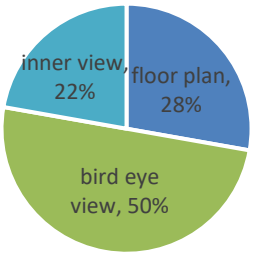

Figure 11. Answer to the question "Which of the visualization mode do you think is most suitable for presenting options?"

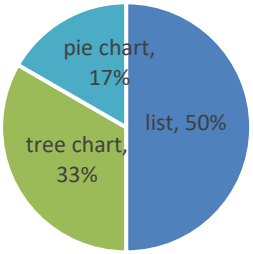

Figure 12. Answer to the question "Which of the graphical presentation do you think is the best for reporting issues in feedback?"

In the end there are also several suggestions for optimizing the communication platform:

- More real time communication in the model would be helpful.
- The authority levels from different users should be distinguished.
- In most of the cases, speedy replies are expected, therefore it would be great if the message notification can be improved and the hint of message priority can be tagged.
- The text should be bigger.

These suggestions are significant indicators for further development of this tool as well as for other similar products.

6 Conclusion

While the market for BIM applications is growing rapidly, there is still no effective working method for architects to propose the variants and discuss with other project participants about design. With the development of adaptive detailing strategies and multi-LOD, it is possible for the domain experts to participate in early design phases and to give suggestions even if there is still missing or vague values in design model. Furthermore, after the literature review on existing BIM based communication tools, the most practical functions, such as the ticket system, are collected and included in this case, whereas the request and feedback functions are embedded as core mechanisms for the communication workflow. Consequently, a BIM based communication platform especially for discussion at early design stages is built based on a specified workflow and in the end validated by a user-study. The result of the user-study shows an overall acceptance of this tool among users, as well as the preferred visualization mode for data in the feedback. These findings could be referred as important hint for further research or for software development in BIM field.

Considering the contribution of this communication platform, it was rewarded in year 2020 as the first prize in the category of Architecture in "Built on IT - Building professions with future" (Auf IT gebaut 2020) federal competition in Germany under the patronage of the Federal Ministry of Economics and Energy [16].

We gratefully acknowledge the support of the German Research Foundation (DFG) for funding the project under grant number FOR2363. We are thankful to the survey participants for their feedback. We thank Ferdinand Tausendpfund GmbH for providing its office building as a sample project.

References

[1] Zahedi A. and Petzold F. Seamless integration of simulation and analysis in early design phases. In Life Cycle Analysis and Assessment in *Civil Engineering: Towards an Integrated Vision: Proceedings of the Sixth International Symposium on Life-Cycle Civil Engineering (IALCCE 2018)*, pages 441, Ghent, Belgium, 2018.

[2] Borrmann A., König M., Koch C. and Beetz J. Building Information Modeling: Why? What? How?, In *Building Information Modeling*, Springer, pages 1-24, 2018.

[3] Abualdenien J., Schneider-Marin P., Zahedi A., Harter H., Exner H., Steiner D., Singh M. M. and Tech M. Consistent management and evaluation of building models in the early design stages. *Journal of Information Technology in Construction*, 25: 212-232, 2020.

[4] Zahedi A., Abualdenien J., Petzold F. and Borrmann A. Minimized communication protocol based on a multi-LOD meta-model for adaptive detailing of BIM models. In *the 26th International Workshop on Intelligent Computing in Engineering*, 2019.

[5] Teufel S. *Computerunterstützung für die Gruppenarbeit*, Addison-Wesley, 1995.

[6] Schapke S. E., Beetz J., König M., Koch C. and Borrmann A. Kooperative Datenverwaltung, In *Building Information Modeling*, Springer Vieweg, Wiesbaden, pages 207-236, 2015.

[7] Zahedi A. and Pezold F. Adaptive Minimized Communication Protocol based on BIM. In *European Conference on Computing in Construction*, Chania, Crete, Greece, 2019.

[8] Turk Z. Communication workflow approach to CIC. In *Computing in Civil and Building Engineering*, pages 1094-1101, 2000.

[9] Lubich H. P. *Towards a CSCW Framework for Scientific Cooperation in Europe*, Springer-Verlag, Heidelberg, 1995.

[10] Winograd T. A language/action perspective on the design of cooperative work. In *Conference on Computer-Supported Cooperative Work*, pages 203-220, Austin, 1986.

[11] Beeson I., & Green, S. Using a language action framework to extend organizational process modelling. In *UK Academy for Information Systems (UKAIS) Conference*, pages 9-11, 2003.

[12] Maaß S. Computergestützte Kommunikation und Kooperation, In *Kooperative Arbeit und Computerunterstützung*, Verlag für Angewandte Psychologie, Göttingen, pages 11-35, 1991.

[13] Zahedi A. and Petzold F. Interaction with analysis and simulation methods via minimized computer-readable BIM-based communication protocol. In *Proceedings of the 37th eCAADe and 23rd SIGraDi Conference*, pages 241–250, University of Porto, Porto, Portugal, 2019.

[14] Gadelhak M., Lang W. and Petzold F. A Visualization Dashboard and Decision Support Tool for Building Integrated Performance Optimization. In *ShoCK!-Sharing Computational Knowledge!-Proceedings of the 35th eCAADe Conference*, 2017.

[15] Ferdinand T. Wir bauen. Mit der Natur zur Kultur. Online: https://www.tausendpfund.group/index.html, Accessed: 20/05/2020.

[16] Kompetenzzentrum R. AUF IT GEBAUT-BAUBERUFE MIT ZUKUNFT. Online: https://www.aufitgebaut.de/startseite/preistraeger-architektur.html, Accessed: 08/06/2020

Decision Support System for Site Layout Planning

A.R. Singh[a], A. Karmakar[a] and V. S. K. Delhi[a]

[a] Department of Civil Engineering, Indian Institute of Technology Bombay, India
E-mail: arsingh@iitb.ac.in, 183040069@iitb.ac.in, venkatad@iitb.ac.in

Abstract -

Construction Site Layout Planning (SLP) is one among the processes that consider decision-making as essential to achieving the desired project performance. In lack of decision support system (DSS), the project planners employ learnings from experience to make decisions that often lead to sub-optimal planning of site, resulting in congestion, safety issues and loss in productivity. Therefore, to mitigate such risks, the SLP targets to identify the temporary facilities (TFs) required to aid the construction and optimally locate these TFs. SLP usually requires all the stakeholders to reach consensus and to aid this a few operations research (OR) models are developed in past studies. While SLP is often viewed as an optimal allocation problem by present research, the decision-making aspect involving multiple stakeholders is understudied. As a result, state-of-art research in modelling and optimal allocation using OR methods are not implemented on site. Therefore, targeting the decision-making in SLP, an approach is demonstrated to enhance the process through efficient exchange of information. This study employs building information modelling (BIM) to make data available for the modelled optimization problem. In addition to this, to foster the decision-making during the SLP task, the study presents an augmented reality (AR) enabled site layout planning decision support system (SLP-DSS) framework to aid the construction practitioners in SLP. The developed DSS with the functionality of AR integrated optimization is designed to make understand the generated solutions to the stakeholders in an efficient manner and targets to ease out the SLP process with a clear perspective exchange.

Keywords -

Augmented Reality; Building Information Modelling; Collaborative Planning; Decision Making; Optimization; Layout Planning; Perspective Exchange; Visualization

1 Introduction and Motivation

Construction site layout incorporates positioning of TFs on a construction site. This task is approached at the initial project phase when information related to the project is scarce. To overcome this limitation, the construction practitioners employ the learnings from previous similar projects [1]. Another challenge comes in the form of site topology and to understand it better, the 2D representation of the site in the form of computer-aided drawings (CAD) is employed. This sort of representation of 3D space requires tailoring of plans and elevations from different CAD sheets. Thus, resulting in additional mental exertion in the process of layout planning. The stakeholders involved in the process of planning site layouts sometime does not have enough experience to understand the 2D site representation. This leads to inaccurate information exchange while discussing SLP making the process of decision making cumbersome. SLP task involves stakeholders with individual goals [2] and the limited site space brings them together to plan for efficient space utilization. Thus, requires an efficient method to plan site layouts collaboratively with optimum space utilization. Moreover, to collaborate effectively, the exchange of perspectives in an efficient manner is a must.

In an attempt to release SLP of some obsolete hindrances in efficient decision-making pertaining to the layouts for the construction site, this study utilizes and demonstrates the applicability of technological advancements like BIM and AR. In addition to approach SLP through these advanced technologies, the research highlights optimization-based solution visualized in AR environment to mitigate the psychological efforts in understanding the generated output results. The utilization of BIM is targeted to address the information requirements to plan site layouts. The developed quantitative approach aided with visual aid is expected to enable the stakeholders to make informed and efficient decisions resulting in enhanced site productivity and a safer work environment.

2 Literature Review

Existing research on layout planning has extensively studied the SLP problem as an optimization problem. The quantitative approach to SLP results into numerical based output, requiring manual interpretation of the obtained results. Considering these challenges posed by optimization-based SLP models proposed in earlier research, a few researchers have attempted to consider DSS for SLP. These efforts were because the resulted output of optimization-based models is of no use until verified. In attempts to develop DSS for SLP, approaches like fuzzy-based multi-criteria model was developed and found useful in terms when the required information is imprecise [1]. Another tacit-based approach was developed to plan site layouts. This was approached utilizing a combination of repertory grid technique and interviews of construction professionals [3]. These both research presented examples of quantitative and learnings from the past based methods, respectively. However, the exchange of perspective while planning site layouts is a prime component of decision-making task; this comes out as a limitation to the existing research. Thus, BIM and AR are utilized to address these impediments to efficient SLP. The former provides input data if the models are prepared to the required level of detail (LOD) and the latter augments the optimal solution of the quantitative approach developed in this study for better exchange of perspective among stakeholders.

2.1 BIM for SLP

The utilization of BIM in the construction industry has been profound in the past decade [4]. In existing SLP concerned studies BIM has been adopted as a source of input data and a few researchers have highlighted LOD 300 as the required level of detail [5]. The data related to the materials required for construction and quantity take-off interested researchers to adopt BIM for layout planning. Another research has demonstrated the implementation of BIM integrated AR to establish efficient collaboration among stakeholders [6]. As BIM is data intrinsic model, its utilization can benefit data-centric tasks like SLP in the construction industry.

2.2 AR for SLP

The development of AR was initially conceptualized as a visual enhanced assistance tool to perform certain tasks. Tasks that require instructions delivered or exchange of perspective were primarily targeted to be benefited from this technology [7]. Implementation of AR to visualize and organize construction worksite was approached utilizing marker-based AR to plan rule base site plan [8].

3 Development of Framework for DSS

The study employs BIM to enable data availability following which the inputs to the optimization module of the DSS allows the generation of results. The BIM model developed to demonstrate the working of the developed DSS conforms LOD 300. The model comprises a structural frame for an industrial setup where the site is adequate to accommodate the required temporary facilities. The temporary facilities required to aid the construction are identified from the quantity take-off generated from the BIM model utilizing visual programming tool Dynamo. The developed BIM model enabled the extraction of data pertaining to cost and the distances from the locations identified as possible options to accommodate the required TFs.

Following the task of acquiring inputs, the mathematical model for the site has been modelled as an optimization problem. The objective function is focused to minimize the material transportation cost along with satisfying the constraints related to the positioning of TFs and restriction on locations available to locate the TFs. In order to minimize the transportation cost, the objective function is modelled as a function of decision variable with coefficient as the product of transportation cost per unit distance 'C_{mq}' and the distance 'D_{lq}' between the points of supply 'l' and demand 'q' as shown in (1. The decision variable 'X_{ml}' is modelled as a Boolean variable representing the position of TFs 'm' at a location 'l'.

$$\text{Min} \sum_{l=1}^{L} \sum_{m=1}^{M} \sum_{q=1}^{Q} C_{mq} D_{lq} X_{ml} \qquad (1)$$

The presented optimization model is adopted from existing research [9] presenting a discrete site layout planning problem. To present a better understanding, the following Figure 1 illustrates the points of material supply 'l' and demand 'q'.

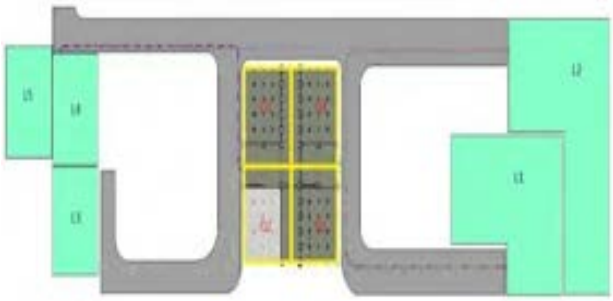

Figure 1. Description of supply and demand points

It indicates that the locations available to accommodate TFs are identified at prior and the continuous site space is divided into isolated areas to position the required TFs. The presented constrain in (2 is modelled to limit each identified location to accommodate a single TF. Similarly, each TF is allowed to occupy a single location on site satisfying the modelled constraint in (3.

$$\sum_{m=1}^{M} X_{ml} = 1 \qquad \text{Where, } \{l=1, 2\ldots L\} \qquad (2)$$

$$\sum_{l=1}^{L} X_{ml} = 1 \qquad \text{Where, } \{m=1, 2\ldots M\} \qquad (3)$$

The modelled optimization model is solved for the optimum value of the decision variable through genetic algorithm (GA). Thus, to obtain the optimum results the crossover and mutation operators are considered in this study. These operators helped in exploring and exploiting the search space in an effort to find the optimal solution. Once the optimal results are achieved, the AR rendering of the solution is generated to visualize the result. This visual aid in the augmented environment is prepared by integrating the code for optimization in the AR development software unity. The following Figure 2 elaborates the steps involved in the development of the AR-BIM enabled decision support system for SLP.

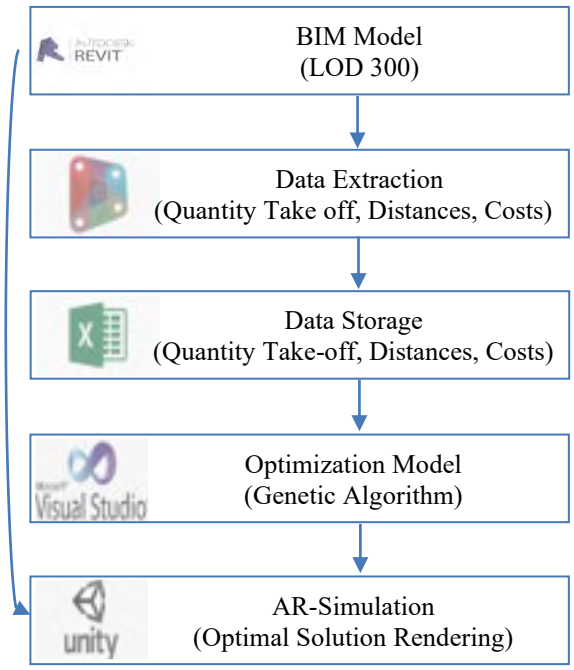

Figure 2. Schematic representation of framework for the proposed DSS

The AR visualization provides a simulation environment to test out the results generated through optimization model. This enhances the effectiveness of the mathematical model by transforming the numerical output of the optimization model to corresponding digital prototypes of the TFs located at the respective obtained locations. Thus, enables the informed decision-making in the process of SLP. A detailed elaboration of the usability of this developed approach is described in the following section.

4 Working of the Developed DSS for SLP

The developed DSS in this study comprises of three key components of any DSS framework i.e. data, model and graphical user interface referred in this research as data, solver and simulation. This section elaborates the approach to obtain efficient results from the developed DSS.

4.1 Data and Solver Component of SLP-DSS

The developed linear flow framework helps in eliminating iterations required for an efficient implementation. This task of developing a support system to aid construction professionals and other stakeholders in making decisions pertaining to SLP could be made as an integral part of the design. If did so, will cater the need of the detailed input data required for the DSS along with providing flexibility to alter certain aspects of design. The presented optimization model in this study targets minimization of the material transportation cost considering actual travel paths on construction site. Thus, for the purpose, the required information related to the materials to be transported, quantities to be handled and the distance travelled by respective material is extracted and stored as input to the optimization model. Table 1 and Table 2 presents the quantity take-off for respective material required for construction and the distance to travel from supply to the demand point on construction site, respectively.

Table 1. Material quantity take-off from BIM

Material	Q_1	Q_2	Q_3	Q_4
M_1 - Reinforcement Steel (Ton)	24.4	24.4	24.4	24.4
M_2 - Quantity of Prefab Steel (Ton)	0	702	0	0
M_3 - Quantity of Concrete (Cubic Meter)	406	405	405	406
M_4 - Quantity of Excavated Soil (Cubic Meter)	287	287	287	287
M_5 - Formwork Material (Ton)	21.5	21.5	21.5	21.5

Table 2. Distance matrix from BIM

	Q_1	Q_2	Q_3	Q_4
L_1	88	108	110	88
L_2	93	114	113	83
L_3	102	82	82	103
L_4	122	100	98	120
L_5	121	101	77	105

Once these inputs to the optimization model are available, a slight modification to the extracted quantities from the BIM model (Table 1) is done to find the required number of trips to be made by the transportation vehicle as shown in Table 3. Following this, the trips are converted to trip cost matrix for unit distance trips and then is multiplied with the distance matrix to obtain the transportation cost. A detailed explanation of the optimization model utilized in this study is available in the existing research [9].

Table 3. Trips required for material transport

Material	Q_1 Trips	Q_2 Trips	Q_3 Trips	Q_4 Trips
M_1	4	4	4	4
M_2	0	88	0	0
M_3	164	164	164	164
M_4	30	30	30	30
M_5	4	4	4	4

Thus, explained the working of the optimization model, the result obtained utilizing genetic algorithm in this research provided a Pareto front to choose a solution. However, the sophisticated approach of mathematical optimization is capable of providing an optimal solution in a reasonable time. The resulted output remains a challenge for the stakeholders discussing site layout if left with the solution as shown in Table 4. The interpretation of the optimal solution would be left upon the mental faculties of the practitioners involved in the task of layout planning. Sometimes these interpretations can be easy as can be perceived in Table 4, but with an increase in the number of materials required or locations available on site can complicate the resultant solution from the optimization model to understand.

Another challenge that is often tackled while planning site layouts is the dynamic nature of construction. This induces relocation of TFs on construction site such that the complexity in planning layouts manifold in multitude.

Table 4. Optimal solution from the optimization model

Optimal Position	Interpretation	Achieved Optimal Cost Unit
$\begin{bmatrix} 0 & 1 & 0 & 0 & 0 \\ 0 & 0 & 0 & 1 & 0 \\ 0 & 0 & 1 & 0 & 0 \\ 1 & 0 & 0 & 0 & 0 \\ 0 & 0 & 0 & 0 & 1 \end{bmatrix}$	M_1 at L_2 M_2 at L_4 M_3 at L_3 M_4 at L_1 M_5 at L_5	84,36,400

4.2 Visualization Component in SLP-DSS

SLP is a data-centric task and efficient results are expected through collaborative planning. Thus, it needed an information management tool along with visual management to aid planning for 3D site space utilization. This study is an attempt to furnish the requirements of the primary components of a DSS. The optimization module is supplemented with the functionality of AR to provide a better understanding of the optimal solutions obtained from the optimization model. Improved visualization is expected to help the stakeholders in presenting thoughts in clear and perceivable manner. The stakeholders involved in the task of SLP jointly come together to fulfil individual objectives due to constraint of sharing space common for all on the construction site. The task is subjected to participation from owner representative, project manager of the main contractor, sub-contractor representatives and site supervisors. This diverse participation with different goals to achieve and varying site experience calls for a common mode to experience each other's perspective. Thus, to enable this, the AR-enabled DSS is proposed in this research. The SLP-DSS in this research is developed as an android application that works with marker-less AR. Upon solving for optimal results in the SLP-DSS solver, the results are internally transferred to the unity platform for analyzing the position of respective TFs on the construction site. This internal information handling is achieved by formulating the optimization approach as part of a visualization script used to render the optimal results of optimization.

The application architecture performs in a cyclic manner as shown in Figure 3, enabling the user to initialize the scene and continue (Figure 3A). Once initialized the required TFs are automatically moved in the site space with coordinates at the origin of the scene and marking all the possible locations available for TFs green. The next step renders the site environment in the field of view of the handheld device used for the

purpose (Figure 3B). The application is provided with a user interface to overlay information in the augmented scene required for the user to run the inbuilt optimization algorithm. Once the run is complete the processor renders the optimal solution while placing the TFs at the optimal locations received from the optimization module (Figure 3C). The corresponding cost associated with the rendered solution is displayed to the user on the interface at the handheld device, along with the allowance to the user to move around the scene and verify the implementation possibility of the proposed solution (Figure 3D).

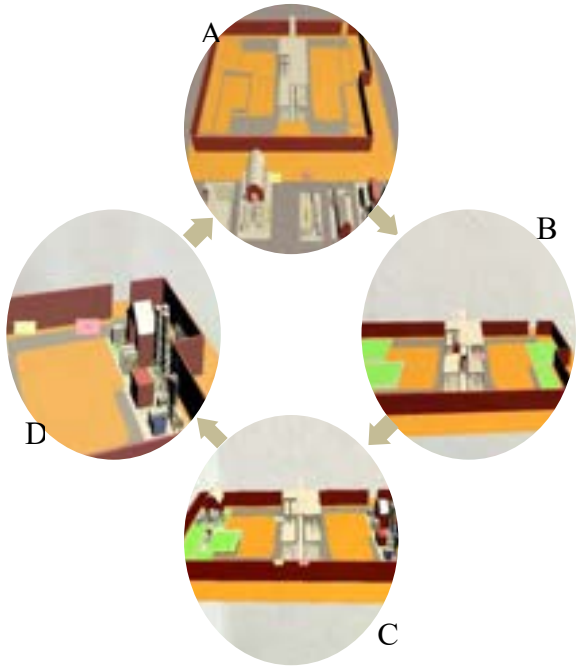

Figure3. Performance of the developed application

If unsatisfied with the results obtained, a rerun is available and the utilization of nature-inspired algorithm GA can be expected to provide another result from the Pareto optimal solutions as shown in Figure 4.

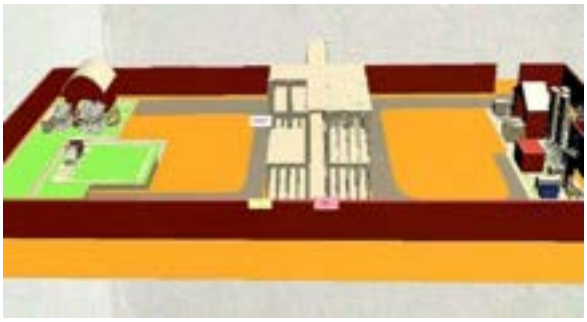

Figure 4. Visual interpretation of the optimal result

5 Limitations

The major limitation to this research comes from the objective function considered as static and discrete site layout example. In order to furnish full functionality of DSS it is proposed to consider other objectives relevant to SLP and the dynamic nature of the site is also needed to be captured. The functionality of the developed application for AR can be distributed among all the stakeholders, where inputs to the augmented scene are possible. This manipulative AR environment will reduce the search space and can provide opportunistic solutions in cases where specific objectives are not modelled as part of the optimization module for SLP-DSS.

6 Conclusion

There exist studies proposing optimization-based approaches to SLP. A few have attempted to come up with a DSS for SLP with a prime focus on the quantitative approach. This study provides a framework of a functional DSS for SLP. The integration of AR for the purpose of visual management is targeted to aid better perspectival exchange among the stakeholders involved in the SLP task. The developed approach illustrates a way forward to make sense of the data available in project designs and the BIM models.

References

[1] C. M. Tam, T. K. L. Tong, A. W. T. Leung, and G. W. C. Chiu, "Site Layout Planning using Nonstructural Fuzzy Decision Support System," *J. Constr. Eng. Manag.*, vol. 128, pp. 220–231, 2002.

[2] X. Song *et al.*, "Reconciling Strategy Towards Construction Site Selection-Layout for Coal-Fired Power Plants," *Appl. Energy*, vol. 204, pp. 846–865, 2017.

[3] H. Abdul-Rahman, C. Wang, and K. S. Eng, "Repertory Grid Technique in The Development of Tacit-Based Decision Support System (TDSS) for Sustainable Site Layout Planning," *Autom. Constr.*, vol. 20, pp. 818–829, 2011.

[4] R. Santos, A. A. Costa, and A. Grilo, "Bibliometric Analysis and Review of Building Information Modelling Literature Published Between 2005 and 2015," *Autom. Constr.*, vol. 80, pp. 118–136, 2017.

[5] S. S. Kumar and J. C. P. Cheng, "A BIM-Based Automated Site Layout Planning Framework for Congested Construction Sites," *Autom. Constr.*, vol. 59, pp. 24–37, 2015.

[6] A. R. Singh and V. S. K. Delhi, "User Behaviour in AR-BIM Based Site Layout Planning," *Int. J.*

Prod. Lifecycle Manag., vol. 11, pp. 221–244, 2018.

[7] T. P. Caudell and D. W. Mizell, "Augmented Reality: An Application of Heads-Up Display Technology to Manual Manufacturing Processes," in *25th Hawaii International Conference on System Sciences*, 1992, pp. 659–669.

[8] X. Wang, "Using Augmented Reality to Plan Virtual Construction Worksite," *Int. J. Adv. Robot. Syst.*, vol. 4, pp. 1729–8806, 2007.

[9] A. R. Singh, Y. Patil, and V. S. K. Delhi, "Optimizing Site Layout Planning utilizing Building Information Modelling," in *36th International Symposium on Automation and Robotics in Construction (ISARC)*, 2019, pp. 376–383.

Factors Affecting the Implementation of AI-based Hearing Protection Technology at Construction Workplace

Yongcan Huang[a] and Tuyen Le[a]

[a]Glenn Department of Civil Engineering, Clemson University, USA
E-mail: yongcah@clemson.edu, tuyenl@clemson.edu

Abstract –
Standard hearing protection devices (HPDs) that reduce noise by strictly passive means are mandatory at construction sites. However, standard HPDs have been proved weaken the audibility of safety-critical sounds thus worsen construction workers' auditory situational awareness (ASA). Therefore, a wearable hearing protection technology that uses artificial intelligence (AI) to amplify safety-critical sounds while greatly attenuating ambient noise would be in great demand for construction safety monitoring. However, little to no study has provided clear evidence on understanding acceptance of the AI-based Hearing Protection Device (AI-HPD) since it is still in the early stages of development. To bridge the gap, this research sets out to identify important factors that need to be incorporated in the design consideration of AI-HPD and investigate users' intention of use which concerns us. The preliminary factor table is firstly generated from critical literature reviews on existing technology adoption theories. Expert reviews help to refine the factor table. With all summarized factors integrated, the final questionnaire of main survey is developed and given out. Through the returned report, the study discusses overall results and points out further study. This study enables researchers and professionals to better understand critical design and implementation considerations for the success adoption of AI-HPD technology in the future.

Keywords –
Construction Safety Monitoring; AI Application; Hearing Protection; Influence Factor

1 Introduction

Situational awareness is associated with safety-related perceptions at construction sites, notifying field staff critical information, for example, the safe distance of field workers from onsite equipment [1]. Recent developments in the field of Artificial Intelligence (AI) have led to a revolution in Architecture, Engineering, Construction (AEC) and Facilities Management (FM) domain. In order to increase situational awareness at construction sites, a number of studies have been carried out to solve practical problems with the help of AI. Kim et al. developed augmented-reality-applied system "Proximity Warning system (PWS)", which set out to prevent users from collisions with objects [2]. In Mardonova & Choi's literature review paper on wearable devices and sensors that enhance workers' situational awareness during mining operations, four types of sensors have been classified accordingly: environmental sensor, biosensors, location tracking sensors and others. Based on related research so far, it can be concluded that situational awareness enhancement is getting more and more attention in both industry and academia [3].

A construction site is such an unpleasant workplace since it mixes up many kinds of sounds beyond comfort level. According to a report from University of Washington [4], construction workers are exposed to multi-level noises because of the equipment they regularly use on-site, such as bulldozers and impact drivers. The average intensity of the noises is well above the 85 dBA in general. However, any sound featuring intensity at 85 dBA or higher is believed to cause ear damage and is great enough to be defined as hazardous. With that said, denoising is a significant technical issue in terms of protecting field workers' hearing. On the other hand, safety-critical sounds at construction sites, varying from acoustic safety cues to human speeches, make great contributions to generating situational awareness that further directs workers' behaviors. Therefore, auditory situational awareness (ASA), referred to situational awareness resourced from auditory signals, has been introduced. Despite that, traditional hearing protection solutions for field workers such as earplugs fail to balance preventing from ear damage and promising ASA. A practical example of construction can interpret this scene. When a carpenter installs a sub floor by connecting it to wooden-frame joints and uses impact driver to put nails in the joint through the sub-floor, the

sound of a successful hitting the joint is different from the missed sound and signals the carpenter a well-done job. However, if the carpenter works with earplugs on, he/she is not able to hear the drilling sound clearly thus fails to give a swift inspection. Additionally, wearable devices are popularly applied to improve situational awareness in industries. As a result, a hearing protection technology in design of wearable device that uses AI to amplify safety-critical sounds while greatly attenuating ambient noise would be in great demand for preserving or augmenting the ASA of construction workers.

Audio signal processing for automated detection guarantees the technology of realizing the AI-based hearing protection device (AI-HPD). A variety of audio signal processing methods employing robust machine learning or deep learning models show prosperous successful potentials to quickly detect auditory safety cues and promise the ASA [5][6][7].These computing advances have been adapted to different contexts, ranging from indoor and public environments [8], medical and health care systems, to working environments [9]. However, when it comes to construction safety, it remains a problem to be addressed. Moreover, little to no study, to the best of our knowledge, has provided evidence on understanding the acceptance of AI-HPD because it stays the early stage of development. In view of the industry's infamous nature of resisting innovation, investigating what controls the successful acceptance of AI-HPD will provide useful information to convince practitioners of its viability.

In this paper, based on construction workers' hearing protection demands and current technical foundation, we envisioned a new AI-based hearing protection device. In an effort to explore user's input, concerns, requirements that are critical to the development of such technology in the future, we firstly listed possible factors according to a systematical literature review of social, physiological, and cognitive knowledge under the topics, for example, innovation adoption, technology acceptance. Then, we revised the factors in ways of introducing an expert panel review where experts from both the industry and the academia are invited to evaluate each factor. Subsequently, we proposed a questionnaire that integrates all reasonable factors after expert panel review and spread it to targeted group, practitioners who have working experiences at construction sites. After retrieving the returned questionnaires, we summarized and described the data and clarified our findings on it. At last, we concluded our work at this stage and pointed out future work.

2 METHOD

2.1 Influence Factors

In system/technology-related research, quite a few frequently used success models and adoption theories are applied to set up connections among multiple levels of practitioners on understanding the feasibility and benefits when an emerging system/technology is about to implemented [10]. Existing studies to date reveal that these basic models and theories have been extensively used across many fields in knowing the technology adoption and implementation, varying from financial services, Internet to education. Construction industry is not an exception. Son et al. took an interest in figuring out a mobile computing device's acceptance by construction professionals. They extended Technology Acceptance Model (TAM) [11] to explore determinants of user satisfaction with the device and link between user satisfaction and perceived performance. In order to determine the success or failure of EPR (Enterprises Resource Planning) system implementation in construction industry, Chung et al. generated a success model by adapting TAM model with Delone and McLean's information systems [12] and integrating them with key project management principles [13]. In analyzing what affects individuals' intention to utilize new technology for the sake of better leading a construction business, Sargent et al. practiced the Unified Theory of Acceptance and Use of Technology (UTAUT) model to examine IT adoption in construction management [14]. In previous studies, researchers followed a general workflow in preparation for confirming those factors controlling the success of a certain technology adoption: choose an original success model or theory, for example TAM, moderate the TAM based on the original model constructs and context-related variables, collect data and test the moderated model. Considering AI-HPD is part of innovation, confirming the factors can start from previous success models and adoption theories. In our study, we firstly put the basic constructs or variables of models in our factor table, like TAM, UTAUT, Delone and McLean Information System Success Model, Technology Organization Environment (TOE) Model [15], Theory of Planned Behavior (TPB) [16]. Secondly, we widely collected more technology adoption investigation documents in regard to the construction industry and also consider broader aspects of society, economy, and organization. By doing so, we developed a preliminary factor table for AI-HPD, which is supposed to be reviewed by the expert panel review and modified according to their comments.

2.2 Expert Panel Review

After the preliminary conceptional model comes into being, the content review by an expert panel is advised. Referring to previous study and sample size calculation, five experts including three researchers and two professionals in practice, with an average of 16-year experience in construction management, were suggested to review the preliminary factor table with regard to AI-HPD [17]. Out of getting sound and valid result, the candidate list for the expert review were selected from databases such as Google Scholar, ResearchGate, and LinkedIn by their academic or occupational relevance to the topic and academic influence. Three associate professors with key word tag Construction Management at Google Scholar respectively from the United States, Japan, China were invited to check the factor table via emails. Two USA-based civil engineers with approximate 20 years on-site working experience accepted the invitation. As a result, the final factor table was generated, as shown in Table 1.

Table 1. Factor table after expert review

No.	Factor	Definition or Scope
1	Participants Demographic Background	Age, institution or company, gender, race, annual income, education level, job title, hearing status, exposed-to-noise experience, hearing protection history
2	Perceived Usefulness	The degree to which a person believes that the use of AI-HPD would enhance his or her personal or job performance
3	Perceived Ease of Use	The degree to which a person believes that AI-HPD would be easy to use
4	Subjective Norms	Perception of important (or relevant) others' beliefs about my use of AI-HPD
5	Resistance to Innovation	The extent to which an individual resists new technology
6	Openness to Data Utilization	The extent to which an individual is comfortable with his or her data of job conditions being used and shared by a certain group while using AI-HPD
7	Hearing Health and Safety Consciousness	Awareness and care of hearing health conditions, and the degree to which hearing health concerns are integrated into an individual's regular work
8	Perceived Economic Constraints	Perception of the economic constraints or consideration of using AI-HPD
9	Perceived Organizational Impact	Perception of the organizational and societal constraints or influence of using AI-HPD
10	Attitude	User's general attitudes towards AI-HPD
11	Familiarity with the Use of AI Assistant	The degree to which the user is familiar with AI assistant
12	Trust	The extent to which an individual believes that using AI-HPD is secure, reliable, effective, and poses no privacy threats
13	Perceived Risks	A combination of uncertainty and seriousness of an outcome in relation to performance, safety, psychological or social uncertainties

2.3 Main Survey

The main survey was conducted in the form of a questionnaire, which consists of three primary sections, includes 79 open- and close-form questions. The first

section introduces fundamental know-how of AI-HPD such as working principles, working modes. After reading the product introduction, participants are expected to answer the trap questions that help to filter out unqualified responses. The trap questions follow the prompts of "I read and understood the introduction section about AI-HPD", "How many modes would the AI-HPD operate", "When using the device under mode 1, you will hear every ambient sound". The second section requests demographic-based information from the survey participants. The third section asks the participants to rate the perceived level of importance for each factor using a five-point Likert scale where 1 represents "Totally disagree" and 5 represents "Totally agree." In particular, the questionnaire survey was designed on the platform of an online tool Qualtrics and distributed to elicit responses from the participants about the importance of the identified factors. At the same time, Amazon Mechanical Turk assisted to identify and reach the targeted construction personnel [18].

In our study, the AI-HPD would offer the following two operation modes.

- **Under the mode 1**, the intelligent filter blocks every sound to the user's ears and only send an alert when a hazard event is detected. The user would not hear anything except for warning alerts.
- **Under the mode 2**, the intelligent filter reduces every sound to under a safe level, but amplifies any critical sounds detected and attenuating unimportant sounds. The user would hear every ambient sound along with a warning alert if any.

Additionally, Intention of Use functions as a very important indicator in testing the participants' acceptance; whether AI-HPD would be accepted or not, which mode would be accepted, whether users would like to recommend it to others, should be focused. Therefore, our survey design subdivides the final Intention of Use into four parts in order to fully reflect the participants' acceptance on AI-HPD, which is specified by following questions, "I intend to use AI-HPD if it is provided by my organization", "I would prefer to use AI-HPD under the condition the device is on the mode of blocking all sounds to my ears and sending me an alert if a hazard event is detected, considering that system might miss an important sound or send a wrong alert", "I would prefer to use AI-HPD under the condition the device is on the mode of reducing all sounds to a safe level, but bypasses and amplifies any critical sounds detected, considering that the system might fail to amplify a critical sound or amplify an unimportant sound", "I will encourage field workers who are exposed to hazardous noises to use AI-HPD for hearing protection". Besides, when setting up questions for factor Perceived Economic Constraints, a filter question "Do you work, or have you ever worked as a business leader of a project" is designed for stopping unqualified participants.

3 Data Description

There were 332 completed responses. An additional 68 participants began the survey but failed to complete it either quitting halfway or being filtered out by trap questions, resulting in a dropout rate of 17% (68/400). The median survey completion time was 437 seconds.

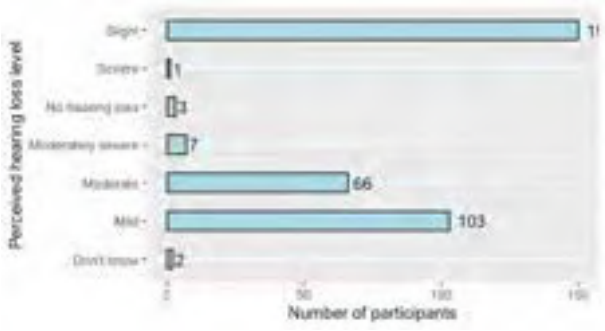

Figure 1. Perceived hearing loss as reported by participants. (N = 332)

3.1 Participant Background Characteristics

Participants ranged from 18 to 69 years old, with median age of 30 (M=32.9, SD=8.9). With all participants positively answering this question, the majority (78.3%) identified as female (N = 260), while 21.7% (N = 72) identified as male. 79.8 % of the participants hold Bachelor or higher degree (N = 265), however, only 1 participant didn't go to high school. Participant' s occupation diverged from business leader to carpenter. Figure 1 shows self-reported level of hearing loss that participants perceived they were suffering, as most participants reported slight or mild hearing loss. Similarly, at least 71.4% (N = 237) of the participants believed they were exposed to noises of different levels during working, as shown in Figure 2. When asked about if they put on hearing protection device whenever there is hazardous noise by Likert scale, the median located at 4 with standard deviation of 1.28, as Figure 3 shows the details. When asked about whether they have heard about any forms of loss caused by the use of hearing protection, the answers were split cleanly between Yes (P = 49.7%, N = 165) and No (P = 50.3%, N = 167), see Figure 4.

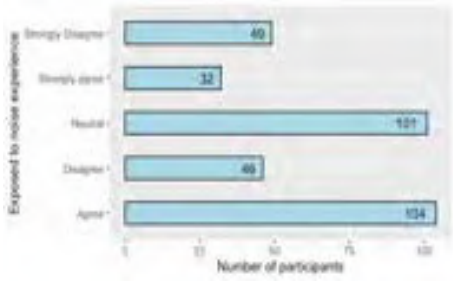

Figure 2. Exposed to noise experience as reported by participants. (N = 332)

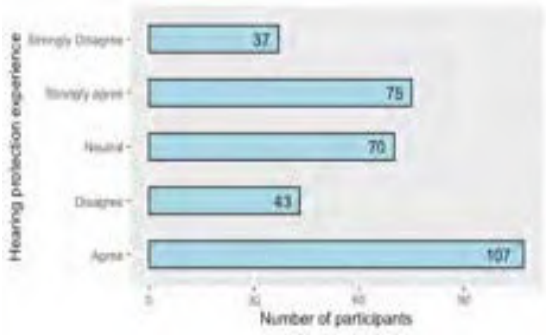

Figure 3. Hearing protection experience as reported by participants. (N = 332)

Figure 4. Heard about any injury case caused by using hearing protection as reported by participants. (N = 332)

3.2 Non-demographic factors and Intention of Use

Responses to non-demographic factors represent participants' attitudes towards AI-HPD under the premise they have understood this technology by browsing the introduction section. On the other hand, these factors, to certain degree, reflect the results of how society, economics, organization shape the way that participants treat such an innovation. Based on this, the data description of non-demographic factors is discussed.

Of Perceived Usefulness, approximate three quarters ("agree" or "strongly agree") of the respondents (P=72.5%, N=241) indicated that AI-HPD would be useful in improving the status-quo of construction sites. Just over 78.2% (N=261) of those who responded agreed that AI-HPD was supposed to be easy to use, concluded from the data of Perceived Ease of Use. In terms of Subjective Norms, 263 of 332 participants believed that people who were meant important to them would suggest them to practice AI-HPD if they got to know about it. As for Resistance to Innovation, different from the whole construction industry which posited a negative attitude towards innovation, almost 72.3% (N=240) of the participants were willing to try new technology. According to the result of Openness to Data Utilization, it's noteworthy that the population (P=61.4%, N=204) of those who positively agreed that job-related data could be used and shared was relatively less, in comparison to other factors. Specifically, only 80 of 332 participants chose "strongly agree" in this case, as shown in Table 2. In regard to Hearing Health and Safety Consciousness, the majority (P=81.3%, N=270) of the questionnaire takers concerned about their health and safety during job. Well under 7% of the participants didn't regard it as a big issue. Three questions were designed to observe Perceived Organizational Impact among the participants. When asked about "the regulations, policies, and procedures on safety in my organization is very strict", at least 241 of 332 believed that safety management was strictly performed in his/her organization. When asked about the hearing protection usage of collogues, by the question "most of my peers working in the field are currently using earplugs or earmuffs whenever required", 205 participants agreed that using earplugs or earmuff for hearing protection normally existed. At this time, the population of those who held neutral attitude rose up to 81 as shown in Table 3, which shows that a certain number of participants didn't have any knowledge about the hearing protection usage of their collogues. In the third question, when asked about "My peers who use earplugs or earmuffs for hearing protection have shown their demand in improving hearing capability", the statistics was very similar to that of the second question, explained by 210 responses of "agree" or "strongly agree" and 75 neutral responses. As for the factor Attitude, over 85.6% (N=284) of participants showed that they liked the idea of AI-HPD. In addition, 237 (P=71.4%) of the participants agreed that AI-HPD would be secure, reliable and efficient in terms of the factor Trust. Moreover, the result of Familiarity with the Use of AI Assistant indicated that most of the participants (P=85.2%, N=283) knew AI assistant well. However, when it came to Perceived Risks, 180 participants perceived that the risks such as misusing personal information, missing important sounds or sending wrong alerts were high. 83 of participants held neutral attitudes, explained by Table 4. This finding revealed that user information management and qualified technology are what concerned users and what we should pay special attention on. Additionally, there were 162 participants recognized as business leaders. More than 80% of them

agreed that their organizations had the funding to afford AI-HPD and 66.7% of them reckoned that the expense of AI-HPD would be high.

Table 2. Openness to Data Utilization as reported by participants. (N = 332)

Openness to Data Utilization	Number of participants	Percent of participants
Strongly disagree	29	8.7%
Disagree	44	13.2%
Neither agree nor disagree	55	16.6%
Agree	124	37.3%
Strongly agree	80	24.1%

Table 3. Perceived peers' hearing protection usage as reported by participants. (N = 332)

Perceived peers' hearing protection usage	Number of participants	Percent of participants
Strongly disagree	15	4.5%
Disagree	30	9.0%
Neither agree nor disagree	81	24.4%
Agree	120	36.1%
Strongly agree	86	25.9%

Table 4. Perceived Risks as reported by participants. (N = 332)

Perceived Risks	Number of participants	Percent of participants
Strongly disagree	14	4.2%
Disagree	55	16.6%
Neither agree nor disagree	83	25.0%
Agree	121	36.4%
Strongly agree	59	17.8%

We examined overall intention of using AI-HPD, and the degree of interest of two modes, and intention of recommending it. Overall intention of use was high, with 79.5% of the participants (N=264) "agree" (scale=4) or "strongly agree" (scale=5) to use AI-HPD. Around 56.6% (scale=4 or 5) of the participants with at least "agree" degree to use mode 1 (users would not hear anything except for warning alerts), while 75% participants show great interest in mode 2 (users would hear every ambient sound along with a warning alert if any), as shown in Figure 5. It was worth noting that participants who rate one mode with high interest may agree or disagree the other mode. However, as far as the acceptance of two modes is concerned, mode 2 seemed to be more popular. The result of intention of recommendation indicated over 83% (N=276, scale=4 or 5) of participants had a strong passion on letting more people know about it.

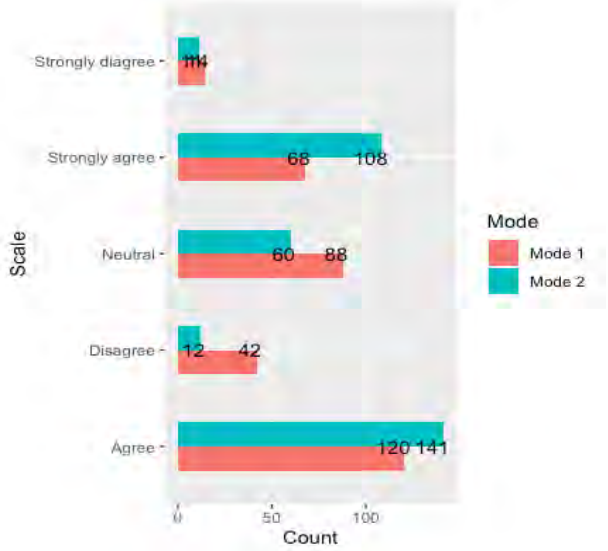

Figure 5. Intention of using Mode 1 and Mode 2

4 Conclusions and Future Work

This paper presents an effort to derive influence factors which control the successful acceptance and implementation of envisioned AI-HPD, a feasible hearing protection technology aiming to improve field worker's operating environments. Significant factors in the realm from social, physiological, economical and construction practice, were confirmed through a review of related literature and expert panel review. In order to further investigate the factors and pre-test workers' intention of using AI-HPD, a survey in the form of a questionnaire was generated, given out and returned with responses. Through describing and discussing the data retrieved, the authors expect this paper to help understand user's input, concerns, requirements that are critical to the development of such technology in the future.

As a result, it can be seen that noises have been an issue to most of the field workers and most of them tried or have been trying to avoid it by taking steps. As for findings from the statistics of non-demographic factors, user information management and qualified technology are what concerned users and where we should pay special attention in post product R&D stage. Quite a few participants believed that organizations they belong to were able to afford the expense of AI-HPD if it was considered; though the expense of AI-HPD was not perceived cheap. This signals us that the economic factors don't need to take up too much consideration when making decisions in the future work. The results of

Intention of Use showed that most people would like to use it; The working mode that enables users hear every ambient sound along with a warning alert if any was more popular, which directs us to focus on amplifying a certain sound in the background of noise in terms of auditory signal processing; large population of them would like to recommend this envisioned technology to their peers.

In future work, there are at least three aspects we should clarify. First, more specific discussions on each identified factor should be practiced. Second, different models or methods are suggested to be applied in analyzing how these factors affect the successful acceptance of AI-HPD and the coefficients of the distinguished factors. Third, the intention of use is made up of three parts, intention of using the technology, intention of choosing mode 1 or 2, intention of recommending the technology. Further data analysis of the subdivisions of intention of use is necessary.

Acknowledgement

This research was funded by the National Science Foundation (NSF) through the Award # 1928550 and the Center for Construction Research and Training (CPWR) through NIOSH cooperative agreement OH009762. The authors gratefully acknowledge NSF and CPWR's support. Any opinions, findings, conclusions, and recommendations expressed in this paper are those of the authors and do not necessarily reflect the views of NSF and CPWR.

References

[1] I. Awolusi, E. Marks, and M. Hallowell, "Wearable technology for personalized construction safety monitoring and trending: Review of applicable devices," *Autom. Constr.*, vol. 85, no. January, pp. 96–106, 2018, doi: 10.1016/j.autcon.2017.10.010.

[2] K. Kim, H. Kim, and H. Kim, "Image-based construction hazard avoidance system using augmented reality in wearable device," *Autom. Constr.*, vol. 83, pp. 390–403, 2017.

[3] M. Mardonova and Y. Choi, "Review of wearable device technology and its applications to the mining industry," *Energies*, vol. 11, no. 3, p. 547, 2018.

[4] N. Seixas and R. Neitzel, "Noise exposure and hearing protection use among construction workers in washington state," *Dep. Environ. Occup. Heal. Sci.*, 2004.

[5] J. Salamon, C. Jacoby, and J. P. Bello, "A dataset and taxonomy for urban sound research," in *Proceedings of the 22nd ACM international conference on Multimedia*, 2014, pp. 1041–1044.

[6] J. Salamon and J. P. Bello, "Deep convolutional neural networks and data augmentation for environmental sound classification," *IEEE Signal Process. Lett.*, vol. 24, no. 3, pp. 279–283, 2017.

[7] J. Cramer, H.-H. Wu, J. Salamon, and J. P. Bello, "Look, listen, and learn more: Design choices for deep audio embeddings," in *ICASSP 2019-2019 IEEE International Conference on Acoustics, Speech and Signal Processing (ICASSP)*, 2019, pp. 3852–3856.

[8] C. Clavel, T. Ehrette, and G. Richard, "Events detection for an audio-based surveillance system," in *2005 IEEE International Conference on Multimedia and Expo*, 2005, pp. 1306–1309.

[9] M. Vacher, D. Istrate, L. Besacier, J.-F. Serignat, and E. Castelli, "Sound detection and classification for medical telesurvey," 2004.

[10] S. Lee, J. Yu, and D. Jeong, "BIM acceptance model in construction organizations," *J. Manag. Eng.*, vol. 31, no. 3, p. 4014048, 2013.

[11] V. Venkatesh and F. D. Davis, "A theoretical extension of the technology acceptance model: Four longitudinal field studies," *Manage. Sci.*, vol. 46, no. 2, pp. 186–204, 2000.

[12] M. E. Jennex and L. Olfman, "A model of knowledge management success," *Int. J. Knowl. Manag.*, vol. 2, no. 3, pp. 51–68, 2006.

[13] B. Chung, M. J. Skibniewski, and Y. H. Kwak, "Developing ERP systems success model for the construction industry," *J. Constr. Eng. Manag.*, vol. 135, no. 3, pp. 207–216, 2009.

[14] K. Sargent, P. Hyland, and S. Sawang, "Factors influencing the adoption of information technology in a construction business," *Australas. J. Constr. Econ. Build.*, vol. 12, no. 2, p. 72, 2012.

[15] H. O. Awa, O. U. Ojiabo, and L. E. Orokor, "Integrated technology-organization-environment (TOE) taxonomies for technology adoption," *J. Enterp. Inf. Manag.*, vol. 30, no. 6, pp. 893–921, 2017.

[16] I. Ajzen, "The theory of planned behavior," *Organ. Behav. Hum. Decis. Process.*, vol. 50, no. 2, pp. 179–211, 1991.

[17] O. A. Bolarinwa, "Principles and methods of validity and reliability testing of questionnaires used in social and health science researches," *Niger. Postgrad. Med. J.*, vol. 22, no. 4, p. 195, 2015.

[18] I. Awolusi, C. Nnaji, E. Marks, and M. Hallowell, "Enhancing Construction Safety Monitoring through the Application of Internet of Things and Wearable Sensing Devices: A Review," in *Computing in Civil Engineering 2019: Data, Sensing, and Analytics*, American Society of Civil Engineers Reston, VA, 2019, pp. 530–538.

Project Work Breakdown Structure Similarity Estimation Using Semantic and Structural Similarity Measures

Navid Torkanfar[a] and Ehsan Rezazadeh Azar[a]

[a] Department of Civil Engineering, Lakehead University, Canada
E-mail: ntorkanf@lakeheadu.ca, eazar@lakeheadu.ca

Abstract –

Reusing of the past information and lessons learned helps practitioners in better management of various aspects of construction projects, such as cost estimation, planning, contracting, and design. Measuring the similarity of construction projects improves the efficiency of the existing information systems in retrieval of relevant cases. It was hypothesized that the Work Breakdown Structure (WBS) of projects contains the necessary information to measure the semantic similarity of construction projects; therefore, WBS can be used as a potential representative of the projects. In this research project, a novel method is proposed to assess the semantic similarity of projects by application of natural language processing techniques. In this method, a new project is compared with the documented as-built projects based on their WBS similarity. This method is implemented using two metrics: (1) node similarity that compares the semantics of all nodes in two WBSs; (2) structural similarity which compares the topology of the work breakdown structures. The proposed system calculates a similarity score between 0 and 1 for each metric and the combination of these two scores provides the final similarity score between a pair of WBSs, thus it could rank the similarity of the documented cases to the new project based on their final scores. Experimental results indicated that the structural similarity produced about 15 percent higher degree of retrieval precision than the node similarity.

Keywords –

Project similarity; Construction project; Work breakdown structure; Natural language processing; Knowledge management

1 Introduction

Effective reuse of gained knowledge from past projects helps managers to complete projects in a timely and economical manner, and with a higher quality [1]. In the construction industry, several methods such as knowledge management techniques and case-based reasoning (CBR) have been applied to reuse past information and experiences. A major step in the knowledge retrieval systems is to index stored data based on several attributes in order to find the most relevant document(s).

Knowledge management systems are IT-based systems that aim to improve the organizational process of knowledge creation, storage/retrieval, transfer, and application [2]. The process of knowledge retrieval is difficult and can result in irrelevant documents [3]. A method was proposed to retrieve relevant information in construction projects by keywords, such as project type and title, through a Google-like function [4].

A CBR system can offer a solution for new problems by recalling a similar past situation(s) [5]. CBR methods have been investigated in different areas of construction research, including cost estimation [6,7], safety [8], and planning [9,10]. In CBR systems, the similarity of cases is compared based on predefined nominal or numerical attributes. Finding the appropriate attributes and assigning weights are among the main challenges in these systems.

A quantitative similarity measurement among construction projects provides a comprehensive metric that can improve the process of retrieving related information. Current practices in similarity measurement of construction projects are limited. These methods distinguish construction projects based on generic factors, such as project size and location or specific user defined attributes, such as number of floors, structural system type or keywords, rather than the entire scope of the project The aim of this research is to fill this gap by proposing a method to compare projects using their WBSs.

WBS is one of the main outcomes of the processes in the scope management of projects [11]. The WBS is used in different project management areas such as time and cost management [11]. The proposed system is the first of the kind attempt to use WBS to measure the

similarity of the project scopes. The metrics for this assessment were developed using NLP techniques. NLP was employed to semantically compare the tasks and services within the WBSs.

1.1 Work breakdown structure (WBS)

WBS is s a hierarchical decomposition of the tasks and services to be carried out by the project team to achieve the project objectives [11]. WBS hierarchy begins with the project name at its highest level. The tasks and services in each level of the hierarchy are subdivided into smaller tasks that must be accomplished to satisfy the higher-level packages (samples in Figure 1). This decomposition continues until the tasks cannot be broken down or are no longer meaningful.

1.2 Semantic similarity measurements

The aim of the studies in NLP area is to enable computers to understand natural language text and speech used in human communications [12]. Measuring the similarity between words and sentences is an NLP technique that has been used in different areas, such as text classification, document clustering, and text summarization [13]. Corpus-based [14] and knowledge-based systems are utilized to semantically measure the similarity of words based on their definitions.

In the knowledge-based systems, semantic similarities are measured based on semantic relations among concepts [15]. These relations are embedded in the semantic networks. WordNet, a lexical database of English, is one of the most popular semantic networks [16]. The hierarchical structure of WordNet contains various semantic relations, such as synonymy, autonomy, hyponymy, and membership. These relations are used to calculate semantic similarities [17].

Wu and Palmer method (WUP) is a procedure to measure the semantic similarities between English words based on the WordNet [18]. In this method, the similarity is measured based on the position of concepts c_1 and c_2 and the position of their lowest common subsumer $lso\ (c_1, c_2)$ in the WordNet hierarchy. For example, Equation 1 calculates the similarity of concepts c_1 and c_2 , where the $len(c_1, c_2)$ is the length of the shortest path between concepts c_1 and c_2, and the $depth$ is the length of the path that connects each concept to the root element [18].

$$sim_{WUP}(c_1, c_2) = \frac{2 * depth(lso\ (c_1, c_2))}{len(c_1, c_2) + 2 * depth(lso\ (c_1, c_2))} \quad (1)$$

2 Method

The proposed method quantifies the similarity between two construction projects by two metrics driven from their WBSs: node similarity and structural similarity. These metrics are calculated based on semantic comparisons of tasks within the two compared WBSs. These semantic comparisons include three measurements: the semantic comparison of nodes, parents of the nodes, and siblings of the nodes.

2.1 Semantic measurements

The tasks in a WBS are composed of several words.

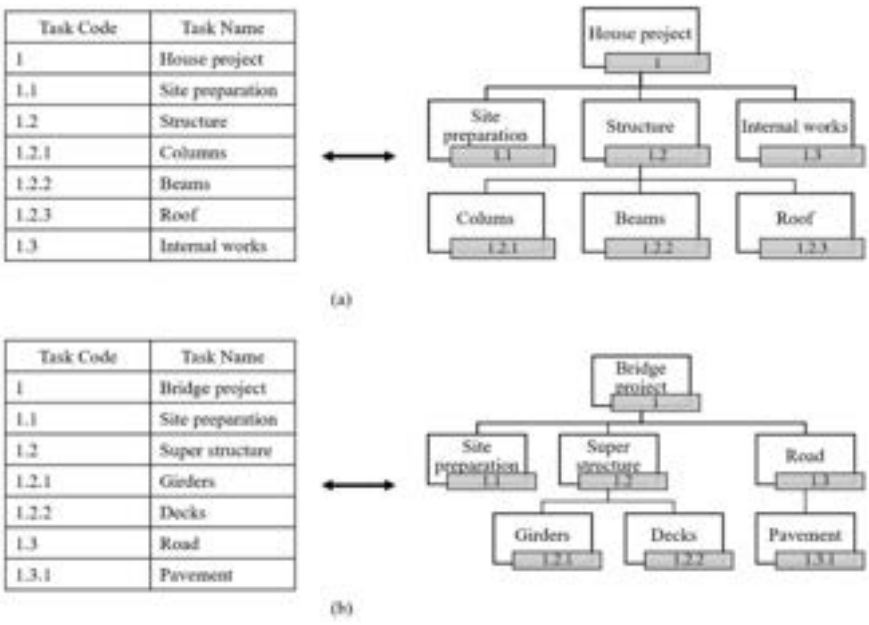

Figure 1. Two simplified work breakdown structures: (a) a House project (b) a Bridge project

The similarity between tasks can be calculated by averaging semantic similarity of their words. This study utilizes Equation 2 [19] to calculate the similarity between $task_i$ and $task_j$. In this equation, the method finds the most similar word for each word (w) in $task_i$ from $task_j$ ($maxSim(w, task_j)_{wup}$) based on Wu and Palmer algorithm [18].

$$sim_{semantic}(task_i, task_j) = \frac{1}{2}\left(\frac{\sum_{w\in\{task_i\}}(maxSim(w, task_j)_{wup})}{\sum_{w\in\{task_i\}} 1} + \frac{\sum_{w\in\{task_j\}}(maxSim(w, task_i)_{wup})}{\sum_{w\in\{task_j\}} 1}\right) \quad (2)$$

2.2 Comparison of nodes

A WBS is made of a hierarchy of nodes containing all the tasks required to complete a project. As shown in Figure 1, each node contains a task name and a task code. The first step in measuring the similarity between two WBSs is to semantically compare the task names. In this study, WBS_N^L represents an entire WBS with N nodes and L levels of hierarchy. Elements of the matrix in Equation 3 represent the semantic similarities between nodes of $WBS_{N_1}^{L_1}$ and $WBS_{N_2}^{L_2}$. In this equation $sim_{semantic}(n_i, m_j)$ equals to the semantic similarity between tasks of nodes n_i and m_j. N_1 and N_2 represent the list of nodes that each WBS contains (N_1: $(n_1, n_2, \dots, n_N)$ and N_2: $(m_1, m_2, \dots, m_M)$).

$$sim_{nodes}(WBS_{N_1}^{L_1}, WBS_{N_2}^{L_2}) = \begin{bmatrix} sim_{semantic}(n_1, m_1) & \cdots & sim_{semantic}(n_1, m_j) \\ \vdots & \ddots & \vdots \\ sim_{semantic}(n_i, m_1) & \cdots & sim_{semantic}(n_N, m_M) \end{bmatrix} \quad (3)$$

2.3 Comparison of node parents

In a WBS, each node is subdivided from an upper-level node which is called the parent of that node. Parent comparison between two nodes measures the semantic similarity of their parents. As shown in Figure 2, each node has a sequence of parents, and the first two parents with a similarity less than a specified threshold are defined as the least similar parents (LSP). The parent similarity, which is calculated using Equation 4, measures the arithmetic mean of semantic similarity of parents which are placed between the intended node and its LSP.

$$sim_{parents}(n_i, m_j) = \frac{\sum_{i=1}^{L_{LSP}-L_n}\left(L_{LSP} - L_{n_i} - (i-1)\right) \times sim_{semantic}(ith\ parents)}{\sum_{i=1}^{L_{LSP}-L_{n_i}}(i)} \quad (4)$$

The matrix in Equation 5 contains the parent similarities between nodes of $WBS_{N_1}^{L_1}$ and $WBS_{N_2}^{L_2}$.

$$sim_{parents}(WBS_{N_1}^{L_1}, WBS_{N_2}^{L_2}) = \begin{bmatrix} sim_{parents}(n_1, m_1) & \cdots & sim_{parents}(n_1, m_j) \\ \vdots & \ddots & \vdots \\ sim_{parents}(n_i, m_1) & \cdots & sim_{parents}(n_N, m_M) \end{bmatrix} \quad (5)$$

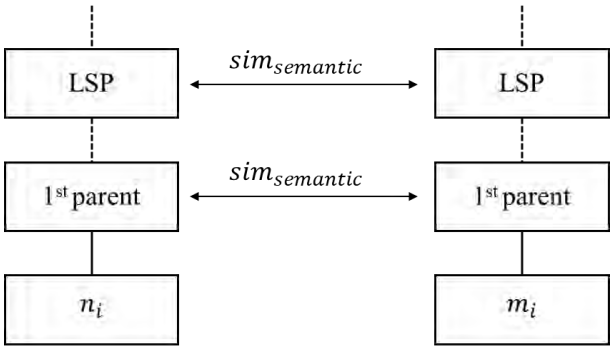

Figure 2. Parent similarity between nodes $\boldsymbol{n_i}$ and $\boldsymbol{m_j}$

2.4 Comparison of node siblings

In a WBS hierarchy, the nodes subdivided from a common parent are called siblings. The sibling similarity between nodes n_i and m_j is calculated by Equation 6 and is the fraction of the number of siblings that were actually matched by the total number of siblings. As shown in Figure 3, any pairs of siblings with a semantic similarity more than a defined threshold are considered matched. The matrix in Equation 7 contains the sibling similarities between nodes of $WBS_{N_1}^{L_1}$ and $WBS_{N_2}^{L_2}$.

$$sim_{siblings}(n_i, m_j) = \frac{|matched_{siblings}(n_i, m_j)|}{|siblings_{n_i}| + |siblings_{m_j}|} \quad (6)$$

$$sim_{siblings}(WBS_{N_1}^{L_1}, WBS_{N_2}^{L_2}) = \begin{bmatrix} sim_{siblings}(n_1, m_1) & \cdots & sim_{siblings}(n_1, m_M) \\ \vdots & \ddots & \vdots \\ sim_{siblings}(n_i, m_1) & \cdots & sim_{siblings}(n_N, m_M) \end{bmatrix} \quad (7)$$

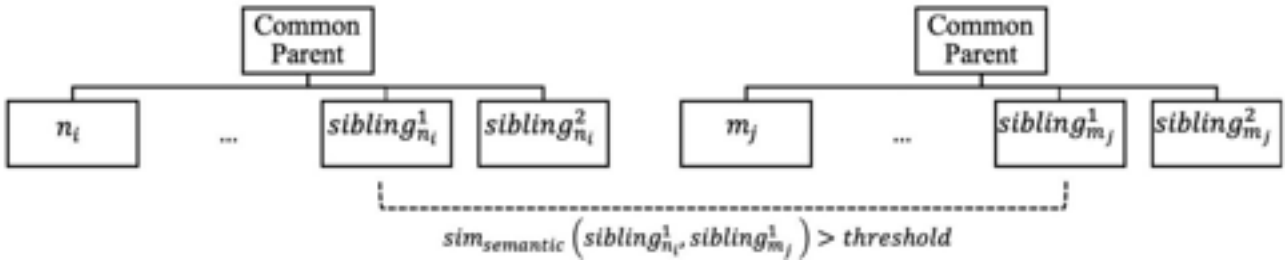

Figure 3. Sibling similarity between nodes $\boldsymbol{n_i}$ and $\boldsymbol{m_j}$

2.5 Mapping of nodes

The average of node, parent, and sibling similarities results in the average similarities (see Equation 8). The matrix in Equation 9 contains the average similarities between nodes of $WBS^{L_1}_{N_1}, WBS^{L_2}_{N_2}$. In this matrix, for instance, the first row includes the similarities between node n_1 from $WBS^{L_1}_{N_1}$, and nodes m_1 to m_M from $WBS^{L_2}_{N_2}$. The node n_1 will be mapped to a node from the second WBS with the highest average similarity. The same procedure will map all the nodes between two WBSs.

Mapped nodes in Equation 10 contain tuples of nodes which are mapped together $(n_i, m_j, sim_{average})$ with their average similarity score (i.e. $sim_{average}$). Mapped nodes and $sim_{average}$ will be used to calculate the similarity scores between two WBSs, as they are utilizied to calculate node similarity and structural similarity scores ($n_i \in N_1$ and $m_j \in N_2$).

$$sim_{average} = \frac{sim_{node} + sim_{parents} + sim_{siblings}}{3} \quad (8)$$

$$sim_{average}\left(WBS^{L_1}_{N_1}, WBS^{L_2}_{N_2}\right) = \begin{bmatrix} sim_{average}(n_1, m_1) & \cdots & sim_{average}(n_1, m_j) \\ \vdots & \ddots & \vdots \\ sim_{average}(n_i, m_1) & \cdots & sim_{average}(n_N, m_M) \end{bmatrix} \quad (9)$$

$$mapped\ nodes = \{(n_i, m_j, sim_{average})\} \quad (10)$$

2.6 Node similarity score

The node similarity score is the arithmetic mean of $sim_{average}$ of the mapped nodes. The node similarity, a score between 0 and 1, is calculated using Equation 11. In this equation, the sum of $sim_{average}$ is divided by the total number of nodes between two work breakdown structures.

$$Node\ similarity\left(WBS^{L_1}_{N_1}, WBS^{L_2}_{N_2}\right) = \frac{2 \times \sum_{(n_i, m_j) \in mapped\ nodes}\left(sim_{avg}(n_i, m_j)\right)}{|N_1| + |N_2|} \quad (11)$$

2.7 Structural similarity score

In the comparison of two WBSs, in addition to the semantic similarity of nodes within the WBS, the structure of hierarchies affects the similarity score as well. The structural similarity [20] was defined based on the graph-edit-distance method [20,21]. Graph-edit-distance is the minimum required operations to alter the structure of one hierarchy to another.

Node deletion and node substitution are two metrics used to derive the graph-edit-distance. In comparison of two WBSs, mapping nodes with a higher degree of similarity requires less effort than mapping nodes with lower similarities. In addition, eliminating the nodes which are not mapped requires an extra effort. Thus, a smaller required effort to change the structures of two WBSs can result in a higher structural similarity. Node deletion measures the required effort to eliminate unmapped nodes. Node substitution is the required effort to link the mapped nodes.

Equations 12 and 13 determine the deletion and substitution efforts between $WBS^{L_1}_{N_1}$ and $WBS^{L_2}_{N_2}$. Equation 12 defines deletion effort (DE) as a ratio of the number of unmapped nodes ($|UN|$) over the total number of nodes. Substitution effort (SE) is calculated in Equation 13 by averaging dissimilarity of the mapped nodes. In other words, a higher degree of similarity between the nodes will result in a lower substitution effort. Arithmetic average of deletion and substitution efforts produces a representative of structural dissimilarity and its complement was determined as a measure of structural similarity as shown in Equation 14.

$$DE\left(WBS^{L_1}_{N_1}, WBS^{L_2}_{N_2}\right) = \frac{|UN|}{|N_1| + |N_2|} \quad (12)$$

$$SE\left(WBS_{N_1}^{L_1}, WBS_{N_2}^{L_2}\right) = \frac{2 * \sum_{(n_i,m_j)\in mapped\ nodes}\left(1 - sim_{average}(n_i, m_j)\right)}{|N_1| + |N_2| - |UN|} \quad (13)$$

$$Structural\ similarity\left(WBS_{N_1}^{L_1}, WBS_{N_2}^{L_2}\right) = 1 - \frac{DE\left(WBS_{N_1}^{L_1}, WBS_{N_2}^{L_2}\right) + SE\left(WBS_{N_1}^{L_1}, WBS_{N_2}^{L_2}\right)}{2} \quad (14)$$

3 Experimental results

Three experts in the project management domain were asked to develop four WBSs for four different construction projects: a bridge construction (steel girder with composite concrete slab), a steel-framed office building, a reinforced concrete-framed residential building, and a road-widening project. Table 1 presents the 12 WBS samples created by these subject matter experts. These samples were utilized to evaluate the performance of the proposed metrics in distinguishing the projects and retrieving the most similar samples.

As was mentioned before, an equal threshold was used in comparison of parents and siblings. To determine the impact of this threshold on the proposed metrics, the results were explored by changing the threshold in the range of 0.5 to 0.8 with 0.05 intervals.

Table 1. Created samples by the experts.

Experts	Developed samples	Represented by
expert 1	$bridge\ construction_1$	B_1
	$concrete\ structure\ building_1$	C_1
	$steel\ structure\ building_1$	S_1
	$road\ maintenance_1$	M_1
expert 2	$bridge\ construction_2$	B_2
	$concrete\ structure\ building_2$	C_2
	$steel\ structure\ building_2$	S_2
	$road\ maintenance_2$	M_2
expert 3	$bridge\ construction_3$	B_3
	$concrete\ structure\ building_3$	C_3
	$steel\ structure\ building_3$	S_3
	$road\ maintenance_3$	M_3

3.1 Retrieval precision and recall

Any retrieved samples resulted from a search process will only fall in one of the following categories: "retrieved and relevant", "retrieved and not relevant", "not retrieved and relevant" or "not retrieved and not relevant" [22]. Recall is the proportion of the retrieved and relevant samples from all the relevant samples [22]. Precision is the proportion of the retrieved and relevant items from all retrieved items [22], as presented in Equation 15.

The samples B_1 , C_1, S_1 and M_1 were chosen to query the database and compute the precision. In each test, one of these samples was compared with all the stored samples in order to retrieve the relevant samples. For instance, the relevant samples to B_1 are B_2 and B_3. In each test, the retrieval process continued until it satisfy the recall score. The results were obtained based on two recall scores of 0.5 and 1. The recall score equals to 0.5 when only one of the two stored relevant samples are retrieved, and it equals to one when both relevant samples are retrieved. For instance, the node similarity scores between B_1 and stored samples are sorted in Table 2. Given that B_1, B_2 and B_3 are developed for the same project, the most relevant sample to B_1 are B_2 and B_3. In this query, assuming recall score is equivalent to 1, all the relevant samples to B_1 (B_2 and B_3) must be retrieved. As a result, the retrieving precision will be equal to 0.67.

$$Retrieving\ precision = \frac{|\{Relevant\ samples\} \cap \{Retrived\ samples\}|}{|\{Retrieved\ samples\}|} \quad (15)$$

Table 2. Comparing B1 with stored samples with a threshold of 0.65

Rank	Query sample	Stored sample	Node similarity score
1	b1	b2	0.64
2	b1	s2	0.56
3	b1	b3	0.48
4	b1	c1	0.47
5	b1	s1	0.40
6	b1	c2	0.39
7	b1	s3	0.35
8	b1	c3	0.34
9	b1	m2	0.13
10	b1	m3	0.13
11	b1	m1	0.05

Figure 4 illustrates the retrieval precision for node similarity and structural similarity scores. It can be concluded that the structural similarity with a threshold between 0.7 to 0.75 results in the highest precision scores.

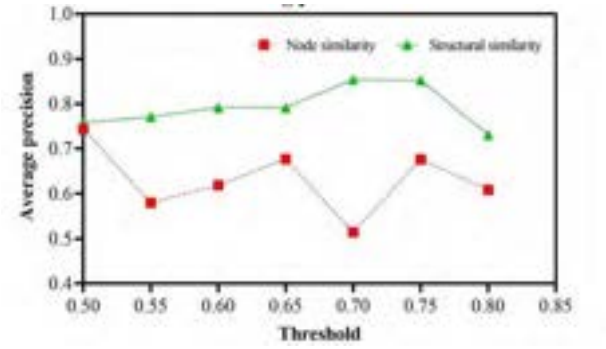

Figure 4. Average precision scores.

3.2 Properties of similarity measures

Symmetry and reflexivity are properties of a similarity measurement [23,24]. A similarity function S: S×S→ [0,1] on a set S, must fulfill two properties that are presented in Equations 16 and 17.

$$Sim(X,Y) = sim(Y,X)\ (Symmetry) \tag{16}$$

$$Sim(X,X) = 1\ (Reflexivity) \quad \forall\, X,Y \in S \tag{17}$$

3.2.1 Symmetry property of work breakdown structure similarity

Symmetry error, calculated using Equation 18, was defined to determine the symmetry fulfillment, in comparing WBS A and B. As illustrated in Figure 5, both node and structural similarity result in low degrees of error of symmetry property, namely the structural similarity error is close to zero.

$$Symmetry\ error = \frac{|sim(A,B) - sim(B,A)|}{average[sim(A,B), sim(B,A)]} \tag{18}$$

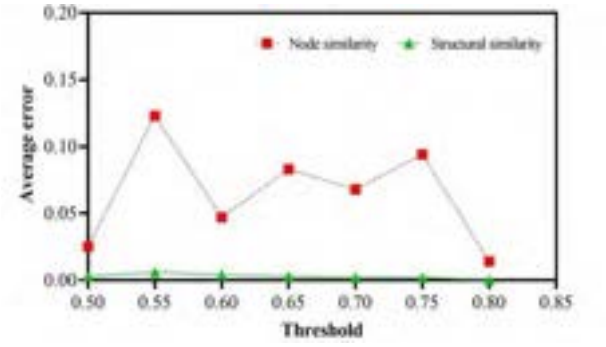

Figure 5. The average of the symmetry errors

3.2.2 Reflexivity property of work breakdown structure similarity

The reflexivity error, calculated using Equation 19, determines the compliance of the node and structural similarities with symmetry property by comparing a WBS to itself. It is evident from Figure 6 that both node and structural similarity result in very low levels of symmetry errors. Specifically, the error for the structural similarity is negligible, indicating better compliance of this metric with the symmetry property.

$$Reflexivity\ error = 1 - sim(A, A) \tag{19}$$

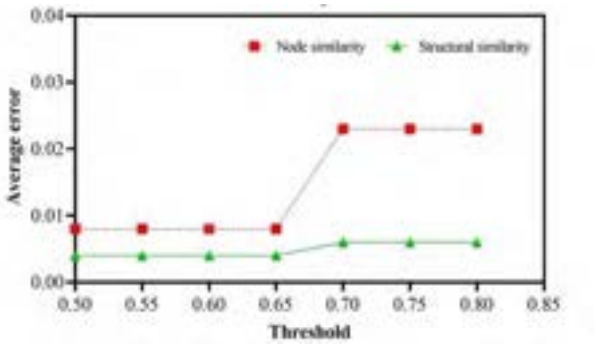

Figure 6. The average of the reflexivity errors

4 Conclusion

A quantitative similarity measurement of construction projects can improve the data retrieval process in knowledge management and case-based reasoning systems. This research utilized the WBS to measure the similarity amongst various construction projects. The WBS theoretically encompasses a significant portion of the tasks and services required to accomplish the project objectives. Thus, the WBS can be used as a comprehensive tool to distinguish constriction projects. The proposed method can be utilized to find the most similar projects and help the project managers use the relevant information and documents of the retrieved projects. This method can also be used as a main metric in exiting knowledge retrieval systems, such as case-based reasoning.

Node and structural similarity metrics were proposed to measure the similarity of construction projects using their WBSs. The results from applying these metrics indicate that the structural similarity performs better than the node similarity in retrieving the relavant samples. Additionally, the results show that the proposed metrics are in compliance with similarity measurement properties.

5 Limitations and future works

To ensure that the work breakdown structures encompass the entire scope of a project, the sample WBSs were developed based on the project management institute guidelines [11]. This approach

might not be fully followed by the practitioners in all construction projects which can limit the performance of the proposed method.

The insufficient number of test samples was another major limitation of this research. The performance of the system can be investigated on a larger sample size. Another limitation of this research was the utilized lexical database, which is WordNet. This is a generic database for English words, in which some of the technical words in the construction domain are not accurately defined. For instance, the word "rebar", which in construction is recognized as reinforcement steel, is not defined in WordNet. This issue can hinder the performance of the metrics in comparing tasks. Thus, there is an opportunity to develop and utilize a semantic network, similar to WordNet, for the construction domain.

6 References

[1] Tserng, H. P., & Lin, Y. C., Developing an activity-based knowledge management system for contractors. Automation in construction, 13(6), 781-802, 2004.

[2] Alavi, M., & Leidner, D. E, Knowledge management and knowledge management systems: Conceptual foundations and research issues. MIS quarterly, 107-136, 2001.

[3] Hahn, J., & Subramani, M., A framework of knowledge management systems: issues and challenges for theory and practice. ICIS 2000 Proceedings, 28 2000.

[4] Tan, H. C., Carrillo, P. M., Anumba, C. J., Bouchlaghem, N., Kamara, J. M., & Udeaja, C. E., Development of a methodology for live capture and reuse of project knowledge in construction. Journal of management in engineering, 23(1), 18-26, 2007.

[5] Kolodner, J. L., An introduction to case-based reasoning. Artificial intelligence review, 6(1), 3-34, 1992.

[6] An, S. H., Kim, G. H., & Kang, K. I., A case-based reasoning cost estimating model using experience by analytic hierarchy process. Building and Environment, 42(7), 2573-2579, 2007.

[7] Raphael, B., Domer, B., Saitta, S., & Smith, I. F., Incremental development of CBR strategies for computing project cost probabilities. Advanced Engineering Informatics, 21(3), 311-321, 2007.

[8] Goh, Y. M., & Chua, D. K. H., Case-based reasoning approach to construction safety hazard identification: Adaptation and utilization. Journal of Construction Engineering and Management, 136(2), 170-178, 2010.

[9] Ryu, H. G., Lee, H. S., & Park, M., Construction planning method using case-based reasoning (CONPLA-CBR). Journal of Computing in Civil Engineering, 21(6), 410-422, 2007.

[10] Mikulakova, E., König, M., Tauscher, E., & Beucke, K., Knowledge-based schedule generation and evaluation. Advanced Engineering Informatics, 24(4), 389-403, 2010.

[11] PMBOK® Guide. Sixth Edition, Project Management Institute, 2017.

[12] Chowdhury, G.G., Natural language processing. Annual review of information science and technology, 37, 51-89, 2003.

[13] Gomaa, W. H., & Fahmy, A. A., A survey of text similarity approaches. International Journal of Computer Applications, 68(13), 13-18, 2013.

[14] Landauer, T. K., & Dumais, S. T., A solution to Plato's problem: The latent semantic analysis theory of acquisition, induction, and representation of knowledge. Psychological review, 104(2), 211, 1997.

[15] Sowa, J. F., Semantic networks. John_Florian_Sowa isi [2012-04-20 16: 51]> Author [2012-04-20 16: 51], 2012.

[16] Miller, G. A., WordNet: a lexical database for English. Communications of the ACM, 38(11), 39-41, 1995.

[17] Meng, L., Huang, R., & Gu, J., A review of semantic similarity measures in wordnet. International Journal of Hybrid Information Technology, 6(1), 1-12, 2013.

[18] Wu, Z., & Palmer, M., Verb semantics and lexical selection. arXiv preprint cmp-lg/9406033, 1994.

[19] Mihalcea, R., Corley, C., & Strapparava, C., Corpus-based and knowledge-based measures of text semantic similarity. In Aaai (Vol. 6, No. 2006, pp. 775-780), 2016.

[20] Dijkman, R., Dumas, M., Van Dongen, B., Käärik, R., & Mendling, J., Similarity of business process models: Metrics and evaluation. Information Systems, 36(2), 498-516, 2011.

[21] Hart, P. E., Nilsson, N. J., & Raphael, B., A formal basis for the heuristic determination of minimum cost paths. IEEE transactions on Systems Science and Cybernetics, 4(2), 100-107, 1968.

[22] Buckland, M., & Gey, F., The relationship between recall and precision. Journal of the American society for information science, 45(1), 12-19, 1994.

[23] Ehrig, M., Koschmider, A., & Oberweis, A., Measuring similarity between semantic business process models. In Proceedings of the fourth Asia-Pacific conference on Comceptual modelling-Volume 67 (pp. 71-80), 2007.

[24] Richter, M. M., Classification and learning of similarity measures. In Information and

Classification (pp. 323-334). Springer, Berlin, Heidelberg, 1993.

ABM and GIS Integration for Investigating the Influential Factors Affecting Wildfire Evacuation Performance

Qi Sun and Yelda Turkan[a]

[a] School of Civil and Construction Engineering, Oregon State University, Corvallis, OR 97331, United States
E-mail: sunq3@oregonstate.edu (Q. Sun), yelda.turkan@oregonstate.edu (Y. Turkan).

Abstract –

Wildfires pose a big threat to human life and property safety. Previous studies on wildfire risk management focused mainly on understanding wildfire behaviour through computer simulations. Effective wildfire risk management also largely depends on the evacuation performance success. Computational tools tend to be the best approach for simulating wildfire evacuation emergencies as well. Therefore, this study proposes a comprehensive simulation framework that integrates Agent-based Modelling (ABM) and Geographical Information Systems (GIS) to efficiently simulate both human behaviour and transportation crowds. In particular, ABM bridges the technical gap between GIS and a multi-agent system (MAS) for simulation design efficiently and effectively. To study the evacuation performance (measured by the number of agents being sheltered or refused to evacuate), our modelling solution enables altering relevant model parameters in wildfire evacuation scenarios. The simulation outputs, as a result, can be used to evaluate the influential factors and further assist in effective evacuation planning. In particular, the following tasks are performed: (1) simulation of the influence of transportation crowds on evacuation performance; (2) evaluation of the effectiveness of public notification on evacuation success; and (3) comparison of the differences among various transportation means as well as their performances during a wildfire emergency. A case study is conducted to verify the simulation framework proposed in this study. The simulation outputs showed that the transportation crowds negatively impact on the evacuation performance, while public notification can enhance resident risk perception, thus assist in the evacuation efficiency. Finally, public vehicles such as public buses have the highest evacuation efficiency compared to other transportation means tested in this study.

Keywords – Wildfire Evacuation Simulation; Agent-based Modeling; Geographical Information Systems

1 Introduction

Wildfires pose a big threat to human life and property safety. The National Interagency Fire Center (NIFC) indicates that, over the past decade, an average of 67,000 wildfires resulted in 7 million acres burned annually [1]. In 2019 alone, there were 4.5 million U.S. homes were identified at high or extreme risk of wildfire, with more than 2 million in California alone [2].

To date, a number of studies have been conducted concerning the simulation of wildfire behavior. Catry et al. [3], for example, studied modeling and mapping the likelihood of wildfire ignition occurrence in Portugal. In [4], Westerling et al. applied statistical approaches to develop models for investigating the wildfire occurrence frequency affected by climate change in California. Linn et al. [5] utilized FIRETEC, a fire growth modeling software, to examine wildfire behavior with regard to different geographical regions. However, modeling wildfire behavior only is insufficient for effective wildfire risk management if both the number of injuries/fatalities and the level of property loss are expected to be minimized.

The success of evacuation performance is a critical factor in wildfire risk management. Due to obvious reasons and ethical concerns, computational simulation tends to be the best approach for studying human evacuation performance and transportation crowds during a wildfire. In addition to fire dynamics, a wildfire evacuation simulation mainly consists of human behavior as well as transportation modules [6]. To that end, this study aims to develop a simulation framework used for simulating both human behavior and transportation crowds simultaneously for wildfire evacuation performance assessment.

The remainder of the paper is organized as follows. Section 2 provides a comprehensive review of the research background. Section 3 details the proposed simulation framework and methodology. The experimental implementation is discussed in Section 4. The final section draws conclusions and offers recommendations for future research.

2 Research Background

A comprehensive review of the relevant literature on wildfire evacuation simulation is provided in this section. Human behavior critical to evacuation performance are also identified.

2.1 ABM and GIS for Evacuation Simulation

In outdoor evacuation scenarios, except for walking, transportation modules typically consist of various transportation means such as bicycles, private or public vehicles. To integrate human behavior and transportation modules into an outdoor evacuation scenario design, Agent-Based Modeling (ABM) technique is commonly used as it provides an environment where agents can be defined as any type of individual simulating their behaviors in mathematical, theoretical, and logical ways [7]. An ABM simulation scenario can reflect agent-to-agent interactions as well as agent-to-environment reactions simultaneously. To date, a number of studies have applied ABM to simulate outdoor emergency scenarios that covered a variety of hazards, including earthquakes [8], tsunamis [9], hurricanes [10], wildfires [11], and so on. Relevant to the study described here, Paveglio and Prato [11] proposed an ABM framework to investigate monetary and non-monetary attributes that influence human behavior and decisions with respect to wildfires. Therefore, it can be concluded that simulating human evacuation reactions and interactions is feasible using an ABM wildfire scenario design.

In addition to simulating human behavior and transportation modules, Geographical Information Systems (GIS) is a tool that can be used for outdoor evacuation simulation as it enables simulating agents' movements and evacuation process by providing the spatial data needed. In [12], Jumadi et al. developed a GIS-ABM simulation model to simulate the volcanic evacuation performance for risk assessment. In this case, ABM bridged the technical gap between the GIS tool and a multi-agent system (MAS) to simulate both human behavior and transportation crowds. Similarly, this study proposes to utilize an integrated ABM - GIS framework to simulate a MAS scenario, and to investigate the influential factors affecting the outdoor evacuation performance during a wildfire.

2.2 Influential Factors Affecting Evacuation Performance

This section provides a review of studies that have assessed wildfire evacuation performance with regard to a variety of human behavior. The following subsections summarize major findings of influential factors affecting human evacuation decisions and related choices in wildfire emergencies.

2.2.1 Public Notification

Public evacuation notification is critical in predicting the decision-making process of evacuees. A telephone questionnaire conducted by Strawderman et al. [13] revealed that, by signal detection theory, reverse 911 warnings had the best performance, and promoted a significantly higher rate of evacuation, compared with other evacuation warning sources. However, evacuees and public safety officials have different perceptions and concerns about the evacuation process [14]. In particular, McLennan et al. reviewed North American research into wildfire evacuation behavior published between 2005 and 2017 and summarized that: (1) even though mandatory evacuation is issued by the police department, many threatened residents are likely to delay evacuating due to the desire to protect their property; (2) some residents who are not on their property may seek to return; (3) warnings that are not sufficiently informative could be another cause for self-delayed evacuation; and (4) residents are likely to engage in information search rather than initiating evacuation actions. Overall, public notification promotes a higher risk-warning efficiency to encourage residents to evacuate. Nevertheless, residents are still likely to refuse to evacuate due to environmental factors and personal factors affecting individual risk perception as well as decision-making that result in evacuation delays.

2.2.2 Risk Perception

Personal factors with regard to risk perception in an emergency are complex and multidisciplinary. Toledo et al. [16] analyzed the influential factors affecting residents' decision-making process during a no-notice wildfire evacuation event that occurred in Haifa, Israel. They found that, in addition to the level of risk that the wildfire event poses to individuals, the influential factors related to household individuals (e.g. initial locations when a wildfire event happened) as well as their relatives (e.g. the number and locations of children or elderly individuals) significantly affect their evacuation decisions and associated movement patterns [16]. Besides, residents' evacuation efficiencies are heavily affected by their knowledge and experience with former wildfires [17], which should be considered in an evacuation scenario design as well.

2.2.3 Risk Mitigation

In addition to risk perception, personal behavior with regard to risk mitigation is another significant factor affecting the decision-making regarding resident evacuation performance. The study by Paveglio et al. [18] revealed that a relatively high proportion of residents are interested in passively defending or sheltering in their homes, with fewer residents favoring evacuation during a wildfire. In particular, resident evacuation preferences

differ significantly due to the forest management strategy. For example, in [11], it was found that in the areas with significantly high rate of forest thinning, the residents chose to stay and actively defend their homes.

In [19, 20], it was found that a higher level of risk mitigation is positively associated with risk perception, including sufficiently informative wildfire information received from local volunteer fire departments, county wildfire specialists, as well as talking with neighbors about the wildfire. To conclude, residents who perceive higher levels of wildfire risk have undertaken higher levels of wildfire-risk mitigation to protect their property. Thus, the relationship between risk perception and risk mitigation undertaken is jointly and mutually represented in our simulation framework design.

2.2.4 Transportation Means

Means of transportation could have a huge impact on evacuation efficiency. In [21], Beloglazov et al. proposed a dynamic modeling approach to simulate the evacuation performance with regard to different evacuation locations. Li et al. [22] investigated the influence of evacuation timing for traffic based on a spatiotemporal GIS approach. In addition to evacuation locations and evacuation timing, movement velocities and loading capacities of various transportation means are significant as well.

Among typical transportation means (e.g. walking, bicycles, private or public vehicles), private or public vehicles account for higher velocities and loading capacities that are meant to have better evacuation performance. Undoubtedly, an efficient transportation network in a wildfire emergency could help residents to evacuate safely. However, frequent occurrence of transportation crowds caused by vehicles occupying the roads could highly impede the evacuation efficiency. Hence, the evacuation efficiency for a variety of transportation means should be further assessed to assist with evacuation strategies and management, and further improve the evacuation success.

2.3 Motivation and Objectives

Understanding the physical and social dynamics imposed by wildfires is fundamental to assessing and mitigating risks for residents [23]. Above all, human evacuation performance is greatly affected by public evacuation warnings, actions, and decisions related to risk perception and risk mitigation, and the variability of transportation means as well as their efficiencies. Those influential factors are critical to evacuation assessment, and pose challenges for modeling an effective wildfire evacuation scenario.

Several studies to date investigated human wildfire evacuation behavior. However, modeling solutions to predict and assess evacuation performance for wildfire scenarios is still at its infancy. Therefore, this paper proposes an evacuation behavior model embedded in an ABM-GIS simulation tool, AnyLogic [24], to simulate and investigate the impact of influential factors summarized in section 2.2. on wildfire evacuation performance.

In particular, (1) the influence of transportation crowds on the evacuation performance is simulated; (2) the effectiveness of public notification on the evacuation success is evaluated; and (3) the differences and efficiencies among various transportation tools during a wildfire emergency are compared. A comprehensive simulation framework, based on the influential factors derived from existing literature on human behavior in wildfires, is introduced to implement the proposed modeling solution. Finally, an experimental case study is conducted to validate the proposed modeling solution using AnyLogic.

2.4 Contribution

The main contribution of this study is a modeling solution for wildfire evacuation simulation in an ABM-GIS simulation framework. To assess evacuation performance (measured by the number of agents being sheltered or refused to evacuate), our modeling solution enables to modify relevant model parameters in wildfire evacuation scenarios. The simulation outputs, as a result, can be used to assess the impacts of influential factors (including the impact of public evacuation warnings, risk perception, risk mitigation, and various transportation means) affecting evacuation performance. Thus, the proposed modeling solution can further assist in safety management and effective evacuation planning for wildfire emergencies. To conclude, this study assesses the evacuation efficiency with regard to human life and transportation crowds in wildfire emergencies, which would ultimately help with wildfire evacuation education and safety strategies.

3 Research Methodology

The proposed simulation framework and modeling solution are introduced in this section. The findings of the recent studies on how to incorporate human wildfire evacuation behavior into an ABM-GIS simulation scenario [13-23] are considered and included in the framework design.

3.1 Simulation Framework

Figure 1 illustrates the simulation framework proposed in this study. The first step is to determine whether there is a wildfire or not. Next, the alert indicator about public evacuation warnings, either positive or negative, divides the scenario into four categories: 1) a true wildfire event and a mandatory evacuation issued by

safety officials (true positive (TP)), 2) a no-notice true wildfire event (true negative (TN)), 3) mandatory evacuation issued for a false wildfire event (false positive (FP)), or 4) neither evacuation alert was issued nor a wildfire occurred (false negative (FN)). These four categories address particular evacuation outcomes, including different evacuation performance for a variety of scenarios.

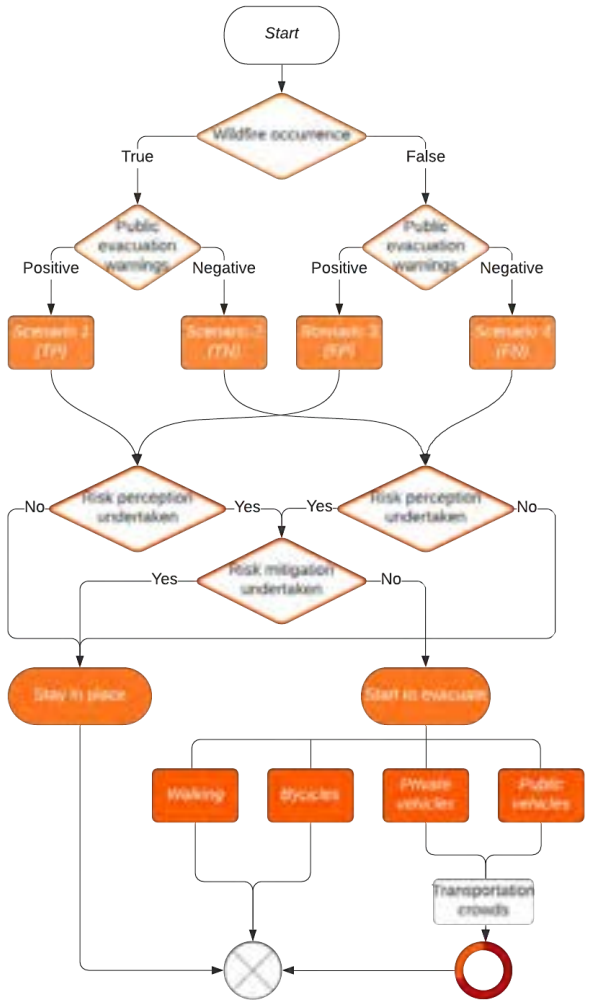

Figure 1. Proposed simulation framework

In the next step, agents' risk perception (true or false) is defined for each scenario. If the agents do not perceive any risk, they will choose to stay in place. The agents who perceive risk will either stay in place to actively defend their homes or start to evacuate. During the evacuation process, vehicles occupying the road may cause transportation crowds. In this case, there will be evacuation delays, which is incorporated in the movement process in our simulation design. The average velocities and capacities of typical transportation means in a wildfire emergency are summarized in Table 1.

Table 1. Designed parameters for various transportation means

	Average velocities (mph)	Common capacities
Walking	3-5	1
Bicycles	12-15	1-2
Public vehicles	30-45	20-50
Private vehicles	40-70	1-5

The final step is to analyze the simulation outputs, which present the number of agents either refusing to evacuate or being sheltered. These numbers can be used to assess agents' evacuation efficiency with regard to the effect of public evacuation warnings, risk perception, risk mitigation, and various means of transportation. Consequently, the impacts of influential factors affecting the evacuation performance are evaluated, which would ultimately help with wildfire evacuation education and safety strategies.

3.2 Modeling Solution

The ABM-GIS wildfire simulation scenario consists of the movement flow module and the geographical module representing the agents' movement process in chosen areas. The modeling software AnyLogic, which embeds the GIS tool, provides a powerful simulation environment, as it enables to simulate agent movement and evacuation process while providing the geographical and spatial data needed.

3.2.1 Modeling Parameters

The movement flow module presents the agent evacuation process. AnyLogic provides users a process modeling library, including various modeling parameters, to define agents' behavior. The agent movement flow in this study is designed based on the simulation framework shown in Figure 1. Hereby, Table 2 introduces several selected modeling parameters including their names, icons, descriptions, and properties of functions.

Table 2. Introduction of modeling parameters [24]

	Description	Function
Source	A starting point of a process flowchart to generate agents.	Define agent location, arrival rate, and quantity, etc.
Select Output	Two output ports to route agents.	Sort agents according to certain criteria.
Select Output5	Five output ports to route agents.	Split the agent flow into different

		transportation means.
Move To	Move agents to a new location.	Define agents' destination and movement speed.
Queue	A queue of agents waiting to be accepted by the next block in the flowchart.	Define the maximum capacity and agent location in a queue.
Sink	An ending point to dispose incoming agents.	Present the number of agents disposed.

3.2.2 The Movement Flow Module

Five agent types are defined in a wildfire scenario, including the residents and four transportation means including walking, bicycles, private vehicles, and public vehicles. By utilizing the process modeling library, the agents' behavior is defined in AnyLogic (Figure 2).

Figure 2. A simplified version of agents' behavior in AnyLogic

At the start of the movement flow, resident agents are sorted based on their judgments about risk perception and risk mitigation undertaken, namely RP and RM. Next, a portion of resident agents, who does not perceive the risk or prefer to self-defend their homes after risk perceived, is disposed to stay in place. The remaining resident agents start to evacuate using one of the four transportation means, which are predefined with different movement velocities and loading capacities summarized in Table 1. It is assumed that transportation crowds (i.e., vehicle flows exceeding the highway capacity) require the agents taking the vehicles to queue to be sheltered. In the meantime, other agents who evacuate by walking or bicycling move toward the shelters identified in the GIS map. AnyLogic allows presenting agents' movements as a 2D/3D animation and counting agents that are disposed by modeling parameters in real-time.

4 Experimental Implementation

To validate the practicality of the proposed modeling solution, an experimental implementation was conducted to simulate a hypothetical wildfire evacuation emergency.

4.1 Experimental Assumptions

4.1.1 Geographical Background

The CampFire in California [25], which occurred in 2018, was used as a geographical background composed of several GIS nodes: (1) the ignition node, namely Creek Camp Road, (2) the shelter node, namely Orland, and (3) four independent scenario nodes, namely Paradise, Oroville, Chico, and Willows, navigated based on their spatial attributes (Figure 3).

Figure 3. Geographical nodes navigated in the GIS tool embedded in AnyLogic

This study assumes the level of wildfire risk for each scenario depending on the spatial distance measured from the ignition node to those scenario nodes. In particular, the town of Paradise is classified as a TP scenario due to its shortest distance to the ignition location, which accounts for the highest level of risk it can be easily detected. Oroville is the second-nearest town that faces a high risk as well, but the risk perceived by residents could be misjudged due to a river close to the node, thus it was classified as a TN scenario. Compared to Oroville, the town of Chico has a lower wildfire risk due to its greater distance from the ignition location, but with higher risk awareness affected by the passing evacuees coming from Paradise. Hence, Chico is chosen to be simulated as a higher possibility for an FP scenario. Finally, the town of Willows is classified as a FN event due to its geographical distance from the ignition location.

4.1.2 Modeling Parameter Setup

For each evacuation scenario, the resident agents are randomly distributed with an arrival rate of one agent per

second and a maximum quantity of 2000 in AnyLogic. The probabilities of select outputs for risk perception and risk mitigation measures undertaken by resident agents vary for different scenarios as shown in Table 3. Besides, this experiment assumes a random distribution for the agent flow split via different transportation means. Furthermore, the traffic flow exceeding a capacity of 100 vehicle agents will trigger transportation crowds, which are represented by agent queues (dashed lines marked in Figure 3).

Table 3. Probabilities of select outputs

	Risk perception undertaken	Risk mitigation undertaken
Scenario 1 (TP)	0.9	0.1
Scenario 2 (TN)	0.1	0.9
Scenario 3 (FP)	0.9	0.9
Scenario 4 (FN)	0.1	0.1

4.2 Simulation Outputs and Analysis

During the simulation, AnyLogic presents the number of agents disposed by modeling parameters in real-time. To evaluate the effectiveness of the proposed modeling solution, test scenarios were developed by adjusting relevant modeling parameters. Hereby, each evacuation scenario was run ten times in order to avoid biased simulation outputs. Simulation outputs with regard to test scenarios are summarized and analyzed in the following subsections.

4.2.1 The Influence of Transportation Crowds

The test scenario was developed with and without the modeling parameter of transportation crowds in order to investigate its influence on agent evacuation efficiency. In particular, the agent evacuation performance is evaluated by the travel time (measured by the modeling time in AnyLogic) for two types of vehicles, i.e., private and public vehicles, in each scenario (Table 4).

Table 4. Travel time (in seconds) for vehicles

	TP	TN	FP	FN
Private vehicles without crowds	2267	1863	2017	1920
Public vehicles without crowds	3983	3189	3463	3301
Private vehicles affected by crowds	7445	6188	7300	6410
Public vehicles affected by crowds	8032	7243	7785	7387

According to the simulation outputs, the evacuation efficiency in each scenario was negatively affected by the transportation crowds due to a longer travel time for both types of vehicles. The queuing time, however, slightly differ among these four scenarios, which have different numbers of vehicles driven through a route as shown in the GIS interface. The simulation outcome, as a result, validate the negative impact of transportation crowds on the evacuation efficiency. In this case, highway capacity must be increased to reduce the occurrence of transportation crowds.

4.2.2 The Effectiveness of Public Notification

To evaluate the effectiveness of public notification, this study used the statistics of disposed agents who stay in place due to not perceiving the risk or perceiving the risk but choosing to stay to defend their homes, as well as the agents who evacuate and reach a shelter using one of the four different transportation means in each scenario (Table 5).

Table 5. Statistics for agents disposed in different scenarios

	TP	TN	FP	FN
Risk not perceived – stay in place	195	1794	174	1825
Risk perceived – stay in place	243	118	1070	27
Walking	120	10	48	11
Bicycles	170	6	80	14
Private vehicles	347	18	165	42
Public vehicles	925	54	463	81

The simulation outputs indicate that public notification has a significant impact on the evacuation decision-making of resident agents. In the scenarios with public notifications (i.e., TP and FP scenarios), the number of agents who perceive the risk is greatly higher compared to the scenarios without notifications (i.e., TN and FN scenarios). Nevertheless, agents in the TP scenario prefer to evacuate after risk perceived and few agents intend to mitigate the risk. Conversely, in the FP scenario, a large portion of agents tend to take actions for risk mitigation instead of evacuating immediately. To conclude, public notification improves resident risk perception, but residents may still refuse to evacuate.

4.2.3 Comparison of Different Transportation Means

In this study, the evacuation efficiency is measured by the evacuation time per agent for different transportation means in each scenario. Several findings are drawn from Table 6: (1) evacuation by walking accounts for the lowest evacuation efficiency; (2) evacuation efficiencies of all transportation means in TP and FP scenarios are greatly higher than the efficiencies in TN and FN scenarios; and (3) evacuation efficiency of

public vehicles is the highest even though their average velocities are slower than private vehicles. One possible explanation is that the loading capacity of public vehicles is the highest, consequently, more agents are loaded and able to approach a shelter at the same time.

Therefore, to improve the evacuation efficiency, it may be helpful to increase the availability of public transportation when evacuating residents in a wildfire emergency.

Table 6. Evacuation efficiency (in %) for different transportation means

	TP	TN	FP	FN
Walking	0.29	0.03	0.12	0.03
Bicycles	1.49	0.05	0.71	0.13
Private vehicles	4.66	0.29	2.26	0.66
(without crowds)	15.31	0.97	8.18	2.19
Public vehicles	11.52	0.75	5.95	1.1
(without crowds)	23.22	1.69	13.37	2.45

5 Conclusions and Future Research

Effective wildfire evacuation planning could help to improve resident evacuation efficiency during a wildfire emergency. Several studies to date focused on studying human behavior and evacuation performance during a wildfire. However, such modeling and simulation solutions to predict and assess evacuation performance in wildfire scenarios are still at their infancy. Therefore, this study proposed a modeling solution, using AnyLogic software, that integrates ABM and GIS to enable simulating and investigating the factors affecting outdoor evacuation performance during a wildfire. To that end, an experimental implementation was conducted to test several wildfire scenarios including: 1) a mandatory evacuation issued by safety officials for a true wildfire event, 2) a no-notice true wildfire event, 3) a mandatory evacuation issued for a false wildfire event, and 4) neither evacuation alert was issued nor a wildfire occurred.

The simulation outputs validated the practicality of our modeling solution. Several major findings are as follows: (1) transportation crowds negatively impact the evacuation performance, (2) public notification can enhance residents' risk perception, thus improve evacuation efficiency, and (3) public vehicles have the highest evacuation efficiency compared to other transportation means evaluated in this study. Several wildfire evacuation management strategies are suggested based on these findings. To conclude, this study assesses evacuation efficiency with regard to human life and transportation crowds in wildfire emergencies, which is expected to help in wildfire evacuation education and safety strategies. The proposed modeling solution provides a novel simulation approach that can used for wildfire safety management and effective evacuation planning for wildfire emergencies.

The proposed simulation framework has several limitations that should be noted. First, human evacuation behavior should be further studied and the modeling solution should be revised by adding or changing relevant modeling parameters to better assess human evacuation performance. Second, AnyLogic software is limited in terms of the number of modeling parameters that can be included in one scenario. Hence, this study fails to add the modeling elements that could simulate those four scenarios simultaneously. Third, due to the limitation of the current ABM modeling technique, this study emphasizes only simulating resident evacuation behavior. However, in reality, wildfire dynamics is a matter that could heavily impact the evacuation performance. To improve the viability of the proposed modeling solution, future studies should: (1) investigate human outdoor evacuation behavior; (2) simulate the interaction between residents living in different geographical regions; and (3) improve the modeling solution to enable simulating the wildfire dynamics and resident evacuation process simultaneously.

References

[1] National Interagency Fire Center (NIFC). Historical Wildland Fire Information. Online: https://www.nifc.gov/fireInfo/fireInfo_statistics.html, Accessed: 31/05/2020.

[2] 2019 Verisk Wildfire Risk Analysis. Online: https://www.verisk.com/insurance/campaigns/location-fireline-state-risk-report/, Accessed: 31/05/2020.

[3] Catry, Filipe X., et al. Modeling and mapping wildfire ignition risk in Portugal. *International Journal of Wildland Fire,* 18(8): 921-931, 2010.

[4] Westerling, A. L., and Bryant., B. P. Climate change and wildfire in California. *Climatic Change,* 87(1): 231-249, 2008.

[5] Linn, Rodman, et al. Studying wildfire behavior using FIRETEC. *International journal of wildland fire,* 11(4) 233-246, 2002.

[6] Ronchi, E., Rein, G., Gwynne, S. M. V., Intini, P. and Wadhwani, R. Framework for an integrated simulation system for Wildland-Urban Interface fire evacuation. *In Proc Int Conf Res Adv Technol Fire Saf* , pages 119-134, 2017.

[7] Railsback, Steven F., and Volker Grimm. Agent-based and individual-based modeling: a practical introduction. *Princeton university press*, 2019.

[8] Bernardini, G., M. D'Orazio, E. Quagliarini, L. Spalazzi. An agent-based model for earthquake pedestrians' evacuation simulation in urban scenarios, *Transp. Res. Proc.* 2 255–263, 2014.

[9] Wang H., Mostafizi, A., Cramer, L.A., Cox, D., Park, H. An agent-based model of a multimodal near-field tsunami evacuation: decision-making and life safety, *Transport. Res. Part C: Emerg. Technol.* 64 86–100, 2016.

[10] Widener, M.J., Horner, M.W., Metcalf, S.S. Simulating the effects of social networks on a population's hurricane evacuation participation, *J. Geogr. Syst.* 15 (2), 2012.

[11] Paveglio, B. and Prato, T. Integrating Dynamic Social Systems into Assessments of future wildfire losses: an experiential agent-based Modeling Approach, *Nova Science Publishers,* 2011.

[12] Jumadi, J, Carver, S. and Quincey, D. A conceptual framework of volcanic evacuation simulation of Merapi using agent-based model and GIS. In: Procedia Social and Behavioral Sciences. *CITIES 2015 International Conference: Intelligent Planning Towards Smart Cities*, 03-04 Nov 2015, Surabaya, Indonesia. Elsevier, pp. 402-409, 2016.

[13] Strawderman, Lesley, et al. Reverse 911 as a complementary evacuation warning system. Natural hazards review 13(1): 65-73, 2012.

[14] Cohn, Patricia J., Matthew S. Carroll, and Yoshitaka Kumagai. Evacuation behavior during wildfires: results of three case studies. *Western Journal of Applied Forestry* 21(1): 39-48 2006.

[15] McLennan, J., Ryan, B., Bearman, C. *et al.* Should We Leave Now? Behavioral Factors in Evacuation Under Wildfire Threat. *Fire Technol* 55, 487–516. https://doi.org/10.1007/s10694-018-0753-8, 2019.

[16] Toledo, Tomer, et al. Analysis of evacuation behavior in a wildfire event. *International journal of disaster risk reduction* 31:1366-1373, 2018.

[17] McLennan, J., Ryan, B., Bearman, C. *et al.* Should We Leave Now? Behavioral Factors in Evacuation Under Wildfire Threat. *Fire Technol* 55, 487–516. https://doi.org/10.1007/s10694-018-0753-8, 2019.

[18] Paveglio, Travis, et al. Understanding evacuation preferences and wildfire mitigations among Northwest Montana residents. *International journal of wildland fire* 23(3): 435-444, 2014.

[19] Champ, Patricia A., Geoffrey H. Donovan, and Christopher M. Barth. Living in a tinderbox: wildfire risk perceptions and mitigating behaviours. *International Journal of Wildland Fire* 22(6): 832-840, 2013.

[20] Brenkert-Smith, Hannah, Patricia A. Champ, & Nicholas Flores. Trying not to get burned: understanding homeowners' wildfire risk–mitigation behaviors. *Environmental Management* 50(6) 1139-1151, 2012.

[21] Beloglazov, A., Almashor, M., Abebe, E., Richter, J. and Steer, K.C.B., Simulation of wildfire evacuation with dynamic factors and model composition. *Simulation Modelling Practice and Theory*, 60, pp.144-159, 2016.

[22] Li, D., Cova, T.J. and Dennison, P.E. Setting wildfire evacuation triggers by coupling fire and traffic simulation models: a spatiotemporal GIS approach. *Fire technology*, *55*(2), pp.617-642, 2019.

[23] Lovreglio, R., Kuligowski, E., Gwynne, S., & Strahan, K. A modelling framework for householder decision-making for wildfire emergencies. *International Journal of Disaster Risk Reduction*, 41, 101274, 2019.

[24] Anylogic. Software. *The AnyLogic Company.*

[25] Baldassari, E. Camp Fire death toll grows to 29, matching 1933 blaze as state's deadliest. *The Mercury News*, 2018.

Streamlining Photogrammetry-based 3D Modeling of Construction Sites using a Smartphone, Cloud Service and Best-view Guidance

R. Moritani[a], S. Kanai[a], K. Akutsu[a], K. Suda[b], A. Elshafey[c], N. Urushidate[d] and M. Nishikawa[e]

[a]Graduate School of Information Science and Technology, Hokkaido University, Japan
[b]Kankyo Fudo Techno Co. Ltd., Japan
[c]Kani Construction Co. Ltd., Japan
[d]Horiguchi-gumi Co. Ltd., Japan
[e]Toho-Engineering Co. Ltd., Japan
E-mail: r_moritani@sdm.ssi.ist.hokudai.ac.jp, kanai@ssi.ist.hokudai.ac.jp, k-suda@bolero.plala.or.jp

Abstract – Three-dimensional (3D) measurement that captures the state of construction sites is key to promoting ICT-supported construction processes. Structure-from-Motion (SfM) and Multi-View Stereo photogrammetry are the best solutions for small and mid-sized construction companies due to their high portability and low cost. However, efficient creation of high-quality 3D dense models using photogrammetry is difficult for site workers because the model quality relies heavily on manually selected camera poses. To address this issue, we propose a photogrammetry process that improves the quality and efficiency of 3D dense model reconstruction to measure construction sites. The proposed process begins with a small initial photo set. Then, a computer-supported best-view guidance system predicts the geometric quality of the dense model, estimates the best target positions for additional photographs using SfM results, and provides workers with that position information. The effectiveness and efficiency of the process and system were evaluated at a real-world construction site. The evaluation demonstrated that the process and system can prevent capturing unnecessary images, improve the efficiency of the on-site photographic work, and generate a dense model with quality assurance. We also found that a smartphone camera is the most suitable device for implementing the process.

Keywords –
Photogrammetry; 3D Modeling; Next-best View; Cloud Service; Smartphone; i-Construction

1 Introduction

In recent years, the "i-Construction" initiative [1], which is intended to improve productivity at construction sites by utilizing ICT, has been promoted at various places in Japan. However, to apply i-Construction initiatives at small and mid-sized construction companies, both the initial and the operating costs of the supporting technologies must be low.

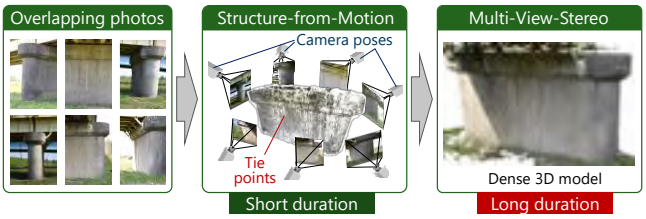

Figure 1. Typical photogrammetry process

Three-dimensional (3D) measurement technology is an essential part of the i-Construction initiative. 3D measurement technology is used to capture the current state of construction sites at various construction stages at high frequency. Currently, terrestrial laser scanners and 3D photogrammetry are used as measurement technologies. Terrestrial laser scanners permit millimeter-accuracy measurements [2]. However, the devices are expensive. In addition, typically, measurement processing is outsourced, which is also expensive. Thus, cost considerations hinder the introduction of laser scanners to small and mid-sized construction companies.

3D photogrammetry [3], shown in Figure 1, is slightly inferior to laser scanners in terms of measurement accuracy. However, it can automatically reconstruct dense 3D models, such as 3D point clouds and textured meshes, from multiple overlapping photos. Photogrammetry can be implemented using UAV-based photography. Consequently, photogrammetry can be

introduced into small and mid-sized construction companies more smoothly than terrestrial laser scanners.

However, introducing photogrammetry and the routine use of high-quality 3D models to monitor construction site activity remains challenging. First, a site worker must take multiple photographs using a heavy, handheld single-lens reflex (SLR) camera. Second, the quality of the dense 3D model reconstructed from the photographs cannot be confirmed on-site because the conventional photogrammetry pipeline requires significant processing time. Moreover, for a given construction site, pre-estimating the camera pose, i.e., the optimal shooting position and orientation, required to capture photographs that can be used to reconstruct a high-quality, dense model is difficult.

To address the various challenges, an innovative photogrammetry process and computer-supported best-view guidance system that can streamline 3D modeling of construction sites is proposed in this paper. The proposed process and the system can be introduced into the everyday activities of small and mid-sized companies by integrating a smartphone, cloud service, and computer-assisted best-view guidance for optimal camera poses. The development of this technology involved both the construction industry and academia, and its effectiveness and efficiency were evaluated experimentally at a real-world construction site.

2 Challenges and Approaches

2.1 Conventional Photogrammetry Process

As shown in Figure 1, the general photogrammetry pipeline to generate a dense 3D model from a set of photographs comprises two steps: Structure-from-Motion (SfM) and Multi-view Stereo (MVS). SfM derives the camera poses and sparse corresponding points, i.e., the so-called "tie points," on real-world objects, and MVS creates a dense 3D model, such as a 3D point cloud or a textured-mesh model, by stereo matching overlapped photographs [3].

SfM processing can be completed in a relatively short time. However, MVS must process all pairs of overlapped photos; therefore, it requires approximately 10 to 50 times more processing time than SfM. For example, for 100 photos, SfM requires only 4 min, while MVS takes 120 min. This example clearly indicates that the MVS step consumes most of the processing time in the photogrammetric 3D model reconstruction process.

As shown in Figure 2, if we attempt to utilize photogrammetry to capture daily progress at a construction sites, the following problems occur.

- The resolution of a 3D model reconstructed by SfM-MVS depends on the resolution of the captured images. Therefore, high-resolution photographs tend to be taken by an SLR camera. However, SLR cameras tend to be large and heavy; carrying and using an SLR camera in complex situations at a construction site, e.g., scaffolding, can be problematic. In addition, with an SLR camera, uploading captured photos via a network is more complicated and less efficient than with a smartphone. Therefore, initially, all captured photos must be stored on the camera's SD memory card. After taking the camera to an office, the 3D model is reconstructed using photogrammetry software. However, this process drops in efficiency because photogrammetry processing cannot be performed during shooting.
- To reconstruct a high-quality, dense model using SfM-MVS, a site worker must carefully consider the importance of capturing overlapping photographs and develop a shooting plan in which the camera poses relative to the object are set appropriately. However, predicting which and how many photos should be taken to reconstruct high-quality models is difficult for the worker. Consequently, defects, such as holes or reduced accuracy in some parts, often appear in the model. To avoid such defects, shooting plans tend to involve a high overlap ratio. However, increasing the number of photographs also increases the MVS processing time.
- To record construction sites using SfM-MVS, it is often necessary to take several hundred to several thousand photographs. With such a large number of photographs, MVS processing can take approximately half a day or even an entire day. Therefore, the quality of the dense model cannot be confirmed on-site immediately after the images are captured. If the model quality is unsatisfactory due

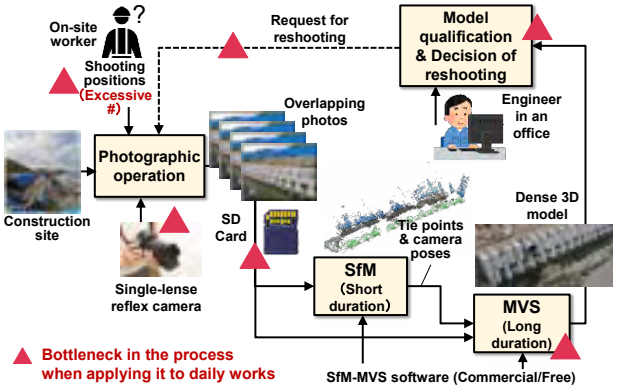

Figure 2. Practical challenges encountered when attempting to apply a conventional photogrammetry process at a construction site

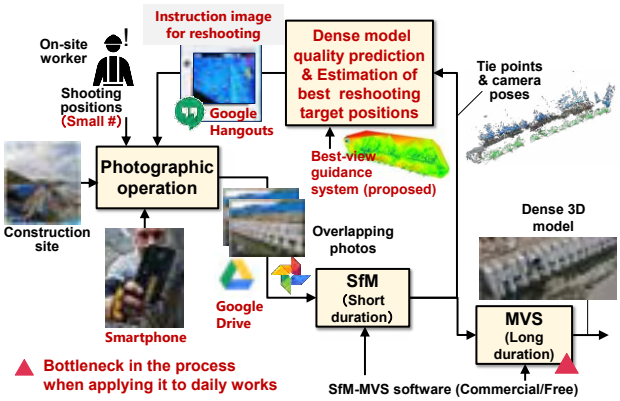

Figure 3. Processing pipeline of the proposed photogrammetry process

to an insufficient number of photographs or unphotographed areas of the site, reshooting will be required, which incurs considerable financial and time costs.

2.2 Proposed Approaches

To address the above problems, the following new photogrammetry process is introduced in this study. The processing pipeline for the proposed process is shown in Figure 3. The process proceeds as follows.

(1) We introduce a smartphone with a high-resolution camera as the device used to capture on-site photographs. Smartphones are lightweight, which makes them suitable for handheld shooting at construction sites. In addition, by utilizing their internet communication function, images can be automatically uploaded to cloud storage (Google Drive) immediately after shooting.

(2) The quality of the dense model that will be reconstructed from the uploaded images is quickly predicted from the SfM results and a computer-supported best-view guidance system. The prediction is based on our developed quality prediction algorithm [4]. The best target positions for additional photo shoots that would improve the quality are estimated in a few minutes by the guidance system connected to the cloud.

(3) The system automatically generates an instruction image in which the marker symbols of these target positions estimated in (2) are superimposed on the photo of the scene saved in the cloud. Furthermore, the instruction image is immediately transmitted to the worker's smartphone at the construction site using a messenger application (Google Hangouts [5]). Then, the worker takes several additional photos according to the target positions on the instruction image and uploads them to the cloud.

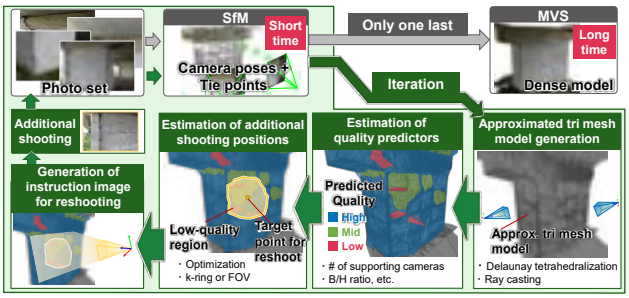

Figure 4. Prediction of the dense model quality and estimation of the best target position for additional shootings

(4) By repeating processes (2) and (3) as often as necessary, a small number of target positions for additional images are estimated only by SfM processing, and additional images are captured according to the target positions. Consequently, the quality of the obtained high-density model is improved successively without requiring multiple MVS processing.

(5) After completing the shooting processes (2)–(4) supported by the best-view guidance system, the time-consuming MVS process is executed only once, and the final dense model is reconstructed. Thus, the MVS process can begin immediately after the required additional images are captured, which improves the overall efficiency of the model reconstruction process.

3 Quality Prediction of Dense Model and Estimation of Additional Shooting Positions

3.1 Approximated Triangular Mesh Model Generation

Figure 4 shows the processing pipeline of the prediction of the dense model quality and estimation of the best target positions to capture additional images. The geometry of the dense model is first approximated by a triangular mesh model generated from the triangulation of tie points created by SfM. The approximation method simplifies a method proposed by Labatut et al. [6] to improve its computational efficiency.

As shown in Figure 5, the triangular mesh generation begins with 3D Delaunay tetrahedralization of 3D tie point set P and creates a set of tetrahedra H. Then, the intersection test is performed between every tetrahedron in P and a set of rays $V_i = \{\boldsymbol{v}_j^i\}\,(\boldsymbol{v}_j^i = \boldsymbol{p}_i - \boldsymbol{c}_j)$ beginning from the projection center of the j-th camera $\boldsymbol{c}_j$ to the i-th visible tie point position $\boldsymbol{p}_i$ $(i \in P)$.

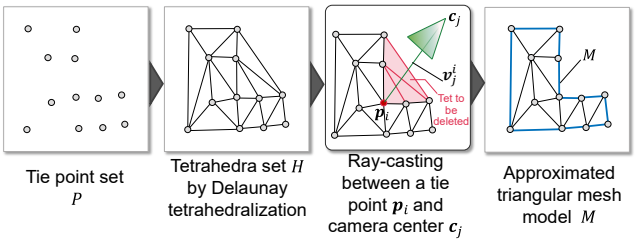

Figure 5. Generation process of the approximated triangular mesh model M

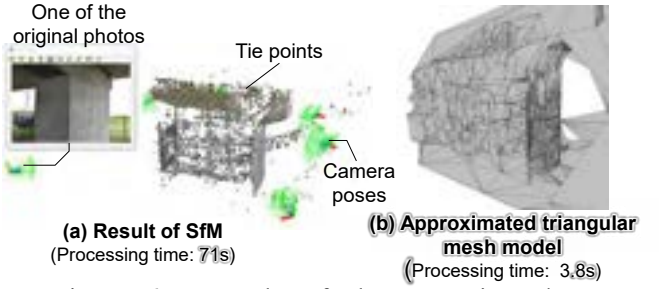

Figure 6. Example of the approximated triangular mesh model M

If a tetrahedron intersects with a ray, it is deleted, and the remaining set of tetrahedra is defined as H'. Finally, we obtain the approximated triangular mesh model M by taking the surface boundary meshes of H'. The algorithm is described in detail in a previous study [4].

Figure 6(a) shows an example of the tie point set P and camera poses generated from 33 original photos of a bridge pier, and Figure 6(b) shows the corresponding approximated triangular mesh model.

3.2 Quality Predictor Estimation

Next, the quality predictors $F_X(i)$ for a dense model are evaluated at a sparse point i ($\in P'$, P': sparce point set) that constitutes the vertex of the approximated triangular mesh model M based on the tie point set P and the camera pose set $E = \{\boldsymbol{e}_j = (\boldsymbol{c}_j, \boldsymbol{\theta}_j)\}$, where $\boldsymbol{\theta}_j (\in R^3)$ is a vector of three Euler angles representing the projection orientation of the j-th camera. The predictor $F_X(i)$ quantifies how accurately the final dense model can be reconstructed around the sparce point $i (\in P')$. The basic idea of the quality predictor was initially proposed by Mauro et al. [7]. Note that we designed different types of predictors based on that study [7].

In the proposed method, the following four quality predictors are evaluated at each sparce point $i (\in P')$.

- **Reliability** $(F_r(i))$. The local geometric quality of the reconstructed dense model around a sparce point i decreases as the n umber of visible cameras $|V_i|$ supporting a point i decreases. Therefore, the *Reliability* predictor of the point i is defined as follows:

$$F_r(i) = |V_i| \tag{1}$$

- **Area** $(F_a(i))$. As the area of a triangle on M enlarges, the reconstruction error of the dense model tends to be large. Therefore, the average area of the triangles on M adjacent to a point i is evaluated as the *Area* predictor defined by as follows:

$$F_a(i) = \frac{1}{|T^i|} \Sigma_{t_j^i \in T^i} area(t_j^i) \tag{2}$$

where T^i denotes a set of triangles adjacent to i.

- **Edge length** $(F_e(i))$. When the object surface to be measured is poorly textured, the edge length of a triangle on M tends to be long and the point clouds generated by SfM become sparce. Thus, the average edge length adjacent to a point i is evaluated as the *Edge length* predictor expressed as follows:

$$F_e(i) = \frac{1}{|D^i|} \Sigma_{j \in D^i} length(e_j^i) \tag{3}$$

where D^i denotes a set of edges connected to i.

- **Baseline and height ratio** $(F_{bh}(i))$. Based on the principle of stereovision, higher-quality reconstruction by MVS is obtained from a correct ratio between the baseline length and height. The baseline length is the distance between two camera positions $\boldsymbol{c}_j$ and $\boldsymbol{c}_k$, and the baseline height is the distance between the space point position $\boldsymbol{p}_i$ and the midpoint of the baseline $\boldsymbol{c'}_{jk}$. It is well known in photogrammetry that the quality of the dense model is related to this ratio [8]. Therefore, the ratio is evaluated as the *Baseline and height ratio* predictor as follows:

$$F_{bh}(i) = \frac{1}{|J_i|} \Sigma_{(j,k) \in J_i} \left(\frac{\|\boldsymbol{c}_j - \boldsymbol{c}_k\|}{\|\boldsymbol{p}_i - \boldsymbol{c'}_{jk}\|} \right) \tag{4}$$

where J_i denotes a set of all possible camera pairs visible from a sparce point i.

The detailed calculation of the indicators is explained in a previous study [4].

To consolidate the four quality predictors into a single indicator representing the degradation of the dense model, first, we converted each of the predictors given by Equations (1–4) to a normalized energy $\in [0,1]$ using the logistic function $L(\,)$ proposed by Mauro et al. [7] and quadratic function $K(\,)$ as follows:

$$E_X(i) = \begin{cases} L(F_X(i) - \mu_X, \sigma_X), & X \in \{a, e\}; \\ 1 - L(F_X(i) - \mu_X, \sigma_X), & X \in \{r\}; \\ 1 - K(F_X(i), \sigma_X), & X \in \{bh\}, \end{cases} \tag{5}$$

where μ_X denotes the average of F_X, σ_X is the standard deviation of F_X, $L(x - \mu, \sigma) = 1/\left(1 + \exp\left(-\frac{2(x-\mu)}{\sigma}\right)\right)$, and $K(x, \sigma) = 1/(1 + (x - 0.5/\sigma)^2)$. In Equation (5), higher energy means that the geometry of the final

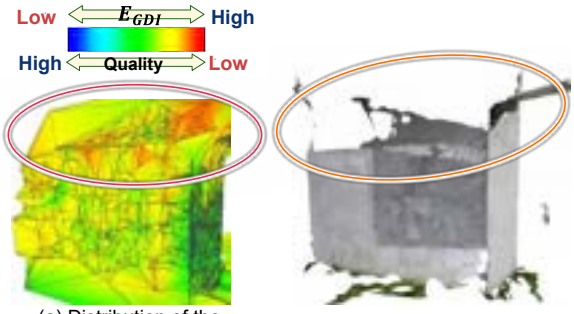

(a) Distribution of the geometry degradation indicators (E_{GDI}) on M

(b) Dense model generated by MVS

Figure 7. Correlation between the distribution of the geometry degradation indicators and the dense model by MVS for original photos

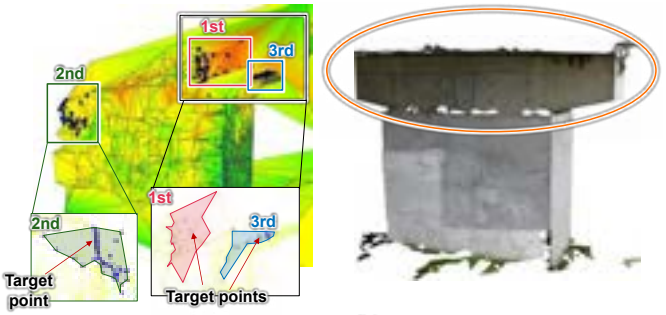

(a) Derived three low-quality regions and the target points ($s = 3$)

(b) Dense model generated from the 33 original photos and 3 additional photos set by MVS

Figure 8. Three target points for additional image capture and the improved dense model obtained used MVS after additional images have been captured

dense model is more degraded.

Finally, the four energy values $E_X(i)$ are aggregated by taking an average to denote a *geometry degradation indicator* at a sparse point i as $E_{GDI}(i)$ as follows.

$$E_{GDI}(i) = \big(E_r(i) + E_a(i) + E_e(i) + E_{bh}(i)\big)/4 \qquad (6)$$

A region with high indicator value $E_{GDI}(i)$ on the approximated triangular mesh model $M^{'}$ indicates that the local region around the sparse point i on the dense model has a more significant possibility of degrading the geometry. It also implies that valid photos are lacking in the region with a high indicator value and that additional image s should be preferentially captured to improve the dense model quality of the region around the point i.

Figure 7(a) shows the distributions of the indicator values $E_{GDI}(i)$ on the approximated mesh model M of the pier shown in Figure 6. The predicted quality of the upper part of the pier is low (red), which suggests that the number of images captured capturing in this area was insufficient. Figure 7(b) shows a dense model generated by MVS from the original 33 photos. In Figure 7(a), the upper parts of the pier shape with high indicator values were not fully reconstructed in the dense model. Thus, it is evident that the quality prediction based on the geometry degradation indicator $E_{GDI}(i)$ is functioning.

3.3 Estimation of Additional Shooting Positions

Low-quality areas on a dense model should be improved by capturing additional images as efficiently as possible. To this end, it is preferable to identify target positions of as many low-quality areas as possible for an additional photo shoot. Therefore, based on the geometry degradation indicator, the target points for the additional photo shoots are selected by an optimization.

First, for every sparce point $i(\in P')$ on the approximated model M, the geometry degradation indicator $E_{GDI}(i)$ value is added as an attribute value w_i. Then, the degree of degradation in the peripheral region of i is estimated both from a target point $j(\in P')$ and from the indicator values of the sparce points i' included in the region near the target point j. A photo shoot to capture additional images should be oriented to cover the areas with the most considerable geometry degradation. Finally, $s$target points for additional photo shoots are derived from the sparce point set P' using the combinatorial optimization and a greedy algorithm. Details of the optimization process are presented in a previous study [4].

Figure 8(a) shows the three low-quality areas and the target points for additional image capture. The areas were derived from the distribution of the geometry degradation indicators in Figure 7(a) with $s = 3$. The indicator values in the areas around the target points are higher than in other areas, and the target points can be placed at the low-quality areas appropriately.

Figure 8(b) shows a dense model reconstructed by MVS from 36 images, including the three additional photos corresponding to the three target points. Compared to the model generated from the 33 initial images in Figure 7(b), the quality of the reconstructed area at the top of the pier increased significantly despite adding only three images. Therefore, the effectiveness of the target point selection algorithm can be confirmed.

4 Case Study

4.1 Evaluation of Reconstruction Qualities

A case study was conducted at a seawall construction site shown in Figure 9 (51 m × 2.4 m) on

Figure 9. Scene of the construction site of wave-dissipating block installations at Toyoura coast

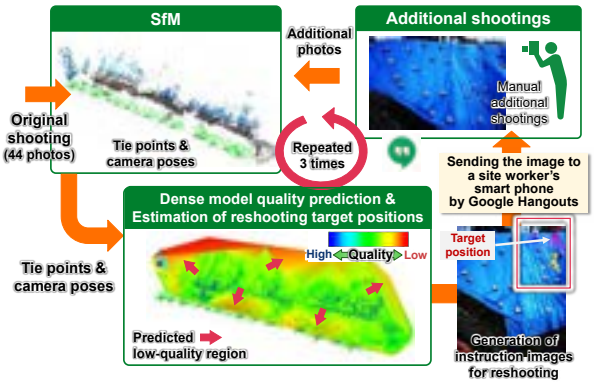

Figure 10. Process flow of the case study

the Toyoura coast in Tomamae-Cho, Hokkaido. The proposed photogrammetry process was performed. The process involved an original photo shoot, dense model quality prediction, on-site best-view guidance, and additional photo shoots to record the installation of wave-dissipating blocks.

To decrease the time required to upload images from a camera to the cloud system, a smartphone (HUAWEI Mate20-Pro) with a built-in high-resolution camera was used. The image resolution was set to 9.7 million pixels to reduce the transfer time, and a wide-angle lens was used. By using a smartphone, captured images could be automatically uploaded to Google Drive immediately. In addition, with this image resolution setting, the upload time could be significantly reduced to within a few seconds per image. Since the SfM and best-view guidance server does not necessarily need to be installed near the construction site, we installed it at the Sapporo campus of Hokkaido University. A high-speed internet connection is available between the university and the construction site on the Toyoura coast.

Figure 10 outlines the process flow of this case study. Forty-four original photos were taken from sparse positions using the smartphone camera by an on-site worker while walking on the top of the wave-dissipating blocks. Next, the next-best target positions to capture additional images were estimated. Then, an instruction image was generated on the server-side and sent to the worker's smart phone. Finally, according to the instruction image, the worker took five to 10 additional photos once and repeated the process of transmitting the images to the server three times. The time required by the process is summarized in Table 1.

Table 1. Processing time in the proposed photogrammetry process

	Total photo # (Additional photo #)	Time for SfM processing	Time for estimating the best target positions	Time for MVS processing
Original	44	**1 min 30 sec**	**3.96 sec**	15 min
1st Addition	49 (5)	**1 min 20 sec**	**4.17 sec**	-
2nd Addition	58 (9)	**1 min 20 sec**	**5.08 sec**	-
3rd addition	68 (10)	**1 min 40 sec**	-	**20 min**

Red Bold： Processing time actually required for the dense model generation using the proposed process

Figure 11 shows the dense model reconstructed by MVS from only the 44 original photos, the estimated best target positions, the corresponding instruction images, and an example of the photos added by the worker. The dense model geometries generated by MVS with those additional images added at each stage are also shown in Figure 11.

As can be seen from Figure 11, it is possible to visually confirm that the 3D model can be generated with relatively good quality even with images captured by the built-in smartphone camera. In addition, using the model quality prediction and estimation of the best target positions to capture additional images, the defects and holes between blocks generated in the model reconstructed from the original images disappeared in the model generated after images were added, and the correct block geometry could be reproduced. The area near the drainage pipes on the upper left of the slope was greatly expanded. As shown in Table 1, estimating the best shooting target position once could be completed in approximately 1.5 min.

From the above results, it is evident that, in a construction site, using a smartphone camera to capture images and as communication device is suitable for 3D photogrammetry measurement in which the model geometry is successively improved. Although the improvement in model quality depends on the number of shots, the result suggested that the proposed process might be able to complete the reconstruction of the dense 3D model on the day that the one-site images were captured.

On the other hand, some areas around the blocks still require additional photo shoots and setting the criteria for terminating these repetitive image capture processes was left as an open problem.

4.2 Estimation of Processing Efficiency

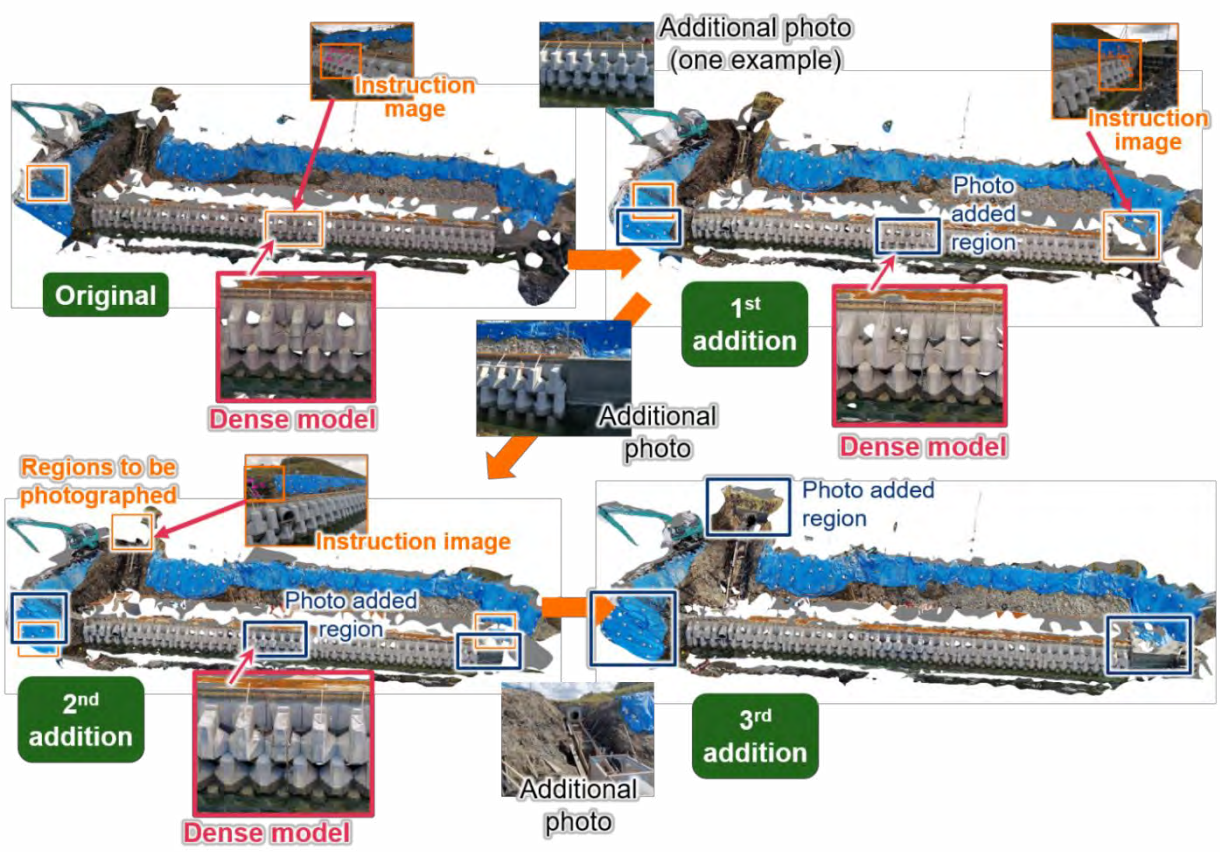

Figure 11. Changes in the dense models by 1st, 2nd, and 3rd addition of images

To quantify how efficient dense model reconstruction using the proposed photogrammetry process is compared to two conventional processes. We compared processing times for the following three approaches.

(1) Conventional photogrammetry with single photo shoot and an excessive number of images. Here, a dense model was reconstructed by performing the SfM-MVS together for approximately 400 images captured at the site.

(2) Conventional photogrammetry with a single additional photo shoot. First, 44 original photos were obtained, and a dense model was generated once by SfM-MVS. Then, the low-quality portions of the dense model were identified manually, and 24 target points for an additional photo shoot were determined. Finally, the SfM-MVS process was re-executed with 68 images to reconstruct a final dense model.

(3) The proposed process. Here, the process started with 44 original images. Then, SfM was performed, target positions to obtain additional images were identified using a computer, and five, nine, and ten photographs were added to the original images. Finally, the dense model was reconstructed by performing MVS only once for the 68 images acquired.

Note, for the processing efficiency comparison, the Toyoura coast construction site was taken as an example (Section 4.1).

The bar chart in Figure 12 shows the comparison results. In estimating the processing time, referring to the values obtained from the construction site of section 4.1, the required shooting time per photograph was estimated to be 15 s. The SfM and MVS processing time per photo was 0.03 and 0.3 min, respectively. Moreover, the time required to estimate the shooting target positions was assumed to be constant at 6 s. Note that the image upload time was included in the shooting time because it was only a few seconds per photo.

As can be seen from the comparison in Fig. 12, process (1) required approximately 3.5 h to reconstruct the dense model from the excessively captured photos. With the proposed process (3), the dense model could be reconstructed in 40 min, which is approximately one-fifth of the time required by process (1).

In addition, since process (1) requires MVS processing of a significant number of images, which takes considerable amount of time, the quality of the dense model cannot be confirmed until the processing is

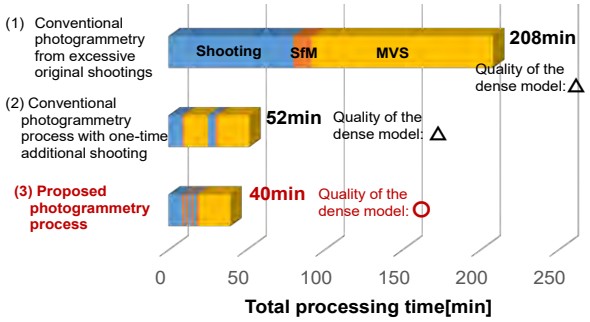

Figure 12. Comparison of the total processing times among (1) conventional photogrammetry process with excessive image capture, (2) conventional photogrammetry process with a single shoot to capture additional images and (3) the proposed photogrammetry process

complete, i.e., approximately 3.5 h after the photo shoot. On the other hand, with the proposed process (3), we estimate that the shooting target positions that reflect the prediction of the dense model quality for the currently captured photos can be fed back to a site worker in approximately 2–3 min after capturing the photo. Thus, it is possible to ensure that all required images are captured and to realize an efficient photo shoot.

Furthermore, in processes (1) and (2), the selection of shooting positions is left to the user; thus, there is no guarantee that the additional photos will improve the reconstructed model's quality. In contrast, with the proposed process (3), since the computer selects the best positions at which additional photos should be taken based on the model quality estimation, it is highly likely that additional images will effectively contribute to the quality improvement of the reconstructed dense model.

5 Conclusion

In this paper, we have proposed a new photogrammetry process that improves the quality and efficiency of dense model reconstruction of construction sites. The proposed process begins with a small original photo set. Then, the computer-supported best-view guidance system predicts the geometric quality of the dense model, estimates the best target positions for additional photo shoots using only SfM results, and feeds back those positions to a site worker. Depending on the number of target positions, the feedback process could complete in 1.5 min. The effectiveness of the proposed process and the system was evaluated at a real-world construction site. As a result, it was found the process and the system could prevent excessive image capture, improve the efficiency of the on-site photo shoots, and generate the dense model with a certain degree of quality assurance. We also found that a smartphone, which can send and receive images to and from the construction site, was the most suitable shooting device for implementing the process.

However, currently, some server-side operations still require manual processing. In the future, we would like to implement fully automated processes that include SfM and best-view guidance on a cloud server.

Acknowledgments

This research was supported by the following grant-in-aid from the Ministry of Land, Infrastructure, Transport, and Tourism in FY2018-19: “Project on the introduction and utilization of innovative technology for dramatically improving the productivity of construction sites: Utilizing data to improve the productivity in construction labor in civil engineering.”

References

[1] Ministry of Land, Infrastructure, Transport, and Tourism. i-Construction (in Japanese). On-line: https://www.mlit.go.jp/tec/i-construction/index.html, Accessed: 10/06/2020.

[2] Riveiro B. and Lindenbergh R. *Laser Scanning: An emerging technology in structural engineering*, CRC Press/Belkema, Leiden, 2019.

[3] Luhmann T., Robson S., Kyle S. and Boehm J. *Close-range Photogrammetry and 3D Imaging (3rd Edition)*, De Gruyter, Berlin/Boston, 2019.

[4] Moritani R., Kanai S., Date H., Niina Y. and Honma R. Quality prediction of dense points generated by structure from motion for high-quality and efficient as-is model reconstruction. *Int. Arch. Photogramm. Remote Sens. Spatial Inf. Sci.*, XLII-2/W13: 95–101, 2019.

[5] Google Hangouts, On-line: https://hangouts.google.com/, Accessed: 10/06/2020.

[6] Labatut P., Pons J.-P. and Keriven R. Efficient multi-view reconstruction of large-scale scenes using interest points, Delaunay triangulation and graph cuts. In *IEEE 11th International Conference on Computer Vision,* pages 1–8, Rio de Janeiro, Brazil, 2007.

[7] Mauro M., Riemenschneider H., Signoroni A., Leonardi R. and Van Gool L.J. A unified framework for content-aware view selection and planning through view importance, In *British Machine Vision Conference*, pages 1–11, Nottingham, U.K, 2014.

[8] Yan L., Fei L., Chen C., Ye Z. and Zhu, R. A multi-view dense image matching method for high-resolution aerial imagery based on a graph network. *Remote Sens.*, 8(10):799, 2016.

Cyber Agent to Support Workers' Decision Making for Mechanized Earthwork

[a]Shigeomi Nishigaki, [b]Katsutoshi Saibara, [c]Takashi Ootsuki, [d]Hirokuni Morikawa
[a] CEO, Mazaran, Co., Ltd. and kick, Co, Ltd., Japan
[b] Senior reseach engineer, Kick, Co., Ltd., Japan
[c]Senior Researcher, Advanced Construction Technology Div.,Research Center for Infrastructure Management, NILIM, MLIT, Japam
[d]Head, Advanced Construction Technology Div.,Research Center for Infrastructure Management, NILIM, MLIT, Japan
E-mail: sleepingbear@c2mp.com, saibara@c2mp.com, ohtsuki-t2sh@mlit.go.jp, morikawa-h573ck@pwri.go.jp

Abstract -

We have been and are doing development and research on construction AI system based on Actor-Critic framework. This paper discusses cyber agents who are computerized agents of mobile entities, which are composed of construction machines, vehicles and workers. Each of the cyber agents would carry with simple function to work together in the Actor-Critic cyberspace. The cyber agents will passively or actively walk through the cyberspace to help for workers to explore and capture critical factors latent in a large amount of information that might go into making decisions. The contents described in this paper might be almost a sublimation of the papers we have submitted to the ISARC for the past decade. This paper is organized as follows. First, this paper describes Actor-Critic framework for construction AI system. Secondly, this paper reports role of cyber agent. Thirdly, this paper explains inference mechanism of abduction reasoning and briefly shows example of inference. Finally, this paper presents further development and research on functions that the cyber agent should carry with in future.

Keywords -

Cyber agent; Humanware; Actor-Critic; Abductive reasoning; SRK model; Subsumption

1 Introduction

We have been and are doing development and research on construction AI system based on Actor-Critic framework (hereinafter called "construction AI") to support workers' decision making for earthworks. Cyber agents are computerized agents of mobile entities, which are composed of construction machines, vehicles and workers (i.e., operators, drivers, foreman, resident engineers, line-manager, and others). Each of the cyber agents would carry with simple function that work together in the actor-critic cyberspace. This cyberspace has three layers structure that consists of knowledge, rule and skill levels (SRK model), and the higher level subsumes lower level with downward commitment and the lower level provokes the higher level with upward activation. The Actor has policy structure to select and take actions, and further the state- or action-value functions to fire signal, sign and symbol. The Critic has functions of edit, calculation and analysis of readings captured by the PoC as explained later.

The cyber-agent will inhabit and passively or actively walk through the cyberspace to help for workers to explore and capture critical factors latent in a large amount of information that might go into making decisions.

The contents described in this paper might be almost a sublimation of the papers we have submitted to the ISARC for the past decade. This paper is organized as follows. First, this paper describes framework of the construction AI system. Secondly, this paper reports role of cyber agent. Thirdly, this paper explains inference mechanism of abduction reasoning and shows example of inference in brief. Finally, this paper reports further development and research on functions that the cyber agent should carry with in future.

2 Framework of Construction AI

Figure 1 shows schematic view of the construction AI system.

Figure 1. Schematic view of construction AI system

The construction AI system consists of the components as described below.

2.1 Points on Construction (PoC)

The PoC takes sensor-based event detection approach to track fleet of construction machines, vehicles and workers which are working together on site. The PoC automatically and real-timely gather a set of readings related to events occurred by the fleet activities [1],[2]. In other words, the PoC looks like a feeler of the cyber agents.

2.2 Geospatial Index based on Space-filling Curve

We use the Hilbert curve that folds one dimensional axis into a 2D space. The Hilbert curve here covers fully minimum bounding box covering working area. A serial number [1, max (number of vertices)] is assigned to each of vertices of the Hilbert curve. The position of the vertices of the Hilbert curve coordinates cell centres of the ground grid, for examples, the position index (i, j) of the corresponding vertex in a 2D array indicates the "i" th vertex in x and the "j" th one in y direction. The serial number might be almost equivalent to zip code in our daily life.

2.3 Database of Readings and Lookup Table of Tuples

Readings are captured by the PoC and then knowledge would be represented by lookup table of tuples. Each of the tuples is composed of code_id, cyber agent name, file name of the readings, proposition, condition, consequent, threshold, effects, belief, w_{ij} and action. The proposition is a parent of conditions and these are organised as a parent - child relationship on a semantic network. In many cases, the condition is expressed as potential cause of failure mode, and the consequent is expressed as potential failure mode in a production rule, which is presented as a disjunction literal and might be a hypothesis.

The threshold is a value above which the condition is true or might take place and below which it is not or might not.

The effect indicates potential effects of failure that forks into two categories "High" and "Hazardous." The former means "Will affect product performance, and some product will have to be scrapped, and rework possible," and the latter means "Will affect workers' safety."

The belief means a posterior probability that is an element of Bayesian Belief Network of the condition and the consequent.

The w_{ij} indicates weight in element [i-th row, j-th column] of Hebbian weight matrix, which represents strength of relationship among the conditions and the consequents or the consequents. The Hebbian weight is defined by the equation (1) [11].

$$w_{ij} = \log \frac{p(y_j, x_i)}{p(y_j) * p(x_i)} \quad (1)$$

In many situations, the consequents might be trouble phenomena happened on site, and otherwise potential failure modes from an action that the cyber agents at the actor component should take as described later.

2.4 Critic Component

Figure 2 shows relationship between the actor component and the critic component. Each of the cyber agents inhabit the critic component, and carries with simple function that could edit, calculate and analyse a set of the readings captured by the PoC. They could set threshold values at the 5% and 95%, or the 1st and the 2nd quantiles of empirical distribution function, and then do quantile processing to convert from the continuous variables to dichotomous ones.

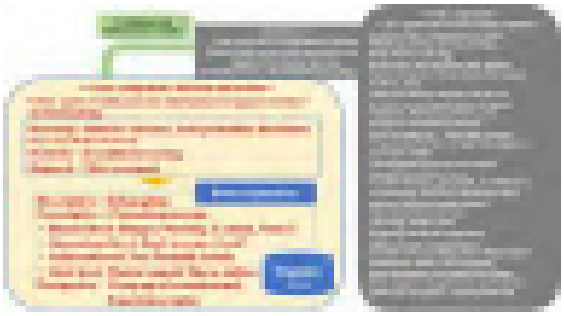

Figure 2. Relationship between actor and critic components

They would hand over their results of calculation and analysis to the cyber agents inhabit the actor component.

2.5 Actor Component

As is shown in Figure 2.4.1, the actor component functions decision and action based on the results received from the critic component. More loosely speaking, the actor component has three mechanisms as follows:

2.5.1 Production rule

Production rule associates a condition or a proposition (if) with the consequent, i.e., a phenomenon or an action (then). Besides, the rule states what cause is most likely to trigger what failure when the consequent might be true.

Strength of production rule indicates firing priority. The production rule is chosen based on the order of

priority predefined by expert experience, or indicated by the calculated Hebbian weight "w_{ij}."

Dichotomous variables received from the critic component would trigger that the cyber agents here would interact with rule-base, that is, listwise production rules and take predetermined action. Besides, each of the cyber agents would carry spatio-temporal analysis model, and functions to generate infographics. The spatio-temporal analysis model would be used to analyse dataset with spatial and temporal property and to visualize a region or points of interest.

2.5.2 Better explanation

The current situation is descriptively depicted by infographics with precaution message might prescriptively be informed as follows:

- Hazard level: Danger, Warning, Caution, Notice,
- Operational level: Bad, Average, Good,
- Achieved level: Not, Partially, Attain, and
- Alert level: Wait or cancel, Take a shelter.

2.5.3 Eligibility trace

The actor produces list-wise infographics with early precautionary messages, and forwards them to the dashboard. Moreover, the visiting of a state or the taking of an action, Hebbian weights are temporary recorded as an eligibility trace. The eligibility trace marks the token (i.e., signal, sign, symbol) associated with the event as eligible for undergoing learning changes. And then, wrap-up of lesson learned would be informed from different person perspectives.

Eligibility trace has two levels: which experiences to store, and which experiences to replay (and how to do so). Here, prioritized experience replay is used to remember and learn from more frequently past experiences [3].

2.6 Dashboard of Remotely Real-time Monitoring System

Figure 3 shows structure of remotely real-time monitoring system.

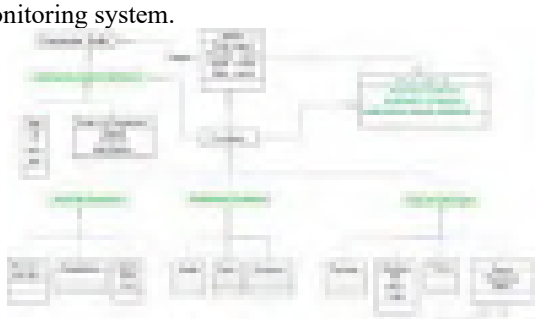

Figure 3. Structure of remotely real-time monitoring system

The dashboard is a visual display on screen of smart phone, PC or other device that are installed at the control or cabin room, and otherwise the operators carry. Information displayed on the dashboard is consolidated and arranged on a single screen so that infographics can be monitored at a glance [2].

2.7 Workers

The workers mean people who are actually working together on site, for examples, operators in cabin room or remote-control room, drivers, foreman, resident engineers, line manager, and others.

3 Role of Cyber Agent

Main role of cyber agents is to pick a set of building block of information at the right level of abstraction and at the right time, and then provide workers with infographics on real time basis. Each of cyber agents with simple functions forms a swarm of them, and interacts with each other. Figure 4 shows schematic view of the cyber agent.

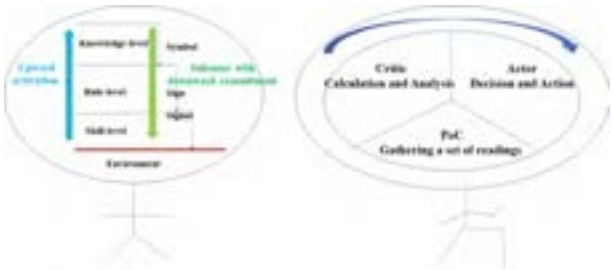

Figure 4. Schematic view of the cyber agent

The actor-critic space, that is, brain of the cyber agent, consists of hierarchy of skill-level. rule-level and knowledge-level （SRK model), and the higher level subsumes lower level with downward commitment and the lower level provokes the higher level with upward activation as shown left in Figure 3.1[4],[5]. At the skill level, signal might distribute from the 1st person point of view. The signal is directly grounded the perception-action coupling with environment. At the rule-level, sign might flow from the 2nd person point of view. The sign is grounded based on social convention, for example, crossing sign "red" means "stop." At the knowledge-level, symbol might propagate from the 3rd person point of view. The symbol has meanings that live in their mind, not in the item itself, for example, flags are symbols for nations. Each of the cyber agents would proceed along cycle of the PoC - the critic - the actor as shown right in Figure 3.1.

Supports for workers' decision making from the 1st, 2nd and 3rd-person point of views are described below.

3.1 The 1st Person Point of View

In general, the 1st person point of view (POV) is used the term that depicts a method to control a radio-controlled machine or vehicle from the operator's or driver's view point. Discussions in this study shall narrow down the eye-hand coordination task regarding to operate construction machine and to drive vehicle from the operator's or driver's view point.

Handling joysticks to operate construction machines or steering wheel in vehicle, either remotely or directly, is an inherently eye-hand coordination task. The eye-hand coordination means to control eye movements with hand movements, and as processing visual representation of the situational views to handle joysticks or to steer control along with the use of proprioception of the hands, or vice versa. In either manned or unmanned operation, the operators' or drivers' performances limited by humanware in their behavioural frameworks, and continuous or intermittent mental workload burden on them. The humanware is defined a function composed of leadership, followership and the reciprocal interaction between the two [6],[7],[8].

Besides, a mechanized earthwork process is separated into several works that are sometime independently and at other time interactively performed by different workers. For examples, road construction includes a series of discretely repetitive operations such as excavating, loading, hauling, dumping, grading, compacting, etc., which are performed by different operators, drivers and other workers, who are belonging to different subcontractors. Consequently, it becomes difficult to gather field data concerning each operation, to grasp their own operations in progress on real time basis, and to understand the "Do's" and "Don'ts" in the whole earthwork process. Here, since workers might reduce their vigilance, they might take physical reactions to startling or unexpected events in the monitors or in front of vehicle, and might not secure the safe, reliable and effective earthwork process.

The cyber agents here would compensate for operator's realistic sensations to enhance spatial awareness by providing workers with physical cues as shown in Figure 5.

It would be significant to provide them with physical cues which would enhance their diagnostic and prognostic capabilities to reflect on their own unsafe behaviour. The information modelling here means a process involving acquisition of field data and feedback of relevant digital representations of physical and functional characteristics of works in progress.

The role of the information modelling is largely grouped in to the followings:
(1) To find signals of overturn, slither, or skid of mobile entity (i.e., machine or vehicle), and then issue alert message. Concretely, the x-, y-, and z-axis acceleration responses are captured and analysed to
- Find signals as to overturn and slither of the mobile entity, and
- Visualize phenomena of rolling, pitching, and vacillation of the mobile entity in order to prognosticate dangerous sections or spots in emergency, and
- Suggest work zone with the driving path to be repaired,
(2) To provide workers with infographics that play role in the following matters:
- Feedback of physical cues related to behaviour of mobile entity, and
- Spatio-temporal visualization of hazards latent in in-situ earthwork process.
(3) To provide oneself with the opportunities to reflect on their own bearings as facing their own works at hand,
(4) To take timely and quickly correct actions based on detailed visibility of appearances and motions of mobile entities in an earthwork process, and accordingly,
(5) To reduce likely mental stress burden on operator and driver in the remote-control or cabin room.

Figure 5. Enhancement of spatial awareness by providing workers with physical cues

3.2 The 2nd Person Point of View

Cyber agents might use push notification service for early precautionary or forced messages to the worker being targeted at, where the use of pronouns: you, your, yours, yourself, yourselves.

The early precautionary messages would hold, referring to ANSI Z535,5 definitions, the levels of early precaution are set as danger, warning, caution, and notice.

The forced message might include changes or stoppage in work order, or evacuation. The forced message could force you to take action in order to prevent undesirable behaviour or events.

3.3 The 3rd Person Point of View

Cyber agents here would pick a set of building block of information at the right level of abstraction, and

produce construction profile at the right time. The construction profile is defined as a set of data to vision characteristics of phenomena being generated along with earthwork in progress and indexes to show their patterns [9],[10]. Figure 6 shows image of cross section and longitudinal analyses. It is expected here to take situational awareness into account in changes and to find any hotspot in spatiotemporal situations.

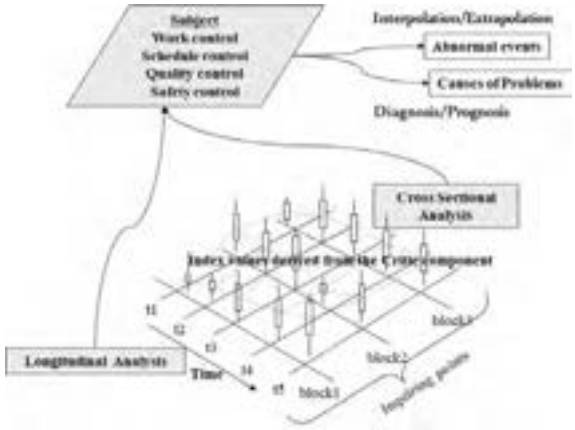

Figure 6. Image of cross section and longitudinal analyses

Based on the above information, the 3rd party people (i.e., resident engineers, line manager and others) would be able to find changes in the situation of work zone or points of interest and to evaluate force account work performed at cross section and toward longitudinal in earthwork progress from the following viewpoints:

- Viewpoint 1: Watch line balance. For example, search unbalance of productive capacity among construction resources;
- Viewpoint 2: Search abnormality in earth work progress. For example, find construction resources that have extra-high production capacity and one in the opposite side;
- Viewpoint 3: Watch state- or action-value of control. For example, find change in mean and variance or shift change in time series, and look at trend of increment or decrement;
- Viewpoint 4: Watch productivity. For example, look at planned versus actual productivity of a work package, and make a comparison between the two. The work package is a group of related tasks within an earthwork process; and
- Viewpoint 5: Look at construction speed based on the following step: first, set base line of earthwork progress; secondly, calculate progress rate in situ, and finally make a comparison between the two.

Infographics could be very helpful for the 3rd people to consider current situation of earthwork in progress from the above viewpoints. The infographics would be displayed on the dashboard of the remotely real-time monitoring system [2].

4 Abduction Reasoning

4.1 Inference Mechanism

The cyber-agent here is a virtual worker who inhabits the cyberspace composed of the actor component and the critic one. The cyber-agent will passively or actively walk through the cyberspace to help workers explore and capture critical factors latent in a large amount of information that might go into making decisions. The cyber agents would utilize abductive reasoning to form threshold value generated by quantile processing of experience probability function, Bayesian Belief Network, Hebbian weight, etc. presented in the tuple, and then inference backwards from consequent to antecedent. The inference is to affirm consequent and then conclude that the condition or the proposition is supposed to be true. In other words, this is inference from the observations to the best explanation, that is, the simplest and most likely conclusion. This inference, however, does not positively verify it.

Figure 7 shows abductive reasoning composition.

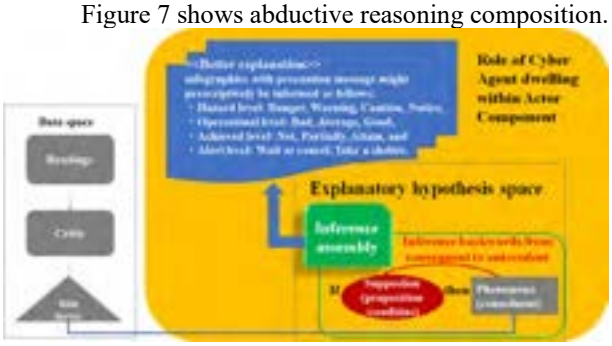

Figure 7. Abductive reasoning composition

4.2 Examples of Abductive Inference

This section shows examples of abductive inference related to dozer operation on highway construction site. First, this section presents a class of the cyber agent. Secondly, composition of tuple is explained. Thirdly, infographics are reported. Finally, Example of abductive inference is briefly shown.

4.2.1 Class of Cyber Agent

The cyber agent is set as a class (ex. R5 in R language). Example of class of dozer is shown below.

```
Bll <- setRefClass(
Class = “dozer ", #character string name for the class.
fields=list(#either a character vector of field names or
a named list of the fields.
maker_name = "character",
model_number = ”integer”,
operating_weight_kg = "numeric",
engine_power _rpm = "numeric",
speed_km/hr = "numeric",
overall_length_mm = "numeric",
```

```
overall_width_mm = "numeric",
overall_height_mm = "numeric",
shoe_width_mm = "numeric",
track_on_ground_mm = "numeric",
ground_contact_area_m2 = "numeric",
ground_pressure_kPa = "numeric",
ground_clearance_mm = "numeric",
),
#named list of function definitions that can be
invoked on objects from this class.
methods =list(
Initialize=function()
  )
)
```

Similarly, each of the required functions is set as a class. A part of the class of the required functions is listed below:

- gg.gauge #progress gauge,
- inflect #Finding local maxima and minima,
- geodetic.distance #distance on the surface of the earth between two points,
- trackDistance #Distance travelled,
- kde2d.weighted #kernel 2D density with weight,
- HampelFilter #median absolute deviation,
- loess (locally weighted scatter plot smooth),
- ses (single exponential smoothing),
- movingAverage,
- LongLatToUTM #Converting lat, long points to UTM meter unit,
- zcr (zero crossing rate),
- PtInPoly #extract points within polygon,
- Hilbert #HilbertCurve,
- force #3-axis acceleration composition value,
- real operational rate of machine by each work-in day,
- body attitude, and
- calculation of polygon area, and so forth.

4.2.2 Composition of Tuple in Lookup Table

As mentioned before, the tuple consists of i code_id, cyber agent name, file name of the readings, proposition, condition, consequent, threshold, effects, belief, w_{ij} and action. This section reports a part of proposition and production rules below.

(1) As for productivity and safety, a part of propositions is listed below.

1. Productivity:
- Reference of productivity per one hour,
- Driving forward or back distance of dozing operation,
- Real operational rate per a day,
- Dumping volume of material per a truck,
- Dozing area performed,
- Performance index (a ratio of the precedent rate to the successive one in each of work cells), Pitch time (time lapsed/production volumne),
- Abnormal observation, and so on.

3. Safety:
- Vehicle uphill/ downhill on a steep slope,
- Jump start; Sudden brake; Sharp turn; Excessive speed,
- Skidding, Overturn,
- Hazards latent in haulage road,
- Proximity Awareness, and so on.

(2) A part of production rules is listed below.

1. Impact and free-fall

Threshold values depends on quantile processing of empirical probability distribution.

If (95% <= the 3-axis acceleration composition value) then it is presumed that strong impact occurred at the longitude and the latitude, and

If (the 3-axis acceleration composition value < 5%) then it is presumed that free-fall occurred at the longitude and the latitude.

2. Dangerous proximity during operating machine when entering into the proximate area of 100 m range from other machine or dangerous spots like those.

3. Dangerous operation:

a) Sudden acceleration or rapid deceleration, when the jerk value of travelling speed gets larger than the predefined threshold value;

b) Turnover risk when finding trend for machine body to lean to crosswise or longitudinal direction and value of rolling or pitching more than 15 degrees; and

c) Defect productivity warning when finding

- Run length of key performance indicator changes in time series more than the threshold "7";

4. Other thresholds are set at the points 5% and 95%, or the 1st and the 3rd quantiles of experience distribution function;

4.2.3 Infographics

Readings in this example are captured by on-board smartphone for dozer. The sampling frequency was one HZ. The array element of the readings consists of [time, longitude, latitude, 3-axis acceleration, 3-axis angular velocity, direction, speed, FB]. The FB is a code that indicates forward, backward, or stopping

Figure 4.2.3.1 shows spatiotemporal trajectory of dozing and compacting In Figure 8, slate blue dashed line means "running trajectory on plane"; Brown dot indicates "spatio-temporal trajectory of running along with the axis of time." It is from Figure 8, we will be able to explore existential changes in spatial and thematic properties of travelling, dozing, and compacting, and also the time lapsed. This trajectory is plotted along with the vertical time axis and with locations on two-dimensional plane of longitude and latitude coordinates. Stopped and/or idling states of machine are dotted vertically along with the time axis. It can be seen from Figure 8 that the stopped and/or idling time is short during dozing and compacting operations. Total distance travelled here was 6030.622 m.

Besides, this infographic can be utilized for a fleet management of several machines, such as backhoes, crawler carriers, dozers, and vibration rollers, and so on. If dotted marks should be plotted at the same time and at the same position, the machine works related to the dotted marks are liable to be interfered with each other.

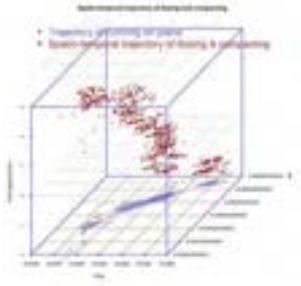

Figure 8. Spatiotemporal trajectory of dozing and compacting

Figure 9 shows index-based Hilbert curve to portray terrain of dozer operation. The Hilbert curve is drawn as following step:
Step 1: Set level=4, then the partition_number=2^leve-1=15; and
Ste 2: Convert longitude and latitude to UTM meter unit; Normalize to range [0,1].

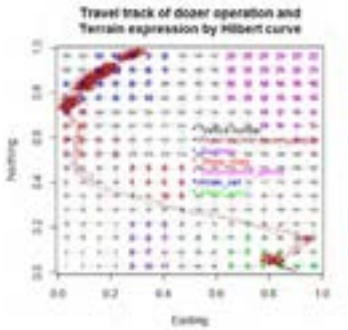

Figure 9. Index-based Hilbert curve

The index-based the Hilbert curve enables us to map multi-dimensional data to one-dimensional sequence values that could be inherently clustered, and then to allow for fast retrieval and storage. As mentioned above, the serial number assigned to the vertices might be equivalent to zip code in our daily life.

4.2.4 Example of abductive inference

The cyber agents could handle many kinds of physical cues to enhance workers' spatial awareness as shown in Figure 5. Due to limitations of space, examples of abduction inference regarding only one part of them are shown below.

Figure 10 and Figure 11 show occurrence spots of sudden acceleration and rapid deceleration while running; and existing of impacts and free-falls on site, respectively.

Some cyber agent might be interested in whether or not impact depends on speed. Here, inference would be proceeded along with the following steps:
Step 1: Set thresholds at the 5% and 95% points of experience distribution function,
Step 2: Generate cross table, that is, contingency table,
Step 3: Do chi-square test,
Step 4: Calculate joint probability and the Hebbian weight.

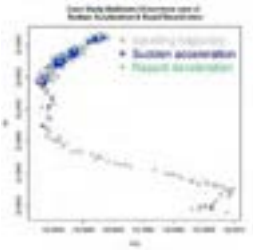

Figure 10. Occurrence spots of sudden acceleration and rapid deceleration while running

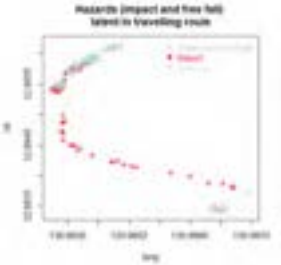

Figure 11. Existing of impacts and free-falls on site.

Figure 12 shows a part of semantic and propagation network related to the issue here.

Figure 12. A part of semantic and propagation network

If the Hebbian weigh might be significant, then the cyber agent would trace upward to the parent node, that is, the hazards latent in haulage road in this case. Otherwise, the cyber agent forgets it. The forget here means “take no-action” but “remember it, in other word, record it.”

The occurrence spots of sudden acceleration and rapid deceleration, and the impact and free-fall are significant, considering the thresholds, respectively, and then the cyber agent would inform workers of that facts, that is, the parent node of them with precaution on the dashboard of the construction AI. The phenomena of sudden acceleration and rapid deceleration is supposed to

be triggered by the dozer operation of "Pushing material" or "Releasing, spreading and compacting material." As for impact and free fall, the workers would investigate the haulage road in situ or review the recorded images of on-board camera for dozer to explore any hazard, for examples, corrugated road surface, pothole, difference in level, cave-in, corrosion, boulder, and so forth, latent in the haulage road.

As for the propagation from sudden acceleration and rapid deceleration to the impact and free-fall, the chi-square test does not show the significance. Moreover, The Hebbian weight values are minus. Consequently, the cyber agent would forget the relationship among the them, that is, "Take no action" but "Remember it."

5 Further Development and Research

The contents described in this paper might be almost a sublimation of the papers we have submitted to the ISARC for the past decade.

Implementation of the cyber agents is yet insufficient and still going on the road. We are required to gain experience of applying the way of thinking about the cyber agents to construction control on site.

For the present, we are scheduled to do further development and research on the following themes:

- Fulfilment of contents built in the tuple, especially, propositions, production rules, belief, Hebbian weights;
- Equipment of existing functions and objects fully with a reference class "setRefClass" in the R language;
- Objectification of abductive inference and to pile up the examples; and
- Experience replay with belief and Hebbian weights propagation.

In closing, we would like to say that any help and suggestions on this study would be heartedly appreciated. We are looking forward to meeting and discussion on the cyber agents with you all at the conference of the ISARC 2021 that will be held in UAE.

References

[1] Shigeomi Nishigaki, Katsutoshi Saibara, et al. Points on construction, 25th ISARC 2008, pp.796-803, 2008.

[2] Shigeomi Nishigakia and Katsutoshi Saibara. Infographics on Unmanned Dozer Operation, 36th ISARC, 2019.

[3] Tom Schaul, John Quan, Ioannis Antonoglou and David Silver. PRIORITIZED EXPERIENCE REPLAY, Cornell University. On line: https://arxiv.org/pdf/1511.05952.pdf

[4] J. Rasmussen. Skills, Rules, and Knowledge: Signals, Signs, and Symbols, and Other Distinctions in Human Performance Models, Vol. SMC-13 , Issue: 3, IEEE Transactions on Systems, Man, and Cybernetics, May-June 1983. On line: https://ieeexplore.ieee.org/document/6313160

[5] R. A. Brooks. A Robust Layered Control System for A Mobile Robot, Artificial Intelligence Laboratory, MIT, A.I. Memo S64, September, 1985. On line: https://people.csail.mit.edu/brooks/papers/AIM-864.pdf

[6] Shigeomi Nishigaki, Jeannette Vavrin, Noriaki Kano, Toshiro Haga. Humanware, Human Error, and Hiyari-Hat: A Template of Unsafe Symptoms, Journal of Construction Engineering and Management. On line: https://ci.nii.ac.jp/naid/80007643885

[7] Nishigaki, S., Vavrin, J., Kano, N., Haga, T., Kunz, J., Law, K.. Humanware, Human Error, and Hiyari-Hat: a Casual-chain of Effects and a Template of Unsafe Symptoms, Centre for Integrated Facility Engineering (CIFE), Stanford University. On line: https://cife.stanford.edu/humanware-human-error-and-hiyari-hat-casual-chain-effects-and-template-unsafe-symptoms

[8] Shigeomi Nishigaki, K.H. Law. Safety problems in On-site Construction Work processes, Automation and Robotics in Construction XI, D.A. Chamberlain (Editor), Elsevier Science B.V., 1994. On line:http://citeseerx.ist.psu.edu/viewdoc/download?doi=10.1.1.470.5795&rep=rep1&type=pdf

[9] Shigeomi Nishigaki, Hitoshi Sugiura, Teiji Takamura, Hiroshi Ogura and Keiji Hatori. Study on Framework of Construction Profile for Collaboration and Intelligent Construction, Vol.14, pp. 287-298, Journal of Applied Computing in Civil Engineering, 2005

[10] Shigeomi Nishigaki, Katsutoshi Saibara, Shigeo Kitahara. Information Modelling on Mechanized Earthwork, the 31st ISARC, 2014. On line: http://www.iaarc.org/publications/2014_proceedings_of_the_31st_isarc_sydney_australia/information_modelling_on_mechanized_earthworks.html

[11] A. Sandberg, A. Lansner, K. M. Petersson, O. Ekeberg. A Bayesian attractor network with incremental learning, pp. 179–194, Network: Comput. Neural Syst. 13, 2002. On line: https://www.researchgate.net/publication/11313800_A_Bayesian_attractor_network_with_incremental_learning

Research on Standardization of Construction Site Time-series Change Information as Learning Data for Automatic Generation of Work Plan of Construction Machinery in Earthworks

Takashi Otsuki[a], Hirokuni Morikawa[b,a], Yushi Shiiba[c], Seigo Ogata[d] and Masaharu Moteki[d]

[a] National Institute for Land and Infrastructure Management, 1, Aasahi, Tsykuba-shi, Ibaraki-ken, 305-0804, Japan
[b] Public Works Research Institute, 1-6, Minamihara, Tsykuba-shi, Ibaraki-ken, 305-8516, Japan
[c] Japan Construction Machinery and Construction Association, 3-5-8, Shibakoen, Minato-ku, Tokyo, Japan
[d] Advanced Construction Technology Center, 2-15-6, Otsuka, Bunkyo-ku, Tokyo, Japan

E-mail: ohtsuki-t2sh@mlit.go.jp, morikawa-h573ck@pwri.go.jp, shiiba@cmi.or.jp, ogata@actec.or.jp, moteki-m@actec.or.jp

Abstract –

For earthwork, whether or not it will be possible to automatically generate a work plan for construction machinery has become the key to realizing autonomous construction of earthworks.

The use of AI is being sought by some researchers for the automatic generation of construction setups. Efforts are being made to utilize the results of construction work plan of construction machinery carried out by skilled engineers as learning data when searching for rules to reproduce construction work plan of construction machinery.

National Institute for Land and Infrastructure Management is considering acquiring work plans of construction machinery data in the MLIT ordering works, and to be going to provide these data. What is required for these data is to reproduce the history of construction progress and explain the reasons for deciding the construction work plan of construction machinery, and to provide those data in a format based on certain rules. We call this approach the examination of data standards for time-series change information at construction sites.

As a starting point, we examined the acquisition method of the topographic shape and the effective display format. We tried the Voxel display as a data format that makes it easy to grasp the amount of construction progress and to add attribute information to each construction point. On the other hand, some experts have pointed out the usefulness of the point cloud data and the surface data generated by connecting the point cloud data in the design of the drainage slope. This paper reports the initiative.

Keywords –

Work plan; Construction machine; earthwork; Learning data; AI

1 Introduction

In Japan, We, the Ministry of Land, Infrastructure, Transport and Tourism (MLIT) has begun to promote the efforts to improve the productivity of construction sites by fully utilizing ICT at construction sites since 2015, under the name "i-Construction" (Figure 1, [1]).

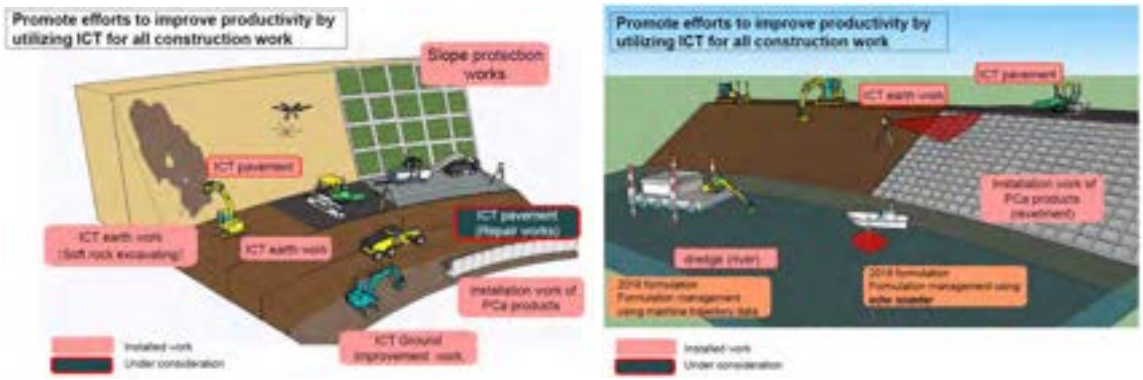

Figure 1. Examples of technologies targeted for introduction [1]

Since then, the following technologies have been utilized in earthwork, paving, dredging, etc.

- Efficient construction survey using ICT.
- A system that provides guidance to construction machine operators about work details.
- Construction machinery that automatically controls the blade edges of buckets and blades such as shovels, graders and bulldozers for shaping slopes and crowns of earthworks.

In the three years up to the end of January 2019, 2,287 cases of ICT utilization work have been carried out in the construction ordered by MLIT [2].

In addition, it is estimated that the amount of work done by humans has been reduced by an average of approximately 30% compared to the past by the full use of ICT in ground surveying, design data correction, construction, work form management/inspection, and electronic delivery [2].

We, National Institute for Land and Infrastructure Management (NILIM; Research department of MLIT) promotes the realization of AI construction machines that can automatically or autonomously construct, and that as a tool for further productivity improvement at construction sites. In order to do so, we started to study the data format for recording the time-series changes at the construction site and providing it in a widely usable form as the learning data for the autonomous construction AI (Figure 2). This paper reports the initiative.

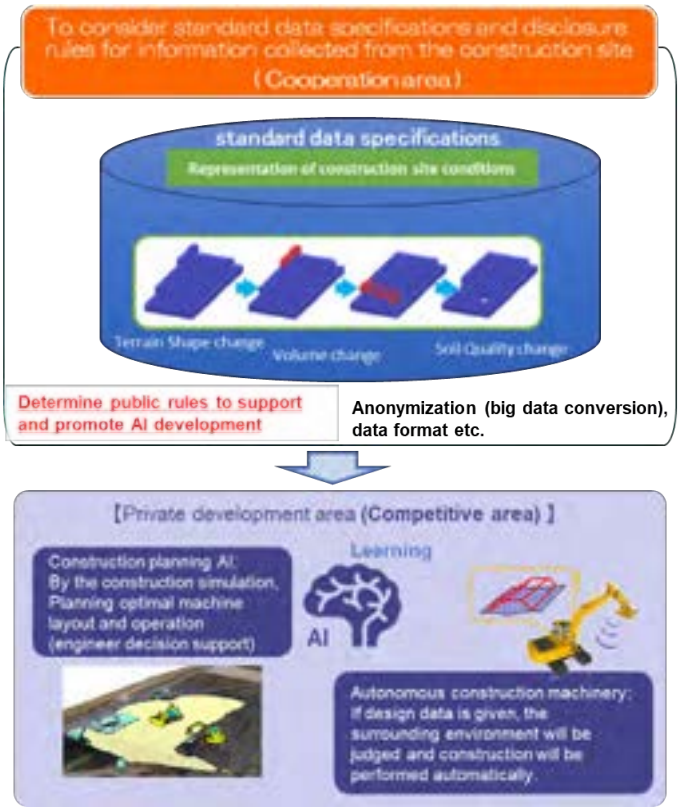

Figure 2. NILIM Project - Overall picture

2 Development status and key to realizing autonomous or automation construction technology

2.1 Current development status

As mentioned above, in earthmoving, semi-automatic control of buckets and blade edges such as shovels, graders and bulldozers has been realized and used for shaping slopes and tops of embankments [3]. Furthermore, some construction companies and construction equipment manufacturers are conducting experiments to operate combined construction of hydraulic excavators, vessel dumps, bulldozers, and vibrating rollers according to a human-defined program. In a closed environment where no one can enter, an excavator scoops up the sand in the sediment storage area, loads it into the dump vessel, moves the dump to the embankment point, dumps it, spreads the bulldozer, and compacts the vibrating roller. A series of work is being attempted [4].

And from a relatively long time ago, automatic calculation of the volume allocation plan has been realized. Compare the current topographic map with the blueprint showing the completed form and calculate the amount of cut and fill at each point. Then, using linear programming or some other method, calculate which embankment is to be filled with which cut so that the transportation cost of the soil is most economical [5].

2.2 The key to realization of autonomous or automatic construction; Development of “automatic generation of construction work plan of construction machinery”

However, based on this volume allocation plan, it is not so easy to calculate where to start and in what order to proceed. In order to move the soil, the difference in the earthmoving machine used (bulldozer, scraper, crawler dump, wheel dump) causes differences in transport efficiency and restrictions on the inclination of the moving path.

In addition, the local procurement costs (rental costs, transportation costs, etc.) of the earthmoving machinery itself to be put into the field will change depending on the site conditions and machine availability information. Many of these constraints exist, and they change depending on conditions such as the weather and economic environment, so if you perform an exact calculation, you will end up with a large-scale model.

When planning these steps with a computer program, it is necessary to examine every possible pattern of the work sequence, evaluate all the patterns, and select the optimum work sequence. This is a so-called "combinatorial optimization problem", and its calculation requires an enormous amount of calculation time compared to the linear programming

method used in soil volume allocation planning. Also, trying to reduce the computational cost of doing so requires a high degree of mathematical manipulation in assigning constraints.

So the bottleneck in automating all earthmoving is the step to achieve the automatic creation of work order plans to execute the volume allocation plan.

(As a program that partially supports work, in the work plan created by humans, the current situation is to calculate the required number of heavy equipment and perform a simulation applying queuing theory.)

3 Study on time series change information of construction site that should be collected as record data of construction execution setup

3.1 Purpose of this study

With the aim of realizing the automatic generation of construction execution setups, which was difficult to achieve with the conventional combination optimization approach, movements aiming for realization using AI are being sought. It is an approach such as using the construction execution setups actually performed by existing humans as learning data, and searching for work rules to reproduce the setups itself.

In order to support this approach, it is necessary to record the actual construction history of the earthwork and collect all the data that would explain the reason for the construction. In addition, it is useful to set certain rules for data collection and data format in order to provide such data in a usable state.

To achieve this, NILIM has begun studying a data standard for time-series change information at construction sites, assuming that this data will be provided.

3.2 Time series change information of construction site to be considered for collection

The most basic information that NILIM considers as time-series information at construction sites (Table 1) is the initial topography and final topography, and the history of changes in topography between them. And, as the constraint information that may have been used when selecting the change process, the ground conditions, usable materials and equipment (size and number of excavators, bulldozers and dumpers, embankment materials, etc.), the maximum number of days allowed for construction, and construction costs.

We will report the results of research and consideration on how to acquire the topographical shape data in Section 3.3, other data in 3.4, and how to link them after 3.5.

Table 1. List of Time series change information of construction site in this paper

	Perspectives of influential elements	Fine details	DATA	Format (unit)	Acquisition timing
Condition of construction machinery	Information for construction machinery management	Machine asset ledger	Construction machinery management records	Text or Numerical value	Annual, renewal
	Position and operating status of construction machinery	Construction machine operation records, location information, location history of work device, etc.	Working time	Date、Time	Secound
			Location log	Latitude/Longitude/ Elevation	Secound
			Operating log	Text or Numerical value	Secound
			Fuel consumption	Numerical value(L)	Day, Hour, Minutes
			Machine sensor log	Text or Numerical value	Secound
	Construction machine maintenance information	Failure code, maintenance history, etc.	Error log	Text or Numerical value	On maintenance or troube occurring
			Maintenance records	Text or Numerical value	On maintenance
	Information for productivity management	Cycle data, payload data, etc.	Construction volume per hour (Calculated by combining other data)		
			Bucket loading capacity	Numerical value(㎥)	On operatiing
Topographical data	Soil volume	Cut volume	Design/Estimation cut volume	Numerical value(㎥)	When starting work
			Actual cut volume	Numerical value(㎥)	On machine operation, UAV surveying
		Fill volume	Design/Estimation fill volume	Numerical value(㎥)	When starting work
			Actual fill volume	Numerical value(㎥)	On machine operation, UAV surveying
	Area	Total area	Design/Estimation area	Numerical value(㎡)	When starting work
			Execution area	Numerical value(㎡)	On machine operation, UAV surveying
		Area for each setting area (construction section)	Design/Estimation area	Numerical value(㎡)	
			Execution area	Numerical value(㎡)	
	Terrain shape	Surface or polygon	Terrain shape or its change	Point cloud、Latitude/Longitude/Elevation	
	Transport distance (outside, inside)	Bull, dump, heavy dump, various scrapers, etc.	Transport distance	Numerical value (km、m)	When starting work
(Geological data)	Soil quality	Clay, silt, sand, gravel, soft rock, hard rock, etc.	Soil type	Text or Index	When measuring
	Rate of change	Loosening rate L, Compaction rate C	Loosening rate	Numerical value(%)	When measuring
			Compaction rate	Numerical value(%)	When measuring
	Specific gravity	1.4～2.1	specific gravity	Numerical	When measuring
	Trafficability	Cone index	Cone index	Numerical	When measuring
	Ripperability	Number of nails	Number of nails	Numerical	When measuring
	Water content	Need for improvement, improvement/aeration yard	Water content	Numerical	When measuring
	Groundwater level	Workability	Presence or absence of groundwater and spring water	0/1	When measuring
(Meteorological and hydrological data)	Considering the number of rainy days and cold regions by region	Area and Weather	Weather	Text or Index	Automatic acquisition/manual input
			AMEDAS data (Regional rainfall information system in japan)	Text or Numerical value	Automatic acquisition
			Cold regions/snowy regions	Text or Index	Automatic acquisition/manual input
	Rainy season/dry season, dry season/normal season		※Present meteorological conditions of the area from past data of AMEDAS		
Construction Site Constraint data	Construction amount limit per day	Cut soil volume (transported soil volume), embankment volume	Cut soil volume (transported soil volume)	Numerical value(㎥)	When starting work or work planning
			embankment volume	Numerical value(㎥)	
	Removal limit of leftover soil	Embankment acceptance conditions and transportation conditions	Limit dump number	Numerical value (number、t)	When starting work or work planning
			Available days/days	Date	
			Available time/number of hours	Time or Time zone	
			Construction volume per hour (Calculated by combining other data)		
	Leveling/adjusting work (cost considerations)	Pile up, landslide, procurable number	Limit machine number	Numerical valeu (Number)	When starting work or work planning
			Available days/days	Date	
			Available time/number of hours	Time or Time zone	
			Construction volume per hour (Calculated by combining other data)		
	Workable time for each area	Securing land, constraints on construction plans	Available days/days	Date	When starting work or work planning
	Workable time constraint	Subdivided according to season, neighborhood, soil disposal conditions, etc.	Available time/number of hours	Time or Time zone	When starting work or work planning
	Secure work space (area)	Separation of heavy equipment that can ensure safety	Machines selected, workload, construction days (process)	Days	When starting work or work planning
			Area of each work area	Area	
	Sky height limit	Overhead line, etc.	Sky height limit	Numerical value(m)、Latitude/Longitude/Elevation	When starting work or work planning
	Construction management standard value data	Quality control, performance control, test/attendance frequency, etc.	Quality control		When starting work or work planning
			Finiish form management		
			test/attendance frequency, etc.		
	Safety management data	Loadable weight of transport machine	Loadable weight of transport machine	Numerical value(%)	When starting work
	Adopting ICT construction equipment construction	3D groundbreaking survey	Organization of construction machinery and surveying equipment to be introduced locally	Text	
		ICT construction machinery		Text	
		3D survey management		Text	
		Others		-	
	Ground improvement	Method	Ground improvement or not	1/0	When confirmed
	Local Soil improvement	Required specifications, materials used, amount added, machinery	Local soil improvement or not	1/0	When confirmed
	Bring-in Soil improvement		Bring-in soil improvement or not	1/0	When confirmed
	Designated construction period		Economic process, last-minute process	Text	
	Limited cost		Limited cost	Text	
	Machines designated for use		Limited Machine for use	Text	

3.3 Survey of technologies for acquisition of basic information (terrain shape data)

The following is the technology for acquiring topographic shapes, which was verified on-site at this time. The description in parentheses at the end is a description of the applied site. The site will be described later.

- UAV photogrammetry (Site A)
- 3D laser scanner (Site B (terrestrial),Site C (with UAV))
- Location history of construction machine work device (Site A, B, C)

These techniques have come to be used for surveys before construction starts and finished work measurements in MLIT ordering work.

The purpose of this survey was to understand the following facts.

- Actual measurement technology that can be used according to site conditions
- Available data area for each measurement technology
- Possibility of extracting topographical shape changes from those data

The field survey was conducted at three sites. The site outline, equipment used, and measurement data are shown.

① Site-A (Figure 3)

At Site A, UAV photogrammetry (about twice a day) and working equipment position history of construction machinery (real time) were used. These are assumed to be the most basic (Figure 4).

The data from the working device position history of the construction machine is, for example, information regarding the history of the blade edge position of the bucket of the hydraulic excavator. The data obtained here is a collection of data on the bottom surface in each range separated by a mesh of a certain size when a series of work is completed at a certain fixed position. In other words, you can acquire and record as data even the breaks for each setup. Utilization of work device position history data seems to be a useful method for grasping work setup.

② Site-B (Figure 5)

From the trial survey at the site A, the usefulness of the working device position history data was confirmed in the scene of utilizing the terrain shape data for grasping the construction execution setup, but at the site B, the problem was also confirmed.

At Site B, it was a site where a steep hill was cut. In order to efficiently carry out the work of loading cut soil into the dump truck to transport the cut soil off-site, the construction company at this site uses the temporarily formed slope for the slope and pushes down the soil to the loading point.

The shape of the pushed-down clod cannot be grasped from the work equipment position history data of construction machinery, so it was necessary to directly measure the terrain

■Site A

Work Type	Embankment widening (River)
Work Outline	Embankment using earth and sand from outside
Machine Configuration	ICT Excavator, ICT Bulldozer, Excavator (normal)
Constructor	Matsuura Construction company (Saitama-pref)
Collaborator	Komatsu Customer Support

Figure 3. Site-A Outline of construction and measure

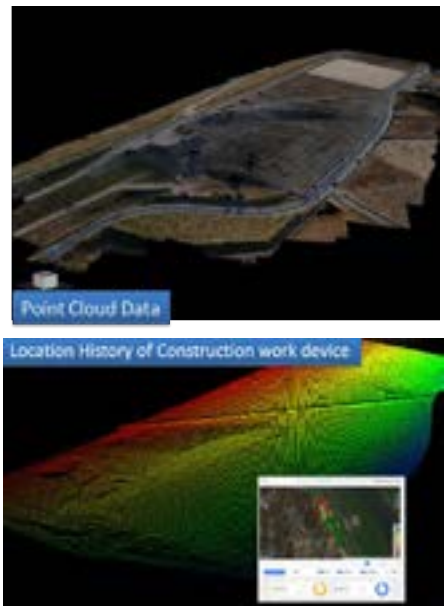

Figure 4. Comparison of point cloud by UAV photogrammetry and Location history of construction work device in Site-A

using UAV photogrammetry or a 3D laser scanner in order to perform this measurement. (Figure 6)

What was even more difficult at this site was the fact that there were roads with heavy traffic in the surroundings and the strong winds made it desirable to refrain from flying UAVs. Therefore, TLS (terrestrial Laser scanner) was used to obtain the topographical shape data.

It took a great deal of effort to change the installation position of the equipment at the site where the height difference was large, and the number of measurements was limited to 4 times per day. (It should be noted that the measurement operators commented that they do not want to carry out such measurements in the future.)

At such sites, it is considered effective to use construction machine-mounted camera images, acquired data from laser scanners, and stationary bird's-eye view camera image data to acquire site conditions.

■Site B

Work Type	Excavation, slope shaping
Work Outline	Excavation of hills, removal of sediment
Machine Configu -ration	ICT Excavator, ICT Bulldozer, Excavator (normal):2
Constru- ctor	Fukuue industry (Kagoshima pref)
Collabor -ator	Sitech Japan, Nippon Caterpillar

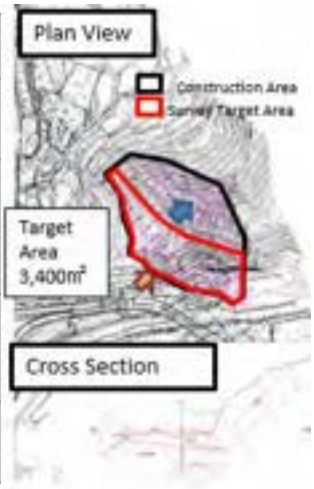

Figure 5. Site-B Outline of construction and measure

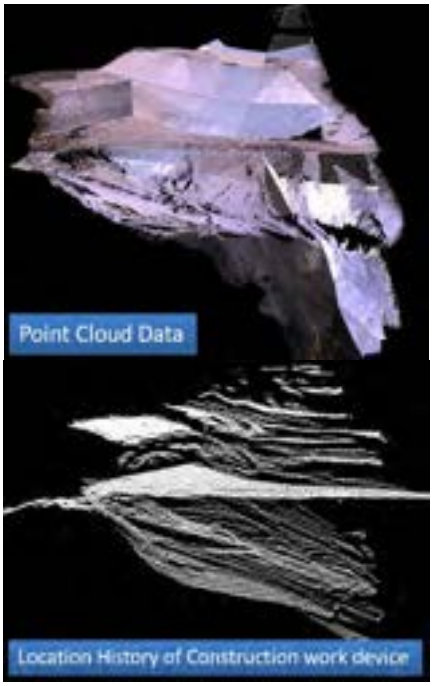

Figure 6. Comparison of point cloud by TLS and Location history of construction work device

③Site-C (Figure 7)

At Site C, we tried to obtain topographical shape data using a 3DLS with UAV. Unlike UAV photogrammetry, it was possible to obtain precise topographical shape data, but it cost about 8 million yen during the survey period. At present, it is difficult to use it from the viewpoint of application of grasping the construction progress. We would like to keep an eye on future technological trends.

Work Type	Road Embankment
Work Outline	Cut, Carry/Dump, Level and compaction
Machine Configu -ration	ICT Excavator, ICT Bulldozer, Articulate Dump(normal)
Constru- ctor	Choho construction(N agano pref)
Collabor -ator	Kobayashi consultant

Figure 7. Site-C Outlines(upper) and Point cloud by LS with UAV

3.4 Survey on the actual status of data recording the progress of daily construction excluding topographical shape data

In grasping the construction execution setup, we investigated the existence of data that can be utilized to confirm from what viewpoint the site decided the machine selection and construction execution setup.

Although daily construction reports are prepared on site, it was confirmed that most of the sites are managed by handwritten or PC text information (Figure 8).

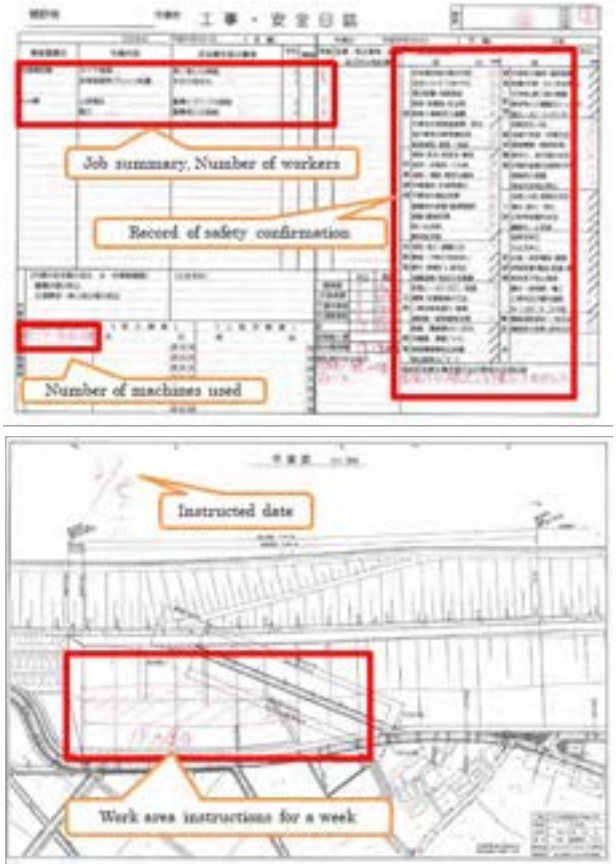

Figure 8. Examples of collected daily reports (upper) and construction instructions (under)

In many cases, the status of safety measures and quality control data are managed by inputting them in files of different styles such as Word and Excel. It is expected to utilize a platform that can handle these data.

System services have been started to centrally provide on-site construction management work, but their use is not yet widespread.

As one of the causes, it is assumed that it is due to the business practice when carrying out the construction work of the construction industry in Japan.

In Japan, the construction contractor, which is the main contractor, works with several companies that do the actual construction work. Also, the combination changes for each individual construction.

As a result, manual data entry can be efficient if different companies use different systems. It is expected that the system side will focus on this point.

3.5 Study on data structure and format of time series change information of construction site collected as record data of construction execution setup

It has been pointed out that the voxel format is useful as a display format of useful topographical shape data in planning the construction execution setup and grasping the progress of the construction.

These papers point out the significance of the following points when performing earthwork with hydraulic excavators and bulldozers [6]-[7].

- Whether the heavy equipment can be moved to the work location
- When planning work, the work volume can be easily grasped by grasping the work in voxel units.
- It is also possible to link quality information such as the material information of the voxel and the degree of compaction.

A further analogy is that when the construction procedure is reproduced later, it is possible to grasp the construction order by associating the starting order of each voxel.

An example of handling data in Voxel is analysis data by CT scan in the medical field. In CT scanning, X-rays are first applied to a fixed human body from various directions, and light is received on the opposite side to obtain transmitted X-ray data. Based on these data, we divide the body into each voxel, construct a simultaneous equation with the transparency of each voxel as a variable, and solve it. In this way, it is a technology that visualizes the internal conditions in three dimensions.

Technology is also being developed to convert the actual patient body data stored in voxel format for the surgery simulator. This has already been used in pre-surgical simulations at medical institutions in Japan [8].

Data retention in Voxel format may contribute to the application of these technologies to the construction side.

It is considered to be useful based on past research and precedents in other fields by converting the acquired topographic shape data into voxels and adding the necessary attributes.

3.6 Trial of data display in voxel display

Using the point cloud data acquired in 3.2, a trial of voxel modeling of the terrain shape was performed.

The voxel model referred to here is a representation of the terrain shape with a set of cubes. Each cube has x, y, z coordinates and is assigned a unique ID. In addition, the side length of a cube can be determined arbitrarily, so it is possible to reproduce terrains of various shapes.

Since this model is created based on the topographic surface data using 3D survey data, it has the feature that a rough ground shape can be visually grasped by the ground model.

Voxels are created by comparing the closest point cloud data with respect to the reference point cloud data and calculating the difference.

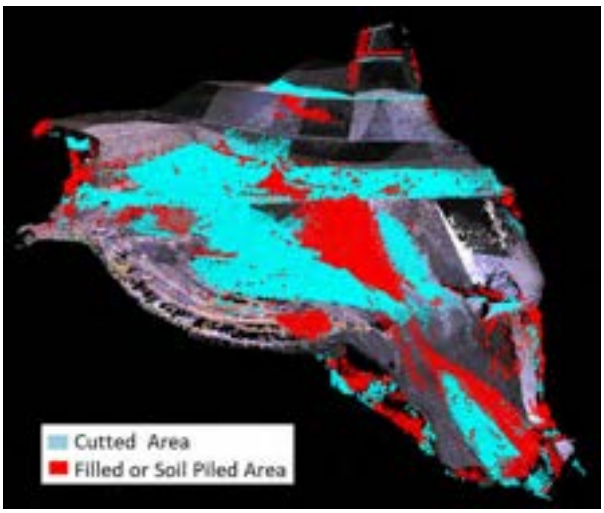

Figure 9. Change amount displayed as voxel on the point cloud data in Site-B

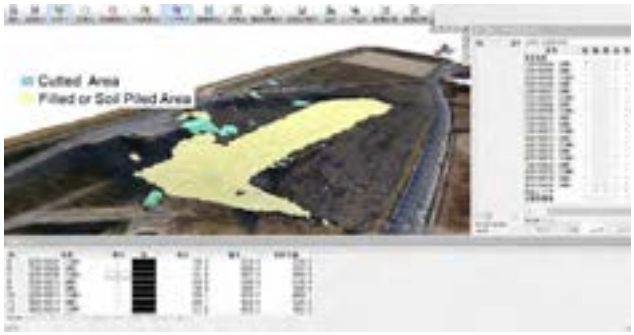

Figure 10. Change amount displayed as voxel on the point cloud data in Site-A

Figure 11. Continuous display of earthwork amount for each day in Site-A

Since software that has the function of changing the mesh width and height of voxels was used, it can be expressed as a cube or a rectangle.

In general, the voxel calculation method can be a one-point method, a four-point average method, a four-point columnar method, a topographic model (TIN) method, or the like. This time, the voxel has a specification that occurs when the difference volume exceeds 1/2 of the voxel volume, and the following method is adopted.

- Mesh width and height: 50 cm Output with voxels on all sides
- Voxel calculation method: 1 point method

By displaying the voxel data overlaid on the point cloud data, it can be seen that the construction part can be effectively extracted (Figure 9, 10).

In addition, the following is displayed separately for each lapse of time (Figure 11).

3.7 Additional discussion on the voxel size and data retention format based on the knowledge obtained from the exchange of opinions with a mechanical earthmoving company for the use of time-series change information at construction sites

Additional discussion on the voxel size and data retention format based on the knowledge obtained from the exchange of opinions with a mechanical earthmoving company for the use of time-series change information at construction sites

We presented these voxel modeled data and asked the construction company that specializes in mechanical earthworks to utilize the time-series change information of construction sites. As a result, the following points were received.

Table 2. Main opinions from earthmoving constructors

	Opinion content
1	I think expressing in voxels is good because attributes can be associated. It is important to consider how the surface water flows. (This is also a provision of MLIT)
2	As earthwork companies, the construction cost is not the best construction plan. In the face of various market constraints, we are planning to make sure that the equipment and human resources that can be arranged will be used without waste. It would be good if we could include things such as constraints.
3	If the construction process can be converted into data, it could be used as a basis for explaining the process to the orderer and for understanding the difficulty of the work.

Among the above points, from the viewpoint of the examination of the voxel model, the point that we should emphasize is that it corresponds to the provision of the inclination angle for drainage regarding the surface finish of earthwork during construction execution setup.

Based on this recognition, the factors affecting the topographical shape were extracted from the precautions for earthwork described in the construction standard specifications, which are applied to the construction ordered by MLIT (Table 3).

Table 3. Main provisions in MLIT specifications related to earthwork topography

Provision Name	Provision Content
1-2-3-3 Embankment	
2. Prevention of embankment sliding	When the embankment is carried out on the ground with the slope steeper than 1: 4, the flat step cutting (minimum width and height are 1.0m and 0.5m) must be carried out, and the embankment and the site board must be closely adhered to prevent the slide, except for the case where the instruction is given.
3. Finished layer thickness	In embankment construction, the finished thickness should be 30 cm or less and compacted flat.
6. Wastewater treatment at the end of work	When the contractor finishes the embankment work or interrupts the work, the contractor must provide a cross slope of about 4% on the surface and compact it evenly to ensure good drainage.

In order to be able to confirm these provisions or regulations with the voxel model, it is necessary to study the size of the voxel. Based on sampling theory, we need to be able to extract less than half the size of the observed object.

It may be necessary to display in a size different from the vertical and horizontal directions, such as 0.5 m or less in the vertical and horizontal directions and 0.15 m or 0.1 m or less in the depth direction, in order to address all of the points pointed out.

When utilizing time series change information at the construction site for accountability to the orderer, it is necessary to consider not only the display format of these data but also the data retention format of the actual voxel model.

Although it is a voxel model, the actual data format may also have a practical idea of having coordinate data of the center point of each voxel and linking the data to it.

The discussion on this point requires further study by grasping the following trends.

- Initiatives for intelligent compaction at FHWA
- Data handling cases in other fields (compared with data capacity from hand rig cases on a computer for large amounts of data)

4 Conclusion

The following findings were obtained in this research.

- Efforts to automate construction work plan of construction machinery will hold the key to the realization of automatic construction in the future.
- To realize the construction work plan of construction machinery support AI, construction history information as learning data is required.
- Construction history information consists of basic time-series data of topographical shape data, quality relations associated with it, and construction constraint data.
- The usefulness of the voxel format as a data display or data storage format.
- Through the trial of voxel display and the exchange of opinions with practitioners based on it, it is necessary to set the voxel size up to 0.5 m in width and height and 0.15 or 0.1 m in height direction along with the effectiveness of the point cloud data.
- Further investigation of data handling precedents in other fields such as consistency with similar efforts in other countries and medical care is effective.

References

[1] Ministry of Land, Infrastructure, Transport and Tourism. Actions toward full utilization of ICT. On-line: https://www.mlit.go.jp/common/001248775.pdf, Accessed: 18/06/2020.

[2] Ministry of Land, Infrastructure, Transport and Tourism. Actions for expanding the spread of ICT construction. On-line: https://www.mlit.go.jp/common/001303213.pdf, Accessed: 18/06/2020.

[3] TOPCON. Machine control system. On-line: https://www.topcon.co.jp/en/positioning/products/product/mc/, Accessed: 18/06/2020.

[4] KAJIMA Corporation: KAJIMA A4CSEL, Kajima Integrated Report 2019, p41, 2020.

[5] N. Okamoto: Construction plan for machine earthwork by a specialized contractor (Japanese), Construction machinery construction, Vol.65 No.9 September 2013

[6] I. Kobayashi, N. Takemoto, A. Takao, H. Yamane, U. Hoshino: Application of Geological Cube Model for the first stage of land design (Japanese), Journal of Civil engineering information utilization technology (JSCE), vol. 18, 10/2009.

[7] Y. Shiiba, S. Ogata, I. Kobayashi, T. Yamanaka: A Proposal on Usage and Application of Data Acquired on the Construction Stage of Construction Management, Proceedings of the First International Conference on Civil and Building Engineering Informatics (ICCBEI 2013）, pp.485-492, 11/2013.

[8] M. Ogata, M. Nagasaka, T. Inui, H. Sakamoto, K. Takanami, K. Yokoyama, Y. Kubota: A Surgical Simulator for Training of Operative Skill Using Patient-specific Data, IPSJ Journal, Vol.53, No.1, pp.421-431, 15/1/2012.

Energy Performance and LCA-driven Computational Design Methodology for Integrating Modular Construction in Adaptation of Concrete Residential Towers in Cold Climates

Sheida Shahi[a], Patryk Wozniczka[b], Tristan Truyens[b], Ian Trudeau[b], Carl Haas[a]

[a]Department of Civil and Environmental Engineering, University of Waterloo, Canada
[b]Entuitive Consulting Engineers, Canada
E-mail: sshahi@uwaterloo.ca, patryk.wozniczka@entuitive.com, tristan.truyens@entuitive.com, ian.trudeau@entuitive.com, chaas@uwaterloo.ca

Abstract –

Adaptation of dated residential towers is an urgent issue due to aging housing infrastructure and growing demand for affordable housing. Computational design methodologies have the potential for facilitating optimized design strategies driven by improved energy performance and reduced life-cycle carbon emissions. Modular Construction (MC) can also increase efficiencies in the design and implementation of building adaptation projects and minimize construction waste. The application of MC in the adaptation of existing buildings is gaining interest with improvements to MC technologies and processes, as well as large-scale adoption. There are currently no frameworks for the integration of MC in the adaptation of complex buildings driven by energy performance and Life Cycle Analysis (LCA). To address this gap, a framework is developed for integrating computational design methodologies and design optimization using energy use and LCA for improving overall building adaptation processes. The building adaptation of Ken Soble Tower in Hamilton, Ontario, is used for the functional demonstration. A set of extension modules are considered, and various adaptation scenarios that conform to set design constraints are evaluated for energy use and LCA. The results of this study prove the practicality of using computational design methodologies for the integration of MC in the adaptation of concrete residential towers and can promote the efficiency of improving existing residential infrastructure.

Keywords –

Computational Design; Modular Construction; Life Cycle Analysis; Building Adaptation

1 Introduction

There is a need for the reconsideration of our status-quo linear approach of design and construction with the inevitable end-of-life option of demolition. Adaptation of existing buildings and infrastructure has increased over the past decade as a response to changing environmental conditions, as well as requirements for reducing energy use and production of construction and demolition waste [1]. For a shift to a circular built environment, there is a need to consider building adaptation, including reuse of buildings and materials, with a focus on modularity, disassembly as a means to facilitate continual loops of resources, products and materials in construction [2]. Modular construction facilitates maintenance, repair and reuse during different life cycle stages of a building and minimizes waste generation during construction and deconstruction [3]. Incorporating modular construction strategies in building adaptation projects, specifically modular extensions to existing buildings can improve the condition of an existing building while preparing it for a circular future in which unnecessary demolition is avoided, and the building modules and materials can enter multiple cycles of use.

The success of modular building projects is directly related to appropriate early decision-making due to the planning and coordination focused nature of modular projects. Morphological and modular form generation is improved by environmental performance feedback in an automated design process [4]. Through early design stage optimization, Kiss and Szalay were able to demonstrate

environmental savings of 60-80% compared to traditional design methods. Life Cycle Assessment (LCA) is an essential factor in evaluating the potential environmental impact of buildings. Design option optimization often considers a limited number of options [5], highlighting the need to consider generative design options and evaluation methods for correct optimization of multiple factors simultaneously. An early-stage design optimization tool for modular extension to existing buildings needs to consider energy performance, life cycle analysis, as well as the design considerations of modular building extensions. This research presents a framework for integrating performance optimization in Modular Construction (MC) for the application of building adaptation projects. The critical aspect of the proposed model is the integration of computational design strategies for simultaneous analysis of MC metrics, energy analysis and life cycle analysis. The Ken Soble Tower retrofitting project in Hamilton, Canada is used as a functional demonstration of the proposed framework.

2 Background

In a traditional building adaptive reuse feasibility and early design process, many uncertain factors need to be taken into consideration. The client's inputs, including project requirements, budget and timeline, are taken into account as well as an analysis of the existing conditions of the building, including building geometry, overall status and areas for improvement. The client information and analysis are processed by the design team to develop design options, to be analyzed by consultants, including energy consultants, LCA consultants and cost consultants. Feedback from consultants is looped back to the design team, and design options are revised intermittently and shared with the client for feedback. This cycle may repeat many times over many months to arrive at possible suitable, non-optimized design options at best.

Compared to traditionally constructed concrete buildings, prefabricated modular construction can reduce environmental impacts, increase on-site productivity and construction quality [6]. Jallion et al. (2009) demonstrated that prefabrication in controlled factory environments has been shown to reduce construction waste by 52 % [7], and reported by other researchers to range typically between 10-15% [8]. Effective assembly of prefabricated modular units can also improve on-site construction conditions, including reduced construction pollution, noise and occupant disruptions, making it an ideal strategy for dealing with occupied existing buildings and urban areas [9]. MC integrates modular design with prefabrication and Design for Manufacture and Assembly (DfMA) [10]. A great potential in quality and productivity is in prefabrication and modularization of buildings and their components [11]. There are multiple levels of modular construction identifies including 1) Components and sub-assemblies (i.e. millwork, fixtures, etc.), 2) Panelling Systems (i.e. exterior cladding), 3) Volumetric Pre-fabricated assembly (i.e. kitchen and bathroom pods), and 4) Pre-fabricated modular units, incorporating complex systems of assembly used in combination to form an entire building [3], [12]. This research focuses on the application of modular units as a complete prefabricated unit ready for assembly.

The current strategies for the design of prefabricated buildings are similar in many ways to the design system common in traditional construction. The design of prefabricated buildings is a systematic process, including considerations in design, manufacture and assembly. The design process for conventional construction does not consider methods and principles for addressing the manufacturing process involved in prefabricated buildings [6]. The design process and precisely, decisions made in the first 10% of projects determine up to 80% of the building operation costs after construction [13]. As MC relies heavily on design accuracy due to the coordination focused nature of their process, the success of a modular project is directly related to appropriate early design decision-making.

Environmental design optimization is the process of considering and evaluating alternatives in the design phase that impact the overall performance of a design. Energy use and LCA are important factors in evaluating the success of a design strategy and the potential environmental impacts of a building. They can be considered adequately in the early stages of design. Parametric and generative design environments also enable optimization of building geometry, allowing the designers to test design variation with immediate building performance feedback [4]. The consideration of multiple factors including cost, energy and life-cycle performance has become common in the past decade in early-stage design. Granadeiro et al. integrate early design stage automation of building envelope design with energy simulation using grammars [14]. Yu et al. used genetic algorithms and design structure matrix (DSM) to support automated spatial organization in the early stages of design [15].

Modular construction has proven advantages in terms of LCA and LCC compared to traditional construction and can contribute to more energy-efficient buildings through the improved quality of construction [16]. Form generation is improved by environmental performance feedback in an automated design process [4]. Despite this, there are currently no studies highlighting a framework for the integration of early-stage design optimization of energy use, LCA for MC, specifically for large-scale building adaptation projects. Energy use and LCA

optimization can be applied using a parametric tool with geometry represented mathematically or as topologies [17] in combination with the application of MC design parameters to design building adaptation scenarios that meet the requirements of modular construction, as well as optimization of environmental metrics.

3 Computational Design Framework

The proposed framework is developed in three stages to integrate a computational design methodology as well as energy and life cycle performance optimizations in MC design processes for building adaptation projects: 1) analysis and parametrization of the existing building, 2) design option generation and simulation and 3) result refinement and optimization. Stage one requires manual work and processing from the user and project designers in processing the existing building and defining parameters. Through a step-by-step analysis of the building, development of design constraints and processing of user inputs, precise design constraints and rules are developed for algorithm input. In the second stage, the developed algorithm generates and analyzes design options for energy use and life cycle performance. Design options that meet the set criteria are displayed in stage three. The framework enables the user to input preferences regarding the generated options, beyond which the algorithm will optimize the options for the defined factors. After optimization, the user can parse through the optimized options and select the most suitable. This framework suggests possibilities for the incorporation of external databases and previously analyzed cases for the development of databases of all feasible solutions leading to a predictive model of performance feeding the results, to be investigated at a later stage of this work. The last two stages of the framework are fully automated and can be processed in real-time (Figure 4).

The developed computational framework is differentiated by geometric simplicity, integration of automated processes and simulation tools and processing of direct manual user input in various stages. Existing computational interfaces, plugins and frameworks are being used in the development of a cohesive tool that integrates existing resources and facilitates integration. The generative design tool is programmed using Grasshopper® visual programming interface and plugins are used within the interface for energy use simulations and optimization. One-Click LCA® is used for preliminary life cycle emission calculations. Future development of the framework will involve the incorporation of external databases and analytical cases, creating a database of feasible solutions over time and developing predictive algorithms (Figure 4).

The Ken Soble Tower in Hamilton, Canada, is selected as a functional demonstration and will be used to demonstrate the functionality of the framework in various stages.

3.1 Stage 1 – Analysis and Parametrization of Existing Building

The first stage in the framework is focused on the analysis of the existing building and parameterization, as well as the development of design constraints. The design constraints are developed by processing the existing building information, defining design parameters and determining user inputs and requirements. Design parameters are defined based on analysis of the existing building, existing site conditions, and planning requirements and restrictions. Design input including adaptation strategies to be considered, such as the extension of the building, recladding of the envelope, re-glazing of the windows and enclosing of existing balconies. In this research, the extension strategy is investigated in the functional demonstration of the Ken Soble Tower.

In the first phase of stage 1, the existing building drawings are analyzed, and the geometry of the existing building, including interior spaces and the building envelope, are modelled. The existing structure is analyzed to determine required design parameters, including structural, environmental and spatial shortcomings of the existing building. The existing building is modelled as zones (Breps) and aggregated into topological complexes. The building geometry is further discretized into panels and elements at the discretion of the project designer.

For efficient MC design, the least number of module variants are required. Development of design constraints early in the process, such as a speculative grid for modular design, will limit the dimensionality of the design problem leading to a heuristic approach and increased accuracy of design options generated. For building an extension, recladding and addition, for example, the following steps are required: 1) building parameters defining modular extension parameters; 2) module parameters including spatial configurations, connection parameters, and growth patterns and restrictions; 3) panel parameters including dimensions of panel divisions, the spatial organization of panels and connection details. To acquire this information, the existing building geometry is analyzed in terms of dimensional and spatial constraints for the extension, and the dimensions of a typical module are determined (**Figure 1**). The typical module dimension and the spatial analysis lead to the determination of rules for “growth.” Figure 1 demonstrates the points of “growth”, and the direction of permitted extension determined by the designer. At the level of the determined module size, panels are broken down and analyzed in terms of joining

conditions that include: 1) attachment of new module to the existing building (*e*), 2) connection of two modules together (*c*) and 3) exterior façade (*f*). Through multiple design exercises, the number of required panel divisions for each panel, panels *a* and *b* are determined for each condition of *e*, *c* and *f*. In the case of the Ken Soble Tower project, the variation of module connections lead to 16 different possible configurations of *e*, *c* and *f* for panel *a,* seven different possible configurations of *e*, *c* and *f* for panel *b* as demonstrated in Table 1. The 23 different panel possibilities result in a total of 22 possible module configurations.

As part of the existing building analysis, the LCA of the existing building is determined considering the existing operational energy use standards. After the modules and panels are determined, use the material take-offs and calculate the life cycle impact, not accounting for energy use for each of the modules separately using One-Click LCA. The combination of these modules will be used in the algorithm to determine the LCA of the combined design options in real-time.

A user input interface using Human UI® for GH® takes into account the preferences of the user regarding various aspects, including budget, number of preferred units, unit size variations, balconies and window placements, etc. An integrated user interface allows for changing initial conditions and input values, selecting modes and paradigms of operation, and integration of user selection and manual search for solutions. User interface – using Human UI® depending on the skill level of a prospective user, one can use Human UI® only or start manipulating the GH® scripts that are part of the framework. The user in our framework is defined as the designer, modeller or client evaluating building adaptation strategies. In our framework, the user can input preferences, review and parse through results and to reconfigure preferences based on project data in real-time. The user inputs and requirements include constraints for the extension, number of additional units required, number of bedrooms per unit and unit square footage as well as environmental goals, including energy efficiency and carbon targets. The building analysis results combined with the input parameters are used to feed the developed algorithm for option generation. The building inputs and analysis, as well as design and user inputs, are combined to create a detailed breakdown of the design constraints (B-3) for the development of the algorithm.

3.2 Stage 2 - Option Generation and Simulation

After defining geometry and selecting strategies, a virtual grid of speculative possibilities is computed. The developed algorithm generates adaptive design options by positioning modules and assigning states based on the information stored in the grid, previously determined in stage 1. The design options are generated using the developed algorithm within GH and Topologic is used to track changes in their topological structure.

Topologic® is a software modelling library enabling hierarchical and topological spatial representations through non-manifold topology [18]. Existing geometry is modelled as Breps (directly modelled or extruded from existing drawings) and then fed as input to the module translating Rhino® 3D Brep object to topologic cells, organizing them and forming topologic complexes. The set of options is generated through a brute force search, being finite and relatively small, allowing for computation and comparison of all the possible options. A topological structure with cells governs the distribution of modules and assignment of states. The generated design options will then be analyzed for energy use and life cycle carbon simultaneously.

The net environmental impacts for each building adaptation design option consider the LCA of the existing building and consideration of the extension of life by 60 years through building adaptation. The LCA of modules and the existing building are calculated in line with EN 15978:2011 standards [19] for LCA Modules A1 to Module D. The energy use of each compiled design option is calculated inside GH® in real-time, using the Honeybee® plugin. Honeybee® supports thermodynamic modelling and creates, runs and visualizes the results of energy models using EnergyPlus® and OpenStudio® simulation engines. The number of extension modules is calculated in Grasshopper® in real-time and calculated using the pre-calculated LCA of each module from stage 1 using the following formula (1):

$$E_{total} = E_i[kgCO_2e] + \sum_M n_M\, E_M\, [kgCO_2e] + U_{total}[kWh](U_{factor}[CO_2e/kWh]) \quad (1)$$

Where E_{total} is total carbon emissions including operational energy use, E_i is the carbon emission of the existing building excluding operational energy use, n is the number modules per module type in each design option, M is the type of module used in the design option, E_M is the emission of type M module excluding operational energy use, U_{total} is the total energy use of the building including existing and extension modules, and U_{factor} is the local emission factor.

3.3 Stage 3 – Result Refinement and Optimization

The results of option generation and simulation is visualized using the Human UI® interface in

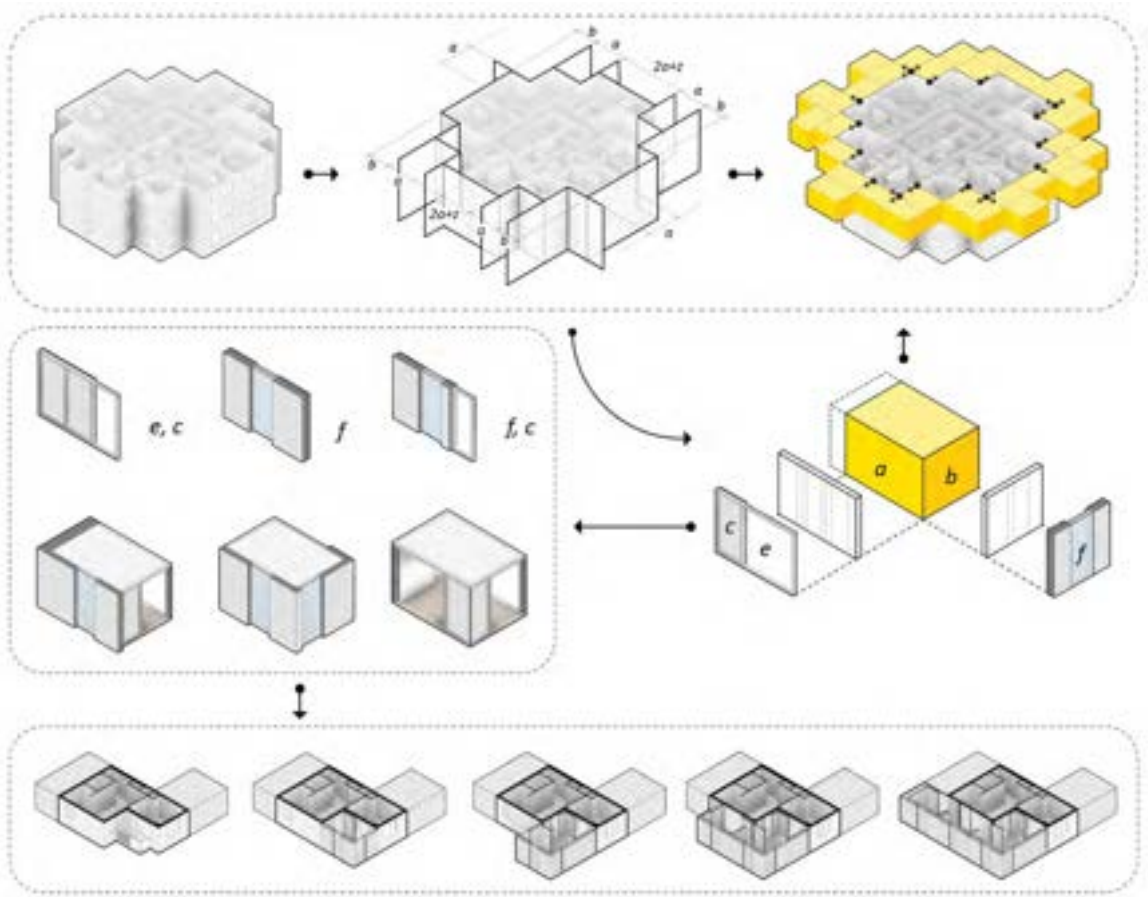

Figure 1. Stage 1 – Parametrization of existing building, determining typical module sizes and panelling configurations, determining possible growth patterns, finalizing module dimensions, and module configurations, determining various module extension options for each existing unit.

Grasshopper®, through which the user can manually review all the generated and evaluated options and refine the search for the most viable option via sliders limiting the scope of the search. After initial refinement user may choose to run a genetic algorithm and optimize further using the selected option as an initial population. The results can be optimized using multi-objective optimization searching for optimal extensions and materials used, based on performance (R-Value), cost or emissions, and refine the distribution of modules.

Octopus®, a multi-objective evolutionary optimization engine, is used within Grasshopper® for optimization of results in stage 3. It allows the search for many goals at once, producing a range of optimized trade-off solutions between the extremes of each target. Octopus® within Grasshopper® is used to optimize material qualities of modules' envelope exploring trade-offs between energy performance and embodied carbon.

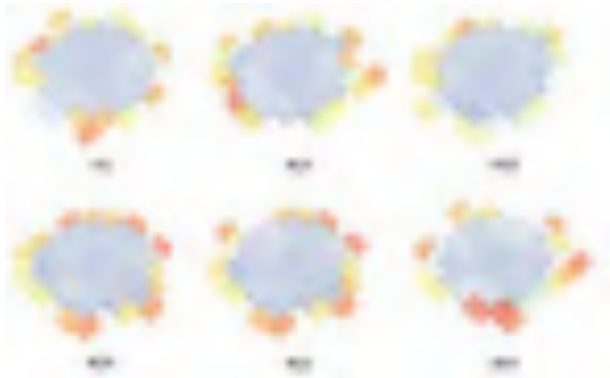

Figure 2. Typical floor plate demonstration of generated design options 1, 14, 16, 97, 24 and 26.

After a predefined amount of iterations of option generations, results are again displayed, and the user can make their final choice and export geometry and data to a predefined format.

From the 100 design option permutations, six designs demonstrate a range of arrangements for a 20-module extension. Figure 2 is a typical floor plate demonstration of the six generated options. Design options 1, 14 and 16 demonstrate similar performance in terms of energy use and LCA. For a 20-module extension, through the generative computational design approach, an 8% saving

of heating energy use and 5% of life cycle carbon emissions was achieved. Design 24 and 26 are similar in overall form. Still, the clustering of modules on one side of option 26, and the resulting reduction in the exposed building envelope, results in option 26 outperforming option 24 by 1,895 kWh of heating energy and 10,619 KgCo2e equivalent of carbon emissions (Figure 3).

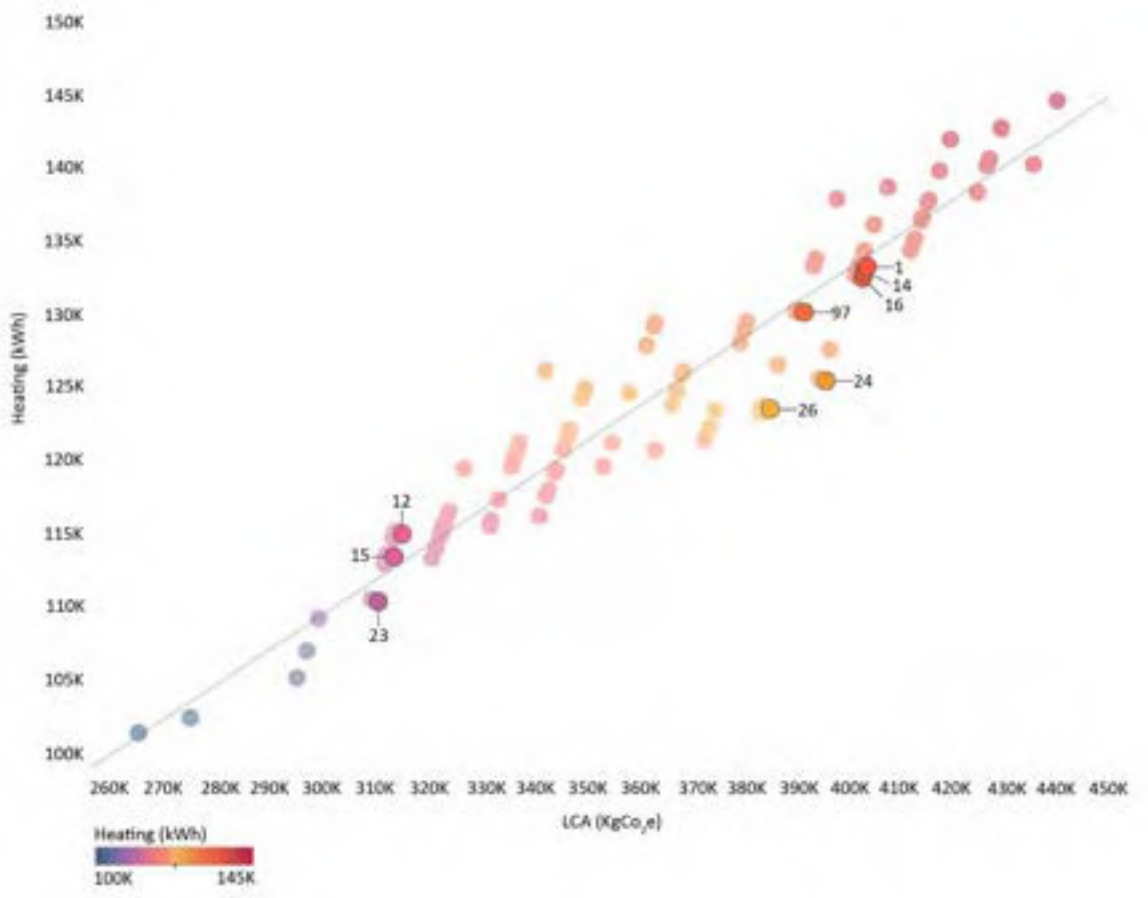

Figure 3. LCA (KgCo2e) and heating energy use (kWh) for 100 design option permutations. Design options are filtered by area of extension – Options 1, 14, 16, 97, 24, 26: 20 module extension (206 m^2) and Options 12, 15, 23: 13 module extension (134 m^2).

4 Conclusion

Adoption of modular construction in building adaptation projects, specifically in extensions to existing buildings, is an essential step in a move to a circular built environment and facilitating the continual use of resources in construction. Parameters and limitations in modular design and the opportunity for design optimization, highlight the importance of incorporating computational design tools in the design of modular buildings. In this paper, a framework is presented for a computational design methodology integrating modular construction in building adaptation projects, while optimizing for energy performance and life cycle impact. The proposed framework is divided into the three stages of analysis and parametrization of the existing building, option generation and simulation and result refinement and optimization. An existing concrete residential building in Hamilton, Canada is used as a functional demonstration of stages one, two and part of stage three of the framework. In stage one, the existing building is analyzed, and a single module size is selected for the extension to the existing building. A grid is developed using rules for module placement, in consideration of the existing building form, interior layouts and required building setbacks. As a result, a growth pattern for the building is determined. The selected module size is broken down into various panelling options that accommodate different module configurations.

An algorithm is developed to generate floor plate module configurations based on the set rules. The energy use and LCA of each design configuration are calculated

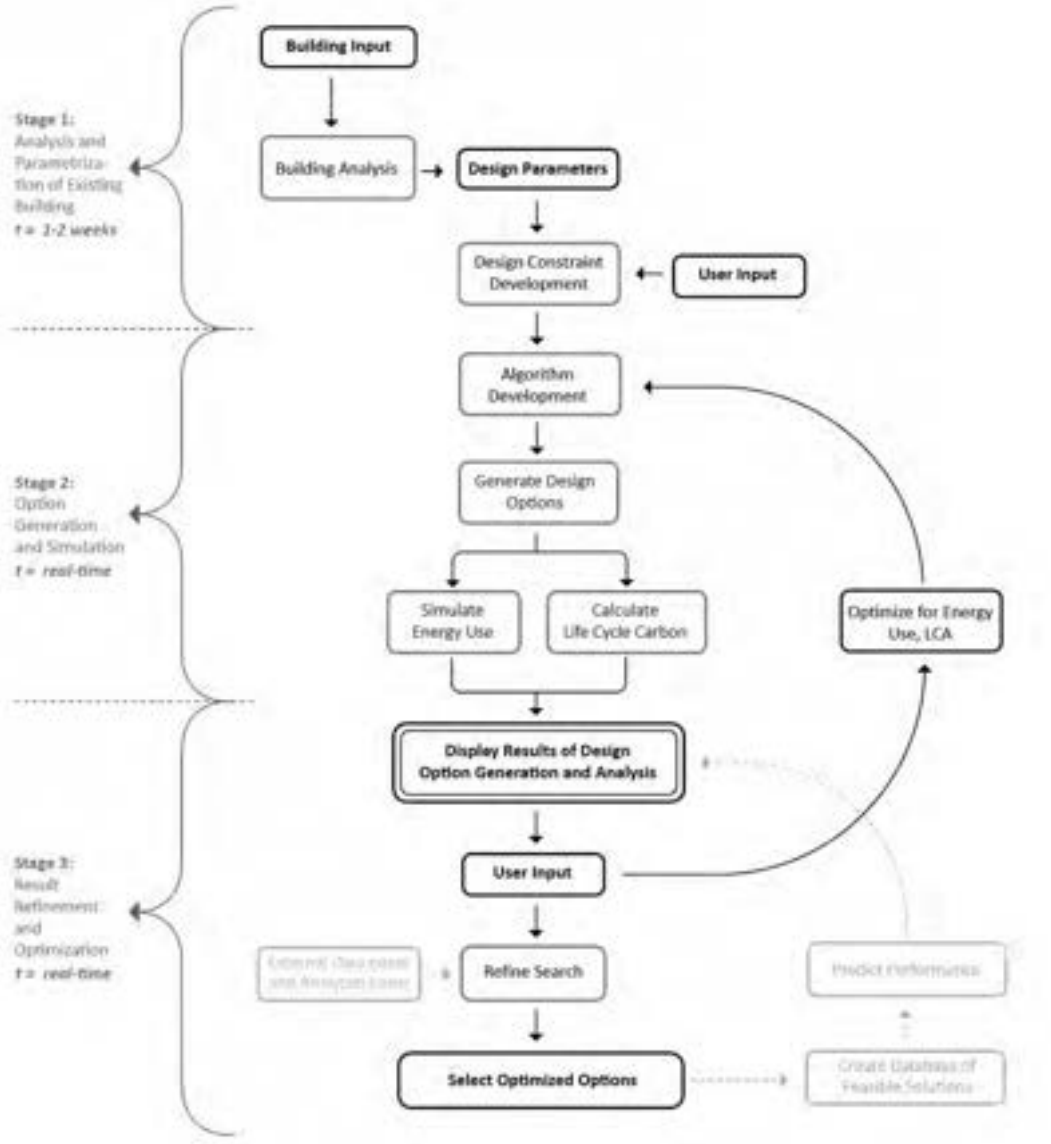

Figure 4. Proposed Computational Design Framework. Framework is separated into the three stages of analysis and parametrization of the existing building, option generation and simulation and result refinement and optimization (the greyed-out portions of the framework are not considered in the functional demonstration and will be pursued in future stages of this work).

simultaneously. A result of 100 permutations ranging from extension of 10 to 20 modules demonstrate the possibility to optimize design option configurations.

The limitations of this research include the exclusion of construction and Life Cycle Cost (LCC) and other environmental factors, such as daylighting, from the optimization model. It is expected that LCC will have a significant impact on design option optimization, and including other environmental factors as part of simulations in stage 2, can increase the quality of generated design options. The design permutations for this research were limited to 100 permutations due to computing limitations. Generating a larger pool of permutations for a single design option will increase the quality and reliability of the design process.

The future of this work will focus on addressing the limitations mentioned and on completing the proposed steps in the framework not investigated in this research. Integration of external databases, linking to other analyzed cases, and the creation of an internal database of feasible solutions will enable the integration of predictive algorithms for enhancing the quality of generated design options.

5 Acknowledgments

This research was supported by the University of Waterloo Department Chair's Supplement Fund and Mitacs Accelerate (Grant No. IT10351). The authors would like to thank the Mitacs industry partner, Entuitive Consulting Engineers, for their support.

References

[1] Pardo-Bosch, F., Cervera, C., and Ysa, T., "Key aspects of building retrofitting: Strategizing sustainable cities," *J. Environ. Manage.*, vol. 248, 2019, doi: 10.1016/j.jenvman.2019.07.018.

[2] Stahel, W. R., "The circular economy," *Nature*, vol. 531, no. 7595, p. 435, 2016, doi: 10.1038/531435a.

[3] Wuni, I. Y. and Shen, G. Q., "Barriers to the adoption of modular integrated construction: Systematic review and meta-analysis, integrated conceptual framework, and strategies," *J. Clean. Prod.*, vol. 249, p. 119347, 2020, doi: https://doi.org/10.1016/j.jclepro.2019.119347.

[4] Holzer, D., "Design exploration supported by digital tool ecologies," *Autom. Constr.*, vol. 72, pp. 3–8, 2016.

[5] Kiss, B. and Szalay, Z., "Modular approach to multi-objective environmental optimization of buildings," *Autom. Constr.*, vol. 111, p. 103044, 2020, doi: https://doi.org/10.1016/j.autcon.2019.103044.

[6] Yuan, Z., Sun, C., and Wang, Y., "Design for Manufacture and Assembly-oriented parametric design of prefabricated buildings," *Autom. Constr.*, vol. 88, pp. 13–22, 2018.

[7] Jaillon, L. and Poon, C. S., "Life cycle design and prefabrication in buildings: A review and case studies in Hong Kong," *Autom. Constr.*, vol. 39, pp. 195–202, 2014.

[8] Xu, Z., Zayed, T., and Niu, Y., "Comparative analysis of modular construction practices in mainland China, Hong Kong and Singapore," *J. Clean. Prod.*, vol. 245, p. 118861, 2020, doi: https://doi.org/10.1016/j.jclepro.2019.118861.

[9] Blismas, N., Pasquire, C., and Gibb, A., "Benefit evaluation for off-site production in construction," *Constr. Manag. Econ.*, vol. 24, no. 2, pp. 121–130, Feb. 2006, doi: 10.1080/01446190500184444.

[10] Wuni, I. Y. and Shen, G. Q., "Critical success factors for management of the early stages of prefabricated prefinished volumetric construction project life cycle," *Eng. Constr. Archit. Manag.*, 2020.

[11] Sharafi, P., Samali, B., Ronagh, H., and Ghodrat, M., "Automated spatial design of multi-story modular buildings using a unified matrix method," *Autom. Constr.*, vol. 82, pp. 31–42, 2017.

[12] Gibb, A. and Isack, F., "Re-engineering through pre-assembly: client expectations and drivers," *Build. Res. Inf.*, vol. 31, no. 2, pp. 146–160, Jan. 2003, doi: 10.1080/09613210302000.

[13] Sharafi, P., Mortazavi, M., Samali, B., and Ronagh, H., "Interlocking system for enhancing the integrity of multi-storey modular buildings," *Autom. Constr.*, vol. 85, pp. 263–272, Jan. 2018, doi: 10.1016/J.AUTCON.2017.10.023.

[14] Granadeiro, V., Duarte, J. P., Correia, J. R., and Leal, V. M. S., "Building envelope shape design in early stages of the design process: Integrating architectural design systems and energy simulation," *Autom. Constr.*, vol. 32, pp. 196–209, 2013, doi: 10.1016/j.autcon.2012.12.003.

[15] Yu, T.-L., Yassine, A., and Goldberg, D., "An information theoretic method for developing modular architectures using genetic algorithms," *Res. Eng. Des.*, vol. 18, no. 2, pp. 91–109, 2007, doi: 10.1007/s00163-007-0030-1.

[16] Lawson, R. M., Ogden, R. G., and Bergin, R., "Application of modular construction in high-rise buildings," *J. Archit. Eng.*, vol. 18, no. 2, pp. 148–154, 2012.

[17] Tugilimana, A., Thrall, A. P., Descamps, B., and Coelho, R. F., "Spatial orientation and topology optimization of modular trusses," *Struct. Multidiscip. Optim.*, vol. 55, no. 2, pp. 459–476, 2017, doi: 10.1007/s00158-016-1501-7.

[18] Aish, R., Jabi, W., Lannon, S., Wardhana, N., and Chatzivasileiadi, A., *Topologic: tools to explore architectural topology*. 2018.

[19] Hosseini, M. R., Rameezdeen, R., Chileshe, N., and Lehmann, S., "Reverse logistics in the construction industry," *Waste Management & Research*, vol. 33, no. 6. SAGE Publications, London, England, pp. 499–514, 2015, doi: 10.1177/0734242X15584842.

A View of Construction Science and Robot Technology Implementation

Hiroshi Yamamoto [a]

[a] Komatsu Ltd.，Office of CTO, Japan
E-mail: hiroshi_05_yamamoto@global.komatsu

Abstract –

In this paper, with an aim to contributing to promotion of this field, the author describes his perspective on desirable future situations, and lists his ideas and matters to be taken into consideration in future efforts, focusing on discussions during 2005-2008. Here, the author proposes promotion of design methods in which construction improvement is incorporated in design, and a proposal that machines should be aiming towards substituting human operators in principle.

Keywords –

Construction Science; Construction production engineering; Robot technology,

1 Introduction

In the field of construction production engineering, construction improvements and efforts to utilize robot technology have been continuously ongoing. However, author believes that there is still an urgent demand to make more improvements.

In author's opinion, the basic concept should be to make people working at construction sites happy. For example, currently there are the following challenges in work sites:

1. How can production technology such as those in manufacturing factories be incorporated?
2. A system that allows individual improvements in high-mix, single-item production, "Multi-product one-type construction production technology"; how can they be diverted and reused?
3. Design improvements found from maintenance and construction: how can the result be effectively fed back to design standard?
4. How can we effectively reach the key points of improvement?
5. How can deaths from accidents be reduced?

In this paper, various images, goals, and approaches are proposed, with the aim to promote construction production engineering.

This paper proposes hypotheses that have not yet been verified or is still under verification. This paper does not cover verification of hypotheses.

2 Towards future construction site

If a work method and software can be described, it can be realized. Author's image of desirable future are outlined as follows.

2.1 Image of approach towards future construction site

2.1.1 Pessimistic and optimistic view in work sites

The population in Japan will inevitably decrease; however, the workload demand will not decrease.

A construction site that uses AI and robot technology with a fewer number of people is eagerly sought in work sites. [1]

2.1.2 How to resolve time-consuming and laborious tasks

- "Consistent data sharing from design to maintenance" is one example of good approach There are various types of support to realize this goal.
- By visualizing overall processes, changes in construction plans, adjusting arrangements / procurement for setup changes, and meetings will become much easier.
- Documents are naturally produced as output if the work process is done properly.

2.1.3 Sharing of fundamental concept that "Unsafe condition should not be allowed"

- Humans should not perform hard or dangerous work.
- Machines should do the hard and dangerous work.
- Danger should be avoided in the plan beforehand.
- Danger should be detected by various data on site.

- Eliminating root causes of human errors that may lead to an accident.

2.1.4 To continue PDCA cycle for technology on-site

- Continue improvement and PDCA (Plan, Do, Check, Action Cycle) on site. (Technology itself, human system, work method, etc.)
- The technology system itself to be also spiraled up with PDCA.
- Technology improvement integrated in the construction project (by the government).
- To be used in construction projects, and to be used in the construction field to improve.
- New technology to be supported, and the site does not stop even in case of unfamiliar or trouble occurring

2.1.5 AI support and growth for people together

- To invite input from AI engineers.
- AI will help us to be safer and the job rewarding.
- AI supports and talks, and people will grow together.
- Substitute hard work for people.

"The risk management method using AI" to be prevalently used.

2.1.6 Construction plans to also co-evolve with people and AI

At the construction site, there are many uncertain factors. There are various factors such as weather, soil quality, human factors, utilization of soil generated by other works, circumstances of supervision and suppliers. Therefore, a robust construction plan is required.

Visualization of progress makes it easier to understand how to improve the construction plan. In this case, there is a procurement system environment and an accounting system environment that allow the construction plans to be changed accurately.

The records of changes/improvements in the construction plan are learned, and the number of cases that have been examined in advance increases every year. (The front loading continues to increase.)

The construction plan should prevent accidents caused by people's carelessness and mistakes.

Reduced uncertainties and variability make them more robust, while improving plan optimization and changing flexibility. By utilizing the work robot, the variation in progress is further reduced.

2.1.7 Valuable labor for workers

Key important aspects are: high income, shortened working hours, an environment to easily take vacations, and safe workplace.

Added-value aspects are: motivated working, comfort of workplace, self-fulfillment, social evaluation, good image, etc.

2.2 Image of future construction structure

2.2.1 Easy to construct, operate and maintain

"Ease of operation/maintenance" and "Easy to make" becomes the evaluation criteria, and the learning/feedback mechanism becomes a business process.

If there is a value that has priority over "ease of maintenance" and "ease of making", it will be clearly stated.

" Maintenance" includes operation, inspection, diagnosis, repair, replacement, restoration, renewal, dismantling, disposal, etc.

The idea of "easiness" is consistent and easy to understand.

Constraints in "ease of maintenance" and "ease of making" will decrease every year due to technological improvements.

"Multi-product one-type construction production technology" will improve year by year.

2.2.2 Evaluation throughout the life cycle

There are measurement items that serve as indicators in inspections and diagnoses.

This index is measured during construction, at the time of completion, and is recorded in the electronic history ledger.

Construction/repair and new technology are evaluated for a long time. Where and who did it, and whether the work done was good or bad will be evaluated later.

This can lead to both pride and shame.

A good company will also benefit in the long run.

2.3 Digitization of the real world

The rules for recording underground data for construction excavation, boring, and geophysical exploration are being developed.

3D terrain models are usually measured with good accuracy.

The current digitalization has the following expected cases.

1. The outline can be designed without a new survey.
2. Depending on the accuracy and accumulation, the survey may be omitted.
3. Fewer modifications needed from design to construction.
4. It can be utilized for automatic operation and road maintenance.
5. We can immediately use the pre-disaster data for disaster recovery

3 Hypotheses for problem solving

3.1 Rules and system design for optimization

Since the rapid growth period, vertical and horizontal division of labor has progressed, and the main body of construction site improvement has become unclear. The people involved were forced to stay within partially limited optimization, which was limited to the area where they could improve themselves.

To expand the scope of optimization, it is necessary to make improvements and change rules across multiple parties. For this purpose, the client (owner) and the government are required to have a certain level of involvement and appropriate system design. Institutional design requires everyone to believe that those who have worked hard and made good ideas are fairly evaluated.

3.2 Various hypotheses for problems and solutions

3.2.1 Designed to improve safety and productivity

When improving material manufacturing and on-site construction, it is advisable to review the design if necessary. At this time, it is desirable to be able to review the conditions that constrain the design.

3.2.2 Overall optimization and information utilization suitable for construction production

Information sharing and collaborative operation are important for overall optimization such as modularization of design, linking of orders and procurement/ plant, linking of transportation/ assembly/ construction.

3.2.3 Strategies for effective factory processing

The method of reducing on-site processing, bringing it into the factory after processing, and then assembling on-site may be effective even in a small scale. Especially, it would be desirable to be able to assemble and install by a machine for small scale.

3.2.4 Process control to ensure productive quality

In order to estimate the degree of quality variation in process confirmation, elucidate the relationship when and what should be measured, and incorporate it into the process.

Particularly in the field of civil engineering, it is expected to utilize ICT such as automatic measurement recording/evaluation and remote attendance, which enables flexible process management and setup adjustment.

It is necessary to discuss how to rationalize the involvement of people, such as the centralized management of a wide area by several people.

3.2.5 Optimization of logistics such as soil

It has been said that the bottleneck of earthworks is the uncertainty of the time, amount and quality of soil. Coordination of excess and deficient soil transportation in construction involves many owners in a wide area, and there are cases in which stockyards and soil improvement are used. It may also be a consideration for the government's construction order plan.

Currently, visualization of transportation is being promoted, and we expect that awareness of issues will be shared.

3.2.6 Improvement of quality/quantity confirmation

Level 4 (L4) is a unit of contract modification (MLIT(Ministry of Land, Infrastructure and Transport) estimation standard in Japan), and the quality/quantity confirmation method is determined. It is easy to improve if this is digitized from the time of occurrence and incorporated into the construction process management in a way that requires as few human hands as possible.

3.2.7 Hierarchical structure of construction/work status

The unit of the state of what you are doing now becomes the unit of motion analysis and the unit of learning (preparation unit of teacher data), and has a hierarchical structure.

"Which state can be changed next?" is an internal description of the state transition in the autonomous case.

3.2.8 Command system of instruction and simulation

Even if both remote and autonomous are used, a command system for construction/work instructions from the control is required.

Construction/work instructions are assumed to have a granularity (unit in a hierarchical structure) that is commensurate with the work unit utilizing autonomy.

It is convenient to use this hierarchical command system for construction simulation.

3.2.9 Blasting machines expected to improve work environment

In the case of improving LCC of steel bridges, it is desirable to repaint with high durability at least at the girder end. For this reason, use of blasting as the substrate adjustment is preferred

For that purpose, it is good to use a blast machine system with few scaffolds and enclosures, less scattering of dust and sewage, a light load on workers' protective clothing and dust masks, and high availability.

4 Transformation of safety philosophy

4.1 Safety philosophy

The number of deaths from construction labor in recent years is about four times the average of other industries on a working population basis. From the standpoint of utilizing robot technology, the safety concept that "unsafety condition should not be allowed. People do not do it" should be rigorously pursued.

In example in Photo 1, this person should not be nearby a hydraulic excavator in the first place. He should not measure the depth of the ditch. The depth of the ditch should be measured by hydraulic excavator.

Again, the points of thinking are shown below.

1. Unsafe condition is not allowed. People should not do unsafe operations.
2. The basic idea is to solve by technology.
3. Some extent of human error is always assumed to occur.

Photo. 1. Simulate close work (by PWRI2003)

The technical points to be pursued are as follows.

1. Substitute by machine
2. Machine/person separation
3. AI avoidance, etc.

4.2 Keeping people away from dangerous work

If area near the machine is dangerous (Photo 1), no one should be present. By using MC/MG (machine control/machine guidance), it is possible to assign the measuring task to machine. (Photo. 2) It is no longer necessary for worker to stand a stick in the ditch to measure ditch depth.

In the future, it is expected that in many situations, people will achieve what they do not need do.

Photo. 2. Depth setting MC

5 Towards an object-oriented construction plan

5.1 Object-oriented CAD

3D CAD design data is composed of parts, and the data structure of parts can be object-oriented. (Fig. 1) In recent years, it has been studied in algorithmic design [2] and parametric model design [3]. The image is as follows. [4]

1. Object modules in Library
2. Object modules make up a structure
3. Object modules link Working standards
4. Design with a combination of Object modules (parts and expansion parametric model).
5. Object modules link Design and Analysis tools
6. Object modules (Parts/group) are written with the context of construction.
7. Object modules link Estimates
8. Object modules link Supply chain management

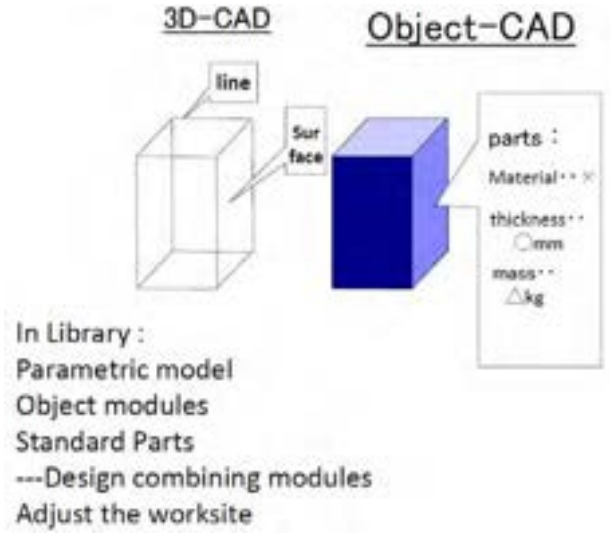

Figure 1. Image of Object oriented CAD

5.2 Expected functional requirements

The evaluation index to be optimized and functions expected from object-oriented CAD are as follows.

1. Object modules in Library
2. Object modules make up a structure
3. Object modules link Working standards
4. It can be solved that construction (/temporary construction) is cheap and quick.
5. It is possible to make a trial design when it consists of only standard parts.
6. It can be solved using environmental evaluation indicators such as energy consumption.
7. Support optimization of setup change
8. Simulation can be performed according to work standard and order.
9. Construction improvement can be described by work standard improvement.
10. Earthwork site rub module can be used.
11. Object modules must Adjust the worksite

6 Conclusion

The author's view on desirable goal and approaches towards the goals was described. In particular, the author presented hypotheses that should be addressed with high priority, with some hypotheses not being discussed for more than 10 years.

This paper lists followings as important aspects to be considered:

1. To share ideas on future construction sites with others.
2. To place high priority and respect on human time, safety and purpose of life.
3. To continue improvement and PDCA on site.
4. To support robust optimization for changes in construction plans and setup changes.
5. Ease of making and ease of maintenance are key indicators in optimization.
6. To set measurement indicators in life cycle
7. To promote digitization in the real world
8. To set rules and system design for optimization
9. To increase production in factory and reduce on-site work
10. Factory products to be handled by machines, not by humans.
11. Monitor process control to ensure productive quality
12. Optimize logistics such as soil
13. Digitization of quantity and quality for each contracted minimum unit
14. To aim for a hierarchical structure of construction/work status
15. To aim for a hierarchical command system of instruction and simulation
16. Unsafe condition should not be allowed.
17. Object-oriented construction plan
18. Object oriented CAD for construction sites
19. How work standard improvements can be diverted and reused

In this paper, author's image, goals, and various hypotheses were presented. It is the author's intention that such information will lead to discussion and promotion in the field of construction production engineering.

The author hopes that further discussions will be deepened and research and development and social implementation will progress toward the future of construction production engineering and robot technology utilization.

References

[1] Hiroshi Yamamoto, Unmanned Construction, The foundation engineering & equipment,,monthly, Vol.46, No.7. 2018.

[2] Naruo Kano, Simulator in building construction, Waseda University Press, 2018.3

[3] E. Hirasawa, N. Aoyama, T. Teraguchi, O. Ashihara, H. Seki, 3D model creation method using parametric model, Civil Engineering Journal, Vol.61 No.3. 2019.

[4] Hiroshi Yamamoto, Construction production technology required for the future, Journal of JCMA, Vol.59 No.1. 2007.

Constructible Design for Off-site Prefabricated Structures in Industrial Environments: Review of Mixed Reality Applications

Ankit Shringi [a], Mehrdad Arashpour [a] and Arnaud Prouzeau [b]

[a]Department of Civil Engineering, Monash University, Australia
[b]Department of Human Centred Computing, Monash University, Australia
E-mail: ankit.shringi@monash.edu, mehrdad.arashpour@monash.edu, arnaud.prouzeau@monash.edu

Abstract –

Studies have shown that early design finalization is important for projects utilizing Off-site Prefabrication and final assembly on site. Freezing engineering design at an early stage has various advantages such as streamlined manufacturing and timely transportation to site as well as timely deployment of adequate resources on site for assembly. However, it is very important to ensure correct design that can be transported, assembled and erected on site in Brownfield Industrial environments. EPC (Engineering, Procurement and Construction) companies have traditionally adopted a "Suit-to-site" approach, where structural members are largely tailored to fit at the site in order to avoid rework. This approach requires mobilization of a large number of resources to site and consumes a lot of time for the fabrication and installation works. Mixed Reality (MR) systems can be used to ensure correct design which can then ensure accurate fabrication and quick installation of structures. This paper reviews the applicability of different MR systems to the concept of Constructible Design for early design finalization in a brown-field Industrial engineering environment. Structural design review is correlated to different tasks of construction that must be performed on the field. Applicability of different components of MR systems is then evaluated for these tasks. This paper finally concludes with selection of suitable MR systems for deign evaluation based on correlation between construction work tasks and components of MR systems.

Keywords –

Design Validation; Augmented Reality; Design Review; Assembly of Structures; Off-site Prefabrication; Constructability Review; Industrial Structures

1 Introduction

Construction in brownfield industrial environments is largely a complex affair due to the large number of variables presented by a pre-existing industrial facility. The rapid shift in construction technology towards prefabrication and assembly at site requires a shift in focus to early design finalization [1]. Any modifications to design at a later stage cannot be incorporated as such changes will lead to major impacts to schedule or budget or both. This is largely due to the fact that changes to a prefabricated module will result in changes to connected modules. Moreover, making modifications or changes at site is time consuming as well as labour intensive - ultimately a costly exercise. In order to ensure a design, a Mixed Reality system could prove to be instrumental with review of a design before its fabrication.

Mixed Reality is a widely accepted term that was first proposed by Milgram et al. and can be expressed as a spectrum with any form of hybrid combination of Virtual Reality (VR) and Augmented Reality (AR) [2] (Fig. 1). Because of its evolution, MR today not only concentrates on graphics and displays but also incorporates various interactions with users including gesture recognition and spatial registration (interaction with surrounding environment). Owing to rapid development of technology in the past decade, differentiation between AR and MR can often be difficult [3]. For this reason, both AR and Augmented Virtuality (AV) - including use of AV on desktop-based systems, are considered as MR for the purpose of this review and their applicability to Brownfield Industrial Construction.

Construction in Brownfield industrial environment, especially for addition of a new facility, expansion of existing plant or re-purposing the process in an existing plant is described as challenging at best. One of the most critical tasks in such a project is to erect structures suited to site conditions in an existing facility within imposed time constraints. Such activities can be made more accurate, quicker and safer if all the structures related to

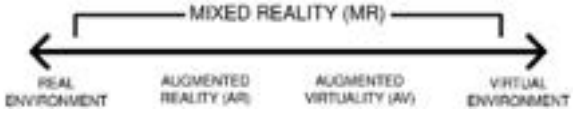

Figure 1. Reality-Virtuality Continuum.
Source: Milgram el al[2]

these activities can be accurately estimated, fabricated off-site and delivered to site for assembly or direct installation.

This paper explores the applicability of Mixed Reality (MR) technologies for early design finalization. The aim of such early design finalization is to arrive at an acceptable level of design accuracy which in turn can facilitate timely fabrication, delivery and installation of tie-in structures thereby avoiding any rework or fabrication work at site. This paper concludes by recognizing See-through Head mounted devices as the most suitable MR systems that can be used to evaluate different work tasks in construction, thereby ensuring a correct design.

2 Review Methodology

For the purpose of review, this paper has been divided into the following sections:

1. Mixed Reality applications
2. Constructability of a Structure and enhancement with MR systems

While discussing the evolution of MR applications, tabulation of features as well as advantages and shortcomings of the more recent and relevant applications has also been done. The purpose of this classification is to then correlate applications with principles of Construction (Work Tasks) in section 4.3. Recommendation of suitable MR systems to reach early design finalization with respect to various facets of design is presented in Section 5.

3 Mixed Reality Applications

3.1 Literature review of work done on Mixed reality in Industrial Construction

Since its conception, Mixed Reality (MR) has been developed to facilitate human-computer interaction. MR has been implemented in devices using various technologies – right from Desktop based applications to Wearable Head Mounted Displays (like the Microsoft Hololens and Google Glass [4] [5]) being used in the Architecture, Engineering, Construction and Owner-operated (AECO) industries.

When it comes to Industrial Construction, Mixed reality has seen applications in areas such as Inspections, Planning and Monitoring of construction work, equipment and material management, training of skilled workers and implementing certain safety management systems. However, MR can also be used to facilitate design reviews of critical structural elements.

Shin et al. reviewed the applicability of Augmented Reality (AR) to various construction tasks in 2008 [6]. The mapping of various construction work tasks and activities to the relevant features of AR systems led to identification of areas where AR can be applied to enhance the performance of activities in their research. Tracking of materials on site for increased efficiency by combining AR with WLAN and GPS information was presented by Behzadan et al. in 2008 [7].

Similarly, Rohani et al. demonstrated the use of Mixed Reality (MR) for development of 4D-CAD based construction management systems [8]. Such systems enable construction managers to visualize the design of a structure along with the reality at a glance and are able to translate this information to provide a powerful management platform for planning and controlling projects. Behzdan et al. explored the use of MR to locate computer-generated graphical information in real world environments [9]. Such information spatially located relative to the user can assist in the performance of various complex engineering tasks.

MR is also being used to train workforce and make some of their tasks easier and/or more efficient. Hou et al. conducted an experiment to analyze the benefits of using AR to train students with no prior experience of piping assembly or using AR [10]. They concluded that AR could increase efficiency, reduce errors as well as optimize cost. Wang et al. conducted research on operating simulation system for tower crane based on VR [11].

Another area where VR has facilitated improvement is engineering reviews - In 2017, Berg et al. reviewed the potency of using VR for early decision making on an industry-based case [12]. The visualization aspect of using VR allowed the design team to make decisions ahead of usual stages and saved them a lot of effort on prototyping. In this aspect, production on assembly lines is akin to that seen in a structural fabrication shop. VR and AR can thus be utilized to foresee and tackle assembly related challenges during design stage rather than do that in field during erection stage. Another research on the same lines by Freeman et al. confirms that use of VR for reviews during design stage can lead to significant improvement in participants ability to understand the geometry of the model correctly, confidently, and quickly, as well as in participants ability to correctly and confidently understand the implications of a proposed design change [13].

These researches are now being applied in field in various areas of construction with the help of new

technological platforms such as Mobile devices (including Mobile Phones and tables), Google Glass, Hololens and Trimble Sitevision [14].

3.2 Understanding MR systems

In order to understand MR systems, it is necessary to understand their components. A recent state-of-the-art review of MR applications in AECO industries by Cheng et al. has a sufficient categorization of components for analysis [3]. The basic categorization of components falls into the following categories – Display, Spatial Registration, User Interaction and Storage.

For the purpose of this review, we will attempt to categorize the components of the following devices:

- Head-mounted See-through displays (likes of Hololens and Google Glass)
- Head-mounted immersive VR displays (like Occulus Rift, Samsung HMD Odyssey Windows Mixed Reality headset)
- Portable Cellphones and Tablets

Table 1 summarizes the categorization of these components. It can be seen from this tabulation that some devices have certain advantages in a particular area that renders them feasible for particular application. For example, Cell phones or Tablets can be used very effectively for outdoor location-based tracking but lack immersive experience which can be crucial when trying to finalize a design and ascertain its feasibility [15]. Similarly, when reviewing a particular structural design which has multiple engineering interfaces involving multiple approving authorities, mobile devices may not make as much sense as use of an immersive display that allows for group interaction - like a Cave display. Another option for group interaction in field would be to use multiple Mixed reality see-through HMD devices like Hololens that can be paired together for group interactions.

3.2.1 Display:

The most important aspect a Mixed Reality system interacts with a user is the way it displays the graphics along with the real-time visuals. Taking into account the devices considered for this review, displays are categorized into the following types:

- ***VR Displays:*** VR displays are usually either Head mounted or immersive CAVE displays connected to a computer and usually used for VR reviews. These displays can be instrumental in remote design reviews also.
- ***Portable Displays:*** Portable displays are actually integrated into portable devices such as Mobile Phones and tablets. These displays employ either LCD or LED displays integrated in the device.
- ***Immersive see-through HMDs:*** Head mounted displays originated back in the early 1980s. The latest development of display technology allows graphic images projected on transparent glass. This gives the user an immersive experience, making virtual graphics seeming as if real, from user's perspective.

3.2.2 Spatial Registration:

Spatial Registration is a feature of MR systems that facilitates "Realistic" experience for the user. The MR system needs to project correct graphics in front of the user's eyes with respect to their motion in real world or in accordance with their commands on a controller device. In order to do this, the device needs to "learn" about its surroundings. This is known as Spatial Registration. The types of spatial registration methods are as follows:

- ***Marker Based:*** Marker-based Spatial registration utilizes a static image also referred to as a trigger photo that a the device scans in order to calibrate its position from the trigger image [16].

Table 1. Categorization of MR System Components

Device Category	Display	Spatial Registration	User Interaction	Storage
See-through HMDs	- Immersive HMD - Immersive Graphic over transparent glass	- Marker Based - Marker-less	- Gestures - Joystick / Controller	- On-board Storage - Cloud storage access
VR Displays	- Immersive HMD	- Marker-less	- Joystick / Controller	- No on-board storage
Portable Cellphones and Tablets	- Portable LCD	- Marker Based - Marker-less - GPS based location tracking	- Touchscreen	- On-board Storage - Cloud storage access

- ***Marker-less:*** Marker-less spatial registration works by accurate measurements of the 6DOF camera pose relative to the real world and matching point features in the current image frame to two spatially separated reference images [17]. This eliminates the necessity for any marker for spatial registration.
- ***GPS Based:*** GPS based spatial registration uses the global position and 3-Dimensional orientation of an MR system in an outdoor environment for calibrating the superimposition of 3D graphics with respect to the real world. This is made possible by use of a GPS tracker and 3DOF orientation tracker in conjunction [9].

3.2.3 User Interaction

In the previous sections we saw how virtual images aligned with the real world. Taking this functionality a step further, MR systems allow the interaction of virtual objects with the real world to simulate real-world collisions, occlusions and interactions [18]. In the context of construction, this interaction can be very helpful when evaluating feasibility of a design or simulating construction or assembly sequences. Modes of interaction available on devices are:

- ***Touch Screen:*** Predominantly used on Mobile MR systems such as Cellphones or Tablets, a Touch Screen allows user to interact by clicking on the projected image on the device. Various gestures such as pinch, pan and rotation can help to interact with the available information.
- ***Joystick or Controller:*** Joysticks or controllers can be used with most MR systems. However, for immersive HMDs, a controller becomes necessary if the display is not transparent (i.e. not see-through) as interactions with real world will not be very intuitive.
- ***Hand Gestures:*** See-through HMDs have a distinct advantage when it comes to user interaction. Combining the marker-less image tracking with the see-through display, the device is able to recognize users' hand gestures and allows interaction of the Virtual Graphics with the real world by executing commands relayed by hand gestures.[4]

3.2.4 Storage

Access to storage on a MR system can enhance its usability in construction industry. This feature enables the device to function independently.

- ***On-board Storage:*** If the device has storage built-in, it is called on-board storage. With on-board storage, virtual models can be directly loaded onto the device and can be accessed in field readily.
- ***Cloud Storage:*** Devices that can access internet via cellular network can use virtual models and other data stored on cloud drives. A clear advantage in this case would be the ability to use a single device on multiple sites as models need not be loaded on to on-board storage or ability to access very large models that are too big for on-board storage drives.

4 Constructability of a Structure and enhancement with MR systems

4.1 Design in a Brownfield Environment

In the context of industrial construction, a brownfield construction site is a site which is either located within an operational facility - such as a capacity expansion project or a new facility being installed to enhance product quality within an operating plant.

The major challenges of a Brownfield Construction Project consist of access through an operational facility, ascertaining location of underground facilities and structures, safety concerns due to an operational facility and schedule related concerns [19]. In order to carry out construction in a safe and timely manner, it makes sense to prefabricate structures off-site and then assemble them with minimum manpower deployment and in minimum possible time.

Also, another issue that arises out of adopting Off-site prefabrication and On-site Assembly is that of customization. Any structure that has been manufactured off-site cannot be modified on site within the scheduled time or budgeted cost [1]. Accuracy of design and fabrication is, therefore, of paramount importance.

4.2 Evaluation of Constructability

Constructability of any structure can be divided into various work tasks that must be completed in order to complete a construction activity [6]. The evaluation of Constructability stems from ability to perform these work tasks as planned and to the design standards. Shin et al. identified work tasks as well as construction activities that can benefit from Augmented Reality based on technology suitability [6]. This study identified the following tasks that benefit from Augmented Reality applications - *Layout, Excavation, Positioning, Inspection, Supervision, Commenting and Strategizing.*

The above mentioned work tasks, in that study, were adopted from J Everett and evaluated against features of AR systems that would enhance the performance of these tasks [20]. Out of the identified tasks, the work tasks that are important for ensuring assembly of prefabricated structures are *Layout, Excavation, Positioning and Strategizing*. Table 2 summarizes the opportunities identified in this study for improvement of work tasks by implementation of MR.

Table 2. Opportunities for evaluating Prefabricated structural design and assembly using Mixed Reality

Work Tasks	Opportunity
Layout and Positioning	Creation of virtual reference points for superimposition on a reviewer's view. This eliminates the need for physical marking the reference points by extensive surveying process to ensure correct location of a structure. This is followed by, projection of a 3D model of prefabricated structure based on reference points. This ensures evaluation of interfaces with existing structures and avoids any last-minute modifications to fit the structure on site (Suit-to-site works)
Excavation	Creation of a 3D reference for superimposition of subsurface structure for a reviewer's view. This will ensure sufficient space for excavation and can ensure constructability of underground structures like foundations.
Strategizing	Projecting 3D image of the complete task can help in visualizing the sequence of various tasks to optimize construction or assembly process and to estimate on-field time of critical machinery.

4.3 Correlation of Work Tasks with MR system features

4.3.1 Layout and Positioning

Fixing layout for the structure being evaluated is largely dependent upon identifying correct reference points on the field and then marking the location of structure with respect to reference points. MR systems can reduce the marking efforts and time required for identifying correct location of a given structure by projecting the virtual image through a MR system. Similarly, Positioning of a virtual 3D image of the structure being evaluated, allows the reviewer to understand its relationship with the surrounding structures and equipment (above ground structures) and also helps to visualize any existing loads that may need to be accommodated into the prefabricated Structure. Refer Table 3 for correlation.

4.3.2 Excavation

In a Brownfield environment with underground structures and facilities, it is very important to be able to visualize the extent of excavation for installation of a structure. Any subsurface structural interfaces that do not come to fore with As-built information can be discovered by an on-site review using an appropriate MR system. This is especially important as foundations need to be ready to receive prefabricated structure for installation. Refer Table 4 for correlation with MR Device Components.

4.3.3 Strategizing

The task of strategizing requires analysis of the actual process of assembly and erection of a prefabricated structure. This process takes into account operations such as logistics, assembly, lifting as well as connecting to any existing interfaces. Strategizing is very different from other work tasks as it is not performed exclusively on site and requires collaboration between different teams. Refer Table 5 for correlation with MR Device Components.

5 Conclusion

Based on Correlation of Work Tasks with MR system features in Section 4.3, we can conclude that see-through HMDs present the best features for reviewing design of prefabricated structure in a brownfield industrial installation. They have the most immersive experience of review - all the while being able to see the real world. They have one of the more accurate spatial registration capabilities which can be further enhanced by use of external attachments to a centimeter level accuracy. User-interaction while using these is very easy and doesn't require any additional device or controller for inputs. These devices can be used for expert reviews as well as collaborative reviews and can help to discover any potential issues for assembly and final installation - thus helping to finalize a structural design much earlier. Another advantage of using these devices for reviewing a critical design is the enhanced customer experience that builds more confidence towards a design firm's capabilities.

Table 3. Correlation of MR System components with work tasks for Layout & Positioning

MR System Components	Work Tasks	Layout & Positioning
Display	VR Display	VR Displays can be used for conducting a Virtual Reality design review or for reviewing any structures remotely when access to a site is restricted [21].
	Portable Display	Device camera is able to produce image of real world on the screen, which is then superimposed with the Virtual image. The only disadvantage with this display is that one hand is occupied with holding the device.
	See-through HMD	These displays have an inherent advantage as the real world is seen through transparent glass and the virtual image is projected on the glass producing an immersive display.
Spatial Registration	Marker-based	A quick and accurate way to calibrate the device camera [22], this technique, however, requires installation of markers on sites. Accordingly, this technique can be adopted for smaller projects.
	Marker-less	Marker-less registration is able to self-calibrate the device to its surroundings by comparing them with pre-captured reference images [17 and thus results in a seamless experience. Also, with marker-less registration, changes to the scene can be detected with the MR system, highlighting any potential clashes.
	GPS-based	GPS based spatial registration on mobile devices has an accuracy of ±10 metres. However, attachments such as Trimble Sitevision are able to enhance the accuracy of measurement and location up to 1 cm [14]. The only disadvantage of using GPS for spatial registration is that it requires clear view of sky and can have issues in tight spaces that experience "Canyon" effect.
User Interaction	Touchscreen	The only disadvantage of using a touchscreen is that it requires use of both hands - one to hold the device and other for interacting with the device.
	Hand Gestures	Identifiable by select MR systems, Hand-gestures can be an excellent way of providing input to a device. Using hand gestures for input also means that both hands are free while not providing any input.
Storage	On-board	On-board storage can be particularly useful when using the device independently and on a remote location devoid of any cellular network or WiFi access. However, this can also be a limiting factor when using large files.
	Cloud	Advantageous when accessing large files and when a single device is used across multiple projects / locations. Needs proper wireless network.

Table 4. Correlation of MR System components with work tasks for Excavation

MR System Components	Work Tasks	Excavation
Display	VR Display	Can only be used for remote reviews. Not suitable to review on-going activity.
	Portable Display	Portable Displays can be used for reviewing interface with subsurface structure but have a narrow field of view since they are small and non-immersive.
	See-through HMD	See through HMDs provide the maximum information in an immersive environment. Reviewing the structural interfaces for excavation using See-through HMDs can help to discover any potential issues [12].
Spatial Registration	Marker-based	Marker-based spatial registration can be effective when reviewing a specific area for interfaces during excavation as it needs pre-installation of markers.

MR System Components	Work Tasks	Excavation
	Marker-less	Marker-less spatial registration would be preferred for evaluation of subsurface structural interfaces as it can identify any changes to the site's surroundings.
	GPS-based	Using GPS-based spatial registration is not particularly accurate to a centimeter level of accuracy. However, if used with enhancements such as Sitevision [14], it can be used to review work done.
User Interaction	Touchscreen	Pinch action on a touchscreen can be used to closely examine a virtual model and may prove to be useful due to limited field of view.
	Joystick / Controller	When reviewing a site remotely, it may be necessary to use keyboard and mouse as controllers to navigate withing the model or recording of the review.
	Hand Gestures	Hand gestures, when coupled with see-through HMDs allow interaction and feedback without use of additional equipment.
Storage	On-board	Particularly useful when using the device independently and on a remote location devoid of any cellular network or WiFi access.
	Cloud	Advantageous when accessing large files and when a single device is used across multiple projects / locations. Needs proper wireless network.

Table 5. Correlation of MR System components with work tasks for Strategizing

MR System Components	Work Tasks	Strategizing
Display	VR Display	Useful for desktop reviews, a VR display like CAVE can be useful in team reviews related to assembly and lifting activities required for erection of a prefabricated modules [12].
	See-through HMD	Some HMDs have collaborative capabilities and can be used for reviewing activities using virtual holograms.
Spatial Registration	Marker-based	Marker-based registration can be used for on-site team reviews.
	Marker-less	Marker-less registration is intuitive and can be used while strategizing. When users are seated around a table, wearing see-through HMDs, the devices can read the table's surface and project holograms for review.
User Interaction	Touchscreen	Large touchscreen displays can be used to convey ideas by marking while carrying out group reviews.
	Joystick / Controller	Keyboard and mice are generally used to navigate within a virtual space. Animations showing performance of important activities may also require user inputs to start, pause and end.
	Hand Gestures	Hand gestures can be useful when carrying out reviews using see-through HMDs. Users can interact with holograms using hand gestures to navigate to different areas of a hologram or to highlight, zoom-in and out of the views.
Storage	On-board	Very important for VR or CAVE reviews as the virtual models require a lot of storage. However, this may not be the apt storage solution for multiple HMDs accessing the same virtual model.
	Cloud	Can be used to ensure currency of the virtual model and also ensures that multiple users can access the same virtual model and review its feasibility.

References

[1] V.W.Y. Tam, C.M. Tam, S.X. Zeng, W.C.Y. Ng, Towards adoption of prefabrication in construction, Build. Environ. 42 (2007) 3642–3654. https://doi.org/10.1016/j.buildenv.2006.10.003.

[2] P. Milgram, F. Kishino, A TAXONOMY OF MIXED REALITY VISUAL DISPLAYS. IEICE Transactions on Information Systems, Vol E77-D, No.12, IEICE Trans. Inf. Syst. E77-D (1994) 1–15.

[3] J.C.P. Cheng, K. Chen, W. Chen, State-of-the-Art Review on Mixed Reality Applications in the AECO Industry, J. Constr. Eng. Manag. 146 (2020) 1–12. https://doi.org/10.1061/(ASCE)CO.1943-7862.0001749.

[4] Microsoft, Microsoft Hololens Development Edition, Online Webpage. (2016). https://www.microsoft.com/en-us/hololens/developers.

[5] Google, Google Glass Enterprise Edition, Google LLC. (2019). https://developers.google.com/glass-enterprise/guides/get-started.

[6] D.H. Shin, P.S. Dunston, Identification of application areas for Augmented Reality in industrial construction based on technology suitability, Autom. Constr. 17 (2008) 882–894. https://doi.org/10.1016/j.autcon.2008.02.012.

[7] A.H. Behzadan, Z. Aziz, C.J. Anumba, V.R. Kamat, Ubiquitous location tracking for context-specific information delivery on construction sites, Autom. Constr. 17 (2008) 737–748. https://doi.org/10.1016/j.autcon.2008.02.002.

[8] M. Rohani, M. Fan, C. Yu, Advanced visualization and simulation techniques for modern construction management, Indoor Built Environ. 23 (2014) 665–674. https://doi.org/10.1177/1420326X13498400.

[9] A.H. Behzadan, V.R. Kamat, Georeferenced registration of construction graphics in mobile outdoor augmented reality, J. Comput. Civ. Eng. 21 (2007) 247–258. https://doi.org/10.1061/(ASCE)0887-3801(2007)21:4(247).

[10] L. Hou, X. Wang, M. Truijens, Using augmented reality to facilitate piping assembly: An experiment-based evaluation, J. Comput. Civ. Eng. 29 (2015) 1–12. https://doi.org/10.1061/(ASCE)CP.1943-5487.0000344.

[11] Y. Wang, D. Chen, H. Dong, B. Wang, Research on operating simulation system for tower crane based on virtual reality, Lect. Notes Comput. Sci. 8351 LNCS (2014) 593–601. https://doi.org/10.1007/978-3-319-09265-2_60.

[12] L.P. Berg, J.M. Vance, An Industry Case Study: Investigating Early Design Decision Making in Virtual Reality, J. Comput. Inf. Sci. Eng. 17 (2017) 1–7. https://doi.org/10.1115/1.4034267.

[13] I. Freeman, J. Salmon, J. Coburn, A bi-directional interface for improved interaction with engineering models in virtual reality design reviews, Int. J. Interact. Des. Manuf. 12 (2018) 549–560. https://doi.org/10.1007/s12008-017-0413-0.

[14] Trimble SiteVision, Trimble SiteVision, (2020). https://sitevision.trimble.com/.

[15] C. Flavián, S. Ibáñez-Sánchez, C. Orús, The impact of virtual, augmented and mixed reality technologies on the customer experience, J. Bus. Res. 100 (2019) 547–560. https://doi.org/10.1016/j.jbusres.2018.10.050.

[16] K. Asai, Role of Head-Up Display in Computer-Assisted Instruction, (2010). http://search.proquest.com/docview/2087160834/.

[17] K. Xu, K.W. Chia, A.D. Cheok, Real-time camera tracking for marker-less and unprepared augmented reality environments, Image Vis. Comput. 26 (2008) 673–689. https://doi.org/10.1016/j.imavis.2007.08.015.

[18] S. Izadi, D. Kim, O. Hilliges, D. Molyneaux, R. Newcombe, P. Kohli, J. Shotton, S. Hodges, D. Freeman, A. Davison, A. Fitzgibbon, KinectFusion: Real-time 3D reconstruction and interaction using a moving depth camera, in: UIST'11 - Proc. 24th Annu. ACM Symp. User Interface Softw. Technol., 2011. https://doi.org/10.1145/2047196.2047270.

[19] S. Nuthanapati, K. Adel, I. Al Awadhi, Civil engineering challenges in brownfield projects - A case study, in: Soc. Pet. Eng. - Abu Dhabi Int. Pet. Exhib. Conf. 2019, ADIP 2019, 2019.

[20] J.G. Everett, Construction automation--basic task selection and development of the CRANIUM, Massachusetts Institute of Technology, 1991.

[21] A. Prouzeau, Y. Wang, B. Ens, W. Willett, T. Dwyer, Corsican Twin: Authoring In Situ Augmented Reality Visualisations in Virtual Reality, in: Int. Conf. Adv. Vis. Interfaces, n.d. https://doi.org/10.1145/3399715.3399743.

[22] H. Kato, M. Billinghurst, Marker tracking and HMD calibration for a video-based augmented reality conferencing system, in: Proc. - 2nd IEEE ACM Int. Work. Augment. Reality, IWAR 1999, 1999: pp. 85–94. https://doi.org/10.1109/IWAR.1999.803809.

Financial Modeling for Modular and Offsite Construction

Tarek Salama [a], Gareth Figgess [a], Mohamed Elsharawy [b], Hossam El-Sokkary[b]

[a] Department of Construction Management, California State University, Sacramento, California, USA

[b] Department of Civil and Construction Engineering, College of Engineering, Imam Abdulrahman Bin Faisal University, Dammam, Kingdom of Saudi Arabia

E-mail: salama@csus.edu, figgess@csus.edu, Mrelsharawy@iau.edu.sa, Hselsokkary@iau.edu.sa

Abstract –

The advantages of using modular and offsite construction compared with the traditional construction methods are numerous due to its efficiency in delivering shorter schedules, lower cost, higher quality, and better safety. However, one of the biggest challenges facing the prefabrication industry today is the inherent difference between financing traditional construction and the upfront capital requirements for modular and offsite construction. Any solution for this problem should introduce better coordination among developers, banks, financial partners, lending institutions, manufacturers, and general contractors. Financing modular construction is challenging as banks are not familiar with the characteristics of this modern industry, and it is all about risk and return. Financing also helps in reducing risk for developers and allows them to undertake projects without having the upfront capital. However, few studies in literature focused on the financial modeling for modular and offsite construction. This paper is presenting a state-of-the-art literature review for current practices concerning financial modeling for modular and offsite construction. This review discusses current challenges for financing this industry, as well as the introduced initiatives by governments to facilitate financing of modular and offsite construction. Conclusions are presented regarding the current practices for funding the prefabrication industry. Furthermore, recommendations are drawn for encouraging the development of prefabricated housing, and its ability in solving the current shortage of housing in different parts of the world.

Keywords –

Instructions; Financial Modeling; Modular; Offsite Construction, Literature Review.

1 Introduction

Shortage of affordable housing for low-income renters is affecting every state and metropolitan area in America. The private market is not producing enough affordable new rental housing to these renters, because rents they can afford do not typically cover development and operating costs for rental housing [1], while public supporting subsidy is absent on this regard. Mayors of Philadelphia, New York and San Francisco confirmed that modular construction is a solution to the housing problem in their cities [2] due to its reported advantages. However, many studies investigated barriers of modular construction to increase its market share [3, 4, 5, 6, 7 &8]. These barriers include 1) modular and offsite construction's negative stigma; 2) lack of evidence for successful application of modular and offsite construction; 3) lack of unified building codes and operational standards for modular and offsite construction; 4) traditional procurement systems does not fit practices of modular and offsite construction; 5) conventional financing tools and cash flow structures does not enable the use of modular construction.

Rahman [3], Smith and Rice [4] listed the difficulty in financing, as one of the main barriers to implement offsite construction, because it requires higher initial capital compared to traditional approach. The Canadian construction innovations report [5] highlighted, cash flow challenges for modular and offsite construction when using the traditional cash flow system and outlined the need to restructure project financing for publicly funded projects to enable the application of modular construction. Salama et al. [6, 7 &8] emphasized the need to create financial models that fit the characteristics of modular construction and to create special conferences for lenders to discuss the different nature of financing modular and offsite construction.

The same studies also suggested to create special lending banks and changing policies for financing modular builders as well as convincing insurance

companies to lower insurance rates for modular buildings. Furthermore, they also recommended universities to design cost management methods and lending programs that consider characteristics of modular construction.
This paper presents a literature review for current practices in financing modular and offsite construction and discusses different initiatives that encourage financing modular builders.

2 Challenges

2.1 Large upfront capital requirements

The production and procurement processes for modular construction require material and overhead costs to equal up to 60 percent of a module's total cost. Hence, manufacturers ask for an upfront payment of around 50 percent at the ordering time to procure materials in short period of time to increase efficiency of manufacturing [9]. This large upfront capital requirements from manufacturers can affect bank reserves, so banks and institutional lenders would ask for any collateral to reserve some money on their equity to avoid scrutiny from regulators [10].

2.2 Perception of ownership

During manufacturing, modules are considered personal property of the manufacturer and it does not become real private property until delivery and assembly onsite [10]. Many banks don't release financing instalments until modules are installed onsite to ensure that their money is utilized in real property. However, manufacturers want to get paid before delivery of modules to avoid the transfer of ownership status from personal to private property which can lead to legal complication to future payment disputes [11]. These differences in understanding for perception of ownership of modules complicate financing instalments and the whole financing structure.

2.3 The immature market

Modular construction developers who lack the experience in this industry, face uncertainty in scheduling and pricing which results in risks' inconsistencies. Banks' evaluations for their projects can change and financing costs would increase for developers [12]. Banks are also concerned regarding project completion if a manufacturer becomes bankrupt.
Few American companies can manage high-rise modular projects, and lack of proven manufacturing would make banks request additional contingency funds to satisfy projects' uncertainty [13]. Immature market affect pricing of manufacturers and it would make it unreliable.

2.4 Progress monitoring for manufacturing

Progress monitoring for manufacturing is hard for modules that can be manufactured simultaneously for multiple projects. Materials allocation is crucial for identifying a collateral to get financing from any bank. Securing financing for modular construction can be more difficult than traditional projects because banks would not prefer the increased risk associated with progress monitoring of manufactured modules [12].

2.5 Lack of support from authorities and financial sector

Lack of support from financial sector is a main challenge for offsite construction due to many reasons like the high profitability of lenders who finance traditional housing [14]. Many offsite manufacturers have to internally finance their projects until the end of manufacturing. Hence, only the most successful builders can manage large-scale projects with reasonable cost. Production of modules can begins six months before delivery of first module on site based on size of different projects, while procurement of materials should start 6-7 weeks before manufacturing [15]. This means modular manufacturer has to pay for materials and then pay for labor during manufacturing of modules while banks release construction financing after delivery of modules to construction site. Depending on project size, modular manufacturer may need $16-$20 million before receiving any financing from lenders [15]. Lack of political will from regulatory authorities to motivate lenders to change their policies is also questionable [14].

2.6 High lending rates

Lending rates for offsite construction are higher than its value for traditional construction because it is a relatively new concept and many banks lack the full understanding of it [16]. However, these rates will be changed by time after more research and development initiatives are undertaken, and higher scale of this market is achieved. For example, a two-year traditional construction project can make the developer pay half of the cost up front for the land and the other half is paid throughout the two years of construction. However, for modular construction project with a compressed project time of one year, the whole payment can be due upfront, while financing could be required for only one year instead of two years. If cost of capital is assumed to be 10 percent, then financing costs would be reduced by 5 percent of the total project cost [16].

2.7 Financial impact and considerations

The potential financial impact from utilizing modular and offsite construction should be investigated

and compared to stick-built construction before project can start. Financial impact is different from a state and country to another and many factors should be studied to assess financial impact such as the high labor cost in some countries. Economic situation for housing market, debt situation, and developer capabilities affect also the financial impact which has to be evaluated before taking a decision to utilize offsite construction [11].

2.8 Transportation and storage costs

Transportation and storage costs are essential for modular and off-site construction. However, lending banks may not consider them while providing construction financing [17]. Additional costs may also face developers such as renting trailers for transportation, and wrapping prefabricated modules to protect them from weathering effects and possible damages. These costs are challenging if project site and manufacturing facility exist in different countries.

2.9 Payment certifications for publicly funded projects

If a modular or offsite construction project is publicly funded, then its schedule of values may not fit with a typical schedule of values developed by the American institute of architects (AIA), which determines monthly progress payments. Some publicly funded projects may not permit some payments certifications in a timely manner due to this challenging fact [18].

3 Modular and offsite construction team

For traditional, modular and offsite construction, clients are developers or building owners, who may be individuals, groups, or representatives for owners. They are motivating building projects by providing funding and determining the required delivery method, as well as construction method utilized, whether prefabricated or not, and the level of required prefabrication with the help of the design team [19]. Relationship between developer and project team for traditional construction is shown in Figure 1 where developer may have contracts with different designers and consultants (e.g. Architect, structural, and civil consultants), and another contract with the general contractor who may hire different subcontractors. For modular and offsite construction, the developer may have a contract with the modular builder as shown in Figure 2 who can manage fabrication and may or may not hire a general contractor to establish building foundation and utilities onsite.

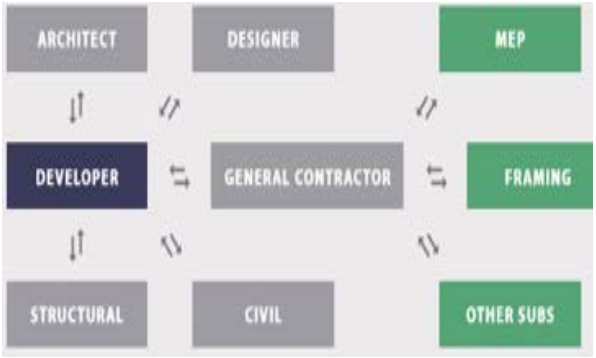

Figure 1. Traditional construction team. Adapted from MBI report [1].

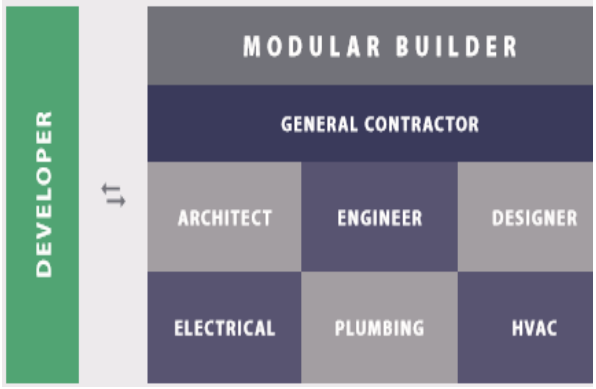

Figure 2. Modular construction team. Adapted from MBI report [1].

4 Financial Modeling

4.1 Financial modeling from developer perspective

Few studies investigated insights of financing offsite construction from developer perspective [11, 20]. Cameron and Carlo [11] conducted a quantitative analysis to assess the impact of utilizing modular construction. Two scenarios were used to measure equity internal rate of return (IRR) – which is the annualized return of investment in any period of time – in a comparison between modular and traditional construction. The first scenario is for a project comprising six buildings constructed as rent development, while the second is for the same project assuming it is constructed for sale. It was concluded that equity IRR increased when utilizing modular construction compared to traditional construction from 35.1% to 47.5% for the first scenario, and from 25.75 % to 27.60 % for the second scenario. Difference between equity IRR of first and second scenarios is attributed to the earned rental income for part of the development. Difference between equity IRR of modular and traditional construction is attributed to flexible phasing of modular construction since for example, two buildings

can be installed onsite to be ready for rental or sale while another building is being manufactured offsite. Shorter schedules of modular construction allows modular developers to reduce interest payments due to the shorter loan period and they can make additional cost savings due to shortened schedules that would reduce the general conditions cost and risk insurance.

Cazemier [20] conducted a comparative financial analysis between a cross laminated timber (CLT) building that utilizes offsite construction technologies, and traditional concrete and steel building in Australia to study economic benefits of using CLT. Feasibility model variables such as sales revenue, land purchase price, construction cost, construction contingency, professional fees, and interest expenses were inputted into EstateMaster software to model their effects on key performance indicators such as development margin, development profit, Return on equity (ROE) – which is the total amount of return receive on original investment –, and IRR. It was concluded that buildings constructed with CLT may result in less development margin, development profit, and ROE, however it will increase equity IRR due to the reduced investment timeline for offsite construction which is the same conclusion of Cameron and Carlo [11]. It was also outlined that any developer will choose between using CLT or traditional buildings based on their investment requirements whether they prefer a greater total amount of return for shareholders on their original investment by the increased ROE, or receive higher annual return of investment by the increase of equity IRR [20]. However, this study is based on using CLT in the Australian market, hence other types of offsite construction such as modular or hybrid construction in other markets like USA or UK might result in different values of ROE and IRR due to the different interest rates, land purchase price, and construction costs in both countries.

4.2 Mortgage financing for consumers

Manufactured housing percentage is nearly 6 % of occupied housing and accounts for much smaller percentage of home loans in the U.S. [21]. Manufactured homes are commonly used in Western and Southern states as shown in Figure 3 [21], and two-thirds of manufactured homes are outside of metropolitan areas in the U.S. Residents of manufactured homes tend to be older and they have lower net worth and incomes compared to residents of traditional homes and they also pay higher loan interest rates than borrowers for traditional homes [21]. Loans for 68 % of manufactured homes are considered “higher-priced mortgage loan” (HPML), which is a definition for loans considered to have high subprime. While only 3% of loans for traditional construction are considered HPMLs [20].

De Mendoza [22] presented a comparison between financial mechanisms for offsite construction in New Zealand and different countries such as USA, Japan, Australia, and Sweden. The main aim of this study is to introduce financial initiatives to encourage offsite construction since New Zealand lacks such financial initiatives where banks do not issue mortgages for manufactured housing.

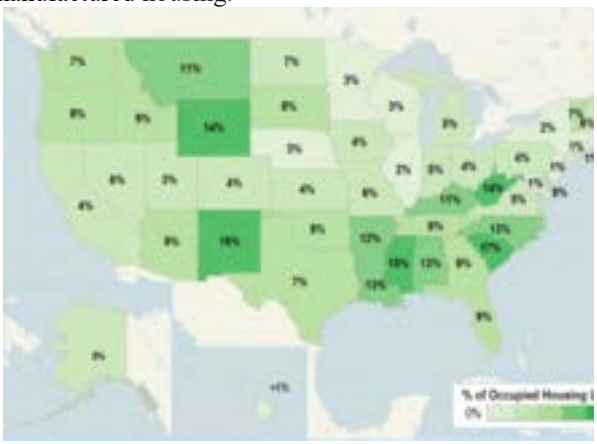

Figure 3. Percentage of manufactured housing of occupied housing units. Adapted from CFPB report [21].

Hence, consumers finance these buildings with chattel/personal loans which are much more expensive than a mortgage. The US consumers’ financing for manufactured homes is based on two types of loans [22]; 1) The chattel loan: which has lower costs at origination, requires more equity for principal payments and it results in higher interest rates and shorter maturities than mortgaging. 2) Manufactured house mortgage: which has lower interest rates than a chattel loan but it would have higher interest rates than traditional construction mortgaging. It has better consumer protections, lower overall costs, and longer maturities. The seven steps for financing modular construction introduced by M&T bank are a good example for manufactured house mortgage [23]. These steps include the creation of a draw disbursement schedule comprising five draws which are disbursed as planned construction milestones are completed. These five draws for construction loan are disbursed for: 1) completion of foundation; 2) delivery of modules onsite; 3) completion of house set; 4) completion of interior /exterior button up and siding; 5) completion of construction. Then, construction loan rollovers to a permanent mortgage when construction is completed. Another innovative financing option is introduced by DIRTT solutions in USA and Canada to lease manufactured homes as leasing cars, where user pays for depreciation of the product during leasing period

[19]. This financial model depends on responsibility of producers/providers for their prefabricated products to be maintained and updated for new leaser after leasing term is expired. While the leaser sets leasing terms with leasing agent as shown in Figure 4.

Manufactured homes in Japan are financed using mortgages which are based on recourse loan contract system [22]. This system is less risky for banks than non-recourse loan system because if borrowers cannot pay for mortgage, they must give up any asset to pay for the loan outstanding, while USA is having a non-recourse loan system in some states, hence borrowers my default on mortgage payments and retain their other assets.

In Australia, banks are conservative in financing manufactured homes [24] because they don't link financing payments to intermediate production stages. Hence, some builders have created other alternatives to ease financing their prefabricated homes. For example, Modscape provides a solution for financing privately the construction, then loan is transferred to consumers using their own bank when project is completed [21]. Other companies established connections with lenders within their group of companies (e.g. TR Homes and Resolve Finance) [22].

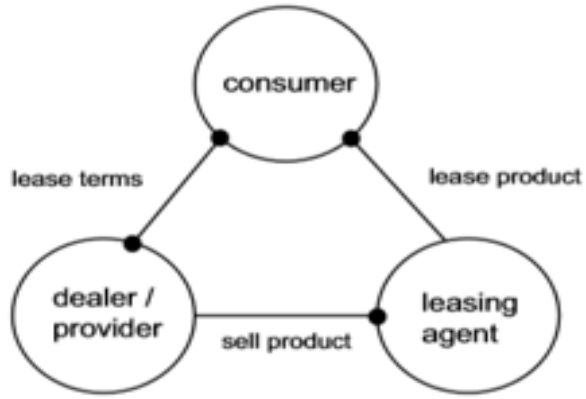

Figure 4. Relationships between providers, leasing agents, and consumers for leasing manufactured housing. Adapted from [19].

5 Recent Advancements

The status of three companies named ZETA factory, Factory OS, and Katerra who worked around the bay area in California illustrate recent developments of modular and offsite construction in USA. The bay area can benefit from offsite and modular construction due to homelessness issues and high prices of real estates in its cities like San Francisco. ZETA factory in Sacramento went out of business in 2016 due to lack of capital after working for 8 years in the market due to issues with ZETA's procurement and ability to deliver projects on schedule [15]. Procurement of materials requires a large upfront capital investment before manufacturing to deliver modules on time. This is challenging for manufacturers, developers and financial partners because each stakeholder has different motivations and constraints. ZETA factory accepted much of its payment after modules were delivered and installed onsite according to the timeline and process of traditional construction. Insufficient capital of ZETA factory led to inability to pay their suppliers in a timely manner and inability to hire personnel for pre-construction activities of the next job. Another developer outlined that many lenders of ZETA factory refused to finance their project, and the lender who agreed at the end needed extensive negotiations and many exceptions to standard bank policies [9]. Hence, the main reasons behind bankruptcy of ZETA factory are the challenges of cash flow management and lack of timely capital [9].

Factory OS and Katerra present a new model an integrated start-ups that develops, designs and builds panelized and modular construction in North America. Both start-ups learned from bankruptcy of ZETA factory and they introduce a recent trend where developers own offsite construction as a response to recent changes in housing market, and both start-ups are supported by venture capital investments from the IT industry in Silicon Valley to solve the homeless problem [2]. Factory OS in Vallejo, California started production in 2018 for a deal required by Google's parent company, Alphabet, to construct 300 apartments with a total value between $25 million and $30 million [25]. Autodesk and Citi bank are also supporting factory floor learning centre at Factory OS which is dedicated to research and education for industrialized construction. This centre is led by Terner centre for housing innovation at UC Berkeley to establish a plan for a new rapid response factory using the best automations to meet demand of quick housing after natural emergencies and disasters. Autodesk is providing software collaboration for design, fabrication and supply chain management, while Citi bank is supporting Factory OS using the initiative of spread products investment technologies (SPRINT) to finance community development projects and affordable housing [26].

Katerra was established in 2015 and built its first manufacturing facility in Phoenix, Arizona after recieving more than $1 billion from the Japanese SoftBank as its major investor, along with other investors such as Foxconn and DFJ, while executives from Amazon and Google joined Katerra's leadership [27]. However, some issues regarding project cost overruns and delayed schedules were reported [27 & 28]. In 2019 Katerra shut down its first factory in Phoenix and laid off 200 workers while some executives were replaced. Then another highly automated manufacturing facility was

built in Tracy, California as a second generation factory for Katerra.

The business models of Factory OS and Katerra as developers and builders follow the business models of Lindbacks in Sweden and Sekisui Heim in Japan who were managing market volatility using their business model for the past 4 decades [2]. Katerra utilized their equipment in Phoenix factory from Sweden's Randek which is nearly identical to the ones used by Lindbacks in Sweden [2] while focusing more in fabrication of panelized construction and Factory OS was focused on volumetric modular construction. Australia's Lend Lease Company is also following the same trend of integrated supply chain to develop, design, and build for multifamily midrise buildings using wood cross-laminated timber (CLT). However, its operations was under review to come up with a new sustainable business model [29].

6 Future Opportunities

Banks are not usually risk-takers and lenders don't consider that offsite construction is affected by both real state and manufacturing risks. Repaying the capital investment of building a manufacturing facility and its ongoing operational expenses affects the business model for offsite construction industry and the expected rate of return. Range of investment cost is based on size of facility and implemented level of automation and it can be between $50 million and $100 million [16]. Cost impact on each project due to this investment can be between 5 % and 15 % of total offsite construction costs [16]. Partnerships and joint ventures are needed with municipalities, general contractors, and IT industry to validate this business model and to reduce any associated risks as well as increasing financing schemes for owners and developers of modular and offsite construction.

In USA, Federal and state funding schemes are introduced to support collaboration between industry and universities to enhance construction productivity for modular and offsite construction [2]. The modular building institute (MBI) is developing a procurement guide for general contractors and modular builders by engaging members of the associated general contractors of America (AGC) to help project teams navigating through lending, bonding, insurance, permitting, and inspection for modular and offsite construction which are different from traditional construction [2].

MBI is also working with an organization named; the housing crisis solutions coalition (HCSC) which believes that federal affordable housing policies, such as low-income housing tax credit (LIHTC) are not efficient. HCSC believes that modular and offsite construction can develop affordable housing quickly to be occupied earlier by low income renters to avoid the need for tax credits. However, some states can offer developers' tax credits as the one presented by State of Virginia for innovative construction processes that develop housing inventory quickly. [1]

A recent action plan was also suggested to the state of Minnesota by industry leaders from around the state to make 10% of multi-family residential developments use offsite construction in Minnesota by 2025 using five steps: 1) Starting multi-sector innovation cohorts to explore challenges and potential of using offsite construction. 2) Promoting learning opportunities to educate lenders, general contractors, and architects about benefits and characteristics of modular and offsite construction. 3) Enhancing local collaboration to fast-track pre-approvals for offsite construction projects. 4) Incentivizing pilot projects using public-private partnership (PPP) which utilize modular and offsite construction. 5) Attracting new modular builders and investors to Minnesota by an economic development campaign [32].

In Australia, the federal government is supporting the advanced manufacturing growth Centre - which is a non-profit advocacy group established in 2015- to issue grants for business development. This centre supports manufacturing companies to increase their capabilities, scope, and scale [2].

In the UK, The housing corporation – which is the non-departmental public organization that funds new affordable housing - started in 2004 to require that 25% of new social housing being funded by the organization should utilize offsite construction. However, government influence on private-sector was limited, and they did not provide direct incentives through planning policy or building regulations [30]. Hence, the housing, communities and local government committee presented a white paper to the parliament in 2017 that recognises the importance of embracing offsite construction to meet UK's plan for building 300,000 homes a year by the mid-2020s [33]. The government response to this white paper was introduced in 2019 outlining many steps to address this issue including their support to financing offsite construction using £236m from the home building fund to support to projects that incorporate offsite construction [34]. As well as establishing an offsite construction working group to address barriers to financing and insurance of offsite construction.

7 Conclusion

This paper presented a literature review for the challenges associated with financing modular and offsite construction, and the current trends in financial modelling from the developer perspective and in mortgage financing for consumers. Recent advancements

in financing modular and offsite construction were also introduced relevant to the new practices of partnering with unconventional financing sources such as venture capitals and IT companies, as well as the cash flow problems incurred by developers. The future opportunities in USA, UK, and Australia were also discussed to present different initiatives developed by organizations and governments to support the use of modular and offsite construction.

It is concluded that a steady demand and support for modular and offsite construction projects could reduce any risks associated with the manufacturing and construction of this industry. Modular and offsite construction projects need to explore new sources of funding and need to develop new sustainable business and financial models.

References

[1] Modular Building Institute (MBI). The U.S. Construction Industry: A National Crisis Looming, *Modular Building Institute*. On-line: https://www.modular.org/documents/document_publication/national-crisis-looming-whitepaper.pdf, 2019.

[2] Smith R., Rupnik I. 5 IN 5 Modular growth initiative research roadmap recommendations, *Modular Building Institute*. https://www.modular.org/documents/document_publication/2018_1019%205in5%20Deliverable.pdf , 2018.

[3] Rahman M.M. Barriers of implementing modern methods of construction. *Journal of management in engineering*, 30(1), pp.69-77, On-line: https://doi.org/10.1061/(ASCE)ME.1943-5479.0000173, 2014.

[4] Smith R. E. and Rice T. Permanent modular construction; process, practice, performance. *Special report from Modular Building Institute*. 48pages, 2015.

[5] Canadian construction innovations (ccinnovations). Challenges and opportunities for modular construction in Canada, *Workshop Summary Report hosted jointly by Concordia University , the Modular Building Institute , Canadian Construction Innovations, and the University of Alberta*, 21 pages, 2015.

[6] Salama T, Moselhi O, Al-Hussein M. Modular Industry Characteristics and Barriers to its Increased Market Share. *Modular and Offsite Construction (MOC) Summit Proceedings*. 1(1), On-line: https://doi.org/10.29173/mocs34, 2018.

[7] Salama T, Moselhi O, Al-Hussein M. Modular Industry Characteristics and Barriers to its Increased Market Share. *Special report published at the website of Modular Building institute*. On-line:https://www.modular.org/documents/document_publication/Modular_Industry_Characteristics_and_Barrier_to_its_Increased_Market_Share.pdf, 2018.

[8] Salama, T. Optimized planning and scheduling for modular and offsite construction. PhD thesis, *department of building, civil and environmental engineering, Concordia University*, *Canada,* 2019.

[9] Galante C, Draper-Zivetz S, Stein A. Building Affordability by Building Affordably: Exploring the Benefits, Barriers, and Breakthroughs Needed to Scale Off-Site Multifamily Construction. *Terner Centre for Housing Innovation, UC Berkeley.* On-line:http://ternercenter.berkeley.edu/uploads/offsite_construction.pdf, 2017.

[10] Maher A. Breaking with tradition. *Special report from AVANA capital.* https://avanacapital.com/wp-content/uploads/Expert-Speak-Finance-HT_MARCH_ISSUE_-2018.pdf , 2018.

[11] Cameron P. J., Carlo N. G. D. Piecing together modular: understanding the benefits and limitations of modular construction methods for multifamily development. *Master of Science thesis in real estate development, Dept. of Architecture, Massachusetts Institute of Technology,* On-line: http://hdl.handle.net/1721.1/42038 , 2007.

[12] Feutz D. The Hurdles to Financing Modular Development. *Cornell Real Estate Review*, *17*(1), p.23, 2019.

[13] Velamati, S. Feasibility, benefits and challenges of modular construction in high rise development in the United States: a developer's perspective, *Master of Science thesis in real estate development, Dept. of Architecture, Massachusetts Institute of Technology*, On-line: http://hdl.handle.net/1721.1/77129 , 2012.

[14] Steinhardt D., Manley K. Exploring the beliefs of Australian prefabricated house builders. *Construction Economics and Building*. 16(2):27-41, On-line: https://doi.org/10.5130/AJCEB.v16i2.4741, 2016.

[15] Stein A. Disruptive Development: Modular Manufacturing in Multifamily Housing. *Master of city planning thesis, department of city and regional planning*, University of California, Berkeley. 2016.

[16] Bertram N., Fuchs S., Mischke J., Palter R., Strube G. and Woetzel J. Modular construction: From projects to products. *McKinsey & Company: Capital Projects & Infrastructure*, pp.1-34, 2019.

[17] Abu-Khalaf A. Overcoming barriers to bringing off-site construction to scale. *Special report by Enterprise Community Partners and funded by JPMorgan Chase Foundation,* On-line:

https://www.enterprisecommunity.org/download?fid=11694&nid=8845, 2019.

[18] American Institute of Architects (AIA). Design for modular construction: an introduction for architects, *Special report by AIA,* On-line: http://content.aia.org/sites/default/files/2019-03/Materials_Practice_Guide_Modular_Construction.pdf , 2019.

[19] Smith, R. E. Prefab architecture: a guide to modular design and construction, *Wiley Publications,* ISBN: 978-0-470-27561-0, 400 pages, 2010.

[20] Cazemier D. Comparing cross laminated timber with concrete and steel: a financial analysis of two buildings in Australia. *Modular and Offsite Construction (MOC) Summit Proceedings*, 2017.

[21] Consumer Financial Protection Bureau CFPB. Manufactured-housing consumer finance in the United States, On-line: https://files.consumerfinance.gov/f/201409_cfpb_report_manufactured-housing.pdf , 2014.

[22] De Mendoza C. Prefabrication: a solution for a NZ housing shortage? *Special report by PrefabNZ,* On-line: http://www.prefabnz.com/Downloads/Assets/Download/9728/1/PrefabNZ%20CnC%20Lit%20Review%20FINAL%20180302.pdf , 2018.

[23] M&T bank. Understanding modular home construction financing: a customer guide, On-line: https://asset.mtb.com/Documents/pdf/modular-home-construction-financing.pdf , 2018.

[24] Boyd N., Khalfan M. & Maqsood T. Off-Site construction of apartment buildings. *Journal of Architectural Engineering*, 19, 51-57, On-line: https://doi.org/10.1061/(ASCE)AE.1943-5568.0000091, 2012.

[25] Kusisto L. Google will buy modular homes to address housing crunch. *The wall street journal*, On-line: https://www.wsj.com/articles/google-bets-on-modular-homes-to-fill-housing-demand-1497448838 , 2017.

[26] Anagnost A. Autodesk invests in Factory OS to advance modular construction, On-line: https://adsknews.autodesk.com/news/autodesk-invests-in-factory_os-to-make-affordable-housing-a-reality , 2019.

[27] Brenzel K. and Jeans D. Warped lumber, failed projects: TRD investigates Katerra, SoftBank's $4B construction startup, *The Real Deal: New York real estate news,* On-line: https://therealdeal.com/2019/12/16/softbank-funded-construction-startup-katerra-promised-a-tech-revolution-its-struggling-to-deliver/ , 2019.

[28] Dodge data and analytics. Prefabrication and modular construction 2020: smart market report, *Special report by Dodge data and analytics*, On-line:https://www.modular.org/documents/public/PrefabModularSmartMarketReport2020.pdf, 2020.

[29] Perinotto T. Future of Lendlease's DesignMake is under review, *the fifth estate,* On-line: https://www.thefifthestate.com.au/business/investment-deals/future-of-lendleases-designmake-is-under-review/, 2019.

[30] Pan W, Gibb AG, Dainty AR. Leading UK housebuilders' utilization of offsite construction methods. *Building research & information*. 1; 36(1):56-67, On-line: https://doi.org/10.1080/09613210701204013, 2008.

[31] Elnaas E. The decision to use off-site manufacturing (OSM) systems for house building projects in the UK, PhD thesis, *University of Brighton*, 2014.

[32] Construction revolution summit. A cross- sector collaboration to reduce the cost of housing by creating an innovation hub for offsite construction, *Summit report and action plan for Minnesota*, On-line:https://static1.squarespace.com/static/5d4b4a44a49c3800010ab89d/t/5edfe7dd5875a7412de91285/1591732195568/Construction_Revolution_Action_Plan.pdf , 2020.

[33] Department for communities and local government. Fixing our broken housing market. *Special report presented to parliament*, On-line: https://assets.publishing.service.gov.uk/government/uploads/system/uploads/attachment_data/file/590464/Fixing_our_broken_housing_market_-_print_ready_version.pdf , 2017.

[34] Ministry of housing, communities and local government. Government response to the housing, communities and local government select committee report on modern methods of construction, *Special report presented to parliament*, On-line: https://assets.publishing.service.gov.uk/government/uploads/system/uploads/attachment_data/file/832176/SC_168_-_modern_methods_of_construction.pdf , 2019.

A Novel Methodological Framework of Smart Project Delivery of Modular Integrated Construction

W. Pan[a], M. Pan[a] and Z.J. Zheng[a]

[a] Department of Civil Engineering, The University of Hong Kong, Hong Kong SAR, China
E-mail: wpan@hku.hk, panmi@connect.hku.hk, zhengzj@connect.hku.hk

Abstract –

Modular Integrated Construction (MiC) is an advanced type of modular construction focusing on addressing high-density high-rise buildings and is adopted as a new policy initiative in Hong Kong. Previous studies have examined the potential for using different methods and technologies to support project delivery in offsite and modular construction. However, there is a lack of systematic exploration and a paucity of examination of smart-tech solutions for MiC project delivery. This paper aims to develop a novel methodological framework of smart project delivery of MiC for achieving a better understanding of the complex process of MiC and ensuring the successful delivery of modular projects. This framework systematically structures the science, methods and technologies at four layers: sensor and data capturing, data storage and analysis, data visualization, and decision making. Drawing on the framework, key functions and technologies are explored through a systematic literature review, theoretical analysis and development, and focus group discussion with stakeholders. The framework provides a methodological basis for developing an integrative smart-tech platform for MiC project delivery. The findings of this paper are informative to practitioners and researchers for gaining a better understanding and implementation of MiC smart project delivery. The findings also contribute insights into the scientific methods and techniques of data capturing, analysis, visualization and use for dealing with complex and dynamic processes of modular building in high-density urban contexts.

Keywords –

Modular Construction; Modular Integrated Construction; Smart Technology; Project Delivery

1 Introduction

Modular construction (MC) has been adopted in many countries with demonstrated benefits including enhanced productivity and quality, improved health and safety, and minimized construction waste [1-3]. In Hong Kong, Modular Integrated Construction (MiC), an advanced type of the MC approach, focuses on addressing high-density high-rise buildings and has been developed as a game-changing approach to innovative building project delivery [4]. In MC and MiC, modules are produced in factories and then transported to sites for installation. It is critical to integrate real-time progress information from the factory production, module transportation and module installation on site, so that project delivery can be well monitored and controlled, achieving just-in-time delivery. However, there is still a lack of systematic exploration and a paucity of examination of smart-tech solutions for modular building project delivery.

This paper aims to develop a novel methodological framework of smart project delivery of MiC for achieving a better understanding of the complex process of MiC and ensuring the successful delivery of modular projects. This framework systematically structures the science, methods and technologies at four layers: sensor and data capturing, data storage and analysis, data visualization, and decision making. Drawing on the framework, key functions and technologies are explored through a systematic literature review, theoretical analysis and development, and focus group discussion with relevant academics and practitioners. The framework provides a basis for developing an integrative smart-tech platform for MiC project delivery. The findings of this paper are informative to practitioners and researchers for gaining a better understanding and implementation of MiC smart project delivery. The findings are also insightful in terms of the scientific methods and techniques of data capturing, analysis, visualization and use for dealing with complex and dynamic processes of modular building in high-density urban contexts.

2 Background

2.1 Modular construction in the world

Modular Construction (MC) is a novel approach to

innovate building construction by using the Design for Manufacture and Assembly (DfMA) theory and advanced manufacturing and logistics technologies. A seminal definition of MC was provided by Gibb [5] as the building approach with three-dimensional (3D) units that enclose usable space and form part of the completed building or structure. MC has been adopted in countries including UK, US, Canada, Germany, Australia and Singapore, with demonstrated benefits including accelerated onsite construction, improved health and safety, enhanced productivity and quality, and minimized construction waste [1-3].

However, the adoption of MC has largely been for houses and low-rises, with only a small number of modular high-rises such as one of 44 floors using steel frame modules in London and another of 40 floors using concrete modules in Singapore [see 6]. There is yet little experience in and scarce knowledge of delivering modular tall buildings. For the small number of modular high-rises, reported benefits and challenges co-existed [1-2]. For example, the project Apex House, a 29-floor modular building in London, was found to have achieved the benefits: (1) 12-month saving in construction duration, (2) on-site waste minimized to 2%, (3) the number of on-site workers reduced to 40, but also encountered issues such as the need for (1) more training for workers in factory as well as on site, (2) enhancement of the capability of module supply chain, and (3) early logistics planning [1]. Another example is the 'B2 Tower' project, a 32-floor residential building in New York, which was completed with severe time and cost overrun and broken project partnership. Attributors to the failure were found to include absence of employee training, lack of a comprehensive plan, insufficient quality control, constraints from labor unions and limited supply chain capability [7].

The merits of and challenges to adopting MC for high-rise buildings are not entirely understood by industry and public [3]. The design, production and construction of modules for high-rises face more technical challenges than for low to medium-rises [2]. The challenges are more significant in high-density maritime cities such as Hong Kong, Singapore, London, New York and Sydney where high-rise buildings are constrained by high-density urban environments and challenged by strong monsoons. However, there is a paucity of examination of MC tall buildings in high-density cities.

2.2 Modular integrated construction in Hong Kong

Modular Integrated Construction (MiC) is based on but advances the MC approach, and is first defined by Pan and Hon [4] as "*a game-changing disruptively-innovative approach to transforming fragmented site-based construction of buildings and facilities into integrated value-driven production and assembly of prefinished modules with the opportunity to realize enhanced quality, productivity, safety and sustainability*." It has recently been adopted as a new policy initiative as stated in the Policy Address 2017 of the Hong Kong Government [8].

The MiC initiative in Hong Kong was set in the Policy Address to mainly address two significant issues facing the construction industry: workforce shortage and very high construction cost. There are several ongoing high-rise MiC pilot projects, including two 17-storey blocks of student residence on a 3-storey podium at The University of Hong Kong and one 16-storey block of staff quarter on a 1-storey podium at The Hong Kong Science Park [9]. These projects adopt the MC systems available in the market within the existing planning and design process and practice. The benefits of MC demonstrated in other countries [1-3] are actually highly consistent and associated with time, cost, quality, safety, sustainability and productivity, and thus should also by large be achievable for MiC in Hong Kong. The potential of MiC to have a transformative impact on the construction industry is also recognized [10]. However, there is a lack of empirical evidence to support the advantageousness of MiC and clear knowledge to guide the successful project delivery that could thereby promote the wide uptake of MiC.

2.3 Previous research related to modular building project delivery

Previous studies investigated the challenges facing the delivery of MC building projects. For example, McGraw-Hill Construction [11] surveyed the American construction industry and their report revealed clients' major concerns such as the early commitment to design and engineering work, the higher requirements for transportation, and the constrained number of suppliers. Yang et al. [12] identified that MiC has many new challenges and more stringent requirements in project delivery than conventional construction methods and other types of offsite approaches. For example, onsite works for MiC depend heavily on integrated modules manufactured offsite, which implies that onsite works are especially vulnerable to poor quality control and delivery delays. There are difficulties identified in logistics control, especially when involving complicated and expensive cross-border transportation for overseas module supply [1]. Decisions to support the successful delivery of MiC projects with optimized performance in time, cost, quality and safety require a clear understanding of the complex process of MiC and leveraging of new technologies.

There have been attempts on the use of smart technologies to support project delivery in MC/MiC. Han

et al. [13] integrated simulation models and post-simulation 3D-visualization techniques for MC to support project managers' precise planning of production process and construction operation. Ramaji and Memari [14] developed information delivery framework for standardizing information exchange mechanisms to facilitate Building Information Modeling (BIM) implementation in modular buildings. Li et al. [15] explored the integration of Radio Frequency Identification (RFID) with BIM in the precast concrete factory for scheduling and supply chain management. Niu et al. [16] examined the potential of integrating Geographic Information System (GIS) and BIM for MiC logistics management. These studies and technology applications are promising for tackling different delivery issues in MiC, but there is still a lack of systematic exploration of integrative smart-tech solutions for MiC project delivery.

3 Research Methods

This paper aims to develop a novel methodological framework of smart project delivery of MiC for achieving a better understanding of the complex process of MiC and ensuring the successful delivery of modular building projects.

The framework was developed through an iterative process including literature review, theoretical analysis and development, and focus group discussion with relevant academics and practitioners. The research process is illustrated in Figure 1. First, the 1st round literature review was done on research works regarding MC/MiC, project delivery frameworks, and relevant smart technologies. Second, by integrating literature review results with theoretical analysis, an initial framework of smart project delivery of MiC was developed. Third, drawing on the initial framework, key functions and technologies were explored through a 2nd round literature review, through which the framework was concretized and refined. Fourth, focus group discussion was conducted with relevant academics and practitioners to verify and further refine the methodological framework with embedded functions and technologies. The details of focus group participants are presented in Table 1. Purposeful sampling was used to select focus group participants to cover MiC clients, contractors, suppliers, relevant government departments, as well as academic and professional bodies who have responsibility for MiC research and consultancy.

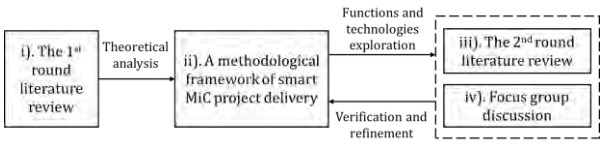

Figure 1. Research process of developing the methodological framework of MiC smart project delivery

Table 1. Participants in focus group discussion

Item	Description	Number
Primary area of practice	Contractor (with ongoing MiC project)	3
	MiC supplier	3
	Client (with ongoing MiC project)	4
	Government and its agencies	3
	Universities and professional bodies	10
Years of experience	6-9	4
	10-19	5
	More than 20 years	14
Total		23

4 A Methodological Framework of Smart Project Delivery of MiC

Successful delivery of construction projects heavily requires the reliable monitoring and control of project performance in terms of cost, time, quality, safety, and environment to satisfy stakeholder requirements via effective communication [17]. While existing literature [17-19] has addressed decision making issues of what and how performance should be measured, this present paper aims to provide a fundamental exploration of the underlying methods and technologies to support decision making in project delivery intelligently.

The proposed methodological framework of smart project delivery of MiC is illustrated in Figure 2, which systematically structures the science and methods at four layers: sensor and data capturing, data storage and analysis, data visualization, and decision making. The key scientific questions to address include:

- What types of information are needed for MiC smart project delivery?
- How such information can be represented and exchanged in various computing models with accuracy to suit different project stages?
- How such information can be analyzed and visualized for decision support?

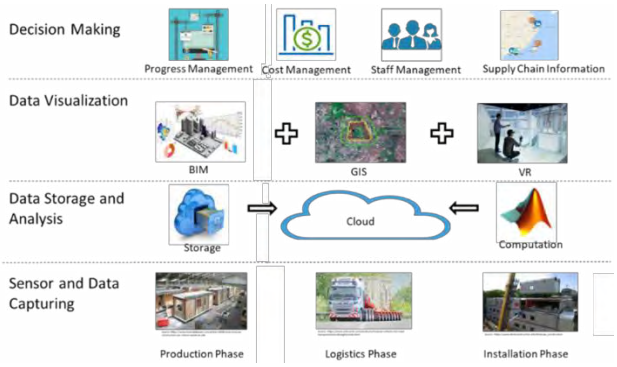

Figure 2. A novel methodological framework of smart project delivery of MiC

Figure 3. Examples of sensors used for MiC smart project delivery in the Greater Bay Area

4.1 Sensor and data capturing

The fundamental layer is sensor and data capturing, which is related to the collection of different types of information during different phases (see Figure 3) to effectively record and track relevant types of information, thereby supporting MiC project delivery.

During the production phase, tagging technologies, such as barcode [20], RFID [20], or Near-field communication (NFC) [21], can be fixed to individual modules for recording production information, e.g. module weight and dimensions, material sources, producers, quality checking and testing records. During the logistics phase, Global Position System (GPS)-based [22] and Bluetooth-based sensors [23] can be used for real-time tracking and tracing of module locations, which can further provide useful information for logistics coordination. During the on-site construction phase, images can be taken by site cameras and drones [24] to capture real-time information on module delivery and installation for efficient site planning and progress monitoring. Besides, different physiological sensors integrated into wearables [25] can be used to monitor fatigue and working conditions of workers for occupational safety and health management, such as electrocardiogram (ECG/EKG) sensors for heart monitoring, electromyography (EMG) sensors for muscle monitoring, and electroencephalography (EEG) sensors for brain monitoring.

Useful insights were obtained through the focus group discussion. Several professionals raised the concern of accuracy requirement (e.g. tracing the module in the factory to the exact on-site location) for selecting suitable sensors. Besides, some participants suggested a life-cycle management perspective that covers the stages from planning through operation and maintenance. In this regard, temperature, humidity, light and pressure sensors can be adopted to monitor the built environment; strain gauges can be used to measure strain on the module structure, thereby monitoring the health condition of the modular building.

4.2 Data storage and analysis

The second layer is data storage and analysis, through which the collected data from using smart sensors can be processed with a cloud-frog-edge computing integrated strategy (see Figure 4).

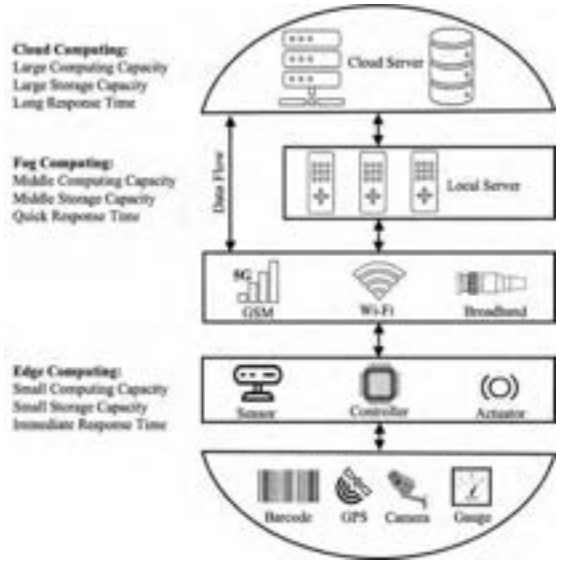

Figure 4. Cloud-frog-edge computing strategy for data storage and analysis

Cloud computing [26], and its extension, fog computing [27] and edge computing [28] can be used for dealing with different data and tasks of MiC. In general, cloud computing [26] is used for tasks that require large computing capacity but allow longer response time; frog computing [26] can be used for tasks that require a middle level of capacity; edge computing [28] is used for tasks that require immediate responses and small computing capacity. For example, in the case of onsite module installation using computer vision to detect the status of the modules, the monitoring task requires immediate responses from video streams and do not require a very large scale of computing compacity, edge computing should therefore be considered. While if the task is like logistic planning that requires large computing compacity on route selection but does not require immediate response, cloud computing should be adopted.

Based on such a data storage and analysis platform, real-time progress monitoring and control function can be developed for MiC projects to achieve just-in-time delivery. Machine learning algorithms can be integrated to predict potential progress delays and risks for better decision making. The concern of platform robustness was also discussed during the focus group meeting, in terms of how to integrate different data sources and extract information for different functions and how to manage and secure big data effectively. It is therefore important to consider information compatibility and design the information exchange schemes.

4.3 Data visualization

The third layer is data visualization, where BIM is the core technique that provides the interface for professionals to access data for project delivery.

The integration of GIS with BIM [16] is recognized as critical in digitalizing the logistics process for logistics planning and decision making. The integration is achievable through building geometry data communication between BIM (e.g. Revit) and GIS (e.g. ArcGIS) platforms for concurrent modelling of buildings. An example is given in Figure 5. Based on the BIM-GIS integration, the transportation and installation status of all modules can be visualized with their location and broader environment information for better logistics management. In addition, augmented reality and virtual reality (AR and VR) [29-31] can be used to enhance BIM for supporting effective execution of construction activities. For example, AR can provide workers with installation details of each type of module in a 3D view, from which workers can easily understand where and how to install a module.

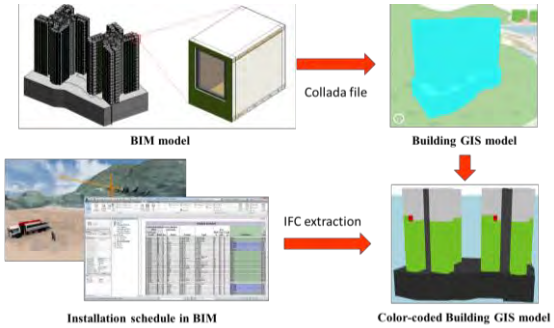

Figure 5. An example of BIM-GIS integration (after [16])

4.4 Decision making

The top layer is decision making, which deals with the managerial issues of how the analyzed and visualized information can be used for data-driven decision support in MiC project delivery. Technically, this layer should involve the design and development of desktop software (e.g. [17]) and mobile application to provide user friendly interfaces for decision making.

From a top-down perspective, identifying key areas of decision making [32, 33] is a preliminary task to support technical design of lower layers. By defining decision criteria and decision making rules, automated monitoring and control can also be achieved.

From a bottom-up view, data visualization can support decision making of stakeholders in an easily understandable manner and provide actionable insights for project delivery. First, decision makers can easily and quickly assess project delivery progress based on visualized data, thereby making timely and informed adjustments. For example, the real-time progress for module delivery can be visualized and compared with the scheduled time to support logistic planning and coordination. Second, different stakeholders can effectively communicate with each other based on data visualization for making joint decisions easier, and also can track the works of other stakeholders to make self-adjustment. Third, alternative plans or different remedial actions for identified issues can be clearly evaluated through data visualization to support decision making.

5 Discussions

The successful delivery of MiC building projects requires accurate and reliable monitoring and control to unleash the full benefits of this “factory assembly followed by on-site installation” [7] construction method for achieving its advantageousness. There are a variety of intelligent methods and technologies available to support MiC smart project delivery. However, how to effectively integrate various methods and technologies to provide

different functions and fulfill stakeholder requirements is still a challenging issue. The developed methodological framework in this paper should address this knowledge gap by providing a systematic approach for understanding many methods and technologies and establishing technical plans for MiC smart project delivery. Table 2 summarizes the examples of methods and technologies with different functions for achieving MiC smart project delivery.

MiC is a very new concept and its feasibility of adoption for high-rise buildings still remains unclear [1]. More research is needed to discover the full potential of MiC and how successful implementation can be achieved. In this regard, the developed methodological framework should support the exploration and examination of best practice for the successful delivery of MiC projects. It provides a benchmarking tool for analyzing different technologies and their integrations to best orchestrate the complex process of MiC project delivery.

From a practical perspective, the developed methodological framework should support the establishment of a workable platform, which could allow optimization for achieving MiC smart project delivery and visualization of the whole process to project stakeholders for better engagement and continuous improvement.

Table 2. Examples of methods and technologies for MiC smart project delivery

Layer	Method and technology	Function
Sensor and data capturing	Barcode, RFID, NFC	Record production information
	GPS, BLE	Track module location
	Camera	Track onsite installation progress
	Physiological sensors	Monitor fatigue and working conditions of workers
	Temperature, humidity, light and pressure sensors	Monitor the built environment
Data storage and analysis	Cloud computing, frog computing, edge computing	Preprocess raw data, match computation tasks with suitable computing capacity, and data storage
Data visualization	BIM	Data manage and exchange center
	GIS	Provide intuitive logistic information
	AR/VR	Assist construction activities
Decision making	Desktop Software, Mobile Application	Interfaces for decision making

6 Conclusions

Modular Integrated Construction (MiC) is an advanced modular construction approach by particularly addressing complex and dynamic high-rise building in high-density urban contexts. It has shown a great potential for the betterment of building construction, but there is still a lack of systematic exploration of how successful project delivery of MiC can be achieved. This paper has developed a novel methodological framework of smart project delivery of MiC. The developed framework systematically structures the science, methods and technologies at four layers: sensor and data capturing, data storage and analysis, data visualization, and decision making. Drawing on the framework, key functions and technologies were explored through a systematic literature review, theoretical analysis and development, and focus group discussion.

The framework provides a basis for understanding different technologies and methods for MiC project delivery. The findings contribute insights into the scientific methods and techniques of data capturing, analysis, visualization and use for dealing with the complex and dynamic processes of modular building in high-density urban contexts. Future study will establish an integrative smart-tech platform based on the developed framework to support project delivery of MiC using real-life projects.

Acknowledgements

The work presented in this paper is supported by a grant from the Research Impact Fund of the Hong Kong Research Grants Council (Project No.: HKU R7027-18) and a grant from the Strategic Public Policy Research Funding Scheme (Project No.: S2019.A8.013.19S) from the Policy Innovation and Co-ordination Office of the Government of the Hong Kong Special Administrative Region.

References

[1] Pan, W., Yang, Y., Zhang, Z. and Chan, S. *Modularisation for Modernisation: A Strategy Paper Rethinking Hong Kong Construction*, HKU CICID and Development Bureau of HKSAR Government, Hong Kong, 2019.

[2] Lawson, R. M., Ogden, R. G. and Popo-Ola, S. Design considerations for modular open building systems. Open House International, 36: 44-53, 2011.
[3] Smith, R. E. *Permanent Modular Construction: Process, Practice and Performance*. Modular Building Institute, 2015.
[4] Pan, W. and Hon, C.K. Modular integrated construction for high-rise buildings. *Proceedings of the Institution of Civil Engineers-Municipal Engineer*, ahead of print, 2018.
[5] Gibb, A. G. *Off-site fabrication: prefabrication, pre-assembly and modularisation*. John Wiley & Sons, 1999.
[6] Wang, Z. and Pan, W. A hybrid coupled wall system with replaceable steel coupling beams for high-rise modular buildings. *Journal of Building Engineering*, 31:101355, 2020.
[7] Pacific Northwest Center for Construction Research and Education (PNCCRE). *Modular prefabricated residential construction: constraints and opportunities*. PNCCRE, University of Washington, USA, 2013.
[8] Chief Executive. *The 2017 Policy Address: Make Best Use of Opportunities, Develop the Economy, Improve People's Livelihood, Build an Inclusive Society*. HKSAR Government, Hong Kong, 2017.
[9] Legislative Council of Hong Kong. *Legislative Council Panel on Development Construction Innovation and Technology Fund*. HKSAR Government, Hong Kong, 2018.
[10] Pan, M., Linner, T., Pan, W., Cheng, H. and Bock, T. Structuring the context for construction robot development through integrated scenario approach. *Automation in Construction*, 114: 103174, 2020.
[11] McGraw-Hill Construction. *Prefabrication and Modularization: Increasing Productivity in the Construction Industry*. McGraw-Hill Construction, Bedford, MA, 2011.
[12] Yang, Y., Pan, M. and Pan, W. 'Co-evolution through interaction' of innovative building technologies: The case of modular integrated construction and robotics. *Automation in Construction*, 107: 102932, 2019.
[13] Han, S. H., Al-Hussein, M., Al-Jibouri, S. and Yu, H. T. Automated post-simulation visualization of modular building production assembly line. *Automation in Construction*, 21: 229-236, 2012.
[14] Ramaji, I. J. and Memari, A. M. Product Architecture Model for Multistory Modular Buildings. *Journal of Construction Engineering and Management*, 142:14, 2016.
[15] Li, C. Z., Zhong, R. Y., Xue, F., Xu, G., Chen, K., Huang, G. G. and Shen, G. Q. Integrating RFID and BIM technologies for mitigating risks and improving schedule performance of prefabricated house construction. *Journal of Cleaner Production*, 165: 1048-1062, 2017.
[16] Niu, S., Yang, Y. and Pan, W. Logistics Planning and Visualization of Modular Integrated Construction Projects Based on BIM-GIS Integration and Vehicle Routing Algorithm. In *2019 Modular and Offsite Construction (MOC) Summit Proceedings*, pp.579-586, 2019.
[17] Cheung, S.O., Suen, H.C. and Cheung, K.K.. PPMS: a web-based construction project performance monitoring system. *Automation in Construction*, 13(3): 361-376, 2004.
[18] Aibinu, A.A. and Jagboro, G.O. The effects of construction delays on project delivery in Nigerian construction industry. *International Journal of Project Management*, 20(8): 593-599, 2002.
[19] Franz, B., Leicht, R., Molenaar, K. and Messner, J. Impact of team integration and group cohesion on project delivery performance. *Journal of Construction Engineering and Management*, 143(1): 04016088, 2017.
[20] Ocheoha, I.A. and Moselhi, O., 2018. A BIM-based Supply Chain Integration for Prefabrication and Modularization. *Modular and Offsite Construction (MOC) Summit Proceedings*, *1*(1).
[21] Chen, K., Xu, G., Xue, F., Zhong, R.Y., Liu, D. and Lu, W., 2018. A physical internet-enabled building information modelling system for prefabricated construction. International Journal of *Computer Integrated Manufacturing*, 31(4-5), pp.349-361.
[22] Zhong, R.Y., Peng, Y., Xue, F., Fang, J., Zou, W., Luo, H., Ng, S.T., Lu, W., Shen, G.Q. and Huang, G.Q., 2017. Prefabricated construction enabled by the Internet-of-Things. *Automation in Construction*, *76*, pp.59-70.
[23] Friesen, M.R. and McLeod, R.D., 2015. Bluetooth in intelligent transportation systems: a survey. *International Journal of Intelligent Transportation Systems Research*, 13(3), pp.143-153.
[24] Ashour, R., Taha, T., Mohamed, F., Hableel, E., Kheil, Y.A., Elsalamouny, M., Kadadha, M., Rangan, K., Dias, J., Seneviratne, L. and Cai, G., 2016, October. Site inspection drone: A solution for inspecting and regulating construction sites. In *2016 IEEE 59th International Midwest Symposium on Circuits and Systems (MWSCAS)*, pp. 1-4, IEEE.
[25] Awolusi, I., Marks, E. and Hallowell, M. Wearable technology for personalized construction safety monitoring and trending: Review of applicable devices. *Automation in Construction*, 85: 96-106, 2018.
[26] Armbrust, M., Fox, A., Griffith, R., Joseph, A.D., Katz, R., Konwinski, A., Lee, G., Patterson, D.,

Rabkin, A., Stoica, I. and Zaharia, M., 2010. A view of cloud computing. *Communications of the ACM*, *53*(4), pp.50-58.

[27] Bonomi, F., Milito, R., Zhu, J. and Addepalli, S., 2012, August. Fog computing and its role in the internet of things. *In Proceedings of the first edition of the MCC workshop on Mobile cloud computing,* pp. 13-16.

[28] Shi, W., Cao, J., Zhang, Q., Li, Y. and Xu, L., 2016. Edge computing: Vision and challenges. *IEEE internet of things journal*, *3*(5), pp.637-646.

[29] Cao, L., Lin, J. and Li, N., 2019. A virtual reality based study of indoor fire evacuation after active or passive spatial exploration. *Computers in Human Behavior*, 90, pp.37-45.

[30] Shi, Y., Du, J., Ahn, C.R. and Ragan, E., 2019. Impact assessment of reinforced learning methods on construction workers' fall risk behavior using virtual reality. *Automation in Construction*, 104, pp.197-214.

[31] Wang, X., Truijens, M., Hou, L., Wang, Y. and Zhou, Y., 2014. Integrating Augmented Reality with Building Information Modeling: Onsite construction process controlling for liquefied natural gas industry. *Automation in Construction*, 40, pp.96-105

[32] Pan, W., Dainty, A. R. and Gibb, A. G. Establishing and weighting decision criteria for building system selection in housing construction. *Journal of Construction Engineering and Management*, 138: 1239-1250, 2012.

[33] Peltokorpi, A., Olivieri, H., Granja, A. D. and Seppänen, O. Categorizing modularization strategies to achieve various objectives of building investments. *Construction Management and Economics*, 36: 32-48, 2018.

Block Chain based Remicon Quality Management

Seungwon Cho[a] , Doyeopo Lee[a] and Chansik Park[a]

[a]School of Architecture and Building Science, Chung-Ang University, Republic of Korea

E-mail: choseungwon@gmail.com, doyeop@cau.ac.kr, cpark@cau.ac.kr

Abstract –

Remicon, an important material constituting the structure of a building, needs an efficient quality management system throughout the entire process from production to delivery, including production management, shipment-transport management, and delivery management, to ensure the required performance by the contractor. Nowadays Remicon factories becoming smart factories and automated form for systematic and accurate management throughout the entire process from production to delivery, including product management, manufacturing facility management, transportation management and quality management based on advanced IT technology and computerization. However, data generated from sensor technology, big data processing technology, and SCM system, which are currently applied to the Remicon factory, are managed through single server management system. A single server has a high possibility of forgery and loss of data, which makes it less reliable for quality management of Remicon.

In this study, we propose a Remicon quality management system based on the hyper-ledger fabric, a private block chain. This is a system that can digitally generate information that needs to be verified by the quality manager to secure the quality of Remicon at each stage of 'mixing-transport-delivery' and share it to all nodes participating in the block chain network to guarantee data reliability. In addition, the Dapp (distributed application) of each node has different ledger access rights. So Remicon manufacturers belonging to different channels do not share sensitive information, but contractors and government can view the status of all Remicon quality management at the construction site.

Keywords –

BlockChain; Remicon; Ready mixed concrete; Quality Management; Concrete

1 Introduction

Ready-mixed concrete (Remicon), which is composed of raw materials, is manufactured by mixing materials according to the pre-designed mixing ratio at the factory. Unconsolidated, flexible concrete, which is Remicon, transported to the construction site within a regulated time and then subjected to a quality evaluation for constructability and durability through quality tests. Remicon, an important material constituting the structure of a building, needs an efficient quality management system in all processes from production to delivery, including production management, shipment-transport management, and delivery management, to ensure the required quality. The general Remicon quality management system manages mixing ratio reports, shipment-entry times, and field test reports based on paper documents. Most of the time, documents are accumulated for a period of time and then batched together and sent to the top, which takes considerable time and energy to organize and computerize the information [1]. This conventional quality management of Remicon can cause various problems. For instance, it is very difficult to informatize the data of the Remicon because when production period, mixing ratio management is completely dependent on the factory. Therefore, the contractor cannot accurately evaluate the Remicon quality [2]. In addition, Remicon has the characteristics of 'Just in Time', so the value as a product is lost after more than 90 minutes, so the supplier must send it to the site according to the date and time requested by the orderer [3]. However, there is no way to determine whether the specified time has been observed [4]. On the other hand, the quality test information is not shared in real time due to insufficient computerization of the quality test of the Remicon. Therefore, even if the one Remicon truck is judged carrying defective product, the defective Remicon continues to produce, and the defective Remicon continuously deliver in the field [2]. Also, it is difficult to check if the quality test inspection report issued by the quality management inspection agency is forged at the construction site, and even if the test report is kept, there is no basis to judge whether the test and inspection

were done if there is no raw data. [5].

Recently, research has been conducted on how to simplify the work by automatically computerizing the quality management data produced by the Remicon to increase the efficiency of the Remicon quality management and share data in real time [1][5][6][7]. For example, a Reimicon production system using an internet network, real-time Remicon delivery-transport management through a location tracking device, and a quality test management system through a mobile device. However, existing information systems are managed through a central server and use a method of storing data in a central database. Centralized servers can operate as a single point of failure (SPoF) vulnerable to security, accessibility and availability [8]. These shortcomings, like Remicon's paper invoice documents, have the potential for concealment and manipulation. In addition, when a concrete defect problem occurs, there is a risk that it is difficult to determine the responsibility of the Remicon factory and contractor [9] through artificial intervention. With this solution, a new way is needed for quality managers to figure out the quality of Remicon without skepticism about the authenticity of Remicon based on reliable quality management data.

2 Related Works

○ General Remicon quality management process

Currently, the Remicon industry is implementing quality management based on paper documents. In general, there are a large number of record registers for document management, which complicates the description and classification, and errors and loss of information occur during documentation. In addition, due to the excessive amount of documents, the documenting work through the manual of the quality manager is burdensome, and the lack of quality management technique makes it difficult to establish history management and evidence data [6].

○ Digitalized Remicon quality management process

In order to solve these problems, large-sized Remicon companies such as Eugene, Sampyo, and Aju have recently built a service model to apply advanced technologies such as information and communication technology (ICT) and artificial intelligence (AI) to the Remicon industry.

Eugene Company has applied Air (Artificial Intelligence for the Remicon industry), a Remicon manufacturing/management system, to domestic plants. It aims to strengthen the competitiveness of autonomous production by improving production efficiency using sensor technology and optimizing logistics using AI.

Aju is building a service model applied with information and communication technologies such as machine learning, chatbots, and robot process automation. The quality manager can automatically check the aggregate usage and check the incoming and outgoing of the Remicon truck by mobile. In addition, it is possible to determine whether quantitative supply between aggregate suppliers is made by replacing paper invoices with electronic invoices.

Sampyo developed a chatbot to check the necessary information such as the Remicon shipment volume, delivery specifications, order quantity, and truck allocation interval in real time. In addition, by establishing an ‘integrated operation system′ that applies ICT technology, it is planning to integrate and manage individual shipments of 26 Remicon factories across the country into 5 regions.

Daewoo E&C introduced the concrete quality management mobile app 'Baroque' to all sites so that the site quality manager can digitize and track the concrete quality test work with the app. Concrete test log

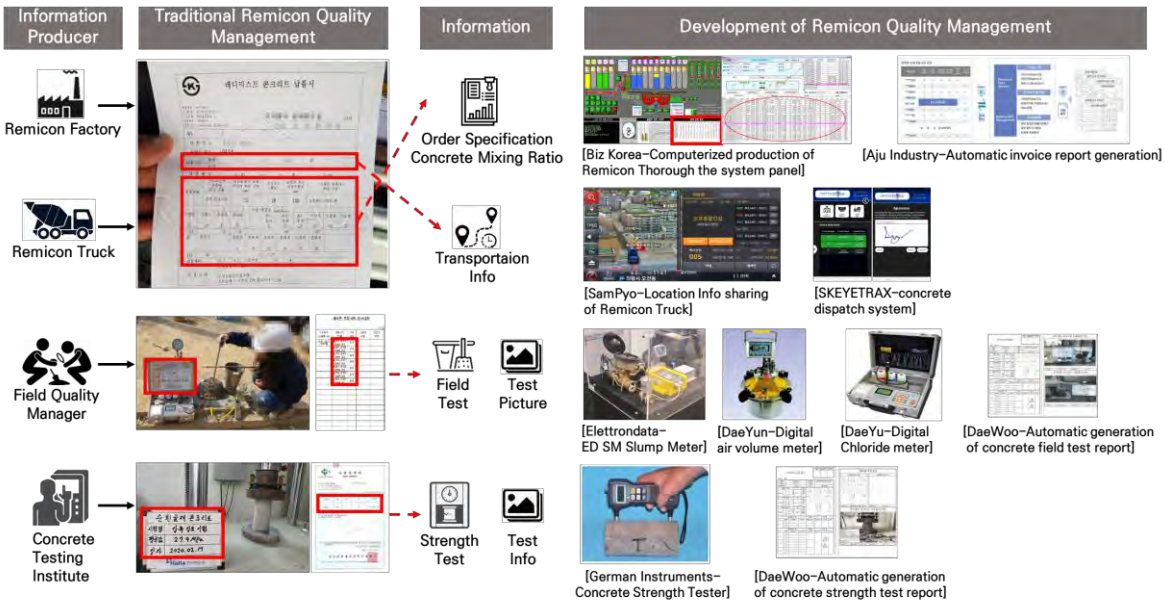

Figure 1. Remicon Quality Management Trend

includes construction site, concrete specification, concrete supplier, slump, air volume, chloride content, compressive strength of 7 and 28 days and test photo.

Biz Korea built their own Remicon quality management system to check material consumption in conjunction with panel and shipment management. In addition, it is possible to check whether the Remicon products are matched by automatically producing the shipping invoice. then, check the weighing error of the panel to manage whether it was produced according to the specifications.

○ limits of Improved Remicon quality management system

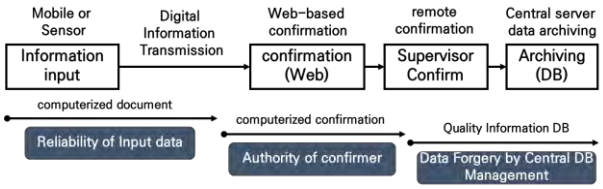

Figure 2. Limits of Improved Remicon Quality Management

Currently, Remicon's quality management is being researched by applying various technologies. It mainly deals with mixing ratio management, delivery management, and on-site quality testing to improve the efficiency of quality management that can occur during the mixing-transport-delivery process. However, the part regarding securing reliability of quality management data generated during the supply chain process of Remicon was found to be insufficient.

The management supervisory authority was keen on whether or not the quality managment of Remicon has been carried out, and in April 2018, the Ministry of Trade, Industry and Energy conducted a “Survey on Eradication of Poor Remicon” to investigate whether the cement content was insufficient or the mixing ratio was manipulated. In addition, in August 2018, the Ministry of Land, Infrastructure and Transport inspected the status of quality management in 779 Remicon factory nationwide to intensively check whether the mixing ratio of Remicon materials was false, and also confirmed whether a quality test was conducted. As such, the emphasis is placed on the reliability of the quality management of Remicon.

○ Research for securing supply chain reliability

Wang, et al studied the transparency and real-time information sharing of PC quality data for each procurement step by utilizing blockchain in the PC (Precast Concrete) Supply Chain section [9].

Abeyratne, S.A conducted a study on the Ready Manufacturing supply chain using blockchain technology to strengthen the reliability of each participants and also mentioned the need to combine blockchain technology with IT technology [10].

A Lanko researched on the efficiency of quality management of procured construction materials by introducing blockchain technology to minimize human intrusion using RFID technology in the procurement process of construction materials and to strengthen the reliability of information [11].

The Mediledger Project was developed by LinkLab and Chronicled to help manage the supply chain of medicines, including transportation of medicines that must comply with trajectory and tracking regulations [12].

N. Nizamuddin applied a blockchain technology to document management to study a system in which various stakeholders can verify and approve documents through a decentralized environment [13].

○ Theoretical considerations

Blockchain-based SCM (Supply Chain Management) is already applied to various industrial groups [14] and researched and proved that it can be sufficiently used in Remicon quality management through use-case. It is not difficult to implement an SCM system for efficient management by connecting individual quality management system at specific stages of mixing, transportation and delivery of the above-mentioned Remicon in one process [15]. Securing the reliability of quality management data using blockchain can be sufficiently approached by collecting and managing computerized data produced by the individual systems mentioned above. This prevents forgery and integrative management of data at the mixing-transport-delivery stage by integrating blockchain data storage with an existing Remicon quality management system rather than creating a new system.

3 Research Scope and Method

Blockchain technology meets the goals of this study with the advantage of sharing data using distributed ledger technology and securing the reliability of stored data. Therefore, this study intends to present a Remicon quality management system using blockchain technology.

In order to ensure the quality of Remicon, the information required by the quality manager is digitally generated and stored in the blockchain distributed ledger. Through this, the framework of the Remicon quality management system that can guarantee the reliability of data will be described.

It analyzes important quality-related data in the remicon production system using the currently developed Internet network, real-time remicon transport time management through location tracking device, and quality test management system through mobile devices.

In addition, it analyzes the data flow that distributes and stores the necessary information through the chaincode running on the blockchain.

4 BlockChain Overview

○ Blockchain

Blockchain is a distributed data storage technology. This structure ensures data integrity, reliability, and cannot be forgery by disclosing and sharing transaction details to all nodes participating in the transaction in a P2P manner without keeping transaction records on a centralized server. There are two main types of blockchain. There is a type (permissionless blockchain) where anyone participates in and verifies transactions, while there is a distributed ledger system where only predetermined participants can access the network (permissioned blockchain)

	Public	Private
Access	Open read/write	Permissioned read and/or write
speed	Slower	Faster
Security	Proof-of-Work/ Proof-of-stake	Pre-approved participants
Identity	Anonymous/pseudonymous	Known identities
Asset	Native assets	Any asset

Figure 3. Difference between Public and Private Blockchain

The permissionless blockchain has the advantage that anyone can participate in transactions and verifications, but does not meet the purpose of this study in that all nodes participating in the network can view the information uploaded to the ledger. The purpose of this study is that the permissioned blockchain that allows only a predetermined participant to access the network (view data) is required in order to set the node authority so that only those concerned with Remicon quality managment can access and input data [16].

○ Hyperledger Fabric

Hyperledger Fabric provides a permissioned network and security by keeping transactions confidential. In addition, it is possible to automate business processes using chaincode and verify the identity of network participants with the MSP function. Therefore, it is possible to clarify the responsibility and network configuration with reliable nodes. In addition, through the Channeling function, the ledger can be released only to authorized participants, thereby preventing indiscriminate data access.

5 BlockChain based Remicon Quality Management System

This chapter describes the development of a Remicon quality management system based on blockchain technology to increase the reliability of stored data. The developed system constructs a Permissioned-Private network using Hyperledger Fabric blockchain technology. Therefore, the important information produced at each stage of the quality management of the Remicon can be distributed and stored so that the quality manager can access the information.

○ system architecture

This system divides the chaincode function according to the type of information produced in each process of mixing-transportation-delivery and distributes the individual information on the quality management of Remicon.

The chain code consists of an insert data function

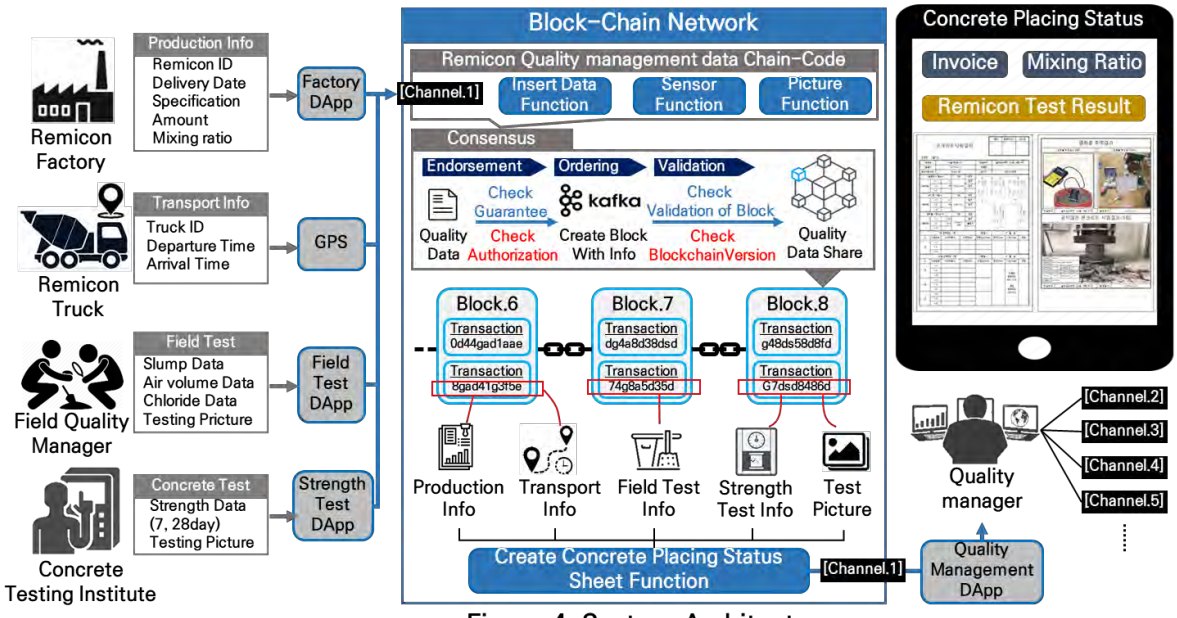

Figure 4. System Architecture

that stores the values input from the Remicon factory, a sensor function that stores GPS data of the Remicon truck and test data, and a picture function that stores pictures of the test process. It is composed of create concrete placing status sheet function for convenient reading by quality manager by reconfiguring mixing ratio information, transportation information, and test information.

Distributed client applications that operate on this blockchain-based Remicon quality management system are divided into Remicon factory, field quality managers, concrete testing institute, and quality manager according to the user's role. In order to use these applications separately for each user, Hyperledger's Membership Service Provide (MSP) function manages the necessary authority (account) to call each function of the chaincode for each user. The authorized user sends data through the application with the corresponding account. The transferred data is verified again through the process of identification and signature verification in the consensus process to verify the reliability of the data produced by the user(quality management data producer).

The Remicon quality management data of each step is called a create concrete placing status sheet function as an application for quality managers after a step of checking an account at the request of the quality manager. Therefore, the stored data is arranged in a certain form and the quality management of the Remicon is provided to the quality manager.

In addition, through the channel MSP, producers of Remicon quality management data can access the corresponding ledger, but not the data of other ledgers. For example, Remicon A factory can judge whether their Remicon has been properly delivered to the ordered site and tested, but cannot see the order history of Remicon B factory belonging to other ledgers. In this way, the quality manager can read the quality managment contents of the Remicon in all ledgers, but it is designed not to share sensitive information among the Remicon factories.

○ Smart Contract architecture

The essence of the transaction is the invoking of a smart contract (chaincode), deployed into the blockchain network to enable interaction with the shared ledger.

Fig 5 illustrated the interaction flow with the chaincode. The client inputs the function name and arguments to initialize the truncation and peers access or modify the ledger via chaincode based on multiple application. Generally, two operations are involved in chaincode: the “init” and “invoke” functions. The “init” function is called when initializing or upgrading chaincode; “invoke” is used in response to transaction proposals to query or update the ledger. In this system, the “invoke” function is composed of eight specific functions: InsertDB, UpdateTransportationTime, UpdateSlump-Test, UpdateAirTest, UpdatePressureTest, Update-Picture and QueryDB.

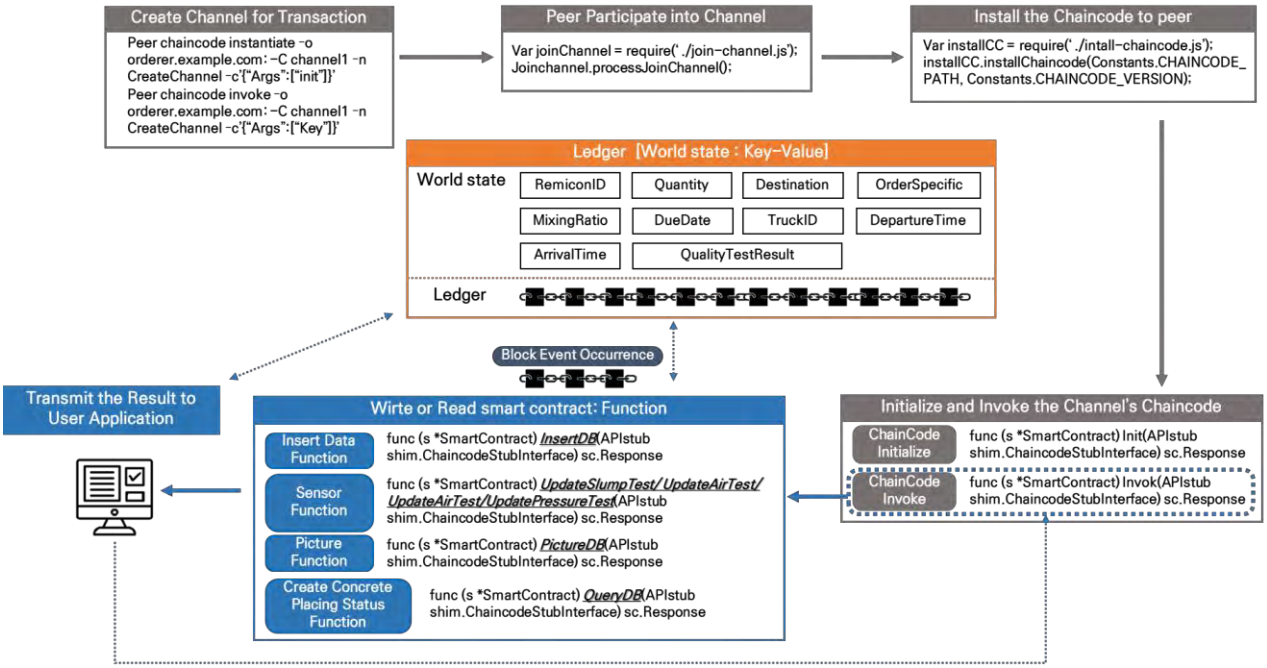

Figure 5. Architecture of Chaincode

Fucntion Name	Invoke Authority	Explaination
InsertDB	Remicon Factory	Input the mixing ratio value into the Remicon mixing control panel
UpdateTransportationTime	Remicon Truck	Input departure and arrival times based on the GPS data of the Remicon Truck
UpdateSlumpTest	Field Quality Manager	Input sensor-based slump data
UpdateAirTest	Field Quality Manager	Input sensor-based Air Volume data
UpdateChlorideTest	Field Quality Manager	Input sensor-based Chloride data
UpdatePressureTest	Concrete Testing Institute	Input sensor-based Compressive Strength of Specimen data
UpdatePicture	Field Quality Manager/ Concrete Testing Institute	Uploade the picture of while tesing Remicon Quality
QueryDB	Quality Manager (Contractor/ Government/ Factory Quality Manager)	All Remicon quality data can be invoked and created in a certain form to be viewed as an application for quality manager.

Figure 6. Explanation of functions

○ Function

The functions and calling authority for storing or viewing Remicon quality management data through the client application are as follows Fig 6.

"QueryDB" function is used to obtain the Remicon quality management data and attributes value. The last seven functions are invoked when Remicon is produced, transported, and delivered, respectively.

6 Features of the Developed Remicon Quality Management System

In general, Remicon quality management checks whether the performance required by the contractor is secured on a document basis. It is difficult to judge the existence of improper quality management records that can be forged. In contrast, the developed blockchain-based Remicon quality management system used computerization and sensors as a way to minimize human intervention when storing mixing ratio reports produced at the mixing stage, compliance with time regulations during transportation, and test data after delivery. Therefore, it reduced human-error and allowed quality manager to view the reliable quality management data in real time.

○ Mixing process

Data for preparing shipping invoices are received from the Remicon panel, which is a system that automatically calculates the mix ratio of Remicon according to the order specifications of the construction company and automatically weighs raw materials. Input RemiconID, Quantity, Destination, Order-Specification, Mixing Ratio, Due date data into Remicon Invoice Info table in charge of Remicon production information in Production Process.

○ Transport process

Departure Time and Arrival Time are recorded in the Transportation Info table in charge of managing transport time information in the transport process by analyzing the GPS data attached to the Remicon.

○ Site Test process

The sensor corresponding to the test info table in charge of the Remicon quality test data put into the delivery process by receiving the slump value, air volume, and chloride content of the Remicon through sensorization of the on-site test equipment. In addition, pictures for each test are transmitted.

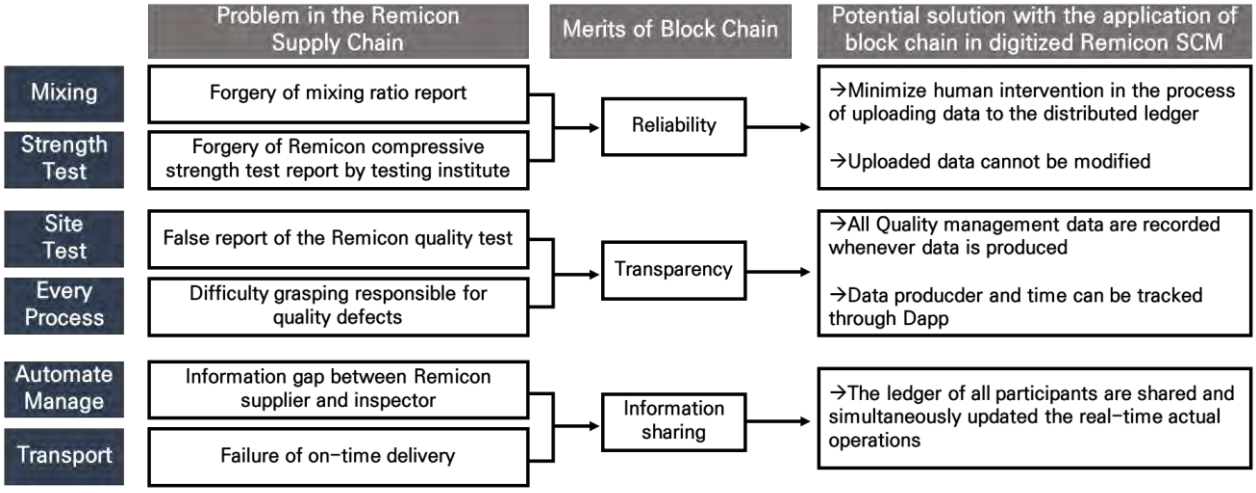

Figure 7. Advantages of System Utilizing Blockchain

○ quality test institution process

The strength of the specimen on the 7th and 28th is measured by the in-house quality testing laboratory or the external quality testing institution. After receiving the data through the strength measurement sensor, record the compressive strength of 7 and 28 days in the Test Info table in charge of the Remicon quality test data in the delivery process. Also, pictures for each test are transmitted.

○ Automation of Remicon quality management documents

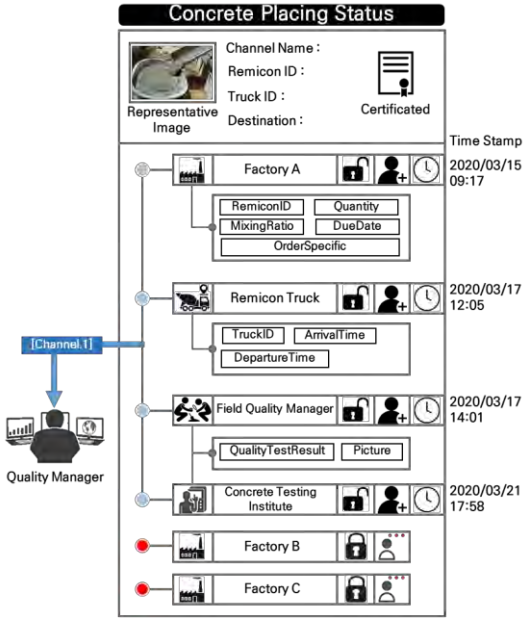

Figure 8. Data Produce Structure

The quality manager (Contractor, Government, Factory Quality Manager) can easily comprehend the status of the quality management of the Remicon by automatically filling in the digital document of the concrete placing status sheet in a certain form by calling all stored Remicon quality management data.

○ Data Base

Fig 9 show indicate what kind of data would be stored in blockchain. Remicon Invoice Info, Transportation Info, and Test Info data produced by each quality management data producer accessing the application with the corresponding account during the quality management process are as follows. The data to be registered in the block chain is Remion ID, quantity, Destination for Remicon, order specification from contractor, mixing ratio of Remicon, due date for delivery, Remicon truck ID, truck Departure-Arrival time, test result(slump, air, chloride, strength) and picture of test. This information is continuously recorded through a step-by-step process, and each data can know who and when stored the information and the account who generates the action. The action execution result is stored in the blockchain in the form of a transaction. By checking the transaction history, it is possible to grasp at what stage there is data forgery, and finally, to ensure the reliability of the Remicon quality management information producing. In addition, the quality manager can view reliable Remicon quality management data.

7 Conclusion

In this study, we proposed to form a trust protocol for quality management through transparent disclosure of quality management details among data producers by utilizing blockchain technology.

The proposed system can prevent the generation of false results by accessing the distributed application used by the producers of Remicon quality managment data at each stage through the corresponding account. In addition, it is meaningful in that it is possible to perform the quality managment of Remicon with integrity, confidentiality and reliability. This ensures transparency through the transaction history of which data is inputted and when data is stored according to the process, and makes it possible to clarify the responsibility even if a concrete defect occurs. since both the contractor and the Remicon factory can share the quality data, the factory can read the field test contents and have confidence in the quality of their product. In addition, the access rights of each blockchain network participant node's ledgers are different, so that remicon factory belonging to different channels do not share sensitive information like how much be ordered or payed, but contractors or national supervisory authorities, etc. can view the status of all remicon quality management at the construction site. it is expected that the national supervisory authority will be able to solve the problem of document forgery/falsification in the process of inspecting whether

	Remicon Invoice Info						Transportaion Info			Test Info
Process	Remicon ID	Quantity	Destination	Order Specfication	Mixing Ratio	Due Date	Truck ID	Departure Time	Arrival Time	Quality Test Result
Production	Remicon.1	6㎥	A Jobsite	25-24-151	[W/C:34.29% , S/a:31.5% , W:6Kg , C:17.5kg , S:26.7kg , G:59.2kg , AE:175g]	2020-06-22				
Trasnportaion	Remicon.1	6㎥	A Jobsite	25-24-152	[W/C:34.29% , S/a:31.5% , W:6Kg , C:17.5kg , S:26.7kg , G:59.2kg , AE:175g]	2020-06-22	Truck.1	2020-06-22 / 06:00	2020-06-22 / 6:50	
Delivery	Remicon.1	6㎥	A Jobsite	25-24-153	[W/C:34.29% , S/a:31.5% , W:6Kg , C:17.5kg , S:26.7kg , G:59.2kg , AE:175g]	2020-06-22	Truck.1	2020-06-22 / 06:00	2020-06-22 / 6:50	[Slump:25 ,Air:4.7% ,Chlorid0:3㎥: ,Mpa(3):30, Mpa(7):182, Mpa(28):358MP] + Picture

Figure 9. DataBase Structure in Blockchain

the quality managment of concrete at the site has been properly performed by reading the concrete placing status sheet of digital document based on trusted data.

In this study, in order to solve the Oracle problem (If information is posted on the blockchain, it is almost impossible to correct it, and forgery is impossible, so if incorrect information is uploaded from the beginning, the information cannot be trusted) when computerizing the Remicon quality management data produced at each stage, it was designed to minimize human intervention. This presupposes the direct transmission and reception of computerized quality management data generated from sensor technology, data processing technology, and SCM systems currently applied to the Remicon industry. In order to connect with the data transmission part of the computerized Remicon quality management system, it is necessary to open and interwork with the system API of the corresponding company, and optimization to meet compatibility is expected. In addition, due to the nature of the blockchain, all quality management data are disclosed, and sensitive concerns that each company's core technology is leaked out should be adjusted.

Acknowledgment

This study was financially supported by the National Research Foundation of Korea (NRF) grant funded by the Korea government Ministry of Science and ICT (MSIP) [No.NRF-2019R1A2B5B02070721] and [No. NRF-2020R1I1A1A01073167].

References

[1] Lee Tae-sik, Research on Invoice Process using RFID at Construction Site, Korean Society of Civil Engineers Regular Conference, 2005-10

[2] Kim Soo-yeon, Design and Implementation of Real-time Mobile Remicon Quality Management Program for Immediate Response to Mixing of Remicon, The Journal of the Korea Internet and Communications Society, Vol. 19, No. 2, 2019-02-16

[3] Chang-Duk Kim, Development of heavy lifting and procurement system for just in time of construction work, Ministry of Construction and Transportation, Korea Institute of Construction and Transportation Technology Evaluation Report, 2004-01

[4] Won-dong Lee, Case study on the efficiency of transportation of ready-mixed concrete through process re-establishment, IE Interfaces vol16 no1 pp44-53, 2003-04

[5] Kim Young-jin, Construction Material Quality Test Result Management System Research Plan, Korea Information Science Society Academic Papers vol39, 2012-06

[6] Moon Ji-hee, Study on Improvement Method of Concrete Quality Test Management Process Using Mobile Technology and Web, Proceedings of the Korean Institute of Architecture Conference vol23, 2003-10

[7] Yoo Jae-kang, Technology for Simplifying Remicon Quality Test Using Smartphone App, Spring Conference of the Korea Concrete Institute, 2019

[8] Han Jun Choi, Utilization of blockchain technology in the healthcare industry, Korea Health Industry Development Institute Health Industry Brief Vol.236, 2017-05-12

[9] Kyung-Hoon Kim, Strategies for securing quality when pouring concrete, Korea Inst Build Construction vol18 no3, 2018

[10] Wang et al, Blockchain-based framework for improving supply chain traceability and information sharing in precast construction, Automation in Construction 111, 2020

[11] Abeyratne S.A, Blockchain ready manufacturing supply chain using distributed ledger, IJRET vol.05 issue.09, 2016-09

[12] A. Lanko, Application of RFID combined with blockchain technology in logistics of construction materials, MATEC Web of Conferences 170, 2018

[13] Mark Crawford, Blockchain: Will it transform the pharmaceutical supply chain?, LOGFILE38, 2018-10

[14] N. Nizamuddin, Decentralized document version control using ethereum blockchain and IPFS, Computer and Electrical Engineering vol.76, 2019

[15] Myung-Hwan Lee, Analysis of Trends in Utilization of Blockchain Technology, Weekly Technology Trend of Information and Communication Technology Promotion Center, 2016-11-16

[16] Jeong Jin-hak, Factory Automation in the Remicon Industry, Journal of the Concrete Institute, Vol. 32, No. 1, 2020-01

[17] Lee Dong-hyuk, Edge Blockchain-Based CCTV Video Privacy Protection Technique, Journal of KITT vol.17 no10 pp101-113, 2019-10-31

A Conceptual Model for Transformation of Bill of Materials from Offsite Manufacturing to Onsite Construction in Industrialized House-building

Raafat Hussamadin[a], Mikael Viklund Tallgren[b], Gustav Jansson, Ph.D.[a]

[a] Department of Civil, Environmental and Natural Resources Engineering, Luleå University of Technology, Sweden
[b] Department of Architecture and Civil Engineering, Construction Management, Chalmers University of Technology, Sweden
E-mail: Raafat.Hussamadin@ltu.se, Mikael.Tallgren@chalmers.se, Gustav.Jansson@ltu.se

Abstract –

Lending inspiration from the manufacturing industry, industrialized house-builders have adopted some of its characteristics such as high standardization of configurable products and manufacturing processes. Standardization of product and information flow within industrialized house-building has shown to beneficially increase offsite manufacturing efficiency. They have however not been able to transfer the increase in efficiency to onsite construction, leading to it being one of the key issues resulting in delays. For offsite manufacturing, previous research has suggested Bill of Material (BOM) as a structure to define information for in manufacturing phases. However, due to the variation in workflow between offsite manufacturing and onsite construction, the structure of a BOM for offsite manufacturing cannot be reused in onsite construction, ultimately resulting in increased data redundancy and recreation.

A conceptual model of a BOM for onsite construction has been developed inspired by Bill of Materials (BOM), Work Breakdown Structure (WBS), Location Breakdown Structure (LBS), Standard Operating Procedure (SOP) and Work Instructions (WI). The conceptual model utilizes space structure LBS to link spaces with SOPs. Furthermore, it also utilizes WBS to link SOPs with WIs.

The BOM for onsite construction is generated by a transformation from offsite manufacturing P-BOM. Streamlining the information flow and transformation between manufacturing and construction phases open the possibility to develop IT-solutions for industrialized house-builders. By developing existing IT-systems to reduce data redundancy, the fragmentation between offsite manufacturing and construction sites could be utilized by reusing existing data. The conceptual model supports multiple information views and allows for information filtering determined by the performed work and project.

Keywords –

Bill of Material; Industrialized House-building; Data Redundancy; Work Breakdown Structure; Location Breakdown Structure; Work Instructions; Information filtering; Offsite Manufacturing; Onsite Construction

1 Introduction

Industrialized house-building (IHB) has been considered as one of possible solutions to achieve the desired increase in effectiveness and efficiency of the construction sector [1]. It has therefore been a major research area in Sweden, where the Swedish construction sector has been a driving force in achieving a substantial development of industrial house-building. IHB has been characterized by high standardization in platforms for basic house types, configurations as well as offsite manufacturing [2]. It has shown several benefits within the construction sector, including assurance of product quality, higher productivity, improved control over manufacturing processes and even improved storage management within onsite construction [3]. IHB has led to an increase in the amount of information produced, handled and gathered around a project [4]. Usage and distribution of information within offsite manufacturing have drastically improved in recent years through a highly integrated offsite engineering, design and manufacturing process [2,3].

IHB could potentially improve the efficiency of onsite logistics, material handling, progress tracking and other onsite activities [3]. To achieve that, its management system must be well integrated with the already existing offsite manufacturing systems. This is however far from reality, where onsite construction is wasting resources searching, sharing or recreating of data,

indicating a clear information flow detachment between prefabrication, assembly and construction site [5].

The degree of redefinition is based on the needed level of flexibility to achieve the desired customer value from the product [6]. Therefore, it is important for the information structure to be flexible according to company needs and clients demands.

Inspired by the manufacturing industry, some companies in the industrialized construction sector have adopted information structures relying on the Bill of Materials (BOM). BOM has the potential to describe the breakdown of a product for IT systems, with the intention of organizing information in a form that makes it usable to visualize multiple information views as well as different phases of a product's life cycle [7,8]. For this, BOM structures need to be integrated with the existing manufacturing systems [3].

The purpose of this study is two-folded. First, explore how BOM could be extended to onsite construction. Secondly, analyze how the extended BOM for onsite construction could reduce data redundancy as well as fragmentation between offsite manufacturing and onsite construction.

2 Research Approach

The study uses Hevner's design science (DS) approach [9], focusing on data collection from five case studies consisting of unstructured interviews, observations and supplemented by a literature review. DS is utilized to research and explore models for onsite BOM, by combining unstructured interviews and observations from case studies to identify practices and structures of construction sites.

Three companies have been observed in the study, two IHB companies (A and B) and one traditional construction company (C). In total these make up five study product cases, two with company A, one with company B and two with company C. A and B have been chosen due to them being the leading IHB companies in Sweden and have during the latter years focused on their processes and information flows, thus represented the leading edge of digitalization of the industry. C is one of the five biggest contractors in Sweden and focuses on construction site digitalization.

The literature review has been an iterative process; each phase of the research has yielded concepts that have been further reviewed and incorporated into the paper, which also has led to further unstructured interviews and discussions. The literature review started out with basic concepts such as the status of Information structures, BOM, Building information modelling (BIM) and Information filtering.

3 Theory

3.1 Information structure & Bill of Materials

A major limitation in current Building Information modelling (BIM) practices is the prevailing activity-based focus of the construction industry, rather than information-centric [10]. Information structures, attributes as well as multiple information views are important for an IT-system to be able to support a variety of construction processes under the life cycle of a building [11]. A way to handle this is through standardization in the form of BOM. Creation of a common information structure and a basis for information flow provides the opportunity for IHB to integrate their products into IT-systems and therefore simplify communication not only within the company itself but also with other companies [7]. BOM can be used to describe the structural breakdown of a product and its relationship with sub-assembly, parts and materials. The BOM has the intention of organizing information so that it can be used in IT-systems under multiple different phases of its life cycle and for a variety of cases by using different information views optimized for each specific task [7,12,13].

When it comes to BOMs in construction, more specifically in IHB, research has exemplified definitions created for design and offsite production phases, there is however little published research on onsite construction within the context of IHB.

Within design and offsite manufacturing, research focuses mainly on Engineering BOM (E-BOM), Manufacturing BOM (M-BOM) and Process BOM (P-BOM) as well as their transformations, see Figure 1. Transformation between these BOM types occurs by modifying the information structure hierarchy, adding or even deleting data from the parent BOM [8]. E-BOM often works as the essential source of information for all other types of BOMs, meaning that all other forms of BOMs are subtypes of an E-BOM [8]. Therefore, it is important to keep E-BOM as the foundation of BOM structure when a transformation occurs.

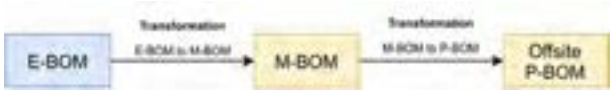

Figure 1. BOM Transformation [7].

Research defines E-BOM as a BOM utilized by designers with the intention to represent the product structure from an engineering viewpoint and is often produced by CAD/BIM systems [14]. M-BOM represents the manufacturing assembly sequence of a product. Its structure is perceived as a series of hierarchical groups and is generated from an E-BOM

transformation, in which additional information of manufacturing sequence is added to the structure [14]. P-BOM is utilized in offsite manufacturing and is generated from an M-BOM transformation with inclusion of detailed process information for assembly of modules and its components [8].

3.2 Location Breakdown Structure

Location Breakdown Structure (LBS), see Figure 2, is a hierarchical structure of spaces that can be used within a project [15,16]. LBS is intended to decompose spaces into smaller units, where each descending level has higher detail of space definition, resulting in a more usable and manageable LBS. Space is a geometrical volume which contains information describing a specific portion of the construction site as well as its relation to other spaces. Different detail levels can be used depending on the needs of each task. Detail planning and finishing related tasks is often preferred to be conducted at the highest level of detail [17]. The highest level in the LBS hierarchy usually represents the construction site of the project, and the lowest level often is represented by apartments. However, it is also possible to have each individual room in the apartment at the lowest level.

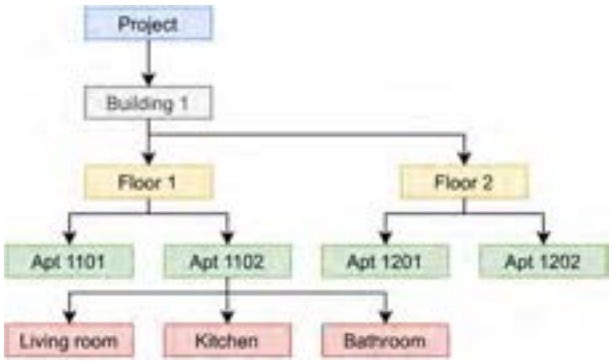

Figure 2. LBS example for a construction project.

3.3 Work Breakdown Structure

Work Breakdown Structure (WBS), see Figure 3, is a project breakdown from the perspective of construction tasks, where the completion of the project is related to the tasks being done [18,19]. WBS is intended to decompose the tasks into smaller tasks that are more manageable by creating a hierarchical structure of tasks [20,21]. Each descending level in the WBS hierarchy represents the subdivision of tasks and an increase in detail of task definition. Usually, the highest level represents the entire project and the lowest level being work packages. It is at work package level that tasks can be assigned to individuals, teams or even contractors [20,22]. WBS must be used with an appropriate level of task detail, as unneeded decomposing will end up requiring additional management efforts and higher cost [20]. Using WBS can improve process management, process definition, scheduling, risk analysis, cost estimation and project organization [21,23].

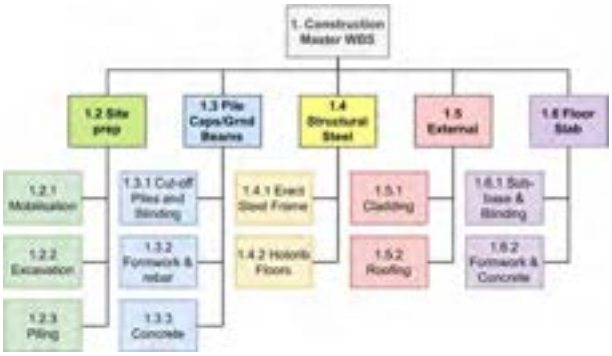

Figure 3. WBS example for a construction project [24].

3.4 Standard Operating Procedure & Work Instruction in construction

Standard Operating Procedure (SOP) is a documented manual of a company's established practices [25]. According to Nakagawa, a well-documented SOP utilizing companies' experience is essential to reach increased construction quality and consistency as well as reduction of scheduling waste, environmental impacts and safety risks [26]. To achieve its goals, a SOP needs to contain information about construction methods, assembly sequence, activity duration, safety instructions and preparatory work [25,26].

Work instruction (WI) is a documented manual of a company's construction methods [27,28]. Traditionally, it is created as text documents containing a list of instructional tasks to guide the assembly process of a building project, it can include shop drawings, 3D models, animations and pictures [29]. A WI includes sequenced instructional description of tasks, safety information as well as a list of resources such as tools and materials [28,29]. To avoid assembly process errors, delays and damaging the credibility of WIs, it is of utmost importance to ensure that WIs are updated in a quick manner [29,30].

4 Conceptual Model Development

The current information structure according to studied cases of offsite P-BOM cannot be reused for onsite construction, with the main reason being the variation in workflow. The industrialized offsite manufacturing and assembly process is done in a factory single assembly line. Components and parts are being assembled while the semi-finished modules are being moved from one workstation to another. Meaning that the factory defines specific workstations in which specific tasks and resources are being used. This enables optimization of tasks and resource management within the factory as well as minimizing the resource usage. Due to spaces being the non-movable components in onsite construction. Instead, it is now the workers and resources that are being moved. While the construction is ongoing, unlike assembly line production, new spaces are becoming available, leading to a more complex and dynamic relation between spaces that needs to be taken into consideration.

This paper proposes the creation of a new BOM for onsite construction, called **onsite BOM**. Onsite BOM aims to improve data sharing by streamlining the information flow process and reducing data redundancy. For that, an onsite BOM is defined, its transformation as well as its dependencies.

4.1 Transformation of BOM

Generally, all forms of BOM transformation are derived from either E-BOM or M-BOM [8]. However, due to the existence of reusable information within offsite manufacturing, and to achieve the aim of reducing data redundancy as well as information recreation, the concept is instead based around a transformation of offsite P-BOM to onsite BOM, see Figure 4. This transformation gives access to information that before was unavailable to the construction site and had to be recreated or modified. From E-BOM, it gets access to information about module types, properties, location of modules as well as components within modules. It even gets access to space data from E-BOM, information used to identify room types, room properties while simultaneously identifying module relations as well as space requirements and limitations. Sequence of module assembly for onsite construction is available from the M-BOM and can be used to identify delivery order of modules, assembly order of modules as well as delivery date estimation to construction site.

Offsite leftover tasks are leftover tasks allocated to onsite construction from offsite manufacturing and the information is available to access from P-BOM to identify additional work instructions required for project completion. Reuse of its data can result in data redundancy reduction as currently this data is manually recreated by site managers as well as skilled workers.

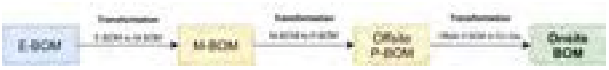

Figure 4. Concept of BOM Transformation from offsite P-BOM to onsite BOM.

4.2 Location Breakdown Structure

To manage and utilize generated spaces within onsite construction a concept of LBS for IHB has been developed from the case study, in which variations of space types and their relation are identified according to needs of IHB.

- The highest level in the LBS hierarchy embodies the whole space that the construction site will occupy, called Product or Project.
- The first descending level in LBS is Buildings, this hierarchy embodies the separate buildings within the product to create a distinction between the building volumes as well as maintain information independently between them.
- The second descending level in LBS is Levels, in which spaces are hierarchically organized with a higher level of detail according to their floor level in the building.
- The third descending level creates a distinction between apartments and stairwells, in which all apartments and stairwells are identified.
- For apartments, the fourth descending level in the hierarchy maintains information about the room, including its room type.
- The lowest descending level in LBS is Modules, it defines the bounding space of modules manufactured offsite and is derived from either Room or Stairwell.

This structure of LBS gives an identified module relation with other modules by identifying which modules create which rooms or stairwell, see Figure 5.

In the concept, Modules have been put as the most detailed level of the space, while they arguably could have been placed under Buildings or even under Levels. Information on Modules are often only required in early stages of onsite construction with exception to offsite leftover tasks, while Levels and Apartments are used from the beginning until completion of construction. Therefore, having the highest level of detail results in it not being required as often when performing construction tasks and can therefore be more often filtered from the information view.

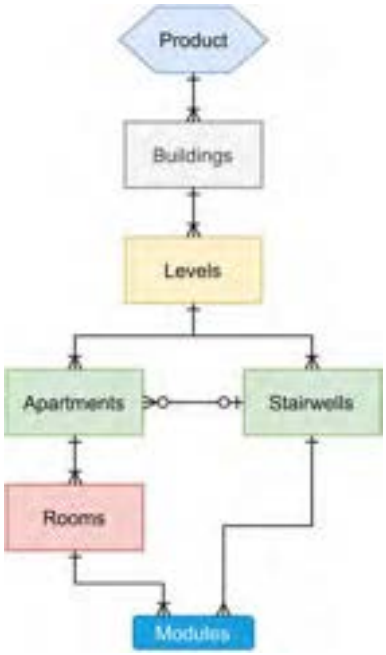

Figure 5. Concept of LBS for IHB projects.

4.3 Relations of BOM for onsite construction

The concept, Figure 6, utilizes the structure of LBS to link spaces with SOPs to create a relation between construction tasks and associated spaces. Each work instruction within a SOP contains information of what spaces it needs to be performed on, with what resources as well as what its space restrictions and requirements are. To put in context, see Figure 6, a SOP is performed for replacement of a window due to a leftover task. It includes two WIs, one for removal of the window and one for its installation, due to it being a leftover task, the SOP is linked to the Module, the highest level of detail, and therefore accessing the available information about the module from offsite P-BOM, including type, dimensions and other specifications of the window.

The concept has spaces as the sole carriers of construction status to establish a communication hub with all other SOPs. The links between WI, SOP as well as LBS ensures a consistent information interoperability between them under all levels of detail. Information interoperability is essential to dynamically modify the sequence of WI and SOPs to adjust according to construction sites continuously changing demands. It is

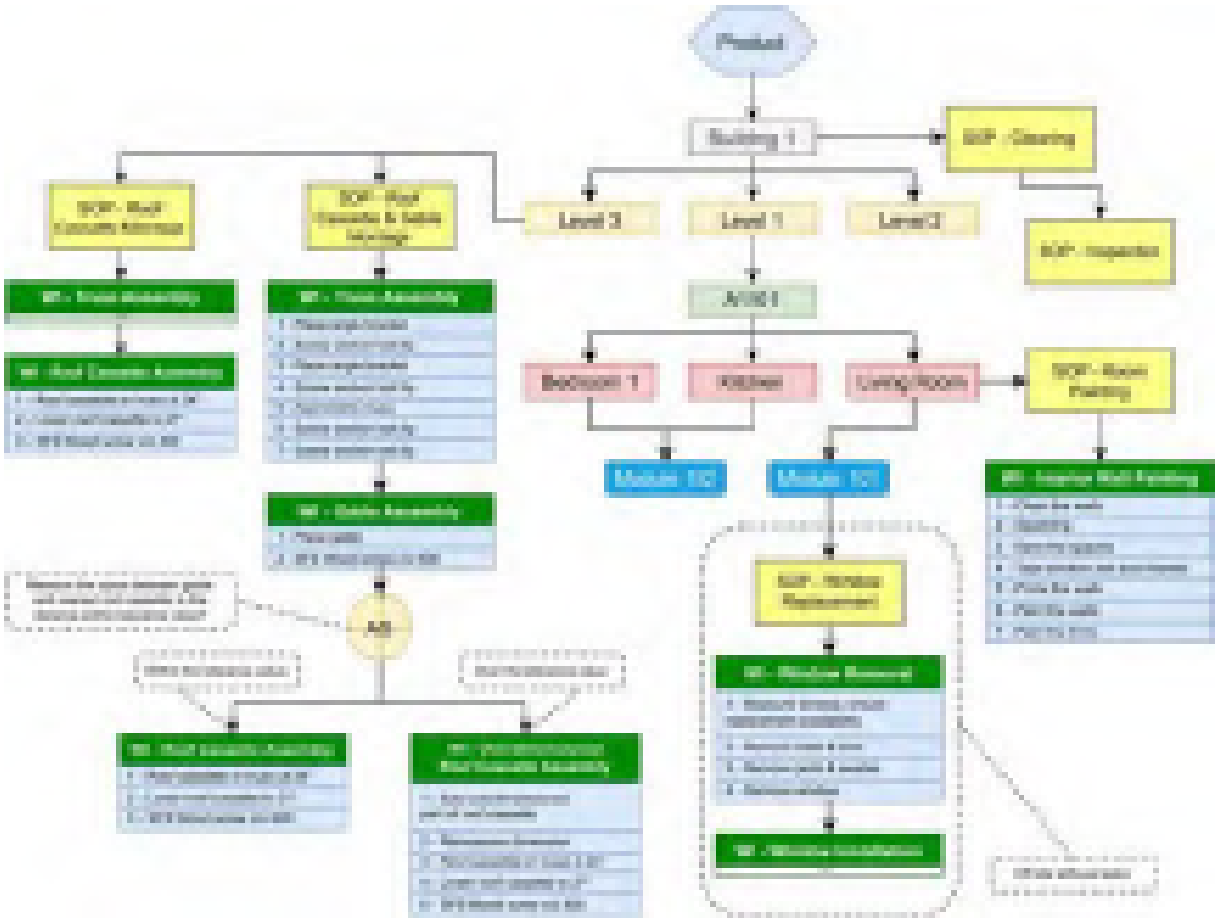

Figure 6. Concept of onsite BOM for IHB projects linking LBS with SOPs, WIs, AS and instructions.

also essential, when looking for an information structure that supports information filtering, as in showing the right amount and type of information to the right target group in information views. Information needs to be interoperable in the information structure for it to be synchronized and filtered to the correct target group. The breakdown structure of information makes filtration possible as it specifies all the existing relations under all levels of detail for the system, therefore showing the ones needed as well as the ones that can be filtered out. The existing types of relation in the concept are: Space – Space, Space – SOP, SOP – WI, SOP – Alternative sequence, Alternative sequence – WI, WI – WI and WI - Instructions.

Alternative sequences (AS), see Figure 6, are alternate WI arrangements within a SOP that can be triggered for foreseeable changes or issues that can be required to conduct a SOP correctly. The study shows that AS changes the sequence of WI within a specific SOP. A SOP has therefore accessibility to information available within its WI sequence and AS. AS consists of a ruleset describing its intentions, multiple alternative WIs and a description of said WIs. It reduces the managerial demands for when modifications are necessary, for example due to weather or construction tolerance related issues that occur commonly. In addition to that, it decreases data redundancy by reducing the need for modification of construction sequence as well as recreation of WI specific for special cases.

The conceptual BOM is built to ensure that SOPs can be assigned to any space independent of its level of detail. This is done by ensuring that available and required information within spaces stay consistent independent of spaces level of detail. Inspired by the hierarchical structure of the decomposed task structure of WBS, a hierarchical structure of SOP, WI and instructions have been developed and later been integrated with LBS. To put in context, see Figure 6, a SOP was developed for roof cassette montage, it has been broken down into two WIs and further into seven and three instructions, respectively.

A SOP is linked to a space either directly or through one of the SOPs it is linked to in a sequence. In cases where a previous SOP exists, that SOP must be fully completed, or as an exception for it to be moved to the next SOP in the sequence. According to theories, a SOP has the requirements of containing a title, description of its usage and step-by-step instructions, known by WIs.

To secure quality of work and safe work procedures, foremen and site managers can use lists of predefined WIs. According to theories and interviews a WIs for onsite construction needs to include an instructional description of itself, safety notes, list of tools, machinery, components, materials, instruction durations, space requirements, space restrictions, number of required skilled workers as well as their work qualifications.

In addition, the study has shown the need to link SOPs to spaces for identification of task locations. AS is required to quickly be able to adjust to constant construction demands and changes. SOPs correlation with WI is designed with intention to reduce data redundancy as well as the need for recreation of said data as the occurring data sharing between SOP and WI.

The concept may achieve this by ensuring that no data redundancy exists between SOP and WI, and that data only exists in a single place with a single owner. Additionally, it aims to ensure that a SOP gets access to all data within its WIs and therefore be able to further generate additional information such as a dynamic list of resources to a changing construction site such as when delays or shortages occur.

5 Discussion & Conclusion

The adopted characteristics of the manufacturing industry, in which most of its engineering and manufacturing is done offsite, this study highlights some major issues with IHB. The existing need of conducting a certain amount of work at the construction site has been a bottleneck, the non-structured information flow has led to data redundancy and fragmentation between offsite manufacturing and onsite construction, further increasing the issues. By usage of BOM structure, this concept aims to improve data integration, reduce fragmentation by streamlining the information flow. Additionally, identifying information types and possible transformation sources of the information to the construction site could ensure that data redundancy can be minimized.

Based on observations, onsite construction in IHB mostly utilizes shop drawings, Excel sheets and to some extent even cloud storage with none of them promoting data integration. Resulting in data redundancy, information is recreated into separate documentation with no bi-directional connections.

A real-time information view opens the possibility of optimizing the construction site and its sequence, by filtering the information and showing only the necessary information to the user. Concept hierarchical structure of level of details opens the possibility to filter information based on a variety of parameters, such as locations, number of skilled workers, their qualifications, etc. Making it possible to generate information views, as an example, a view for a painter, in which the painter gets access to information displaying SOPs and WIs associated with tasks they are qualified to and is ready to be performed.

Leftover tasks were a common occurrence that worsened the situation for construction sites by increasing the demand for communication between

onsite and offsite. Non-standardization of the tasks and information availability has resulted in site manager's not being able to optimize the workflow or assign teams for conducting these tasks, ordering of replacement components and parts has been a demanding process. Therefore, we believe that transformation of BOM to onsite BOM would facilitate the work of the site manager, since the factory can potentially utilize the transformation to allocate leftover tasks with SOPs and resources, thus reducing data redundancy and data fragmentation between offsite and onsite. Furthermore, transparency of SOP and WI communication has the possibility of reducing the risk of construction errors.

Onsite BOM has the potential to simplify the process of maintaining and updating SOPs as well as WIs within a construction. This is done through standardizing of information flow and information requirements between offsite manufacturing and onsite construction as well as the whole company in general. A combination of the information structures of WBS, LBS, SOPs and WIs has shown the potential to manage the information flow by BOM for onsite production.

6 Acknowledgement

This research study was made in the research project Connected Building Site funded by the Swedish Governmental Agency for Innovation (VINNOVA). Connected Building site is a testbed on digitization of construction with a focus on site planning, production and supply. We thank interviewees as well as construction companies for their incentive and effort.

References

[1] Uusitalo P, Stehn L, Brege S, Wernicke B. Reciprocal dynamic effectiveness for industrialized house builder. In: European Operations Management Association Conference 2017, EurOma 2017, Edinburgh, Scotland, July 1-5, 2017. 2017.

[2] Lessing J, Brege S. Industrialized Building Companies' Business Models: Multiple Case Study of Swedish and North American Companies. J Constr Eng Manag. 2018;144(2).

[3] Čuš-Babič N, Rebolj D, Nekrep-Perc M, Podbreznik P. Supply-chain transparency within industrialized construction projects. Comput Ind [Internet]. 2014 [cited 2020 May 28];65(2):345–53. Available from: http://dx.doi.org/10.1016/j.compind.2013.12.003

[4] Jonsson H, Rudberg M. Classification of production systems for industrialized building: A production strategy perspective. Constr Manag Econ [Internet]. 2014 [cited 2020 May 28];32(1–2):53–69. Available from: https://www.tandfonline.com/action/journalInformation?journalCode=rcme20

[5] Andersson N, Lessing J. Industrialization of construction: Implications on standards, business models and project orientation. Organ Technol Manag Constr an Int J. 2020;12(1):2109–16.

[6] Lidelöw H, Olofsson T. The Structure and Predefinition of the Industrialized Construction Value Chain. In: ICCREM 2016: BIM Application and Offsite Construction - Proceedings of the 2016 International Conference on Construction and Real Estate Management. 2016. p. 117–25.

[7] Mukkavaara J, Jansson G, Olofsson T. Structuring information from BIM: A glance at bills of materials. In: ISARC 2018 - 35th International Symposium on Automation and Robotics in Construction and International AEC/FM Hackathon: The Future of Building Things. 2018.

[8] Jung SY, Kim BH, Choi YJ, Choi HZ. BOM-centric product data management for small and medium manufacturing enterprises. Proc Int Des Conf Des. 2014;2014-Janua:1799–810.

[9] Hevner Alan R, Hevner AR. A Three Cycle View of Design Science Research. Vol. 19, Scandinavian Journal of Information Systems. 2007.

[10] Boton C, Rivest L, Forgues D, Jupp J. Comparing PLM and BIM from the product structure standpoint. In: IFIP Advances in Information and Communication Technology. 2016. p. 443–53.

[11] Zhou C, Liu X, Xue F, Bo H, Li K. Research on static service BOM transformation for complex products. Adv Eng Informatics. 2018 Apr 1;36:146–62.

[12] Guoli J, Daxin G, Tsui F. Analysis and implementation of the BOM of a tree-type structure in MRPII. J Mater Process Technol. 2003;139(1-3 SPEC):535–8.

[13] Meng XJ, Ning RX, Zhang X, Song Y. Research on integration platform based on PDM for networked manufacturing. In: IEEM 2007: 2007 IEEE International Conference on Industrial Engineering and Engineering Management. 2007. p. 573–6.

[14] Xu HC, Xu XF, He T. Research on transformation engineering BOM into manufacturing BOM based on BOP. In: Applied Mechanics and Materials. 2008. p. 99–103.

[15] Seppänen O, Kenley R. Performance

measurement using location-based status data New view at construction logistics View project Lean Design Management and Scheduling View project [Internet]. 2016 [cited 2020 May 17]. Available from: https://www.researchgate.net/publication/228367623

[16] Mourgues C, Fischer M. A product / process model-based system to produce work instructions. Manag IT Constr Constr Tomorrow. 2010;

[17] Kenley R, Harfield T. Reviewing the IJPM for WBS: The Search for Planning and Control. Procedia - Soc Behav Sci. 2014;119:887–93.

[18] Jung Y, Woo S. Flexible work breakdown structure for integrated cost and schedule control. J Constr Eng Manag. 2004;130(5):616–25.

[19] Makarfi Ibrahim Y, Kaka A, Aouad G, Kagioglou M. Framework for a generic work breakdown structure for building projects. Constr Innov [Internet]. 2009 [cited 2020 Jun 12];9(4):388–405. Available from: www.emeraldinsight.com/1471-4175.htm

[20] Ibrahim YM, Kaka AP, Trucco E, Kagioglou M, Ghassan A. Semi-automatic development of the work breakdown structure (WBS) for construction projects. Proc 4th Int SCRI Res Symp Salford, UK. 2007;133–45.

[21] Siami-Irdemoosa E, Dindarloo SR, Sharifzadeh M. Work breakdown structure (WBS) development for underground construction. Autom Constr. 2015;58:85–94.

[22] Kenley R, Harfield T. Location Breakdown Structure (LBS): a solution for construction project management data redundancy. Proc Int Conf Constr a Chang World. 2014;11.

[23] Brotherton SA, Fried RT, Norman ES. Applying the Work Breakdown Structure to the Project Management Lifecycle. PMI Glob Congr Proc. 2008;1–15.

[24] Construction Project WBS - Examples to Get You Started | Plan Academy [Internet]. [cited 2020 May 28]. Available from: https://www.planacademy.com/construction-project-wbs-examples/

[25] Nakagawa Y, Shimizu Y. Toyota Production System Adopted by Building Construction in Japan 817 TOYOTA PRODUCTION SYSTEM ADOPTED BY BUILDING CONSTRUCTION IN JAPAN. Vol. 12, Proceedings IGLC. 2004.

[26] Nakagawa Y. Importance of standard operating procedure documents and visualization to implement lean construction. In: 13th International Group for Lean Construction Conference: Proceedings. 2005. p. 207–15.

[27] Li D, Mattsson S, Salunkhe O, Fast-Berglund A, Skoogh A, Broberg J. Effects of Information Content in Work Instructions for Operator Performance. Procedia Manuf [Internet]. 2018;25:628–35. Available from: https://doi.org/10.1016/j.promfg.2018.06.092

[28] Mourgues C, Fischer M, Kunz J. Method to produce field instructions from product and process models for cast-in-place concrete operations. Autom Constr [Internet]. 2012;22:233–46. Available from: http://dx.doi.org/10.1016/j.autcon.2011.07.007

[29] Serván J, Mas F, Menéndez JL, Ríos J. Using augmented reality in AIRBUS A400M shop floor assembly work instructions. AIP Conf Proc. 2012;1431(April):633–40.

[30] Mourgues C, Fischer M, Hudgens D. USING 3D AND 4D MODELS TO IMPROVE JOBSITE COMMUNICATION – VIRTUAL HUDDLES CASE STUDY. In: CIB 24th W78 Conference & 14th EG-ICE Workshop & 5th ITC@ EDU Workshop,. 2007. p. 91–7.

Study on the Level Concept of Autonomous Construction in Mechanized Construction

Hirokuni Morikawa[b,a], Takashi Otsuki[a]

[a] National Institute for Land and Infrastructure Management, 1, Aasahi, Tsykuba-shi, Ibaraki-ken, 305-0804, Japan
[b] Public Works Research Institute, 1-6, Minamihara, Tsykuba-shi, Ibaraki-ken, 305-8516, Japan
E-mail: morikawa-h573ck@pwri.go.jp, ohtsuki-t2sh@mlit.go.jp

Abstract –

With a focus on mechanical earthworks, automation of limited operations is progressing with regard to driving operations such as hydraulic excavators, bulldozers, and compaction rollers. The Ministry of Land, Infrastructure, Transport and Tourism is promoting public works that positively utilizes automated construction equipment and the like for the purpose of improving productivity at construction sites.

In the future, it is expected that the scope of automation of construction machinery will expand due to further technological advances such as AI and IoT. In that discussion, it is instructive to note that the classification of automation driving in automobiles serves as the basis for discussion of technology diffusion. Regarding automated construction machinery as well, in considering the promotion of the introduction of this technology into society, we believe that it is useful to formulate a concept at the autonomous construction level.

In this paper, while referring to cases such as classification of automation driving in automobiles, while paying attention to the differences between automatic running of vehicles and autonomous construction of construction machines, a conceptual draft of the level of autonomous construction by construction machines is proposed. In addition to showing the results of the study, the additional study issues that became clear in the study process are shown.

Keywords –

Autonomous; Construction; Level concept; Construction machine

1 Present situation for ICT in mechanized construction field and necessity of roadmap or concept of level for realization of automatic construction

1.1 Short history of introducing construction machinery and Machine control.

Mechanization of construction work has progressed in crane work and earthwork. After the Meiji Restoration, electric shovels were developed in Japan in the 1940s and were mainly used in large-scale earthwork sites [1].

In Japan, the mechanization of construction work has been rapidly promoted since the Second World War. In order to improve the supply capacity for the enormous demand for infrastructure, the construction machinery used by the United States during the war were paid off to japan government and construction industry, and then and then through technical cooperation with overseas companies, domestic construction machinery manufacturing took place again. Nowadays, several construction machinery manufacturers in Japan are competing to contribute to mechanization of construction sites in the world (Figure 1, [1]) [2],[3].

Since the 1980s, in the midst of rapid anxiety about the aging of the working population, automation and autonomy were sought for earthwork, which was the

Kobe Steel (1930) Komatsu(1943) SCM(1961) Hitachi(1965))

Figure 1. Example of construction machinery manufactured by a Japanese manufacturer [1]

most mechanized construction field.

Around 1990, hydraulic excavator manufacturers developed and commercialized semi-automatic hydraulic excavators. Operating a hydraulic excavator is a difficult operation in which the operating levers of the boom, arm, and bucket are moved simultaneously. However, with this semi-automatic product, the system automatically assists the hydraulic valve by the operator only operating the arm operation lever, and the bucket blade edge moves linearly for shaping.

Unfortunately, the economic downturn caused a recession and many workers returned to the construction site, so these did not lead to large sales.

Then, taking advantage of the spread of GNSS technology, an information presentation technology was developed that assists construction machine operators to visually confirm the difference between the cutting edge and the topographical design information. In the 2000s, these were called machine guidance systems in Japan and have been introduced in hydraulic excavators and bulldozers. (In Europe, this is called "Machine Control".)

Nowadays, semi-automated technology and its combination are used to provide hydraulic excavators and bulldozers that assist shaping operations at any place in the construction site using 3D design information and real-time position information. In Japan, this is called 3D machine control [4]-[7].

Figure 2. Concept of future vision for construction work [9]

Also, within a limited environment, trials have been made to automatically construct embankments by operating a plurality of such construction machines programmatically [8].

The Ministry of Land, Infrastructure, Transport and Tourism of Japan has set a future vision of realizing automatic construction in order to increase the production per worker in the construction field amid the rapid aging of the population (Figure 2, [9]).

1.2 Present situation for ICT in mechanized construction field and necessity of roadmap or concept of level for realization of automatic construction.

On the other hand, there are some differences in the understanding and evaluation of the actual situation of the developed semi-automated level among the parties concerned. Both the overestimation and the underestimation have caused cases in which the introduction of users is hindered and the policy making of the administrative agencies promoting the utilization becomes difficult.

The public works orderer wants to utilize these technologies to facilitate the supervision and inspection work such as step confirmation during construction. However, there are concerns that such misunderstandings will cause difficulties.

Please note that the content presented in this paper is not the official view of the Japanese government at this point, but is a report at the stage of consideration as a national research institute.

2 Investigation study on roadmap and technical level concept classification of automation driving

First, we reviewed the progress of the study on the roadmap for realizing automation driving in Japan (Figure 3, [10])

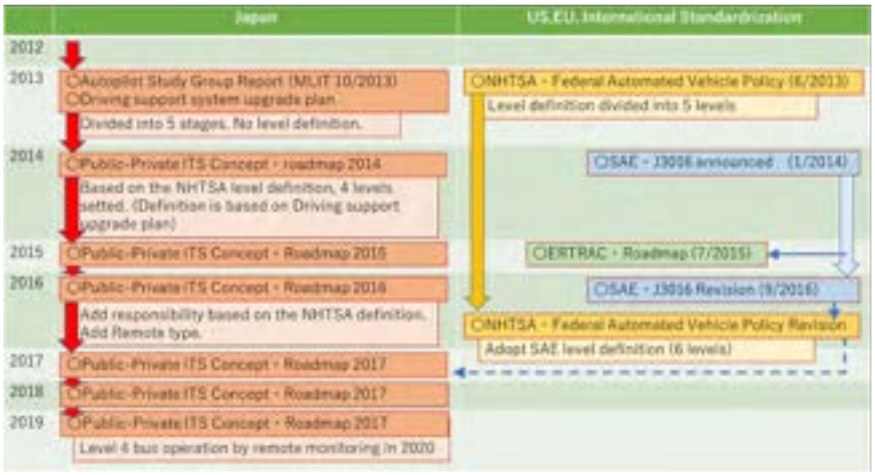

Figure 3. Movement around definition of autonomous driving level [10]

In Japan, the "Autopilot Study Group" established by the Ministry of Land, Infrastructure, Transport and Tourism held discussions and compiled the "Driver Assistance System Advancement Plan" in 2013. After that, with the Cabinet Secretariat as the secretariat, the Prime Minister's top meeting: Advanced Information and Communication Network Society Promotion Strategy Headquarters was launched, and at that meeting the roadmap for realizing automation driving is being

discussed. At that meeting, the first version of the "Public-Private ITS Concept/Roadmap" was formulated in 2014.

In the discussion there, the definition by the US Department of Transportation NHTSA and the discussion on the ERTRAC/Roadmap were investigated, and the definition of automation driving was referenced. With the aim of defining the concept of level classification and refining the scope of the roadmap, representatives of automobile manufacturers, government officials, and other parties continue to hold discussions and update the roadmap every year. Discussions and revisions were also held in response to the drastic revision of SAE/J3016 in 2016.9.

In Japan, a system that automatically stops the traveling vehicle by detecting people or objects was introduced due to the technological development of several manufacturers. For that reason, the terms "safe driving support system" and "automation driving system" existed before. The discussion of correspondence and consistency between those terms and the terms defined in the discussions such as NHTSA was an important issue.

In addition, a service was offered to reduce automobile insurance costs in response to the introduction of these systems. For this reason, the concept of responsible relationship between the driver and the safe driving support system installed in the automobile was also discussed.

In automation driving, what role the driver and self-driving car should share, and how to organize the components of the task of driving were important subjects of the discussion.

In the 2016 revision of SAE/J3016, these issues were organized as DDT, OEDR, DDT fallback, ODD, etc.

The roadmap for automation driving in Japan also follows this concept.

These conceptual arrangements have contributed greatly to clarifying the evaluation of technical contents as well as the definition of automation driving (Table.1, [11]).

Based on these discussions, revisions to the concept and roadmap of automation driving in Japan have been made. This has led to deepening of discussions and progress of work mainly in the following points.

- Clarification of manufacturers' priority development products and enhancement of management strategies
- Discussion from the perspective of how automation driving can help solve social issues
- Clarification of use cases that should be preceded
  (* Mobile services in depopulated areas (Level 4 bus operation by remote monitoring, etc.)
- Discussion on how much resources the government should devote to the social introduction of self-driving cars.
  (*Positioning of advanced driving systems for safe driving, etc.)
- Revision of relevant laws and regulations by the government
  (*Revision of technical standards for automobiles and consideration of new formulation)
- Adjustment of existing laws and regulations for experiments in real environments
  (* Clarification of necessity of road use permission rules by police, review to enable experiments of remote monitoring vehicles)

Table 1. Elements Concept [11]

Element		Definition or Meaning
DDT	Sustained lateral and vehicle motion control	Sustained lateral and vehicle motion control
	OEDR (Object and Event Detection and Response)	The subtasks of the DDT (dynamic driving task) that include monitoring the driving environment (detecting, recognizing, and classifying objects and events and preparing to respond as needed) and executing an appropriate response to such objects and events (i.e., as needed to complete the DDT and/or DDT fallback
DDT fallback		Complete action or Response to when DDT operation is difficult to continue (i.e. Transiton to Minimal Risk condition)
ODD (Operational Design Domain)		The specific operating domains in which the ADS (Automated driving systems) is designed to function.

3 Conceptual study of autonomous construction level in construction machinery that is becoming more automated

3.1 Arrangement of element concepts that are the basis of level division

-The survey and consideration in the previous section confirmed that the role played by the roadmap is effectively useful for the social introduction of technology. In addition, useful points were confirmed regarding the roadmap and level conceptual studies for the automation of construction work.

In particular, it is effective to sort out the concepts of DDT, Vehicle control motion, OEDR, Fallback, and ODD, and we took steps to sort out this point of view regarding automation of construction work.

Table 2. Elements Concept of Automation construction and comparison with Automation driving one

Automation driving		Automation construction		
Element		Element name		Definition or Meaning
DDT	Sustained lateral and vehicle motion control	TASK	Control work device	Control of work device of construction machine (including movement of construction machine)
DDT	OEDR (Object and Event Detection and Response)	TASK	OEDR	Detection of the changes of work objects and terrain shapes and procedure changes due to changes in them
DDT fallback		Task fallback		What to do if the construction machine system cannot control the task (Site Condition change, Changes in soil quality etc)
—		Work area setting / Task allocation		Construction execution planning or setup
ODD (Operational Design Domain)		ODD		(Site Condition change, Changes in soil quality etc)

Table.2 is the corresponding concept that we have examined (Table.2).

Here, as a new element, we propose to add "Work area setting/Task allocation" separately from “DDT”.

It is because that we define automatic construction in mechanical earthworks as changing the existing terrain to the terrain shape shown in the design drawing of the area without human intervention.

If you think in that way, the construction setup will emerge as the next necessary element after the above Task (corresponding to DDT) and fallback.

For example, if the automatic excavator digs the ground all the way to the surface of the design shape, the dump may create a slope that cannot carry the soil. In order for the work to proceed properly, it is necessary to determine the order of the excavation work positions of the excavator and the depth at which each is to be excavated in stages.

In addition, when performing construction with a bulldozer, just because the ground at that point needs to be excavated, the construction does not proceed simply by pushing down the cutting edge. If you do not set up a plan for where to push the soil and carry it, that is, the traveling route, the work will not proceed.

From this perspective, we added the construction setup as the adding new element.

However, we recognize that there is room for further discussion on these points. For example, an already developed car navigation system is responsible for searching for the movement from the current position to the destination in automation driving. And this car navigation is outside the scope of the roadmap (Figure 4, [12]).

Considering the current location as the current topography and the destination as the design drawing, considering how to reach it is equivalent to route selection, so there may be a way of thinking that the construction setup is outside the roadmap.

Since the proposals in this paper are tentative, we expect many opinions.

3.2 Tentative plan of level division concept in automatic or autonomous construction

Based on the above concept of functional elements and whether they are shared by people or systematization, we propose the level divisions concept (Table.3).

The outline of the six levels and the descriptive definition of each level follows the table of automobiles. Of course, this division depends on the combination of the realization of each element, so the level division also changes depending on how the element is considered.

In addition, between level2 and level3, we set level2.9 as the realization of automation with a single construction machine among the components of level3.

It is level 3 after level 2 when it is classified as a commercial level. However, among the development factors required before reaching Level 3, automatic excavation of hydraulic excavators is being realized in research. We think that it is necessary to realize Level 3 after Level 2 in order to have a significant meaning in practical use. However, level 2.9 may also be useful as a practical category when performing embankment compaction as a single task.

In addition, referring to the discussion on the roadmap for automation driving in Japan, we described the technologies that have already been realized and the technologies that are expected in the future at each level.

In Japan, the semi-automatic control of the shovel is called MC, and please note that it is different from Europe. In Japan, a system that gives guidance to operators is called MG.

The automatic embankment construction system at the dam site realized at Kajima corporation was set to level 3, but this may be a point of discussion.

Furthermore, similar to the discussion on the roadmap for automation driving in Japan, the safety equipment introduced to prevent accidents where construction machinery comes into contact with people on-site was not included in the table. This is an area where it seems to be highly effective as a utilization destination of AI for image analysis based on deep learning, which has undergone remarkable technological innovation these days. However, this is because the highest level was

organized from the viewpoint of a realization route to autonomous construction that does not involve people on-site.

We think that this point is also subject to debate, depending on how to utilize the roadmap and considering the possibility of human intervention at the site of autonomous construction.

Table 3. Level Concepts of Automation or Autonomous Construction

Level	Name or Narrative Definition	Task		Task fallback	Work area setting / Task allocation	ODD	Product
		Control work device	OEDR				
0	Non automation The work area of each operator is determined by the instruction of the foreman, and each operator controls construction machine in the allocated area, using finishing stake as a guide.	Operator	Operator	Operator	Foreman/ On-Site Agent	n/a	
1	Work Support The foreman (or on-site agent) divides the work range, and in that work range, each operator controls construction machine based on work device position information obtained from sensor and inputted 3D design digital data.	Operator (with position information support)	Operator	Operator	Foreman/ On-Site Agent	Limited	Machine Control In Japan, called "Machine Guidance"
2	Work Device Control Assistance The foreman (or on-site agent) divides the work range, and in that work range, the operator controls construction machine basically, the control system assist its control based on work device position information obtained from sensor and inputted 3D design data .	Operator and System	Operator	Operator	Foreman/ On-Site Agent	Limited	"Semi-auto" In Japan, called "Machine control" [4]-[7]
2.9	Work Device Control Automation The foreman (or on-site agent) divides the work range, and in that work range, control system controls construction machine to work based on work device position and current terrain information obtained from sensor and the inputed 3D design digital data. When the work is completed, it is in a standby state automatically.	System	System (Monitored by Operator)	Fallback-ready Operator	Foreman/ On-Site Agent	Limited	Multiple realization cases at the research stage. (Hydraulic Excavator, Wheel Loader) [13],[14]
3	Semi-auto combination construction The foreman (or on-site agent) divides the work range basically, and system assist. And in that each work range, the control system controls construction machine to work, the operator supervise those machines. Automatic stop when it is difficult to continue appropriate work.	System	System (Monitored by Operator)	Fallback-ready Operator	Foreman / On-Site Agent and System	Limited	KAJIMA corporation "A^{4}CSEL" called "Quad accel" [8]
4	Conditional automatic construction The system is used to perform work plans from the planned completion (design drawings) and work division to each construction machine in the work that consists of only specific conditions and specific work types. Each construction machine carries out work autonomously and autonomously.	System	System	System	System	Limited	
5	Automatic construction Automation of construction in all case.	System	System	System	System	Un-limited	

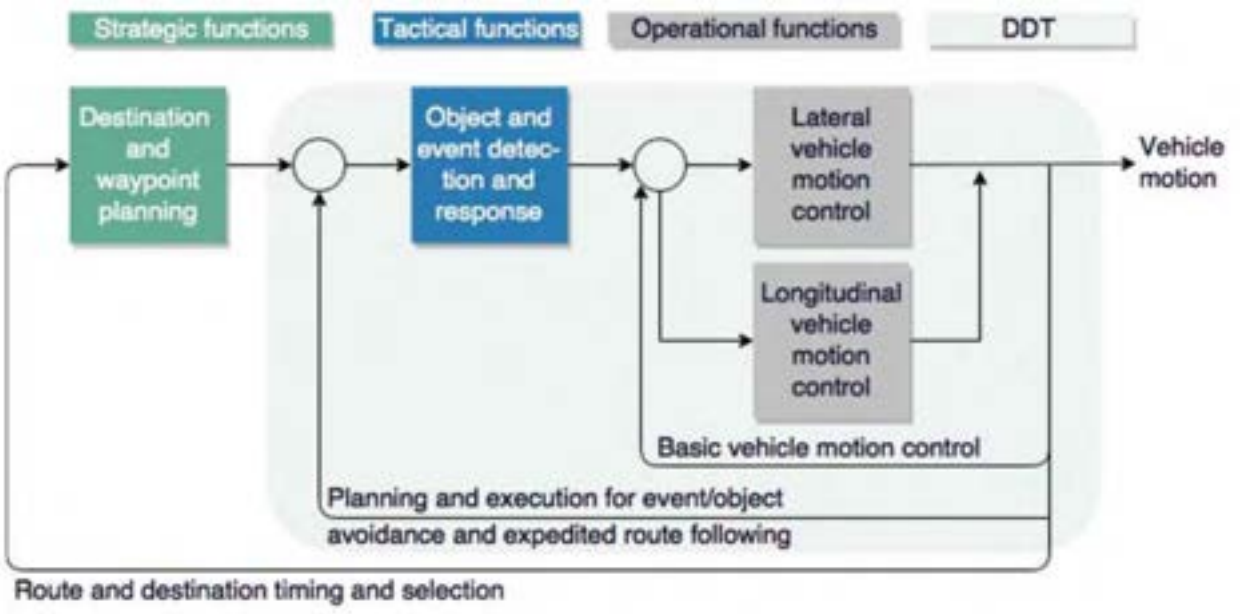

Figure 4. Functional component classification according to SAE J 3016 [12]

4 Additional study issues clarified in this study process

4.1 Need for automatic generation system of construction execution setup (Between Level2 and Level3)

At the construction site, the person in charge of the construction and the work team leader who receives the work instructions from the person in charge of the construction decide the work place and work goals for the day and work plans. Further, in many cases, detailed work preparation is left to the operator himself, and his know-how has not been formalized. It became clear that a solution to this point was required.

Note that a large amount of learning data is required when it is assumed that this problem will be solved by AI.

NILIM is considering the need for an approach by AI as a system to realize this function. In addition, we are conducting activities to collect on-site data as learning data for construction setup creation support AI. This will be announced in another paper (Figure 5).

4.2 Necessity of roadmap composition with "improvement of safety at construction site" as policy objective

The goal of the autonomous construction movement in Japan is to let the machines do what they can do, as a countermeasure for labor shortages in the construction industry.

However, the cause of the labor shortage in the construction industry is that the construction industry is dangerous. Further, in order to realize a completely safe machine earthwork, it is beneficial to construct an on-site environment where people do not mix with heavy equipment. This final goal matches the definition of automatic construction set above.

Also, by setting a roadmap with safety as the main goal, it is possible to put the technology of safety measures at the time of contact between people and construction machinery on the roadmap.

The above-mentioned person detection technology will be required when a third party enters the construction site even if autonomous construction is realized in which workers and construction machinery do not coexist in the future.

Due to these advantages, it is useful to construct a roadmap that aims to realize safety in order to realize automatic construction.

4.3 Necessity of refining the level concept when assuming development

In this level conceptual study, autonomous construction of machine earthworks was assumed, and it was expanded to other types of work in level 5. However, in addition to this positioning, the work of earthmoving also differs depending on the type of machine adopted, so it is necessary to make detailed the level classification that assumes them.

To this end, it may be useful to proceed with the discussion from the perspective of developing the hierarchy of ideas that correspond to the original ODD in more detail, based on the correspondence relationship of DDT.

(*We are aware that the Public Works Research Institute of the National Research and Development Agency is working on this point, and we are exchanging opinions. I would like to ask you to continue your studies.)

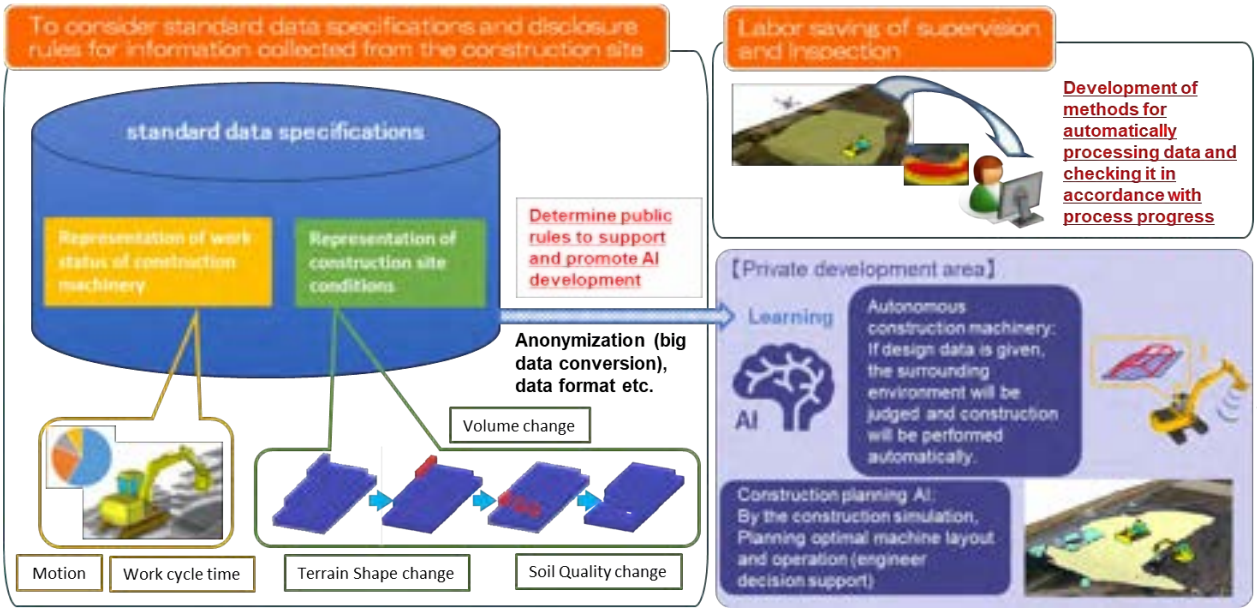

Figure 5. NILIM project outline

4.4 International terminology issues

In addition, there are some confusions among Japanese stakeholders due to differences in terms such as MC in Europe and Japan.

In the future, when broadly discussing the roadmap and the concept of level, it is necessary to make efforts to organize the term definitions between countries.

However, it may be difficult to make a complete agreement because there are differences in the construction sites and backgrounds of construction in each country.

5 Conclusion

① The following effects were confirmed as the roles of the automation driving realization roadmap.

1) Clarification of manufacturers' priority development products and enhancement of management strategies
2) ・Discussion from the perspective of how automation driving can help solve social issues
3) Clarification of use cases that should be preceded
4) (* Mobile services in depopulated areas (Level 4 bus operation by remote monitoring, etc.)
5) Discussion on how much resources the government should devote to the social introduction of self-driving cars.
6) Revision of relevant laws and regulations by the government
7) Adjustment of existing laws and regulations for experiments in real environments

② Based on the discussion on automatic operation, we created a draft of Level classification based on the concept of functional elements in automatic construction and the current technical situation. As a concept of functional elements, the category of 3) is newly added.

1) Task (Concepts corresponding to "DDT")
   ① Control work device
   ② OEDR (Object and Event Detection and Response)
2) Task fallback
3) Work area setting / Task allocation : Construction execution planning or setup (Additional element candidates not in automation driving)
4) ODD (Operational Design Domain)

③ Based on the concept of functional elements of Automation Driving and the current state of technology, a draft for Level Concept was created.

④ The following additional considerations were confirmed from these processes.

1) Need for developing construction execution setup setup generation system. (Between Level2 and Level3)
2) Necessity of roadmap composition with "improvement of safety at construction site" as policy objective.
3) Necessity of refining the level concept when assuming development
4) International terminology issues

The definition of automatic construction, functional elements, and level conceptual divisions shown in this paper are all in the trial stage. Opinions from interested parties are

welcome. In response to those, further discussion will be deepened in the future.

References

[1] Masaharu Ikuta: Hydraulic Excavator Technology Systematization Study, National Science Museum Technology Systematization Survey Report, Vol.22, 2015.

[2] Mietsugu Kato: Construction mechanization history, p.8, 1982.

[3] Naoki Okamoto: History and recent status of mechanical earthwork, Mechanization of construction, September, 2005.

[4] KOMATSU. Achieved the world's first intelligent machine control Started the introduction of ICT hydraulic excavator. On-line: https://home.komatsu/jp/press/2014/product/1187708_1572.html, Accessed: 18/06/2020.

[5] Hitachi Construction Machinery. Market introduction of the ICT hydraulic excavator ZX200X-5B, which is the core of the computerized construction solution. On-line: https://www.hitachicm.com/global/jp/news-jpn/press/16-04-18j/, Accessed:18/06/2020.

[6] KOMATSU. World's first fully automatic blade control function installed] Decided to introduce the medium-sized ICT bulldozer to the market. On-line: https://home.komatsu/jp/press/2013/product/1187925_1566.html, Accessed:18/06/2020

[7] TOPCON. Machine control system. On-line: https://www.topcon.co.jp/en/positioning/products/product/mc/, Accessed: 18/06/2020.

[8] KAJIMA Corporation: KAJIMA A4CSEL, Kajima Integrated Report 2019, p41, 2020.

[9] Ministry of Land, Infrastructure, Transport and Tourism. Robotics and AI technology. On-line: https://www.mlit.go.jp/sogoseisaku/constplan/sosei_constplan_tk_000028.html,Accessed: 26/05/2020.

[10] Cabinet Secretariat IT Comprehensive Strategy Office. Movement around the definition of automatic driving level and future actions (draft), 2016.

[11] Society of Automotive Engineers International: Taxonomy and Definitions for Terms Related to Driving Automation Systems for On-Road Motor Vehicles J3016_201806, p.19, 2018.

[12] Society of Automotive Engineers (SAE). SAE international taxonomy and definitions for terms related to on-road motor vehicle automated driving systems, levels of driving automation, Springer; 2014.

[13] Hiroshi Yamamoto, Masaharu Moteki, Takashi Ootsuki, Yuji Yanagisawa, Akira Nozue, Takashi Yamaguchi, Shin'ichi Yuta: Development of the Autonomous Hydraulic Excavator Prototype Using 3-D Information for Motion Planning and Control, Transactions of the Society of Instrument and Control Engineers, Vol.48, No.8, pp.488-497, 2012

[14] Shigeru Sarata, Nobuhiro Koyachi, Takashi Tsubouchi, Hisashi Osumi, Masamitu Kurisu, Kazuhiro Sugawara: Development of Autonomous System for Loading Operation by Wheel Loader, ISARC2006, pp.466-471

Mask R-CNN Deep Learning-based Approach to Detect Construction Machinery on Jobsites

H. Raoofi[a] and A. Motamedi[b]

[a]Department of Construction, École de Technologie Supérieure, Canada
[b]Department of Construction, École de Technologie Supérieure, Canada
E-mail: Ali.Motamedi@etsmtl.ca

Abstract –

In the construction industry, there is often a need to identify and localize assets and activities on the jobsite to assess and improve the performance of their associated processes. Traditional methods for monitoring construction activities are costly and time-consuming. Excavators and dump trucks are among the most common assets used in the construction industry. Consequently, accurately monitoring their activities can reduce time and increase the efficiency of progress monitoring.

With the presence of cameras on jobsites and the advancement of methods based on artificial intelligence and computer vision, progress monitoring activities can be automated. Furthermore, by using techniques such as deep learning, a wider range of data resources can be processed, and oftentimes more accurate results can be produced for the purpose of object detection.

This research proposes a computer-vision approach that utilizes a Mask Region Based Convolutional Neural Network (Mask-RCNN) to detect excavators and dump trucks in a construction site. This research investigates an innovative technique to achieve high accuracy object detection using relatively small datasets. To overcome the problem of overfitting and improve generalization, a pre-trained model based on a Microsoft COCO dataset is used as a network that presumably has already been trained to distinguish basic features. Finally, the model is further fine-tuned to minimize validation loss.

Keywords –

Computer Vision; Artificial Intelligence; Deep Learning; Mask R-CNN; Construction Monitoring; Progress Management

1 Introduction

An efficient and effective workforce improves the time and cost performance of construction projects [1, 2]. Accurate progress monitoring, safety management, and quality control activities require skilled labor with adequate supervision, which in turn increases time and project costs.

With the advancement of methods based on artificial-intelligence, computer vision and deep learning, the abovementioned activities could be automated, leading to time and cost reductions. Specifically, there is a growing trend to use computer vision approaches to detect construction machinery from video outputs. These technologies could help project managers to access more accurate data in order to monitor construction assets, facilitate progress management and manage site safety.

To address this need, a region-based deep learning architecture called Mask R-CNN is utilized in this study to detect and segment excavators and dump trucks in the images from jobsites using a relatively small dataset.

The main objective of this research is to develop an improved deep-learning-based network to enhance the accuracy of predictions and decrease the processing time. The study's sub-objectives are to:

1. Develop a network for automatic detection of machinery (i.e. excavators and dump trucks) on construction sites from captured videos based on machine learning algorithms.
2. Train and validate the network on a small dataset.
3. Fine-tune the network's parameters to further increase its performance.

2 Related Works

AI techniques can assist project managers in monitoring and analyzing job site activities [2, 3, 4, 5, 6, 7]. Furthermore, AI approaches can be used for safety management to monitor and reduce risks [8, 9, 10, 11, 12].

Machine learning techniques can be deployed to detect construction machinery on jobsites. Project managers can utilize the information about these assets to increase the efficiency and safety of the projects.

Deploying an Unmanned Aerial Vehicle (UAV), Kim et al. [13] presented a visual monitoring method that

could automatically measure proximities among construction vehicles and workers. They localized objects using a deep neural network, YOLOv3, and developed an image rectification method that facilitates the measurement of actual distances from a 2D image. Struck-by hazards around workers could be detected with this method, making timely intervention possible. YOLOv3 provides bounding boxes for detected objects, but it is unable to generate pixel-level masks.

In another study, Kim et al. [14] developed a vision-based method to classify equipment operations in video data. The framework consists of four stages: equipment tracking, individual action recognition, interaction analysis and post-processing. The hybrid detector used in this study consists of ferns and a random forest classification algorithm, which uses a sliding window to propose bounding boxes and cannot provide shape data.

To detect dense multiple vehicles from UAV, Guo et al. [15] presents a deep learning approach that uses a single-stage detection (SSD) algorithm with orientation-awareness and integrates it with a developed feature fusion module. Similar to YOLOv3, the SSD algorithm is unable to provide pixel-level mask data for the detected objects.

3 Methodology

In this research, two common classes of construction vehicles, namely excavators and dump trucks, are studied. Due to the unavailability of open datasets, a dataset of 341 annotated images of excavators and dump trucks is created to train the proposed network. In order to develop a high-quality dataset of these heavy machineries in construction sites, public domain images were gathered through Google Image® and Flicker®. Some 269 images are used for the network training, while 72 images are assigned to the evaluation process. VGG Image Annotator (VIA) [16] is used to annotate the images of the dataset to provide the ground truth for the training process (Figure 1).

Figure 1. Data annotation using VIA [16]

Since the size of the dataset is relatively small, pre-trained weights for the MS COCO dataset are used as a transfer learning technique to overcome overfitting problem and increase the accuracy.

3.1 Instance Segmentation

In this study, an instance segmentation technique called Mask R-CNN is used, which can provide pixel-level boundaries for each detected object. Mask R-CNN has a new ability to segment objects in addition to classification and detection, compared with its predecessor Faster R-CNN [17].

As illustrated in Figure 2, first, the feature map of the entire image is extracted using a ResNet-101 architecture as a convolutional backbone. Then, a Region Proposal Network (RPN) analyzes the developed feature map and proposes candidates for object bounding boxes. To resolve Faster R-CNN's problem regarding the pixel-to-pixel misalignment between network inputs and outputs, a quantization-free layer called Region of Interest (RoI) Align is utilized, which preserves spatial locations. After fixing the misalignment problem of the bounding-box candidates, using fully connected (FC) layers, the network can classify objects and recognize bounding boxes and in parallel, a convolutional layer unit predicts masks that are applied separately to each RoI [17].

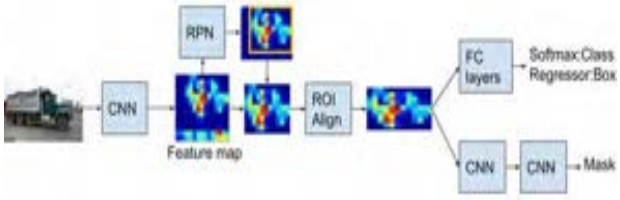

Figure 2. Mask R-CNN architecture

3.1.1 Loss Function

A multi-task loss is defined on each RoI as the sum of the classification loss (L_{cls}), the bounding-box loss (L_{box}), and the mask loss (L_{mask}) [17].

$$L = L_{cls} + L_{box} + L_{mask} \quad (1)$$

3.2 Training Method

As shown in Table 1, the hardware setting is Laptop ROG Strix GL502VS with a NVIDIA GTX 1070 8GB GPU. It has an Intel Core i7 7700HQ as CPU processor and 16GB of RAM. Concerning the limitation of GPU memory, we use 1 image per GPU for each mini-batch and each epoch consists of 100 steps.

Table 1. Hardware setting

ROG Strix GL502VS	
CPU	Intel Core i7 7700HQ

GPU	NVIDIA GTX 1070 8GB
RAM	16GB

Matterport's implementation [18] of Mask R-CNN on Python 3, Keras, and TensorFlow is used. The backbone of our network is ResNet-101 and we utilize only one class of data augmentation in our training phase, which consists of horizontally flipping 50 percent of the images. As described in section 3, pre-trained weights on MS COCO are used as our initial network weights. We adapted a multi-phase training strategy to fine-tune our results. In the first phase (first 5 epochs), only the top layer (heads) of our developed network was trained with the learning rate (lr) of 0.001. Next, for epoch 6 to 15, ResNet stage 4 and up were trained with lr of 0.001, while the rest of the layers are frozen. In the third step, for epoch 16 to 30, ResNet stage 3 and up were trained and lr decreased to 0.0001. In the final phase (epoch 31 to 40), all layers of ResNet were trained with lr of 0.00001. Table 2 presents the specifications of the developed multi-phase training.

Table 2. Multi-phase training specification

Phase	Epochs	Training layers	lr
I	1-5	Only top layer	0.001
II	6-15	ResNet stage 4 and up	0.001
III	16-30	ResNet stage 3 and up	0.0001
IV	31-40	ResNet all layers	0.00001

3.3 Metrics for Evaluating Performance

The network's performance is evaluated and quantized using two metrics: Average precision (AP) and inference time, which is the amount of time the network requires to do the prediction.

3.3.1 Average precision (AP)

According to the definition of Pascal VOC 2010 [19], for a specific value of Intersection over Union (IoU), the AP measures the precision/recall curve at recall values (r_1, r_2, etc.) when the maximum precision value drops. The AP is then computed as the area under the curve by numerical integration [20].

$$AP = \sum (r_{n+1} - r_n)\, p_{interp}(r_{n+1})$$
$$p_{interp}(r_{n+1}) = \max_{\tilde{r} \geq r_{n+1}} p(\tilde{r}) \quad (2)$$

The metric mAP is the average of AP over a range of IoU from 0.5 to 0.95 at intervals of 0.05 (AP@ [.5:.95]) [20].

3.3.2 Detecting Threshold

To eliminate network predictions having a low confidence score, only detected instances above the threshold level of 0.9 are considered in the final results.

4 Results

Over the 40 epochs of training the network, the minimum validation loss function took place at epoch 38 with a value of 0.1889. Figure 3 illustrates the loss function of the network at each epoch. As shown in Table 3, the total training time was 68 minutes on 1 GPU.

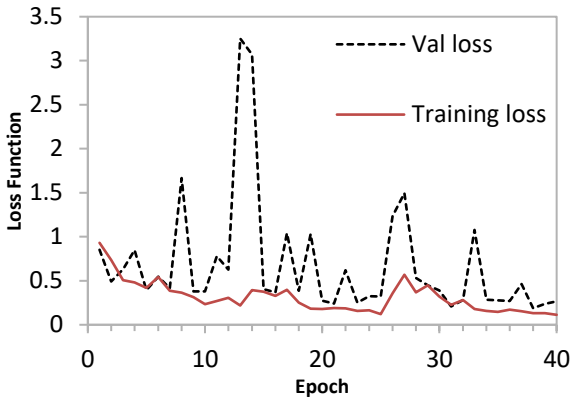

Figure 3. Loss function at each epoch

Table 3. Training time

Phase	Training time
I	7 min
II	24 min
III	48 min
IV	68 min

4.1 Metrics Results

The results of the average precision of the network predictions are reported in Table 4.

Table 4. Average precision results

Average precision	
AP_{50}	0.8792
AP_{75}	0.7438
mAP	0.5984

The inference time is calculated by averaging the time required to segment 10 images, which amounted to 3173 ms with the current hardware setting.

4.2 Examples of network predictions

As illustrated in Figure 4 and Figure 5, the network's performance was excellent for the classification task with a confidence score nearly equal to 1, while keeping a reasonably high-performance level on segmentation with

an IoU measured above 0.85.

Figure 4. Excavator example (Confidence score/IoU), network prediction (red line) vs. ground truth (green line)

Figure 5. Truck example (Confidence score/IoU), network prediction (red line) vs. ground truth (green line)

Although the developed network performs with a good level of accuracy on most testing images, there are some situations in which the network segments the instances weakly. For example, if there is an occlusion in the image, as illustrated in Figure 6, the network has difficulty recognizing the proper boundaries of the occluded objects. For example, in the case of Figure 6, the IoU for the excavator was as low as 0.485.

Another condition that dramatically affects the network's performance is low illumination. As shown in Figure 7, the overall lighting in the image is low. The network confidence score associated with the truck was consequently below the detecting threshold of 0.90, which means the truck cannot be detected by the network.

Figure 6. Example of Occlusion (Confidence score/IoU), network prediction (red line) vs. ground truth (green line)

Figure 7. Poor illumination example

5 Discussion

A deep learning model is developed to segment excavators and trucks utilizing a relatively small dataset of public domain images.

By using a small dataset, complications arise in the training process as the network faces challenges such as overfitting. Transfer learning, data augmentation, and fine-tuning techniques were used to decrease the effect of overfitting and increase the accuracy of results.

To deal with the challenges associated with occlusion and low lighting, it is proposed that a larger training dataset should be created to enhance the network's performance. In this study, the use of data augmentation is limited to flipping, yet the use of a conclusive data augmentation that deals with occlusion and lighting should be considered in future studies.

With the current hardware setting, the inference time was measured as 3173 ms, which is high for real-time applications. By using a more powerful hardware setting, the inference time could be decreased. Additionally, other implementations of Mask R-CNN should be tested to avoid slow performance related to weak network implementation.

6 Conclusion

In this study, a deep learning model was developed to accurately detect and segment two types of construction machineries. The network's performance resulted in an average precision of 0.8792 and inference time of 3173 ms, using a relatively small dataset and a transfer learning technique.

The pixel-level segmentation approach can provide the spatial information about objects. Compared with the previous approach relying on bounding boxes to measure proximities between vehicles, the generated pixel-level masks increase the accuracy of the proximity calculations related to safety control and decrease false safety alarms.

The number of vehicle classes in the proposed model could be increased to include a broader range of machineries and could be used to efficiently manage construction assets and monitor safety on jobsites.

The network performs poorly when objects are occluded or poorly lit. In future studies, it is proposed that a larger and more diverse dataset be used to overcome problems such as occlusion and poor lighting. Further work is also needed to study the effect of data augmentation on the network performance when it faces occlusion or illumination challenges.

References

[1] Ghanem AG, AbdelRazig YA (2012) A Framework for Real-Time Construction Project Progress Tracking. Earth & Space 2006 1–8.

[2] Luo H, Xiong C, Fang W, Love PED, Zhang B, Ouyang X (2018) Convolutional neural networks: Computer vision-based workforce activity assessment in construction. Automation in Construction 94:282–289.

[3] Son H, Choi H, Seong H, Kim C (2019) Detection of construction workers under varying poses and changing background in image sequences via very deep residual networks. Automation in Construction 99:27–38.

[4] Fang Q, Li H, Luo X, Ding L, Rose TM, An W, Yu Y (2018) A deep learning-based method for detecting non-certified work on construction sites. Advanced Engineering Informatics 35:56–68.

[5] Fang W, Ding L, Zhong B, Love PED, Luo H (2018) Automated detection of workers and heavy equipment on construction sites: A convolutional neural network approach. Advanced Engineering Informatics 37:139–149.

[6] Lee Y-J, Park M-W (2019) 3D tracking of multiple onsite workers based on stereo vision. Automation in Construction 98:146–159.

[7] Ayhan BU, Tokdemir OB (2019) Predicting the outcome of construction incidents. Safety Science 113:91–104.

[8] Luo X, Li H, Yang X, Yu Y, Cao D (2018) Capturing and Understanding Workers' Activities in Far‐Field Surveillance Videos with Deep Action Recognition and Bayesian Nonparametric Learning. Computer-Aided Civil and Infrastructure Engineering. 34:333–351.

[9] Ding L, Fang W, Luo H, Love PED, Zhong B, Ouyang X (2018) A deep hybrid learning model to detect unsafe behavior: Integrating convolution neural networks and long short-term memory. Automation in Construction 86:118–124.

[10] Mneymneh BE, Abbas M, Khoury H (2017) Automated Hardhat Detection for Construction Safety Applications. Procedia Engineering 196:895–902.

[11] Fang Q, Li H, Luo X, Ding L, Luo H, Rose TM, An W (2018) Detecting non-hardhat-use by a deep learning method from far-field surveillance videos. Automation in Construction 85:1–9.

[12] Fang W, Ding L, Luo H, Love PED (2018) Falls from heights: A computer vision-based approach for safety harness detection. Automation in Construction 91:53–61.

[13] Kim D, Liu M, Lee S, Kamat VR (2019) Remote proximity monitoring between mobile construction resources using camera-mounted UAVs. Automation in Construction 99:168–182.

[14] Kim J, Chi S, Seo J (2018) Interaction analysis for vision-based activity identification of earthmoving excavators and dump trucks. Automation in Construction 87:297–308.

[15] Guo Y, Xu Y, Li S (2020) Dense construction vehicle detection based on orientation-aware feature fusion convolutional neural network. Automation in Construction 112:103124.

[16] Dutta A, Zisserman A (2019) The VIA Annotation Software for Images, Audio and Video. In: Proceedings of the 27th ACM International Conference on Multimedia. ACM, New York, NY, USA, pp 2276–2279.

[17] He K, Gkioxari G, Dollár P, Girshick R (2017) Mask R-CNN. In: 2017 IEEE International Conference on Computer Vision (ICCV). pp 2980–2988.

[18] Abdulla W (2017) Mask R-CNN for object detection and instance segmentation on Keras and TensorFlow. GitHub repository, https://github.com/matterport/Mask_RCNN

[19] Everingham M, Van Gool L, Williams CKI, Winn J, Zisserman A (2010) The PASCAL Visual Object Classes Challenge 2010 (VOC2010) Results.

[20] Hui J (2019) mAP (mean Average Precision) for Object Detection. In: Medium. On-line: https://medium.com/@jonathan_hui/map-mean-

average-precision-for-object-detection-
45c121a31173. Accessed 14 Dec 2019.

Implementation of Unsupervised Learning Method in Rule Learning from Construction Schedules

B.Y. Ryoo[a] and M. Ashtab[b]

[a] Department of Construction Science, Texas A&M University, United States
[b] College of Architecture, Texas A&M University, United States
E-mail: bryoo@tamu.edu sokratis10@tamu.edu

Abstract –

The construction industry has insufficient utilization of standard work and workload. Generally, scheduling for construction projects follows the common sense of the industry. The sequencing of activity and its duration estimation is highly dependent on the experience of the experts who are assigning them to the project, and it is a considerable barrier for automating scheduling process.

To overcome this challenge, the FP-Growth algorithm, which is an automated unsupervised learning tool, applied to create a platform for the acquisition of knowledge from actual construction schedules which are the outcome of experienced experts. The main advantage of this method in comparison to supervised learning models is the fact that it can generate contractor-specific rules from a given schedule and also identify a variety of potential path when it is applied for multiple projects which are similar to each other. The main contribution of FP-Growth Algorithm to this research is in finding association rules between sets of activities and identifying recurrent patterns in the sequence of activities, their duration, logical relationship (FF, SS, SF, FS) and specifications in different sections of construction projects.

The model applied on schedules of two case studies with different occupational function and structural material. The model substantiated to be capable of learning and identifying various rules including activity durations, predecessor activity and logical relationship and lead times that can happen in between two related activities.

Keywords –

Unsupervised Learning; Construction Scheduling; Rule Learning; Machine Learning; Association rules; FP-Growth Algorithm

1 Introduction

Construction project schedules are heavily replying to schedulers' expertise and corporate scheduling approaches.

Also the construction industry always faces delays and change orders.[1] Poor planning, lack of flexibility during change orders and inconsistent resource allocation are the leading causes of delay, which are instigated directly by deficiencies in scheduling practice. The main goal in scheduling is to set a baseline for activity relationships and their duration while considering optimized tradeoffs between time, cost and resources. The scheduling process mostly based on personal experience of planners and lacks standardized sets of work items. The complex nature of the scheduling process with the presence of logical and resource-based constraints makes it difficult for project planners to generate the optimum schedule persistently [2]. Hence, construction management practice needs more dynamic and integrated schedules.

Previous works on the issue mainly focus on small and partial sets of activity for projects and try to find a mathematical solution to optimize time while meeting all the resource and cost restraints of projects [3]. The common shortcoming for all of these studies is that they applied in large scale and real-life projects. The main approach to overcome this gap and simplify the scheduling problems could be binding sets of activities together and assign single values of constraint to them [4]. Another way is generating association rules based on the sequence of activities and use them as constants while generating a schedule based on mathematical models. While the majority of the solutions for automating schedules focus on supervised learning which has to establish probabilistic hypothesis to generate a single solution for similar scheduling, this research implements the Frequent Pattern Algorithm(FP-Growth algorithm) to absorb different possibilities and sequences that can be performed to create a schedule. FP-Growth Algorithm identifies association rules among activities which can be different from project to project and instead of having a model with given premises, the model learns contractor specific rules. The main benefit of using FP-Growth over other pattern finding methods is the fact that it is compatible with confined groups of datasets which

would be the case for current research [5]. After shaping the constants for the schedule genetic algorithm would be implemented to optimize time for the rest of the project based on its tradeoff with resource and cost.

2 Related Researches

Time overrun is one of the significant barriers to project success. There are a plethora of factors contributing to the intensification of this problem. Some studies investigated the factors which are instigating delays and their importance to tackle the negative effects of them on schedules. According to Zidane and Andersen [1] who implemented a broad literature review on the issue, poor planning and scheduling, resource shortage and poor decision making in change orders are the most repeated factors in altering construction project time globally. Different strategies had been applied to improve each problem.

In addressing resource-constrained scheduling, many scholarly works focused basically on using mathematical optimization tools. Adeli [6] defines an optimization function for minimizing direct cost based on the maximum acceptable time for a transportation project and applies artificial neural networks to generate a solution for the target function. Toklu [7] uses sets of concrete-related activities for applying Genetic Algorithm as the time minimization tool which sets on the stage for other papers to implement a genetic algorithm for scheduling problems. Dawood and Sriprasert [8] had continued the path adding time-space confliction alongside the resource constraint as a variable to the mathematical model of optimizing time according to cost. In another significant approach to the problem, Birjandi and Mousavi [4] differentiated between a set of activities that can be bind together and other activities in the schedule in modelling and formulating their target function for optimization. There has been plenty of similar researches conducted based on optimizing cost time relation through the application of some alterations using Genetic Algorithm and stochastics [9-16].

Koo, et al. [17] concentrate on rescheduling practice by developing an anthological hierarchy for categorizing critical path activities based on the level of effect they got from resource constraint during the project and also their effect on their successor activities. Building information modelling also applied as a tool to automate data generating in some of the recent works where tasks which are driven from BIM models are subject to optimization to reach the time-cost-efficient solution.

Faghihi, et al. [3] focused on sequencing activities for a limited set of activities in the steel structure model while Chen, et al. [18] developed a comprehensive module to generate a full schedule of the project through linking it with resource and cost data.

Reviewed works are containing valuable solutions to address scheduling problems, but they all share a common gap. They generate a single solution for a dynamic problem of creating schedules and using stochastic models for considering uncertainties to run their model. This is due to the complexity of calculations for mathematical models when they engage with a plethora of activities and their intensified logical relations. Alongside that, they put aside the current practice by trying to generate schedules with any kind of input from historical data from contractors. Hence, the schedules generated in this manner are not expandable to complex projects in commercial, residential sections of the construction industry. Figure1 summarizes the problems and gaps that have been identified in this research.

Figure1.

The construction scheduling automation literature

FP-Growth algorithm has the potential to ease both problems. By extracting rules from current schedules and apply them as constants, uncertainty and thus, the complexity of mathematical models can decrease. Furthermore, the FP-Growth algorithm has the potential to mine project-specific rules schedule by schedule and integrate the knowledge of experts with generated results.

The current study focuses on generating knowledge from real-life project schedules. Identifying patterns in a sequence of activities as association rules inside a project and assessing the significance of them could be the missing step in generating automated schedules.

3 Research methodology and Data preparation

As discussed, the scheduling practice in the construction industry lacks consistency and flexibility, and both problems could be alleviated through automation. Automation can be considered as sequencing activities or allocating resources. The current article aims

to reduce the complexity of automation in generating schedules, by suggesting rules which are driven through investigating contractor schedules and reduce variables and give more certainty to optimizing models. Unsupervised learning has the ability to capture underlying knowledge), which is specific to each schedule. To be more specific FP-Growth algorithm as an unsupervised learning tool is capable of mining durations and relationships of activities in a project-specific manner.

FP-Growth's main contribution to the research was it is ability in Finding frequency among features and attribute relationships which were both needed in finding a chain of activities that would be repeated in each floor or work sections.

The research uses two construction schedules as the case studies to examine the possibility of extracting association rules from them which draw a certain and meaningful sequence of activities. The first project was a multi-story hotel building with a concrete structure (CASE 1), and the second one was a 3-story commercial building with steel structure (CASE 2).

For extracting association rules and their significance, there are multiple options in the unsupervised machine learning realm. The FP-Growth Algorithm selected as the data available were confined. While the FP-Growth Algorithm works with nominal variables, it fits with the type of data that can be extracted from schedules.

3.1 Preparing data for the FP-Growth algorithm

The next step was transforming the available schedule into a decent input for FP-Growth Algorithm. The schedules included activities identification number (ID), description, start date, finish date, predecessor activity or activities and duration. Furthermore, logical relationships and sequences like Finish-to-Start (FS), Start-to-Start (SS), Start-to-Finish (SF), Finish-to-Finish (FF) gathered to be mined and provide more practical rules.

While the FP-Growth Algorithm works with nominal variables, it fits with most of the attributes except duration, which is a continuous value. By rounding all times into an integer, this problem solved as well. The main challenge here was to identify the type of activities from the description section.

3.1.1 Attribute extraction from descriptions

Each project had a specific routine in the description section. For CASE 1 schedule, the description part had a systemic approach. The operational part separated into three main parts. The building had 14 stories above ground and description was based on the level of the building, the activity, and the section of work on that level which can be extracted in excel and put into three different attributes. The predecessor for each activity also located and expanded in the same row. Table1 shows attributes extracted from CASE 1 and their range.

For CASE 2 dataset available had an attribute as activity types like contracts, procurement, structure, foundations, interior, paving and etc. In each group of activities with the same type, the extraction of attributes of section, level and type from the description part was the challenging part due to inconsistency in naming activities. So, as an instance in the foundation to extract attributes from activities, the tags created based on possible foundation types. The first step was to know what is the foundation type and how it is named description section. Tags such as Drill, Drilled, Pier, Shaft, Caisson, Mat, Grade, Grade Beam, Slab on grade, footing, strip, spread checked on data set and the results showed that the building uses drilled piers and grade beams for the foundation. Here due to lack of enough datasets, general knowledge of construction work played a role in guessing tags. By having more datasets, text mining can come to help in not only in generating tags but also in creating trees of activities which are connected based on tags. Table2 shows attribute extracted from activities with foundation type and their variety and range in CASE 2.

Table 1. Attributes extracted from CASE 1

Attribute	Range
Activity	
Duration	Integer (weeks)
Activity/ PRE-Requisite	
Type	MB(Mobilization), EX (Excavation), C.R. (Crane), SG (Slab on grade), CS(Concrete) R.B.(Rebar), FR (Framing)
Section	1,2,3, ALL
Level	B2-L14
Spec	PR (pouring), FT (footing) FR (framing) SC (stress cable)
Logic	Finish-to-Start (FS) Start-to-Start (SS) Start-to-Finish (SF) Finish-to-Finish (FF)

PRE-Requisite	
Level Difference(D)	Integer
Lag	Integer (hours)

Table 2. Attributes extracted from CASE 1

Attribute	Range
Activity	
Duration	Integer (weeks)
Activity/ PRE-Requisite	
Element/area of Work	Piers Grade beams Elevator Slab on Grade Under Slab
Section	1,2,3, ALL
Level	N/A for foundation
Spec	Pour Cure Forms(edge) Forms (Carton) Waterproof Electrical Plumbing Reinforcing Strip/lift Excavation Backfill
Logic	Finish-to-Start (FS) Start-to-Start (SS) Start-to-Finish (SF) Finish-to-Finish (FF)
PRE-Requisite	
Level Difference(D)	Integer
Lag	Integer(hours)

3.1.2 Attribute extraction from sequences

For each activity, there might be a predecessor or successor activities in a given schedule. So, extracting attributes from predecessor or successor has already done except the possible connection between predecessor or successor and the activity itself. The logic of connection (i.e., Finish-to-Start, Start-to-Start, Finish-to-Finish and Start-to-Finish) and lags were ones which already provided in the schedules. Furthermore, there are some locational dependencies which can happen between activities. So, to consider that, Level (i.e., floor) difference (i.e., Level D) attribute defined as subtraction of level in which activity takes place, and the level predecessor needs to be done. To monitor sections, section-relation attribute defined. As there are only three of them in each CASE, all six possible connections considered as a different value of the attribute.

Hence, for a given activity, attributes extracted for itself and also for its predecessor shape a row of feature for it. If activities have multiple predecessors, a new row of feature would be considered for the attributes of the same activity and the other predecessor. So, for example for and activity with four predecessors there would be four rows of features in the dataset which is subject to be analyzed by the FP-Growth algorithm. It is evident that while covering activities and their predecessors, its precisely the same job in the reverse direction if the study would focus on the activities and their successors. Hence, to eliminate the unnecessary data and keep dataset consistent only the predecessor relations considered as the basis.

3.2 Implementation of FP-Growth Algorithm

In the previous section, the activities and each of their predecessor analyzed and expanded into a row of features. FP-Growth algorithm implemented to figure out if there is a significant pattern among the rows of features, While all the attributes could get finite values (either it is integer or string), an operator used to transfer or nominal variables into binominal. Dummy encoding used to separate columns for each value of a single attribute to make it more flexible to use in the FP-Growth model. Furthermore, the model applied to sets of activities with the same attribute of type in both CASE 1 and CASE 2 to give more realistic results. The process of data preparation and modelling has done in RapidMiner Studio®. The overall process has shown in Figure 2.

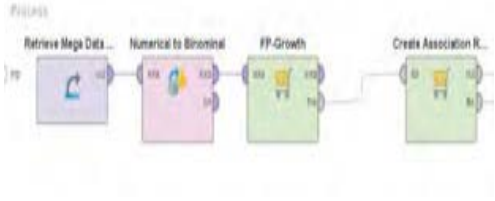

Figure2.

Process of implementing FP-Growth in Rapid mining

The association rules which are driven from the FP-Growth Algorithm are containing premises and conclusions. Premises are the constant parts that we would always have in our datasets. Conclusions are that might vary when the data changes. In this case activity, spec and detail are the constant part, and the parts that are needed to get defined as conclusions are the duration of activity and its predecessor logic, type, Level D. So, the rule generation followed the same logic by separating different activity types.

This process repeated for all the sections of both projects and CASE 1 concrete pouring and framing generated some rules and in CASE 2 foundation and structure came out with some rules that will be discussed in section 4.

4 Data Analysis

The first group of activities that generated meaningful association rules were framings in CASE 1. The main reason for that was the fact that the framing activities repeated in 14 levels without any sectional consideration. The first step was applying FP-Growth to all row of features with framing (i.e., FR) as their activity type. Here the main output is not all the created rules but just identification of most repetitive values in each attribute. The most repetitive values were as below:

As it is discussed in section 3 section, specification and type of activity (i.e., Activity Section, Activity Spec, Activity Type) and also the type, section and specification of predecessor and its logical relationship (i.e., SS/FS/FF/SF PRE Requisite Spec, SS/FS/FF/SF PRE Requisite Section, SS/FS/FF/SF PRE Requisite Type) alongside the Lag (i.e., SS/FS/FF/SF PRE Requisite lag) would be components of one rows of attributes in the dataset generated from the schedule.

Activity Section = ALL,
Activity Spec = IN,
Activity Type = FR,
SS PRE Requisite Lag = 0,
SS PRE Requisite Level D = -5,
SS PRE Requisite Section = 2,
SS PRE Requisite Spec = PR
SS PRE Requisite Type = CS
FS PRE-Requisite Lag = 14 days,
FS PRE-Requisite Level D = 1,
FS PRE-Requisite Section = ALL,
FS PRE-Requisite Spec = IN,
FS PRE-Requisite Type = F.R.
Duration = 3(weeks)

Before reporting rules resulted from the implementation of the FP-Growth algorithm, it is necessary to mention that the association rules are frequent if-then patterns which can be found through a data set and significance of them in identifying recurrent patterns are related to *support* and *confidence criteria.* Support is an indication of how frequently the items appear in the data. Confidence indicates the number of times the if-then statements are found true.

As the first endeavour for finding association rules, the search was for the attributes that could be bind together in the framing section. To make that happen the attributes connections with FR (framing) attribute evaluated. Initial interpretation for the outputs was the fact that the framing had taken place without any further section separation inside each level. It had happened at the same time for a single level. (Activity sec=All).

Premise:
Activity Type = FR
Conclusion:
Activity Section = ALL, Activity Spec = IN
(Confidence:1, Support:1)

So, for any given activity with FR (framing) type, its section and spec would be as of ALL and IN (interior). While doing more detailed rule mining, these three attributes could be considered as one for framing related rows of features and bind together as the general premise in the next steps.

Further looking there are two frequent predecessors for Framing activities in CASE 1. The first one has a Start-to-Start logic and is among pouring activities from the floors above. Second, framing activities from lower floors which has a Finish-to-Start logical sequence with the desired activity. While the framing activities take place in similar square feet in most levels, the duration could also be mined as three weeks (Duration=3) which is not a rule but a valuable taking for indicating the rate crews would work on that.

Premise:
Activity type= FR,
Activity Section = ALL,
Activity Spec = IN
Conclusion:
Duration=3weeks
(Confidence:1, Support:0.923)

After figuring out which attributes are the most frequent in framing rows of feature, a more specific FP-Growth algorithm had performed separately on the row of features in framing with FS predecessor and also SS predecessor. Given rows with FR. as the type and SS as

the logic of relation and putting them in the premise section of creating association rules, the first significant rule was as below:

Premise:
Activity type= FR,
Activity Section = ALL,
Activity Spec = IN
Conclusion:
FS PRE-Requisite Lag = 14 days,
FS PRE-Requisite Level D = 1,
FS PRE-Requisite Type = F.R.
(Confidence:.0.8, Support:0.923)

Given rows with FR as the type and FS as the logic of relation and putting them in premise section of creating association rules the first significant rule was as below:

Premise:
Activity type= FR,
Activity Section = ALL,
Activity Spec = IN
Conclusion:
SS PRE Requisite Lag = 0,
SS PRE Requisite Level D = -5,
SS PRE Requisite Section = 2,
SS PRE-Requisite Type = CS
(Confidence 0.9, support:0.583)

Based on the analysis on this section for any given framing activity that would be inside and will not be done on sections in each level. Furthermore, for nearly most of the FR activity, there is the FR predecessor with the Finish-to-Start relationship in one level lower. There would be a 2-week lag between predecessor and successor in this case

Finally, for nearly half of framing activities (support=0.583) there is CS (concrete for structure) predecessor with Start-to-Start logic which happens in Section two and six-level higher than the level that activity takes place, without any lags.

The second part of CASE 1, which generated meaningful rules was pouring concrete, and the schedule was gathered all the related tasks (forming, reinforcing and pouring) into one single item.The process which has applied for the framing section utilized here as well. First, the most repetitive attributes identified from applying the FP-Growth algorithm to all rows of features in CS (concrete of structure) section.

Activity Spec = PR
Activity Type = CS
FS PRE-Requisite Lag = 0
SS PRE Requisite Level D = 0
Duration = 2weeks
FS PRE-Requisite Level D = 1
FS PRE-Requisite Spec = PR
FS PRE-Requisite Type = CS
SS PRE-Requisite Lag = 0
SS PRE-Requisite Level = NA
SS PRE-Requisite Logic = NA
SS PRE-Requisite Section = 0
SS PRE-Requisite Spec = NA
SS PRE-Requisite Type = NA

Before starting any further analysis, the frequent attributes show that there is not any Start-to-Start predecessor for pouring activities while all the extracted frequent values for that are showing NA (not applicable). Hence, the main focus here remains with Finish-to-Start predecessors.

The first part was searching attributes that could be bind with activity type (CS). Implementing FP-Growth here gave us the following results.

Premise:
Activity Type = CS
Conclusion:
Activity Spec = PR
(Confidence:1, Support:1)

The duration of activities proved to be minable in the CS section while the pouring parts were in equal square feet and setup.

Premise:
Activity Type = CS
Activity Spec = PR
Conclusion:
Duration = 2
(Confidence:0.8, support:0.972)

The level difference and Lag and also type predecessor and the support rate of them also evaluated by putting them in the conclusion section of FP-Growth algorithm while considering Activity type (CS) and specs (PR) as the premises.

Premise:
Activity Type = CS
Activity Spec = PR
Conclusion:
FS PRE-Requisite Level D = 1
FS PRE-Requisite Type = CS
SS PRE-Requisite Lag = 0
(Confidence:0.9, support:0.889)

This indicates that for nearly most of CS activity, there is a CS predecessor with the Finish-to-Start relationship in one level lower. There would be no lag between predecessor and successor in this case. All the CS activities have PR (pouring) specification, which directly relates with the setup that schedule uses in gathering all forming, reinforcing and pouring as one

activity.

CASE 2 undergone the same process FP-Growth Algorithm and for foundation section, main rules were as below:

Premise:
Element= Piers,
Type= Pour,
Logic = FS,
Conclusion:
Element P=Pre1-Cage
(Confidence: 1.000, support: 0.375)

Here our model identified for any pier pouring activity there would be predecessor containing pier cage with Finish-to-Start relation to that. The reason for the decrease in support ratio is the fact that in CASE2, the four kinds of logic between activities put in separated rows of features. So, the initial ratio divided into each logic. For example, the support rate for the appearance of Element=Piers and Logic = FS is 0.625.

For the grade beams, the model came up with association rules as below:

Premise
Element=Grade Beams
Conclusion
Element P=Pre1-Grade Beams
(Confidence:1.000, support: 0.890)

Premise:
Element=Grade Beams,
Element P=Pre1-Pour
Conclusion:
Logic = FS
(Confidence: 0.917, support: 0.890)

5 Findings and conclusion

Implementation of the FP-Growth algorithm for CASE1 and CASE2 had a variety of notable findings. In CASE1 due to abbreviations in the work description and consistent way of naming activities make data mining relatively easy comparing CASE2, which had more descriptive titles as its activities' names.

Furthermore, unlike the successful experience of extracting duration for activities in CASE1, the model experienced lower confidence rates in extracting durations in CASE2. The main reason for that was more repetitive and typical activities in CASE1 with the sequence of activities remaining the same in each floor. For buildings with a lower number of floors, the only possible way is gathering group of similar projects and create full rows of features for them to mine duration.

In learning the logical relationship between activities and their Lag, the model performed well in both cases and generated meaningful rules. Start-to-Start and Finish-to-Start relationships between activities were identified as the most informative rules because they were addressing the connection between varying types and specifications in most cases which could be the cornerstone in shaping a masterplan. For example, FP-Growth algorithm learned SS relationship between framing and pouring five floors away from each other in the CASE1, which could be a significant barrier if it has not been put into consideration in master and detailed planning.

The model was performing better over CASE2 in identifying the sequence of activities ending in a specific element. The main reason for that could be the detailed description of each activity in their name column. The rules were found showed the pier cage as the predecessor of pouring for the pier. Also, pouring the pier was a predecessor for grade beam related activities with excavation specification. The reason for that was the broad details provided in naming each activity. The rules generated from CASE2 could be used to complete in between any two milestones which are identified for masterplans with activities.

To conclude, the research shows the possibility of generating rules in micro and macro scale from historical data and real-life schedules. Generated rules could minimize the uncertainty of mathematical models for scheduling as they can function as constant features in them. Also, by having hundreds of similar schedules, the standardization of construction work can happen through generated rules from more descriptive schedules. The results also have the capability to be used in generating alternative schedules Further uses of the results of current research could be in reducing uncertainties in scheduling process which can help to optimize the projects' cost-time tradeoffs which are highly dependent on the mathematical model. By having more learned rules that their frequency and certainty had been evaluated, the initial schedule could be set up and the allocation of resource with the goal of optimizing time-cost function happen for remaining activities.

References

[1] Y. J. T. Zidane and B. Andersen, "The top 10 universal delay factors in construction projects," *International Journal of Managing Projects in Business,* vol. 11, no. 3, pp. 650-672, 2018.

[2] J.-B. Yang and P.-R. Wei, "Causes of delay in the planning and design phases for construction projects," *Journal of Architectural Engineering,* vol. 16, no. 2, pp. 80-83, 2010.

[3] V. Faghihi, A. Nejat, K. F. Reinschmidt, and J. H. Kang, "Automation in construction scheduling: a review of the literature," (in

English), *Int J Adv Manuf Tech,* vol. 81, no. 9-12, pp. 1845-1856, Dec 2015.

[4] A. Birjandi and S. M. Mousavi, "Fuzzy resource-constrained project scheduling with multiple routes: A heuristic solution," *Automation in Construction,* vol. 100, pp. 84-102, 2019.

[5] M. Kavitha and S. T. Selvi, "Comparative Study on Apriori Algorithm and Fp Growth Algorithm with Pros and Cons," *International Journal of Computer Science Trends and Technology (I JCS T)–Volume,* vol. 4, 2016.

[6] H. Adeli, & Karim, A., *Construction scheduling, cost optimization and management*, 1st ed. London: CRC Press, 2001.

[7] Y. C. Toklu, "Application of genetic algorithms to construction scheduling with or without resource constraints," (in English), *Can J Civil Eng,* vol. 29, no. 3, pp. 421-429, Jun 2002.

[8] N. Dawood and E. Sriprasert, "Construction scheduling using multi‐constraint and genetic algorithms approach," *Construction Management and Economics,* vol. 24, no. 1, pp. 19-30, 2006.

[9] S. Chand, Q. Huynh, H. Singh, T. Ray, and M. Wagner, "On the use of genetic programming to evolve priority rules for resource constrained project scheduling problems," *Information Sciences,* vol. 432, pp. 146-163, 2018.

[10] M. Đumić, D. Šišejković, R. Čorić, and D. Jakobović, "Evolving priority rules for resource-constrained project scheduling problem with genetic programming," *Future Generation Computer Systems,* vol. 86, pp. 211-221, 2018.

[11] H. Seidgar, M. Kiani, and H. Fazlollahtabar, "Genetic and artificial bee colony algorithms for scheduling of multi-skilled manpower in combined manpower-vehicle routing problem," (in English), *Prod Manuf Res,* vol. 4, no. 1, pp. 133-151, Aug 25 2016.

[12] G. Campos Ciro, F. Dugardin, F. Yalaoui, and R. Kelly, "Open shop scheduling problem with a multi-skills resource constraint: a genetic algorithm and an ant colony optimization approach," *International Journal of Production Research,* vol. 54, no. 16, pp. 4854-4881, 2015.

[13] Z. Irani and M. M. Kamal, "Intelligent Systems Research in the Construction Industry," (in English), *Expert Syst Appl,* vol. 41, no. 4, pp. 934-950, Mar 2014.

[14] V. Faghihi, K. F. Reinschmidt, and J. H. Kang, "Construction scheduling using Genetic Algorithm based on Building Information Model," *Expert Syst Appl,* vol. 41, no. 16, pp. 7565-7578, 2014.

[15] M. Chen, S. Yan, S.-S. Wang, and C.-L. Liu, "A generalized network flow model for the multi-mode resource-constrained project scheduling problem with discounted cash flows," *Engineering Optimization,* vol. 47, no. 2, pp. 165-183, 2014.

[16] R. H. A. El Razek, A. M. Diab, S. M. Hafez, and R. F. Aziz, "Time-cost-quality tradeoff software by using simplified genetic algorithm for typical repetitive construction projects," *World academy of science, engineering and technology,* vol. 37, pp. 312-320, 2010.

[17] B. Koo, M. Fischer, and J. Kunz, "Formalization of construction Sequencing rationale and classification mechanism to support rapid generation of Sequencing alternatives," (in English), *Journal of Computing in Civil Engineering,* vol. 21, no. 6, pp. 423-433, Nov-Dec 2007.

[18] S. M. Chen, F. H. Griffis, P. H. Chen, and L. M. Chang, "Simulation and analytical techniques for construction resource planning and scheduling," (in English), *Automation in Construction,* vol. 21, pp. 99-113, Jan 2012.

Evaluation of Spalling in Bridges Using Machine Vision Method

Eslam Mohammed Abdelkader[a,b], Osama Moselhi[a], Mohamed Marzouk[b] and Tarek Zayed[c]

[a]Department of Building, Civil, and Environmental Engineering, Concordia University, Canada
[b]Structural Engineering Department, Faculty of Engineering, Cairo University, Egypt
[c]Department of Building and Real Estate, the Hong Kong Polytechnic University, Hong Kong
E-mail: eslam_ahmed1990@hotmail.com, moselhi@encs.Concordia.ca, mm_marzouk@yahoo.com, tarek.zayed@polyu.edu.hk

Abstract –

The growing number of bridges and their deteriorated conditions on one hand and the budget squeeze for their repair and rehabilitation on the other call for automated detection of defects and smart methods for condition rating of these bridges. This paper presents a newly-developed standalone computer application for automated detection and evaluation of spalling severities in reinforced concrete bridges. The application is coded in C#.net and makes use of an early developed model for detection of surface defects. The method is applied in two tiers, in the first tier, a single-objective particle swarm optimization model is developed for detection of spalling based on Tsallis entropy function. The second tier is devised for evaluation of spalling severities. It generates a comprehensive representation of the bridge deck image using Daubechies discrete wavelet transform feature description algorithm. The second tier also encompasses a hybrid artificial neural network-particle swarm optimization model for accurate prediction of spalling area; circumventing the drawbacks of the gradient descent algorithm. The developed method was tested using 60 images from three bridge decks in Montreal and Laval in Quebec, Canada. Results indicate significant superiority in area prediction accuracies; achieving mean absolute percentage error, mean absolute error and relative absolute error of 6.12%, 56.407 and 0.393, respectively. The developed method is expected to assist transportation agencies in performing more accurate condition assessment of concrete bridge decks and accordingly assist them in developing optimum maintenance plans.

Keywords –

Image; Reinforced Concrete Bridges; Spalling; Single-objective Optimization; Tsallis entropy; Daubechies discrete wavelet transform; artificial neural network

1 Introduction

Bridges are viral elements in infrastructure systems. Meanwhile, they are vulnerable to severe deterioration agents such as freeze-thaw cycles, excessive distress loads due to traffic overload, sulfates, alkali-silica reaction, poor construction practices, etc. It was reported that 26% of the bridges in Canada are experiencing medium to very poor severity levels. They are expected to suffer a further degradation in their condition ratings resulting from the increase of backlog of intervention actions [1-2]. There are two main reasons for the significant deterioration of bridges which are: the decrease in the public investment, and the high age of bridges. The investment in bridges is below the required level to maintain the age of bridges constant, whereas the age of bridges increased by 3.2 years from 21.3 years in 1985 to 24.5 years in 2007. Bridges in Quebec have the highest average age followed by Nova Scotia. Conversely, Prince Edward Island's bridges have the lowest average age. In this context, the average age of bridges on Quebec, Nova Scotia, and Prince Edward Island are 31, 24.5, and 15.6, respectively [3].

In the light of forgoing, it is essential to assess the structural condition ratings of bridges in order to maintain them within acceptable performance levels. The use of machine vision technologies has emerged in the last few years because they enable more efficient and cost effective assessment of structural components than visual inspection. Spalling is an important surface defect that is larger and deeper than scaling. It is created as a result of corrosion of steel reinforcement and it affects the durability and structural integrity of reinforced concrete bridges [4]. In this regard, the present study proposes a novel method for the evaluation spalling in reinforced concrete bridges. It is expected that the developed method will enable decision makers in improving accuracy, reducing cost and minimizing the inherent subjectivity of the visual

inspection process of reinforced concrete bridges.

2 Literature Review

Several machine vision-based methods were developed for the purpose of evaluating of surface defects in bridges. Ho et al. [5] developed a method for surface damage detection in cable-stayed bridges. In the developed method, median filter and histogram equalization were applied to improve the quality of captured images. The captured images were then projected onto principal component analysis sub-space. Mahalanobis square distance was then utilized to detect the existence of defects through computing the distance between the projection of input image and all the trained images. Noh et al. [6] proposed a method for the detection of cracks using fuzzy C-means clustering. In it, a set of morphological operations were employed to better reveal the characteristics of cracks and remove noise from the background. This encompassed dilation operation, manually-tuned masks and connected-component labelling. It was highlighted that the developed method could achieve higher recall and precision when compared against other edge detection-based methods.

Mohammed Abdelkader et al. [7] introduced a two-stage multi-objective optimization-based method for the sake of detection of crack images in reinforced concrete bridges. In it, invasive weed optimization algorithm was employed to find the optimum thresholds capitalizing on Kapur entropy function and Renyi entropy function. It was found that the developed method could achieve mean-squared error, peak signal to noise ratio and structural similarity index of 0.0784, 11.4831 and 0.9921, respectively. Talab et al. [8] proposed an approach for the detection of cracks in images based on a combination of edge-detection and histogram-based algorithms. Sobel filter was first applied to detect the edges of crack. Then, Otsu algorithm was utilized to classify the image into cracking pixels and background. It was deduced that the proposed approach could achieve clear and accurate identification of cracks with no noise.

Otero et al. [9] introduced five-stage algorithm for the detection of cracks. Anisotropic diffusion filter was applied to smooth the image while preserving cracking details. Sobel algorithm was utilized to extract cracking edges from the image. The resulted images from Sobel algorithm were processed using active contours technique for the segmentation of cracks. A group of morphological operations were then applied to remove noise blobs. It was highlighted that the developed algorithm could deal with transversal, longitudinal and alligator cracks. Liu et al. [10] presented a method for the detection of cracks in concrete structures capitalizing on multi-scale enhancement and visual features. Multi-scale enhancement algorithm supervised by gradient information was utilized to filter out noise from the images. A combination of Sobel operator and adaptive threshold segmentation was used to binarize the enhanced images. Closing and small area removal morphological operations were then used to integrate the fragmented cracks and remove the noises. It was found that the developed method could eventually achieve higher true positive rate when compared against Otsu and morphology-based algorithm in addition to percolation model-based algorithm.

Wang et al. [11] introduced an algorithm for crack detection of concrete bridges. In it, adaptive filter o size 3×3 was employed multiple times to remove any superimposed noises. Then, contrast enhancement was applied to the processed images to retain detailed information of the target crack as much as possible. An integration of Otsu threshold segmentation and modified Sobel operator were used to detect cracking pixels present in the image. It was inferred that the developed algorithm could achieve absolute error of 0.02 mm in the detection of cracking width. Pavithra et al. [12] developed an image processing-based method for the detection of cracks in concrete structures. Median filter was employed to remove salt and pepper noise that corrupts the images. Threshold segmentation was applied to separate the cracking pixels from the background. Erosion and dilation morphological operations with manually tuned structuring elements were applied to better detection the details of cracks. The outputs from Grey-level co-occurrence matrix alongside statistical features of the images were used as an input to the cascaded random forest classifier for cracking detection. The developed method was able to achieve a detection accuracy of 98%.

Shehata et al. [13] developed two models for the estimation of cracking width using feed and cascade forward back propagation artificial neural network models. Each crack was divided into segments and the maximum width of each segment was computed. It was reported that feed forward back propagation artificial neural network provided higher prediction accuracies achieving mean absolute testing error of 10.3%. Andrushia et al. [14] presented a method for structural concrete crack detection using a combination of image processing algorithms. Anisotropic diffusion filter was first employed to smooth the input images. The filtered images were then fed into the six sigma statistical method to separate the foreground cracking pixels from the background. The developed method outperformed some state of the art methods accomplishing mean squared error, peak signal to noise ratio and mean structural similarity of 62.41, 35.63 and 0.923, respectively. Jain and Sharma [15] proposed an

automatic system for the detection of severity levels of cracks. After applying histogram equalization and contrast enhancement, the processed images were segmented using K-means clustering algorithm. Different settings of K-means clustering were investigated, whereas it was found that random initialization with Euclidean distance provided better results. A fuzzy inference system was then devised for crack risk prediction based on aggregated score.

3 Proposed Method

The primary objective of the present study is to develop a computerized platform for the automated detection and severity assessment of spalling in reinforced concrete bridges. This research study extends on a method earlier developed by the authors for the recognition of surface defect type in the image [16]. The flowchart of the proposed method is depicted in Figure 1. In this context, the framework houses five main modules, namely data prep-processing, automated detection, feature extraction, automated evaluation and method validation. It should be mentioned that the spalling detection and assessment of its severities are described and validated separately. In the first module, the input true-color image RGB is transformed to the grayscale image to accelerate the computational process, whereas the intensity values of the gray level image are varying from 0 to 255. The images are resized to 200×200 to better capture the details and characteristics of spalling present in the images.

The performance of machine vision algorithms depends on the quality of the input images which may be corrupted with noise during acquisition and transmission phases. Noise is undesirable random fluctuations in the color and brightness of the image. In this context, the proposed method utilizes Frost filter to remove noises from the input images while retaining the fine details and edges of the object of interest. Frost is an exponentially weighted average filter that employs local statistics to reduce separate and multiplicative noises. It is based on computing an image coefficient of variation which is equal to the ratio of local standard deviation to the local mean of the noisy filter. Frost filter can be mathematically expressed as follows [17-18].

$$R\hat{}(\tau) = \sum_{n\times n} K\alpha e^{-\alpha|t|} \quad (1)$$

Such that;

$$\alpha = \frac{4}{n\sigma\hat{}^2} \times \frac{\sigma^2}{I^2} \quad (2)$$

$$t = |X - X_o| + |Y - Y_o| \quad (3)$$

Where;

K denotes a normalizing constant. $\sigma\hat{}^2$ stands for the image coefficient of variation. σ^2 denotes the local variance. n represents the moving kernel size. I represents the local mean.

Processing of defects images in reinforced concrete bridges is a challenging task because of their complexity, low contrast, color distortion and non-uniform illumination. In this regard, the proposed method utilizes min-max gray level discrimination approach for the sake of improving the contrast of images. This is accomplished through increasing the gray level intensities of the spalling pixels meanwhile decreasing the intensities of the non-spalling pixels [19].

The second module is designated for automated detection of spalling. Image segmentation is one of the basic and critical operations used to analyze the retrieved images in pattern recognition applications. It is the process of dividing the image into non-overlapping multiple segments based on some attributes such as color, intensity and texture. In this regard, optimization-based method proved their efficiency in dealing with complex image segmentation problems in various applications [7]. In the present study, bi-level thresholding is applied to segment the spalling images by designing a single-objective particle swarm optimization model that aims at maximizing Tsallis entropy of the image. The output of this module is a single threshold T that classifies the image pixels into two classes: the spalling (foreground) and surface (background).

The third module is the feature extraction of the captured images. It comprises the use of Daubechies discrete wavelet transform. It decomposes the input original image into four sub-images via high-pass and low-pass filters. The four quadrant sub-bands are called HH_n, LL_n, HL_n and LH_n. For instance, LL_n is generated through employing low-pass filter for both rows and columns. LH_n is generated through employing low-pass filter for rows and high-pass filter for columns [20-21]. The fourth module is the automated assessment of spalling severities. The proposed method ($ANN - PSO$) utilizes particle swarm optimization algorithm for both parametric and structural training of back propagation artificial neural network. This involves autonomous optimizing the weights of artificial neural network and its best possible architecture. In this context, artificial neural network is trained through formulating a variable-length single-objective optimization problem which encompasses a fitness function of minimization of mean absolute percentage error of spalling area. The optimized artificial neural network is then appended and adopted to simulate the testing dataset for its performance evaluation. Particle swarm optimization algorithm is a widely-recognized meta-heuristic that proved its efficiency in dealing with complex and

diverse optimization problems such as allocation of irrigation water [22], resource-constrained project scheduling [23] and damage detection using vibrational data [24].

The automated detection model is validated through comparison against Otsu algorithm. It is an unsupervised algorithm that is used to segment an image by maximizing the variance between the segmented classes [25]. The performance of the automated assessment model is evaluated against the back propagation artificial neural network for its validation.

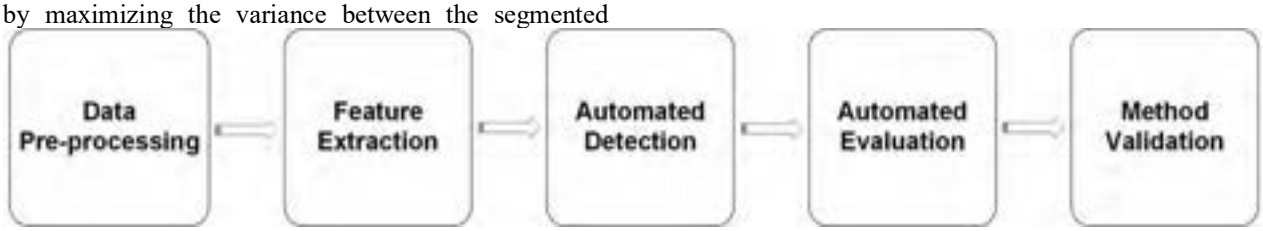

Figure 1. Main modules of the developed spalling detection model

4 Method Development

This section describes the basic computational procedures of Tsallis entropy algorithm and particle swarm optimization algorithm.

4.1 Tsallis Entropy

Assume an image I that contains L gray-levels $\{0, 1, 2, 3, \dots \dots . L-1\}$. Tsallis entropy can be defined using Equation (4) [26-27].

$$S_q = \frac{1 - \sum_1^k (P_i)^q}{q - 1} \quad (4)$$

Where;

k represents the total number of possibilities in the system. q denotes Tsallis entropy or entropic index.

Tsallis entropy of a whole system can be described based on the pseudo additive entropic rule as shown in Equation (5).

$$S_q^{A+B} = S_q^A + S_q^B + (1-q) S_q^A S_q^B \quad (5)$$

Tsallis entropy of the two classes C1 and C2 can be computed using Equations (6) and (7), respectively. Tsallis entropy is computed based on the calculation of the probabilities of occurrence of the gray levels P_i, whereas $\sum_{i=0}^{L-1} P_i = 1$

$$S_q^{C1}(T) = \frac{1 - \sum_{i=0}^{T-1} \left(\frac{P_i}{P^{C1}}\right)^q}{q-1}, P^{C1} = \sum_{i=0}^{T-1} P_i \quad (6)$$

$$S_q^{C2}(T) = \frac{1 - \sum_{i=T}^{L-1} \left(\frac{P_i}{P^{C2}}\right)^q}{q-1}, P^{C2} = \sum_{i=T}^{L-1} P_i \quad (7)$$

Where;

$S_q^{C1}(T)$ and $S_q^{C2}(T)$ represent Tsallis entropy of the two classes C1 and C2, respectively.

Thus, the objective of the optimization problem is to find the gray threshold T , which maximizes Tsallis entropy of the segmented classes as per Equation (8).

$$F(T) = \max \left(S_q^A + S_q^B + (1-q) S_q^A S_q^B\right) \quad (8)$$

4.2 Particle Swarm Optimization

Particle swarm optimization is a population-based meta-heuristic that was first introduced by Eberhart and Kennedy. The basic computational stages of particle swarm optimization algorithm are depicted in Figure 2 [28-29]. It is inspired by the social behaviour of migrating flock of birds. Each candidate solution is called "particle" and a population of randomly positioned particles in the search space is called "swarm". Each particle in the multi-dimensional solution space is characterized by its position and velocity. During each iteration in the evolution process, each particle monitors its current position, the best position it achieved and its own flying velocity. The position and velocity of each particle is updated according to its own best flying experience and the best position achieved by the entire swarm. In this regard, the position of the best particle in the swarm is obtained based on the pre-defined fitness function(s). The computational procedures of particle swarm optimization algorithm combines local and global search which helps in providing a proper balance between exploration and exploitation. The positions and velocities of the swarm of particles in the trajectory are updated as follows.

$$v_i(t+1) = w \times v_i(t) + c_1 \times r_1 \times (pbest_i(t) - x_i(t)) + c_2 \times r_2 \times (gbest(t) - x_i(t)) \quad (9)$$

$$x_i(t+1) = x_i(t) + v_i(t+1) \quad (10)$$

Where;

$x_i(t)$ and $x_i(t+1)$ denote the position of the i-th particle in iteration t and $t+1$, respectively. $v_i(t)$ and $v_i(t+1)$ represent the velocity of the i-th particle in iteration t and $t+$, respectively. $pbest_i$ is the individual local best position that particle i achieved so far. gbest stands for the global best position achieved by the entire swarm. c_1 and c_2 are two acceleration coefficients that denote cognitive learning, and social parameters, respectively. They enable controlling the global and local guides. r_1 and r_2 represent two uniformly distributed random numbers searching search for better solutions along the direction towards the personal best and global best. w refers to the inertia weight. It is advised to start with a large inertia factor and then it decreases within the evolution process to enable both global and local explorations.

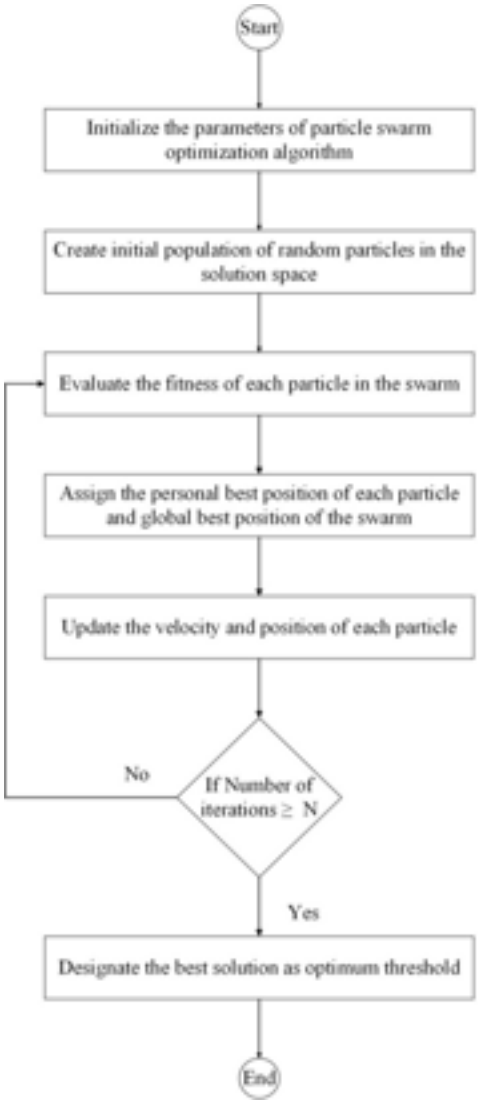

Figure 2. Flowchart of particle swarm optimization algorithm

5 Method Implementation

A dataset comprising of 60 real-world images are used as an input to experiment the proposed method such that 50 images are used for training while the remaining 10 images are used for testing. These images are captured from bridge decks in Montreal and Laval, Canada using Sony DSC-H300 digital camera of 20.1 megapixel resolution. All the calculations and optimization algorithms took place on a laptop with an Intel Core i7 CPU, 2.2 GHz and 16 GB of memory. Sample of the spalling images used is presented in Figure 3.

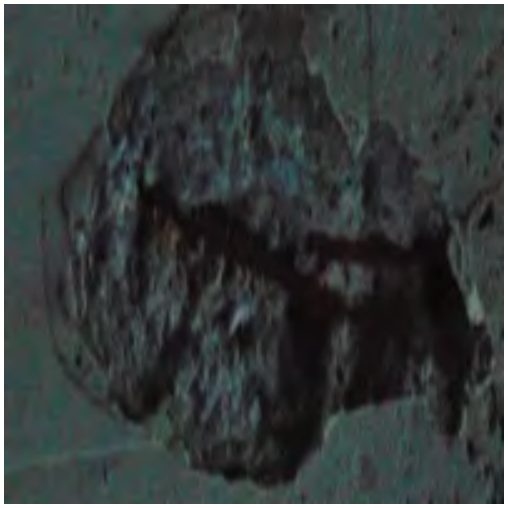

(a) Image "A"

(b) Image "B"

Figure 3. Sample of the spalling images

In the automated spalling detection model, Tsallis entropy index is assumed 0.5. With respect to the particle swarm algorithm in this model, the number of iterations and the initial population size are assumed 30 and 10, respectively. The cognitive learning and social parameters are assumed 2 while the inertia factor is assumed 0.5. Figure 4 demonstrates the segmented image of spalling after the application of the single objective particle swam optimization-based segmentation method alongside the segmented image after the implementation of Otsu algorithm. As can be seen, the developed detection model successfully recognized the spalling. However, Otsu algorithm failed to discriminate the spalling pixels from the background causing a lot of distortion in the image.

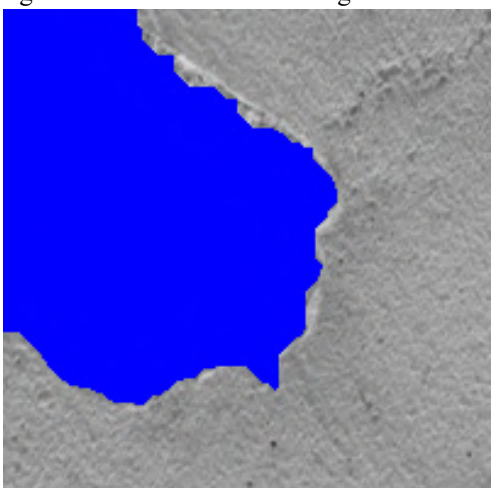

(a) Segmented image using the developed detection model

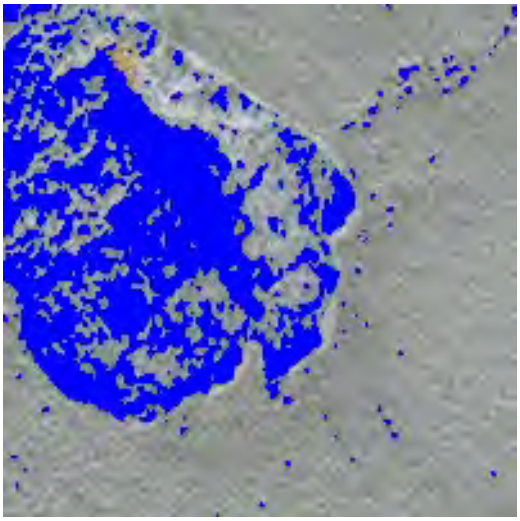

(b) Segmented image using Otsu algorithm

Figure 4. Visual representation of spalling detection models

At the level of spalling evaluation, the ANN – PSO model is composed of one output neuron for the prediction of spalling area. The optimization parameters of the developed ANN – PSO model are recorded in Table 1. It is found that the optimum numbers of hidden layers and hidden neurons are one and two, respectively. Tangent sigmoid is the optimum transfer function. A comparative analysis between the ANN – PSO model and the back propagation artificial neural network is presented in Table 2. The comparison is carried out using mean absolute percentage error (MAPE), mean absolute error (MAE) and relative absolute error (RAE). It can be inferred that the developed assessment model substantially outperformed the conventional artificial neural network through reducing MAPE, MAE and RAE by 76.65%, 71.47% and 71.43%, respectively.

Table 1. Optimization parameters of the developed **ANN – PSO** model

Parameter	Corresponding value
Minimum number of hidden layers	1
Minimum number of hidden neurons	1
Maximum number of hidden layers	10
Maximum number of hidden neurons	10
Initial population size	200
Number of iterations	400
Cognitive learning	2
Social parameter	2
Inertia weight	0.5

Table 2. Performance comparison between the spalling evaluation models

Model	MAPE	MAE	RAE
ANN – PSO	6.12%	56.407	0.393
Artificial neural network	26.21%	197.756	1.376

6 Conclusion

Routine visual inspections are mandatory to build condition assessment models. Nevertheless, they are prone to subjective judgments. This can lead to inaccurate deterioration models and intervention actions. In this context the present study introduces a novel two-tier method for the automated detection and evaluation of spalling in reinforced concrete bridges.

Results obtained from the visual comparison demonstrated superiority of the spalling segmentation model of the developed method. It was able to establish

well-separated thresholds as well as more compact and homogenous clusters. On the other hand, Otsu algorithm failed to detection spalling pixels in the image. With regard to the spalling evaluation, it was concluded that the developed spalling evaluation model managed to reduce of the prediction error by values ranging from 71.43% to 76.65% with reference to the artificial neural network. Accordingly, the developed method can be deployed as an efficient tool to provide safer, productive and more reliable inspection of reinforced concrete bridges.

References

[1] Felio, G. Canadian Infrastructure Report Card. Canadian Construction Association, Canadian Public Works Association, Canadian Society for Civil Engineering, and Federation of Canadian Municipalities, Canada. <www.canadainfrastructure.ca/downloads/Canadian_Infrastructure_Report_2016.pdf> (06.05.2016), 2016.

[2] Mohammed Abdelkader, E., Moselhi, O., Marzouk, M. and Zayed, T. Condition Prediction of Concrete Bridge Decks Using Markov Chain Monte Carlo-Based Method, *7th CSCE International Construction Specialty Conference Jointly with Construction Research Congress*, Canada, 1-10, 2019.

[3] Viami International Inc. and the Technology Strategies Group. *Market Study for Aluminium Use in Roadway Bridges*, 1-29, Montreal, Canada, 2013.

[4] Mazzotta, F., Lantieri, C., Vignali, V., Simone, A., Dondi, G. and Sangiorgi, C. Performance evaluation of recycled rubber waterproofing bituminous membranes for concrete bridge decks and other surfaces. *Construction and Building Materials*, 136:524–532, 2017.

[5] Ho, H., Kim, K, Park, Y. and Lee, J. An efficient image-based damage detection for cable surface in cable-stayed bridges. *NDT & E International,* 58:18–23, 2013.

[6] Noh, Y., Koo, D., Kang, Y. M., Park, D. G. and Lee, D. H. Automatic crack detection on concrete images using segmentation via fuzzy C-means clustering. *Proceedings of the 2017 IEEE International Conference on Applied System Innovation: Applied System Innovation for Modern Technology,* Japan, 877-880, 2017.

[7] Mohammed Abdelkader, E., Moselhi, O., Marzouk, M. and Zayed, T. A Multi-objective Invasive Weed Optimization Method for Segmentation of Distress Images *Intelligent automation and soft computing*, 1-20, 2019.

[8] Talab, A. M. A., Huang, Z., Xi, F. and Haiming, L. Detection crack in image using Otsu method and multiple filtering in image processing techniques. *Optik*, 123:1030–1033, 2016.

[9] Otero, L. D., Moyou, M., Peter, A. and Otero, C. E. Towards a Remote Sensing System for Railroad Bridge Inspections: A Concrete Crack Detection Component. *Proceedings of IEEE SOUTHEASTCON*, United States of America, 1-4, 2018.

[10] Liu, X., Ai, Y. and Scherer, S. Robust Image-based Crack Detection in Concrete Structure Using Multi-scale Enhancement and Visual Features. *2017 IEEE International Conference on Image Processing*, China, 2304-2308, 2017.

[11] Wang, Y., Zhang, J. Y., Liu, J. X., Zhang, Y., Chen, Z. P., Li, C. G., He, K. and Yan, R. Research on Crack Detection Algorithm of the Concrete Bridge Based on Image Processing. *Procedia Computer Science*, 154:610–616, 2018.

[12] Pavithra, D., Saranya, T., Prakash, K. and Soundarya, G. Electronic Crack Detection On Concrete. *International Journal of Advanced Science and Engineering Research*, 3:515–521, 2018.

[13] Shehata, H. M., Mohamed, Y. S., Abdellatif, M. and Awad, T. H. Crack width estimation using feed and cascade forward back propagation artificial neural networks. *Key Engineering Materials*, 786:293–301, 2018.

[14] Andrushia, D., Anand, N. and Arulraj, P. Anisotropic diffusion based denoising on concrete images and surface crack segmentation. *International Journal of Structural Integrity*, 11:395–409, 2019.

[15] Jain, R. and Sharma, R. S. Predicting Severity of Cracks in Concrete using Fuzzy Logic. *International Conference on Recent Innovations in Electrical, Electronics and Communication Engineering*, India, 2976–2982, 2018.

[16] Mohammed Abdelkader, E., Moselhi, O., Marzouk, M. and Zayed, T. (2020). "Hybrid Elman Neural Network and Invasive Weed Optimization Method for Bridge Defects Recognition, *Submitted to: Journal of the Transportation Research Board*.

[17] Kulkarni, S., Kedar, M. and Rege, P. P. Comparison of Different Speckle Noise Reduction Filters for RISAT-1 SAR Imagery. *International Conference on Communication and Signal Processing*, India, 537-541, 2018.

[18] Dhanushree, M., Priyadharsini, P., Sharmila, T. S. Acoustic image denoising using various spatial filtering techniques. *International Journal of Information Technology*, 11:659-665, 2019.

[19] Hoang, N. Detection of Surface Crack in Building Structures Using Image Processing Technique with an Improved Otsu Method for Image Thresholding, *Advances in Civil Engineering,* Article ID 3924120, 10 pages, 2018.
[20] Waqas, U. A., Khan, M. and Batool, S. I. A new watermarking scheme based on Daubechies wavelet and chaotic map for quick response code images. *Multimedia Tools and Applications*, 79:6891–6914, 2020.
[21] Devi, T. K. and Sakthivel, P. Pipelined Direct Mapping Method based Low Power VLSI Architecture for the 4-Tap Wavelet Filter. *Asian Journal of Applied Science and Technology*, 1:76–79, 2017.
[22] Noory, H., Liaghat, A. M., Parsinejad, M. and Haddad, O. B. Optimizing Irrigation Water Allocation and Multicrop Planning Using Discrete PSO Algorithm. *Journal of Irrigation and Drainage Engineering*, 138:437–444, 2012.
[23] Koulinas, G., Kotsikas, L. and Anagnostopoulos, K. A particle swarm optimization based hyper-heuristic algorithm for the classic resource constrained project scheduling problem. *Information Sciences*, 277:680–693, 2014.
[24] Kang, F., Li, J. J. and Xu, Q. Damage detection based on improved particle swarm optimization using vibration data. *Applied Soft Computing Journal*, 12:2329–2335, 2012.
[25] Khairuzzaman, A. K., and Chaudhury, S. Multilevel Thresholding using Grey Wolf Optimizer for Image Segmentation. *Expert Systems With Applications*, 86:64–76, 2017.
[26] Mishra, S., and Panda, M. Bat Algorithm for Multilevel Colour Image Segmentation Using Entropy-Based Thresholding. *Arabian Journal for Science and Engineering*, 43(12):7285-7314, 2018.
[27] Bhandari, A. K., Kumar, A., and Singh, G. K. Tsallis Entropy Based Multilevel Thresholding for Colored Satellite Image Segmentation using Evolutionary Algorithms. *Expert Systems With Application*, 42(22):8707-8730, 2015.
[28] Kennedy, J. and Eberhart, R. Particle swarm optimization. *Proceedings of the IEEE International Conference on Neural Networks*, Australia, 1942–1948, 1995.
[29] Li, F., Gong, Y., Cai, L., Sun, C., Chen, Y., Liu, Y. and Jiang, P. Sustainable land-use allocation: A multiobjective particle swarm optimization model and application in Changzhou, China. *Journal of Urban Planning and Development*, 144:1-11, 2018.

Improving Construction Project Schedules before Execution

John Fitzsimmons[a], Ying Hong[b] and Ioannis Brilakis[b]

[a]Laing O'Rourke, United Kingdom
[b]Department of Engineering, University of Cambridge, United Kingdom
E-mail: jpf36@cam.ac.uk, yh448@cam.ac.uk, ib340@cam.ac.uk

Abstract –

The construction industry has been forever blighted by delay and disruption. To address this problem, this study proposes the Fitzsimmons Method (FM method) to improve the scheduling performance of activities on the Critical Path before the project execution. The proposed FM method integrates Bayesian Networks to estimate the conditional probability of activity delay given its predecessor and Support Vector Machines to estimate the time delay. The FM method was trained on 302 completed infrastructure construction projects and validated on a £40 million completed road construction project. Compared with traditional Monte Carlo Simulation results, the proposed FM method is 52% more accurate in predicting the projects' time delay. The proposed FM method contributes to leveraging the vast quantities of data available to improve the estimation of time risk on infrastructure and construction projects.

Keywords –

Construction Schedule; Machine Learning; Project Delay; Critical Path Method

1 Introduction

At present, around £100bn is spent in the UK each year on infrastructure investments [1], making the delivery of infrastructure 70% of the total spending on the National Health Service. By 2030 it is estimated that around £19bn a year will be wasted on the avoidable costs generated by poorly delivered infrastructure projects [2]. This is a worrying trend in an age where populations are aging and productivity in the UK economy has stagnated [3]. Experts estimate that for every £1 invested in infrastructure, the benefit to the economy is £2.841 [4]; the money wasted on poorly delivered infrastructure would equate to as much as £35bn per year in unrealised economic benefit. The cost to the global economy would be $620bn each year, if the trend were extrapolated worldwide [5], with around $1.1tn of potential loss. While delays are only part of the picture, it has been argued that they are among the most significant culprits in undermining the successful completion of infrastructure investment [6,7].

Recent research used machine learning methods to predict project delay, including naïve Bayesian [8], Bayesian Belief Network [9] and logistic regression [10]. In practice, some software packages (e.g. Deltek Acumen Fuse) enable users to pre-define delay factors and its correlations while modelling risk. However, the analysis of these packages is still inarticulate and does not have a strong evidentiary basis.

This research aims to create a more objective and evidence-based framework for schedule risk analysis, given the theoretical limits and incompatible software in risk analysis. The proposed solution – the FM Method simulates risks on the critical path and predict project delay. Hence, the proposed method can provide the project manager and schedulers insights about the potential risks of their planning before execution, thus enable effective planning.

This paper starts with reviewing literature ineffective planning and project duration prediction, followed by the proposed FM method, analysis results of FM method and a discussion of analysis results. The conclusion is summarised at the end.

2 Literature Review

This section provides a comprehensive review in construction project delay estimation. This section starts with a review in schedule quality, followed by commonly used methods in predicting construction delay. Research gaps and questions are summarised at the end.

2.1 Schedule Quality

Late project delivery is affected by many factors either internally or externally, from engineering design to project management [11]. External factors including weather [12,13] and macroeconomic conditions [14] being unpredictable and uncontrollable. Whereas addressing internal factors, and in particular schedule quality [15], can significantly reduce the chance of late delivery [16]. A quality schedule uses expected outputs,

resource and space constraints, and technical expertise to determine an optimal and achievable schedule of activities. Subjectivity and uncertainty hinder the production of quality schedules.

Schedulers estimate time-risk on construction projects and allocate time contingency for high-risk activities to minimise the possibility of project delay in common practice. However, the estimation of time-risk on construction projects is done subjectively, largely by experience, and the penetration of academic concepts into the realm of common practice is negligible [17,18]. Including time continency is one of the trickiest areas of project planning, as it deals with a level of uncertainty which can be challenging to calculate and understand without detailed knowledge of historical records [19].

2.2 Predicting construction delay

The most traditional way to detect project delay in the practice is the Critical Path Method (CPM) [17,20]. CPM connects a series of construction tasks with defined dependency links to create a directed acyclic graph (DAG) network. Programme Evaluation and Review Technique (PERT) is a variant of CPM that accounts uncertainty with Beta distribution [21,22]. Azaron et al. [23] look at refining the bounds of the project duration risk by introducing the concept of a dynamic Markov PERT model. The approach estimates societal factors such as war, strikes and inflation to make activity durations non-static over time. However, it is an untested model, but it begins to link external factors, deterministic CPM, PERT, and correlation together in an interesting way.

To add covariance and correlation effects to PERT and MCS, Ökmen et al. [24] construct a system called Correlated Schedule Risk Analysis (CSRAM), which uses simple subjective inputs on a range of project risks including weather, soil conditions, labour productivity, and material/resource availability factors. However, CSRAM does not address the crucial problem of subjectivity and opinion-based analysis, a factor commonly associated with disputes in contracts [25,26]. Furthermore, the empirical evidence that this technique is scalable and works across a range of projects types is lacking.

Recent researchers predict project delay using machine learning methods (e.g. Artificial Neural Network (ANN)) based on influencing factors (including the project manager's experience). Kog et al. [27] create a neural network for determining schedule performance from extraneous project factors, including project manager's experience and monetary incentive to the designer. Attal [28] used the overall duration and cost of highways projects to train a series of ANN to determine the key project features to be used in a duration prediction model. Hola et al. [29] take a more specific approach, using ANN to predict earthworks durations. Similarly, Bhokha et al. [30] predicted the duration of building construction using ANN.

A promising solution to the problem of co-variance and project uncertainty is the Bayesian Network (BN) approach. A BN is a probabilistic DAG network, with nodes representing outcomes and arcs, or links, representing the conditional relationships between the nodes [31]. In this respect, they are very similar to construction schedules, where each task could be considered a node and each logic link a conditional dependence relationship. BN has been successfully used in several fields, including medical diagnoses [32] and modelling of complex interactions including operational risk [33], environment [34], and road traffic accidents [35]. Consequently, several recent studies have proposed a framework for using BNs to enhance schedule risk analysis [36–38].

2.3 Research gaps and questions

Three research gaps are identified through extensive literature: (1) it is not known how well the subjective risk analysis studies scale up to large infrastructure projects – they either set out an untested framework or use small sample projects to demonstrate accuracy; (2) the studies which use data have done so at a macro level, which does not allow risk simulation and assessment of a baseline schedule to be undertaken; (3) natural language processing techniques have not yet been optimised for construction industry language. In essence, the research problem left unsolved is that there is no unified approach which seeks to model uncertainty in project schedules using historical data to validate all of the inputs into the process.

This study aims to answer the following research questions: (1) What techniques can be employed to prepare historical construction schedule data for prediction model training? (2) What effect will the application of these techniques, combined with prediction modelling have on the accuracy of time-risk simulation models?

3 Proposed Method

This section provides the proposed method. It starts with an overview of the methods. This study proposes a framework - Fitzsimmons (FM) Method for simulating schedule risk which combines the strengths of Bayesian Networks, Support Vector Machines and Monte Carlo Simulation to simulate project outcomes. Figure 1 presents an overview of the proposed FM method. This study targets an analysis risk of the critical path statically, not dynamically. Therefore, the change of critical path is not evaluated in this model. The following subsections explain the proposed FM methods

in detail.

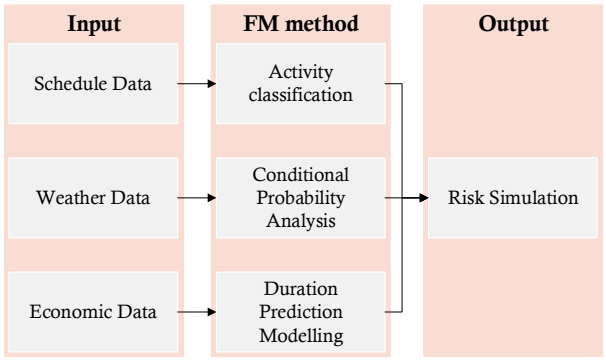

Figure 1. Overview of the proposed method

3.1 Word Embedding

Word embedding (Word2Vec) was used to add semantic meaning to the words in each task description. The two neural network architectures identified for this purpose were Skip-gram and Continuous bag-of-words (CBOW) embeddings. CBOW and Skip-gram are recent methods that learn word embedding representation and predict target words from context [39], but work inversely [40]. CBOW predicts target words from source text words; while, Skip-gram predicts source text words from target words [40].

It is unavoidable that there are similar activities, in terms of its functionality; for example, 'pour concrete for ring beam' and 'concrete ring beam'. Since distinguishing the semantic differences between activities remains challenging, this study clustered activities into topics using Gaussian Mixture Modelling (GMM). GMM is a probabilistic model for representing normally distributed subpopulations within an overall population [41]. The most common and well-used topic modelling methods are Latent Dirichlet Allocation (LDA) [42] and Latent Semantic Analysis (LSA) [43]. These models have been shown to work well for large corpora and documents, where keywords may appear several times [44]. Whereas, the average construction task description length is 5-10 words, rendering LDA/LSA largely ineffective. Hence, this study employed GMM to cluster construction activities. The optimal number of clusters was determined by using topic coherence as a reference. After several iterations of the test, it was difficult to determine a precise optimum number of topics.

3.2 Bayesian Probability

This study measures activity duration deviation, rather than activity delayed duration, to simulate the project duration. Early finished activity may also lead to project duration variation. Activity duration deviation is estimated as follows:

$$Duration\ deviation = \left(\frac{Actual\ duration}{Original\ duration} - 1\right) \times 100\% \quad \text{Eq. (1)}$$

In this study, BN is used to estimate the probability that each activity duration will deviate based on its characteristics and position within the CPM network in this study. The probability of activity duration deviation derived will be used as input in the next step. Figure 2 presents a simplified BN that estimates the probability of activity duration deviation.

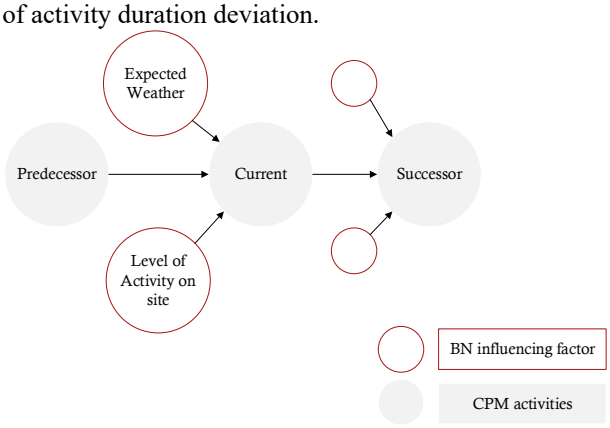

Figure 2. Simplified BN

3.3 Support Vector Machines

Support Vector Machines (SVM) is a classification method which distinguishes classes via solving a constrained quadratic programming problem and inserting a hyperplane [45]. SVM is used to predict the duration growth percentage of activity. Different from BN, SVM estimates the duration deviation of the current activity. Except for the probability of duration deviation derived above, SVM inputs also include the level of concurrent activity, estimated duration, and previous activity duration deviation. The dataset was split into train and test subset with a ratio of 80/20%, to avoid overfitting, to train an accurate SVM.

SVM, in this study, predicts the duration growth percentage of activity, as highlighted earlier. A task of 200 days and a task of 2 days could both find a prediction of 400% duration increase, but with different levels of impact to project delay. Therefore, this study calibrates duration growth percentage into a relative number as compared to the activity's duration. Eq. (2) explains the duration growth percentage calibration:

$$\tilde{Y} = (2 \times \hat{Y} \times \delta \times \mu)/(2 \times \delta \times \mu + \hat{Y} \times \delta \times ED) \quad \textit{Eq. (2)}$$

Where $\tilde{Y}$ is the calibrated duration growth of a given activity,

$\hat{Y}$ is the predicted duration growth of a given activity by SVM,

δ is the standard deviation of all durations in the project being simulated,

μ is the mean activity duration for the project being simulated,

ED is the estimated duration of the given activity.

3.4 Risk simulation

The simulation algorithm intended to calculate the average finishing position of each task over a nominal number of simulation iterations. This gives a time-distributed profile of tasks that can be used as the output of the risk analysis simulation. It is conceptually based on the Monte Carlo Simulation algorithm but with uncertainty and SVM to predict the deviation parameters. A beta distribution is used to determine the final duration deviation factor, to ensure that the duration uncertainty parameters change from one simulation iteration to the next. This distribution is parameterised by the SVM model prediction. The author chose this method to capture the strengths of MCS and PERT in modelling duration uncertainty. This model can be described as truly dynamic. With each iteration, the SVM input values will change and the duration deviation estimate will change with them, giving a broader range of possible values for the duration of each task.

4 Data Collection and Analysis Results

4.1 Data Collection and Pre-processing

The schedule data was collected from two construction and engineering firms. One of the organisations is a tier one contractor who directly delivers large infrastructure projects on behalf of public and private sector clients. The other is a schedule management consultancy that provides services to clients and contractors in several engineering disciplines. Both were requested to provide as-built schedules and initial baseline schedules for infrastructure projects regardless of the project outcome. The files were provided in the software-native Primavera P6 '.XER' format.

In total 560 project files were collected, of which 302 were valid. Some were invalid due to corrupt native files or a lack of 'actual versus planned' information. Figure 3 below shows the split by project discipline, with a relatively broad range of projects included. In total 444,173 tasks were added to the dataset, using an algorithm which interrogated the native schedule files and extracted any useful information into a large data file in '.txt' format. For context, a simple analysis of 'task count vs. project value' suggests that every 1,000 tasks represent £20m in project value. This indicates that the database may be equivalent to as much as £8.9bn in completed infrastructure.

This study pre-processed activity names to secure accuracy, before feeding activity names into analysis models. Pre-processing steps include tokenisation, lemmatisation, stemming and removing stop words. Tokenisation is a process that transforms text into tokens which are readable in a computer language [46]. Lemmatisation and stemming are used to reduce the effects of inflectional form and words' morphology [47]. Stop words (e.g. 'and', the') and punctuation was removed, to get eliminate the unmeaningful words.

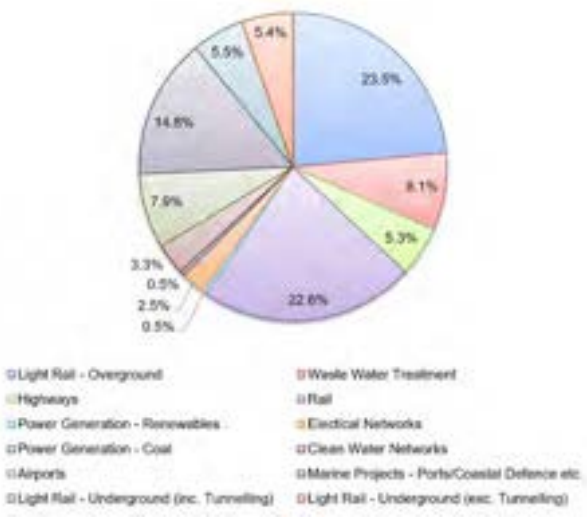

Figure 3. Data Distribution

4.2 Analysis Results

After pre-processing, data were fed into the proposed FM method. The following subsections summarise analysis results of each step from word embedding to simulation results.

4.2.1 Word Embedding

The first step in the proposed FM method represents construction activities' names with word vectors and clusters similar activities into topics. This study used Word2Vec to represent construction activities names with word vectors, as highlighted in Section 3.1. The hyperparameters of the Word2Vec model are the number of training iterations, the context window length, and the vector size [48]. A range of 5, to 50 iterations was tested with no significant improvement in performance, so the default value of 5 iterations was used. The context window of 8 was selected based on the average concatenated task description and section heading length. The default vector size of 100 was used, which is suggested by literature [49,50]. In total 5,496 unique words were used in the embedding process, training across a raw dataset of 3.1 million co-occurring words.

Following that, similar activities are clustered into topics using word vectors as input. Topic modelling is an unsupervised learning method and determining the number of clusters is challenging. This study used the coherence score to determine the optimal number of

clusters. It is found that the score settles between 10 and 25 topics, with higher scores towards 20 by plotting the coherence score. Intuitively, this feels appropriate. The design manual for roads and bridges [51] has 16 volumes; if more topics are allowed for procurement, rail and mechanical & electrical trades, then 20 is reasonable.

4.2.2 Activity Duration Deviation

The SVM kernel selected was the radial basis function (RBF), which enables the SVM to perform well with high-dimensional non-linear data. The results of the activity duration growth percentage are summarised in Figure 4. The mean value of activity duration growth percentage is 114% with a standard deviation of 631%. The result indicates that on average, activities are delayed for 114%, as compared with its original duration.

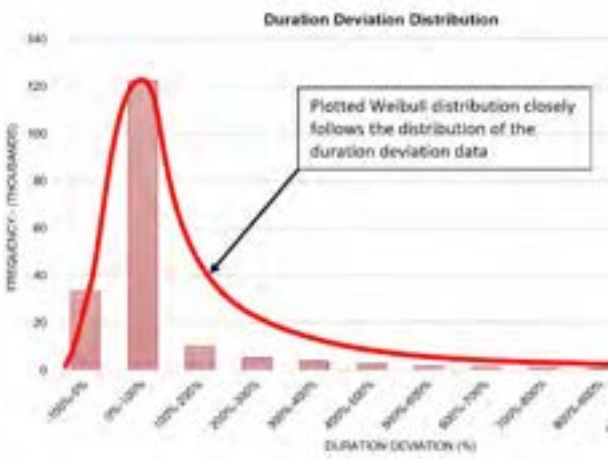

Figure 4. Distribution of Duration Deviation

Using variations about the mean is not the optimum way to simulate activity by activity variance, as shown in Figure 4. The value is heavily skewed by a few extremely high variance numbers, which in normal circumstances might be considered outliers. The issue with treating this as a normal distribution problem is that the data will never be normally distributed. Schedule duration growth works such that most samples sit around the 0% growth point – the 'quicker than planned' activities are bounded at -100%, whereas increased durations have no upper boundary. This makes deciding what constitutes an outlier a particularly difficult activity as normal conventions, involving excluding data over a certain standard deviation (σ) threshold, cannot be meaningfully applied to datasets with large right-skewed distribution tails. The activity duration deviations appear to more closely represent a Weibull distribution as discussed by [52]. Perhaps an approach to modelling duration risk which instead selects duration deviation from a Weibull rather than a normal distribution would be a more appropriate methodology.

Significantly, the high variability was smoothed to give estimates with an average variance of around +68% against the original duration estimate, when using SVM with a radial basis function kernel to predict the variance in an activity. The SVM results predict that some activities could finish earlier, and some activities could be late for 1,500%, which is more than enough to raise a red flag to those looking for significant risks.

The accuracy of SVM results is 80% in predicting whether an activity is delayed, on time or early on the test set. The SVM model predicts a standard prediction error of 122% of activity duration. This may seem extreme, but in a very random training set with a standard deviation of 870%, this is remarkably accurate.

4.2.3 Risk Simulation

The last step is the risk simulation. The case study used was selected randomly and excluded from model training. The selected case study is a port renovation work with a contract value at £40M in the UK. This project finished 26 weeks later than its originally estimated duration. The key risks in this project were that the piling on the existing dock – the ground conditions and existing substructure - were unknown, as well as the condition of the existing aging structures. These were additionally subject to tidal working constraints, which exacerbated the delays experienced because of the realisation of the above risks.

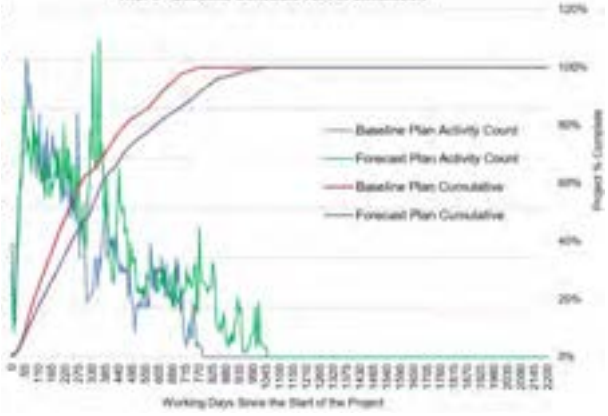

Figure 5. Baseline schedule vs FM simulation

MCS was run first, using inarticulate risk parameters derived from the literature review (best case = 90%, most likely = estimated duration, worst case = 130%). Following that, the proposed FM method was run to estimate the project finishing time and compare results with the MCS results. The MCS results suggested that the project will delay for 1 week; whereas results of the FM method suggested that the project will delay for 38 weeks, which is 52% more accurate than MCS results.

Figure 5 shows a comparison of the baseline schedule and the FM simulation over project completion. In addition, the FM method output has succeeded in assigning large time delays to the piling works and tidal interface works, so in this case study it can be considered a relative success.

4.3 Results Interpretation

The case studies and hypothesis test indicate that the proposed FM risk simulation methodology is significantly more accurate than the state of practice – Monte Carlo Simulation. The standard prediction error was 35 weeks for MCS and 12 weeks for the FM. This suggests that the FM could be 52% more accurate than a standard MCS model. Despite these promising results, the error for the simulation of 12 weeks is still very high and the SVM model prediction standard error is also very high at 122% of the activity duration. There is ample scope to improve on the predictive accuracy of this model, although it may require a good deal more high-quality data than what has been gathered in this research.

It is also apparent from the case study that the risk simulation methodology is unable to detect some of the most significant reasons for project delay; namely: changes to scope, problems with land access, and unexpected existing site conditions. It is difficult to see from the available literature how this might change in the future, but the mitigating factor for contractors is that the time and costs associated with much of those types of delays should be recoverable through standard out-of-court contractual claim mechanisms. This would remain a highly significant problem for project promoters. The evidence is also compelling that construction activities experience delays greater than those commonly allowed for in schedule risk analysis practice.

5 Discussion

This study proposed an FM method which integrates BN and SVM to predict project completion time under uncertainty. This study focuses on analysing activities on the critical path to predict project duration. A domain-specific task classification model for construction schedule data has been demonstrated. This is an approach which combines unsupervised machine learning – word embedding – with Gaussian mixture models and has been adapted from methods intended to topic model social media, revealing promising if imprecise results. Bayesian Networks are used to calculate the conditional probabilities associated with the independent and duration deviation variables. Using tables of these conditional probabilities the problem is turned into a simpler Naïve Bayes or converging Bayesian Network to calculate the probability of a task changing from its original estimated duration. MCS results suggest that the project will delay for 1 week; whereas results of FM method suggest that the project will delay for 38 weeks, which is 52% more accurate than MCS results.

In summary, there is no single technique that can be applied to the complex task of measuring risk in a noisy sequence of construction operations, using only the data contained within a Gantt chart schedule. Understanding how multiple techniques can be employed to add meaning to a construction schedule dataset, however, is a useful contribution towards leveraging the vast quantities of data available to improve the estimation of time risk on infrastructure and construction projects. Using these techniques, machines can learn about highly complex construction projects without being explicitly programmed, which presents some exciting opportunities for construction practice.

The topic modelling techniques proposed in this research could be used for a range of other purposes including automatic schedule alignment of costs and 3D objects in 5D modelling. Similar natural language techniques could also be used to monitor sentiment across a company's portfolio of projects, delivering a contemporaneous health check. Construction schedules are possibly the most up-to-date and comprehensive records on large construction projects; harnessing the value of the data they contain is a significant area of opportunity.

6 Conclusion

This research presents a new framework for construction schedule risk analysis. It represents the first approach to use machine learning to pre-process noisy construction schedules for a novel hybrid application of Bayesian Networks (BN) and Support Vector Machines (SVM). The proposed solution (the Fitzsimmons Method) was trained and tested on large infrastructure projects. The FM method looks at the delay risks before project execution and simulates the delay risks on the critical path. Hence, the proposed method provides the project manager and schedulers insights about the potential risks of their planning. The method is built on the work of several studies describing how machine learning can be used to approach the problem of understanding construction schedules. It has been shown that using large datasets to train prediction models can lead to superior simulation results on a limited sample, doing so with a technique eminently scalable to larger datasets and higher numbers of test projects. In tackling the problems associated with construction schedule data, some valuable contributions have been made to research around applied artificial

intelligence. The proposed method is limited to predict the delay of critical path statically. Future research can investigate the incorporation of dynamic modelling to facilitate a real-time project delay prediction.

References

[1] HM Infrastructure and Projects Authority, National Infrastructure Delivery Plan 2016-2021, 2016.

[2] Mace Insights, Social Value: Underpinning our future legacy, (2017) 1–6.

[3] ONS, Construction output in Great Britain: August 2019, Off. Natl. Stat. (2019).

[4] HM Treasury, National Infrastructure Plan 2014, 2014. https://doi.org/10.4324/9781351203111-4.

[5] Oxford Economics, Global Infrastructure Outlook, 2017.

[6] B. Flyvbjerg, M. Garbuio, D. Lovallo, Delusion and deception in large infrastructure projects: two models for explaining and preventing executive disaster, Calif. Manage. Rev. 51 (2009) 170–194.

[7] F. Beckers, N. Chiara, A. Flesch, J. Maly, E. Silva, U. Stegemann, A risk-management approach to a successful infrastructure project, Mckinsey Work. Pap. Risk. (2013) 18.

[8] A. Gondia, A. Siam, W. El-Dakhakhni, A.H. Nassar, Machine Learning Algorithms for Construction Projects Delay Risk Prediction, J. Constr. Eng. Manag. 146 (2020) 4019085. https://doi.org/doi:10.1061/(ASCE)CO.1943-7862.0001736.

[9] V.T. Luu, S.-Y. Kim, N. Van Tuan, S.O. Ogunlana, Quantifying schedule risk in construction projects using Bayesian belief networks, Int. J. Proj. Manag. 27 (2009) 39–50. https://doi.org/https://doi.org/10.1016/j.ijproman.2008.03.003.

[10] P.C. Anastasopoulos, S. Labi, A. Bhargava, L. Mannering Fred, Empirical Assessment of the Likelihood and Duration of Highway Project Time Delays, J. Constr. Eng. Manag. 138 (2012) 390–398. https://doi.org/10.1061/(ASCE)CO.1943-7862.0000437.

[11] B. Mulholland, J. Christian, Risk Assessment in Construction Schedules, J. Constr. Eng. Manag. 125 (1999) 8–15. https://doi.org/10.1061/(ASCE)0733-9364(1999)125:1(8).

[12] P.F. Kaming, P.O. Olomolaiye, G.D. Holt, F.C. Harris, Factors influencing construction time and cost overruns on high-rise projects in Indonesia, Constr. Manag. Econ. 15 (1997) 83–94. https://doi.org/10.1080/014461997373132.

[13] O. Moselhi, D. Gong, K. El-Rayes, Estimating weather impact on the duration of construction activities, Can. J. Civ. Eng. 24 (2011) 359–366. https://doi.org/10.1139/l96-122.

[14] K. Honek, E. Azar, C.C. Menassa, Recession Effects in United States Public Sector Construction Contracting: Focus on the American Recovery and Reinvestment Act of 2009, J. Manag. Eng. 28 (2012) 354–361.

[15] M.A. Bragadin, K. Kähkönen, Safety, Space and Structure Quality Requirements in Construction Scheduling, Procedia Econ. Financ. 21 (2015) 407–414. https://doi.org/10.1016/s2212-5671(15)00193-8.

[16] M. Elzomor, R. Burke, K. Parrish, G.E. Gibson, Front-End Planning for Large and Small Infrastructure Projects: Comparison of Project Definition Rating Index Tools, J. Manag. Eng. 34 (2018).

[17] CIOB, Managing the risk of delayed completion in the 21st Century, (2009).

[18] J.I. Ortiz-González, E. Pellicer, G. Howell, Contingency management in construction projects: A survey of spanish contractors, 22nd Annu. Conf. Int. Gr. Lean Constr. Underst. Improv. Proj. Based Prod. IGLC 2014. (2014) 195–206.

[19] S.A. Mubarak, Construction project scheduling and control, John Wiley & Sons, 2015.

[20] P.D. Galloway, Survey of the construction industry relative to the use of CPM scheduling for construction projects, J. Constr. Eng. Manag. 132 (2006) 697–711.

[21] J. Fortin, P. Zieliński, D. Dubois, H. Fargier, Criticality analysis of activity networks under interval uncertainty, J. Sched. 13 (2010) 609–627. https://doi.org/10.1007/s10951-010-0163-3.

[22] B. Gładysz, D. Skorupka, D. Kuchta, A. Duchaczek, Project Risk time Management - A Proposed Model and a Case Study in the Construction Industry, Procedia Comput. Sci. 64 (2015) 24–31. https://doi.org/10.1016/j.procs.2015.08.459.

[23] A. Azaron, S.M.T. Fatemi Ghomi, Lower bound for the mean project completion time in dynamic PERT networks, Eur. J. Oper. Res. 186 (2008) 120–127. https://doi.org/10.1016/j.ejor.2007.01.015.

[24] O. Ökmen, A. Öztaş, Construction Project Network Evaluation with Correlated Schedule Risk Analysis Model, J. Constr. Eng. Manag. 134 (2008) 49. https://doi.org/10.1061/(ASCE)0733-9364(2008)134:1(49).

[25] J. Levin, Relational incentive contracts, Am. Econ. Rev. 93 (2003) 835–857.
[26] S. Mitkus, T. Mitkus, Causes of Conflicts in a Construction Industry: A Communicational Approach, Procedia - Soc. Behav. Sci. 110 (2014) 777–786. https://doi.org/10.1016/j.sbspro.2013.12.922.
[27] Y.C. Kog, D.K.H. Chua, P.K. Loh, E.J. Jaselskis, Key determinants for construction schedule performance, Int. J. Proj. Manag. 17 (1999) 351–359. https://doi.org/10.1016/S0263-7863(98)00058-1.
[28] A. Attal, Masters Thesis - Development of neural network models for prediction of highway construction cost and project duration, Ohio University, 2010.
[29] B. Hola, K. Schabowicz, Estimation of earthworks execution time cost by means of artificial neural networks, Autom. Constr. 19 (2010) 570–579. https://doi.org/10.1016/j.autcon.2010.02.004.
[30] S. Bhokha, S.O. Ogunlana, Application of artificial neural network to forecast construction duration of buildings at the predesign stage, Eng. Constr. Archit. Manag. 6 (1999) 133–144.
[31] M. Scutari, Learning Bayesian networks with the bnlearn R package, ArXiv Prepr. ArXiv0908.3817. (2009).
[32] D. Nikovski, Constructing Bayesian networks for medical diagnosis from incomplete and partially correct statistics, IEEE Trans. Knowl. & Data Eng. (2000) 509–516.
[33] R.G. Cowell, R.J. Verrall, Y.K. Yoon, Modeling operational risk with Bayesian networks, J. Risk Insur. 74 (2007) 795–827.
[34] P.A. Aguilera, A. Fernández, R. Fernández, R. Rum\'\i, A. Salmerón, Bayesian networks in environmental modelling, Environ. Model. & Softw. 26 (2011) 1376–1388.
[35] J. De Oña, G. López, R. Mujalli, F.J. Calvo, Analysis of traffic accidents on rural highways using Latent Class Clustering and Bayesian Networks, Accid. Anal. & Prev. 51 (2013) 1–10.
[36] M. Fineman, Improved risk analysis for large projects: Bayesian networks approach, 2010.
[37] L. Jun-yan, Schedule Uncertainty Control: A Literature Review, Phys. Procedia. 33 (2012) 1842–1848. https://doi.org/10.1016/j.phpro.2012.05.293.
[38] V. Khodakarami, A. Abdi, Project cost risk analysis: A Bayesian networks approach for modeling dependencies between cost items, Int. J. Proj. Manag. 32 (2014) 1233–1245. https://doi.org/10.1016/j.ijproman.2014.01.001.
[39] J. Pennington, R. Socher, C. Manning, Glove: Global vectors for word representation, in: Proc. 2014 Conf. Empir. Methods Nat. Lang. Process., 2014: pp. 1532–1543.
[40] T. Mikolov, K. Chen, G. Corrado, J. Dean, Efficient estimation of word representations in vector space, ArXiv Prepr. ArXiv1301.3781. (2013).
[41] C. Bishop, Pattern Recognition and Machine Learning, Springer-Verlag New York, 2006.
[42] D.M. Blei, A.Y. Ng, M.I. Jordan, Latent dirichlet allocation, J. Mach. Learn. Res. 3 (2003) 993–1022.
[43] S. Deerwester, S.T. Dumais, G.W. Furnas, T.K. Landauer, R. Harshman, Indexing by latent semantic analysis, J. Am. Soc. Inf. Sci. 41 (1990) 391–407.
[44] D. Mimno, H.M. Wallach, E. Talley, M. Leenders, A. McCallum, Optimizing Semantic Coherence in Topic Models, Proc. 2011 Conf. Empir. Methods Nat. Lang. Process. (2011) 262–272. https://doi.org/10.1037/1082-989X.12.1.105.
[45] T. Joachims, Making large-Scale SVM Learning Practical, in: Adv. Kernel Methods - Support Vector Learn., 1999.
[46] C.D. Manning, M. Surdeanu, J. Bauer, J.R. Finkel, S. Bethard, D. McClosky, The Stanford CoreNLP natural language processing toolkit, in: Proc. 52nd Annu. Meet. Assoc. Comput. Linguist. Syst. Demonstr., 2014: pp. 55–60.
[47] N. Habash, O. Rambow, R. Roth, MADA+ TOKAN: A toolkit for Arabic tokenization, diacritization, morphological disambiguation, POS tagging, stemming and lemmatization, in: Proc. 2nd Int. Conf. Arab. Lang. Resour. Tools (MEDAR), Cairo, Egypt, 2009: p. 62.
[48] R. Řehůřek, models.word2vec – Word2vec embeddings, Gensim. (2019).
[49] R. Das, M. Zaheer, C. Dyer, Gaussian lda for topic models with word embeddings, in: Proc. 53rd Annu. Meet. Assoc. Comput. Linguist. 7th Int. Jt. Conf. Nat. Lang. Process. (Volume 1 Long Pap., 2015: pp. 795–804.
[50] V.K. Rangarajan Sridhar, Unsupervised Topic Modeling for Short Texts Using Distributed Representations of Words, (2015) 192–200. https://doi.org/10.3115/v1/w15-1526.
[51] DMRB, Design Manual for Roads and Bridges (DMRB), Standardsforhighways.Co.Uk. (2019).
[52] Y.H. Abdelkader, Evaluating project completion times when activity times are Weibull distributed, Eur. J. Oper. Res. 157 (2004) 704–715. https://doi.org/10.1016/S0377-2217(03)00269-8.

Automated On-Site Quality Inspection and Reporting Technology for Off-Site Construction(OSC)-based Precast Concrete Members

S.J.Lee[a] , S.W. Kwon[b] , M.K. Jeong[c] , S.M. Hasan[d] , A. Kim[e]

[a] Department of Convergence Engineering for Future City, SungKyunKwan University, Republic of Korea
[b] School of Civil, Architectural Engineering and Landscape Architecture, Sungkyunkwan University, Republic of Korea (corresponding author)
[c] Department of Convergence Engineering for Future City, SungKyunKwan University, Republic of Korea
[d] Civil, Architectural and Environmental Systems Engineering, SungKyunKwan University, Republic of Korea
[e] Department of Convergence Engineering for Future City, SungKyunKwan University, Republic of Korea

E-mail: sjlee8490@naver.com, swkwon@skku.edu, dufguf147@naver.com, s.mobeenhasan@gmail.com, aksovius@naver.com

Abstract

Recently, Off-Site Construction (OSC) is being actively applied to improve productivity by efficient factory-based production method rather than on-site production.

In OSC-based construction process, problem is the accurate quality inspection for the members produced in the factory is carried out but the quality inspection for the members shipped from the factory and brought to the site is not performed properly. The existing problem in OSC-based Precast Concrete member site detection is on-site workers have to check the members directly, which is very time-consuming and expensive, and the detection accuracy is low. In addition, quality inspection is performed only in the unit of sample, not all members

This study classifies the major detection items of PC members by analyzing the importance of all the detection items of PC members based on the PC member quality checklist that workers have used for on-site detection of PC members.

The items that can automatically detect the damage of PC members are derived, and the types of damage necessary for the detection of each member such as deformation, crack, and wear are classified.

Then, in order to apply the automatic detection technique, the data according to the damage type is collected respectively, and the damaged part is automatically detected through the machine learning. The detected damaged area is reclassified according to the degree of damage. Finally, based on the degree of damage, the status of the member is automatically identified and automatically reported to the checklist.

Keywords –

Off-Site Construction(OSC); Precast Concrete member; Artificial Intelligence; Automated Quality Inspection

1 Introduction

1.1 Background and objectives of the research

Recently, the construction industry has introduced "Off-Site Construction (OSC)", which is a factory-based production method, rather than an existing site-oriented production method, to increase productivity and efficiency of work and to enhance the competitiveness of the construction industry. OSC is a method in which members, parts, and pre-assembled parts are produced in advance in a factory, and then transported to a site where such construction materials will be assembled and building will be constructed. In the process of OSC-based construction, accurate quality inspection is performed on parts produced in factories. However, the exact quality test has not been performed on the members that have been transported from the factory and brought into the field. The existing problem in OSC-based PC member field test is that it takes a lot of time and money and the test accuracy is poor because workers have to test the members brought into the field after being checked with the naked eye. In addition, due to the lack of manpower in the field, only the sample units are being tested. Members shipped from the

factory may be damaged or get defected during transportation to the site. Therefore, it is essential to test the quality of the imported material in the field. In order to detect the breakage or defect of the member, recently, studies on image-based defect detection, such as concrete cracking and surface defect detection of electronic components, have been actively conducted using one of deep learning technologies, the Convolutional Neural Network (CNN). In addition, several researches have been conducted on quality inspection automation support systems using mobile devices such as Smart phones and tablet PC to support efficient quality inspection and management of construction and buildings by field workers. Therefore, in this paper, research was conducted to support more efficient and accurate test of field workers on PC members brought into the site. The main concepts of the automatic quality test & reporting system presented in this study are as follows. First, it prevents errors that may occur due to the manual writing of the PC member test checklist that workers are using during the existing inspection. Second, it prevents the loss of the test checklist and the detection by the subjective judgment of the worker. Third, the test results are automatically recorded and saved in a quality checklist through a mobile device-based quality test system. Finally, it assists field workers to figure out the quality status of PC members according to damage criteria.

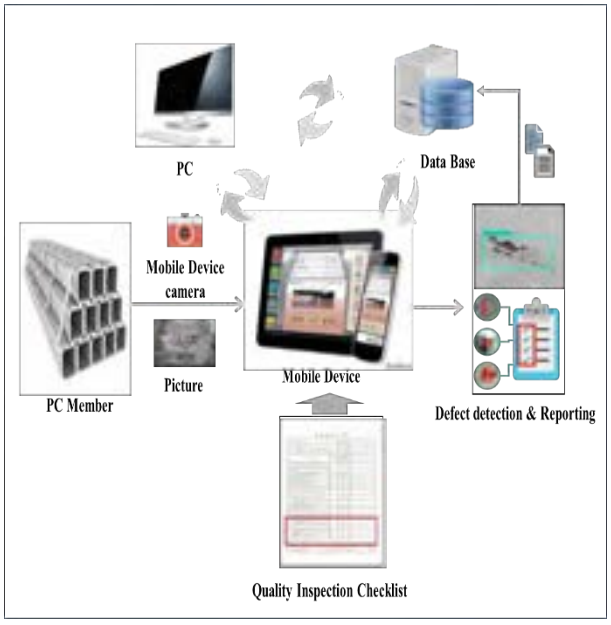

Figure 1. Conceptual diagram of automatic quality inspection reporting system

1.2 Study method and procedure

This study was conducted by the following procedures. First, the quality test automation support system using mobile devices such as Smart phones and tablet PC to support defect detection through AI technology-based image learning and efficient quality inspection and management of construction and buildings by field workers. Second, all test items in the collected PC member test checklist were analyzed to classify the main test items to be tested in the field. Third, when A.I technology is applied based on the main test items classified above, items that can be tested for member damage are automatically reclassified. In addition, the member's damage types such as breakage and cracks were classified to enable automatic defect testing of the member. Fourth, in order to apply AI-based automatic test technology, data according to the type of damage was collected and the member's damaged area was automatically detected through deep learning. In order to classify the detected damage sites in more detail, damage criteria according to the degree of damage were established. Lastly, the quality of the member is found according to the damage criteria, and a configuration diagram of an automatic quality test system based on a mobile device capable of automatic reporting is presented.

2 Analysis of previous studies

2.1 Automatic quality defect detection using A.I technology

In the past, quality test of structures or members has been performed by the operator's eyes. The quality test by the operator's naked eye takes a lot of work time and manpower, and the subjective judgment of the worker can be involved, so there is a problem of objectivity and reliability. Recently, to solve this problem, deep learning technology has been applied to perform more efficient and accurate quality tests on various objects such as concrete structures such as buildings, roads, bridges, tunnels, and electronic products. In order to perform such an automatic quality defect test, research on image-based defect detection using a convolutional neural network (CNN), one of deep learning technologies, has been actively conducted.

Kim[1] carried out a study to detect cracks in concrete ground structures by applying deep learning and image processing techniques.

Lee[3] re-learned Inception-v3, one of the deep learning neural network models, using concrete crack photography, and carried out a study to recognize and visualize cracks in concrete photography using the retrained model.

Jung[5] applied deep learning and image processing technologies to recognize cracks in concrete and conducted research on algorithms that testers can check for crack width and length information.

In Kim's research[2], deep learning models that are actively used in recent image analysis fields for image-based concrete crack detection are classified into four types (image classification model, object detection model, shape refinement model, and instance refinement model). This study compared and analyzed the performance of crack detection of representative models of ResNet-101, Faster R-CNN, DeepLab, and Mask R-CNN.

Choi[4] carried out a study on the detection of defects on the surface of electronic components by using a convolutional neural network (CNN) for the inspection of surface defects of electronic components with high detection difficulty and insufficient learning data.

As a result of analyzing the previous studies, most of the studies that automatically recognize or detect the presence or absence of a concrete surface defect on the existing structure or member have been actively carried out, but researches on automatic quality defect detection for quality testing of members are still insufficient.

Table 1. A.I-based automatic quality defect detection related research

Research area	Research subjects
CNN- based crack detection	Crack detection of concrete ground structures using deep learning and image processing techniques
	Visualization of information on the width and length of cracks in concrete using deep learning and image processing technology
CNN-based crack detection	Comparison and analysis of crack detection performance of deep learning models (ResNet-101, Faster R-CNN, DeepLab, Mask R-CNN)
CNN-based damage detection and classification	Detection of surface defects in electronic components using a convolutional neural network (CNN)
	Damage detection and classification of damage in sewer pipes using a convolutional neural network (CNN)

2.2 Automated quality inspection using IT technology

During test activities such as quality inspection, safety inspection, etc. for construction work or buildings, field workers should be familiar with various test information such as design drawings, specifications, and inspection items. They write the completed items directly on the checklist, and write a report after the test activity. In order to solve the inefficiency and inconvenience caused by the repetitive work of these workers, in recent years, workers in the field use a mobile device such as a Smartphone or a tablet PC during the test activity. For more efficient and accurate test quality test automation, several studies have been conducted.

Yoon[7] has established and prototyped a quality inspection system for the temporary construction, which is the basis for the development of an electronic work support system based on the construction test information, so that the quality of the construction work can be improved by accessibility of necessary information and the systematic inspection is performed through automation of inspection work. Research was conducted to develop the type.

In order to improve the efficiency of quality inspection, Choi[10] carried out a study on the development of a quality inspection system for a temporary construction in connection with BIM that can automate related tasks and systematically store and manage various quality inspection information.

In order to enable mobile devices to be used for safety during building safety inspection, Ko[6] carried out a research to develop a prototype for regular inspection of buildings by deriving the existing safety

inspection practical problems and core required functions.

Oh[8] carried out a study to collect information on the quality inspection and defect management of apartments in real time using PDA and the web, and through this, it is an apartment quality inspection and defect management system that enables efficient business processing among related actors and support for generational history management.

Seo[9] carried out a study on the 'automated levitation railroad facility automatic inspection system'. to improve the maintenance efficiency and advancement of the magnetic levitation railway using the vision system, check the main inspection items of the track facilities, and automatically analyze the data to detect abnormal points and provide the user with location information of abnormal points.

As a result of analyzing the previous studies, the researcher found that several studies have been conducted on the quality inspection automation for the ongoing construction or completed facilities, but studies on the automation of the quality test to check the quality of the member to be assembled before construction starts, such as OSC-based PC construction are still insufficient.

Table 2. Automated quality detection using IT technology

Research area	Research subjects
Automated construction information management	Prototype research for development of electronic work support system based on construction inspection information
	Development of quality inspection system based on rule-based temporary construction in connection with BIM
Automated defect inspection	Development of prototype for periodic inspection application using mobile devices
	Development of PDA and web-based apartment housing quality inspection and defect management system
Automated Safety inspection	Development of Vision-based magnetic levitation railroad facility automatic inspection system

3 Analysis of PC Member Quality Checklist

3.1 Derivation of main inspection items for PC Member

In this study, a PC member test checklist was collected from a PC member specialist to develop automatic PC member quality test reporting technology.

The quality test of the PC member produced in the factory is based on the test checklist items as shown below. After the test is over, members with no abnormalities are brought to the construction site by a transport vehicle by attaching a test checklist. As the members brought into the site are likely to have been damaged or damaged during loading or transportation, so the field workers perform a quality test on the members one again. Workers carry check construction name, member code, manufacturing year, month, date, product inspection mark, crack,

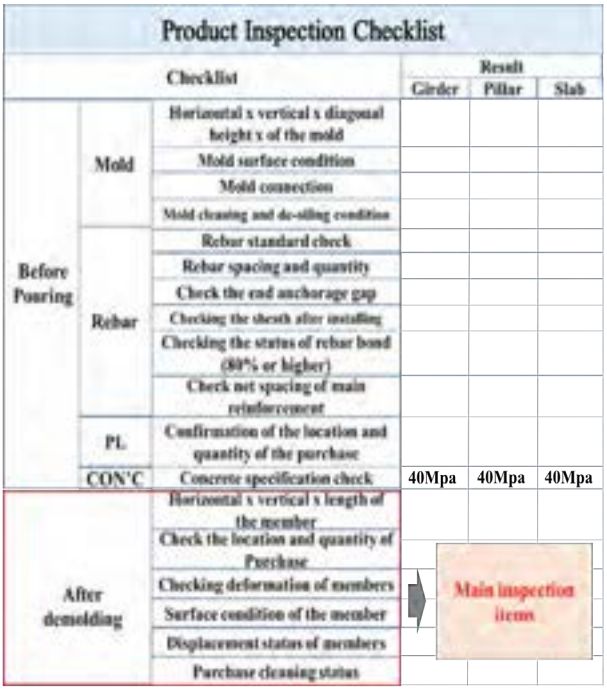

Figure 2. PC member quality inspection checklist

breakage, deformation, etc. in accordance with the PC Construction Standard Specification. Therefore, the main items to be tested in the field according to the specifications of the PC construction standard specification were classified as shown in the following figure2.

3.2 Deriving inspection items that can be measured using A.I technology

In order to support more efficient and accurate quality testing by on-site quality test workers, items that can be automatically tested for quality among the main items of the quality checklist derived above were classified as the following table3.

Table 3. Inspection items by A.I

Checklist	Check items
After demolding	Horizontal x vertical x length of the member
	Surface condition of the member
	Displacement status of members

4 Automatic quality inspection based on A.I

4.1 Classification of damage types and establishment of damage criteria

In this study, in order to check the surface condition of a member among testable items by applying deep learning technology, the member's damage type was classified into cracking and breaking. Later, in order to train the CNN model, which is one of the deep learning techniques, each image data of cracks and fractures was collected. The image data was secured through photographs of Google images and concrete cracks existing on the inside and outside walls, floors, and road surfaces of buildings. In addition, in the case of damage criteria for the quality condition of PC members, if the crack width exceeds 0.3mm based on the contents specified in the PC construction standard specification, it was classified as Class 1 crack, if 0.2~0.3mm, classified as Class 2 crack, and if 0.2mm or less, such fine cracks, it was classified as Class 3 crack. In the case of damage, the damage criteria was established by classifying the damage to the 1st class damage if the joint part was damaged by 200mm or more, the second class damage if the edge of the base plate was damaged, and the third class damages for other damages.

Table 4. Damage types and criteria

Damage Type	Rating	Rating criteria
Crack	Class 1	Crack width exceeds 0.3mm
	Class 2	Crack width 0.2~0.3mm
	Class 3	Crack width 0.2mm or less
Breakage	Class 1	Damage to joints over 200mm
	Class 2	Breakage of the edge of the bottom plate
	Class 3	Damage other than Class 1 and 2

4.2 CNN-based image learning and defect detection

After collecting the image data for each type of damage, the image was modified by resizing and labeling each image to enable image learning through CNN. Afterwards, image learning was performed using Faster R-CNN model, which has high test accuracy and high detection speed, among several CNN models. 500 images were used for training image data and 100 images were used for test image data. As a result of learning and testing of Faster R-CNN, it was identified that cracking and fracture recognition and detection are possible as follows. In addition, a study was carried out to enable detailed visualization of defects by applying an algorithm to visualize numerical values for the width and length of the crack.

The deep learning algorithm for automatic member defect test is largely divided into a stage of learning the damage image, a stage of extracting the damage feature (length and width of the crack), and a stage of visualizing the damage information. Defect detection is visualized through the calculation of the

pixel for the damaged part and the damage type detection through the Canny Edge Detector in the damage feature extraction step. Based on this, member quality test results are output along with the check of the test checklist items.

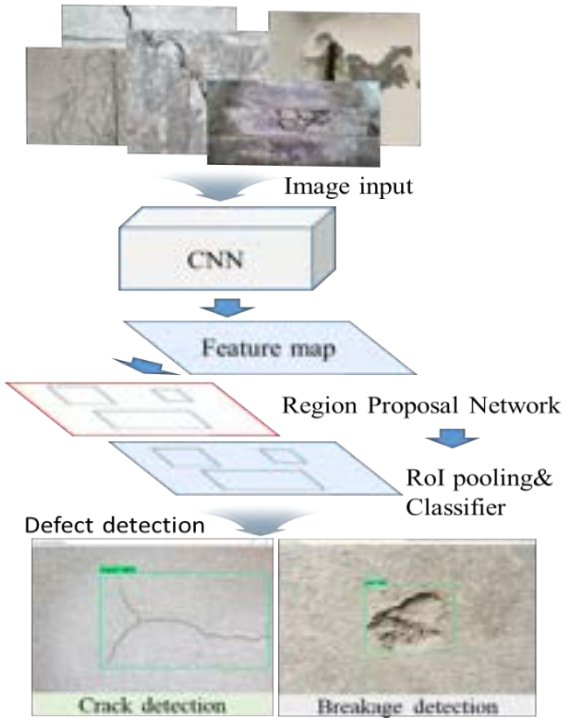

Figure 3. Automatic crack and breakage detection

5 Automatic quality inspection reporting system

The configuration of the automatic quality test reporting system is as follows. First, set the member to be tested. Second, run the camera App mounted on the tester's mobile device to take an image of the target member. Third, defects are detected and visualized through image analysis. Fourth, after a

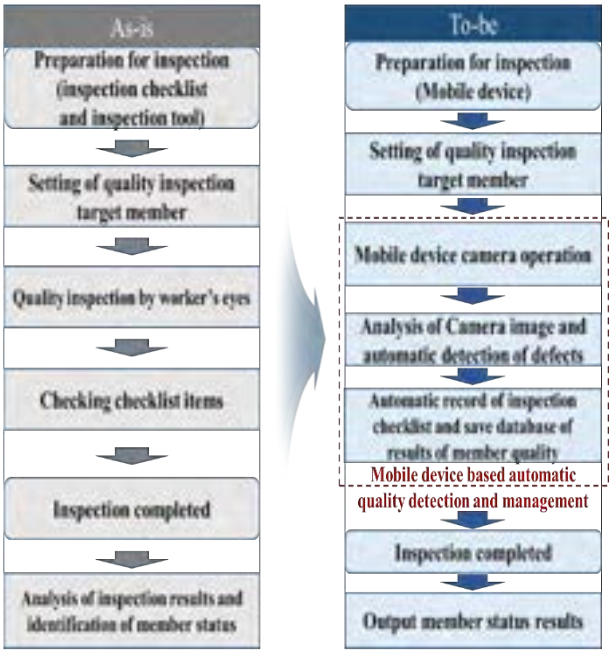

Figure 5. As is – To be Process of Quality Inspection Work

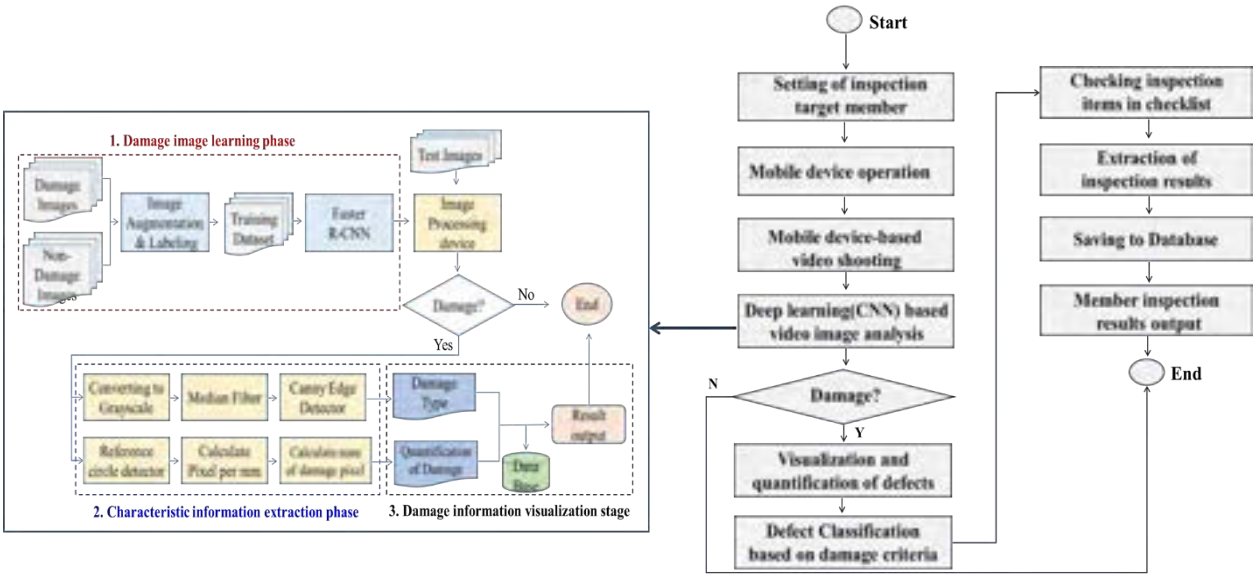

Figure 4. Member defect automatic detection algorithm

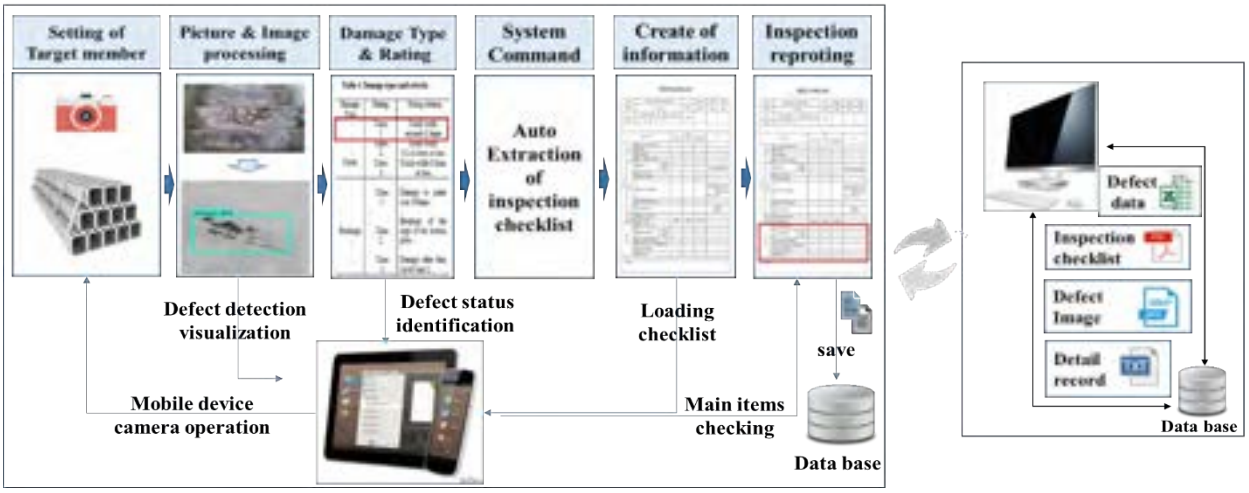

Figure 6. Automatic quality inspection reporting system

defect is detected, a test checklist is automatically loaded in the mobile device system. Finally, the main items in the checklist are checked. After the check is completed, the test checklist file is saved in the database. Test related data can be converted into file formats such as xls, pdf, jpg, txt, etc., and shared and stored in the worker PC.

Therefore, it is possible to automate member damage detection and test checklist inspection through a mobile device-based automatic quality test reporting system.

6 Conclusions

In this study, the researchers proposed an automatic quality test reporting technology to increase the test efficiency and accuracy of field quality testers for OSC-based PC members. In order to implement the automatic quality test technology, the damage type of the PC member was classified into cracks and breaks, and image learning was conducted using the deep learning model Faster R-CNN. In addition, damage criteria were established based on the PC construction standard specifications to figure out the quality status of PC members. Through the automatic quality test reporting technology of this study, on-site testers can more easily detect damages such as cracks and breakages of PC members, and finally identify the member status according to the damage criteria.

In the future, in order to complete the automatic quality test reporting technology suggested in this study, it is necessary to add a process of technology verification and feedback with workers through practical system development and field application. In addition, since this study only discovered cracks and breaks on the member surface when applying A.I technology, it is expected that the quality test method for the deformation of the member itself, such as bending or warping of the member, can be completed through further study.

Acknowledgment

This work is supported by the Korea Agency for Infrastructure Technology Advancement(KAIA) grant funded by the Ministry of Land, Infrastructure and Transport (Grant 20ORPS-B158109-01)

References

[1] Kim, Ah-Ram, Kim Donghyeon, Byun, Yo-Seph, and Lee, Seong-Won, Crack Detection of Concrete Structure Using Deep Learning and Image Processing Method in Geotechnical Engineering. Journal of the Korean geotechnical society, Vol.34, No.12, pp. 145 ~ 154, 2018

[2] Byunghyun Kim, Geonsoon Kim, Soomin Jin, and Soojin Cho, A Comparative Study on Performance of Deep Learning Models for Vision-based Concrete Crack Detection according to Model Types Journal of the Korean Society of Safety, Vol. 34, No. 6 pp. 50-57, 2019

[3] k·Yang, Gyeong-Mo·Lee, Jemyung·Lee, Jong-Hyuk·Jeong, Yeong-Joon·Lee, Jun-Gu·Choi and Won, Recognition and Visualization of Crack on Concrete Wall using Deep Learning and Transfer Learning, Journal of the Korean Society of Agricultural Engineer, Vol. 61, No. 3, pp. 55-65,

2019
[4] Hakyoung Choi, and Kisung Seo, CNN Based Detection of Surface Defects for Electronic Parts, Journal of Korean Institute of Intelligent Systems, Vol. 27, No. 3, pp. 195-200, 2017
[5] Jung, Seo-Young Lee, Seul-Ki Park, Chan-Il Cho, Soo-Young and Yu, Jung-Ho, A Method for Detecting Concrete Cracks using Deep-Learning and Image Processing, Journal of the Architectural Institute of Korea Structure & Construction Vol.35 No.11, 2019
[6] Ko, Kyujin, Oh, Sanghoon and Lee, Chansik, Application Prototype Development for the Building Safety Periodic Inspection, JOURNAL OF THE ARCHITECTURAL INSTITUTE OF KOREA Structure & Construction 32(1), 2016
[7] Yoon, Soo-Ho, Choi, Chang-Hoon, Han, Choong-Hee and Lee, Junbok, A Study on Development of Electronic Performance Support System Prototype for Improving the Efficiency of Quality Inspection of Temporary Work, KJCEM 20. 2. 013~027, 2019
[8] Oh, Se-Wook, Kim, Young-Suk, Development of PDA and Web-based System for Quality Inspection and Defect Management of Apartment Housing Project, Journal of Korea Institute of Construction Engineering and Management, Vol. 6, No. 1, 2005
[9] Il Seo, Kyoung-Bok Lee, Seok-Kyun Jang,m Jin-Gi Beak, A Study on the Development of Insepction System for Maglev Track Facilities, The Korean Society For Railway, 2013
[10] Choi Chang-Hoon, Development of BIM Integrated Rule-based Quality Inspection System for Temporary Works, Doctoral dissertation at Kyung Hee University's Graduate School, 2020
[11] Ranz,J. Monitoring of the curing process in precast concrete slabs: An experimental study. Construction and Building Materials, 122,406–416, 2016.
[12] Newell, S., Hajdukiewicz, M., and Goggins, J., Real-time monitoring to investigate structural performance of hybrid precast concrete educational buildings. Journal of Structural Integrity and Maintenance (TSTR), 1(4), 147–155, 2016
[13] Nguyen,T.,Venugopala,T.,Chen, S., Sun,T.,Grattan, K.T Taylor, S. E., and Long, A. E. ,Fluorescence based fibre optic pH sensor for the pH 10–13 range suitable for corrosion monitor-ing in concrete structures. Sensors and Actuators B: Chemical, 191, 498–507, 2014
[14] Uva,G.,Porco,F.,Fiore,A. and Porco,G, Structural monitoring using fiber optic sensors of a pre-stressed concrete viaduct during construction phases. Case Studies in Nondestructive Testing and Evaluation, 2,p.27–37, 2014
[15] Valero, E. and Adán, A, Integration of RFID with other technologies in construction. Measurement, 94, 614–620, 2016
[16] Wu, P., Low, S. P. and Jin, X, Identification of non-value adding (NVA) activities in precast concrete installation sitestoachieve low-carbon installation. Resources, Conservation and Recycling, 81,60–70, 2013
[17] Oskouie, P., Becerik-Gerber, B. and Soibelman, L. Automated measurement of highway retaining wall displacements using terrestrial laser scanners. Automation in Construction, 65,86–101, 2016
[18] Ožbolt, J., Bošnjak, J., Periškić, G. and Sharma, A. 3D numerical analysis of reinforced concrete beams exposed to elevated temperature. Engineering Structures, 58, 166–174, 2014

The Impact of Integrating Augmented Reality into the Production Strategy Process

Hala Nassereddine[a], Dharmaraj Veeramani[b], and Awad Hanna[c]

[a]Department of Civil Engineering, University of Kentucky, USA
[b]Department of Industrial and Systems Engineering, University of Wisconsin–Madison, USA
[c]Department of Civil and Environmental Engineering, University of Wisconsin–Madison, USA
E-mail: hnassereddin@wisc.edu, raj.veeramani@wisc.edu, ashanna@wisc.edu

Abstract –

Although execution is generally the phase during which challenges faced by the construction industry become apparent, it only represents the tip of the iceberg. Execution depends on the effectiveness of construction planning and control – an area identified by researchers as in need of improvement. Production Strategy is a fundamental step and a critical component of production planning and control where decisions are collectively made to properly allocate and deploy resources to achieve project objectives. The Production Strategy Process (PSP) involves a massive information transfer and requires a high level of communication between the project team members. The increased complexity and sophistication of construction projects along with the rapid advances in emerging technologies has fueled construction companies' interest in technology as a source of innovation. One technology that has gained great interest in recent years is Augmented Reality (AR). AR, a pillar of the fourth industrial revolution, offers powerful capabilities to enable the next generation of PSP and provides companies significant opportunities to maintain their vitality and competitive edge. This research investigated the integration of AR with PSP and the impact that AR can have on the process. An AR-enabled PSP prototype was developed for the Microsoft HoloLens headset and was validated on an ongoing construction project. The results showed that AR has the highest impact on PSP in three areas, namely analytical, tracking, and informational.

Keywords –

Augmented Reality; Prototype; Production Strategy; Re-engineering

1 Introduction

While the importance of the construction industry as a main contributor to the prosperity of nations has been well documented, volumes have been written about the long-standing challenges facing this industry. The daunting decline in productivity, cost and schedule overruns, costs of rework and waste, loss of information when design documents are translated into construction documents, and inability to execute according to the plan are, to name a few, some of the major challenges that researchers have been investigating [1].

One common trait with the above-mentioned problems is that they all occur during execution, which depends on the effectiveness of production planning and control systems – an area identified by researchers as in need for improvement [2].

Construction researchers noted that major issues in production planning and control are caused by the 1) inadequacy of traditional project management theory and 2) improper applications of information technologies (IT) [3]–[5], [2], [6]. Inspired by innovations in manufacturing, the application of Lean Production and the advancements in Information and Communication Technologies (ICT) have been at the core of addressing the deficiencies in the traditional planning and control system. New innovative production planning and control systems such as the Last Planner® System (LPS) emerged and were empowered with the integration of Building Information Modeling (BIM) [7]. While the implementation of LPS results in a more predictable workflow, a greater degree of team-building, respect, and reliable delivery of tasks, the system does not presuppose any specific work structure [8]. Researchers have investigated a location-based work structure, namely Takt-Time Planning. Takt is a German word that means 'beat' or 'rhythm' and is a Lean concept used to establish flow [9].

The complementary nature of Takt-Time Planning and LPS was investigated and studied by various researchers. The concepts of Takt-Time Planning were then added to the LPS in the form of a new stage, named Production Strategy [10].

Production Strategy is an integral part of production

planning and control and is essential to developing a reliable and balanced production plan [11]. [1] noted that The Production Strategy Process (PSP) involves a massive information transfer and requires a high level of communication between the project team members.

The increased complexity and sophistication of construction projects along with the rapid advances in emerging technologies has fueled construction companies' interest in technology as a source of innovation [12]–[15]. One technology that has gained great interest in recent years is Augmented Reality (AR). AR, a pillar of the fourth industrial revolution, is described as both an aggregator of information and an information publishing platform which allows users a spectrum of capabilities to 1) passively view displayed information, 2) actively engage and interact with published content, and 3) collaborate with others in real-time from remote locations [1]. AR offers powerful capabilities to enable the next generation of PSP and provides companies significant opportunities to maintain their vitality and competitive edge. This paper builds on the work of [1], which proposed an AR-enabled PSP future state.

2 Research Objective and Methodology

This research investigated the integration of AR into PSP and the impact AR can have on the process. The methodology employed to achieve the research objective consists of 1) reviewing the current state of PSP and its challenges, 2) exploring the capabilities of AR, 3) identifying how the AR capabilities can address PSP challenges, 4) developing an AR-enabled PSP prototype for the Microsoft HoloLens headset, and 5) validating the prototype on an ongoing construction project through a survey and analyzing the impact of AR on PSP.

3 Production Strategy Process

3.1 Current State

[8], who noted that LPS does not presuppose any specific work structure, indicated that work structuring happened before project control – i.e., before lookahead planning could occur. [10] introduced PSP as the third step of LPS. Therefore, Production Strategy is implemented after the project team has set the expectations for the project in Master Schedule level (step 1) and has broken down the project into phases (such as overhead, exterior) and identified the activities to be carried out in each phase in the Phase Scheduling level (step 2). The Production Strategy level is where the project teams collectively develop a production plan for each phase. [7], [1] interviewed subject matter experts on PSP and provided a detailed explanation of the process. The authors explained that PSP consists of a prerequisite step and five other principal steps.

The prerequisite step highlights the importance of collaboration among the project team which consists of the General Contractor and Trade Partners (also known as Subcontractors). PSP is, thus, best implemented on an Integrated Project Delivery (IPD) project. The five steps consist of:

- Step 1 – Perform sequence and flow analysis of a phase: Project team reviews 2D construction drawings for a certain phase and agree on the sequence of construction activities and identify the direction of the flow.
- Step 2 – Gather information: The General Contractor conducts one-on-one meetings with the last planners of individual Trade Partners and ask them to 1) highlight on the 2D construction drawings how much work they can perform in one day (daily production), and 2) to group the highlighted daily productions into production areas with five days' worth of work.
- Step 3 – Develop Common Areas: The General Contractors collect the documents produced in Step 2 from each last planner, overlays them, and attempts to identify common production areas.
- Step 4 – Define Production Areas: The General Contractor works with each last planner to ensure that the scope of work within the developed common areas can be completed within five days. Depending on the situation, the last planner might need to adjust their production information or the General Contractor might need to adjust the common areas.
- Step 5 – Validate the Production Strategy: The General Contractor shares the initial production plan with all Trade Partners and solicit their feedback. The production plan is then revised and updated.

3.2 Current Challenges

[7] noted that PSP is information-dense, lengthy, and iterative and identified 11 challenges associated with the current process, namely:

- Collaboration: The lack of effective visual rendering in the traditional 2D drawings does not support collaboration.
- Communication: 2D drawings, unlike 3D models, do not embed detailed information on building components, which can result in misunderstanding and miscommunication among different stakeholders, leading to inefficiencies in the PSP.
- Decision-making: Specific information needs to be extracted from these drawings and processed to

formulate the necessary knowledge for making decisions and taking actions. The nature of the existing PSP does not support the rapid and right decision-making.

- Detection of Errors: 2D drawings do not allow for efficient design coordination, which can lead to inaccurate production input.
- Documentation: The documentation of the current PSP is decentralized where necessary data is often stored in various forms across different devices or locations.
- Efficiency: The one-on-one meetings with the last planners of each activity and the iterative process to develop common production areas and balance the workflow are time-consuming.
- Information Access: A variety of information and data is needed to feed the production plan. Project Participants often need to review multiple documents and software to access the needed information. For example, while 2D drawings are useful to illustrate the spatial arrangement of a project, numerical information is often not represented.
- Information Flow (Navigation): 2D drawings and paper-based information storage that planners rely on often hinder information flow.
- Input Accuracy: Some information depicted on the 2D drawings may not be current or consistent, which complicates the decision-making process of PSP participants. Therefore, when last planners highlight their daily production capacity, they are not provided with the actual quantity of their daily production.
- Interpretation of Plans (Spatial Cognition): 2D drawings present an individual view that is subject to individual interpretation.
- Safety: It is not easy for engineers to discuss and identify construction safety problems and considerations based on 2D drawings.

4 Opportunities to integrate AR

4.1 AR Capabilities

[16] explained that opportunities for supporting a process with Information technology (IT) fall into nine categories. The opportunities to integrate AR – an emerging and promising technology in the realm of IT – into PSP can be also grouped into those nine categories, defining the capabilities of AR, as explained (in alphabetical order) below:

- Analytical: Data analytics and AR build off one another. AR can provide real-time in-situ information visualization of multi-dimensional data [17]. AR brings a new dimension to present and visualize and interact with big data. The technology also offers a new medium that supports users in analyzing data [18]. AR enhances the perception of the user which leads to a better cognition and an enhanced understanding of the environment. Better cognition results in more processed information, wider understanding, and more effective learning leading to more successful and accurate decisions. AR supports the decision-making process by displaying the needed information and enhancing collaboration between those involved in the process [19].
- Automation: AR systems allow the automation of processes. Information can be automatically generated in real-time and displayed onto the real environment [20].
- Disintermediating: With the transition to the digital era, technologies such as AR has the potential to disrupt industries and intermediate and disintermediate processes [21]. AR overcomes the big hurdles of data capture, storage, processing, and integration and therefore creates a new kind of disintermediation.
- Geographical: One of the greatest potentials of AR is the development of new types of collaborative interfaces. AR can be employed to enhance face-to-face and remote collaboration where remote participants can be added to the real world. AR enables a more natural co-located collaboration by blending the physical and virtual worlds to increase shared understanding. Researchers identified five key features of collaborative AR environments: 1) Virtuality – objects that don't exist in the real world can be viewed and examined; 2) Augmentation – real objects can be augmented by virtual annotations; 3) Cooperation – multiple users can see each other and cooperate naturally; 4) Interdependence – each user controls their own independent viewpoints; and 5) Individuality – Displayed data can be different for each viewer [22].
- Informational: AR overlays digital content and contextual information onto real scenes which increases the perception the user has of reality. Furthermore, information can be captured from the user and saved for later analysis [23].
- Integrative: AR is a new source of context-rich data that allows the user to connect the dots between cross-functional teams [24].
- Intellectual: AR supports tacit knowledge exchange. A remote expert can transfer their tacit knowledge through AR via demonstration. Graphics, audio, and video could be used to effectively transfer tacit expert knowledge through AR [25].

- Sequential: AR systems support the performance of activities/tasks in parallel. This is also enabled with the remote collaboration feature that AR provides [20].
- Tracking: AR can visualize BIM data along with the real world of each construction activity and therefore, the status of the activity (complete, in progress, delayed) can be monitored and tracked, allowing the generation of an automatic report to check the progress of an activity [26].

4.2 Matrix of AR capabilities and PSP Challenges

Once the capabilities of AR have been identified, ways of integrating AR to overcome the challenges of the current PSP listed in the previous section are discussed. The nine impact areas laid the foundation for exploring opportunities to address the challenges encountered in the current process. A matrix was created to identify how each challenge will be addressed using the AR impact areas (as shown in Table 1). A detailed description of how AR can address each challenge is provided as follows:

- Collaboration: AR can be used to create a unique collaborative experience. Co-located users can see shared virtual objects (3D and 2D) that they can interact with. AR has the potential to augment the face-to-face (local) collaborative experience and to enable remotely stationed people to feel that they are virtually co-located [27]. AR allows multiple users to be actively engaged in the PSP.
- Communication: [28] reported that AR facilitates communication and discussion of engineering processes in real-time. AR supports the broadcasting of the user's view into a different screen allowing other users to freely exchange information.
- Efficiency: [29] showed that AR can improve performance time and mental effort in collaborative design review. AR can be a proactive approach that enables efficient re-planning [26].
- Decision-Making: [30] stated that using AR can result in better planning by reducing wastes of overproduction, waiting, unnecessary movement, and unnecessary inventory. AR can be used to make a well-informed decision on resource allocation and dynamic adjustment. AR has the capability to process real-time graphics which allows the user to process data faster and more effectively [31].
- Detection of errors: [30] mentioned that the integration of AR and BIM allows subcontractors to immediately recognize the interdependencies between activities. BIM provides the capabilities to identify activities and their interdependencies, and AR serves a visualization tool that provides a context for the work that needs to be performed in the field. AR also displays singular and integrated views in real-scale, context, and time and allows the planners to accurately recognize design errors, which can, therefore, minimize repeated work.
- Information Access: While BIM aims to consolidate and archive all relevant information related to the project, the merge of AR with BIM improves the information search and access. Users can also filter the 3D model by enabling and disabling different construction phases, levels, activities, and components. Users can also select elements in the 3D model and extract information corresponding to that element. Furthermore, an AR system can be connected to other databases that contain other planning and relevant information that the user can search for and extract.
- Information flow: Replacing 2D drawings and paper-based information storage with data-rich 3D models projected using AR facilitates a seamless flow of information from one stage to the other, providing planners with the needed information at the right time.
- Input Accuracy: AR allows the last planners to better recognize inter-relationships and links between activities. Furthermore, information can be associated with each element, and the user can select a certain component and visualize and read its corresponding information (such as properties, the material used, geometry, etc.). BIM can identify the interdependencies between the various activities, and AR offers a powerful visualization tool to supply such information to the last planner who is directly involved in the execution phase. AR can make the interdependencies between activities more explicit [26].
- Interpretation of Plans: AR can display any chosen single view or integrated view into the real view of the user. The challenge to construct a mental model can be alleviated with AR because 3D models are visualized [26].

Table 1. Matrix of AR Impact Areas and PSP Challenges

	C1	C2	C3	C4	C5	C6	C7	C8	C9
Collaboration	✓		✓	✓	✓	✓	✓		
Communication			✓	✓	✓	✓			
Decision-Making	✓				✓		✓		
Detection of Errors	✓				✓		✓		✓
Documentation		✓			✓	✓	✓		✓
Efficiency		✓	✓			✓		✓	
Information Access		✓			✓	✓			✓
Information Flow						✓			✓
Input Accuracy	✓	✓			✓		✓		
Interpretation of Plans	✓				✓		✓		
Safety Integration	✓				✓		✓		✓

*C1 – Analytical | C2 – Automation | C3 – Disintermediating | C4 – Geographical | C5 – Informational | C6 – Integrative | C7 – Intellectual | C8 – Sequential | C9 – Tracking

5 Prototype Development and Implementation

Developing a prototype is a way to simulate and test the operations of the new process [16]. Instead of describing the new process, prototyping allows the user to visualize and experience it. The prototype developed in this research is a small-scale, quasi-operational version of the AR-enabled PSP.

The AR-enabled PSP prototype is developed for the HoloLens, one of the most widely anticipated display devices for the AR market. Additionally, a study conducted by [32] surveyed 128 construction professionals and showed that Microsoft HoloLens is the device that is most commonly used in construction.

The cross-platform Unity 3D game engine was used to build a proof-of-concept of the AR-enabled PSP. Developing for the Microsoft HoloLens requires the use of the Universal Windows Platforms (UWP) to create 3D (holographic) applications. Such applications use Windows Holographic Application Program Interface (API). Therefore, Microsoft recommends the use of Unity to create 3D applications for the HoloLens.

The 3D model used for the prototype was a Navisworks model of an ongoing healthcare project that was acquired from a construction company. The model had a Level of Devolvement (LOD) 350. From the moment the 3D model was acquired to the time when the validation phase would take place, it was anticipated that the construction team would be developing the production strategy of the overhead to the third floor of the project. Therefore, a series of selection sets were created in Navisworks to only show the overhead work of the third floor. Figure 1 shows the first view that is displayed to the user and consists of the user menu and the section of the 3D model that was used.

Figure 1. User's First View of the menu and the 3D model

6 Prototype Validation

Once the prototype was fully developed and implemented, it was validated on the ongoing healthcare project. A short presentation was delivered to participants to introduce them to the research topic, review the steps of the PSP, explain the technology (AR), outline the research objective, and provide an overview of the demonstration software. Participants were also provided with short tutorial videos that demonstrated the functionalities of the prototypes and asked to familiarize themselves with the software and its capabilities. In addition, the means of interacting with

the prototype (gaze and air-tap, and tap and hold gestures) were explained and demonstrated to the participants.

Participants were first asked to test the prototype and were then asked to complete a survey to capture their feedback. Physical and digital copies of the survey were distributed and a total of 20 surveys were obtained.

6.1 Participants Information

Participants were asked to select their age category. 45% of participants were between 18 and 34 years, 35% between 35 and 44 years, 15% between 45 and 54, and the remaining 5% between 55 and 64. Participants were also asked to specify their current job title. 5 out of the 20 participants are Project Managers and 3 participants are Field Engineer. Single responses were collected from participants with the following titles: Project Engineer, Project Technology, Virtual Design and Construction (VDC) Specialist, Project Manager/BIM Manager, Steamfitter Foreman, Foreman, Mechanical/Electrical/Plumbing (MEP) Coordinator, Senior Project Manager, Director of Production Planning and Innovation, Production Engineer, BIM Coordinator, Member of the Performance and Innovation Resources Team.

The respondents' expertise in construction ranged from 2 years to 27 years, with average expertise of over 13 years. Collectively, the respondents totaled 248 years of experience in construction. During their years of experience in the construction industry, the number of projects that the participants worked on ranged from 2 to over 100 projects. Out of these projects, participants were asked to identify the number of projects on which they have been involved in PSP. The respondents' experience with PSP ranged from 1 project to over 20 projects.

6.2 Technology (AR) Evaluation

The survey included two sets of questions to solicit participants' opinions and feedback regarding the capabilities of AR as a promising technology in PSP. The first set of questions asked participants about their level of agreement with four statements using a five-point scale of strongly disagree (1), disagree (2), undecided (3), agree (4), and strongly agree (5). The results displayed in Figure 2 show that, on average, respondents agree that AR enhances their cognitive understanding of the process, facilitates the decision-making process, provides the user with the needed and desired type of information, and allows for a natural way to interact with the displayed information.

The second set of questions asked participants to rate the impact of the nine AR capabilities on PSP using a five-point Likert scale of very low (1), low (2), moderate (3), high (4), and very high (5). The results are reported in Table 2.

k-means cluster analysis was then performed to identify the capabilities that have the highest impact on PSP. Cluster analysis is a statistical method used to group data by comparing each candidate AR capability, for example, to the other AR capability already in the cluster. If the difference between the candidate AR capability and the other AR capability already in the cluster is significant, then the candidate AR capability is assigned to a different cluster.

The cluster analysis grouped the nine AR capabilities into three clusters based on the participants' average impact, with each cluster encompassing three areas. The three areas of Cluster 1 are the areas where AR has the highest impact on PSP and are as follows: Analytical (3.95), Tracking (3.79), and Informational (3.74).

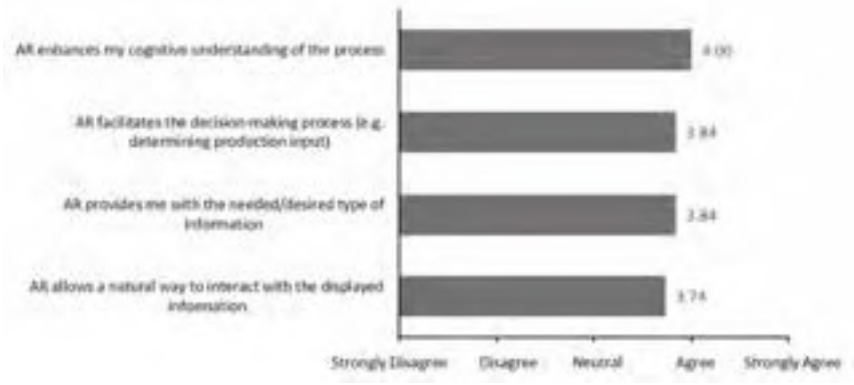

Figure 2. Technology (AR) Evaluation Criteria

Table 2. Clustered Table of the impact of AR Capabilities on PSP

AR Capability	Explanation	Average Impact	Clusters
Analytical	Improving the analysis of information and decision making	3.95	
Tracking	Closely monitoring process status and objects	3.79	Cluster 1
Informational	Capturing process innovation for purposes of understanding	3.74	
Geographical	Coordinating process across distances	3.63	
Integrative	Coordinating between tasks and processes	3.58	Cluster 2
Sequential	Changing process sequence or enabling parallelization	3.47	
Automation	Reducing human labor from a process	3.16	
Disintermediating	Eliminating intermediaries from a process	3.16	Cluster 3
Intellectual	Capturing and distributing intellectual assets	3.05	

6.3 User Experience

Another question in this section asked respondents to describe their experience using the AR-Enabled PSP. Figure 3 shows that participants saw this experience as engaging, interesting, innovative, fun, and easy.

Figure 3. User Experience (generated with WordItOut)

7 Conclusions

As interest in AR continues to grow, this paper explored the impact of AR on PSP – an information-intensive process. The current state of PSP and its challenges were first reviewed. Then, nine AR capabilities were discussed and a matrix was developed to explain how these capabilities can address the PSP challenges. Next, an AR-enabled PSP prototype was developed for the HoloLens and validated on an ongoing healthcare project. Twenty construction practitioners were asked to test the prototype first and then completed a short survey. Survey results showed that participants agreed on average that AR enhances their cognitive understanding of the process, facilitates the decision-making process, provides them with the needed and desired type of information, and allows for a natural way to interact with the displayed information. According to participants, the average impact of the AR capabilities varies between high and moderate with Analytical, Tracking, and Informational being the areas with the highest impact (cluster 1). Overall, participants saw this experience as engaging, interesting, innovative, fun, and easy and recognized the value AR can add to the PSP.

While this paper focused on integrating AR into the production planner process, further studies can build upon this work and study the integration of AR throughout the entire production planning and control system.

8 Acknowledgments

The authors would like to thank The Boldt Company for their continuous support throughout this research effort and for partially funding this project. The authors would also like to thank Parker Schroeder for helping in implementing the AR-enabled PSP.

9 References

[1] Nassereddine H. Veeramani D. and Hanna A. Augmented Reality-Enabled Production Strategy Process. *In Proceedings of the International Symposium on Automation and Robotics in Construction*, 36:297–305, 2019.

[2] Sriprasert E. and Dawood N. Next generation of construction planning and control system: the LEWIS approach*Z. Turk, & R. Scherer, eWork and eBusiness in Architecture, Engineering and Construction,* pp. 175–182, 2002.

[3] Koskela L. Application of the new production philosophy to construction. Stanford University Stanford, 1992.

[4] Ballard H. G. The last planner system of production control. Ph.D. Thesis, University of Birmingham, 2000.

[5] Koskela L. An exploration towards a production theory and its application to construction. *Technical Research Centre of Finland*, 2000.

[6] Dave B. S. Koskela L. Improving information flow within the production management system with web services. *In Proceedings of the 18th Annual Conference of the International Group for Lean Construction*, pp. 445–455, 2010.

[7] Nassereddine H. M. Design, Development and Validation of an Augmented Reality-Enabled Production Strategy Process for the Construction Industry. The University of Wisconsin-Madison, 2019.

[8] Ballard G. and Tommelein I. Current Process Benchmark for the Last Planner System, 2016.

[9] Liker J. K. The Toyota way: 14 management principles from the world's greatest manufacturer. New York: McGraw-Hill, 2004.

[10] Ebrahim M. Berghede K. Thomack D. Lampsas P. Kievet D. and Hanna A. A Framework of Five-Stream Production System for Megaprojects, presented at the 25th Annual Conference of the International Group for Lean Construction, pp. 729–736, 2017.

[12] El Jazzar, M., Piskernik, M. and Nassereddine, H. Digital twin in construction: an empirical analysis. In *EG-ICE 2020 Proceedings: Workshop on Intelligent Computing in Engineering*, pages 501–510, Berlin, Germany, 2020.

[13] Bou Hatoum, M. and Nassereddine, H. Developing a framework for the implementation of robotics in construction enterprises. In *EG-ICE 2020 Proceedings: Workshop on Intelligent Computing in Engineering*, pages 453–462, Berlin, Germany, 2020.

[14] Nassereddine, H., Schranz, C., Bou Hatoum, M., & Urban, H. A comprehensive map for integrating augmented reality during the construction phase. In *Creative Construction e-Conference 2020*, pages 56–64, Budapest, 2020.

[15] Nassereddine H., El Jazzar M. and Piskernik M. Transforming the AEC industry: a model-centric approach. In *Creative Construction e-Conference 2020*, pages 13–18, Budapest, 2020.

[16] Davenport T. H. Process innovation: reengineering work through information technology. Harvard Business Press, 1993.

[17] ElSayed N. A. Thomas B. H. Smith R. T. Marriott K.and Piantadosi J. Using augmented reality to support situated analytics. *In 2015 IEEE Virtual Reality (VR)*, pp. 175–176, 2015.

[18] Luboschik M.Berger P.and Staadt O. On spatial perception issues in augmented reality based immersive analytics. *In Proceedings of the 2016 ACM Companion on Interactive Surfaces and Spaces*, pp. 47–53, 2016.

[19] Székely Z. Application of augmented reality in support of decision making for authorities, 2015.

[20] Verlinden J. Horváth I. and Nam T.J. Recording augmented reality experiences to capture design reviews. *International Journal on Interactive Design and Manufacturing (IJIDeM)*. 3(3):189–200, 2009.

[21] Miller R. and Custis K. Disruption. Digitalization. Disintermediation. Transportation and logistics in the coming decade, 2017.

[22] Billinghurst M. and Kato H. Collaborative augmented reality. *Communications of the ACM*, 45(7):64–70, 2002.

[23] Diaz C. Hincapié M. and Moreno G. How the type of content in educative augmented reality application affects the learning experience. *Procedia Computer Science*. 75: 205–212, 2015.

[24] Biron J. and Lang J. Unlocking the Value of Augmented Reality Data. *MIT Sloan Management Review*, 2018.

[25] Aromaa S. Väätänen A. Aaltonen I. and Heimonen T. A model for gathering and sharing knowledge in maintenance work. *In Proceedings of the European Conference on Cognitive Ergonomics 2015*, 2015.

[26] Wang X. and Love P. E. BIM+ AR: Onsite information sharing and communication via advanced visualization. *In Proceedings of the 2012 IEEE 16th International Conference on Computer Supported Cooperative Work in Design (CSCWD)*, pp. 850–855, 2012.

[27] Lukosch S. Billinghurst M. Alem L. and Kiyokawa K. Collaboration in augmented reality. *Computer Supported Cooperative Work (CSCW)* 24(6):515–525, 2015.

[28] Dong S. Behzadan A. H. Chen F. and Kamat V. R. Collaborative visualization of engineering processes using tabletop augmented reality. *Advances in Engineering Software*, 55:45–55, 2013.

[29] Wang X. and Dunston P. S. Comparative effectiveness of mixed reality-based virtual environments in collaborative design. *IEEE Transactions on Systems, Man, and Cybernetics, Part C (Applications and Reviews)*, 41(3):284–296, 2011.

[30] Wang X. Love P. E. D. Kim M. J. Park C.-S. Sing C.P. and Hou L. A conceptual framework for integrating building information modeling with augmented reality*Automation in Construction*vol. 34:37–44, 2013.

[31] Waly A. F. and Thabet W. Y. A virtual construction environment for preconstruction planning. *Automation in construction*, 12(2):139–154, 2003.

[32] Nassereddine H. Hanna A. S. and Veeramani D. Exploring the Current and Future States of Augmented Reality in the Construction Industry. *Handbook of augmented reality*, Springer, pp. 47–63, 2020.

Automatic Detection of Air Bubbles with Deep Learning

Takuma Nakabayashi[a], Koji Wada[b] and Yoshikazu Utsumi[b]

[a]Technical Research Institute, Obayashi Corporation, Japan
[b]Construction Robotics Division, Obayashi Corporation, Japan
E-mail: nakabayashi.takuma@obayashi.co.jp, wada.koji@obayashi.co.jp, utsumi.yoshikazu@obayashi.co.jp

Abstract –

Recently, the demand for base-isolated structures has been increasing, especially in Japan. For reliable construction of seismic isolation devices, contractors must ensure that the area ratio of the air bubbles occupying the backside of the base plate does not cross the threshold, which is decided by the structural designer. However, the backside of the base plate can include larger and more air bubbles than ordinary concrete surfaces as it is difficult to pour concrete into the foundation properly. Additionally, the inspection process includes many time-consuming tasks. Therefore, it normally takes about one week or longer after concrete work to perform the inspection.

We present a method to automate the tasks relating to inspection, including image preprocessing, air bubble extraction, and calculation of the area ratio of the air bubbles, using conventional image processing and a convolutional neural network (CNN) to speed up the inspection.

While CNN normally requires a significant amount of training data to achieve high performance, it is generally difficult to collect such a large amount of high-quality data. We have conducted thorough accuracy inspections to evaluate the appropriate amount of training data required. Additionally, we have verified the effect of data augmentation and compared the performance of certain typical CNN architectures.

As a result, our method has obtained results that are close to those of manual inspection by a skilled inspector. We can conclude that our method can reduce the overall inspection time by 50% compared to conventional methods.

Keywords –

Base-Isolated Structure; Concrete; Visual Inspection; Air Bubble; Bug Hole; Machine Learning; Deep Learning; Image Processing

1 Introduction

The demand for seismic base isolation has increased due to the number of earthquakes experienced across the world, especially in Japan. Seismic isolation devices are installed at specific levels of the building in a base-isolated structure to reduce the tremble caused by earthquakes. As shown in Figure 1, seismic isolation devices are installed on the base plate, which is set on the base-isolated foundation. To integrate the base plate into the foundation correctly, it is necessary to pour concrete with the base plate in place, as shown in Figure 2. This pouring process could lead to the formation of air bubbles underneath the base plate, which should be avoided. As these bubbles negatively affect adhesion, their area ratio should be decreased to increase the adhesion force. However, the removal of the base plate is not allowed during the construction phase to check for the presence of air bubbles. Therefore, a full-scale construction field test is required before the base-isolated foundation work.

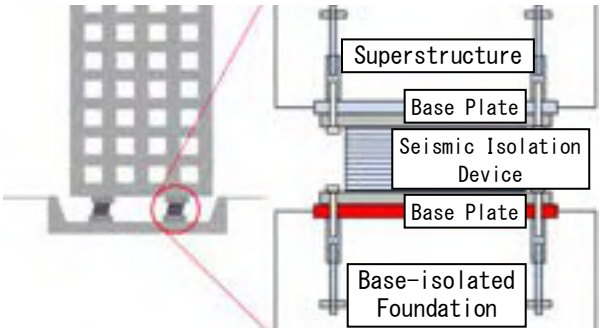

Figure 1. Cross-section of base-isolated foundation

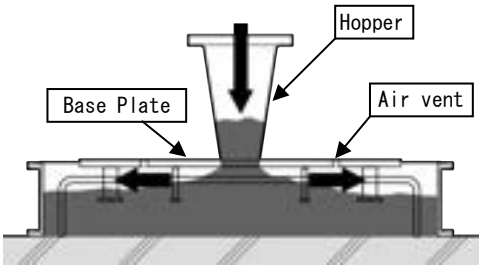

Figure 2. Methodology to cast concrete underneath a baseplate

A field test is conducted to inspect whether the ratio of the area of the air bubbles to that of the concrete surface satisfies the criteria that are generally set by structural designers. According to [1], the criteria for the ratio of the area of air bubbles is defined as less than 10%, which differs for each project. We need to locate air bubbles and measure each bubble's maximum diameter and area to calculate the area ratio. As there can sometimes be over 1000 air bubbles, the entire inspection process is time consuming and work intensive.

The purpose of the field test is to confirm whether the planned workflow of the base-isolated foundation is appropriate. Base-isolated foundation work can begin when the result of the field test is verified. However, if the field test does not pass the criteria, the concrete placement plan must be reconsidered. Naturally, the field test must also be repeated.

This study introduces a method to automate the entire inspection process in the field test using conventional image processing and a convolutional neural network (CNN). Additionally, we have conducted many accuracy inspections to evaluate the appropriate amount of training data and to determine which architecture is suitable for the considered purpose. The remainder of this paper is organized as follows: related works are reviewed in Section 2, the conventional inspection method is presented in Section 3, the proposed method is introduced in Section 4, the experiments and results at the actual site are described in Section 5, and the conclusions are presented in Section 6.

2 Related Work

Many technologies have been developed to improve productivity in concrete work [2]. Their scope is not restricted to construction as they can be applied to inspection. Visual inspection is one of the important examinations in concrete work. Prasanna et al. [3] developed an automated crack detection algorithm for robot inspection.

As in the present study, previous research has used CNN and other machine learning approaches to tackle this issue. Cha et al. [4] developed a crack damage detection method based on a CNN architecture. They mentioned that CNN is more robust than conventional approaches, such as the Canny and Sobel edge detection methods. Gang et al. [5] tested certain typical CNN architectures for tunnel crack detection. As listed here, many studies have focused on automatic crack detection systems.

However, certain studies have also focused on automatic air bubble detection on the concrete surface. Yoshitake et al. [6] developed a method for tunnel lining. Gang et al. [7] developed a CNN-based method and compared it to Otsu's thresholding method and Laplacian of Gaussian (LoG) algorithm. They concluded that their method was more robust against various light conditions. Fujia et al. [8] tested a popular CNN architecture for semantic segmentation, which is a major field in computer vision. The goal of semantic segmentation is to classify the class labels at the pixel level.

In contrast to prior studies, this study specifically focuses on the concrete surface of the backside of the base plate in base-isolated structures, rather than the concrete surfaces on more classical architectural elements, such as walls and columns. The backside of the base plate normally includes more air bubbles than the surfaces of other architectural elements, as it is difficult to vent the air from the bottom of the base plate properly. Additionally, it is not possible to check how the concrete is being filled during the construction owing to the base plate structure. Therefore, the bottom of the base plate can include many air bubbles, of sizes larger than those on ordinary concrete surfaces. In a report focusing on the detection of air bubbles at the bottom of the base plate, Mitani [9] and Katoh [10] evaluated the accuracy of their method, which connected 2 CNN architectures that were used for object detection and semantic segmentation. However, the main targets of most object detection methods based on CNN are the objects, which are along the XY coordinates. This is due to the manner in which object detection methods are trained. In the training process, they normally evaluate if they properly detect the target objects by using bounding boxes that are along the XY coordinates. In contrast, air bubbles are multi-oriented objects. Therefore, they can be impediments in the training process as their bounding boxes can cover a wide area of the concrete surface and may intersect with other air bubbles.

In contrast, as semantic segmentation methods generally do not depend on the axes on which target objects are based. Thus, we only used a CNN architecture for semantic segmentation to deal with various types of air bubbles. Additionally, this paper presents a method to automate the entire inspection and air bubble detection processes. Here, we employ conventional image preprocessing approaches, followed by semantic segmentation with a CNN structure, to detect air bubbles accurately. Each of these processes will be explained in Section 3.

3 Conventional Inspection Method

In the field test, according to the construction plan, concrete work is conducted at the beginning, after which the base plate is removed. Marking work is then

completed as a preparation for the area ratio calculation (Figure 3). If the area ratio satisfies the criteria, the construction site can proceed to the actual construction phase. The area ratio calculation in conventional inspection is composed of the following steps.

1. Color the air bubbles red by hand using markers. (Figure 4)
2. Take a picture of each grid.
3. Preprocess pictures, through keystone correction, cropping, and resizing of each picture using an image processing software.
4. Color the areas that are not on the backside of the base plate, as this is outside the scope areas of the inspection. (Figure 4)
5. Automatically extract the colored air bubbles identified in step 1 using the software. If necessary, correct the extracted results manually.
6. Exclude the air bubbles that are less than the specified diameter. (Figure 4)
7. Repeat steps 3 to 6 for each grid.
8. Automatically calculate the area ratio of the air bubbles against the area of the concrete surface.

It is important to note that certain tasks need to be carried out carefully. To perform accurate automatic extraction in step 5, it is necessary to color the air bubbles accurately in Step 1, and then take a picture from the front of the concrete surface as much as possible in Step 2. Although keystone correction in Step 3 is necessary irrespective of how carefully the pictures are taken, the lower the distortion, the higher the obtained image quality. The areas identified as out of scope in Step 5 indicate locations that can be ignored. These not only include the outside of the backside of the base plate but also on bolts, air vent holes, and pressure inlets. As shown in Figure 4, these areas are colored using different colors so that they are ignored during the color extraction process in Step 8. Additionally, a negligible minimum diameter is normally set for this inspection. The air bubbles that are smaller than the minimum diameter need to be colored in Step 6 (colored black in Figure 4). After all the grids are processed completely from Steps 1 to 6, the area ratio can be automatically calculated by using the color extraction method.

The conventional inspection method involves a lot of manual work. Additionally, the number of pictures to be processed can reach up to 100 per specimen. Further, if the construction site has multiple design types of base-isolated foundations, the field test must be conducted for each design. Thus, the tests need to be performed by a skilled inspector to hasten the entire process. However, despite having a skilled inspector for the field test, the process takes about a week after the completion of concrete work to obtain the test results when using the conventional inspection method.

Figure 3. Concrete specimen and marking work

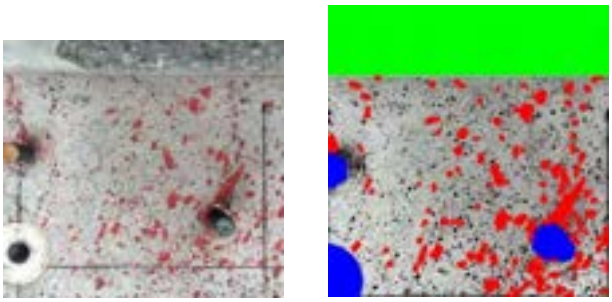

Figure 4. Before preprocessing (Left), result of preprocessing (Right)

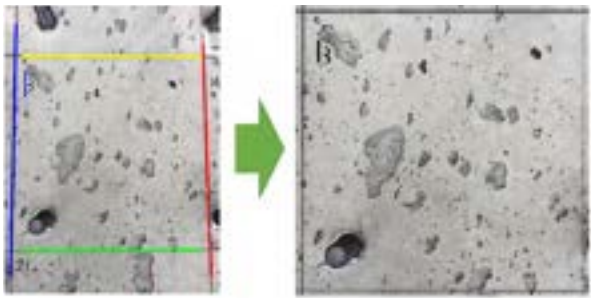

Figure 5. Example of processed marking recognition, keystone correction, and cropping

4 Methodology

4.1 Automation of preprocessing using a conventional image processing method

The preprocessing described in Step 3 in the previous section includes keystone correction, cropping, and resizing. This is necessary to calculate the area ratio in the real scale from a photograph. The preprocessing is performed manually using an image processing

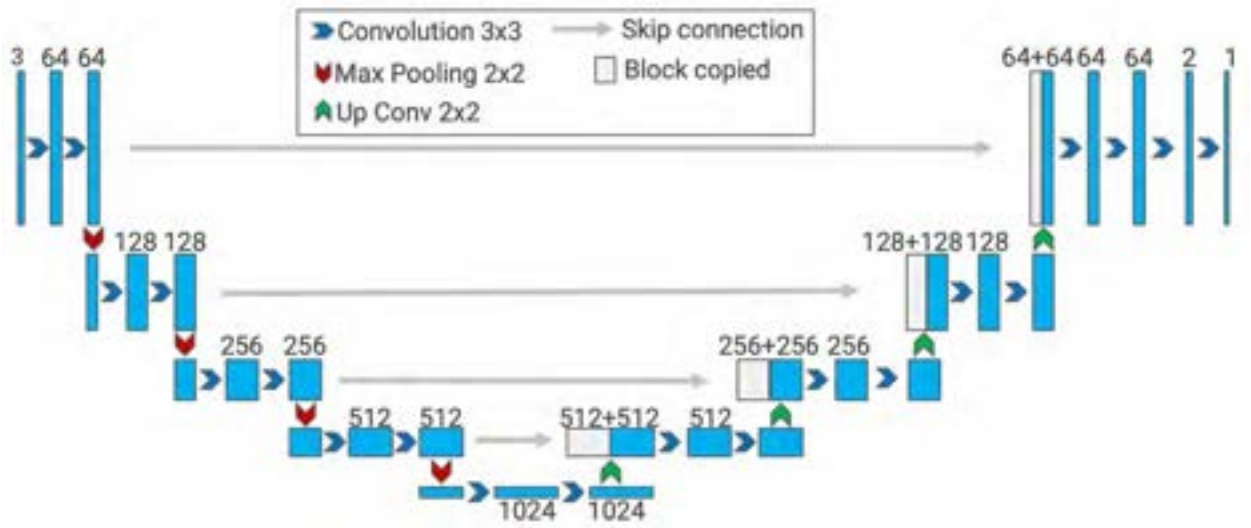

Figure 6. Network architecture based on U-Net. Each number describes the number of channels in each convolutional layer.

software. This process takes about one day, even for a skilled inspector.

To automate the keystone correction process, it is first necessary to recognize the marked grids automatically. In this study, we use a template-matching algorithm to achieve this. The template-matching algorithm can detect the areas in the image that have a pattern similar to the pattern of the input template. We prepared simple vertical and horizontal templates to detect the grids. As a result, the algorithm can detect the grid lines as four different colored lines, as shown on the left side in Figure 5.

Keystone correction utilizes the results of template matching. It needs to calculate the conversion matrix from a perspective image to an orthogonal image. It uses the four corner points detected by template matching for this. As a result, we obtain a square image that does not contain the perspective distortions, as shown on the right side in Figure 5.

The image is then resized to the specified resolution. This process clarifies the relationship between the pixels and the real scale. The resolution used in this study was set to 2000 px.

4.2 Automation of air bubble detection using a CNN

In this study, a U-Net-based architecture is utilized for automatic bubble detection. The U-Net was designed for semantic segmentation, which won the International Symposium on Biomedical Imaging (ISBC) cell tracking challenge in 2015 [11]. Semantic segmentation is a typical task in the machine learning field and is performed to classify images in pixel units.

As shown in Figure 6, the U-Net is mainly composed of two symmetry paths for encoding and decoding, where each path is composed of multiple layers of CNN blocks. Each layer has a connection from the encoding path to the decoding path. The connections contribute to maintaining a wide context in each focus area. The U-Net was originally designed for biomedical image segmentation, but its simple architecture can be utilized for many purposes, including air bubble detection. Therefore, we adopt the U-Net as the base architecture of our method.

CNN is a type of neural network that normally consists of many convolutional layers. Each layer has many filters, and each filter can be trained to extract various types of image features. In contrast to CNN and recent learning-based algorithms, conventional image processing algorithms are not robust in diverse environments. Several studies referenced in Section 2 report that CNN is more robust to changes in the light environment than conventional image processing algorithms.

Although CNN is more accurate and robust, its

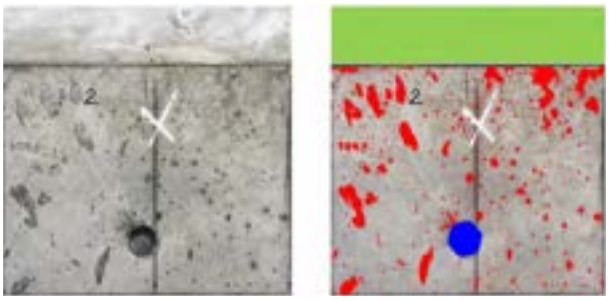

Figure 7. Sample pair of training data

training process needs a large amount of training data. Additionally, U-Net belongs to a supervised training algorithm, indicating that the training dataset needs to have not only images but also labels that describe the classes to which each pixel in the image belongs. Therefore, we collected a large amount of data, as shown in Figure 7.

While a learning-based algorithm is used for air bubble detection, the postprocessing, including calculation of each air bubble's maximum diameter and area, uses the thresholding and contour extraction method. As mentioned in Section 3, small air bubbles that have maximum diameters less than the specified length are ignored in the inspection. In Section 5.2, the negligible diameter is set to 5 mm.

5 Experiments

5.1 Basic Experiments

We evaluated different combinations of datasets to identify a suitable amount of training data to obtain a high-performance trained model. We collected 452 images from 4 construction sites, with varying characteristics and light environments. Additionally, four images from each construction site were used as test data. Therefore, in total, 436 training data points and 16 test data points were considered. Each image was divided into smaller images, as processing high-resolution images requires a large GPU memory. Thus, the resolution was set to 512 px.

Precision, recall, intersection over union (IoU), and F1 scores were used as metrics to evaluate each result. Equations (1), (2), (3), and (4) define these metrics. Figure 8 describes each value of the equations, such as true positive (TP), true negative (TN), false positive (FP), and false negative (FN). In this study, we assign

$$Precision = \frac{TP}{TP + FP} \quad (1)$$

$$Recall = \frac{TP}{TP + FN} \quad (2)$$

$$IoU = \frac{TP}{TP + FP + FN} \quad (3)$$

$$F1\ Score = \frac{2Precision * Recall}{(Precision + Recall)} \quad (4)$$

		Actual	
		Positive	Negative
Predicted	Positive	True Positive (TP)	False Positive (FP)
	Negative	False Negative (FN)	True Negative (TN)

Figure 8. Confusion matrix used for the evaluation

Table 1. Training Dataset

Dataset	Site 1	Site 2	Site 3	Site 4	Total
S1	10	10	10	10	40
S2	30	30	30	30	120
S3	60	60	59	60	239
S4	223	94	59	60	436

Table 2. Results of Each Dataset (N = 16)

Dataset	Precision	IoU	Recall	F1 Score
S1	0.803	0.687	0.835	0.812
S2	0.874	**0.769**	0.869	**0.868**
S3	**0.888**	**0.769**	0.856	**0.868**
S4	0.839	0.763	**0.897**	0.863
Otsu	0.686	0.563	0.786	0.712

the greatest importance to the F1 score, as it can evaluate not only precision but also recall.

We prepared four datasets, as shown in Table 1, to evaluate the effect of the amount of training data. Table 2 presents the results obtained using the datasets. According to the results, the result of S2 was almost the same as that of S3 and slightly better than that of S4. The result indicates that 30 images from a construction site can contain most of the patterns in the construction site. Additionally, we evaluated Otsu's automatic image thresholding [12] as a baseline result of conventional image processing. The result is shown at the bottom of Table 2. The result is lower in all metrics compared to the results of our method, even if the dataset is as small as S1. This means that air bubbles are not always darker than concrete surfaces and have various characteristics.

To improve the results, we additionally conducted a study using data augmentation (DA). DA is known as the general technique to improve the results of machine learning algorithms. It includes a wide variety of manipulations, but we used only simple image processing methods, such as rotation, mirroring, expansion, contraction, color channel shifting, brightness, and random crop. The results are shown in Table 3. It increased the F1 score by 0.024. The result shows that DA can work well in our domain as well as in the other domains.

Table 3. Results of Data Augmentation (N = 16)

Dataset	Precision	IoU	Recall	F1 Score
S4	0.839	0.763	**0.897**	0.863
S4+DA	**0.885**	**0.800**	0.895	**0.887**

5.2 Additional Experiments

In addition to the experiments presented in the previous section, we conducted several experiments to identify the generalization of the trained model and

prepared additional datasets, as shown in Table 4.

S4 was the same as the dataset used in the previous section. S5 included the data from S4 in addition to the data from Site 5, 6, 7, and 8, and S6 included data from S5 in addition to data from Site 9.

Table 4. Training dataset for generalization test

Dataset	Site 1–4	Site 5–8	Site 9	Total
S4	436	0	0	436
S5	436	494	0	960
S6	436	494	32	992

In this test, four images from Site 9 were used as the test data. Site 9 was not included in S4 and S5 and was included only in S6. To clarify the results, we used a simpler DA approach, such as slight rotation, expansion, contraction, mirroring, and random crop, in this test.

As shown in the result in Table 5, the higher the number of training data points, the more accurate the result. However, while S5 had almost the same number of training data points as S6, the result was not at the same level. This means that obtaining good results requires more diverse data or data from the construction site where our method was planned to be use.

Table 5. Results against test data from Site 9 (N=4)

Dataset	Precision	IoU	Recall	F1 Score
S4	0.726	0.615	0.792	0.756
S5	0.724	0.684	**0.927**	0.809
S6	**0.913**	**0.823**	0.894	**0.902**

Additionally, to evaluate the capabilities of different architectures, PSPNet [13] and DeepLabv3+ [14] were compared to the U-Net-based architecture. Both PSPNet and DeepLabv3+ are known for their well-designed architectures that enable them to exploit a broad image context. In this study, ResNet-101 [15] was used as the backbone architecture for PSPNet and DeepLabv3+.

We used the S6 dataset to train all the architectures during the test. Additionally, four images from 8 construction sites were used as test data, totaling 32 data points for the test. We also used a simple DA, similar to that used in the previous test.

As shown in Table 6, our U-Net-based architecture obtained the highest F1 score. This was almost the same as the results for S2, S3, and S4, as described in Table 2.

Table 6. Results of Architecture Comparison Including Negligible Air Bubbles (N = 32)

	Including negligible air bubbles			
Architecture	Precision	IoU	Recall	F1 Score
U-Net based	0.873	**0.768**	**0.869**	**0.865**
PSPNet	0.885	0.643	0.698	0.774
DeepLabv3+	**0.916**	0.704	0.754	0.821

Table 7. Results of Architecture Comparison Ignoring Negligible Air Bubbles (N = 32)

	Ignore negligible air bubbles			
Architecture	Precision	IoU	Recall	F1 Score
U-Net based	0.864	0.687	0.770	0.803
PSPNet	0.860	0.710	**0.805**	0.819
DeepLabv3+	**0.909**	**0.715**	0.770	**0.821**

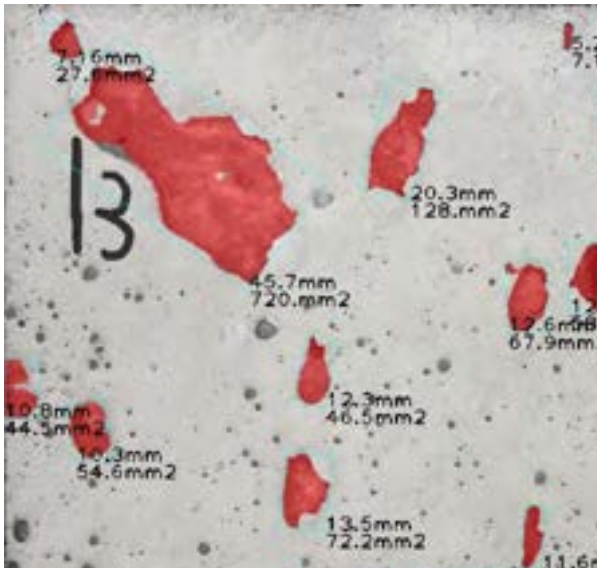

Figure 9. Result of the proposed method

However, while our U-Net-based architecture can detect almost all the smaller air bubbles, we found that it sometimes did not work well against larger air bubbles. Therefore, we reevaluated the results while ignoring the negligible air bubbles. As mentioned earlier, the negligible length was set to 5 mm. Table 7 shows the results, and Figure 9 shows the predicted result.

It can be seen that when the negligible length is ignored, the results change significantly. The recall of PSPNet was increased by 0.097, indicating that it was good at detecting larger air bubbles but not smaller ones. However, the recall of our U-Net-based architecture declined by 0.139. This reveals how well this architecture worked against small air bubbles. Additionally, Table 7 shows that our U-Net-based architecture maintained a comparative F1 score in this study.

From these results, we found that the dataset used in this paper needs not only the capability of detecting details, but also the capability of wide perception. For future work, continuous exploration of CNN architectures will be required to achieve higher performance.

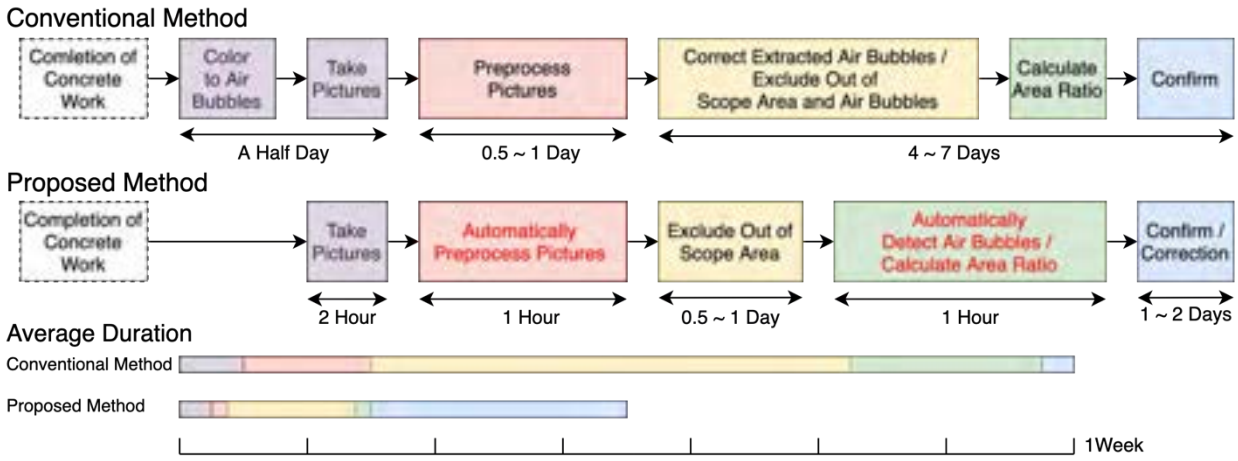

Figure 10. Workload Comparison between Conventional Method and Proposed Method, assuming that 100 pictures have to be processed.

5.3 Workload Comparison between the Conventional Method and Our Method

In this section, the workload between the conventional method and the proposed method is compared to evaluate the effect of the proposed method. The best-performing model in Section 5.1 was used for air bubble detection.

Figure 10 shows the workflow and workload of the conventional method and the proposed method. As shown here, the conventional method generally took approximately one week. The main tasks in the conventional method included preprocessing images and coloring of the air bubbles by hand. However, these manual steps were avoided in our method. At this moment, the predicted results still contain some false detections. However, as mentioned earlier, the U-Net based architecture works well against smaller air bubbles.

Therefore, in this comparison, the inspector did not have to care about the smaller air bubbles. The area ratio was obtained with a high degree of accuracy by correcting the oversight of large air bubbles. The surface of the base-isolated foundation used in this comparison has 64 grids. Considering these grids, the area ratio obtained manually was 6.19%, and that calculated by our method, with oversight correction, was 6.56%. Additionally, the oversight correction took less than 2 hours since the inspector only focused on correcting the oversight of large air bubbles.

Although the performance of our method needs to be improved, we have confirmed that it is effective in reducing the overall inspection time. Additionally, regarding the automation of preprocessing, we found that it worked almost perfectly for the expected situation where the grid was marked. Although it sometimes does not work well when including traces of the base plate's boundary, we conclude that it contributes to improving the speed of the preprocessing step.

From the above results, we conclude that our method can reduce the overall inspection time by 50%.

6 Conclusion

In this study, we developed a method to automate concrete surface inspection of a base-isolated structure. This paper presented a method that uses conventional image processing algorithms and a learning-based algorithm. Conventional image processing algorithms, such as template matching, thresholding, and contour extraction, were used for preprocessing and postprocessing of the images. For the learning-based algorithm, we used a U-Net-based architecture for automatic air bubble detection.

In the experiments, we evaluated the performance of our method, recording a best F1 score of 0.887. When the salient false detections are corrected by hand, the difference between the area ratio calculated using our method and the area ratio calculated manually by a skilled inspector was 0.37%. Furthermore, the workload between the conventional method and our method was compared. As a result, although the results predicted using our method needed to be corrected by hand, our method can reduce the overall inspection time by 50%.

In conclusion, this paper demonstrates the promising performance of the proposed method. While there is still room for improvement in terms of performance, this paper shows that our approach can automate the entire inspection process. There are many other promising CNN architectures and techniques available to improve

the performance. Accordingly, future work should focus on exploring better architectures and correcting more training data.

References

[1] JSSI Menshin Kouzou Sekou Hyojun 2017 [JSSI Construction standard of base isolation structure 2017], The Japan Society of Seismic Isolation, pp.84, 2017.

[2] Gharbia. M., Chang-Richards. Y. A., and Zhong. R., Robotic Technologies in Concrete Building Construction: A Systematic Review, 2019 Proceedings of the 36th ISARC, pp. 10-19, 2019.

[3] Prasanna. P., et al., Automated Crack Detection on Concrete Bridges, in IEEE Transactions on Automation Science and Engineering, vol. 13, no. 2, pp. 591-599, 2016.

[4] Cha. Y.-J., Choi. W. and Büyüköztürk, O., Deep Learning-Based Crack Damage Detection Using Convolutional Neural Networks. Computer-Aided Civil and Infrastructure Engineering, 32: 361-378. 2017.

[5] Gang. L., Biao. M., Shuannhai. H., Xueli. R., and Qiangwei. L., Automatic Tunnel Crack Detection Based on U-Net and a Convolutional Neural Network with Alternately Updated Clique, Sensors. 20. 717, 2020.

[6] Yoshitake. I., Maeda. T., and Hieda. M., Image analysis for the detection and quantification of concrete bugholes in a tunnel lining, Case Studies in Construction Materials, Vol. 8, pp. 116-130, 2018.

[7] Gang. Y., Fujia. W., Yang. Y., and Yujia. S., Deep-Learning based bughole detection for concrete surface image," Advances in Civil Engineering, vol. 2019, 2019.

[8] Fujia. W., Gang. Y., Yang. Y., and Yujia. S., Instance-level recognition and quantification for concrete surface bughole based on deep learning. Automation in Construction. vol. 107, 2019

[9] Mitani. K., and Katoh. Y., Study on evaluation for surface air of concrete by DeepLearning. Part1 : Outline and Surface Air Detection, Summaries of technical papers of annual meeting, Architectural Institute of Japan, pp. 1227-1228, 2019.

[10] Katoh. Y., and Mitani. K., Study on evaluation for surface air of concrete by DeepLearning. Part 2 : Estimation of binary image of surface air and filling, Summaries of technical papers of annual meeting, Architectural Institute of Japan, pp. 1229-1230, 2019.

[11] Ronneberger. O., Fischer. P. and Brox. T., U-net: Convolutional networks for biomedical image segmentation, Medical Image Computing and Computer-Assisted Intervention (MICCAI), Springer, LNCS, Vol.9351, pp. 234–241, 2015.

[12] Otsu. N, A Threshold Selection Method from Gray-Level Histograms, IEEE Transactions on Systems, Man, and Cybernetics, Vol.9, 1979

[13] Zhao. H., Shi. J., Qi. X., Wang. X. and Jia. J., Pyramid Scene Parsing Network, 2017 IEEE Conference on Computer Vision and Pattern Recognition (CVPR), Honolulu, HI, pp. 6230-6239, 2017.

[14] Chen. L., Zhu. Y., Papandreou, G., Schroff, F., and Adam, H., Encoder-Decoder with Atrous Separable Convolution for Semantic Image Segmentation. ArXiv, https://arxiv.org/pdf/1802.02611.pdf, Accessed: 06/03/2020

[15] He, K., Zhang, X., Ren, S., and Sun, J., Deep Residual Learning for Image Recognition. 2016 IEEE Conference on Computer Vision and Pattern Recognition (CVPR), pp.770-778, 2016

Using a Virtual Reality-based Experiment Environment to Examine Risk Habituation in Construction Safety

Namgyun Kim[a] and Changbum R. Ahn[b]

[a]Department of Architecture, College of Architecture, Texas A&M University, Texas, USA
[b]Department of Construction Science, College of Architecture, Texas A&M University, Texas, USA
E-mail: ng1022.kim@tamu.edu, ryanahn@tamu.edu

Abstract –

A majority of safety accidents in construction workplaces stem from workers' unsafe behaviors. Such unsafe behaviors are often caused by "risk habituation," the tendency to underestimate a risk after previous repeated exposure to similar hazardous situations. Understanding the risk habituation process in construction is critical for intervening and preventing the unsafe behaviors that it causes, but the approaches adopted in previous studies, which are retrospective and self-evaluative, pose challenges to gaining an unbiased understanding of the factors affecting this habituation process. In this context, this study exploits virtual reality (VR) as an experimental tool to examine the risk habituation process in construction and demonstrates the validity of the approach. A VR model that engages a subject in a road reconstruction project is designed and developed, and then is used to repeatedly expose subjects to struck-by hazards and warning signals for such hazards. The results from the pilot experiment indicate that the developed VR model is effective in replicating and accelerating the risk habituation process, thereby allowing researchers to more expeditiously study the factors influencing risk habituation process.

Keywords –

Construction safety; Risk habituation; Virtual reality; Unsafe behavior; Safety training

1 Introduction

"Habituation" is the decline of a response to a repetitive stimulus [1]. Similarly, the capability of a stimulus to elicit a response can be diminished when the stimulus occurs repeatedly [2]. Such habituation can result in workers being less cautious about stimuli associated with hazards in workplaces when the stimuli present, and therefore to workers engaging in unsafe behaviors [3]. This problem is relevant to the construction industry, where workers have been found to be prone to becoming habituated to hazards after exposure to repeated hazardous situations [4] at construction sites. Workers who are habituated to hazards tend to underestimate risks and put themselves at jeopardy of being in an accident [5]. This behavioral phenomenon is called "risk habituation" [6], and is considered one of the main causes of workers' unsafe behavior. Many researchers and practitioners are dedicated to understanding why and how workers underestimate risk and engage in unsafe behaviors, but previous studies have mostly relied on the capability of subjects to recall when they were in hazardous situations. Consequently, the results can be biased and cannot clearly explain the developmental process of risk habituation [7–11]. Furthermore, it is extremely difficult to control moderating and influencing factors in risk habituation in field experiments, due to their potential to harm subjects [12]. In this context, this study aims to design and evaluate the validity of a virtual reality (VR) model as an experimental tool to examine an individual worker's risk habituation process.

2 Background

Around 80–90% of all workplace accidents are caused by workers' unsafe behavior [9,13,14]. Previous studies have shown that an individual's risk perception significantly affects his/her unsafe behaviors at construction sites. Repeated exposure to hazards in the workplace can cause a bias to form in workers' risk perception [15]. Even if workers properly identify hazards, they may engage in risky behavior due to improper perception and evaluation of risk [16]. Irizarry and Abraham [17] examined the factors influencing the risk perception of ironworkers, and their results indicate that long tenure in working experience at workplaces is correlated with unsafe behavior caused by bias in workers' risk perception. Majekodunmi and Farrow [4] investigated the risk perception of lift truck operators. Their results indicate that repeated exposures cause workers to become accustomed to the hazards related to their tasks. While these studies indicate that risk

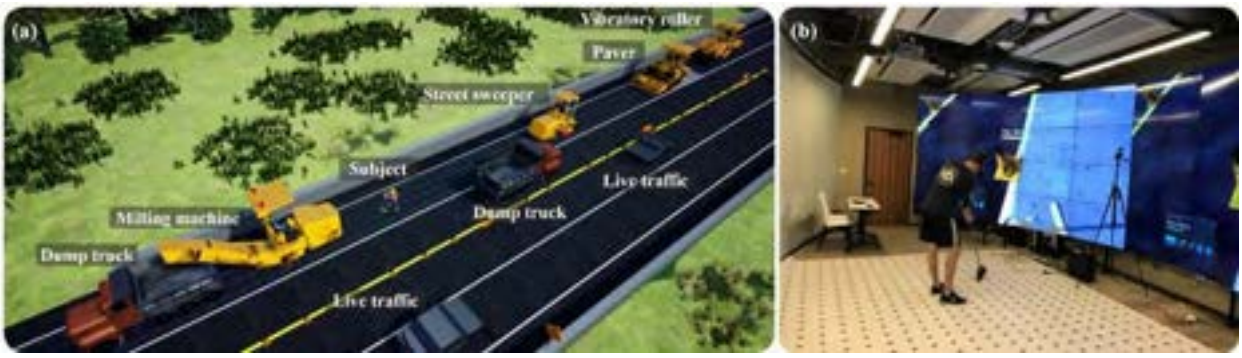

Figure 1. Experimental environment: (a) the landscape of the immersive virtual road construction environment, (b) the Building Information Modeling-Computer Aided Virtual Environment (BIM-CAVE)

habituation is one of the factors causing unsafe behaviors, a knowledge gap still exists as to which specific personal and situational factors critically influence the development process of risk habituation and how this development process can be intervened in, due to the methodological limitations of the approaches adopted in the previous studies, which were uniformly retrospective and self-evaluative.

With the recent development of virtual reality (VR) technologies, VR has emerged as an experimental tool for examining workers' unsafe behaviors. VR-based safety interventions in previous studies have enabled researchers to expose subjects to virtually replicated hazardous situations without any actual risk. Albert et al. [18] showed that as a safety intervention platform, VR can provide close-to-reality simulations. Thus, workers can evaluate the risks of hazard very similarly in the VR environment as in a real environment. Moreover, VR enables researchers to analyze workers' behaviors in near real-time. Many researchers have therefore utilized VR to investigate construction workers' behavior in dangerous situations. For instance, Hasanzadeh et al. [19] attempted to observe a roofer's risk-taking behavior in the virtual environment (VE) and demonstrated that a group of roofers with more safety protection took more risks than other groups in the VE. Shi et al. [20] utilized a VR model as an experimental tool in order to show the effect of accident experiences on workers' fall risk behavior. To this end, this study exploits VR as an experimental tool to address uncertainty in construction workers' risk habituation processes. An immersive VE for road construction is developed to expose workers to repetitive hazardous situations. Leveraging data acquired from subjects' physical responses to hazards in the VE, this paper demonstrates the approach's validity as an experimental tool to examine an individual worker's risk habituation.

3 Methodology

The objective of this study has been accomplished in three phases. An immersive virtual road construction environment was built and a cyber-physical interactive system that synchronizes the actual movement of a subject with a virtual movement in the VE was developed. A pilot experiment was then conducted to observe and evaluate how the risk habituation process in the VE develops. The data from the pilot experiment was analyzed to identify the relationship between repeated exposures to hazards and subjects' responses to repetitive hazards in the VE.

3.1 Designing the Scenario

A road maintenance workplace in which subjects would be part of an asphalt milling crew was selected for the VE development scenario (Figure 1-a), as such a scenario is high-risk and likely to cause risk habituation in the VE. Road construction and maintenance work repeatedly exposes workers to struck-by hazards such as working adjacent to live traffic and heavy construction equipment; 532 workers were killed at road construction work zones between 2011 and 2016 in the United States [21]. The proposed VR model focuses specifically on the construction equipment risk, with a subject at risk of being struck by a dump truck, street sweeper, or other piece of heavy construction machinery.

A normal asphalt removing, and paving work process was modeled in the VE. As the first step of the process, a milling machine removes the surface asphalt of a highway and loads the millings onto a fleet of dump trucks to haul off-site. As part of the cleaning crew, a subject then follows closely behind the milling machine and carefully sweeps the surface to remove debris. Behind the subject, a street sweeper moves back and forth

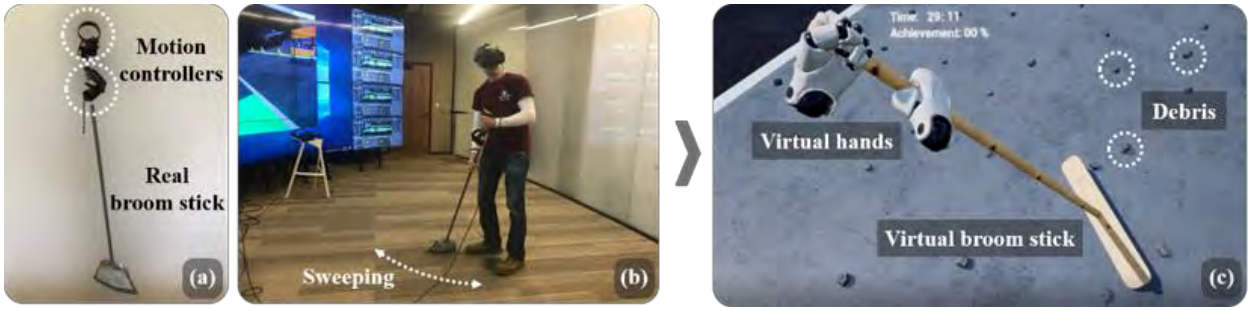

Figure 2. Cyber-physical interactive system for hand-movement synchronization; (a) Motion controllers on real the broomstick, (b) sweeping in the real world, (c) debris on the surface in the VE

continuously. After that, the paver will lay down asphalt, and a vibratory roller will move forward. Next to the lane where the asphalt maintenance takes place, a fleet of dump trucks intermittently moves to supply materials. Live commuter traffic takes place also within the construction work area. In this VE, the various pieces of road construction equipment (e.g., the milling machine, roller, and other machinery) expose each subject to the risk of a struck-by accident and allow researchers to observe subjects' responses to repeated hazards.

3.1.1 Immersive Virtual Road Construction Environment Modeling

Unreal Engine 4 (UE4) was adopted to develop an immersive virtual road construction environment. UE4 offers various project templates, allowing researchers to rapidly develop a VE. All models used in this study are drawn using Maya and 3dStudioMax. Then, all aspects of an immersive virtual environment were created using UE4 with a graphical user interface in order to induce risk habituation in subjects while working in close proximity to live traffic and heavy equipment in the VE.

3.1.2 Hazards and Non-Player Characters (NPC) Setup

Life-threatening hazards in highway construction sites (e.g., adjacent live traffic, heavy construction equipment, and a fleet of dump trucks moving near workers) were simulated in the VE. All the interactive components in the VE respond to behaviors of a subject. Behind a subject, the street sweeper moves back and forth at a constant speed. An alarm sounds as the street sweeper moves forward in order to notify its proximity to a subject. The movement of the sweeper is subject to the distance between a subject and the street sweeper, and repeatedly endangers a subject to struck-by accident. Next to the lane where the road maintenance takes place, dump trucks intermittently pass by very close to the subject, with accompanying warning alarms. These movement cycles of the sweeper and dump trucks will continue while the subject performs the task.

3.1.3 Cyber-physical Interactive System

The level of immersiveness in any VE plays a crucial role in VR-based safety training [22]. Feeling the VE as a real working environment is an important factor in VR-based safety training [23]. To achieve the necessary high level of immersiveness, a cyber-physical interactive system was applied. Motion controllers for a Head Mounted Display (HMD) were attached to a real broomstick (Figure 2-a), and the movements made by a subject sweeping in the real world is then linked to the broomstick in the VE (Figure 2-b). This physical interaction addresses the limitations of previous VR-based safety research that did not consider the influence of actual human body movements in a VE [8]. Moreover, in order to realize a high level of fidelity, around 1,000 pieces of debris were placed on the road in the VE. This debris is responsive to each subject's sweeping movements in the VE. The goal of the subject is to remove all debris and clean the entire surface of the road by sweeping with the broomstick (Figure 2-c).

3.2 Risk Habituation Measurement

In this study, habituation is defined as the decline of a subject's hazard-checking behavior and the increase of the number of deviations in the working lane. For the purpose of observing the risk habituation development process, this model monitors hazard-checking behaviors of a subject and documents the distance to the hazard when a subject undertakes a hazard-checking action as a precautionary action. Hazard-checking behaviors are defined as any movement the subject makes to look for hazards (Figure 3-a); the measurement system that detects subjects' hazard-checking behavior is validated by comparison with video recordings of the experiments. The system documents the distance between the subject and the sweeper when such checking behavior is sensed. In addition, the system records the movement trajectory of subjects in order to detect the moment when a subject deviates from the working lane, regardless of the risk of being struck by the truck. The analysis of the movement

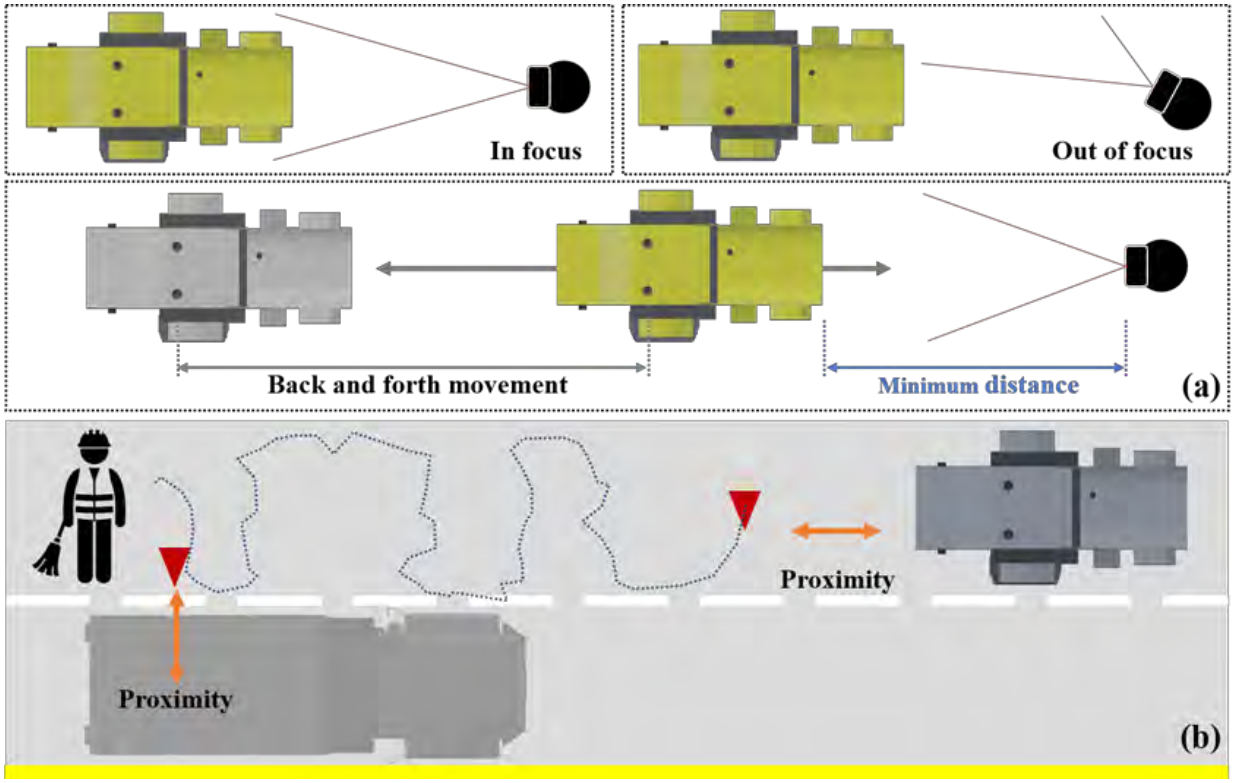

Figure 3. Unsafe behavior measurement system; (a) detecting the hazard-checking behavior, (b) recording the movement trajectory of a subject

trajectory allows researchers to identify when and how a subject becomes habituated to the risk of being struck by accident (Figure 3-b). The location of a subject is collected with a peak frequency of 30 Hz.

3.3 Pilot Experiment Conditions and Procedures

A pilot experiment was performed in the Building Information Modeling-Computer Aided Virtual Environment (BIM-CAVE) at Texas A&M University (Figure 1-b). Three subjects who are graduate students in the department of construction science were recruited for a pilot experiment; none of the subjects had any prior hands-on experience with road construction maintenance work. The following instructions were given: 1) the subjects should follow the milling machine, 2) the subjects should sweep away all the debris from the working lane, and 3) the subjects should pay attention to approaching equipment and warning signals for safety purposes. Completing the overall task in the VE took around 20 minutes, and once a subject ignored the hazards more than 10 times, the experiment was discontinued since this was perceived as a signal that the subject had become habituated to the risk in the VE. A follow-up interview on the perceived immersiveness of the environment was conducted after the experiment.

4 Results and Findings

By analyzing the data directly acquired from the subjects' hazard-checking behaviors, the process of subjects' risk habituation in the VE was observed. Figure 5 demonstrates a relationship between the number of cycles and checking distances of the respective subjects, and the distance between the sweeper and a subject at the moment when s/he undertook an action to check the approaching sweeper at each cycle. The dashed blue lines indicate the designed minimum distance between the sweeper and a subject. If the subject didn't check the sweeper's position until the minimum distance was reached, this was regarded as unsafe behavior. The data points marked with black in the graphs indicate subjects' unsafe behaviors. The highlighted parts of each graph represent the moment where the subjects' unsafe behaviors rapidly increased and give an opportunity to identify which subjects became accustomed to the hazard more quickly than the others. All distances were measured employing Unreal units, the default measure of length within the Unreal Engine environment; one Unreal unit equals one centimeter.

Table 1. Analysis of subjects' hazard checking behaviors in the VE

Subject #	Mean distance	F	p-value	Slope of the line	Correlation coefficient
Subject #1	984.356	10.106	0.003	- 10.023 ± 2.024	-0.459
Subject #2	939.512	32.628	< 0.001	- 14.345 ± 2.021	-0.670
Subject #3	1096.837	44.628	< 0.001	- 54.176± 2.074	-0.818

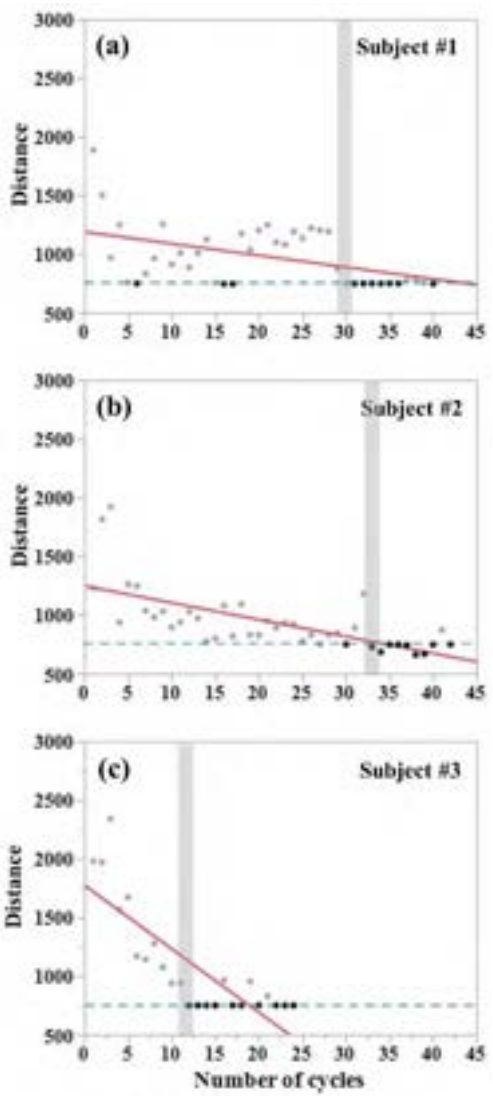

Figure 4. The distance to the street sweeper when subjects checked the proximity of the equipment

To measure the strength and direction of the linear relationship between two variables, the Pearson correlation coefficient, referred to as Pearson's r, was employed. Table 1 shows that there is a statistically significant correlation between checking distances and the number of exposures to the hazard. The checking distance and the number of exposures are moderately negatively correlated in the data from Subject #1 ($r(39) = -.46$, $p = .003$) and Subject #2 ($r(41) = -.67$, $p < .001$), and strongly negatively correlated in the data from Subject #3 ($r(22) = -.82$, $p < .001$). At the beginning of experiment, all subjects immediately responded to the warning sounds and looked back to check the source of warning alarm. However, as the number of cycles (i.e., the number of exposures to the hazard) increased, subjects responded more slowly, and the checking distances gradually decreased in all three subjects. The correlation coefficient and slope of the line of Subject #3 show the strongest negative linear relationship among three subjects. Subject #3 ignored the hazard 10 times out of 22 times. This indicates that Subject #3 became habituated to the hazard more quickly than other subjects (Figure 4). After the experiment, the subjects reported how they felt and why they ignored the hazard. Subjects answered that they no longer paid attention to the hazards and began to act dangerously from the moment when they focused on the completion of the task and started to This debris is responsive to each subject's sweeping movements in the VE believe the surrounding hazards would not hurt them. Interestingly, Subject #1 relayed that he totally ceased to hear the alarm sound of the sweeper when he felt time pressure and started to think about how to finish the task more quickly.

The movement trajectories of subjects were plotted (Figure 5) in order to examine how close the subject moved to the truck when the truck was passing by in the neighboring lane. The highlighted points are the moments where the subject crossed over the lane regardless of the risk of being hit by the truck. Subject #1 relayed the fact that although at the beginning of the experiment he had been thinking about the hazard related to trucks, he unconsciously crossed the lane to sweep debris on the road. This result showed that analyzing the movement trajectory can help in detecting unconscious unsafe behaviors of subjects in the VE. Although the sample size was small and further studies are necessary to confirm these findings, the results of the experiment indicate that repeated exposure to hazards in a VE can lead to subjects' risk habituation, highlighting the utility of VR as an experimental tool in examining safety behaviors.

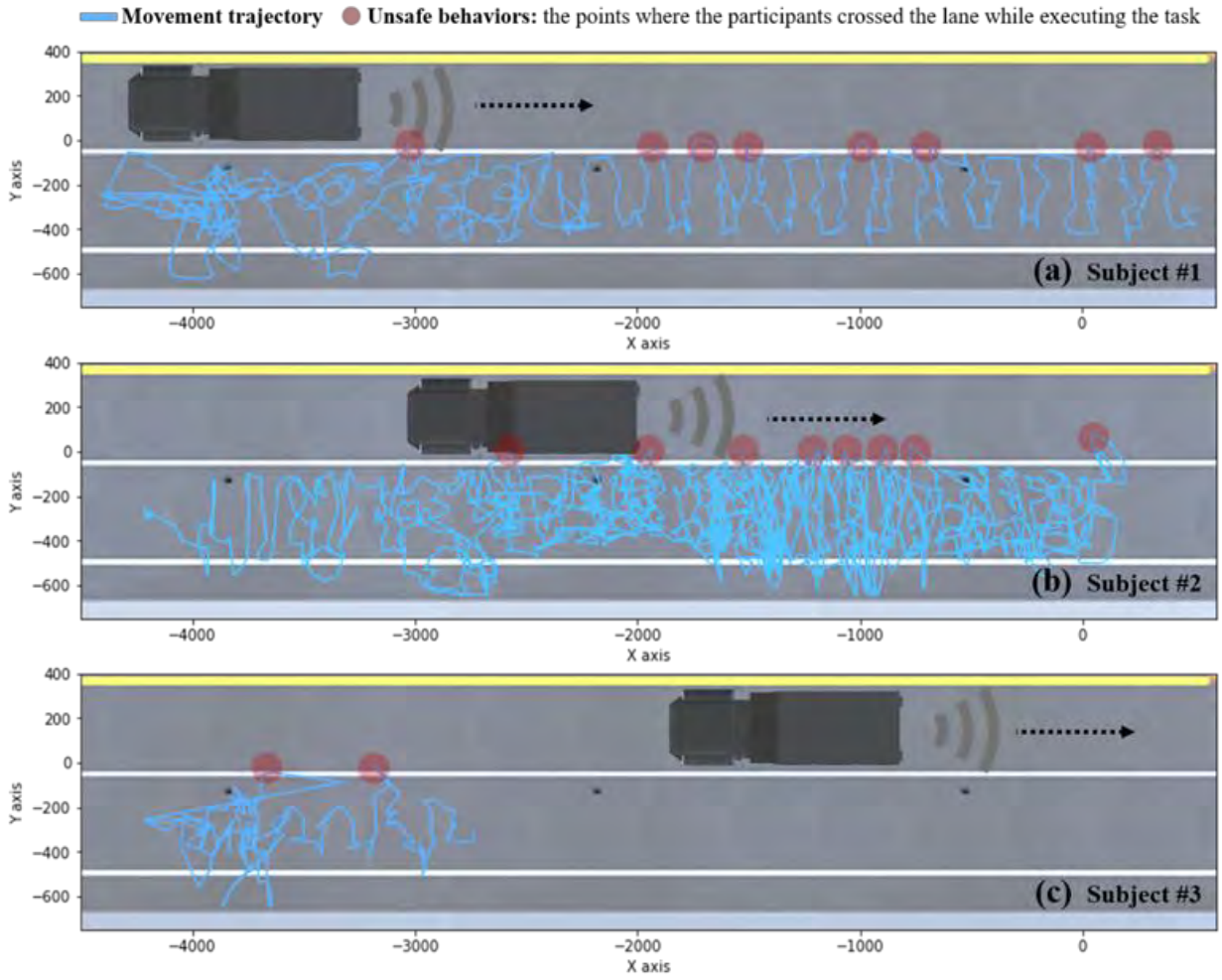

Figure 5. Movement trajectory analysis

5 Conclusion

The results of the experiment indicate that the designed VR model is capable of observing an individual's risk habituation process. Although there were individual differences, all subjects became habituated to repeated hazards in the virtual road construction environment. After a certain period of time, subjects began to ignore the proximity of the construction equipment behind of them and began to cross the lane in pursuit of finishing their cleaning task, regardless of the risk of being struck by the truck. This highlights the opportunities available in analyzing behavioral responses of construction workers to hazards in an immersive virtual construction environment. For example, a similar such VR model could provide a chance to investigate which personal factors (e.g., working experiences, injury experiences, and personalities) and situational factors (e.g., safety rules, the behavior of other personnel in working groups) affect workers' unsafe behavior in construction. Future work will also examine VR-based intervention mechanisms to prevent construction workers from becoming habituated to hazards and engaging in unsafe behaviors that might cause life-threatening accidents at construction sites.

References

[1] D. Bukatko, M.W. Daehler, Child development: A thematic approach, Nelson Education, 2012.

[2] A.R. Lebbon, S.O. Sigurdsson, Behavioral perspectives on variability in human behavior as part of process safety, J. Organ. Behav. Manag. 37 (2017) 261–282.

[3] K. Bogard, T.D. Ludwig, C. Staats, D. Kretschmer, An industry's call to understand the contingencies involved in process safety: Normalization of deviance, J. Organ. Behav. Manag. 35 (2015) 70–80.

[4] A. Majekodunmi, A. Farrow, Perceptions and Attitudes Toward Workplace Transport Risks: A Study of Industrial Lift Truck Operators in a London Authority, Arch. Environ. Occup. Health. 64 (2009) 251–260. https://doi.org/10.1080/19338240903348238.

[5] E. Blaauwgeers, L. Dubois, L. Ryckaert, Real-time risk estimation for better situational awareness, IFAC Proc. Vol. 46 (2013) 232–239. https://doi.org/10.3182/20130811-5-US-2037.00036.

[6] P. Slovic, Perception of risk, Science. 236 (1987) 280–285. https://doi.org/10.1126/science.3563507.

[7] J. Bohm, D. Harris, Risk Perception and Risk-Taking Behavior of Construction Site Dumper Drivers, Int. J. Occup. Saf. Ergon. 16 (2010) 55–67. https://doi.org/10.1080/10803548.2010.11076829.

[8] C. de-Juan-Ripoll, J.L. Soler-Domínguez, J. Guixeres, M. Contero, N. Álvarez Gutiérrez, M. Alcañiz, Virtual Reality as a New Approach for Risk Taking Assessment, Front. Psychol. 9 (2018). https://doi.org/10.3389/fpsyg.2018.02532.

[9] M. Hallowell, Safety risk perception in construction companies in the Pacific Northwest of the USA, Constr. Manag. Econ. 28 (2010) 403–413. https://doi.org/10.1080/01446191003587752.

[10] M. Kreyenfeld, S. Bastin, Blurred Memory, Deliberate Misreporting, or "True Tales"? How Different Survey Methods Affect Respondents' Reports of Partnership Status at First Birth, (2013) 36.

[11] Sun Cenfei, Ahn Changbum Ryan, Bae Junseo, Johnson Matthew, Monitoring Changes in Gait Adaptation to Identify Construction Workers? Risk Preparedness after Multiple Exposures to a Hazard, Constr. Res. Congr. 2018. (n.d.) 221–230. https://doi.org/10.1061/9780784481288.022.

[12] J.R. Bartels, D.H. Ambrose, S. Gallagher, Analyzing Factors Influencing Struck-By Accidents of a Moving Mining Machine by using Motion Capture and DHM Simulations, SAE Int. J. Passeng. Cars - Electron. Electr. Syst. 1 (2008) 599–604. https://doi.org/10.4271/2008-01-1911.

[13] HSE (Health and Safety Executive), Strategies to promote safe behavior as part of a health and safety management system, (2002).

[14] K. Yang, C.R. Ahn, M.C. Vuran, H. Kim, Collective sensing of workers' gait patterns to identify fall hazards in construction, Autom. Constr. 82 (2017) 166–178. https://doi.org/10.1016/j.autcon.2017.04.010.

[15] J. Inouye, Risk perception: Theories, strategies, and next steps, Itasca IL Campbell Inst. Natl. Saf. Counc. (2014).

[16] Tixier Antoine J.-P., Hallowell Matthew R., Albert Alex, van Boven Leaf, Kleiner Brian M., Psychological Antecedents of Risk-Taking Behavior in Construction, J. Constr. Eng. Manag. 140 (2014) 04014052. https://doi.org/10.1061/(ASCE)CO.1943-7862.0000894.

[17] J. Irizarry, D.M. Abraham, Assessment of Risk Perception of Ironworkers, J. Constr. Res. 7 (2006) 111–132. https://doi.org/10.1142/S1609945106000499.

[18] Albert Alex, Hallowell Matthew R., Kleiner Brian, Chen Ao, Golparvar-Fard Mani, Enhancing Construction Hazard Recognition with High-Fidelity Augmented Virtuality, J. Constr. Eng. Manag. 140 (2014) 04014024. https://doi.org/10.1061/(ASCE)CO.1943-7862.0000860.

[19] S. Hasanzadeh, Understanding Roofer's Risk Compensatory Behavior through Passive Haptics Mixed-Reality System, Comput. Civ. Eng. (2019) 9.

[20] Y. Shi, J. Du, C.R. Ahn, E. Ragan, Impact assessment of reinforced learning methods on construction workers' fall risk behavior using virtual reality, Autom. Constr. 104 (2019) 197–214. https://doi.org/10.1016/j.autcon.2019.04.015.

[21] Bureau of Labor Statistics, Fatal occupational injuries by selected characterisitics, (2017).

[22] I. Jeelani, K. Han, A. Albert, Development of Immersive Personalized Training Environment for Construction Workers, in: Comput. Civ. Eng. 2017, American Society of Civil Engineers, Seattle, Washington, 2017: pp. 407–415. https://doi.org/10.1061/9780784480830.050.

[23] R. Sacks, A. Perlman, R. Barak, Construction safety training using immersive virtual reality, Constr. Manag. Econ. 31 (2013) 1005–1017. https://doi.org/10.1080/01446193.2013.828844.

Towards a Computational Approach to Quantify Human Experience in Urban Design: A Data Collection Platform

Keundeok Park and Semiha Ergan

Tandon School of Engineering, New York University, the USA
E-mail: kp2393@nyu.edu, semiha@nyu.edu

Abstract –

Design features that form urban settings such as greenery, height of buildings, and variation in the building façade (materials, color, and proportion) are known to have effects on how people experience environments. As the urban population grows and shifts to urban settings for living (e.g., 82% of people live in cities in the US), understanding the impact of urban environments on human experience becomes more essential. Previous studies to capture human experience in urban settings have been limited due to the labor-intensive and manual process of data collection (i.e., field surveys). Due to limited quantified data on urban design features, previous methodologies were constrained to a few neighborhoods, hence lacked generalizability across regions. Advancements in technologies such as GIS, computer vision, and data-driven methodologies and accessibility to large image sets on urban settings provide opportunities to eliminate the labor-intensive process of data collection. With the help of technologies, it is possible to quantify how people experience cities. This study leverages such advancements and aims to develop an automated approach for quantifying human experience toward built environments regarding their restorative impact on citizens. Towards this aim, within the context of this paper, we provide the details of a web-based crowdsourcing platform developed for the data collection at urban scale. We combine Geographic Information System (GIS), Google Street View (GSV), and JavaScript libraries to build the platform to capture the responses of participants on the restorative impact of the environments displayed to them as images. Based on the geolocation information obtained from GIS, we collected high resolution 360° GSV images within New York City (NYC) and used them to collect responses of citizens on structured questions tailored to the scope of the study. The crowdsourcing platform enables participants to evaluate the overall restorative impact of environments given in a 360° image, and to specify areas and design features influencing their evaluation. To quantify the influential design features on responses, we use semantic segmentation, and perform statistical analysis on the dataset to examine the impact of each urban design feature on the overall restorative impact. The approach will be presented for researchers to integrate GIS, Google API, and libraries to pull massive urban data for research study necessitating a good representation of the built environment as inputs. The outcomes will guide practitioners in urban redevelopment projects about urban design features that are influential.

Keywords –

Urban design; Restorative environments; Computer vision; Semantic Segmentation; Crowdsourcing; GIS; Google Street View

1 Introduction

The indoor and outdoor built environment has a strong association with restorativeness, which directly impacts mental fatigue, stress indicators, and quality of life of individuals [1-5]. As the urban population grows (82% of Northern American people are living in cities), the stress level of the urban residents has increased because of reduced space and overcrowding accompanied with urbanization [6]. With the aim to improve the quality of life, many researchers have been focusing on studying the impact of the built environment on human perception, including the restorativeness of the environment on people [7-9]. Various studies under this umbrella evaluated the relationship between the built environment and people's experience (e.g., preference, feeling of safety, stress/anxiety) and behavioral changes (e.g., reduction/increase in physical activities) in urban settings [1-6,10]. Their studies evaluate the built environment at micro and macro scales, including understanding the effect of various urban design elements, such as buildings, streets, and urban design blend as a whole. Majority of such empirical studies utilized Geographic Information System as a tool to quantify properties of such elements in the built environment (e.g., urban density, building height),

resulting in many street level design elements (such as the presence of street furniture, type of building façade) being omitted due to the hardship of data collection and representation format in existing data sources, mostly being shapefiles. In order to reflect street level elements as impacting factors on human experience, more recently, few studies have utilized urban street imagery and machine learning algorithm. These studies used urban street images that are prelabeled by people indicating how they feel about the environment in the images to predict people's perception (e.g., safety, excitement) about a given environment [11-15]. However, previous studies used non-panoramic and low-resolution images, which lacked rich visual information to give realistic experience of streets. In addition, what lacked in those approaches are the assessment of individual contributors of the type and amount of urban design elements on the resulting influence. Such information is essential for urban designers/practitioners to shape the urban settings with clear knowledge on how they will positively influence people's experience in an area.

Hence, in this work, we propose the details of a data collection platform that will enable (a) capturing rich geometric and visual information from multiple perspectives in a given area, and (b) correlating the overall experience of people in that area with the type and quantified properties of urban design elements that make up that area.

2 Literature review

This study is at the intersection of (a) previous studies that evaluated urban design elements on their restorative impacts on people, (b) metrics defined for measuring restorative capability of an environment, (c) data collection methods to measure impact of urban settings on people, and (d) contemporary and large image sets from urban settings.

2.1 Urban design elements and their impact on human experience

This work focuses on the restorativeness impact of the built environment on human experience, which is defined as the potential to recover and increase cognitive, physical, and mental capacity of people [27,34]. The effects of restorative environments on physical, social, and mental well-being has been examined extensively by studies in environmental psychology domain [3, 33].

Kaplan & Kaplan (1989) established the attention restoration theory and the value of nature on psychological restoration [27]. Based on that, studies in environmental psychology domain have empirically proved that not only the natural environment but also the presence of certain elements in the built environment have restorativeness effect on people. Examples of these urban design elements are provided in Table 1. Due to the high population density of cities, this potential of restorative environments in urban settings is significant.

Table 1. Urban design elements that were studied for restorative impact of the built environment

	Urban design elements	Reference
Built environment	Height of buildings	[4,5,28]
	Presence of socialization places such as cafés and restaurants	[25,26]
	Width of streets	[28]
	Visual complexity (e.g., the number of signages, dis/continuity of building façade style)	[23]
	Presence of landmarks and historical buildings	[24,27]
Natural environ-ment	Presence and amount of water bodies around	[23,25]
	Presence and amount of vegetation (e.g., trees, flowers, plants) around	[4,5,16-18]

2.2 Metrics defined for measuring restorative capability of an environment

One of the first studies that aim at measuring restorative impact of an environment is by Hartig et al. (1997). Perceived Restorativeness Scale (PRS) suggested by that study has been used to capture restorative quality of environments in environmental psychology studies. PRS was designed to measure the restorative quality of environments by capturing four psychological aspects - which are Being-away (being away from daily concerns), Fascination (capacity to drag people's attention), Coherence (clear order of the physical arrangement of design elements), and Compatibility (match between people's goals and availability of required activity in the place). The original version of PRS composes of 11 scale (0-10) and 26 questions. After Hartig et al. (1997) suggested PRS, several researches have made efforts to make shorter versions of PRS questionnaire and prove the usability of new versions of questionnaires [5,11,21,22]. In this study, to adopt a user-friendly and a shorter version, we adopted PRS questionnaires as used in Lindal & Hartig (2013) to capture being-away and fascination of built environments in urban settings. Due to characteristics of an online crowdsourcing platform, the shorter version of questionnaire is more appropriate for the participants' convenience and the reliability of the collected information.

2.3 Data collection methods utilized in literature

Previous studies are mainly empirical studies that aim to define the urban design elements that affect the restorative impact of a neighborhood. Such studies examine the direct and indirect effects of physical urban design elements (e.g., building height, presence of greenery and vegetation, bench) on streets on restorativeness, measured through a combination of metrics such as the feeling of openness, being away, fascination, compatibility, and complexity [4,16-18]. The data collection efforts that provide the required inputs for these studies can be mainly grouped under three categories: (1) field experiments, which include taking trips to areas of interest and conducting interviews with participants [19,20]; (2) image auditing, which includes using static street images with varying context (e.g., commercial area vs. historical place, residential area vs. parks and recreational areas) and comparing people's responses [21,24]; and (3) 3D modeling, which includes generating digital replica of an urban location with controlled objects in a scene and asking questions to participants regarding their perception of the area [4,16].

Each one of the described categories has specific limitations: field experiments are labor intensive, image auditing is manual for quantitative analysis of each urban design element on a scene, and 3D modeling is time-consuming to get realistic representation in virtual worlds. Besides the limitations that are specific to each category, they share a common limitation that hinders the extension and generalization of research outcomes, because of the fact that they could only focus on a specific urban area in these labor-intensive data collection processes. Hence, to alleviate the limitations in the existing data collection processes and enable collection of massive and rich data on urban settings, we describe a data collection platform that can merge several data sources, slice, and extract geometric and location information of areas with rich contextual data.

2.4 Contemporary and large image datasets that are generated to measure human experience in urban settings

A few recent studies focused on understanding human perception on the aesthetic preferences of people in urban settings using images and data-driven methods [29-31]. Although these studies differ in the urban evaluations, they are worth mentioning here because of the large datasets generated for similar purposes. Being one of them, the Aesthetic Visual Analysis (AVA) dataset has 250,000 images with semantic annotation (e.g., cityscape, landscape, architecture, etc. already labeled) and ratings of people on the images about how aesthetic they find [29]. Using the AVA dataset, some of the studies examined the possibility of machines mimicking human perception toward the selection of places (represented as images) with high aesthetic appeals [30,31]. Beyond this dataset, a few research studies have generated image sets on human perception in street level urban environments [11-15,32]. Place Pulse project by MIT Media Lab collected human perception regarding safety, wealth, boring, beauty, depressing, and livability using 100,000 images from 56 cities by comparing two street images and selecting better image in terms of being safer, wealthier, less boring, more beautiful, less depressing, and more livable [11,12]. The image ratings are through pairwise comparison of two static images, which show the place only from one viewpoint and without disaggregating the images into influential urban design elements on human perception The data platform presented in this paper eliminates these limitations by enabling (a) capturing high-resolution 360° panorama images of locations of interests, and (b) annotations on images for defining the influential objects in assigned ratings by participants.

The results of previous studies that utilize such image datasets to predict human perception indicate that visual representations captured in images are reflective of human perception and are promising to study urban design through leveraging image datasets. Previous studies also provide a point of departure about the strong indication that a machine can mimic human perception in an urban environment if presented with structured and large data. With the overall aim to have an empirical study on quantifying human restorativeness on urban environments, this paper provides the data collection platform developed to provide the required input of well-structured and large datasets for such studies. The structure of data is maintained through disaggregation of captured images to primitive urban design elements and quantifying their influence on the overall human experience.

3 Urban-scale data collection platform

In this section, we provide the details of the platform by introducing the major components of this platform and how they function and interact with each other. Major components of the platform are explained based on their roles in forming the image database (part 1 in Figure 1) and in capturing participants input in the crowdsourcing phase of the data collection (part 2 in Figure 1).

3.1 Overview

An overview of this platform is provided in Figure 1. First, the urban image database for images from areas of interests should be captured, which includes Geographic

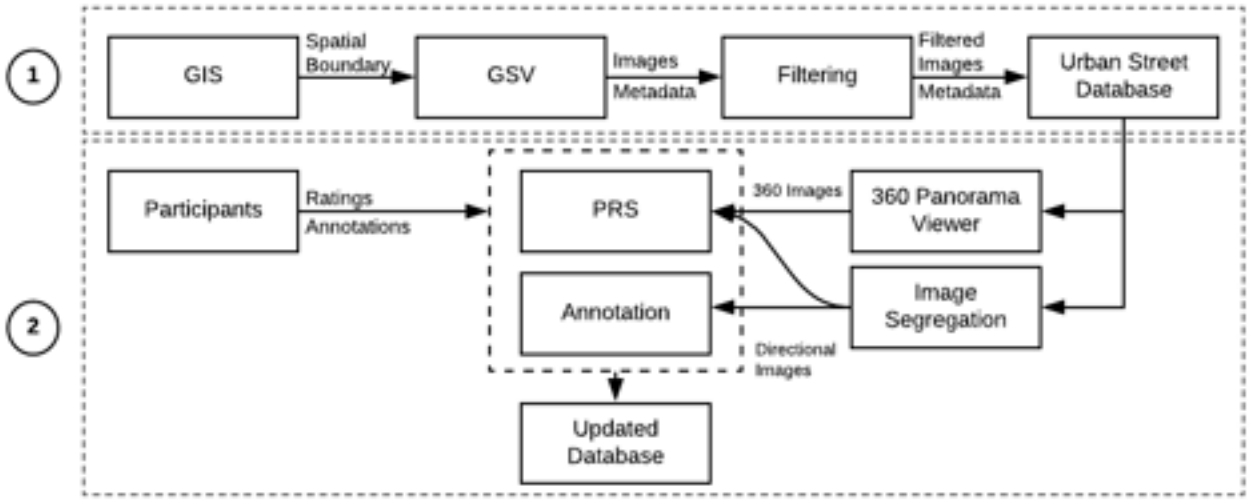

Figure 1. Components of the data collection platform and their interactions.

Information Systems (GIS) and Google Street View (GSV) APIs. The images are stored for locations represented with global latitude and longitude information of a specific location in Google's database and retrieved by a point by point request through Google API. Therefore, to request images through Google API, we need to (1) set the spatial boundary of interest using GIS, (2) generate a large number of points within the boundary in GIS, and (3) request the images and metadata (i.e., panoID, geographic coordinate) through Google API. During this request, all types of images from GSV including the ones about indoor environments are also retrieved. Therefore, a filtering component has been integrated in the platform that use semantic segmentation and unsupervised learning to eliminate images that are irrelevant (as detailed in section 3.4).

The images that stand out after the filtering are stored in our database and ready for use in part 2 of the platform (labeled with #2 in Figure 1). This part deals with capturing and storing response of citizens, who participate in the crowdsourcing based data collection. The data to be collected includes the ratings of people on restorative impact of the environment displayed on a set of randomly assigned 360˚ images and the associated unidirectional images (i.e., an image from front, back, left, right of a selected field of view) along with the annotations on images that define sections that were influential in participant ratings (see details in section 3.3). Ratings are captured through a 1-5 Likert on the perceived restorativeness scale (PRS) (detailed in section 2.2). In summary, the data collection platform enables to capture: (1) GSV image, (2) segmentation output of the image, (3) crowdsourced ratings on 360˚ and each directional image, and (4) annotations of influential urban design elements present in an image (Figure 2).

The following subsections provide further details of these components and their functions over the example implementation in New York City.

3.2 Populating the Urban Street Image Database

GSV is an open data source that provides street imagery and its metadata, which can be requested by a panoID or geographic coordinate. In the platform presented here, 360˚ panorama images are captured from Google Street View (GSV) in equirectangular projection, which is a 360˚ panorama image representation format providing a 360˚ horizontally and 180˚ vertically stitched image (Figure 4). Extracting the related images for a

Figure 2. Data captured and stored through the platform for one image.

neighborhood of interest, first a spatial boundary is defined in GIS. An example boundary (near Washington Square Park, NYC) is provided in Figure 3. We generate a number of points in GIS (represented as latitude and longitude) within this boundary and request GSV images

and their metadata for each point generated. As a result, generated points within the specified boundary are matched with available GSV data as shown in Figure 3. As part of the metadata, there is "panoID" which is the unique key representing a street view image. Using "panoID", 360˚ panorama GSV images are retrieved in this platform.

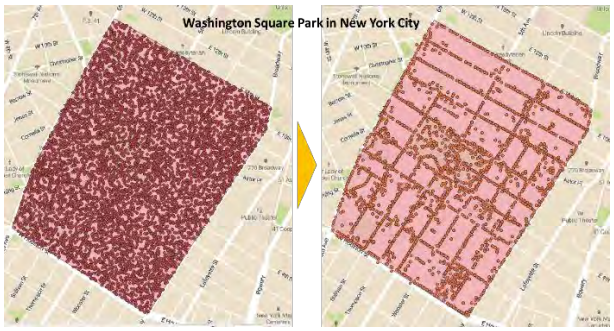

Figure 3. Illustration of a spatial boundary selection and mapping of GSV metadata within the boundary. Left: generated points by GIS; Right: obtained images.

Using this process, it is possible to populate a large image dataset for a neighborhood of interest without the need for time consuming manual image collection. The image resolution we obtained is 8192 × 4096, which is the same quality of 4K 360˚ camera and 4K content in VR device, surpassing the problems in previous data collection efforts resulting in low resolution images (640x640) and lack of visual details. For testing of this platform, we captured 2,628 images from NYC Washington Square Park area.

3.3 Projecting images and annotation

Equirectangular image is a popular format to store and convey 360˚ panorama images. However, the image is not intuitive to human perspective because it is projected as a single flat image with 360˚ horizontal and 180˚ vertical coordinate in the image (Figure 4). Therefore, to use the equirectangular image in the platform, the image needs to be converted to a perspective projection image.

Figure 4. Equirectangular image

Firstly, to capture entire human experience in the place at the first page, we used a 360˚ panorama viewer. We used open source panorama viewer Pannellum, which is built using web programming language (Figure 5). Next, we extracted unidirectional images from equirectangular images (Figure 6). The selected field of view are looking front, right, left, back and up along the street.

Figure 5. Equirectangular image projected in a 360˚ panorama viewer.

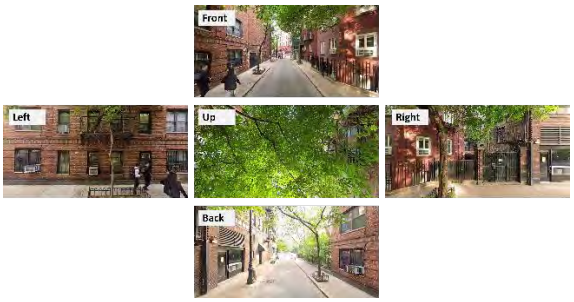

Figure 6. Unidirectional images (Front, left, up, right, bottom along the street) extracted from the equirectangular image shown in Figure 5.

To facilitate capturing parts of an image that were influential to a participant's ratings on restorative impact of that image, we set HTML canvas that allow users to draw rectangles on sections in images (Figure 7). The rectangular shapes on canvas are stored as images during the data collection process, which will be segmented further in the data analysis phase for quantifying urban design elements.

Figure 7. Annotation capability in the platform.

3.4 Filtering out irrelevant images

The automated population of images from GSV in a spatial boundary could result in extracting images that are stored in GSV but not representing street views. To eliminate such irrelevant images from the image database, this data collection platform has a filtering component that utilize semantic segmentation and unsupervised learning to classify indoor and outdoor images. During the initial step of populating the urban image dataset, points generated could match to images that are representing indoor environments. In order to exclude the images related to indoor environments, we used semantic segmentation and unsupervised learning. Semantic segmentation enables us to parse images and assign a class label (i.e., flower, tree, building, car) by pixel level and unsupervised learning facilitates clustering based on the segmentation output (objects in the image). Since the indoor environment has distinct object compositions from outdoors, one of the clusters represents the indoor images. For semantic segmentation, we utilized the HRNetV2 model, which is a neural network based model developed by Sun et al. (2019) as a segmentation model [35]. Since the objects appearing in indoor and outdoor images are distinguished (i.e., indoor: chairs, floor, ceiling, refrigerator, as shown in Figure 8; outdoor: cars, trees, sky, buildings, as shown in Figure 9), the unsupervised learning algorithm can learn the difference between indoor and outdoor images based on the information from the output of semantic segmentation of the image without label. Figure 8 and 9 show segmentation results for images captured indoors and outdoors, respectively.

Figure 8. Sematic segmentation of an image from indoors. Top: original image; Bottom: segmented image, where each colour represents a different category of objects.

The performance of the filtering process has been tested using the images captured in Washington Square Park boundary as a testbed. For the testbed we generated,

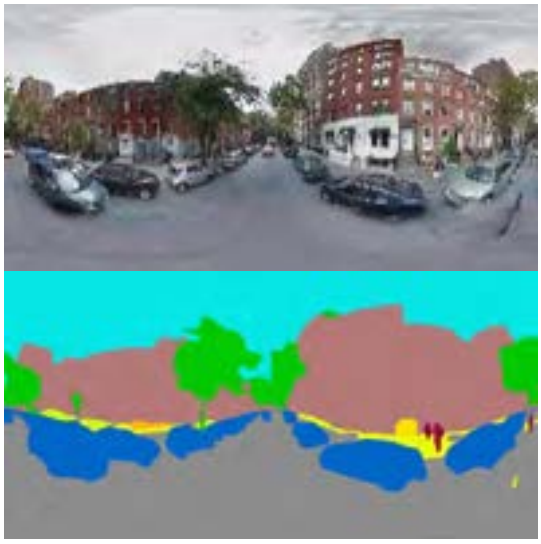

Figure 9. Semantic segmentation of an image from outdoors. Top: Original image; Bottom: Segmented image, where each color represents a different group of objects.

We eliminated 406 images from the original urban street image set from Washington Square Park. The overall accuracy of the model to classify indoor/outdoor images was 99.23% and the only error was on Type I (i.e., outdoor predicted as indoor) as 5% (Table 2).

Table 2. Accuracy of indoor/outdoor classification model.

Actual class / Prediction	**Indoor**	**Outdoor**
Indoor	**386**	20
Outdoor	0	**2,222**
Accuracy	**99.23%**	

3.5 Crowdsourcing to capture citizen ratings

PRS to measure restorativeness impact of a location and 360˚ panorama GSV images were integrated and implemented as part of a questionnaire in a crowdsourcing platform to capture the restorative quality of places in urban settings. The crowdsourcing platform was developed by utilizing JavaScript and SurveyJS for generating the survey forms and integrates to the urban street database generated. The questionnaire composes of six pages, where each page has the same PRS questions (Figure 10). A participant will be given a 360˚ panorama image (same as a GSV in Google Maps) on the first page, and the rest of the pages will show the unidirectional images (along the street: front, right, left, back, up). The reason for collecting responses for each disaggregated image is since the PRS ratings of the 360˚ panorama image includes contributions of each disaggregated image. Additionally, in each unidirectional view of the

location (e.g., front), participants are asked to select areas that were influential in their ratings of that location's restorative capacity as annotations on the image.

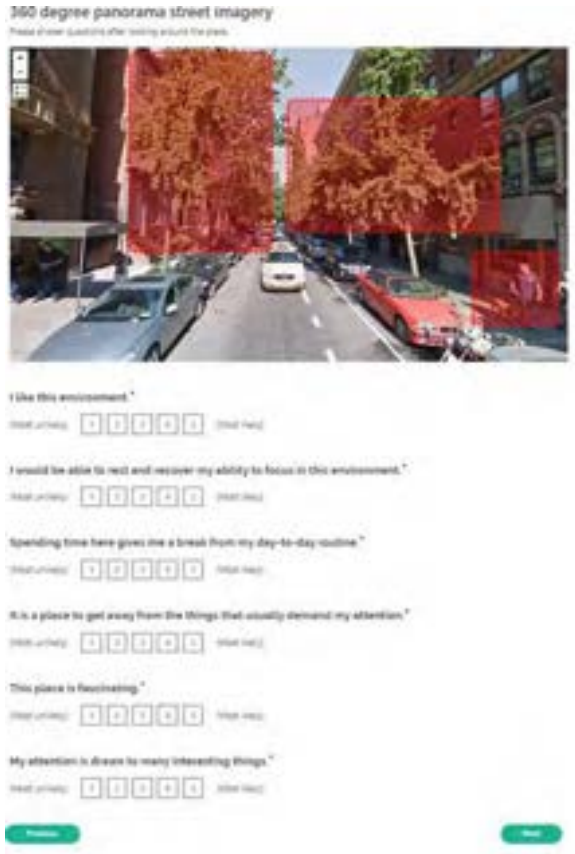

Figure 10. Crowdsourcing part of the platform.

This information is captured and used to update the images stored in the filtered database. Figure 11 shows examples of images stored in the urban image dataset through the utilization of the platform.

Figure 11. Examples of collected 360˚ panorama images

4 Conclusion and Future Work

We developed a data collection platform that integrates GIS, GSV, and a crowdsourcing module to enable capturing of massive and high-resolution urban scale image sets that are rich in visual information. The platform also enables marking urban design elements present in images and relating them to citizen ratings captured through the crowdsourcing component. We implemented this platform and developed measurement tools to capture a sense of restorativeness towards urban street images. The platform uses semantic segmentation and unsupervised learning to classify images to exclude indoor images retrieved from GSV.

The collected data is anticipated to be used to identify the urban street elements affecting perceived restorativeness as a future work. Finally, we expect that this platform will be utilized in other interdisciplinary studies since the database and platform have the potential to be extended to capture other aspects relevant to urban studies possibly expanding with other GIS data such as census data, land use data, and building data as needed.

References

[1] Ergan, S., Shi, Z., & Yu, X. Towards quantifying human experience in the built environment: A crowdsourcing based experiment to identify influential architectural design features. *Journal of Building Engineering*, 20, 51-59, 2018.

[2] Hartig, T., Korpela, K., Evans, G. W., & Gärling, T. A measure of restorative quality in environments. *Scandinavian housing and planning research*, 14(4), 175-194, 1997.

[3] Evans, G. W. The built environment and mental health. *Journal of urban health*, 80(4), 536-555, 2003.

[4] Lindal, P. J., & Hartig, T. Architectural variation, building height, and the restorative quality of urban residential streetscapes. *Journal of Environmental Psychology*, 33, 26-36, 2013.

[5] Stigsdotter, U. K., Corazon, S. S., Sidenius, U., Kristiansen, J., & Grahn, P. It is not all bad for the grey city–A crossover study on physiological and psychological restoration in a forest and an urban environment. *Health & place*, 46, 145-154, 2017.

[6] Srivastava, K. Urbanization and mental health. *Industrial psychiatry journal*, 18(2), 75, 2009.

[7] Kaplan, S., Bardwell, L. V., & Slakter, D. B. The restorative experience as a museum benefit. *Journal of Museum Education*, 18(3), 15-18, 1993.

[8] Staats, H., Kieviet, A., & Hartig, T. Where to recover from attentional fatigue: An expectancy-value analysis of environmental preference. *Journal of environmental psychology*, 23(2), 147-157, 2003.

[9] Fornara, F., & Troffa, R. Restorative experiences and perceived affective qualities in different built and natural urban places. *e*, 1-10, 2009.
[10] Lee, S, Sung, H. & Woo, A. The spatial variations of relationship between built environment and pedestrian volume: Focused on the 2009 Seoul pedestrian flow survey in Seoul, Korea. *Journal of Asian Architecture and Building Engineering*, 16(1): 147-154, 2018.
[11] Salesses, P., Schechtner, K., & Hidalgo, C. A. The collaborative image of the city: mapping the inequality of urban perception. *PloS one*, 8(7), 2013.
[12] Dubey, A., Naik, N., Parikh, D., Raskar, R., & Hidalgo, C. A. Deep learning the city: Quantifying urban perception at a global scale. *In European conference on computer vision*, 196-212. Springer, Cham, 2016 October.
[13] Naik, N., Philipoom, J., Raskar, R., & Hidalgo, C. Streetscore-predicting the perceived safety of one million streetscapes. *In Proceedings of the IEEE Conference on Computer Vision and Pattern Recognition Workshops*, 779-785, 2014.
[14] Naik, N., Raskar, R., & Hidalgo, C. A. Cities are physical too: Using computer vision to measure the quality and impact of urban appearance. *American Economic Review*, 106(5), 128-32, 2016.
[15] Porzi, L., Rota Bulò, S., Lepri, B., & Ricci, E. Predicting and understanding urban perception with convolutional neural networks. *In Proceedings of the 23rd ACM international conference on Multimedia*, 139-148, 2015 October.
[16] Lindal, P. J., & Hartig, T. Effects of urban street vegetation on judgments of restoration likelihood. *Urban forestry & urban greening*, 14(2), 200-209, 2015.
[17] Lin, Y. H., Tsai, C. C., Sullivan, W. C., Chang, P. J., & Chang, C. Y. Does awareness effect the restorative function and perception of street trees?. *Frontiers in psychology*, 5, 906, 2014.
[18] Hernández, B., & Hidalgo, M. C. Effect of urban vegetation on psychological restorativeness. *Psychological reports*, 96 (3), 1025-1028, 2005.
[19] Roe, J., & Aspinall, P. The restorative benefits of walking in urban and rural settings in adults with good and poor mental health. *Health & place*, 17(1), 103-113, 2011.
[20] Gatersleben, B., & Andrews, M. When walking in nature is not restorative—The role of prospect and refuge. *Health & place*, 20, 91-101, 2013.
[21] Herzog, T. R., Maguire, P., & Nebel, M. B. Assessing the restorative components of environments. *Journal of Environmental Psychology*, 23(2), 159-170, 2003.
[22] Wang, X., Rodiek, S., Wu, C., Chen, Y., & Li, Y. Stress recovery and restorative effects of viewing different urban park scenes in Shanghai, China. *Urban forestry & urban greening*, 15, 112-122, 2016.
[23] Han, K. T. Responses to six major terrestrial biomes in terms of scenic beauty, preference, and restorativeness. *Environment and Behavior*, 39(4), 529-556, 2007.
[24] Karmanov, D., & Hamel, R. Assessing the restorative potential of contemporary urban environment (s): Beyond the nature versus urban dichotomy. *Landscape and Urban Planning*, 86(2), 115-125, 2008.
[25] Korpela, K., & Hartig, T. Restorative qualities of favorite places. *Journal of environmental psychology*, 16(3), 221-233, 1996.
[26] Rosenbaum, M. S., Sweeney, J. C., & Windhorst, C. The restorative qualities of an activity-based, third place café for seniors: Restoration, social support, and place attachment at Mather's--More than a café. *Seniors Housing & Care Journal*, 17(1), 2009.
[27] Kaplan, R., & Kaplan, S. *The experience of nature: A psychological perspective*. CUP Archive, 1989.
[28] Masoudinejad, S., & Hartig, T. Window view to the sky as a restorative resource for residents in densely populated cities. *Environment and behavior*, 52(4), 401-436, 2020.
[29] Xue, W., Zhang, L., & Mou, X. Learning without human scores for blind image quality assessment. *In Proceedings of the IEEE Conference on Computer Vision and Pattern Recognition,* 995-1002, 2013 June.
[30] Talebi, H., & Milanfar, P. Nima: Neural image assessment. *IEEE Transactions on Image Processing*, 27(8), 3998-4011, 2018.
[31] Choi, J. H., Kim, J. H., Cheon, M., & Lee, J. S. Deep learning-based image super-resolution considering quantitative and perceptual quality. *Neurocomputing*, 2019.
[32] Liu, L., Silva, E. A., Wu, C., & Wang, H. A machine learning-based method for the large-scale evaluation of the qualities of the urban environment. *Computers, Environment and Urban Systems*, 65, 113-125, 2017.
[33] Hartig, T., & Staats, H. The need for psychological restoration: A determinant of environmental preference. *Journal of Environmental Psychology*, 26, 215–226, 2006.
[34] Herzog, T. R., Black, A. M., Fountaine, K. A., & Knotts, D. J. Reflection and attentional recovery as distinctive benefits of restorative environments. *Journal of environmental psychology*, 17(2), 165-170, 1997.
[35] Sun, K., Zhao, Y., Jiang, B., Cheng, T., Xiao, B., Liu, D., Mu, Y., Wang, X., Liu, W., & Wang, J. High-resolution representations for labeling pixels and regions. *In Proceedings of the IEEE Conference on Computer Vision and Pattern Recognition*, 2019.

Investigation of Changes in Eye-Blink Rate by VR Experiment for Incident Detection at Construction Sites

Shunsuke Hamasaki[a], Mizuki Sugimoto[a], Ryosuke Yajima[a], Atsushi Yamashita[a], Keiji Nagatani[a] and Hajime Asama[a]

[a]School of Engenerring, The University of Tokyo, Japan

hamasaki@robot.t.u-tokyo.ac.jp, m-sugimoto@robot.t.u-tokyo.ac.jp, yajima@robot.t.u-tokyo.ac.jp, yamashita@robot.t.u-tokyo.ac.jp, keiji@i-con.u-tokyo.ac.jp, asama@robot.t.u-tokyo.ac.jp

Abstract -

Productivity and safety are in a trade-off relationship, and the improvement of the safety management system of construction sites is a pressing issue. Therefore, it is important to know and analyze information about incidents at real construction sites. However, it is difficult to gather information about these incidents from workers' self-reports. Therefore, in this research, we take an approach to view the workers as the sensors distributed in construction site and detect these incidents with the reaction of the workers. Biological signals such as heart rate, sweating, and muscle activity are the signals generally used to detect an emotional reaction; however, requiring workers to attach electrodes to their body during work is not suitable. Thus, we focused on blinks since they can be detected without electrodes attached to the skin. This study aims to investigate changes that occur in human blinks during an incident at a construction site. For safety purposes, this study used VR technology to simulate an incident at a construction site. During the simulation, an image of the subject's eyes was taken by the camera installed in the head-mounted display. The results of this study suggest that humans who face an incident have lower blink rates because they gaze at the cause of the incident.

Keywords -

Blink; Construction sites; Head-mounted display; VR

1 Introduction

Focusing on current industrial accidents in Japan, the number of fatalities in the construction industry accounts for more than 30% of fatal accidents in all industries. The number of fatalities due to accidents in construction industries has been on a downward trend; however, the decline has stagnated over the last decade. This shows that ensuring the safety of workers at construction sites is an important and urgent theme. On the other hand, improvement in labor productivity is also an urgent challenge. In many situations, productivity and safety are in a trade-off relationship. For instance, the areas, where workers and construction machines are active, are often separated for safety reasons in construction sites. However, restricting movable ranges too narrowly for safety reasons would adversely affect work efficiency. This means development of technologies for improving safety without lowering efficiency is necessary.

Figure 1. Concept of the final goal

To improve safety without lowering efficiency, identifying when danger occurs at the construction site is of utmost importance. It is also generally said that there are many "incidents" behind the serious accidents that cause fatalities. Thus, the motivation for our study is to collect information on these incidents. At many construction sites, these incidents are currently collected through reports from workers. However, these are uncertain methods because they are subjective on the worker's memory.

There are two possible methods for detecting incidents from construction sites. One is by observing the entire construction site using cameras or LiDAR, and the other is through the measurement of workers. In this study, we focused on the latter method.

A previous study detected incidents through the measurement of workers via heart rate variability. This method is also actively conducted, especially for detecting stress [1], sleepiness and fatigue[2], and the feeling of "traffic near-miss" (surprising)[3, 4] among car driver subjects using heart rate and other indicators. Heart rate is related to a person's mental state. During tension, the sympathetic nervous system is more dominant resulting to higher heart rates. However, it is generally known that the heart rate increases not only during mental tension but also during exercise and work. Furthermore, attaching many electrodes to field workers is not considered as a suitable method. Therefore, we focused on the element of eye blinks.

Blinking is associated with various factors such as prevention of corneal dryness, eye purification, eyelid muscle refreshment, and mental conditions such as anxiety and tension/attention[5]. A study relates blinking to stress in driving and using a personal computer[6, 7]. Blinking is not only measured by electrodes attached to the skin, but a method has also been developed for measuring it from images, which is suitable for this study since it is a non-contact procedure.

The aim of this study is to detect incidents that occur at construction sites. We aim to detect them by measuring blinks of workers when faced with dangerous incidents. Figure 1 shows our concept. As the first step, it is necessary to investigate what kind of changes human blink shows when human experiences a dangerous incident. This study uses VR technology as a safety precaution during the simulation of such incidents.

2 Method

VR technology was used to simulate the incident. Specifically, the subject wore a head-mounted display while viewing the VR image. A small camera was also installed in the head-mounted display to observe the state of blinking during the experiment.

Simple image processing was performed to detect the state of blinking. Since the camera was fixed to the head-mounted display, the position of the eyes can be easily specified manually. First, the brightness and contrast were adjusted for the obtained image, including the eye region. Next, the edges of the upper and lower eyelids were clearly visualized by bilateral smoothing and adaptive binarization. After image processing, the number of blinks was counted visually. Similarly, the high-speed opening and closing of the eyelids that occurred during 100-200 ms was considered to be a "blink". Figure 2 shows an example of this simple image processing.

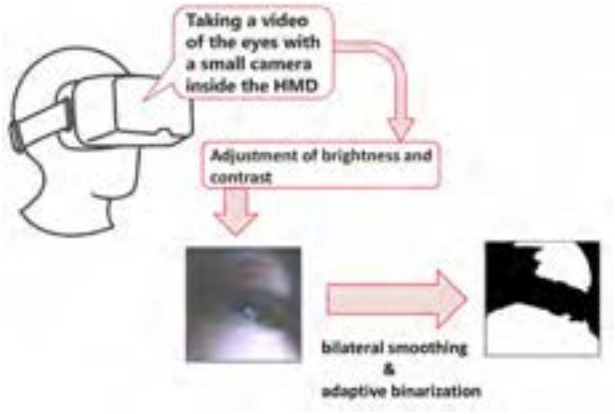

Figure 2. Simple image processing to blink detection

For comparison, we calculated the blink rate, which represent the number of blinks per minute. We compared the blink rate both when the incident is occurring and not occurring.

3 VR Experiment

3.1 Outline of Experiment

In this experiment, participants watched the simulation environment of the construction site through a VR video. During the simulation, an image of the subject's eyes was taken by the camera installed in the head-mounted display. In order to know the scene where the subject perceived danger, a gamepad was used and the subject was instructed to press a button during a dangerous scene.

3.2 VR video

The videos shown to the subject in the VR experiment must reproduce the incident. We focused on incidents related to collision of construction machines and humans, which is a very common accident at construction sites. To prepare videos that are impressive to the subjects, we used reverse playback. We carefully brought the construction machine and the 360-degree camera close to each other and shot a video of the construction machine moving away from the high-speed 360-degree camera.

We prepared the following four types of incident VR videos:

- Two types of incident videos in which the hydraulic excavator goes backwards without noticing the presence of the worker and almost comes into contact with the worker. There are two types of stop positions: (i) long-distance backward and (ii) short-distance backward.
- Two types of incident videos in which the hydraulic excavator turns unaware of the presence of the worker, and the tip of the bucket almost comes into contact with the worker. There are two types of distances to the excavator: (i) Long-distance turning and (ii) Short-distance turning.

For that incident VR video, we compared the blink rate before and after the incident occurs. However, discrepancies may arise when subjects expect that an incident will occur.

Therefore, we prepared four types of VR videos where incidents do not occur.

- One type of non-incident scene where the hydraulic excavator is stationary at a sufficient distance from the worker (stand by).

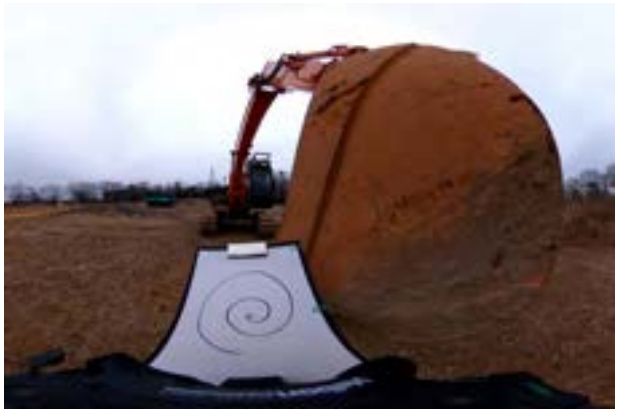

Figure 3. Sample Scene of a VR Video

Figure 4. Two cameras installed inside the head-mounted display

- One type of non-incident scene where the hydraulic excavator turns in the opposite direction from the worker (non-accidental turning).
- One type of non-incident scene where the hydraulic excavator moves forward and away from the worker (forward).
- One type of non-incident scene where the hydraulic excavator crosses at a distance far enough from the worker (crossing).

In addition, we prepared the videos so that the subject could see the paper near the subject's hand. This replicates a scene where the subject is working at the site while looking at the paper, such as progress schedule charts. The subjects were instructed in advance to look at the paper in front of them while paying attention to the construction machines as if they were in a construction site. These eight types of images were about one-minute long each and presented to the subjects in random order. An example scene of the prepared VR videos is shown in Fig. 3.

All these VR videos were shot at the Public Works Research Institute. We used Theta V from Richo and ZAXIS120 from Hitachi Construction Machinery as the 360-degree camera and hydraulic excavator, respectively.

3.3 Experimental Equipment

The head-mounted display used in the experiment was Vive COSMOS from HTC. This included headphones for the audio output of the virtual environment.

The two small cameras installed inside the head-mounted display were Raspberry Pi Camera Module V2. To capture a wider area inside the head-mounted display, the lens of the cameras was replaced with a 195 属 wide-angle lens. Two cameras were controlled by the Raspberry Pi 3B with a frame rate of 30 fps. This frame rate was selected since blinks are generally captured between 150 and 200 ms. To synchronize the VR video presentation and camera control, an integrated experimental environment was constructed using Unity.

The inside of the head-mounted display is shown in Fig. 4 where the two red circles are the cameras. Since the inside of the head-mounted display is sufficiently dark, the camera does not interfere with the subject's VR watching.

3.4 Participants

Three healthy male volunteers took part in the experiment and supplied informed consent. This study was approved by the research ethics committee of the University of Tokyo.

4 Results and Discussion

The results of the VR experiment are shown in Fig. 5. The blue bar stands for the average of subjects' blink rate before the incident occurs, while the red bar stands for the average of subjects' blink rate during the incident. The timing of the incident was determined from the video once the heavy equipment started to move.

Three results excluding short-distance backward revealed that the blink rate during the incident tended to be lower than that in the safe state. First, we must consider the reason why the blink rate did not decrease in Short-distance backward. Interestingly, the blinks that seemed to be voluntary were concentrated in the results of one subject which shows the higher blink rate. This is considered to be the reason for the higher average of blink rate in Short-distance backward. Voluntary blinks caused by some reasons unrelated to VR incidents such as eye itching become noise in this experiment. Hence, increasing the number of subjects and performing statistical processing are recommended to potentially eliminate noise unrelated to VR incidents.

Next, we discuss the decreasing tendency observed in

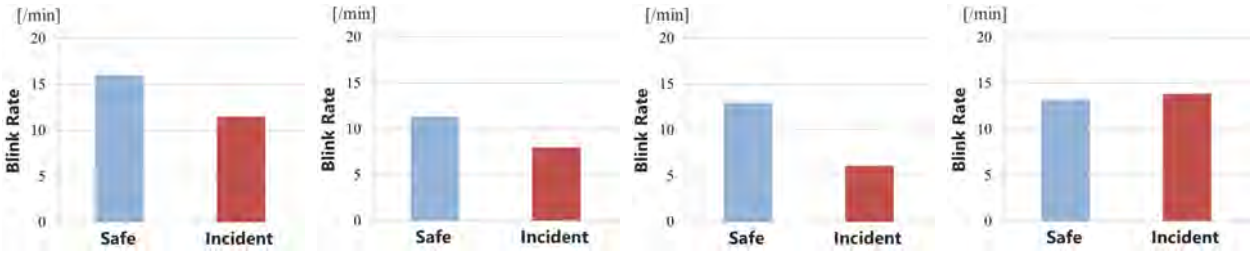

(a) Long-distance turning (b) Short-distance turning (c) Long-distance backward (d) Short-distance backward

Figure 5. Blink rate during incident and safe time

the three graphs. The first possibility is that the blink rate gradually decreases while watching a VR video for one minute. In other words, the blink rate is high until subjects adjust to the brightness of the VR image, and it decreases as they adjusted to it. Therefore, we calculated the blink rate in the "stand-by" condition where subject is farthest from the incident by dividing one minute into 10 seconds each (0-10 s, 10-20 s, 20-30 s, 30-40 s, 40-50 s, and 50-60 s). According to the results of the calculation, the blink rate under the stand-by condition remained almost constant. Therefore, this consideration was excluded. From this, it was considered that the decrease in the blink rate shown in the three graphs is related to the incident.

Another possible cause for the decreasing trend is that the subjects gazed at the cause of the incident (excavator). It is well known that the blink rate of a person who is gazing at something decreases, and this can explain the decreasing trend properly. The purpose of this study was to examine changes that occur in human blinks when humans experience an incident at a construction site. The results of this research suggest that humans during an incident have lower blink rates because they gaze at the cause of the incident.

During application of this approach for incident detection at construction sites, it is necessary to make a distinction between blink rate reduction due to incidents from those due to gaze irrelevant to incidents. In this case, a combination of saccades and facial expressions is considered effective.

5 Conclusion

In this study, we investigated the changes that occur in human blinks when humans experience an incident at a construction site. The VR experiment was performed using a VR video simulating an incident scene. Our results suggest that humans during an incident have lower blink rates because they gaze at the cause of the incident. However, increasing the number of subjects is recommended to further verify the suggestions obtained in this study.

References

[1] J. Healey and R. W. Picard: "SmartCar: detecting driver stress", Proceedings 15th International Conference on Pattern Recognition. ICPR-2000, Vol. 4, pp. 218-221, 2000.

[2] M. Patel, S. K. L. Lal, D. Kacanagh and P. Rossiter: "Applying neural network analysis on heart rate variability data to assess driver fatigue" Expert Systems with Applications, Vol. 38, Issue 6, pp. 7235-7242, 2011.

[3] Masayasu Tanaka, Fumiaki Obayashi, Toshiya Arakawa, Shinji Kondo and Kazuhiro Kozuka: "Detection of Driver's Surprised State Based on Blood Pressure and Consideration about Sensitivity of Surprised State", Proceeding of the 2nd International Conference on Intelligent Systems and Image Processing 2014, pp. 56-60, 2014.

[4] Toshiya Arakawa, Masayasu Tanaka, Fumiaki Obayashi, Shinji Kondo and Kazuhiro Kozuka: "Probability of Driver's State Detection Based on Systolic Blood Pressure", Proceeding of 2015 IEEE International Conference on Mechatronics and Automation (ICMA), pp. 2106-2111, 2015.

[5] J. A. Stern, L. C. Walrath and R. Goldstein: "The Endogenous Eyeblink", Psychophysiol, Vol. 21, No. 1, pp. 22-33, 1984.

[6] R. Mork, H. K. Falkenberg, K. I. Fostervold and H. M. S. Throud: "Visual and psychological stress during computer work in healthy, young females-physiological responses" International Archives of Occupational and Environmental Health, Vol. 91, pp. 811-830, 2018.

[7] C. S. Hsieh and C. C. Tai: "An Improved and Portable Eye-Blink Duration Detection System to Warn of Driver Fatigue" Instrumentation Science and Technology, Vol. 41, Issue 5, pp. 429-444, 2013.

BIM-Aided Scanning Path Planning for Autonomous Surveillance UAVs with LiDAR

Changhao Song [a], Kai Wang [a] and Jack C.P. Cheng [a]

[a]Department of Civil and Environmental Engineering, The Hong Kong University of Science and Technology, Hong Kong SAR
E-mail: csongae@connect.ust.hk, kwangaw@connect.ust.hk, cejcheng@ust.hk

Abstract –

An Unmanned Aerial Vehicle (UAV), equipped with a Light Detection And Ranging (LiDAR) scanner, can collect high-accuracy point cloud data of facilities in cluttered indoor environment. Recent developments in aerial robotics have demonstrated navigation through designated waypoints, yet little has been investigated on the trajectory to complete a full scan of the environment. This study develops an automated approach to integrate scan planning and trajectory generation of a LiDAR-carrying UAV. The proposed approach converts an as-designed Building Information Model (BIM) into an occupancy map, where a set of waypoints are generated with a greedy algorithm. The shortest collision-free path to traverse all the waypoints is computed with the A* algorithm and Genetic Algorithm (GA). After that, the straight-line segments are transformed into a minimum snap trajectory formed of piecewise polynomials. The planned trajectory is validated with both a MATLAB numerical solver and a Hardware-In-the-Loop (HIL) simulation in the Unreal Engine 4.

Keywords –

UAV; LiDAR; BIM; Hardware-in-the-loop; Motion planning

1 Introduction

Terrestrial Laser Scanning (TLS) is commonly used in the Architecture, Engineering, Construction and Facility Management (AEC/FM) industry for site inspection, progress tracking and model generation. Traditional ways of TLS involve selection of scanner locations and registration of multiple point clouds. This process is usually conducted manually by surveyors, which is time-consuming and subject to coverage issues [1]. A wise approach is to integrate a Light Detection And Ranging (LiDAR) scanner with a ground or aerial robot, making it a versatile and efficient tool for Mobile Laser Scanning (MLS). An Unmanned Aerial Vehicle (UAV), owing to its autonomy and flexibility, is a good choice for the platform, especially in cluttered environments where the walkability is poor. In recent years, research in LiDAR-carrying UAVs has demonstrated robustness in Simultaneous Localization And Mapping (SLAM), as well as autonomous navigation in unknown environments [2]. However, most existing methods focus on navigation through a sequence of designated waypoints, while it is difficult to achieve an autonomous flight. The missing segment is planning for the essential waypoints to explore the environment and complete a full scan. This problem can be effectively addressed when prior knowledge of the environment is available, such as the design information of buildings and facilities.

This study is proposed to close the loop of scan planning and UAV path finding, with the aim of facilitating a fully autonomous flight for LiDAR-carrying UAVs. It starts from an as-designed Building Information Model (BIM), which retains the geometric and semantic information of a facility and is compatible with various data formats [3]. The sensor model is constructed based on an existing product [4] to represent the perception range, Field of View (FOV), and Level of Detail (LOD). A greedy algorithm is designed to iteratively maximize the coverage of the planned waypoints, followed by a Traveling Salesman Problem (TSP) to solve for an optimal path that consists of straight-line segments. This serves as a guiding path, which is transformed into a minimum snap trajectory with Quadratic Programming (QP).

The planned trajectory is validated first with a MATLAB numerical solver, before conducting a Hardware-In-the-Loop (HIL) simulation with the Robot Operation System (ROS) [5] and Unreal Engine 4 (UE4) [6]. The HIL simulation builds on our previous work [7] with an extension of automated control input. The intended scene is a cluttered indoor environment filled with Mechanical, Electrical and Plumbing (MEP) components.

This paper is organized as follows: section 2 provides a comprehensive review of the related studies

on LiDAR-carrying UAVs. Section 3 illustrates the proposed methodology on scan planning and trajectory generation, followed by the simulation environments and results in section 4. In closing, the conclusion and future work will be presented in section 5.

2 Literature Review

2.1 Scan Planning

The purpose of scan planning is to ensure coverage of the target objects while minimizing the cost of time or energy. Compared with traditional TLS, a mobile LiDAR scanner automatically enforces overlapping between consecutive scans for registration. However, similar techniques can be applied for visibility analysis and occlusion handling. For example, Argüelles-Fraga et al. [8] developed a method to parametrize the influencing factors of scan accuracy, based on a circular cross-section tunnel. Biswas et al. [1] proposed a BIM-oriented approach to determine optimal scanner locations that maximize the covered surfaces while considering occlusions between components. Wang et al. [9] presented a greedy algorithm to iteratively generate scanner locations around concrete specimens. While the above-mentioned studies aim at planning for fixed scanner locations, an integrated framework was proposed in [10] to generate waypoints of LiDAR-carrying UAVs and connect them with the shortest path. This study provides a clear outline to plan for scanning paths, yet little has been discussed on trajectory generation and flight control for detailed implementation.

2.2 Localization and Mapping

Localization is a critical issue for UAVs in an indoor environment, where GPS signals are not available. It is often combined with mapping to form a SLAM problem. The objective of localization is to obtain the 6-DoF (Degrees of Freedom) state estimation, including 3 positions (x, y, z) and 3 orientations (yaw, pitch, roll). This can be achieved with internal sensor suites, including Inertial Measurement Units (IMUs), LiDAR scanners, monocular and stereo cameras. IMUs are easily accessible, lightweight sensors that measure acceleration and angular velocity at high frequency. They are usually fused with other sensory data to produce odometry. LiDAR-based solutions, such as LOAM [11], outperform vision-based methods in terms of cumulative drifts. However, the demand for payload limits their application in Micro Aerial Vehicles (MAVs). There are also methods that take advantage of both types, such as V-LOAM [12], which is ranking the top on the KITTI odometry benchmark [13].

SLAM problems can be solved with filter-based algorithms, such as the commonly used Extended Kalman Filter (EKF), Unscented Kalman Filter (UKF) [14] that deals with highly nonlinear models and particle filter [15] that can handle non-Gaussian distributions. In recent years, it is a growing trend to switch from filters to graph optimization, integrated with loop closure to reduce cumulative drifts. Such examples include ORB-SLAM [16] and VINS [17].

2.3 Motion Planning

In UAV motion planning, the term “path” and “trajectory” are often used interchangeably. According to [18], a path can be a continuous curve or discrete line segments connecting two positions, while a trajectory refers to a path parametrized with time *t*. In this paper, we use “path” to denote straight-line segments connecting waypoints, and “trajectory” for high-degree polynomials to be followed by a UAV.

The objective of UAV path planning is to determine the shortest collision-free path that connects the take-off position, a sequence of waypoints, and the landing position. Path planning problems can be solved efficiently with sampling-based methods, which generate random samples and connect to a search graph. Examples include Probabilistic Road Map (PRM), Rapid-exploring Random Tree (RRT), and RRT* [19] which converges to optimality as samples increase. Search-based methods, such as Dijkstra’s algorithm and A* algorithm, are also frequently used to find the optimal path from a search graph. A* is an extension of Dijkstra’s algorithm that evaluates each search node with a heuristic function before accessing it. As shown in [20], search algorithms can be combined with sampling methods to enable real-time processing.

To transform a path into a trajectory, the simplest approach is to solve for the polynomial parameters with respect to *t*, by setting waypoint constraints. However, a UAV trajectory is supposed to be safe and feasible, at least twice differentiable to produce velocity and acceleration. Mellinger and Kumar [21] formulated the trajectory as an optimization problem to minimize energy consumption and solved with Quadratic Programming (QP). Richter et al. [19] extended their work to an unconstrained QP and ensured safety by adding intermediate waypoints. A different technique was proposed by Chen et al. [22] that generates flight corridors formed by safe regions, and constrain the trajectory within it.

3 Methodology

This section describes the proposed methods and implementation. An overview of the framework is illustrated in Figure 1. The planning phase consists of four steps: (1) map construction, (2) waypoint

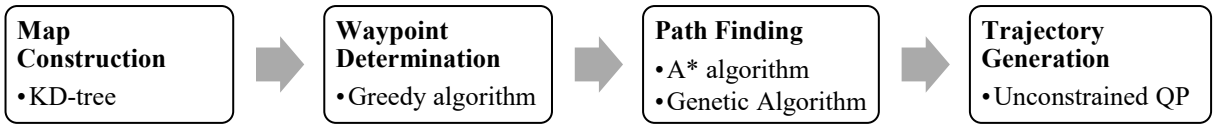

Figure 1. Workflow of the planning phase

determination, (3) path finding and (4) trajectory generation, which are detailed in 3.1-3.4, respectively. The target facility is a water treatment plant located in Tai Po, Hong Kong SAR. It is a cluttered indoor area filled with MEP components, such as pipelines and valves. One set of the pipelines, which is part of the duplicated layouts, is extracted as the test area. The planning phase is implemented in MATLAB, followed by the simulations in section 4.

3.1 Map Construction

The UAV motion planning is performed on an occupancy grid map, where each cell is attached with a label, indicating obstacles or free space. The map is constructed based on an as-designed BIM of the target object, as shown in Figure 2. The model is exported as an OBJ file with an add-in [23] of Revit, and meshed in CloudCompare [24] to produce a reference point cloud, displayed in Figure 3. The reference point cloud consists of evenly distributed points, covering the surface of the objects. It is represented with the KD-tree data structure, which enables fast K-Nearest Neighbor (KNN) search for computing safe distance. An empty voxel grid is created with resolution s, and a KNN search is applied between the grid points and the reference point cloud. Depending on the nearest neighbor distance d, and the safe threshold θ_d, each cell in the voxel grid is labeled as obstacle ($d < 0.5s$), safe region ($d > \theta_d$), or buffer zone. Considering the scale of the facility, s and θ_d are determined as 0.5m and 1m, respectively. This completes the construction of the occupancy grid map.

Figure 2. The as-designed BIM of the target components in Revit

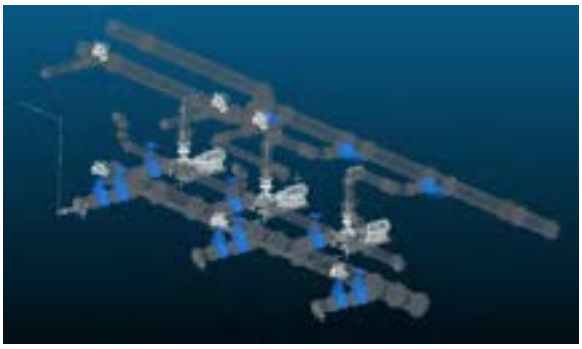

Figure 3. The meshed point cloud in CloudCompare. Surface density = 1000. RGB entries are obtained from the texture.

3.2 Waypoint Determination

The objective of waypoint determination is to bridge the problem of traditional TLS with that of LiDAR-carrying UAVs. A greedy algorithm was proposed in [9] that maximizes the number of covered surfaces at each selection. However, this method is not model-based and works only for concrete specimens. In this study, we adopt a similar idea that tries to achieve the local optimum when generating each waypoint and iterate until the requirements are satisfied. Besides, we describe the coverage based on the LiDAR model and consider occlusion handling.

3.2.1 LiDAR Model

The sensor model in this paper is constructed based on an existing product, RS-LiDAR-32 [4], of which the specifications are listed in Table 1. Geometrically, the sensor coverage can be described as the volume between two conic surfaces, bounded by the sphere of perception range (Figure 4). Given the LOD requirement δ and angular resolution θ, the perception range L should be reduced according to Equation (1):

$$L = \delta/\theta \quad (1)$$

In this case, the smallest element has a diameter of 5cm. Considering the typical measurement error of ±2cm and the worst-case resolution 0.4°, the perception range is determined as 4m to ensure detection of the pipes. As for the FOV, UAVs will not stay horizontal during the flight because the pitch, roll angles change according to the x-y motion. Therefore, the vertical FOV can be reduced to account for the inclination. In this study, the

reduction is taken as 10%.

Table 1. RS-LiDAR-32 specifications

Horizontal FOV	360°
Vertical FOV	–25° ~ +15°
Horizontal Resolution	0.1°/ 0.2°/ 0.4°
Vertical Resolution	≥ 0.33°
Range	200m
Range accuracy (typical)	±2cm

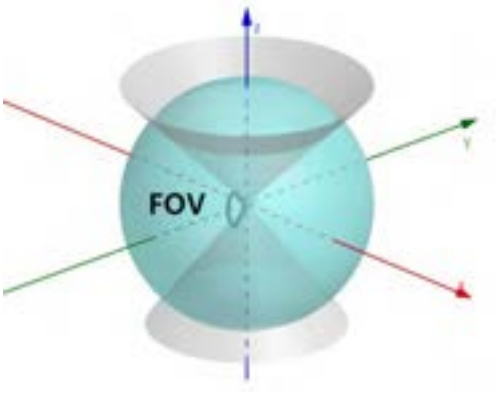

Figure 4. Coverage of the LiDAR model. The donut shape bounded by two conic surfaces (FOV) and a sphere (perception range)

3.2.2 Greedy Algorithm

The greedy algorithm is designed to generate a set of waypoints by maximizing the number of newly covered cells at each iteration, until the stopping criteria are met. The algorithm takes all the occupied cells (i.e. obstacles) as the target to be covered, and the safe regions as potential waypoints. A greedy search is applied to determine the safe cell with maximum coverage and add to the waypoint list. Detailed procedures are illustrated in Algorithm 1. The coverage examination is explained as follows.

For each safe cell, the range search is applied to return all the target cells within the sphere of perception range. This is also achieved with the KD-tree structure. After that, the sphere is reduced according to the FOV with Equation (2), where γ is the angle between the vector **u** from the safe cell to the target cell, and the body frame z-axis **z**. This represents the volume sandwiched between two conic surfaces from the vertical FOV, as illustrated in Figure 4.

$$\gamma = \cos^{-1}\left(\frac{\boldsymbol{u}\cdot\boldsymbol{z}}{\|\boldsymbol{u}\|\|\boldsymbol{z}\|}\right) \in \frac{\pi}{2} - FOV \tag{2}$$

The occlusion handling is realized with similar techniques. The vector **l**, which connects the safe cell with an obstacle cell, is checked against **u**. When Equation (3) and (4) are both satisfied, the ray to the target cell is considered as occluded by the obstacle. These equations indicate the cylindrical volume centered around **u**, with radius 1/2 of the grid size. An illustration is available in Figure 5. The occlusion check is applied for the obstacle cells within the spherical range. When all the obstacles return false, the target cell is considered as within the coverage.

$$h = \frac{\|\boldsymbol{l}\times\boldsymbol{u}\|}{\|\boldsymbol{u}\|} < \frac{1}{2}s \tag{3}$$

$$p = \frac{\|\boldsymbol{l}\cdot\boldsymbol{u}\|}{\|\boldsymbol{u}\|} \in (0, \|\boldsymbol{u}\|) \tag{4}$$

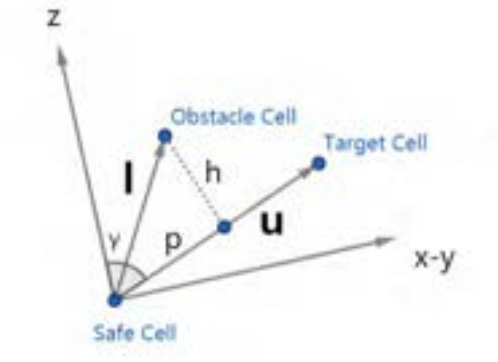

Figure 5. Illustration of Equation (2), (3) and (4). γ is the angle between **u** and **z**, h is the point-to-line distance and p is the projection of **l** on **u**

Algorithm 1 Greedy algorithm

```
i ← 0
waypoints ← empty()
uncovered_map ← obstacles
while i < max_iteration
   max_coverage ← empty()
   max_cell ← null
   for cell in safe_region
      sphere ← range_search(cell, uncovered_map, L)
      cone ← reduce_by_FOV(sphere)
      coverage ← reduce_by_occlusion(cone)
      if coverage > max_coverage
         max_coverage ← coverage
         max_cell ← cell
      end if
   end for
   uncovered_map ← uncovered_map \ max_coverage
   waypoints ← waypoints ∪ max_cell
   i ← i+1
   if max_coverage < quit_threshold
      break
   end if
end while
return waypoints
```

3.3 Path Finding

After a set of waypoints are determined, the problem is to compute an optimal path to traverse all of them. According to [10], this can be formulated as a TSP and solved efficiently with Genetic Algorithm (GA). We adopt similar techniques to solve for a collision-free path that ensures the shortest summed Euclidean distance. However, this path contains straight-line segments and sharp turns that are unsuitable for flight control. Therefore, it serves as the waypoint constraints for trajectory generation.

To form the TSP, a cost matrix is required to represent the pairwise path cost between the nodes. In this problem, it is constructed with the A* algorithm, which is applied on every pair of the waypoints. The occupancy map is treated as a search graph, where the successors of a cell are generated from the 26 adjacent cells. The heuristic function is taken as the Euclidean distance to the goal, which is guaranteed to be admissible.

After the cost matrix is obtained, the GA is implemented as follows:

1. The initial population is generated with random permutation of the waypoints, in bit arrays.
2. The tournament selection is applied to obtain a set of parents based on the fitness function, which is the summed path cost of the ordered sequence.
3. Three operations are applied to produce the next generation: (1) copy: select a member and copy directly to the next generation. (2) crossover: select two parents to produce offspring. Here, the order crossover operator is used, which takes a subset from parent 1, and arrange the remaining bits according to their order in parent 2. (3) mutation: select a member and randomly switch two bits in it.
4. Iterate from step 2, until N generations.

For this study, a population size of 1000 is applied on a set of 10 waypoints. The rate of copy, crossover and mutation are 9%, 90% and 1%, respectively. The optimal solution first appeared after 9 generations.

3.4 Trajectory Generation

The UAV trajectories are usually represented as piecewise polynomials parametrized with time *t*, in three dimensions, respectively. To ensure kinodynamic feasibility, the trajectory is subject to the derivative constraints which come from the specified end derivatives, and the continuity constraints which ensures smoothness. The expression in one dimension is shown in Equation (5) and (6), where the trajectory is an N-degree polynomial with M pieces:

$$f(t) = \begin{cases} f_1(t) = \sum_{i=1}^{N} p_{1,i}(t-T_0)^i & T_0 \le t \le T_1 \\ f_2(t) = \sum_{i=1}^{N} p_{2,i}(t-T_1)^i & T_1 \le t \le T_2 \\ \vdots & \\ f_M(t) = \sum_{i=1}^{N} p_{M,i}(t-T_{M-1})^i & T_{M-1} \le t \le T_M \end{cases} \quad (5)$$

$$\text{s.t.} \quad \begin{cases} f_j^{(k)}(T_j) = x_{T,j}^{(k)} \\ f_j^{(k)}(T_j) = f_{j+1}^{(k)}(T_j) \end{cases} \quad (6)$$

To solve for the polynomial parameters $p_{j,i}$, we refer to the method in [21], which formulates the trajectory as an optimization problem: the objective is to minimize the fourth order derivative (i.e. snap) of the trajectory, subject to the continuity constraints and derivative constraints. Equation (7) and (8) illustrate the problem definition in vector form, where **p** is the collection of polynomial parameters and **Q** is the Hessian matrix, $\mathbf{A_{eq}}$ and $\mathbf{d_{eq}}$ are the collection of constraints. The minimum snap trajectory is a seventh degree (N=7) piecewise polynomial, which optimizes the least energy consumption. The variable **p** can be solved with QP.

$$\begin{aligned} \text{min.} \quad & J = \int_o^T \left(f^{(4)}(x)\right)^2 dx \\ & = \begin{bmatrix} \boldsymbol{p_1} \\ \vdots \\ \boldsymbol{p_M} \end{bmatrix} \begin{bmatrix} \boldsymbol{Q_1}(T_1) & & \\ & \ddots & \\ & & \boldsymbol{Q_M}(T_M) \end{bmatrix} \begin{bmatrix} \boldsymbol{p_1} \\ \vdots \\ \boldsymbol{p_M} \end{bmatrix}^T \\ & = \boldsymbol{p^T Q p} \end{aligned} \quad (7)$$

$$\text{s.t.} \quad \boldsymbol{A_{eq}} \begin{bmatrix} \boldsymbol{p_1} \\ \vdots \\ \boldsymbol{p_M} \end{bmatrix} = \boldsymbol{d_{eq}} \quad (8)$$

However, direct optimization of polynomial parameters is numerically unstable, because the values are usually very small as time *t* increases. Therefore, we adopt the method in [19] to reformulate the problem as an unconstrained QP. A mapping matrix **M** is constructed to transform the variable from polynomial parameters **p** into the end derivatives **d**. Additionally, a binary selection matrix **C** containing 1s and 0s is constructed to separate the fixed derivatives $\mathbf{d_F}$ and free derivatives $\mathbf{d_P}$. The derivative constraints and continuity constraints are automatically enforced by the selection matrix. In this way, the problem is transformed into an unconstrained QP. The composition matrix in the middle can be further split according to the size of $\mathbf{d_F}$ and $\mathbf{d_P}$, as shown in Equation (9) and the close-form solution is obtained with Equation (10). The optimized end derivatives are transformed back to polynomial parameters to compute the trajectory.

$$J = \begin{bmatrix} \boldsymbol{d_1} \\ \vdots \\ \boldsymbol{d_M} \end{bmatrix} \boldsymbol{M^{-T} Q M^{-1}} \begin{bmatrix} \boldsymbol{d_1} \\ \vdots \\ \boldsymbol{d_M} \end{bmatrix}^T = \begin{bmatrix} \boldsymbol{d_F} \\ \boldsymbol{d_P} \end{bmatrix}^T \boldsymbol{C M^{-T} Q M^{-1} C^T} \begin{bmatrix} \boldsymbol{d_F} \\ \boldsymbol{d_P} \end{bmatrix} = \begin{bmatrix} \boldsymbol{d_F} \\ \boldsymbol{d_P} \end{bmatrix}^T \begin{bmatrix} \boldsymbol{R_{FF}} & \boldsymbol{R_{FP}} \\ \boldsymbol{R_{PF}} & \boldsymbol{R_{PP}} \end{bmatrix} \begin{bmatrix} \boldsymbol{d_F} \\ \boldsymbol{d_P} \end{bmatrix} \quad (9)$$

$$\boldsymbol{d_P^*} = -\boldsymbol{R_{PP}^{-1} R_{FP}^T d_F} \quad (10)$$

To construct the Hessian matrix **Q** and mapping matrix **M**, the time duration T_i for each segment is required. In this study, the time is allocated according to the Euclidean path cost, based on the predefined average velocity at 1m/s. Another critical issue in trajectory generation is that the piecewise polynomial may deviate from the collision-free guiding path. To reinforce safety, collision check is performed along the trajectory with KNN search. The positions at each timestamp are checked against the nearest obstacle cell. The midpoint of guiding path segments will be added as an intermediate waypoint if collision is detected.

4 Validation

This section describes two separate experiments to validate the planned trajectory. The first one is performed in MATLAB with the numerical solver ode45. A simple PID controller is implemented to realize the motion control. The second experiment is an HIL simulation in the UE4 environment, where a physical flight controller is employed to communicate with the simulator. Details are explained in 4.1 and 4.2, respectively.

4.1 MATLAB simulation

The UAV trajectories are executed with a flight controller, which takes in the desired states and true states of the UAV at each moment to produce the desired motor output. The planned trajectory is published in a stream of state vectors $[x, y, z, v_x, v_y, v_z, \psi, \theta, \varphi, \omega_x, \omega_y, \omega_z]^T \in R^{12}$, with a fixed frequency. It was demonstrated in [21] that the full state vector can be reduced to the 3D position and yaw angle $[x, y, z, \psi]^T$, due to the differential flatness property. For this study, only the 3D position is enforced while the yaw planning is left as future work. A PID controller is constructed following the nested loops in [25], where the position control lies in the outer loop and influence the attitude control in the inner loop. The governing equation is shown in Equation (11), where **e**(t) is the error between the desired state and true state. The control output **u**(t) is

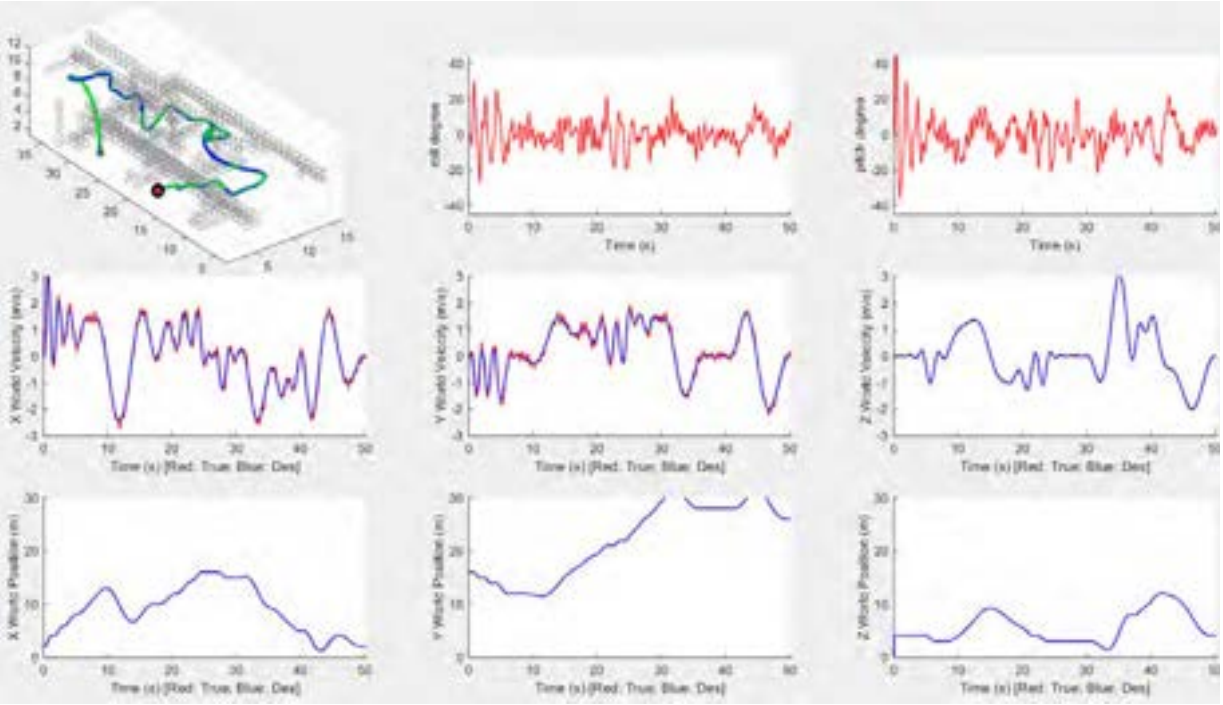

Figure 6. Simulation results in MATLAB. In subplot (1), the planned trajectory and the ground truth trajectory are plotted with green and blue curves, respectively. The grey cells indicate the obstacles. In (2)-(9), the desired states and the true states are plotted with blue and red curves, respectively. For the roll and pitch angle, the desired values are not commanded, but determined by the horizontal motion, instead.

related to the Force and Moment with the Newton-Euler equations, as shown in Equation (12) and (13). The weight *mg* and moment of inertia matrix **I** are determined according to the UAV model in [26]. The gain parameters K_p and K_d are tuned manually, while the Integral term is omitted for simplicity. During the simulation, the desired states are the input from the trajectory generator, while the true state is computed with the ode45 solver, based on rigid body dynamics.

$$\boldsymbol{u}(t) = \ddot{\boldsymbol{x}}^{\boldsymbol{des}}(t) + K_d\dot{\boldsymbol{e}}(t) + K_p\boldsymbol{e}(t) \tag{11}$$

$$m\ddot{\boldsymbol{p}} = \begin{bmatrix} 0 \\ 0 \\ -mg \end{bmatrix} + \boldsymbol{R} \cdot \begin{bmatrix} 0 \\ 0 \\ \Sigma F_i \end{bmatrix} \tag{12}$$

$$\boldsymbol{I} \cdot \begin{bmatrix} \ddot{\Phi} \\ \ddot{\theta} \\ \ddot{\psi} \end{bmatrix} + \begin{bmatrix} \omega_x \\ \omega_y \\ \omega_z \end{bmatrix} \times \boldsymbol{I} \cdot \begin{bmatrix} \omega_x \\ \omega_y \\ \omega_z \end{bmatrix} = \begin{bmatrix} \Sigma M_x \\ \Sigma M_y \\ \Sigma M_z \end{bmatrix} \tag{13}$$

The simulation result is plotted in Figure 6, where subplot (1) is a 3D view of the trajectory and (2)-(9) are the UAV states against time.

4.2 HIL simulation

The UE4 is an advanced game engine that provides highly realistic virtual environment. Besides, it enables a wide range of robotics applications, such as navigation, computer vision, deep learning, etc. This is the main reason why it is selected as the platform for experiment. The HIL simulation is carried out based on our previous work [7], in which a software pipeline was developed to integrate UE4 with ROS. The former provides the physics engine and high-quality sensor data, while the latter contains abundant packages for robotics perception and odometry. The communication between them is realized with the ROS master.

In this simulation, the as-designed BIM of the target facility is exported in FBX format and then imported into UE4 to create a scene, as shown in Figure 7. The planned trajectory is coded into a script as a stream of messages with timestamp, position and orientation. The script is passed into the UE4 server through an API layer, AirSim [27]. The trajectory is executed with a hardware flight controller, Pixhawk 4 [28], which subscribes desired states and ground truth states from the UE4 environment and publish motor outputs to the UAV model. A screenshot during the simulation is displayed in Figure 8.

5 Conclusion and Future Work

This paper presents an integrated framework to bridge the robotics problem of UAV navigation with the civil engineering application of as-built point cloud generation. The framework comprises BIM-aided map construction, waypoint-based scan planning, static path planning, and dynamic trajectory generation. These techniques are verified with a numerical simulation and a highly realistic HIL simulation. The results demonstrated that the motion planning algorithms can deal with complex environments with MEP components.

The proposed framework can be improved in several aspects. First, the yaw planning for trajectory can be completed, which is critical for vision-based odometry and navigation. Secondly, the quality of scanning is not evaluated. This can be addressed by setting a LiDAR sensor model into the UE4 environment to perform a virtual scan. Furthermore, it is promising if the framework can run in parallel with ROS to achieve real-time application. This is possible with the MATLAB ROS Bridge and it is expected to conduct a real-world experiment in future.

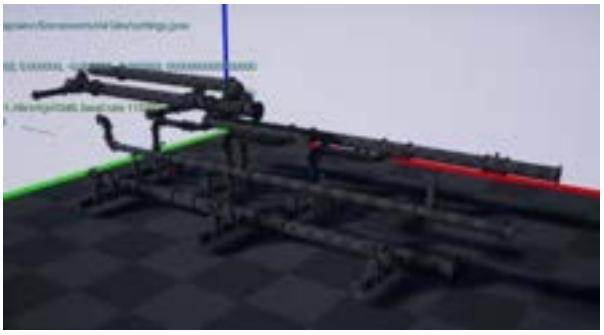

Figure 7. The scene constructed from the FBX file in UE4.

Figure 8. Trajectory following with the Pixhawk 4 flight controller.

References

[1] Biswas H. K., Bosché F., and Sun M. Planning for scanning using building information models: A novel approach with occlusion handling. In *Symposium on Automation and Robotics in Construction and Mining (ISARC 2015),* 2015.

[2] Gao F. et al. Flying on point clouds: Online trajectory generation and autonomous navigation for quadrotors in cluttered environments. *Journal of Field Robotics,* vol. 36, *(4),* pp. 710-733, 2019.
[3] Shirowzhan S. et al. BIM compatibility and its differentiation with interoperability challenges as an innovation factor. *Autom. Constr.,* vol. 112, pp. 103086, 2020.
[4] RS-LiDAR-32. Online: https://www.robosense.ai/rslidar/rs-lidar-32. Accessed: 12/06/2020
[5] Quigley M. et al. ROS: An open-source robot operating system. In *ICRA Workshop on Open Source Software,* 2009.
[6] Unreal Engine 4. Online: https://www.unrealengine.com/en-US/?lang=en-US. Accessed: 12/06/2020
[7] Wang K. and Cheng J. C. Integrating hardware-in-the-loop simulation and BIM for planning UAV-based as-built MEP inspection with deep learning techniques. In *Proceedings of the 36th International Symposium on Automation and Robotics in Construction,* 2019.
[8] Argüelles-Fraga R. et al. Measurement planning for circular cross-section tunnels using terrestrial laser scanning. *Autom. Constr.,* vol. 31, pp. 1-9, 2013.
[9] Wang Q., Sohn H., and Cheng J. C. Automatic as-built BIM creation of precast concrete bridge deck panels using laser scan data. *J. Comput. Civ. Eng.,* vol. 32, *(3),* pp. 04018011, 2018.
[10] Bolourian N. and Hammad A. LiDAR-equipped UAV path planning considering potential locations of defects for bridge inspection. *Autom. Constr.,* vol. 117, pp. 103250, 2020.
[11] Zhang J. and Singh S. LOAM: Lidar odometry and mapping in real-time. In *Robotics: Science and Systems,* 2014.
[12] Zhang J. and Singh S. Visual-lidar odometry and mapping: Low-drift, robust, and fast. In *2015 IEEE International Conference on Robotics and Automation (ICRA),* 2015.
[13] Geiger A. et al. Vision meets robotics: The kitti dataset. *The International Journal of Robotics Research,* vol. 32, *(11),* pp. 1231-1237, 2013.
[14] Jung J. et al. Development of kinematic 3D laser scanning system for indoor mapping and as-built BIM using constrained SLAM. *Sensors,* vol. 15, *(10),* pp. 26430-26456, 2015.
[15] Özaslan T. et al. Inspection of penstocks and featureless tunnel-like environments using micro UAVs. In *Field and Service Robotics,* 2015.
[16] Mur-Artal R., Montiel J. M. M., and Tardos J. D. ORB-SLAM: a versatile and accurate monocular SLAM system. *IEEE Transactions on Robotics*, vol. 31, (5), pp. 1147-1163, 2015.
[17] Qin T., Li P., and Shen S. Vins-mono: A robust and versatile monocular visual-inertial state estimator. *IEEE Transactions on Robotics,* vol. 34, *(4),* pp. 1004-1020, 2018.
[18] Yang L. et al. A literature review of UAV 3D path planning. In Proceeding of the 11th World Congress on Intelligent Control and Automation, 2014.
[19] Richter C., Bry A., and Roy N. Polynomial trajectory planning for aggressive quadrotor flight in dense indoor environments. In *Robotics Research* (pp. 649-666), Springer, Cham, 2016.
[20] Gao F. and Shen S. Online quadrotor trajectory generation and autonomous navigation on point clouds. Presented at the 2016 IEEE International Symposium on Safety, Security, and Rescue Robotics (SSRR), 2016, pp. 139–146.
[21] Mellinger D. and Kumar V. Minimum snap trajectory generation and control for quadrotors. Presented at the 2011 IEEE International Conference on Robotics and Automation, 2011, pp. 2520–2525.
[22] Chen J., Liu T., and Shen S. Online generation of collision-free trajectories for quadrotor flight in unknown cluttered environments. Presented at the 2016 IEEE International Conference on Robotics and Automation (ICRA), 2016, pp. 1476–1483.
[23] Revit OBJ converter. Online: https://visionworkplace.com/products/obj-converter-for-autodesk-revit. Accessed: 12/06/2020.
[24] CloudCompare. Online: https://www.danielgm.net/cc/. Accessed: 12/06/2020.
[25] Michael N. et al. The grasp multiple micro-uav testbed. *IEEE Robotics & Automation Magazine,* vol. 17, *(3),* pp. 56-65, 2010.
[26] Mellinger D., Michael N., and Kumar V. Trajectory generation and control for precise aggressive maneuvers with quadrotors. *The International Journal of Robotics Research,* vol. 31, *(5),* pp. 664-674, 2012.
[27] Shah S. et al. Airsim: High-fidelity visual and physical simulation for autonomous vehicles. In *Field and Service Robotics,* 2018.
[28] Meier L. et al. PIXHAWK: A micro aerial vehicle design for autonomous flight using onboard computer vision. *Autonomous Robots,* vol. 33, *(1-2),* pp. 21-39, 2012.

Research on a Method to Consider Inspection and Processing for Atypical Wood Members Using 3D Laser Scanning

Shunsuke Someya [a], Yasushi Ikeda [b], Kensuke Hotta [c], Seigo Tanaka [d], Mizuki Hayashi [e], Mitsuhiro Jokaku [e] and Taito Takahashi [a]

[a]Research & Development Institute, Head Office, Takenaka Corporation, Japan
[b]Ph.D, Keio University SFC, Japan
[c]Keio University SFC, Japan
[d]1ft-Seabass, Japan
[e]Construction Project Office, Nagoya Branch Office, Takenaka Corporation, Japan
Email: someya.shunsuke@takenaka.co.jp, yasushi@sfc.keio.ac.jp, hottakensuke@keio.jp, seigo@1ft-seabass.jp, hayashi.mizuki@takenaka.co.jp, joukaku.mitsuhiro@takenaka.co.jp, takahashi.taito@takenaka.co.jp

Abstract –

The purpose of this research is to use digital technology to streamline operations and improve construction when using non-uniform building materials with discrete and differing forms, such as those used in traditional wooden buildings. Taking irregular timber procurement as a model use case, we formulated a method of utilizing 3D scanning technology to facilitate inspection and processing considerations.

Keywords –

Traditional building; Wood; BIM; 3D laser scanner; Point cloud

1 Introduction

Recent years have seen the wider construction industry in Japan look to the use of cutting-edge technologies in construction work as a possible means of increasing productivity. For example, the Ministry of Land, Infrastructure, Transport and Tourism has begun a set of initiatives, called "i-Construction," to promote the use of digital technologies. At the same time, given the growing problem of the declining number of construction workers with advanced skills, new construction methods are needed to mitigate the loss of human resources and these advanced skills. Some examples exist of research into construction management or processing building materials method utilizing digital technology. One is a research project by Kano et al., who are exploring a method to automatically ascertain the progress of PCa projects using 3D laser scanners during the construction stages [1]. In terms of research into the machining of building materials, Takabayashi et al. have reported on a method of generating machining paths for regular, uniform timber using robotic arms [2]. One of the key points proposed in these research projects is a technology to measure the shape of the PCa member and the lumber processed accurately. The authors have focused herein on digitizing material geometry accurately as one technical issue commonly found in the above research and other initiatives to refine craftsmanship and manufacturing through digital technology. Construction is the process of assembling building materials to match design information. By digitizing the shape of the building material accurately throughout each phase of the production process, this technique should allow for using complex simulations and automated control of machinery during subsequent construction steps.

The focus in this research is on renovation projects involving traditional wooden buildings as the most suitable use case. This is because the parts used are not mechanically machined such as those seen in industrial products, but those in which the processing steps must accommodate the unique geometry and form of each tree. Shrines, temples, castles and other ancient structures were built in Japan long ago, with many such traditional buildings remaining in existence and of high value today. While wooden buildings today generally use machined timber such as laminated wood and CLT, traditional Japanese wooden buildings tend to, for instance, employ a single timber log for columns or beams and exceptional skills are required throughout the entire production process, from procurement to processing and assembly.

Accordingly, we chose to treat the procurement phase, which marks the start of the manufacturing process, as a case study and propose a method to assist inspection work. This method employs 3D scanning technology to

digitize the timber geometry during the inspection phase. We also propose a method of converting the data into a lightweight and general-purpose format, reflecting the assumption that the shape data would be used when considering how to process the timber in subsequent work phases.

2 Current Workflow

We begin by enumerating some of the aspects of the procurement and processing process in traditional Japanese wooden building conservation and renovation projects.

In terms of the procurement process, the timber supply chain is very unique and since the timber used in traditional wooden structures is generally a single piece from a single tree, the materials involved tend to be large. Many of these pieces of timber are over 5m long and weigh upwards of 1 ton. Construction companies lack the commercial flow and know-how to purchase large pieces of timber within a short time, making it difficult for construction companies to purchase materials directly from timber owners. Consequently, construction companies must themselves purchase from specialist wood suppliers. The construction company communicates the design specifications to the suppliers and the suppliers collect pieces of timber that meet these specifications on the contractor's behalf. Timber obtained from the supplier in line with the above is generally rough, with only the bark removed and processed into square or round shapes. Since the cross-sectional dimension and curvature of this timber is unique in each case, construction companies inspect the merchandise at the warehouse to determine its fitness for a specific portion of the architectural design, ultimately purchasing only those pieces that pass this check. The current inspection covers points like shape, such as length and cross-sectional dimensions; aesthetics, such as color and scratches; and physical properties, such as Young's modulus. For shape inspections, 1:1 scale printed drawings are laid under the timber to check the size and the details are checked via tape measure, while aesthetic inspections are conducted visually by the design supervisor. In many cases, special measuring instruments are used to ascertain the physical properties. In addition, the inspector also relies on visual particularities, such as the shape, knots, barks caught inside and rots to infer the internal condition of the wood and determine whether it is fit for use. Given the considerably advanced skills and timber processing experience this entails, construction companies sometimes assign carpenters to handle inspections. The construction company asks the carpenter to cut the timber down to match the desired dimensions and cut the surface to ensure a consistent cross-sectional shape. Any pieces that are intended to connect to other parts must be further processed in detail.

The process by which the shape of the timber changes is shown in Figure 1.

3 Creation of Inspection Assistance and Data Conversion Methods

Two methods, to facilitate inspection work and convert the data into a lightweight and general-purpose format are explained in detail.

3.1 Inspection Assistance Methods

The timber shape is digitized accurately in advance and automatically screened by the program, so the inspection itself takes place minimizing the number of people involved and with maximum accuracy. The technical requirements for implementing our proposed method are as follows:

3.1.1 Digitization of Timber Shapes

First, a 3D laser scanner is used to digitize the timber geometry accurately as shown in Figure 2. This is because it is a machine that can measure the shape of objects very precisely, rendering them as a collection of points with three-dimensional coordinates. Many commercially available products of this type can measure target objects up to ten meters away with error tolerance to within 2 to 3 mm, making it sufficiently accurate to facilitate timber inspection and processing. The data obtained is a collection of point data described by seven

Trees in the forest | Timbers after felling | Timber at inspection | Timber after processing

Figure 1. Process by which the shape of a timber changes

text strings: three-dimensional coordinates (x, y, z), laser reflection (intensity) and color information (R, G, B). This is generally referred to as a point cloud. Next, two data processing schemes are implemented to generalize the point cloud data and perform registration such that it is converted into a general-purpose format for editing by common programs using most commercially available software.

3.1.2 Automation Program for Inspections

Next, we developed a new program used to automate the inspection of timber geometry. To replace conventional inspection work with programmatic processing, the main functions required are: (1) automatic generation of the required dimensions, (2) superimposition (overlaying) of design blueprints. We developed a program to meet the following requirements to utilize timber point cloud data for the purposes described above:

a) Ability to read point cloud data

b) Point cloud data display function

Most pass/fail criteria are expressed numerically, such as dimensions and the position of the dimensions to be measured is determined in a horizontal or vertical projection plane relative to the timber. We opted to display the point cloud data in three two-dimensional perspectives, rather than three-dimensional views, namely: plan, elevation and cross-section.

c) Automatic sorting and alignment of point cloud data

The timber orientation is crucial. Cross-sectional cut surfaces, which always includes two sections, are referred to as the "koguchi," or cut end, with the root side referred to as the "motokuchi," and the other, the "suekuchi." A lot of pine timber is bent as a characteristic of the material and when using wood, the curvature generally faces upward, as a building material to the extent possible the area closest to the "motokuchi". Accordingly, the location of the "motokuchi," "suekuchi," and bend must be determined, even when measuring the dimensions. The program we developed is designed to automatically arrange the timber rendering in the above desired orientation when importing the cloud point data. This process involves first generating a 3D bounding box for the cloud point data and arranging it on the plan view such that the long side of this rectangular solid is horizontal. Next, we compare the two point cloud sections closest to the two faces on the short side and determine that the larger and smaller areas correspond to the "motokuchi" and "suekuchi" respectively, arranging them such that the "motokuchi" is on the right side in the plan view. Finally, all point clouds in the bounding box are compared to the point clouds for the cut ends and the point clouds in the bounding box are positioned so as to appear higher up in the plan view.

d) Automatic display of dimension lines and figures

We referred to the inspection sheets used in actual inspections and discussions with designers, contractors and shrine carpenters, to indicate which dimensions should be used to determine a pass or fail. We used this insight to develop the program such that it automatically generates the exterior dimensions and those implicated in downstream processing, to facilitate timber inspection. The processing dimensions indicate where the timber (in its raw state during inspection) should be cut to obtain the desired piece. This cutting process is referred to as "kidori." The bend is a key criterion during assembly and calculated based on the shape obtained after the "kidori" process. When viewing the external timber lines in a plan view, the two long sides form the arcs of a curved line and represent the "mukuri," calculated as the largest vertical distance from the straight line obtained by connecting both ends. The names and dimensions of each part of the timber are shown in Figure 3.

・Outer dimensions of the timber: width and height of both cut ends, length of timber

・Timber dimensions: length from the "motokuchi" and "suekuchi" sides to the location of the "kidori," length of timber after "kidori" cutting (design length), camber value after "kidori," and the width and height of both cut ends after "kidori"

e) Overlaid display of blueprint data

For items for which determining the dimensional values is difficult, the system superimposes the cloud point data with cross-sectional lines from the blueprint when displayed in plan view and these cross-sectional lines indicate the sections on which other cut materials

Figure 2. 3D laser scanner

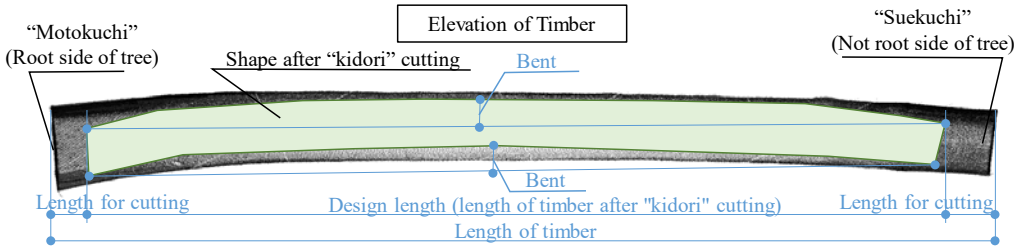

Figure 3. Names and dimensions of each part in timber

intersect. Given that timber does not comprise perfectly straight lines or curves, it must be checked prior to assembly to verify whether it will properly intersect and connect with other pieces.

3.2 Data Compaction and Generalization Method for 3D Scan Data

We propose a method of converting point cloud data into a lightweight, general-purpose format such that the geometry data of the timber obtained in Section 3.1 can continue to be used in subsequent processes.

We focused on using this solution in the context of considering how to process wood after it is procured. This process presumes the use of the tool to simulate, using a CAD program, how timber would be processed and machined for subsequent use. The cloud point data is converted into a more lightweight polygon mesh.

To that end, we employed both the following algorithms to convert the data to meet those requirements:

3.2.1 Culling Point Clouds Using Octrees

When generating polygon mesh data from point cloud data, we first mechanically generate triangles using the point clouds as vertices. Therefore, creating lightweight polygon mesh data requires culling points to a more even approximation. However, point cloud data is a collection of points measured by laser radially around a 3D laser scanner, which means even the same piece of timber can exhibit considerable variation in point density depending on the scan location. Accordingly, an even thinning method using octrees is used to simplify the non-uniform point cloud data. Octrees are a representational method of dividing a target space evenly on a grid; we believed that leaving single point data within the cells of a subdivided space would help us obtain evenly culled cloud point data as shown in Figure 4.

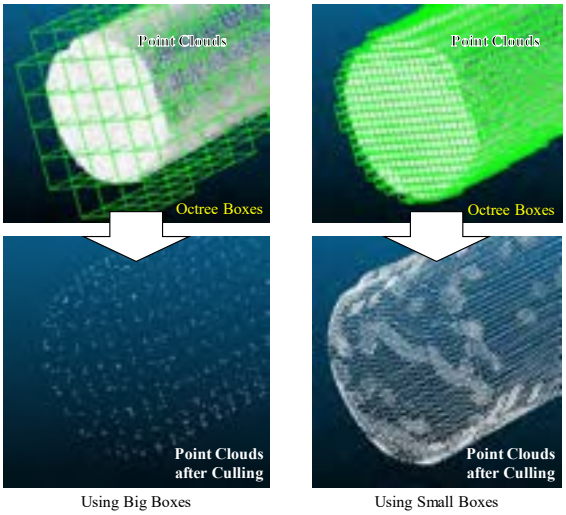

Figure 4. Examples of culling points by octrees

3.2.2 Smoothing Using Poisson's Equation

When creating a polygon mesh using the culled point cloud, one issue is noise within the point clouds, which is then calculated as part of the vertices, resulting in irregularities that differ from the actual shape. The laser scanning process functions by estimating the distance from time and phase differences caused by laser reflection, which implies that some noise is inevitable due to airborne dust or dirt on the equipment. Therefore, we allowed for the generation of polygon mesh containing some noise, then minimized its impact by smoothing the mesh. Specifically, we adopted a smoothing algorithm using Poisson's equation, as announced by Kazhdan et al. [3]. This is the process of calculating the average plane of the neighboring faces, preventing sharp irregularities and smoothing the entire surface as shown in Figure 5. We believe that this step allows for generating a polygon mesh that is minimally affected by mechanical noise. The resulting polygon mesh is archived in STL format. We opted to use STL because it is a universal intermediate file format commonly used in 3D CAD software in architectural systems and simulation and analysis software in other fields.

In this research, we tested the effectiveness of these methods in actual projects, the outcomes of which re detailed in the next section.

4 Application to the Project

4.1 Project Overview

An actual project to restore a traditional wooden building is adopted in this paper as its theme.

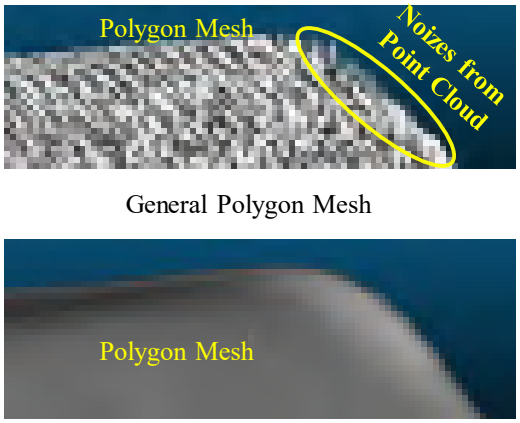

Figure 5. Smoothing polygon mesh

About 2,323 trees covering a volume of about 2,000 ㎥ were used as the materials for the mainframes; mainly Hinoki cypress and pine and square and round pieces of timber depending on the part. These were then processed into materials by carving out one column or beam from each tree.

The following is an explanation of the inspection tasks to serve as the model case for inspection. First, the timber to be inspected was laid on the ground in the direction for which its warp is parallel. The exposed parts in this state, which specifically constitutes both ends of the cut section comprising roughly 3/4 of the sides of the timber, are subject to inspection. In this instance, a blueprint of the designed cross-section with the original dimensions was laid between the timber and ground as necessary to compare the shapes. This process was carried out for all the timber and to move it and turn it over smoothly, the timber to be inspected was laid out on the ground by the day before the inspection, whereupon the timber that had already been inspected was moved and stacked in the stockyard in order. The new methods were then applied as part of this workflow.

4.2 Ways of Applying the Proposed Methods

4.2.1 Objectives

The first objective involved automatically executing inspections related to shape beforehand. The second objective involved archiving the point cloud data obtained as light and general data to be utilized in post-inspection processes.

4.2.2 Targets of Application

The targets were about 500 poles of round pine timber to be used as material for the main frame. This is because they had the most complex and unique shapes among the materials to be used, presenting the most significant potential impact of consequently applying the proposed methods.

4.2.3 Application Period and Location

The application took place between January 2019 and March 2020 in Iwate Prefecture, Japan.

4.2.4 Equipment Used

・3D laser scanner (FARO Focus 3D S120)
・Point cloud editing software (FARO SCENE)
・Developed inspection assistance program
・A software package to execute algorithms to cull and generalize point clouds: Cloud Compare (free software)

4.2.5 Ways of Application to the Project

1. Inspection Assistance Methods

Each timber block had its shape 3D scanned twice. The first was when the timber was laid out the day before the inspection and the second was when the timber was turned over after the inspection and moved to the stock-yard. To avoid missing any measurements, each timber block was scanned from two to four positions and the state of the timber pieces the day before the inspection is shown in Figure 6. There were two reasons for scanning the timber twice. The first was to scan the surface as a minimum requirement for automatic inspection prior to human inspection. Even if this is done beforehand, there are not enough surfaces exposed when pieces of timber are stacked and it was considered feasible to inspect the shapes when the timber is laid out on the ground. The second reason was to avoid adding steps to the usual procedures. To utilize the data from the scans in later processes, data is required for all the timber surfaces. However, the considerable effort would be needed to do so before the inspection, as a forklift would be needed to move and rotate the timber. Therefore, the second scan was carried out when the remaining surfaces would be exposed during the usual workflow.

The point cloud data scanned from multiple directions was registered using dedicated auxiliary software and converted to point cloud data in PTS format, which is a

Figure 6. Statement of timbers the day before inspection

general intermediate file format, after being separated into files for each timber block.

Subsequently, the inspection assistance program was used on the point cloud data for each timber block to automatically generate the following dimensions while also overlapping the designed cross-section data.

・Outer dimensions of the timber: The width and height of the cross-section at both ends and the length of the timber

・Dimensions after processing: The design length and the distance between both ends of the materials carved out of the timber, the warp of the materials and the width and height of the cross-sections at both ends of the materials

To add, regarding the length between both ends when carving out the materials from the timber, the initial value was 250mm from the root side of the timber, which was set as a standard rule for the project because the pieces of timber ordered are 500 mm longer than the design.

2. Data Compaction and Generalization Method

The process of simulation the processing shape of the timber by the construction department on a post-process using polygon mesh data, using the popular computational design software programs Rhinoceros and Grasshopper. The processing flow was set up to first apply the processing rules written in the programming language to the 3D timber data before processing and then automatically generating the log shape after processing. To implement this processing flow, the 3D data to be input should be general-purpose surface data and the file size must be 10 MB or less. Since the point cloud data obtained do not meet this requirement, we attempted to transform the data obtained with the method proposed in the previous section.

As the target polygon mesh data specifications, the vertices of the triangular meshes comprising the data were set at intervals of about 10 mm. The reason is that after interviewing a designer who is considering machining and a carpenter, when considering machining with characteristic distortions and scratches on the timber surface in mind, the data suffices provided irregularities of 10 mm or more are expressed, because the conclusion has been obtained.

Specifically, since timber used in traditional wooden construction is often around 7,000 mm long, point cloud data at 9.6 mm intervals can be obtained by dividing with $9^3 = 729$ grids.

Then, a polygon mesh was generated using this point cloud as its apex and the surface was smoothed using Poisson's equation. These processes were carried out by combining multiple features available in the free software package CloudCompare.

The results of applying the above processes are explained in the following chapter.

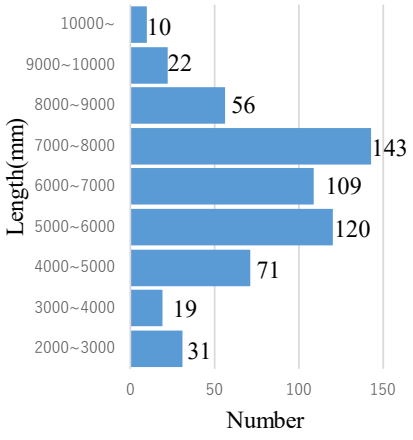

Figure 7. Statement of timbers the day before inspection

5 Results and Discussion of Applying the Proposed Method

First, we will describe the results of 3D scanning of timber. We accompanied timber inspections to apply this method during a 32-day period between January 2019 and March 2020 and performed 3D scans of all 581 logs of round timber including re-inspection. The number of logs by length is shown in Figure 7. The shortest log was 2,350 mm and the longest was 16,968 mm, with a median length of 6,800 mm. The results of the inspection assistance method using these data and of the data compaction and generalization method are described and discussed in the following section.

5.1 Results and Discussion of Applying the Inspection Assistance Method

First, we will describe the results of testing this method on one representative timber log. A timber log 7,130 mm long, which is close to the overall median length and shaped similarly to many other logs, was selected as the test log and will hereinafter be referred to as the sample log. The first 3D scan was performed a day before the inspection, with the sample log laid out on the floor next to four other logs. The 3D scan was performed from seven positions around the five logs to reduce shielding as much as possible. The equipment positioning during the measurement is shown below. Four plastic balls, 145 mm in diameter, were placed around the log to serve as benchmarks during the registration process and laser scanning was performed at a resolution of 5,120pt/360°. This density corresponds to intervals of about 4 mm at a distance of 10 meters. Next, the data for the sample log were

extracted from the obtained point cloud data with point cloud editing software and saved in PTS format. Then, the inspection assistance program we developed was used to automatically generate the dimensional values required for inspection. The specific inspection items and dimensional values generated with the program are shown below. Inspection items: Length of 6,800 mm or more, W×H of the cross-section on the root side of the log of 550 x 550 mm or more and warpage within 150 mm ± 30 mm. The automatically calculated values included a length of 7,044 mm, a cross-section of 728 x 663 mm and warpage of 139 mm, which met the acceptance criteria. In addition, a cross-sectional layout view was superimposed on the point cloud data, so that one inspector could make a preliminary evaluation, even for shapes that could not be expressed numerically. Consequently, the conventional process of comparing the log with a full-sized paper diagram placed under the timber log at inspection could be omitted for this sample log. The preliminary inspection using this program is shown in Figure 8.

We will discuss the results of using this inspection assistance method by assessing the required man-hours. 20 minutes per log are required for the usual inspection. The inspection time is shortened by 10 minutes by omitting any comparison to a full-sized drawing paper. Conversely, the 3D scanning and data processing carried out by a single engineer requires about 30 minutes per log. The above approach shortened 50 man-minutes out of 160, or about 31%.

In addition, the use of this method created added value that were inexpressible numerically. At the request of a highly skilled craftsman, we were able to confirm dimensions and shapes that were not assessable when inspecting the actual timber log in advance. There are two specific points, the first of which is warpage. The inspection items include confirming the parts that can be measured on the outside of the log. Using the point cloud data, we could measure warpage from the inside of the timber to the top, which is more important for construction. The second point is the cross-sectional shape of the timber when processed. In this case, we could assess the virtual cutting surface using the point cloud data, which demonstrates how a highly skilled craftsman can perform more sophisticated work when using this digital technology.

5.2 Results and Discussion of Applying Data Compaction and Generalization Method

We will describe the results of testing this method on the sample log. The point cloud data obtained in (1) are described as a text array of (x, y, z, intensity, R, G, B). The point cloud data of the sample log comprised 1,097,310 data points of heterogeneous density with a file size of 67 MB. As a first step, a three-dimensional octree

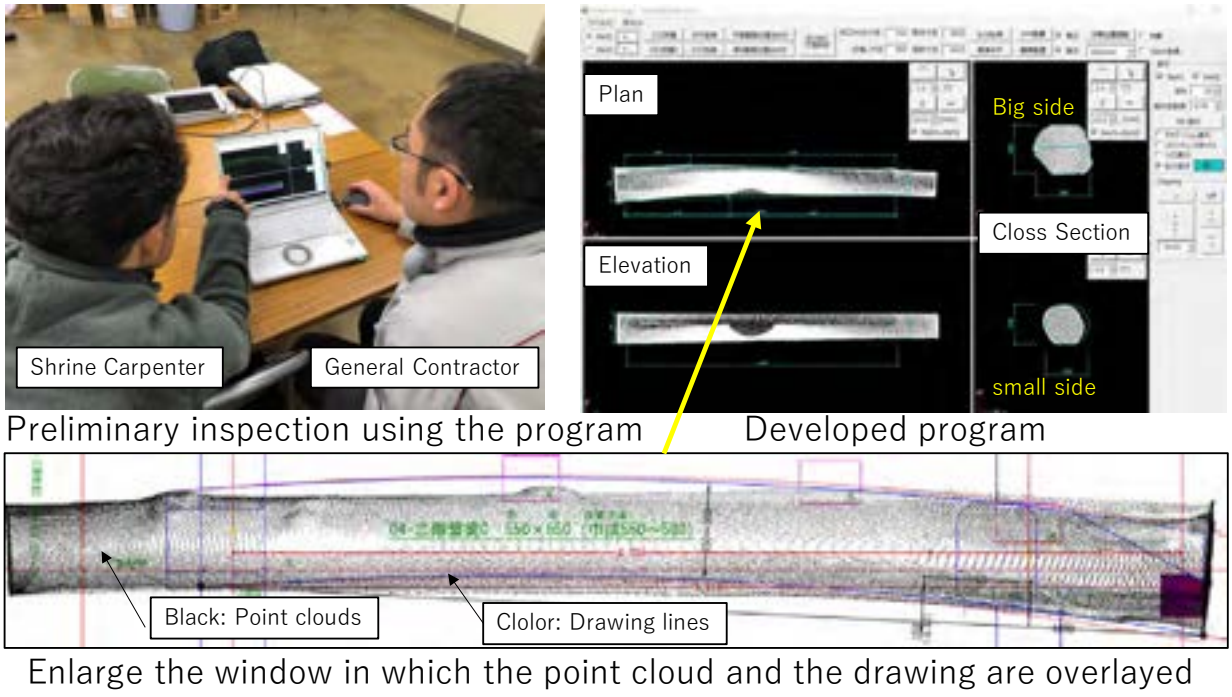

Figure 8. Statement of timbers the day before inspection

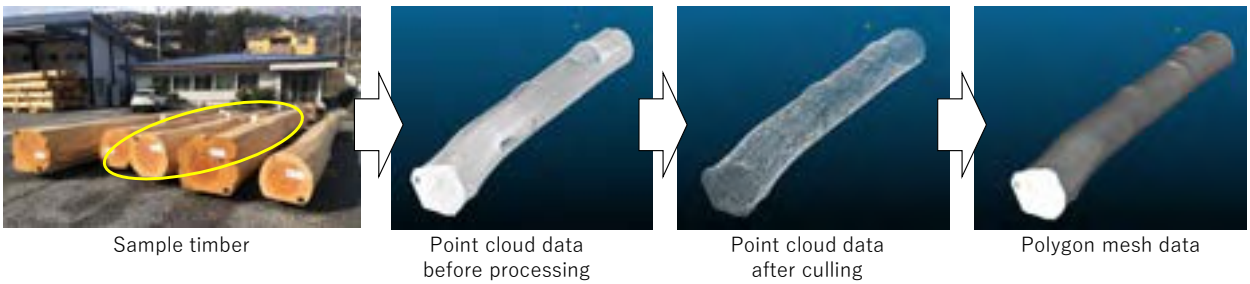

Figure 9. Procedure of data conversion for sample timber

was generated by dividing the data into 93 areas and only one point was left in the center of each area, reducing the data evenly to a density of about 10 mm intervals. Next, a polygon mesh comprising triangles and with each of these points as vertices was mechanically generated and the surfaces smoothed using Poisson's equation to produce polygon mesh data of the desired quality. When the data was saved in the STL format, the file size could be reduced by 88.4% to 7.6 MB. The data conversion procedure is shown in Figure 9.

The data created by the above procedure could be used for processing simulation, as shown in Figure 10. Specifically, the cross-sectional shape is defined as a regular hexagon inscribed in a circle of diameter 550 mm and timber is cut along the center line in the long axis direction. Usually, simulations are done with a simple BIM model for design purposes, but with our method, the real shape of the timber log could be used to plan more precise processing and extract potential issues. This demonstrates that compacting and generalizing the data obtained in (1) can enable more sophisticated work, including in later work stages.

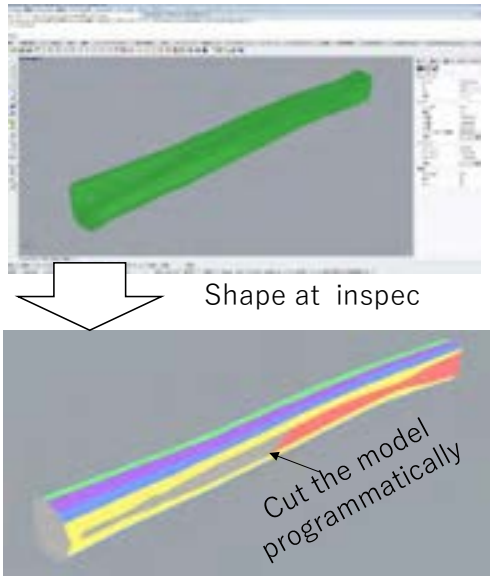

Figure 10. Processing simulation after inspection

6 Conclusion

In this study, we proposed a method to assist inspection using 3D scans of building material shapes and a data compaction and generalization method to facilitate use of these data in subsequent work stages. We also verified the effectiveness of these methods by applying them to a traditional wooden castle restoration project. Our results showed that the method helped save about 4,000 man-hours involved in inspecting building materials and that converting the obtained data into polygon mesh data about 90% smaller in size made them amenable for use in subsequent processing simulations. Our results also suggested the feasibility of a highly skilled craftsman using this digital technology to perform more sophisticated work than with conventional methods.

In future, we aim to investigate ways to efficiently manage the relationship between these data to use data obtained with such digital technologies more efficiently in the overall architectural workflow and improve construction.

References

[1] Naruo K., et al., Automated Recognition of Work Progress at a Construction Site Judgment of Erection Work Progress for Precast Concrete Components, J. *Archit. Plann.*, AIJ, Vol. 80 No. 715, pp. 2081-2090, Sep., 2015

[2] Hiroki T., et al., Study on Tool Path Generation for Wood Processing Using Articulated Robot, *AIJ J. Technol.,* AIJ, Vol. 22, No. 51, pp. 813-816, Jun., 2016

[3] Kazhdan M., et al., Screened poisson surface reconstruction, *ACM Transactions on Graphics (ToG)*, 32(3), pp. 1-13, 2013

Generative Damage Learning for Concrete Aging Detection using Auto-flight Images

T. Yasuno[a] , A. Ishii[a] , J. Fujii[a] , M. Amakata[a] , Y. Takahashi[a]

[a]Research Institute for Infrastructure Paradigm Shift, Yachiyo Engineering, Co. Ltd, Japan
E-mail: {tk-yasuno, akri-ishii, jn-fujii, amakata, yt-takahashi}@yachiyo-eng.co.jp

Abstract –

In order to monitor the state of large-scale infrastructures, image acquisition by autonomous flight drones is efficient for stable angle and high-quality images. Supervised learning requires a large dataset consisting of images and annotation labels. It takes a long time to accumulate images, including identifying the damaged regions of interest (ROIs). In recent years, unsupervised deep learning approaches such as generative adversarial networks (GANs) for anomaly detection algorithms have progressed. When a damaged image is a generator input, it tends to reverse from the damaged state to the healthy state generated image. Using the distance of distribution between the real damaged image and the generated reverse aging healthy state fake image, it is possible to detect the concrete damage automatically from unsupervised learning. This paper proposes an anomaly detection method using unpaired image-to-image translation mapping from damaged images to reverse aging fakes that approximates healthy conditions. We apply our method to field studies, and we examine the usefulness of our method for health monitoring of concrete damage.

Keywords –

Auto-flight monitoring; Aging detection; Image-to-image translation; Concrete infrastructure

1 Introduction

1.1 Related Works

Starting from a climbing robot for inspection in 2000 [1], there has been much research on autonomous robotics for infrastructure inspection [2];for example, bridge crack detection [3] using unmanned aerial vehicles (UAVs), and so forth. After the deep learning revolution in 2014 [4], vision-based infrastructure inspection techniques have been researched using deep learning algorithms [5]. UAVs as autonomous robotics and vision-based deep learning techniques have been combined for powerful inspection applications [6]-[9].

In the field of infrastructure inspection, there are useful algorithms to detect damages such as object detection tasks and semantic segmentation. However, from a supervised learning standpoint, the damaged class is a rare event and the dataset including such events is always imbalanced, and hence, the number of rare class images is very small. When deteriorations are more progressed, the less events that occurred to enable image collection. Because of this scarcity of damaged data, it is difficult to improve the accuracy of supervised learning in infrastructure inspection. This is one of the hurdles to overcome our underlying problems for infrastructure aging detection for data mining from supervised learning approaches. Instead, this paper proposes an unsupervised deep learning method for aging detection.

Since 2014, the original generative adversarial network (GAN) paper has been cited more than 21,400 times to date (August 14, 2020). Starting from GAN's invention in 2014, the field of GAN has been growing exponentially. Over 500 papers have been published on the topic [10]. GANs may be used for many applications: not just fighting breast cancer or generating human faces, but also 62 other medical GAN applications published until the end of July 2018 [11].

Furthermore, unsupervised deep learning approaches such as the generative adversarial network for anomaly detection algorithms have progressed [12]. When a damaged image is a generator input, it tends to reverse from the damaged state to the health-like state image. Using the distance of distribution between the real damaged image and the generated reverse aging health-like image, it is possible to detect the concrete damage automatically from unsupervised learning.

In the field of infrastructure, there are synthetic augmentation studies to map from the structure edge label to damaged images such as concrete crack and rebar exposure [13]. Here, the conditional GAN framework pix2pix [14] is one of the most successful one that uses paired images, but the image-to-image relationship, i.e., the one-to-one relationship, is a strong constraint for dataset preparation. In particular, we could not collect any unseen damaged image not yet experienced.

In contrast, the CycleGAN framework is flexible for the case of mapping unpaired images from domain-A to domain-B. Even if each number of domain images is different, the CycleGAN framework enables the optimization of end-to-end unsupervised learning. This paper proposes an anomaly detection method using the unpaired image-to-image translation framework CycleGAN, mapping from damaged raw images to reverse aging images as a fake that approximates health conditions. We apply our method to field studies conducted on two dams in Japan.

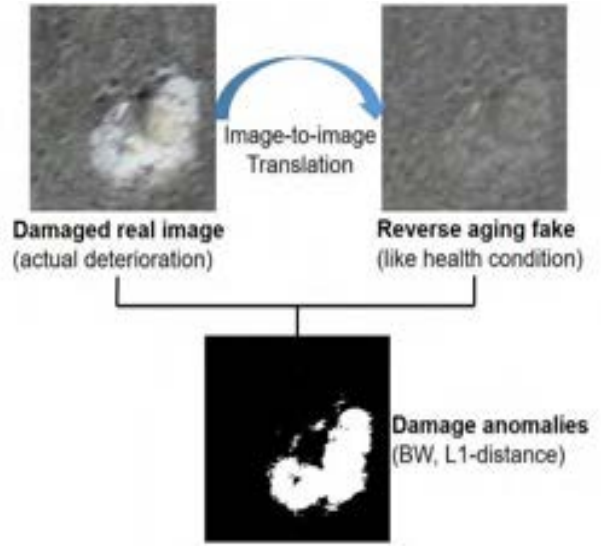

Figure 1. A proposed method using unsupervised generative learning and L1-distance detection.

1.2 Unsupervised Aging Detection Workflow

Figure 1 shows an overview of our method using unsupervised generative learning and L1-distance anomaly detection. This method consists of three mainly workflow so as to detect aging infrastructures.

1. Prepare unpaired images dataset: extract from drone images into unit size images and divide two subgroups with damaged and healthy conditions.
2. Train generators and discriminators to optimize the objective function of CycleGAN network mapping functions reverse aging (forward) and deterioration (backward), and cycle consistency.
3. The damage anomalies are visualized by adapting the noise threshold to compute the L1-distance between the real damaged image and the fake output that approximates the health condition using the reverse aging generator.

2 Generative Damage Learning Method

2.1 Unpaired Dataset Preparation

Auto-flight images captured by a drone have 43 images with a pixel size of 6,000 × 3,000 at the upper left side of dam-1 in the Kanto region. In this study, we set the unit size to 256 × 256. Without loss of resolution, we are able to resize the original size to 5,888 × 2,816 because the resized width is 256 multiplied by 23 and the resized height is 256 multiplied by 11, without any remaining surplus. This method of preparation results in 10,879 unit images.

Second, we classified two groups: a damaged group with damaged regions of interest (ROIs) made up of 4,549 unit images, and a health condition group without any damage made up of 6,325 unit images. Furthermore, we classified four groups 1) health condition without damage (3,852), 2) damaged image (279), 3) blurred (353), and 4) repaired region image (69).

Thus, we create an unpaired image dataset based on the minimum number 222 that contains domain-D (damaged) and domain-H (healthy). The domain-D contains pixel elements of both ROIs and background. Similarly, regarding dam-2 in Tohoku region, the auto-flight drone image has a size of 6,000 × 4,000 pixels, from which we extracted 12,600 unit images of size 256 × 256. This leads to another unpaired image dataset of 237 images.

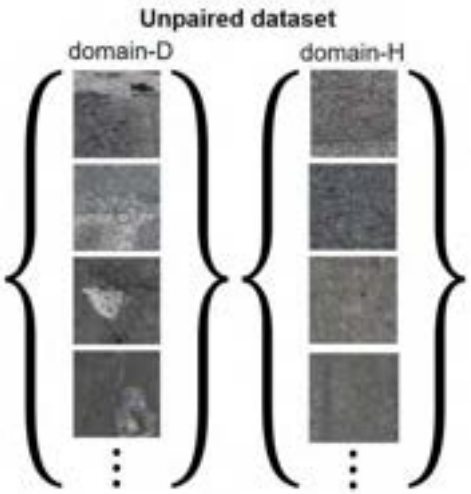

Figure 2. Unpaired images dataset: domain-D (damaged) to domain-H (healthy) translation using CycleGAN.

2.2 Damaged-to-Normal Image Translation: Reverse Aging via CycleGAN

Figure 3 shows an overview of our applied CycleGAN framework mapping the “reverse aging” (forward) function R : D →H and the “deteriorated aging” (backward) function F : H →D.

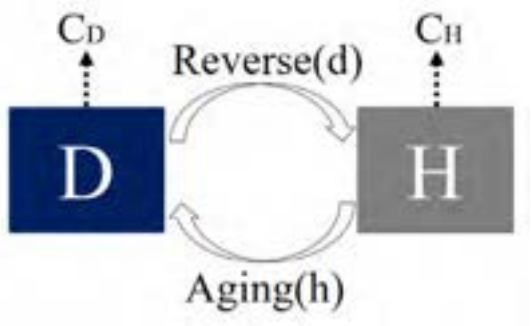

Figure 3. Our applied CycleGAN model mapping functions R : D →H and F : H →D. Discriminator function C_D classifies whether the image is a real damaged image or a generated fake one, and C_H discriminates whether it is a real health condition image or a fake output image.

As Equation (1) shows, for each image d from domain D, the image translation cycle should be able to return d to the original damaged image. This is reverse aging (forward) cycle consistency.

$$d \to R(d) \to A\big(R(d)\big) \approx d. \quad (1)$$

Similarly, as Equation (2) shows, for each image h from domain-H, both translation cycles R and A should also satisfy aging (backward) cycle consistency.

$$h \to A(h) \to R\big(A(h)\big) \approx h. \quad (2)$$

Equation (3) represents the full objective function that consists of the reverse aging adversarial loss mapping R : D →H and discriminator C_H ; the aging adversarial loss mapping F : H →D and the discriminator C_D , and the cycle consistency loss to prevent learned mappings R and A from contradicting each other as follows:

$$\mathcal{L}(R, A, C_D, C_H) = \mathcal{L}_{GAN}(R, C_H, D, H) + \mathcal{L}_{GAN}(A, C_D, D, H) + \lambda\, \mathcal{L}_{cyc}(R, A), \quad (3)$$

where λ controls the relative importance. More detailed numerical representation and network architectures of the generator and discriminator are shown as references [16].

2.3 De-noise Anomaly Detection L1-distance

Using the prediction output (health conditions as a fake output) and the input real damaged image, we propose an anomaly detection based on L1-distance. In order to detect damage anomalies as a ROI signal (large difference), another background noise (small difference) is reduced using the background noise threshold ϵ as a hyper parameter. A larger difference means the deteriorated damage, in contrast a small difference stands for the background noise, such as stain and moss-grown concrete surface. Furthermore, we try to perform blob analysis, such as area open, dilate image, and clear border analysis. This paper computes the next seven steps of image processing as follows:

1. Predict reverse aging output (healthy as a fake prediction) using a trained generator
2. Transform RGB into grayscale of real and fake
3. Centralize the median and set the absolute value
4. Visualize damage anomalies more than the background noise threshold ϵ , which is the maximum peak vector, exceeds the median
5. Area open to delete four connected elements less than 0.3ϵ (background noise threshold)
6. Dilate image with structural element “octagon”
7. Clear image border where the regions are more blight than neighbors with eight connected

3 Applied Results

3.1 Dataset of Auto-flight images

Table 1 shows the case study field of two dams in Japan from which we collected images of the concrete surface via an auto-flight drone. Dam-1 took 20 years at an early deterioration stage on the public service timeline. In contrast, Dam-2 is located in one of the snowfall regions of Japan, and consequently, 62 years passed so that several large damages have occurred in appearance.

Table 1. Dam field profile to data collect by Auto-flight

Profile	Dam-1	Dam-2
Form	Gravity Concrete dam	Arch Concrete dam
Height	156.0 m	94.5 m
Length of Levee	375.0 m	215.0 m
Service years	20 years	62 years
Region	Kanto	Tohoku

3.2 Early Damage Study: 20 years

3.2.1 Training Damaged-to-health Image Reverse Aging Translation

Figure 4 shows the training process of discriminator loss using the CycleGAN framework in the Kanto region, where the loss values are transformed into the moving average within an interval of 300 iterations and plots after skipping every 10 iterations. This discriminator classifies whether an image is the real image in the domain-H (health condition) or if it is a predicted fake output. At approximately 15,000 iterations, the discriminator recognizes the generated fake image, but after 40,000 iterations, the fake image often fools the discriminator because the generated image approaches the real health condition. This testing took 17 hours.

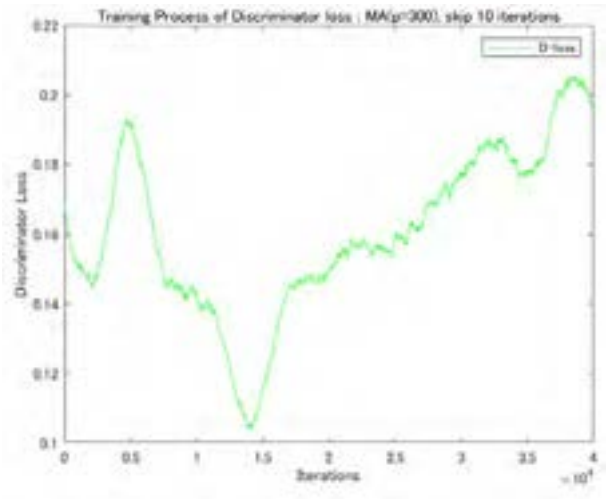

Figure 4. Training process of discriminator loss using CycleGAN framework in the Kanto region.

Figure 5 shows the training process of generator loss using the CycleGAN framework in the Kanto region. This generator transforms from domain-D (damaged) into domain-H (health condition). After 40,000 iterations, the generator approaches a minimum level.

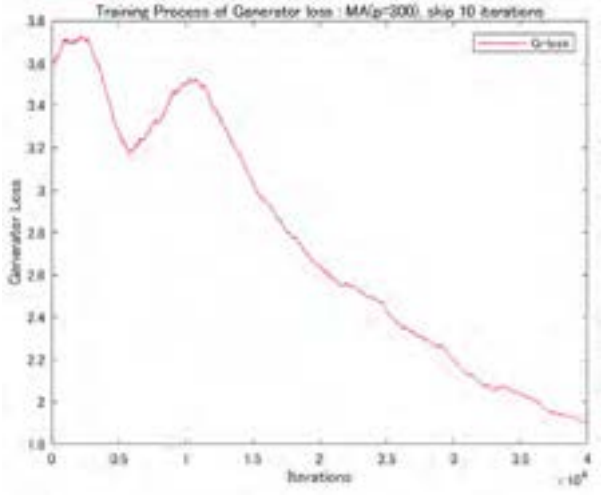

Figure 5. Training process of generator loss using CycleGAN framework in the Kanto region.

3.2.2 Anomaly aging detection using L1-distance between raw image and predicted fake

Figures 6 to 9 show the output results of dam-1, such as damaged image (upper-left) and reverse aging "health condition fake" (upper-right) that were translated using trained generator mapping from damaged to health conditions. Both the real damaged and reverse aging fake output are subtracted into a gray-scaled L1-distance mask output (bottom). Although a small noise level remains, our method can detect phenomena such as exfoliation, isolated stone, and sand leak. In particular, Figure 9 shows that sand leak damage is not yet recognized.

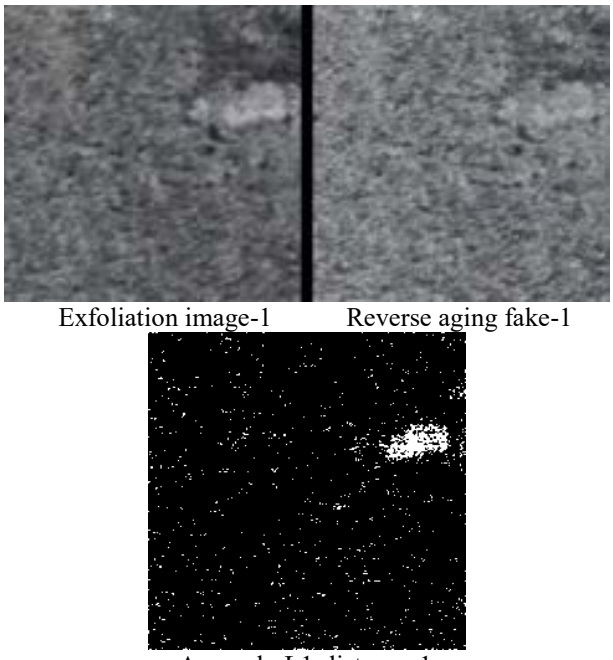

Exfoliation image-1 Reverse aging fake-1

Anomaly L1-distance-1

Figure 6. Exfoliation image (upper-left) and reverse aging "health condition fake" (upper-right) translated using trained generator mapping from damaged to normal image. Grayscale L1-distance mask output (bottom).

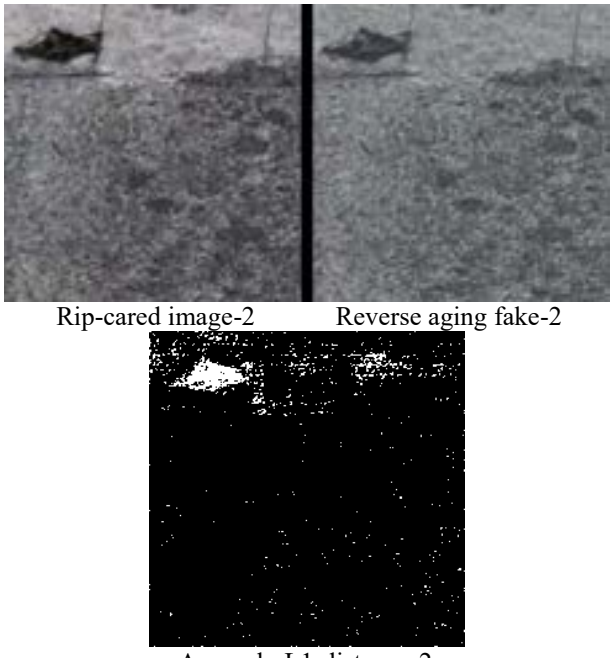

Rip-cared image-2 Reverse aging fake-2

Anomaly L1-distance-2

Figure 7. Rip cared image (upper-left) and reverse aging "health condition fake" (upper-right) translated using trained generator mapping from damaged to normal image. Grayscale L1-distance mask output (bottom).

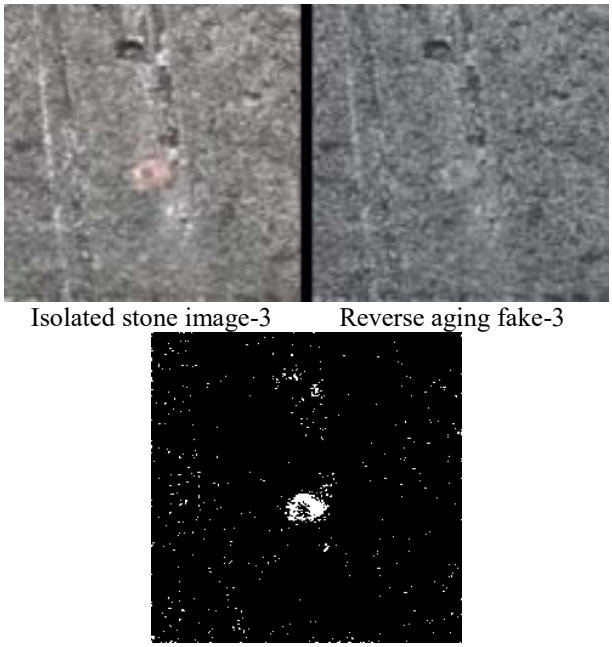

Isolated stone image-3 Reverse aging fake-3

Anomaly L1-distance-3

Figure 8. Pre-cause pop-out isolated stone image (upper-left) and reverse aging "health condition fake" (upper-right) translated using trained generator mapping from damaged to normal image. Grayscale L1-distance mask output (bottom).

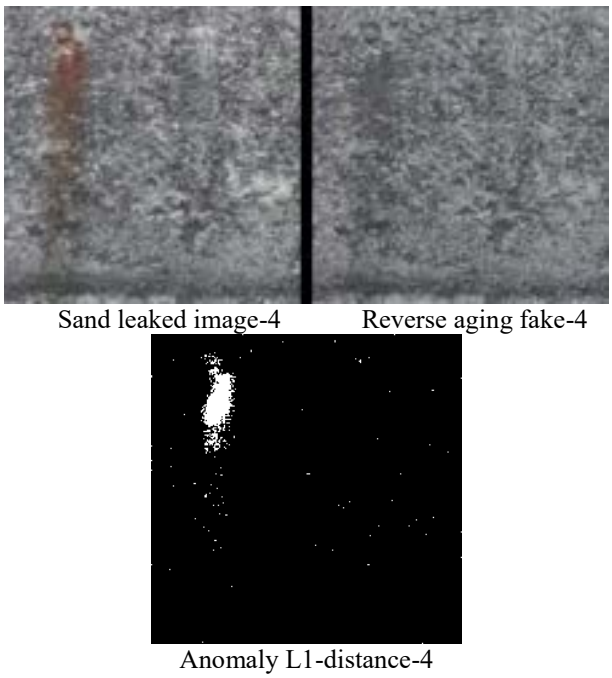

Sand leaked image-4 Reverse aging fake-4

Anomaly L1-distance-4

Figure 9. Sand leak image (upper-left) and reverse aging "health condition fake" (upper-right) translated using trained generator mapping from damaged to normal image. Grayscale L1-distance mask output (bottom).

We learn a lesson from this dam-1 case that was 20 years old. Even if the inspection target class is a rare event, by using "reverse aging" generator, any damage anomalies could be detected. In studying a dam over a period of 20 years, our method is useful for "rip care" on the early deterioration stage, such as sand leak and exfoliation, so as to avoid subsequent progressive damage at the prognosis of concrete structures.

3.3 Cold Damage Study: 62 years

3.3.1 Training Damaged-to-health Image Reverse Aging Translation

Figure 10 shows the training process of discriminator loss using the CycleGAN framework in the Tohoku region, where the loss values are transformed into the moving average within an interval of 300 iterations and plots after skipping every 10 iterations computing. This discriminator classifies whether it is a real image in the domain-H (health condition) or if it is a predicted fake output image. After 20,000 iterations, the discriminator repeats to fool the output image because the generated image approaches the real health condition. It took 17 hours to complete this training process.

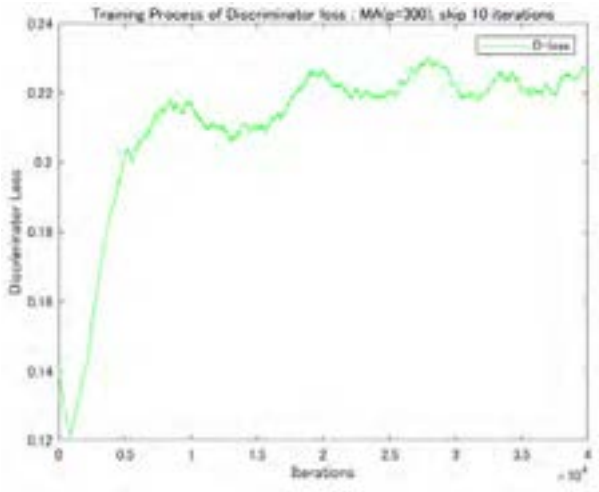

Figure 10. Training process of discriminator loss using CycleGAN framework in the Tohoku region.

Figure 11 shows the training process of generator loss using the CycleGAN framework in the Tohoku region. This generator maps from domain-D (damaged) into domain-H (health condition). After 30,000 iterations, the generator approaches a stable level.

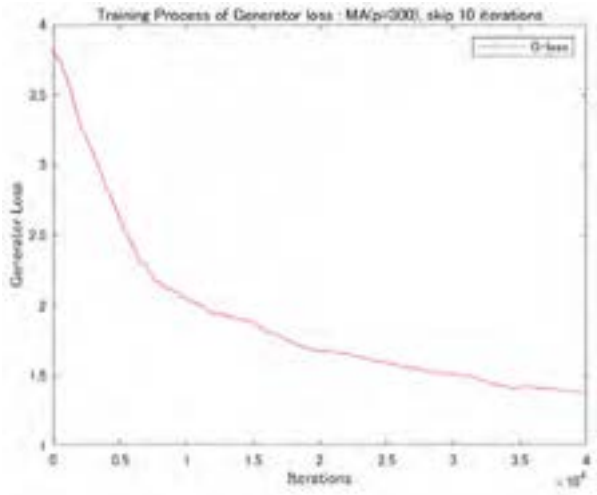

Figure 11. Training process of generator loss using CycleGAN framework in the field of Tohoku region.

3.3.2 Anomaly aging detection using L1-distance between raw image and predicted fake

Figures 12 – 15 show the detection studies conducted on dam-2, similar to those on dam-1; the damaged image (upper-left) and reverse aging "healthy fake" output (upper-right) were translated using trained generator mapping from damaged to health condition image. Both the real damaged and healthy fake output are subtracted into a gray-scaled L1-distance mask output (bottom).

Pop-out crater-born image-1 Reverse aging fake-1

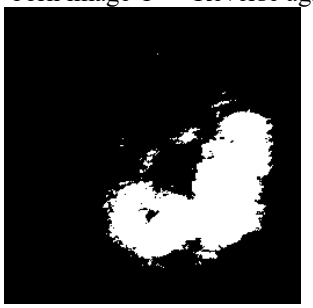

Anomaly L1-distance-1

Figure 12. Pop-out crater born image (upper-left) and reverse aging "health condition fake" (upper-right) translated using trained generator mapping from damaged to normal image. Grayscale L1-distance mask output (bottom).

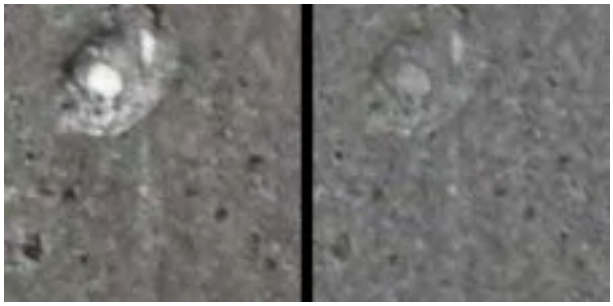

Soft stone pop-out image-2 reverse aging fake-2

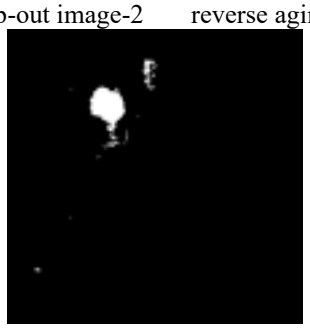

Anomaly L1-distance-2

Figure 13. Soft stone pop-out image (upper-left) and reverse aging "health condition fake" (upper-right) translated using trained generator mapping from damaged to normal image. Grayscale L1-distance mask output (bottom).

Crater-like pop-out image-3 Reverse aging fake-3

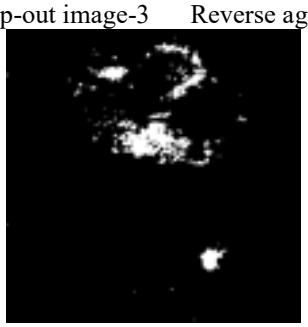

Anomaly L1-distance-3

Figure 14. Crater-shape pop-out image (upper-left) and reverse aging "health condition fake" (upper-right) translated using trained generator mapping from damaged to normal image. Grayscale L1-distance mask output (bottom).

Small pop-out image-4 Reverse aging fake-4

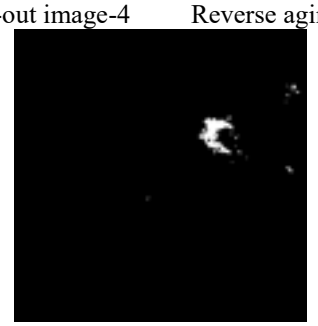

Anomaly L1-distance-4

Figure 15. Small pop-out image (upper-left) and reverse aging "health condition fake" (upper-right) translated using trained generator mapping from damaged to normal image. Grayscale L1-distance mask output (bottom).

4 Concluding Remarks

4.1 Contributions and Lessons

This paper proposed an anomaly detection method using the unpaired image-to-image translation framework CycleGAN, mapping from damaged raw images to reverse aging predicted fake output as healthy conditions. We apply our method to field studies conducted on two dams, one at its early stages and aged 20 years on the public service, and another one aged 62 years, which is located in a cold region. The CycleGAN framework is flexible because this input only requires an unpaired image dataset such as raw images including a damaged ROI and health raw images without damage. This is a data-mining merit instead of the paired image algorithm, such as that of pix2pix.

In addition to the merit of more flexible dataset, our generative unsupervised approach does not require annotation works supervised for any classes, such as damaged ROIs and background. After we prepare to extract a unit size image and divide a damaged group with another health group, we can use unsupervised deep learning to perform end-to-end training to create an image-to-image translator mapping from the damaged domain to the health (normal) domain. Even if the inspection target class is a rare event, using a "reverse aging" generator, any damage anomalies could be detected. Based on our case studies, in a dam deteriorating over 20 years, our method is useful for "rip care" on the early deterioration stage on the public service of concrete structures, such as sand leak and exfoliation, so as to delay the later progressive damage.

4.2 Future Works

It is necessary to optimize a background noise threshold for visualizing the target signal of damage anomalies, and for computing the L1-distance between a damaged image and predicted fake output that approximates healthy condition. This study only considered two case studies of concrete structures. In the future, we will gain further experience with another service periods (e.g. 40 years), much moisture damp locations, steel materials, and another infrastructures such as bridges and tunnels. We will create damage anomaly scores using the L1-distance based on the generator of GAN, in addition to featurematching based on the discriminator. We will also attempt to build another framework that contains a parallel encoder for more efficient damage detection.

Acknowledgments We would like to thank Shinich Kuramoto and Takuji Fukumoto for providing practical deep learning MATLAB resources.

References

[1] Balaguer C., Gim'enez A., Pastor J., et al., A climbing autonomous robot for inspection applications in 3D complex environments, *Robotica*, 18, pp287-297, 2000.

[2] Liu D.K., Dissanayake G., Miro J.V., Waldron K.J., Infrastructure robotics: research challenges and opportunities, 31st International Symposium on Automation and Robotics in Construction and Mining (ISARC), 2014.

[3] Phung M.D., Dinh T.H., Hoang V.T., et al., Automatic crack detection in built infrastructure using unmanned aerial vehicles, 34th International Symposium on Automation and Robotics in Construction (ISARC), 2017.

[4] Sejnowski T.J., *The Deep Learning Revolution*, MIT press, 2018.

[5] Xu S., Wang J., Shou W., Computer vision technique in construction, operation and maintenance phases of civil assets: a critical review, 36th International Symposium on Automation and Robotics in Construction (ISARC), 2019.

[6] Kucuksubasi, F., Sorguc A.G., Transfer learning-based crack detection by autonomous UAVs, 35th International Symposium on Automation and Robotics in Construction (ISARC), 2018.

[7] McLaughlin E., Charron N., Narasimhan S.,

Combining deep learning and robotics for automated concrete delamination assessment, 36th International Symposium on Automation and Robotics in Construction (ISARC), 2019.
[8] Gopalakrishnan K., Gholami H. et al., Crack damage detection in unmanned aerial vehicle images of civil infrastructure using pre-trained deep learning model, International Journal for Traffic and Transport Engineering, 8(1), pp1-14, 2018.
[9] Yasuno T., Fujii J. Amakata M., Pop-outs segmentation for concrete structure prognosis indices using UAV monitoring and per-pixel prediction, Proceedings of 12th International Workshop on Structural Health Monitoring 2019.
[10] Hindupur A., The GAN zoo, On-line: https://github.com/hindupuravinash/the-gan-zoo. Accessed: 15/6/2020.
[11] Kazeminia S. et al., GANs for medical image analysis, https://arxiv.org/pdf/1809.06222.pdf.
[12] Schlegl T., Seebock P., Waldstein S.M. et al., Unsupervised anomaly detection with generative adversarial networks to guide marker discovery, Proceedings of IPMI 2017.
[13] Yasuno T., Nakajima M., Sekiguchi T., Synthetic image augmentation for damage region segmentation using conditional GAN with structure edge, 34th Journal of Society for Artificial Intelligence, 2020.
[14] Isola, P., Zhu J-Y. et al. : Image-to-image Translation with Conditional Adversarial Network, CVPR, 2017.
[15] Zhu J-Y., Park T., Isola P. et al., Unpaired image-to-image translation using cycle-consistent adversarial networks, arXiv:1703.10593v6, 2018.
[16] Gonzalez R.C., Woods R.E., *Digital Image Processing*, 3rd edition, Prentice Hall, 2008.
[17] Langr J., Bok V., *GANs in Action, Deep Learning with Generative Adversarial Networks, Manning*, 2019.
[18] Foster D., *Generative Deep Learning : Teaching Machines to Paint, Write, Compose and Play*, O'reilly, 2019.

Evaluation of Drainage Gradient using Three-dimensional Measurement Data and Physics Engine

Kosei Ishida[a]

[a]Department of Architecture, Assistant Professor, Doctor of Engineering, Waseda University, Tokyo, Japan
E-mail: k_ishida@waseda.jp

Abstract –

The shape of a building can be recorded through various technologies, such as three-dimensional (3D) laser scanners and photogrammetry. The 3D measurement technology facilitates the mensuration of unevenness of a reinforced concrete structure, horizontality of the floor, and drainage gradient. In particular, measuring devices with a tilt sensor (e.g., 3D laser scanners) allow the evaluation of the horizontality of buildings using point cloud data. In this study, a method is introduced to evaluate the drainage gradient using 3D polygon data and a physics engine. The point cloud data were acquired via a 3D laser scanner and converted into polygon data. The polygon data were imported into a virtual space through the physics engine. Subsequently, the drainage capacity was evaluated by placing water particles on the polygon data and observing their movement according to the physics engine. The aim of this procedure is to evaluate the inclination angle of all parts of a building (e.g., rooftop) and develop a method for identifying the locations where puddles can frequently occur. Our simulation software was created using Unity and NVIDIA FleX. In this research, a simulation was conducted in which the polygon data were imported into the developed software, and the drainage situation was predicted.

Keywords –
3D laser scanner; Point cloud; 3D surface; Drainage gradient; Physics engine

1 Introduction

1.1 Background and Related Work

Point cloud data are composed of a set of points containing information related to three-dimensional (3D) coordinates and colors. However, because the data are only composed of points, they are usually converted into 3D models and building information modeling (BIM) data. Alternatively, data analysis is applied to point cloud data, for example, comparing the horizontal plane information with the point cloud data to analyze floor flatness. Accordingly, several researchers have examined evaluation methods using 3D point clouds, shape recognition of point clouds, and automatic conversion of point clouds into BIM data.

In the construction industry, approximately half of the studies on the application of point cloud data are based on 3D model reconstruction [1], and a quarter involve geometry quality inspection [1].

The automatic segmentation of point cloud data into building parts (e.g., walls and columns) acquired by a laser scanner has been investigated [2]. Research on reconstructing point cloud data into a 3D model has been performed by creating BIM data for buildings [3] and other civil engineering structures, such as tunnels [4]. Studies on creating BIM data according to the level of development (LOD) specification using point cloud data have also been explored [5]. In some studies, point cloud data and parametric modeling are combined [6]. For example, one study performed a dimensional quality assessment of the rebar of a reinforced concrete element based on point cloud data. [7]. In recent years, methods for directly performing structural calculations from point cloud data have been explored [8]. A system implemented for floor flatness compliance control given a set of point clouds and a 3D BIM model has also been proposed [9].

1.2 Research Aim

Point cloud data contain considerable amounts of information. For example, surface dirt and deterioration of buildings can be observed based on point cloud data. Furthermore, because the accuracy of 3D laser scanners has improved, it is possible to analyze the drainage gradient using the data acquired by the scanner. A 3D laser scanner can measure even the slightest unevenness in an actual building.

In several recent studies, methods for automatically converting point cloud data into a 3D model or BIM data have been investigated. The general BIM data exhibit a smooth shape of walls and floors. Therefore, the 3D shape information of the building included in the point cloud data is typically lost after conversion into BIM data. Point cloud data contain the exact shape and color

information in the real world; hence, these data include richer information than the BIM data of the LOD 500 level.

The purpose of this study is to utilize the shape information contained in point cloud data. Our research aims to devise a mechanism to evaluate drainage performance by combining a 3D surface converted from point cloud data and a physics engine.

The objectives of this study are summarized as follows:

(1) Devise a procedure to create a 3D model for analyzing drainage capacity
(2) Verify water particle movement on a 3D surface model using the physics engine
(3) Conduct validation of the drainage capacity analysis results by comparing against actual measurement data

2 Drainage gradient evaluation method using 3D measurement data and physics engine

2.1 Drainage Gradient Evaluation Procedure Using Point Cloud Data and Physics Engine

The evaluation method for the drainage gradient using point cloud data and the physics engine involves the following three steps:

(1) Measurement using a 3D laser scanner
(2) Creation of a simulation model based on point cloud data
(3) Evaluation of the drainage gradient using a physics engine

The point cloud data of a building that are obtained using a 3D laser scanner cannot be employed for simulation that uses a physics engine. Accordingly, we have formulated a procedure for converting point cloud data into information that can be applied to such a simulation.

The procedure for converting point cloud data is shown in Fig. 1. Two 3D models are used to evaluate the drainage gradient using point cloud data and a physics engine. The first type of 3D model is a surface model converted from point cloud data; the second is a 3D model of a sewer created from point cloud data and field surveys.

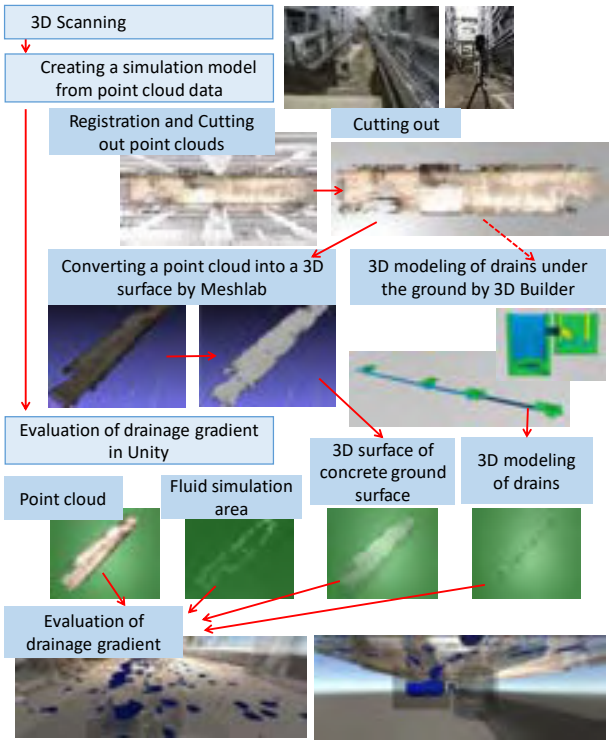

Figure 1. Evaluation procedure of drainage gradient using 3D measurement data and physics engine

2.2 Level of graphical information acquired from point cloud data

Point cloud data contain rich information; to utilize this information, the data are usually analyzed and converted into another data format. In this study, we categorized the level of graphical information acquired from point cloud data. This classification is summarized in Table 1.

A point cloud is composed of 3D coordinates, color, and brightness. We can observe the shape and color of a building as well as the stains and wet spots on its surface based on the color of the point cloud.

The data containing the information extracted from the point cloud data for analysis are derived by examining the 3D coordinates of the point cloud data. For example, there are certain amounts of data containing information on the distance of a point from a horizontal plane that represent this distance in terms of color.

The 3D surface is composed of data obtained by converting point cloud data into polygon data. In this study, objects in motion were used based on the physics engine.

The simulation model is a 3D model that implements various simulations. It is composed of a 3D surface converted from point cloud data, a simulation area, point cloud data, and 3D models. The simulation model is employed to estimate the drainage capacity using actual measurement data.

Table 1. Level of graphical information acquired from point cloud data

Level definition	Image
Point cloud data Point cloud data is composed of 3D coordinates, color, and brightness.	
Point cloud data analyzed to extract information These are data created by analyzing the 3D coordinates of the point cloud data.	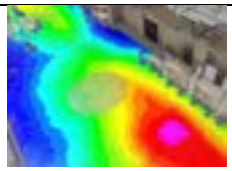
3D surface These data are obtained by converting point cloud data into polygon data. In this study, the data are used for moving objects based on the physics engine.	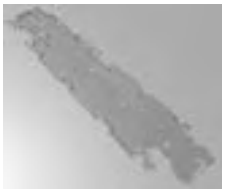
Simulation model This is a 3D model that can be employed in various simulations.	

2.3 Creation of the Simulation Model from Point Cloud Data

2.3.1 Procedure for Creating a Simulation Model from Point Cloud Data

To create a model for simulation, we organized three types of 3D data by analyzing and converting point cloud data. These three types consist of "point cloud data analyzed to extract information" and "3D surface," as summarized in Table 1. Additionally, we created "a 3D model of drains under the ground." However, underground drains cannot be measured using a 3D laser scanner. Therefore, after examining the point cloud, we estimated the position of these drains and created a 3D model to represent them.

Four positions were scanned with the 3D laser scanner; Fig. 2 presents a photograph of these measurements. The acquired point cloud data of the campus building are shown in Fig. 3. These data were used to create the simulation model employed in this study.

The procedure for creating a 3D surface from the point cloud data is detailed below:

(1) Register several scanning data
(2) Cut out the point cloud data on the floor
(3) Convert the point cloud data into a 3D surface model

Figure 2. Measurement scheme in experiment

Figure 3. Acquired point cloud data of campus buildings

2.3.2 Registering and Cutting Out Point Clouds

We registered the point cloud data and removed the floor point cloud data to convert them into a 3D surface model; the cutoff point cloud data are depicted in Fig. 4. The installation positions of the 3D laser scanner are denoted as A, B, C, and D. The point cloud data captured from these four positions are illustrated in Fig. 5. The data were classified into four colors (i.e., red, blue, yellow, and green) corresponding to the point cloud data acquired from these four locations.

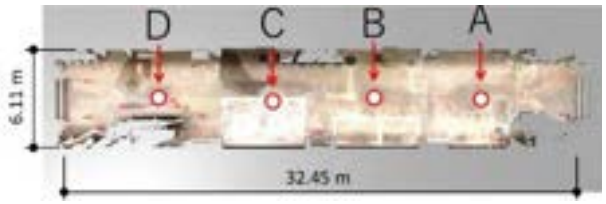

Figure 4. Installation positions of 3D laser scanner

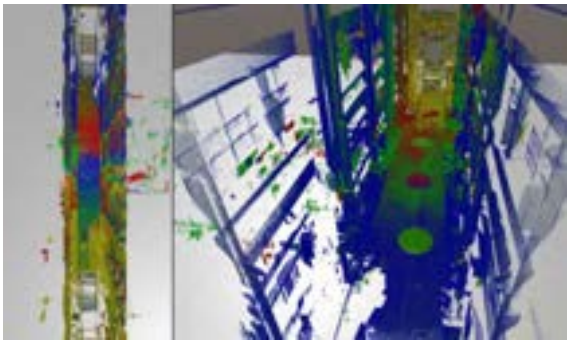

Figure 5. Point cloud data captured from four measurement positions

2.3.3 Measurement of Concrete Floor Flatness Using a 3D Point Cloud

The slope of the concrete slab is obtained from the point cloud data, and the location of the local minimum point is then analyzed, as presented in this section. Water accumulates in locations with low elevation. Therefore, it is essential to analyze the position of the local minimum point to compare the Z-coordinate values with the surroundings.

The analysis of the position of this minimum point was performed according to the procedure shown in Fig. 6. First, as shown in Fig. 6(a), the point cloud on the floor is extracted. The point cloud is placed on the XY plane in a 5-cm square grid, and the average value of the Z coordinate of the point cloud in the grid is calculated. Next, one grid is selected, as shown in Fig. 6(c), and the elevation based on the Z coordinate is compared with the surrounding grids of 11 × 11 cells. If the Z coordinate of the selected grid has the smallest value in the 11 × 11 cells, then that position is defined as the local minimum point.

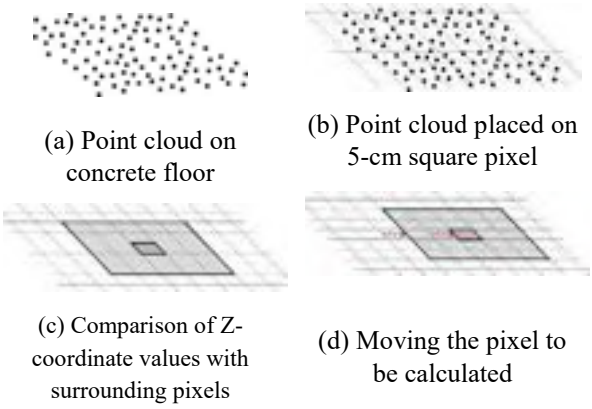

(a) Point cloud on concrete floor

(b) Point cloud placed on 5-cm square pixel

(c) Comparison of Z-coordinate values with surrounding pixels

(d) Moving the pixel to be calculated

Figure 6. Calculation procedure of local minimum point position on concrete slab surface by point cloud data

The analysis results of the flatness of the concrete floor slab are presented in Fig. 7, which illustrates the inclination of the concrete slab towards the four drain covers. The positions and elevations of the local minimum point on the concrete slab are shown in Fig. 8.

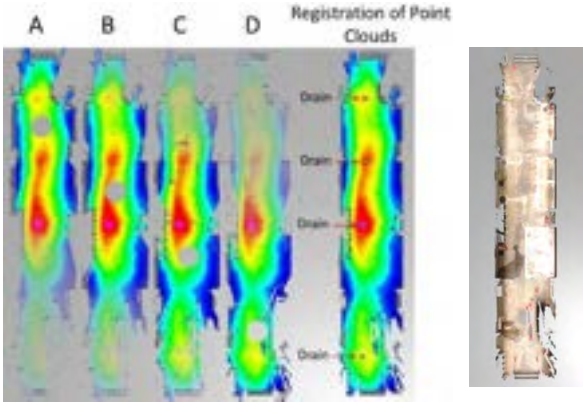

Figure 7. Measurement of concrete floor flatness using 3D point cloud data

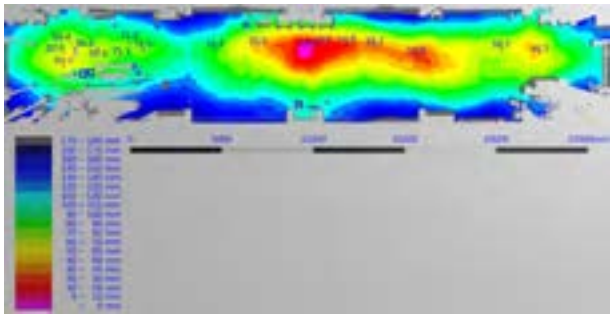

Figure 8. Positions and elevations of local minimum points on concrete slab extracted by point cloud data analysis

2.3.4 Point cloud data conversion into 3D surface model

The point cloud data shown in Fig. 4 were used to convert the point cloud into a 3D surface model through MeshLab [10]. The point cloud data consist of 6.67 million points, which were reduced to a density of point clouds at intervals of 2 cm. Thereafter, the point cloud data contained 525,000 points. Subsequently, the point cloud data were converted into mesh data. Furthermore, hole filling was performed using mesh data. Finally, the data compression process was conducted until the number of faces in the mesh data was 50,000.

2.3.5 3D Modeling of Underground Drains

We were unable to measure the shape of the drainage and sewer under the concrete slab using a 3D laser scanner. Therefore, the drain cover position from the point cloud data was extracted, and the shape of the drainage and sewer was estimated. Subsequently, a 3D model of the drainage and sewer was created using “Microsoft 3D Builder,” as shown in Fig. 9.

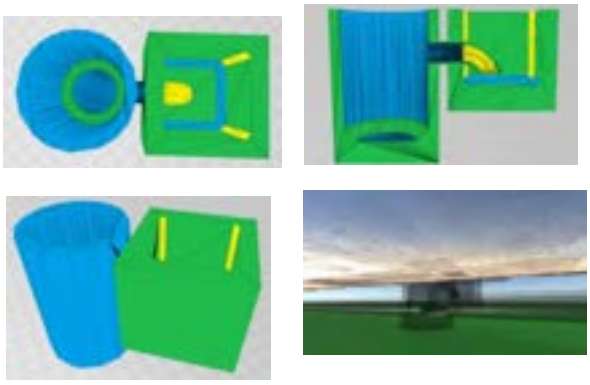

Figure 9. 3D modeling of underground drains by 3D Builder

2.3.6 Simulation Model for Analyzing Drainage Capacity

We created a 3D model and a simulation model to evaluate the drainage capacity. The 3D model contains four types of 3D shape data, as shown in Fig. 10.

(1) color point cloud
(2) fluid simulation area
(3) 3D surface of concrete floor surface
(4) 3D model of underground drains

In this study, fluid flow simulations were performed using the NVIDIA FleX for Unity [11]. Therefore, a 3D object, which can engage with the fluid "particles", was used to convert the point cloud on the concrete floor into a 3D surface.

The 3D model of the drain was placed below the 3D surface of the concrete floor. Four holes on the 3D surface were created according to the position of the drain cover. Water particles flow through the holes in the drain cover into the 3D surface and move inside the 3D model of the drain.

The fluid simulation area is defined as a wall-shaped object. A 3D model with the wall-shaped object of the fluid simulation area is presented in Fig. 11. This area can prevent the flow of water particles from the periphery of the 3D surface.

In addition, a colored point cloud was employed to observe the dirt and water wet spots on the concrete floor.

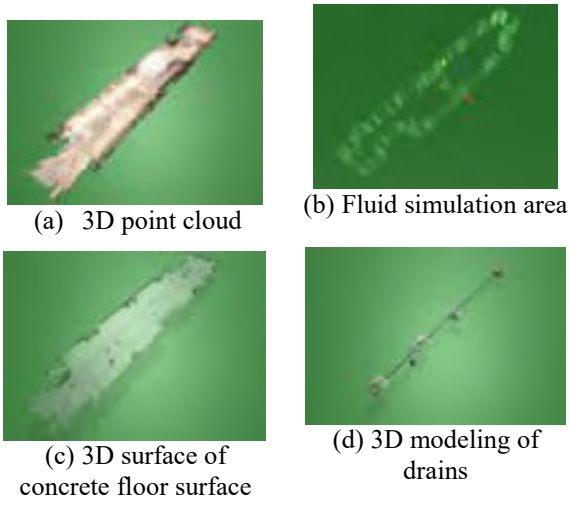

(a) 3D point cloud (b) Fluid simulation area

(c) 3D surface of concrete floor surface (d) 3D modeling of drains

Figure 10. Four types of 3D shape data for evaluating water flow

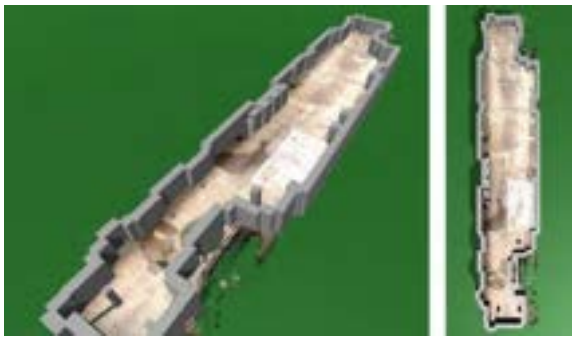

Figure 11. 3D shape data for analyzing drainage capacity

2.4 Verification of water particle movement on 3D surface model using a physics engine

The simulation model demonstrated in Fig. 11 was used to evaluate whether the water particles moved according to the principles of the physics engine. A part of the concrete slab measured in this study was wet due to water draining from the air conditioner, as illustrated in Fig. 12 (a). The water particles were generated according to the positions of the drainage of the air conditioner, thereby evaluating the water particle movement.

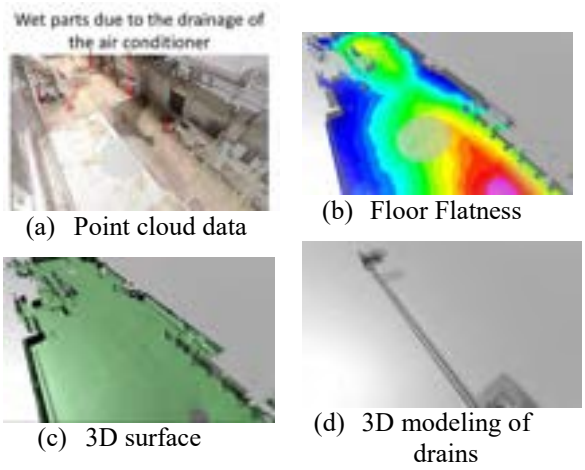

(a) Point cloud data (b) Floor Flatness

(c) 3D surface (d) 3D modeling of drains

Figure 12. Simulation model for verification of water particles movement using physics engine

The simulation was performed in Unity, and NVIDIA FleX was used to achieve water movement. The simulation for generating water particles in Unity and moving them onto the 3D surface is shown in Fig. 13. The water particles created by NVIDIA FleX for Unity in the 3D measurement model are shown in Fig. 14. The diameter of the simulated water particles is 0.03 m.

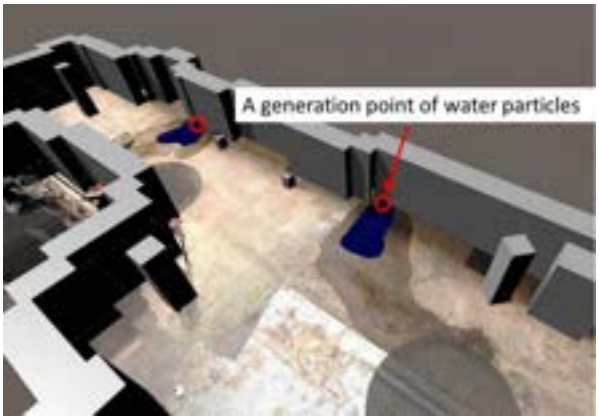

Figure 13. Simulation for predicting drainage flow

Figure 14. Water particles generation by NVIDIA FleX for Unity on 3D measurement model

The evaluation results of the drainage gradient using 3D measurement data and the physics engine are presented in Fig. 15. We confirmed that the water objects flowed on the wet parts of the concrete floor. Using the visualization data that analyzed the distance of each point from the horizontal plane and represented the distance in color, we confirmed that the water objects were flowing along the low positions of the concrete floor rather than on the surrounding area.

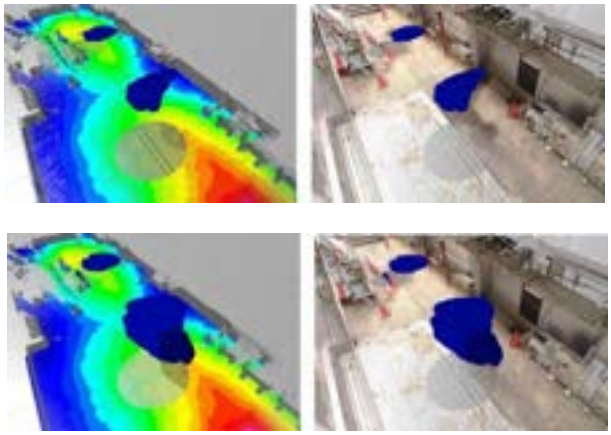

Figure 15. Drainage gradient evaluation result using 3D measurement data and physics engine

3 Results and Discussion

3.1 Evaluation of drainage capacity when water is uniformly generated.

A 3D measurement model was used to evaluate the drainage capacity. The results are presented based on a uniform distribution of water particles. Water particles with a diameter of 0.03 m are uniformly generated on the upper surface of the simulation model. The movement of these particles, according to gravity and their flow from the drain, was observed. The image in Fig. 16 (a) indicates that our system uniformly generated water particles.

These uniformly generated water particles on the concrete floor moved to a location with a lower elevation than the surrounding area. Thereafter, the water dropped into the drainage channel, reducing the amount of water on the floor. However, some water particles did not drain and instead remained on the concrete floor. The image in Fig. 16 (b) illustrates the accumulated water particles in the section where the gradient is low.

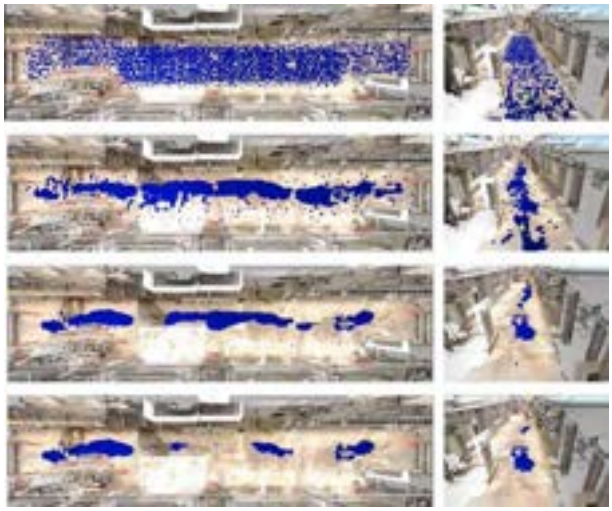

(a) Evaluation progress and results

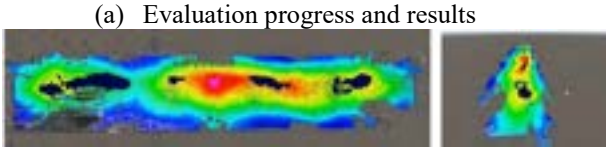

(b) Evaluation results and concrete floor flatness

Figure 16. Evaluation of drainage capacity when water is uniformly generated

3.2 Situation of drains and sewers under concrete floor slab

In the simulation (Fig. 16), it was observed that water particles flowed into the drain and through the sewer. As shown in Fig. 17 (a), the water particles flowed to the drain located above the concrete ground floor. Moreover, Fig. 17 (b) shows that the water particles flowed into the drain and sewer under the concrete floor slab.

(a) Situation above the concrete ground floor

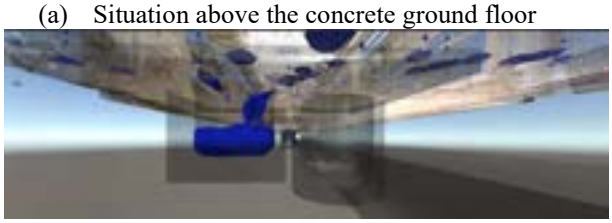

(b) Situation of water particles flowing through drains and sewers under concrete floor slab

Figure 17. Water objects falling into drain

As shown in Fig. 18, the water particles were stored in a storm drain consisting of a catch basin and sand traps. It was confirmed that the water particles flowed into the sewer through the outlet trap when the catch basin was full.

Figure 18. Water particles accumulating in drainage drain and flowing into sewer pipe

3.3 Verification of Drainage Capacity Analysis Results Using Actual Measurement Data

The simulation results of the drainage gradient were investigated using 3D measurement data and a physics engine. These were compared with the actual situation of floor drainage. First, the locations of the remaining water objects were compared with the unevenness of the concrete floor. The dotted line in the image in Fig. 19 (a) denotes the position of the valley line on the concrete floor. The figure shows that the water objects remain near the valley line of the concrete floor with a small slope value.

The locations of the minimum point elevation on the concrete slab are shown in Fig. 20. If the elevation is minimum at a 55 × 55 cm area, then this can be defined as the minimum elevation point. Considering the results shown in Figs. 19 and 20, it can be observed that water tends to remain at a point relatively lower than the surroundings.

(a) Drainage gradient evaluation results with point cloud data

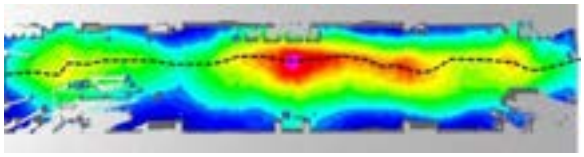

(b) Concrete floor flatness and position of the valley line

Figure 19. Location of remaining water objects and valley line of concrete floor

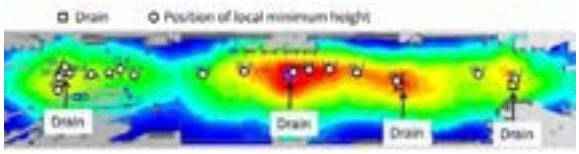

Figure 20. Position of local minimum elevation

The image on the left side of Fig. 21 depicts the condition of the actual concrete floor after the rain. The image on the right side represents the condition of the virtual concrete floor after the water particles have been drained. In observing the concrete floor state after the rain in the actual world, and based on the simulation results, it can be confirmed that water accumulates along the valley line portion, as shown in Fig. 19.

From Fig. 21, it was confirmed that the simulation results based on the measurement data were accurately analyzed to a certain extent.


Figure 21. Conditions of concrete floor after rain in actual world and after water particles are drained in virtual world

4 Conclusion

In this study, a 3D surface was created from the data obtained by converting point cloud data. The data representing the concrete floor contained 6.67 million points. However, the use of 3D surfaces reduced the number of faces to 50,000. The size of the concrete floor measured by the 3D laser scanner was 32.45 × 6.11 m, as depicted in Fig. 4. We reproduced the concrete floor, of an area of approximately 200 m², with a 3D surface composed of 50,000 faces. This 3D surface with a reduced data size was used to verify that the drainage gradients could be evaluated.

Furthermore, we reproduced the drainage and sewage channel under the concrete slab using a 3D model, which was used in combination with the 3D surface in the drainage simulation. It was confirmed that the water particles properly flowed inside the drains and sewers.

Ultimately, this study verified that the drainage gradient could be evaluated using a 3D measurement model and physics engine.

References

[1] Qian Wang and Min-Koo Kim. Applications of 3D point cloud data in the construction industry: A fifteen-year review from 2004 to 2018. *Advanced Engineering Informatics*, 39:306–319, January 2019.

[2] Jong Won Ma. Thomas Czerniawski. Fernanda Leite. Semantic segmentation of point clouds of building interiors with deep learning: Augmenting training datasets with synthetic BIM-based point clouds. *Automation in Construction*, 113, Article 103144, May 2020.

[3] Jaehoon Jung. Cyrill Stachniss. Sungha Ju. Joon Heo. Automated 3D volumetric reconstruction of multiple-room building interiors for as-built BIM. *Advanced Engineering Informatics*, 38:811–825, October 2018.

[4] Yun-Jian Cheng. Wen-Ge Qiu. Dong-Ya Duan. Automatic creation of as-is building information model from single-track railway tunnel point clouds. *Automation in Construction*, 106, Article 102911, October 2019.

[5] Ruodan Lu. Ioannis Brilakis. Digital twinning of existing reinforced concrete bridges from labelled point clusters. *Automation in Construction*, 105, Article 102837, September 2019.

[6] Luigi Barazzetti. Parametric as-built model generation of complex shapes from point clouds. *Advanced Engineering Informatics*, 30(3): 298–311, August 2016.

[7] Min-Koo Kim. Julian Pratama Putra Thedja. Qian Wang. Automated dimensional quality assessment for formwork and rebar of reinforced concrete components using 3D point cloud data. *Automation in Construction*, 112, Article 103077, April 2020.

[8] László Kudela. Stefan Kollmannsberger. Umut Almac. Ernst Rank. Direct structural analysis of domains defined by point clouds. Computer Methods in Applied Mechanics and Engineering, 3581, Article 112581, January 2020.

[9] Fr´ed´eric Bosch´e. Emeline Guenet. Automating Surface Flatness Control using Terrestrial Laser Scanning and Building Information Models. *Automation in Construction*, 44: 212–226, August 2014.

[10] MeshLab, Online: https://www.meshlab.net/, Accessed: 27/06/2020

[11] NVIDIA FleX for Unity (1.0 BETA). Online: https://assetstore.unity.com/packages/tools/physics/nvidia-flex-for-unity-1-0-beta-120425, Accessed: 27/06/2020

Stakeholder Perspectives on the Adoption of Drones in Construction Projects

V.P.C. Charlesraj and N. Rakshith

RICS School of Built Environment, Delhi NCR 201313 India
E-mail: vpcharlesraj@ricssbe.edu.in, rakshithn.mc18n@ricssbe.edu.in

Abstract –

Drones or Unmanned Aerial Vehicle (UAV) and services based on them have been used globally in various sectors including but not limited to construction, real estate, e-commerce, agriculture, utilities & energy, financial services, and media & entertainment. Use of such robots have a potential to reduce the cost & time and increase safety & productivity among other benefits. The use of drones is increasing in India and the UAV market is expected to grow at a CAGR of 18% during 2017-2023 in terms of revenue. While the use of drones is primarily in defence sector compared to commercial use, it has been reported that drone-based solutions are being explored in agriculture, energy & utilities, insurance, infrastructure, media & entertainment and mining in India. Hence, there exists a need to investigate the level of awareness, application, benefits and barriers of using drones in Indian construction.

The primary objective of this study is to investigate the level of awareness and the application of drones among the key stakeholders in Indian construction through questionnaire survey-based quantitative research among key stakeholders. The study revealed there is high level of awareness of drones and low level of usage in Indian construction. The overall pattern in the data revealed that the respondents have rated most of the indicators highly important. Following are the top-rated attributes: Drones must be experimented before using it in the construction projects (relevance); Surveying (application); Drones provide real time updates from the site (benefit); Weather related issues (barrier) and Health and Safety (KPI). It has been observed that there is statistically significant difference in perception among contractors, consultants and clients with respect to relevance & application of drones and not so for benefits, barriers & impact on KPI.

Keywords –

Awareness; Drones; Indian construction; Unmanned Aerial Vehicle (UAV)

1 Introduction

The construction industry globally is worth 10 Trillion Dollars per annum. The countries around the world spend around 9-15% of the Gross Domestic Product on the construction sector. But the construction industry is very fragmented and unorganized. The construction industry is facing huge challenges compared to other sectors. There is a serious performance outfall observed over the decades in the construction industry [1].

The challenges such as lack of performance, low productivity of labours, lack of data collection and documentation, cost over runs of the project, lack of adoption of technology, delays in project completion, safety issues on site, lack of quality, lack of innovation, high expenses and management issues are observed in the construction industry [2]. The industry suffers with severe shortage of labours, lack of adoption of new technology, lack of performance due to decreased productivity [3]. Disasters such as one created by COVID-19 pandemic demand change in working conditions in addition to unavailability of resources.

One of the ways to overcome these challenges in construction operations is to implement automation and robotics to improve the performance [4]. Construction industry is labour dependent and robotics & automation has shown potential improvement in the productivity and quality of the construction projects [5]. The emerging technologies such as Building Information Modelling (BIM), Internet of Things (IOT), Light Detection and Ranging (LIDAR) and robots like bricklaying machine, glazing machine, Unmanned Aerial Vehicle or drones, autonomous ground vehicles, robotic 3d printing can be used to increase the productivity, reduce the cost over-runs and delays in the project. So there is need for adopting the innovative technologies for the development of the construction industry [4,6].

Drones or Unmanned Aerial Vehicles (UAV) can be adopted as potential solution to the challenges faced by the construction industry. While the use of drones in India is primarily in defence sector compared to commercial use, it has been reported that drone-based solutions are being explored in agriculture, energy &

utilities, insurance, infrastructure, media & entertainment and mining in India. The regulation on the use of drones in India has been released very recently. Adoption of drone technology is in its formative stage in Indian construction. Hence there is a need to investigate the adoption of drones in Indian construction. It has been attempted to study the level of awareness & adoption of drones in Indian construction and assess the perspectives of various key stakeholders.

2 Literature Review

2.1 Drones

Drones or UAVs also known as Remotely Piloted Aircraft (RPA) are the aircrafts which operates without the requirement of onboard human pilot and are controlled by remotes [7]. Drones vary in the sizes and can be equipped with various accessories. The various parts of drones include frame for supporting the components of drone, propeller and engine which constitutes propulsion system for lift off, battery which acts as power source, electronic and communication system which is used to control drone [8] . The drones are attached with sensors which are used for the alignment and positioning. Manual interference of the pilot is not required due to these sensors[9].

2.2 Types of Drones

Based on the vehicle mass principle the drones can be classified as "heavier than air" drones in which the drone uses aerodynamics and propulsive thrust, "Lighter than air" drones in which the drones which uses the principle of buoyancy. Wing type and rotor type come under the "Heavier than Air" drones. Wing and rotor are further divided as wing type multirotor, fixed-wing, flapping wing, single-rotor and fixed wing hybrid[10]. Based on take-off and landing it is further divided into two types as horizontal take-off and landing(HTOL) and vertical take-off and landing(VTOL)[11].

The classification of drones based on total weight including payload in India is shown in Table 1 [12]:

Table 1. Types of Drones

Sl. No	Type	Payload
1	Nano	≤250 Grams
2	Micro	>250 Grams and ≤ 2Kg
3	Small	>2 kg and ≤ 25 Kg
4	Medium	>25 Kg and ≤ 150 Kg
5	Large	> 150 Kg

2.3 Regulations on Drones in India

The Director General of Civil Aviation (DGCA) has released a policy on regulation of drones on 27th August and came into effect on 1st December 2018 in India [12]. The policy briefs about the classification and restriction on drones. The operators must obtain license Unique Identification number and Unmanned Aircraft Operation permit.

Any drones imported to India have to obtain Equipment Type Approval (ETA) from Department of Telecommunication. Except Nano drone all the other drone categories should apply for DGCA clearance

Unique Identification Number (UIN)

All the drones except Nano Drones must obtain the Unique Identification Number (UIN) from the DGCA.

Unmanned Aircraft Operator Permit (UAOP)

The civil drone operators must obtain the permit from the DGCA. The DGCA should provide the permit within seven days of the application submitted date. The validity of the permit is for five years from the date of issue and should not be transferred.

Drones owned by government institutions are not required to get a permit. Nano drones operating below 50 ft and micro drones operating below 200 feet are exempted from taking permit and Micro drones. All the drones must be within the Visual Line of Sight of the Operator. The maximum height allowed for the drones for various categories is as follows: Nano drone-50 ft, Micro drone-200 ft, Small, Medium, Large drones-400 ft above ground level.

2.4 Application of Drones in Construction

It has been reported that drones have been used in various activities such as damage assessment and building maintenance [13], land surveying [9,14], Safety inspection [15-17], 3-D modelling [18-20], building inspection [21], drone assembly [22,23], monitoring of progress [24], site inspection and management [25], facility management [26,27], and 3-D printing [28].

2.5 Benefits and Barriers

A study of benefits of using drones in construction sites reported that *safety inspection* and *accessibility to inaccessible location* are the top benefits [29]. Some of the critical barriers to the use of drones are *limited battery life* and *weather-related issues* [30].

2.6 Summary

The "Global Construction 2030" states that the construction industry will grow by 85% by 2030. Construction industry is purely dependent on labour,

work and materials involved in construction change. Use of robots in construction can have advantages such as higher safety by deploying machines for dangerous jobs, high quality, increased productivity, and reduction in costs [31].

The technology adoption rate in the construction industry is lagging compared to other industries and usage of these technologies is proving challenging for the management [15,17]. The traditional techniques are replaced by drones and they provide enhanced performance and early accomplishment of tasks [32]. The drones are needed in various aspects for the development of the industry [6]. With limited literature on drones in Indian construction and the potential application is humongous, there is a need to investigate the adoption of drones in Indian construction. Hence, this study is aimed at assessing the awareness of the drone technology in and analyse the perceptions of key stakeholders on the relevance, application, benefits, barriers of using drones in construction and the impact of the same on the Key Performance Indicators (KPI) of projects. The scope of this study is limited to Indian construction and the stakeholders involved are Clients, Contractors and Consultants.

3 Research Methodology

The primary research methods used to achieve the intended objectives are literature review and questionnaire survey-based quantitative study. An in-depth literature review in the field of drones in construction has been attempted to identify the variables of study (relevance, application, benefits, barriers and KPI) and the indicators as presented in Figure 1.

3.1 Experimental Design

A questionnaire instrument has been designed for the quantitative study and deployed online. The questionnaire contained seven sections with questions related to the respondent's profile, awareness, relevance, application, benefits, barriers and KPI. Five-point Likert scales (of agreement and value) are used to measure the indicators of the variables identified. The questionnaire also had a cover note and two informative short videos for clarity and benefit of the respondents.

Target population for this study are clients, contractors and consultants in Indian construction industry. Stratified sampling is used.

Descriptive statistics is used for data analysis. *Relative Importance Index (RII)* is used to rank the indicators to understand the relative importance as perceived by the stakeholders. *ANOVA analysis* is used to check the statistical significance of the perceived differences between clients, contractors and consultants. Cronbach Alpha is used for internal consistency and data reliability for analysis.

3.2 Data Collection

The questionnaire instrument is deployed on Google Forms and the enquiries are sent to over 100 prospective Indian respondents (clients, contractors & consultants) through Email, LinkedIn, and over phone. There are 75 valid responses received, which includes coincidentally 25 each from the three stakeholder groups after continuous follow-up in a span of 4 weeks.

4 Data Analysis, Results and Discussion

The data collected is screened and codified for further analysis.

4.1 Data Analysis

Cronbach Alpha is used to evaluate the internal consistency of the instrument and reliability of the data collected for further analysis. The calculated Cronbach Alpha values are presented in Table 2. It is observed that all the values are greater than 0.8 (except for KPI), which is very good, and the data collected is reliable for further analysis.

Descriptive data analysis is conducted to understand the profile of the respondents and awareness levels. *Relative Import Index (RII)* is computed for all the indicators and ranked overall and within stakeholder groups for observation. *ANOVA* test have been conducted to check for statistical significance in difference in opinion of respondent groups.

4.2 Results

Among the 75 respondents 88% belonged to private sector and rest to public sector. Majority of the respondents (~70%) are from large organisations base on turnover (>INR2500M) and number of employees (>250). It has been observed that 12, 32 & 56% of respondents represent top, middle & operations management in their respective organisation. It is also interesting to note that most of the respondents (76%) less than 5 years of experience and 15 & 8% of respondents having an experience of 5-10 & 10-20 years respectively (Figure 2). A little fraction of them have more than 20 years of experience.

4.2.1 Awareness and Use of Drones

The results of the analysis on the awareness and use of drones are shown in Figure 3 and 4. The results show that 83% of the respondents were aware of drone and 17 % of them were unaware. Among the respondents who are aware of drones, 85% of them have not used drones and 15% of them have used drones in various operations.

Code	Relevance of drones [R]
R1	Drone is an emerging robot in the field of construction
R2	Automation and robotics have an impact on construction industry
R3	Drones have potential uses in the construction industry
R4	It is simple for me to use the existing drone technology
R5	Drone are compatible to the construction industry
R6	Drones are still in inception stage in implementing when it comes to construction
R7	Drones must be experimented before using it in the construction projects
R8	Drones are difficult to handle and require a skilled personnel to handle it

Code	Application [A]
A1	Surveying
A2	Inspection
A3	3-D Modelling
A4	3-D Printing
A5	Drone Construction
A6	Progress Reporting
A7	Safety Monitoring
A8	Facility Management
A9	Logistic and Tracking
A10	Emergency Response and Accessibility
A11	Advertising and Marketing

Codes	Benefits of drones [B]
B1	Drones provide real time updates from the site
B2	Drones can fly to inaccessible areas and hazardous areas
B3	Drones decrease the cost of projects
B4	Drones can carry out the work faster
B5	Drones provide easier access to data to professionals of different department
B6	Drones create new job opportunities and add value to construction
B7	Drones help in accurate and enhanced data collection
B8	Drones help in effective communication
B9	Drones reduce the safety risks
B10	Drones improve the productivity
B11	User friendliness and Eco

Codes	Barriers of drones [BA]
BA1	Loss of Data and Signal
BA2	Limited Payload and Battery life
BA3	Weather related issues
BA4	Acquisition and maintenance cost
BA5	Owner and Management support
BA6	Accidents and interference in sites
BA7	Air traffic restriction and regulation
BA8	Requirement of skilled professional
BA9	Privacy Issues

Codes	Key Performance Indicators [K]
K1	Cost
K2	Time
K3	Quality
K4	Health and Safety
K5	Stakeholder Satisfaction

Figure 1. Indicators of Relevance, Application, Benefits, Barriers and KPI

Table 2. Cronbach Alpha

Variable	Questions	Cronbach Alpha
Relevance	Q1-Q8	0.87
Application	Q9-Q19	0.90
Benefits	Q20-Q30	0.88
Barriers	Q31-Q39	0.79
KPI	Q40-Q44	0.57
Overall	Q1-Q44	0.94

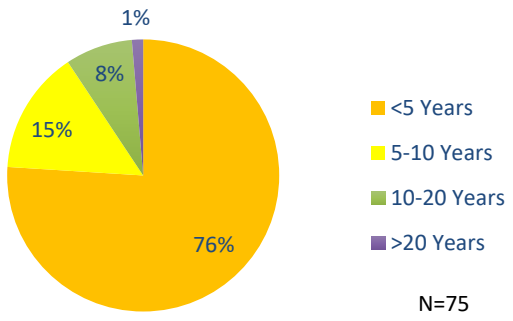

Figure 2. Experience of Respondents

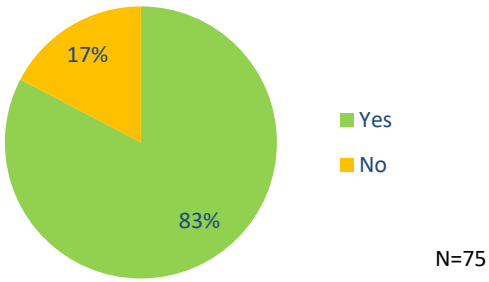

Figure 3. Awareness on Drones

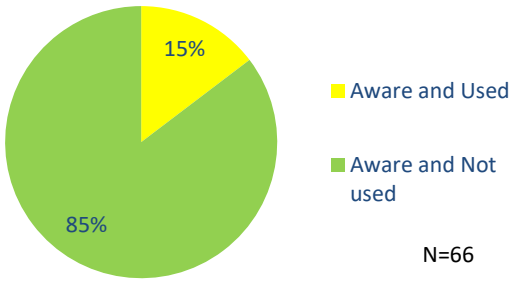

Figure 4. Awareness and Usage Chart

4.2.2 Relative Importance of Indicators (Overall)

RII has been calculated for all the indicators of chosen variables (Figure 1) using the data from all the respondents. RII along with the frequency distribution of individual ratings of indicators is presented variable-wise in Figure 5. The overall pattern in the data and RII revealed that the respondents have rated most of the indicators highly important. The top-rated indicators within the chosen variables are presented in Figure 6.

4.2.3 Relative Importance of Indicators (within stakeholder groups)

Indicators of the chosen variables are ranked using RII that is calculated based on the responses from three difference stakeholder groups (C1-Contractors, C2-Consultants and C3-Clients) in order to compare the perspectives of these groups on the relative importance. The results are presented in Table 3(a-e). The pattern in the results indicate there are differences in the relative importance of the indicators.

Table 3. Relative importance of indicators (within stakeholder groups)

a) Relevance

	C1	Rank	C2	Rank	C3	Rank
R1	**0.73**	**2**	**0.77**	**2**	**0.70**	**2**
R2	0.70	4	**0.74**	**3**	0.63	5
R3	**0.72**	**3**	0.67	7	0.66	4
R4	0.70	4	0.63	8	0.62	6
R5	0.70	4	0.71	5	**0.70**	**1**
R6	**0.74**	**1**	0.70	6	0.66	4
R7	**0.73**	**2**	**0.78**	**1**	**0.69**	**3**
R8	**0.74**	**1**	0.73	4	0.66	4

b) Application

	C1	Rank	C2	Rank	C3	Rank
A1	**0.77**	**2**	**0.79**	**1**	**0.77**	**1**
A2	0.70	5	**0.74**	**3**	0.66	7
A3	0.67	6	0.73	5	0.69	5
A4	0.64	7	0.68	7	0.70	4
A5	0.62	8	0.71	6	0.62	8
A6	**0.77**	**2**	0.74	4	**0.72**	**3**
A7	**0.75**	**3**	**0.79**	**1**	**0.74**	**2**
A8	0.67	6	0.73	5	0.67	6
A9	0.70	5	0.71	6	0.66	7
A10	**0.78**	**1**	**0.78**	**2**	**0.74**	**2**
A11	0.72	4	0.66	8	0.66	7

c) Benefits

	C1	Rank	C2	Rank	C3	Rank
B1	**0.78**	**2**	**0.79**	**1**	**0.79**	**1**
B2	**0.79**	**1**	0.74	4	**0.73**	**2**
B3	0.62	10	0.69	7	0.66	6
B4	0.62	10	0.69	7	0.66	6
B5	0.70	8	0.74	4	0.70	4
B6	0.67	9	0.74	4	**0.71**	**3**
B7	**0.77**	**3**	**0.76**	**2**	**0.73**	**2**
B8	0.73	5	0.73	5	0.70	4
B9	0.74	4	**0.75**	**3**	0.70	4
B10	0.72	6	0.73	5	0.68	5
B11	0.71	7	0.72	6	0.70	4

d) Barriers

	C1	Rank	C2	Rank	C3	Rank
BA1	0.72	8	0.70	5	**0.72**	**3**
BA2	0.76	4	**0.73**	**3**	0.65	7
BA3	**0.81**	**1**	**0.77**	**1**	0.71	4
BA4	0.75	5	**0.74**	**2**	0.68	6
BA5	0.74	6	**0.77**	**1**	**0.78**	**1**
BA6	0.73	7	0.71	4	**0.76**	**2**
BA7	**0.77**	**3**	0.70	5	0.70	5
BA8	**0.78**	**2**	**0.74**	**2**	**0.72**	**3**
BA9	0.71	9	0.70	5	**0.72**	**3**

e) Impact on KPI

	C1	Rank	C2	Rank	C3	Rank
K1	0.70	4	0.72	3	**0.72**	**3**
K2	0.67	5	0.68	5	0.64	5
K3	**0.72**	**3**	**0.74**	**2**	**0.75**	**1**
K4	**0.76**	**2**	**0.75**	**1**	**0.74**	**2**
K5	**0.82**	**1**	**0.72**	**3**	0.66	4

C1-Contractors C2- Consultants C3-Clients

4.2.4 ANOVA Analysis

It has been attempted to test this difference in perceived relative importance among Contractors, Consultants and Clients is by chance or statistically significant using ANOVA analysis at 5% significance level. The test results are shown in Table 4.

Table 4. ANOVA Analysis

Variables	F	p-value	F-crit
Relevance (R)	4.553	**0.011**	3.011
Application (A)	3.134	**0.044**	3.007
Benefits (B)	2.075	0.126	3.007
Barriers (BA)	2.948	0.053	3.009
KPI (K)	1.379	0.253	3.020

It can be noted that p-value is less than 0.05 for variables Relevance (R) and Application (A) that implies that there is statistically significant difference in perception among C1, C2 & C3. There is no significant difference with respect to other three variables.

4.3 Discussion

While high level of awareness is a welcome sign, low levels of actual usage must be looked in to by promoting the benefits/drivers and addressing the barriers. It is also supported in the higher ratings for relative importance for various indicators. Top rated relevance *Drones must be experimented before using it in the construction projects* (R7) implies that there is a need to demonstrate the use/benefits of drone through use cases. The most relevant applications for drones are *Surveying* (A1), *Emergency Response and Accessibility* (A10) and *Safety Monitoring* (A7). Necessary action plans may be drawn

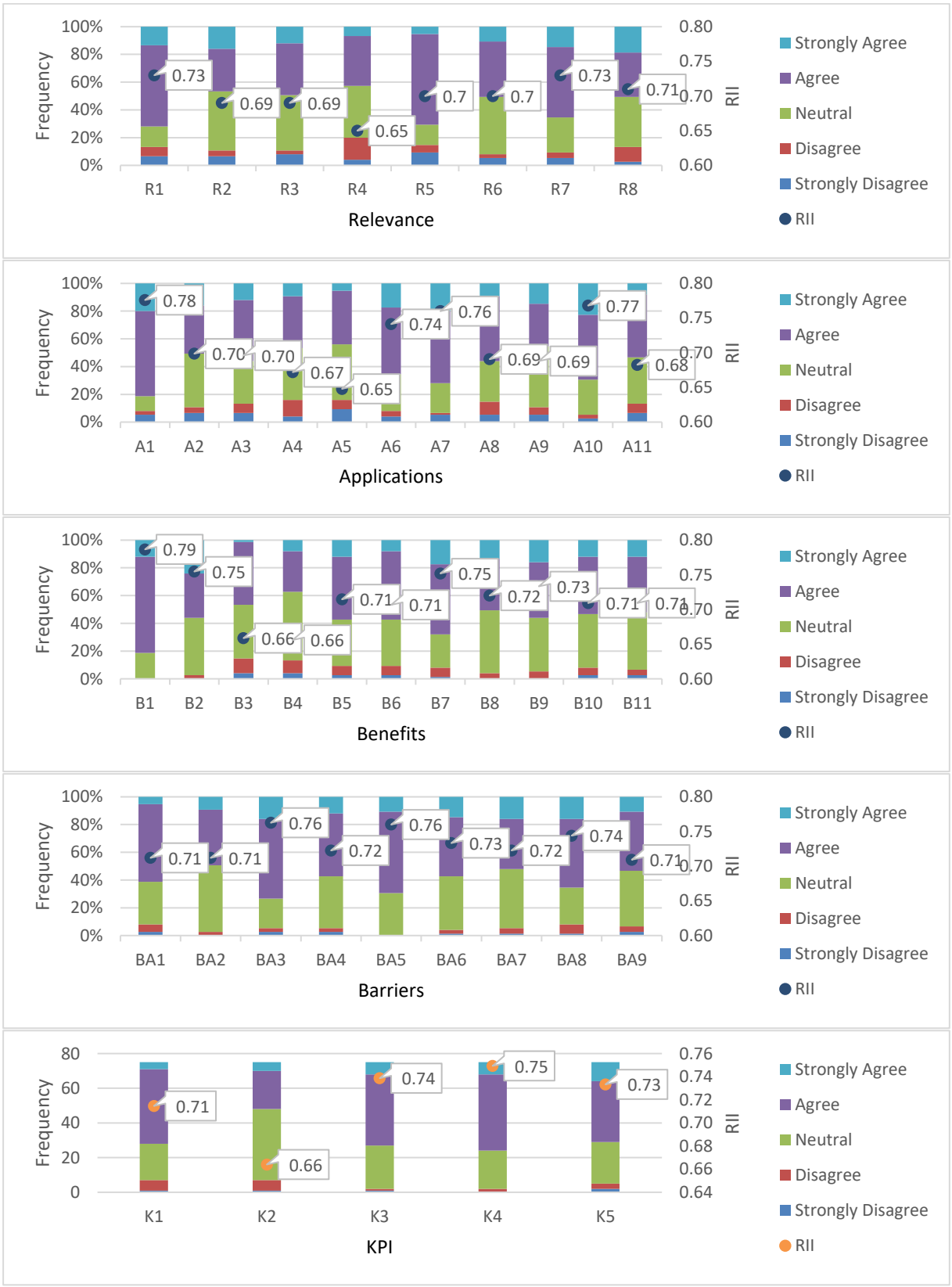

Figure 5. Frequency distribution & RII of indicators (overall)

Code	Variables/Indicators	RII	Rank
	Relevance		
R7	Drones must be experimented before using it in the construction projects	0.73	1
R1	Drone is an emerging robot in the field of construction	0.73	1
R8	Drones are difficult to handle and require a skilled personnel to handle it	0.71	2
	Application		
A1	Surveying	0.78	1
A10	Emergency Response and Accessibility	0.77	2
A7	Safety Monitoring	0.76	3
	Benefits		
B1	Drones provide real time updates from the site (through video)	0.79	1
B2	Drones can fly to inaccessible areas and hazardous areas	0.75	2
B7	Drones help in accurate and enhanced data collection	0.75	2
	Barriers		
BA3	Weather related issues	0.76	1
BA5	Owner and Management support	0.76	1
BA8	Requirement of skilled professional	0.74	2
	Key Performance Indicators		
K4	Health and Safety	0.75	1
K3	Quality	0.74	2
K5	Stakeholder Satisfaction	0.73	3

Figure 6. Top rated indicators based on RII (overall)

by the professional organisations & educational institutions to instil the skills required. The highly rated benefits are *Drones provide real time updates from the site* (B1), *Drones can fly to inaccessible areas and hazardous areas* (B2) and *Drones help in accurate and enhanced data collection* (B7). This information may be of great value for the construction contractors and drone operators. The key barriers for the adoption of drones in Indian construction are: *Weather related issues* (BA3), *Owner and Management support* (BA5) and *Requirement of skilled professional* (BA8). The project managers and drone manufacturers/operators may find this information useful to plan their business/project objectives. *Health and Safety* (K4), *Quality* (K3) and *Stakeholder Satisfaction* (K5) are the most important KPIs impacted by the use of drones. These are in line with the demands of changing business environment.

5 Summary and Conclusions

Efficient project delivery is a continuous challenge in construction. With growing complexity and uncertainty in project environments, it more prudent to promote innovate solutions to overcome the challenges and create value for the stakeholders involved. Automation and robotics have been promising in efficient and safer construction projects. However, the uptake of robot technology such as drones/UAV is slow in Indian construction. It has been attempted to study the level of awareness & use of drones as well as benefits, barriers & impact on the KPIs.

It has been observed that there is high level of awareness of drones and low level of usage in Indian construction. The overall pattern in the data revealed that the respondents have rated most of the indicators highly important. Following are the top-rated attributes: *Drones must be experimented before using it in the construction projects* (relevance); *Surveying* (application); *Drones provide real time updates from the site* (benefit); *Weather related issues* (barrier) and *Health and Safety* (KPI). ANOVA analysis revealed that there is statistically significant difference in perception among contractors, consultants and clients with respect to relevance & application of drones and not so for benefits, barriers & impact on KPI.

The sample size of the groups is limited in this study and a larger sample size may unfold results that can be generalised with much more confidence. It is worth investigating the relationship between the application, benefits, barriers an KPIs for more insight. Also, a detailed study among public & private clients shall be useful in formulating strategies for greater adoption of drones.

6 References

[1] Loganathan, S., Srinath, P., Kumaraswamy, M., Kalidindi, S. N. and Varghese, K. Identifying and addressing critical issues in the Indian construction industry: Perspectives of large building construction clients. J. Constr. Dev. Ctries., 22:121–144, 2017.

[2] Ofori, G. Construction in developing countries: A research Agenda. J. Constr. Dev. Ctries., 11:1–16, 2006.

[3] Bogue, R. What are the prospects for robots in the construction industry? Ind. Rob., 45:1–6, 2018.

[4] Okpala, I., Nnaji, C. and Awolusi, I. Emerging Construction Technologies: State of Standard and Regulation Implementation. ASCE International Conference on Computing in Civil Engineering 2019, Atlanta, USA, 153–161, 2019.

[5] Davila Delgado, J. M., Oyedele, L., Ajayi, A., Akanbi, L., Akinade, O., Bilal, M. and Owolabi, H. Robotics and automated systems in construction: Understanding industry-specific challenges for adoption. J. Build. Eng., 26:100868, 2019.

[6] Mosly, I. Applications and Issues of Unmanned Aerial Systems in the Construction Industry. Int. J. Constr. Eng. Manag., 6(6):235–239, 2017.

[7] Rao, B., Gopi, A G., and Maione, R. The societal impact of commercial drones. Technol. Soc., 45:83–90, 2016.

[8] Kardasz, P. and Doskocz, J. Drones and Possibilities of Their Using. J. Civ. Environ. Eng., 6(3):1000233, 2016.

[9] Siebert, S. and Teizer, J. Mobile 3d mapping for surveying earthwork using an unmanned aerial vehicle (UAV) system. Automation in Construction, 41:1-14, 2014.

[10] Liew, C. F., DeLatte, D., Takeishi, N. and Yairi, T. Recent Developments in Aerial Robotics: A Survey and Prototypes Overview. Robotics, ArXiv, abs/1711.10085, 2017.

[11] Singhal, G., Bansod, B. and Mathew, L. Unmanned Aerial Vehicle Classification, Applications and Challenges: A Review. Preprint, doi:10.20944/preprints201811.0601.v1 1–19, 2018.

[12] MOCA, Govt of India. Drone ecosystem policy road map. < https://digitalsky.dgca.gov.in/ > 2019.

[13] Zhou, S. and Gheisari, M. Unmanned aerial system applications in construction: a systematic review. Constr. Innov., 18:453–68, 2018.

[14] Li, Y. and Liu, C. Applications of multirotor drone technologies in construction management. Int. J. Constr. Manag., 19:401–412, 2018.

[15] Irizarry, J., Gheisari, M. and Walker, B. N. Usability assessment of drone technology as safety inspection tools. Electron. J. Inf. Technol. Constr. 17:194–212, 2012.

[16] Gheisari, M. and Esmaeili, B. Unmanned Aerial Systems (UAS) for Construction Safety Applications. Construction Research Congress 2016, CRC 2016, San Juan, Puerto Rico, 2642-2650, 2016.

[17] Melo, R. R. S., Costa, D. B., Álvares, J. S. and Irizarry, J. Applicability of unmanned aerial system (UAS) for safety inspection on construction sites. Saf. Sci., 98:174–185, 2017.

[18] Anwar, N., Najam, F., Amir Izhar, M. and Ahmed Najam, F. Construction Monitoring and Reporting using Drones and Unmanned Aerial Vehicles (UAVs). The Tenth International Conference on Construction in the 21st Century (CITC-10), Colombo, Sri Lanka, 2018.

[19] Yamazaki, F., Matsuda, T., Denda, S. and Liu, W. Construction of 3D models of buildings damaged by earthquakes using UAV aerial images. Proceedings of the Tenth Pacific Conference on Earthquake Engineering Building an Earthquake, Sydney, Australia, 2015.

[20] Iglesias, L., De Santos-Berbel, C., Pascual, V. and Castro, M. Using small unmanned aerial vehicle in 3D modeling of highways with tree-covered roadsides to estimate sight distance. Remote Sens., 11:2625, 2019.

[21] Entrop, A. G. and Vasenev, A. Infrared drones in the construction industry: Designing a protocol for building thermography procedures. Energy Procedia, 132:63–68, 2017.

[22] Latteur, P., Goessens, S., Mueller, C. T., Kawaguchi, K., Ohsaki, M., Takeuchi, T., Goessens, S. and Mueller, C. Masonary Construction with drones. IASS Annual Symposium, Spatial Structures in the 21st Century, Tokyo, Japan, 2016.

[23] Lindsey, Q., Mellinger, D. and Kumar, V. Construction of cubic structures with quadrotor teams. Robot. Sci. Syst., 7:177–84, 2012.

[24] Lin, J. J., Han, K., Golparvar-Fard, M., A Framework for Model-Driven Acquisition and Analytics of Visual Data Using UAVs for Automated Construction Progress Monitoring, International Workshop on Computing in Civil Engineering, Austin, Texas, 2015.

[25] Bryan, Hubbard., Heng, Wang., Michael, Leasure., Tim, Ropp., Tamara, Lofton. and S, H. Feasibility Study of UAV use for RFID Material Tracking on Construction Sites. 51st ASC Annu. Int. Conf. Proc., 669–676, 2015.

[26] Ezequiel, C. A. F., Cua, M., Libatique, N. C., Tangonan, G. L., Alampay, R., Labuguen, R. T., Favila, C. M., Honrado, J. L. E., Canos, V., Devaney, C., Loreto, A. B., Bacusmo, J. and Palma, B. UAV aerial imaging applications for post-disaster assessment, environmental management and infrastructure development. Int. Conf. Unmanned Aircr. Syst. ICUAS 2014, 274–283, 2014.

[27] Curran, M., Spillane, J. and Clarke-Hagen, D. Urban Development and Construction Project Management Issues considering External Stakeholders. In Proceedings of the RICS COBRA Conference, 1-8, 2018.

[28] Hunt, G., Mitzalis, F., Alhinai, T., Hooper, P. A, and Kovac, M. 3D printing with flying robots. Proc. - IEEE Int. Conf. Robot. Autom., Hong Kong, 4493–4499, 2014.

[29] Calantropio, A. The use of UAVs for performing safety-related tasks at post-disaster and non-critical construction sites. Safety, 5(4), 64: 1-12, 2019.

[30] Golizadeh, H., Hosseini, M. R., Edwards, D. J., Abrishami, S., Taghavi, N. and Banihashemi, S. Barriers to adoption of RPAs on construction projects: a task–technology fit perspective. Constr. Innov. 19:149–69, 2019.

[31] Elattar, S. M. S. Automation and Robotics in Construction: Opportunities and Challenges. Emirates J. Eng. Res., 13:21–6, 2008.

[32] Opfer, N. D. and Shields, D. R. Unmanned aerial vehicle applications and issues for construction. ASEE Annu. Conf. Expo. Conf. Proc., Indianapolis, 2014.

Examination of Efficiency of Bridge Periodic Inspection Using 3D Data (Point Cloud Data and Images)

Tatsuru Ninomiya[a] , Mami Enomoto[a] , Mitsuharu Shimokawa[a] ,

Tatsuya Hattori[a] and Yasushi Nitta[b]

[a] Public Works Research Institute
[b] Ministry of Land, Infrastructure and Transport
E-mail: sentan@pwri.go.jp

Abstract –

Many of Japan's bridges built during the period of high economic growth are deteriorating and require proper maintenance. However, due to the shortage of specialist in the field of civil engineering as well as the declining birthrate and aging population, the current bridge periodic inspection the proximity visual inspection and the preparation of inspection reports require a lot of work by each inspection engineer. To promote bridge inspection using robots such as UAVs, we have been improving efficiency in on-site inspection and the documentation of inspection results. The current challenges in this effort are the management of a vast number of images, image analysis and damage detection, and the accurate recording of damage locations. In this report, we present the results of the accuracy test of 3D bridge data generated by Structure from Motion (SfM) and explain the management of images using 3D data.

Keywords –

Bridge maintenance; Bridge periodic inspection; Inspection robot(UAV); Structure from Motion(SfM); 3D data(Point cloud data)

1 Introduction

Many Japanese bridges constructed during the period of high economic growth are aging and require proper maintenance. Due to the shortage of specialist in the field of civil engineering as well as the declining birthrate and aging population, realization of more efficient bridge inspection is an urgent issue for proper maintenance of bridges.

Bridge periodic inspections every five years in Japan require a lot of labor, time and cost, and for on-site visual inspection and preparation of inspection reports. MLIT (Ministry of Land, Infrastructure, Transport and Tourism) which manages bridges, has published Guidelines For Using New Technology for the purpose of streamlining bridge inspections, and is actively promoting the use of inspection robots.

In that case, it is necessary to efficiently perform, Managing the tremendous amount of images acquired from robots, Recognizing degradation in image, and Accurate recording of degradation position.

In recent years, UAVs and computer vision have been utilized in various fields of civil engineering.[1] Among these technologies, we focused on SfM, which automatically estimates the shooting position and shooting direction of images shot continuously in 3D space, generates 3D data of the shooting target.

In this paper, in order to improve efficiency the field work and record creation work of the bridge periodic inspection, we report the status of the examination up to now regarding bridge inspection using 3D data.

2 Research Content

In order to verify the possibility of bridge inspection using robots and 3D data, we examine the following three processes for the South Loop Bridge on the site of PWRI(Public Works Research Institute).

1. Efficient image shooting by a bridge inspection robot
2. Generation of 3D data of bridge by SfM
3. Image management method using 3D data

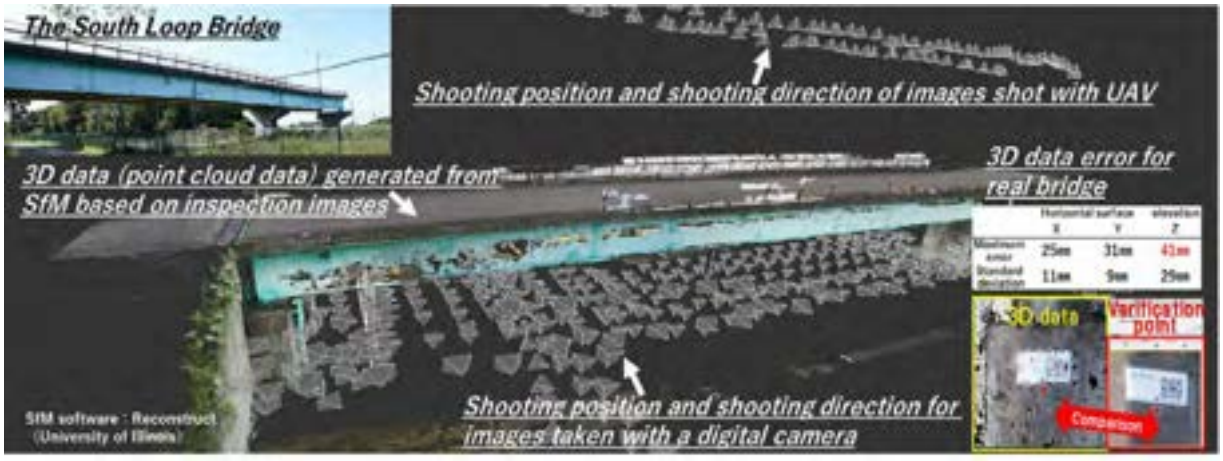

Figure 1. 3D data of South Loop Bridge generated from SfM

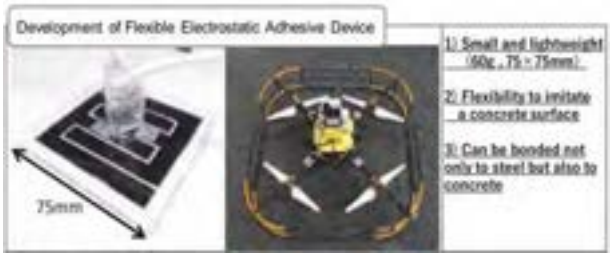

a) Development of infrastructure inspection system using semi-autonomous multi-copter equipped with flexible electrostatic adhesive device

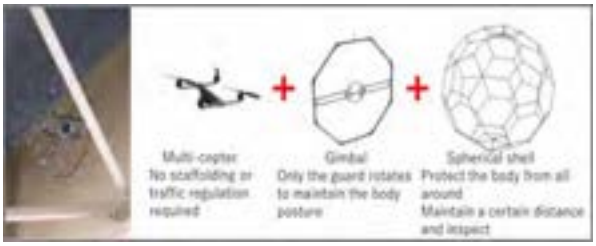

b) Development of UAV for Observing and Hammering Aged Bridges at Short Range

Figure 2. Example of bridge inspection robot developed by SIP[3]

3 Generation of 3D Data and Image Management Using Images of Bridge Inspection Robots (UAVs, etc.)

3.1 Accuracy Verification of Generated 3D Data

In this paper, the bridge was shoot with a UAV (Phantom4Pro made by DJI) and a digital camera (α7R2 made by SONY). It was confirmed that the 3D data of the bridge can be generated by SfM from the shooting image and that the position and direction of the captured image can be expressed in the 3D space. 'Figure 1'

The coordinates of the verification points on the actual bridge obtained from the survey criteria and the coordinates of the verification points on the 3D data were compared. The error of all verification points was within 5 cm, which satisfied the quality control standard defined by MLIT. 'Figure 1' [2]

3.2 Applicability to Bridge Inspection Robot

Figure 1 shows 3D data generated from images of general UAVs and digital cameras. Furthermore, by utilizing the robots specialized for advanced bridge inspection developed by the Cabinet Office's SIP (Cross-ministerial Strategic Innovation Promotion Program), more detailed bridge photography can be performed. 'Figure 2' [3]

By generating 3D data from the images taken by such a bridge inspection robot, it becomes possible to manage images taken of the damage conditions inside members and girders.

3.3 Management Example of Image Shooting Position Using 3D Data

3.3.1 Bearing

As shown in 'Figure 3 a)', the area around the bearing is often complicated due to abutments, floor slabs, main girders, and various piping. This area is generated as 3D data by SfM, and the shooting

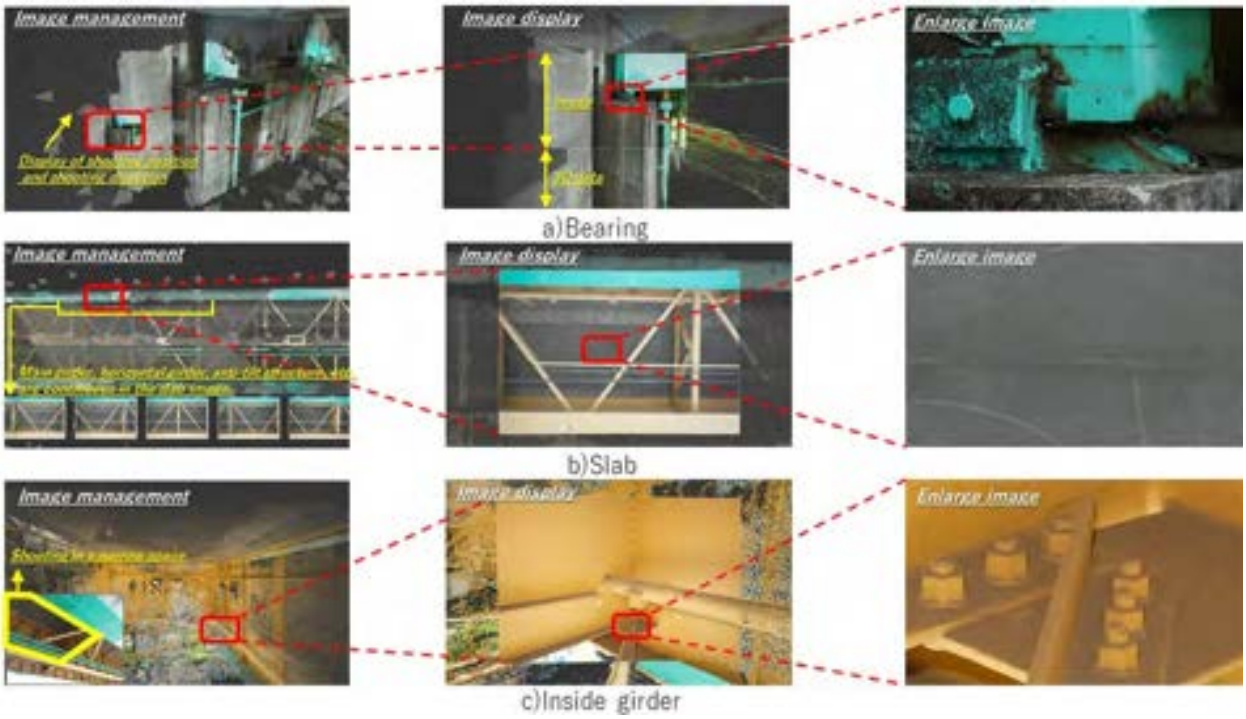

Figure 3. Image management example using 3D data

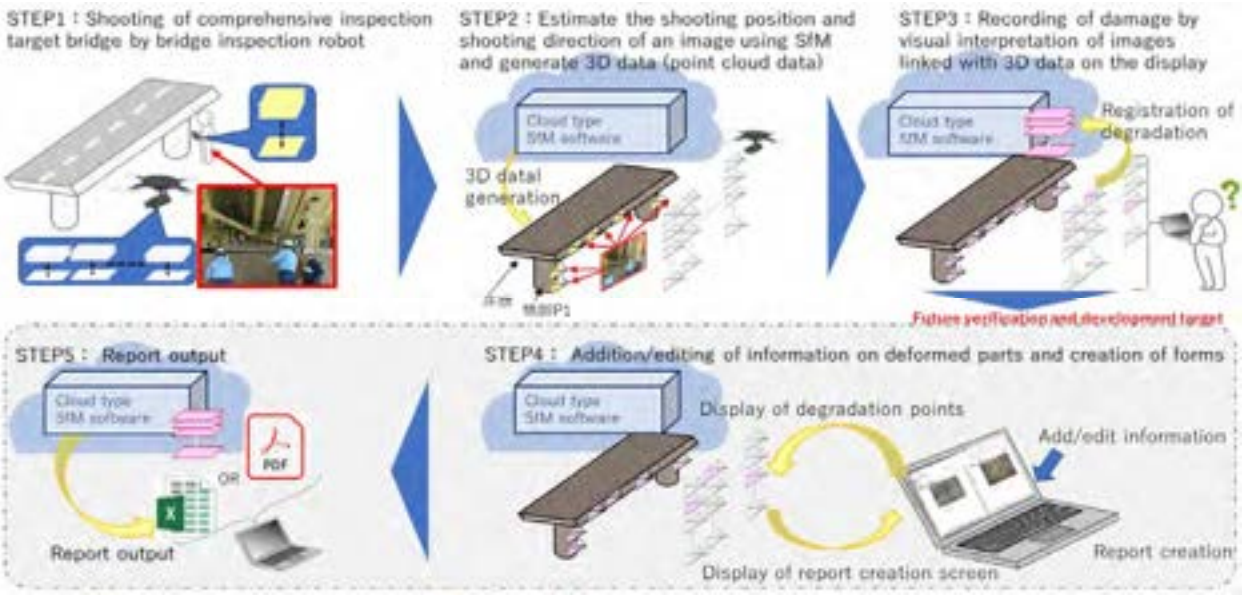

Figure 4. Bridge periodic inspection method utilizing 3D data

position and direction of the image can be expressed as a quadrangular pyramid in 3D space.

When the image of the bearing is displayed, it is displayed so as to match the 3D data, and the accuracy of the automatically estimated shooting position and shooting direction can be confirmed.

3.3.2 Slab

As shown in 'Figure 3 b)', the inspection results of slab in the current bridge inspection are managed by span. When the slab is continuously and comprehensively photographed, slab, main girders, horizontal girders, and the like are repeated, so a large number of images with the same contents are stored,

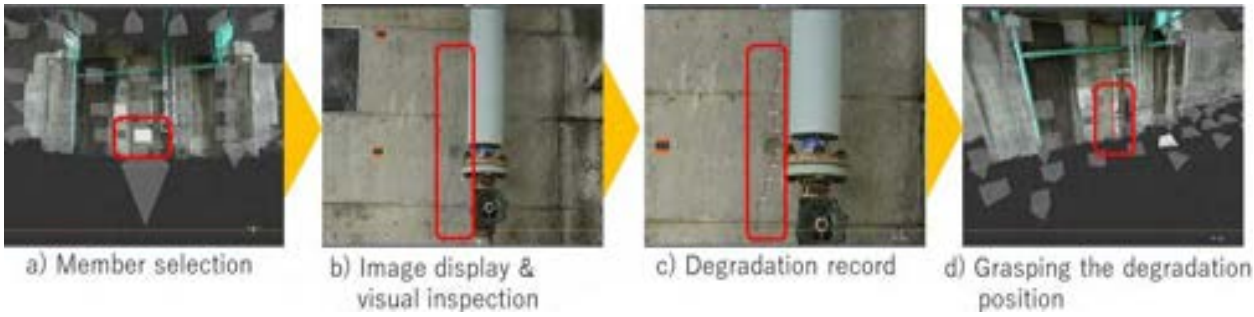

Figure 5. Visual confirmation of image degradation and recording example

and it becomes difficult to estimate the shooting positions of them later.

However, SfM's automatic image shooting position estimation and automatic association of 3D data with images can improve the efficiency of such continuous-image management.

3.3.3 Inside Girder

As shown in 'Figure 3 c)', It is difficult to manually record the image inside girder in the image shooting direction. The reason is that the shooting is focused on checking the condition of slab, the main girder, the anti-tilt structure, etc., and that the shooting is performed in a narrow space surrounded by the main girder and the horizontal girder.

By automatically estimating the shooting direction of the image with SfM, it is possible to manage the image of only the local part such as the bolt inside the girder and the corrosion condition of the anti-tilt structure.

4 Bridge Periodic Inspection Utilizing 3D Data

4.1 Proposal of Bridge Periodic Inspection Method Utilizing 3D Data

Based on the examination results to date, we propose a bridge periodic inspection method that uses 3D data generated by SfM as a solution to the problem which are Efficiency of inspection work, recording accuracy of deformed position of bridge inspection. 'Figure 4' This study does not limit the generation of 3D data, the estimation of the shooting position, direction of images to SfM in consideration of future technological development and development of this inspection method.

Since this inspection method generates 3D data by SfM, it is premised and important that robots shoot a comprehensive image of the bridge. After that, the inspection engineer will visually inspect only the areas where the degradation can be confirmed from the images taken by the bridge inspection robot and the areas where it was difficult to take images. The characteristics of the inspection method are as follows.

4.1.1 Efficiency Improvement of Visual Inspection for Actual Bridge

When the degradation of the member is confirmed on the image, the position of it can be grasped by referring to 3D data. In addition, an engineer will visually inspect the actual bridge depending on the condition of the degradation.

Therefore, it is possible to narrow down the scope of visual inspection on-site by the engineer in advance in the office.

4.1.2 Enhancing the Record of Changes in Visual Inspections by Engineers

The scope of visual inspection by the engineer is narrowed down, and more detailed degradation inspection can be performed on the degradation, so the contents of the recording of the degradation status are enriched.

4.1.3 Upgrading of Degradation Management by Utilizing 3D Data

By managing images and degradations by associating them with the three-dimensional data of the bridge, the shooting position and shooting direction will become clear, and it will be possible to guide the degradation shooting with the same angle of view in later years. In addition, by comparing images having the same shooting angle of view, it is possible to contribute to highly accurate progress grasp of aged deterioration.

4.2 Degradation Recording Example on Image

One of the merits of utilizing 3D data in bridge inspection is the possible to check and record the state of degradation on images managed in association with 3D data.

After 3D data is generated from the image by SfM,

the image of the member to be confirmed is displayed, and the content of the degradation is recorded on the image for which the degradation can be confirmed. ‘Figure 3 a)~c)’ The degradation is recorded in association with the 3D data, and the position of the degradation can be grasped on 3D data even when the image is not displayed. ‘Figure 3 d)’

5 Summary

This paper reported the research results on the method of utilizing 3D data for the purpose of improving the efficiency of periodical bridge inspection. As a concrete content, the basic verification result of the 3D data accuracy of the bridge generated by SfM was shown, and the image management method using the 3D data was proposed. This paper is summarized as follows;

1. We proposed a bridge periodic inspection method using 3D data as a solution to the problems of bridge inspection (many image management, accurate recording of degradation position) when using robots.
2. It was shown that the 3D data of bridges generated by SfM from the images taken continuously and automatically by UAV satisfy the quality control standards set by MLIT.
3. We proposed an image management method and a degradation confirmation method using 3D data. The feasibility of periodical bridge inspection using 3D data was also shown by introducing application examples.

The information generated by the proposed method in this paper, such as a set of image angles and perspectives and 3d structure by SfM, has not been applied in bridge inspection phase. Utilizing those infomation to improve the whole management cycle, which is not limited to the inspection, will contribute to improvement of the productivity in the entire construction field. Future research contents assume points listed below;

1. Confirmed to the bridge manager and the inspection engineer "Recording method for image degradation and expression method on 3D data" and "Delivery standard and management method for products of bridge periodical inspection utilizing 3D data" To do. Based on the results, we will study the workflow, functional requirements and related standards for social implementation.
2. It takes a great deal of effort to grasp the degradation on the image because the engineer performs visual inspection. Therefore, we will study support technologies that can efficiently detect degradations from images (automatic extraction of degradations by AI, emphasis on degradations by image processing).
3. By managing the images at the time of completion using this method, we will examine the utility of this method during emergency inspections such as grasping the displacement and degradation of the bridge structure after an earthquake.

References

[1] Youngjib Ham. Kevin K.Han. Jacob J Lin and Mani Golparvar Fard. Visual monitoring of civil infrastructure systems via camera-equipped Unmanned Aerial Vehicles (UAVs), a review of related works， Visualization in Engineering， 4 Article number: 1， 2016.

[2] Mitsuharu Shimokawa. Yasushi Nitta. Tatsuru Ninomiya and Yoichi Tanaka. Consideration on 3D management of bridge inspection image, Construction and Construction Machinery Symposium， pages 177–188， 2019.

[3] Cabinet Office. Infrastructure Maintenance, Renovation and Management, Cabinet Office, 2017.

Experimental Result of Third-person View Generation using Deliberately Delayed Omni-directional Video

A. Sakata[a] , Y. Hada[a] , R. Hojo[a] , M. Munemoto[a] ,
Y. Takeshita[b] , T. Asuma[b] , and S. Kitahara[b]
[a]Kogakuin University
[b]Kumagai Gumi Co., Ltd.
E-mail: am20033@ns.kogakuin.ac.jp, had@cc.kogakuin.ac.jp, am19050@ns.kogakuin.ac.jp, am19055@ns.kogakuin.ac.jp, yoshito.takeshita@ku.kumagaigumi.co.jp, tsubasa.asuma@ku.kumagaigumi.co.jp, skitahar@ku.kumagaigumi.co.jp

Abstract –

This study developed a system that generates video from a view following a robot, using composition CG of the present position of the robot using deliberately delayed video on the robot for displaying the current position and orientation of the robot. The proposed view generation method overcomes the disadvantage of conventional methods because it always has a close-up view, and has the advantage of the video making it easy to understand the area around the robot. In this study, we verified the advantage of this method experimentally using a crawler carrier and the robot, and addressed some problems.

Keywords –

Past image; Remote control; Bird's-eye view

1 Introduction

When a disaster occurs, unmanned construction is used for recovery and investigation using a construction machine in a safe area. In general remote-control and unmanned construction, the pilot controls using the subjective view sent to the pilot's terminal by a camera on a construction machine, or a third-person view sent by a camera installed in the surroundings. Subjective view has the advantage that it can be seen in front of the construction machine at all times, and third-person view has the advantage that it is easy to determine when the construction machine is about to hit obstacles. However, subjective view and bird's-eye view videos have parts that cannot be seen or are difficult to see. The purpose of this research was to develop a system that generates video from a view behind the robot by composition CG of the present position of the robot, using deliberately delayed video from the robot.

2 Related research

2.1 Classification and advantage of camera view

In remote control, camera images are used to understand the environment of the construction machine.

Here, we classify the installation positions of the cameras and the obtained images, and describe the advantages and disadvantages thereof.

- Subjective view

Generally, the camera is installed in the driver's seat of the construction machine, and a subjective image is taken as if the operator is looking forward from the driver's seat. A typical obtained image is shown in Figure 1.

Subjective images are realistic and easy for the operator to imagine, and the device is simple and fully contained in the construction machine; thus, the usage cost is low. However, the general camera can only retrieve limited information because its viewing angle is narrower than the human viewing angle. Thus, there are cases where multiple cameras are installed or a fisheye camera with a wider viewing angle is used [1].

Figure 1. Example of subjective view

- Swingable subjective view

In a previous study, the attachment of a swing mechanism was attached to the camera to allow the operator to check the sides and back to overcome the narrow viewing angle of subjective images [2]. However, it is not possible to change the large view such as leaning forward to check the rear like in a manned vehicle, and the viewing angle is limited. In addition, the swing mechanism is operated separately; VR technology can be used to simplify this[3].

- Fixed third-person view

In unmanned construction, the condition of the construction site and the positional relationship of the construction machine therein are important. Thus, it is common to install cameras on pipe scaffolding or prefabricated scaffolding for a broad third-person view. An image from a typical fixed third-person-view video is shown in Figure 2. The third-person-view video may have a sensational discrepancy between the operation and the movement of the construction machine, because it does not always face the same direction as the construction machine; therefore, it requires skill to operate. For example, the right crawler must be moved to turn the construction machine in Figure 2 to the left. In addition, when the distance between the camera and the construction machine is large, the construction machine in the image may appear small, or another object may appear between the two, hiding the construction machine. Furthermore, the installation cost of the camera is high, and installation of the camera itself may be impossible immediately after a disaster.

Figure 2. Representative fixed third-person view video

- Third-person view from mobile robotsthird-person view

In some disaster response robots, a rod is extended backward on the robot and a camera is installed in a high position on the tip of the rod to obtain a third-person-view video of the robot surroundings. A typical image is shown in Figure 3. In this case, the orientation of the robot and the position and orientation of the camera always match, and it is easy to grasp the surroundings subjectively. Toda et al. obtained a bird's-eye view from the top in real time by mooring a balloon on the robot instead of a stick, and looking down at the robot from the camera installed on the balloon [4]. Nagatani and others also moored a drone on a construction machine [5]. These methods increase the total height, which includes that of the camera. Moreover, they limit the usable environment because it is necessary to physically separate the camera from the center of the robot. Further, there is the drawback that the image is very shaky owing to the effects of rotation, vibration, and wind of the construction machine because the robot moves away from the center of rotation.

The technology of artificially generating a bird's-eye view image by synthesizing a plurality of camera images mounted on a robot on a plane has been applied practically by automobile manufacturers. An example of the one put into practical use is the around view monitor of Nissan Motor Co., Ltd [6]. Sato et al. applied this method to unmanned construction equipment [7]. Shimizu et al. applied this method and made it possible to move the view [8].

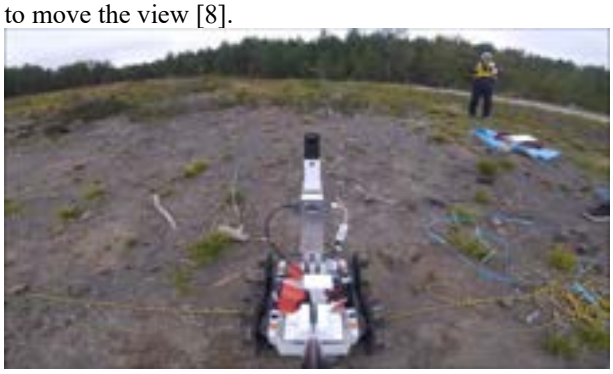

Figure 3. Representative moving third-person view video

2.2 Fixed third-person view using past image method

Shiroma et al. saved a still image acquired by a camera mounted on a robot, and synthesized a CG that matched the position of the robot in the still image in the save history to view the robot from the position where the still image was acquired; they proposed a method to generate an imaginary bird's-eye view [9]. In addition, Kinoshita et al. eliminated the narrow viewing angle by shooting still images using an omni-directional camera [10]. Figure 4 shows the outline and Figure 5 shows the generated third-person-view image.

The fixed third-person-view generation method using previous images involves obtaining the fixed third-person-view view by using previous still images captured by the robot. That is, if the only moving object in the image is the robot, the still image once taken is used as the background, and the moving robot draws the CG according to the position and orientation

information. This method has the merit that the amount of communication and the associated communication delay can be reduced because moving image transfer is not required.

In contrast, the image obtained by this method has a fixed third-person-view, and thus there is the problem that the size of the image decreases as the robot moves away. To solve this, it is necessary to retake a still image when a certain distance is reached. In addition, moving objects such as humans and other robots are perceived as stationary, because moving objects other than robots are not assumed.

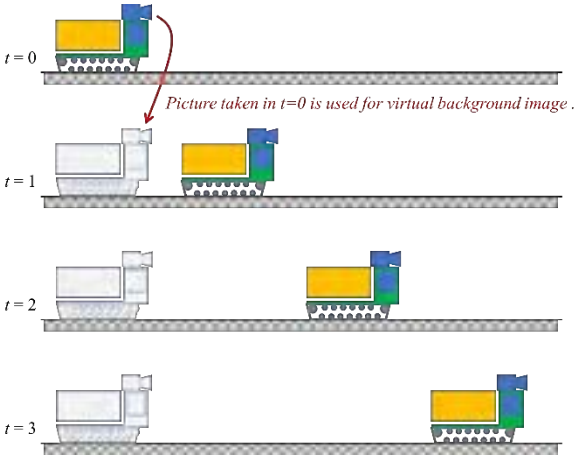

Figure 4. Overview of past image method

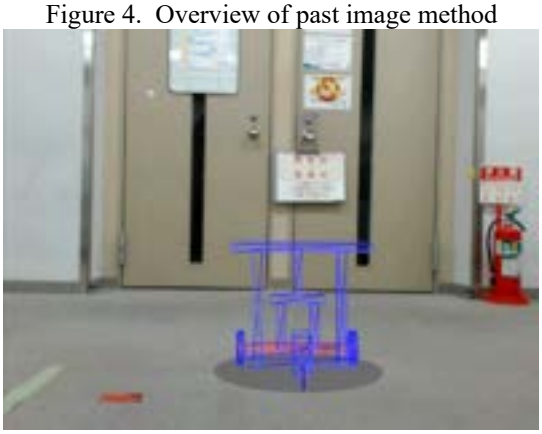

Figure 5. Third-person view image by past image method

3 Tracking third-person view video method

3.1 Proposal of tracking third-person video method

We extended the idea of the fixed third-person-view generation method using past images from an omni-directional camera developed by Kinoshita et al. We used a moving image instead of a still image, and intentionally delaying this to create a CG image at the robot's current position. We proposed a method of generating a moving view in which a camera positioned behind a robot is followed by continuous drawing [11]. Figure 6 shows the outline. In this paper, this is called a tracking bird's-eye view view. In the case of the fixed bird's-eye view image described above, the drawing position of the robot and its size change. However, in this method, it is always drawn in a fixed size in the center of the screen; thus, it has the advantage of being easily drivable. In contrast, in the proposed method, the amount of communication is not reduced because moving images are used. Although the moving object is reflected, it is a delayed moving image and does not correctly reflect the movement of the object.

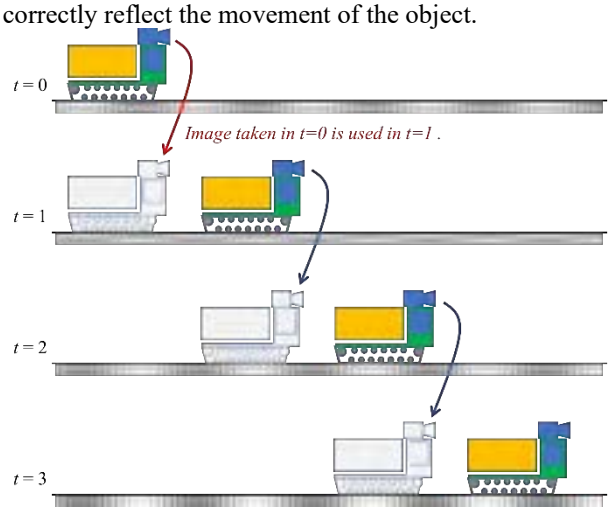

Figure 6. Overview of tracking third-person view method

3.2 Generation method of tracking third-person view video method

The generation procedure of this method is shown as follows.

1. The robot saves the current time and the position and orientation of the robot along with the moving image.
2. A moving image and robot position and orientation that meet the conditions are selected. There are two possible conditions to select.
   A) Fixed time delay—Selection of the latest moving image where the difference between the current time and the shooting time of the image is more than a certain value.
   B) Fixed distance delay—Selection of the latest moving image where the distance between the current position and the shooting position of the image is a certain distance or more.
3. The robot sends the current position/orientation of the robot, the selected moving image, and the position and orientation at the time of image capture to the operator terminal.

4. The CG reflecting the current position and orientation of the robot is superimposed on the moving image received by the operator side, and displayed on the screen. The current direction of the robot is cut from the moving image when drawing so that the CG of the robot is always centered.

3.3 System configuration

Figure 7 shows the system configuration of this research. The upper left side of the dotted line shows the processing performed by the robot side, and the upper right side shows the processing performed by the operator side. These are the contents of the software. The lower part of the dotted line shows the required hardware. The system on the operator side calculates the relative position and orientation from the shooting point from the current position and orientation received from the system on the robot side and the position and orientation at the time of shooting the moving image, and synthesizes the CG of the robot with the moving image. The positional relationship between the self-position estimation sensor, the omni-directional camera, and the robot must be obtained before the experiment. The position where CG is combined with the moving image is calculated as follows. Figure 8 shows an example of robot behavior. Position/posture P_{pc} of the camera at the time of shooting when the position/orientation of the robot center at the time of shooting is the origin, position/posture P_{pr} of the robot center at the time of shooting, sensor position/posture P_{ps} at the time of shooting, current position/posture P_{nr} of the robot center, The current position/orientation P_{ns} of the sensor is defined as follows.

$$P_{pc} = (x_{pc}, y_{pc}, z_{pc}, yaw_p, pitch_p, roll_p)$$
$$P_{pr} = (x_{pr}, y_{pr}, z_{pr}, yaw_p, pitch_p, roll_p)$$
$$P_{ps} = (x_{ps}, y_{ps}, z_{ps}, yaw_p, pitch_p, roll_p)$$
$$P_{nr} = (x_{nr}, y_{nr}, z_{nr}, yaw_n, pitch_n, roll_n)$$
$$P_{ns} = (x_{ns}, y_{ns}, z_{ns}, yaw_n, pitch_n, roll_n)$$

The relative position of the position and orientation of the camera, the position and orientation of the robot center, and the position and orientation of the sensor are fixed because they are fixed to the robot. Also, assuming that the directions of the camera, sensor, and robot are the same, the yaw, pitch, and roll values are the same. Therefore, the position and orientation P_{rs} of the sensor viewed from the center of the robot and the position and orientation P_{sc} of the camera viewed from the sensor are defined as follows.

$$P_{rs} = (x_{rs}, y_{rs}, z_{rs}, 0,0,0)$$
$$P_{sc} = (x_{sc}, y_{sc}, z_{sc}, 0,0,0)$$

When the robot moves as shown in Fig. 8, the vector from the camera at the time of shooting to the center of the robot after the movement is obtained by the following procedure.

1. Obtain the position and orientation of the camera during shooting from the position and orientation of the sensor during shooting

$$P_{pc} = P_{ps} + P_{sc}$$

2. Obtain the coordinates of the current robot center from the current sensor position and orientation and the sensor position and orientation seen from the robot center

$$P_{nr} = P_{ns} - R_y R_p R_r P_{rs}$$

However, $R_y R_p R_r$ is the following formula.

$$R_y = \begin{bmatrix} \cos(yaw_n - yaw_p) & -\sin(yaw_n - yaw_p) & 0 & 0 & 0 & 0 \\ \sin(yaw_n - yaw_p) & \cos(yaw_n - yaw_p) & 0 & 0 & 0 & 0 \\ 0 & 0 & 1 & 0 & 0 & 0 \\ 0 & 0 & 0 & 1 & 0 & 0 \\ 0 & 0 & 0 & 0 & 1 & 0 \\ 0 & 0 & 0 & 0 & 0 & 1 \end{bmatrix}$$

$$R_p = \begin{bmatrix} \cos(pitch_n - pitch_p) & 0 & \sin(pitch_n - pitch_p) & 0 & 0 & 0 \\ 0 & 1 & 0 & 0 & 0 & 0 \\ -\sin(pitch_n - pitch_p) & 0 & \cos(pitch_n - pitch_p) & 0 & 0 & 0 \\ 0 & 0 & 0 & 1 & 0 & 0 \\ 0 & 0 & 0 & 0 & 1 & 0 \\ 0 & 0 & 0 & 0 & 0 & 1 \end{bmatrix}$$

$$R_r = \begin{bmatrix} 1 & 0 & 0 & 0 & 0 & 0 \\ 0 & \cos(roll_n - roll_p) & -\sin(roll_n - roll_p) & 0 & 0 & 0 \\ 0 & \sin(roll_n - roll_p) & \cos(roll_n - roll_p) & 0 & 0 & 0 \\ 0 & 0 & 0 & 1 & 0 & 0 \\ 0 & 0 & 0 & 0 & 1 & 0 \\ 0 & 0 & 0 & 0 & 0 & 1 \end{bmatrix}$$

3. Obtain the current position/orientation P_{pcns} of the robot center with the position/orientation of the camera as the origin

$$P_{pcns} = P_{ns} - P_{pc}$$

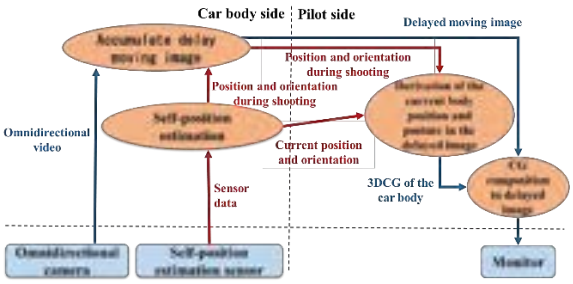

Figure 7. System Configuration

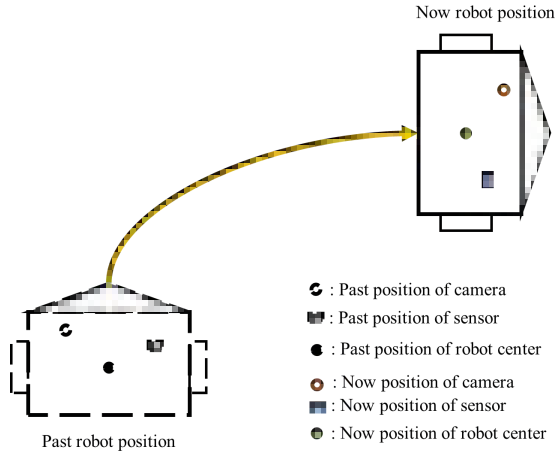

4 Figure 8. An example of robot behavior Experiment of generating a third-person view video

4.1 Video generation experiment using construction machinery

4.1.1 Purpose

Using the proposed method, we attempted to generate a tracking third-person-view image from the moving image of the omni-directional camera acquired while traveled the crawler carrier equipped with the implemented robot side system and the information of RTK positioning.

4.1.2 Data acquisition robot side system

Figure 9 shows the robot system used to acquire the data. The installed camera is the omni-directional camera which name is " RICOH THETA V ".

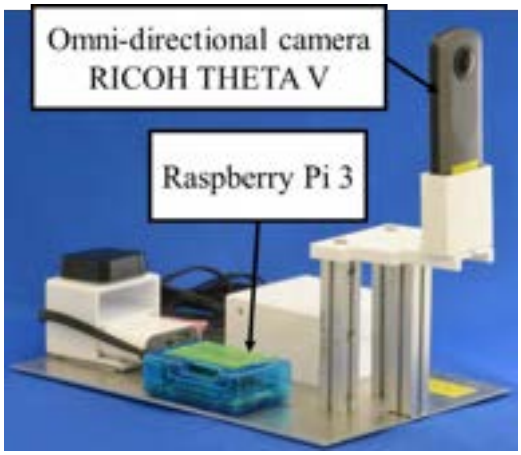

Figure 9. Data acquisition robot side system

4.1.3 Content

The robot side system shown in Figure 10 was installed in a crawler carrier IC 120 manufactured by KATO WORKS. Figure 10 shows the dimensions of the crawler carrier, and Figure 11 shows the camera installation position. The position of the crawler carrier was determined using the data of RTK positioning.position In this experiment, only the position of the crawler carrier and the moving image of the omni-directional camera were acquired during operation, and the video was generated offline. The condition for moving image selection during image generation was the fixed time delay described in 2(a) in section 3.2.

Figure 10. IC120 dimensions

Figure 11. Camera's position

4.1.4 Results and discussion

The video in Figure 12 was generated offline from the data acquired during the experiment. The video is available at https://youtu.be/HMjuIucaNg4. The

generated image confirms that the rough movement of the CG of the construction machine matches the movement of the actual construction machine, and that the view follows the CG. As a result, we demonstrated that it is possible to generate a third-person view image from the image of the vehicle-mounted camera. There was a problem in that the view sometimes caught up with CG when the construction machine speed decreased. This is probably because the delay time was constant and the distance to the camera changed depending on the speed of the crawler carrier. There was a further problem that the CG skidded and oscillated. It is considered that this is because the shooting time of the moving image and the acquisition time of the position and orientation were not correctly synchronized.

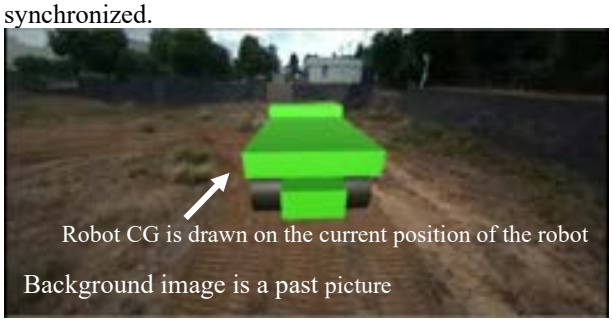

Figure 12. Video generated in an experiment using a crawler carrier

4.2 Video generation experiment using a small dolly

4.2.1 Purpose

Based on the experiment detailed in the previous section, we attempted to solve the problem by improving the system. The video was generated in real time to check for practical problems.

4.2.2 Implementation on a robot for running experiments

We implemented the system on Beego, a small indoor vehicle shown in Figure 13. The installed camera is the omni-directional camera which name is " RICOH THETA S ".The odometry obtained from the number of tire rotations was used to acquire the position and orientation of Beego.

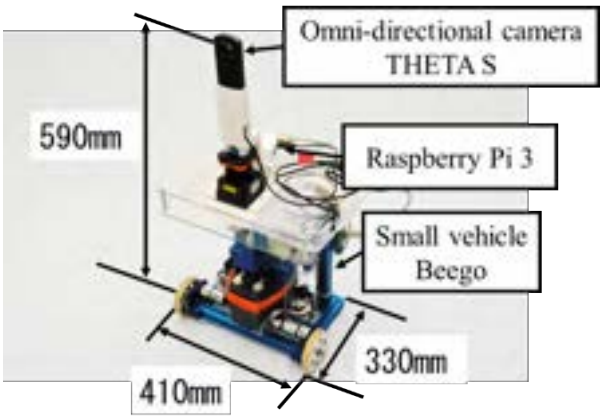

Figure 13. Mounted small vehicle

4.2.3 Content

We generated a tracking third-person-view image with the improved system. In the experiment, the vehicle traveled from the position shown in Figure 14 along a 2-m square perimeter, drawn as a dashed black line. The turns were made on the spot or without stopping. The image selection condition for moving image generation was the constant distance delay (75 cm) described in Procedure 2(a) in Section 3.2.

Figure 14. Indoor experimental environment

4.2.4 Results and discussion

An image from the video generated in real time while driving is shown in Figure 15; the video is available at https://youtu.be/GBiFHKc6bh0. From the generated image shows that the camera position changed according to the robot's moving and stopping, we confirm that the position change of the camera also changed with the speed and stopping of the robot. From this, we succeeded in keeping the distance between the robot and the camera constant. However, the CG was drawn at a different position to the actual position. When the CG bent inward from the actual robot position, especially when it turned smoothly without stopping, it was inflated and drawn outside. A visual check confirmed that the actual robot position and the CG position were shifted by a maximum of approximately 106 cm. And, the stop position was offset by about 5 cm

in the direction of travel. It is considered that this is because the operation of the program is slow, and the delay of the program is unintentionally added to the intentional delay.

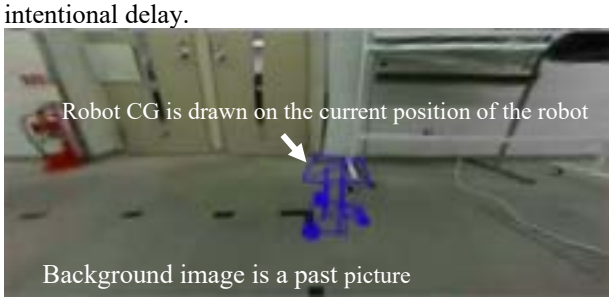

Figure 15. Video generated in an experiment using a small vehicle

5 Summary and outlook

This paper described a method to generate a video that follows the robot from the back, using the camera on the robot, by intentionally superimposing the CG of the robot on the delayed video. We implemented a tracking view generation method. We conducted experiments using two types of robots—a construction machine and a small vehicle—and confirmed the basic operation. From the experimental results, we prove that the third-person view image can be generated from the image of the camera on the robot according to the theory, and it was confirmed that the distance between the robot and the camera can be fixed. A mounting problem caused a phenomenon in which the actual position of the robot and the position of the CG caused an error and the CG skid. As a result, in addition to the intentionally generated delay, there was an unintentional delay in the program.

In the future, we plan to reduce the delay in the system to more accurately superimpose CG. In addition, we aim to demonstrate the superiority of this research by performing a subject experiment using the generated tracking bird's-eye-view image and other images.

References

[1] Kyohei Yoshida, Fuminori Hibino, Yasutake Takahashi, and Yoichiro Maeda, “Development and Evaluation of Human Pointing Navigation System Using Spherical Vision System on Mobile Robot”, Proceedings of 27th Fuzzy System Symposium, WC3-1, 2011. [in Japanese]

[2] Tomoki Tajiri, Rei Ogami, Yogo Takada, and Tadao Kawai, “Supporting of Safe Walking at a Crossing by Using a Small Mobile Robot with Cameras”, Proceedings of the 2012JSME Conference on Robotics and Mechatronics, 1A2-G09, 2012. [in Japanese]

[3] Takashi Kato. and Jun Ueno. “Development of realistic type remote control system using the HMD”. Proceedings of The 16th Symposium on Construction Robotics in Japan, p2-4, 2016. [in Japanese]

[4] Koki Toda, Naoya Maeda, Motoko Kanegae, Yuta Sugiura, Masaahiko Inami, and Maki Sugimoto, “Real time visual operational support interface to display a third-person view of a camera suspended from a floating ballon”, Proceedings of JSME annual Conference on Robotics and Mechatronics 2013, 1P1–P01, 2013. [in Japanese]

[5] Chikushi S, Moriyama Y, Fujii H, Tamura Y, Yamakawa H, Nagatani K, Sakai Y, Chiba T, Yamamoto S, Chayama K, Yamashita A and Asama H (2020), "Automated Image Presentation for Backhoe Embankment Construction in Unmanned Construction Site", In IEEE/SICE International Symposium on System Integration (SII)., pp. 22-27, 2020.

[6] “Intelligent Around View Monitor | NISSAN | Technology Development initiatives”. https://www.nissan-global.com/JP/TECHNOLOGY/OVERVIEW/iavm.html .

[7] Takaaki Sato, Alessandro Moro, Hiromitsu Fuji, Kazuya Sugimoto, Akira Nozue, Yoichi Mimura, Katsumi Obata, Atsushi Yamashita, and Hajime Asama, “Development of Virtual Bird’s-eye View System in Unmanned Construction,” Proceedings of the 19th Robotics Symposia, 346-352, 2014. [in Japanese]

[8] Seiya Shimizu. Masami Mizutani. and Tohru Tsuruta. “Development of Wraparound View System for Vehicles”. Proceedings of The Journal of The Institute of Image Information and Television Engineers Volume 68 Issue 1, pp. J24-J29, 2014. [in Japanese]

[9] Naoji Shiroma, Georges Kagotani, Maki Sugimoto, Masahiko Inami, and Fumitoshi Matsuno, “A Novel Teleoperation Method for a Mobile Robot Using Real Image Data Records,” Proceedings of the 2004 IEEE International Conference on Robotics and Biomimetics, pp. 233-238, 2004.

[10] Himuro Kinoshita, and Yasushi Hada，“Research on Remote Control of Robots Using Omnidirectional Past Images,” The 34th Annual Conference of The Robotics Society of Japan, 2D1-05, 2016. [in Japanese]

[11] Yuya Kaneko and Yasushi Hada, “Third person view generation for remote control robot,” Japan Society of Mechanical Engineers Kanto Student Council 58th Student Graduation Research Presentation, 206, 2019.

Construction Operation Assessment and Correction using Laser Scanning and Projection Feedback

A. Pevzner[a], S. Hasan[b], R. Sacks[b] and A. Degani[a,b]

[a]Technion Autonomous Systems Program, Technion – Israel Institute of Technology, Haifa, Israel
[b] National Building Research Institute, Faculty of Civil and Environmental Engineering, Technion – Israel Institute of Technology, Haifa, Israel
E-mail: salexpoz@campus.technion.ac.il, saed.hasan@campus.technion.ac.il, cvsacks@technion.ac.il, adegani@technion.ac.il

Abstract –

Lean construction (LC) and Building Information Modeling (BIM) support an integrated vision for short cycle plan-do-check-act cycles of planning and control in construction. However, operations control tasks, such as delivery of design information to the field, monitoring, progress evaluation and error detection are still largely manual and thus time-consuming, costly and error-prone. Innovations in construction technologies can be applied to reduce cycle time, waste, construction errors and the rework that necessarily follows. In this context, we propose application of a projection and scanning technology to provide workers with real-time information and feedback regarding the quality and accuracy of their handiwork. The goal is to achieve proper quality in the first iteration, with fully automated inspection, and no rework.

As a proof-of-concept, we demonstrate the system using an example of wall plastering. The result of plaster application is difficult to measure in conventional means, and errors are difficult to detect. Our system monitors the progress of the procedure (Field-to-BIM), evaluates the surface flatness and projects corrections onto the surface itself, after optimizing with respect to industry standards and tolerances (BIM-to-Field). We demonstrate the concept in an experimental setup using a Trimble™ TX8 laser scanner and an angled adjustable projector. The results show high precision detection of wall flatness deviations, of up to 2 mm accuracy.

Keywords –

Building information modeling; construction; technologies; Data acquisition; Sensing/recognition; Human Machine interaction

1 Introduction

Lean construction (LC) and Building Information Modelling (BIM) support an integrated vision for short cycle plan-do-check-act cycles of planning and control in construction [1]. LC aims to maximize the value and eliminate the wastes in the construction process while BIM supports closer collaboration among project teams during the design and construction phases. Yet thorough implementation of the potential remains elusive because manual methods of information delivery from BIM-to-field *(a process to automatically transfer product and/or process information from BIM environment to construction field)*, and of monitoring operations in the field and reporting the data to the Information Technology (IT) systems (Field-to-BIM: *a process to automatically collect/collate raw data from construction field, to interpret the data and store situational awareness information in BIM environment*), are costly, time-consuming and error prone.

IT, BIM and other construction technologies (3D scanners, sensors and cameras, etc.) can be applied to automate these information delivery and collection tasks. Especially noticeable is three-dimensional laser scanning technology which is widely used around the construction industry in tasks like mapping buildings and creating detailed as-built models, deterioration tracking, quality assurance and progress monitoring. Laser scanners provide fast, extremely detailed, easily manageable information about their surroundings in the form of point clouds. These data can then be processed for useful as-built information to be recorded and organized. Point cloud processing is possible using proprietary software tools but unfortunately, their abilities are limited and sometimes not accurate enough. Where the use of laser scanners is task-specific, the algorithmic support must be tailored to meet the unique requirements.

In this paper we demonstrate the use of terrestrial laser scanning technology and image projection as a proof-of-concept for parallel, short cycle time control of a construction operation. Figure 1 summarizes the flow of the presented proof-of-concept demonstration. The specific use-case is a wall plastering operation, and the demonstration includes monitoring and quality assessment. We implement our algorithmic approach to track the progress of construction while detecting errors and suggesting corrections, all in near to real-time. We showcase the positive effect of information transfer from site to BIM using laser scanners and data processing, and from BIM-to-field by projecting our results, in the form of images, using standard projectors. We demonstrate our results with a small-scale experiment, performed in a rectangular room, defining one of its walls as our target wall.

2 Related Work

The following sub-sections discuss the implementation of construction tech and computer vision for on-site data collection, monitoring, and information projection.

2.1 Construction Technology Integration for Automated Site Monitoring Systems (Field-To-BIM Data Gathering)

The construction industry, to date, has many construction technologies innovations. Many research papers have discussed a variety of technologies with potential for improving operation control. Lee and Choi presented a study of combination between laser scanning and imagery for building reconstruction purposes [2]. Shih and Wang reported a laser scanning system for controlling the dimensional compliance of finished walls [3]. Gordon, Lichti et al. discussed the results of using the laser scanning for structural health monitoring [4]. Biddiscombe discussed the uses of laser scanning for controlling as-built dimensions [5].

Akinci, Boukamp et al. used spatial raw data gathering from the construction field, integrated the collected data into the project models, and developed a formalism for pro-active QA/QC construction for defect detection [6]. Ordóñez, Arias et al. proposed an image-based approach for controlling dimensions of flat elements, but it requires significant human input [7]. Bhatla, Choe et al. used a 3D laser scanner to capture and record the site progress data. The results were proven as more accurate than traditional site progress tracking [8].

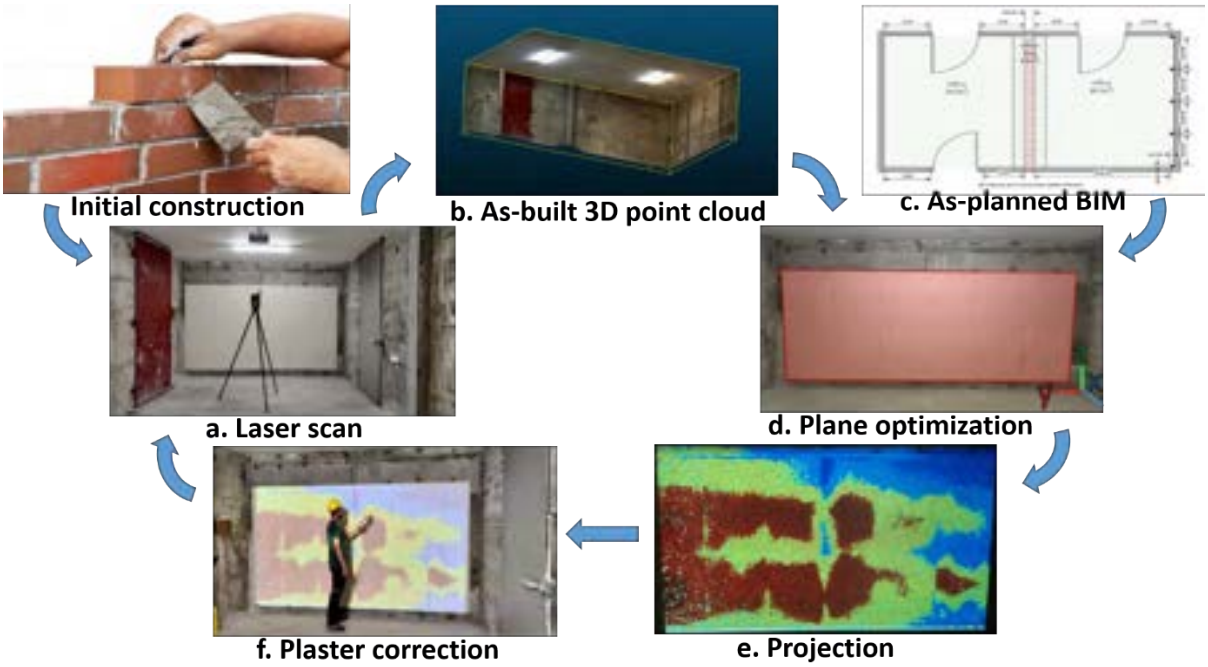

Figure 1. Flow of proof-of-concept demonstration. (a) Begin by scanning for progress detection, (b) obtain high accuracy as-built point cloud, (c) compare to the as-planned BIM data and detect errors, (d) cost optimization, (e) output projection, (f) correction of errors in accordance with image projection on the wall. Repeat scanning for updating status and next flow iteration until reaching termination at satisfactory conditions.

Braun, Tuttas et al. presented a test case of on-site progress tracking and recording. The presented work discussed ways to transfer collected raw progress data to BIM workspace using point cloud technology for construction control purposes [9].

Pučko, Šuman et al. presented a method where site works are constantly monitored, instead of scanning of a whole building under construction from time to time [10]. As a result, the as-built BIM model is continuously updated during the construction cycle. The presented method depends on low precision 3D scanning devices which are small enough to fix on workers' helmets and on the active machinery as well. The 3D scanning devices allow workers to capture the workspace and work that has been done, inside and outside of the building, in real-time. The recorded data include workers' locations and capturing time. The captured point-clouds were imported to 4D as-built BIM models. Then, the comparison between 4D as-built model with 4D as-planned model enabled identification of the differences between both models and the deviations from the time schedule as well.

Current approaches to control surface flatness are inefficient. Bosché and Guenet proposed an automatic surface flatness control process using laser scanning and BIM [11]. Their approach applied straightedge and F-Numbers methods. Their experiments demonstrated the suitability of laser scanning for standard dimensional controls and validated its quality and efficiency benefits vis-à-vis traditional measurement approaches. Valero, Forster et al. presented a method for automated defect detection and classification in ashlar masonry walls using laser scanning and machine learning [12]. The algorithm they developed identifies material defects and discoloration. Neither of these methods included in-situ feedback to the workers, as our system does.

Clearly, laser scanning technology is one of the leading methods for spatial data gathering. Past success encouraged us to choose this technology for our experiments.

2.2 BIM and Construction Technology Integration for Information Management

BIM and construction technology integrated applications are still not very common. Alizadehsalehi and Yitmen [13] and Patraucean et al. [14] discussed the impact of the combination of data capturing techniques with BIM in construction companies; both discussed the point cloud based method for creating as-built BIM models. The results show that site surveying for work done on site could be prepared in less time and more accurately by overlaying as-designed BIM models with 3D as-built captured BIM models, than by manual surveying.

Bosché, Ahmed et al. discussed the value of integrating Scan-to-BIM and Scan-vs-BIM techniques for construction monitoring [15]. They used laser scanning and BIM in a unified approach for automated mapping of as-built vs. as-planned MEP works to monitor earned value (work done), and to assist in delivering as-built BIM models from as-designed ones (performance measurement). Among the incremental improvements of their approach: (1) recognition and identification of objects not built at their as-planned locations; and (2) consideration of pipe completeness in the pipe recognition and identification metric.

Kim, Chen et al. presented a navigation and object recognition method that was implemented and tested with a custom-designed mobile robot platform, which uses multiple laser scanners and a camera to sense and build a 3D environment map [16]. The study shows that the 3D colour-mapped point clouds of construction sites generated were of sufficient quality to be used for many construction control applications such as construction progress monitoring, safety hazard identification, and defect detection.

Kopsida and Brilakis have evaluated different methods for reality augmentation by BIM model information and came to the conclusion that sparse 3D data leads to the most robust results when as-built and as-planned information overlay is requested for progress management [17].

2.3 Construction Technology Integration for Product and Process Information Transfer (BIM-To-Field)

To date, Augmented Reality (AR) has rarely been applied to construction control. However, it has the potential to improve the efficiency and quality of construction work by providing digital content on top of physical surface views to assist teams in the field [18]. Different approaches to integration of BIM and AR in construction have been proposed. Yang and Ergan discussed integration of BIM and AR, showing how semantic information can be transferred from a BIM platform to an AR system to improve the user visualization interface [19]. Williams, Gheisari et al. proposed an approach for BIM model translation to be used in a mobile AR application, which improves the direct use of BIM information through AR on-site [20].

Degani et al. presented an integrated BIM-Robot-AR system with self-localization method using data from distance sensors to find the probable pose (position and orientation) of system in an identified space [18]. The study showed the accuracy of self-localization and the system's feasibility for accurate projection of BIM model data directly onto physical surfaces in the field. In this work, we extend the capability of that system, focusing on two-way communication of information, from BIM-to-field and from field-to-BIM.

3 Methodology and Algorithms

3.1 Initial Assumptions

To reduce extra effort for unlikely scenarios, a few assumptions were made. The main assumption, regarding the operational area, is a rectangular shaped room. The room is assumed to have four walls, a ceiling and a floor, six planes in total, all perpendicular (or parallel) to each other. The origin of the coordinate system is assumed to lie within the room, in the geometric center. It is also assumed to be almost empty, without furniture or clutter. These assumptions help organize the initial conditions and partially assure consistency in the point clouds received after scanning the operational area. In previous work, we have demonstrated the ability to localize a moving AR projector using Markov localization [18]. In this work, we simplify by assuming a static projector in a known location.

3.2 Laser Scan Pre-Processing

To achieve satisfactory conditions for working with the point cloud recorded by the laser scanner, each scan needed to be pre-processed. Each scan was acquired from two scanning stations and registered manually. The use of two scanning stations enhanced the overall accuracy of the scanned data. The stations were located opposite one another, one on each side of the operation room. Combining two scans roughly evens out the point density of the entire cloud, since the point spacing grows linearly with the distance between the scanned object and the laser scanner. Using Trimble Realworks™, the point clouds of the two stations were manually registered together and aligned with the X, Y and Z axes. Later, the alignment is manually refined as discussed in the next section. The point cloud was down-sampled by a factor of 10, yielding a dataset that was easy to work with without compromising accuracy. A RANSAC algorithm was applied on the points and a normal was estimated for each point based on 10 of its nearest neighbors [21]. This normal represents the plane on which the point is assumed to lie. Finally, the point cloud's center of mass was calculated by averaging all the X, Y and Z coordinates of the points. With two stations, each with its own deviations, we could refine the alignment between the two. In the next section, we will describe the process of wall detection. This is needed for two reasons: first, we impose no requirements or constraints on the position and orientation of the laser scanner during the scans; second, as we are capturing the status of the operation at partial progress, with possible errors already present on site, we can use the as-planned information only as reference while making sure the detection of walls, errors and progress status are correct.

3.3 Wall Detection

Once the point cloud had been pre-processed, the walls were detected, and a specific target wall was identified. The walls, or planes, of the point cloud were detected using a clustering algorithm, K-means [22]. The clustering algorithm receives the normals of the points as input. The points were then divided into six clusters. Each cluster represented one of the walls, the floor, or the ceiling. The algorithm also assigns a center of mass (COM) to each group, which is not necessarily a member of the cluster. This COM was then validated by averaging all X, Y and Z arguments of the normal of the points related to each cluster. The central normal of each cloud, at this stage, has slight deviations from the absolute Cartesian axes. This can be fixed effortlessly by calculating a transformation between the absolute axes and the current plane normals. This transformation was then applied to the entire point cloud, aligning it with the absolute coordinate system of the as-planned information. For simplicity's sake, the experiment focused on a single, randomly chosen wall called the 'target wall'. The wall was identified by its ID output of the k-means algorithm and separated from the point cloud. At this stage, all elements of the room are known and identified. Any construction progress made with respect to previous scans can be updated and registered. The process is detailed in algorithm 1.

Algorithm 1: Wall Detection

Input:
- Scan of the room [PCL file]
- Target wall normal vector [float vector]

Output: Target wall point cloud aligned to wanted vector

Constants:
- NUM_OF_WALLS
- WALL_NORMALS

```
Mean_PCL = avg{ PCL (x), PCL (y), PCL (z)}
Displacement = -1* Mean_PCL
Normals = find_normals(PCL)
Normals = rotate normals towards Mean_PCL
Walls = cluster(Normals, num_of_walls)
for wall_index :=1 to num_of_walls:
   normal := avg{ Normals (x), Normals (y), Normals (z)}
Rotation = angle(normal(1), const_normal(1))
PCL = translate and rotate(Displacement, Rotation)
for wall_idx := 1 to num_of_walls:
   if wall_normal == target wall normal
      target_wall_idx = wall_idx
target_wall_ PCL = PCL (wall_idx)
rotate (target_wall_PCL [0,0,1])
```

3.4 Plane Optimization

Two main features of our proposed system are error detection and correction. After detecting the error, a cost assessment must be performed for the repair operation. To estimate this cost, we must know how different the current state is from the desired, optimal one, i.e. how

severe the detected errors are. Note that the optimal result does not necessarily conform to the originally designed state defined in the BIM model. In certain situations, considering underlying deviations from the original design, such as deviations in the concrete or block face, an optimal result may be one that can be achieved economically while still satisfying design performance conditions (such as planarity, verticality). The decision needs to be made simultaneously with the construction operation. As part of our proof-of-concept experiment, we are dealing with monitoring and correcting plaster application. Our goal is to supply real time improvement suggestions and we want it to be optimal in terms of cost. A tight constraint we face is the fact that the wall must be perpendicular to the floor. In 3D terms, we are left with two degrees of freedom for plane adjustments, keeping the plane's normal parallel to the floor. Figure 2 shows in top view, the exaggerated features of the wall surface with a blue line and the red line is the optimal plane.

As can be seen in Figure 2a, one option is to move the plane along its normal, basically controlling the "d" parameter of the plane equation. The equation of a plane in the three-dimensional space is:

$$ax + by + cz + d = 0 \qquad (1)$$

In Figure 2b and Figure 2c the second degree of freedom is presented – rotating the plane about the Z axis. Each one of the two described changes in the plane's location results in a different topography of protrusions and depressions. Figure 2d shows the grid of cost calculation. The calculations are demonstrated in algorithm 2.

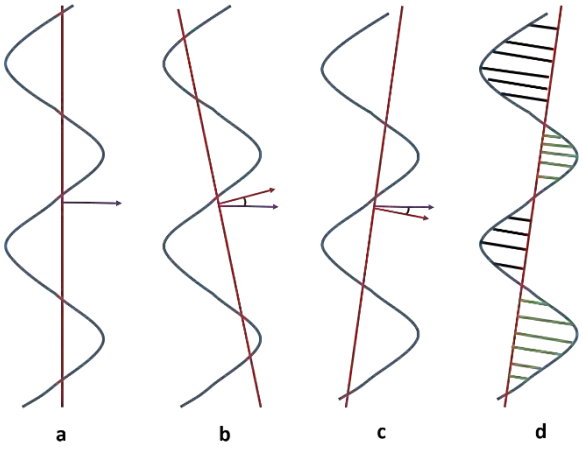

Figure 2. Surface flatness optimization. (a) Nominal plane, (b) rotated plane to positive angle limit, (c) rotated plane to negative angle limit, (d) visualization of grid for cost calculations.

Algorithm 2: Cost Optimization

Input:
- Target wall point cloud [PCL file]
- Nominal plane [plane parameters]
- Filling up cost [float number]-FU_cost
- Shaving off cost [float number]-SO_cost

Output: optimal plane [plane parameters]
Constants:
- Target wall absolute normal vector-TWANV
- Industry tolerance-IT
- Design constraints-DC

```
DC_vec := [0:0.001:DC]
IT_vec := [-IT:0.001:IT]
Optimal_plane := Nominal_plane
Fill_up_cost := 0
Shave_off_cost := 0
Cost_TOT = max(FU_cost,SO_cost)*num_of_ PCL _pts
for D in DC_vec:
   for Angle in IT_vec:
      Curr_plane := [Angle, D]
      Fill_TOT = (num_wall_points > curr_plane)*FU_cost
      Shave_TOT = (num_wall_points< curr_plane)*SO_cost
      Curr_cost := Fill_up_cost_TOT + Shave_off_cost_TOT
      If Curr_cost < Cost_TOT:
         Cost_TOT = Curr_cost
         Optimal_plane = Curr_plane
```

4 Experiment

4.1 Experimental Setup

The experimental setup includes a rectangular, 32 m^2 room (8 m x 4 m), a laser scanner (Trimble™ TX8) and a standard projector. As can be seen in Figure 3, the room has bare, unfinished walls, a convenient state for benchmarking the accuracy of the laser scanner. The room is rectangular, and all of its parameters are in accordance with the initial assumptions given in section 3.1. The purpose of the experimental setup is to construct a proof-of-concept system that can monitor, assess, and evaluate a wall plastering operation. The system is required to perform in near real-time and provide a complete start-to-end solution. System demands include progress monitoring and surface quality assessment by error detection and optimal error correction. Three visual steps of the flow can be seen in Figure 4.

4.1.1 Indistinguishable Discrepancies

A reasonable assumption is that errors of plaster application are difficult to notice with the naked eye. Imperfections will usually be due to gradual straying from a desired plane, without rough changes or noticeable edges.

Figure 3. Experimental room

In these cases, our system is most useful, which was the motivation of this experiment. This experiment is performed in the same room, but with a target wall with thin cardboard sheets attached to it as shown in Figure 5a. The sheets are fixed adjacent to one other and cover most of the surface of the wall. The main purpose of the setup was to simulate a gradual drift of the plaster surface instead of rough, highly visible discrepancies. The target wall imperfections were also taken into consideration, but their effect was negligible as the optimal plane placement is fixed with respect to absolute X, Y and Z global coordinates.

4.2 Experimental Flow

The experiment is used to show the full extent of the construction operation. The main target of our proof-of-concept experiment was to demonstrate the cycle of construction work monitoring, error detection, error correction and status update. The experiment comprised a few stages, which are discussed in the next subsections.

4.2.1 First Scan

The first scan was performed to calibrate and prepare the system. Two scanning locations ("stations") were used as described in section 3.2. Each scan was performed with highest accuracy setup of the laser scanner. For the Trimble™ TX8, used in this work, the point spacing at 30 m is 5.7 mm. Each scan took about 10 minutes. Both stations were registered using a proprietary software tool that receives manual input – the user needs to mark three pairs of locations on both scans. The same scan setup was performed twice, both in an illuminated environment and in complete darkness. The scans were compared, and the results were similar - both point clouds met the requirements of section 3.2 and had equal errors. In accordance with sections 4.1.1 and 4.1.2, a wall was chosen for demonstration purposes and two types of plaster lookalikes were applied.

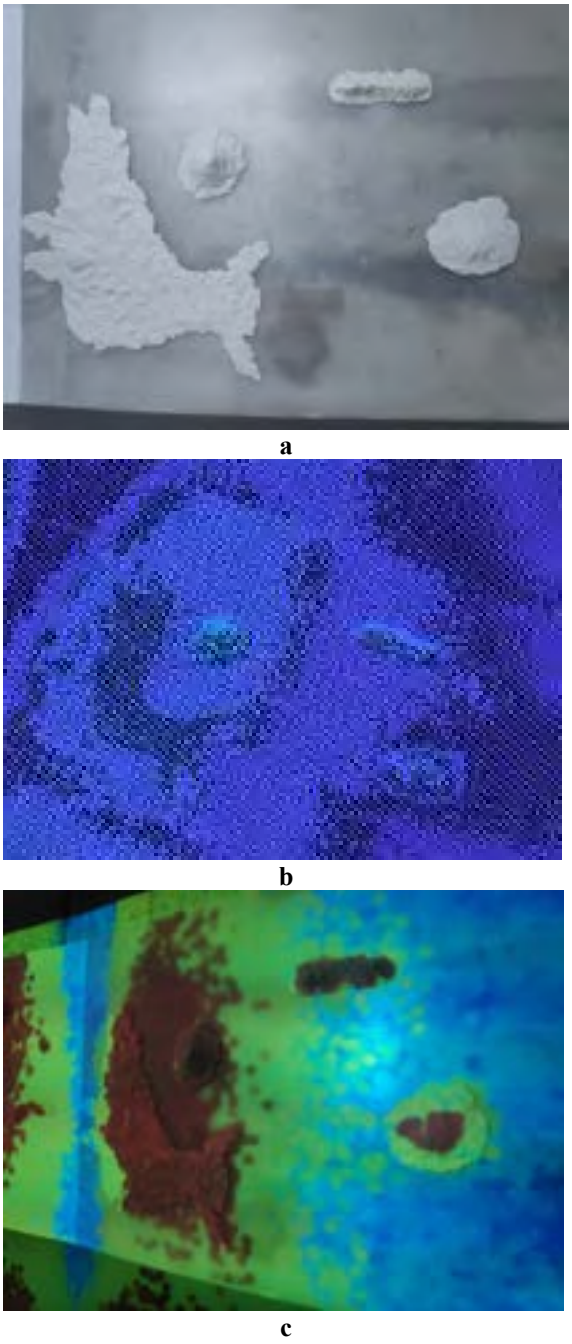

a

b

c

Figure 4. Using modelling clay to simulate discrepancies in the wall. (a) Hand sculptured modelling clay, (b) point cloud of the target wall, (c) projection on the target wall.

The cardboard sheets were placed on the wall to simulate low frequency plaster irregularities and the play dough was placed to simulate rough inaccuracies and to benchmark the laser scanner accuracy. People find it difficult to identify small inaccuracies in a plastered wall. This is why the cardboard setup was chosen for the rest of the experiment.

a

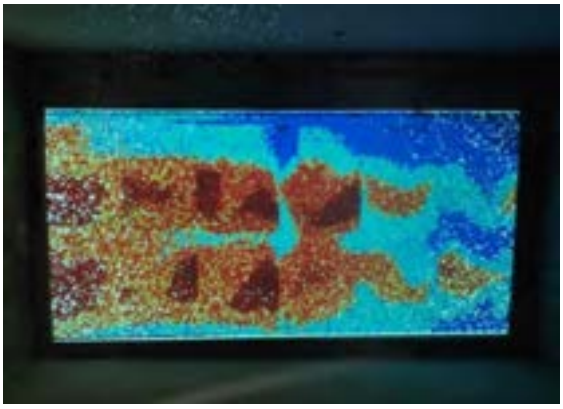

b

Figure 5. (a) Using cardboard sheets attached to a target wall to simulate minor discrepancies in the wall, (b) error correction projection on target wall.

4.2.2 Data Processing

Data processing was performed as described in sections 3.2 and 3.3. After extracting all the points of the working wall, a mean normal was calculated and a plane was fitted by this normal. This was the nominal plane that identified the current baseline target wall from which the optimization calculations could start.

4.2.3 Optimization

After making sure that the nominal plane was perpendicular to the plane of the floor, an optimization process was initiated. With the current state of the target wall, an optimal plane was derived from the optimization process. In some areas the optimal plane was "submerged" in the target wall and in others – raised above it. This was evident in the projected image as different areas had different colors.

4.2.4 Projection

A topographic map was produced, relative to the direction of the optimal plane normal. A manual calibration of the projector's location was done in order to project the image on the wall with the correct perspective. We have previously demonstrated the ability to localize a projector based on an image captured by a camera in a known location [18]. As can be seen in Figure 5b all areas on the target wall that needed to be shaved off were colored in shades of red and the ones that needed to be filled up with plaster were colored in blue. The color map helped with visualizing 3D data in a 2D image. The gradient of colors was equally spread between the "highest top" and the "lowest bottom". All the high contrast areas that can be seen in Figure 5b are edges between sheets of cardboard or between a sheet of cardboard and the wall itself.

4.2.5 Additional Iterations

The cardboard sheets were flattened to simulate a flattening procedure in accordance with the projection. The room was then scanned once again, with identical parameters as the previous time. The second cycle was about finer detail correction, in comparison to the first one. The scan was similarly processed, and another complete flow cycle was carried out, resulting in a new heat map. The heat map was projected using the same static projector and both iterations included high precision projection accuracy with offsets no more than 1 cm. Within the projected image, the measured errors had a mean of 2 mm. The projection process was not optimized and can be improved in future executions. This procedure can be repeated as often as needed, terminating once the work complies with some predetermined accuracy threshold.

5 Conclusion

In this work we have successfully demonstrated practical implementation of a conceptual short cycle of construction control composed of progress monitoring, error detection and optimal error correction. We have planned and carried out a small-scale experimental setup dealing with wall plastering assessment.

The experiment indicated that maximal accuracy is within reach and is restricted only by the capabilities of the hardware in use, i.e. laser scanner. In our model and scan setup we were able to achieve 2 mm accuracy of scan that was reflected on the measured results. We have iterated over two complete cycles of the flow, improving the plastering quality with every iteration. In each cycle we measured the distance between the projected elements and the real ones before mending the work.

We assume that the principles demonstrated by our proof-of-concept experiment can be applied to other

construction operations, and that our bi-directional workflow can help automate operations. We stress that from a technological perspective, each task must be treated in a different manner with appropriate algorithms. The robustness of the specific implementation is restricted to the task at hand and cannot be easily transferred to other construction tasks. We plan to integrate automated localization for the projector in future work.

Acknowledgment

This research was supported by the Ministry of Science & Technology, Israel.

References

[1] R. Sacks, M. Radosavljevic, and R. Barak, "Requirements for building information modeling based lean production management systems for construction," *Autom. Constr.*, vol. 19, no. 5, pp. 641–655, Aug. 2010.

[2] I. Lee and Y. Choi, "Fusion of terrestrial laser scanner data and images for building reconstruction," 2004.

[3] N.-J. Shih and P.-H. Wang, "Using point cloud to inspect the construction quality of wall finish," *Proc. 22nd eCAADe Conf.*, pp. 573–578, 2004.

[4] S. J. Gordon, D. D. Lichti, M. P. Stewart, J. Franke, and P. Cloud, "Modelling Point Clouds for Precise Structural Deformation Measurement."

[5] P. Biddiscombe, "3D laser scan tunnel inspections keep expressway infrastructure project on schedule," 2005.

[6] B. Akinci, F. Boukamp, C. Gordon, D. Huber, C. Lyons, and K. Park, "A formalism for utilization of sensor systems and integrated project models for active construction quality control," *Autom. Constr.*, vol. 15, no. 2, pp. 124–138, Mar. 2006.

[7] C. Ordóñez, P. Arias, J. Herráez, J. Rodríguez, and M. T. Martín, "Two photogrammetric methods for measuring flat elements in buildings under construction," *Automation in Construction*, vol. 17, no. 5. Elsevier, pp. 517–525, 01-Jul-2008.

[8] A. Bhatla, S. Y. Choe, O. Fierro, and F. Leite, "Evaluation of accuracy of as-built 3D modeling from photos taken by handheld digital cameras," *Autom. Constr.*, vol. 28, pp. 116–127, Dec. 2012.

[9] A. Braun, S. Tuttas, A. Borrmann, and U. Stilla, "A concept for automated construction progress monitoring using BIM-based geometric constraints and photogrammetric point clouds," *J. Inf. Technol. Constr.*, vol. 20, pp. 68–79, 2015.

[10] Z. Pučko, N. Šuman, and D. Rebolj, "Automated continuous construction progress monitoring using multiple workplace real time 3D scans," *Adv. Eng. Informatics*, vol. 38, pp. 27–40, Oct. 2018.

[11] F. Bosché and E. Guenet, "Automating surface flatness control using terrestrial laser scanning and building information models," *Autom. Constr.*, 2014.

[12] E. Valero, A. Forster, F. Bosché, E. Hyslop, L. Wilson, and A. Turmel, "Automated defect detection and classification in ashlar masonry walls using machine learning," *Autom. Constr.*, vol. 106, p. 102846, Oct. 2019.

[13] S. Alizadehsalehi and I. Yitmen, "The Impact of Field Data Capturing Technologies on Automated Construction Project Progress Monitoring," in *Procedia Engineering*, 2016, vol. 161, pp. 97–103.

[14] V. Pətrəucean, I. Armeni, M. Nahangi, J. Yeung, I. Brilakis, and C. Haas, "State of research in automatic as-built modelling," *Adv. Eng. Informatics*, vol. 29, no. 2, pp. 162–171, Apr. 2015.

[15] F. Bosché, M. Ahmed, Y. Turkan, C. T. Haas, and R. Haas, "The value of integrating Scan-to-BIM and Scan-vs-BIM techniques for construction monitoring using laser scanning and BIM: The case of cylindrical MEP components," *Autom. Constr.*, vol. 49, pp. 201–213, Jan. 2015.

[16] P. Kim, J. Chen, J. Kim, and Y. K. Cho, "SLAM-driven intelligent autonomous mobile robot navigation for construction applications," in *Lecture Notes in Computer Science (including subseries Lecture Notes in Artificial Intelligence and Lecture Notes in Bioinformatics)*, 2018, vol. 10863 LNCS, pp. 254–269.

[17] M. Kopsida, "BIM Registration Methods for Mobile Augmented Reality-Based Inspection Cloud-based Building Information Modelling (CBIM) View project Automation in Construction View project," 2016.

[18] A. Degani, W. B. Li, R. Sacks, and L. Ma, "An Automated System for Projection of Interior Construction Layouts," *IEEE Trans. Autom. Sci. Eng.*, vol. 16, no. 4, pp. 1825–1835, Oct. 2019.

[19] X. Yang and S. Ergan, "Evaluation of visualization techniques for use by facility operators during monitoring tasks," *Autom. Constr.*, vol. 44, pp. 103–118, Aug. 2014.

[20] G. Williams, M. Gheisari, P.-J. Chen, and J. Irizarry, "BIM2MAR: An Efficient BIM Translation to Mobile Augmented Reality Applications," *J. Manag. Eng.*, vol. 31, no. 1, p. A4014009, Jan. 2015.

[21] M. A. Fischler and R. C. Bolles, "Random sample consensus: A Paradigm for Model Fitting with Applications to Image Analysis and Automated Cartography," 1981.

[22] J. MacQueen and others, "Some methods for classification and analysis of multivariate observations," in *Proceedings of the fifth Berkeley symposium on mathematical statistics and probability*, 1967, vol. 1, no. 14, pp. 281–297.

OpenBridgeGraph: Integrating Open Government Data for Bridge Management

Jia-Rui Lin[a,b]

[a]Department of Civil Engineering, Tsinghua University, China
[b]Tsinghua University-Glodon Joint Research Center for Building Information Modeling, Tsinghua University, China
E-mail: lin611@tsinghua.edu.cn

Abstract –

Due to limited funds, road authorities around the world are facing challenges related to bridge management and the escalating maintenance requirements of large infrastructure assets. Nowadays, many government organizations have published a variety of data to enable transparency, foster applications, and to satisfy legal obligations. Open governments data like bridge data, weather data would help to better assess the condition of bridges for maintenance purpose and allocation of funds. However, these data sets are fragmented in different systems or formats, and their value in bridge management are not fully explored. This paper proposes a graph-based bridge information modeling framework to integrate open government data for bridge management. The framework represents bridge inventory data as a labeled property graph model and extends the model with weather data. Implementation of the framework employs python scripts for data processing, and neo4j database for data management. The framework is demonstrated using data from national bridge inventory (NBI) and national oceanic and atmosphere administration (NOAA). The results show that the proposed framework can potentially facilitate the integration and retrieval of public government data, and effectively support and provide services to bridge management. Scripts and used data are also shared on GitHub to foster future explorations.

Keywords –

Bridge management; Open government data; Bridge information modeling; Graph database; Data retrieval; Knowledge.

1 Introduction

As essential infrastructures for transportation, bridges are widely seen in both cities and rural areas. Since most of the bridges have been built for decades, the deterioration of structural assets and more specifically, deficiencies related to ageing bridges have become a common problem throughout the world[1]. Given that theirs conditions are getting worse year by year, there is a huge demand for resources and funds to maintain bridges every year. For instance, UK has more 160,000 bridges and it will cost about £180 m to maintain or repair bridges in England only according to previous research[2].

Due to limited funds, it is hard to fulfill the escalating maintenance requirements, and the road authorities have to make decisions wisely to avoid potential structural failures. Thus, structural condition assessment and rating are always utilized to choose bridges that with the worst conditions[1, 3]. This calls for a national bridge database[2] as well as bridge management systems, to estimate costs of bridge maintenance accurately. Thus, National Bridge Inventory is established as a unified database to analyze bridges and judge their conditions, for safety and management purposes[2] in the United States since 1968. And similar databases are later created in other countries.

Usually, typical bridge maintenance scenarios like risk evaluation or condition rating require not only structural characteristics, inspections but also other factors such as environmental parameters[4]. However, environmental parameters such as temperature, precipitation are not included in the national bridge databases like NBI. And environmental data are still missing in most of the bridge management systems[2] such as Pontis[5] in the United States, DANBRO in Denmark. Lack of environmental data will lead to inaccurate assessment of bridge conditions and impact the decision-making process.

Recently, many government organizations have published a variety of data to enable transparency, foster applications. For example, the public sector information directive in Europe, the open data initiative in 2009 in the United States, are proposed and open government data portals such data.gov.uk, data.gov, and data.gov.sg are provided for citizens and stakeholders[6]. The Federal

Highway Administration (FHWA) of the U.S. Department of Transportation has opened the NBI database for public access[7]. While there are also quite a few datasets related to environmental data available from national oceanic and atmosphere administration (NOAA)[8]. Integration of all these datasets will bring new opportunities for bridge management and maintenance.

However, to the best knowledge of the author, few attentions have been paid to integration of open government data for bridge maintenance. Therefore, this research explores how to integrate open government data and how to use them for bridge management purpose. First of all, research methodology and framework are proposed in section 2. Then, a labeled property graph model is introduced to model bridge inventory data and environmental data in section 3, procedures and scripts for integration of open government data to create the graph model are also explained in this section. While section 4 demonstrates how to use the established graph model in various data retrieval scenarios related to bridge management. Finally, benefits of the proposed method and potential future works are concluded and discussed in section 5.

2 Framework

As mentioned above, various government data have been opened for public access, and more open data will be accessible in the future. However, these data are usually represented in different formats. To integrate heterogeneous data from different sources, graph based data model are preferred than relational data model according previous investigations[9].

Thus, this research utilized a similar approach based on labeled property graph. As shown in Figure 1, the proposed framework consists of five steps, namely, data collection, graph modeling, graph creation, model extension and application, which are explained in detail as follows.

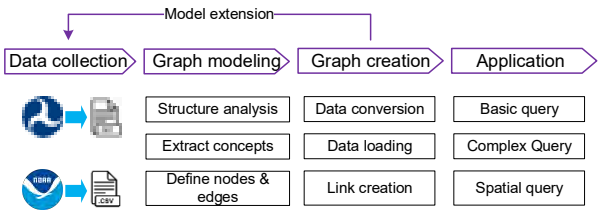

Figure 1. Workflow of the proposed framework

1. **Data collection:** first of all, bridge information from opened bridge databases like the NBI database[7] are downloaded as text files similar to csv format, and environmental data is also obtained from the website such as the NOAA[8] as csv files.
2. **Graph modeling:** considering that the data types, property names and values are encoded and represented with different rules, for instance, NBI database is recorded and encoded following this guide[10], structure of the collected data are analyzed. Then, key concepts as well as their properties are extracted by analyzing corresponding guides on data formatting. At last, key concepts are modeled as nodes of a graph, with their names or classes attached as labels, and relationships between concepts are represented as edges.
3. **Graph creation:** to create the defined graph model in the previous step, a data conversion process is firstly implemented based on python scripts. Then, all data are loaded into a graph database called neo4j, and links between datasets from different sources with neo4j cypher scripts if needed.
4. **Model extension**: since more open data could be accessed, they could be integrated in the graph model through model extension. Generally, engineers or developers could follow the same way as the above-mentioned 3 steps, and the same concepts used in different models and links between different concepts should be identified to merge different data sources and connect different concepts together.
5. **Application**: finally, the created graph is demonstrated with different data retrieval scenarios. In this research, basic query showing the capacity of graph database, complex query for finding bridges linking two states, and spatial query to get environmental data from nearest weather stations of a bridge are provided.

3 Graph-based Modeling of Bridge and Environmental Information

3.1 Concept Graph Model

Following the above-mentioned framework, a concept graph model in Figure 2 is first established for bridge management purpose.

In the middle of Figure 2, concept Bridge is used to represent basic information of a bridge. Structure type, year built, length, and a few other properties defined in NBI database are included in Bridge. Instead of taken all data related to a bridge into a single row as NBI database did, Route, Feature, Traffic, Navigation, Inspection, SpecialInspection, and Improvement are introduced as new concepts. Route stands for a road a bridge carries, and Features are rivers, creeks, etc., that a bridge intersects. Traffic and Navigation capture properties related to traffic loads (i.e., cars, trucks, buses) and navigation control on waterway. Within these two concepts, average daily traffic, vertical and horizontal

clearance of navigation are usually considered properties. Meanwhile, Inspection and SpecialInspection are also introduced to model data related to bridge inspections. Date of inspection, inspection frequency as well as category of special inspections like underwater inspection, fractural inspection is considered in the data model. Finally, improvements made to a bridge are also modeled as Improvement in the proposed model. Cost, date and other properties of improvements are considered.

Moreover, the concepts State, County, and Agency are also introduced to represent state, county a bridge locates in and the agency which the bridge belongs to. According to the NBI database, states are also responsible for the maintenance of bridges, and thus a relationship ResponsibleFor is defined.

To better illustrate the proposed graph model, an exemplary graph of bridge inventory which shows most of the previously mentioned concepts and relationships are provided in Figure 3.

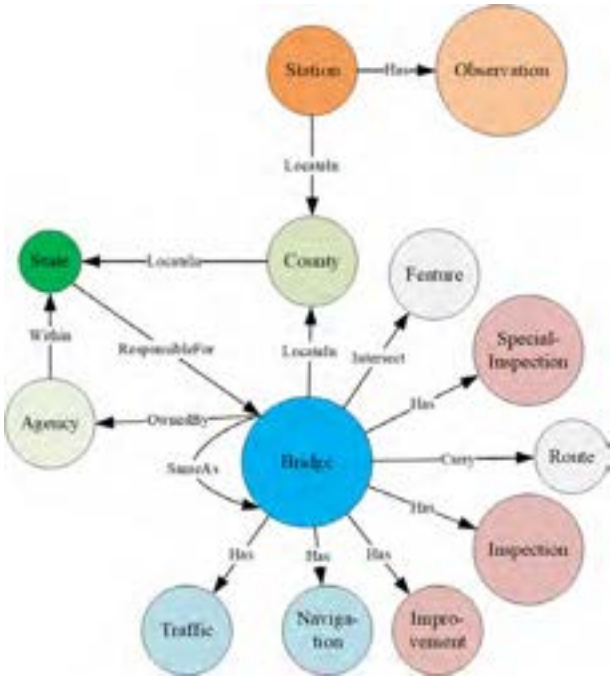

Figure 2. Concept graph model for bridge management

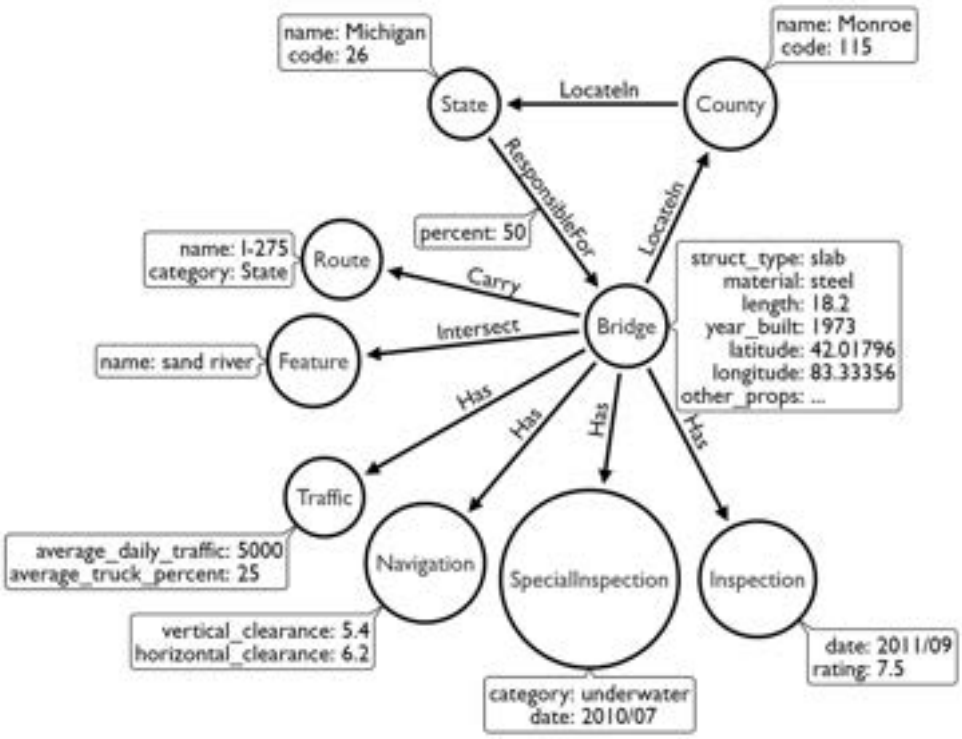

Figure 3. Exemplary Graph of Bridge Inventory

At the top of Figure 2, two concepts, Station, and Observation, are introduced to model environmental from NOAA. Station captures the ID, name, latitude, longitude, and elevation of a weather station, while Observation represents a few environmental features such as temperature, precipitation, wind, observed at a curtained time. And a Has relationship is used to model the relationship between Station and Observation. In this way, an exemplary graph model as shown in Figure 4 could obtained based on raw data from NOAA website.

Note that the Has relationship defined in the graph model is not only used to link bridges and inspections, features, navigations, but also used to connect weather stations and their observations. This is where graph model shows its power. Another benefit of labeled graph model is that relationships can also have properties, as ResponsibleFor relationship does in Figure 3, which is quite straightforward for engineers.

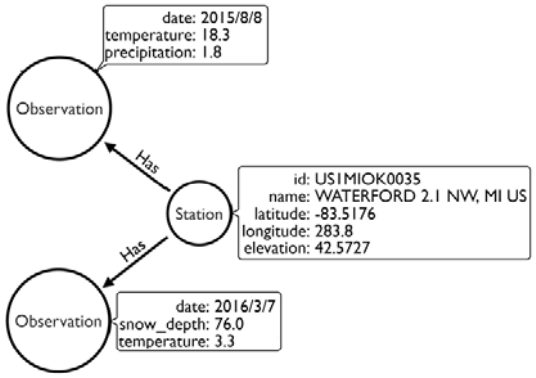

Figure 4. Exemplary Graph of Climate Data

3.2 Data Integration and Graph Creation

To convert multiple source data into the proposed graph model, a data integration and graph creation method is adopted in this research.

Firstly, to transform a data row containing all data related to bridges into different concepts, data mapping rules are defined based on python scripts. Figure 5 shows how to map NBI data tables to Bridge concept and ResponsibleFor relationship of the graph model. According to the upper part of Figure 5, label of the Bridge concept followed by NBI properties used to generated its ID are firstly provided. Then, how to map each column of the NBI data table to properties of the Bridge concept is then defined. Similarly, label and property mapping configurations of relationship ResponsibleFor are defined at the bottom part of Figure 5. Meanwhile, labels as well as NBI properties used to created IDs of source and target concepts are also provided, which links between different concepts can be further created.

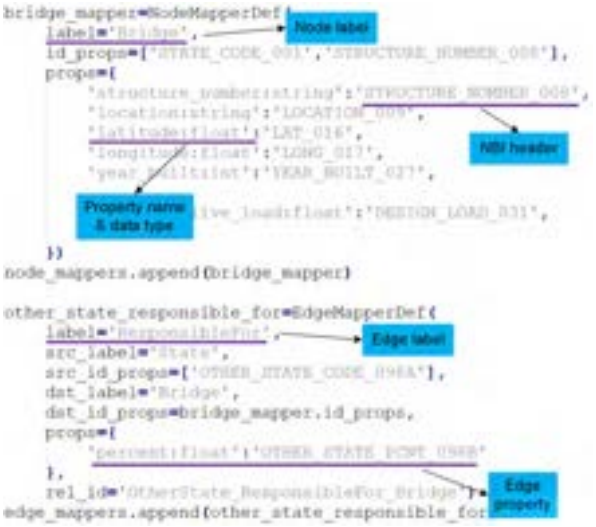

Figure 5. Mapping scripts to create graph model

In addition, since data values of the NBI database are encoded following specific rules, python scripts to decode and convert the data are also needed. For example, latitude and longitude are encoded as a string with 6 digits in the NBI database, and degree, minute, second are represented by the first two digits, the middle two digits, and the last two digits respectively. In this way, python scrips to convert the string to a float number representing the latitude and longitude in radian is provided in Figure 6. Another example shown in Figure 6 is the python script used to convert the year information represented with a two digits string in the NBI database.

```
def get_latlong(raw_val):
    degree=float(raw_val[:-6])
    minute=float(raw_val[-6:-4])
    second=float(raw_val[-4:])/100.0
    return degree+minute/60.0+second/3600.0

def get_date(raw_val):
    month=int(raw_val[:-2])
    year_str=raw_val[-2:]
    if int(year_str[0])<3:
        year=int('20'+year_str)
    else:
        year=int('19'+year_str)
    return datetime.datetime(year,month,1)
```

Figure 6. Scripts to convert NBI properties

Therefore, with defined mapping rules and data conversion scripts, bridge information of the NBI database are converted to different csv files, each of which persists data of a concept or a relationship of the proposed graph model.

Then, the generated csv files could be loaded in neo4j database and the graph is established. As shown in Figure 7, bridge information could be imported with the csv

loading script of neo4j, and nodes representing bridges are automatically created.

```
LOAD CSV WITH HEADERS FROM
"file:///Bridge.csv" AS row merge
(n:Bridge{id:row.id}) on match set
n+=row on create set n=row;

LOAD CSV WITH HEADERS FROM
"file:///State_To_Bridge.csv" AS row
match (s:State{id:row.src_id}),
(d:Bridge{id:row.dst_id}) merge (s)-
[r:ResponsibleFor]→(d) on match set
r+={percent:row.percent} on create
set r={percent:row.percent};
```

Figure 7. Data loading scripts

Furthermore, once nodes representing bridges and states are created, the ResponsibleFor relationship can also be created by loading corresponding csv files with script provided in Figure 7.

Following the same way, data tables obtained from the NOAA website could also be converted and imported into neo4j database, thereby creating data nodes and relationships related to environmental data.

If connections exist between data nodes generated with different datasets, extra rules could be defined based on neo4j script. For example, if ID of concept ConceptA from a dataset equals a property PropB of concept ConceptB generated by another dataset, then the following script in Figure 8 could be used to create the relationship RelAtoB.

```
match (a:ConceptA),(b:conceptB) where
a.ID=b.PropB create (a)-[:RelAtoB]→(b)
```

Figure 8. Data script to create relationships

4 Demonstration

Following the previously mentioned workflow, this research build a graph model based on data retrieved from the NBI and NOAA website. Specifically, NBI data of Michigan state from 2011 to 2016 and Wisconsin state in 2016 as well as environmental data in Michigan and Ohio state from 2015/1/1 to 2016/12/31 are utilized. In addition, codes and names of all states and counties are also included when creating the graph. At last, there are 190, 525 nodes with 13 labels and 283, 616 relationships with 8 labels created in total. Details of nodes and relationships are listed in Table 1.

According to Table 1, it is concluded that there are 25, 410 bridge inventories carrying 1, 509 routes and intersecting with 6, 955 features in total. While 30, 737 inspections, 1, 506 special inspections as well as 3, 879 improvements were made from 2011 to 2015. In other words, about 1.27 inspections were made for each bridge on average and only 15.26% of them were improved during this period, reflecting that there is a huge demand of funds for bridge maintenance.

Table 1. Number of Nodes and Relationships in Generated Graph Model

Category	Label	Amount
Node	State	52
Node	County	3, 228
Node	Agency	26
Node	Bridge	25, 410
Node	Route	1, 509
Node	Feature	6, 955
Node	Traffic	25, 747
Node	Navigation	15, 952
Node	Improvement	3, 879
Node	Inspection	30, 737
Node	SpecialInspection	1, 506
Node	Station	179
Node	Observation	75, 345
Relationship	LocateIn	28, 628
Relationship	OwnedBy	25, 411
Relationship	Within	26
Relationship	ResponsibleFor	25, 513
Relationship	Carry	25, 413
Relationship	Intersect	25, 438
Relationship	Has	153, 166
Relationship	SameAs	21

To further illustrate how the established graph could be used for various data retrieval scenarios. Due to limited content of this paper, three scenarios are chosen to show basic query, complex query and spatial query capacity of the neo4j graph database.

4.1 Scenario 1: Query Data Related to Bridges

Top of Figure 9 shows a basic query retrieving bridges and all nodes they direct to. In the query, putting noting in the square brackets means matching all relationships, and the arrow implies that only relationships directing from bridges to other nodes are considered. To limit the results within 25, graph shown at the middle of Figure 9 is obtained.

Figure 9. Query bridges and its connected data

It is found that there are 3 bridges built in the year of 1932, 1980, and 2000 respectively, and two of them carry the same route. Meanwhile, a special inspection considering fracture critical details is also conducted when inspecting the bridge built in 1932. In this scenario, it is quite easier to retrieve all information related to a bridge with a simple query. It is also possible to match certain nodes connected with a specific relationship by specifying the relationship's label in the square brackets.

4.2 Scenario 2: Query Bridges Linking Two States

Furthermore, it is also possible to retrieve bridges linking two states. Query shown at the top of Figure 10 generates a small graph at the bottom of Figure 10.

As illustrated in Figure 10, two bridges connecting Michigan state and Wisconsin state are identified with the query. Since the NBI database assigns different unique numbers to bridges located in different states, there are two bridge nodes representing the same bridge in Figure 10. It is also illustrated in Figure 10 that the bridges are maintained together by the two states.

In this way, it is possible to query bridges carrying the same route, intersecting with the same feature, or owned by the same agency.

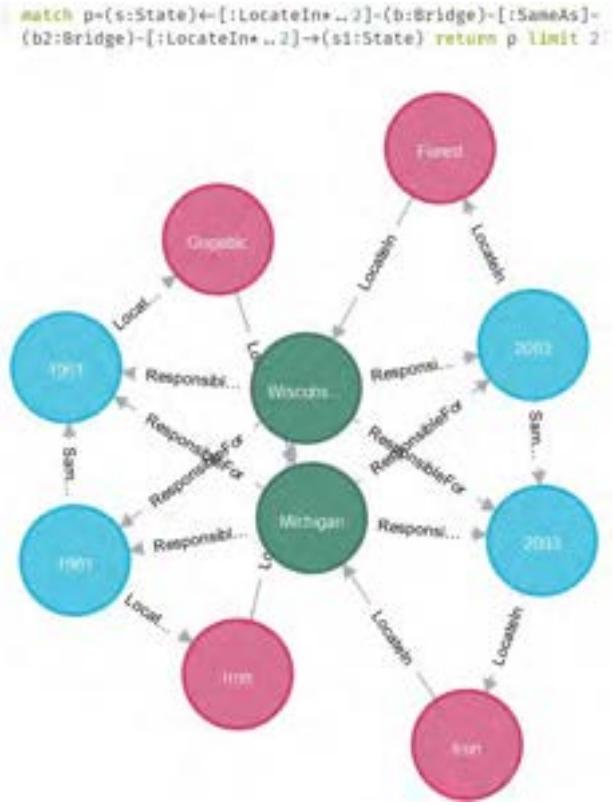

Figure 10. Bridges linking two states

4.3 Scenario 3: Query Nearby Environmental Data of Bridges

At last, given that longitude and latitude of bridges and weather stations are available in the created graph database, it is also possible to retrieve nearby environmental data of a bridge. For example, Figure 11 shows a query retrieving temperature and precipitation observed by nearby weather stations of a bridge for underwater inspection purpose. And part of the results of the query are listed in Table 2

```
match p=(b:Bridge)-[:Has]→
(ins:SpecialInspection{category:'underwater inspection'}),
q=(s:Station)-[:Has]→(o:Observation) where ins.date>o.date
and o.precipitation>0 and exists(o.temperature) return
b.structure_number,ins.date,o.temperature,o.precipitation,di
stance(b.loc_point,s.loc_point)/1000 as distance order by
distance limit 5
```

Figure 11. Query nearby environmental data of bridges for special inspection

It is found that underwater inspection of bridge No. 000000000011328 is conducted on 2015/4/1 and the temperature and precipitation observed by the nearest weather station (about 5.92 km away) at the same day are 1.7℃ and 0.3mm respectively. While similar results could be also obtained for the other two bridges.

In this way, researchers, engineers, and road authorities could extract environmental data from weather stations, thereby developing better model for condition evaluation and making wise decisions for bridge maintenance.

Table 2. Nearby environmental data of bridges for special inspection

Bridge No.	Date	Temperature/℃	Precipitation/mm	Distance/km
000000000011328	2015/4/1	1.7	0.3	5.92
B27007400000000	2015/11/1	6.1	3.8	24.05
000000000011884	2015/4/1	-2.2	0.3	27.90

5 Discussion

In this work, a framework integrating multi-source open data for bridge management and maintenance is proposed and demonstrated in a few scenarios.

The framework is validated with data collected from the NBI database and the NOAA website, since they are the public available and could be accesses easily. Despite this, it is possible and easy to adapt the proposed framework for integrating other bridge databases and data sources. For example, bridge database of the UK could be accessed from data.gov.uk, then the same workflow proposed in Figure 1 can be directly used to create a graph model for bridge management and maintenance. Similarly, open weather data could also be integrated with the same way. Moreover, except for bridge data and environmental data, as other open data is published, it is also possible to further extend the established graph model and continuously integrate more data sources.

With the proposed framework and graph model, it is possible for the managers to query related bridge information, environmental data as well as their connections for bridge management purpose. In this way, decision-makers could take open government data as a supplement of their private data to further improve bridge maintenance process. For example, a manager could take a target bridge operated by the agency he/she belongs to, query bridges that have similar states and environmental conditions with the target bridge from the graph database, and by comparing the retrieved bridges with the target bridge, he/she could get insights on how to improve the inspection and maintenance decisions.

However, when conducting this research, it is also found that the quality and richness of open government data still need further improvements. Detailed inspection information, other factors such as geotechnical stability, subsurface conditions are still not available from open data sources. Thus, it is recommended that the governments as well as other data providers should open more data if possible, and an approach that integrating both open data and private data for bridge maintenance are suggested.

6 Conclusions

As the government keeps opening data for public access, there is a trend in integrating multisource open data to foster applications and innovations in different areas. However, though bridges are essential for delivering goods and people around the urban and rural ear and there is a huge demand of funds for bridge maintenance, value of open government data for bridge management has not been explored yet.

This research investigates how to integrate the bridge information and the environmental data opened by the government based on graph modeling for bridge maintenance. A labeled graph model and python scripts for data conversion and integration are proposed. Demonstration in different scenarios show the flexibility and feasibility of the proposed framework. With the proposed method, it is possible to query various data related to bridges and retrieve environmental data nearby bridges, which are valuable for flood risk assessment, vulnerability, damage modeling [5] and decision-making, etc.

In the future, stakeholders are encouraged to open more data, such as data of highway network, traffic data collected by mobiles or sensors, which could be integrated and innovative application in bridge management would emerge quickly. In addition, it is also recommended to integrate both open data and private data as they could complement each other, thus bridge managers could make better decisions for bridge maintenance purpose.

What's more, to foster more explorations and applications, scripts used for data conversion and graph creation as well as a few exemplary graph queries are shared through GitHub:

https://github.com/smartaec/OpenBridgeGraph. Other researchers could access and modify the scripts for their further works.

Acknowledgement

This research is supported by the Tsinghua University Initiative Scientific Research Program (No. 2019Z02UOT), the Natural Science Foundation of China (No. 51908323), and the Beijing Natural Science Foundation (No. 8194067). The author also thanks Prof. Kincho Law (Stanford University) for his valuable comments.

References

[1] Rashidi M., Samali B. and Sharafi P. A new model for bridge management: Part A: condition assessment and priority ranking of bridges. *Australian Journal of Civil Engineering*,14(1):35-45, 2016.

[2] Pregnolato M. Bridge safety is not for granted-a novel approach to bridge management. *Engineering Structures*,196:109193, 2019.

[3] Aktan A., Farhey D., Brown D., Dalal V., Helmicki A., Hunt V. and Shelley S. Condition assessment for bridge management. *Journal of Infrastructure Systems*, 2(3):108-117, 1996.

[4] Wang H., Hsieh S., Lin C. and Wang C. Forensic diagnosis on flood-induced bridge failure. I: Determination of the possible causes of failure. *Journal of Performance of Constructed Facilities*, 28(1):76-84, 2014.

[5] Thompson P., Small E., Johnson M. and Marshall A. The Pontis bridge management system. *Structural Engineering International*, 8(4):303-308, 1998.

[6] Attard J., Orlandi F., Scerri S. and Auer S. A systematic review of open government data initiatives. *Government Information Quarterly*, 32(4):399-418, 2015.

[7] FHWA. National Bridge Inventory. On-line: https://www.fhwa.dot.gov/bridge/nbi.cfm, Accessed: 14/03/2020.

[8] NOAA. Climate Data Online. On-line: https://www.ncdc.noaa.gov/cdo-web/, Accessed: 14/03/2020.

[9] Yoon B., Kim S. and Kim S. Use of graph database for the integration of heterogeneous biological data. *Genomics & informatics*, 15(1):19-27, 2017.

[10] FHWA. *Recording and Coding Guide for the Structure Inventory and Appraisal of the Nation's Bridges*. Washington, D.C., 1995.

Five-dimensional Simulation of Bridge Engineering Based on BIM and VR

K. C. Wang[a], S. H. Tung[a], W. C. Chen[a], and Z. C. Zhao[a]

[a]Department of Construction Engineering, Chaoyang University of Technology, Taiwan
E-mail: wkc@cyut.edu.tw, s10811614@gm.cyut.edu.tw, xxx56618@gmail.com, g90253@gmail.com

Abstract –

Building information modeling (BIM) is a rapidly developing technology used in the construction industry. Many construction companies have implemented BIM into their construction processes for executing various construction management tasks, including four-dimensional (4D) progress simulation and cost control. However, 4D progress simulation has not been simultaneously integrated and compared with cost control thus far. With the execution of this simultaneous task, the relationship among project progress, construction cost, and project components can be explored. Moreover, currently, when conducting a cost review, discretionary adjustments cannot be performed based on an actual site implementation. To this end, in this study, first, the quantities of each of the cost items are calculated using BIM and are matched with the corresponding construction progress. The quantities of each of the cost items can, therefore, be included in each construction progress report. Next, BIM is integrated with the construction cost and the project schedule to generate an S curve concurrently with the 4D simulation. By using the S curve, cost control can be performed according to construction progress. In addition, the proposed model can be presented clearly by using virtual reality (VR).

Finally, this study explore the feasibility of the proposed model by applying it to a bridge construction project. The results indicate that the cost of each stage can be clearly determined using the proposed model. When a cost item is unclear, it can be compared with the simulated construction progress. Coordination and management can be performed, and any gaps therein can be filled early to increase the efficiency of the management process.

Keywords –

Building Information modeling; Virtual Reality; Five-dimensional Simulation

1 Introduction

Building information modeling (BIM) is a rapidly advancing technology in the construction industry. Numerous manufacturers use BIM to manage operations during construction, such as four-dimensional (4D)[1,2] progress simulations and cost control. Progress schedules are linked with BIM components by using 4D progress simulations. Accordingly, BIM models are progressively developed according to the progress schedules, which enable examinations of crucial matters and management items during each operation. Cost estimation entails quantity calculations using BIM models, which link the unit price of each work item and distribute the cost of items to corresponding operations[3]. This allows users to determine the daily costs incurred from various operations and plot a cumulative cost curve (S-curve) [4].

Despite the prevalent use of 4D progress simulations and cost control in construction companies, they have yet to be integrated together to simultaneously determine the relationships between progress, costs, and building components. Thus, when conducting cost reviews, construction companies cannot account for actual situations at the construction site or make adjustments accordingly. Therefore, this study integrated each cost item and its corresponding BIM model into 4D simulation task lists and integrated construction costs and schedules to generate S-curves. This enabled real-time simulation of construction progress by using the models and control costs by using S-curves. In addition, virtual reality (VR) was used to clearly present the models.

2 Literature Review

2.1 BIM 4D Progress Simulations

Generally, 4D simulations are effective auxiliary tools for construction planning and monitoring and help convey construction-related information. Early detection of conflicting construction items and process problems can help construction companies save considerable

money. Communication during meetings can help clarify problems, discuss issues related to construction interfaces, facilitate the attribution of responsibility, save communication time, and reduce wasted time resulting from misunderstandings. 4D simulations offer visual information to no construction personnel, and BIM provide easy-to-understand information that allows them to solve problems during preconstruction, diminish construction risks, control progress, and plan and review the planning of building interfaces and circulation. By using 4D simulation visual technology, construction companies can quickly understand relevant situations, which allows them to save communication time, reduce construction errors, enhance efficiency, and lower costs [5].

2.2 BIM-based Five-Dimensional Cost Control

Replacing traditional two-dimensional (2D) design processes with those that involved the integration and visualization of three-dimensional (3D) parameters and objects substantially reduces the number of drawings used. Moreover, this reduces the amount of work overseen by entry-level staff, which effectively integrates human resources and streamlines manpower costs. Construction schedules and costs are closely related, and 4D schedule planning enables managers to accurately monitor construction quality and progress, thereby controlling construction costs. Although effective in many respects, traditional 2D drawings are ineffective in presenting the number and areas of 3D space in houses. Five-dimensional (5D) cost estimates can be employed to perform detailed estimation of areas and material costs by using drawings. Specifically, this approach considers construction companies' budgets and material unit prices, accurately estimates construction costs, and reduces material estimation costs [6].

2.3 BIM and VR Integration

Intrgrating BIM and VR is a revolutionary breakthrough in the construction industry. BIM enhances authenticity, motion capture precision with VR plugins, and display resolution. BIM+VR has been promoted in the construction and construction marketing fields and enable the integration of BIM and VR systems. Such system integration prevalently used in the construction design industry. Promoting BIM+VR is possible because of advances in computer and Internet technology, which offer the construction industry enhanced computing power and effective software–hardware connections. Applying a BIM+VR system in construction projects and construction marketing is the result of increased investments in relevant systems by the construction industry and the public's improved consumption power [7].

3 5D Simulation of BIM+VR-Based Bridge Construction

3.1 BIM Model Building

This study entered various building dimensions from 2D drawings into Revit to generate 3D models. In general, each building component is separated during the drawing process to allow users to click on the building components separately during component scheduling (i.e., when selecting components and their corresponding operations) and design (Figure 1).

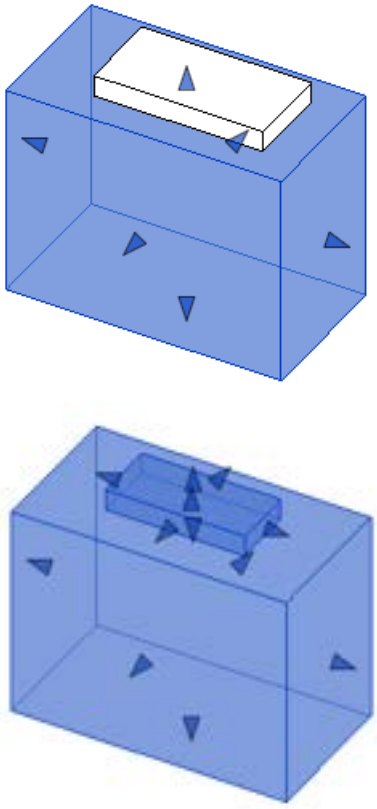

Figure 1. Difference between models with and without separated components

3.2 Number of Various Components and Cost Calculations

The concrete cost is determined by calculating the concrete required using the BIM model and multiplying

this number by the concrete unit price. The template cost is determined by calculating the surface area (using the BIM model) and multiplying this number by the concrete formwork unit price.

Because rebars are not drawn when building the models, the rebar cost is determined by calculating their lengths by using the rebar distribution diagram, multiplying these numbers by their corresponding unit weights, and multiplying the total weight by the unit price. The same calculation method are employed to determine the costs of other materials.

3.3 BIM Models Integrated with Construction Schedules: 4D Simulations

In this study, work items that needed to be completed in the progress schedule network diagram were first identified because numerous work items were completed prior to actual construction. Because this study only investigated the actual construction, work items that were completed before and after the construction process were removed. According to the progress schedules, work items and their corresponding components were integrated into a task list to adjust parameters such as construction time, animation speeds, animation effects, and illumination level to ensure that the 4D simulations ran smoothly.

3.4 3.4. Costs Integrated with 4D Simulations: 5D Simulations

The cost of each component previously calculated is entered into each progress schedule item. This allows users to know the total work item costs when performing 4D simulations. The users learn of these costs by selecting the construction shapes desired and examining the cost curves generated. The construction schedule–cost integration process is described as follows:

(1) The construction schedules and costs are integrated into an Excel sheet.
(2) The costs are entered as the material costs in actual construction schedules.
(3) The construction shapes in the left column of the 4D simulations are selected to generate cost curves.

3.5 VR and 5D Cost Control Integration

For managers to oversee the construction of a building as if they have participated in the construction process in person and review the construction progress, this study displayed the 5D simulation results in VR environments. By using the VR function of Fuzor along with external hardware devices, handles, and a VR head-mounted display, users can observe 4D VR simulation models to simulate authentic construction processes.

External drive equipment that connects the built-in VR functions of Fuzor with external VR drivers (e.g., STEAMVR.GeForce) include Sony PlayStation, Sony VR, and HTC Vive head-mounted displays. Users who do not have this equipment at their disposal could have used a smartphone with easily accessible VR glasses to enjoy the VR experience.

4 Case Study

4.1 Case Descripting

This study use a cable-stayed bridge as a case project. The cable-stayed bridge investigated is near the National Freeway 1 Daya Interchange, spanned Provincial Highway 74, and connected to Shuinan Economic and Trade Park in Taiwan. The sketchup model of case project is shown in Figure 2.

Figure 2. The sketchup model of case project

4.2 BIM Model Construction

The bridge was drawn in four stages: the drawing of the pier foundation, bridge roads, main tower, and steel cables. When drawing the bridge, the Revit group was turned on, and the computer-aided design drawings of each component were imported. Subsequently, the extrusion function was used to draw the bridge according to the construction shapes desired and elevations set. All components had to be drawn separately when drawing the bridge.

The bridge roads drawn were divided into six segments, and the components were drawn using the cross-sections of the roads. Because the bridge was not straight but curved, this study developed bridge roads through the sweeping method in Revit.

The main tower comprised 14 steel components that were drawn separately before being put together. The left and right sides each had seven components,. Similar to the bridge roads, the components were developed using the sweeping method. The main tower model is shown in Figure 3.

Figure 3. The BIM model of the main tower

Steel cables were found on all four sides of the bridge. Each side of the bridge contained 24 steel cables for a total of 96 steel cables. The steel cables were drawn using built-in components of Revit. Because some road surfaces were tilted or had turns and because steel cables in different sections varied in length, the cables on the four sides were drawn individually, and the cable lengths and locations had to be adjusted. Finally, the pier foundation, bridge roads, main tower, and steel cables were integrated, as presented in Figure 4.

Figure 4. The BIM model of the integrated model

4.3 Number of Each Component and Cost Calculations

The bridge was built using steel and reinforced concrete, and the upper and lower parts were constructed using steel and reinforced concrete, respectively. Calculations revealed that the quantities of concrete, rebars, concrete formwork, road steel plates, and main tower steel plates used were 15,722.3 m^3, 2,081,987.6 kg, 3,882.2 m^2, 844,062.3 kg, and 945,862.2 kg, respectively.

Revit was used to calculate the volume of the building components, from which the quantity could be determined. The components calculated included full-casing foundation piles, foundations (e.g., precast and self-filling concrete), piers, top beams, steel roads, parapets, asphalt concrete, the steel main tower, and the concrete formwork.

4.4 Costs of Performing Calculations Through BIM

After obtaining the quantity of each component by using these calculations, this study searched for the unit price of each component by using the unit price database prepared by the Public Construction Commission. The two variables were multiplied to derive the costs. The costs of concrete, rebars, the concrete formwork, road steel plates, and the main tower steel plates were NT$33,803,035, NT$41,639,753, NT$1,071,484, NT$145,321,869, and NT$28,375,866, respectively.

4.5 BIM Models Integrated with Construction Schedules: 4D Simulations

To clearly grasp the overall construction progress on the dates specified by construction companies, the construction progress schedules shown in the network diagram can be viewed. This enables users to learn about the schedules, float time, and progress of each work item and facilitate subsequent 4D simulations, as displayed in Figure 5.

Figure 5. Parts of the schedule of the case project

After displaying the overall construction progress by using Project, users are required to enter the names and durations of the construction work items in the BIM model by using the Fuzor 4D model task creation menu. Next, 4D simulations are generated (Figure 6), which allows overall construction progress to be observed visually. After entering the schedules for all models, users can preview 4D simulation results in advance and produce smoother 4D simulation animations by adjusting parameters such as the animation speed and illumination level. 4D simulation animations are produced using Fuzor through the following three steps:

(1) Add simulation items: Select the function “4D simulation model” in the menu and turn on the function “4D simulation.” Then, add new items for subsequent scheduling.
(2) Set construction dates: Set the overall construction start and completion dates. For instance, in this study, the “start date” and “completion date” were set as “September 23, 2017” and “October 19, 2019,”

respectively.

(3) Add model parameters: After importing the model into Fuzor, click on the models to be scheduled and set the work items and construction dates to facilitate 4D simulations for each work item according to their schedules.

Figure 6. 4D simulation

4.6 Costs Integrated with 4D Simulations: 5D Cost Control

Costs are integrated with 4D simulations to produce BIM 5D simulations. The cost of each work item is incorporated into 4D simulations to form cost curves, which allows them to be generated when each work item was implemented, and corresponding costs are simulated. 5D simulations are performed using Fuzor through the following two steps:

(1) Enter work item costs:When entering costs in 4D simulations, the costs of the component are used as the material cost of the work items. For example, the cost of hoisting the steel bridge in this study was 28,375,866. Work item costs could also be entered using Project or Excel, as shown in Figure 7.

(2) Display cost curves: After entering costs in 4D simulations, select the function “construction shape” to generate cost curves. Cost curves are also displayed during 4D simulations, as illustrated in Figure 8.

Figure 7. Work item costs

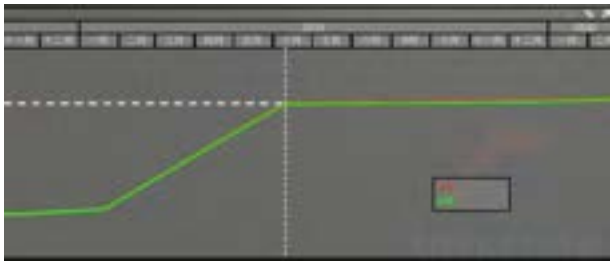

Figure 8. Progress curves of cumulative cost

4.7 5D Simulations Displayed as VR

In this study, mobile phones were placed in VR Boxes, and joysticks were used to move around in the VR environment and present the results of integrating VR and 5D simulations. In general, 5D simulations are displayed through VR through the following three steps:

(1) Initiate connection: Connect to a mobile phone by using Riftcat2.0 and turn on VRidge in the phone to connect it to a computer, as shown in Figure 9.

(2) Place a mobile in a VR Box (as shown in Figure 10) and click the option “connect” in Riftcat2.0 to connect it to VR.

(3) After opening Fuzor Project, use the VR button to connect the VR environment to the VR Box for viewing, as shown in Figures 11 and Figure 12.

Figure 9. Link the phone and the computer

Figure 10. VR Box

Figure 11. VR environment on the computer screen.

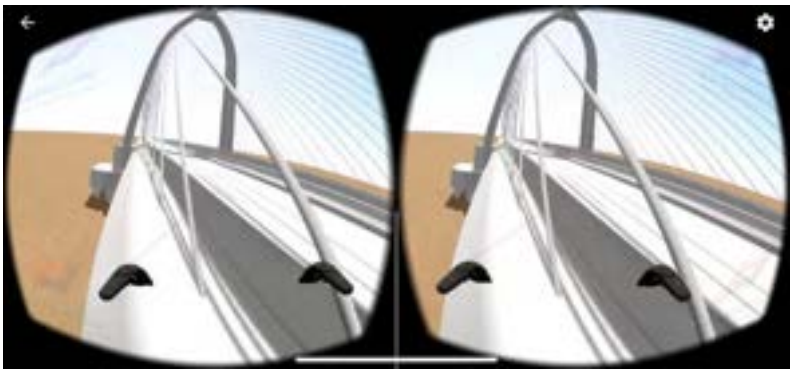

Figure 12. VR environment on the mobile screen.

5 Conclusion

5.1 Benefits of Applying Cost Curves

This study combined 4D simulations and costs to display 5D simulations. 4D simulations enable constructions to be viewed as animations, and construction progress costs are viewed as cost curves. Comparing the simulated cost curves with actual cost curves allows identifying actual construction progress and construction costs. This enabls construction companies to determine whether they are ahead or behind schedule on the basis of the discussions and revisions made to elevate construction quality.

5.2 5D Animation Simulations Integrated with VR

Although the group method can be adopted to create bridge models by using Revit and incorporated the models into projects, 4D simulations exhibit the following problem: Only one 4D simulation can be performed for identical components in different work items. Therefore, different component groups must be created for different work items to enable 4D simulations for all work items.

In addition, although higher-standard VR equipment (such as HTC Vive) can produce superior and immersive experiences, it requires using VR sensors, head-mounted devices, and a computer connection, rendering it unfeasible in specific locations. By contrast, this study used VR Box, connected it to a laptop computer and mobile phone, and placed the mobile phone in a VR Box to display the VR, which effectively elevated the applicability of VR displays.

References

[1] Choi, B., Lee, H. S., Park, M., Cho, Y. K. and Kim, H. Framework for work-Space Planning Using Fou-

Ddimensional BIM in Construction Project. Journal of Construction Engineering and Management (ASCE). 140(9):1-13, 2014.

[2] Lopez, R., Chong, Y., H., Wang, X. and Graham, J. Technical Review ： Analysis and Appraisal of Four-Dimensional Building Information Modeling Usability in Construction and Engineering Projects. Journal of Construction Engineering and Management (ASCE).142(5):1-6,2016.

[3] Zhang, R.and Liang, C. Research on Construction Schedule Control Based on Critical Chain Method and BIM.Journal of Applied Science and Engineering Innovation (ACSS).5(2):47-50,2018.

[4] Jrade, A. and Lessard, J. An Integrated BIM System to Track the Time and Cost of Construction Project: A Case Study.Journal of Construction Engineering,page 1-10,2015.

[5] Chen, H. Y. Guideline Development of BIM/4D Applications for Owners . National Central University Electronic Theses & Dissertations. Thesis,2019.

[6] Chen, Y. X.,Lai, M. H.,Li, Y. W.and Wu, Y. Z. Architect firm BIM technology introduction and effectiveness analysis. Civil and Ecological Engineering Seminar. Page 1-6, Kaohsiung , 2012.

[7] Concord Tech Co .,Ltd. Guangci social housing On-line:https://www.ctc.com.tw/web/Home/NewsInfo ?key=698860839777&cont=158945.

Digital Twinning of Railway Overhead Line Equipment from Airborne LiDAR Data

M.R.M.F. Ariyachandra[a] and Ioannis Brilakis[a]

[a] Department of Engineering, University of Cambridge, United Kingdom
E-mail: mfa47@cam.ac.uk, ib340@cam.ac.uk

Abstract –

The automated generation of geometry-only digital twins of Overhead Line Equipment (OLE) system in existing railways from point clouds is an unsolved problem. Currently, this process is highly reliant upon manual inputs, needing 10 times more labour hours than scanning the physical asset. The resulting modelling cost counteracts the expected benefits of the digital twin. We tackle this challenge using a novel model-driven method that exploits the highly regulated and standardised nature of railways. It starts by restricting the search for OLE elements relative to point clusters of the railway masts. The resulting point clusters of the OLE elements are then converged with various parametric models of different catenary configurations to verify the presence of OLE elements and to find the best possible fit. The method outputs a geometry-only digital twin of the OLE system in Industry Foundation Classes (IFC) format. The method was tested on an 18 km railway point cloud and achieves overall detection rates of 93.2% F1 score for OLE cables and 98.1% F1 score for other OLE elements. The accuracy of the generated model is evaluated using distance-based metrics between the ground truth model and the automated model. The average modelling distance is 3.82 cm Root Mean Square Error (RMSE) for all 18 km data.

Keywords –

Overhead Line Equipment (OLE); Geometric Digital Twin (gDT); Point Cloud Data (PCD)

1 Introduction

Cost overruns are a worldwide phenomenon for railway projects, irrespective of the size and the contract value. The average cost overruns account for 29% projects' engineer estimates for rail and road projects in Europe and the United Kingdom (UK) [1], [2]. For example, the London Docklands Light Rail project is currently overrunning by over £1 billion in costs and three years [3] in duration. These cost and time overruns are common partly due to the absence of Information and communications technology (ICT) sector-level data management for construction/upgrade and maintenance of railways. Specifically, the absence of any form of a digital representation of railways caused by the extensive time required for collecting and processing raw data into working models makes it challenging to upgrade railways.

We argue that the need to create and maintain up-to-date digital twins of railways is an opportunity that should not be missed. Digital twins are expected to bring significant benefits to time, cost and quality parameters of railway projects [4]. These benefits include an 80% reduction in time, 10% through clash detection and 40% elimination of unbudgeted change [5], [6]. Yet, the current cost of creating and maintaining the digital twins greatly counteracts the perceived benefits of the digital twin. The non-canonical shapes in railways require 95% of the total modelling hours for manual shape customisation and fitting processes [7]. The automation of the twinning process will reduce the modelling time and ultimately save costs. We presented a method for generating railway masts as a first step to tackling this challenge [8], which also presented a method for removing the majority of the vegetation and other noise data from the input Point Cloud Data (PCD). The current paper addresses the next step; a method to automatically generate Geometric Digital Twin (gDT)s of railway Overhead Line Equipment (OLE) systems from airborne LiDAR data.

2 Overhead Line Equipment (OLE)

We define the following components as OLE elements (Figure 1).

- Connecting beam - Connects two masts of the same pair together.
- Contact cable - Transmits power to the train by a pantograph. They lie in the lowest height among all overhead cables and shall not be placed less than 5.8 m from the ground [9]. The contact cable runs in a zig-zag path above the track to avoid wearing a

groove in the pantograph. The zigzag known as the 'stagger' - is generally achieved using 'pull-off' arms attached to the support structures.

- Auxiliary cable – Placed between the catenary and contact cables, functions as a buffer and reduces the fluctuation of the cables.
- Catenary cable - Supports the contact cable and located immediately above auxiliary cables.
- Cantilever - Consists of horizontal and vertical metal tubes, connects catenary cables to masts. It supports the catenary projecting from a single mast on one side of the track.

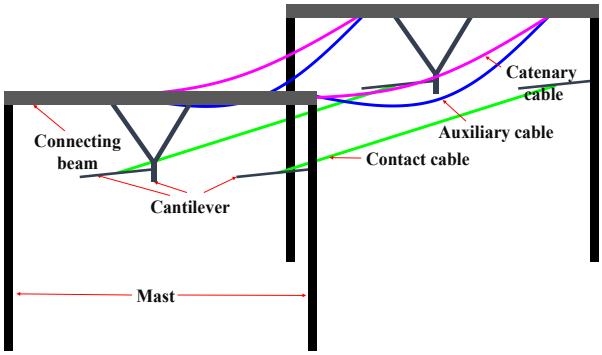

Figure 1. OLE elements

3 Research Background

3.1 Contact, Auxiliary and Catenary Cables

The process of converting PCD into gDTs of cables involves three steps: (1) Extraction of cable points, (2) Clustering single cable points, and (3) 3D cable fitting. Methods for cable extraction and clustering include: (1) Statistical analysis of PCDs based on height, density or number of pulses, etc. [10]–[14] (2) Hough transform and clustering based on two-dimensional (2D) image processing [11], [15], [16] (3) Supervised classification based on metrical and distribution features between points [13], [17]–[19]. Verification of detected cables is performed using a simplified model to fit into detected cables in the planar horizontal view [20] or by the usage of the Random Sample Consensus (RANSAC) algorithm combined with intensity values [21] or a polynomial function to fit the model [22]. We review each of these for cables in both railways and roads.

3.1.1 Statistical Analysis of PCDs Based on Height, Density or Number of Pulses

Jwa and Sohn [23] converted the cloud into voxels and detected cables using the linearity of the element. The method also used point density and segmentation analysis to differentiate roof edges, fences and other linear assets from cables and to group the points into catenary and contact cables. However, their method highly depended on the point density and the size of the voxel. The method did not work well when the cloud had data gaps, vegetation encroachment, and bundled cables. Cheng et al. [10] used a similar approach following KD trees and a polynomial function for clustering and 3D model fitting. The main limitation was they ignored the sagging posture of cables. Also, the method was influenced by frequent occlusions by trees or buildings, ambient conditions such as the temperature and the ageing of spans. The high detection and clustering accuracies were also attributed to the high point density of the data.

Zhu and Hyyppa [11] used statistical analysis considering height, point density and histogram thresholds and image processing methods to extract cables considering geometric properties. However, the thresholds highly relied on the point density and their dataset had a clear cut-off edge between cables and trees. In the majority of cases, OLE cables are not located at a distance away from the surrounding trees and other pole-like objects. A similar approach was used in Guan et al [14] to differentiate road and off-road points and to extract power-transmission cables/power tower points from the latter, followed by the extraction of individual power-transmission cables via Hough transform and Euclidean distance clustering. Finally, a 3D object fitting was done using linear and hyperbolic cosine functions. However, the method was sensitive to the point density of their PCD and did not work well for a different point cloud. Following previous methods, Cserép et al. [13] used height analysis to filter ground points and then used intervals along a selected axis with a point counter assigned to each interval to remove outliers. Finally, the method extracted cable points using using a density analysis and 3D voxels. Yet, their method could not reconstruct those cables into 3D models as the density algorithms removed some cable points as well.

3.1.2 Hough Transform, and Clustering Based on 2D Image Processing

Liu et al. [15] used statistical analysis and an improved Hough transform [24], to segment and to detect cable points. However, the thresholds were sensitive to the point density of the PCD and further work is needed to map the detection results to original 3D data and fit the curves to cable points. The method used in Sohn, Jwa and Kim [16] segmented cable points using Markov Random Field (MRF) classifier, which classifies power cables from other linear assets. The locations of pylons were used to detect cable span, within which cables are modelled with catenary curve models in 3D using the piecewise model growing. Yet this method assumed that the cables were parallel.

3.1.3 Supervised Classification Based on Metrical and Distribution Features between Points

Kim and Sohn [17] used Random Forests classifier as a supervised classification method to detect five key object classes which include cables, pylons, building, vegetation and low objects. They used 2D Hough Transform to 2D points of cables obtained by projecting 3D points onto a horizontal plane. A similar approach has been used in Wang et al. [19] by filtering cables using the height relative to the other objects. Then, the multi-scale spherical neighbourhoods are used to capture the anisotropy and details of cable topology structure. Next, metrical and distribution features were used to enhance classification accuracy. Finally, using Support Vector Machine (SVM) they classified cable points. However, both methods were unable to perform well when cables become the only object of interest as all the feature-based classifiers were highly attributed to the five class objects they considered. Furthermore, these methods only classified but not reconstructed 3D models of any of the class objects.

Following the same classification process, Guo et al. [18] used an improved RANSAC algorithm that includes similarity detection. A powerline between a span was segmented into neighbourhood cubes. Then the points within the cubes were projected onto planes to detect the similarities amongst the planes. At last, they detected cables using the inliers selected by RANSAC. However, the accuracy of the method was sensitive to the sparseness of the data and did not work well for a different point cloud. For instance, if there are few or no points on the cables, data are classified as vegetation by default. Also, cables were split into several pieces or categorised as false negatives when parts of the cables are being obscured by vegetation or when there were few points along a section of the line.

3.2 Cantilevers and Connecting beams

There are only two methods exist that detect cantilevers from PCD in Pastucha [25] and Rodríguez et al. [26] and no methods exist that detect connecting beams. In Pastucha [25], the method used the pattern of the points; a cross above the track to indicate the presence of cantilevers using RANSAC algorithm. All model points are classified as the catenary system in the case of positive authentication. Yet, the high detection rates were attributed to the trajectory of the mobile scanner and the density of the PCD. Besides, all the geometrical distances and properties of the objects should be manually entered by the end-user. Rodríguez et al. [26] detected points of cantilevers using a range search algorithm to filter the highest set of points relative to the points on the catenary cable. However, they could not validate the method since the data set was too small, so it only contained one cantilever.

3.3 Gaps in Knowledge

Cable scene complexity including data gaps, vegetation encroachment [11], [18], and bundled cables affected the accuracy of the results of the existing OLE elements detection methods [10], [23], [26]. Majority of methods were sensitive to the size of the voxels used [23], the setting of thresholds, point density [10], [11], [14], [15], [18] and to ambient conditions such as the temperature and the ageing of spans [10]. A few studies disregarded the sagging of the cables [10], while some assumed cables as a set of small straight-line segments [13], [23] and that cables are always parallel [16]. These methods were unable to distinguish cables from other straight lines such as building roof edges, fences and tree stems [23]. Also, these methods did not perform well when reconstructing 3D models of OLE elements as the initial filtering removed some of the OLE elements points as well [13]. Finally, one of the methods used to detect cantilevers considered a very small dataset which only contains one cantilever and the method did not contain any validation process [26]. OLE elements are very thin, hence often represented with few or no points. The detection of OLE elements is a very hard problem also due to the presence of vegetation. These factors render the methods discussed for OLE elements detection ineffective. Also, the gDT generation for OLE systems in existing railways is almost missing in the literature.

4 Proposed Solution

4.1 Scope

Our method focuses on typical double-track railways that represent 70% of the existing and under construction railways in the UK [27]. Railways are a linear asset type; therefore, their geometric relations remain roughly unchanged often over very long distances. Close inspection of railway PCD validates this effect, with repeating geometrical features such as; (1) the special relations between masts, cables and the rails remain fairly unchanged along the railway [9], (2) the connections between masts and the cables are placed in regular intervals (roughly 50-70m intervals), (3) the main axis of the masts (Z-axis) is roughly perpendicular to the track direction (X-axis) (error tolerance is 11° [9]) and (4) masts are always positioned as pairs throughout the rail track.

4.2 Overview

It is often the case that there are few to no points on the OLE elements in a railways PCD due to the small

size of the cables compared to the size of the asset. This is expected and likely to occur no matter what scanning technology is used. This creates obstacles that hinder the robustness of OLE elements reconstruction. We argue that the strengths of model-driven strategies (providing fast geometrical models without visual deformations [28]) are strong in the scenarios with very low point densities meaning the model-driven methods can create the gDTs of OLE elements despite poor densities and sparseness of the PCD. Hence, our method proposed a fitting of pre-defined parametric assemblies to the point segments obtained using previously sorted mast position coordinates [8]. This proposed method is a re-iterative method throughout the track; it exploits the railway geometric relations mentioned in section 4.1 and railway topology as key factors. The workflow of the proposed method is illustrated in Figure 2.

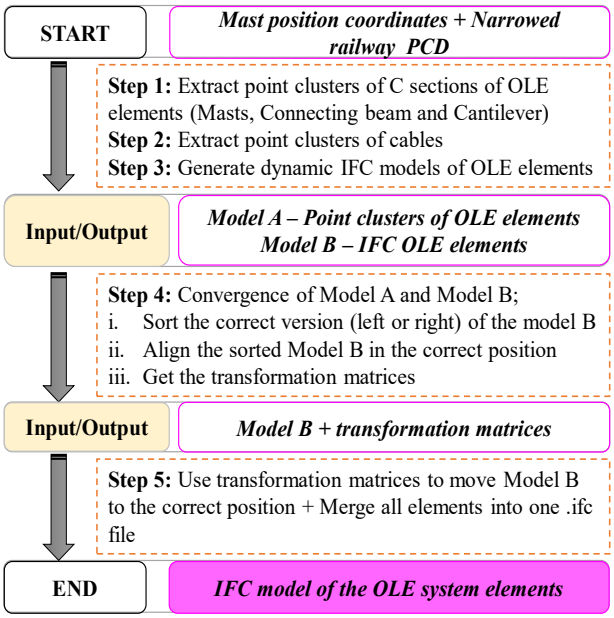

Figure 2. The workflow of the proposed method

4.3 Extract Point Clusters of OLE Elements – Model A

4.3.1 Point Clusters of Other OLE Elements – C Sections

Initially, we extract point clusters of the OLE system includes two railway masts, the connecting beam and the cantilever. This unit is hereafter known as 'C section'. We use a crop box filter to extract the point segment of the C section. The crop box filter automatically extracts all the data inside of a given box, by removing any points that lie outside the specified range along the specified field.

In our proposed method we have set three fields, which refer to intervals along the X, Y and Z directions. The limits are defined relative to the mast coordinates so that the filter extracts any points according to the given direction and the limits. Specifically, the X range is experimentally set to 1.0 m in the direction along the track length. This range has been set relative to the X coordinates of masts to include the width of the mast allowing 0.7 m of a buffer window. The Y range is the distance between two masts of the same pair, calculated using Y coordinates of the two masts and the experimentally set buffer window of 0.6 m, in the direction along the track width. The Z range is experimentally set to 9.5 m (height of the mast) in the direction along the mast. We have experimentally eliminated 0.23 m from the ground plane to remove ground points as it would suffice to extract the C section without shortening the mast. In this paper, we haven't illustrated the graphs representing calculations for these parameters due to limited space. This finally gives resulting point segments of C sections along the track.

4.3.2 Point Clusters of Cables

We use an improved RANSAC algorithm to extract point clusters of cables. The method starts by determining Bounding Boxes (BB) using mast position coordinates along the track to crop the input PCD such that the resulting pieces are relatively straight enough for any further processing. The general RANSAC could not detect cables as lines due to few or no points on the cables.

Hence, we initially up-sampled the points on cables to improve line detection. The up-sampling was done along the track direction (Figure 3) with defined intervals along either side of the actual points. The track direction is not constant along a particular direction due to the varying horizontal and vertical elevations along the track. To determine the track direction prior to up-sampling, we calculate the range between minimum and maximum of X and Y values of each BB and sort the general track direction along the X-axis if the X range > Y range and vice versa (Figure 4).

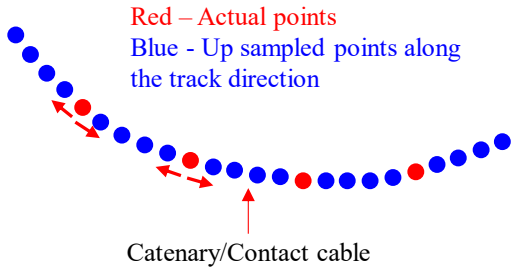

Figure 3. Upsampling along the track direction

Next, we use two pre-processing steps prior to the RANSAC algorithm to improve line detection and to reduce the computational cost.

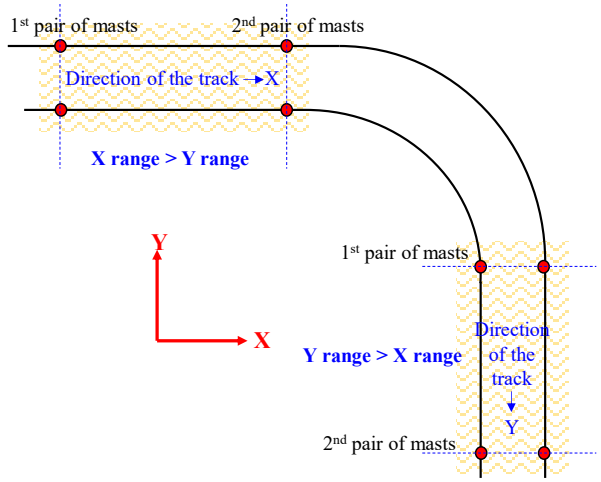

Figure 4. Determining general track direction

Firstly, we remove the ground plane to eliminate all ground points. This ensures all points on the ground are removed prior to further calculations. This significantly reduces the points for faster computational performance and reduces the number of false positives that would be caused by the lines on the ground. Secondly, we get the XY projection of the cloud. This allows projecting the catenary shapes of the catenary and auxiliary cables into straight lines so that RANSAC can detect those cables despite its curved shape. We then detect cables as lines using RANSAC and classify cables based on the heights of the lines relative to the track structure. The detected cables along with the previously extracted C sections are hereafter known as 'Model A'.

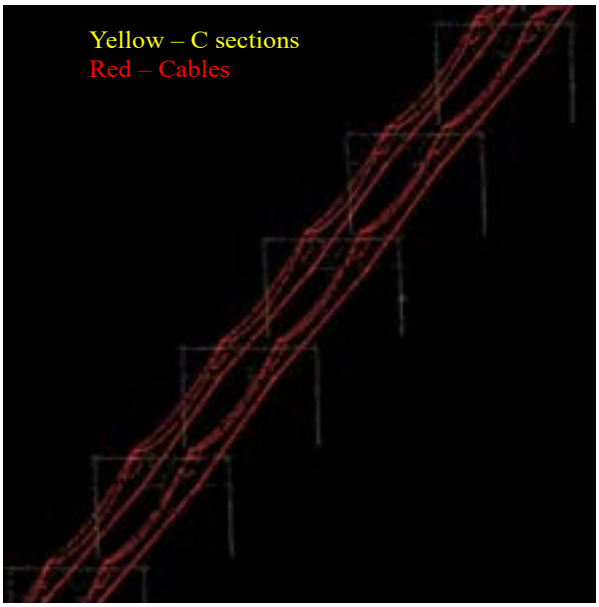

Figure 5. Point clusters of OLE elements – Model A

4.4 Generate Dynamic IFC Models of the OLE System

We design a parametric OLE system model; hereafter known as 'Model B' using standard railway electrification guidelines [9] to represent the geometry of the real OLE elements. This model preserves geometrical properties of the elements, such as angles between the different elements, relative distances compared to each element of the system. The model developed during this research is much simpler compared to the real OLE system as the model is limited only for the elements defined at the beginning of this paper. This limited number of elements simplifies the task of adjusting the model while the resulting model is still suitable to reconstruct the geometric shape of the OLE system.

The orientation of Model B constantly changes from left to right along the track due to the stagger occur in the OLE system. However, this alignment might change if the track is not perfectly straight so that we cannot assume the orientation of the model. Hence, we have created 10 variations of Model B, compatible with the left and right versions of the 5 types of the OLE configurations exist in UK railways [9]. Figure 6 illustrates only one of those configurations due to the limited space. Note that on the actual model, two of these configurations (from the same type) are connected with cables.

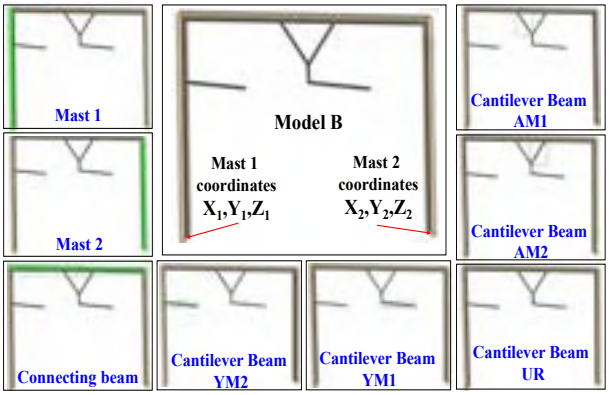

Figure 6. The left-to-right orientation of one of the OLE configurations

We define each of the OLE elements using extruded area solid definition in IFC format. We use the standard cross-sectional dimensions given on Network Rail standards [9] to define the 2D area profile for each element. The extruded area solid defined the extrusion of a 2D area; here defined as the section profile, by two attributes. One is the extruded direction, defining the direction in which the profile is to be swept. The other attribute is the distance over which the profile is to be swept. For each OLE element, we define these distances using either standard height (for masts) or length (for

every other OLE element). The extruded direction and relative angles are derived considering the position and the orientation of each element relative to mast positions.

4.5 Convergence of Model A and Model B

Iterative closest point (ICP) algorithm aims to find the transformation between a point cloud and its reference cloud, by minimizing the square errors between the corresponding entities. We use this algorithm to converge Model B to Model A. Initially, we set Model A as the reference cloud; is kept fixed while the left and right orientations of Model B are source clouds. We first convert Model B into .pcd files and then these source clouds are transformed to find the best match with the reference – Model A. The ICP iteratively revises the transformation of Model B to minimize the distance to the Model A, such as the sum of squared differences between the coordinates of the matched pairs. Hence, by using ICP we first sort the correct orientation (left or right) of OLE configuration as the correct orientation ideally has the minimum sum of squared differences between the coordinates of the target and reference clouds. Once we sorted the correct orientation, our method then converges the sorted model on to the correct position and finally gives transformation matrix which provides the corresponding translation vector and rotation matrix of the Model B (model) relative to Model A (point cluster). Finally, we moved .ifc format of the Model B to the correct position using the resulting transformation matrices of the previous step and finally merged all units (including two C sections and cables) into one file to get the final IFC model of the OLE elements.

Figure 7. The convergence of Model A and Model B

5 Experiments

5.1 Ground Truth Data and Results

We used the rail track located in-between 's-Hertogenbosch and Nijmegen in the Netherlands and specifically a piece of the railroad track that is approximately 18 km long, to test our proposed method. The size of this file was over 100 GB hence too large to process with the machines available in terms of processor and memory capacity. We address this challenge by splitting the data file into three sub PCDs as D1, D2 and D3 each length around 6 km. We also manually generated two sets of Ground Truth (GT) datasets consist of three sub-datasets each per one railway PCD;

GT A: This set is created by manually extracting point clusters of C sections and cables along the rail track. They are used to compare against the automatically detected point clusters of OLE elements.

GT B: The set is created by manually creating the OLE systems models. They are used to compare against automatically generated gDTs of OLE elements.

We implemented the solution with the Point Cloud Library (PCL) version 1.8.0 using C++ on Visual Studio 2017, in a laptop (Intel Core i7-8550U 1.8GHz CPU, 16 GB RAM, Samsung 256GB SSD).

Table 1 illustrates the results of the point cluster extraction and Figure 8 demonstrates the results of the automated gDTs compared to GT B. The detection of OLE elements needed an average of 35 seconds per km. Generation of dynamic IFC models and conversions took 16 seconds per km, while the convergence required 51 seconds per km. Finally, the transformation only took 0.2 seconds per km. Hence, the processing time of the proposed method was on average 103 seconds/km.

6 Evaluation

6.1 Evaluation of point cluster extraction

We used performance metrics; precision (Pr) and recall (R) and F1 score (F1) as; True Positive (TP) - OLE elements were correctly detected as OLE elements, False negatives (FN) - OLE elements were not detected as OLE elements and False Positives (FP) - other objects were detected as OLE elements, to measure the performance step 1 and 2. The average detection accuracy for C sections was 98.1% F1 score and for cables 93.2% F1 score (Table 1).

6.2 Evaluation of the OLE system gDTs

We used cloud-to-cloud (C2C) distance evaluation to detect changes between GT B and the automated ones. Initially we converted the GT B and the automated gDTs into .pcd files. Then we computed the Root Mean Square Error (RMSE) between each unit of automated gDT of OLE elements (consists of two C sections and cables) and corresponding GT B model (Figure 8). The average model distance between the two for all 18 km was 3.82 cm RMSE.

Table 1. Performance metrics for OLE elements point cluster extraction

	Performance metrics for C section extraction						Performance metrics for cables extraction					
Dataset	TP	FP	FN	Pr	R	F1	TP	FP	FN	Pr	R	F1
D1	104	0	2	100%	98.1%	99.0%	101	1	4	99.0%	96.2%	97.6%
D2	86	0	4	100%	95.6%	97.7%	77	8	12	90.6%	86.5%	88.5%
D3	90	0	5	100%	94.7%	97.3%	84	3	10	96.6%	89.4%	92.8%
Average				*100%*	*96.2%*	*98.1%*				*95.6%*	*91%*	*93.2%*

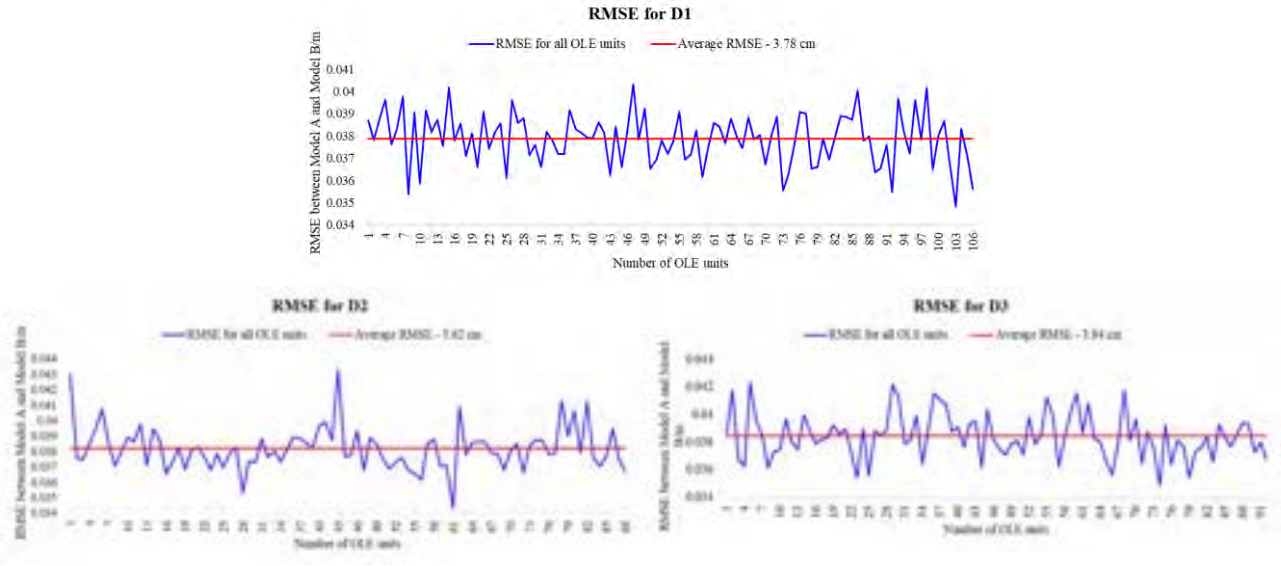

Figure 8. RMSE values for three datasets D1, D2 and D3

method that exploits the highly regulated and standardised nature of railways to generate gDTs of OLE elements for existing railways from PCD. Compared to existing methods, the proposed method is more consistent, less liable to human errors. The method was tested on an 18 km railway point cloud and achieves overall detection rates of 98.1% (F1 score) and 93.2% (F1 score) for point cluster detection of C sections and cables respectively. The accuracy of the automated gDTs of OLE elements was evaluated by minimising the mean Euclidean distance between the ground truth model and the automated one. The average RMSE of the model for all 18 km equals to 3.82 cm.

8 Acknowledgements

We express our gratitude for Fugro NL Land B.V. who provided data for evaluation. The research leading to these results has received funding from the Cambridge Commonwealth, European & International Trust and Bentley Systems UK Plc. We gratefully acknowledge the collaboration of all academic and industrial project partners. Any opinions, findings and

9 References

[1] K. B. Salling and S. Leleur, "Accounting for the inaccuracies in demand forecasts and construction cost estimations in transport project evaluation," *Transp. Policy*, vol. 38, pp. 8–18, 2015.

[2] S. Vick and I. Brilakis, "Road Design Layer Detection in Point Cloud Data for Construction Progress Monitoring," *J. Comput. Civ. Eng.*, vol. 32, no. 5, 2018.

[3] P. E. D. Love, D. D. Ahiaga-Dagbui, and Z. Irani, "Cost overruns in transportation infrastructure projects: Sowing the seeds for a probabilistic theory of causation," *Transp. Res. Part A Policy Pract.*, vol. 92, pp. 184–194, 2016.

[4] B. Fanning, C. M. Clevenger, M. E. Ozbek, and H. Mahmoud, "Implementing BIM on Infrastructure: Comparison of Two Bridge Construction Projects," *Pract. Period. Struct. Des. Constr.*, vol. 20, no. 4, 2015.

[5] C. Eastman, K. Liston, R. Sacks, and K. Liston, *BIM Handbook*. 2008.

[6] C. Furneaux and R. Kivvits., "BIM – Implications for Government.," *Constr. Innov.*, no. 5, pp. 1–43, 2008.

[7] M. R. M. F. Ariyachandra and I. Brilakis, "Understanding the challenge of digitally twinning the geometry of existing rail infrastructure," in *12th FARU International Research Conference (Faculty of Architecture Research Unit)*, 2019.

[8] M. R. M. F. Ariyachandra and I. Brilakis, "Detection of Railway Masts in Air-Borne LiDAR Data," *J. Constr. Eng. Manag.*, 2020.

[9] Network Rail, "Catalogue of Network Rail Standards." 2018.

[10] L. Cheng, L. Tong, Y. Wang, and M. Li, "Extraction of Urban Power Lines from Vehicle-Borne LiDAR Data," *Remote Sens.*, vol. 6, no. 4, pp. 3302–3320, 2014.

[11] L. Zhu and J. Hyyppa, "The use of airborne and mobile laser scanning for modeling railway environments in 3D," *Remote Sens.*, vol. 6, no. 4, pp. 3075–3100, 2014.

[12] H. Guan, J. Li, Y. Zhou, Y. Yu, C. Wang, and C. Wen, "Automatic Extraction of Power Lines From Mobile Laser Scanning Data," pp. 918–921, 2014.

[13] M. Cserép, P. Hudoba, and Z. Vincellér, "Robust Railroad Cable Detection in Rural Areas from MLS Point Clouds," *Free Open Source Softw. Geospatial Conf. Proc.*, vol. 18, no. 1, 2018.

[14] H. Guan, Y. Yu, J. Li, Z. Ji, and Q. Zhang, "Extraction of power-transmission lines from vehicle-borne lidar data," *Int. J. Remote Sens.*, vol. 37, no. 1, pp. 229–247, 2016.

[15] Y. Liu, Z. Li, R. Hayward, R. Walker, and H. Jin, "Classification of Airborne LIDAR Intensity Data Using Statistical Analysis and Hough Transform with Application to Power Line Corridors," *2009 Digit. Image Comput. Tech. Appl.*, no. May, pp. 462–467, 2009.

[16] G. Sohn, Y. Jwa, and H. B. Kim, "AUTOMATIC POWERLINE SCENE CLASSIFICATION and RECONSTRUCTION USING AIRBORNE LIDAR DATA," *ISPRS Ann. Photogramm. Remote Sens. Spat. Inf. Sci.*, vol. 1, no. September, pp. 167–172, 2012.

[17] H. B. Kim and G. Sohn, "Point-based classification of power line corridor scene using random forests," *Photogramm. Eng. Remote Sensing*, vol. 79, no. 9, pp. 821–833, 2013.

[18] B. Guo, Q. Li, X. Huang, and C. Wang, "An improved method for power-line reconstruction from point cloud data," *Remote Sens.*, vol. 8, no. 1, pp. 1–17, 2016.

[19] Y. Wang, Q. Chen, L. Liu, D. Zheng, C. Li, and K. Li, "Supervised Classification of Power Lines from Airborne LiDAR Data in Urban Areas," *Remote Sens.*, vol. 9, no. 8, p. 771, 2017.

[20] M. Arastounia, "Automatic Classification of LiDAR Point Clouds in A Railway Environment," *Univ. Twente, Netherlands*, 2012.

[21] M. Neubert *et al.*, "Extraction of railroad objects from very high resolution helicopter-borne LIDAR and ortho-image data," 2008.

[22] S. Zhang, C. Wang, Z. Yang, Y. Chen, and J. Li, "Automatic Railway Power Line Extraction Using Mobile Laser Scanning Data," *ISPRS - Int. Arch. Photogramm. Remote Sens. Spat. Inf. Sci.*, vol. XLI-B5, no. July, pp. 615–619, 2016.

[23] Y. Jwa and G. Sohn, "A piecewise catenary curve model growing for 3D power line reconstruction," *Photogramm. Eng. Remote Sensing*, vol. 78, no. 12, pp. 1227–1240, 2012.

[24] L. A. F. Fernandes and M. M. Oliveira, "Corrigendum to 'Real-time line detection through an improved hough transform voting scheme' [Pattern Recognition 41 (1) 299-314] (DOI:10.1016/j.patcog.2007.04.003)," *Pattern Recognit.*, vol. 41, no. 9, p. 2964, 2008.

[25] E. Pastucha, "Catenary system detection, localization and classification using mobile scanning data," *Remote Sens.*, vol. 8, no. 10, 2016.

[26] A. Sánchez-Rodríguez, M. Soilán, M. Cabaleiro, and P. Arias, "Automated inspection of Railway Tunnels' power line using LiDAR point clouds," *Remote Sens.*, vol. 11, no. 21, 2019.

[27] Eurostat, "Railway transport - length of lines, by number of tracks," 2019.

[28] F. Tarsha-Kurdi, T. Landes, P. Grussenmeyer, and M. Koehl, "Model-driven and data-driven approaches using LIDAR data: Analysis and comparison," *PIA 2007 - Photogramm. Image Anal. Proc.*, pp. 87–92, 2007.

A Shared Ontology for Logistics Information Management in the Construction Industry

Yuan Zheng[a], Müge Tetik[a], Seppo Törmä[b], Antti Peltokorpi[a], Olli Seppänen[a]

[a]Department of Civil Engineering, Aalto University, Finland
[b]VisuaLynk Oy, Finland
E-mail: yuan.zheng@aalto.fi, muge.tetik@aalto.fi

Abstract –

Logistics management plays an essential role in supporting the primary activities in manufacturing industries. Similarly, in the construction industry, logistics operations are a crucial part that directly influence the construction operations. Construction operations management requires various stakeholders to collaborate through effective communication and prompt information sharing. However, logistics management in construction is often challenged by insufficient information management, lack of formalized information standards and poor information interoperability among heterogeneous systems. Semantic Web technologies advance information management support and improve information interoperability. In this research, we present a domain-level ontology as a common information reference for standardizing and integrating construction logistics information, and finally to improve the efficiency and transparency of logistics information management. The proposed ontology provides information interoperability between logistics management and construction workflow management. The ontology was evaluated by automatic consistency checking and answering the competency questions (CQs) via SPARQL queries. Furthermore, we used actual schedule and material delivery data of a construction project to evaluate the proposed ontology to see if it could support the material kitting logistics practice. We provide a valid ontology that is able support the logistics information management for the construction. The research is limited to providing a single example application of the ontology. Future research should focus on extending the ontology for different specific solutions to yield standardized information management for construction operations.

Keywords –

Information; Construction logistics; Ontology; Construction operations

1 Introduction

Construction industry differs from the other industries because of the temporary project-specific organizations and strong interdependencies between the firms, materials and construction activities [1]. Fragmented construction supply chain makes it difficult to control the construction operations. Logistics practices support these operations and improve construction projects in terms of cost, schedule and planning [2]. Recently, logistics operations in the construction industry have been gaining importance. Logistics solutions are an important element for successful completion of the projects [3] and logistics specialists can improve on-site logistics to a large extent [4]. Due to the benefits of logistics in construction projects, companies are motivated to develop their own logistics processes [5].

During construction projects, significant amount of information is exchanged among the project partners. Construction logistics depend on detailed data and decisions about operations on-site and material needs [6]. Successful delivery of the materials is an important condition that affects the workflow and performance of the projects [7]. To achieve that, coordination is needed between the material supply chain and on-site operational decisions [6]. The logistics information should properly collaborate with the corresponding construction workflow to coordinate the logistics process to perform the operations. Because forecasting material deliveries is directly related to construction schedules, change in the material delivery impacts the execution of schedules [8]. Thus, accurate and timely information flow is required to manage the construction logistics activities efficiently [9].

Construction logistics can be considered complex due to the multiple stakeholders and fragmented tasks that are involved in the process [10]. Therefore, effective information exchange for communication and coordination among different stakeholders are vital for improving the management of the construction logistics process. This requires advanced information

formalization and interoperability among the stakeholders and various information systems.

However, there is no adequate information management standard that could formalize the information from the construction logistics process. A gap exists for linking the on-site construction operation information with the supporting logistics process. In the information management domain, ontology tries to provide a definite classification of entities [11]. In terms of information systems, Semantic Web technology supports representing, obtaining and utilizing knowledge [12]. This research is based on the hypothesis that the advancements in Semantic Web technology can help alleviate the information bottleneck in construction logistics. Determining the information requirements for logistics operations is significant to develop logistics practices. Mapping construction logistics with ontology would bring opportunities for interoperating logistics information with digitized situational awareness systems to improve construction workflow management.

In this research, we present an ontology as a common information reference for linking the material logistics information with the construction workflow. We describe a possible conceptual map design for the logistics and product data flow in construction. Moreover, we extend the ontology to a domain specific level presenting kitting logistics practice information. Kitting is one of the recently developed industrialized JIT-based logistics practices in which requirements for information management are obvious. In the following, we present background for construction logistics, kitting practice and ontology. Then, we describe our methodology and present our findings based on the proposed ontology. Lastly, we provide discussion and conclusion.

2 Background

This research combines two research streams: 1) Material logistics in construction; and 2) Semantic Web, ontology and their applications in the construction and logistics domains. In kitting logistics practice, the information requirements are evident and straightforward. Hence, combining these two research streams: developing an ontology for kitting practice could result in an application where all the information requirements are ready to be utilized in any construction project.

2.1 Material logistics in construction

Logistics practitioners face integration problems regarding the material and logistics information in their operations. In the construction industry, only about 40% of deliveries are fulfilled with the correct amount, time, location and information [13]. However, most of these activities are still managed by humans. Materials could be purchased too late causing delays or too early and getting damaged in poor storage conditions on-site [4]. Delivering materials to the site without a timely notice causes extra material handling and labour cost [14]. Proper logistics management requires complete and accurate information regarding the materials and delivery that is communicated between the project parties.

Construction logistics is an inherent part of construction projects [15]. It impacts important aspects of construction projects such as cost, completion time and plan accuracy [2]. A great deal of energy is spent on coordinating fragmented operations, procuring the required goods and other resources, coordinating materials and resources on the construction site [16]. Problems associated with such mistakes could be prevented via proper logistics management [7].

2.1.1 Kitting as an information-intensive logistic practice

Kitting is a logistics solution that was originally used in the manufacturing industry. It represents delivering the products or components organized, packed and as one package [17]. Figure 1 illustrates the kitting process; the materials that are delivered to the logistics center from the material suppliers are kitted and delivered to the work locations. It has been proposed that the practice could be used in the construction industry as well [18][19]. Recently, Tetik et al. [20] conducted research on the applicability and impacts of using kitting in the construction industry. Construction workers spent around 20% of their time moving materials and equipment to the installation location [21]. Thus, the workers on-site spend less time searching for or moving the materials when the materials are delivered to the assembly location as pre-sorted kits.

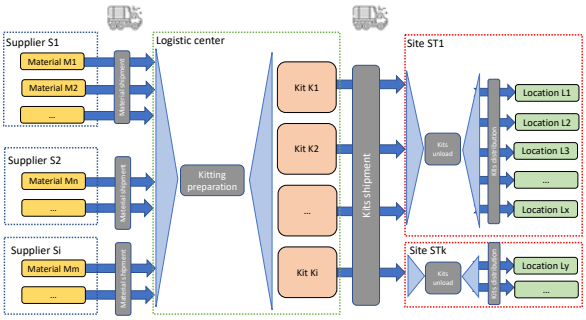

Figure 1. Kitting process

Kitting logistics practice is usually utilized with logistics centers and Just-in-time (JIT) delivery. Information required for kitting practice should be available to properly apply this solution. Currently, it requires manual efforts to collect and integrate this information during the planning phase of the projects.

Used together with logistics center and JIT delivery, improvements on waste and cost reductions as well as

increase in production rates are possible with kitting practice [21][22]. Kitting logistics practice required a smooth information flow between operations [23]. Said and El-Rayes [6] proposed an automated construction logistics optimization system to minimize the logistics costs and integrate the project and supplier data. It could be integrated with kitting practice to ensure material and spatial requirements. Logistics centers can be configured to track materials via using information systems [8]. These advancements create potential for automation. Potential of kitting logistics practice in the construction industry motivates mapping this solution on ontology to generate future opportunities in terms of standardizing the information flow and improving efficiency.

Based on available literature on kitting in the manufacturing industry, information requirements for kitting are number of kits [24], information about the parts [25], item numbers and quantities as well as assembly location [26]. Based on the information we obtained for the use case from a renovation project, we determined that the information relevant to the kitting practice includes material type, quantity, unit, supplier, kitting date, delivery date, kit (name/number), task and location that the kit will be used. This information needs to be explicitly available to apply the kitting solution.

2.2 Ontology and its applications in AEC industry

Ontology originates from the philosophy domain and is recently widely adopted in the domains of computer science and engineering. Gruber [27] defined ontology as "an explicit formal specification of a conceptualization". In other words, ontology is a formal conceptualization of domain knowledge that formally defines the concepts (classes), properties and the interrelationships between the concepts, which thus could share common understanding of the structure of information and domain knowledge [28][29].

In the Architectural, Engineering, and Construction (AEC) domain, numerous efforts of ontology development have been made to solve the problems of data integration [30], knowledge management [31][32], and information utilization [30][33]. Construction is known as an information-intensive industry. The benefit of the ontology-based approach is that construction information can be stored and reused under a systematic information management framework. Moreover, with the machine-readable representation, ontology is able to make the information and knowledge accessible to both humans and computers for further computer-aided construction management tools [34].

Meanwhile, in terms of the logistics and supply-chain domain, ontologies have also been considered a solution for managing the logistics knowledge and information. Daniele and Pires [35] suggested ontologies are able to improve the enterprise interoperability in the logistics domain. A logistics ontology was developed by Lian et al. [36]to semantically represent the logistics situation. Hendi et al. [37] introduced a logistics ontology as a core of logistics optimization framework to support the logistics management. Although these ontologies efforts provided conceptualization of the general logistics process, they are insufficient to specifically expand to the construction domain.

Developing an ontology for construction logistics could improve the information management by accurately specifying the information needs for materials and on-site as well as logistics center activities required to successfully perform the construction tasks. However, currently there are no ontologies that specifically represent the construction logistics process information, nor ontological works that create the links between construction and logistics ontologies. Thus, an ontology is developed for construction logistics in this study.

3 Methodology

Our chosen methodology is design science. Design science identifies a real-world problem and proposes and evaluates a solution to this problem [38]. Thus, we use design science to develop a solution to represent logistics practices in the construction industry with ontology to solve the practitioners' problems regarding logistics information integration.

Development of the proposed ontology requires its design to be described and desirably implemented. The scope of this paper does not include a real-life case implementation. However, we provide validation of the ontology and evaluate the ontology based on a real-life construction project's schedule and material information. Multiple data resources were used to develop and validate the ontology. We used document analysis and public materials to form an example use case. We used a planned project schedule from a company to realize the use case. We obtained the schedule and material list per kits of a renovation project. We used required material and kit information to answer the competency questions. The ontology was validated using competency questions and automatic consistency checking.

3.1 Ontology development approach

To develop such ontology, an ontology development approach is established initially. The ontology development approach in this research is a hybrid approach that draws mainly on METHONTOLOGY [39] and the approach by Grüninger and Fox [40]. The major steps of the ontology development approach are shown in the following Figure 2.

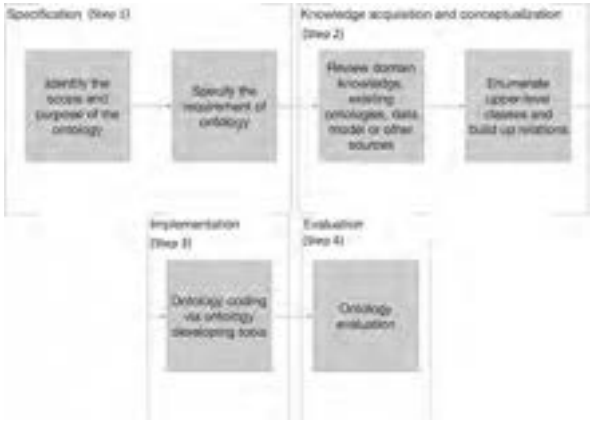

Figure 2. Ontology development process

3.1.1 Specification

The first step of the ontology development process is specification, which aims to first specify the scope and the purpose of the ontology by answering the following specification questions [39]:

What is the purpose? The purpose of the developed ontology is to formalize and structure the logistics information and simultaneously coordinate with the construction process information to improve the information exchange of the construction logistics operation.

What is the scope? The ontology is focusing on the construction logistics process and information flow of the material delivering. Meanwhile, the ontology is designed to be a higher-level ontology that only contains the higher-level concepts and relations of the construction logistics process.

Based on the scope and purpose, the requirement of the ontology can be identified with a list of competency questions. The competency questions (CQs) are a more detailed specification of the ontology requirements [40], that can be used to formalize the ontological model, concepts, hierarchy and relations. In this research, a workshop, consisting of participants from 17 Finnish AEC firms, was organized to define the CQs in compliance with the content of information that is required by all the stakeholders involved in the construction logistics (Table 1). The workshop showed that a material batch is an essential unit of analysis in logistics operations.

Table 1 A list of Competency Questions for the ontology

1.	What is the content of the material batch?
2.	When the material batch should be delivered?
3.	What is the status of the material batch? (packaged, shipped, received, used)
4.	Was the material batch delivered as planned?
5.	What is the corresponding activity of the material batch?
6.	What is the location of the corresponding activity of the material batch?
7.	Who is the responsible worker or firm of the corresponding activity of the material batch?
8.	What is the location of the material batch on site?

These questions were also used for further ontology evaluation to check if the ontology covered the desired content and if it can represent the domain knowledge.

3.1.2 Knowledge acquisition and conceptualization

After defining the ontology requirements specification, the second step of the ontology development process is to determine what domain knowledge for the ontology should be acquired and how it should be represented [39]. In this phase, relevant domain knowledge of the construction process and logistics process were reviewed. This is followed by the conceptualization process that all relevant terms of the concepts, class hierarchy, class properties including their range and domain in the ontology are defined to construct the ontological model.

3.1.3 Implementation

In terms of further implementation and application, the ontology should be implemented with a machine-readable format. This comprises the third step of the ontology development process (see Fig.2). In this research, the ontology was coded using Semantic Web Ontology Language (OWL) by using the Protégé environment. OWL is a computational ontology language that is designed for ontology development, which is a W3C recommended ontology language [41].

3.1.4 Ontology evaluation

Ontology evaluation aims to check whether developed ontology is satisfied with the specifications, fulfils its intended purpose and meets all the requirements, which consists of verification and validation [34]. In this research, the ontology evaluation consisted of automated consistency checking (verification), answering the competency questions based on a practical case example (validation). In the following sections, we present our results, namely the proposed ontology and its evaluation.

4 Findings: construction logistics ontology

In this section, the Digital Construction Logistics Ontology (DCL-Onto) that is developed based on the previously discussed approach is presented in detail as a

('12,&K#XM'#'?),2)&*+%#+>#&M'#+%&+,+A.#*1#4*17211'4#*%#&M'#>+,,+P*%A#1'7&*+%K#

G=>! ;$.3:3)/@#:%63B(:%

D*A2('# !#*,,21&()&'1# &M'# +%&+,+A*7),# / +4',K# $%# &M'#=8FIH%&+B# "#$%&%&'#)('# 21'4# &+# ('0('1'%&# &M'# 6)1*7#7,)11'1# P*&M*%#&M'#4+ /)*%# +>#7+%1&(27&*+%#)%4#,+A*1&*71#0(+7'11'1K# _ +('+?'(B#&M'#=8FIH%&+#7)%#6'#1264*?*4'4#*%&+#&P+# /)0+(#0)(&1K XM'#>*(1&#0)(&#*1#&M'#7+%1&(27&*+%#0(+7'11#0)(&B#PM*7M#)* / 1#&+#0(+?*4'#)%#)61&()7&*+%#+>#&M'#7+%1&(27&*+%#0(+7'11#+%#)#A'%'(*7#,'?',#)%4#1&(27&2('#&M'#*%>+(/)&*+%#+>#&M'#7+%1&(27&*+%#+0'()&*+%#&+#('?'),#&M'#7+%1&*&2&'1#+>#)7&2),#7+%1&(27&*+%#)7&*?*&*'1K#XM'#1'7+%4#0)(&*1#&M'#,+A*1&*71#0(+7'11#0)(&B#PM*7M#)* / 1#&+#>+(/),*L'#&M'#*%>+(/)&*+%#)%4#'%&*&*'1#*%#&M'#7+%1&(27&*+%#,+A*1&*71#0(+7'11# ?*)# ?)(*+21# ,+A*1&*71# 1.1&' / 1# 6.# / 2,&*0,'#1&)G'M+,4'(1K# XM'#,+A*1&*71# 0(+7'11#*1# ('A)(4'4#)1#)%#'T&'%1*+%# +># &M'# A'%'(),# 7+%1&(27&*+%# 0(+7'11K#_ ')%PM*,'B#&M'#*%&'()7&*+%#+>#&P+#0)(&1#7)%#6'#21'4#>+(#7++(4*%)&*%A#&M'#7+%1&(27&*+%#,+A*1&*71#0(+7'11#P*&M#&M'#+%I1*&'#7+%1&(27&*+%#+0'()&*+%1K#D2(&M'(/ +('B#&M'#10'7*>*7#)00,*7)&*+%#>+(#&M'#G*&&*%A#0()7&*7'#*1#),1+#4'?',+0'4#*%#&M'#,+A*1&*71#0)(&&#&+#'T' / 0,*>.#&M'#21)A'#+>#&M'#4'?',+0'4#+%&+,+A.K#

$%#&M'#7+%1&(27&*+%#0(+7'11#0)(&B#&M'# /)*%#'%&*&*'1#9)1#4'0*7&'4#P*&M#&M'#4''0#6,2'#7+,+2(#*%#D*A2('#!<#*%7,24'#Y2*,4*%A# @,' / '%&B# 3A'%&B# @[2*0 / '%&B# F+7)&*+%B#$%>+(/)&*+%# 8+%&'%&# @%&*&.B# f(+20B# 37&*?*&.#)%4#8+%1&()*%&&K#XM'1'#0(+?*4'#)#A'%'(*7#,'?',#)61&()7&*+%#+%#7+%1&(27&*+%# '%&*&*'1# &M)&# *%?+,?'# *%# &M'# 7+%1&(27&*+%#0(+7'11K# XM'# 0(+0+1'4# +%&+,+A.# 7+%1*4'(1# &M'#7+%1&(27&*+%#0(+7'11#)1# 7+%1&*&2&'4# 6.# 1'?'(),# 4+ /)*%#'%&*&*'1B# *%7,24*%A#)7&*?*&*'1B# ,+7)&*+%1B#)A'%&1B#'[2*0 / '%&B# /)&'(*),# 6)&7M'1B#)%4# *%>+(/)&*+%# 7+%&'%&#'%&*&*'1K# 37&*?*&.#('>'(1#&+#)#120'(7,)11#>+(#),,# P+(G#+(#)AA('A)&*+%1# +># P+(G1# &M)&#)('# 7)((*'4# +2&# *%# &M'#7+%1&(27&*+%# 0(+7'11K# 37&*?*&*'1#),1+# M)?'# 0('7'4'%7'#(',)&*+%1# P*&M# +&M'(#)7&*?*&*'1K# H60'7&# 37&*?*&.# *1#)#1267,)11# +>#37&*?*&.# PM*7M# M)1# &M'#&)(A'&# +>#)#7'(&)*%#+60'7&K#XM'('>+('B#F+A*1&*71#0(+7'11#*1#)#1267,)11#+>#&M'#H60'7&#37&*?*&.# PM+1'# &)(A'&# +60'7&1#)('# _)&'(*),#Y)&7M'1K##

#

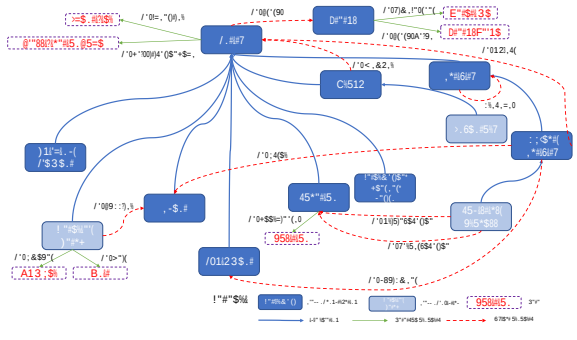

D*A2('#!K#H%&+,+A*7),# / +4',#+>#=8FIH%&+#

G=<! H(25(?($./$)% .'(% @3$?.5"@./3$% :3)/?./@?%253@(??%

XM'# /)*%# 7+%7'0&1# +># &M'# 7+%1&(27&*+%# ,+A*1&*71#0(+7'11#)('#7+,+2('4#P*&M#&M'#,*AM&#6,2'#7+,+2(#*%#D*A2('#!K#XM'#,+A*1&*71#0(+7'11#0)(&#*1#4'1*A%'4#&+#6'#)6,'#&+#('0('1'%&#&M'#'11'%&*),#,+A*1&*71#*%>+(/)&*+%#P*&M#)#>+(/),#2%*>*'4#1&(27&2('K#XM'#,+A*1&*71#0(+7'11#0)(&#7+ / 0(*1'1#&P+# /)*%#126I7+ / 0+%'%&1K#XM'#>*(1&#*1#&M'#*%>+(/)&*+%#)6+2&#&M'#,+A*1&*71#0(+7'11#)%4#&M'#1'7+%4#*1#&M'#0(+427&#*%>+(/)&*+%#+>#&M'# /)&'(*),#6)&7M'1K#D*A2('#U#*,,21&()&'1#&M'#G*&&*%A#,+A*1&*71#1+,2&*+%i1#+%&+,+A.# / +4',#*%#4'&)*,K#*( )$&*%)+!,%$#*1#)#-*./0#&M)&#7+%1*1&1#+>!123'%4)+!567&4$'!+># /)&'(*),1# &M)&#)('# 7+,,'7&'4# >(+ / # ( )$&*%)+8)$42&'K#9#:&#$.*3!7+%1*1&1#+>#( )$&*%)+8)$42&'K#XM'#*%>+(/)&*+%#+%# PM*7M# /)&'(*),1#&M'#G*&#7+%1*1&1#*1#+6&)*%'4#>(+ / #&M'#9#;.*<)$%.#!567&4$'=!

G=E! CF#:"#./3$%3I%.'(%3$.3:3)A%

U9S9R! !4$+.&$-'('+/#-#$0/'3('50'>-/,(

8+%1*1&'%7.#7M'7G*%A#)*/ 1#&+#*4'%&*>.#7+%&()4*7&+(.#>)7&1#*%#)%#+%&+,+A.#6)1'4#+%#='17(*0&*+%#F+A*7#9=F<#0(*%7*0,'1B# 127M#)1# ,+A*7),# 7+%>,*7&1# +(# *%7+%1*1&'%&#7,)11'1K#8+%1*1&'%7.#7M'7G*%A#*1#'%)6,'4#6.#='17(*0&*+%#F+A*7# (')1+%'(1B# PM*7M#)('#)6,'# &+# 0'(>+(/ # ?)(*+21#)2&+ /)&'4#*%>'('%7*%A# 1'(?*7'1# QU:S K# $%# &M*1# ('1')(7MB#7+%1*1&'%7.# 7M'7G*%A# +># &M'# 0(+0+1'4# +%&+,+A.# P)1#7+%427&'4#21*%A#&M'#d',,'&#PM*7M#*1#)#d(+&oAo#62*,&I*%#=F#(')1+%'(K#d',,'&#*1#)%#+0'%I1+2(7'#H^FI=F#(')1+%'(#&M)&#*1#)6,'#&+#1200+(&#&M'#(')1+%*%A#+>#7M'7G*%A#&M'#+%&+,+A.#7+%1*1&'%7.#QU!SK#XM'#('12,&#+>#&M'#)2&+ /)&*7#7+%1*1&'%7.#7M'7G*%A#>+(#&M'#=8FIH%&+#*1#&M)&#&M'#+%&+,+A.#*1#7+%1*1&'%&#)%4#7+M'('%&#&M)&P*&M+2&#,+A*7),#7+%>,*7&1K##

U9S9Q! !/#@0%-/,($50('+.10$0/'3(=40#$-+/#(

$%#&'(/1#+>#=8FIH%&+B#)#1'&#+>#8m1#>+(#*&1#7+%>+(/)%7'#)('#0('4'>*%'4#8m1#*%#&M'#0('?*+21#g_'&M+4+,+A.h#1'7&*+%K#$%#&M*1#('1')(7MB#&M'#0(+7'42('#+>#)%1P'(*%A#8m1#P'('#7+%427&'4#)1#)#&)1GI6)1'4#'?),2)&*+%#6.#)%1P'(*%A#&M'#10'7*>*'4#8m1#6)1'4#+%#&M'#*%1&)%7'#4)&)#+>#&M'#>+,,+P*%A#0()7&*7),#7)1'#)%4#21*%A#&M'#-d35mF#d(+&+7+,#)%4#5=D#m2'(.#F)%A2)A'#9-d35mF<#>+(#[2'(.*%A#)%4#('&(*'?*%A#&M'#*%>+(/)&*+%#&+#)%1P'(#1) / 0,'#[2'(*'1#6)1'4#+%#&M'#0()7&*7),#*%>+(/)&*+%#*%#&M'#>+,,+P*%A#21'#7)1'K#

V#0('&#0(

X+#?'(*>.#&M'#7+?'()A'#+>#&M'#+%&+,+A.#)%4#),1+#?),*4)&'#&M'#21)6*,*&.#+>#&M'#+%&+,+A.#&+P)(41#0()7&*7),#7+%1&(27&*+%#,+A*1&*71#7)1'1B#)#21'#7)1'#'T)/0,'#P)1#>+(/ '4#6)1'4#+%#)%#)7&2),#7+%1&(27&*+%#,+A*1&*71#7)1'#&M)&#)00,*'4#&M'#G*&&*%A#/'&M+4K#$%#&M*1#7)1'B#&M'#0()7&*7),#7+%1&(27&*+%#0(+0'7&#)00,*'4#&M'#&)G&#0,)%%*%A#)%4#7+%&(+,,*%A#/'&M+4#QUUSB#)%4#&M'#,+A*1&*71#0(+7'11#+>#&M'#

/)&'(*),# *1# 7++(4*%)&'4# P*&M# &M'# &)G&# 0,)%#)%4#)7&2),# 0(+A('11# +%# &M'# 1*&'K# XM'# +6&)*%'4# 1&)&*7#*%>+(/)&*+%# 1+2(7'1# *%7,24'# &M'# 7+%1&(27&*+%# 0(+0'7&#17M'42,'#)%4# /)&'(*),# G*&# *%>+(/)&*+%B# / +('+?'(B# &M'# 0(+0'7&#0(+A('11# *%>+(/)&*+%#)%4# 7+((('10+%4*%A# 204)&'4# /)&'(*),#4',*?'(.#17M'42,'#)(')#),1+#)7[2*('4K#3%# 'T&'%1*+%#+>#&M'#+%&+,+A.#>+(#&M'#G*&&*%A#0(+7'11#7)%#6'# 1''%#*%#D*A2('#UB#*%# PM*7M#)# ( )$&*%)+! >%$#*1#4'>*%'4#&+# ('0('1'%&# &M'# /)&'(*),# G*&1# &M)&#)('# A(+201# +># /)&'(*),# 6)&7M'1K#3,,#&M'#*%>+(/)&*+%# P*,,#6'#*%&'A()&'4#6)1'4#+%# &M'#+%&+,+A.K#

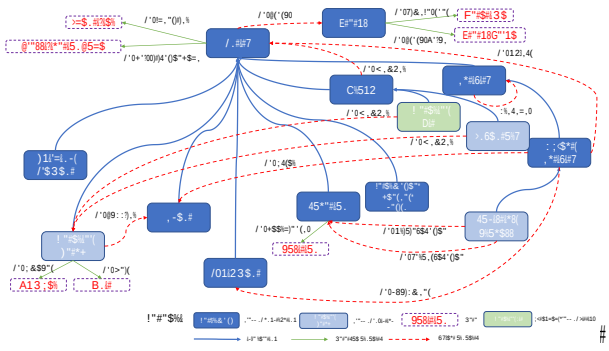

D*A2('#UK#=8FIH%&+#'T&'%1*+%#>+(#&M'#G*&&*%A# 0()7&*7'#

XM'# 4)&)# P'('# /)%2),,.# /)00'4# P*&M# 4'?',+0'4# +%&+,+A.#*%#&M'#H0'%#5'>*%'#1+>&P)('#)%4#&M'%#7+%?'(&'4# &+#5'1+2(7'#='17(*0&*+%#D() / 'P+(G#95=D<#>+(/)&#6)1'4# +%#&M'#+%&+,+A.K#-261'[2'%&,.B#&M'#5=D#A()0M#P)1#1&+('4# *%#&M'#f()0M#=Y#1+>&P)('K#$%#&M'#f()0M#=Y#'%?*(+% / '%&B#)#1'&#+>#-d35mF#[2'(*'1#P'('#7+%427&'4#PM*7M#)*/1#&+#)%1P'(#&M'#8m1#>+(#'?),2)&*%A#&M'#+%&+,+A.K#XM'#[2'(.# ('12,&#7)%#6'#1''%#*%#X)6,'#:B#*%#PM*7M#&M'#8m1#+>#&M'# +%&+,+A.#P'('#10'7*>*7),,.#4'>*%'4#6)1'4#+%#&M'#0()7&*7),# 7)1'B#)%4#&M'#[2'(.#('12,&1#)('#>*&&'4#P*&M#&M'#0()7&*7),# 4)&)K##

X)6,'#:#&#-0'7*>*'4#8m1#)%4#)%1P'(1#6)1'4#+%#&M'#7)1'#

8+/0'&'%7.#m2'1&*+%1!		3%1P'(1#
RK!	^M)&#*1#&M'#7+%&'%&#+>#&M'#	>%%+$.! ?@A! BC!
	! "#$%&"'() "#*+(, -n#	6)D'!
:K!	^M'%#&M'#! "#$%&"'() "#*+(	BE=F@=B@FG!
	, -#1M+2,4#6'#4',*?'('4n#	!
!K!	^M)&#*1#&M'#1&)&21#+>#	H&+%:&*&I!
	! "#$%&"'() "#*+(, -n#	
UK!	^)1# ! "#$%&"'( ) "#*+(, -(	J*/&!
	4',*?'('4#)1#0,)%%'4n#	
VK!	^M)&#*1#&M'#1&)&21#+>#&M'#	9#!0*.D*&''!
	7+((('10+%4*%A#)7&*?*&.#+>#	!
	! "#$%&"'() "#*+(, -n#	
WK!	^M'('#*1#,+7)&*+%#&M'#	K0)*$<&#$B!
	_)&'(*),#Y)&7M#R:#1M+2,4#	
	6'#4',*?'('4#6)1'4#+%#&M'#	
	,+7)&*+%#+>#&M'#	
	7+((('10+%4*%A#)7&*?*&.n#	
"K!	^M+# *1# &M'# ('10+%1*6,'#	L)*0&#$&*!
	P+(G'(# +(# >*(/ # +># &M'#	
	7+((('10+%4*%A#)7&*?*&.# +>#	
	&M'# /)&'(*),#6)&7Mn#	
ZK!	^M)&#*1#&M'#,+7)&*+%# +>#&M'#	K0)*$<&#$B!
	/)&'(*),#6)&7M#+%#1*&'n#	

#

;! <*9)(99*&#+

$%# &M*1# ('1')(7MB#)#%+?',# +%&+,+A.#>+(#7+%1&(27&*+%# ,+A*1&*71#P)1#0(+0+1'4K#XM'#4'?',+0'4#+%&+,+A.#/)G'1#*&# 0+11*6,'#>+(#M2/)%1#&+#2%4'(1&)%4#)%4#/)7M*%'1#&+#21'# &M'# *%>+(/)&*+%# ('[2*('4# >+(# 7+%1&(27&*+%# ,+A*1&*7# +0'()&*+%1#)%4#&M'*(#/)%)A'/'%&K#XM'#+%&+,+A.#4'>*%'1# &M'# *%>+(/)&*+%# ('[2*(' / '%&1# &+# 0(+0'(,.# *%&'A()&'#)# ,+A*1&*71#1+,2&*+%#*%#0()7&*&*+%'(1i#0()7&*7'1#*%#&M'#0(+0'7&K# Y.# M)?*%A# &M'# ('[2*('4# *%>+(/)&*+%#)?)*,)6,'B# 0()7&*&*+%'(1#7)%# 2&*,*L'#&M'#+%&+,+A.#*%# &M'*(#,+A*1&*71# 1.1&'/1#&+# *%&'A()&'#&M'#*%>+(/)&*+%# &()%1>'((('4#>(+/# &M'*(#0)(&%'(1#)%4#/)&'(*),#1200,*'(1#P*&M#&M'#0(+0'7&I 10'7*>*7#*%>+(/)&*+%K#_)7M*%'I('4)6,'#>+(/)&#/)G'1#*&# 0+11*6,'#&+#)2&+/)&'#&M'#0()7&*7'#*%#&M'#>2&2('K#

31#M)1#6''%#4'/+%1&()&'4#*%#&M'#21'#7)1'#0)(&B#&M'# 0(+0+1'4#+%&+,+A.#*1#)6,'#&+#>+(/),*L'#)%4#*%&'A()&'#&M'# *%>+(/)&*+%# ('A)(4*%A# 7+%1&(27&*+%# ,+A*1&*71K# D2(&M'(/+('B#*&#7)%#6'#'%?*1*+%'4#>(+/#&M'#7)1'#&M)&#&M'# +%&+,+A.#7)%#6'#21'4#*%#>2(&M'(#)00,*7)&*+%1#>+(#0,)%%*%A#)%4#7+%&(+,#+>#7+%1&(27&*+%#,+A*1&*71#0(+7'11'1B#127M#)1# &M(+2AM#*%>+(/)&*+%#('&(*'?),K#XM'#0(+0+1'4#+%&+,+A.# 7)%# 6'# 21'4# >+(#*%>+(/)&*+%# 1&)%4)(4*L)&*+%#)%4# *%&'A()&*+%#&+#1200+(&#1','7&'4#,+A*1&*71#0()7&*7'1B#127M#)1# G*&&*%A# P*&M# a$X# 4',*?'(.#)%4# 7+%1+,*4)&*+%# 7'%&'(1B# &+P)(41#>2,,.#*%421&(*),#,+A*1&*71#1.1&'/1K##

8+%?'%&*+%),#/'&M+41#*%#7+%1&(27&*+%#M)?'#(')7M'4# &M'*(#,*/*&1B#)%4#)2&+/)&*+%#)%4#(+6+&*71#6'7+/'# +/%*0('1'%&#*%#+2(#4)*,.#,*?'1#QUVSK#]'%7'B#*&#*1#?),2)6,'# &+#('0('1'%&#,+A*1&*71#*%>+(/)&*+%#P*&M#)%#+%&+,+A.#&+# A'%'()&'#+00+(&2%*&*'1#>+(#7+%1&(27&*+%#,+A*1&*71#%0(7'11'1B#127M#)1# G*&&*%A#P*&M#a$X#4',*?'(.#)%4#7+%1+,*4)&*+%#7'%&'(1B# &+P)(41#>2,,.#*%421&(*),#,+A*1&*71#1.1&'/1K##

D+(#&M'#4*A*&),#&()%1>+(/)&*+%#+>#&M'#7+%1&(27&*+%# *%421&(.B# '1&)6,*1M*%A# &M'# *%>+(/)&*+%# 1&)%4)(41# *1# 1*A%*>*7)%&#QUWSK#XM'#+%&+,+A.#4'?',+0/'%&#7+%&(*62&'1# &+#4'&'(/*%*%A#&M'#*%>+(/)&*+%#('[2*(' / '%&1K#XM21B#&M'# 4'?',+0'4#+%&+,+A.#7)%#6'#21'4#)%4#>2(&M'(#4'?',+0'4#&+# 7++(4*%)&'#&M'#7+%1&(27&*+%#,+A*1&*71#)%4#*%&'A()&'#&M'# *%>+(/)&*+%#('[2*('4#&+#0'(>+(/#&M'1'#)7&?*&*'1#>(+/# 4*>>'('%&#%>+(/)&*+%#1+2(7'1#*%?+,?'4#*%#)#1&)%4)(4#P).K##

=! >&#)5(9*&#+

$%# &M*1# 1&24.B# P'#M)?'#4'17(*6'4#)%# +%&+,+A.#>+(# ,+A*1&*71# +0'()&*+%1# *%# &M'# 7+%1&(27&*+%# *%421&(.K# XM'#

ontology can be applied to specific logistics solutions. We have provided a use case example to illustrate the application of the ontology in a project setting. The research was limited to not having a real project application of the ontology. Since there was not a logistics system in use to our knowledge that operates with a full kitting logistics information model, it was not possible to obtain enough data to test the ontology from a real project. Future work should focus on implementing the developed ontology in real-life applications. Moreover, for future research, an ontology-based solution needs to be developed taking advantage of computing technologies to support the logistics management practices.

References

[1] Segerstedt, A., Olofsson, T., Bankvall, L., Bygballe, L.E., Dubois, A. and Jahre, M. Interdependence in supply chains and projects in construction. *Supply chain management: an international journal*, 15(5):385-393, 2010.

[2] Sullivan, G., Barthorpe, S. and Robbins, S. *Managing construction logistics*. John Wiley & Sons, 2011.

[3] Sobotka, A., Czarnigowska, A. and Stefaniak, K. Logistics of construction projects. *Foundations of civil and environmental engineering*, 6:203-216, 2005.

[4] Sundquist, V., Gadde, L.E. and Hulthén, K. Reorganizing construction logistics for improved performance. *Construction management and economics*, 36(1):49-65, 2018.

[5] Browne, M. The challenge of construction logistics. *In: G. Lundesjö, ed. Supply chain management and logistics in construction*. London: Kogan Press, 9–24, 2015.

[6] Said, H. and El-Rayes, K.Automated multi-objective construction logistics optimization system. *Automation in Construction*, 43:110-122, 2014.

[7] Vrijhoef, R. and Koskela, L. The four roles of supply chain management in construction. *European journal of purchasing & supply management*, 6(3-4):169-178, 2000.

[8] Hamzeh, F.R., Tommelein, I.D., Ballard, G. and Kaminsky, P. Logistics centers to support project-based production in the construction industry. In *Proceedings of the 15th Annual Conference of the International Group for Lean Construction (IGLC 15)* , page 181-191, 2007.

[9] Titus, S. and Bröchner, J. Managing information flow in construction supply chains. *Construction innovation*, 5(2):71-82, 2005.

[10] Omar, B. and Ballal, T. Intelligent wireless web services: context-aware computing in construction-logistics supply chain. *Journal of Information Technology in Construction*, 14(Specia):289-308, 2009.

[11] Smith, B. Ontology. In *The furniture of the world*, page 47-68. Brill Rodopi, 2012.

[12] Sheth, A.P. and Ramakrishnan, C. Semantic (Web) technology in action: Ontology driven information systems for search, integration, and analysis. *IEEE Data Engineering Bulletin*, 26(4):40, 2003.

[13] Thunberg, M. and Persson, F. Using the scor model's performance measurements to improve construction logistics. *Production Planning and Control*, 25(13–14):1065–1078, 2014.

[14] Ying, F., Tookey, J. and Roberti, J. Addressing effective construction logistics through the lens of vehicle movements. *Engineering, construction and architectural management*, 21(3):261-275, 2014.

[15] Dotoli, M., Epicoco, N., Falagario, M., Costantino, N. and Turchiano, B. An integrated approach for warehouse analysis and optimization: A case study. *Computers in Industry*, 70:56–69, 2015.

[16] Ekeskär, A. and Rudberg, M. Third-party logistics in construction: the case of a large hospital project. *Construction management and economics*, 34(3):174-191, 2016.

[17] Bozer, Y.A. and McGinnis, L.F. Kitting versus line stocking: A conceptual framework and a descriptive model. *International Journal of Production Economics*, 28(1):1-19, 1992.

[18] Hanson, R. and Brolin, A. A comparison of kitting and continuous supply in in-plant materials supply. *International Journal of Production Research*, 51(4):979-992, 2013.

[19] Tanskanen, K., Homström, J., Elfving, J. and Talvitie, U. Vendor-managed-inventory (VMI) in construction, *International Journal of Productivity and Performance Management*, 58(1):29-40, 2009.

[20] Tetik, M., Peltokorpi, A., Holmström, J. and Seppänen, O. Impacts of an assembly kit logistic solution in renovation projects: a multiple case study with camera-based measurement. *25th Annual EurOMA Conference*, Budapest, Hungary, 2018.

[21] Strandberg, J. and Josephson, P.E. What do construction workers do? Direct observations in housing projects. In *Proceedings of 11th Joint CIB International Symposium Combining Forces, Advancing Facilities management and Construction through Innovation*, pages 184-193, 2005.

[22] Tetik, M., Peltokorpi, A., Seppänen, O., Viitanen, A. and Lehtovaara, J. Combining Takt Production with Industrialized Logistics in Construction. In *Proceedings of 27 th Annual Conference of the International. Group for Lean Construction (IGLC)*, pages 299–310, Dublin, Ireland, 2019.

[23] Tetik, M., Peltokorpi, A., Seppänen, O., Leväniemi,

M., Holmström, J. Kitting Logistics Solution for Improving On-Site Work Performance in Construction Projects. *ASCE Journal of Construction Engineering and Management*, In Press.

[24] Balakirsky, S., Kootbally, Z., Kramer, T., Madhavan, R., Schlenoff, C. and Shneier, M. Functional requirements of a model for kitting plans. In *Proceedings of the Workshop on Performance Metrics for Intelligent Systems*, pages 29-36, 2012.

[25] Balakirsky, S., Kootbally, Z., Kramer, T., Pietromartire, A., Schlenoff, C. and Gupta, S. Knowledge driven robotics for kitting applications. *Robotics and Autonomous Systems*, 61(11):1205-1214, 2013.

[26] Hua, S.Y. and Johnson, D.J. Research issues on factors influencing the choice of kitting versus line stocking. *International Journal of Production Research*, 48(3):779-800, 2010.

[27] Gruber, T.R. Toward principles for the design of ontologies used for knowledge sharing. *International journal of human-computer studies*, 43(5-6):907-928, 1995.

[28] Noy, N.F. and McGuinness, D.L. Ontology development 101: A guide to creating your first ontology, 2001.

[29] Zhang, J. and El-Diraby, T.E. Social semantic approach to support communication in AEC. *Journal of computing in civil engineering*, 26(1):90-104, 2012.

[30] Anumba, C.J., Pan, J., Issa, R.R.A. and Mutis, I. Collaborative project information management in a semantic web environment. *Engineering, Construction and Architectural Management*, 15(1):78-94, 2008.

[31] Lima, C., El-Diraby, T. and Stephens, J. Ontology-based optimisation of knowledge management in e-Construction. *Journal of Information Technology in Construction*, 10(21):305-327, 2005.

[32] Ding, L.Y., Zhong, B.T., Wu, S. and Luo, H.B. Construction risk knowledge management in BIM using ontology and semantic web technology. *Safety science*, 87:202-213, 2016.

[33] Pauwels, P., Zhang, S. and Lee, Y.C. Semantic web technologies in AEC industry: A literature overview. *Automation in Construction*, 73:145-165, 2017.

[34] Zhou, Z., Goh, Y.M. and Shen, L. Overview and analysis of ontology studies supporting development of the construction industry. *Journal of Computing in Civil Engineering*, 30(6):04016026 1-14, 2016.

[35] Daniele, L. and Pires, L.F. An ontological approach to logistics. *Enterprise interoperability, research and applications in the service-oriented ecosystem, IWEI*, 13:199-213, 2013.

[36] Lian, P., Park, D.W. and Kwon, H.C. Design of logistics ontology for semantic representing of situation in logistics. In *Second Workshop on Digital Media and its Application in Museum & Heritages (DMAMH 2007)*, pages 432-437, IEEE, 2007.

[37] Hendi, H., Ahmad, A., Bouneffa, M. and Fonlupt, C. Logistics optimization using ontologies, 2014.

[38] Peffers, K., Tuunanen, T., Rothenberger, M.A. and Chatterjee, S. A design science research methodology for information systems research. *Journal of Management Information System*, 24 (3):45-77, 2007.

[39] Fernández-López, M., Gómez-Pérez, A. and Juristo, N. Methontology: from ontological art towards ontological engineering. From: *AAAI Technical Report SS-97-06*, 1997.

[40] Grüninger, M. and Fox, M.S. Methodology for the design and evaluation of ontologies, 1995.

[41] Hitzler, P., Krötzsch, M., Parsia, B., Patel-Schneider, P.F. and Rudolph, S. OWL 2 web ontology language primer. *W3C recommendation*, 27(1):123, 2009.

[42] El-Gohary, N.M. and El-Diraby, T.E. Domain ontology for processes in infrastructure and construction. *Journal of Construction Engineering and Management*, 136(7):730-744, 2010.

[43] Sirin, E., Parsia, B., Grau, B.C., Kalyanpur, A. and Katz, Y. Pellet: A practical owl-dl reasoner. *Journal of Web Semantics*, 5(2):51-53, 2007.

[44] Frandson, A., Berghede, K. and Tommelein, I.D. Takt time planning for construction of exterior cladding. In *Proceeding of 21st Ann. Conf. of the Int'l Group for Lean Construction*, 2013.

[45] Bock, T. The future of construction automation: Technological disruption and the upcoming ubiquity of robotics. *Automation in Construction*, 59:113-121, 2015.

[46] Andersson, N. and Lessing, J. Industrialization of construction: Implications on standards, business models and project orientation. *Organization, Technology and Management in Construction: an International Journal*, 12(1):2109-2116, 2020.

Visualization of the Progress Management of Earthwork Volume at Construction Jobsite

Hajime Honda[a] , Akifumi Minami[b], Yoshihiko Takahashi[c], Seishi Tajima[d], Takashi Ohtsuki[e], Yushi Shiiba[f]

[a]Topcon Corporation, [b]Kinoshita Construction Co. Ltd., [c]Akasakatec Inc., [d]Kobayashi Consultant Co. Ltd., [e]National Institute for Land and Infrastructure Management, [f]Japan Construction Method and Machinery Research Institute.

E-mail: hhonda@topcon.com

Abstract –

In recent years, the use of intelligent construction equipment with sensors attached to construction heavy equipment used in civil engineering earth work has become commonplace. Sensors provide a variety of information on construction equipment, and this information is used to control the cutting edge of construction equipment called machine control and machine guidance. On the other hand, it is also possible to use the information obtained from the sensors in a wide range of applications to manage the construction progress at civil engineering sites. In this study, a network-based cloud system for soil volume progress management in the actual construction site was verified.

Keywords –

Intelligent Construction Equipment; Network system; As-built data; Construction Progress Management

1 Introduction

In civil engineering earth work sites, it is common to control the progress of construction in terms of soil quantity, volume. This is because construction volume is usually contracted by each material volume, and therefore the site manager daily wants to know the volume as soon as possible during construction. However, it is difficult to realize a means of accurately measuring the daily progress volume, for example, in the case of an excavation site, the construction volume is generally estimated from the average load capacity of the dump trucks used to haul the excavated soil and the number of hauls of dump trucks to be taken out of the construction site. In other words, there is no general method for accurately ascertaining the construction volume. Then, the purpose of this study is to obtain the daily progress volume by using the bucket cutting edge history information calculated based on the information from sensors attached to heavy equipment, and to make the progress of the construction work visible so that the site manager can easily understand the situation on the site.

2 System Configuration

The system used in this study was the X-53x Excavator machine guidance system of Topcon Corporation [1]. The system consists of the following, and the configuration of the system is shown in Figure 1.

(a)Tilt sensor 4pcs.
(b)Display
(c)Controller
(d)GNSS, Global Network Satellite System, antenna 2pcs.
(e)Communication routers to connect to the server
(f)Cloud Server of Data collection and management system, Sitelink3D [2]

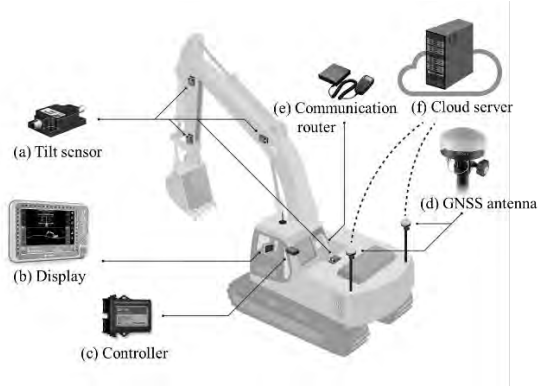

Figure 1. The configuration of the system

3 Construction Site

The construction site of this study was a civil engineering project to excavate and remove sediment

from the dam's lake bottom during the winter in order to increase the dam's water storage capacity, this was ordered by Nagano Prefecture and the contractor was Kinoshita Construction Co. Ltd. and the excavation work took 51 days. The planed excavation volume was 53,000 m^3 and the area was 24,000 m^2, and work was carried out by the three-layer bench-cut method. In terms of soil quality, it was mainly sandy soil that was easy to excavate, although some boulders appeared during the last phase of the work. A picture of the construction site is shown in Figure 2.

Figure 2. Construction site photo

4 System principle

The Excavator machine guidance system uses the angle information detected by angle sensors attached to the Boom, Arm, Bucket and Body of the Excavator and the coordinate information detected by the two Global Navigation Satellite System (GNSS) antennas, respectively, to measure in real time the coordinates of the Bucket cutting edge of the Excavator, generally the coordinates at the center, Pc(Xc,Yc,Zc) or the coordinates at right and left ends points Pr(Xr,Yr,Zr) and Pl(Xl,Yl,Zl) of the bucket. The coordinates measurement points are shown in Figure 3. The system displays the difference in height between the measured data and the design data in the z-coordinate (elevation) by comparing it with the three-dimensional design data entered into the system beforehand. The Excavator operator can see the difference between the cutting edge and the design surface, and the system is used for guidance in construction. The display image is shown in Figure 4.

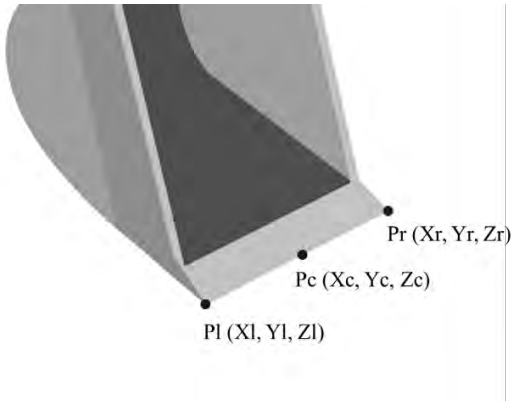

Figure 3. The coordinate measurement points of bucket cutting edge

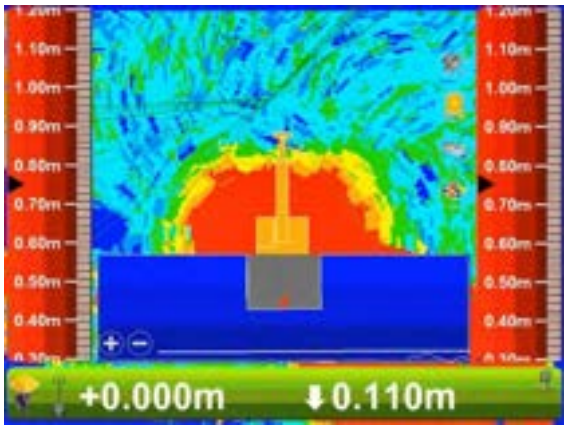

Figure 4. Display image

By using the cloud data collection and management system, Sitelink3D system, in this study, the coordinate data of the bucket cutting edge are transmitted through the mobile phone line in real time and stored on the server. The bucket cutting edge data stored on the server is automatically processed on the server and can be output as gridded mesh data. This data enables us to grasp the 3D shape of the construction site. It is also possible to calculate the daily construction volume, the excavation volume, by calculating the daily differences in the 3D geometry processed on the server. The Sitelink3D system can output grid mesh data and construction volumes as daily reports, allowing the site manager to visually grasp the day's construction results on a daily basis.

5 System Accuracy Verification

The purpose of this study was to verify the accuracy of the system in order to numerically verify the output construction volume. In terms of hardware accuracy, the errors of each sensor contribute to the system accuracy. In this study, the RTK, Real Time Kinematic, method was adopted as a method of GNSS, coordinate

measurement. RTK is one of the most accurate surveying methods for surveying moving objects in real time, with a 2-3 cm error in coordinating detection. In this study, a multi-GNSS type antenna was used to improve the stability of the detection of GNSS satellites, which can detect Japan's Quasi-Zenith Satellite System (QZSS), satellite. On the other hand, since the angle detection error of the angle sensor cannot be directly converted to the coordinate measurement error, the accuracy of the machine guidance system is generally discussed in terms of the total system error including the GNSS coordinate measurement error. It was confirmed that the system was calibrated prior to the start of construction, and that the coordinate measurement error was within ±5 cm as specified in the Accuracy Verification Test Procedure of the Ministry of Land, Infrastructure and Transport [3].

Next, I describe the error of gridding to represent the 3D shape of the construction site. The grid data consist of the Z-coordinates extracted when gridded with X and Y coordinates of a certain interval on the plane through which the line of the bucket cutting edge passes. Figure 5 shows an image of the grid data.

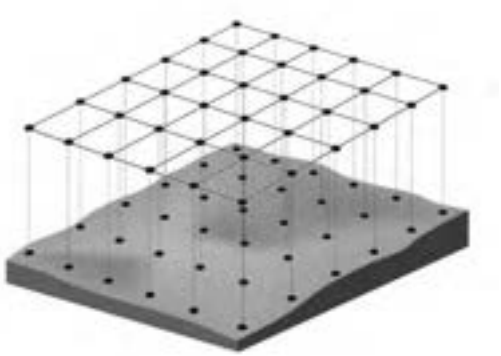

Figure 5. Image of Grid data

In this study, grids were created at 20 cm intervals in the X and Y directions. The grid data are different from the actual 3D shape because it is a polygon shape. The line of the bucket cutting edge is a straight line, so there is no error in the gridding process. On the other hand, it can be understood geometrically that the error in the direction of bucket rotation is small if the bucket moves in a flat plane, but the error is large if the bucket moves steeply. Here, I discuss the error when only the bucket is in rotational motion as a typical movement. The bucket used has a length of 1.5 m, so the rotational motion draws the shape of an arc of 1.5 m radius. On the other hand, the grid is represented by the z-coordinate, which is the arc divided by 20 cm. Figure 6 illustrates the difference.

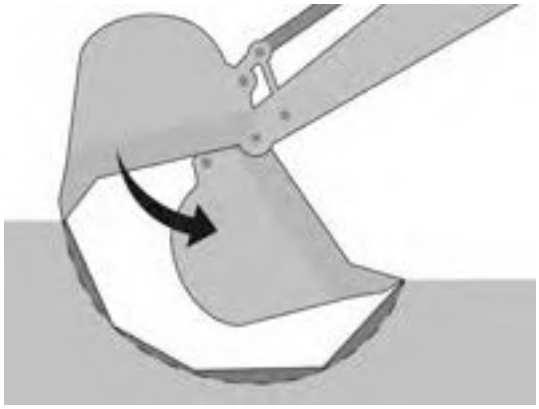

Figure 6. Image of gridding errors

The calculated volume error is the difference between the total area of the arc area and the area to be clipped by the grid data. For a turning radius of 1.5 m, this difference is calculated to be about 2%. The error of the volume by gridding process is assumed to be a typical value of 2%.

On the other hand, if we assume that the volume error is at most 5 cm larger than the error in the z-direction after the calibration adjustment, the volume error will contribute to that error in the depth direction. The volume of soil excavated at this site is 53,000m^3 and the area is 24,000m^2, and the average depth of excavation is 2.2m. The contribution of the system's error of 5 cm in the z-direction to the volume was calculated to be 0.05m / 2.2m = approx. 2%. Based on the above, we can estimate that the error in the overall volume calculation results due to gridding and system errors in this study is up to about 4%.

6 Obtained Data

The data obtained from the daily construction history of the Bucket cutting edge are grid data processed by 20 cm on the server. On the other hand, before the start of construction, the 3D point cloud data of the entire construction site is acquired by the UAV laser surveying, and the TIN, Triangulated Irregular Network, data, which represents the 3D shape of the construction area converted from the point cloud data, are acquired. The pre-construction TIN data are uploaded to the cloud server, and since this study is an excavation site, the current construction site shape can always be virtually formed on the server by updating the 3D shape data when the elevation of the bucket cutting edge of excavator passes lower than the pre-construction TIN shape.

7 Soil Weight Measurement System

In this study, in addition to the machine guidance

Excavator, a soil weighting system was introduced at the same time. The LOADEX100[4] of Topcon Corporation, which directly measures the weight of the soil held by the bucket by using hydraulic data obtained from the hydraulic sensor of the Excavator. This measurement data are sent to Akasakatec Inc's cloud-based soil management system, VasMap[5], which manages the weight of the soil per truck and the daily transport of the soil. The purpose of introducing LOADEX100 is to be able to accurately measure the amount of soil held by the bucket, which was not known before, and to be able to manage the exact weight of each dump truck loaded with soil. The acquired data are recorded digitally on a cloud server, allowing to know directly the daily hauling weight. In the past, the only way for dump trucks to avoid violating the Road Traffic Law by overloading was to load less than the truck's load capacity by considering the margin, but this system will allow for maximum efficiency in loading. As a result, the cost is reduced by enabling more efficient vehicle dispatch compared to the conventional method, contributing to increased productivity. In this study, the soil weight calculated from LOADEX100 was measured daily; however, since construction history data are measured in volume, the daily moisture content of the soil was measured and the soil weight was converted to volume as a reference for progress of volume measurement.

8 Data Reference

Three methods were used as references for the data to be obtained in this study. One is the periodic surveying with UAV laser scanner by a surveyor every two weeks and, in which the final shape is measured by a ground-based laser scanner. The survey results were used to evaluate the 3D grid data. Another one was to evaluate the volume calculated from the aforementioned weight measurements system, and the last one is volume calculations based on the conventional method by dump truck operation times.

9 Visualization

9.1 As-built Shape

The 3D as-built shape obtained from the grid data is shown in Figure 7. This figure shows the overall shape of the construction site, which allows the site manager to grasp the 3D shape of the site using information obtained from the cloud without actually going to the site. In addition, by comparing with the design data, it is possible to easily identify the un-constructed areas and the volume of un-constructed work.

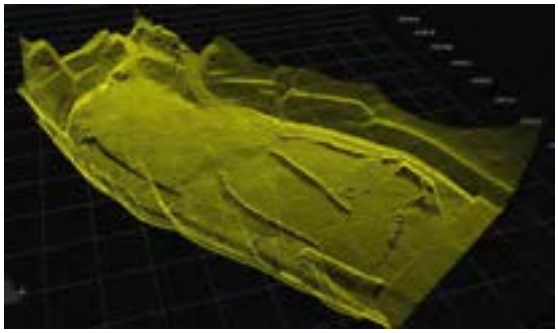

Figure 7. A sample of 3D as-built shape

9.2 Cut Volume

An example of a volume report output from the cloud data collection and management system Sitelink3D is shown in Figure 8.

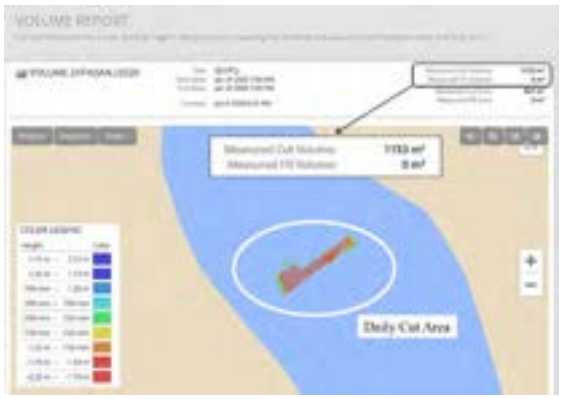

Figure 8. A sample of volume report output

In this report, the cutting depth of excavation in the area is shown in color as a daily report. In addition, the volume of cut volume for the day is displayed in quantity. By simply looking at this report, the site manager can get an idea of the cutting area and cut volume for the day.

The cumulative data obtained from this cut volume report is shown in Figure 9. The graph in the figure shows the cut volume based on bucket cutting edge history and laser 3D surveying, a soil volume measurement system, and the conventional method based on the number of dump truck hauls as a reference, all at the same time. This graph shows that the cumulative total based on the bucket cutting edge history data is not much different from the three references mentioned above. Finally, for the actual construction volume of 55,000 m^3 calculated from the laser survey, on the other hand, the calculated volume obtained from the bucket cutting edge history was 55,640 m^3, which is an actual difference of about 1.2%.

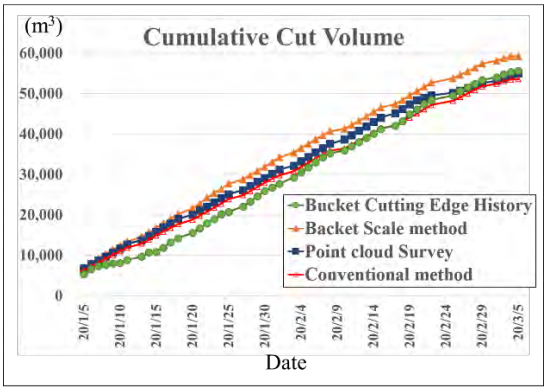

Figure 9. The cumulative cut volume data

10 Consideration

By conducting this study, we found the following. The accuracy of calculated volume of obtained from the historical data of the bucket cutting edge is approximately 1.2% of the total quantity of construction on site, this is consistent with the assumed system error mentioned above. However, if we focus on the daily construction volume, the volume cannot be accurately calculated when the history of the bucket cutting edge does not represent the construction shape due to the appearance of megaliths during the construction process, or when the excavated soil is temporarily placed in the field. Therefore, we feel that it is necessary to evaluate it in terms of numbers over a certain period of time. It has also been reported that accurate volume cannot be calculated even when the bucket edge is pierced into the ground at an acute angle without excavation due to accidental mishandling [6].

11 Conclusion

The historical data of the bucket cutting edge of the machine guidance excavator was used to visualize its construction progress. The volume quantities obtained from the historical data were accurate enough to track the daily construction progress. As a result, daily surveying work, for example, which was originally done as an additional work, can be greatly reduced by using the construction history data. From a productivity standpoint, not only does it reduce the workload of field agents at civil engineering sites, but it can also be used as a tool to more accurately assess the situation.

References

[1] Website of Topcon Corporation. On-line: https://www.topcon.co.jp/positioning/products/product/mc/excavator-system.html, Accessed: 15/06/2020.

[2] Website of Topcon Corporation. On-line: https://www.topcon.co.jp/positioning/products/product/mc/Sitelink3D_J.html, Accessed: 15/06/2020.

[3] Ministry of Land, Infrastructure, Transport and Tourism of Japan, Accuracy Verification Test Procedure, 2019.

[4] Website of Topcon Corporation. On-line: https://www.topcon.co.jp/positioning/products/product/mc/excavator-system.html#LOADEX100, Accessed: 15/06/2020.

[5] Website of Akasakatec. Inc. On-line: https://www.akasakatec.com/products/software/vasmap/, Accessed: 15/06/2020.

[6] Komoto Y, Nakamura K and Taira H, Verification of Practical Effectiveness of final shape Management of the Intelligent excavator by using bucket cutting edge history. *The symposium of Japan Construction Machinery and Construction Association*, 2019.

Incentivizing High-Quality Data Sets in Construction Using Blockchain: A Feasibility Study in the Swiss Industry

Jens J. Hunhevicz[a], Tobias Schraner[a] and Daniel M. Hall[a]

[a]Department of Civil, Environmental & Geomatic Engineering, ETH Zurich, Switzerland
E-mail: hunhevicz@ibi.baug.ethz.ch, tobias.schraner@alumni.ethz.ch, hall@ibi.baug.ethz.ch

Abstract –

Data sets are often incomplete and low-quality at the end of a construction project. This creates rework or hinders opportunities to use data during future activities of the facility lifecycle (e.g. facility management, renovation, demolition). This research prototypes and evaluates a novel process to use blockchain and smart contracts in construction projects to incentivize high quality data sets. The proposed solution is defined in collaboration with construction professionals. The process traces and saves project data while incentivizing participants to create high-quality data sets through reward tokens. To validate the process, an Ethereum-based blockchain prototype is developed. A simple case study is conducted in collaboration with local industry professionals to simulate how the prototype can function in a typical design bid build process used in Switzerland. The early findings and possible subsequent research steps are presented. Overall, it was found that such a blockchain based incentive systems has the potential to not only incentivize high-quality data sets, but also change the way of tendering and related construction processes.

Keywords –

Blockchain; Incentives; Data Management; Construction Projects

1 Introduction

As digitalization in the construction industry increases adoption of building information modeling (BIM) and other digital tools, there are new opportunities to better optimize and manage the operations, maintenance, and deconstruction over a facility lifecycle. The oft-mentioned goal is to create a real time digital twin of the asset.

However, usually digital data sets at the conclusion of construction projects are of low-quality. There can be many reasons for this, such as poor documentation in the first place, difficulties to find the data, or low reliability of the information [1]. When not done properly, the operations team must reconstruct a vast amount of the "as-built" or "as-is" BIM at great time and expense.

To avoid this, construction project teams should seek to handover complete, high-quality data sets at the end of the project. The data gathering should take place from as early on in the project as possible [2]. This challenge is not only technological but also process related [3]; it is important to also consider personal and organizational incentives to provide the data in the first place [4].

Blockchain is seen as a technology to improve transparency and collaboration in construction [5]. Blockchain can track transactions over time and store them in a trustworthy, distributed manner. It enables the building of trust between transacting parties and devices. Blockchain also offers the potential to decrease transaction time and reduce costs associated with intermediaries [6]. Most blockchains can execute *smart contracts,* which are code protocols running on top of a blockchain. On more sophisticated platforms like Ethereum [7], touring complete smart contracts can be used to automate workflows through predefined functions (often conditional if… then... statements), as well as to create so-called *tokens* to represent different kinds of transferable value. Since these tokens represent value, incentive systems can be designed to influence the human behavior when interacting with the created blockchain based process.

In the broader blockchain research space, there is much interest in this topic of crypto-economic systems design – i.e. creating a blockchain-based incentive system among multiple parties to align them towards a higher level goal [8]. For example, Zavalokina et al. [9] investigate a blockchain reward system for maintaining high-quality records for used cars in Switzerland. However, in reviews of proposed use cases for blockchain in the construction context, cryptoeconomic systems design is less often mentioned than other potential use-cases [10]. Only two studies have proposed use-cases where a token is used to incentivize multidisciplinary design teams [11,12]. Having said that, crypto-economic incentive systems could be a novel opportunity to tackle existing challenges of integrating technology and processes in the fragmented construction

industry [13].

This paper introduces a use case of crypto-economic system design to incentivize complete, high-quality data sets at the handover of construction projects. The novel solution proposes smart contracts and tokens to create a trustworthy track-record of data drops, to automate information flow activities, and to incentivize participants in the construction process to share high quality data sets.

2 Methodology

The systems design was conducted in collaboration with construction industry professionals. Research began with a preliminary feasibility study in collaboration with the blockchain workgroup of the buildingSMART chapter Switzerland. The group consisted of construction professionals with diverse backgrounds such as owner, architect, BIM manager, engineer, supplier, contractor, and facility manager. Over the course of one year, the group of industry professionals and researchers held monthly workshops to discuss various aspects of implementing blockchain in the proposed use case.

First, the group discussed the information flow and information categories needed to create a complete data set (chapter 3.1). At the same time, the group defined a use case demonstration (chapter 3.2) and construction process (chapter 3.3) to simplify and focus the investigations. The prototype consists of a basic house represented by a simple BIM model. The home should be procured and constructed using the design bid build (DBB) construction process that is typical in Switzerland.

After the process and data flow for the use case was defined, a first blockchain implementation was prototyped with Ethereum smart contracts (chapter 3.4). Finally, the potential incentive system for high quality data was described (chapter 3.5).

To validate the design, the workgroup participants were then asked in a subsequent workshop about their opinion of the solution (chapter 4). The early results are discussed regarding limitations, opportunities and future research areas for implementation of such a system (chapter 5).

3 Use Case

3.1 Information Flow

To design the subsequent blockchain prototype to incentivize complete data sets, there needs to be an understanding of the information that is typically shared and relevant for later use phases. In the mentioned workshops, potential information categories and relevant data fields were identified. Furthermore, expectations regarding high quality data sets in the scope of this use case were discussed.

3.1.1 Information Categories

Two information categories were identified throughout the workshop: technical and commercial information. Technical information was defined as data important for the subsequent use phase and later recycling of the elements. Commercial information is defined as data relevant and needed during the actual construction process and to control the process for data capturing.

Technical Information

For technical information, various efforts categorize important information for facility management. The data structure for the prototype was based in part on the data fields of the Construction Operation Building Information Exchange (COBie) [14]. COBie is an information exchange specification that defines a consistent structure about a projects facilities, spaces, floors, systems, installed equipment, and related documentation. It was developed especially for asset data without geometric information, which make it very convenient for the later blockchain prototype. Even though COBie represents a first step in the direction of addressing life cycle data challenges related to facility management, it still faces many challenges [2,3].

Commercial Information

For commercial information, the project workflow and the project participants provide the backbone of the process. During the workshops and prototype implementation, commercial data about the project was vital to design the blockchain system. Without this information, the smart contracts would not know from whom and when to request and reward data drops.

The commercial information required was identified during the workshops. Most of the commercial information comes from the tendering process. This also includes the associated prices and quantities of the items in question and the information about the bidding contractors such as insurances and declarations. In addition, information about the project's progression as well as deadlines or contractual information is important. This includes the documentation of decisions, the confirmations for tendering, and the final selection of tendered offers.

3.1.2 High Quality Data Sets

The workshops identified three attributes necessary for high quality data sets: completeness, correctness, and structure. *Completeness* is necessary to ensure that all information is stored. However, completeness should be balanced with complexity. A focus on the important data reduces cost and complexity in the process, since typical

buildings or infrastructure exists for many years. This is especially true for expensive systems such as blockchains. As little data as possible to create a complete date set should be saved. *Correctness* is important in order to draw the right conclusions from the information. Incorrect information can lead to subsequent mistakes and/or costly reconstruction of data. *Structure* is crucial to organize data for later use. Without a standard structure (naming, file type, database) the retrieval and processing will be challenging. The challenge is to fulfill these three attributes as best as possible through the blockchain based workflow and incentive system.

3.2 Use Case Demonstrator

To investigate the described use case in a realistic context, a simple house demonstrator is created using openBIM. The demonstrator has four elements: a door, wall, floor, and pump (Figure 1). These four elements represent the typical diversity of building components (e.g. make-in-place products, semi-finished products, and finished products). The demonstrator acted as a base to investigate the construction processes and related data to build these.

Figure 1. Demonstrator with four elements: floor, wall, door, and pump.

3.3 Construction Process

To start the investigation, a typical design bid build (DBB) process for Switzerland was analyzed for the use case demonstrator together with the buildingSMART Switzerland focus group, resulting in the process diagram pictured in Figure 2. The DBB process was chosen since it is still the most commonly used project delivery model in Switzerland. Furthermore, it simplified the communication with the construction experts, because they were all familiar with it.

Because the process scope should be as focused as possible, some simplifications were made. First, only four stakeholders were considered: the owner, planner, contractor, and supplier. In reality, many more stakeholders exist, including numerous sub-contractors. However, the most important interactions and tasks can be demonstrated with these four stakeholders. Second, some of the contractor tasks are compressed to keep the process diagram as short as possible.

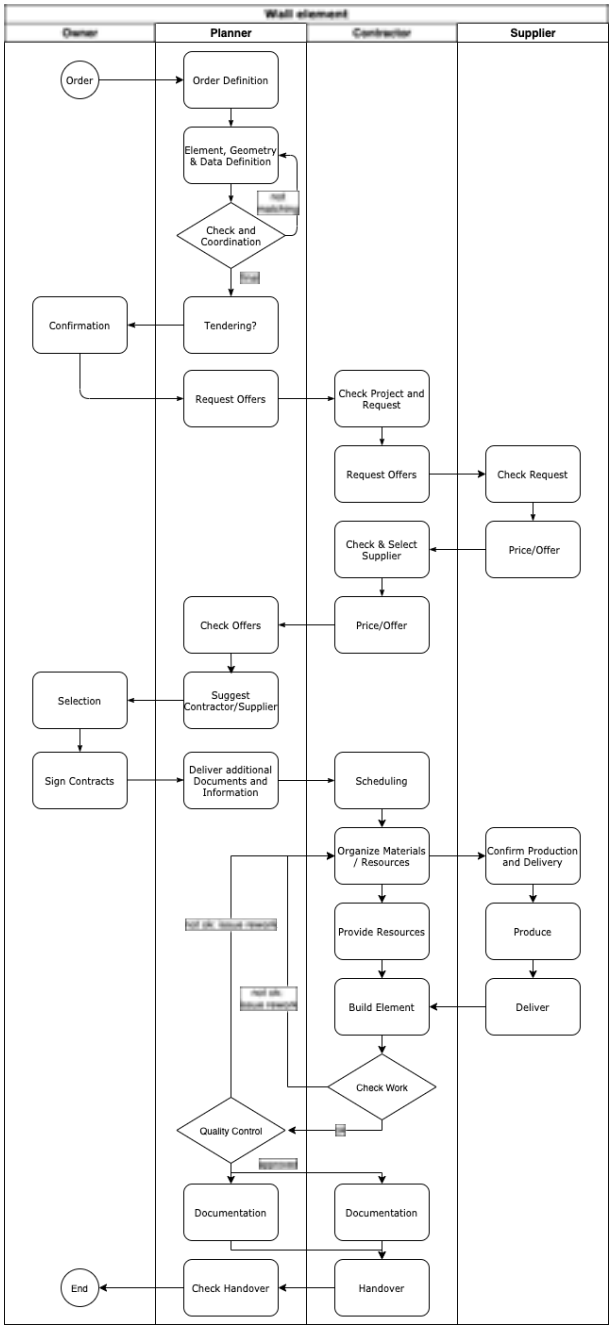

Figure 2. Process diagram of the construction process for the wall element of the demonstrator.

3.4 Prototype

A preliminary blockchain prototype was developed in order to test the feasibility of such a system. The focus was only on the first part of the construction process (see Figure 2): the project phase of element definition and tendering until the contract is signed (Figure 3). Furthermore, the supplier was not considered in the prototype; it is assumed the functions of the supplier

would be similar to the ones of the contractor. The prototype was developed for the Ethereum blockchain. Ethereum was the first blockchain that introduced touring-complete smart contracts [7]. These smart contracts can encode logic that will be executed when the according functions are called. Furthermore, they can hold and save data on the blockchain. The feature of smart contracts is essential for the proposed use case. Although there are many other blockchains that support smart contracts nowadays, Ethereum is still the biggest network with vast documentation available. It should be noted that there is no claim that Ethereum is the only blockchain framework for this use case. The proposed logic could be implemented on any other system that supports smart contracts.

3.4.1 Smart Contract Logic for Workflow

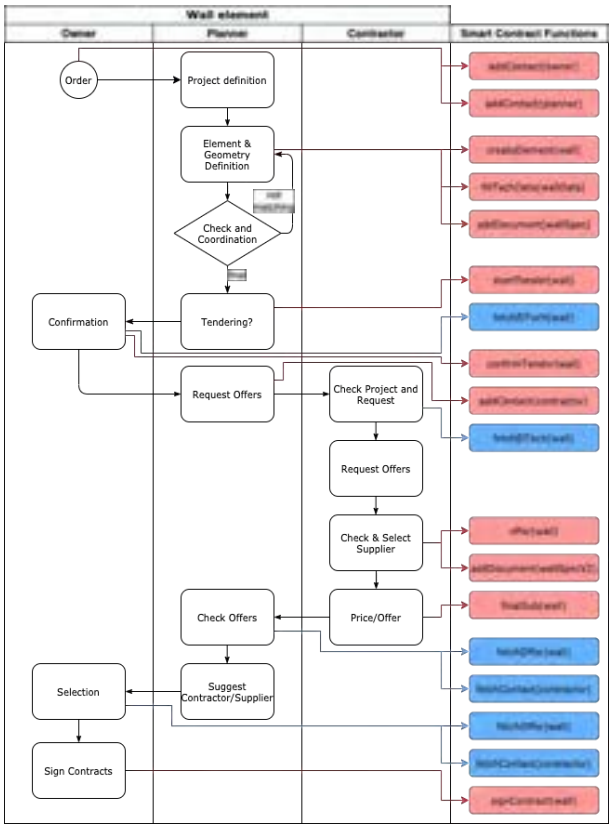

Figure 3. Workflow for the built prototype with smart contract functions. Red: write functions; Blue: view-functions to retrieve information.

The workflow pictured in Figure 3 was realized by coding the related functions for each necessary transaction into a smart contract. To write and test the smart contract in the Ethereum-specific language Solidity (https://solidity.readthedocs.io), the brower-based open-source tool Remix (https://remix.ethereum.org/) was used. Remix allows for fast writing and testing of the smart contract functions through an integrated JavaScript compiler that simulates the Ethereum virtual machine environment.

The smart contract includes different functions. Through so-called "state variables" the process order is defined. The variable is changed if a project step is completed. This is a very restrictive approach, because the next phase can only be started when the previous step has been completed. Each construction element contains these state variables, and the smart contract only allows to execute the associated functions. For example, if an element is in the state *ReleasedForTender*, only then can the owner confirm by calling the function *confirm()*, which would put the element into the subsequent state *Confirmed*. The function *offer()* would for example fail, since this is not the next workflow step. Furthermore, the smart contract logic ensures that functions can only be called by the correct parties. Each party has their own network address to identify itself. With the associated private key (similar to a password) the stakeholders can identify themselves and sign transactions, e.g. the execution of a specific function.

3.4.2 Data Structure

The data structure for the prototype has been defined based on the identified categories in chapter 3.1.1. The storage type *struct* was used in Solidity to store the information. A *struct* for both the technical information and commercial information was defined, which means it defines the data fields that need to be filled in during the work flow. If multiple entries are expected for one field, arrays are used. The *struct* is then applied to each element or product in the construction project. This was found to be the best suited solution because the BIM-based tender process is based upon each individual BIM element.

Different functions take care of filling the information related to the various data drops in the process. This is displayed in Figure 4. For example, the function *confirm()* only alters the state variable through the contractor signing that function. In contrast, the function *createElement()* called by the designer takes all the design parameters as input and stores them in the respective struct entries. The different data drops can be defined including who will need to do the data drop by calling the respective function and when this function can be called. The different view functions allow to retrieve and validate the information.

Finally, a *struct* for contact information was defined (Figure 4). This allows to save additional information about the stakeholder next to their Ethereum address. With only the public address-string (e.g. 0x25213E8E0964a98A017Ebbf36c633eFd006fe2ce), it is hard to see in reasonable time who belongs to which address.

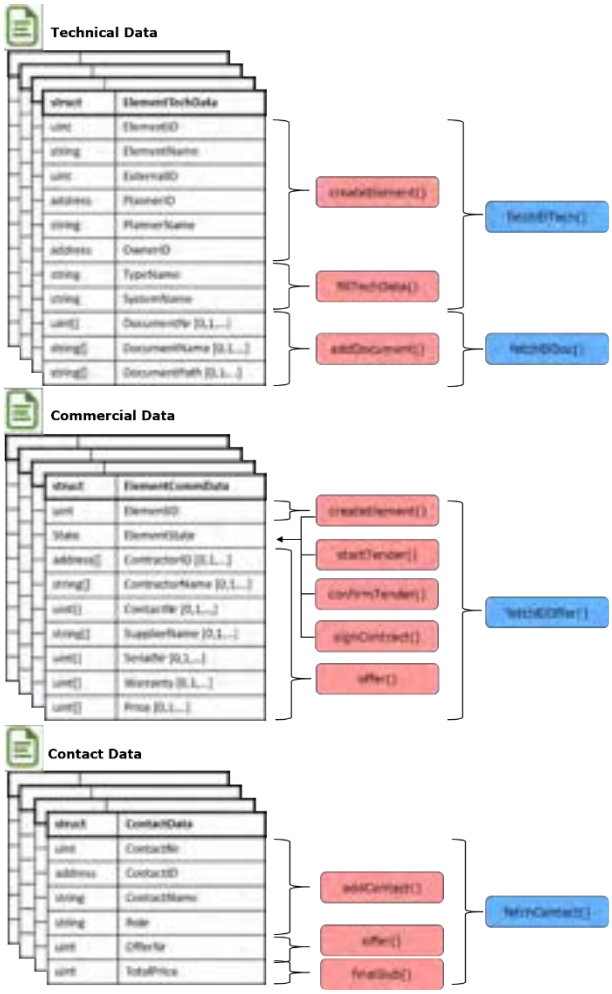

Figure 4. The data *struct*'s used in the prototype: technical, commercial, and contact. The functions modify the respective elements when called.

3.5 Possible Incentive Structure

The implemented prototype allows to build a blockchain-based incentive system along the introduced work flow. Tokens can be issued, transferred or burned together with the introduced blockchain function (see Figure 3). As briefly explained in the introduction, blockchain-based tokens represent value containers that could be used for currency, reputation, securities, or other value types [15,16]. Tokens are also coded through smart contracts. In the case of Ethereum, the most used token-types are called ERC20 (fungible) and ERC721 (non-fungible). Depending on the use case, both tokens types could be useful.

Figure 5 presents a schematic view on a possible structure. The idea is to incentivize data suppliers to only write high-quality data. This mainly applies to the correctness of data. To some extent, the smart contracts already take care on the structure and completeness aspect, since they force the actors to input the data as specified in the workflow rules and defined data fields. However, the quality of that data could be still low. As a solution, an additional role in the process of a data verifier can check the data transactions and confirm the quality. For now it is not further defined who will take on this role, but in general every capable stakeholder could do this. If the data quality is good, the data supplier receives some kind of reward token.

The challenge is then to design the right incentive system out of countless possible combinations. For this construction case, the authors imagine either financial rewards (tokens for micropayments or a stake in the project) or a reputation system (tokens represent reputation). Also a combination of both and/or multi token system is possible. Different solutions are part of the ongoing research. They should then be carefully tested to exclude possibilities of cheating or negative side effects. It is important that all actors in the system are incentivized in the intended way. Next to the considered construction participants, this also applies to the role of the data verifiers.

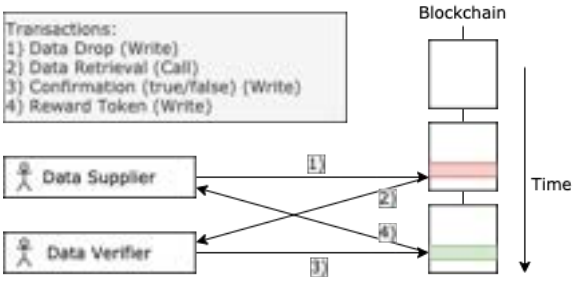

Figure 5. Schematic representation of the imagined incentive system to achieve high quality data sets.

4 Participant Assessment

The prototype implementation and ideas on how to incentivize high quality data sets through tokenization were presented to the buildingSMART workgroup. A first brainstorming session took place for each of the stakeholder's role in the system and potential benefits and drawbacks associated to it. The insights will be used in future research to iteratively improve the incentive system design. The following presents some preliminary insights and feedback from the participants.

All participants agreed that the blockchain based process can add value to today's working practice. The strict nature of smart contracts and the transparency of the process could already mitigate many of today's challenges regarding data structure and information completeness. Furthermore, the participants saw the blockchain-based incentive system as promising to

incentivize correct content (either through financial or reputational rewards), but also to potentially create a self-sustaining infrastructure. The construction professionals wondered who would pay for such a system, either in terms of transaction fees (in public blockchain network) or the overhead for the infrastructure and maintenance (private blockchain network) (see Hunhevicz and Hall [10] for more information on different blockchain network types). While in the first case the fees could be covered by each individual party (similar to post stamps for official sharing of documentation nowadays), the second case would need to be financed out of the system (e.g. through participation fees) or by the stakeholders. An independent funding source not related to one project stakeholder would support the adoption of such a system also across projects. The system should ideally be opt-in and attract the users through the associated benefits. The participants agreed that this would be the better option than forced participation through powerful parties, e.g. the owner. However, the exact design of the system – including both the incentive for high-quality data and the financing of the system – was seen as not straightforward and a major future challenge for adoption.

Overall, the participants perceive the system in two different ways. Some see the system as a project-specific implementation. Others considered it a market-wide system. This is surprising because the research initially targeted a data management system for a construction project. However, a market-wide integration would affect the tendering process and ultimately lead to a market protocol on which competitive offers for construction projects can be automatically managed in a transparent way. This could be done based on the reputation system where reputation can be derived from past data saved on the blockchain. Market-wide consequences of incentive systems might need to be considered in future research.

Furthermore, the need for privacy of sensitive information becomes apparent (especially from the viewpoint of suppliers and contractors). This creates potential issues with data visibility and privacy on public blockchain systems.

The owner was considered to be the stakeholder to benefit most from such a solution. Potential benefits include the higher data quality for the operation, more transparency for data and process analysis, fewer disputes, simplified contract signing (transaction signatures), more competition in tendering leading to better prices, price transparency, and subjective selection criteria for choice of contractor (in case of a reputation system).

Finally, it was challenging to identify if the perceived advantages by the workgroup stem really from the blockchain-based (incentive) system, or the more structured documentation process in general. There is need for future work to identify what can be achieved with conventional data structures and technologies, but better data management – and what can be achieved only with a fully-implemented cryptoeconomic system design for complete data sets.

5 Discussion

Since blockchain-based incentive systems for construction projects is a new concept, there is potential and challenges alike. The following sections discuss the limitations in this paper and point to future research work for improvement.

5.1.1 Use Case

The considered use case focuses on the DBB construction process in Switzerland with only a very limited amount of stakeholders. This should be extended and generalized for future implementation.

Also, a better differentiation between construction elements should be considered. Typical unfinished products and elements that need to be completed on site involve more stakeholders. In contrast, finished and prefabricated products could be ordered directly from the supplier. All these different possibilities would need to be captured. The process was conceptually developed for all four elements of the demonstrator, but it turned out that the project steps are largely identical for the different elements. They might differ though in the amount of needed suppliers to provide the products. For a use case of supply chain traceability, this would be important. But for the investigated use case of incentivizing data sets, the amount of suppliers is conceptually not further relevant to showcase the functionality. Having said that, this could change for scalability of the solution later on.

Finally, the implemented information flow, data categories, and high-quality data attributes are based on the workshop discussions. There should be more investigation on each aspect on the state of the art. Therefore, the chosen structure (based on COBie in the technical case) should be seen as a starting point to identify important information attributes, not as a final recommendation. Furthermore, the data categories might need to be extended. One example could be a definition of the required material information to track and implement a circular economy for building elements.

5.1.2 Blockchain Prototype

The main point of the prototype was to investigate if and how such a system could be implemented with the available tools. The implemented logic and functions will need to be refined.

In the future, investigations should target how to create the user interfaces (e.g. web based front end application) to conveniently interact with the system. Also, the smart contracts would need to be optimized to

better capture ownership properties, optimize gas consumption (i.e. cost for computation on-chain) to save on costs, allow for updatability of the contract, and comply with the latest coding best practice for security reasons.

All the data is currently saved on-chain, which is known to be very expensive and potentially creates issues with storage size down the road. A future solution could store part of the data off-chain with notarization on the blockchain. While this would allow to check whether data is changed, data would still need to be fetched off-chain. This complicates the use of smart contracts and is sometimes referred to as the "oracle-problem."

A public permissionless system (Ethereum) is used because the system is intended to exist thoughout the long life cycle of the facility. The Ethereum network incentives contributors to maintain it independently of who uses the network. This avoids efforts required to run a private network server infrastructure over such long time durations. However, there are many possible DLT design options available [10]. A more detailed investigation on the best suitable system should be part of future research. This should be also aligned with current construction and BIM software.

Finally, there are still challenges related to privacy protection of on-chain data (especially in public blockchains) and how to deal in general with the very strict nature of smart contracts in the context of processes that require some flexibility.

5.1.3 Incentive System

This paper introduces an initial incentive system concept. While the imagined incentive mechanism seems promising to motivate stakeholders to provide correct data drops, there is need for future research to study different and specific incentive systems for the introduced purpose based on financial, reputation, or other possible tokenized reward structures. As a starting point, a better understanding of each stakeholder's position and motivation in the system is important. It is also possible that there needs to be specific roles associated with the incentive system, e.g. the mentioned data verifiers. More investigation is needed on how to properly reward stakeholders for their work.

6 Conclusion

The paper proposes an innovative way to incentivize high-quality data sets in construction through blockchain based process management linked to reward systems. It makes use of blockchain to combine technological aspects of data management with personal and organizational aspects to share data in the first place.

The prototype demonstrates how such a solution can be built, as well as technical challenges that still remain. The most important include scalability, on-chain data storage, privacy of sensitive data in public systems, and the coding of smart contracts to remain somewhat adaptable to different construction processes.

The main area of future research is related to the design of possible incentive systems. Many combinations exists that should be assessed and validated. Furthermore, implications to the construction process and markets should be investigated. There could be consequences of beyond one construction project on general market forces and project delivery practices.

Also, the proposed system would benefit from a more detailed analysis on the effect of different parts of the proposed blockchain implementation on high-quality data sets. A blockchain based process without any tokenized incentive system might already benefit the structure and completeness aspects of data sets with data transparency and automation through smart contracts. Having said that, this alone might be also achievable through conventional IT solutions. The need for blockchain in this case should be carefully assessed.

The proposed incentive system has the potential to improve data correctness and completeness at the conclusion of a construction project. The use of such tokenized incentive systems would be a strong argument to use blockchain as a technological tool, since its real strength applies to (semi/automatic) value transactions in an environment with low trust.

Overall, blockchain-based incentive systems show promise to align construction stakeholders. This study intended to showcase this with a concrete example on how blockchain and smart contracts can enable a trustworthy track-record of data drops, automation of information flow related activities, as well as a token-based incentive for participants in the construction process to share high quality data sets.

Acknowledgment

The authors would like to thank the construction professionals of the blockchain group in the buildingSMART chapter Switzerland for their valuable insights and support during the workshops; special thanks for their efforts are given to Enrico Cristini, Erik de Ruiter, Tobias Jörn, Arthur Loosen, Daniel Schwarz, and Thorsten Strathaus.

References

[1] T. Jylhä, M.E. Suvanto, Impacts of poor quality of information in the facility management field, Facilities. 33 (2015) 302–319. https://doi.org/10.1108/F-07-2013-0057.

[2] S. Jawadekar, S. Lavy, A Case Study of Using

BIM and COBie for Facility Management, Int. J. Facil. Manag. 5 (2014). https://staging-media.thebimhub.com/user_uploads/user_uploads/110-597-1-pb.pdf.

[3] A. Alnaggar, M. Pitt, Lifecycle Exchange for Asset Data (LEAD): A proposed process model for managing asset dataflow between building stakeholders using BIM open standards, J. Facil. Manag. 17 (2019) 385–411. https://doi.org/10.1108/JFM-06-2019-0030.

[4] R. Liu, R.R.A. Issa, Issues in BIM for Facility Management from Industry Practitioners' Perspectives, in: Comput. Civ. Eng., American Society of Civil Engineers, Reston, VA, 2013: pp. 411–418. https://doi.org/10.1061/9780784413029.052.

[5] B. Penzes, Blockchain technology: could it revolutionise construction?, Institution of Civil Engineers, 2018. https://www.ice.org.uk/news-and-insight/the-civil-engineer/december-2018/can-blockchain-transform-construction (accessed December 30, 2018).

[6] W. Viryasitavat, L. Da Xu, Z. Bi, A. Sapsomboon, Blockchain-based business process management (BPM) framework for service composition in industry 4.0, J. Intell. Manuf. (2018) 1–12. https://doi.org/10.1007/s10845-018-1422-y.

[7] V. Buterin, Ethereum: A Next-Generation Smart Contract and Decentralized Application Platform, White Pap. (2014). https://github.com/ethereum/wiki/wiki/White-Paper (accessed August 27, 2018).

[8] B.S. Voshmgir, M. Zargham, Foundations of Cryptoeconomic Systems, (2019) 1–18. https://epub.wu.ac.at/id/eprint/7309.

[9] L. Zavalokina, F. Spychiger, C.J. Tessone, G. Schwabe, Incentivizing Data Quality in Blockchains for Inter-Organizational Networks – Learning from the Digital Car Dossier, Thirty Ninth Int. Conf. Inf. Syst. (2018) 1–17. https://doi.org/10.5167/uzh-157909.

[10] J.J. Hunhevicz, D.M. Hall, Do you need a blockchain in construction? Use case categories and decision framework for DLT design options, Adv. Eng. Informatics. 45 (2020) 101094. https://doi.org/10.1016/j.aei.2020.101094.

[11] M. Mathews, D. Robles, B. Bowe, BIM+ Blockchain: A Solution to the Trust Problem in Collaboration?, CITA BIM Gather. 2017. (2017) 11.

[12] A. O'Reilly, M. Mathews, Incentivising Multidisciplinary Teams with New Methods of Procurement using BIM + Blockchain, Conf. Pap. (2019). https://arrow.dit.ie/bescharcon/31 (accessed June 11, 2019).

[13] J.J. Hunhevicz, D. Hall, Crypto-Economic Incentives in the Construction Industry, (2020). https://www.research-collection.ethz.ch:443/handle/20.500.11850/420837 (accessed August 10, 2020).

[14] E. William East, N. Nisbet, T. Liebich, Facility Management Handover Model View, J. Comput. Civ. Eng. 27 (2013) 61–67. https://doi.org/10.1061/(ASCE)CP.1943-5487.0000196.

[15] M.M. Dapp, S. Klauser, M. Ballandies, Finance 4.0 Design, (2019). https://doi.org/10.3929/ETHZ-B-000331093.

[16] W. Mougayar, Tokenomics — A Business Guide to Token Usage, Utility and Value, (2017).

A Holistic Framework for the Implementation of Big Data throughout a Construction Project Lifecycle

Makram Bou Hatoum[a], Melanie Piskernik[b], and Hala Nassereddine[a]

[a]Department of Construction Management and Civil Engineering, University of Kentucky, USA
[b]Institute of Interdisciplinary Construction Process Management, Technical University of Vienna, Austria
E-mail: mbh.93@uky.edu, melanie.piskernik@tuwien.ac.at, hala.nassereddine@uky.edu

Abstract –

As the world witnesses the fourth industrial revolution, construction remains a newcomer that lags in its adoption of technological innovations. The information-intensive nature of the construction industry, coupled with its multidisciplinary nature, has pushed construction to enter the era of Big Data and has provided fertile ground for research on Big Data. Numerous efforts have been undertaken to investigate the use of Big Data and its impact on construction. This paper builds on the existing body of knowledge and explores the implementation of Big Data throughout the different phases of a construction project. By synthesizing the extant research corpus, this empirical study provides insights into the current state-of-adoption of Big Data throughout the lifecycle of a construction project, its sources, capabilities, and benefits. The findings of this paper are combined into a Big Data Framework that summarizes the "what, how, where, and why" of Big Data implementation in the construction industry.

Keywords –

Big Data; Adoption Framework; Construction Industry; Project Lifecycle; Benefits; Use-Cases.

1 Introduction and Background

Industries worldwide are currently in the midst of the fourth wave of technological advancement, known as Industry 4.0. This wave of advancement is a collection of various technologies that promote innovation in industries through the convergence of humans, technology, and information [1]. The construction industry is not an exception to the pervasive digital revolution. The industry deals with sheer volumes of data arising from different disciplines throughout the different phases of a project.

Despite the information-intensive nature of the construction industry, it remains slower than other industries in harnessing the power of data [2]. Researchers have identified various barriers that prevent construction from fully exploiting information and communication technologies (ICT) and harvesting construction data. Example of barriers include the highly fragmented nature of the industry, the temporary nature of projects, the uniqueness and complexity of construction projects, the inadequate coordination and collaboration between stakeholders, the lack of ICT knowledge and skills, the lack of standardization, the challenge to change organizational culture, and the unclear return on investments [3].

The above-mentioned barriers pose a multi-dimensional challenge that can be tackled from different aspects. One aspect that this paper explores is ICT. Research in the industry showed that data captured through ICT can be used to address crucial issues associated with cost, planning, risk management, safety, progress monitoring, and quality control [4]. This collected data is the major source of Big Data, which, compared to small data sets or sampling, can help to draw a fuller, more trustworthy picture in all areas of construction [4].

Big Data in construction can be defined by five different attributes: volume, variety velocity, value, and veracity (5V's). The interdisciplinary nature of the construction industry produces large, heterogeneous, and dynamic construction data, which mirrors the volume, variety, and velocity attributes of Big Data [5]. Moreover, primary sources of Big Data in construction generate data in large volumes, numerous formats – including images and AutoCAD and Revit enabled files, and in near real time [6]. As for value and veracity, these two attributes are conveyed through the ability to extract information from construction's Big Data and detect and analyze patterns and trends [7].

Primary sources of Big Data in construction include 1) people who are continuously generating and sharing information, 2) IT-enabled construction equipment that gather, share and store data, and 3) internal Information Technology (IT) systems such as Building Information Modeling (BIM), planning and procurement software [8].

The vast accumulation of data from these sources, especially from BIM, has been studied by numerous

researchers. BIM serves as a starting platform to adopt Big Data approaches. [9] stated that Big Data is essential in "bridging BIM and building" (BBB), where technologies such as radio-frequency identification (RFID), cameras, Geographic Information System (GIS), global positioning system (GPS), and Augmented Reality (AR) capture real-time information from real-life physical project processes and synchronize it with BIM to track construction and generate as-built models. The authors developed a BBB conceptual framework that uses data beyond the construction phase of a project and generates architectures of real RFID-enabled BIM systems for prefabricated housing productions. In another study conducted by [10], BIM was extended to "dynamic BIM", an innovative approach which stores information from the early phases of the project through facility management, with a cloud-based system framework to effectively retrieve required information for various applications by Big Data analysis based on parallel processing of large data sets.

This integration of BIM and Big Data was classified by [11] as an example of a technological factor that drives Big Data adoption in the construction industry. Another example of a technological factor considered by the same study is the advantage of information derived from Big Data analysis such as decision making, planning, and simulations. The study also noted two other factors that drive the adoption of Big Data: organizational factors which reflect Big Data's ability to improve design and execution efficiencies and project management capabilities, and environmental factors which represent the availability of construction related technology that can collect, store, analyze and visualize Big Data [11] . Moreover, data that is being collected and stored by construction stakeholders can be analyzed to continuously assess and improve stakeholders' management maturity by generating new types of holistic and adaptive maturity models [12]. For example, social network analysis (SNA) and text mining techniques can be used to recognize patterns of communication within the organization and among project stakeholders, and evaluate the extent to which documents reflect project management processes [12].

In addition to the aforementioned drivers, Big Data presents new opportunities for construction firms to innovate and improve current construction processes [13]. Big data can empower project progress monitoring and optimize resources allocation by providing new ways to simplify the detection of performance deviations and give stakeholders more time for corrective actions on ongoing projects. This capability can be also extended to future projects by allowing stakeholders to build their knowledge to thoroughly understand the adopted practices [13].

To examine the status of Big Data research in construction, [6] performed an extensive study that analyzed Big Data research in construction and mapped out its orientation. The authors found that Big Data studies mostly focused on utilizing Big Data on construction projects to monitor progress and performance, enhance time and cost management, and inform better decisions. The authors also noted that other studies focused on site safety and worker safety behavior, energy management of buildings, decision-making framework design, and resource management and tracking during construction [6].

This paper builds on the existing body of knowledge and synthesizes previous research efforts into a framework that holistically summarizes the implementation of Big Data in the construction industry. To achieve the research objective, the study starts by first identifying applications of Big Data throughout the lifecycle of a construction project – from conceptual planning to demolition. Next, ten major benefits of adopting Big Data in the construction industry are extracted and discussed. Finally, a holistic framework that summarizes the "what, how, where, and why" of Big Data implementation in the construction industry is proposed.

2 Big Data Applications throughout the Construction Project Lifecycle

Numerous research efforts were reviewed and examined to extract potential applications of Big Data throughout the lifecycle of the construction project. The project phases used in this paper are those discussed by [14] who divided the project lifecycle into seven phases: concept planning, design, pre-construction, construction, commissioning, operation and maintenance, and demolition.

Throughout the review of the extant literature, the authors noted that some project phases were discussed interchangeably, namely conceptual planning and design, and construction and commissioning. Thus, this research grouped the seven phases into five stages, discussed below, to accommodate the Big Data literature.

2.1 Stage 1: Conceptual Planning & Design

A project lifecycle begins with conceptualizing the project and developing the design. During this stage, geospatial, a type of Big Data , can provide planners and designers with important information about the project location, infrastructure, public spaces and resources [8], [15]. [16] added that Big Data can also offer insights from previous projects about future residents, their behavior, and preferences, thus facilitating stakeholders' understanding of end-users' needs by and designing the project for optimization.

[17] discussed that Big Data can be integrated with BIM and online social networks to select sustainable energy solutions capable of optimizing the project performance. This can enhance project design and is particularly valuable for green buildings. Simulations can also be generated with Big Data to evaluate various design alternatives for space and efficiency, creating a new approach for producing innovative designs [16].

Another application of Big Data in the project early phases is found in the bidding process of traditional projects. Tender price evaluation is one of the central challenges that owners face during bidding. While owners collect project cost data from all bids, this information is generally not used after a bid is awarded. To take advantage of historic data, project cost data need to be stored in the cloud. Then, Big data algorithms can be designed and generated to mine the stored data and allow the evaluation of tender prices in real-time [18]. Stakeholders can also use Big Data to estimate their profit. [19] indicated that the company or industry benchmarks currently used to estimate profit are not accurate as they do not reflect project-specific variations. The authors argued that the architecture Big Data makes it possible to quickly examine large amounts of project data, identify underlying trends, and understand the dependence between profit margins and project attributes.

2.2 Stage 2: Pre-Construction Planning

The second stage is pre-construction planning, which includes planning the construction phase of the project. The effectiveness of this stage relies on the proper use of all available knowledge needed to develop an execution plan [20]. Big Data collected from similar historic projects can be analyzed and used to ensure the robustness of the project plan by reducing uncertainty and allowing more accurate forecasts, projections, and planning [20]. Pattern analysis, simulations, and trend analysis are three approaches that are frequently used to analyze data during pre-construction planning and aim to assess implications of current issues and decisions, detect early warnings and threats that can impact project performance, consider consequences of design assumptions, and simulate future scenarios [20].

Another application of Big Data in this stage focuses on predicting the behavior of stakeholders and analyzing the reliability of their commitments, their level of collaboration, and readiness to share knowledge [20].

Moreover, historic and new data collected during this stage can be used to simulate different construction activities and tasks, and thus, improving project performance. These simulations become very critical when automating activities or tasks, as the effect of automation on safety, productivity, and parallel-occurring tasks need to be carefully analyzed [13].

2.3 Stage 3: Construction & Commissioning

The third stage discussed in this paper includes the construction and commissioning phases of a project. Most Big Data applications in this stage are used in capturing real time or near-real time data to track project progress and create as-built 3D models [9]. [21] reviewed different applications that use computer visual techniques for monitoring and analyzing activities performed on construction sites. These visual techniques are found to have the ability to analyze static images, time lapse photos and visual streams. [22] proposed an application that uses 4D plan BIM and 3D as-built point clouds models to track construction progress. The point clouds were generated from site photologs using structure-from-motion techniques.

Real time data can also be gathered using as built-in smartphone sensors to collect equipment-related data. The status of an equipment, i.e. off, idle, or busy, and the type of work performed, i.e. dumping or scoping, can be analyzed to assist construction personnel to better utilize the equipment, inform better decisions, and ultimately, have better control of the project [23]. Moreover, [24] indicated that setting laser scanners and video cameras on blind spots across the construction site allows the collection of new data that can be beneficial to equipment operators, by providing them with 3D workspace data, automatic object recognition, and rapid 3D surface modeling in near real time.

In addition to sensors, applications of IT are also being embedded into construction machinery. An example of such applications include machine-to-machine (M2M) [25]. M2M can be used on construction machines to recommend overhauls for construction end users on site at the optimum timing. This data can also help manufacturers better understand and transform their business models, thus creating enhanced machinery.

[26] explored a Big Data application for real time construction quality monitoring application to provide timely collection and analysis of data from ongoing activities. The application is a real time construction quality monitoring method for storehouse surfaces of reinforced cement concrete (RCC) damps using GPS, global navigation satellite business techniques, sensor technology, and network transmission technology.

[27] proposed an enterprise integrated data platform (EIDP) to overcome challenges such as poor interoperability of data and inaccurate manual entries between the business management and the project management, showcasing the value of Big Data for construction companies.

Applications of Big Data have been also explored for earthwork processes. [28] combined photogrammetry and video analysis for measuring the exact machinery productivity and determine site-specific performance factors. Photogrammetry was used to determine the

volume of excavated soil, while video analysis was used to generate statistics such as loading and idle times.

Big data can also be used for human resources and labor. For example, [29] used Big Data to analyze worker behaviors in a metro construction in China. The study formed a behavioral risk knowledge base by combining vital unsafe behavior in multiple dimensions with the work breakdown structure of the construction. Then, the knowledge base, with the assistance of mobile applications and surveillance cameras, was used to detect unsafe behavior, analyze the factors affecting this behavior by Job Hazard Analysis (JHA), and match it with the predefined unsafe behaviors using Vector Space Model (VSM). All this information was also stored in a Big Data cloud platform and sorted by a Hadoop Distributed File System (HDFS).

2.4 Stage 4: Operation & Maintenance

The fourth stage includes the operation and maintenance phase of a project lifecycle. With properly installed technologies like RFIDs and sensors, facility managers can obtain the exact location and details of different building components to simplify monitoring, inspection and maintenance [9]. Beyond that, using BIM models and Internet of Things (IoT), Big Data can be generated for buildings to provide geometric and semantic information as well as state of building elements, all of which can be used to represent buildings within a virtual GIS environment for city monitoring and management applications [30].

Big Data that includes building information, in particular energy efficiency, has become one of the main concerns for a sustainable society. Despite the existence of current challenges – like analyzing accumulated data in a short time – Big Data analysis can be the solution for understanding energy consumption behavior and improving energy efficiency in the construction sector [31]. A successful example includes the analysis of energy consumption, environmental measures, and occupancy information using Big Data Analytics techniques to study building performance and visualize it on a building performance comparison application [32], [33]. This application was designed to handle large volumes of data with a user interface platform to change the options of the desired analysis. [34] reviewed sustainable construction management strategies that use quantitative Big Data approaches to monitor, diagnose, and retrofit the dynamic energy performance of buildings in use.

2.5 Stage 5: Demolition

The last stage of a project is demolition. Big Data gathered from construction waste management indicators, especially in the demolition of a project, can assist in managing the disposal of the deconstructed materials and reduce the waste generation of the contractor [4]. Examples of performance indicators include waste generation rates, costs associated with waste collection, storage, transportation and recycling, and revenues and savings from selling waste [35]. This data can also be beneficial for the public, where the government can use Big Data to manage construction wastes, and monitor air and noise pollution from construction activity [36].

3 Benefits of Big Data

Big data has a wide range of applications throughout the project lifecycle, as highlighted in the previous section. Various research efforts have also discussed the benefits that Big Data can offer to the construction industry. These potential benefits are discussed below and are summarized in Table 1:

- Enable data driven simulations and solutions for different on-site construction activities to optimize construction site layout and resource allocation [16], [17], [37]
- Enable the delivery of the right information such as project location, surrounding environment including traffic and parks, and infrastructure overview [15], [18]
- Enable the monitoring and assessment of various facility performance areas, specifically energy, and thus empowering facility managers to perform their work more efficiently [7], [30], [32]–[34], [38], [39]
- Enhance decision-making by accessing and analyzing previously collected data and identifying trends and patterns [3], [4], [7], [37]
- Enhance the flow of information between project stakeholders and across project phases. For example, this can be achieved with the applications that track real time or near-real time construction status and update as-built models for downstream players [7], [12], [37], [40]
- Facilitate collaboration and communication between stakeholders, which is of great importance, especially at the early stages of the project to align stakeholders' interests. Increase collaboration and communication ensure that all stakeholders have a clear understanding of the scope of work and expected outcomes [17], [20], [25], [37], [41]
- Improve project control including the location and status of labor, equipment, material and tools [21], [23]–[25], [28], [29], [42]
- Improve the accuracy of forecasting and promote better predictability, specifically during pre-construction planning where construction tasks can be simulated before execution to identify and remove barriers and constraints [7], [13], [17]–[20],

[36], [37], [43]
- Optimize project environmental performance, particularly waste management, during construction and demolition [4], [36], [44]
- Support electronic information management systems to centralize information throughout the project lifecycle [41], [45]

Table 1. Benefits of utilizing Big Data in Construction

Code	Benefits
B1	Enable data-driven simulations
B2	Enable the delivery of the right information
B3	Enable the monitoring and assessment of facility performance
B4	Enhance decision-making
B5	Enhance information flow
B6	Facilitate collaboration and communication between stakeholders
B7	Improve project control
B8	Improve the accuracy of forecasting and predictability
B9	Optimize environmental performance
B10	Support electronic information management systems

4 Big Data Framework

The culminating effort of this research is a holistic framework that provides an overview of the implementation of Big Data in the construction industry. Such technology frameworks can guide the adoption of technology in different construction firms and companies, develop implementation roadmaps, and revolutionize the construction industry to warrant project success [46]–[49]. The framework, illustrated in Figure 2, consists of four layers. At the core, the 5V's are outlined, representing the prerequisites of *what* is considered Big Data. The second layer discusses *how* Big Data is enabled. Data needs to be first properly collected from multiple sources including sensors, surveillance cameras, Radio-Frequency Identification (RFID) tags, laser scanners, Geographic Information Systems (GIS), operating documents, Global Positioning Systems (GPS), and BIM models, to name a few. Data can be collected throughout the project lifecycle when designing, planning, performing risk analysis, forecasting, among other activities. Next, Big Data engineering transpires where the captured data is processed and stored for current and future usage. Then, collected data is harnessed using different analytics forms such as data mining, statistics, and machine learning [5]. The third layer of the holist framework illustrates *where* Big Data is used and encompasses the seven phases of the project lifecycle introduced earlier in the paper. The size and color of the circles representing the phases is proportional to the frequent mention of the phase in the literature review. It can be shown from Figure 2 that Big Data applications in Construction, Commissioning, and Operation and Maintenance (i.e. stages 3 and 4) are frequently explored in the current body of knowledge. Finally, the fourth layer of the framework captures the reasons *why* Big Data should be implemented in construction and presents the 10 benefits identified in this study.

To illustrate how the framework can be utilized, a case study conducted by [9] about the use of Big Data to produce prefabricated housing is discussed. During the design stage, teams use BIM to completely design the project and extract the components that should be constructed and purchased. The BIM model can also show locations of auto-ID technologies to turn components into Smart Construction Objects that can communicate with each other and the end users. Another technology that was frequently used is RFID models and tags. RFID tags can carry information about the production of the prefabricated components and their status (such as: manufacturing, in-storage, delivery or received). Production of the prefabricated components can work in parallel with the "as-planned" schedule and the updated BIM model. Once the components reach the construction site, they are assembled and installed which is also reflected in the BIM model allowing the project team to track the progress of the work and develop the as-built model. This model will be transferred to both the commissioning and operation and maintenance stage, or facility management, which can help them easily identify one component form the other, monitor their performance, and simplify repair work. This data is also useful during the final stage, demolition, where the RFID tags used earlier in the project can show the location, design, and status of every component, allowing stakeholders to better plan for demolition and manage the generated waste. The use of Big Data throughout the different phases of the project leads to all the ten benefits discussed in Table 1.

Figure 1. Big Data Holistic Framework

5 Conclusions, Limitations and Further Studies

The adoption of Big Data is integral to the construction industry. This paper performed a thorough and comprehensive review of Big Data adoption in construction. This review was summarized in a framework that shows the "what, how, where, and why" of the Big Data implementation in the construction industry. As revealed in the framework, the existing research corpus shows that the proper adoption of Big Data is possible throughout the entire lifecycle of a construction project. By using the right sources to gather Big Data, the proper engineering practices to process and store this data, and the appropriate analytics to explore it, the construction industry can achieve major benefits.

The proper implementation can revolutionize the industry, promoting high-fidelity collaboration among construction players, enabling stakeholder-driven analysis, enhancing decision-making, increasing transparency and information exchange, and enhancing project performance. Moreover, the framework of this study reveals that most studies targeted the construction, commissioning, operation and maintenance phases of the construction project.

The findings of this framework are limited by the research body reviewed in this paper. Further interviews with subject matters experts can be pursued to explore new applications, challenges, and benefits of Big Data adoption that the existing literature has not yet covered. Further research efforts can also explore more Big Data use-cases and applications in the less-discussed project phases such as demolition. More research can also focus on connecting these Big Data applications across the project phases to enable the industry's biggest potential.

References

[1] Sawhney A, Riley M., and Irizarry J. *Construction 4.0: an innovation platform for the built environment*. Routledge, New York, 2020.

[2] Nassereddine, H., Veeramani, D., and Hanna, A.

Augmented reality-enabled production strategy process. In *ISARC. Proceedings of the 36th International Symposium on Automation and Robotics in Construction*, pages 297-305, Banff, Canada, 2019.

[3] Martínez-Rojas M., Marín N. The role of information technologies to address data handling in construction project management. *Journal of Computing in. Civil Engineering*, 30(4):04015064, 2016.

[4] Lu W., Webster C., Peng Y., Chen X. and Chen K. Big Data in construction waste management: prospects and challenges. *Detritus*, 4:129-139, 2018.

[5] Bilal M., Oyedele L.O., Qadir J., Munir K., Ajayi S.O., Akinade O.O., Owolabi H.A., Alaka H.A., and Pasha M. Big Data in the construction industry: A review of present status, opportunities, and future trends. *Advanced Engineering Informatics*, 30(3):500–521, 2016.

[6] Ismail S.A., Bandi S., and Maaz Z.N. An Appraisal into the Potential Application of Big Data in the Construction Industry. *International Journal of Built Environment and Safety*, 5(2), 2018.

[7] Ekambaram A., Sørensen, A. Ø., Bull-Berg H., and Olsson N. The role of Big Data and knowledge management in improving projects and project-based organizations. *Procedia Computer Science*, 138:851–858, 2018.

[8] Sørensen, A. Ø., Olsson N., and Landmark A.D. Big Data in Construction Management Research. *SINTEF*, 3:405-416, 2016.

[9] Chen K., Lu W., Peng Y., Rowlinson S., and Huang G.Q. Bridging BIM and building: From a literature review to an integrated conceptual framework. *International Journal of Project Management*, 33(6):1405–1416, 2015.

[10] Chen H.M. and Chang K.C. A Cloud-based System Framework for Storage and Analysis on Big Data of Massive BIMs. *In ISARC. Proceedings of the 32nd International Symposium on Automation and Robotics in Construction*, pages 1-8, Oulu, Finland, 2015.

[11] Ram J., Afridi N.K., and Khan K.A. Adoption of Big Data analytics in construction: development of a conceptual model. *Built Environment Project and Asset Management*, 9(4):564-579, 2019.

[12] Williams N., Ferdinand N.P., and Croft R. Project management maturity in the age of Big Data. *International Journal of Managing Projects in Business*, 7(2):311–317, 2014.

[13] Skibniewski, M. and Golparvar-Fard, M. Toward a science of autonomy for physical systems: Construction. *arXiv preprint arXiv*: 1604.03563, 2016.

[14] Nassereddine, H. *Design, Development and Validation of an Augmented Reality-Enabled Production Strategy Process for the Construction Industry*. The University of Wisconsin-Madison, 2019.

[15] Lee J.G. and Kang M. Geospatial Big Data: Challenges and Opportunities. *Big Data Research*, 2(2): 74–81, 2015.

[16] Loyola M. Big data in building design: a review. *Journal of Information Technology in Construction* (ITcon), 23:259-284, 2018.

[17] Redmond A., El-Diraby T., and Papagelis M. Employing an Exploratory Research Stage to Evaluate Green Building Technologies for Sustainable Systems. *In Proceedings of the International Conference on Civil, Structural and Transportation Engineering*, paper 291, Ottowa, Canada, 2015.

[18] Zhang Y., Luo H., and He Y. A system for tender price evaluation of construction project based on Big Data. *Procedia Engineering*, 123:606-614, 2015.

[19] Bilal M., Oyedele L.O., Kusimo H.O., Owolabi H.A., Akanbi L.A., Ajayi A.O., Akinade O.O., Delgado J.M.D. Investigating profitability performance of construction projects using big data: A project analytics approach. *Journal of Building Engineering*, 26:100850, 2019.

[20] Caron F. Data management in project planning and control. *International Journal of Data Science*, 1(1):42-57, 2015.

[21] Yang J., Park M.W., Vela P. A., and Golparvar-Fard, M. Construction performance monitoring via still images, time-lapse photos, and video streams: Now, tomorrow, and the future. *Advanced Engineering Informatics*, 29(2):211-224, 2015.

[22] Han K.K., and Golparvar-Fard, M. Appearance-based material classification for monitoring of operation-level construction progress using 4D BIM and site photologs. *Automation in Construction*, 53:44–57, May 2015.

[23] Akhavian R. and Behzadan A.H. Construction equipment activity recognition for simulation input modeling using mobile sensors and machine learning classifiers. *Advanced Engineering Informatics*, 29(4):867–877, 2015.

[24] Wang C. and Cho Y.K. Smart scanning and near real-time 3D surface modelling of dynamic construction equipment from a point cloud. *Automation in Construction*, 49:239–249, 2015.

[25] Vanzulli, B. Kosaka, M. and Matsuda, F. Servitization in a construction machinery industry by using M2M and cloud computing systems. In *2014 11th International Conference on Service Systems and Service Management (ICSSSM)*, pages 1-6, Beijing, China, 2014.

[26] Liu Y., Zhong D., Cui, B., Zhong G., and Wei Y. Study on real-time construction quality monitoring of storehouse surfaces for RCC dams. *Automation in Construction*, 49:100-112, 2015.

[27] You Z. and Wu C. A framework for data-driven informatization of the construction company. *Advanced Engineering Informatics*, 39:269-277, 2019.

[28] Bügler M., Ogunmakin G., Teizer J., Vela P.A., and Borrmann A. A comprehensive methodology for vision-based progress and activity estimation of excavation processes for productivity assessment. In *Proceedings of the 21st International Workshop: Intelligent Computing in engineering (EG-ICE)*, Cardifff, Wales, 2014.

[29] Guo H., Luo H., and Yong L. A Big Data-based workers behavior observation in China metro construction. *Procedia Engineering*, 123:190-197, 2015.

[30] Isikdag U. BIM and IoT: A Synopsis from GIS Perspective. *The International Archives of Photogrammetry, Remote Sensing and Spatial Information Science*, 40(2/W4):33-38, 2015.

[31] Koseleva N. and Ropaite, G. Big Data in building energy efficiency: Understanding of Big Data and main challenges. *Procedia Engineering*, 172:544-549, 2017.

[32] Ioannidis D., Fotiadou A., Krinidis S., Stavropoulos G., Tzovaras D., and Likothanassis S. Big Data and visual analytics for building performance comparison. *In IFIP International Conference on Artificial Intelligence Applications and Innovations*, pages 421-430, Springer, Cham, 2015.

[33] Ioannidis D., Tropios P., Krinidis S., Stavropoulos G., Tzovaras D., and Likothanasis S. Occupancy driven building performance assessment. *Journal of Innovation in Digital Ecosystems*, 3(2):57-69, 2016.

[34] Hong, T., Koo C., Kim J., Lee M., and Jeong K. A review on sustainable construction management strategies for monitoring, diagnosing, and retrofitting the building's dynamic energy performance: Focused on the operation and maintenance phase. *Applied Energy*, 155: 671-707, 2015.

[35] Yuan, H. Key indicators for assessing the effectiveness of waste management in construction projects. *Ecological Indicators*, 24:476-484, 2013.

[36] Chen X. and Lu W.S. Scenarios for applying Big Data in boosting construction: A review. *In Proceedings of the 21st International Symposium on Advancement of Construction Management and Real Estate*, pages 1299-1306, Springer, Singapore, 2018.

[37] Deutsch R. Leveraging data across the building lifecycle. *Procedia Engineering*, 118:260-267, 2015.

[38] Hashem I.A.T., Chang V., Anuar N.B., Adewole K., Yaqoob I., Gani A., Ahmed E. Chiroma H. The role of Big Data in smart city. *International Journal of Information Management*, 36(5):748-758, 2016.

[39] Ahmed V., Tezel A., Aziz Z., and Sibley M. The future of Big Data in facilities management: opportunities and challenges. *Facilities*, 35(13/14):725-745, 2017.

[40] Luboschik M., Berger P., and Staadt O. On spatial perception issues in augmented reality based immersive analytics. *In Proceedings of the 2016 ACM Companion on Interactive Surfaces and Spaces*, pages 47-53, 2016.

[41] Kähkönen K. and Rannisto J. Understanding fundamental and practical ingredients of construction project data management. *Construction Innovation*, 15(1):7-23, 2015.

[42] Teizer J. Status quo and open challenges in vision-based sensing and tracking of temporary resources on infrastructure construction sites. *Advanced Engineering Informatics*, 29(2):225-238, 2015.

[43] Safa M. and Hill L. Necessity of Big Data analysis in construction management. *Strategic Direction*, 35(1):3-5, 2019.

[44] Lu W., Chen X., Peng Y., and Shen L. Benchmarking construction waste management performance using Big Data. *Resources, Conservation and Recycling*, 105:49-58, 2015.

[45] Curry E., O'Donnell J., Corry E., Hasan S., Keane M., and O'Riain S. Linking building data in the cloud: Integrating cross-domain building data using linked data. *Advanced Engineering Informatics*, 27(2):206-219, 2013.

[46] Bou Hatoum, M. and Nassereddine, H. Developing a framework for the implementation of robotics in construction enterprises. In *EG-ICE 2020 Proceedings: Workshop on Intelligent Computing in Engineering*, pages 453–462, Berlin, Germany, 2020.

[47] El Jazzar, M., Piskernik, M. and Nassereddine, H. Digital twin in construction: an empirical analysis. In *EG-ICE 2020 Proceedings: Workshop on Intelligent Computing in Engineering*, pages 501–510, Berlin, Germany, 2020.

[48] El Jazzar, M., Piskernik, M. and Nassereddine, H. Transforming the AEC industry: a model-centric approach. In *Creative Construction e-Conference 2020*, pages 13–18, Budapest, 2020.

[49] Nassereddine, H., Schranz, C., Bou Hatoum, M., & Urban, H. A comprehensive map for integrating augmented reality during the construction phase. In *Creative Construction e-Conference 2020*, pages 56–64, Budapest, 2020.

Automatic Analysis of Idling in Excavator's Operations Based on Excavator-Truck Relationships

Chen Chen[a], Zhenhua Zhu[b], and Amin Hammad[c]

[a]Department of Building, Civil and Environmental Engineering, Concordia University, 1515 Sainte-Catherine Street West, Montreal, QC H3G 2W1

[b]Department of Civil and Environmental Engineering, University of Wisconsin - Madison, Madison, United States, WI 53706

[c]Concordia Institue for Information Systems Engineering, Concordia University, 1515 Sainte-CatherineStreet West, Montreal, QC H3G 2W1

E-mail: chen.chen@mail.concordia.ca, zzhu286@wisc.edu, hammad@ciise.concordia.ca

Abstract –

Excavators and trucks are important equipment for earthmoving work, which have major contributions to construction productivity. In order to control the work efficiency and productivity of earthmoving equipment, computer-vision (CV) methods have been proposed to monitor equipment operations from site surveillance videos. Existing methods can recognize equipment activities to estimate the working time and idling time; however, they are limited in analyzing the reasons behind the equipment idling and low productivity. Therefore, this research proposes a method to identify the main reasons that cause excavators and trucks idling by analyzing their interactive operations. In this method, the relationships between the excavator and the surrounding truck(s) in each group are analyzed to identify the potential reasons that cause the excavator's idling. The proposed method was validated with a video from construction site and the test results showed its effectiveness and efficiency.

Keywords –

Excavator; Interactive operation; Idling reasons

1 Introduction

Heavy equipment is one of three major resources in construction projects along with labor and material [1]. Efficient use of equipment is critical for construction cost control and time saving [2]. One way to increase the efficiency of equipment operation is reducing its idling time. When the equipment is idling, it has no contribution to production, and adds no value to the construction project. Therefore, minimizing idling time is important to improve the efficiency and productivity of construction equipment.

As cameras are recently installed to monitor construction sites, an increasing number of research studies have been focused on monitoring equipment work productivity by automatically analyzing surveillance videos with computer vision (CV)-based methods. Current research work has been focused on estimating equipment's productivity by identifying its states, such as working, moving and idling. However, existing methods did not fully consider the interactive relationships between different pieces of equipment, such as excavators and trucks, which is important for productivity analysis. This research aims to provide a CV-based method for identifying idling reasons of excavators based on the interaction analysis between excavators and trucks from construction surveillance videos. First, the activities of the excavators and trucks are identified using convolutional neural networks (CNN). Then, work groups of excavators and trucks are clustered. Finally, the relationships between each excavator and the surrounding truck(s) are analyzed to identify potential reasons that cause the idling. The proposed method has been tested in a case study and the results indicate that the average accuracy of the idling reasons identification is 93%.

2 Background

In recent years, CV technologies have been widely used for automatic construction equipment operation monitoring and efficiency measurement. In the early stage, researchers focused on developing methods to accurately detect and localize target equipment in video frames. Kim and Zou [3] used color space to detect and localize the excavator in video frames. Emarzadeh et al. [4] concatenated both HOG and the Hue-Saturation colors as descriptors, and used Support Vector Machine (SVM) classifiers to detect excavators, trucks and workers from site surveillance videos. In addition to the

previous work of equipment detection and localization, researchers developed methods for equipment operation monitoring. For instance, some researches attempted to monitor the excavators' operations by recognizing their activities. Gong et al. [5] and Golparvar-Fard et al. [6] used motion features extracted from consecutive video frames, and classified the features with SVM to recognize excavators' activities, such as hauling, dumping, swinging, etc. Instead of using feature-classification-based activity recognition, other researchers developed activity recognition based on context information extracted from images. Kim et al. [8] considered the sequential relationship of the excavator's activities in its work cycle, and used CNN and Long-Short Term Memory (LSTM) network to recognize digging, dumping and hauling activities. Instead of using activity recognition, Soltani et al. [8] detected different components (e.g. dipper, boom and body), and extracted the excavator's 2-dimensional (2D) skeleton from the poses of the detected components. For the productivity estimation, Chen et al. [9] proposed a framework which integrated detection, tracking, and a 3D CNN to recognize multiple excavators' activities (e.g. digging, swinging, loading, and idling). By analyzing the activity information, the number of cycles and the productivity of the excavator are calculated.

The literature review shows that existing research mainly focused on excavator's productivity estimation and operation monitoring. Idling is one of the main factors that causes excavator's low productivity; However, deducing the potential reasons of idling has not been deeply investigated using CV. In order to reduce idling time of excavators and increase their productivity, it is necessary to identify the potential reasons that causes excavators idling. This paper aims to fill the research gap in existing works, and focuses on identifying the potential reasons of idling.

3 Methodology

The methodology for idling reasons identification of excavators is shown in Figure 1, which contains three main steps. First, the excavators and trucks are detected and tracked to get their locations and activities in video frames. Second, excavators and trucks are clustered to analyze their interactive work states. Third, the idling reasons of the excavators are classified into four different cases based on the number, activities and locations of trucks, as well as the interactive work states of the excavators and trucks, which are calculated in the previous steps. The details of these three steps are introduced in the following sub-sections. The methodology of this paper is based on the assumption that the equipment does not have mechanical problems and all the operators have no health issues that may cause idling. These potential reasons of idling are beyond the scope of this paper.

3.1 Identification of excavators and trucks locations and activities

In the first step, detection and tracking methods are used to extract equipment's types and coordinates of bounding boxes in *K* video frames. YOLO-v3 [10] detector and multi-object deep Simple Online and Real-Time (SORT) tracker [11] are applied in this study for equipment detection and tracking, respectively. The YOLO-v3 and deep SORT are selected for their performance of high accuracy and speed in both CV and applications in the construction domain. Following the detection and tracking, the working and idling states of excavators and trucks are recognized using the method proposed by Chen et al. [9].

3.2 Excavator and truck clustering

The second step is to cluster excavators and trucks into different groups. In the real earthwork operations, excavators usually work with nearby trucks. Therefore, excavators and trucks are clustered based on their distances in video frames. First, the number of excavators *M* and trucks *N* are obtained from detection results. Second, the distance in pixels between each truck and each excavator in frame k (d_k) is calculated using Equation (1).

$$d_k = \sqrt{(y_k^e - y_k^t)^2 + (x_k^e - x_k^t)^2} \quad (1)$$

where (x_k^e, y_k^e), (x_k^t, y_k^t) are the centroid coordinates of excavator and truck in frame k, respectively. Accordingly, each truck is grouped with the nearest excavator. If the distance between the truck and the excavator is larger than the threshold, the truck will not be included in the group. The threshold is calculated using Equation (2).

$$Threshold\ (\mu) = 0.5 \times (w_k^e + w_k^t) \quad (2)$$

where w_k^e, w_k^t are the widths of bounding boxes of excavator and truck, respectively, in frame k.

3.3 Idling reasons identification

The third step is to identify the potential reasons why excavators are idling. These reasons are summarized into four cases, as shown in Table 1. For each idling excavator, the number of trucks n in the same group is calculated. If there is no truck in the group, the reason of the idling is classified into Case 1, which indicates that the excavator is waiting for a truck.

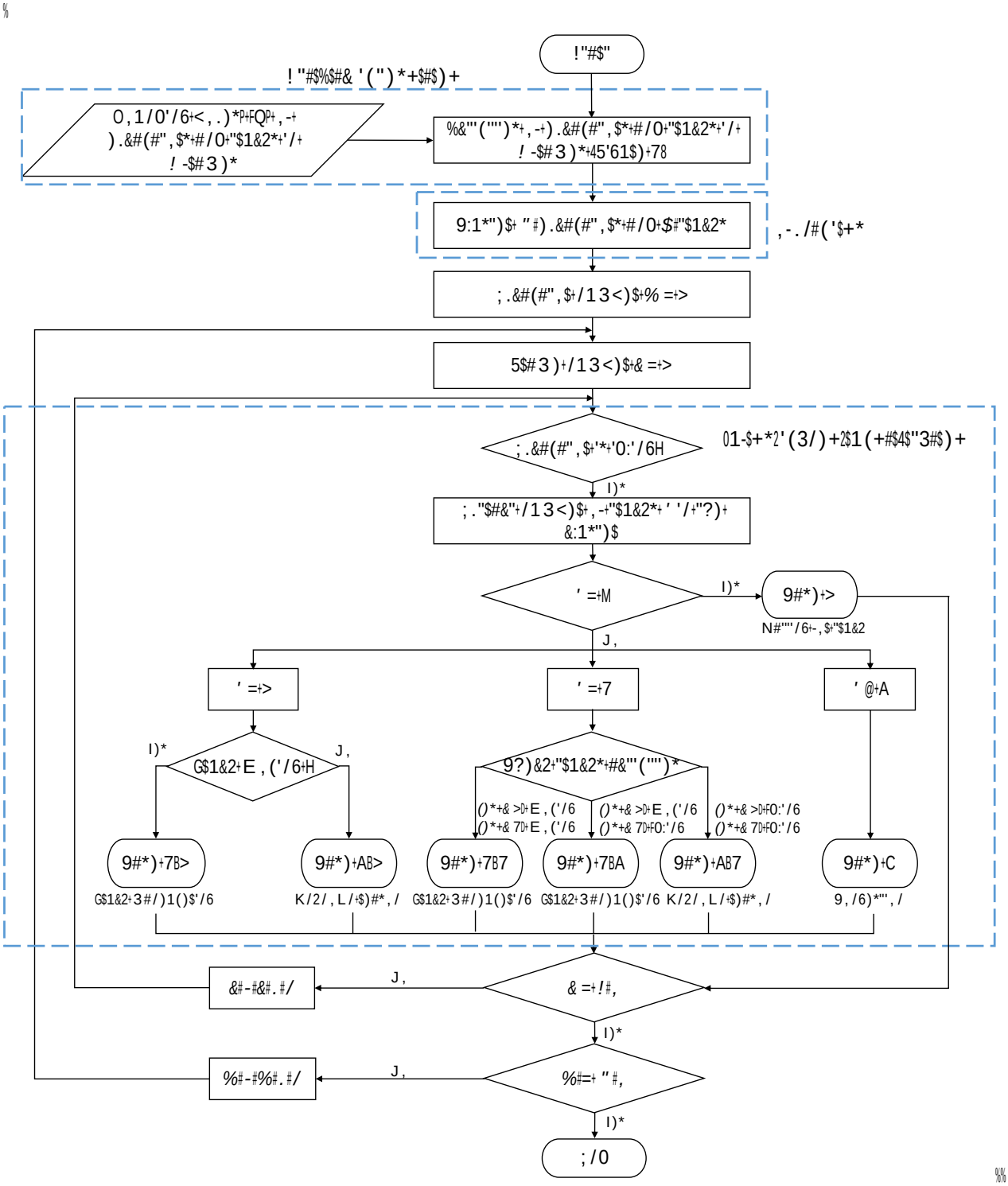

_+A3)(%F%_-,T8$*)#%,?%#$(%1),1,2(5%0(#$,5,-,A/

When there is only one truck in the group, the idling reason is determined by the activity of the truck. If the truck is moving, the reason is classified to into Case 2, which indicates that the excavator is waiting for the truck maneuvering to the loading position. Otherwise, there could be different reasons that cause excavator's idling as explained above. Therefore, in this condition, the reason of excavator's idling is classified into Case 3 (unknown reason). For Case 2 and Case 3, there are subcases depending on the number of trucks. When there are two trucks identified in the group, the activities of trucks have three conditions: both trucks are moving, one is moving and the other is idling, or both trucks are idling. These different conditions of trucks' activities could lead to two reasons of excavator's idling. If at least one of the two trucks is moving, the reason is classified into Case 2 (i.e. truck maneuvering). If both trucks are idling, the reason of excavator's idling is unknown, which is Case 3. When there are more than three trucks in the group, the idling of the excavator is classified into Case 4, which indicates too many trucks causing site congestion around the excavator.

Table 1. Potential reasons of the excavator idling

Case		Potential reasons
Excavator idling	Case 1	Excavator is waiting and there is no truck
	Case 2	Several trucks are maneuvering
	Case 3	Unknown reasons (e.g. operator, mechanical problem, safety issue)
	Case 4	Congested site with many trucks

4 Implementation and case study

In this section, the implementation of the proposed method is introduced, and three case studies are provided to demonstrate the performance of the proposed method. A computer with two NVIDIA GeForce GTX 1070 GPUs @ 3.4 GHz, 64 GB DDR, and Windows 10 system was used for the implementation.

4.1 Training and testing

First, to get the locations of the excavators and trucks in video frames, the YOLO-v3 detection model was trained to detect excavators and trucks in the video frames. A dataset containing 1,191 images of excavators and trucks (1,071 excavators, 871 trucks) was created to train the detector. In the training process, the learning rate is set to 0.1, and an Adam optimizer was used to adjust the learning rate during each epoch. The batch size was set to 6. It took about 10 hours with the validation loss not decreasing after 350 epochs. Then, the detection model was tested on the test dataset with 300 images (362 excavators, 421 trucks). The test results are shown in Table 2. The average accuracy of the detection is 82%, which shows that the model has a good ability to identify excavators and trucks in video frames.

Table 2. Detection results

Confusion matrix	Predict class			Model performance		
	Excavator	Truck	None	Precision (%)	Recall (%)	Accuracy (%)
Excavator	337	2	23	98	93	
Truck	6	303	112	99	72	
Average						82

4.2 Case study

In this section, a video of about 62 min of earthmoving work was used for testing. The video has the resolution of 1920 × 1080 pixels and the frame rate of 30 fps (110,914 image frames). In this video, one excavator has 2,645 s idling time and 1,052 s working time. The idling and working states of the excavator and trucks were identified based on the method explained in Section 3.1. The step of the sliding window was selected as 100 frames for both excavators and trucks idling states identification. The thresholds α and μ of the excavator were selected as 7 pixels and 2% of average bounding box areas. The threshold of trucks was selected as 10 pixels without considering the bounding box's area changing. The comparison of ground truths and estimated results are shown in Figure 2. The estimated idling and working times are 2,612 s and 2,085 s, respectively. The error rates are 1.2% and 3.1%.

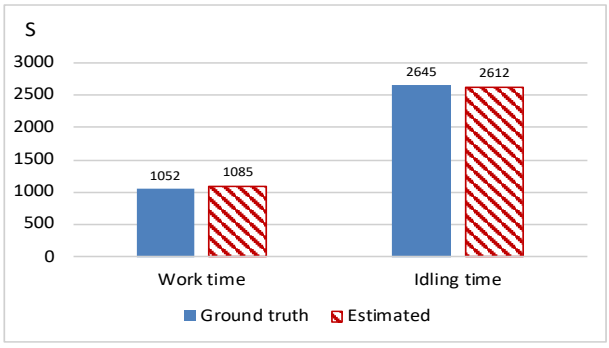

Figure 2. Estimated excavator idling and working time with ground truth

The idling time of the excavator was further analyzed to identify the reasons that caused excavator's idling. In this video, there are three kinds of reasons of excavator's idling: Case 1, Case 2 and Case 3. The accuracy of the estimated results of these three cases are 99%, 82%, and 98%, respectively as shown in Figure 3.

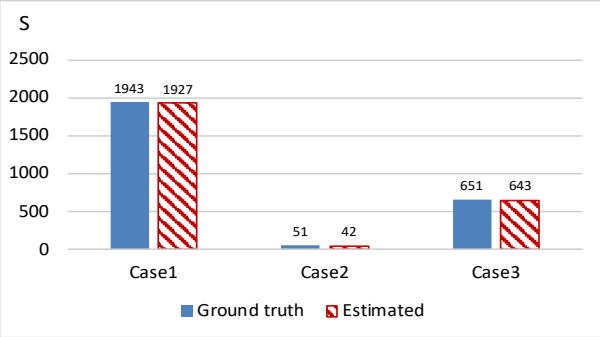

Figure 3. Results of idling reasons analysis with ground truth

The results show that the identification of Case 2 has the maximum error rate of 18%. The errors are mainly due to the failure of detection of partial appearances of trucks as can be seen in Figure 4. This case appeared from time T = 2,535 s to T = 2,540 s and T = 3,153 s to T = 3,156 s, which decreased the estimated moving time of trucks. If the errors of the detection results are excluded, the accuracy of these Cases 1-3 are 100%, 97%, and 99%, respectively.

The results of Case Study 1 show that during 62 min earthmoving work, the excavator's idling time is 60% of total operation time. The proportion of each case is shown in Figure 5. Among these three cases, Case 1 consumes 74% of the total idling time, which indicates a limited number of trucks were arranged to work with the excavator. By observing the video, it could be noticed that the average cycle time of trucks is about 20 min, and Loading time per truck is about 4 min. In the earthmoving work, more trucks should be arranged to cooperate with the excavator to reduce its idling time, since the utilization cost of the excavator is higher than truck. Therefore, to keep the excavator working at capacity, more trucks are required.

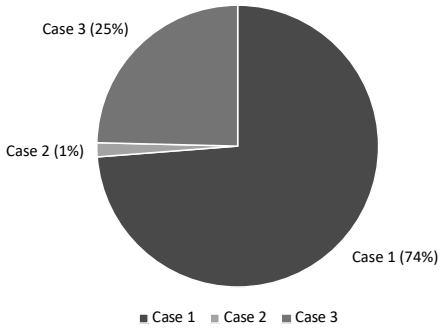

Figure 5. Percentage of the reasons for idling

Case 3 consumes 25 % of the total idling time. From the video time T = 51 s to T = 520 s, it can be observed that the operator of the excavator left the equipment, as shown in Figure 6(a). From T = 3,159 s to T = 3,358 s, it can be observed that two persons were talking near the excavator, and the excavator started to work after they left, as shown in Figure 6(b).

Figure 4. Example of lost detection for the partial truck

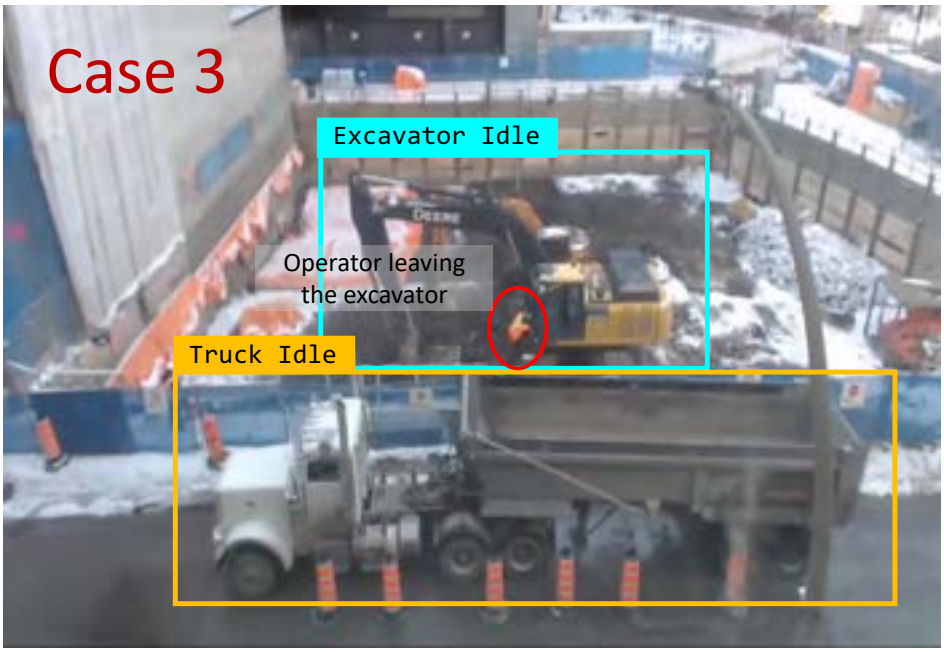

(a) Operator leaving the excavator

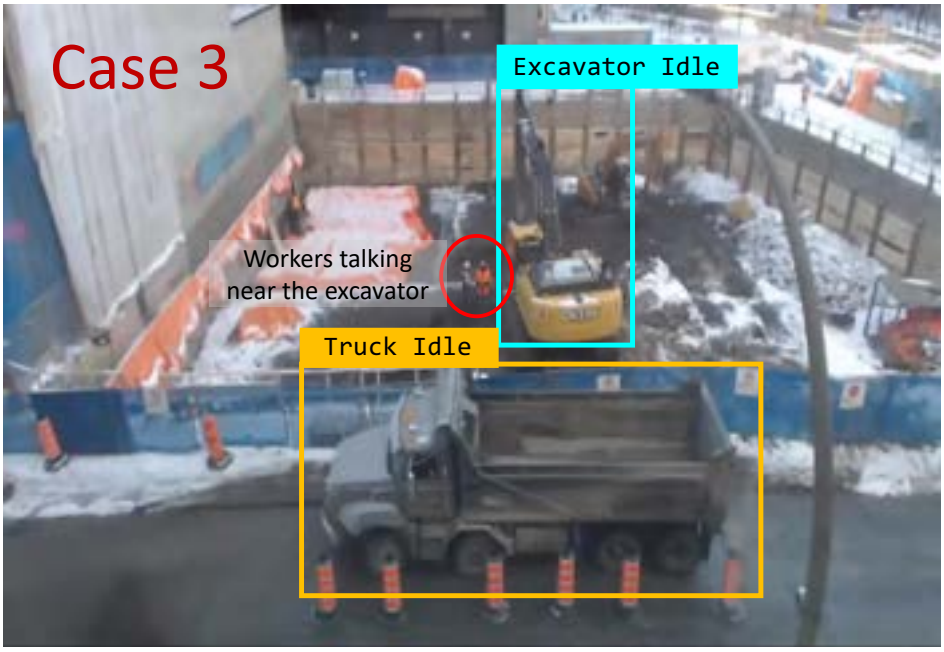

(b) People talking near the excavator

Figure 6. Examples of Case 3

5 Conclusion and future work

This paper developed a novel CV-based method to automatically identify the idling reasons of excavator and truck based on their interactive work states. To the best knowledge of the authors, this is the first attempt to classify the reasons of equipment's idling into detailed categories using CV. The proposed method provides an efficient solution to explore the reasons of low productivity from site surveillance videos, which could contribute to the better understanding of the earthmoving productivity under complex construction site conditions.

References

[1] Zou, J., Kim, H. Image processing for construction equipment idle time analysis, in: *Proceeding of 22nd International Symposium on Automation and Robotics in Construction (ISARC)*, National Institute of Standards and Technology, Ferrara, Italy.

[2] Edwards, D., Holt, G. A model for calculating excavator productivity and output costs. Engineering, *Construction and Architectural Management*, 2000, 1, 52-62.

[3] Zou, J., Kim, H. Using hue, saturation, and value color space for hydraulic excavator idle time analysis, *Journal of Computing in Civil Engineering*, 21 (4) (2007) 238–246.

[4] Memarzadeh, M., Golparvar-Fard, M., Niebles, J. C. Automated 2D Detection of construction equipment and workers from site video streams using histoframs of oriented gradients and colors, *Automation in Construction*, 32(2013)24-37.

[5] Gong, J., Caldas, C.H., Gordon, C. Learning and classifying actions of construction workers and equipment using bag-of-video-feature-words and Bayesian network models, *Advanced Engineering Informatics*, 25 (2011) 771–782.

[6] Golparvar-Fard, M., Heydarian, A., Niebles, J.C. Vision-based action recognition of earthmoving equipment using spatio-temporal features and support vector machine classifers, *Advanced Engineering Informatics*, 27 (2013) 652–663.

[7] Kim, J., Chi, S. Action recognition of earthmoving excavators based on sequential pattern analysis of visual features and operation cycles, *Automation in Construction*, 104 (2019), 255-264.

[8] Soltani, M., Zhu, Z., Hammad, A. Skeleton estimation of excavator by detecting its parts, *Automation in Construction*, 82 (2017) 1–15.

[9] Chen, C., Zhu, Z., Hammad, A. Automated excavators activity recognition and productivity analysis from construction site surveillance videos, *Automation in Construction*, 110(2020)103045.

[10] Redmon, J., Farhadi, A. YOLOv3: An incremental improvement, 2018, arXiv:1804.02767 [cs.CV].

[11] Nicolai, W., Alex, B., Paulus, D. Simple online and realtime tracking with a deep association metric, *2016 IEEE International Conference on Image Processing (ICIP)*, IEEE, 2016, pp. 3464–3468.

Construction 4.0: A Roadmap to Shaping the Future of Construction

Mahmoud El Jazzar[a], Harald Urban[b], Christian Schranz[b], and Hala Nassereddine[a]

[a]Department of Civil Engineering, University of Kentucky, USA
[b]Department of Civil Engineering, Technical University of Vienna, Austria
E-mail: meljazzar@uky.edu, harald.urban@tuwien.ac.at, christian.schranz@tuwien.ac.at, hala.nassereddine@uky.edu

Abstract –

The construction industry is forecast to grow from its already impressive size to unprecedented new heights. This significant expansion, along with the increased complexity and sophistication of construction projects, has placed more pressure on construction companies to maintain their vitality and grow in the modern market. As the fourth wave of technological advancements, known as Industry 4.0, continues to evolve, it becomes imperative for construction companies to adopt new technology to remain competitive – much like the Darwinian mantra, the companies must adapt or die. Although the construction industry is often labeled as conservative regarding potential advancements in technology, it has been experiencing a growing use of a wide range of 4.0 technologies. Using insights gained from the existing literature, this paper explores the current state of Construction 4.0 and discusses a four-layer implementation of Construction 4.0 in the industry. Seven Construction 4.0 technologies are first discussed, their integration throughout the project lifecycle is presented in a roadmap, their integration and connectivity with one another are outlined in an interaction roadmap, and the requirements necessary for achieving the 4.0 transformation are articulated. A case study is finally presented to showcase the proposed implementation plan.

Keywords –
Construction 4.0; Implementation; Roadmap; Integration; Interactions

1 Introduction

The construction industry sits at a crossroads. It is economically vital to the prosperity of nations, and a key player that affects our everyday lives. Yet, the construction industry lags behind other major industries in its adoption of technological advances [1]. Nassereddine et al. [2] noted that the complex nature of the construction industry and its heavy reliance of information require the adoption of new and emerging technologies. Challenges facing the construction industry span a multitude of reasons including the dauting decline in productivity, shortage in the workforce, low levels of research and development (R&D), and the inefficient and insufficient transfer of knowledge from project to project [3], add more pressure on construction to move from an industry that has resisted emerging technology to one that is embracing it. One industry that has been a source of innovation in construction is manufacturing [4]. From the many practices that construction has adopted from manufacturing, this paper focuses on the concepts of Industry 4.0.

Industry 4.0, a term coined by the German Federal Government to highlight the fourth industrial revolution [5], can be defined as "a new technological age for manufacturing that uses cyber-physical systems and Internet of Things, Data and Services to connect production technologies with smart production processes" [6]. Montgomery and Norman [7] noted that manufacturing has passed through three different revolutions before reaching Industry 4.0, namely, revolutions, mechanization, electrification, and digitalization. Schwab [8] explained that Industry 4.0 is the stage that enables the full integration between people and digitally controlled machines with the help of internet and information technology (IT). Lu [9] added that industry 4.0 supports the growth and evolution of various fields and industries. The automotive industry has greatly benefited from Industry 4.0, where manufactured cars are being 40% controlled by electronics [10]. The health sector has also taken full advantage of Industry 4.0 in creating new diagnostic methods and technologies to sequence genes [11].

The industry is said to transform the lifecycle process of products and production systems by increasing the connectivity and interaction among parts, machines, and humans [10]. This transformation is enabled and driven by nine fundamental technological advances, also referred to as pillars: autonomous robots,

Augmented Reality, Simulations, the cloud, Big Data and analytics, the Industrial Internet of Things, cybersecurity, additive manufacturing, and horizontal and vertical system integration [12]. It should be noted that the technology itself is not powering Industry 4.0: while most of the nine pillars are not entirely new to manufacturing, it is the full integration of these building blocks and their connectivity across the borders that define Industry 4.0 [3].

The construction industry has also experienced a radical transformation and made great strides in changing its status quo and embrace technological advancements [13],[14],[15]. Influenced by the gains that resulted from the fourth industrial revolution, researchers in construction began investigating the potential of integrating Industry 4.0 into construction. While construction is often compared to manufacturing, the former is approaching and embracing Industry 4.0 from a different direction [12]. Recently, the term "Construction 4.0" emerged in the 21st century construction research corpus [16]. The interest in Construction 4.0 is fueled by the development of various technologies, the drastic change in the needs of owners, the shift towards mass customization, and the need for green construction and sustainability [16].

Through a thorough literature review, this paper introduces a four-layer implementation plan and begins by discussing Construction 4.0 and seven of its most commonly cited technologies, namely: iBIM, AR, VR, robotics, 3D printing, AI, and drones. As a construction 4.0 approach is seen as a two-level integration effort: 1) integration of a Construction 4.0 technology throughout the construction project lifecycle and 2) integration and connectivity of Construction 4.0 technologies, each of those levels is examined in this paper. A roadmap for the integration of Construction 4.0 technologies across the project lifecycle is created and an interaction map of Construction 4.0 is developed. The requirements for achieving Construction 4.0 are also discussed. Finally, a case study is presented to highlight how Construction 4.0 can be realized by showcasing the four layers put forth in the paper.

2 Construction 4.0

According to the European Industry Construction Federation (FIEC), "Construction 4.0" is the counter part of industry 4.0 in the Architecture, Engineering & Construction (AEC) industry and it refers to the digitalization of the construction industry [17].

Rastogi [16] stated that the main goal of construction 4.0 is to create a digital construction site that monitors progress throughout the life cycle of a project by using different technologies. The adoption of Construction 4.0 will not only change the construction process, but it will change the organization and project structures, shifting the fragmented construction industry into an integrated industry [17].

2.1 Construction 4.0 Technologies

To understand the various layers of Construction 4.0, it is important to first understand the technologies that are enabling this transformation. While the existing research corpus discusses various Construction 4.0 technologies, this paper focuses on seven Construction 4.0 technologies that have been frequently cited. A brief introduction to each of these technologies is provided below:

Integrated Building Information Modeling (iBIM) is considered the higher level of traditional BIM and consists of three elements: (1) the integration architecture which defines major layers of iBIM and how they are interconnected, (2) the product model which defines the content and function of the object's behavior, and (3) the process model which identifies the interaction scheme and mechanism between model objects [18].

Augmented Reality (AR) is both an information aggregator and a data publishing platform that allows the user to (1) passively view displayed information, (2) actively engage and interact with published content, and (3) collaborate with others in real-time from remote locations [19]. AR is gaining increased momentum in the construction industry, and various use-cases are being explored and tested throughout the project lifecycle, such as promoting AR-enabled production planning [13] and enabling remote expert system [20].

Virtual Reality (VR) is a step further than AR on the spectrum of virtuality. VR creates a virtual and immersive experience for the user through headsets with 360-degree visions, allowing the user to experience a completely different environment. Li et al. [21] categorized the use of VR in construction into the hazard identification, which allows construction teams to sense, analyze, and extract potential dangers, and safety training and education, in which construction workers will train in a safe environment in comparison to on-site training, which might be expensive and hazardous.

Robotics uses machines that can perform or replicate human actions. While robotics has been widely used in manufacturing and aerospace, construction is following suit and is using robotics, mainly in the vertical construction sector [22]. This technology is heavily used in construction assembly work, especially for high rise buildings. SMART system developed by SHIMIZU in Japan, for instance, was used to construct more than 30 stories of an office building [23]. Additionally, different construction tasks such as painting, brick overlaying, and earthwork can be performed by robots [24].

3D printing, also known as additive manufacturing, is the process of creating a complex, physical 3D object from a CAD model. 3D printing has undergone 25 years of research and development, and as a result, the technology is currently used in different industries such as aerospace, automobile, and medical [25]. The construction industry is also exploring the use of 3D printing, mainly for small and medium-sized applications at the time being [26]. This technology is showing great potential for large scale implementations; however, a number of challenges such as layering effect which results in uneven surfaces with voids, tensile strength issues associated with the lack of steel reinforcement need to be overcome before the industry embrace this technology [27].

Artificial Intelligence (AI) is a term used to describe a machine that replicates the human cognitive functions [28]. One of the main components of AI is machine learning, where a machine learns from a set of data using statistical methods. According to a study by McKinsey & Company, AI is starting to gain momentum in construction [29]. The study highlighted three main current AI applications: (1) project scheduling optimization which is achieved by continuously testing a large number of plan alternatives and selecting the better option, (2) image recognition and classification which can be used to identify issues related to safety on site and to collect the information for future learning, (3) enhanced analytic platforms which collect and analyze building machine data and building sensor data to predict any issues related to maintenance.

Drones, also known as Unmanned Aerial Vehicles (UAVs), are unpiloted small sized aircrafts that are remotely controlled. In early 2006, drones were mainly used for military applications [30]. In recent years, their use in construction and other industries has been on the rise [31]. The construction industry is mainly employing drones for inspection and monitoring during surveying, construction, and facility management [32].

2.2 Construction 4.0 Roadmap

The first level of the Construction 4.0 integration efforts takes a lifecycle view for the integration of Construction 4.0 technologies. A project moved from its early planning phase, to design, construction, and then facility management. A technology is used to its full potential when it is integrated throughout the construction project lifecycle, where applicable [33].

For instance, several studies including [34], [35], [20] identified potential use-cases of AR throughout the project lifecycle. The blue, solid bars of AR in Figure 1 reflect the AR applications that have been tested and used on construction projects and the green, hatched bars represent the potential benefits of additional AR use-cases that are being explored.

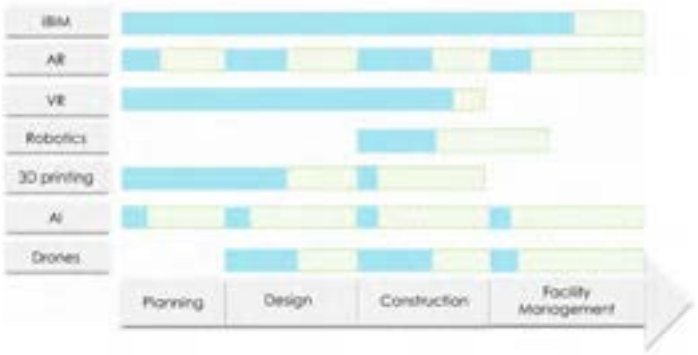

Figure 1. Construction 4.0 Envisioned Roadmap
(The solid blue bars represent the current use of a construction 4.0 technology
and the green hatched green bars represent the projected use of a construction 4.0 technology)

2.3 Construction 4.0 Interaction

The second level of the integration efforts demands an increased connectivity and interaction of Construction 4.0 technologies [36]. Aleksandrova et al. [37] noted that the full integration of digital technologies is a radical transformation in construction that creates a united digital ecosystem.

A scan of the literature on Construction 4.0 and its associated technologies was performed to identify current and future potential interactions. A map was then developed (Figure 2) to outline those interactions and illustrate potential synergistic efforts.

iBIM and AI can be thought of as core technologies

of Construction 4.0 and the impetus to connectivity [37]. Copper [38] added that BIM and cloud-based common data environment (CDE) are central to Construction 4.0 framework: BIM carriers the simulation feature that is a core component for Industry 4.0, and CDE acts as the data warehouse for all information related to construction project over its life cycle. BIM and CDE establish a single platform that helps integrate all of the construction project phases and link the physical and cyberspace [3]. Thus, allowing the implementation of Construction 4.0.

Some of the interactions outlined in Figure 2 are extracted from the existing construction research corpus, while others are extracted from adjacent industries, such as aerospace and medical, and are interactions yet to come to construction. For instance, Wake et al. [39] discussed the interaction between 3D printing and AR technology in a healthcare environment. The authors used these two technologies on a patient with a kidney tumor. A 3D printing transparent kidney model with the ability to color the tumor zone was first created. Then, an AR kidney model of the patient was created. These models were used before and during the operation to aid in the robotic partial nephrectomy operation.

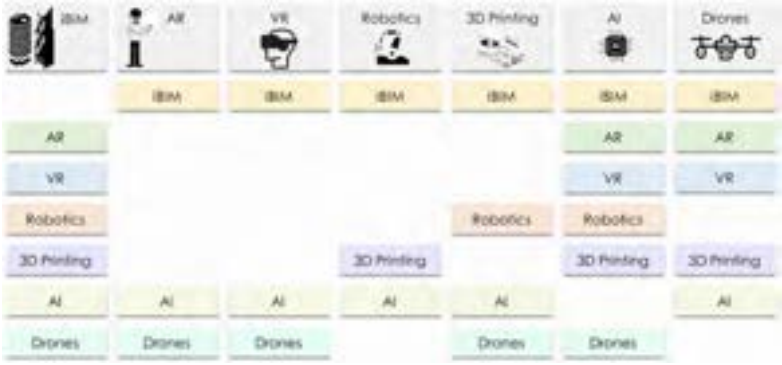

Figure 2. Interaction Map of Construction 4.0 technologies
(graphics downloaded from https://www.freepik.com/)

2.4 Construction 4.0 Requirements

Embracing Construction 4.0 entails several challenges that have been discussed by construction researchers. Industries are normally averse to change, and therefore it is initially resisted until it can be perceived as a guaranteed opportunity. Several authors [38], [40], [41] noted that the construction industry is no stranger to the resistance of change.

Researchers pointed out that the multidisciplinary nature and uniqueness of the construction industry results in an unclear understanding of the value proposition of Construction 4.0 technologies. In the past construction companies often relied on a project-thinking approach when managing construction projects. The shift to Construction 4.0 requires a change of the thinking-approach and the processes. The development of digital technologies and their adaption to the construction company's needs is highly dynamic, tailorable, and expensive. Additionally, when new technologies are introduced, employees and workers will need extra training. Therefore, construction companies will generate a surplus value only if the new technologies are integrated within the company's processes and can be used across projects. The switch to Construction 4.0 requires a process-oriented mindset, as opposed to the traditional project-oriented approach. However, this mindset shift pushes construction companies to digitize their existing processes, posing an additional challenge for two reasons: (1) existing process have mostly been designed before current digital tools were available, and (2) not every process can be directly digitized. Therefore, all existing processes have to be re-engineered to accommodate the shift in the mindset and support the 4.0 transformation of construction companies.

Figure 3 shows a general process to implement new digital technologies in a construction company, as required for the transition to Construction 4.0. Prior to re-thinking a process, the actual process must be first recorded and analyzed to explore how and where the technology(ies) could be used. A thorough analysis and documentation of the "status quo" of the existing process is crucial to successfully manage the technological changes. Assessing current processes helps in identifying the relevant decision-making structures and cost relevant process steps. The process-oriented approach also forms the basis for the identification of waste and inefficiencies in the company, and thus, becomes a prerequisite for the application of Lean management in the company.

Once the existing process has been investigated, the potential for innovation and integration of technologies, along with efficiency enhancement analysis, is assessed next. This includes an application analysis of the different technologies of interest, as well as the digital tools that are already in use. The structural needs as well as the existing barriers to innovation have to be identified. The structural needs include the aforementioned aspects of implementing the various Construction 4.0 technologies in the construction companies. Other considerations for companies to think of are the high investments associated with adopting technologies, the need to additional human resources, and R&D investments, all of which poses a major financial barrier.

For a successful transition to Construction 4.0, a construction company needs a vision of the digitization change process which fits the company's needs. This is especially important since Construction 4.0 goes beyond technology alone. It includes a change in the mindset of the all people involved (from field personnel to management) as well as of the processes in consideration. Hence, a clear vision, which is supported by these people, is important. Only when these requirements are met, companies can make the transition from the traditional project-thinking to process-thinking.

This shift also changes the organization and infrastructure of many companies i.e. their partners. Another consideration to address is the long-standing problem of longitudinal fragmentation that renders stakeholders nearly powerless to pilot their companies through this change [42]. Over the past decade, the construction industry has made significant changes to its structure as organizational changes have already been applied to companies which implement Lean management. The importance of some traditional departments decreases significantly, whereas some new departments emerge.

In addition to the challenges associated with moving construction towards a process-thinking industry, the lack of global standards and framework for implementation is another roadblock. Furthermore, Construction 4.0 heavily relies on various Information Technology (IT) systems, and, therefore, concerns related to data and cybersecurity must be addressed and stringent security standards must be put forth. Legal and contractual issues need to be also discussed to allocate risks among stakeholders.

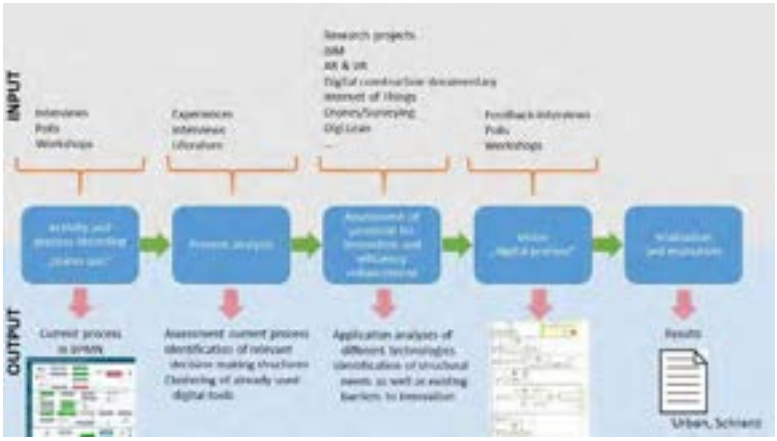

Figure 3. Process to implement Construction 4.0

3 A Case Study of the Two-Level Construction 4.0 Integration

To illustrate the two-level construction 4.0 integration, a case study where many of the previously discussed Construction 4.0 technologies act as a cross-linked system is presented.

Figure 4 shows a generalized data path for a future cross-linked system. All begins with a BIM model, which is created in a native modeling environment, like Revit or ArchiCAD. For a general use, the model is exported as an Industry Foundation Classes (IFC) file to a collaborative data environment on a BIM server. This export allows the model to be used in several of the previously discussed Construction 4.0 technologies. After exporting the model to a smartphone or tablet, the site supervisor and/or inspector (referred to hereinafter as user) can benefit from the visualization and interaction with the model on the smart device when e.g. inspecting a Heating, Ventilation, and Air Conditioning (HVAC) system. QR codes or RFID chips attached to a building component connect the smart device with the manufacturer's database of the building component.

This enables the user to access specific product data, which can be also transferred via BIM Collaboration Format (BCF) to the BIM server and, hence, back into the native BIM model. This two-way communication leads to a closed loop data transfer. Moreover, the manufacturer data, also referred to as semantic data, can be transferred to an .xml database that is then connected with the component's Globally Unique Identifier (GUID) in the BIM model. This information can be then retrieved by facility managers. This is especially valuable for maintenance- and safety-technical relevant data and leads to component-referenced manufacturer data.

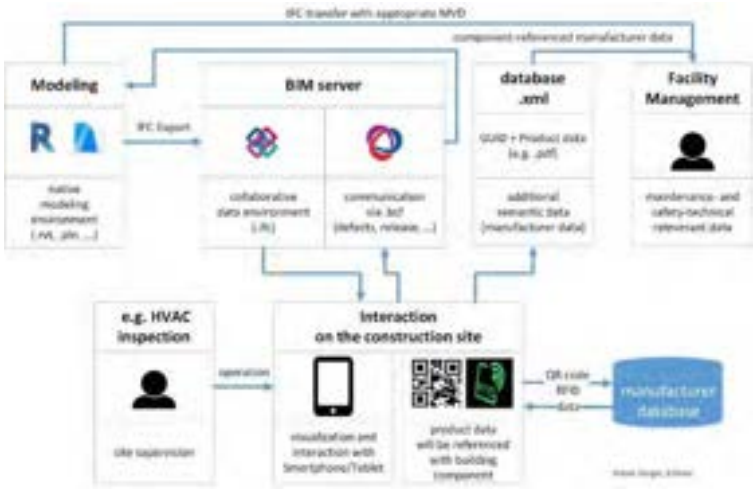

Figure 4. On-site inspection: closed-loop data transfer in a generalized form

For example, the BIM model normally contains the general specifications for a required fire protection flap. After the installation of the fire protection flap, the specific product data can be transferred into the BIM model. Then, the correct maintenance requirements for this product are available for the facility management. Another option is the usage of an IFC transfer with an appropriate MVD (Model View Definition) directly from the BIM model.

This closed-loop data transfer not only works during the construction phase, but also in the later operation and maintenance phase. Each time one or more building components are replaced, the new product data is transferred into the central BIM model.

Another technology that can be considered is Augmented Reality (AR). The authors worked on different use-cases for AR in Construction 4.0 [34], [43]. AR is one of the emerging technologies which has a great potential to transform the construction industry. The aforementioned closed-loop data transfer can be used with several AR use-case, e.g. for monitoring the progress of the construction site, visualizing augmented drawings or construction systems in the field, as well as conducting on-site inspection. In one of the research projects of the authors, AR-AQ-Bau [44], a specific AR use-case for on-site inspection has been developed. In this case, the BIM model was also exported to a BIM server and then an AR model was created using the game-engine Unity. The site supervisor can use this AR model to control the HVAC system on the construction site. The control can happen before the HVAC system is built, to check for instance, whether there is enough space for movement in front of inspection hatch. After the HVAC system is installed, the site inspection can monitor and check if everything is built correctly. This process or application not only works for HVAC but for the whole construction. In the AR device, the site inspection marks every defect or deficiency in the construction. Hence, the position of the defect in the building is stored in the AR model. Additionally, a description (text or audio) of the defect as well as photos can be added. All this information is then transferred back into the BIM model via BCF. On one hand, this helps to keep a record of all defects in a building and, on the other hand, improves the repair of existing defects. Additionally, the AR tool for site inspection is also very invaluable for the facility management during the operation phase.

The scan of QR-codes or RFID becomes easier with AR devices. After scanning the tag, the AR devices can be connected with the manufacturer's database and can retrieve the specific product data of the built-in component. This data is then transferred to the BIM model or another specific database (as described before).

4 Conclusions and Future Work

The fourth wave of technological advancement (Industry 4.0) and the digital transformation at its helm are pushing industries worldwide to embrace newer technologies to continue to remain competitive. Although the construction industry is not leading this change, it is not an exception to the digital revolution. The unique nature of the construction industry provides fertile ground for research on digitizing the industry and the term Construction 4.0. This research builds on the existing construction research corpus and discusses four layers of Construction 4.0 implementation. The first layer consists of the understanding the technologies associated with Construction 4.0. This research discussed seven frequently cited technologies, namely: iBIM, AR, VR, robotics, 3D printing, AI, and drones. The second and third layers defined the two-level of integration needed to implement Construction 4.0. The second layer presents a roadmap that outlines the integration of each of the seven technologies across the construction project lifecycle. The roadmap is a depiction of the current state-of-practice of the technologies and an outlook into future developments. The third layer offers insights into how the seven technologies can be connected and integrated together. An interaction matrix is developed to outline the relationships between the different technologies. It should be noted that the two-level integration cannot happen across the board, but rather only when applicable. The implementation of these three layers is only enabled when the fourth layer is realized. The fourth layer encompasses a set of requirements that construction companies must consider. At the core of these requirements is the necessary shift to process-thinking. Construction stakeholders must have the right mindset to pilot their companies through the disruptive Construction 4.0 storm. Finally, a case-study is presented to discuss the four-level implementation outlined in the paper. Future research efforts can extend on the seven technologies discussed in the paper and introduce additional elements of Construction 4.0. Additional research is also needed to verify the interactions between all the Construction 4.0 technologies.

References

[1] Osunsanmi O. T., Aigbavboa C. and Oke A. Construction 4.0: The Future of the Construction Industry in South Africa. *International Journal of Civil and Environmental Engineering*, 12:7, 2018.

[2] Nassereddine H., El Jazzar M. and Piskernik M. Transforming the AEC industry: a model-centric approach. In *Creative Construction e-Conference 2020*, pages 13–18, Budapest, 2020.

[3] Sawhney A., Riley M. and Irizarry J. Eds. *Construction 4.0: an innovation platform for the built environment*. Abingdon, Oxon , New York, NY: Routledge, 2020.

[4] Koskela L. *Application of the new production philosophy to construction*, volume 72. Stanford university, Stanford, 1992.

[5] Osunsanmi O., Aigbavboa C., Oke A. and Ohiomah I. Construction 4.0: Towards Delivering of Sustainable Houses in South Africa. In *The Creative Construction Conference 2018*, pages 147-156, Slovenia , 2018.

[6] MacDougall W. Industrie 4.0-Smart Manufacturing For The Future. *Germany Trade & Invest*, 2014.

[7] Montgomery D. and Norman J. The Future for Construction Product Manufacturing Digitalisation, Industry 4.0 and the Circular Economy.Online:http://thenorrisgroup.com/learning/files/edia_manager/original/106.pdf,Accessed: 31/05/ 2020.

[8] Schwab K. The Fourth Industrial Revolution. *The World Economic Forum*, 2016.

[9] Lu Y. Industry 4.0: A survey on technologies, applications and open research issues. *The Journal of Industrial Information Integration*, 6:1-10, 2017.

[10] Manohar N. Industry 4.0 and the digital transformation of the automotive industry. Online:https://www.automotiveworld.com/articles/industry-4-0-digital-transformationautomotive-industry,Accessed: 31/05/2020.

[11] Thuemmler C. and Bai C. *Health 4.0: How virtualization and big data are revolutionizing healthcare*, Springer, 2017.

[12] Klinc R. and Turk Ž. Construction 4.0 – Digital Transformation of One of the Oldest Industries. *Economic and Business Review*, 2019.

[13] Nassereddine H., Veeramani D., and Hanna A. Augmented Reality-Enabled Production Strategy Process. In *The 36th International Symposium on Automation and Robotics in Construction*, Banff, AB, Canada, 2019.

[14] Bou Hatoum, M. and Nassereddine, H. Developing a framework for the implementation of robotics in construction enterprises. In *EG-ICE 2020 Proceedings: Workshop on Intelligent Computing in Engineering*, pages 453–462, Berlin, Germany, 2020.

[15] El Jazzar, M., Piskernik, M. and Nassereddine, H. Digital twin in construction: an empirical analysis. In *EG-ICE 2020 Proceedings: Workshop on Intelligent Computing in Engineering*, pages 501–510, Berlin, Germany, 2020.

[16] Rastogi D. S. Construction 4.0: The 4th Generation Revolution. In *the Indian Lean Construction Conference 2017*, page 12, 2017.

[17] García de Soto B. Agustí-Juan I. Joss S. and Hunhevicz J. Implications of Construction 4.0 to the workforce and organizational structures. *The*

International Journal of Construction Management, 1-13, 2019.

[18] Abdalla J. A. and Eltayeb T. M. An Integrated Building Information Model (iBIM) for Design of Reinforced Concrete Structures. In *the 17th International Conference on Computing in Civil and Building Engineering*, page 8, 2018.

[19] Nassereddine, H., Schranz, C., Bou Hatoum, M., & Urban, H. A comprehensive map for integrating augmented reality during the construction phase. In *Creative Construction e-Conference 2020*, pages 56–64, Budapest, 2020.

[20] Urban H., Schranz C., and Gerger A. BIM auf Baustellen mit Augmented Reality (BIM on the construction site with Augmented Reality). 10:192-196, 2019.

[21] Li X., Yi W., Chi H.-L., Wang X. and Chan A. P. C. A critical review of virtual and augmented reality (VR/AR) applications in construction safety. *Automation in Construction*, 86:50-162, 2018.

[22] Liu B. Construction robotics technologies 2030. 2017.

[23] Amediya F. Robotics and Automation in Construction. 2016.

[24] Bogue R. What are the prospects for robots in the construction industry?. *The Industrial Robot*, 45:1-6, 2018.

[25] Chua C. K. and Leong K. F. *3D Printing and Additive Manufacturing 4th ed*. World Scientific, 2014.

[26] Rouhana C., Aoun M., Faek F., EL Jazzar M. and Hamzeh F. The Reduction of Construction Duration by Implementing Contour Crafting (3D Printing). 2014.

[27] Tay Y. W. D., Panda B., Paul S. C., Noor Mohamed N. A., Tan M. J. and Leong K. F. 3D printing trends in building and construction industry: a review. *The Virtual and Physical Prototyping*, 12:261-276, 2017.

[28] Rao S. The Benefits of AI In Construction. On-line:https://constructible.trimble.com/construction-industry/the-benefits-of-ai-in-construction,Accessed: 31/05/ 2020.

[29] Blanco J., Fuchs S., Parsons M. and Ribeirinho M. Artificial intelligence: Construction technology's next frontier. On-line: https://www.mckinsey.com/industries/capital-projects-and-infrastructure/our-insights/artificial-intelligence-construction-technologys-next-frontier, Accessed: 31/05/ 2020.

[30] Nisser T. and Westin C. Human factors challenges in unmanned aerial vehicles (uavs): A literature review. 2006.

[31] Irizarry J. and Costa D. B. Exploratory Study of Potential Applications of Unmanned Aerial Systems for Construction Management Tasks. *Journal of Management in Engineering,* 32:0501-6001, 2016.

[32] Zaychenko I., Smirnova A. and Borremans A. Digital transformation: the case of the application of drones in construction. *MATEC Web of Conferences*, 193:50-66, 2018.

[33] Eadie R., Browne M., Odeyinka H., McKeown C. and McNiff S. BIM implementation throughout the UK construction project lifecycle: An analysis. *Automation in construction*, 36: 145–151, 2013.

[34] Goger G., Piskernik M. and Urban H. Studie: Potenziale Der Digitalisierung Im Bauwesen. *WKO*, 2018.

[35] Nassereddine H. M. Design, Development and Validation of an Augmented Reality-Enabled Production Strategy Process for the Construction Industry. The University of Wisconsin-Madison, 2019.

[36] Rüßmann M., Lorenz M., Gerbert P. Waldner M. Justus J., Engel P. and Harnisch M. Industry 4.0: The future of productivity and growth in manufacturing industries. *Boston Consulting Group*, 9:54-89, 2015.

[37] Aleksandrova E., Vinogradova V. and Tokunova G. Integration of digital technologies in the field of construction in the Russian Federation. *Engineering Management in Production and Services*, 11:38-47, 2019.

[38] Cooper S. Civil Engineering Collaborative Digital Platforms Underpin the Creation of 'Digital Ecosystems'. In *Proceedings of the Institution of Civil Engineers - Civil Engineering*, 171:14-14, 2018.

[39] Wake N., Bjurlin M. A., Rostami P., Chandarana H. and Huang W. C. Three-dimensional Printing and Augmented Reality: Enhanced Precision for Robotic Assisted Partial Nephrectomy. 116:227-228, 2018.

[40] Nassereddine, H., Hanna, A., Veeramani, R. Exploring the Current and Future States of Augmented Reality in the Construction Industry. In *The Eleventh International Conference on Construction in the 21st Century (CITC-11)*, London, 2019.

[41] Oesterreich T. D. and Teuteberg F. Understanding the implications of digitisation and automation in the context of Industry 4.0: A triangulation approach and elements of a research agenda for the construction industry. *Computers in industry*, 83:121-139, 2016.

[42] Fergusson K. J. and Teicholz P. M. Achieving industrial facility quality: Integration is key. *Journal of management in engineering*, 12:49-56, 1996.

[43] Gerger A., Schranz C. and Urban H. Neue Möglichkeiten Durch Den Einsatz von Augmented Reality Im Kontext Digitaler Bauvorhaben. City of Vienna, 2020.

[44] Urban, H. and Schranz C. AR-AQ-Bau - Use of Augmented Reality for Acceptance and Quality Assurance on Construction Sites. On-Line:https://nachhaltigwirtschaften.at/en/sdz/projects/ar-aq-bau.php,Accessed: 31/05/ 2020.

Deep Learning-based Question Answering System for Proactive Disaster Management

Yohan Kim[a], Jiu Sohn[a], Seongdeok Bang[a], Hyoungkwan Kim[a*]

[a]Department of Civil and Environmental Engineering, Yonsei University, Seoul, Korea

E-mail: homez815@yonsei.ac.kr, jiujohn@yonsei.ac.kr, bangdeok@yonsei.ac.kr, hyoungkwan@yonsei.ac.kr

Abstract –

As climate change increases the frequency and intensity of natural disasters, proactive disaster management is needed to reduce the damage caused by the natural disasters. Existing reports that record the scale, damage, and response of natural disasters can be used as references for proactive disaster management. However, it is labor-intensive and time-consuming to manually find the necessary information from a number of reports. Thus, this study proposes a natural language processing (NLP)-based question answering system (QA system) for proactive disaster management using the existing reports. This study is focused on paragraphs retrieval, which retrieves paragraphs that have a high similarity to a given question based on the word embedding. The National Hurricane Center's Tropical Cyclone Reports are used to evaluate the proposed method.

Keywords –

Deep Learning; Disaster Management; Natural Language Processing; Question Answering System

1 Introduction

Natural disasters have negative impacts on infrastructure such as structural failure. In recent years, as the frequency and intensity of natural disasters have increased due to the impact of climate change, the importance of disaster prevention has increased [1].

Analyzing historical data and extracting the necessary information can help disaster prevention. With the advancement of deep learning and natural language processing, many studies for information extraction use unstructured data such as text data. Wang and Taylor proposed a method for detecting urban emergencies using Twitter data and topic modelling techniques [2]. Sit et al. conducted a study to identify disaster-related tweets using deep learning, natural language processing, and spatial analysis [3]. Ragnini et al. proposed a data analysis method for disaster response and recovery using Twitter and sentiment analysis [4].

The Question Answering system (QA system) provides users with answers for questions regarding the data. The QA system is useful in finding the necessary information in a large amount of data. Chan and Tsai proposed a dialogue system that combines a QA module and a knowledge base for emergency operations [5]. Tsai et al. proposed a chatbot system called Ask Diana that provides users with water-related information [6].

Social media data, mainly used in previous studies, can satisfy the need of big data for deep learning models. However, they contain inaccurate or unnecessary data. Previous studies that proposed QA systems were mostly focused on extracting keywords. This keyword-based information is intuitive, but it is difficult to grasp the context of the information.

In this study, we propose a QA system for proactive disaster management. The purpose of the proposed system is to provide users with the necessary information to reduce the damage to the infrastructure caused by natural disasters, especially tropical cyclones. In this study, the Tropical Cyclone reports provided by the National Hurricane Center are used. Since tropical cyclones are one of the major weather phenomena that cause enormous damage to infrastructure, they are chosen as the subject of disaster management. We conduct paragraphs retrieval, one of the steps in the QA system, and represent its results.

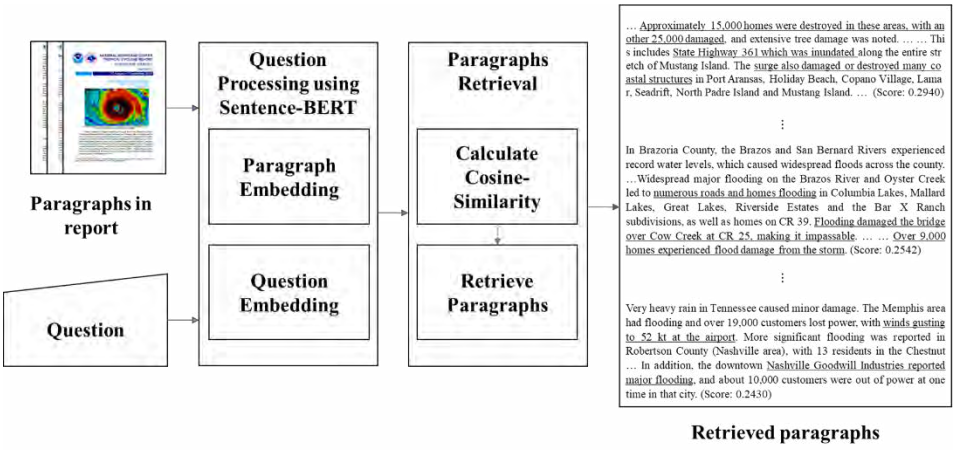

Figure 1. Overview of the proposed paragraphs retrieval in the QA system

2 Paragraphs retrieval using sentence-BERT

2.1 BERT and sentence-BERT

In the past, deep learning models mainly used in natural language processing were Recurrent Neural Network (RNN) models such as Long Short-Term Memory (LSTM) and Gated Recurrent Unit (GRU). The performance of RNN models is excellent, but they have a vanishing gradient problem. When the input sequence is long, the prediction accuracy is decreased by the vanishing gradient problem. To solve the vanishing gradient problem, Sutskever et al. proposed a seq2seq model using the attention mechanism [7]. In the Seq2seq model, the output word is predicted considering all the input words of an encoder. The purpose of the Attention mechanism is to improve the accuracy of prediction by focusing on the part of the input words associated with the predicted word. Vaswani et al. proposed a model called Transformer consisting of an encoder and a decoder using only the attention mechanism [8].

Bidirectional Encoder Representations from Transformers (BERT) [9] is a language representation model developed by Google based on Transformer. BERT is pre-trained with a large amount of Wikipedia and BookCorpus data using unsupervised learning. At the time of the publication, BERT achieved the state-of-the-art from 11 NLP tasks, including Question Answering tests [9].

Sentence-BERT is a model proposed by Reimers and Gurevych [10]. The existing BERT model is a word-based language representations model, and each word that passes the BERT has a dimension of 512. Tasks such as similarity comparison, clustering, and information retrieval take too much computational cost. To solve this problem, Sentence-BERT performs word-embedding in sentence or higher units.

2.2 Paragraphs retrieval

A QA system typically consists of three steps: 1) Question processing, 2) Document and Passage Retrieval, 3) Answer extraction [11]. A paragraph has one subtopic and is a unit that can be clearly classified within the whole text. Therefore, in this study, retrieval is performed on a paragraph basis. In particular, paragraphs retrieval is performed using sentence-BERT and the results are presented. These results show that sentence-BERT can be used in a QA system for proactive disaster management. Figure 1 shows the framework of this study.

2.3 Tropical cyclone reports

As mentioned above, this study uses public data to ensure data reliability, focusing on the tropical cyclones. To this end, Tropical cyclone reports provided by the National Hurricane Center (nhc.noaa.gov) are used. 12 reports, including the Hurricane Harvey report, and 404 paragraphs in them are used for this study.

3 Experiments and Results

To conduct the experiment, the 12 reports provided by the National Hurricane Center were reformatted into paragraphs and saved as Microsoft Excel file. Question embedding and paragraph embedding were performed using the Sentence-BERT. Using the cosine similarity, the similarity score between the question embedding and each paragraph embedding was calculated and the top five paragraphs with high scores were retrieved. Table 1 is the result of paragraphs retrieval on the Hurricane Harvey report. This study uses the same

Table 1. Results of paragraphs retrieval on the Hurricane Harvey report; underlined parts show the information regarding infrastructure damage.

Question	Top 5 most similar paragraphs in reports
What infrastructure has been damaged and What kind of damage has happened to the infrastructure?	Near the initial landfall location in Texas, wind damage was extreme in Aransas County, Nueces County, Refugio County and the eastern part of San Patricio County. Approximately 15,000 homes were destroyed in these areas, with another 25,000 damaged, and extensive tree damage was noted. … … This includes State Highway 361 which was inundated along the entire stretch of Mustang Island. The surge also damaged or destroyed many coastal structures in Port Aransas, Holiday Beach, Copano Village, Lamar, Seadrift, North Padre Island and Mustang Island. … … (Score: 0.2940)
	Major-to-record flooding occurred in Liberty County along the Trinity River with numerous roads inundated including FM 787. Many homes and subdivisions were either cut off or inundated, specifically north of the city of Liberty and in the Grenada Lakes Estates subdivision. … … High flows caused significant scouring of the state 105 (business) road; other roads were washed out as well, with bridge washouts or closures observed in many parts of the county. At least 1,000 homes were damaged in the county. (Score: 0.2636)
	In Brazoria County, the Brazos and San Bernard Rivers experienced record water levels, which caused widespread floods across the county. The hardest hit communities were in Baileys Prairie, Richard and West Columbia. Widespread major flooding on the Brazos River and Oyster Creek led to numerous roads and homes flooding in Columbia Lakes, Mallard Lakes, Great Lakes, Riverside Estates and the Bar X Ranch subdivisions, as well as homes on CR 39. Flooding damaged the bridge over Cow Creek at CR 25, making it impassable. … … Over 9,000 homes experienced flood damage from the storm. (Score: 0.2542)
	Major lowland flooding occurred in Matagorda County along the Tres Palacios River. Many roadways were under water, and homes in the El Dorado Country, Oak Grove, and Tres Palacios Oaks subdivisions flooded. Major flooding also occurred on the Colorado River at Bay City as levees were overtopped by 2 ft of water. High flows from the Colorado and Tres Palacios Rivers impacted river navigation for several weeks. Roughly 2,900 homes were damaged in the county. (Score: 0.2469)
	Very heavy rain in Tennessee caused minor damage. The Memphis area had flooding and over 19,000 customers lost power, with winds gusting to 52 kt at the airport. More significant flooding was reported in Robertson County (Nashville area), with 13 residents in the Chestnut Flats Apartment near the Nashville Fairgrounds evacuated due to the high water. In addition, the downtown Nashville Goodwill Industries reported major flooding, and about 10,000 customers were out of power at one time in that city. (Score: 0.2430)

uses the same question for all of the 12 reports. Examples of infrastructure damage information with in paragraphs are shown in Table 1.

Table 2 shows the results of paragraphs retrieval. all of the paragraphs retrieved from four reports (Harvey, Ingrid, Irma, and Issac) include information about infrastructure damage. In the other eight reports (Alex, Bill, Cindy, Dolly, Hermine, Imelda, Lee, and Michael), only a few paragraphs include infrastructure damage information. This is because the total number of paragraphs with infrastructure damage information in the eight reports was less than 5. In brief, the paragraphs retrieval has been performed well in all the reports.

Table 2. Results of paragraphs retrieval (the number of paragraphs showing infrastructure damage information / the preset number of paragraphs retrieval)

Tropical Cyclone	Result
Alex	1/5
Bill	2/5
Cindy	1/5
Dolly	1/5
Harvey	5/5
Hermine	1/5
Imelda	3/5
Ingrid	5/5
Irma	5/5
Isaac	5/5
Lee	2/5
Michael	2/5

Table 3 shows two paragraphs with different similarity scores. The one with higher score (0.2189) shows no information related to infrastructure damage, whereas the one with lower score shows infrastructure damage information. It seems to be because many words related to damage were used such as *"flood"* and *"death"*, even if there are no words related to infrastructure. This problem could be solved by fine-tuning for text classification using labeled data.

4 Conclusion

In this study, a paragraphs retrieval model, one of the steps in the QA system for proactive disaster management, was proposed and the experimental results were represented. The proposed model well retrieved the paragraphs including infrastructure damage information for all the 12 reports. The retrieved paragraphs can be used as an input in the next module (the answer extraction model) of the QA system. The proposed methods are expected to help disaster prevention and reduce the damage to the infrastructure.

Table 3. Retrieved paragraphs of the Hurricane Lee report; underlined parts show the information regarding infrastructure damage.

Paragraphs
Paragraph not including infrastructure damage information (Score: 0.2189)
Media reports indicate that flooding largely related to the remnants of Lee was responsible for at least 12 additional deaths in the eastern United States; seven people in Pennsylvania, four in Virginia, one in Maryland, and one in Georgia. Nearly all of these deaths occurred when individuals tried to cross flooded roadways in vehicles or were swept away in flood waters.
Paragraph including infrastructure damage information (Score: 0.1565)
Most of the damage from Lee was the result of storm surge or freshwater flooding. Storm surge flooding from Lake Pontchartrain <u>inundated more than 150 houses</u> in Jefferson and St. Tammany Parishes in Louisiana. Minor storm surge flooding was also reported outside the hurricane protection levees in St. Bernard and Orleans Parishes. Freshwater flooding was reported in low-lying areas of southeastern Louisiana and southern and central Mississippi. Several roads were inundated by floodwaters in Hancock, Jackson, and Harrison Counties Mississippi, while in Neshoba County in the central portion of the state, <u>35 roads were damaged with 5 of those completely washed out</u>.

Acknowledge

This work was supported by the National Research Foundation of Korea (NRF) grant funded by the Ministry of Science and ICT (No. 2018R1A2B2008600) and the Ministry of Education (No. 2018R1A6A1A08025348).

References

[1] Field, C. B., V. R. Barros, D. J. Dokken, K. J. Mach, M. D. Mastrandrea, P. R. Mastrandrea, and L. L. White. "Intergovernmental panel on climate change. Climate change 2014: Impacts, adaptation, and vulnerability." In *Contribution of Working Group II to the Fifthe Assessment Report of the Intergovernmental Panel on Climate Change*. Cambridge University Press Cambridge/New York, 2014.

[2] Wang Y. and Taylor J. E. "DUET: Data-driven approach based on latent Dirichlet allocation topic modeling." *Journal of Computing in Civil Engineering* 33.3: 04019023, 2019.

[3] Sit M. A., Koylu C., and Demir I. Identifying disaster-related tweets and their semantic, spatial and temporal context using deep learning, natural language processing and spatial analysis: a case study of Hurricane Irma. *International Journal of Digital Earth*, 12(11), 1205-1229, 2019.

[4] Ragini J. R., Anand P. R., and Bhaskar V. Big data analytics for disaster response and recovery through sentiment analysis. *International Journal of Information Management*, 42, 13-24, 2018.

[5] Chan H. Y., and Tsai M. H. Question-answering dialogue system for emergency operations. *International Journal of Disaster Risk Reduction*, 41, 101313, 2019.

[6] Tsai M. H., Chen J. Y., and Kang S. C. Ask Diana: A Keyword-Based Chatbot System for Water-Related Disaster Management. *Water*, 11(2), 234, 2019.

[7] Sutskever I., Vinyals O., and Le Q. V. Sequence to sequence learning with neural networks. In *Advances in neural information processing systems*, pages 3104-3112, Montreal, Canada, 2014.

[8] Vaswani A., Shazeer N., Parmar N., Uszkoreit J., Jones L., Gomez A. N., Kaiser L. and Polosukhin, I. Attention is all you need. In *Advances in neural information processing systems,* pages 5998-6008, Long Beach, CA, USA, 2017.

[9] Devlin J., Chang M. W., Lee K., and Toutanova K. Bert: Pre-training of deep bidirectional transformers for language understanding. arXiv preprint arXiv:1810.04805, 2018.

[10] Reimers N., and Gurevych I. Sentence-bert: Sentence embeddings using siamese bert-networks. arXiv preprint arXiv:1908.10084, 2019.

[11] Jurafsky D. Speech & language processing. Pearson Education India, 2000.

Overall Utilization of Information and Communication Technologies in Excavation Work and Management at Yoneshiro-gawa River, A First-class River

Tatsuro Masu[a] ,Akihiro Ishii[b] , Fumihiro Tamori[b], Hanako Hatakeyama[b], Yutaka Suzuki[c], Satoshi Shirato[c], Yurie Abe[c]

[a]Policy Planning and Coodination Divixion for Public works Project, Policy Bureau, MLIT.JP
[b]OHMORI CONSTRUCTION Co., Ltd., Japan
[c]NOSHIRO work office of River and National Highway,Tohoku Regional Development Bureau, MLIT.JP
E-mail: masu-t82ac@mlit.go.jp, akhr-ishii@om346.co.jp

Abstract -

We obtained various effects about 'Efficiency, Quality, Safety, Improving the work environment and Human resource development' through overall utilization of Information and Communication Technologies (hereinafter referred to as ICTs) in the excavation work and management at Yoneshiro-gawa River, a first-class river.

At the topographic surveying stage, we used the UAV and made three-dimensional topographical data. At the excavation stage (most excavations are under water), we used the machine controlled system and at the same time introduced a new system by which we could automatically grasp the amount of excavation (finished work). At the delivery stage, we could automatically get a predetermined form showing the work done by the excavation.

Keywords -

Overall utilization of ICTs; Underwater excavation; New system using excavation history data; New-3K [Kyuyo:salary, Kyuka:vacation, Kibo:hope]

1 Introduction

Recently in Japan, due to the effects of global climate change, we are facing severe and frequent disasters and need to take measures to prevent floods. In general, short-term measures are to cut and remove trees along the river and to excavate the bottom of the river in order to improve the flow of water in the river.

As one such measure against flood, we implemented the flood control project of cutting and removing the trees and excavating the bottom of the river in the Yoneshiro-gawa River at Noshiro city, Akita prefecture, Japan. In the process of this project, we used various ICTs. In particular, the use of 3D-machine controlled system in excavation work in muddy water was effective for efficiency and safety. On the other hand, we discovered the difficulty of understanding new rules on the usage and the management of these new technologies.

2 Construction overview

We cut the trees in an area of 300,000m2. And in part of the area where the trees were cut and removed, we set up a pilot area. This area was dug down to a certain depth, so it is difficult for trees to grow up in this area. The area was designed so that usually there is water, and once it rains and the water level rises, the mud at the bottom of the area is washed away. To construct this pilot area, we utilized various ICTs. (Figure 1, 2)

The construction project was done from 3th April 2019 to 31th January 2020. The cost was 250,000,000JPY. The supervisor was NOSHIRO work office of River and National Highway, Tohoku Regional Development Bureau, MLIT.JP. The contractor was OHMORI CONSTRUCTION Co., Ltd.

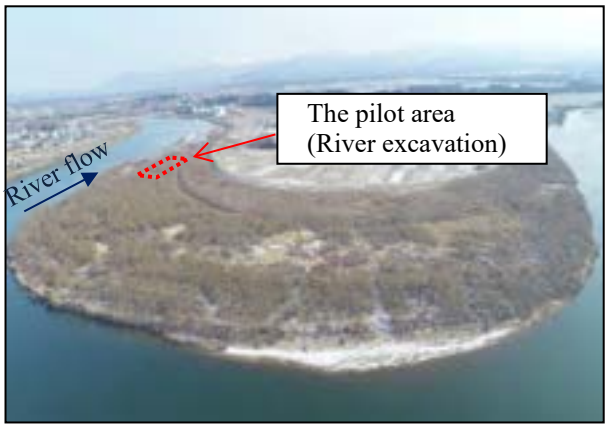

Figure 1. View of construction site (Before work)

2.1 Utilization status of ICTs in Construction

At the construction area we utilized several ICTs through the process of topographic survey, excavation and delivery.

Figure 2. The pilot area (River excavation) (After work)

2.1.1 3 dimensional survey

At the area of river excavation we utilized the UAV and took many photographs (700 photos) from the air(Figure 3,4). And many photographs (689 photos) were converted to 3 dimensional topographic data by the software(Table 1). And the 3 dimensional data were used for next excavation process.

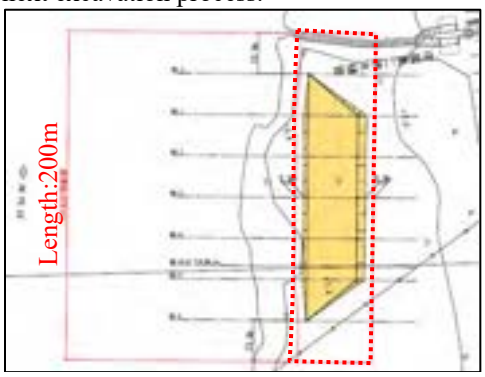

Figure 3. The area of 3D survey

Figure 4. The UAV surveying
(UAV, monitor, flight control system)

Table 1. Equipment and software used

UAV	EAMS ROBOTICS UAV-E470SU1
Software of Photogrammetry	Agisoft Metashape
Software of 3D design	SITE-Scope Sitec3D (KENSETSU SYSTEM)

2.1.2 3 dimensional excavation

At the process of the river excavation (volume: 5,400m3) we utilized 3 dimensional machine controlled system. We didn't need elevation stakes, markers which are usually installed on site to show operator how much to excavate. Especially, because it was difficult to see the status of excavation in the muddy water, it was much more useful to use this 3 dimensional machine controlled system (Figure 5). In the clear water, operator and surveyor could see the status of the ground and check certain situation, but on the other hand in muddy water, they couldn't see nothing about the ground.

Table 2. Construction Information

Type	Earthwork River excavation
Place	R4.4k+80m- R4.6k+40m
Volume_ Excavation	5,400m3

Figure 5. ICT construction (3D-machine control)
(Appearance Guidance and the monitor which shows the excavation status in operation room)

2.1.3 Management of the excavation

By using the machine controlled system, we introduced a new system by which we could automatically grasp the amount of excavation required.

The system is that the position data of the bucket is converted to the data of the amount of excavation (finished work) and then sent to the clouded server and stored. And the data is automatically compared to the design date and shows the difference by colors, green color is completed and red is not. (Figure 6)

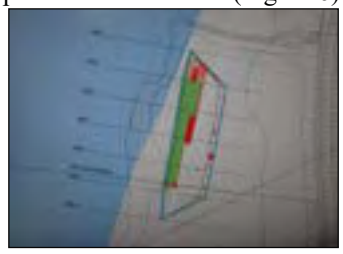

Figure 6. The monitor which shows instantly the excavation status at office connected to the site via internet

We could use this data for the management of excavation work. Previously, we needed to survey the level of the ground after finishing the excavation works to grasp the amount of the work. But by using this system, we need not to do such these survey and recording in the field required. (Figure 7)

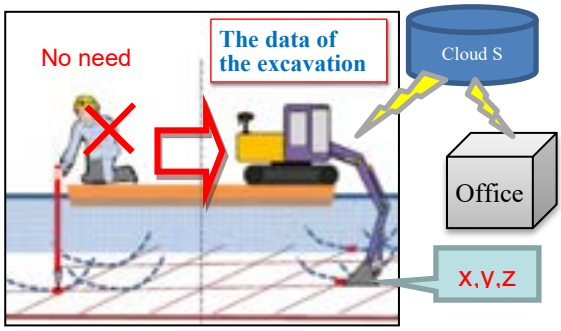

Figure 7. The image of the comparison of the previous method and new one

3 Analysis of effects and challenges

Through these works by using ICTs, we obtained effects about the efficiency, the quality, the safety, the improving of the work environment and the human resource development.

3.1 Quantitative analysis of the effect

In order to measure the effect on efficiency, we investigated the amount of work in each work that utilized ICTs. The amount of work was calculated as the total number of each work times multiplied by the number of each workers related. The amount of work by the normal method was calculated on the basis of the work experienced in the past, assuming the normal work.

Through all process the efficiency increased by 20%. The efficiency increased in each processes of the survey, the3dimensional design, the excavation and the inspection. But because of the growth of the data, the efficiency declined in the electronic delivery process. (Figure 8)

By the way, the average efficiency of 17 construction sites (excavation work) in Japan last year (2019s) increased 15%. (Figure 9) It shows that our work was more effective.

Figure 8. The efficiency of our work (Upper: Normal method, Lower: Utilize ICT)

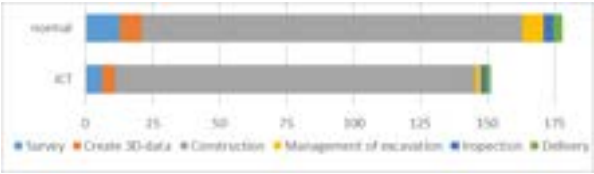

Figure 9. The average efficiency of 17 works (Upper: Normal method, Lower: Utilize ICT)

3.2 Quantitative analysis of the quality

The accuracy of excavation work passed all standard values. (Table 3)

- ✓ The average of finished height was -20mm, thought the standard value was +-40.
- ✓ And both the maximum and minimum value passed enough. Etc.

Table 3. Results of the accuracy

Mesurement Item			Standard value	In-house value
Flat Field elevation difference	Average	−20mm	±50	±40
	Maximum	57mm	±300	±240
	Minimun	−137mm	±300	±240
	Number of data	3880	over1point／m2 (3750points)	over1point／m2 (3750points)
	Area	3750㎡	—	—
	Number of failed data	0	within0.3% (11points)	within0.3% (11points)
Slope Field elevation difference	Average	−6mm	±70	±56
	Maximum	70mm	±300	±240
	Minimun	−144mm	±300	±240
	Number of data	1152	orer1point／m2 (928points)	over1point／m2 (928points)
	Area	928㎡	—	—
	Number of failed data	0	within0.3% (3points)	within0.3% (3points)

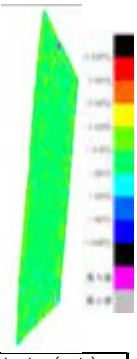

	Number of data within the standard value (ratio)		
	80～50%	50～20%	20%～
Variation at flat	0/3880 (0.0%)	102/3880(2.6%)	3778/3880(97.3%)
Varietion at slope	0/1152 (0.0%)	48/1152(4.1%)	1104/1152(95.8%)

3.3 Quantitative analysis of effect

We conducted a questionnaire survey on satisfaction with ICTs utilization at each 5 processes. Especially, "The management of the amount of excavation work" was the best score. And "The 3 dimensional excavation work" was the second best. The others were middle score (Figure 10). This means that the system (explained in 2.1.3), which can catch and record the data of the status of construction automatically, is much more useful than the usual method that surveyor need to survey many times constantly.

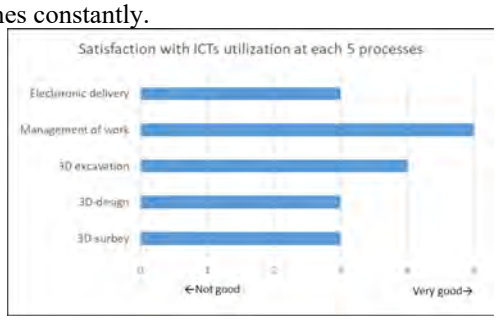

Figure 10. Satisfaction with ICTs utilization at each process

3.4 Other effects

In addition to the above, we obtained the following effects through utilization of several ICTs in this project.

1. The pictures taken by UAV made it easy to understand the whole view of the construction, so we could use it as a reference material for the meetings among the parties concerned.
2. We have improved safety as we have reduced the work done near construction machinery.
3. Young staffs were familiar with digital devices and could easily use them. (Perhaps enjoying!) This mean that we could assign young employees who don't have enough civil engineering skills this work. And this work could be done at home, so it is more efficient.

Figure11. Young staff easily used 3 dimensional data

3.5 Challenges to effectiveness

On the other hand, there were several challenges to effectiveness through the utilization of ICTs.

1. The new rule of the management of excavation work was newly created, so it was difficult to understand.
2. The excavated riverbed changed easily due to changes in water level, and the accuracy of the finished work required was normal. By relaxing the required accuracy, there is a possibility that productivity will be further improved.
3. This time, it was not a place with water flow, but when excavating in a river with water flow, a method of confirming the completed shape will be needed.

4 To conclude

Through the use of ICT in a series of processes, a certain level of efficiency and quality improvement has been achieved as a whole. Since it is a new technology and a new relationship, it is expected that the effects will be further improved by getting used to it. At that time, in order to promote the spread to smaller-scale construction, it is desirable to develop human resources for engineers who work together with both the public and private sectors.

The UAV survey this time was on flat land, but in the future it will help to expand the range of UAV utilization by developing the know-how and data for implementation on undulations and slopes.

Finally, increasing the opportunities for young people including women to play active roles by improving the work environment is very important in Japan, where the declining birthrate (declining young employee) and aging population are becoming issues. Especially in the construction industry, which was said to be 3K (KITSUI:hard, KITANAI:dirty, KIKEN:dangerous), the declining birthrate (declining young employee) and aging population are outstanding. Therefore, it is highly desired that the introduction of ICT will expand the opportunities for young people to play active roles and realize the new 3K (KYUYO:salary, KYUKA;vacation, KIBO:hope).

References

[1] Procedure for calculating the amount of work done for earthwork using construction history data (Ministry of Land, Infrastructure and Transport, March 2019)

[2] Kozuka K, Okajima T and Morikawa K.Verification of the Applicability of ICT-based River Dredging Work. *Civil engineering journal*, pages 20-23, 03/2020.

[3] Ryuichi I, Hisatoshi T and Genzaburo M. AS-BUILT MANAGEMENT USING THE EXECUTION HISTORY OF CONSTRUCTION MACHINES IN PAVEMENT CONSTRUCTION: *JSCE Proceedings* F3 Vol.73, No.2, I_416-I_423, 2017.

Weakly Supervised Defect Detection using Acoustic Data based on Positive and Negative Constraints

Jun Younes Louhi Kasahara[a], Atsushi Yamashita[a], Hajime Asama[a]

[a]Department of Precision Engineering, The University of Tokyo, Japan
E-mail: louhi@robot.t.u-tokyo.ac.jp

Abstract -

Concrete structures are heavily used in most modern societies and the population of structures in need of inspection is rapidly growing. On the other hand, the manpower for inspection is decreasing. This has brought into focus the need for automated inspection methods for concrete structures. The hammering test is a popular method for inspection that uses the sound resulting from a hammer impact on the surface of the structure for defect detection. Previous methods largely employed machine learning approaches for the automation of the hammering test. Weakly supervised methods used positive queries answers on sample pair similarity: a human user was questioned on the similarity of pairs of hammering samples and similar pairs were used to transform the feature space. However, it can be expected that dissimilar pairs would also be gathered in this process. Therefore, in the present paper is proposed a method for weakly supervised defect detection in concrete structures using hammering with both positive and negative answers to queries. After the initial feature space transformation based on positive query answers, another feature space transformation is introduced based on negative query answers. Experiments in laboratory conditions showed the effectiveness of the proposed method.

Keywords -

Defect detection; Infrastructure inspection; Weak supervision; Acoustic data; Clustering

1 Introduction

Concrete structures are featured heavily in most modern societies. This is especially true for social infrastructures such as tunnels, highways and bridges. Due to various factors ranging from simple aging to damage caused by environmental conditions, concrete structures require regular and careful inspection. This is a critical aspect for social infrastructures due to their large number of users, for which safety is of utmost concern [1]. Recent events such as the collapse of the Sasago tunnel in Japan [2] or the collapse of the Morandi bridge in Italy [3] have emphasized the issues caused by an ever-increasing population of aging structures facing an ever-decreasing population of workers tasked with inspection work.

Figure 1. A human inspector conducting the hammering test on the wall portion inside a tunnel. The hammer is used to hit the surface of the concrete structure and the returned sound used to assess the presence of defect beneath the surface.

One popular inspection method for concrete structures is the hammering test, illustrated in Figure 1. It consists in a human inspector using a simple hammer to hit the surface of the structure and assessing the presence of defects beneath the surface from the impact sound. Due to both its simplicity and non-destructive nature, it is widely popular. However, it requires a skilled human inspector to be able to distinguish impact sounds resulting from defect portions of the structures. Due to the manpower shortage and the population of structures in need of testing, the hammering test in its current, traditional form, is not effective. Therefore, the automation of the hammering test is highly sought after and has attracted much focus in recent years [4][5][6].

Previous works have mainly employed machine learning approaches to tackle this issue. Supervised learning approaches use training data to train classifiers to distinguish defect and non-defect sounds. In [7], a Neural Network was used with a Radial Basis Function in order to detect defects in concrete bridges by the sound of dragging chains. In [8], Time-Frequency Analysis was employed together with Ensemble Learning and achieved accurate classification of hammering samples into defect and non-defect classes. Furthermore, classification of defects samples into shallow and deep classes was also achieved. Supervised learning approaches often boasted remarkable per-

formance. However, they are limited by the availability of adequate training data. Indeed, if the training data does not correspond to the actual tested concrete structure, difficulties arises when attempting to produce a good model. Since concrete is an aggregate, each structure is unique and therefore, besides the fact that generating training data is a human labor intensive task, adequate training data may only be obtainable on site, i.e., on the very tested structure. This severely limits the practicability of such approaches.

Unsupervised learning methods, characterized by the fact that they to not require training data, offer an interesting alternative to this issue. In [9], clustering was used on Fourier spectrum of hammering samples with a correlation distance. In [10] and [11], clustering of audio hammering samples was considered along each hammering sample's hit location using a camera. Unsupervised learning approaches successfully bypassed the practical issue caused by training data. However, they generally have lacking performance compared to supervised learning methods in their optimal conditions. Furthermore, Unsupervised Learning approaches also incorporate strong priors, which requires careful consideration in the design phase.

Between supervised and unsupervised learning methods, weakly supervised approaches aims to combine the best of both worlds by only requiring *weak supervision*, i.e., a form of supervision which is less informative but also presents less burden on the human user than generating training data. In [12], an initial framework for the automation of the hammering test based on pairs of hammering samples a human user has indicated as similar was proposed. In [13], this initial framework was reinforced by the addition of hammering samples' hit location using a camera. In [14], an active query scheme was proposed to ensure more consistent weak supervision quality. Good results were obtained. However, only positive answers to queries were considered in those works: weak supervision is gathered from human users, through queries on sample pair similarity. Positive answers to such queries, i.e., the sample pair is similar, are known as *must-links*. Negative answers, i.e., the sample pair is dissimilar, are known as *cannot-links*. It is realistic to assume that the human user is limited in the number of queries it can answer to and while approaches such as [14] attempted to maximize the number of obtained must-links through active query, all the queries resulting in must-links cannot be ensured. This means that there will inevitably be cannot-links generated during the query process, which are not taken advantage of in previous work regarding automation of hammering test.

Therefore, in this paper, the objective is to achieve defect detection in concrete structures using acoustic data with both positive and negative answers to queries.

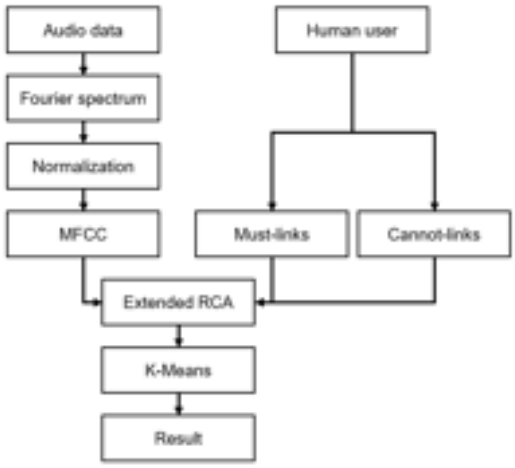

Figure 2. Overview of the proposed method.

2 Method

2.1 Overview

An overview of the proposed method is shown in Figure 2. The input, audio data, is first pre-processed: this involves a conversion to Fourier spectrum, normalization and conversion to Mel-Frequency Cepstrum Coefficients (MFCC). Then, weak supervision, provided by a human user under the form of must-links and cannot-links, is used to conduct a transformation of the feature space to match the human user's notion of similarity. Finally, separation between defect and non-defect samples is conducted by clustering using K-Means.

2.2 Initial Feature Space

Hammering samples are initially collected as audio segments. The first step of the processing is conversion to Fourier spectrum. Given a sound sample defined by $\mathbf{x} = (x_1, ..., x_d)$, its Fourier spectrum $\mathbf{a} = (a_1, ..., a_d)$ is calculated. Next, since there is no assumption about regularity of the input, i.e., the hammer strike is not assumed to be of constant force, a normalization to zero mean and unit variance is conducted as in (2), with $\bar{a}$ being the mean of the components of a_i as defined in (1).

$$\bar{a} = \frac{1}{d}\sum_{i=1}^{d} a_i, \tag{1}$$

$$a_i = \frac{a_i - \bar{a}}{\sqrt{\frac{\sum_{i=1}^{d}(a_i-\bar{a})^2}{d-2}}}. \tag{2}$$

In [10], the MFCC feature space was shown to be a good feature space for discrimination of defect hammering samples. MFCC are hand-crafted feature vectors originally

build for speech recognition and popular across several fields dealing with audio data [15, 16]. MFCC are suited for hammering samples because they emulate the human hearing and the human hearing is able to discriminate defect hammering samples from non-defect hammering samples.

To compute the MFCC, first the periodogram estimate of the power spectrum is computed. Then, what are known as Mel filterbanks, a set of N_{filter} triangular filters equally spaced in the Mel scale, are applied. The Mel scale is an empirical scale tuned to the sensitivity of the human cochlea, as in (3) with f the frequency in Hertz. The logarithm of the resulting N_{filter} energy values are further processed by Discrete Cosine Transform to finally obtain MFCC.

$$M(f) = 1125 * \ln(1 + \frac{f}{700}). \tag{3}$$

For the sake of clarity, in the remainder of this paper, the MFCC feature vector of a hammering sample will simply be noted as $\mathbf{x}$.

2.3 Weakly Supervised Feature Space Transformation: Extended Relevant Component Analysis

The feature space defined by MFCC is a good one for separating defect and non-defect hammering samples. However, improvements can be achieved by further transforming the feature space to match the human user's notion of similarity according to answers provided to queries. Those answers to queries can come in two forms: pairs of samples the human user considers similar are called must-links whereas pairs of samples the human user considers dissimilar are called cannot-links.

The previous work [14] only employed must-links through Relevant Component Analysis (RCA). RCA is a weakly supervised metric learning method initially proposed in [17]. While the authors in [17] puts the fact that RCA is only based on must-links as an advantage, as must-links are easier to generate compared to cannot-links, in practice it can be reasonably expected that the human user answering queries would be limited in the number of queries he can answer to, rather than in the number of must-links he can provide. This means that the querying process is very likely to produce cannot-links along must-links. Therefore, not using cannot-links to contribute to the feature space transformation is wasteful.

Extended RCA is an extension of the original RCA initially proposed in [18]. The feature space transformation matrix build upon must-links $\mathcal{M}$ differs slightly from what is used in RCA, as shown in (4). This allows to build a similar transformation matrix on the set of cannot-links C as well, as in (5).

$$\hat{\mathbf{C}}_{\mathcal{M}} = \frac{1}{2|\mathcal{M}|} \sum_{(\mathbf{x}_i, \mathbf{x}_j) \in \mathcal{M}} (\mathbf{x}_i - \mathbf{x}_j)(\mathbf{x}_i - \mathbf{x}_j)^T, \tag{4}$$

$$\hat{\mathbf{C}}_{C} = \frac{1}{2|C|} \sum_{(\mathbf{x}_i, \mathbf{x}_j) \in C} (\mathbf{x}_i - \mathbf{x}_j)(\mathbf{x}_i - \mathbf{x}_j)^T, \tag{5}$$

$$\mathbf{y}_i = \hat{\mathbf{C}}_C^{1/2} \hat{\mathbf{C}}_{\mathcal{M}}^{-1/2} \mathbf{x}_i, \quad 1 \leq i \leq N. \tag{6}$$

Therefore, given a dataset containing N samples, each sample $\mathbf{x}_i$ is first linearly transformed to $\mathbf{y}_i^{'} = \mathbf{C}_{\mathcal{M}}^{-1/2} \mathbf{x}_i$, using must-links, and then linearly transformed again to $\mathbf{y}_i = \mathbf{C}_C^{1/2} \mathbf{y}_i^{'}$, using cannot-links this time, as in (6). The transformation based on $\hat{\mathbf{C}}_{\mathcal{M}}$ aims to reduce the within-class scatter while the transformation based on $\hat{\mathbf{C}}_C$ aims to increase the between-class scatter.

2.4 Clustering

After the weakly supervised feature space transformation described in the previous section, separation of hammering samples between defect and non-defects is conducted using K-Means [19]. K-Means is simple iterative clustering algorithm that aims to achieve a partitioning of the dataset by minimizing the variance of each cluster S_k. Algorithm 1 shows a pseudo-algorithm of K-Means.

3 Experiments

Experiments were conducted in laboratory conditions using concrete test blocks containing simulated defects. The used setup is illustrated in Figure 3. The blocks were hit on several locations, once per location, using a KTC UDHT-2 hammer (head diameter 16 mm, length 380 mm, weight 160 g). This hammer is commonly used in actual inspection sites. Audio recording was done using a Behringer ECM8000 microphone fixed roughly at 0.5 m from the concrete test block and coupled with a Roland

Algorithm 1: Pseudo-algorithm of K-Means.

Data: Dataset D of N samples $\mathbf{y}_i$,
number of clusters K
Result: Partition of D into K clusters
Initialization:
Initialize cluster centroids $\mathbf{c}_1$,$\mathbf{c}_2$,...,$\mathbf{c}_K$ randomly;
while termination criterion not met **do**
Assign samples:
for each sample $\mathbf{y}_i$
$l_i \rightarrow \underset{k}{\text{argmin}} \|\mathbf{y}_i - \mathbf{c}_k\|^2$
Update centroids:
for each centroid $\mathbf{c}_k$
$\mathbf{c}_k \rightarrow \frac{1}{|S_k|} \sum_{\mathbf{y}_i \in S_k} \mathbf{y}_i$
end

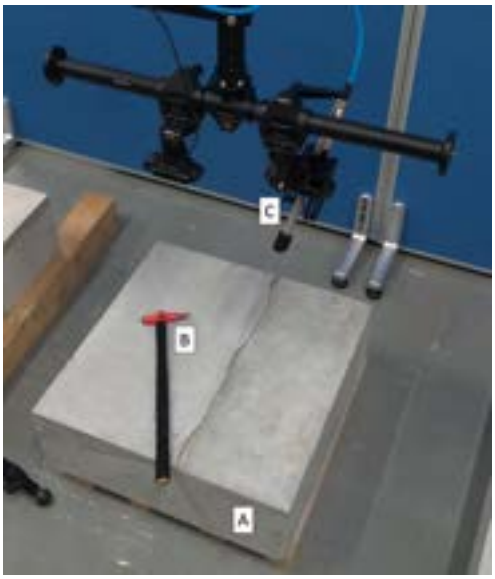

Figure 3. The experimental setup in laboratory conditions with (A) a concrete test block containing a simulated defect, (B) a hammer and (C) a microphone to record the hammering sound.

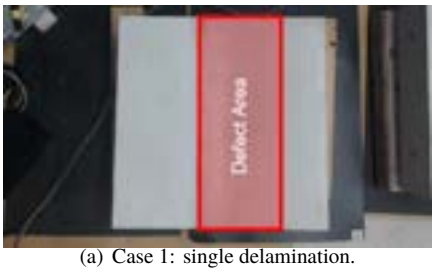

(a) Case 1: single delamination.

(b) Case 2: dual delaminations.

Figure 4. Concrete test blocks used in laboratory experiments containing man-made defects. Defect areas are therefore precisely known and indicated by light red overlays.

UA-25EX sound board at 44.1 kHz. MFCC were computed with $N_{filter} = 26$ and 10 coefficients. 30 queries were allowed for each run.

Two scenarios were considered, those are the same as featured in [14] and the setting $K = 2$ was used for both:

- Case 1: single delamination. This dataset contains 462 samples: 272 non-defects and 190 defects. The delamination is at an angle of 30 degrees.
- Case 2: dual delaminations. This dataset contains 270 samples: 155 non-defects and 115 defects. Two delaminations are present, both at an angle of 15 degrees.

A picture for both cases is provided in Figure 4.

4 Results and Discussion

In Table 1 is reported the average number of must-links and cannot-links obtained out of 30 queries over 50 runs. About half of the queries effectively resulted in cannot-links, which are essentially wasted queries for previous approaches. Since sample pairs were queried randomly, the ratio of must-links and cannot-links reflected approximately the datasets' ratio of defect/defect, non-defect/non-defect pairs and defect/non-defect pairs.

In Figure 5 are reported the average performance obtained over 50 runs in both considered cases for the approach of [12] and the proposed method. Error bars correspond to one standard deviation. The performance was measured using the Rand index [20]. The Rand index is a common measure of performance for clustering methods and is essentially a ratio of correctly clustered sample pairs over the total number of sample pairs in the dataset. It ranges between 0 and 1, with higher values of Rand index indicating the better clustering.

For both Case 1 and Case 2, it can be noticed that the proposed method achieved better clustering on average than the method of [12]. The spread of the output seems to be also narrower for the proposed method, indicated by lower values of standard deviation. This is especially noticeable for Case 2. This is certainly due to the increased number of constraints used in the feature space transformation by the proposed method, defining more precisely the target feature space.

The performance of the method of [12] on Case 1 is significantly lower than reported in the initial publication. This is due to the difference in number of effective must-links: while 20 must-links were allowed in [12] whereas in the present paper 30 queries were allowed, resulting in about only 15 must-links in average. This indicates that, depending on the dataset, a significantly larger number of queries is potentially required to obtain the desired number of must-links.

With the same number of must-links, the proposed method, that makes use of cannot-links as well, does perform better. However, the performance increase enabled by the additional feature space transformation computed based on cannot-links does not bring as much improvement

Table 1. Average number of constraints of each type over 50 runs for 30 allowed queries.

	Number of allowed queries	Average number of obtained must-links	Average number of obtained cannot-links
Case 1: single delamination	30	15.01	14.99
Case 2: dual delaminations	30	15.41	14.59

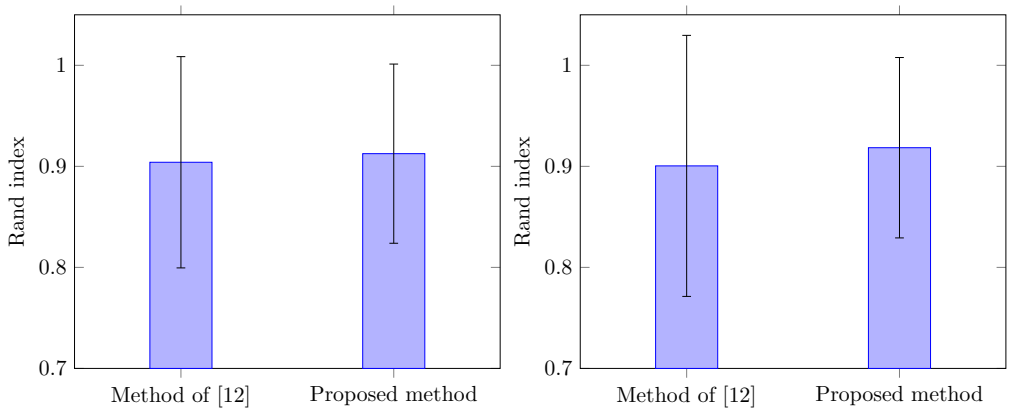

(a) Case 1: single delamination. (b) Case 2: dual delaminations.

Figure 5. Performance of the method of [12] and the proposed method. Average over 50 iterations reported, error bars correspond to one standard deviation. 30 queries were allowed and random seeding was used for each run.

per constraint compared to must-links. This potentially indicates that must-links are more informative and better suited for fine-tuning the feature space, at least within the RCA framework.

5 Conclusion

In the present paper was proposed a method for defect detection in concrete structures using acoustic data based on both positive and negative constraints. Using Extended RCA, an additional feature space transformation based on negative constraints was conducted following the first feature space transformation using positive constraints. Experiments in laboratory conditions using concrete test blocks showed that the proposed method achieved better results more consistently than the previous method that only used positive constraints.

As future work, we would like to further study the influence of negative constraints on the final feature space. As unavoidable by-products of the querying process, cannot-links should be employed to maximize the data provided by the human user. However, a straight inclusion of those negative constraints in the RCA framework might not be their only use. For example, negative constraints obtained early in the query process could be used in the selection process for the next sample pair to query the human user on.

Acknowledgments

This work was supported in part by the Japan Construction Information Center (JACIC) foundation. The authors thank Prof. Hiromitsu Fujii, Department of Advanced Robotics, Chiba Institute of Technology for his valuable help. The authors also thank the Institute of Technology, Tokyu Construction Co., Ltd. for their precious help and cooperation.

References

[1] Keiji Nagatani and Yozo Fujino. Research and development on robotic technologies for infrastructure maintenance. In Journal of Robotics and Mechatronics, volume 31, pages 744–751. Fuji Technology Press Ltd., 2019.

[2] BBC News. Japan Sasago tunnel collapse killed nine. [web page]. https://www.bbc.com/news/world-asia-20576492, 2012. Accessed: 2019-04-11.

[3] BBC News. Italy bridge collapse: Genoa death toll rises to 43. [web page]. `https://www.bbc.com/news/world-europe-45241842`, 2018. Accessed: 2019-04-11.

[4] Yusuke Takahashi, Satoru Nakamura, Yasuichi Ogawa, and Tomoya Satoh. Velocity control

mechanism of the under-actuated hammering robot for gravity compensation. In Proceedings of the International Symposium on Automation and Robotics in Construction (ISARC), volume 34. IAARC, 2017.

[5] Satoru Nakamura, Yusuke Takahashi, Daisuke Inoue, and Takao Ueno. The variable guide frame vehicle for tunnel inspection. In Proceedings of the International Symposium on Automation and Robotics in Construction (ISARC), volume 34. IAARC, 2017.

[6] Yusuke Takahashi, Satoshi Maehara, Yasuichi Ogawa, and Tomoya Satoh. Concrete inspection systems using hammering robot imitating sounds of workers. In Proceedings of the International Symposium on Automation and Robotics in Construction (ISARC), volume 35. IAARC, 2018.

[7] Gang Zhang, Ronald S. Harichandran, and Pradeep Ramuhalli. An automatic impact-based delamination detection system for concrete bridge decks. In NDT & E International, volume 45, pages 120–127. Elsevier, 2012.

[8] Hiromitsu Fujii, Atsushi Yamashita, and Hajime Asama. Defect detection with estimation of material condition using ensemble learning for hammering test. In Proceedings of the International Conference on Robotics and Automation (ICRA), pages 3847–3854. IEEE, 2016.

[9] Jun Younes Louhi Kasahara, Hiromitsu Fujii, Atsushi Yamashita, and Hajime Asama. Unsupervised learning approach to automation of hammering test using topological information. In ROBOMECH Journal, volume 4, pages 13–23. Springer, 2017.

[10] Jun Younes Louhi Kasahara, Hiromitsu Fujii, Atsushi Yamashita, and Hajime Asama. Clustering of spatially relevant audio data using Mel-frequency cepstrum for diagnosis of concrete structure by hammering test. In Proceedings of the International Symposium on System Integration (SII), pages 787–792. IEEE, 2017.

[11] Jun Younes Louhi Kasahara, Hiromitsu Fujii, Atsushi Yamashita, and Hajime Asama. Fuzzy clustering of spatially relevant acoustic data for defect detection. In Robotics and Automation Letters, volume 3, pages 2616–2623. IEEE, 2018.

[12] Jun Younes Louhi Kasahara, Hiromitsu Fujii, Atsushi Yamashita, and Hajime Asama. Weakly supervised approach to defect detection in concrete structures using hammering test. In Proceedings of the International Conference on Consumer Electronics (GCCE), pages 997–998, 2019.

[13] Jun Younes Louhi Kasahara, Hiromitsu Fujii, Atsushi Yamashita, and Hajime Asama. Complementarity of sensors and weak supervision for defect detection in concrete structures. In Proceedings of the International Symposium on System Integration (SII), pages 1–6. IEEE, 2020.

[14] Jun Younes Louhi Kasahara, Atsushi Yamashita, and Hajime Asama. Acoustic inspection of concrete structures using active weak supervision and visual information. In Sensors, volume 20, page 629. Multidisciplinary Digital Publishing Institute, 2020.

[15] Todor Ganchev, Nikos Fakotakis, and George Kokkinakis. Comparative evaluation of various MFCC implementations on the speaker verification task. In Proceedings of the International Conference on Speech and Computer (SPECOM), volume 1, pages 191–194. International Speech Communication Association, 2005.

[16] Meinard Müller. Information retrieval for music and motion. Springer, 2007.

[17] Aharon Bar-Hillel, Tomer Hertz, Noam Shental, and Daphna Weinshall. Learning distance functions using equivalence relations. In Proceedings of the International Conference on Machine Learning (ICML), pages 11–18, 2003.

[18] Dit-Yan Yeung and Hong Chang. Extending the relevant component analysis algorithm for metric learning using both positive and negative equivalence constraints. In Pattern Recognition, volume 39, pages 1007–1010. Elsevier, 2006.

[19] Stuart Lloyd. Least squares quantization in PCM. In Transactions on Information Theory, volume 28, pages 129–137. IEEE, 1982.

[20] William M Rand. Objective criteria for the evaluation of clustering methods. In Journal of the American Statistical Association, volume 66, pages 846–850. Taylor & Francis Group, 1971.

Road Maintenance Management System Using 3D Data by Terrestrial Laser Scanner and UAV

Satoshi Kubota[a], Ryosuke Hata[a], Kotaro Nishi[b], Chiyuan Ho[b], and Yoshihiro Yasumuro[a]

[a]Department of Civil, Environmental and Applied Systems Engineering, Kansai University, Japan
[b]Department of Civil, Environmental and Applied Systems Engineering, Graduate School of Kansai University, Japan
E-mail: skubota@kansai-u.ac.jp

Abstract –

In road maintenance, it is necessary to construct an environment that manages 3D data and maintenance information for its effectivity and efficiency. Engineers should be able to use 3D data not only for virtually reviewing the design of a facility, but also for analyzing building operations and performance. Using 3D data will thus improve the efficiency of operations and maintenance.

The primary objective of this research is to support road maintenance work using 3D data by combining point cloud data of terrestrial laser scanning (TLS) and unmanned aerial vehicles (UAV) with photogrammetry. TLS and photogrammetry technologies were used to survey pavement, landform, and bridge of road structures.

This research evaluated the accuracy of the usage of point cloud data by TLS and photogrammetry for road maintenance. This method can be used to check potholes and surface irregularities on pavement that can be easily and quickly confirmed by management. To evaluate the accuracy of 3D data of the bridge, we compare the 3D data with its design conditions. The 3D data describes the structure with high accuracy.

The 3D data could be used to develop a road maintenance management system that accumulates data and refers to the inspection results and repair information. The system can link inspection results and recondition information with the point cloud data for display, storage, and reference, facilitating the management of road cracks and areas for repair. The prototype system was developed using Skyline Terra Explorer Pro. It was visualized constructed 3D data on temporal sequence.

Keywords –

Three-dimensional Data; Point Cloud Data; Terrestrial Laser Scanning; Unmanned Aerial Vehicle; Road Maintenance; Information System

1 Introduction

Roads must be safe and maintained in good condition. Maintenance management is an essential operation that must be carried out effectively for maintaining, repairing, and rehabilitating roads. It is important to protect roads from large-scale damage and to carry out road maintenance in order to maintain services for the public. In addition, it is necessary to accumulate information produced during the entire life cycle of a road in order to analyze problems and solutions within a temporal sequence and to maintain roads strategically and effectively. In Japan, much road infrastructure was built over fifty years ago. Due to progressive deterioration in road infrastructure, ensuring proper maintenance of overall facilities to avoid potential problems is currently an important issue. In particular, in order to avoid or reduce substantial loss, deal with an emergency, prevent damage, perform emergency disaster control, and carry out disaster recovery, road administrators must maintain roads more efficiently. In current maintenance work, road administration facilities are represented on a 2D map, which is not suitable for pothole repair, inspection, or annual overhaul. Locating and analyzing a position can be difficult when using such a map.

There are many reported cases of damage to aging road structures. Existing structures are generally maintained rather than rebuilt, but blueprints and completion drawings may be unavailable for road structures that have been in service for a long time, and existing drawings may no longer reflect the current situation, hindering inspections and repairs [1]. To realize appropriate road maintenance, it is important to share information among all stakeholders, and easily shared 3D data with high visual fidelity are effective means toward this end. A road management system comprises functions for planning, design, construction, maintenance, and rehabilitation of roads. A fundamental requirement of such a system is the ability to support the modeling and management of design and construction information, and to enable the exchange of such

information among different project disciplines in an effective and efficient manner.

With the introduction of unmanned aerial vehicles (UAVs) and terrestrial laser scanners (TLS) in the "i-Construction" policy being promoted by the Japanese Ministry of Land, Infrastructure, Transport and Tourism, there will be increased use of 3D data in the future. Dense point cloud data were generated using three and over pictures which taken same points [2], [3]. Agarwal et al. and Frahm et al. were constructed 3D city by automated reconstruction [4], [5]. The 3D point cloud data are constructed on the basis of the Structure from Motion (SfM) range-imaging technique of photogrammetry using video camera data. The accuracy of 3D model by SfM were evaluated by several researches [6]. And, the generated point cloud data which measured the objects from several measurement points are integrated for representing the accurate objects. The integration method of point cloud data is iterative closest point method (ICP) [7], globally consistent registration method of terrestrial laser scan data using graph optimization [8], curve matching [9], [10], and automated registration using points curve [11].

However, there are outstanding issues related to TLS measurements. In particular, selection of appropriate measurement positions is difficult, data loss can occur, and increasing the number of measurements to obtain more detailed data increases measurement and data-processing times. Further, maintenance management systems for use of the generated 3D data are still under development. Data processing software differs according to the equipment used, and data storage can be complex.

In this study, we performed TLS, UAV, and camera measurements on road pavement, bridges, and slopes with the aim of realizing 3D data for road maintenance. We also devised a method for constructing 3D data for structures lacking existing drawing information. To do this, we attempted measurement methods and data generation for constructing highly accurate 3D data for a bridge from a small number of measurements. We also investigated functions for collectively managing the generated 3D data and visualizing results of inspecting the 3D data.

2 Use Cases of 3D Data

There are a number of survey methods for constructing 3D data using laser imaging detection and ranging (Lidar; laser profiler), laser-based photogrammetry, mobile mapping system, terrestrial laser scanning, and photogrammetry using a camera by UAV. Combining these survey methods according to site situations and structures enables surveys of civil infrastructure and construction of 3D point cloud data. It is necessary to understand the characteristics and specifications of the specific measurement instruments and choose suitable point cloud data for a use case for a road maintenance site.

In this research project, terrestrial laser scanning and UAV-based photogrammetry are used for usage scenes as shown in Figure 1. Usage scene 1 visualization of inspection results; Usage scene 2 visualization of damage on the structures; Usage scene 3 information management of inspection and damage; Usage scene 4 landslide; Usage scene 5 superposition of 3D data.

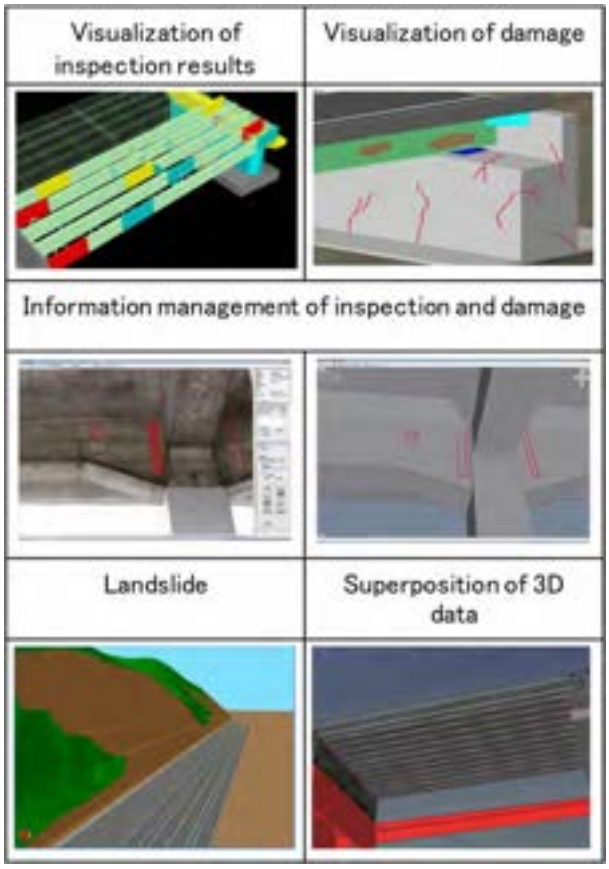

Figure 1. Usage scenes of 3D data

3 Measurement and Construction of On-site 3D Data

3.1 3D Data Measurements Using Multiple Devices

In addition to TLS and UAV images as used in our previous study [12], here we used SfM technologies to generate point-cloud data from camera images and combined the images and data to generate high-density 3D data. Equipment used were a laser scanner (Focus

3D X 330; FARO), a UAV (Inspire2 with mounted Zenmuse X5S camera; DJI), and a handheld camera (GoPro Hero6 Black; GoPro, Inc.).

3.2 Pavement Surface Measurement and 3D Data Construction

We performed TLS measurements in September 2019 on paved surfaces along the Shiraito Highland Way in Karuizawa, Nagano Prefecture. The Focus 3D X330 can perform high-density measurements of road surfaces over a range of about 10 m [12], so we measured 16 points at 20-m intervals based on an approximate 10-m radius, and constructed 3D data using the FARO SCENE data processing software. Figure 2 shows the 3D data of the pavement. To reduce the burden of image-joining tasks, we used triangular cones at 10-m intervals as targets during measurements. This reduced time required for joining tasks as compared with data construction in our previous study [12], but it was difficult to specify points in the 3D point-cloud data. In future studies we will investigate use of planar objects such as spheres and cylinders as feature points when combining images.

In combination with data collected in 2018, 3D data were constructed for a road length of about 580 m in Figure 3. The average error for point-to-point distances for joining locations in the measurement data was 4.7 mm, which was better than the accuracy of 8 mm required in this study. As reference points within the measurement range, we used slopes calculated from horizontal and vertical distances listed in the Shiraito Highland Way Toll Road Reference Point Survey and measured points near the reference points in the point cloud data. Comparing the obtained gradients showed differences of less than 0.5%, indicating that the gradients were essentially the same.

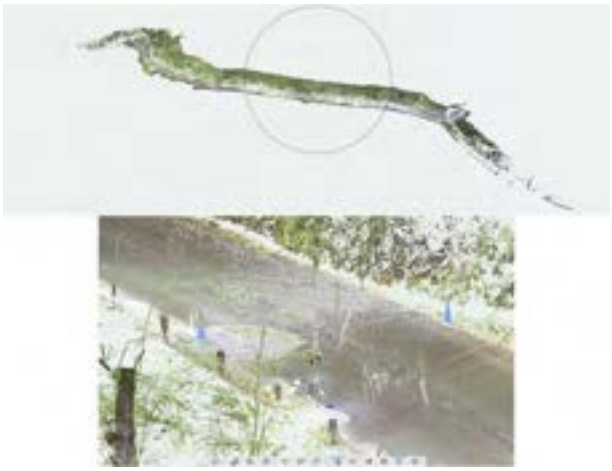

Figure 2. Joined road surface data

Figure 3. Joined FY2018 and FY2019 3D measurement data

3.3 Slope Measurement and 3D Data Construction

UAV measurements was performed in September 2019 on slopes of the Shiraito Highland Way in Karuizawa, Nagano Prefecture. Video images were extracted at 1-s intervals, and used the Metashape software package (Agisoft) to perform SfM processing on a computer with an Intel Core i9-9900X CPU, an NVIDIA GeForce RTX2070 GPU, and 64 GB RAM. The open-source point-cloud editing software package CloudCompare was used to overlay data constructed in FY2017, 2018 [12], and 2019 and performed differential analysis. Figure 4 shows the results, which indicate that the amount of accumulated sediment in the upper part decreased and that in the lower part increased in 2018 as compared to 2017, suggesting that sediment is flowing downward over time.

3.4 Bridge Measurement and 3D Data Construction

Measurements using TLS, UAV, and on-ground cameras were performed in July 2019 at the Warazuhata Bridge in Sennan, Osaka. We performed TLS measurements at six locations around the bridge, and combined data measured from pairs of diagonal points across the bridge with the 3D data constructed by SfM processing of images captured by the UAV and the camera in Figure 5. The upper figure of Figure 5 shows 3D data created by combining TLS and UAV photogrammetry. The lower figure shows 3D data created by combining data created from TLS and handheld camera images. As a result, we were able to provide data for the superstructure and the abutment sections, which were missing in the 3D data constructed from the two-sites TLS measurements, and we could construct 3D data showing the bridge length and width. For the bridge length and width, we compared measurement results in the 3D data constructed from the six TLS measurements with design specifications from the Kishiwada Civil Engineering Office and with on-site measurements. Table 1 shows the results, which suggest that the 3D bridge data constructed in this study has a

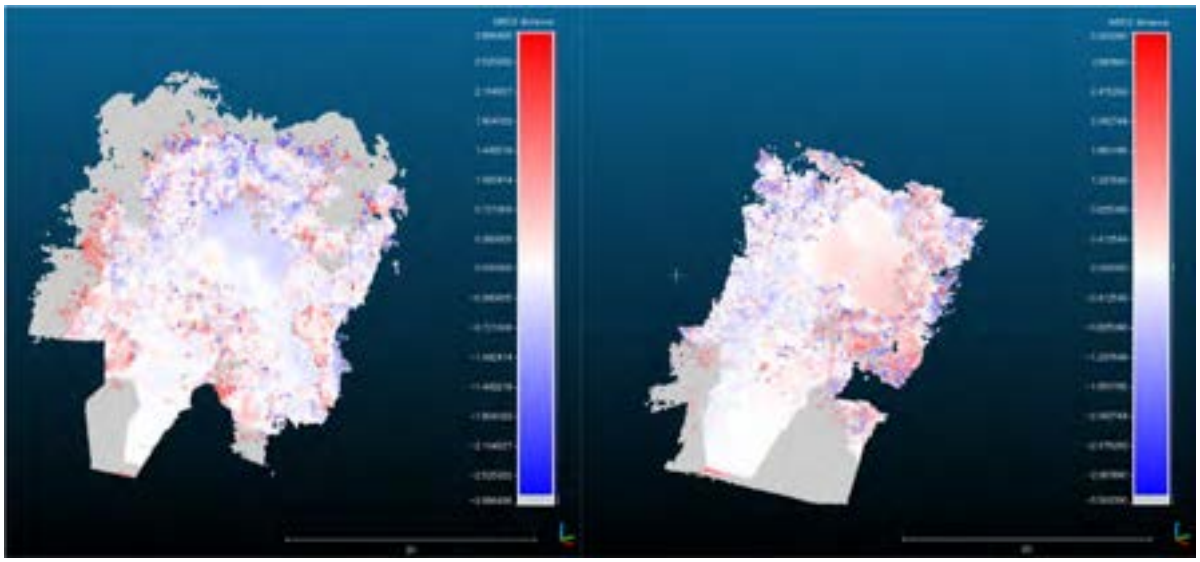

Figure 4. Differential data for (upper) FY2017 and 2018 and (lower) 2018 and 2019

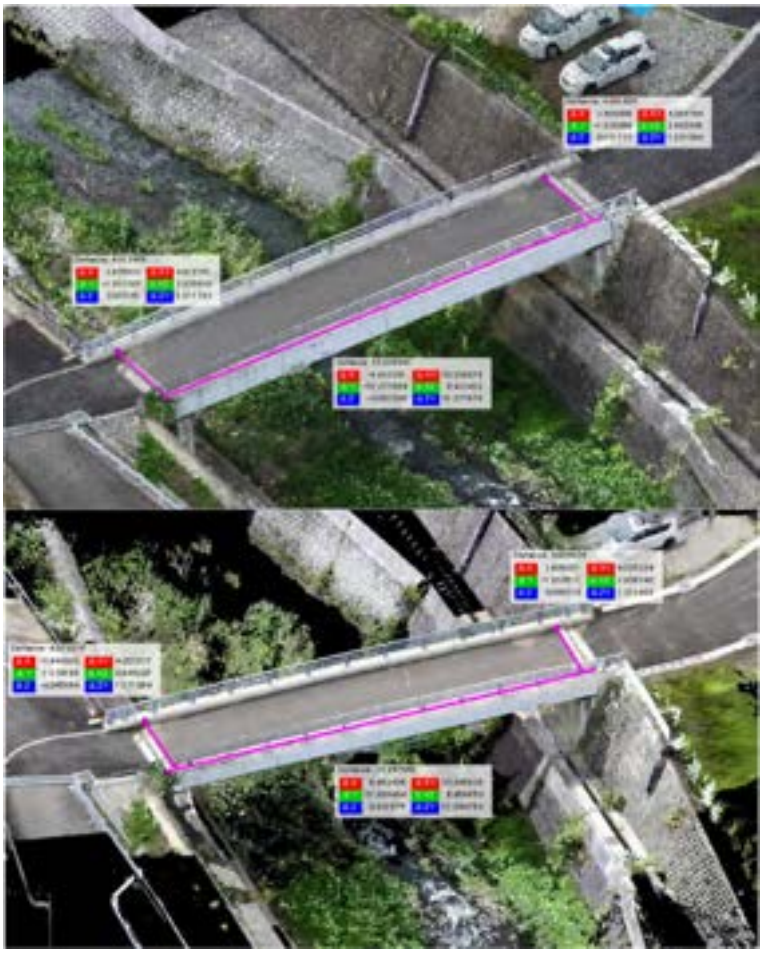

Figure 5. (Upper) 3D data combining TLS and UAV photogrammetry and (lower) 3D data combining data created from TLS and handheld camera images

level of development of around 200 as indicated in the level of development for three-dimensional model in civil engineering (Draft) [13].

The time required for TLS measurements at six locations was about 2 hours, while the time for two locations was about 40 min. In contrast, the UAV photography time was about 15 min including preparation and GoPro shooting time was about 10 min, suggesting their potential for shortening on-site measurement times.

To construct 3D data with location information, in November 2019 we took a series of photographs with a GoPro camera capable of acquiring location information at an unnamed bridge in Niigata City, Niigata Prefecture, and performed SfM processing to construct 3D data in Figure 6. Selecting an arbitrary point in the 3D data shows the latitude and longitude for that point. The data do not have the ground control points. The data were set using the latitude and longitude of GPS of GoPro camera. We arranged it using aerial photograph.

Table 1. Comparison of measured lengths and widths

	Length (m)	Width (m)
Design specifications	22.200	4.000
On-site measurement	22.253	4.025
TLS (6 locations)	22.258	4.013
TLS (2 locations) and UAV	22.229	4.052
TLS (2 locations) and camera	22.247	4.024

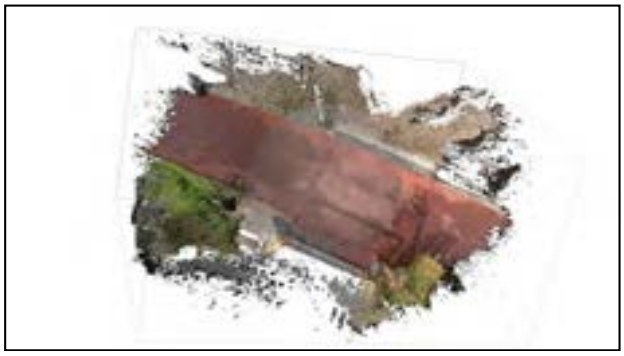

Figure 6. 3D data from SfM processing for a bridge

4 GIS Visualization of 3D Data

The 3D point cloud data for the road pavement surface and the bridge could be used to develop a road maintenance management system that accumulates data and refers to the inspection results and repair information in three dimensions.

An information system for road maintenance is proposed in this research project. This chapter discusses the information system, which uses point cloud data based on the definition of an information system. By definition, an information system collects, processes, transfers, and utilizes information in its own domain. Figure 7 depicts the definition of a road maintenance information system using point cloud data. A road maintenance system was considered based on the definitions within an information system. The road maintenance system can link inspection results and recondition information with the point cloud data for display, storage, and reference, facilitating the management of road cracks and areas for repair. In future work, point cloud data will be used to identify changes in the shape and condition of damage through spatial and temporal management.

Figure 7. Definition of road maintenance management system

4.1 Information Collection

Point cloud data for road infrastructure are collected using terrestrial laser scanning and UAV-based photogrammetry. In addition, maintenance and operation data, such as for inspection, rehabilitation, and repair, are collected on-site for the system.

4.2 Information Processing

Point cloud data generated by TLS contain noise data concerning trees and vegetation on a road. In information processing, such objects should be removed in order to represent road structures accurately. terrestrial laser scanning's survey range is confined to the visible range and the scan range of the scanner; therefore, it contains blind spots that are not represented

by the point cloud data cloud. Accordingly, surveyors need to move the scanner to multiple locations across a number of points in time. UAVs can acquire photographs or videos in-flight. Such visual records are used for SfM software and translated point cloud data. In addition, the point cloud data are colorized for visualization.

4.3 Information Transmission

TLS and UAV-based photogrammetry each have distinct characteristics with respect to survey time cost, scan range, and accuracy. Wide area and high precision point cloud data are generated by combining each set of data units. In addition, in this process, structural members and surface data, such as a triangulated irregular network, are extracted and generated in accordance with the purpose of usage. Furthermore, it is also possible to compare two different temporal data units for analysis.

4.4 Usage of Information

In this research project, instead of a surface model, point cloud data are used for road maintenance. A road maintenance information system is proposed, which has functions for detecting cracks and superimposing photographs based on point cloud data. In addition, a function is needed for reflecting inspection and repair events that have been represented on a two-dimensional map displayed on a smart device onto 3D point cloud data on-site. In the road maintenance system, the inspection result and repair information can be linked with 3D point cloud data and displayed, stored, and referenced. It is easy to detect road cracks and spots in need of repair. In addition, it is possible to determine changes in shape and damage using temporal management of point cloud data.

We arranged the constructed 3D data using absolute GIS coordinates, storing these data with corresponding inspection results. This should allow road managers to better grasp topographical information for the surrounding area and to store positional coordinates for stored locations, leading to more efficient maintenance. By road managers performing regular inspections and confirming and comparing 3D data before and after a disaster, this function can be applied to grasping the damage situation. We used Terra Explorer Pro (Skyline Software Systems) as GIS software for displaying 3D data. Absolute coordinates for road pavement and slopes were given using the “Align two clouds by picking (at least 4) equivalent points pairs” function in Cloud Compare and displayed on a 3D map. Because 3D data for the Warazubata Bridge did not have position coordinates and thus could not be displayed at an arbitrary position, we manually set latitudes, longitudes, and altitudes in reference to aerial photographs. Regarding the 3D data for the unnamed bridge in Niigata, comparing bridge positions on Google Earth showed no significant differences for latitude and longitude, but there were large displacements for altitudes, causing the 3D data in the map display to appear as if floating in air. We therefore corrected positions in reference to aerial photographs. Displaying the 3D data on a map confirmed cracks in the paved surface, and 3D data from two different periods could be displayed in Figure 8 and 9. These figures show the registration function of the system for accumulating the inspection and damage information on the point cloud data.

Figure 8. 3D Road surface data display in the system

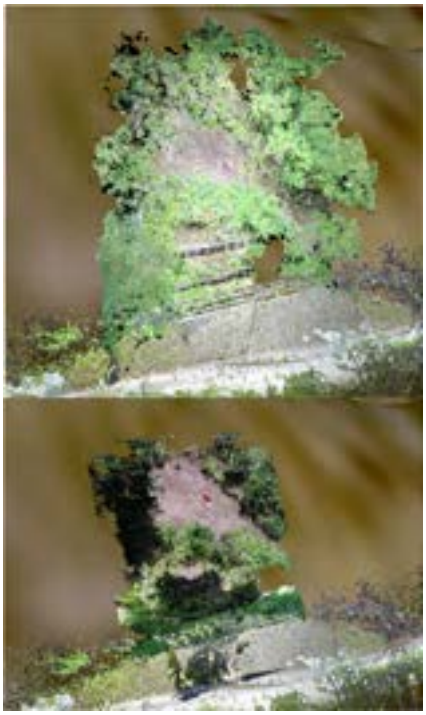

Figure 9. 3D land form data display in the system

5 Conclusion

In this study, we investigated a system for using TLS, UAV, and cameras to construct 3D data for road pavement, slopes, and bridges. The system provides absolute coordinates, displays them on a 3D map, and can store and reference inspection results at any location. Future tasks will include improving the efficiency of overlaying 3D data constructed in different years by setting positioning points during measurements, and creating 3D data with positional information for measurements of sediment runoff.

Acknowledgements

The part of this work was supported by Japan Society for Promotion of Science (JSPS) Grants-in-Aid for Scientific Research (20K04652), Japan Digital Road Map Association, and the Kansai University Grant-in-Aid for progress of research in graduate course, 2020.

References

[1] Ministry of Land, Infrastructure, Transport and Tourism, *Proposals for implementation of measures against road deterioration*. 2014.

[2] Furukawa, Y. and Ponce, J., Accurate, dense, and robust Multiview stereopsis, *IEEE Transactions on Pattern Analysis and Machine Intelligence*. 32(8): 1362-1376, 2010.

[3] Hirschmuller, H., Stereo processing by semiglobal matching and mutual information, *IEEE Transactions on Pattern Analysis and Machine Intelligence*, 3(2): 328-342, 2008.

[4] Agarwal, A., Snavely, N., Simon, I., Seitz, S. and Szeliski, R., Building Rome in a day, In *ICCV09*, pages 72-79, 2009.

[5] Frahm, J.M., Fite-Georgel, P., Gallup, D., Johnson, T., Raguram, R., Wu, C., Jen, Y.H., Dunn, E., Clipp, B., Lazebnik, S. and Pollefeys, M., Building rome on a cloudless day, In *ECCV10*, pages 368-381, 2010.

[6] Remondino, F., Del, P.S., Kersten, T.P. and Troisi, S., Low cost and open source solutions for automated image orientation – a critical overview, *Lecture Notes in Computer Science*. 7616, pages 40-54, 2012.

[7] Besl, P. J. and McKay, H. D., A method of registration of 3-D shapes, *IEEE Transaction Pattern Analysis and Machine Intelligence*. 14(2): 39-256, 1992.

[8] Pascal, W. H., Wegner, J. D. and Schindler, K., Globally consistent registration of terrestrial lase scans via graph optimization, *ISPRS Journal of Photogrammetry and Remote Sensing*. 109: 126-138, 2015.

[9] Grune, A. and Akca, D. Least squares 3D surface and curve matching, *ISPRS Journal of Photogrammetry and Remote Sensing*. 59: 151-174, 2005.

[10] Yang, B. and Zang, Y., Automated registration of dense terrestrial laser-scanning point clouds using curves, *ISPRS Journal of Photogrammetry and Remote Sensing*, 95: 109-121, 2014.

[11] Yang, B., Dong, Z., Liang, F. and Liu, Y., Automated registration of large-scale urban scene point clouds based on semantic feature points curves, *ISPRS Journal of Photogrammetry and Remote Sensing*. 113: 43-58, 2016.

[12] Kubota, S. and Ho, C.Y., Creation of three-dimensional data for road maintenance using several measurement instruments. *Journal of Japan Society for Fuzzy Theory and Intelligent Informatics*, 31(6): 867-875, 2019.

[13] The committee for standardization of civil infrastructures, *The level of development for three-dimensional model in civil engineering (Draft)*. 2017.

Traffic Regulation Technology by Movable Barriers

Toshiharu Tanikawa[a] and Tohya Okishio[b]

[a] Deputy Director General, Kanto Regional Head Office, East Nippon Expressway Company Limited, Japan
[b] Nexco-East Innovation &Communications Company Limited, Japan
E-mail: t.tanikawa.aa@e-nexco.co.jp, t.okishio.aa@e-nexco.co.jp

Abstract –

Approximately a half century has passed since the construction of expressways in Japan, and expressways have become decrepit over the decades. In order to ensure safety and security of expressways for the next generation, expressway companies have been carrying out large-scale renewal works of bridges and tunnels (hereinafter collectively the "renewal works" and individually a "renewal work").

Because renewal works are carried out while vehicles pass by the side of work zones, various types of safety equipment have been used to regulate traffic lanes such as rubber road cones, more rigid temporary barriers and so forth. However, speeds of passing vehicles are fast and, if a vehicle accidentally enters a work zone, rubber road cones cannot prevent from a vehicle entry which endangers workers' lives.

Therefore, East Nippon Expressway Company Limited (hereinafter "NEXCO EAST") group adopted traffic regulation technology by movable barriers, the Road Zipper System (hereinafter "the RZS"), for renewal works. Using the RZS is aimed at improving workers' safety by prevention of accidental vehicle entries and alleviating traffic congestion by more efficient traffic regulation.

This paper examines effects of the RZS introduction, enhancement of safety and prevention of traffic congestion associated with the use of the RZS in traffic regulations and lane reconfigurations according to the time of day, as well as future developments.

Keywords –

expressway; traffic regulation technology; traffic regulation for construction works; lane regulation; lane management; movable barriers; Road Zipper System; safety and security; traffic congestion alleviation; traffic congestion prevention

1 Introduction

The RZS is the lane management system by a Barrier Transfer Machine (hereinafter "BTM") transferring crash-tested barriers from one side to another (Figure 1).

The RZS is a system from a company in the USA, Lindsay Transportation Solutions LLC (hereinafter "LTS"). Nexco-East Innovation & Communications, one of NEXCO EAST group subsidiaries, is appointed to sell and lease BTMs and related products to expressway companies in Japan, based on a formal agreement with LTS.

Figure 1. BTM working situation abroad

An overview of the RZS is transfer of barriers from one side to another through an S-shaped conveyor mounted at the sides and bottom of a BTM (Figure 2 and 3).

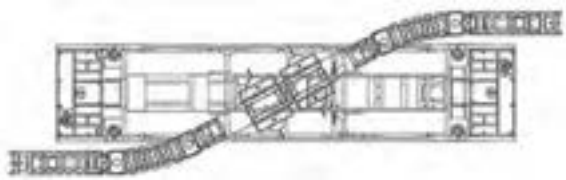

Figure 2. BTM Conceptual Diagram [1]

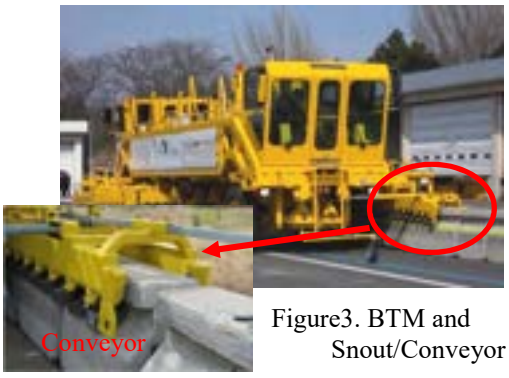

Figure3. BTM and Snout/Conveyor

There are three types of barriers used in the RZS. The main barrier is Concrete Reactive Tension System (hereinafter "CRTS") which is composed of reinforced concrete. (Figure 4).

Other than CRTS, there is a steel barrier called a Variable Length Barrier (hereinafter "VLB") which extends and contracts to adjust a shape and vertical grade of road and is set at regular intervals in alignment of CRTSs (Figure 5). The final component is a crash cushion installed at ends of the CRTS barrier alignment so as to absorb impact of a vehicle crash (hereinafter "Absorb") (Figure 6). There does exist different options within the RZS, but the systems deployed in Japan currently are referenced above and illustrated below.

Figure 4. CRTS

Figure 5. VLB

Figure 6. Absorb

2 Examination for RTS introduction

NEXCO EAST conducted a demonstration experiment on Joban Expressway from April through July in 2016 so as to confirm and examine effectiveness of the RZS for its future introduction in Japan (Figure 7).

Figure 7. Demonstration Experiment
(Left: rubber road cones Right: the RZS)

From the experiment, two results turned out superiority of the RZS in comparison to conventional equipment, rubber road cones.

The outcomes were found from image analyses; lanes were regulated by rubber road cones and the RZS respectively on the expressway, and three fixed cameras on over bridges and tracking cameras set up on a car for cone installation and a BTM captured vehicles' behavior while the vehicles were passing by the regulated lanes.

One result is the ratio of drivers' avoidance behavior to keep a distance from regulation equipment during installment and removal at night by the RZS was approximately 15% lower than by rubber road cones.

Another is the ratio of drivers stepping on the brakes while lanes were regulated at night by the RZS also turned out to be lower than the one of rubber road cones (Figure 9).

Those two results show the RZS ensures a higher level of safety and security towards vehicles and drivers.

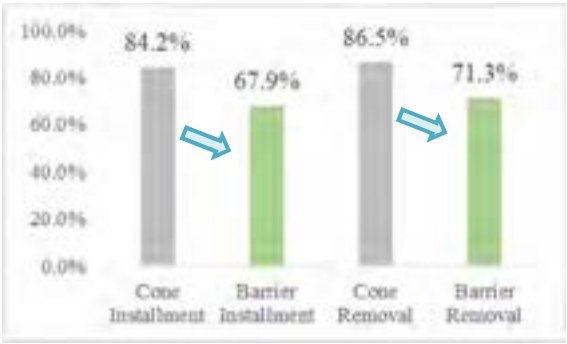

Figure8. Comparison of drivers' avoidance behaviour between uses of rubber road cones and the RZS barriers during instalment and removal [2]

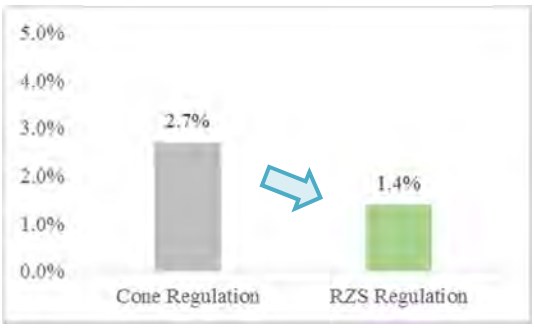

Figure 9. Comparison of drivers' actions of stepping on the breaks between uses of rubber road cones and the RZS barriers [2]

Consequently, NEXCO EAST fully introduced and utilized the RZS for traffic regulations for construction works in some projects such as construction of Tokyo-Gaikan Expressway and additional lane construction of Kan-etsu Expressway in Kanto Regional Head Office. In addition, the RZS has been used in several renewal works for regulating and opening lanes quickly and efficiently, and assuring safety and security.

The next chapter shows concrete examples of full introduction and utilization of the RZS with backgrounds, processes and evaluations.

3 Full introduction and utilization of the RZS

3.1 A renewal work of Shimamatsugawa Bridge of Hokkaido Expressway

Sapporo Operation Office, Hokkaido Regional Head Office of NEXCO EAST utilized the RZS for lane managements and regulations in order to alleviate traffic congestion in a renewal works, the project of floor slab replacement, at Shimamatsugawa Bridge.

About 47 years had passed since the Bridge opened and the Bridge severely deteriorated due to anti-freezing agents and some other influences.

3.1.1 Outline of the project site

The Shimamatsugawa Bridge is located between Eniwa Interchange (Interchange is used as an entrance and exit of an expressway. hereinafter "IC") and Kitahiroshima IC of Hokkaido Expressway (Figure 10).

The section between the two ICs is an important route and part of expressways in Hokkaido because it connects New Chitose Airport, the gateway of Hokkaido, and Sapporo, a major city.

A daily traffic volume of both up and down lanes between the two ICs is approximately 40,000.

Figure10. Location of Shimamatsugawa Bridge [3]

3.1.2 Traffic Regulation Examination

Since the section of the project site is considered to be important, it is difficult to close both up and down lanes for a long term. Therefore, the method regulating a down lane and dividing into two-way traffic was adopted while the floor slab replacement of up lanes were carried out.

Regarding to traffic characteristics in the section on Monday through Saturday, traffic volume rises in the morning on the up lane from Sapporo to New Chitose Airport, and the peak time is mostly at around 7 am.

This is associated with passengers using New Chitose Airport and commercial vehicles which are mainly from Sapporo. On the other hand, traffic volume increases in the afternoon on the down lane from New Chitose Airport to Sapporo, frequently at around 6 pm.

As clearly shown, there is a significant difference of hourly traffic volume between up and down lanes; the volume of one lane at peak time on both lanes surpass a traffic capacity (1,400 unit per hour) therefore it was predicted traffic congestions would happen every single day (Figure11).

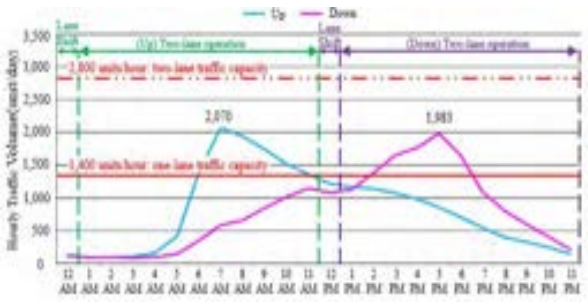

Figure11. Hourly traffic volumes of the up and down lanes between Eniwa IC and Kitahiroshima IC on weekdays [3]

On the purpose of traffic congestion prevention, three traffic lanes were ensured on the down lane by narrowing the width of road shoulder from 1.25m to 0.5m and traffic lanes from 3.50m to 3.25m.

A combination of two lanes and one lane for the up and down lanes were shifted by time of day from Monday through Saturday depending on the traffic characteristics (Figure 12).

Traffic volume of the up lane in Sunday afternoon does not go below the one-lane traffic capacity, hence two lanes were open operated as the up lanes so as to ensure access punctuality to New Chitose Airport.

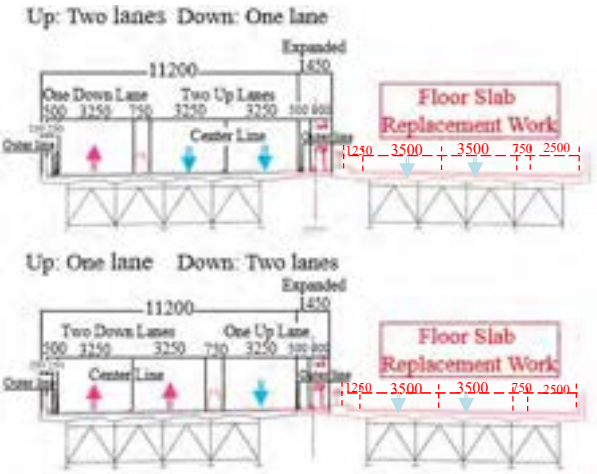

Figure12. Lane management cross-section view (unit: mm) [3]

With regard to daily lane shifting in two-way traffic, traffic administrator had an opinion towards a usage of conventional regulation equipment, rubber road cones, as temporary central median for two-way traffic regulation: there is a high risk of head-on vehicle collision in the heavy traffic section.

In addition, it is impossible to shift lanes by rubber road cones without expressway closure. In order to resolve and adjust the problem, the RZS was put on the table to ensure safety of vehicles and streamline lane regulation work since the RZS have proven records of lane managements and shifts in other countries.

The regulation plan of the renewal work was reviewed and changed to the one by the RZS: using temporary medians composed of barriers and transferring them by time of day for lane shifts. In the end, with the consent of traffic administrator, the RZS was adopted for the first time in Japan to regulate traffic by shifting lanes from one to two and vice versa on the expressway.

3.1.3 Traffic Regulation Operation by the RZS

Traffic regulations were implemented during the period from May 29th to July 12th, 2018, except for Sundays, by shifting the number of up and down lanes between 12 pm and 1 pm and 12 am and 1 am in a day by transferring temporary center median composed of barriers (Figure13 and 14).

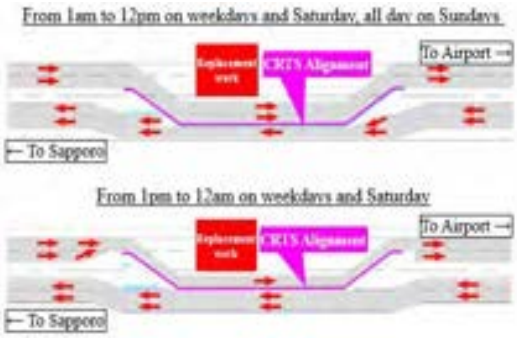

Figure13. Illustration of lane shiftting [3]

Figure14. Lane shifted by the RZS

3.1.4 Result of Traffic Regulation by the RZS

The results of traffic regulation by the RZS came out as follows.

- If conventional two-way traffic regulation was implemented, the estimated number of days and maximum length of traffic congestion during the project period would be 37 days and 18 km on the up lane and 27 days and 18 km on the down lane, while the actual occurrences of traffic congestion were 0 days and 0 km on the up lane and 6 days and 3.4 km on the down lane.
- On holidays, the estimation of number of days and the maximum length of traffic congestions were 5 days and 14 km on the up lane and 6 days and 8 km on the down lane. However, the actual number of days and maximum length were 0 day and 0km on the up lane and 6 days and 5.1km on the down lane.

The RZS contributed to safety of drivers by alleviation of traffic congestion compared to prediction both on weekdays and weekends, and reduction of major accidents by blocking breakthrough of temporary central medians.

3.2 A renewal work of Takase Bridge of Hokuriku Expressway

Nagaoka Operation Office, Niigata Regional Head Office of NEXCO EAST used the RZS for lane management and regulation in the project of floor slab replacement of Takase Bridge on the up line of Hokuriku Expressway in the direction to Nagaoka. About 40 years had passed since the Bridge opened and the Bridge had faced severe deterioration.

3.2.1 Outline of the project site

Takase Bridge is located right before diverging lanes of Nagaoka Junction between Nagaoka Junction and Nakanoshimamitsuke IC of Hokuriku Expressway (Figure15).

The Bridge includes a ramp (a speed change lane) of Hokuriku Expressway bound for Toyama therefore three-lane width was ensured at the site.

Figure15. Location of Takase Bridge [4]

3.2.2 Traffic Regulation Examination

The traffic volume in this section is relatively large and a cross section traffic volume of approximately 32,000 vehicles. In the case that floor slab replacement work is carried out on an up line, that up line is normally closed and two lanes on a down line are used as two-way traffic: one lane for the up and another for the down. However, it was highly predicted severe traffic congestions would happen on both of the one up and one down lane at this project site, which also requires large-scale traffic regulations.

Thus, in order to take an advantage of three-lane width of this Bridge, the floor slab replacement work was divided into three steps based on each of three traffic lanes (Figure16) and the width was reduced from 3.5m to 3.25m; two traffic lanes remained open while one lane was under the replacement work.

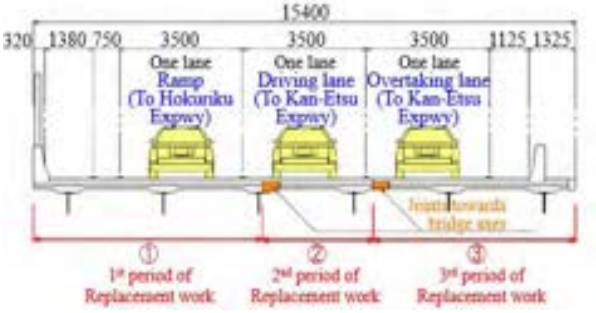

Figure16. Replacement work steps (unit: mm) [5]

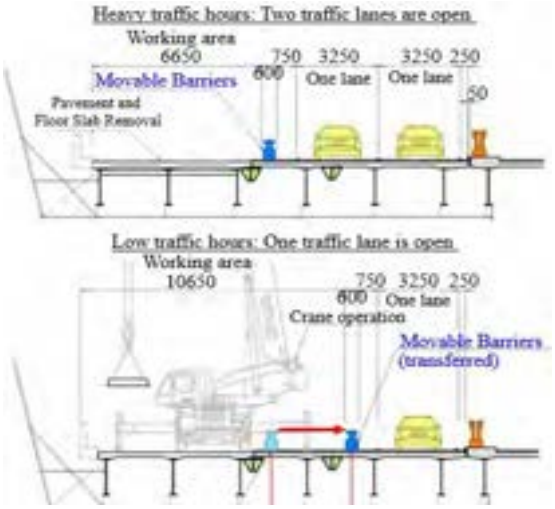

Figure17. Lane management based on hourly traffic volumes (unit: mm) [5]

By using this method, two lanes were always open while any lane was under the replacement work. Moreover, two lanes were closed for operation by a crane which requires larger working area, during time of low traffic volume, and lanes were shifted on a daily basis depending on the time of day (Figure17).

3.2.3 Traffic Regulation Operation by the RZS

For implementation of traffic regulations from the end of August to the mid of November, 2018, two driving lanes were secured from 7 am to 12 pm: the time period when hourly traffic volume is heavy on weekdays from Monday to Saturday. During the other time period from 12pm to 7 am, only one lane was open for traffic and the replacement work proceeded in the two closed lanes.

On holidays, two lanes were open from 7 am to 8 pm and one lane was designated as a traffic lane from 8 pm to 7 am the following day by RZS (Figure18 and 19).

Figure18. Traffic Management by the RZS

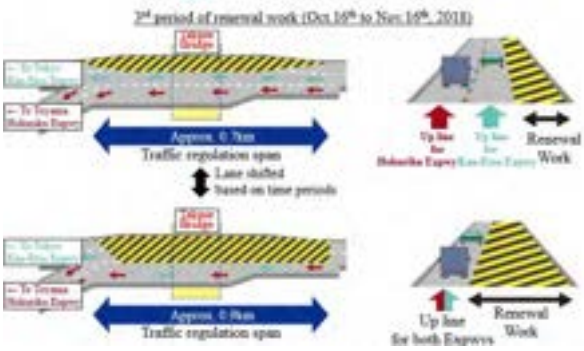

Figure19. Traffic regulation by the RZS in the 3rd period of renewal work [5]

This renewal work was completed within the scheduled period although it was difficult to manage a work process by the influence of rain on works accompanying the replacement work due to many rainy days.

During the project period, traffic congestions occurred twice and both were relatively small in scale: one is 3.0km at maximum for 30 minutes on Wednesday, September 26th and another is 1.7km at maximum for 2 hours on Saturday, October 6th.

From the perspective of congestion by traffic regulation for construction works, impacts on drivers was minimized and there were no breakthrough of temporary central medians and no major accident; hence, the RZS contributed to safety of drivers and workers..

3.3 The RZS implementation by another company, Central Nippon Expressway Company Limited

Although NEXCO EAST introduced the RZS for the first time in Japan, RZS is also used by Tokyo Regional Head Office of Central Nippon Expressway Company Limited (hereinafter "NEXCO CENTRAL") so as to regulate traffics in renewal work of Tomei Expressway.

They introduced the RZS in order to prevent serious accidents caused by breaking through temporary central medians, and to shorten a period of time for installment and removal of barriers used as the medians. Two examples of projects are listed below.

- Renewal work in 2017 (Numazu IC – Fuji IC, Tomei Expressway)
  Regulation: Two-way regulation by day and night
  Project: Floor slab replacement work of Akabuchigawa Bridge (down line)

- Renewal work in 2018 (Susono IC – Fuji IC, Tomei Expressway)
  Regulation: Two-way regulation by day and night
  Project: Floor slab replacement work of Kaminagakubo Bridge (up line) and Ashitaka Bridge (up line)

4 Future Developments

4.1.1 More uses and developments of the RZS

Currently, the RZS is being used in a number of renewal projects and construction works by NEXCO EAST and NEXCO CENTRAL.

In addition, Kansai Regional Head Office of West Nippon Expressway Company Limited is also planning traffic regulations for construction works and lane managements by the RZS for a renewal work of Chugoku Expressway. The uses of RZS on expressways has been promoted across Japan.

4.1.2 Modification of BTM for further safety and efficiency

Meanwhile RZS is widely used on expressways, there are also several challenges. One is a size of a BTM; RZS has been used a lot in other countries including America and expressways, highways and roads in those countries consists of more and wider traffic lanes compared to those in Japan.

Examples of BTM dimensions are in Table 1 and actual machines are shown in Figure19 and 20.

Table 1. RTS BTM dimensions

Element	BTM for traffic regulation for construction works [(Numbers) are without conveyors]
Width	4.32m (2.54m)
Length	14.8m (12.8m)
Weight	22t (20t)

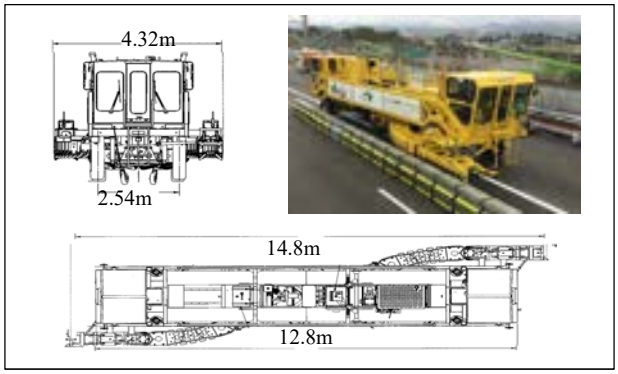

Figure 19. BTM for traffic regulation for construction works [1]

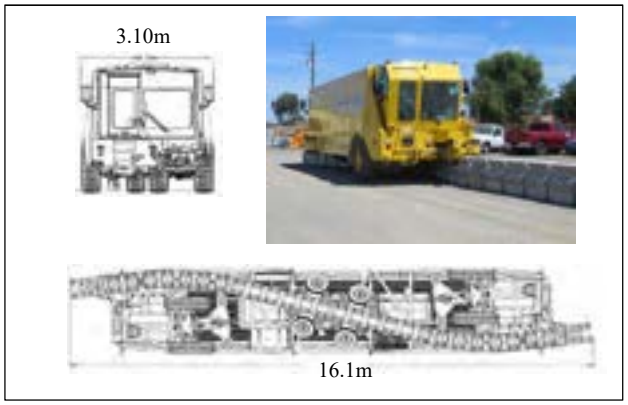

Figure 20. BTM for permanent lane management [1]

Other than a BTM for construction applications, there are other BTM models used for permanent lane management. Some have a width that fits within a traffic lane in Japan. However, the weight is heavier than 25t therefore investigation and confirmation about safety to pass through bridges and other road structures is necessary.

As a result, it does take time and effort to transport such a BTM.

In addition, the BTM exceeds general limits required by law for dimensions of vehicles in Japan therefore conveyors must be removed and transported by a special low-floor trailer, which also requires additional time, effort and expense.

Hence, in order to utilize RZS more safely and efficiently in Japan, after a request from NEXCO EAST, LTS agreed to and currently develop the new model "N-Class", a downsized BTM (named after NEXCO Group), for consideration of the machine size that the BTM fits and drives in the regulated area for construction (within the width of one driving lane) without removing conveyors and can be transported by a normal low-floor trailer rather than a special one.

5 Conclusions

The number of renewal works are expected to increase more and more in the future so as to ensure the safe use of expressways. However, there have been many accidents due to incursions of general vehicles into area regulated for construction works; hence, it is important to ensure safety of construction works in regulated area on heavy traffic lanes for a long span of time.

At the same time, it is necessary to carry out works in traffic regulation area more efficiently during limited time periods such as at night time with the low volume of traffic. It is believed that the RZS will contribute to improvement of safety and efficiency of traffic regulation for construction works

, and will be utilized by more companies and organizations as a measure to ensure safety and alleviate traffic congestion through development and improvement of the RZS.

References

[1] A drawing of BTM owned by LTS

[2] NEXCO EAST. A research paper. *Verification of vehicles' behavior towards lane regulation for construction works on Joban Expressway for RZS utilization*. 2016

[3] NEXCO EAST Hokkaido Regional Head Office. Explanatory material for a renewal work of Shimamatsugawa Bridge of Hokkaido Expressway. 2018

[4] Geospatial Information Authority of Japan. Map in English (captured and edited by Tohya OKISHIO). https://maps.gsi.go.jp/multil/index.html#8/36.102376/140.042725/&base=pale2&ls=pale2%7Chillshademap%2C0.1%7Cchuki_eng&blend=0&disp=111&lcd=chuki_eng&vs=c1 Accessed: 09/06/20

[5] NEXCO EAST Niigata Regional Head Office. Explanatory material for a renewal work of Takase Bridge of Hokuriku Expressway.2019

Development and Verification of Inspection Method for Concrete Surface utilizing Digital Camera

Shungo Matsui[a], Yoshimasa Nakata[b], Shitashimizu Hidenori[c], Nakatsuiji.Ryota[d], Takeshi Ueda[e], and Naoki Maehara[f]

[a] West Nippon Expressway Engineering Kansai Co.,Ltd., Japan
[b] West Nippon Expressway Innovation Co.,Ltd., Japan
[c] West Nippon Expressway Engineering Kansai Co.,Ltd., Japan
[d] West Nippon Expressway Engineering Kansai Co.,Ltd., Japan
[a] West Nippon Expressway Co.,Ltd., Japan
[f] West Nippon Expressway Co.,Ltd., Japan
E-mail: s_matsui@w-e-kansai.co.jp, y.nakata@w-nexco-inv.co.jp, h_shitashimizu@w-e-kansai.co.jp, r_nakatsuji@w-e-kansai.co.jp, t.ueda.ac@w-nexco.co.jp, n.maehara.aa@w-nexco.co.jp

Abstract –

Currently, road managers are required to maintain and renew road assets that are rapidly aging and damaged. On the other hand, due to the ever-increasing road assets, social problems such as cost reduction and shortage of engineers in maintenance and renewal are occurring. In particular, the "Road Bridge Periodic Inspection Procedure" was formulated in June 2014, and the periodic inspection is based on close-up visual inspection once every five effore, which requires enormous expenses and personnel. Therefore, efficient and economical inspection by applying non-destructive inspection technology is strongly required. For this reason, NEXCO West Japan Group has developed a digital camera inspection system (hereinafter referred to as Auto-CIMA) for the purpose of enhancing the structure inspection and improving efficiency.

Keywords –

Digital camera; Non-destructive inspection; Inspection; Crack;

1 Introduction

Auto-CIMA is a system that acquires high-definition images from digital cameras in order to grasp and inspect the state of concrete structures. Auto-CIMA can automatically paste the high-definition images that have taken and digitally check the surface condition of concrete. In addition, cracks and their widths (widths more than 0.1 mm can be visually confirmed in the image) and lengths can be automatically extracted, and the secular change of cracks can be grasped by accumulated data.

According to the verification from the development to the present, the inspection using Auto-CIMA has a condition that it is inefficient, but it does not require adjustment work or high place work by inspection, so it is economically advantageous. It has also been confirmed that the same inspection results as the close-up visual inspection can be obtained by combining with an inspection method that captures internal damage such as floating or peeling of concrete by infrared inspection.

Currently, we are verifying the applicability of Auto-CIMA as one of the inspection methods for periodical inspection, and it is expected that the efficiency of inspection using Auto-CIMA will be improved in the future. Here, I will report the outline.

2 Auto-CIMA

2.1 Overview of Auto-CIMA

Auto-CIMA is an inspection method that grasps the condition of the concrete surface of a bridge by acquiring high-definition images with a digital camera. The captured high-definition images are automatically pasted together and expanded in a plane, and the surface condition of the concrete can be confirmed on the digital image from the expanded image. Furthermore, cracks and their widths and lengths can be automatically extracted, and secular changes in cracks can be grasped by accumulated data. The Auto-CIMA shooting is aimed at a concrete plane and can shoot up to a distance of 40 m. Under this shooting distance condition, cracks with a width of more than 0.2 mm can be automatically extracted, and cracks with a width of more than 0.1 mm can be confirmed visually with a digital image. Table 1 shows the targets and specifications of Auto-CIMA.

Table 1. Targets and specifications of Auto-CIMA

target	specification
Hollow slab bridge	Shooting distance:2m～40m
Box-girder bridge	Shooting angle:Within 45°
Abutment	Shooting renge:Horizontal Within ±45°
Pier	Vertical Within ±30°

2.2 Features of Auto-CIMA

①Automatic shooting

Auto CIMA can photograph concrete planes by automatically operating a digital camera with an electric pan head shown in Fig. 1 on a PC. The shooting range for one shot is ±45° on the long side and ±30° on the short side, and the dimensions differ depending on the shooting distance. The shooting plan (shooting angle of view and direction) shown in Figure 2 is automatically set by setting the shooting range and shooting accuracy (0.5mm/pixel in NEXCO West Japan) on the PC. This eliminates erroneous measurement during shooting as much as possible.

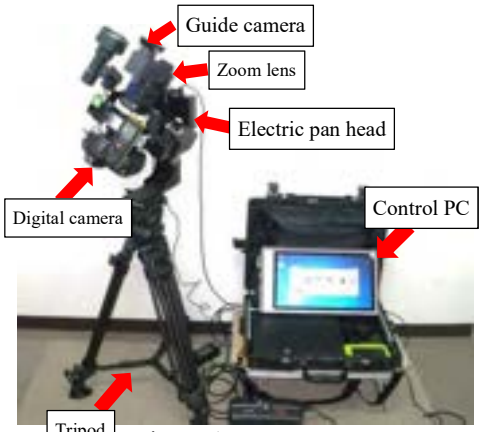

Figure 1. Auto CIMA

Figure 2. Shooting plan

②Image composition

Auto-CIMA can easily check the shooting status of automatically shot images (Fig. 3 (a)). Images that are out of focus due to obstacles such as electric wires during automatic shooting can be re-shot with manual shooting. It is difficult to recognize as a single image due to the color unevenness of the image composition. Therefore, the captured images are stitched together with high precision by image processing. (Fig. 3(b)). Since this high-definition image composition requires processing on a high-performance PC, it is performed indoors rather than immediately after shooting.

a) Simple pasting image b) High-precision stitched image

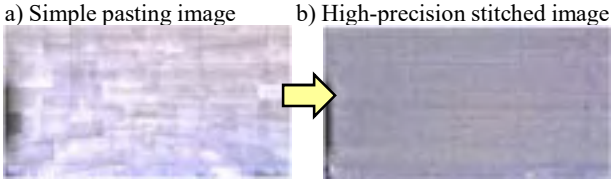

Figure 3. Automatic stitching image

③Automatic crack detection

The automatic crack detection on the concrete surface image uses an algorithm (line matching) to detect cracks as "continuous with lines". Compared with the binarization and contour detection generally used for image processing, dirt on the concrete surface is eliminated as much as possible, and it is specialized for crack detection as shown in Figure 4. Since the accuracy of the captured image is 0.5 mm/pix, the crack detection accuracy can recognize a 0.2 mm wide crack.

3 Application to visual inspection

The application of Auto-CIMA to proximity visual inspection was verified for the following four items.

①Inspection rate

Auto-CIMA is installed under the inspection target to perform the inspection, so there are some parts that cannot be photographed due to obstacles etc. We calculated the inspection rate for each bridge (see below) and verified the inspection range with Auto-CIMA.

Inspection rate (%):
Inspection area by Auto-CIMA (m^2) / Total inspection area (m^2)

②Inspection result

By comparing the visual inspection results with the Auto-CIMA inspection results, we verified whether it could be applied as an alternative method of visual inspection. In addition, Auto-CIMA can inspect only the damage appeared on surface, so the internal damage was inspected by the infrared thermography inspection.

③Cost and capacity

It was feared that Auto-CIMA inspection had lower work capacity than visual inspection. Therefore, in order to confirm the scope of application of Auto-CIMA, we compared and verified the cost and work capacity of visual inspection and inspection by Auto-CIMA.

④Application effect

We compared the work abilities of visual inspection with inspection combining Auto-CIMA and infrared rays (hereinafter, non-destructive inspection) to verify the effect of introducing non-destructive inspection.

3.1 Inspection rate verification

The scope of application was verified for the three bridges shown in Table-2. Table-3 shows the inspection rates for Auto-CIMA inspection for each bridge. The inspection rate of the superstructure was about 50% at the end span and about 100% at other spans due to the influence of obstacles (slopes, trees). The inspection rate for substructures is 0% for abutments and about 80% for piers, as in superstructures. As a result, it was confirmed that the inspection by Auto-CIMA can be applied to about 65% of the entire bridge.

Table 2. Target bridge(Inspection range verification)

Bridge	Type	Span	Shooting distance	Shooting area	Underpass
Bridge A	PC Box-girder	5span	30m	12,705㎡	River and road
Bridge B	PC Box-girder	5span	10～30m	12,296㎡	River and road
Bridge C	PC Box-girder	4span	10～30m	6,137㎡	Train

Table 3. Inspection rate (Inspection by Auto-CIMA)

	Inspection rate					
	Bridge A		Bridge B		Bridge C	
substructure	A1	0.0%	A1	0.0%	A1	0.0%
	P1	54.6%	P1	72.7%	P1	80.2%
	P2	96.3%	P2	62.7%	P2	74.1%
	P3	94.2%	P3	56.1%	P3	69.3%
	P4	62.7%	P4	69.1%	A2	0.0%
	A2	0.0%	A2	0.0%		
superstructure	A1-P1	45.4%	A1-P1	64.1%	A1-P1	81.9%
	P1-P2	100.0%	P1-P2	95.2%	P1-P2	100.0%
	P2-P3	100.0%	P2-P3	100.0%	P2-P3	100.0%
	P3-P4	100.0%	P3-P4	86.9%	P3-A2	95.7%
	P4-A2	47.7%	P4-A2	64.9%		
			average		65.5%	

3.2 Inspection results verification

From the bridges that were visually inspected, we selected RC hollow floor slab bridges and PC box girder bridges where blind spots are less likely to occur during shooting, and verified the inspection results for 12 bridges with 62 spans. The deformation detected by each inspection method was classified into the following patterns, and it was verified whether the nondestructive inspection could be applied as an alternative method with the same accuracy as the precision visual inspection. Table 4 shows the verification results.

Pattern A:
Damage found at the same position and in the same area as the visual inspection

Pattern B:
Damage that was confirmed by visual inspection but not by non-destructive equipment inspection

Pattern C:
Damage not confirmed by visual inspection but newly confirmed by non-destructive inspection

Table 4. Verification result of inspection result

Found damages		quantity	Match rate	Remark
Proximity inspection		229	-	
Non-destructive inspection	PatternA	224	97.8%	
	PatternB	5	2.2%	all delamination
	PatternC	353	-	

As a result of the verification, out of 229 deformations visually confirmed, 5 cases (Pattern B) were not confirmed by non-destructive inspection (concordance rate 97.8%). The damage that could not be confirmed by non-destructive inspection was delamination (no change in appearance) as shown in Fig. 4, and no damage could be confirmed by inspection by infrared thermography. We could not confirm it because it was lurking deeper than the range that could be confirmed by infrared thermography.

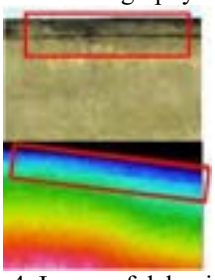

Figure 4. Image of delamination

In addition, nondestructive inspection (Pattern C) confirmed 353 new damages. Of these, 239 were confirmed by Auto-CIMA and 116 by infrared thermography. The new damage identified by Auto-CIMA was a crack. Since the inspection is performed with a high-definition visible image, it can be confirmed more accurately than the visual inspection, and it is considered that the inspection accuracy has improved. Especially, it seems to be very useful for the inspection of PC structures, etc. where cracks have a great influence on the soundness.

On the other hand, the damage newly confirmed by infrared thermography is characterized in that the damaged part can be seen due to the temperature difference. Therefore, a temperature difference occurs depending on the surface condition and the surrounding environment, and a sound part was erroneously detected as a damaged part. When it is judged that the sound part is damaged, it is judged to be worse than the original soundness in judging the soundness of the bridge, and it is judged that repair is necessary even if the bridge is not necessary to be repair. .. However, in most case spalling needs to be repaired, appears with surface damage such as cracks and rust. Since cracks and rust have been confirmed by Auto CIMA, there is no major change in soundness judgment.

Based on the above, as a result of non-destructive inspection, 97.8% of visual inspection damage was detected, and all damage that could not be confirmed was delamination, which was considered to be outside the detection range of infrared thermography. With non-destructive inspection, almost all visual inspection damage was detected, and soundness quality was obtained by using visible and infrared images together.

3.3 Cost and capacity verification

Cost and capacity verifications were performed on the bridges shown in Table 4 which were selected from RC hollow floor slabs and PC box girder bridges that are less prone to blind spots. In the verification, the inspection cost required for visual inspection and non-destructive inspection was compared with the number of inspected persons, and the applicable range of the inspection method was examined. The inspection cost was calculated by comparing the personnel cost with the cost required for the inspection (traffic regulation cost, machine cost, driver cost, security personnel cost, etc.). The number of inspectors was calculated by comparing the total number of inspectors engaged in on-site work and office work. In non-destructive inspection, as shown in Fig. 5, there are areas that cannot be inspected due to blind spots. Therefore, we decided to cover the range that cannot be confirmed by non-destructive inspection with visual inspection and add inspection cost. The verification results are shown below.

Table 4. Target bridge (Cost and capacity verification)

Bridge	Bridge Type	Span	Inspection size	Bridge	Bridge Type	Span	Inspection size
Bridge A	PC	2	108m	Bridge G	RC	7	108m
Bridge B		1	24m	Bridge H		9	24m
Bridge C		1	90m	Bridge I		2	90m
Bridge D		9	348m	Bridge J		6	348m
Bridge E		5	202m	Bridge K		5	202m
Bridge F		3	115m	Bridge L		3	115m

Figure 5. Blind spot range

① Comparison of inspection cost and number of inspectors

Table 6 shows the comparison result of the inspection cost and the number of inspectors between visual inspection and non-destructive inspection, and the consideration from the comparison of the inspection cost and the number of inspectors. The comparison results were calculated by arranging the percentage of nondestructive inspection when the visual inspection was taken as 100%. It also summarizes the under-girder height of each bridge and the characteristics at the time of inspection (necessity of traffic regulation, etc.).

【Consideration】

①Comparison of inspection costs

- For bridges with small spans and visual inspection in one day, nondestructive inspection always requires one more day to cover areas that cannot be inspected due to blind spots. Therefore, visual inspection is inexpensive. (Bridge A, Bridge B, Bridge C)
- For bridges with low under-girder height and no traffic restrictions, visual inspection costs are low. (Bridge D)
- For bridges that require traffic regulation, the cost of non-destructive inspection will be lower than visual inspection due to the impact of regulatory costs. (Bridge F, Bridge G, Bridge H, Bridge I)
- If the height under the girder is high, the inspection cost will be lower than the non-destructive inspection even if traffic regulation is not required for visual inspection. (Bridge J)
- The cost of non-destructive inspection of bridges at rampway is kept low because of complicated traffic regulations and time-consuming inspection. (Bridge K, Bridge L)

Table 6. Comparison result (Cost and capacity verification)

Bridge	Cost ratio (Non-destructive/visual)	personnel ratio (Non-destructive/visual)	Height under girder	Characteristic
Bridge A	178%	281%	16m	Visual inspection only for 1 day
Bridge B	122%	140%	10m	Visual inspection only for 1 day
Bridge C	126%	175%	15m	Visual inspection only for 1 day
Bridge D	108%	130%	6m since	The height under the girder was low and the visual inspection did not require traffic regulation.
Bridge E	93%	252%	Aithough 10m	The height under the girder was low and visual inspection required traffic regulation.
Bridge F	91%	158%	20m	Traffic regulation and bridge inspection vehicle required for visual inspection.
Bridge G	79%	148%	20m	Traffic regulation and bridge inspection vehicle required for visual inspection.
Bridge H	71%	525%	24m	Traffic regulation and bridge inspection vehicle required for visual inspection.
Bridge I	71%	92%	17m	Traffic regulation and bridge inspection vehicle required for visual inspection.
Bridge J	74%	138%	20m	The height under the girder was high and no traffic regulation was required for visual inspection.
Bridge K	37%	77%	25m	Visual inspection needs a lot of manpower due to a rampway bridge where the crossing condition is complicated.
Bridge L	21%	43%	26m	Visual inspection needs a lot of manpower due to a rampway bridge where the crossing condition is complicated.

②Comparison of number of inspectors

- At almost all bridges except rampway bridge visual inspection require less number of inspectors. (Bridge A-H, Bridge J)
- Due to the complexity of crossing condition roads, the number of non-destructive inspectors on rampway bridges is low. (Bridge K, Bridge L)
- Higher heights under the girder increase the efficiency of non-destructive inspection and may reduce the number of non-destructive inspectors due to traffic regulations. (Bridge I)

②Scope of non-destructive inspection

Table 7 shows the inspection methods that should be applied, which were confirmed by the verification conducted so far. The inspection method to be applied was decided by giving priority to the inspection cost. Furthermore, the under-girder height less than 10m was defined as “low”, more than 10m as “high”.

The bridges that were confirmed to be suitable for visual inspection were "bridges with short visual inspection days" and "bridges with low under-girder height that do not require visual traffic regulation". Non-destructive inspection is desirable for “rampway", "bridges that require traffic regulation under the bridges" and "high under-girder height bridges under the bridges".

Table 7. Applicable inspection

Inspection conditions			Comparison item		Applicable inspection
			personnel	cost	
Short visual inspection date			×	×	Visual inspection
Rampway bridge			○	○	Non-destructive
Height under-girder	low (Less than 10m)	No traffic regulation	×	×	Non-destructive
		Traffic regulation	×	○	Non-destructive
	high (10m or more)	No traffic regulation	×	○	Non-destructive
		Traffic regulation	×	○	Non-destructive

3.4 Application effect verification

The effect of introducing nondestructive inspection was verified by comparing that for visual inspection alone with the number of inspection days for introducing nondestructive inspection. The number of days of comparative inspection was confirmed by the number of days of bridge inspection within the jurisdiction of the Kansai branch of NEXCO West Japan. A non-destructive inspection was conducted on bridges that meet the conditions of Auto-CIMA shown in Table 1.

The verification results are shown in Table-8.

Table 8. Inspection days

Inspection method	Inspection days	Reduction rate
Visual inspection	12,463 days	−
Non-destructive inspection	10,136 days	18.7%

As a result of verification, if non-destructive inspection is introduced, numbers of days necessary for inspection will be shortened from 12,463days to 10136days, that is the efficiency will be improved by 20%.

4 Conclusion

As a result of the verification, the non-destructive inspection using Auto-CIMA confirmed the same inspection result as the visual inspection, and was confirmed to be applicable as an alternative method of visual inspection. In addition, we were able to confirm cracks in more detail than humans and improve inspection results.

Regarding the efficiency of the inspection, there were some areas where the inspection could not be performed due to blind spots, but with the introduction, the efficiency is expected to be improved by about 20%. However, depending on the conditions, the efficiency of the inspection may decrease, and it is necessary to be careful such as limiting the inspection target.

In the future, we will consider the development of guidelines and the use of automatic CIMA in the field to realize efficient and advanced bridge maintenance management.

MLIT's Initiatives for Promotion the Efficient Construction and Inspection by using new Technologies such as AI and Robots in Japan.

Kenichi Watanabe

Deputy Director for AI and Robotics for Construction and Maintenance, Policy Planning and Coordination Division for Public Works Project, Policy Bureau, The Ministry of Land, Infrastructure, Transport and Tourism, Government of Japan
E-mail: watanabe-k2q2@mlit.go.jp

Abstract –

The Ministry of Land, Infrastructure, Transport and Tourism (MLIT) is promoting the use of drones and other robots to improve the construction and management processes and improve the efficiency of infrastructure inspections, and is preparing an AI development environment that supports "human judgment." Specifically, MLIT is preparing "teaching data" which necessary for AI development and provides it to AI developers. In order to create an annotation rule for preparing teaching data, MLIT have started the working group of Industry-academia-government collaboration and are proceeding with discussions. At present, teaching data for cracks in bridges and tunnels has been prepared. MLIT is going to realize future advanced inspection, such as accumulating and using high-definition photographs with positional information taken by robots and inspection records in a 3D model. This will be possible to grasp the secular change of damage and deformation easily.

Keywords –

AI; Inspection; Teaching data; Drone; Bridge; Tunnel

1 Introduction

Currently, many of Japan's infrastructure is aging, while there is increasing risk of natural disasters such as typhoons and floods due to climate changes related to global warming. Japanese people are also in the face of challenges such as low birthrate and aging population. Under such situation, maintenance of infrastructure needs to be performing more effective and efficient, while the development and introduction of robot technology which support the work is required to proceed rapidly and intensively.

Therefore, MLIT and the Ministry of Economy, Trade and Industry (METI) in Japan have considered the needs of robots in a situation of social infrastructure survey, construction, maintenance and disaster management, including different needs from other industry fields in Japan and overseas such as IT, manufacturing, and so on. In order to consider measures for practical application such as clarifying the development and introduction fields of robots in, the "Next Generation Social Infrastructure Robot Development and Introduction Study Group" was established on July 16, 2013, "Next Generation robots for infrastructure development and introduction priority areas (5 key areas)" was formulated on December 25, 2013 (as shown in Figure.1).

Figure 1. Next Generation social infrastructure for robot development and introduction priority areas (5 key areas)

Therefore, MLIT had decided to establish "the on-site robot verification committee for the next generation social infrastructure" (hereinafter referred to as "the on-site verification committee") in 2014 February, to experiment on-site for the purpose of evaluating the robots. It was also the purpose to facilitate the development and introduction robots in the maintenance and disaster management field of social infrastructure.

The on-site verification committee had 5 subcommittees, 3 as the maintenance (the bridge, the tunnel, and dams and river), and 2 as the disaster

management (the disaster investigation and the emergency restoration). Experiments were conducted for each of the five priority areas.

The robots for maintenance of social infrastructure can take photographs which can detect damages of infrastructure such as cracks or corrosion. This can reduce the time which an engineer work on-site, and this can be also expected to reduce the time lost due to traffic closed for construction or inspection. But it is needed for an engineer to look at each photo for detecting the damage.

For further improving the efficiency of inspection work, it can be worth considering that creating three-dimensional model which shows the overall structure of the inspection object from inspection photos and organizing large amounts of photos on the 3D model. It can be also useful for grasping the changing over time of the infrastructure. Furthermore, it can be an efficient technique for such inspection to create and use artificial intelligence (AI) which can automatically detect damages on infrastructure from inspection photos.

In this paper, I show you “Initiatives and results of the on-site verification committee” in section 2,” Efforts to further improve the efficiency of inspection work” in section 3, and “Conclusion” in section 4.

2 Initiatives and results of the on-site verification committee

In fiscal year 2014 and 2015, MLIT had researched various robot technologies like drones or ROV related to five priority areas (FY2014: 67 techs, FY2015: 70 techs). MLIT had taken technological verification and evaluation for improving and promoting these technologies. For disaster management, two years verification and evaluation initiatives have made these robot techs to be used in site. On the other hand, the robot techs for the maintenance had many difficulties on achieving inspection efficiency and accuracy which were required, so it was decided to continue the verification and evaluation initiatives beyond year.

In FY2016 and FY2017, the situation and performance level to be achieved for practical use were set, while some of these robot techs were re-verified and re-evaluated the accuracy and the economic efficiency caused by shortening of work time (FY2016: 16 techs, FY2017: 16 techs). Figure 2 shows examples of the verified robot techs.

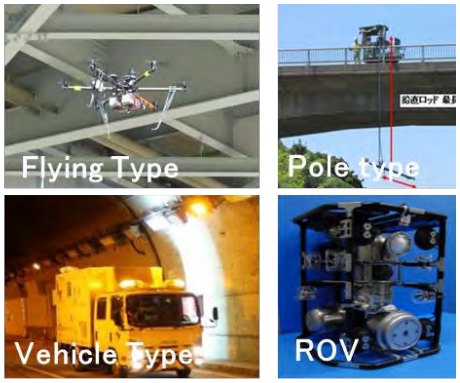

Figure 2. Examples of the verified robot techs

In FY2018, MLIT have written the manuals which described the method to use these robot techs in each situation such as bridge maintenance or disaster investigation. It has made the robot techs to be used in site.

The manual regarding road (bridge, tunnel) maintenance is described in detail below.

2.1 Road (Bridge, Tunnel) Maintenance Manual Using Robots

For the road infrastructures in Japan, The Ministerial Ordinance Revising Part of Road Law Enforcement Regulations has been issued and enforced in 2014 behind the rapid increase in aging road infrastructures. Therefore, regular inspections of road bridges and tunnels are conducted once every five years by close visual inspection, while evaluating its healthiness in stages.

The first round of inspections was completed in FY2018, and the road bridge periodic inspection guideline was revised in 2019, February through discussions on the revision of the periodic inspection guideline by the Road Subcommittee of the Council for Social Capital Development Road Subcommittee . The road tunnel regular inspection procedure was revised in March of the same year.

In addition, in the process up to the revision of the periodic inspection procedure, the direction was shown to utilize these technologies for periodic inspections. “Inspection support technology” such as infrastructure inspection robots will be determined by a professional engineer who has the knowledge and skills which are necessary for inspection of the parts, members, scope, and purpose of using these technologies.

Therefore, MLIT has established standard performance evaluation items that show the performance of inspection support technology, and then "the catalog" was made in 2019 February for the performance values submitted by the developer through

on-site verification.

Moreover, "the guideline" was compiled in same time. For professional engineers of the order and the contractor, the guideline shows the process of decision making to use these technologies on periodic inspection work.

3 Efforts to Further Improve The Efficiency of Inspection Work

The inspection support technology, shown in above section, can take photographs from which a professional engineer can detect damages of infrastructure such as cracks or corrosion. This can reduce the time which a professional engineer work on-site like marking with chalk or measuring with crack scale, and this can be also expected to reduce the time lost due to traffic closed for construction or inspection. However, it is needed for a professional engineer to look at each photo for detecting the damage.

For further improving the efficiency of inspection work, it can be worth considering that creating 3D model which shows the overall structure of the inspection object from inspection photos and organizing large amounts of photos on the 3D model. It can be also useful for grasping the changing over time of the infrastructure. Furthermore, it can be an efficient technique for such inspection to create and use AI which can automatically detect damages on infrastructure from inspection photos.

Two methods that MLIT is currently studying about AI are shown in below.

3.1 Damage Representation above 3D model

In the current inspection work in Japan, the contractor is not needed to deliver all of the photographs taken by inspection support technology, and it is often enough to deliver the photographs of the places where damage is recognized and damage information with the form defined.

The inspection support technology can take high quality and large images which can use to generate a 3D model. If it could record and accumulate accurate damage location above such 3D models, deformation of aging structure changing over time can accumulate inspection records of the structure in comparable form. The more information amount of inspection results is, the more useful diagnosis by a professional engineer can be expected.

The deliverable for making 3D model needs photos which show shape and location of damages, metadata of positional information of taken photos, and damage shape data added to the 3D model. If the standard which defined these data items and specification did not exist, it might make a situation that the damage 3D model only depended on the application which was used and managed the data. Incompatible and discontinuous data might store in that cases.

Therefore, MLIT have stipulated common data items and specifications related to the data required to create a 3D model. MLIT have also shown the method how to deliver the result of inspection through an application that creates a 3D model from photos taken by inspection support technology. So, " 3D deliverables manual for tunnel or bridges by inspection support technology (image measurement technique) " have created in 2019, March.

MLIT is going to verify the 3D model creation method using photographs are taken through the periodic inspection work. MLIT is also going to revise the manual while researching the inspection scene in which we can use 3D model efficiently. Through these initiatives, MLIT leads inspection work to improve.

I will explain the 3 types of deliverables that are defined in this manual: "inspection photo", "damage shape data", "Inspection photo metadata".

Each of the details are as follows.

3.1.1 Inspection Photo

This is raw data of photos taken by inspection support technology. For creating 3D model, photos should be taken not only of the damaged part but also whole of the structure including the sound part.

It is necessary for inspection photos to carry out appropriate quality control based on shooting condition which defined to secure the accuracy. In this manual, the conditions of inspection photos taken will be described referring to shooting conditions for teaching data which is essential to create AI. (As shown in Table 1.)

Table 1. Conditions for taking photos for the preparation of teaching data for bridges

When a crack of 0.1mm width is detected, the width shall be 0.3mm/pixel or less.
The field of view size should be determined according to the camera used.
Field of view size in longitudinal direction (mm) = Number of camera pixels in longitudinal direction x 0.3mm
Size of vertical field of view (mm) = Number of camera pixels in vertical direction x 0.3mm

	specification	points to remember
Camera model	Mirrorless camera or equivalent	Necessary to ensure stable image quality
		Sensor size: APS-C or larger
		Do not use contrast AF
		Necessary for depth of field
ISO sensitivity	ISO200 or less	Increasing the ISO sensitivity may smooth the image and make it impossible to detect cracks
Lap rate	Overlap and side-lap percentages are both over 30%	Necessary for compositing to the planar development
Shooting angle	Confronting directly (in principle)	Depends on the environmental conditions, but generally up to 10 degrees

3.1.2 Damage Shape Data

This is the information of damage position, shape, and area. When we create this data, we can choose two methods: 3D model or the layer structure drawing file

(2D). The damage shape data on 3D model is expressed by 3D polylines (cracking, etc.), a polygon (corrosion, free lime, etc.) which are described on 3D-CAD.

On the other hand, the damage shape data based on the layer structure drawing file (2D) is created by showing polylines and polygons indicating damage on 2D drawing that is superimposed with a layer structure that can be separated from the inspection photos. This corresponds to the data delivered as a damage diagram in the conventional inspection record.

3.1.3 Inspection Photo Metadata

This is the text data (CSV file) in which describes the information of coordinate system in which inspection target structure is located, and of the position coordinates and angle of inspection photo or camera.

The position coordinates and angle information are necessary to express at which position and angle the photo exists in 3D space. Representation methods of this information can be 3types: (1) center position coordinates and angle of the inspection photo, (2) center position coordinates of the camera and angle, and (3) four corner coordinates of the inspection photo.

This manual defines the representation methods of these metadata, and one example is shown in Table2.

Table 2. Conditions for taking photos for the preparation of teaching data for bridges

Item	Input condition	Description
Position Coordinate Entry Method	Required	Enter 0 if the positional coordinates are the center positional coordinates of the photo, 1 if it is the center positional coordinates of the camera, and 2 if it is the four corner coordinates of the photo.
Position Coordinate	Required (When the positional coordinate input method is "0")	XYZ coordinates (x, y, z) to show the center position of the inspection photo. Eulerian angle (α, ß, γ) or quaternion (q0, q1, q2, q3) that represents the slope of the inspection photo.
	Required (When the positional coordinate input method is "1")	XYZ coordinates for the center position of the camera (x, y, z) Eulerian angles (α, ß, γ) or quaternions (q0, q1, q2, q3) that represent the inclination of the camera.
	Required (When the positional coordinate input method is "2", 3 points or more)	XYZ coordinates (xUR, yUR, zUR, xUL, yUL, zUL, xDR, yDR, zDR, xDL, yDL, zDL) of the four corners of the inspection photo (top right, top left, bottom right, bottom left)

3.2 Automatic Interpretation of Damage Using AI

As previously described, from many photos obtained using the current inspection support technology, damage of structure has been read by hand. By utilizing AI, this damage reading procedure can be done automatically. It can be also a great help for the work of those who create inspection records. A future image of inspection procedure is shown in Figure 3.

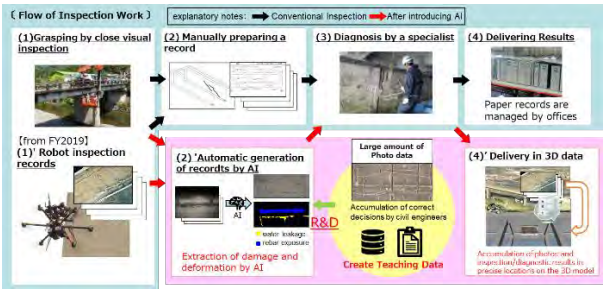

Figure 3. Future Images of Inspection Procedure

In conventional inspection procedure, a professional engineer needs to get closer to the structure to be inspected and check with his/her own eyes. So, inspection records (output) have been created from the visual information (input).

If this procedure is going to be achieved by AI, first, it will be needed to create the teaching data which is based on photos (input) and records(output) which have been acquired and made by a professional engineer.

These teaching data contains the tacit knowledge and know-how of the professional engineers of inspection. AI learning algorithm needs to learn based on teaching data like these.

The learned AI can infer results from inputs, so it can automatically interpret damages of the structure to be inspected from photos acquired by inspection support technology. To develop such AI, and to improve automatic interpretation by such AI to higher precision, it is necessary to prepare a large amount of teaching data. The teaching data is created by simply tagging (annotating) where in the photo acquired by inspection the damage is on the photo.

The inspection photo is owned by the manager of the structure like MLIT, and annotating requires the knowledge and skills of inspection professional engineers. So that, MLIT prepares teaching data as a cooperative area. MLIT is confident that this initiative can be a great help for firms to create AI needed in the fields of inspection.

An image of AI learning and utilization is as shown in Figure 4.

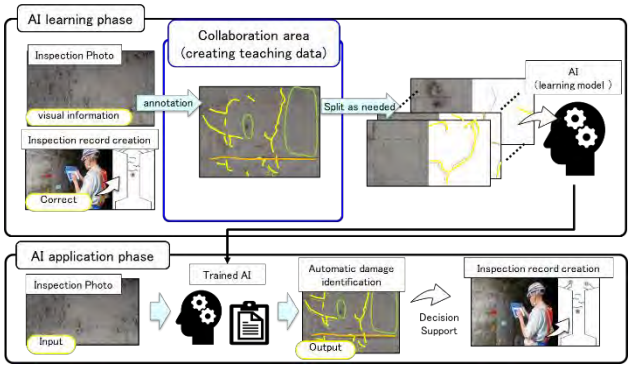

Figure 4. An image of AI learning and utilization

MLIT is considering the establishment of "AI Development Support Platform" for the purpose of creating teaching data, giving the data to AI developers, and evaluating the performance of the developed AI (Figure 5).

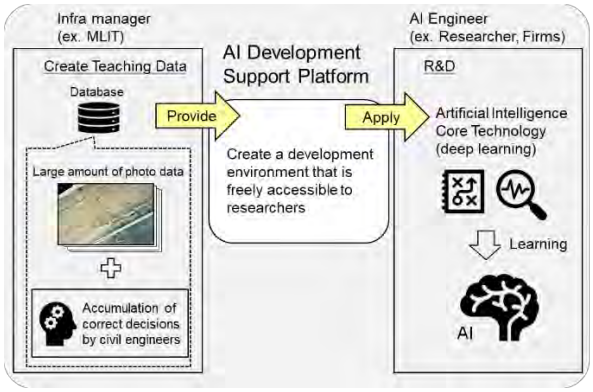

Figure 5. Outline of AI development Support Platform

MLIT have established the industry-academia-government collaboration working group for AI towards the establishment of the platform. In this WG, MLIT and WG members have considered a good quality and efficient way to create and deliver teaching data, and examined the ideal way of a data infrastructure that facilitates the acquisition, storage, analysis, and utilization of inspection data.

This WG has been held 3 times so far. The WG members have discussed specifications for the original photo used as teaching data, specifications of annotations, rules regarding provision of teaching data, sharing of schedule for future teaching data provision and prototype AI development, opinions exchange on prototype teaching data, and review of specifications of teaching data.

In addition, in order to improve the accuracy of AI, it is necessary to accumulate more inspection photos. MLIT is going to verify how to take a picture of the structure based on the technological progress of inspection support technology continuously, and "3D deliverables manual for tunnel or bridges by inspection support technology (image measurement technique) " should be revised as appropriate.

4 In Conclusion

In Japan, the skilled worker in construction site is decreasing, the infrastructure is aging, and it is important to maintain existing infrastructure effectively and use them longer.

MLIT initiatives will contribute a variety of inspection support technology development in the robot market, supporting the work of professional engineers in infrastructure inspection, accelerating the development and introduction of robots, and further improving the efficiency and sophistication of the overall infrastructure maintenance management.

MLIT will be contributing to the improvement of productivity of construction industry, while grasping the trend of technology seeds and worksite needs by the social implementation of new technology on construction site.

References

[1] MLIT, Measures to deal with aging roads On-line: https://www.mlit.go.jp/road/sisaku/yobohozen/yobohozen.html, Accessed: 15/June/2020.

[2] MLIT, Robots and AI technology On-line: https://www.mlit.go.jp/sogoseisaku/constplan/sosei_constplan_tk_000028.html, Accessed: 15/June/2020.

[3] MLIT, About the preparation working group for the “AI Development Support Platform” On-line:https://www.mlit.go.jp/sogoseisaku/constplan/sosei_constplan_tk_000034.html, Accessed: 15/June/2020.

Track Similarity-based Typhoon Search Engine for Disaster Preparedness

C.M. Hsieh[a], C.Y. Ho[b], H.K. Kung[b], H.Y. Chan[c], M.H. Tsai[c] and Y.C. Tsai[d]

[a]Department of Economics, National Taiwan University, Taiwan
[b]Department of Geography, National Taiwan University, Taiwan
[c]Department of Civil and Construction Engineering, National Taiwan University of Science and Technology, Taiwan
[d]School of Big Data Management, Waishuanghsi Campus, Soochow University, Taiwan
E-mail: b06303059@ntu.edu.tw, b06208030@ntu.edu.tw, b06208001@ntu.edu.tw, d10705005@mail.ntust.edu.tw, menghan@mail.ntust.edu.tw, pecutsai@scu.edu.tw

Abstract –

Plenty of variance lies in the development stage of a typhoon, including its location, direction, and surrounding meteorological conditions. Affected by such numerous contributing factors, it is not always easy for nowaday technology to make accurate typhoon forecasts. The experiences from the past typhoons may provide decision-makers with sufficient information to anticipate potential damage and thus develop appropriate strategies. The typhoon track plays a vital role in selecting appropriate historical cases based on the need to grasp the situation during the disaster preparedness phase. This paper summarizes our published journal article, which proposed an algorithm to compare the similarity between the current typhoon forecast track and all the typhoon tracks of the western North Pacific in the past. Based on the forecast track points of the current typhoon, the algorithm suggests a list of historical typhoons with the highest similarity in tracks. Hence, the tracks and the disastrous area of those historical typhoons can be used as crucial alerts and hints for disaster preparedness. Inside the algorithm, the mechanism follows the Recentness Dominance Principle, which is elaborated in our published journal article. The principle states that the more recent the forecast track point is, the higher the weight that it possesses and thus should be emphasized. For implementation, the study develops a user-friendly front-end interface that synchronizes the latest forecast typhoon tracks from six major meteorological institutions automatically, including CWB, HKO, JMA, JTWC, KMA, and NMC. The result comes with a convenient and concise search engine that assists decision-makers in finding similar historical typhoon records.

Keywords –

typhoon track similarity; search engine; user interface design; disaster preparedness; decision support

1 Introduction

Precise response strategies to typhoons rely on accurate forecasts. However, plenty of variance lies in the development stage of a typhoon, including its location, direction, and surrounding meteorological conditions. Affected by such numerous contributing factors, it is not always easy for nowaday technology to make accurate typhoon forecasts, causing the difficulties of developing precise strategies.

The experiences from the past typhoons may provide decision-makers with sufficient information to anticipate potential damage and thus develop appropriate strategies for precaution. The damage of a typhoon, caused by the winds and rainfall, is regarded as a consequence of the interaction between the typhoon and the land. Such interactions are affected by typhoon tracks, making the track a critical factor for disaster reduction of typhoon events. Based on the need to predict and grasp the situation, during the disaster preparedness phase, the typhoon track plays a vital role in selecting appropriate historical cases. Decision-makers may anticipate the impact of an upcoming typhoon by utilizing the historical typhoon records with similar tracks.

The categorization of historical typhoon tracks helps to analyze the patterns of damage caused by different typhoons. For example, the Central Weather Bureau (CWB) of Taiwan has determined nine categories of tracks of typhoons that invades Taiwan [1]. The CWB has also linked the behavior of wind and rainfall of typhoons with different tracks to different regions in Taiwan [1], supporting decision-makers to figure out the

potential damage of upcoming typhoons.

This paper summarizes our published journal article [2], which proposes a track similarity algorithm to compare the similarity between an upcoming typhoon forecast track and all the tropical cyclones (TCs) in the western North Pacific (WNP) in the past. A comparison model, which is the core of the algorithm, was first developed in our preliminary work [3], and in the present study, we further explore the details of the model and complete the comprehensive algorithm. We also developed a new information display panel featuring auto-importing forecast data. A literature review of typhoon databases is presented in Section 2, including a discussion of our preliminary work. The algorithm and its detailed discussion are discussed in Section 3. The design and implementation of the new panel are described in Section 4. More information can be found in the journal article [2].

2 Literature Review

Many studies about typhoons focus on forecast model performance. Classical prediction techniques are climatological or dynamic with different considerations. For example, Lee et al. [4] developed a climatology model for predicting rainfall at different areas for a specified typhoon center location. On the other hand, some recent studies discuss data-driven approaches to typhoon forecasts. For example, Rüttgers et al. [5] utilized a generative adversarial network (GAN) with satellite images for typhoon track predictions. Although precise forecasts support decision making, the deduction of damage from the distribution of rainfall and wind is not explicit and requires expertise. Also, forecasts cost computation time, hindering immediate reactions to emergencies. Hence, utilizing past typhoon records for developing quicker response strategies may be useful for decision-makers.

The experiences from the past typhoons may provide decision-makers sufficient information to anticipate potential damage and thus develop appropriate strategies for precaution. Wu and Kuo [6] states that significant mesoscale variations in weather are derivative from the interaction of typhoons and the complicated topography in Taiwan. Also, Huang et al. [7] has investigated the relationship between typhoon track, rainfall patterns, and flood peak time, concluding that that preferable rainfall types vary by typhoon tracks. For the preparedness and the emergency response phase of typhoon events in Taiwan, decision-makers seek the status of the disaster, the response strategies, and other relevant data of similar past typhoons for decision making support [2].

Several databases for TCs in the western North Pacific WNP have been developed, including the Taiwan Typhoon Database of CWB [8] and the Digital Typhoon Database of the National Institute of Informatics (NII) of Japan [9]. Such databases feature filtering by time, pressure, wind, rainfall, intensity, etc. However, searching by TC track is not commonly provided. The Taiwan Typhoon Database allows searching by the track categories proposed by the CWB, but the actual category that a forecast track belongs to still requires the users' determination. The task of track matching is less intuitive for users due to the lack of explicit integration with forecast and historical records.

T-search, a real-time historical typhoon search engine, was introduced by the authors to assist relevant personnel to intuitively search and review the historical typhoon information and efficiently develop corresponding response strategies [3]. A track similarity comparison model was also developed in the work. It also provided an intuitive cross-platform user interface for retrieving the historical typhoon records. T-search has been validated by a usability test and a three-year field test coordinated with the government of Taiwan. The real case study has shown that T-search enhances the accessibility to typhoon records. However, the preliminary work did not discuss the usage of each parameter in the comparison model, making the parameter setting without baseless. Also, the large number of typhoon records and track points resulted in long calculation times for the track similarity algorithm. Further, the system only allowed users to input the forecast data manually instead of automatically import, thus reducing the convenience of the system.

3 Methodology

This paper summarizes our published journal article [2], which proposes an algorithm to compare the similarity between an upcoming typhoon track forecast and all the past TC tracks in the WNP. The proposed algorithm is composed of the comparison model developed in the preliminary work [3] and a ranking strategy. In the present study, we decompose the comparison model into a static sector and a dynamic sector, propose a strategy to enhance the efficiency of the computation and set an order to ensure the discrimination of similarity. Also, the Recentness Dominance Principle (RDP) is introduced based on the presumption of the high uncertainty of the typhoon's direction during development [2]. The RDP states that those later user-specific track points are more relevant than the earlier ones, and thus their relative weighting should be increased. We extend elaborates on the preliminary work and provides the definition and interpretation of the time weighting. More information can be found in the journal article [2].

3.1 Comparison Model

The comparison model selects the most similar historical typhoon track for the user-specific track of the forecasted typhoon through track comparison and matching. For each past typhoon, the model calculates the similarity based on points of tracks, valid regions given by the user, time, etc., for the user-specific track points and quantifies scores for comparison. The similarity of the forecasted typhoon and each historical typhoon is calculated with Equations (1) and (2):

$$similarity(i) = \sum_{k=1}^{M}(1 + kw) \times \delta_k = \sum_{k=1}^{M}\delta_k + w\sum_{k=1}^{M} k \times \delta_k \quad (1)$$

$$\delta_k = \begin{cases} 1, d_{jk} < R_k \\ 0, otherwise \end{cases} \quad (2)$$

M is the number of the user-specific track points. k is the index of the user-specific track points starting from 1. i is the index of the historical typhoons. j is the index of the closest track point of the historical typhoon i to the user-specific track point k. w is the time weighting of all the user-specific points, which determines the importance of each point. The binary variable δ_k represents whether the historical typhoon track point j falls in the given valid region of the user-specific track point k. The valid regions corresponding to the user-specific track points are designed to restrict the distances between a forecast track point and historical track points, denoted as d_{jk} in Equation (2). At least one point of each historical typhoon track should lie within the valid region set by the user-specified radius, denoted as R_k in Equation (2), or the similarity scores of the typhoons are zero since they are determined to be too far.

For discussing the roles of k and w, Equation (1) is divided into the static sector and the dynamic sector. The static sector refers to the constant part constant part ($\sum_{k=1}^{M}\delta_k$), while the dynamic sector refers to the second component ($w\sum_{k=1}^{M} k \times \delta_k$). In the static sector, only the valid regions of the given track points are of concern, indicating that how many given track points of a forecast typhoon a historical typhoon passes. The dynamic sector includes time as a factor in the model by multiplying the time series (k) by the time weighting (w). The adjustment to the given time weighting emphasizes the importance of time of the track points.

Both the static sector and the dynamic sector impact the result of similarity comparison. An example is shown in Figure 1, with one typhoon passing through the last three input points with the score of $3 + 12w$, and the other passes through the first three input points and the last input point with the score of $4 + 11w$. In this case, the first typhoon has a higher static sector than the second, but if the time weighting w is greater than one, the second typhoon eventually obtains higher similarity. Hence, it is essential to discuss the usage of time weighting for a comprehensive explanation.

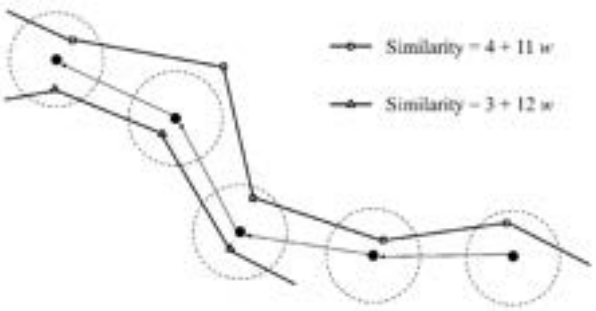

Figure 1. An example of two typhoon tracks for the similarity comparison demonstrating the impact of the dynamic sector [2].

3.2 Recentness Dominance Principle

The Recentness Dominance Principle states that the more recent the forecast track point is, the higher the weight that it possesses and thus should be emphasized [2]. Since a TC direction is highly uncertain during its developing stage, we tend to emphasize the importance of later track points by giving higher weightings to them. Following the RDP, the time weighting should be changed when more track points are given. The similarity score of a historical typhoon may be distorted in some circumstances if the time weighting is not adequately set following the RDP or does not correlate with the number of given track points.

For ensuring the RDP, we introduce the global recentness dominance time weighting (gRDW) and the individual recentness dominance time weighting (iRDW). They are obtained by the following approach (Equations (3) and (4)):

$$\widehat{w} = \max\{w_i : i = 1..|P|\} \quad (3)$$

$$w_i = \frac{s_{i,b} - s_{i,a}}{d_{i,a} - d_{i,b}} \forall \left(s_{i,a} + d_{i,a}w, s_{i,b} + d_{i,b}w\right) \quad (4)$$

$$P \equiv (s_a + d_a w, s_b + d_b w) \forall a, b \in \mathbb{N}(s_a > s_b \wedge d_a < d_b) \quad (5)$$

The value of gRDW (denoted as $\widehat{w}$ in Equation (3)) determines the number of the indeterministic score pairs (denoted as P in Equations (3) and (4)), which are defined in Equation (5). A properly specified value of gRDW eliminates the indeterministic score pair that contravenes RDP, and the similarity scores can then be calculated. In this study, the model equalizes the score of each score pair to obtain iRDW (denoted as w_i in

Equations (3) and (4)) for simplicity. To emphasize the recentness, the model takes the maximum of the set of iRDW as gRDW.

The dynamic sector of the model constructs a gRDW that ensures the dominance of recentness. To discuss the effect of setting different values of time weighting, we relax RDP by allowing users to set the preferred time weighting. Seven special weight groups are divided, giving different interpretations of the time weighting. One of the weight group, when w equals gRDW, is the critical value to ensure RDP. The remaining six groups are:

Over gRDW: $w \in (gRDW, \infty)$. In this case, the outcome of the similarity model remains identical to the outcome's time weighting set as gRDW, showing that exaggerating RDP generates the same result.

Positive related time weighting: $w \in (0, gRDW)$. In this case, the time weighting determines whether the impact of the dynamic sector can defeat the static sector, providing a trade-off between the two sectors. The closer values are to gRDW, the more influential the recentness.

Static sector: $w = 0$, only presenting the static sector's score. It eliminates the dynamic sector, presenting the neat summation of the historical typhoon track passing through the valid regions of the user-specific track points.

Negative related time weighting: $w \in (-1, 0)$. The recentness is proportionally decreased in this case, making older typhoons more important than recent typhoons.

Repulsion force weighting: $w = -1$. In this case, the comparison model reduces to $(\sum_{k=1}^{M}(1-k)$. Mathematically, the similarity score must not be greater than zero, referring to select historical typhoons who pass through none ($M = 0$) or only the first ($k = 1$) of the given points.

Reverse similarity: $w \in (-\infty, -1)$. In this case, the model simply eliminates all the historical typhoons that pass through the user-specific track points.

Setting time weightings with the six groups may not provide proper search results since they are obtained by relaxing the RDP. The actual usage of non-RDP time weighting is not yet clarified; however, the discussion of the behavior of search results with time weightings of different groups potentially provides insight for further usage.

3.3 Ranking Strategy

For the distinction of similarity between the historical typhoon tracks and the user-specific track, the ranking strategy is in five steps as follows:

1. Total similarity score;
2. Dynamic sector;
3. Static sector;
4. Month disparity;
5. Year gap.

First, the model sorts the past typhoons by the computed similarity scores with the user-specific track using Equation (1). The similarity score considers RDP by utilizing the time weighting assigned to each given track points with higher values for later points, indicating that the score is an index of general similarity. When the scores of some historical typhoons are equally matched, the dynamic sectors are compared first, and then the static sectors are compared, which reaffirms that RDP does matter. If the ranks still make no difference, the algorithm keeps comparing by the disparity of months, and the gap between the present year and the year of each historical typhoon. Finally, the comparison result should be clear.

4 Implementation

This study re-designs and develops a user-friendly interface that automatically synchronizes the latest forecast typhoon tracks from six major meteorological institutions of TCs in the WNP. The interface is implemented in the form of a web application, consisting of a front-end panel that displays the information and a back-end server that handles the data retrieving and the similarity comparison.

All required typhoon data are collected from the meteorological institutions. For the historical typhoons, the system utilizes the historical best track data of TCs in the WNP provided by the Japan Meteorological Agency (JMA), the regional specialized meteorological center of the WNP, and the South China Sea [10], as the references of similarity calculation. The TC data in the jurisdiction of the JMA since 1951 are retrieved from the JMA website. The system parses the raw data and extracts the approximately 1700 typhoons with the contained approximately 65,000 coordinates.

Meanwhile, typhoon track forecasts, the input of the system, are retrieved from several meteorological institutions that provide forecasts of present typhoons in the WNP. In this study, the real-time forecasts are obtained from the Integrated Multi-Agency Tropical Cyclone Forecast, which provides comprehensive information about current typhoon forecasts from several meteorological institutions, including the CWB, the Hong Kong Observatory (HKO), the JMA, the Joint Typhoon Warning Center (JTWC) of the US, the Korea Meteorological Administration (KMA), and the National Meteorological Center (NMC) of China [11].

Figure 2. The information display panel and the query result using Typhoon Maysak (2020).

The information display panel contains a map view built with OpenLayers libraries and a control panel for inputting track points. The system provides two input modes:

Center auto-import, which offers real-time feeds and forecasts of current typhoons provided by the meteorology institutions;

Manual input, which allows users to complete comparisons between any desired tracks and historical typhoon tracks by either keying in coordinates or clicking on the map view.

The integration of multi-institution forecasts allows the decision-maker to choose the exact institution as the forecast data provider considering the need. By auto-importing the forecast typhoon track, the time cost for manual input is reduced, and the accuracy of the track data is also improved.

Figure 2 illustrates the overview of the information display panel and the result using Maysak (2020) as an example. The control panel on the right lists all active TCs in the WNP and available forecasts from different meteorological institutions for users to select. In the case of Figure 2, the user selects the forecast data provided by CWB. After auto-import, the map view illustrates the forecast typhoon track points and all the valid regions. Next, the user activates the query. The system starts calculating, finds the most similar historical typhoons, and demonstrates the tracks of the selected historical typhoons on the map view. The control panel also lists the selected historical typhoons and directly links to the Taiwan Typhoon Database of CWB. With the support of the panel, it is convenient for decision-makers to review the historical typhoon records efficiently. The damages caused by typhoons can thus be forecast, and the response strategies such as evacuations and pump pre-allocations can be executed on time. More information can be found in the journal article [2].

5 Conclusions

This study has improved the preliminary work and developed a new information display panel featuring auto-importing forecast data, coming with a convenient and concise search engine that assists decision-makers in finding similar historical typhoon records. In this paper, summarized from our published journal article [2], we have discussed the details of the comparison model and completed the ranking strategy. In addition, we have stated the time weightings as a vital role of controlling the impact of time of each track point for the similarity algorithm. The use of RDP has been proposed regarding the effect of the number of track points. Furthermore, the effect of varying time weightings potentially provides insight for decision-makers to modify the time weighting for different purposes based on the need or their profession. We have also developed a new information display panel, featuring both the manual-input method and the center auto-import method to forecast track data, reducing the required time to import data and the possibility of making mistakes in

the exact locations of the track points. Several forecasters are additionally integrated into the system, providing various choices for the decision-makers. More information can be found in the article [2].

In future work, the algorithm's insufficiency of only considering track points as input should be solved. Since there are numerous factors that affect the damage of a typhoon, taking other factors such as the intensity of typhoons into consideration may enhance the search engine to get a better search result that meets up to the current scenario. Also, the algorithm can be adapted to utilize ensemble forecasting to comprehensively demonstrate forecasting uncertainty and support the decision-makers to evaluate the risk of different circumstances.

Acknowledgment

We thank Shih-Chung Kang, Yih-Chi Tan, Jihn-sung Lai, James Yichu Chen, Cheng-Hsuan Yang, and Tzong-Hann Wu of National Taiwan University; and Wei-Chyuan Shieh and Chun-Nan Chen of the Meteorological Application and Development Foundation for their contribution to the preliminary work.

References

[1] Central Weather Bureau. Faq for typhoon. On-line: https://www.cwb.gov.tw/V8/E/K/ Encyclopedia/typhoon/. Accessed: 01-06-2020.

[2] Tsai M.H., Chan H.Y., Hsieh C.M., Ho C.Y.,. Kung H.K, Tsai Y.C., and Cho I.C. Historical typhoon search engine based on track similarity. *International Journal of Environmental Research and Public Health*, 16(24):4879, 2019. doi:10.3390/ijerph16244879.

[3] Tsai M.H., Chen J.Y. and Kang S.C. T-search: A cross-platform searcher for historical typhoon events. *Journal of the Chinese Institute of Civil and Hydraulic Engineering*, 31(4):351–360, 2019.

[4] Lee C.S., Huang L.R., Shen H.S. and Wang S.T. A climatology model for forecasting typhoon rainfall in taiwan. Natural Hazards, 37(1):87–105, 2006. doi:10.1007/s11069-005-4658-8.

[5] Rüttgers M., Lee S., Jeon S. and You D. Prediction of a typhoon track using a generative adversarial network and satellite images. *Scientific Reports*, 9(1):6057, 2019

[6] Wu C.C. and Kuo Y.H. Typhoons affecting taiwan: Current understanding and future challenges. *Bulletin of the American Meteorological Society*, 80(1):67–80, 1999.

[7] Huang J.C., Yu C.K., Lee J.Y., Cheng L.W., Lee T.Y. and Kao S.J. Linking typhoon tracks and spatial rainfall patterns for improving flood lead time predictions over a mesoscale mountainous watershed. *Water Resources Research*, 48(9), 2012. doi:10.1029/2011WR011508.

[8] Central Weather Bureau. Typhoon database. Online: https: //rdc28.cwb.gov.tw/TDB/. Accessed: 22-072019.

[9] National Institute of Informatics. Digital typhoon: Typhoon images and information. Online: http:// agora.ex.nii.ac.jp/digital-typhoon/. Accessed: 02-10-2019.

[10] Japan Meteorological Agency. Rsmc tokyo - typhoon center. Online: https: //www.jma.go.jp/jma/jma-eng/jma-center/rsmc-hp-pub-eg/RSMC_HP.htm. Accessed: 01-10-2019.

[11] Typhoon2000.com. Integrated multi-agency tropical cyclone forecast. Online: http://www. typhoon2000.ph/multi/. Accessed: 01-10-2019.

Cracks Detection using Artificial Intelligence to Enhance Inspection Efficiency and Analyze the Critical Defects

Fawaz.Habbal [a], Abdualla.AlNuaimi [b], Mohammed.Alshamsi [c], Saleh.Alshaibah [c], Thuraya.Aldarmaki [c],

[a]Department of Management College of Business,
International learning institute, United Arab of Emirates
[b]Ministry of Infrastructure Development, United Arab of Emirates
[C]Sheikh Zayed Housing Program, United Arab of Emirates
E-mail: fawaz.habbal@iqli.net, Abdulla.alnuaimi@moid.gov.ae, mohammed.alshamsi@szhp.gov.ae, saleh.alshibah@szhp.gov.ae, thuraya.aldarmaki@szhp.gov.ae

Abstract –

Cracks are one of the significant criteria utilized for diagnosing the disintegration of solid structures. Normally, a structural designer with specific information would assess such structures by checking for breaks outwardly, outlining the aftereffects of the examination, and afterward getting ready to investigate information based on their discoveries. A review technique like this is not without a doubt, as it requires manual chronicle of upwards of a few hundred thousand splits individually. However, it additionally cannot precisely identify the length and state of the breaks. To handle the issue, the industry has progressively looked toward utilizing AI detection to conduct a direct based assessment. Researchers are as of now building up a mobile-based intelligence equipped with AI analytics for recognizing splits and different imperfections, which will upgrade the proficiency of the investigation process and enhance the emergency response towards users. This study aims to provide an insight on the most efficient crack detection method by comparing several techniques. It was found out that the hybrid technique was the most efficient method to detect cracks. This technique combines the positive points from both the artificial neural network (ANN) and artificial bee colony (ABC) to come up with a more proper entirely new method.

Keywords –
Cracks Detection; Inspection Enhancements; AI Detection; Cracks Deep Learning; Buildings Defects

1 Introduction

Structural systems in civil engineering are exposed to deterioration and damage during their service life. Damage is defined as a weakening of the structure which may cause undesirable displacements, stresses, or vibrations to the structure leading to sudden and catastrophic consequences. Damage that severely affects the safety and functionality of the structure and detection of it at an early stage can increase safety and extend its serviceability. Thus detection of damage is one of the most important factors in maintaining the integrity and safety of structures.

Visual inspections have always been the most common approaches used in detecting damage on a structure. However, these inspection techniques are often inadequate for assessing the health state of a structure especially when the damage is invisible to the human eyes. Thus, in many situations to ensure structural integrity, it is desirable to monitor the structural behavior when damage is not observable. Some numerical techniques such as the finite element method, artificial neural networks, genetic algorithm, and fuzzy logic have been applied increasingly for damage detection with varied success [1].

In recent decades there has been an increasing interest in using neural networks to predict and estimate the damage in structures. ANNs can be considered as an Artificial Intelligence (AI) technique and the structure of an ANN bears a very approximate similarity to the human brain. ANNs are employed when the relationship between the input and output is complicated or when the application of another available technique requires long computational time and the effort is very expensive [2].

ANNs are a powerful tool used to solve many real-life problems. They can learn from their experience to improve their performance and to adjust themselves to changes in the environment.

Damage detection as an inverse problem can be identified using ANNs from the measured responses under the excitation of the structure. The inverse problem is defined as the determination of the internal structure of a physical system from the system's measured behavior or identification of the unknown input that gives rise to a

measured output signal. The neural network can be trained to recognize the characteristics of an undamaged structure as well as those of the structure with elements of varying degrees of damage. The trained neural network will then have the ability to identify the location and the extent of damage of individual elements [3].

There are four levels of damage identification consisting of determination of the presence of damage in the structure, determination of damage location, and determination of the severity of damage [4]. The fourth level that is the prediction of the remaining service life of the structure is associated with fatigue life and fracture mechanics and will not be addressed in this review. In this paper, a review of the literature for damage identification and structural health monitoring based on measured dynamic properties by using ANNs during the last two decades is presented.

While there are a number of literature that discuss about crack detection methods, none of them provides a direct comparison between the methods to find out the one that has the best efficiency and accuracy rate. This is an important point that needs to be resolved as it may help designers to come up with the most efficient design from the very beginning to anticipate cracks on different surfaces. This is why this study aims to close this gap as a contribution to the field of research with the purpose to provide an insight for future researches, particularly within the crack detection discourse.

2 Literature Review

2.1 Cracks Development

Different types of engineering structures, including concrete surfaces, can have fatigue stress which can lead to creating cracks. This results in a reduction of local stiffness and can also result in material discontinuities. If such measures can be detected in an early manner, then proper actions can be taken to prevent any sort of damage and failure. Cracks on the concrete surface are one of the indications where users will be able to see the degradation of the overall structure. Manual inspection is often used for inspecting the crack properly [5].

In such a method, the sketch is prepared manually, and any sort of conditions related to irregularities are kept in record. However, there are shortcomings of using such a manual approach since this can be subjected to the knowledge and experience of the specialist who is investigating the case. To tackle the issue, the Artificial Intelligence-based system gets more popular now.

This is an objective-based practical solution. Using Artificial Intelligence, it is possible to identify the crack specifically. Such actions have prompted the creation of Cracks deep learning.

2.2 Cracks Detection through Artificial Intelligence

When the solid structures disintegrate, then there is a case of developing cracks. The structural designer is the person responsible for providing such information that will look for cracks.

The Artificial Intelligence or AI system is improving regularly. With its regular evolution process, the system is used on different cracks detection process. Some systems are used to find structural damage that can exist in major infrastructure, including- dams, skyscrapers, nuclear reactors, bridges, and other buildings defects.

This technique focuses on using video technology and examines it frame by frame to look for any sort of cracks. Artificial Intelligence (AI) is mainly used to track the cracks from one frame to another. A specific operator remains who reviews the specific frames of the video to find the cracks and understand what actions are needed.

AI detection technology helps to reduce any accidents or deaths. It focuses on the computer doing the hard work and gives the human operator specific information related to the cracks [6].

2.3 Cracks Detection Process

It has been known that if there is any tiny crack in the nuclear reactor or any other infrastructure, then it could lead to catastrophic consequences.

There could be cataclysmic consequences in high risk and sensitive areas, such as- nuclear reactors if there is unidentified or under-identified structural damage. The use of Artificial Intelligence helps to create an automatic crack detection system to find out cracks properly and not to misidentify the small scratches.

Therefore, the technicians are required to review the videos frame by frame basis. The process itself is time-consuming and there could be human errors as well [7].

It can be considered a tedious task to inspect any cracks manually. It is both complex and very time-consuming. In some cases, such actions can also pose a greater danger. Therefore, authorities are now moving towards AI detection that will help them to look for buildings' defects or cracks detection.

In such cases, there has also been the use of drones that look fly around the structures, capture the live feed to the AI algorithm so that it can find the right images and also classify them into cracks or non-cracks region [8].

In terms of deep learning, one of the challenging things is network training. There are several parameters involved in this and it also requires a huge level of data for training purposes. Some techniques are considered to be efficient whereas some others are not. There is a technique known as per-pixel window-sliding which can be used for crack detection. This process is considered extremely inefficient and could also contribute to a much

higher level of cost. However, there is an alternative to using the per-pixel window-sliding where users will be able to utilize the Convolutional Neural Network or CNN for pre-selection purposes that will help to divide the full-size image into few image blocks. Inspection enhancements procedures are also used to properly understand cracks detection. To process the cracks accurately, there have been propositions to use CNN for block-level crack detection [9].

2.4 Cracks Classifications

Cracks classification is considered to be an approach through which specific crack type can be found using machine learning algorithms. Crack detection normally identifies or looks towards the presence of a crack. On the other hand, cracks classification deals with the crack classification based on feature which has been extracted from the crack region [10]. It is essential to understand the type of cracking that has been identified. Therefore, the classification of such cracks is needed to be understood. After detecting the crack in the pre-processing phase, the next step involves the detection and classification of the type of cracks in the overall processing phase. The right kind of classification model is therefore important in such cases. These cracks can be classified into seven different categories as in the following- Alligator cracking, hair cracking, multi cracking, diagonal cracking, block cracking, longitudinal cracking, and transverse cracking [11].

2.5 Shapes of Crack

The form and size of the crack can sometimes indicate the underlying problem. Cracking can be horizontal, vertical, stepped, cogged, or a combination of all these. When assessing cracks, the width of the crack is often more important than the length of the crack.

Stepped cracks tend to follow the lines of horizontal and vertical joints in buildings, such as beds of mortar between bricks or blocks and may indicate structural movement.

Vertical cracks may indicate that structural components such as bricks or blocks have failed and so can be a sign of significant stresses within the building structure.

Table 1. Damage to Walls caused by the movement of Slabs and Footings, and other Causes [10]

Application	Data Analytics
< 0.1 mm	Hairline cracks
< 1 mm	Fine cracks that do not need repair
< 5 mm	Cracks noticeable but easily filled. Doors and windows stick slightly.
5 mm to 15 mm (or a number of cracks 3 mm or more in one group)	Cracks can be repaired and possibly a small amount of wall will need to be replaced. Doors and windows stick. Service pipes can fracture. Weather tightness often impaired.
15 mm to 25 mm but also depends on number of cracks	Extensive repair work involving breaking-out and replacing sections but also depends on walls, especially over doors and windows. Window and door frames distort. Walls lean or bulge noticeably, some loss of bearing

Cracks that are wider at the top or the bottom may indicate that there has been foundation movement, with the direction of the widening indicating the likely direction of the movement.

Horizontal cracks may indicate that an element such as a wall is failing, and this may present a safety concern.

3 Research Methodology

3.1 Study Using ML

In this work, the authors develop an ML algorithmic framework for failure detection and classification merging a pattern recognition (PR) scheme and ML algorithms applied to a damage and fatigue phase-field model. The authors consider an isothermal, linear elastic, and isotropic material under the hypothesis of small deformations and brittle fracture.

We simulate the phase-field model using Finite Element Method (FEM) and a semi-implicit time-integration scheme to generate time-series data of damage phase-field ϕ and degradation function

$$g(\emptyset)=(1-\emptyset)2$$

From virtual sensing nodes positioned at different locations across a test specimen. The authors introduce a PR scheme as part of the ML framework, in which time-series data from FEM node responses are considered as a pattern with a corresponding label. The authors define multiple labels for "no failure", "onset of failure" and "failure" of the test specimen based on tensile test load-displacement curve and damage threshold concept. Once

the patterns representing different states of the material are identified, the proposed ML framework employs k-nearest neighbor (k-NN) and ANN algorithms to detect the presence and location of failure using such patterns. In this study, the authors consider different failure types to further assess the performance of the framework. Also, by introducing noise to the time series data, the authors ascertain the robustness of the proposed framework with noise-polluted data, leading to the effective use in failure analysis under high sensitive/uncertain parameters and operators. The findings from this study will pave a way for the development of novel data-driven failure prediction frameworks, which can efficiently establish a link among the classification results (i.e., accuracy) and different phase-field model parameters, thus enabling the computational framework to identify those parameters affecting model's accuracy and updating them to achieve the best performance.

3.2 Cracks Modes

Various studies over the last decade have indicated that a beam with a breathing crack, i.e., one which opens and closes during oscillation, shows nonlinear dynamic behavior because of the variation in the structural stiffness which occurs during the response cycle. On the other hand, the effect of moving loads and masses on structures and machines is an important problem both in the field of transportation and in the design of machining processes. A moving load (or moving mass) produces larger deflections and higher stresses than does an equivalent load applied statically.

These deflections and stresses are functions of both time and speed of the moving loads. It is, therefore, essential to detect and control damages in structures subjected to a moving mass. Very few studies have been reported in the literature that deals with moving load or moving mass problems under the effect of cracks.

Diagnosing a cracked component by examining the vibration signals is the most commonly used method for detecting this fault. The fault detection is possible by comparing the signals of a machine running in normal and faulty conditions.

Depending on the crack's size and location, the stiffness of the structure is reduced and, therefore, so are its natural frequencies compared to the original crack-free structure. This shift in natural frequencies has been commonly used to investigate the crack's location and size.

Vibration analysis can also be carried out using Fourier transform techniques like Fourier series expansion (FSE), Fourier integral transform (FIT), and discrete Fourier transform (DFT). Identification and diagnosis of a crack in inaccessible machine members have gained importance in now a day using vibrational analysis and artificial intelligence technologies. Using a modern technology sensor is placed near the inaccessible internal machine component. The piezoelectric transducer of the sensor produces a vibrational signal which is transformed using Wavelet Transformation technology.

These signals are time and frequency-dependent. After extracting fault features, a proper artificial neural network is implemented for aiding of the fault classification. An intelligent fault diagnosis system is performed throughout combing the approach to fault diagnosis with an artificial neural network. An artificial neural network is proved as a reliable technique to diagnose the condition of a rotating member. In general, the cracks present in the beams are not always open or close condition. It always varies from time to time depending upon the situation. If the loads are static like load due to dead weight, the load of the beam, etc. and if the deflection is more than the vibration amplitude then the crack becomes an open crack, otherwise it will be breathing crack.

Beams are one of the most commonly used structural elements in several engineering applications and experience a wide variety of static and dynamic loads. Cracks may develop in beam-like structures due to such loads. Considering the crack as a significant form of such damage, its modeling is an important step in studying the behavior of damaged structures.

Knowing the effect of crack on stiffness, the beam or shaft can be modeled using either Euler-Bernoulli or Timoshenko beam theories. The beam boundary conditions are used along with the crack compatibility relations to derive the characteristic equation relating to the natural frequency, the crack depth, and location with the other beam properties.

4 Results & Evaluation

The form and size of the crack can sometimes indicate the underlying problem. Cracking can be horizontal, vertical, stepped, cogged, or a combination of all these. When assessing cracks, the width of the crack is often more important than the length of the crack.

The accuracy of the classifications was evaluated through an analysis of the confusion matrices, this being the most commonly used method to validate this type of model. This matrix contains information based on the percentages of observed and estimated data for each object is classified, in which different parameter that indicates the precision of the classification can be calculated [14]. The parameters that arise from the error matrix and the formula to calculate them are as follow:

Precision $$P = \frac{\sum_{i=1}^{m} x_{ii}}{N}$$

Accuracy $$P_A = \frac{x_{ii}}{x_{\sum i}}$$

Precision $$U_p = \frac{x_{ii}}{x_{i\sum}}$$

Coefficient Analysis

$$K = \frac{N \sum_{i=1}^{m} x_{ii} - \sum_{i=1}^{m} x_{i\sum}\ x_{\sum i}}{N^2 - \sum_{i=1}^{m} x_{i\sum}\ x_{\sum i}}$$

Where m = Total number of classes, N = Total number of pixels in the m reference classes, x_ii= elements of the main diagonal of the confusion matrix, x_∑i= sum of the pixels of reference class i and x_(i ∑)= sum of the pixels classified as class i.

4.1 Cracks Detection Using ANN Method

There are different classical methods which are used for cracks detection. One of the methods was known as an artificial neural network method. Bakhary (2007) considered applying Artificial Neural Network or ANN towards damage [12]. During the person's investigation, a certain type of ANN model has been created to apply towards Rosenblueth's point estimate method. This method has been verified through the simulation process of Monte Carlo. There has also been an estimation of the statistics of the stiffness. After that, the probability of damage existence was done and calculated based on the probability density function of the current undamaged and damaged states. Such a developed approach was applied to detect simulated damage in a steel frame model and another concrete [13].

There has been the use of ANN or Artificial Neural Networks by different researchers so that they identify the damage location properly and also by getting severity from different types of input as well as output variables. They help to provide an efficient tool in terms of pattern recognition. There have been several studies [10].

ANN and it has been concluded from most of the studies that the Artificial Neural Network or ANNs can provide the correct level of damage identification. This is especially true when the overall structural damage and the related changes in vibration properties are simulated numerically and they are considered error-free. Nonetheless, this needs to be noted that during practice, there could be uncertainties in the overall FE model parameters and there could be some modeling errors that are known to be inevitable [10].

The overall existence of having modeling error in the FE model because of the inaccuracy of physical parameters and structural properties may end up in vibration parameters. Furthermore, having measurement error in the data which is normally used as testing data in the ANN model can also be considered unavoidable. ANN prediction efficiency is mostly dependent on the accuracy of both these components. The existence of such types of uncertainties can also result in a false and inaccurate type of ANN predictions. Therefore, the authors can understand that there should be proper analysis related to the reliability of the Artificial Neural Networks or ANN models for any sort of structural damage detection.

4.2 Cracks Detection by Hybrid Technique

Research has brought in a new method so that the location as well as crack depth on any structure can be identified. One such method is known as a hybrid neuro-genetic technique. In this case, feed-forward multi-layer neural networks are trained through the process of backpropagation to learn about the input-output relation of the whole system [5]. After that, the researchers used a genetic algorithm to find out the different locations of the crack as well as its depth so that the difference from the measured frequencies can be minimized. Using neural networks for damage detection has been developed for many years. This is because they can cope with the different structural damage analysis without considering any intensive computation. Neural networks are considered to be a potential approach through which users will be able to understand and detect the structural damage. For such researches, it is required to have both the modal frequencies and the modal shapes as well for ensuring the neural network training so that the authors can understand more about the structural damage detection [10].

4.3 Discussion

Out of the described methods, the hybrid technique of crack detection provided the most accurate results in detecting cracks with at least 18% of accuracy above the other methods. This is seen as a great outcome from a crack detection method, which may ensure a significant enhancement in terms of identifying and fixing cracks on different surfaces.

In terms of deep learning, one of the challenging things is network training. There are several parameters involved in this and it also requires a huge level of data for training purposes. Some techniques are considered to be efficient whereas some others are not. There is a technique known as per-pixel window-sliding which can be used for crack detection [11]. This process is considered extremely inefficient and could also

contribute to a much higher level of cost. However, there is an alternative to using the per-pixel window-sliding where users will be able to utilize the Convolutional Neural Network or CNN for pre-selection purposes that will help to divide the full-size image into few image blocks. Inspection enhancements procedures are also used to properly understand cracks detection. To process the cracks accurately, there have been propositions to use CNN for block-level crack detection [5].

5 Conclusion

Cracks occur when solid structures disintegrate. These include concrete surfaces in which crack detection methods could help identifying any type of cracks, including transversal, longitudinal, and pothole. The challenge for this procedure would be network training, in which several parameters are involved in the determination of the location and severity level of the cracks. This study found out that the hybrid crack detection technique provides more accurate and reliable outcomes due to the fact that it combines both the ANN and ABC algorithms to help the designers locating and analyzing cracks. It is expected that this finding may contribute in answering several questions over the accuracy and reliability of various crack detection methods as well as help providing an appropriate response to the growing discourse over the field of research.

Acknowledgment

This research is financially supported by the Sheikh Zayed Housing Program in United Arab of Emirates and International Group of Innovative Solutions. Special thanks for Jamila Al Fandi, Dhoha Al Hamodi, Aesha Aleghfeli, Maryam Al Rayssi, Ahmed Al Ali

References

[1] Abella, B.M., Rubio. L. and Rubio, P. (2012), "A non-destructive method for elliptical cracks identification in shafts based on wave propagation signals and genetic algorithm", Smart Struct. Syst., 10(1), 16-20.

[2] Hakim, S.J.S. and Abdul Razak, H. (2013b), "Adaptive Neuro Fuzzy Inference System (ANFIS) and Artificial Neural Networks (ANNs) for structural damage identification", Struct. Eng. Mech., 45(6) 779-802

[3] Li, Z.X. and Yang, X.M. (2008), "Damage identification for beams using ANN based on statistical property of structural responses", Comput. Struct., 86, 64-71.

[4] Rytter, A. and Kirkegaard, P. (1997), "Vibration based inspection using neural networks, Structural damage assessment using advanced signal processing procedures", Proceedings of the DAMAS 97, University of Sheffield, UK.

[5] Mohan, A., & Poobal, S. (2018). Crack detection using image processing: A critical review and analysis. Alexandria Engineering Journal, 57(2), 787-798.

[6] Bucklin, S. (2019). AI Technology Improves Critical Crack Detection. Retrieved from Communications ACM: https://cacm.acm.org/news/237484-ai-technology-improves-critical-crack-detection/fulltext

[7] Purdue. (2019). AI technology improves critical crack detection in nuclear reactors, bridges, buildings. Retrieved from Phys: https://phys.org/news/2019-06-ai-technology-critical-nuclear-reactors.html

[8] Thielemans, L. (2018). How users can detect cracks in concrete bridges using deep learning. Retrieved from Raccoons: https://blog.raccoons.be/detecting-cracks-in-bridges-using-deep-learning

[9] Zhang, K. (2019). DEEP LEARNING FOR CRACK-LIKE OBJECT DETECTION. Retrieved from Digital Commons: https://digitalcommons.usu.edu/cgi/viewcontent.cgi?article=8747&context=etd

[10] Sitara, S. N., Kavitha, S., & Raghuraman, G. (2018). Review and Analysis of Crack Detection and Classification Techniques based on Crack Types. *International Journal of Applied Engineering Research, 13*(8), 6056-6062.

[11] Ahmadi, A., Khalesi, S., & Bagheri, M. R. (2018). Automatic road crack detection and classification using image processing techniques, machine learning and integrated models in urban areas: A novel image binarization technique. *Journal of Industrial and Systems Engineering, 11*, 85-97.

[12] Bakhary, N., Hao, H., & Deeks, A. (2007). Damage detection using artificial neural network with consideration of uncertainties. *Eng. Struct., 29*(11), 2806-2815.

[13] Parhi, D., & Choudhury, S. (2011). Analysis of smart crack detection methodologies in various structures. *Journal of Engineering and Technology Research*, 139-147.

[14] Clarke. F. R. Constant-ratio rule for confusion matrices in speech communication. Journal of the Acoustical Society of America. 1957,29,715-720.

Smart Tunnel Inspection and Assessment using Mobile Inspection Vehicle, Non-Contact Radar and AI

Toru Yasuda[a] , Hideki Yamamoto[a], Mami Enomoto[b] and Yasushi Nitta[c]

[a]Transportation Infrastructure Div., Pacific Consultants Co.,Ltd, Japan
[b]Advanced Technology Research Team, Public Works Research Institute, Japan
[c]Policy Planning and Coordination Division for Public Works Project, Ministry of Land, Infrastructure and Transport and Tourism, Japan
E-mail: tooru.yasuda@os.pacific.co.jp, hideki.yamamoto@tk.pacific.co.jp, enomoto-m574bs@pwri.go.jp, nitta-y92qx@mlit.go.jp

Abstract –

We have developed a mobile survey vehicle with a high-precision laser scanner measurements for deformation analysis, 20 video cameras for damage assessment on lining surface such as cracks and water leakage, and also a non-contact radar to detect lining thickness and cavity behind lining.

In this paper, we report the development of a non-contact radar survey system mounted on a mobile inspection vehicle to detect inner defects and cavities behind lining concrete, and examination of efficiency of utilizing an integrated diagnosis system to assess the soundness comprehensively as well as value of compiling database of various unsoundness conditions including inner defects by a 3D visualizing technology.

It supports the technical experts to evaluate the diagnosis and the cause of the damage in the tunnel. It contributes to efficient damage detection for tunnel inspection based on AI (Artificial Intelligence) and 3D visualization of various damage conditions, including inner defects.

Keywords –
Tunnel inspection; Mobile survey technology; Non-contact radar; Lining defects and cavity detection; 3D visualization; Artificial Intelligence

1 Introduction

Human visual inspection of road tunnels has been a common practice used in routine maintenance procedure to ensure its safety. It, however, has some problems; it requires traffic restrictions on at least one lane, and it is hard to make a fair judgement in dark and narrow spaces.

We have overcome some of the problems, by developing a mobile survey vehicle with a high-precision laser scanner measurements for deformation analysis, 20 video cameras for damage assessment on lining surface such as cracks and water leakage, as explaining the overview of the inspection vehicle in next section.

Our next challenges are to dispense hammering test of unnecessary normal parts. We introduced non-contact radar to detect lining thickness and cavity behind lining, and developed an inspection technology detecting the inner defects in concrete lining using rapidly scannable non-contact radar as a complement of hammering test. With non-contact radar system, which allows the vehicle to survey at 50km/h, concrete lining thickness and its back cavity has successfully detected.

In addition, in this paper, we examined efficiency of utilizing an integrated diagnosis system to assess the soundness comprehensively as well as value of compiling database of various unsoundness conditions including inner defects by a 3D visualizing technology. With the acquired data, analysis engineers overlay the result on the 3D model and integrate information such as position synchronized images, deformation contours, cavities and inner defects. It is expected to support the technical experts to evaluate the diagnosis and the cause of the deformation in the tunnel. By recording those damages in digital format, progressiveness can be correctly and accurately tracked off. After the first survey measurements, the cause and progress of damage is continuously monitored. It contributes to efficient damage detection for tunnel inspection based on AI (Artificial Intelligence) and 3D visualization of various damage conditions, including inner defects.

2 Overview of Mobile Inspection Vehicle

An overview of this mobile inspection vehicle is shown in Figures 1, 2. The following measurement data and functions are available for the tunnel inspection.

1. Laser Tunnel Surveys and Deformation mode analysis: The high-precision laser scanner with 1 million points/second is used to obtain high-density data, which enables us to objectively determine the

lining shapes and the deformation of the lining (deformation mode, joints, and level differences of cracks).

2. Tunnel Image surveys and Soundness assessment: Image of wall surface taken while travelling at 50-70km/h, the cracks of 0.3 mm or more can be identified. It is possible to draw an objective and accurate damage map, and to identify the progressive of unsoundness conditions and to estimate the causes of damage.
3. Radar Tunnel Surveys Cavity Evaluation: Non-contact radar system to detect lining thickness, back cavities, and inner defects (while travelling at 50km/h). The system aims to quickly detect hazard locations with thin lining and cavities [1]. This is the world's first radar antenna capable of high-speed detection with a separation of about 3 m. The details of the functions and development are indicate in next section.

The results obtained from these results can be used to support efficient close visual inspection and hammering test, and plan detailed inspections and repairs.

3 Development of Mobile Non-contact Radar

3.1 Radar for Inspection of Lining Thickness and Cavities behind Lining Concrete

3.1.1 Principles of radar survey

The principles of subsurface radar survey are those of indirect survey, which applies the physical characteristics of EM waves that reflect at boundaries between different substances.

Due to the damping nature of a substance, when an EM wave propagates through a medium, its energy is absorbed and the amplitude reduced as a result. Because of this, the general characteristics are that the reflected waves coming from deep locations lack adequate strength and thus are undetectable on radar records. This damping effect is closely interrelated with frequency; the greater the frequency the greater the damping effect, and vice versa. Therefore, to have a deeper survey depth, it is necessary to set a lower frequency.

On the other hand, a lower frequency which leads to a lower resolution, making it difficult to identify small configurations. There is thus a conflicting relationship; obtaining a high resolution requires high frequencies, while achieving a larger survey depth requires low frequencies (See Table 1). Because of this

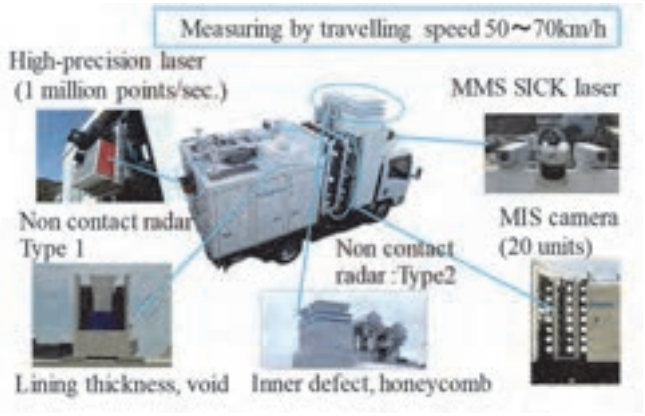

Figure 1. System of MIMM-R

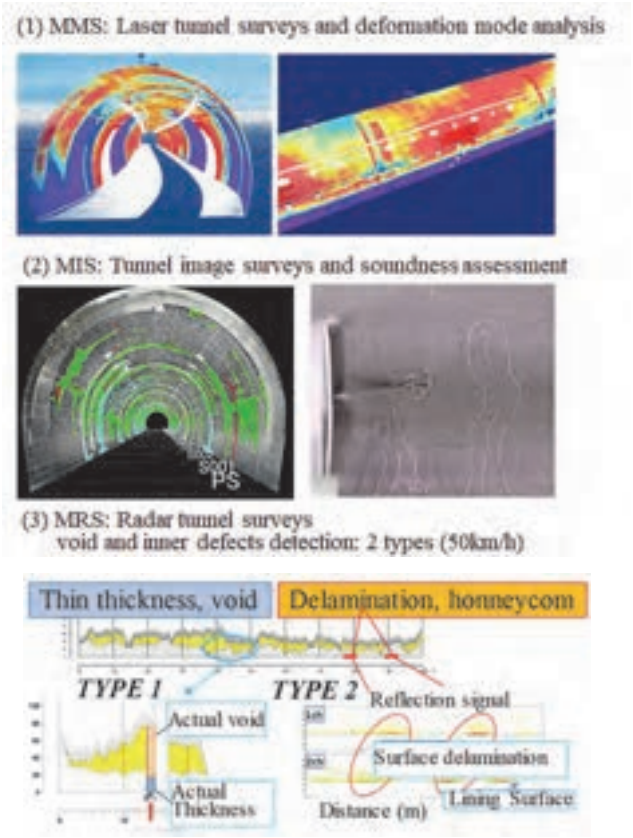

Figure 2. Function of MIMM-R

Table 1. Frequency and resolution

	High frequency	Med frequency	Low frequency
Frequency	1000GHz~	900～300MH	~300GHz
Detectable depth	~0.3m	~1.0m	~1.8m
With rebars	ctc 100mm	ctc 300mm	ctc 500mm
Depth image	Shallow		Deep
Resolution image	Fine		Rough

dependency of EM wave characteristics on frequency, an appropriate frequency should be selected according to the purpose and the target of a survey.

In improving the non-contact radar system to be applicable to tunnels, particular attention was given to the following two issues [2] .

3.1.2 Approx. 3m distance from the target in the non-contact radar system

The non-contact radar system makes it difficult to analyze the patterns of reflected waves further away from the target due to the damping and diffusion of EM waves. Based on the principles analysis that takes into account the polarity and coefficient of EM wave reflection as shown in Figure 3, the team managed to resolve the issue of reduction in detection performance in the non-contact radar system.

In the case of contact antennas, the diffusion characteristics of EM waves also caused difficulties in keeping an adequate distance. The contact-type bow tie antenna has no directionality and low sensitivity, and therefore should be touched with the target. On the other hand, the newly adopted horn antenna has a high directionality and high sensitivity, allowing to set a greater distance of 3m.

3.1.3 Realization of high-speed inspection

Improvement of the controller was necessary to obtain the same amount of data as the contact type while travelling at a speed of 50km/h or faster. To handle the extreme speed of EM waves, a sampler is used to divide a single trace, obtain the divided pieces and then reconstruct the same single trace shape. Data collection at a 50km or faster was made possible by enhancing the sampling speed, and speeding up the analog/digital converter.

3.1.4 Evaluation of Practical Use

To determine the practicability, past adequacy survey results obtained for a tunnel using the contact-type antennas and those by drilling were compared to the data obtained with the non-contact radar system, the differences of which were then analyzed and evaluated.

Regarding Sample shown in Figure 4, Data A and B were obtained with a conventional contact-type radar system and the newly developed non-contact radar system, respectively. The figure shows that they yielded more or less the same results.

The data obtained with the non-contact system were then compared to the actual lengths measured in a boring survey, which proved to have a high correlation as shown in Figure 4. Next, the analytical results for the radar survey were compared to the actual measurements taken by boring. These results show that the accuracy is generally 80-90%, which is sufficient for practical use.

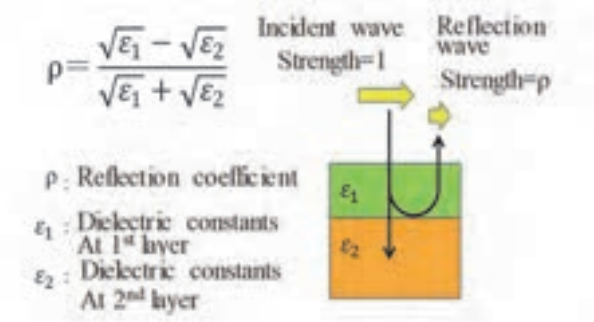

Figure 3. Concept of polarity and coefficient of reflection

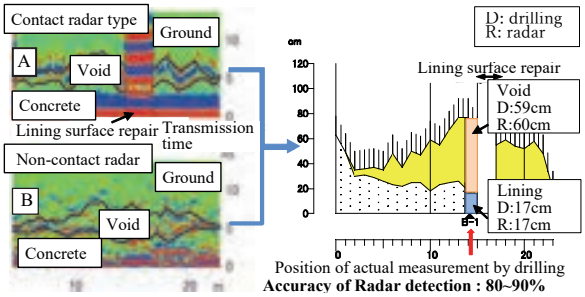

Figure 4. Comparison of results obtained by radar type and comparison with actual drilling

Figure 5. Targets of inner defects

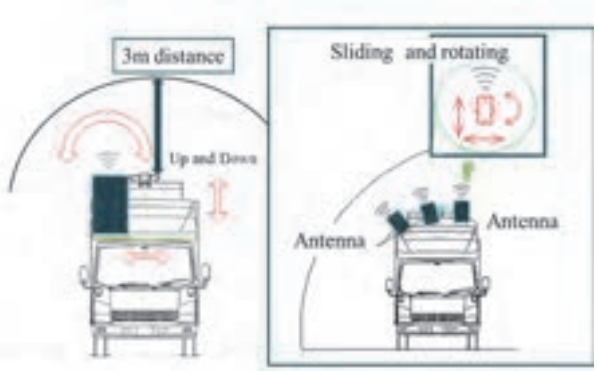

Radar for detecting of lining thickness and cavity behind lining

Radar for detecting of inner defection (New developing radar)

Figure 6. 2 types of radar systems

3.2 Radar for Inner Defects Detection

3.2.1 Development Background and Target

In the field of SIP (Cross-ministerial Strategic Innovation Promotion Program in Japan) infrastructure maintenance, renewal and management technology, we have developed the technology under the theme of "Development of Internal Defect Inspection Technology and Integrated Diagnosis System for Tunnel Lining Using High-Speed Non-contact Radar" (completed in fiscal year 2016), and have achieved good results in the development of radar for internal defects as a support system for percussion inspection [2] [3].

Of various irregularities found in tunnel lining concrete, exfoliation of block pieces is regarded important in tunnel management because it gives direct impacts on users, and the timing of its occurrence is difficult to predict. In particular, certain inner defects including discontinuous joint loosening, honeycombs and poor material quality that do not involve cracking, water leakage or level differences on the surface are extremely difficult to detect unless a proper hammering test is carried out. Survey vehicles could not detect these inner defects if they were of the non-contact type and travelling at a high speed. Such inner defects often occur around and along joints, as shown in Figure 5. Given these, for the radar system designed for inner defects detection, the target size of areas to be surveyed was set at 5cm and 1m in the longitudinal and transversal directions, respectively.

The antennas of five domestic and five overseas companies were investigated prior to the development of the radar antenna. The results of the survey showed that a maximum separation of about 1 m is the limit for the existing antennas to detect defects in concrete. In road tunnels, a separation of about 3 m is required to allow for a driving survey without traffic control, due to constraints caused by clearance limit and obstacles such as signs and jet fans. As a result, this led to the development of an original antenna.

3.2.2 Verification Results

Figure 6 shows the schematic diagrams of the two types of radar systems, figure 7 shows the installation and measurement status of the internal defect radar antenna. The antenna specifications are shown in Table 2, and the verification results of the developed antenna are shown in Figure 8.

The results of the verification are as follows; internal cavities of known size and location were accurately detected in the full-scale test model of New Bridge at Nagoya University. The depth of the search for cavities, surface delamination and honeycomb in the lining concrete is about 20 cm, and the developed

Figure7. Installation and Measurement of Internal Defect Radar Antenna

Table2. Specifications of Internal Defect Radar Antenna

Specifications		Remarks
primary detecting target	Void in lining	Mainly used to detect for void e.g., in the tunnel lining
Maximum detectable distance	4m	The distance to the wall is assumed to be about 3 m
Pitch resolution	0.075m	In concrete: 0.025m
Maximum detecting speed	25m/s	Actual speed: 25[m/s]/Number of antennas used
Radar system	FM-CW	Separate antenna system for transmission and reception
Centre frequency	3Ghz	—
Bandwidth	2Ghz	—
Signal Processing and Display	The received signals can be aggregated in the direction of the vehicle's motion by the synthetic aperture process. Outputs the distance to the wall and reflection intensity. It is possible to evaluate whether the reflected signal is due to a cavity or metal.	

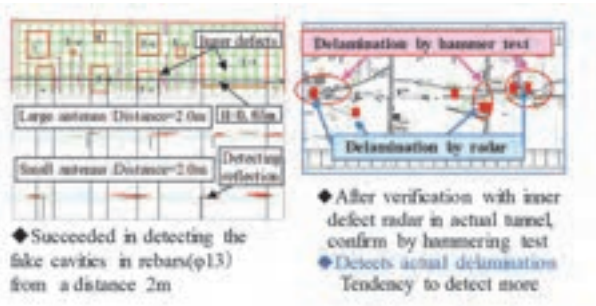

Figure 8. Verification results of radar system

method can support efficient inspection by screening the problem areas before the hammering test.

4 Damage Detection with AI

4.1 Damage Detection Using Deep Learning Based Semantic Segmentation

In the post-processes of measurement, it requires a lot of time and efforts to manually detect damages and record them on a damage map. In order to reduce manual efforts, we have applied deep learning and semantic segmentation models [4] [5]. In particular, it is expected that the semantic segmentation models can be improved to practical detection of degradation [6].

4.1.1 Training dataset

Using 200 spans of tunnel inspection images, annotate three types of damages; water leakage, free lime and cracks. In our previous studies, discrepancies between the damage on the inspection photographs and the annotation data, It could be affected its low accuracy of detection. In this study, we annotated the degradation in pixel level.

4.1.2 Model Architecture

The damage detection network is built on the SegNet, which is deep convolutional encoder-decoder architecture designed for multi-class pixel-wise segmentation and developed by members at the University of Cambridge, UK.

4.2 Experimental evaluation

To evaluate the performance of the model, out-of-sample images are used for inputs, and detects water leakage, free lime, cracks. Figure 9 shows the results and its ground truth.

4.2.1 Evaluation for water leakage and free lime detection

As a result of water leakage and free lime detection, it assumed that simple degradation are mostly extracted. However, the degradation where the damages are compounded or covered by a repair net tend to fail to be detected.

4.2.2 Evaluation for crack detection

Although cracks that are clearly visible in the images are generally detected, narrow cracks and those that were difficult to distinguish from chalks or shadows were over detected.

On the assumption that the model trained with various types of cracks in the images can extract cracks in all sizes and conditions, however the trained network has failed to converge and resulted in over detection.

By examining the cause of failure, the initial model

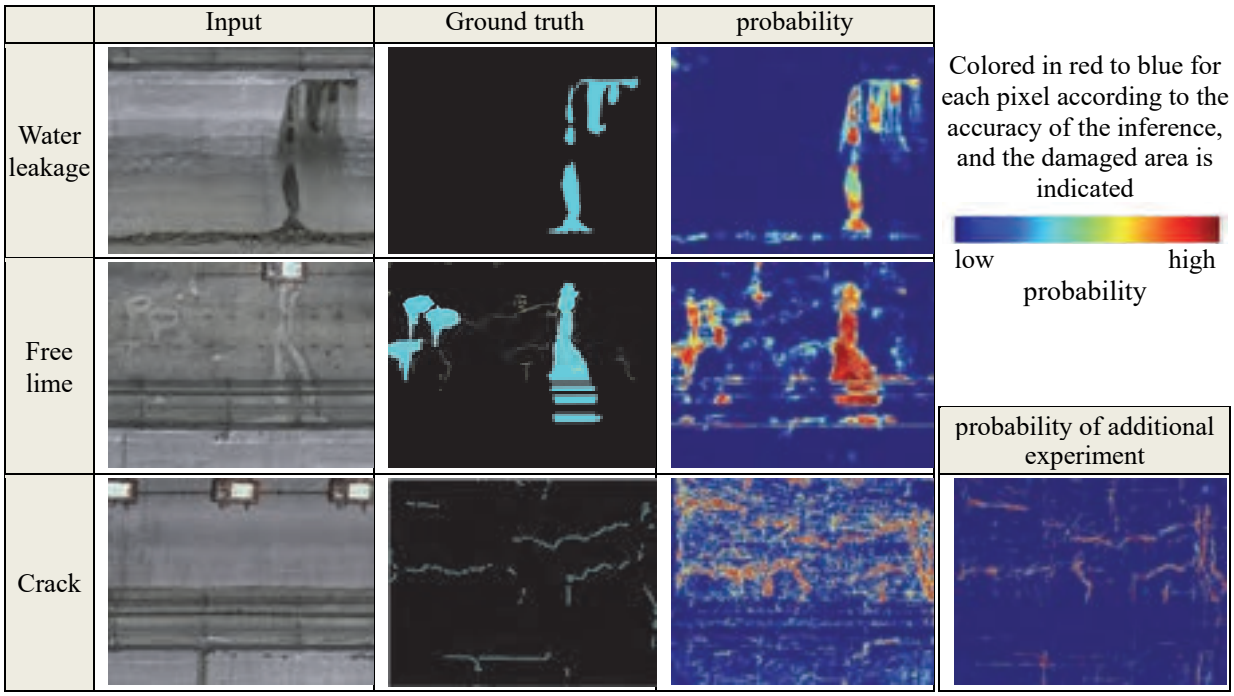

Figure 9. Results of damage detection using AI

has trained with a mixture of images in various qualities. The images in low quality could be a cause of non-convergence in the training process. In additional experiment, new training data has been set only with high-quality images, and it has achieved successful training process. The bottom right image in figure 9 shows the result from the retrained model, which has been achieved the desired performance.

5 Visualization in 3D

The mobile inspection vehicle is capable of not only image measurement also geometry measurement by built-in laser scanners. It enables to construct 3D model based on the point clouds of the laser, and to generate composite images and obtain the deformation position in synchronized accurate position. Figure 10 shows the 3D model including deformation information.

The image layer and deformation map layers are superimposed on 3D model based on coordinates and positions of the laser point cloud.

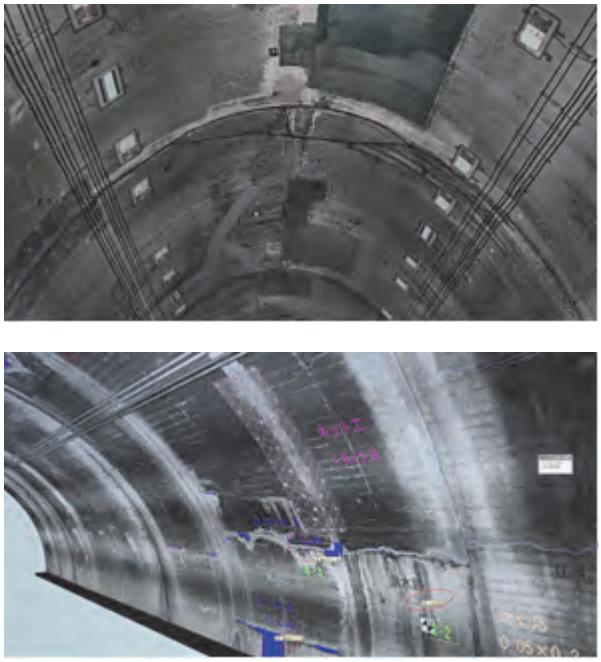

Figure 10. 3D models（bottom: damage map）

6 Development of Integrated Diagnosis System

To support diagnosis evaluation, it is necessary to comprehensively analyze not only images but also data from laser and radar units;

(1) Detecting degradation, such as cracks, water leakage and free lime, from acquired images

(2) Identifying deformation mode and damaged position by utilizing laser point clouds, estimating the cause of the deformation mode, and identifying progressive degradations

(3) Detecting lining thickness and cavity behind concrete lining with analyzing acquired data from radar units

To diagnose correctly and certainly, a system which is capable of intuitively displaying details of those information is needed. The integrated diagnosis system to assess the soundness comprehensively and compiling a database of various unsoundness conditions, including inner defects by a 3D visualizing technology. The overview of the integrated diagnostic system is shown in figure 11. The integrated diagnostic system has the functions listed below.

(1) Point clouds analysis: Automatic detection of construction joints, extraction of cross-sectional shapes and span axes for each span, deformation mode analysis

(2) Damage map generator: Lining surface images are combined with the positional information of point clouds to create a damage map of cracks and leaks.

(3) Radar measurement analysis: The results of measurement and analysis of internal defects, lining thickness and cavity can be synchronized with the point cloud information and displayed in 3D, contour, longitudinal and transverse views.

(4) 3D visualization: A function to support the estimation of the cause of deformation and diagnosis by displaying the results of image, laser, and radar analysis in 3D and superimposing them on each other.

(5) Database: Stores images and records of multiple tunnels and inspection, deformation and countermeasure history.

To develop the function that detect progressive degradations, measuring the difference in relative position of the detected degradation in two different years. Also, the system has export function that allows integrate the both in 2D and 3D visualized result into other database systems, which make it possible to use the analyzed data for linking to BIM models. The system analyzes and visualizes the obtained data in 3D, and also visualizes and exports in 2D when necessary. These results are used to optimize the priority of the implementation of countermeasures, budget allocation, and to provide support services for facility management.

7 Conclusions

While visual inspection requires human labors to manually judge by sight, the integrated diagnosis system, which effectively utilize technologies, supports visual inspection to improve the efficiency of diagnosis, to extract deformation objectively and accurately, and to draw damage maps efficiently.

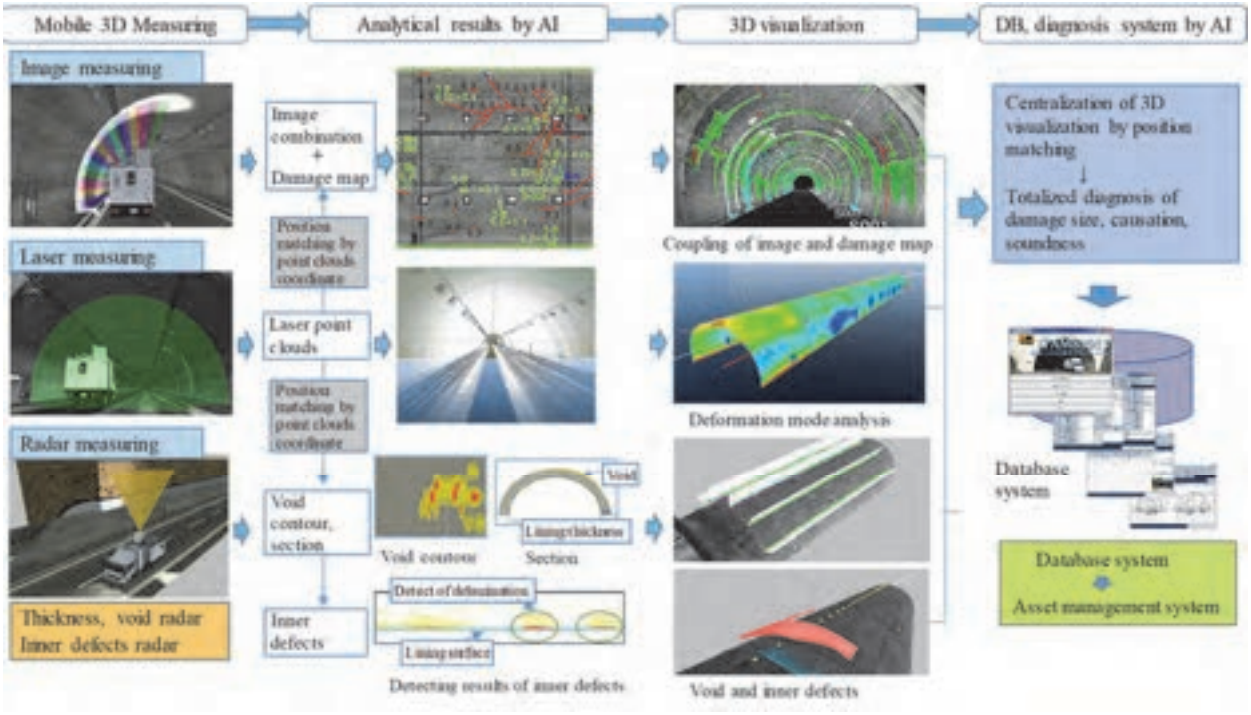

Figure 11. Totalized diagnosis and asset database system using 3D visualization and AI

It is not suitable to completely replace humanity to technologies, since it is responsible to human to make judgements to ensure the safety. However, it is sufficiently possible to use the results from the mobile measurement and its analytical data to conduct effective human visual inspection. The Usage of mobile inspection vehicle before conducting a human visual inspection, will reduce the cost and time involved in the overall workflow. Pre-inspection by the vehicle extract areas that requires attention at visual inspection and hammering tests. The visualization in 3D supports to understand integrated information of cameras, lasers and radars, and to appropriately judge the diagnosis and soundness.

The application of AI to inspection and diagnosis is in the development, although some results have been achieved. It will be our next challenges to improve accuracy of damage detection, reliability of evaluation and quality. Also, as a supportive technology for overall maintenance management, we will work towards the establishment of the system and the achievement of safe and secure society through smart tunnel management.

References

[1] Yasuda T., Yamamoto H. and Kitazawa R., High Speed Non-Contact Radar for Tunnel Lining Thickness and Cavity Detection at 50 km/h, *Construction Method and Machinery,* Vol.66 No.12、2014.

[2] Yasuda T. Tunnel Inspection Technology using Rapidly Scannable Non-contact Radar, EASEC-14, Ho Chi Minh City, Vietnam, January 6-8, 2016

[3] Summary of Research on SIP Research and Development, *SIP (Cross-ministerial Strategic Innovation Promotion Program in Japan Cabinet Office)*, http://www.jst.go.jp/sip/dl/k07/booklet_2017_A4.pdf, pp28-29

[4] Enomoto M. Fujiwara H. Matsubara K., Shigeta Y.,and Yasuda T. Development of AI-based Damage Extraction Model for Road Facilities, *Presentation of the 2018 Construction Consultant Services Research*, 2018

[5] Kawashiro K., Emomoto M., Yasuda T. and Yoshioka M., A Study on Damage Extraction in Tunnels by Deep Learning, *Proceedings of the 81st IPSJ Conference (4), Information Processing Society of Japan* pp.381-382, 2019

[6] Kawashiro K., Yasuda T., Emomoto M. and Kuge S., A Study on Damage Extraction in Tunnels by Semantic Segmentation, *The 74th Annual Academic Lecture CS10-20, Japan Society of Civil Engineers*, 2019

Applications of Building Information Modeling (BIM) in Disaster Resilience: Present Status and Future Trends

S. Khanmohammadi[a], M. Arashpour[a] and Y. Bai[a]

[a]Department of Civil Engineering, Monash University, Australia
E-mail: sadegh.khanmohammadi@monash.edu; mehrdad.arashpour@monash.edu; yu.bai@monash.edu

Abstract –

Natural disasters such as bushfires, wildfires, hurricanes, earthquakes, and floods cause significant socioeconomic losses with associated damages to communities. From 2005 to 2014, the worldwide damage caused by disasters has been more than US$1.4 trillion, with 0.7 million deaths and 1.7 billion people affected. In order to reduce the negative impacts of disasters and strengthening communities, the disaster resilience topic has been receiving increased attention to maximize the ability of communities to adapt and recover fast. Disaster resilience can benefit from Building information modeling (BIM) as an effective tool to facilitate informed decision-making. This article provides a comprehensive review of the existing literature on BIM applications in disaster resilience. Past research studies are categorized by the year of publications, type of disasters (fire, earthquake, flood), phase of the disaster (mitigation, preparedness, response, recovery), and target groups (buildings, infrastructures). The paper aims to provide a holistic review of research trends and patterns, emerging technologies, benefits, challenges and limitations, and research gaps.

Keywords –

BIM; Building information modeling; Bushfire; Disaster; Earthquake; Evacuation; Fire; Flood; Resilience; Review

1 Introduction

Based on the report of the United Nations Office for Disaster Risk Reduction (UNDRR), the number of disasters associated with natural hazards has increased over the past two decades. Consequently, communities should be prepared to recover from the impacts of disasters. A disaster-resilient community should withstand a natural hazard with a tolerable level of losses and adopts mitigation actions consistent with the desired level of protection [1]. The number of scientific research studies on disaster resilience has increased dramatically in recent years as shown in Figure 1.

Integration of disaster resilience and Building information modeling (BIM) provides an effective tool to help decision-makers visualize what is to happen in a simulated environment [2]. Similar to research on disaster resilience, the number of studies on BIM has increased over the past 20 years as presented in Figure 1. Although many BIM applications have been explored in the literature, applications for disaster resilience is scarce.

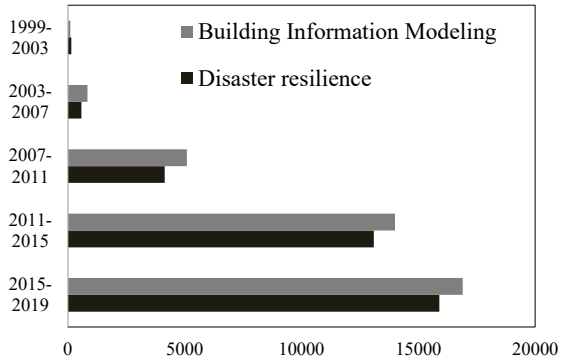

Figure 1. Number of publications on "Disaster resilience" and "Building Information modeling" in Google Scholar during the past 20

This research carries out a systematic review of the relevant literature with the following objectives: (1) classification of papers on BIM applications for disaster resilience; and (2) scoring the papers based on relevance; and (3) categorizing the selected papers based on the type and phase of disasters; and (4) identifying the research gaps in the literature, and outlining the potential future research directions.

Following the introduction, section 2 describes the research methods adopted in this paper. Section 3 provides an overview of the current literature on BIM applications for disaster resilience. The detailed BIM applications are categorized and described in Section 4. Section 5 outlines the identified research gaps and opportunities for future research. Finally, the conclusion is presented in Section 6.

2 Research methodology

The review method was informed by the Preferred Reporting Items for Systematic Reviews and Meta-Analyses (PRISMA) guidelines [3]. In the first step, about 30 BIM review papers were assessed, and the papers on the disaster resilience area were shortlisted. In the second step, two search attempts were conducted to find relevant studies. The keywords of the first attempt comprised building information modeling, BIM, and resilience, which resulted in finding 63 papers. In the second attempt, keywords such as building information modeling, BIM, disaster, flood, hurricane, tornadoes, volcanic, wildfire, earthquake, tsunami, and storm were utilized, and 251 research studies were found. The studies found in the two attempts were merged and the duplicated papers removed. In the next step, the evaluation of article titles was conducted to find the most suitable papers. Consequently, the outcome contains 123 papers.

In order to select the most appropriate papers, a selection system was needed. The selection system of these papers considered four important paper quality indexes such as authors' expertise, paper citations, and journal quality. Indexes are described as below:

- **Authors' expertise:** The authors' expertise is a critical index for the quality of the paper. The h-index of authors can be a good measure in order to show their expertise.
- **Publication date:** new publications can demonstrate the trends of current research; thus, they are more interesting for researchers. The current paper reviews papers that have been published during 2007-2020.
- **Paper citations:** Number paper citations are a measure of validity. Papers published before 2018 without at least 10 citations were excluded from this review.
- **Paper type:** Only books and journal publications are considered in this review paper.

All 123 papers are evaluated based on the above indexes. Consequently, 42 papers are detected as the most relevant papers that should be reviewed in this paper. Using the abovementioned approach, a comprehensive analysis of the literature was conducted. The comprehensive literature review provides useful information about identified gaps and opportunities for future research. The process is demonstrated in Figure 2.

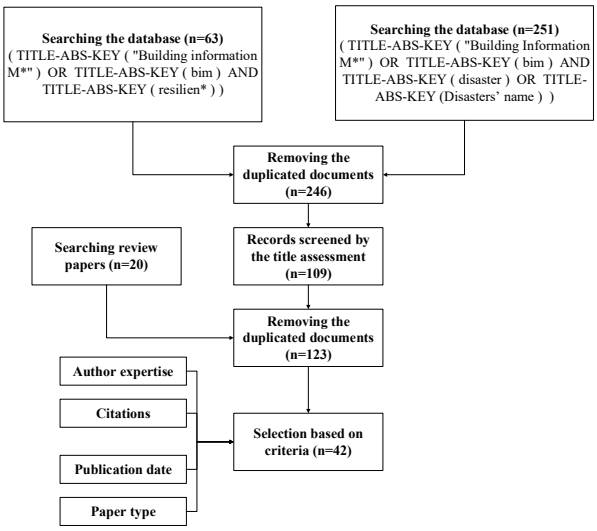

Figure 2. The process of the systematic review

3 Analysis of publications

The database of the nominated papers contains articles published from 2007 to 2020. However, about 39 percent of the selected papers are published after 2019. This means that the attention to the BIM applications for disaster resilience has been increased. Most of the selected papers has not been reviewed by the past review papers. Only 4 papers [4]–[6] among 44 papers have been reviewed by Tang et al. [7]. The selected papers have been published in 25 different journals. The journals with more than one included paper and their research impact are shown in Table 1. Based on the database of selected articles, an analysis was performed on the content of the article titles and abstracts to identify the most occurring topics. VOSviewer was utilized in this paper. Constructing and viewing bibliometric maps can be done by VOSviewer. The size of the label and the circle of an item is determined by the weight of the item. In addition, the distance between the two circles reveals the relatedness and similarity between them. The lighter colors show more recent papers as the graph guide. The output of VOSviewer is shown in Figure 3.

Table 1 Top journals in BIM applications for disaster resilience

No.	Journal name	No. of papers	CiteScore 2018
1	Automation in Construction	13	6.35
2	Advanced Engineering Informatics	5	5.72
3	Journal of Computing in Civil Engineering	4	2.55
4	Water (Switzerland)	2	2.66

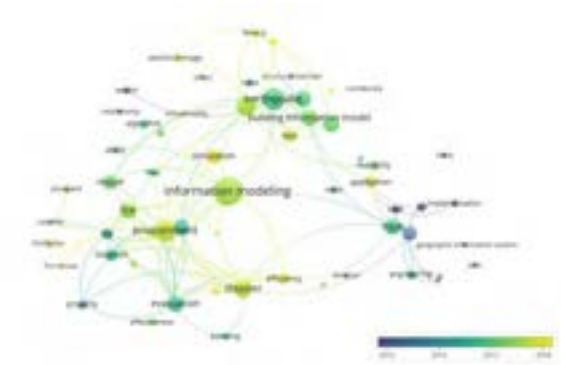

Figure 3. Main research areas in BIM applications for disaster resilience and its trends

4 Discussion

The database of the papers contains the most outstanding papers on BIM applications for disaster resilience. The BIM applications can be categorized based on the phase of the disaster. Four disaster phases (preparedness, mitigation, response, and recovery) are considered in this paper. Disaster preparedness is persuading organizations to realize the hazard that has to be faced. Loss reduction by identifying the risk assessment is disaster mitigation. Disaster response is associated with the post-disaster situation and it contains actions such as damage assessment and evacuation. Post-disaster activities that restore or improve the pre-disaster conditions can be defined as disaster recovery [8]. In addition to disaster phases, the selected papers analyzed the BIM applications based on disaster types. The database comprises the application of BIM for fire, earthquake, and flood.

4.1 Fire

Based on the publication date, it can be mentioned that the BIM application for fire response is the first BIM application for disaster resilience. Structural fires are common urban disasters. Traditionally, the 2-D maps guided people to find the exit routes in emergencies such as the fire in buildings. The outdated approach has a few critical limitations. For instance, it is possible that people cannot interpret 2-D maps correctly. The BIM applications for fire are generally related to preparedness, mitigation, and response phases.

4.1.1 Pre-disaster rescue route planning

BIM can be an appropriate tool for visualizing and providing insight. Pre-disaster rescue route planning concentrated on finding the shortest route. GIS historically utilized for finding the evacuation routes. However, in order to information transformation, Isikdag et al. [9] presented a combination of BIM and GIS to find the rescue routes. Li et al. [6] designed an algorithm for finding the location of trapped occupants at building fire emergency scenes based on BIM and GIS integration. A graphical interface for user interaction is provided by the model. Chi et al. [10] proposed that evacuation regulation can be done based on static rescue routes evaluation and BIM models. Designers can check their design by the proposed methodology, and revise it if it is mandatory. The distance of the exit routes is assumed as the longest possible distance.

4.1.2 Dynamic rescue route planning

Not only should the rescue route be short, but also it must be safe and obstacle-free. These rescue routes may be changed during the disasters based on the fire condition. Consequently, rescue routes should be determined dynamically. In most cases, firefighters lose a great amount of valuable time to get familiar with the site. BIM-based 3D model can help them to find invaluable information about the building easily. Shiau et al. [11] create a web-based fire control system based on BIM. The characteristics of the building material are accessible in the 3D map. A lot of fire detectors and monitors are available in the building, and their information is integrated by the 3D map. Firefighters could find the best relief program based on the material type around the fire location. Wang et al. [12] utilized BIM as a comprehensive building information model to provide real-time guidance for fire evacuation. The shortest evacuation routes generated by the A* search algorithm. The results of the path finding algorithm should be safe with no obstacles. Users can show the result of the path finding on their mobile devices using virtual reality. In addition, the developed methodology can propose a suitable path for disabled evacuees. Yoon et al. [5] presented a smartphone-based, in-building emergency response assistance system that can provide useful information about the location and physical status of victims. The location of the victims can be determined by Wi-Fi signals of the smartphone. The status of the victims is assessed by asking themselves or sensors in their phones.

Happening a disaster in a surrounding building may block a few entrances and exits and change the navigation routes. To remedy this problem, Tashakkori et al. [13] proposed a model that considers the information about the interiors and exteriors of the building in the fire management system. Chen et al. [14] integrated Internet of Things (IoT) technology and BIM in order to monitor the real-time situation during a fire disaster. The system controls the LED guide pointers to help evacuees find the best routes. Chen et al. [15] integrated network analysis with building information modeling (BIM) to help responders can find the rescue routes by using the developed graph. The route selection

procedure is a function of distance, risk of the disaster, and people congestion in this study. Chou et al. [16] developed a framework of dynamic evacuation procedures for departments. The best fire rescue paths are calculated based on the shortest path algorithm. Bluetooth sensor outputs show the information of temperature and smoke of routes. The best routes are updated based on this information.

4.1.3 Evacuation route considering human behavior

The crowding effect should be considered in rescue route planning as well. For this goal, human behavior is required. Cheng et al. [17] considered the individual characteristics (e.g., confusion and nervousness in an emergency event) in the mobile guidance device of the proposed BIM-based model. Marzouk et al. [18] present a framework to help managers to plan for labor evacuation in construction sites. BIM and agent-based simulation are utilized in the mentioned framework. The Evacuation Simulation Model contains an agent-based simulation approach to simulate the labor evacuation considering labor behavior. Mirahadi et al. [19] developed a tool that is named EvacuSafe. EvacuSafe can be useful to increase the evacuation safety performance by considering fire risk and population crowd risk. It comprises an agent-based model to predict the behavior of the residents. Ma et al. [20] a fire emergency management system based on the BIM platform. The developed system can consider the behavior of evacuees during fire disasters. People can find optimal paths such as obstacle-free and minimum distance by using technologies. Then, they will select their way. The fire management system effectively manages fire disasters based on fire conditions and people's behavior.

4.2 Earthquake

Earthquake is the second disaster type which can be managed by BIM. Earthquakes are major threats to many societies across the world [21]. Early research studies tried to prove the applicability of BIM for enhancing the seismic resilience of buildings. A research study by Welch et al. [22] is devoted to investigating the possible BIM application in seismic resilience area. Welch et al. [22] argue that BIM application for earthquakes can be classified into 3 groups. First, BIM comprises detailed information about building for seismic risk assessments. Second, BIM can be combined with structural health monitoring to protect critical buildings such as hospitals. Third, BIM can pave the roads of information communication in the emergency shutdown in order to efficiently make decisions to identify, prioritize, and manage risks. In this paper, the research studies on BIM application for earthquakes are classified anticipating the as-damage BIM model, design guidance, search and rescue application, and fire due to the earthquake. Anticipating the as-damage BIM model, and design guidance belongs to the preparedness and mitigation phases. However, search and rescue applications, and fire due to the earthquake belong to the response phase.

4.2.1 Anticipating as-damaged BIM model and loss estimation

To calculate the building strength accurately and demonstrate the anticipated damages after earthquakes, Anil et al. [23] developed an as-damaged BIM model. This model contains strength analysis and visual assessment including structural analysis models, building geometry and specification, material properties, reinforcement information, and damage records. The earthquake damages are predicted based on FEMA 306 guideline. The approach to forecasting the as-damage BIM model of a building based on its as-built BIM model is described by Ma et al. [24]. In addition, Zeibak-Shini et al. [25] anticipated the as-damaged model by developing an algorithm to assess the location and damage of each component of reinforced concrete frames with masonry infill walls. Ma et al. [26] forecasted the damage sequence information of a building based on BIM. Zhang et al. [27] highlighted the fact that due to hidden structural elements, building deflection evaluation after earthquakes is difficult and cost-intensive. On the other hand, this task plays an important role in occupant safety and should be determined. Sensors are able to solve this problem and provide updated information about building deflection. The output of the sensors can be easily visualized for users by using BIM.

Xu et al. [28] developed a BIM-based seismic loss evaluation based on FEMA guidelines. Consequently, decision-makers are able to observe the distribution of damage and loss in a virtual walkthrough. Considering the fact that FEMA guidelines require detailed information to predict building damages. In addition, the building components in the BIM model may have various levels of development (LODs). Xu et al. [29] found that some components may not have enough detailed information for analysis based on FEMA guidelines. They developed a framework to estimate the seismic loss of a model with various-LOD BIM data considering uncertainties. Vitiello et al. [30] implemented a BIM model in order to determine the most cost-effective retrofit intervention that can be determined based on the seismic loss estimation of each intervention.

BIM can be used in the design procedure as well. Non-structural building elements play an important role in performance-based earthquake engineering. Perrone

et al. [31] developed a tool for the seismic design of non-structural building elements based on BIM. It is shown that the BIM model information eases the seismic design procedure of sprinkler piping systems. Furthermore, the finite element analysis needs accurate geometric characteristics of building elements. This accurate information can get available by BIM. Ren et al. [32] introduced a framework that can conduct a finite element simulation for a building based on BIM.

4.2.2 Search and rescue application and post-disaster fire

Traditionally, rescuers should enter the damaged building to collect information. This task is dangerous and time-consuming. Bloch et al. [33] provided a BIM approach in order to help search and rescue teams after earthquakes. The interior of the damaged building is estimated using the as-built and as-damaged BIM model. The developed framework can accelerate the procedure and save the search and rescue teams. Xu et al. [34] taught inhabitants how to survive in earthquakes by visualizing non-structural damages. 3D information BIM model of the building is the basis of the structural analysis and Virtual Reality analysis.

Fire disasters are common after seismic disasters. In most modern buildings, fire sprinkler systems are installed in order to protect the building against fire. However, sprinkler systems may sustain damages due to earthquakes. The effect of the spread of the fire owing to sprinkler systems damages is studied by Xu et al. [35]. In addition, Lu et al. [36] developed a simulation framework of indoor post-earthquake fire based on BIM. In this study, the post-earthquake fire, building damages, fallen debris are estimated. Considering the damages and fire conditions, the rescue route can be determined in a virtual reality scenario. The results can be used as a training tool for building occupants.

4.3 Flood

The third frequent disaster type in BIM research studies is flood disasters. Due to climate change, the number of flood hazards has been increased recently. In addition, high settlement density highlighted the risk of economic losses due to floods. The BIM application for flood hazards are more recent and are mentioned in below. Most of BIM applications for flood hazards are related to preparedness, mitigation disaster phases.

4.3.1 Damage assessment

The flood damage assessment should be done for each building separately. This requirement needs detailed information about buildings. BIM model is able to satisfy this condition based on Amirebrahimi et al. [37]. Based on this study, the effect of the flood on the building can be calculated and visualized. Amirebrahimi et al. [38] completed the past study by integrating BIM and geographic information systems (GIS). Considering the fact that the most application of GIS is related to an outdoor and large-scale geographical feature, and the most application of BIM is associated with indoor objects, BIM and GIS integration is a proper combination for flood damage assessment. BIM is responsible for building information, and GIS is responsible for flood information. Lyu et al. [39] recommended that BIM and GIS integration can be a suitable tool for city managers in order to assess the flooding hazards.

BIM has been used to investigate the impact of a dam on the downstream by Rong et al. [40]. The dam discharge and flood routing are simulated by BIM. The downstream flood risk is evaluated by simulating the dam operation under different water levels. The treats due to the reservoir flood discharge for the building is analyzed. The results of a case study show that reservoir flood discharge is a treat for a city on the downstream. Moreover, the potential flooding hazards for coastal cities can be anticipated by BIM. Traditional approaches utilize 2D modeling for flood hazards. However, their results are not appropriate for vertical fluctuations. Rong et al. [41] integrated BIM and GIS to simulate the wave propagation more realistically based on high-resolution topography data. The proposed methodology can provide detailed information about flooding hazards such as flood extent, axial velocity, and vortex structures, etc.

4.3.2 Real-time monitoring

BIM is capable to use in real-time monitoring the flood hazards. Edmondson et al. [42] developed a BIM model that comprises smart sensors. The BIM model can predict floods by real-time monitoring and reporting of sewer asset performance. This approach can be used in order to evaluate the risk of inundation of metro systems due to flooding hazards. Lyu et al. [43] presented a framework that comprises GIS and remote sensing. In this research paper is recommended that the integration of GIS, Global Positioning System (GPS), and BIM can is a tool for visual management of 3D geographic spatial location information. Consequently, managers can monitor the risks of inundations in the metro tunnel dynamically.

In addition to real-time monitoring of the water level, BIM can be used in real-time monitoring of the water diversion projects to find the defections. Insufficient inspection and late problem detection may lead to disastrous results. Liu et al. [44] proposed a framework to optimize the inspection process. Unmanned aerial vehicle (UAV) and BIM integration are used in the proposed framework. The BIM model is dynamic and it comprises timely-updated safety information. The

model is shown in the Web environment.

4.4 General : Post-disaster construction

Biagini et al. [45] proposed utilizing BIM for the restoration of historical buildings. The main concern for the restoration of historical buildings is an on-site intervention. In order to efficient on-site intervention, a complete information plan should be provided for executing the restoration plan. Tradition restoration methods provided 2D maps that generally comprise insufficient information. BIM allows users to build a 3D model of the historical buildings and link a variety of information to it. The post-disaster construction permits can be facilitated by BIM. Nawari et al. [46] proposed a framework that can accelerate the construction process after a disaster. BIM and Blockchain integration can be utilized in any transaction related to post-disaster construction. Consequently, extra processing fees, paperwork, and the time required to issue building permits can be eliminated. Messaoudi et al. [47] developed a BIM-based virtual permitting framework that is able to improve the efficiency of obtaining the construction permit in Post-Disaster recovery efforts. Determining the type of the construction permit, applying the newly developed permitting framework, and deciding about the result of the permit is the main procedure of the framework. Moreover, Pizzi et al. [48] utilized BIM to ease the reconstruction process after an earthquake. The main tasks of the BIM model are (1) compliance with regulatory (2) contextual modeling of various disciplines (3) clash detection among different disciplines (4) coordinating building documents. All BIM application for disaster is demonstrated in Figure 4.

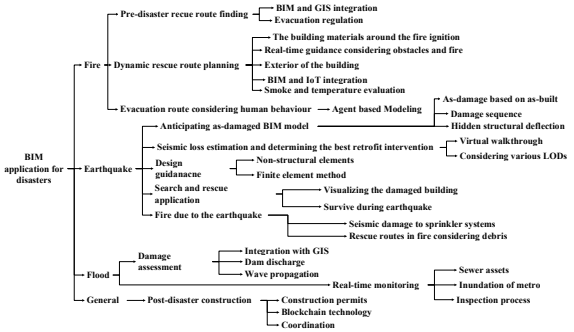

Figure 4. BIM application for disasters

5 Research gaps and future directions

Increasing the number of natural disasters makes disaster resilience an interesting research area these years. New technologies such as BIM has a great capability to enhance the resilience of the communities. After reviewing the relevant literature, existing research gaps have been detected. First, past studies have concentrated on fire, earthquakes, and floods. However, the resilience of the communities against other disaster types such as wildfires, hurricanes, and storms can be enhanced by BIM. For instance, the real-time monitoring of wildfire and bushfire stratus can be a helpful tool to reduce negative impacts. West et al. [49] argued that effective training procedures can increase the resilience of the community against wildfire and bushfire. As stated before, BIM is an ideal tool for training procedures. Second, the BIM application recovery and reconstruction process can be expanded. For example, the demolition process of damaged buildings is a critical task that can be hard without new technologies. BIM application for the demolition process is neglected in past studies. Third, most of the past studies on BIM application for disaster resilience are qualitative. More quantitative research approaches can be useful for decision-makers.

6 Conclusion

BIM applications in order to enhance disaster resilience are reviewed and classified in this paper. In order to conduct an unbiased analysis of the literature, this paper employed Preferred Reporting Items for Systematic Reviews and Meta-Analysis (PRISMA). BIM application for resilience enhancement due to fire, earthquake, and flood are studied by past researchers. Past studies generally emphasized on information transformation and visualization as two critical characteristics of BIM. Fire in buildings and finding the appropriate rescue routes, earthquake and flood damage assessment and visualizing the damages have been studied in the past. BIM can guide people to find short and safe rescue routes and prevent crowding. Earthquake damages and losses can be anticipated and visualized by BIM. Flood damage assessment can be done by integrating BIM and GIS. Findings show BIM applications have advanced in recent years but there is room for improvement when it comes to quantitative approaches. Furthermore, it is suggested that future studies could utilize the BIM application for other disasters such as bushfires. For instance, real-time monitoring, one of BIM applications, can be utilized to visualize and assess the risk of bushfire disasters. Real-time monitoring can be facilitated by using BIM and IoT integration. The findings are expected to provide useful insights to researchers in this context.

References

[1] D. Mileti, *Disasters by design: A reassessment of natural hazards in the United States.* Joseph Henry Press, 1999.

[2] C. M. C. Eastman *et al.*, *BIM handbook: A guide to building information modeling for owners, managers, designers, engineers and contractors.* John Wiley & Sons., 2011.

[3] D. Moher *et al.*, "Preferred reporting items for systematic reviews and meta-analyses: The PRISMA statement," *Ann. Intern. Med.*, vol. 151, no. 4, pp. 264–269, Aug. 2009.

[4] A. Y. Chen and J. C. Chu, "TDVRP and BIM integrated approach for in-building emergency rescue routing," *J. Comput. Civ. Eng.*, vol. 30, no. 5, Sep. 2016.

[5] H. Yoon, R. Shiftehfar, S. Cho, B. F. Spencer, M. E. Nelson, and G. Agha, "Victim Localization and Assessment System for Emergency Responders," *J. Comput. Civ. Eng.*, vol. 30, no. 2, Mar. 2016.

[6] N. Li, B. Becerik-Gerber, B. Krishnamachari, and L. Soibelman, "A BIM centered indoor localization algorithm to support building fire emergency response operations," *Autom. Constr.*, vol. 42, pp. 78–89, Jun. 2014.

[7] S. Tang, D. R. Shelden, C. M. Eastman, P. Pishdad-Bozorgi, and X. Gao, "A review of building information modeling (BIM) and the internet of things (IoT) devices integration: Present status and future trends," *Automation in Construction*, vol. 101. Elsevier B.V., pp. 127–139, May 01, 2019.

[8] G. P. Cimellaro, *Urban resilience for emergency response and recovery*, vol. 41. Cham: Springer, 2016.

[9] U. Isikdag, J. Underwood, G. Aouad, and N. Trodd, "Investigating the role of building information models as a part of an integrated data layer: A fire response management case," *Archit. Eng. Des. Manag.*, vol. 3, no. 2, pp. 124–142, 2007.

[10] J. Choi, J. Choi, and I. Kim, "Development of BIM-based evacuation regulation checking system for high-rise and complex buildings," *Autom. Constr.*, vol. 46, pp. 38–49, 2014.

[11] Y.-C. Shiau, Y.-Y. Tsai, J.-Y. Hsiao, and C.-T. Chang, "Development of building fire control and management system in BIM environment," *Stud. Informatics Control*, vol. 22, no. 1, pp. 15–24, 2013.

[12] B. Wang, H. Li, Y. Rezgui, A. Bradley, and H. N. Ong, "BIM based virtual environment for fire emergency evacuation," *Sci. World J.*, vol. 2014, 2014.

[13] H. Tashakkori, A. Rajabifard, and M. Kalantari, "A new 3D indoor/outdoor spatial model for indoor emergency response facilitation," *Build. Environ.*, vol. 89, pp. 170–182, Jul. 2015.

[14] X.-S. Chen, C.-C. Liu, and I.-C. Wu, "A BIM-based visualization and warning system for fire rescue," *Adv. Eng. Informatics*, vol. 37, pp. 42–53, 2018.

[15] A. Y. A. Y. Chen and T. Huang, "Toward BIM-Enabled Decision Making for In-Building Response Missions," *IEEE Trans. Intell. Transp. Syst.*, vol. 16, no. 5, pp. 2765–2773, Oct. 2015.

[16] J.-S. Chou, M.-Y. Cheng, Y.-M. Hsieh, I.-T. Yang, and H.-T. Hsu, "Optimal path planning in real time for dynamic building fire rescue operations using wireless sensors and visual guidance," *Autom. Constr.*, vol. 99, pp. 1–17, 2019.

[17] M.-Y. M. Y. Cheng, K.-C. K. C. Chiu, Y. M. Y.-M. Hsieh, I.-T. T. Yang, J. S. J.-S. Chou, and Y.-W. Y. W. Wu, "BIM integrated smart monitoring technique for building fire prevention and disaster relief," *Autom. Constr.*, vol. 84, pp. 14–30, Dec. 2017.

[18] M. Marzouk and I. A. Daour, "Planning labor evacuation for construction sites using BIM and agent-based simulation," *Saf. Sci.*, vol. 109, pp. 174–185, 2018.

[19] F. Mirahadi, B. McCabe, and A. Shahi, "IFC-centric performance-based evaluation of building evacuations using fire dynamics simulation and agent-based modeling," *Autom. Constr.*, vol. 101, pp. 1–16, 2019.

[20] G. Ma and Z. Wu, "BIM-based building fire emergency management: Combining building users' behavior decisions," *Autom. Constr.*, vol. 109, 2020.

[21] A. M. Major, "The utility of situational theory of publics for assessing public response to a disaster prediction," *Public Relat. Rev.*, vol. 24, no. 4, pp. 489–508, 1999.

[22] D. P. Welch, T. J. Sullivan, and A. Filiatrault, "Potential of Building Information Modelling for seismic risk mitigation in buildings," *Bull. New Zeal. Soc. Earthq. Eng.*, vol. 47, no. 4, pp. 253–263, 2014.

[23] E. B. Anil, B. Akinci, O. Kurc, and J. H. Garrett, "Building-information-modeling-based earthquake damage assessment for reinforced concrete walls," *J. Comput. Civ. Eng.*, vol. 30, no. 4, 2016.

[24] L. Ma, R. Sacks, R. Zeibak-Shini, A. Aryal, and S. Filin, "Preparation of Synthetic As-Damaged Models for Post-Earthquake BIM Reconstruction Research," *J. Comput. Civ. Eng.*, vol. 30, no. 3, 2016.

[25] R. Zeibak-Shini, R. Sacks, L. Ma, and S. Filin, "Towards generation of as-damaged BIM models using laser-scanning and as-built BIM:

First estimate of as-damaged locations of reinforced concrete frame members in masonry infill structures," *Adv. Eng. Informatics*, vol. 30, no. 3, pp. 312–326, 2016.

[26] L. Ma, R. Sacks, and R. Zeibak-Shini, "Information modeling of earthquake-damaged reinforced concrete structures," *Adv. Eng. Informatics*, vol. 29, no. 3, pp. 396–407. 2015.

[27] Y. Zhang and L. Bai, "Rapid structural condition assessment using radio frequency identification (RFID) based wireless strain sensor," *Autom. Constr.*, vol. 54, pp. 1–11, 2015.

[28] Z. Xu, H. Zhang, X. Lu, Y. Xu, Z. Zhang, and Y. Li, "A prediction method of building seismic loss based on BIM and FEMA P-58," *Autom. Constr.*, vol. 102, pp. 245–257, 2019.

[29] Z. Xu, X. Lu, X. Zeng, Y. Xu, and Y. Li, "Seismic loss assessment for buildings with various-LOD BIM data," *Adv. Eng. Informatics*, vol. 39, pp. 112–126, 2019.

[30] U. Vitiello, V. Ciotta, A. Salzano, D. Asprone, G. Manfredi, and E. Cosenza, "BIM-based approach for the cost-optimization of seismic retrofit strategies on existing buildings," *Autom. Constr.*, vol. 98, pp. 90–101, 2019.

[31] D. Perrone and A. Filiatrault, "Automated seismic design of non-structural elements with building information modelling," *Autom. Constr.*, vol. 84, pp. 166–175, 2017.

[32] X. Ren, W. Fan, J. Li, and J. Chen, "Building Information Model–based finite element analysis of high-rise building community subjected to extreme earthquakes," *Adv. Struct. Eng.*, vol. 22, no. 4, pp. 971–981, 2019.

[33] T. Bloch, R. Sacks, and O. Rabinovitch, "Interior models of earthquake damaged buildings for search and rescue," *Adv. Eng. Informatics*, vol. 30, no. 1, pp. 65–76, 2016.

[34] Z. Xu, H. Zhang, W. Wei, and Z. Yang, "Virtual scene construction for seismic damage of building ceilings and furniture," *Appl. Sci.*, vol. 9, no. 17, 2019.

[35] Z. Xu, Z. Zhang, X. Lu, X. Zeng, and H. Guan, "Post-earthquake fire simulation considering overall seismic damage of sprinkler systems based on BIM and FEMA P-58," *Autom. Constr.*, vol. 90, pp. 9–22, 2018.

[36] X. Lu, Z. Yang, Z. Xu, and C. Xiong, "Scenario simulation of indoor post-earthquake fire rescue based on building information model and virtual reality," *Adv. Eng. Softw.*, vol. 143, 2020.

[37] S. Amirebrahimi, A. Rajabifard, P. Mendis, and T. Ngo, "A framework for a microscale flood damage assessment and visualization for a building using BIM–GIS integration," *Int. J. Digit. Earth*, vol. 9, no. 4, pp. 363–386, 2016.

[38] S. Amirebrahimi, A. Rajabifard, P. Mendis, and T. Ngo, "A BIM-GIS integration method in support of the assessment and 3D visualisation of flood damage to a building," *J. Spat. Sci.*, vol. 61, no. 2, pp. 317–350, 2016.

[39] H.-M. Lyu, G.-F. Wang, J. S. Shen, L.-H. Lu, and G.-Q. Wang, "Analysis and GIS mapping of flooding hazards on 10 May 2016, Guangzhou, China," *Water (Switzerland)*, vol. 8, no. 10, 2016.

[40] Y. Rong, T. Zhang, L. Peng, and P. Feng, "Three-dimensional numerical simulation of dam discharge and flood routing in Wudu reservoir," *Water (Switzerland)*, vol. 11, no. 10, 2019.

[41] Y. Rong, T. Zhang, Y. Zheng, C. Hu, L. Peng, and P. Feng, "Three-dimensional urban flood inundation simulation based on digital aerial photogrammetry," *J. Hydrol.*, 2019.

[42] V. Edmondson, M. Cerny, M. Lim, B. Gledson, S. Lockley, and J. Woodward, "A smart sewer asset information model to enable an 'Internet of Things' for operational wastewater management," *Autom. Constr.*, vol. 91, pp. 193–205, 2018.

[43] H.-M. Lyu, S.-L. Shen, A. Zhou, and J. Yang, "Perspectives for flood risk assessment and management for mega-city metro system," *Tunn. Undergr. Sp. Technol.*, vol. 84, pp. 31–44, 2019.

[44] D. Liu, J. Chen, D. Hu, and Z. Zhang, "Dynamic BIM-augmented UAV safety inspection for water diversion project," *Comput. Ind.*, vol. 108, pp. 163–177, 2019.

[45] C. Biagini, P. Capone, V. Donato, and N. Facchini, "Towards the BIM implementation for historical building restoration sites," *Autom. Constr.*, vol. 71, pp. 74–86, 2016.

[46] N. O. Nawari and S. Ravindran, "Blockchain and Building Information Modeling (BIM): Review and applications in post-disaster recovery," *Buildings*, vol. 9, no. 6, 2019.

[47] M. Messaoudi and N. O. Nawari, "BIM-based Virtual Permitting Framework (VPF) for post-disaster recovery and rebuilding in the state of Florida," *Int. J. Disaster Risk Reduct.*, vol. 42, 2020.

[48] E. Pizzi, M. Acito, C. Del Pero, E. Seghezzi, V. Villa, and E. S. Mazzucchelli, *Technical-scientific support for the definition of the project for the reconstruction of school buildings involved in seismic events*. 2020.

[49] S. West, D. C. Visentin, A. Neil, R. Kornhaber, V. Ingham, and M. Cleary, "Forging, protecting, and repairing community resilience informed by the 2019–2020 Australian bushfires," *J. Adv. Nurs.*, vol. 76, no. 5, pp. 1095–1097, 2020.

Integrating BIM- and Cost-included Information Container with Blockchain for Construction Automated Payment using Billing Model and Smart Contracts

Xuling Ye, Katharina Sigalov and Markus König

Department of Civil and Environmental Engineering, Ruhr-University Bochum, Germany
E-mail: xuling.ye@rub.de, katharina.sigalov@rub.de, koenig@inf.bi.rub.de

Abstract –

Payment issues are necessary in the construction industry, often manifested by high levels of arrears and long-term payment delays. An automated payment could be a solution to speed-up the payment process after successful completions. In this paper, a framework is proposed for the automated payment via Building Information Modeling (BIM), Linked Data, Smart Contract and Blockchain technologies. Geometrical and payment-related data are stored as BIM-based linked data. Linked Data technology connects a BIM model with its related Bill of Quantities (BoQ) and Quantity Take-Off (QTO). Based on the transparency, traceability and collaboration of the Blockchain technology, an automated payment can be secured. To integrate such an information container with Blockchain for the automated payment, an additional information model called Billing Model (BM) is proposed. Thereby, each Billing Unit (BU) stores one or more construction work tasks with a related payment and a related due date. Together with the corresponding Smart Contract rules, the BM can automate payment via a Blockchain. Several aspects of improvement and further development are discussed in the end.

Keywords –

Billing Model; Building Information Modeling (BIM); Information Container; Blockchain; Smart Contracts

1 Introduction

Low margins and relatively low productivity have been the issues of the construction industry for decades [1]. The main reason for this lies in the low degree of digitization within the construction sector despite the increasing scale and complexity of construction projects. Relying mainly on drawings or paper-based documentation does no longer satisfy the increasing needs of construction projects. In addition, unsatisfactory software interoperability in the Architecture, Engineering and Construction (AEC) industry makes coordination between clients and contractors unnecessarily difficult. As a result, no single source can provide an integrated, real-time view of project design, costs or schedules. To make things worse, Caldas et al. [2] state that a large amount of construction documents, which necessarily contain graphical and non-graphical information that must be communicated between project team members, are needed to describe the characteristics, specifications and execution plans of building products, such as drawings, specifications, schedules and cost estimates.

These problems of contract management in construction can be reduced by applying newly available digital technologies and working methods. Building Information Modeling (BIM) has become a widely accepted solution for making the whole lifecycle of a construction project digital. By integrating “cost” into a BIM model, budget and cash flow planning and cost controlling can be enabled. After the implementation of smart contract applications by Ethereum [3], non-currency data can be stored in the Blockchain. Based on the transparency, traceability and collaboration of the Blockchain technology, it could be a good solution to enable digitalization of the contract management and the automation of the payment process.

However, because of the traceability of Blockchains, the data stored in a Blockchain will be repeatedly copied and stored in different blocks, even when modifications are only slight. As a result, the data storage of Blockchains is extremely expensive [4]. Moreover, because of the consensus mechanism and verification of Blockchains, the transaction speed is relatively slow compared to central network systems. It is time-consuming and arduous to store all the data of a construction project entirely in the Blockchain and therefore not worth the effort.

According to the points mentioned above and the available technologies, this paper presents a concept for the generation and application of an information

container (BIM Contract Container or BCC for short), which is to be used as a basis for automatic payment transactions in the construction industry. For this purpose, a billing model is introduced, which is the basis for the creation of a smart contract.

2 Related Work

2.1 Digital Models in Construction

By integrating "cost" into the BIM model, a cost budget and the corresponding financial representations can be instantly generated. The purpose of using BIM for cost is to provide accurate and reliable cost estimation based on the digital 3D model, and eliminate errors caused by manual measurements or estimations [5]. To exchange digital building models for building constructions, the Industry Foundation Classes (IFC) were developed and standardized internationally by buildingSMART [6]. With the help of the IFC, geometric and semantic building information can be exchanged independently of the manufacturer. The Bill of Quantities (BoQ) are created for the tendering and awarding of construction works [7]. An international standard for the description of BoQ information does not yet exist. Nevertheless, there is a standardized format for data exchange, which was created in Germany by the Joint Committee Electronics in Construction (GAEB) with the GAEB XML standard [8]. The GAEB XML format has been proposed to serve the agreement of a German uniform exchange standard for service specification and thus to support all requirements for electronic processes concerning public notice, contracting and accounting in the execution of construction works [8]. The building model can be used to determine quantities that are assigned to the individual BoQ elements. The calculation of the individual quantities based on the components of the BIM model is called Quantity Take-Off (QTO).

In recent years, some formats have been developed in order to use and exchange information from various data sources (often files). For this purpose, the individual data sources are described and linked using metadata. The links are saved explicitly. Data sources, metadata and links are generally referred to as information containers. In the simplest case, an information container comprises only one data source without links. If the data sources are in the form of files, the data exchange of an information container is realized as an archive file (e.g. as a zip file). The BIM-LV container according to DIN SPEC 91350, for example, enables standardized data exchange between digital building models and digital service specifications [9]. DIN EN ISO 21597-1 defines a similar approach to building and exchanging linked information using linked data concepts [10]. An information container according to DIN EN ISO 21597-1 is described using the Resource Description Framework (RDF) [11]. ISO 21597-1 was developed for the standardized data exchange of linked data sources using a generic information container format as shown in Figure 1. A container includes a header file "index.rdf" in the top-level folder. A container shall have at least three folders. The "Ontology resources" folder may be used to store ontologies providing the object classes and properties that shall be used to specify the contents of and links between the documents within the container. The "Payload documents" folder and "Payload triples" folder may contain nested folders to allow groups of associated digital resources to be held together and referenced as a group (e.g. a building information model with its associated reference files or a set of linked spreadsheet documents). A container according to ISO 21597-1 can also be used to exchange data and forms the information basis for the approach presented here. Building models, BoQs and QTOs are linked with the help of a container and used in the creation of a billing model.

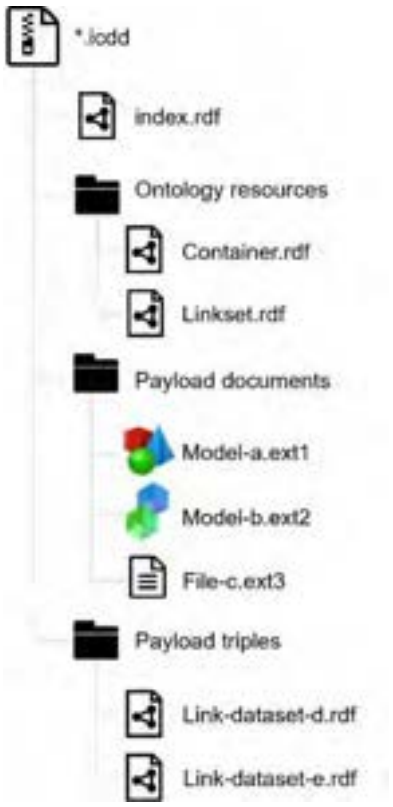

Figure 1. The structure of an information container according to DIN EN ISO 21597-1

2.2 Blockchain and Smart Contract

Blockchain is a distributed ledger technology, where "distributed" is managed by a decentralized peer-to-peer (P2P) network [12] and "ledger" is realized as an

electronic database comprising a chain of blocks [13]. In this network, the transactions are verified, validated and combined into blocks. The blocks are then chained together. Thus, the procedure is based on a chained block structure that grows linearly. The data in the Blockchain is immutable and cannot be manipulated or deleted. Blockchain has the following key characteristics: decentralisation, persistency, anonymity and auditability [14].

The Blockchain concept was developed from the Bitcoin technology first proposed by the pseudonymous Satoshi Nakamoto in 2008 [15]. However, the Bitcoin (i.e. the origin of Blockchain) was a non-programmable system suitable only for cash transactions. The situation starts to change after smart contracts come into the stage of Blockchain. The smart contract, first proposed by Szabo in 1996 [16], is a digital agreement which self-executes itself. Since Buterin et al. [17] have embedded smart contracts in their Ethereum Blockchain system in 2014, Blockchain has become a platform with programmable applications. This way, more possibilities and more applications in more fields than just finance have come to the Blockchain stage. However, due to the limited Blockchain storage and relatively slow transaction speed, it is does not make sense to store all the project-related data in the Blockchain as mentioned above. Many researchers suggest the notion of off-chain data storage, which is a conventional or a distributed database to store the data outside of the Blockchain. For example, Xu et al. [18] propose an architecture using Blockchain for connecting application layer within off-chain data and off-chain control.

In the construction industry, a great deal of research has been done on using Blockchains due to their enormous potential. For example, Li et al. [19] reviewed 73 papers from 2014 to 2018 on the applications of Blockchains in the construction industry. The reviewed applications lie in smart energy, smart cities and the sharing economy, smart government, smart homes, intelligent transport, building information modelling (BIM) and construction management, as well as business models and organizational structures. In 2020, Kasten [20] pointed out that research related to Blockchain applications in engineering or manufacturing has been growing fast after 2016, especially in data validity (e.g. BIM). In particular, Shojaei [21] states that smart contracts can provide a new type of work breakdown structure, which can automate the process of compliance and payment. Moreover, Li et al. [22] emphasize that smart contracts are one of the key complementary concepts to BIM, which can represent the construction project requirements in a computable way and automate contract clauses. However, Eschenbruch et al. [23] point out that using smart contracts in construction contract and payment automation still faces many legal issues.

3 Methodology

This paper proposes a framework for automated contract, invoice and billing management, as shown in Figure 2. The framework focuses on automating the payment between clients and contractors. The payment-related transactions are no longer defined in a paper-based construction contract, but rather mapped in a smart contract. Each payment-related transaction can be considered as a billing unit, and billing units must be defined in a digital way so that an automated payment can take place. For this purpose, billing units contain information about the construction work items and building elements and are based on the information from the BIM model, the BoQ and the QTO. All billing units together compose a billing plan, which together with the BIM model, the BoQ and the QTO is referred to as a billing model.

A billing model is generated accordingly, and serves as a data basis for smart contracts. The billing model, in collaboration with the smart contract, enables the automation of the delivery and acceptance process. If the client checked and confirmed a construction task reported by the contractor, the payment will be automatically transferred from the client bank to the contractor bank. A Common Data Environment (CDE), as an off-chain storage, handles all the payment-related files. For this purpose, a BIM Contract Container (BCC) is used, which contains all payment-relevant data (i.e. the BIM model, the BoQ with QTO and the billing model). For a secure and resource-efficient storage of the information in a Blockchain, only the URLs and hash values of the files stored in the CDE are used. The following three subsections detail how to filter payment-related transactions from a construction contract to a smart contract, how to generate a billing model, and how to automate the payment.

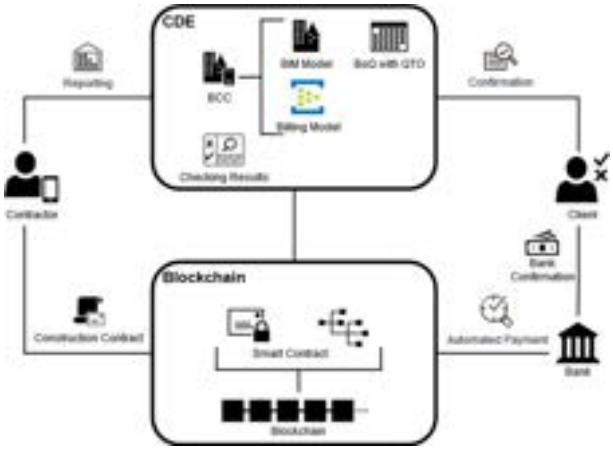

Figure 2. The overview of the proposed framework

3.1 Construction Contract to Smart Contract

Due to the complexity and the legality of a construction contract, a smart contract will not be able to replace a construction contract completely. The starting point is to filter out the payment-related transactions from the conventional construction contract. On the one hand, this is about the services and billing units to be provided and, on the other hand, the remuneration assigned to them. The payment-related data can be obtained via the BoQ and QTO. Based on a BIM model and a BoQ with QTO, a corresponding billing model is created, which is then automatically processed via smart contracts. Hash values of the smart contract, the BIM model and the BoQ with QTO are included in the paper contract to identify the billing basis of the contract.

Once confirmed, any contractually relevant data cannot be changed unnoticed. All subsequent modifications or extensions must be agreed between the contracting parties, and be stored as an update of all the former versions. The relationships from a construction contract to a smart contract can be viewed in Figure 3. With the help of completion notifications of the contractor and confirmations of the client, payment instructions are automatically sent to the involved banks and payments are performed out immediately. Such processing modalities or processes are expressed in the smart contract with if-then relationships.

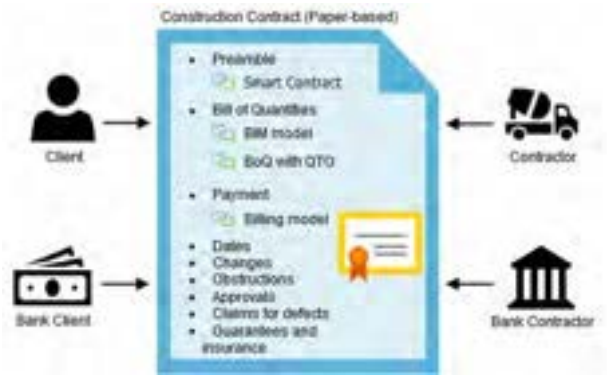

Figure 3. Integration of a smart contract into a construction contract

3.2 Billing Model

In order to automate payment transactions, a billing model has been developed based on the BIM model. Depending on the type of contract used and the underlying service description, the billing model can have different contents. In this context, a billing model is equivalent to a digital payment plan. The basis for the preparation of the payment plan is a service specification (i.e. a BoQ with QTO), which is linked to the BIM model. A service specification contains hierarchically structured elements, whereby the smallest element is a quantity split. The payment plan consists of billing units that can be clearly identified by a generated unique ID. Each billing unit contains one or more construction work items from the underlying service description with a total amount to be paid and a completion date. If the billing unit is completed and accepted on schedule, the contractor will get the agreed payment of the billing unit.

The used XML Schema Definition (XSD) of a billing model is visualized in Figure 4. A billing model consists of general billing model information (*BMInfo*) and several billing unit(s). Each billing unit contains one or more items, and the items may contain sub-items. Each item could be a single element or a group of service specification elements. In addition to the items, each billing unit stores short and long descriptions, the total quantities, the unit and the total price. The *CompletionDate* of a billing unit indicates the latest completion date of all the construction work tasks in this billing unit.

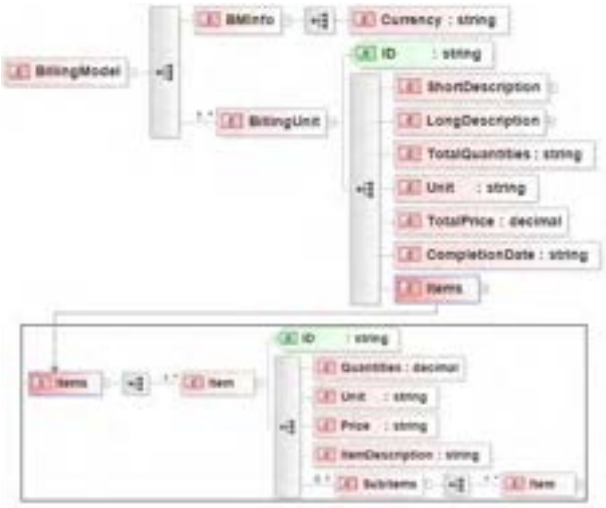

Figure 4. Visualization of the XML Schema Definition (XSD) of a billing model

To generate a Billing Model, a software tool as shown in Figure 5 has been implemented. A BIM model can be imported in the form of a BIM-LV container (Figure 5a), which contains IFC files (i.e. BIM models), GAEB files for service specification (i.e. BoQs with QTOs) and the LinkSet files to build up the links between IFC files and GAEB files. In this way, by selecting an element of the BIM model (Figure 5b), the corresponding linked BoQ item (Figure 5c) will also be selected. Multiple BoQ items in the GAEB Parser can be selected and formed as the items of a billing unit in the billing model (Figure 5d). The overall quantities, unit and total price of a billing unit are automatically generated based on the information of selected items. To successfully generate a billing unit, the

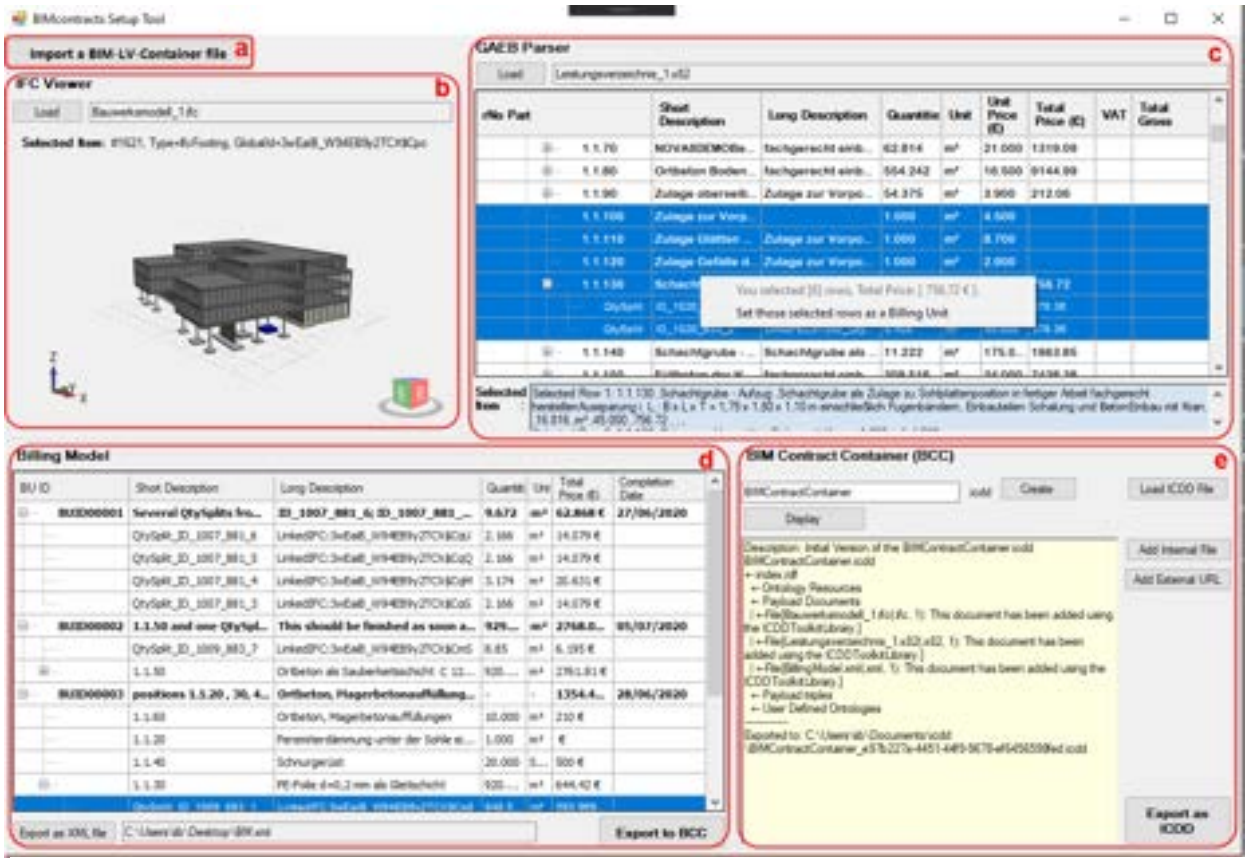

Figure 5. Implemented prototype for generating a billing model and a BIM Contact Container (BCC): (a) "Import a BIM-LV-Container file" button, (b) the IFC Viewer component, (c) the GAEB Parser component, (d) the Billing Model component and (e) the BIM Contract Container (BCC) component.

client needs to fill in the short description and the completion date of the billing unit. The long description of a billing unit is formed by the IDs of the selected items by default, which can be modified by the client. If an item is selected, all its sub-items will be selected and become the sub-items of the selected item in the billing unit (Figure 5d). When an item is linked with an IFC element, its long description in the billing model will display the *GlobalID* of the linked IFC element. For data exchange, an XML-based data format of billing models has been developed. Such an XML-format billing model can be directly exported to a BIM Contract Container (BCC) using the framework presented in Hagedorn [25]), or stored as an XML file. A generated billing unit in XML format is shown in Figure 6.

Figure 6. A billing unit generated via the software tool shown in Figure 5.

3.3 BIM Contract Container (BCC)

An information container (called the BIM Contract Container, or BCC for short), which contains the list of services (i.e. the BoQ with QTO), the digital building model (i.e. the BIM model) and the agreed billing model, can be generated via the software tool (Figure 5e). The loaded IFC file and GAEB file are automatically added to the container. The agreed billing model can be exported to this container afterward (as introduced in section 3.2). In this way, a BCC is generated accordingly.

The BCC's folder structure is shown in Figure 7. The content of such a BCC is stored in a ZIP64 encoded folder with the extension .icdd. The RDF index file includes the overall description. It contains all necessary documents and link sets of the container. The building model ("BuildingModel.ifc") is considered as an internal document and therefore its referenced file is stored inside the "Payload documents" subfolder. Its assigned format is IFC2x3. The BoQ and QTO ("BoQ_gaebxml.x86") and the billing model ("BillingModel.xml") are also stored in the "Payload documents" subfolder. Apart from these documents, the container description also refers to linksets, which includes the linking for the BoQ and billing model. The contents are therefore defined in two separated files named "BoQLinks.rdf" and "BillingUnitLinks.rdf", and stored inside the "Payload triples" subfolder.

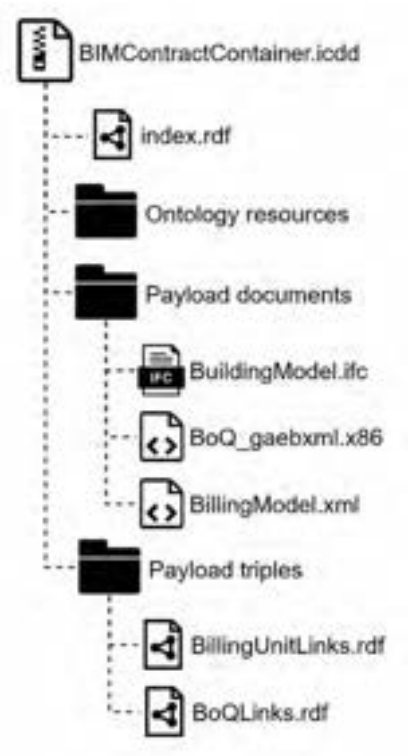

Figure 7. The folder structure of the BCC

3.4 Billing Process

Subsequently, based on the individual construction works and calculated quantities, a schedule and time planning can be made, taking into account the design and the building site. For this purpose, individual activities are defined, connected and saved as a network plan. The durations can be determined, for example, considering the selected construction methods and calculated quantities. The components of the BIM model are then linked to the individual activities using the calculated quantities.

A billing process with corresponding rules is created for each billing unit and stored in the smart contract. Such a billing process can be instantiated for each billing unit in the smart contract and linked to the digital billing unit of the billing model stored in the BCC. A simple and defect-free process for a billing unit is shown in Figure 8. The actions (start of construction works, report of the completion, checking and acceptance, execution of the payment and confirmation of the payment) are viewed as a sequential process.

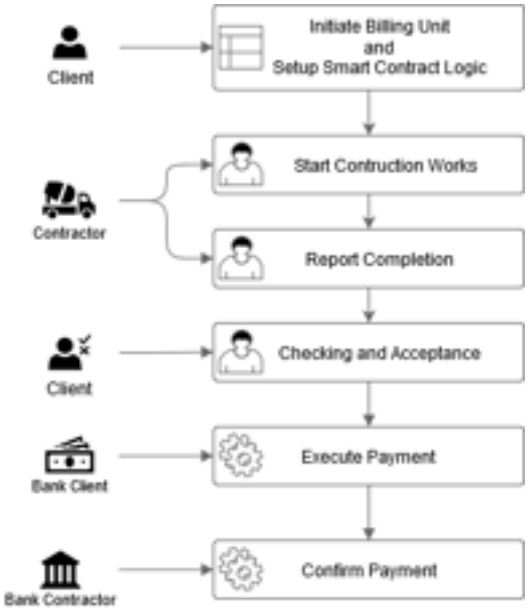

Figure 8. A defect-free process of a billing unit via BCC and smart contract logic

After the client finishes the "Checking and Acceptance" process, the possible smart contract logic as shown in Figure 9 can be executed. The values of *CompletionDate*, *isPartialPaymentAllowed*, *RejectionThreshold* and *Penalty* are predefined in the smart contract based on the construction contract and the billing unit, while the values of *FinishedDate* and *AcceptanceRate* are obtained via the actual acceptance process. When the contractor reports completion, its *FinishedDate* will be recorded. This *FinishedDate* can be

compared with the *CompletionDate* set in the billing unit. The acceptance results of the client can be represented as *AcceptanceRate*. Only if the contractor completed the works as scheduled (i.e. the *FinishedDate* not later than the *CompletionDate*) and the client fully accepted the works (i.e. the *AcceptanceRate* is 100%) will the contractor get fully paid. If the contractor did not finish the work as scheduled, he/she will either get the payment with a penalty deducted or be refused to be paid altogether. If it is allowed to have partial payments and the value of *AcceptanceRate* is more than the *RejectionThreshold*, the contractor can get a partial payment. In other cases, the client refuses to pay.

```
if(FinishedDate <= CompletionDate)
{
   if(AcceptanceRate == 1.0)
   {
      Payment Execution;
      PaymentStatus = "Fully Paid";
   }
   else if(isPartialPaymentAllowed == true
     && RejectionThreshold < AcceptanceRate < 1.0)
   {
      Payment = Payment*AcceptanceRate;
      Payment Execution;
      PaymentStatus = "Partial Paid";
   }
   else{PaymentStatus = "Payment Refused";}
}
else if(AcceptanceRate == 1.0)
{
   Payment = Payment - Penalty;
   Payment Execution;
   PaymentStatus = "Paid With Penalty";
}
else{PaymentStatus = "Payment Refused";}
```

Figure 9. A smart contract logic for the "Execute Payment" step

4 Conclusion and Outlook

Digitization is widely considered as the solution for the optimization and automation of processes in the construction industry. However, the current practice of a construction project still relies on paper contracts and conventional communications, which are time-consuming and non-transparent. This paper presents a framework for simplification and automation of payments during the construction process by combining the BIM contract container (BCC) with smart contracts. All the project-required data (i.e. the BIM model, the BoQ with QTO, and the billing model) are stored and linked in the BCC. The BCC is stored in an off-chain storage (i.e. CDE), while the sensitive and important information (e.g. the hash values of the documents stored in the CDE, results of acceptance procedure and payments) is safely stored and recorded in the Blockchain. Integration of the billing model and smart contract automates the payments between the client and the contractor during acceptance procedures.

This study has several limitations. First, the subcontractors are not taken into account in this study. Moreover, to define the smart contract rules, there are a lot of logic and legal issues to be settled, which are not handled in this study. Finally, the payment procedure during a construction process is more complex and has more factors to be considered in the future.

Acknowledgment

This work is part of the BIMcontracts research project which is funded within the scope of the "Smarte Datenwirtschaft" technology program run by the German Federal Ministry for Economic Affairs and Energy. The Ruhr-Universität Bochum, Universität Duisburg-Essen, FREUNDLIEB Bauunternehmung GmbH & Co. KG, Kapellmann und Partner Rechtsanwälte mbB and adesso SE (Consortium leader) are involved in the consortium. The authors would like to express their gratitude to the support and funding for the project activities. A further acknowledgement is addressed to the FREUNDLIEB Bauunternehmung GmbH & Co for the provided BIM models and construction data.

References

[1] Agarwal R., Chandrasekaran S. and Sridhar M. Imagining construction's digital future. *McKinsey Productivity Sciences Center*, 2016.

[2] Caldas C. H., Soibelman L. and Han, J. Automated classification of construction project documents. *Journal of Computing in Civil Engineering*, 16(4): 234–243, 2002.

[3] Buterin V. A next-generation Smart Contract and decentralized application platform. *Ethereum White Paper*, 3:37, 2014.

[4] Eberhardt J. and Tai S. On or off the blockchain? Insights on off-chaining computation and data. In *European Conference on Service-Oriented and Cloud Computing,* pages 3–15, Springer, 2017.

[5] Chen C., Tang L. C. M., and Jin Y. Development of 5D BIM-Based Management System for Pre-Fabricated Construction in China. In *International Conference on Smart Infrastructure and Construction 2019 (ICSIC) Driving data-informed decision-making*, pages 215–224, ICE Publishing, 2019.

[6] buildingSMART. Industry Foundation Classes (IFC). Online: https://www.buildingsmart.org/standards/bsi-standards/industry-foundation-classes/, Accessed: 16/05/2020.

[7] Brook M. Estimating and Tendering for Construction Work. *Butterworth-Heinemann,*

Oxford, 2008.

[8] GAEB. GAEB data exchange XML. Online: https://www.gaeb.de/en/products/gaeb-data-exchange/, Accessed: 17/05/2020.

[9] DIN SPEC 91350: 2016-11: Linked BIM data exchange comprising building information model and specified bill of quantities. Online: https://www.beuth.de/en/technical-rule/ din-spec-91350/263151122, Accessed: 17/05/2020.

[10] DIN EN ISO 21597-1:2018-10 – Draft: Information container for data drop - Exchange specification - Part 1: Container Online: https://www.beuth.de/en/draft-standard/din-en-iso-21597-1/293151537, Accessed: 17/05/2020.

[11] W3C. Resource Description Framework (RDF) Model and Syntax Specification. Online: https://www.w3.org/TR/PR-rdf-syntax/ Overview.html, Accessed: 17/05/2020.

[12] Dorri A., Steger M., Kanhere S. S. and Jurdak R. Blockchain: A distributed solution to automotive security and privacy. *IEEE Communications Magazine*, 55(12): 119–125, 2017.

[13] Bahga A. and Madisetti V. K. Blockchain platform for industrial internet of things. *Journal of Software Engineering and Applications*, 9(10): 533, 2016.

[14] Zheng Z., Xie S., Dai H.N., Chen X. and Wang H. Blockchain challenges and opportunities: A survey. *International Journal of Web and Grid Services*, 14(4): 352–375, 2018.

[15] Nakamoto S. Bitcoin: A peer-to-peer electronic cash system. Online: http://bitcoin.org/bitcoin.pdf, Accessed: 19/05/2020.

[16] Szabo N. Smart Contracts: building blocks for digital markets. *EXTROPY: The Journal of Transhumanist Thought*, (16), 18:2, 1996.

[17] Buterin V. A next-generation Smart Contract and decentralized application platform. *Ethereum White Paper*, 3:37, 2014.

[18] Xu X., Pautasso C., Zhu L., Gramoli V., Ponomarev A., Tran A.B. and Chen S.: The blockchain as a software connector. In *2016 13th Working IEEE/IFIP Conference on Software Architecture (WICSA)*, pages 182–191, IEEE, 2016.

[19] Li J., Greenwood D. and Kassem M. Blockchain in the built environment and construction industry: A systematic review, conceptual models and practical use cases. *Automation in Construction*, 102: 288–307, 2019.

[20] Kasten J.E. Engineering and Manufacturing on the Blockchain: A Systematic Review. *IEEE Engineering Management Review*, *48*(1): 31–47, 2020.

[21] Shojaei A. Exploring applications of blockchain technology in the construction industry. *Interdependence Between Structural Engineering and Construction Management*, 2019.

[22] Li J., Kassem M., Ciribini A. L. C. and Bolpagni M. A proposed approach integrating DLT, BIM, IOT and smart contracts: Demonstration using a simulated installation task. In *International Conference on Smart Infrastructure and Construction 2019 (ICSIC) Driving data-informed decision-making*, pages 275–282, ICE Publishing, 2019.

[23] Eschenbruch K., Gross D. and König M. Auf dem Weg zum digitalen Bauvertrag - Automatisierung des Zahlungsverkehrs im Bauwesen mittels BIM und Smart Contracts (BIMcontracts). *Bauwirtschaft 1/2020*, 2020.

[24] xBimTeam. XbimWindowsUI. Online: https://github.com/xBimTeam/XbimWindowsUI, Accessed: 25/06/2020.

[25] Hagedorn P. Implementation of a Validation Framework for the Information Container for Data Drop. *Tagungsband 30. Forum Bauinformatik*, pages 147–155, 2018

An Agent-based Framework for Evaluating Location-based Risk Score in Indoor Emergency Evacuation

Tianlun Cai[a], Hong Zheng[a], Jiamou Liu[b], Yupan Wang[b] and Vicente Gonzalez[c]

[a]School of Computer Science and Technology, Beijing Institute of Technology, China
[b]School of Computer Science, University of Auckland, New Zealand
[c]Civil and Environmental Engineering, University of Auckland, New Zealand

E-mail: kojiharufish@163.com, jiamou.liu@auckland.ac.nz, hongzheng@bit.edu.cn, ywan980@aucklanduni.ac.nz, v.gonzalez@auckland.ac.nz

Abstract -

The evaluation of indoor risks is a paramount issue in building design and construction. Conventional methods that rely on handcrafted rules or drills are insufficient for this task as they either fail to accurately depict the sophisticated spatial attributes and people's cognition abilities or are not suitable during the design phase of the building. This paper puts forward a novel computational framework with a reinforcement learning-based paradigm to automatically assess the evacuation risk posed by the indoor space through intelligent agents. Our model focuses on the agent's exploration behaviours as it gains knowledge to locate the optimal path from an initial location to an exit. The cost of this knowledge acquisition process is then used to capture the risk posed by the initial location of the building. The work aims to shed new light on utilizing agent-based techniques in evaluating building safety.

Keywords -

Indoor risk evaluation; Reinforcement learning; Agent-based evacuation; Computational framework

1 Introduction

The evaluation of indoor risks posed by emergency situations such as fire and earthquake has been a critical issue in building design and construction management. Imagine a situation where a designer is planning the interior space of a building. It is important to identify potential emergency situations and assess the level of risks of the designed indoor layout before commencing development. One of the key safety criteria is how effective the interior layout enables building occupants to evacuate during an emergency. A well-designed interior layout should in principle enable people in the building to quickly find optimal evacuation pathways and escape, thereby greatly reducing human casualty. Yet, to characterise the indoor environment and hazards, a huge amount of variables need to be taken into consideration that includes not only the spatial features of each interior location, placement of structural and non-structural elements, but also people's behavioural and cognitive traits. This demands an objective, cost-effective, and general method to assess indoor risks which differentiate risks of different indoor locations, truthfully reflect the spatial features, and are not biased by human input.

So far, however, most commonly used methods to evaluate indoor space risks rely on fixed sets of well-defined criteria, e.g., the equations in SFPE handbook of fire protection engineering [1]. It is easy to see that limitation with this common practice: In a building with complex indoor layout structures, applying a set of prescriptive rules to evaluate risks is deemed to be too coarse to account for the differences among the spatial features of the locations, and the erratic and complex behaviours of building occupants [2]. Another common way to evaluate evacuation effectiveness is by conducting evacuation drills. However, this approach introduced various issues related to ethical, practical, and financial constraints [3]. For example, drills will hardly recreate the sense of urgency in a real-world emergency and the effectiveness of evacuation drills greatly relies on whether people actively engage in the training. Moreover, conducting evacuation drills has one obvious shortcoming: we can only perform evacuation drills after the entire interior layout has been developed. Thus, it is not a suitable way to reveal potential risks during the design phase [4].

A desirable scheme for assessing indoor evacuation effectiveness during the building design phase must satisfy the following:

1. Firstly, as the evaluation should take place during the design phase where no physical involvement of human participants is possible, the scheme should exploit computerised modeling and simulation techniques to achieve its goals.

2. Secondly, the evacuation process's effectiveness relies on the evacuees' physical and mental ability. Therefore the assessment must be carried out based on the behavioural patterns of evacuees.

3. At the design phase, however, no input will be avail-

able on the specific features of the building occupants. It is therefore desirable for the risk assessment to be independent from the features of any specific evacuee. Similarly, the specific emergency situation that triggers the evacuation may greatly impact the evacuation process. Therefore, the assessment should also be independent from any specific emergency situation. In summary, the output of the assessment would be a form of *risk score* that measures the level of safety guaranteed by the indoor environment given the interior building layout in a generic setting.

4. Then, as an indoor environment has complex layout structure and locations may have vastly different spatial features, it is important to have a location-based risk assessment where risk scores are associated with individual location points. This has the result of a type of "heat map" that visually illustrates areas of potential hazards in the building where building occupants may face a greater level of risks.

5. Lastly, the scheme should be sufficiently general so that it can be applied to different layout plans and reveal their differences.

This paper proposes a novel framework for computing risk scores of indoor locations given a layout plan. The risk score reflects in a generic sense how much the interior layout supports effective evacuation of a building occupant from a specific location spot. The computation is agent-based in the sense that reinforcement learning (RL), commonly seen in the development of artificial intelligence agents, as an integral part of risk assessment. RL has demonstrated wide applicability in improving the performance of AI systems in many fields [5, 6]. Yet, to the authors' knowledge, our work is the first to incorporate RL in building risk assessments. The aptness of the RL paradigm in our setting lies in the fact that we model an evacuee as a reward-driven decision-maker, i.e., an agent who can assess the physical space while finding an optimal evacuation pathway.

In a nutshell, our framework defines the risk score using the efficiency of an agent – which is initialised with no knowledge regarding the building layout – in finding the optimal evacuation path through exploring the indoor environment. This framework has the following advantages:

Firstly, by applying machine learning algorithms on evacuees who have no prior knowledge regarding the indoor layout, the behaviours of the evacuees are generated in run-time through their interactions with the indoor environment. This avoids handcrafted behaviours of evacuees, thereby giving an unbiased evaluation of the effectiveness of evacuation.

Then, as we let the same agent start its exploration from all location points in the indoor environment, the obtained scores can be compared with each other in an objective way. Through this, one can easily generate a unified heat map of the indoor layout.

Thirdly, the proposed risk score takes into account the cognitive aspect of the agent by focusing on the dimension of *knowledge acquisition*. In other words, the risk score of a location point is defined as the cost for an evacuee who starts from the location points to identify the optimal evacuation path through repeated simulated exploratory evacuation. A location that facilitates higher safety is seen as one that incurs the lower cost of knowledge acquisition, while a more risky location is one where an evacuee needs to spend a lot more effort finding the optimal evacuation path. In comparison with other classical methods for evacuating location-based evacuation effectiveness such as computing the distance between a location and the nearest exit, our formulation is more realistic as it takes into account the behavioural aspect of evacuees and thus is a more reliable and robust safety index.

It is important to note that, while our formulation of the risk score is based on a simulation of evacuation behaviours of an evacuee, the aim of this model is not to mimic the actual evacuation during an emergency scenario [7]. To do that, many factors such as dynamics of the physical space during an emergency (e.g., fire), people's reaction to crowd movements (e.g., herding, stampede, etc.), as well as behavioural traits such as panic and altruism need to be addressed. Our work does not address these factors, as they are specific to particular emergency situations.

2 Related work

2.1 Building Safety Evaluation

The most standard practice to evaluate building safety is to adhere to a set of rigid rules which lays out best practices in building design. One of the main weaknesses of such approaches is that it is not able to accurately and deeply depict the erratic and complex behaviour and movement pattern of evacuees in a building under urgent conditions. Therefore, modeling and simulating emergency evacuation is essential to provide valuable insights about building safety and evacuation management [8].

In 1998, Ming [9] proposes a fire safety assurance approach including the fire safety assessment method for high-rise buildings in Hong Kong. In 1999, Ming [10] proposes a fuzzy fire safety assessment approach based on fire risk ranking techniques. The research at this stage carries out an emergency safety assessment on the completed buildings, the purpose is to evaluate the emergency safety risks of the buildings and formulate appropriate rectification plans to ensure the safety of the buildings.

Since the 2000s, researchers have shifted their attention towards the evaluation of building safety in real emer-

gency situations. In 2001, Ellingwood [11] studied the emergency safety of buildings under earthquake disasters. In 2008, Anagnostopoulos et al. [12] studied the post-earthquake emergency safety assessment of the building and provided support for the post-disaster rescue work plan. Carrying out research in a real emergency play an important role in reducing casualties and property losses under various disaster conditions.

In recent years, it has become a new research direction to carry out safety evaluation on design and construction stage. In 2010, Gangolells et al. [13] discussed the safety considerations of building construction at the design stage using a risk analysis method, aiming to reduce construction risks in advance. In 2011, Oien K et al. [14] conducted a research on the theoretical basis of building safety evaluation, which provided an important reference for subsequent research. In addition, based on the behaviour of people in the building under emergency evacuation conditions, carrying out building emergency safety evaluations to serve the safe evacuation of people under emergency evacuation conditions has become the focus of relevant research. In 2018, Bahr [15] conducted extensive discussions on the safety engineering and risk assessment of system based on practical methods in his work.

2.2 Evacuation modeling

We now review theories and models for evacuation simulation.

Flow-based models. Flow-based models use the density of nodes in flows to simulate the features of the people flow. Henderson [16] firstly argued that the behaviour patterns of pedestrian crowds are similar to gases or fluids. Bradley [17] applied Navier–Stokes equations to describe the motion of high-density pedestrian crowds. Helbing et al. [18] summarised that for medium and high-density pedestrian crowds, its motion patterns are very similar to fluids. For instance, people's footprints in snow look similar to streamlines of fluids. Flow-based models could apply the complete network model to develop the optimal evacuation plan in terms of the minimum evacuation time. However, the main restriction of flow-based models is it makes wrong assumptions of people's homogeneity. These assumptions make this type of model difficult to simulate people's different physical abilities, behaviour patterns, and characters. That is, the sociological factors of group decision-making processes that play a crucial rule in all emergency evacuation scenarios could not be simulated and defined in flow-based models.

Cellular automata. Cellular automata evacuation models involve discretization space and model people's evacuation process by single individual cells. One of the earliest cellular automata evacuation models was proposed by Perez et al. [19]. Daoliang et al. [20] applied a two-dimensional cellular automata model to simulate the evacuation dynamics of occupants. Yu and Song [21] proposed a model to simulate pedestrian counter flow in an corridor considering the surrounding environment. Kirchner et al. [22] proposed a stochastic cellular automata model to simulate the friction effects and clogging phenomenons in the crowd during the evacuation process.

Due to the simple shape of grids and predefined behaviour rules of evacuees, cellular automata models hardly to simulate unique characteristics and behaviour patterns for different types of evacuees, like women or kids. Therefore, most of the complex sociological factors among evacuees cannot be simulated in cellular automata models.

Agent-based models. An agent-based model is a system that comprises many intelligent agents which can be used to build heterogeneous characteristics and behaviour patterns. Instead of a global goal, each of the agents has a local goal to achieve [23]. Camillen et al. [24] evaluated different evacuation strategies in closed spatial environments, they demonstrated that due to the dynamic environment, traditional simulation models are difficult to simulate the evacuation process accurately. Only agent-based models are able to capture the dynamic characteristics of certain closed spatial environments properly. More recently, Sumam et al. [25] focused on the impacts of various evacuation behaviours and determined their efficiency in terms of the final evacuation rate. Yang et al. [26] present a prototype that uses agent-based modeling to simulate deep foundation pit evacuation in the presence of a collapse disaster. Şahin et al. [27] proposed an approach which combines a multi-agent model with fuzzy logic to simulate common human and group behaviour during safety evacuation. Kasereka et al. [28] proposed an intelligent Agent-Based Model enabling the modeling and simulation of the evacuation of people from a building on fire. Gonzalez et al. [29] propose a simulation model to find out optimum evacuation routes during a tsunami using Ant Colony Optimization (ACO) algorithms.

3 A New Agent-based Framework for Assessing Risk Score

We describe our computational framework to assess the risk score given input layouts. A prototype of our framework is implemented using the NetLogo platform. NetLogo is a programmable agent-based modeling environment designed and authored by Wilensky [30]. The physical space in a NetLogo environment is realised by a set of *patches* that represent location points. An agent is a special entity in the framework which can be in a patch at any given time instance. The NetLogo platform has built in function that enable us to define the states, perception and decision making functionalities of the agent, before letting the agent to start its simulated runs, i.e., evacuation

in the building.

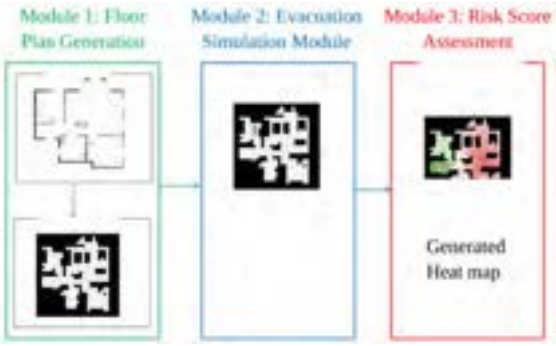

Figure 1. Framework of our approach, with three main modules.

Broadly speaking, our framework consists of three main modules (as shown in Figure1): the floor plan generation module, evacuation simulation module, and risk score assessment module.

First, the indoor space is represented by a digital model that is to be processed by the NetLogo platform. This digital model captures the interior layout and regions that are reachable by the evacuee. The many spatial attributes of the interior layout are represented in the floor plans, such as pathways, exits, corridors, furniture, etc. This digital representation is going to serve as the input to the next module which performs RL algorithm to assess the evacuation risk and generate risk scores.

The second module is the core part of the framework and it simulates the exploratory behaviour of an evacuee in the building. The main idea is we focus on the exploration behaviours of the agent as it gains knowledge in order to locate the optimal path from an initial location to an exit. This corresponds to a process of knowledge acquisition. As discussed above, the cost of the knowledge acquisition process is then used to capture the risk posed by the initial location of the building.

The third module is used to generate risk scores. In particular, we apply the evacuation simulation assuming the evacuee starts from every location points of the physical space. In this way, this module will generate a risk score for every location point. Using these risk scores, one may derive an overall risk score for the entire floor plan, that is, a quantitative measurement of the input floor plans' safety level in terms of emergency evacuation. Moreover, we will generate a heat map based on each patches' risk score.

3.1 Module 1: Floor Plan Generation

The first module performs preliminary processing of floor-plans: we label the inaccessible areas (like walls or large cabinets) and the exits, and then import the modified floor plan. The system will generate a virtual plan base on the coloured floor-plan. Figure 2 shows the coloured original real-world floor-plan of a hospital and the generated virtual plan in Netlogo separately. The black patches represent the inaccessible area, and the white patches represent the accessible area, that is agents could arbitrarily move in white areas. Finally, the blue patches represent the exits.

Figure 2. The coloured original real-world floor-plan of a hospital (left) and the digital representation in Netlogo (right).

3.2 Module 2: Evacuation Simulation Module

The main task performed by this module is to assess the evacuation risk posed by the indoor space automatically. Here we use one of the well-known machine-learning paradigm, reinforcement learning (RL), to model a person's cognitive behaviours. An RL agent is a reward-driven decision-maker who's able to adjust behaviours and improve performance based on the external environment through repeated trial-and-error. In this way, RL aims to mimic the cognitive process of operant conditioning in humans and animals. Imagine someone starting from an arbitrary location in a building that aims to escape the building by finding the nearest exit. Suppose that this person has no knowledge regarding the physical space. The person may explore the space by conducting *trials*, i.e., walking in the indoor area until reaching an exit point, or coming to a location that has already been visited in the same trial. Within each trial, certain knowledge is developed by the person that indicates how easy it is to find the nearest exit from this location.

To realise the exploration and learning process above, we formalise the evacuation situation using finite *Markov decision processes* (MDP): An MDP is a tuple $\langle \mathcal{S}, \mathcal{A}, \delta, r \rangle$ where $\mathcal{S}$ is the finite set contain all the states, $\mathcal{A}$ is the finite set contain all the actions, $\delta : \mathcal{S} \times \mathcal{S} \times \mathcal{A} \to [0, 1]$ is the dynamic function, $r : \mathcal{S} \times \mathcal{A} \to \mathbb{R}$ is the reward function. The goal of MDPs is to determine a policy $\pi : \mathcal{S} \mapsto A$, a function which maps states to actions, with the maximum

expected reward:

$$\arg\max_{\pi} \mathrm{E}\left[\sum_{t=0}^{T-1} r\left(s_t, a_t\right)\right] \tag{1}$$

where $s_{t+1} = \delta\left(s_t, a_t\right), a_t = \pi\left(s_t\right)$ and T is a final time step.

In our setting, the MDP represents the indoor environment of the agent. The set $\mathcal{S}$ of states represents the set of all patches in the digital representation of indoor space. Note that there are only three types of patches in our digital floor-plan layout: black (inaccessible area), white (accessible area), and blue (exits). Agents are only able to walk on the white patches. The action set $\mathcal{A}$ consists of four elements: up, down, left, and right. We assume that these actions will deterministically causes the agent to move from one white patch to another patch in the respective direction. If the target patch is a black wall, the agent will stay put in this time step. An policy directs the agent's movements. To realise the knowledge acquisition process, we assume that the MDP is unknown to the agent, and through a model-free RL algorithm, the agent iteratively improves its knowledge regarding the environment by keeping track of a *valuation function*.

This scenario can be handled by a well-established RL algorithm, *Q-learning*. Q-learning has been the most widely-used approach with demonstrated efficiency and reliability guarantee [31]. The key idea of Q-learning is incrementally approximating the valuation (Q) function of each state-action pair based on the rewards received. To be more specific, in each round, the *Q-value* will be updated from Q_t to Q_{t+1} base on old value (i.e., Q_t) and the maximum Q-values of the next state (i.e., s_{t+1}) using a temporal difference mechanism:

$$\begin{aligned} Q_{k+1}\left(s_t, a_t\right) = & Q_k\left(s_t, a_t\right) \\ & + \alpha\left(r_t + \gamma \max_a Q_k\left(s_{t+1}, a\right) - Q_k\left(s_t, a_t\right)\right) \end{aligned} \tag{2}$$

We now introduce the work flow of the safety assessment module below: A *path* is a contiguous sequence of patches $p_1, p_2, \ldots, p_\ell$ where every patch p_i where $1 \leq i < \ell$ is white and p_{i+1} is reachable from p_i by one of the moves. From a patch p, the *shortest path* to exit is the path that starts from p and ends at an exit that contains the least number of patches.

Our agent performs *trials* to explore the indoor area from every white patch p. In each *trial*, the agent starts by initialising the $Q(s, a)$-values to 0 for every patch s and action $a \in \mathcal{A}$. As the agent traverses through the patches, it will update its Q-value as defined above. When the agent arrives at the exit patch, the module checks whether the agent has found a shortest path to the closest exists in terms of its Q-values for each patch-action pair. If no shortest path is identified based on the Q-value, we will start a new trial from the starting patch; on the other hand, if the shortest path has been identified, the module will record the total number of patches this agent has walked through during the all the trials which started from the same initial patch p, this number is denoted by C_p.

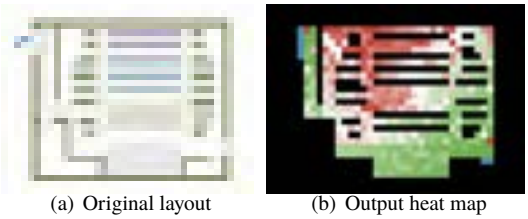

(a) Original layout (b) Output heat map

Figure 3. Original layout and heat map of an theater. Retrieved May 22, 2019, from `https://www.cadpro.com/draw-floor-plans/`

3.3 Module 3: Risk Score Assessment

For any white patch $p \in \mathcal{S}$, let d_p be the length of the shortest path that starts from p. To account for the impact made by different sizes of the floor plan (i.e., the number of patches $|\mathcal{S}|$), we divide C_p by d and set:

$$\sigma_p = C_p / p \tag{3}$$

We define this value σ_p as the *risk score* of the patch p.

We will generate a heat map base on each patches' risk score. We calculate the overall average of σ_p and denote the result σ as the *risk score* of the entire indoor space. We try to use this risk score σ to make the indoor location-based risk quantitative and allow people to judge the configuration of the floor plan as a whole.

4 Experimental Validation

Parameters setup. We apply frequently-used parameters in Q-learning here. In the following experiments, we set ϵ as 20%, α equal to 0.2, γ equal to 0.9, respectively. Here $\epsilon = 20\%$ means random actions are taking 20% in all actions for the agent's behaviour. We set the path reward -1 to correspond to the time cost during the exploration, and we set the exit-reward to 10 as the reward of finding the exit. Since the Q-learning process is non-deterministic, the choice of the agent's move is not the same in each episode, so we run our model 20 independent episodes for each experiment.

4.1 Case Study 1: A Theater

Figure 3 is a floor plan of a theater[1]. Here, we execute our program on this floor plan and output the heat map. The area near the exit door have a relatively low output risk score (green area), which means such areas are easy to evacuate; meanwhile, the areas far from the exit get high output risk score. This result is matching our expectation and common sense. Moreover, the top left corner is covered with dark red. The reason is there are too many obstacles (i.e., chairs.) around. So it is difficult to quickly evacuate from this area in an emergency situation. If a shooter stormed into this theater and starting hurt people, this dark red area might become a dead-end corner. The heat map shows that our prototype program can judge and measure the safety of different sub-areas. From this heat map, we could get some useful design suggestions: we might need to open an exit door at this red area for safety concerns.

One main advantage of our framework is, we could calculate sub-area risk score base on the risk score of each patch. For example, the risk score of the green left-bottom corner is 471; the risk score of the red left-top corner is 1466; the average risk score value of the whole theater is 848.6. This makes our program has more flexibility and capability. We could only focus on the important part of the building which we are interested in.

4.2 Case Study 2: Auckland Hospital

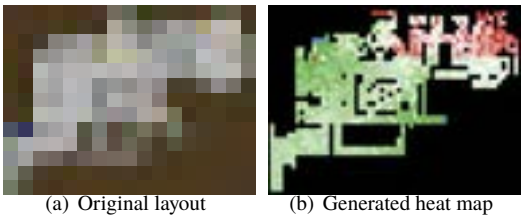

(a) Original layout (b) Generated heat map

Figure 4. Original layout and generated heat map of Auckland hospital [32]

Figure 4 shows the original layout and generated heat map of one floor of Auckland hospital, respectively [32]. There are six exits in the original map, as shown in Figure 4(a). Now we remove four of them and generate corresponding heat map, as shown in Figure 4(b), and see what difference it will make. From the graph, we can see the map was separated into two different parts: the left part got two exits and fewer obstacles. Therefore, it has a much lower risk score; the right part has a very complex layout, many obstacles around, some narrow corridors, and dead ends. So we can guess there should be some exits in the red part, just like the original layout. This case study shows that our program does have some ability to understand the structure information embedding in the floor plans.

[1]retrieved May 22, 2019, from `https://www.cadpro.com/draw-floor-plans/`

4.3 Case Study 3: Rational Configuration Design

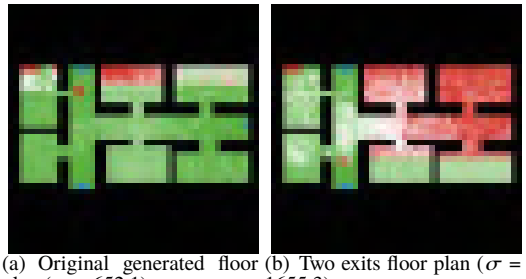

(a) Original generated floor plan (σ = 652.1) (b) Two exits floor plan (σ = 1655.3)

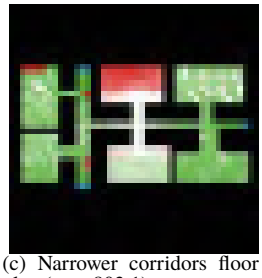

(c) Narrower corridors floor plan (σ = 803.1)

Figure 5. Rational configuration design

This case study aims to demonstrate that our framework has the potential to provide decision support to designers by allowing flexible adjustment to the indoor layout and observing the resulting risk score. For this, we manually generate an artificial indoor environment that consists of several rooms linked by two corridors. We imagine the situation where a designer is facing a number of design decisions that include setting the number of exists and adjusting the width of the corridors. By applying our model, the designer is able to predict the likely impact to risk scores of the interior space of tuning these parameters.

The number of exits. We first check the difference of the risk score by varying the number of exits. We apply the control variate method here, which means the only thing we change is the number of exits. Figure 5(a) shows the orignal floor plan with six rooms and three exits. The risk score σ is 652.1.

Now we reduce the number of exit to two and rerun our program. We give the output heat map in Figure 5(b). Now the floor plan has a much higher risk score: σ = 1655.3. From the heat maps we generated, we could have some insight view of the whole layout of the current building,

like if a certain area has a relevantly high risk score, we might consider adding an exit in this area. The more exit we have, the lower risk score we will achieve. We could set up a proper threshold risk score value to balance the risk score σ and the number of exits.

The width of corridors. We then check how the width of corridors affects the risk score of a floor plan. We reduce the width of the original vertical corridors from four grids to two grids and the original horizontal corridors from four grids to a single grid, as shown in Figure 5(c). By comparing the original floor plan, we find that the narrower corridors floor plan has a higher risk score: σ = 803.1 compared to the original risk score: σ = 652.1. This means narrower corridors make people difficult to evacuate, especially for the two rooms in the middle. This experiment is causing alarm that we must not use the main corridors for storage or rebuild the corridor without permission. We should keep all escape route free and unobstructed evacuation from the premises.

5 Conclusion

The evaluation of indoor risks is a paramount issue in building design and construction. This paper puts forward a novel computational framework to automatically assess the evacuation risk posed by the indoor space through intelligent agents. In particular, we model a person's cognitive process when exploring the indoor space in search for an exit, and then capture the risk using the cost of such process. Such an automated process to evaluate the safety conditions of indoor spaces could help evaluate the risk without deploying safety inspectors or conducting an evacuation drill. Our framework is a cost-effective solution than rule-based risk evaluation or evacuation drills since we perform the evaluation procedure in a simulation environment instead of requiring expensive expertise or conducting an evacuation drill in real buildings. Our framework has also high flexibility because the evaluation procedure could be conduct at any stage of construction, even in the sketch stage, if deemed necessary. Our case studies show that the proposed framework can understand the structure information embedded in the floor plan and offer some reference suggestions for structural design and risk evaluation.

We believe that the proposed method provides a new perspective to evaluating building safety through the lens of computational agents. There are many ways to extend the current work. Future studies could consider a dynamic environment where multiple agents interact through exploring the environment. We also could extend our prototype to the multi-agent system to provide insights into the mechanisms and interactions for panic and crowding under urgent situations. From an application perspective, the idea proposed in the paper can be developed as a plug-in in a building information management (BIM) system that automate the evaluation of evacuation risks.

References

[1] Morgan J Hurley, Daniel T Gottuk, John R Hall Jr, Kazunori Harada, Erica D Kuligowski, Milosh Puchovsky, John M Watts Jr, CHRISTOPHER J WIECZOREK, et al. *SFPE handbook of fire protection engineering*. Springer, 2015.

[2] Margrethe Kobes, Ira Helsloot, Bauke De Vries, and Jos G Post. Building safety and human behaviour in fire: A literature review. *Fire Safety Journal*, 45(1): 1–11, 2010.

[3] Steve Gwynne, Edward R Galea, M Owen, Peter J Lawrence, and L Filippidis. A review of the methodologies used in the computer simulation of evacuation from the built environment. *Building and environment*, 34(6):741–749, 1999.

[4] Xiaoping Zheng, Tingkuan Zhong, and Mengting Liu. Modeling crowd evacuation of a building based on seven methodological approaches. *Building and Environment*, 44(3):437–445, 2009.

[5] Gerald Tesauro, Rajarshi Das, Hoi Chan, Jeffrey Kephart, David Levine, Freeman Rawson, and Charles Lefurgy. Managing power consumption and performance of computing systems using reinforcement learning. In *Advances in Neural Information Processing Systems*, pages 1497–1504, 2008.

[6] Barret Zoph and Quoc V Le. Neural architecture search with reinforcement learning. *arXiv preprint arXiv:1611.01578*, 2016.

[7] Gabriel Santos and Benigno E Aguirre. A critical review of emergency evacuation simulation models. 2004.

[8] João E Almeida, Rosaldo JF Rosseti, and António Leça Coelho. Crowd simulation modeling applied to emergency and evacuation simulations using multi-agent systems. *arXiv preprint arXiv:1303.4692*, 2013.

[9] Siu Ming Lo. A building safety inspection system for fire safety issues in existing buildings. *Structural Survey*, 16(4):209–217, 1998.

[10] Siu Ming Lo. A fire safety assessment system for existing buildings. *Fire technology*, 35(2):131–152, 1999.

[11] Bruce R Ellingwood. Earthquake risk assessment of building structures. *Reliability Engineering & System Safety*, 74(3):251–262, 2001.

[12] S Anagnostopoulos and Marina Moretti. Post-earthquake emergency assessment of building damage, safety and usability—part 1: Technical issues. *Soil Dynamics and Earthquake Engineering*, 28(3): 223–232, 2008.

[13] Marta Gangolells, Miquel Casals, Núria Forcada, Xavier Roca, and Alba Fuertes. Mitigating construction safety risks using prevention through design. *Journal of safety research*, 41(2):107–122, 2010.

[14] Knut Oien, Ingrid Bouwer Utne, and Ivonne Andrade Herrera. Building safety indicators: Part 1–theoretical foundation. *Safety science*, 49(2):148–161, 2011.

[15] Nicholas J Bahr. *System safety engineering and risk assessment: a practical approach*. CRC press, 2018.

[16] LF Henderson. The statistics of crowd fluids. *nature*, 229(5284):381, 1971.

[17] GE Bradley. A proposed mathematical model for computer prediction of crowd movements and their associated risks. In *Proceedings of the International Conference on Engineering for Crowd Safety*, pages 303–311, 1993.

[18] Dirk Helbing, Illes J Farkas, Peter Molnar, and Tamás Vicsek. Simulation of pedestrian crowds in normal and evacuation situations. *Pedestrian and evacuation dynamics*, 21(2):21–58, 2002.

[19] Gay Jane Perez, Giovanni Tapang, May Lim, and Caesar Saloma. Streaming, disruptive interference and power-law behavior in the exit dynamics of confined pedestrians. *Physica A: Statistical Mechanics and its Applications*, 312(3-4):609–618, 2002.

[20] Zhao Daoliang, Yang Lizhong, and Li Jian. Exit dynamics of occupant evacuation in an emergency. *Physica A: Statistical Mechanics and its Applications*, 363(2):501–511, 2006.

[21] YF Yu and WG Song. Cellular automaton simulation of pedestrian counter flow considering the surrounding environment. *Physical Review E*, 75(4):046112, 2007.

[22] Ansgar Kirchner, Katsuhiro Nishinari, and Andreas Schadschneider. Friction effects and clogging in a cellular automaton model for pedestrian dynamics. *Physical review E*, 67(5):056122, 2003.

[23] Michael Wooldridge. *An introduction to multiagent systems*. John Wiley & Sons, 2009.

[24] Francesca Camillen, Salvatore Caprì, Cesare Garofalo, Matteo Ignaccolo, Giuseppe Inturri, Alessandro Pluchino, Andrea Rapisarda, and Salvatore Tudisco. Multi agent simulation of pedestrian behavior in closed spatial environments. In *2009 IEEE Toronto International Conference Science and Technology for Humanity (TIC-STH)*, pages 375–380. IEEE, 2009.

[25] Mary Idicula Sumam and K Vani. Agent based evacuation simulation using leader-follower model. 2013.

[26] Weilong Yang, Yue Hu, Cong Hu, and Mei Yang. An agent-based simulation of deep foundation pit emergency evacuation modeling in the presence of collapse disaster. *Symmetry*, 10(11):581, 2018.

[27] Coşkun Şahin, Jon Rokne, and Reda Alhajj. Human behavior modeling for simulating evacuation of buildings during emergencies. *Physica A: Statistical Mechanics and its Applications*, 528:121432, 2019.

[28] Selain Kasereka, Nathanaël Kasoro, Kyandoghere Kyamakya, Emile-Franc Doungmo Goufo, Abiola P Chokki, and Maurice V Yengo. Agent-based modelling and simulation for evacuation of people from a building in case of fire. *Procedia Computer Science*, 130:10–17, 2018.

[29] Eric Forcael, Vicente Gonzalez, Francisco Orozco, Sergio Vargas, Alejandro Pantoja, and Pablo Moscoso. Ant colony optimization model for tsunamis evacuation routes. *Computer-Aided Civil and Infrastructure Engineering*, 29(10):723–737, 2014.

[30] Wilensky. *Wilensky*. Uri, NetLogo (and NetLogo User Manual), Center for Connected Learning and Computer-Based Modeling, Northwestern University, 1999. URL `http://ccl.northwestern.edu/netlogo/`.

[31] Richard S Sutton and Andrew G Barto. *Reinforcement learning: An introduction*. MIT press, 2018.

[32] Lin Ni, Vicente Gonzalez, Jiamou Liu, Anass Rahouti, Libo Zhang, and Bun Por Taing. An agent-based approach to simulate post-earthquake indoor crowd evacuation. In *International Conference on Principles and Practice of Multi-Agent Systems*, pages 568–575. Springer, 2018.

A Framework for Camera Planning in Construction Site using 4D BIM and VPL

Si Van-Tien Tran[a], Ahmed Khairadeen Ali[a], Numan Khan[a], Doyeop Lee[a] and Chansik Park[a*]

[a]School of Architecture and Building Science, Chung-Ang University, Seoul 06974, Korea
E-mail: Tranvantiensi1994@gmail.com, ahmedshingaly@gmail.com, numanpe@gmail.com, doyeop@cau.ac.kr, cpark@cau.ac.kr,

Abstract –

With the recent rapid advancement of vision technologies, recognized research widely applies to resolve the construction industry's remaining problem as known quality, cost, time, and safety. However, there are few studies on how to place visual devices for effectively collecting images/videos on construction activities. This study proposes a framework for camera planning using 4D BIM and visual programming language (VPL) that considers construction's nature. A case study was also implemented, whose results reveal the proposed method's enormous potential in camera positioning, simulation, and schedule installation.

Keywords –

4D BIM; Camera planning; Visual data; Visual Programming Language

1 Introduction

Currently, construction managers still face the provision of quality, safety, time, and cost reduction projects. For these purposes, researchers have studied many different approaches aimed at achieving a higher level of automation throughout the project cycle. Computer vision technology (CST) has been one of the past decade's main directions, which has proven to be cost-effective, accurate, and easy to implement. The utilization of CST reveals in four main categories including (1) construction progress monitoring [1–3] , (2) quality control [4–6], (3) logistic (material, equipment,.etc.) [3,7,8], (4) safety management [9–12].

How to get visual data has become one of the critical and challenging questions for CST's success in the construction industry. Accordingly, it should be considered from the planning stage. First, it is the choice of data collection equipment that fits the job's needs. Recent innovations include making portable cameras such as smartphones, 360-degree camera devices, and UAVs accessible. These camera systems have led to an unparalleled rise in the number of images and videos routinely taken at construction sites [13]. Besides, fixed cameras still account for a large part of their usage through cost and real-time monitoring. The planner needs to choose which camera systems adapts to the condition of the project. For instance, the identification and tracking of construction-related workers' progress require a fixed camera for real-time monitoring. Therein, a high-resolution camera as a 360-degree camera is necessary to detect the wall's crack in the inspection process. Second, schedule planning is needed regarding the placement of installing the camera. Choosing locations with progress in mind will avoid unnecessary reinstallation for cameras and other monitoring equipment.

In the field of construction, Albahri [14] attempted to find an optimal positioning of cameras in indoor buildings using Building Information Modeling (BIM). Camera placement optimization also studies by Kim in the construction project. However, these studies have omission the changeable of constraints due to scheduling during construction progress. It leads that even project planner has camera placement plan, but they do not know when they can install during construction progress.

Building information modeling (BIM) has become an essential step to the digital management of construction projects, helping facility and construction managers with decision making [15]. 3D BIM can automatically provide the geometrical and nongeometrical attributes of these elements to be considered in the optimization camera placement process. Moreover, when integrating with scheduling into 3D model, as known, 4D BIM can provide visual the change of constraints.

This paper aims to propose a framework for camera installation planning that applying 4D BIM and Visual Programming Language (VPL). The proposed framework consists of four steps as "predefine camera parameter," "Camera Placement Optimization," "Installation Plan," "Visualization." The remaining of this work includes the following. Section 2 reviews the related study; section 3 defines the objective of research; then, the proposed framework is explained in section 4. A case study is implemented for evaluation following section 5. Finally, the author summarizes the method and discussion.

2 Literature Review

2.1 Camera Placement Problem in Construction management

Visual data acquisition is an essential first step in applying computer vision in the construction site. Depending on the quality of the data collection, the results of image processing-based may be the difference. Therefore, useful guidance for camera installation is crucial to the success of the subsequent adopt computer vision algorithm in the construction industry [1].

In practice, camera positioning is generally performed manually, relying on experts' expertise or observations [15]. Manual processes make camera placement time-consuming and cost-effective. Several researchers have made efforts to solve the Art Gallery Problem (AGP) [16]. In the field of construction, various researches put effort into solving this issue with a different objective. Kim [17] proposed the hybrid simulation-optimization of camera placement on construction job sites. Contributes in (1) interviewing expert to the identification of critical concern when installing fixed cameras, (2) developing a systematic framework for camera placement, and (3) visualization and quantification of the camera system network. While Yang [18] applied dynamic programming and developed general algorithms to the camera coverage and cost problems.

While the previous works showed promising results in seeking optimal camera configurations, there are still elements remaining concern. Camera type selection relies on the purpose of the visual data needed. Furthermore, the camera installation plans need to determine related to the progress of the project.

2.2 BIM and Visual Languages

Eastman [19] described BIM as a digital representation of the building process that simplifies interacting and exchanging information within a digital structure. The BIM model application was applied to a wide range of construction aspects, including improved safety, efficiency in the management of quality, and the optimization of project times and costs. In the indoor buildings, Albahri [15], for example, attempted to find an optimal camera positioning via BIM. Visual Programming Languages support utilization BIM easily. It adopted in different studies recently, such as KBIM code [20] or Khan [21], uses BIM to optimize fire extinguishing installations.

After conducting a review of current studies, this paper aims to develop a camera installation planning framework using 4D BIM and VPL that takes into account the characteristics of the construction industry.

3 Propose Framework

The goal of this study is to (1) select the type of camera which is fixed or portable system according to task intended in the schedule, (2) deliver the amount and position of the camera for the specific working space (following scheduling), (3) integrate the camera installation plan into BIM 4D, and (4) simulate the view of the camera in BIM.

Following the objective, the author proposes the framework for camera planning in construction, as illustrated in Figure **2**. It comprises four steps that are "predefine camera parameter," "Camera Placement Optimization," "Installation Plan," "Visualization."

3.1 Step 1- Predefine Camera Parameter

4D BIM extracts the working space for each activity and schedules information. The planner should pick the camera style proper to the activity information, based on the visual data's intent. In this article, the author selects two common camera forms as a (1) fixed camera, which hangs on the wall for surveillance to detect and monitor much of the manual construction operation. And (2) portable camera, for easy inspection of quality. In our research, we choose the 360-degree camera representing for portable system.

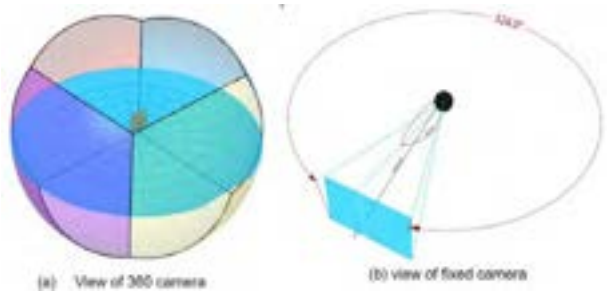

Figure 1. The view of the camera

After choosing the type of camera, the need to consider is to determine the camera's coverage, from which can calculate the number of cameras needed for an activity working area. Figure 1 shows the working area of 360-degree cameras and fixed cameras.

3.2 Step 2- Camera Placement Optimization Module (CPOM)

In step 2, the CPOM converts mathematical information to computer-readable data using visual programming tools. First, this module includes determining the number of cameras and these placements. The following formulas are utilized for calculation.

(1) The number of the camera (N) using for specific

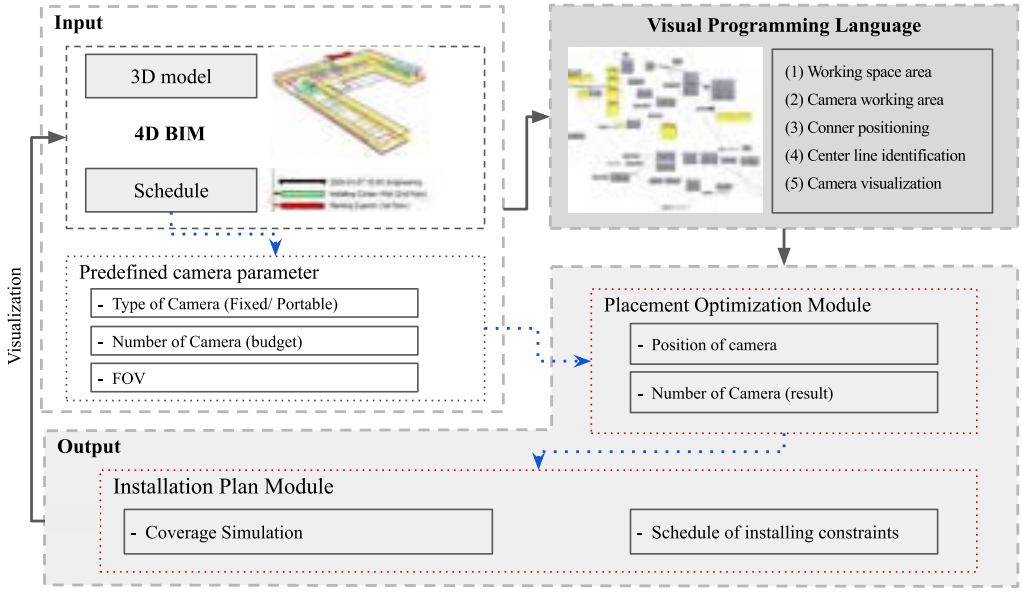

Figure 2. The framework for camera installation planning in construction

activity working area (i).

$$N_i = \frac{\text{volume of activity working area}}{\text{Camera working area}}$$

The camera position is represented by the values of X, Y, and Z coordinates. The (X, Y) variable is coordinated in the 2D working area, while Z is the camera's height.

(2) $0 \leq Z \leq H$ (H- the height of the wall)

The author analyzes two kinds of cameras (fixed and portable cameras) to assess the camera location. Following O'Rourke's theory [16], the fixed cameras were placed in the corner of the activity working area. For the portable camera, the software uses VORONOI grid logic to create the optimized centerline working field. Then the place is set to lay at the centerline.

3.3 Step 3- Installation Plan

After completing step 2, the planner made a final inspection by simulating camera network activity. It helps planners visually predict the monitoring area. This simulation also allows planners to adjust camera position and visibility. Due to construction nature, the construction process has not completed a number of potential camera installation locations identified in step 2. For example, the potential wall that has camera placement is construction. Therefore, the need to schedule cameras installation according to activity progress. Camera planning can also be beneficial in considering moving completed work areas to operating areas. It contributes to cost savings for contractors and still perform best.

3.4 Step 4- Visualization

Finally, the camera position and installation plan can be visualized in 4D BIM. The information can be communicated with related work crews (safety manager, supervisor) in a construction job site in various channels, including mobile devices.

4 Case study

To validate the proposed framework's applicability, the authors performed a case study planning for sample building's interior work. In the case study, the progress of constructing three rooms is evaluated, shown in Figure 3. The initial stage of the camera plan is conducting in Figure 4. The planners (1) insert the 3D model and room space volume box. Then, they (2) choose the camera type for usage purposes. For each type of camera, the permeameter inputs are the difference. The 360-degree camera can be adjusted by the height from the ground, range of view. With the fixed camera, the planner can choose the Conner position, height from the ground, rotation angle, and the working window. After visual programming analyzing, the results are illustrated in Figure 6.

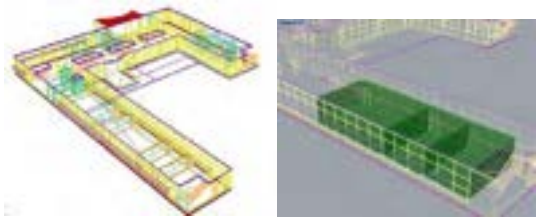

Figure 3. The case study project

Figure 4. Input information

Figure 6(a) shows the results of 360-degree camera placement. Therein, the blue range is the visible view, and the red area is block view in Figure 5, and 6(b) describes the camera view simulation. The schedule of camera planning also presents in Figure 4 as the day installation.

Figure 5. Fixed camera simulation

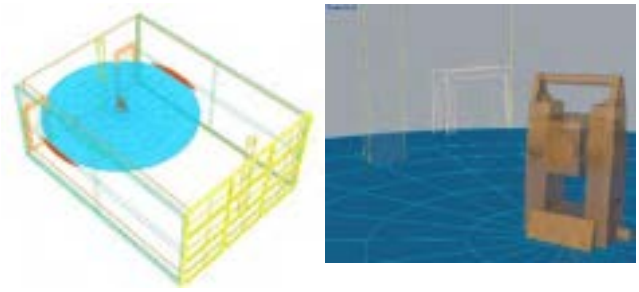

Figure 6. 360-degree camera coverage result

5 Discussion and conclusion

Establishing camera installation planning to collect visual data based on dynamic construction site requires significant manual and labor-intensive tasks. Most construction provides original installation plans without considering the progress. The study proposed a framework for camera installation planning using 4D BIM and VPL. To validate the proposed framework's applicability, the case study was conducted considering the project's construction planning. The results showed camera selection after task purpose. The system also visualizes the camera plan in 4D BIM, simulating camera view. Proper camera placement is expected to collect adequate video/image data quality and successfully support vision-based monitoring tasks.

Several research challenges need improvement. For example, the study considers the level of detail following the weekly or monthly schedule. Moreover, the case study uses two task monitoring and quality inspection. Future studies need to examine activity-based visual data. Moreover, the delay is a critical issue when implementing the construction phase. It may affect camera installation plans.

Acknowledgment

This work is supported by the Korea Agency for Infrastructure Technology Advancement (KAIA) grant funded by the Ministry of Land, Infrastructure and Transport (Grant 20SMIP-A158708-01).

References

[1] Kim C, Kim B, Kim H. 4D CAD model updating using image processing-based construction progress monitoring. Autom Constr 2013;35:44–52. https://doi.org/10.1016/j.autcon.2013.03.005.

[2] Kropp C, Koch C, König M. Interior construction state recognition with 4D BIM registered image sequences. Autom Constr 2018;86:11–32. https://doi.org/10.1016/j.autcon.2017.10.027.

[3] Yang J, Park MW, Vela PA, Golparvar-Fard M. Construction performance monitoring via still images, time-lapse photos, and video streams: Now, tomorrow, and the future. Adv Eng Informatics 2015;29:211–24. https://doi.org/10.1016/j.aei.2015.01.011.

[4] Lin KL, Fang JL. Applications of computer vision on tile alignment inspection. Autom Constr 2013;35:562–7. https://doi.org/10.1016/j.autcon.2013.01.009.

[5] Kazemian A, Yuan X, Davtalab O, Khoshnevis B. Computer vision for real-time extrusion quality monitoring and control in robotic construction. Autom Constr 2019;101:92–8. https://doi.org/10.1016/j.autcon.2019.01.022.

[6] Zhang X, Zhang J, Ma M, Chen Z, Yue S, He T, et al. A High Precision Quality Inspection System for Steel Bars Based on Machine Vision. Sensors 2018;18:2732. https://doi.org/10.3390/s18082732.

[7] Golparvar-Fard M, Heydarian A, Niebles JC. Vision-based action recognition of earthmoving equipment using spatio-temporal features and support vector machine classifiers. Adv Eng Informatics 2013;27:652–63. https://doi.org/10.1016/j.aei.2013.09.001.

[8] Dimitrov A, Golparvar-Fard M. Vision-based material recognition for automated monitoring of construction progress and generating building information modeling from unordered site image collections. Adv Eng Informatics 2014;28:37–49. https://doi.org/10.1016/j.aei.2013.11.002.

[9] Deng Y, Luo H, Hong H, Deng H. BIM-based Indoor Positioning Technology Using a Monocular Camera 2017. https://doi.org/10.22260/ISARC2017/0142.

[10] Zhang M, Shi R, Yang Z. A critical review of vision-based occupational health and safety monitoring of construction site workers. Saf Sci 2020;126:104658. https://doi.org/10.1016/j.ssci.2020.104658.

[11] Seo J, Han S, Lee S, Kim H. Computer vision techniques for construction safety and health monitoring. Adv Eng Informatics 2015;29:239–51. https://doi.org/10.1016/j.aei.2015.02.001.

[12] Fang Q, Li H, Luo X, Ding L, Luo H, Li C. Computer vision aided inspection on falling prevention measures for steeplejacks in an aerial environment. Autom Constr 2018;93:148–64. https://doi.org/10.1016/j.autcon.2018.05.022.

[13] Lin JJ, Golparvar-Fard M. Visual data and predictive analytics for proactive project controls on construction sites. Lect. Notes Comput. Sci. (including Subser. Lect. Notes Artif. Intell. Lect. Notes Bioinformatics), vol. 10863 LNCS, Springer Verlag; 2018, p. 412–30. https://doi.org/10.1007/978-3-319-91635-4_21.

[14] Zhang Y, Luo H, Skitmore M, Li Q, Zhong B. Optimal Camera Placement for Monitoring Safety in Metro Station Construction Work 2018. https://doi.org/10.1061/(ASCE)CO.1943-7862.0001584.

[15] Albahri AH, Hammad A. Simulation-Based Optimization of Surveillance Camera Types, Number, and Placement in Buildings Using BIM 2017. https://doi.org/10.1061/(ASCE)CP.1943-5487.0000704.

[16] O'rourke J. Art gallery theorems and algorithms. vol. 57. Oxford University Press Oxford; 1987.

[17] Kim J, Ham Y, Asce AM, Chung Y, Chi S, Asce M. Systematic Camera Placement Framework for Operation-Level Visual Monitoring on Construction Jobsites n.d. https://doi.org/10.1061/(ASCE)CO.1943-7862.0001636.

[18] Yang X, Li H, Huang T, Zhai X, Wang F, Wang C. Computer-Aided Optimization of Surveillance Cameras Placement on Construction Sites. Comput Civ Infrastruct Eng 2018;33:1110–26. https://doi.org/10.1111/mice.12385.

[19] Eastman CM, Eastman C, Teicholz P, Sacks R, Liston K. BIM handbook: A guide to building information modeling for owners, managers, designers, engineers and contractors. John Wiley & Sons; 2011.

[20] Kim H, Lee J, Shin J, and JC-J of CD, 2019 undefined. Visual language approach to representing KBimCode-based Korea building code sentences for automated rule checking. Elsevier n.d.

[21] Khan N, Ali AK, Tran SVT, Lee D, Park C. Visual language-aided construction fire safety planning approach in building information modeling. Appl Sci 2020;10. https://doi.org/10.3390/app10051704.

Safe and Lean Location-based Construction Scheduling

Beidi Li [a], Carl Schultz [a], Jürgen Melzner [b], Olga Golovina [a], and Jochen Teizer [a]

[a] Department of Engineering, Aarhus University, Denmark
[b] Hochschule für angewandte Wissenschaften Würzburg-Schweinfurt, Germany
E-mail: beidi.li@eng.au.dk; cschultz@eng.au.dk; teizer@eng.au.dk; juergen.melzner@fhws.de

Abstract –
Based on case studies within the construction industry, the application of location-based construction scheduling and utilizing software-based rule checking has delivered promising research results. We first explain a path on how the lessons from existing work practices can be used in digitalizing construction processes. This includes the objective of describing how the digital transformation of construction drawings and work break down structures lead to safe and lean work environments that crews – according to occupational laws and regulations – should face.

To achieve this objective, we present our ongoing work towards a unifying formal (logic-based) domain model that consists of: (1) a semantically rich ontology of construction schedules, work breakdown structures, and safety concepts; (2) rules for undertaking construction activities that avoid unsafe and wasteful situations.

This paper displays the case study of a newly built fire station for validation of the developed prototype. This experience illustrates that safe and lean allocation of work crews can be planned before construction starts. The outlook presents it's potential in future applications in the construction industry, e.g. resource allocation, as well as in research, e.g. automated work progress tracking by comparing actual vs. planned data.

Keywords –
Building Information Modeling (BIM); construction safety and health; fall protection; lean construction scheduling; prevention through design and planning; resource allocation; rule checking

1 Introduction

All project stakeholders that facilitate design, planning, construction and operation play a vital role in achieving project objectives for cost, schedule and quality. However, few recognize that design and planning can play a critical role for the safety, health and well-being of construction workers, maintenance staff or users during an entire project life-cycle. Although significant research has been undertaken in occupational construction safety, health and well-being, human-assisted software tools for detection and prevention of hazards embedded in construction schedules hardly exist in practice.

Example: Figure 1 illustrates a building information model (BIM) of a (real) building under construction. The roof panels were planned to be installed in sequence. One particularly ubiquitous hazard is that of a *fall* hazard: falls on construction sites account for approximately one third of all fatalities and numerous more severe accidents leading tragically to loss of life, serious and minor injuries [1].

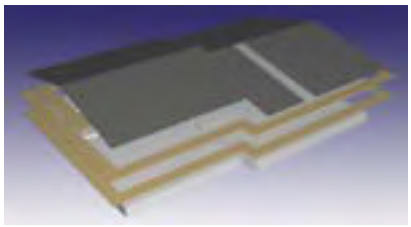

Figure 1. 4D BIM of roof panels under construction.

The edge of a working platform on which workers are occupied with a task that has a drop of more than approximately 2m is widely deemed to be categorized as a hazardous leading edge in many of the world's construction safety codes. In such situations, a fall protection system may prevent a worker from colliding with the ground, structure, or any other obstacle during a free fall and limit the impact force on the body of the worker during fall arrest.

Unfortunately, few projects utilizing BIM model fall protection (e.g., guardrails, safety nets, and covers for holes or openings on roofs) and personal protective equipment (PPE) (e.g., harnesses, lanyards, and temporary anchor points) are not part of the standard object libraries in commercial BIM software. Furthermore, a user-friendly software component to plan the use of PPE that is easy to use, fast, and perhaps can consider work progress, in brief here called a safety analysis system that assesses safety code compliance over the project schedule, does not exist.

Moreover, leading edges can be further distinguished based on the geometry of the work platform (i.e., in this

example the steepness of the roof's slope, and the location of the edge relative to the slope), and tasks or next activities in a construction schedule.

As shown in Figure 2, in time step t_1 the first roof panel is installed, creating four leading edges (one edge on each side of the panel). In the very next time step t_2 the next roof panel is installed, causing the rightmost leading edges from t_1 to disappear (a transient edge). In contrast, the upper leading edge in t_1 will remain until the very last roof panel is installed on the far side of the roof (a persistent edge), and the leftmost edge and lower edge are permanent, and will still exist even when the building is completed (permanent edges).

Edges are further distinguished based on their position on the slope: the upper edge being at the top of the slope is dealt with differently than the lower edge at the bottom of the slope where preventative measures employ safety nets for catching workers, material and/or tools that may accidentally slide down and fall off the roof.

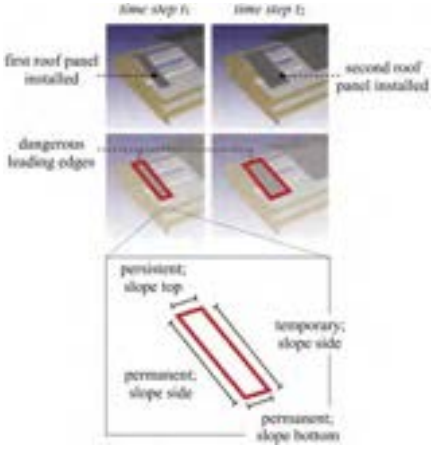

Figure 2. Part way through a construction plan. Roof panels are being installed sequentially in time steps t_1 and t_2. The dangerous leading edges that exist in each partially constructed state are distinguished based on the geometry of the roof slope, and the temporality of the leading edge based on the next construction task in the plan.

In general, measures to prevent fall hazards on roofs include installing fall protection and workers using PPE, or combinations of both. Depending on the type of work, the leading edge is always protected using a fall protection system. Workers without sufficient instruction or training and the right supervision often disregard wearing a personal fall arrest system [2].

Importantly, 4D building information models (4D BIM) are often *incomplete* in that the designer has omitted certain key pieces of information, e.g. the particular order in which roof panels will be installed. It makes it difficult to assess whether a safety code is complied with or not at a particular time step. This motivates the role of **default reasoning** in safety analysis, so that we might assert by default certain details that are missing from an incomplete BIM, and **hypothetical reasoning** that uses what-if scenarios to abduct missing information that would result in a particular situation, e.g. *"Suppose that the roof has to be completed in 5 workdays, can we fill in the blanks in the construction schedule in a way that meet with the availability of the crew and safety and health resources?"* Thus, we require:

- a semantically rich domain model of different features in a 4D BIM (such as leading edges and the refining semantic categories);
- a knowledge base of formal rules that can take a 4D BIM, analyze it, and augment it with these new concepts, injected as new, special kinds of *objects* in the model; and
- a reasoning engine that can take hypothetical statements about construction plans and missing details in the BIM and identify and mitigate resulting safety hazards using adequate methods that are consistent with safety codes and typical construction practices.

2 Related work

Work on roofs is highly dangerous and proper precautions are needed to control the risk. The main causes of death and injury are falling from roof edges or openings, through fragile roofs and through skylights. Many accidents could be avoided if the most suitable equipment was used and those doing the work were given adequate information, instruction, training and supervision. Roof work requires careful planning, particularly where work progresses along the roof. Sloping roofs require scaffolding to prevent people or materials falling from the edge. Another issue is that the small size and economic pressure of roofing companies often does not allow the execution of such best practices.

While Prevention through Design (PtD) concepts have been practiced for many years [3], most of the existing risk mitigation approaches are done manually, and are thus prone to error or not performed at the right time [4]. Several other key reasons contribute to such unacceptable practices: (a) the disconnect in a fragmented construction industry does not allow owners, architects, engineers, contractors and subcontractors to exchange their respective competent knowledge within the disciplines via an open, shareable platform, thus causing poor designs and unsafe execution and (b) the process of preventing hazards starts too late, often in the construction planning phase only, and involves safety and health experts who have to manage multiple projects at the same time.

More recently, research on Job Hazard Analysis (JHA) [5] and safety rule checking [6-8] that can automatically detect and resolve known hazards embedded in individual work activates have been introduced.

However, there is still a wide gap in standardization of safety concepts and software tools and a lack of strong requests from project owners and contractors to demand such solutions. An extensible, intuitive to apply, integrated suite of safety analysis software tools for construction is currently still missing. In part, the reasons are the complex, dynamic nature of construction projects and the multifaceted roles of its stakeholders. Aligning design intent with construction schedules and allocating resources (labor, material, equipment) is a demanding task. *Lean* in the field of construction safety refers to designing safe workplace, for example, using virtual construction models that attempt to bring construction process and safety product information to the job face [10]. Although research has shown that the creation of automated construction schedules is possible based on a priori knowledge about processes of activities and historical crew data, process related safety information has been left out so far for the majority of potential applications [11].

3 Methods

3.1 SafeConDM: an Ontology of Construction Safety

An example illustrates the German construction safety regulation for fall prevention (Figure 3) [12]. Similar to other countries, the code states that a guardrail must be installed at a leading edge if a worker could fall more than 2m, or a covering must be applied if the drop in a hole on the work platform is greater than 9 m^2.

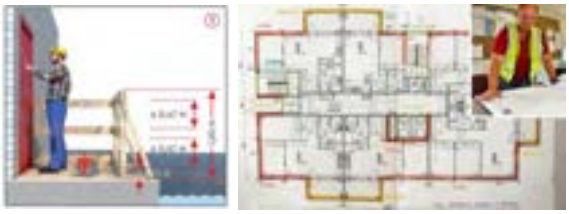

Figure 3. Examples: Safety regulation for fall prevention [12] (left) and manual hazard identification and mitigation (right).

To detect and prevent, for example, a fall-from-height hazard and apply a protective guardrail system, in an ideal case, a designer would design-out the hazard (so it does not appear during construction or later in maintenance). In reality, a safety engineer manually identifies the hazardous locations on a paper-based drawing (e.g., colors in Figure 3 indicate types and locations where protective equipment needs to be installed) or substitutes unsafe construction methods with a safer method (e.g., instead of workers using ladders that can tilt, workers should apply a scissor lift platform).

We aim to develop software tools that can automatically assess such codes on a given BIM of a construction site. BIMs are an object-oriented formal representation of buildings, including classes such as door, wall, or slab. Furthermore, in the field of *construction planning*, 4D BIM is used to model how a BIM is planned to be erected in a series of discrete time steps, i.e. a 4D BIM is equivalent to a sequence of partially constructed BIMs that represent the building under construction.

Our approach has been developed based on previous research in ontological and logic-based approaches to Construction Safety including [5,6]. To illustrate this, we integrate our approach into a broader existing ontological framework for construction safety. Figure 4 illustrates the *construction safety ontology* by Zhang et al. [5] extended with new (abstract) classes: spatial artefact and hazard space [13]. The authors hereby distinguish the following three modelling layers:

1) *Construction Product Model:* building products and relations, such as doors, walls, stories, slabs;
2) *Construction Process Model:* the construction plan including resources (equipment, materials, labor);
3) *Construction Safety Model:* construction safety knowledge (potential hazards, regulations, mitigating steps).

We define pertinent spatial artefacts [14] that capture semantic information about regions of empty space based on construction site activities, and human perception and behavior (movement, visibility, falling spaces, activity, etc.). Similarly, we model hazards as spatial artefacts whose existence and (geometric) definition is often a simple expression involving topological relations and geometric operations between regions (intersection, union, offset etc.), i.e. the *algorithm* for hazard detection is often as simple as clash detection. Spatial artefacts are modeled on the same ontological level as any other object in the product model, i.e. they inherit from the abstract class Product.

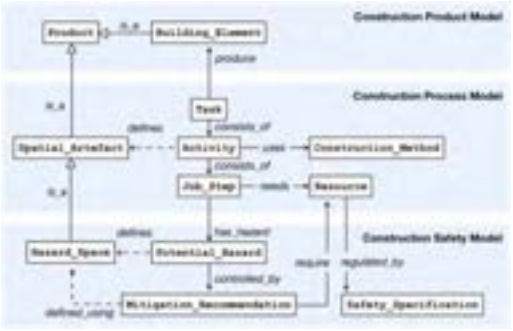

Figure 4. Construction Safety Ontology from [5] extended with spatial artefacts to create SafeConDM [13].

3.2 The shape of meaningful *empty spaces* in construction safety

Consider the region of empty space around an object such as a fuse box or valve; this region is meaningful

because a person must be located in that region to perform a particular act (e.g., operate on the fuse box). The geometry of this *functional space* region depends on properties of the person (consider electrician, mechanic, etc.), the task, and the object. Agents (e.g., workers and vehicles) have a movement space which are the regions in which they can move (travel) within. Excavators and other heavy equipment have an *operational space* required for rotating and depositing dug up material. People and sensors have *range spaces* (which can be further refined into: *visibility space, hearing space, reach space*), and so on. These are examples of spatial artefacts, a modeling approach that was initially developed for human centered architectural analysis [14-18].

The idea is that human behavior and experience is formally modelled as regions of empty space in which those behaviors and perceptual experiences take place. By doing this, behavior and experience (such as where a person needs to stand to see a particular object, i.e. *visibility space*) can be *represented* as "objects" in a BIM, on the same ontological level as other building objects such as doors, walls, slabs, and so on. Moreover, they can be *reasoned about* in a similar way to other BIM objects that instead have a material extension, e.g. clash detection can now be used to reason about whether a worker is in danger of a heavy vehicle strike by finding the intersection between the worker's *movement space*, the o*perational space* of the vehicle, and the *blind spots* of the vehicle operator seated in the cab. Concretely, in a BIM such as IFC, spatial artefacts form an abstract class that is a subclass of *IfcSpace*.

Example. Consider the previously discussed natural language code about a specific fall hazard: *"A platform that has a leading edge to a drop of more than 2m must be secured by a guardrail."*

We define a new spatial artefact called *Fall Space*, parametrically defined as: the region in which a person will fall by at least height `DANGEROUS_DISTANCE`, i.e. in the German code example the parameter is set to 2m. The dangerous platform edges can now be precisely, formally defined as: "where a *Movement space* horizontally meets (touches) a *Fall Space*".

There are a number of desirable properties of using spatial artefacts from a knowledge engineering perspective: the formalization is (a) very faithful to the original natural language code (semantics only, without any additional clauses for speeding up rule checking which would clutter the formalization and obscure the intended meaning), (b) easy to understand and verify by other planners (transparent); (c) directly applies to different contexts without changing the declarative statement that formalizes the code (portable), i.e. the geometry of Fall Space is customized according to the project and context, whereas the concept dangerous edge as defined above does not need to change. Importantly, this provides a uniform approach for modelling a large range of human-centered concepts (movement, visibility, performing tasks etc.) that can seamlessly be integrated within a BIM, and are effective "building blocks" for formalizing a broad range of hazards in a clear and transparent way.

In Tables 1 and 2 we list the spatial artefacts that we use to define fall hazards. We develop two new classes of spatial artefacts: *Falling spaces* and *Hazard spaces*. We ground the geometry of the spatial artefacts in our models based on the specific context of construction. We encode rules about hazards as the spatial definition of specific (subclasses of) hazard spaces.

Table 1. Construction site spatial artefacts

Spatial Artefact	Description
Movement space	Regions in which an agent (e.g., construction worker, manager, and visitor) can travel.
Movement corridor	Specific pathways along which a group of agents (e.g. crowds) is moving.
Functional space	Region in which an agent must be located to perform a given function or use a given object.
Work area	Area where an agent is occupied with a given task (e.g. electrician working on a fuse box).
Range space	Regions carrying information about how an object can be detected by an agent.
Visibility space	Region in which there is an unobstructed line of sight to a given object.
Blind spot	Region to which a vehicle operator has obstructed line of sight.
Fall space	Region in which an object or agent will fall by a dangerous distance.
Broad fall space	Region through which an agent can (easily) fall.
Narrow fall space	Region that is too narrowly shaped for an agent to (easily) fall through, but through which equipment and material could fall, or in which an agent's ankle could get stuck or sprain.
Operational space	Region that an object or vehicle may occupy to perform a given function.

3.3 Reasoning about hazards in construction

4D BIM introduces time to model a (possibly incomplete) construction plan. We encode this in Answer Set Programming (ASP) using two new predicates. Each element can optionally be assigned to a symbolic time step *construct/2*. The set of time steps form a partial order through an intransitive relation *next/2*: given time steps t_i, t_j then the interpretation of *next*(t_i, t_j) is that t_j occurs directly after t_j such that there does not exist time step t_k where *next*(t_i, t_k) and *next*(t_k, t_j). The temporal relation *before/2* between time steps is the transitive closure of *next/2*. Finally, 4D BIMs express temporal dependencies between elements: *dependency/2* between two BIM elements *A*, *B* means that element *A* must be constructed before *B*.

The following code snippet describes a series of slabs s_1, s_2, s_3 optionally assigned a time step, and their temporal dependencies. ASP derives the partial order *before/2* and the total order *next/2* of time steps.

Table 2. Construction safety hazards defined as spatial artefacts.

Subclass of hazard spaces	Hazard category	Description	Spatio-temporal definition
Fall hazard space	Slips, trips and falls	A person in these regions is at risk of falling from a dangerous height.	Intersection of movement spaces and broad fall spaces.
Sprain ankle hazard space	Slips, trips and falls	A person in these regions is at risk of twisting their ankle by walking into a small hole.	Intersection of movement spaces and narrow fall spaces.
Falling object hazard space	Struck by	A person in these regions may get hit by a falling object (e.g. tools, materials).	Subset of movement spaces that is directly below a narrow fall space (e.g. their vertical projection overlap).
Falling material corridor	Struck by	A person in these regions is at risk of being hit by an object falling from an active work area directly above.	Subset of movement spaces that is directly below the intersection of narrow fall space and work area.
Travelling vehicle strike hazard space	Struck by	A person in these regions is at risk of being hit by a moving vehicle.	Intersection of vehicle movement space (or corridor) and worker movement space (or corridor).
Operating vehicle strike hazard space	Struck by	A person located in these regions is at risk of being struck by a heavy vehicle in operation.	Intersection of vehicle operational space and worker movement space. The presence of blind spots further increases the risk.
Electrocution hazard space	Electrocution	A person located in these regions is at risk of electrocution.	Functional space of fuse box.

```
construct(s1, 1).
construct(s2, 3).
construct(s3, 4).
timestep(1..5).
before(T1, T2):-
   timestep(T1), timestep(T2),
   T1 < T2.
-next(T1, T3):-
   before(T1, T2), before(T2, T3).
next(T1, T2):-
   before(T1, T2), not -next(T1, T2).
dependency(S1, S2) :-
   construct(S1, T1), construct(S2, T2),
   before(T1, T2).
```

3.4 Evaluating consistency

Given a declarative formal encoding of construction safety codes, we can evaluate the consistency of such statements on a given BIM using off-the-shelf solvers that have spatial reasoning support; we opt for using a logic programming paradigm where the knowledge base consists of Horn clause rules of the form: $h \leftarrow b_1,\ldots, b_n$, where proposition h is true (the rule head) if propositions $b_1,\ldots, b_n$ are all true (the rule body). Horn clauses strike a balance between being sufficiently expressive to capture logical IF-THEN relationships between symbolic terms, while still being computable (unlike full first-order logic). We specifically use ASP, a logic- programming paradigm developed within the artificial intelligence community, that supports both deduction and other forms of non-monotonic reasoning (including default reasoning and hypothetical reasoning) and is computationally efficient. Similar to Prolog, ASP has a knowledge base of facts and rules of the form: "*Head :- Body.*" meaning that if the Body is true, then the Head must also be true. Rules with no Head are ASP integrity constraints, written as "*:- Body.*" meaning that the Body must not be true (i.e. as a logical expression: Body implies False). Head and Body expressions consist of literals, representing propositions that can be either True or False, and ASP reasoning engines are specifically designed to rapidly find combinations of deduced facts that are consistent with all given domain rules (referred to as models or answer sets).

We have extended the base language of ASP beyond propositions so that a set of consistent facts must also be spatially consistent, e.g. a 2D point can never be both inside, and outside, of a given polygon [19]. We use our extension of ASP that also supports spatial reasoning, called ASPMT(QS) [19], by encoding a building information model and derived artefacts as ASP facts, encoding the inference of hazards and responses as ASP rules and constraints, and implementing safety checking via ASP's answer set search. We have implemented ASPMT(QS) based on clingo [20], a complete ASP system composed of a grounder (gringo) and a solver (clasp).

Example. The following ASPMT(QS) rule states that, for all movement spaces that meet flush (touch horizontally) with a fall space in the same time step, then deduce a fall hazard space object. In this example, fall hazard spaces are modeled as the intersection of movement spaces and fall spaces, offset by a threshold of 200mm.

```
fall_hazard_space(H, Time) :-
   timestep(Time),
   movement_space(M, Time),
   fall_space(F, Time),
   topology(externally_connected, M, F),
   H_ = intersection(M,F),
   H = buffer(H_, 200).
```

We then derive the semantic refinements of fall hazard spaces based on their temporal duration in the construction plan. Firstly, a part of a fall hazard space (H) at timestep T is defined to be *permanent* (Hp) if it is still

there in the final timestep (Te), i.e. it is the intersection between fall hazard space H at time T, and a fall hazard space He in the final timestep Te:

```
permanent_fall_hazard_space(Hp, T) :-
   timestep(T),
   timestep(Te), not next(Te, _),
   fall_hazard_space(H, T),
   fall_hazard_space(He, Te),
   Hp = intersection(H, He).
```

Conversely, a part of a fall hazard space (H) at time step T is temporary (Ht) if it does *not* exist in the final time step (Te), which is computed by subtracting the final fall hazard spaces (He) from H:

```
temporary_fall_hazard_space(Ht, T) :-
   timestep(T),
   timestep(Te), not next(Te, _),
   fall_hazard_space(H, T),
   fall_hazard_space(He, Te),
   Ht = difference(H, He).
```

A temporary fall space is *transient* at T if it disappears in the very next time step Ti:

```
transient_fall_hazard_space(Ht, T) :-
   timestep(T), next(T, Ti),
   temporary_fall_hazard_space(H, T),
   temporary_fall_hazard_space(Hi, Ti),
   Ht = difference(H, Hi).
```

A temporary fall space is *persistent* at T if it still exists in the very next timestep Ti:

```
persistent_fall_hazard_space(Hp, T) :-
   timestep(T), next(T, Ti),
   temporary_fall_hazard_space(H, T),
   temporary_fall_hazard_space(H_, Ti),
   Hp = intersection(H, Hi).
```

Similarly, movement spaces are created as the volume 2m directly on top of slabs, subtracted by walls, columns and other movement obstacles. Fall spaces are the volume of space between the top surface of each object, and the next surface directly above (or the "sky") with the lower 2m subtracted. For this first prototype we simplified the calculation of movement spaces as the top surface of slabs subtracted by movement obstacles (columns and walls with voids where windows and doors will be placed), and we simplified fall spaces by taking a 2D bounding box of the site on each building floor and subtracting the slabs on that floor.

Note: The final time step Te is identified as the time step that does **not** have any *next* time step, i.e. "not next(Te,_)". In ASP underscore refers to an "anonymous" variable that does not need to be named. In the above rules, we assimilate object IDs to their geometric representation in ASP's internal geometry database. Moreover, topology relations and Boolean operations on polygons (intersection, difference, buffer) are evaluated using external Python libraries (Polygon, PyClipper) and non-linear real arithmetic solver *z3*.

4 Case study and results

A fire station is a structure or other area for storing firefighting apparatus such as fire engines and related vehicles, personal protective equipment, fire hoses and other specialized equipment, extended the nature of fire emergencies. Fire stations around the world also provide an important role in training volunteering or professional fire fighters or search and rescue personnel on site and educating the public regarding fire and safety (Figure 5). Most fire or Emergency Medical System (EMS) stations are municipally owned and usually require public bidding. In rural areas, many firefighters contribute labor time, increasing the potential risk on such projects.

Construction budgets and schedules respectively vary by the project. Due to the large number of such buildings, preference is given to systems design and functionality (which can be repeated once available).

The fire station model in this case study consists of a building with several levels. We focus on the roof aggregate consisting of 24 panels and 1 chimney opening. The chimney is added after the roof panels are installed. Supposing the roof is installed in the anti-clockwise order from the lower right corner, we assign each panel with a time step ranging from 1 to 24 (Figure 5). ASP then identifies fall hazard spaces (permanent, transient and persistent) at each time step. Moreover, permanent and persistent fall hazards are mitigated depending on the location of fall hazard spaces with respect to the slope, e.g. leading edges on the bottom of the slope require safety nets to capture falling objects, leading edges on the top or the side of the slope require guardrails, small openings on the slope require a cover (Figure 5). Table 3 shows fall hazard spaces and mitigation measures at 3 representative time steps.

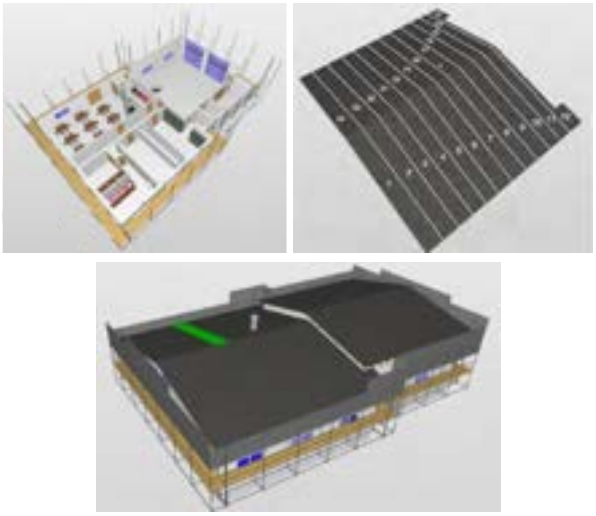

Figure 5. Main functions of a fire station on first floor (top left), order of roof panel installation (top right),3D view of the fire station model incl. protective safety nets on scaffolding with a single highlighted roof panel.

Table 3. Identified fall hazard spaces and proposed mitigation measures at t = 5, 19, and 24. Permanent (red), transient (green), and persistent (purple) fall hazards; Non-transient fall hazards are mitigated using a combination of safety nets (orange), guardrails (blue), and coverings (pink).

	t = 5	t = 19	t = 24
Fall hazard spaces		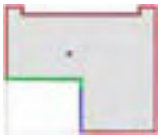	
Mitigation measure			

Figure 6 shows the quantity of safety protection materials needed at each time step. While these quantities were automatically generated, it shows a nearly linear demand for safety nets. Midway the project (t = 13) the peak of demand for guardrail is reached (panels on the other side of the roof allow removal of earlier installations). The demand for coverings becomes a non-null constant at t = 17 when the roof panel with one sole opening (for the later installation of the chimney) is installed and requires protection.

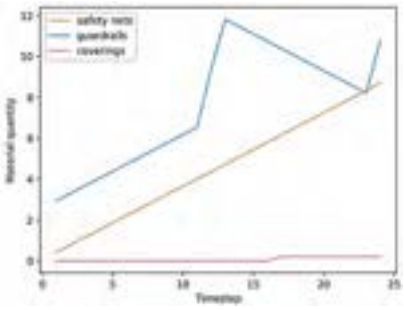

Figure 6. Requirement of safety protection equipment as roof panels are installed successively.

Providing a project manager or a safety engineer with such visual and quantitative information can impact decision making. Noteworthy examples are: (a) understand the location of fall risks associated to specific tasks in a construction schedule and (b) ordering the right quantities of protective equipment when needed. In a further step, if done continuously throughout a project, responsible personnel can seek forecasts of potential demands of (fall) protection resources and align with proper construction methods. On this particular project, due to the roof covering the entire and relatively small building area, resource leveling would not offer much potential savings [21]. However, depending on the amount of time needed to install one roof panel, an alternative fall arrest system (e.g., lanyard and energy absorber instead of guardrails, safety nets, and a hole cover) could be employed to protect the workforce who is installing the roof panels [22].

In this paper, we natively integrate an internal geometry database within ASPMT(QS) to manage large amounts of complex geometric data. To do this, we generate the polyhedral mesh representation of BIM objects via our modified version of IfcConvert (IfcConvert+). ASPMT(QS) then retrieves object geometries and deduces spatial artefacts using previously defined rules. Table 4 presents model statistics and ASPMT(QS) runtime. Compared to previous research [6,9] the runtime has significantly improved to a level where practitioners could apply it.

Table 4. Model statistics and runtime.

Number of BIM objects		1273
Average number of vertices		35
Number of spatial artefacts	Movement spaces	24
	Fall spaces	30
	Fall hazard spaces	66 (of which: 24 permanent, 22 transient, 20 persistent)
Time to generate 3D meshes from IFC via IfcConvert+		340 seconds (1218 meshes; total of 870k triangles)
Time to generate all spatial artefacts		0.181 seconds

5 Conclusion

We have presented a work in progress domain model of safety concepts on a construction site, and an approach for reasoning about safety compliance and mitigation strategies that integrates with 4D BIM construction schedules using Answer Set Programming (ASP) extended to natively support spatial reasoning. A key feature of our approach is the role *spatial artefacts* for representing and reasoning about semantically rich regions of worker perception, behavior and activities. We demonstrate this modeling approach with *fall hazards*, spatial regions where a worker is at risk of falling from a dangerous height. We refine fall hazard spaces according to their position in relation to building elements (e.g. with respect to a sloped roof) and temporal persistence (according to the 4D BIM construction schedule). These refinements are critical for reasoning about alternative mitigation plans that make tradeoffs against cost and construction progress (*lean* construction), particularly when 4D BIMs are incomplete, such as the installation of guard rails or safety nets. Our empirical evaluation on a real 4D BIM shows that our approach runs fast enough to be practical to use on large 4D BIMs.

In our future work we are expanding the scope of hazards to include a wide range visuo-locomotive features that are critical to safety in construction. In order to demonstrate further competitiveness over existing approaches, future testing may focus on highly complex 4D BIMs. Monitoring as-planned vs. as-built situations may yield further insights in how technology [23,24] or

combinations thereof can assist future decision making in construction safety and health planning and mitigation.

References

[1] OSHA (Occupational Safety and Health Administration) (2015). Commonly used statistics, https://www.osha.gov/data/commonstats.

[2] Choi, S. (2006). "Fall Protection Equipment Effects on Productivity and Safety in Residential Roofing Construction." *Construction Research,* 7 (1/2) 149-157, doi.org/10.1142/S1609945106000578.

[3] Toole, M., Gambatese, J.A., Abowitz, D.A. (2017). Owners' role in facilitating prevention through design. *Professional Issues in Engineering Education and Practice*, 143 (1) 04016012, doi.org/10.1061/(ASCE)EI.1943-5541.0000295.

[4] Teizer, J. (2016). Right-time vs real-time pro-active construction safety and health system architecture. *Construction Innovation,* 16 (3), 253-280, http://dx.doi.org/10.1108/CI-10-2015-0049.

[5] Zhang, S., Boukamp, F., and Teizer, J. (2015). "Ontology-Based Semantic Modeling of Construction Safety Knowledge: Towards Automated Safety Planning for Job Hazard Analysis (JHA)", *Automation in Construction*, Elsevier, 52, 29-41, http://www.itcon.org/2015/19.

[6] Zhang, S., Teizer, J., Lee, J.-K., Eastman, C., Venugopal, M. (2013). "Building Information Modeling (BIM) and Safety: Automatic Safety Checking of Construction Models and Schedules", *Automation in Construction*, 29, 183-195, http://dx.doi.org/10.1016/j.autcon.2012.05.006.

[7] Melzner, J, Zhang, S., Teizer, J., Bargstädt, H.-J. (2013). "A case study on automated safety compliance checking to assist fall protection design and planning in building information models", *Construction Management and Economics*, 31(6), 661-674, https://doi.org/10.1080/01446193.2013.780662.

[8] Sulankivi, K., Teizer J., Kiviniemi, M., Eastman, C.M., Zhang, S., Kim, K. (2012). "Framework for Integrating Safety into Building Information Modeling." *Proc. of CIB W099*, Singapore, 93-100.

[9] Schwabe, K., Teizer, J., König, M. (2019). "Applying rule-based model-checking to construction site layout planning tasks", *Automation in Construction*, 97, 205-219, https://doi.org/10.1016/j.autcon.2018.10.012.

[10] Zhou, W., Whyte, J., Sacks, R. (2012). "Construction safety and digital design: A review." *Automation in Construction*, 22, 102-111, https://doi.org/10.1016/j.autcon.2011.07.005.

[11] Teizer, J., Melzner, J., Wolf, M., Golovina, O., König, M. (2017). "Automatisierte 4D-Bauablaufvisualisierung und Ist-Datenerfassung zur Planung und Steuerung von Bauprozessen", Bauingenieur, Springer, ISSN 0005-6650, 129-135.

[12] BG Bau (2019) Absturzsicherungen auf Baustellen. https://www.bgbau.de/fileadmin/Medien-Objekte/Medien/Bausteine/b_100/b_100.pdf.

[13] Schultz, C., Li, B., Teizer, J., (2020). Towards a Unifying Domain Model of Construction Safety: SafeConDM. *EG-ICE* (accepted for publication).

[14] Bhatt, M., Schultz, C., Huang, M. (2012). "The shape of empty space: Human-centred cognitive foundations in computing for spatial design." *IEEE Symposium on Visual Languages and Human-Centric Computing*, 33–40.

[15] Schultz, S., Bhatt, M. (2012). "Multimodal spatial data access for architecture design assistance." *AI for Engineering Design, Analysis and Manufacturing*, 26 (2) 177–203.

[16] Schultz, C., Bhatt, M. (2012) "Towards a Declarative Spatial Reasoning System." *20th European Conference on Artificial Intelligence*.

[17] Bhatt, M., Schultz, C, Huang, M. (2012). "The Shape of Empty Space: Human-Centred Cognitive Foundations in Computing for Spatial Design." IEEE Symposium on Visual Languages and Human-Centric Computing. Innsbruck, 33–40.

[18] Bhatt M., Freksa C. (2015). "Spatial Computing for Design -an Artificial Intelligence Perspective." *Studying Visual and Spatial Reasoning for Design Creativity*. doi.org/10.1007/978-94-017-9297-4_7.

[19] Walega, P., Schultz, C., Bhatt, M. (2017). "Non-monotonic spatial reasoning with Answer Set Programming Modulo Theories." *Theory and Practice of Logic Programming*. 17 (2) 205–225.

[20] Gebser, M., Kaminski, R., Kaufmann, B., Ostrowski, M., Schaub, T., and Wanko, P. (2016). "Theory solving made easy with clingo 5." *Technical Communications of the 32nd Intl. Conference on Logic Programming*, 52, 2:1-2:15.

[21] Cheng, T., Yang, J., Teizer, J, Vela, P.A. (2010). "Automated Construction Resource Location Tracking to Support the Analysis of Lean Principles." 18th IGLC, Haifa, Israel, 643-653.

[22] OSH-Wiki (2020). Fall arrest systems. https://oshwiki.eu/wiki/Fall_arrest_systems#Types_of_fall_arrest_systems_and_main_components.

[23] Zhang, S., Teizer, J., Pradhananga, N., Eastman, C. (2015). "Workforce location tracking to model, visualize and analyze workspace requirements in building information models for construction safety planning", *Automation in Construction*, 60, 74-86, http://dx.doi.org/10.1016/j.autcon.2015.09.009.

[24] Getuli, V., Capone, P., Bruttini, A., Isaac, S. (2020). "BIM-based immersive Virtual Reality for construction workspace planning: A safety-oriented approach." *Automation in Construction,* 114, https://doi.org/10.1016/j.autcon.2020.103160.

Don't Risk Your Real Estate

Actions to Realize Efficient Project Risk Management using the BIM Method

M. Eilers, C. Pütz, M. Helmus, A. Meins-Becker

Chair of Construction Management, University of Wuppertal, Germany
E-mail: eilers@uni-wuppertal.de, puetz@uni-wuppertal.de

Abstract –

At the beginning of a construction project, cost, time and quality are defined, which must be adhered to throughout the entire construction process. Compared to other industries, risk management in the construction industry is often treated negligently. Risk management is rather an additional documentation task than an effective project management and controlling instrument. However, systematically applied risk management and successfully implemented counter-measures offer the opportunity to significantly increase the result of the construction project. Information gained from an efficient risk management system can automatically be used as empirical values for subsequent projects, thus increasing the achievement of quality, cost and time targets in the long term. The application of the BIM method opens up new possibilities in terms of the automatic linking of risk management information to other processes, which have not been exploited to date.

The research project "BIM-based risk management" examines the application of risk management in construction projects on the basis of literature research, numerous interviews with experts and an online survey. The content of the analysis is the strategy of companies in implementing the classic phases of the project risk management process consisting of risk identification, risk assessment, risk control and risk monitoring. The result shows, that there is no consistent systematic approach to the use of risk management systems in the construction industry. Individual approaches, such as the use of Excel templates to identify risks, are being implemented, but there is no linking of information across projects or departments, which means that the great potential of project risk management is not sufficiently exploited.

On this basis, the research project develops an ideal-typical process for the application of risk management in construction projects. The resulting BIM use case risk management shows how this information can be automatically generated and made available via the BIM process.

Keywords –

risk management; Building Information Modeling; project risk management; risk management process; information delivery; Data linkage; Information controlling; Risk

1 Procedure and principles

Within the framework of the research project "Measures for the implementation of an efficient project risk management by using the BIM method" of the chair of Construction Management of the University of Wuppertal, solutions are being developed how the information linkage associated with the application of the BIM method can be used to improve risk management. The classical risk management process (see Fig. 1) based on DIN ISO 31000 is a sub-area of project management which is implemented over all life cycle phases of a project, involving all project participants and involving different business units. Together, the project participants identify potential opportunities and risks for the project at an early stage and take proactive countermeasures by means of the process steps of identification, assessment, control and monitoring. The risk management cycle is a continuous process. This means that the cycle is constantly repeated in the course of project processing [1]. Only project risk management is considered in the project. The aim of project risk management is to increase the transparency of risks in a construction project and to derive and evaluate measures to reduce unknown parameters and determine realistic target figures. This leads to a higher achievability of the project goals in terms of costs, deadlines and quality. Project risk

management is distinct from corporate risk management, whose overriding goal is to maintain the company.

In the research project, which has been running since January 2019, the current application of risk management in construction projects was first examined. In view of the ever-increasing demands for a partnership approach to projects between client and contractor, the project deliberately considers both sides and in particular their interfaces in terms of risk management.

Through numerous expert interviews and an online survey, the strategy of companies in implementing the project risk management process was analysed. When looking at the existing risk management processes in terms of the flow of information, level of detail and responsibilities, differences in the approaches to risk management and the priority given to the issue became apparent.

2 Risk management

The term risk refers to the deviation from project goals caused by influences on productivity. The project objective is to complete a project on time, within budget and in line with quality standards [2]. The term risk includes both positive and negative deviations from targets. The positive deviation from goals is called opportunity, the negative deviation is called danger [3]. Since mainly the negative deviations can cause construction delays and cost increases, the term risk is used in this paper to refer to the negative deviation in particular. For the correct application of a risk management system it is necessary to create an awareness of risk management in the company, the organization or the department. A risk management system must be integrated within the company or the organization or project at various organizational levels. On the one hand, it must be integrated at the normative level, where the goals of the company or project are defined. An implementation on a strategic level, determines the risk strategy to achieve the defined goals. The risk management system, the focus of this paper, is implemented at the operational level [4].

The risk strategy defines the objectives to be achieved by risk management. The risk strategy must contain the following specifications [5]:

- The type of risks to be taken
- The level of risk tolerance
- The limit of the risk-bearing capacity
- The time limit in which the risks are dealt with
- Specifications on the risk management process

DIN ISO 31000 specifies a process structure for risk management, see Figure 1 [6].

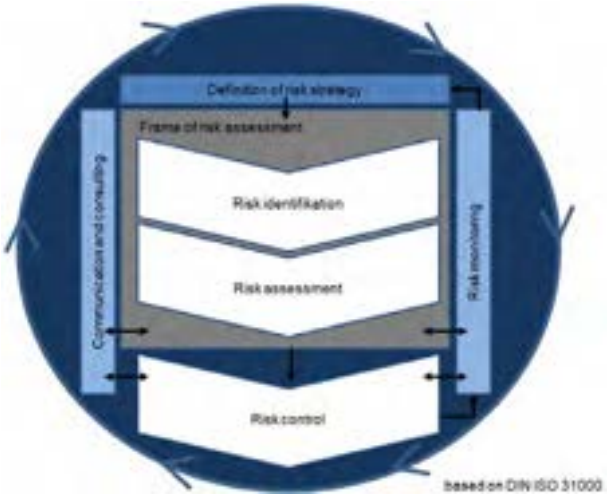

Figure 1. risk management process

The core of this process structure is transparency and openness. The process can only be successfully implemented if risks are not covered up, but are addressed openly. However, risk assessment and treatment cannot be carried out without defining an area of application, the context and setting risk criteria, see Figure 1. Throughout the cycle, continuous communication, documentation and review is required [7]. The risk management cycle is a continuous process. This means that the cycle is repeated in the course of project processing. The reason for this is that risks can change or new ones arise as the project progresses [8].

In the course of the risk management process, communication and consultation means that expertise from a wide range of fields is taken into account in the risk management process and that, as a result, different perspectives are considered in the identification, assessment, control and monitoring process. This also serves to obtain the necessary information required for risk management. Communication and consultation should take place between all those involved in the project or company [9].

Continuous monitoring and review of the existing risk management system is necessary to ensure the quality and effectiveness of risk management. In order to communicate the results of risk management, it is necessary to document risk management on an ongoing basis. This can provide information that is necessary, for example, for decision-making [10].

In order to apply a risk management process, the scope, context and criteria must be defined. This means that a risk strategy is defined as described above [11]. The definition of the scope includes a specification of the risk management processes and tools used and the necessary

means and responsibilities. A definition of the cycle of involvement and an analysis of interfaces with other projects and stakeholders are also part of the definition of the scope [12].

In addition, the environment in which the defined objectives are to be achieved must be analysed. The environment has a significant influence on the design of risk management. The external and internal relationships are defined. External interrelationships include, for example, political, legal and social aspects, whereas internal interrelationships include responsibilities and roles in the company or project [13].

Risk criteria are necessary for risk assessment. Therefore, they must also be considered. Risks can be assessed from a variety of perspectives within the company or organization, such as individual sub-projects of a major project or different levels within an organization. Since the approach and procedures differ depending on the viewpoint, criteria must be defined for risk assessment. For example, the type, extent and measurement of effects and the decision-making criteria for risks are defined [14].

3 Steps of the risk management process

The environment of all risk management processes is the risk strategy. This is used to formulate objectives and framework conditions. The next steps are the sub-processes identification, assessment, control and monitoring. Continuous controlling, careful documentation and regular communication and advice complete the risk management control loop [15].

3.1 Identification

The aim of risk identification is to identify all existing risks that could jeopardise the achievement of objectives. In risk identification, a distinction is made between cause, event and effect. A cause results in an event that has an impact on the project objectives. This distinction is important because countermeasures for dealing with risks can only be developed if the cause of the effect is known [16].

With regard to the method of risk identification, a distinction is made between the type of recording, the time of recording and the integration of the identification into the structure of the company or project [17].

It is important to complete the risk identification before starting the analysis [18].

3.2 Assessment

In the course of the risk assessment, the probability of occurrence and the extent of damage of a risk are estimated. This can be qualitative (e.g. low, medium, high) as well as quantitative (e.g. 50%, €50,000 loss). Based on the risk assessment, it can then be decided whether or not the identified and assessed risks are handled in the following ways[19]:

- No further action is taken
- Options for risk treatment exist
- Whether further analysis is needed for understanding
- The existing control system must be maintained
- project objectives may need to be adjusted if necessary.

For this purpose, the risks that are to be treated with the highest priority must first be determined.

The assessment of risks can be divided into gross and net assessment. In the net risk assessment, only the residual risk is assessed with a countermeasure. The gross risk is therefore the purely assessed risk. The gross risk thus represents the entire extent of the risk, whereas the net risk only shows the residual risk after countermeasures. It is assumed, however, that the countermeasures to reduce the scope of the risk occur to the extent assessed [20].

3.3 Control

In the risk management process step, countermeasures are developed to deal with the risks. The effectiveness of the selected countermeasures is then assessed. If the remaining residual risk remains too high, a further or, if necessary, new countermeasure is defined. This results in an iterative process [21].

How a risk is treated depends on the risk behaviour of the company or project and the risk strategy that has been defined [22]. A basic distinction is made between cause-related and effect-related measures [23]. Cause-related measures reduce the probability of a risk occurring, whereas effect-related measures reduce the extent of damage [24].

A distinction is also made between active and passive measures. Active measures contribute to reducing the probability of occurrence and/or the amount of damage, thereby changing the risk structure. Passive measures, on the other hand, aim to minimize the extent of damage. An attempt is made to compensate for the occurrence of a risk [25]. The combination of several coping measures is also possible and common in order to keep the residual risk low [26].

A distinction is made between five different risk management strategies [27]:

- Avoidance
- Reduction
- Transmission
- Insurance
- Acceptance

With regard to the order of priority of the application of coping measures, there is no fixed order. This must be determined individually. All measures depend on the cost-benefit ratio, but also on the time schedule, the qualitative dependencies and the applicability.

3.4 Monitoring

As already explained, communication and consultation, recording and reporting, as well as monitoring and reviewing are also part of the risk management cycle according to DIN 31000, and these components of the cycle should take place at all stages of the process [28].

The risk management process of a company or project must always be reviewed. This part of the risk management process is therefore also called risk controlling [29]. On the one hand, risk controlling serves to determine whether the desired effectiveness of the management measure has been achieved. On the other hand, it serves the right insight if a risk has to be re-evaluated or a countermeasure is not effective. It must also be checked whether a risk no longer exists, for example, due to a change in planning, and whether the change in planning gives rise to new individual risks [30].

4 Study on the application of risk management in the construction industry

In order to gain an insight into the application of risk management in construction practice from the perspective of the client and the construction company, expert interviews and an online survey were launched by the University of Wuppertal. The structure of the web-based survey corresponds to that of the expert interview.

The online survey was completed at the end of September 2019. 249 participants took part in the survey. Among the participants are 50 construction companies, 47 private builders, 34 planning/architectural offices, 31 participants from the field of consulting, 25 public builders, 6 experts, 3 from the craft sector and 54 from other fields. The findings of the survey are summarized below.

4.1 Positive approaches visible in practice

Around 60% of the companies surveyed implement risk management in accordance with a uniform company-wide risk strategy. Risks are identified for the first time at the acquisition stage or at the start of a project and are continued through the subsequent project phases. Risks are usually recorded in Excel applications or the company's own software applications. Communication channels for risk management are generally short and, thanks to open discussion cultures, there are few fears of communicating risks.

The interviewed experts recognize advantages for the project business through risk management: Risks that are recognized early have a positive influence on the further course of the project. Costs are saved, customers are retained and experience and improvement potential for follow-up projects is generated. There is improved control of costs and cost transparency throughout the entire construction phase, and through the integration of the risk management system, all those involved are able to improve the reliability of deadlines and costs.

4.2 Identified problem areas

Instead of uniform guidelines for dealing with risks and a systematic approach, a good third of companies rely purely on the experience of their employees.

Risks are considered in greater depth in the bidding phase, but are neglected in the execution phase. When assessing risks, the effects of deadlines are usually not taken into account in the offer. Risk assessment is largely intuitive and is shaped by the experience of the individual employee. The risk assessment usually ends with the acceptance and is not continued until the end of the warranty. Companies often have clear divisions between the departments of acquisition and project execution or planning and implementation on the client side. After project completion, the knowledge gained is only transferred to a few colleagues in discussions at communication level. None of the companies carries out a systematic evaluation of the risks after project completion and a systematic transfer of this information to subsequent projects.

4.3 Conclusion of the study

Overall, it became clear that risk management is by no means accorded importance in every company. For about half of the companies surveyed, risk management hardly plays a role in their projects. The cost and schedule of a project is usually determined by higher authorities and the project participants lack the necessary room for maneuver. There is potential for a stabilisation of risk management processes: Regular identification of risks, adjustment of assessments and linking to other processes have so far hardly been used to make risk management more effective. There is often no consistent systematic approach to the use of risk management systems. It is more a combination of individual approaches, which are not sufficiently linked and therefore information is lost or not fully used. In view of the imbalance of many current major projects, the potential of an industry-wide application of risk management processes is evident here.

5 Outlook using BIM

The mentioned research project has the aim to show the development possibilities of risk management into the method BIM. Therefore, the participants of the study were asked for which use cases and to what extent they currently use the BIM method to generate integration potentials for risk management. The survey showed that BIM is already being used in companies. The most frequently used use case is the use case of 3D modelling and collision check. The 3D modelling is set up in the planning phase and attributes are defined to support the prefabrication process. In addition, the models are used to generate carcass and fit-out dimensions, which serve as a basis for the bill of quantities and costing. Schedules and costs are usually not yet linked in the respondents' BIM models. In some companies, there are also company specifications to digitalize the complete planning and construction processes. Tablets are also often used for construction site operations. These enable access to the documents, checklists and work aids in the cloud. In addition, barcodes are sometimes stuck into every room on the construction site and the site manager has the option of calling up the attributes and information important for the room via tablet. The complete defect management is generated daily via the tablet of the site manager and the information stored in the cloud. The areas of construction site logistics, modularization, systematization of construction products and components are currently the focus of integration into the execution. In addition, some of the construction companies also want to use their project model for later operation and extract an as-built model from the data and attributes. The aim is to use BIM to create a complete digitalization of the processes from the construction site or project. As a use case, construction companies have their own focus such as quantity take-off, calculation and quality assurance on the construction site. Developers usually use BIM to focus on 3D coordination. Documentation is an important use case for all parties involved. A market analysis of risk management software carried out in parallel to the surveys also revealed, that there is currently no BIM-capable offering, for example with an ifc interface.

5.1 Process modelled risk management

As the study shows, risk management is currently regarded and implemented as a separate process in most companies. There is currently no link to other project processes such as scheduling or cost planning. To be able to use the advantages of the BIM method for risk management, the process must first be linked to the other project processes.

The first step in linking with the BIM method in the research project is therefore to model the risk management processes and link them to the other project processes. For this purpose, the risk management process described in chapter 2 and 3 was created/modelled with the help of the Business Process Modelling Notation 2.0 (BPMN 2.0). Figure 2 shows an extract of the process and gives an overview of the type of modeling.

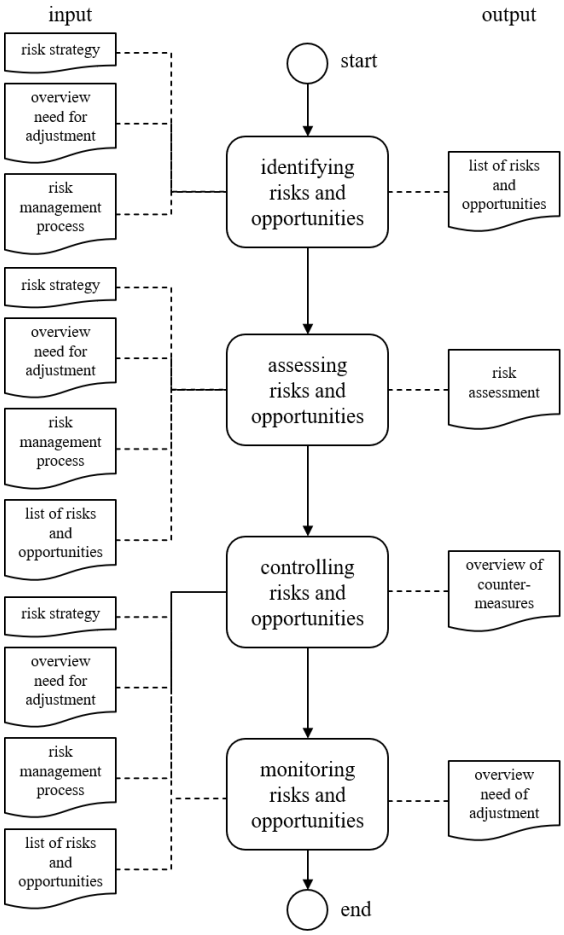

Figure 2. risk management process in BPMN 2.0

Each step of the risk management process shown in Figure 2 is broken down in more detail in further levels of the process model. The process "Identifying risks and opportunities" is divided, for example, into the process steps "Describing risks/opportunities", "Defining a short description", "Determining the cause and effect of the risks" and "Assigning a risk/opportunity category". In this way, all process steps are linked to one another and clearly presented.

In a second step, the modelled risk management processes are then linked to the other processes of the shown project, for example, cost control. In this way, it becomes clear at which point in the project, risks must be identified, assessed and controlled on the one hand, and which processes provide information in order to better

assess risks on the other. Figure 3 shows an example of this information linkage.

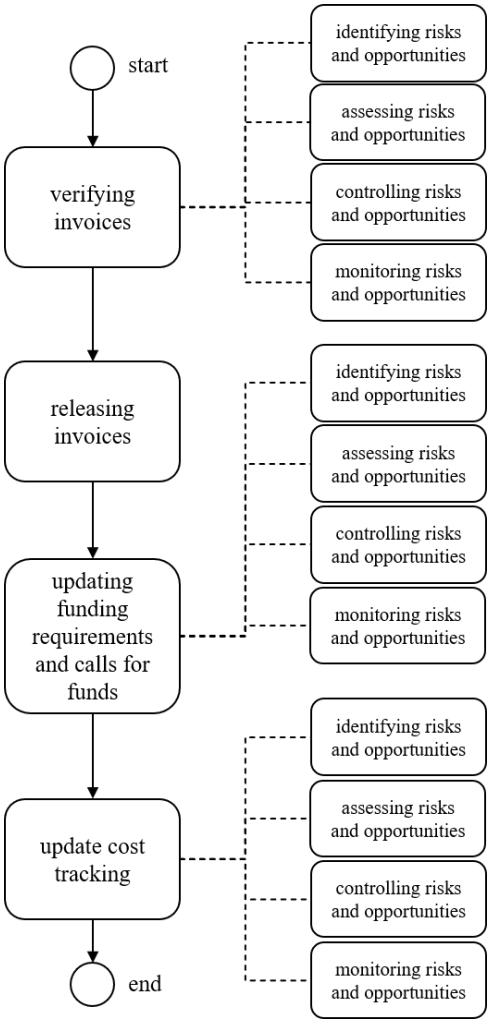

Figure 3. risk management processes linked to the process of cost management

The risk management process is represented on the process level, in which the methods and digital tools of a construction project are applied. The documents required for the risk management process in this section are formulated at a deeper, more detailed level.

The created risk management process now serves as a support process for the process steps in a construction project over the complete life cycle phase. In the further course of the research project, critical paths/processes in a construction project are analysed and the support process is integrated into them. This resulted in an overview of the critical processes for the different phases and from the point of view of the client and the construction company. Helpful tools and documents are formulated for each of these processes. The overview serves to link and identify potentials for the application of BIM.

6 Outlook research project BIM-based risk management

Processes have to be concretized, digitalized in the companies and responsibilities defined. Forms in the company and in the individual project phases must be digitalised and linked to software options. Checklists and required documents should be maintained regularly through experience and market adjustments and should be centrally stored for each employee.

In the further course of the research project, which will run until the beginning of 2021, optimization possibilities will be worked out based on the results of the survey so far and further potentials will be identified by using digital tools. A short self-check was developed for companies interested in a check of their own risk management processes. By ticking off the points, both approaches already successfully applied are made clear and ideas for further potential are offered.

In the coming months, a possible integration of the Building Information Modeling (BIM) method will be examined. To this end, the first step will be to link the risk management processes with the other processes of a construction project. The resulting process model will then show which information from the project activities should be used for risk management and, vice versa, which information is generated by risk management for the further course of the project. The BIM method is intended to enable a structured collection of risk management data. With increasing planning accuracy, the linking of information can be continued down to the component level. The linking of identified risks with components of the digital building model in the realization phase, promotes the integration and thus the acceptance of risk management and visualizes its advantages for the project result. The principle of the BIM method "first plan - then build" allows an early consideration of risks already from the planning phase to increase the reliability of deadlines, costs and quality.

References

[1] Hoffmann W., Risikomanagement (p. 24). Springer Vieweg, Berlin, [Heidelberg], 2017.

[2] Girmscheid G., Strategisches Bauunternehmensmanagement, Prozessorientiertes integriertes Management für Unternehmen in der Bauwirtschaft (p. 703). Springer, Berlin, Heidelberg, 2010.

[3] Hoffmann W., Risikomanagement (p. 2). Springer Vieweg, Berlin, [Heidelberg], 2017.
[4] Girmscheid G., Strategisches Bauunternehmensmanagement, Prozessorientiertes integriertes Management für Unternehmen in der Bauwirtschaft (p. 698). Springer, Berlin, Heidelberg, 2010.
[5] Romeike F., Risikomanagement (p. 39). Springer Fachmedien, Wiesbaden, 2018.
[6] DIN Deutsches Institut für Normung e.V., Risikomanagement – Leitlinien (ISO 31000:2018) (p. 16). Beuth Verlag GmbH, Berlin, Oktober 2018.
[7] Hoffmann W., Risikomanagement (p. 18). Springer Vieweg, Berlin, [Heidelberg], 2017.
[8] Hoffmann W., Risikomanagement (p. 24). Springer Vieweg, Berlin, [Heidelberg], 2017.
[9] DIN Deutsches Institut für Normung e.V., Risikomanagement – Leitlinien (ISO 31000:2018) (p. 17). Beuth Verlag GmbH, Berlin, Oktober 2018.
[10] DIN Deutsches Institut für Normung e.V., Risikomanagement – Leitlinien (ISO 31000:2018) (p. 16). Beuth Verlag GmbH, Berlin, Oktober 2018.
[11] Hoffmann W., Risikomanagement (p. 20). Springer Vieweg, Berlin, [Heidelberg], 2017.
[12] DIN Deutsches Institut für Normung e.V., Risikomanagement – Leitlinien (ISO 31000:2018) (p. 18). Beuth Verlag GmbH, Berlin, Oktober 2018.
[13] Romeike F., Risikomanagement (p. 36). Springer Fachmedien, Wiesbaden, 2018.
[14] Hoffmann W., Risikomanagement (p. 22). Springer Vieweg, Berlin, [Heidelberg], 2017.
[15] Hoffmann W., Risikomanagement (p. 18). Springer Vieweg, Berlin, [Heidelberg], 2017.
[16] Girmscheid G., Strategisches Bauunternehmensmanagement, Prozessorientiertes integriertes Management für Unternehmen in der Bauwirtschaft (p. 753). Springer, Berlin, Heidelberg, 2010.
[17] Girmscheid G., Strategisches Bauunternehmensmanagement, Prozessorientiertes integriertes Management für Unternehmen in der Bauwirtschaft (p. 756). Springer, Berlin, Heidelberg, 2010.
[18] Girmscheid G., Strategisches Bauunternehmensmanagement, Prozessorientiertes integriertes Management für Unternehmen in der Bauwirtschaft (p. 751). Springer, Berlin, Heidelberg, 2010.
[19] DIN Deutsches Institut für Normung e.V., Risikomanagement – Leitlinien (ISO 31000:2018) (p. 19). Beuth Verlag GmbH, Berlin, Oktober 2018.
[20] Diederichs M., Risikomanagement und Risikocontrolling (p. 139). Verlag Franz Vahlen, München, 2018.
[21] DIN Deutsches Institut für Normung e.V., Risikomanagement – Leitlinien (ISO 31000:2018) (p. 21). Beuth Verlag GmbH, Berlin, Oktober 2018.
[22] Girmscheid G. and Busch T.A., Projektrisikomanagement in der Bauwirtschaft (p. 67). Beuth Verlag GmbH, Berlin, 2014.
[23] Girmscheid G. and Busch T.A., Projektrisikomanagement in der Bauwirtschaft (p. 71). Beuth Verlag GmbH, Berlin, 2014.
[24] Diederichs M., Risikomanagement und Risikocontrolling (p. 172). Verlag Franz Vahlen, München, 2018.
[25] Hoffmann W., Risikomanagement (p. 43). Springer Vieweg, Berlin, [Heidelberg], 2017.
[26] Girmscheid G. and Busch T.A., Projektrisikomanagement in der Bauwirtschaft (p. 67). Beuth Verlag GmbH, Berlin, 2014.
[27] Girmscheid G. and Busch T.A., Projektrisikomanagement in der Bauwirtschaft (p. 67). Beuth Verlag GmbH, Berlin, 2014.
[28] DIN Deutsches Institut für Normung e.V., Risikomanagement – Leitlinien (ISO 31000:2018) (p. 17). Beuth Verlag GmbH, Berlin, Oktober 2018.
[29] Girmscheid G. and Busch T.A., Projektrisikomanagement in der Bauwirtschaft (p. 76). Beuth Verlag GmbH, Berlin, 2014.
[30] Girmscheid G. and Busch T.A., Projektrisikomanagement in der Bauwirtschaft (p. 76-77). Beuth Verlag GmbH, Berlin, 2014.

Introduction of the New Safety Concept "Safety2.0" to Reduce the Risk of Machinery Accidents

Hidesato Kojima[a] , Takaya Fujii[a] , Yasushi Mihara[a] and Hiroaki Ihara[a]

[a]Shimizu Corporation, Japan
E-mail: h_kojima@shimz.co.jp, f-takaya@shimz.co.jp, mihara.yas@shimz.co.jp, h.ihara@shimz.co.jp

Abstract –

In order to dramatically improve the productivity and safety of tunnel construction, we are developing a new construction production system "Shimizu Smart Tunnel". Based on the concept of "Digital Twin", it utilizes data sensing technology and information communication technology to acquire all kinds of data from people, machines and environment at construction sites. Using the data, we have implemented "Safety 2.0" that realizes collaborative safety technologies between humans and machines and "Safeguard support system" that reduces human error. We introduced a "Human-Machine contact risk reduction system" at actual sites.

Keywords –

Safety2.0; collaborative safety; risk reduction system; Safeguarding Supportive System

1 Introduction

Japan is facing the problem of a declining birthrate and an aging population and a decline in the working-age population. In the construction field, the number of engineers and skilled workers has decreased, and the construction production system has to be changed. In 2017, construction-related casualties accounted for about 30% of all industries, of which more than 70% of fatal accidents were related to falls, construction machinery and dropped loads.[1] The rate of work-related fatalities per 100,000 workers in each country shows that in some countries the rate is lower than in Japan. (Figure 1) [2] Especially in the UK, the rate of decline is very large. We have to learn from the West how to improve occupational safety. [3],[4]

The Ministry of Land, Infrastructure, Transport and Tourism has announced "i-Construction," which utilizes new technologies such as digital data acquisition, ICT, IoT, AI, and robotics. By 2025, it aims to improve productivity by 20% and solve problems in the construction sector. The Ministry of Health, Labor and Welfare aims to realize a society where people can work in good health and peace of mind in a safe environment free from occupational accidents. In 2022, it has set a target to reduce the number of work-related fatalities in the construction industry by more than 15%. [5] The Ministry of Economy, Trade and Industry has announced "New Robot Strategy" in 2015, aiming to strengthen and spread the use of robots, to popularize them, and to acquire international standards.

A robot is defined as a machine that has three elements: sensor, intelligence/control system, and drive system. Construction machinery, like automobiles, is expected to accelerate remote unmanned operation, automatic operation, and robotization.

In this paper, we report the results obtained through the practical introduction and trial of the human-machine contact risk reduction system to the construction site.

Figure 1. Comparison Occupational Fatality Rate (per 100,000 people). Processing based on [2].

2 Improved safety and productivity

In the construction field, it is required that humans and machines work together to ensure work safety.

2.1 The Concept of Safety 2.0

The human-machine collaborative work consists of a human area, a machine area, and a collaboration area. Here, Safety 2.0 is explained. (Figure 2) [6],[7],[8]

Safety0.0 is a state in which there is no concept of machine safety in the machine domain and it is a hazard to humans, and the collaborative domain is also the hazard domain. A state in which we try to ensure overall safety with only human safety technology. Safety1.0 is a state where the concept of machine safety has been introduced into the machine domain, and together with human safety technology, each ensures safety. The principle of isolation and suspension is established by fool proof and fail safe. Safety 2.0 is a state in which a collaborative safety mechanism that shares information using ICT is incorporated in each area of man and machine, enabling safe work in the area of collaboration.

In the construction field, it is difficult to realize the principle of "Isolation and Suspension" in the construction field, and the avoidance of residual risk is in the state of Safety 0.0, which largely depends on human safety technology.

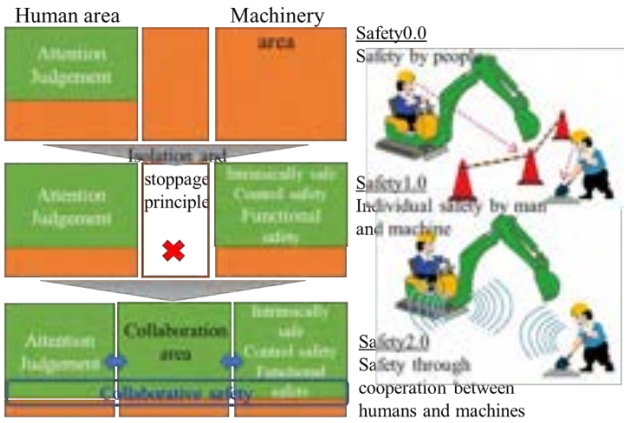

Figure 2. The Concept of Safety 2.0

2.2 Safeguarding Supportive System

In the international standard ISO12100, risk reduction measures for ensuring safety are based on an essentially safe design, safeguarding measures, and a three-step method based on provision of information on use. However, measures to avoid residual risk depend on human safety technology, and human error leads to serious occupational accidents.

There is a misunderstanding that human error can be avoided by attention, education/training/motivation, and multiple checks. The error occurrence rate of a person increases when the consciousness mode is fatigued, strained, or unsteady. Moreover, even if a person understands the work standard and can execute it, there is a case where the improvement of the productivity is prioritized, and the work standard is not intentionally observed. People must be aware that they have the property of causing an error.[9]

Dr.SHIMIZU et al. have reported comprehensive safety management that incorporates a "Safeguarding Supportive system" that prevents human error by combining appropriate ICT equipment.[10],[11]

In contracting duties, construction workers are required to constantly anticipate changes in the surrounding environment and residual risk and implement appropriate protection measures in addition to the original skill implementation.

The relationship between the hazard and the occurrence of harm and the "Safeguarding Supportive system" is shown in Figure 3.

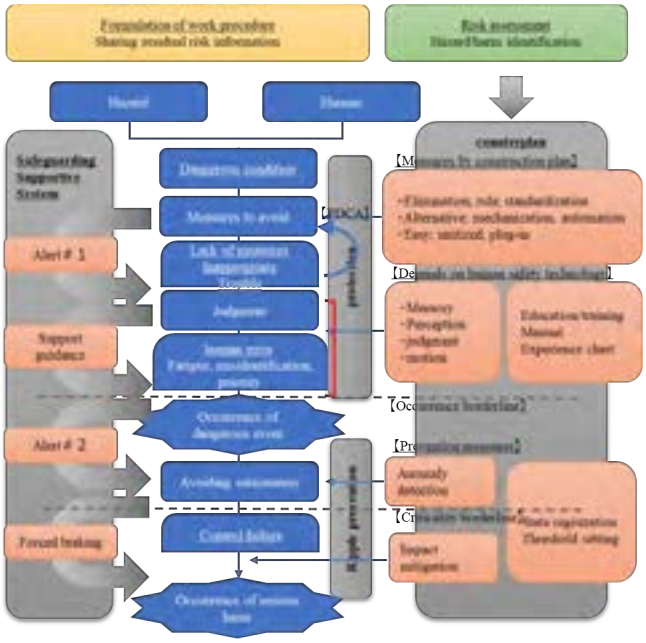

Figure 3. The relationship of harm and the "Safeguarding Supportive system"

2.3 Shimizu Smart Tunnel

Shimizu Corporation is advancing digital reform of its construction production system. In the field of civil engineering, in 2016, we started the development of "Shimizu Smart Tunnel". This system is based on the concept of "Digital Twin". (Figure 4)

In the physical space, various sensors, control devices and communication devices are installed on people and machines, and material supply, position and orientation of people and machines, movement status, condition, work environment, safety and quality, engineers and skilled labor Workers and production process information are aggregated on a digital platform

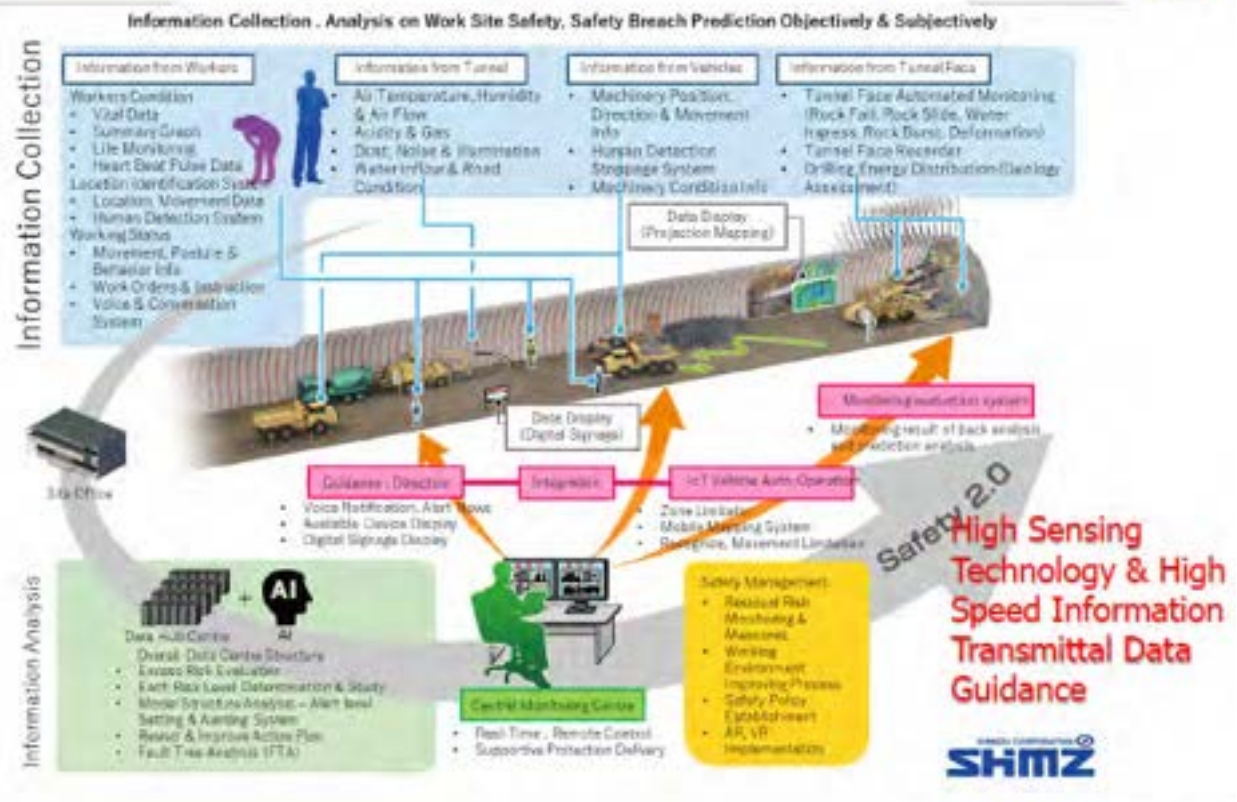

Figure 4. The Concept of Shimizu Smart Tunnel

in cyberspace. It is equipped with a support system that provides feedback to the site in real time through AI analysis and simulation analysis of information that changes moment by moment.

In tunnel construction, the collapse of the face and the contact between people and machines lead to serious disasters. The Shimizu Smart Tunnel will incorporate a safety support system to eliminate these serious disasters.

3 A Practical Approach

The development team of the safety support system selected the actual construction site and tried to introduce Safety2.0 from Safety1.0 by the practical approach.

3.1 Preparation

The safety support system development team held a workshop with experts. In addition, we investigated the safety awareness of the people concerned at all tunnel sites of Shimizu Corporation and reviewed and created safety teaching materials. we learned the following lessons.

- It is important to understand the concept of machine safety and prerequisites.
- It is necessary to rebuild an appropriate safety philosophy through appropriate risk assessment.
- Framework is important to implement and function Safety 2.0.

3.2 Goal Setting

The goals were set as follows.

- Development of a risk assessment method that is compatible with machine safety.
- Site managers and workers understand the concept of safety system.
- Site managers and workers should learn how to operate the safety system and adjustment procedures.
- Obtain "Safety 2.0" certification for the implemented safety system.

3.3 Scope of Development

In general, the construction of mountain tunnels is a cycle work that repeats blasting and mechanical excavation work, mucking work, steel support work, concrete spraying work, and rock bolt installation work. Within 100m from the face (tunnel excavation surface),

the machines will be replaced, and the work will continue day and night. The composition of the machines used in the construction is decided at the time of formulating the construction plan, but the risk was extracted by applying a new risk assessment method to the site already in operation.

The development target was set to "mucking work" from the viewpoint of developing "collaborative safety between humans and machines", and we developed the " Human-Machine contact risk reduction system".

3.4 Zoning of Work Areas

The work area for "mucking work" has been divided into a working zone, a moving zone, and a parking zone. The mucking work of excavated soil is performed in a working zone within a range of 100 m from the face.

The tire shovel, which has started from the parking zone about 230 m from the face, travels in the moving zone of about 100 m and enters the working zone. The tire shovel puts the excavated soil scraped by the hydraulic excavator into the hopper near the rear of the working zone. The tire shovel collaborates with the hydraulic excavator to repeat loading into the hopper and finish the mucking work. After that, the tire shovel exits the working zone and retreats to the parking zone to complete the work.

The work area moves forward as the tunnel excavation progresses.

3.5 Risk Extraction

The risks extracted in the mucking work are the following four items that occur irregularly.

- Unauthorized workers enter the working zone and come into contact with operating machines.
- In the work zone, the driver who gets off the machine contacts another machine in operation.
- A machine starting from the parking lot comes into contact with people around
- The retreating machine comes into contact with the person who was in the parking lot.

3.6 Piloting a “Human-Machine contact risk reduction system”

3.6.1 System Component

A directional receiver was placed at the boundary between the working zone and the moving zone, and a normal receiver was placed every 10 m in the moving zone and the parking zone, and the whole was divided into 14 blocks. And a receiver was installed on the ceiling of the machine driver's seat. It receives the BLE (Bluetooth Low Energy) transmitted by the driver and monitors the presence of leaving the machine. Two transmitters are installed for each person and machine. The transmitter transmits a BLE signal that identifies the individual. The receiver installed in the tunnel mine configures a mesh network with multiple units, and the received BLE signal is stored in the cloud server from the Gateway via the on-site network. In the cloud, the positional relationship between the person and the machine is specified from the collected information, and the difference from the set permission state is determined. When an abnormality is detected, an alert signal is transmitted to the warning lighting device. The warning lighting device is arranged at the boundary between the working zone and the moving zone. When the PLC (Programmable Logic Controller) receives an alert signal, it immediately emits a loud alarm and simultaneously projects a blinking red and white LED beam light on the face. (Figure 5,6)

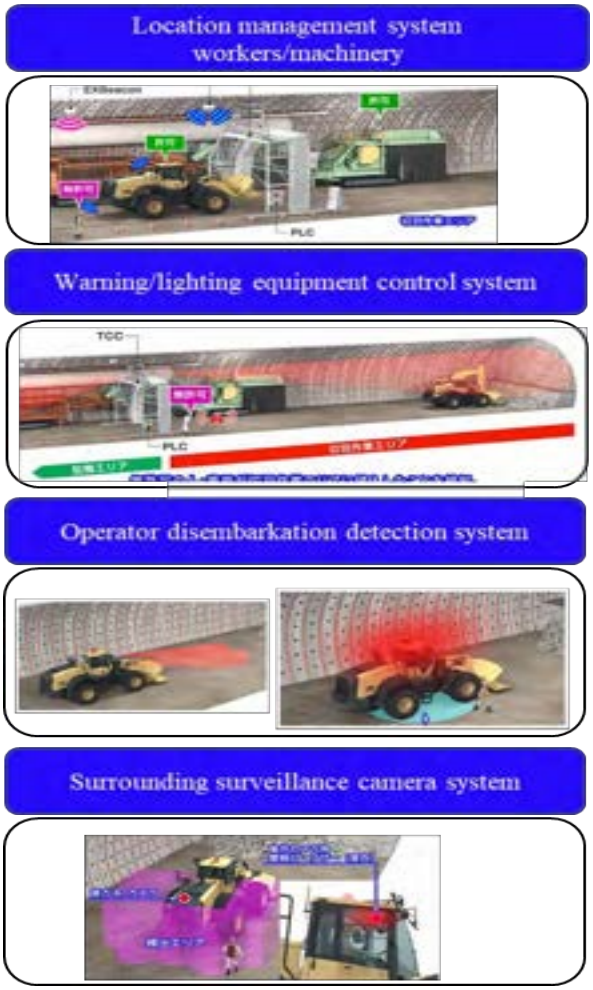

Figure 5. Human-Machine contact risk reduction system

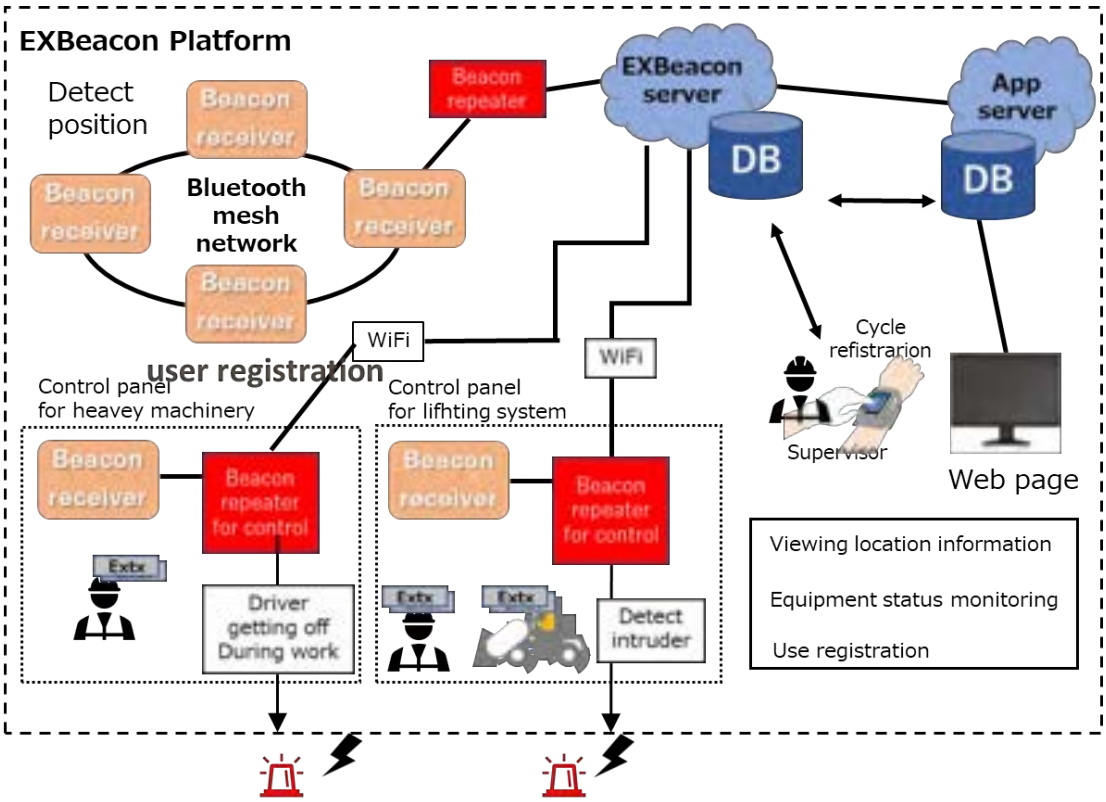

Figure 6. System block diagram

3.6.2 Site of Application

This system was introduced to the construction of the Kumamoto Route 57 TAKIMUROZAKA Tunnel West (first stage) construction (high standard road, construction extension = 2,679m, excavation section = 107m2).

3.6.3 Rules of Operation

- The site manager should register the mucking work permission ID and combination conditions before the work.
- Daily inspection of the system should be carried out by all supervisors and workers before starting work.
- The person in charge of monitoring carries the control tablet.
- The person in charge of monitoring switches the safety system to the "mucking mode" during mucking work.
- When the warning lighting system is activated, the machine operator makes an emergency stop.
- The person in charge of monitoring cannot cancel the alarm until the cause of the alarm is eliminated.
- The site manager collects the number of reports, IDs, and logs to inform workers and improve work.

3.6.4 Procedure for Adjusting the Safety System

Since a large machine is installed inside the tunnel mine under construction and the machine operates in a narrow work zone, the radio wave system tends to be unstable. Even in this introduction, several malfunctions occurred. There was a big difference between the ID position reproduced in the cyber space on the cloud and the position in the actual physical space, causing the ID position to move confusion in the tunnel in the cyber space. Further, at the boundary between the work zone and the moving zone, there was a false detection that a worker in the moving zone was in the working zone.

BLE transmission/reception in a tunnel mine is apt to cause multipath due to the reflection of the machines located in the mine and the moving machines. Even if the reception strength is weak, if the number of BLE transmission receptions fluctuates, it may be erroneously determined that there is a transmitter in the vicinity. The safety system adjustment procedure was established for these problems.

Step1. Divide the adjustment scene into whether the machine is operating or not.

Step2. In a static environment where there is no machine operation, repeat the receiver placement verification at intervals of 50 cm, analyze the radio wave intensity characteristics, and determine the optimal installation position.

Step3. In a dynamic environment with machine operation, analyze the radio wave strength characteristics and determine the optimum combination of reception strength thresholds.

3.6.5 Implementation Process Framework

Generally, when introducing a new system to the field, it is important to understand the theory, foster appropriate operation methods and improvement consciousness, and share consciousness with the development team. If the site manager and workers have a voluntary intention, they will succeed. is there. The education of safety concept and the new system by the development team was repeated using animated videos. A dedicated instructor was assigned to the site to practice the operation confirmation and inspection methods of the new system equipment at "On Job Training (OJT) ". OJT was repeatedly carried out for the mechanical and electrical engineering staff because the procedure for eliminating false positives requires specialized technical knowledge to analytical the radio characteristics and reset thresholds.

3.6.6 Effects of Introduction

Here, the introduction effects are summarized.

- Unauthorized entry into the work zone and disembarking from the driver's machine could be quickly shared as a risk.
- The warning from the warning lighting device surely guided the stoppage of the machine operation, and the risk of being overlooked became zero
- The loud alarm and the intense red and white flashing projection caused psychological strain on the machine driver, and the initial action of the machine stop for the risk occurrence was accelerated.
- Workers began efforts to prevent short-circuiting work violations. This is because warning issuance leads to a reduction in work efficiency. Intentional disembarkation from the machine in the work zone was reduced.
- The frequency of cleaning and checking not only the equipment that constitutes the safety system but also the machine itself has been improved. In addition, they became more sensitive to machine failures and reduced the frequency of repairs.
- The safety system operation at the installation site has received level 1 certification from IGSAP (Safety Global Promotion Organization) as a technical measure that complies with Safety 2.0. [12]

4 Conclusion

This paper has seen a trial example of a safety system for collaborative safety for human-machine collaboration. The risk assessment in the construction field was reviewed based on the flow of machine safety.

The concept of coordinated safety (Safety 2.0) and Safeguarding Supportive system was highly evaluated by workers and field managers who work on the front lines of the field. “We understand the need, and I feel that productivity will be improved by the support system.” (Figure 7)

Figure 7. Warning by blinking LED light

It is expected that robot technology will continue to evolve in the future, and a more advanced production system will be constructed in which humans, machines, and the environment will be firmly connected by IoT and IoP (Internet of Process). Standards, standards, rules and frameworks are important for maximizing the Safety 2.0 effect with a Safeguarding Supportive system.

References

[1] Japan Federation of Construction contractors; Measures to prevent construction labor accidents Special activity leaflet https://www.nikkenren.com/anzen/iinkaianzen.html

[2] Japan Industrial Safety & Health Association; Country information/international relations > Overseas information by field > Health and safety statistics (by country) ; https://www.jisha.or.jp/english/index.html https://www.jisha.or.jp/international/field/disaster.html(Japanese)

[3] Kikkawa,N., Ohdo,K., Toyosawa,Y., Hiraoka,N., Hamashima,K., and Shimizu,S.; Proposal on safety and health issues in the construction industry and future policy from the viewpoint of safety science in the mechanical field, Proceedings (Safety Issues) of JSCE, 2019.1.

[4] Supervised by Mukaidono,M. Safety Technology Application Research Group, Safety Technology of Machine Systems in the Age of Internationali-zation, Nikkan Kogyo Shimbun, 2000.4

[5] Ministry of Health, Labour and Welfare; “The 13th Industrial Accident Prevention Plan”, 2019.2
[6] Ikuo Maeda;Masaki Nobuhiro;Takayoshi Shimizu; Kazuya Okada;Masao Dohi; Shigetoshi Fujitani; Koji Inada;Toshihiro Fujita, New concept of safety to realize improvement of higher productivity and safety in an environment of human-robot collaboration, and proposal of the, ISR 2018; 50th International Symposium on Robotics, 20-21 June 2018, Munich, Germany
[7] Nikkei Business Publications; Safety2.0 Project, Safety2.0 – Concept, 2015 (in Japanese).
[8] Mukaidono,M.; Safety in construction industry from the viewpoint of safety studies; Road construction (in Japanese) , 2019.11.
[9] Supervised by Haga,S.; Research Institute for Safety, Inc.;Human Error Theory and Counter-measures, 2018.05
[10] Shimizu,S., Otsuka,H., Hamashima,K., Tsuchiya,M., Umezaki,S., Fukuda,T. and Hojo,R.; Machinery Safety ― Supportive protective system(SPS)(Risk Reduction Effectiveness of SPS in Integrated Manufacturing Systems (IMS)) Proceedings of the Japan Society of Mechanical Engineers,2018.4
[11] Shimizu,S., Hojo,R., Hamashima,K. and Umesaki,S.; Safeguarding Supportive System - Necessity of comprehensive safety management by Safety of Desin, 2019.6
[12] Ariyama,M.; Toward social implementation of Safety 2.0 (collaborative safety); Safety and health (in Japanese), 2019.8.

Applying ANN to the AI Utilization in Forecasting Planning Risks in Construction

Fawaz.Habbal [a], Firas.Habbal [a], Abdulla.Alnuaimi [b], Anwar.Alshimmari [b], Nawal.AlHanaee [b], Ammar.Safi [b]

[a]Department of Management College of Business,
International learning institute, United Arab of Emirates
[b]Ministry of Infrastructure Development, United Arab of Emirates
E-mail: firas.habbal@iqli.net, fawaz.habbal@iqli.net, Abdulla.alnuaimi@moid.gov.ae, anwar.alshimmari@moid.gov.ae, nawal.alhanaee@moid.gov.ae, ammar.safi@moid.gov.ae

Abstract

A long-standing problem in the field of automated reasoning is designing systems that can describe a set of actions (or a plan) that can be expected to allow the system to reach the desired goal. Artificial Intelligence (AI) techniques provide the means to generate plans and to reason with as well as provide explanations from stored knowledge. However, these methods, which employ little domain knowledge and are originally used in AI for planning, proved inadequate for complex real-life problems such as project planning. As a result, more recent research adopts the knowledge engineering methodology as an efficient approach for developing planning systems. This paper highlights the limitations of existing project planning tools. It also illustrates the power of AI techniques in the construction planning domain through a summary and critique of previous and current research in AI planning. It then concludes with a suggested approach for development. From the study, it was found out that a proper application of the AI technology requires full support in form of a Data Bank, which, unfortunately, becomes one of the most significant hurdles in its adoption. To deal with this limitation, it is recommended to adopt the ANN.

Keywords –

Risks Planning; Construction Planning; Risks forecasting; Neural Network; Support Vector Machines

1 Introduction

Utilization of artificial intelligence in planning involves the use of a planner generator which follows the sequence of actions for presenting the solution of a problem. Artificial intelligence can provide a powerful tactic for managing the risks and ambiguities in construction planning. Utilization of artificial intelligence can be efficient when employed in different phases of construction which involves estimation of production, management of risks, and plan schedules. With the recent development in the construction industry, different artificial intelligence systems have been used and widely applied for forecasting risks [1]. The economics of the developed countries can be improved and fulfil the crucial role of the construction sector. Time, cost, and quality performance the construction project my years though successful construction projects. The duration of the construction project can be a problem as accurate predictability is hard to be achieved. It is not the cause the construction process usually faces many factors that sometimes involve unpredictable variables that can be the result of various factors [2]. These variations or changes usually hinders the completion of projects in the estimated time and become the reason to lead the way towards the latest in the process of construction [3].

The prediction of risk regarding the construction project is based on both internal and external sources which upon identification can help the project managers to have a clear and accurate forecast for the effective management approach towards the construction project. Construction projects are complex and dynamic [4]. Providing an efficient tool for the analysis of the factors which are involved in the risk can provide an accuracy of determining the factors in the construction projects. Recently several models of artificial intelligence have been applied in different fields of engineering and science. Various studies included and researched on the involvement of various artificial intelligence models for the completion and conduction of the research regarding construction project management [5]. Different artificial intelligence methods are being used in the forecasting of the final project duration and risks.

2 Literature Review

2.1 Decision trees

Morgan and Sonquist (1963) dealt with the automatic interaction detection and proposed a fresh method for the regression and analysis of data which is being recognized as decision tree learning [6]. Breiman et al., (1984) also suggested the idea of the algorithm that majorly consisted of 2 phases; In the 1st phase, this solution space is separated with a binary or multi-way split. in the second phase, to every node of partition, a constant model is applied. these well-known procedures are subjected to two pitfalls which are named as overfitting and selection bias. and this method is collectively known as classification and regression trees [7]. This method is not perfect as the overfitting problem emerged as a result of the lack of significance of statistical data. Although some of the information is maximized to divide the decision tree, there is no other significant method of determining whether the split is justified or not. Another major limitation of this processing includes the selection bias which is derived from the fact that most points are preferred.

To upgrade the shortcomings or trees, another method known as bagging predictors was introduced. It involves the arrangement of different trees on the bootstrap on the test set giving us the final estimation by the prediction of average values from each tree. To remove the barriers in begging predictions another method known as random forests were introduced which involves the selection of random numbers of the predictors from each split [8].

Despite the fact that there have been a number of literature that attempt to discuss about AI application, there is none discussing about how ANN may help project managers establish and maintain proper Data Bank. Thus, this is where this study is attempting to fill as it looks to close this gap in the field of research.

2.2 AI Limitation

The limitation of this increase includes their instability even when there is a small difference in the learning data. Selection of the variables and cut points for the selected variables hang on the observations made in the learning sample. If there is a change in the first splitting variable due to a minor change in the learning data, then there is a probability that the structure of the entire tree might have been altered. Therefore it can be concluded that the single predictions have a high variability rate [9].

2.3 Construction simulation

Most of the construction projects involve repetitive activities such as the movement of the projects. If the decisions taken goes in the wrong direction they can cost a lot of expense along with time and energy. while if the project planning involved the right decisions at the right planning state a substantial time, money, effort, and energy can be spared. Due to the stochastic nature of the process of construction, the data collected from the preceding experiences and projects can help in the elimination of errors and risks. Because planning engineers can make an improved evaluation of expected productivity rates [10]. In the traditional method, the planning engineers manually add and adjust the productivity record for the establishment of expected values and figures. Due to the rising complexity and size of the project decision making and planning were becoming inaccurate because of human errors. To ease this complexity of estimation introduction of simulation, pickney has helped in various operational and managerial projects. it is a powerful tool that is being used as artificial intelligence in the systems for the prediction and accuracy of estimations regarding the construction processes.

Although construction simulation is a potent tool that is being applied by various companies for resource planning, designing, and analysis of the construction method. It is still dependent upon the human corrections as it only estimates depending upon the data which is being saved and processed in this system. As it cannot make any assumptions irrespective of the data. Therefore, it does not provide complete independence [11].

2.4 Productivity Assessment

These days productivity management is considered a key concern regarding the management of projects in the industry of construction. As the project varies, the level of productivity regarding construction also varies according to the atmospheric and organizational situations. the impact of factors affecting the productivity of the project is considered important in the productivity estimations. These factors can affect both positively and negatively on productivity. Human factors, weather conditions, change orders, and materials management can be the possible factors for determining the productivity rate of any construction project. At the initial step in the creation of a model for the productivity estimation identification of these factors can lead to better planning utilizing artificial intelligence because AI can predict possible risks through effective calculations [12].

Moselhi et al. [13], Introduced a supportive system that was able to make the decision named WEATHER for the prediction of climatic conditions regarding the efficiency of operations during the construction. This model was developed to make the estimations in the construction productivity to have a better prediction regarding activity durations and patterns of weather to

improve the planning and scheduling of the model to reduce the risk which can affect productivity. Moslehi et al. [14] then utilized the simulation system in 57 different projects to check the impact of changes during construction projects.

It was then discovered that there is a straightforward correlation between labor components of change orders and production damage in all kinds of projects. These predictions from then are being used in the estimation of losses regarding the changes.

2.5 Artificial Neural Network – ANN

ANN is a mathematical model that is being used to search for the finding the patters among t eh huge datasets when during the construction planning there are complicated relationships found between inputs and outputs. Through ANN attempts are made to stimulate and make it able to function and operate as a human neural network system. One of the major achievements is the capability to learn from the mistakes and this system due to this ability is approaching the heights of perfection. As ANN Act like a black box and cannot be used for the explanation of the reasoning process Therefore it can be restricted to the areas where there is no need for the explanation. It is well suited to the problems where the value of input-output relations is not being researched [15].

In recent years ANN has been widely used in the forecasting and prediction of the models which are being used in the construction industry. Researches are being made in different areas of construction management which includes cash flow predictions, risk analysis, optimization of resource, and construction productivity assessment.

2.6 Fuzzy Logic

As compared to ANN fuzzy logic was developed and introduced to resolve the necessity for systematic reasoning that can improve conform to human logic. Fuzzy logic is aimed at connecting the input space to an output space. Fuzzy models have their basic rule which contains the list of all the rules. Through the parallel evaluation, the inference procedure is performed. In different areas and fields of construction management, the concept of fuzzy reasoning is being applied. Car and Tah [16], used the fuzzy model to relate and address the risk assessment and analysis. They explained that risk information of a specified project is based on the items and procedures which are to be utilized during the process. These items are catalogued and are customized for each project. Therefore, the results would be according to the requirement of that project. The implementation of fuzzy logic makes the use of descriptive linguistic variables for the description of risks and their associated consequences.

Zhang et al. [17], demonstrated the relevance of fuzzy logic in discrete event simulation. The fuzzy simulation uses the fuzzy sets to explain the quantity of the resources which are required for the activation of an activity. These activities are regarded as constants incorporating the fuzzy logic rule to control the stimulation of behaviors. They further explained that the length of the construction project changes with the change in amounts of supplies implicated in the procedure of action. Fuzzy simulations give an alternative to the uncertainties of the models by contemplating the dynamic characters of the operations being done during construction in real-time situations. The results of experiments depict that flexibility in demand regarding the resources can have a positive effect on productivity which is being practiced at construction sites.

Paek et al. [18], implemented a multi-criteria methodology of decision-making with the use of a fuzzy-logic system for the selection of a design or build proposal. To reduce the cost of construction and reduction of time and money, several design projects are introduced and proposed in opposition to the traditional methods for the building. However, for this purpose there is a need to maximize the degree of technical factors and minimizing the cost of construction, the evaluation method is filled with uncertainties. To remove or minimize these uncertainties, this study was aimed at utilizing the criteria of decision-making method with efficient usage of a fuzzy logic system. This system is introduced to assist in making the decision which is a better-suited design proposal to satisfy the needs and requirements regarding the physical and environmental conditions along with the reduction of cost.

Fuzzy logic and ANN both complement each other. ANN can learn from the data, but its limitation involves the unavailability of explanation regarding the value of the input-output mapping process. Fuzzy reasoning offers a systematic reasoning procedure which is more compatible and closer to human logic and intuition. But its limitations include the need to make itself to adopt techniques of self-regulation to differentiate it from other areas. The constraints of these two procedures led to the introduction and development of another AI system known as a neuro-fuzzy system. Hybrid intelligent systems include the term neuro fuzzy as the fusion of both techniques i.e. ANN and fuzzy logic [19]. This fusion led to overcome the restrictions of both techniques as the shortcoming of one technique is covered by another. Although the utilization of neuro-fuzzy technique is being practiced it still is not common.

2.7 Genetic Algorithm

Genetic algorithm (GA) is it mattered which is developed by the optimization of artificial intelligence

base techniques, which imitates the natural mechanism of evolution. The genetic algorithm has boosted the structure optimization and parameter fine-tuning procedure of neuro-fuzzy systems. An evolutionary approach is used to find the solution to problems for finding the best options for a potentially better future. In GA random individuals are selected for the production of a population which then evolves itself through the evolutionary procedure in a natural way by mutating and altering the properties of a population. The performance of every representative of the population depends on some standards of fitness. These fitness criteria then determine the basis on which the next generation is selected and which characters are to be migrated in the next generation [20].

Due to advancements in technology AI has made its way in every field of life including construction planning and risk management along with better decision making to minimize the costs and effects of the variables. AI has enabled the planning engineers to go for more complex construction plans minimizing the efforts, costs, and errors regarding construction projects. These days the use of hybrid systems which includes the use of artificial intelligence can enhance the accuracy and productivity of the construction operations and projects. Further modifications in the upgrade of these systems are making its marks in these systems predicting the variables with much more accuracy and precision. The limitations of artificial intelligence or systems including AI is sticking of these systems to the data provided. Even the hybrid systems like neuro-fuzzy systems are unable to follow the rules through which the human intuition can be proposed. In other words, it can be interpreted as it functions like neural networks as a black box without having a clear interference of human thinking procedures. The method for the selection of variables is not conducted even in the advanced systems of AI for the selection of input variables which are necessary for the specification of neutral or deteriorating factors [21]. The major restriction of AI is its inability to make decisions as it is still dependent upon the humans for the data entry. It only analyzes and interprets the data that is being fed to the system. But still, these limitations cannot deny the usefulness of its use in various engineering fields and especially in construction planning which is helping this industry by minimizing the risks of aftershocks from the variables.

3 Research Methodology

Because of the risk management, the executives have become a fundamental strategy in the advancement of any development venture; by and by, its usage includes the utilization of the essential ideas, for example, "Hazard" and "Vulnerability". These ideas are regularly befuddled and used like equivalent, in any event, when they are unique as seen in Figure 1.

Risks: are recognizable and quantifiable potential occasions or factors; from which, negative (perils) or positive (possibilities) results may happen 250.

Vulnerability: alludes to obscure and unforeseeable occasions or factors; which no measurement or practically no distinguishing proof is conceivable.

Subsequently, it's essential to separate between these two ideas; a large portion of the dangers are conceivable to recognize and control, they can be arranged in Perils and Possibilities, while vulnerabilities are consistently startling and additionally not quantifiable. Figure 1 presents the conduct of vulnerability and hazards through the diverse venture stages. At the early stages, the vulnerability has a significant impact on the venture condition than dangers; therefore, as the task progress along the improvement stages, the nearness of risks become higher than the vulnerability, or the most part since vulnerabilities are distinguished and measured as explicit undertaking dangers. A short time later they are overseen to accomplish the undertaking possibilities and to keep away from its risks.

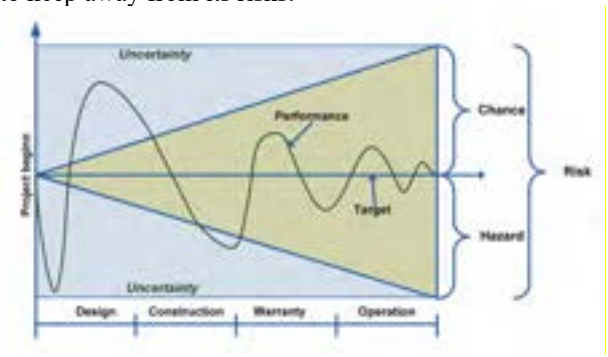

Figure 1. Risks & Uncertainty

3.1 Risks Evaluation Methods

Risks examination strategies manage the assessment of dangers; Risks measurement implies that probabilities can be related to anticipated qualities or results; nonetheless, its adequacy relies upon the past strides in the RMP because those means are the establishment of the entire procedure. The arranging procedure for executing Risk the board is a critical stage, it gives the chance to the venture and hazard supervisors to clarify and depict in subtleties what chance administration is about, why it is imperative to have a risk group, what is normal from them and what are the expectations. Consequently, threat reporting and verbal exchange play a crucial function beneath the threat analysis process; it is also an outstanding chance to discover with the crew any doubts or questions about the threat management method and also a risk for convincing the project stakeholders, the executives and the relaxation of the

crew about the advantages of imposing a serious quantitative risk analysis.

Risk analysis is the most important milestone for performing an advantageous quantitative assessment. All these processes outline the requirements to be attended on the search of inputs and the definition of stochastic fashions and their functions; consequently, the utilization of quantitative strategies like Monte Carlo Simulation shall turn out to be a requirement for danger analysis. Checklists are in most cases used for threat identification; they are necessary and beneficial for the identification but not sufficient for the analysis.

3.2 Artificial Neural Networks

Although this approach is relatively new in the business world, the unique idea used to be developed in the '60s together with the algorithms and some theoretical approaches. Nevertheless, the lack of ability with the computers´ processors stored this technique in the shadow for many years. ANNs comprise their structure, exclusive sections of layers, the middle ones generally are known as the hidden layers. The conceptual process of ANNs is conformed of an enter vector, a switch function, and an output vector (see Figure 5).

The switching characteristic with its limits is very frequently referred to as a "black box", this is due to the fact at this phase an inside system for adjusting and calculating new weight for the network is performed and this system is now not found by means of the designer.

The foremost gain of ANNs is that the entire process (training and testing) mimics the human's intelligence reasoning. In different words, it learns via the experience: Once an excellent database is developed, the chances to acquire dependable predictions with ANNs are very feasible.

One instance of the practicability of the ANNs is the Neuronal Risk Assessment System (NRAS) developed by using Maria-Sanchez. 254 This approach indicates a very practical manner for implementing ANNs for assessing the risks in infrastructure projects. The essential goal of the gadget is to decide the contingency quantity based on unique mission risks. The consequences exhibit the capabilities of ANNs to mimic the data, offering a wonderful new strategy for performing chance analysis. In addition, in modern times it is feasible to discover business reachable ANN tools.

3.3 Support Vector Machines

The SVM is a technique from the synthetic Genius that has proven excessive attainable for its applicability in the threat analysis. Vapnik defines this technique as a statistical mastering theory; [22] it works below the identification, screening, and separation of the information in hyperplanes primarily based in a support vector. In this form, the information is categorized in various dimensions (hyperplanes); as a 2d step simulations are done via growing statistics internal of the numerous hyperplanes. The SVM lets in to research from a described database and from this gaining knowledge of the procedure to forecast feasible results, in this form it is possible to perform simulations with a greater legal responsibility derivate from the studying process.

From these three techniques SVM represents a very promising technique because it allows us to examine from the statistics and simulating besides assumptions (like MCS); the simulation is primarily based on the recognized hyperplanes, which make bigger certainty. However, the technique is based on the synthetic talent theory and requires a considered quantity of facts to operate its learning process.

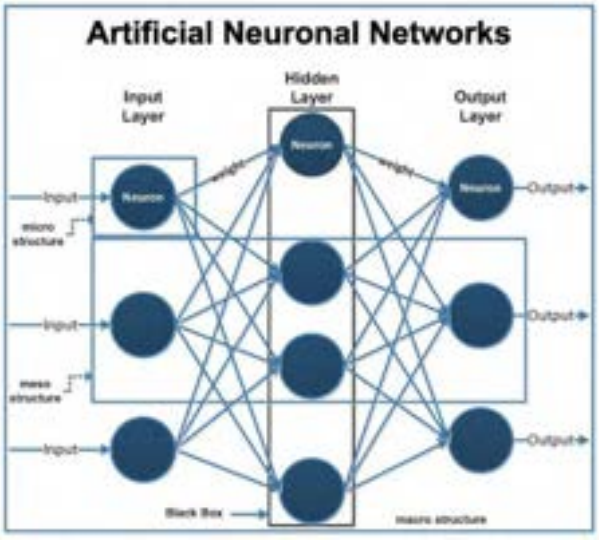

Figure 2. Artificial neuronal Networks Functionality

4 Experiment

The Support Vector Machine ought to emerge as a methodology of the synthetic intelligence that will be used in the chance analysis; it lets in a first step to perform a studying system to display screen and separate the before amassed data in hyperplanes. As 2d step, it implements a simulation system in order to convey probabilities to the anticipated danger or value. But the utilization of danger analysis in the praxis relies upon the availability of the required tools to operate this kind of evaluation for the threat evaluation practitioners. Until these days there is no commercial application of the SVM, therefore for its employment is crucial to create computer programs.

Thus the mixture of ANNs and MCS shall emulate its functionality, from existing commercial programs. The downside of MCS is the use of assumptions in its

procedure. This can lead to dispersion will increase with the inputs and in the corresponding delivered results, or in in the worst case, into blunders and misconceptions; for example, when the threat analyst does now not have ample experience, can create ambiguous surroundings to the whole process and this can affect the excellent and outcomes of the complete implementation.

MCS allows simulating dangers but the inputs nevertheless need to be described as a section of the qualitative analysis. Better inputs can be observed through ANNs: They enable predicting values from defined records banks; therefore it represents an essential useful resource for the definition of inputs for the MCS. Consequently, the mixture of both strategies shall minimize the opportunity of mistakes, by means of defining the initial values with the ANNs and the use of MCS for the simulation process.

ANNs are one of the new strategies from the synthetic Genius discipline that have emerged and observed its applicability in risk analysis. It has two key steps for enforcing in danger management. However, a vast database is wished in order to educate and check the network. Different network designs can be done and for some algorithms, the training and trying out process can be extra effortlessly done if the design is environmentally friendly and practical.

4.1 ANNs Prediction

The software of the ANNs needs a facts bank of the advantageous ability relying on the relevant criteria. For lack of measured web site facts, it was created based totally on the components and values through the ability of the addition technique in building machines. The statistics bank includes a wide variety of 12 criteria; via the formulation, we can decide the "exact" end result (important for the check of the ANNs) of the superb capacity. For each of the 12 standards a range was determined and thru the utilization of a random generator quantity one thousand one-of-a-kind result combos have been created, having the end result and criteria a direct relation.

The textual content criteria have been created with the utilization of numerical facts and they were replaced with text for its checking out in ANNs. At the give up each and every system was once deleted, final just the numbers and text without any relation rule, for the assessment of the ANNs.

ANNs estimate the manufacturing-based totally in the Data Bank, the regular manner with the aid of ANNs is as seen in Figure 3. The Data Bank needs to be elaborated and loaded into the ANN program, the impartial and dependent criteria must be specified.

The second step is to get to know the method (training) for the ANNs has to be described properly with error tolerance. Afterward, when gaining knowledge of the procedure is concluded, the trained ANN ought to be examined for its liability. When the checking out system is efficiently achieved, the prediction takes place.

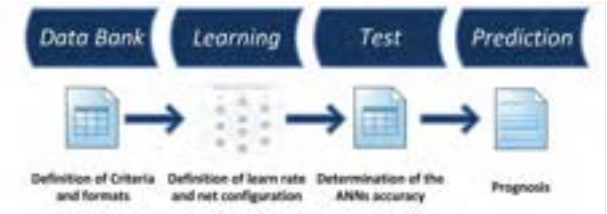

Figure 3. Artificial neuronal Networks Functionality

For the present instance, two results/outputs were searched. It is necessary to remark that these two consequences had been acknowledged through the formula, for that reason it was once extensive to affirm how dependable had been the outcomes produced through the ANNs.

5 Conclusion

The utilization of the ANNs collectively with the MCS permits increasing the simplicity in the data with the aid of identifying the inputs for the simulation process. The studying manner contained in the ANNs permits to decrease the variant (maximum and minimum values used with the distribution functions and for this reason in the histograms) delivered by means of the MCS. This system mimics the human procedure. Each and every deliberation carried out through experts, resumes the comparison of similar standards and experiences from completed comparable situations reproduces this contrast system with excessive liability. Pondering by the different facet does now not permit to function such dependable quantitatively valuation; the subsequent utilization of MCS lets into combination editions in a smaller range collectively as correlations with different criteria. Finally, the MCS grants better hazard evaluation and reliable quantification of risks.

Another advantage is that the learning process approves to encompass concerns of uncertainty. In the presented instance each result was once created for the checking out of the ANNs.

When actual facts are collected, they represent real results. For this reason, the ANNs will analyze to simulate the issues of uncertainties and would provide results that could be nearest to reality.

An important hurdle for the ANNs is the required Data Bank. One of the most attribute houses of the development enterprise is the specialty of each and every infrastructure project; therefore, the variations in the standards are not constant or similar in many cases. This may complicate the improvement of an accountable Data Bank. On the other hand, the consideration of text and

uncertainty influences in the amassed criteria may additionally even confer simpler tasks and flexibility once a Data Bank is created. The mixtures of these two threat evaluation techniques possess an outstanding possibility for imposing threat administration with the use of defined databases. The project managers typically remember in specialist support for deciding price estimates, project planning, sources needed, etc. ANNs are the perfect system to furnish this understanding as soon as an ideal database is available. For example, if a set of fees estimate statistics is available, then an ANN can be constructed based on that records and complete price predictions can be gained whilst simulating the networks.

References

[1] F., & Zayed, T. Simulation-based construction productivity forecast using neural-network-driven fuzzy reasoning. *Automation in Construction*, *65*, 102-115, 2016

[2] Chan, A.P. Time-cost relationship of public sector projects in Malaysia. Int. J. Proj. Manag. 19, 223–229, 2006.

[3] Assaf, S.A.; Al-Hejji, S. Causes of delay in large construction projects. Int. J. Proj. Manag. 24, 349–357, 2006.

[4] Gondia,A.;Siam,A.;El Dakhakhni,W.;Nassar,A.H.MachineLearningAlgorithmsforConstructionProjects Delay Risk Prediction. J. Constr. Eng. Manag. 146, 04019085, 2020.

[5] Elazouni,A.ClassifyingConstructionContractorsUsingUnsupervised-LearningNeuralNetworks. J.Constr. Eng. Manag. 132, 1242–1253, 2006.

[6] Morgan, J. and Sonquist, J. Problems in the analysis of survey data, and a proposal. Journal of the American Statistical Association, 58:415–434, 1963.

[7] Breiman, L., Friedman, J., Olshen, R., and Stone, C. (1984). Classification and regression trees. Wadsworth International Group, 1984.

[8] Breiman, L. Random forests. Machine Learning, 45:5–32, 2001.

[9] Wauters, M., & Vanhoucke, M. A comparative study of Artificial Intelligence methods for project duration forecasting. *Expert systems with applications*, *46*, 249-261, 2016.

[10] Chan,A.P.C.;Chan,D.W.Developing bench mark model for project construction time performance in Hong Kong. Build. Environ. 2004, 39, 339–349

[11] Yaseen, Z. M., Ali, Z. H., Salih, S. Q., & Al-Ansari, N. (2020). Prediction of risk delay in construction projects using a hybrid artificial intelligence model. *Sustainability*, *12*(4), 1514

[12] Park, H. S. Conceptual framework of construction productivity estimation. *KSCE Journal of Civil Engineering*, *10*(5), 311-317, 2006.

[13] Moselhi, O., Gong, D., & El-Rayes, K. Estimating weather impact on the duration of construction activities. *Canadian Journal of Civil Engineering*, *24*(3), 359-366, 1997.

[14] Moselhi, O., Leonard, C., & Fazio, P. Impact of change orders on construction productivity. *Canadian journal of civil engineering*, *18*(3), 484-492, 1991.

[15] Elwakil, E. *Knowledge discovery based simulation system in construction* (Doctoral dissertation, Concordia University), 2011.

[16] Carr, V., & Tah, J. H. M. A fuzzy approach to construction project risk assessment and analysis: construction project risk management system. *Advances in engineering software*, *32*(10-11), 847-857, 2001.

[17] Zhang, H., Tam, C. M., & Shi, J. J. Application of fuzzy logic to simulation for construction operations. *Journal of computing in civil engineering*, *17*(1), 38-45, 2003.

[18] Paek, J. H., Lee, Y. W., & Napier, T. R. (1992). Selection of design/build proposal using fuzzy-logic system. *Journal of Construction Engineering and Management*, *118*(2), 303-317.

[19] Jang, J. S., & Sun, C. T. Neuro-fuzzy modeling and control. *Proceedings of the IEEE*, *83*(3), 378-406, 1995.

[20] Seng, T. L., Khalid, M. B., & Yusof, R. Tuning of a neuro-fuzzy controller by genetic algorithm. *IEEE Transactions on Systems, Man, and Cybernetics, Part B (Cybernetics)*, *29*(2), 226-236, 1999.

[21] Mirahadi, F., & Zayed, T. Simulation-based construction productivity forecast using neural-network-driven fuzzy reasoning. *Automation in Construction*, *65*, 102-115, 2016.

[22] Vapnik, Vladimir N. 1995. The nature of statistical learning theory. New York : Springer, 1995. 0-387-94559-8 .

Development of A Mobile Robot pulling An Omni-directional Cart for A Construction Site

Yusuke Takahashi[a] , Yoshiro Hada[a] and Satoru Nakamura[a]

[a]Tokyu Construction Co.,Ltd.
E-mail: takahashi.yuusuke [@] tokyu-cnst.co.jp

Abstract -

We have been researching a mobile robot that pull a cart with equipment to improve productivity at construction sites. In this field of research, a cart having front wheels as swivel wheels and rear wheels as rigid wheels have been used. However, at the construction site, in many cases, wheels of a cart have only swivel wheels in order to easily transport them in a narrow space. We aimed to be able to transport a minimum width of 1200 mm by pulling this cart by a robot. However, when this cart is pulled using a simple 1-axis connection, there is no guarantee that a cart will follow the same trajectory as a robot. For example, a cart will move significantly out of the trajectory of a robot as it turns a curve. At this time, it is expected that a cart will collide with the building under construction or the materials placed on the site. This paper describes the results of a theoretical and experimental confirmation of the features of a cart and examination of its solution.

Keywords -

AGV; Mobile robot; Omni-directional cart

Figure 1. A mobile robot.

1 Introduction

In Japan, the workers involved in the construction industry are aging. It is expected that many workers will retire in 10 years and there will be a shortage of workers. Therefore, in this research, we decided to aim at improving the productivity of the construction site by automating the transfer work by pulling a cart with a mobile robot. We assumed that we would transport the aisles of Japanese buildings, and targeted aisles of 1200 mm or more. Therefore, the robot needs to use a small size.

There are several methods for transporting materials by a robot. For example, there is a method in which a robot pulls a cart with materials[1][2][3]. In this case, the robot can be made smaller and lighter than the material. Therefore, there is a possibility of traveling on the target passageway. On the other hand, it is necessary to control the traveling of a robot in consideration of the movement of a cart. There is a method to put materials on a robot[4]. In this case, controlling the running of a robot is simple. However, in order to realize stable running, the weight of the robot needs to be larger than the weight of the material, and a robot tends to be large. Therefore, it may not be possible to travel on the target passage. For the above reasons, the method of pulling a cart was selected in this research.

In order to control the traveling of a robot, it is necessary to theoretically verify the motion characteristics of a cart. There are theoretical researches about a cart with front wheels as swivel wheels and rear wheels as rigid wheels[5][6][7][8][9]. On the other hand, an omni-directional cart which is a slewing wheel for all the wheels is used in a construction site. The reason is that the materials are manually transported even in a narrow way. There are few theoretical researches on this cart. In this research, this omni-directional cart is connected to a robot to improve the convenience. However, when this cart is pulled using a simple 1-axis connection, a cart deviates from the trajectory of a robot. Therefore, it is expected that a cart will collide with surrounding buildings and materials. In order to reduce such a risk, this research theoretically examined the movement of a cart during a curve. In addition, in order to confirm that this theoretically result is useful, we conducted a traction experiment and compared the results.

2 A mobile robot

This chapter describes a robot. A robot used in this research are shown in the Figure 1 and the specifications are shown in the Table 1. This robot is jointly developed by Tokyu Construction Co.,Ltd. and THK Co.,Ltd. A bumper and an LRF（Laser Range Finder） are installed in front of the robot to automatically stop working when

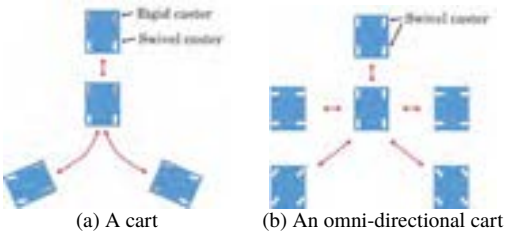

(a) A cart (b) An omni-directional cart

Figure 2. The motion characteristics of a cart.

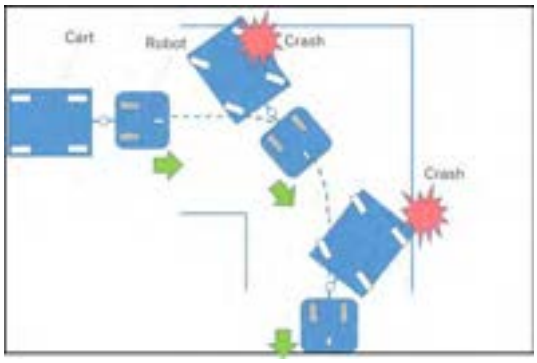

Figure 3. Behavior of an omni-directional cart on curve.

an operator or an obstacle approaches. A cart connects to the back of this robot.

3 An omni-directional cart

A cart with only swivel wheels has the characteristics of being able to move in all direction. Therefore it is hereinafter referred to as an omni-directional cart. On the other hand, a cart with front wheels as swivel wheels and rear wheels as rigid wheels is hereinafter referred to as cart. First, the motion of characteristics of an omni-directional cart are described in this chapter. Second, the results of theoretically examining the motion of a cart when traveling on a curve are described.

3.1 Characteristics of an omni-directional cart

The motion characteristics of a cart are shown in the Figure 2-(a), and the motion characteristics of an omni-directional cart are shown in the Figure 2-(b). From a Figure 2-(a), a cart can move in a front-back direction, but cannot move in a lateral direction unless wheels skid. When moving diagonally, there is a characteristic that a curve is drawn. However, as shown in a Figure 2-(b), an omni-directional cart can move in the lateral direction in addition to the front-back direction. These features of an omni-directional cart benefit when traveling in a narrow space on a construction site. When this cart is pulled using a simple 1-axis connection, a cart moves in all directions. It means that a cart will move significantly out of the trajectory of a robot as it turns a curve. For example, when connecting a cart as shown in a Figure 2-(a), a cart can move in the same trajectory as a robot. This is because the inertial force acting on a cart during the curve balances the frictional force generated on a rigid wheel and the road surface. On the other hand, when using a cart shown in the Figure 2-(b), the direction of the wheel changes, so the frictional force with the road surface becomes very small. Therefore, it is expected that a cart will swing outward due to inertial force as shown in Figure 3. At this time, it is expected that a cart will collide with the building under construction or the materials placed on the site.

Table 1. Specification of a robot.

Size	W600mm × D800mm × H400mm
Weight	120 kg
Speed(MAX)	0.5 m/s
Running time	8 hours

3.2 Motion model of a cart

The motion of an omni-directional cart on the curve was theoretically examined. In this research, it is assumed that a robot travels at a constant velocity $\dot{\phi}$ on a curve with radius r at coordinate x-y. A omni-directional cart is towed using a simple 1-axis connection. The model of this system is shown in Figure 4.

The force balance for a robot is expressed by the following equation.

$$M_1\ddot{x} = F_x - T_x \tag{1}$$

$$M_1\ddot{y} = F_y - T_y \tag{2}$$

The force balance for a cart is expressed by the following equation.

$$M_2\frac{d^2}{dt^2}(x + l_2\sin\theta) = T_x \tag{3}$$

$$M_2\frac{d^2}{dt^2}(y + l_2\cos\theta) = T_y \tag{4}$$

$$I_2\ddot{\theta} = T_y l_2\sin\theta - T_x l_2\cos\theta \tag{5}$$

Transform Equation (1) and (2).

$$T_x = -M_1\ddot{x} + F_x \tag{6}$$

$$T_y = -M_1\ddot{y} + F_y \tag{7}$$

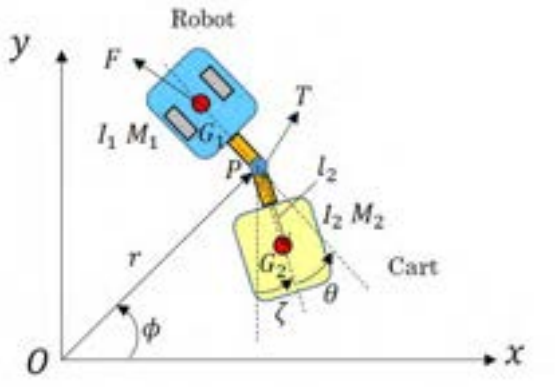

M_1 : The mass of a robot. [kg]
I_1 : The moment of inertia of a robot. [kg・m^2]
F : The tractive force of a robot. [N]
M_2 : The mass of a cart. [kg]
I_2 : The moment of inertia of a cart. [kg・m^2]
T : The force exerted on a cart by a robot. [N]
l_2 : The PG_2 distance. [m]
θ : Relative angle between robot and cart. [rad]
ζ : The direction of a cart. [rad]
r : The turning radius of a robot. [m]
ϕ: The angle of P. [rad]

Figure 4. A Model of the system.

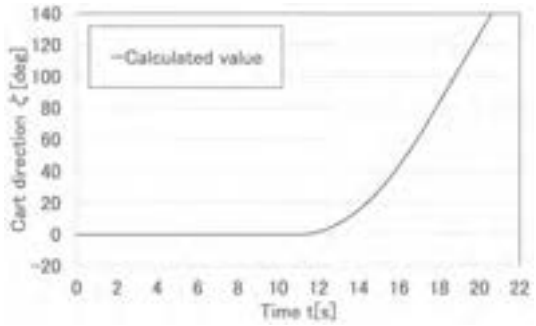

Figure 5. Direction of an omni-directional cart on the curve (Calculated value).

Table 2. Specification of the calculation.

M_2	150 kg
I_2	142 kg·m^2
l_2	0.90 m
r	2.00 m
$\dot{\phi}$	0.25 rad/s

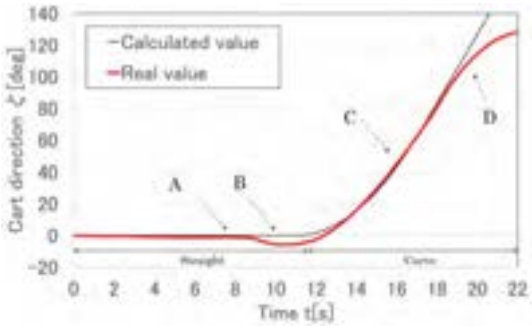

Figure 6. Direction of an omni-directional cart on the curve (Calculated value vs Real value).

From Equation (3) and (4), the following Equation can be obtained.

$$M_2(\ddot{x} - l_2 \sin\theta\dot{\theta}^2 + l_2 \cos\theta\ddot{\theta}) = T_x \tag{8}$$

$$M_2(\ddot{y} - l_2 \cos\theta\dot{\theta}^2 + l_2 \sin\theta\ddot{\theta}) = T_y \tag{9}$$

Substitute Equation (8) and (9) into Equation (5).

$$M_2 l_2 \cos\theta\ddot{x} - M_2 l_2 \sin\theta\ddot{y} + (I_2 + M_2 {l_2}^2)\ddot{\theta} = 0 \tag{10}$$

Transform Equation (10) with respect to $\ddot{\theta}$.

$$\ddot{\theta} = -\frac{M_2 l_2}{I_2 + M_2 {l_2}^2}(\ddot{x}\cos\theta - \ddot{y}\sin\theta) \tag{11}$$

To analyze the motion of a cart, we should solve Equation(11) for θ. However, it is difficult to get analytical solution because this equation is non-linear. Therefore, we analyze it numerically by the Euler method. The pitch width is

$$\Delta t = t_{n+1} - t_n \tag{12}$$

and we can get numerical solution as follows.

$$\dot{\theta}_2(t_{n+1}) = \dot{\theta}_2(t_n) + \ddot{\theta}_2(t_n)(t_{n+1} - t_n) \tag{13}$$

$$\theta_2(t_{n+1}) = \theta_2(t_n) + \dot{\theta}_2(t_n)(t_{n+1} - t_n) \tag{14}$$

When initial conditions are following Equations.

$$\dot{\theta}_2(t_0) = \dot{\theta}_2(0) = 0 \tag{15}$$

$$\theta_2(t_0) = \theta_2(0) = 0 \tag{16}$$

The motion of the robot is expressed by following equations.

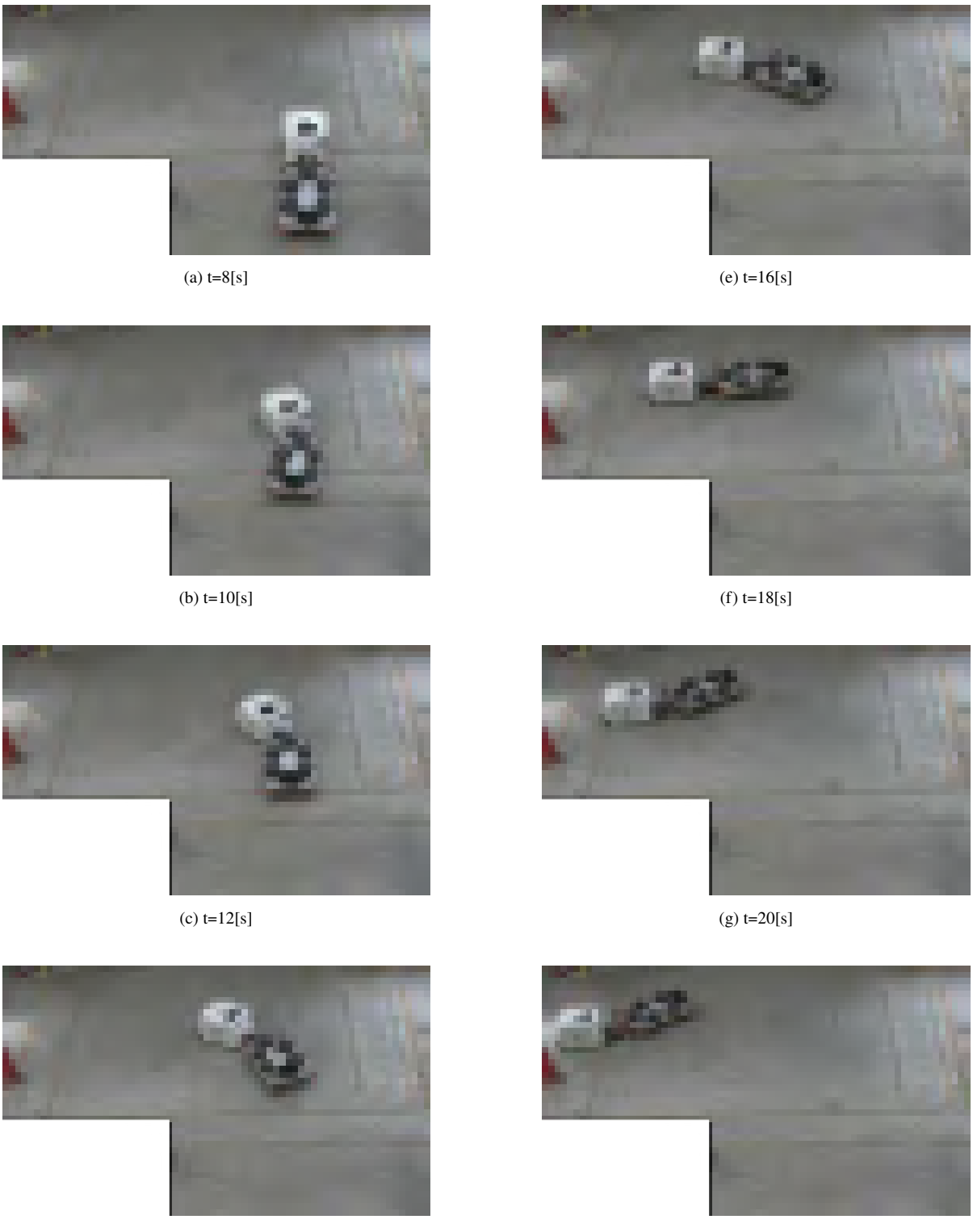

(a) t=8[s]

(e) t=16[s]

(b) t=10[s]

(f) t=18[s]

(c) t=12[s]

(g) t=20[s]

(d) t=14[s]

(h) t=22[s]

Figure 7. Behavior of a cart during experiment.

$$x = r\cos\phi \tag{17}$$

$$y = r\sin\phi \tag{18}$$

The second derivative of Equation (17) and (18) is as follows.

$$\ddot{x} = -r\dot{\phi}^2\cos\phi \tag{19}$$

$$\ddot{y} = -r\dot{\phi}^2\sin\phi \tag{20}$$

Robot turns at a constant speed.

$$\ddot{\phi} = 0 \tag{21}$$

A cart direction ζ is expressed by the following Equation.

$$\zeta = \phi - \theta \tag{22}$$

We performed a simulation as shown in Figure 3, and assuming first a straight(0s∼12s), next a curved at 90deg (12s∼18s), and finally a straight(18s∼22s). The parameters used the conditions in the table 2. The result of the simulation is shown in the figure 5. It was theoretically found that the direction of a cart gradually increased as the curve started, and a cart sways over 90 deg at t=17s.

4 Comparison of a pulling experiment and a simulation result

An omni-directional cart was connected to the robot and the behavior of a cart on the curve was observed. In this chapter, the conditions of the experiment and the experimental results are explained.

4.1 Experimental conditions

In this experiment, a robot and an omni-directional cart were connected by a simple 1-axis connector. The experimental conditions were the same run as the simulation under the table 2. An IMU(Inertial Measurement Unit) was attached to the back of a cart. This sensor is equipped with geomagnetic sensor and can measure the direction ζ of the cart.

4.2 Experimental results and consideration

The experimental results are shown in Figure 6. Furthermore, the state of the experiment is shown in Figure 7. For comparison, Figure 5 is overlaid on Figure 6. In Figure 6, we divided into 4 sections and compared a experimental result with a simulation result. That is, Section A (0s∼9s): Straight, Section B (9s∼12s): Transition from straight to curve, Section C(12s∼18s): Curve, Section D(18s∼22s): Transition from curve to straight.

At first, the experimental value and the calculated value were almost the same in the section A(Figure 7-(a)). Next, there was a difference between the experimental and calculated values in the section B(Figure 7-(b)). Since the connecting point between a cart and a robot (Figure 4 - point P) is away from the robot's reference point (Figure 4 - point G_1), it is considered that the turning of a robot moved the connecting point to the outside and the direction of a cart changed. The experimental value and the calculated value were almost the same in the section C(Figure 7-(c)∼(f)). Finally, there was a difference between the experimental and calculated values in the section D(Figure 7-(g)∼(h)). As a result of confirming the actual operation of a robot and a cart, it was found that the cause was that a robot and a cart mechanically contacted with each other and the movement of a cart was suppressed. Such a phenomenon may damage a robot or cause a cart to collide with surrounding materials and buildings.

We considered that there are three ways to solve this problem. The first is a method of attaching a rigid wheel to an omni-directional cart. However, this method may lose convenience at a construction site. Moreover, an accident may occur due to forgetting to attach the parts. The second method is to add a spring/damper to the connecting device. By this method, there is a possibility that the behavior of a cart swinging outward can be suppressed. The third is a method of devising the traveling control of a robot. For example, it is conceivable that the inertial force can be reduced by decelerating as much as possible during a curve, and the swing of a cart can be suppressed.

5 Conclusion

In this research, we aimed to improve the productivity of a construction site by automating by pulling a cart with a robot. When pulling a cart by a robot, it was important to develop it in consideration of the motion of a cart. For this reason, first, we theoretically examined the motion characteristics of an omni-directional cart when traveling on a curve. As a result, it was found that the direction of a cart gradually increased as it began to curve and swayed outward. Next, we conducted the pulling experiment and observed the behavior of a cart. As a result, it was found that the same tendency as the theory was shown in the curve section. On the other hand, after the end of the curve, there was a discrepancy between the calculated value and the experimental value due to the touch of a cart. In order to solve the problem of an omni-directional cart that a robot greatly deviates from the trajectory of a robot in the curve, a method of attaching a swivel wheel to an omni-directional cart, a method of adding a spring/damper to the connecting device, and a method of driving control

of a robot was considered. In the future, we will set the target trajectory of a cart based on this calculated value and examine these methods.

6 Acknowledgements

In conducting this research, we received a lot of advice from THK Co.,Ltd.（Hitoshi Kitano, Tetsuya Sakagami, Akihiro Iimura, Tsubasa Usui, Takashi Naito, Syota Arakawa, Kosei Mochizuki, Hirokazu Tatsuzuki）regarding the development of the robot and the control system as well as the experiments. We would like to express our gratitude to them.

References

[1] S. Sekhavat, F. Lamiraux, J.P. Laumond, G. Bauzil, and A. Ferrandy. Motion planning and control for Hilare pulling a trailer: experimental issues. IEEE Transactions on Robotics and Automation, Vol.15, Issue.4, pp.640-652. Aug 1999.

[2] PLAMEN PETROV. Nonlinear Backward Tracking Control of an Articulated Mobile Robot with Off-Axle Hitching. Proc. of the 9th WSEAS international conference on Signal processing, robotics and automation, pp.269-273, 2010.

[3] Ali K. Khalaji and S. A. A. Moosavian. SWITCHING CONTROL OF A TRACTOR-TRAILER WHEELED ROBOT. International Journal of Robotics and Automation, Vol.30, No.2, 2015.

[4] Jun-tao Li, and Hong-jian Liu. Design Optimization of Amazon Robotics. Automation, Control and Intelligent Systems, Vol.4, Issue.2, pp.48-52. Apr 2016.

[5] Xuanzuo Liu, Anil K. Madhusudhanan, and David Cebon. Minimum Swept-Path Control for Autonomous Reversing of a Tractor Semi-Trailer. IEEE TRANSACTIONS ON VEHICULAR TECHNOLOGY, VOL. 68, NO. 5, May 2019.

[6] Ali Keymasi Khalaji, and S. Ali A. Moosavian. Modified transpose Jacobian control of a tractor-trailer wheeled robot. Journal of Mechanical Science and Technology 29 (9) pp. 3961-3969, 2015.

[7] Ali Keymasi Khalaji, Mojtaba Rahimi Bidgoli and S Ali A Moosavian. Non-model-based control for a wheeled mobile robot towing two trailers. Proceedings of the Institution of Mechanical Engineers Part K Journal of Multi-body Dynamics, 229(1), Feb 2014.

[8] Bai Li, Youmin Zhang, and Tankut Acarma. Trajectory Planning for a Tractor with Multiple Trailers in Extremely Narrow Environments. 2019 International Conference on Robotics and Automation, IEEE, May 2019.

[9] Oskar Ljungqvist, Daniel Axehill, and Henrik Pettersson. On sensing-aware model predictive path-following control for a reversing general 2-trailer with a car-like tractor. International Conference on Robotics and Automation, IEEE, Feb 2020.

Developing a Windshield Display for Mobile Cranes

Taufik Akbar Sitompul[ab], Simon Roysson[a] and José Rosa[c]

[a]Mälardalen University, Västerås, Sweden
[b]CrossControl AB, Västerås, Sweden
[c]Beneq Oy, Espoo, Finland

Email: taufik.akbar.sitompul@mdh.se, srn17002@student.mdh.se, jose.rosa@beneq.com

Abstract -

Modern heavy machinery, including mobile cranes, are increasingly equipped with information systems in the form of head-down displays that present supportive information. Due to the physical presence of head-down displays, they are usually placed far away from operators' line of sight, thus the information is unintentionally overlooked. This paper investigated the use of transparent displays in mobile cranes, which enables supportive information to be presented near operators' line of sight without fully obstructing their view. We developed both virtual and physical versions of the transparent display, which show information related to the lifting capacity and its influencing factors. The virtual version was developed using the Unity game engine with the data from the official load charts for a specific mobile crane model were incorporated into the mobile crane simulation. The physical version was made using off-the-shelves items, such as glasses, LEDs, super glues, insulated copper wires, and an Arduino. We then connected the virtual transparent display with its physical counterpart using an asset called Uduino, which enabled the Unity game engine to send data to the Arduino. The result in this study showed that the virtual transparent display and its real counterpart were functioning as what we intended. The developed prototype would be used in future user evaluations, thus we could determine to what extent this approach would affect the operators' performance and experience.

Keywords -

Human-machine interface; Head-up display; Transparent display; Prototype; Mobile cranes; Heavy machinery.

1 Introduction

Cranes are one kind of heavy machinery specifically used for lifting and moving objects from one place to another. Cranes come in different types, such as mobile cranes and tower cranes. Operating a crane is a complex task that continuously demands significant cognitive workload from the operator [1, 2]. When lifting a load, the operator has to remain cautious, as the crane's parts or the lifted load may collide with nearby people or structures. The operator also needs to ensure that the operation is always done within permissible conditions, such as permitted load weight or wind speed, thus the crane's balance can be maintained [3]. Crane-related accidents can harm lives and properties of both workers and non-workers [3, 4].

Modern cranes are increasingly installed with information systems in the form of head-down displays that provide supportive information to the operator [3]. The head-down display is usually placed far from operational areas, since the presence of the display can obstruct the operator's view. However, this placement makes the supportive information is unintentionally overlooked by the operator. The benefit of having such supportive information is diminished if the operator does not use it.

In this study, we explored another way of presenting supportive information in mobile cranes through the use of transparent displays, which emit their own light but look transparent when the light is off. This way, the supportive information can be presented near line of sight, without obstructing the operator's view. Mobile cranes were chosen as the use case, since they were responsible for around 70% of all crane-related accidents [4]. Looking at the causation factors, human errors contributed about one-third of total accidents, where the main reason was due to operators used the crane beyond the permissible operational limits. Here, we focused on visualizing information related to the lifting capacity and the factors that influence it as the information presented on the transparent display. These kinds of information were chosen as they play vital role for performing safe lifting operations [5]. Similar information can also be found on the Load Moment Indicator (LMI) system, which is commonly installed in various types of cranes [3].

2 Related Work

Many studies have been done to investigate new ways for visualizing information to the operator of heavy machinery, including mobile cranes. Although the proposed approaches vary from one study to another, the common ones are projecting the information on the windshield or directly on the object of interest (see Sitompul and Wallmyr [6] for the review). However, most of the studies were conducted in simulations, and thus it is difficult to determine to what

extent the proposed approaches would work in real machines.

There were several studies that tried to build the physical visualization system, which could be deployed in real machines. In the context of mobile cranes, Fang et al. [2] investigated the use of bigger head-down displays, where the operator could see multiple views around the machine, as well as the supportive information. In the context of tractors, Fernandez et al. [7] explored the use of head-mounted displays, where the information, such as navigation and which areas that have been treated, can be shown as it appeared directly on the object of interest. Still in in the context of tractors, Palonen et al. [8] also used a head-mounted display, but they probed on how to visualize the environment that was occluded by the machine's part, thus the operator could observe blind spots around the machine. There were three studies that explored the cabin's windshield as a place to visualize the information. Both Rakauskas et al. [9] and Englund et al. [10] respectively used a projection head-up display to present the information on the windshield of snowplowers and forest harvesters. In the context of off-shore cranes, Kvalberg [11] considered using a transparent display that could be installed on the windshield.

Based on the studies mentioned above, it is still difficult to decide which approach as the most suitable one due to two main reasons. Firstly, the studies were often limited to technical evaluations only, except for Rakauskas et al. [9], Englund et al. [10], and Fang et al. [2] who carried out some user evaluations in their studies and each evaluation was for a different kind of heavy machinery. Therefore, more studies are still needed to determine to which extent the proposed approaches could benefit the operator. Secondly, each option has its own advantages and disadvantages. Although Fang et al. [2] found that the operators performed better when using the bigger head-down display compared to when the operators had no support, the operators still commented that the bigger head-down display was still considered too small and the presence of the display could also obstruct their view. Head-mounted displays are another option that allows the operator to see the information exactly within the line of sight, but this approach could be ergonomically uncomfortable for the operator, especially for long-hour usages [12]. In addition, considering that the operator is required to wear a protective helmet, wearing multiple head gears may not be a viable option for the operator. Both projection head-up display and transparent displays are the other two options, as the operator could see the information without wearing additional equipment. The main drawback of projection head-up displays is the projected information may deteriorate in bright environments [13]. On the contrary, transparent displays are strong against external light, but they are still limited in terms of colors, as only green and yellow are currently available [14]. In addition, the information being shown is static to what has been determined when the display was manufactured.

Figure 1. The transparent display prototype for off-shore cranes that was made by Kvalberg [11]. The light-emitting diodes (LEDs) were manually controlled by setting two values on the computer program: one for the indicator and one for the limit. The LEDs that formed the 5-digit numbers were lit to visualize the value of the indicator. The LEDs that formed a triangle warning were lit if the indicator value was higher than the limit value.

Taking into account the fact that all proposed approaches are still in the exploratory stage, as well as both advantages and disadvantages of each proposed approach, we were interested to further explore how transparent displays could be utilized in mobile cranes, similar to what Kvalberg [11] has done (see Figure 1). In our prior study [5], we have determined what kinds of information that should be presented on the windshield, how the information should be visualized based on the capability of transparent displays, and gathered feedback from six mobile crane operators regarding this proposed approach. Although the operators perceived the effort of bringing information closer their line of sight positively, our prior study was still limited to the operators' understanding on the proposed information visualization and where to place the information on

the windshield. There is a need for high-fidelity prototypes, which could later be used to evaluate the proposed visualization approach in certain scenarios. Therefore, it would be possible to determine to what extent this visualization approach would improve or hinder the operators' performance and experience.

3 The Prototype

In this study, we developed both virtual and physical transparent displays that act as a replica of each other. Both virtual and physical displays visualized the information related to the lifting capacity, such as the boom length, the load radius, and the lifting percentage. Based on our prior study [5], we found that these kinds of information are essential for performing safe lifting operations and the operators would also like to have them to be presented on the windshield. The remaining of this section describes how both virtual and physical transparent displays were developed.

3.1 The Simulation

To speed up the development, we used an available mobile crane simulation that was purchased from Unity Asset Store [15]. Therefore, we did not have to develop everything from scratch. The simulation has two fully functioning mobile cranes that can be played immediately, but the one that we used in this study was the one named 'HTR1045' in the downloaded project (see Figure 2). Although not the exact replica, the virtual mobile crane in the simulation has a close resemblance with the Liebherr's LTC 1050-3.1 compact mobile crane [16]. A notable difference is the boom of the LTC 1050-3.1 crane has five telescopic booms, while the boom of the virtual mobile crane only has four telescopic booms. The virtual environment was made of a flat ground without additional weather conditions. We kept this initial setup, since a mobile crane should be operated on the flat ground and permissible weather conditions due to safety reasons [17, 18].

Since we aimed to develop a prototype that could be used in certain scenarios, it is important that the presented information on the transparent display is not arbitrary and the information is shown based on the run-time situation. To do so, we had to continuously measure the machine status, such as the boom length, the load radius, the lifting capacity, and the lifting percentage. As the virtual mobile crane has a close resemblance to the Liebherr's LTC 1050-3.1 crane, we used its two official load charts [16, pp. 23 and 29] as the source of information on how the lifting capacity of the virtual mobile crane should change based on the boom length and the load radius. Two load charts were used, since the LTC 1050-3.1 crane can be used using the 4.8-tonne counterweight or the 6.5-tonne counterweight.

Figure 2. The virtual mobile crane and the virtual environment used in this study.

The rest of this subsection describes the modifications that we have made on the initial simulation.

3.1.1 Establishing a Metric Measurement in the Simulation

Based on the original code in the initial simulation, the Unity coordinates were often multiplied by 3.6 to define the length of one meter inside the simulation. However, the reason behind this decision was unknown and we had to establish a constant metric system in the simulation, since the load charts in [16, pp. 23 and 29] were documented in meters. From the load charts, the maximum boom length for the LTC 1050-3.1 crane is 36 m. Instead of using the unknown conversion rate, we defined a new conversion rate by dividing the maximum boom length of the virtual mobile crane measured in Unity coordinates with the LTC 1050-3 crane's maximum boom length, which gave us a conversion rate of 0.88264784. By multiplying Unity coordinates with the new conversion rate, we were able to establish another constant metric that defines the length of one meter in the simulation. This calculation was always used for measuring the boom length and the load radius.

3.1.2 Storing the Values from the Load Charts into the Simulation

We stored the values from two load charts in [16, pp. 23 and 29] directly into the simulation, which enabled the virtual transparent display to automatically find the specific information that should be presented. To automatically find the values based on load charts during the run-time, a lifting capacity class was made, which acted as the look-up table for the lifting capacity. As the values were taken from the load charts, the class comprised of

three fields: boom length, load radius, and their corresponding lifting capacity. Boom length and load radius were represented as arrays, while the corresponding lifting capacity was represented as a matrix. To determine the corresponding lifting capacity, the indexes of the arrays were used as the table representation of a load chart, where both boom length index and load radius index decide the lifting capacity value. `CurrentLengthIndex` and `CurrentRadiusIndex` were set to be the active index values based on the current state of the virtual mobile crane. Both indexes were managed by `GetBoomLengthIndex()` and `GetRadiusIndex()` methods that took the values of the current boom length and the current load radius of the virtual mobile crane. For example, when the boom was extended to 36 m, then the index value was set to 10 (note that the index value started from 0). If we used the load chart for the 6.5-tonne counterweight [16, pp. 23], when `CurrentLengthIndex` was 10 and `CurrentRadiusIndex` was 7, then the lifting capacity was 8 tonnes. The `GetLoadCapacityInTonnes()` method then looked up the values in the lifting capacity matrix based on the values of `GetBoomLengthIndex()` and `GetRadiusIndex()`. See Figure 3 for an illustration that shows how the lifting capacity class works.

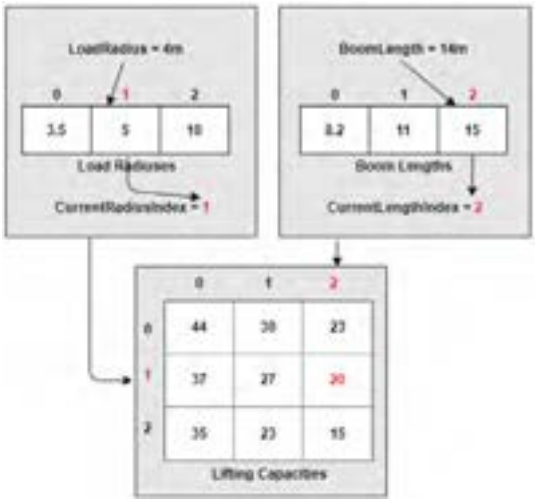

Figure 3. An illustration that shows how the lifting capacity class works inside the simulation. The numbers in red color indicate the activated indexes. The class automatically finds the lifting capacity value based on the indexes of both boom length and load radius.

As the load charts contained the values for some of the states of boom length and load radius, the lifting capacity class could show the lifting capacity for the states documented in the load charts only. Due to this limitation, we automatically set the lifting capacity to the next available state when the boom length or the load radius were between two documented states in the load charts, as shown in Figure 3. This decision was made, since setting the lifting capacity to the next available set would make the lifting capacity to be slightly lower than the actual one, and thus more preferable from safety point of view.

3.1.3 Adding the Virtual Transparent Display into the Simulation

We added a graphical user interface (GUI) into the simulation, which served as the virtual transparent display (see the right image in Figure 4). The virtual transparent display was designed based on the revised version of one of visualization concepts that we designed and evaluated in our previous study [5]. Three kinds of information are shown on the virtual transparent display: (1) the current boom length, (2) the current load radius, and (3) the lifting percentage (see the left image in Figure 4). The lifting percentage was calculated by dividing the weight of the lifted load with the lifting capacity for the current state of boom length and load radius, and then multiplied by 100.

Based on the measurement of boom length and load radius described in Section 3.1.1, the values of boom length and load radius could be in decimals, but the virtual transparent display only shows the values of boom length and load radius in integers, as shown in the left image in Figure 4. If the decimals are between 0.1 and 0.5, the values are automatically rounded down. If the decimals are between 0.6 and 0.9, the values are automatically rounded up.

As illustrated in the left image in Figure 4, the lifting percentage is visualized using ten blocks, where each block indicates that 10% of the lifting capacity has been used. Since each block indicates 10% of the lifting percentage, one block is turned on if the lifting percentage is anywhere between 0.1% and 10.0%. For example, when the lifting percentage is 20.1%, then the first three blocks from the bottom are turned on. The operator needs to ensure that the top block is not turned on, since that means the virtual mobile crane is approaching its limit and the risk of tipping over is high.

3.2 The Physical Transparent Display

Our approach for making the physical transparent display was similar to what Kvalberg [11] has done for the transparent display prototype in off-shore cranes (see Figure 1). We used WS2812b light emitting diodes (LEDs), which allowed us to control the LEDs individually. A WS2812b LED has four pins, where one pin is for the supply voltage, one pin for the ground, one pin for the input signal, and another pin for the output signal [19]. We initially wanted to use the 2 mm x 2mm LEDs, since that means we could use glasses with smaller dimension. However, we later found that those LEDs were too small

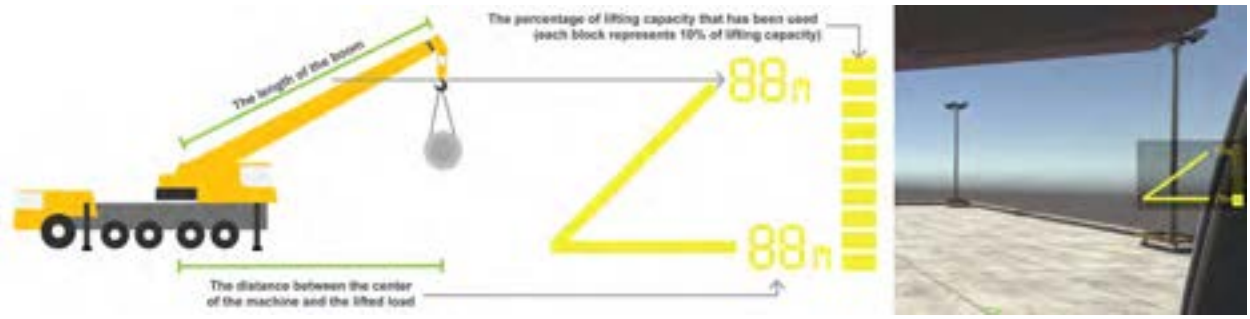

Figure 4. The left image shows the meaning for each kind of information shown on the virtual transparent display. The right image shows how the virtual transparent display looks like inside the simulation.

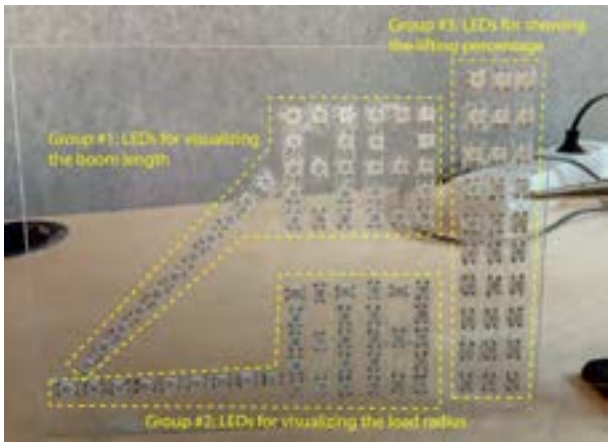

Figure 5. The LEDs were attached on a glass and arranged in a way that resembled the design of the virtual transparent display. The LEDs were divided into three groups and each group was assigned to visualize specific kinds of information.

to be soldered manually. We then decided to use the same type of LEDs, but the dimension was 5 mm x 5mm. The LEDs were then attached using a superglue to a glass with dimension of 20 cm x 12 cm and thickness of 1 mm. The connection between one LED to another was done using insulated copper wires with diameter of 0.1 mm. We used 102 LEDs and arranged them in a way that the LEDs would resemble the design of the virtual transparent display (see Figure 5).

We used an Arduino Mega2560 microcontroller and a FastLed library [20] for controlling the LEDs. To make the control simpler, we divided the LEDs into three groups, where each group was respectively assigned to visualize the information about the boom length, the load radius, and the lifting percentage (see Figure 5). Each group of LEDs was connected to one specific pin on the Arduino. For the number of LEDs that we used for the physical transparent display, the power supply from the USB cable was enough to power all the LEDs, thus we did not use an external power supply in this study. Although the LEDs used for the physical transparent display could display any color by changing the values of red, green, and blue (RGB) on each LED, we decided to use the yellow color since real transparent displays are available in yellow or green only [14].

3.3 Connecting the Simulation with the Physical Transparent Display

We used an asset called Uduino, which was purchased from Unity Asset Store [21], to connect the physical transparent display with the virtual one. Uduino enabled the Unity game engine to send data to Arduino via a USB cable. In this study, the Unity game engine was continuously sending the data about the boom length, the load radius, and the lifting percentage to Arduino. Based on the input data, Arduino automatically decided which LEDs that should be turned on or turned off. For example, if the virtual transparent display shows that the boom length is 10 m, the physical transparent display should turn on several LEDs in the group that visualize the boom length, so that the number 10 can be formed. The same thing also applies for visualizing the load radius. Specifically for the lifting percentage, the first two bottom rows of the LEDs are turned on if the lifting percentage is 20%.

4 Result

In this section, we present two examples that demonstrate the integration between the virtual transparent display and its physical counterpart. The examples shown in this section were taken when the virtual mobile crane was using the 4.8-tonne counterweight and lifting a 1-tonne load. Note that it was possible to manually adjust the brightness of the LEDs. We found that the LEDs were

Figure 6. The examples that show the integration between the virtual transparent display and its physical counterpart. The examples were made when the virtual mobile crane was using the 4.8-tonne counterweight and lifting a 1-tonne load. The left image shows the boom length was 19 m, the load radius was 14 m, and the lifting capacity was 20% used. The right image shows that the boom length was 36 m, the load radius was 30 m, and the lifting capacity was 90% used.

quite bright for indoor environments, thus we decided to use only 10% of the brightness in this study.

The left image in Figure 6 shows that the boom length and the load radius of the virtual mobile crane were respectively 19 m and 14 m. The lifting capacity for that state of boom length and load radius was 6.3 tonnes. Since the virtual mobile crane was lifting a 1-tonne load, the lifting capacity was 15.87% used. Based on the setting of the virtual transparent display, which is described in Section 3.1.3, the first two rows of LEDs from the bottom were turned on.

Similar to the previous example, the right image in Figure 6 shows that the boom length and the load radius of the virtual mobile crane were respectively 36 m and 30 m. The lifting capacity for that state of boom length and load radius was 1.2 tonnes. Since the virtual mobile crane was lifting a load with the same weight, the lifting capacity was 83.3% used, and thus the first nine rows of LEDs from the bottom were turned on.

5 Conclusion and Future Work

In this paper, we have developed a prototype that consisted of a virtual transparent display and its physical counterpart. The kinds of information were shown and how they were visualized were determined based on the result of our earlier study [5]. The virtual transparent display was hosted in a mobile crane simulation developed in the Unity game engine, which was a modified version of an available mobile crane simulation. The physical transparent display was made using off-the-shelves items, such as glasses, LEDs, super glues, insulated copper wires, and an Arduino to control which LEDs that should be turned on or turned off. The virtual transparent display was connected with its physical counterpart using an asset called Uduino, which enabled the Unity game engine to communicate with Arduino. The information shown on the prototype was not arbitrary, as the relevant data were imported from the official load charts, and the information was shown based on the run-time state of the virtual mobile crane, which are in contrast to the prototype developed by Kvalberg [11]. The developed prototype in this study was shown to be functioning as what we intended.

The study in this paper was limited to the development of the virtual transparent display and its counterpart. Due to the ongoing pandemic situation, we were unable to involve mobile crane operators to obtain their feedback on the developed prototype. In the future, the developed prototype would be evaluated in two possible settings. The first setting is where we could evaluate the physical transparent display in real mobile cranes using the Wizard-of-Oz method [22], where another person would control the virtual mobile crane, while trying to mimic what the operator is doing when performing lifting operations using the real mobile crane. According to the operator's view, the information presented on the physical transparent display would appear to resemble the status of the real mobile crane. Therefore, it would still be possible to carry out the evaluation without actually using or modifying any existing system in the mobile crane. However, we nonetheless need to adapt the lifting capacity in the simulation according to the load chart of the real mobile crane that would

be used, thus the presented information remains relevant for the operator. The second setting is to conduct a user evaluation in the mixed reality environment, where the transparent display is physical, but the environment is virtual and projected to the wall, similar to the mixed reality setup used by Wallmyr et al. [23]. In this case, we need to further modify the virtual environment in the simulation, thus the lifting scenario inside the simulation could resemble the real-world scenario.

Finally, the information shown using the virtual transparent display and its physical counterpart in this study was based on the LTC 1050-3.1 crane and its official load charts. It is possible to use a different mobile crane model as the use case, given that the 3D model that resembles such mobile crane and its official load charts are available. The proposed approach could also be modified and applied to excavators, since excavators also have the concept of lifting capacity and load charts provided by manufacturers [24].

6 Acknowledgments

This research has received funding from the European Union's Horizon 2020 research and innovation programme under the Marie Skłodowska-Curie grant agreement number 764951.

References

[1] Yihai Fang, Yong K. Cho, and Jingdao Chen. A framework for real-time pro-active safety assistance for mobile crane lifting operations. *Automation in Construction*, 72:367 – 379, December 2016. ISSN 0926-5805. doi:10.1016/j.autcon.2016.08.025.

[2] Yihai Fang, Yong K. Cho, Frank Durso, and Jongwon Seo. Assessment of operator's situation awareness for smart operation of mobile cranes. *Automation in Construction*, 85:65 – 75, January 2018. ISSN 0926-5805. doi:10.1016/j.autcon.2017.10.007.

[3] Richard L. Neitzel, Noah S. Seixas, and Kyle K. Ren. A review of crane safety in the construction industry. *Applied Occupational and Environmental Hygiene*, 16(12):1106–1117, November 2001. doi:10.1080/10473220127411.

[4] M. F. Milazzo, G. Ancione, V. Spasojevic Brkic, and D. Valis. Investigation of crane operation safety by analysing main accident causes. In Lesley Walls, Matthew Revie, and Tim Bedford, editors, *Risk, Reliability and Safety: Innovating Theory and Practice*, pages 74–80. Taylor and Francis, London, UK, 2017. ISBN 9781138029972.

[5] Taufik Akbar Sitompul, Rikard Lindell, Markus Wallmyr, and Antti Siren. Presenting information closer to mobile crane operators' line of sight: Designing and evaluating visualization concepts based on transparent displays. In *Proceedings of Graphics Interface Conference 2020*, GI '20, Toronto, Canada, 2020. Canadian Human-Computer Communications Society. URL `https://openreview.net/pdf?id=WWxviNxYwoc`.

[6] Taufik Akbar Sitompul and Markus Wallmyr. Using augmented reality to improve productivity and safety for heavy machinery operators: State of the art. In *the 17th International Conference on Virtual-Reality Continuum and Its Applications in Industry*, VRCAI '19, New York, USA, 2019. ACM. doi:10.1145/3359997.3365689.

[7] Javier Santana-Fernández, Jaime Gómez Gil, and Laura Del-Pozo-San-Cirilo. Design and implementation of a GPS guidance system for agricultural tractors using augmented reality technology. *Sensors*, 10 (11):10435–10447, 2010. doi:10.3390/s101110435.

[8] Tuomo Palonen, Heikki Hyyti, and Arto Visala. Augmented reality in forest machine cabin. *IFAC-PapersOnLine*, 50(1):5410 – 5417, 2017. doi:10.1016/j.ifacol.2017.08.1075. 20th IFAC World Congress.

[9] Michael E Rakauskas, Nicholas J Ward, Alec R Gorjestani, Craig R Shankwitz, and Max Donath. Evaluation of a dgps driver assistive system for snowplows and emergency vehicles. In *International Conference of Traffic and Transport Psychology*, pages 257–272, Nottingham, UK, 2005. Elsevier.

[10] Martin Englund, Hagos Lundström, Torbjörn Brunberg, and Björn Löfgren. Utvärdering av head-up display för visning av apteringsinformation i slutavverkning. Technical report, Skogforsk, 2015. URL `https://www.skogforsk.se/cd_4e530/contentassets/710b3f2be7a340bd87f4841c72ee302f/utvardering-av-head-up-display-for-visning-av-apteringsinformation-i-slutavverkning.arbetsrapport-869-2015-1.pdf`.

[11] Jonas Loe Kvalberg. Head-up display in driller and crane cabin. Master's thesis, Norwegian University of Science and Technology, 2010. URL `http://hdl.handle.net/11250/260185`.

[12] Álvaro Segura, Aitor Moreno, Gino Brunetti, and Thomas Henn. Interaction and ergonomics issues

in the development of a mixed reality construction machinery simulator for safety training. In *International Conference on Ergonomics and Health Aspects of Work with Computers*, pages 290–299, Berlin, Germany, 2007. Springer. doi:10.1007/978-3-540-73333-1_36.

[13] Phillip Tretten, Anita Gärling, Rickard Nilsson, and Tobias C. Larsson. An on-road study of head-up display: Preferred location and acceptance levels. *Proceedings of the Human Factors and Ergonomics Society Annual Meeting*, 55(1):1914–1918, 2011. doi:10.1177/1071181311551398.

[14] Adi Abileah, Kari Harkonen, Arto Pakkala, and Gerald Smid. Transparent electroluminescent (EL) displays. Technical report, Planar Systems, 1 2008. URL https://www.planar.com/blog/2008/3/27/transparent-electroluminescent-display-whitepaper.

[15] Unity Asset Store. Crane simulator v.2 (designer), 2020. URL https://assetstore.unity.com/packages/3d/vehicles/land/crane-simulator-v-2-designer-150285.

[16] Liebherr. Technical data - compact crane ltc 1050-3.1, 2019. URL https://www.liebherr.com/external/products/products-assets/916432/liebherr-260-ltc-1050-3-1-td-260-00-\defisr11-2019.pdf.

[17] Safe Work Australia. General guide for cranes, December 2015. URL www.safeworkaustralia.gov.au/system/files/documents/1703/general-guide-for-cranes.pdf.

[18] Labour Department. Code of practice for safe use of mobile cranes, September 2017. URL https://www.labour.gov.hk/eng/public/os/B/MobileCrane.pdf.

[19] Worldsemi. WS2812b intelligent control led integrated light source. URL https://cdn-shop.adafruit.com/datasheets/WS2812B.pdf.

[20] FastLED Animation Library. Fast, easy LED library for Arduino. URL http://fastled.io/.

[21] Unity Asset Store. Uduino - arduino and unity communication, simple, fast and stable, may 2020. URL https://assetstore.unity.com/packages/tools/input-management/uduino-arduino-and-unity-communication-simple-fast-and-stable-78402.

[22] Aaron Steinfeld, Odest Chadwicke Jenkins, and Brian Scassellati. The oz of wizard: Simulating the human for interaction research. In *Proceedings of the 4th ACM/IEEE International Conference on Human Robot Interaction*, HRI '09, page 101–108, New York, USA, 2009. ACM. doi:10.1145/1514095.1514115.

[23] Markus Wallmyr, Taufik Akbar Sitompul, Tobias Holstein, and Rikard Lindell. Evaluating mixed reality notifications to support excavator operator awareness. In *Human-Computer Interaction – INTERACT 2019*, pages 743–762, Cham, Switzerland, 2019. Springer. doi:10.1007/978-3-030-29381-9_44.

[24] Strategic Forum for Construction. Lifting operations with excavators, 5 2008. URL https://www.cpa.uk.net/sfpsgpublications.

Development of Simple Attachment for Remote Control (DokaTouch)

Kazuki Sumi[a]

[a]Fujiken co., Ltd.

E-mail: sumi@fujiken-co.jp

Abstract –

The development of the DokaRobo series for remotely controlling construction equipment began in 2007, and life-size humanoid robots (The DokaRobo No. 1 and 2) were developed. The DokaRobo series is installed in the driver's seat and can be easily installed by a single adult. After repeated tests and interviews with users, it was realized that the robot needs to be frequently switched between remote control and manned operation, and it is desirable to have a remote control unit that can be manned even when it is installed. The compact retrofit device "DokaTouch" was developed based on the concept that it would improve the work in the bad environment if an ordinary construction machine could be remote-controlled more easily. In this paper, the present configuration and functions of the DokaTouch are explained, and its application to the future construction site is reported.

Keywords –
Unmanned Construction Machinery; Internet; LTE

1 Introduction

In recent years, large-scale natural disasters have been occurring frequently, and there is a need for urgent and rapid recovery work to save lives and prevent secondary disasters. In addition, remotely operated construction equipment that can be used in a wide range of areas with multiple units is also needed. The greatest advantage of remotely operated construction machinery is that it can safely carry out unmanned construction work in adverse environments, such as disaster areas. However, it is also desirable to have an operator on board the machine for emergency or detailed work that is difficult to do by remote control. Therefore, it is necessary to secure the passenger space even if the remote control device is installed. In order to solve this problem, we have developed a remote-controlled construction machine by installing a compact actuator unit for each control device.

The system must be able to transport, install, and operate the equipment easily and smoothly to respond to emergencies such as disasters. In addition, it is necessary to reduce the discomfort of remote control by faithfully reproducing the operation with low latency. The biggest advantage of DokaTouch is that it is compact, lightweight, and highly functional, and can be used with general-purpose construction equipment that can be procured on site. In addition, the system allows the operator to use not only the operator's eye view from the cockpit, but also the overhead view of the machine. The operator can work remotely from a distance via the Internet, and can also use a control device that feeds back the sound, vibration and posture of the construction equipment.

DokaTouch is aiming to create an economical and easy-to-use remote control system by eliminating custom-made parts as much as possible. In the case of Internet connection, it is possible to monitor the operation status and assist the pilot, which will improve safety and reduce the shortage of operators. The inexpensive and highly functional control device "DokaTouch" will be widely used for construction work during normal operations. It can be used on a daily basis to speed up the recovery process in the event of a disaster.

This paper introduces an attachment-type remote-control actuator, "DokaTouch," which can be attached to the operating levers and pedals of general-purpose construction machinery to enable remote control.

2 Purpose of Development

Currently, remote control of construction equipment is meant to enable rapid recovery work in places where human life is at risk in the event of a disaster. To achieve this goal, the system must be able to respond to emergencies, but it is not realistic to have a dedicated

machine on standby for training in the event of a disaster, which is costly and unpredictable. In the future, we may see remote-controlled aircraft deployed to every corner of the country. Until then, it is necessary to install and use remote control devices whenever necessary.

Familiarity with the operation of a remote-controlled machine is a very useful experience in case of disaster. A remote-controlled system for on-site construction would be a good preparation for disaster response without special training. Therefore, a safe, easy-to-use, and inexpensive system is needed. Each disaster site has different conditions, and the working procedures and types of equipment used are different. For example, various types of machines such as excavation, loading, transportation, and land preparation will be required. The following is a list of requirements for the remote control system of construction machinery.

(1) Lightweight and easy to install, easy to transport the main body, and about half a day's installation time for two people.

(2) Easy to handle, general-purpose machines can be used as they are.

(3) Easy to set up and positional calibration can be done in a short time.

(4) The 3D image is easy to work with and to understand the site conditions.

(5) Compatible with various types of construction equipment, mainly shovels, but also crawler dumps, bulldozers, bulldozers and uneven terrain carriers.

(6) No radio qualification and application is required to use it.

(7) It is compatible with WIFI and internet connection.

3 Configuration of Dokatouch

3.1 Hardware Configuration

DokaTouch enables remote control of construction machinery by attaching an actuator to the control lever, pedal, switch, etc. and controlling them simultaneously. Fig 1 shows the photo of the backhoe. The retrofit actuators are compactly attached to the levers for both hands and feet. Fig. 2 shows a picture of the manned operation. Fig.3 shows the DT1 for a single axis. Fig.4 shows the DT2 for for two axis.

Since DokaTouch is a unit module, it does not require assembly work and can be used immediately by attaching it to each operating device. The drive unit is mainly a rotary type servo motor, but a stepping motor or linear actuator can also be used depending on the conditions of use. In addition to the drive unit, the system consists of a control unit, a communication unit, and a power supply unit, which is installed and fixed at the rear of the driver's seat. The power supply unit is powered by 24V DC from the battery of the construction equipment. A sub-battery can also be installed as an auxiliary power source. The frame of the drive unit is made of aluminum or CFRP (carbon fiber reinforced plastic) for a lightweight, strong structure. The use of CFRP prevents deformation due to impact and absorbs shocks during operation, transportation, installation and removal. Table 1 shows the specifications of DokaTouch.

Various types of DokaTouch are available, and they can be used for various types of construction machinery. Table 2 shows the various types of DokaTouch. The multi-functional joystick can also be used.

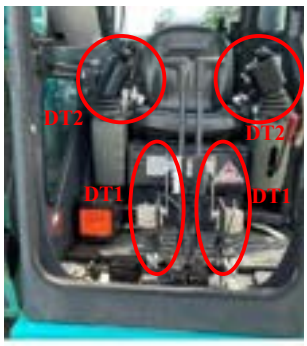

Figure 1. DokaTouch

Figure 2. With Operator

Figure 3. DT1

Figure 4. DT2

Table 1. Specification

Item	Content
Size	B300mm × L300mm × H250mm
Weight	1Axis : 1kg-3kg , 2Axis : 2kg-5kg
Power	DC24V , 300W(max)
Actuator	Servomotor , Stepping motor
Flame	Aluminum , Duralumin , CFRP

Table 2. Type of DokaTouch

TYPE	Operation part	Operation
DT1	Lever	1 Axis
DT2	Lever	2 Axis
DT3	Lever	3 Axis
DTP	Pedal	1 Axis
DTH	Handle	1 Axis
DTK	Rotary switch	3 Points
DTD	Dial	Any position
DTS	Push-button switch	1 Axis
DTR	Relay switch	1 Axis

3.1.1 SW Servo Type

Several servo motors are mounted on the upper part of the joystick, and each switch is pressed by a lever connected to each servo horn. Fig.5 shows the small servo motor attached to the switch.

Pros:

- Good response time.
- The servo motor allows a stepless setting.
- Installation is easy when using a servo unit.
- Each switch is equipped with an individual servo motor and can be operated simultaneously.

Cons:

- Difficult to operate with the switch installed. (Lighter servos with back drives can be used.)

3.1.2 Thumb Robot Type

The joystick is operated with a 3-axis robot attached to the top of the switch. Fig.6 shows a joystick with a thumb-robot attached.

Pros:

- Multiple switches can be operated by indicating their positions.
- The servo motor allows a stepless setting.
- Manned operation is possible with the device attached. (The device is placed in a position where it will not interfere with button operation.)

Cons:

- Simultaneous operation of multiple buttons is not possible.
- Responsiveness is not as good as that of the direct-attached servo motor type.

3.1.3 Wire Actuation Type

A wire-driven switch operating device is attached to the top of the switch on the joystick. Fig.7 shows the wire-driven joystick.

Pros:

- The light weight of the device makes it resistant to vibration.
- The servo motor can be used for a stepless setting.
- The servo motor unit can be made waterproof.
- Easy installation and removal of the device.
- Can be operated while mounted.

Cons:

- Responsiveness is worse than the direct servo motor type due to the elongation of the wire.
- Wiring space is required.

Figure 5. SW Servo Type

Figure 6. Thumb Robot Type

Figure 7. Wire Actuation Type

3.2 System Configuration

The system configuration of DokaTouch is shown in Fig.8. The edge PC processes the camera image and communicates with the network. The microcomputer acquires sensor data from IMU, etc., and controls the actuator based on the operator's operation information. The microcomputer is connected to the edge PC via serial communication. The network configuration of DokaTouch is shown in Fig.9. DokaTouch is connected to the server on the Internet, and it can be accessed by

any device that can use a browser, regardless of whether it is a PC or a smartphone. WebRTC is used for the video system, and MQTT is used for the operation commands, and the HTTP server is used for the GUI.

ired.

3.3 Software Configuration

The main control unit consists of an edge PC and a microcontroller, and various functions can be added to the system. This system has the following functions.

- Control the robot using a joystick, and remote control via the Internet.
- Remote control through the Internet.
- Grasping the posture of construction machinery using a gyro sensor attached to the robot.
- Camera tracking using a gyro sensor attached to the operator's head.
- 3D display of binocular camera images using a head-mounted display.

tion.

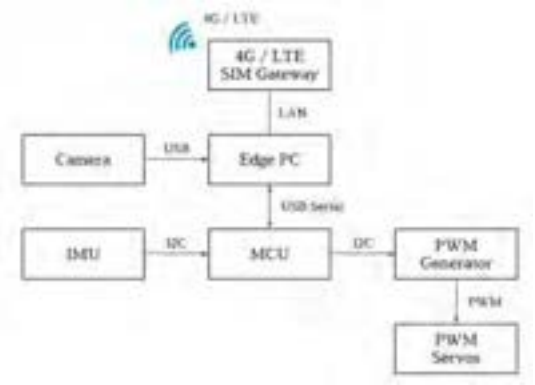

Figure 8. System Configuration

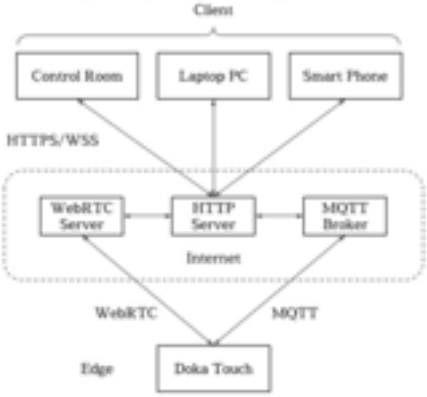

Figure 9. Software Configuration

4 Features of DokaTouch

DokaTouch can be installed in the driver's seat of general-purpose construction equipment when and where it is needed. This system allows work to be performed by remote control from a safe location. The features of this system are safety, small size and lightweight, and high performance.

4.1 Hardware Configuration

A small servo motor of 60 watts or less is used to ensure safe operation. The main drive unit uses one or two DC servomotors with a maximum torque of 100kg-cm, connected and linked to each other. One servo motor is used for each axis, and multiple axes can be used by combining units. The standby current at startup is 2A or less, and about 12A at maximum during operation. The turn-on/off of the safety lever of the machine is controlled by a separate circuit. In an emergency, the safety lever can be operated independently..

4.2 Software Safety

A software multi-safety system is used. To ensure safe operation, several measures are taken. First, each servo motor can be set to have a range of motion. To prevent the levers and pedals from rotating at unexpected angles and damaging the motors, the rotatable angle range is set for each servo motor in advance. This value is stored in the flash memory in each servo motor. Next, the maximum torque setting is set at a lower value for joints that do not require the torque of the servo motor to prevent the possibility of damaging surrounding objects when they move in an unexpected manner. Finally, as a countermeasure for communication errors, a function to stop at a safe position if communication is lost is provided.

4.3 Easy Install

Each device is small and light enough to be carried in the driver's seat by one person. The weight of the single-shaft type is about 2 kg, and the weight of the two-shaft type is about 4 kg. This is because it would be difficult for more than one person to work on the narrow driver's seat when it is installed over a door on one side. Since the equipment is dispersed, it can be transported in a small storage case in a car. Each device is fixed by using the armrest support part of the driver's seat and lever mounting bolts. Because they are attached to the existing levers as attachments, there is no need to remove any parts and no need to modify them. It takes one person about half a day to complete the installation and about two hours to dismantle it..

4.4 High Functionality

Our goal is to be able to use general-purpose machines at the site, regardless of the manufacturer or model. At present, the system can be installed on most of the backhoes, and we are planning to install it on the bulldozers and rugged terrain vehicles in the near future.

4.4.1 Any manufacturer or model

The conventional method of installing a device on the driver's seat makes it difficult to adapt to various types of construction machinery because the position of the levers (distance, height, and direction) is different for each machine. DokaTouch solves this problem by installing an actuator module directly to each lever. In addition, DokaTouch is very small, less than 300mm wide and 300mm long, so that it can be operated by a manned operator even when the equipment is installed.

4.4.2 User Friendly Interface

The remote-control unit is equipped with two operating levers (boom, arm, bucket, and slewing lever), two traveling levers (to move the crawler when moving), and button switches (to activate various operating motions). The maneuvering lever is controlled so that the target position of the work lever on the actual machine is calculated in response to the angle of fall and the operation is the same as at the time of boarding. Depending on the status of communication, there may be a delay, so the operator must pay attention to the delay. The gyroscope is installed in DokaTouch, and it is possible to prevent the machine from tipping over while working by grasping the inclination of the machine.

As an option, a bilateral operation system can be implemented, such as a rigid steering lever if the machine is in a dangerous condition. In addition, by attaching angle sensors to the operator's shoulders and arms, a master-slave operation system can be implemented to synchronize the arm movements with the bucket.

The operation situation from the control room is shown in Fig.10.

4.4.3 Easy calibration

Since the positions of levers and pedals must be taught to the operator after installation of the DokaTouch, positional calibration can be easily performed by the teaching function. After the machine is started up, the positions of the work lever, the traveling lever, and the foot pedal for the actual machine are taught by hand in the calibration mode. If the neutral position is fixed, move the movable range of each lever back and forth, left and right, and instruct it. After that, check if the operation is within the range of motion.

4.4.4 3D Head Mounted Display

Two FullHD (1920×1080) cameras are mounted on the head, which are converted to 3D images by a special device and transmitted. By using composite images, the amount of data can be reduced and the delay can be reduced. If the image is displayed on a head-mounted display, it is possible to feel a three-dimensional effect, which makes it easy to judge perspective and unevenness. By displaying the simulated image on the display, when an abnormality is detected, the part of the display changes to yellow or red depending on the alarm level, making it possible to check the abnormality while operating the system. Fig.11 shows a combined image from the binocular cameras. This image is displayed on the head-mounted display for each eye.

The camera head, which corresponds to the human head, has three axes of pitch, roll, and turn, and the gyroscope on the pilot's head enables the viewpoint tracking. The gyroscopic sensor on the head enables the pilot to track his or her viewpoints. A picture of the stereo camera is shown in Fig. 12.

4.4.5 Can be Operated via the Internet

The heavy equipment is equipped with a SIM that enables the use of mobile phone networks (4G/LTE). Therefore, if the machine is installed in an area where a mobile phone network is available, users can operate the machine from anywhere in Japan where they can access the Internet. Since the remote control and video transmission radios use the wireless LAN standard, no qualifications or licenses are required for radio operation.

4.4.6 Record and Play Mode

On a construction site, similar tasks may be repeated many times. To reduce the burden on the remote operator, a motion program can be created by recording the position data of the operating lever during the operation. For repeated operations, it is possible to activate the appropriate work motion to assist in the maneuvering.

Figure 10. Operation Room

Figure 11. Stereo Camera Images

Figure 12. Head Mounted Display

5 Issues and Future Development

At present, the efficiency of remote control by DokaTouch is about half of the efficiency of on-board operation. For the improvement of the efficiency, it is necessary to reduce the delay in operation and visual information between the operator and the actual device. Therefore, it is necessary to provide a reliable communication line. In order to supplement the visual information, the information of distance and ups and downs to be able to judge the working position and the surrounding situation is necessary. For this purpose, it is effective to display information on the screen from the operator's eye view of the camera or by installing a distance sensor or rangefinder on the machine itself. It is also possible to combine this information with XR (Mixed Reality) to provide an efficient work environment. By attaching sensors to the bends, it is possible to improve the operating environment while providing feedback on the condition of the construction machinery.

In the future, we must develop a system that is compatible with CIM (Construction Information Modeling) and allows multiple construction machines to work together.

6 Conclusion

We have developed DokaTouch, which can be remote-controlled safely and efficiently from anywhere in Japan, for use in dangerous construction work. DokaTouch is a compact and lightweight device that can be attached to each control unit of a general-purpose construction machine, and is equipped with an advanced software system. In the future, the system will be developed to control multiple construction machines and be expected to be used for various construction tasks.

References

[1] ROBO-ONE Committee, *Bipedalism evolving with ROBO-ONE How to build a robot*, Ohm Co.

[2] Kusanagi Yohei, *Japanese Makers*, Gakken Educational Publishing Co.

[3] Kazuki Sumi and Wataru Yoshizaki:, *Development of a Remotely Operated Dual-Arm Bipedal Robot (HRM2)*, Proceedings of the 14th Construction Robot Symposium

Preliminary Development of a Powerful and Backdrivable Robot Gripper Using Magnetorheological Fluid

Sahil Shembekar[a], Mitsuhiro Kamezaki[b], Peizhi Zhang[a], Zhouyi He[a], Ryuichiro Tsunoda[a], Kenshiro Otsuki[a], Hiroyuki Sakamoto[c], and Shigeki Sugano[a]

[a] Department of Modern Mechanical Engineering, Waseda University, Japan
[b] Research Institute for Science and Engineering, Waseda University, Japan
[c] Nippon Paint Holdings Co. Ltd., Japan
E-mail: sahilshembekar@akane.waseda.jp, kame-mitsu@aoni.waseda.jp, pzcsmc@gmail.com, hezhuoyi96@gmail.com, tsunoryu@ruri.waseda.jp, otsuki@fuji.waseda.jp, hiroyuki.sakamoto@nipponpaint.jp, sugano@waseda.jp

Abstract –

Currently, humans work in high-risk environments such as earthwork sites with construction machine. Such works are expected to be replaced by robots, but autonomous technologies of current robots are not sophisticated enough to deploy to such tasks. Thus, it is reasonable to use robots that can assist humans in cumbersome tasks and dangerous situation. These robots must have high repeatability, speed, power, and safety. As a preliminary study on human assistive robots, this paper designs and develops a powerful and backdrivable robot gripper. To provide powerful output suitable for construction works, we adopt an oil-hydraulic-driven actuator. To provide backdrivability for geometric and mechanical adaptability, we adopt magnetorheological fluids (MRFs), which can change its apparent viscosity, quickly, continuously, and reversibly, based on the strength of the applied magnetic field, as the working fluids in the actuation system. MRF largely affects the dynamic range of viscosity and response time, so we develop special type of MRF suitable for construction works. We then develop a small size vane type rotary actuator that consists of a passage in the vane and an electromagnetic circuit to efficiently apply the magnetic field to MRF passing through the passage. The backdrivability can change based on the current applied to the coil and output torque can change based on the flow rate from the pump to the electro-hydrostatic actuator. Finally, we develop a robot gripper (similar to the size of human hands) with two fingers (three interconnected joints) actuated by one MRF actuator. From preliminary evaluation experiments, we confirmed that the developed robot gripper could change backdrivability and output torque depending on the coil current and pump flow rate.

Keywords –

Robot gripper; Magnetorheological fluid (MRF); Electro-hydrostatic actuator (EHA)

1 Introduction

Robot grippers and manipulators have been extensively researched in the past decades and they have become one of the most popular research topics in robotics. This is due to the fact that there is a wide demand of robot grippers in the field of industrial robots, medical field, and for humanoid robots. Generally, robot grippers are involved in the task of grasping of objects. However, it is not just limited to that. If the robot gripper is attached to a manipulator, it can be used for object manipulation and pick and place operation as well.

Robot grippers have different classification types. They can be classified based on the number of fingers, which includes robot gripper with two fingers [1], three fingers [2] with some even commercially available. Also, there are flexible [3] or multiple fingers [4], [5], and the most famous ones in the recent days is the grain filled flexible ball gripper (universal gripper) [6]. Another type of classification is based on actuation system. The grippers can be classified as tendon driven, pneumatic [7], vacuum [8], [9], electric, and hydraulic. Each has its own advantages and disadvantages as described in Table 1.

From Table 1, we can understand that the hydraulic actuation system provides high force output. This is useful for construction machinery and heavy-duty operation. However, in case of a sudden collision, we need to ensure safety which can be achieved through backdrivability. In most robotic systems, backdrivability is introduced with the use of series-elastic actuators [10]. The major problem in using this is the difficulty in design of elastic elements to damp the oscillations. By considering the problems, we use a different type of hydraulic system called electro-hydrostatic actuator (EHA) [11]. The principle involves using same number of pumps with actuator. This system provides ease of maintenance due to its modality and backdrivability due to absence of valves. This principle has been used in knee joint of robot [12],

Table 1. Different types of actuation system

Actuation type	Merits	Demerits
Tendon driven	Low weight	Complex to control, loosening of tendon with high force (low durability)
Pneumatic	Small size, low weight	Complex to control, high cost
Vacuum	Versatility	Cannot be used for complicated objects
Electric	Low cost, easy to control	Low force output
Hydraulic	High force output	High maintenance cost

wearable robot [13], and tendon driven hand [14]. We combine the advantages of EHA system with a different type of functional fluid called magnetorheological fluid (MRF).

Construction and heavy-duty operations which are currently being performed by human operators often involve cumbersome tasks and dangerous environments that are potential risks for the operators. The barrier to the automation of such tasks has been the development of versatile, powerful, and efficient grasping tools, i.e., robotic grippers. Grippers are also very useful for the teleoperation applications [15] where the human is moved away from an unsafe environment. Therefore, in these types of applications, it is reasonable to develop robot grippers. These robots must have high repeatability, speed, power, and most importantly, they need to be safe. As a preliminary study on human assistive robots, in this paper, we discuss the design and development of a powerful and backdrivable robot gripper which can be used to assist on-site human workers. As discussed previously, the backdrivability is essential to provide for safety. When a system is backdrivable, it can be pushed back to its initial position which will help in situation when there is an occurrence of collision.

To provide powerful output suitable for construction works, we adopt an oil-hydraulic-driven actuator. To provide backdrivability for geometric and mechanical adaptability, we adopt magnetorheological fluids (MRFs) as the working fluids in the actuation system. MRFs are a functional fluid that can changes its apparent viscosity, quickly, continuously, and reversibly, based on the strength of the applied magnetic field. MRFs largely affect the dynamic range of viscosity and response time, so we also discuss the use of special type of MRF which is suitable for application in construction robots because most of the current commercially available MRF is not suitable for robotic applications, and then we develop several MRFs suitable for robot grippers. Subsequently, we develop a small size vane type rotary actuator that consists of a passage in the vane and an electromagnetic circuit to efficiently apply the magnetic field to MRF passing through the passage. The backdrivability can change based on the current applied to the coil and output torque can change based on the flow rate from the pump to the electro-hydrostatic actuator (EHA) system. The EHA system gives us the merits of the electrical system of ease of control and hydraulic/hydrostatic system gives us the high force output. Finally, we develop a robot griper (similar to the size of human hands) with two fingers and the finger has three inter-connected joints actuated by one MRF actuator. The main advantages of our gripper are:

- High power output
- Safety due to backdrivability
- Ease of control and robustness

From preliminary evaluation experiments, we confirmed that the developed robot gripper could change backdrivability and output torque depending on the coil current and pump flow rate of the functional fluid.

The rest of this paper is organized as follows. Section 2 describes the functional fluid and design of actuation system and gripper. Section 3 reports the experiments that were conducted and describes the results that were obtained. Section 4 draws conclusions and discusses possible future work.

2 Design of Robot Gripper

In this section, we explain about the design of robot gripper with high output force and backdrivability. We make three distinction while describing the design process (i) functional fluid, (ii) actuation system, and (iii) gripper design.

2.1 Functional Fluids

The commercially available products are MRF-122EG, MRF-132DG, and MRF140-CG, respectively, and all these MRF are manufactured by LORD Corporation [16]. We previously developed compliant linear device using MRF [17]. They are differentiated by the number of magnetic substances present inside the oil suspension. When the commercially available MRFs are kept ideal for long time, in the system or outside the system, the magnetic substances inside it settle down. The settling takes place due to the gravitational force and leads to stability and dispersibility issues in MRF. Due to these issues, the MRFs cannot guarantee the reliability when precise control is needed. To overcome these shortcomings, we have developed a special anti-sedimentation type MRF. This MRF is more stable, more powerful, and hence more suitable for next generation human-coexistence robots. We discuss its development and related experiments in [18]. We use this anti-sedimentation type

MRF as the functional fluid for the actuation system.

2.2 Actuation System

We use an EHA system which consists of various components. Firstly, we have made a hydraulic vane type rotary actuator. The actuator uses MRF as functional fluid. The actuator provides a rotation of up to 90°. The upper drawing of Figure 1 shows the internal structure of the actuator. There are two ports, one inlet and one outlet. Both ports are connected to a single bidirectional hydraulic pump via a connector. The pump is responsible for pushing the MRF in and out of the actuator. Inside the actuator we have a vane which rotates when it is pushed by the fluid. We have a small space above the vane shaft. This gets filled with MRF and create a low friction fluid seal. This seal is created by fluid being always presented in the small gap at high pressure. When we fill the fluid inside the actuation system, we ensure that high pressure is maintained in it. Solid seal and no seal approaches have been tried before and they have resulted in problems such as low power, poor backdrivability, oil leakage etc. Hence, in our approach with this new type of seal, we overcome the above problems and achieve high response rate as well.

We have a small extension on the side of the actuator which is made of soft Magnetic Steel (KM-31) whereas, the rest of the actuator is manufactured using Aluminium (A2017). On this extension, we wound a coil to create an electromagnet which can switch ON/OFF using a control strategy. We use MRF as functional fluid which can change its rheology with the application of electromagnetic field as discussed in Section 2.1. Depending on the strength of the magnetic field, the fluid will change its properties. When the magnetic field is high, the flow rate is slow. When the magnetic field is low, the flow rate is high. The strength of magnetic field and flow rate are inversely proportional. The direction of the flow of MRF inside the actuator is solely controlled by direction of rotation of the bidirectional pump. However, the flow rate of MRF is controlled by both, the bidirectional pump and also the strength of the magnetic field. The system has high backdrivability because the end effector of the actuator can be pushed back to its original position in case of a contact with any obstacle.

The size of the actuator is 41 mm x 75 mm x 45 mm. The pump is connected to the rotary actuator using a connector. This connector is specially designed to have two ports to fill the MRF in the actuation system at high pressure. The bidirectional pump that we use is TFH-080 a small axial piston pump by Takako Inc. We selected it because it is small in size and produces a displacement of 0.80 cm^3 which is sufficient for our application. We use a small brushless DC motor which rotates the pump shaft in clockwise or anti-clockwise direction as per our need. We use Faulhaber BP4 with a planetary gearhead of type

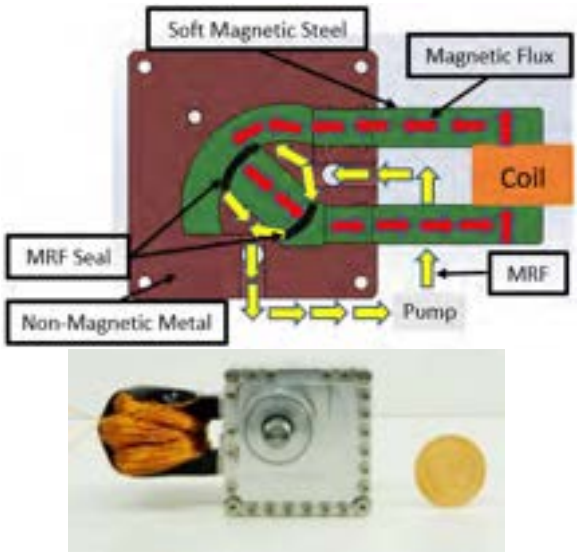

Figure 1. Vane type rotary actuator

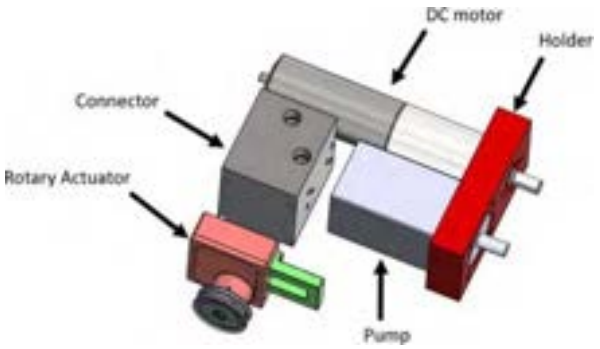

Figure 2. Exploded view of actuation system

32/3R. The pump and the brushless DC motor are attached to a holder and connected using timing pulley and belt. The exploded view of the actuation system is given in Figure 2.

2.3 Gripper Design

For the gripper, we developed two identical fingers. We designed this gripper with the following goals in mind:

- Efficient transmission of torque from actuator shaft to fingertip.
- Maximum contact between object and finger for an adequate grasp.
- Ability to grasp variety of objects.

The idea is to ensure that the object gets grasped by contact between the distal phalanx and the proximal phalanx with the extra support provided by the palm cavity created by the arrangement of the fingers in front of each other. The finger is designed using a six-bar linkage mechanism. The primary actuation is provided by a shaft

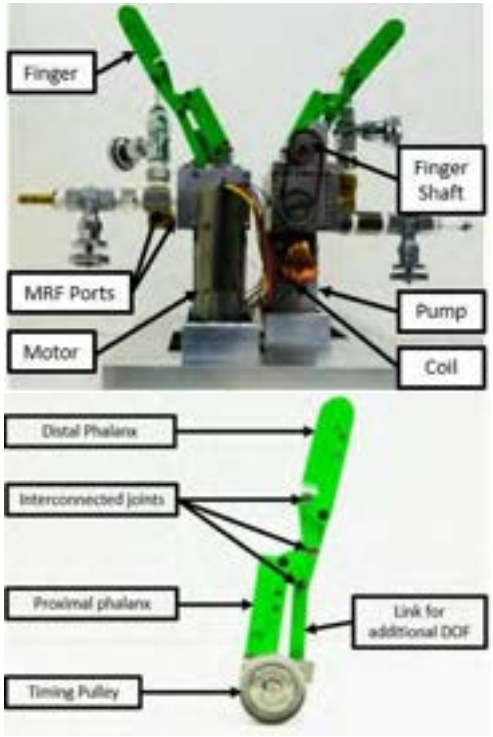

Figure 3. Gripper and finger design

which is connected to the actuator shaft via a timing pulley and belt. There is a holder which serves the dual purpose of supporting the shaft for free rotation and also as mechanical stoppage for finger. The stoppage ensures that the finger does not open beyond the angle of 120° when we want to use it for grasping objects. There is another link at the back of the finger which is responsible for transfer of actuation to the distal phalanges (fingertip). We use a clamp link to connect it with the main actuation shaft. For each of the fingers we achieve a two-degree-of-freedom (DOF) operation with one actuator. A robot gripper with fingers resembling the human finger is designed. Each finger has two phalanges giving two DOF because the motion of the proximal phalanx is directly coupled to the motion of the distal phalanx via a link. This is how we achieve underactuation. Figure 3 shows the gripper and the finger design.

For the rotation/ movement of link, we use hinge pin with ring which rotates over a bushing made of polyacetal resin. The hinge pin and bushing arrangement ensures that play maintained between the links is minimum. The links are made using Zortrax M200 Plus three-dimension (3D) printer.

3 Experiments and Results

We conducted two type of tests; torque test and grasping test. The first test is to evaluate the torque output at the actuator shaft. The second one is the grasping test in which we show the grasping operation of the gripper and evaluate the size limit in which the gripper can operate.

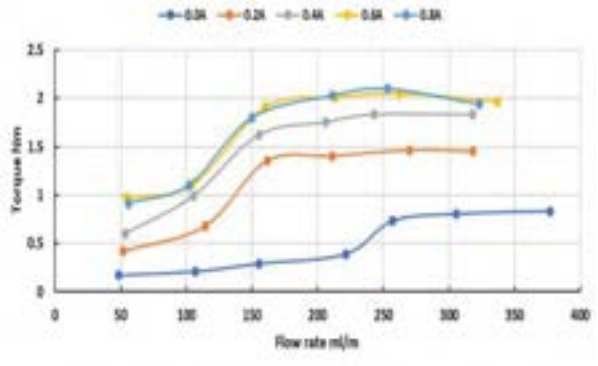

Figure 4. Torque v/s Flow rate

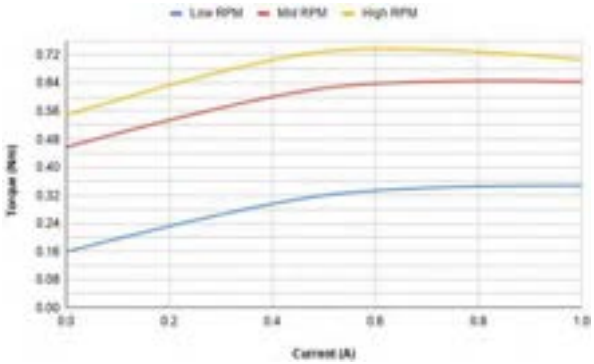

Figure 5. Torque v/s current

3.1 Torque Test

For this test, we measure the static torque at the actuator shaft by changing the speed of motor rotation. With pressure sensors, we measure the flow rate of the MRF inside the system. We plot the graph of torque (Nm) v/s Flow rate (ml/m). We use current control to switch On/Off the magnetic field. When the current is high the electromagnetic field is higher and vice-versa. We record values for the graph for current at 5 stages; 0 A, 0.2 A, 0.4 A, 0.6 A, and 0.8 A. We observe that the flow rate increases with increase in the speed of motor. The result is a non-linear relationship between torque and flow rate as shown in Figure 4. Also, we observe that the torque increases as we increase the current in the coil. This happens due to solidification of MRF inside the system. More force is required to achieve same flow rate when the MRF in the system has been solidified due to electromagnetic field. In Figure 4, we also observe a slight decrease in torque output at higher current and a state of stagnation after the achievement of a certain flow rate. We perform another torque test at a constant speed as we increase the current to electromagnet, as shown in Figure

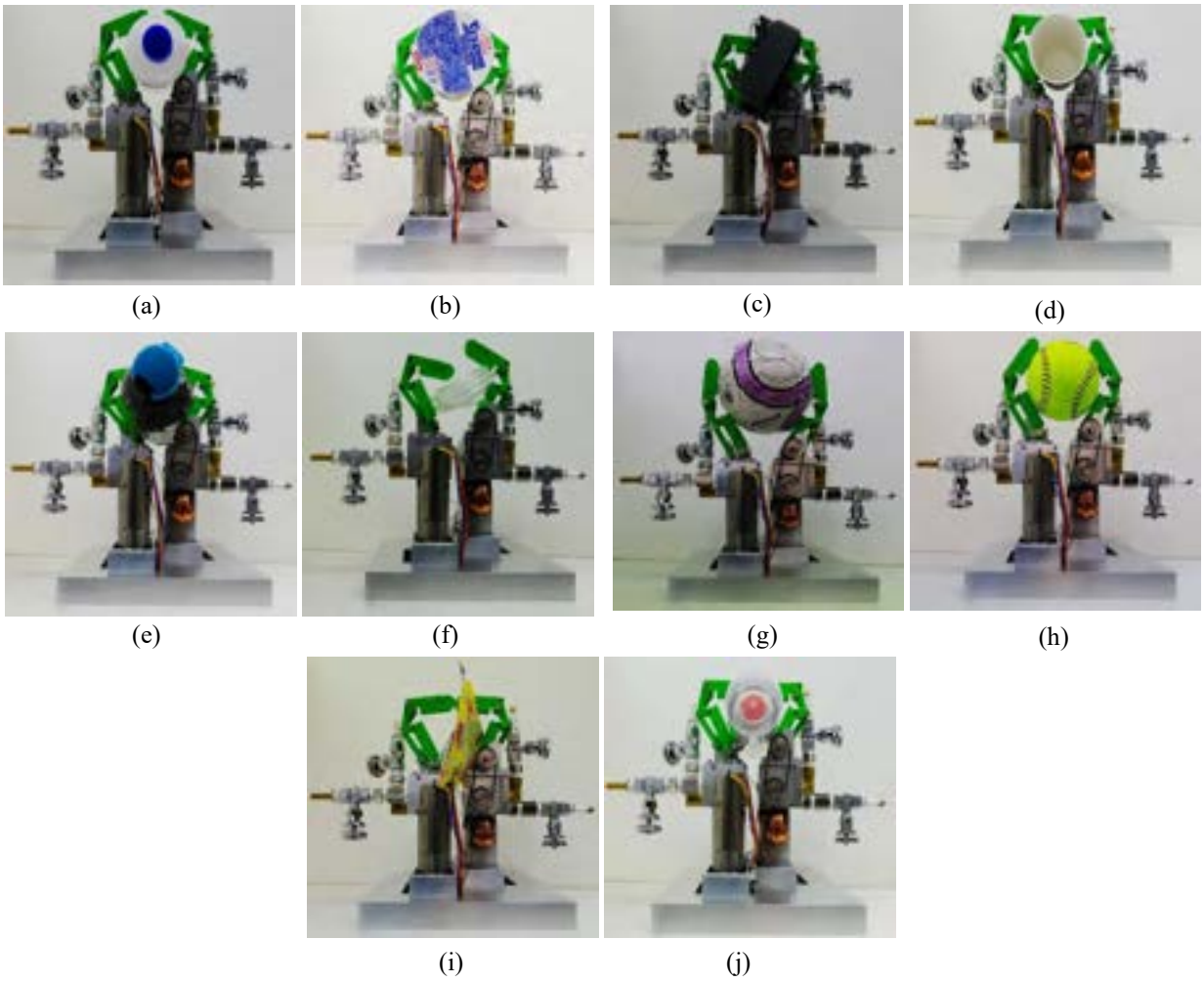

Figure 6. (a) small bottle, (b) cup noodles, (c) multi-meter, (d) cup (e), water bottle, (f) folded tube, (g) small football, (h) baseball, (i) detergent, and (j) spray can

5 to verify our observations. From the tests, we can conclude that the actuator can achieve a maximum torque output of 2.1 Nm.

3.2 Grasping Test

We perform the grasping test using different type of objects. Some of the objects that we used are (a) small bottle, (b) cup noodles, (c) multi-meter, (d) cup, (e) water bottle, (f) folded tube, (g) small football, (h) baseball (i), detergent , and (j) spray can, as shown in Figure 6. Our desired goal of grasping objects which are heavy is achieved. In some cases, like small objects which are heavy, the gripper is unable to grasp them. We believe that the reason this happens is because the size of the finger is large which renders grasping ineffective. Also, sometimes there is a difficulty in the grasping of objects which have a smooth exterior. The texture of the 3D printed distal phalanges causes this issue. With the use of an anti-skid tape on the phalanges, we solved this problem. We also tried removing object without opening the grasp. We did this to demonstrate reaction of the gripper for the condition in which object hits an obstacle/ collision during the process of grasping or pick and place. The gripper held on to the object based on the threshold value that we decided for constant grasping.

4 Conclusion and Future Works

This paper presented a robot gripper using electro-hydrostatic actuator (EHA) system. With the EHA system we combine the advantages of high power of hydraulic system with ease of control of electric system. As functional fluid, instead of using oil and conventional hydraulic fluid we use magnetorheological fluid (MRF) whose viscosity can be controlled by varying the magnetic field. We used a special type of MRF which is

suitable for robotics applications. Through this, we achieve speed and stiffness variation in finger motion. We explained the internal structure of the actuation system, the design of the finger and its working. We achieve backdrivability because of the design of our hydraulic actuation system. Hence, the system is safe. We performed Torque test and grasping test to verify our design and its functioning.

In future, we plan to work on a few key points. Firstly, to reduce the size of finger to increase the dexterity of object grasping and manipulations. This will help in making the gripper more robust. Also, we plan to use tactile sensors on phalanges. The sensor data can be analyzed and trained to be used for the purpose of object recognition in future applications.

Acknowledgement

This research was supported by the New Energy and Industrial Technology Development Organization (NEDO) and the Research Institute for Science and Engineering (WISE), Waseda University.

References

[1] Robotiq Corporation. 2 finger robot gripper. Online: https://robotiq.com/products/ 2f85-140-adaptive-robot-gripper, Accessed: 23/06/2020.

[2] S. Backus and A. Dollar. An adaptive three-fingered prismatic gripper with passive rotational joints. *IEEE Robotics and Automation Letters*, 1(2):668–675, July 2016.

[3] B. Homberg, R. Katzschmann, M. Dogar, and D. Rus, Haptic identification of objects using a modular soft robotic gripper. In *Proc. IEEE/RSJ Int. Conf. Intelligent Robots and Systems*, pp.1698–1705, Hamburg, Germany, 2015.

[4] F. Ilievski, A. Mazzeo, R. Shepherd, X. Chen, and G. Whitesides. Soft robotics for chemists. *Angewandte Chemie*, 123(8):1930–1935, 2011.

[5] H Iwata and S. Sugano. Design of anthropomorphic dexterous hand with passive joints and sensitive soft skins. In *Proc. IEEE/SICE Int. Sympo. System Integration (SII)*, pp.129–134, Tokyo, Japan, 2009.

[6] J. R. Amend, E. M. Brown, N. Rodenberg, H. M. Jaeger, and H. Lipson. A positive pressure universal gripper based on the jamming of granular mate- rial. *IEEE Transactions on Robotics*, 28(2):341–350, April 2012.

[7] R. Deimel and O. Brock. A compliant hand based on a novel pneumatic actuator. In *Proc. IEEE Int. Conf. Robotics and Automation*, pp. 2047–2053, Karlsruhe, Germany, 2013.

[8] E. Brown, N. Rodenberg, J. Amend, A. Mozeika, Steltz, M.R. Zakin, H. Lipson, and H. M Jaeger. Universal robotic gripper based on the jamming of granular material. In *Proc. the National Academy of Sciences of the United States of America*, volume 107(44), pp. 18809–18814, 2010.

[9] S. Li, J. J. Stampfli, H. J. Xu, E. K. Malkin, E. V. Diaz, D. Rus, and R. J. Wood. A vacuum-driven origami "magic-ball" soft gripper. In *Proc. Int. Con. Robotics and Automation*, pp. 7401–7408, Montreal, Canada, 2019.

[10] M. Diftler, J. Mehling, M. Abdallah, N. Radford, L. Bridgwater, A. Sanders, R. Askew, D. Linn, J. Yamokoski, F. Permenter, R. Piatt B. Hargrave, R. Savely, and R. Ambrose. Robonaut 2 - the first humanoid robot in space. In *Proc. IEEE Int. Conf. Robotics and Automation*, pp. 2178–2183, Shanghai, China, 2011.

[11] J. Bobrow and J. Desai. Modeling and analysis of a hightorque, hydrostatic actuator for robotic applications. *Experimental Robotics*, 139(1):215–228, Jan. 2006.

[12] H. Kaminaga, J. Ono, Y. Nakashima, and Y. Nakamura. Development of backdrivable hydraulic joint mechanism for knee joint of humanoid robots. In *Proc. IEEE Int. Conf. Robotics and Automation*, pp. 1577–1582, Kobe, Japan, 2009.

[13] H. Kaminaga, T. Amari, Y. Niwa, and Y. Nakamura. Development of knee power assist using backdrivable electro-hydrostatic actuator. In *Proc. IEEE/RSJ Int. Conf. Intelligent Robots and Systems*, pp. 5517–5524, Taipei, Taiwan, 2010.

[14] T. Kang, H. Kaminaga, and Y. Nakamura. A robot hand driven by hydraulic cluster actuators. In *IEEE-RAS Int. Conf. Humanoid Robots*, pp. 39–44, Madrid, Spain, 2014.

[15] S. N. Yu, J.K. Lee, S.H. Kim, B.S. Park, K.H. Kim and I.J. Cho. Experimental Study of Tele-Operation Devices for the Remote Handling System in a Pyroprocessing Facility. *Proc. Int. Symp. Automation and Robotics in Construction,* pp. 866–874*,* Montréal, Canada, 2013.

[16] LORD Corporation. On-line: https: //www.lord.com/products-and-solutions/active-vibration-control/industrial-suspension-systems/magneto-rheological-mr-fluid, Accessed: 25/06/2020.

[17] G. A. Dominguez, M. Kamezaki, and S. Sugano. Proposal and preliminary feasibility study of a novel toroidal magnetorheological piston. *IEEE Transactions on Mechatronics*, 22(2), 657–668, April 2017.

[18] P. Zhang, M. Kamezaki, K. Otsuki, H. Zhuoyi, H. Sakamoto, and S. Sugano. Development of anti-sedimentation magnetorheological fluids and its implementation to MR damper. In *Proc. IEEE/ASME Int. Conf. Advanced Intelligent Mechatronics*, pp. 400–405, Hong Kong, 2019.

Development and Application of a Fire Resistive Covering Spraying Robot to Building Construction Site

Yuichi Ikeda[a], Hirofumi Segawa[a], and Nobuyoshi Yabuki[b]

[a] Technical Research Institute, Obayashi Corporation, Japan
[b] Division of Sustainable Energy and Environmental Engineering, Graduate School of Engineering, Osaka University, Japan
E-mail: ikeda.yuichi@obayashi.co.jp, segawa.hirofumi@obayashi.co.jp, yabuki@see.eng.osaka-u.ac.jp

Abstract –

Although the amount of building construction in Japan is not expected to decrease in the next few years, there has been a decrease in the number of fire resistive covering workers over the years. In this study, to overcome the shortage of construction workers, we developed a spraying robot for fire resistive covering. Optical sensors such as LiDARs and cameras may not work efficiently in dusty environments under spraying; therefore, we proposed a spraying method that would feasibly work without using them.

The robot is composed of traveling, lifting, and traversing devices, and a robot arm; it can move autonomously if a map of the working area is created in advance. We carried out several experiments to obtain the optimum spraying work data for each beam size in advance. Having the optimal spraying work data for each beam size, and grasping the position error and posture of the robot, the robot can spray accurately when sensing data for spraying is not available. By registering the work data in the work list according to the stop position and beam size, the robot can automatically spray multiple beams continuously.

We applied the developed robot to a building construction. After spraying, the shape of the sprayed covering was measured using a LiDAR, which verified the thickness. The specific gravity was observed to be higher than the regulation, and the quality was equivalent to that of workers. The spraying speed was approximately 80% of that of workers. In the future, the robot will have the potential of attaining the same construction speed as workers by making various improvements to it, as well as making it spray automatically.

Keywords –

Building Construction Robot; Fire Resistive Covering; Construction Automation; LiDAR

1 Introduction

In recent years, there has been a remarkable shortage of construction workers in Japan[1]. In particular, the number of workers for fire resistive covering spraying work in Japan has been significantly reduced because of poor working environments. In past study, the authors conducted a basic experiment of fire resistive covering spraying automatically using a robot arm and confirmed that the quality of fire resistive covering sprayed by the robot arm was equivalent to that sprayed by skilled workers[2]. As a next step, we developed a fire resistive covering spraying robot (hereinafter, spraying robot), and tested spraying. Subsequently, the spraying robot was applied in a construction site. This thesis describes the its development and results of its application.

2 Robot Development

2.1 Past Development Cases

In Japan, over 30 years ago, several companies had been developing spraying robots. Skilled workers taught those robots spraying motion and they could not move to the spraying position easily. However, the development was interrupted because the construction performance of robots were lower than workers[3]. There were various reasons for this, including the low level of technology at the time and the high cost of development and so on. In recent years, the robot arm has become cheaper, easier to use and an environment for easy development has been established. On the other hand, SLAM in the field of autonomous mobile robot has become available to anyone. There are two major methods of SLAM. One is a method using vision and the other is a method using shape matching with point cloud data. Both methods have been used in the construction field in recent years[4][5]. Therefore, we

decided to start the development of the spraying robot in-house.

2.2 Robot Specifications

In order to replace a spraying worker with a robot, we assumed the work system shown in Figure 1. We set a high technical level goal where the robot could move, align and spray automatically by itself rather than be operated remotely by a dedicated operator.

The developed robot is shown in Figure 2, and its specifications are shown in Table 1. Table 1 shows the applicable construction sites. The targets of the robot's spraying are the girders and beams on the standard floors of middle or high-rise buildings. The robot is relocated to the upper floors by a crane or a construction elevator. The size and weight of the robot are such that it can be loaded on the platform of the construction elevator (2500kgf class). Because the robot sprays for girders and beams at a raised place, a lifting device is indispensable. Because widening the spraying area improves work efficiency, we install a traversing device that can move in the beam direction. In the case of large spans (more than 20 m), the maximum girder height is 1.5 m and the floor height is about 4.5 m; therefore, the workable floor height is set to 5.5m with some margin. We install to a travelling devise four mecanum wheels that can be finely adjusted in all directions when positioning the spraying robot. This is because the robot may move slightly in all directions.

2.3 Robot Control

The parameters involved in the spraying control of the robot include spraying distance, moving speed, pitch, and angle. The set value varies depending on the part of beams (lower flange bottom, its top, its edge, web, upper flange bottom, its edge), and changes according to the required fire resistive time specification of the fire resistive covering (specified coating thickness). We created a program that automatically assigns these control parameters to each beam size (beam height, beam width, plate thickness), and automatically creates robot work files. If we have structural design data in advance, it is possible to create spraying work files for all girders and beams of any construction without teaching by skilled workers.

We conducted an experiment in advance to evaluate the optimum parameters that could be used to effectively spray each part of the girders and beams in terms of quality. The spraying robot moves to the set girder and beam locations and aligns to them within a threshold. The working data of the spraying robot is corrected according to its stopping position error. The robot was operated on these principles.

If we create the map data of working area based on the distance data of the surrounding shape acquired by the two 2D-LiDARs installed at the diagonal corners of the robot and the initial position of the robot is specified, the position and direction of the robot are determined by SLAM. It can be calculated in the map using a

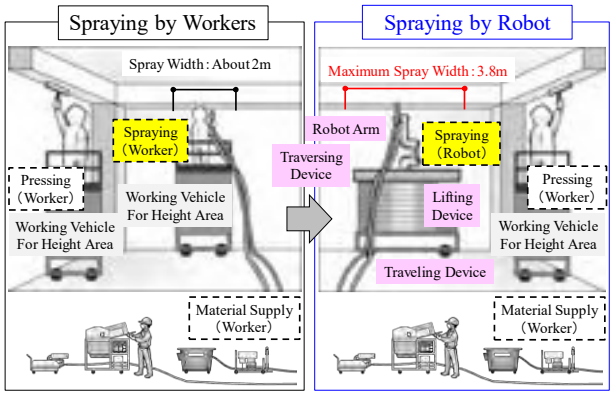

Figure 1. Spraying by Workers and Robot

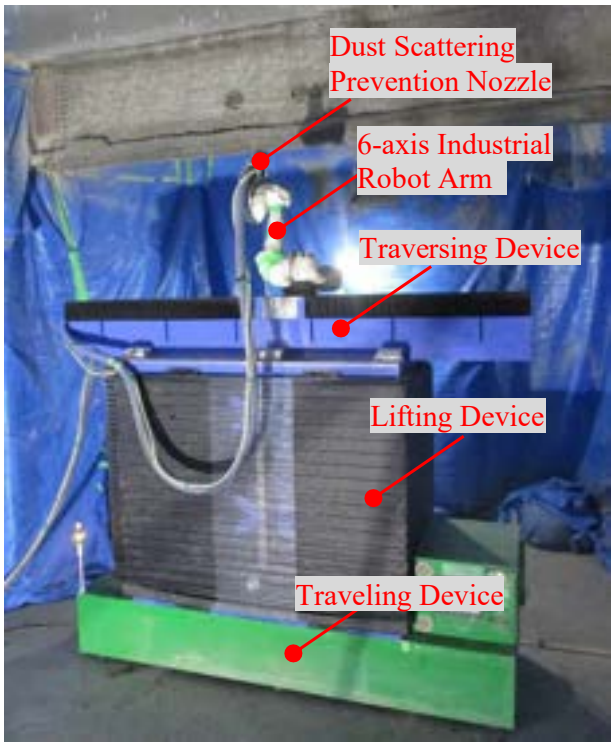

Figure 2. Fire Resistive Covering Spraying Robot

Table 1. Specifications of Spraying Robot

Structure	Traveling device, Lifting device, Traversing device, 6-axis Robot arm
Size	3.3 x 1.15 x 1.5 m
Weight	2350 kg
Workable floor height	5.5 m or less
Workable beam height	1.5 m or less
Maximum Spray Width	3.8 m or less

commercially available dedicated sensor.

2.4 Safety

Two 2D-LiDARs are installed to set the protection area and the alarm area; the robot stops when something breaks in the protection area, it slows down when in the alarm area. Additionally, a bumper sensor is attached around it to stop the robot when it contacts something. The situation when entering the set area and the operating status of the robot are clearly indicated by two warning lights, melody, alarm sound, etc, to make it easier for the surroundings to be understood.

2.5 Environmental Consideration

When spraying the fire resistive covering, a large amount of unwound rock wool discharged from the nozzle is scattered and suspended. For robots, there is a high risk that the scattered material will enter the joints and precision parts of the equipment and cause malfunctions. Therefore, to create an environment friendly to robot spraying, we developed the dust scattering prevention nozzle shown in Figure 3. By enclosing the discharged rock wool in a water mist, this nozzle can significantly reduce the amount of dust scattering and contribute to the stable operation of the robot. The results obtained from measuring the amount of dust scattering in the construction test confirmed that the amount was reduced to approximately one-third of the conventional spraying nozzle used by workers.

2.6 Spraying Experiment

After developing the robot, spraying experiments were carried out a few times at an in-house facility to confirm the thickness, and specific gravity of coverage sprayed by the robot. In the spraying experiments, the formation of high-quality coatings on each part of the H-section steel that is assumed to be a beam at a construction site, confirmed the robot control conditions proper. We also conducted an automatic construction test of the robot. Automatic construction is a series of spraying flow, in which the robot moves autonomously from the starting point to the spraying position, and after automatic alignment, sprays the fire resistive covering. In this test, we confirmed the optimum threshold value for the positioning error of the traveling device.

3 Application to a Construction Site

3.1 Purpose of Application

To collect the actual construction data, the robot sprayed the fire resistive covering on the girders and beams of a building construction site. Here, the actual construction data refers to the confirmation of sprayed quality, work efficiency, and verification of effectiveness of automatic construction.

Figure 4 shows steel girders and beams before spraying by the robot. Figure 5 shows the floor plan of the girders and beams to be sprayed, and Figure 6 shows the robot layout during spraying a girder. The spraying target was a total of thirty girders and beams with a floor height of 3.64 m and 1-hour fire resistive specifications. For both the girders and beams, the spraying area was divided into three to five parts on one side in the beam direction and sprayed at a total of six to ten positions on both of their sides. In each beam, a robot was placed on a line offset parallel to the center line, a traveling device ran in the girder or beam direction, and coating was sequentially sprayed onto the beam surface. The automatic construction procedure is shown below. The construction status is shown in Figure 7 and Figure 8.

1) Create a map of the construction area
2) Create a route for the autonomous movement of the

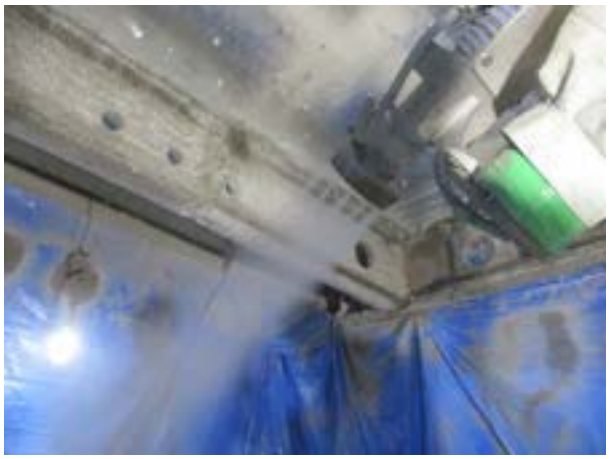

Figure 3. Dust Scattering Prevention Nozzle

Figure 4. Steel Girders and Beams Before Spraying

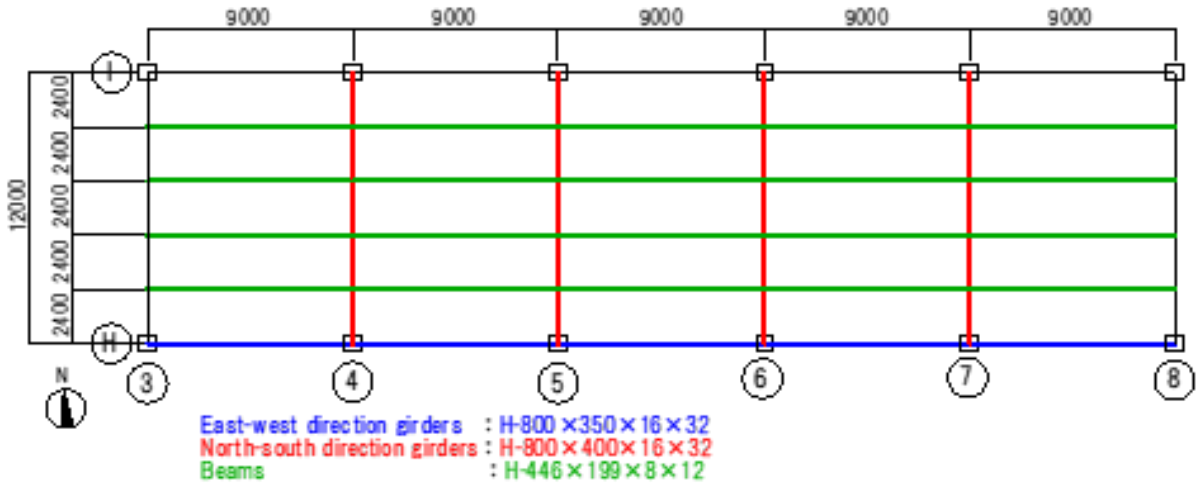

Figure 5. Plan View of Spraying Area

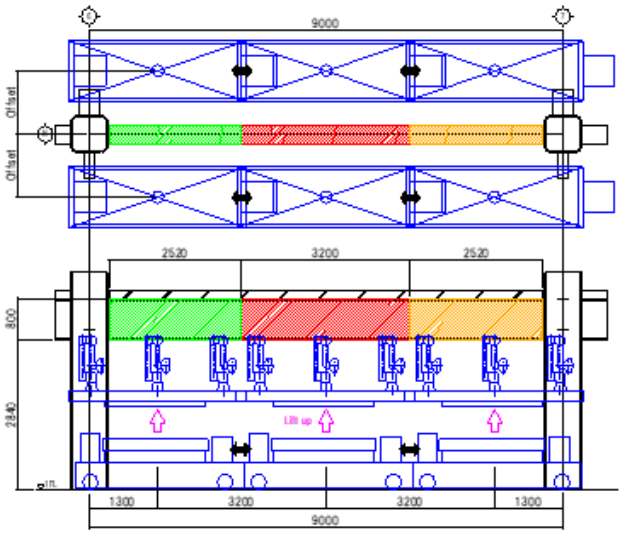

Figure 6. Robot Placement During Spraying a Girder

Figure 7. Autonomous Movement and Alignment of Robot

Figure 8. The Robot Under Spraying

robot, taking into consideration the layout of the girders and beams within the site.

3) Robot moves autonomously
4) Automatic alignment after moving to the spraying position
5) Spraying on one side of girders and beams
6) Spraying on the other side of girders and beams
After that, repeat 3) to 6)
7) Pressing sprayed fire resistive covering using trowel (by a worker)

3.2 Performance Assessment

We measured the fire resistive covering thickness and specific gravity of the sprayed covering after it was pressed by a worker using a trowel. The result of spraying girders and beams after pressing is shown in Figure 9. Two types of methods were used to obtain the measurements: randomly using a measuring pin, and overall using a laser scanner. Figures 10 and 11 show the measuring pin and laser scanner, respectively. The specific gravity of the sprayed covering was calculated

from the weight of the sample taken from the dry sprayed covering.

Figure 9. Girders and Beams After Sprayed

Figure 10. Measuring Pin

Figure 11. Laser Scanner

3.3 Application Results

3.3.1 Effect of Automatic Construction

To confirm the effect of automatic construction, we performed both automatic and manual construction. Automatic construction is a series of automatic running, automatic alignment, and automatic spraying. In manual construction, remote control is used to run, and align, whereas automatic control is used to spray. The construction efficiency between automatic and manual construction was compared.

3.3.2 Construction Quality

Figures 12 and 13 show the histogram and normal distribution of the measurement results of the covering thickness using a measuring pin. The average covering thickness was 45-50 mm, and both were well above the 1-hour fire resistive limit of 25 mm. The specified thickness of the girder and beam measurement points were exceeded at 97% or more.

Figures 14 and 15 show the measurement results of the covering thickness using laser scanners (typically between lines 4 and 5, and between lines 6 and 7 at the site). We obtained the measurements before spraying

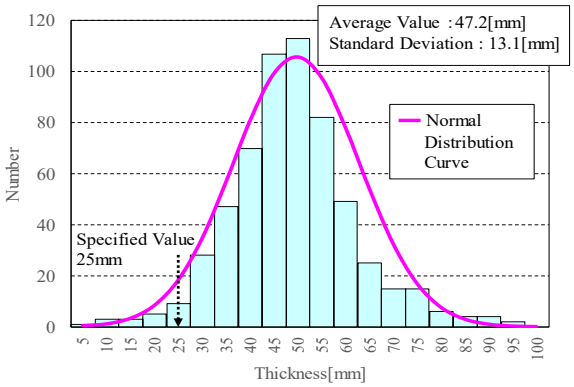

Figure 12. Results of Covering Thickness Measurement Using Measurement Pin (Girder)

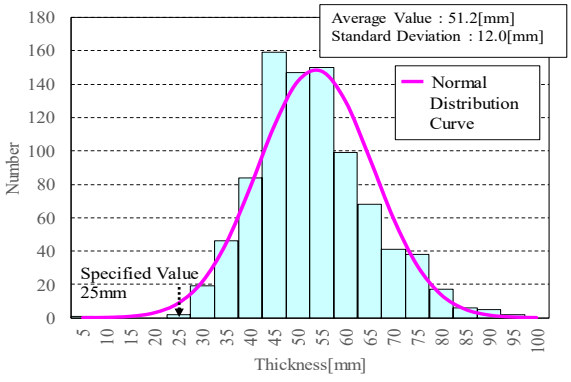

Figure 13. Results of Covering Thickness Measurement Using Measurement Pin (Beam)

the steel girders and beams, using a laser scanner. After spraying, we measured the surface of the covering again. After post processing the point cloud data, we calculated the difference between the point cloud data before and after spraying using software called CloudCompare. The heat map of the covering thickness calculated by this softwear is a view oriented from southwest to northeast. In these figures, the areas less than 25 mm of the an hour fire resistant specification are displayed in blue and the darkest green, and all other colors represent 25 mm thickness or more. A thickness less than 25 mm was found around the sleeves and around the stiffener of the north-south girder and beam joint, most of the other parts had a specified thickness of 25 mm or more. These data are consistent with the covering thickness measurements obtained using the measuring pin. After spraying using the robot, areas with insufficient thickness were repaired by workers.

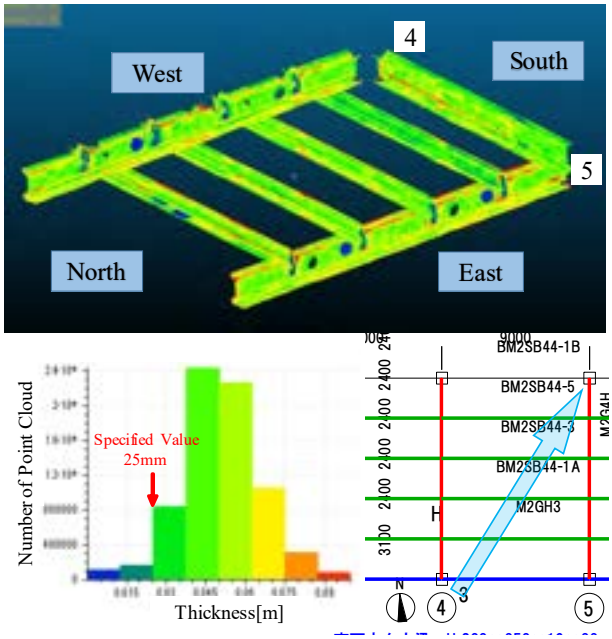

Figure 14. Results of Covering Thickness Measurement Using Laser Scanner (Between line 4 and 5)

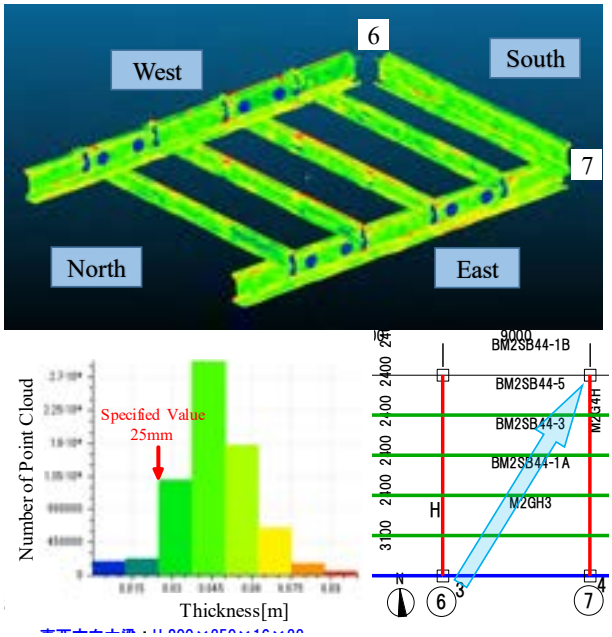

Figure 15. Results of Covering Thickness Measurement Using Laser Scanner (Between line 6 and 7)

The specific gravity measurement results were approximately 0.35-0.40, which did not fall below the construction management standard value of 0.28, during the entire construction period. There was no difference observed between the robot's manual construction and manual construction in both the coating thickness and specific gravity.

3.3.3 Working Time and Work Efficiency

Figure 16 shows the sprayed area per day of the automatic and manual construction. In this figure, the sprayed area per day of conventional spraying by a worker was set to 1. The sprayed area of the automatic construction was approximately 80% and the manual construction was approximately 50% of a skilled worker.

Figures 17 and 18 show the results of the automatic and manual construction, respectively. These figures shows the time ratio of spraying (=mondatory work), preparation/movement/alignment/nozzle cleaning (=subordinate work) and meeting/breaks (=other) when the time from beginning the work to the end of work is 100%. In manual construction, it took a lot of time to move and position the robot manually, and the spraying time per day (the net time when the material was discharged) was maintained at about 20%. In automatic construction, the spraying time per day was approximately 45%, which was an increase by roughly 25% compared to the manual construction. On the other hand, as shown in Figure 16, the sprayed area per day in automatic construction is around 80% of the necessary to reduce the time devoted to cleaning.

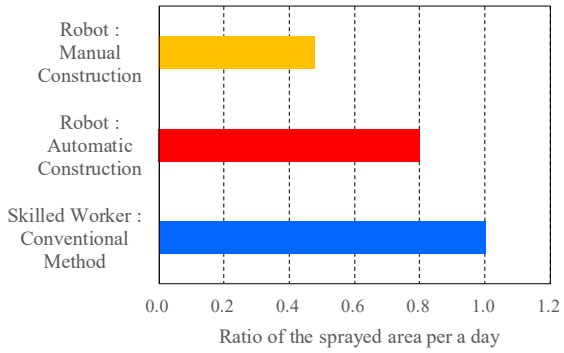

Figure 16. Comparison of Sprayed Area per Day

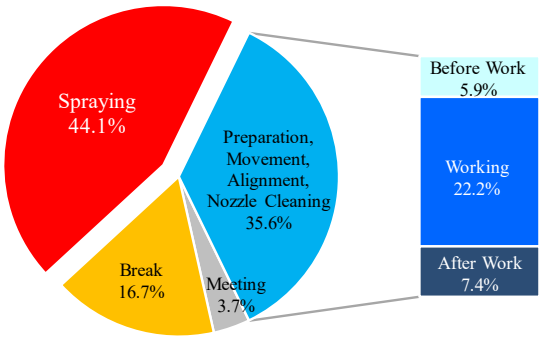

Figure 17. Working Time Analysis per Day (Automatic Construction)

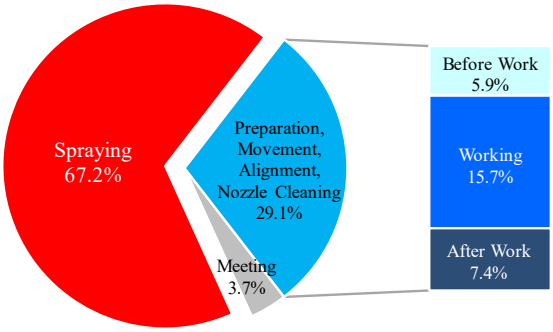

Figure 18. Working Time Analysis per Day (Automatic Construction with Improvement Plan)

4 Discussion

First, regarding the movement and alignment of the spraying robot, both were performed automatically and manually, and compared. Consequently, compared to the manual operation, the sprayed area per day in the automatic operation was improved by 70%. This indicates that work efficiency cannot be improved because movement and alignment take time by manual operation. So, it is essential for the spraying robot to travel automatically and to align automatically.

Next, regarding the measurement of the coating thickness, the measuring pin and the laser scanner were used in two ways. The normal distribution and average value of the covering thickness showed approximately the same value. From these results, the effectiveness of the measurement of the covering thickness by the laser scanner was verified. Because measurement using the measuring pin is manual work, a lot of man-power is required for post-processing. On the other hand, measurement using the laser scanner requires a long time for post-processing; moreover, it takes long time to obtain the results although most of the work is done automatically. From these strengths and weaknesses, work efficiency can be improved significantly by using the measuring pin to measure a part of area, getting immediate results, and obtaining the measurements later the rest of whole area by using laser scanners.

Finally, we describe the future productivity improvement. The nozzles were easily clogged with material, making the cleaning time long; thus, work efficiency did not improve. In the future, we plan to develop a new nozzle that does not require nozzle cleaning. It is also expected that this will improve work efficiency and exceed the sprayed area per day of skilled workers.

5 Conclusion

In this study, to save on labor in fire resistive covering work, a fire resistive covering spraying robot that sprays the fire resistive cover was developed through experiments and was applied at a construction site. The following findings were obtained.

1) The fire resistive covering sprayed by the robot at the construction site achieved quality results that satisfied the specified values for thickness and specific gravity.
2) The sprayed area per day of robot automatic construction is 1.7 times higher than that of manual construction. The effectiveness of automatic construction was confirmed.
3) Because it was necessary to secure the cleaning time of the spray nozzle, the sprayed area per day of automatic construction was approximately 80% of that of a skilled worker.
4) In the future, by developing a spray nozzle that does not easily get clogged by rock wool materials, and performing automatic construction, it will be possible to improve the sprayed area per day to a level equivalent to that of a skilled worker.

References

[1] https://www.mlit.go.jp/common/001174197.pdf#search=%27%E5%9B%BD%E4%BA%A4%E7%9C%81+%E8%B3%87%E6%96%99+201703213+%E5%BB%BA%E8%A8%AD%E6%A5%AD%E3%81%AE%E7%8F%BE%E7%8A%B6%E3%81%AB%E3%81%A4%E3%81%84%E3%81%A6%27(in Japanese)： Accessed: 30/08/2020.

[2] Segawa H. Ikeda Y. and Sakagami H, Basic Test for Automated Spraying Work for Fire Protection (in Japanese). *Report of OBAYASHI Corporation Technical Research Institute*, No.83:1-4, 2019. https://www.obayashi.co.jp/technology/shoho/083/2019_083_34.pdf: Accessed: 15/06/2020.

[3] Yoshida T, A Short History of Construction Robots Research and Development in a Japanese Company, *23th International Symposium on*

Automation and Robotics in Construction, pages 188-193, 2006

[4] Khashayar Asadi, Hariharan Ramshankar, Harish Pullagurla, Aishwarya Bhandare, Suraj Shanbhag, Pooja Mehta, Spondon Kundu, Kevin Han, Edgar Lobaton and Tianfu Wu, Building an Integrated Mobile Robotic System for Real-Time Applications in Construction, *35th International Symposium on Automation and Robotics in Construction*, 2018

[5] Jingdao Cheu, Yong K. Cho, Real-time 3D Mobile Mapping for the Built Environment, *33th International Symposium on Automation and Robotics in Construction*, 2016

A Cable Driven Parallel Robot with a Modular End Effector for the Installation of Curtain Wall Modules

K. Iturralde[a], M. Feucht[a], R. Hu[a], W. Pan[a], M. Schlandt[a], T. Linner[a], T. Bock[a], J.-B. Izard[b], I. Eskudero[b], M. Rodriguez[b], J. Gorrotxategi[b], J. Astudillo[b], J. Cavalcanti[c], M. Gouttefarde[c], M. Fabritius[d], C. Martin[d], T. Henninge[e], S. M. Normes[e], Y. Jacobsen[e], A. Pracucci[f], J. Cañada[g], J.D. Jimenez-Vicaria[h], C. Paulotto[h], R. Alonso[i], L. Elia[i]

[a]Chair of Building Realization and Robotics, Technical University of Munich, Germany
[b]TECNALIA, Basque Research and Technology Alliance (BRTA), Spain
[c]LIRMM, CNRS, France [d]IPA, Fraunhofer, Germany
[e]nLink, Norway [f]Focchi Spa, Italy [g]Vicinay-Cemvisa, Spain
[h]Acciona, Spain [i]R2M Solution, United Kingdom
E-mail: kepa.iturralde@br2.ar.tum.de

Abstract –

The installation of curtain wall modules (CWMs) is a risky activity carried out in the heights and often under unfavorable weather conditions. CWMs are heavy prefabricated walls that are lifted normally with bindings and cranes. High stability is needed while positioning in order not to damage the fragile CWMs. Moreover, this activity requires high precision while positioning brackets, the modules, and for that reason, intensive survey and marking are necessary. In order to avoid such inconveniences, there were experiences to install façade modules in automatic mode using robotic devices. In the research project HEPHAESTUS, a novel system has been developed in order to install CWMs automatically. The system consists of two sub-systems: a cable driven parallel robot (CDPR) and a set of robotic tools named as Modular End Effector (MEE). The platform of the CDPR hosts the MEE. This MEE performs the necessary tasks of installing the curtain wall modules. There are two main tasks that the CDPR and MEE need to achieve: first is the fixation of the brackets onto the concrete slab, and second is the picking and placing of the CWMs onto the brackets. The first integration of the aforementioned system was carried out in a controlled environment that resembled a building structure. The results of this first test show that there are minor deviations when positioning the CDPR platform. In future steps, the deviations will be compensated by the tools of the MEE and the installation of the CWM will be carried out with the required accuracy automatically.

Keywords –

Automation; On-site; Robotics; Facade

1 Introduction

The European construction sector constitutes an immense market. It is one of the main industrial employers in the European Union, contributing about 9% of its GDP, with an annual turnover of more than €1,500 million and a direct workforce of 18 million people [1]. Despite the fact that the construction sector is a fairly traditional sector, trends such as smart construction, involving advanced materials, innovative processes and concepts and green approaches, are becoming more noticeable.

The curtain wall modules (CWMs) are the building envelope technological system which represents the boundary condition between indoor and outdoor environment with the goal to guarantee and preserve the designed building performances. For this purpose, the as-built façade needs to guarantee the correct installation of the CWMs to achieve the performance assessed by project specs detailed in the design phase and validated with tests conducted under EN 13830. This critical but fundamental moment of installation phase requires a full accomplishment of operative instructions to guarantee the performance achievement with a strict accuracy of its component installation. Indeed, because the CWM setting is a millimetric activity due to the absolute position of façade, the installation process and regulations guarantee that the as-built façade corresponds to the design. For this reason, even if some mechanical regulations are possible through specific façade's components (bolts, screws, anchors), installers today have a central role. In addition to the installation operations to guarantee the correct setting of the CWM in line with project specs, other relevant issues related to site activities need to be managed such as risk control,

preservation of the safety of personnel involved, and correct maintenance of the equipment used. The safety of personnel involved in all site activities (not only the one responsible for façade) is the most crucial aspect. The safety procedures are independent of specific building components, but related to general principles to be pursued for each activity during site operations based on national and local norms. In this frame, façade related risks (e.g., lifting materials, equipment placement, exclusion zones, falling restrain for personnel and material, weather condition during lifting operations) are some of the risks to be considered during CWM installation to preserve the safety operation of the site activities. In this scenario, to pursue the quality of installation while reducing its risk to preserve the site personnel's safety, automation through robot is an opportunity worth being investigated.

In order to cope with these issues, different robots for installing, painting, cleaning, delaminating, maintaining and inspecting any kind of facade were developed in the past. More specifically, several robotic devices have been classified for façade module installation [2]. Besides these single task robots, on-site factories like ABCS [3] and SMART [4, 5] developed techniques for installing fully prefabricated façade modules during the erection of new buildings. Apart from façade modules, there were experiences in on-site assembly of walls like in the Rocco project, in this case, for assembling building blocks [6]. Lee et al. [7] developed a robot on top of a platform that helps the human operator to handle a CWM. The most recent instance of the installation of a façade module with a robot dates to a manually operated robotic crane [8]. Test results show that in worst case the achieved repeatability of handler end-effector positioning is 7.0 mm. This result might not be sufficient for the installation of CWMs. Regarding the cable robots for installing façade elements, a tendon suspended platform robot was envisioned [9], but the definition degree of that solution did not show further detail, especially regarding the necessary cranes to support the loads and forces of the cables. Moreover, that solution did not show any type of on-board tools.

Cable-driven parallel robots (CDPR) are a subclass of parallel robots [10]. Instead of rigid links, they use cables to manipulate a mobile platform. The principle is to drive a mobile element in up to 6 degrees of freedom (DOF) by attaching cables to the mobile element and by synchronously controlling their length from a base frame with winches. At least 6 cables are required for controlling all 6 DOFs of the load, while often no more than 8 cables are used for better performance. The most well-known example of such robots is aerial cameras for stadiums [11] working with 3 DOF and 4 cables, and the first concept for manipulating all DOFs of a load dates back to the 1990s [12]. Today, they have already proven their benefits, in particular for large scale industrial applications [13, 14, 15]; indeed, the principle of a CDPR can be adapted to move heavy payloads over large dimensions. For the same reasons, CDPRs have being theorized in the past for several construction applications, from manipulating elements, contour crafting, to building inspection [9, 16].

In the HEPHAESTUS project, a redundantly constrained cable robot was built. The redundancy of using eight cables to control the six degrees of freedom of the platform increases the available workspace volume. Only few related works involving cable robots in the field of construction can be found. In [17], a concept for a cable robot for large-scale assembly of solar power plants is introduced. In [18], a cable robot concept for a contour crafting system is described. In [19, 20], cable-robots for automated brick laying can be found.

The work performed within the HEPHAESTUS project [21] features for the first time that a CDPR is designed, built and deployed specifically for the construction sector, with the primary purpose of installing CWMs, which encompasses two main tasks: bracket installation and module installation. The advantages of cable robots in HEPHAESTUS are their large workspace, high payloads, reconfigurability and modular components, which make it easily transportable.

2 Concept description

The aforementioned tasks (bracket installation and module placement) require high relative and absolute accuracy. To accomplish such accuracy, it is necessary to foresee the precision of the CDPR, which was estimated to have a tolerance of 40 mm [22] in previous phases. Therefore, in previous stages of the project, it was foreseen that there would be two means for installing the CWM: the CDPR for the rough positioning and the Modular End Effector (MEE) along with its tools for the fine positioning.

2.1 CDPR

From a geometrical point of view, a CDPR is an association of cables of variable lengths linking a drawing point attached to base frame, and a fixing point attached to the mobile element or platform. How these drawing and fixing points are positioned in space, respectively in the general frame and the mobile platform frame, and how they are connected together formulate a configuration.

2.1.1 CDPR calculation

The geometrical design of the CDPR presented in Figure 1 can be summarized as the definition of the following parameters: (i) number of cables, (ii) geometry of the structure, (iii) geometry of the platform, and (iv) cable configuration. Based on previous studies indicating

that CDPRs driven by eight cables have appropriate performances [23], this number of cables was chosen. The parameters (ii) and (iii) are defined by the positions of the drawing points and attachment points respectively (see Figure 1). The cable configuration (iv) defines the pairs of drawing and attachment points that are connected by cables. Therefore, significant efforts in the design of this CDPR were dedicated to the definition of an appropriate set of parameters (ii), (iii) and (iv).

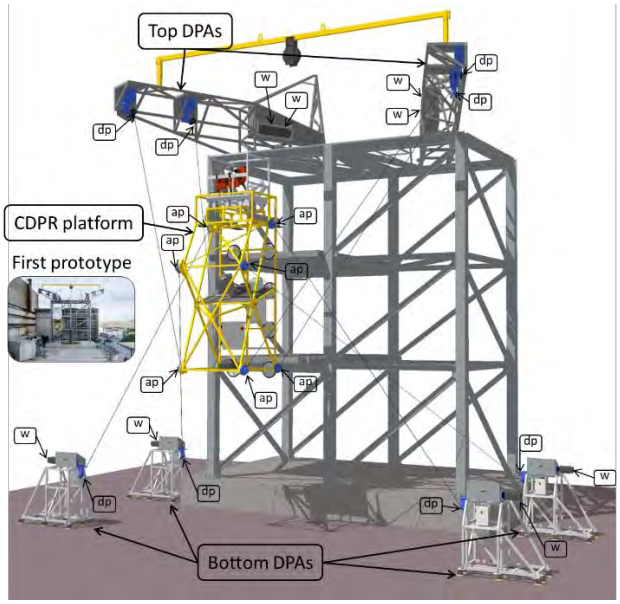

Figure 1. Hephaestus CDPR prototype

The abstract goal of finding an appropriate set of parameters was formulated as an optimization problem. The cost function of the proposed optimization problem is the maximal cable tension, directly linked to the Safe Working Load (SWL), obtained during operation across the building facade. The choice of this cost function is motivated by the direct relationship between the SWL and the cost of the machine. Minimizing the SWL leads to minimizing the maximal loads that are applied on the mechanical parts of the CDPR and, therefore, the cost is minimized. In addition, the constraints of the optimization problem include the positioning accuracy which should meet the precision necessary for the installation of the CWMs. Further details on the geometrical optimization of the Hephaestus CDPR prototype can be found in [24].

2.1.2 CDPR hardware

The Hephaestus CDPR is composed of 7 subassemblies. The first set of subassemblies provides the means of controlling the lengths of the cables. These subassemblies are fixed to the building, which works as the base frame for the robot. They are called drawing point assemblies (DPA in Figure 1) and come in two types. The first type is fixed at ground level, materializing the lower drawing points (dp in Figure 1) of the proposed configuration (one per assembly). The second type is attached to the building top slab. Each top DPA materializes two among the top drawing points. There are, therefore, two top DPAs and 4 bottom DPAs (see Figure 1).

Each drawing point need a winch, a swivel pulley at the location of the drawing point, and a force sensor for monitoring the cable tension. The components are the same for all drawing points. The travelling sheave winches (VICINAY winches WB21.L30S.1: SWL 15.7 kN, drum torque 2128 Nm, velocity 30 m/min, cable travel 16m, see w in Figure 1 and Figure 2) are powered by a servomotor with brake and absolute multi-turn encoder integrated, associated to a gearbox and wire rope spooling mechanism synchronized with the grooved drum.

The swivel pulley installed at the theoretical location of the drawing point rotates around a vertical axis; it guides the cable towards the matching fixing point. The force sensor is embedded in the shaft of the sheave directing the cable from the winch to the swivel pulley. The steel wire rope is a Ø11mm non-rotating cable with a minimum breaking load of 115.5 kN.

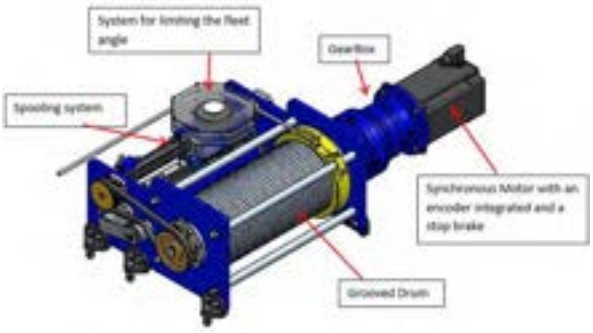

Figure 2. CAD view of the VICINAY Winch WB21.L.30S.1

The mechanical structure of the DPAs is designed in order to transfer the load from the swivel pulleys and the winches to the anchoring elements. They were designed to show a displacement of less than 50 mm at the drawing point location when loaded with the winches' SWL. Steel anchorage plates are embedded during the construction of the concrete building in the third (top) slab. The supporting structures are later welded to these anchorage plates in the correct position so that the DPA are in the correct coordinates with the required tolerances, with the drawing point positions being monitored continuously by a surveyor with a total station

Another CDPR subassembly is the platform (see Figure 1 and Figure 5). It features the 8 fixing points

placed accordingly to the dimensions set in the configuration, as well as the various tools and power systems for the MEE. The total weight of the fully loaded platform reaches 1460 kg, in which 350 kg accounts for the carried CWM.

The norms applied during the design are ISO 4301, ISO 16625 and FEM 1.001. All elements have been designed with a safety factor of at least 5.6 in order to match the M5 mechanism group requirements.

The final CDPR subassembly is a weatherproof electrical cabinet housing the central control unit. It features the servomotor drives, the associated power units, the central PLC where the central control is implemented, and the associated inputs and outputs acquisition system. The cables towards the platform (data and power) are directed to it by means of a cable chain mechanism fixed to a beam installed between the two top DPAs.

2.2 MEE and its components

The MEE is the set of tools that performs each of the activities necessary for installing the CWM onto the structure of the building. The MEE is fixed to the CDPR platform (see Figure 5). In the case of the HEPHAESTUS project, two main activities need to be performed. First, there is the fixation of the bracket onto the concrete slab. This task is achieved by a robotic arm. Second, there is a placement of the CWM modules onto the brackets. This task is achieved by a vacuum system attached to the CDPR platform that picks a CWM from an inclined magazine and releases the CWM when it is placed onto the brackets.

2.2.1 Robotic arm and its tools

Selected tools need to be manipulated by the robot in order to mount brackets to hold the CWM to the building. The most versatile method is in-situ mounting and this was the chosen approach in this project. The list of actions needed to be handled by the robot is concluded: drilling of holes for anchor bolts, picking and placement of bracket over holes, picking and placement of anchor bolts in holes, setting of bolts into holes, and tightening of anchor bolts nuts to set torque. A Universal Robots UR10e was selected as the tool manipulator. This was done based on previous experience with this robot and its possibilities and limitations, specifically regarding drilling in concrete. The robot arm also allows for excellent adaptability to changes based on underway project learnings. The arm was mounted on a custom structure made of profiled aluminum bars. A tool-changer system was integrated to give the robotic arm the possibility to manipulate a variety of tools.

Four tools were put together to achieve the needed customized functionality: 1) the drilling tool, 2) the bracket picker and holder, 3) the setting tool with a hammer function, and 4) a tool to torque the nut of the anchor.

The cycle is completed by the robotic arm returning to the bracket holder, and releasing the vacuum and magnets from the slab and bracket correspondingly, before the bracket holder is returned to the tool dock.^

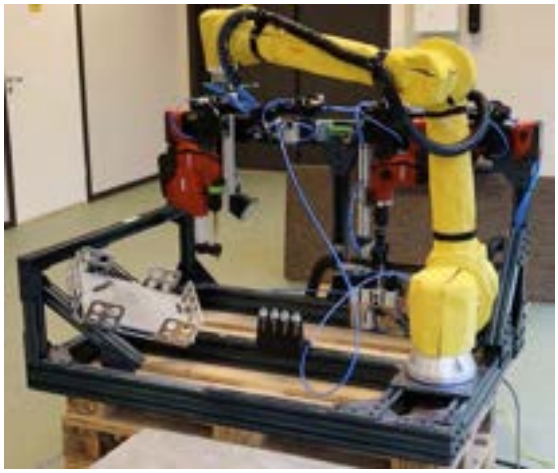

Figure 3. Robotic arm and its tools before mounting on the CDPR platform.

2.2.2 Stabilizer of the robot's frame

One of the issues regarding the accuracy of the robotic arm relied on the stability of the frame that hosts the robotic arm and its tools while performing tasks.

For achieving such needs, a linear system with vacuum cups was defined, tested and prototyped. This linear system was conceived for hosting forces of up to 1500N.

Figure 4. Stabilizer of the robot's frame prototype during the opening of the stabilizers.

The linear system consisted on two subsystems: the linear actuators and the machined steel profiles (see Figure 4) that run along the rails with the help of carriers.

2.2.3 Vacuum Lifting System for picking and placing the CWM

The Vacuum Lifting System (VLS) is capable for

picking and placing the CWM of 350kg during operations that require inclined plans.

The VLS is designed to grip, in vertical position, a CWM of the aforementioned mass, with a smooth glass surface, and a surface A_{zx} of 5.1m² . The CWM is a parallelepiped with three different faces $A\,(A_{yz}, A_{zx}, A_{xy})$ perpendicular to x, y, z axes with values $A = (0.68 \quad 5.1 \quad 0.3)^T m^2$ and showing a maximum aerodynamic coefficient c_a at 1.32. It would be possible to work in both dry and wet states, without ice, with the friction coefficient being estimated 0.2 (μ in *(3)*). The VLS is dimensioned to lift a load greater than or equal to twice its design load with the minimum relative vacuum pressure q_r. Finally, the altitude should be at least 900m from sea level, the temperature between -5 to 40 ºC, and accordingly the wind pressure q_w during service is estimated lower than 125N/m² and the vacuum differential pressure q_r at least equal to 600 mbar. The system creates a grip force f_g between the surfaces of the CWM and those of the $n = 8$ suction cups, showing a diameter d of Ø360 mm. The total load solicitation vector $\boldsymbol{s}$ is the sum of: the CWM mass m multiplied by gravity vector g, and by acceleration $j = (1\ 1\ 1)$ m/s² due to the movement, and the forces due to the wind action f_w, each factorized with the applicable partial safety coefficients ($\gamma_p = 1.1$), which are expressed as follows:

$$f_g = n\frac{\pi \cdot d^2 \cdot q_r}{4} = 48.86\ kN \qquad (1)$$

$$f_w = c_a \cdot q_w A = (112 \quad 841 \quad 50)^T N \qquad (2)$$

$$s = \left(\frac{m(g+j)}{\mu \cdot (1\ 1\ 1)^T} + \frac{\gamma_p \cdot f_w}{(\mu \quad 1 \quad \mu)^T}\right) = \begin{pmatrix} 2.52 \\ 2.52 \\ 20.8 \end{pmatrix} kN \qquad (3)$$

The current VLS design is validated by f_g being greater than twice any component of $\boldsymbol{s}$.

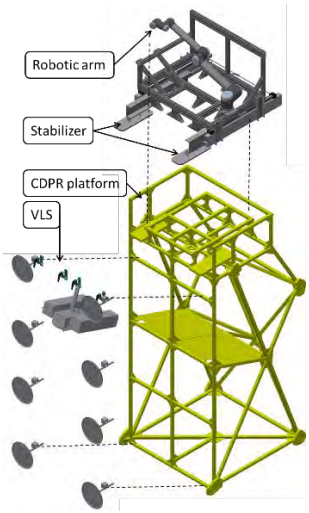

Figure 5. location of the MEE on the platform.

The VLS, and its warnings and safety measures are connected to the Beckhoff control and therefore it can be activated automatically as explained in the next section.

2.3 Control system

In Figure 6, the scheme of the hardware and wiring of the HEPHAESTUS robot is shown. The system consists of 4 PCs in total. Starting from the left side in the scheme, a standard PC is used to execute a software tool to automate the façade panel installation. This tool commands the steps in the correct order to mount the facade modules. Furthermore, it provides a GUI for the operator to control the whole HEPHAESTUS robot. It is connected to a total station via TCP/IP, which can measure the absolute pose of the cable robot platform and to the IPC on which the cable robot controller is running. The cable robot controller is based on the TwinCAT 3 software from BECKHOFF [25]. It consists of a soft-PLC and a motion controller. The latter can either be a Beckhoff CNC, or an advanced motion controller. The IPC is connected via WLAN (CANopen) to the Radio Control, via Ethernet (EtherCAT) to the safety sensors, I/Os, force sensors and drives.

Furthermore, the IPC has an Ethernet (EtherCAT) interface to the IPC of the MEE, which is integrated within the EtherCAT network as an EtherCAT slave. On the MEE IPC a PLC is implemented to control the MEE system consisting of the ROS-PC to control the UR-Robot, the stabilizer, and the vacuum system.

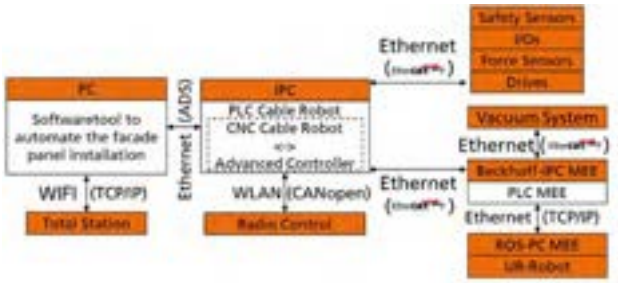

Figure 6. Scheme of the hardware and wiring of the HEPHAESTUS cable robot.

The main application controls the interactions between the user and the main controller. The application UI shows cable robot data, such as cable tensions, and each state the robot is performing in real time. It also allows the user to intercept each state, pausing the operation, or to stop the task. It is connected to the cable robot controller, allowing the user to move the cable robot and see the state the cable robot and the MEE are in at any moment, allowing the user to operate and control it, and the total station controller, allowing the user to obtain position and rotation measures at will.

A precise kinematic model is necessary in order to guarantee a satisfying positioning accuracy of the CDPR. Since the pose of the platform is computed based on the winch motor positions, cable sagging and elongation may be considered [26]. Among other aspects related to the position tracking control for CDPRs, these are still ongoing research subjects addressed in this project.

2.4 State Machine

The main controller is designed to operate as a state machine that controls all the individual controllers. Likewise, it is designed to work separately from the UI, merging the real time environment with the UI thread, and it controls all the error controllers to broadcast individual error signals. There are two main operations that the robot must do in order to complete the CWM installation successfully: first drill and set the brackets in the correct positions, and then set the CWMs in the corresponding brackets. To do both of them there are several states that the controller must follow, each one of them linked to a specific controller (cable robot control, MEE control or total station control). Each state, as shown in the simplified state machine diagram (see Figure 7), has an optional breakpoint where the user can stop the operation if a malfunction is detected. Besides these two main operations, the state machine contains also the semi-automatic initialization states of the total station.

3 Prototyping and tests

The first demonstration tests were performed in TECNALIA facilities in Derio, Basque Country (Spain). Once all the components of the demonstrator were installed, the operation of all the components (motors, movement of the robot, positioning in relation with the steel structure, sensor, etc.) was verified. This was the first time the different elements of the robot (winches with cable pulling on the platform/base) and the higher-level control of the robot that makes the coordination of the winches were put together.

3.1 Building structure used for the demonstration

For this purpose, a steel structure has been erected matching the foreseen dimensions of the demonstration building: 10.2m high, 8.80m wide, and 2.7m deep. Two concrete slabs have been installed at the first and second floor to perform all tests required for installing one CWM.

The steel structure has features to accommodate the top DPAs on the top floor; the bottom DPAs are directly anchored to the ground (Figure 1).

The higher platform empty weight more than expected and the SWL lower than originally planned (respectively 1110 kg instead of 910 and 15.7kN instead of 20) led to the nominal transit positions of the top row of panels not being accessible. The transit distance for the top floor panels therefore needed to be reduced from 600 to 450 mm.

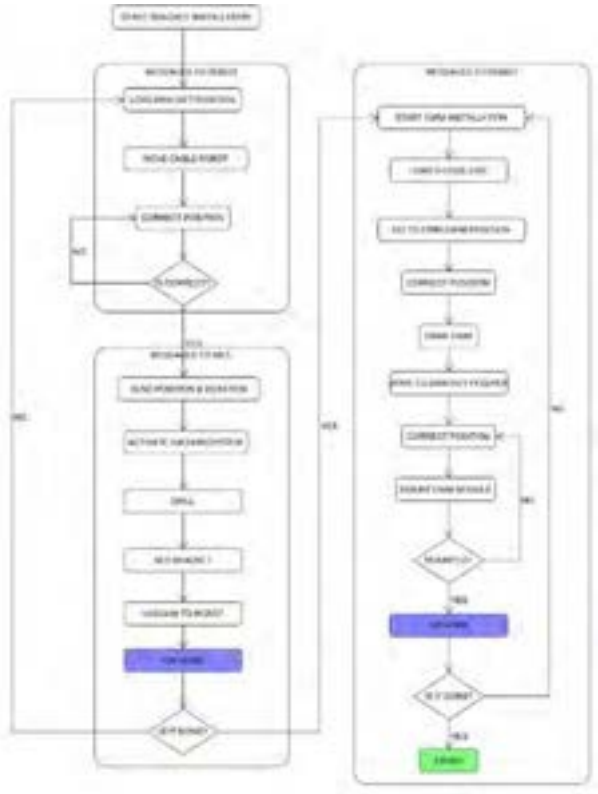

Figure 7. Simplified state machine diagram

3.2 Installation of the CDPR

After the erection of the building, the DPAs, mobile platform and control cabinet were brought to the building site. The top DPAs (2500kg each) were installed on the building top floor by the means of a mobile crane. The bottom DPAs (1100kg each) can be moved around using a forklift. Once the DPAs have been installed, calibration must be carried out.

Calibration of the drawing point positions is performed thanks to the integration of total station targets onto the swivel pulley assemblies. Each swivel pulley assembly features 4 targets; their positions are used to build a local frame to reconstruct the current position of the associated drawing point. In order to calibrate the full system, apart from the A and B points, there are 3 Leica 360º targets [27] attached to the cable robot platform in order to track it on the move, 3 Leica 20x20 mm reflectors attached to the cable robot platform in order to calibrate the origin point of the MEE with respect to the cable robot platform frame, and at least 3 Leica 20x20

mm reflectors to triangulate the building from the total station. It is highly advisable to calibrate all the prism and reflectors at the same time to achieve best possible accuracy.

The calibration procedure has been performed at the same time as the installation of the DPAs, with the drawing point positions being monitored continuously by a surveyor with a total station. The objective was to have the DPAs installed as close as possible to their theoretical positions: the distance to the theoretical positions was measured at maximum 19mm.

3.3 Results

The first results of the demonstration show a better performance than expected in previous phases of the research project (see Figure 8 and check video in [21]). The maximum position error of the CDPR is about 20mm and the max orientation error about 0.8deg. Moreover, the preliminary results show a promising repeatability (with an accuracy of 1-2 mm) of the CDPR while moving the platform within the workspace. However, more tests are necessary to define better this parameter. The deviations in respect to the desired position were supposed to be adjusted by the MEE while fixing the brackets. However, due to time constrains during the installation of the CDPR and the MEE, some calibration issues appeared and the transformed of the MEE with regard to the 0,0,0 point of the building was not achieved properly. For that reason, some deviations occurred during the placement of the bracket. This is a topic that will be improved in the next phase.

Figure 8. MEE and CDPR in operation as in [21]

4 Conclusions and future work

The first test of a CDPR for installing CWMs was achieved with better than expected results. However, there are still some points that need to be improved:

- Improve the calibration of the MEE in regards with the building in order to achieve a better accuracy.
- The detection of the CWM while it stands on the magazine and measuring its location.
- Detection of the brackets that are already fixed on the building slab in order to adjust, if necessary, the CDPR path while placing the CWM.

In order to seek for future commercialization, a market research was carried out which found a growing awareness from building owners and residents about comfort and health as well as political and economic drivers (e.g: nZEB and other EU directives, incentive schemes and favorable tax regimes, especially for green construction). Technological innovations will complete these drivers, making investors, policymakers and professionals (i.e. architects, designers as well as façade manufacturers) accelerate the adoption of construction robots. Therefore, the goal is that in the coming years the innovations mentioned in this paper will reach the market with the following exploitable results: i) CDPR for vertical works: suitable for handling, moving and placing CWMs; ii) MEE: including several tools to automate the insertion of a connector onto the building´s structure; iii) curtain wall adapted to robotic installation: for fixing elements of the CWM to slab; CWM to bracket; and connection between CWMs; and iv) Hephaestus system: as an integrated solution for handling and installing CWMs. To facilitate commercialization of new device categories, standards can do the following:

1. Standardize the components and interfaces from which it is made in order to allow for faster development and efficient supply chains ("interoperability").
2. Standardize the processes and infrastructures surrounding the new technology or product/service.
3. Ensure quality and efficiency of the technology and/or its development processes in order to minimize the risks for the involved stakeholders.

During a final demonstration stage of the project, the robot will complete the installation of a set of CWMs covering part of the façade of a demo building particularly built and enabled for these activities. This demo building has been erected in the machinery park owned by ACCIONA and is located in Noblejas, Toledo (Spain), so that the performance of the cable robot can be demonstrated in a real construction environment. The emo building was erected with three floors and a total height of 10.2 m, and the façade is 8.5m wide. To access the various floors of the demo building during demonstration activities, a staircase has been installed on the back side of the building where no facade panels will be installed. The Hephaestus system will be validated, among other performance indicators, in terms of time required to complete the operations for the CWM placing, the accuracy, the efficiency and the usability for workers of the construction sector. Also, special care will be taken in order to fulfil the safety requirements and recommendations for these robotic operations.

Acknowledgements

This project has received funding from the European Union's Horizon 2020 research and innovation programme under grant agreement No 732513.

References

[1] European Commission, "Construction. Internal Market, Industry, Entrepreneurship and SMEs," [Online]. Available: https://ec.europa.eu/growth/sectors/construction_en [Accessed 10 June 2020].

[2] Bock T. and Iturralde K., "Automated and Robotic Process Lifecycle of Prefabricated Facades," in Neue Entwicklungen im Betonbau, Beuth Verlag GmnH, 2019, pp. 117-129.

[3] Obayashi-Corporation, Director, ABCS Riverside Sumida Bachelor Dormitory Documentary Video. [Film]. 1993.

[4] Miyakawa H., Ochiai J., Oohata K., and Shiokawa T., "Application of automated building construction system for high rise office building," in Proceedings of 17th International Symposium on Automation and Robotics in Construction, Taipei, Taiwan, 2000.

[5] Maeda J., "Development and Application of the SMART System," in Automation and Robotics in Construction, Elsevier Science B.V., 1994, pp. 457-464.

[6] Gambao E., Balaguer C., Barrientos A., Saltaren R., and Puente E., "Robot assembly system for the construction process automation," in Proceedings of International Conference on Robotics and Automation, Albuquerque, USA, 1997.

[7] Lee S.Y., Gil M., Lee K., Lee S and Han C., "Design of a ceiling glass installation robot," in Proceedings of 24th International Symposium on Automation and Robotics in Construction, Madras, 2007.

[8] Činkelj J., Kamnik R., Čepon P., Mihelj M. and Munih M., "Closed-loop control of hydraulic telescopic handler.," Automation in Construction, 19(7), pp. 954-963., 2010.

[9] Thompson C. and Campbell P.J., "Tendon suspended platform robot". U.S. Patent Patent 5,585,707, 17 December 1996.

[10] Cone L., "Skycam - an aerial robotic camera system", Byte, vol. 10, no. 10, pp. 122-132, 1985.

[11] Albus J., Bostelman R. and Dagalakis N., "The NIST Robocrane," Journal of Robotic Systems, vol. 10, no. 5, pp. 702-724, 1993.

[12] Pott A., Cable-driven parallel robots: theory and application, Springer, 2018.

[13] Gouttefarde M., Collard J.-F., Riehl N. and Baradat C., "Geometry selection of a redundantly actuated cable-suspended parallel robot," IEEE Transactions on Robotics, vol. 31, no. 2, pp. 501-510, 2015.

[14] Pott A., Mütherich H., Kraus W., Schmidt V., Miermeister P. and Verl A., "IPAnema: A family of Cable-Driven Parallel Robots for Industrial Applications," Cable-Driven Parallel Robots, 2013.

[15] Culla D., Gorrotxategi J., Rodríguez M., Izard J.-B. and Hervé P.-E., "Full Production Plant Automation in Industry Using Cable Robotics with High Load Capacities and Position Accuracy," Iberian Robotics conference, pp. 3-14, 2017.

[16] Izard J.-B., Gouttefarde M., Baradat C., Culla D. and Sallé D., "Integration of a parallel cable-driven robot on an existing building façade, " Cable-Driven Parallel Robots, pp. 149-164, 2013.

[17] Pott A., Meyer C. and Verl A., "Large-scale assembly of solar power plants with parallel cable robots," in (41st International Symposium on Robotics) and ROBOTIK 2010 (6th German Conference on Robotics) VDE, 2010.

[18] Bosscher P., Williams II R. L., Bryson L. S. and Castro-Lacouture D., "Cable-suspended robotic contour crafting system," Automation in Construction, pp. 45-55, 2007.

[19] Vukorep I., "Autonomous big-scale additive manufacturing using cable-driven robots," in Proceedings of the International Symposium on Automation and Robotics in Construction, Taiwan, 2017.

[20] Bruckmann T., Reichert C., Meik M., Lemmen P., Spengler A., Mattern H. and König M., "Concept Studies of Automated Construction Using Cable-Driven Parallel Robots," Cable-Driven Parallel Robots. Springer, Cham, pp. 364-375, 2018.

[21] R2M Solutions, "Hephaestus - EU H2020 Project," 2017. [Online]. Available: http://www.hephaestus-project.eu/ [Accessed 10 June 2020].

[22] Taghavi M., Iturralde K. and Bock T., "Cable-driven parallel robot for curtain wall modules automatic installation," in 35th International Symposium on Automation and Robotics in Construction , Berlin, 2018.

[23] Gouttefarde M., Lamaury J., Reichert C. and Bruckmann T., "A Versatile Tension Distribution Algorithm for n-DOF Parallel Robots Driven by n + 2 Cables," IEEE Trans. Robot., vol. 31, no. 6, p. 1444–1457, 2015.

[24] Hussein H., Santos J.C. and Gouttefarde M., "Geometric Optimization of a Large Scale CDPR Operating on a Building Facade," in IEEE International Conference on Intelligent Robots and Systems, 2018.

[25] Beckhoff. [Online]. Available: https://www.beckhoff.de/default.asp?twincat/twincat-3.htm [Accessed 09 June 2020].

[26] Izard, J. B. et al., "On the improvements of a cable-driven parallel robot for achieving additive manufacturing for construction", Cable-Driven Parallel Robots, Springer, pp. 353-363, 2018.

[27] Leica. [Online]. Available: http://www.surveyequipment.com/PDFs/leica-white-paper-surveying-prisms.pdf [Accessed 09 June 2020].

Bi-Directional Communication Bridge for State Synchronization between Digital Twin Simulations and Physical Construction Robots

C. J. Liang[a], W. McGee[b,c], C. C. Menassa[a,c] and V. R. Kamat[a,c]

[a]Department of Civil and Environmental Engineering, University of Michigan, USA
[b]School of Architecture, University of Michigan, USA
[c]Robotics Institute, University of Michigan, USA

cjliang@umich.edu, wesmcgee@umich.edu, menassa@umich.edu, vkamat@umich.edu

Abstract -

Collaborative robot (co-robots) are being increasingly deployed on construction sites to assist human workers with physically demanding work tasks. However, due to inherent safety and trust-related concerns, human-robot collaborative work is subject to strict safety standards that require robot motion and forces to be sensitive to proximate human workers. Robot simulations in online digital twins can be used to extend designed construction models, such as BIM, to the construction phase for real-time monitoring of robot motion planning and control. Robots plan work tasks and execute them in the digital twin simulations allowing humans to review and approve robot trajectories. Once approved, commands can be sent to the physical robots to perform the tasks. This paper discusses the development of a system to bridge robot simulations and physical robots in construction and digital fabrication. The Robot Operating System (ROS) is leveraged as the primary framework for bi-directional communication and Gazebo is used for robot simulations. The virtual robots in Gazebo receive work tasks from a BIM model to plan their trajectories, and then send the commands to the physical robots for execution. The system is implemented with a digital fabrication case study with a full-scale mobile KUKA KR120 six-degrees-of-freedom robotic arm mounted on a track system for an additional degree-of-freedom, and evaluated by comparing the pose between the physical robot and the virtual robot. The results show a high accuracy of the pose synchronization between two robots, which provide the opportunity for further deploying to real construction sites.

Keywords -

Digital Twin; Co-robots; Robot Operating System; Human-robot Collaboration

1 Introduction

Due to the 3D characteristics of construction work (dull, dirty, and dangerous) [1], construction sites can be hazardous and harmful working environments for human workers. The construction industry ranks the highest in occupational injuries and fatalities across all U.S. industries [2]. Robots deployment on construction sites can help relieve these issues [3]. For instance, the construction robot can group with human workers on job-site to assist with physically demanding tasks, while human workers focus on the work process plan and decision-making [4]. However, such human-robot collaborative work suffers from safety and trust-related concerns [5, 6], and is subject to strict safety standards [7]. For example, the robot must be restricted for speed and force while collaborating with nearby human workers. A real-time human and robot tracking system can ensure safety by providing the information of the robot state to human workers [8].

The Digital Twin (DT) offers opportunities to virtually mimic the conditions of the physical (real) environment in allowing for a cyber-physical system (CPS) [9] where information of the current and forecasted future states of the robot can be displayed [5]. Figure 1 shows the physical robotic arm and its Digital Twin. Madni et al. [10] defined four levels of Digital Twin (Pre-Digital Twin, Digital Twin, Adaptive Digital Twin, and Intelligent Digital Twin) based on the level of intelligence. The Adaptive Digital Twin combines user interface and machine learning with normal DT, whereas the Intelligent Digital Twin further utilizes reinforcement learning to process the state in a partially observed and uncertain environment.

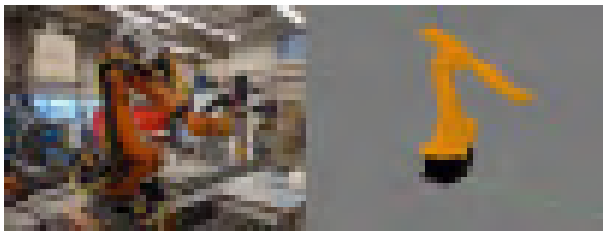

Figure 1. The physical robotic arm (left) and its Digital Twin (right).

One of the major aspects of the DT is the synchro-

nized model [11]. The DT first constructs the virtual model based on the physical environment, then records and tracks the changes in the physical environment and reflects them in the virtual model. The virtual model can be extracted from the designed construction model such as BIM or scanned 3D point cloud of the as-built environment [12, 13]. On the other hand, a communication mechanism is required to synchronize the data between the physical environment and the virtual model [9]. The communication is bi-directional so that the virtual model can reflect the changes of the physical environment, and the user can determine the next steps in the virtual model and send the command to the physical environment.

To address the issue of human-robot collaboration in construction work, we develop an online Digital Twin system to bridge the virtual robot and physical robot in construction and digital fabrication. We utilize Robot Operating System (ROS) [14] to construct the framework of the system and create a robotic arm model representing the physical robotic arm in Gazebo simulation environment [15]. In terms of bi-directional communication, we use MQTT [16] to connect the virtual robotic arm with the physical robotic arm. The mechanism of checking the synchronization between the physical robotic arm and the virtual twin is also developed. The proposed framework can be adapted to any robotic arm models reflecting physical robots. We implement the system in a fabrication laboratory with a full-scale mobile KUKA KR120 six-degrees-of-freedom robotic arm, and evaluate by comparing the pose of the physical robotic arm with the virtual robotic arm.

2 Related Work

Digital modeling methods, such as 3D visualization or BIM, are used in the construction industry for design, management, and operation throughout the building life cycle [17, 18]. These modeling methods document the project information and provide a platform for stakeholders to record changes, collaborate and resolve conflicts [19, 20]. In order to achieve a high-quality collaboration, the model must be fully synchronized with the physical environment. It is time and cost prohibitive to manually update the model [21]. Thus, existing research focuses on automatically generating and updating the 3D model [22]. Collecting the 3D point cloud is one of the methods for generating the 3D model of the indoor environment [23]. This type of method requires a registration method for obtaining 3D points from camera or laser scanner [24, 25, 26], and then applies segmentation method to separate objects and reconstructs the semantic model [27, 28]. Object recognition algorithms are also applied to identify different objects in the point cloud [29, 30].

A similar approach can be used to integrate a construction robot with digital modeling methods for visualization and task planning [31]. For example, Yang et al. [32] utilized BIM and robot path planner to find and visualize the construction process of the modular construction. However, these types of systems are typically not synchronized between the virtual model and physical robot and require further adaption [33, 1]. The robot Digital Twin (DT) system developed in this work fulfills the demand for real-time data exchange, which is wildly utilized in the manufacturing industry, digital fabrication, and human-robot collaboration assembly [34, 35]. For example, Naboni and Kunic [36] used DT for complex wood structure manufacturing and assembly. Furthermore, by combining with other techniques such as Augmented Reality, the synchronization and communication mechanism of robot DT system can be improved [37].

3 Robot Digital Twin System

The proposed online robot Digital Twin system is shown in 2 and consists of three modules: the physical robot module, the virtual robot module, and the communication module. First, the virtual robot module includes the Digital Twin for visualizing the robot and the motion planner for planning the trajectory and solving the inverse kinematics (IK). Second, the physical robot module includes the real robotic arm and the embedded sensors for measuring joint angles. Finally, the communication module includes the MQTT communication protocol for data exchange and synchronization. The system is developed in Robot Operating System (ROS) since it is the meta-operating system that provides a message exchange mechanism between platforms across a network. For instance, the motion planner in the virtual robot module plans a trajectory and then sends the control commands to the DT robot for execution and visualization. Figure 3 shows the data exchange between each platform. The detailed description of each module is provided in the following subsections.

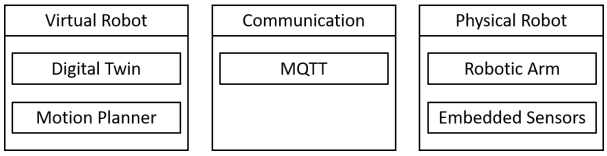

Figure 2. The framework of the online robot Digital Twin system.

3.1 Virtual Robot Module

We use ROS Gazebo and rviz to develop the DT in the virtual robot module on a Linux PC [15, 38]. The Gazebo is a real-world physics simulator that creates a world and

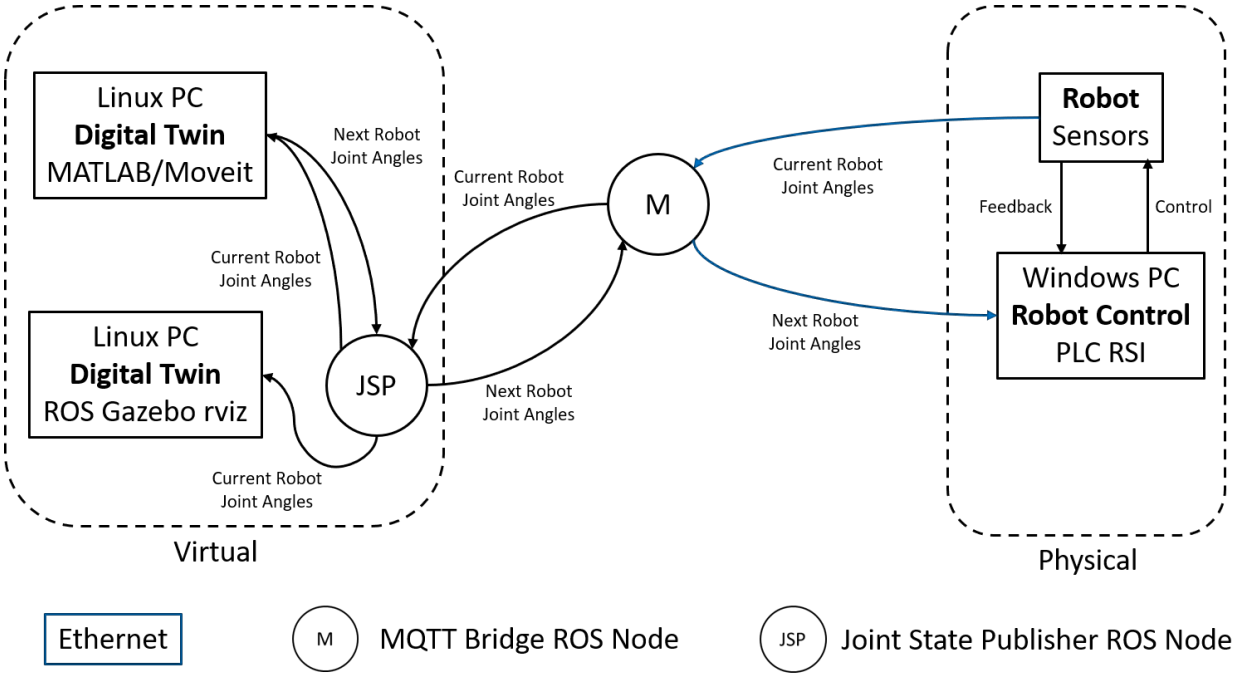

Figure 3. The flowchart of the data exchange and each platform.

simulates the robot, whereas the rviz is visualization software that can read and display the data from Gazebo or real-world sensors. The robotic arm model is imported to the Gazebo and rviz, as shown in Figure 4. The joint angles of the robotic arm are exchanged between the two programs to ensure synchronization.

In order to plan the specific construction task or motion, a motion planner is required in the module. Either MATLAB or MoveIt! can be used as the motion planner to achieve the task [39]. The Robotic System Toolbox in MATLAB can plan the trajectory and solve the inverse kinematics of the robot. However, it suffers from the latency issue and is not fast enough for real-time planning purpose. On the other hand, the MoveIt! is a motion planning package for ROS, which plans the motion inside rviz and sends to Gazebo. Figure 4 top shows the interface of the MoveIt! motion planning in rviz. The start state, goal state, and time parameters can be customized and determined by the user as input to the motion planner. The result of the motion planning will then be demonstrated in rviz and sent back to Gazebo for execution. Both MATLAB and MoveIt! can be run on the same Linux PC as the DT, or run on a different PC and connected through network.

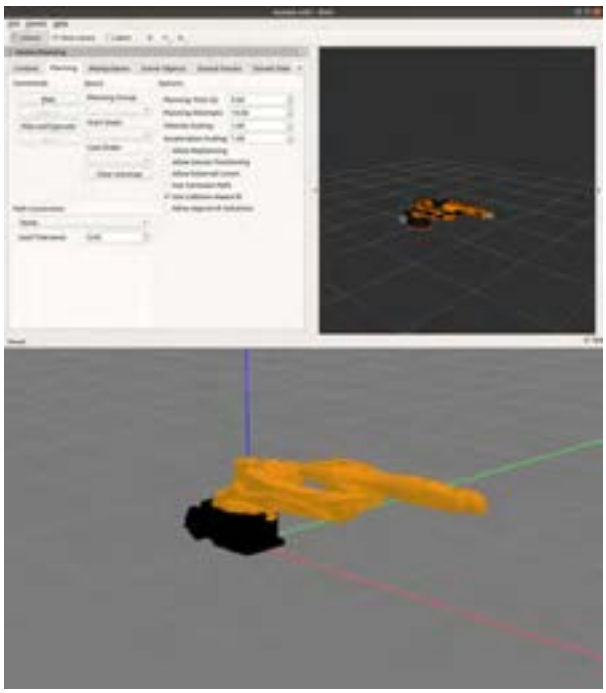

Figure 4. The robotic arm in Gazebo (bottom) and rviz with MoveIt! package (top).

For the data exchange, only the current robot joint angles and the next robot joint angles are displayed within the virtual robot module. Both Gazebo and rviz read the current robot joint angles to visualize the robot state. The MATLAB or MoveIt! package read the robot joint angles, determine the next robot joint angles, and send back to Gazebo and rviz for execution. The joint state publisher (JSP) is the ROS node for publishing the current robot

state to different ROS nodes, including the current robot joint angles from the physical robot module.

3.2 Physical Robot Module

We utilize the KUKA KR120 robotic arm on the track system as the physical robot for the DT system, as shown in Figure 5. In the current version of the online DT system, the track system is not included in the virtual robot module. The programmable logic controller (PLC) and robot sensor interface (RSI) are running on a Windows PC to control the robotic arm and retrieve the sensor data. The embedded encoders on the robotic arm are used to measure the joint angles and read by the RSI. After activating the robotic arm, the system first records the current robot joint angles as the origin of the robot for robot controlling purpose. Once the physical robot receives the next joint angles from the virtual robot, it will calculate the differences of the joint angles and then uses the recorded origin to control the robotic arm in the relative mode. The robot control command and the sensor measurement are two data exchanges inside the physical robot module, as shown in Figure 3 right side.

Figure 5. The KUKA KR120 robotic arm for the physical robot module.

3.3 Communication Module

Finally, the communication module links the virtual robot module and the physical robot module. We use MQTT communication protocol for data exchange between ROS system in the virtual robot module and the PLC in the physical robot module. The MQTT communication protocol is capable of real-time communication and thus is suitable for smooth robotic control. We develop an MQTT Bridge ROS node (M) to connect the MQTT to the ROS system, as shown in the middle of Figure 3. The MQTT Bridge node is run on the same Linux PC as the DT system to exchange the joint angles with JSP node and connect with PLC in the physical robot module through Ethernet. The data exchange frequency in the MQTT Bridge is set to be 250 Hz to ensure the transmission speed and avoid jitter effects on the robotic arm.

The joint angles of the robotic arm are the main data stream exchanged in the MQTT bridge ROS node. Figure 6 illustrates the data structure and exchange process in the MQTT bridge ROS node. The data stream concatenates the robot joint angles from A1 to A6 with a plus-minus sign and comma. Each joint angle is rounded to three decimal places and pads zeros to the left. Thus, the length of the data is consistent and easily retrieved by PLC. After receiving the joint angles data from the virtual robot module through the ROS topic, the system first converts the data to python string for easy storage and access. Next, the data is converted to the MQTT string type and sent to the physical robot module. This process can also avoid the garbled text issue when directly converting from the ROS topic to the MQTT string type. The data stream from the physical robot module is also processed with the same procedure and data structure and sent to the virtual robot module.

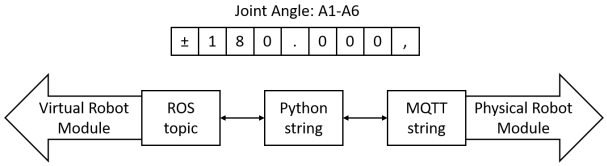

Figure 6. The data structure and exchange in the MQTT Bridge ROS node.

When exchanging the data between the virtual robot module and the physical robot module, the system must ensure the control commands are executed completely and the pose of the physical and virtual robot is synchronized. We develop a robot pose checking algorithm to confirm the synchronization between the two robotic arms. Algorithm 1 shows the pseudo-code of the pose checking algorithm (PCA). The algorithm takes the current virtual robot pose $\theta_{virtual}$, current physical robot pose $\theta_{physical}$, and the next robot pose θ_{next} as input. First, the PCA calculates the difference of $\theta_{virtual}$ and $\theta_{physical}$. If the difference exceeds the pre-defined threshold, the next joint angle θ_{next} will be assigned with the current joint angles $\theta_{virtual}$ to ensure the physical robot can reach the desired joint angles. The trajectory also needs to be re-planned to reflect the new current joint angles. On the other hand, if the difference does not exceed the threshold, the robot will simply execute the next joint angles.

Algorithm 1 Pose Checking Algorithm

procedure NEXT POSE($\theta_{virtual}, \theta_{physical}, \theta_{next}$)
  $diff(\theta) \leftarrow |\theta_{virtual} - \theta_{physical}|$
  if $diff(\theta) > threshold$ **then**
    $\theta_{next} \leftarrow \theta_{virtual}$
    Re-plan the trajectory based on θ_{next}
  else
    $\theta_{next} \leftarrow \theta_{next}$
  end if
  return θ_{next}
end procedure

4 Experiment and Results

4.1 Experiment

The online robot Digital Twin system is implemented and deployed in the Digital Fabrication Laboratory at the Taubman College of Architecture and Urban Planning at the University of Michigan. Two KUKA KR120 robotic arms are the target physical robots, as shown in Figure 1 and Figure 5. To evaluate the proposed system, we conduct an experiment to verify the pose between the physical robot and its DT are synchronized during trajectory execution. Figure 7 shows the procedure of the online robot Digital Twin system experiment. One reaching task trajectory is prepared and executed in MATLAB and Gazebo DT, then the joint angles are sent to the physical robot. Figure 8 shows the planned reaching task trajectory (pink line) in MATLAB. We use the embedded encoders on the KUKA robotic arm to measure and record the joint angles of the physical robot.

4.2 Results

The joint angles of the physical robot and the virtual robot are recorded and compared with each other. Figure 9 shows the results of the virtual and physical robot joint angles. Each line represents the angle of each joint (A1, A2, A3, A4, A5, and A6) in radians. The trajectory from the virtual robot consists of 1,500 waypoints and the measurement from the physical robot includes 18,802 data points. The result showed that the line of each joint angle had the same trend in two robots, which demonstrated the consistency of the synchronization between the two robots.

To further evaluate the accuracy of the synchronization, we calculate the average error and the maximum error of each joint angle between the two robots. Table 1 lists the result of the average and the maximum joint angle error. The average errors of each joint angle are less than 2.4e-05 in radians and the maximum errors of each joint angle are less than 2.1e-05 in radians. These results indicate that the synchronization of the virtual and the physical robot demonstrated high accuracy. The proposed pose checking

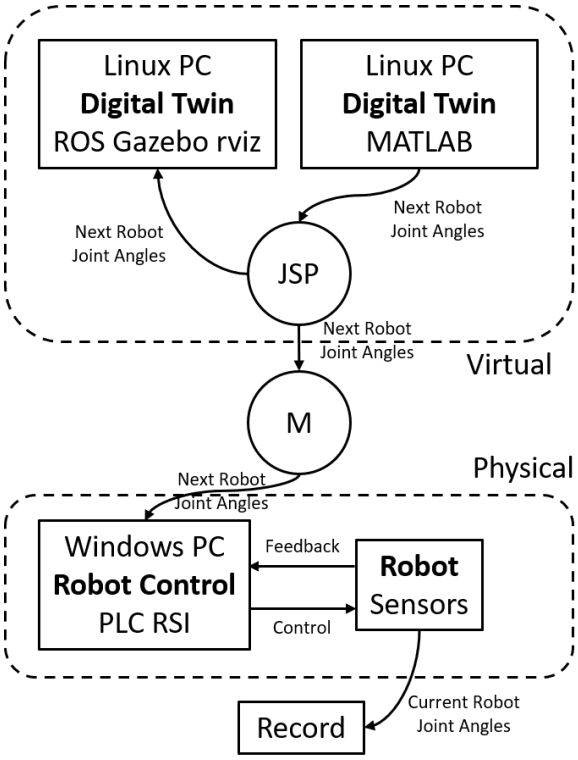

Figure 7. The procedure of the online robot Digital Twin system experiment.

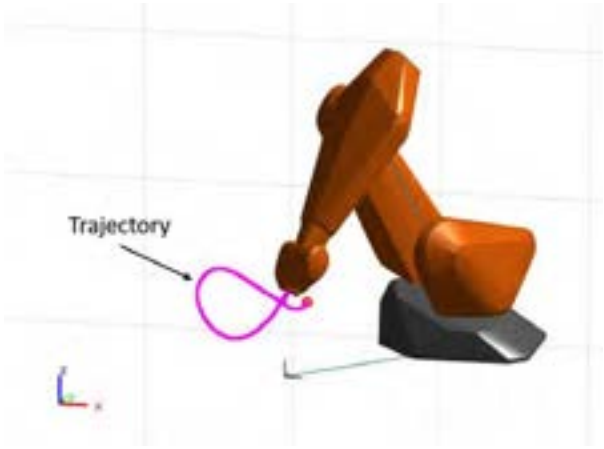

Figure 8. The planned reaching task trajectory (pink line) in MATLAB.

algorithm (PCA) also helped minimize the latency during the transmission.

5 Conclusion

This paper presented the initial development of the online robot Digital Twin system for human-robot collabo-

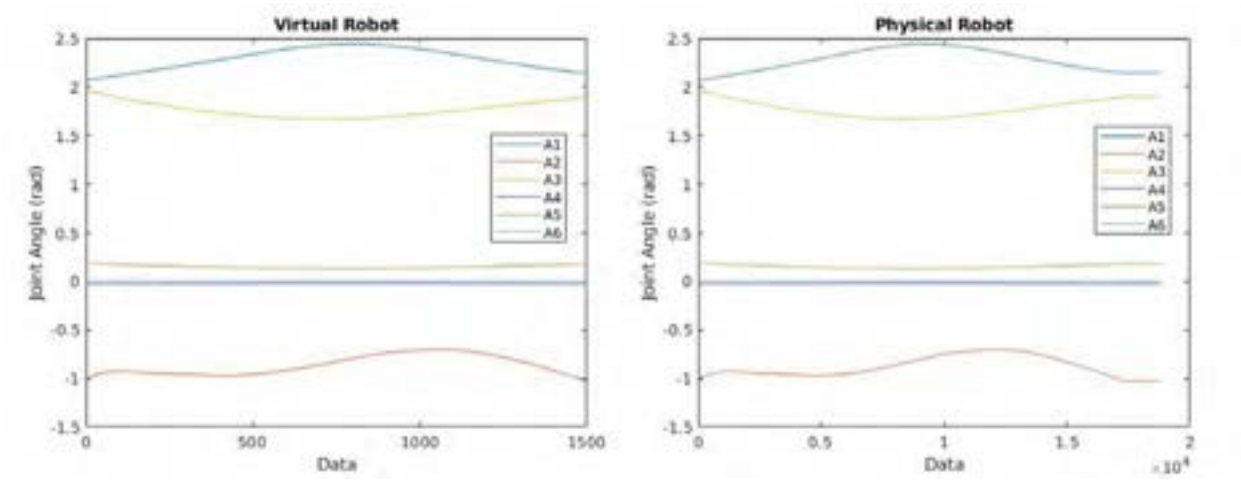

Figure 9. The results of the virtual and physical robot joint angles.

Table 1. The average and the maximum joint angle error between the virtual and the physical robot.

Joint	Average Error (rad)	Maximum Error (rad)
A1	1.5269e-06	1.7232e-06
A2	1.9848e-06	2.2391e-06
A3	2.2334e-05	2.0717e-05
A4	2.2993e-07	2.8146e-07
A5	6.2252e-06	7.0128e-06
A6	4.3442e-06	3.9486e-06

ration in the construction and digital fabrication. The system includes the virtual robot module, the physical robot module, and the communication module. We leveraged ROS Gazebo and rviz to develop the virtual robot module, i.e., Digital Twin of the physical robot, and connect to the physical robot module through MQTT Bridge in the communication module. The joint angles of the robotic arm are exchanged and synchronized between two robots. We also utilized MATLAB or MoveIt! package to plan and control the robotic arm in the virtual robot module, then send the command to the physical robot module for execution. In addition, we developed a pose checking algorithm (PCA) to ensure the pose of the two robots were synchronized.

The system was implemented and deployed on a KUKA KR120 robotic arm in the digital fabrication laboratory. Although we developed the system for the specific KUKA robotic arm, it can be easily adapted to other robot models. We evaluated the system by comparing the joint angles between the virtual and physical robot in a planned trajectory, and calculated the average and maximum errors. The results showed that the proposed online robot Digital Twin system could plan the robot trajectory inside the virtual environment and execute it in the physical environment with high accuracy. In ongoing work, we are designing the user interface for displaying the information of the physical robot in Digital Twin. We are also developing the robot planning mechanism such that the robot can first demonstrate the planned trajectory inside Digital Twin before executing by the physical robot. The human can thus expect the movement of the robot in advance and approve the task. Finally, we are designing and conducting more case studies for evaluating the proposed online robot Digital Twin system.

References

[1] Kurt M. Lundeen, Vineet R. Kamat, Carol C. Menassa, and Wes McGee. Autonomous motion planning and task execution in geometrically adaptive robotized construction work. *Automation in Construction*, 100:24–45, 2019. doi:10.1016/j.autcon.2018.12.020.

[2] BLS. Census of fatal occupational injuries (CFOI) - current and revised data, 2018. URL `https://www.bls.gov/iif/oshcfoi1.htm`.

[3] Ci-Jyun Liang, Vineet Kamat, and Carol Menassa. Teaching robots to perform construction tasks via learning from demonstration. In *Proceedings of the International Symposium on Automation and Robotics in Construction (ISARC)*, pages 1305–1311, Banff, Canada, May 2019. IAARC. doi:10.22260/ISARC2019/0175.

[4] Ci-Jyun Liang, Vineet R. Kamat, and Carol C. Menassa. Teaching robots to perform quasi-repetitive construction tasks through human demonstration. *Automation in Construction*, 120:103370, 2020. ISSN 0926-5805. doi:10.1016/j.autcon.2020.103370.

[5] Amos Freedy, Ewart DeVisser, Gershon Weltman, and Nicole Coeyman. Measurement of trust in human-robot collaboration. In *Proceedings of the International Symposium on Collaborative Technologies and Systems*, pages 106–114, Orlando, FL, USA, May 2007. IEEE. doi:10.1109/CTS.2007.4621745.

[6] Sangseok You, Jeong-Hwan Kim, SangHyun Lee, Vineet Kamat, and Lionel P. Robert. Enhancing perceived safety in human–robot collaborative construction using immersive virtual environments. *Automation in Construction*, 96:161–170, 2018. doi:10.1016/j.autcon.2018.09.008.

[7] Timo Salmi, Jari M. Ahola, Tapio Heikkilä, Pekka Kilpeläinen, and Timo Malm. Human-robot collaboration and sensor-based robots in industrial applications and construction. In Henriette Bier, editor, *Robotic Building*, pages 25–52. Springer International Publishing, 2018. ISBN 978-3-319-70866-9.

[8] Carlos Morato, Krishnanand N. Kaipa, Boxuan Zhao, and Satyandra K. Gupta. Toward safe human robot collaboration by using multiple kinects based real-time human tracking. *Journal of Computing and Information Science in Engineering*, 14(1):011006, 2014. doi:10.1115/1.4025810.

[9] Shohin Aheleroff, Jan Polzer, Huiyue Huang, Zexuan Zhu, David Tomzik, Yuqian Lu, Yuan Lin, and Xun Xu. Smart manufacturing based on digital twin technologies. In Carolina Machado and J. Paulo Davim, editors, *Industry 4.0: Challenges, Trends, and Solutions in Management and Engineering*, page 77. CRC Press, 2020. ISBN 978-0-8153-5440-6.

[10] Azad M. Madni, Carla C. Madni, and Scott D. Lucero. Leveraging digital twin technology in model-based systems engineering. *Systems*, 7(1):7, 2019. doi:10.3390/systems7010007.

[11] Yuqian Lu and Xun Xu. Resource virtualization: A core technology for developing cyber-physical production systems. *Journal of Manufacturing Systems*, 47:128–140, 2018. doi:10.1016/j.jmsy.2018.05.003.

[12] Tim Delbrügger, Lisa Theresa Lenz, Daniel Losch, and Jürgen Roßmann. A navigation framework for digital twins of factories based on building information modeling. In *Proceedings of the IEEE International Conference on Emerging Technologies and Factory Automation (ETFA)*, pages 1–4, Limassol, Cyprus, September 2017. IEEE. doi:10.1109/ETFA.2017.8247712.

[13] Matthew Q. Marshall and Cameron Redovian. An application of a digital twin to robotic system design for an unstructured environment. In *Proceedings of the ASME International Mechanical Engineering Congress and Exposition*, page V02BT02A010, Salt Lake City, UT, USA, November 2019. ASME. doi:10.1115/IMECE2019-11337.

[14] Open Robotics. Robot Operating System, 2018. URL `https://www.ros.org/`.

[15] Open Robotics. Gazebo, 2019. URL `http://gazebosim.org/`.

[16] Roger A. Light. Mosquitto: server and client implementation of the MQTT protocol. *Journal of Open Source Software*, 2(13):265, 2017. doi:10.21105/joss.00265.

[17] Vineet R. Kamat and Julio C. Martinez. Large-scale dynamic terrain in three-dimensional construction process visualizations. *Journal of Computing in Civil Engineering*, 19(2):160–171, 2005. doi:10.1061/(ASCE)0887-3801(2005)19:2(160).

[18] Robert Eadie, Mike Browne, Henry Odeyinka, Clare McKeown, and Sean McNiff. BIM implementation throughout the UK construction project lifecycle: An analysis. *Automation in Construction*, 36:145–151, 2013. doi:10.1016/j.autcon.2013.09.001.

[19] Alcinia Z. Sampaio and Edgar Berdeja. Collaborative BIM environment as a support to conflict analysis in building design. In *Proceedings of the Experiment@International Conference (exp.at'17)*, pages 77–82, Faro, Portugal, June 2017. IEEE. doi:10.1109/EXPAT.2017.7984348.

[20] Tzong-Hann Wu, Feng Wu, Ci-Jyun Liang, Yi-Fen Li, Ching-Mei Tseng, and Shih-Chung Kang. A virtual reality tool for training in global engineering collaboration. *Universal Access in the Information Society*, pages 1–13, 2017. doi:10.1007/s10209-017-0594-0.

[21] Sebastian Ochmann, Richard Vock, Raoul Wessel, and Reinhard Klein. Automatic reconstruction of parametric building models from indoor point clouds. *Computers & Graphics*, 54:94–103, 2016. doi:10.1016/j.cag.2015.07.008.

[22] Hesam Hamledari, Brenda McCabe, Shakiba Davari, and Arash Shahi. Automated schedule and progress updating of IFC-based 4D BIMs. *Journal of Computing in Civil Engineering*, 31(4):04017012, 2017. doi:10.1061/(ASCE)CP.1943-5487.0000660.

[23] Yong Xiao, Yuichi Taguchi, and Vineet R. Kamat. Coupling point cloud completion and surface connectivity relation inference for 3D modeling of indoor building environments. *Journal of Computing in Civil Engineering*, 32(5):04018033, 2018. doi:10.1061/(ASCE)CP.1943-5487.0000776.

[24] Lichao Xu, Chen Feng, Vineet R. Kamat, and Carol C. Menassa. An Occupancy Grid Mapping enhanced visual SLAM for real-time locating applications in indoor GPS-denied environments. *Automation in Construction*, 104:230–245, 2019. doi:10.1016/j.autcon.2019.04.011.

[25] Chen Feng, Yong Xiao, Aaron Willette, Wes McGee, and Vineet R. Kamat. Vision guided autonomous robotic assembly and as-built scanning on unstructured construction sites. *Automation in Construction*, 59:128–138, 2015. doi:10.1016/j.autcon.2015.06.002.

[26] Frédéric Bosché, Mahmoud Ahmed, Yelda Turkan, Carl T. Haas, and Ralph Haas. The value of integrating Scan-to-BIM and Scan-vs-BIM techniques for construction monitoring using laser scanning and BIM: The case of cylindrical MEP components. *Automation in Construction*, 49:201–213, 2015. doi:10.1016/j.autcon.2014.05.014.

[27] Andrey Dimitrov and Mani Golparvar-Fard. Segmentation of building point cloud models including detailed architectural/structural features and MEP systems. *Automation in Construction*, 51:32–45, 2015. doi:10.1016/j.autcon.2014.12.015.

[28] Vladeta Stojanovic, Matthias Trapp, Rico Richter, Benjamin Hagedorn, and Jürgen Döllner. Towards the generation of digital twins for facility management based on 3D point clouds. In *Proceedings of the ARCOM 34th Annual Conference*, pages 270–279, Belfast, UK, September 2018.

[29] Chao Wang and Yong K. Cho. Smart scanning and near real-time 3D surface modeling of dynamic construction equipment from a point cloud. *Automation in Construction*, 49:239–249, January 2015. doi:10.1016/j.autcon.2014.06.003.

[30] Jacob J. Lin, Jae Yong Lee, and Mani Golparvar-Fard. Exploring the potential of image-based 3D geometry and appearance reasoning for automated construction progress monitoring. In *Proceedings of the ASCE International Conference on Computing in Civil Engineering (i3CE)*, pages 162–170, Atlanta, GA, USA, June 2019. ASCE. doi:10.1061/9780784482438.021.

[31] Vineet R. Kamat and Julio C. Martinez. Dynamic 3d visualization of articulated construction equipment. *Journal of Computing in Civil Engineering*, 19(4):356–368, 2005. doi:10.1061/(ASCE)0887-3801(2005)19:4(356).

[32] Cheng-Hsuan Yang, Tzong-Hann Wu, Bo Xiao, and Shih-Chung Kang. Design of a robotic software package for modular home builder. In *Proceedings of the International Symposium on Automation and Robotics in Construction (ISARC)*, pages 1217–1222, Banff, AB, Canada, May 2019. IAARC. doi:10.22260/ISARC2019/0163.

[33] Kurt M. Lundeen, Vineet R. Kamat, Carol C. Menassa, and Wes McGee. Scene understanding for adaptive manipulation in robotized construction work. *Automation in Construction*, 82:16–30, 2017. doi:10.1016/j.autcon.2017.06.022.

[34] Cunbo Zhuang, Jianhua Liu, and Hui Xiong. Digital twin-based smart production management and control framework for the complex product assembly shop-floor. *The International Journal of Advanced Manufacturing Technology*, 96(1):1149–1163, 2018. doi:10.1007/s00170-018-1617-6.

[35] Arne Bilberg and Ali Ahmad Malik. Digital twin driven human–robot collaborative assembly. *CIRP Annals*, 68(1):499–502, 2019. doi:10.1016/j.cirp.2019.04.011.

[36] Roberto Naboni and Anja Kunic. A computational framework for the design and robotic manufacturing of complex wood structures. In *Proceedings of the Education and Research in Computer Aided Architectural Design in Europe and Iberoamerican Society of Digital Graphics, Joint Conference*, volume 7, pages 189–196, Porto, Portugal, September 2019. doi:10.5151/proceedings-ecaadesigradi2019_488.

[37] Yi Cai, Yi Wang, and Morice Burnett. Using augmented reality to build digital twin for reconfigurable additive manufacturing system. *Journal of Manufacturing Systems*, In Press, May 2020. doi:10.1016/j.jmsy.2020.04.005.

[38] ros-visualization. ROS 3D Robot Visualizer, 2020. URL `https://github.com/ros-visualization/rviz`.

[39] David T. Coleman, Ioan A. Sucan, Sachin Chitta, and Nikolaus Correll. Reducing the barrier to entry of complex robotic software: a MoveIt! case study. *Journal of Software Engineering for Robotics*, 5(1): 3–16, 2014. doi:10.6092/JOSER_2014_05_01_p3.

Parallel Kinematic Construction Robot for AEC Industry

M. Klöckner[a], M. Haage[a], K. Nilsson [b], A. Robertsson[c], R. Andersson[d]

[a]Department of Computer Science, Lund University, Sweden
[b]Cognibotics AB, Lund, Sweden
[c]Department of Automatic Control, Lund University, Sweden
[d]AChoice AB, Malmö, Sweden

E-mail: maike.klockner@cs.lth.se, mathias.haage@cs.lth.se, klas@cognibotics.com, anders.robertsson@control.lth.se, ronny.andersson@achoice.se

Abstract –

This article reports work-in-progress of a parallel kinematic robot development for construction with main focus on the concept phase. We assume the weight distribution of the proposed structure enables integration of robotic components into construction equipment while enabling tailoring of important characteristics such as accuracy, stiffness and workspace toward application needs. We describe challenges as well as kinematics, simulation and an experimental setup for evaluating performance of the proposed concept in a construction experiment using a concrete build system.

Keywords –

Parallel kinematic manipulator; Construction robotics; Concrete build system

1 Introduction/preliminary work

The community building sector in Sweden has an annual turnover of around SEK 500bn with 500,000 employees in 20,000 companies. However, productivity development is very low and has been for a long time. Low profitability and the absence of strong drivers of change are preserving the sector. For instance, in mass production of reinforcement, plasterboard, insulation, steel profiles and concrete, one person hour produces material for more than 50 m² of exterior wall with high profitability. At the same time experience show that for finished (built) exterior walls, one person hour has often only produced less than 1 m², this independent of construction material, whether, prefabricated or site-built. Swedish and international efforts to improve productivity in construction have often landed in prefabrication of composite components and building information modeling (BIM). However, the success of trying to increase productivity and profitability through this approach has been limited, mainly due to compound product complexity, inability to handle variations in deliveries, high fixed services and best widespread fragmentation in a project-based construction process [1].

In the manufacturing industry, customer focus, digitization and use of robots enabled mass customization and increased productivity. However, in the construction sector, the degree of automation is very small and in principle none of the players work with flexible customer-based production. Investments have been made but large-scale solutions have failed. The utilization of robots in the construction sector is limited by adaptation to the construction site, rapid and agile change of work steps and that the sector needs a balanced and small-scale collaboration between man and machine at the construction site. Today, the construction sector has about 3 times the number of accidents and load-related illnesses compared to other operations in Sweden, and the situation makes it difficult to improve the working environment and safety as well as to reduce both climate and environmental impact. Recent literature surveys support these findings and list hampering factors such as lack of interoperability, tolerance management, experts, power and communications as well as design for human installation procedures, high initial investment and risk for subcontractors, immature technology, unproven effectiveness, and low R&D budgets, among others [2, 3, 4]. At the same time, there are indications that automation is needed in AEC for continued growth [5].

To target these issues at a national level a Swedish center for construction robotics [1] is being formed in collaboration with the Swedish concrete industry. The center aims to develop, adapt and demonstrate automation solutions for construction before being put to use at construction sites, and act as a knowledge

[1] Swedish national center for construction robotics, http://www.lth.se/digitalth/byggrobotik/

transfer channel from academia to Swedish industry within construction robotics. Efforts now being carried out in associated national research projects aims to demonstrate a feasible automated construction system for small concrete house production in Sweden. The hypothesis is that the use of small-scale robotics gives feasible construction automation. Two robot automation approaches are being tested: utilization of off-the-shelf industrial robot arms from the manufacturing industry for automation of in-situ processes, and utilization of parallel kinematic manipulators (PKMs) for use in-situ and for prefabrication processes.

The type of PKMs put forward in this article fit, in our opinion, well for automation of construction tasks. The weight distribution of the robot with mass concentrated to stationary parts suits well for integration into construction equipment. Corresponding light-weight arm systems can be tailored toward processes in important robot characteristics such as accuracy, stiffness, and workspace.

This article describes our experimental setup and motivation behind selection of the two robot types as candidates for construction work, as well as reporting work-in-progress regarding development of PKMs for construction. The rest of the article is outlined as follows: a test process is described (masonry using the Finja Exakt build system[2]). This is followed by a short description of the off-the-shelf robot system (important as we plan for comparison of performance between the systems). Then a general overview of parallel kinematic manipulators is given to illustrate the machine concept, followed by work-in-progress reporting on initial steps we needed for adaptation to construction experiments. Currently open problems regarding integration, safety and interaction are then discussed briefly. Last, future work and current conclusions end the article.

2 Masonry process

The targets for experiments in current projects are processes needed for small concrete house construction, such as shown in Figure 1.

This particular house type is constructed using a build system based on a refined type of concrete blocks. The process of placing the blocks to form the outer walls is not that time consuming (about two days manual labor by two persons), but it is heavy and non-ergonomic work involving a total lifting of several tons of material during short time. Fully or partially replacing manual labor in this specific process would remove a strenuous work task. From a robot automation point-of-view the process contains most challenges that need to be addressed for robot application on-site, such as safety, calibration, performance, workspace, etc. Furthermore, commercial automation solutions exist (HadrianX [6], SAM100 [7]) as well as research prototypes (in-situ fabricator [8,9]) for benchmarking and comparisons.

Figure 1. House type targeted for masonry robot automation

2.1 Manual masonry process

The Finja Exakt system consists of a family of insulated blocks that are available on pallets of around 40 blocks per pallet. The system consists of a number of blocks to handle different situations such as corners, windows and doors. The weight of individual blocks vary between 15 and 20 kg. Blocks are stacked in layers of 200 mm including a 3 mm thin layer of Exakt mortar, with possibility of a half layer of 100 mm. The length of an individual block is around 600 mm. The Exakt system exists in three different widths, 290, 350 and 400 mm. We limit ourselves to consider only the 350 mm width for experiments.

The manual process is specified in Finja Exakt manuals[3]. The steps involved are visualized in Figure 2; starting from a slab and a blueprint, the first layer of blocks is layed down with care taken to accurate placement of openings and care taken to achieve an even layer height. Mortar is applied using a special tool for application (white box). Every few layers (not each layer) reinforcement is applied. Custom block sizes needed for corners and openings (windows and doors), are solved by on-site sawing of blocks, see Figure 3.

[2] Finja Exakt system, https://youtu.be/S6NdghrdLkI

[3] Finja Exakt build system manuals (see link "arbetsanvisning" (Swedish for work manual), https://www.finja.se/produkter/block/isolerblock-exakt?id=16292060

Figure 2. Steps in the masonry process with Finja Exakt block system; first layer (top left), application of mortar (top right), application of reinforcement (bottom left) and customization for cabling (bottom right).

Figure 3. Finja Exakt Block with corner block (left) and on-site customization of sawing block (right).

3 Research contribution

Within this paper we show our recent work-in-progress towards building a construction robotics lab including a PKM and an industrial arm robot to explore robotic aspects of construction processes. Our main contribution belongs to the development of the PKM and to the final development of the process customized industrial arm robot for construction tasks. Next to the robot development our contributions comprise in investigating application aspects of construction processes. These aspects include e.g., logistics, material flow, safety, collaboration, and risks. The first process we explore the mentioned aspects for is masonry.

4 Industrial construction robot

Industrial robot arms were originally developed for long series manufacturing, typically batch production in automobile industry, with the robot specializing in dirty and dangerous processes, such as welding and painting, as well as highly repetitious tasks such as pick- and place operations. The main important characteristics being high repeatability and low cycle time. An industrial robot is typically placed in a well-organized cell within a production line. In construction the most similar environment is in prefabrication where similar thinking may apply, though with different materials. Prefab wood house production already has automation solutions involving robotics. For prefab concrete the main application so far seems to be 3D printing, but then featuring large Gantry structures built to scale. For on-site production there are several factors to consider:

The environment is less structured than in a traditional robot cell, furthermore it may be unique for each new construction site. Figure 4 shows a typical small house slab cramped with construction material and cabling.

In the construction context considered, adoption to the blueprint typically happens at centimeter tolerance. Blocks are also allowed a few millimeters of placement tolerance since a grouting process evens out small errors. Accumulation of errors are not tolerated. On-site robot systems need efficient on-site calibration methods and/or accurate positioning sensing.

Mobility is probably required unless prefabrication on-site is sufficient (it very well may be) since the house is much larger than the workspace of the typical robot arm. In such case, the form factor of the robot and mobile platform should fit standard openings in the construction and adhere to pressure limitations posed by slab or use workarounds such as distributed steel plates. A small form factor also needs to ensure stability to allow utilization of robot performance.

Figure 4. Typical small house slab cramped with construction material and cabling

The protection class of the robot system needs to handle the on-site conditions, which includes abrasive materials and weather conditions. Most current industrial robot brands are available in IP67 editions which however is not enough leading to the need for protective clothing.

Opposed to manipulating a material flow through a cell, the robot system needs to adopt to the less structured material logistics on the construction site, or to enforce more structure to suit the automation process.

Safety, interaction and collaboration are important subjects. They are therefore given a separate section later in this paper.

The concept to be tried out is integration of an off-the-shelf industrial robot arm with an off-the-shelf piece of construction equipment as mobile platform, similar to what is seen recently in literature (the in-situ fabricator). Unlike the fabricator we will put focus on integration of the robot system into an automation system including considerations for the build system used. The system will be used for comparison with the PKM robot described next.

5 Parallel kinematic machines (PKMs)

Parallel kinematic machines (PKMs), classified as robots whose arms have concurrent prismatic or rotary joints in so-called closed kinematic loops, differ from the standard serial manipulators in several important aspects and complementary broadens the applicability and use of robots [10]. With a significantly higher stiffness in relation to the inertia/moving mass, PKMs typically either show up in (I) industrial pick-and-place systems where the very high accelerations due low moving mass – for so called delta and cable robots the actuators could be mounted in the stationary frame and thus get low moving mass – one gets significantly shortened cycle times in comparison to what is achievable with serial manipulators at the corresponding energy budget. or (II) are used in industrial applications where the high stiffness and/or positioning accuracy are required; different machining operations such as grinding, deburring and cutting, where structures like Stewart-Gough platforms or different gantry manipulators provide beneficial configurations. Parallel kinematic structures are also quite common in active or passive fixtures. Cable driven robots have emerged during the last decade and one can find examples from suspended camera system in sport stadiums to large wire robots in industrial settings [11]. An often-advocated shortcoming of PKMs is the smaller workspace with respect to the footprint of the robot, compared to the typical serial manipulators, and the risk of collisions between PKM-links/cables and obstacles within the workspace. However, whereas this may be true in many industrial applications, the masonry of walls is a task where the workspace is very suitably tailored to a new PKM structure. Furthermore, the strength, stiffness, and positional accuracy of the PKM within this workspace makes it a competitive alternative. The Gantry-Tau PKM was developed for achieving a large, open workspace for structures in e.g., the aerospace and windmill industry where the reconfigurability concept encompassed and integrated calibration as important part of the concept [12]. Further development of the latter PKM-concept is an important step towards efficient use in AEC applications.

5.1 PKM for masonry

Here we present work-in-progress to adapt a PKM structure to automate the selected masonry process (see Chapter 2.1). Our work so far considers kinematic aspects (e.g. workspace, stiffness) and mechanical aspects (e.g. joints, drive concepts) as well as guidelines and standards relevant for collaborative robots [12, 13, 14]. The lab sized PKM is part of the experimental setup we build (Figure 5).

The work scenario contains: the PKM placed parallel to the wall we want to build at some distance from the wall. The end effector will be utilized for pick and place of blocks. Our first experiment will include pick and place of blocks with no humans in the robot cell with no collaboration taking place. Since we need Exakt mortar as a first layer a human will applicate one layer of Exakt mortar while the robot stops completely. Thereafter the robot will pick a block from a palette and place it at the needed position for building a wall. After placing one layer of blocks the robot stops again and the human applicates the next layer of Exakt mortar. As a next step the robot starts to perform pick and placement of next block layer and so on. Parallel to these experiments we will perform experiments with the industrial construction robot with regard to automated

Exakt mortar application which will be later adapted into the PKM experiments.

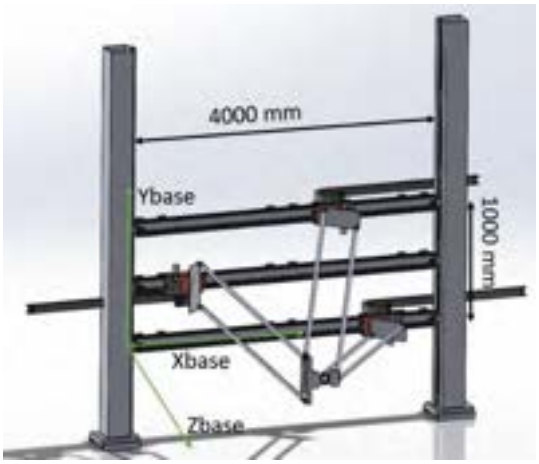

Figure 5. CAD of lab sized PKM with coordination system and wrist dummy

PKM development has so far been divided into four main parts. At a first step we investigate the basic PKM mechanism and structure to realize the translatory movement (basic PKM - translatory movement). In a second step we investigate the wrist, the end effector and the drive concept for the end effector to realize the rotatory movement with modular parts, adaptable for different applications (advanced PKM - rotatory movement). In a third step we have to investigate movable support structure to bring our PKM in a full sized version to the construction side or other relevant application places (support structure). The fourth step includes implementation of safety and interaction for human robot collaboration. This division into four parts (translatory movement, rotatory movement, support structure, safety and interaction) is very important since our aim is to bring the PKM into different application areas with different human robot interaction levels. Further explanations contain the PKM development regarding the translatory movement and the implementation of safety and collaboration.

5.2 Basic PKM – translatory movement

The basic PKM for construction tasks (Figure 6) consists of three kinematic chains. Each chain includes an actuator, which is realized by motor driven carts moving on tracks. A total of six links is used. These links have fixed length and are connected to the carts and the wrist in a 2-2-2 configuration. Joints used for the connections are at this stage spherical joints with a tilting angle of +/-45 deg. Two of the carts are placed on one side and the third cart is placed on the other side in comparison to the wrist. By this configuration we are already able to realize the three translatory degrees of freedom (DOF). The wrist itself consists of a support platform, where the fixed length links are connected to and of a tool platform with which we realize the rotational DOFs.

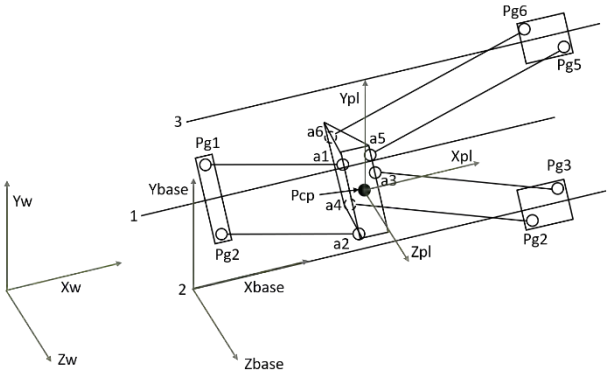

Figure 6. Schematic construction PKM for translatory movement with notation for variables and parameters

Since the wrist transmits the translatory movement and realizes the rotational DOF it has a key function in our PKM. Furthermore, the chosen connection points from links and wrist have a high impact on stiffness. The best regarding stiffness is to choose the distances between the links as big as possible.

For figuring out the best combination of distances between tracks, length of links and distances between links in dependency of workspace we realized the kinematic modeling. The kinematic model contains a defined cubic workspace in which we proof the reachability of the platform center point (Pcp). Further we described the inverse kinematics from Pcp over connections links/wrist (a1, a2, …, a6) to connection links/carts (Pg1, Pg2, …, Pg6) to carts. After this we calculated the intersection points of the links with the tracks to check if there are intersection points in the defined areas along x-axis. In case of intersection points we had to figure out which of the intersection points are valid. Moreover, we had to proof the angles between the links and the wrist and the links and the carts. We did this because we used spherical joints with +/- 45 deg tilting angle. After this procedure we found out which points in space are reachable with our configuration. Figure 7 shows reachable workspace in green for a PKM with 4000 mm tracks, 500 mm distances between tracks in y-direction, length links 2 and 3 = 1722 mm, length links 1 = 1648 mm. With this configuration it will be possible to build a wall with length = 1,8 m

and height = 1,5 m which will be appropriate for our experimental setup. For later use of the PKM on the construction site calculations will be adapted to design an upscaled version.

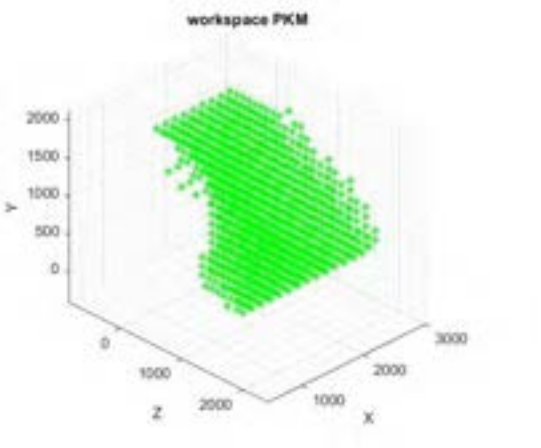

Figure 7. Result workspace calculation – Reachable points in space of platform center point for translatory movement

Due to the fact, that we want to perform first experiments to evaluate stiffness, torsion and workspace with the calculated parameters, we decided to build a downscaled version with parts to realize translatory movement (Figure 8).

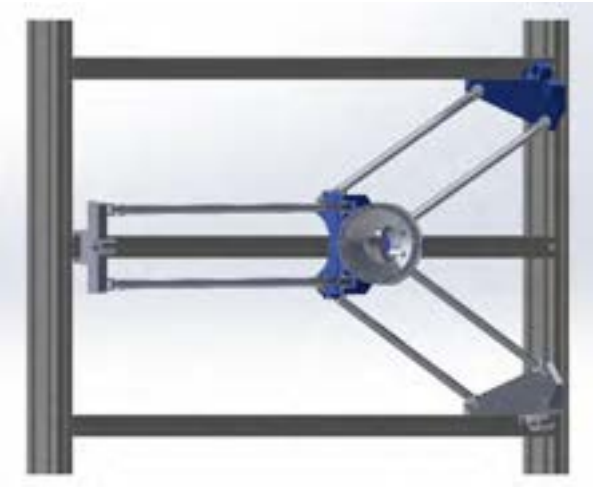

Figure 8. CAD PKM – designed for downscaled version

To fasten up the mentioned process, we designed the downscaled version of the PKM for first experiments with 3D-printed and out-off the shelf made parts and a functional support structure (Figure 9).

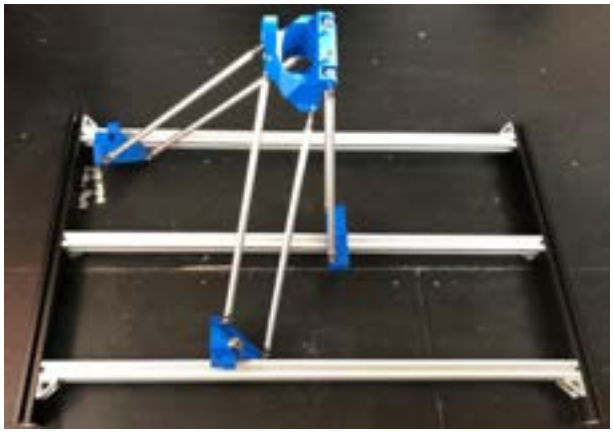

Figure 9. Realized downscaled PKM with 3 DOF

6 Experimental setup

Our experimental setup in the construction lab will contain the PKM placed parallel to the wall to build as well as a palette of blocks with the aim to perform pick and place experiments of blocks (Figure 10). Not shown in the picture, but planned, is the industrial arm application on the opposite side of the wall to perform experiments regarding pick and place, gluing and sensor integration. Since safety and interaction will be needed already in the lab, we will start to integrate some safety features in the shown application, which is described in the next chapter.

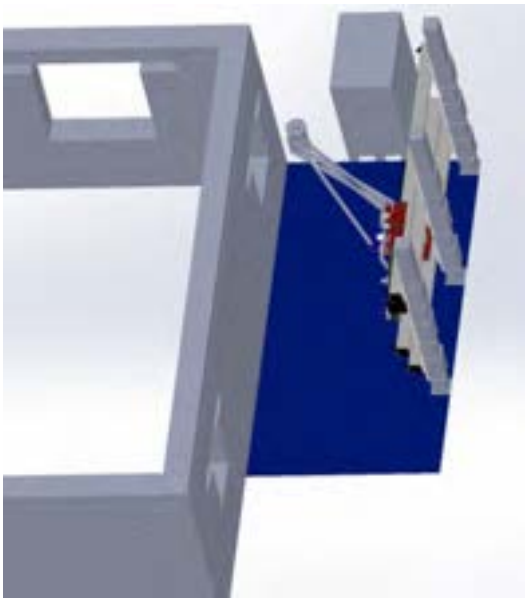

Figure 10. Experimental setup for PKM

6.1 Safety & interaction

The machine directive needs machines to fulfill stated requirements before they are considered safe for use. Traditional industrial robot cells disallow human presence during autonomous operation and ensure this situation by surrounding the cell with safety systems. Another approach is represented by collaborative robots where a limit in allowable utilized energy allow humans to work in close collaboration with the machine despite autonomous operation. The unstructured and perhaps changing environment on the construction site pose challenges for safe autonomous robot automation.

How can and must safety look like on construction site? Different approaches:

- Physical protection
- Disallowing human presence
- Supervised operation
- Detection of human presence

By limiting access to the robot structure itself by, for instance, providing an enclosure for the robot it is easier to limit access during operation. Approaches to small mobile robot factories often suggest enclosure of the robot in a container. Enclosing the entire work area (all or part of the construction site) for autonomous work provides safety by disallowing human presence altogether. Supervision of the operation at all times with personnel equipped with dead man's switch and emergency stops. Automatic detection techniques of human presence, such as laser planes. But this requires an uncluttered environment (no occlusions) for robust operation. There is no obvious option. This remains an open problem.

Another consideration is human interaction with the robot system. In a masonry automation system, examples could be refilling of mortar, requiring a human to get close to the robot system, or division of labor between a human and machine in the masonry process. These issues also remain open problems.

7 Future Work

Developing the drive concept for the wrist and the end effector as well as building the PKM in the lab. Part of the masonry process will be tested with the robot structure (the path for pick and place blocks). Moreover, we will carry out a feasibility study regarding the pick and place application of the blocks. Parallel to this realization we will create a simulation of the whole process. We will use this simulation to figure out cycle times in dependency of all process elements (robot, palette bricks, wall). Other work for next year contains implementing the gluing/cement application process as well as the needed hardware (pump, pipes, tool) for this process. We want to realize a tool changing system with which we can change between a gripper and a saw or a combination tool consisting of a gripper and a saw. We further need a block fixing station for sawing and a measuring system to define the needed length of the blocks before sawing. Another future process will be plastering.

8 Conclusion

With this paper we have shown work-in-progress of a parallel kinematic robot development for construction with main focus on the concept phase. There are many open questions and challenges remaining, some of them listed in this article. Robot challenges include large workspace, efficient calibration procedures, safety concepts, and human-machine interaction ability with regard to construction workers.

9 Acknowledgements

The authors gratefully acknowledge the support received from Boverket/"Innovativt Bostadsbyggande" (#6438/2018) and VINNOVA/"Innovativ Agile Construction for globally improved sustainability" (ACon 4.0 #2019-04750) as well as the support received from Robert Larsson (Cementa AB), Petra Jenning (Fojab), Cognibotics AB and Miklos Molnar (LTH). These projects provided the opportunity to investigate the use of parallel kinematic manipulators in construction applications and to develop a parallel kinematic manipulator for specific construction tasks.

References

[1] Aitchison M., Tabrizi T. B., Beim A., Couper R., Doe R., Engstrom D., ... & Nelson, J. *Prefab housing and the future of building: product to process*. Lund Humphries, 2018.

[2] Bock T. The future of construction automation: Technological disruption and the upcoming ubiquity of robotics. *Automation in Construction*, 59, 113-121, 2015.

[3] Buchli J., Giftthaler M., Kumar N., Lussi M., Sandy T., Dörfler K., & Hack N. Digital in situ fabrication-Challenges and opportunities for robotic in situ fabrication in architecture, construction, and beyond. *Cement and Concrete Research*, 112, 66-75, 2018.

[4] Pivac M., & Pivac M. Fastbrick robotics. Online: https://www.fbr.com.au/, Accessed: 15/06/2020.

[5] Podkaminer N., & Peters L. Construction robotics, Online:https://www.construction-robotics.com/sam100/, Accessed: 15/06/2020.

[6] Sandy T., Giftthaler M., Dörfler K., Kohler M., & Buchli J. Autonomous Repositioning and Localization of an in situ Fabricator. *In Proceedings of the International Conference on Robotics and Automation*, pages 2852-2858, Stockholm, Sweden, 2016.

[7] Lussi M., Sandy T., Dörfler K., Hack N., Gramazio F., Kohler M., & Buchli J. Accurate and Adaptive In situ Fabrication of an Undulated Wall using On-Board Visual Sensing System. *In Proceedings of the International Conference on Robotics and Automation*, pages 3532-3539, Brisbane, Australia, 2018.

[8] Delgado J. M. D., Oyedele L., Ajayi A., Akanbi L., Akinade O., Bilal M., & Owolabi H. Robotics and automated systems in construction: Understanding industry-specific challenges for adoption. *Journal of Building Engineering*, *26*, 100868, 2019.

[9] Saidi K. S., Bock T., & Georgoulas C. Robotics in construction. In *Springer handbook of robotics* (pp. 1493-1520). Springer, Cham, 2016.

[10] Merlet J.P. *Parallel Robots,* 2nd ed. Springer Science & Business Media, 2006.

[11] ISO Robots and robotic devices - Collaborative robots. ISO 15066, 2016.

[12] ISO Safety of machinery – General principles for design – Risk assessment and risk reduction. ISO12100, 2010.

[13] ISO Safety of machinery – Safety-related parts of control systems – Part 1: General principles for design. ISO 13849-1, 2015.

[14] Pott A. *Cable-driven Parallel Robots: Theory and Applications,* Springer Berlin Heidelberg, 2018.

[15] Online: http://www.smerobot.org, Accessed: 15/06/2020.

Design-to-Robotic-Production and -Assembly for Architectural Hybrid Structures

H. Bier [a], A. Hidding [a] and M. Galli [a,b]

[a] Robotic Building Lab, Faculty of Architecture, DUT, The Netherlands
[b] Digital Production Research Group, Faculty of Technology, AUAS, The Netherlands

E-mail: h.h.bier@tudelft.nl

Abstract –

The Design-to-Robotic-Production and -Assembly (D2RP&A) process developed at Delft University of Technology (DUT) has been scaled up to building size by prototyping of-site a 3.30 m high fragment of a larger spaceframe structure The fragment consists of wooden linear elements connected to a polymer node printed at 3D Robot Printing and panels robotically milled at Amsterdam University of Applied Science (AUAS). It has been evaluated for suitability for assembly on-site without temporary support while relying on human-robot collaboration. The constructed architectural hybrid structure is proof of concept for an on- and off-site D2RP&A approach that is envisioned to be implemented using a range of robots able to possibly address all phases of construction in the future.

Keywords –

Architecture; computational design; optimization; robotic production; robotic assembly

1 Design-to-Robotic-Production and -Assembly

Design-to-Robotic-Production and -Assembly (D2RP&A) links design to materialization by integrating all (from functional and formal to structural, environmental, etc.) requirements in the design of building components. It establishes the framework for robotic production at building scale. The main consideration is that in architecture and building construction the factory of the future will employ building materials and components that can be robotically processed and assembled. D2RP&A processes incorporate material properties in design, control all aspects of the processes numerically, and utilize parametric design principles that can be linked to the robotic production.

The developed 1:1 prototype (Figure 1) is a 3.30 m high fragment of a larger structure and consists of variously sized wood elements (linear members and panels) that are milled according to functional, structural, and acoustic requirements and a 3D printed polymer node. The employed D2RP&A approach builds up on knowledge and know-how developed at Robotic Building (RB) Delft University of Technology (DUT) since 2014 [1]. It combines off-site additive and subtractive D2RP with on-site human-robot D2RA (Figure 2) and the challenge has been the integration of various D2RP&A techniques.

Figure 1. Prototype of the hybrid structure built in laboratory conditions

The architectural approach relies on principles such as continuous variation and material hybridity. While continuous variation implies that the structure is defined as adaptive mesh with high-low resolution tessellation

(with patterns varying in size and shape (Figure 3) and volumes transitioning into surfaces and vice versa), material hybridity emerges from combining wood and polymer-based elements.

2 Material hybridity

Buildings consists of various material systems. In a first iteration a series of studies exploring connections between multiple materials have been implemented. Materials considered were wood, recycled wood, reinforced Polypropylene and various steels.

2.1 3D printed nodes

Complex nodes connecting many linear wood beams are usually designed for maximal loads and are not optimized in terms of shape or structural strength for global and local requirements. The proposed additive D2RP approach aims to optimize nodes and a first polymer node (Figure 1) has been generated by connecting several linear elements in such a manner that a sequence for assembly without temporary support using robots is achievable. A second metal node (Figure 2) has been developed aiming to exploit and advance, respectively, knowledge developed in clay [1] and polymer [5] 3D printing. This knowledge combines structural optimization with adaptive material design and optimized robotic paths for printing without support material.

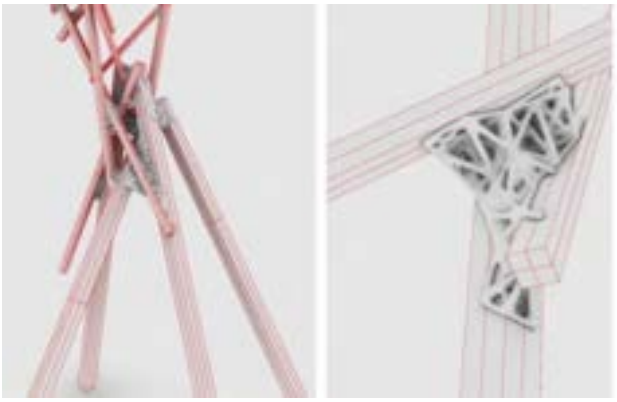

Figure 2. Optimised structural node for metal printing

2.2 Wooden spaceframe and panels

As a carbon-neutral renewable resource the wooden spaceframe consisting of linear elements with various sizes has been designed to explore D2RP&A at relatively large scale using a 3D printed node. The spaceframe is designed to accommodate paneling that together address structural and acoustic requirements and are produced by employing a packing procedure and milling (Figure 3). The panels were designed to be mounted on the structure and for the purpose of this proof-of-concept exercise they were rationalized to rectangular shape.

3 D2RP for Material Hybridity

Material hybridity requires taking into consideration various material performances. Thus, D2RP needs to integrate several requirements for materials, tools, and procedures in design.

3.1 3D Printing

The linear wooden elements of the spaceframe are connected by 3D printed nodes, which can reach a high level of complexity due to the employed additive D2RP process. The nodes are from glass-fiber reinforced Polypropylene and various steels. The produced 1:1 reinforced Polypropylene prototype is a proof of concept illustrating the flexibility of the joint to allow for connections of large-scale wooden elements of varying sizes placed in diverse angles. The node connects three large timber pieces of 140x140 mm. While 3D printing of polymer components using structural optimization and adaptive material design to fine tune stiffness has been extensively explored, 3D printing with various steels and the combination with another material such as linear wood elements needs further investigation.

In the next iteration, the goal is to structurally optimize the spaceframe in order to achieve a highly efficient distribution of nodes and linear elements. The thickness of the linear elements is then chosen according to the structural analysis in order to minimize material, and reduce the total weight of the structure. The reduction of the weight leads to a further reduction in stresses in the linear elements, and therefore smaller elements can be used and nodes are customized to fit local and global stiffness requirements. This D2RP process is run in Karamba, Grasshopper where several safety factors can be considered, such as overall and material safety factors that will compensate for the structural irregularities of the wooden elements.

3.2 3–4D Milling

The basic panels were produced at Amsterdam University of Applied Science (AUAS) by employing a

packing procedure that allowed to pack linear elements of various sizes within the bounding box, which for the purpose of the exercise were rationalized to rectangles (Figure 4). Since the panels had to integrate acoustic and structural considerations, they were structurally optimized using Karmaba in order to minimize material usage. Furthermore, they were acoustically optimized. In order to increase interior comfort, it is important to decrease direct reflection and thus, create a scattering geometry in order to transform noise into ambient background sound. Large flat surfaces generate strong specular reflection, which is unwanted. In addition to absorption, the goal is to achieve diffused or scattered sound waves by manipulating overall geometry and surface treatment.

The surface treatment of the panels (Figure 3) addresses sound waves in two ways: One addresses the mid-high frequency range, where the global shape of the prototype diffuses or scatters the sound in the chosen frequency range. The other addresses the higher frequencies, which are effectuated by the detailed surface treatments. The sharp edges cause diffraction, therefore increasing the absorption coefficient for the higher frequency sounds. By tuning the surface treatment, the scattering and the absorption coefficients can be controlled and surfaces can be shaped to match the acoustic requirements of the space.

The 6-axis robotic arm can reach further and approach the material at more angles than a 3, 4, or 5 axis milling machines thus facilitating performative geometries. A larger cylindrical bit was used to remove the material efficiently, while for the small-scale surface textures resulted a smaller bit was used (Figure 4).

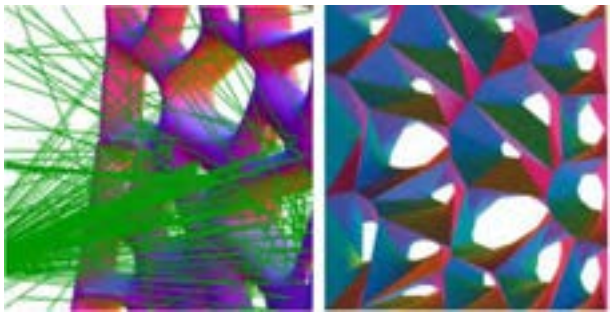

Figure 3. Acoustic simulation on specific surface tectonic

The acoustic simulations have been implemented in Acoustic Shoot, Grasshopper. This plugin imitates the acoustic ray tracing process. The next step is to create accurate surface textures according to the requirements and to predict their behaviors using more accurate mathematical models. The current ray tracing simulations do not take into consideration the behavior of the different wavelengths, when compared to the dimensions of the surface textures. Furthermore, conducting physical measurements is paramount for determining the absorption and scattering coefficients locally, based on local surface details.

Figure 4. Panels with integrated acoustic and structural performance robotically produced at AUAS

4 D2RP&A on - and off - site

D2RP implied prefabrication of building components using robotic additive and subtractive production systems for 3D printing nodes and 3-4D milling surface tectonics of panels.

D2RA on-site implied at this stage that the assembly focused only on the spaceframe with the 3D printed node not the panelling ‘Figure 1’. D2RA required some level of human-robot interaction. While robotic stacking of linear elements in controlled environment (Figure 5) has been explored in a previous project [2], the assembly of freestanding structures needed and still needs investigation with respect to identifying the sequence of operations as well as challenges for human-robot interaction while reducing use of temporary support. Similar to strategies and concepts for large-scale projects developed at ETHZ [3] a multiscale production system was proposed that employs building component optimization based on geometry analysis, structural and acoustic optimization.

The process is based on a human-robot on-site production approach wherein the material, in this case timber, is brought to the site together with the robotic production setup. The production strategy involves robots that cut the elements and place them in space based on their specific angle and connection point, and the humans fix i.e. screw the elements in place. The spaceframe, panels and joints are thus prefabricated and are assembled on site with help of robots. The size of the structure is in this case restricted to the size of the robot reach and the height of the truck on which the robots are fixed [4].

The challenge is to choreograph the interaction between humans and robots employing machine learning

(ML) and computer vision techniques, such as OpenCV and DNN in order to find nodes' location, detect the related linear elements, pick and transfer them with a gripper to the intended location, while considering obstacle avoidance (human safety). The idea is that a human will navigate the arm with the hand, and in order to move it from the intended location, which is near the node to its final location, which is next to the node.

The proposed D2RP&A approach is still work in progress, and the proof of concept presented in this paper has been implemented using various mapping, modeling, simulating, and prototyping techniques that identified challenges that need to be tackled.

Figure 5. Huma-robot stacking of linear elements tested in lab conditions

5 Conclusion

The space frame fragment is proof of concept for a hybrid on- and off-site D2RP&A approach that is envisioned to be implemented using a range of robots and in collaboration with humans. Challenges of the envisioned on- and off-site construction process are various from HRC to environment related challenges involving rough terrain, wind, rain, dust, and temperature fluctuations. Previous projects such as the Factory-on-the-Fly by Odico [6] or In-situ Fabricator by ETH Zurich [4] have tackled some of the challenges, however, the question of how on- and off-site approaches need to be combined and human-robot collaboration needs to be choreographed, require further exploration. While all these projects transported the robotic arms in containers that could either open up or could be completely removed, the integration of design, production, and assembly as HRC processes and the handling of outdoor unstructured environments requires further specification.

The project presented in this paper identifies a series of processes from design to production and assembly that require integration. It challenges the fragmented, inefficient, and expensive processes of today's building construction practice and proposes novel multi-performative D2RP&A strategies. While some aspects of these strategies have been developed only conceptually, others have been already modelled, simulated or prototyped. The next step is the development of the HRC approach, which relies on practical methods facilitating collaborative sawing [8], collaborative polishing [9], etc. and involving Artificial Intelligence (AI) that enables physical collaboration between robots and humans. Furthermore, other materials such as circular wood and steel are considered. The ultimate goal is to advance data-driven design approaches for the robotic production and assembly of mass customizable multi-material building components and deploy HRC techniques for testing the blueprint of future robotic building.

Acknowledgments

This paper has profited from the contribution of students and researchers from the Robotic Building Lab at TU Delft and Digital Production Research Group at AUAS. The presented project could not have been implemented without the support of industrial partner 3D Robot Printing.

References

[1] H. Bier (ed.), *Robotic Building, Springer's Adaptive Environments Book Series Vol. 1*, 2018

[2] Y. Chiang, H. Bier and S. Mostafavi, *Design to Robotic Assembly: An Exploration in Stacking*, Frontiers in Digital Humanities, Vol. 5, 2018.

[3] P. Eversmann, *Digital Fabrication in Education: Strategies and Concepts for Large-Scale Projects.* On-line: https://www.researchgate.net/publication/322316908_Digital_Fabrication_in_Education_Strategies_and_Concepts_for_Large-Scale_Projects Accessed: 20/06/2019.

[4] M. Galli, *Architecture for Disaster Relief - D2RP System for Disaster Management*. On-line: http://rbse.hyperbody.nl/index.php/project12:P63

[5] V. Helm, J. Willmann, F. Gramazio, and M. Kohler, *In-Situ Robotic Fabrication: Advanced Digital Manufacturing Beyond the Laboratory* in F. Rohrbein et al. (eds.), Gearing Up and Accelerating Cross-Fertilization between Academic 63 and Industrial Robotics Research in Europe, Springer Tracts in Advanced Robotics 94, DOI: 10.1007/978-3-319-02934-4_4, 2014 Science, Engineering and Humanities and Social Sciences references

[6] A. Hidding, H. Bier, Q. Wang, P. Teuffel, G. Senatore, *Structural Adaptation through Stiffness Tuning,* Spool: Cyber-physical Architecture Issue 2, 2019

[7] Odico, 2017, *Factory-On-The-Fly*. On-line: https://odico.dk/en/technologies#factory-on-the-fly

[8] Peternel, Tsagarakis and Ajoudani. A Human-Robot Co-Manipulation Approach Based on Human Sensorimotor Information. In IEEE Transactions on Neural Systems and Rehabilitation Engineering, vol. 25, no. 7, pages 811-822, 2017.
[9] Peternel, Tsagarakis, Caldwell and Ajoudani. Robot adaptation to human physical fatigue in human–robot co-manipulation. In Autonomous Robots 42, pages 1011–1021, 2018.

Design and Synthesis of the Localization System for the On-site Construction Robot

Wen Pan[a], Rui Li[b], and Thomas Bock[a]

[a] Chair of Building Realisation and Robotics, Technical University of Munich, Germany
[b]School of Automation, Chongqing University, Chongqing, P.R. China
E-mail: wen.pan@br2.ar.tum.de, raysworld@outlook.com, thomas.bock@br2.ar.tum.de

Abstract – Building tasks that carry out on the building façade, such as painting, cleaning, and maintenance are often to be described as dangerous, dirty, and demanding. Recently, researchers and institutes are developing autonomous and semi-autonomous On-site Construction Robots (OCR) for those aforementioned applications. The most of façade working OCR is either suspended or supported by the secondary structure. The biggest challenges for these types of methods are obtained stability while carrying out the task against external elements such as wind and inertia caused by the step motors. There are very limited resources that discuss positioning and stabilizing methods. In this paper, a novel localization system for OCR will be introduced, which is based on the on-site construction robot commissioned by The Construction Industry Council Hong Kong (CIC) and developed by the Chair of Building Realization and Robotics (br2) at Technical University of Munich (TUM). The research presents the preliminary concept of a stabilization method that can be adopted on most of the suspended OCR type. The proposed system will localize the initial position, alter the OCR into the correct working pose, and secure the system to place. At the time of this writing, it is only limited to the conceptualization and proof of concept of the system. The control scheme is validated in simulation. The proposed approach is expected to be expanded into other applications in the future.

Keywords –
Construction robotic; localization; Stabilization

1 Introduction

To adopt automation and robotic technology with the aim to augment human performance is not a new concept in the construction industry. In fact, since the late 1970s and the early 1980s, many research institutions, universities, and construction machinery companies have conducted research and development (R&D) initiatives. In the early 1980s, Japan's construction industry started to face a shortage of skilled workers due to the fact that working condition of conventional construction sites was considered dirty, dangerous and difficult by the young generation. The construction industry had begun to fall behind the manufacturing industry [1]. Until today, there are over 150 Single-Task Construction Robots (STCRs). Most of the systems were developed to be used on the construction site. Each type of robot was designed to focus on a particular on-site work task. In general, automation and robotic technologies are often referred to as a solution to solve many profound industry-related issues, such as declining productivity, skilled labour shortage, safety, and quality. The increased popularity of robots is expected with improved economic incentive and wider applicability [2]. Some construction processes can be automated while others not, even the one that can be automated in the other sector, such as manufacturing sector might not be realized in the construction context. For instance, the construction sector is fundamentally different from that in the manufacturing sector in many aspects. The difference can be reflected in the following characteristics including working environment, distribution of materials, the allocation of the robot and human function, skill sets, and information transformation [3]. Therefore, to develop a practical application for the construction industry the system designers must be proficient in traditional construction methods, building structure, engineering management and other disciplines, and understand the auxiliary knowledge about microelectronics, mechanical design, manufacturing, and automation, so interdisciplinary teaching and cooperation in the field of construction robotics is essential.

There are increasing demands of working in great heights, due to the popularity of high-rise buildings. Yet, high-rise construction often prone to issues that affiliated with working in great heights. In this paper, the author will use the multifunctional façade finishing robot that was developed through the consulting project commissioned by the Construction Industry Council Hong Kong (CIC) as a case study. When the proposed

OCR system is suspended in great heights and to be exposed in the external environment. It is vital for the system to maintain stability while operation, and to position itself securely and accurately. This paper will focus on the development of a practical solution that can potentially address the challenges associated with localization, stabilization, and positioning tasks in respect of the suspended type of OCR system. The method can be adjusted and adopted when executing a similar development.

2 Background

Many construction tasks require labour to perform repetitive motions while to be suspended in great heights. For instance, cleaning task for high-rise buildings fitted with glazing curtain wall system, painting for high-rise building façade, and various maintenance tasks that need to be carried out from building façade. As mentioned earlier, working in heights imposes considerable safety hazards. It may sound contradictory but in the construction industry, on-site operational health and safety are one of the most critical areas that the industry trying to improve and very often overlooked. Construction accidents are influenced by multiple circumstances, such as workplace organization, equipment, training, risk awareness, and individual attitude. Hence, in many cases, it is hard to predict or to prevent accidents from happening. According to research regards to contributing factors in construction accidents, falling from heights is one of the biggest contributors to construction-related accidents [4]. In addition, working in heights also increases the opportunities of suffering other types of injuries, such as slips, trips due to unpredictable working condition. Many tasks involve working in heights are usually physically demanding even for the fit and younger workers [5]. Evidently, many developed economies in the world experience the aging workforce due to demographic changes. For instance, in Hong Kong, approximately 25.83% of the workers are above 50 years of age. Compared to a younger worker, workers 50 years and over will expose themselves to a higher risk of injury [6].

Consequently, researchers have been developing OCRs that provide full or partial replacement of the tasks that used to perform entirely by human. Automation does not offer all the solutions to the identified challenges, yet can provide an alternative method that enhances human performance and improve on-site operational [7]. In principle, façade OCRs can be divided into three main functions include rendering, cleaning, and inspection. The examples of some of the applications can be seen in Table 1 .

Table 1. Examples of the applications in on-site construction robot

Manufacturer	Robot	Country	Application	localization method	Façade type
Taisel	Exterior wall painting	Japan	Rendering	Guide rail	Vertical, flat
Kajima	Façade inspection robot	Japan	Tile façade inspection	Parapet, wall clamps and supported by cables	Vertical, flat
Fraunhofer, SIRIUS	Glazing curtain wall cleaning robot	Germany	Façade cleaning	Wheels and cables	Protruding
Louvre, Robosoft	Glazing curtain wall cleaning robot	France	Façade cleaning	Vacuum cups	Vertical, flat

The aforementioned systems also demonstrate various localization methods that have been adopted for a diverse range of application. Each system were tailor made for a specific configuration of building design that means the system is not applicable to be used for other buildings. Along with high operational costs, and complexity, many systems are not be able to commercialize successfully.

CIC commissioned the Chair of Building Realization and Robotics (br2) at Technical University of Munich (TUM) to research and develop construction robots and automation strategies that are tailor-made for the Public Housing Construction (PHC) sector in Hong Kong. As part of the project, the project team have to identify the requirements of the stakeholders, functional, non-functional requirements, and the circumstances of the construction site. There are other factors could also influence on the final decisions, such as technological, social, political, and economical. The project has been divided into six stages. The first phase consists of initial research, literature review, preselection, and proposing use case scenarios. The second stage includes an online survey, questionnaires, and on-site visit. The third stage is co-creation workshops. The fourth stage is concept development and detailed design of the proposed system. The fifth stage includes the construction of the mock-up and discussion of dissemination and exploitation strategies. The final stage is to develop a roadmap that provides a guideline on how to execute the remaining project a short-, mid-, and long-term basis. In the end, the Multifunctional Façade and Exterior Finishing Robot were chosen to be developed as a stimulator to the PHC industry. During the development stage, the project team have identified numbers of issues, in which the system positioning, stabilization imposes serious implication on the overall performance of the proposed OCR.

3 Research challenge and objective

Diverse localization methods were adopted in the façade application OCRs that have been developed in the past. However, they were designed to operate on the specific type of building façade. For instance, the Taisel exterior wall painting robot is positioned with guide rails. The guide rails are not an additional fixture for the building, yet the architect was made aware that the exterior wall painting robot will be equipped, hence the guide rail was included as part of the design feature of the façade to accommodate the robot. Evidently, the façade OCRs is tend to be developed and operated on specific type of façade and to manage unique configuration and material.

According the research, the project team realised that the existing façade OCRs are not applicable to the PHC façade type. This is due to the complexed geometry shape of the façade design. The external façade is constructed with prefabricated concrete panel. As shown in Figure the prefabricated concrete façade (PCF) element consists of two major protruding sections, both are designed to support air-conditioning equipment. The edge at the bottom of the panel overshadowing the floor level below, especially during the hottest hour of the day. Another function of the overhanging edge is to divert rainfalls during the subtropical monsoon seasons in Hong Kong. The advantage is that the PCF is identical for every elevation of the building.

Figure 1. Typical public housing construction type

Because of the complexed shape, a high level of accuracy is required for the painting task, in particular to keep an even paint coverage throughout every sections of the PCF. When dealing with a flat surfaces, this requirement is achievable even with the conventional supporting solution, such as suspended working platform that is often referred as gondola. The gondola is suspended by cables, which supported by wall clamps that installed to the parapet wall. When hanging in mid-air, it is very difficult to keep the gondola in absolute stable motion, due to wind, inertia, and movements caused by the operator. In the case of CIC project, as part of the design requirement, the proposed OCR was developed based on the conventional gondola platform that is widely used in Hong Kong construction industry for various façade tasks. The system need to be stable and retain levelled with the reference wall surface prior to carry out painting task and to ensure the required functional performance can be achieved.

The main challenge faced by the proposed OCR is how to design a system that is capable of self-diagnose the position, and to keep the working platform stable during operation. The primary design objectives of the system are, first, the system is to be expected to come to a stop once the system reaches the correct position. Second, after stopping, the system needs to remain stationary and to keep perfectly horizontal to the building façade. Third, the system should able to detect moments caused by either the external force or the momentum of itself. Once displacement has been detected, the system is required to correct the position automatically.

The proposed localization method presents the following improvements to the existing method. The design will not require any temporary or permanent additional fixtures and fittings other than the one has been used in a conventional manner. With a minor adjustment to the design, the system can be adapted to a large variety of building façade. The improved stability will accommodate a variety of automated applications, which demands an immobilized working condition. In terms of semi-automated application, human labour will also benefit from a stationary working platform to avoid the risk of occupational injuries. The next section will describe the development method in detail [8].

4 Method

The proposed Multifunctional Façade and Exterior Finishing Robot is based on the design of conventional gondola, the additional frame below the gondola hosts the robot end-effector, the space between the frame structure constitutes the robot working trajectory. Supported by the common roof supporting system, the robot can descend from the top to the bottom of a high-rise building while executing a task. Two electric motors near the hoisting devices on top of the robot are used to actuate the up and down movement. Through the addition of various sensors, the ultimate goal is to achieve a fully automated façade processing robot system. The robot system is highly modularized, meaning that the shape and size of the robot can be easily changed in accordance with the design of the target buildings, see Figure 1.

The localization system compresses of counterbalance design. It is compatible with all types of prefabricated façade panels used in Hong Kong PHC sector. The system consists of three subsystems, which include a detection system, stabilization system, and final

positioning system [8].

1. **Detection system**: equipped with two linear actuators that provide moment along X and Z-axis. A limit switch module is installed at the end of the X-axis.

2. **Stabilization system**: consists of three rotation servo actuators interconnected with counterbalance bars. At the tip of the final link a clamping device along with pressure sensors are installed. In addition, an inner industrial vacuum suction device is equipped in between the clamps.

3. **Final positioning system**: comprised off two retractable vacuum suction cups, they are able to secure the system to the final position. They are also able to withstand wind loads under normal circumstances.

All three subsystems can be adjusted when applied to another building and only minimum setup time is needed.

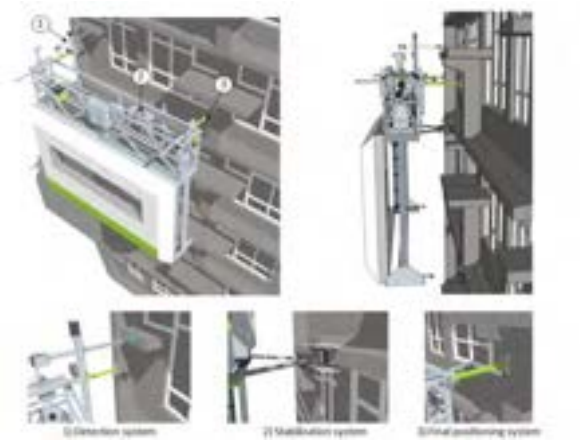

Figure 1. The design of the localization system

4.1 The design of the localization system

4.1.1 The mechatronic design and the kinematics of the system

The kinematic model of the localization system is shown in Figure 2. Based on the Denavit-Hartenberg (D-H) convention, the coordinate transformation between two consecutive link frames $\{i-1\}$ to $\{i\}$ can be defined as:

$$^{n-1}T_n = \mathrm{Rot}_{x_{n-1}}(\alpha_{n-1}) \cdot \mathrm{Trans}_{x_{n-1}}(a_{n-1}) \cdot \mathrm{Rot}_{z_n}(\theta_n) \cdot \mathrm{Trans}_{z_n}(d_n), \quad (1)$$

where $\mathrm{Rot}_{x_{n-1}}(\alpha_{n-1})$ defines a rotation of angle α_{n-1} around the x_{n-1} axis, and $\mathrm{Trans}_{x_{n-1}}(a_{n-1})$ defines a translation of a_{n-1} along the x_{n-1} axis. The transformation matrix $^{n-1}T_n$ is a composition of rotations and translations to move from a frame $\{i-1\}$ until it coincides with the frame $\{i\}$.

Accordingly, the D-H parameters for this model is shown in Table 2, where d means the offset along previous z to the common normal, θ means the angle about previous z, from old x to new x, a means the length of the common normal (Assuming a revolute joint, this is the radius about previous z), and α means the angle about common normal, from old z axis to new z axis [8] and [9].

Table 2. The D-H parameters of the localization system model

α_{n-1}	a_{n-1}	θ_n	d_n
$-pi/2$	0	0	d_1
$pi/2$	0	$-pi/2$	d_2
$-pi/2$	0	0	d_3
$pi/2$	0	$\theta_4 + pi/2$	0
$pi/2$	0	θ_5	0

With the D-H parameters, the transformation matrix from the robot base frame to the end-effector can be calculated using joint variables. The end-effector pose can be obtained by multiplying the transformation matrix as follows:

$$^0T_e = {}^0T_1\,{}^1T_2\,{}^2T_3\,{}^3T_4\,{}^4T_5\,{}^5T_e, \quad (2)$$

where $^{n-1}T_n$ is the transformation matrix as shown in (1).

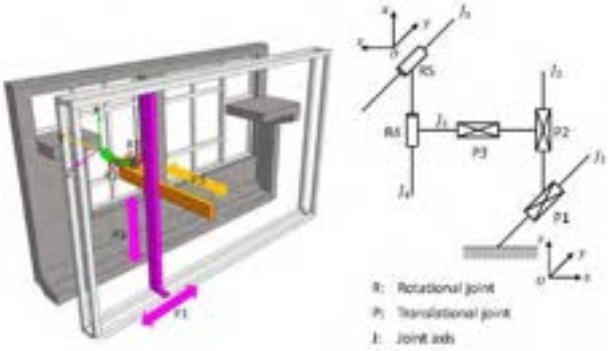

Figure 2. Kinematic structure of the localization system.

4.1.2 The work principle of the design

The localization process can be divided into six steps.

Step 1: Robot descends along the cable operated by the conventional step motor. The system will stop descending when the limit switch make contact with the protruding feature of the PCF.

Step 2: Due to inertia and external forces, at this moment the system may swing swiftly. The system is

designed so the stabilization system is aligned with the overhanging edge of the PCF. The stabilization system will be reaching out and press onto the surface of the edge. Once the pressure sensor detects even force has been distributed across the sensor the clamping device will retract and form a firm grasp to the edge, while the inner suction cup secures the system in place [8].

Step 3: once the system is stabilized, the stabilization system detects if the position is horizontally aligned with the PCF façade, if it is not, then the system will correct the position by using impedance control method.

Step 4: The robot extends the retractable vacuum grippers toward the wall at the proper length, then to grasps the wall to fix its position.

Step 5: the robot will detect any deviation between the real position and the ideal one. If there is any deviation the system will offsets, and the step three and four will be repeated.

Step 6: after the painting application has been complicated. The vacuum suction cups and clamps will be unfastened. The system is ready to decent to the lower floor level.

4.2 The control of the localization system

To achieve the above processes, several controllers for the localization system should be designed. Based on whether the robot will interact (have contact) with the target building, the controllers are divided into two categories: position controller and force controller. The former guides the robot to a precise position, while the latter attempts to maintain a compliant contact between the robot and the environment. We take the stabilization system as the example to illustrate how to achieve the stabilization with the abovementioned controllers.

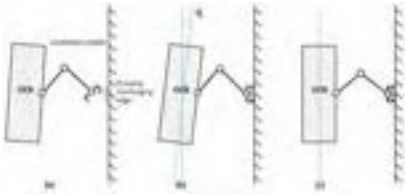

Figure 3. The three phases of the localization system (LS) for stabilization. (a) The LS moves towards its front direction to get in touch with the building wall; (b) The LS attaches its end with the wall and fixes its pose; (c) The LS eliminates the pose error.

As shown in Figure 2, the goal of the stabilization system is to find the wall, attach the gripper with the wall and finally adjust the pose of the robot. To achieve that, the following control laws are adopted [8].

4.2.1 The proportional-derivative (PD) control law

The dynamics of the robot system can be described in the form of the equation

$$M(\theta)\ddot{\theta} + C(\theta,\dot{\theta})\dot{\theta} + N(\theta,\dot{\theta}) = \tau, \quad (3)$$

where $\theta \in \mathbb{R}^n$ is the set of configuration variables for the robot and $\tau \in \mathbb{R}^n$ the torques applied at the joints, and M, C, and N are the inertia, Coriolis and gravity-related matrix, respectively. In practice, the robot is controlled by τ.

Before the localization system starts to act, and after it holds the wall firmly, the system should always keep a high precision for the movement or keep itself exactly where it is. This could be achieved with the PD controller:

$$\tau = -K_v\dot{e} - K_p e, \quad (4)$$

where $e = \theta - \theta_d$, and θ_d defines the desired configuration of the robot. K_v and K_p are positive definite matrices indicating the coefficients of the PD controller. For second-order systems, the relationship between K_v, K_p and the damping D of the system can be described as

$$D = \frac{K_d}{2\sqrt{K_p}}, \quad (5)$$

which helps to provide an initial value to adjust the expected response of the system [8].

4.2.2 The impedance control law

During the states where the robot and the wall are in contact, the robot should prevent rigid collisions between itself and the wall. In that case, the PD controller, which only targets at moving to the goal position in joint space, will not fulfil the requirement. We need to redesign a controller to provide a compliant force in the task space. When contact occurs, the robot should handle the contact in a soft, compliant way.

In such case, the dynamics of the robot system in the task space can be rewritten as

$$M_x(\theta)\ddot{x} + C_x(\theta,\dot{\theta})\dot{x} + N_x(\theta,\dot{\theta}) = J^{-\top}\tau + F_a, \quad (6)$$

where x is the pose of the end-effector in task space, J is the Jacobian and F_a is the external force applied to the end-effector. The postscript of M_x, C_x, and N_x indicates that the matrix is an equivalent of the matrix expressed in task space with

$$M_x(\theta) = J^{-\top}M(\theta)J^{-1} \quad (7)$$
$$C_x(\theta,\dot{\theta}) = J^{-\top}C(\theta,\dot{\theta})J^{-1} - M_x(\theta)\dot{J}J_a^{-1} \quad (8)$$
$$N_x(\theta,\dot{\theta}) = J^{-\top}N(\theta,\dot{\theta}). \quad (9)$$

Still, the robot is controlled by τ:

$$\tau = J^{\top}(\theta)\big[M_x(\theta)\ddot{x} + C_x\big(\theta,\dot{\theta}\big)\dot{x} + N_x\big(\theta,\dot{\theta}\big) - F_a\big]. \quad (10)$$

Then the desired acceleration trajectory $\ddot{x} = a$ can be designed in the task space. Regarding the contact force, a dynamic impedance model can be expressed as

$$M_d(\ddot{x} - \ddot{x_d}) + D_d(\dot{x} - \dot{x_d}) + K_d(x - x_d) = F_a, \quad (11)$$

where $x_d(t)$ and $x(t)$ are the desired/real motion, respectively. M_d, D_d, and K_d are the desired inertia, damping and stiffness, respectively. In this case, if a soft and compliant contact is desired, it can be achieved by choosing

$$a = \ddot{x}_d + M_d^{-1}[D_d(\dot{x}_d - \dot{x}) + K_d(x_d - x) + F_a]. \quad (12)$$

Substituting Eq. (10) into Eq. (12), there will be

$$\begin{aligned}\tau = M(\theta)J^{-1}(\theta)\{&\ddot{x}_d - \dot{J}(\theta)\dot{\theta} \\ &+ M_d^{-1}[D_d(\dot{x}_d - \dot{x}) \\ &+ K_d(x_d - x)] + C(\theta,\dot{\theta})\dot{\theta} \\ &+ N(\theta,\dot{\theta}) \\ &+ J^{\top}(\theta)[M_x(\theta)M_m^{-1} - I]F_a\}.\end{aligned} \quad (13)$$

Further, if M_d is chosen as

$$M_d = M_x(\theta) = J^{-\top}(\theta)M(\theta)J^{-1}(\theta), \quad (14)$$

then the control law becomes

$$\begin{aligned}\tau = M(\theta)J^{-1}(\theta)\{&\ddot{x}_d - \dot{J}(\theta)\dot{\theta}\} + C\big(\theta,\dot{\theta}\big)\dot{\theta} \\ &+ N\big(\theta,\dot{\theta}\big) \\ &+ J^{\top}(\theta)[D_m(\dot{x}_d - \dot{x}) \\ &+ K_m(x_d - x)],\end{aligned} \quad (15)$$

which do not require the contact force F_a feedback anymore. With Eq. (15), the compliant motion which limits the contact forces at the end-effector could be achieved [8].

4.3 Simulation of the proposed system

4.3.1 Setup of the simulation

The proposed localization system is verified in robot simulation environment ROS (Robot Operating System) + Gazebo. Gazebo is an open-source 3D robotics simulator, which is widely applied in robotics research area. In this simulation, it is hoped that the validity and effectiveness of the design could be verified.

4.3.2 Process of the simulation

To proceed, a simplified robot model is firstly established in Gazebo. Following the link-joint relationship of the robot, the model is expressed in sdf format [10]. The size of the model and the corresponding inertia property are set as the measured value in the CAD designing software. Finally, a Gazebo plugin is programmed to send the joint commands from the controller to the simulator. A framework structure is depicted in Figure 3.

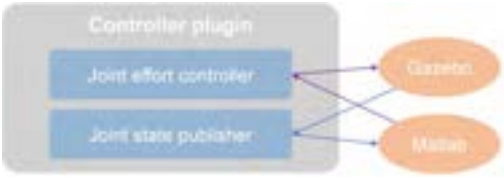

Figure 4. The framework structure of the simulation. The simulation is implemented in Gazebo. The controller is designed in Matlab. Using ROS communication mechanism, Matlab receives the current joint states from Gazebo, determines the joint efforts and sends them to Gazebo to achieve the final movement.

4.3.3 Data analysis

For the first stage, after fine-tuning the parameters for the PD controller, it could drive the localization system (LS) to the standby state fast and steady. For the second stage, the impedance controller could guide the robot to the right direction and achieve the contact with a very soft impact, see Figure 5.

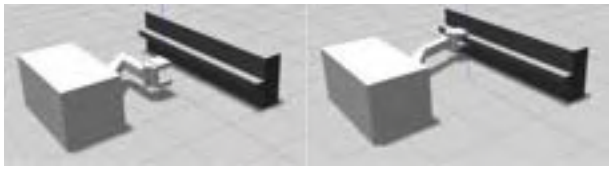

Figure 5. The localization process in the simulation. Left: the standby state. Right: the grasping process.

5 Future work

At the time of this writing, the proposed stabilization system is still under the Proof of concept (PoC) stage. There still many tasks and will take time and extensive tests to develop them into a practical application. The following tasks need to take into consideration when further developing the proposed system.

- For the detection system: to select the appropriate sensor technology for the specific construction operation environment. For example, a laser sensor may be sensitive to dust particles or reflective surfaces such as glazing and metal, but on the other hand, a gyroscope sensor may require high precision of the reference façade.
- For the stabilization system: it is necessary to develop an active and passive compliant control method to eliminate the external influence (i.e. the

wind, an unexpected collision).

- For the final positioning system: it is necessary to develop a robust position controller to guide the end-effector docking position.

It is crucial to test the localization system before the final pilot runs to reduce the risk of system failure, damage, or safety hazards. To test the effectiveness of the localization system, it is necessary to build a fully functional simulation or prototype that can be used for laboratory testing as well as pilot testing [8].

6 Conclusion

The paper proposed an innovative localization system for the Multifunctional Façade and Exterior Finishing Robot that developed in the CIC project. The proposed system consists of three subsystems, which include a detection system, stabilization system, and final positioning system. The objectives of the localization system including to assist the robot to localize the initial position, current the robot's position into the accurate operation pose, finally to grasp the façade and secure the robot to place. In order to achieve a fully functional application, several controllers for the localization system should be designed. As a PoC, two controllers were developed and described in the paper: position controller and force controller. The localization system was developed based on PD control law, the impedance control law was used to avoid rigid collisions between the robot and the façade. The controllers are designed in Matlab. Using ROS communication mechanism method, and simulated by using Gazebo simulator. As mentioned earlier, at the time of this writing, the proposed localization system limited to the conceptualisation. A fully functional robot application and extensive pilot testing are necessary to develop the PoC further.

Acknowledgements: The authors would like to sincerely thank the Construction Industry Council Hong Kong (CIC) for initiating and funding part of this research.

Rui Li is with School of Automation, Chongqing University. He was also with Informatics 6, Technical University of Munich. The work is partly supported by Zhejiang Lab Open Program (2019MC0AS04) and National Natural Science Foundation of China (Grant No. 61703400, 61702516)

References

[1] Gann, R.G. Innovation in the Japanese Construction Industry: A 1995 Appraisal. National Institute of Standards and Technology Special Publication 898, 1996.

[2] Cousineau, L. and Miura, N. Construction robots: the search for new building technology in Japan. ASCE Publications, 1998.

[3] Everett, J. G., & Slocum, A. H. Automation and robotics opportunities: construction versus manufacturing. Journal of construction engineering and management, 120(2), 443-452, 1994.

[4] Haslam, R. A., Hide, S. A., Gibb, A. G., Gyi, D. E., Pavitt, T., Atkinson, S., & Duff, A. R. Contributing factors in construction accidents. Applied ergonomics, 36(4), 401-415, 2005.

[5] Gibb, A., Leaviss, J. and Bust, P. Older construction workers: needs and abilities. In Procs 29th Annual ARCOM Conference (pp. 2-4), 2013.

[6] Maertens, J.A., Putter, S.E., Chen, P.Y., Diehl, M. and Huang, Y.H.E. 12 Physical Capabilities and Occupational Health of Older Workers. The Oxford handbook of work and aging, p.215, 2012.

[7] Lia, R. Y. M., & Leung, T. H. Leading safety indicators and automated tools in the construction industry. In ISARC. Proceedings of the International Symposium on Automation and Robotics in Construction (Vol. 34). Vilnius Gediminas Technical University, Department of Construction Economics & Property, 2017.

[8] Pan, W. Methodological development for exploring the potential to implement on-site robotics and automation in the context of public housing construction in Hong Kong. (Unpublished doctoral dissertation). Technical University of Munich, Germany, 2020.

[9] Hartenberg, Richard Scheunemann; Denavit, Jacques. Kinematic synthesis of linkages. McGraw-Hill series in mechanical engineering. New York: McGraw-Hill. p. 435, 1965.

[10] SDFormat. On-line: http://sdformat.org/, Accessed: 04/05/2020.

Online Synchronization of Building Model for On-Site Mobile Robotic Construction

S. Ercan Jenny[a], H. Blum[b], A. Gawel[b], R. Siegwart[b], F. Gramazio[a] and M. Kohler[a]

[a]Department of Architecture, ETH Zurich, Switzerland
[b]Department of Mechanical and Process Engineering, ETH Zurich, Switzerland

ercan@arch.ethz.ch, hermann.blum@mavt.ethz.ch, abel.gawel@mavt.ethz.ch, rsiegwart@ethz.ch, gramazio@arch.ethz.ch, kohler@arch.ethz.ch

Abstract -

This research presents a novel method for a data flow that synchronizes building information with the robot map and updates building components to their "as-built" states, in order to facilitate an on-site mobile construction process. Our experiments showcase mobile mapping and localization of a robotic platform featuring segmentation, plane association and quantitative evaluation of deviations. For the users of the on-site mobile robotic system, we present a suitable interface that allows for task level commanding and the selection of target and reference building components (i.e. walls, floor, ceiling). Additionally, this interface seamlessly integrates the online workflow between building construction and the robot map, updating the target building components to their "as-built" states in real time and providing a visual representation of additional task-specific attributes for building components in the robot map, in addition to geometries. This is presented as a first step toward integrating users of the system into the proposed robotic workflow to develop decision-making strategies for fitting building tasks to local references on-site.

Keywords -

On-Site Mobile Construction; Localization; Construction Robotics; Building Model; As-Built; Deviation Analysis; Robotic Construction Workflow with User Interaction

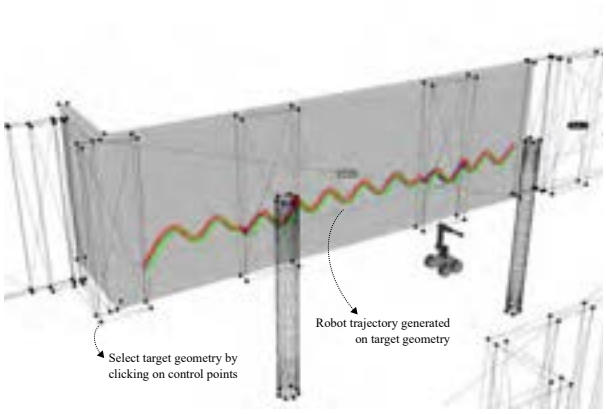

Figure 1. Robot trajectory representing the building task, generated on selected target geometry.

1 Introduction

Robotic technologies are widely applied in the off-site prefabrication of building components, where the strength of high-tech assembly lines can yield their full potentials: robots and work-pieces are in fixed locations with constant conditions, and building components can be mass-produced without the need to dynamically adapt the process. However, the majority of building tasks are executed directly on construction sites. In contrast to off-site prefabrication, on-site building construction often deals with dynamically changing conditions of large scale building components in spatially complex and cluttered environments. Furthermore, on-site work inherently generates deviations from the "as-planned", which is the state of the design as it should be. This requires craftsmen to register the differences and adapt the building tasks according to the "as-built" condition, which is the state of the construction as it is [1].

To facilitate an on-site construction cycle in an unbroken digital chain, a mobile construction robot must be able to understand the context within which it is working: it must localize itself via a robot map, both globally and locally, in reference to the already built components and the task being executed. In addition, it must be able to detect and understand any divergences between "as-planned", and "as-built" conditions. To achieve this in an on-site robotic construction process, a key challenge is linking the building information to the mobile robot's internal representation of the world (referred to as a robot map) and perception of its surroundings, using on-board sensing. This information is often represented as point clouds where the underlying geometric relationships are unknown. Such linkages between the building information and the mobile robot allow to cope with any divergences and the associated inaccuracies of the building materials and components, and to apply decision-making strategies while executing building tasks. To facilitate this link, there must be a flow of data between the complex building information and the construction robot.

In this paper we present:

- An online digital workflow between the building model and robot perception

- A suitable interface that allows the users of the on-site mobile robotic system to fit building tasks to local references on-site
- Real-time adaptation of the building components (i.e. walls) with respect to measured "as-built" state

2 State of the Art

Recent developments indicate an increased use of mobile robots on jobsites to monitor, track progress[1], or register differences[2]. Still, the problem of how to manage the flow of data between mobile robots that build and the complex building information is an emerging topic. Early automation attempts in the 1990s sought to replace manual processes with robotic building technologies in the construction sector, and resulted in early-stage mobile construction robots such as [2, 3, 4, 5], all of which lacked the hardware ability to interface to the complex building information. An early attempt to have a mobile construction robot with a limited interface using integrated sensing abilities, for localizing itself with respect to the building components for executing building tasks on-site is exemplified in [6], but still not enabling real-time adaptation of building components.

A large amount of research is dedicated to automated modelling of "as-built" states of building components [7, 8], and localizing camera and laser sensors in a Building Information Model (BIM) as well as tracking construction progress [9, 10, 11, 12, 13, 8]. While these works show an integration of BIM with static and mobile sensing, the assumption is that the "as-built" status reflects the "as-planned" status and the problem of progress tracking is then defined as detecting the presence or absence of discrete building components. In this paper, we address the challenge of having an online data flow for an on-site mobile construction process by detecting and communicating metric deviations, such as walls being placed several cm differently than "as-planned". Detection of such metric deviations enable the adaptation of building models beyond mere presence or absence of building components.

Current research in the field, such as [14, 15], has put forward novel approaches for software interfaces that facilitate the adaption of "as-planned" building information in an on-site mobile construction process. In the case of [14], for the task of automated brick-laying, the planned geometries of two pillars are fitted to the robot map, and their as-built location is extracted to generate the robot tasks for fabricating a brick wall between them in a mobile robotic construction process. In the case of [15], a similar approach is implemented locally. By tracking visual features of the geometry that is being built, each discrete steel member is registered with stereo vision and locally corrected, all facilitated by the interface between the robot perception and the building information during the execution of the building task. These works demonstrated the feasibility and necessity of deviation measurements to adapt and execute construction tasks online, but they were limited to specific pre-programmed geometries and tasks.

It has not been demonstrated so far to establish an online data flow for an integrated robotic construction process and a flexible work area selection directly on job sites, localizing the construction robot both globally and locally in reference to the already built components (local references such as walls, floor, ceiling). With this research, we propose the online deployment of the building model into the robotic construction process, aiming to introduce a real-time method to plan a robotic workflow by fitting building tasks to local, selected references on-site, via a suitable interface.

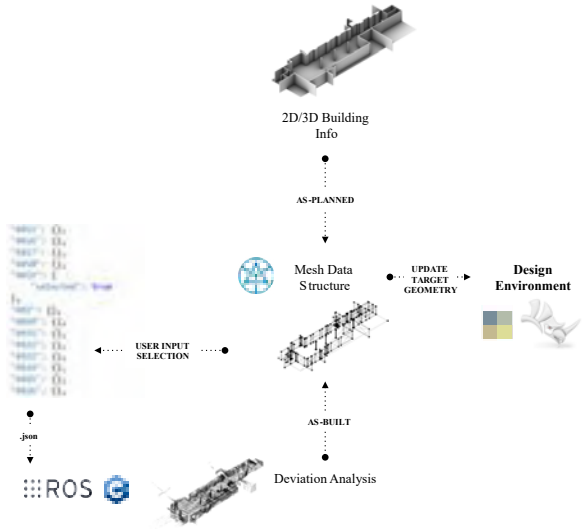

Figure 2. Overall workflow.

3 Method

Towards a generalized workflow, our method considers an abstraction where a building task is executed (i.e. as a robot trajectory) on a selected target geometry. To execute such a task, the robot requires poses of the trajectory in a local coordinate frame, which we anchor at given reference geometries. In this section, we describe a method that can execute such a task although the location and orientation of the target mesh faces (belonging to a target geometry), with respect to the reference mesh faces (belonging to reference geometries), may diverge from the "as-planned" state.

The procedure for the proposed method consists of the

[1] https://www.doxel.ai/
[2] https://www.scaledrobotics.com/

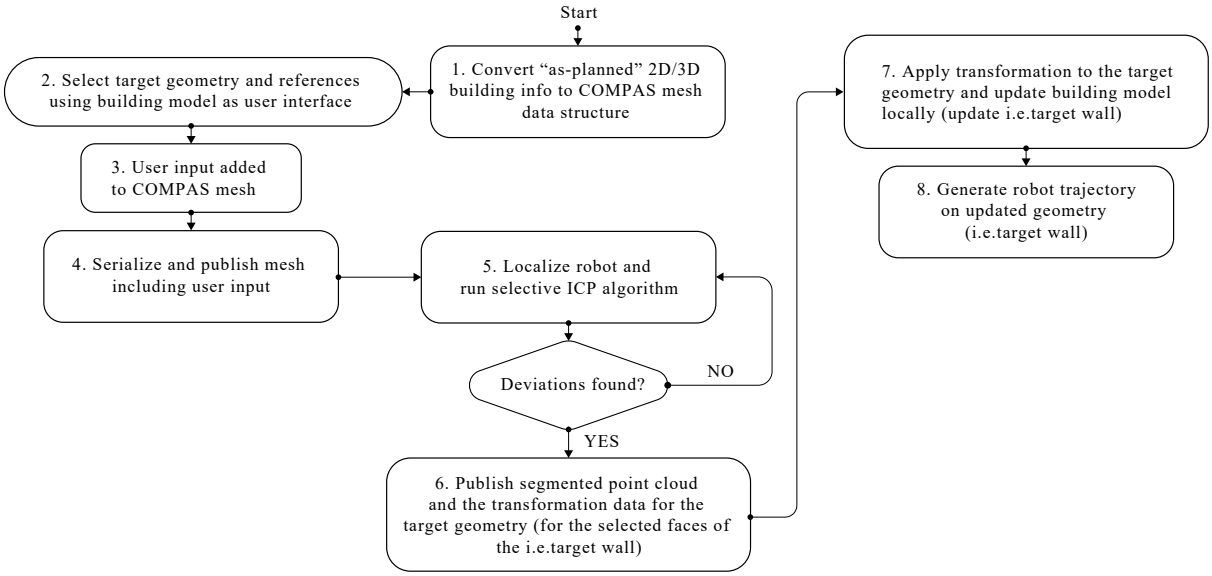

Figure 3. The procedure for the proposed method.

following steps (Figure 3): Firstly, the mesh data structure representing the building components is generated from the “as-planned” 2D/3D building information, as described in subsection 3.1. Secondly, the user selects the target geometry and the references by clicking on the control points for bounding the areas of interest, and the program executes necessary steps to find the target and reference mesh faces that contain all given points as vertices. This is then included in the mesh data structure via labeling the target mesh faces as "selected" and the reference mesh faces as "reference", as described in subsection 3.2. Following this, the mesh data structure containing the user input is serialized and published as a message in the ROS environment running the robot controller. Next, the robot is localized and the ICP algorithm is executed on-site, as described in subsection 3.3, using local references (coined selective ICP) [16]. The calculated transformation is published back and imported into the building model. As described in subsection 3.4, the transformation is applied to the target geometry and the building model is updated locally in the design environment. Finally, the robot trajectory representing the building task is generated on the "as-built" target wall. These steps are also shown in an accompanying video[3].

3.1 Building Model Data Structure

A schematic overview of the data representation communicated to the robot is shown in Figure 4. This

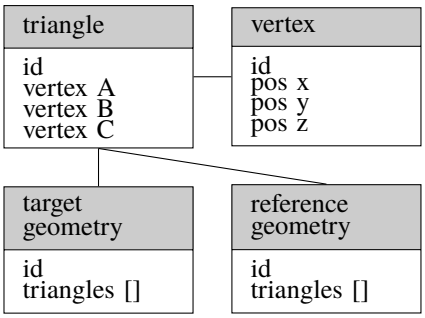

Figure 4. Data representation communicated between the building model and the robot.

data representation is initially generated from the "as-planned" 2D/3D building information, using the open-source, Python-based computational framework COMPAS[4] and visualised in 3D modeling software Rhino (Figure 2). It contains the mesh data structure of the COMPAS framework that allows for storing and adapting geometry and topology, aiming to represent the continuously changing building information and the robot trajectory (representing the building task) in relation to *target geometries*, i.e selected faces of the target wall. Like this, robot trajectory planning and generation from the design environment is aligned with the "as-built" state and the robot map (Figure 1). The communication between the robot controller - running in a ROS[5] environment - and the Python-based

[3] https://youtu.be/pu4hb_nZNUw

[4] https://github.com/compas-dev/compas

[5] https://www.ros.org/

design environment is established using the ROS Bridge library roslibpy[6]. Additionally, the kinematic model of the mobile robot is visualized in the design environment using the COMPAS FAB package of the COMPAS framework. This allows users to visualize the current robot state and task status in relation to the building model in the later stages of the process as well (such as i.e. feedback- based plaster spraying - that comes after Step 8 of the procedure shown in Figure 3) - which is not included within the scope of this paper.

3.2 Building Model as User Interface

The building model described in 3.1 - with the necessary abstraction level - is used directly on-site for task level commanding and for the selection of the target geometries and the necessary references, which are the relevant faces of the neighboring meshes, constraining the work area for the building task in the x, y and z axes. Firstly, the user selects the target geometry by clicking on the control points (located on the corners of the geometries) for bounding the area of interest (Figure 1), and the program executes necessary steps to find the target mesh faces that contain all given points as vertices. The same steps are repeated for the selection of the references. Next, the selected vertices are labeled in the mesh data structure, which is then serialised and communicated to the robot.

3.3 Robot Localization

The robot localizes against the building model using measurements from the 3D LiDAR described in subsection 4.1. In this way, the user provides an initial coarse alignment during robot start-up. The robot subsequently aligns the LiDAR scan with a sampled point cloud from the mesh as described in [17], using the Iterative Closest Point (ICP) algorithm [18]. To increase accuracy and overcome ambiguities, the alignment is constrained to a few *reference mesh faces* [16]. Here, these reference mesh faces are selected through the interface described in subsection 3.2 and communicated to the robot as described in subsection 3.1. Consequently, all LiDAR scans are aligned to the selected reference frame when measurements on the *target mesh faces* are extracted.

3.4 Adapting the Building Model to As-Built

When the robot is localized, deviations between "as-planned" and "as-built" can be measured on the target geometry. Candidate planes from the LiDAR scan are extracted in order to find the plane associated to the target geometry. Given measured distances d_{it} between points i on the candidate plane c and the target plane t, we associate planes by:

$$\arg\min_{c} \ \lambda_1 \min_{i} d_{it} + \lambda_2 \frac{1}{N} \sum_{i} d_{it} + (1 - \lambda_1 - \lambda_2)\,\mathrm{rot}(c, t)$$

where λ_1, λ_2 are tuning weights. The geometric transformation between "as-planned" and "as-built" can then be found as the translation between the plane centroids and rotation $\mathrm{rot}(c, t)$ between the face normals of the target geometry. As the current sensor setup does not allow the measuring of points over the whole height of the building components (i.e. walls), the z coordinate of the centroid cannot be estimated and therefore the z translation is not considered in the experiments. Upon detection of the geometric transformation, it is applied to the target geometry and the building model is updated locally.

Figure 5. Mobile robotic platform used in our experiments, here with an additional arm mounted.

4 Experiments

Experiments are presented in three subsections. The first subsection describes the robotic platform; the second subsection showcases the online selection of references and the work area and the third section focuses on the deviation detection and update of the target geometries locally in the building model. All experiments are conducted at a parking garage, which is set up as a mock construction scene at ETH Zurich.

4.1 Robotic Platform

The experiments are conducted on our open-source robotic platform[7] that consists of a wheeled base with LiDAR and IMU sensors, as shown in Figure 5. The platform's capabilities of high-accuracy manipulation [17] and

[6] https://github.com/gramaziokohler/roslibpy

[7] https://github.com/ethz-asl/eth_supermegabot

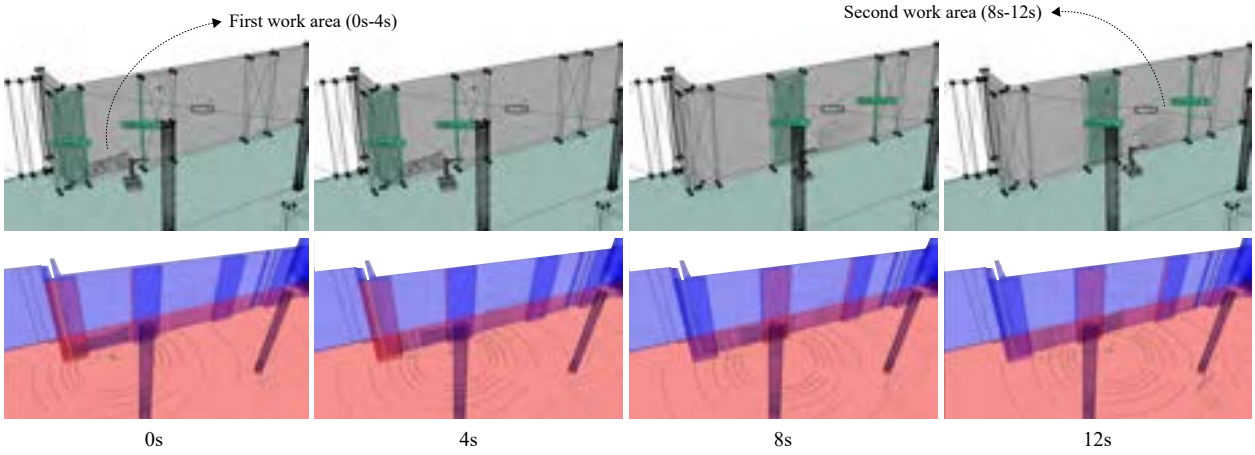

Figure 6. Top row: Online selection of references and work area. Bottom row: Robot map and perception.

localization in cluttered environments [16] were validated in earlier works. Since no manipulation for the execution of the building task is tested within the scope of this paper, the robotic arm was not mounted on the mobile platform in our experiments.

The LiDAR sensor used has an accuracy of 2 cm, 16 beams, and an opening angle of 30°, leading to height measurements on target walls of approximately 1 m. The scope of this work is therefore not a precise deviation analysis or sensing benchmark, which is out of the capabilities of the used sensors, but the demonstration of an integrated online workflow. The demonstrated workflow is not specific to the sensors used here, and can in fact be applied to any robotic platform that has the capability to localize in a robot map and to measure spatial information on selected geometries.

4.2 Online Selection of References and Work Area

In the first set of experiments, steps 1-4 of the procedure shown in Figure 3 are tested in order to showcase the initial steps of the online data flow proposed for synchronizing building information and the robot map. Initially, for the first work area shown in Figure 6, relevant references X, Y, and Z are selected, where X refers to the reference constraining the work area in the x-axis, and Y and Z, refer to the ones constraining the work area in the y and z axes. Without the need to reload a new building model to the robot off-site, the references are shifted on-site (as described in subsection 3.2) to the ones shown in Figure 6, at 8s. This successfully demonstrates a flexible, online method for work area selection to execute a building task (i.e. plaster spraying), for which fitting to relevant and local references on-site is crucial.

4.3 Deviation Detection and Update

In the second set of experiments, steps 1-8 of the procedure shown in Figure 3 are tested in order to showcase the update of building components to their as-built states for tolerance handling to facilitate an on-site construction process. For a selected set of target geometries shown in Figure 7, Walls 1-3, the same set of references X, Y, and Z (shown in Figure 7) are selected as described in subsection 3.2, constraining the work areas in x, y, and z axes to execute the selective ICP algorithm on-site. Robot trajectories are then generated on updated target geometries.

Table 1. Geometric transformations calculated for the target geometries, resulting from deviation detection: Translation of the mesh face centroid and rotation of the mesh face normal

Target	X Translation	Y Translation	Rotation
Wall 1	−30 ± 11 mm	−23 ± 34 mm	1.1 ± 1.4°
Wall 2	−13 ± 1 mm	−109 ± 1 mm	2.0 ± 1.4°
Wall 3	−5 ± 50 mm	36 ± 42 mm	0.9 ± 0.1°

5 Results

In all conducted experiments, the robot correctly associated its measurements to the selected target geometry and was able to provide associated sensor readings in the form of a point cloud, in addition to a parametric analysis of the deviation. This is important, as it allowed for updating the target geometry and for adapting the robot trajectory, representing the building task. The geometric transformations calculated for each target geometry are presented in Table 1.

Within the scope of this paper, the experiments focused

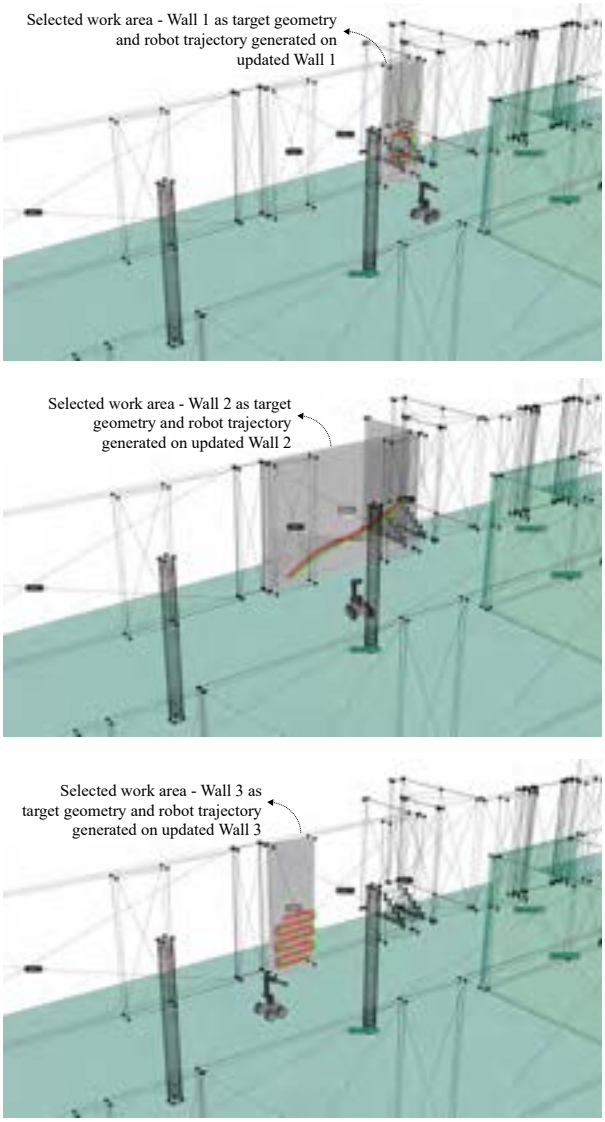

Figure 7. Deviation detection on selected target geometries, Walls 1-3, and generation of robot trajectories on updated target geometries.

on demonstrating the online workflow of the robotic construction system. In order to assess achievable degrees of precision, tests will be performed with higher-quality sensors on the robotic platform, and results will be compared to a ground truth site survey derived from measurements with a tripod system.

6 Conclusion and Outlook

In this paper, we present the first implementation steps of a novel method for an online data flow to synchronize building information with the robot map for facilitating an on-site construction process in an unbroken digital chain. This is established via linking the generation of robot trajectories, representing the building tasks, to the "as-built" states of selected building components directly on-site. Within the experiments presented in this paper, this is achieved by updating the target geometries in the building model, via the selective ICP algorithm executed directly on-site. Online deployment of the building model as an interface for including human actors into the robotic construction process is also tested, introducing a flexible method to plan a robotic workflow by fitting building tasks to local references on-site. However, these experiments do not extend to the actual execution of the tasks, which involve i.e. feedback-based plaster spraying, grinding, chiseling, etc. For these steps, in-process robot trajectory adaptation will be established with continuous process control, using visual feedback for acquisition of the current state of target geometries i.e. spraying, chiseling, and grinding surfaces. The overarching goal of this research is the development of a digital toolbox, so that the compatibility of the proposed workflow can be tested on different mobile robotic platforms deployed for on-site construction.

Within the scope of the experiments presented in this paper, the proposed method facilitated the digitization of crucial task information, i.e. selection of relevant references for building tasks for importation back into the building model and robot map. In further development, we will explore methods of dispatching task-specific instructions via different types of interfaces and experiment with on-site robotic workflows based on human collaboration and aim to further leverage the strengths of both humans and robots, enhancing the capabilities of digital construction processes.

Acknowledgements

We would like to thank Julian Stiefel for his contributions on mobile robotic deviation analysis. This work was partially supported by the Swiss National Science Foundation (SNF), within the National Centre of Competence in Research Digital Fabrication (NCCCR DFAB) and by the HILTI group.

References

[1] Pingbo Tang, Daniel Huber, Burcu Akinci, Robert Lipman, and Alan Lytle. Automatic reconstruction of as-built building information models from laser-scanned point clouds: A review of related techniques. *Automation in construction*, 19(7):829–843, 2010.

[2] Jurgen Andres, Thomas Bock, Friedrich Gebhart, and Werner Steck. First results of the development

of the masonry robot system rocco: A fault tolerant assembly tool. In Denis A. Chamberlain, editor, *Automation and Robotics in Construction XI: Proceedings of the Eleventh International Symposium on Automation and Robotics in Construction (ISARC)*, pages 87–93, Brighton, UK, May 1994. International Association for Automation and Robotics in Construction (IAARC). ISBN 9780444820440. doi:10.1016/B978-0-444-82044-0.50016-3.

[3] D. Apostolopoulos, H. Schempf, and J. West. Mobile robot for automatic installation of floor tiles. In *Proceedings of IEEE International Conference on Robotics and Automation*, volume 4, pages 3652–3657 vol.4, 1996.

[4] Ronie Navon. Process and quality control with a video camera, for a floor-tilling robot. *Automation in Construction*, 10:113–125, 11 2000. doi:10.1016/S0926-5805(99)00044-8.

[5] G. Pritschow, M. Dalacker, J. Kurz, and M. Gaenssle. Technological aspects in the development of a mobile bricklaying robot. In Eugeniusz Budny and Anna McCrea, editors, *Proceedings of the 12th International Symposium on Automation and Robotics in Construction (ISARC)*, pages 281–290, Warsaw, Poland, June 1995. International Association for Automation and Robotics in Construction (IAARC). ISBN 9788386040025. doi:10.22260/ISARC1995/0034.

[6] V. Helm, S. Ercan, F. Gramazio, and M. Kohler. Mobile robotic fabrication on construction sites: Dimrob. In *2012 IEEE/RSJ International Conference on Intelligent Robots and Systems*, pages 4335–4341, 2012.

[7] Tomás Werner and Andrew Zisserman. New techniques for automated architectural reconstruction from photographs. In *European conference on computer vision*, pages 541–555. Springer, 2002.

[8] Khashayar Asadi, Hariharan Ramshankar, Mojtaba Noghabaei, and Kevin Han. Real-time image localization and registration with bim using perspective alignment for indoor monitoring of construction. *Journal of Computing in Civil Engineering*, 33(5): 04019031, 2019.

[9] Frédéric Bosché. Automated recognition of 3d cad model objects in laser scans and calculation of as-built dimensions for dimensional compliance control in construction. *Advanced engineering informatics*, 24(1):107–118, 2010.

[10] Viorica Pătrăucean, Iro Armeni, Mohammad Nahangi, Jamie Yeung, Ioannis Brilakis, and Carl Haas. State of research in automatic as-built modelling. *Advanced Engineering Informatics*, 29(2):162–171, 2015.

[11] Christopher Kropp, Christian Koch, and Markus König. Interior construction state recognition with 4d bim registered image sequences. *Automation in construction*, 86:11–32, 2018.

[12] YM Ibrahim, Tim C Lukins, X Zhang, Emanuele Trucco, and AP Kaka. Towards automated progress assessment of workpackage components in construction projects using computer vision. *Advanced Engineering Informatics*, 23(1):93–103, 2009.

[13] Kevin Han, Joseph Degol, and Mani Golparvar-Fard. Geometry-and appearance-based reasoning of construction progress monitoring. *Journal of Construction Engineering and Management*, 144(2): 04017110, 2018.

[14] Kathrin Dörfler, Timothy Sandy, Markus Giftthaler, Fabio Gramazio, Matthias Kohler, and Jonas Buchli. Mobile robotic brickwork. In *Robotic Fabrication in Architecture, Art and Design 2016*, pages 204–217. Springer, 2016.

[15] Manuel Lussi, Timothy Sandy, Kathrin Doerfler, Norman Hack, Fabio Gramazio, Matthias Kohler, and Jonas Buchli. Accurate and adaptive in situ fabrication of an undulated wall using an on-board visual sensing system. In *2018 IEEE International Conference on Robotics and Automation (ICRA)*, pages 1–8. IEEE, 2018.

[16] Hermann Blum, Julian Stiefel, Cesar Cadena, Roland Siegwart, and Abel Gawel. Precise robot localization in architectural 3D plans. June 2020.

[17] Abel Gawel, Hermann Blum, Johannes Pankert, Koen Krämer, Luca Bartolomei, Selen Ercan, Farbod Farshidian, Margarita Chli, Fabio Gramazio, Roland Siegwart, et al. A fully-integrated sensing and control system for high-accuracy mobile robotic building construction. In *IEEE/RSJ International Conference on Intelligent Robots and Systems (IROS 2019)*, 2019.

[18] Paul J Besl and Neil D McKay. Method for registration of 3-d shapes. In *Sensor fusion IV: control paradigms and data structures*, volume 1611, pages 586–606. International Society for Optics and Photonics, 1992.

A Methodology to Monitor Construction Progress Using Autonomous Robots

S. A. Prieto [a], B. García de Soto [a] and A. Adán [b]

[a] S.M.A.R.T. Construction Research Group, Division of Engineering, New York University Abu Dhabi (NYUAD), Experimental Research Building, Saadiyat Island, P.O. Box 129188, Abu Dhabi, United Arab Emirates

[b] 3DVC&R Laboratory, University of Castilla-La Mancha, 13005 Ciudad Real, Spain

E-mail: Samuel.Prieto@nyu.edu, garcia.de.soto@nyu.edu, Antonio.Adan@uclm.es

Abstract –

In recent years, new technologies have improved the monitoring of construction progress by using the as-planned BIM of a building and comparing it with the current state of construction (i.e., the as-is model) to identifying differences and generating a progress report. However, in most cases, the different components required for the progress reports are still done by human operators. Those inspections typically consist of time-consuming and repetitive processes, making them a great candidate for automation, which can improve the quality of the methods used to monitor and assess the progress of buildings during the different construction phases.

This study proposes the development of an autonomous robot equipped with different sensors to collect data that can be used to conduct an automatic assessment of the state of construction, improving the current tedious and error-prone data collection and documentation processes. The proposed methodology is divided into three components: 1) Development of a robotic system able to navigate through construction sites in an autonomous way, 2) Data collection, and 3) Comparison of as-is with as-is conditions to identify discrepancies and generate a progress report. This paper focuses on the first two elements of the process.

The proposed robot is equipped with a 3D Terrestrial Laser Scanner (TLS). In addition, a robotic arm with a gripper is included so the robot can interact with different elements to achieve an autonomous robust robotic system. To test the autonomous navigation of the robot (including obtaining the optimal path through the building), the actions of the robotic manipulator, and the generation of the progress report, a simulation test was developed under the framework ROS (Robotic Operating System).

Keywords –

Progress Monitoring; Autonomous Robot; IFC; Inspection; Scan to BIM

1 Introduction

During the last years, new technologies have made the assessment and inspection of buildings much more efficiently and with better quality. However, in many cases, these inspections and assessments are still done by human operators who can induce errors in the process. Thus, a typical manual inspection entails time-consuming and repetitive processes that are usually carried out by two operators. This all leads to that, after some time, the operator is more susceptible to making mistakes and, therefore, might report a wrong assessment. The importance of the construction in the last years has brought to the table a need to automate and improve the quality of the methods used to assess buildings along with the different phases of construction projects.

By using an autonomous robot equipped with different sensors, an automatic assessment and inspection system can be used to perform this task, improving its quality and making it a much faster process.

The proposed methodology is divided into three components: a) development of a robotic system that can navigate through construction sites in an autonomous way (navigation and localization algorithms), b) data collection and c) analysis to quantify installed items, comparing as-is with as-planned conditions (BIM and project schedule). The work presented in this paper focuses on the two first components and provides details of the autonomous robotic system.

1.1 Previous work

The rising popularity of BIM models has allowed construction professionals to plan in a much more organized way all the construction processes before actual construction begins. However, up to this date, there is still a gap in how to keep track of the actual progress of construction tasks in an efficient way.

Photography and visual inspection are nowadays the most common way to compare the as-built model with

the BIM reference (i.e., as-planned model). That means that someone has to collect all the images through the construction site and later inspect them in order to generate a report. In general, this process is very tedious, time-consuming, and human dependent, meaning it can lead to inaccuracies and subjective assessment regarding the actual state of construction.

With the development of terrestrial laser scanning (TLS) technologies, some of these reports are now being generated by using 3D point clouds [1]–[3] instead of visual inspection or 2D photographs [4], [5]. This process has significantly improved the way the as-built model is compared with the as-planned BIM model, with the point cloud containing a much higher density of data and, therefore, allowing the operator to inspect the building in more detail. However, a higher amount of data implies longer time requirements for the inspection and report generation. In addition, this 3D data collection is still supervised and handled by a human operator, which again is a very time-consuming process.

Research has already been done regarding the data processing stages [6], [7], improving the autonomous data analysis characteristic of the process. Automatic segmentation algorithms are able to analyze the raw data coming from the 3D point clouds and identify the different structural elements of the building [7]–[13]. Some of them focus on general aspects of the building, such as the recognition of large indoor spaces [7]. Others concentrate on particular structural elements such as the detection and identification of cylindrical components [13], which can later be used in order to assess the proper location and type of the installed components. The use of additional information such as thermographic data [14] can also be used in order to identify the structural elements. This way, an automatic report can be generated by comparing the generated as-built model with the as-planned BIM [3], [15]–[17].

However, few approaches deal with the automation of the data collection process. By automating the data acquisition, the whole process can become completely autonomous, and the system would be able to automatically collect the data, generate the model, and create a report to assess the progress of the building. Adan et al. [18] propose an autonomous system in order to gather data from the building and to generate an as-is model; however, it does not take into account the as-planned BIM model. Ibrahim et al. [19] present an autonomous robotic platform able to collect 3D geometric and RGB data from the building. The data acquisition process has to consider that the quality of the data must be good enough in order to process the information and generate the model [20]. Therefore, a good strategy has to be designed, considering the fact that the BIM model of the building is available, which can be used to obtain the floor plans in order to plan a valid path.

The method proposed in this paper fulfills the aforementioned requisite, hence becoming a fully autonomous system that automatically collects data using the existing (as-planned) BIM model, navigates through multi-story buildings, collects and processes data to generate a progress (as-is) model of the building, and later compares the as-is model with the as-planned model in order to generate a progress report of the building by identifying discrepancies found in terms of quantities, dimensions, locations, etc.

The scope of the work presented in this paper focuses on the autonomous collection of the data. It does not consider the generation of the as-is model and the progress report. The rest of this paper is organized as follows. Section 2 presents the proposed robotic system and an overview of the main points from the data collection process. Section 3 gives a preview of the work conducted by the authors related to the model generation and automatic comparison between the as-planned and as-is models with the ultimate goal to generate progress reports in an automatic way. Section 4 shows the experimental tests for the navigation and data collection in a simulated environment. Finally, Section 5 summarizes all the work.

2 Robotic system and data collection

This section addresses key elements of the robotic system and the overall process of the collection of data that would be used for the generation of the as-is models.

2.1 Robotic system

This section presents the different aspects related to the required characteristics of the mobile platform. Due to the complexity of the approach, a well-designed and equipped robotic platform is necessary. The platform is mainly composed of three elements, the mobile robot, the sensors, and the actuators. An example is shown in Figure 1.

2.1.1 Mobile robot

First, the locomotion aspect. Robots used in construction are usually limited to either tracks, legs, or outdoor all-terrain wheels [21], [22]. These locomotive systems are efficient when it comes to moving through rough terrain; on the other hand, they are not very precise, and they can be difficult to control in small indoor scenarios. However, means and methods of construction, as well as construction materials, have evolved during the last few years, making construction sites more approachable to robotic systems. For example, drywall is widely used for indoor construction, which, when compared to using bricks or any other conventional construction method, does not generate that much debris or dust.

(a) (b)

Figure 1. (a) Robotic platform based on Robotnik Kairos with UR10-e, (b) 3D scanner (Leica BLK 360)

Therefore, all-terrain locomotion systems are no longer necessary to achieve optimum navigation through a construction environment. Omni-wheels or any other kind of holonomic system would allow the robot to achieve much higher levels of control and precision, without sacrificing freedom of movement through the construction site.

2.1.2 Sensors

One of the key aspects is the localization system of the platform. GPS or any other satellite-based localization systems are widely used for outdoor scenarios, achieving a reliable and precise real-time position of the robot. Since our project is aimed to work indoors, this is not a valid option. Visual-based localization systems would need to have markers installed through the construction site. Since the approach is designed for the robot to be working in different stages of the construction process, this environment might be in constant change, which would not make the installation of visual markers a reliable method. Since the BIM model of the building will be available, information from the floor plans will be used in conjunction with LiDARs in order to obtain a precise and real-time position of the robot.

The type of data that the robot needs to collect includes, but is not limited to, structural geometry data of the building, thermal information, colored visual information, and surface reflectance information. Therefore, several sensors, such as 3D scanners, thermal cameras, and RGB-D cameras, are needed. The 3D scanner could be similar to the Leica BLK 360 (Figure 1b), which provides 3D geometric data, RGB color data, and thermal infrared data. This scanner also has a wide FOV of 360° (horizontal) / 300° (vertical) and a range of up to 60 m, which for most interior applications is more than enough. The ranging accuracy is 4 mm @ 10 m / 7 mm @ 20 m. Owing to its reduced size and weight (165 mm in height and 100 mm in diameter, and 1 Kg), this is a good scanner candidate for a mobile robotic platform.

2.1.3 Actuators

Finally, in order to facilitate a fully autonomous behavior on the scene, the robot will need to interact with the environment (e.g., obstacle removing, door opening, elevator access). To do this, a robotic arm with a suitable gripper is placed at the base of the robot. Given the platform will move through an inhabited construction site, populated with other construction workers, it is a must that this system complies with the collaborative robot background. This means the robot must be safe enough to be able to work side by side with human beings. The chosen robot arm, UR10-e, belongs to the spectrum of collaborative robots.

2.2 Navigation and data collection

The overview of the entire process is shown in Figure 2. This subsection presents the different elements related to 'Part 1: Flor plan extraction' and 'Part 2: Autonomous navigations & Data acquisition'.

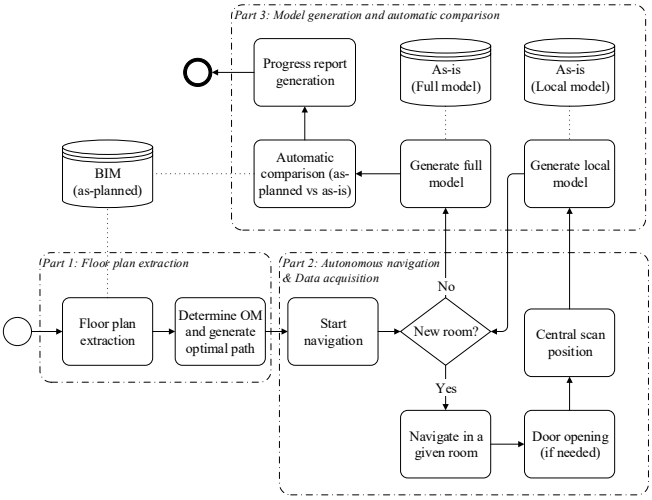

Figure 2. Overview of the navigation and data collection process

2.2.1 Floor plan extraction

All valuable information extracted during the 3D data processing stages is used for the positioning and secure navigation of the mobile robot. This consists of the following stages.

2.2.2 Optimal path generation

The only input the system is getting from the very beginning is the Industry Foundation Classes (IFC) file of the building. This file contains all the information related to the BIM model. A proper methodology to

understand the structure of the file needs to be developed to automatically extract the information needed for each one of the stages (Figure 3).

Since a single file can describe multiple buildings, the first distinction that can be found inside an IFC file is the building tag. Under the building tag, there are multiple levels or stories of the building. Within the same level or story, all the defined spaces can be extracted, that is, all the different rooms and corridors inside the same floor. Lastly, the rooms and connections between the different spaces can be identified (Figure 3).

One of the main things to be considered in order to extract the information from the IFC file is the type of information present in it. The definition of the spaces, for example, can be provided in different ways in the tag IFCSHAPEREPRESENTATION [23]. There are multiple types of representation, but they can be separated into three main blocks: 2D curve representations, solid model representations, and surface model representations. The ideal scenario is the one where all the available representations can be found within the same file, in order to access each, one of them depending on the kind of information that needs to be extracted.

At this point, all the information required to proceed with the first step in the process has been extracted. Now, in order to provide the robot with a safe and approximate representation of the scene, an obstacle map (OM) of the current floor needs to be generated. This will guarantee safe navigation. The OM is obtained from the accumulated point cloud and the current floor plan (i.e., map).

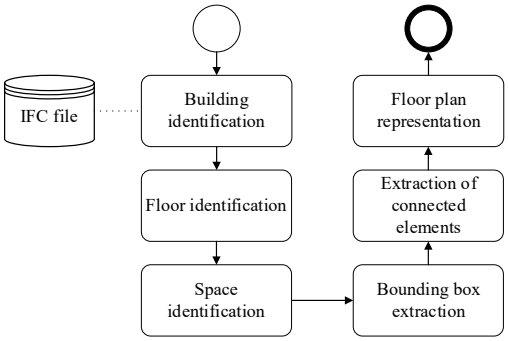

Figure 3. Structure within the IFC file in order to extract the floor plan representation.

In order to alleviate the post-processing stages, the 2D curve representation would be of a suitable type to extract the 2D floor plan (i.e., map) from the IFC file. If the IFC file does not contain a curve type representation, the 3D solid model or face representation (BREP) could then be used to generate the 2D map. Figure 4 shows a 2D curve representation and a BREP representation extracted from two different IFC files.

With the 2D representation of the floor plan extracted, a morphological set of operations are applied in order to generate a binary occupancy map, that is, the OM of the robot.

The robot will always begin the autonomous data acquisition process in the center of a room, indicated by the user as an input. In order to visit the other rooms on the same floor, a global navigation algorithm generates a room visiting schedule. According to this schedule, the robot moves towards the closest non/visited following room, updating on each iteration the list of visited rooms (Figure 5). More details on the generation of this schedule can be found in [18].

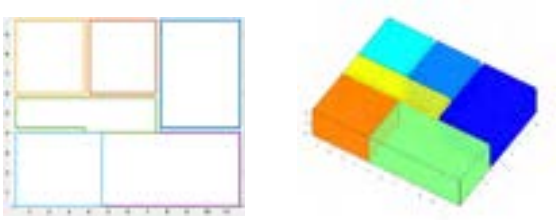

(a) (b)

Figure 4. (a) 2D and (b) BREP representations extracted from the IFC.

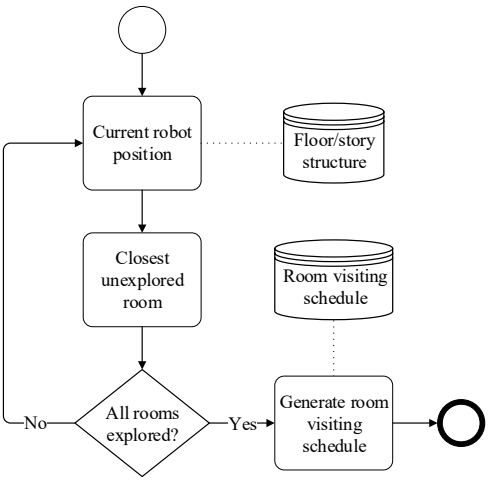

Figure 5. Generation of room visiting schedule.

The generated path needs to make sure that the robot visits all the individual rooms of the building, maximizing the coverage of all the structural elements present in the construction site.

This OM gets updated with each single scan performed by the robot before moving to the next goal, in order to add all the obstacles not present in the floor plan extracted from the IFC file.

2.2.3 Autonomous navigation

In addition to obtaining the map, the robot needs to know its position inside the map. This is accomplished

by matching the data points provided by the LiDARs with a horizontal slice obtained from the point cloud at the height of these LiDARs, combining it with the boundaries of the 2D floor plan extracted from the IFC file. This is done using an Adaptive Monte Carlo Localization (AMCL) algorithm [24].

The path planning algorithm then yields an off-line theoretical path that the robot must follow by moving towards the different locations based on the existing BIM model. This path will have different stages. First, the robot needs to exit the current room, and therefore a path towards the exit door will be generated. Once the robot is in front of the door, it has to determine whether the door is either open or closed. This can be achieved by reading the front LiDAR data in order to detect a void. If the door is closed, a door opening approach will be executed. If the door is open, a second path will then be generated towards the entry room of the next room in the visiting schedule. Again, a procedure that detects the state of the door will be executed, with the door opening approach performed if needed. The third and last path in the sequence aims to lead the robot towards the center of the room in order to perform the next scan.

The NAVFN path planning algorithm will be used for the robot to navigate between goals. It is the most common global planner used in ROS (Robotic Operating System). This path planner is based on the Dijkstra's algorithm [25] approach.

If the robot encounters a closed door on its way to the final goal, it will begin a door opening approach. Since the coordinates of the door are already known from the IFC file, the robot will position itself in front of the door, in order to perform a detailed scan of the center section to detect the doorknob. Once the doorknob has been detected and the main parameters that define the door have been identified, the robot can safely open the door and continue its path towards the center of the room. A more detailed explanation of the door opening process can be found in [26].

The localization and the autonomous navigation would be implemented first in a simulated environment and then transferred to the real robot. This paper only focuses on the simulation part.

2.3 Data acquisition

As previously stated, every time the robot enters a new room, it performs a new scan from the center of the room. Of course, this will vary depending on the shape of the room. For example, corridors are treated as rooms by the algorithm, but due to the geometry of corridors, if the length of the room is larger than the maximum range of the 3D scanner, more than one scan will be needed to obtain the full geometry. That is why some factors need to be taken into account in order to compute the number of scans needed to digitize the room in its entirety. These factors depend mainly on the size of the room, the range of the scanner, and the shape of the room itself (concave or convex rooms).

The 3D scanner provides not only geometric data but also RGB, reflectance, and thermal information. This means that the generated point clouds have different layers of information, which will be used in subsequent 3D data processing stages.

In addition, all the data is progressively registered using the localization data coming from the robot. This position is obtained by fusing the data coming from the wheels odometry (read by the wheels' encoders), the Inertial Measurement Unit (IMU), and the output from the AMCL using the LiDARs. Also, all the data is time-stamped for further inspection. This data is registered for each room (in case multiple scans were needed for a single room), resulting in multiple raw local models representing different rooms of the current floor.

The resulting raw data is an accumulated point cloud of the whole building or a global model composed of all the singular 3D point clouds obtained in the different rooms. This accumulated point cloud includes all the sub-layers containing information about the surface reflectance, the 3D geometry, the RGB data, and thermal information captured by the cameras embedded in the Leica BLK 360.

3 Model generation and automatic comparison

After completing all the tasks indicated in Section 2, the raw data acquired is not structured in any way. Semantic meaning to all the collected data through the different stages of the process needs to be added. This is where the as-is model generation comes in place. Due to space constraints, only key components of these elements form the overall process are presented below.

3.1 As-is model generation

The segmentation process is aided by the fact that a semantic model of what the building is supposed to look like (i.e., as-planned BIM model) is available. Therefore, the raw data only needs to be fitted to the already existing model.

In order to do that, the first thing is to identify the envelope of each space. That is, a BREP representation of the current state of the building. For that, the BREP representation obtained from the BIM model in earlier stages will be used. With the obtained geometric faces, the raw 3D data obtained from the building is fitted to the planes defined by the BIM model, locating which ones have or do not have data. This will determine whether the plane has been constructed or not.

Based on the existent data, it can be determined which of these faces is present in the current model and those that are not.

3.2 Autonomous progress report

With the as-is model generated from the raw data obtained, the evaluation of the progress of construction can be done. With the semantic information for the main elements of the building, such as walls, ceilings, columns, floors, as well as secondary elements like doors, windows, and wall-mounted objects, a progress report can be generated. This progress report would contain, amongst other things, the percentage of completion of all these elements with respect to the planned schedule.

4 Experimental test

This section summarizes the experimental tests for the navigation and data collection under the framework ROS using the robot simulation software Gazebo and Blensor in a simulated construction environment.

4.1 Simulation test

In the current state of the research, the first part of the approach has been tested in simulation, successfully extracting the information from the IFC file and achieving autonomous navigation throughout the simulated environment.

Given the widespread use of BIM, there are plenty of available resources with different IFC files presenting different characteristics. For the current test, a simple two-story building was used. Given we are only testing the automatic IFC feature extraction and the autonomous navigation, the test focused on just the first story of the building, since the movement between floors is not the goal of this paper.

Multiple software is used in order to perform these simulations. First and foremost, Revit is used in order to inspect the IFC file and modify the state of the simulated building if needed (Figure 6a). For the robot simulation stages, the Gazebo simulation tool, natively working in ROS, was used (Figure 6b). This platform can test the different approaches regarding the robot, such as the localization and autonomous navigation or the door opening techniques. In order to obtain simulated 3D data, the Blensor add-on for the Blender software [27] is used. Finally, MATLAB is used to extract the features, control the robot, and process the obtained data.

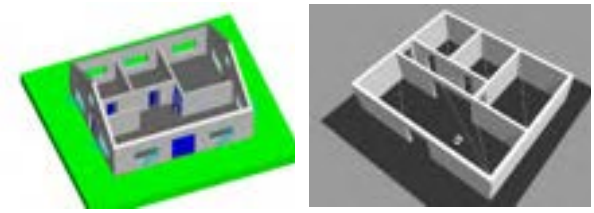

(a) (b)

Figure 6. (a) Visualization in Revit of the IFC file of the tested building. (b) The same model inserted in Gazebo.

Once the building has been simulated with the information from the IFC file, the outline geometry of each one of the spaces within the floor is extracted from the IFC file. The location and size of each one of the openings (i.e., doors) are included in this map containing the previous information, and after applying an infill morphological operation to the void spaces between the different outline of the spaces, an OM map for the robot is generated (Figure 7).

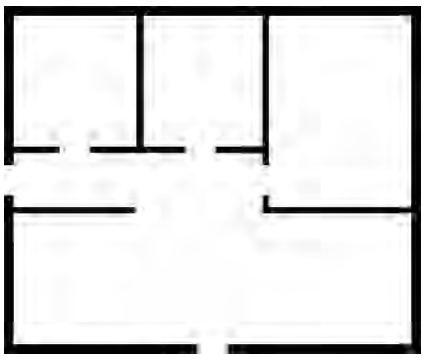

Figure 7. Obstacle map obtained from the information retrieved in the IFC file.

By using the obstacle maps and the inter-room navigation algorithm, the robot can autonomously visit the entire floor. Figure 8 shows the robot autonomously planning a path to navigate through the different rooms. In this figure, the cloud of small red arrows surrounding the robot represents the uncertainty in the position of the robot. That is why in its initial position (Figure 8a), the uncertainty is bigger than in the following positions, where the robot has already navigated through the scene and fully identified its localization. The local costmap calculated by the local planner is represented by the blue cells surrounding the obstacles. Figure 9 shows the accumulated raw data collected by the robot after performing a 3D scan in each of the visited rooms.

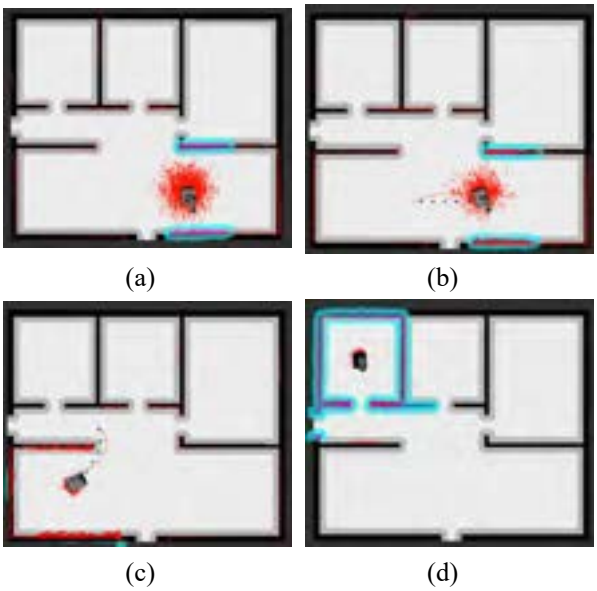

(a) (b)

(c) (d)

Figure 8. Scenes representing different stages of the simulation process. (a) First initial position of the robot. (b) and (c) Robot moving towards the next goal, where the path generated by the global planner (red line) can be seen. (d) Robot completely localized within the map.

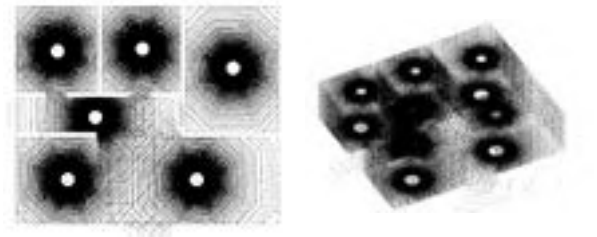

(a) (b)

Figure 9. Top (a) and 3D (b) view of the raw data collected by the robot at the end of the process.

5 Conclusions and outlook

This paper presents the early stages of what aims to be an autonomous approach to perform inspections during the construction process in order to generate a progress report automatically.

Given a generic IFC file, a methodology to automatically extract all the different elements of a building has been presented.

A test, under simulation conditions, has been conducted on an IFC file of a two-floor building. Our system computes 2D obstacle maps, takes simulate 3D data of the rooms, and provides safe autonomous navigation of the robotic platform.

Ongoing work focuses, on the one hand, on developing new 3D data processing algorithms, in order to provide a semantic as-is 3D model of a multi-floor building. On the other hand, we aim to establish a procedure that easily compares as-planned to as-is 3D models and automatically generate a building progress report. This work also includes testing the findings from the simulation using the proposed robotic system in a real-world environment.

References

[1] C. Feng, Y. Xiao, A. Willette, W. McGee, and V. R. Kamat, “Vision guided autonomous robotic assembly and as-built scanning on unstructured construction sites,” *Autom. Constr.*, 2015.

[2] C. H. P. Nguyen and Y. Choi, “Comparison of point cloud data and 3D CAD data for on-site dimensional inspection of industrial plant piping systems,” *Autom. Constr.*, 2018.

[3] C. Kim, C. Kim, and H. Son, “Automated construction progress measurement using a 4D building information model and 3D data,” *Autom. Constr.*, 2013.

[4] L. Klein, N. Li, and B. Becerik-Gerber, “Imaged-based verification of as-built documentation of operational buildings,” *Autom. Constr.*, 2012.

[5] A. Bhatla, S. Y. Choe, O. Fierro, and F. Leite, “Evaluation of accuracy of as-built 3D modeling from photos taken by handheld digital cameras,” *Autom. Constr.*, 2012.

[6] V. Pətrəucean, I. Armeni, M. Nahangi, J. Yeung, I. Brilakis, and C. Haas, “State of research in automatic as-built modelling,” *Adv. Eng. Informatics*, vol. 29, no. 2, pp. 162–171, Apr. 2015.

[7] I. Armeni *et al.*, “3D Semantic Parsing of Large-Scale Indoor Spaces (a) Raw Point Cloud (b) Space Parsing and Alignment in Canonical 3D Space (c) Building Element Detection Enclosed Spaces.”

[8] P. Tang, D. Huber, B. Akinci, R. Lipman, and A. Lytle, “Automatic reconstruction of as-built building information models from laser-scanned point clouds: A review of related techniques,” *Automation in Construction*. 2010.

[9] F. Wang, X. Xi, C. Wang, Y. Xiao, and Y. Wan, “Boundary regularization and building reconstruction based on terrestrial laser scanning data,” *2013 IEEE Int. Geosci. Remote Sens. Symp. - IGARSS*, no. 41271428, pp. 1509–1512, 2013.

[10] H. Son and C. Kim, “Automatic segmentation and 3D modeling of pipelines into constituent parts from laser-scan data of the built

environment," *Autom. Constr.*, 2016.

[11] H. Son, C. Kim, and C. Kim, "3D reconstruction of as-built industrial instrumentation models from laser-scan data and a 3D CAD database based on prior knowledge," *Autom. Constr.*, 2015.

[12] Y. Zhuang, X. Lin, H. Hu, and G. Guo, "Using scale coordination and semantic information for robust 3-D object recognition by a service robot," *IEEE Sens. J.*, vol. 15, no. 1, pp. 37–47, 2015.

[13] F. Bosché, M. Ahmed, Y. Turkan, C. T. Haas, and R. Haas, "The value of integrating Scan-to-BIM and Scan-vs-BIM techniques for construction monitoring using laser scanning and BIM: The case of cylindrical MEP components," *Autom. Constr.*, 2015.

[14] S. Lagüela, L. Díaz-Vilariño, J. Martínez, and J. Armesto, "Automatic thermographic and RGB texture of as-built BIM for energy rehabilitation purposes," *Autom. Constr.*, 2013.

[15] A. K. Patil, P. Holi, S. K. Lee, and Y. H. Chai, "An adaptive approach for the reconstruction and modeling of as-built 3D pipelines from point clouds," *Autom. Constr.*, 2017.

[16] K. J. Shrestha and H. D. Jeong, "Computational algorithm to automate as-built schedule development using digital daily work reports," *Autom. Constr.*, 2017.

[17] M. Bueno, F. Bosché, H. González-Jorge, J. Martínez-Sánchez, and P. Arias, "4-Plane congruent sets for automatic registration of as-is 3D point clouds with 3D BIM models," *Autom. Constr.*, 2018.

[18] A. Adán, B. Quintana, S. A. Prieto, and F. Bosché, "An autonomous robotic platform for automatic extraction of detailed semantic models of buildings," *Autom. Constr.*, vol. 109, no. April 2019, p. 102963, 2020.

[19] A. Ibrahim, A. Sabet, and M. Golparvar-Fard, "BIM-driven mission planning and navigation for automatic indoor construction progress detection using robotic ground platform," *Proc. 2019 Eur. Conf. Comput. Constr.*, vol. 1, pp. 182–189, 2019.

[20] D. Rebolj, Z. Pučko, N. Č. Babič, M. Bizjak, and D. Mongus, "Point cloud quality requirements for Scan-vs-BIM based automated construction progress monitoring," *Autom. Constr.*, 2017.

[21] B. R. K. Mantha and B. Garcia de Soto, "Designing a Reliable Fiducial Marker Network for Autonomous Indoor Robot Navigation," in *36th International Symposium on Automation and Robotics in Construction, ISARC 2019.*, 2019, pp. 74–81.

[22] B. R. K. Mantha, B. Garcia de Soto, C. C. Menassa, and V. R. Kamat, "Robots in indoor and outdoor environments," in *Construction 4.0: An Innovation Platform for the Built Environment*, 1st Editio., A. Sawhney, M. Riley, and J. Irizarry, Eds. Routledge, London, 2020, pp. 307–325.

[23] "Building Smart foundation." [Online]. Available: https://www.buildingsmart.org/. Last access 15/06/2020.

[24] S. Thrun, *Probabilistic Robotics. Communications of the ACM.* 2002.

[25] E. W. Dijkstra, "A note on two problems in connexion with graphs," *Numer. Math.*, vol. 1, no. 1, pp. 269–271, 1959.

[26] S. A. Prieto, A. Adán, A. S. Vázquez, and B. Quintana, "Passing through Open/Closed Doors: A Solution for 3D Scanning Robots," *Sensors*, vol. 19, no. 21, p. 4740, Oct. 2019.

[27] M. Gschwandtner, R. Kwitt, A. Uhl, and W. Pree, "BlenSor: Blender sensor simulation toolbox," *Lect. Notes Comput. Sci. (including Subser. Lect. Notes Artif. Intell. Lect. Notes Bioinformatics)*, vol. 6939 LNCS, no. PART 2, pp. 199–208, 2011.

Digital Twin Technology

Utilizing Robots and Deep Learning

Fuminori Yamasaki

iXs Co., Ltd. , Japan
E-mail: yamasaki@ixs.co.jp

Abstract

Recently 3D management solution utilizing BIM/CIM is expected for construction and inspection management. Especially for inspection utility, big data such as huge number of inspection pictures and sounds should be managed with location data of taking data and should be taken with high quality and resolution on 3D world. This paper describes the total solution for 3D management system using Robots and AI technology.

Keywords –

BIM/CIM; Robot; Deep Learning; 3D

1 Introduction

In recent years, the deterioration of social backbone in terms of industrial infrastructure and social infrastructure has become a social problem. It has become necessary to solve many problems such as increase in the number of inspection and repair locations, aging of workers engaged in maintenance and management and decline in the number of employees, and pressure for reducing the maintenance and management cost. Especially for social infrastructure, in 2014, it became a requirement to carry out close-up visual inspection once in every 5 years for maintenance and management of all bridges, which are said to be 720,000 in total in Japan. In the case of close-up visual inspection conducted by workers based on the old inspection procedure, it is expected that continuing sound maintenance and management in future will be difficult.

As a solution in this situation, various new technologies such as the use of robots and drones and automatic extraction of damage by deep learning are being examined. In addition, research and development of three-dimensional unification technology for the integrated management of enormous amount of information obtained by robots and drones is also underway.

On the other hand, the initiative of i-Construction is underway in the field of construction and civil engineering, and by using BIM/CIM (Building Information Modeling / Construction Information Modeling), three-dimensional models are linked and developed in a series of processes such as planning, research, design, construction, and management, and a mechanism for sharing information at each stage has been developed [1].

In the present paper, in light of the above background, as a method for sustainable infrastructure maintenance and management, we developed a mechanism that uses digital twin technology, automatically extracts damage from various data acquired by inspection robots with deep learning, and associates them with a time axis on a 3D drawing. In addition, by assuming a case of a structure where drawings are lost or a case where there are attached equipment not reflected in the drawings, we also worked on methods such as CAD conversion from three-dimensions points group data obtained by 3D scanner and photogrammetry.

2 Digital twin technology

The digital twin technology [2] proposed by Professor Michael Grieves of the University of Michigan in 2002 is a technology that reproduces the real world in real time in a digital space in a linked manner. It is a technology that makes it possible to contribute to preventive maintenance by using acquired data, such as understanding the current situation digitally and making changes and predictions by conducting various simulations.

For the digital twin in infrastructure maintenance, first of all, it is important to obtain the latest shape and configuration of the structure, and it is necessary to accurately model attached equipment and repair marks that are not yet reflected in the construction drawings. On the other hand, a system that induces third party damage and that increases social losses such as traffic

congestion when taking measures such as suspension of sharing in data acquisition is not desirable. At the same time, it is also necessary that is a method for making a complex structure into a detailed three-dimensional structure.

Especially in the case of a large-scale structure, when trying to restore a complex structure in the digital space with an accuracy that contributes to infrastructure maintenance and management, if 3D restoration is done from continuous images with 90% overlap by a drone etc. using photogrammetry technology, the data size of the restored data becomes huge because thousands of images of a few MB size each are joined. The joining process itself takes a lot of time, and at the same time, there are some problems to be solved before putting it into practical use, for example, it requires a high-performance PC for viewing the restored data.

Therefore, in infrastructure maintenance and management, it is necessary to acquire data for understanding the latest shape and configuration of the structure and data of inspection quality required for maintenance and management, and it is necessary to acquire and restore data with the accuracy required for each of them.

In the present paper, the data for understanding the shape and configuration is acquired at a resolution that will allow understanding the shape and configuration, and the data size is further compressed by CAD. Moreover, the inspection data for checking cracks in concrete is acquired at a resolution that can detect the cracks of 0.1 mm size. After that, these data is merged for solving the above problems.

Figure 1 shows a panoramic view of the steel plate girder bridge, and Figure 2 shows a 3D points group obtained by mounting a 3D scanner on the robot Turrets (Figure 3) [3] that can access the girder of the steel plate girder bridge from the back of the bridge.

Figure 1. Three-dimensional point groups model of the whole bridge view

Figure 2 . Three-dimensional point groups model in bridge girder

Figure 3. Flange-suspended type inspection robot Turrets

3 Damage extraction by using AI

Recently, AI has been used in various scenarios such as crack extraction of concrete and corrosion extraction of steel structure by using deep learning. Even in infrastructure maintenance and management, the Ministry of Land, Infrastructure, Transport and Tourism is playing a central role for making preparations such as rolling out the "AI development support platform" [4].

As for extracting cracks in the concrete, from the high-quality camera images taken, cracks are extracted by using semantic segmentation, and the cracks are then displayed in different colors according to the crack width and crack length. It is expected that because of this the inspection staff will not miss the inspection of cracks (Figure 4) and it will shorten the preparation of crack diagrams when preparing inspection records (Figure 5).

Turrets is equipped with a high-definition camera that can detect cracks of 0.1 mm size, and it is also equipped with a lighting device to obtain appropriate photographic images even in dark environments. Therefore, it is possible to obtain pictures with good image quality.

Figure 4. Bridge deck crack extraction image

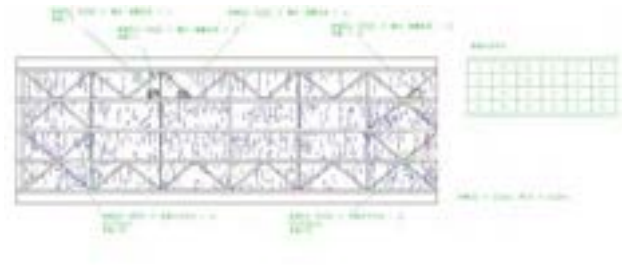

Figure 5. Inspection record

On the other hand, in the case of damage such as corrosion, after the target site is identified, deep learning and image processing technologies are used to automatically calculate the corrosion position, corrosion area, etc.

By associating these deterioration data with 3D drawing data with a time axis, the inspection staff can accurately understand the current state of the structure from a remote location, and it becomes possible to correctly diagnose the state of the structure.

In addition, since it has a time axis, the reusability of data is high, and it is easy to observe changes over time, which can contribute to the planning of future repairs.

4 Three-dimensional model and BIM / CIM conversion

Various types of data for structures including photographic images obtained by robots are often large amounts of data when compared to that of conventional inspections conducted by inspection staff. Therefore, if the various data obtained are randomly stored, the reusability will be poor, and it will take a lot of time to organize the data, which will reduce the advantages of using a robot.

One of the advantages of using robots is that the position information obtained from the sensors used to control the robots can be used as self-position information, and it can be associated with the acquired data to automatically organize the data. In addition, by managing the acquired data with position information in three dimensions, it is possible to intuitively overlook the damage situation in the entire structure compared to the two-dimensional management as shown in Figure 5.

On the other hand, in i-Construction, which is being promoted in the field of construction and civil engineering, integrated three-dimensional data management by using BIM / CIM is progressing. Therefore, integrating maintenance and management information into BIM / CIM not only offers the advantage that the data obtained in maintenance and management operations can be intuitively managed in three dimensions, but it also allows integrated management of design and construction data and maintenance and management data. In that respect, it is very effective that it can be used to estimate the cause of damage.

Give that, a mechanism was developed for unifying the robot's self-position and the BIM / CIM coordinate system, managing various data obtained by the robot in the BIM/CIM coordinate system, and then correlating them with the attribute data IFC (Industry Foundation Classes) used in BIM/CIM. In addition, it is often difficult to correlate with BIM/CIM data when the robot acquires self-position, for example, in the case of structures with old construction without BIM/CIM drawings, structures with attached equipment not reflected in the drawings, and structures that were repaired.

Recently, there is a measuring device called 3D scanner that can acquire the surrounding conditions with high precision in a three-dimensional points group. A method to make a new BIM/CIM by using this was also developed.

Figure 6 shows the Turrets (Figure 3) equipped with a three-dimensional scanner that is scanning while moving over the structure. It was possible to obtain the three-dimensional points group data shown in Figure 1 and Figure 2 by combining the multiple points group data at each measurement position obtained here.

In addition, Figure 7 and Figure 8 show the results of surface estimation from the obtained three-dimensional points group data and CIM conversion.


Figure 6. Turrets equipped with a three-dimensional scanner

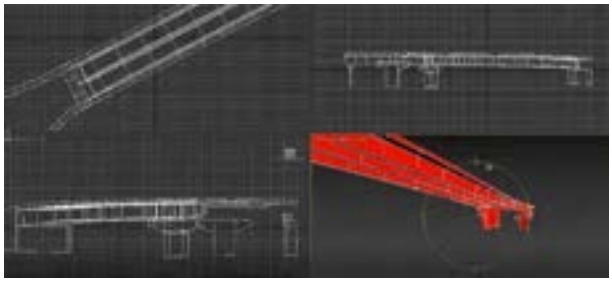
Figure 7. CIM conversion from three-dimensional points group data

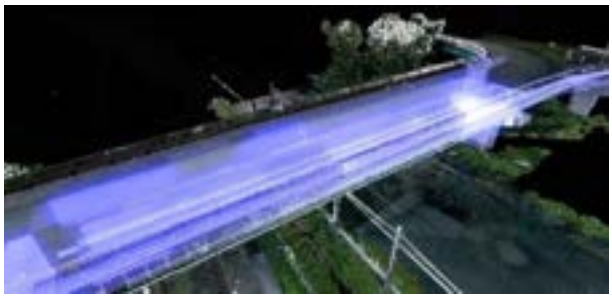
Figure 8. Superimposing three-dimensional points group data and CIM

5 Data superposition for digital twin

Up to the previous section, by correlating various data acquired by the robot with position information, it became possible to automatically extract and automatically measure the damage by using image processing technology and AI such as deep learning. In addition, by mounting a 3D scanner on the robot, three-dimensional points group data of the structure was acquired and converted into CIM. Since all of these data are managed in the BIM / CIM coordinate system, and the acquired data were superimposed on the three-dimensional points group so that they could be correlated with the IFC, which is the attribute data, and the damage condition could be intuitively understood.

Superimposition of the acquired images calculates the shooting position of the robot (camera center) from the postures of each joint of the robot, converts it to the BIM/CIM coordinate system, and measures the distance up to the shooting surface with the sensor mounted on the robot. Furthermore, the image size at that distance is estimated from the camera parameters, and its neighboring points are searched and correlated from the three-dimensional points group.

By the above processing, it became possible to arrange the images on the three-dimensional points group as shown in Figure 9.


Figure 9. Image superposition on three-dimensional points group data

At this time, since the damage in the image is extracted by deep learning etc. and displayed on the image, the worker can intuitively understand the damage location on the three-dimensional points group on which the image is superimposed (Figure 10).


Figure 10. Digital twin data

In addition, since these images associated with IFC can also be associated with other data described in IFC during design and construction, it is expected to contribute to preventive maintenance such as investigating the cause of damage occurrence and estimating future growth of damage from the relationship with design values, materials, and

completion inspection data.

6 Conclusion

In the paper, as one of the methods that effectively contribute new technologies such as robots and deep learning to infrastructure maintenance and management work, a digital twin technology based three-dimensional integrated management method was proposed. It is expected that future technological innovations will facilitate appropriate maintenance and management of the infrastructure, where aging has become a social problem.

However, while each technology is expected to be labor-saving, some problem have been pointed out such as the enormous data size and some operational issues like subsequent browsing of the data. Therefore, in this paper, we acquired the data with the required accuracy according to the purpose, converted it into three-dimensional data, and developed a sustainable infrastructure maintenance and management method by making it compliant with BIM/CIM.

In particular, as the number of skilled inspection personnel is expected to decrease in the future, it is necessary to propose to asset owners the diagnostic information that contributes to preventive maintenance from these new technologies. By setting up a mechanism that can correlate the acquired data and the position information and manage this information with a time axis, it is expected that efforts will be made for automation of diagnosis in the future.

In the future, we would like to deepen the digital twin technology that would allow inspection personnel to properly diagnose the infrastructure by accumulating data at various times for structures constructed in various environments.

References

[1] Ministry of Land, Infrastructure, Transport and Tourism, On-line:http://www.mlit.go.jp/tec/i-construction/index.html, Accessed: 04/06/2020.

[2] Michael Grieves: Digital Twin, Mitigating Unpredictable, Undesirable Emergent Behavior in Complex Systems (Excerpt)

[3] Fuminori Yamasaki, Norihisa Haneda: Bridge inspection robot with Compound eye camera, RSJ2015.

[4] Ministry of Land, Infrastructure, Transport and Tourism, On-line: https://www.mlit.go.jp/sogoseisaku/constplan/sosei_constplan_tk_000034.html,Accessed:04/06/2020.

Real-Time Process-Level Digital Twin for Collaborative Human-Robot Construction Work

X. Wang[a], C. J. Liang[a], C. C. Menassa[a,b], and V. R. Kamat[a.b]

[a]Department of Civil and Environmental Engineering, University of Michigan, USA
[b]Robotics Institute, University of Michigan, USA

wangix@umich.edu, cjliang@umich.edu, menassa@umich.edu, vkamat@umich.edu

Abstract -

Widespread use of autonomous robots in on-site construction has been limited because it is impractical to preprogram robots to perform quasi-repetitive tasks due to the relatively loose work tolerances and deviations of as-built work from the project design. Robotization of field construction work must thus be conceived as a collaborative human-robot endeavor capable of planning and improvising during the performance of construction tasks. Although humans can control robot motion through teleoperation, it is often impractical due to the range of a robot's motion and associated safety issues arising from heavy or large construction materials. An intuitive and safe bi-directional interface is thus needed to enable construction robots to seamlessly interact with and partner with human co-workers. This paper proposes a framework that allows human-robot interaction and collaboration within a real-time, process-level, immersive virtual reality (VR) digital twin that is created by combining the as-designed BIM model and the evolving as-built workspace geometry obtained from on-site sensors. Humans can use the digital twin to remotely demonstrate a task plan to the robot. The robot understands the communicated objectives and plans its motion to complete the task, which is communicated back through the system for human evaluation and approval before the robot executes the task. A case study involving imperfect rough carpentry (i.e., stud framing) and a 6DOF KUKA drywall-installing robot arm is conducted to demonstrate and evaluate the digital twin system.

Keywords -

Improvisation; Digital twin; Virtual reality; Human-robot interaction

1 Introduction

The construction industry is one of the largest sectors of the economy, accounting for up to 13% of GDP worldwide [1]. However, as one of the most labor-intensive industries, the construction industry is suffering from shortage and aging of the labor force [2, 3]. On one hand, the construction site is unstructured and dynamic. On the other hand, the construction work imposes considerable physical demands on workers. These facts lead to high fatality and injury rates in construction workers [4, 5]. In addition, the productivity of the construction industry has barely increased over the past few decades [6]. More recently, the outbreak of the Covid-19 pandemic has caused serious economic impact and schedule delays on construction projects since it is hard to maintain social-distancing while working in close proximity on construction sites [7]. This has highlighted the need for construction techniques that can allow workers to perform tasks remotely, allowing for reduction in the number of on-site workers or their physical separation while on site.

Robots can manipulate heavy objects and could potentially relieve construction workers from excessive physical demand, alleviate labor shortage, increase productivity, and promote remote construction. Although robots have already boosted the productivity of several industries, some attributes of the construction industry inhibit the wide application of construction robots [8]. First, the unique and static nature of the construction product requires robots being able to move to the workspace, accurately localize themselves, and conduct a series of different actions on the product [9, 10]. Second, the unstructured construction site limits the workspace of the robot and adds to the difficulty of robot motion planning and localization [11, 12]. Third, the moving workers, components, and construction equipment require robots to be able to comprehensively perceive the environment and make quick responses [13].

In addition, construction work has relatively loose tolerances [14, 15]. The evolving as-built structure and some construction materials may deviate from designed geometry, which requires adjustment of high-level task plans accordingly [16]. Although the recent development of artificial intelligence algorithms allows robots to be programmed with adaptability, it is not cost-effective or practical to equip and program construction robots with such high perception ability and adaptivity to cope with all potential issues on construction sites [17]. Human-robot collaboration (HRC) combines human beings' cognitive ability with robots' competency in power, speed, and accuracy, and has thus become a promising solution for robotizing construction work.

Several HRC methods have been adopted in the construction industry. An intuitive method for collaborative human-robot construction is to lead the robot by directly applying forces to the robot or the object carried by the robot through physical contacts, such as MULE135 (Material Unit Lift Enhancer) [18] and curtain wall installation robot [13]. It relieves construction workers from high physical stress while retains their operation agility. However, it still requires human workers to be present alongside the robot. Considering the needs of performing construction work remotely, several teleoperation techniques have been proposed for construction robotics, such as joysticks [19], haptic devices [20], wearable sensors [21], and vision detection systems [22]. Although teleoperation can protect workers from potential dangers on-site, operating robots with multiple degrees of freedom (DOFs) requires expertise. The robot is moving at the same time as human operation and the human needs to figure out and lead the robot through the full manipulation path. There are also safety issues caused by the limited perception of working environments [13]. Recently, the emergence of commercial head-mounted devices promoted the application of immersive virtual reality (VR), augmented reality (AR), and mixed reality (MR) in HRC. For example, VR has been used to study worker reactions while sharing workspaces with robots and AR has been used to give worker instructions to cooperate with robots [23, 24]. Therefore, a safe and intuitive HRC interface for construction robots that takes advantage of immersive technologies and allows remote operation is proposed.

The objective of this paper is to propose a real-time, process-level, immersive VR digital twin for intuitive and remote human-robot collaborative construction work. The human worker performs high-level decision making and supervision in an immersive VR digital twin of the construction site. The robot is responsible for detailed motion planning and task execution on-site. The detailed motion plan and robot status information are visualized in VR for human approval before actual execution. A case study involving imperfect rough carpentry (i.e., stud framing) and a 6DOF KUKA drywall-installing robot arm is conducted to demonstrate and evaluate the digital twin system. The construction site and robot arm are emulated in the Gazebo simulator that allows rapid prototyping of robotic tasks and direct subsequent transfer of the methods to the corresponding real robotic platforms [25].

2 Collaborative Human-Robot Construction System

Figure 1 gives an overview of the proposed collaborative human-robot construction framework. The human worker interacts with the robot through an immersive VR interface developed in Unity3D. The Oculus Rift S VR headset and the Oculus Touch controllers are used to create the VR experience. The immersive VR interface is connected to the robot operation environment (i.e. the construction site environment in which the robot performs the task) via the Robot Operating System (ROS) as the computational core. The computational core is responsible for computation and data processing. It also acts as the communication tool between the human and the robot. In this section, the immersive VR interface and the computational core are discussed in detail. The operation environment is discussed later in the case study.

2.1 Immersive VR interface

2.1.1 Immersive VR environment

The immersive VR environment is the digital twin of the construction environment. There are two common methods of developing the VR model of a construction site. One of them is to use the 3D CAD model, such as Building Information Modeling (BIM) [26]. It is fast and convenient to be loaded as a VR scene but it cannot reflect actual construction site environment since the built structure could deviate from design and there would be obstacles stacking on-site during construction. Another method is to construct point clouds from laser scanners or RGBD cameras [27]. However, it takes significant computational resources to construct the point cloud of a construction site and use it in VR. Therefore, this research uses a combination of the as-design BIM model and as-built point clouds of workspace obtained from the sensors to create the VR digital twin of the construction site (Figure 2).

The general construction site environment is generated from the BIM model. For the non-critical components, the BIM models are directly loaded and used in VR. It creates a realistic construction environment VR experience. The non-critical components indicate components that are outside the robot workspace or components that are inside the robot workspace but their deviations from design do not influence user decision making and robot execution processes. The BIM models of the critical components are set as semi-transparent so that the user can visualize how the structure is designed and supposed to be built.

Meanwhile, the robot workspace is captured by RGBD cameras placed on the construction site. The RGBD images are sent to the computational core for processing and then transferred to Unity3D for visualization in VR in near real-time. The point cloud overlays the semi-transparent as-design BIM model so the differences between the as-design and as-built geometry can be inspected. Point clouds can also capture the dynamic conditions in robot workspace, such as workers and obstacles, and show it in the VR. The human worker can view the as-built workspace conditions for decision making, such as deciding how and where to install the next component.

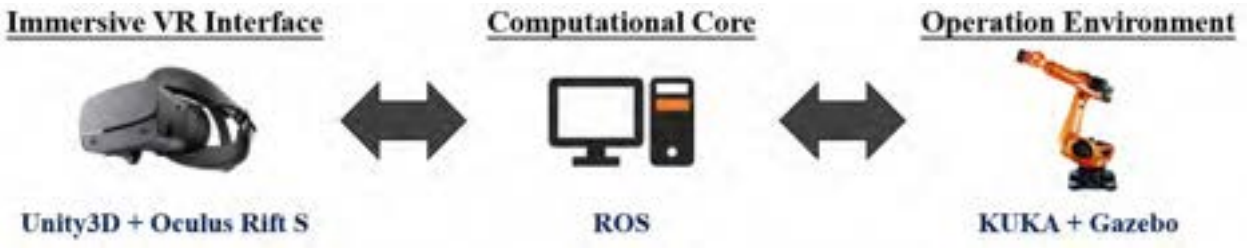

Figure 1. Collaborative human-robot construction system overview

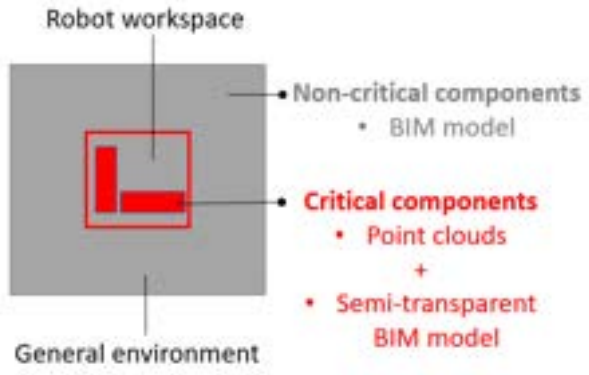

Figure 2. Immersive VR environment construction

2.1.2 Robot digital twin model

There are two full-scale robot models in the VR scene, which overlap with each other in the original state. One of them shows the planning state of the robot. It is used to visualize the robot motion plan (Figure 3(a)). The other one shows the actual state of the robot for execution status visualization (Figure 3(b)). The two robot models are referred to as the "planning" robot and the "execution" robot respectively in the rest of this paper. The KUKA robot arm model is built in Unified Robotics Description Format (URDF) in the ROS computational core, which has the same size and configuration as the actual robot [28]. The model is then transferred from ROS to be loaded as a game object in VR using the ROS# library [29]. The VR robot models preserve the kinematic and dynamic properties of the robot and can be controlled by subscribing messages from the computational core.

2.1.3 Interactive VR elements and functions

One of the advantages of immersive VR is that the user can have realistic experience while overcoming some restrictions of the real world. For example, users can receive extra information that they cannot directly achieve from the real world, such as the comparison between the as-design and as-built geometry, and overcome some real-world constraints, like gravity.

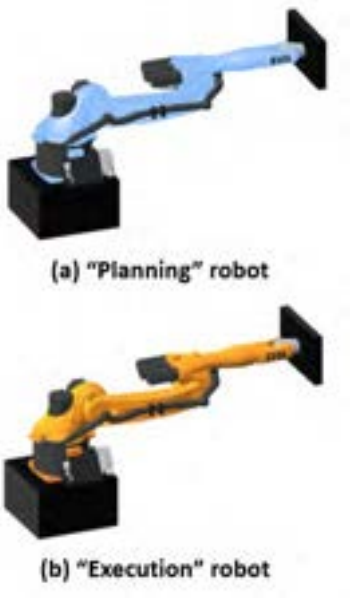

Figure 3. VR robot models (a) "planning" robot (b) "execution" robot

Our digital twin system includes several interactive VR elements. An interactive billboard with two functions has been developed. First, it shows the user system messages that cannot be directly obtain even from the actual construction environment, such as warning messages from ROS. Second, the billboard can also be used as an input device inside VR where the user can give commands to the system by interacting with the buttons on the screen. Users' sight could easily be occluded in complex construction environments. Therefore, instead of fixing the billboard to one location, our system allows users to manipulate it with the VR controller and adjust its pose and view at their convenience. The billboard can be suspended in the air as how it has been placed. As the environment changes, users can always put the billboard at a new desirable position. Some interactive construction materials have been created for pick-and-place related tasks, which can also be grabbed and suspended in the air, for the user to perform high-level task planning. It should be noted

that although the paper mainly discussed pick-and-place related cases, the system can be generalized to many construction tasks by adding customized interactive elements and functions.

2.2 Computational Core

ROS has been used as the system computational core. ROS is an open-source system that combines a variety of tools and software libraries for robot operation [30]. It can communicate with Unity3D, Gazebo, and the actual robot. In our system, ROS is also responsible for sensor data processing, motion planning, and robot control besides communication.

2.2.1 Communication

The system communication framework is shown in Figure 4. ROS# is used for communication between ROS and Unity3D [29], and *gazebo_ros_pkgs* is used to interface Gazebo with ROS [31]. As the program starts, Gazebo starts to constantly publish sensor data and robot states to ROS. In the meantime, ROS processes the sensor data and publish the processed data and robot states to Unity3D, which is then visualized as the point cloud and the state of the "execution" robot in VR. Based on the point cloud, the user develops the task plan and sends it to ROS after confirmation. ROS then generates a collision-free motion plan accordingly.

The motion plan is sent back to Unity3D and is visualized by the user on the "planning" robot. If the user is not satisfied with the motion plan, they can either adjust their task plan or request another motion plan from ROS which in turn generates a new motion plan in response. Upon user approval, a message is sent to ROS which converts the motion plan into execution commands to control the actual robot. As the actual robot executes the work, updated robot state messages are received by ROS and Unity3D. The "execution" robot in VR moves accordingly.

2.2.2 Sensor data processing

Several Microsoft Kinect cameras are placed on the virtual construction site in Gazebo to capture robot workspace. The RGBD images captured are converted into point clouds. Point clouds from different cameras are transformed into the world frame based on respective camera positions and rotations and then concatenated into one single point cloud. The point cloud is then downsampled with the voxel grid filter. Finally, it goes through the self-filtering process. Self-filter removes visible parts of the robot from the point cloud based on the current robot state.

2.2.3 Motion planning

After receiving the user-specified task plan, the corresponding end-effector pose is calculated. The robot then plans a trajectory to that pose so that both the robot itself and the object carried by the robot do not collide with the environment. The motion planning is conducted by MoveIt, a robotics manipulation platform in ROS [32]. The point cloud after processing discussed earlier is further processed by OctoMap into a 3D occupancy grid map of the environment [33]. The Open Motion Planning Library is used as the motion planner and the Flexible Collision Library is used for collision detection [34, 35]. The inverse kinematics is calculated by the Kinematics and Dynamics Library numerical jacobian-based solver [36]. The joint velocity and acceleration limits are taken into consideration to time-parameterize the generated path. After that, the time-parameterized path is sent to Unity3D as separate states for visualization on the "planning" robot.

2.2.4 Robot Control

When the user approves the trajectory plan in VR, ROS will be notified with an approval message. The *ros_control* package is then used to convert the approved trajectory plan into robot control commands [37]. It obtains joint state data from the encoders of robot actuators and generates output with PID controllers to robot actuators.

2.3 Case Study

A drywall installation case study with a 6DOF KUKA robot arm that is capable of real construction work has been conducted to evaluate the immersive digital twin system. The user guides the robot arm to pick up a drywall panel placed on the ground near the robot and place it on a wall frame that is built with deviations from design. Figure 5 shows the robot operating environment in Gazebo, which represents the actual construction site, and its VR digital twin in Unity3D. Three Microsoft Kinect cameras are used to capture the robot workspace environment in Gazebo.

Figure 6 shows the point cloud before and after processing. Points on the ground panel are also removed with the RANSAC plane segmentation algorithm. In VR, a drywall panel is set to be the interactive construction component, which is in the same shape as the actual drywall. The user will first observe the wall frame geometry from the point cloud and decide how to install the drywall panel onto the frame. The user can then demonstrate the task plan by grabbing the interactive panel and placing it at the desired installation position. The buttons on the interactive billboard provide options for fast and accurate adjustment of the orientation of the interactive panel.

The robot will first pick up the drywall panel on the floor and then wait for the user to specify the task plan. The

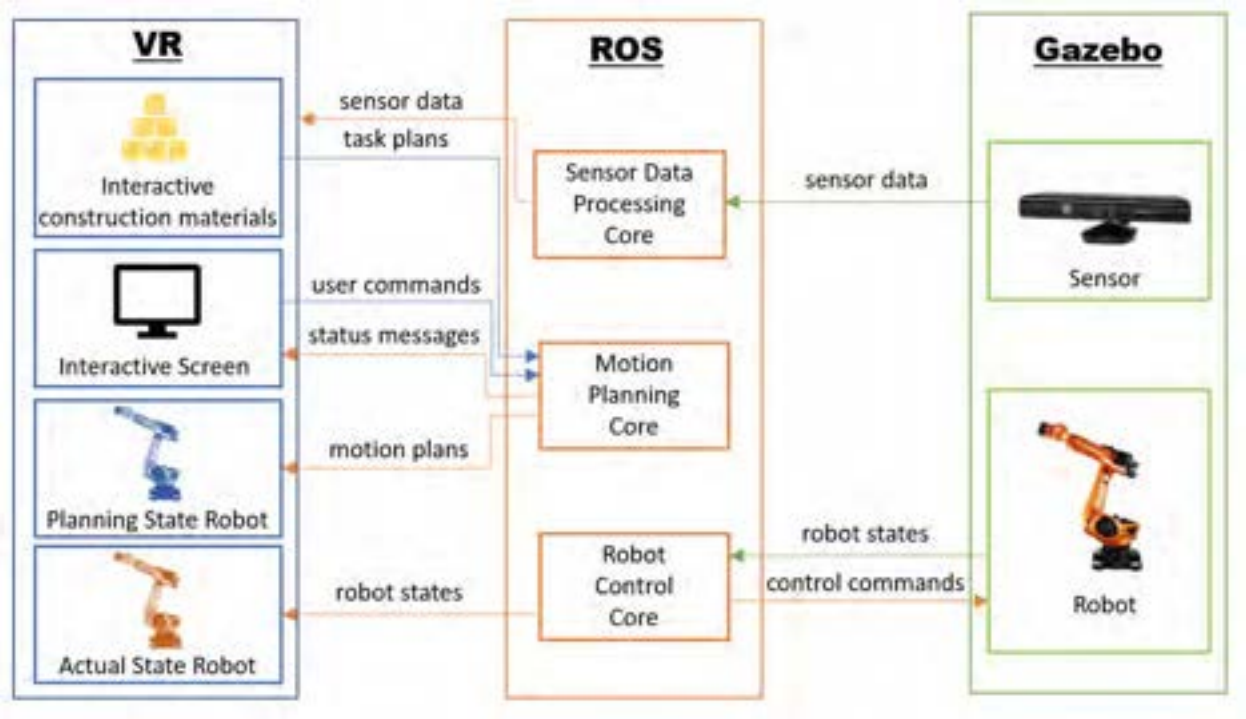

Figure 4. System communication framework

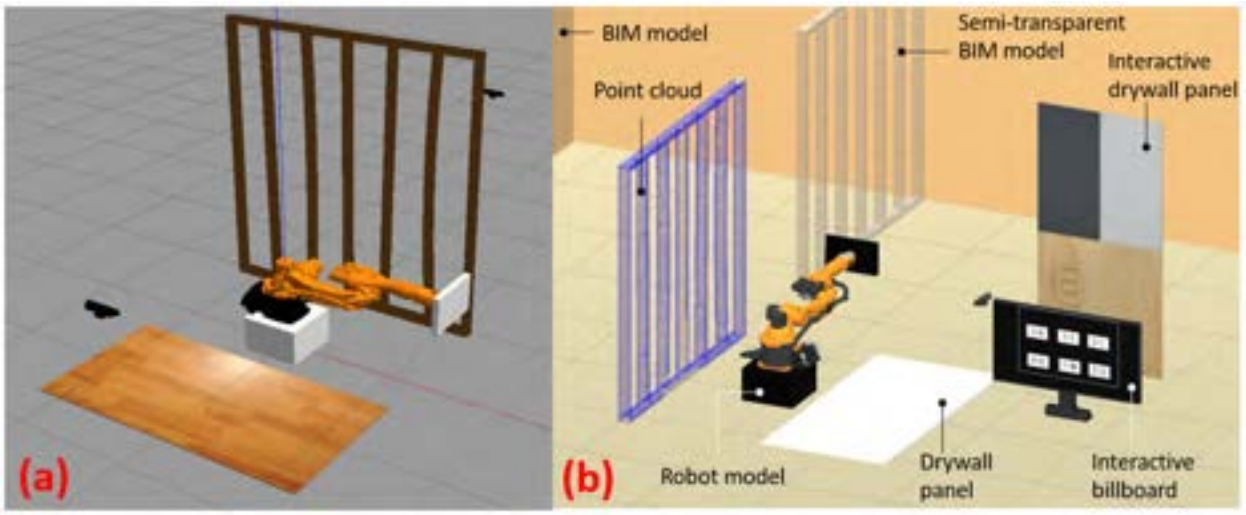

Figure 5. (a) Robot operation environment (b) VR environment

user can know whether the robot has successfully picked up the panel from the billboard and the panel will change color after being picked up. After the user confirms the task plan, ROS starts to develop the detailed motion plan to place the panel to the user-specified position while sending planning status messages (e.g. in progress, success, reasons of failure) to the user via the billboard. After motion planning, the "planning" robot demonstrates the plan to the user while the actual robot stays still (Figure 7).

Upon approval, ROS controls the actual robot to execute the approved motion plan and update the user with execution status messages. At the same time, the "execution" robot is synchronized with the actual robot by subscribing to the actual robot state messages so that the user can perceive actual robot status from VR (Figure 8).

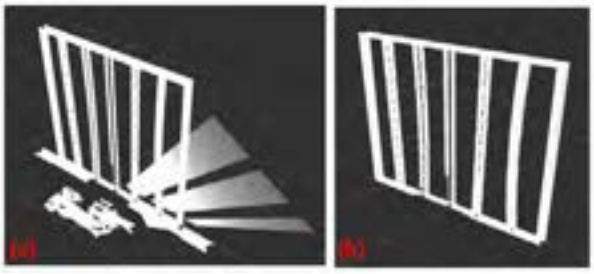

Figure 6. Point cloud (a) before processing (b) after processing

Figure 7. "Planning" robot demonstrating motion plan

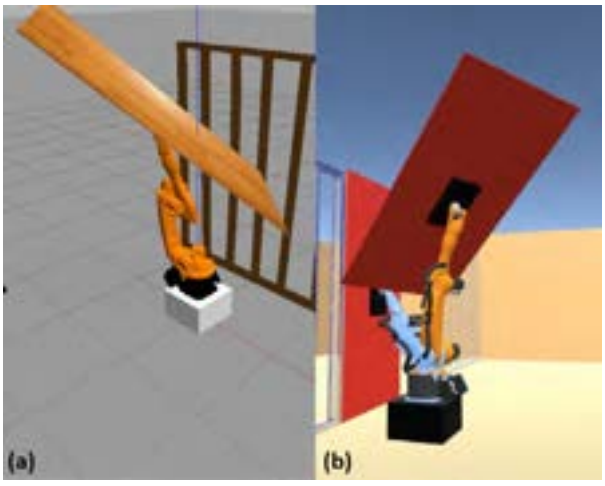

Figure 8. Synchronized movement of (a) actual robot and (b) execution robot

3 Conclusion

In this study, a real-time, process-level, immersive digital twin system for collaborative human-robot construction work is proposed. The system has several advantages. First, human workers can visualize construction site conditions and collaborate with the robot remotely, which protects them from potential dangers on the construction site. Second, the communication network allows the human worker and the robot to exchange task plans and status information in near real-time. Third, it allows the human worker to improvise high-level construction plans based on as-built construction site geometry. Last, the robot develops its motion plan and carries out physical construction work on-site, which significantly reduces human workload. In ongoing work, our research team is experimenting with real robots and implementing the immersive digital twin system with mobile robot arms.

Acknowledgements

The authors would like to acknowledge the financial support received from the U.S. National Science Foundation (NSF) CBET 1638186 and CBET 1804321. Any opinions and findings in this paper are those of the authors and do not necessarily represent those of the NSF.

References

[1] Jan Mischke Maria João Ribeirinho Mukund Sridhar Matthew Parsons Nick Bertram Filipe Barbosa, Jonathan Woetzel and Stephanie Brown. Reinventing construction: A route to higher productivity. On-line: `https://www.mckinsey.com/~/media/McKinsey/Industries/Capital%20Projects%20and%20Infrastructure/Our%20Insights/Reinventing%20construction%20through%20a%20productivity%20revolution/MGI-Reinventing-construction-A-route-to-higher-productivity-Full-report.ashx`, 2017.

[2] Meiyin Liu. *Video-Based Human Motion Capture and Force Estimation for Comprehensive On-Site Ergonomic Risk Assessment*. PhD thesis, 2019.

[3] CJ Liang, VR Kamat, and CC Menassa. Teaching robots to perform construction tasks via learning from demonstration. In *ISARC. Proceedings of the International Symposium on Automation and Robotics in Construction*, volume 36, pages 1305–1311. IAARC Publications, 2019.

[4] CPWR. The construction chart book. On-line: `https://www.cpwr.com/publications/research-findings-articles/construction-chart-book`, 2018.

[5] CJ Liang, KM Lundeen, W McGee, CC Menassa, S Lee, and VR Kamat. Stacked hourglass networks for markerless pose estimation of articulated construction robots. In *35th International Symposium on Automation and Robotics in Construction*, 2018.

[6] Juan Manuel Davila Delgado, Lukumon Oyedele, Anuoluwapo Ajayi, Lukman Akanbi, Olugbenga Akinade, Muhammad Bilal, and Hakeem Owolabi. Robotics and automated systems in construction: Understanding industry-specific challenges for adoption. *Journal of Building Engineering*, 26:100868, 2019.

[7] ENR. Construction loses 975,000 jobs in april, due to covid-19 impacts. On-line: `https://www.enr.com/articles/49333-construction-loses-975000-jobs-in-april-due-to-covid-19-impacts`, 2020.

[8] Kurt M Lundeen, Vineet R Kamat, Carol C Menassa, and Wes McGee. Scene understanding for adaptive manipulation in robotized construction work. *Automation in Construction*, 82:16–30, 2017.

[9] Toshio Fukuda, Yoshio Fujisawa, Fumihito Arai, H Muro, K Hoshino, Kenji Miyazaki, and K Uehara. A new robotic manipulator in construction based on man-robot cooperation work. In *Proc. of the 8th International Symposium on Automation and Robotics in Construction*, pages 239–245. Citeseer, 1991.

[10] Chen Feng, Yong Xiao, Aaron Willette, Wes McGee, and Vineet R Kamat. Vision guided autonomous robotic assembly and as-built scanning on unstructured construction sites. *Automation in Construction*, 59:128–138, 2015.

[11] Xing Su and Hubo Cai. Enabling construction 4d topological analysis for effective construction planning. *Journal of Computing in Civil Engineering*, 30 (1):04014123, 2016.

[12] Lichao Xu, Chen Feng, Vineet R Kamat, and Carol C Menassa. An occupancy grid mapping enhanced visual slam for real-time locating applications in indoor gps-denied environments. *Automation in Construction*, 104:230–245, 2019.

[13] Seungyeol Lee and Jeon Il Moon. Introduction of human-robot cooperation technology at construction sites. In *ISARC. Proceedings of the International Symposium on Automation and Robotics in Construction*, volume 31, page 1. IAARC Publications, 2014.

[14] Ci-Jyun Liang, Vineet R Kamat, and Carol C Menassa. Teaching robots to perform quasi-repetitive construction tasks through human demonstration. *Automation in Construction*, 120:103370, 2020.

[15] Colin Milberg and Iris Tommelein. Role of tolerances and process capability data in product and process design integration. In *Construction Research Congress: Wind of Change: Integration and Innovation*, pages 1–8, 2003.

[16] Kurt M Lundeen, Vineet R Kamat, Carol C Menassa, and Wes McGee. Autonomous motion planning and task execution in geometrically adaptive robotized construction work. *Automation in Construction*, 100: 24–45, 2019.

[17] Yap Hwa Jen, Zahari Taha, and Lee Jer Vui. Vr-based robot programming and simulation system for an industrial robot. *International Journal of Industrial Engineering*, 15(3):314–322, 2008.

[18] Construction Robotics. Mule. On-line: `https://www.construction-robotics.com/mule/`, Accessed: 06/01/2020.

[19] Kyungmo Jung, Baeksuk Chu, Shinsuk Park, and Daehie Hong. An implementation of a teleoperation system for robotic beam assembly in construction. *International Journal of Precision Engineering and Manufacturing*, 14(3):351–358, 2013.

[20] P Chotiprayanakul, DK Liu, and G Dissanayake. Human–robot–environment interaction interface for robotic grit-blasting of complex steel bridges. *Automation in Construction*, 27:11–23, 2012.

[21] Dongmok Kim, Jongwon Kim, Kyouhee Lee, Cheolgyu Park, Jinsuk Song, and Deuksoo Kang. Excavator tele-operation system using a human arm. *Automation in construction*, 18(2):173–182, 2009.

[22] Ying-Hao Yu, Chun-Hsien Yeh, Tsu-Tian Lee, Pei-Yin Chen, and Yeu-Horng Shiau. Chip-based real-time gesture tracking for construction robot's guidance. In *ISARC. Proceedings of the International Symposium on Automation and Robotics in Construction*, volume 31, page 1. IAARC Publications, 2014.

[23] Sangseok You, Jeong-Hwan Kim, SangHyun Lee, Vineet Kamat, and Lionel P Robert Jr. Enhancing perceived safety in human–robot collaborative construction using immersive virtual environments. *Automation in Construction*, 96:161–170, 2018.

[24] Pedro Tavares, Carlos M Costa, Luís Rocha, Pedro Malaca, Pedro Costa, António P Moreira, Armando Sousa, and Germano Veiga. Collaborative welding system using bim for robotic reprogramming and spatial augmented reality. *Automation in Construction*, 106:102825, 2019.

[25] Nathan Koenig and Andrew Howard. Design and use paradigms for gazebo, an open-source multi-robot simulator. In *2004 IEEE/RSJ International Conference on Intelligent Robots and Systems (IROS)(IEEE Cat. No. 04CH37566)*, volume 3, pages 2149–2154. IEEE, 2004.

[26] Jing Du, Zhengbo Zou, Yangming Shi, and Dong Zhao. Zero latency: Real-time synchronization of bim data in virtual reality for collaborative decision-making. *Automation in Construction*, 85:51–64, 2018.

[27] Qian Wang, Jingjing Guo, and Min-Koo Kim. An application oriented scan-to-bim framework. *Remote sensing*, 11(3):365, 2019.

[28] kuka - ros wiki. On-line: `http://wiki.ros.org/kuka`, Accessed: 06/01/2020.

[29] ros-sharp. On-line: `https://github.com/siemens/ros-sharp`, Accessed: 06/01/2020.

[30] Morgan Quigley, Ken Conley, Brian Gerkey, Josh Faust, Tully Foote, Jeremy Leibs, Rob Wheeler, and Andrew Y Ng. Ros: an open-source robot operating system. In *ICRA workshop on open source software*, volume 3, page 5. Kobe, Japan, 2009.

[31] gazebo_ros_pkgs - ros wiki. On-line: `http://wiki.ros.org/gazebo_ros_pkgs`, Accessed: 06/01/2020.

[32] Sachin Chitta, Ioan Sucan, and Steve Cousins. Moveit![ros topics]. *IEEE Robotics & Automation Magazine*, 19(1):18–19, 2012.

[33] A Hornung, KM Wurm, M Bennewitz, C Stachniss, and W Burgard. An efficient probabilistic 3d mapping framework based on octrees armin hornung. *Autonomous Robots Journal. Springer*, 2013.

[34] Ioan A Sucan, Mark Moll, and Lydia E Kavraki. The open motion planning library. *IEEE Robotics & Automation Magazine*, 19(4):72–82, 2012.

[35] Jia Pan, Sachin Chitta, and Dinesh Manocha. Fcl: A general purpose library for collision and proximity queries. In *2012 IEEE International Conference on Robotics and Automation*, pages 3859–3866. IEEE, 2012.

[36] Ruben Smits, H Bruyninckx, and E Aertbeliën. Kdl: Kinematics and dynamics library, 2011.

[37] Sachin Chitta, Eitan Marder-Eppstein, Wim Meeussen, Vijay Pradeep, Adolfo Rodríguez Tsouroukdissian, Jonathan Bohren, David Coleman, Bence Magyar, Gennaro Raiola, Mathias Lüdtke, and Enrique Fernández Perdomo. ros_control: A generic and simple control framework for ros. *The Journal of Open Source Software*, 2017.

Research and Development of Construction Technology in Social Cooperation Program "Intelligent Construction System"

Shota CHIKUSHI[a], Jun Younes LOUHI KASAHARA[a], Hiromitsu FUJII[b], Yusuke TAMURA[c], Angela FARAGASSO[a], Hiroshi YAMAKAWA[a], Keiji NAGATANI[a], Yonghoon JI[d], Shinji AOKI[e], Takumi CHIBA[e], Shingo YAMAMOTO[e], Kazuhiro CHAYAMA[e], Atsushi YAMASHITA[a] and Hajime ASAMA[a]

[a]The University of Tokyo, Japan
[b]Chiba Institute of Technology, Japan
[c]Tohoku University, Japan
[d]Japan Advanced Institute of Science and Technology, Japan
[e]Fujita Co., Ltd. Japan
E-mail: chikushi@robot.t.u-tokyo.ac.jp, louhi@robot.t.u-tokyo.ac.jp, hiromitsu.fujii@p.chibakoudai.jp, y.tamura@srd.mech.tohoku.ac.jp, faragasso@robot.t.u-tokyo.ac.jp, yamakawa@susdesign.t.u-tokyo.ac.jp, keiji@i-con.t.u-tokyo.ac.jp, ji-y@jaist.ac.jp, shinji.aoki@fujita.co.jp, takumi.chiba@fujita.co.jp, syamamoto@fujita.co.jp, chayama@eae.co.jp, yamashita@robot.t.u-tokyo.ac.jp, asama@robot.t.u-tokyo.ac.jp,

Abstract -

This paper presents the developments achieved via the Social Cooperation Program "Intelligent Construction System," from three primary perspectives: environmental measurements, improvements in remote operability, and improvements in efficiency and automation of remote operation. For improvements in remote operation, environmental measurements of the disaster sites are critical. Therefore, a method to integrate the data from drones and ground-based vehicles in order to generate 3D maps was proposed. Another method for estimating the changes in soil volumes through a 3D map based on drone data was also proposed. Finally, to estimate the trafficability in disaster sites, a cone index-based method employing spectral images was proposed. Improving remote operability is essential to facilitate improved working conditions for operators. Considering this, a method providing human operators with a bird's-eye view of remotely operated machinery from any perspective was proposed. Additionally, to avoid the tumbling of remotely operated machinery, a running stability presentation method was proposed; this method presented the human operator with a tumble risk index. For improving efficiency and automation, an automatic camera control method, based on requirements of construction machine operators, was proposed. Using this method, the need for a dedicated human camera operator could be bypassed. Furthermore, for the automatic measurement of construction time and content, a method based on deep learning and using cameras for recognizing the actions of construction machinery was proposed. Preliminary experiments on some of the proposed methods in real environments yielded promising results.

Keywords -

Intelligent construction system; Environmental measurement; Improving remote operability; Automation; Efficiency improvement

1 Introduction

Japan experiences several earthquakes and volcanic eruptions as it is located on a crustal deformation zone. Moreover, the country also experiences heavy rainfall due to its dense forests (accounting for approximately 70% of the country's area). Such environmental conditions result in several natural disasters such as lava and debris flows due to volcanic eruptions, landslides caused by earthquakes, and flooding of rivers due to heavy rainfall. In the event of such natural disasters, it is necessary to promptly conduct appropriate investigations and restoration activities in order to prevent any further damage. However, disaster sites, i.e., the areas affected by these natural disasters, present a certain amount of risk due to secondary disasters. Disaster recovery efforts should be implemented soon after a disaster. Thus, considering the potential risk of secondary collapses or disasters, remotely controlled robots and remote-operated construction machinery are employed, which allows the human operators to work from a safe distance. However, such methods are associated with low work efficiencies, and they also prolong the time required for disaster recovery efforts. Therefore, a more efficient and intelligent construction system is necessary. For this purpose, a Social Cooperation Program "Intelligent Construction System" was organized by The University of Tokyo and Fujita Co., Ltd, in October 2017. The goal of this program was to research, develop, and establish an intelligent construction system for the inspection of infrastructures as well as for repair and disaster recovery efforts. This program focuses on utilizing in-

telligent construction technology achieved via advanced equipment, such as unmanned ground vehicles (UGVs) (including remote controlled robots and unmanned construction machines), drones, and information and communications technology.

This paper presents the advancements achieved via the Social Cooperation Program "Intelligent Construction System," from three main perspectives: environmental measurements, improvements in remote operability, and improvements in efficiency and automation of remote operation. For the environmental measurements, we introduce methods for generating 3D maps, estimating changes in soil volume, and determining trafficability. To improve remote operability, we introduce methods for providing a bird's-eye view of remote-operated machinery and for avoiding the tumble of UGVs. Finally, for the improvements in efficiency and automation, we introduce methods for presenting images via automatic control of external cameras and recognizing the actions of construction machinery.

2 Environmental measurement

2.1 Generation of 3D map with scale and slope information

At a disaster site, the topography and surrounding environment vary with respect to time. Therefore, unmanned construction machines should be operated based on the disaster scenes measured over a wide area as well as real-time data regarding changes in topography and surrounding environments. Therefore, studies have been conducted on environment map generation using UAVs [1]. To better understand the different conditions of a disaster site, we are developing a 3D map generation method that integrates data measured via drones and unmanned construction equipment [2]. By integrating the data acquired from drones and the inertial measurement unit (IMU) sensors mounted on UGVs, this proposed approach generates a 3D map comprising scale and slope information, as shown in Figure 1.

In addition, to monitor the ground information of disaster sites, we are developing a method to estimate the variations in soil volumes [3]. The ground at disaster sites is altered due to the gradual unloading of landslides and sediments. With regard to this, the proposed method compares a local map after terrain change with a global map prior to terrain change, in order to obtain the changes in soil volume as a 3D.

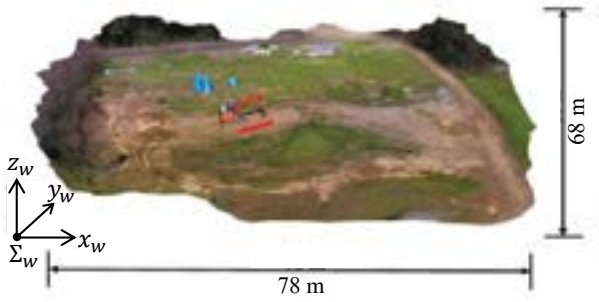

Figure 1. 3D map with scale and slope information

2.2 Trafficability judgment of UGV by ground measurement

Disaster sites can comprise soft soils, which cannot be traversed using UGVs, because such vehicles can get stuck and tumble in soft soils. Therefore, several researchers have studied the judgement the trafficability of UGVs [4]. However, no studies have focused on the non-contact judgement of trafficability with soft ground having a cone index of less than 200 kN/m^2, such as a landslide disaster site, as a target. Therefore, to ensure safe operation of UGVs at disaster sites, we are developing a method for judging the trafficability of UGVs without contact, based on the cone index [5]. The cone index is determined by the soil type and its water content. For this method, ground surfaces are evaluated via a multispectral camera, and the soil type and water content of the ground are estimated. The cone index is calculated based on these estimation results and used to determine the trafficability of UGVs.

3 Improving remote operability

3.1 Bird's-eye view image presentation

Remote-operated UGVs are effective for disaster recovery and inspection work in environments that are difficult for people to enter. When working with a remote-operated UGV, it is necessary to present an image to the operator. If the operator is presented with multiple camera images, the effectiveness of recovery or inspection efforts can be degraded. A single video depicting the surrounding environment is more effective. Therefore, several studies have been conducted on image presentation for improving the remote operability of UGVs [6]. To ensure improved operability, to view the remote-operated UGV as a single image, under this project, we are developing a bird's-eye view image that can be viewed from any angle. The proposed method generates a bird's-eye view image by using a laser range sensor and multiple fish-eye cameras mounted on a UGV [7]. The proposed method involves measuring the surrounding environment using a laser range sensor and generates a 3D mesh model of the wall. The wall is assumed to be perpendicular to the ground. A bird's-eye view image in an indoor environment is generated by projecting the image acquired from each fisheye camera on the generated 3D mesh model. By presenting a single bird's-eye view image, it is possible to recognize the rel-

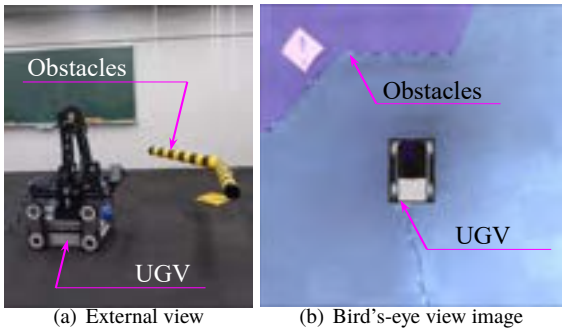

(a) External view (b) Bird's-eye view image

Figure 2. Obstacles presentation on bird's-eye view image

ative positions of the UGV and the wall and to improve remote operability in an indoor environment.

Furthermore, the path of the UGV can be obstructed by obstacles. Information regarding the relative positions of the UGV and obstacles can be effective for obstacle avoidance. Therefore, we are also developing a bird's-eye view image depicting the obstacles, as shown in Figure 2 [8]. This method generates a bird's-eye view image with a fish-eye camera mounted on the UGV. In addition, the surrounding environment is measured using the distance sensor mounted on the UGV. Finally, the obstacle is presented in the bird's-eye view image by integrating the different types of information. By presenting a single bird's-eye view image, it is possible to recognize the relative position of the UGV and the obstacle and to improve remote operability.

These methods involve measuring the distance to the object with a sensor. However, we are also researching a method to estimate the depth from only image information [9]. In this study, high- and low-spatial-frequency features were extracted from two images with different viewpoints, and two types of features with different frequency features were extracted. We generated a single feature by mixing these two different features. Finally, the depth was estimated via depth regression based on a single feature.

3.2 Tumble avoidance

When driving on the uneven grounds of a disaster site, it is necessary to avoid tumbles. However, it is difficult for operators to avoid tumbles using only information from the UGV's onboard sensor feedback. Therefore, several researchers have studied the tumble avoidance of UGVs [10]. We are currently developing a UGV running stability visualization method [11]. This method calculates the "stability" of a UGV using 3D ground surface information acquired via environmental measurements, through a

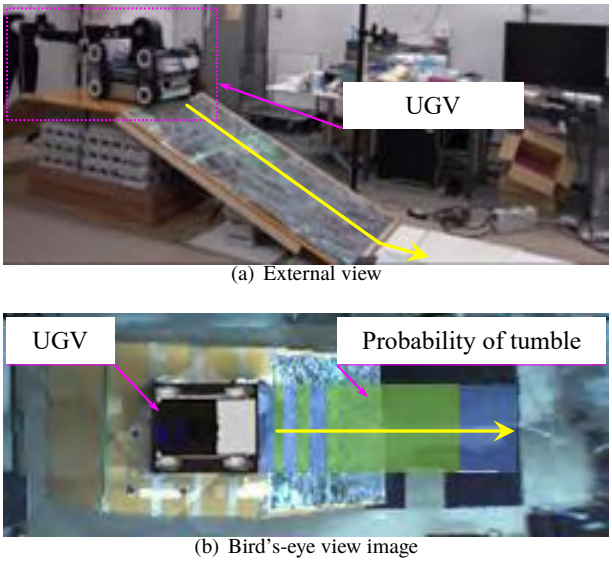

(a) External view

(b) Bird's-eye view image

Figure 3. Presentation of the probability of tumble

dynamics simulation. Thereafter, the probability of a tumble along the route selected by the operator is presented, as shown in Figure 3. In addition, we are constructing a method for the autonomous avoidance of tumbling; in this method, a manipulator mounted on the UGV is autonomously controlled to mitigate any detected tumbles. This method prevents the UGV from tumbling by moving its center of gravity via the autonomously controlled manipulator. Accordingly, the posture of the UGV is altered and its stability is improved.

4 Improvement of efficiency and automation

4.1 Image presentation by automatic control of external camera

During the embankment work of unmanned construction, the operator operates unmanned construction machinery based on external camera images. In such cases, the unmanned construction machine and the external camera are operated by the machine operator and the camera operator, respectively. Such an arrangement can lead to operation-related issues, because the camera operator may not present the view required by the machine operator. Several studies have been conducted on image presentation for remote construction [12].We are currently developing a method for the automatic control of external cameras [13]. In this method, to present the images desired by the machine operator, the video presented to the machine operator, the operator's gaze, and the machine operator's voice were recorded and analyzed, in an actual unmanned construction site. Based on the results, the required speci-

Figure 4. Automatic control External camera image

fications of the external camera image were extracted. The proposed method automatically controls the pan, tilt, and zoom of external cameras based on the extracted requirements for embankment work. Thus, appropriate external camera images are automatically presented to the machine operator, based on the construction requirements, as shown in Figure 4. Equivalent results were obtained for work time and visibility through a comparison between the image obtained using the proposed method and the image operated by the camera operator.

4.2 Hydraulic excavator action recognition

For effective management of construction machineries, it is essential to quantitatively determine the operation times and actions of these machineries. There are several studies on the action recognition of hydraulic excavators based on images [14]. In previous research, the action of the hydraulic excavator was recognized via deep learning, based on learning from actual hydraulic excavator videos. However, collecting a large amount of video data of actual hydraulic excavators is a significant challenge. To improve generalization, it is necessary to collect a large amount of data on hydraulic excavators of different sizes, colors, and shapes. Therefore, we are developing a method for recognizing the actual hydraulic excavator action via deep learning using simulation data of the hydraulic excavator action as a training dataset [15]. This method involves creating the data for recognizing the action of a hydraulic excavator in the dynamics simulation. We focused on three actions—digging, piling, and turning. These actions are learned based on simulation data. Then, a video filter is used for each data point to address the gap between the simulation data and the actual data. As a result, the action is recognized with an accuracy of 53.7%. This result shows the effectiveness of the proposed video filter, which is more than 20% higher than the action recognition result obtained using CNN+LSTM under the same data condition.

5 Conclusion

This paper presents the advancements resulting from the Social Cooperation Program "Intelligent Construction System" for environmental measurements, improvements in remote operability, and improvements in efficiency and automation of remote operation. For the environmental measurements, we introduced methods for generating 3D maps, estimating variations in soil volumes, and determining trafficability. For the improvement of remote operability, we introduced methods for presenting a bird's-eye view of remote-operated machinery and for the tumble avoidance of UGVs. For improving efficiency and automation, we introduced methods for presenting appropriate site images via automatic control of external cameras and for recognizing the actions of construction machinery.

As future efforts, we plan to validate the proposed methods at actual construction sites. In addition, we aim to further improve the construction efficiency, reduce manual labor, and improve intelligent construction.

References

[1] Darren Turner, Arko Lucieer and Christopher Watson: An automated technique for generating georectified mosaics from ultra-high resolution unmanned aerial vehicle (UAV) imagery, based on structure from motion (SfM) point clouds, *Remote Sensing*, 4(5), 1392-1410, 2012.

[2] Yuyang Shao, Yonghoon Ji, Hiromitsu Fujii, Keiji Nagatani, Atsushi Yamashita and Hajime Asama: Estimation of Scale and Slope Information for Structure from Motion-based 3D Map, *Proceedings of the 2017 IEEE/SICE International Symposium on System Integration (SII2017),* pages 208-213, Taipei, Taiwan, 2017.

[3] Yuyang Shao, Yonghoon Ji, Hiromitsu Fujii, Shingo Yamamoto, Takumi Chiba, Kazuhiro Chayama, Yusuke Tamura, Keiji Nagatani, Atsushi Yamashita and Hajime Asama: Estimation of Soil Volume Change Using UAV-based 3D Terrain Mapping, *Proceedings of the 2017 SICE Systems and Information Division,* pages 247-250, Hamamatsu, Japan, 2017.

[4] Roemi Fernández, Héctor Montes and Carlota Salinas: VIS-NIR, SWIR and LWIR Imagery for Estimation of Ground Bearing Capacity, *Sensors,* 15(6), 13994–14015, 2015.

[5] Norihiro Yamauchi, Shota Chikushi, Yusuke Tamura, Hiroshi Yamakawa, Keiji Nagatani, Hiromitsu Fujii, Yuya Sakai, Takumi Chiba, Shingo Yamamoto, Kazuhiro Chayama, Atsushi Yamashita and Hajime Asama: Estimation of Cone Index from Water Content and Soil Types Obtained from Hyperspectral Images, *Proceedings of the 2019 IEEE 8th Global Conference on Consumer Electronics (GCCE2019),* pages 999-1002, Osaka, Japan, 2019.

[6] Terrence Fong and Charles Thorpe: Vehicle Teleoperation Interfaces, *Autonomous Robots,* 11(1), 9-18, 2001.

[7] Ren Komatsu, Hiromitsu Fujii, Yusuke Tamura, Atsushi Yamashita and Hajime Asama: Free Viewpoint Image Generation System Using Fisheye Cameras and a Laser Rangefinder for Indoor Robot Teleoperation, *ROBOMECH Journal,* 7(15), 1-10, 2020.

[8] Yasuyuki Awashima, Ren Komatsu, Hiromitsu Fujii, Yusuke Tamura, Atsushi Yamashita and Hajime Asama: Visualization of Obstacles on Bird's-eye View Using Depth Sensor for Remote Controlled Robot, *Proceedings of the International Workshop on Advanced Image Technology 2017 (IWAIT2017),* pages 1-4, Penang, Malaysia, 2017.

[9] Ren Komatsu, Hiromitsu Fujii, Yusuke Tamura, Atsushi Yamashita and Hajime Asama: Octave Deep Plane-sweeping Network: Reducing Spatial Redundancy for Learning-based Plane-sweeping Stereo, *IEEE Access,* 7, 150306-150317, 2019.

[10] Miyahara Keizo, Itakura Satoshi, Chen Junbai and Osuka Koichi: Stability Analysis Method for Off-road Vehicles, *Proceedings of the 2019 58th Annual Conference of the Society of Instrument and Control Engineers of Japan (SICE2019),* pages 1-6, Hiroshima, Japan, 2019.

[11] Yasuyuki Awashima, Hiromitsu Fujii, Yusuke Tamura, Keiji Nagatani, Atsushi Yamashita and Hajime Asama: Safeness Visualization of Terrain for Teleoperation of Mobile Robot Using 3D Environment Map and Dynamic Simulator, *Proceedings of the 2017 IEEE/SICE International Symposium on System Integration (SII2017),* pages 194-200, Taipei, Taiwan, 2017.

[12] Mitsuhiro Kamezaki, Junjie Yang, Hiroyasu Iwata and Shigeki Sugano: Visibility Enhancement using Autonomous Multicamera Controls with Situational Role Assignment for Teleoperated Work Machines, *Journal of Field Robotics,* 33(6), 802-824, 2016.

[13] Shota Chikushi, Yushi Moriyama, Hiromitsu Fujii, Yusuke Tamura, Hiroshi Yamakawa, Keiji Nagatani, Yuya Sakai, Takumi Chiba, Shingo Yamamoto, Kazuhiro Chayama, Atsushi Yamashita and Hajime Asama: Automated Image Presentation for Backhoe Embankment Construction in Unmanned Construction Site, *Proceedings of the 2020 IEEE/SICE International Symposium on System Integration (SII2020),* pages 22-27, Honolulu, USA, 2020.

[14] Jinwoo Kim and Seokho Chi: Action recognition of earthmoving excavators based on sequential pattern analysis of visual features and operation cycles, *Automation in Construction,* 104, 255-264, 2019.

[15] Jinhyeok Sim, Jun Younes Louhi Kasahara, Shota Chikushi, Hiroshi Yamakawa, Yusuke Tamura, Keiji Nagatani, Takumi Chiba, Shingo Yamamoto, Kazuhiro Chayama, Atsushi Yamashita and Hajime Asama: Action Recognition of Construction Machinery from Simulated Training Data Using Video Filters, *Proceedings of the 2020 IAARC 37th International Symposium on Automation and Robotics in Construction (ISARC2020),* pages 1-5, Kitakyushu, Japan, 2020.

Automated Framework for the Optimisation of Spatial Layouts for Concrete Structures Reinforced with Robotic Filament Winding

R. Oval[a], E. Costa[b], D. Thomas-McEwen[a], S. Spadea[c], J. Orr[a], P. Shepherd[b]

[a]Department of Engineering, University of Cambridge, United Kingdom
[b]Department of Architecture and Civil Engineering, University of Bath, United Kingdom
[c]School of Science and Engineering, University of Dundee, United Kingdom

rpho2@cam.ac.uk

Abstract -

Concrete is a major contributor to the environmental impact of the construction industry, due to its cement content but also its reinforcement. Reinforcement has a significant contribution because of construction rationalisation, resorting to regular mats or cages of steel bars, despite layout-optimisation algorithms and additive-manufacturing technologies. This paper presents an automated framework, connecting design and fabrication requirements for the optimisation of spatial layouts as of reinforcement of concrete structures, by the means of robotic filament winding.

Keywords -

Automated construction; Concrete structures; Reinforced concrete; Strut-and-tie models; Layout optimisation; Wound reinforcement; Digital fabrication; Additive manufacturing; Robotics; Robotic filament winding; 3D winding; Coreless winding; Trajectory planning

1 Introduction

This paper presents research on the automated reinforcement of concrete structures, investigated in the framework of the research project *Automating Concrete Construction* (ACORN) [1, 2].

1.1 Context

The construction industry is responsible for nearly 50% of the UK's carbon emissions [3]. More specifically, concrete construction is the main culprit, with more than 5% of the carbon emissions worldwide. The environmental impact of reinforced concrete stems from the amount of cement as well as the amount of reinforcement [4]. Layout optimisation applied to strut-and-tie models can find optimised tensile reinforcement for various concrete elements [5, 6]. However, these optimised layouts are not affordable, or even feasible, without significant post-rationalisation to build such reinforcement from stiff bar elements. Extreme rationalisation resorts to the use of standardised reinforcement bars, mats and cages, which require a higher amount of material and energy to produce. However, the use of advanced fabrication strategies and additive manufacturing, combined with robotics, provides an opportunity to automate the fabrication of complex optimised layouts of reinforced concrete structures using flexible filament materials.

1.2 Literature review

Short fibres can improve durability, provide a minimum tensile reinforcement against cracking and isotropic strengthening [7]. However, short fibres do not reinforce specific directions to carry high local tensile stresses based on an optimised layout. Reinforcement mats can carry higher tensile stresses, but the use of non-optimal, homogeneous and orthogonal meshes demands more material, and their placement is hard to automate, requiring patching and overlapping to map large-span plates or shells with double curvature [8, 9]. High, local, oriented tensile capacity can be provided by long fibres, or filaments [10]. Moreover, filaments are suitable for automated additive manufacturing [11], as commonly proven in the automotive industry to produce composite parts thanks to robotic filament winding [12]. For instance, the technology FibreTEC3D [13, 14], developed by Daimler and CIKONI, winds spatial layouts to produce mechanically-optimised components. In the construction industry, Spadea *et al.* [10] wound shear reinforcement for concrete beams using a rotating mandrel as core and Prado *et al.* [15] wound filaments to form composite shells using robotic arms holding boundary frames, instead of using a core. Filament winding of tensile reinforcement offers the flexibility to produce complex but optimised shapes and is suitable for automation using robotic arms. Moreover, achieving coreless winding removes the constraint of laying the filament on the surface of a core object, whose fabrication can be saved.

1.3 Outline

This paper presents an automated framework for the optimisation of tensile reinforcement for concrete structures that are suitable for robotic filament winding. Section

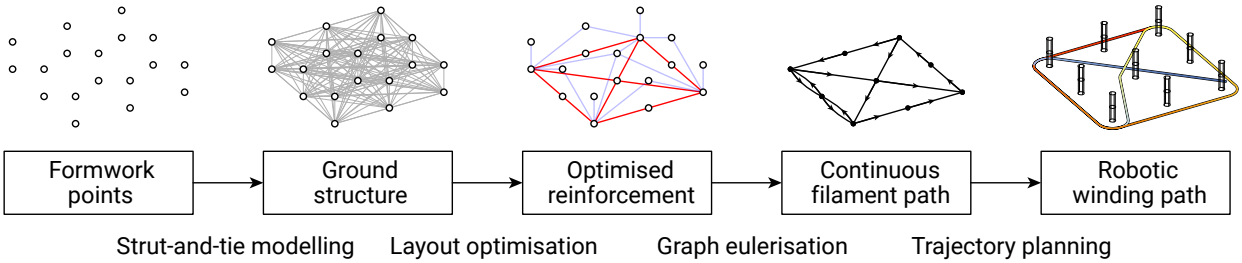

Figure 1. Workflow for the robotic filament winding of tensile reinforcement for concrete structures, including fabrication-informed generation, optimisation and rationalisation.

2 presents the automated framework, taking into account the constraints of the formwork system during the process of structural optimisation and the additive-manufacturing strategy for fabrication rationalisation. Section 3 applies this framework to a standard, benchmark plate with numerical results comparing the material quantities before and after rationalisation.

2 Automated framework

The workflow, illustrated in Figure 1 and detailed in this section, includes structural optimisation and rationalisation informed by fabrication requirements according to the following steps:

1. Define the winding points in the formwork system;
2. Generate a ground structure based on these points, which includes all the admissible winding passes;
3. Optimise the layout of this ground structure to obtain a strut-and-tie model with a minimal amount of tensile reinforcement;
4. Rationalise the tensile layout for robotic filament winding by creating a continuous path using graph Eulerisation;
5. Generate the trajectory for robotic winding around the formwork elements.

2.1 Formwork system

For coreless winding of a spatial layout made of a flexible filament, winding points are necessary for anchoring and deviating the filament and for tensioning it before concreting.

Such winding points can be included in the formwork of any structural system, such as beams, plates or shells, as illustrated in red in Figure 2. These elements must be designed according to the formwork strategy, be it rigid timber frame or flexible membrane, for instance. Stiff pins that can transmit the shear forces of the tensioned filament to the formwork can be reused, by covering them with a sliding lost cap and by removing them before demoulding, and the resulting void subsequently grouted.

The higher the density of these elements, the more diverse the range of potential reinforcement layouts, although these elements have a cost in terms of production time and material consumption. The position of these winding points serve as input for structural optimisation, informed by the available design space.

2.2 Structural optimisation

The structural design of the reinforcement for concrete structures is based on layout optimisation using a strut-and-tie model.

Strut-and-tie models are discrete stress fields use to design concrete structures as a set of compressive struts and tensile ties for the given support and load conditions. Their justification is based on the lower-bound theorem of plasticity. While concrete plays the role of the compressive struts, the reinforcements act as tensile ties. Structural analysis of the strut-and-tie model provides the stresses and the necessary cross-sections of tensile reinforcement. This model can include any combination of lines connecting the winding points in the formwork system, which can all be built using filament winding.

In this combinatorial design space of tensile ties, some layouts are more efficient and therefore require less reinforcement. The search through this space of feasible layouts is performed using layout optimisation [16, 17]. Such methods minimise the amount of material, which is equivalent to the total load path LP, which is the sum of the force F_i times the length L_i in each edge i over the entire set of edges E:

$$LP = \sum_{i \in E} |F_i| L_i$$

.

Minimising the amount of tensile reinforcement is equivalent to minimising this load path, when the location, magnitude and direction of the external forces is the

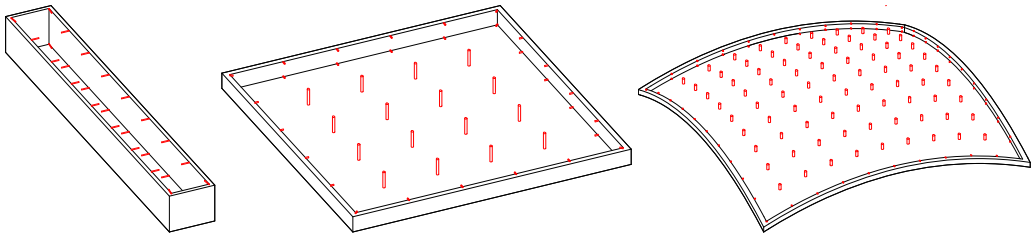

(a) Beam (b) Plate (c) Shell

Figure 2. Formwork system with winding points, using elements in red to anchor and deviate the flexible filament.

same. Indeed, according to Maxwell's theorem [18], the algebraic load path, which comprises the tensile part T and the compressive part C, only depends on the applied loads:

$$\sum |F_T| L_T - \sum |F_C| L_C = \sum \underline{\mathbf{P}} \cdot \underline{\mathbf{r}},$$

with $\underline{\mathbf{P}}$ the external loads and $\underline{\mathbf{r}}$ their position vectors from any arbitrary reference point. Since the algebraic load path is constant for a given set of loads, decreasing the total volume of material decreases in equal volume the compression material and the tension material.

Therefore, global layout optimisation provides the minimum reinforcement.

After optimisation, the discrete cross-section A_f of the filament must be included. For each tensile element, the force F_T is retrieved to find the necessary number n of filament passes that must constitute this element to take this force, based on the filament tensile strength f_f:

$$n = \left\lceil \frac{F}{A_f \cdot f_f} \right\rceil.$$

The lower the filament cross-section, the lower the loss of material due to the rounding up and oversizing, but the higher the number of passes and the production time.

As the initial ground structure was informed by the location of the winding points in the formwork, the resulting structurally-optimised layouts include only passes that can be realised by the filament. Even though significant post-processing is not necessary, a rationalisation step is required to obtain a continuous path through the tensile reinforcement layout. This specific continuity requirement prevents from multiple interruptions of the filament-based fabrication process, whether manually or robotically wound.

2.3 Fabrication rationalisation

From the optimised layout, a continuous path for filament winding must be computed that respects the required number of passes per tensile element. From this continuous path, a robotic trajectory is generated that winds the reinforcement around the winding points of the formwork.

However, the existence of such a continuous path is not guaranteed for any graph of nodes and edges. Here, the graph consists of the winding points as nodes and the tensile elements as edges. Since some edges require multiple passes to achieve the necessary filament cross-section, the algorithm is applied to a multi-graph, where multiple edges can connect the same pair of nodes. For each pair of nodes requiring n passes, n edges connect the pair of nodes in the graph.

Figure 3a shows an Eulerian graph with a closed circuit, marked with arrows, that visits each edge of the graph exactly once. This strong constraint of a circuit can be relaxed to an open path, as the wound filament does not need to close. Such a graph is called a semi-Eulerian graph, as in Figure 3b with path extremities marked with white nodes. However, some graphs do not have such paths nor circuits, such as the one in Figure 3c.

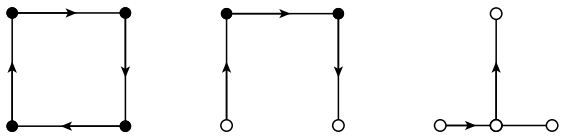

(a) (b) (c)

Figure 3. Eulerian properties of graphs: (a) an Eulerian graph with a cycle, (b) a semi-Eulerian graph with a path and (c) a graph without path visiting each edge exactly once.

The problem of finding a path can be solved with Eulerisation algorithms, which convert graphs into Eulerian graphs, which have the property of containing a circuit, or closed path, that visits each edge of the graph exactly once. The Eulerisation problem is also called the Chinese Postman Problem (CPP) [19]. The CPP searches for edges to add to obtain a circuit. In Figure 4, Eulerisation of the graph yields two Eulerian graphs. To minimise the amount

of material for needed reinforcement, the one that corresponds to a minimal length of added edges is retained. This algorithm is adapted to perform semi-Eulerisation to find a continuous path by considering different path extremities, highlighted in white in Figure 5, resulting in more semi-Eulerian graphs, with fewer edges added due to rationalisation.

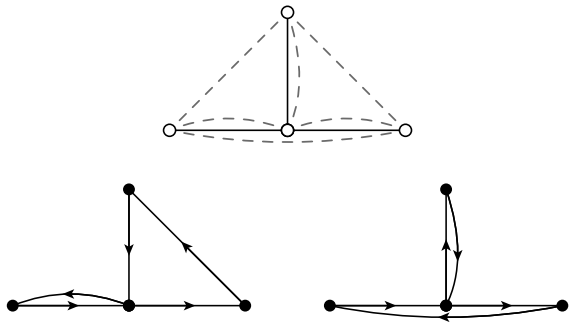

Figure 4. Eulerisation of a graph by adding edges to find a closed circuit.

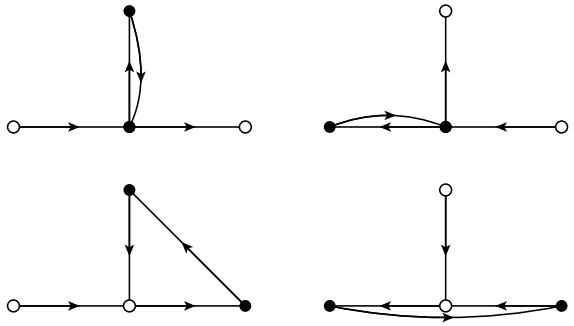

Figure 5. Semi-Eulerisation of a graph by adding edges to find an open path.

However, because the tensile parts can form disconnected graphs, and because other edges in the ground structure represent other potential winding passes, the Rural Postman Problem (RPP) [20] is used, which is a generalisation of the CPP. The RPP, also called priority-constrained CPP, finds a circuit that visits each required edge exactly once and potentially visits optional edges of the graph to form a circuit or path. Here, the required edges are the tensile edges and the optional edges are all the edges of the ground structure.

While the CPP is NP-complete, the RPP is NP-hard. Therefore, multiple algorithms exist to solve this problem based on heuristics. Here, the sub-paths are found for each disconnected component first, using a CPP algorithm. Then, as shown in Figure 6, these sub-paths, simplified as black edges, are iteratively connected in a greedy approach by adding the shortest optional path, highlighted in red, among all the possible ones, until they form a general path that connects all the sub-paths.

As a result, a continuous path is found through the tensile part of the optimised strut-and-tie model, taking into account the number of passes per edge.

From the continuous path, a trajectory for robotic winding around the formwork points is obtained.

The bulk of the formwork elements informs the offset of the lines connecting the axes of these elements. The orientation of the offset takes into account the relative positions of the elements along the winding path. Figure 7 shows how from a path, in black, connecting winding elements, in white, the trajectory, in red, alternates on the right- and left-hand sides based on the successive path turns. The trajectory passes by the opposite side of the next element: winding from element $i-1$ to i, the filament goes to the right-hand side of the path at the element i if the next element $i+1$ is on the left-hand side, and vice versa.

Vertical sliding along the elements is assumed to be prevented.

The robotic trajectory computation completes this automated workflow to obtain an optimised layout to wind reinforcement in concrete structures around formwork points.

3 Structural application

This automated workflow is applied to a classic plate as a benchmark, though more complex shapes can be considered, as long as winding points are provided during the fabrication process.

3.1 Parameters

The plate is a 5m x 5m square, has a thickness of 20cm, is supported vertically at its bottom four corners and is loaded at the top surface with a uniform downward vertical load of 5 kN/m^2. The concrete is considered to be C30/37 with a compressive strength f_c=30MPa. The filament is considered to be Fibre-Reinforced Polymer with a tensile strength f_f=1500MPa and a cross-section A_f=4.3mm^2 [21]. The winding points in the formwork are organised in a 6 x 6 x 2 array of 72 nodes, corresponding to a spacing of 1m in-plane and 0.2m vertically, as shown in Figure 8 with the results of the automated workflow.

3.2 Results

The ground structure, shown in grey in Figure 8a, connects all the pairs of the 72 winding points, highlighted as white dots, to each other, representing all the $\binom{72}{2}$=2556 edges that can be potential filament paths. Only edges shorter than 3m are shown for clarity.

The optimised strut-and-tie model in Figure 8b shows the support reactions in green, the external loads in orange,

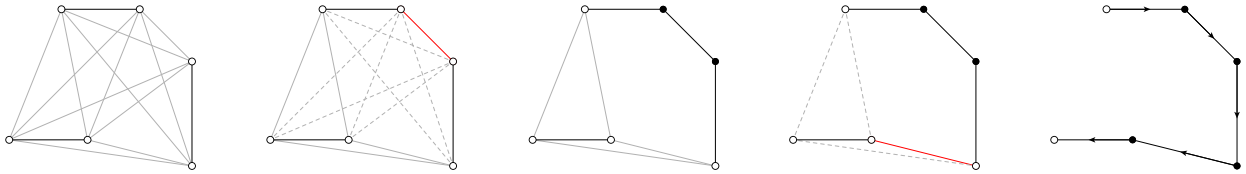

Figure 6. Semi-Eulerisation of a disconnected graph by finding first sub-paths, in black, and then connecting them with the shortest optional paths, in red.

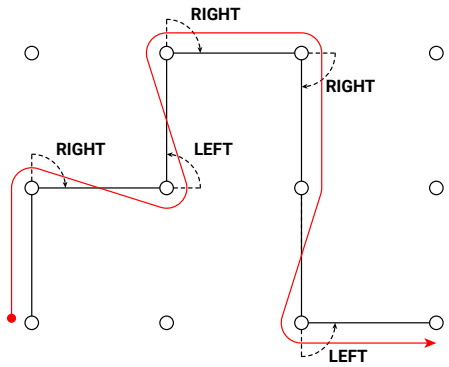

Figure 7. Winding trajectory, in red, from the filament path, in black, alternating between the right- and left-hand sides.

the compressive struts in blue and the tensile ties in red. The cylindrical elements are sized based on the internal forces and corresponding material strengths. The tensile load path amounts to 3266kN.m, or a theoretical material volume of CFRP of 0.00218m^3. A grid of winding points with an XY spacing of 50cm gives 3004kN.m, or 8% less, and an XY spacing of 25cm gives 2870kN.m, or 12% less, but also more than 3 times and 12 times the number of formwork elements, respectively. These results are summarised in Table 1.

Table 1. Tensile load paths for different densities of formwork winding points

winding node spacing [cm]	tensile load path [kN.m]	nb. of winding nodes [-]
100	3266 (100%)	72
50	3004 (92%)	242
25	2870 (88%)	882

Once computed the number of passes per tensile element, the filament volume is 0.00241m^3, an increase of 11%, for a total filament length of 561m. The graph in Figure 8c illustrates the continuous filament path generated after semi-Eulerisation. The colours and thicknesses illustrate the number of passes per edge, ranging from thin green edges with 1 pass to thick red edges with 10 passes. The filament volume is then 0.00246m^3, an additional increase of 2%, for a total filament length of 572m that can be wound in one go. Eventually, the total increase of material volume from the initial, optimal strut-and-tie model including the winding points to the filament path amounts to 13%. Table 2 summaries the material quantities at the different steps of the optimisation and rationalisation workflow.

The continuous curve in Figure 8d represents the path of the extremity of the robot end-effector winding the filament around the formwork elements. The path time is plotted as a colour gradient from red to blue, from an extremity to the other of the job. The material increase due to the bulkiness of the formwork elements is not taken into account.

Table 2. Reinforcement material quantities after each step of the optimisation and rationalisation workflow

step	volume [m^3]	increase [-]
layout optimisation	0.00218	-
discrete sizing	0.00241	+11%
graph eulerisation	0.00246	+2%
total		+13%

3.3 Discussion

This case study shows the application of a digital framework for the optimisation of structurally-sound and fabrication-informed reinforcement layouts. The numerical results predicting the material quantities highlight the trade-offs between the theoretical optimal design and the feasible sub-optimal design. The waste of material due to winding (2%) is low compared to the waste due to using a limited number of winding points in the formwork (around 10%) and compared to oversizing due to the use of a single cross-section for the filament (11%). These parameters, number of winding points and discrete filament cross-section, also have an impact on the production time, due to assembly/disassembly time of the formwork and winding time of the robot, respectively. A physical prototype of a structural element with a specific formwork system will allow the evaluation of this impact. The specific setup will introduce additional constraints, related to

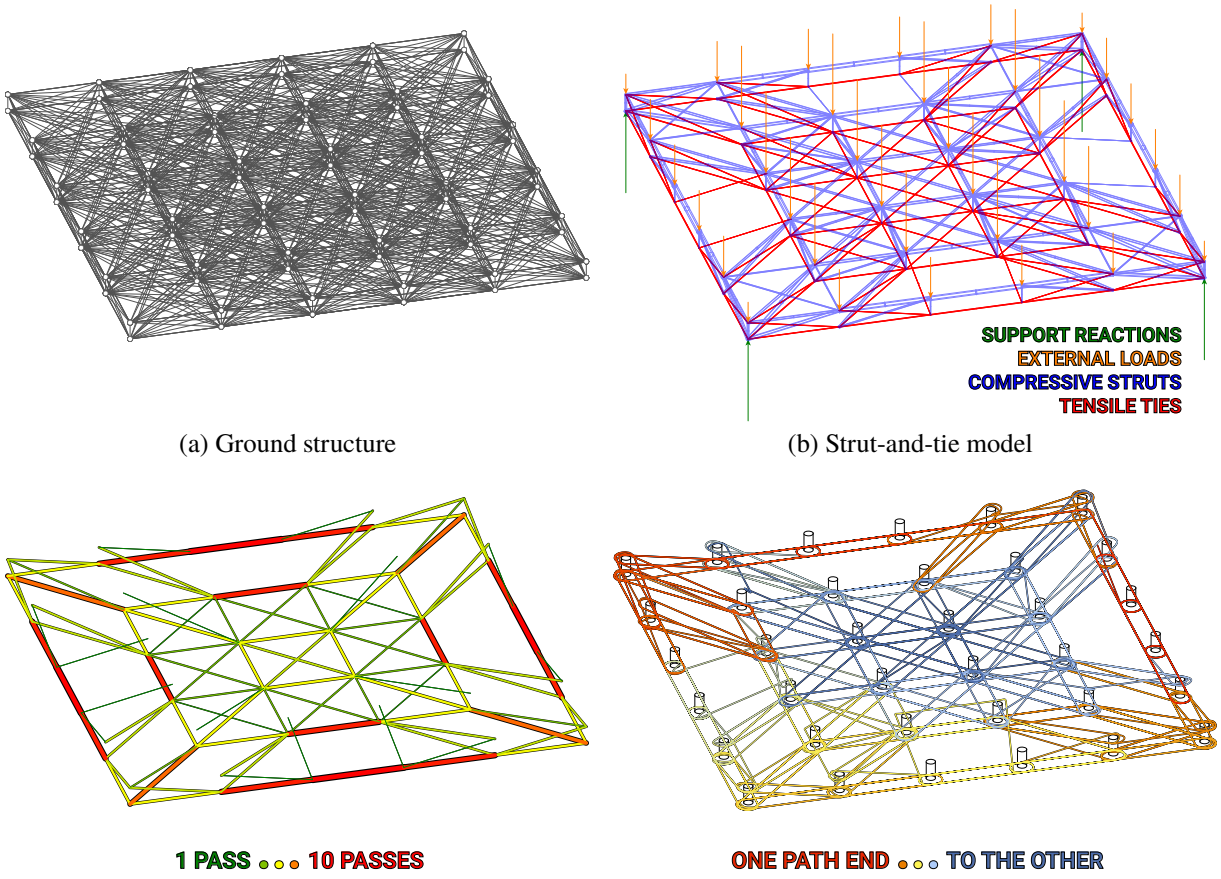

(a) Ground structure

(b) Strut-and-tie model

(c) Connectivity graph

(d) Winding path

Figure 8. Automated optimisation and rationalisation of a reinforcement layout suitable for robotic filament winding applied to a concrete plate of 5m x 5m x 20cm.

reach possibilities and the collision risks, which will need to be integrated into this automated workflow.

4 Conclusion

Advanced fabrication technology should enable the production of optimised reinforcements, instead of resorting to standardised and inefficient cages or mats, which significantly contribute to the environmental impact of reinforced-concrete structures. This paper presented an automated framework for the design of optimised reinforcement layouts for concrete structures that are suitable for robotic filament winding. Its application to a reinforced-concrete slab highlight the impact of the rationalisation steps and some of their parameters. Further work consists of:

- parametric studies on the spacing of the formwork points for winding, the filament cross-section, as well as layout simplification, to reduce the production time with controlled deviation from the optimal tensile reinforcement;
- physical prototypes with detailing of the formwork system and its winding points, exact generation of the robotic tool-path and inverse kinematics that prevents clashes, with the sequencing of the winding from the bottom layer to the top layer of the reinforcement layout;
- material and structural testing to understand the behaviour of this system, including the bonding between concrete and reinforcement; and
- life-cycle assessment to compare the whole-life cost of this approach with traditional methods, as comparing only embodied material can be misleading, without taking into account production waste and energy.

Acknowledgements

The *Automating Concrete Construction* (ACORN) research project is funded by UKRI through the ISCF Transforming Construction programme, grant number EP/S031316/1.

References

[1] ACORN: Automating Concrete Construction, 2019. URL `http://automated.construction/`. Accessed on 15/06/2020.

[2] Eduardo Costa, Paul Shepherd, John Orr, Tim Ibell, and Robin Oval. Automating Concrete Construction: Digital design of non-prismatic reinforced concrete beams. In *2nd RILEM International Conference on Concrete and Digital Fabrication (DigitalConcrete 2020)*, 2020.

[3] Department for Business Innovation & Skills (BIS). Estimating the amount of CO2 emissions that the construction industry can influence - supporting material for the Low Carbon Construction IGT Report, 2010.

[4] Hashem Alhumayani, Mohamed Gomaa, Veronica Soebarto, and Wassim Jabi. Environmental assessment of large-scale 3D printing in construction: A comparative study between cob and concrete. *Journal of Cleaner Production*, 2020.

[5] Jorg Schlaich, Kurt Schäfer, and Mattias Jennewein. Toward a consistent design of structural concrete. *PCI journal*, 1987.

[6] Jackson L Jewett and Josephine V Carstensen. Experimental investigation of strut-and-tie layouts in deep RC beams designed with hybrid bi-linear topology optimization. *Engineering Structures*, 2019.

[7] ACI Committee: State of the art report on fiber reinforced concrete, ACI 544.1R-82. Technical report, American Concrete Institute, Detroit, 2006.

[8] Tomás Méndez Echenagucia, Dave Pigram, Andrew Liew, Tom Van Mele, and Philippe Block. A cable-net and fabric formwork system for the construction of concrete shells: Design, fabrication and construction of a full scale prototype. *Structures*, 2019.

[9] Will Hawkins, John Orr, Paul Shepherd, and Tim Ibell. Design, construction and testing of a low carbon thin-shell concrete flooring system. *Structures*, 2019.

[10] Saverio Spadea, John Orr, Antonio Nanni, and Yuanzhang Yang. Wound FRP shear reinforcement for concrete structures. *Journal of Composites for Construction*, 2017.

[11] Ma Quanjin, MRM Rejab, MS Idris, Nallapaneni Manoj Kumar, and MNM Merzuki. Robotic filament winding technique (RFWT) in industrial application: A review of state of the art and future perspectives. *International Research Journal of Engineering and Technology*, 2018.

[12] Ginger Gardiner. Filament winding, reinvented, 2018. URL `https://www.compositesworld.com/articles/filament-winding-reinvented`. Accessed on 15/06/2020.

[13] Niklas Minsch, Matthias Müller, Thomas Gereke, Aandreas Nocke, and Chokri Cherif. Novel fully automated 3D coreless filament winding technology. *Journal of Composite Materials*, 2018.

[14] Niklas Minsch, Matthias Müller, Thomas Gereke, Andreas Nocke, and Chokri Cherif. 3D truss structures with coreless 3D filament winding technology. *Journal of Composite Materials*, 2019.

[15] Marshall Prado, Moritz Dörstelmann, Tobias Schwinn, Achim Menges, and Jan Knippers. Coreless filament winding. In *Robotic Fabrication in Architecture, Art and Design 2014*. Springer, 2014.

[16] Linwei He, Matthew Gilbert, and Xingyi Song. A Python script for adaptive layout optimization of trusses. *Structural and Multidisciplinary Optimization*, 2019.

[17] Alemseged Gebrehiwot Weldeyesus, Jacek Gondzio, Linwei He, Matthew Gilbert, Paul Shepherd, and Andrew Tyas. Adaptive solution of truss layout optimization problems with global stability constraints. *Structural and Multidisciplinary Optimization*, 2019.

[18] William F Baker, Lauren L Beghini, Arkadiusz Mazurek, Juan Carrion, and Alessandro Beghini. Structural innovation: combining classic theories with new technologies. *Engineering Journal-American Institute of Steel Construction*, 2015.

[19] Ozlem Comakli Sokmen, Seyma Emec, Mustafa Yilmaz, and Gokay Akkaya. An overview of Chinese Postman Problem. In *3rd International Conference on Advanced Engineering Technologies*, 2019.

[20] Horst A Eiselt, Michel Gendreau, and Gilbert Laporte. Arc routing problems, part ii: The rural postman problem. *Operations research*, 1995.

[21] Saverio Spadea, John Orr, and Kristin Ivanova. Bend-strength of novel filament wound shear reinforcement. *Composite Structures*, 2017.

Adopting Off-site Manufacturing, and Automation and Robotics Technologies in Energy-efficient Building

Wen Pan [a], Kepa Iturralde [a], Rongbo Hu [a], Thomas Linner [a] and Thomas Bock [a]

[a] Chair of Building Realisation and Robotics, Technical University of Munich, Germany
E-mail: wen.pan@br2.ar.tum.de, kepa.iturralde@br2.ar.tum.de, rongbo.hu@br2.ar.tum.de, thomas.linner@br2.ar.tum.de, thomas.bock@ br2.ar.tum.de

Abstract –

Delivering energy-efficient buildings or settlements has become a popular topic amongst architects, engineers, and building engineering physicists. There are many methods for improving building energy performances, both for new build projects and for retrofitting existing buildings. However, the construction industry faces some profound challenges to satisfy the increasing demand for energy-efficient buildings or other solutions and to be able to offer them at an affordable cost. A holistic approach has been adopted to validate whether automation robotics and off-site manufacturing technologies can yield positive changes in the delivery of energy-efficient buildings. This paper emphasizes the potential transformations and possible impacts on the design, construction, and installation process of an energy-efficient building once the advanced technologies are implemented. This paper also highlights case studies in multiple on-going or past European Union (EU) Horizon 2020 research projects as well as private projects to demonstrate the applicability and technical feasibility of the proposed solution. The scenario proposed was used to demonstrate how to apply the proposal in a large-scale residential building project. In addition, the findings from this study will serve as proof of the concept of a larger research project, or as an inspiration for the construction industry to execute energy-efficient building projects in the future.

Keywords –

Prefabrication; Construction robotic; Energy-efficient building

1 Introduction

At present, and in the near future, the build environment has many implications for peoples' lives in Europe. The construction industry consists of a complex value chain and supply chain yet is also one of the major contributors to CO2 emissions and consumes a substantial amount of energy. Building activities consumes up to 40% of the total EU energy usage [1]. Recently, decarbonisation has become a popular topic so new policies and research initiatives are aiming to improve the overall energy consumption rates in new builds and existing building stocks. Many building activities belong to a construction project and the energy consumption rates differ between each activity across the entire building life cycle. For instance, the building operational phase consumes the most energy, which is why it is the area researchers and the extended industries are focused most. However, due to the complexity and fragmentation of construction tasks, it is very challenging to improve the overall performance of an energy-efficient building if it only addresses the operational phase and ignores the others. This paper provides a comprehensive insight into how prefabrication, construction automation, and technology integration have the potential to enhance entire segments of an energy-efficient building value chain from the design stage to the end of the building life cycle. The paper features several EU Horizon 2020 research projects that validate the proposed solutions. These proposed solutions are an emphasis on the design, energy product integration, and construction processes in both new build and renovation projects. Introducing innovative methods and technologies to the construction industry requires cross-disciplinary collaboration between stakeholders, allowing interdisciplinary interaction and promoting collaborative work throughout the building life cycle. In addition, the featured solutions for energy-efficient building construction or renovation can be used as a proof of concept (PoC) for a larger research project within the respective parties [2].

2 Energy-efficient building construction strategy

It is difficult to form a definition that would easily summarize the building construction process, let alone an energy-efficient building construction project. Building construction consists of various phases and tasks; each task involves specific skill sets, tools, and methods.

Buildings are designed, constructed, or located in different styles, materials, locations, respectively, and also sometimes have different functions. Occupants also change over the entire building life cycle. Ultimately, an energy-efficient building should consume less energy yet retain the same performance for as long as possible. To achieve maximum adaptability and flexibility, a building should be designed as a system rather than a collection of individual parts, which creates high levels of inefficiency. More flexibility in design also means the building can easily adapt to potential changes in requirements and demands. The designer should consider all the building phases regarding building energy consumption and evaluate how the energy performance could be influenced by each construction phase throughout the building life cycle.

In general, the building life cycle consists of four stages, including the planning stage, the building stage, the operational stage, and the decommissioning stage. The planning stage includes building site selection, obtaining a building permit, a regulation submission, building material selection, and general organization. The building stage involves logistics, site preparation, construction, site clearance, and building commissioning. Each construction method will have distinct energy requirements and the choice of construction method can instantly influence many aspects within the building phase, such as the selection of construction tools, management method, scheduling, and cost structure. The operational phase consists of usage, repair, maintenance, and upgrades of the building. Based on research, the operational phase uses up to 36% of the total energy consumption in the building life cycle. Moreover, a building should be designed to accommodate the selected technologies as well as to ease the repair and maintenance processes [3]. The decommissioning phase covers disassembly, large-scale alteration, demolition, and recycling. The waste generated by the construction sector is astronomical. In terms of an energy-efficient building, the building should be ungraded and reutilized rather than disposed of in a landfill site. Moreover, to achieve an energy-efficient design, the designer should take into account the embodied energy in the building lifecycle, which means being aware of the energy consumption associated with each building process, i.e., production, design, construction, operation, maintenance, and repair [4].

A reduction of building energy consumption in building construction as well as in existing building stock is a vital part of the EU sustainable development strategies. Thus, the European Commission has set up relevant policies and directives that are aimed towards supporting energy-efficient buildings. For instance, Energy Performance of Buildings Directive (EPBD) was set up in 2002 [5], an Energy Policy for Europe was announced in 2007 [6], Energy 2020 was enacted in 2009, and Energy Performance of Building Directive was published in 2010 [7]. Due to building processes involving many stakeholders, implementing innovative building technologies requires an extensive cross-disciplinary approach along with strong public-private-partnerships in order to develop a feasible roadmap and applicable solutions for developing an energy-efficient building.

3 Challenges and barriers

The energy-efficient building development has been divided into the following stages: design, building structure, building envelope, construction process, end of life, integration, and cross-disciplinary collaboration. This section will evaluate the challenges and barriers imposed by each of these stages.

The main challenges during the design stage are how to involve every key stakeholder from the earliest phase of the project as well as how to enhance interactions of the stakeholders to achieve cost-effective solutions. The main barrier associated with these challenges is a lack of a holistic approach for organizing construction tasks related to energy-efficient buildings. There are ample opportunities for miscommunication or a lack of communication between key stakeholders. Many stakeholders are reluctant to adopt Information and Communication Technology (ICT) tools and many of the regulations regarding energy-efficient building are complex and varied across the EU. The challenges that relate to the building structure stage are reducing the overall level of embodied CO2 level in all buildings and utilising building structures more effectively. The barrier associated with these challenges is how difficult it is to integrate innovative energy production products with existing building structures. Regarding improving the performance of the building envelope, the main challenges are improving the building envelope energy performance in both new builds and existing buildings, interconnecting innovative materials and technology with the existing envelope, complying with the regulations, and easing the installation process by using alternative construction methods, such as prefabrication. The barriers associated with the building envelope stage are fourfold. First, there is a lack of development in energy-efficient building envelopes. Second, most of the commercialized products are driven by local building code and investments. Third, there are high costs involved in industrialized systems and they are still not wildly accepted. Finally, the compatibility between the innovative technology and the existing building envelope is low. The main challenges and barriers related to the construction process include labour-intensiveness, inadaptability, and lacking innovation and a skilled

workforce. The construction sector is slow in adopting prefabrication and the initial investments for implementing an innovative construction method are high [8]. Understanding what the most feasible solution is for transferring the industry from traditional building demolition to deconstruction, upgrading, reusing, and recycling is the main challenge for a building's end of life management. The main barriers with these are a lack of innovative recyclable construction material, the costs of building material recycling being high, and limited institutional, as well as technological, support for deconstruction. The next section summarizes numerous on-going or past European Union (EU) Horizon 2020 research projects to investigate the practicable solutions for the aforementioned challenges. The selected projects also inspired the design of the proposed systems that shall be described in the later section.

4 Methods

Developing energy-efficient buildings or settlements still faces many challenges so it is essential to transform the barriers associated with each challenge into innovation opportunities for the designer to consider during each construction stage. The selected case studies provide a comprehensive insight into technology integration, prefabrication, and automated installation technology, and are focused on either new builds or renovations of a residential building, see Figure 1.

4.1 Case studies

4.1.1 Zero-Plus

The ZERO-PLUS project was commissioned by the European Union's Horizon 2020 Research and Innovation Programme under Grant Agreement No. 678407 [9]. In brief, the overall aim of the ZERO-PLUS project is to achieve near-zero and positive energy settlement by using innovative and cost-effective energy production products in Europe. The project consists of four case study countries: the United Kingdom (UK), Italy, France, and Cyprus, which cover various climatic regions in Europe. In the Cyprus case, the Freescoo system is an innovative desiccant evaporative cooling air conditioning system developed by SolarInvent in Italy. According to the structural features of the case study building, an installation wall was developed to simulate the installation processes of the Freescoo system, which can be installed either externally or integrated into the building envelope. The installation wall is comprised of galvanized strut channels, fixture profiles, roof panels, insulation panels, HPL stratified laminated cladding panels, and a maintenance access door. The installation wall components were prefabricated in Italy and then shipped to Cyprus, and the installation took three days to complete. There were two main lessons learned from the Freescoo case study. First, the system was too heavy for manual handling so the optimum method would be integrating the system with the wall element and hoisting it into place using a crane. Second, the installation time was slow due to many smaller loose parts, which could impose challenges when installing the system at extreme heights or while standing on a suspended working platform. Nevertheless, the ZERO-PLUS demonstrates that energy technology can be integrated with a building façade and that prefabrication technology could potentially improve product quality as well as improve installation processes incrementally.

4.1.2 BERTIM

BERTIM was also funded by the European Union's Horizon 2020 Research and Innovation Programme under Grant Agreement No. 636984 [10]. The objectives of the project were to enhance a building retrofitting process by deploying an integrated timber frame façade module system and to develop an efficient manufacturing method for the timber façade. The timber façade module uses prefabricated windows, heating, ventilation, and air conditioning (HVAC) systems, and insulation materials were integrated ingeniously. The design, manufacturing, installation, and life cycle management systems were supported by an advanced Building Information Modelling (BIM) application. One of the challenges when installing an additional layer of the façade element on an existing building was that the installation surface was not completely flat or level. To solve this issue, an innovative interface design was proposed, which consisted of three components: one part connected to the surface, another part fastened with the façade module, and a middle piece sandwiched between the two parts. An existing building, located in one of the Tecnalia's testing facilities in Derio, Basque Country, Spain, was used as the pilot project to validate the logistics, the installation process, and the thermal performance of the BERTIM project. The project demonstrates the benefits of using prefabrication technology in a renovation project. In addition, the innovative interface connectors developed during the project enabled accurate installation results and revealed the potential of implementing automated installation methods by using construction robotics.

4.1.3 Hephaestus

Hephaestus was also founded by the European Union's Horizon 2020 Research and Innovation Programme under Grant Agreement No. 732513 [11]. The key objective of the project was to improve the glazing wall installation process by adopting an innovative Cable-driven parallel robot (CDPR). The CDPR consists of five components, which include the

CDPR structure, the CDPR body, the modular end-effector (MEE), the loading bay, and the control station. The CDPR can be installed on a roof structure or on a floor level that can support the weights and force of the system, respectively. The optimal installation location of the CDPR varies and depends on the individual building's load-bearing structure. The CDPR enjoys great manoeuvrability across the vertical plane of the building due to the eight winches and pulleys located on the top and ground levels. The MEE is divided into upper and lower sections. The upper MEE enables the system to detect rebar positions, drill, install fixtures, and fasten the fixtures in the correct position. The lower MEE is equipped with a vacuum system that is used for picking and placing the curtain wall element as well as the stabilization system. The pilot project was carried out from late December 2019 to early January 2020 at the Tecnalia facilities in Derio, Basque Country, Spain. During the pilot project, the overall performance of the CDPR was evaluated, but because the project isn't over yet, there are still some challenges that have to be solved (i.e., calibration time, size of the different components, etc.). Hephaestus has greatly inspired the proposed design that will be described in the later section. First, the project is a useful starting point case that can be augmented by adopting automation and robotic technologies. Second, the project provides a systematic approach and features applicable integration of software, sensors, and hardware in the context of the curtain wall installation. Third, the project demonstrates that CDPR is able to pick up and position large, heavy building components and is relatively highly accurate.

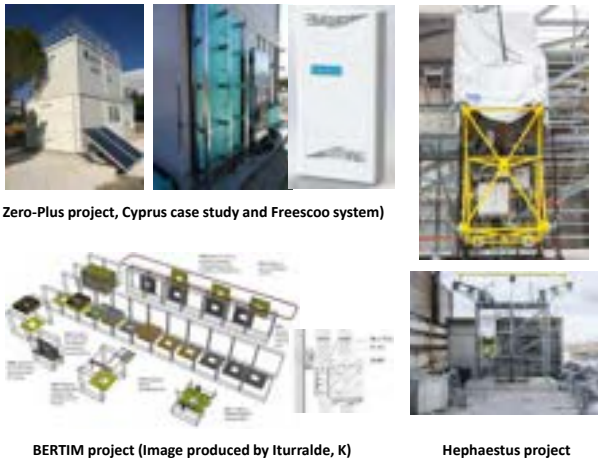

Figure 1. Top left: Zero-Plus, Bottom left: BERTIM, and Right: Hephaestus

5 System development

The demand for energy-efficient buildings are increasing in Europe and fulfilling the demand must be done either through new build projects or renovations of existing housing stocks. Conventional construction activities associated with new build project or renovation projects, however, are often inefficient, labour-intensive, and impose a high level of health risks to the workers. A novel construction system that focuses on the construction of a low-rise residential building by using prefabricated building components and assembled by automated on-site construction system is proposed in this section. Energy production technology is merged with the prefabricated façade module to ease the installation and maintenance processes by using construction robotic technology that was inspired by the aforementioned projects.

A prefabricated, fully assembled building system was used as a case study building for developing the proposed on-site assembly factory. The system is commercialized in China and it consists of the precast foundation system, structural frames, steel bracing system, precast external wall panel, precast internal wall panel, precast floor panel, precast canopy, precast roof panel, and precast stairwell. The prefabrication rate of the system is over 95% and, during on-site assembly, scaffolding is no longer required.

The proposed semi-automatic construction system features an on-site factory equipped with CDPRs that could travel on preassembled rails. The proposed on-site factory consists of ten key parts, see Figure 2.

1. On-site factory structural frame: the structural frames will arrive on-site as steel components and will be assembled by a spider crane.
2. Cable robot structure: the cable robot structure supports winches, pulleys, and cable routing systems and there are two branches of the structure that support two connecting planes.
3. Winches and pulleys: the winches and pulleys are installed on the cable robot structure and the lower supporting structure and in principle, the payloads should be more than 2.5 tons.
4. CDPR: there are two sets of CDPRs installed on either plane of the on-site factory that are equipped with a vacuum platform that is able to hold and position the precast external wall panels.
5. Lower supporting system: the lower supporting system supports the lower winches and pulleys and is equipped with a rotating set of rail wheels that is similar to the system used on trams or trains while the dimension of the wheels will be determined by the specification of the track gauge.
6. Temporary rail: the temporary rail track will be laid in a similar manner as traditional railway tracks but will depend on ground conditions, project budgets, and time as to whether the rail track will be laid on wooden sleepers or precast concrete track supports.
7. Gantry crane: the function of the overhead gantry

crane is to hoist and position precast floor and roof panels, but it is retractable, so it can reach out to the picking area.

8. Control room: the control room contains the main electrical cabinet, control units, power supply, and operator stations and is fully waterproof and highly mobile.
9. Temporary stabilization pillar: the stabilization pillar consists of two parts, the underground precast concrete footing, and over-ground pillar and he on-site factory structure will be connected to the over-ground pillar while it is in operation.
10. Temporary horizontal stabilizer: the horizontal stabilizer is used to provide additional strength of the on-site factory structure, but it can be disassembled and exchange to the working plane where the CDPR is not installed.

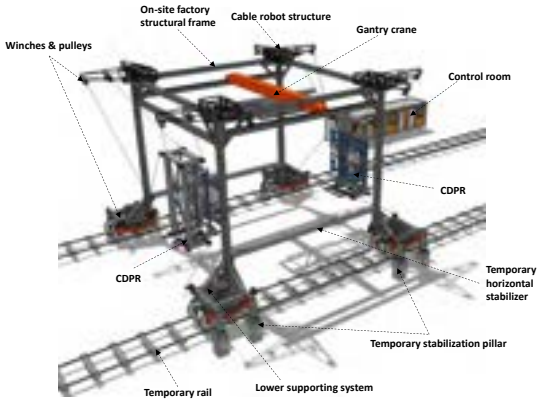

Figure 2. The proposed CDPR

The site will be prepared according to the construction plan. Once the location is confirmed, the precast concrete footings will be installed and the steel structure of the building will be assembled manually with assistance from the spider crane. Meanwhile, the precast external walls, floor panels, internal walls, and roof panels will be delivered and stored on-site. The on-site factory structure will arrive on-site partially assembled. The entire on-site factory structure, winches and pulleys, cable robot structure, and gantry crane will then be assembled and the temporary stabilization pillar is to be connected to the precast concrete footings. At this point, the on-site factory is stabilized and the CDPR can be installed and calibrated. Then the precast external wall panels are picked up from the picking position. The CDPR positions the wall panel at the correct installation position. The worker will carry out the final positioning and fastening task while the precast floor panels and internal wall panels are installed by using the overhead gantry crane. Figure 2 and Figure 3 demonstrate how the CDPR would operate at the front elevation of the building. Once the front wall panel is installed, the CDPR will be dismantled and reassembled on the side plane of the on-site factory. To cope with various weather conditions, the roof opening of the on-site factory can be covered with a waterproofing material. The direction of the temporary rail depends on the construction site configuration, but can be longitudinal or transversely. In addition, once the assembly task has been completed, the on-site factory shall be towed by the lorry to the next assembly location. The visualization of the building and the settlement are shown in Figure 3.

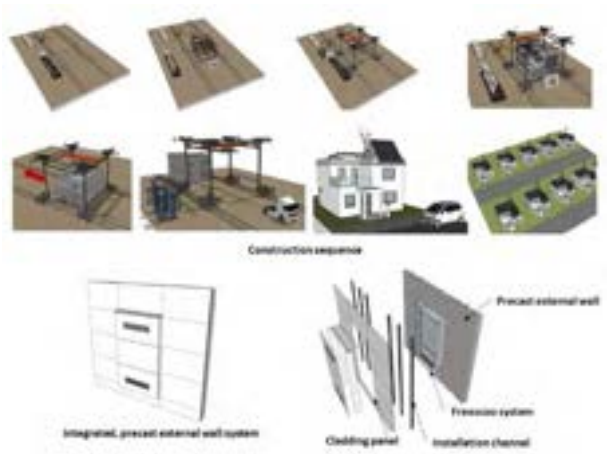

Figure 3. The construction sequence and the integrated precast external wall system

The proposed system features an integrated, precast external wall system, which is integrated with the energy production products. To demonstrates the design, the Freescoo system is utilized as an example. The integrated external system consists of four components, including the precast concrete wall panels, the Freescoo system, the installation channels, and the cladding panels. In the proposed scenario, the integrated wall system is installed by the CDPR and the installation channels along with the cladding panels are installed by the worker once the building structure is completed. The design provides proof that to ease repair and maintenance activities, a building should be designed as sequential parts and components. Energy production systems and mechanical systems can be integrated with the building envelope so as to be accessed, disassembled, and serviced separately.

At the time of this writing, the design presented in this scenario has been developed only as a conceptual idea to demonstrate the overall concept. The drawbacks and specific issues that need to be taken into consideration while continuing to develop the conceptual idea are:

- The construction site needs to be relatively level. If the slanted level of the site is too great, the site is not suitable to adopt the proposed design.
- The temporary rail requires additional groundworks, (i.e., increased construction time and costs) so

achieving economy of scale is key.
- The on-site factory might take significant time to assemble and calibrate, therefore the time spent on assembling the on-site factory needs to be taken into consideration when planning the project.
- New health and safety legislation is required when introducing human-robot collaboration for on-site assembly tasks.

6 Future work and recommendations

The outcomes from the Hephaestus project demonstrated the potential of implementing automation and robotic technologies for improving the overall performance of a specific construction task. The results from the BERTIM and Zero-Plus project indicate that the adoption of prefabricated façade elements and the integration of energy production technology can improve the installation process as well as renovation tasks over the building lifecycle. The proposed system in the paper encapsulated the outcomes of the three projects to embrace building prefabrication and construction automation in the context of energy-efficient settlement construction. To continue developing the PoC, there are still many obstacles and challenges. First, building prefabrication technology has not been wildly accepted by the conventional construction industry. Second, initial investments are high and the operation might be limited geographically. Third, the construction task involves many stakeholders and the construction industry is known to be one of the most fragmented industries, making the adoption of a new building method, material, or technology extremely challenging, highlighting the significance of cross-disciplinary collaboration. An energy-efficient building should be designed as an open building system rather than a single-use permanent structure to be disposed of once the building life runs out. The initial costs of construction automation may be high, nevertheless, the embedded costs over the building life cycle will decrease incrementally due to higher construction quality and easier repair and maintenance procedures [8]. To further develop the proposed concept requires financial assistance, policy incentives, and institutional support from the construction industry and government bodies. Furthermore, the proposed design shall serve as a foundation for a larger research project in the future, when the design, production, installation, management, operation, and human-robot collaboration can be validated through lab testing and pilot projects.

7 Conclusion

The paper proposed an innovative semi-automatic construction system in conjunction with an integrated, precast external wall system with an aim to improve construction efficiency and quality and to enhance building performance throughout the entire building life cycle. The proposed system was inspired by investigating several selected European Union (EU) Horizon 2020 research projects. Each project provided specific insight on how to implement prefabrication and construction automation technology in the context of energy-efficient settlement construction. The proposed construction system is based on the concept developed in the Hephaestus project. The system incorporates a CDPR equipped with a concrete vacuum end-effector, overhead gantry crane, and control room, supported by a structural frame. The system functions like an on-site construction factory, and moreover, it travels on temporary rails that follow a pre-planned construction master plan. Unfortunately, there are also challenges imposed by the industry to further developing the PoC. Some of the issues and barriers cannot yet be verified, such as the construction industry's reluctance to change, the lack of development in the energy-efficient building envelope and integration methods, the lack of skilled labour, and awareness of cross-disciplinary knowledge. Furthermore, using the proposed concept to inspire the construction industry and focusing on solving energy-efficient buildings with innovative, practical, and feasible approaches could bridge the gap between academia and the construction industry.

Acknowledgements:

This research has received funding from the European Union's Horizon 2020 Research and Innovation programme under Grant Agreement No. 732513.

References

[1] Bean, F. et al. Future-proof Buildings for all Europeans - A Guide to Implement the Energy Performance of Buildings Directive. Buildings Performance Institute Europe (BPIE) 76, 2019.

[2] Moseley, P. EU support for innovation and market uptake in smart buildings under the horizon 2020 framework programme. A journal article. Buildings, 7(4), p.105, 2017

[3] Koukkari, H., Brangança, L. Review on the european strategies for energy-efficient buildings. International Journal of Sustainable Building Technology and Urban Development 2, 87–99, 2011.

[4] Yüksek, I., Karadayi, T.T. Energy-Efficient Building Design in the Context of Building Life Cycle, in: Energy Efficient Buildings. InTech, Janeza Trdine 9, 51000 Rijeka, Croatia, p93, 2017.

[5] Hogeling, J. and Derjanecz, A.The 2nd recast of the Energy Performance of Buildings Directive (EPBD). EU Policy News, A Journal article. Rehva Journal, pp.71-72, 2018.
[6] An Energy Policy for Europe. On-line: https://eur-lex.europa.eu/legal-content/EN/TXT/?uri=LEGISSUM%3Al27067#:~:text=A%20European%20Energy%20Policy%20will,competitive%20and%20more%20sustainable%20energy, Accessed: 14/05/2020.
[7] Energy performance of buildings directive. On-line: https://ec.europa.eu/energy/topics/energy-efficiency/energy-efficient-buildings/energy-performance-buildings-directive_en, Accessed: 05/05/2020.
[8] Bock, T. and Linner, T.Robotic industrialization. Cambridge University Press, 32 Avenue of the Americas, New York, NY 10013-2473, USA, 2015.
[9] ZERO-PLUS. On-line: http://www.zeroplus.org/, Accessed: 23/05/2020.
[10] BERTIM. On-line: http://www.bertim.eu/index.php?option=com_content&view=featured&Itemid=111&lang=en, Accessed: 22/05/2020.
[11] Hephaestus. On-line: https://www.hephaestus-project.eu/, Accessed: 21/05/2020.

Analysis on the Implementation Mechanism of an Inspection Robot for Glass Curtain Walls in High-rise Buildings

Shiyao Cai[a], Zhiliang Ma[a] and Jianfeng Guo[b]

[a]Department of Civil Engineering, Tsinghua University, China
[b]Glodon Company Limited, China
E-mail: mazl@tsinghua.edu.cn

Abstract –

With a growing number of high-rise buildings, glass curtain walls are widely used. In the long-term service of such curtain walls, the safety problems arise, such as cracks and spontaneous breakages of glass. Therefore, they need regular inspections to prevent accidents. Current inspection work for glass curtain walls in high-rise buildings mostly depends on manpower and conventional tools such as ropes and gondolas, which exhibit poor performance and safety risks for the workers to operate in the high-elevation working environment. Thus, there is an urgent need for inspection robots to improve efficiency and reduce safety risks. As a preceding work for the development of an inspection robot for glass curtain walls, this paper investigates the existing publications of the robots for the façade works and analyzes the implementation mechanism of an inspection robot for glass curtain walls.

Keywords –

Inspection robot; High-rise building; Glass curtain wall; Work mechanism

1 Introduction

In recent years, the number of the world's high-rise buildings is growing rapidly. Glass curtain walls are widely used in high-rise buildings because they can enhance the appearance of the buildings by creating a beautiful façade, as well as allow the filtration of natural light into the building. For example, in 2018, the annual output of tempered glass in China was about 470 million square meters and more than 40% are used in glass curtain walls [1]. However, the wide usage of glass curtain walls also brings safety risks. The glass curtain wall system has the potential of failure, which may lead to falling of glass fragments. Since most high-rise buildings with glass curtain walls are located in downtown areas with large people and traffic flow, the accidents of glass falling would be devastating. Therefore, the glass curtain wall inspection of high-rise buildings is necessary.

The conventional method of glass curtain wall inspection in high-rise buildings mainly depends on manpower with ropes, gondolas and winch systems. However, it is costly and inefficient with safety risks for workers in high-elevations.

In a broader range, the interest in wall inspection of high-rise buildings is increasing in recent years and there have been studied exploring automatic methods to replace human workers to conduct the inspection work, such as developing inspection robots. These studies can be divided into two categories:

(1) Unmanned Aerial Vehicles (UAV) with visioning methods to detect visible cracks. For example, Liu et al. [2, 3] developed a bat-like inspection robot with abilities of flying and adhesion to save power and prolong the time of endurance. Bulgakov et al. [4] proposed control algorithms to stabilize the UAV for high quality captured images. However, photography by UAVs is not allowed in many cities around the world, which limits the applications of the research results based on UAVs.

(2) Wall climbing robots with visioning methods for wall inspection. For example, Muthukumaran and Ramachandraiah [5] developed a pneumatics based wall-climbing robot for façade inspection. The robots in this category have both technical feasibility and the potential of applications. However, there is only a small number of studies in this category and many of them deal with the bonding situation of the wall tiles rather than the quality of glass curtain walls. Besides, many studies only focused on the development of mechanical parts, without an in-depth analysis of the inspection method and the user demands.

Therefore, this paper aims to focus on the inspection robots based on wall climbing platforms and systematically analyze and summarize their implementation mechanisms for glass curtain wall inspection in high-rise buildings. The remainder of the paper is organized as follows. Section 2 introduces the method of this study. Section 3 proposes the requirements of an inspection robot for glass curtain

walls based on an analysis of the glass curtain wall failure. Based on the requirements, Section 4 analyzes the implementation mechanisms according to the existing literature and discusses their features for the implementation of an inspection robot for glass curtain walls. Finally, the paper is concluded in Section 5.

2 Method

In this study, a literature review was conducted firstly in two aspects: (1) the essential information of the working environment of inspection robots and the knowledge of safety inspection of glass curtain walls. (2) the development of related robotic systems in both academic research and existing products in the market.

As the number of studies on wall climbing-based inspection robots is small, the literature retrieval in the second step was not limited to inspection robots but also expanded to other robots for façade works. First, since this study focuses on wall climbing-based inspection robots, the literature related to wall climbing robots also needs to be reviewed. Second, since wall-climbing robots can also be used for other façade maintenance works in high-rise buildings, particularly for façade cleaning and in most cases, the key technologies of a façade inspection (or cleaning) robot include climbing mechanisms and inspection mechanisms (or cleaning mechanisms) [6], hence the experience of façade cleaning robots can be a reference for inspection robots, so the literature of façade cleaning robots is also reviewed.

The literature retrieval was conducted in both Scopus and CNKI (China National Knowledge Infrastructure). The two databases were selected because Scopus covered a large range of literature in the field of construction robotics [6] and CNKI is the largest database of Chinese literature. The search keywords included “high-rise”, “robot*”, “curtain wall”, “façade”, “safety”, “inspection”, “climbing”, “maintenance”, and “cleaning” (in both English and Chinese). The asterisk (*) is a wildcard character that denotes a fuzzy search. Then a preliminary screening process was conducted successively to exclude the papers from irrelevant areas (e.g., biology, medicine, agriculture, etc.). By reading the titles, we successively filtered out unrelated papers and finally obtained 91 papers, including 71 ones about robot development and 20 ones about glass curtain wall inspection. Then we read the abstracts of each paper and selected the most related and important content for further reading.

Besides, we also referred to some Chinese national standards and industry standards for basic concepts of the glass curtain wall such as Terminology for Curtain Wall (GB/T 34327-2017), Standard for Testing of Engineering Quality of Glass Curtain Walls (JGJ/T 139-2001), and Test Method for the Defects of Glass – Photoelastic Scanning Method (GB/T 30020-2013).

The investigation of existing products in the market was also conducted by searching on the Internet with search engines including Google and Baidu. As a result, 15 products were found, which are all façade cleaning robots.

Both the analysis on the requirements and that on implementation mechanism are very much crucial for developing an inspection robot for glass curtain walls. Thus, the former is conducted based on the results of (1) because it needs our knowledge on both the related robotics and the inspection of the glass curtain wall. The latter is conducted based on the result of the former with the help of the results of (2) because it is a feasible way to build the implementation mechanism instead of building it from scratch.

Due to space limitation, this paper focuses on the following two points, i.e., requirement analysis of the inspection robot for glass curtain walls and analysis on its implementation mechanisms.

3 Requirement analysis of the inspection robot

3.1 Working environment of the inspection robot

The working environment of the inspection robot depends on the surface conditions of the glass curtain walls. A glass curtain wall system of a high-rise building consists of glass panels and a supporting system. The supporting systems are usually metal frames, such as aluminum frames and steel frames. According to the exposure of the supporting frames, the glass curtain wall systems can be categorized as exposed framing glass curtain wall, hidden framing glass curtain wall, and semi-exposed framing glass curtain wall, i.e., the horizontal/vertical frames are exposed and the frame in the other directions are hidden [7]. Besides, there are also other types of supporting systems, such as glass rib supporting curtain walls and point-supported glass curtain walls [7]. However, these supporting systems have no ledges at the external side of the curtain walls. For the climbing robots working on the façades of the buildings, the exposed frames are larger obstacles and the seams between glass panels are smaller ones, which need to be considered in the design of the climbing mechanisms.

In some cases, the façades of the buildings are not flat but curved. However, the glass panels are still flat but the panels are connected with small angles [8]. Therefore, in these cases, the climbing mechanism should be specially designed for the robot to cross from one panel to another.

3.2 Failure of glass curtain walls

The failure of the glass curtain walls on the high-rise buildings can be divided into two categories [9]: (1) Failure I is the partial failure of the aging components, including the spontaneous breakage of the glass under temperature stress or installation stress, the bonding failure because of the aging of the seals, the corrosion of metal fittings, etc. The most common one is the spontaneous breakage of the glass under temperature stress or installation stress. The characteristics of this failure type are as follows: the failure points cannot be easily found; the failure has a high probability to lead to accidents; the accidents caused by this type of failure will lead to serious damages and casualties without warning to people on the ground. (2) Failure II is the failure of the entire structure after large impacts from external forces such as typhoons, earthquakes, and fires. In these cases, one or more materials of the curtain wall reach their bearing capacity. This type of failure is caused by force majeure in a short time with great damage and low probability.

The prevention of accidents caused by Failure II depends on structural reliability, which is decided by design, construction and usage according to the standards. However, the prevention of accidents caused by Failure I depends on management and maintenance. In fact, most accidents of glass curtain walls were caused by Failure I. Therefore, this paper focuses on the inspect tasks on the detection of Failure I.

The spontaneous breakage of the glass (Failure I) can be explained as follows [1, 10]. Tempered glass for curtain walls has many internal defects, which are formed in production, processing, installation, and application. These defects will lead to stress concentrations. When these stress concentrations are combined with other environmental loads such as wind loads, vibration loads, and temperature loads, the local strength of the glass might exceed the capacity and the glass might break spontaneously. Although it is difficult to detect the defects, the stress concentrations can be detected with a specific instrument.

Some studies mentioned about using the visioning technology in inspection robots to detect visible cracks on the building façade [5, 11]. However, these studies are aimed at the cracks on other materials rather than glass panels. Actually, for the tempered glass, the spontaneous breakage happens before visible cracks are formed.

Therefore, the inspection robot needs the ability to detect the stress concentration of the glass panels.

3.3 Requirement analysis

Based on the above analysis and the usage scenarios of the inspection robot for glass curtain walls, the basic requirements include the following five points. Moreover, requirements 1-4 are for wall climbing and requirements 5-6 are for inspection.

1. Safe and reliable climbing mechanisms on the surface of the glass curtain wall. The climbing robot should attach to the glass panels safely with reliable protection methods. It should have the ability to move horizontally and vertically on the glass so that it can cover all the working areas.
2. Identification of the surrounding environment and obstacles. Multiple sensors and an intelligent control system are needed to identify the situation of the environment, especially the obstacles. Most obstacles are predictable ones such as the frames of the curtain wall, the information of which needs to be input preliminarily into the control system. Meanwhile, the control system also needs to consider the unpredictable obstacles that the robot might meet and the corresponding identification algorithms.
3. The ability to cross or avoid obstacles. After the detection of obstacles, the robots should have the corresponding methods to cross them safely and quickly. If there is an unpredictable obstacle that cannot be crossed, the robot should avoid it and record the situation and corresponding position.
4. Motion control. To realize the movement and cross the obstacles, motion control needs to be precise and instant to ensure safety. Besides, the sensors need to detect deviations and the control system needs to correct the motion direction.
5. Efficient inspection methods. Sensors are needed to identify the internal stress concentration of the glass panels.
6. The ability to record and export the inspection results. After the inspection on each panel of the curtain wall, the robot should record the results, especially the problems and the corresponding positions. When the inspection work is finished, the results need to be export to a computer.

4 Analysis on the implementation mechanisms of the inspection robot

The inspection robot should contain two parts, i.e., the climbing part and the inspection part. The most critical issue for developing it is to design the mechanism for each part.

4.1 Climbing mechanism

After reading the abstracts and important content of the 71 papers about robots of wall climbing, cleaning, and inspection in high-rise buildings, as well as the introduction materials of the 15 products of façade

cleaning robots, we found the climbing mechanisms of façade cleaning robots are most valuable references to this study. The reasons are as follows: (1) as mentioned in Section 1, the number of papers on glass curtain wall inspection robots is small and many of them are based on UAVs or deal with wall tiles rather than glass panels; (2) although the research on wall-climbing robots proposed various mechanisms such as legged robots, biomimetic robots, and robots with dry adhesive materials on the footpads, they are still at the stage of laboratory prototype with low practicability.

Based on an analysis of the related robots for façade works, they can be divided into two categories, i.e., robots with and without built-in guide rails, which have different climbing mechanisms.

For robots with built-in guide rails, the climbing mechanism is based on the guide rails. For example, Lee et al. [12] proposed a robotic system for façade cleaning (Figure 1), which consists of a horizontal-moving robot (HMR) performing cleaning, a vertical-moving robot (VMR) for transporting the HMR to each floor, and a winch module to move the VMR to the target floor. Both the HMR and VMR are connected with the rails and move on the building façade by gliding along the rails. A communication network is built for information transmission among the robots and the monitors. The power source of the system is DC batteries installed on the robots.

For robots without built-in guide rails, the core mechanism of climbing mainly includes the techniques of adhesion to the wall and that of locomotion.

There are two most commonly used adhesion techniques that have the maturity to be implemented in on-site prototypes. One is using suction cups. As shown in Figure 2, the suction cups can not only provide adhesion but are also "feet" of the robot, which can be organized into several groups. The groups of suction cups can adhere to the glass and release alternatively and the released ones can retract and move on to the next position so that the robot can realize locomotion and cross the obstacles. Another method is using vacuum fans to extract the air to create a vacuum between the robot and the wall surface for adhesion, as shown in Figure 3.

Various types of locomotion were designed for climbing robots and the common ones implemented in on-site prototypes include footed/legged, wheeled, and cable-driven. The footed/legged robots usually use suction cups for adhesion as mentioned above. The wheeled and cable-driven ones can work with suction cups or vacuum fans for adhesion, as shown in Figure 3-5. For cable-driven robots, the cables can provide different functions. For example, in Figure 4, the robot can move in all directions based on the cables. In Figure 5, the robotic system consists of a robot and a rooftop gantry, which are connected with cables. In this system, the cables are only responsible for the vertical movement and the horizontal movement is realized by the rooftop gantry moving along the pre-installed tracks. The cables can also transfer data and provide power.

Figure 1. A robotic system with built-in guide rails [12]

Figure 2. A robot with suction cups [13]

Figure 3. A wheeled robot with a vacuum fan [14]

Table 1 summarizes the climbing mechanisms mentioned above and compares their advantages and disadvantages. The guide rail-based robot has high efficiency because it can cover a large area and the motion path is very clear. It also has high safety and robustness because the connection between the robot and the guide rail is reliable. However, it is not versatile because it is based on the built-in guide rail of the

building and its dimensions depend on the design of the building. The footed/legged robot with suction cups is flexible to cross obstacles by releasing and retracting the feet/legs alternatively. However, it needs a more complicated design of the gait and corresponding algorithms for movement. Wheeled and cable-driven robots with suction cups or vacuum fans are both easy to control and agile in movement but incapable of crossing large obstacles. The cable-driven robot has higher safety because the cables can protect the robot from falling once the adhesion fails. However, its versatility is limited by auxiliary tools such as pre-installed pulleys and rooftop gantry. Besides, it is difficult to deal with curved façades.

Figure 4. A cable-driven robot [15]

Figure 5. A robot with a rooftop gantry [16]

Table 1. Comparison of the basic climbing mechanisms

Climbing mechanism	Advantages / Disadvantages
Guide-rail based	High efficiency High safety and robustness
	Limited versatility
Footed/legged with suction cups	Flexible to cross obstacles
	Complicated design of gaits and moving algorithms
Wheeled with suction cups or vacuum fans	Easy to control Agile in movement
	Hard to cross large obstacles
Cable-driven with suction cups or vacuum fans	Easy to control Agile in movement High safety
	Hard to cross large obstacles Limited versatility

4.2 Inspection mechanism

According to the analysis in Section 3.2, the critical part of glass curtain wall inspection is the detection of stress concentrations.

The instrument to detect stress concentrations already exists and is named photoelastic scanner, as shown in Figure 6 [17]. In manual inspection, the photoelastic scanner is handheld and placed close to the surface of the glass. Then the photoelastic image of the glass will be transmitted to a computer through a wireless communication network. When a photoelastic scanner is placed close to the surface of the glass, it can take images based on the reflection of polarized light on the glass surface. Since the glass is a photoelastic material, which is isotropic in general but anisotropic at the positions of stress concentrations, the stress concentrations in the glass will result in spots in the image, which can be easily observed by people or identified by image processing [18]. Thus the photoelastic scanner can be implemented in inspection robots for glass curtain walls. A robotic device with a sensor for distance detection should be designed on the robot to move the photoelastic scanner and place it close to the glass surface for inspection.

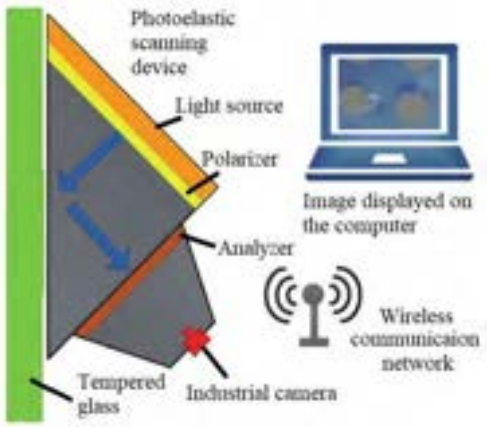

Figure 6. A photoelastic scanner for tempered glass inspection [17]

5 Conclusion

With a growing number of high-rise buildings, the glass curtain wall is widely used and its safety problem is concerned. To improve the safety and efficiency of glass curtain wall inspection, inspection robots are needed. As a preceding work of the robot development, this paper investigates the existing publications of the robots for the façade works. Based on the essential information above, six requirements of the inspection robot were proposed, in which four requirements are for wall climbing and the other two are for inspection. Then

based on a literature review, the climbing mechanisms of a glass curtain wall inspection robot were summarized and compared. The inspection mechanism based on a photoelastic scanner and its potential to be implemented in the inspection robot were analyzed.

The results of this paper can be a valuable reference for further development of glass curtain wall inspection robots, as well as other robots for façade maintenance.

Acknowledgments

The study has been supported by the Tsinghua - Glodon Joint Research Center for Building Information Modeling.

References

[1] Wang, W. Application of photoelastic scanning method in defect detection of existing curtain wall glass. *Guangdong Architecture and Civil Engineering.*, 26(7): 90-93, 2019. DOI: 10.19731/j.gdtmyjz.2019.07.023. (in Chinese).

[2] Liu, Y., Sun, G. and Chen, H. A micro robot with the ability of fly and adhesion: Development and experiment. In *Proceedings of IEEE International Conference on Robotics and Biomimetics (ROBIO)*, pages 2413-2414, Phuket, 2011. DOI: 10.1109/ROBIO.2011.6181663.

[3] Liu, Y., Chen, H., Tang, Z. and Sun, G. A bat-like switched flying and adhesive robot. In *Proceedings of IEEE International Conference on Cyber Technology in Automation, Control, and Intelligent Systems (CYBER)*, pages 92-97, Bangkok, 2012. DOI: 10.1109/CYBER.2012.6392533.

[4] Bulgakov, A., Emelianov, S., Bock, T. and Sayfeddine, D. Control of hovering altitude of a quadrotor with shifted centre of gravity for inspection of high-rise structures. In *Proceedings of International Symposium on Automation and Robotics in Construction and Mining (ISARC)*, pages 762-767, Sydney, Australia, 2014. DOI: 10.22260/ISARC2014/0103.

[5] Muthukumaran, G. and Ramachandraiah, U. Modelling and realization of pneumatics based wall climbing robot for inspection applications. *International Journal of Engineering and Technology*, 8(5): 1999-2007, 2016. DOI: 10.21817/ijet/2016/v8i5/160805418.

[6] Cai, S., Ma, Z., Skibniewski, M. J. and Bao, S. Construction automation and robotics for high-rise buildings over the past decades: A comprehensive review. *Advanced Engineering Informatics*, 42: 100989, 2019. DOI: 10.1016/j.aei.2019.100989.

[7] General Administration of Quality Supervision, Inspection and Quarantine of the People's Republic of China. *Terminology for Curtain Wall (GB/T 34327-2017)*. Standards Press of China, Beijing, China, 2017.

[8] Zhang, H., Zhang, J. and Zong, G. Requirements of glass cleaning and development of climbing robot systems. In *Proceedings of International Conference on Intelligent Mechatronics and Automation*, pages 101-106, Chengdu, China, 2004. DOI: 10.1109/ICIMA.2004.1384170.

[9] Wu, Y. The key technical research of existing glass curtain wall inspection and identification base on the glass falling. *Guangdong Architecture and Civil Engineering.*, 3: 45-48, 2013. DOI: 10.19731/j.gdtmyjz.2013.03.015. (in Chinese).

[10] Bao, Y. and Liu, Z. Mechanism and criterion of spontaneous breakage of tempered glass. *Journal of Inorganic Materials*, 31(4): 401-406, 2016. DOI: 10.15541/jim20150444. (in Chinese).

[11] Aliakbar, M., Qidwai, U., Jahanshahi, M. R., Masri, S. and Shen, W. M. Progressive image stitching algorithm for vision based automated inspection. In *Proceedings of International Conference on Machine Learning and Cybernetics (ICMLC)*, pages 337-3432017. DOI: 10.1109/ICMLC.2016.7860924.

[12] Lee, Y. S., Kim, S. H., Gil, M. S., Lee, S. H., Kang, M. S., Jang, S. H., Yu, B. H., Ryu, B. G., Hong, D. and Han, C. S. The study on the integrated control system for curtain wall building façade cleaning robot. *Automation in Construction*, 94: 39-46, 2018. DOI: 10.1016/j.autcon.2017.12.030.

[13] Zhang, H., Zhang, J., Wang, W., Liu, R. and Zong, G. A series of pneumatic glass-wall cleaning robots for high-rise buildings. *Industrial Robot*, 34(2): 150-160, 2007. DOI: 10.1108/01439910710727504.

[14] Akinfiev, T., Armada, M. and Nabulsi, S. Climbing cleaning robot for vertical surfaces. *Industrial Robot*, 36(4): 352-357, 2009. DOI: 10.1108/01439910910957110.

[15] Kite Robotics. Online: http://www.kiterobotics.com/, Accessed: 15/06/2020.

[16] Elkmann, N., Kunst, D., Krueger, T., Lucke, M., Böhme, T., Felsch, T. and Strüze, T. *SIRIUSc — Facade cleaning robot for a high-rise building in Munich, Germany. Climbing and Walking Robots*. Springer, Berlin, Heidelberg, 2005. ISBN: 978-3-540-22992-6.

[17] Liu, X. The technology of spontaneous breakage risk detection and prediction for tempered glass. *China Building Materials*, 3: 104-106, 2017. DOI: 10.16291/j.cnki.zgjc.2017.03.019. (in Chinese).

[18] Bao, Y., Zhou, H., Qiu, Y., Liu, X., Wan, D. and Wang, X. Experimental research on glass defect inspection technology based on photoelasticity. *China Building Materials Science & Technology*, S2: 147-150, 2010. (in Chinese).

Application of Robots to the Construction of Complex Structures using Standardized Timbers

Yi Leng[a], Xingyu Shi[a,b] and Fukuda Hiroatsu[a]

[a]Department of Environmental Engineering, University of Kitakyushu, Japan
[b] iSMART, Qingdao University of Technology, China
E-mail: winer386493@gmail.com, sxy@qut.edu.cn , fukuda@kitakyu-u.ac.jp

Abstract –
For thousands of years, the human construction process was mainly done by hand. In an era when automation technology is so mature, although some components of building components can be produced industrially, on-site construction and special component production still require a lot of manpower. But no matter how skilled the workers are, more or less mistakes will occur during the construction process, which wastes a lot of material waste and energy waste, especially when dealing with increasingly complex digital designs. Using a robot instead of manually completing the construction process will be the solution to these problems. Currently, most ideas for robot construction are dealing with non-standard components in the field, this will cause a lot of problems, first of all, it will extend the construction cycle, and secondly, it will generate a lot of waste. This article proposes a new construction workflow using standardized timbers. Spatial information for each piece of wood is communicated directly to a robot fabricator. The robot, equipped with various tools, can accurately position and assemble timbers. This workflow has the potential to improve the sustainability, time, cost, and quality of construction.

Keywords –
Robotic Fabrication; Parametric Design; Standardized Timber; Spatial Structure

1 Introduction

Fukuda Building Technology Lab and iSMART Qingdao were able to leverage their previous research into mass standardized timber and robotic fabrication, combining expertise across laboratory in two month effort. Fukuda Building Technology Lab and iSMART Qingdao fabricated a wooden arch in modules(using 840 pieces of timber and 3155 nails) at Qingdao University of Technology iSMART Robotic Center, used over 26 hours to fabricate 8 parts of the structure and were then shipped and assembled at the exhibition venue where it stole the show with its complex structure and huge volume, topping out at 2.25 meters tall and 4*4 meters wide.

The success of the wooden arch marks a major step forward for automation construction application and sustainable application of robotic fabrication. Because it shows the possibility of applying standardized timber to complex spatial structures, and the use of wood allows for a sustainable, renewable material to displace concrete or steel to reduce carbon footprint. The use of robotics simplifies the construction process, allows to constructed faster and precisely. Designed construction process and use of standardized timber simplifies the works of workers allows the undergraduates who have only received simple construction training and complete safety training to easily complete the construction work.

In the future, iSMART and Fukuda Lab seeks to optimize these workflows and implement into their projects, ensuring a better solution of robotic construction.

1.1 Problem Statement

Robotic is an old and new field in architecture industry. The importance of developing technology to increase the productivity of the construction industry has been proposed in the late of 20th century[1-3]. Over the decades, many studies have also emphasized the necessity of implementing robotic technology.[4] Whether in China or Japan the population aging and declining labor force have become a serious problem, the aging workforce and the increasing complexity of construction shows that traditional construction methods have gradually shown inadequacies [5]. Although many studies have been implemented and various of technologies have been developed but application of robotics still limited and behind other industries. High cost, unskilled worker and lack of research funding make robotic technology not widely used in the construction industry.

Considering application of Robotic Timber Construction(RTC)research is still in initial stage, and

high cost and high construction difficulty is the main problem. Fukuda Lab and iSMART used uniform standardized timber to displace customized wood and optimized the man-machine collaboration workflow. Significantly reduced costs and the skill requirements of workforce.

2 Robot Setup

A 6-axis KUKA kr30/60/HA robot applied in this experiment. The robot is operated at a speed of 2 meters/s, vertical range of activity from +35° to -135° and large turning range of 185˚ in both directions.

2.1.1 Tool Setting

In order to optimize the construction process 3 tools are equipped, those tools are mounted to one shared base to allow for rapid positioning. These tools include(Fig 1):

- A customized pneumatic suction sucker for gripping wood with a maximum payload of 8kg.
- A customized laser emitter for locating the nailing point and glue area of each piece of wood.
- A customized pneumatic suction gripper for fixing the wood to allow the workers can finish the glue and nailing.

A pneumatic calibration table is set next to the reclaimer to recalibrate the position as each timber is processed.

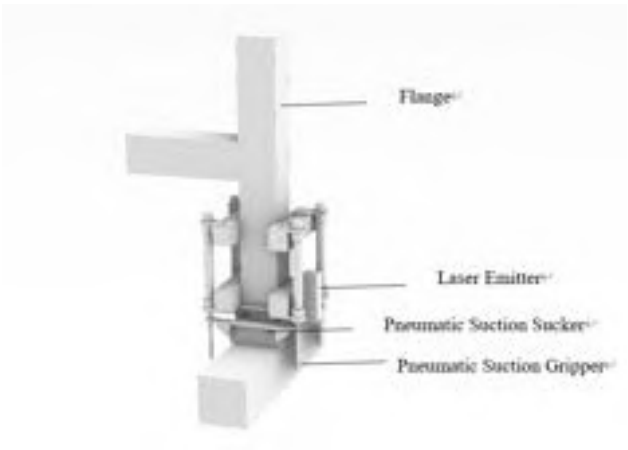

Figure 1. Customized Tools

2.1.2 The Robot Work Area

The work area measures 2.35 meters wide by 2.5 meters long and by 3.56 meters tall dictating the maximum construction area of robot. Laid out in a sector fashion, the area has two parts, the first being for material stacking and the other for construction. Each part is linked with safety control system of the robot and activates an emergency stop if limit or error occurs during robot operation. A safety operator is configured with the smart pad during each construction operation for collaborative operation(Fig 2). If an emergency occurs, the machine can be manually stopped. Positioned next to the material stacking area, a positioning frame is resting in a appropriate allows reposition each piece of wood to ensure that the center coordinates of them are accurate.

Figure 2. Safety Operator

2.1.3 Wood selection

A series of investigations in attempt to select suitable wood for RTC process. After comparing all kinds of the timber in Qingdao and Fukuoka lumberyards, our solution was to side on a low-cost approach using Japanese Hinoki as it is a popular construction material and it is reliable and easily machined. We use (50*100*650 mm) wooden bricks as construction material, the uniform size reduces processing costs and allows stacking without sorting, reducing construction difficulty.

2.2 Design program

A 4-sided symmetrical wooden arch were explored within the 5*5 meters area of the booth at the exhibition hall, with the basic theme of two sets of symmetrical construction units(Fig 3). Grasshopper was used to divide those 4 units into 8 construction team and divide the surfaces in to the center plane of timber, modeled in Rhinoceros 3d into its individual elements and generate.

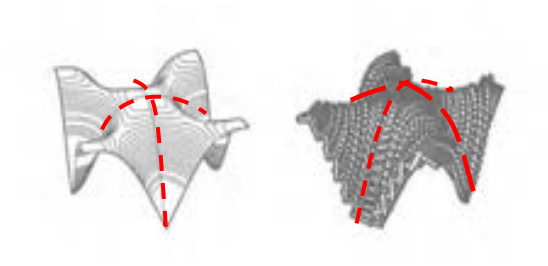

Figure 3. Model of the design

a nailing-gluing pattern needed to connect them. The positioning of nailing points and glued range of the digital model was automated using the custom script for Grasshopper. The nailing points and the glued area are mapped to the joints of the wooden blocks in the form of point coordinates. Primary parameters of divided surface geometry script, used to adjust the position of the nailing point and the size of the glue area:

- Timber Thickness
- Timber Length
- Timber Width
- Timber Rotation Angle

Using the custom script for Grasshopper, surfaces of the construction team are divided into polyline contours every timber thickness along the y axis (The default y direction in the software three-dimensional space.). Polylines are divided into lines based on timber length. According to the timber width and timber length, rectangular profiles are extruded along the resulting linear. Using KUKA|plc plugin for Grasshopper provide input data by design output subsequently by assembly. These input data include:

- Timber Thickness
- Timber Center Plane
- Timber Center Lines
- Nailing Points Plane
- Gluing Area Line
- Press Points Plane

Rotate the whole structure 90 degrees along the y-axis as the construction form. Timber geometry organized by construction order.

Using the Grasshopper Gluing area script, the overlapping area of the two layers of timber are offset inward by 15mm to generate the glued area. Primary parameters of Grasshopper Nailing points script, used to generate the nailing points planes:

- The Maximum Diameter of The Glue Range
- Nail Collision Radius
- Nail Length
- Glue Range Center Points

Using the Grasshopper gluing area script, glue range are showed visible, adjusting timber length and rotation angle to optimize the glue area to a suitable size and a suitable shape (quadrilateral), 4 terminal points of glue range are identified for primary rail and laser emitter, moved by the order of endpoints along the length from both endpoints. All endpoints are assigned to geometry and organized by construction order as glue range. Two nail points are selected by the maximum distance between the glue area minus the upper and lower nail collision range (to avoid conflicts) and assigned to each primary rail. All nails are assigned to geometry and organized by construction order as nail-points. The center points of two glue range center points which on the same timber are assigned to each primary rail as the press points (Fix the wood for nailing and gluing).

Figure 4. Geometry nailing points and gluing range

2.3 RTC Process

The KUKA|plc plugin is applied to transform outputs from the design script into construction process and outputting robotic commands for execution. The Softwire used for RTC process are:

- Rhinoceros 3D (modelling)
- Grasshopper(scripting)
- KUKA|plc Plugin (robot communication and simulation)

An accurate simulation of RTC was created for a visual understanding of work process of the RTC, and adjust main parameters in time according to simulation results.

OBJECTIVE	ROBOT MOVEMENT	IMAGE
1. Get Timber From Stack	· Select Timber in Order · Turn on Air Pump · Get Timber from Stack	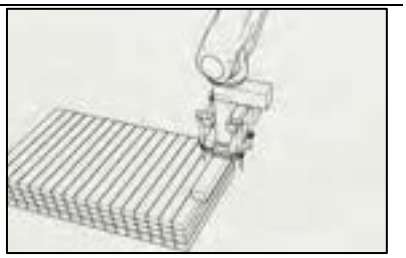
2. Calibrate Timber	· Place Timber on Calibrator · Calibrate Timber · Pick up Timber	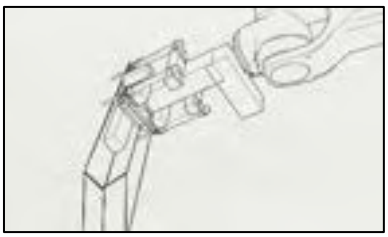
3. Place Timber on Site	· Place Timber on Site · Release Air Pump · Move to Safe Distance	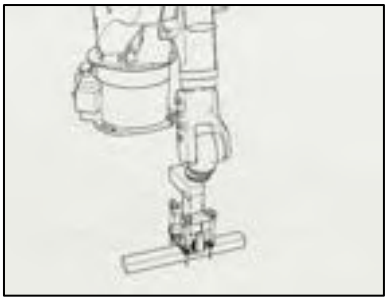
4. Draw Gluing Range With Laser	· Move to Gluing Start Point · Turn on Laser · Transform Robot Speed to 0.2m/s · Move Along Endpoints · Turn off Laser	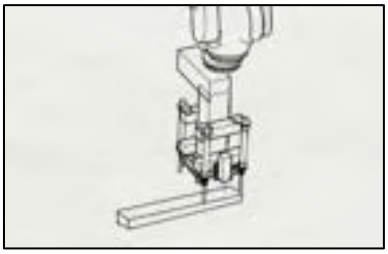
5. Draw Nailing points With Laser	· Move to First Nailing Point · Turn on Laser · Move to Second Nailing Point · Turn off Laser · Transform Robot Speed to 2m/s	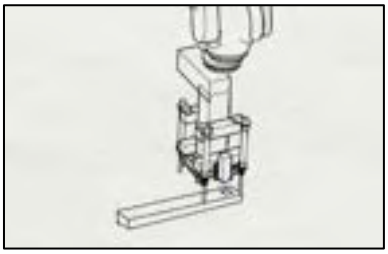
6. Fixe Timber	· Move to Center Point · Turn on Gripper · Nail and Glue Timber · Turn off Gripper	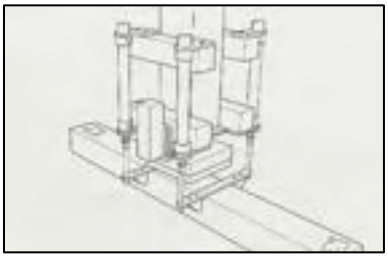

The script generates whole process of RTC. Standardized Timber allows the stacks don't need order, using the calibration device also allows the wood place unprecise, reduced the difficulty of placing stacks. Output construction data is oriented and centered to build site, that gives the designer a visual understanding of the structure which will be built. A series of subroutines are programmed outlining the overall construction process.

2.4 On-site Assembly

Limitation of robot arm length, manual handling, transportation and assembly logistics were factored which limited the size of each construction part could be. The constraints are that every part should be its longest length not greater than 2 meters and its height not greater the 1.5 meters. That ensured that every part fabricated by the robot could be lifted and moved by 6 people into a moving truck and erected on site. Every part was drawn a crossover line with neighbouring part, that aided in precisely aligning modules together. This simple modular technique was designed to allow for non-skilled worker to easily assemble complex structure with basic tools.

3 Result

Using the parametric workflow was necessary to managing the mass data of 840 individual timber with 3155 nails. The relation of the digital model allowed for this big data to be flexible, changing as the tests affirmed or rejected our initial setting. After completing the construction work, 4 construction units (Fig 5) were moved and assembled in the exhibition hall (Fig 6). The overall appearance is a smooth arch, consistent with expectations. The strong visual impact made by the huge volume. Using standardized timber placed along a hyperbola allowed audiences to visually obtain surface information.

Figure 5. One construction unit

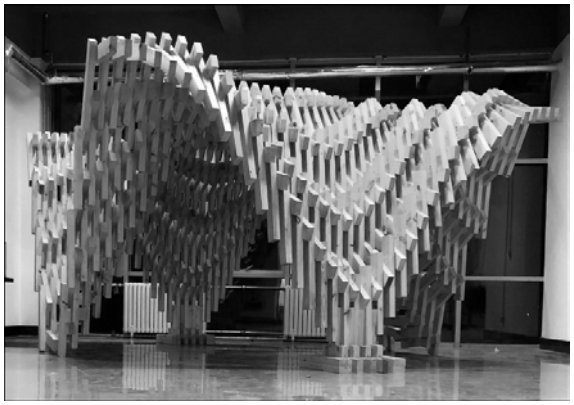

Figure 6. Construction Result

3.1 Speed of Construction

Every steps of the construction were gradually sped up to maximum capabilities without affecting performance and quality. Each step of pick up the timber to nailing it in place would take per 1 minutes 42 seconds. For the total of 840 members, total construction time amounted to 24 hours, and it takes 2 hours to assemble.

3.2 Human-Robot Coordination

Despite the automated nature of the RTC process, there were a few manual processes involved during fabrication and post fabrication. 840 standardized timber supplied from the lumber yard came in size of 50*100*650 millimeter stacked on site. 3115 nails nailed by non-skilled labour. with the nail-points and glue-range marked by robot, the work of nailing and gluing were very easy and non-skilled labour can finish the work with simple training.

3.3 Calibration

Every tool was carefully measured in and calibrated of optimal performance to untilize the high precision of the robot. Integration tool's TCP (Tool Center Point) was measured in with an accuracy of 0.01mm-0.05mm. The sucker went through a series of optimizations, gripping vacuum pressure and crawl speed reached the expected value. As for the Laser, adjusted the distance from the timber surface to 5mm which is the best focal distance to burning wood surface for mark the nail-points and glue-range. The speed of laser process was running to 0.2m/s, provided clear marking (Fig 7).

Figure 7. Mark of glue-range and nail-points

4 Conclusion

The success of the wooden arch marks a major step forward for application of robotics. Because it used the standardized timber to construct a complex hyperbolic structure. The use of standardized timber allows for a widely available, renewable material to displace steel and concrete to reduce a building carbon footprint, in the same time, allowed to reduce the material cost and processing cost. The use of robot allows the resulting optimized with millimeter precision. Human-Robot coordination allows non-skill labour involved in construction, alleviated the social problem of shortage of experienced workers. The communication between the digital model and the robot allows for a seamless translation from design to constructed on-site.

5 Future Research

Fukuda Lab and iSMART will seek ways to implement this workflow into real projects. Due to time and technology limitations, nailing and gluing process have not been automated in this experiment, the project used generous tolerances to finish within the deadline. Future research will optimize workflow, automate and integrate the nailing and gluing process into the current process.

In the future, iSMART and Fukuda Lab seeks to optimize these workflows and implement into their projects, ensuring a better solution of robotic construction.

Acknowledgements

This research was funded by iSMART Qingdao and Fukuda Building Technology Lab and supported by the following partners: Fukuda Hiroatsu, Gao Weijun, Qing Chuan, Zhu Guanqi, Xu Dawei, Jiang Zhuoqun, Alex Kalachev, Shi Xingyu, Yue Xu, Members of 4th Digital Tectonics International Workshop of iSMART Qingdao.

References

[1] T. Bock and T. Linner. *Construction Robots*, ISBN: 9781107075993. Cambridge University Press, New York, USA, 2016.

[2] T. Bock and T. Linner. *Site Automation*, ISBN: 9781107075979. Cambridge University Press, New York, USA, 2016.

[3] J. Paulson and C. Boyd. Automatation and robotics for construction. *Constr.Eng.Manage*, 111(2):190–207, 1985.

[4] T. Bock. The future of construction automation: Technological disruption and the upcoming ubiquity of robotics. *Autom. Constr*, 59(7):113–121, 2015.

[5] H. Hasan and A. Reddy and A. TsayJacobs. Robotic Fabrication of Nail Laminated Timber. In *36th International Symposium on Automation and Robotics in Construction*, 1210–1216, Banff, Alberta, Canada, 2019.

A Preliminary Comparison Between Manual and Robotic Construction of Wooden Structure Architecture

Lu Wang [a], Hiroatsu Fukuda [b], and Xinyu Shi [c]

[a]Faculty of Environmental Engineering, The University of Kitakyushu, Kitakyushu, Fukuoka, Japan
[b]Faculty of Environmental Engineering, The University of Kitakyushu, Kitakyushu, Fukuoka, Japan
[c]DAM Laboratory, iSMART, Qingdao University of Technology, Qingdao, China
E-mail: garfield13yp@gmail.com, fukuda@kitakyu-u.ac.jp, sxy@qut.edu.cn

Abstract –

The participation of robots in building construction is already a global trend. Compared with the actual construction with a large number of manual participation at this stage, the stability of the robot construction process will greatly affect construction efficiency and construction accuracy. As a future material carrier for building industrialization, robot construction has promoted the realization process of customized production and intelligent on-site construction. How to coordinate the robot platform, tool end development, building materials, construction tasks and on-site environment for the complex on-site construction environment and mass production needs The relationship between the optimization of robot construction technology will become an important step in the future development of building industrialization.

This paper focuses on the actual case, through the simulation of a built-in residential reconstruction, from the design process, the actual construction process to the final result, exploring the possibility of robots participating in the construction of residential buildings. It is hoped that the construction performance of the on-site construction will be improved through the participation of robots.

Keywords –

Robot construction; KUKA robot; Wooden structure architecture

1 In Situ Fabrication

1.1 Application Status of Robotic in Architecture

Since the construction industry has begun deploying robotic technologies for digital fabrication processes, this direction has mostly been focused on integrating industrial-type robots into off-site prefabrication processes [1]. By contrast, no enabling robotic technology exists today that allows robotic systems to be integrated into in situ construction processes right on the building site. This is mainly because in comparison with robotic prefabrication, robotic in situ fabrication faces fundamental technological challenges.

First, buildings are large in scale. In contrast to prefabricating sub-assemblies of a building with stationary robotic systems off-site, in situ robotic systems must be able to fabricate large-scale assemblies at their final location.

Second, building sites are poorly structured. As opposed to operate within structured factory conditions, in situ robotic systems must be able to accurately fabricate large-scale assemblies irrespective of the uncertainties prevalent on-site.

At the same time, the construction site has a strong dynamic, the task and the surrounding environment are prone to system changes, in a large, unstructured on-site environment, robot also face fundamental challenges of mobility and robotic manipulation. The accompanying questions of locomotion, planning, self-localization, workpiece-localization, mapping as well as guaranteeing accuracy and repeatability are only partially solved to date [4].

The in situ construction project aims to bring robotic fabrication out off the laboratory environment directly to the construction sites. The long-term goal is to use context-aware, collaborative mobile robotics to manufacture the high-accuracy fabrication of large-scale building structures [4,5].

Integrating in situ fabrication into architectural planning and building construction workflows can ensure constant information exchange between the design and the construction processes. Ultimately, the goal is to develop an adaptable and accurate fabrication process for building components on site and enable a novel digital fabrication system.

This paper will focus on the possibility of implementing robot construction in actual construction and compare it to traditional construction methods to

explore the advantages and disadvantages of different construction methods.

At the same time, this paper uses two different types of construction robotics for on-site construction simulation: stationary robotic and mobile robotic, and analyzes their different focuses, advantages and disadvantages.

1.2 Type of the Robotic System

The challenge of accuracy in robotic in situ building construction directly correlates with the type of robotic system used. The construction robotics has two main types: stationary robotic systems and mobile robotic systems [5]. And mobile robotic systems also have three types. this division is irrespective of the robotic system's customisation for tasks-specific operations, or the material system used [3].

The fabrication of building components usually requires the absolute positioning of the end electronic components of the robot in a global workspace. This allows the material to be deposited in absolute positions, thereby keeping the fabricated components consistent with the CAD model. Therefore, depending on the type of robot system used, there are various methods to deal with the challenges of absolute positioning [5].

This paper will use two types of construction robots to simulate the construction of the target building, and then compare the advantages and disadvantages of the two types of robots through the construction method and construction efficiency.

1.3 Mapping, Alignment and Localization

The construction site is an uncertain environment induced from multiple sources. The building site, localization and materially induced uncertainties [4].

Regarding the various uncertainties on the construction site, the robotic system used for on-site construction must perform sensing tasks at multiple levels before and during the ongoing fabrication process. The process are as follows:

The first step is mapping and alignment. Before the fabrication, the building site needs to be mapped by the robot from a central location. the corresponding robot's sensing system must obtain a set of measurement values for the entire construction site environment or certain entities therein. Then, these acquired data are fused to construct a 3D reference map of the measurement space. In the one-time calibration step, the reference drawing is aligned with the CAD model of the construction site, and the transformation between them is estimated based on this.

Then is localization. During the fabrication process, the robot must sense and estimate its position on the construction site. For this localization process, the reference mapping created in the previous mapping step serves as a source of information. This known map is used as a reference to estimate the transformation of the robot pose respectively.

The last step is fabrication survey: During the fabrication process, the robot must also check the structure being built. Since the fabrication survey is local, it is always performed with the currently estimated robot pose [5]. This survey allows the robot to perceive uncertain material behavior and record the geometric deviation from the fabricated structure relative to its reference geometry.

Mapping, alignment and localization largely guarantees the accuracy of the robot's in situ fabrication process. Especially for mobile robotics, the relative changes in the robot's position during the construction process can easily cause errors in the construction results. Therefore, mapping, alignment and localization is particularly important throughout the construction process. In the following experiments, the mapping, alignment and localization process needs to be considered during the construction process using mobile robotic.

2 Application of KUKA robot in wooden structure architecture

2.1 Research Purposes

The target building is a wooden house that has been designed and built by students. Here we will study how to use robots to replace part of the manual to build a building when facing the same target building. Finally, through the comparison of the number of participants, construction efficiency, construction accuracy and construction difficulty, the difference and the advantages and disadvantages between the two construction methods are finally obtained.

2.2 Overview of the Building

This is a two-story building constructed by wood construction, covering an area of 32.1 square meters (see Fig.1).

Previous studies have planned complex plans for free-form modeling. Previous studies have planned complex plans for free-form modeling. The construction will use 105mm timber, which is not designed for free-form design as previously studied.

Therefore, in order to improve the constructability and research constructability at the time of design, the plan is set as a simple form, and the module is set to 105 mm timber multiple (105 x 9 = 945 mm) for overall design.

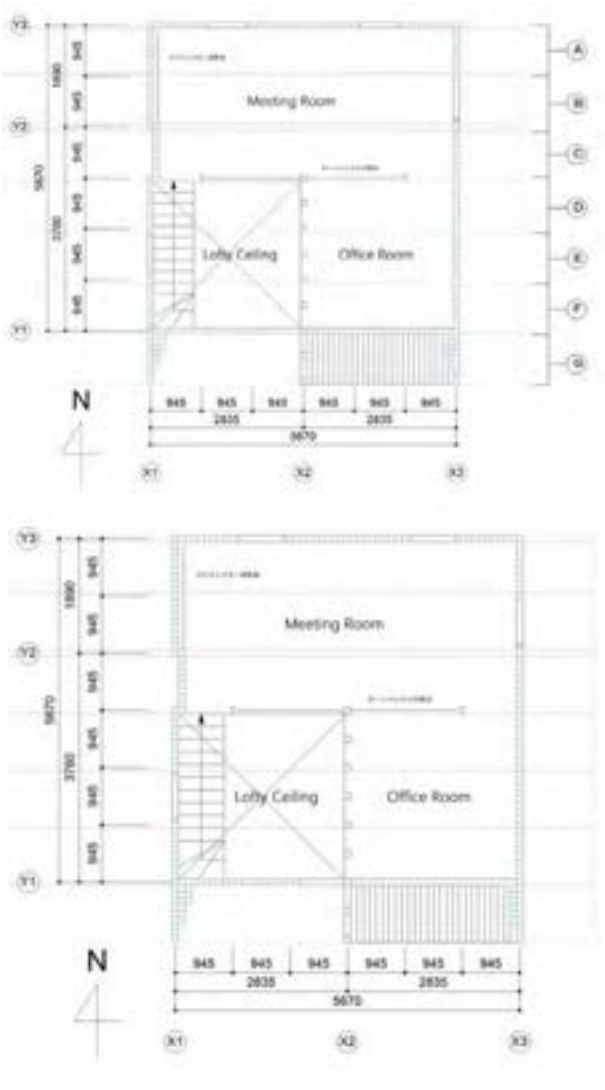

Figure 1. First and second floor plan of the wooden building.

2.3 Design Methods

The parametric design software RHINO is used as the design platform, and the simulation is built using the grasshopper on it. Most importantly, Kuka | prc software [3] of the KUKA robot can run on the grasshopper platform, effectively converting the design graphics into a language that the robot can recognize. At the same time, compared with traditional design software, the digital design platform can effectively improve the design efficiency in the design stage. Especially for modular residential buildings, digital modeling can more effectively formulate the rules between modules, which is convenient for modeling and later modification.

2.4 Construction Procedure

The human construction building was completed by students by hand. Construction efficiency is affected by many factors when building by manual work. Because the construction depends on manual work, the constructor has a decisive influence on the construction efficiency. First of all, the construction efficiency largely depends on the construction experience of the constructor. Secondly, construction difficulty of construction objects will also affect efficiency. Since the construction work is located outdoors, the construction efficiency is also affected by the weather.

For robot construction, two types of robots, stationary robotic and mobile robotic, are used. The KR90-KR150 R3700K KUKA robot is used in both constructions (see Fig.2).

The two types of robots in this construction are this KUKA robots equipped with a span of 3.7m, plus a Y-axis slide and the other equipped with a mobile base.

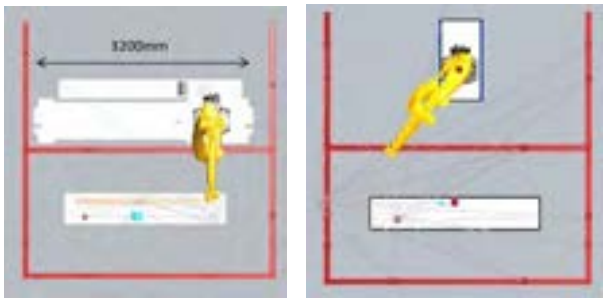

Figure 2. KR90-KR150 R3700K KUKA Robot with Y-axis slide and with a mobile base.

2.5 Robot Building Process

2.5.1 Comparison of Unit Assembly

These three construction methods are different in the construction unit assembly. In comparison, the number of units when the fabrication with mobile robot is the smallest, which simplifies the overall assembly steps after the completion of the later unit construction.

The completed unit, like unit A of Figure 3, is first erected perpendicular to the ground. The other units take the same action. Then, the completed unit B is connected with the unit A, and then the unit C is connected to the unit B in turn, and so on, until the units are spliced together. The building finally uses the crane to erect the units and erect them, then fixes the erected units to the anchor points of the foundation.

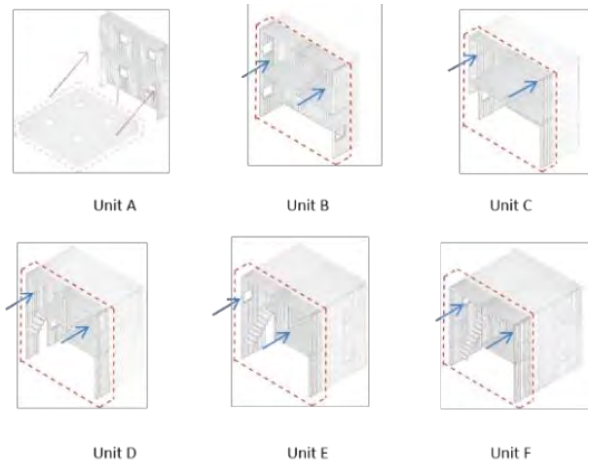

Figure 3. Unit assembly of human construction building

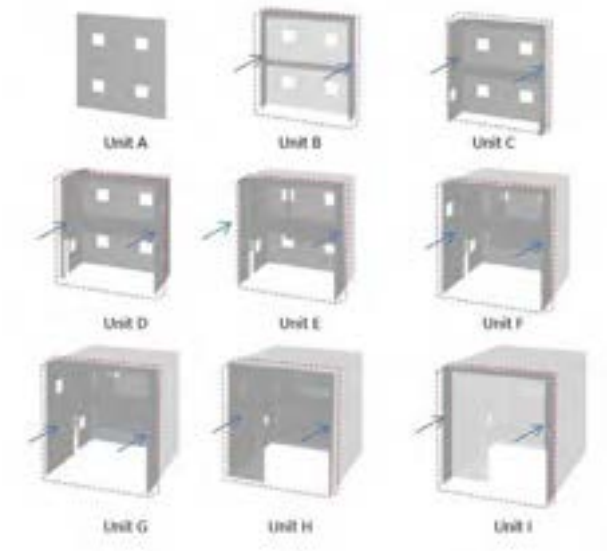

Figure 4. Unit assembly of stationary robotic construction building

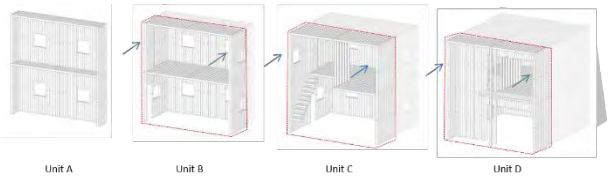

Figure 5. Unit assembly of mobile robotic construction building

For stationary robotic construction (see Fig.4), each unit is composed of eight layers during construction. The robot moves directionally through the y-axis slide, and a complete unit can be built each time. During the construction of mobile robotic construction (see Fig.5), each unit is built in two parts, so that the robot can complete the construction of sixteen floors in one positioning, and the construction of each unit needs to be displaced once.

The specific construction of each building unit, the construction mode of the stationary robotic construction and mobile robotic construction are also different (see Fig.6 and Fig.7).

Figure 6. Unit composition of stationary robotic construction building

Figure 7. Unit composition of mobile robotic construction building

2.5.2 Comparison of Construction Procedure

Construction efficiency is affected by many factors when building by manual work. Because the construction depends on manual work, the constructor has a decisive influence on the construction efficiency. The construction efficiency largely depends on the construction experience of the constructor. Also, the construction difficulty of construction objects will also affect efficiency. Since the construction work is located outdoors, the construction efficiency is also affected by the weather (see Fig.8).

Figure 8. Live photos of human construction building

The purpose of using robots in the construction field is to minimize the amount of manual use in the construction process.

So first of all, we will see which construction steps are replaced by robots in the reconstruction of the target building (see Fig.9 and Fig.10).

Grab timber: In the robot construction step designed with grasshopper software, the robot operation step begins with grabbing timber from the timber stacking

point. First of all, how to select the timber stacking point is very important. The appropriate starting point for grabbing should be at an appropriate position between the robot and the building object. Considering the length of the timber, it should be ensured that the stacked timber will not affect the operation of the robot, nor will it collide with the subsequent building.

Glue: The joint method of this construction mainly adopts an adhesive connection. Each of the intersecting timbers is coated with an adhesive. This process of applying the adhesive is also done by the robot. A glue tank is arranged between the timber stacking place and the building object, and the glue tank is provided with a glue roller. When the timber contacts and moves, the glue in the glue tank can be automatically applied. After the robot arm grabs the timber from the timber stacking place, it stops at the beginning of the glue tank and then descends and brings the timber into contact with the glue roller. And then drag the timber to move, so that the contact surface of the timber is coated with glue. Similarly, the setting of the position of the glue tank also ensures the continuity of the robot's operation.

Timber construction: After completing the steps of grabbing and applying the glue to the timber, the robot arm then places the timber in the designated position of the design. This is also the most critical step in the entire construction process. In order to ensure the smooth construction process, in the design stage, the order of the robot construction should be considered. Compared with manual construction, the construction method operated by the robot arm greatly improves the accuracy and precision of the construction.

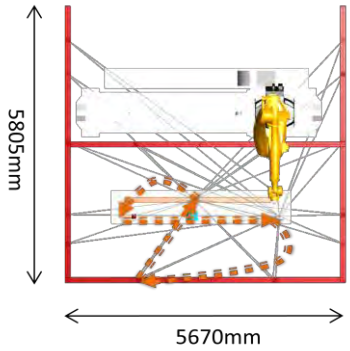

Figure 9. A process diagram of stationary robot construction

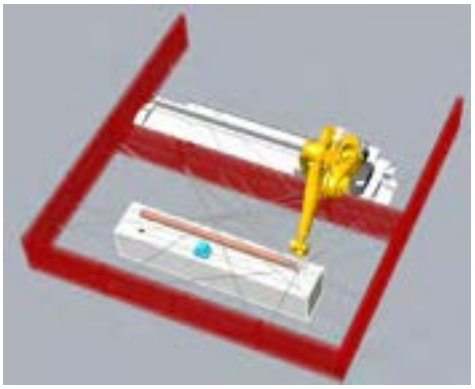

Figure 10. Schematic diagram of stationary robot work

For the construction process of mobile robots, a displacement of the robot is also included in the construction process of each unit, and each movement of the robot requires a localization (see Fig.11 and Fig.12). For this purpose, the robot is equipped with an end effector consisting of a vacuum gripper for pick and place routines and a laser range finder for sensing.

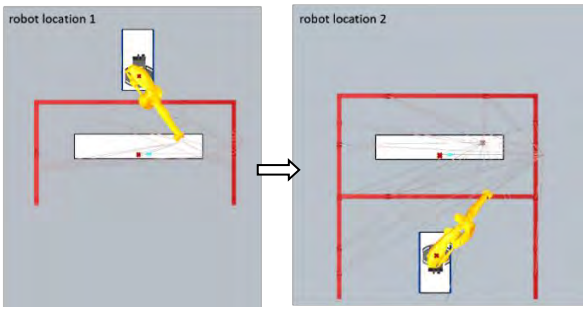

Figure 11. Fabrication sequence for mobile fabrication

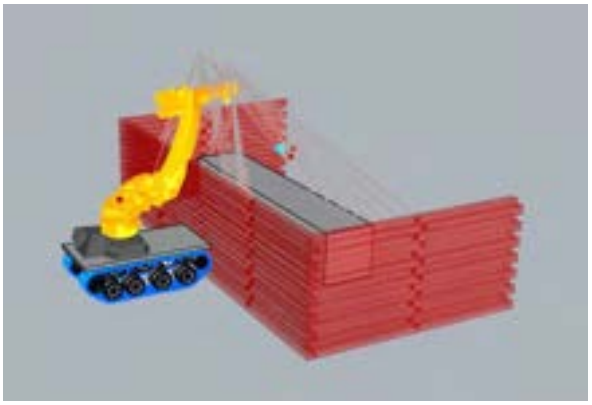

Figure 12. Schematic diagram of mobile robot work

3 Construction Evaluation

The construction evaluation is the focus of this comparative test. It aims to compare the advantages and

disadvantages of the two ways of building a wooden house by comparing the human construction with the robot construction. Next, the efficiency of both parties is evaluated mainly from the aspects of time efficiency evaluation, human efficiency evaluation, and construction quality evaluation.

Time efficiency is an important manifestation of the efficiency of a project, so time efficiency evaluation is the focus of this comparison. When the other conditions are the same, the time is shortened, which means that the overall efficiency of the project is increased, thereby greatly shortening the construction period, saving time and labor costs. This makes sense for any building project.

The first is the efficiency evaluation of human construction building.

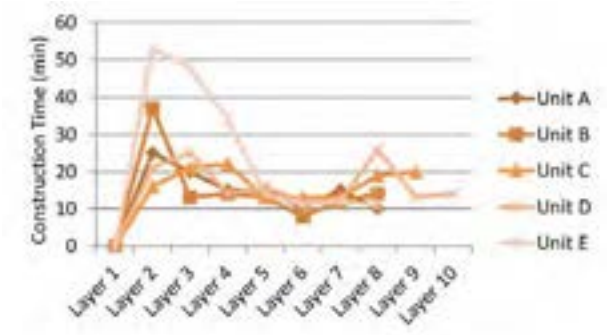

Figure 13. The layer construction time of each unit by human construction building

In the production of each unit (see Fig.13), the shortest production time is the sixth layer of unit B, about 8 minutes. In addition, the longest production time is the second layer of unit E is 53 minutes, as shown in figure 10. One of the reasons for this difference is the number of people working. There are 8 people in unit B, 2 in the first half of the work in Unit E, and 3 in the second half of the work in unit E. This is the reason for the difference in working hours. The number of people involved in the construction will directly affect the construction time.

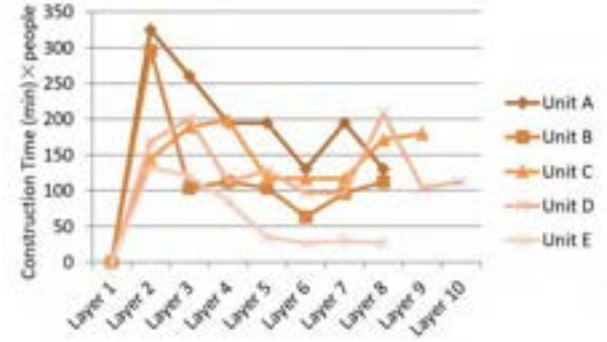

Figure 14. The layer construction time × people of each unit by human construction building

Compared with unit E, unit A has the lowest efficiency and unit E has the highest efficiency (see Fig.14).

First, it can be concluded that in this construction, each unit does not need too many people, and three people work at the same time with the highest efficiency.

Secondly, unit A is the first group of construction units, and the construction workers are unfamiliar with the construction process, resulting in inefficiency.

This proves that in the manual construction, the factors of the workers have a great influence on the construction efficiency.

Then is the efficiency evaluation of stationary robot construction building.

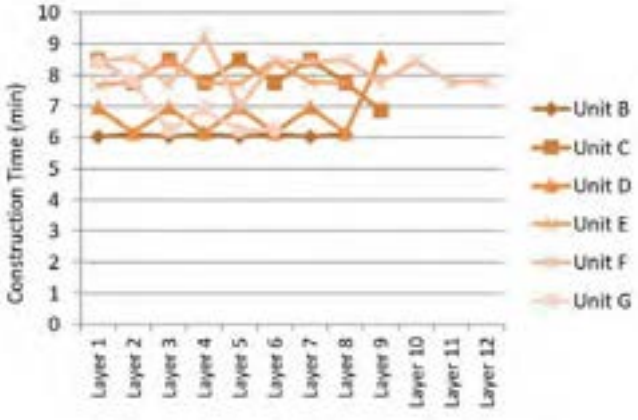

Figure 15. The layer construction time of each unit by stationary robot construction building

In the design of the grasshopper, every step of the whole process of the construction has been considered, so the time required for the robot to build can be directly calculated by the program.

The efficiency of the robot construction is stable, and the difference in construction time is only because the number of timbers that need to be built on each layer is different.

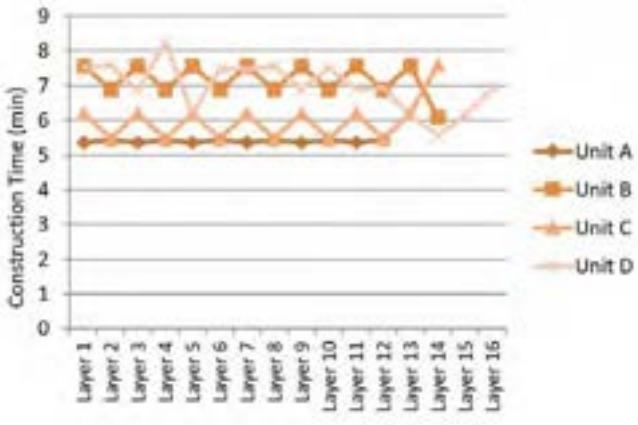

Figure 16. The layer construction time of each unit by mobile robot construction building

The comparison shows that the robot construction time is shorter than the human construction time, the efficiency is higher, and it is more stable and will not be affected by the number of people.

The difference in the time of each layer between the two robot construction methods is mainly caused by the different robot construction steps (see Fig.15 and Fig.16).

Here, the construction time of each layer of the mobile robot does not include the time required for the displacement and repositioning of the robot during the construction of each unit.

Table 1. Each unit and production time by human construction

Time(min)	Unit A	Unit B	Unit C	Unit D	Unit E
Total Time	115	111	137	153	183
Average Build Time Per Layer	14.38	13.88	14.63	15.75	22.88
Per Layer Builds Time	16.3				

Table 2. Each unit and production time by stationary robot construction

Time(min)	Unit B	Unit C	Unit D	Unit E	Unit F	Unit G
Total Time	49	72	61	63	98	42
Average Build Time Per Layer	6.07	7.98	6.78	7.92	8.17	6.97
Per Layer Builds Time	7.31					

Table 3. Each unit and production time by mobile robot construction

Time(min)	Unit B	Unit C	Unit D	Unit E
Total Time	86	100	84	112
Average Build Time Per Layer	5.36	7.16	5.98	7.00
Per Layer Builds Time	6.38			

The comparison clearly shows that the robot construction time is nearly 1/2 less than the human construction time, as shown from Table 1 to Table 3. Therefore, the construction of robots has a significant effect on the improvement of construction time efficiency.

4 Conclusion

stationary robots and mobile robots are usually suitable for different construction environments. For the target building, two sets of different types of robot simulation construction are designed to verify that facing a medium-sized wooden residential building, under the existing conditions, the simulation can be carried out by both stationary robots and mobile robots, and the two types of robots Construction, its efficiency and accuracy are much higher than manual construction. stationary robots and mobile robots are usually suitable for different construction environments. The construction of the two ways of robotic construction under the existing simulation conditions also has advantages and disadvantages. In future research, it is equally important to find conditions suitable for the construction of different types of robots.

The focus of this research is to compare the advantages and disadvantages of the same wooden structure, human construction and robot construction in software modeling, construction, and construction results. It is hoped that the construction performance of the on-site construction will be improved through the participation of robots. From the comparison results, the construction time efficiency evaluation, human efficiency evaluation, and construction quality evaluation of the robot construction are significantly improved compared with the human construction. Therefore, it is considered practical to study the use of robots in the field of building construction.

Compared with stationary robots, mobile robots have more advantages in actual building construction. And for the in situ processing tasks of various functions to further optimize the mobile robot, future research must target real-time sensing and complex dynamic overall control methods.

References

[1] Stylianos Dritsas, Gim Song Soh. Building robotics design for construction. Design considerations and principles for mobile systems, Springer Nature Switzerland AG 2018.

[2] Volker Helm, Michael Knauss. Additive Robotic Fabrication of Complex Timber Zurich: Park Books, pp. 364–377, 2014

[3] Jonas Buchli and Markus Giftthaler. Digital in situ fabrication - Challenges and opportunities for robotic in situ fabrication in architecture, construction, and beyond. Cement and Concrete

Research, 112 (2018) 66–75, 2018
[4] Markus Giftthaler. Towards a Unified Framework of Efficient Algorithms for Numerical Optimal Robot Control. Ph.D. thesis, DISS. ETH NO. 25168. 2018
[5] Kathrin Doerfler. Strategies for Robotic In situ Fabrication. Ph.D. thesis, Diss. ETH No. 25276. 2018
[6] Markus Giftthaler, Timothy Sandy, Kathrin Dörfler, Ian Brooks, Mark Buckingham. Mobile Robotic Fabrication at 1:1 scale: the In situ Fabricator, arXiv:1701.03573v1 [cs.RO] 13 Jan 2017.
[7] Jan Willmann, Michael Knauss, Tobias Bonwetsch, Anna Aleksandra Apolinarska. Robotic timber construction — Expanding additive fabrication to new dimensions, Automation in Construction 61 (2016) 16-23.
[8] Philip F. Yuan, Hua Chai, Chao Yan. Robotic Fabrication of Structural Performance-based Timber Grid-shell in Large-Scale Building Scenario, POSTHUMAN FRONTIERS: Data, Designers, and Cognitive Machines, pp. 196–205, 2016.
[9] Philipp Eversmann, Fabio Gramazio, Matthias Kohler. Robotic prefabrication of timber structures: towards automated large-scale spatial assembly, pp. 1:49–60, Constr Robot 2017.

Towards 3D Perception and Closed-Loop Control for 3D Construction Printing

Xuchu Xu, Ruoyu Wang, Qiming Cao, Chen Feng

Tandon School of Engineering, New York University, Brooklyn, NY 11201, USA

{xuchu.xu, ruoyuwang, qimingcao, cfeng}@nyu.edu

Abstract -

With the expanding size of additive manufacturing products, research pioneers start to explore 3D printing in the construction field. For 3D construction printing, quality means safety, cost, and efficiency. However, it is challenging to ensure quality via defect detection and deviation correction during the construction printing process. Conventionally, defect and deviation still rely on the quality check after printing is completed or on-site manual monitoring, which could cause either a waste of material and time to abort printing or lagging adjustment for printing settings after obvious defect appeared. To overcome these challenges, we propose a point-cloud-based approach for real-time 3D construction printing defect detection using a 3D camera and cloud-to-plane distance to evaluate printing layer integrity and compare printing results with CAD models. We also define different types of defects and deviations that can cause printing failure. Additionally, we feedback detection output into a closed-loop controller for updating the printhead motion. Our experiments show this joint printing and detection process handling various defects and deviations.

Keywords -

3D Construction Printing; Point Cloud Comparison; Defect Detection; Close-loop Control

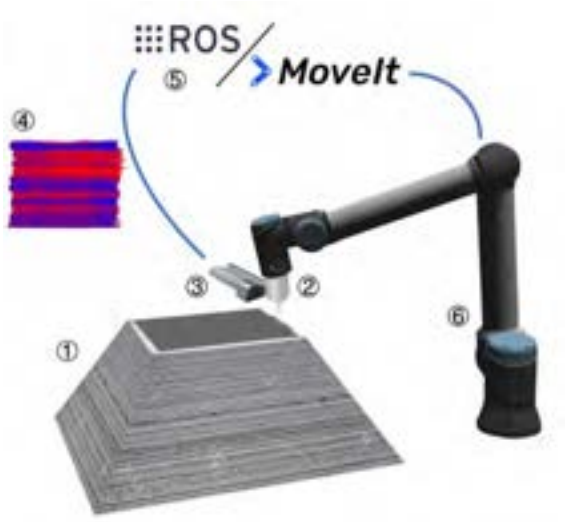

Figure 1. Illustration of our setup. 1. Concrete printing model. 2. Print head. 3. 3D perception sensor. 4. Color-coded printing error. 5. Control system. 6. Robot arm. During the printing process, the 3D perception sensor updates error feedback to the control system for defect and deviation correction.

1 Introduction

During the last several decades, additive manufacturing (AM), also widely known as 3D printing, demonstrated an incredible ability to assist designers and engineers prototype and produce rapidly. Recently, the study of 3D construction printing has rapidly risen as a new active area in the AM communities. A key challenge in 3D construction printing is monitoring the output quality and in real-time automatically adjusting the printhead control to reduce deviation and avoid structure collapse. To achieve this, 3D perception should to be tightly coupled into the printing process, since we need to evaluate not only each layer's integrity but also the evolving structure's shape deviation from the CAD model.

To acquire 3D shape data, traditional sensors, like multi-beam Lidar [1, 2], firmly occupy the high-end manufacturing and research of 3D perception. Although it could provide highly accurate point cloud data, a notable drawback of this type sensor is the excessive cost. Another limitation of this sensor in 3D printing is the difficulty of point cloud segmentation in post-processing due to their spare coverage on the printing output. To overcome these drawbacks, a different approach is to combine Time-Of-Flight (TOF) sensor with RGB camera. Microsoft Azure Kinect (Kinect) benefit from its high resolution TOF sensor, which has a balanced cost and performance. Kinect could provide precise and densely distributed point cloud data with RGB information that help us extract useful points while easily excluding the insignificant background. Moreover, we can observe the printer's extruder from Kinect's RGB camera in real time, which monitors material without interrupting the printing process.

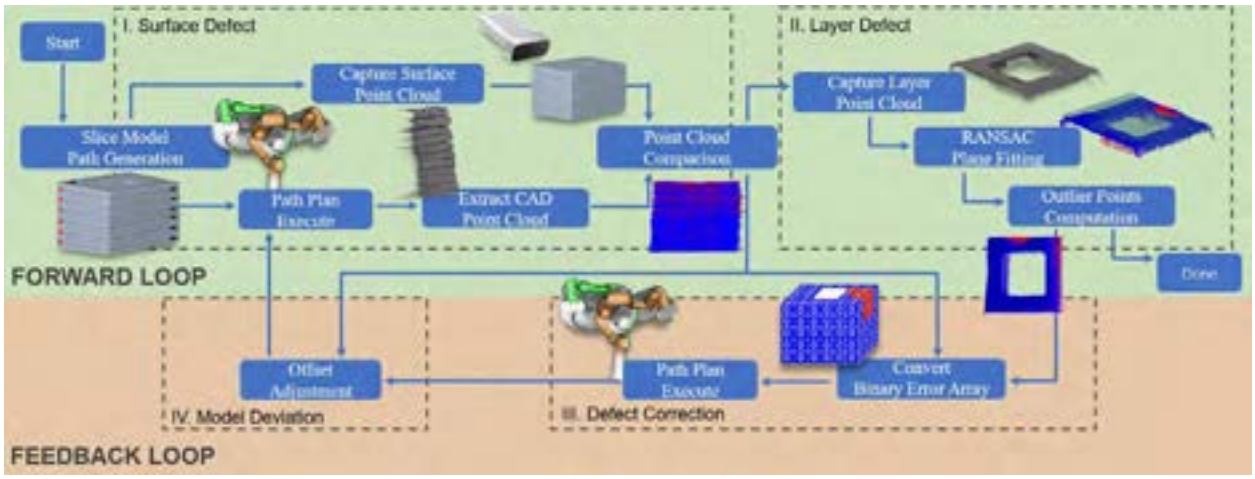

Figure 2. Our workflow. I. Simultaneous surface defect detection and 3D printing. II. Defect detection after printing the current layer. III. Error feedback. IV. Error adjustment from the current to the next layer.

With dense RGB point cloud data, we will measure surface defect and shape deviation compared with the corresponding point cloud which is generated from the CAD model. Cloud-to-plane (C2P) [3] distance is the error metric we adopt for measuring the difference between two point clouds. By projecting error vectors along the unit normal vector of the local plane, this metric could evaluate shape deviation and trigger with preset tolerances the online printing correction through feedback control.

In this paper, we propose an online approach for increasing the quality of 3D construction printing using a 3D camera and feedback control. To this end, we designed two experiments testing several different types of defects and deviation. Due to COVID-19 pandemic and facility closure, one of our experiment, closed-loop 3D printing, was only conducted in the simulation environment. The following are our main contributions in this paper:

- We define three types of printing error in 3D construction printing, includes layer defect and deviation, surface defect, and model deviation.
- We propose a novel approach for closed-loop 3D construction printing that could help us correct defects during the printing process.
- We implement a cloud-to-plane shape deviation error assessment between the point cloud captured by the 3D camera and that generated from the CAD model.
- We design two experiments to demonstrate our approach under different printing error scenarios.

2 Related Works

Our approach is mainly involved in three major research domains: 3D construction printing, defect detection and closed-loop control printing. As our previously mentioned, point cloud matching algorithm employed to find corresponding points between two point clouds and help us to calculate the error rate between them. Therefore, we will expand to discuss related research and approaches in these three areas.

3D Construction Printing. Different from other 3D printing types, construction 3D printing needs more consideration in product transportation, material property, printing quality and even aesthetic requirement. Crump et al. [4], as inventor of fused deposition modeling (FDM) technology, opened the gate of 3D printing. His method slices 3D objects to 2D layers and prints by CNC based machine. Although his approach initially used polymer filament, this method is also applicable to use other materials in different regions, such as AM with concrete material. Contour crafting [5, 6], present by Khoshnevis, is one of approach which employed for 3D construction printing. This approach sets a side trowel on the side of the extruder to smooth the apparent finish texture produced by the printing process. Buswell et al. [7] proposed the concept of Freeform Construction, which brings 3D printing into mega-scale rapid manufacturing. He aims to divide the building into a mega-scale section that could rapidly produce in the factory and assemble at the construction site. Recently, Keating et al. [8] demonstrated a mobile printing platform called Digital Construction Platform (DCP). DCP used a KUKA robot arm to research the printing position instead of the gantry-base fixed platform. Also, the author of DCP uses two-component polyurethane closed-cell foam to ensure printing material curing in a short period of time. 3D construction printing is not only a popular topic in the research area but also favored by the construction industry. WinSun [9], a Chinese 3D print-

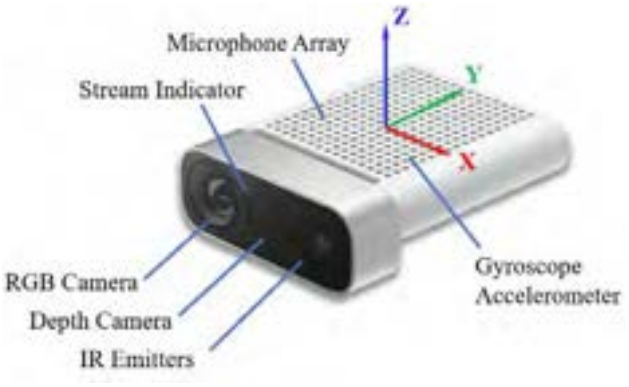

Figure 3. Microsoft Azure Kinect. We use RGB camera, Depth camera and Gyroscope in the following experiments.

ing industry leader company, developed multiply property material and successfully applied 3D printing to the construction field. Therefore, we need to explore a reliable method to real-time monitor the quality of 3D printing.

Defect Detection. Currently, defect detection methods of 3D Printing fall in two different domains, scanning based and vision based. Scanning based methods usually use a TOF sensor or with additional auxiliary equipment. Benefit form scanning whole model, these type methods could inspect detailing defects, such as tiny surface crack and local deformation. One of the obvious drawbacks is time-consuming, that these methods required a screening window to scan each layer during the printing process. Moreover, the calibration and preciseness of auxiliary equipment will directly affect the final accuracy. Lin et al. [10] used a sliding window to detect filling situations by a laser scanner, which attaching with printer extruder. Liu et al. [11] used a camera to measure the target surface assisting with a line laser and linear translation stage. Image based methods only rely on different types of cameras. Holzmond et al. [12] demonstrated real time defect monitor system that compares layer point cloud with a model cross section by using a dual camera under different light sources. Shen et al. [13] proposed a feature based surface defect detection approach by contour comparison. There are also some vision based methods combined with neural network [14, 15]. The downside is that these methods require a large amount of data, especially labeled data for supervised learning. Moreover, most of the methods above are implemented in polymer FDM 3D printing. Either point cloud of one single layer is too sparse or model defects is difficult to be accurately captured online. Therefore, all of the above methods only detect defects after printing and can not correct error during printing process.

Closed-loop Control Printing. Nowadays, researchers have not only focused on developing new 3D printing technology, but also hoped to improve the quality and automation level of 3D printing, which reducing the degree and impact of human factors. Different types of 3D printing have disparate limitations and drawbacks which need to overcome. For the ink-jet printer, Lu et al. [16] proposed a feedback controller for finding the best droplet location to minimize the edge shrinkage effect. Guo et al. [17] incorporated feedback measurements to a predictive control algorithm for avoiding edge shrinking, unreliable dimensions and uneven surfaces. Altın et al. [18] developed a spatial iterative learning control framework that involves discrete Fourier transforms and iterative learning control to improve part's build quality from a single layer toward the relationship between two layers. For laser metal deposition (LMD) printing, Sammons and his colleagues [19] present a stabilizing layer-to-layer controller to track and compensate for the deposition process. When we ask why closed-loop control is so important in 3D printing, especially used in manufacturing, we need to understand that the nature of 3D printing is repetitive motion. The quality of the current layer is highly dependent on the previous layer, such as integrity, flatness and support structure.

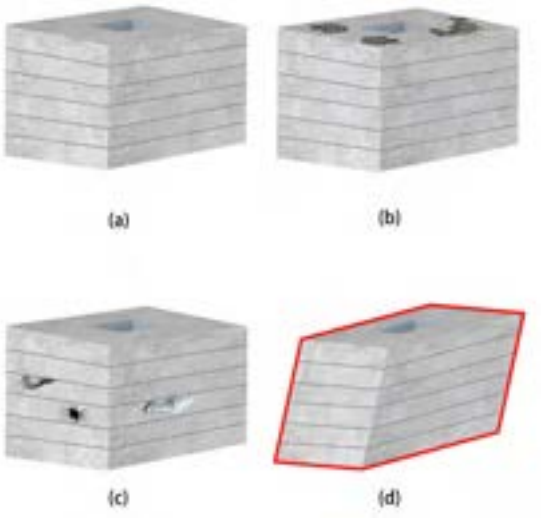

Figure 4. Defect and Deviation Diagram: (a) Ground Truth; (b) Layer Defect and Deviation; (c) Surface Defect; (d) Model Deviation.

3 Method

As shown in Figure 2, the entire 3D printing processing workflow is divided into four phases. Phase 1 is mainly composed with the regular 3D printing process and surface defect detection, which also includes layer deviation detection. Phase 2 includes our original steps, which are layer defect detection after each layer printing. Phase 3 aims to integrate the error output of phase 1 and 2, then following to repair the model. The goal of phase 4 is to

compensate for model shape deviation by adjusting offset. The detail of the explanation and discussion will present in section 3.2.

3.1 Hardware Platform

Perception Sensor. Microsoft Azure Kinect, Figure 3, is a fusion sensor that provides an RGB camera, infrared sensor, depth sensor, gyroscope with accelerometer and microphone array. The reason why we chose Kinect as perception sensor in our approach is that it preset synchronization and calibration-free transformation between each sensor. The depth sensor model in our research is set as WFOV 2x2 binned. The nominal range accuracy of Kinect is less than 11mm in the distance range of 0.25-2.88m [20]. It provides 512x512 resolution with 0.5m to 5m operating range and 120 degrees field of interest in the dual-axis, accurate and dense enough for our purpose.

3D Printing Platform. Universal Robot 10e (UR10e) [21] is a 6-DOF collaborative robot arm that could handle up to 10 kg payload in a 1.3 meters radius and 360 degrees workspace. We designed a concrete print head with a center mixer and attachment for Kinect. The center mixer could rotate clockwise to feed material and the opposite direction to block material. We prepared fast setting mortar mix as our printing material.

Control and Simulation Environment. In order to better observe printing process, ensure safety environment and prevent hardware damage, we use ROS [22] with Moveit [23] in the Gazebo environment to simulate the printing path. Moreover, we use Gazebo simulation world and physics engine for simulating and demonstrating the closed-loop control experiment in section 4.3.

3.2 Defect and Deviation Detection.

When the failure of the 3D printing model occurs, defect and deviation will appear in some places of our model. Therefore, we need to clarify what is defect and what is deviation. In this paper, we define a defect as missing the integrity of the printing layer or material overfill and underfill on the printing model surface. Similarly, the deviation is defined as the contour or shape error.

We divide the defect and deviation generated in 3D construction printing into the following three categories:

Layer Defect and Deviation. Since the printing model is stacked up by multiply concrete layers, it is necessary to check the defect and contour deviation of each layer. The cause of layer defect is either the interruption of feeding material or the impurities contained in the material, such as air bubbles. Layer deviation is caused by path planning error or robot arm control accuracy and noise.

We use RANSAC to fit a plane, $\hat{P}_L$, based on the points in the point cloud, S_L, captured from the Kinect sensor.

$$\begin{aligned} S_L &= \{(x, y, z)\} \\ \hat{P}_L &= \{(x, y, z) | \hat{A}x + \hat{B}y + \hat{C}z + \hat{D} = 0\} \end{aligned} \tag{1}$$

By calculating the point to plane distance, d_i, of each points in the point cloud, we uses an error index array, $e(d_i)$, to record those outliers which compare with the preset tolerance, λ.

$$d_i = \frac{|\hat{A}x_i + \hat{B}y_i + \hat{C}z_i + \hat{D}|}{\sqrt{(A^2 + B^2 + C^2)}} \tag{2}$$

$$e_L(d_i) = \begin{cases} 1 & |d_i| \geq \lambda \\ 0 & |d_i| < \lambda \end{cases} \tag{3}$$

Surface Defect. The surface of the 3D printing model is formed by stacking the sides of the layer. Hence, the obvious layer texture can be observed on the model surface. During the printing process, due to changes in the print head's motion speed or angle rotation, it will cause the material to accumulate at some particular positions, thus forming a class of overfill defect. Unlike overfill, underfill is happened at the gap between roaster path and contour path. Additionally, the local collapse by lacking support will also cause surface underfill.

In order to slice the CAD model for outputting each layer's outer surface, we export the CAD design file to STL format. During printing operation, we subscribe ROS message which present Kinect's position in global coordinate system by calculating robot's forward kinematics. After that, we use this position to map points cloud into Kinect coordinate system. By applying Iterative Closest Point (ICP) algorithm, we identify corresponding point, p_i, for each point, $\hat{p}_i$, between CAD point cloud and scanning point cloud respectively. We minus p_i and $\hat{p}_i$ to get error vector. Then we project the error vector along the unit norm vector N_p on point p_i in reference point cloud P. Therefore, the C2P error distance, d_i, is finally computed as,

$$d_i = \min_{\forall p_i \in P_s} (|\hat{p}_i - p_i| \cdot N_p) \tag{4}$$

Once we have the C2P error distance, we apply (3) to compute point cloud error array.

Model Deviation. Even our printing model avoiding previous errors, we may still fall short of our printing results. The shape deviation we discuss here refers to the misalignment between layers. To provide misalignment bias to feedback control system, here we choose absolute error distance instead of error index array in (3).

$$e_M(d_i) = \begin{cases} d_i & |d_i| \geq \lambda \\ 0 & |d_i| < \lambda \end{cases} \tag{5}$$

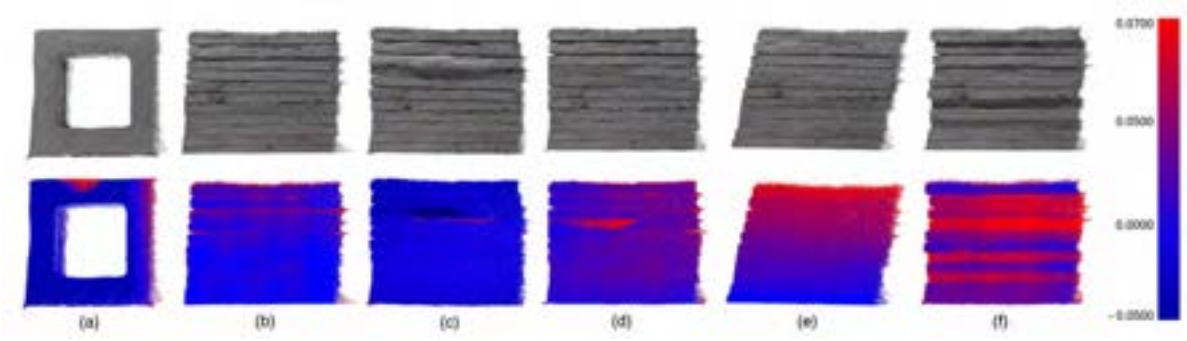

Figure 5. Task 1 results: (a) Layer Defect; (b) Surface without Defect and Deviation; (c) & (d) Surface Defect; (e) & (f) Model Deviation. Top: RGB point cloud captured by Kinect. Bottom: visualization of C2P error between scanned point cloud and CAD. Signed error is color coded from red (positive) to blue (negative).

3.3 Closed Loop Control

As we mentioned in the beginning of this section, we explain and discuss in detail for the each phase setup and process below:

Phase 1. First of all, we directly export the design model from CAD drawing software and save it in STL format. Then we send this STL file to ROS Additive Manufacturing (RAM) for 3D slicing and path generation. We import each layer path from RAM output into ROS MoveIt! to perform path planning. This step helps us to ensure UR10e avoiding self-collision. Once MoveIt! does not detect any collision, it will send the trajectory to UR10e and execute.

At the same time, our point cloud comparison algorithm is also working as a ROS node during the printing process. By subscribing pose message, ROS transfer the position of UR10e's end effector to point cloud generation. In our algorithm, we compute the Kinect observation frame and generate the reference point cloud under the current frame. On the other side, the Kinect sensor continuously captures depth images of the layer surface and transmits it back to our algorithm in real-time. When UR10e completes printing each layer, our approach will go through the ICP algorithm to register the scanning point cloud to reference point cloud and calculate the C2P distance to output the error-index array.

Phase 2. During exporting error-index array in phase 1, UR10e move forward to the next phase, which set Kinect to capture the top view of each layer. By converting RGB to HSV color space, we able to easily segment layer's points from the scanning point cloud. Subsequently, we apply the RANSAC algorithm to fit a plane from those layer's points and output as the planar equation format. The manipulation of the planar equation can help us check multiple layer defects. We check the layer's level corresponding to the horizontal datum. We also find the outlier compare with our preset distance to find the defect position

Figure 6. Task 1 results. Left: RGB point cloud captured by Kinect. Right: visualization of Layer Deviation between scanning point cloud and CAD file. Signed error is color coded from red (positive) to blue (negative).

on the layer plane. The same as phase 1's last step, the algorithm outputs the error-index array to provide feedback information.

Phase 3. In the previous two phases, we got error-index arrays. In the feedback loop, we first convert them into binary error-index arrays to indicate the makeup position for MoveIt! path planning. During MoveIt! execute the trajectory path, we able to correct layer deviation before concrete curing by setting the different angles of side trowel. Moreover, for those defect positions, the print head will re-feed concrete with adjusted side trowel.

Phase 4. Benefit from error array provided in phase 1, the final phase is able to estimate the offset between the current layer and previous layers on each axis direction. In this step, we regard the previous layer as an integral base and only discuss the relationship between the current layer and the base. Applying compensation could help us avoid systematic bias, even compensates control noise for certain special position.

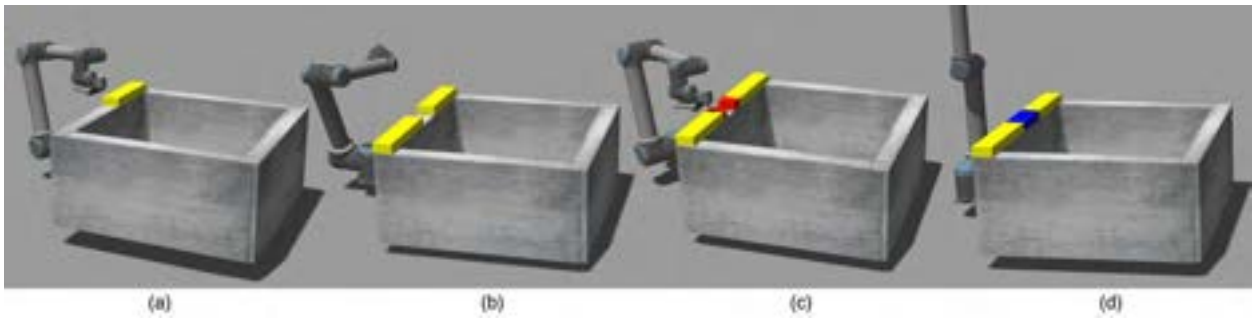

Figure 7. Task 2 experiment process: (a) Normal Printing without Defects; (b) Printing Complete; (c) Mark Defect Area; (d) Complete Defect Correction.

4 Experiments

Our experiment is designed as two tasks, static detection test, and simulation of 3D construction printing. The first task, static detection, aims to demonstrate our approach worked as normal defect detection in a static environment. We will show the three different defects and deviations, which defined in section 3.2. For the second task, we will present our complete approach including defect detection with feedback control during real-time printing. Due to research facility closure and limited available equipment, this experiment will be present in the simulation world by Gazebo.

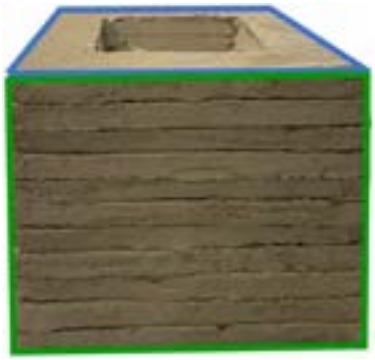

Figure 8. Eleven-layer concrete cubic. Top (Blue): Layer without defect and deviation. Front (Green): Surface without defects.

4.1 Experiments Setup

In Task 1, we are looking for a model that would demonstrate errors as mentioned in section 3.2. For better simulate the product of 3D construction printing, including material property and texture, we made serval half inches concrete planes by concrete-water mixture in a ratio of 9:1. We superimposed these concrete planes to build a cubic shape model. Here, each concrete plane represents corresponding layer in the real printing process. Therefore, we finally got a cube that is 6.5 inches high and 8.5 inches in both depth and width. Each concrete plane has two sides of fixed length and 90 degrees angle, the same as our CAD design. The other two sides are designed to contain different deviation and defect, such as material overfill or layer deviation. We can simulate the errors under various situations by adjusting the placement and order of concrete planes, just like we designed in advance.

In Task2, we setup a UR10e robot with a combination of a simple print head an kinect in Gazebo's simulation environment. To prevent the robot arm hitting the ground, we set the UR10e on a 0.7m high box. Similarly, the printing platform also raised 0.4m accordingly. In this task, our goal is to use the Kinect to capture the layer defect caused by interrupt feeding material during the printing process. Since there is no fluid setting in Gazebo, we made a plugin that will follow the print head position to place thin yellow boxes from the waiting area to the target location in real time. We randomly deleted one segment of materials in the waiting area. Therefore, UR10e will interrupt printing even robot arm is still moving. By using the depth camera plugin, we convert the depth image to a point cloud and use it as the feedback input of our approach. After the printing complete, our plugin will mark the defect position in red first and turn blue after defect correction.

4.2 Defect and Deviation Detection

Figure 5 and Figure 6 present the experiment results in task 1. For Figure 5, RGB point cloud images in the top row demonstrate the concrete cubic that we see in the real world. The images in the bottom row show the difference between printing model and CAD design by presenting in heat map. As scale bar shows, the red regions represent the shrinkage of the model, which means that these regions do not meet the designed size. Similarly, the dark blue areas tell us that the printing exceeds CAD design. As mentioned in section 3.2, tolerance is always a necessary consideration in the engineering world. We set 0.5cm as

the tolerance, λ, in (3) and (5).

The images in column (a) are captured by Kinect from top to bottom after completing each layer. We can see that there are only slight traces in the top image, even it will not be noticed, if the observer does not look closely. However, after generating RGB point cloud, we can easily segment our target, concrete cubic, from the background by color space change. The heatmap below makes us more intuitive to see the defects that are difficult to detect with naked eye or image based detection approaches. There is a shrinkage area at the top of the model. In the actual printing process, the reason of causing this type failure could be the interruption of feeding material. Furthermore, we can also determine the layer deviation at the same time. In Figure 6, the red area presents layer deviation exceeding the boundary of the CAD design model.

Column (b) in Figure 5 shows an ideal 3D printing model that we can see that the entire point cloud is the blue color. Columns (c) and (d) simulate two types of surface defects, overfill and underfill, respectively. In the top image of column (c), we can see a prominent material overflow part in the middle of our printing model. When we applied our method, the dark blue zone is the detection of the overfill area. The note that the underfill depth in column (d) is only 0.7 cm, but our approach still can accurately detect it. For model deviation detection, we simulate two types of control error, columns (e) and (f), that cause to misalignment between neighbor layers. Column (e) simulates the printing drift, which usually occurs in the control systems with accumulated errors. We choose random noise for offset error and make the detection in column (f).

4.3 Closed-loop Control Printing

As Figure 8 shown, our goal is to print a 1 meter cubic. The initial experiment randomly deletes material for an arbitrary length. After confirming that our experiment plan is feasible in the simulation environment, we change the range of the interrupted material to check the limitation of our approach. Starting from 20cm, we found, when the length is less than 2.4cm, our method cannot detect surface defects. Note that we follow the specs entirely from the Microsoft Kinect website to set the parameters in Gazebo depth camera plugin.

5 Conclusion

In this paper, we proposed a front-end closed-loop control approach for 3D construction printing. We also explored the feasibility of using point cloud based defect defection for the construction size printing model. Comparing to other methods, our approach demonstrates a high performance defect detection method with a cost-effective sensor. As the experiments we showed, we believe that our proposed approach has great potential in the field of 3D construction printing.

Limitations and Discussions. An obvious limitation of our approach is that the detection accuracy will significantly decrease as a shrink of the printing model size. Generally, a smaller model will require higher performance and resolution of the 3D perception sensor to detect detail defects. Since the model size of 3D construction printing is large enough, and even a single layer could be easily captured by Kinect. Therefore, this is the main reason why we propose our method for defect detection in 3D construction printing.

Future Work. Our future work is aiming to bring out the real 3D printing product by using our approach. Furthermore, we believe that our work can ultimately help construction workers improve their safety and construction quality, help customers achieve their ideal designs, and reduce material waste to protect our environment.

Acknowledgment

The research is supported by NSF CPS program under CMMI-1932187.

References

[1] Velodyne lidar. https://velodynelidar.com/.

[2] Ouster lidar. https://ouster.com/.

[3] Dong Tian, Hideaki Ochimizu, Chen Feng, Robert Cohen, and Anthony Vetro. Geometric distortion metrics for point cloud compression. In *2017 IEEE International Conference on Image Processing (ICIP)*, pages 3460–3464. IEEE, 2017.

[4] S Scott Crump. Apparatus and method for creating three-dimensional objects, June 9 1992. US Patent 5,121,329.

[5] Behrokh Khoshnevis. Automated construction by contour crafting—related robotics and information technologies. *Automation in construction*, 13(1):5–19, 2004.

[6] Behrokh Khoshnevis, Dooil Hwang, Ke-Thia Yao, and Zhenghao Yeh. Mega-scale fabrication by contour crafting. *International Journal of Industrial and Systems Engineering*, 1(3):301–320, 2006.

[7] Richard A Buswell, Rupert C Soar, Alistair GF Gibb, and A Thorpe. Freeform construction: mega-scale rapid manufacturing for construction. *Automation in construction*, 16(2):224–231, 2007.

[8] Steven J Keating, Julian C Leland, Levi Cai, and Neri Oxman. Toward site-specific and self-sufficient robotic fabrication on architectural scales. *Science Robotics*, 2(5):eaam8986, 2017.

[9] Winsun. http://www.winsun3d.com/En/Product/.

[10] Weiyi Lin, Hongyao Shen, Jianzhong Fu, and Senyang Wu. Online quality monitoring in material extrusion additive manufacturing processes based on laser scanning technology. *Precision Engineering*, 60:76–84, 2019.

[11] Zhen Liu, Suining Wu, Qun Wu, Chenggen Quan, and Yiming Ren. A novel stereo vision measurement system using both line scan camera and frame camera. *IEEE Transactions on Instrumentation and Measurement*, 68(10):3563–3575, 2018.

[12] Oliver Holzmond and Xiaodong Li. In situ real time defect detection of 3d printed parts. *Additive Manufacturing*, 17:135–142, 2017.

[13] Hongyao Shen, Weijun Sun, and Jianzhong Fu. Multi-view online vision detection based on robot fused deposit modeling 3d printing technology. *Rapid Prototyping Journal*, 2019.

[14] Tianjiao Wang, Tsz-Ho Kwok, Chi Zhou, and Scott Vader. In-situ droplet inspection and closed-loop control system using machine learning for liquid metal jet printing. *Journal of manufacturing systems*, 47:83–92, 2018.

[15] Wentai Zhang, Akash Mehta, Prathamesh S Desai, and C Higgs. Machine learning enabled powder spreading process map for metal additive manufacturing (am). In *Int. Solid Free Form Fabr. Symp. Austin, TX*, pages 1235–1249, 2017.

[16] Lu Lu, Jian Zheng, and Sandipan Mishra. A layer-to-layer model and feedback control of ink-jet 3-d printing. *IEEE/ASME Transactions on Mechatronics*, 20(3):1056–1068, 2014.

[17] Yijie Guo and Sandipan Mishra. A predictive control algorithm for layer-to-layer ink-jet 3d printing. In *2016 American Control Conference (ACC)*, pages 833–838. IEEE, 2016.

[18] Berk Altın, Zhi Wang, David J Hoelzle, and Kira Barton. Robust monotonically convergent spatial iterative learning control: Interval systems analysis via discrete fourier transform. *IEEE Transactions on Control Systems Technology*, 27(6):2470–2483, 2018.

[19] Patrick M Sammons, Michelle L Gegel, Douglas A Bristow, and Robert G Landers. Repetitive process control of additive manufacturing with application to laser metal deposition. *IEEE Transactions on Control Systems Technology*, 27(2):566–575, 2018.

[20] Azure kinect dk hardware specifications. https://docs.microsoft.com/en-us/azure/kinect-dk/hardware-specification.

[21] Ur10e collaborative industrial robot arm. https://www.universal-robots.com/products/ur10-robot/.

[22] Ros: The robot operation system. https://www.ros.org/.

[23] Moveit! https://moveit.ros.org/.

Robotics Autonomous Surveillance Algorithms for Assessing Construction Automation and Completion Progress

Firas.Habbal [a], Abdualla.AlNuaimi [b], Dhoha.Alhmoudi [c], Mariam.Alrayssi [c], Ahmed.Alali [c],

[a]Department of Management College of Business,
International learning institute, United Arab of Emirates
[b]Ministry of Infrastructure Development, United Arab of Emirates
[C]Sheikh Zayed Housing Program, United Arab of Emirates
E-mail: firas.habbal@iqli.net, Abdulla.alnuaimi@moid.gov.ae, dhoha.alhmoudi@szhp.gov.ae,
mariam.alrayssi@szhp.gov.ae, ahmed.alali@szhp.gov.ae

Abstract –

Exact development progress estimation has been demonstrated to be basic to the accomplishment of a structure venture. The techniques for robotized development progress estimation proposed in past examinations have certain constraints in light of fragmented informational collections. The principle target of this research was to create a precise, basically completely mechanized strategy for development progress estimation utilizing a 360□ cameras and 3D information with LiDAR technology to detect site plan by remote-detecting innovation. The cameras at that point select the parameter settings that best fulfill the relegated contending solicitations to give high goals perspectives on the stage accomplishments. We propose using robotic scanning with AI analytics to tackle the plaster stage and the camera parameter determination issues continuously. The adequacy of the proposed framework is approved in both reproduction and physical test. The consequences of the proposed progress estimation technique can be utilized as contribution for development progress representation and enhance the inspections timeframe.

Keywords –
Construction Robotics; Inspections Enhancements; AI Detection; Internal Mapping; Autonomous Inspection

1 Introduction

Robots and mobile platforms have recently begun to solve many of the goals for remote sensing. Mobile laser scanning devices have enabled the identification and classification of roadside objects [1].

Human-mounted solutions, like backpacks equipped with laser scanners, allow for human-in-the-loop navigation of indoor spaces [2]. These mobile solutions afford operators access to previously inaccessible regions that stationary systems cannot sense.

Autonomous and semi-autonomous mobile remote sensing platforms, including robots, further improve the flexibility that mobile sensing offers. Robotic agents can operate without the need of constant human presence and input [3][4]. Therefore, environments can be remotely sensed without involving or endangering humans, making surveying safer and more efficient. Many robotic platforms outperform their human counterparts in similar sensing and mapping tasks as well [5], which increases the reliability and accuracy of produced geospatial intelligence. This process of simultaneously localizing a robot in its surroundings and mapping these surroundings is known as Simultaneous Localization and Mapping (SLAM). The fine level details and autonomy afforded by SLAM robots have contributed to the ubiquity of these platforms as mobile and adaptable exploration solutions.

One result of the increased use in robotic remote sensing platforms is a greater portfolio of environments and spaces that can be explored. Urban and subterranean environments pose a unique challenge because they typically feature tight spaces and are often poorly lit. Additionally, underground caves are often rocky and difficult to traverse. Nonetheless, robots have been produced to explore these spaces. Urban-focused robots use three-dimensional (3-D) lidar to scan areas due to the high failure rate of visible-light dependent cameras [6][7]. As a result, robots can produce highly detailed maps for the precise environments for which they are selected, including deep mines and archaeological sites [8].

The goal is to provide the warfighter a cost-effective solution that provides situational awareness, in near real-time, of building interiors and Subterranean (SubT) environments. In order to address the gaps listed above, merging a mapping technology with a robotics platform that has limited computational and power resources will need be done successfully.

However, most commercially available LIDAR systems are designed for use outdoors, specifically for

high-resolution aerial imaging and mapping applications. As a result, they tend to be large, heavy, power-hungry, data bandwidth intensive, and expensive and not suitable for integration on a robotics platform. Also, the amount of data collected is quite large (gigabits) and requires post-processing (days). In the last few years, the automotive industry's push for autonomy has resulted in a number of industries producing SWaP-C sensors that should be suitable for a robotics platform and still be capable of surveying and mapping underground structures and the interior of buildings.

This capability would provide the warfighter with data intelligence to develop situational understanding and support troop maneuverability. Utilizing these commercial off the shelf (COTS) low-power sensors to provide a near real-time solution has yet to be implemented, and the benefits provided when compared to their larger, expensive, and power-hungry counterparts are unrealized.

In regards to the robotics platform, the Maneuver Center of Excellence (MCoE) SubT equipment list has a variety of robot platforms, including the Firstlook and Packbot 510. Both of these robots are equipped with cameras, but neither system generates point clouds of the environment. In addition to the cost of the robotics platform, additional revenue is also required for mapping sensors (i.e., GeoSLAM ZEB-REVO or Carnegie Robotics Multisense). However, these sensors merely sit atop the robotics platform and do not leverage the robot's on-board sensors for enhanced positioning and localization. The robotics platform that is being leveraged for this report is the Army Ground Vehicle Robot (GVR-BOT) Gen 1.1 platform. This platform is the reference design standard for Project Manager (PdM) Unmanned Ground Vehicle. By combining the robot's localization and positioning sensors with the mapping solution, highly accurate data can be generated.

2 Literature Review

2.1 Robotics Surveillance

The construction industry is known to be a major economic sector. However, it is also dealt with different types of inefficiencies as well as low productivity. Robotics autonomous surveillance is a solution that has the potential to address such types of shortcomings. Delgado stated that robotics and subsequent automated systems can revolutionize and also provide several advantages to the overall construction industry [9]. Construction is considered to be a labour-intensive sector. Nonetheless, it can also be stated that the Robotic System automation can help to become very effective in other sectors as well for labour cost reduction and at the same time, look for productivity and quality improvement.

2.2 Robotics Automation

Different types of Construction Robotics exist in the construction industry. These can be group into 4 general categories. This include off-site prefabrication systems, on-site automated and robotic systems, drones and autonomous vehicles, and exoskeletons. The adoption of such robotic mechanisms can be largely attributed to the successful use of robots in the automotive manufacturing industry of Japan. Construction works need to be completed soon as significant financial matters are involved. However, this process can be automated as Artificial Intelligence (AI) can consider proper measures that will improve the situation related to robotics involvement in construction [9].

2.3 Factors of Robotics Automations

This is evident that there is a cost for the client for robotics adoption in their whole process. Governments are considered to be the major clients of all the construction and infrastructure companies. Furthermore, the public spending amount in the infrastructure can have a big influence as well in terms of adopting new technologies. The construction companies operate in a highly competitive market. If we consider that price is the only criteria for selection, then the construction companies can significantly consider reducing the overall profit margins in an aggressive manner. This type of manner will increase confrontational behaviour as well as restrict those people from alternative thinking [10].

2.4 Technical Factors

There is also case where different practical factors can limit the overall robotics related implementation. These factors can be attributed to the technical limitations that reside within the current technologies and also some other work-related factors.

The challenge in this case is the high complexity that remains within the construction tasks which also have effects on the usability and effective of the robotic automated solutions [9]. Construction robotics, with the help of AI detection and internal mapping, can consider construction automation and inform about completion. This type of autonomous inspection will bring results within a short period of time. To improve the quality of such inspections, it is preferred to have inspections enhancements in place [9].

A construction work consists of many stages. With AI detection and other latest technologies, it is possible to know about construction automation and completion period. The progress will help the stakeholders to make relevant decisions that will have an impact at the direct workflow.

2.5 Adaptation Process

There is a certain level of complexity in the overall construction process and hence, sufficient preparation is necessary for adaptability. All the participants who work in the construction process needs to be considered in the overall adaptation process. The autonomous inspection will help time and cost for the companies and help them focus on the core issues. The adaptation process of the robotic automation can take place through step by step process [11].

2.6 Robotics in Construction Automation

The robotic technology performance is on the rise rapidly and therefore, this can complement the construction process's automation and completion progress monitoring. Nonetheless, to conduct the operations flawlessly, workers need to have mechatronic and robotic training as well as qualifications [9]. The stakeholders and the decision makers can think about automation and integration of different advanced technologies in the construction field. This can be done when the guidelines are properly followed and considered into the thinking process.

Robotics can work in different forms and it has also been considered for augment abilities. There are working exoskeleton available which will not only help to enhance the wearer's mobility but also make them much stronger. This will make those people less prone towards any type of work-related injuries. These wearables eliminate major stress as well as damage that can result from being involved in physical labor too often [11].

Robotics and automation play a crucial role in the construction sector. It is also to be noted that there should be high technology of Research & Development to be used because of the dynamic and unstructured nature of the overall construction environment. There are several robotics automations which are used in the construction area and they include- fireproofing spray robot, wall finishing robot, steel beam positioning manipulator, spray coating robot, and ceiling panel positioning robot. In terms of the civil work, there are also the use of different types of robot, such as- semi autonomous robot, concrete crusher, demolition robot, robot for all jobs etc. Each of these robots have different purposes that they serve [12].

2.7 Robotics in Construction

The primary role of automated techniques in the construction sector is to develop a multidimensional as well as a comprehensive costs and benefits analysis which is related to some certain robotic application. The success in this regard can be analysed through the process of technical as well as economic feasibility. The technical feasibility is an ergonomic evaluation of the steps that help to complete the given work task. It also considers the analysis related to the robot control and process monitoring requirements [9].

Through the process of Robotics and Automation, we have also seen an increase in the overall occupational safety issue. Using robotics and its automation help especially in the case of dangerous zones. There are several automated systems which may help in working for the dangerous zones for the humans. This type of automation helps to reduce the labour related injuries and also keep company cost at a minimum. There is an increase in quality that is evident as well because of the robotics autonomous surveillance algorithms. These operations are carried out with less variability in comparison to the human workers [13].

The automation system possesses a greater control towards the whole production process. We are able to detect the problems easily and for different stage as well. Through this process, it gets easier to understand if there is a correct functioning of the system happening or not. The robotics automation gives greater control towards the final result and this can be controlled in an efficient way by look at the steps of the overall process individually.

3 Research Methodology

3.1 Lidar Automation

The method of simultaneous localization and mapping (SLAM) using a light detection and ranging (LiDAR) sensor is commonly adopted for robot navigation. However, consumer robots are price sensitive and often have to use low-cost sensors. Due to the poor performance of a low-cost LiDAR, error accumulates rapidly while SLAM, and it may cause a huge error for building a larger map. To cope with this problem, this paper proposes a new graph optimization-based SLAM framework through the combination of low-cost LiDAR sensor and vision sensor. In the SLAM framework, a new cost-function considering both scan and image data is proposed, and the Bag of Words (BoW) model with visual features is applied for loop close detection. A 2D map presenting both obstacles and vision features is also proposed, as well as a fast relocation method with the map.

Experiments were taken on a service robot equipped with a low-cost LiDAR and a front-view RGB-D camera in the real indoor scene. The results show that the proposed method has better performance than using LiDAR or camera only, while the relocation speed with our 2D map is much faster than with traditional grid map.

Localization and navigation are the key technologies of autonomous mobile service robots, and simultaneous

localization and mapping (SLAM) is considered as an essential basis for this. The main principle of SLAM is to detect the surrounding environment through sensors on the robot, and to construct the map of the environment while estimating the pose (including both location and orientation) of the robot.

3.2 SLAM Detection

LiDAR can detect the distance of the obstacles, and it is the best sensor to construct a grid map, which represents the structure and obstacles on the robot running plane. The early SLAM research often used LiDAR as the main sensor. Figure 1 shows the obstacles near the robot, marked in red dots. SLAM has the ability to detect moving objects as well. Table 1 shows the angle and distance from the obstacle shown in figure 1.

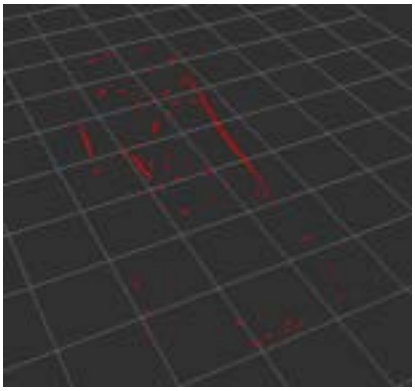

Figure 1. Obstacles Detection

Table 1. Angle and Obstacles

Angle	Distance
-179	2.691
-143	2.124
-107	0.901
-71	0,655
-35	2.679
1	1.872
36	0.963
72	0.643
108	0.703
144	1.344
180	0.729

Extended Kalman filter (EKF) was applied to estimate the pose and of the robot, but the performance was not ideal. For some strong nonlinear systems, this method will bring more truncation errors, which may lead to inaccurate positioning and mapping. Particle filter approaches were introduced because they can effectively avoid the nonlinear problem, but it also leads to the problem of increasing the amount of calculation with the increase of particle number. In 2007, Grisetti proposed a milestone of LiDAR-SLAM method called Gapping based on improved Rao-Blackwellized particle filter (RBPF), it improves the positioning accuracy and reduces the computational complexity by improving the proposed distribution and adaptive re-sampling technique.

As an effective alternative to probabilistic approaches, optimization-based methods are popular in recent years. In 2010, Kurt Konolige proposed such a representative method called Karto-SLAM, which uses sparse pose adjustment to solve the problem of matrix direct solution in nonlinear optimization. Hector SLAM proposed in 2011 uses the Gauss-Newton method to solve the problem of scanning matching, this method does not need odometer information, but high precision LiDAR is required. In 2016, Google put forward a notable method called Cartographer by applying the laser loop closing to both sub-maps and global map, the accumulative error is reduced. Figure 2 shows the map generated using hector slam. This map is saved and then used in navigation to avoid the walls. The dark black boxes shown in figure 2 shows the room boundaries.

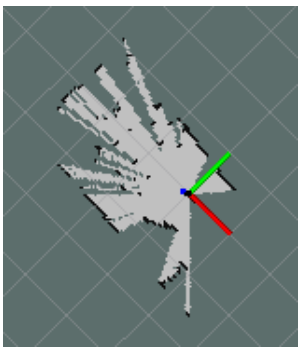

Figure 2. Map generated using Hector SLAM

3.3 Traditional Grid Map

Occupy grid map is wildly used in LiDAR-SLAM, it is a simple kind of 2D map that represents the obstacles on the LiDAR plane:

$$Mgrid = \{mg(x, y)\},$$

where mg(x, y) denotes the possibility if the grid (x, y) is occupied. Generally, the value of mg(x, y) can be 1 (the grid (x, y) is occupied) or 0 (the grid (x, y) is not occupied).

Feature map is another kind map generated by most feature-based Visual-SLAM approaches; it can be represented as:

$$Mfeature = \{f(x,y,z)\},$$

where f(x,y,z) denotes that on the world position (x,y,z), there is a feature f(x,y,z), for real applications, f (x, y, z) could be a descriptor to the feature in a dictionary like BoW.

As a result, a feature map is a sparse map which only has value on the position which has features. This makes a feature map is reliable for localization, but not good for navigation and path-planning.

3.4 360 degree Cameras

In photography, a 360-degree camera is a camera with a visual field of the entire sphere or simply a camera with the ability to capture a 360-degree field of view in the horizontal plane. Such cameras are a highly appreciated in instances when large visual field coverage is desired, such as in robotics or panoramic photography.

Most cameras have a field of view that ranges from a few degrees to almost 180 degrees or sometimes slightly larger than this. It implies that such cameras have the ability to capture the light falling onto their focal points through a sphere. On the contrary, a 360-degree camera covers a full sphere and has the ability to capture light falling from all directions onto the focal point. In actual application, however, most 360 degrees cameras can cover almost a full sphere along the equator, but with the exclusion of the bottom and top of the sphere. Should they cover the full sphere, including the top and the bottom, the rays will not meet at a single focal point.

3.5 Robotic Computer Vision

360-degree cameras are used in robotics to solve simultaneous localization and mapping as well as for visual odometry. With the ability to capture a 360-degree field of view, the 360-degree cameras lead to better optical flow, feature matching and feature selection in robotics.

The 360-degree camera would be used to take pictures of the rooms constructed. That will be used later on to determine the stage the wall is in. It can take the picture of the whole room in one go, and then the program can differentiate different walls in the room.

Figure 3. 3 stages of construction

After taking the picture, the program will use AI to determine the stage the wall is on and then evaluate the progress of the construction. Figure 4 shows the three stages of construction that are Blocks, Plaster and Primer. After determining the stage of all walls in the house, the program can evaluate the progress of house completion.

4 Results & Findings

For each classified scene, a confusion matrix was generated, used to examine commission and omission errors, the accuracy of the producer, and the classification in general. In turn, the K was calculated, which computes the agreement between the classified image and the observed reality due solely to the accuracy of the classification, deleting the agreement that would fit simply wait by chance. How much is K close to 100% how much is the classification accuracy good.

Table 1 below provides a detailed information from the used images in the training and testing with each results classification accuracy.

Table 2. Learning Model Classifications Accuracy

Dataset	Amount	Confusion Matrices	Classifier Behaviour Testing
Training	Class plaster 540	Class one-one 99%	Class with plaster 98%
		Class one-two 1%	Class without plaster 99%
	Class without plaster 540	Class two-two 100%	
Testing	Class plaster108	Class one-one 100%	Class with plaster 100%
		Class one-two 100%	
	Class without plaster 108	Class two-two 0%	Class without plaster 100%

Acknowledgment

This research is financially supported by the Sheikh Zayed Housing Program in United Arab of Emirates and International Group of Innovative Solutions. Special thanks for Jamila Al Fandi, Aesha Aleghfeli, Mohamed Al Shamsi, Saleh Al Shehi, Thuraya Al Darmaki.

References

[1] Lehtomäki, Matti, et al. "Object classification and recognition from mobile laser scanning point clouds in a road environment." IEEE Transactions on Geoscience and Remote Sensing 54.2 (2015): 1226-1239.

[2] Wen, M. (2016). Using the Monte Carlo Localization Algorithm to Allow for Effective Indoor Navigation.

[3] Tsubouchi, T., Tanaka, A., Ishioka, A., Tomono, M., & Yuta, S. (2004). A SLAM based teleoperation and interface system for indoor environment reconnaissance in rescue activities. In 2004 IEEE/RSJ International Conference on Intelligent Robots and Systems (IROS)(IEEE Cat. No. 04CH37566) (Vol. 2, pp. 1096-1102). IEEE.

[4] Quin, P., Paul, G., & Liu, D. (2017). Experimental evaluation of nearest neighbor exploration approach in field environments. IEEE Transactions on Automation Science and Engineering, 14(2), 869-880.

[5] Ekvall, S., Jensfelt, P., & Kragic, D. (2006, October). Integrating active mobile robot object recognition and slam in natural environments. In 2006 IEEE/RSJ International Conference on Intelligent Robots and Systems (pp. 5792-5797). IEEE.

[6] Niemeyer, J., Rottensteiner, F., & Soergel, U. (2014). Contextual classification of lidar data and building object detection in urban areas. ISPRS journal of photogrammetry and remote sensing, 87, 152-165.

[7] Wang, W., Huang, W. W., & Zhen, J. (2011). Pictometry oblique photography technique and its application in 3D city modeling. Geomatics & Spatial Information Technology, 3.

[8] Guo, S., He, Y., Shi, L., Pan, S., Tang, K., Xiao, R., & Guo, P. (2017). Modal and fatigue analysis of critical components of an amphibious spherical robot. Microsystem Technologies, 23(6), 2233-2247.

[9] Delgado, R., You, B. J., & Choi, B. W. (2019). Real-time control architecture based on xenomai using ros packages for a service robot. Journal of Systems and Software, 151, 8-19.

[10] Wickens, C. D., Sebok, A., Li, H., Sarter, N., & Gacy, A. M. (2015). Using modeling and simulation to predict operator performance and automation-induced complacency with robotic automation: a case study and empirical validation. Human factors, 57(6), 959-975.

[11] Balaguer, C., & Abderrahim, M. (Eds.). (2008). Robotics and automation in construction. BoD–Books on Demand.

[12] Kulik, M., Hrin, O., & Volkova, O. (2019). Aspects of the use of roboted systems for optimization of construction processes. Ways to Improve Construction Efficiency, 1(39), 208-215.

[13] Ha, Q., Santos, M., Nguyen, Q., Rye, D., & Durrant-Whyte, H. (2002). Robotic excavation in construction automation. IEEE Robotics & Automation Magazine, 9(1), 20-28.

Oscillation Reduction for Knuckle Cranes

Michele Ambrosino[a], Arnaud Dawans[b], Brent Thierens[a], Emanuele Garone[a]

[a]Service d'Automatique et d'Analyse des Systèmes, Université Libre de Bruxelles, Brussels, Belgium
[b]Entreprises Jacques Delens S.A., Brussels, Belgium

Michele.Ambrosino@ulb.ac.be, adawans@jacquesdelens.be, Brent.Thierens@vub.be, egarone@ulb.ac.be

Abstract -

Boom cranes are among the most common material handling systems due to their simple design. Some boom cranes also have an auxiliary jib connected to the boom with a flexible joint to enhance the maneuverability and increase the workspace of the crane. Such boom cranes are commonly called knuckle boom cranes. Due to their underactuated properties, it is fairly challenging to control knuckle boom cranes. To the best of our knowledge, only a few techniques are present in the literature to control this type of cranes using approximate models of the crane. In this paper we present for the first time a complete mathematical model for this crane where it is possible to control the three rotations of the crane (known as luff, slew, and jib movement), and the cable length. One of the main challenges to control this system is how to reduce the oscillations in an effective way. In this paper we propose a nonlinear control based on energy considerations capable of guiding the crane to desired sets points while effectively reducing load oscillations. The corresponding stability and convergence analysis is proved using the LaSalle's invariance principle. Simulation results are provided to demonstrate the effectiveness and feasibility of the proposed method.

Keywords -

Knuckle Cranes; Robotics; Oscillation Reduction; Underactuated Systems; Nonlinear Control

1 Introduction

Cranes are material handling machines which are used in different industries (i.e., construction, manufacturing, shipbuilding and freight handling) for transporting heavy materials that humans cannot handle. Cranes have the capability of moving the load vertically and horizontally, either along a straight or a curved path. Nowadays, most cranes are manually operated by skilled operators. In this paper we focus on the design of an effective automatic control to obtain accurate positioning and reduce the swing of the load.

Cranes come in various sizes and designs to perform different tasks. Depending on their dynamic properties they can be classified as gantry cranes and rotary cranes. Gantry cranes can be further classified into overhead cranes and container cranes. Rotary cranes can be classified into tower cranes and boom cranes [1].

In this paper we will focus on a so called 'knuckle boom' crane which is one of the most common type of boom crane. Boom cranes are characterized by a first boom that can rotate around two orthogonal axes (e.g. slew and luff motions). From the free end of the boom, a payload is suspended using a hoisting rope. The length of the hoisting rope can be driven using a winch. A boom crane can move the payload in the 3D space using the luff and slew movements of the boom and the hoisting of the payload. Such cranes are commonly used in construction sites [2]. Boom cranes can also have more than one boom. Common variant of the boom crane has an auxiliary jib connected to the boom to enhance the maneuverability. Such boom cranes are the knuckle boom cranes (see Fig. 1). In this paper we present for the first time a complete mathematical model for this kind of crane which takes into account not only the three main rotations (e.g. luff, slew, and jib movement), but also the cable dynamic and the payload oscillations.

As all cranes, knuckle cranes are nonlinear systems with complicated underactuated dynamics. Underactuated systems [3] are commonly found in several areas and applications, such as robotics, aerospace systems, marine systems, flexible systems, mobile systems, and locomotive systems. The condition of underactuation refers to a system with more DoF (number of independent variables that define the system configuration) to be controlled, than actuators (input variables). This restriction implies that some of the configuration variables of the system cannot be directly commanded, which highly complicates the design of control algorithms. In particular for the proposed model of knuckle crane the non-actuated variable are the swing angles of the payload, whereas the four actuated variable will be the three main rotation (i.e. luff, slew, and jib movements) and the length of the cable.

Cranes can be controlled using different control laws depending on their operations, which usually involve the process of gripping, lifting, transporting the load, lowering, and releasing the load. A damping capacity of the system plays a significant role towards the precision motion

performance. The control schemes developed for cranes can mainly be categorised into open loop and closed loop techniques [4]. Control schemes based on a combination of open and closed loop techniques have also been proposed. Input shaping is one of the most used open loop techniques, mostly based on a linearized system, that can be applied in real time, mainly for control of the oscillations of the payload. Anti-swing crane controls using input shaping have been widely implemented in the literature [5]-[6]. Concerning closed loop techniques, Proportional Integral Derivative (PID) control laws have been proposed for instance in [4], where the authors proposed a position control of a gantry crane system. A state feedback controller has been implemented in [7] for a boom crane system in order to control the load sway angles in the vertical and horizontal boom motions, as well as in the vertical and horizontal boom angles. In [8] the authors present a constrained control scheme based on the ERG framework for the control of boom cranes. In [9] a model predictive control (MPC) approach was used for a boom crane in order to reduce the swing angles as much as possible.

Compared with the other kinds of cranes like boom cranes, the study of knuckle cranes is still at an early stage with much less reported control strategies. In [10] the authors focus on controlling mobile electro-hydraulic proportional valves to move the crane to a desired position. In [11] the authors solve the problem of controlling knuckle crane through the inverse kinematics without take into account the dynamic of the cable and the payload. In [12] an anti-sway control is shown which is performed by simplifying the dynamic model and assuming that the tip of the crane can be controlled directly.

To the best of our knowledge, no research has been carried out to develop a detailed mathematical model and develop a control strategy taking into account the strongly nonlinear nature of this type of crane. In this paper we advance the state of the art of the knuckle crane by introducing for the first time a complete mathematical model in which we takes into account all of the degrees of freedom (DoF) that characterize this type of system (i.e. the three rotations, the length of the rope and the payload swing angles) and proposing novel control strategy designed directly on the nonlinear model.

The rest of this paper is organized as follows. In Section 2, the dynamic model of the knuckle crane and the control objectives are provided. In Section 3, the proposed controller is designed, and the corresponding stability analysis is provided in detail. Section 4 shows the results of the simulations regarding the proposed control strategy.

Figure 1. Model of a knuckle crane [1].

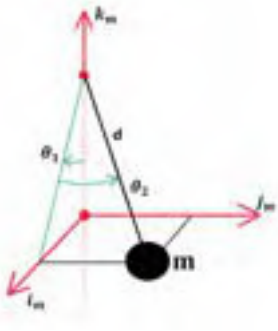

Figure 2. Payload swing angles.

2 Dynamic Model

A schematic view of knuckle crane is shown in Fig.1. The knuckle crane consists of a first boom of length l_b and mass m_b connected to the tower with one revolute joint. The auxiliary jib of length l_j and mass m_j is linked to the first boom by a revolute joint. For the sake of simplicity in this paper, both of these two links are considered to be rigid. The cable is supposed to be massless and rigid, thus the lifting mechanism can be represent as a prismatic joint. The payload of mass m can be represented as lumped mass. The two swing angles of the payload are represented in the Fig.2.

The configuration of the crane can be represented by six generalized coordinates, in which, α is the slew angle of the tower, β is the luff angle of the boom, γ is the luff angle of the jib, d is the length of the rope, θ_1 is the tangential pendulation mainly due to the motion of the tower and θ_2 is the radial sway mainly due to the motion of the boom.

To simplify the ensuing analysis, the following abbreviations are used: $S_\alpha \triangleq \sin(\alpha), S_\beta \triangleq sin(\beta), S_\gamma \triangleq \sin(\gamma), S_{\theta_1} \triangleq \sin(\theta_1), S_{\theta_2} \triangleq \sin(\theta_2), C_\alpha \triangleq \cos(\alpha), C_\beta \triangleq \cos(\beta), C_\gamma \triangleq \cos(\gamma), C_{\theta_1} \triangleq \cos(\theta_1), C_{\theta_2} \triangleq \cos(\theta_2)$.

The dynamic model of the knuckle crane is obtained by using the Lagrange method [13]. Firstly, we need to express the system kinematic energy $T(t)$, which consists of three parts, the boom kinematic energy $T_t(t)$, the jib

kinematic energy $T_j(t)$, and the payload kinematic energy $T_p(t)$. Then, the system potential energy $U(t)$ consists of the boom gravity energy $U_t(t)$, the jib gravity energy $U_j(t)$, and the payload gravity energy $U_p(t)$. Next, the Lagrange function is constructed as

$$\begin{aligned} L(t) &= T(t) - U(t) \\ &= T_b(t) + T_j(t) + T_p(t) - U_b(t) - U_j(t) - U_p(t), \end{aligned} \tag{1}$$

where

$$\begin{aligned} T(t) = \frac{1}{8}(m_B((l_B C_\beta S_\alpha \dot{\alpha} + l_B C_\alpha S_\beta \dot{\beta})^2 + (l_B C_\alpha C_\beta \dot{\alpha} \\ -l_B S_\alpha S_\beta \dot{\beta})^2 + l_B^2 C_\beta^2 \dot{\beta}^2)) + \frac{1}{2}(m_J((l_B C_\beta S_\alpha \dot{\alpha} + l_B C_\alpha S_\beta \dot{\beta} \\ +\frac{1}{2}(l_J C_\gamma S_\alpha \dot{\alpha}) + \frac{1}{2}(l_J C_\alpha S_\gamma \dot{\gamma}))^2 + (l_B C_\alpha C_\beta \dot{\alpha} + \frac{1}{2}(l_J C_\alpha C_\gamma \dot{\alpha}) \\ -l_B S_\alpha S_\beta \dot{\beta} - \frac{1}{2}(l_J S_\alpha S_\gamma \dot{\gamma}))^2 + (l_B C_\beta \dot{\beta} + \frac{1}{2}(l_J C_\gamma \dot{\gamma}))^2)) \\ +\frac{1}{2}(m((C_{\theta_2} S_\alpha S_{\theta_1} \dot{d} - C_\alpha S_{\theta_2} \dot{d} + l_B C_\beta S_\alpha \dot{\alpha} + l_B C_\alpha S_\beta \dot{\beta} \\ +l_J C_\gamma S_\alpha \dot{\alpha} + l_J C_\alpha S_\gamma \dot{\gamma} - C_\alpha C_{\theta_2} \dot{\theta_2} d + S_\alpha S_{\theta_2} \dot{\alpha} d \\ +C_\alpha C_{\theta_2} S_{\theta_1} \dot{\alpha} d + C_{\theta_1} C_{\theta_2} S_\alpha \dot{\theta_1} d - S_\alpha S_{\theta_1} S_{\theta_2} \dot{\theta_2} d)^2 + (l_B C_\beta \dot{\beta} \\ -C_{\theta_1} C_{\theta_2} \dot{d} + l_J C_\gamma \dot{\gamma} + C_{\theta_2} S_{\theta_1} \dot{\theta_1} d + C_{\theta_1} S_{\theta_2} \dot{\theta_2} d)^2 \\ +(S_\alpha S_{\theta_2} \dot{d} + l_B C_\alpha C_\beta \dot{\alpha} + l_J C_\alpha C_\gamma \dot{\alpha} \\ -l_B S_\alpha S_\beta \dot{\beta} - l_J S_\alpha S_\gamma \dot{\gamma} + C_\alpha S_{\theta_2} \dot{\alpha} d + C_{\theta_2} S_\alpha \dot{\theta_2} dv \\ +C_\alpha C_{\theta_2} S_{\theta_1} \dot{d} + C_\alpha C_{\theta_1} C_{\theta_2} \dot{\theta_1} d - C_{\theta_2} S_\alpha S_{\theta_1} \dot{\alpha} d \\ -C_\alpha S_{\theta_1} S_{\theta_2} \dot{\theta_2} d)^2)) + \frac{1}{2} I_{tot} \dot{\alpha}^2 + \frac{1}{2} I_B \dot{\beta}^2 + \frac{1}{2} I_J \dot{\gamma}^2, \end{aligned} \tag{2}$$

$$\begin{aligned} U(t) = gm(l_B S_\beta + l_J S_\gamma - C_{\theta_1} C_{\theta_2} d) + gm_J(l_B S_\beta \\ +\frac{1}{2} l_J S_\gamma) + \frac{1}{2} g l_B m_B S_\beta, \end{aligned} \tag{3}$$

The equations of the motion of the crane are derived using the Lagrange's equation

$$\frac{d}{dt}\left(\frac{\partial L(q,\dot{q})}{\partial \dot{q}}\right) - \frac{\partial L(q,\dot{q})}{\partial q} = \zeta, \tag{4}$$

where $\mathrm{q} = [\alpha, \beta, \gamma, d, \theta_1, \theta_2]^T \in \mathbb{R}^6$ represents the system state vector, and $\zeta = [u_1, u_2, u_3, u_4, 0, 0]^T \in \mathbb{R}^6$ represents the control input vector.

The dynamic model of a knuckle crane (see Fig. 1) can be written as:

$$M(q)\ddot{q} + C(q,\dot{q})\dot{q} + F(\dot{q}) + g(q) = \begin{bmatrix} I_{4x4} \\ 0_{2x2} \end{bmatrix} u. \tag{5}$$

The matrices $\mathrm{M(q)} \in \mathbb{R}^{6x6}$,$C(q,\dot{q}) \in \mathbb{R}^{6x6}$,$F(\dot{q}) \in \mathbb{R}^6$ and $\mathrm{g(q)} \in \mathbb{R}^6$ represent the inertia, centripetal-Coriolis, air dynamic friction [14], and gravity. The system matrices (see Appendix for the detailed description) are defined as follows:

$$M(q) = \begin{bmatrix} m_{11} & m_{12} & m_{13} & m_{14} & m_{15} & m_{16} \\ m_{21} & m_{22} & m_{23} & m_{24} & m_{25} & m_{26} \\ m_{31} & m_{32} & m_{33} & m_{34} & m_{35} & m_{36} \\ m_{41} & m_{42} & m_{43} & m_{44} & 0 & 0 \\ m_{51} & m_{52} & m_{53} & 0 & m_{55} & 0 \\ m_{61} & m_{62} & m_{63} & 0 & 0 & m_{66} \end{bmatrix}, \tag{6}$$

$$C(q,\dot{q}) = \begin{bmatrix} c_{11} & c_{12} & c_{13} & c_{14} & c_{15} & c_{16} \\ c_{21} & c_{22} & c_{23} & c_{24} & c_{25} & c_{26} \\ c_{31} & c_{32} & c_{33} & c_{34} & c_{35} & c_{36} \\ c_{41} & c_{42} & c_{43} & 0 & c_{45} & c_{46} \\ c_{51} & c_{52} & c_{53} & c_{54} & c_{55} & c_{56} \\ c_{61} & c_{62} & c_{63} & c_{64} & c_{65} & c_{66} \end{bmatrix}, \tag{7}$$

$$g(q) = \begin{bmatrix} 0, g_2, g_3, g_4, g_5, g_6 \end{bmatrix}^T. \tag{8}$$

$$F(\dot{q}) = \begin{bmatrix} 0, 0, 0, 0, f_1, f_2 \end{bmatrix}^T, \tag{9}$$

Although the equation of motion (5) is quite complicated, it has several fundamental properties that can be exploited to facilitate the design of the controller. The two main properties that will be exploited in the next section are:

Property 1. The matrix

$$\frac{1}{2}\dot{M}(q) - C(q,\dot{q}),$$

is skew symmetric which means that

$$\zeta^T \left[\frac{1}{2}\dot{M}(q) - C(q,\dot{q})\right]\zeta = 0, \quad \zeta \in \mathbb{R}^6$$

Property 2. The gravity vector (8) can be obtained as the gradient of the crane potential energy (3), i.e., $g(q) = \frac{\partial U(q)}{\partial \dot{q}}$.

2.1 Control objective

The aim of the control is to move the crane to the desired position and to dampen the swing angles of the load as much as possible.

The control objective can be described mathematically as

$$\begin{aligned} \lim_{t\to\infty}[\alpha(t), \beta(t), \gamma(t), d(t), \theta_1(t), \theta_2(t)] = [\alpha_d, \beta_d, \gamma_d, d_d, 0, 0], \\ \lim_{t\to\infty}[\dot{\alpha}(t), \dot{\beta}(t), \dot{\gamma}(t), \dot{d}(t), \dot{\theta_1}(t), \dot{\theta_2}(t)] = [0, 0, 0, 0, 0, 0], \end{aligned} \tag{10}$$

where $\alpha_d, \beta_d, \gamma_d, d_d$ are the desired references for the actuated states.
In our development we will consider the following reasonable assumptions.

Assumption 1 *The payload swings satisfy the following inequality* $|\theta_{1,2}| < \frac{\pi}{2}$.

Assumption 2 *The cable length is always greater than zero to avoid singularity in the model (5):* $d(t) >, \forall t \geq 0$.

3 Control Design and Stability Analysis

The control strategy proposed in this paper consists of a nonlinear control law based on energy consideration. The corresponding stability and convergence analysis is demostrated by using the LaSalle's invariance principle.

In order to develop our control law, we started to considered the energy of system (2)-(3), wich is

$$E(t) = \frac{1}{2}\dot{q}^T M(q)\dot{q} + mgd(1 - C_{\theta_1}C_{\theta_2}), \tag{11}$$

where the first term is the kinetic energy of the crane, whereas the second term represents the payload potential energy. Based on (11), we can define the following Lyapunov function candidate:

$$\begin{aligned} V(t) = &\frac{1}{2}\dot{q}^T M(q)\dot{q} + mgd(1 - C_{\theta_1}C_{\theta_2}) \\ &+\frac{1}{2}k_{p\alpha}e_\alpha^2 + \frac{1}{2}k_{p\beta}e_\beta^2 + \frac{1}{2}k_{p\gamma}e_\gamma^2 + \frac{1}{2}k_{pd}e_d^2, \end{aligned} \tag{12}$$

where $e_\alpha, e_\beta, e_\gamma, e_d$ are the error signals defined as:

$$e_\alpha = \alpha_d - \alpha, \quad e_\beta = \beta_d - \beta, e_\gamma = \gamma_d - \gamma, \quad e_d = d_d - d. \tag{13}$$

Differentiating the equation (12) with respect to the time and using (5) we obtain

$$\begin{aligned} \dot{V}(t) = &\dot{\alpha}(u_1 - k_{p\alpha}e_\alpha) \\ &+\dot{\beta}(u_2 - k_{p\beta}e_\beta - gl_B C_\beta(m + \frac{1}{2}m_B m_J)) \\ &\dot{\gamma}(u_3 - k_{p\gamma}e_\gamma - gl_J C_\gamma(m + \frac{1}{2}m_J)) \\ &+\dot{d}(u_4 - k_{pd}e_d + mgC_{\theta_1}C_{\theta_2} + mg(1 - C_{\theta_1}C_{\theta_2})) \\ &-d_{\theta_1}C_{\theta_2}^2|\theta_1|\,\dot{\theta}_1^2 - d_{\theta_2}|\theta_1|\,\dot{\theta}_2^2. \end{aligned} \tag{14}$$

In order to cancel the gravitational terms and keep $\dot{V}(t)$ non-positive, the following controller is designed:

$$u_1 = k_{p\alpha}e_\alpha - k_{d\alpha}\dot{\alpha}, \tag{15}$$

$$u_2 = k_{p\beta}e_\beta - k_{d\beta}\dot{\beta} + gl_B C_\beta(m + \frac{1}{2}m_B m_J), \tag{16}$$

$$u_3 = k_{p\gamma}e_\gamma - k_{d\gamma}\dot{\gamma} + gl_J C_\gamma(m + \frac{1}{2}m_J), \tag{17}$$

$$u_4 = k_{pd}e_d - k_{dd}\dot{d} + mg, \tag{18}$$

where $k_{p\alpha}$, $k_{p\beta}$, $k_{p\gamma}$, k_{pd}, $k_{d\alpha}$, $k_{d\beta}$, $k_{d\gamma}$, $k_{dd} \in \mathbb{R}$ are positive control gains.
Substituting (15)-(18) into (14), one obtains

$$\begin{aligned} \dot{V}(t) = &-k_{d\alpha}\dot{\alpha}^2 - k_{d\beta}\dot{\beta}^2 - k_{d\gamma}\dot{\gamma}^2 \\ &-k_{dd}\dot{d}^2 - d_{\theta_1}C_{\theta_2}^2\dot{\theta}_1^2 - d_{\theta_2}\dot{\theta}_2^2 \leq 0, \end{aligned} \tag{19}$$

The following theorem describes the stability property of the crane using the proposed control law (15)-(18).

Theorem 1 *Consider the system (5)-(9). Under Assumptions 1-2, the controller (15)-(18) makes every equilibrium point (10) satisfying Assumptions 1-2, asymptotically stable.*

Proof: As already seen, the derivative of the Lyapunov function candidate (12) is (19) which is negative semidefinite.

At this point let Φ be defined as the set where $\dot{V}(t) = 0$, i.e.

$$\Phi = \{q, \dot{q} | \dot{V}(t) = 0\}. \tag{20}$$

Further, let Γ represent the largest invariant set in Φ where the Assumptions 1-2 are verified. Based on (19), it can be seen that Γ is the set such that:

$$\begin{aligned} &\dot{\alpha} = 0, \dot{\beta} = 0, \Rightarrow \ddot{\alpha} = 0, \ddot{\beta} = 0, \\ &\dot{\gamma} = 0, \dot{d} = 0, \Rightarrow \ddot{\gamma} = 0, \ddot{d} = 0, \\ &\dot{\theta_1} = 0, \dot{\theta_2} = 0, \Rightarrow \ddot{\theta_1} = 0, \ddot{\theta_2} = 0, \\ &\dot{e}_\alpha = 0, \dot{e}_\beta = 0, \Rightarrow e_\alpha = \phi_1, e_\beta = \phi_2, \\ &\dot{e}_\gamma = 0, \dot{e}_d = 0, \Rightarrow e_\gamma = \phi_3, e_d = \phi_4, \end{aligned} \tag{21}$$

where $\phi_{1,2,3,4}$ are constants to be determined.
Combining (21) with (15)-(18) and (5), we obtain the conditions:

$$\begin{aligned} k_{p\alpha}e_\alpha &= 0, \\ k_{p\beta}e_\beta &= 0, \\ k_{p\gamma}e_\gamma &= 0, \\ -gmcos\theta_1 cos\theta_2 &= -mg + k_{pd}e_d, \\ gmdcos\theta_2 sin\theta_1 &= 0, \\ gmdcos\theta_1 sin\theta_2 &= 0. \end{aligned} \tag{22}$$

From the first three equations of (22),we will have that

$$k_{p\alpha}e_\alpha = 0 \Rightarrow e_\alpha = 0 \Rightarrow \phi_1 = 0 \Rightarrow \alpha = \alpha_d, \tag{23}$$

$$k_{p\beta}e_\beta = 0 \Rightarrow e_\beta = 0 \Rightarrow \phi_2 = 0 \Rightarrow \beta = \beta_d, \tag{24}$$

$$k_{p\gamma}e_\gamma = 0 \Rightarrow e_\gamma = 0 \Rightarrow \phi_3 = 0 \Rightarrow \gamma = \gamma_d. \tag{25}$$

From the last two equations of (22), due to Assumption 2, one can be obtained that:

$$\begin{aligned} cos\theta_2 sin\theta_1 = 0, \\ cos\theta_1 sin\theta_2 = 0, \end{aligned} \tag{26}$$

The following conclusion can be achieved:

$$\theta_1 = \theta_2 = (k\pi) \vee \frac{(2k+1)}{2}\pi, \quad k \in \mathbb{Z}. \tag{27}$$

However, due to Assumption 1, the only acceptable solution will be:

$$\theta_1 = \theta_2 = 0. \tag{28}$$

By inserting the (28) in the forth equation of (22), one can conclude that:

$$k_{pd} e_d = 0 \Rightarrow e_d = 0 \Rightarrow \phi_4 = 0 \Rightarrow d = d_d, \tag{29}$$

□

Remark 1 *Other types of cranes such as overhead cranes, boom cranes, tower cranes etc, have similar dynamic characteristics to a knuckle cranes. Accordingly, the controller proposed in this paper may be adapted to all these underactuated system.*

4 Simulation Results

In order to demonstrate the effectiveness of the proposed strategy, in this section we simulate the knuckle crane in Fig. 1. The practical performances of the proposed control approach are compared with a linear quadratic regulator (LQR) obtained by linearization.The physical parameters are selected as follows: $m_b = 2kg$, $m_j = 3kg$, $m = 1k$, $l_b = 5m$, $l_j = 4m$.
The parameters for the control law (15)-(18) are the following:$k_{p\alpha} = 30, k_{p\beta} = 10, k_{p\gamma} = 10, k_{pd} = 1, k_{d\alpha} = 50, k_{d\beta} = 30, k_{d\gamma} = 50, k_{dd} = 10$.
For the LQR control approach, first, the crane dynamics is linearized around the equilibrium point, and then, the following weight matrices have been chosen to stabilize the plant: $Q = diag\{25, 400, 450, 200, 1, 1, 1, 1, 1, 1, 120, 120\}$ and $R = diag\{0.1, 0.1, 0.1, 1\}$.

As one can see in Figg. 3-4-5 both controllers successfully move the crane towards the desired angular positions. Although the LQR controller moves the first three degrees of the cranes (tower, boom, and jib angles) slightly faster than the method presented in this paper, one can notice that our method produces much less oscillations of the load (see Figg.7-8) and of the cable (see Fig. 6) , resulting in an overall faster and safer stabilization of the load. It is worth noting that in both methods, the input profiles and maximum values are almost similar. This values are well within the typical limits of the crane actuators.

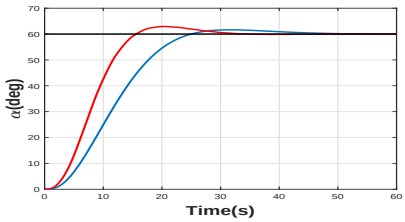

Figure 3. Tower angle α. Black line: Desired reference. Blue line: Nonlinear controller. Red line: LQR.

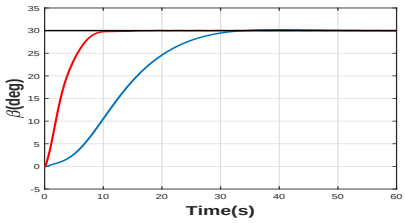

Figure 4. Boom angle β. Black line: Desired reference. Blue line: Nonlinear controller. Red line: LQR.

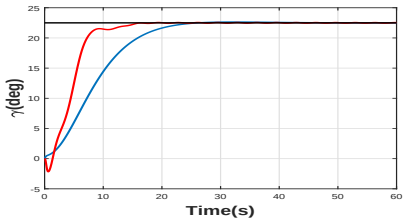

Figure 5. Jib angle γ. Black line: Desired reference. Blue line: Nonlinear controller. Red line: LQR.

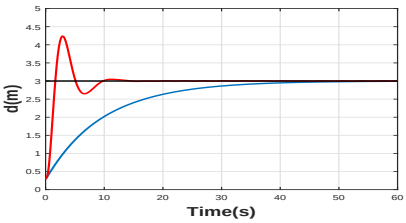

Figure 6. Rope length. Black line: Desired reference. Blue line: Nonlinear controller. Red line: LQR.

5 Conclusion

This paper proposed a nonlinear control scheme for the control of knuckle crane. The main contribution of this article is that for the first time a detailed mathematical model is shown where the complexity of this type of sys-

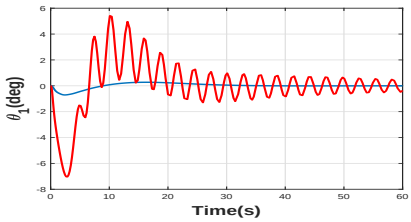

Figure 7. Payload angle θ_1. Blue line: Nonlinear controller. Red line: LQR.

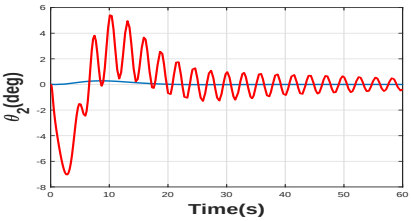

Figure 8. Payload angle θ_2 Blue line: Nonlinear controller. Red line: LQR.

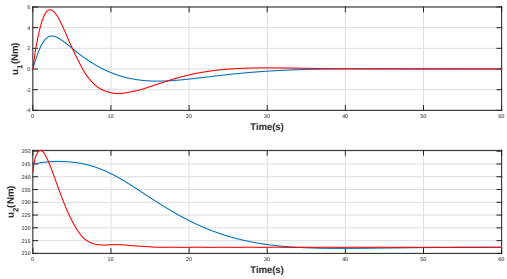

Figure 9. Control inputs u_1 & u_2. Blue line: Nonlinear controller. Red line: LQR.

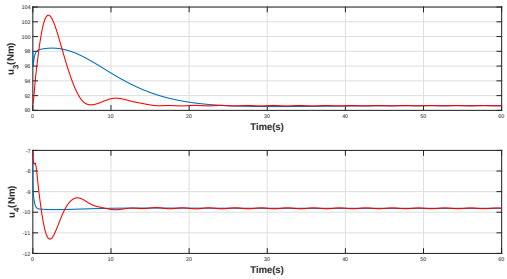

Figure 10. Control inputs u_3 & u_4. Blue line: Nonlinear controller. Red line: LQR.

tem emerges. Furthermore, the proposed control is based directly on the nonlinear system avoiding linearization. Despite the complexity of the model, the proposed control scheme is able to guide the crane towards a desired reference and ensuring that the non-actuated variables (i.e., θ_1 and θ_2) go to zero in a fast way.

Appendix

The nonzero entries of the system matrices $M(q)$, $C(q,\dot{q})$, $F(\dot{q})$ and $g(q)$ are define as follows:

$$m_{11} = I_{tot} + d^2m + A_1C_\beta^2 + A_2C_\gamma^2 + A_3C_\beta C_\gamma$$
$$+2A_4dC_\beta S_{\theta_2} + 2A_5dC_\gamma S_{\theta_2} - d^2mC_{\theta_1}^2C_{\theta_2}^2$$
$$m_{22} = A_1 + I_B \quad m_{33} = A_2 + I_J \quad m_{44} = m$$
$$m_{55} = dmC_{\theta_2}^2 \quad m_{66} = dm \quad m_{12} = m_{21} = A_4dC_{\theta_2}S_\beta S_{\theta_1}$$
$$m_{13} = m_{31} = A_5dC_{\theta_2}S_\gamma S_{\theta_1} \quad m_{14} = m_{41} = C_{\theta_2}S_{\theta_1}(A_4C_\beta + A_5C_\gamma)$$
$$m_{15} = m_{51} = dC_{\theta_1}C_{\theta_2}(A_4C_\beta + A_5C_\gamma + dmS_{\theta_2})$$
$$m_{16} = m_{61} = -dS_{\theta_1}(dm + A_4C_\beta S_{\theta_2} + A_5C_\gamma S_{\theta_2})$$
$$m_{23} = m_{32} = \frac{1}{2}(A_3C_{\beta-\gamma}), m_{24} = m_{42} = -A_4(S_\beta S_{\theta_2} + C_\beta C_{\theta_1}C_{\theta_2})$$
$$m_{25} = m_{52} = A_4dC_\beta C_{\theta_2}S_{\theta_1}$$
$$m_{26} = m_{62} = -A_4d(C_{\theta_2}S_\beta - C_\beta C_{\theta_1}S_{\theta_2})$$
$$m_{34} = m_{43} = -A_5(S_\gamma S_{\theta_2} + C_\gamma C_{\theta_1}C_{\theta_2})$$
$$m_{35} = m_{53} = A_5dC_\gamma C_{\theta_2}S_{\theta_1} \quad , m_{36} = m_{63} = -A_5d(C_{\theta_2}S_\gamma - C_\gamma C_{\theta_1}S_{\theta_2})$$
$$c_{11} = 2d\dot{d}m - A_2\dot{\gamma}S_{2\gamma} - A_1\dot{\beta}S_{2\beta} + 2A_4\dot{d}C_\beta S_{\theta_2}$$
$$+2A_5\dot{d}C_\gamma S_{\theta_2} - A_3\dot{\beta}C_\gamma S_\beta - A_3\dot{\gamma}C_\beta S_\gamma$$
$$-2d\dot{d}mC_{\theta_1}^2C_{\theta_2}^2 + 2A_4d\dot{\theta}_2C_\beta C_{\theta_2} + 2A_5d\dot{\theta}_2C_\gamma C_{\theta_2} - 2A_4d\dot{\beta}S_\beta S_{\theta_2}$$
$$-2A_5d\dot{\gamma}S_\gamma S_{\theta_2} + 2d^2\dot{\theta}_1mC_{\theta_1}C_{\theta_2}^2S_{\theta_1} + 2d^2\dot{\theta}_2mC_{\theta_1}^2C_{\theta_2}S_{\theta_2}$$
$$c_{12} = A_4\dot{d}C_{\theta_2}S_\beta S_{\theta_1} + A_d\dot{\beta}C_\beta C_{\theta_2}S_{\theta_1} + A_4d\dot{\theta}_1C_{\theta_1}C_{\theta_2}S_\beta - A_4d\dot{\theta}_2S_\beta S_{\theta_1}S_{\theta_2}$$
$$c_{13} = A_5\dot{d}C_{\theta_2}S_\gamma S_{\theta_1} + A_5d\dot{\gamma}C_\gamma C_{\theta_2}S_{\theta_1} +$$
$$A_5d\dot{\theta}_1C_{\theta_1}C_{\theta_2}S_\gamma - A_5d\dot{\theta}_2S_\gamma S_{\theta_1}S_{\theta_2}$$
$$c_{14} = \dot{\theta}_1C_{\theta_1}C_{\theta_2}(A_4C_\beta + A_5C_\gamma) - C_{\theta_2}S_{\theta_1}(A_4\dot{\beta}S_\beta + A_5\dot{\gamma}S_\gamma)$$
$$-\dot{\theta}_2S_{\theta_1}S_{\theta_2}(A_4C_\beta + A_5C_\gamma)$$
$$c_{15} = dC_{\theta_1}C_{\theta_2}(\dot{d}mS_{\theta_2} - A_4\dot{\beta}S_\beta - A_5d\dot{\gamma}S_\gamma + d\dot{\theta}_2mC_{\theta_2})$$
$$+\dot{d}C_{\theta_1}C_{\theta_2}(A_4C_\beta + A_5C_\gamma + dmS_{\theta_2}) - d\dot{\theta}_1C_{\theta_2}S_{\theta_1}(A_4C_\beta$$
$$+A_5C_\gamma + dmS_{\theta_2}) - d\dot{\theta}_2C_{\theta_1}S_{\theta_2}(A_4C_\beta + A_5C_\gamma + dmS_{\theta_2})$$
$$c_{16} = -dS_{\theta_1}(\dot{d}m + A_4\dot{\theta}_2C_\beta C_{\theta_2} + A_5\dot{\theta}_2C_\gamma C_{\theta_2} -$$
$$A_4d\dot{\beta}S_\beta S_{\theta_2} - A_5\dot{\gamma}S_\gamma S_{\theta_2}) - \dot{d}S_{\theta_1}(dm + A_4C_\beta S_{\theta_2} +$$
$$A_5C_\gamma S_{\theta_2}) - d\dot{\theta}_1C_{\theta_1}(dm + A_4C_\beta S_{\theta_2} + A_5C_\gamma S_{\theta_2})$$
$$c_{21} = \frac{1}{2}(\dot{\alpha}S_\beta(2A_1C_\beta + A_3C_\gamma + 2A_4dS_{\theta_2})) +$$
$$\frac{1}{2}(3A_4\dot{d}C_{\theta_2}S_\beta S_{\theta_1}) + \frac{1}{2}(A_4d\dot{\beta}C_\beta C_{\theta_2}S_{\theta_1}) +$$
$$\frac{1}{2}(3A_4d\dot{\theta}_1C_{\theta_1}C_{\theta_2}S_\beta) - \frac{1}{2}(3A_4d\dot{\theta}_2S_\beta S_{\theta_1}S_{\theta_2})$$

$$c_{22} = \frac{1}{4}(A_3\dot{\gamma}S_{\beta-\gamma}) + \frac{1}{2}(A_4\dot{d}(C_\beta S_{\theta_2} - C_{\theta_1}C_{\theta_2}S_\beta)) + \frac{1}{2}(A_4 d\dot{\theta}_2(C_\beta C_{\theta_2} + C_{\theta_1}S_\beta S_{\theta_2})) - \frac{1}{2}(A_4 d\dot{\alpha}C_\beta C_{\theta_2}S_\beta) + \frac{1}{2}(A_4 d\dot{\theta}_1 C_{\theta_2}S_\beta S_\beta), \quad c_{23} = -\frac{1}{4}(A_3 S_{\beta-\gamma})(\dot{\beta} - 2\dot{\gamma}))$$

$$c_{24} = \frac{1}{2}(A_4\dot{\beta}C_{\theta_1}C_{\theta_2}S_\beta) - A_4\dot{\theta}_2 C_{\theta_2}S_\beta - \frac{1}{2}(A_4\dot{\beta}C_\beta S_{\theta_2}) + A_4\dot{\theta}_1 C_\beta C_{\theta_2}S_\beta + A_4\dot{\theta}_2 C_\beta C_{\theta_1}S_{\theta_2} + \frac{1}{2}(A_4\dot{\alpha}C_{\theta_2}S_\beta S_\beta)$$

$$c_{25} = A_4\dot{d}C_\beta C_{\theta_2}S_\beta + \frac{1}{2}(A_4 d\dot{\alpha}C_{\theta_1}C_{\theta_2}S_\beta) + A_4 d\dot{\theta}_1 C_\beta C_{\theta_1}C_{\theta_2} - \frac{1}{2}(A_4 d\dot{\beta}C_{\theta_2}S_\beta S_\beta) - A_4 d\dot{\theta}_2 C_\beta S_\beta S_{\theta_2}$$

$$c_{26} = A_4 d\dot{\theta}_2 S_\beta S_{\theta_2} - \frac{1}{2}(A_4 d\dot{\beta}C_\beta C_{\theta_2}) - A_4\dot{d}C_{\theta_2}S_\beta + A_4\dot{d}C_\beta C_{\theta_1}S_{\theta_2} - \frac{1}{2}(A_4 d\dot{\beta}C_{\theta_1}S_\beta S_{\theta_2}) - A_4 d\dot{\theta}_1 C_\beta S_\beta S_{\theta_2} - \frac{1}{2}(A_4 d\dot{\alpha}S_\beta S_\beta S_{\theta_2}) + A_4 d\dot{\theta}_2 C_\beta C_{\theta_1}C_{\theta_2}$$

$$c_{31} = \frac{1}{2}(\dot{\alpha}S_\gamma(2A_2C_\gamma + A_3C_\beta + 2A_5 dS_{\theta_2})) + \frac{1}{2}(3A_5\dot{d}C_{\theta_2}S_\gamma S_{\theta_1}) + \frac{1}{2}(A_5 d\dot{\gamma}C_\gamma C_{\theta_2}S_{\theta_1}) + \frac{1}{2}(3A_5 d\dot{\theta}_1 C_{\theta_1}C_{\theta_2}S_\gamma) - \frac{1}{2}(3A_5 d\dot{\theta}_2 S_\gamma S_{\theta_1}S_{\theta_2})$$

$$c_{32} = -\frac{1}{4}(A_3 S_{\beta-\gamma})(2\dot{\beta} - \dot{\gamma}))$$

$$c_{33} = \frac{1}{2}(A_5\dot{d}(C_\gamma S_{\theta_2} - C_{\theta_1}C_{\theta_2}S_\gamma)) - \frac{1}{4}(A_3\dot{\beta}S_{\beta-\gamma}) + \frac{1}{2}(A_5 d\dot{\theta}_2(C_\gamma C_{\theta_2} + C_{\theta_1}S_\gamma S_{\theta_2})) - \frac{1}{2}(A_5 d\dot{\alpha}C_\gamma C_{\theta_2}S_{\theta_1}) + \frac{1}{2}(A_5 d\dot{\theta}_1 C_{\theta_2}S_\gamma S_{\theta_1})$$

$$c_{34} = \frac{1}{2}(A_5\dot{\gamma}C_{\theta_1}C_{\theta_2}S_\gamma) - A_5\dot{\theta}_2 C_{\theta_2}S_\gamma - \frac{1}{2}(A_5\dot{\gamma}C_\gamma S_{\theta_2}) + A_5\dot{\theta}_1 C_\gamma C_{\theta_2}S_{\theta_1} + A_5\dot{\theta}_2 C_\gamma C_{\theta_1}S_{\theta_2} + \frac{1}{2}(A_5\dot{\alpha}C_{\theta_2}S_\gamma S_{\theta_1})$$

$$c_{35} = A_5 dd C_\gamma C_{\theta_2}S_{\theta_1} + \frac{1}{2}(A_5 d\dot{\alpha}C_{\theta_1}C_{\theta_2}S_\gamma) - \frac{1}{2}(A_5 d\dot{\gamma}C_{\theta_2}S_\gamma S_{\theta_1}) - A_5 d\dot{\theta}_2 C_\gamma S_{\theta_1}S_{\theta_2} + A_5 d\dot{\theta}_1 C_\gamma C_{\theta_1}C_{\theta_2}$$

$$c_{36} = A_5 d\dot{\theta}_2 S_\gamma S_{\theta_2} - \frac{1}{2}(A_5 d\dot{\gamma}C_\gamma C_{\theta_2}) - A_5\dot{d}C_{\theta_2}S_\gamma + A_5\dot{d}C_\gamma C_{\theta_1}S_{\theta_2} - \frac{1}{2}(A_5 d\dot{\gamma}C_{\theta_1}S_\gamma S_{\theta_2}) - A_5 d\dot{\theta}_1 C_\gamma S_{\theta_1}S_{\theta_2} - \frac{1}{2}(A_5 d\dot{\alpha}S_\gamma S_{\theta_1}S_{\theta_2}) + A_5 d\dot{\theta}_2 C_\gamma C_{\theta_1}C_{\theta_2}$$

$$c_{41} = d\dot{\theta}_2 mS_{\theta_1} - d\dot{\alpha}m - A_4\dot{\alpha}C_\beta S_{\theta_2} - A_5\dot{\alpha}C_\gamma S_{\theta_2} + d\dot{\alpha}mC_{\theta_1}^2C_{\theta_2}^2 + \frac{1}{2}(A_4\dot{\theta}_1 C_\beta C_{\theta_1}C_{\theta_2}) + \frac{1}{2}(A_5\dot{\theta}_1 C_\gamma C_{\theta_1}C_{\theta_2}) - \frac{1}{2}(3A_4\dot{\beta}C_{\theta_2}S_\beta S_{\theta_1}) - \frac{1}{2}(A_4\dot{\theta}_2 C_\beta S_{\theta_1}S_{\theta_2}) - \frac{1}{2}(3A_5\dot{\gamma}C_{\theta_2}S_\gamma S_{\theta_1}) - \frac{1}{2}(A_5\dot{\theta}_2 C_\gamma S_{\theta_1}S_{\theta_2}) - d\dot{\theta}_1 mC_{\theta_1}C_{\theta_2}S_{\theta_2}$$

$$c_{42} = A_4\dot{\beta}C_{\theta_1}C_{\theta_2}S_\beta - (A_4\dot{\theta}_2 C_{\theta_2}S_\beta)/2 - A_4\dot{\beta}C_\beta S_{\theta_2} + \frac{1}{2}(A_4\dot{\theta}_1 C_\beta C_{\theta_2}S_{\theta_1}) + \frac{1}{2}(A_4\dot{\theta}_2 C_\beta C_{\theta_1}S_{\theta_2}) - \frac{1}{2}(A_4\dot{\alpha}C_{\theta_2}S_\beta S_{\theta_2})$$

$$c_{43} = A_5\dot{\gamma}C_{\theta_1}C_{\theta_2}S_\gamma - \frac{1}{2}(A_5\dot{\theta}_2 C_{\theta_2}S_\gamma) - A_5\dot{\gamma}C_\gamma S_{\theta_2} + \frac{1}{2}(A_5\dot{\theta}_1 C_\gamma C_{\theta_2}S_{\theta_1}) + \frac{1}{2}(A_5\dot{\theta}_2 C_\gamma C_{\theta_1}S_{\theta_2}) - \frac{1}{2}(A_5\dot{\alpha}C_{\theta_2}S_\gamma S_{\theta_1})$$

$$c_{45} = d\dot{\theta}_1 m(S_{\theta_2}^2 - 1) - \frac{1}{2}(\dot{\alpha}C_{\theta_1}C_{\theta_2}(A_4C_\beta + A_5C_\gamma + 2dmS_{\theta_2})) - \frac{1}{2}(A_4\dot{\beta}C_\beta C_{\theta_2}S_{\theta_1}) - \frac{1}{2}(A_5\dot{\gamma}C_\gamma C_{\theta_2}S_{\theta_1})$$

$$c_{46} = \frac{1}{2}(A_4\dot{\beta}(C_{\theta_2}S_\beta - C_\beta C_{\theta_1}S_{\theta_2})) + \frac{1}{2}(A_5\dot{\gamma}(C_{\theta_2}S_\gamma - C_\gamma C_{\theta_1}S_{\theta_2})) - d\dot{\theta}_2 m + \frac{1}{2}(\dot{\alpha}S_{\theta_1}(2dm + A_4C_\beta S_{\theta_2} + A_5C_\gamma S_{\theta_2}))$$

$$c_{51} = 2d^2\dot{\theta}_2 mC_{\theta_1}C_{\theta_2}^2 - \frac{1}{2}(d^2\dot{\theta}_2 mC_{\theta_1}) + \frac{1}{2}(A_4\dot{d}C_\beta C_{\theta_1}C_{\theta_2}) + \frac{1}{2}(A_5\dot{d}C_\gamma C_{\theta_1}C_{\theta_2}) - \frac{1}{2}(3A_4 d\dot{\beta}C_{\theta_1}C_{\theta_2}S_\beta) - \frac{1}{2}(A_4 d\dot{\theta}_1 C_\beta C_{\theta_2}S_{\theta_1}) - \frac{1}{2}(A_4 d\dot{\theta}_2 C_\beta C_{\theta_1}S_{\theta_2}) - \frac{1}{2}(3A_5 d\dot{\gamma}C_{\theta_1}C_{\theta_2}S_\gamma) - \frac{1}{2}(A_5 d\dot{\theta}_1 C_\gamma C_{\theta_2}S_{\theta_1}) - \frac{1}{2}(A_5 d\dot{\theta}_2 C_\gamma C_{\theta_1}S_{\theta_2}) + 2d\dot{d}mC_{\theta_1}C_{\theta_2}S_{\theta_2} - \frac{1}{2}(d^2\dot{\theta}_1 mC_{\theta_2}S_{\theta_1}S_{\theta_2}) - d^2\dot{\alpha}mC_{\theta_1}C_{\theta_2}^2S_{\theta_1}$$

$$c_{52} = \frac{1}{2}(A_4\dot{d}C_\beta C_{\theta_2}S_{\theta_1}) - \frac{1}{2}(A_4 d\dot{\alpha}C_{\theta_1}C_{\theta_2}S_\beta) - A_4 d\dot{\beta}C_{\theta_2}S_\beta S_{\theta_1} - \frac{1}{2}(A_4 d\dot{\theta}_2 C_\beta S_{\theta_1}S_{\theta_2}) + \frac{1}{2}(A_4 d\dot{\theta}_1 C_\beta C_{\theta_1}C_{\theta_2})$$

$$c_{53} = \frac{1}{2}(A_5\dot{d}C_\gamma C_{\theta_2}S_{\theta_1}) - \frac{1}{2}(A_5 d\dot{\alpha}C_{\theta_1}C_{\theta_2}S_\gamma) - A_5 d\dot{\gamma}C_{\theta_2}S_\gamma S_{\theta_1} - \frac{1}{2}(A_5 d\dot{\theta}_2 C_\gamma S_{\theta_1}S_{\theta_2}) + \frac{1}{2}(A_5 d\dot{\theta}_1 C_\gamma C_{\theta_1}C_{\theta_2})$$

$$c_{54} = -\frac{1}{2}(\dot{\alpha}C_{\theta_1}C_{\theta_2}(A_4C_\beta + A_5C_\gamma)) - \frac{1}{2}(A_4\dot{\beta}C_\beta C_{\theta_2}S_{\theta_1}) - \frac{1}{2}(A_5\dot{\gamma}C_\gamma C_{\theta_2}S_{\theta_1})$$

$$c_{55} = \frac{1}{2}(d\dot{\alpha}C_{\theta_2}S_{\theta_1}(A_4C_\beta + A_5C_\gamma + dmS_{\theta_2})) - \frac{1}{2}(A_4 d\dot{\beta}C_\beta C_{\theta_1}C_{\theta_2}) - \frac{1}{2}(A_5 d\dot{\gamma}C_\gamma C_{\theta_1}C_{\theta_2})$$

$$c_{56} = \frac{1}{2}(d\dot{\alpha}C_{\theta_1}(dm + A_4C_\beta S_{\theta_2} + A_5C_\gamma S_{\theta_2})) + \frac{1}{2}(A_4 d\dot{\beta}C_\beta S_{\theta_1}S_{\theta_2}) + \frac{1}{2}(A_5 d\dot{\gamma}C_\gamma S_{\theta_1}S_{\theta_2})$$

$$c_{61} = \frac{1}{2}(3A_4 d\dot{\beta}S_\beta S_{\theta_1}S_{\theta_2}) - \frac{1}{2}(d^2\dot{\theta}_1 mC_{\theta_1}) - A_4 d\dot{\alpha}C_\beta C_{\theta_2} - A_5 d\dot{\alpha}C_\gamma C_{\theta_2} - \frac{1}{2}(A_4 d\dot{d}C_\beta S_{\theta_1}S_{\theta_2}) - \frac{1}{2}(A_5 d\dot{d}C_\gamma S_{\theta_1}S_{\theta_2}) - \frac{1}{2}(A_4 d\dot{\theta}_1 C_\beta C_{\theta_1}S_{\theta_2}) - \frac{1}{2}(A_4 d\dot{\theta}_2 C_\beta C_{\theta_2}S_{\theta_1}) - \frac{1}{2}(A_5 d\dot{\theta}_1 C_\gamma C_{\theta_1}S_{\theta_2}) - \frac{1}{2}(A_5 d\dot{\theta}_2 C_\gamma C_{\theta_2}S_{\theta_1}) - 2d\dot{d}mS_{\theta_1} + \frac{1}{2}(3A_5 d\dot{\gamma}S_\gamma S_{\theta_1}S_{\theta_2})$$

$$c_{62} = \frac{1}{2}(A_4 d\dot{\theta}_2 S_\beta S_{\theta_2}) - A_4 d\dot{\beta}C_\beta C_{\theta_2} - \frac{1}{2}(A_4 d\dot{d}C_{\theta_2}S_\beta) + \frac{1}{2}(A_4 d\dot{d}C_\beta C_{\theta_1}S_{\theta_2}) - \frac{1}{2}(A_4 d\dot{\theta}_1 C_\beta S_{\theta_1}S_{\theta_2}) + \frac{1}{2}(A_4 d\dot{\alpha}S_\beta S_{\theta_1}S_{\theta_2}) + \frac{1}{2}(A_4 d\dot{\theta}_2 C_\beta C_{\theta_1}C_{\theta_2})$$

$$c_{63} = \frac{1}{2}(A_5 d\dot{\theta}_2 S_\gamma S_{\theta_2}) - A_5 d\dot{\gamma} C_\gamma C_{\theta_2} - \frac{1}{2}(A_5 d\dot{d} C_{\theta_2} S_\gamma) + \frac{1}{2}(A_5 d\dot{d} C_\gamma C_{\theta_1} S_{\theta_2}) - A_5 d\dot{\gamma} C_{\theta_1} S_\gamma S_{\theta_2} + \frac{1}{2}(A_5 d\dot{\alpha} S_\gamma S_{\theta_1} S_{\theta_2}) + \frac{1}{2}(A_5 d\dot{\theta}_2 C_\gamma C_{\theta_1} C_{\theta_2})$$

$$c_{64} = \frac{1}{2}(A_4 \dot{\beta}(C_{\theta_2} S_\beta - C_\beta C_{\theta_1} S_{\theta_2})) + \frac{1}{2}(A_5 \dot{\gamma}(C_{\theta_2} S_\gamma - C_\gamma C_{\theta_1} S_{\theta_2})) + \frac{1}{2}(\dot{\alpha} S_{\theta_1} S_{\theta_2}(A_4 C_\beta + A_5 C_\gamma))$$

$$c_{65} = \frac{1}{2}(d^2 \dot{\alpha} m C_{\theta_1}) - d^2 \dot{\alpha} m C_{\theta_1} C_{\theta_2}^2 + \frac{1}{2}(A_4 d\dot{\alpha} C_\beta C_{\theta_1} S_{\theta_2}) + \frac{1}{2}(A_4 d\dot{\beta} C_\beta S_{\theta_1} S_{\theta_2}) + \frac{1}{2}(A_5 d\dot{\gamma} C_\gamma S_{\theta_1} S_{\theta_2})$$

$$c_{66} = \frac{1}{2}(d\dot{\alpha} C_{\theta_2} S_{\theta_1}(A_4 C_\beta + A_5 C_\gamma)) - \frac{1}{2}(A_5 d\dot{\gamma}(S_\gamma S_{\theta_2} + C_\gamma C_{\theta_1} C_{\theta_2})) - \frac{1}{2}(A_4 d\dot{\beta}(S_\beta S_{\theta_2} + C_\beta C_{\theta_1} C_{\theta_2}))$$

$$g_2 = \frac{1}{2} g l_B cos\beta(2m + m_B + 2m_J),$$

$$g_3 = \frac{1}{2} g l_J cos\gamma(2m + m_J), \quad g_4 = -gmcos\theta_1 cos\theta_2,$$

$$g_5 = gmdcos\theta_2 sin\theta_1, \quad g_6 = gmdcos\theta_1 sin\theta_2$$

$$f_1 = d_{\theta_1} C_{\theta_2}^2 |\theta_1| \dot{\theta}_1, \qquad f_2 = d_{\theta_2} \theta_2 | \dot{\theta}_2$$

where the following auxiliary variables are defined: $A_1 = l_B^2 m + (l_B^2 m_B)/4 + l_B^2 m_J$, $A_2 = l_J^2 m + (l_J^2 m_J)/4$, $A_3 = 2 l_B l_J m + l_B l_J m_J$, $A_4 = 2 l_B m$, $A_5 = 2 l_J m$

References

[1] Keum-Shik Hong and Umer Shah. *Dynamics and Control of Industrial Cranes*. 01 2019. ISBN 978-981-13-5770-1. doi:10.1007/978-981-13-5770-1.

[2] M. Ambrosino, M. Berneman, G. Carbone, A. Dawans, and E. Garone. Modeling and control of a 5-dof boom crane. In *ISARC. Proceedings of the International Symposium on Automation and Robotics in Construction*, 2020.

[3] Javier Moreno-Valenzuela and Carlos Aguilar-Avelar. *Motion control of underactuated mechanical systems*. Springer, 2018.

[4] Liyana Ramli, Z. Mohamed, Auwalu M. Abdullahi, H.I. Jaafar, and Izzuddin M. Lazim. Control strategies for crane systems: A comprehensive review. *Mechanical Systems and Signal Processing*, 95:1 – 23, 2017. ISSN 0888-3270. doi:https://doi.org/10.1016/j.ymssp.2017.03.015.

[5] Joshua Vaughan, Jieun Yoo, Nathan Knight, and William Singhose. Multi-input shaping control for multi-hoist cranes. pages 3449–3454, 2013.

[6] Daichi Fujioka and William Singhose. Input-shaped model reference control of a nonlinear time-varying double-pendulum crane. pages 1–6, 2015.

[7] Huimin Ouyang, Guangming Zhang, Lei Mei, Xin Deng, and Deming Wang. Load vibration reduction in rotary cranes using robust two-degree-of-freedom control approach. *Advances in Mechanical Engineering*, 8(3):1687814016641819, 2016. doi:10.1177/1687814016641819.

[8] M. Ambrosino, A. Dawans, and E. Garone. Constraint control of a boom crane system. In *ISARC. Proceedings of the International Symposium on Automation and Robotics in Construction*, 2020.

[9] E. Arnold, O. Sawodny, J. Neupert, and K. Schneider. Anti-sway system for boom cranes based on a model predictive control approach. 3:1533–1538 Vol. 3, 2005.

[10] Petter Krus and Jan-Ove Palmberg. Vector control of a hydraulic crane. 09 1992. doi:10.4271/921659.

[11] Henrik Pedersen, B Nielsen, Torben Andersen, Michael Hansen, and P Pedersen. Resolved motion control of a hydraulic loader crane. pages 145–154, 01 2003.

[12] Yingguang Chu, Filippo Sanfilippo, Vilmar Æsøy, and Houxiang Zhang. An effective heave compensation and anti-sway control approach for offshore hydraulic crane operations. *2014 IEEE International Conference on Mechatronics and Automation, IEEE ICMA 2014*, 08 2014. doi:10.1109/ICMA.2014.6885884.

[13] I. Fantoni, R. Lozano, and Sc Sinha. Non-linear control of underactuated mechanical systems. *Applied Mechanics Reviews - APPL MECH REV*, 55, 01 2002. doi:10.1115/1.1483350.

[14] Menghua Zhang, Xin Ma, Xuewen Rong, Rui Song, Xincheng Tian, and Yibin Li. An enhanced coupling nonlinear tracking controller for underactuated 3d overhead crane systems: Enhanced coupling nonlinear tracking controller. *Asian Journal of Control*, 20, 10 2017. doi:10.1002/asjc.1683.

Bridge Inspection with Aerial Robots and Computer Vision: A Japanese National Initiative

Jacob J. Lin[a], Amir Ibrahim[a], Shubham Sarwade[a], Mani Golparvar-Fard[a]
Yasushi Nitta[b], Hirokuni Moirkawa[b], and Yoshihiko Fukuchi[c]

[a] University of Illinois at Urbana-Champaign, USA
[b] Ministry of Land, Transport, Infrastructure and Tourism, Japan
[c] Autodesk Inc., USA

jlin67@illinois.edu

Abstract -

Fast and accurate inspection of elevated structures is imperative for sustaining the increasing traffic flow o n deteriorating bridges. Despsite their importance, today's inspection processes still require dedicated equipment, impact traffic flow, a nd e xpose i nspection p ersonnel t o s afety concerns. The advent of Unmanned Aerial Vehicles (UAVs) and the ability to position a camera close to elevated highway structures presents an opportunity to perform inspections quickly, safely and effectively. Towards this goal, we present an end-to-end system for robotic bridge inspection. Our system is structured around integrated methods to (a) create UAV flight m issions; (b) e valuate a ccuracy a nd completeness of data collection plans; (c) generate 3D models of the structures of interest; (d) detect surface distresses in 3D; and (e) generate inspection reports in compliance with the requirements of highway agencies. We present results on validating each algorithm and the system as a whole. We also share lessons learned from an owner's perspective on deploying this system for bridge inspection in Japan particularly around procedures for documenting, communicating, and following up on bridge inspectors' recommendations.

Keywords -

Bridge Inspection; Deep Learning; Structure from Motion; Aerial Robots; Computer Vision

1 Introduction

The discovery of fractures in steel members of Kisogawa Ohashi Bridge and Honjo Ohashi Bridge in 2007, yet again raised alarms about the deterioration and fragile state of the infrastructure in Japan. By March 2019, deficient or functionally obsolete bridges constitute 9.6% of all the 700,000 road bridges in Japan [1]. Japan's geography creates additional risks associated with natural disasters. Thus, evaluating as-is conditions of Japan's bridges and infrastructure assets is more important than many other places around the world.

Today's bridge inspection practices are expensive and can be disruptive to ongoing traffic. Onsite documentations are also time-consuming and assessments can be inconsistent. This means additional data collection may be necessary in many cases, while resource allocation is always challenging. The advent of agile aerial platforms with the ability to carry digital cameras, along with a greater awareness of the technology has created an cost-effective alternative to conduct bridge inspection in a quick, safe and effective manner. Application of aerial platforms resolves issues of access and traffic disruptions. Also, cloud-based analysis lowers the need for onsite engineer visits, reducing cost associated with inspection. As such, the Ministry of Land, Infrastructure, Transport and Tourism (MLIT) in Japan launched an initiative in 2015 with the aim of leveraging advanced robots and artificial intelligence technologies to improve productivity in construction and infrastructure inspection tasks.

Because of the MLIT initiative as well as similar ones in the United States, a large body of work has emerged from the industry and academia which focuses on computer vision and visualization methods to process, analyze and share inspected drone data. Much of these efforts has focused on improving one step in the process, rarely offering an insight or recommendation on how various techniques can be applied in an integrated manner to streamline the data collection, analytics, and reporting in an end-to-end fashion. While there are promising computer vision methods such as 3D reconstruction, image classification, object detection and semantic segmentation that can been applied to bridge inspection processes, yet their adaptability as part of an end-to-end system has not been investigated.

To address the existing gaps in knowledge, we present an integrated end-to-end system for robotic bridge inspection consisting of five integrated methods: (a) creation of flight missions for data collection; (b) evaluation of flight missions based on requirements of inspection and visual quality of collected data; (c) 3D reconstruction of elevated structures; (d) automated detection and localization of surface distresses in 3D; and (e) report generation in compliance with owner requirements. We validate each underlying algorithm and the end-to-end system as a whole. We also share best practices on documentation, communication and following up on bridge inspection recommendations based on deploying our system on 30 bridge inspection projects in Japan and the United States.

2 Related Work

A large body of work in the literature has focused on robotic infrastructure inspection. In this section, we discuss the most recent methods and their gaps in knowledge:

2.1 Model-driven Data Capture using UAVs

Visual data collection with the UAVs has many applications including surveying, inspections, safety and progress monitoring. Based on whether models are used as *a priori*, these methods can be categorized into two classes: (1) Conventional methods that focus on ensuring minimum overlap between collected images to generate complete 3D point clouds; and (b) model-driven methods which use 3D CAD or BIM as *a priori* to simulate and evaluate the 3D visual coverage of structures and in turn reduce safety risks associated with the UAVs. Flight plans with waypoints sampled at a safe offset distance from the structure [2] and the utilization of 4D BIM for path planning in construction monitoring use-cases [3] are examples of these model-driven approaches. Our method builds on these model-driven path planning methods, but it also enables verifying and planning for requirements such as preserving line-of-sight to UAVs, or orthogonality of camera viewpoints against the structure during data capture.

2.2 Image-based 3D reconstruction

Structure from Motion (SfM) and Simultaneous Localization and Mapping (SLAM) algorithms have been widely used as 3D reconstruction techniques to generate high fidelity 3D point cloud and mesh models using images or videos collected with aerial robots. These techniques allow for better organization of collected data by identifying locations and viewpoints of images relative to 3D models. While these techniques have matured over the past decade, nevertheless they can still result in *incomplete* and *inaccurate* models. To address these issues, recent efforts such as [4] propose simulators or empirical metrics to examine quality of data collection and their impact on 3D reconstruction. Nonetheless, these studies have been validated in contexts which are not relevant to data collected from varying heights and viewpoints relative to elevated structures. Tools that can generate elevation or under-deck orthoviews are also required for inspection reports, however current 3D reconstruction pipelines do not produce such deliverables.

2.3 Metrics for visual quality assurance

The percent overlap between collected images, the resolution of bridge elements in each image, and the quality of 3D reconstruction are three key parameters that influence the accuracy of automated condition assessment system. Model-driven flight paths have been deployed to improve the quality of collected visual data [2] but these methods lack quality assurance capabilities. [5, 6] show parameters such as proximity of camera to the bridge elements and orientations of the collected images, which can impact accuracy of defect detection and appearance-based classification of structural components. To evaluate accuracy of 3D reconstruction in simulation environments, metrics such as (a) visibility per element and (b) redundancy in visibility have been introduced by [7]. Metrics such as Ground Sampling Distance (GSD) have also been employed to guarantee resolution of 3D reconstruction before image capture is conducted [8]. In this study, we build upon previously studied visual quality assurance metrics and investigate new metrics focusing on defect detection such as perpendicularity of image viewpoints while achieving a specific GSD per inspection target.

2.4 Defect Recognition, Severity Assessment and Mapping

Computer vision methods can be used on site images to detect and classify surface defects such as crack, spalling, exposed rebar, efflorescence and corrosion. Particularly, deep learning-based approaches have shown promising results in the recent years. Deep Convolutional Neural Network (CNN) architectures such as VGG, AlexNet, ResNet and MetaQNN for single and multi-class defect classification [8] have resulted in exceptional results (e.g., VGG architecture achieved 70.61% for multi-class defect classification) but these method do not predict defect regions and at best, they only focus on a Single-class defect detection. [9, 10, 11, 12] in among the few works that has investigated feasibility of an end-to-end framework for bridge inspection, however no previous work has considered multi-class defect detection and localization within a 3D context. Localizing defect in 2D and 3D is essential for assessing seriousness of defects and to prioritize maintenance operations.

2.5 Virtual inspection and report generation

There is plenty of work in the literature on generating 3D point clouds of bridges and detection of multiple type of defects; nevertheless there are still many components missing to enable an end-to-end robotic inspection; i.e., (a) Comparative views of point clouds and images over time, (b) interactive orthoviews generated automatically, and (c) ability to view images overlaid on 3D point clouds through an interactive interface, similar to ones implemented for project controls [13], are much needed. 3D measurements and annotations could also be enabled through a visual interface for defect severity assessment purposes. These tools and systems can automate and significantly improve how owner-compliance reports are generated. The work in

[9, 14] demonstrate methods to generate reports utilizing BIM of bridges. However, creating BIM from point clouds is not a trivial task and is often cost-prohibitive for large number of bridges in need for inspection.

In the following, we present an end-to-end solution that addresses these gaps in knowledge. Our solution has been deployed by the MLIT in Japan and other bridge owners and operators in the United States.

3 Method

We propose a new end-to-end system for robotic inspection (see Figure 1). Each step in our system's is discussed in the following sections:

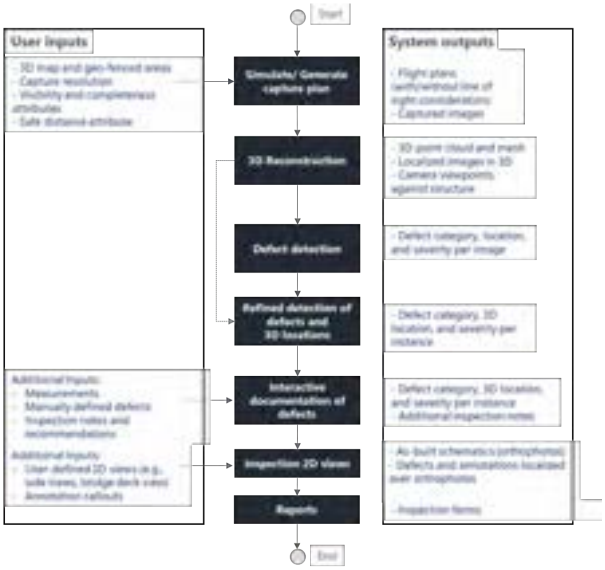

Figure 1. A new end-to-end system of bridge inspection, with relevant user inputs and expected outputs.

3.1 Model-driven Visual Data Inspection

Automatic visual data collection is the first step in our end-to-end bridge inspection system. To achieve this, we developed a web-based virtual environment with client-server architecture for fast and easy access to aerial data collection missions and automatic 3D flight plans generation. The user sets the inspection region with a 2D satellite map and specified the data collection parameters to generate the 3D flight p lan. The p arameters c onsidered the requirements of the data collection, such as altitudes of bridge deck underside and topside, waypoints offset distance from the structure, drone and camera settings, the field of view to keep line-of-sight during flight execution and the required overlap between image frames. The generated flight p lan i s s liced i nto m issions t o a ccount for line-of-sight requirements and the drone's battery life.

The 3D virtual environment is used to render the flight mission alongside BIM/reality models of the bridge for evaluation and communication. This allows adjustments to the flight mission parameters for improving visual coverage and safety. Execution is supported via an iOS mobile application adapted from a previous study [3].

3.2 Quality Evaluation and Feedback on Data Collection Plan

We developed four metrics to define the visual quality of bridge inspection data with regards to the requirements of bridge inspection data: (1) visual coverage completeness of inspection region; (2) redundancy of observations of bridge elements across images needed for accurate 3D reconstruction; (3) target pixel resolution or GSD needed for precise defect detection; and (4) canonical orientation of camera against bridge elements for minimal distortion and required pixel resolution. Redundancy in observations is used for cross-referencing detection across images, which improves detection reliability.

A priori 3D model needs to be generated to perform the flight mission simulation. Without previous capture, we perform a 3D reconstruction from synthetic images extracted from 3D terrain map platforms to create *a priori* model. Using this model, the simulation can estimate: (1) the visibility of each element in each data frame; (2) redundant visibility of elements across all data frames; (3) the average pixel resolution of each element in every frame; and (4) the relative orientation of each element to each frame. The elements are rendered in the virtual environment by a simulated camera with the parameters of the actual camera used for data collection. In the evaluation of visibility and redundant visibility of elements, an element ID color-coding scheme is implemented, and an element's visibility is determined by whether the number of back-projected pixels of the corresponding color exceeds a user-defined threshold in a frame.

A similar approach is applied to estimate pixel resolution of an element in each frame with color-coding based on the depth of the element. The relative orientation of each element to each data frame is estimated in the final simulation. We utilize the surface normal shader to render elements' surface normals as RGB colors. The results of the simulation are provided to the user visually for flight plan adjustment.

3.3 Image-based 3D modeling

We developed different 3D reconstruction methods to address the issues that appear more frequently for bridges. These issues include incompleteness, misregistration, and curvature (drift). The 3D reconstruction pipeline follows an extension of previous studies [15], which include Structure from Motion (SfM) algorithm, patch-based multi-

view reconstruction and mesh modeling steps. However, point cloud misregistration often occurs in bridges due to the repetitive bridge structures in typical SfM process. To resolve the ambiguity in the feature matching process, we introduced a feature clustering mechanism that utilizes GPS coordinates extracted from image metadata to reduce the misregistration. To mitigate point clouds curvature caused by the radial distortion ambiguity, we implemented the camera model [16] that estimates the intrinsic matrix including the distortion coefficient. In the final mesh modeling process, a *digital depth model* is generated to allow users to create orthographic views from any user-defined view necessary for inspection (e.g., under the deck view or side view). The *digital depth model* is presented in the form of a raster image with pixels representing depth value arranged in rows and columns. The images are stitched together along the seam lines with the correction of radial and depth distortion utilizing the digital depth model.

3.4 Damage Detection, Localization and Mapping

We use the Faster-RCNN architecture [17] and present a new algorithm to detect, localize, and determine the 3D spatial mapping of each type of damage. The detection output is a predicted label with its bounding box and score. In our new method, these outputs are projected into the 3D point clouds and back-projected to all related images to analyze intersected area and then fed into the 3D spatial mapping algorithm to determine final labels for each fragment in the 3D point cloud (Fig. 2).

Faster-RCNN includes a Region Proposal Network (RPN) and an object detection network Fast-RCNN, which shares a backbone CNN to form a unified network. The backbone CNN architecture is initialized with a pretrained network (e.g., VGG, Alexnet, ResNet) and fed with input images to extract feature maps. The RPN utilizes the feature maps to generate region proposals by sliding a network with fully-connected $n \times n$ spatial windows, which are output as a lower-dimensional (512 for VGG, 1024 for Resnet) vector and fed into box-regression and box-classification layers. Translation and scale-invariant outputs are achieved using k anchor boxes set as a grid, and k regions are predicted simultaneously. Anchors are associated with three scales and three aspect rations and are generated at the center of the sliding window. Loss function for training of RPN is computed using eq. 1 with a binary class label assigned to each anchor box, where positive labels have Intersection over Union (IoU) over 70% with ground truth. The Feature Pyramid Network (FPN) utilizes deep CNN pyramidal feature hierarchy to build a semantically rich feature pyramid from low to high levels to both learn local and spatial features.

$$L\{d_i\},\{t_i\} = \frac{1}{N_{cls}} L_{cls} d_i, d_i^* + \lambda \frac{1}{N_{reg}} d_i^* L_{reg} t_i, t_i^* \quad (1)$$

where, i is the index of the anchors, d_i the corresponding predicted probability and the ground truth label d_i^* the binary classification of the anchor. t_i is the coordinate of the bounding boxes where t_i^* denotes the ground truth box associated with the positive anchor. L_{cls} is the classification loss and L_{reg} is the regression loss, while these two terms are normalized to N_{cls} and N_{reg} by batch size and total anchor locations.

3.5 3D Spatial Mapping

The 3D spatial mapping developed in this study helps eliminate the annotation and prediction inconsistencies. We utilize computer graphics techniques and camera projection matrices estimated in 3D reconstruction to localize the same damages. All defect bounding boxes from each data frame are projected to 3D space and back-projected to any images that contain the corresponding region. Ideally, all such back-projected boxes should perfectly align with the same defect, but due to errors in projection and defect detection, that is not the case. To address such errors and increase detection precision, we present an algorithm to identify the most probable back-projected boxes for each defect.

Three user-defined parameter thresholds are used for this purpose. An IoU threshold is used to identify bounding box clusters within a user-defined 3D spatial distance to limit reprojection error. Clustered bounding boxes over a threshold count are then processed by performing a greedy Non-maximum suppression (NMS) to choose the most probable box. This approach is first applied to the ground-truth bounding boxes obtained from annotations and then to the predicted detection bounding boxes. Ground-truth bounding box clusters with lower box count than the threshold are kept, and detection box clusters with lower box count than the threshold and lower IoU than the threshold are removed. Similar approach is also applied to the detection process.

3.6 Interactive Web-based Viewers for Inspection

The interactive web-based viewer is extended from [13] with added components specifically developed for the purpose of bridge inspection. In our system, the octree structure stores a point cloud in different hierarchical levels of detail for efficient rendering. The system automatically loads the points inside the user's field of view via a lazy scheme to reduce the loading speed.

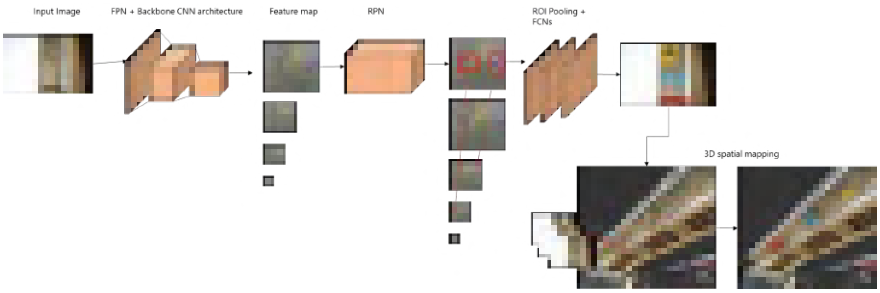

Figure 2. The network architecture. Feature maps extracted from backbone Resnet50, FPN are input to RPN. Bounding boxes with labels and scores as output from classifier mapped in 3D environment is re-injected to finalize prediction.

In addition to visual data collection planning and capture quality evaluation, the virtual walkthrough provides the necessary measurement capabilities for inspection. The image-based measurement tools utilize raycasting to find the closest point and backproject the point using the camera intrinsic, extrinsic to the image. We improved the raycasting accuracy by implementing a cylindrical ray with a radius r to get accurate results when the point cloud is sparser with varying depth. The web-based viewer also provides a non-linear transformation from 3D point clouds to 2D orthophoto using feature matches, estimated depth, and gravity direction from 3D reconstruction. A 4D (3D+time) point cloud timeline is formed chronologically by the capture date with the images, point clouds. Side-by-side or overlaid image comparison interface over time is also enabled by finding the closest image and transform it into the same coordinates using McMillan & Bishop warping method.

Per-pixel distance values are used to warp pixels to their correct location for the current camera position. Side-by-side or overlay views enable observation of defect progression over time and severity assessment for the inspectors.

3.7 Report Generation

Bridge inspection results are summarized in necessary reporting forms that (a) present schematic views of various bridge components and relative location and severity of defects; and (b) defect images as well as their associated inspection info. Our process leverages defect information and associated attributes already mapped in the 3D point cloud to speed up the generation of such reports. An image with a pin is automatically attached to the reports with associated information. These are exported as excel sheets with hyperlinks to the 3D location in the viewer. The related information includes properties such as severity, notes, inspector's name, and GPS location. Inspectors can easily access all the information that needs to be used to assess the defect from these excel sheets that follow owner reporting guidelines (fig. 3).

Our surface mapping tool creates 2D orthophoto from different viewpoints, facilitates the schematic drawing creation with more information than the traditional. The 2D orthophoto with the analysis of the inspected structure provides the overall status of the bridge in a short glance.

Figure 3. Examples of inspection forms (left) that require bridge elevation view to illustrate defect location and (right) detailed description of each defect with additional notes

4 Technical Validation

We validated the developed end-to-end system through 30 bridge inspection projects in Japan and the United States. In this section we present a couple of these projects for the purpose of demonstrating our results, mainly we show the qualitative and quantitative findings of deploying the new system to two Japanese bridge inspection projects. For each of the later projects, we focused on automatic defects detection for one of the bridge's spans covering the underside and lateral sides of the inspection region. Accordingly, detailed results for each stage of the inspection workflow are presented as follows.

4.1 Data Collection

The first step of bridge inspection system is using the developed web-interface to select the inspection region for each of the bridges, such region is selected by navigating a 2D map to the project location and using satellite images to define the boundary of the region. Next we set the data collection parameters as discussed in the method section, for instance, we provide an example of the parameters set for one of the bridges in Table 1.

Table 1. Flight plan parameters

Parameter	Value
Top offset	6 m
Bottom offset	3 m
Sides offset	4 m
Images overlap	80%
Drone battery life	20 mins
Drone speed	25 kph
Line-of-sight FOV	90°
Aerial platform	DJI Phantom4

The developed flight planning interface automatically generates a 3D flight plan with missions covering the top, lateral and under sides of the bride structure. The total flight distance and flight-time for the plan are 2,200 meters and 79 minutes respectively. We provide a visual representation for the later flight plan in Figure 4 which shows the 3D missions along with as-is point cloud model of the bridge.

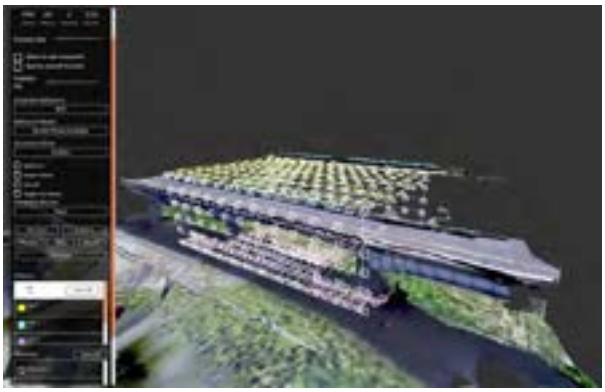

Figure 4. Generated 3D flight plan with top, bottom and one of the side missions visualized in unique colors.

4.2 Visual Quality Evaluation

Feedback for the visual quality of the data collection plan is presented in Figure 5 which provides an example of the visual feedback for visibility, resolution and orientation evaluations. For such task, the bridge mesh was divided into fine fragments that are color-coded to show the visual quality value for each fragment.

The visual evaluation criteria are set according to the requirements for bridge inspection, the later criteria and results of the evaluation feedback are shown in Table 2. 13 fragments found to be outside the acceptable criteria which happen to be on the ground and outside the inspection scope. In future iterations of the tool, we plan to remove these elements from the resolution evaluation process, thus, revisions and further modifications to the flight plan were not needed.

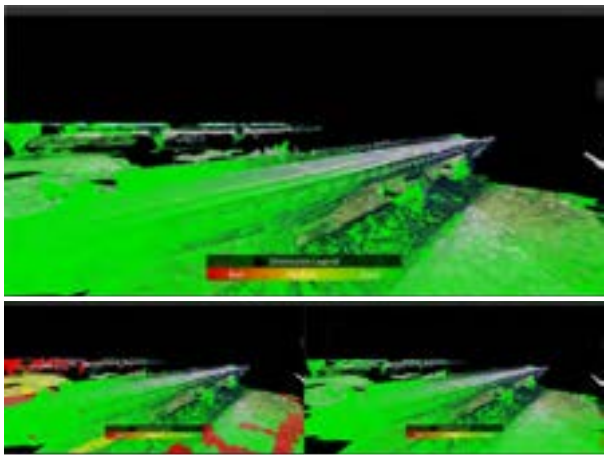

Figure 5. Color-coded visual feedback for data collection plan. (top) visibility evaluation, (bottom-left) resolution evaluation, and (bottom-right) orientation evaluation. The red region, being outside scope of evaluation, is ignored.

Table 2. Flight plan evaluation results

Metric	Criteria	# of elements	% of elements
Visibility	Not met ($<$ 3 observations)	13	16.88%
	Acceptable ($3-8$ observations)	3	3.90%
	Satisfactory ($\geq$ 8 observations)	61	79.22%
Resolution	Not met ($>$ 0.01 m/pix)	11	14.29%
	Acceptable ($0.005-0.01$ m/pix)	0	0.00%
	Satisfactory (≤ 0.005 m/pix)	66	85.71%
Orientation	Not met ($>45°$)	1	1.30%
	Acceptable ($15-45°$)	2	2.60%
	Satisfactory ($\leq 15°$)	74	96.10%

4.3 Damage Localization, Detection and Mapping

4.3.1 Dataset preparation and annotations

The image dataset was created from inspection images captured for the two bridges, the defects in these images were labelled into five common defect classes, namely: crack, spalling, efflorescence, corrosion stains and exposed rebar. For the annotation process, we extended Computer Vision Annotation Tool (CVAT) by integrating the collected dataset and specifying new labels. The inspection images were annotated by experts and validated by two reviewers per each annotation job following the quality assurance/control process in [18]. A total of 30 engineering experts served as annotators and reviewers in this study. Attributes of the resulted dataset are detailed in Table 3. For defect detection, the dataset was split into training and testing datasets with the 80/20 convention. A total of 653 images with 14,302 defect instances were used for training and 89 images with 4804 object instances for testing.

Table 3. Results from the annotation process and detection

Defect Class	Number of annotations	AP (%)	w/Mapping AP (%)
Spalling	5,013	84.6	85.3
Exposed rebar	1,545	84.5	85.2
Corrosion stains	3,310	74.1	74.9
Efflorescence	1,944	57.6	61.1
Crack	5,779	49.2	53.2

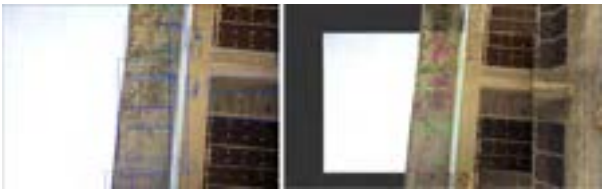

Figure 6. (Left): Results of the localization bounding-boxes for defects in green with projected boxes from other frames -generated through 3D mapping process- colored in blue; (Right) the final localized bounding boxes -after 3D mapping process- overlaid on registered image in 3D point cloud context.

4.3.2 Experimental Results and Discussions

FasterRCNN architecture was implemented using pytorch framework and was fine-tuned with MS-COCO object detection model to expedite initial training with six object classes including defects mentioned earlier and the background. The model was trained from scratch for each layer with the Stochastic Gradient Descent (SGD) optimizer. The learning rate was set using cosine annealing schedule cycling between 1e-5 to 1e-2 in every 10 epochs to avoid local minimum and overfitting. Results of the detection are shown in Fig. 6.

Average Precision (AP) is then calculated by dividing count of true positive detections over all positive detections and is used to evaluate the detection results. The average precision values from the detection are summarized in Table 3. NMS removes some detection boxes not meeting threshold earlier defined leading to reduced total detections. NMS parameters were fine-tuned to balance trade-off for best result.

3D spatial mapping was found to increase the AP for crack and efflorescence by more than 4% with improvements in all defect types (Table.3). Detection results are also continuously improved through user inputs provided through the interactive web viewer such as verification of correct defects and adding missing detections for documentation and reporting by expanding dataset and detection model retraining.

4.4 Web-based Viewer and Inspection Reports

We adopted Charette test method [19] to evaluate the user's feedback about the web-viewer and report generation process. The validation works by evaluating *effectiveness*, *repeatability*, and *reliability* of our method, which measure productivity improvement, performance of system under different inspection conditions and users. These were measured qualitatively through interviews and observations from MLIT practitioners interacting with the system. We have provided training and guidelines for bridge inspectors, transportation professionals and civil engineers to perform virtual inspection tasks. Users expressed through the training that time required for defect localization and creating reports using corresponding images was significantly reduced. Users also expressed that the output generated can be easily transformed to actionable format which is vital for effective bridge maintenance.

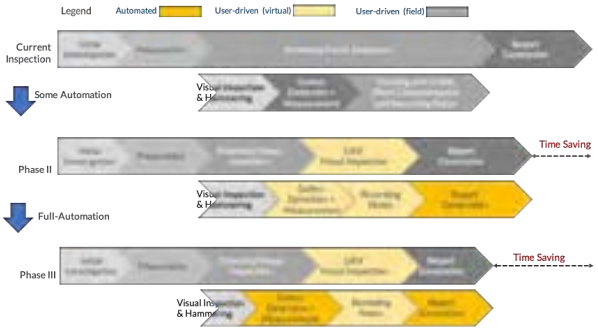

Figure 7. The MLIT in Japan has outlined a three-phase path towards a fully automated bridge inspection process, where more automation is introduced one step at a time. Currently, Phase II is in full testing mode with the solution presented in this paper.

5 Discussion - Gradual Transition to a Fully Automated System

The components of the presented system were deployed on bridge inspection projects in Japan and the United States. Based on discussion and interviews with bridge inspectors, Japan MLIT has decided to engage in a gradual transition from their current workflow to full automation, due to the many components, bridge owners, and engineering personnel involved. Fig. 7 shows MLIT's plan and perceived benefit from this transition.

In the current workflow, inspectors spend significant time measuring, capturing and organizing damages and related information. Phase II will involve automating data collection and report generation processes consisting of the robotic solutions that collect and process the data in the web-based system. The system will also actively improve the automatic defect detection through (a) user input of correcting and adding missing detections, and (b) retraining of detection model on a timely basis over more massive ground truth datasets. Phase III will introduce automated pre-analysis of bridge condition, 3D reconstruction, defect

detection, and report generation. Analyzed data will be used for verification of condition and to perform physical examinations on the field. Full adaptation of automation by Phase III is expected to cause substantial time savings (30% based on Charettes) and cost-savings in the inspection process. A reliable defect detection component is an essential step towards Phase III.

We have shown in this study that the data collection process improves the visual quality of collected data to meet MLIT inspection and report generation requirements. Future work will focus on improvements of the flight plan optimization by eliminating user manual inputs, the evaluation process by removing simulated fragments that are not in the inspection scope, the detection model by phased rollouts of improved models, and expansion of ground-truth dataset with a generalized distribution of defect shapes, colors and incorporating 3D geometry information in the detection process.

6 Conclusion

We presented an end-to-end system to automate robotic bridge inspection process with integration of flight mission generation, assessment of visual quality of collected data, ensuring accuracy and completeness of reconstructed reality model, 3D reconstruction for elevated structures, automated detection and localization of damages and report generation. Our proposed system shows the connections between components and how robotic bridge inspection solutions can be streamlined systematically and gradually. We introduced the phase-based implementation of detection models that enables continuous improvement and active learning over time through dataset expansion and user input. Our holistic approach through the proposed end-to-end system connects the dots between the components of robotic bridge inspection for the MLIT in Japan. We plan to implement this system across 100s of bridges in the coming year.

References

[1] MLIT. Annual Road Maintenance Report, 2019. URL https://www.mlit.go.jp/road/sisaku/yobohozen/pdf/h30/1-2.pdf.

[2] Henk Freimuth and Markus König. Planning and executing construction inspections with unmanned aerial vehicles. *Automation in Construction*, 96:540–553, 12 2018. ISSN 09265805. doi:10.1016/j.autcon.2018.10.016.

[3] Amir Ibrahim, Dominic Roberts, Mani Golparvar-Fard, and Timothy Bretl. An Interactive Model-Driven Path Planning and Data Capture System for Camera-Equipped Aerial Robots on Construction Sites. *International Workshop for Computing in Civil Engineering (IWCCE 2017)*, pages 117–124, 2017.

[4] Yuting Chen, Jiansong Zhang, and Byung-Cheol Min. Applications of BIM and UAV to Construction Safety. In *7th CSCE International Construction Specialty Conference, Laval, QC, Canada*, pages 1–7, 2019.

[5] R. S. Adhikari, O. Moselhi, and A. Bagchi. Image-based retrieval of concrete crack properties for bridge inspection. *Automation in Construction*, 39:180–194, 2014. ISSN 09265805. doi:10.1016/j.autcon.2013.06.011. URL http://dx.doi.org/10.1016/j.autcon.2013.06.011.

[6] J.J. Jacob J. Lin, Kevin K.K. Han, and Mani Golparvar-Fard. A Framework for Model-Driven Acquisition and Analytics of Visual Data Using UAVs for Automated Construction Progress Monitoring. In *Computing in Civil Engineering 2015*, pages 156–164, 2015. ISBN 978-0-7844-0794-3. doi:doi:10.1061/9780784407943.

[7] Amir Ibrahim and Mani Golparvar-Fard. 4D BIM Based Optimal Flight Planning for Construction Monitoring Applications Using Camera-Equipped UAVs. In *Computing in Civil Engineering 2019*, pages 217–224, 2019. doi:10.1061/9780784482438.028.

[8] Yahui Liu, Jian Yao, Xiaohu Lu, Renping Xie, and Li Li. DeepCrack: A deep hierarchical feature learning architecture for crack segmentation. *Neurocomputing*, 338:139–153, 4 2019. ISSN 18728286. doi:10.1016/j.neucom.2019.01.036.

[9] Guido Morgenthal, Norman Hallermann, Jens Kersten, Jakob Taraben, Paul Debus, Marcel Helmrich, and Volker Rodehorst. Framework for automated UAS-based structural condition assessment of bridges. *Automation in Construction*, 97:77–95, 1 2019. ISSN 09265805. doi:10.1016/j.autcon.2018.10.006.

[10] Mohamad Alipour, Devin K. Harris, and Gregory R. Miller. Robust Pixel-Level Crack Detection Using Deep Fully Convolutional Neural Networks. *Journal of Computing in Civil Engineering*, 33(6):4019040, 11 2019. doi:10.1061/(ASCE)CP.1943-5487.0000854. URL https://doi.org/10.1061/(ASCE)CP.1943-5487.0000854.

[11] Allen Zhang, Kelvin CP Wang, Yue Fei, Yang Liu, Siyu Tao, Cheng Chen, Joshua Q. Li, and Baoxian Li. Deep Learning–Based Fully Automated Pavement Crack Detection on 3D Asphalt Surfaces with an Improved CrackNet. *Journal of Computing in Civil Engineering*, 32(5):4018041, 9 2018. doi:10.1061/(ASCE)CP.1943-5487.0000775. URL https://doi.org/10.1061/(ASCE)CP.1943-5487.0000775.

[12] Young-Jin Cha, Wooram Choi, and Oral Büyüköztürk. Deep Learning-Based Crack Damage Detection Using Convolutional Neural Networks. *Computer-Aided Civil and Infrastructure Engineering*, 32(5):361–378, 5 2017. ISSN 1093-9687. doi:10.1111/mice.12263. URL https://doi.org/10.1111/mice.12263.

[13] Jacob J. Lin and Mani Golparvar-Fard. Visual data and predictive analytics for proactive project controls on construction sites. In *Lecture Notes in Computer Science (including subseries Lecture Notes in Artificial Intelligence and Lecture Notes in Bioinformatics)*, volume 10863 LNCS, pages 412–430. Springer Verlag, 6 2018. ISBN 9783319916347. doi:10.1007/978-3-319-91635-4_21.

[14] Dušan Isailović, Vladeta Stojanovic, Matthias Trapp, Rico Richter, Rade Hajdin, and Jürgen Döllner. Bridge damage: Detection, IFC-based semantic enrichment and visualization. *Automation in Construction*, 112:103088, 4 2020. ISSN 09265805. doi:10.1016/j.autcon.2020.103088.

[15] Mani Golparvar-Fard, Feniosky Peña-Mora, and Silvio Savarese. Automated Progress Monitoring Using Unordered Daily Construction Photographs and IFC-Based Building Information Models. *Journal of Computing in Civil Engineering*, 29(1):04014025, 1 2015. ISSN 0887-3801. doi:10.1061/(ASCE)CP.1943-5487.0000205. URL http://ascelibrary.org/doi/10.1061/%28ASCE%29CP.1943-5487.0000205.

[16] Duane C. Brown and Duane C. Brown. Close-range camera calibration. *PHOTOGRAMMETRIC ENGINEERING*, 37(8):855–866, 1971. URL http://citeseerx.ist.psu.edu/viewdoc/summary?doi=10.1.1.14.6358.

[17] Shaoqing Ren, Kaiming He, Ross Girshick, and Jian Sun. Faster R-CNN: Towards Real-Time Object Detection with Region Proposal Networks. *IEEE Transactions on Pattern Analysis and Machine Intelligence*, 39(6):1137–1149, 6 2017. ISSN 01628828. doi:10.1109/TPAMI.2016.2577031.

[18] Kaijian Liu and Mani Golparvar-Fard. Crowdsourcing Construction Activity Analysis from Jobsite Video Streams. *Journal of Construction Engineering and Management*, 141(11):04015035, 11 2015. ISSN 0733-9364. doi:10.1061/(ASCE)CO.1943-7862.0001010. URL http://ascelibrary.org/doi/10.1061/%28ASCE%29CO.1943-7862.0001010.

[19] Mark Clayton, John Kunz, and Martin Fischer. The charrette test method. Technical report, 1998.